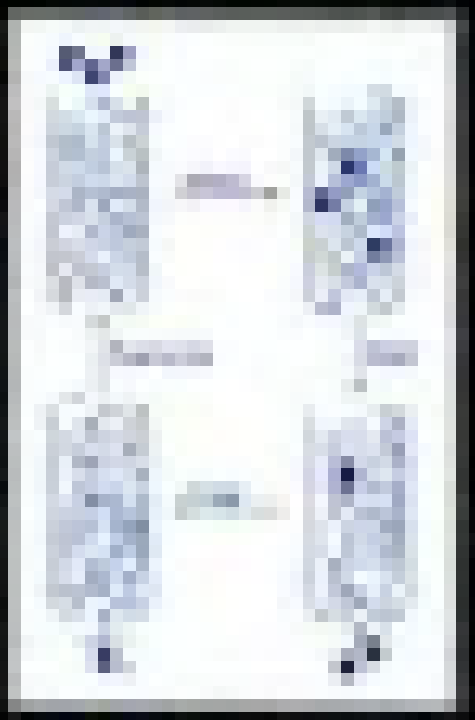
Handbook of HPLC



edited by
Barry Boyes
Greg Bynum
Peter Schoenmakers
Rod Simpson

PREFACE

During the last decade, high-performance liquid chromatography (HPLC) has become the analytical method of choice for product separation, purification, and detection in many areas such as pharmaceuticals, biotechnology, environmental monitoring, and applied research.

The development and availability of HPLC columns of different geometries and various stationary phases have been accompanied by the development of rugged and reliable HPLC instrumentation, the performance of which is now compatible with that of the modern, highly efficient columns.

Many excellent, but specialized, books devoted to both HPLC theory and applications have been published. This handbook encompasses all the aspects of the method, presented in four parts: fundamentals, HPLC techniques, instrumentation, and applications. Part I, fundamentals, covers the HPLC theory that is necessary to understand in order to successfully practice the method. Part II, HPLC techniques, discusses different HPLC modes—reversed-phase HPLC and ion-exchange, size exclusion HPLC among others—and critically addresses their applicability and limitations, with the emphasis on how to select an appropriate technique to achieve desirable solutions. Part III, instrumentation, describes the principles and practical operations of modern HPLC equipment: pumps, detectors, injection devices, and data handling systems. Part IV, applications, covers a comprehensive array of the HPLC applications in different areas of industry and applied research. All the chapters contain extensive lists of tables and references.

CONTENTS

Preface iii

Contributors ix

Part I. Fundamentals

1. Retention and Selectivity 1
Andreas Rizzi

2. The Mechanisms and Importance of Zone-Spreading 55
Robert Tijssen

3. Principles of Detection 143
Wim Th. Kok

4. Capillary Electrophoresis 169
Herbert E. Schwartz And Bart J. Wanders

5. Programmed Analysis 193
Peter Schoenmakers

6. Computers and Liquid Chromatography 233
J. Strauters

Part II. HPLC Techniques

7. Size Exclusion Chromatography 273
Howard G. Barth

8. Reversed-Phase HPLC: Preparation and Characterization of Reversed-Phase Stationary Phases 293
Charles A. Doyle And John G. Dorsey

9. Normal-Phase Liquid Chromatography 325
Marcel Caude And Alain Jardy

10. HPLC of Ions: Ion-Exchange Chromatography 365
Robert E. Smith

11. Ion Chromatography by HPLC 413
Donald J. Pietrzyk

12. Hydrophobic Interaction Chromatography of Biopolymers 463
Ziad El Rassi

13. Affinity Chromatography 483
David S. Hage

Part III. HPLC Instrumentation

14. Mobile-Phase Delivery Systems for HPLC 499
Robert L. Stevenson

15. Liquid Chromatography Detectors 531
Raymond P. W Scott

16. Injection Devices 559
Richard A. Henry

17. Tandem Liquid Chromatography Systems 581
Raymond P. W. Scott

18. Temperature Control in Analytical High-Performance Liquid Chromatography 607
Joel K. Swadesh

19. Collection Devices 617
Gordon S. Hunter

Part IV. HPLC Applications

20. HPLC Application of Drugs in Biological Samples 629
James T. Stewart

21. HPLC Applications for Chiral Pharmaceutical Analysis 669
Curt Pettersson And Bengt-Arne Persson

22. HPLC Applications in Biotechnology 695
John C. Ford

23. HPLC Applications in Food and Nutritional Analysis 753
Kenneth A. Berg And Carlos E. Cuevasa

24. HPLC Analysis of Surfactants 789
Thomas M. Schmitt

25. HPLC Applications to the Analysis of Ions and Inorganic Species 805
Charles A. Lucy

26. HPLC Application to Polymer Analysis 831
Sadao Mori

27. HPLC Applications in Physicochemical Measurements 859
Klára Valkó

28. HPLC Applications in Art Conservation 903
Suzanne M. Halpine

29. Sample Handling and Analysis of Organic Pollutants (Pesticides and Phenols) in Water Matrices by HPLC 929
Silvia Lacorte, David Puig, And Damiá Barceló

Index 975

1

Retention and Selectivity

Andreas Rizzi

University of Vienna, Vienna, Austria

I. PRINCIPLES OF DISTRIBUTION AND ADSORPTION

Chromatographic separation can be attained for compounds that migrate at different speeds through a "chromatographic bed." The phenomenon of different migration velocities is based on different *retentions* of the migrating compounds ("separands" or "analytes") caused by the elementary process of different distributions of the separands between two phases: a mobile phase and a stationary phase.

In liquid chromatography (LC), the mobile phase is a liquid. The corresponding stationary phases consist predominantly of solid surfaces. These surfaces can be the original support materials themselves, or they may consist of various chemical structures attached to the support materials. (Such modifications are discussed in detail later.) This type of chromatography is addressed as *liquid–solid chromatography* (LSC). [In the physicochemical treatment, the total stationary phase, beyond the surface of the adsorbent, is considered to also include the first adsorbed layers of the mobile phase.]

In a different type of chromatography, which nowadays is used only in very few practical applications of classic chromatography [1,2], the stationary phase is also a liquid, which is adsorbed as a bulky film onto a solid support. Stationary liquid-phase and mobile liquid–phase are immiscible; their equilibrium composition is interrelated by the tie-lines (connodes) of the miscibility gap. Mobile and stationary phases employed are usually at least ternary mixtures, occasionally including polymeric components [1]. This type of chromatography is addressed as *liquid–liquid chromatography* (LLC). In "ideal" LLC the influence of the surface on the partition equilibrium is negligible. Partition between two liquid phases is also the basis of countercurrent chromatography [3]. In this technique, the liquid stationary phase is not adsorbed onto any support material, but the liquid mobile phase moves through the stationary liquid (e.g., in the form of upstreaming liquid bubbles or by motion in a helical coil). All commonly used experimental techniques use density differences between the two liquid phases as driving forces for phase movement.

To distinguish between the LSC and LLC distribution equilibria, one can call the first one an adsorption equilibrium, the second one a partition equilibrium.

A. Retention Factor and Distribution Coefficients

Chromatographic separation is based on a continuous sequence of equilibrium distribution steps that cause the analytes to migrate at different speeds through the chromatographic bed. Their migration velocity is given by the fundamental equation:

$$u_i = u_0 \left(\frac{1}{1 + k_i} \right) \tag{1}$$

where u_0 is the average migration velocity of the mobile-phase components, and k_i the *retention factor* or *capacity factor* of the considered component. The retention factor is equal to the *distribution coefficient* of the compound i between a stationary (superscript s) and a mobile (superscript m) phase in terms of *masses* m, or *moles* n.

$$k_i = \frac{m_i^s}{m_i^m} = \frac{n_i^s}{n_i^m} \tag{2}$$

The term $1/(1 + k_i)$ reflects the fraction of analyte molecules present in the mobile phase, or—equally—the fraction of time each analyte molecule spends in the mobile phase. The corresponding fraction of time every analyte molecule spends in the stationary phase is given by $k_i/(1 + k_i)$.

From the migration velocity of a component [see Eq. (1)] the *retention time*, t_{Ri}, of the considered component is obtained by

$$t_{Ri} = \frac{r^2 \pi \varepsilon_m L}{u_0} (1 + k_i) = t_{R0}(1 + k_i) \tag{1b}$$

where r is the inner diameter of the column and L its length, ε_m the porosity of the column bed (about 0.7–0.8) and t_{R0} the holdup time of a nonretained compound (e.g., eluent component). This equation evaluates the retention factor values from the measured retention time values according to

$$k_i = \frac{t_{Ri}}{t_{R0}} - 1 \tag{1c}$$

The holdup time of a nonretained compound is expected to slightly change with the composition of the mobile phase owing to the adsorbed solvent layer (see later in this chapter) [4]. To achieve accurate values for t_{R0} one has to make sure that the used marker component is really unretained. Frequently, the detector signals resulting from eluent components injected in concentrations differing from the eluent composition are used for this purpose. Particularly, the accurate calculation of very low retention factors needs an accurate determination of t_{R0} values.

Conventionally, distribution constants can also be defined in terms of other units; for instance, ${}^cK_i$, which stands for the distribution coefficient in terms of molar concentrations, c; and ${}^xK_i$, which is the distribution coefficient in terms of mole fractions x.

$${}^cK_i = \frac{c_i^s}{c_i^m} \tag{3a}$$

$${}^xK_i = \frac{x_i^s}{x_i^m} \tag{3b}$$

${}^cK_i$ is interrelated with the retention factor k_i by

$$k_i = {}^cK_i q \tag{4a}$$

where q is the phase ratio. In LLC, q is defined as the ratio of stationary phase volume V^s to mobile-phase volume V^m. In LSC, q is the ratio of the surface area A^s to mobile-phase volume V^m. (When using c_i^s in mol/m^2, ${}^cK$ in LSC has the dimension of [m^{-1}].)

$$q^{(\mathrm{LLC})} = \frac{V^s}{V^m} \qquad \text{and} \qquad q^{(\mathrm{LSC})} = \frac{A^s}{V^m} \tag{4b}$$

For strongly diluted analyte solutions, the analyte concentration is related to its mole fraction by the following approximate relation:

$$x_i \approx c_i v \tag{5a}$$

where v is the mean molar volume of the considered phase.

From Eq. (5a), the retention factor can be related to the distribution coefficient in terms of mole fractions ${}^xK_i$ by Eq. (5b)

$$k_i = {}^xK_i \frac{v^m}{v^s} q = {}^xK_i \frac{n^m}{n^s} \tag{5b}$$

v^m and v^s indicating the mean molar volume of the indicated phases, and n^m and n^s the respective mole number. In LSC, v^s represents the mean surface area occupied by 1 mol of the predominantly adsorbed solvent.

Selectivity in chromatography is discussed in terms of the *selectivity coefficient* (or *separation factor*) between a pair of components $r_{j,i}$, which is defined as the ratio of the capacity factors of the two compounds considered j and i.

$$r_{j,i} = \frac{k_j}{k_i} \tag{6}$$

Table 1 summarizes the basic definitions of the various distribution coefficients and the equations interrelating them with the retention factor.

Table 1 Definition Equations for Retention Factor and Various Other Forms of Distribution Coefficients

Distribution coefficient	Symbol	Definition	Relations
Retention factor, capacity factor, mass distribution coefficient	k_i	$k_i = \frac{m_i^s}{m_i^m} = \frac{n_i^s}{n_i^m}$	
Distribution coefficient in units of molar concentrations	${}^cK_i$	${}^cK_i = \frac{c_i^s}{c_i^m}$	$k_i = {}^cK_i q$
			$q^{(\mathrm{LSC})} = \frac{A^s}{V^m}$
Distribution coefficient in mole fractions	${}^xK_i$	${}^xK_i = \frac{x_i^s}{x_i^m}$	$k_i = {}^xK_i \frac{n^m}{n^s}$ [a]
Separation factor, selectivity coefficient	$r_{j,i}$	$r_{j,i} = \frac{k_j}{k_i}$	
		$r_{j,i} = \frac{{}^cK_j}{{}^cK_i} = \frac{{}^xK_j}{{}^xK_i}$	

[a]For strongly diluted analyte solutions.

B. Distribution Coefficients and Chemical Potentials in Solutions

The thermodynamic equilibrium condition for the distribution of an analyte between two phases (denoted by the superscripts m and s) is that the chemical potentials of the analyte μ_i, in the two phases are equal. (Throughout this volume, the index i indicates the analyte.)

$$\mu_i^m = \mu_i^s \tag{7}$$

In liquid mobile phases the chemical potential of a component is related to its concentration (mole fraction) by Eq. (8):

$$\mu_i^m = \mu_i^{o,m} + RT\ln x_i^m\gamma_i^m = \mu_i^{o,m} + RT\ln a_i^m \tag{8}$$

where $\mu_i^{o,m}$ is the chemical potential of the compound i in a standard state, and γ_i^m is the *activity coefficient* of the compound i. The numerical value of the activity coefficient is dependent on the chosen standard state and varies with the composition of the phase. The product of x and γ is called the activity a.

If we consider a partition equilibrium between two liquid phases, the chemical potential in the liquid stationary phase is described by an analogous equation, replacing the superscript m by s. When choosing the pure analyte as the standard state, as is most frequently done when dealing with nonelectrolytes and organic compounds in mixed solvents [5], the standard-state potential $\mu_i^{o,m}$ becomes equal in both liquid phases. From Eqs. (7) and (8) it then follows that in equilibrium

$$x_i^m\gamma_i^m = x_i^s\gamma_i^s \tag{9}$$

The *partition coefficient between two liquid phases* is then obtained as

$${}^xK_i = \frac{x_i^s}{x_i^m} = \frac{\gamma_i^m}{\gamma_i^s} \tag{10}$$

The partition of analytes between two liquid phases is thus seen to be totally governed by the magnitude of the activity coefficients which, in turn, are determined by the excess Gibbs free energies g^E, associated with the intermolecular interactions in solutions. The free energy comprises enthalpic and entropic contributions. At this stage, it is important to realize two points: (1) The lower the activity coefficients of the analytes in a given phase, the higher is their "affinity" for this phase; and (2) the activity coefficients of any component in a solution change on variation of the solution's composition, and so does the partition coefficient ${}^xK_i$ (Eq. 10). A qualitative discussion on activity coefficients will be given in Section I.D. Before a deeper discussion on activity coefficients, however, an equation analogous to Eq. (10) will be derived for adsorption equilibria, which enables us to understand the role of solvent components in LSC systems.

C. Distribution Coefficients in Adsorption from Solution

Most theories of adsorption from solution onto solid surfaces start from a monolayer-type adsorption model and the fundamental assumption of a displacement reaction. In this displacement reaction, it is assumed, for a surface in equilibrium with a liquid phase, that, upon adsorption of a further component, a corresponding number of adsorbed molecules (e.g., solvent molecules) have to be desorbed. Such a displacement reaction involves analyte components as well as all the different solvent components in a mixture [6–8]. In the basic theories, *energetic homogeneity* of the surface (i.e., equal adsorption energy of a compound on all sites of the surface) is frequently assumed.

Equation (11) gives the displacement reaction by which a compound i (e.g., an analyte i or a solvent component) is adsorbed onto the surface displacing a component A (e.g., a solvent component) from the adsorbed state.

$$i^m + \nu_{i,A}A^x \leftrightarrow i^s + \nu_{i,A}A^m \tag{11}$$

The superscripts s and m indicate here the compounds being in the surface phase and the liquid bulk phase, respectively. The stoichiometric number of molecules involved in this reaction depends on the relative sizes of the surface areas occupied per mole of the different compounds. This is accounted for by introducing stoichiometric factors ν into Eq. (11).

The displacement reaction [see Eq. (11)] can be described by the corresponding equilibrium constant $K_{i,A}$ (indicating, that compound i displaces compound A). $K_{i,A}$ is called the *competitive adsorption constant.*

$$K_{i,A} = \frac{x_i^s (x_A^m)^{\nu_{i,A}}}{x_i^m (x_A^s)^{\nu_{i,A}}} \tag{12a}$$

To keep the treatment simple we assume equal stoichiometric numbers (i.e., $\nu_{i,A} = 1$) in the following discussion. This results in

$$K_{i,A} = \frac{x_i^s x_A^m}{x_i^m x_A^s} \tag{12b}$$

The competitive adsorption constant measures the relative strength of adsorption of two compounds competing for the adsorption sites. From Eq. (11) follows that $K_{A,i} = 1/K_{i,A}$. The higher the competitive constant $K_{A,i}$, the stronger is the displacing power of the solvent component A relative to the component i.

If we introduce the simple boundary condition that the sum of mole fractions in each phase is 1 (and keeping in mind that $K_{A,i} = 1/K_{i,A}$) rearrangement of Eq. (12) yields an equation for the *adsorption isotherm* of component i.

$$x_i^s = \frac{x_i^m}{(x_i^m + K_{A,i}x_A^m)} \tag{13}$$

The adsorption isotherm correlates the concentration (mole fraction) of a compound at the surface (stationary phase) with its concentration in the bulk phase (mobile phase). From the adsorption isotherm the distribution coefficient of the compound ${}^xK_i$, between the surface and the bulk phase is readily obtained and is given as a function of the analyte concentration in the bulk phase.

$${}^xK_i = \frac{1}{(x_i^m + K_{A,i}x_A^m)} \tag{14}$$

For very dilute analyte solutions Eq. (14) simplifies to

$${}^xK_i = \frac{1}{K_{A,i}x_A^m} \approx K_{i,A} \tag{15}$$

so that the adsorption isotherm becomes linear in the region of strong dilution.

$$x_i^s = K_{i,A}\, x_i^m \tag{16}$$

The graph of the adsorption isotherm for a binary mixture according to Eq. (13) is shown in Fig. 1 choosing various values of the competitive adsorption constant $K_{i,A}$. The shown isotherms illustrate two important points: (1) If we consider that the two competing components are two solvent components, then the isotherm illustrates the preferential coverage of the surface by the stronger adsorbed solvent component as dependent on its concentration in the liquid bulk phase. This component will exhibit high mole fractions in the adsorbed layer x^s, even at rather low concentrations in the bulk phase x^m. (2) When we consider that the minor component is the analyte, then the isotherm illustrates how the slope and, thus, the

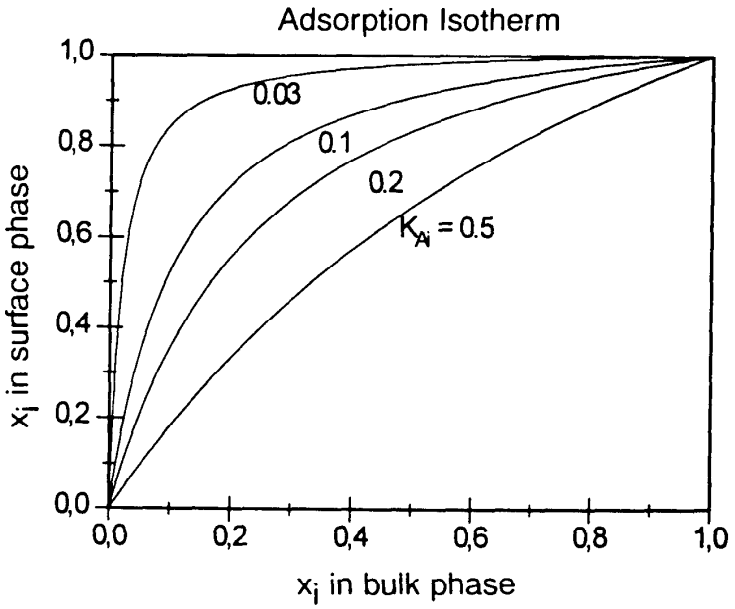


Figure 1 Adsorption isotherms for the stronger-adsorbed component in a binary liquid mixture according to Eq. (13). Competitive adsorption constants, $K_{A,i}$, are 0.5, 0.2, 0.1, and 0.03, respectively.

distribution coefficient of the analyte between the two phases decreases with increasing analyte concentration in the bulk phase.

An analogous treatment for mixed mobile phases yields Eq. (17) when introducing some (minor) approximations.

$$^{x}K_i = \frac{1}{\Sigma_n(K_{n,i}x_n^m)} \tag{17}$$

The subscript n indicates the solvent components and i the analyte. This equation describes the influence of solvent composition on analyte distribution in liquid–solid systems, assuming competitive adsorption. The equation shows, that the competitive effect of a solvent component, n, is stronger, if the corresponding competitive adsorption constant $K_{n,i}$ and the concentration of this component in the bulk phase x_n^m are higher. On the basis of this equation the predominant influence of eluent components with high competitive adsorption constants on the retention of analytes can be understood.

The only basis for Eq. (17) was the competitive adsorption of solution components, as described by the displacement reactions within a monolayer model. To obtain a more complete description of adsorption from solution, one must account for changes in solvation associated with the adsorption process (i.e., for changes in the activity coefficients of the components on adsorption). This is done by replacing all mole fractions in Eq. (17) by the corresponding activities [see Eq. (8)], yielding Eq. (18).

$$^{x}K_i = \left(\frac{\gamma_i^m}{\gamma_i^s}\right)\frac{1}{\Sigma_n[K_{n,i}x_n^m(\gamma_n^m/\gamma_n^s)]} \tag{18}$$

In this equation, γ_i^s stands for the activity coefficient of the compound i in the adsorbed layer, accounting for intermolecular interactions of compound i with those solvent molecules that form this adsorption layer and that partially surround the adsorbate. Generally, γ_i^m and γ_i^s differ in their values because the solvent composition in the bulk phase is different from that in the adsorbed layer (see Fig. 1). This is a consequence of the preferential adsorption of the

solvent components with the highest adsorption constants (usually called *modifiers*) according to the fundamental concept of competitive adsorption.

Activity coefficients in the surface layer cannot easily be assessed numerically [9,10]. However, the preferential adsorption of solvent components implies that, in most instances (and with the exception of very low modifier concentrations), the surface activity coefficients of analytes do not change much with the modifier concentration in the bulk phase. This is unlike the corresponding mobile-phase activity coefficient of the analyte.

Accounting for the stoichiometric factors $\nu_{n,i}$ for each pair of components in the solution [see Eq. (11)] (and introducing further approximations) results in an equation analogous to Eq. (18), in which each (solvent-associated) term of the sum in the denominator is powered by the corresponding stoichiometric factor $\nu_{n,i}$. The approximate size of the stoichiometric numbers cannot be assessed by the ratio of the molecular volumes of the adsorbates, for generally a preferential orientation of the adsorbates on the surface must be assumed. Because of this preferential orientation, the stoichiometric factors will often not be as different from unity as might be expected simply on the base of the molecular volumes.

Heterogeneity of the surface relative to adsorption energies of various sites has been accounted for in a more refined model [11]. This, however, is much more complex and thus beyond the scope of the present chapter. The energetic heterogeneity of surfaces may play an important role at very low concentrations of modifiers in the eluent.

D. Solvation of Analytes: Activity Coefficients in Mixed Liquid Phases

Distribution equilibria in LLC and LSC are governed, to a great extent, by the activity coefficients of the analytes, as has been indicated by Eqs. (10) and (18). Activity coefficients account for deviations from ideal mixing behavior in liquid mixtures; they are related to the partial molar excess Gibbs free energy in a mixture g_i^E [5] by

$$\ln \gamma_i = \frac{g_i^E}{RT} \tag{19}$$

Activity coefficients of analytes reflect the strength of intermolecular interactions between analyte and solvent components in comparison with the strength of interaction between the solvent components and analyte components themselves. They further account for differences in the sizes of the molecules in the mixture. In this sense, activity coefficients incorporate contributions arising from both enthalpies and nonideal entropies of mixing.

The numerical value of the activity coefficient of a compound in a liquid mixture is a function of the composition of the mixture, including the mole fraction of the component under consideration. For chromatographic discussions, the most important component is the analyte, which most often appears in very dilute solution. It is thus useful to discuss the activity coefficient of analytes at high dilution. At very low concentrations of analyte ("infinite dilution") γ assumes a (constant) value, defined as the *limiting activity coefficient.*

Activity coefficients can be experimentally obtained from vapor pressure or solubility data. At infinite dilution and with volatile analytes, they are usually obtained by headspace analysis. These measurements require a considerable experimental effort if the systems of interest are more complex than simple binary or ternary mixtures. Activity coefficient data for such simple mixtures are addressed here to illustrate the correlation between the chemical structures of the components in a liquid and the approximate magnitude of their activity coefficients.

1. Approximate Magnitude of Activity Coefficients

Table 2 lists limiting activity coefficients for simple binary systems collected from the literature [19,20, and Refs. in 18]. The table illustrates the variation of activity coefficients with analyte and solvent structure.

Table 2 Activity Coefficients of Analytes at Infinite Dilution in Pure Solvents at 25°C

Analyte	Solvent	γ_i^∞	Analyte	Solvent	γ_i^∞
Effect of functional groups					
Ethanol	Heptane	49.0	Heptane	Ethanol	16.0
Acetone	Heptane	7.4	Heptane	Acetone	7.1
Benzene	Heptane	1.5	Heptane	Benzene	2.7
Acetone	Ethanol	2.3	Ethanol	Acetone	2.1
Benzene	Ethanol	6.6	Ethanol	Benzene	12.9
Ethanol	Water	3.5	Water	Ethanol	2.5
Acetone	Water	7.8	Water	Acetone	6.9
Benzene	Water	2,400	Water	Benzene	386
Pentane	Water	10,000	Water	Pentane	2,080
Effect of CH_2 groups in homologous compounds					
Ethanol	Water	3.5	Water	Ethanol	2.5
1-Propanol	Water	11.7			
1-Butanol	Water	48.2	Water	1-Butanol	3.8
1-Pentanol	Water	169			
1-Octanol	Water	11,000	Water	1-Octanol	4.5
1-Decanol	Water	210,000			
Benzene	Water	2,400	Water	Benzene	386
Toluene	Water	9,800			
Ethylbenzene	Water	42,000			
Pentane	Water	10,000			
Hexane	Water	34,000			
Heptane	Water	110,000	Water	Heptane	1,188
Octane	Water	420,000			
Ethanol	Heptane	49.0			
1-Butanol	Heptane	37.1			
Benzene	Heptane	1.5	Heptane	Benzene	2.7
Toluene	Heptane	1.4			
Effect of molecular shape and mole volume					
1-Propanol	Water	11.7			
2-Propanol	Water	6.5			
1-Butanol	Water	48.2			
2-Butanol	Water	24.7			

Source: Refs. 18–20.

The following simple rules are illustrated by the data in this table:

1. The more similar the mixture components are in terms of their chemical structure and "polarity," the lower are the (limiting) activity coefficients γ^∞.
2. In aqueous systems the dominant contribution to γ^∞ results from the CH_2 groups in the analyte. The logarithm of γ^∞ increases about linearly with the number of CH_2 groups in the analyte or with the size of the hydrophobic moiety in the analyte. [The dominant contribution of CH_2 groups to the activity coefficients in aqueous eluents is of great importance for the understanding of retention in reversed-phase chromatography, which is discussed in detail later in this chapter. It is a widely used form of liquid chromatography, in which the stationary phase has a low polarity, whereas the mobile phase is a highly polar, usually *aqueous* liquid mixture.]

3. In ethanol as solvent (and methanol and acetonitrile as well, although not shown in the table) the contributions of CH_2 groups in the analyte to γ^∞ are much smaller. A fairly linear increase of the logarithm of the activity coefficients with the number of CH_2 groups in the analyte (*n*-alkanes, *n*-alcohols, ketones, esters, and such) is observed not only in pure water, but also in mixed aqueous–alcohol (methanol, ethanol) mixtures. The slopes of these lines are significantly lower compared with pure water.

A physicochemical discussion of the data in Table 1 is given in the following:

The transfer of molecules from the pure state (the *pure state* is the usual standard state for nonelectrolytes with $\gamma = 1$) to the state of strong dilution in a surrounding solvent is almost always associated with a net need for free energy. In these cases, the activity coefficients for the analytes are greater than 1. In rare cases only, in which the energy gain by interactions between unequal mixing partners is greater than the mean value of energy associated with interactions between equal partners, activity coefficients are less than 1. Such strong solvation effects can be observed if hydrogen bridges can be formed or acid–base interactions can occur between unequal molecules, but not between equal ones.

For the mixing of liquid components, three steps may be distinguished conceptually. These are associated with either a gain in or a need of energy.

1. Energy is needed to eliminate the analyte molecules from their molecule clusters. The amount of energy required is proportional to the energy of vaporization of the analyte.
2. Energy is needed to break up the solvent structure to accommodate the incoming analyte. This energy demand is dependent on the strength of intermolecular interactions *between solvent molecules* and is further dependent on the size of the incoming analyte.
3. Energy is gained from the interaction of the analyte with the surrounding solvent molecules.

The breaking of the solvent structure for the uptake of the analyte compound is energy-consuming. The strong interaction between water molecules used as solvent is of particular importance. It can be seen as the dominant cause of the large activity coefficients in aqueous solutions found for those analytes for which this energy demand cannot be compensated by the energy gain resulting from the intermolecular interactions between the analyte and water. This is true for analytes with large nonpolar structures and no or only few polar moieties. The high net demands in free energy needed for the mixing of those nonpolar compounds with water is the reason for the so-called hydrophobic effect, which is of great importance in chromatography. The larger the structure within the analyte that has no energy-gaining interaction with water (*hydrophobic structures*), the higher the activity coefficients of the analyte. This is illustrated by Table 2.

2. The Solubility Parameter Model

Semiempirical equations based on concepts of molecular thermodynamics have been applied to mixed liquid systems to make predictions for the variation of activity coefficients with eluent composition [5,12–15] and to correlate activity coefficients with the chemical structure of analytes [16,17]. Several equations of varying complexity have been derived for these purposes. Some of these have been used for the calculation of limiting activity coefficients to study retention and selectivity in chromatographic systems. For this purpose the parameter sets have been previously optimized for the region of infinite dilution [18]. A detailed discussion of these topics cannot be given in this chapter. However, we will briefly discuss a concept, which is particularly illustrative for the purposes here and was developed long ago by G. Scatchard and J. Hildebrand; the concept of *solubility parameters* [12].

The main aspect of this concept is that the energy in a pure liquid is fully characterized by its *cohesive-energy density*, which is approximately equal to the energy of complete vaporization (to the ideal gas state), ΔU_i^V, divided by the molar volume of the liquid, v_i.

$$C_{i,i} = \frac{\Delta U_i^V}{v_i} \tag{20}$$

The square route of the cohesive energy density is the so-called solubility parameter δ_i.

$$\delta_i = \sqrt{C_{i,i}} \tag{21}$$

The cohesive energy density is rather low in liquids in which the molecules have no dipole moment and are not able to undergo charge–transfer interactions. Typical examples are alkanes and other molecules of low polarity. On the other hand, the cohesive energy density is high in liquids in which the molecules exhibit dipoles or hydrogen-bonding groups. A collection of solubility parameters of pure liquids is given in Table 3.

The main assumption within this concept is that an analogous total cohesive energy density can be defined for liquid mixtures. This is thought to be built up from contributions of interactions between equal molecules $C_{i,i}$, and nonequal molecules $C_{i,j}$, weighted by the probability of their occurrence. The $C_{i,j}$ values are approximately calculated by means of a mixing rule, which gives $C_{i,j}$ as a function of $C_{i,i}$ and $C_{j,j}$. The fascination of this concept lies in this particular aspect (i.e., that by means of this mixing rule, mixture data can be calculated and predicted from pure component data only). The choice of the equation for the mixing rule, however, is one of the most decisive points in the solubility parameter concept. Calculating $C_{i,j}$ simply as the geometric mean of the pure component values is a good approximation

Table 3 Solubility Parameters of Various Solvents

	δ (cal/cm^3)$^{1/2}$	
Solvent	25°C	20°C
Perfluorinated alkanes	6.0	
Neopentane	6.2	
n-Pentane	7.1	
n-Hexane	7.3	
n-Heptane	7.4	
Cyclohexane	8.2	
Carbon tetrachloride	8.6	
Toluene	8.9	
Benzene	9.2	
Styrene	9.3	
Chloroform	9.2	9.87
Acetone		10.51
Methylene chloride	9.8	10.68
Diethyl ether	7.4	
Diisopropyl ether		7.60
Ethyl acetate		9.57
THF		9.88
1,4-dioxane		10.65
n-Propanol		12.27
2-Propanol		12.37
Acetonitrile		13.14
Ethanol		13.65
Methanol		15.85
Water		25.52

Source: Refs. 12 (25°C); 21 (20°C).

only for nonpolar liquids. The introduction of more sophisticated mixing rules [21,22] requires much more pure component data and destroys the advantage of simplicity of the concept. In its simple version the solubility parameter concept is, however, well suited for a semiquantitative discussion of solvent effects on activity coefficients [23,24].

The equation for the activity coefficient of a component in a binary mixture according to the simple version of the solubility parameter concept reads:

$$RT \ln \gamma_1 = v_1 \Phi_2^2 (\delta_1 - \delta_2)^2 \tag{22}$$

Where v is the molar volume of the compound indicated, and Φ the volume fraction (volume %). The corresponding equation for γ_2 is obtained by a mutation of indices. For the limiting activity coefficient the equation reads:

$$\ln \gamma_1^{\infty} = \frac{v_1}{RT} (\delta_1 - \delta_2)^2 \tag{23}$$

With Eq. (23), activity coefficients are always larger than or equal to 1. This is a consequence of the simple geometric mixing rule at the basis of this equation. The nonideality of the mixture is characterized by the difference of the solubility parameters of the mixing components $(\delta_1 - \delta_2)$. As $(\delta_1 - \delta_2)$ does not change much with temperature, $\ln \gamma_i$ is proportional to $1/T$. The accuracy of this simple equation is not very sound. A much more refined model [21,22] gives better agreement at the expense of much higher requirements for pure component data. With better mixing rules, γ_i values less than 1 can also be obtained.

Regular solution concepts intrinsically assume that the excess entropy of mixing and the excess volume are zero, $s^E = 0$ and $v^E = 0$. However, to account for great differences in the sizes of the molecules, $s^E = 0$ is commonly replaced by the s^E value calculated by the Flory–Huggins equation [5]:

$$s^E = \Sigma_n x_n \ln \left(\frac{\Phi_n}{x_n} \right) \tag{24}$$

and Eq. (25) gives the entropic contribution to the activity coefficient that must be added to the enthalpic contribution in Eq. (23).

$$\ln \gamma_i^{S\infty} = \ln \left(\frac{v_i}{v} \right) + 1 - \left(\frac{v_i}{v} \right) \tag{25}$$

the v stands for the mean molar volumes of the mixture; $\ln \gamma_i^{S\infty}$ is always less than zero $(\gamma_i^S < 1)$.

3. Multicomponent Eluents

A standard example in chromatography is the situation for which the analyte is present at a very low concentration in a mixture of at least two eluent components. A frequent question is how the activity coefficient of the analyte changes with the mobile-phase composition.

A simple equation for the calculation of activity coefficients in multicomponent mixtures is

$$\ln \gamma_i^{\infty[\text{mix}]} = \Sigma_n \Phi_n \ln \gamma_i^{\infty[n]} - v_i \Sigma_n \Sigma_{<m} A_{n,m} \Phi_n \Phi_m \tag{26}$$

where the index i indicates the analyte, and n and m the eluent components. $A_{n,m}$ is an intermolecular interaction parameter between the solvent components. The first term of Eq. (26) is the weighted sum of the activity coefficients in the pure eluent components. The second term accounts for the solvent–solvent interactions. (Pairs of solvent components are counted only once, therefore $n < m$.) These solvent–solvent interactions are responsible for deviations from simple additive (linear) behavior. [Eq. (26) is the two-suffix Margules equation generalized for multicomponent mixtures. It is one of the most simple equations used for the calculation of activity coefficients in liquid mixtures. It accounts for the interactions between

each pair of components in the solution by only a single parameter $A_{1,2}$. These interaction parameters can be evaluated starting from experimental limiting activity coefficient data in *binary* mixtures. By knowing these parameters multicomponent mixtures (with not too different solvent components) can be treated in an approximate way. $A_{1,2}$ is obtained by means of the following equation: $\ln \gamma_1^{\infty} = v_1 A_{1,2}$.]

For a binary eluent this equation reads:

$$\ln \gamma_i^{\infty[\mathrm{mix}]} = \Phi_1 \ln \gamma_i^{\infty[1]} + \Phi_2 \ln \gamma_i^{\infty[2]} - v_i A_{1,2} \Phi_1 \Phi_2 \tag{27}$$

$A_{1,2}$ is rather small for solvent components similar in polarity (i.e., about 0.45 for the pair water–methanol, and 1.0 for the pair water–ethanol). In an eluent composition range for which the product $\Phi_1\Phi_2$ does not change much (e.g., between 30 and 70% (v/v) of each component) an approximately linear relation between $\ln \gamma^{\infty}$ and the volume fraction of either component is obtained.

Figure 2 shows the calculated graphs for the limiting activity coefficients of the analytes benzene and toluene in mixed solvents consisting of water–methanol, water–ethanol, and water–acetonitrile. The calculation is based on experimental limiting-activity coefficient data taken from the literature. With acetonitrile as the organic solvent component (modifier) the

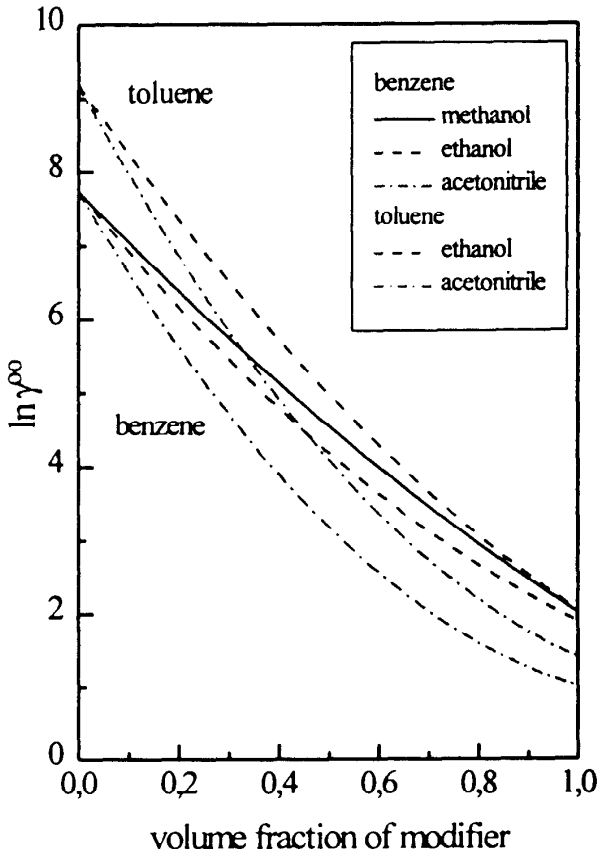


Figure 2 Calculated graphs according to Eq. (27) for limiting-activity coefficients of benzene and toluene in mixed solvents consisting of water–methanol, water–ethanol, and water–acetonitrile. The calculations are based on experimental limiting-activity coefficients of the analytes in the pure solvent components and the limiting-activity coefficients of the solvent components in the pure partner solvent [16,18,20]. Assumed mole–volume ratios: analyte/methanol: 3; analyte/ethanol: 2; and analyte/acetonitrile: 2.

deviations from linearity are more significant. The shown dependence is commonly expected for analytes with a significant hydrophobic moiety, which is better solvated by the alcoholic (organic) eluent component. Experimental data for *n*-alcohols and ketones show an approximately linear decrease of $\ln \gamma^{\infty}$ values with increasing concentration of methanol in water; and an at least continuous decrease is found for most hydrophobic analytes.

With charged analytes, such a linear dependence cannot be expected across the whole concentration range, as the solvation of the charge becomes decisive. For *small ions* without a large hydrophobic moiety, the solvation of charge becomes worse when increasing the content of organic modifier in the eluent, and thus, the activity coefficient increases. If the charged analytes also contain large hydrophobic moieties, this trend for small ions is overlaid by the opposite trend typically observed with hydrophobic analytes. In these cases, the relationship between the activity coefficient and the modifier concentration may exhibit a minimum.

If we again refer to the simple solubility parameter model for calculating activity coefficients in multicomponent mixtures, the equation for the analyte component i reads [5]:

$$\ln \gamma_i^{\infty} = \frac{v_i}{RT} (\delta_i - \delta^*)^2 \tag{28a}$$

where

$$\delta^* = \Sigma_n \Phi_n \delta_n \tag{28b}$$

In the context of chromatography, δ^* may be interpreted as the solubility parameter of a chromatographic phase (mobile or stationary). When assigning such (phase-)solubility parameters to both phases, the following expression is obtained for the retention factor:

$$\ln k_i = \frac{v_i}{RT} [(\delta_i - \delta^m)^2 - (\delta_i - \delta^s)^2] + \ln q \frac{v^m}{v^s} \tag{29a}$$

or

$$\ln k_i = \frac{v_i}{RT} [(\delta^m + \delta^s - 2\delta_i)(\delta^m - \delta^s)] + \ln q \frac{v^m}{v^s} \tag{29b}$$

The entropic Flory–Huggins contribution is neglected for simplicity.

The equation for the selectivity coefficient now becomes (assuming $v_i \approx v_j$)

$$\ln r_{j,i} = \frac{2v_i}{RT} [(\delta_i - \delta_j)(\delta^m - \delta^s)] \tag{30}$$

Two general rules can be derived from these equations:

1. Retention as well as selectivity increase exponentially with the difference between the solubility parameters of the mobile and stationary phases.
2. Retention, but not necessarily selectivity, becomes small when the solubility parameter of the analyte is approximately equal to the arithmetic mean of the solubility parameters of the two phases. (Solubility parameters of analytes are not easily obtained. A very *approximate* value can be assessed on the basis of polarity and size of the hydrophobic structures in the analyte; polar compounds exhibiting higher, hydrophobic compounds lower, values as shown in Table 3.)

These rules have been pointed out by Schoenmakers et al. [23] and can be used as a guideline for selecting optimum eluent compositions.

E. Summary

The basic considerations given in this section result in the following conclusions:

1. Retention in LSC is determined by the distribution equilibria between the stationary surface phase and the mobile liquid bulk phase.
2. Two primary phenomena determine the strength of retention. First, the competitive adsorption of analyte and all solvent components; second, the solvation of the analytes in the mobile phase. Both phenomena are dependent on the composition of the mobile phase. An approximate equation [see Eq. (18)] correlates the retention factor of a compound with the eluent composition.
3. Equation (17) accounts for the competitive adsorption alone, and Eq. (26) presents a simple equation for activity coefficients of analytes in mixed mobile phases.
4. Semiempirical models such as the solubility parameter model may be useful for understanding deviations from a linear (ideal) relation between retention ($\ln k_i$) and mixture composition (volume fractions) as dependent on the chemical structure (polarity) of the mixture components.

II. EQUATIONS FOR CHROMATOGRAPHIC ELUENT SELECTION

For the purpose of eluent optimization in chromatography the general form of Eq. (18), describing competitive adsorption from solution and accounting for changes in the activity coefficients in both phases, is commonly not needed. For many commonly used phase systems in chromatography (discussed later in this chapter), it happens that various *simplifying approximations* can be introduced to obtain more simple equations that are easier to handle. There are systems in which the phenomena of competitive adsorption are dominant and most decisive and, conversely, others for which the solvation phenomena are dominant. Which type of simplifications and approximations are appropriate is, therefore, primarily dependent on the type of the surface and the mobile phase employed.

A. Predominance of Competitive Adsorption Phenomena

The predominance of competitive adsorption phenomena is assumed when employing polar surfaces, such as silica gels, and a polar eluent component (modifier) is added to an otherwise nonpolar solvent. This type of phase system is usually referred to as *normal-* or *straight-phase*. In this instance, several approximations can be introduced, on the base of which significant simplifications of Eq. (18) can be obtained. The course of these simplifications is shown in Table 4.

The first three assumptions can be widely accepted and yield Eq. (31), giving the retention factor as dependent on the eluent composition.

$$\ln k_i = \{\ln q - \ln K_{2,i}\gamma_i^s v^s\} + \ln(\gamma_i^m v^m) - \ln x_2^m \tag{31}$$

The term in the first bracket is constant, the two following terms change with mobile-phase composition.

For a further simplification one needs an additional approximation [see assumption 4 in Table 4], which works across a certain limited concentration range of the modifier. Its introduction yields an equation that is linearly dependent on the mobile-phase composition.

$$\ln k_i = \{\ln q - \ln K_{2,i}\gamma_i^s v^s + b_{0i}\} - (1 + b_{1i}) \ln x_2^m \tag{32a}$$

1. The slope in this equation is seen not to equal unity, except when b_{1i} is equal to zero (i.e., when γ_i^m is constant across the composition range). This is despite that Eq. (18) was

Table 4 Assumptions and Approximations Used to Simplify Eq. (18)

Assumptions	Approximation	Simplified equation
Assumption 1[a]	$K_{2,i}x_2^m >> K_{1,i}x_1^m \cdots$	$\Sigma_n(K_{n,i}x_n^m) \approx K_{2,i}x_2^m$
Assumption 2[b]	$\frac{\gamma_2^m}{\gamma_2^s} \approx$ const.	${}^xK_i = \left(\frac{\gamma_i^m}{\gamma_i^s}\right)\left[\frac{1}{K_{2,i}x_2^m}\right]$.
Assumption 3[c]	$\gamma_i^s \approx$ const. $v_i^s \approx$ const.	${}^xK_i = \left(\frac{\gamma_i^m}{\text{const.}}\right)\left[\frac{1}{K_{2,i}x_2^m}\right]$.
	$\ln k_i = \{\ln q - \ln K_{2,i}\gamma_i^s v^s\} + \ln(\gamma_i^m v^m) - \ln x_2^m$ Eq. (31)[d]	
Assumption 4[e]	$\ln(\gamma_i^m v^m) = b_{0i} - b_{1i} \ln x_2^m$	
	$\ln k_i = \{\ln q - \ln K_{2,i}\gamma_i^s v^s + b_{0i}\} - (1 + b_{1i}) \ln x_2^m$ Eq. (32)	
	simplified to a two-parameter equation	
	$\ln k_i = \{\text{const.}\} - (1 + b_{1i}) \ln x_2^m$	
	$\ln k_i = \ln k_i^{[2]} - S_i \ln x_2^m$ Eq. (33)	

[a]*Assumption 1*: Solvent component 2 (the "modifier") is much more strongly adsorbed than the other solvent component(s) (here identified as components 1, 3, and so on). *Physical meaning* thereof: The surface will be covered by a solvent layer consisting, to a high extent, of molecules of component 2. The modifier will be the main competitor for the adsorption of analytes.

[b]*Assumption 2*: The variation of the activity coefficient ratio of the predominantly adsorbed *solvent component* (γ_2^m/γ_2^s), with eluent composition is neglected, and this constant value is included in the competitive adsorption constant $K_{2,i}$. *Comment*: This approximation is expected to be appropriate with the exception of very low modifier concentrations only.

[c]*Physical meaning*: The composition of the solvent layer at the surface changes only very moderately on changing the mobile-phase composition, owing to the preferential adsorption of the modifier. The activity coefficient of the adsorbed analyte (surrounded by the molecules of the adsorbed solvent layer), γ_i^s, as well as v^s will thus be largely independent of the eluent composition.

[d]For the conversion from distribution coefficients to retention factor see Eq. (5b).

[e]*Assumption 4* implies a linear dependence of $\ln(\gamma_i^m v^m)$ with $\ln x_2^m$. This assumption allows one to attain a significant further simplification toward a linear equation. *Comment*: This approximation might be critical. Equations for activity coefficients in mixed solvents based on molecular thermodynamics do not predict a linear dependence of $\ln \gamma$ on $\ln x_2^m$ (or the logarithm of the volume fraction, Φ_2^m) of a strongly solvating eluent component. However, experimental capacity factor data correlating $\ln k_i$ with $\ln x_2^m$ in typical straight-phase solvent mixtures show, across the usually considered range of moderator concentrations, approximately linear graphs [27–29,39]. This approximation can be accepted thus across certain limited ranges of modifier concentration and, particularly, for those (not too polar) analytes and modifiers for which γ_i^m does not change dramatically with eluent composition.

based on the assumption of equal surface areas per adsorbed molecule for all adsorbates ($\nu_{A,i} = 1$).

2. The equation shows that for analytes covering equal surface areas per mole, selectivity can be gained by varying the eluent composition only if the b_1 values of the analytes are different (i.e., the mobile-phase activity coefficients vary differently with composition).
3. When accounting for different surface areas covered per mole of the different components by stoichiometric factors $\nu_{n,i}$ [see Eq. (11)] a size parameter $\nu_{2,i}$ has to be introduced into Eq. (32a), attaining Eq. (32b) after certain approximations.

$$\ln k_i = \{\ln q - \ln K'_{2,i}\gamma_i^s v^s + b_{0i}\} - (\nu_{2,i} + b_{1,i}) \ln x_2^m \qquad (32b)$$

The size parameter thus affects the slope of Eq. (32b), and therewith, the way in which the

selectivity varies with eluent composition. (Again, one should be aware that the size parameters for surface adsorption do not directly reflect molecular size ratios in bulk liquids.)

An equation essentially analogous to this linear Eq. (32) was proposed nearly three decades ago by Soczewiński [25,26] on the basis of experimental evidence. This equation reads in its most popular form:

$$\ln k_i = \ln k_i^{[2]} - S_i \ln x_2^m \tag{33}$$

where $k_i^{[2]}$ is the hypothetic (extrapolated) retention factor of the analyte in pure eluent component 2 (strongest adsorbed component). S_i has been considered mainly as a surface area parameter.

In this form Eq. (33) is the most commonly used equation for practical chromatographic purposes when working in the straight-phase mode with polar adsorbents. It is used for high-performance (HP)LC as well as (equilibrium) TLC. For the purpose of data correlation, $\ln k_i^{[2]}$ and S_i can be treated as best-fit parameters in a simple linear regression procedure. Such a strategy allows one to optimize eluent composition and separation conditions based on very few experimental data. For chromatographic systems operated with polar stationary phases and mobile phases of low polarity (typical straight-phase chromatography), a fairly good description of experimental data is usually provided by this equation [27–29], at least when modifier concentrations are not too low. An example showing steroid derivatives as analytes with heptane–diethyl ether and heptane–ethyl acetate mobile phases is given in Fig. 3. However, there are other systems in which deviations from linearity are more significant.

At approximately the same time as Soczewiński, Snyder developed his equations for competitive adsorption of solvent components [30–33]. Snyder's theoretical approach is fundamentally based on a displacement model. The adsorption strength of a solvent is characterized by a solvent-strength parameter ε^0, which scales the solvent strengths in relation to

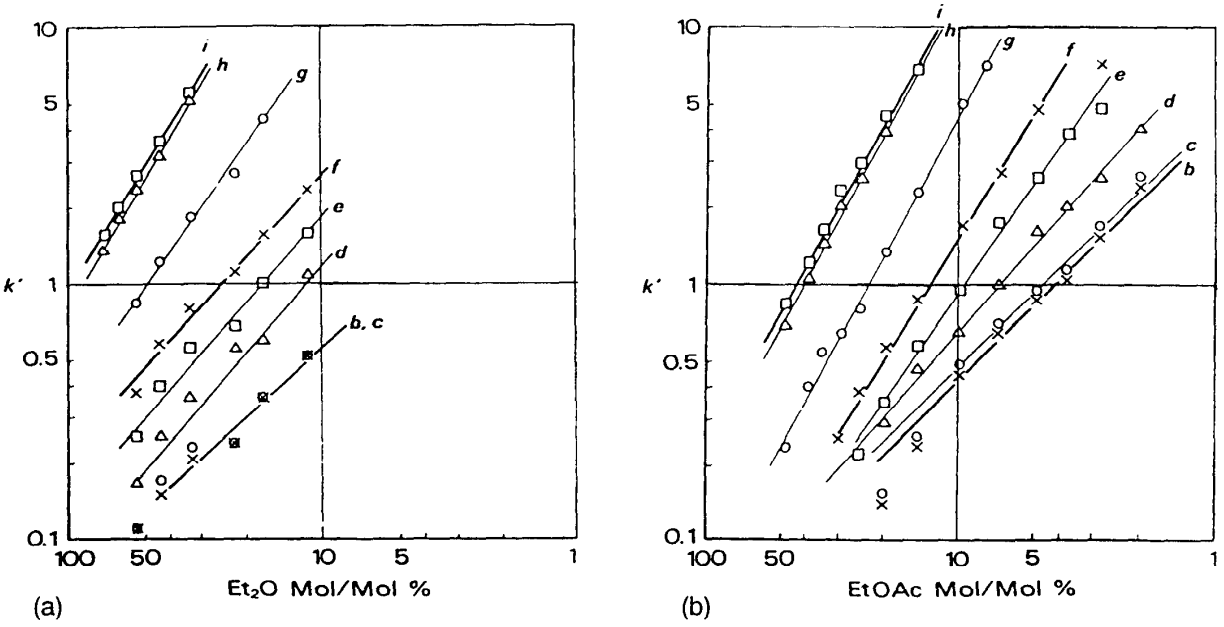


Figure 3 Retention factors in dependence on the mole fraction of the stronger-eluting eluent component in a double logarithmic plot. Stationary phase: silica; mobile phases (a) heptane–diethyl ether, and (b) heptane–ethyl acetate. The symbols represent monosubstituted cholestane derivatives, the curves are linear regression lines (analyte samples: *b*, 3β-acetoxy-5α-cholestane; *c*, 3β-acetoxy-5-cholestene; *d*, 3β-tosyloxy-5-cholestene; *e*, 5β-cholestan-3-one; *f*, 5α-cholestan-3-one; *g*, 4-cholesten-3-one; *h*, 5-cholesten-3β-ol; *i*, 5α-cholestan-3β-ol). (From Ref. 27.)

that of *n*-pentane (for which $\varepsilon^0 = 0$). The solvent strength parameters are dependent on the type of surface used and correspond conceptually to the competitive adsorption constants of the solvents (e.g., $K_{2,1}$, $K_{3,1}$, ···) discussed earlier [see (12)]. A large number of ε^0 values have been published, some of which are listed in Table 5.

Snyder's equation reads:

$$\log K_i = \log V^s + \alpha'(S_i^0 - A_i\varepsilon^0) \tag{34}$$

Where K_i is the distribution coefficient in units of molar concentrations and V^s is the volume of the adsorbed solvent layer ($\log V^s$ lies between -0.9 and -1.5 [42]); α' is a surface-activity parameter (between 0.7 and 1 for most of the polar adsorbents), A_i is the relative surface area covered by an analyte molecule ($A_i' = 6$ for benzene), S_i^0 and ε^0 are adsorption energies: S_i^0 of the analyte and ε^0 of the eluent per unit surface area, both relating to $\alpha' = 1$. For the most commonly used eluent components in straight-phase chromatography, the ε^0 values can be obtained from tables, allowing the chromatographer to establish an eluotropic series (i.e., a rank order of solvents according to increasing elution strength) for different adsorbents and to predict changes in retention by varying the solvent. For mixed eluents, a mixing rule for solvent strength parameters is given from which analyte retention can be calculated on the base of pure solvent parameters.

$$\varepsilon_{12}^0 = \varepsilon_1^0 + \left(\frac{1}{\alpha' n_2}\right) \log\{x_2 10^{[\alpha' n_2(\varepsilon_2 - \varepsilon_1)]} + 1 - x_2\} \tag{35}$$

n being a molecular size parameter. Introduction of this mixing rule leads to Eq. (36a)

Table 5 Eluent Strength Parameters, ε^0, for Some Selected Solvents

	Eluent strength	
Eluent	Silica	Alumina
n-Pentane	0.00	0.00
n-Hexane	0.01	0.01
n-Heptane	0.01	0.01
Cyclohexane		0.04
Carbon tetrachloride	0.11	0.18
Diisopropyl ether		0.28
Benzene	0.25	0.32
Chloroform	0.26	0.40
Methylene chloride	0.32	0.42
Tetrahydrofuran	0.35	0.45
Diethyl ether	0.38	0.38
Ethyl acetate	0.38	0.58
Dichloroethane		0.49
Dioxane	0.49	0.56
Acetonitrile	0.50	0.65
n-Propanol		0.82
Ethanol		0.88
Methanol	0.73	0.95
Water		Very large

Source: Refs. 30 and 34.

$$\log k_i = \text{const.} - \left(\frac{A_i}{n_2}\right) \log(1 + C_{1,2}x_2) \tag{36a}$$

with

$$C_{1,2} = 10^{[a'n_2(\varepsilon_2 - \varepsilon_1)]} - 1 \tag{36b}$$

Snyder's equation simplifies to Eq. (33) on introducing the approximation $C_{1,2}x_2 >> 1$. The treatment is based exclusively on competitive adsorption; changes in the analyte solvation (activity coefficients) with changes in the eluent composition are not accounted for. In further work Snyder also dealt with the effects of surface heterogeneity [32,33].

Other equations accounting for the dependence of capacity factors on solvent composition (in straight-phase chromatography) have been developed by Scott and Kucera [35] and by Jandera and Churacek [36]. Scott and Kucera started from the observation that at modifier concentrations higher than about 2%, silica surfaces are completely covered by the more strongly adsorbed polar eluent component. At these higher modifier concentrations the activity of the surface is constant, and retention is assumed to be governed mainly by changes in the activity coefficients in the mobile phase. This concept results in the following equation:

$$\left(\frac{1}{k_i}\right) = \left(\frac{1}{k_i^{[1]}}\right) + \left\{\left(\frac{1}{k_i^{[2]}}\right) - \left(\frac{1}{k_i^{[1]}}\right)\right\} x_2^m \tag{37}$$

The numbers in the superscripts indicate pure solvent conditions. It has been shown [37] that this equation can formally be transformed into Synder's and Soczewinski's equation [see Eq. 33), although the two models start from completely different concepts. (Despite the great merits of such equations for the correlation and interpolation of experimental data, it has become quite clear that the accuracy of theoretical concepts cannot be tested by evaluating the ability of these equations to correlate chromatographic retention data. The additional assessment of activity coefficient data provides more insight into the different sources of observed retention effects [38,39].)

B. Dominant Solvation Phenomena

In several chromatographic systems, the change in retention factors with eluent composition is governed mainly by significant changes in the mobile-phase activity coefficients of the analytes. This is typically observed with hydrophobic supports and with aqueous–organic-mixed eluents (i.e., reversed-phase chromatography). [In Sec. I.D, it was shown that activity coefficients of analytes exhibiting (large) hydrophobic structures are (very) high in water and much lower in organic solvents. The strong decrease in the activity coefficients of such analytes on addition of organic eluent component becomes thus the predominant effect. This large effect on activity coefficients observed in aqueous solutions is different from the much smaller effects observed with hydrophobic analytes (with polar functional groups) in straight-phase chromatography with organic eluents of rather low polarity. There, the activity coefficients are not very high, the changes in activity coefficients on variation of the eluent composition are thus not as dramatic as in RPLC. This situation thus justifies the use of different approximations for the two types of chromatography.] In these instances, it is more useful to start from Eq. (26) than from Eq. (18). If we assume that the surface-layer composition does not change much with eluent composition ($\gamma_i^s \sim$ constant) within a limited concentration range, the following equation can be derived from Eq. (26) [40]:

$$\ln k_i^{[\text{mix}]} = \Phi_1 \ln k_i^{[1]} + \Phi_2 \ln k_i^{[2]} - v_i A_{1,2} \Phi_1 \Phi_2 \tag{38}$$

$A_{1,2}$ is an interaction parameter *between solvent components*, as discussed in the previous section. It is related to the solubility parameters mentioned before and to the limiting activity coefficients by

$$A_{1,2} = \frac{1}{RT}(\delta_1 - \delta_2)^2 = \frac{1}{v_1} \ln \gamma_1^{\infty} \tag{39}$$

Equation (38) can also be written as

$$\ln k_i^{[mix]} = \ln k_i^{[1]} - [\ln k_i^{[1]} - \ln k_i^{[2]} + v_i A_{1,2}]\Phi_2 + v_i A_{1,2}\Phi_2^2 \tag{40a}$$

This relation proved to be very useful for eluent optimization in reversed-phase–type systems using alcohols, acetonitrile, and tetrahydrofuran (THF) as moderators. Within a moderate concentration range of modifier (e.g., between 30 and 70% (v/v)), the product $\Phi_1\Phi_2$ does not change much and an approximately linear relation between $\ln k_i$ and the volume fraction of the stronger solvating eluent component is often observed across such a limited range. This is illustrated by experimental data on noncharged analytes given in Fig. 4 and 5. In these instances and for the purpose of curve-fitting and interpolation, Eq. (40a) can be further simplified by neglecting the term quadratic in the volume fraction. With empirical parameters a_0, a_1 (and a_2) Eq. (40a) reads

$$\ln k_i^{[mix]} = a_{0,i} - a_{1,i}\,\Phi_2 + (a_{2,i}\Phi_2^2) \tag{40b}$$

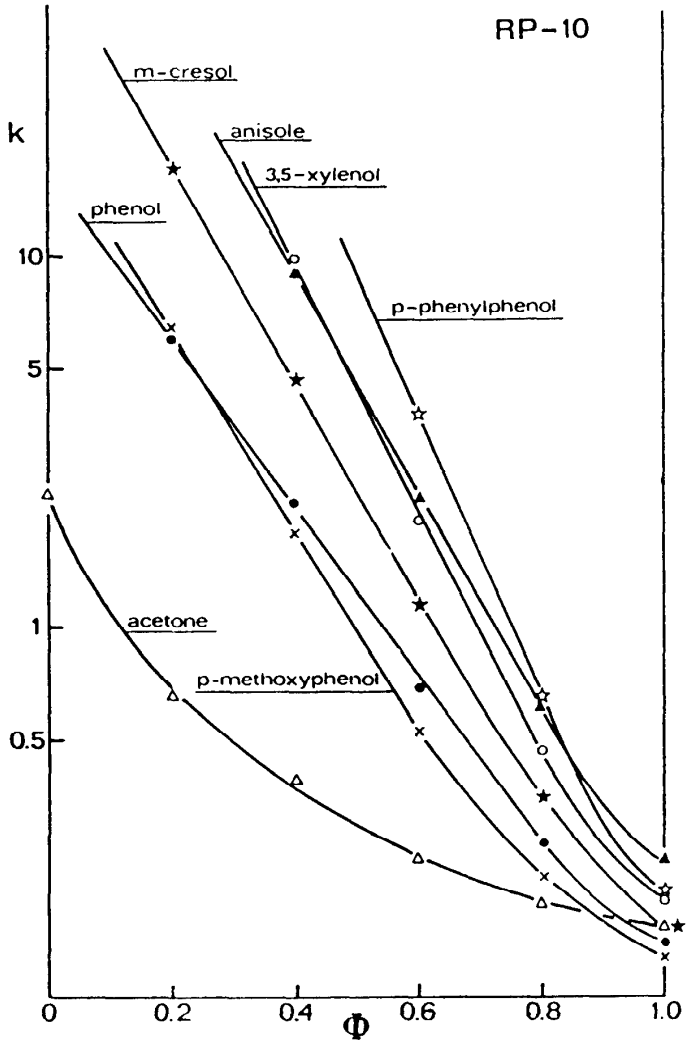


Figure 4 Logarithm of retention factor as dependent on the volume fraction of methanol in water–methanol-mixed mobile phases. Stationary phase: decylsilica. The symbols represent experimental data on substituted phenols. (From Ref. 54.)

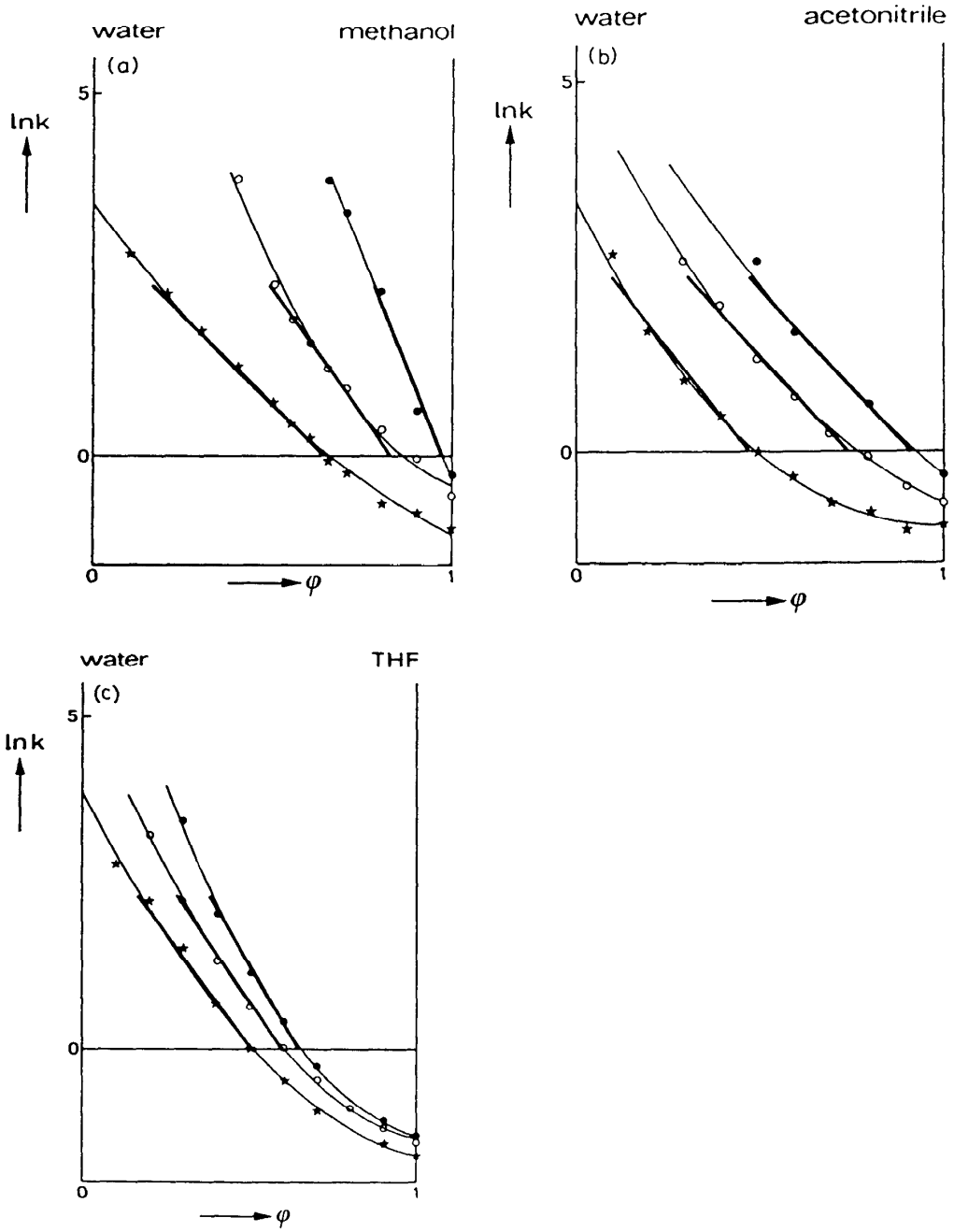


Figure 5 Logarithms of retention factors as dependent on the mole fraction of the organic modifiers in the water–modifier-mixed mobile phases. Modifiers: (a) methanol, (b) acetonitrile, (c) tetrahydrofuran; stationary phase: octadecylsilica. The symbols represent the experimental data on ● naphthalene, ○ anisole, and ★ phenol; curves are obtained by simulation. (From Ref. 41.)

For eluent pairs with larger $A_{1,2}$ values (greatly different solubility parameters) the deviation from linearity becomes significant. With charged analytes, the simple linear relation is usually not observed, as discussed earlier. At low and high moderator concentrations, even the quadratic equation [see Eq. (40a)] is not very reliable: At low moderator concentrations, because the structure of the hydrophobic surface commonly changes by folding of the alkyl ligand under these conditions. At high moderator concentrations, and with many silica-based

materials, adsorption of analyte on unmodified silica sites also becomes important, causing a mixed retention mechanism.

For analytes of approximately equal molar volumes, the dependence of the selectivity coefficient (separation factor) on the composition according to Eq. (40a) is given by Eq. (41).

$$\ln r_{j,i}^{[\text{mix}]} = \Delta \ln k_i^{[1]} - [\Delta \ln k_i^{[1]} - \Delta \ln k_i^{[2]}]\Phi_2 \tag{41}$$

Selectivity changes with eluent composition in reversed-phase systems are mainly governed by the differences in the (logarithms of the) retention factors of the analytes in pure water, $\Delta \ln k^{[1]}$. This is because the differences in the retention factors in pure modifiers $\Delta \ln k^{[2]}$ (methanol, ethanol, acetonitrile, tetrahydrofuran) are usually much smaller than those in pure water.

C. Summary

For *straight-phase systems* (polar stationary phases operated by mobile phases of low polarity) the competitive adsorption of analyte and solvent components plays the predominant role determining the retention factors dependent on eluent composition. With these systems and with not too polar analytes and modifiers, equations that follow the form of Eq. (33) can be used for data correlation.

For *reversed-phase systems* (nonpolar stationary phases operated by aqueous–organic eluents), the change of solvation of analytes in the mobile phase plays the dominant role. With these systems (and with the usual modifiers methanol, ethanol, acetonitrile, and uncharged analytes) equations following the form of Eq. (40a) can be used for data correlation across the most frequently applied concentration ranges.

III. CHEMICAL STRUCTURE OF SURFACES AND RETENTION

The type and strength of the prevailing intermolecular interactions between analyte, stationary phase, and eluent components are determined by the chemical structure of these partners. Retention of analytes will be discussed in this chapter in the context of the chemical structures of

The stationary phase with its particular functional groups
The analyte
The mobile-phase constituents

Particular attention will be given in this chapter to the stationary phases.

A. Support Materials in Liquid Chromatography

Many features of stationary phases are essentially determined by the support material. Support materials can be used as adsorbents themselves. However, the surface of the support material is usually modified either by chemical reaction or by deposition of polymer layers. The stationary phase onto which adsorption of analytes takes place is then determined primarily by these chemical modifications or coatings. Nevertheless, the support material often still influences adsorption, for chemical modification rarely covers all the adsorption sites of the support material.

The most important support materials in HPLC are listed as follows:

Inorganic materials	Silica gel (SiO_2)
	Alumina (Al_2O_3)
	Porous, graphitized carbon (PGC)
Cross-linked synthetic organic polymers	Polystyrene–divinylbenzene copolymers (PS–DVB)
	Polyacrylamide (PAA) and hydrophilic derivatives thereof
Carbohydrate based polymers	Agarose
	Cellulose (especially as supports for affinity chromatography)

There are a few other support materials that are employed for particular purposes, such as hydroxylapatite for protein chromatography and acetylated or benzylated cellulose for chiral separations in preparative LC. However, silica and the organic polymers together cover most of the today's LC applications.

For the characterization of chromatographic support materials, physical and chemical parameters are of interest. *Physical parameters* are the porosity, pore size, the size and rigidity of the particle and, to a minor extent, its shape. *Chemical parameters* are the polarity of the material, its acid–base behavior, its stability toward solvents and "extreme" pH values in aqueous eluents, and—very importantly—the possibilities for it to be modified by chemical reactions.

1. Physical Parameters

Silica and polymeric particles for chromatography can be produced within very narrow size ranges, with spherical symmetry, and with a defined porosity. The particle porosity of totally porous silica particles is close to 0.72 in most instances [42], leading to a total column porosity of approximately 0.80. The porosity of PS–DVB copolymers depends on the degree of cross-linking, which is determined by the percentage of DVB present. The degree of cross-linking also determines the rigidity of the particles. Silica as well as polymeric particles can also be produced as small nonporous particles (1- to 3-μm–particle diameter) or with a thin porous layer around a nonporous core [43,44]. The specific surface areas (i.e., the surface areas per unit weight of support material) are much smaller in these latter examples. These materials offer significant advantages for fast separations [45] and for separations of biopolymers, for which diffusion pathways should be kept small.

The mean pore diameter of a material affects the specific surface area and, thus, the phase ratio [see Eq. (4)]. This correlation between pore diameter and specific surface area of a sorbent is illustrated in Table 6 for some contemporary commercial silica materials. A broader overview is given elsewhere [47]. Materials for which the surface is modified by chemical reaction (or is to be modified by the user) need a certain minimum pore diameter to allow fast mass transport in the pores. Octadecyl (C_{18})-modified particles, for instance, have mean pore diameters usually no smaller than 100 Å. For adsorption chromatography of polymeric analytes, such as proteins, on porous particles, wide-pore materials, with mean pore sizes from 300 to 1000 Å are used, as these pores are accessible for large analytes. The specific surface areas of wide-pore particles are low.

There are new strategies under development that allow one to synthesize a continuous chromatographic bed without particle structure as "rigid rods" or "monoliths." Such materials promise low-peak dispersion even at high-flow velocities.

Table 6 Physical Data on Silica Gel Materials for Analytical HPLC

Material name	Mean pore diameter (Å)	Specific surface area (m^2/g)	Specific pore volume (mL/g)
LiChrosorb	60	500	0.75
(Merck)	100	300	1.0
	100-RP-18	300	—
LiChrospher	60	700	0.85
(Merck)	100	400	1.25
	100 RP-18	350	1.25
	300 RP-18	80	1.0

Source: Ref. 46.

2. Silica Gels

Silica gels for chromatography are amorphous gels with a very polar surface. The main surface groups existing in materials that have not been heat-treated above 500°C are isolated free silanol groups, vicinal silanol groups that form hydrogen bonds with each other, and silanols that bind water by hydrogen bonding [42]. These surface groups are illustrated in Fig. 6. The total concentration of free silanols in amorphous gels is about five groups per 100 $Å^2$ corresponding to about 8 $\mu mol/m^2$ [47,48]. It varies, however, depending on the preparative procedure.

Silanol groups are *weakly acidic* with pK_a values close to 5–6, depending on their structure (and on the composition of the surrounding mobile phase). They are strong adsorption sites for polar compounds, offering hydrogen-bonding, acid–base, and dipole–dipole interactions. Bare silica is the most common adsorbent used in normal (straight)-phase chromatography. The different surface groups shown in Fig. 6 are clearly not equivalent relative to the Gibbs energy of analyte adsorption. Silica surfaces are thus *energetically heterogeneous*. Further, traces of metals may be a source of chelating interactions. Controlling the silica material in this respect was decisive for improving energetic homogeneity.

The presence of adsorption sites with different adsorption free enthalpies causes the adsorption isotherms to significantly deviate from a linear configuration, even in the range of strong dilution. As a consequence, the resulting peak form becomes nonsymmetrical, exhibiting tailing in the presence of strong heterogeneity. Energetic heterogeneity of acidic silica materials might cause particular problems with basic analytes.

Silanol groups can easily be derivatized by proper chemical reactions to yield stable surface-modified adsorbents, as discussed later. The stability of silica gel toward acids and bases is limited. Aqueous mobile phases with a low content of organic modifier should have

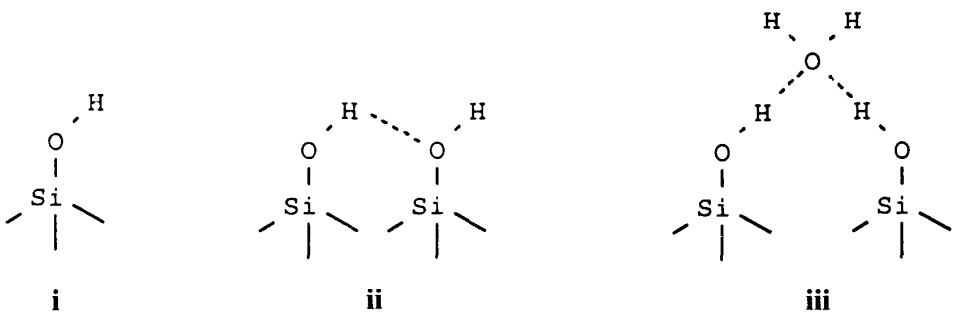


Figure 6 Illustration of the main surface groups of silica gels: (i) isolated free silanol group; (ii) vicinal silanol groups; (iii) silanols binding water. (According to Ref. 42.)

a pH in the range of 2.5–8.5. (Specially treated materials tolerate pH values up to 9; similarly at high organic modifier concentrations, the stability of silica is increased.)

3. Other Inorganic Materials

Alumina (Al_2O_3) is a polar, *basic* material that exhibits about six hydroxyl groups per 100 Å^2. Because of the Lewis-acidic sites of the Al ion, unsaturated compounds are more strongly adsorbed onto alumina than on silica. The specific surface areas are between 100 and 200 m^2/g, pore volumes about 0.2–0.3 mL/g, and mean pore diameters between 100 and 200 Å [47]. Alumina has been less frequently employed as adsorbent in analytical HPLC than has silica. It cannot be derivatized as easily as silica, but chemical modification of the surface can be achieved by coating the surface of the particle with polymeric layers, which will then be the material interacting with the analyte [49]. With aqueous eluents, Al_2O_3 exhibits improved stability at higher pH values than does silica, and it offers weak cation-exchange properties.

Porous graphitized carbon (PGC) [50] is a hydrophobic material with a rigid surface structure. It is usually operated in a reversed-phase mode.

4. Organic Polymers

Organic polymeric support materials are most frequently used with attached functional groups appropriate for a special type of chromatography. Although these attached groups are the decisive interaction sites, the chemical structure of the support itself is of significant relevance, particularly for its hydrophobicity or hydrophilicity. Strongly hydrophobic support polymers, such as polystyrene–divinylbenzene, can be distinguished from hydrophilic materials, such as polyacrylamides, polymers of hydroxy-substituted acrylamides, and agarose (and, for low-pressure LC, also cellulose). The stability of these materials across a wide range of pH is excellent, which makes them excellently suited for ion-exchange chromatography, even under harsh conditions. The energetic heterogeneity of these materials is less troublesome than that of silica gels. An extensive discussion of the recent significant developments in polymeric support materials is given elsewhere [51].

5. Modification of Support Materials

The support material itself serves directly as the stationary phase only in the particular instances of silica and alumina particles used in the normal-phase mode and PGC in the reversed-phase mode. In the other applications of LC, the support materials are submitted to a chemical modification of the surface. Three different modification methods can be chosen.

1. *Chemical bonding of ligands* to the support material. This can be performed by chemically derivatizing certain (reactive) groups at the surface (i.e., the silanol groups of silica, the hydroxyl groups of carbohydrate supports, or the aromatic CH groups of PS-DVB polymers) with activated ligands.
2. Deposition of a *polymer layer* onto the surface of the support. The polymer is then the stationary phase interacting with the analyte. It depends on the thickness, structure, and density of this layer, whether or not the support material contributes (at least partially) to the retention phenomena. This method is frequently used when employing chiral polymers, and it is a way to modify alumina supports.
3. A combination of these two modes yields a third one, which involves chemically immobilized polymer networks fixed at the surface of the support material.

The most important types of modifications are the following:

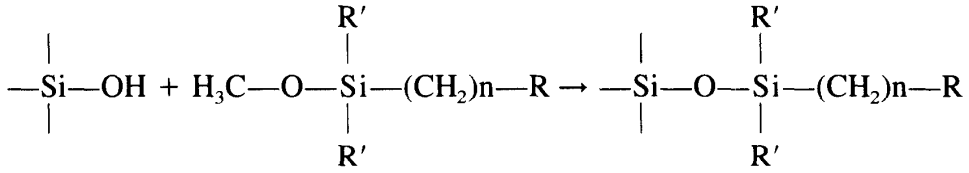
Type of ligand	Modification of the surface	Type of chromatography
Hydrophobic ligands (alkyl chains)	Nonpolar surface	Reversed-phase chromatography
Acidic or basic groups	Charged groups at the surface	Ion-exchange chromatography

Type of ligand	Modification of the surface	Type of chromatography
Various functional groups	Functionalized surfaces or deactivated surfaces	Various types of chromatography Size exclusion chromatography
Chiral molecules	Chiral stationary phases	Chiral chromatography
Affinity ligands[a]	Affinity phases	Affinity chromatography

[a]Large molecules offering strong (shape-) specific interactions with certain types of analytes, including biopolymers.

The chemistry of modifying support materials is considered here primarily relative to its effect on the eventual retention characteristics of the newly generated stationary phase. Here, several parameters are of relevance: (1) The chemical structure of the introduced ligand (e.g., hydrophobic ligand, ion-exchange group, affinity–ligand, chiral selector); (2) the extent of modification defines the number of newly introduced specific ligands, as well as the coverage of original adsorption sites; (3) the chemistry of immobilization; the introduced linking groups may provide relevant interaction with analytes; (4) the length, flexibility, and polarity of the spacer, linking the functional group with the support material.

Chemical immobilization on silica gels is frequently based on the shown reaction of methoxysilanes with the silica support material to give *siloxanes* [42]. An analogous reaction is obtained when starting from clorosilanes.



Starting from difunctional- or trifunctional-silanes, additional binding to the surface and between the ligands may be achieved. The modified phases obtained by using a trifunctional agent (they are sometimes referred to as "polymeric" phases) are sometimes less defined than those of a monofunctional agent. A detailed discussion of various immobilization reactions and the hydrolytic stability of the products is given elsewhere [42].

The foregoing reaction is a standard reaction to immobilize alkyl-ligands onto the surface, yielding alkyl-siloxanes of various chain lengths. Frequently used chain lengths are those with 8 (octylsilica) or 18 (octadecylsilica) carbon atoms. It is also possible to immobilize phenyl ligands and functional groups, such as amino, carboxylic, cyano, or diol groups. These are usually positioned at the end of a short alkyl chain, known as a spacer (Fig. 7).

With the introduction of potentially reactive groups, such as epoxide or thiocyanate groups, subsequent reactions can be carried out. Such reactions are needed for the immobilization of larger molecules (e.g., for the preparation of chiral stationary phases or affinity phases. The length and chemical structure of the spacer, whether it is hydrophobic or carries hydrophilic groups, can be of certain relevance. Procedures to prepare modified phases will be subject of a more extensive discussion later (see Chap. 8). It is addressed here primarily under the aspect of naming the parameters relevant for the final retention properties of stationary phases.

When reacting silica with alkyl ligands to achieve materials for reversed-phase chromatography, the degree of derivatization and coverage of the reactive surface groups does not reach 100%. It depends on the procedure and reaction conditions and is less than 90%. Thus, on any stationary phase, a certain percentage of *unmodified silanols* is still available. Some of these may be accessible for the analyte molecules. At the uncovered accessible silanol groups all interactions typical for bare silica can take place. Such interactions are especially

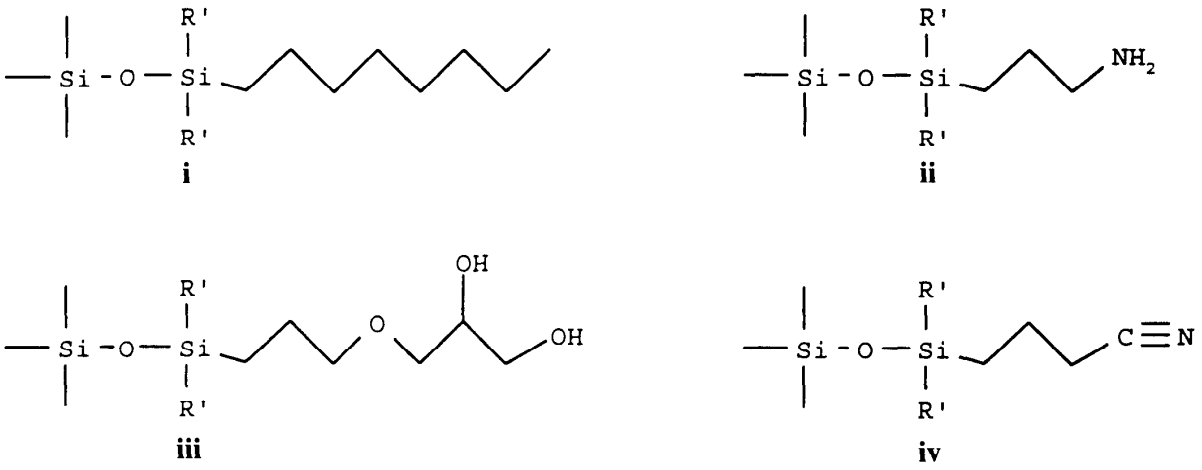


Figure 7 Chemical structure of functional ligands immobilized on silica surfaces: (i) octylsiloxane, (ii) aminopropylsiloxane, (iii) diol-substituted propylsiloxane, (iv) cyanopropylsiloxane.

strong with basic analytes. A consequence of this heterogeneity of the surface can be considerable peak tailing. Size and type of the side groups R′ on the Si-atom shown in the foregoing reaction are of considerable relevance for the features of the new surface in this context.

Various treatments of the surfaces allow minimization of the peak tailing and surface heterogeneity: (1) Performing a further, so-called end-capping reaction to improve the coverage with nonpolar ligands as well as to better shield residual polar sites and make them inaccessible; (2) covering the surface by depositing a polymeric layer; (3) using highly purified and deactivated support silica material; (4) dynamic deactivation of the (acidic) silanols by adding weakly soluble basic additives in low concentrations (about 0.1%) to the eluent. Such basic additives are strongly adsorbed at the most energetic surface sites. Triethylamine and octylamine are typically used for this purpose. Because of different deactivation treatments, alkylsiloxane phases may exhibit significant differences in their properties (retention, peak shape, or efficiency), particularly with basic analytes. Polymer-based materials are more homogeneous in this respect and thus may be more consistent.

Support materials without and with chemical modifications frequently employed in the various modes of chromatography are summarized in Table 7.

B. Normal-Phase Liquid Chromatography

In the normal-phase liquid chromatography (NPLC) mode of operation a *polar stationary phase* is operated with a *mobile phase of low polarity*. Interactions between polar groups in the analyte (e.g., hydroxy, keto, amino, amido, ether, ester, or mercapto groups) and the polar sites of the surfaces dominate the retention. The adsorbent material employed is bare silica material, with few exceptions. [Amino–alkyl-modified and diol-modified silica in nonaqueous medium used for the separation of carbohydrates is such an exception.] Its polar and acidic silanol groups are able to undergo dipole, hydrogen-bonding, and acid–base interactions with analytes exhibiting corresponding structural features. These interactions of the analytes with the surface are competed by the eluent components, particularly the polar eluent components ("modifiers") exhibiting functional groups similar to the analyte. Frequently used modifiers are 1-propanol, 2-propanol, butanol, diethyl ether, diisopropyl ether, methyl-*t*-butyl ether, dichloromethane, ethyl acetate, and other such. According to the magnitude of the competitive adsorption constants (or, equivalently, the eluent-strength parameters given in Table 5), an *eluotropic series* can be established:

alkanes < chloro alkanes < ethers ~ esters < alcohols < methanol < water

Table 7 Schematic Overview on Types of Stationary Phases Frequently Employed in HPLC

Mode of chromatography	Stationary phase		Mobile phase
	Support material[a]	Modifications	
Straight-phase	Silica	None	Nonpolar
	Alumina	None	
	Silica	Aminoalkyl	
Reversed-phase	Silica	Alkyl	Mixed aqueous–organic
	Silica	Phenyl, cyanoalkyl	
	PS–DVB	Alkyl	
	PGC	None	
Ion-exchange	Silica, PS–DVB, Hydrophilic PAAs	Aminoalkyl, Carboxyalkyl, Sulfonylalkyl	Aqueous
Affinity	Silica, Agarose, cellulose, PST/DVB, PAA	Various ligands, Various spacers	Aqueous
Hydrophobic interaction	Silica	Dimethyl, short alkyl, alkyldiol	Aqueous salt solution
Chiral	Silica	Various chiral ligands Chiral polymer coatings	Aqueous or organic nonpolar
Size-exclusion	Silica	Alkyldiol	Aqueous or organic nonpolar
	Carbohydrates	None	Aqueous
	Derivatized PAA	None	Aqueous

[a]PST/DVB, polystyrene–divinylbenzene copolymer; PAA, polyacrylamide; PGC, porous graphitized carbon.

In the NPLC mode and with the mentioned modifiers the phenomena of competitive adsorption controls the retention. Eqs. (33) and (36), correlating the logarithm of the capacity factor with the logarithm of the mole fraction x_2 of the modifier (stronger-eluting eluent component), are of great use for these systems.

$$\ln k_i = \ln k_i^{[2]} - S_i \ln x_2^m \tag{33}$$

Although in experiments a strictly linear dependence is not always found over the entire range of modifier concentration, the linear approximation serves as a useful tool for practical optimization of mobile-phase conditions, except at very low modifier concentrations.

In NPLC systems with silica surfaces, water can be a particularly strong competitor, which influences retention even at very low concentrations (in the range of 10–100 ppm). At these concentrations, water is often present even in "pure" solvents (particularly in polar modifiers). The role of water has to be considered in more detail, for water can form more than one adsorbed layer at the surface of silica [53]. At rather low concentrations (up to about 10% of the saturation concentration in a nonpolar eluent) water acts primarily as a strong competitor for the adsorption of polar analytes [10,38]. In this low-concentration range, an increase in the water content leads to a strong decrease in retention. The water content in nonpolar eluents thus must be controlled extremely carefully to achieve reproducible chromatographic conditions. At water concentrations higher than about 15% of the saturation concentration in the nonpolar eluent, the competitive strength of water becomes smaller, as multilayer-type ad-

sorption (of water) starts to take place. It is thus recommended, to operate NPLC systems with nonpolar eluents that are *saturated to about 30% with water.* This makes the system more reproducible and may speed up phase equilibration.

Nonpolar mobile phases containing a few percent of polar modifiers are also the eluent of choice for several types of sophisticated stationary phases with immobilized chiral molecules designed for enantiomer resolution. With such phases, the normal-phase mode of operation (indicating in this context simply the use of mobile phases of low polarity) is advantageous, if dipole interactions and charge transfer interactions (hydrogen-bonding, acid–base interactions, π–π interactions involving aromatic structures) are significant for retention and for chiral recognition. Under normal-phase conditions these interactions are not overshadowed, as they are in polar and protic eluents.

C. Reversed-Phase Liquid Chromatography

In the reversed-phase-chromatographic mode a *nonpolar surface* is operated with a polar, usually mixed *aqueous–organic mobile phase.* RPLC is the most commonly used mode for analytes that can be dissolved in mixed aqueous–organic eluents. The main materials used as stationary phases are alkyl-modified silica and alkylated PS–DVB polymers (the alkyl ligands attached to the aromatic rings).

The driving forces for retention in RPLC are (1) dispersive interactions between the nonpolar surface ligands and the nonpolar components of the analyte, and (2) the "hydrophobic effect" (i.e., the tendency to minimize the disturbance of the water structure). This latter, mobile-phase–associated effect can be understood and described as the change of the analyte's activity coefficient on adsorption, and it is the main effect in most instances of RPLC [39]. RPLC is especially suitable for the separation of analytes that exhibit different activity coefficients in water (aqueous solutions), either because of the different sizes of their hydrophobic structures or of different numbers of polar groups. Particularly strong selectivity is commonly obtained for compounds differing in the number of aliphatic and aromatic carbon groups. RPLC is not as highly selective as NPLC relative to different polar groups.

The adsorption of the analyte is schematically understood as the hydrophobic part, "stacking" in between the hydrophobic alkyl ligands attached to the surface. In this way the contact area with water is minimized, for both the alkyl ligands and the analyte. Orientation of the stacked analyte is expected to occur in such a way that hydrophilic groups are positioned outside the hydrophobic chains, thus being well-solvated by the aqueous eluent. A schematic picture of such stacking of analytes into the ligands has been given by Berendsen [54] and is shown in Fig. 8.

The alkyl-chain length of the ligands strongly influences the retention factor as far as the contact area between analyte and surface is dependent on the chain length. The $\ln k_i$ increases linearly with the number of CH_2 groups of the alkyl chains up to a number of 6 to 18 CH_2 groups [54], dependent on the size of the analyte. Above this number the $\ln k_i$ values are fairly constant. This critical number of CH_2 groups is higher for larger analytes (between 10 and 18) and close to 6 for small ones [54].

The most frequently used modifiers to tune retention in RPLC are methanol (MeOH), ethanol (EtOH), acetonitrile (ACN), and tetrahydrofuran (THF), all of which are miscible with water over the entire concentration range. The dependence of retention factors on the eluent composition is largely determined by the change in the activity coefficient of the analytes in the mobile phase with the addition of modifier, rather than by an increase in the competitive effect [39]. The eluotropic strength of the modifiers increases according to

$$\text{methanol} < \text{ethanol} \sim \text{acetonitrile} < \text{tetrahydrofuran}$$

With modifier concentrations between 30 and 70% v/v, the logarithm of the capacity factor decreases approximately linearly with increasing volume fraction (i.e., volume percent) of the modifier (see foregoing discussion).

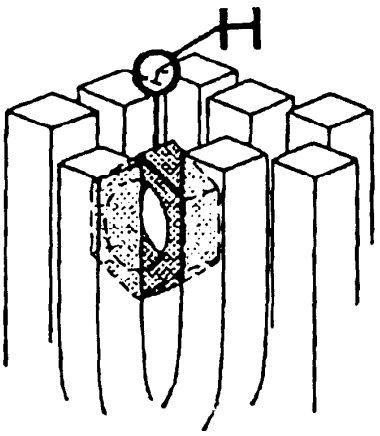


Figure 8 Schematic representation of adsorption of analytes (phenol) by chemically bonded alkyl chains, according to Berendsen. (From Ref. 54.)

$$\ln k_i = a_{0,i} - a_{1,i}\,\Phi_2 \tag{40b}$$

More detailed analyses frequently show slightly concave lines, in agreement with the quadratic term in Eq. (40b), neglected in the foregoing equation. Because of this not strictly linear dependence the best fit parameter $a_{0,i}$ in the Eq. (40b) is thus not identical with $\ln k_i^{[\text{water}]}$. Best-fit parameters $a_{0,i}$, determined by linear regression in aqueous systems with different modifiers, are usually not identical. The extrapolations *to very low moderator concentrations* face an additional, fundamental problem as the hydrophobic alkyl ligands tend to minimize their contact area with water by folding and clustering. This results in a reduction of the accessible surface area and, thereby, in considerable deviations from linearity (at very low moderator concentrations). Thus, $\ln k_i^{[\text{water}]}$ values obtained by extrapolations have to be used with care, although they might be quite useful for optimizing sample enrichment and preparation protocols using solid-phase extraction.

Hydrophobic (i.e., reversed-phase type) adsorption of analytes also takes place to a considerable extent with adsorbents not primarily designed for RPLC; for instance, with some ion-exchangers, affinity phases, and chiral phases operated with aqueous eluents. With ion-exchange materials based on hydrophobic polymers, such as PS–DVB, the hydrophobic adsorption of analytes onto the support material may be significant. Long alkyl chains serving as spacers for the immobilization of functional groups may also act as hydrophobic adsorption sites. Undesired hydrophobic interactions with the spacer can be avoided by choosing spacers containing hydroxyl groups. Cyanoalkyl ligands behave very similarly to alkylsiloxanes in RPLC, again indicating that mobile-phase effects are dominant.

Porous graphitized carbon (PGC) is an RPLC adsorbent with a very high hydrophobicity. To achieve wetting of the surface, the eluents need a certain percentage of organic modifier. The rigidity of the surface, which has no dynamic arrangement of ligands, as in the alkylsiloxanes, offers particular advantages for the discrimination of geometric isomers [55].

D. Ion-Exchange Chromatography

Ion-exchange chromatography (IEC) is a method for the separation of charged analytes, using *electrostatic interactions* between analyte ions and charged groups immobilized at a surface. IEC is operated with buffered aqueous or aqueous–organic mobile phases. In the common mode of operation; the coulombic interactions are used to attract and, thus, retain oppositely charged analytes at charged surfaces. In a special mode of operation, called ion-exclusion chromatography, surface charge and analyte charge are equally signed.

Ion-exchange groups typically employed in IEC are summarized in Table 8.

Strong ion-exchange groups are permanently charged, independent of the pH of the mobile phase. *Weakly acidic* or *weakly basic ion-exchange groups* are charged only in certain pH ranges (i.e., pH $\geq$ pK_a + 1 for weakly acidic ion-exchange groups and pH $\leq$ pK_a − 1 for weakly basic ion-exchange groups). The number of charged groups and, thus, the capacity of the weak exchanger, can be changed by varying the pH (near their pK_a values). Weak ion-exchange materials loose their charges in certain pH ranges, a feature that can be used for the rapid and complete elution of analytes that are otherwise strongly adsorbed. Commonly, weak exchange materials are used for the chromatography of strong acids or bases, and strong exchange materials are used for weak acids and bases.

For the analysis of weakly acidic or weakly basic analytes, the most important mobile-phase parameter is the pH. The differences between the pH value of the buffer solution and the pK_a values of the analytes determine their degree of ionization and, therewith, the retention. Variation of the pH in the range near the pK_a is a very powerful instrument for tuning the separation selectivity. This is the subject of a more detailed discussion on secondary equilibria in Sec. V.

The strength of analyte retention by the electrostatic interaction in solution is dependent on the *concentration* of the *ions of equal charge* as the analyte (e.g., buffer ions), for these act as competitors for the charged interaction sites. In a double logarithmic plot the retention factors decrease approximately linearly with increasing concentration of the equally charged buffer ions, in agreement with the expectations [see Eq. (33)]. The slope of this line is determined by the ratio of charges carried by the analyte and the competitive counter ions (to the exchange group)

$$\ln k_i = \ln k_i^{[*]} - |z_n/z_i| \ln c_n \tag{42}$$

where n indicates the counterion and i the analyte, z represents the charge number, and $k_i^{[*]}$ the retention factor of the analyte at an arbitrary unit concentration of the counterion. Different slopes, implying changes in selectivity with varying counterion concentration, are observed for differently charged analytes.

With permanently charged analytes, variation of the pH is not particularly effective for tuning retention and selectivity. For such analytes the type of counterions employed may affect the retention considerably. The relative eluotropic strength of frequently used counterions in the order of increasing displacing power is [24]:

$$F^- < OH^- \text{ (with strong IEC)} < \text{acetate} < \text{formiate} < Cl^- < SCN^- < SO_4^{2-} < \text{citrate}^{3-}$$

for anions and

Table 8 Ion-Exchange Groups Used in IEC

Type of exchanger	Ion-exchange group	pH range when fully charged[a]
Cation-exchanger		
Strongly acidic	$-SO_3H$	0–14
Weakly acidic	$-COOH$,	>6.0
	$(-OH)$[b]	Not specified
Anion-exchanger		
Strongly basic	$-NR_3^+$	0–14
Weakly basic	$-NH_2$, $-NR_2$	<8.0

R, methyl-, ethyl-group

[a]At least 1 pH unit above the pK_a value of weakly acidic ion-exchange groups and 1 pH unit below the pK_a value of weakly basic ion-exchange groups.

[b]Hydroxy groups of support material.

$$Li^+ < H_3O^+ < Na^+ < NH_3^+ < K^+ < Cu^{2+} < Ca^{2+} < Me^{3+}$$

for cations. It is clear that the displacing power of the counterions increases with their charge.

The counterion concentration and, generally, the *ionic strength* of the mobile phase influences the retention in various ways: (1) by an increased competitive effect owing to a higher ion concentration; and (2) through its influence on the pK_a values of the analytes, with an increased ionic strength resulting in a decreased dissociation of the analyte. Both increased competitive adsorption and decreased dissociation lead to reduced capacity factors with increasing counterion concentration and ionic strength in IEC.

Ion-exchange materials are either based on silica or on organic polymer supports. The type and hydrophobicity of the support material, as well as the type and length of the spacer are essential parameters in establishing either a pure ion-exchange mechanism or a mixed mechanism, which includes hydrophobic adsorption. This may have a significant influence on the selectivity and on the separation. When hydrophobic adsorption occurs, the role of organic modifiers in mixed eluents is equal to that in RPLC. The *pH stability* is another decisive aspect for the selection of a suitable support material. Silica particles are unstable outside the range of pH 2.5 to about 8.5—depending to some extent on the concentration of organic modifier in the solution. In addition, siloxane bonds are sensitive to hydrolysis at extreme pH values. Polymeric support materials are stable from pH 0 to 14, and their binding chemistry is not as sensitive to hydrolysis at extreme pH as observed with siloxanes.

Ion-exchange chromatography is particularly well suited for the separation of proteins, because the risk of denaturing and refolding of the protein on interacting with the charged groups at the surface is small. When separating labile proteins, the hydrophobicity of the support must be low. Otherwise, the proteins may be denatured and lose their biological activity when being adsorbed onto hydrophobic sites of the surface, or with the addition of organic modifiers required for their elution from hydrophobic supports. Type, length, and flexibility of the spacer may play an important role in this context. Thus, ion-exchange materials have been developed in which several charged groups are present on long spacers [56]. By this design hydrophobic adsorption can be avoid, while attaining a high flexibility of the interacting site of the stationary phase. These so-called tentacle-type ion-exchange materials are of special benefit for protein chromatography. It has also been observed with other types of modified phases (e.g., in chiral ligand-exchange chromatography) that long and flexible spacers provide a higher efficiency owing to fewer steric constraints on the transition state in the adsorption–desorption path [57].

Immobilization of charge at the surface does not require chemical bonding of charged groups. Molecules containing acidic or basic groups and long alkyl chains can be used as mobile-phase additives in very low concentrations. They are adsorbed from the mobile phase onto alkylsilica-type surfaces, forming a "dynamically generated" ion exchanger. The mobile-phase concentration of these additives must be below their critical micellar concentration. Additives with short hydrophobic chains and with a charge complementary to that of the analyte are called *ion-pairing agents*. It depends on the length of the hydrophobic chain of the additive (in other words, on the activity coefficient of the additive in the mobile phase) whether the additive is predominantly in the mobile phase (forming an ion-pair with the analyte, which is subsequently adsorbed), or whether the additive is predominantly adsorbed onto the surface (forming a dynamically generated ion-exchange layer, onto which the analyte is adsorbed). In principle, the mechanism is the same. There is an inclination to address this mechanism as a secondary equilibrium.

IV. STATIONARY PHASES FOR SPECIAL TYPES OF CHROMATOGRAPHY

Ligands of special and analyte-tailored chemical design immobilized at the surface are used to create stationary phases for *affinity chromatography* and for the separation of *enantiomeric*

compounds. Specially deactivated surfaces, exhibiting (very) weak or practically no interactions with the analytes are employed for *hydrophobic–interaction chromatography* and for *size-exclusion chromatography*, respectively.

A. Affinity Chromatography

Affinity chromatography (AFC) is a separation method especially designed for the separation of biomolecules and biopolymers. It usually involves separations in which an ensemble of strong interactions effects strong and shape-specific binding of the analyte. Immobilized ligands and target analytes need to possess structurally complementary interacting moieties. This phenomenon is frequently addressed by the term *bioaffinity*. All types of interactions can be involved, even fast and reversible chemical reactions between analyte and ligand. AFC covers a broad spectrum of ligands and substrates. A list of frequently employed ligands is given, together with the corresponding group of target analytes in Table 9.

Immune affinity, enzyme–substrate affinity, nucleotide–protein affinity, and other affinity principles have been exploited. The following main types of affinity ligands can be identified: (1) immobilized protein A or G for binding antibodies; (2) immobilized antibodies for highly selective (specific) adsorption of immunogenic proteins; (3) dyes for adsorption of proteins, especially of enzymes binding to purine nucleotides; (4) immobilized ligands that mimic substrate molecules or cofactors for the separation of enzymes; (5) immobilized lectins for binding glycosylated proteins and peptides; (6) immobilized metal ions for adsorption of proteins rich in histidine and phosphorylated proteins and peptides; (7) immobilized boronic acid for binding planar *cis*-diolic groups of carbohydrates, nucleic acid components, and *o*-disubstituted diphenols; and (8) nucleotide sequences for binding complementary RNA or nucleic acid-binding proteins [58–60]. [Although a specific binding between ligand sites and analyte is the basis of retention, the structure and length of the spacer may have some influence on the accessibility of the active sites and, thus, on eventual features of an AFC phase.]

Elution from the affinity support is effected either by changing (frequently lowering) the pH (effective if electrostatic interactions are involved) or by adding high concentrations of

Table 9 Commercially Available Types of Affinity Phases for Liquid Chromatography[a]

Ligands	Target analytes
Protein A, protein G	Antibodies, IgG subclasses
Dyes	Nucleotide-binding and NADP-dependent enzymes
2′5′-ADP; 5′-AMP	NADP- and NAD-dependent dehydrogenases
Lectines	Carbohydrates, glycoproteins, membrane proteins, glycolipids; (specific for certain sugars)
Heparin	Coagulation factors, lipoproteins, lipases, steroid receptors, DNA-binding proteins, growth factors
Avidin	Biotinylated proteins
Imminodiacetic acid (IDA)	Histidine-rich proteins, phosphorylated proteins
Phenylboronic acid	*cis*-Vicinal diols in sugars, nucleotides, glycopeptides, glycoproteins, catecholamines
Oligo (dT)	mRNA
Oligo nucleotides	Nucleic acid-binding enzymes
Denatured DNA	Proteins binding to DNA

[a]All mentioned phases are available with ligands immobilized on cross-linked agarose beads (with particle diameters ≥30 μm) suited for "fast protein liquid chromatography" (FPLC). Some are available also based on silica or highly cross-linked polymers suited for use under high pressure (HPLC).

salts (NaCl up to 1 M) or chaotropic agents to the eluent. Such agents reduce the hydrogen-bonding as well as the hydrophobic interactions. Typically used chaotropic agents are urea, thiourea, sodium thiocyanate, and guanidine hydrochloride, applied in concentrations between 1 and even 6 M. (In higher concentrations there is a risk of denaturation of labile proteins.)

Affinity chromatography is primarily used for the enrichment of the target analytes and for their specific isolation from all other substances, which are not retained, in a sample. Separation between similarly retained substances using this method is not entirely practicable. AFC is operated most frequently in a yes/no mode, which implies strong specific retention (and enrichment) of the target compound, followed by prompt desorption and elution using as little eluent volume as possible. Such separations do not rely on high plate numbers and high peak capacities, as offered by small particles in HPLC. Less rigid support materials, with larger particle sizes and with lower pressure limits, based on agarose beads are frequently used for the preparation of AFC phases used in so-called fast-protein liquid chromatography (FPLC).

B. Chiral-Stationary Phases

Chiral stationary phases (CSPs) are the main tool for separating enantiomers by HPLC. A particular chiral phase is effective for only a certain kind (family) of chiral analytes, because there has to be a high degree of structural correspondence between the chiral *selector* (chiral stationary phase in this instance) and the *selectand* (chiral analyte to be separated). With chiral stationary phases, the chiral selector is either immobilized on a support material as a chiral surface ligand, or it is coated in the form of a chiral polymer. Several mechanisms of chiral recognition are described in the following. From these different mechanisms, a list containing the main groups of stationary phases can be given (Table 10).

An alternative strategy for chiral separation involves chiral selectors that are not immobilized onto a solid support, but are added to the mobile phase, in which they act through a secondary equilibrium. This will be discussed in Sec. V. The molecular mechanisms of steric recognition are very similar in both strategies.

Discrimination (recognition) of enantiomers is possible if the Gibbs free energies of the interaction with a chiral selector are different for the two enantiomeric selectands. Enantiomeric recognition needs an ensemble of interactions between at least three points of the selector and three points of one of the retained enantiomeric selectands (analytes) [61,62]. A schematic drawing illustrating selector–selectand interactions is given in Fig. 9. Interactions in this context can be attractive as well as repulsive, and steric hindrance (for adopting an optimum interaction position) is often a main factor. Generally, all types of attractive interactions between selector and selectand can be used for chiral recognition (i.e., dipole–dipole, charge–transfer, electrostatic, dispersive, or hydrophobic interactions). The strength and relative importance of these various interactions are influenced by the eluent composition. Nonpolar organic eluents enhance dipole–dipole and charge–transfer interactions, whereas aqueous eluents induce hydrophobic interactions. The main types of interactions needed to achieve stereorecognition thus determine the type of mobile phase to be employed. For the mobile phase, a distinction can be made between a normal-phase and a reversed-phase mode chiral chromatography. One must remember that, although the interactions between selector and analyte may be dominated by one type of interaction, chiral recognition always needs a set of interactions.

Various classification schemes have been proposed for chiral separations. To distinguish between mechanisms, the following may be useful.

1. Chiral recognition by the formation of 1:1 complexes between a surface-immobilized selector and a selectand in a broad sense, covering the following types of complexes.
   a. *Host–guest complexation* resulting in inclusion complexes between chiral analytes and chiral host molecules. Cyclic oligosaccharides (cyclodextrins) [63,64], chiral

Table 10 Commercially Available Types of Chiral Stationary Phases for HPLC

Selector	Mobile phase	Support material
Chiral host phases		
α-, β-, and γ-cyclodextrins	Aqueous (organic)	Chemically immobilized onto silica support
Derivatized cyclodextrins	Aqueous, organic	
Crown ethers	Aqueous	
Macrobiotics (e.g., vancomycin V)	Aqueous	
Chelation phases		
Amino acid–Cu^{2+}	Aqueous	Immobilized onto silica or polymer resins
Charge-transfer phases		
Chiral π-electron acceptors	Nonpolar organic	Immobilized onto silica
Chiral π-electron donators		
Chiral polymers		
Cellulose triacetate	Alcohols	Materials themselves (swollen microcrystalline)
Cellulose tribenzoate		
Cellulose esters	Nonpolar organic	Coated (or bonded) onto silica or aminopropyl-silica
Cellulose carbamates		
Amylose carbamates		
Helical poly(triphenylmethyl methacrylate)		
Chiral-derivatized polyacrylamides		
Proteins		
Serum albumins (BSA, HSA)	Aqueous	Chemically bonded to silica (or physically adsorbed)
Glycoproteins (AGP)		
Ovomucoid, cellulase		

crown ethers, and chiral macrocylic antibiotics are frequently used selectors in this group. All of these offer a variety of different interactions (hydrophobic, hydrogen-bonding, dipolar interactions, and in some cases electrostatic). These stationary phases are operated predominantly with mixed aqueous–organic mobile phases.

b. *Chelate complexation* involving an optically pure chiral selector, a central metal ion (most often Cu^{2+}) and the chiral analyte in the form of a ternary complex [65,66]: [chiral selector ligand–metal–chiral analyte].
Chiral discrimination is achieved if the two diastereomeric complexes

[(*R*)-selector–metal–(*S*)-analyte]
[(*R*)-selector–metal–(*R*)-analyte]

differ in their Gibbs energy of complex formation. Here, different binding strengths (retention factors) of the analyte enantiomers with the immobilized selector are observed. These stationary phases are operated with aqueous mobile phases.

c. *Charge–transfer complexes*, in which charge–transfer interactions of various types are decisive for stereorecognition. These include π–π interactions between activated (electron-rich) and deactivated (electron-poor) aromatic rigs, hydrogen-bonding, and acid–base interactions [67,68]. These interactions are emphasized in nonpolar eluents. Therefore, the mentioned separations are carried out in nonpolar organic mobile phases, which contain a few percent of a more polar modifier to tune retention.

2. Chiral recognition using *chiral polymers*. These polymers are usually carbohydrate-, polyacrylate-, or polyacryamid-based, and are coated (and fixed) onto the surface of the

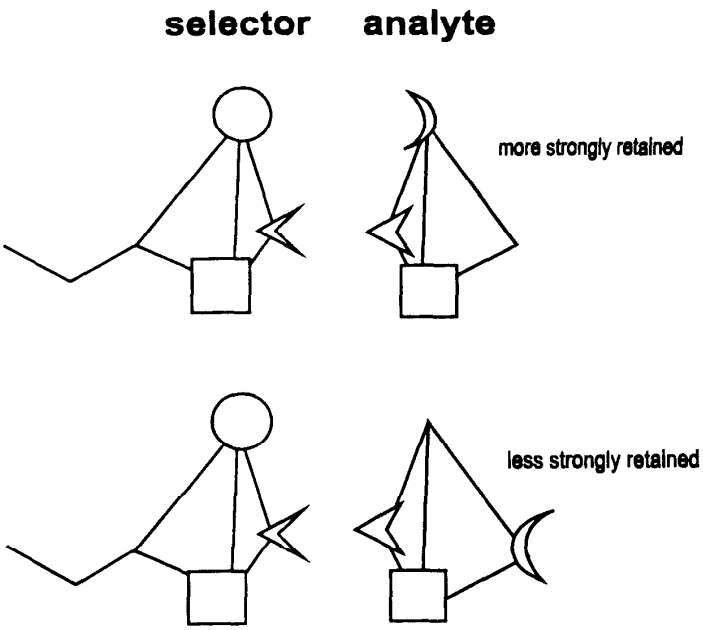


Figure 9 Schematic representation of interactions between an optically pure immobilized selector and enantiomeric analytes. Better correspondence of interaction sites results in stronger retention. Enantiorecognition requires at least three interactions with one enantiomer and a different strength of at least one interaction comparing the enantiomers.

support materials [69–71]. With some chiral or helical polymers, a surrounding of the analyte by the network, in a manner similar to an inclusion mechanism, is envisaged. In other cases, some kind of 1:1 complex between analyte molecules and the monomer units of the polymer appears to be the key to stereorecognition. Charge–transfer interactions are of significant importance, with most of these polymers, especially with those phases using substituted celluloses and amyloses. Eluents are predominantly nonpolar.

3. Chiral recognition by interactions with receptor-type sites of proteins [72,73]. Aqueous eluents are used for this.

A more detailed discussion of separation mechanisms, structures of selectors, mobile phases, separation conditions and optimization strategies is given elsewhere (see Chap. 21). The use of chiral selectors as mobile-phase additives; that is, the formation of diastereomeric complexes of the various types discussed in the foregoing (host–guest, chelate, and charge–transfer complexes) between the analytes and a sufficiently soluble selector in the mobile phase is briefly discussed in Sec. V.

C. Hydrophobic-Interaction Chromatography

Hydrophobic-interaction chromatography (HIC) is a separation method used primarily for the *separation of proteins* under mild conditions. HIC is carried out under reversed-phase conditions and with increased salt concentrations. When compared with usual RPLC, however, the density of alkyl ligands immobilized at the stationary phase is much lower for this purpose (about 10% of the usual RP materials) and very short alkyl chains are used (methyl to butyl, phenyl, polyether, or diol) [51]. Moreover, concentrations of the organic modifier in the aqueous phase are zero or only very small to minimize protein denaturing.

The retention mechanism in HIC is based on the decreased solubility of proteins at high concentrations of certain salts (particularly ammonium and sodium sulfate) in the mobile phase. Weak, mainly hydrophobic, interactions of outer protein regions with the short surface

ligands contribute to the retention. High salt concentrations strengthen these interactions and cause a reduced solubility of the proteins. The proteins are eluted with gradually decreasing salt concentrations during the run (e.g., from 0.5 to 1 M ammonium sulfate to 20 mM buffer solution).

The hydrophobicity of the surface ligands affects the retention. However, frequently polar surfaces can be used as well. (For these, the selectivity arises mainly from different solubilities in the salt solution.) Retention depends on the number of hydrophobic amino acids in the peptide or protein, on the clustering of hydrophobic regions, and on the folding of the protein. HIC thus discriminates according to the hydrophobicity of the outer protein regions. Salts usually employed in HIC are ammonium and sodium sulfate. Starting concentrations might be as high as 40% of the saturation levels.

D. Size-Exclusion Chromatography

Size-exclusion chromatography (SEC) is a separation method that discriminates according to the size of analyte molecules, it is employed particularly for the separation of polymers. [Size-exclusion effects can sometimes also be observed with small molecules. In swelled gels, such as triacetylated cellulose used as chiral discrimination media, analytes with bulky groups are excluded, whereas even larger planar aromatic compounds can easily access the adsorption sites.] A pure size-exclusion mechanism is characterized by the absence of any retention. Rather, separation in SEC is based on a selective "acceleration mechanism" by selective exclusion. Depending on the shape and size of the polymeric molecules, different percentages of the pore volume in the porous particles is accessible to the analytes, leading to differences in the total migration time through the column. Large molecules are eluted first, small analytes later. In pure size-exclusion chromatography using inactive surfaces, the last peak does not elute after t_{R0}, the migration time of the solvent molecules. In regular adsorption chromatography, this would be the beginning of the elution from the column.

Silica-based materials with wide and controlled pore size and deactivated (e.g., by immobilized diolic groups) can be used, as well as cross-linked gels, such as dextrines, dextrans, agarose, or synthetic three-dimensional cross-linked hydrophilic polymer gels, such as polyacrylates or polyacryl amides. The selectivity of the SEC materials is determined by the pore diameter. To minimize any retention of analytes, the stationary phase should have a polarity equal to that of the mobile phase.

Size exclusion chromatography has a wide application in protein separation and characterization of protein aggregation under mild conditions. It is extensively used for these purposes. It is also a method for getting rid of high salt concentrations after ion-exchange or affinity chromatography, with all these methods being operated with aqueous eluents. SEC is also frequently used for the separation and characterization of organic (synthetic) polymer samples, in these instances, using organic eluents, particularly THF.

V. USE OF SECONDARY CHEMICAL EQUILIBRIA

Secondary equilibria are of great importance in chromatography because they allow the chromatographer to introduce and control selectivity in a very effective way. They are most important in those instances for which the *species* in equilibrium *exhibit different retention* on the stationary phase. Even a small shift in the equilibrium can then result in strong changes in retention factors. The major equilibria involved in chromatography are as follows:

1. Acid–base equilibria controlling the dissociation and protonation of the analytes
2. Ion-pairing equilibria
3. Complex formation equilibria involving metal binding
4. Complex formation equilibria of the host–guest type

Different species may exhibit differently strong interactions with the stationary phase (i.e., different adsorption constants) and, in addition, different activity coefficients in the mobile phase [see Eq. (18)]. For equilibria in which neutral and ionic species are in equilibrium (e.g., with acid–base and many chelate-formation equilibria) the general case is that $\gamma_i^{(\text{ionic})\infty} \neq \gamma_i^{(\text{neutral})\infty}$. [Considering the chromatography of weakly acidic and weakly basic analytes: The electrostatic interactions with charged (ion-exchange) groups at the surface (and thus the retention of analytes) take place only with those analyte species that are charged at the pH of the mobile phase. In RPLC, hydrophobic adsorption (and retention) is usually lower for the charged analyte species.] Examples in which secondary equilibria have a significant influence on retention and selectivity are collected in Table 11.

A. Acid–Base Equilibria

Acid–base equilibria are extremely important in chromatography when aqueous mobile phases are used. They determine the degree of dissociation of weakly acidic groups and the degree of protonation of weakly basic groups, whether these groups are constituents of the analyte, constituents of the stationary phase (e.g., weak ion-exchanging groups or the silanol groups of the support material), or constituents of the buffer, or whether they belong to the matrix components of the sample. In all these instances, the pH of the aqueous mobile phase determines the position of the equilibrium and thus the retention and separation of the analytes.

1. pK_a Values and the Degree of Dissociation and Protonation

For weak acids or weakly acidic moieties within a molecule HA, which undergo dissociation in water according to the equilibrium

$$HA + H_2O \leftrightarrow H_3O^+ + A^- \tag{43}$$

with the equilibrium constant K_a,

$$K_a = \frac{[A^-][H_3O^+]}{[HA]} \tag{44}$$

the *degree of dissociation* α^d is defined as

Table 11 Secondary Chemical Equilibria Frequently Employed in HPLC

Analytes	Mobile phase	Stationary phase	Type of chromatography
Dissociation and protonation equilibria			
Acidic compounds	Aqueous	Anion-exchanger	IEC
		Alkyl–silica	RPLC
Basic compounds	Aqueous	Cation-exchanger	IEC
		Alkyl–silica	RPLC
Ion-pairing equilibria			
Charged analytes	Aqueous + ion-pairing reagent	Alkyl–silica	RPLC
Chelate complexation equilibria			
Charged ligands	Aqueous + metal ion	Alkyl–silica	RPLC
Metal ions	Aqueous + charged ligand	Ion-exchanger	IEC
		Alkyl–silica	RPLC
Host–guest complexation			
Organic compounds	Aqueous + host molecule	Alkyl–silica	RPLC

$$\alpha^d = \frac{[A^-]}{\{[A^-] + [HA]\}} \tag{45}$$

where square brackets symbolize the molar concentrations of the species. Combining the two equations yields the fundamental Eq. (46).

$$\alpha^d = \frac{1}{\{1 + [H_3O^+]/K_a\}} = \frac{1}{1 + 10^{(pK_a - pH)}} \tag{46}$$

This equation shows that the degree of dissociation is determined by the difference between the pH value of the mobile phase and the pK_a value of the compound.

An analogous formalism can be given for the *degree of protonation* α^p of weakly basic moieties B, according to the equilibrium (written here as deprotonation)

$$HB^+ + H_2O \leftrightarrow H_3O^+ + B \tag{47}$$

with the equilibrium constant K_a,

$$K_a = \frac{[B][H_3O^+]}{[HB^+]} \tag{48}$$

In this case, α^p is defined as

$$\alpha^p = \frac{[HB^+]}{\{[HB^+] + [B]\}} \tag{49}$$

B being the unprotonated basic species and HB^+ the protonated (acidic) species. The degree of protonation is given by Eq. (50).

$$\alpha^p = \frac{1}{\{1 + K_a/[H_3O^+]\}} = \frac{1}{1 + 10^{(pH - pK_a)}} \tag{50}$$

The graphs showing the degree of dissociation and protonation, respectively, according to the Eqs. (46) and (50) are given in Fig. 10. When the pH equals the pK_a, the degree of dissociation or protonation is ½. α^d and α^p change significantly only in a range of about 2 pH units on either sides of the pK_a value. Outside this range any changes in pH have a marginal influence on the dissociation or protonation and thus on the retention factor.

The pK_a values of many compounds of interest (analytes and buffer compounds) can be found in tables in the literature [76]. Given these data and with a certain chemical intuition one can very approximately "predict" pK_a values of homologous, analogous, and similar compounds not found in the tables. This might be quite useful during the development of a chromatographic method. Table 12 collects pK_a ranges typically found for some acidic and basic groups and Table 13 gives a collection of pK_a values for various selected molecules taken from the literature [76]. The table illustrates the influence of the molecular structural environment on the pK_a values of acidic and basic groups.

The K_a values given in tables are equilibrium constants in water under conditions of strong dilution (with very few exceptions). It is important to realize that a high ionic strength of the solution, and particularly the presence of organic solvents, substantially affect the value of K_a. The presence of buffer salts causes a shift in the pK_a, usually favoring the charged species (i.e., decreasing pK_a values for acids, increasing them for bases). The shift in pK_a values with the addition of organic solvent components is much stronger. Usually the pK_a values of acids become larger, indicating weaker dissociation [76]. With mobile phases containing high concentrations of organic modifiers, this pK_a shift can be more than 2 units [77]. Particularly, acetonitrile causes a significant increase in the pK_a values of acids, because it reduces the solvation of the anionic species. The dielectric constants of the solvent components play an important, but not exclusive, role in this context. Because the solvation of the charged species is critical, the ability of the solvent component to form hydrogen bridges or other charge–

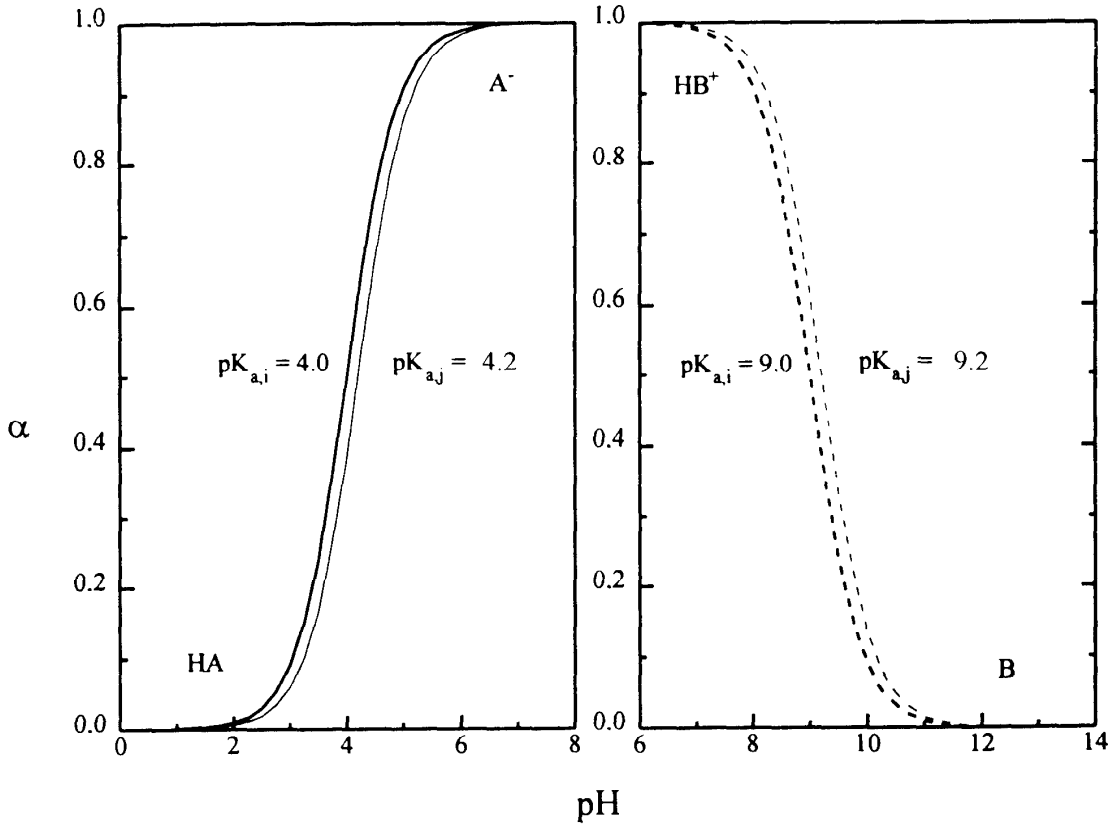


Figure 10 Degree of dissociation for two weak acids (pK_a = 4.0 and 4.2; left) and degree of protonation for two weak bases (pK_a = 9.0 and 9.2; right) as a function of pH.

Table 12 pK_a Ranges of Weakly Acidic and Protonated Weakly Basic Groups at 25°C

Moieties	Molecular environment	pK_a
–COOH	Carboxylic acids	4.5–5.0
	α-Amino acids	1.8–2.5
	α-Amido acids	3.5–4.0
–OH	Aliphatic	12–15
	Phenolic	9–10
	Mono-nitrophenols	7–8
$-NH_2$, –NHR, $-NR_2$	Aliphatic	9–11.5
	Aromatic[a]	4.5–5.5
	α-Amino acids	9–10
NH aromatic	[b]	5–6.5
$-CONH_2$, –CONHR	Amides	~0 to −1

[a]Such as aniline.
[b]Such as pyridine.

Table 13 pK_a Values in Water at 25°C

Acids	pK_{a_1}	pK_{a_2}	Protonated bases	pK_{a_1}	pK_{a_2}
Acetic acid	4.756		Ammonia	9.3	
Propionic acid	4.87		Triethylamine	10.75	
Octanoic acid	4.89		Trimethylamine	9.80	
Trifluoroacetic acid	0.52		Diethylamine	10.84	
Trichloroacetic acid	0.66[a]		Benzylamine	9.34	
Phenoxyacetic acid	3.17		Piperidine	11.12	
Phenylacetic acid	4.31		Pyrrolidine	11.31	
Benzoic acid	4.20		1,2-Diaminoethan	9.92	6.86
Methanol	15.5		Aniline	4.87	
Ethanol	15.5		*N*-Methylaniline	4.85	
Glucose	12.46		*o*-Chloroaniline	2.66	
Fructose	12.27		Pyridine	5.23	
Phenol	9.99		2-Methylpyridine	6.00	
o-Chlorophenol	8.56		Quinoline	4.90	
o-Nitrophenol	7.23		Isoquinoline	5.40	
2,4-Dinitrophenol	4.07				
2,4,6-Trinitrophenol	0.42				
1-Naphthol	9.39		Urea	0.10	
2-Mercaptoethanol	9.72		Thiourea	−1	
Oxalic acid	1.25	3.81	Acetamide	−1.4	
(−) Tartaric acid	3.03	4.37			
meso-Tartaric acid	3.17	4.91			
Citric acid	3.16	4.76			
		6.40			
Phthalic acid	2.94	5.43			
Amino acids					
	Acidic group			Basic group	
Glycine	2.35			9.78	
Alanine	2.34			9.87	
Phenylalanine	2.2			9.3	
Tryptophan	2.5			9.5	
Tyrosine	2.2	9.1		10.1	
Asparagine	2.1			8.7	
Arginine	1.8			9.0	12.5
Lysine	2.2			9.0	10.5
Histidine	1.8			6.0	9.3
Aspartic acid	2.0	3.9		10.0	

[a]Data refer to 20°C.
Source: Ref. 76.

transfer interactions with the charged species can be even more important. The pK_a shifts induced by the increased ionic strength and by the organic solvent components are dependent on the particular dissociation reaction and on the analyte structure. Thus, buffer concentration, ionic strength, and solvent composition may influence the selectivity of acid–base equilibria.

2. Influence of pH on Retention Factor and Selectivity Coefficient

According to the acid–base equilibrium, an acidic or basic analyte may exist in the form of several species in both phases. The retention factor k_i is defined in these instances as *total capacity factor* (i.e., the ratio of the total amounts of the analyte species in the two phases) [79].

$$k_i = \frac{\text{total amount of analyte species in the stationary phase}}{\text{total amount of analyte species in the mobile phase}} \tag{51}$$

To illustrate a simple, but frequently encountered case in chromatography, we assume a dissociation equilibrium of a monoprotic acid (equilibrium constant K_a) and distribution equilibria for two species (with the retention factors k_{HA} and k_{A^-}) to be operative in a chromatographic system:

$$\begin{array}{ccc} HA^m + H_2O & \xleftrightarrow{K_a} & A^{-m} \\ \downarrow k_{HA} & & \downarrow k_{A^-} \\ HA^s & & A^{-s} \end{array}$$

The superscripts m and s again indicate the species present in the mobile and stationary phase, respectively.

For these equilibrium reactions, the total capacity factor including all species k_i is

$$k_i = q \frac{[HA]^s + [A^-]^s}{[HA]^m + [A^-]^m} \tag{52}$$

q is the phase ratio (A^s/V^m) as usual.

Inserting Eq. (45) for the degree of dissociation and using equations analogous to Eq. (2) for the capacity factors of the species k_{A^-} and k_{HA}, the final equation [Eq. (53a)] is obtained for acidic and Eq. (53b) for basic analytes.

$$k_i = k_{A^-}\alpha_i^d + k_{HA}(1 - \alpha_i^d) \tag{53a}$$

$$k_i = k_{HB^+}\alpha_i^p + k_B(1 - \alpha_i^p) \tag{53b}$$

This equation indicates that the total retention factor is the weighted sum of the retention factors of the various species of the analyte. The weighting factors for charged species are the degree of dissociation and protonation, respectively. In many cases of ion-exchange chromatography with organic ions, hydrophobic adsorption of the charged analyte species takes place together with the ion-exchange mechanism. This is particularly true when using hydrophobic support materials or long hydrophobic spacers. Equation 53 accounts for both types of retention. The two special cases, for which either ion-exchange or reversed-phase mechanism are by far predominant will briefly be illustrated in the following.

(a) Ion-Exchange Mechanism. With a pure ion-exchange mechanism, the capacity factor of weakly acidic and weakly basic analytes simply increases proportionally to the degree of dissociation of the acids α_i^d, and the degree of protonation of the bases α_i^p, respectively. α_i^d as well as α_i^p are indicated here by α_i.

$$k_i = k_i^{IEX}\alpha_i \tag{54}$$

where k_i^{IEX} indicates the capacity factor of the fully dissociated or protonated analyte (k_{A^-} or k_{HB^+}). The variation of k with the pH of the eluent according to Eq. (54) for weakly acidic ($pK_a = 4.0$) and weakly basic compound ($pK_a = 9.0$) is given by the graph in Fig. 11.

The corresponding selectivity coefficients are given by:

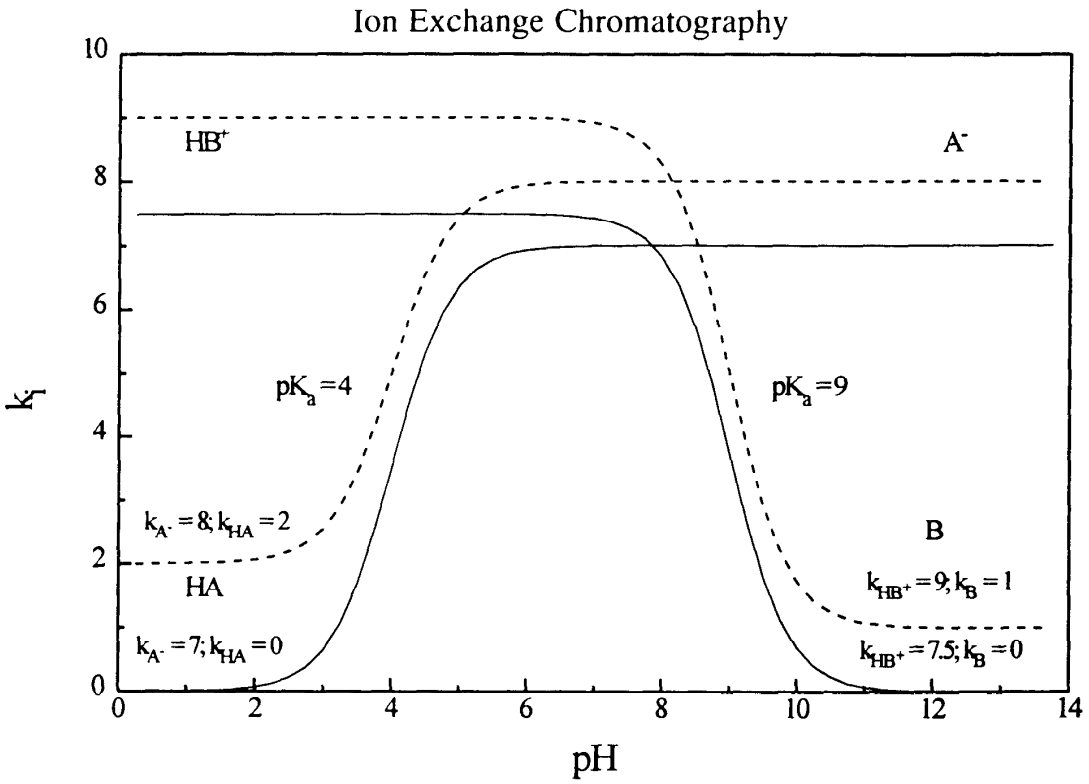


Figure 11 Calculated capacity factors of weak acids (pK_a = 4.0) and weak bases (pK_a = 9.0) as a function of pH. The pure ion-exchange mechanism is illustrated by the solid lines with $k_{HA} = 0$ and $k_B = 0$. The two other lines show a mixed retention mechanism, including slight retention of the uncharged species.

$$r_{j,i} = \left[\frac{k_j^{IEX}}{k_i^{IEX}}\right]\left[\frac{\alpha_j}{\alpha_i}\right] \tag{55}$$

Selectivity may result from both factors: (1) *different strength of interactions* of the fully charged analytes with the charged surface groups resulting in $[k_j^{IEX}/k_i^{IEX}] \neq 1$, and (2) from *different degrees of dissociation* (or protonation) at the chosen pH value, when $[\alpha_j/\alpha_i] \neq 1$. $[\alpha_j/\alpha_i]$ as a function of the pH is simply obtained by substituting Eqs. (46) and (50) for α, and is given by Eq. (56a) for acidic and (56b) for basic compounds.

$$\left[\frac{\alpha_j^d}{\alpha_i^d}\right] = \frac{[1 + 10^{(pK_{ai} - pH)}]}{[1 + 10^{(pK_{aj} - pH)}]} \tag{56a}$$

$$\left[\frac{\alpha_j^p}{\alpha_i^p}\right] = \frac{[1 + 10^{(pH - pK_{ai})}]}{[1 + 10^{(pH - pK_{aj})}]} \tag{56b}$$

The corresponding graphs exhibiting the variation of the degree of dissociation (protonation) with pH for slight differences in the pK_a values of two analytes are shown in Fig. 12.

For achieving optimum separation factors one must consider the following:

1. If selectivity results from differences in the k^{IEX} values only, the greatest selectivity is obtained at pH values at which the analytes are fully charged.
2. The selectivity arising from differences in the pK_a values of the analytes is highest (see Fig. 12) when the charge of the analytes is lowest. (In this region, however, there is only

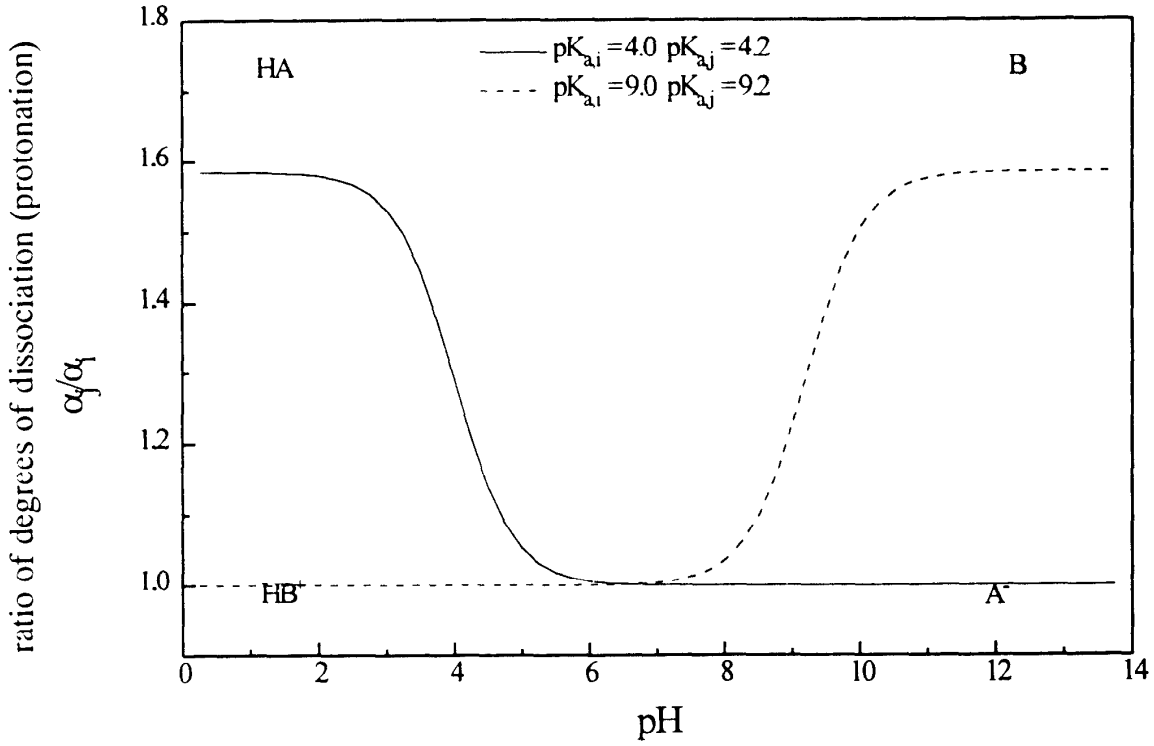


Figure 12 Calculated selectivity coeffcients based solely on differences in the pK_a values for ion-exchange chromatography. The solid line shows the ratio of the degrees of dissociation for two weak acids with pK_a values of 4.0 and 4.2. The dashed line shows the ratio of degrees of protonation for two weak bases with pK_a values of 9.0 and 9.2.

low retention in pure IEC. Maximum resolution can thus be exploited in the region near the pK_a value. In this region, however, it is essential to ensure close pH control to obtain adequate precision.)

When the k^{IEX} as well as the pK_a values differ between analytes, the pH optimum lies in between the extreme cases mentioned. However, inversion of elution order can happen in this region too, depending on the k^{IEX} and pK_a pairs of the analytes. For a mixed ion-exchange–hydrophobic adsorption mechanism Eq. (53) must be used for calculating retention and optimizing selectivity, depending on the pH of the eluent.

(b) Reversed-Phase Mechanism. Again, in RPLC, differently charged species are usually differently strongly retained. They generally exhibit not only different interactions with the surface, but also different activity coefficients in the mobile phase. As hydrophobic adsorption of neutral species is usually higher, the retention factors of weakly acidic analytes retained by an RP mechanism decrease with increasing dissociation of the analytes.

$$k_i = k_i^{\text{neutral}}(1 - \alpha_i) + k_i^{\text{ionic}}\alpha_i \tag{57}$$

where k_i^{neutral} and k_i^{ionic} indicate the capacity factors of the nondissociated (nonprotonated) neutral and the dissociated (protonated) ionic analyte, both according to a hydrophobic adsorption mechanism. The variation of the retention factor with pH according to Eq. (57) for an acidic and a basic analyte is given by the graph in Fig. 13. [The form of the curves is general for acidic and basic analytes. A combination of the curves for acids and bases will be obtained for zwitterionic analytes.]

The equation for selectivity coefficients is given by:

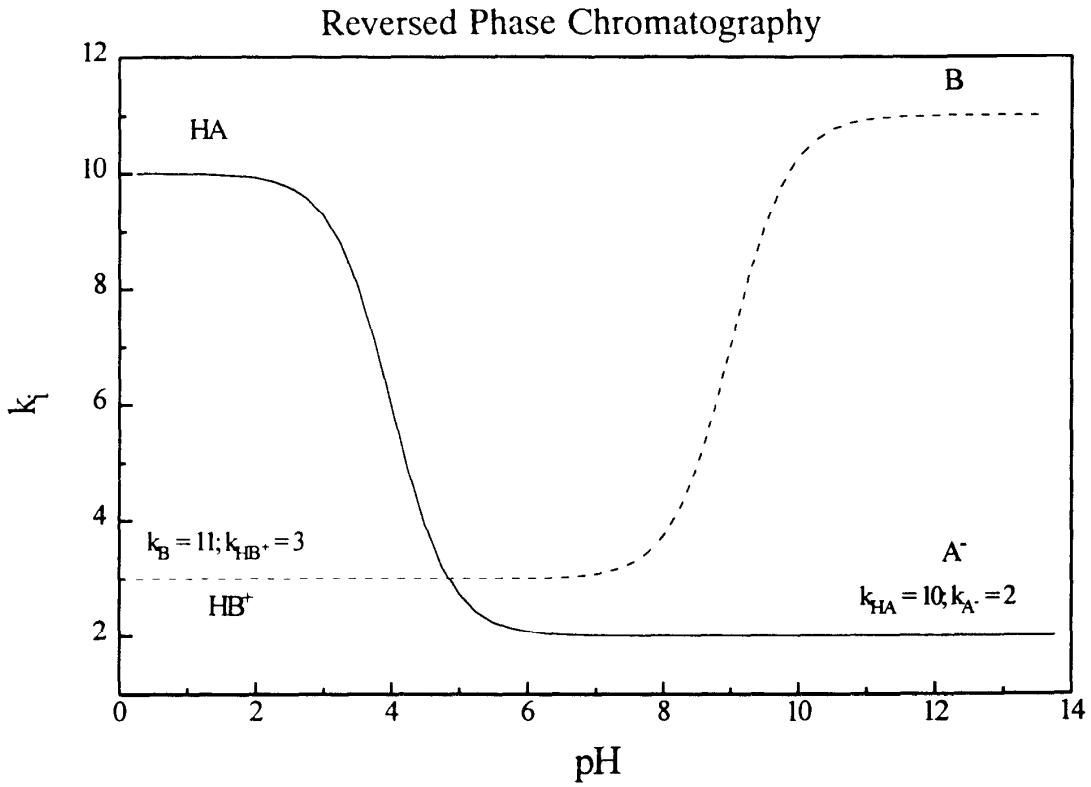


Figure 13 Calculated capacity factors of a weak acid (pK_a = 4.0; solid line) and a weak base (pK_a = 9.0; dashed line) as a function of pH. A mixed retention mechanism is assumed, in which the charged species are slightly retained.

$$r_{j,i} = \frac{[k_j^{\text{neutral}}(1 - \alpha_j) + k_j^{\text{ionic}}\alpha_j]}{[k_i^{\text{neutral}}(1 - \alpha_i) + k_i^{\text{ionic}}\alpha_i]} \tag{58}$$

If the adsorption of the ionic species is very low, Eq. (58) simplifies to

$$r_{j,i} = \left[\frac{k_j^{\text{neutral}}}{k_i^{\text{neutral}}}\right]\left[\frac{1 - \alpha_j}{1 - \alpha_i}\right] \tag{59}$$

Again, selectivity results either from different interaction strength with the surface (i.e. $[k_j^{\text{neutral}}/k_i^{\text{neutral}}] \neq 1$), or from different degrees of dissociation at the chosen pH value (i.e. $[(1 - \alpha_j)/(1 - \alpha_i)] \neq 1$). Figure 14 shows the graphs corresponding to Eq. (59). The agreement between experimental curves and the simulated curves is usually excellent.

(c) Electrophoresis. Electrophoresis, particularly when carried out in narrow (25- to 100-μm) capillaries (capillary electrophoresis; CE) and with applied voltages of 10–30 kV is a high-performance separation method that is based on the different fast migrations of charged compounds (dissolved in a buffered electrolyte solution) in the applied electric field. The migration velocity of a compound u_i is proportional to the electric field strength E in the capillary.

$$u_i = \mu_i E \tag{60}$$

The migration velocity under unit field strength is called *electrophoretic mobility* (μ_i). The mobility of a permanent ion or of a fully dissociated weakly acidic (fully protonated

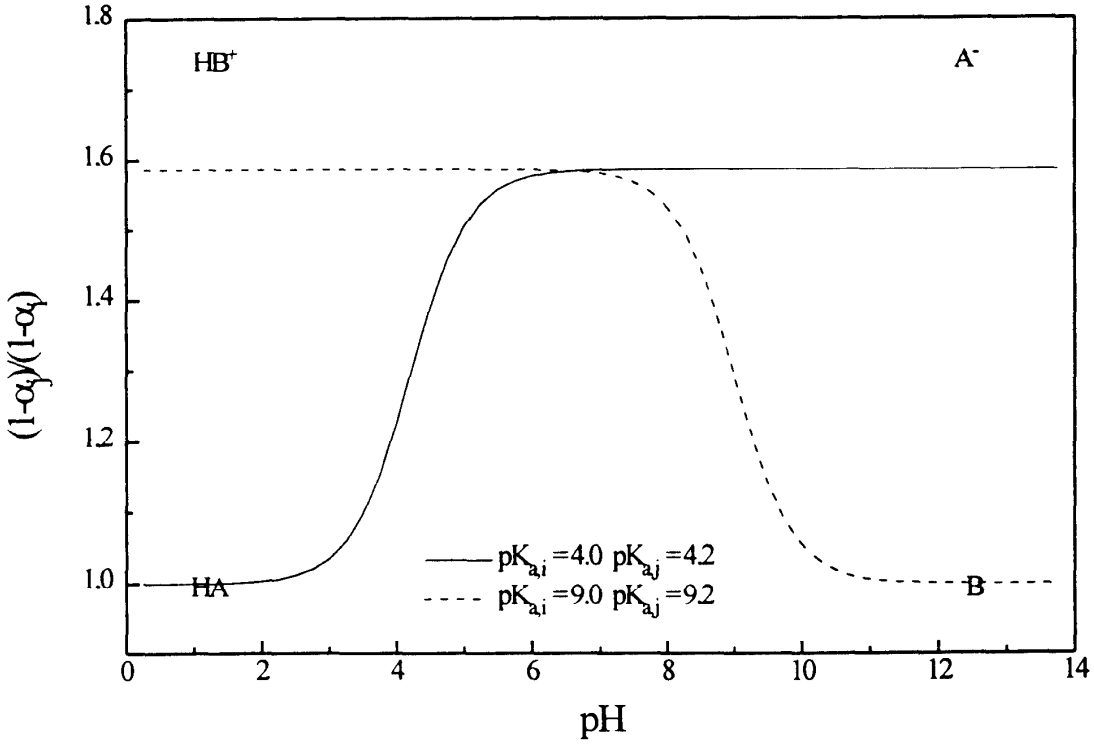


Figure 14 Calculated selectivity coefficients based solely on differences in the pK_a values for reversed-phase chromatography. The solid line shows the ratio of the degrees of nondissociation for two weak acids with pK_a values of 4.0 and 4.2. The dashed line shows the ratio of degrees of nonprotonation for two weak bases with pK_a values of 9.0 and 0.2.

weakly basic) analyte under the given ionic strength conditions of the solution is called the *actual mobility* (μ_i^{act}). The mobility that is decisive for the migration velocity of nonpermanent ions in electrophoretic systems, is the *effective electrophoretic mobility* (μ_i^{eff}), given by the actual mobility μ_i^{act} times the degree of dissociation (or protonation).

$$\mu_i^{eff} = \mu_i^{act}\alpha_i \tag{61}$$

The selectivity coefficient in capillary electrophoretic systems is defined by the ratio of the effective mobilities:

$$r_{j,i} = \left[\frac{\mu_j^{eff}}{\mu_i^{eff}}\right] = \left[\frac{\mu_j^{act}}{\mu_i^{act}}\right]\left[\frac{\alpha_j}{\alpha_i}\right] \tag{62}$$

With this definition the *resolution* in CE is obtained proportional to $(r_{j,i} - 1)$ and thus completely analogous to chromatography $R_{j,i} = (1/4)(r_{j,i} - 1)\sqrt{N_i}$.

In systems with electroosmotic flow (EOF) the electrophoretic mobility of the ions have to be corrected by the "mobility" resulting from the EOF, yielding "apparent" mobilities. The selectivity coefficients are then given as the ratio of the apparent mobilities.

Differences in the pK_a values of analytes are the major sources for selective separations in electrophoresis. The curves given for the ratio $[\alpha_j/\alpha_i]$ in Fig. 12 are equally valid for electrophoretic separations. For analytes of equal actual mobilities ($\mu_j^{act} = \mu_i^{act}$) maximum selectivity is again obtained in the region of low charge. In these instances, however, the migration times become long and peak dispersion is increased. In capillary electrophoresis, where several 100,000 theoretical plates can be achieved, very subtle differences in the pK_a

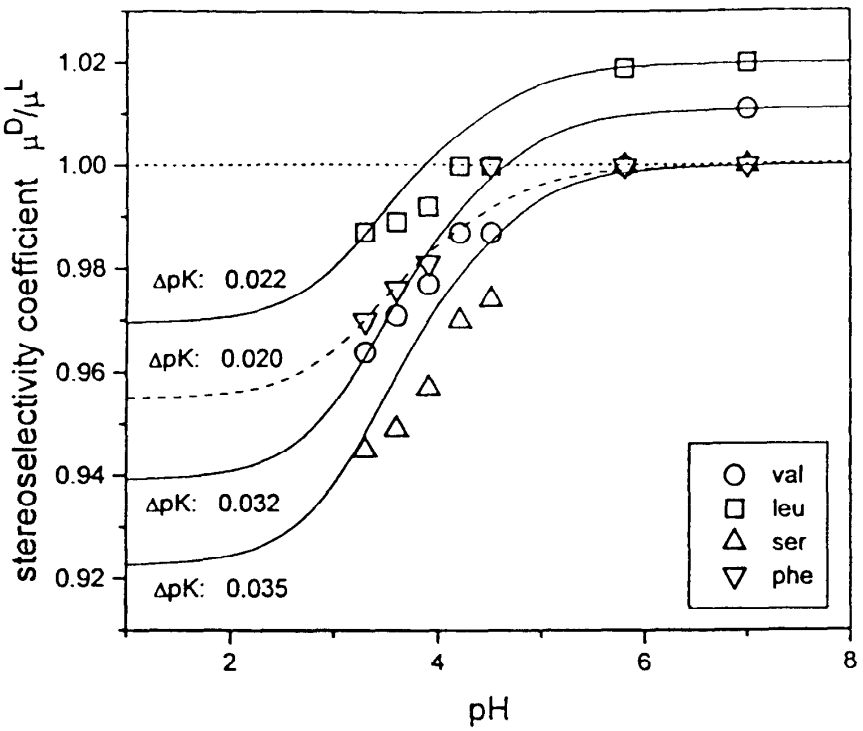


Figure 15 Stereoselectivity coefficients as dependent on the pH for four selected DBT-derivatized amino acids. The symbols represent the experimental data; curves are obtained by simulation using ΔpK_a values between the diastereomeric amino acid derivatives as given in the figure (DBT, dibenzoyl-tartaric acid). (From Ref. 78.)

values of two compounds, down to less than 0.01 units can be used to achieve separation. This is illustrated by data on (diastereomeric) derivatized amino acids given in Fig. 15.

3. Acid–Base Equilibria Involving Mobile and Stationary Phases

(*a*) *Buffer Systems.* Table 14 shows pK_a values of some buffers frequently used in chromatography. For CE a great number of further buffers are commonly used. Buffer systems should be chosen such that the pH value to be maintained by the buffer does not deviate from the pK_a value (or one of the pK_a values) of the buffer constituent(s) by more than 1 unit. The primary criterion for the selection of buffer systems is the pK_a range covered. However, other

Table 14 Dissociation Constants (pK_a values) of Buffer Compounds Frequently Employed in HPLC

Buffer	pK_{a1}	pK_{a2}	pK_{a3}
Phosphate	2.12	7.21	12.32
Citrate	3.16	4.74	6.40
Formate	3.75		
Acetate	4.75		
MES	6.15		
Glycylglycine	8.25		
Borate	9.24		

features, such as volatility, solubility, UV-absorbance, and chelating potential, may also be of great relevance. In CE, zwitterionic buffers are often preferred to avoid excessive heat production by buffer-induced conductivity.

(*b*) *Silanol Groups of the Support Material.* Acid–base equilibria in the stationary phases involve the silanol groups of silica gel, which exhibit pK_a values (in water) of about 5–6.5. Again, these values are shifted to higher values in the presence of high concentrations of organic solvent components, especially solvents, such as acetonitrile, that have low solvation power for anions. The dissociation of silanols affects (to an extent dependent on their accessibility) the retention of basic compounds in RPLC by offering cation-exchange sites.

The dissociation of silanol groups in aqueous environments causes the formation of an electric double layer constituted of the negatively charged surface and the positively charged layer of the solvated cations (H_3O^+, Na^+, K^+) that maintain the charge balance [80,81]. The potential difference (ζ-potential) between the surface and the layer is dependent on the degree of dissociation of the silanol groups, on the dielectric constant, and on the ionic strength of the solution, as well as on the concentration of organic solvent components.

The existence of an electric double layer with solvated counterions is the cause of a bulk flow, which arises with the application of an electric field. This bulk flow is called electroosmotic flow (EOF). It has been extensively used and studied in capillary electrophoresis. The (linear) flow velocity of the EOF u^{EOF} increases linearly with an increase in the ζ-potential and can thus be influenced by the eluent and particularly its pH value.

$$u^{EOF} = \frac{E\zeta\varepsilon}{\eta} \tag{63}$$

E being the electric field strength, ε the dielectric constant of the solution, and η its viscosity. The EOF can be used for the nonselective transport of (charged and uncharged) analytes in CE. The flow profile of the EOF is very flat (plug profile) and is thus not a source of peak-broadening. This is in contrast with the situation with parabolic flow profiles generated in pressure-driven chromatographic systems, such as HPLC (see Chap. 2). A chromatographic mode, in which the mobile phase is not driven by pressure, but electrically (by generating a sufficiently high EOF), has been established under the name capillary electrochromatography (CEC) [82]. Obviously, the dissociation of silanol groups of support particles plays a major role in this technique.

(*c*) *Ion-Exchange Groups.* The frequently used weak ion-exchange groups $-CH_2-COOH$ and the primary, secondary, and tertiary amino groups, $-CH_2-NH_3^+$, $-CH_2-RNH_2^+$, and $-CH_2-NR_2H^+$, exhibit pK_a values within the ranges shown in Table 12. Weakly acidic cation-exchangers should be operated at pH values no lower than about 6.5; weakly basic anion-exchangers not above pH values of about 7.5–8. If the pH value of the mobile phase used is too close to the pK_a value of the exchange groups, the number of charged groups available at the surface and, hence, the capacity factors of the analytes, may vary, with even small variations in the pH of the eluent. Such a situation would not allow a robust method to be established.

Strongly acidic groups (sulfonic acid) or strongly basic groups (quaternary ammonium) do not loose or change their charge in a pH range of 0–14. Hence, weakly acidic or weakly basic analytes are frequently separated using strongly basic or strongly acidic exchange materials. Conversely, strongly acidic or strongly basic analytes are typically separated using weakly basic or weakly acidic exchangers.

B. Complexation Equilibria

Complexation equilibria are very useful to establish (or improve) selectivity in liquid chromatography and particularly in electrophoresis. Chelate complexation, ion-pairing, and host–guest equilibria have been successfully employed [79,83,84].

Table 15 Secondary Chemical Equilibria and the Fundamental Equations Describing Capacity Factors and Electrophoretic Mobilities (middle column) and Position of Equilibrium (last column)

	General equation	
	$k_i = k_i^I \varphi_i^I + k_i^{II} \varphi_i^{II}$	—
	Acid–base equilibrium	
IEC/RPLC	$k_i = k_i^{ion} \alpha_i + k_i^{nonionic}(1 - \alpha_i)$	$\alpha_i^d = (K_{a_i}/[H_3O^+])/\{1 + K_{a_i}/[H_3O^+]\}$ [a]
CZE	$\mu_i = \mu_i^{ion} \alpha_i$	$\alpha_i^p = ([H_3O^+]/K_{a_i})/\{1 + [H_3O^+]/K_{a_i}\}$
	Ion-pairing	
RPLC	$k_i = k_i^{IP} \beta_i + k_i^{nonpaired}(1 - \beta_i)$	$\beta_i = ([IP]K_i^{IP})/\{1 + [IP]K_i^{IP}\}$
	Chelate complexation	
RPLC/IEC	$k_i = k_i^{cplx} \beta_i + k_i^{free}(1 - \beta_i)$	$\beta_i = ([L]K_i^{cplx})/\{1 + [L]K_i^{cplx}\}$ [b]
CZE	$\mu_i = \mu_i^{cplx} \beta_i + \mu_i^{free}(1 - \beta_i)$	
	Host–guest complexation	
RPLC	$k_i = k_i^{cplx} \beta_i + k_i^{free}(1 - \beta_i)$	$\beta_i = ([CD]K_i^{cplx})/\{1 + [CD]K_i^{cplx}\}$
CZE	$\mu_i = \mu_i^{cplx} \beta_i + \mu_i^{free}(1 - \beta_i)$	
	Micellar partitioning	
MEKC	$\mu_i = \mu_i^{mic} \beta_i + \mu_i^{free}(1 - \beta_i)$	$\beta_i = (k_i^{mic})/\{1 + k_i^{mic}\}$

α_i^d, degree of dissociation; α_i^p, degree of protonation; β_i, degree of complexation.

K_{a_i}, acid dissociation constant; K_i^{IP}, constant for ion-pairing; K_i^{cplx}, complexation constant; k_i^{mic}, distribution coefficient into micelle.

[IP], concentration of ion-pairing reagent; [L], concentration of chelating ligand; [CD], concentration of host molecule (e.g., cyclodextrin).

MEKC, micellar electrokinetic chromatography.

[a]For monoprotic acids.

[b]For 1:1 binary chelate complexes.

The influence of the equilibrium constants on the retention (or the migration in electrophoresis) can be understood in a manner analogous to that described before for acid–base equilibria. A prerequisite to achieve separation by means of complexation equilibria is, once again, that different species must show different retention (or migration when considering CE). As shown by Eqs. (51) and (53) the total capacity factor of an analyte can be evaluated by adding the contributions of the various species in equilibrium, weighted by the fraction of the analyte present as these species. In the simple case of two species, the former equations can be written more generally [Eq. (64a)].

$$k_i = k_i^I \varphi_i^I + k_i^{II} \varphi_i^{II} \tag{64a}$$

where *I* and *II* indicate the different species of the analyte in equilibrium and φ_i^I and φ_i^{II} are the weighting factors quantifying the relative amount of the indicated species in equilibrium; for instance, φ_i^I stands for the degree of dissociation, protonation, or for the degree of complexation, ion-pair formation, and such, and φ_i^{II} measures the probability of finding the nondissociated, unprotonated, or uncomplexed species. The selectivity coefficients can be obtained accordingly.

With simple secondary equilibria involving only two species, Eq. (64a) is widely applicable. The analogous equation giving the net mobility in capillary electrophoresis is obtained by replacing the capacity factors in Eq. (64a) by the effective electrophoretic mobilities, μ^{eff}:

$$\mu_i = \mu_i^I \varphi_i^I + \mu_i^{II} \varphi_i^{II} \tag{64b}$$

Table 15 provides a collection of various modifications of the general Eqs. (64a) and (64b) adapted to the particular equilibria encountered. (A treatment of *diprotic acids* and zwitterionic

compounds is given elsewhere [83].) The φ values for the species are obtained from the equilibrium constants by a quite uniform formalism. It can be seen that the previously discussed Eq. (53) is a special case of Eq. (64). Because φ depends on the concentration of the complexing additive (reagent), the selectivity coefficient will also be dependent on the additive concentration. Depending on the k^I and k^{II} (μ^I and μ^{II}) values of the analyte species maximum values are found in the selectivity versus additive concentration curves.

1. Ion-Pairing and Chelation Equilibria

Various cases of complexation equilibria can be distinguished, depending on, whether the complex is adsorbed more strongly onto the stationary phase than the noncomplexed species, or whether it is adsorbed more weakly. A frequent situation found is that a neutral complex is formed from a charged analyte, X_i^{n-}, and an oppositely charged mobile-phase additive, Y^{n+}.

$$\begin{array}{ccc} X_i^{n-} + Y^{n+} & \xleftrightarrow{K_i^{cplx}} & X_iY \\ \downarrow k_i^{free} & & \downarrow k_i^{cplx} \\ X_i^{n-s} & & X_iY^s \end{array} \tag{65}$$

Such a situation is often given with ion-pairing and chelate formation equilibria (see following Examples A1 and A2). Other examples for which different equilibria are involved are also indicated.

		Mode	Examples
Neutral complex more strongly adsorbed	($k_i^{cplx} > k_i^{free}$)	RPLC	Ion-pairing (see A1) Chelate complexes (see A2)
Noncomplexed (charged) species more strongly adsorbed	($k_i^{cplx} < k_i^{free}$)	IEC	Chelate complexes (see B)
Charged complex more strongly adsorbed	($k_i^{cplx} > k_i^{free}$)	IEC	Inorganic complexes (see C)

For all the mentioned types of complexes—and in complete analogy to the acid–base equilibria—the selectivity between two analytes can arise from two factors:

1. The retained species (e.g., the analyte–additive complexes) may exhibit different capacity factors, $k_i^{cplx} \neq k_j^{cplx}$.
2. The complexation constants K^{cplx}, may be different: $K_i^{cplx} \neq K_j^{cplx}$.

See the equations in Table 15.

Typical examples for the mentioned situations are given in the following:

Example A1: *Ion-Pairing*

Ion-pairing equilibria are usually employed in aqueous environments using RPLC. Typical ion-pairing additives to the mobile phases are tetraalkyl ammonium cations and trifluoroacetate anions. An example will be given, in which diastereomeric ion-pairs of enantiomeric analytes are separated in organic mobile phases using straight-phase chromatography.

Example A2: *Chelate Complexes Strongly Retained*

Chelate complexes can be formed between heavy metal ions (particularly Cu, Zn, Pb, or other) and analytes that contain structural groups that may form a coordinative binding with

these metal ions. Such groups are typically carboxy, amino, amide, and mercapto-groups, and to a lesser extent also hydroxy and ether groups. Strong binding is often observed for ligands containing two such complexing groups (bidentate ligands); for example, α-amino acids, α-hydroxy acids, diamines, and such.
With divalent metal ions ternary complexes are frequently formed between one metal ion and two ligand ions.

$$2L^- + Me^{2+} \leftrightarrow [L - Me - L] \tag{66}$$

Strong retention for neutral complexes can be used to determine either the ligand or the metal ion. The nonanalyte partner is introduced as an additive to the mobile phase. Chelating buffer ions (such as phosphate, acetate, citrate, ammonium) act as competitors for the complexing reaction between metal and ligand, thereby reducing the degree of complexation. Complexation constants are highly dependent on the pH of the solution, because, nearly always, weakly acidic and weakly basic groups are involved.
Chelate complexation involving ternary complexes can be successfully applied to separate enantiomers [65,66,85–87]. Such an example is discussed in Example D.

Example B: *Chelate Complexes More Weakly Retained*

The analyte–additive complex formed may be more weakly adsorbed onto the stationary phases than the noncomplexed species. Selectivity can be gained mainly by the selectivity of the complex formation reaction (i.e., different complexation constants for different analytes). A well-known example is the HPLC separation of rare-earth elements by complexation with α-hydroxyisobutyric acid [89]. The complexation constants decrease in the order Yb > Ho > Dy > Gd > Eu > Nd > Ce > La. The strongest complex (Yb) is eluted first when using an cation-exchange stationary phase.

Example C: *Charged Complexes Retained*

A classic example of preparatively used separations of metal cations is the selective formation of negatively charged chloride complexes in solutions with high concentrations of hydrochloric acid and the separation of the complexes by anion-exchange chromatography (using inert polymeric supports because of the extreme pH conditions) [90].

$$n\mathrm{Cl}^- + \mathrm{Me}^{m+} \leftrightarrow [\mathrm{MeCl}_n]^{(n-m)-}$$

Example D: *Diastereomeric Chelate Complexes for Enantiomer Separation*

Enantiomeric analytes, $A^-_{(R)}$ and $A^-_{(S)}$, which are bidentate ligands that can be incorporated [by the ligand-exchange reaction; Eq. (67)] into ternary complexes with the added metal ion and the added optically pure selector ligand $S_{(S)}$, form two types of complexes that are diastereomeric to each other.

$$\begin{aligned} [S_{(S)}\text{–Me–}S_{(S)}] + A^-_{(S)} &\leftrightarrow [S_{(S)}\text{–Me–}A_{(S)}] + S^-_{(S)} \\ [S_{(S)}\text{–Me–}S_{(S)}] + A^-_{(R)} &\leftrightarrow [S_{(S)}\text{–Me–}A_{(R)}] + S^-_{(S)} \end{aligned} \tag{67}$$

Figure 16 shows schematically two diastereomeric complexes formed between L-proline (as selector) and an L- and D-amino acid, respectively.

The two equilibrium constants for the two ligand–exchange reactions are $K^{\mathrm{cplx}}_{(S,S)}$ and $K^{\mathrm{cplx}}_{(S,R)}$, respectively. Complexed enantiomers can be separated by simple chromatographic means, without a need for chiral stationary phases, if either the complexation constants for the two diastereomeric complexes differ ($K^{\mathrm{cplx}}_{(S,S)} \neq K^{\mathrm{cplx}}_{(S,R)}$), or if the adsorption equilibrium onto the surface is sufficiently different for the two diastereomeric complexes ($k^{\mathrm{cplx}}_{(S,S)} \neq k^{\mathrm{cplx}}_{(S,R)}$).

Analogous equilibria have been used with optically pure ion-pairing additives, $IP^+_{(S)}$ [Eq. (68)]:

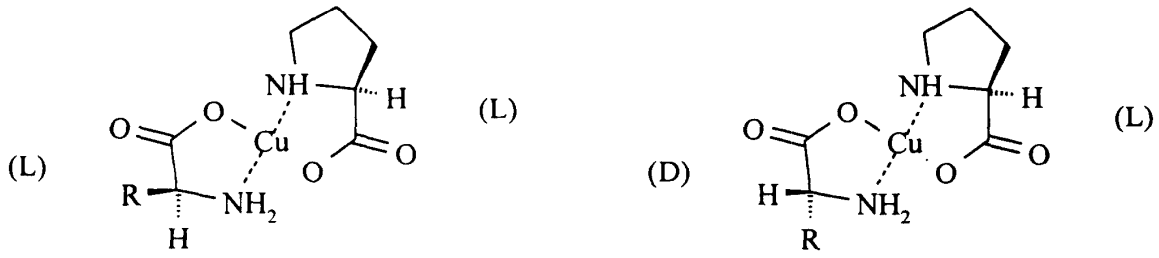


Figure 16 Schematic drawing of the two diastereomeric chelate complexes formed between L-proline and an (L)- and (D)-amino acid enantiomer, respectively. (According to Ref. 65.)

$$A^-_{(S)} + IP^+_{(S)} \leftrightarrow A_{(S)}\text{–}IP_{(S)}$$
$$A^-_{(R)} + IP^+_{(S)} \leftrightarrow A_{(R)}\text{–}IP_{(S)} \qquad (68)$$

The two equilibrium constants for the two ion-pairing reactions are $K^{IP}_{(S,S)}$ and $K^{IIP}_{(S,R)}$, and the capacity factors of the two diastereomeric ion-pairs are $k^{IP}_{(S,S)}$ and $k^{IP}_{(S,R)}$. In these instances, nonpolar mobile phases are employed [88] for the separation of the diastereomeric ion-pairs.

2. Host–Guest Complexation Equilibria

Host–guest complexation equilibria are frequently used for the separation of isomers and particularly enantiomers. For this purpose chiral host molecules are employed. By far the widest used chiral hosts are the cyclodextrins. [Cyclodextrins are cyclic oligosaccharides consisting of six, seven, or eight glucose units, cyclically connected by a 1,4-glycoside linkage. Depending on the number of glucose units they are called α-, β-, and γ-cyclodextrins, respectively.] Cyclodextrins are added as chiral selectors to the mobile phase in HPLC or to the background electrolyte in CE.

These host–guest equilibria are the main tool for introducing enantioselectivity in capillary electrophoresis [91] and are extensively used there. The electrophoretic mobilities of charged analytes decrease more, the higher the degree of complex formation with the (uncharged or oppositely charged) cyclodextrin host. Strong complexation results in slow migration velocity. Native and various derivatized (neutral or charged) cyclodextrins are commercially available (e.g., fully or partially methylated, hydroxyalkylated, carboxymethylated, and other). Derivatized forms offer additional types of interactions between analyte and selector that might contribute to improved enantiorecognition or—if the derivatives are charged—can act as a "carrier." Further chiral additives employed, particularly in CE, are chiral crown ethers and macrocylic antibiotics (for the applicable equations see Table 15).

Analysis by HPLC with cyclodextrins is commonly performed in an aqueous environment by RP-type chromatography. The rather polar native (underivatized) cyclodextrin as well as the host–guest complexes formed with the analytes are only very weakly adsorbed under typical reversed-phase conditions. The higher the degree of complex formation the less is the observed retention factor. The elution sequence is thus opposite to that obtained with surface-immobilized cyclodextrins (chiral stationary phases). This might offer considerable advantages with certain separation problems.

C. Partition Equilibria into Pseudophases

Partition equilibria into micellar pseudophases are elegantly used in CE. This technique is called micellar electrokinetic chromatography (MEKC) [92] and will be described in Chap. 4. It is mentioned here, because effective mobilities in micellar systems can be calculated using the simple Eq. (64b). The weighting factors for a simple partition equilibrium are given

in Table 15. To show the analogy of all equations, the partition coefficient into the pseudophase k_i^{mic}, may be considered equal to the product of the equilibrium constant for the partition reaction K_i^{part} multiplied by the concentration of the micelle [MIC].

$$k_i^{mic} = [MIC]\ K_i^{part} \tag{69}$$

Charged micelles are a main tool for separating neutral analytes in CE. Selective migration of neutral analytes in such electrophoretic systems arises from selective partitioning of the analytes between the electrolyte and the (migrating) micellar pseudophase.

REFERENCES

1. W Müller. Eur J Biochem 155:203, 1986.
2. M Cichna, P Markl, JFK Huber. J Pharm Biomed Anal 13:339–351, 1995.
3. WD Conway. Countercurrent Chromatography, Apparatus, Theory and Applications. New York: VCH Publishers, 1990, Chap. 5–7.
4. GE Berendsen, PJ Schoenmakers, L de Galan, G Vigh, Z Varga-Puchony, J Inczédy. J Liq Chromatogr. 3: 1669, 1980.
5. JM Prausnitz. Molecular Thermodynamics of Fluid-Phase Equilibria. Englewood Cliffs, NJ: Prentice-Hall, 1969, p 181.
6. DH Everett. Trans Faraday Soc 60:1803–1813, 1964.
7. DH Everett. Trans Faraday Soc 61:2478, 1965.
8. J Ościk. Adsorption. Warsaw, Poland: PWN-Polish Scientific Publishers, 1982, p. 109.
9. AL Myers. AIChE J 29:691, 1983.
10. A Rizzi. J Chromatogr 348:1–25, 1985.
11. W Rudziński, J Narkiewicz-Michalek, R Schöllner, H Herden, WD Einicke. Acta Chim Hung 113:207–224, 1983.
12. JH Hildebrand, JM Prausnitz, RL Scott. Regular and Related Solutions. New York: Van Nostrand Reinhold, 1970.
13. GM Wilson. J Am Chem Soc 86:127, 1964.
14. H Renon, JM Prausnitz. AIChE J., 14:135, 1968.
15. DS Abrams, JM Prausnitz. AIChE J. 21:116, 1975.
16. EL Derr, CH Deal. Ind Chem Eng Symp Ser 32:40, 1969.
17. A Fredenslund, RL Jones, JM Prausnitz. AIChE J. 21:1086, 1975.
18. A Rizzi, JFK Huber. Ind Eng Chem Process Design Dev 20:204–210, 1981.
19. GJ Pierotti, CH Deal, EL Derr. Ind Eng Chem Addendum ADI 5782 51:95, 1959.
20. A Fredenslund, RL Jones, JM Prausnitz. AIChE J 21:1086 (suppl), 1975.
21. R Tijssen, HAH Billiet, PJ Schoenmakers. J Chromatogr 122:185, 1976.
22. BL Karger, LR Snyder, C Eon. J Chromatogr 125:71, 1976.
23. PJ Schoenmakers, HAH Billiet, L de Galan. Chromatographia 15:387–398, 1982.
24. PJ Schoenmakers. Optimization of Chromatographic Selectivity, a Guide to Method Development. Journal of Chromatography Library, vol 35. Amsterdam: Elsevier, 1986.
25. E Soczewiński, G Matysik. J Chromatogr 32:458, 1968.
26. E Soczewiński. Anal Chem 41:179, 1969.
27. S Hara, Y Fujii, M Hirasawa, S Miyamoto. J Chromatogr 149:143–159, 1978.
28. E Soczewiński, J Jusiak. Chromatographia 14:23–31, 1981.
29. S Hara, K Kunihiro, H Yamaguchi, E Soczewiński. J Chromatogr 239:687, 1982.
30. LR Snyder. Principles of Adsorption Chromatography. New York: Marcel Decker, 1968.
31. LR Snyder. Anal Chem 46:1384, 1974.
32. LR Snyder, H Poppe. J Chromatogr 184:363–413, 1980.
33. LR Snyder, JL Glajch. J Chromatogr 248:165–182, 1982.
34. DL Saunders. J Chromatogr Sci 15:372, 1977.
35. RPW Scott, P Kucera. J Chromatogr 112:425, 1975.

36. P Jandera, J Churáček. J Chromatogr 91:207, 1974.
37. J Narkiewicz, M Naroniec, M Borowko, A Patrykiejew. J Chromatogr 157:1–5, 1978.
38. JE Paanakker, JC Kraak, H Poppe. J Chromatogr 149:111, 1978.
39. EJ Slaats, JC Kraak, WJT Brugman, H Poppe. J Chromatogr 149:255, 1978.
40. RW Perry, PF Tiley. J Chem Soc Faraday Trans I 74:1655, 1978.
41. PJ Schoenmakers, HAH Billiet, L de Galan. J Chromatogr 185:188, 1979.
42. KK Unger. Porous Silica, Its Properties and Use as Support in Column Liquid Chromatography. J Chromatogr Library, vol 16, Amsterdam: Elsevier, 1979.
43. J Ugelstad, L Soderberg, A Berge, J Bergstrom. Nature 303:95, 1983.
44. C Huber, P Oefner, G Bonn. J Chromatogr 599:113–118, 1992.
45. C Huber, P Oefner, G Bonn. Chromatographia 37:653, 1993.
46. ChromBook. Darmstadt: Merck KGaA, 1995.
47. H Engelhardt, H Elgass. Liquid chromatography on silica and alumina as stationary phases. In: C Horváth, ed. High Performance Liquid Chromatography, Advances and Perspectives, vol 2, New York: Academic Press, 1980, pp 57–111.
48. K Unger. Angew Chem 84:331, 1972.
49. G Schomburg. LC–GC 6:36, 1988.
50. JH Knox, B Kauer, GR Millward. J Chromatogr 352:3, 1986.
51. R Eksteen. Column selection in high performance liquid chromatography. In: ED Katz, ed. High Performance Liquid Chromatography: Principles and Methods in Biotechnology. Chichester: John Wiley & Sons, 1996.
52. B Feibush, MJ Cohen, BL Karger. J Chromatogr 282:3, 1983.
53. C Souteyrand, M Thibert, M Caude, R Rosset. J Chromatogr 262:1, 1983.
54. GE Berendsen, L de Galan. J Chromatogr 196:21, 1980.
55. B Kauer. LC–GC 8:468, 1990.
56. C Jansen. In: MERCK-Spektrum (Darmstadt) Sonderheft Chromatographie. 1991, p 71.
57. B Feibush, MJ Cohen, BL Karger. J Chromatogr 282:3, 1983.
58. RK Scopes. Protein Purification Principles and Practice, 2nd ed. New York: Springer Verlag, 1987.
59. TM Phillips. Adv Chromatogr 29:293, 1989.
60. A Rizzi, I Maurer-Fogy. Sample preparation. In: ED Katz, ed. High Performance Liquid Chromatography: Principles and Methods in Biotechnology. Chichester: John Wiley & Sons, 1996, pp 271.
61. CE Dalgliesh. J Chem Soc 3940, 1952.
62. VR Meyer, M Rais. Chirality 1:167, 1989.
63. WL Hinze, TE Riehl, DW Armstrong, E DeMond, A Alak, T Ward. Anal Chem 57:237, 1985.
64. SH Lee, A Berthod, DW Armstrong. J Chromatogr 603:83, 1992.
65. VA Davankov, AA Kurganov, AS Bochkov. Adv Chromatogr 22:22, 1983.
66. VA Davankov. J Chromatogr A 666:55–76, 1994.
67. WH Pirkle, TC Pochapsky. Chem Rev 89:347, 1989.
68. CJ Welch. J Chromatogr A 666:3–26, 1994.
69. G Blaschke, W Fraenkel, W Bröker. Angew Chem Int Ed Engl 25:830, 1986.
70. Y Okamoto, M Kawashima, K Yamamoto, K Hatada. Chem Lett 739, 1984.
71. Y Okamoto, Y Kaida. J Chromatogr A 666:403–419, 1994.
72. J Hermansson. Trends Anal Chem 8:251, 1989.
73. SG Allenmark, S Andersson. J Chromatogr A 666:167–179, 1994.
74. Y Kato. Adv Chromatogr 26:97–116, 1992.
75. PL Dubin. Adv Chromatogr 31:119–152, 1992.
76. A Albert, EP Serjeant. The Determination of Ionization Constants, A Laboratory Manual, 3rd ed. London: Chapman & Hall, 1984.
77. E Kenndler, P Jenner. J Chromatogr 390:169–184, 1987.

78. W Schützner, S Fanali, A Rizzi, E Kenndler. J Chromatogr A 719:411–420, 1996.
79. BL Karger, JN LePage, N Tanaka. Secondary chemical equilibria in high-performance–liquid-chromatography. In: C Horváth, ed. High-Performance–Liquid Chromatography, Advances and Perspectives, vol. 1. New York: Academic Press, 1980, p 113.
80. SFY Li. Capillary Electrophoresis—Principles, Practice and Applications. Journal of Chromatography Library. Amsterdam: Elsevier Scientific, 1992.
81. HC Hamann, W Vielstich. Elektrochemie I. Weinheim: Verlag Chemie, 1985.
82. H Yamamoto, J Baumann, F Erni. J Chromatogr 593:313, 1992.
83. WR Melander, C Horváth. Reversed-phase chromatography. In: C Horváth, ed. High-Performance–Liquid Chromatography, Advances and Perspectives, vol 2. New York: Academic Press, 1980, p 229.
84. S Terabe, K Otsuka, H Nishi. J Chromatogr A 666:295–319, 1994.
85. W Lindner, JN LePage, G Davies, DE Seitz, BL Karger. J Chromatogr 185:323–344, 1979.
86. S Lam, F Chow, A Karmen. J Chromatogr 199:295–303, 1980.
87. E Grushka, R Leshem, C Gilon. J Chromatogr. 255:41–50, 1983.
88. C Pettersson, E Heldin. Ion-pair chromatography in enantiomer separations. In: G Subramanian, ed. A Practical Approach to Chiral Separations by Liquid Chromatography. Weinheim: Verlag Chemia, 1994, p 279.
89. JA Tielrooy, JC Kraak, TJM Maessen. Anal Chim Acta 176:161–174, 1985.
90. Y Marcus, AS Kertes. In: Ion Exchange and Solvent Extraction of Metal Complexes. London: John Wiley & Sons, 1969.
91. S Fanali. J Chromatogr 474:441–446, 1989.
92. S Terabe, K Otsuka, K Ichikawa, A Tsuchiya, T Ando. Anal Chem 56:111–113, 1984.

2

The Mechanisms and Importance of Zone-Spreading

Robert Tijssen

University of Amsterdam, Amsterdam, The Netherlands

I. INTRODUCTION

Chromatography, by definition, is a separation methodology for multicomponent sample mixtures, based on the selective movement (or differential migration) of individual component zones of the sample. An essential feature of chromatographic separations is that the components of the sample are transported through a separating medium, often within the closed environment of a tubular column. The differences in interaction with the medium lead to a selective redistribution of the component zones from a commonly shared region or zone at the start after injection, toward largely individual regions inside or outside the separating medium. In the latter event, elution from the separation column takes place and the appearance of individual component zones in time can be recorded, with the aid of a detector, as the chromatogram. The goal of the separative operation is to obtain a more or less complete separation of the original mixture in its individual chemical constituents. This is achieved by subjecting solute molecules to *regions with different velocity*, thereby creating velocity differences which, for different components, lead to selective movement of the respective zones. In chromatography, solutes are distributed selectively between the stationary- and mobile-phase regions inside the separation column, and separation occurs because the mobile-phase region undergoes a flowing movement relative to the immobile stationary region. If the mobile-phase region were stopped in its movement from time to time, as happens, for example, in countercurrent distribution (CCD) in a train of discrete extraction vessels, full thermodynamic equilibrium partitioning of solute molecules between the two phases would be obtained within a finite time interval. This is caused by the fairly rapid movement of individual molecules (e.g., by diffusion), which creates the possibility for exchange of molecules between the phases. In chromatography, however, where the mobile phase is flowing continuously, mass exchange between the phases may be rapid, and equilibrium may be approached, but never reached. This is because the continuous flow disturbance of the mobile-phase region of the zone, possibly with the exception of the zone's center [1] (see Sec. II.C). Consequently, the peak center will move under equilibrium conditions, the very reason why the migration equations for retention times or volumes are validly written in terms of equilibrium concentrations c^* and equilibrium partition coefficients K^* (see Chap. 1).

This chapter is dedicated to the memory of J. Calvin Giddings (1996 †).

Furthermore, the migration of individual molecules in sample zones through the separating medium occurs at almost the same speed because zone integrity for each component is largely maintained in the chromatogram. Indeed, narrow peaks can be obtained, especially for smaller solute molecules that rapidly diffuse through the phase regions. Thus, a quick shuttling of molecules between both regions, prevents molecules in the moving regions from getting far ahead of molecules in stationary regions. Although in the strict sense, equilibrium partitioning can never be obtained in chromatographic techniques, rapid mass exchange actually leads to a condition of *virtual* or *near equilibrium.*

However, small differences in the individual velocities of the molecules within each component zone lead to a spread in residence times. This is called band-, zone-, or peak-broadening or, alternatively, dispersion. It stems from the universal and unavoidable thermodynamic inclination toward disorder. This results in the observed peak shapes and widths, which may oppose the separation obtained between zones.

Giddings, in his masterpiece textbook [1], phrased the intricate balance between selectivity and opposing blurring of zones as follows: *Separation is the art and science of maximizing separative transport relative to dispersive transport.*

In other words, although the displacement of the components should be selective (i.e., different for all components), we need to limit the dispersive transport of the molecules within each zone to acceptable levels to obtain sufficient resolution. It is thus clear that the control of dispersive transport has a major influence on the efficiency of chromatographic separations. Without understanding the underlying transport phenomena (mainly flow transport and viscous and diffusive phenomena) modern analytical separation techniques, such as chromatography and electrophoretic techniques, would not be capable of performing simultaneous fractionation of over 100 components in one single analysis.

The most useful criterion for the effectiveness of separation of *two* components is the *resolution,* which is conveniently defined as the ratio of the distance between the centers (or peak tops) of the two component zones to the average zone width. Because resolution differs for each pair of components, it cannot be considered a universal and characteristic measure for separation performance. For that purpose, better criteria have been evolved, such as *plate height, number of (theoretical) plates, separation speed,* and *peak capacity.* These criteria are less dependent on the differences between analyte components and, thus, can be considered as useful figures of merit for different systems and operating conditions. The subject of the present chapter is to relate the mentioned criteria to physically meaningful transport mechanisms, to obtain insight into the optimization of chromatographic separations. It is possible to base the discussion on a thermodynamic point of view, realizing the fundamental role of the chemical potential in both selectivity (partitioning between phases) and transport phenomena (diffusion) [1,2]. Here we take a simpler approach, which is intended to provide a qualitative feeling for the subject, rather than striving after quantitative and exact results. The same applies for the use of the formal mass balance equations [see e.g., Ref. 1] that fully describe the chromatographic processes that occur after injecting a sample pulse into the separation system. Here, we take a more practical (stochastic) approach based on *random-walk models,* which is easier to understand and leads to the same result as the exact solutions.

Furthermore, we restrict ourselves to the more common chromatographic techniques that apply a tubular separation column (either open or filled with packing particles), thereby precluding flat bed systems, such as paper and thin-layer chromatography.

II. MEASURES OF EFFICIENCY: PEAK SHAPE, RESOLUTION, AND PLATE HEIGHT

A. Peak Shape: Basic Form

The containment of zone-spreading, with a view to avoid overlap and cross-contamination with neighboring zones, is a major goal of chromatographic science. This requires an under-

standing of the processes responsible for the dispersion of injected sample concentration pulses in chromatographic systems, which are transported with the mobile phase to the end of the system. If we designate the longitudinal or axial coordinate with z, $z = 0$ is the beginning of the system (entrance of the column) and $z = L$, where L is the column length, is the location of the end of the system where elution of the zones takes place.

The linear mobile-phase velocity u_m which is responsible for the axial movement of the zones, should be carefully defined, depending on the structure of the system. The latter can be an open tube or a packed-bed system. The easiest definition follows directly from the column volume $V_c = A_c L$ and the column cross-sectional area $A_c = V_c/L$ that is flushed with mobile phase at a flow rate F, and we have $u_{sup} = F/A_c$ which is called the *overall* or *superficial velocity* [15], as it does not show any information on the local velocity inside the column. For example, a packed bed may consist of porous particles which depending on their pore structure and extent of filling with stationary phase, are either accessible (sometimes even allowing real flow) or inaccessible for the mobile phase. In the normal situation, flow occurs solely through the interstices between the packing particles (or open corespace in tubes), which is called the *interstitial velocity* u_0, that can be obtained from the superficial velocity by correcting for the fraction of open-pore area (ε_0) in the column cross section A_c. ε_0 is called the *interstitial porosity* and is defined as the ratio of interstitial pore volume (V_0) and column volume (V_c), $\varepsilon_0 = V_0/V_c$. Consequently $u_0 = F/\varepsilon_0 A_c$, but in practice, values for this velocity are usually obtained from the residence time of an injected concentration pulse of a solute that does not interact with the stationary medium, a so-called inert or nonretained solute. If injection takes place at $z = 0$ and it takes a time t_m for this solute zone to reach the end of the system, the associated linear velocity $u_m = L/t_m$ can be identified as the actual mobile-phase velocity within the interparticle interstices u_0, provided that mobile-phase and inert solute molecules cannot enter the interparticle pore space. If they do so, the residence time of the inert component will be extended in proportion to the available intraparticle pore space, and we should write: $t_m = t_0 + t_{m,i}$, where subscript i refers to the interior intraparticle and accessible pore space (with volume $V_{m,i}$ and internal porosity based on the total column volume V_c, $\varepsilon_i = V_{m,i}/V_c$) and subscript 0 to the exterior interparticle space (volume V_0 and interstitial porosity $\varepsilon_0 = V_0/V_c$). If we define the fraction $\phi = \varepsilon_0/\varepsilon_{tot} = \varepsilon_0/(\varepsilon_0 + \varepsilon_i)$, as the volume fraction of mobile phase that occupies movable interparticle space, we have, in general, that the mobile-phase velocity u_m as obtained from t_m is related to the actual interstitial velocity u_0, as $u_m = \phi u_0$. Indeed u_m is only identical with u_0 for $\phi = 1$, (i.e., $\varepsilon_i = 0$). We will come back to this situation in treating porous particles in particular (see Secs. II.E.4.d and II.E.4.g), and restate that the usual definition of velocity in chromatography is based on $u_m = L/t_m$.

At the start of the chromatographic process, at time $t = 0$, components to be separated are injected as one common narrow concentration pulse $c(z = 0, t = 0)$ at the beginning of the separation column, located at the longitudinal (or axial) coordinate $z = 0$. We intend to keep the initial zone as narrow as functionally possible, because we do not want the final zone to be unnecessarily wide (see under Extracolumn Broadening, Sec. II.F).

Mathematically, the narrow starting band can conveniently be approximated by a so-called line- or δ-function which, in effect, represents an infinitely narrow zone with unit area. These initial and almost line-like zones evolve during transport through the column by random diffusion or diffusion-like processes (dispersion) into diluted and slightly broadened zones that can be described by the well-known bell-shaped normal distribution or gaussian function (Fig. 1):

$$c(z, t) = c_{max} \exp(-\zeta^2/2\sigma_z^2) = (\text{constant}/\sigma_z^{1/2}) \exp(-\zeta^2/2\sigma_z^2) \quad (1)$$

where c_{max} is the maximum concentration encountered at the zone center that travels with the average zone velocity u_z ($u_z \leq u_m$, caused by interaction with the retentive stationary phase) along the axial z-coordinate (column axis). Here $\zeta = z - z_z = z - u_z t$, the axial coordinate

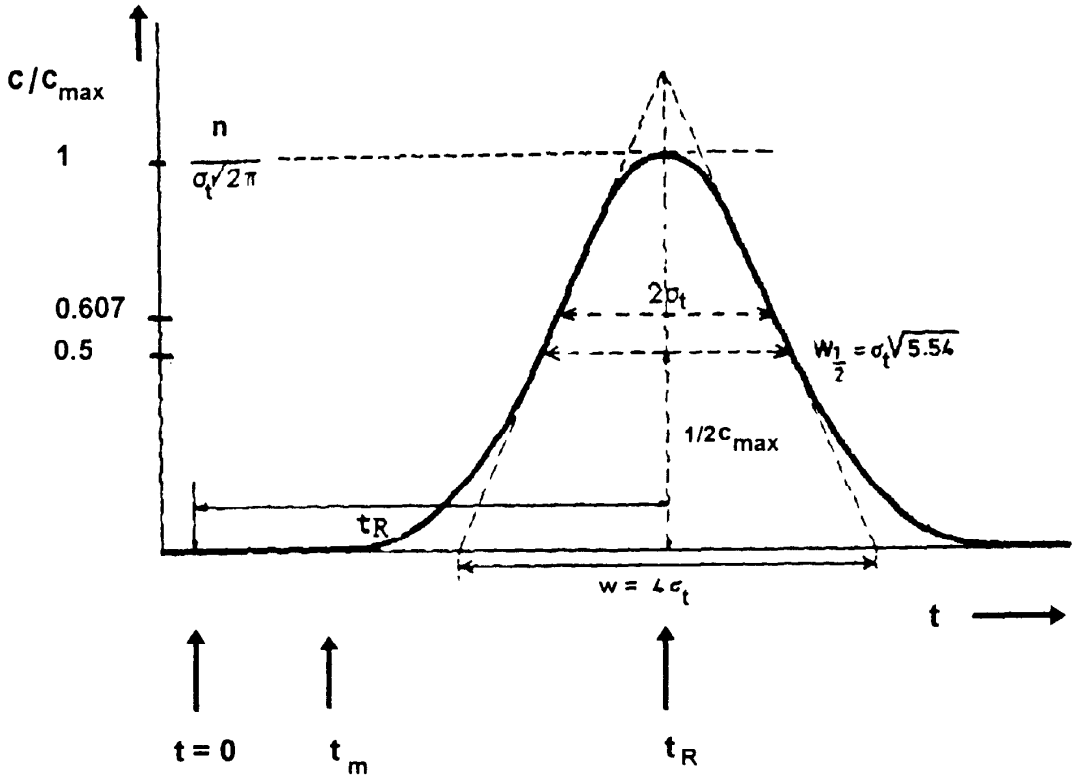


Figure 1 Characteristics of a gaussian peak; injected amount is n mol per unit area of the cross section of the column.

for the zone center at $z_z = u_z t$ and σ_z is the standard deviation of the concentration distribution in distance units, whereas σ_z^2 represents its variance. Both these latter parameters are measures of the width of the zone that is obtained at the baseline by triangulation of the gaussian function as $4\sigma_z$, whereas the zone width at $0.607c_{max}$, the position of the inflection points, equals $2\sigma_z$. In the forthcoming we will see how standard deviation and variance can be related to dispersive processes stemming from diffusive, convective, and mass-transfer phenomena. Here, it suffices to recognize that zone or peak widths can be characterized by the standard deviation of the concentration distribution, a measure for the continuously outward spreading and blurring of the zone around its center as the separation process advances. Hence, σ_z is a function of place and time: $\sigma_z = \sigma_z(z, t)$.

The gaussian expression, by the way, is also an exact solution to the mass balance equation, so our informal approach yields a good answer. Equation (1) for $t = 0$ becomes infinitely narrow (as $\sigma_z \rightarrow 0$) and thus obeys the necessary starting condition of the δ-function form at the beginning. If we normalize the expression to unit area (i.e., it is valid for 1 mol of substance per unit area of cross section), the constant can be obtained, and for n mol per unit area in Eq. (1) becomes:

$$c(z, t) = \{n/[\sigma_z(2\pi)^{1/2}]\} \exp\{-(z - z_z)^2/2\sigma_z^2\} \tag{2}$$

For practice, it is more convenient to replace the local or spatial distribution with the time distribution function at the moment of elution (*residence* or *retention time*) of the zone center $t_R = L/u_z$ using the relations $z = u_z t$ and $\sigma_z = u_z \sigma_t$, where σ_t is the standard deviation around the peaktop at $t = t_R$ in time units:

$$c(z = L, t) = \{n/[\sigma_t(2\pi)^{1/2}]\} \exp\{-(t - t_R)^2/2\sigma_t^2\} \tag{3a}$$

or

$$c(z = L, t) = c_{max} \exp\{-(t - t_R)^2/2\sigma_t^2\} \quad (3b)$$

These important expressions for peak or zone shape yield detailed information on how the original injection pulse becomes broader and lower in concentration (dilution) with the passage through the column (i.e., with time).

It can be shown that 95.6% of the total area of the gaussian distribution lies between $t_R - 2\sigma_t$ and $t_R + 2\sigma_t$ for which reason we may (albeit arbitrarily) take a total of $4\sigma_t$ as the *effective width* of the zone (see Fig. 1). Observe that this effective zone width is the same as that obtained from triangulation of the peak by drawing the tangents through the inflection points at both sides of the distribution. In modern practice, detector signals are often digitally recorded, and the determination of peak top (for the retention time) and peak width can easily be automated. Ideally (but not usually in practice) this is done by calculation of the mean (or center of gravity); namely, the first moment (for a gaussian located on the peak center line) and the second central moment around the mean (equal to the variance σ_t^2). Higher moments can, in principle, be obtained as well, but for symmetrical and often for gaussian peak shapes this is useless because the third moment (an indication for asymmetry) equals zero and the excess (or flattening) of the zone, as obtained from the fourth moment, is also zero. Higher moments are thus of interest only for asymmetrical (fronting or tailing peaks; see Sec. II.F). The accurate determination of these higher moments is far from trivial, and it is often not possible in view of signal-to-noise problems. In practice, only the two lowest moments can be obtained with sufficient accuracy.

B. Theoretical Plate Concept

In the foregoing we found that the efficiency of chromatographic separations largely depends on the peak or zone widths of the components to be separated, and as the measure for that, we obtained the effective width of the zone, which is determined by the standard deviation σ of the concentration distribution. To optimize the separation conditions, for example, with a view to reduce analysis time (= residence or retention time of the last peak) to required values (e.g., fast separations in process analysis), fundamental insight should be obtained in the processes that occur in chromatographic columns.

The pioneers in this field (Martin and Synge [3]) took the approach of comparing the zone-broadening in chromatography with that obtained in other separation techniques in which components are partitioned between two phases, notably extraction by countercurrent distribution (CCD) and distillation. In the latter techniques, it was customary to express the efficiency of the separation in terms of so-called plates, discrete geometric vessels in which forced interphase mass exchange of the components to be separated was intended to produce thermodynamic equilibration. This equilibrium could be characterized by a well-defined partition coefficient K^*, representing the ratio of the concentration of the component of interest in the two phases. In CCD, the plates are real extraction vessels, in which the upper liquid phase with its dissolved components is discontinuously transported toward the next vessel, where a new equilibration takes place. In distillation, the plates do not correspond to the physical plates possibly present in the distillation column, but are fictive plates, called *theoretical plates* that represent nothing but a characteristic for the zone-spreading observed, just as found in the foregoing paragraph for the effective zone width.

In effect the only analogy between chromatography (as a continuous process) and CCD (discontinuous process) is the partitioning of components between two immiscible phases. In CCD, equilibrium partitioning is strived for and largely achieved, whereas in chromatography, owing to the continuous flow of mobile phase, potentially obtained equilibrium partitioning is, in fact, never actually achieved (possibly with the exception of the center of a zone [1]). However, the resulting zone widths can be *described* in both cases by the theoretical plate number. For chromatography, this number is then the necessary number of fictive plates that would result in the same width as if the separation column were artificially divided into

equilibrium cells or plates. Each cell is then allotted a certain finite length (called *theoretical plate height*) in which the components spend a finite time sufficient to achieve equilibrium with the two phases. There is nothing against such an artificial model, as long as one realizes that the plate number is just another descriptor for the efficiency. Indeed, smaller plates imply a more efficient exchange of components between the two phases, and the more plates there are in a column, the more efficient the separation and the narrower the component zones. This is why historically the number of theoretical plates in a chromatographic column has become the accepted measure of column efficiency.

It should be clear, however, that the only process that compares well between chromatography and CCD is the slowness of interphase mass transfer, which implies that the contribution of all other physical processes, such as diffusion and convection, is interpreted as if it were stemming from that equilibration. Thus, plate theory, as such, does little to explain how operating conditions, such as column geometry (open or packed, straight or coiled), properties of the packing and the stationary phase, and the mobile-phase velocity and its properties, influence the efficiency of a column. The plate concept is useful for the description of peak- or zone-broadening and for the notion that each plate represents a kind of *dwell time* for components. The notion of this dwell time is useful, not so much in the sense of achieving equilibrium, as originally intended, but to look at the process of distribution between phases as being incremental. This picture is plausible if we consider that partitioning of a component between two phases with a measurable partition coefficient K implies a dynamic process during which molecules of the component spend specific *average local* dwell times in both phases, per interchange jump τ_s and τ_m, and for the total residence in the two-phase system t_s and t_m, respectively. These average dwell- or residence times of molecules are necessarily related to the chance of finding molecules of the partitioning component in each of the phases. Hence, the ratio of the number of molecules in both phases, and that is nothing but the capacity factor k, also equals the ratio of *average total residence* times:

$$k = K(V_s/V_m) = \frac{\text{(amount component in stationary phase)}}{\text{(amount component in mobile phase}} = \frac{\text{(time spent in stationary phase)}}{\text{(time spent in mobile phase}} = t_s/t_m \tag{4}$$

This equation forms the link between the static equilibrium properties (K from thermodynamics, and the phase ratio $\varphi = (V_s/V_m)$, as installed in the column) and the dynamic chromatographic quantities (time constants) that allow for the kinetics of equilibration.

Thus, on a molecular scale and speaking in terms of averages, the chromatographic transport of molecules through the two-phase system comprised of a mobile phase and a stationary phase may be viewed as being discontinuous. The discontinuity lies in the sense that molecules, on the average, spend an infinitesimal time τ_s in the stationary phase, during which time no axial transport occurs. This is followed by phase exchange (desorption) and an infinitesimal time τ_m spent in the mobile phase, during which molecules flow together with those of the mobile phase (convective transport with linear velocity u_m) through the system. The larger the k, the more time molecules spend in the stationary phase and the longer it takes to travel the distance of the complete column length L (i.e., the longer the residence time t_R).

Thus, the picture arises that molecules of partitioning components travel stepwise discontinuously through the column and reach the column exit to elute only after a large number of n_t transfers between the stationary and mobile phases during the retention time t_R. The latter is composed of n_t times the infinitesimal residence times τ_s and τ_m in the respective phases:

$$t_R = n_t(\tau_s + \tau_m) = t_s + t_m = t_m(1 + k) \tag{5}$$

This is the well-known retention equation which can alternatively be expressed in retention volumes rather than retention times:

$$V_R = Ft_R = V_m + KV_s = V_m(1 + k) \tag{5a}$$

The present discontinuous model implies that molecules are axially transported during the short times τ_m that they spend in the flowing mobile phase, covering a step or transfer length $\ell = L/n_t$ while also $\ell = u_m\tau_m$. The number of transfers n_t is analogous to the number of extraction vessels in CCD or the number of theoretical plates in distillation or absorption columns in chemical technology. Likewise, the step or transfer length ℓ is analogous to the height of a transfer unit (HTU) or height equivalent of a theoretical plate (HETP). As such, it should be considered a useful measure for the efficiency of the column (bearing in mind the obvious differences between chromatography and the technological processes). Again, it is stressed that being only a descriptor for zone broadening, plate numbers as such do not give an indication of how to improve the observed efficiency, nor do they allow us to predict the effect of operational changes and to optimize separations.
Yet, we will make a twofold use of this plate theory analogy:

First, we keep on using the nomenclature of plates and plate heights, not in the least for historical reasons.
Second, we can use the notion of step length in the coming discussion for the description of additional effects, such as diffusion and convection, which will finally lead to a situation where we can predict the influence of operating conditions and find their optimum values.

C. Random-Walk Processes, Variance, Diffusion, and Plate Height

Without derivation (but basically by expanding Newton's binomium $(p + q)^N$ [see, e.g., Ref. 4] we give here the result for zone-spreading (in terms of variance) in CCD after n_t absorptions and desorptions of the partitioning component equilibrating with a capacity ratio k; that is, a fraction $1/(1 + k)$ in the mobile solvent and a fraction $k/(1 + k)$ in the stagnant solvent, just as in chromatography:

$$\sigma^2 = n_t \tag{6a}$$

Here, σ^2 is the dimensionless variance expressed in numbers of vessels around the mean position of the zone located in vessel number $n_tk/(1 + k)$. If we transpose this result to chromatography in a column of length L and a step length ℓ, we obtain the result $\sigma^2 = n_t = L/\ell$ or in units of distance:

$$\sigma_z^2 = n_t\ell^2 = L\ell \tag{6b}$$

The importance of the result lies in that the spread of a distribution originating from a stepwise process can be found from the product of the number of steps n_t (more general N) and the step length squared ℓ^2 (more general λ^2); so,

$$\sigma_z^2 = N\lambda^2 \tag{7}$$

Processes that obey this relation are stochastic and so-called random-walk processes [see, e.g., Refs. 1,5]. Examples thereof are the drunken-man's walk and the thermal motion (molecular diffusion) of molecules and particles (Brownian motion). In the following we will make use of this relation in various other occasions (e.g., for eddy-diffusion). First of all, we will apply Eq. (7) to molecular diffusion.

1. Diffusion and Dispersion

Molecules as well as colloidal particles are subject to all kinds of forces, but notably to strong collisional forces from contacts with neighboring molecules or particles (thermal motion), as becomes observable for particles in Brownian motion. The well-known fickian diffusion equations [1,2,5] describe how, whenever concentration gradients exist, there will be a movement

to eliminate the gradient by the molecular transport mechanism called *diffusion* at a rate that is determined by the *diffusion coefficient* $\boldsymbol{D}$. $\boldsymbol{D}$ can be related to the average velocity $\langle v \rangle$ of the molecules and their free path length λ (the distance molecules are apart) as $\boldsymbol{D} = \frac{1}{2}\lambda\langle v \rangle$, a typical random-walk process. We consider first the simplest case of one-dimensional particle movement either to the right or to the left along a line in the z-direction, with equal probabilities and equal fixed diffusional steps of length λ. The total net displacement z in time t is the total sum Σ of all steps z_i ($i = 1 - N$), N being the number of steps with length $z_i = \pm\lambda$, with equal probability. Hence, the total net or mean displacement $\langle z_i \rangle = \Sigma z_i = 0$ (no net displacement), while each z_i has the mean square or variance of $\langle z_i^2 \rangle = \lambda^2$, and so after N of such steps it follows that $\sigma_z^2 = N\langle z_i^2 \rangle = N\lambda^2$, the expected random-walk result from Eq. (7). The number of steps N is found from the total time t and the step time τ_λ as $N = t/\tau_\lambda$. Diffusional steps are taken with an average velocity of the molecule $\langle v \rangle$, which thus have a step time $\tau_\lambda = \lambda/\langle v \rangle$. If now the diffusion coefficient is *defined* as being $\boldsymbol{D} = \frac{1}{2}\lambda\langle v \rangle$ or alternatively $\boldsymbol{D} = \lambda^2/(2\tau_\lambda)$, we arrive at

$$\sigma_z^2 = 2\boldsymbol{D}t \tag{7a}$$

or

$$\lambda^2 = 2\boldsymbol{D}\tau_\lambda \tag{7b}$$

The second alternative, Eq. (7a) is valid for the microscopic scale, whereas the first alternative is the macroscopic version. This most important result is also found from the formal solution to Fick's second law (the mass balance equation) for a δ-pulse concentration profile as the starting profile; that is, Eq. (2), with variance according to Eq. (7a).

The latter equation, which we will use many times in the following, reflects how peak width for diffusional or diffusion-like processes increases with time; namely, as a square root function [see Eq. (7a)] belonging to gaussian-shaped concentration distributions [see Eq. (2)]. Experimentally observed gaussian peak shapes do not stem from molecular diffusion alone. Other zone-broadening mechanisms are often random processes, which also lead to gaussian profiles, and we may describe the total resulting gaussian spreading as an *apparent diffusion or dispersion process with an effective diffusion or dispersion coefficient*, which is related to σ as described by Eq. (7a); so,

$$\boldsymbol{D}_{\text{eff}} = \sigma_z^2/(2t) \tag{7c}$$

After a fundamental statistical law we can, if several *independent* random processes contribute to the total zone-spreading, add the individual variances. Thus, the total variance becomes

$$\sigma^2 = \Sigma\,\sigma_i^2 = \sigma_1^2 + \sigma_2^2 + \sigma_3^2 + \cdots \tag{8}$$

and it follows that the effective total dispersion coefficient is additive in the same way:

$$\boldsymbol{D}_{\text{tot}} = \Sigma\,\boldsymbol{D}_i = \boldsymbol{D}_1 + \boldsymbol{D}_2 + \boldsymbol{D}_3 + \cdots \tag{8a}$$

Mechanisms of individual diffusion or dispersion processes will be further discussed in Sec. II.E.

2. Theoretical Plates

In Eqs. (6) and (7) the transfer or step number represents the role of the longitudinal coordinate in chromatography, and in words, it reads that the variance obtained is proportional to that number and thereby to the distance traveled along the column length dimension z. Physically speaking, this is not quite an unexpected phenomenon, because we can explain this by reasoning that if the length of the steps double, the final distance of a randomly walking molecule from its starting position will also double. Clearly, the average deviation in the displacement distances (i.e., σ) can also be expected to double; thus, it is proportional to the step length λ.

In contrast to this linear dependence on λ, there is no linear dependence on the number of steps N. The rationale for this is that the ongoing random-walk is as likely to send a molecule arriving at some distance z backward toward the origin as it is to send it onward to larger z values. Thus, previous displacements are often cancelled, and this results in a less than proportional increase of the standard deviation with N.

The fundamental processes that cause zone-broadening are generally of such a random nature, as we will see in the following. The random-walk result [Eqs. (6)–(8)] is, hence, precisely what is found in the practice of paper and thin-layer chromatography, during which the initially tiny spot of sample deposited at the start, smears out into larger blots exactly according to the foregoing rule. The same applies to all column-based forms of chromatography, but there we cannot look inside the column to directly observe the local zone variance, and we have to wait for the eluting zone at the column outlet at $z = L$.

Just for the convenient proportionality between variance and elapsed distance, the *theoretical plate height* in chromatography is defined as the proportionality constant H:

$$\sigma_z^2 = Hz \tag{9}$$

or, expressed in time units and at the position of the column exit ($z = L = u_z t_R$, and $\sigma_z = \sigma_t u_z$; so, $\sigma_t^2 = (H/L)t_R^2$):

$$H = \sigma_z^2/L = L(\sigma_t/t_R)^2 \tag{9a}$$

The associated *number of theoretical plates* n_{th} is now logically found from the number of theoretical plate heights that fit into the column length L:

$$n_{\text{th}} = L/H = (t_R/\sigma_t)^2 \tag{9b}$$

From Eqs. (9) and (9a) it follows that the width of a component zone increases with the distance, or time traveled, in the system, and the final extent of spreading depends on values of H or n_{th}. The theoretical plate number (often simply called plate number) is the relative zone-broadening per unit length of the system and, stressed once more, it is a valuable measure for the quality (read *efficiency*) of a chromatographic system. In actual fact, the theoretical plate number and plate height thus conveniently defined, do not reflect the exact meaning of plates in the technological mass-transfer processes, such as CCD or distillation [so H(chromatography) $\neq$ HETP (distillation)]. It is true, however, that the key proportionality between variance and distance [see Eq. (9)] is valid in both staged and discontinuous systems, and the nomenclature is so much accepted that is not useful to try and change it now. It is better to retain the nomenclature of plates for historical continuity, and to realize ourselves that the quantities plate height and plate number are just characteristics that describe zone-spreading. We can then make use of the possibility to compare many diverse separation techniques on a common basis.

For that purpose, Sec. II.E is devoted to finding the contributions to plate height for all types of random-walk mechanisms, including the partitioning process itself.

If we take molecular diffusion in the mobile phase as the simplest example, we know from Eq. (7a) that $\sigma_z^2 = 2\boldsymbol{D}_m t_m$, where $\boldsymbol{D}_m$ represents the molecular diffusion coefficient of the analyte solute in the mobile phase. As $H = \sigma_z^2/L$ and $L/t_m = u_m$, we find: $H_{D,m} = 2\boldsymbol{D}_m t_m/L$ or

$$H_{D,m} = 2\boldsymbol{D}_m/u_m = B/u_m \tag{10}$$

Depending on the accessibility of the intraparticle pore space (see the discussion in Sec. II.A), we should realize that, in fact, it is the time t_0, the time spent in the interstitial mobile phase, that should have been used here (during time $t_{m,i}$, molecules are stagnant and no axial diffusion occurs), and so the interstitial velocity $u_0 = u_m/\phi$ is the one that actually appears in the plate height expression for axial diffusion:

$$H_{D,m} = 2\boldsymbol{D}_m/u_0 = B\phi/u_m \tag{10a}$$

This shows that the plate height stemming from diffusive (or diffusion-like dispersive processes) is inversely proportional to the flow velocity. For dispersive processes, Eqs. (10) and (10a), cast in the general form:

$$H = 2\boldsymbol{D}_{\text{eff}}/u_z \tag{10b}$$

can be used as an alternative definition of H, as is not uncommon in technological sciences. By virtue of the fact that H is proportional to $\boldsymbol{D}$ and σ^2, the total H value for a combination of independent dispersive processes can be found as the sum of the individual contributions to H, in complete analogy with Eqs. (8) and (8a):

$$H_{\text{tot}} = \Sigma H_i = H_1 + H_2 + H_3 \ldots \tag{10c}$$

3. The Central Role of Velocity Differences and Near Equilibrium

We have found in the foregoing that chromatographic separations depend on the *velocity differences* present in the system between mobile and stationary phase, and the differential partitioning of components between these velocity regions. Although fundamentally necessary, these velocity differences also introduce departures from equilibrium. With ongoing flow, equilibrium concentrations are never reached, with the exception of the zone maximum. Instead, what can be expected from the fact that the mobile phase sweeps solute molecules with it from upstream, is that the *actual* position of these molecules will be *ahead* of the equilibrium position.

It is true that rapid exchange (mainly by diffusion) between the two phases largely diminishes the deleterious effect of nonequilibrium on zone-spreading. Indeed, peaks are generally quite narrow. However, there remain subtle departures from equilibrium with major consequences. This is most clearly seen by investigating the trailing and leading parts of a migrating concentration zone. In a small volume element at the front edge, arriving solute molecules come in from more concentrated regions near the zone center and inflowing solution transported with the mobile-phase velocity u_m overtakes regions of lower solute concentration. Thus, this part of the zone, which moves as a whole with a zone velocity *lower* than u_m, is enriched in comparison with the equilibrium concentration c_m^*. The excess $\Delta c_m = c_m - c_m^*$ will be quickly transported to the stationary phase, driven by the tendency to reach a new equilibrium; however, this is not an instantaneous process. It is being driven by molecular diffusion and requires a finite time to be realized. During that time, a more-enriched mobile phase is flowing into the volume element and, again, the equilibration is out of balance. The actual concentration of the solute in the mobile phase, ahead of the zone center, will remain higher than the equilibrium concentration.

For a volume element in the tail of the zone, the situation is just reversed: the concentration of solute in the incoming mobile phase is lower than the equilibrium concentration. The concentration deficiency Δc_m is being partly compensated by desorption of the solute from the stationary phase. However, continued dilution by less-concentrated mobile phase, again prevents the attainment of equilibrium. Here, the concentration is slightly lower than the equilibrium value, and for the zone, as a whole, the actual concentration profile is slightly shifted relative to the equilibrium profile, the shift being in the upstream direction throughout the zone. Because the resulting excess nonequilibrium concentration Δc_m is small in comparison with the concentration c_m itself, we can speak of near-equilibrium conditions, but we will show that the effect of these small deviations from equilibrium are definitely significant. Qualitatively, this can be predicted already from the present reasoning, by realizing that chromatographic transport [see Eq. (4)] is governed by the ratio of concentrations in both phases. This is expressed as the partition coefficient $K = c_s/c_m$, (or $K^* = c_s^*/c_m^*$, which is valid for equilibrium; i.e., for the zone center). Because of the excess concentration in the mobile phase in the front part of the zone, the front will move faster than the zone center. The opposite is true for the rear of the zone, where the deficiency in concentration in the mobile phase leads

to a slower movement than the zone center. Thus, the front and tail of the zone pull away from each other, which is essentially leading to band-broadening.

Unequal displacement velocities for different solutes are fundamentally necessary to obtain successful chromatographic separations. However, from the foregoing, the ideal of obtaining equal velocities for all molecules of the same solute is impossible to reach: differential migration of zones is accompanied by unwanted, but unavoidable, effects that "tear" the zones apart along the column axis. Although we have to minimize this band- or zone-broadening effect to obtain effective resolution of component zones, it should be realized that these dispersion effects cannot be fully eliminated, for the underlying flow-induced displacement is also needed for separation.

The partitioning process is dynamic (i.e., molecules move continuously in and out of the phase regions). Therefore, the described zone-spreading will be limited if the equilibration time t^*, necessary for exchanging molecules between phases, is small. Minimization of this time (e.g., in diffusing systems by reducing the dimensions, application of thin liquid layers, and small porous particle sizes) is of eminent importance.

To express the foregoing zone-spreading mechanism quantitatively in terms of plate height, we can again make use of the random-walk model, now supported by the knowledge that the assumption of near-equilibrium (i.e., small values of Δc_m) is realistic. Hence, rather than account for all possible multiple transfers of molecules between possible velocity regions, we can concentrate on the average case of near-equilibrium, at which solute molecules are partitioning between only two possible velocities, u_m in the mobile phase and u_s in the stationary phase (in actual practice almost always zero), thereby acquiring an overall zone velocity u_z somewhere in between u_m and u_s. We treat this case with the random-walk model, which will be applied to all possible mechanisms of zone-broadening, in Sec. II.E. We will close this section by deriving a simplistic, but generally applicable, relation for the plate height caused by the foregoing two-region velocity random walk.

A molecule will be present in the high-velocity region of the mobile phase only during some average equilibration time t^*, after which exchange toward the low- (or zero-) velocity region of the stationary phase occurs by a diffusional or similar transport mechanism. During that time, the molecule will overtake the average of the zone by the velocity difference $\Delta u = u_m - u_z$. Thus, it gains a distance of $\lambda = \Delta u t^*$ relative to the zone center. Obviously, we may use this gain as the step length in a random-walk process of transferring molecules back and forth between the two velocity conditions. The same step, in the opposite direction is valid for a molecule staying in the stationary phase. The number of steps (forward and backward) is found from the number of times t^* fits into the total process time t_R. Hence, $N = t_R/t^*$, which can also be written as $N = (L/u_z)/t^*$, because from Eq. (7), $\sigma_z^2 = N\lambda^2$, the zone variance obtained is $\sigma_z^2 = [(L/u_z)/t^*](\Delta u t^*)^2 = (\Delta u/u_z)^2 L u_z t^*$, and the plate height is thus:

$$H = \sigma_z^2/L = (\Delta u/u_z)^2 u_z t^* \tag{11}$$

Although approximate, this relation between H and practical parameters, such as velocities, is key to the understanding and optimization of band-broadening in chromatographic systems.

It is seen that two effects are responsible for zone-broadening: first, the equilibration time t^* (or alternatively the characteristic length $\ell^* = u_z t^*$) and, second, the relative velocity difference $(\Delta u/u_z)$, a measure for the nonuniformity of flow in the system. Because the square of the velocity factor occurs in Eq. (11), the velocity differences experienced by component molecules are of utmost importance for the extent of zone-spreading. In our first assumption the velocities are given specific and constant values, but the dimensionless constant $(\Delta u/u_z)$ does not change with, for example, the flow rate, nor would it change if there were more than one velocity (a velocity profile) in each phase: the ratio $(\Delta u/u_z)$ remains constant.

In Sec. II.E this important cause of band-broadening is treated further. Here, we observe that it may be tempting to reduce the plate height by minimizing the velocity term $(\Delta u/u_z)^2$, but the separation does require differential flow and might result with a reduced separation power. Besides diffusion, there are other types of flow dispersion that add to the plate height

without influencing the selectivity; namely, flow differences between flow channels in packed columns, or velocity profiles within one channel (or open column). Especially when flow differences do not contribute to the selectivity, but do contribute to the plate height, we must be aware of the possibilities to reduce their influence (e.g., by preparing more uniform packings or by using electro-osmotic flow—with a very flat profile—instead of pressure-driven flow). The latter may produce very pronounced velocity profiles, such as the well-known parabolic Poiseuille profile in open tubes. Some means to minimize these band-spreading mechanisms will be discussed later (see Sec. II.E and IV).

Equation (11) also clearly shows that the plate height increases in proportion to the average velocity u_z of the component zone. Hence, it is expected that H values can be reduced by lowering the flow rate. Although this is true in many practical situations, lower flow rates lead to longer retention times and, thus, affect the separation speed. In practice, some compromise should be found between efficiency and analysis time. This we will treat in the section on optimization (see Sec. IV).

The last and most important term in Eq. (11) is the equilibration time t^*, the time required for the exchange of solute molecules between different velocity states, either within one phase (velocity profile) or between phases. Mechanisms contributing to t^* are molecular diffusion, hydrodynamic phenomena, and perhaps interfacial kinetics at the phase boundary. In the simplest case, diffusion over a characteristic distance, for example, the liquid thickness δ_s of a stationary phase film, can cause an equilibration time, which is estimated as

$$t_D^* = \delta_s^2/2\boldsymbol{D} \tag{12}$$

with which Eq. (11) takes the form

$$H = (\Delta u/u_z)^2 u_z(\delta_s^2/2\boldsymbol{D}) \tag{13}$$

From this it follows that H is small if the diffusion coefficient is large, but that H increases quadratically with the characteristic thickness δ. This, for example, is the very reason why in high-performance liquid chromatography (HPLC)-packing materials are used with particles as small as 1–5 μm in diameter.

D. Resolution and Peak Capacity

Zonal differential migration methods, such as chromatography, are so successful in practice because their separation power can be increased by using ever-longer columns. In fact, every required separation, however difficult, can in principle be obtained, given time and column material. This is thanks to the fundamental random-walk property that σ increases only in proportionality with $L^{1/2}$, whereas the separation distance between zone centers of two components is proportional with L.

As said in the introduction, the important index of success for an analytical separation is the *resolution Rs*, defined as the ratio of the distance between the centers of two specific component zones and the average zone width. Defined in this way the *Rs* parameter characterizes the extent of overlap of the chosen component zones. If we use the average effective zone width $w = 4\sigma$, *Rs* can be defined as:

$$Rs = \frac{\text{(distance between zones)}}{\text{(average effective zone width)}} = \frac{z_2 - z_1}{\frac{1}{2}(w_1 + w_2)} = \frac{z_2 - z_1}{2(\sigma_{z,1} + \sigma_{z,2})} \tag{14}$$

For close-lying components with similar properties, the σ values are almost the same, and we can use the average σ value, to obtain:

$$Rs = \Delta z/4\sigma_z = \Delta t_R/4\sigma_t \tag{14a}$$

which clearly shows the two competing aspects of a chromatographic separation: the sepa-

ration distance achieved by the primary separating process (nominator) is opposed by the blurring action of the zone-broadening (denominator).

To obtain an impression of the meaning of numerical values of this *Rs* parameter, we prepared the following list (Table 1), which is based on a pair of gaussian zones of equal σ:

As seen from the peak area overlap, satisfactory resolution can be said to correspond to *Rs* values in the range of 1–1.5, but this partly depends on the peak height ratio. As a rule of thumb, we speak of *baseline separation* in those cases where $Rs \geq 1.5$, and *sufficient separation* (in many cases) for $Rs \geq 1$. Two distinct peak maxima can be found only for $Rs \geq 0.5$. In many practical situations, separations with *Rs* larger than 1 but smaller than 1.5 are adequate (*sufficient*), and are considered as being *optimal*. If the chromatogram shows higher resolution, optimization toward faster analyses or shorter columns can be applied (see Sec. IV).

Resolution is not a global criterion of separation, for it differs for each component pair. Yet *Rs* does confirm that resolution is enhanced with increasing column length or retention time as the nominator rises in proportion with L or t, whereas the denominator increases only with $L^{1/2}$ or $t^{1/2}$. At some value of L or t, a sufficient resolution is achieved, and any further increase in column length or retention time is unnecessary and inefficient.

This procedure of optimization of separation conditions is largely a matter of optimization of the zone-spreading (i.e., of σ or alternatively, of the number of *required plates*). The latter is easily incorporated in the relation for *Rs*; by using the foregoing equations for *Rs*, σ, and H (or n_{th}) we find:

$$Rs = \Delta z/4\sigma_z = \Delta u_z t/4u_z\sigma_t = \tfrac{1}{4}(\Delta u_z/u_z)(n_{th})^{1/2} \tag{14b}$$

where again the dualistic nature of the *Rs* factor shows from the occurrence of two parts in the RHS of Eq. (14b); that is, the relative zone–velocity difference ($\Delta u_z/u_z$), which causes zone separation by selective transport, and the efficiency $(n_{th})^{1/2}$ which opposes complete separation. In the Sec. IV we will derive more complex relations between *Rs*, migration times, and plate numbers, but here we present one more practical expression for *Rs*. This is based on the experimental observation [see e.g., Ref. 6] that in chromatograms the peak width often increases linearly with increasing retention time:

$$\sigma_t \approx \bar{\omega} t'_R = \bar{\omega} t_s = \bar{\omega} k t_m \tag{15}$$

where t'_R is the net retention time (i.e., the retention time of the component minus the residence time of the mobile phase molecules (dead time) or retention time for unretained components). This just equals the residence time of component molecules in the stationary phase $t_s = kt_m$, because all molecules spend the same time t_m in the mobile phase. Substitution in the expression for *Rs* then yields

$$Rs = (1/2\bar{\omega})[(\alpha - 1)/(\alpha + 1)] \approx (1/4\bar{\omega}) \ln \alpha \tag{16}$$

Here, α is the *relative retention* or *selectivity* expressed as $\alpha = k_2/k_1$, a most fundamental

Table 1 Properties of the Resolution Factor

Distance Δt	Resolution *Rs*	Peak height ratio	Area overlap (%)
6σ	1.5	1 : 1	0.13
4σ	1.0	1 : 1	2.28
6σ	1.5	3 : 1	0.30
4σ	1.0	3 : 1	3.30
6σ	1.5	10 : 1	3.30

thermodynamic quantity, which relates to the difference in standard chemical potentials of the two components of interest. Thus, α is at the very basis of the separation. Again, the two factors of selectivity and zone-spreading that rule *Rs* are apparent in Eq. (16).

The constant $\bar{\omega}$ in Eqs. (15) and (16) represents the rate at which the zone width in a chromatogram increases with retention time, and can be related to plate numbers by substituting Eq. (15) into the definition of plate height *H*:

$$\bar{\omega} = \sigma_t/t'_R = (t_R/t'_R)(H/L)^{1/2} = [(1 + k)/k]n_{th}^{-1/2} = n_{eff}^{-1/2} \tag{17}$$

(assuming close-lying peaks and using $k = k_2$) where n_{eff} is the *effective plate number*, based on net retention times, rather than total retention times:

$$n_{eff} = (t'_R/\sigma_t)^2 = n_{th}[k/(1 + k)]^2 = 1/\bar{\omega}^2 \tag{17a}$$

There is some virtue in using the effective plate number instead of the theoretical plate number, because in chromatograms the nonretained components often show the highest numbers of plates, but they cannot be separated easily. This drawback is not incorporated in the effective plate number: for unretained compounds $k = 0$, and so $n_{eff} = 0$, indicating a useless chromatographic condition. Yet, there is no reason for replacing the theoretical plate by the effective plate, other than that equations are simpler through the absence of some functions of k or $(1 + k)$. The theoretical plate height remains the only one with a physical meaning, so we prefer to keep using it.

Certain equations are quite elegant when expressed in terms of effective plates; for example, Eq. (16) becomes

$$Rs = \tfrac{1}{2}[(\alpha - 1)/(\alpha + 1)]n_{eff}^{1/2} \approx \tfrac{1}{4}[(\alpha - 1)/\alpha]n_{eff}^{1/2} \approx \tfrac{1}{4}(\ln)\ \alpha n_{eff}^{1/2} \tag{18}$$

while the associated expression with n_{th} would show an additional factor of $k/(1 + k)$. Also, trends in *Rs* (e.g., when studying temperature effects) are closely followed by the same trend in n_{eff}, which is not true for n_{th}. In addition, the relation for the *required number of plates* necessary to obtain a resolution of, say, $Rs = 1$ from Eq. (18), is more elegant in terms of n_{eff}:

$$(n_{eff})_{ne} = 16[\alpha/(\alpha - 1)]^2 \tag{19}$$

than in terms of n_{th}, which expression contains an additional factor of $[(1 + k)/k]^2$. We will make use of these equations later in Sec. IV. Here it suffices to say that Eqs. (14) through (19) allow the calculation of the required length of column necessary to obtain a specified resolution between component pairs, provided that retention data (in terms of k, or α) and zone-broadening data (in terms of plate height or plate number) are known.

The concept of effective plates is also useful to introduce another way of judging the performance of a chromatographic system; that is, the idea of looking at the *total number of peaks* or *zones* separable, rather than focusing on the resolution of specific pairs of components. One parameter to be used then, is the *peak capacity* n_c, representing the maximum number of separated zones or peaks that fit into the separation system (from $z = 0$ to $z = L$) or chromatogram (from $t = t_m$ to $t = t_{R,c}$, the time of the last peak), with a specified resolution between adjacent peaks, say $Rs = 1$. Because we already know that peak width increases during the course of a chromatogram at a rate specified by the parameter $\bar{\omega} = n_{eff}^{-1/2}$ (from Eq. 17), we readily obtain n_c from:

$$n_c = (t_{R,c} - t_m)/4\langle\sigma_t\rangle \approx t_{R,c}/2\sigma_{t,c} = 1/2\bar{\omega} = \tfrac{1}{2}n_{eff}^{1/2} \tag{20}$$

by which the effective plate number is determined for the last peak. This is in approximate agreement with more exact expressions as derived by Giddings [1]. In gas chromatography literature, the peak capacity is also termed *Trennzahl* [6].

If we do not neglect the dead time relative to the last retention time, Eq. (20) is modified by a factor $\ln(t_{max}/t_{min})$ [1]. This factor significantly reduces peak capacity when there is a

limited retention window, such as in size exclusion chromatography (SEC; typically ln 2 = 0.69), but causes enhanced peak capacities (typically ln 50 = 3.9 for gas and liquid chromatography and for field flow fractionation [1]). These equations clearly illustrate the importance of obtaining high plate numbers. Therefore, we should be aware of all aspects that potentially contribute to zone dispersion and their underlying fundamental transport processes.

E. Mechanisms of Zone-Broadening

Zone- or peak-broadening potentially occurs in the entire chromatographic system, both inside and outside the separation column, the latter particularly during injection and detection. These latter two processes will be discussed later in the Sec. II.F. Here, we will treat the mechanisms of broadening inside the column, by following molecular migration and by describing individual mechanisms by the random-walk model.

Possible mechanisms one can think of are the following:

1. Longitudinal molecular diffusion in both phases
2. Combined flow differences and lateral diffusion (convective dispersion) in the mobile phase
3. Sorption and desorption between phases

These will be treated in this order in the following sections.

We will close this section by reviewing the literature on the subject to guide the reader through various alternative expressions available for the description of band-broadening.

1. Longitudinal Molecular Diffusion

After the preparations made in Secs. II.C.1 and II.C.2, the contribution of molecular diffusion to the total zone-broadening process in longitudinal directions, is straightforward. The never-ending thermal motion of molecules within each phase will cause these molecules to move backward and forward in the axial flow direction in a random manner. Because in the axial direction, concentration gradients are present [the concentration profile $c(z, t)$ of Eqs. (1) and (2)], molecular diffusion, characterized by the diffusion coefficient $\boldsymbol{D}$, tends to eliminate these gradients and thus, contributes to further peak-broadening. On the basis of the fundamental diffusion–dispersion Eq. (7a), we derived Eqs. (10) and (10a), for the plate height caused by molecular diffusion in the mobile phase: $H_{D,m} = 2\boldsymbol{D}_{\text{eff},m}/u_z = B/u_m$.

For clarity we remark that the *effective diffusion* coefficient is smaller than the *free* molecular diffusion coefficient by a factor $(1 + k)$; that is, $\boldsymbol{D}_{\text{eff},m} = \boldsymbol{D}_m/(1 + k)$. Just as for migration by flow through the two-phase system, diffusional transport is also retarded by the partitioning process. Obviously, the constant B refers to the molecular diffusion coefficient in the mobile phase $\boldsymbol{D}_m$. Because molecules of all components (including the mobile phase itself and nonretarded ones with $k = 0$) stay in the mobile phase for the same residence time t_m, this contribution to plate height is the same for all components, the only difference being the value of the individual diffusion coefficients.

At this point we should make a difference between packed and open tubular columns. The solid particles in packed columns create numerous obstructions to the streamlines of the flow and also to the diffusional pathways, preventing flow and diffusion in straight lines. Molecules have to go around these obstructions and are thus retarded in the axial direction by an *obstruction factor* γ ($\gamma < 1$), first introduced by van Deemter et al. [7]. Hence, the obstructed diffusion coefficient $\gamma_m\boldsymbol{D}_m$ should replace the free molecular diffusion coefficient $\boldsymbol{D}_m$ in the foregoing, and we obtain

$$H_{D,m} = 2\boldsymbol{D}_{\text{eff},m}/u_z = 2\gamma_m\boldsymbol{D}_m/u_m = B/u_m \tag{21}$$

where

$$B = 2\gamma_m\boldsymbol{D}_m \tag{21a}$$

For open tubular (or capillary) columns $\gamma = 1$, but for packed columns, the obstruction, "tortuosity" or labyrinth factor γ_m is less than 1, and is experimentally found in the region $\gamma_m = 0.6 - 0.75$. Giddings [5] found on a theoretical basis that $\gamma_m \approx 0.6$ for well-packed columns, whereas from inspection of many published experimental data we find a correlation with the interparticle porosity ε_0 as follows:

$$\gamma_m = 0.45 + 0.55\varepsilon_0 \tag{21b}$$

Diffusion in gases is much faster than in liquids, and so particularly in gas chromatography (GC) the longitudinal diffusion process is of importance. The pioneers in describing plate heights in terms of physically meaningful processes, such as diffusion and flow phenomena, van Deemter et al. [7], were mainly concerned with GC, and thus described only one longitudinal diffusion term in their plate height equation. For those times where longitudinal diffusion in the stationary phase is also of importance, such as in liquid–liquid chromatography (LLC), we should add an additional longitudinal diffusion term

$$H_{D,s} = 2\boldsymbol{D}_{\text{eff},s}/u_z = 2k\gamma_s\boldsymbol{D}_s/u_m \tag{22}$$

where, again by the partitioning process $\boldsymbol{D}_{\text{eff},s} = k\gamma_s\boldsymbol{D}_s/(1 + k)$. The capacity factor k in the nominator arises from the fact that now, in Eq. (7a) the time for diffusion is $t_s = kt_m$.

Here, the obstruction factor in the stationary phase is added for completeness, but that factor will be even more difficult to determine than its counterpart in the mobile phase, because the geometry of stationary liquid layers on and within porous packings is largely unknown. Yet, if diffusion in both the mobile and stationary phases is significant, the resulting plate height contributions should be added to yield:

$$\begin{aligned} H_D = 2\boldsymbol{D}_{\text{eff}}/u_z &= H_{D,m} + H_{D,s} = 2\gamma_m\boldsymbol{D}_m/u_m + 2k\gamma_s\boldsymbol{D}_s/u_m \\ &= [2\gamma_m\boldsymbol{D}_m/u_m](1 + \xi k) = B/u_m \end{aligned} \tag{23}$$

where for two liquids (LLC) $\xi = [\gamma_s\boldsymbol{D}_s/\gamma_m\boldsymbol{D}_m] \approx 1$. For a liquid–solid phase system with adsorption onto a solid surface $\boldsymbol{D}_s \approx 0$ and so $\xi \approx 0$; likewise in GC and SFC $\xi \rightarrow 0$ because now $\boldsymbol{D}_m >> \boldsymbol{D}_s$ and, to all intents and purposes,

$$H_D = [2\gamma_m\boldsymbol{D}_m/u_m] \tag{23a}$$

Only, for liquid–liquid systems, we find

$$H_D = [2\gamma_m\boldsymbol{D}_m/u_m](1 + k) \tag{23b}$$

a rather overlooked result, because almost always Eq. (23a) is reported in the literature. For axial diffusion, the omittance of the correction factor $(1 + k)$ is hardly of any practical value (probably the reason for its general neglect) because the absolute values of $H_{D,s}$ are very small in LC compared with the other contributions to zone-broadening. However, for radial diffusion (see Sec. II.E.2), which is important in suppressing flow unevenness, the correction may be of value. Because modern LC is very often carried out with chemically bonded layers grafted onto the surface of solid particles, and the diffusion within these layers is largely unknown, the correction factor $(1 + k)$ in Eq. (23b) may or may not be valid in the majority of HPLC analyses. It should be applied strictly only to LLC.

As a result, omitting the $(1 + k)$ factor in Eq. (23), B is a constant, $2\gamma_m\boldsymbol{D}_m$. Hence, the contribution of longitudinal diffusion to plate height, called "the B term" ever since van Deemter, is inversely proportional to the flow velocity. This logical result means that for the practice of chromatography, mobile-phase velocities should be chosen such that the B term is of less importance than the other contributions to plate height. In GC this is easily achieved by the choice of relatively high velocities (on the order of 1–10 cm/s), whereas in LC, diffusion coefficients are generally too small to produce significant contributions from diffusion at the practical liquid flow velocities used (on the order of 1–10 mm/s).

2. Convective Dispersion in the Mobile Phase

Chromatographic separations, especially in LC, occur mainly in packed beds (i.e., a tubular column filled with particulate materials). When preparing these columns, the particles of the packing acquire a random arrangement, usually with an interstitial porosity of $\varepsilon_0 \approx 0.40$. In such beds, flow encounters obstruction by the very presence of the particulate obstacles, and molecules follow a tortuous path through the bed. The interstitial channels between the particles show a highly variable cross section, very narrow in regions where particles touch each other, and widening up in the regions in between those successive contact points. When approaching such constrictions in the flow path, flowing volume elements slow down considerably owing to increasing viscous forces, whereas much higher velocities are possible in the regions where flow channels widen. Thus, local velocities vary strongly, depending on the size of the interstices, the proximity to a particle surface, and the continuous blocking of the flow channel by successive particles. Molecular movement through such beds is possible only when molecules avoid the obstacles by moving around them in all possible radial and longitudinal directions, and there are no straight pathways. The process of this movement is highly erratic and can best be considered a random process of splitting the flow lines around the particles. Such a process is subject to modeling by statistical models, such as the random-walk. As a consequence of the local velocity differences and the potentially different lengths of the flow lines, a spread in residence times is expected. Because we deal with numerous particles (the number of particles with size d_p that fits in the column length L/d_p, easily reaches values of 2×10^4 to 5×10^6), and with open connections from all directions of the flow paths the mentioned velocity differences will smooth out. Overall, a nearly plug-like flow, with an average velocity u_m, is expected in columns that are packed randomly and well. The resulting small residual velocity differences from local streamline-splitting has been termed *eddy diffusion* in older literature, although *convective dispersion* might be a much better term in view of the hydrodynamic background of the phenomenon.

This contribution to zone-spreading has resulted in much controversy in the literature over the years. In GC, it is always small and, therefore, not amenable to precise determination. As a consequence, different results have been reported: the contribution of this process to plate height can be positive, absent, or occasionally, even negative.

In LC the influence of the packing is often much more pronounced, and the gap between the van Deemter theory and experiment has been filled by incorporating the aforementioned irregular flow phenomena on a small scale (approximately that of the particle size) as well as flow unevenness throughout the column cross section [1,5,11,12]. The relative magnitude of hydrodynamic processes, such as eddy diffusion and molecular diffusion, is the key to understand the experimental findings on peak-broadening in packed columns. The scales on which velocity differences in packed beds occur ranges from the subparticle scale to the scale covering the entire column cross section. On the small side of this scale, we distinguish intraparticle (pore flow inside particles), interparticle (flow in interstitial channels), and extra-particle, short-range, interchannel (flow in nearby, but differing, channels) regions. Then, through regions consisting of, say 10–100 particles (long-range interchannel effects), we finally have transcolumn (velocity profiles covering the whole cross section) and wall effects (depletion of particles near the wall as a result of the relative loose packing next to the solid wall). We will treat some of the more important processes in the following sections.

(*a*) *Convective Dispersion: Eddy Diffusion or Streamline-Splitting.* On a scale of several particle diameters, unevenness of flow may occur in nearby channels because of differences in shape, openness (packing irregularity), obstructions, or other. The resulting spreading in residence times is called eddy diffusion, and can best be pictured as a form of streamline-splitting. Molecules that approach a particle have to choose their way around the particle, either on the left, upper, lower, or right side (or somewhere in between), and in the worst case, the molecules are stuck momentarily in front of the particle. Thus, in the flow process of traversing one particle layer of thickness d_p, the average particle size, with zone velocity

u_z, the difference in traversed distance is at most d_p, which we can interpret as the step length $\ell_{e,z} = d_p$ in a random-walk process in the longitudinal direction z. The total process involves $N = L/d_p$ particle layers and, hence, by using the random-walk rule [see Eq. (7)], the variance of this process is $\sigma^2_{e,z} = (L/d_p)d_p^2 = Ld_p$, and the associated dispersion coefficient $\boldsymbol{D}_{e,z}$, from Eq. (7a) and plate height $H_{e,z}$, from Eq. (9) or (10a) are found as

$$\boldsymbol{D}_{\text{eff},e,z} \approx \tfrac{1}{2} d_p u_z = \lambda_{e,z} d_p u_z \tag{24}$$

and

$$H_{e,z} = 2\boldsymbol{D}_{\text{eff},e,z}/u_z = 2\lambda_{e,z} d_p = A \tag{24a}$$

where $\lambda_{e,z}$ is a constant representing the regularity of the packing. In experiments the constant A is often found in the range of several particle diameters, and $\lambda_{e,z}$ ranges from 1 (very well packed) to 10 (faulty packing). This eddy diffusion contribution was first introduced by van Deemter et al. [7], and since has been called the A term of the plate height relation with velocity, H_{tot} versus u_m, which is called the van Deemter equation. Although this A term is small and of the order of several particle diameters, especially in modern LC with particle sizes as low as 1 μm, other contributions to plate height may also be very small, and so this contribution, in effect, sets the upper limit attainable for the column efficiency. Because this A term is constant (i.e., independent of the velocity) in this limiting condition where the other broadening contributions are also small, high velocities are allowed and fast separations are possible without reducing column efficiency too much (see later Sec. IV on optimization).

(*b*) *Convective Dispersion and Molecular Diffusion.* In general, the flow pattern through packed beds is very uneven. As such, this would lead to very broad chromatographic peaks, which is not so in practice. What happens, is that lateral (or radial) mass transfer (directed along the radial coordinate r), perpendicular to the main flow direction (longitudinal or axial coordinate z), causes radial mixing of flowing elements. The faster the radial mixing, the more flowing elements will achieve the average velocity, and the more zone-spreading will be reduced. On the other hand, the farther apart in the cross-sectional regions concomitant with different average flow velocities, the larger the distance over which lateral or radial mass transfer has to occur to relax the dispersing effect of the uneven flow. For example, wall effects and uneven, nonrandom packing are dominant contributors to mobile-phase dispersion.

Molecular diffusion in the radial directions is the first contributor to lateral mass transfer, and just as in longitudinal diffusion (see Sec. II.E.1), this can be described by the obstructed diffusion coefficient $\boldsymbol{D}_{m,R} = \gamma_m \boldsymbol{D}_m$. However, molecular diffusion is not the only process transferring molecules from one flow channel to another. In the former section, we found that molecules have to find their ways around the particles of the packing by streamline-splitting. In this process, molecules not only take steps in the longitudinal direction, which lead to the eddy diffusion effect, but also in the radial direction (Fig. 2). Any molecule or fluid element in the flow coming up against a particle of the packing is forced to go around it and, in doing so, it moves sideways in the lateral or radial direction. This, in fact, is radial mass transfer, now of a hydrodynamic origin. In the older literature, this is referred to as *anastomosis* [12], a physiological phenomenon that describes the complex interconnections of blood capillaries. Hiby [19] shed some light on the nature of convective dispersion in an interesting experiment in which a "thread" of colored dye solution was introduced (comparable with an injected zone in a column) perpendicular to the flow direction of water on a two-dimensional water table used to visualize flow phenomena. The water table was provided with solid cylinders as a model for a packed bed, and after some time, in which the thread was deformed strongly by the streamline-splitting around the cylindrical obstacles in creeping flow, the flow was reversed. It then appeared that streamline-splitting *without diffusion* was *reversible* as the thread was restored in its original position. Obviously, streamline-splitting leads to broadening of zones, but is a deterministic, directional, and reversible process, and it is not a random mixing or dispersion phenomenon, such as diffusion, which is acting in all directions and

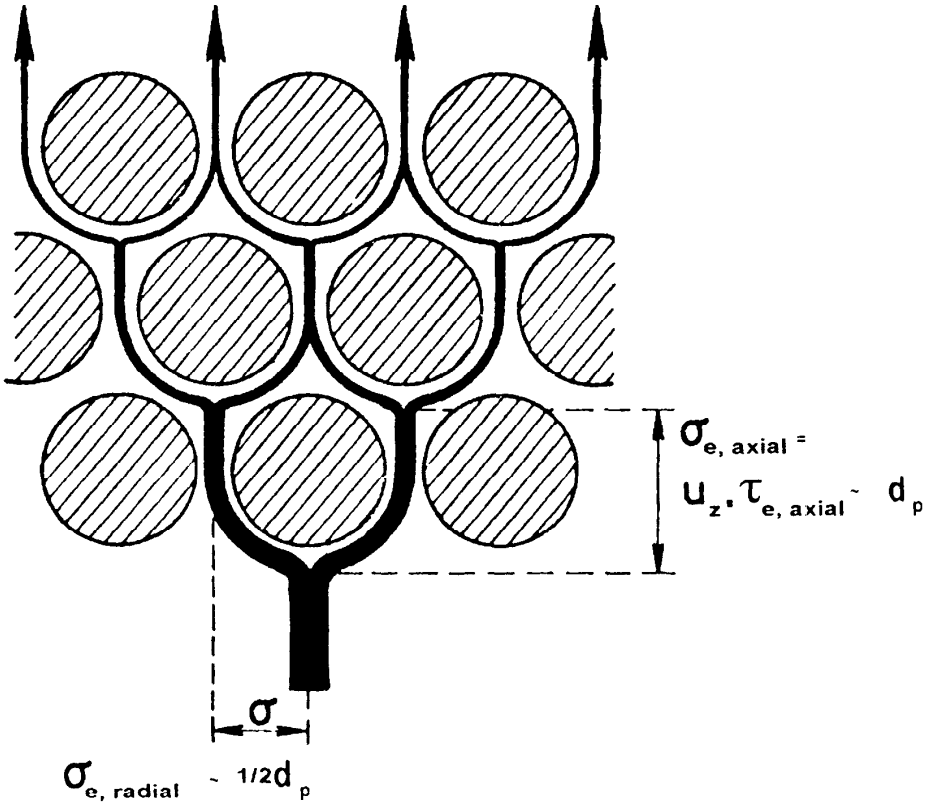


Figure 2 Axial and radial eddy–diffusion steps at higher velocities: At lower velocities streamlines do not separate from particle surface, and the radial step length becomes smaller.

chaotic as well as irreversible. It thus appears, that only the combined action of diffusion and streamline-splitting can be interpreted as a mixing or dispersion process, in other words the displacement of molecules by streamline-splitting allows mixing over larger distances than molecular diffusion alone would be capable of. The convective process thus helps diffusion to mix or disperse molecules over larger distances. Hence, for the description of the total effect we should be looking for an effective dispersion coefficient that consists of two parts, the always present obstructed diffusion and a dispersion coefficient that describes the displacement of the streamlines.

The latter convective radial dispersion mechanism can be described by a random-walk model, with a resulting dispersion coefficient that will be additive [see Eq. (8a)] to the effective obstructive diffusion coefficient introduced before to obtain the total effect of radial mass transfer from both diffusion and convective (or hydrodynamic) dispersion.

In the random-walk process for radial convective dispersion, radial displacement steps $\ell_{e,R}$ are smaller than the axial displacement steps (see Fig. 2) and amount to approximately $\ell_{e,R} = \frac{1}{2}d_p$. The steptime $\tau_{e,R} = d_p/u_z$ and, as in axial eddy diffusion, the dispersion coefficient $\boldsymbol{D}_{\text{eff},e,R}$ for this process is found from Eq. (7a) as

$$\boldsymbol{D}_{\text{eff},e,R} = (\ell_{e,R})^2/(2\tau_{e,R}) \approx (1/8)d_p u_z = \lambda_{e,R} d_p u_z \tag{25}$$

where the dimensionless constant $\lambda_{e,R}$, just as its longitudinal counterpart, depends on the geometry of the packing. The value found here with the random-walk approach, $\lambda_{e,R} = 1/8$, closely resembles the one found by one of the models of Giddings [5]. Johnson [13] obtained $\lambda_{e,R} = 1/11$ from a very refined model for hydrodynamic-spreading effects in packed beds. The value found by Johnson is close to those determined experimentally, at least at higher-flow velocities. At lower flows, we can imagine that the radial step length is reduced to values

$<½\ d_p$ because flowlines tend to follow the particle surface more closely (creeping flow), and detach themselves at the backside of the particle, rather than at the upper, right, left, or lower side. The latter is true only for increased velocities, where flow lines stay the distance d_p apart and detach from the surface after streamline-splitting around the particle, because (still laminar) vortices are formed right behind the particle. Actually, $\lambda_{e,R}$ describes the correlation between the positions of molecules before and after the particle and the streamline-splitting process, and in creeping flow the correlation is complete (the molecule returns to its same position as before, and $\lambda_{e,R}$ would become zero). The correlation becomes ever less at higher velocities owing to the randomization by flow phenomena, such as the vortex formation. Behind the particle, in large-scale flow visualization experiments, effects such as this are clearly demonstrated in technological science literature.

Indeed, Gunn [14] summarizes many literature data such that $\lambda_{e,R} = 1/11$ for $\mathbf{Re}_p > 200$ and $\lambda_{e,R} = 1/40$ for $\mathbf{Re}_p < 1$. Here $\mathbf{Re}_p = ud_p/\nu$ the *Reynolds number* [15], based on the particle size (with ν being the kinematic viscosity, which is the "normal" dynamic viscosity η divided by the density ρ; that is, $\nu = \eta/\rho$). At intermediate velocities fitting the Gunn data yields:

$$1/\lambda_{e,R} = 11 + 29\ \exp(-\mathbf{Re}_p/25) \tag{25a}$$

The values of 1/16–1/30, as reported by Sie and Rijnders [11], based on different geometric models of randomly packed spheres, fit nicely into the range covered by Eq. (25a). It should be stressed that in modern LC, for which particle sizes are as small as several micrometers, it is hardly possible to reach values for the Reynolds number in excess of 1, and so, for practical reasons, it is very safe to adopt a constant value for $\lambda_{e,R}$, being 1/40, the limiting value of Eq. (25a).

Not surprisingly, a correlation has also been reported between the constant $\lambda_{e,R}$ and the column/particle size ratio Ω (defined as $\Omega = R_c/d_p$, where R_c is the column radius), probably caused by the fact that wall effects (particle depletion) are more pronounced in columns with a smaller number of particles in the cross section. Fahien et al. [15] report that

$$\lambda_{e,R} = \Omega^2/[8\Omega^2 + (155/4)] \tag{25b}$$

Equation (25b) was experimentally obtained for technological-scale packed columns, for which the packing structure can easily differ from that in modern analytical-scale packed columns. Yet the limiting value of 1/8 for large values of Ω (i.e., small particles, as in modern practice) is close to the values found in analytical columns at very high flow rates and equals the random-walk value. Although there may be some virtue in relations such as Eq. (25b), Ω values <50 are seldom applied in modern analytical separation columns and wall effects are thus expected to be practically absent.

Summarizing, we have found two contributions to radial mass transfer in packed columns, and we are left with adding these together to obtain the total radial dispersion coefficient:

$$\boldsymbol{D}_{\text{eff},R} = \boldsymbol{D}_{eff,m,R} + \boldsymbol{D}_{eff,e,R} = [\gamma_m \boldsymbol{D}_m + \lambda_{e,R} d_p u_m]/(1 + k) \tag{26}$$

or, in the absence of partitioning (and this is usually reported in the literature):

$$\boldsymbol{D}_R = \boldsymbol{D}_{m,R} + \boldsymbol{D}_{e,R} = \gamma_m \boldsymbol{D}_m + \lambda_{e,R} d_p u_m \tag{26a}$$

The $\boldsymbol{D}_R$ is seen to be dominated by molecular diffusion at low-flow rates, whereas at high-flow velocities the hydrodynamic dispersion from radial eddy diffusion takes over.

In GC, for which molecular diffusion coefficients are relatively large (about 10^{-1} cm^2/s), radial eddy diffusion will seldom be of influence, except for very high velocities and large particles, which are increasingly rare. Thus, Eq. (26) and Eq. (26a) are of direct interest only for LC techniques.

In LLC [see Eq. (23)], owing to the presence of stationary phase, a diffusion correction factor for diffusion with partitioning, $(1 + \xi k)$ should be added to the first term on the RHS of Eq. (26), thereby almost eliminating the factor $1/(1 + k)$ present there, but this is reported nowhere in the literature. So the correct formulation, but *only for LLC* is that:

$$\mathbf{D}_{R,\text{eff,LLC}} \approx \gamma_m \boldsymbol{D}_m + \lambda_{e,R} d_p u_m/(1 + k) \tag{26b1}$$

or:

$$\boldsymbol{D}_{R,\text{LLC}} = \boldsymbol{D}_{R,\text{eff,LLC}}(1 + k) \approx \gamma_m \boldsymbol{D}_m(1 + k) + \lambda_{e,R} d_p u_m \tag{26b2}$$

In the following we will use Eq. (26a) as the simpler and more generally applicable version, but for LLC Eq. (26b) should be used. In view of the importance of the extent of radial dispersion for suppressing the deleterious effects of velocity profiles over the cross section of the column (see following section), it can be of value to use Eq. (26b) when appropriate.

What has been said in the foregoing on radial dispersion throughout the porous structure of a packed column, will be equally valid for the radial dispersion *within* porous particles, *provided that these particles are permeable to flow*; that is, *perfusion*. Many contemporary porous packing particles are susceptible to flow to a certain extent, but pressure drop across a small particle is very low and the associated flow is seldom helpful in enlarging mass transfer within these porous particles. Only at very high velocities, and especially for large (polymeric) solutes, intraparticle convective mixing can be observed [55], because a small permeation velocity is then sufficient to dominate over the very small diffusion coefficients of macromolecules. We will return to this point in Sec. IV.B on size exclusion chromatography, and will discuss there the possibility of electrodriven permeation through porous particles [56].

As a footnote, we remark that in the literature [1,4,5,11–13], there are many controversial viewpoints on the validity of Eq. (26), (i.e., the simple summation of a diffusive and a convective mass transfer mechanism). Giddings [1,5] made a point in observing that summation of random-walk variances, as in Eq. (26) and based on the statistical rule Eq. (8), is valid only for *independent random processes* in which the step length and the step number are mutually independent. This being true, we should look at the combined effect of flow and diffusion again. Both random-walks occur in steps that originate from the same axial velocity differences and, following Giddings: "a random step undertaken by the flow process can be cut short by rapid diffusional exchange, and a normal diffusion-controlled step can be cut short by flow exchange. Diffusion and flow clearly do not have independent random walks."

Subsequently, Giddings idea to allow only *additivity of the number of random steps* initiated by both processes, rather than adding their variances, is erroneous, because the two processes must necessarily then be placed in time, one after the other, whereas actually the flow and diffusion act at the same time. In the latter, and more appropriate case, statistics again allow the summation of variances, rather than only the steps, when provided the independence of the two processes. As the driving forces and the manifestations of both processes are quite different and independent (see foregoing), there is no reason to doubt the independence, and we prefer the additivity of variances above the restricted additivity of steps. Indeed, Giddings' reasoning, which resulted in a so-called coupling of flow and diffusion terms, qualitatively explained many experiments in which it was shown that plate heights originated by mobile-phase effects, did not grow to infinity with ever increasing flow rates, but rather, leveled off in concave plots towards the velocity axis. We will show, in the footmarks of Littlewood [12], Sie and Rijnders [11], and Johnson [13], that the same explanation can be based on the present reasoning, with Eq. (26) as the result. Thus, it remains uncertain whether the generalizations in the coupling theory are correct, but it is certain that this theory fails in the limiting condition of infinite

velocity, for which it predicts zero plate height. This cannot be true based on first principles and many experiments at very high velocities. It is reassuring that the present approach does not lead to this situation and correctly predicts a finite plate height (see the next section).

(*c*) *Convective Dispersion from Velocity Profiles and Radial Dispersion.* In Sec. II.C.3 we discussed the general effect of velocity differences on zone-broadening in chromatographic systems, be they velocity differences within one phase (to be treated further in this section) or velocity differences between the two phases (see following Sec. II.E.3). The resulting plate height for any velocity difference Δu has been found, and it is described by Eq. (11).

Here, we concentrate on the velocity differences possible within one phase, logically the mobile phase. In the former section we described the unevenness of flow through packed beds and the potential existence of transcolumn velocity differences and wall effects. For these kinds of flow differences, there exists a continuously changing velocity throughout the column cross section, just as in open tube flow, for which the well-known parabolic flow profile after Poiseuille is valid [1,4–6,8,10,12,15]. In packed columns, less pronounced, but significant profiles over the entire column cross section can be observed, sometimes made visible, through injection of colored components, as bands in glass columns [see e.g., Ref. 11]. As seen in the former section, radial mass transfer mechanisms are active to counteract the deleterious broadening resulting from velocity profiles alone. This radial mixing quickly smoothes out the velocity differences, but now the distance to be covered is larger and approximates that of the column radius R_c. The equilibration time required for sufficient mixing of all velocity states over the distance R_c is [see Eq. (7a)] on the order of

$$t^* = \tau_{\Delta u} \approx R_c^2/2\boldsymbol{D}_{R,\text{eff}} \tag{27}$$

Here, the following is tacitly assumed:

1. The stationary phase is evenly distributed throughout the cross section over which the velocity differences occur (this is not true for open tubular columns, which need a different approach; see Sec. II.E.4.e).
2. Molecules in the cross section are averaged effectively over all velocity states by at least *twice crossing* the distance (R_c) that minimum and maximum velocity are apart. This is not unreasonable, as has been proved by Taylor [16], Aris [17], and Gill et al. [27] who derive that the dimensionless residence time $\mathbf{Fo} = (\boldsymbol{D}_R/\boldsymbol{R}_c^2)t$, the so-called Fourier-number (for an introduction to dimensionless quantities see Sec. II.E.4.b) should be in excess of about 0.8. This actually means that radial mixing of molecules throughout the cross section is considered complete only after much more than $2 \times 0.8 = 1.6$ (so say at least two) passes [one pass requires time τ after Eq. (27)]. If this condition of (relatively) long residence times is obeyed, this has the effect that all concentration differences within phases are smeared out effectively; thus, in a cross section only small concentration differences occur, a basic assumption in the Taylor [16], Aris [17], and Golay [10] theories, but also in Giddings' nonequilibrium theory [1,5]. Precise experiments (see, e.g., Ref. [26]) show that indeed for $\mathbf{Fo} > 0.8$, Taylor–Aris–Golay dispersion is valid, but that at smaller Fourier numbers a correction factor of about 1.3 $\mathbf{Fo}^{0.5}$ should be applied to the expected dispersion coefficients (and thus plate heights). For further comments on this see Sec. II.E.4.e.

We proceed our reasoning, which is approximate anyhow, by using Eq. (27).

For packed columns then, with $u_{\max}$ being the local maximum velocity of the profile and $\langle u_m \rangle$ the *average* or mean velocity now required, we obtain a maximum velocity difference in the mobile phase of $[u_{\max} - \langle u_m \rangle]$ causing the zone-broadening. Within the mobile phase, transport by flow is reduced by the factor $1/(1 + k)$ by virtue of the equilibration with the present stationary phase. Hence, the effective velocity difference is $\Delta u = [u_{\max} - \langle u_m \rangle]/(1 + k) = \Delta u_{\max}/(1 + k)$ and we find with Eqs. (11) and (27):

$$H_m = \tfrac{1}{2}(\Delta u_{\max}/\langle u_m\rangle)^2(R_c^2/\boldsymbol{D}_R)\langle u_m\rangle = 2(\kappa R_c^2/\boldsymbol{D}_R)\langle u_m\rangle \tag{28}$$

where $\boldsymbol{D}_R = \boldsymbol{D}_{R,\text{eff}}(1 + k)$ and $\kappa = \tfrac{1}{4}(\Delta u_{\max}/\langle u_m\rangle)^2$. The latter may be called the *velocity profile factor*, for it strongly reflects the spreading influence (note the quadratic dependence) of the velocity difference within the moving phase. Actually, we should have taken the local velocity differences at each radial position r, to find by integration over the column cross section an average value for κ. This exercise, while using the exact mass balance equations, was first carried out by Taylor [16], Aris [17], and Golay [10] for open tubular columns, and later for packed columns by Littlewood [12], Johnson [13], and Sie and Rijnders [11]. The present author treated both open and packed columns [18], and the plate height equation (28) was always found to represent spreading from all kinds of velocity profiles, including the symmetrical Poiseuille profile and the strongly asymmetrical profiles found in helically coiled spiral tubes. In open tubular columns, all theoretical approaches agree in the value of $\kappa = 1/48$, for the underlying strongly pronounced parabolic flow profile. In packed columns, more flat profiles often exist, sometimes even almost flat and plug-like in modern well-packed columns, so that less peak-broadening from velocity differences is found, which reflects in smaller values for κ. Indeed, several literature searches on experimental data for κ, yield values in the range 10^{-1} to 10^{-6}, the smallest value almost approaching the ideal of $\kappa = 0$. This would be present in exact plug-flow, such as in turbulent flow where $\Delta u_{\max} = 0$ (all axial velocities are the same and equal to the average velocity). We stress that under normal chromatographic conditions, turbulent flow can never occur, because Reynolds numbers are far too small [15]. The flat velocity profile that is ideally present in packed columns simply arises from the chaotic streamline-splitting described before. It is illustrative to obtain some numerical values for the foregoing radial-mixing process. For example, in modern LC columns, for which packings are used with particles as small as 1–5 μm, radial transport by eddy diffusion is not able to cover the whole cross-sectional area. This follows from Eqs. (27) and (26b) if we substitute pertinent values of the parameters for a 15-cm LLC column packed with 5-μm particles: the radial squared distance travelled $\langle r^2\rangle = 2\boldsymbol{D}_{R,\text{LLC}}t = 2[\gamma_m\boldsymbol{D}_m(1 + k) + \lambda_{e,R}d_p\langle u_m\rangle]t \approx 2\lambda_{e,R}d_p\langle u_m\rangle t = 2\lambda_{e,R}d_pL \approx 2 \times (1/40) \times (5 \times 10^{-4}) \times 15 = 3.75 \times 10^{-4}$ cm^2 (i.e., a linear distance of $\langle r\rangle = 0.2$ mm is covered, far less than the column radius of about 1–2 mm). For a central injection of sample onto the column axis, this would imply that component molecules do not reach the wall regions before eluting from the column. Thus, the column would be effectively infinite in diameter, and potential wall effects (see next section) could be circumvented. In daily practice, samples are not centrally injected, but are spread across the column cross section, and wall effects, if present, will still be of importance.

The chaotic nature of this type of radial flow is less prominent if fewer particles are available in the cross section to randomize the flow. Thus, we expect that velocity profiles become more prominent if the column/particle aspect ratio $\Omega = R_c/d_p$ becomes smaller. This is exactly what is found in experiments [11–13], supported by the theoretical modeling after Johnson [13]. That author proves on the basis of a porosity profile near the wall, that the velocity profile factor κ for an isotropic bed depends on Ω as:

$$\kappa\Omega^2 = 0.11 \qquad (\text{for } \Omega > 50) \tag{29}$$

which agrees very well with the experimental observations [11], and is applicable to the range of modern column/particle sizes. So, for an average number of particles in the cross section exceeding about 50 or 100, the velocity profile factor κ is a simple quadratic function of the aspect ratio. Johnson also has good arguments to predict that for $\Omega < 50$ the constant 0.11 in Eq. (29) is no longer constant and becomes a function of Ω, which shows a minimum of about 0.02 at an aspect ratio $\Omega \approx 1$–2. This is borne out in experiments [13], but for the practice of chromatography, for which aspect ratios Ω in excess of 100 are customary, only Eq. (29) is of importance.

With this in mind, we can write from Eqs. (28) and (29) that

$$H_m = 2(\kappa R_c^2/\boldsymbol{D}_R)\langle u_m\rangle = 0.22(d_p^2/\boldsymbol{D}_R)\langle u_m\rangle = C_m\langle u_m\rangle \tag{30}$$

which is confirmed by many experimental data in both LC and GC. The general trend is thus that the plate height decreases quadratically with particle size, which is one of the main reasons for the choice of particles in the size range of 1–5 μm in HPLC.

Equation (30) describes how transcolumn velocity profiles, if present, give rise to plate height contributions, which are, in a first approximation, linear in the mobile-phase velocity (proportionality factor C_m). This is as expected: the larger the velocity, the larger (and in proportion) the velocity differences. This so-called C_m term contribution was not present in the original van Deemter equation [7], but was later added [20] in analogy with the situation in open tubular or capillary columns for GC [8,10,17,18], in which this term is of great importance. In GC, the plate height arising from these mobile-phase effects is strictly linear in velocity, at least for straight (or loosely coiled) columns. In packed columns for GC, the term is generally small relative to other ones and does reflect the goodness of the packing and packing procedure. For example, if the spread in particle sizes is too large, during packing so-called segregation may occur (i.e., the smaller particles are located preferentially in the central regions of the packing, whereas the larger particles are located more toward the wall regions. Johnson [13], for example, reports that in his experiments particle size increases about quadratically with the radial coordinate toward the wall, and the associated velocity profile, with higher velocities in the wall regions, resulted in $\kappa \approx 0.15\ \Omega^{-1}$ instead of Eq. (29). As a result H_m, from Eq. (30), becomes large and dependent on R_c (rather than being independent) and proportional to d_p (rather than to d_p^2). On the other hand, wall effects by particle depletion from the wall regions results in plate height contributions proportional to d_p^2, but independent of R_c. This is of eminent importance for preparative chromatography, in which wide-bore columns are generally used.

Especially in LC, the H_m term contribution leads to the well-known curved and no longer linear plate height plots as a function of velocity (H vs. $\langle u_m \rangle$), owing to the velocity-dependent radial dispersion coefficient from Eq. (26). In LC, the velocity profile factor is always small (except for badly packed columns with, e.g., short-range effects by porosity differences), owing to the choice of small-particle sizes [see Eq. (29)], and segregation and wall effects are generally negligible. Yet, the denominator of the plate height expression for H_m, $\boldsymbol{D}_R$ in Eq. (30), is far smaller than in GC (owing to smaller particle sizes). The resulting plate height may still be appreciable relative to all other contributions, because the molecular diffusion coefficient is far smaller than in GC and on the order of 10^{-5} to 10^{-6} cm^2/s. Second, radial dispersion from eddy diffusion effects is small, and becomes larger only at higher velocities. As we have seen, the latter is velocity-dependent and so yields a concave H versus $\langle u_m \rangle$ plot under all practical LC conditions (see Sec. II.E.4).

One last property of Eq. (30) to discuss is that it does not contain any dependence on the partition equilibrium. Thus, the contribution of plate height stemming from mobile effects, is basically the same for retained ($k > 0$) and nonretained ($k = 0$) components. This is true (see the Sec. II.E.4.e, on capillary columns) if the stationary phase is very evenly distributed over the column (i.e., not only should each cross section contain the same amount of stationary phase, but this should also be homogeneously smeared out throughout the cross section). This is seen, on a macroscopic scale, as almost true for packed columns filled with finely dispersed particles, but on a subparticle scale, this is no longer valid. On this scale, component molecules spend finite times τ_m in the flowing phase, without contacting any stationary phase that could be imagined to be present as a coated film on the walls (or inside pores) of the packing particles. The situation very much resembles that in open tubular or capillary columns, in which the stationary phase is located at the wall of the tube, and the core of the mobile phase region does not actually meet the stationary phase. Rather, it flows along the phase interface and interphase mass-transfer proceeds only by radial diffusion perpendicular to the interface. Later (see the next section and Sec. II.E.4.e) on capillary columns, we will see that under such conditions, the C_m term becomes dependent on the capacity ratio k, through some function $f(k)$, such that Eq. (30) is written as:

$$H_m = 2f(k)(\kappa R_c^2/D_R)\langle u_m\rangle = C_m(k)\langle u_m\rangle \tag{30a}$$

In Eq. (30a) the C_m term now also contains the partitioning effect [so $C_m = C_m(k)$] through the factor $f(k)$, still to be specified (see following section).

Here, we continue with extending the idea that a packed bed separation column may be assumed to be equivalent to a bundle of capillary columns, of uniform size, with internal coating of stationary phase on their walls. This concept has proved to be of great help in the study of flow through packed beds in technological sciences [15], using so-called capillaric models for flow through the interparticle interstices. Because these irregularly shaped interstitial pores are not cylinders, it is better to consider the effective pore diameter as being $d_{\text{eff,pore}} = 4R_h$, where R_h represents the *hydraulic radius*. The latter concept is generally used in engineering sciences [15] to represent the characteristic size of interstitial pores in packed beds, such that the pressure drop versus flow relation is uniquely defined (see Sec. III). The hydraulic radius is found from the definition: R_h = {[volume of (interstitial) pore space filled with fluid]/[surface area of (interstitial) pore space in contact with fluid]} = {porosity (ε_0)/ specific surface area (S_v)}, where both ε_0 and S_v are practical and experimentally measurable characteristics of porous materials. In separation science R_h has been successfully applied to describe the average effective size of intraparticle pores, such as those used for the steric separation of macromolecules with size exclusion chromatography (SEC; formerly called gel permeation chromatography or GPC) [2,37]. The same applies to the interparticle pore space that is used for exclusion and separation of macromolecules and particulates in hydrodynamic chromatography (HDC) [2], formerly called separation by flow. We recognize that for real capillary flow in a tube with radius R_c, the hydraulic radius $R_h = \pi R_c^2/2\pi R_c = R_c/2$ and, thus, $d_c = 2R_c = 4R_h$. For spherical particles of the packing in a packed bed column with an average particle diameter d_p, S_v simply reads: $S_v = 6(1 - \varepsilon_0)/d_p$, whereas often for random packings, interstitial porosity $\varepsilon_0 \approx 0.40$. Thus, the hydraulic radius can be obtained from

$$R_h = \varepsilon_0/S_v = (d_p/6)[\varepsilon_0/(1 - \varepsilon_0)] = (R_p/3)[\varepsilon_0/(1 - \varepsilon_0)] \approx (2/9)R_p = (1/9)d_p \tag{31}$$

If we now imagine that the packed bed can be represented by parallel tubes with radius $R_{c,h}$, based on the hydraulic radius R_h, such that $R_h = R_{c,h}/2$ (the same relation as for real tube flow, see foregoing) we have

$$R_{c,h} = 2R_h = (d_p/3)[\varepsilon_0/(1 - \varepsilon_0)] \approx (2/9)d_p \tag{31a}$$

Note that, as a rule of thumb, the fictive diameter $d_{c,h} = 4R_h \approx (4/9)d_p$ almost equals the particle radius R_p. This relation between hydraulic–radius-based channel size and particle size causes the well-known Poiseuille pressure–flow relation [15] (see Sec. III), to be valid for both the packed bed and the fictive hydraulic tube flow. Hence, a tube with a (fictive) radius $R_{c,h} = 2R_h \approx (2/9)d_p$ shows the same flow characteristics as a packed bed with particle size d_p using Eq. (31) for R_h.

Thus, we may replace in Eq. (30) the original column radius R_c by the fictive and hydraulic–radius-based tube radius $R_{c,h}$ to find:

$$H_m = 2(\kappa_{c,h}R_{c,h}^2/D_R)\langle u_m\rangle \approx 2\kappa_{c,h}([(2/9)d_p]^2/D_R)\langle u_m\rangle \approx 0.1\kappa_{c,h}(d_p^2/D_R)\langle u_m\rangle = C_m\langle u_m\rangle \tag{32}$$

Only for real tube flow when both radii are the same, then $R_{c,h} = 2R_h = R_c$, and Eq. (32) should approach the result for the C_m term after Golay [10] and Aris [17] in straight capillary tubes, where $\kappa = 1/48$ (see Sec. II.E.4.e). Using this value as a first approximation leads to

$$H_m \approx 0.002(d_p^2/D_R)\langle u_m\rangle = C_m\langle u_m\rangle \tag{32a}$$

which differs by only a factor of 5 with the original estimation of this effect by van Deemter [20] (see next section).

3. Sorption and Desorption: The Stationary-Phase Contribution

For this last contribution to the plate height that we will consider, we refer once more to the random-walk model, in which we first have to find the exact step length λ and the number of steps N, that a molecule takes once it partitions into the stationary phase and, thus, takes a step backward relative to the zone center. Likewise, when desorbed, it moves faster than the zone center and thus takes a step ahead. After each desorption of a molecule from the stationary phase, the distance covered in the mobile phase is the step $\ell = \langle u_m \rangle \tau_m$, but because we are looking for the final spread *around the mean position at the zone center* we have to subtract the distance covered by that center $\ell_z = u_z \tau_m$ to find the relative step forward: $\lambda = \ell - \ell_z = \tau_m(\langle u_m \rangle - u_z) = \ell k/(1 + k)$.

A molecule that stays behind during the time $\tau_s = k\tau_m$ in the stationary phase also steps behind the zone center with the same step length $|\lambda| = |\ell - \ell_z| = |\tau_s(0 - u_z)| = k\tau_m u_z = \ell k/(1 + k)$. A molecule thus chooses in $N = 2n_t = 2(L/\ell)$ steps (desorption and absorption steps) a step λ either forward or backward relative to the zone center, and the associated spreading after the random-walk rule Eq. (7) is $\sigma_z^2 = N\lambda^2 = 2L\ell[k/(1 + k)]^2$, from which the plate height for this partitioning process is obtained as:

$$H_{\text{part}} = \sigma_z^2/L = 2\ell[k/(1 + k)]^2 = 2[k/(1 + k)]^2\langle u_m \rangle \tau_m$$
$$= 2[k/(1 + k)^2]\langle u_m \rangle \tau_s = C\langle u_m \rangle \tag{33}$$

This result, another so-called C term, reflects the contribution to plate height accounting for the slowness of mass transfer of a molecule traversing one phase to reach the other in a characteristic finite time τ_m or τ_s. It is also called the *nonequilibrium term* after Giddings [1,5] for reasons explained in Sec. II.C.3, from which we already expected the proportionality (factor C) with the flow velocity. Here, it is revealed that the step length $\ell = \langle u_m \rangle \tau_m$ is the main parameter of interest for the plate height associated with the partitioning process.

Assuming for the moment that *slow diffusion in the mobile phase* would account for this mass-transfer term, and using the capillaric model for that phase, as discussed in the previous section, we can find the required expression for τ_m as: $\tau_m = R_{c,h}^2/2\boldsymbol{D}_R$, and so from Eq. (33):

$$H_{m,\text{part}} = 2[k/(1 + k)]^2\langle u_m \rangle \tau_m$$
$$= 2[k/(1 + k)]^2\langle u_m \rangle (R_{c,h}^2/2\boldsymbol{D}_R)$$
$$\approx 0.05[k/(1 + k)]^2\langle u_m \rangle (d_p^2/\boldsymbol{D}_R) = C_{m,\text{part}}\langle u_m \rangle \tag{33a}$$

which differs by only a factor of 5 with the quoted result obtained by van Deemter [20] in his extended plate height equation. He estimated the numerical factor to be 0.01, rather than 0.05, based on technological correlations for mass transfer. Littlewood [12] suggests the numerical value of the constant to be 0.025, whereas Giddings [5] obtains a constant of $(1/6) \times (1/16) = 1/96$, almost identical with the original van Deemter result. Ever since van Deemter, this particular contribution to plate height, which is small in packed columns for GC, but important in capillary columns and also in LC, is called the C_m term. With this result, we have also found the function $f(k) = [k/(1 + k)]^2$ to be used in Eq. (30a) in the previous section. In the specific case of capillary columns, $f(k)$ is slightly more complex, but still a ratio of quadratic functions of k, as has been proved by Golay [10] and Aris [17]. We proceed on that topic in Sec. II.E.4.e.

In addition to the C_m term, a logical stationary-phase contribution to plate height occurs if mass transfer by diffusion is slow. For that, we can use $\tau_s = k\tau_m$, instead of τ_m, as the characteristic time to escape from the stationary phase, as seen in Eq. (33):

$$H_{s,\text{part}} = 2[k/(1 + k)^2]\langle u_m \rangle \tau_s = C_s\langle u_m \rangle \tag{33b}$$

This so-called C_s term of the plate height equation differs in its functionality in k from the

earlier C_m term, and contains the characteristic time spent in the stationary phase as the time constant.

For adsorption chromatography, this time constant τ_s represents the average time for detachment of molecules from adsorption sites at the surface of the stationary phase. For a linear, first-order detachment reaction, with rate constant k_d, τ_s equals $1/k_d$, and the associated C_s term readily follows from Eq. (33b) as

$$H_{s,\text{ads}} = 2[k/(1 + k)^2]\langle u_m\rangle\tau_s = 2[k/(1 + k)^2]\langle u_m\rangle/k_d = C_{s,\text{ads}}\langle u_m\rangle \tag{33c}$$

A closely related contribution to plate height from adsorption, after Horvath and Lin [25], will be met in Sec. II.E.4.d.

In absorption or partition chromatography, desorption from the absorbing liquid that serves as the stationary phase involves diffusional transport from the interior regions toward the surface at the phase boundary where molecules can be transferred to the other phase. As was done earlier [see Eq. (12)] for this process, we can estimate the characteristic time from δ_s, the average film thickness or depth of pores filled with liquid, and the diffusion coefficient $\boldsymbol{D}_s$ to find $\tau_s \approx \delta_s^2/2\boldsymbol{D}_s$. The resulting C_s term reads:

$$H_{s,\text{part}} \approx [k/(1 + k)^2]\delta_s^2\langle u_m\rangle/\boldsymbol{D}_s = C_{s,\text{part}}\langle u_m\rangle \tag{33d}$$

It can be proved in more exact models [5,10,12,17,18] that, for a uniform film of thickness δ_s, a configuration factor $q_c = (2/3)$ is valid in Eq. (33d), whereas values for other geometries are given. The original numerical geometrical form factor $(8/\pi^2)$, as found by van Deemter et al., has been later corrected in (2/3), for a stationary phase present as a film. The final expression for H_s in film partition chromatography thus reads:

$$H_{s,\text{part}} = (2/3)[k/(1 + k)^2]\delta_s^2\langle u_m\rangle/\boldsymbol{D}_s = C_{s,\text{part}}\langle u_m\rangle \tag{33e}$$

Giddings [5] proves that for several other geometries in which a stationary phase may be present, such as the rod (as in paper chromatography), and the spherical porous particle (with stagnant pores, e.g., an ion-exchange bead), geometric form factors can be generalized, such as q_c, which replaces (2/3) in Eq. (33e) to yield:

$$H_{s,\text{part}} = q_c[k/(1 + k)^2]\delta^2\langle u_m\rangle/\boldsymbol{D}_s = C_{s,\text{part}}\langle u_m\rangle \tag{33f}$$

Here the form factor q_c can be found from $q_c = 2/(n' + 1)(n' + 3)$, such that for the

Uniform film, thickness δ_s:	$n' = 0$, $q_c = 2/3$, and $\delta = \delta_s$
Cylindrical porous rod, diameter d:	$n' = 1$, $q_c = 1/4$, and $\delta = d/2$
Spherical porous particle, diameter d_p:	$n' = 2$, $q_c = 2/15$, and $\delta = d_p/2$
Contact place (saddle surface) between particles coated with liquid:	$n' = 3$, $q_c = 1/12$, and $\delta \approx d_p/2$

Interestingly, a collection of randomly sized pores behaves as a continuous film in this approach. The spherical porous particle in particular is of interest for later discussion (see Sec. II.E.4.g).

Next to the fact that the H value obtained is proportional to the flow velocity of the mobile phase (the larger the velocity, the larger the disturbance of equilibrium), this result shows that plate height in partition chromatography is favored by reducing the dimensions of the stationary phase regions as much as possible (note the quadratic dependence on δ_s). The result for the C_s term as given by Eq. (33e) is also found in the more formal approaches cited [1,5,10,12,17,18], in which the exact mass balance equations were solved. This proves the reliability and applicability of the present approach proposed by Giddings [1,5], based on random-walks, rather than continuous processes.

In fact, the only particular geometry where the spatial distribution ("shape" or geometry) of a stationary liquid is exactly known to be a thin layer or film, is in capillary or open tubular columns, mainly used in GC [8], but more recently also applied in LC [9].

The exact solution to the mass-balance equation in this circular–cylindrical geometry has been first given by Golay [10], and as said, his result for the sorption process matches precisely with Eq. (33e), which can alternatively be expressed in terms of the open column radius R_c as

$$H_{s,\text{part}} = (1/6)\{k/[(1 + k)]^2\}R_c^2\varphi^2\langle u_m\rangle/\boldsymbol{D}_s = C_{s,\text{part}}\langle u_m\rangle \tag{33g}$$

where $\varphi = (V_s/V_m)$, the phase volume ratio of stationary and mobile phases. Golay [10] has produced the same result.

4. Alternative Expressions and Additional Forms of Broadening

In the foregoing, expressions have been derived for the main mechanisms that cause broadening of the chromatographic zones migrating through (often packed) separation columns. In this section, we describe possible methods to characterize the efficiency of columns by expressing the *total* plate height as a function of mobile-phase velocity. This was first done by van Deemter et al. [7] and has been used since then to optimize separation speed and power.

(*a*) *Packed Columns: The van Deemter Equation.* When we summarize the foregoing, we arrive at the conclusion that several important mechanisms contribute to the total plate height of zones to be separated, which by virtue of the additivity rule for independent processes [see Eq. (10c)] can be summed up to obtain the total plate height. These mechanisms are as follows:

1. Molecular (obstructed) longitudinal diffusion in both phases: Eq. (23) B term
2. Convective dispersion in the mobile phase: By axial eddy diffusion or streamline-splitting: Eq. (24a) A term
3. Convective dispersion in the mobile phase: By combined convection and lateral dispersion: Eq. (33a) C_m term
4. Sorption and desorption from the stationary phase or nonequilibrium: Eqs. (33b–g) C_s term

In partition chromatography, we arrive at the so-called extended van Deemter equation, which basically relates plate height to velocity as:

$$H_{\text{tot}} = A + B/\langle u_m\rangle + (C_m + C_s)\langle u_m\rangle \qquad \text{for } \phi = 1 \tag{34}$$

where, in fact (see Sec. II.A) $\langle u_m\rangle$ is meant to be the interstitial velocity u_0, and so should contain, in the general case of porous packing particles, the inverse porosity fraction ϕ^{-1} as a prefactor to each $\langle u_m\rangle$. This is rarely shown in literature, so we follow the custom to write only $\langle u_m\rangle$ instead of $\phi^{-1}\langle u_m\rangle$, but stress that Eq. (34) is valid only for nonaccessible porous particles ($\phi = 1$) (see Secs. II.E.4.d and II.E.4.g for further comments). It is always safe in practice to obtain $\langle u_m\rangle$ from u_0 (i.e., from the residence time t_0 of an excluded nonretained solute as L/t_0).

In Eq. (34) the following constants occur:

$$A = 2\lambda_{e,z}d_p \tag{34a}$$

$$B = 2\gamma_m\boldsymbol{D}_m \tag{34b}$$

$$C_m = 0.05[k/(1 + k)]^2(d_p^2/\boldsymbol{D}_m) = f'(k)(d_p^2/\boldsymbol{D}_m) \tag{34c1}$$

$$C_s = (2/3)[k/(1 + k)^2](\delta_s^2/\boldsymbol{D}_s) = g'(k)(\delta_s^2/\boldsymbol{D}_s) \tag{34c2}$$

Hence, there appears a total C term of magnitude:

$$C = C_m + C_s = f'(k)(d_p^2/\boldsymbol{D}_m) + g'(k)(\delta_s^2/\boldsymbol{D}_s) \tag{34c3}$$

In the molecular diffusion B term, van Deemter accounted for only mobile (in his case gaseous) phase diffusion, whereas in the C_m term radial diffusion ($\boldsymbol{D}_m$) rather than dispersion

(D_R) is used. In the following, we will incorporate the extended expressions as found before, but here we stress that the original van Deemter equation has been the key to the development of modern efficient separation columns. Although a quantitative agreement between experimental data and the theoretical expectation could not always be obtained, the relation as given in Eq. (34), shows many qualitatively correct trends in describing changes in operating conditions and is in use up to the present day.

For example, the van Deemter equation, being hyperbolic in velocity (Fig. 3), correctly describes the occurrence of a minimum plate height H_{min} at the velocity at which the B/u and Cu-terms ($C = C_m + C_s$) are equal:

$$H_{min} = A + 2[BC]^{1/2} \tag{35a}$$

The specific velocity where this maximum efficiency is found, is called the optimum velocity u_{opt} such that

$$u_{opt} = [B/C]^{1/2} \tag{35b}$$

This is illustrated in Fig. 3. We note that the optimum velocity is a specific velocity for the transition between different processes controlling dispersion; namely, the diffusion-controlled process described by B, and the flow-controlled process described by C. We will return to this matter shortly, at the introduction of dimensionless quantities.

The other column variables, such as the amount of stationary phase and its thickness, partition equilibrium and capacity factor, type of mobile phase, and so on, are contained in the factors A, B, and C and thus are also amenable to optimization. For that purpose, from experimental chromatograms at different velocities, one plots plate heights as obtained from peak widths (σ_t) and retention times (t_R) from Eq. (9a) versus the average mobile-phase velocity $\langle u_m \rangle$. The slope of the asymptotic tangent to the highest velocity datapoints represents the total C term, the possible intercept of the asymptote at zero velocity represents the A term, and the remainder is interpreted as the B term, inversely proportional to the flow velocity. To obtain B values easily, a plot of $(H - A)\langle u_m \rangle$ versus $\langle u_m \rangle^2$ should give almost straight

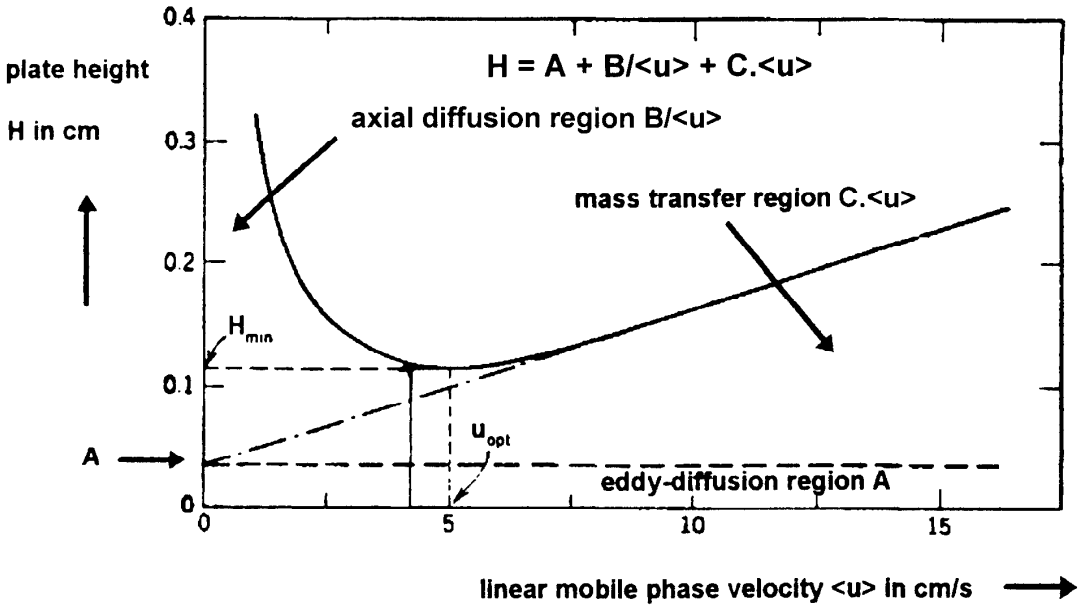


Figure 3 van Deemter plot of plate height H versus average mobile-phase velocity $\langle u \rangle$: Optimum velocity conditions with minimum plate height and regions of the three contributions to plate height are indicated.

lines, giving access to B as the intercept at zero velocity (slope C). Also helpful is a plot of $(H - A)/\langle u_m \rangle$ versus $(1/\langle u_m \rangle^2)$ which gives B as the slope and C as the intercept. In HPLC we usually work at higher velocities than optimal (see Sec. IV) so that the B term is not observed in practice.

Careful experimentation leads to the view that, despite all efforts to improve on the van Deemter equation over the last 30 years, zone dispersions in chromatographic columns are most accurately described by this equation, in terms of the physical properties of the column, especially near the optimum velocity. This optimum, however, is not always used in practice for good reasons (see Sec. IV on optimization), and in those practical working conditions, the original equation is not always the best choice. Its simplicity still makes it attractive to predict dispersion in chromatographic columns and useful for column design.

Typical experimental values for the various terms in packed column GC and LC (for normal liquids) are collected in Table 2. Note that the dimensions of the different terms reflect their background: the A term is a length parameter, just as plate height, because it stems from flow around particles of size d_p; the B term is a transport coefficient (length squared over time) because of the underlying diffusion coefficient; the C terms are inverse seconds because of the equilibration time constants τ that molecules spend in both phases.

The optimum conditions for separation efficiency (minimum plate height) are closely connected to column variables, such as particle size and stationary phase thickness. Practically useful expressions for optimum performance, which contain these variables are obtained from Eqs. (35a,b). Optimum plate height is found as:

$$H_{\min} = 2\lambda_{e,z} d_p + 2\{2\gamma_m[f'(k)d_p^2 + g'(k)\delta_s^2(\boldsymbol{D}_m/\boldsymbol{D}_s)]\}^{1/2} \tag{36a}$$

With realistic estimations for the constants $\lambda_{e,z} \approx 1/2$, $\gamma_m \approx 2/3$, and using $f'(k) = 0.05k/(1 + k)^2 \approx 0.05 \times 0.2 = 0.01$ for the k range of 0.4–4 (maximum is $0.05 \times 0.25 = 0.0125$ at $k = 1$), while approximating (for $k = 2$) $g'(k) = (2/3)[k/(1 + k)]^2 = (2/3)(1/0.05)kf'(k) = (40/3)k \times 0.01$, with ≈ 0.3 in the same k range, we obtain:

$$H_{\min} \approx d_p + 2\{0.013d_p^2 + 0.4\delta_s^2(\boldsymbol{D}_m/\boldsymbol{D}_s)\}^{1/2} \tag{36b}$$

or

Table 2 Experimental Values for Various Terms in Packed Column GC and LC

	Packed column	
Quantity	Gas chromatography	Liquid chromatography
Velocity (cm/s)	10	0.2
Column length (cm)	200	25
Column radius R_c (cm)	0.2	0.2
Diffusion coefficient $\boldsymbol{D}_m$ (cm^2/s)	10^{-1}	10^{-5}
Diffusion coefficient $\boldsymbol{D}_s$ (cm^2/s)	10^{-5}	10^{-5}
Stationary film thickness (μm)	5	1[a]
Particle size d_p (μm)	100	5
A term (cm)	10^{-2}	10^{-3}
B term (cm^2/s)	1.5×10^{-1}	2×10^{-5}
C_m term (1/s)	10^{-2}	10^{-3}
C_s term (1/s)	4×10^{-3}	2×10^{-4}
Total plate height (cm)	10^{-1}	1.5×10^{-3}
Minimum plate height $H_{\min}$ (cm)	10^{-1}	10^{-3}
Optimum velocity u_{opt} (cm/s)	2	10^{-1}

[a]Valid for LLC only; LSC and reversed-phase HPLC have no, or quite different, phase dimensions.

$$H_{min} \approx d_p[1 + \{0.05 + 1.6(\delta_s/d_p)^2(\boldsymbol{D}_m/\boldsymbol{D}_s)\}^{1/2}] \quad (36c)$$

from which the fundamentally great importance of particle size is clear: minimum plate height and thus maximum performance is proportional to particle size. This is the very reason why HPLC with particle sizes as small as 5 μm or less has been developed. Equation (36c) shows that in LC where $(\boldsymbol{D}_m/\boldsymbol{D}_s) \approx 1$, the approximate value of minimum plate heights obtainable in a well-packed column for moderately retained substances is of the order of particle size or slightly above. This is a useful rule of thumb for assessing the quality of a column, and LC columns with optimum plate heights less than $1.5d_p$–$2d_p$ can be considered as good.

We also see that the relative loading of a column with stationary phase, by the factor $\mathbf{d}^2 = (\delta_s/d_p)^2$ is of some importance for high performances: the thinner the layer of stationary phase, the better the efficiency, but there is a practical limit in choosing ever-decreasing film thicknesses because of potential adsorption onto the particles of the packing, which should be avoided. For example, in GC, packed columns are loaded with 5–15% w/w of stationary phase onto the packing particles. For spherical particles the ratio (mass stationary phase)/(mass particle) $= 6(\delta_s/d_p)(\rho_s/\rho_p) \approx 0.15$, where ρ is the density. The density ratio $(\rho_s/\rho_p) \approx 0.25$ and so $\mathbf{d} = (\delta_s/d_p) \approx 0.1$. With this, Eq. (36c) becomes

$$H_{min} \approx d_p[1 + \{0.05 + 0.016(\boldsymbol{D}_m/\boldsymbol{D}_s)\}^{1/2}] \quad (36d)$$

For the optimal velocity we find

$$u_{opt} = \{[2\gamma_m \boldsymbol{D}_m]/[f'(k)(d_p^2/\boldsymbol{D}_m) + g'(k)(\delta_s^2/\boldsymbol{D}_s)]\}^{1/2} \quad (37a)$$

or

$$u_{opt} = 1.15(\boldsymbol{D}_m/d_p)\{[0.01 + 0.3(\delta_s/d_p)^2(\boldsymbol{D}_m/\boldsymbol{D}_s)]\}^{-1/2} \quad (37b)$$

With again a fixed $\mathbf{d} = (\delta_s/d_p) \approx 0.1$:

$$u_{opt} = 1.15(\boldsymbol{D}_m/d_p)\{[0.01 + 0.003(\boldsymbol{D}_m/\boldsymbol{D}_s)\}^{-1/2} \quad (37c)$$

We now see that a.o. the (dimensionless) ratio of diffusion coefficients, $\mathbf{D} = (\boldsymbol{D}_m/\boldsymbol{D}_s)$, determines the optimum conditions, to a large extent. Here we have to discriminate between GC and LC because the diffusion in gases is some four orders of magnitude faster than that in liquids. In GC, we thus have $\mathbf{D} = (\boldsymbol{D}_m/\boldsymbol{D}_s) \approx 10^{-1+5} = 10^4$ from which $u_{opt,GC} \approx 0.2(\boldsymbol{D}_m/d_p) \approx 0.2(10^{-1}/10^{-2}) = 2$ cm/s, a realistic value in practice. Also it is predicted from Eq. (36d) that $H_{min,GC} \approx 14d_p \approx 10^{-1}$ cm, which is a common finding in GC with packed columns.

The situation in LC is quite different as $\mathbf{D} = (\boldsymbol{D}_m/\boldsymbol{D}_s) \approx 1$ and from Eq. (37c) $u_{opt,LC} \approx 10(\boldsymbol{D}_m/d_p) \approx 10(10^{-5}/5 \times 10^{-4}) = 0.2$ cm/s, an order of magnitude less than in GC and, again, a realistic value in LC practice. If we rearrange the last equality into $\mathbf{v}_{opt,LC} = u_{opt,LC}(d_p/\boldsymbol{D}_m) \approx 10$, we observe that this group $(ud_p/\boldsymbol{D})$ is a *dimensionless* (so-called reduced, see next section) velocity, which in daily practice of LC reaches the optimum value of 3–7, not far from the foregoing estimated value of 10. Also we find for $H_{opt,LC} \approx 1.26d_p$, a slightly optimistic [$(1.4–2)d_p$ would better reflect practice], but not an unrealistic value. These results prove how well the van Deemter equation can be used in predicting efficiencies of chromatographic columns and how it can be used to optimize operating conditions.

Yet, there are many possible criticisms and, not surprisingly, a number of alternatives have been proposed. In comparing these alternatives it is very convenient to do this in terms of *dimensionless quantities or characteristic numbers.*

(*b*) *Dimensionless Parameters and Reduced Plate Height.* Dimensionless quantities and parameters are attractive because they have a general validity, and are helpful in the formulation of corresponding states. For example, the well-known *Reynolds number* **Re** = (velocity times typical length over kinematic viscosity) [15] is a universal measure for the status of hydrodynamic flows: in tubular flow channels and **Re** < 2000, flow can generally be consid-

ered laminar, whereas for **Re** > 2000 turbulence sets in for all possible tube sizes, whether they are short, long, narrow, or wide. Here we observe a principle of *corresponding states* for flow processes.

It does, however, make a difference if the flow tube is packed, because the characteristic length parameter becomes the particle size. In open tubes **Re** is based on the diameter of the tube ($\langle u \rangle d_c/\nu = 2\langle u \rangle R_c/\nu$) and in packed columns on particle size ($\langle u \rangle d_p/\nu$), where $\nu = \eta/\rho$ is the kinematic viscosity [for gases $\nu \approx 10^{-1}$ and for normal liquids $\nu \approx 10^{-2}$ Stokes (1 St = 1 cm^2/s = 10^{-4} m^2/s) and η is the (common) dynamic viscosity (in poise: 1 P = 1 dynes/cm^2 = 0.1 Pa s).

Another dimensionless quantity we have already met in the foregoing is the dimensionless time or Fourier number, $\mathbf{Fo} = \boldsymbol{D}_m t/R^2$. This quantity separates for example short and long time regions, such that in the short-time region nonstationary (i.e., time-dependent) processes occur, whereas for long times, stationary equilibrium processes are described. This aspect becomes important, for example, in using very fast flows or using relatively large-scale apparatus by which equilibration becomes problematic (see, for example, Sec. II.E.4.e on open tubular columns).

In the foregoing we observed that maximum efficiency is strongly dependent on particle size [see Eq. (36d)], whereas the optimal velocity, which separates the low-velocity diffusional region and the high-velocity hydrodynamic mass-transfer region, seems to be determined by the value of $(\boldsymbol{D}_m/d_p)$. The latter ratio with dimension length/time can be considered as a critical velocity $u_{crit} = (\boldsymbol{D}_m/d_p)$, a fundamental parameter for every packed column in characterizing the transition in the mobile phase of diffusion- and flow-controlled processes. Both H_{min} and u_{opt} are further dependent on two more dimensionless ratios, $\mathbf{d} = (\delta_s/d_p)$ and $\mathbf{D} = (\boldsymbol{D}_m/\boldsymbol{D}_s)$. It thus is logical to define next to these ratios the following dimensionless quantities:

$\mathbf{h} = H/d_p$ (so-called reduced plate height)

$\mathbf{v} = \langle u \rangle (d_p/\boldsymbol{D}_m)$ (so-called reduced velocity)

Here, particle size d_p provides a scale for the goodness of the efficiency in terms of **h** (**h** >> 1 is bad), and the critical transition velocity $u_{crit} = (\boldsymbol{D}_m/d_p)$ provides a scale for the relative importance of diffusion- and flow-controlled processes in the mobile phase in terms of **v**. Just as the Reynolds number, **v** is a basic measure for the *state of flow*, relative to the fundamental velocity u_{crit} and is thus more characteristic than the absolute value of the flow velocity itself. Indeed, for $\langle u_m \rangle = u_{crit}$ (i.e., **v** = 1), the plate height is close to the particle size, and it is logical to scale plate height in multiples of d_p, as is done by the definition of reduced plate height.

We remark also that the reduced velocity is closely related to the dimensional number called after Peclet and used in technological sciences as a measure for the extent of dispersion. By definition [15] the Peclet number is found from **Pe** = (velocity times characteristic length)/(dispersion coefficient). In the case of diffusion and flow through packed beds with characteristic particle size d_p, we find the molecular diffusion based (or sometimes called fluid mechanical) Peclet number $\mathbf{Pe_m} = \langle u_m \rangle d_p/\boldsymbol{D}_m$, which is identical with our reduced velocity **v**.

For completeness we introduce another pair of dimensionless numbers; namely, the particle size-based Reynolds number $\mathbf{Re_p} = \langle u_m \rangle d_p/\nu$, and the Schmidt number $\mathbf{Sc} = \nu/\boldsymbol{D}_m$, which together constitute the $\mathbf{Pe}_m$ number:

$$\mathbf{v} = \mathbf{Pe_m} = \langle u_m \rangle d_p/\boldsymbol{D}_m = (\langle u_m \rangle d_p/\nu)(\nu/\boldsymbol{D}_m) = \mathbf{Re_pSc}$$

The Schmidt number (for gases **Sc** $\approx$ 1, and for normal [i.e., low molecular mass] liquids **Sc** $\approx 10^3$) is responsible for allowing corresponding states even between gases and liquids. In technology the Peclet number is generally used for all dispersive processes that can be described by a dispersion coefficient $\boldsymbol{D}$, and reads $\mathbf{Pe} = \langle u \rangle d/\boldsymbol{D}$ which, in fact, is a dimen-

sionless inverse plate height: if we take $\langle u \rangle = u_z$, $d = d_p = 2R_p$ (in packed columns) or $d = d_c = 2R_c$ (in open tubes) and recall that by one definition $H = 2\boldsymbol{D}/u_z$, then:

$$\mathbf{Pe} = \langle u \rangle d/\boldsymbol{D} = (\langle u \rangle / 2\boldsymbol{D}) 2d_p = 2d_p/H = 2/\mathbf{h} \text{ (packed columns)}$$

and

$$\mathbf{Pe} = \langle u \rangle d/\boldsymbol{D} = (\langle u \rangle / 2\boldsymbol{D}) 2d_c = 2d_c/H = 2/\mathbf{h} \text{ (open columns, with } \mathbf{h} = H/d_c = H/2R_c)$$

We thus see that if the Peclet number were based on the length of the columns (L), rather than on the size of the packing or the diameter of the column, we would obtain the plate number $n_{\text{th}} = L/H = \frac{1}{2}\mathbf{Pe}_{\text{L}}$ where $\mathbf{Pe}_{\text{L}} = \langle u \rangle L/\boldsymbol{D} = 2n_{\text{th}}$.

These relations provide the key between chromatographic and technological nomenclature, and it is seen that a plot of H versus $\langle u \rangle$ in chromatography is analogous with a plot of $1/\mathbf{Pe}$ versus $\mathbf{ReSc}$ in technology.

An example of the use of such dimensionless numbers in technology is the well-known correlation between axial Peclet numbers and dimensionless velocity $\mathbf{Re}_{\mathbf{p}}\mathbf{Sc}$ for axial dispersion in packed bed systems; for example, the one after Hiby [19] for nonretained zones:

$$1/\mathbf{Pe} = \gamma_m/\mathbf{Re}_{\mathbf{p}}\mathbf{Sc} + \lambda_1/[1 + \lambda_2/(\mathbf{Re}_{\mathbf{p}}\mathbf{Sc})^{1/2}]$$

where $\lambda_1 = 0.65$, $\lambda_2 = 7.0$. Although obtained for both gases and liquids, later results question the accuracy for liquids [14]. We will return to this correlation later in Sec. II.E.4.d, but observe here already that the plot $1/\mathbf{Pe}$ versus $\mathbf{Re}_{\mathbf{p}}\mathbf{Sc}$, the analog of the H versus $\langle u \rangle$ plot in chromatography, is curved by virtue of the velocity-dependent denominator in the Hiby correlation, and thus the van Deemter equation, which is linear in velocity, is not supported in technological sciences.

With reduced variables we are able to formulate a corresponding-states principle for the efficiency of all chromatographic separation columns of the same type (packed or open). For example, for all well-packed columns we can rearrange the van Deemter equation into:

$$\mathbf{h} = H/d_p = \underbrace{2\lambda_{e,z} + 2\gamma_m/\mathbf{v} + f'(k)\mathbf{v}}_{\text{Mobile-phase terms}} + \underbrace{g'(k)\mathbf{d}^2\mathbf{D}\mathbf{v}}_{\text{Stationary-phase term}} \tag{38}$$

We observe that for all mobile-phase processes, $\mathbf{h}$ is only a function of $\mathbf{v}$ (with some packing parameters), and dependencies on d_p and $\boldsymbol{D}_m$ are no longer present. Thus, for packings with the same packing parameters, $\mathbf{h}$ versus $\mathbf{v}$ relations for the mobile phase contributions will be almost the same, irrespective of whether it concerns GC or LC which, in an absolute sense, differ vastly in diffusion and particle size characteristics. It is the strength of dimensionless parameters to unify the momentous consequences of these extremes into one single (corresponding-states) trend.

If we now plot $\mathbf{h}$ versus $\mathbf{v}$ for well-packed columns with small stationary phase terms in both GC and LC we observe that, indeed, nearly superimposing curves are obtained that define a kind of norm band into which $\mathbf{h} - \mathbf{v}$ plots for any useful column should lie. Significant differences observed with a plot above this high performance band should disqualify the column based on poor efficiency (Fig. 4).

(*c*) *To Couple or Not to Couple*? In Figure 4, dimensionless plate heights as a function of dimensionless velocity yields superimposing curves in both LC and GC, but on closer inspection, the GC curves are residing in the lower-velocity regions (say $\mathbf{v} < 20$) and the LC curves are mainly in the higher-velocity regions (say $\mathbf{v} > 10$). This is because diffusion in gases is very much faster than in liquids and the van Deemter B term, representing axial diffusion, comes into play much more easily in GC than in LC. This becomes very clear particularly when plotting the original plate height data in dimensional, rather than dimen-

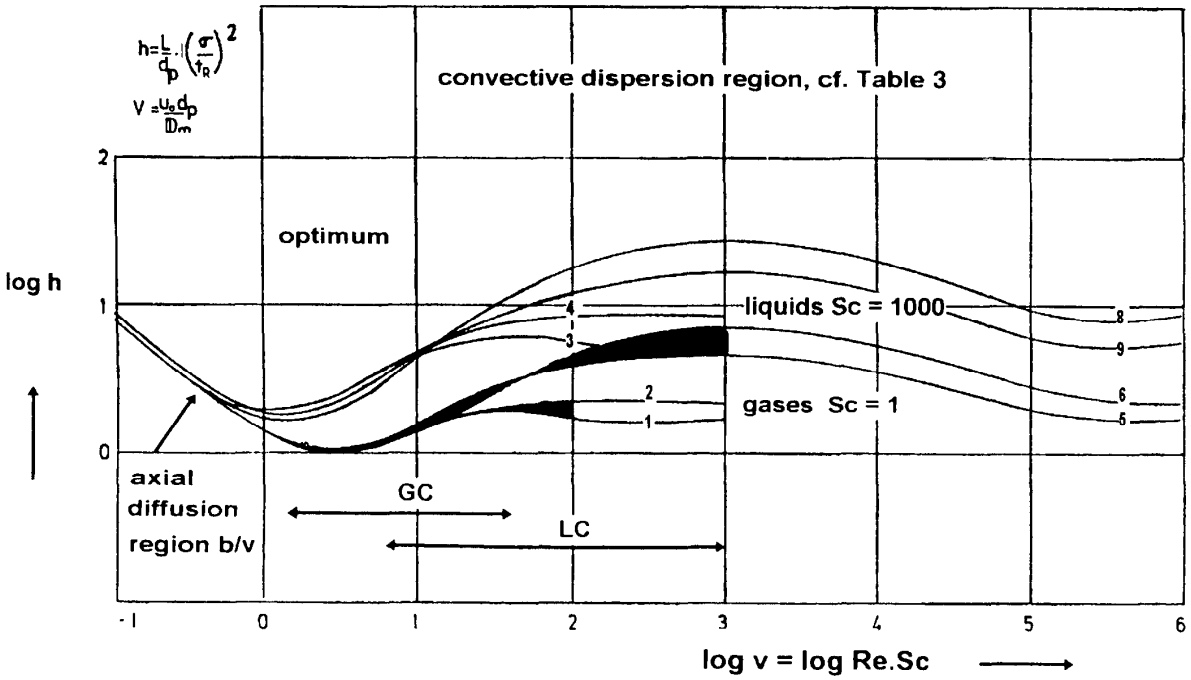


Figure 4 Reduced plate height plot: Bands for packed high-performance columns (1–2 for GC, 5–6 for LC) and nonretained solutes; poorly-packed columns have plots above the shaded bands (3–4 for GC, 8–9 for LC; log $v > 3$ in engineering science).

sionless parameters H versus $\langle u \rangle$: the plate height curves for LC and GC columns remain of quite similar form (as should be, because they follow the same equation), but they are set apart widely along the velocity scale (see Table 2, the velocity scales differ an order of magnitude). On further inspection of the dimensionless (but also the common) efficiency plots, it appears that the rising branch of the curve at higher velocities is not always as straight as might be expected from the C terms (proportional to $\langle u \rangle$) in the van Deemter equation. As mentioned in Sec. II.E.2.b, Giddings [1,5] was the first to reject the idea of an additive contribution of hydrodynamic "eddy" diffusivity and mobile-phase diffusion-controlled processes ("mass transfer"). Given the additivity of step numbers in the statistical description of both effects, thereby implying that these effects are not independent, he arrived at a so-called nonadditive *coupling* of both effects as follows:

$$H = B/\langle u_m \rangle + \underbrace{\{1/[(1/A) + (1/C_m\langle u_m \rangle)]\}}_{\text{Mobile-phase coupling term}} + C_s\langle u_m \rangle \tag{39a}$$

or in reduced terms, while writing $C_m = \omega d_p^2/D_m$ where ω is a constant of the order of 1 [see Eq. (34)],

$$\mathbf{h}_{\text{coupling}} = \underbrace{2\gamma_m/\mathbf{v}}_{\text{Longitudinal molecular diffusion}} + \underbrace{1/[(1/2\lambda) + (1/\omega\mathbf{v})]}_{\text{coupling term}} + \underbrace{g'(k)\mathbf{d}^2\mathbf{D}\mathbf{v}}_{\text{Stationary-phase term}} \tag{39b}$$

Mobile-phase terms

This *coupling equation* indeed yields curved plate height plots at higher velocities, which can never be obtained from the van Deemter equation. In Sec. II.E.2.b, we objected against this

idea of mutual dependence of the mobile-phase processes, and we add to that the failure of the coupling equation's mobile-phase term in the limit of low-velocities lim $H(\langle u_m \rangle \rightarrow 0) = \lim 1/[(1/A) + 1/(C_m\langle u_m \rangle)] = 0$ to reflect the actual observation of a finite and constant limiting H value. Therefore, rather than following a suspicious statistical argument, we follow the line of thought already outlined in Sec. II.E.2.b. There we applied the physically sound reasoning to add the dispersion coefficients in the radial direction, stemming from both diffusional and hydrodynamic sources, just as we add dispersion coefficients (also in the van Deemter equation) in the longitudinal direction. This reasoning is generally accepted in technological sciences and hydrology and leads to results quite comparable with those predicted by Giddings' coupling theory: concave plate height plots toward the velocity axis are predicted. Following this line of thought, first applied by Littlewood [12], Sie and Rijnders [11], and Johnson [13], we should replace the C_m term after van Deemter [see Eq. (34c1)] by the one that contains the radial dispersion coefficient $\boldsymbol{D}_R$ instead of the molecular diffusion coefficient. We derived that particular mobile-phase term earlier as Eq. (28), which with the expression for the radial dispersion coefficient, Eq. (26a) shows the desired coupling effect-like structure:

$$H_m = 2(\kappa R_c^2/\boldsymbol{D}_R)\langle u_m \rangle = 2\kappa R_c^2\langle u_m \rangle/(\boldsymbol{D}_{e,R} + \boldsymbol{D}_{m,R})$$
$$= 2\kappa R_c^2\langle u_m \rangle/(\lambda_{e,R} d_p\langle u_m \rangle + \gamma_m \boldsymbol{D}_m) \tag{40a}$$

or:

$$H_m = 2(\kappa R_c^2/\boldsymbol{D}_R)\langle u_m \rangle = 1/[(\lambda_{e,R} d_p/2\kappa R_c^2) + (\gamma_m \boldsymbol{D}_m/2\kappa R_c^2\langle u_m \rangle)] \tag{40b}$$

Although the same structure $\{1/[(1/A_R) + (1/C_m\langle u_m \rangle)]\}$ seen in the coupling Eq. (39) can be recognized, there is the difference that here A_R is strictly assigned to *radial* eddy diffusion, whereas the coupling equation does not separate axial and radial directions.

Again we see the occurrence of the critical velocity, $u_{crit} = (\boldsymbol{D}_m/d_p)$, defined earlier in the case of longitudinal dispersion. The critical velocity now appears also in the radial direction, which is the direction of interest for the mobile-phase dispersion terms in the denominator of Eq. (40). Again, for high diffusivities, such as in GC, lateral transport is predominantly due to molecular diffusion ($\gamma_m \boldsymbol{D}_m$ is of the order of 6.10^{-2} cm^2/s) as convective diffusivity under normal GC conditions ($\langle u_m \rangle \approx 10$ cm/s and $d_p \approx 10^{-2}$ cm; asee Table 2) amounts to only about an order of magnitude less (say 2.5×10^{-3} cm^2/s). As a result, in GC the mobile-phase term, Eq. (40) is generally almost linear in velocity: $H_m = 2(\kappa R_c^2/\gamma_m \boldsymbol{D}_m)\langle u_m \rangle$, the very reason that the original van Deemter equation is so valuable in GC practice. It requires high velocities and large packing particles to observe the characteristic concave curvature of the plate height plot H versus $\langle u \rangle$ [see, e.g., Refs. 11,12]. This is one of the reasons why the discussion on coupling lasted so long. If the liquid-phase mass transfer term C_s, on the other hand, is not negligible in comparison with the mobile-phase term, plate height plots will always be linear with velocity at higher velocities, another reason why the van Deemter theory was often found to be satisfactory. Then again, for lightly loaded columns, with relatively large particles in thin columns (e.g., $\leq$1-mm ID), the C_s term vanishes in comparison with C_m, and the curvature in the H versus $\langle u \rangle$ plot becomes visible owing to the radial dispersion in the denominator of the C_m term. This is true in so-called microcolumns and packed capillary columns, where plate height can be approximated by $H_{micro,GC} = A + B/\langle u_m \rangle + C_m\langle u_m \rangle$. The optimum conditions, at which velocity is low and radial dispersion is dominated by diffusion, are found from Eq. (35) as

$$H_{microGC,min} = A + 2[BC_m]^{1/2} \approx 2\lambda_{e,z} d_p + 4\kappa^{1/2} R_c \tag{41a}$$

and

$$u_{microGC,opt} = [B/C_m]^{1/2} \approx \gamma_m \boldsymbol{D}_m/\kappa^{1/2} R_c \tag{41b}$$

At the higher velocities in excess of $u_{microGC,opt}$, plate height in these columns is largely determined by the mobile-phase convective term C_m where the velocity profile factor κ is

relatively large because of small $\Omega = R_c/d_p$ values (R_c is small) and approximates that in open tubular columns (see Sec. II.E.4.e; i.e., $\kappa_{\text{microGC}} \approx 1/50$).

This is large compared with normal-sized (ID > 2-mm) columns but the reduction in plate height from the small diameters (factor R_c^2 in the C_m term) more than offsets the increased κ value, which makes this type of column more efficient than conventional (up to 6-mm–ID) columns, and allows us to still attain good efficiencies at high speeds. Note, that for higher velocities, the convective diffusivity becomes ever more important and for very high velocities the velocity profile (C_m) term does become independent of the velocity and levels off to a plateau value of $\lim H(\langle u\rangle \rightarrow \infty) = 2\kappa R_c^2/\lambda_{e,R} d_p$. It is seen that zone-broadening by the velocity differences is entirely determined by the hydrodynamics of the packed bed, the typical condition in which the classic concept of eddy diffusion has its full physical meaning.

This is exceptional in GC (because of the fast molecular diffusion), but in LC it is easier to attain. Here, for typical LC conditions ($d_p = 5\ \mu\text{m} = 5.10^{-4}$ cm, and $\langle u_m\rangle = 0.2$ cm/s, convective radial diffusivity will be about 2.5×10^{-6} cm^2/s, not too different from the molecular diffusivity in liquids (see Table 2). Indeed, at the transition velocity of $\langle u_{m,\text{trans}}\rangle = \gamma_m \boldsymbol{D}_m/\lambda_{e,R} d_p \approx 0.5$ cm/s the two processes become equivalent, and the typically curved plate height plot is obtained. This is most clearly seen in the dimensionless representation of the mobile phase term H_m in Eq. (40):

$$\mathbf{h}_m = H_m/d_p = 2\kappa\Omega^2/(\lambda_{e,R} + \gamma_m/\mathbf{v}) \approx 0.11/(\lambda_{e,R} + \gamma_m/\mathbf{v}) \tag{42}$$

The total plate height can now be represented as:

$$H = H_{e,z} + H_D + H_m + H_s = A + B/\langle u_m\rangle + \{1/[(1/A_R) + (1/C_m\langle u_m\rangle)]\} + C_s\langle u_m\rangle$$

$$\{1/[(1/A_R) + (1/C_m\langle u_m\rangle)]\}: \text{Mobile-phase convective dispersion term} \tag{43a}$$

or in reduced parameters:

$$\mathbf{h} = H/d_p = 2\lambda_{e,z} + 2\gamma_m/\mathbf{v} + f(k)2\kappa\Omega^2/(\lambda_{e,R} + \gamma_m/\mathbf{v}) + (2/3)g(k)\mathbf{d}^2\mathbf{D}\mathbf{v} \tag{43b}$$

$2\lambda_{e,z} + 2\gamma_m/\mathbf{v}$: longitudinal "eddy" + molecular diffusion; $f(k)2\kappa\Omega^2/(\lambda_{e,R} + \gamma_m/\mathbf{v})$: Convective dispersion; $2\lambda_{e,z} + 2\gamma_m/\mathbf{v} + f(k)2\kappa\Omega^2/(\lambda_{e,R} + \gamma_m/\mathbf{v})$: Mobile-phase terms; $(2/3)g(k)\mathbf{d}^2\mathbf{D}\mathbf{v}$: Stationary-phase term

where $f(k)$ and $g(k)$ are functions of k, replacing $f'(k)$ and $g'(k) = (3/2)g(k)$ in the foregoing. Figure 5 shows the reduced plate height plot and the different contributors to total plate height. In the normal working range for GC $\langle u_m\rangle$ is far smaller than 100 cm/s (i.e., $\mathbf{v} << 10$), whereas for LC $\langle u_m\rangle$ is in the range of 0.1–1 cm/s and so $10 < \mathbf{v} < 100$. These are clearly different working ranges in the dimensionless plot. In LC the molecular diffusion is seldom significant, whereas in GC, the convective dispersion region is seldom in operation.

This does not mean, however, that in LC curved H versus $\langle u\rangle$ plots should necessarily occur. This very much depends on the choice of the experimental conditions and parameters and, in actuality, a van Deemter type of efficiency plot can often be observed [see, e.g., Ref. 21].

In our derivation, the convective dispersion term is not dependent on the partition equilibrium and, thus, should not contain a function of k. However, this is only true if the stationary phase is distributed very evenly throughout the column cross section. This may not always be true in practice. Indeed, experimentally one may observe a slight k-dependence of the mobile phase convective dispersion term as predicted in the extended van Deemter equation. For that reason, we added the function $f(k)$ in Eq. (43b), which is still to be determined. Presently we remark that it is not uncommon, not even in LC [21], to use the result for $f(k)$

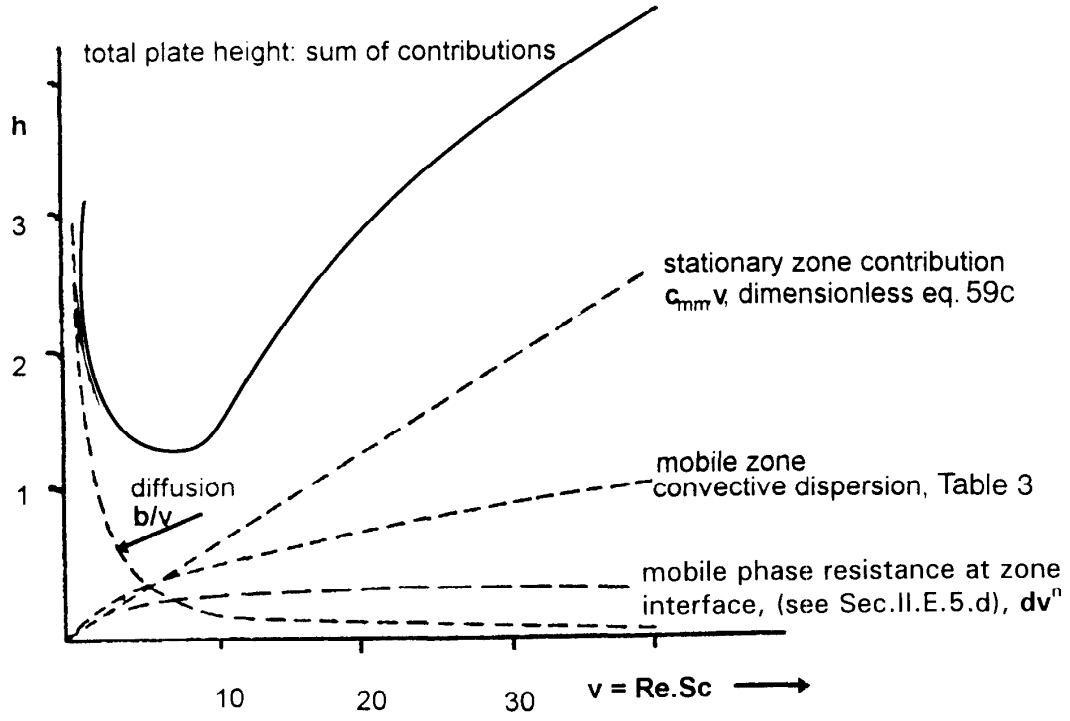


Figure 5 Reduced plate height plot, showing the most important contributions.

valid for capillary columns (see Sec. II.E.4.e) in which the stationary phase is supposed to be present as a thin film at the column wall. This idea arises from the capillaric models for packed beds as described in Sec. II.E.2.c.

Although the mathematical structure of the coupling Eq. (39b) and our result Eq. (43a,b) is identical, there are several more or less important differences.

The A *Term.* In the coupling equation, there is no explicit term for the longitudinal eddy diffusion or streamline-splitting along the column axis. Only if $C_m\langle u_m\rangle \rightarrow 0$ (i.e., either for $\mathbf{v} \rightarrow 0$, or in the ideal case, if there are no velocity profile effects in the mobile phase) there appears a constant A term. This term, however, both in Giddings' theory and in our approach, reflects the hydrodynamic contribution to *radial* mass transfer, called A_R in Eq. (43). Giddings' coupling theory thus does not provide a specific term for this realistic effect that is also recognized in technological and hydrological sciences. As said before, many experiments in these and also in chromatographic sciences support the existence of a constant A term also if $\mathbf{v} \rightarrow 0$. Hence, we prefer the relation in Eq. (43) over the coupling Eq. (39b).

The Mobile Phase Term as a Whole. It should be pointed out, however, that Giddings' coupling theory [1,5] does provide more than one coupling term stemming from mobile-phase dispersion processes for velocity differences on different scales in the column cross section. The complete coupling equation reads:

$$\mathbf{h}_{\text{coupling}} = 2\gamma_m/\mathbf{v} + \Sigma_i \{1/[(1/2\lambda_i) + (1/\omega_i\mathbf{v})]\} + (2/3)g(k)\mathbf{d}^2\mathbf{D}\mathbf{v} \tag{44}$$

Longitudinal diffusion — Coupling terms — Mobile-phase terms — Stationary-phase term

Here, the summation Σ_i is over all possible velocity differences that might arise in the column cross section, such as:

i = 1, for molecules that travel faster in the center of narrow interstitial flow channels than at the walls of those channels, caused by intrachannel velocity profiles (so-called transchannel effect [1,5])

i = 2, for molecules that move faster (or slower) in surrounding but neighboring channels, because of differences in shapes, widths, obstructions, and such, in the channel of interest (so-called short-range interchannel effect)

i = 3, for molecules that undergo faster (or slower) transport in neighboring regions (covering some tens to hundreds of particles) owing to local packing irregularities, which may cause open voids or local porosity differences (stemming, e.g., from segregation of different-sized packing particles; so-called long-range interchannel effect)

i = 4, for molecules that can penetrate potentially present pores within porous packing particles, in which intraparticle transport is necessarily slower than in the wider interstitial channels outside the particles (so-called transparticle effect)

i = 5, for molecules near the column wall, at which packing density is generally lower than in the center of the packing (extending at least over several particle layers from the wall); consequently, higher velocities occur (so-called transcolumn or wall effect)

All the listed velocity differences contribute potentially to zone-broadening, and each is treated by Giddings in the described way of coupling the processes of flow and diffusion "in concert" as Giddings phrases it. The constants λ_i and ω_i, reflecting the geometry of the packing on the different scales, are undoubtedly different for the mentioned regions over which the velocity differences exist, and each effect, when treated as an independent random-walk, generates its own and additive coupled plate height term.

None of these effects will produce a single, constant longitudinal effect to be identified as the eddy diffusion term A, and because there is no way to distinguish between them (the effects show a gradual overlap, rather than being discrete and separate) we prefer the description of velocity profile effects in one single mobile-phase term, with the velocity profile factor κ representing the overall velocity differences, and combined diffusional and convective radial mass transfer that counteracts the spreading from the velocity profile.

In fact, our expression for C_m is a good model for the unknown ω value for transcolumn processes in Giddings' theory, the more important of the foregoing terms.

Dependence of the Mobile-Phase Terms on Partitioning. A difference between Eqs. (43) and (44) is further seen to be the factor $f(k)$ in Eq. (43), which is not present in the total coupling equation [see Eq. 44]. This is a result of the derivations as made by the coupling theory, which, see the foregoing listing of effects, concerns everything in the mobile phase except the *distribution of stationary phase.* As mentioned before, and as will become very clear in the section on capillary columns (see Sec. II.E.4.e), uneven distribution of stationary phase in a cross section will result in a dependence of the velocity profile term of k. What is more, many experiments in LC [see, for example, Ref. 21] show a distinct k-dependence of the mobile-phase term. This is, probably, caused largely by the presence of dead end or stagnant pores within porous packing particles. Here, mobile phase is present and molecules trapped in these pores are also stagnant. Thus, these pores represent a kind of *stationary* (in fact, *stagnant mobile*) *phase*, where partitioning (with a partition coefficient $K = 1$) takes place with the surrounding flowing mobile phase. Trapped molecules can, however, escape only with a limited transfer rate, which is solely based on strongly hindered (in the tortuous pores) diffusion in the mobile phase. This would introduce an additional C term, C_{mm}, which is definitely dependent on k, and not easily distinguished from C_m (see Sec. II.E.4.g). It should be stressed here, that the existence of these dead end pores filled with stagnant mobile phase can also play a positive role, notably in GC. If these pores were totally filled with stationary liquid, the transfer of solute molecules toward the surrounding flowing mobile gas phase would take dramatically longer and a large zone-broadening would result.

In conclusion of this section, we prefer the use of the physically well-supported Eq. (43) over the coupling Eq. (44), noting that the original success of the coupling theory by describ-

ing the potentially concave curvature of plate height plots, is equally well explained by Eq. (43). In a more simple representation we may write Eq. (43) in a dimensional form related to the van Deemter equation, still reflecting the velocity and partitioning dependence of the mobile-phase terms, now grouped together in the $C'_m(\langle u_m\rangle,k)$ term:

$$H = A + B/\langle u_m\rangle + [C'_m(\langle u_m\rangle,k) + C_s(k)]\langle u_m\rangle \tag{45}$$

(*d*) *Pragmatic Approximate Equations for Plate Height.* In view of the relative complexity mainly of the expressions for plate height stemming from mobile-phase effects, chromatographic workers, especially in the field of LC, have tried over the years to simplify matters with some success, often based on empirical relations for extraparticle mobile-phase mass transfer in technological and chromatographic sciences.

Table 3 gives an overview of equations describing the mobile phase effects that appeared since 1956, including the ones discussed in the foregoing, in a dimensionless form for easy comparison.

Ideally, **a**, **b**, and **c** are constants related to the reduced coefficients present in eddy diffusion, molecular diffusion, and mobile-phase dispersion, but in using these functions as fitting functions to experimental data, they loose their physical meaning.

To complete the foregoing equations, the stationary-phase contribution, to be represented by a C term proportional in $\mathbf{v}$, so $\mathbf{c}_s\mathbf{v}$, should be added to each of the equations to obtain total reduced plate height. In view of a potential C_{mm} term, representing the effect of stagnant mobile phase within porous packings (see Sec. II.E.4.g), both the Huber equation and the Horvath equation are supplied with further terms to be represented as $\mathbf{dv}^{1/2}$ (Huber) and $\mathbf{dv}^{2/3} + \mathbf{ev}$ (Horvath). For example, the complete Huber equation reads:

$$\mathbf{h} = \mathbf{b}/\mathbf{v} + \mathbf{a}/[1 + (\mathbf{a}/\mathbf{c})\mathbf{v}^{-1/2}] + \mathbf{c}_s\mathbf{v} + \mathbf{dv}^{1/2} \tag{46a}$$

This equation is largely based on correlations for mass transfer in packed bed systems as provided by physical technology literature [15]. The second term can be based on the correlation after Hiby [19], which has been already cited in Sec. II.E.4.b:

$$1/\mathbf{Pe} = \gamma_m/\mathbf{Re}_p\mathbf{Sc} + \lambda_1/[1 + \lambda_2/(\mathbf{Re}_p\mathbf{Sc})^{1/2}] \qquad \lambda_1 = 0.65,\ \lambda_2 = 7.0 \tag{50}$$

We have already mentioned that the plot $1/\mathbf{Pe}$ versus $\mathbf{Re}_p\mathbf{Sc}$, the analog of the H versus $\langle u\rangle$ plot in chromatography, is curved by virtue of the velocity-dependent denominator in the Hiby correlation. Qualitatively this corresponds to the observation of concave H versus $\langle u\rangle$ plots, notably in LC. Quantitatively, however, although Eq. (50) was obtained for both gases and liquids, later results question the accuracy especially for liquids [14]. In addition, a further dimensionless correlation for the mass-transfer coefficient in the process of equilibration between phases, leading to the $\mathbf{dv}^{1/2}$ term, was used by Huber; namely, the Thoenes correlation. The latter is known to exhibit a large uncertainty (a factor of 4 is no exception) and, moreover,

Table 3 Equations Describing Plate Height Relations for Mobile-Phase Effects

Authors	Equation (number)		Ref.
van Deemter et al.	$\mathbf{h} = \mathbf{a} + \mathbf{b}/\mathbf{v} + \mathbf{cv}$	(38a)	7,20
Giddings	$\mathbf{h} = \mathbf{b}/\mathbf{v} + \mathbf{a}/[1 + (\mathbf{a}/\mathbf{c})\mathbf{v}^{-1}]$	(39c)	1,5
Huber and Hulsman	$\mathbf{h} = \mathbf{b}/\mathbf{v} + \mathbf{a}/[1 + (\mathbf{a}/\mathbf{c})\mathbf{v}^{-1/2}]$	(46)	22
Sie and Rijnders, Johnson, and Littlewood	$\mathbf{h} = \mathbf{a} + \mathbf{b}/\mathbf{v} + \mathbf{a}_R/[1 + (\mathbf{a}_R/\mathbf{c})\mathbf{v}^{-1}]$	(43c)	11,13 12
Snyder	$\mathbf{h} = \mathbf{cv}^n$, with $0.3 < n < 0.7$	(47)	23
Knox et al.	$\mathbf{h} = \mathbf{b}/\mathbf{v} + \mathbf{cv}^{1/3}$	(48)	24
Horvath and Lin	$\mathbf{h} = \mathbf{b}/\mathbf{v} + \mathbf{a}/[1 + (\mathbf{a}/\mathbf{c})\mathbf{v}^{-1/3}]$	(49)	25

if valid, it is to be used only for high Reynolds numbers much larger than 10 [15], whereas for LC, in particular, but also for GC, the velocity working range leads to $\mathbf{Re}_p < 1$. Better correlations, supported by theoretical arguments have since become available [15], and these would yield quite different velocity dependencies; namely, proportionality with $\mathbf{v}^{2/3}$ [as found by Horvath; see Eq. (49)], rather than with $\mathbf{v}^{1/2}$. Hence, it is no surprise that based on careful experiments [see, e.g., Ref. 21] the Huber equation can be discarded. Only occasionally, over a relatively small velocity range, one can obtain a satisfactory fit of experimental data with a Huber-type equation of the form:

$$H = A + B/\langle u_m \rangle + C\langle u_m \rangle + D\langle u_m \rangle^{1/2} \tag{51}$$

where it should be questioned whether the coefficients have any physical meaning in the light of the derivations given in the foregoing. The C term reflects contributions from mass transfer in the stationary phase, which for porous materials incorporates stagnant mobile-phase regions inside the particles of the packing. Because the Horvath equation is very similar to the Huber equation [see Eq. 46], except for the improved exponent of the power function of $\mathbf{v}$, the same reasoning applies to Eq. (49). Yet, especially for nonretained solutes, or in the absence of a stationary phase and at not too elevated velocities, the Horvath equation is almost identical with the Knox equation. It has been used in several theoretical studies (e.g., in supercritical fluid chromatography; SFC [33]), and it was valid in the practice of LC [26,28]. Because this equation is the most extended one, also offering a term for intraparticle stagnant mobile-phase phenomena and a kinetic term representing resistance for solute binding or adsorption, we will give the extended Horvath and Lin equation here for completeness and in the dimensional form to see the details:

$$\begin{aligned} H = {} & 2\gamma_m \boldsymbol{D}_m/u_0 && \text{(axial molecular diffusion)} \\ & + 2\lambda d_p u_0^{1/3}/[u_0^{1/3} + \omega(\boldsymbol{D}_m/d_p)^{1/3}] && \text{(convective dispersion)} \\ & + \beta(\psi + k + \psi k)^2 d_p^{5/3} u_0^{2/3}/[(1+\psi)^2(1+k)^2 \boldsymbol{D}_m^{2/3}] && \text{(resistance at interface of moving and stagnant mobile phase)} \\ & + (\psi + k + \psi k)^2 d_p^2 u_0/30\gamma_i \boldsymbol{D}_m (1+\psi)^2(1+k)^2 && \text{(intraparticle diffusion resistance)} \\ & + 2k^2 u_0/(1+\psi)(1+k)^2 \varphi_a k_a && \text{(kinetic resistance for adsorptive solute binding} \end{aligned} \tag{49a}$$

Here the new symbols have the following meaning:

$\gamma = (\theta/\psi)$, where θ is an alternative tortuosity factor, and ω, λ, and β are additional structural packing parameters.

$\psi = (\varepsilon_i/\varepsilon_0) = [(1/\phi) - 1]$ is another porosity fraction representing the ratio of intraparticle and interstitial mobile phase volumes $(V_{m,i}/V_0)$.

φ_a is the phase ratio defined as the concentration of surface adsorption sites onto the packing per unit volume of mobile phase.

k_a is the rate constant for adsorption.

Note further the correct use of the interstitial velocity $u_0 = L/t_0$ of actual moving mobile phase (see Sec. II.A).

According to Horvath and Lin [25], for LC systems with particle sizes smaller than 3–5 μm, the kinetic sorption term will outweigh all the other terms. This conclusion is rather uncertain, however, for the mechanism and kinetics of solute sorption onto and from the stationary phase are largely unexplored. Giddings' treatment of the underlying kinetics yields different results [1,5; see also Eq. (33c)] and experimental verification of the Horvath equation, on the whole, has no favorable outcome for this relation [21,31,35].

Equally uncertain in their connection to the underlying physical phenomena, but far more practical, are the equations of Snyder and Knox [Eqs. (47) and (48), respectively], which

simply "save the phenomena" by fitting the observed data in a power function. The assumption here is that column design can effectively be based on an accurate *description*, rather than a prediction, of the plate height plot. By using the reduced variables **h** and **v**, these equations are very practical versions of the principle of corresponding states connected through these variables, as discussed in Sec. II.E.4.b. Indeed, in LC, the Knox equation in particular, is renowned in its ability to describe the effect of particle size on plate height for many different packing materials and, literally, serves as an extremely valuable tool for assessing the quality of a packed column. For instance, in well-packed columns for LC the reduced minimum plate height (see Sec. II.E.4.a) should be close to 1.5–2 and the associated reduced optimum velocity in the range of 3–7. For the more practical velocities in excess of the optimum value, the Knox equation adequately describes the general curvature observed in the plate height plot. If represented on a logarithmic basis (i.e., as log **h** vs. log **v**), the plot becomes linear, with a slope in the vicinity of 0.3–0.4 [Snyder, in older days and for less optimal packings, reports 0.3–0.7; see Eq. (47)].

The power 1/3 in the mobile phase term obviously approximates the complex "coupling" (as Giddings phrases it) or convective dispersion phenomena, leading to the curvature in the **h** versus **v** plots. The neat and fixed value of 1/3 = 0.33, may in practice vary between 0.30–0.40 [35]. The experimental fit, rather than the a priori estimation of constants such as **a**–**e**, obscures physical insight, but on the other hand, we do have an accurate description and no further doubts about complexities, such as the role of partitioning [via $f(k)$, for example] and the influence of stagnant mobile phase in porous packings.

The latter power functions after Snyder and Knox are, in principle, also found in GC, provided that velocities are high to very high, such as to reach sufficiently large reduced velocities (which is not easy in rapidly diffusing gases). Dedicated experiments at high velocities and using large particles, yielded values that could be represented by n = 0.45–0.60 for porous packings, and n = 0.25–0.35 for nonporous packings, very much in agreement with LC. We will return to the differences between porous and nonporous packings in Sec. II.E.4.g.

After first treating the case of open tubular columns in the next section, we will return to the Knox and Snyder equations in Sec. IV, because they can play a useful role in the kinetic and time optimization of separations. Also, after treating the capillary column case, we are able to appreciate some additional alternative expressions for the plate height curve in packed columns, as obtained from adaptation of the capillary column expressions.

(*e*) *Open Tubular or Capillary Columns*: *The Golay Equation.* The only geometry that can be analyzed exactly on flow and diffusional mass-transfer phenomena is that of *capillary* columns, which ideally possess a straight and open tubular (usually circular–cylindrical) geometry, and in which the stationary phase is coated and distributed evenly as a film (or a chemically bonded polymeric network) onto the column perimeter.

This type of column has largely replaced the packed columns in modern GC, in view of their favorable *separation speed.* Open columns are able to produce large plate numbers (low plate heights) in relatively short analysis times (see Sec. IV on optimization). Lately, after solving difficult practical problems, such as detection and preparation of stationary phases in open columns with extremely small dimensions, open columns are even becoming of interest for LC [9,50–53]. However, open tubular LC (OTLC) is still in its infancy and in an experimental research stage.

In comparison with the situation in packed columns, the description of flow and mass-transfer phenomena in open tubular columns are relatively easy, especially if the geometry of the flow channel is simple and symmetrical, as in the circular–cylindrical straight columns. This is exactly the type of column used in practice, although a slight curvature is always present because of loose (relative to the column diameter) coiling of the capillary columns that are too long (several meters up to say 100 m) to fit in normal GC ovens. This coiling,

although potentially affecting flow and dispersion phenomena [5,18,26; see under Sec. II.F.2.b], is of little practical interest under common-operating conditions.

First then, looking at the flow condition in open tubular channels, it is immediately clear that in the absence of obstacles all flow lines are straight and parallel to the column axis, strongly opposed to the situation in packed columns as described in the foregoing. The first obvious consequence of this is that molecular diffusion is unobstructed; hence, the obstruction factor γ equals unity, and the axial diffusion contribution to plate height is simply found from

$$H_{D,\text{cap}} = 2\boldsymbol{D}_m/\langle u_m\rangle = B_{\text{cap}}/\langle u_m\rangle \tag{52a}$$

or

$$\mathbf{h}_{D,\text{cap}} = H_{D,\text{cap}}/d_c = 2/\mathbf{v}_{\text{cap}}, \qquad \text{with } \mathbf{v}_{\text{cap}} = \langle u_m\rangle d_c/\boldsymbol{D}_m = \mathbf{ReSc} \tag{52b}$$

Equally logical is the absence of an eddy diffusion term in the total plate height equation. The flow velocity profile, however, is very pronounced and yields a large C_m term contribution to plate height. The velocity profile properties, as a result of the radial symmetry of the column, can be calculated from first principles [15]. It is parabolic and known as the *Poiseuille profile*:

$$u_m(r) = u_{\max}[1 - (r/R_c)^2] \qquad \text{with } u_{\max} = u_m(r = 0) = 2\langle u_m\rangle \tag{53}$$

The center line velocity $u_{\max}$, identifies the maximum velocity in the profile, which exactly equals 2 times the mean velocity. At the column wall ($r = R_c$), the velocity becomes zero, as slip of the fluid at the wall is not supposed to be present.

We are now interested in the zone-spreading of a thin solute zone introduced as a flat concentration pulse evenly distributed throughout the cross section of the tube at the entrance ($z = 0$) of the column, through the action of the velocity differences in the profile. It is clear that molecules present at or near the center line, rapidly move away in the axial direction from the molecules near the column wall that have lower velocities, even down to zero at the exact position of the column wall. It is illustrative to take as an example an average velocity of 1 cm/s (low for GC but high for LC), which implies that the maximum velocity difference in the zone amounts to 2 cm/s. Hence, every second the zone widens by at least 2 cm, a growth rate that would make it impossible to obtain any useful efficiency of the column after a typical retention time of several minutes or longer: the sample zone fills as if it were the complete column over its entire length on elution of the first, fast-moving molecules on the center line. The strongly asymmetrical and tailing peak shapes (better called *residence time distributions*) under these conditions can be calculated [15], but have no practical meaning in chromatography.

Hence, a very strong zone-broadening would occur were it not that the molecular diffusion, which acts equally in all directions, also mutually exchanges molecules in the radial direction throughout the cross section, thereby more or less averaging out all velocity differences. The faster this happens, the less zone-broadening is originated. In GC, with gaseous mobile phases, relatively wide capillaries can be used in view of the fast molecular diffusion. The smaller the column ID, the more efficient radial diffusion maintains zone integrity, and the more efficient separations can be provided. In LC, as a consequence of the very limited diffusional mixing, we can foresee that extremely small diameters should be used. This is all the more true because radial molecular diffusion is the only mass-transfer mechanism present in these open tubular systems. Convective mechanisms in the radial sense, such as eddy diffusion in packed systems, is absent. Thus, in the open systems we cannot, as with packed systems, make unlimited use of increased flow velocities to generate enhanced radial mixing and counteract zone-broadening owing to velocity profiles. The only effect of increased velocities would be a larger spreading as the velocity differences increase in proportion with the velocity.

For this purpose the earlier mentioned dimensionless time expressed as the Fourier number ($\mathbf{Fo} = \boldsymbol{D}t/R_c^2$) is a good measure for the limiting velocities to be used: residence or

retention times should never be shorter than the equilibration time necessary to either allow partitioning between phases or to exchange molecules between velocity extremes at least two or more times (see Sec. II.E.2.c). We will come back to this shortly.

To quantify the present reasoning, we may use the results obtained in Secs. II.C.3 and II.E.2.c, where generalized expressions for convective dispersion from combined velocity differences and radial dispersion were derived. For that purpose Eq. (11) can be used, with an equilibration time based solely on molecular diffusion [i.e., $\tau_{\Delta u} = R_c^2/2\boldsymbol{D}_m$; in contrast with Eq. (27) for packed columns, see later discussion], the time needed for diffusion to cross the average distance (column radius R_c) that velocity extremes are apart, to obtain

$$H_{m,\text{cap}} = \tfrac{1}{2}(\Delta u_{\max}/\langle u_m\rangle)^2[R_c^2/\boldsymbol{D}_m(1 + k)]\langle u_m\rangle$$
$$= 2(\kappa R_c^2/\boldsymbol{D}_m)f(k)\langle u_m\rangle \tag{54}$$

where $\kappa = \tfrac{1}{4}(\Delta u_{\max}/\langle u_m\rangle)^2$, the same *velocity profile factor* as introduced in Sec. II.E.2.c, and $f(k) = 1/(1 + k)$. Equation (54) is identical with Eq. (28) once we realize that the relative maximum velocity difference (in the axial direction) $\Delta u/\langle u_m\rangle$ is the same as before and equal to $\Delta u/\langle u_m\rangle = [u_{\max} - \langle u_m\rangle]/[\langle u_m\rangle(1 + k)] = (\Delta u_{\max}/\langle u_m\rangle)/(1 + k)$. However, the situation for radial diffusion is different, because the stationary phase is now situated at the inside column wall perimeter and, thus, is not present in the core of the tube. Hence, the effective radial dispersion coefficient in Eq. (28) is not influenced by the presence of stationary phase, and the retention factor $1/(1 + k)$ drops out to obtain $\boldsymbol{D}_{R,\text{eff}} = \boldsymbol{D}_m$, and Eq. (54) is found.

An important difference with packed columns is thus the occurrence of a factor $f(k) = 1/(1 + k)$ in the expression for the plate height from velocity profiles over the column cross section, as a logical result from the even distribution of stationary phase in packed systems, compared with the uneven one in open columns. Hence, the important result is obtained that mobile-phase zone-spreading becomes dependent on the capacity factor in open tubular columns.

As a first approximation for κ we can calculate the average value for $\tfrac{1}{4}(\Delta u_{\max}/\langle u_m\rangle)^2$ using the Poiseuille expression Eq. (53) for $u(r)$ to obtain $\langle\kappa\rangle = 1/12$. This cannot be more than a first guess, because it is based on the maximum velocity difference alone, and we should actually have taken the local velocity differences at each radial position r, to find, by integration over the column cross section, an average value for κ. This exercise, while using the exact mass-balance equations, has been carried out first by Taylor [16] (in the absence of a stationary phase, or for $k = 0$), Aris [17], and Golay [10] (for coated open tubular columns and $k \neq 0$), later followed by Giddings [1,5] and the present author [18]. The plate height equation [see Eq. (54)] represents spreading not only caused by the symmetrical Poiseuille profile, but also for all kinds of other profiles, such as a flat profile for turbulent flow, and even strongly asymmetrical profiles, as found in helically and tightly coiled spiral tubes [18]. In the open tubular columns, all theoretical approaches agree in the value of $\kappa = 1/48$, for the underlying strongly pronounced parabolic flow profile. Our first approximation $\langle\kappa\rangle = 1/12$ is thus off by a factor of 4, but more interestingly, the exact approach yields a final form of $f(k)$ that is quite different from our simple $1/(1 + k)$; that is,

$$f(k) = (1 + 6k + 11k^2)/(1 + k)^2 \tag{54a}$$

a function with limiting values of 1 (for $k = 0$; the Taylor case) and 11, the maximum value for $k \to \infty$. This function shows that the partition equilibrium strongly influences the zone-broadening by convective diffusion in the mobile phase. For strongly retained substances ($k > 10$) it yields an order of magnitude larger plate heights than at low k. The resultant C_m term for convective diffusion in capillary columns is thus very important and reads:

$$H_{m,\text{cap}} = C_{m,\text{cap}}\langle u_m\rangle = (1/24)f(k)R_c^2\langle u_m\rangle/\boldsymbol{D}_m \tag{54b1}$$

or in dimensionless terms and taking along all mobile phase effects:

$$\mathbf{h}_{m,\text{cap}} = H_{m,\text{cap}}/2R_c = 2/\mathbf{v}_{\text{cap}} + (1/96)f(k)\mathbf{v}_{\text{cap}} \quad (54b2)$$

An important assumption in the derivation of this result, is that mass transfer between and inside phases is sufficiently fast to reach equilibrium, as was expressed by the Fourier number requirement $\mathbf{Fo} > 0.8$ (see Sec. II.E.2.c). Gill et al. [27], in a most thorough analysis of the situation, prove that not only the dimensionless time or Fourier number is limiting, but quite logically also the Peclet number $\mathbf{Pe}_m = 2\langle u_m\rangle R_c/D_m$ (i.e., our reduced velocity $\mathbf{v}$). They solved the exact mass balance equations to find the concentration profile of a migrating zone in the absence of stationary phase (or $k = 0$) for all possible values of $\mathbf{Pe}_m = \mathbf{v}$ and $\mathbf{Fo}$. Their solutions include the Taylor, Aris, and Golay result Eq. (54d), proved to be valid in the domain $\mathbf{Pe}_m = \mathbf{v} > 20$ and $\mathbf{Fo} > 0.8$. In addition they also provide solutions in all other $\mathbf{v}$–$\mathbf{Fo}$ domains, which can be summarized in our notation as follows:

$$\mathbf{h}_{m,\text{cap}} = 2/\mathbf{v}_{\text{cap}} + 0.014\mathbf{Fo}^{0.55} \quad \text{for } \mathbf{Fo} < 0.6 \quad (54c)$$

$$\mathbf{h}_{m,\text{cap}} = 2/\mathbf{v}_{\text{cap}} + (1/96)\mathbf{v}_{\text{cap}} \quad \text{for } \mathbf{Fo} > 0.8 \text{ and } \mathbf{v}_{\text{cap}} > 20 \quad (54d)$$

$$\mathbf{h}_{m,\text{cap}} = 2/\mathbf{v}_{\text{cap}} \quad \text{for } \mathbf{v}_{\text{cap}}\mathbf{Fo}^{1/2} < 1 \quad (54e)$$

Here, for completeness, Eq. (54d) is the Taylor–Aris–Golay solution, valid within a large, yet restricted $\mathbf{v}$–$\mathbf{Fo}$ domain. Equation (54e) is the pure diffusion solution (i.e., only the B term), which is of no practical use for chromatography, just as the pure convection solution (spreading from the velocity profile in the absence of radial diffusion which results in a very broad and tailing peak).

To summarize the domains in which Eqs. (54c–e) are valid we can construct the approximate graph as seen in Figure 6. The figure clearly shows the region where the Taylor–Aris–Golay approximation is valid, the usual working area for chromatography.

The last contribution to the plate height in capillary columns is the mass-transfer term C_s from the stationary phase. Ideally, this phase is distributed as a uniform film of thickness δ_s on the inside column wall. If this is true and if the column radius is not too small, the stationary phase can be treated as a flat film, for which the classical C_s term after van Deemter et al. is already available, Eq. (34c2). We thus arrive at an expression for the total plate height for capillary columns, named after Golay:

$$\begin{aligned} H_{\text{cap}} = \Sigma_i H_i &= B_{\text{cap}}/\langle u_m\rangle + C_{m,\text{cap}}\langle u_m\rangle + C_s\langle u_m\rangle \\ &= 2\boldsymbol{D}_m/\langle u_m\rangle + (1/24)f(k)(R_c^2/\boldsymbol{D}_m)\langle u_m\rangle + (2/3)g(k)(\delta_s^2/\boldsymbol{D}_s)\langle u_m\rangle \end{aligned} \quad (55a)$$

or

$$\mathbf{h}_{\text{cap}} = H_{\text{cap}}/2R_c = 2/\mathbf{v}_{\text{cap}} + (1/96)f(k)\mathbf{v}_{\text{cap}} + (2/3)g(k)\mathbf{d}_{\text{cap}}^2\mathbf{D}\mathbf{v}_{\text{cap}} \quad (55b)$$

where, as before, $\mathbf{d}_{\text{cap}} = (\delta_s/d_c) = (\delta_s/2R_c)$ and $\mathbf{D} = (\boldsymbol{D}_m/\boldsymbol{D}_s)$.

Just as for packed columns, plate height first decreases hyperbolically at (very) low velocities owing to molecular diffusion in the mobile phase (for LLC, to be extended with that for the stationary phase as well, see Sec. II.E.1). In contrast, at higher velocities, plate height increases linearly with velocity, caused by both C terms. Somewhere in between, at moderate velocities in GC practice and at very low velocities in LC practice, plate height obtains a minimum value, indicating maximum efficiency at a specific optimal velocity. This behavior is analogous to that of the van Deemter equation.

Especially for capillary columns in GC, one of the considerable advantages in practice is that the contribution from the stationary phase is almost negligible because very thin films are used: δ_s/d_c is often chosen to be $<1/300$, which in actual practice means that $\delta_s = 0.1$–$1\ \mu\text{m}$. If we also try to apply capacity factors as large as possible, the stationary phase contribution term C_s is further reduced by the function $g(k) = k/(1 + k)^2$, which has its maximum at $k = 1$ and tends to zero for both $k \rightarrow 0$ and large k. This situation is strongly

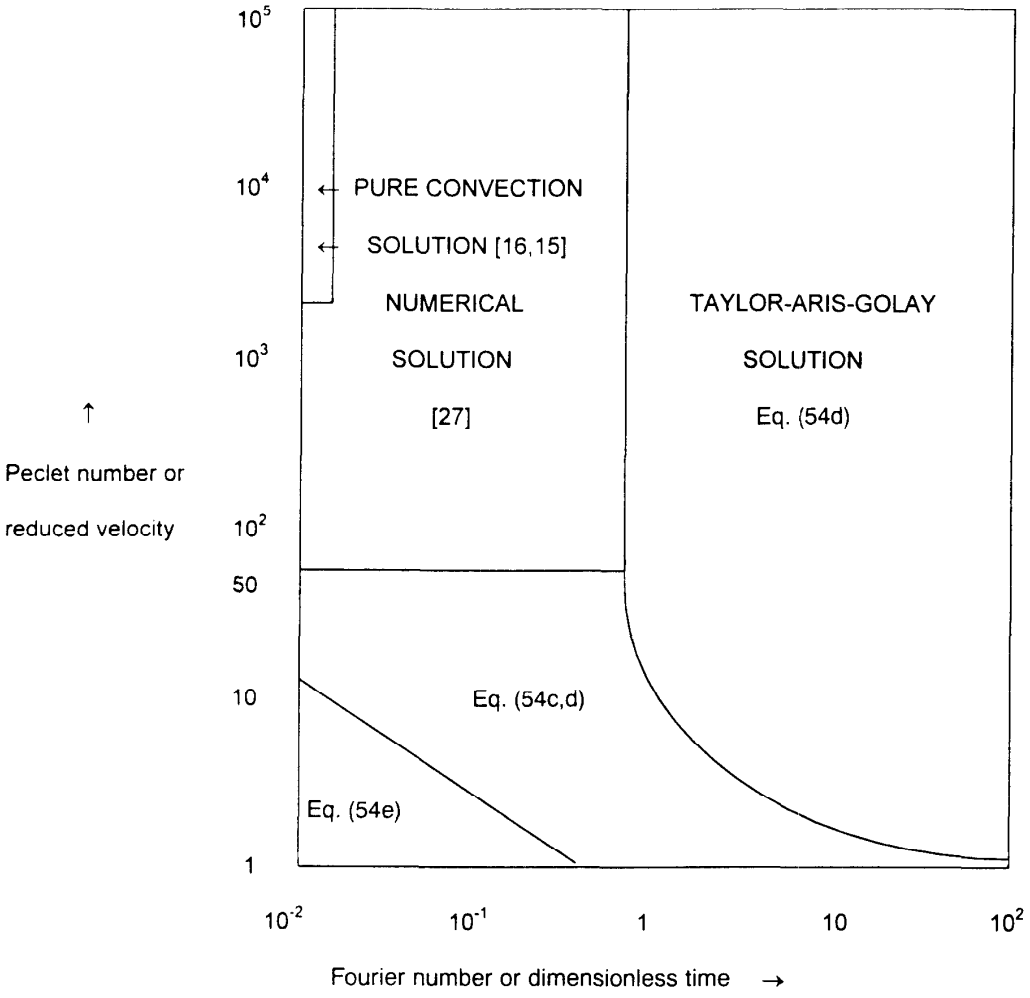


Figure 6 Dimensionless velocity versus dimensionless time domains in which different plate height equations are valid for $k = 0$. The preferred region is the upper right Taylor–Aris–Golay region.

different when relatively thick layers of stationary phase are used, in specific cases in GC and OTLC.

If the C_s term is negligible, the optimum conditions for capillary GC columns can be estimated from Eqs. (35a) (without the A term), and (35b) to yield:

$$H_{\min,\text{cap}} = 2[B_{\text{cap}}C_{m,\text{cap}}]^{1/2} = R_c[f(k)/3]^{1/2}$$

and

$$\mathbf{h}_{\min,\text{cap}} = (1/2)[f(k)/3]^{1/2} \tag{56a}$$

while:

$$u_{\text{opt,cap}} = [B_{\text{cap}}/C_{m,\text{cap}}]^{1/2} = (D_m/R_c)[48/f(k)]^{1/2}$$

and

$$\mathbf{v}_{\text{opt,cap}} = 2[48/f(k)]^{1/2} \tag{56b}$$

Hence, there is a clear dependence on the capacity factor k:

$k = 0$	$H_{\text{min,cap}} = 0.58R_c$	$\mathbf{h}_{\text{min,cap}} = 0.29$	$u_{\text{opt,cap}} = 6.9(D_m/R_c)$	$\mathbf{v}_{\text{opt,cap}} = 13.9$
$k = 1$	$H_{\text{min,cap}} = 1.22R_c$	$\mathbf{h}_{\text{min,cap}} = 0.61$	$u_{\text{opt,cap}} = 3.3(D_m/R_c)$	$\mathbf{v}_{\text{opt,cap}} = 6.6$
$k = 2$	$H_{\text{min,cap}} = 1.45R_c$	$\mathbf{h}_{\text{min,cap}} = 0.73$	$u_{\text{opt,cap}} = 2.8(D_m/R_c)$	$\mathbf{v}_{\text{opt,cap}} = 5.6$
$k = 5$	$H_{\text{min,cap}} = 1.68R_c$	$\mathbf{h}_{\text{min,cap}} = 0.84$	$u_{\text{opt,cap}} = 2.4(D_m/R_c)$	$\mathbf{v}_{\text{opt,cap}} = 4.8$
$k = 10$	$H_{\text{min,cap}} = 1.79R_c$	$\mathbf{h}_{\text{min,cap}} = 0.89$	$u_{\text{opt,cap}} = 2.2(D_m/R_c)$	$\mathbf{v}_{\text{opt,cap}} = 4.4$
$k = \infty$	$H_{\text{min,cap}} = 1.91R_c$	$\mathbf{h}_{\text{min,cap}} = 0.96$	$u_{\text{opt,cap}} = 2.1(D_m/R_c)$	$\mathbf{v}_{\text{opt,cap}} = 4.2$

The situation becomes more complicated when the resistance to mass-transfer term in the stationary phase becomes relevant; for example, in OTLC and GC using thick films (>0.5 μm), notably of polar gum or immobilized stationary phases, in which the diffusion coefficients are much smaller than in phases that are not immobilized. In capillary GC using such phases, especially with thick films up to 5 μm, the C_s term may be of the order of C_m or even larger. Other complications may arise in capillary columns with "rough" walls such as in support-coated and whisker-walled open tubular columns; however, the Golay equation can, as an approximation, be used here as well.

Thus, we see that for any extent of retention, and for small resistances to mass transfer in the stationary phase, the minimum plate height is not likely to exceed the column diameter, which implies reduced plate heights of close to 1. For $k > 1$ the optimum reduced velocity in open tubular columns is about 5. In a dimensional sense, converting $\mathbf{v}$ to u, this implies that when working with mobile phases that allow fast diffusion of solutes, the absolute value of the (optimum) working velocity is higher than with slowly diffusing solutes in more viscous mobile phases. This is of eminent importance for GC, in which the use of light gases, such as hydrogen or helium as the carrier gas, allows faster analysis. Diffusion coefficients are about 4 times higher than with nitrogen as the carrier, which yields 2 times faster optimal velocities, and correspondingly shorter analysis times. H_{min} values are more or less independent of the nature of the carrier gas, as long as C_s contributes little or nothing to plate height. Thus, the faster analyses with the light carrier gases at optimum conditions are not more efficient. At velocities other than u_{opt}, the identity of the mobile phase is important in determining the C_m term. At higher velocities, carrier gases of relatively high molecular mass will yield relatively high H values, because of larger C_m values.

The ratio of optimum velocity and minimum plate height is a characteristic analysis time $t_{a,\text{max}} = u_{\text{opt}}/H_{\text{min}}$, or in reduced terms $\tau_{a,\text{max}} = \mathbf{v}_{\text{opt}}/\mathbf{h}_{\text{min}}$. This is the time necessary to produce maximum efficiency and thus maximum resolution (see Sec. II.D) from the column. Note, by the way, that this characteristic time is closely related to the C terms: $t_{a,\text{max}} = u_{\text{opt}}/H_{\text{min}} = 2(C_m + C_s)$ for both the Golay and van Deemter type of equations.

With Eq. (56a,b) we find

$$t_{a,\text{max}} = (R_c^2/D_m)[f(k)/12] \qquad \text{and} \qquad \tau_{a,\text{max}} = f(k)/48$$

This characteristic time for maximum resolution sets a natural lower limit to the *practical analysis time* (the retention time of the last component), which [apart from a retention factor $1/(1 + k)$] is determined by the optimum velocity. Indeed, lowering the velocity below u_{opt} would lead to a strong increase of the plate height by molecular diffusion (the B term becomes important) and thus to a loss in resolution at the additional cost of an increased residence, retention or analysis time $t_a = t_R > t_{a,\text{max}}$. With an increase in the mobile-phase velocity, we find some room for improvement (i.e., lowering the analysis time), because from the Golay and van Deemter equations, and from the retention equation using $L = \langle u_m \rangle t_m = n_{\text{th}} H$ it is found that:

$$t_a = t_R = t_m(1 + k) = (L/\langle u_m \rangle)(1 + k) = n_{\text{th}}(H/\langle u_m \rangle)(1 + k)$$

which shows that *for practical purposes it is the ratio of plate height and mobile-phase*

velocity, rather than plate height alone, that determines the analysis time. If we define the *separation speed* as $Ss = n_{th}/t_a$ we have:

$$\begin{aligned} Ss = n_{th}/t_a &= (L/H)/[t_m(1 + k)] = 1/[(H/\langle u_m\rangle)(1 + k)] \\ &= 1/[\{(A/\langle u_m\rangle) + B/\langle u_m\rangle^2 + (C_m + C_s)\}(1 + k)] \\ &\approx 1/[(C_m + C_s)(1 + k)] \end{aligned} \tag{57a}$$

for sufficiently high velocities. This shows that for Golay- and van Deemter-type equations, the separation speed is constant and *independent of the mobile-phase velocity.*

At the optimum conditions at minimum plate height, the separation speed would have been:

$$\begin{aligned} Ss_{min} &= 1/[(H_{min}/u_{opt})(1 + k)] \\ &= 1/[A\{(C_m + C_s)/B\}^{1/2} + 2(C_m + C_s)][(1 + k)] \\ &\approx 1/[2(C_m + C_s)(1 + k)] \end{aligned} \tag{57b}$$

for the usual case of small (or nonexistent, as in the capillaries) A values. This separation speed, under optimum conditions, is seen to be a factor of 2 smaller than the separation speed at velocities, well above the optimum velocity. As a consequence, the fastest operation of a column does not correspond to working at or near the optimum conditions, the latter being of interest only for maximum performance irrespective of analysis time. We should, however, realize that working at elevated velocities will not necessarily lead to lower resolutions, notwithstanding the increase in plate height, because the use of longer columns or columns with smaller IDs, would yield a gain in theoretical plates, compensating for the loss in plate height. Obviously, we should make a distinction between maximizing the resolution (especially for complex samples, resolution or peak capacity is often inadequate) and optimizing the retention time if resolution is adequate.

In the first case, it is clear that the plate number should be maximized by decreasing the plate height to its minimum value; for example, by using longer columns (mile long capillaries have indeed been designed to yield some 10^6 theoretical plates). Here, we should realize that the optimum mobile-phase velocity determines the maximum plate number and the (minimum) time required to obtain a specific separation. A strong means to improve resolution is to increase the selectivity α, as shown in Eq. (18); for example, by changing the stationary phase or by changing operating conditions, such as the temperature. This and the process of optimization of resolution and time, will be discussed further in Sec. IV, but here we mention that redesigning the column to greater lengths or smaller diameters, combined with higher velocities implies that higher inlet pressures are needed to transport the mobile phase through the system. Hence, it is obvious that pressure limitations will ultimately determine the maximum separation speed.

In the early days of capillary chromatography, the late 1950s, this aspect of pressure sometimes led to hilarious discussions at conferences. For example, a quote from the 1960 Edinburgh Symposium on Gas Chromatography reads [29, p. 198]:

> J.H. Knox: The point is that if you double your pressure drop across the column you could use it more efficiently by redesigning the column.
>
> C.P. Quinn: Yes, I agree again, you can carry on in this way trying first one and then improving the other and so on, ad infinitum. However, as far as our own practical experience is concerned, we have always found that the *pressure drop across the column is not the thing which limits us, but in fact it is the size of the capillary*, or the size of the support particles, which is in the end the limiting factor. So when Dr. Knox gets to the end of his capillary columns and has got them so small that he cannot breathe down them, we shall double our pressure and do it twice as fast. I am afraid that is all I can say.

Alas, discussions at contemporary conferences are not equally inspired. Maybe this is a good reason for no longer including them in conference proceedings. This is a pity, however, because quotes such as the foregoing show us the heart of the matter, which in this case is the complexity of optimization beyond the use of the accepted optimum conditions H_{min} and u_{opt}. History has awarded both speakers in their own right.

The key to further optimization has been miniaturization of sizes down to the micrometer level in both packed and open systems, but the available pressure has also become a limiting factor at levels of several hundred bars. Not only pressure as such, but also, especially for gaseous and supercritical mobile phases used as carriers in GC and SFC, compressibility effects play an important role in the further discussion of kinetic optimization (see Sec. IV) for both packed and capillary columns.

(f) Plate Height in Packed Columns Using the Golay Equation. In Sec. II.E.4.d, we discussed all kinds of pragmatic alternative expressions for plate height in packed columns, and here we continue the discussion, for there are possibilities and pregnant preferences of authors to use plate height equations, based on the foregoing Golay equation for open tubular or capillary columns and also for packed columns, both in GC and in LC.

It was Golay himself who opened the discussion in this direction by comparing his results directly with those of van Deemter. Golay concentrated on the C_s term, but Purnell et al. [29,30] argued that packed columns may be considered as a bundle of capillaries, the radius of which can be reasonably approximated by the particle radius of the packing. They thus adopted the Golay equation [see Eq. (55)] and used it rather successfully for characterizing and optimizing packed columns in GC. The general conclusion of Bohemen and Purnell [31] was that in packed column GC the following equation is useful:

$$H = 1.5dp + 2\gamma \boldsymbol{D}_m/\langle u_m\rangle + (3/2)f(k)(\langle u_m\rangle(d_p^2/\boldsymbol{D}_m) + (2/3)g(k)\langle u_m\rangle(\delta_s^2/\boldsymbol{D}_s) \tag{58a}$$

In LC, Scott et al. [21,31] tested a variety of equations, among which are the ones in Table 3, but also the van Deemter equation in a Golay adaptation. It was observed that, notwithstanding that good fits with experimental data could be obtained with most equations, physically meaningful values for the coefficients in the A, B and C, terms could be assigned to only the modified van Deemter–Golay equation in the following form (written in our notation):

$$\begin{aligned} H = A + B\phi/\langle u_m\rangle + (C\phi^{-1})\langle u_m\rangle = {} & 2\lambda d_p + 2\gamma\phi \boldsymbol{D}_m(1 + k_0/\mathbf{D})/\langle u_m\rangle \\ & + [(1/24)f(k_0)\chi \\ & + (2/3)g(k_0)\mathbf{d}^2\mathbf{D}]\phi^{-1}(\langle u_m\rangle d_p^2/\boldsymbol{D}_m) \end{aligned} \tag{58b}$$

The new symbols are k_0 (a modified retention factor) and χ (a correction factor), which will be discussed in the following.

Here, we retained the notation in the usual velocity $\langle u_m\rangle$, while in the equations naturally the interstitial velocity $u_0 = \phi^{-1}\langle u_m\rangle$ occurs, where ϕ represents the fraction of mobile phase that actually moves in the interstitial pores between particles that have an internal porosity ε_i contributing to the total bed porosity $\varepsilon_{tot} = \varepsilon_0 + \varepsilon_i$, so $\phi = \varepsilon_0/\varepsilon_{tot}$. As usual $\langle u_m\rangle$ is found from the residence time t_m of a nonretained low molecular mass marker solute that penetrates both interstitial and intraparticle pore space: $\langle u_m\rangle = L/t_m$. Both the interstitial velocity u_0 and the modified retention factor k_0 replacing the conventional capacity factor k, are found from the retention time t_0 of a completely excluded (from the intraparticle pores) solute, such as a high molecular mass standard compound of a nonadsorbed polymer (for instance a polystyrene standard with molar mass 83,000), $u_0 = L/t_0$ and $k_0 = (t_R - t_0)/t_0$. Note, that we now have two equivalent expressions for the retention time:

$$t_R = t_m(1 + k) = t_0(1 + k_0)$$

In this way, the packing particle as a whole, including pores filled with mobile phase (but

excluding the skeleton; see Sec. II.E.4.g), is considered as the stationary phase or, better, as the stationary "region" or "zone" [32]. Stagnant mobile phase within the particles, would contribute to the common dead time t_m as measured with a (totally permeating, but nonretained) low molecular mass marker. The ratio L/t_0 is thus a true measure of the interstitial mobile-phase velocity u_0. This is indeed the velocity that was meant to occur in all our equations so far, because we tacitly assumed that all internal pore space was occupied by a stationary phase, rather than a mobile phase. The usual L/t_m ratio yields an average velocity smaller than u_0, as t_m includes time spent in the intraparticle stagnant pores. The difference between the two values $k_0 = (t_R - t_0)/t_0$ and $k = (t_R - t_m)/t_m$ may be appreciable, as shown by Scott et al. [21,31–33]. For modern Partisil and Zorbax columns, for example, $k_0 \approx 2k$. This is not quite unexpected as, from the definitions of k_0 and k we find that $k_0/k = [(t_R - t_0)/(t_R - t_m)](t_m/t_0)$. With $t_R = t_m + t_s = t_0 + t_{m,i} + t_s$, where $t_s = kt_m$, and again $\varepsilon_{tot} = \varepsilon_i + \varepsilon_0$ and $\phi = \varepsilon_0/\varepsilon_{tot}$, (see Sec. II.A), we see that $k_0/k = 1 + [(1/\phi) - 1][(1 + k)/k]$ or $k_0 = (1 + k - \phi)/\phi$. For $\varepsilon_i = 0$ (nonporous particles) $\phi = 1$ and $k_0 = k$, but for typical porous particles we have $\varepsilon_i \approx \varepsilon_0$, $\phi = \frac{1}{2}$, and so $k_0 = k + (1 + k) = 1 + 2k$, which approaches $2k$ for large k values.

It is dangerous to simply replace k with k_0 without a solid fundamental background, as done by Scott in the modified van Deemter–Golay equation [see Eq. (58b)]. However, in the next section, where we will treat this issue of porous particles further, it is proved from first principles that the substitution is correct.

The counterpart of Eq. (58b) in references [21,31] contains the original, but outdated geometric factor $8/\pi^2$ after van Deemter, but we prefer the use of the modified van Deemter and Golay C_s terms with the factor 2/3, as used by Purnell et al. [29,30] in Eq. (58a). We also added a correction factor χ, accounting for the fact that the effective capillaric radius in packed beds is not exactly the particle diameter, as was assumed by Scott et al. The effective radius is better estimated from our earlier discussion on the hydraulic radius concept [see Sec. II.E.2.c, Eq. (31a)], as $R_{c,h} \approx (2/9)d_p$. From this treatment, we expect a value of $\chi \approx (2/9)^2 = 0.05$. Equation (58a) for GC shows, however, an experimental value of $\chi = 3/2$, much larger than expected. Hence, the result of Scott et al., Eq. (58b), is suspect in its estimation of the numerical factor in the C_m term.

(*g*) *Plate Height from Porous Particles.* The notion of stationary phase (region, or zone) is necessary in the case of porous particles with stagnant mobile phase in the pores. The latter play a role in the residence time of all molecules, including mobile-phase molecules (t_m vs. t_0). Because there is slow and possibly strongly hindered molecular diffusion in the tortuous pores containing stagnant mobile phase, notably in LC, we may expect the occurrence of an additional C term. We designate this as C_{mm}, because it concerns partitioning of solute molecules between two types of mobile-phase regions; namely, the interstitial and truly mobile region and the stagnant intraparticle region, with a partition coefficient of 1 at the "interface" between the two regions. Indeed, in the literature, a poor agreement is found between experimental and theoretical contributions to the plate height stemming from the stationary phase (= region; C_s term), especially for packing materials such as Partisil and Zorbax. A significant contribution from stagnant mobile phase may, therefore, be suspected.

The mobile phase potentially present in stagnant pores is not moving; therefore, it constitutes part of the stationary phase. Hence, as proposed by Scott [21,31], the term *moving phase* should be used for the fraction of the phase that actually moves, whereas the term *static phase* would be appropriate for the fraction that is trapped in the pores. Thus, the retention equation should read, as in the former section: $t_R = t_0 + t_{m,i} + t_s$, where $t_m = t_0 + t_{m,i}$ as always indicates the total residence time in the mobile phase, including t_0 in the interstitial, moving region and $t_{m,i}$ in the static region inside the porous particles.

The true practical situation in LC is even more complicated because exclusion of larger solute molecules can easily occur, especially for silica-based materials with pore diameters ranging from as low as 1–3 Å, to as much as 1500–3000 Å. Open pores with diameters less

than the solute size are inaccessible. Size exclusion chromatography (SEC, formerly called gel permeation chromatography; GPC) is based on this principle. This technique is used mainly for macromolecular species [2,37], but the principle acts equally on smaller-sized molecules (see Chap. 7).

Indeed, Aldehai et al. [33] showed that, on a Zorbax C_8 reversed-phase column, retention times of both small ions and larger hydrocarbons decreased with the molecular volume or size of the analytes, which is the signature of selectivity based on size exclusion. The total volume of mobile phase present in the column was 2.78 mL, whereas the total interstitial volume was estimated as 1.91 mL. The static intraparticle pore volume thus amounts to 0.87 mL, while the volume of stationary phase present was reported as 0.40 mL. The relative values of volumes are probably representative for silica-based packings, but may differ from one type of packing material to another. Even if we ignore further complications, such as inaccessibility of stationary phase by blocking of small pores in the grafting process of chemically bonded phases for HPLC, and also composition differences of multicomponent mobile phases for RPLC inside and outside the packing particles, the present reasoning indicates that it is not easy to define the fundamental properties (such as the different volumes) of porous packings, thereby obscuring the physical meaning of observed retention and dispersion data. This was the very reason to introduce the capacity factor $k_0 \approx 2k$ based on treating the entire particle as the stationary phase, instead of k, which is based on the "liquid" stationary phase within the particle alone.

Let us assume that packings of porous particles into a column volume V_c are to be characterized as being subdivided into the three regions introduced earlier:

1. An interstitial, moving volume fraction $\varepsilon_0 = V_0/V_c$
2. A stagnant intraparticle fraction $\varepsilon_i = V_{m,i}/V_c$ (note that $V_m = V_0 + V_{m,i}$)
3. A stationary phase volume fraction $\varepsilon_s = V_s/V_c$, complemented by:
4. The remainder of the column volume to be attributed to the skeleton of the porous particles.

The latter ranges in practice from $\varepsilon_{sk} = 0.1$ (in GC packings) to 0.6 (for solid nonporous LC packings). Of course, the fraction $\varepsilon_p = V_p/V_c = (V_c - V_0)/V_c = (1 - \varepsilon_0)$ is the volume fraction occupied by the particles as a whole, and we have the relations: $\varepsilon_0 + \varepsilon_i = \varepsilon_{tot}$, representing the total porosity $[(V_m/V_c) = (V_{m,i} + V_0)/V_c]$ of the column, whereas $\varepsilon_i + \varepsilon_0 + \varepsilon_s + \varepsilon_{sk} = 1$. ε_s ranges in practice from 0.01 to 0.10, ε_0 is invariably about 0.4, and so ε_i ranges from 0 to 0.5, and ε_{tot} from 0.4 to 0.9, depending on the pore volume. Components are distributed between the mobile and the stationary phase fluids with the equilibrium partition coefficient $K^* = c_s^*/c_m^*$, but also between the moving and the stagnant mobile phases. For small molecules, the latter occurs with a partition coefficient 1; hence, the concentration in the intraparticle stagnant mobile phase equals that in the interstitial space. Long before the proposal by Scott et al. it was custom in technical sciences to define the *apparent partition coefficient* K_{app} based on the partitioning of compounds between regions inside the "whole particle," which was treated as the stationary zone [fraction $\varepsilon_p = (1 - \varepsilon_0)$] and the region outside the particle, that was treated as the mobile zone (fraction ε_0), and we find:

$$K_{app} = [(c_s V_s + c_m V_{m,i})/V_p]/c_m = [(\varepsilon_i + K^* \varepsilon_s)/(1 - \varepsilon_0)]$$

Also, the *apparent retention factor* $k_{app} = K_{app} V_p/V_0 = K_{app}(1 - \varepsilon_0)/\varepsilon_0 = (\varepsilon_i + K^* \varepsilon_s)/\varepsilon_0$, based on partitioning between the moving fraction of the mobile phase (ε_0) and the whole particle as the stationary phase (including the skeleton), can be found in terms of these volume fractions or porosities ε. The customary chromatographic capacity factor k can also be expressed in terms of porosities as $k = K^*(V_s/V_m) = K^*(\varepsilon_s/\varepsilon_{tot}) = K^* \varepsilon_s/(\varepsilon_i + \varepsilon_0)$, and so we find: $k_{app} = (k/\phi) + [(1/\phi) - 1] = (1 - \phi + k)/\phi$, which is identical with k_0 as seen by Scott et al., see the former section (as before $\phi = \varepsilon_0/\varepsilon_{tot} = \langle u_m \rangle/u_0 = (1 + k)/(1 + k_0)$. Hence, the simple substitution of $k_0 \approx 1 + 2k$ is justified to express our results in terms of $k_{app} = k_0$.

We will now proceed to apply the exact mass-balance equations to yield an exact solution for the concentration profile of the component zone [7, and references therein]. Subsequent application of correlations between dimensionless mass-transfer numbers [15] for spherical particles then yields the contribution of slow and obstructed diffusion in the tortuous stationary particle region ($\gamma_{i,p}\boldsymbol{D}_{i,p}$) as an additional C term, which we call the C_{mm} term because of the partitioning between two regions of mobile phase. This contribution reads:

$$H_{mm} = (1/30)[\varepsilon_0/(\varepsilon_i + \varepsilon_s)][k_0/(1 + k_0)]^2(u_0 d_p^2/\gamma_{i,p}D_{i,p}) \tag{59a}$$

The diffusion factor $\gamma_{i,p}\boldsymbol{D}_{i,p}$ can be assumed to be determined by diffusion through the mobile phase in the pores along $\gamma_{i,p}\boldsymbol{D}_{i,p} \approx \gamma_{i,p}\boldsymbol{D}_m$, which applies to GC packings where $\boldsymbol{D}_m$ is large and renders the C_{mm} term small for all practical purposes. In LC, however, $\gamma_{i,p}\boldsymbol{D}_{i,p}$ will most likely be determined by diffusion in both phases, which may lead to a distinct contribution to plate height. Notably in RPLC, this term is present and is smaller than anticipated by the diffusion in the stationary phase alone.

We can express the C_{mm} contribution in our usual notation with $\langle u_m \rangle$ and k as:

$$H_{mm} = C_{mm}\langle u_m \rangle = (1/30)[\varepsilon_0/(\varepsilon_i + \varepsilon_s)](1/\phi)[(1 - \phi + k)/(1 + k)]^2(\langle u_m \rangle d_p^2/\gamma_{i,p}\boldsymbol{D}_{i,p}) \tag{59b}$$

where, as before, ϕ is the fraction of total mobile phase that occupies interparticle space: $\phi = \varepsilon_0/(\varepsilon_0 + \varepsilon_i) \approx (\varepsilon_0/\varepsilon_{tot})$ and $\langle u_m \rangle$ is the usual mean mobile-phase velocity $\langle u_m \rangle = L/t_m$. Note, that for lightly loaded porous particles $\varepsilon_s \to 0$, and the factor $[\varepsilon_0/(\varepsilon_i + \varepsilon_s)] \approx \varepsilon_0/\varepsilon_i = \phi/(1 - \phi)$, and Eq. (59b) becomes:

$$H_{mm} = C_{mm}\langle u_m \rangle = (1/30)\{[(1 - \phi + k)/(1 + k)]^2/(1 - \phi)\}(\langle u_m \rangle d_p^2/\phi_{i,p}\boldsymbol{D}_{i,p}) \tag{59c}$$

This equation has also been derived within the framework of the nonequilibrium theory after Giddings [5] elegantly expressing the ϕ-function as: $(1 - \phi\boldsymbol{R})^2/(1 - \phi) = [1 - \phi/(1 + k)]^2/(1 - \phi)$ with $\boldsymbol{R} = 1/(1 + k)$.

The problem of describing combined internal partitioning and resistance to mass transfer in porous particles has been exhaustively treated by Grubner [36]. A common assumption in flow processes is that the flowing fluid does adhere to the wall (zero velocity and so-called no-slip). Thus, for the mobile phase at the particles surfaces, Grubner introduced a stagnant film coating, with mobile phase around the porous particle, which is used as the interface between moving and stationary regions. Partitioning at this interface is governed by the partition coefficient $K_{m,i} = c_{m,i}/c_{m,0}$ over the volumes $V_{m,i}$ and V_0, which approaches 1 for small molecules, as the interparticle solute concentration in the moving phase $c_{m,0}$ equals that inside the porous particles in the intraparticle stagnant phase $c_{m,i}$. This is not true for larger molecules, which, as a result of their discrete sizes, will be partly excluded from intraparticle pore space by the principle of size exclusion chromatography (SEC) [2,37]. Hence, it is more general to allow explicitly for partitioning governed by size exclusion at the interface of the particle and proceed with Grubner's analysis to include the final partitioning of solute molecules with the stationary phase provided by a stationary fluid at the walls of the intraparticle pores, or by adsorption onto those walls. If we denote the associated partition coefficient with K_s, the resulting plate height for the total diffusion-controlled process for spherical particles, as obtained by Grubner, using the method of statistical moments, as introduced by Aris [17], reads in our notation:

$$H = A + B/u_0 + (1/30)[k_0/(1 + k_0)]^2[\phi/K_{m,i}(1 - \phi)]\,(u_0 d_p^2/\boldsymbol{D}_R) + \text{kinetic terms} \tag{59d}$$

which is identical with the foregoing results for the C term [see Eqs. (59b,c)] for $K_{m,i} = 1$. However, if exclusion occurs and $K_{m,i} = K_{SEC} < 1$, while at the same time $K_s = 0$ is assumed (no sorption at the porous particles, as is the ideal case for SEC), we have

$$H_{SEC} = C_{SEC}\langle u_m \rangle = (1/30)[k_0/(1 + k_0)^2](1/\phi)(\langle u_m \rangle d_p^2/\boldsymbol{D}_R) \tag{59e}$$

where $k_0 = K_{SEC}\,\psi$, with $\psi = \varepsilon_i/\varepsilon_0 = V_{m,i}/V_0$ is the alternative void fraction introduced before in the Horvath equation [see Eq. (49a)] and representing the ratio of intraparticle and extraparticle (interstitial) pore volume: $\psi = (1/\phi) - 1$ or $\phi = 1/(1 + \psi)$. As a result we may write:

$$H_{SEC} = C_{SEC}\langle u_m\rangle = (1/30)[K_{SEC}\psi/(1 + K_{SEC}\psi)^2]\phi^{-1}(\langle u_m\rangle d_p^2/\boldsymbol{D}_R) \tag{59f}$$

a well-known relation for SEC zone dispersion, generally cited in the literature [37].

For completeness, we note that the Horvath equation [see Eq. (49a)] which contains the C_{mm} term expressed in terms of ψ rather than in ϕ, is exactly identical with the present results, [see Eqs. (59a–f)], and it shows the same dependence on particle size, velocity, and diffusion as all earlier expressions, including the numerical factor 1/30.

Without going into the mathematical details of the derivation of Eqs. (59), we can obtain some insight into its character, by looking at the very basis of the phenomenon of partitioning between inter- and intraparticle void space. So much is clear, that slow (strongly hindered) intraparticle diffusion with a diffusion coefficient $\boldsymbol{D}_{\text{eff},p} = \gamma_{i,p}\boldsymbol{D}_{i,p}$ occurs in the pores of particles, which are assumed to be spherical. In a three-dimensional spherical geometry, the random-walk approach for diffusion, leading to the relation in Eq. (7a), which is valid in the one-dimensional case, is slightly altered because three-dimensional diffusion takes place in six rather than two directions; namely, in the $\pm\ x$, the $\pm\ y$, and the $\pm\ z$ directions. For a number of $N = t/\tau$ steps of length λ, with step time τ and occurring with equal probabilities (1/6) for all directions, the mean square displacement should be equal for all directions, so $\langle x^2\rangle = \langle y^2\rangle = \langle z^2\rangle = N\lambda^2/3$. The diffusion coefficient $\boldsymbol{D}$ remains by definition (see Sec. II.C.1) the same for all directions; for example $\langle x^2\rangle = 2\boldsymbol{D}t$ and so the mean square spatial distance $\langle r^2\rangle = \langle x^2\rangle + \langle y^2\rangle + \langle z^2\rangle = N\lambda^2 = 6\boldsymbol{D}t$, and the three-dimensional diffusion coefficient contains the factor 6 instead of 2 and reads: $\boldsymbol{D} = \langle r^2\rangle/6t = N\lambda^2 = \lambda^2/6\tau$ [2].

Hence, for a step length of the order of the radius of a spherical particle, the characteristic intraparticle step time τ_{mm} is: $\tau_{mm} \approx R_p^2/6\boldsymbol{D}_{i,p}$. The exact solution for diffusion without convection from the mass-balance equation represented by Fick's second law [15] for a spherical geometry yields the same result, only replacing the constant 6 by $\pi^2 \approx 10$. Hence,

$$\tau_{mm} \approx R_p^2/10\gamma_{i,p}\boldsymbol{D}_{i,p} = d_p^2/40\gamma_{i,p}\boldsymbol{D}_{i,p} \tag{60}$$

which is to be considered a characteristic equilibration time between moving and stagnant regions of the mobile phase. The associated time τ_0, the step time spent in the moving interstitial region, is then found from the partitioning of solute molecules with a partition coefficient of 1 over the interstitial and intraparticle mobile-phase regions [i.e., $\tau_0/\tau_{mm} = 1 \times V_0/V_{m,i} = \phi/(1 - \phi)$]. The associated plate height contribution from this zone-broadening effect is found from using Eq. (11) for a general velocity difference. In the present situation, the latter is determined by the difference between the interstitial (maximum) velocity $u_0 = \phi\langle u_m\rangle$ and the zone velocity, and reads $\Delta u = u_0 - u_z$. Hence, the step length of molecules in the moving mobile phase $\ell_{mm} = u_0\tau_0$, whereas that for the zone in the same time $\ell_z = u_z\tau_0 = \langle u_m\rangle\tau_0/(1 + k) = \phi(u_0\tau_0)/(1 + k) = [\phi/(1 + k)]\,\ell_{mm}$. Following the same reasoning that led to Eq. (33), a molecule chooses in $N = 2L/\ell_{m,i}$ exchange steps during transport through the whole system, either a relative step length $\lambda_{mm} = \ell_{mm} - \ell_z = \ell_{mm}[1 - \phi/(1 + k)]$ forward or backward relative to the zone center, and the associated spreading after the random-walk rule Eq. (7) is $\sigma_z^2 = N\lambda^2 = 2L\ell_{\text{mm}}[1 - \phi/(1 + k)]^2$, from which:

$$\begin{aligned} H_{mm} &= 2\ell_{mm}[1 - \phi/(1 + k)]^2 = 2[1 - \phi/(1 + k)]^2 u_0\tau_0 \\ &= 2[1 - \phi/(1 + k)]^2\langle u_m\rangle\tau_{mm}/(1 - \phi) \\ &= \{[1 - \phi/(1 + k)]^2/(1 - \phi)\}\langle u_m\rangle d_p^2/40\gamma_{i,p}\boldsymbol{D}_{i,p} = C_{mm}\langle u_m\rangle \end{aligned} \tag{61}$$

within a factor of 4/3 (1/40 instead of 1/30) equal to the exact result of Eq (59c). The difference in the constant may be attributed to the fact that the constant 1/40 has been derived

for diffusion without convection, whereas the exact solution to the mass balance equations does include convection.

F. Broadening and Peak Shape from Nonideal and Extracolumn Processes

In the preceding discussion we assumed a priori that the concentration distribution of the migrating bands and the eluting zones from the separation column would possess the ideal gaussian character that will lead to symmetrical and bell-shaped peaks in the chromatograms. On careful inspection of the detection signals obtained in practice, often peak shapes are either symmetrical, but nongaussian or asymmetrical (often tailing or backward-skewing and sometimes fronting or forward-skewing) and peaks are wider than expected. Thus the gaussian shape is, at best, an approximation in greater or lesser degree and we envisage that these deviating peak shapes may arise from two sources:

1. From the separative and transport mechanisms within the column itself
2. From extracolumn contributions in the connected apparatus.

For the first source, we can think of neglected but potentially active phenomena such as nonidealities connected with the partitioning and broadening mechanisms, such as

1. Interfacial resistance at the phase boundary, replacing the assumed equilibrium condition
2. Concentration effects (nonlinear partitioning isotherms, thermal and sorption effects, viscosity of the injected sample, concentration-dependent diffusion)
3. Compressibility of phases
4. Mixed retention mechanisms (e.g., additional nonlinear [and slow in its kinetics] adsorptive interactions of solute and column material, or even reactions occurring)
5. A badly packed or deteriorated column containing voids in the packing structure.

Some of these effects may be circumvented (for example, by choosing different operating conditions such as lower concentrations, lower pressures, elevated temperatures, or adding modifiers to suppress adsorption), or minimized (by producing more column efficiency), but others are not.

For the second source, extracolumn contributions in the connected apparatus to the column may easily interfere, to produce broader and asymmetrical peaks that elute from the column as such. Examples of such contributions are

1. Nonideal connectings: too long connecting capillary lines, leakage of mobile phase, and remaining dead volumes or corners
2. Broadening from injection (e.g., a too large injection volume, a nonsharp input distribution, a too viscous sample solution or dead volumes)
3. Broadening from detection and data-handling systems (e.g., a too large detection cell volume, dead corners in the cell, or even nonlinearity of the detector response, and too large time constants of detectors and data systems)

Often these sources of additional band-broadening are to be avoided (fast electronic data systems, check on dead volumes and short connections), but sometimes the required detection principle (with a large cell for instance) or the geometric conditions to be met (leading to long connecting lines) are imperative.

1. Broadening from Nonidealities in the Partitioning

(*a*) *Nonequilibrium at the Phase Boundary: Interfacial Resistance.* Since the early days of chromatography, workers in the field have objected to the common assumption that partition equilibrium is present at the exact position of the phase boundary. Especially liquid–liquid chromatography, with two potentially partly miscible liquid phases, and the advent of HPLC

in later years for which chemically bonded phases are used as the retentive stationary layer, have made clear that it is necessary to redefine the spatial extent of both phases, because there is no clear interface that separates both domains. In the latter case, the chemically modified surface of the carrier particles is grafted with chain-like molecules with different lengths (C_8 and C_{18}, for example), with different surface coverages (from isolated flexible chains to "hairy" polymer brushes), and with varying capabilities to include molecules of the mobile phase itself, so that a pure and separate stationary phase no longer exists. Rather, a continuous change of concentrations exists if we look perpendicular onto the solid interface, for both stationary-phase chain segments, mobile-phase constituents, and solute molecules. In a review on this matter [39], it has been shown that a hydrodynamic layer thickness, rather than a geometric condition, defines the existence of a stationary phase next to a moving mobile phase. The same situation, probably to another extent, may be present at liquid–liquid interfaces, with mutual penetration of molecules from one phase to the other.

In these situations, rather than postulating equilibrium to exist at the "interface," it seems more appropriate to remove the equilibrium condition and treat mass transfer in this region as being driven by concentration differences and a kinetic adsorption and desorption process, with rate constants k_a and k_d that represent the mass-transfer velocity such that the partition coefficient is now given by $K = k_a/k_d$. Advocates of this approach [for a short introduction see Ref. 40], among which Giddings [5], derive an additional term in the plate height equation, analogous to the one valid for adsorption [see Eq. (33c)]. For capillary chromatography this contribution reads:

$$H_{\text{interface}} = [k/(1 + k)^2]\langle u_m\rangle/k_d = C_{\text{interface}}\langle u_m\rangle \tag{62a}$$

Although the physical meaning of the desorption constant is still a matter of debate, it is possible to approximate this mass transfer coefficient by using Gidding's nonequilibrium theory [5], to find that [40]:

$$k_d \approx (R_c/C_m)[k/(1 + k)] \tag{62b}$$

and so, the interfacial resistance C term in the plate height equation is strongly connected to the mobile-phase convective dispersion C_m term as we know it from the foregoing treatment:

$$C_{\text{interface}} \approx C_m[k/(1 + k)] \tag{62c}$$

With this additional C term, the total plate height Eq. (55a) becomes extended to:

$$\begin{aligned} H_{\text{cap}} = \Sigma_i H_i &= B_{\text{cap}}/\langle u_m\rangle + C_{m,\text{cap}}\langle u_m\rangle + C_{\text{interface,cap}}\langle u_m\rangle + C_s\langle u_m\rangle \\ &= 2\boldsymbol{D}_m/\langle u_m\rangle + (1/24)h(k)R_c^2\langle u_m\rangle + (2/3)g(k)(\delta_s^2/\boldsymbol{D}_s) \end{aligned} \tag{62d}$$

where $h(k) = f(k)[(1 + 2k)/(1 + k)]$ replaces $f(k)$ in the original Golay equation. From this, it appears that for almost the whole k range the C_m term is increased by a factor approaching 2 at high k values ($k > 10$), which certainly cannot be ignored. A decisive study on the subject of interfacial resistance still has not been performed; but the available experimental data [40] clearly points in favor of the proposed additional term.

(*b*) *Peak Shape and Partitioning.* Although the presence of an overlapping nonresolved second component should always be considered, often asymmetrical peak shapes can be attributed to concentration effects in the partitioning mechanism, and to a far lesser extent, to adsorption, chemical reactions, and extracolumn band-spreading. Concentration effects are at the very basis of chromatographic separations, both in the partitioning process and the transport processes governing the peak dispersion. When considering the effect of concentration, one should realize that the overall concentration of migrating zones falls as the band proceeds: the rate of the fall is rapid at first and reduces toward the column exit, where the detector is measuring the outlet concentrations, which are thus always smaller than those inside the column. Hence, even if the outlet concentration may be infinite dilution, the inside column

concentration and, especially, the near inlet concentration, may be well in the finite concentration range. If so, the developed asymmetry near the inlet will remain in the concentration profile during further migration, only reduced to some extent by the mixing effect inherent with zone dispersion. As a result, we should not allow the inlet concentration, rather than the outlet concentration to be in excess of some limiting concentration value, yet to be specified.

(*c*) *Curvature of Partitioning Isotherms.* The partition coefficient $K = c_s/c_m$, representing the slope of the so-called partition isotherm $c_s = c_s(c_m)$ is constant for any partition equilibrium at infinite dilution. In practice the linearity of the isotherm, and so the constancy of K, is limited to some restricted concentration range, above which deviations occur. The curvature of the isotherm at higher concentrations than the mentioned threshold value of the linear range, is either toward (*concave*, or *Langmuir*-type) or directed away from (*convex*, or *anti-Langmuir*) the abscissa c_m. The background behind this is that, at elevated concentrations, molecules of the solute are ever more subject to interactions with molecules of their own kind (solute–solute), rather than with solvent molecules (solute–solvent) alone, as is true at infinite dilution. Because the interactive forces for solute–solute and solute–solvent contacts may be appreciably different, the solute molecules may show an increased preference for one of the phases, thereby influencing the ratio c_s/c_m. As a result, the partition ratio $K = c_s/c_m = c_s(c_m)/c_m = K(c_m)$ becomes concentration-dependent, and we should reserve the term *partition coefficient* only for infinite dilution. If we realize now that the partition ratio determines the zone velocity of partitioning components as $u_z = \langle u \rangle/(1 + K\varphi)$, it is seen at once that the zone velocity also becomes a function of concentration, which, depending on the curvature of the isotherm, increases (concave isotherm) or decreases (convex isotherm) with concentration. As within the migrating component zone the concentration is approaching zero (infinite dilution) at the very rear and the front of the zone, and shows a maximum concentration somewhere in between near the zone center, it becomes apparent that the different regions of a component zone may migrate at different velocities through the column. For a concave isotherm, the partition ratio in the center is smaller and the zone center moves faster than the more diluted parts near the bottom of the concentration profile, which produces a tailing peak on elution. For a convex isotherm, the opposite is true and the resulting peak shape is fronting. Partition isotherms cannot be expected to be linear over a solute concentration range of more than say 0.01 mol fraction, although this depends on the system at hand. Given the amount of phases present, this easily sets a limit to the maximum permissible sample size if isotherm linearity is to be maintained. In practice this limit is typically on the order of 0.01 μmol (i.e., 0.001 mg or μL of liquid solute of assumed molecular mass 100).

2. Peak Widths in Apparatus

The principal places that the apparatus can contribute to the zone dispersion are the injector, column frits and connectors, connecting tubes and fittings, the detector, and the data-handling system. Sternberg [38] has given a comprehensive survey of these extracolumn contributions to zone-spreading. The residence times of the component zone in each of the mentioned contributing parts as well as in the column can be considered as independent and so their means and variances will be additive, as has been done with intracolumn contributions before:

$$\sigma^2_{\text{peak}} = \sigma^2_{\text{inject}} + \sigma^2_{\text{column}} + \sigma^2_{\text{detect}} + \sigma^2_{\text{connect}} = \sigma^2_{\text{column}} + \sigma^2_{\text{extracolumn}}$$

Experimentally there are two methods to obtain the extracolumn band-broadening of the chromatographic system: a linear extrapolation method using σ^2_{peak} as a function of retention time; and a "zero" length column method where the column is removed from the system and replaced by a very short connecting capillary. Obviously, the latter method ignores the contribution of column frits and connectors, whereas additional broadening from the connecting capillary is introduced. Furthermore, because the pressure drop is lowered, short residence times and the resulting very narrow peaks offer experimental difficulties; this approach is very demanding and not recommended. A modification of this method, experimentally more at-

tractive, is to use, in place of the short connection, a relatively long open tubular column with known length and internal diameter. Here, σ^2_{column} is exactly known from the Taylor, Aris, and Golay equation (see Sec. II.E.4.e), so that by subtraction $\sigma^2_{peak} - \sigma^2_{column} = \sigma^2_{extracolumn}$ becomes known.

The first method using linear extrapolation is based on the fact that the column contribution to the peak variance can be expressed in terms of retention times and the true column efficiency in terms of the number of theoretical plates. By definition $n_{th} = (t_R/\sigma_{column})^2$; hence, $\sigma^2_{column} = t_R^2/n_{th}$. If this is inserted into the foregoing equation, it is seen that then a plot of σ^2_{peak} against t_R^2 will be linear, with a slope determined by n_{th} and an intercept value on the vertical σ^2_{peak} axis representing $\sigma^2_{extracolumn}$. This method is relatively straightforward and yields good results if the solutes used have sufficiently large retention (say $k > 5$).

Obviously, it is our purpose to carry out chromatography such that the extracolumn contribution is minimized, to maximize the efficiency of the final separation. However, by virtue of the foregoing statistical rule for which variances σ^2 rather than peak widths (or standard deviations σ) are summed, there is some actual room for allowing extracolumn dispersion. For example, if we require that the influence of extracolumn dispersion on the peak widths (so on σ) is less than several (say 2) percent, we have that $\sigma_{column} \geq 0.98\sigma_{peak}$, and so $\sigma^2_{column} \geq 0.96\sigma^2_{peak}$, which leaves for the extracolumn contribution: $\sigma^2_{extracolumn} \leq 0.04\sigma_{peak}$, implying that $\sigma_{extracolumn} \leq 0.2\sigma_{peak}$. Hence, a criterion to be proposed so that extracolumn dispersion does not to contribute significantly (about 2%) to the overall peak width is approximately:

$$\sigma_{extracolumn}/\sigma_{peak} \leq 0.2 \tag{63a}$$

or in words and applied to injection, for example: the inlet bandwidth should not exceed about one-fifth of the final outlet zone width, which ensures that

$$1 \leq \sigma_{peak}/\sigma_{column} \leq 1.02 \tag{63b}$$

As a result of this estimation, extracolumn dispersion can be allowed to have an appreciable contribution of about 20% of the total dispersion, without influencing the final peak width significantly. Equation (63a) allows the calculation of the minimum plate height or plate number required to fulfill the criterion.

Injectors and detectors in the chromatographic setup represent dead volumes (V), which are swept with the flow velocity F produced by the solvent-propelling system, often a pump. The characteristic time spent by the mobile phase and the solute molecules in that dead volume is the time constant $\tau_V = V/F$, the time needed to flush the volume once. An estimate of the variance of this process can be obtained, provided we know something about the extent of internal mixing within the volume.

(*a*) *Injection.* For example, if the volume V is ideally mixed [15,38], the variance σ_t^2 is simply τ^2, and the concentration profile leaving the dead volume and serving as the inlet profile for the column on injection, for example, is an exponentially decaying (tailing) profile, proportional to $\exp[-t/\tau]$ and such that after time τ concentration has been lowered by the factor $1/e$, as compared with the maximum concentration. As another example, handheld syringe injections are observed to yield almost symmetrical gaussian-like injection profiles (with base width $4\sigma_t \approx \tau$, and so $\sigma_t^2 \approx \tau^2/16$). Another interesting example is that of the plug, or block injection profile, which can be envisaged to occur in modern sample loop injector valves, where ideally a discrete plug of sample solution is displaced by a fresh mobile phase and is pushed as an undisturbed plug onto the top of the column. For such an ideal plug profile, the variance σ_t^2 can be calculated to be $\tau^2/12$ [15,38].

Although the elution profile of a solute leaving a sample valve is largely controlled by the geometry of the sample volume (sudden changes in diameters or cross sections are large contributors), contemporary sample injectors are so carefully designed that there is no danger of any other contribution (in unions and such) than the injected volume itself. Hence, in a

first approximation, assuming plug-like injection, we can apply the criterion of Eq. (63a) to find the maximum permissible injection volume from the perspective of dispersion (rather than from the concentration effects discussed in Sec. II.F.1). From Eq. (63a), together with the known variance of plug injections $\sigma^2_{inject} = \tau^2_{inject}/12$, we find that $\tau_{inject}/\sqrt{12} \leq \sigma_{peak}/5$, and because $\tau_{inject} = V_{inject}/F$, we have finally,

$$V_{inject} = F\tau_{inject} \leq 0.69\, F\sigma_{peak} \tag{64a}$$

or with $V_R = Ft_R$ is the retention volume of the solute, and $n_{th} = (t_R/\sigma_t)^2$ is the number of theoretical plates for the solute peak:

$$V_{inject} \leq 0.69 V_R/\sqrt{n_{th}} \tag{64b}$$

This equation, apart from the necessarily arbitrary slightly different numerical constant, is identical with that originally proposed by van Deemter et al. [20] for the maximum allowable injection volume. For illustration purposes the following table can be made for HPLC columns:

Column type	ID	Peak variance $(\mu L)^2$	Peak volume (μL)
Conventional packed	4.6 mm	20–2000	15–175
Small-bore packed	1–2 mm	1–25	4–20
Packed capillary	0.2–0.5 mm	10^{-3} to 10^{-1}	0.2–0.8
Open tubular	5–15 μm	10^{-8} to 10^{-3}	10^{-4} to 10^{-2}

from which, with the aid of criterion Eq. (64a), the maximum allowable injection volume can be estimated, or alternatively, with criterion Eq. (64b) the required number of theoretical plates necessary to have an insignificant injection broadening.

This estimation heavily relies on the assumption of plug-like injection volumes, and the actual situation in modern loop-type injectors differs quite significantly from that. In actual practice a more or less pronounced tail in the injection profile is almost unavoidable because sample loops consist of small-diameter, open channels in which very pronounced velocity profiles exist, comparable with the parabolic Poiseuille profile in open tube flow. Thus, in general, the displacement is not exactly plug-like (which requires a flat velocity profile with equal velocities throughout the cross section of the loop), but the resulting tails in the solute zones can be effectively cut off by rapidly switching back of the sample valve, just before the sample loop is totally flushed (so $t < \tau$). The internal mixing process resembles the situation already discussed in open tubular columns, and for sufficiently long tubing a parabolic velocity profile together with radial diffusion determines convective dispersion after the Taylor, Aris, and Golay model, discussed in Sec. II.E.4.e. Although it is questionable whether in the relatively short loop-type channels, the suddenly starting flow of mobile phase at the moment of injection has reached its quasistationary state where it is fully developed, it is illustrative to explore the potential contribution to peak dispersion in the light of the mentioned theories and, also, for the contribution to be expected in the longer connecting tubes, often present between column and detector, for instance.

A very practical way to establish the maximum allowable injection volume is to perform a number of injections with increasing sample size. Usually, a more or less linear relation with a constant offset at very low volumes $\boldsymbol{a}$, followed by a slight curvature and increased peak width (slope $\boldsymbol{K}$) at increasing injection volumes is obtained when plotting the observed standard deviation σ_{peak} versus the sample volume V_{inject}, and an approximate description can be given as:

$$\sigma^2_{\text{peak},V} = \boldsymbol{a}^2 + \boldsymbol{K}^2 V^2_{\text{inject}} \tag{65}$$

Here, $\boldsymbol{a}^2$ is nothing but the extracolumn variance caused by fittings, connecting tubing, and detector, whereas $\boldsymbol{K}$, is a quality parameter for the injector valve, that cannot be smaller than $1/\sqrt{12} = 0.29$ (for the plug injection) and is typically found in the range of 0.70–0.35, but may reach values of 1 as a conservative estimation.

For conventional packed columns (ID = 4.6 mm) and for a k value of 2 and $\boldsymbol{K} = 1$, the maximum allowable injection volume then amounts to about 50 μL. This amount is much reduced in short, efficient columns and especially for narrow-bore columns that are designed to yield little dilution of the sample (which may be limited, as in a clinical analysis). As a rule of thumb, one should inject large volumes onto wide and long columns, especially for large capacity factors, and small volumes in all opposite cases. In this way, relatively small dilution factors of about 3 can normally be obtained.

(*b*) *The Connecting Tubes.* Especially in HPLC, owing to the slow molecular diffusion in liquids, the dead volume present in connecting tubes between the different parts of the apparatus may contribute essentially to the observed zone-broadening. Given the slow diffusion, it will be clear from the start that wide tubing should be avoided whenever possible: molecular diffusion alone will not then be able to achieve sufficient mixing of regions with different velocities, resulting in inefficient mass transfer and broad zones.

It should be realized, however, that changes in tube diameter are even more serious sources of band-spreading and asymmetry, as such changes create dead pockets (i.e., regions of recirculating flow outside the main flow stream). Molecules trapped in these circulations cannot escape except by (again slow) molecular diffusion, and thus these corner regions act as diffusion or mixing chambers. As described for injection, these mixing chambers modify the concentration profile more or less exponentially, leading to serious tailing and broadening of peaks. As a result one should always carefully design the connecting line between the several parts of the system, using as short as possible and as thin as possible tubing, but with an eye for changes in the diameter. Thus, occasionally, it may be more profitable to use wider tubing, avoiding the diameter changes, than to stay with IDs as small as possible.

More quantitatively, the connecting tubes (and with a well-designed injector, also the internal volume of the valve) can be treated with the Taylor, Aris, and Golay expression as discussed in Sec. II.E.4.e. For a nonretained component ($k = 0$) and neglecting the B term for axial molecular diffusion, which is slow, we are left with the C_m term describing the convective dispersion of solutes in (parabolic) cylindrical flow channels. From Eq. (55a), we then have $H_{\text{conn}} = \sigma^2_{z,\text{conn}}/L_{\text{conn}} \approx (1/24)R^2_{\text{conn}}\langle u_{m,\text{conn}}\rangle/\boldsymbol{D}_m$, or expressed in terms of the flow velocity $F = \langle u_{m,\text{conn}}\rangle \pi R^2_{\text{conn}}$:

$$\sigma^2_{z,\text{conn}} \approx (FL_{\text{conn}})/(24\pi \boldsymbol{D}_m) \tag{66a}$$

This result implies that, given a fixed and small diffusion coefficient for liquids (of about 10^{-5} cm^2/s), both flow F and tube length L are prime factors in determining the spreading caused by connecting tubes: for F in the range of 0.1–1 mL/min, each centimeter of tubing, *irrespective of its diameter*, adds to the variance in length units by about 2–20 cm^2. More practical is the variance in terms of volumes, for which we have to multiply the length-based variance with the cross section (πR^2_{conn}) squared:

$$\sigma^2_{V,\text{conn}} \approx \pi R^4_{\text{conn}}(FL_{\text{conn}})/(24\boldsymbol{D}_m) \tag{66b}$$

Here, the role of the tube radius and the length becomes apparent, for example, with a flow rate of 1 mL/min ($F = 1/60$ cm^3/s), and a connecting tube with a length of 10 cm and a tube radius of ¼ mm, we find with 10^{-5} cm^2/s for the diffusion coefficient, that $\sigma^2_{V,\text{conn}} \approx 2.9 \times 10^{-2}$ cm$^3 \approx 30$ μL. This is passable for conventional packed columns, but certainly not for small-bore and other types of minicolumns (see the listed peak volumes in the former section).

In general we can find limiting dimensions for the connecting lines by requiring that the standard deviation does not exceed one-fifth of the total standard deviation, as expressed by Eq. (63a), to find that

$$R_{conn}^4 L_{conn} \leq (1/25) H_{column} L_{column} \varepsilon^2 \pi R_{column}^4 (24 D_m)/F \tag{67a}$$

where F is the common flow rate in both connection tubing and column, and $\varepsilon \approx 0.4$ is the interparticle porosity of the column. If we assume that a minimum length of connecting tubing of say $L_{conn} = 10$ cm is needed and the minimum flow rate is set, relatively short, but not unusual, column lengths are chosen, and ε is taken as ≈ 0.40, except for the open tubular case where $\varepsilon = 1$, this condition yields the following results for maximum tubing diameter in the divers column types:

Column type	ID	L (cm)	F_{min}	H_{column}	$R_{conn}/R_c \leq$	$R_{conn} \leq$
Conventional packed	4.6 mm	10	0.5 mL/min	25 μm	0.062	0.14 mm
Small-bore packed	1–2 mm	10	2 μL/min	10–25 μm	0.2	0.10–0.25 mm
Packed capillary	0.2–0.5 mm	30	0.1 μL/min	15–50 μm	0.61–0.82	0.06–0.21 mm
Open tubular	5–25 μm	100	0.02 μL/min	10–30 μm	1.75–2.31	4.4–29 μm

Hence, as a rule, open tubulars can safely be connected with tubing of the same size, whereas packed columns should be connected with tubing far smaller, say a factor of 2/3–2/30, the smaller factor being valid for conventional packed columns.

Low Dispersion Connecting Tubes. An alternative for the straight open tubes commonly used as connecting lines, is the use of tubing that introduces enhanced radial mixing to break up the deleterious effect of the parabolic flow profile in straight, open-flow channels. Here two approaches are possible: by tightly coiling the connecting tube around a thin bar into a helical shape [18], or by using so-called serpentine tubing for which the length of the tube is folded in a tight zig-zag shape [21]. In both types, the underlying idea is to introduce strong radial convection to assist the slow radial diffusion in the mass-transfer process of averaging out of velocity profiles. In a sense, it resembles the eddy–diffusion phenomenon in packed beds, where radial dispersion is also partly convective as discussed in Sec. II.E.2.

For coiled tubing, the radial convection is originated simply by the main stream velocity that is continuously forced to follow the curved path along the coil length. In such curved paths, centrifugal forces arise and generate a so-called secondary flow in the tube cross section, perpendicular to the main flow direction. A strong circulation arises and, just as in stirring in teacups or in the exchange process in coiled heat exchangers, mass transfer is enhanced in radial directions, thereby sampling all axial velocities. At very low velocities secondary flow is already strong enough to improve on molecular diffusion in the radial direction by a factor of 4, but the real gain in mixing and, thereby, reducing band-spreading occurs at higher velocities. The common rising C term branch of the plate height curve H versus $\langle u \rangle$ at sufficiently high velocities goes through a maximum and even declines toward very small plate height values, indicating that radial mixing is very powerful and able to prevent bands from much axial broadening. A drawback of this secondary flow-mixing mechanism, however, is that linear velocities should be unpractically high to profit fully from the reduced band-spreading. For example, in usual 0.25-mm–ID connecting tubing for conventional columns, the transient velocity at which plate height goes through its maximum lies close to $\langle u_m \rangle \approx$ 30–40 cm/s and velocities of 100 cm/s are needed to obtain the very low plate heights required. At low velocities, more practical for normal HPLC, say <2 cm/s, the gain in plate height is only the mentioned factor of 4.

In this respect, serpentine tubes with the same (original) ID and a small amplitude zig-zag of about 0.5 mm, are more effective at the lower velocities. The underlying flow mechanism is largely unknown, but it is clear that it cannot be fully developed into pronounced velocity profiles and, at each bend in the serpentine, potentially present secondary flows are generated and reversed from one bend to the next. Above 100 cm/s, serpentine and coiled tubing behave almost identical in dispersion reduction toward low values of H. An attractive feature of serpentine tubing is that it preserves part of the gain in mixing toward lower velocities, losing only a factor of 2 in plate height, on lowering the velocity. However, at the more practical velocities of say $\langle u_m \rangle \leq 10$ cm/s, plate heights in both types of tubing again become equal. At this velocity of 10 cm/s and expressed in volumes, for instance, the variance per unit length is 0.10 $(\mu L)^2/cm$ for both coil and serpentine tubing, which compares very favorably with the 5 $(\mu L)^2/cm$ valid for the straight tubing of the same ID at this velocity.

(*c*) *The Detector.* In detectors we distinguish three types of band-broadening, some of which not only broaden the eluting zone but add also a tailing one:

1. Connecting tubing for the column and the measuring cell with a certain dead, but flushed volume behave the same as described in the former section. In some exceptional cases, where on-column detection is applied (e.g., in microcapillary LC where column volumes are far less than present in any available detector cell) no discrete cell is present and the detector signal is generated in an extension of the column itself [see, e.g., Refs 2,9]. Taylor dispersive broadening is then valid for the combined column and detector.
2. Generally, detector geometry often involves sudden changes in cross section, creating dead corners, notably in the measuring cell, and this leads to spreading associated with tailing. Modern detector cells are designed with small detection volumes (1–10 μL), but still, in contemporary apparatus, detectors contribute the most significant of the extracolumn terms, which is caused mainly by the presence of this detector cell volume effect. As a result we can use the same reasoning as we did for the injector and describe the detector effect as the response to a block-like concentration pulse, with a width connected to the cell volume V_{detect}. Again the time constant for this process is of the order of V_{detect}/F and analogous to Eq. (65) we write:

$$\sigma^2_{peak,V} = \boldsymbol{b}^2 + \boldsymbol{K}^2 V^2_{detect} \tag{68}$$

where $\boldsymbol{b}$ now represents the extracolumn contributions from injection, connectings and such; $\boldsymbol{K}$ has the same meaning as before and can be given a value smaller than $1/\sqrt{12}$. When written in time units: $\sigma^2_{peak,t} \approx (1/12)(V_{detect}/F)^2$ it becomes clear that increasing the flow rate through the detector (possibly with the aid of an additional makeup flow) results in a decrease in the peak residence time in the cell and, hence, in a decrease of its extracolumn-broadening contribution, albeit at the expense of sensitivity. As a general rule the detector does not change the standard deviation of the incoming concentration pulse by ore than 1.7% if $\sigma_{peak} \leq 2.5.V_{detect}$ [15,38].
3. Detectors and data systems can also cause additional zone-broadening owing to the finite time they require to respond to their input functions. As a result of this slow response, peaks in chromatograms may be deformed [38] into delayed, lower, wider, and tailing peaks. The delay can, in a first approximation, again be measured by the time constant τ_{det}, which is defined as the time for the output signal to rise exponentially to $1/e$ times the height (63.2%) of an instantaneous step function change in input. One, more practical way of measuring the overall time constant of the readout system is to measure the time constant only for the tail of the peak, which is nearly exponential [38].

The peak position at the center of gravity then shifts according to $t_R + \tau_{detect}$ (t_R being the original position) at least for $\tau_{detect}/\sigma_{peak,t} \leq 0.2$ [38]. It appears that the peak maximum follows the declining tail of the original (assumed gaussian) function, becomes lower, and as

a result, because the peak area remains constant, the peak broadens and shows tailing. The variance of the resulting peak can again be estimated from the additivity rule: $\sigma^2_{\text{peak},t} = \sigma^2_t + \tau^2_{\text{detect}} = \sigma^2_t[1 + (\tau_{\text{detect}}/\sigma_t)^2]$, where σ_t is the original standard deviation. For small $\tau_{\text{detect}}/\sigma_{\text{peak},t}$ (say again ≤ 0.2) this allows the following approximation: $\sigma_{\text{peak},t} \approx \sigma_t[1 + \frac{1}{2}(\tau_{\text{detect}}/\sigma_t)^2]$ and at most only 2% deviation in σ. Hence, the rule is to keep detector time constants as small as possible and in any event, smaller than one-fifth the standard deviation of the nonretained peak.

III. FLOW PHENOMENA AND COMPRESSIBILITY EFFECTS

Flow processes, as becomes apparent from the foregoing discussions, constitute a major mechanism of transport and even separative transport. Its magnitude, its cross-sectional distribution, but also its nature (laminar) and direction (axial, radial, circulating, or other) largely determine the success of separations. As a result, to fully characterize flow transport, we need to know the flow velocity u_m at every position in the system. For simple flow systems, such as open tubes, velocity can be calculated analytically by first principles, but for packed beds, which are rather more complex, the velocity distributions can be estimated only by simplified models for the bed, or by statistical methods.

Description of flows in general, requires the knowledge of forces that play a role in the mechanical transport of all fluid elements that together constitute the fluid volume in motion. These forces are of different origin:

1. Pressure forces, or electrical forces deriving from a gradient (in pressure and voltage, respectively) that causes different forces on the different sides of the fluid elements, and thus, a net force and movement in one (often the axial) direction. Capillarity (the wetting of surfaces in vacant capillaries) is also used as a method to obtain flow.
2. Viscous forces resulting from the drag forces that occur from sliding one fluid element past another.
3. External forces, such as gravitation, and centrifugation (e.g., in coiled tubes).

As is well-known, in HPLC pumps are often used because of their precise control of flow, but in recent years electro-osmotic flow drive has been applied ever more frequently and is a promising way to propel liquids. In methods for which flow is not confined by a column, such as in paper and thin-layer chromatography, flow is usually driven by capillaric forces.

The final aim of the following short treatment of flow phenomena is to find out how pressure limitations influence the kinetic optimization of chromatographic columns relative to the time of analysis, which is logically required to be as short as is convenient.

A. Pressure–Flow Relations

The characteristics of pressure drive (being the common way to obtain liquid flows) are best illustrated first for steady fluid flow in (thin and long) capillary tubes, so-called Poiseuille flow. This provides an easy model for flow calculations, not only for regular open tubes, but also for irregular interstices in packed beds (as already used in Sec. II.E.2.c).

1. Flow in Capillaries

Flow in a capillary tube can be originated and maintained by a steady pressure difference Δp between the inlet and outlet of the channel, in which, for horizontal tubes or sufficiently high-pressure difference, gravitational and other external forces can be neglected. At application of Δp, the fluid rapidly accelerates to a steady flow rate at which viscous drag forces are just balancing the applied pressure (or hydrostatic) forces. The viscous forces, resisting the fluid motion, are proportional to the contact area A_f between sliding fluid elements (or layers) and the velocity gradient or *shear rate*, which is nothing but the velocity difference Δu_m between

adjacent sliding layers at a distance Δr apart. In differential terms: $\tau_f = -du_m/dr$ (where r is the radial coordinate perpendicular to the direction z of flow), and the proportionality constant η between the viscous force F_f and both quantities mentioned is called the viscosity: $F_f = \eta A_f \tau_f$. Viscosities of liquids are generally a hundred times larger than those of gases, and roughly $\eta_{liq} \approx 0.3 - 3$ cP (1 poise (P) = 1 g/cm s and the viscosity of water is 0.01 P = 1 cP), while $\eta_{gas} \approx 0.9 \times 10^{-4}$ to 2×10^{-4} P (0.9 for hydrogen and 1.9 for helium). In the intermediate region between gases and liquids of so-called supercritical fluids (see Sec. IV.B.1), viscosities are also in between the limiting values for gases and liquids.

When we make the force balance in a circular cylindrical tube with radius R_c and length L, and equate the viscous and pressure forces, we find that in the steady equilibrium situation at which both forces are equal but opposite, that on any coaxial cylinder of thickness dr and with contact area $2\pi R_c L$ the velocity gradient reads: $-(du_m/dr) = \Delta p r/2\eta L$. This differential equation can be integrated to obtain Eq. (53)

$$u_m(r) = u_{max}[1 - (r/R_c)^2]$$

with

$$u_{max} = u_m(r = 0) = 2\langle u_m \rangle = \Delta p R_c^2/4\eta L \tag{69a}$$

which expresses the velocity profile as being strongly pronounced and bullet-shaped (parabolic), as obtained originally by Poiseuille [15]. The total volumetric flow through the capillary tube is found by multiplication of the average linear velocity and the total cross-sectional area of the tube:

$$F = \langle u_m \rangle \pi R_c^2 = \pi \Delta p R_c^4/8\eta L \tag{69b}$$

an equation known as the *Hagen–Poiseuille equation*, which shows that the volumetric flow is proportional to the fourth power of the tube radius. This equation holds over a wide range of practical conditions for chromatography, from the region of diffusional flow onward to the point at which turbulence would set in ($Re > 2000$), hardly ever practiced. Note, that the Poiseuille relations represent a kind of Ohm's law for fluid flow, rather than for electrical flow: in both examples of linear transport, it is stated that the flow (or current) obtained is proportional to the applied pressure (or voltage). The proportionality constant represents a resistance, which in engineering sciences [15] traditionally is represented by the inverse of a resistance; that is, a conductivity or *permeability* B, such that the superficial average velocity (equal to flow rate F over cross section A) is proportional to the pressure gradient:

$$\langle u_m \rangle = -B(dp/dz) = B(\Delta p/L) \tag{69c}$$

and retaining the influence of viscosity, this can be written as

$$\langle u_m \rangle = (B_0/\eta)(\Delta p/L) \tag{69d}$$

where $B_0 = \eta B$ is called the *specific permeability* with dimension (length) squared. Indeed, for open tube flow in circular–cylindrical channels, $B_0 = R_c^2/8$ after Poiseuille. Note, that for gravitational flow the pressure gradient $\Delta p/L$ should be replaced by the hydrostatic quantity ($\rho gL/L = \rho g$).

Thus, from the foregoing we see that pressure-driven flow is strongly inhibited by small tube (or pore) diameters, a logical event because of the large specific surface area of small capillaries. Also, it can be concluded that linear velocities required for efficient chromatographic separations, are obtained only at the cost of some finite pressure crop, which in practice, may reach the limits of safety in the apparatus. Thus, we cannot generate any velocity we want at will, and we should always take pressure limitations into account.

For completeness and later use for field flow fractionation techniques (see Sec. IV.B.4), we give here the result for flow in a thin and relatively wide rectangular flat channel where

the confining walls are apart over the distance (often height) w, with x as the lateral coordinate measuring the distance from the lower wall and perpendicular to z:

$$u_m(x) = 4u_{max}[(x/w) - (x/w)^2]$$

with

$$u_{max} = u_m(x = \tfrac{1}{2} w) = (3/2)\langle u_m \rangle \tag{69e}$$

2. Flow Through Packed Columns

In Sec. II.E.2, we described the chaotic nature of flow through packed beds, but also pointed out that the interstices between the particles of the packing through which the actual flow occurs can be treated as a bundle of more or less parallel capillaries. In this capillaric model for the bed, the hydraulic radius $R_h = \tfrac{1}{2}R_c$ takes over the role of the capillary lateral dimension (see Eqs. 31) and it seems logical to proceed with this model to also describe the pressure drop in packed bed systems. Referring to the former section, we expect then that the ohmic permeability law Eq. (69) is also valid for packed bed systems and, indeed, the empirical equation relating pressure drop and flow through unconsolidated packed media, known as Darcy's law [15], is widely accepted as the fundamental relation for flow such that again, flow velocity is proportional to the pressure gradient, as expressed by Eq. (69c). Because in packed beds only the fraction ε_0, the porosity determined by interstitial pore space, is available, the velocity in Eq. (69c), being the volumetric flow rate over the total cross-sectional area of the flow channel, is actually the superficial velocity. The true interstitial velocity in packed beds, pertaining to the *free* cross section, rather than the total cross section (equal for only open flow systems), is thus $\langle u_m \rangle = F/\varepsilon_0 A$ and so, for packed beds, Darcy's law reads

$$\langle u_m \rangle = (B_0/\varepsilon_0 \eta)(\Delta p/L) \tag{70a}$$

Here, we may estimate B_0 on the basis of the hydraulic radius somewhat similar to [see Eq. (31a)] $R_{c,h}^2/8 = (1/8)(d_p/3)^2[\varepsilon_0/(1 - \varepsilon_0)]^2 = (d_p^2/72)[\varepsilon_0/(1 - \varepsilon_0)]^2$, which for the common value for $\varepsilon_0 \approx 0.40$ becomes $\approx d_p^2/225$, if the capillaric analogy would be valid. We should not forget that the interstitial capillaries, which are in no way straight, go around the particles and so the actual length traveled by fluid elements in the bundle of capillaries is longer by some tortuosity factor, than the column length L. If we retain L in Darcy's law, this should be reflected in a larger numerical constant of approximately $\sqrt{2}$ in B_0, rather than 72. The expected proportionality between linear velocity and particle size squared, is borne out in practice, both in engineering sciences [15] and in chromatography [1,5,12,34], with only the numerical constant being different (slightly larger than expected) and somewhat dependent on the type and shape of the particle. The *Kozeny–Carman* equation

$$\langle u_m \rangle = (d_p^2/180)[\varepsilon_0/(1 - \varepsilon_0)]^2(\Delta p/\eta L) \tag{70b}$$

is often found to be valid in practice. On comparison of Eqs. 70a and 70b, we find that the specific permeability obeys

$$B_0 = (d_p^2/180)[\varepsilon_0^3/(1 - \varepsilon_0)^2] \tag{70c}$$

which for well-packed columns, with $\varepsilon_0 \approx 0.40$, is practically $B_0 \approx d_p^2/1000$, in agreement with many chromatographic data, although the numerical factor of 1000 may differ somewhat for different packings, and in HPLC may drop to lower values (< 500), especially for packed capillary and other micropacked column types. One reason for this could be the decreased density of the packing in these minicolumns, but there also might be an influence of the intraparticle porosity ε_i present in some packing materials, either as stagnant or as permeable pore space. As in practice, $\langle u_m \rangle$ is always measured from the residence time of an inert and

nonretained solute, $\langle u_m \rangle = L/t_m = F/(\varepsilon_0 + \varepsilon_i)A = F/\varepsilon_{tot}A$, this intraparticle porosity should enter the foregoing equations. We then find

$$\langle u_m \rangle = (d_p^2/180)[(\varepsilon_0^3/\varepsilon_{tot})/(1 - \varepsilon_0)^2](\Delta p/\eta L) \tag{70d}$$

$$B_0 = (d_p^2/180)[(\varepsilon_0^4/\varepsilon_{tot})/(1 - \varepsilon_0)^2 \tag{70e}$$

For silica packings, the internal pore volume is independent of the particle size and ε_{tot} will be constant, but larger than 0.4. In recent years, it has become habit to express the column pressure–flow characteristic in terms of *flow resistance*, rather than in terms of its permeability. The inverse of the specific permeability is a good measure for a *flow resistance parameter* ϕ_f, and thus,

$$B_0 = \varepsilon_0 d_p^2/\phi_f \text{ or } \phi_f = \varepsilon_0 d_p^2/B_0 \tag{71a}$$

with which a more comprehensive flow–velocity equation is found as

$$\langle u_m \rangle = L/t_m = (d_p^2/\phi_f)(\Delta p/\eta L) \tag{71b}$$

where in the practice of HPLC the following flow resistances are observed:

Conventional packed	$\phi_f = 500$–10^3
Small-bore packed	$\phi_f = 500$–10^3
Packed capillary	$\phi_f = 300$–10^3
Semipacked capillary	$\phi_f = 50$–300
Open tubular	$\phi_f = 32$

Note that the looser the packing the less resistance, finally approaching that of open tubes that have the smallest resistance. Flow resistance factors are important for the further optimization of separations and columns (see Sec. IV), for they partly determine the required pressure drop that is a natural limiting factor in speeding up analyses:

$$\Delta p = \phi_f \langle u_m \rangle \eta L)/d_p^2 \tag{71c}$$

This result also shows the importance of the choice of particle sizes: for a given linear velocity pressure increases rapidly with decreasing particle size.

B. Compressibility Effects on Flow and Plate Height

Gases, liquids, and supercritical fluids, all behave the same according to the universal flow relations discussed in the foregoing. But as said, they differ substantially in some physical constants, such as the difference in viscosity, by a factor of about 100. As a result, for gases, the same velocity can be reached in the same flow channel with a pressure difference that is roughly 100 times smaller than that required for liquids; supercritical fluids require some intermediate pressure drop.

Another difference is the extent of compressibility of the mentioned fluids: gases are highly compressible, whereas liquids are virtually noncompressible, only about 10% for pressures exceeding 1000 bar. Supercritical fluids have an intermediate position again, but with the further complication that viscosity is also pressure-dependent [see Sec. IV.B.1 and Ref. 34]. In GC with an ideal gas as the carrier, the density of the mobile phase is proportional to the pressure and, thus, expansion during its movement along the column length not only leads to an increasing linear velocity, but also to changing diffusion coefficients and (for SFC) viscosities.

To determine the pressure and velocity changes along the column length, we should replace the overall pressure gradient $\Delta p/L$ by its local value at position z, this being $-dp(z)/dz$ (negative because pressure decreases in the positive z direction). Darcy's law, and also Poiseuille's flow relation in open tubes, can then be integrated simply by use of the ideal

(Boyle's) gas law in the form $p(z)\langle u_m(z)\rangle$ = constant. For example the product of local pressure and velocity equals that at outlet conditions: $p(z)\langle u_m(z)\rangle = p(z = L)\langle u_m(z = L)\rangle = p^0\langle u_m^0\rangle$, where the superscript zero indicates outlet conditions (often atmospheric). Because for gases, viscosity is pressure-independent, integration is possible over the column length to find that:

$$t_m = \int_0^L dz/\langle u_m(z) = (1/p^0\langle u_m^0\rangle) \int_0^L p(z)dz = L/\langle u_m^0\rangle j \tag{72}$$

where, as expected, a correction factor j, connected with the average pressure $\langle p\rangle$ appears. For $\langle p\rangle$ it is found that

$$\langle p\rangle/p^0 = (2/3)[(P^3 - 1)/(P^2 - 1)] = 1/j \qquad (P = p_i/p^0) \tag{73a}$$

whereas the pressure and velocity profiles along the column are represented by

$$\begin{aligned} z/L &= (p_i^2 - p^2)/[p_i^2 - (p^0)^2] \\ &= [P^2 - (p/p^0)^2]/(P^2 - 1) = [p^2 - (1/j^2)]/(P^2 - 1) \end{aligned} \tag{73b}$$

where p_i is the inlet pressure $p(z = 0)$. The factor $j = (3/2)[(P^2 - 1)/(P^3 - 1)]$ is called the James and Martin pressure correction factor, sometimes also denoted by the symbol f_2, which not only applies to retention volumes and times but also to several terms of the plate height equations. The factor is 1 at zero pressure drop, but quickly drops to reach the value 0.75 at $P = 1.62$, and at high pressure drops can be approximated by $j = 3.2/2P$ ($P > 3$) and $3/2P$ ($P > 10$) and at low pressure drops by $1/j = \frac{1}{2} + \frac{1}{2}P$ ($P < 1.5$ better than ½%). The same relation is valid for the average velocity: $\langle u_{m,av}\rangle = L/t_m = \langle u_m^0\rangle j$. The pressure gradient $-dp/dz$ is now found as

$$-dp(z)/dz = \tfrac{1}{2}\, p^0(P^2 - 1) \tag{73c}$$

by which, for example, Darcy's law in compressible fluids can be written in terms of the experimentally available outlet flow F^0 or the interstitial outlet flow velocity $\langle u_m^0\rangle = F_0\pi R_c^2/\varepsilon_0$ as:

$$\langle u_m^0\rangle = \tfrac{1}{2}\,(B_0p^0/\varepsilon_0\eta L)(P^2 - 1) \tag{73d}$$

An influence of pressure drop on plate height can also be expected, because diffusion coefficients ($p\boldsymbol{D}_m = p^0\boldsymbol{D}_m^0$ for ideal gases) as well as local velocities (see foregoing) are pressure-dependent in gases. Hence, rather than using $H = \sigma_z^2/L$, we should write for the local plate height at position z: $H(z) = \partial[\sigma_z^2(z, p)]/\partial z$. This expresses the plate height dependence on the axial coordinate. Furthermore, we expect that the standard deviation (most easily seen if expressed in terms of volumes) is pressure-dependent, $\sigma_z = \sigma_z(z, p)$ and behaves as $p\sigma = p^0\sigma_0$ = constant for ideal gases. If so, then also, $(p\sigma)^2$ = constant, and we have for the partial differential to pressure; $\partial[\sigma_z^2(z, p)]/\partial[p(z)]^2 = -\sigma_z^2(z, p)/p^2(z)$; hence, the total differential for the variance becomes $d\sigma_z^2/dz = H(z) - [\sigma_z^2(z, p)/p^2(z)][d(p^2)/dz$, and so after integration from $z = 0$ (where $\sigma = 0$ is assumed) to $z = L$

$$\sigma_z^2(z = L) = (1/p^0)^2 \int_0^L p^2(z)H(z)dz$$

and because plate height is always measured in practice at $z = L$ after retention time t_R (which depends on the average velocity $\langle u_m\rangle = \langle u_m^0\rangle j$, rather than on the outlet velocity $\langle u_m^0\rangle$) we find the final corrected plate height $\boldsymbol{H}$:

$$\boldsymbol{H} = L[\sigma_t(t = t_R)/t_R]^2 = (j^2/(p^0)^2L) \int_0^L p^2(z)H(z)dz \tag{73e}$$

If the integral is evaluated for the extended van Deemter equation [see Eq. (34)], the result when expressed in terms of the outlet velocity is

$$H = [A + B^0/\langle u_m^0\rangle + C_m^0\langle u_m^0\rangle]g(P) + C_s\langle u_m^0\rangle j(P) \tag{73f}$$

where the superscript zero indicates outlet conditions. A and C_s have the same meaning as in Eq. (34), and B^0 and C_m^0 contain the diffusion coefficient D_m^0 (valid under outlet-pressure conditions) instead of D_m as in Eq. (34). Again, $j = j(P)$ is the James–Martin correction and $g(P)$ is another pressure correction term, named after its originator (Giddings) and equal to

$$g(P) = (9/8)[(P^4 - 1)(P^2 - 1)/(P^3 - 1)^2, \qquad \text{with } 1 \leq g(P) \leq 9/8 \tag{73g}$$

$g(P)$, sometimes denoted as f_1 is clearly smaller (and so often neglected) than $j(P)$, but this is expected as the A term in the van Deemter equation, as such, does not depend on pressure, whereas the pressure dependencies in the B and C_m terms cancel because of the presence of the ratio D_m/u_m, which is also pressure-independent. Only in the C_s term, where u_m appears without cancellation by a diffusion coefficient, the large pressure correction by the j-factor is found. The same result (without A term) is found for the pressure dependence of the Golay equation for open tubular columns. Pressure dependence in SFC, as said, is more complicated, as will be further illustrated in Sec. IV.B.1.

C. Electrodrive and Electrokinetic Chromatography

Electro-osmotic flow is flow induced by an electrical potential applied across the length of a packed bed column, or a capillary tube, filled with an aqueous electrolyte solution. This type of flow results from the way ions are distributed near the channel walls. These walls, being insulators, acquire a surface charge either by adsorption of ions from solution or by the dissociation of surface functional groups, such as silanols on silica surfaces that produce a negative charge. As a result of these surface charges, oppositely charged ions (so-called counterions) are attracted and these gather into a cloud that is more concentrated nearer the surface. This region is called the electrical double layer, which is very thin, typically 10 nm. The potential at the boundary between the charged surface and the diffuse part of the double layer is called the zeta (ζ) potential, typically smaller than 100 mV. The excess free positive ions in the diffuse cloud form something similar to a charged sheath that surrounds the bulk of electrolyte. When an electrical field is applied parallel to the wall, these counterions will be pulled along the surface, thereby dragging along the enclosed aqueous solution with them, thus generating bulk flow. Electro-osmotic flow is rather counterproductive in electrophoretic methods, because it causes bands to broaden. However, electro-osmotic flow is beginning to play an ever more constructive role in CZE and also in chromatographic methods [41–43]. This is mainly caused by the nature of the electro-osmotic flow which is plug-like in the main part of the bulk, and only shearing within the diffuse part of the double layer, which is very thin. Thus, plug flow, rather than pronounced (for example, parabolic) velocity profiles occur, which is very attractive, as we know, to obtain little peak-broadening. The velocity with which the bulk liquid migrates is given by

$$u_{eo} = \varepsilon_m \zeta E/\eta \tag{74a}$$

where ε_m is the dielectric constant of the (mobile-phase) solution and E the potential gradient (in V/cm). Typically $\varepsilon_m = 80 \times 8.84 \times 10^{-14}$ F/cm (water), $E = 30$ kV/25 cm, and $\zeta = 30$ mV; with $\eta = 0.01$ P, we find that $u_{eo} = 0.64$ mm/s, is a very practical and useful value. As a result, we can expect that very efficient chromatography would be possible in not only open, but also packed columns of any diameter (note, that column dimension does not appear in u_{eo}), because axial diffusion is the only mechanism left for axial spreading. Consequently, the ultimate efficiency for plug flow

$$n_{th} = L/H = Lu_{eo}/2D_m \tag{74b}$$

becomes an attractive goal to reach in separation sciences. For example, there is no dependence on column diameter, the efficiency becomes higher at higher velocities and is better for higher molecular mass solutes with lower diffusion coefficients, this in strong contrast with traditional pressure-driven chromatography.

This is too optimistic, and the observed column efficiency is substantially lower than predicted by Eq. (74b) owing to experimental limitations. First, column length, internal diameter, and applied field are dependent variables because of the Joule heating of the electrolyte which, in turn, causes parabolic flow profiles to appear as a result of viscosity differences in the cross section. The most effective means to optimize heat removal and minimize temperature gradients across the column diameter is to reduce the column diameter. Thus, again, for high efficiencies, small column diameters should be used to maintain the plug flow profile, and problems with extracolumn-broadening (mainly sample injection width) arise. Furthermore, analyte sorption at the column wall, or at the matrix of the packing, yields large (chromatographic partitioning-like) additional plate heights.

In addition, for chromatographic separations to be achieved in this type of columns, suitable solvents for many divers sample types are necessary that still have large enough dielectric constants to maintain electro-osmotic flow, and this is somewhat problematic. Moreover, a stationary phase should be incorporated, which gives typical problems. In several innovative papers Terabe et al. [41] introduced the incorporation of a pseudostationary phase as one component of the electrolyte, thereby inventing micellar electrochromatography (MEC). In a CZE system, they added micelle-forming surfactants (sodium dodecyl sulfate; SDS) in the carrier liquid to obtain the pseudostationary phase of micelles at a concentration above its critical micelle concentration (CMC). Whereas the carrier liquid moves at the electro-osmotic velocity, micelles are retarded by opposing electrophoretic forces. Thus, the micellar phase is not a distinct stationary phase in the conventional sense, nor is it immobilized. Yet, these micelles have the ability to absorb foreign species, including ions and also neutral components. Thus, injected analytes distribute themselves by partitioning between the bulk carrier and the micelles, which move at different velocities, and chromatographic separation occurs. Neutral solutes that do not distribute themselves into the micelles show no "retention" and elute corresponding to the electro-osmotic flow. Analytes with a strong distribution toward the micelles, elute at the micelles position and everything else elutes in between these extremes, which creates a retention window. Hence, all of the sample elutes by using MEC, one of the advantages of the method that adds to the high efficiency of CZE that is preserved.

Later, and inspired by this work, Knox [42,43] proposed another variety of electrodrive chromatography (EDC). Instead of micelles a solid colloidal material, such as silica-based particles smaller than a micron, is foreseen to provide another type of moving pseudostationary phase. Although this variety has not yet been tested experimentally, the other and more conventional variety for which the silica particles are traditionally fixed in position within a packed bed column, has already shown some promise. This concept was put forward long before the inception of CZE, but had to wait until experimental progress in CZE made it feasible to apply electrodrive to packed bed columns for HPLC. Not until after the bubble-formation problem and column instability were solved, were the significant advantages of this approach made visible in recent years [42,43]:

1. Plug flow also prevails in the interparticle interstices in packed beds, and thus dispersion owing to the nonuniform flow phenomena within and between the channels, termed eddy–diffusion in the foregoing and represented by the A term, is much decreased, and perhaps even more important, velocity and thus dispersion does not depend on the width of the channels and column.

2. Another very decisive advantage is that particles of smaller size than traditionally, say less than 1 μm, are feasible. The lower limit has not yet been assessed experimentally, but it is now far into the submicron range, probably limited only by the effect that the double layers of opposing walls are going to overlap on evermore decreasing particle size and,

thereby, (hydraulic radius) channel size. If this happens, the plug profile will again be distorted into a pronounced parabolic flow profile and the advantage of EDC is lost.

We will return to electrodrive in Sec. IV.B.2 for application in SEC.

IV. OPTIMIZATION: WHAT THE FOREGOING IS ALL ABOUT

In this section, we focus on the application of plate height theory to use it for the characterization of different experimental chromatographic systems (including packed and open columns under different pressure conditions) with a view to optimizing chromatographic separations. We should proceed to apply all elements of the foregoing in obtaining not only sufficient separation performance of columns, but also to accomplish this in a reasonable and, preferably, shortest time possible.

The requirements that (1) a sufficient and defined resolution should be obtained, and (2) analysis time should be minimized and defined are generally accepted as main goals to reach because it is of no use to have a more than sufficient resolution between the components of interest. In that case the analysis time can be lowered, and the analysis becomes faster. Vice versa, if analysis times are long, we may obtain resolutions that are better than required for the sample of interest, which is not effective.

In stating these requirements, it becomes clear that high efficiency of columns requires low plate heights, which can best be obtained in columns with either small particles or in open columns with very small internal diameters. It is at once clear then that the smaller these dimensions, the higher the pressure drop required to operate the columns with a sufficiently high linear velocity, which should always be in excess of the optimum velocity. As a result, we envisage two limitations beforehand: a particle–size-limited case and a pressure-limited situation.

In addition to these main criteria of a defined resolution needed within a minimum analysis time, one could also formulate other important criteria, such as (3) analysis should require a minimum and defined solvent consumption, and (4) analysis should be optimized toward trace amounts. Next to the dilution of samples in the apparatus (and so on plate height) requirement (4) strongly depends on the detector properties and will not be treated here. Requirement (3) can be of utmost importance when routine analyses are performed and large amounts of expensive solvents are traditionally used; for instance in SEC, which sometimes also offers toxic and environmental problems. Biomedical analysis (e.g., of total cell contents) offers other examples for which solvent consumption by miniaturization is important. We will come to that in Sec. IV.B.2 on SEC.

Two approaches for optimization of separations are possible:

1. The simple approach is to optimize only to obtain higher resolutions, for example, for complex samples with inadequate peak capacity found in trial runs.
2. The more involved optimization toward faster analysis, also called kinetic optimization.

For example, 1, optimization of separation toward higher resolution, the discussion in Sec. II.D on the separation resolution factor Rs applies fully. Concerning the influence of column efficiency, Eqs. (14b) and (18) show that Rs is dependent on the square root of the (effective) plate number: $Rs \approx \frac{1}{4}[(\alpha - 1)/\alpha]n_{\text{eff}}^{1/2}$, and so, $Rs \div \sqrt{n_{\text{th}}} = \sqrt{(L/H)}$. Thus, resolution in general is improved by obtaining smaller plate heights and using columns with greater lengths. In Sec. II.E.4 we discussed the minimum plate height H_{min} to be obtained at the optimum velocity u_{opt} [see Eqs. (35) through (37)]. From that it follows straightforwardly that $H_{\text{min}} \div d_p$, which implies that one should design columns with as small as possible packing particles (or tube diameters, for open columns). This is an important aspect of modern chromatography, also advantageous for separation speed (see the next section), but it is no use to lower particle size and associated plate heights to values at which extracolumn-broadening becomes overruling. An increase in length is these cases is possible, producing

more plates, but this will increase analysis times to perhaps unacceptable levels. If stationary-phase effects are important, reduction of the film thickness is clearly profitable, and increasing the diffusion in the stationary phase is also to be considered, which can be realized by increasing the temperature, for example: indeed, high-temperature LC can be very profitable. Many chromatographic systems are run above the optimum flow velocity to achieve faster separations, if resolution allows for that.

As discussed in Sec. II.E.4.e, maximum resolution can be obtained only under optimum velocity conditions, Yet, because the resolution factor Rs depends only on the square root of plate number, there is still some freedom to chose velocities near or around the optimum velocity, as given by Eq. (35). As a rule of thumb, we may state that more than 80% of the maximum resolution, as obtained at the optimum velocity, is preserved over almost a decade in velocities: $(1/3)u_{opt} \leq \langle u_m \rangle \leq 3u_{opt}$. Even at velocities as high as $\langle u_m \rangle = 10u_{opt}$, only 50% loss in resolution occurs because of the smooth and gentle curvature of the plate height plot around its minimum:

$$H/H_{min} = \tfrac{1}{2}[(\langle u_m \rangle / u_{opt}) + (u_{opt}/\langle u_m \rangle)] \tag{75a}$$

and so,

$$Rs/Rs_{max} = \{\tfrac{1}{2}[(\langle u_m \rangle / u_{opt}) + (u_{opt}/\langle u_m \rangle)]\}^{1/2} \tag{75b}$$

This slow loss of resolution on increasing the velocity, is the very reason why so often velocities are chosen well above the optimum value, to reduce analysis times (provided that the analysis time equals at least a necessary time $t_a \geq t_{ne}$ to obtain any sufficient resolution see the next section).

A. The Approach to Faster Analyses: Kinetic Optimization

The fundamental starting point for time optimization is naturally the retention time required for the sample to migrate through the column of length L with n_{th} theoretical plates ($L = n_{th}H$), as discussed in Sec. II.E.4.e. There it was shown that the analysis time t_a, taken as the retention time of (logically the last) component is proportional to the number of plates and the *ratio* of plate height and linear velocity $n_{th}(H/\langle u_m \rangle)$, rather than on plate height itself. For that reason, separation speed $Ss = n_{th}/t_a$ was introduced in that section to provide a good measure for comparing the performance of separation columns, Eq. (57a). Alternatively, we may formulate this in terms of the resolution factor itself to obtain, with the aid of Eqs. (14) through (18):

$$t_a = t_R = n_{th}(H/\langle u_m \rangle)(1 + k) = 16\, Rs^2[\alpha/(\alpha - 1)]^2[(1 + k)^3/k^2](H/\langle u_m \rangle) \tag{76a}$$

and for velocities far above the optimum velocity, $H/\langle u_m \rangle = C$ (including mobile and stationary phase contributions); hence, we obtain:

$$\boldsymbol{Rss} = Rs^2/t_R = (1/16C)/[\alpha/(\alpha - 1)]^2[(1 + k)^3/k^2 \tag{76b}$$

which shows that the pragmatic parameter $\boldsymbol{Rss} = Rs^2/t_R$, which is easily established in practice, is a constant independent of operating variables, such as pressure drop, length, and velocity and, thereby, a good parameter to mutually compare columns of one kind. This is not at all surprising, as we know from Eq. (18) that Rs is related to the effective plate number: $Rs \approx \tfrac{1}{4}[(\alpha - 1)/\alpha]n_{eff}^{1/2}$, and so the meaning of the quantity $\boldsymbol{Rss} = Rs^2/t_R$ is nothing but an effective plate number per unit time, and so, $\boldsymbol{Rss} \div n_{eff}/t_R \div Ss$ represents just as does $Ss = n_{th}/t_R$, the separation speed of the system, indeed a useful characteristic. We will make use of that property later in this section.

If we consider that for sufficient resolution $Rs = 1 = \text{constant}$, the foregoing Eqs. (76) determine a characteristic and *required* analysis time t_{ne}, which defines the minimum analysis time to obtain sufficient resolution. Times longer than t_{ne} are wasteful and unnecessary,

whereas times shorter than t_{ne} do not yield the required and sufficient resolution (conclusions that are valid provided that the constant C term of the van Deemter or Golay equations applies, and thus for velocities higher than optimal). t_{ne} together with the linear flow velocity $\langle u_m \rangle$ now determine the necessary column length L_{ne} ($= \langle u_m \rangle t_{ne}$), or alternatively, at a fixed and chosen length L, the required flow velocity. Thereby, the required number of effective plates, as given by Eq. (19) are also fixed: $L = n_{th}H = n_{eff}H_{eff}$, where H_{eff} is the effective plate height, as based on the net retention time $t'_R = t_R - t_m$ and so $H_{eff} = L(\sigma_t/t'_R)^2$. As a result Eq. (76a) for $Rs = 1$ can be written as

$$t_a \geq t_{ne} = n_{th,ne}C(1 + k) = n_{eff,ne}C(1 + k)^3/k^2 \tag{76c}$$

for velocities in far excess of the optimum velocity, and for the van Deemter–Golay-type of plate height curves. Note that $C \div d_p^2$, and so the eminent importance of small particles in reducing both plate heights and analysis time once more becomes visible. Also note that in LC curved plate height plots are often obtained (see Sec. II.E.4.c) for which no constant C term is valid, and the dependence on particle size is less than quadratic, see later.

Equation (76c) further predicts that analysis time increases with required plate number and, consequently, any step that will reduce this plate number will also reduce time. This calls for high relative selectivities for peak pairs of interest. Because of the close relation between Rs, α, and n_{eff} from Eq. (18), it requires a tremendous number of (effective) plates for closely eluting components with close-lying peaks in the chromatogram. In this event the relative retention $\alpha \approx 1$, and Eq. (18) then shows that up to 10^5–10^6 plates are necessary for $Rs = 1$:

$n_{eff,ne}$	160,000	6,800	1,940	940	575
α	1.01	1.05	1.10	1.15	1.20

This illustrates that the quest for large plate numbers is necessary only for very difficult separations of closely related components that almost coelute. It also proves that it is very profitable to obtain, sometimes only slightly, better selectivity in the separation: a change of α from 1.01 to 1.02, so only 1%, saves some 400% in required plates and about 100% in Rs. Thus, one should always first try to increase α-values by a change in operating conditions (temperature and phase ratio) or in the phase system (modifiers or packing).

Also, the retention factor $(1 + k)^3/k^2$ should be limited (i.e., k should be kept small enough, on the one hand, but not too small, on the other) because otherwise, the required plate number becomes too large. By differentiation, it can be easily shown that this retention function has a minimum at $k = 2$. Thus, an optimum analysis time requires small k values of about $k = 2$, say in the range 1.5–5. It is illustrative to calculate some values for the required analysis time: for optimum k, and about 1000 effective plates needed ($\alpha = 1.14$), and from C term values from Table 2, we see that in GC, $t_{ne} \approx 1$ s, whereas that for LC is an order of magnitude larger, say 10 s. Even for more difficult separation problems requiring some 10^5 effective plates, analysis times should not be much longer than 1 min (GC) and 10 min (LC). Modern column types are so well designed that, indeed, these limits are now approached. Deviations from this, and so longer analysis times, are no exception, however, because either too long columns are used or the k range is not optimal.

Another factor in the minimization of analysis time is the C term of the plate height plot, or better the ratio $H/\langle u_m \rangle$. Hence, according to Eq. (76c), the analysis time is shorter for smaller $H/\langle u_m \rangle$ values, and for a van Deemter–Golay-type plate height curve (omitting the A term), this ratio reads $H/\langle u_m \rangle = B/\langle u_m \rangle^2 + C$, which clearly has its smallest possible value (C) for increased velocities $\langle u_m \rangle \rightarrow \infty$. However, because of the gentleness in the curvature of the plate height plot around its minimum [see Eq. (75a)], we also have that

$$(H/\langle u_m \rangle)/(H_{min}/u_{opt}) = \tfrac{1}{2}\{1 + (u_{opt}/\langle u_m \rangle)^2\} \tag{77a}$$

which implies that for $\langle u_m \rangle = 2u_{opt}$ almost the limiting value of ½ is reached for this function. As a result, it is not useful to reduce t_{ne} by increasing the linear velocity above values of 2 times the optimum value for the velocity. If it proves to be possible in practice to achieve still sufficient resolution after increasing the velocity above this factor of 2, it clearly means that the analysis time has not yet reached the lower value of t_{ne}, possibly by the use of a too long column for the present analysis.

The separation problem at hand is only then optimally solved when a column length is chosen such that with the installed velocity of 2 times the optimum velocity, the last component elutes just in the minimum time t_{ne}, and $Rs = 1$ is obtained. In that case:

$$L_{opt} = 2u_{opt}t_{ne}/(1 + k) \tag{77b}$$

This amounts for optimum k, in GC (see Table 2) and the same t_{ne} values as before (1–60 s) to optimal column lengths of 1.3–80 cm, and in LC (t_{ne} = 1–10 min) to 4–40 cm, well in the range of modern practice. Yet, it proves that for not-too-difficult separations, the choice for standard sized (in LC 10, 15, 25, or 30 cm), commercially available columns, might be quite overdone, which leads to too long analysis times.

In the foregoing it has become clear that optimum analysis can be expected only after careful design of the column and its operating conditions, among which are the linear velocity, the column length, and the C term, or H/u ratio. All three of these aspects are recognized to depend on the particle size as well as on the pressure drop necessary.

In the tendency to produce and use ever smaller particles to obtain better resolution, taking into account all aspects of the former discussion, two limits should be carefully considered:

1. Velocity should not fall (by more than one-third) below the optimum velocity.
2. The associated pressure drop necessary should not grow higher than a specified limit, determined by the apparatus and safety aspects.

Clearly, plate heights and pressure–flow relations come together here and should be treated in a combined procedure, which is called kinetic optimization.

1. The Pressure Limitation

Pressure comes into play naturally if we treat the required analysis times obtained from the foregoing as being determined by the column length and the applied linear velocity: $t_{ne} \leq t_a = L/u_z = L/\langle u_m \rangle(1 + k)$. In Sec. III we treated pressure–flow phenomena on the basis of Darcy's law [see Eq. (70)], which we can substitute into the analysis time equation to find (with specific permeability approximated by $B_0 \approx d_p^2/1000$):

$$t_a \approx 10^3(\eta/\Delta p)(L/d_p)^2(1 + k) \tag{78}$$

This clearly shows that for a given (maximum) pressure drop analysis times can be shorter the larger the particles: the column resistance to flow is then less. Alternatively, at the same t_a with larger particles, longer columns can be used, producing more plates and permitting more difficult separations. Hence, for fast analyses large d_p values are requested, but on the other hand, for enhanced plate height, smaller particles are better, and we have two conflicting demands to solve: the particle and the pressure limitations.

First we investigate the pressure limitation. For long columns used for difficult separations, owing to pressure limitations as well as the high plate numbers required, velocities are not far removed from the optimum velocity. Pressure in connection with plate height and column length can be explicitly written by substituting Darcy's law in the (van Deemter-type, only with B and C terms) plate height equation and realizing that column length $L = n_{th}H$, also contains plate height. If we solve these two equations with two unknowns (H and $\langle u_m \rangle$) for the ratio $H/\langle u_m \rangle$, which we know to be the determining factor for the speed of analysis,

we find that a characteristic and critical pressure drop Δp_{crit} occurs that is determined by the molecular diffusion B term (which comes into play at too-low velocities) and the required number of plates:

$$H/\langle u_m \rangle = C[1 - (\Delta p_{crit}/\Delta p)]^{-1} \qquad \text{with} \qquad \Delta p_{crit} = \eta n_{th} B/B_0 \tag{79}$$

where $B = 2\gamma D_m$ and $B_0 \approx d_p^2/10^3$. This relation replaces the limiting value $H/\langle u_m \rangle = C$ that was used before.

The critical pressure drop is the one that should be present anyway to complete the separation within a finite time, which is seen if we substitute Eq. (79) in the expression for the analysis time:

$$t_a \geq t_{ne} = n_{th}(1 + k)(H/\langle u_m \rangle) = n_{th}C(1 + k)[1 - (\Delta p_{crit}/\Delta p)]^{-1} \tag{80}$$

which replaces Eq. (76c), the latter being valid only far removed from the optimum velocity. We see that for $\Delta p_{crit}/\Delta p \rightarrow 1$, analysis time becomes infinite. Consequently, only pressures (or better pressure drops) in excess of the critical one are to be used; but then, how large are the critical values? From Eq. (79) we obtain for liquids that $\Delta p_{crit} \approx 2 \times 10^3 \times (2/3) \times 10^{-2} \times 10^{-5}\, d_p^{-2} n_{th,ne} = 1.33 \times 10^{-4}\, d_p^{-2} n_{th,ne}$. Hence, for modern packings with 5-μm particles, critical pressure expressed in bars (multiplication factor 10^{-6}) amounts to $\Delta p_{crit} \approx 5 \times 10^4\, n_{th,ne}$ (bar) and the required number of plates determines proportionally the final pressure limitation. For these and smaller particles we then find

$n_{th,ne}$	10^3	10^4	10^5	10^6	
Δp_{crit} (bar)	0.5	5	50	100	for $d_p = 5$ μm
Δp_{crit} (bar)	1.5	15	150	1.5×10^3	for $d_p = 3$ μm
Δp_{crit} (bar)	3.3	30	300	3×10^3	for $d_p = 2$ μm
Δp_{crit} (bar)	1.3	130	1.3×10^3	1.3×10^4	for $d_p = 1$ μm

and we see that the common limiting pressure for LC apparatus of about 400 bar limits separations either in number of plates to be obtained (each plate requires some minimal pressure drop), or in length, and it is also clear that for difficult separations requiring many plates, not-too-small particles should be chosen, because they require very large pressures.

The situation for compressible fluids is analogous, but sightly more complicated. For completeness we give without proof, the result for the critical pressure drop in ideal gases for GC, assuming a constant C term again, that is altered as compared with incompressible liquids:

$$t_a \geq t_{ne} = n_{th}C(1 + k)[1 - (\Delta p_{crit}/\Delta p)^2]^{-1} \tag{81a}$$

with

$$\Delta p_{crit,GC} = (\eta n_{th,ne} B^0/B_0)^{1/2} = (3.10^3 \eta n_{th} \gamma D_m^0 p^0)^{1/2}/d_p \tag{81b}$$

Both the required plate number (now in the square root) and the particle size (now inversely proportional) have less influence than in liquids. Numerical values are then found from $\Delta p_{crit} \approx 1.41 \times 10^{-4}\, (n_{th,ne})^{1/2}/d_p$ (bar) and for common particle sizes of 100 μm, critical values are seen to be lower than those for liquids by a factor of about 10. The following table yields some values for the different particle sizes and the plate numbers required:

$n_{th,ne}$	10^3	10^4	10^5	10^6	
Δp_{crit} (bar)	0.2	0.7	2.2	7.1	for $d_p = 200$ μm
Δp_{crit} (bar)	0.4	1.4	4.5	14	for $d_p = 100$ μm
Δp_{crit} (bar)	0.9	2.8	8.9	28	for $d_p = 50$ μm
Δp_{crit} (bar)	1.8	5.6	18	57	for $d_p = 25$ μm

The pressure limit for GC apparatus is far lower than that for LC, and amounts to say 20 bar, which implies that the standard 100-μm packings are capable of producing some million plates without too many problems. This picture is slightly optimistic for compressible fluids, because in GC e.g., it is not uncommon that the C_m term, rather than the pressure-independent C_s term, is the more important C term. In that case, taking into account the pressure dependence of the C term also through the diffusion coefficient ($C_m \div 1/\boldsymbol{D}_m \div p/\boldsymbol{D}_m^0 p^0$), the pressure function in Eq. (81a) changes such that $t_a \div p[1 - (\Delta p_{crit}/\Delta p)^2]^{-1}$, which happens to be a function with a minimum at pressure $p = p_{opt} = \Delta p_{crit}\sqrt{3}$. Hence, in GC, there is an optimum pressure drop and an associated practical optimum gas velocity, above which the separation speed $H/\langle u_m \rangle$ drops, and analysis times increase relative to that optimum. Thus, we conclude that in GC pressures should be chosen carefully and not too high, with a view to the practical optimum gas velocity.

This situation differs from that in LC for which analysis times continuously decrease and separation speed increases on increasing pressure, up to the critical pressure value: so, in LC pressures should be chosen as high as possible.

2. The Particle Size Limitation

The role that particle size plays in this game among pressure, analysis time, and resolution is complex and, as said, may impair another limiting condition. In the foregoing discussion, particle size appears both in the efficiency terms ($C \div d_p^2$) and in the pressure–flow terms (Δp and Δp_{crit} are both $\div d_p^2$ as well), and it is a matter of substitution to find that analysis times are dependent on d_p, as follows: $t_a \div d_p^4/(d_p^2 - \frac{1}{2}\boldsymbol{P}^2)$, where $\boldsymbol{P}$ is a constant. This function, just as in GC for pressure, has also an optimum that can be found by differentiation, and the associated *optimum particle* size is:

$$d_{p,opt} = \boldsymbol{P} = [4 \times 10^3 \eta\gamma \boldsymbol{D}_m n_{th,ne}/\Delta p]^{1/2} \approx 1.63 \times 10^{-5}(n_{th,ne}/\Delta p)^{1/2} \tag{82}$$

where Δp is the pressure in bar, which according to the former section, should be chosen at its maximum, so $\Delta p \approx 400 \times 106$ and $d_{p,opt} = 8.16 \times 10^{-7}(n_{th,ne})^{1/2}$. We remark that the velocity that is associated with the optimum condition given here is just the optimum velocity u_{opt}. Additionally, we note that the optimal particle size increases with required plate number (i.e., *difficult separations require larger particles, longer columns, and longer times*). This relation implies that for 10^4 theoretical plates, the optimum particle size at 400 bar pressure yields the required resolution on a column packed with 0.8-μm particles. The following table illustrates the situation at different levels of theoretical plates required:

$n_{th,ne}$	10^3	10^4	10^5	10^6	
$d_{p,opt}$ (μm)	0.26	0.82	2.6	8.2	at Δp = 400 bar
$L_{pract,opt}$ (cm)	0.27	2.7	27	269	
$t_{a,pract,opt}$(s)	2.7	27	270	2.7×10^3	

where column length and analysis times should also have been *calculated*, but are based here on actual practice, where velocities lower than 0.1 cm/s can and will rarely be used. The calculated values will be shown later, see the next section.

The present result implies that contemporary 3- to 5-μm particles and column lengths up to 30 cm are quite optimal and some 10^5 plates should be obtained in a matter of 5–10 min, which is a too optimistic value. The quest for ever-smaller particles below the micron range is a quest for faster analyses, but as seen in the table, unpractically short columns and analysis times will result.

In summary of this informal approach, we conclude that LC techniques are able to produce many plates, especially when given time, but that on the other hand, also fast analysis is possible with short columns packed with fine particles. In short, the separation speed $Ss = n_{th}/t_a \div \langle u_m \rangle / H$ of LC increases with mobile-phase velocity.

This is also valid for compressible fluids; for example, in GC with ideal gases, but then compressibility again plays a decisive role. We can illustrate that by using the result of Eq. (76b); that is, that the separation speed, expressed as $\boldsymbol{Rss} = Rs^2/t_R$ i.e., the number of [effective] plates per second is a characteristic constant for the separation system at hand, so that the required analysis time to obtain sufficient resolution ($Rs = 1$) becomes simply:

$$t_a \geq t_R = 1/\boldsymbol{Rss} = \text{constant} \tag{83a}$$

Hence, a specific retention time should be used to obtain the desired resolution, and so, at a certain chosen column length, a specific pressure drop should be maintained, the larger the drop the longer the column. Furthermore, for gases $t_a \approx t_R = L/u_z \div L/\langle u_{m,av} \rangle$, with (see Sec. III)

$$\langle u_{m,av} \rangle = L/t_m = \langle u_m^0 \rangle j = \tfrac{1}{2}\,(B_0 p^0/\eta\varepsilon_0 L)(P^2 - 1) \tag{83b}$$

which for large P becomes: $\langle u_{m,av} \rangle \approx (3/4)(B_0 p^0 P/\eta\varepsilon_0 L)$. The associated column length L is obtained from Eq. (83b) as:

$$L = \{\tfrac{1}{2}\, B_0 p^0/\eta\varepsilon_0 \boldsymbol{Rss}(1 + k)][(P^2 - 1)j]\}^{1/2} \tag{83c}$$

Now suppose we have achieved the desired separation in time t_a in a column of length L, maintaining a gas velocity $\langle u_m^0 \rangle$, and we are willing to shorten the column. Because t_a should be kept constant, from Eq. (83a), the velocity should then be lowered, which is obtained by a smaller inlet pressure. The limiting condition in further shortening the column is that the velocity should not fall below the optimal velocity $\langle u_{m,opt}^0 \rangle = \sqrt{(B^0/C)} = \sqrt{(2\gamma \boldsymbol{D}_m^0/C_s)}$, provided that the stationary phase-broadening is dominating. The resulting minimal column length is then:

$$\begin{aligned} L_{opt} &= u_z t_a = \langle u_{m,av,opt}^0 \rangle t_a/(1 + k) \\ &= \langle u_{m,opt}^0 \rangle j/\boldsymbol{Rss}(1 + k) = \sqrt{(2\gamma \boldsymbol{D}_m^0/C_s)}\, j/\boldsymbol{Rss}(1 + k) \end{aligned} \tag{83d}$$

and the associated pressure drop follows from equating L in Eqs. (83c,d):

$$P^3 - 1 = 6\gamma \boldsymbol{D}_m^0 \eta\varepsilon_0/C_s B_0 p^0 \boldsymbol{Rss}(1 + k) \tag{83e}$$

Although more complicated than with incompressible liquids, the same trend appears that lower pressures are needed for larger particles and for higher separation speeds, whereas columns can be made as short as determined by the product of optimal velocity and analysis time required.

The one correction we should make to the foregoing discussion for incompressible liquids in LC is evidently the use of the van Deemter-type plate height expressions. Indeed, especially in LC, plate height plots are curved toward the velocity axis, and the proportionality between plate height and velocity (as reflected by the C terms) is no longer valid. As a result, the separation speed, determined by $n_{th}/t_R \div \langle u_m \rangle / H$ is no longer constant, but depends on the velocity (t_{ne} becomes ever shorter at higher velocities), and this has serious consequences for the optimization process at velocities far removed from the optimum velocity. The limiting cases discussed in the foregoing remain valid because the conditions are near optimal, but in the practice of LC, one often operates at velocities much higher than optimal, and the picture changes accordingly.

We will illustrate this by using the pragmatic plate height equation after Snyder and Knox (see Table 3), which in dimensional form and omitting the B term reads: $H \approx C\langle u_m \rangle^n$, where

n = 0.3–0.4 in practice, and we may often approximate the power by the value 1/3. Retaining the power as n, separation speed $n_{th}/t_R \div \langle u_m \rangle / H = (1/C)\langle u_m \rangle^{1-n}$ (i.e., because $n < 1$, separation speed increases with velocity in LC practice) quite in contrast with the van Deemter-type results discussed previously. Separation speeds of about 100 effective plates per s are obtained in modern LC practice, using particles as small as 1 μm. Because of the small particles and the high velocities aimed for, pressure becomes limiting again; finally, according to foregoing discussion, limited by the optimum conditions.

Far removed from these optimum conditions, the relation between generated plates, analysis time, velocity, length, and pressure, using the Snyder–Knox plate height equation is easily found as:

$$n_{eff} = (1/C)(B_0 \Delta p/\eta)^{(1-n)/2} t_a^{(1+n)/2} k^2/(1 + k)^{(5+n)/2} \tag{84a}$$

or for n = 1/3:

$$n_{eff} \approx (1/C)(B_0 \Delta p/\eta)^{1/3} t_a^{2/3} k^2/(1 + k)^{8/3} \tag{84b}$$

This relation has the following properties:

1. *Influence of pressure*: $n_{eff,ne} \div (\Delta p)^{1/3}$, which is rather weak, and implies that it is not useful to enhance the pressure limit of the apparatus above the present, say 500 bar, except for a very large pressure limit increase of say one order of magnitude (if that were at all technically possible).
2. *Influence of particle size*: Because $C \div d_p^2$ (but smaller powers than 2, down to 1.5, are also reported in literature) and $B_0 \div d_p^2$ (again smaller powers down to 1.8 are reported), the ideal dependence on particle size is $n_{eff} \div d_p^{-4/3}$ (which is often found, but powers up to −0.95 have been reported).
3. *Influence of column length*: $L \div \langle u_m \rangle t_m \div (\Delta p/\eta)^{1/3} n_{eff}^{2/3} d_p^4$, and so, for a fixed required plate number reduction of particle size has a very strong effect on the required column length (fourth power), allowing even lower pressures to be used than with larger particles, and indeed in columns, packed with 5- and 3-μm particles, effective plate numbers of 5×10^4 or so are obtained in short columns at moderate pressure.
4. *Influence of retention*: $n_{eff} \div k^2/(1 + k)^{(n+5)/2}$, which is a function with an optimum at $k = 4/(n + 1)$. In van Deemter-type plate height plots, with n = 1, the classic optimum earlier obtained is at k_{opt} = 2, whereas that for n = 1/3 is found at k_{opt} = 3, not too different from the former value, again at moderate retention.

3. Kinetic Optimization Using Reduced Variables

Because reduced quantities are eminently suited to compare columns under different operating conditions, it is logical to use the plate height and pressure–flow expressions in reduced forms. In earlier sections we introduced for that purpose the reduced plate height $\mathbf{h} = H/d_p$, the reduced velocity $\mathbf{v} = \langle u_m \rangle d_p/\boldsymbol{D}_m$, while the dimensionless column flow resistance parameter $\phi_f = \Delta p d_p^2/\eta \langle u_m \rangle L = \Delta p d_p^2 t_m/\eta L^2$ is a measure for the resistance to flow of mobile phase that takes into account column length L, particle diameter d_p, and viscosity of the eluent η.

Suppose, again, that a desired separation at a certain velocity has been achieved, generating the required number of plates at the expense of a certain pressure drop. Faster separation would be possible if $t_R > t_{ne}$, but only at the cost of increased pressure: first of all, pressure increases in proportion with $\langle u_m \rangle$, but because plate height increases also, the length should be increased to produce the needed $n_{th,ne}$ plates. This enhanced length requires a further increase in pressure drop, and we can go on to the pressure limit of the apparatus working at the optimum velocity, as described before in the pressure-limited situation that had first been envisaged by Knox for GC, as cited in Sec. II.E.4e.

The logical next question is then whether additional gains in speed can be obtained by varying the particle size. Although we know the answer to that from the former section, we

want to see how this can be formulated in reduced variables, and we now write Eq. (80) for the analysis time in a reduced form:

$$t_a \geq t_{ne} = n_{th}(1 + k)(H/\langle u_m \rangle) = n_{th}(1 + k)(\mathbf{h}/\mathbf{v})(d_p^2/\boldsymbol{D}_m) \tag{85a}$$

This shows the expected and strong influence of particle size immediately: for a given velocity and plate height in the dimensionless plate height plot, **h/v** is a given value and analysis time is quadratically connected to d_p. Hence, the expected approach to faster analysis by reducing particle size becomes clear at once. Although reduced particle size requires increased pressure drop, we can gain speed more effectively by reducing d_p, but at constant **v**. Again, the reduction in d_p is then limited by the available pressure drop to maintain the optimum $\mathbf{v}_{opt}$ through the column. We know the length is required to be

$$L_{ne} = n_{th,ne}H = n_{th,ne}\mathbf{h}d_p \tag{85b}$$

and this allows us to calculate the analysis time as

$$t_a \geq t_{ne} = \phi_f(n_{th,ne}\mathbf{h})^2\eta/\Delta p = E(n_{th,ne})^2\eta/\Delta p \tag{85c}$$

where, by definition, $E = \phi_f\mathbf{h}^2$, and is called the *separation impedance* [43], which can also be written as

$$E = (1/\eta)(t_m/n_{th})(\Delta p/n_{th}) \tag{85d}$$

which represents the elution time per plate, the pressure drop per plate, and a correction for viscosity. This quantity E is a kind of ultimate figure of merit for LC columns, which characterizes how favorable the compromise between speed, efficiency, and pressure drop is. It represents the difficulty of achieving a certain separation, and as such, it should be minimized for optimum performance, for this is produced by columns that combine a low flow resistance and minimum dispersion at low pressures.

The notion of the separation impedance is by no way new, and goes back to the early days of (gas) chromatography, namely, to 1958, when for capillary GC Golay introduced an analogous concept, called the *column performance factor* [10]. Yet, its practical use was delayed until Knox [43] stressed its value in comparing columns. Typical values for E (and the other dimensionless quantities) for different column types used in LC are shown in Table 4.

As it is a dimensionless parameter, the impedance of well-packed columns should be independent of the column internal diameter, and this is seen for all packed columns, be they conventional, small-bore, or packed capillary columns. The lower flow resistance in the se-

Table 4 Typical Values for E, and Other Dimensionless Quantities, for Different LC Column Types

Column type	$\mathbf{h}_{min}$ (reduced minimum plate height)	$\mathbf{v}_{min}$ (reduced minimum velocity)	ϕ_f (dimensionless flow resistance)	**E** (separation impedance)
Conventional packed	1.5–3	3–5	500–10^3	2×10^3–10^4
Small-bore packed	1.5–3	3–5	500–10^3	2×10^3–10^4
Packed capillary	1–3	1–5	150–10^3	3×10^2–2×10^3
Semipacked capillary	2–3	3–5	50–300	150–2×10^3
Open tubular capillary	0.5–1.5	4–30	32	32–50

quence: small-bore packed, packed, semipacked, and open tubular capillary reflects the reduction in packing density (ε_0 from 0.4 → 1).

Equation (85d), also known as the *Knox equation*, shows that generally the smallest possible reduced plate height that can be generated at the upper operating limit of pressure should be sought. In practice, this means that well-packed columns with minimal stationary- and mobile-phase contributions should be prepared so that the **h** versus **v** curve is as low-lying as possible.

We then calculate the best choice for a column packed with a particular particle size, which should follow from rearranging Eq. (71b) and substituting $n_{th}H$ for L and subsequently $H\langle u_m\rangle$ by $\mathbf{hv}D_m$:

$$d_p^2 = (\phi_f \eta_{th,ne} D_m/\Delta p)\mathbf{hv} \tag{86}$$

which, for the optimum conditions $\mathbf{hv} = \mathbf{h}_{min}\mathbf{v}_{min}$, is an analogue of Eq. (82) for d_{opt}, now using reduced variables. Basically, Eq. (86) and the optimization procedure outlined here is independent of the specific plate height equations chosen to represent column performance. In using the optimal conditions, however, the choice of the plate height equation becomes important, because the optima for van Deemter type equations or Snyder–Knox equations are quite different. Modern packings with 0.75- to 1-μm particles used, for example, in HDC (see Sec. IV.B.3), in the absence of chromatographic partitioning, appear to yield such low-lying plate height plots that C terms are virtually zero, and at sufficiently high velocities, almost a constant plate height is obtained [44], $\mathbf{h} \approx 1.4$, which can be interpreted as an A term. Here, we have no realistic optimum, and separating speed increases with velocity almost ad infinitum, limited only by the extracolumn broadening.

In all other cases, the shortest analysis time with given backpressure, a required plate number, and using optimum particle sizes is obtained when we work at the mininum of the plate height plot, as was also found without using reduced variables. This may be called the *kinetic optimum*, which is very easy to find if we can assume that all columns have virtually the same reduced plate height plot as indicated before. This happens to be true in practice, and the "universal" reduced plate height equation

$$\mathbf{h} = \boldsymbol{B}/\mathbf{v} + \boldsymbol{C}\mathbf{v}^{1/3} + \boldsymbol{D}\mathbf{v} \tag{87}$$

appears in recent reviews as being valid for moderate retention (say $k \approx 3$) and with $\boldsymbol{B} \approx 1.5$, $\boldsymbol{C} \approx 0.8$–1, and $\boldsymbol{D} \approx 2 \times 10^{-2}$ to 5×10^{-2}. Note again, that Eq. (86), when written for the "universal" optimum conditions ($\mathbf{h}_{min} \approx 2$ and $\mathbf{v}_{min} \approx 3$ for all packed columns) yields

$$d_{p,opt} = [(\phi_f \eta n_{th,ne} D_m/\Delta p)\mathbf{h}_{min}\mathbf{v}_{min}]^{1/2} \tag{88}$$

and predicts the occurrence of the following optimum particle sizes for a maximum backpressure of 400 bar, a viscosity of 10^{-2} poise (= 10^{-3} Pa s), $\phi_f = 10^3$, and $k = 0$ (for the nonretained component), so:

$n_{th,ne}$	10^3	10^4	10^5	10^6	
$d_{p,opt}$ (μm)	0.4	1.2	3.5	12	at Δp = 400 bar
L_{opt} (cm)	8×10^{-2}	2.5	78	2.5×10^3	
$t_{0,opt}$ (s)	0.14	14.1	1414	1.41×10^5 = 1.6 days	

the same trend as estimated before [from Eq. (82)], but more pronounced, because here we did not limit the velocity to practical values of about 0.1 cm/s.

Present particle technology allows the availability of submicron particles (as small as about 0.2 μm), but in pressure-driven systems, both the associated analysis times of less than

1 s and column lengths shorter than 1 mm are not feasible in practice with a view to the extracolumn-broadening. Yet, the state of art is not at all inefficient, for we are halfway between the pressure- and particle–size-limited situations working with 1–2 μm particles and obtaining 10,000 or so plates in a matter of 30–60 min. Poppe [45], in a recent review, concludes that the state-of-art HPLC column is not far from the best packed and pressure-driven column.

Further conclusions to be drawn from this result are the following

1. For the high-plate numbers required, the pressure-limited situation prevails, but particle sizes of 3–20 μm are readily available. However, in this range the table shows that high-resolution HPLC requiring 10^5 or more plates cannot be expected to be performed in reasonable analysis times. This becomes clear from realizing that, for the too high plate numbers required, the velocity is forced back into the diffusion region of the plate height curve, where plate height goes up again at lower velocities and column length has to be increased even farther to compensate this diffusion effect. We asymptotically reach the critical pressure drop, as discussed earlier, and it is an easy exercise to calculate the reversed concept of the critical plate number that can be achieved, given a maximum pressure, such that plate height is diffusion controlled ($H = 2\gamma \boldsymbol{D}_m/\langle u_m \rangle$). The required length then is $L = n_{\text{th,ne}}H$, and the critical pressure drop and critical plate number are found as

$$\Delta p_{\text{crit}} = 2\phi_f \eta n_{\text{th,ne}} \gamma \boldsymbol{D}_m / d_p^2 \tag{89a}$$

another form for the critical pressure than that in Eq. (79), and

$$n_{\text{th,crit}} = \Delta p_{\max} d_p^2 / 2\gamma \boldsymbol{D}_m \eta \phi_f \tag{89b}$$

Thus, the smaller the particles, the smaller the plate number obtained. This has been found experimentally in both GC and LC: in LC, using 1.4-μm particles, plate numbers in excess of 3×10^4 are problematic. Higher pressures up to 5×10^3 bar have been proposed and used [46] to give some room for improvement, but the pressure gain is limited (third-power root), and the practical difficulties high.

2. The other extreme of very fast chromatography, for low-resolution separations in short times (process analysis, for example), requires the newest generation of particles, but also a brand new generation of equipment, with virtually no contribution to band-broadening.

In the foregoing, the usefulness of the notion of the reduced parameters and variables is illustrated in the unavoidable outcome that invariably we are unable to avoid the Knox pressure and particle limitations, and LC research, since the early 1980s, has sought ways to circumvent these barriers.

One approach has been to use "microcapillary"-packed LC in columns with smaller diameters (often using fused-silica tubes, which are so successful in capillary GC) and enhanced permeabilities by reducing the packing density. Table 4 proves that this has some success in obtaining better separation impedances. It also proves that open tubular LC with pressure drive is the more promising variety in this direction of development and, indeed, OTLC has gained some advocates [9,47]. This interest, mainly inspired by the widespread proliferation of capillary GC, has some funding in the column resistance factor ϕ and the separation impedance E, which on substituting the column diameter d_c for the particle size d_p in the foregoing equations, are both 32 (i.e., OTLC combines the lowest flow resistance with the best separation performance of all pressure-driven systems). Unfortunately, this concept fails notably because of the difficult detection aspect. The gain in efficiency and speed obtained is largely at the expense of detectability and dynamic range of the ultraminiaturized system [45,47]. This has to do with the fact that $E = 32$, a required plate number of 10^5, and a maximum pressure of 400 bar at a reduced minimum plate height of 1, yields a necessary open tubular ID of less than a micrometer. This implies a volume standard deviation of less than 1 pL and detection in such volumes can be accomplished in practice only with laser-induced fluorescence detection [9] or on-column UV absorption detection [48]. Apart from

the detection problem, the hurdle of preparing suitable stationary phases has to be taken, which is by no means trivial [9]. As a result, pressure-driven OTLC columns are currently reasonably practical only with diameters in the range of 3–5 μm, which is rather far off the kinetic optimum, especially for plate numbers fewer than some 5×10^4.

The only alternative to obtain high efficiencies without the price paid in terms of unattractively high pressures is the use of electrodrive instead of pressure drive, as mentioned in Sec. III.c. For the separation of neutral substances, this requires the presence of electro-osmotic flow, with the main advantages of plug-like velocity profiles (which do not cause convective peak-broadening) and independence of the channel diameters (at least if chosen such that heat transport through the liquid is fast enough, usually true when diameters are smaller than say 75 μm). Knox and Grant [49] described these advantages precisely, and both Tsuda et al. [50] and Poppe et al. [51] were the first to apply these ideas in actual electrodrive open tubular LC columns with narrow bores and a retentive phase deposited at the wall.

Because the occurrence of the unavoidable C term arising from stationary-phase contributions, albeit that the total C term is slightly less than in pressure-driven OTLC, it is of the same order of magnitude. Again small diameters (3–10 μm) should be chosen, and the same problem as found in the pressure-driven case, that of detection, occurs. Incidentally, the maximum plate number obtained is that determined by Eq. (55a) and amounts to about 10^6 plates.

In their pioneering paper on CE, Jorgenson and Lukacs [52] proposed the use of electrodrive in packed columns for LC (also called capillary electrochromatography; CEC), which are about 75-μm ID and packed with micrometer-sized silica-based particles. Here, substantially less miniaturization is present, no detection problem arises while the plug-flow is preserved. Knox et al. [47,49] drew attention to the fact that in electrodrive-packed column chromatography particle size can be reduced much farther than in pressure-driven systems, again because flow is independent of the channel diameter. This would produce much smaller C terms and open up the way to fast and efficient separations. Rozing et al. [53], for instance, obtained in this way an impressive 10^5 plates within 20 min, presently quite impossible to obtain in pressure-driven systems. Yet, stable electro-osmotic flows are difficult to maintain, and the advantage of electrodrive seems to become less important at higher plate numbers, as their critical plate numbers are limited to the range of 3×10^5 to 5×10^5 [45]. For the excessively high plate numbers needed, the only technique of choice would be pressure-driven OTLC with critical plate numbers as high as 10^7, but with the mentioned drawback of small peak volumes.

B. Kinetic Optimization of Separation Methods for Macromolecules

One of many famous statements by Giddings [54] reads:

> The difference between macromolecular chromatography and small-molecule chromatography, from a fundamental point of view, is considerably greater than the difference between gas and liquid chromatography.

This is a consequence of the chain-like structure of macromolecules that results in their characteristic physicochemical properties, such as limited solubility, slow diffusion, high viscosity, and shear-dependent flow. For chromatographic separations, the typical macromolecular behavior (diffusion and flow properties) are of importance for zone-broadening, and this is why they deserve a short, but separate treatment.

Because of the finite sizes of macromolecules, and the almost chemical identity of polymer molecules of one species, separation of macromolecular homologues is based mainly on size separation principles, rather than on the enthalpic interactions that cause selectivity in small-molecule chromatography [for a review of the separation mechanisms in macromolecular chromatography, see, e.g. Refs. 2, 37].

Because of the inherent properties of polymers, such as no volatility and solubility in liquid solvents, LC techniques are of special interest for polymer separations. Among the LC techniques, size exclusion chromatography (SEC; formerly called gel permeation chromatography [GPC]) is by far the most widely used analysis technique for polymers. It is a powerful and universally applicable technique for polymer characterization, separating macromolecules in solution according to their sizes, based on the exclusion of finite-sized solutes from the solid walls of pore space present in packed LC columns. Currently, SEC is a useful and comfortable routine method for the determination of the molecular mass distribution (MMD), which is an important characteristic for polymer properties in general. One of the problems accompanying SEC separations is the occurrence of relatively large zone-spreading, originated by the slow and hindered diffusion of macromolecules in pore space; thereby, the separation speed of SEC methods is limited. The pertinent equations for the efficiency of SEC have already been given, in particular in Sec. II.E.4.g on porous particles. All given optimization procedures are as valid for LC as for its subtechnique SEC, the main difference being the low numerical value of the molecular diffusion coefficients of polymers. In Sec. IV.B.2 we will describe how, by the introduction of convection (either pressure- or electrically driven), mass transfer within a porous medium can be strongly improved [55,56]

Although there is no single other method of analysis more effective in the characterization of polymeric materials, especially when SEC is combined with dividers specific and selective detectors (light scattering, viscometry, and infrared spectrometry) particulate materials (among which polymeric micelles and other colloidal species) and very large macromolecules do not lend themselves to SEC analysis. For these materials other separation techniques are being developed, such as hydrodynamic chromatography (HDC) [2,44] and a family of field flow fractionation (FFF) techniques [1]. In the next sections, a short description is given of zone-broadening in some of these techniques.

Because supercritical fluid chromatography (SFC) bridges the gap between small-molecule chromatography and macromolecular chromatography, we start with a short description of dispersion in (compressible flow) SFC.

1. Kinetic Optimization of Compressible Supercritical Fluid Chromatographic Methods

The position of supercritical fluid chromatography (SFC) between GC and LC from a kinetic point of view has been thoroughly discussed by Cramers et al. [34]. The differences between SFC, GC, and LC are determined largely by the pure fluid properties, such as density, polarity, diffusivity, and viscosity, of the mobile phase. In the supercritical region, both pressure and temperature exceed critical values, Carbon dioxide, with a critical pressure of 72.9 bar and a critical temperature of 31.3°C is by far the most used supercritical carrier, either pure or modified with other more polar solvents. Depending on the choice of the working pressure and temperature conditions, the density of CO_2 ranges from about $\rho = 0.1$ to 0.96 g/mL. By changing the density, the solvating power of supercritical fluids is much greater than that of gases and, therefore, can be used for the separation of involatile and high molecular mass samples, unsuited to GC. Indeed, in the analysis of hydrocarbon waxes in petrochemistry, substances with carbon numbers up to say 120 (molecular mass of about 1500) can be analyzed.

Concerning column efficiency, two important aspects determine the differences between SFC and the other chromatographic techniques: the transport properties, such as diffusion and viscosity, and the compressibility. Diffusivity for CO_2 ranges from 10^{-3} cm^2/s at low density to 10^{-4} cm^2/s at high density, thereby approaching typical liquid diffusivities of 10^{-5} cm^2/s, but still an order of magnitude faster. This has consequences for the efficiency and separation speed of SFC separations, which can be appreciated from the equations given in the foregoing that have a general applicability. Typical minimum plate heights in packed column SFC and LC are very similar, but this maximum efficiency in SFC is achieved at linear velocities five

to ten times greater than for LC. Thus, SFC separations can be achieved in much shorter times than in LC.

In obtaining these higher separation speeds, the viscosity plays a role and that for CO_2 ranges from gas-like values of 0.02 cP at low densities to values of 0.1 cP at high densities, typically an order of magnitude less than the typical liquid viscosity of about 1 cP.

From this short discussion, it becomes clear how complicated the situation is in SFC, for density, pressure, and temperature not only determine the efficiency of the separation, but also have an influence on the selectivity, and these conditions should thus be chosen very carefully.

For open tubular SFC, and for the moment, omitting pressure drop influences and compressibility effects, as described in Sec. III, separation speed can be derived on the basis of the equations given in Secs. II and IV [see also Ref. 34]. For typical values for the reduced plate height $\mathbf{h} = 4.5$ and velocity $\mathbf{v} = 45$, it follows that with $\phi_f = 32$, $\boldsymbol{D}_m = 10^{-4}$ cm^2/s, and $\eta = 0.1$ cP (CO_2 at 40°C and 200 bar), pressure drop is relatively small. Even with 8-μm–ID columns, 10^4 plates are achieved with a pressure drop of only 10 bar (so inlet pressure is 210 bar, outlet pressure 200 bar). Thus the kinetic parameter $n_{th}/\Delta p$ (plates per bar pressure drop) amounts to 10^3. A 50-μm ID column, showing even less flow resistance, then yields some 4×10^4 plates per bar and difficult separations are basically possible.

With such fluids, the solvating and transport properties and, thus in principle, both retention and efficiency, are a function of pressure and, therefore, also vary along the column length. Hence, a large pressure drop would give rise to a density gradient along the column, which will slow the migration of the components. In extreme cases, the migration could eventually even stop, and the problem will have to be solved by pressure- or density-programming techniques.

For packed columns in SFC, with $\phi_f = 1000$, $\mathbf{h} = 3$, $\mathbf{v} = 10$, the analogous calculation yields that, for particle sizes of 5 μm, 83 plates per bar will be obtained, and for 10-μm particles, 333 plates per bar will be obtained under the foregoing conditions. Thus, open columns in SFC allow much higher plate numbers to be achieved than packed columns, the maximum being dependent on the maximum allowable pressure crop. In the case of SFC, this maximum pressure drop is determined by fundamental aspects concerning the influence of pressure on retention and efficiency, rather than on instrument design aspects that would allow high pressure drops. Furthermore, the pressure gradient in SFC can be obtained from the observation that density gradients along the columns are almost linear [34].

The effects of pressure drop for gases has been treated in Secs. III and IV, but in SFC, aside from changes in local plate height, velocity, and diffusivity, the change in local partition coefficient in the pressure and density gradient along the column length should also be incorporated. For that Cramers et al. used a correlation with experimental data in the form $\ln k = \boldsymbol{a} + \boldsymbol{b}\rho + \boldsymbol{c}\rho^2$, which typically, may lead to a change (increase) in capacity factor by a factor of about 3–5 along the column. In SFC, no analytical expressions describing the effects of compressibility (for gases leading to the James–Martin factor j and the Giddings factor g, see Sec. III) can be derived because no universal equation of state (such as Boyle's law for gases) is available. In a numerical calculation [34], it was shown that in SFC with a linear density gradient along the column and assuming a constant density-independent value for $\boldsymbol{D}_m/u_m$, the mentioned "pressure" correction factors can be modified as

$$j_{SFC} = 2/(1 + \Re) \tag{90a}$$

and

$$g_{SFC} = (4/3)(1 + \Re + \Re^2)/(1 + \Re)^2 \tag{90b}$$

where $\Re$ replaces the pressure ratio in gases by the inlet/outlet density ratio in SFC: $\Re = (\rho_i/\rho^0)$. A density drop of 20% (i.e., $\Re = 1.2$) appears to be a reasonable estimate for maximum permissible density drop under average practical conditions. In that case $j_{SFC} \approx 0.9$ and $g_{SFC} \approx 1.01$, both close to unity. This implies that the expansion of fluid along the column

length in SFC does not significantly increase the plate height. Hence, the decompression effect in SFC is very low when compared with GC. As a consequence, analysis time in SFC in open columns reduces proportional to the square of the column diameter, the same as in open tubular LC. From the Golay equation for the plate height, and for unretained solutes, one can expect to obtain 10^5 plates in a 10-μm–ID open column with a length of 29 cm at the optimum velocity, requiring a pressure drop of only 0.45 bar at 160 bar inlet pressure (temperature 70°C) and a residence time of 30 s. For retained solutes [34], the effects of the pressure drop on the retention time and the plate height for this 10-μm column can already begin to appear at the optimum velocity, and they increase to significant losses for higher velocities. As a result, open tubular SFC is limited to columns with IDs wider than approximately 10 μm.

In packed columns for SFC, when using the Horvath and Lin plate height equation, with significant pressure drops across the column, the increase in the capacity factor will cause a significant increase of the plate height along the column [34], which is important especially for capacity factors lower than 5.

2. Kinetic Optimization of SEC

Peak capacity in SEC techniques is limited by two factors: The first, and obvious one, is that of the limited retention window of the technique. Based on the exclusion principle, solutes with a size exceeding that of the intraparticle pores are present only in the interstitial pore space and elute in the exclusion limit, defined by the (minimum) residence time t_0 connected with the interstitial velocity $u_0 = L/t_0$. At the other extreme of small-sized molecules (for instance also solvent molecules) that completely penetrate the intraparticle pore space, residence time is determined by the (maximum) time t_m, which is connected with the average velocity $\langle u_m \rangle = L/t_m$. Hence, all solutes with sizes in between these limits elute in the restricted retention window from t_0 to t_m, which can be connected with the pertinent porosities of interparticle and intraparticle pore spaces (see the discussions in Secs.II.A and II.E.4.g).

The second reason for limited peak capacity in SEC is found in the large broadening of zones. For SEC, the pertinent equations that describe peak-broadening have been obtained in Sec. II.E.4.g. From that, it is clear that intraparticle mass transfer in SEC must be of great influence, because of the slow diffusion of macromolecular solutes. All equations given in Sec. IV on optimization of LC separations in general remain valid, and so we can derive that the peak capacity, from Eq. (20), is given approximately by $n_c \approx \frac{1}{2}n_{th}$, which is seen to depend solely on the number of plates available. As said, SEC is not particularly efficient, small plate numbers are generally obtained, and peak capacity is typically restricted to 20–50, considerably smaller than can be obtained with other HPLC systems.

To increase the number of plates in SEC, we should obtain smaller plate heights, preferably at increased velocities, because of required limited analysis times (i.e., we should increase the separation speed). In a pioneering paper, van Kreveld and van den Hoed [55], showed that on increasing the linear velocity and, thereby, the pressure drop across the column, certain silica-based packings for SEC showed plate height plots that were strongly curved toward the velocity axis. This can be elegantly interpreted such that, at these higher velocities, the increased pressure gradient causes permeative flow through the porous particles of the packing. If true, the radial dispersion coefficient present in the plate height expression [see Eq. (59f)] can indeed be interpreted as consisting of a diffusional part plus a convective part, according to Eq. (26a). If this convective contribution to mass transfer within the porous particles would be large enough, then, notably for slowly, diffusing macromolecular solutes, this term can be significant in reducing plate height. From Ref. [55] and using Eq. (26) to interpret the plate height data, we obtain that, for a series of polystyrene (PS) standards of different molecular mass and known molecular diffusion coefficients in the free solvent tetrahydrofuran (THF), a strongly hindered molecular diffusion in the pores takes place. The obstruction factor is a strong function of molecular mass (and thus size) and ranges from an expected value of 0.7 for a small molecule, such as toluene, to 0.12 for PS 160,000.

In addition, the convective term amounts to an effective value of zero for toluene, which means that the intraparticle flow is too small to approach the values for molecular mass transport by diffusion, which is (relatively) large for the small molecule of toluene—2.44×10^{-5} cm^2/s [55]. Hence, for toluene, mass transfer is still dominated by molecular diffusion, which is not strongly obstructed either. As a result the plate height plot of toluene is of the van Deemter type, and almost straight, as predicted by Eq. (59f) if we use $\boldsymbol{D}_m$, rather than $\boldsymbol{D}_R$.

Significantly differing results are obtained for the PS solute, for which the obstructed molecular diffusion coefficient of 4.7×10^{-8} cm^2/s [55] is easily dominated by the convective contribution of 8.3×10^{-8} cm^2/s $\langle u_m \rangle$. At a velocity of about 0.5 cm/s convective and molecular contributions are already equal, and the increased convective dispersion at increasing velocity, yields a strongly curved plate height plot analogous with that obtained in the coupling and Knox and Snyder equations. The latter, however, describe the combined influence of diffusion and convection in the interstitial pore space, whereas in the present example, the same for intraparticle pore space is observed.

The plate height plot for polystyrenes even levels off to a plateau value ($H = 5$ cm), for which radial convective dispersion dominates obstructed diffusion by a factor of 10, and the plate height should indeed become independent of the velocity according to Eq. (59f), where now $\boldsymbol{D}_R$ is also proportional with velocity, and the velocity dependence cancels.

(*a*) *Kinetic Optimization of Electrically Driven Capillary SEC.* In electrically driven chromatography (see Secs. III.C and IV.A), fused silica-packed capillary columns are used to propel the mobile phase by electro-osmosis, rather than by pressure forces. The attractive feature of this is the occurrence of an almost flat velocity profile, which seldom gives rise to axial convective dispersion contributions to plate height, even if solutes do not diffuse (or flow) very fast in radial directions. This is nowadays frequently demonstrated, and it is promising to extend this idea to SEC separations, especially in view of the low diffusivity of macromolecules. The results of "perfusion"-type increased intraparticle mass transfer is a further inspiration to investigate the possibilities of electrodrive SEC (EDSEC), because it is basically simple to generate flow through a porous medium with open-ended pores by electro-osmosis. It simply requires a layer of counterions (Stern layer) next to the solid walls of the pores and a potential gradient applied across the column length, as explained in Sec. III.C.

In most cases, SEC is applied to synthetic polymers in industrial environments. These polymers are mainly neutral (noncharged), and sometimes it is somewhat of a problem to find a suitable solvent for such compounds. Virtually all of the CEC studies have been performed in aqueous mixtures as the solvent, which are largely unsuited for SEC of synthetic polymers. The latter are generally hydrophobic and do not dissolve in solvents other than organic liquids. These solvents exhibit a relatively small dielectric constant and, as a consequence, the dissolution of ions becomes difficult. Recently [56], the feasibility of EDSEC using dimethylformamide (DMF) as the solvent, with a relatively large dielectric constant, was demonstrated, however, by using 100-μm–ID capillary columns, with about 31-cm length of packing (3- and 5-μm particles). For the small-molecule marker toluene, when using these columns both with electrodrive and under pressure drive, the obtained plate height plots are as expected. At low velocities in both cases, axial molecular diffusion (the B term) rules the plate height and the reduced minimum value of $\mathbf{h} \approx 2$ is obtained, indicating a well-packed column. For polystyrenes of different molecular masses, this behavior is quite different. First of all, the B term is not reached for all velocities above 0.05 mm/s, because of the low diffusion coefficients. Second, under pressure drive, the plate heights of a small PS molecule (mass 2200 Da) and a larger one (43,900 Da) appear to be significantly larger than for toluene, owing to broadening after the C term. Plate heights up to 80 μm are found at velocities of about 0.4 mm/s, and smaller the smaller the molecular mass. This is as expected, because molecular diffusion rules the intraparticle mass transfer, the faster the transfer, the lower the mass. Under electrodrive, the plate heights of the mentioned PS solutes almost coincide, and the average

trend is a rather flat and low-lying plate height plot, with h values not exceeding 25 μm at the velocity of 0.4 mm/s. Obviously, the gain in efficiency of about a factor of 3, can be explained by the aforementioned phenomenon of intraparticle convection through the pores. This flow is the same for small and large PS molecules, suggesting that molecular diffusion in the pores for all masses is largely overruled by the generated electro-osmotic convection within the particles, and thus leads to the same low and identical plate heights. If true, the perfusion under electrodrive is far larger than under pressure drive, and so the gain in efficiency and separation speed is far larger than discussed in the former section.

An accompanying effect is that under electrodrive, the actually moving volume of the mobile phase is increased; consequently, the stagnant or stationary volume is reduced. As a result, the retention times of polymeric solutes increase if intraparticle flow is allowed, because less retardation in the stagnant volume occurs. This was predicted by Giddings, in 1965 [5] and is actually observed [56] that under electrodrive the retention window is even less wide than in classic pressure-driven SEC. This would lead to a smaller peak capacity, but this is largely compensated for by the increased efficiency. One further observation [56] is that the retention window can be influenced by the ion strength of the mobile phase. This further supports the present reasoning, because electro-osmotic flow depends on the double-layer thickness, which increases in thickness with decreasing ionic strength. Eventually, at very low ionic strengths, the double layer of adjacent walls of the pore space overlap and no electromigration is possible within the particles. Indeed the experimental retention window diminishes with increasing salt concentration, as expected, and in favor of the electroperfusion mechanism.

Although the same columns under pressure drive are less efficient, they show the largest retention window, and the 100-μm columns can actually be used to do pressure-driven SEC. The achievement is that the special-packing procedure [56] enables the preparation of minisized columns that actually have useful efficiencies. This, in itself, is rather important for routine SEC methods because with by the small column cross sections, solvent consumption can be reduced by a factor of about 2000. This is especially important when toxic or expensive solvents are to be used. Admittedly, the plate heights in these packed capillary minicolumns are higher by a factor of 1.5–2 than those of standard-sized 4.6-mm–ID classic packed columns, but they are still very useful for practice.

3. Kinetic Optimization of Hydrodynamic Chromatography

Hydrodynamic chromatography (HDC) is another separation method for macromolecules, and is especially suited for samples that cannot be handled by SEC (particulates, micelles, and such). The basic mechanism of HDC separation, similar to SEC, is based on exclusion from solid walls, with the extension of the presence of a distinct velocity profile [2]. Here electrodrive is of far less interest, and the supposedly dead-end pores in SEC and the slow mass transfer by diffusion is replaced by open-ended pores and strong convective mixing. As a result, HDC is expected to be far more efficient than SEC which, with certain restrictions, has proved to be true [57]. The open-ended pore space can be found in the interstitial space in packed bed columns (packed column HDC; PHDC), or in actual open but microcapillary tubes (microcapillary HDC; MHDC). The latter can be obtained and used in diameters down to the micrometer level and, for PHDC, the dimension of the flow channel is determined by the hydrodynamic radius, as discussed in Sec. III, and amounts to a radius of about $(1/4.5)d_p$.

Under pressure drive, the flow profile in such channels may be assumed to be parabolic, and for geometric reasons, large solutes are excluded from the slow streamlines close to the wall. Thus, these larger solutes sample higher velocities in the flow profile than smaller solutes, and by this hydrodynamic effect a separation occurs, during which large solutes elute before smaller ones, just as in SEC. It has been proved [57] that HDC methods are rather nonselective in comparison with SEC, but the gain in efficiency is so large that HDC methods can easily compete with those of SEC. Note, incidentally, that, in SEC columns packed with contem-

porary small particles with sizes below 5 μm, the HDC mechanisms are active in the interstitial pore space for large enough solutes. This, for example, is also true in the columns discussed in the former section, so that a mixed SEC–HDC mechanism is active, and the retention window is widened.

Concerning the efficiency of HDC columns, the discussion in Secs. II, III, and IV, on general packed columns is valid. Indeed, workers with PHDC and nonporous packing particles [44,57] report the validity of, for example, Giddings' coupling equation [see Eq. (39c)] with **a** = 1.4 and **c** = 1. This represents, outside the diffusion region of the B term, an almost flat-lying plate height plot that is approximated by $H = 1.4d_p$; in fact, a constant plate height determined by eddy diffusion. The low and velocity-independent plate height is the large achievement here, ensuring high separation speeds in PHDC [57].

In MHDC, the situation is slightly more complex, but can conveniently be described by a modification of the Golay equation. The modification is twofold:

1. By the exclusion from the wall of the supposedly circular–cylindrical tube, radial diffusion distances are smaller for large solutes than for small ones.
2. Again, by the exclusion from the wall, large solutes sample only higher velocities in the profile, but at the same time there is a smaller maximum velocity difference.

Provided that we are still allowed to use the free bulk diffusion coefficient (hence, ignoring possible hydrodynamic effects of the nearby walls on diffusion [15]) it is easy to correct for both of these effects and to obtain a corrected Taylor–Aris–Golay convective dispersion C term of the form:

$$H_{m,\mathrm{MHDC}} = [R_c^2\langle u_m\rangle/24\boldsymbol{D}_m][1 - \lambda_{\mathrm{HDC}}]^6 \tag{91}$$

where λ_{HDC} is the aspect ratio of the analyte size and column size: $\lambda_{\mathrm{HDC}} = R_a/R_c$. From the Stokes–Einstein equation [15], the diffusion coefficient of spherical analytes is inversely proportional to the analyte size, so we may estimate $\boldsymbol{D}_m$ by $\boldsymbol{D}_m = \Xi/R_a$ where Ξ is a constant, depending on temperature and viscosity. For PS in THF and from light-scattering experiments [55], we obtain for example $\Xi = 4.73 \times 10^{-13}$ cm^3/s. Regardless, with the Stokes–Einstein relation being valid, we prove that the peak width in the course of an MHDC chromatogram depends rather much on the residence time. If we designate the latter in the dimensionless form τ_{HDC} = (residence time of the solute)/(residence time of a small-molecule marker) = t_a/t_m, then we obtain from Eq. (91) for the peak variance in time units:

$$\sigma_{t,\mathrm{HDC}}^2 = (R_c^3 t_m/24\Xi)[1 - (\tau_{\mathrm{HDC}})^{1/2}]\tau_{\mathrm{HDC}}^6 \tag{92}$$

which is a strong function on τ. Its mean value is found by integrating over τ, and the average standard deviation of a MHDC peak in time units amounts to approximately

$$\langle\sigma_{t,\mathrm{HDC}}\rangle \approx (1/4)(R_c^3 t_m/24\Xi)^{1/2} \tag{92a}$$

From this result we obtain the peak capacity of MHDC chromatograms as the number of peaks with width $4\sigma_t$, that fit into the total chromatogram (extending from $\tau_{\mathrm{HDC}} \approx 0.6$ to 1), to find that for PS in THF:

$$n_{c,\mathrm{HDC}} \approx 10^{-6}(t_m/R_c^3)^{1/2} \tag{92b}$$

which is seen to be a strong function of the column radius. For a column radius of 1 μm, this result implies that 10 peaks can be accommodated into the chromatogram in a matter of 1-min–analysis time. If we want to accommodate 100 peaks, the same column requires an analysis time of about 1 h. Another example is calculated for the smallest ID ever reported in experiments [2]; $R_c = 0.6$ μm. Here we calculate that in an analysis time of 1 h, 200 peaks (with a lower limit of $M = 2600$) are baseline resolved in a column of length $L = 325$ cm at the expense of 326 bar inlet pressure. The lower mass limit occurs because the toluene peak, used to obtain the t_m value is rather wide by axial diffusion in this long time. The

calculated upper mass limit of the solute eluting at $\tau_{HDC} = 0.6$, amounts to 62×10^6, which indicates that MHDC is basically suited for analysis of very high molecular mass polymers, unsuited for SEC.

For a required analysis time of 1 min, the result is that (again taking the same mass range) 23 peaks are baseline resolved in a column of only 5.42 cm length, requiring a pressure drop of only 5.44 bar. These calculated results prove the high separation speed of MHDC separations, but the extracolumn dispersion as well as the problematic (on-column) detection still prevent routine application of MHDC.

4. Kinetic Optimization of Field Flow Fractionation

Field flow fractionation is an instrumental analysis technique for the characterization of particulate and macromolecular analytes, introduced by Giddings [5] in 1967. It took some decades to overcome the difficulties to design efficient instrumentation, but the last decade saw an impressive upsurge in FFF methods and applications [for a review see Ref 58].

The FFF methods resemble the LC methods in many respects, and the underlying mechanisms can be treated in the same way as described in the foregoing. There are two main differences, the first being that in FFF techniques packed columns are never used, and second, that perpendicular to the main flow in the open slit-like FFF channels, an additional external force is applied. The latter force or field is the basic mechanism for separation in FFF, and it can be of many different kinds: gravitational or centrifugal, electrical, flow-based, or thermal, to name the more important ones.

Retention and efficiency in FFF methods can be calculated exactly from first principles, because of the neat geometry of the separation channels, and many interesting applications are based on these theoretical achievements, largely put forward by Giddings [1,58].

Although LC and FFF have much in common, it is outside the scope of this chapter to review separation efficiencies and separation speeds obtained in FFF methods, and the reader is referred to the pertinent literature [1,58]. A comparison between SEC, HDC, and FFF relative to these aspects is available [57].

APPENDIX: ABBREVIATED LIST OF SYMBOLS*

$c(z,t)$	concentration function or profile in space and time
c_m^*	equilibrium concentration in the mobile phase
c_s^*	equilibrium concentration in the stationary phase
Δc_m	extent of nonequilibrium concentration
H	height equivalent of a theoretical plate, $H = \sigma_z^2/L = L(\sigma_t/t_R)^2 = 2D/u_z$
k	capacity factor $k = K(V_s/V_m) = t_R'/t_m$
K^*	equilibrium partition coefficient, $K^* = c_s^*/c_m^*$
L	column length
ζ	axial coordinate moving with the zone center, $\zeta = z - u_z t$
z	longitudinal coordinate along the column axis
z_c	coordinate of the zone center
ℓ	step length, height of a transfer unit, $\ell = \langle u_m \rangle \tau_m$
n_t	number of transfers between stationary and mobile phases after the retention time t_R
n_{th}	number of theoretical plates, $n_{th} = (t_R/\sigma_t)^2 = L/H$
n_{eff}	effective plate number, $n_{eff} = (t_R'/\sigma_t)^2$
n_c	peak capacity, number of peaks with baseline separation fitting in the chromatogram ("Trennzahl")
N	general symbol for number (of steps, and such)

*Contact chapter author directly for a complete list of symbols.

t_R	retention or residence time $t_R = t_m(1 + k) = L/u_z$
t'_R	net retention time, $t_R = t_R - t_m$
t_m	residence time of mobile phase and unretained components, "dead" time
t_s	time spent in the stationary phase
t^*	equilibration time
$\langle u_m \rangle$	average mobile-phase linear velocity
u_z	zone velocity, $u_z = \langle u_m \rangle/(1 + k)$
α	relative retention or selectivity, $\alpha = k_2/k_1$
$\varphi = (V_s/V_m)$	phase ratio of stationary and mobile phases
σ_t	standard deviation around the peak top in time units
σ_t^2	variance around the peak top at in time units
τ_s	infinitesimal time spent in the stationary phase per absorption step
τ_m	infinitesimal time spent in the mobile phase per desorption step
λ	general symbol for step length; also geometric constant in eddy diffusion
D	diffusion or dispersion coefficient
D_m	molecular diffusion coefficient
ℓ^*	characteristic length for equilibration
Rs	resolution factor, $Rs = \Delta z/4\sigma_z = \Delta t_R/4\sigma_t$
Ω	column/particle size ratio, $\Omega = R_c/d_p$

REFERENCES

1. JC Giddings. Unified Separation Science. New York: Wiley–Interscience, 1991.
2. R Tijssen. In: F Dondi, G Guiochon, eds. Theoretical Advancements in Chromatography and Related Separation Techniques. NATO-ASI vol C 383. Dordrecht: Kluwer Academic Press, 1992, pp. 397–441.
3. AJP Martin, RLM Synge. Biochem J 25:1358, 1941.
4. E Wicke. Chromatographie im Rahmen der Trennverfahren. Ber Bunsenges 69:761, 1965.
5. JC Giddings. Dynamics of Chromatography. New York: Marcel Dekker, 1965.
6. R Kaiser. Chromatographie in der Gasphase, I, II, III; Hochschultaschenbücher 22, 23, 24. Mannheim: Bibliographisches Institut, 1966.
7. JJ van Deemter, FJ Zuiderweg, A Klinkenberg. Chem Eng Sci 5:271, 1956.
8. ML Lee, FJ Yang, KD Bartle. Open Tubular Columns in Gas Chromatography: Theory and Practice. New York: John Wiley & Sons, 1984.
9. R Swart, JC Kraak, H Poppe. Chromatographia 40:587 1995; J Chromatogr 732: 201, 1996; 670:25, 1994; 689:177, 1995; TrAC, 16:332–342, 1997.
10. MJE Golay. In: DH Desty, ed. Gas Chromatography 1958. New York: Academic Press, 1958, pp. 36–53.
11. ST Sie, GWA Rijnders. Anal Chim Acta 38:3, 1967.
12. AB Littlewood. Gas Chromatography, Principles, Techniques, and Applications, 2nd ed. New York: Academic Press, 1970.
13. GW Johnson. Axial Dispersion from Flow Non-Uniformities in Packed Beds. PhD dissertation, Rensselaer Polytechnic Institute, Troy, NY, 1967.
14. DJ Gunn. Trans Inst Chem Eng (Chem Eng) 46:CE153, 1968; 47:T-351, 1969; 49:241, 1971.
15. RB Bird, WE Stewart, EN Lightfoot. Transport Phenomena. New York: Wiley Interscience, 1960.
16. GI Taylor. Proc R Soc A 219:186, 1953; A 223: 446, 1954; A 225: 231; 473, 1954.
17. R Aris. Proc R Soc, A 235: 67, 1956.
18. R Tijssen, RT Wittebrood. Chromatographia 3:525, 1970; 5:286, 1972.
19. JW Hiby. In: PA Rottenburg, ed. Proceedings Symposium on Interaction between Fluids and Particles. London: Inst Chem Eng, 1962, p. 317.
20. JJ van Deemter. 2nd Informal Symposium GC Discussion Group. Cambridge, September 1957.

21. RPW Scott. Liquid Chromatography Column Theory. Separation Science Series, Chichester: Wiley, 1992.
22. JFK Huber, JARJ Hulsman. Anal Chim Acta 38:305, 1967; JFK Huber. J Chromatogr Sci 7: 85, 1969.
23. LR Snyder. J Chromatogr Sci 7:352, 1969.
24. JN Done, GJ Kennedy, JH Knox. In: ES Perry, ed. Gas Chromatography 1972. London: Applied Science, 1973; JH Knox, JF Parcher. Anal Chem 41:1599, 1969.
25. C Horvath, HJ Lin. J Chromatogr 126:401, 1976; 149:43, 1978.
26. SD Kolev. Anal Chim Acta 308:36–66, 1995.
27. V Ananthakrishnan, WN Gill, AJ Barduhn. Am Inst Chem Eng J 11:1063–1072, 1965.
28. HE Schwartz, PJ Barthel, SE Morring, HH Lauer. LC–GC 5:490, 1987.
29. JH Purnell, CP Quinn. In: RPW Scott, ed. Gas Chromatography 1960 London: Butterworths, 1960. pp. 184–198.
30. J Bohemen, JH Purnell. J Chem Soc 360:2630, 1961.
31. ED Katz, K Ogan, RPW Scott. J Chromatogr 270:29; 51, 1983.
32. JH Knox, RPW Scott. J Chromatogr 282:297, 1983.
33. A Aldehai, DE Martire, RPW Scott. Analyst 114:869, 1989.
34. CA Cramers, PJ Schoenmakers, H-G Janssen. In: F Dondi, G Guiochon, eds. Theoretical Advancements in Chromatography and Related Separation Techniques. NATO–ASI vol C 383. Dordrecht: Kluwer Academic Press, 1992, pp. 289–314.
35. FH Arnold, HW Blanch, CR Wilke. J Chromatogr 330:159, 1985.
36. O Grubner. In: JC Giddings, RA Keller, eds. Advances in Chromatography, vol 6. New York: Marcel Dekker, 1968, pp. 173–209.
37. WW Yau, JJ Kirkland, DD Bly. Modern Size-Exclusion Liquid Chromatography. New York: Wiley–Interscience, 1979.
38. JC Sternberg. In: JC Giddings, RA Keller, eds. Advances in Chromatography, vol 2. New York: Marcel Dekker, 1966, pp. 205–270.
39. R Tijssen, PJ Schoenmakers, MR Böhmer, LK Koopal. J Chromatogr A 656:135–196, 1993.
40. R Tijssen, JPA Bleumer, ALC Smit, ME van Kreveld. J Chromatogr 218:137–165, 1981.
41. S Terable, K. Otsuka, T. Ando. Anal Chem 56:111, 1984; 57:834, 1985; 61:251, 1989.
42. JH Knox, IH Grant Chromatiographia 24:135, 1987; 26:329, 1988.
43. JH Knox, P Bristow. Chromatographia 10:279, 1977.
44. G Stegeman, JC Kraak, H Poppe. J Chromatogr 634:149, 1993.
45. H Poppe. J Chromatogr A 778: 3–21, 1997.
46. J MacNair, and JW Jorgenson. 20th ISCLC Symposium, San Francisco, 1996, Abstr L-0012.
47. JH Knox, MT Gilbert. J Chromatogr 186:405, 1979.
48. R Tijssen, J Bos, ME van Kreveld. Anal Chem 58:3036, 1986.
49. JH Knox Chromatographia 26:329, 1988; JH Knox, IH Grant. Chromatographia 32:1991, 1991; 24:135, 1987.
50. T Tsuda, K Nomura, and G Nakawa. J Chromatogr 248:241, 1982.
51. GJM Bruin, PPH Tock, JC Kraak, H Poppe. J Chromatogr. 517:557, 1990.
52. JW Jorgenson, KD Lukacs. J Chromatogr. 218:209, 1981.
53. MM Dittmann, GP Rozing. J Chromatogr A 744:63, 1996.
54. JC Giddings, J Gas Chromatogr 14:413–419, 1967.
55. ME van Kreveld, N van den Hoed. J Chromatogr 83:111, 1973.
56. E Venema, JC Kraak, H Poppe, R. Tijssen. Electrically driven capillary size exclusion chromatography. Accepted for publication in Chromatographia.
57. G Stegeman, AC van Asten, JC Kraak, H Poppe, and R Tijssen. Anal Chem 66:1147–1160, 1994.
58. JC Giddings. Science 260:1456, 1993.

3

Principles of Detection

Wim Th. Kok

University of Amsterdam, Amsterdam, The Netherlands

I. INTRODUCTION

After the column, the detector may be considered the most important part of a high performance liquid chromatography (HPLC) system. The detector translates the changes in the chemical composition of the column effluent during the chromatographic run into an electrical signal. This signal can then be recorded or digitized and processed to give the required information about the sample composition.

The choice of the detector to be used depends on several sample-related factors: the chemical properties of the analytes, the desired range of sample concentrations to be determined, the complexity of the sample matrix, but also on the chromatographic system used for the separation. The requirements imposed on the separation and the detection for a specific analytical problem are complementary: the higher the quality of detection in terms of selectivity and sensitivity, the less demands are put on the separation system, and vice versa.

Since the emergence of HPLC, a considerable research effort has been devoted to the development and improvement of detectors, based on a variety of physicochemical principles. Still, only a few types of detectors have found general application [1]. Ultraviolet–visual light absorbance, fluorescence, and refractive-index detectors are used in all modes of liquid chromatography, electrochemical or amperometric detectors in reversed-phase chromatography, and conductivity detectors are used mainly in ion (exchange) chromatography. In this chapter the principles and characteristics of these detectors will be discussed. Other types of detectors are used mostly in special applications or in research laboratories. Several of these detectors will be treated briefly.

II. REQUIREMENTS FOR AND CHARACTERIZATION OF DETECTORS

Several general factors should be considered when a detector and a specific separation system are selected. These are, for instance, the allowed detector contribution to peak broadening, the lower and upper limits of the concentration of the sample components that have to be determined, and the required selectivity. Such considerations may be used in both directions. A separation system can be selected to suit a specific detector, or a detector is chosen that is suitable for a specific separation system.

A. Peak Broadening

The variance of a peak (σ^2), as registered after a chromatographic separation, can be considered the sum of independent contributions from the different parts of the system [2]. The main contributions are those from the injector, the column, and the detector:

$$\sigma_{tot}^2 = \sigma_{inj}^2 + \sigma_{col}^2 + \sigma_{det}^2 \quad (1)$$

The peak-width contributions σ may be expressed in units of time or volume. In general, column and detector are chosen such that the detector contribution to σ_{tot}^2 is only a minor part (e.g., 10% for the unretained peak) of the total, to minimize the loss of resolution. The value of σ_{det} in volume units is usually of the same order as the geometric volume of the detector cell, but it can be larger when the flow patterns in the cell are unfavorable (dead corners). Especially for miniaturized systems, the contribution of connecting tubing cannot always be neglected.

In the last years there has been a trend in HPLC to use columns with a smaller diameter than the traditional 4.6 mm, mostly to cut the costs for mobile-phase solvents and for environmental reasons [3]. It will be clear that the requirements for the detector volume become more stringent when the separation system is miniaturized. In Table 1 maximum values of V_{det} are given for some typical column dimensions. For most commercial (UV-absorbance) detectors, special small-volume cells are available for use with microbore columns or packed capillaries.

B. Sensitivity and Detection Limits

Detectors can be concentration-sensitive, when they produce a signal that depends on the concentration of an analyte in the detector cell (in moles per liter), or mass flow-sensitive, when the signal depends on the mass flux of analyte to the detector (in moles per second). Examples of the former type are the optical detectors and the conductivity detector, and of the latter type the mass spectrometer. Most amperometric detectors behave somewhere in between the two types.

In principle, the sensitivity S_i of a concentration-sensitive detector for a specific analyte i is defined as the increase of the output voltage with an increase in the concentration of the analyte in the detector cell $c_{i,det}$:

$$S_i = \frac{dV_{out}}{dc_{i,det}} \quad (2)$$

For a mass-sensitive detector, the corresponding expression is

$$S_i = \frac{dV_{out}}{d\phi_i} \quad (3)$$

Table 1 Detection Volume Requirements for Different Column Types

Column type	Length (mm)	Diameter (mm)	V_{det} (μL)
Conventional	250	4.6	10
Microbore	150	2.0	1
Packed capillary	150	0.3	0.02
Open capillary	1000	0.01	0.0002

where ϕ_i is the mass flux of i. Often the output of a detector is not (or in only a limited region) proportional to the analyte concentration or mass flux. This means that the detector sensitivity can depend on the concentration or mass flux of the analyte. Because the output voltage is easily amplified or attenuated, the foregoing definitions of the sensitivity are not particularly useful in practice. The output voltage is usually translated into a value for the physical parameter that is being measured. However, with some detector types (e.g., fluorescence detectors) this translation is not straightforward, in which case a comparison of different instruments is difficult.

A better method to compare different detection modes and instruments is by the limit of detection (LOD) or "minimum detectability" for a certain analyte. In principle, the *LOD* may be defined as that concentration (or mass flux) that gives a signal (peak) that will be recognized as such with a probability of 50%. In HPLC, the LOD is related to the obtained peak heights and to the noise on the baseline output of the detector (the signal/noise ratio). To determine the LOD, the noise N (i.e., the peak-to-peak amplitude of the baseline detector signal) must be measured. The sensitivity is then determined with a standard solution of low concentration and the LOD is calculated as

$$\text{LOD} = 2 \cdot \frac{N}{S_i} \tag{4}$$

A factor of 3, instead of 2, in this equation is also often used.

For a proper determination of the noise N, its frequency distribution has to be considered. This is illustrated in Figure 1. In Figure 1a, a chromatographic signal is shown that is accompanied by a relatively high baseline noise. Still, even when the noise amplitude is almost as

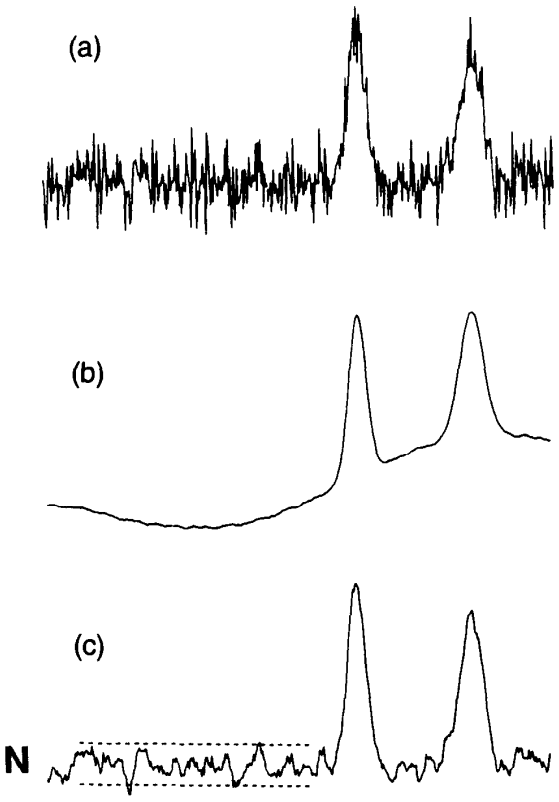


Figure 1 Types of noise in chromatographic signals: (a) high-frequency noise; (b) low-frequency noise or drift; (c) midfrequency noise and determination of the peak-to-peak noise level (N).

high as the peaks, any experienced chromatographer could recognize the peaks and determine their heights and areas with reasonable accuracy. Therefore, the peaks are certainly above the detection limit. This is because the frequency of the noise is high compared with the "rate of change" of the signal in the peaks. Before the determination of noise and LOD, the signal may be filtered to eliminate a large part of the noise. This can be done with an electronic or digital low-pass filter. To avoid distortion of the peaks by the filtering, the time constant τ of the filter should be lower than the standard deviation σ_t (in time units) of the peak of interest. With a first-order filter (e.g., a simple RC-circuit), τ should be at most equal to 0.1 σ_t. With more sophisticated higher-order filters, sometimes applied in the electronics of the detector or as a software routine in a data-processing program, a higher value of τ can be chosen that gives a more efficient elimination of the high-frequency noise without significant peak distortion.

In Figure 1b, the baseline instability has a lower frequency than the peaks. In this case it is reported as drift, rather than as noise. Again, any chromatographer, integrator, or software package should find the peaks and determine their areas correctly. When the noise is measured over a limited time span (e.g., ten times the peak width) low frequency drift will have no influence on the determination of N. In Figure 1c the proper way to measure the peak-to-peak noise is indicated.

If one follows the foregoing reasoning, the LOD for a concentration-sensitive detector is obtained in units of concentration in the detector cell, which is how detectors should be characterized. However, the sensitivities and detection limits reported in the literature are often related to the analyte concentration in the sample or to the amount (in grams or moles) of analyte injected into the HPLC system. This affects the reported LOD by factors independent of the detectors, such as the injection volume and the column dispersion. Unfortunately, there is no generally accepted convention to report detection limits in HPLC.

A parameter related to the LOD is the *lower limit of determination.* This is usually defined as that sample concentration (or injected mass) that yields a relative standard deviation of 10% for the results (peak heights or areas) of individual analyses. In contrast with the LOD, the lower limit of determination can be defined only for the total analytical procedure; it is not a good parameter for characterizing detectors.

C. Linearity

There is no strict demand that the detector signal should increase linearly with the analyte concentration, as long as the relation between these two parameters is predictable and reproducible. For the commonly used absorbance detector, for instance, the measured quantity—the intensity of the light transmitted through the optical cell—decreases exponentially with the analyte concentration. A linearly dependent signal (output voltage) is obtained only after electronic transformation. However, linear behavior simplifies calibration and quantification. Moreover, a linear calibration plot is often an indication that the system is functioning properly.

Frequently, nonlinear behavior of a detector starts above a certain analyte concentration or mass flux. A distinction can be made between the linear and the dynamic range of a detector [4]. The *upper limit* of linearity is usually defined as that sample concentration (or amount injected) at which the sensitivity is decreased by 5%, compared with the sensitivity at low concentrations. The *linear range* is the ratio of the upper limit of linearity and the LOD. A wide linear range is of importance when minor and major sample components have to be determined simultaneously.

The upper limit of the *dynamic range* is that concentration or mass flux which, when increased, does not give a higher signal: the sensitivity, as defined in Eq. (2) or (3), has dropped to zero, and the detector is saturated. In Figure 2 the relations between the LOD and the linear and the dynamic ranges are illustrated.

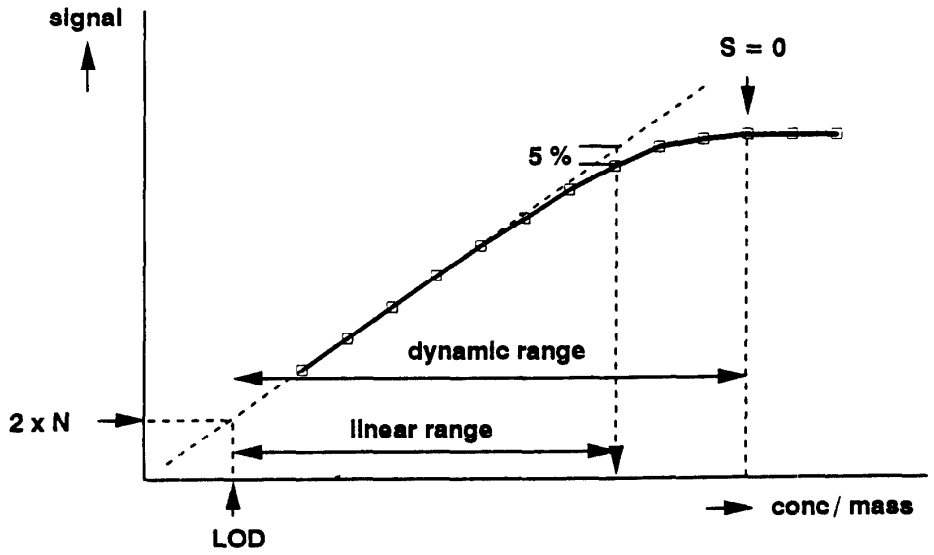


Figure 2 Determination of the limit of detection, the linear range and the dynamic range of a detector.

D. Selectivity

With some detectors most analytes give a signal: These detectors are called universal. Other detectors respond to only certain classes of analytes: these detectors are called selective. Whether a universal or a selective detector should be used is largely determined by the analytical requirements and the sample composition. There is also an effect by the separation system; the more selective the detector, the lower the demands on column performance. Therefore, the selectivity of a detector cannot be strictly defined. A comparison between different detector types can be made in general terms only.

III. UV–VIS ABSORBANCE DETECTION

The general applicability and ease of operation of the UV-vis absorbance detector have made it the most popular detector in HPLC. It measures the absorbtion of monochromatic light by the solute according to the well-known Lambert–Beer law:

$$I = I_0 \cdot 10^{-\epsilon bc} \tag{5}$$

where I is the intensity of the light transmitted through the detector cell, I_0 the light intensity in the absence of the analyte, ϵ the molar absorptivity of the analyte at the wavelength used, b the optical path length of the cell, and c the concentration of the analyte in the cell. The signal is electronically linearized so that the absorbance ($-\log I/I_0$) can be registered directly. Signals are usually expressed in (dimensionless) absorbance units (AU).

The linearity of the absorbance with the concentration of the analyte holds only for monochromatic light, with one fixed value of ϵ for the analyte. In most detectors, light with a certain spectral bandwidth (about 2–5 nm) passes the optical cell. When the ϵ value of the analyte is not constant over this range, nonlinearities occur at high-absorbance values. In practice, however, a more serious problem at high absorbances is the increased noise level. Because of the low intensity of the transmitted light, shot noise (the counting statistics of the photons detected) and electronic noise of the photodetector and the amplifier become more important. Another aspect to be considered in this context is the background absorbance of the mobile-phase constituents. With a strongly absorbing solvent, the light intensities are

decreased and so are the signal/noise ratios. Most organic solvents used in HPLC are sufficiently transparent above a certain wavelength. This limit may be expressed as the cutoff wavelength, at which the absorbance is 1 AU in a 1-cm cell for the pure solvent. In Table 2, cutoff wavelengths are given for several solvents commonly used in HPLC. More extensive lists have been published [5]. In practice, the cutoff wavelength is strongly dependent on the quality (purity) of the solvent used. Also, background absorbance may be caused by other mobile-phase constituents, such as buffers and detergents [6].

A. Single- and Variable-Wavelength Detectors

Optical cells are usually cylindrical, with quartz windows at both ends to allow detection in the 190- to 650-nm range. For most commercial instruments, cells are available with a volume of approximately 8 μL for conventional columns and 1-μL flow cells are available for microbore columns. Single-wavelength detectors are equipped with a discharge lamp. The 254-nm line of a mercury lamp is often used for detection, for at this wavelength, many aromatic compounds show a strong absorption. Variable-wavelength detectors are equipped with tungsten or deuterium lamps and with gratings to select the wavelength. The bandwidth of the selected light is approximately 2–5 nm. Modern automated instruments offer the possibility of changing the wavelength during the run, so that each peak can be detected at its optimum wavelength. Light intensities are usually measured by a solid-state photodiode. Typical sources of detector noise are variations in the refractive index of the solvent, caused by temperature and pressure changes, and lamp fluctuations. The latter factor can be largely eliminated by using a double-beam configuration, with a reference cell filled with air or with the mobile phase.

With modern instruments, the noise level is close to 5×10^{-5} AU. For a typical analyte with a molar absorptivity of 10^4 M^{-1} cm^{-1}, using a 1-cm cell, the LOD is 1.5×10^{-9} M in the cell. If we assume a relative molecular mass of 200 for the analyte, a 100-μL injection volume and a fivefold dilution of the sample in the column, this is equivalent to 1 pmol or

Table 2 UV Cutoff[a] Wavelengths λ_{min} of Mobile-Phase Solvents of Ultrapure Quality

Solvent	λ_{min} (nm)
Acetone	330
Acetonitrile	190
Chloroform	245
Cyclohexane	200
Dichloromethane	235
Diethyl ether	215
Dimethylformamide	270
1,4-Dioxane	215
Ethanol	210
Ethyl acetate	260
n-Hexane	190
Methanol	205
2-Propanol	210
Tetrahydrofuran	220

[a]The *cutoff* is defined as the wavelength at which the absorbance is 1 AU in a 10-mm cuvette.

0.2 ng injected. Because the linearity of an absorbance detector stretches to 1 or 2 AU, the linear range exceeds four orders of magnitude.

The selectivity of UV absorbance detection strongly depends on the wavelength used. Close to the minimum wavelength of 200 or 190 nm, most (organic) analytes absorb light and the detector is almost universal in this range. With increasing wavelength the selectivity is increased.

B. Multiple Wavelength Absorbance Detection

Two principally different methods exist to measure and record complete absorbance spectra during a chromatographic run. In some instruments, a rapidly rotating or vibrating grating is placed in front of the optical cell, thereby providing the possibility to scan a range of wavelengths in approximately 1s. The signal of the photodetector is measured as a function of time during a measuring cycle. The latter can be related to the wavelength of the light transmitted through the cell.

The other approach is to use a diode array for detection (DAD). Here, the full polychromatic light of the lamp passes through the optical cell before it is dispersed on a grating. The dispersed light strikes an array of 200–500 equidistant light-sensitive diodes, each corresponding to a specific wavelength (range). Every diode of the DAD is part of an electronic circuit, with a capacitor that is discharged to an extent proportional with the light's intensity. During every measuring cycle, which lasts less than 1 ms, the diodes are recharged. The amount of electric charge necessary to do this is taken as a measure of the light intensities at the different wavelengths during that cycle. The intensity data are stored, after conversion into absorbance values.

In Figure 3, the optical arrangements of the rapidly scanning detector and the diode-array detector (DAD) can be compared. The performance of the two types of instruments, in terms of detection limits, is approximately equal, but still slightly worse than that of a single-wavelength instrument. With the scanning method, the detection limits suffer from the short sampling time for every wavelength. With a DAD, the lower signal/noise ratios may be related to the smaller size of the photodiodes in comparison with those used in single-wavelength instruments. By "bunching" the signals for different wavelengths or different measuring cycles during data processing, these disadvantages can be reduced. Despite the slightly inferior detection limits, multiwavelength detection has rapidly become very popular for various reasons. The main areas of application are the following:

1. *Peak-purity assessment*: When two compounds elute very close together within one peak, this can be recognized by the differing spectra recorded on the two flanks, provided the two compounds have different absorption spectra.
2. *Deconvolution of unresolved peaks*: When two peaks are not completely separated, their respective areas can be calculated by deconvolution of the signal using the spectra of the pure compounds. The precision of this method depends on how different the spectra are.
3. *Peak identification*: Even though the information content of a UV spectrum is not very high and these spectra are dependent on the solvent composition, the spectrum of a peak recorded during the chromatographic run can be used as an aid in the identification of an unknown compound. Libraries of spectra, stored in the memory of the data-processing unit, can be used for comparison. Differences between the recorded and library spectra will always exist, owing to small differences in the solvent, the presence of minor interferences, and detector noise. Methods exist to express the similarity of spectra in a single numeric value (a matching factor).
4. *Peak tracking*: One of the problems in (automated) optimization of separations is the identification of the peaks when the order of elution of the compounds changes. With multiwavelength detection, this can easily be achieved.

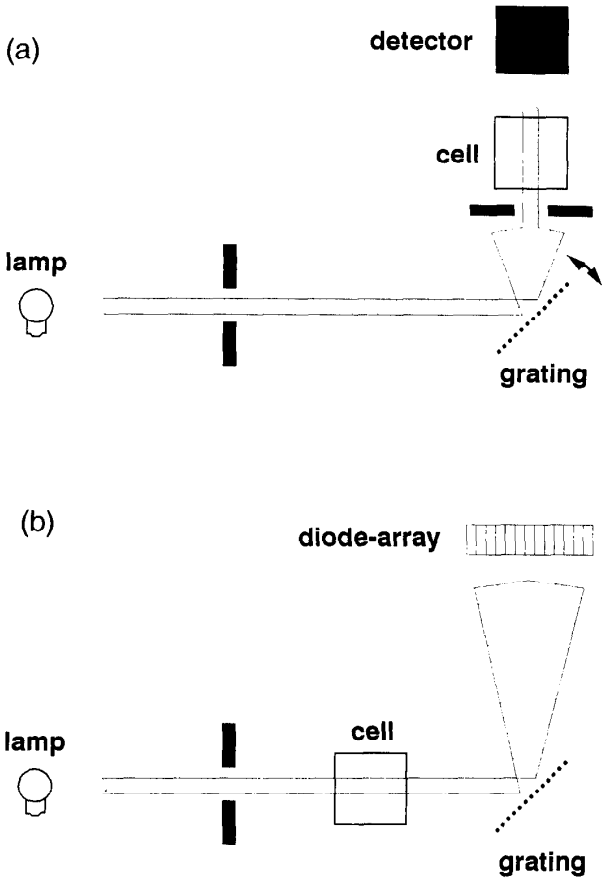


Figure 3 Optical arrangements for multiple wavelength detection: (a) rapidly scanning detector; (b) diode-array detector.

When multiwavelength data are used for peak identification or deconvolution purposes, care should be taken that the detector behaves linearly (i.e., that the absorbance stays well below 1 AU).

The development of methods and programs for data processing in multiwavelength detection is still progressing strongly. Different techniques for graphic representation of the recorded signals are employed, such as three-dimensional (3-D) plots or contour plots (Fig. 4). For the quantitative interpretation of the experimental results, however, such plots are of little value.

IV. FLUORESCENCE DETECTION

Fluorescence detection is based on the property of certain molecules to emit light after excitation by UV radiation. Molecules are promoted to an excited state by absorption of a photon. First, a fraction of the absorbed energy is dissipated without radiation until the lowest singlet energy level of the electronic state is reached. Subsequently, after typically 1–100 ns, the molecule falls back to one of the vibrational energy levels of the ground state, emitting a photon (Fig. 5). From this principle of fluorescence, it follows that the emitted light is always of a longer wavelength than the excitation light and that the photons are emitted in a random direction. The emission spectrum (i.e., the variation in the wavelength of the emitted light) is usually rather broad.

Fluorescence is a rather rare phenomenon, rendering it one of the most selective detection methods for HPLC.

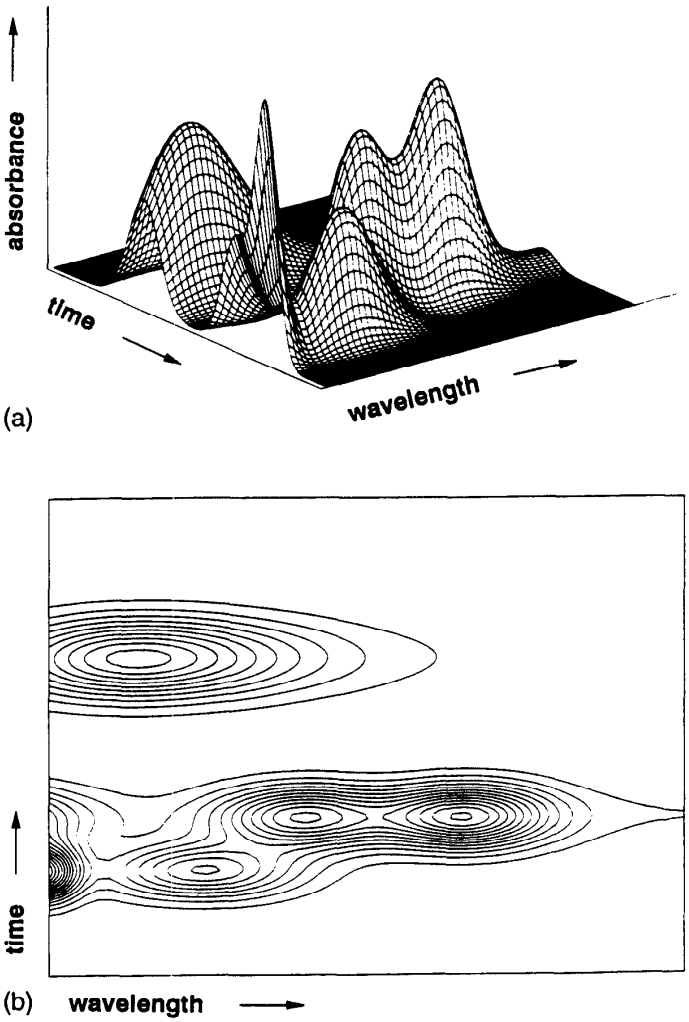


Figure 4 Graphic representation of multiwavelength data: (a) 3-D plot; (b) contour plot.

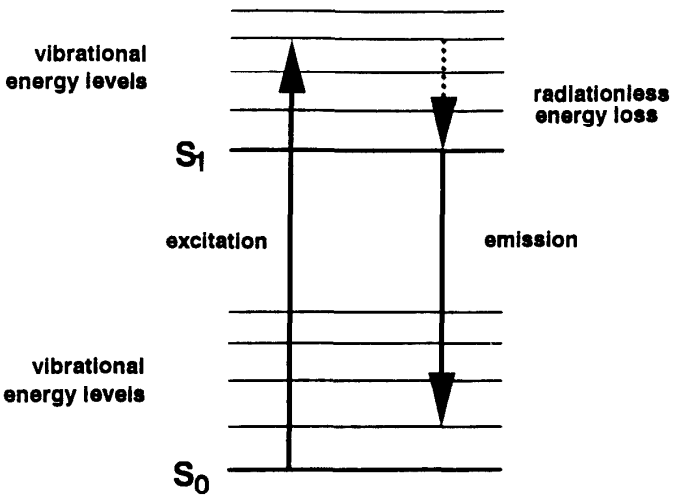


Figure 5 Energy diagram of the fluorescence process.

A. Fluorescence Yields

Generally, the emission of a photon is only one of the pathways for the dissipation of energy by an excited molecule. The quantum efficiency of fluorescence (ϕ_f) for a compound is given by

$$\phi_f = \frac{k_f}{k_f + \Sigma k_i} \tag{6}$$

where k_f is the rate constant of the fluorescence process and k_i represents those of the alternative (radiationless) routes. Although quantum yields of 1 have been observed, a compound with a ϕ_f of 0.1 can readily be considered "highly" fluorescent. The fluorescence properties of a compound are difficult to predict on the basis of its molecular structure; moreover, they also depend on the solvent. However, some general trends can be formulated.

1. A reasonable to high degree of fluorescence is often found for highly conjugated organic molecules, especially when they have a rigid, planar structure.
2. The fluorescence of organic ring structures is often enhanced by the incorporation of heteroatoms in the ring.
3. Substitution of electron-donating groups in aromatic molecules enhances fluorescence, whereas electron-withdrawing groups decrease fluorescence.
4. The presence of heavy-atom (chloride, bromide) substituents decreases the fluorescence efficiency.
5. The fluorescence of a specific molecule is sometimes stronger in a polar than in a nonpolar solvent.

The presence of other solutes in the solvent can strongly decrease the fluorescence by a process called quenching—the promotion of radiationless pathways of energy dissipation. Dissolved oxygen and large ions (metals, bromide) are notorious for this. Therefore, careful purification and degasing of the mobile phase is necessary when fluorescence detection is used. Another source of concern is the presence of "invisible" quenchers in the sample. When such compounds coelute with the analytes of interest, highly inaccurate and irreproducible results may be obtained.

B. Instrumentation

The intensity I_{det} of the emitted light striking the photomultiplier tube in a fluorescence detector is given by Eq. (7).

$$I_{det} = q \cdot I_0 \cdot (1 - 10^{-\epsilon bc}) \cdot \phi_f \tag{7}$$

where q is the efficiency of the instrument for the collection of the emitted light, I_0 the intensity of the excitation radiation in the optical cell, and ϕ_f the fluorescence yield of the analyte molecules. The factor $(1 - 10^{-\epsilon bc})$ in Eq. (7), where ϵ is the extinction coefficient of the analyte at the excitation wavelength, represents the fraction of the light absorbed by the analyte in the optical cell. For low absorbances the absorbed fraction approaches 2.3 ϵbc. Therefore, the fluorescence signal is [approximately] linear only at low analyte concentrations. Nonlinearities can also be caused by the absorption of emitted light when its wavelength is in an absorption band of the analyte.

From Eq. (7), it is clear that the instrumental requirements for a high sensitivity are a strong radiation source and an efficient collection of the emitted light. In commercial instruments high-pressure mercury lamps or (pulsed) xenon arcs are used as high-intensity excitation sources. The appropriate wavelength is selected using a band-pass filter or a grating. With the former, higher intensities can be obtained, whereas the latter offers greater selectivity. The

desired emission wavelength range is also selected with a filter or a grating. With a hemispherical mirror or a 2π arrangement, the emitted light can be collected with a high efficiency. To obtain a low background signal, it is especially important to eliminate the excitation wavelength and overtones thereof by spectral filtering or spatial resolution. A laser is often used as the excitation source in miniaturized HPLC, with packed or open capillary columns. With a laser, a high light intensity can be focused on a small detection volume. A part of the (fused-silica) capillary is used as the optical cell. A disadvantage of laser-induced fluorescence (LIF) is that at the wavelengths of reasonably priced lasers (i.e., above 600 nm) only a few specially designed molecules exhibit fluorescence.

The fluorescence signal of the analytes is always measured against a certain background signal. This background is caused by scattering of the excitation radiation on the walls of the flow cell, by fluorescent impurities in the solvent, and by Raleigh and Raman scattering of the solvent. The noise on the background signal largely determines the LODs that can be obtained. These can still be one to three orders of magnitude lower than with absorbance detection.

C. Precolumn Fluorescence Labeling

Because fluorescence is a rather rare phenomenon, the applicability of this detection mode is limited if we restrict ourselves to native fluorescence. However, to profit from the inherent selectivity and sensitivity, numerous reagents have been developed with which certain classes of compounds can be made fluorescent before chromatographic separation [7]. Most of these precolumn derivatization schemes involve the covalent addition of a fluorescent moiety to a specific functional group of the analyte molecules. Criteria for the development or selection of a derivatization reagent include the following:

1. The derivative should have a high fluorescence quantum yield at an excitation wavelength for which a strong source (lamp or laser) is available.
2. The labeling should proceed selectively with one type of functional group.
3. The derivatization reaction should yield a single, well-defined, stable product.
4. The excess of nonreacted reagent should either be nonfluorescent, or should be easily separable from the derivatized analytes.

Many labeling reagents are commercially available; some of those more frequently used are listed in Table 3.

Table 3 Reagents for Precolumn Fluorescence Labeling

Reagent	Analytes	λ_{ex} (nm)	λ_{em} (nm)
o-Phthalic anhydride (OPA)	Primary amines, thiols	340	455
Fluorescamine	Primary amines	390	475
Dansyl chloride (Dns-Cl)	Primary and secondary amines	350	530
9-Fluorenylmethyl chloroformate (FMOC)	Primary and secondary amines	260	305
Naphthyl isocyanate	Hydroxy compounds	310	350
Dansylhydrazine (Dns-H)	Aldehydes and ketones	365	505
Anthryldiazomethane (ADAM)	Carboxylic acids	365	412
N-Acridinyl maleimide (NAM)	Thiols	355	465

D. Postcolumn Derivatization

A derivatization to make analytes fluorescent can also be performed postcolumn (i.e., after the separation). In Figure 6, a common setup for postcolumn derivatization is shown schematically. A reagent solution is added to the column effluent by a second pump. After mixing, the solution passes a reactor, where a certain amount of time, as determined by the volume of the reactor and the total flow rate, is allowed for the reaction to proceed before the reaction products are detected. Postcolumn derivatization has two major advantages over precolumn methods:

1. If multiple reaction products are formed for one analyte, only one peak will still be obtained.
2. Reproducible results can be obtained, even when the reaction is not complete or when the products are unstable, because the reaction time is highly reproducible.

However, the possibilities for application of a certain reaction postcolumn are more limited. A first prerequisite is that the (nonreacted) reagent itself is not fluorescent. Moreover, the reaction conditions (solvent, temperature) should be compatible with the separation system, and the reaction time is limited owing to peak broadening in the reactor.

The quality of a reactor design can be quantified by the ratio of the extra peak broadening it causes and the reaction time it provides. For fast reactions, with a reaction time up to 1 min, a simple piece of tubing is usually used as the reactor. To reduce the dispersive effect of the parabolic flow profile in the tube, it can be coiled or "knitted." The secondary radial flow patterns in such a tube help diminish the effect of velocity differences between individual analyte molecules.

Alternative approaches to postcolumn derivatization have been studied intensively [8]. These include photochemical and electrochemical derivatization and the use of immobilized enzymes or antibodies.

V. REFRACTIVE INDEX DETECTION

The refractive index (RI) detector is the most universal detector available for LC. It was one of the first LC detectors developed. Compared with other detector types, however, its detection limits are poor. Therefore, an RI detector is now used only when other methods fail.

With an RI detector, the difference in refractive index is measured between the pure mobile phase and the solution containing an eluted compound. The relation between the refractive index n and the concentration or volume fraction of an analyte is nonlinear, but for low analyte concentrations, it is linear to a good approximation:

$$n = n_0 + k \cdot (n_i - n_0) \cdot C_i \tag{8}$$

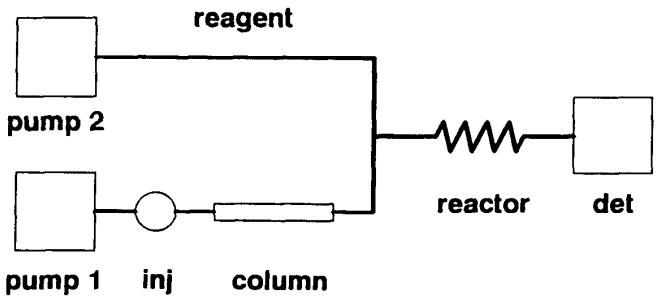


Figure 6 Setup for postcolumn derivatization.

where n_0 is the refractive index of the pure solvent, n_i that of the pure analyte, and C_i the volume fraction of the analyte. The constant k is usually not far from unity. RI differences between solvent and solute $(n_i - n_0)$ are often in the range 0.1–0.2. Only when an analyte has exactly the same RI as the solvent, then no response is obtained.

A. Optical Principles

In commercially available instruments, different optical principles are applied. The most common are the diffraction-type and the reflection or Fresnel-type RI detector. In both types, a light source in the visible range is used, as well as photocells for the measurement of light intensities. A simplified scheme of the optical system of a diffraction-type instrument is shown in Figure 7a. The light passes through two prism-shaped flow-cells, one filled with "pure" mobile-phase solution, and one flushed by the column effluent. When the two solutions differ in refractive index, the light beam is deflected at the wall between the two optical cells, with the angle depending on the RI difference. Detection can be performed in the differential mode by measuring the difference in light intensity on two photocells.

The Fresnel-type detector is shown schematically in Figure 7b. A light beam is directed at the sample cell under an angle close to the critical one. Although most of the light is reflected on the wall–solution interface, a small part of it is deflected; its intensity is strongly dependent on the refractive index of the solution. The deflected beam hits the backside of the cell, which is grained to give a diffuse backscatter. The backscattered light is collected with a lens on a photodetector. The intensity of the detected light depends on the refractive index in a complicated manner.

A third type of RI detector uses interference as the measuring principle. The light of a source is split into two beams, one going through a reference cell and one through the sample cell. The beams are combined again before they hit the photodetector. Because the optical path lengths in the cells depend on the refractive index of the solutions, a shift of the interference pattern and, consequently, of the measured light intensity, is observed when the refractive index of the sample solution changes.

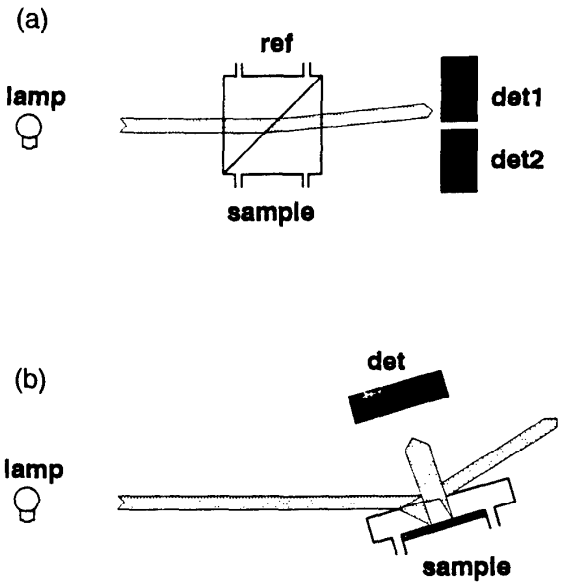


Figure 7 Optical arrangements for RI detection: (a) diffraction system; (b) reflection system.

B. Performance and Applications

One of the most critical factors that affect the performance of an RI detector is the stability of the temperature of the sample and the reference cells. Refractive indices are strongly dependent on the temperature. Any temperature difference between the effluent and the (stagnant) reference solution will give rise to a large offset signal. Therefore, proper thermostating is essential. One of the strategies developed to reduce these problems is the differential technique. The column effluent is passing through two cells in series, with a small time delay. The signals measured from the two cells are subtracted, so that a time-differentiated signal is obtained. From this, the chromatogram is easily reconstructed. The advantage of this system is that it is easier to keep the two cells at identical temperatures than to keep one cell at a fixed temperature. Also, pressure fluctuations caused by pump variations are leveled out.

With modern RI instruments, noise levels of approximately 3×10^{-9} RI units can be realized. Because the sensitivity for most compounds is close to 10^{-3} units/% (v/v), detection limits are near 0.1 mg L^{-1} in the cell. For a conventional LC system, this corresponds to 10–100 ng/injection. A typical cell volume of a commercial instrument is 10 μL. The RI detectors are less suited for miniaturized systems.

Despite the relatively high-detection limits, the RI detector is still the norm for several applications. Compounds lacking a chromophoric group in the workable wavelength range, such as sugars, can be detected by RI. One of the favorable characteristics of RI detection is the similarity of response for compounds of the same type. In size-exclusion chromatography, RI detection can often be used for the determination of molecular mass distributions, because the signal is directly proportional to the volume fraction irrespective of the molecular size.

VI. ELECTROCHEMICAL DETECTION

Electrochemical detection can be based on measurement of the voltage between electrodes (potentiometry), or of a current passing an electrode (amperometry). Sometimes conductometry, measuring the electrical conductance of a solution, is also referred to as an electrochemical technique. However, because in conductometry the electrochemical (electrode) processes are secondary and a bulk property of the solution is measured, we prefer to discuss this technique separately.

Potentiometric detection is not often applied in combination with HPLC: potentiometric sensors are usually too insensitive and too slow to monitor the column effluent. Moreover, potentiometry is often too selective for what is, in principle, a multicomponent technique. Therefore, the term electrochemical detection (ECD) is usually reserved for amperometric detection.

Electrochemical detection is based on the transfer of electrons between oxidizable or reducible molecules in solution and a solid conductor, the working electrode. In amperometry, the rate of electron transfer (the current) is measured. An inherent advantage of ECD is that the measured quantity is already an electrical signal, which makes the instrumentation relatively simple. Because ECD requires a conductive mobile phase, it is almost exclusively used in reversed-phase HPLC.

A. Principles of Operation

By exchange of one or more (n) electrons with an electrode surface, an oxidator in solution can be reduced or a reductor can be oxidized:

$$\mathrm{Ox(aq)} + n\ \mathrm{e^-(electrode)} \rightleftharpoons \mathrm{red(aq)}$$

The direction and rate of this electrode process depends on the difference of the electric potential between the electrode and the solution: an increase in the electrode potential promotes oxidation of a reductor, a change in the opposite direction promotes reduction. Because

the potential difference between electrode and solution cannot be directly controlled or measured, the electrode potential is set relative to a reference electrode, which supposedly has a constant (although unknown) potential difference with the solution.

The rate of the electrochemical reaction is monitored by measuring the current through the working electrode. In the electrochemical process as a whole, three consecutive steps can be discerned, the rates of which are all proportional to the concentration of the oxidator or reductor in the solution.

1. Transport of the analyte molecules to the electrode surface by convective diffusion
2. Transfer of electrons between the analytes in the solution and the electrode surface
3. Transport of the reaction products away from the electrode surface

Either the first and third step (mass transport) or the second step (electron transfer) can be rate-limiting. The rate of mass transport is determined mainly by the flow cell geometry, the rate of electron transfer by the applied electrode potential.

To determine the optimal detection potential for an analyte, a so-called hydrodynamic voltammogram can be recorded (Fig. 8). Chromatograms of standard solutions are recorded with the detection potential at different values. When a low potential is applied to the electrode, the electron transfer is slow and the sensitivity is low. When the potential is increased, the rate of the electrode reaction and, consequently, the peak height increase exponentially. Above a certain potential, however, the transport of the analyte toward the electrode surface becomes the limiting factor, and a constant peak height is reached. This maximum current, i_{lim}, is proportional to the concentration of the analyte in the bulk solution. The detection potential is usually chosen at a value that is just high enough to obtain the maximum current. This optimal potential depends on the chemical properties of the analyte, on the solvent composition (the pH being important), and on the electrode material.

The selectivity of ECD depends on the potential applied. The higher the potential (or the more negative for reductive detection), the more sample constituents will be detected. The potential range that can be used is limited by electrochemical decomposition of the solvent, which causes a high background current. Usually, this is more problematic for negative potentials, so that most applications of ECD involve oxidative detection. Typical compounds

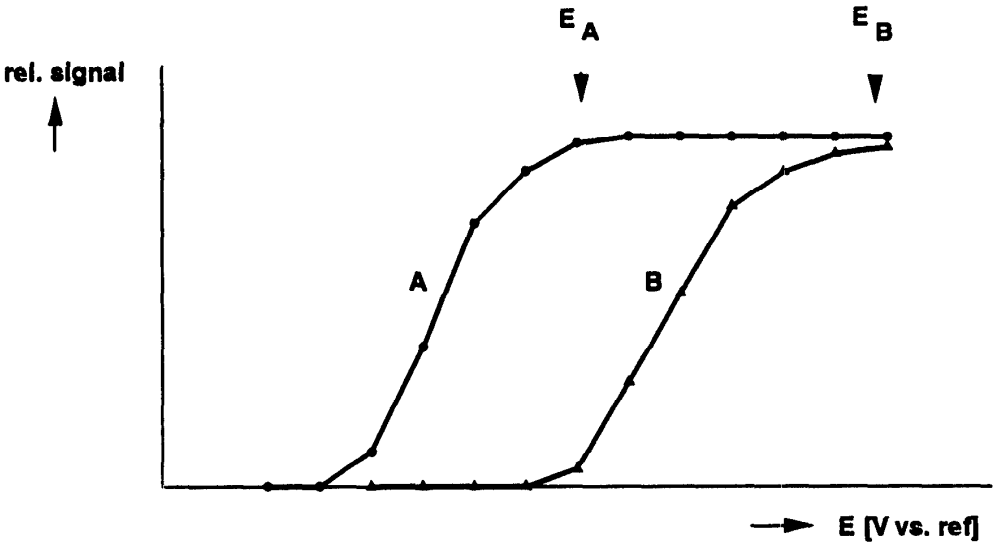


Figure 8 Hydrodynamic voltammograms of two oxidizable compounds A and B: At working electrode potential E_A, only A will be detected; at E_B both compounds will yield maximum sensitivity.

detected in the oxidative mode are catechol derivatives (neurotransmitters), phenols, and aromatic amines. An extra problem in reductive detection is interference owing to the reduction of oxygen dissolved in the mobile phase or the sample.

B. Electrode Materials, Flow-Cells, and Instrumentation

The most widely used material for the working electrode in ECD is glassy carbon, which is a solid, nonporous-type carbon, produced by thermal decomposition of a polymeric material. Relatively high electrochemical reaction rates are often observed on glassy carbon; hence, a moderate detection potential can be applied for many classes of compounds. Because of its smooth, nonporous surface, deactivation of the electrode by adsorption of reaction products or sample-matrix constituents is less problematic than with most other materials.

Mercury, applied as a thin film on gold, is used as electrode material for reductive ECD. The reduction of water from the mobile phase is a very slow process on mercury; therefore, more negative potentials can be applied with mercury than with other electrode materials.

To obtain a high sensitivity in ECD, the flow cell used should provide an effective transport of analytes from the column effluent to the electrode surface. Two different types of flow cells are commercially available: thin-layer cells and porous electrode cells. In the former, the column effluent flows through a thin channel over the solid electrode surface. The current i_{lim} with such a thin-layer cell is given approximately by Eq. (9)[9].

$$i_{lim} = 1.47\, nF \left(\frac{d^{2/3} \cdot A_{el}^{2/3} \cdot \phi^{1/3}}{b^{2/3}} \right) C_0 \tag{9}$$

where F is the Faraday constant, D the diffusion coefficient of the analyte, c_0 its concentration in the cell, A_{el} the surface area of the electrode, b the thickness of the channel, and ϕ the flow rate. In commercial cells, with the usual values for A_{el}(1–10 mm^2) and b(25–100 μm), the conversion of the analyte is only 1–10%. An increase in the electrode area would increase the sensitivity (with $A_{el}^{2/3}$). However, because the noise is usually proportional to the electrode area, a lower signal/noise ratio would be obtained.

Complete conversion of the analyte, with maximum sensitivity, can be obtained with a porous electrode cell. In the commercially available cells the working electrode is a packed bed of carbon particles. A high mass-transfer rate is obtained when the column effluent percolates through the bed. For a complete (coulometric) conversion the minimum required bed length depends on the linear flow velocity in the cell. For a given cell this implies that coulometric conversion may not be obtained when the flow rate is too high. A coulometric cell gives the highest possible sensitivity. However, owing to the large internal surface area of a porous electrode, signal/noise ratios are inferior to those obtained with thin-layer cells.

The advantage of a coulometric system is that, in principle, calibration is not necessary. The amount of analyte eluted from the column can be calculated directly from the peak area using Faraday's law, provided that the number of electrons exchanged per molecule is known. This can be an important advantage when the pure compounds are not available for calibration (e.g., in metabolic studies).

In a flow cell, three electrodes are present: the working electrode, the reference electrode, and a counter- or auxiliary electrode. The counter-electrode is used to prevent the electric current from passing through the reference electrode, for this could change its potential. A potentiostat automatically adapts the counterelectrode potential to accommodate the current through the working electrode, while keeping the working electrode potential at the desired value relative to the reference. With modern instrumentation, currents in the nanoampere and picoampere ranges are easily measured. To keep the noise level low, adequate electromagnetic and thermal shielding of the cell is required. For easily oxidizable compounds, detection limits as low as 0.1 pmol can be obtained in a conventional LC system.

C. Selectivity Enhancement in ECD

At the low concentration levels that can be measured, the selectivity of ECD can be insufficient for complex samples, such as biological fluids. One of the techniques developed to increase the selectivity is dual-electrode detection [10]. For this, two working electrodes are installed in series in the flow cell. These operate at different potentials. When, for instance, the first electrode is used to oxidize compounds eluted from the column, the second electrode can be used to reduce back the reaction products. Only those compounds for which the electrochemical process is reversible will give rise to a signal at the second electrode. The chromatogram obtained with the second electrode can be considerably less complex than that of the first electrode. The sensitivity obtained with the second electrode, however, is usually lower, because the reaction products of the first electrode are only partially converted at the second one.

Another way to use a dual-electrode system is with the first working electrode in the shielding mode. This electrode is then operated at a lower potential than the second one, which is the measuring electrode. Interfering compounds with a low oxidation potential are removed from the solution at the first electrode. In this way the second electrode is "shielded." Again, the chromatogram recorded with the second electrode becomes less complex. To obtain the high efficiency of this shielding, the first electrode should be porous.

Another way to increase the selectivity of ECD is to use special electrode material [11]. In most applications of ECD an electrode material is selected that is as inert as possible (e.g., glassy carbon). However, for certain classes of analytes special electrodes can be used that play an active role in the electrochemical process. Thiol compounds, for instance, can be detected with a mercury (film) electrode. In the oxidation process, a mercury compound is formed. Because this is energetically favorable, the thiol compounds can be detected at a much lower potential than with a carbon electrode. According to a similar principle, silver electrodes are used for the detection of inorganic ions that form complexes or insoluble salts with silver ions, and copper electrodes are used for the detection of amino acids.

Much research effort is being devoted to the development of chemically modified electrodes [12]. Selectively permeable films of polymeric materials can be applied on the electrode surface to increase the selectivity of detection. Redox catalysts can be bound to promote the oxidation or reduction of certain classes of compounds. The ultimate selectivity is obtained by modification of an electrode with an enzyme, catalyzing the oxidation or reduction of eluted substrates, or producing an electroactive substance, such as hydrogen peroxide. Incompatibility of the enzyme with the mobile phase and the electrode lifetime are the main factors limiting the application of enzyme modified electrodes.

D. Pulsed-Amperometric Detection

Pulsed-amperometric detection (PAD) has become a valuable technique for the determination of sugars [13]. Sugars are not easily oxidized electrochemically, but with a gold or platinum working electrode and a high-pH solvent, they can be detected. The gold or platinum surface is believed to have a catalytic effect on the electrochemical reaction. If the electrode were to be operated at a constant potential, the sensitivity would rapidly drop to zero owing to deactivation of the electrode material and adsorption of reaction products on the surface. Therefore, a repeating cycle of potential pulses has to be used. In a typical 1-s cycle, three potential levels are applied. First, the sugars are adsorbed on the electrode surface at a negative potential. Then, the potential is changed to a small positive value, at which the adsorbed compounds are oxidized, and the current is measured. Finally, a high potential is applied, at which the gold or platinum surface itself is oxidized. In this way the electrode is cleaned before a new cycle starts. In Figure 9 an example of the use of PAD is shown.

The use of PAD is a robust technique, for electrode pollution, often a problem in ECD, is prevented. However, owing to the high background current associated with the potential

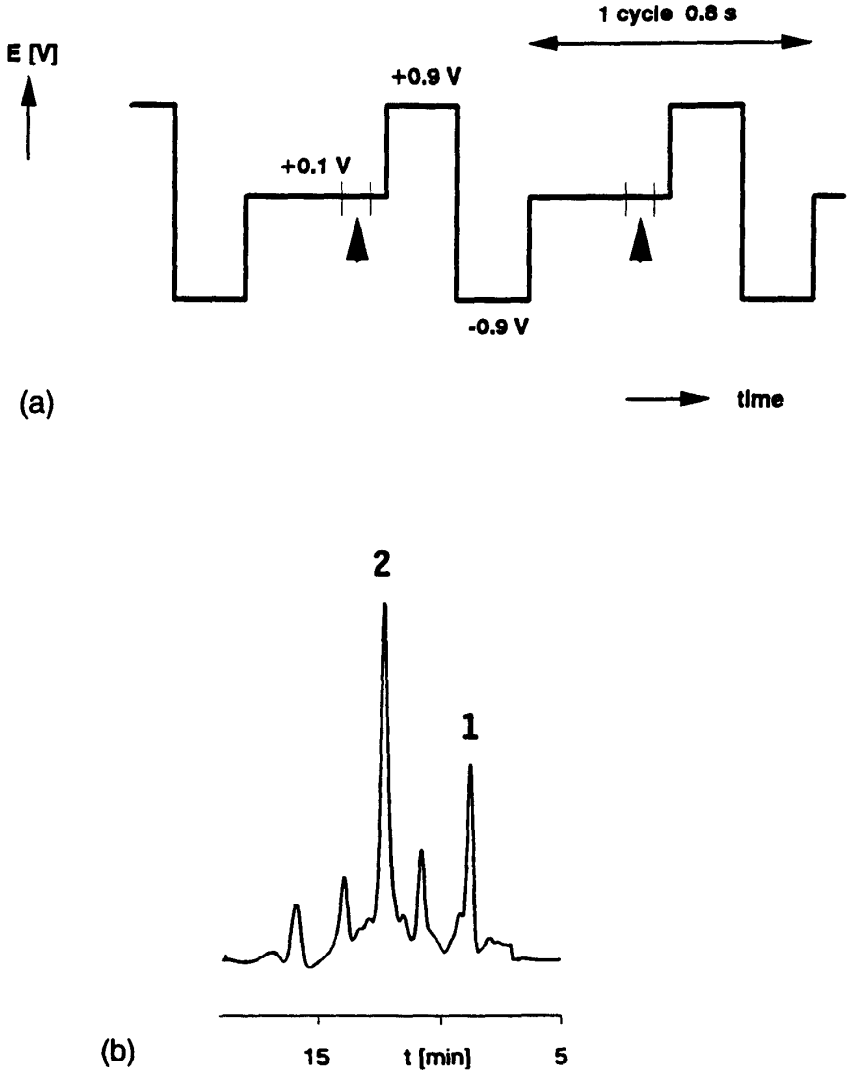


Figure 9 Detection of sugars with PAD: (a) cycling of the applied potential, the arrow indicates the current sampling time; (b) chromatogram of a urine sample containing the exogenic sugars cellobiose (1) and rhamnose (2), separated on an ion-exclusion column.

pulses, the limits of detection are two or three orders of magnitude higher than with constant-potential ECD.

VII. CONDUCTIVITY DETECTION

A. Principle of Operation

In ion-exchange chromatography the elution of analyte ions causes a change in the electrical conductivity of the column effluent. The solution conductance k is the sum of the contributions of the different ionic species present in the solution:

$$k = \Sigma_i \lambda_i^0 \cdot C_i \tag{10}$$

where λ_i^0 is the equivalent conductivity of ion i. Changes in the column effluent composition can be monitored by measuring the current passing two parallel platinum or stainless steel

electrodes in a flow cell when an alternating (AC) voltage, with an amplitude of a few volts, is applied between them. The voltage function can be a sine or a square wave. With a constant (DC) voltage over the electrodes, no current would be measured, because in the absence of electroactive components in the cell, electric charge cannot be transferred between the electrodes and the solution. However, when the applied voltage is changed, a transient current will be measured owing to the charging of the electrode surface. The electrode surface and the electrolyte solution layer in its proximity constitute an electrical double layer that behaves as a capacitor. The two sensing electrodes and the conducting solution between them in the flow cell can be modeled as a series circuit of two capacitors C_{el} and a resistance R_{sol}. The current i_{AC} measured in such a circuit when an alternating sine-wave voltage V_{AC} is applied is:

$$i_{AC} = \frac{V_{AC}}{R_{sol} + (1/\pi f C_{el})} \tag{11}$$

where f is the frequency (in hertz) of the sine wave. By using a high-frequency voltage source (usually about 1 kHz), the influence of the electrode processes can be minimized (i.e., fC_{el} becomes larger) and the current measured will reflect mainly the resistance of the solution. Because R_{sol} is, by definition, inversely proportional to the conductivity, the current measured at high frequencies is approximately proportional to k:

$$i_{AC} \approx q \cdot k. \tag{12}$$

The proportionality constant q is determined by the amplitude of the applied AC voltage, by the size of the electrodes, and by the geometry of the flow cell. However, at high analyte concentrations the linearity between the measured current and the conductivity of the solution may be lost because the term representing the capacities in Eq. (11) can no longer be neglected.

B. Suppression Systems

Because in ion chromatography an electrolyte solution is used as the mobile phase, conductivity changes owing to the elution of sample ions should be measured against a high background. This affects the detection limits, even when the conductivity measurement itself can be performed with high precision. There are three ways to reverse this effect.

The first strategy is simply to use a buffer of low concentration. This usually implies that a column with a low capacity must be used to avoid excessive analysis times. The second way to reduce the negative effects of a high background signal is by electronic suppression. This can be achieved, for instance, by a differential measurement with two electrode pairs in series in the cell. The time lag between the currents measured with the two electrode pairs results in a differentiated signal, from which the original chromatogram may easily be reconstructed. Baseline drift and other disturbances that are slow relative to the chromatographic process can be eliminated.

The third strategy is to use a chemical suppression system. Chemical suppression is based on the replacement, after the separation, of strong ions of the buffer by hydrogen or hydroxide ions, which then bind with the weak buffer ions to form neutral molecules. In anion chromatography, for instance, a sodium hydrogen carbonate buffer is often used. In an on-line suppression system after the separation column the sodium cations are replaced by hydrogen ions. Because of the acid–base reaction

$$H^+ + HCO_3^- \rightarrow CO_2 + H_2O$$

the background conductivity is suppressed. When (strong) anions elute, the sensitivity can even be increased because Na^+ are replaced by more mobile H^+ ions. Correspondingly, when

in cation chromatography, for example, a diaminopropionic acid (DAP)–HCl buffer is used as a mobile phase, the chloride ions can be exchanged for hydroxide ions in the suppression system. The background conductivity is then decreased by the reaction

$$DAPH^+ + OH^- \rightarrow DAP + H_2O$$

It is clear that to maintain the sensitivity for analyte ions, they should not be neutralized by hydrogen or hydroxide ions. This means that the analytes should be stronger acids or bases than the buffer species used in the mobile phase. Three different systems for chemical background suppression have been developed.

The oldest chemical suppression system [14] consists of a small ion-exchange column after the separation column. For anion separations, a high-capacity cation exchanger in the H^+ form is used as packing material for the suppression column; for cation separations an anion exchanger in the OH^- form is used. After a certain period of use the resin becomes saturated with the strong buffer ions, and the suppression column has to be regenerated.

A second chemical suppression system is based on dialysis through a semipermeable membrane. The column effluent is led through a hollow fiber or over a flat membrane of the appropriate ion-exchange material, with a solution of a strong acid or hydroxide on the other side. The exchange of buffer ions takes place by (passive) diffusion through the membrane. The suppressant solution is stirred or circulated to promote a high-exchange yield and as complete a suppression of the background conductivity as possible. The membrane material is not permeable for oppositely charged analyte ions; therefore, these are not lost from the system. An advantage of this method, compared with the use of a suppression column, is that regeneration is not required. Only the acid or hydroxide solution at the "outside" of the membrane system must be refreshed regularly.

The third, and most recent, development in this field is a suppression system based on electrodialysis [15]. The column effluent is led through a thin channel between two ion-exchange membranes. The exchange of strong buffer ions for hydrogen or hydroxide ions is promoted by an electric field applied between the solutions on the "outsides" of the membranes. Pure water can be used as regenerant solution, with the required hydrogen or hydroxide ions being electrolytically generated. The advantages claimed for this system are a more effective background suppression and the greater speed of the process. The latter factor makes it possible to use a smaller channel, giving a correspondingly smaller contribution to peak broadening. The detection cell itself can be made very small, so that this type of conductivity detection becomes compatible with miniaturized HPLC.

With proper suppression of the background, detection limits for simple inorganic ions are about 1×10^{-7} to 5×10^{-7} mol L^{-1} in the sample, depending on the sample matrix and the column used. Chemical suppression systems have been strongly protected by patents; consequently, their commercial availability has been limited to one supplier (Dionex). Instrument suppliers using electronic suppression have claimed detection limits of the same order of magnitude with isocratic elution. A suppression system is a prerequisite for the application of gradient elution.

VIII. DETECTORS FOR POLYMER ANALYSIS

Size-exclusion chromatography, and related separation techniques, are used to determine the molecular mass distribution of homogeneous polymer samples[1] of synthetic or biochemical origin. The most frequently used detectors for routine analysis are the RI and the UV-vis absorbance instruments. Because these detectors do not give molecular size information,

[1]In this context, "homogeneous" refers to the usual assumption in SEC that detection sensitivity is independent of molecular mass. The chemical composition is assumed to be constant (and the polymer sample homogeneous) throughout the molecular mass range.

parameters describing the molecular mass distribution of a polydisperse sample can be determined only from the elution profile obtained. This requires calibration of the separation system using standards with a narrow size distribution (see Chap. 7). The translation of the elution profile into a mass distribution is facilitated by the generally uniform sensitivity of the RI and the UV-vis detectors for similar polymer molecules of different sizes when their concentrations are expressed in mass per volume. Because of this uniform behavior, calibration of the sensitivity can usually be performed with only a few mono- or polydispersed samples of known total concentration.

Several detectors have been developed especially for polymer analysis. Some of these allow information to be obtained on the molecular mass, and other size parameters of eluting fractions, when their signals are combined with the signal of a concentration-sensitive detector. In this way the molecular mass distribution of a polydisperse sample can be determined without the need for size calibration of the separation system with monodisperse standards.

A. Evaporative Detectors

The evaporative light-scattering detector (ELSD), or mass detector, is a relatively simple and inexpensive detector that offers an alternative to the use of RI detectors [16]. In this instrument, the column effluent is pneumatically nebulized from a needle. The droplets formed are transported by a stream of air or nitrogen gas through a heated (100–250°C) compartment, in which the solvent is evaporated. The resulting solid particles, which contain the nonvolatile material eluted from the column, are transported to the optical unit, where they pass a beam of light from a small laser or a polychromatic lamp. Part of the incident light is scattered from the particles, and the intensity of the reflected light is measured with a photosensitive device.

The intensity of light scattered from small solid particles can be expressed as:

$$I_{sc} = kI_0 \left(\frac{n^2 - 1}{n^2 + 2}\right)^2 \left(\frac{NV^2}{\lambda^4}\right) \tag{13}$$

where I_0 is the intensity of the incident light, n the refractive index of the solid particles, N the number of particles per unit volume, V the volume of a particle, and λ the wavelength of the light. The proportionality constant k in Eq. (13) depends on the geometry of the optical unit.

Equation (13) shows that, to a first approximation, the signal of a mass detector will be proportional to the square of the mass flux of analyte eluting from the column. The number of droplets formed in the nebulizer per unit of time (determining N) can be assumed to be constant, and the mean volume of the resulting solid particles V is proportional to the concentration of nonvolatile material dissolved in the column effluent. However, in practice, the relation between the signal and the concentration of analyte is more complicated than suggested by Eq. (13). An explanation for this behavior may be that the nebulization process is affected by the presence of polymers in the solution, because of changes in the viscosity. At different analyte concentrations the mean droplet size may be different, giving rise to a different number of particles N. Moreover, the efficiency of the transport of droplets through the evaporation chamber may depend on their mean size. Regardless, the behavior of the mass detector is inherently nonlinear, and when it is used for the determination of molecular mass distribution a careful calibration of its sensitivity is necessary. When the molecular mass range of a sample is calculated from a peak profile, without accounting for the nonlinear behavior of the detector, the polydispersity will be strongly underestimated.

The mass detector can be regarded as a universal detector for polymers. Still, differences in sensitivity can be expected for different solvents (owing to different nebulization characteristics) and different types of polymers (owing to the influence of the refractive index). It can be used with aqueous mobile phases containing volatile buffers, but generally, its performance, in terms of signal/noise ratios, is superior with organic solvents. The limits of

detection are about 10–100 ng/injection. Because all solvent is evaporated before the actual detection, there is no baseline drift during gradient elution.

B. Light-Scattering Detection

Various detectors have been developed based on the Rayleigh scattering of laser light by polymers in solution. When light passes through a solution, it induces temporary dipoles in its molecules. The induced dipoles begin emitting light in phase with the incident light, but in different directions. This phenomenon is known as Rayleigh scattering. The intensity of the scattered light depends on the size and concentration of the scattering molecules and on the angle of the incident light beam. For polymer molecules with a size smaller than the wavelength of the light in the medium λ_m, the scattered light intensity, measured under an angle θ, at a distance z, from the illuminated volume of polymer solution, is given by Eq. (14) [17].

$$I_{SC} = \frac{I_0}{z^2} \cdot \frac{2\pi^2}{N_A \cdot \lambda_m^4} \cdot \left(\frac{d(n/n_0)}{dc}\right)^2 \cdot (1 + \cos^2\theta) \cdot P(\theta) \cdot M \cdot C \tag{14}$$

where I_0 is the intensity of the incident light, N_A Avogadro's number, M the molecular mass of the dissolved polymer molecules, and c their concentration (in mass per volume). The factor $d(n/n_0)/dc$ in Eq. (14), the dependency of the relative refractive index of the solution on the polymer concentration, is a measure of the polarizability (dipole induction) of the polymer molecules. $P(\theta)$ in Eq. (14) is called the size–shape factor. For very small molecules $P(\theta)$ approaches 1; for larger molecules it is given by Eq. (15).

$$P(\theta) = \frac{1}{1 + [(16\pi^2/3)(r_g^2/\lambda_m^2)\sin^2(\theta/2)]} \tag{15}$$

where r_g is the radius of gyration of the polymer molecules. Figure 10 is a diagram showing the angular dependency of the scattering intensity for polymer molecules of different sizes.

From Figure 10, it is clear that, at low angles, the scattering intensity is highest and is least influenced by the size of the polymer molecules. Therefore, low-angle laser–light-scattering (LALLS) detectors have been developed for polymer characterization [18]. To ob-

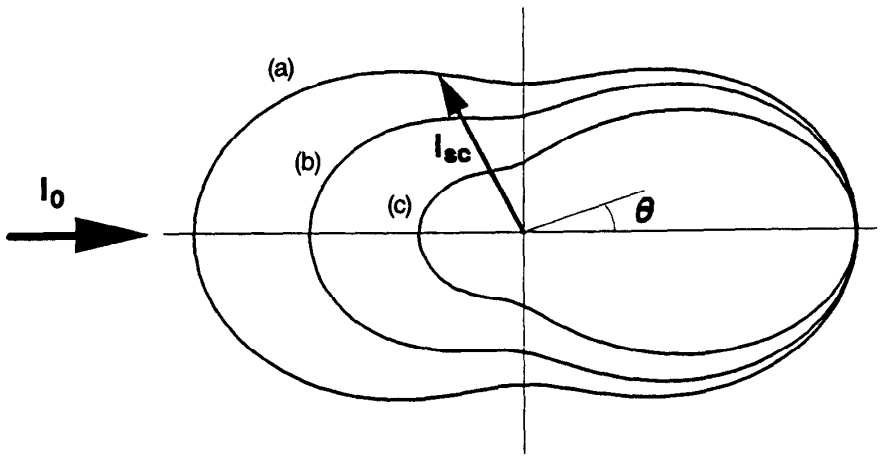


Figure 10 Diagram showing the dependency of the scattered light intensity on the angle, with the incident beam θ and the radius of gyration r_g of the polymer molecules. The relative-scattering intensity is indicated by the distance of the lines from the origin. λ_m = 500 nm; r_g = 0 (a); 50 (b); and 100 (c) nm.

tain a high sensitivity, an intense light source, for instance, the 633-nm line of a He–Ne laser, is focused on a small volume of sample solution. The scattered light is detected at an angle of 3°–5°. The signal obtained from an LALLS detector is proportional to the product of the concentration and the molecular mass of the polymer in the column effluent [see Eq. (14)]. Combined with the signal of an RI detector connected in series, the molecular mass distribution can be obtained directly, without size calibration. For this type of calculation, it is important to know precisely the time delay between the two detectors: otherwise, the results are strongly biased [19].

Polymer molecules of biological origin, such as proteins, are usually compact and small compared with the wavelength of visible light. Therefore, the size–shape factor (P) of these molecules often approximates unity for all detection angles. For these molecules a right-angle (RALLS) detector is sometimes used. Although the sensitivity is lower with a right-angle optical system, an advantage, compared with LALLS, is that the interference by large particles (dust or gas bubbles) is strongly reduced. For RALLS a conventional LC fluorescence detector can be used [20].

With a multiangle laser–light-scattering (MALLS) detector, the scattered light intensity is simultaneously measured under different (fixed) angles using a series of photodetectors. After correction for the background Rayleigh scattering of the solvent, the radius of gyration of the eluting fractions can be obtained from the angular dependency of the signals measured. From this signal, in combination with that of a concentration-sensitive detector, the molecular mass and size distributions of polydisperse samples can be calculated. In terms of detection limits, the LALLS and MALLS detectors give approximately similar results [21]. In return for the additional expenses of a MALLS detector, qualitative information on the sample can be obtained.

C. Viscosity Detectors

The viscosity η of a solution containing a low concentration of a polymer depends on its molecular mass M according to Eq. (16).

$$\eta = \eta_0[1 + (kM^a c)] \tag{16}$$

where η_0 is the viscosity of the pure solvent and k is a constant depending on the type of polymer. The exponent a in the equation depends on only the quality of the solvent for the given polymer; it varies from 0.5 for a θ-solvent, to 0.8 for a good solvent. In combination with a concentration-sensitive detector, a viscosimeter yields information on the molecular mass (distribution) of a sample. Size calibration is not necessary when the Mark-Houwink constants (k and a) are known.

In a viscosity detector for liquid chromatography, the pressure drop is monitored across a piece of narrow capillary, through which the column effluent flows. At a constant flow rate, the pressure drop is proportional to the solution's viscosity. To eliminate pressure variations caused by pump pulsations and temperature changes, a differential setup is used, with a second restriction capillary after a large reservoir, in which eluting peaks are strongly diluted. A relatively high sensitivity can be obtained with a four-capillary setup that resembles a Wheatstone bridge [22].

The simple principle of viscosity detection is not reflected in the price of commercial devices.

IX. OTHER DETECTORS

A. Infrared Detection

Infrared (IR) spectra have a high content of structural information. Therefore, it appears attractive to use IR spectrometry for detection and peak identification in HPLC. The main

problem to be addressed in coupling an IR spectrophotometer to a chromatographic system is the absorbance of radiation by most solvents used as mobile phases. In the past, only off-line measurements were possible when using dispersive scanning IR spectrometers to identify eluted peaks. The time-consuming scanning, necessary to obtain a reasonable sensitivity, prevented on-the-fly application. With the advent of relatively low-cost Fourier-transform (FT) instruments, however, it became possible to apply on-line FT–IR detection [23].

Interfaces using a flow cell with IR transparent windows are commercially available. The flow cell thickness should be small (about 0.2 mm) because of the high absorbance of the solvents. However, in most applications of LC–FTIR an interface is used that eliminates the solvents before detection of the analytes takes place. In such interfaces, the column eluate is deposited on a moving substrate. In the delay time before the actual detection takes place the mobile phase can be evaporated. A quality parameter of the interface is the extent to which droplets of column effluent spread on the substrate before the solvent is completely removed: too much spatial spreading results in a loss of resolution.

B. Optical Activity Detection

For the determination or recognition of optically active compounds a polarimetric [24] or a circular dichroism [25] detector can be used. Polarimetric detection is based on the change of the plane of polarization of light when transmitted through an optical cell containing a chiral compound. In a polarimetric detector two perpendicular polarizers are used: one before and one after the cell. In the absence of a chiral species, the light intensity on the photodetector is minimal. The rotation of the polarization plane caused by the presence of a chiral compound causes an increase in the transmitted light's intensity, which is to a first approximation, proportional to the concentration of the chiral compound.

Circular dichroism detection is based on the difference of absorption by a chiral species of left-circularly and right-circularly polarized light. The light from the source (an Ar laser) is directed onto an electrooptic modulator, then through the cell and onto the photodetector with a lock-in amplifier tuned to the modulation frequency.

The problem with both detectors is the small magnitude of the optical rotation effects. Detection limits are high, even with large optical cells.

C. Radiochemical Detection

Radioactivity detection has the inherent advantage of a high selectivity. However, its combination with LC is not straightforward, because the time-consuming counting process (necessary for high signal/noise ratios) is not compatible with fast separations. In the past, off-line detection was usually applied, the counting being performed on collected fractions of the effluent. More recently, flow-through detection system have become commercially available [26].

The most important radioisotopes for biomedical and pharmaceutical research (^{3}H, ^{14}C, ^{35}S, or ^{32}P) are β-emitters. Nuclear radiation from the active sample constituents is absorbed in liquid or solid scintillator materials. The energy is converted into photons with wavelengths in the range of 350–600 nm, which can be detected with a photomultiplier tube. Liquid scintillators are a cocktail of an organic solvent, a fluorophor, and a detergent or other solubilizer. This mixture is delivered by a reagent pump and mixed with the column effluent before it enters the counting device. The latter is usually a light-transparent tube held between two photomultipliers. Solid scintillation materials include granular anthracene, special inorganic glasses, and fluorophor-doped plastics. The flow cell can be constructed as a transparent cell packed with finely divided scintillation material, as a capillary made of plastic scintillator, or as a transparent tube encapsulated in an external scintillator. The choice of the flow cell volume is a compromise between effective counting and excessive peak broadening.

D. Gas-Phase Detectors

Despite all effort put into the development of sensitive detectors for HPLC, their performance in terms of mass sensitivity is still inferior to that of many simple detectors for gas chromatography (GC). Therefore, the coupling of GC detectors to HPLC is under investigation by several research groups. These investigations have focused on the development of suitable interfaces, in which the mobile-phase solvents can be evaporated. The proliferation of micro-LC has facilitated the construction of interfaces that do not require splitting of the column effluent. The couplings of electron-capture detectors (ECD) [27], flame-ionization detectors (FID) [28], and thermionic or nitrogen–phosphorus detectors (NPD) [29] have been reported.

X. COMPARISON OF DETECTOR PERFORMANCES

With the five main types of detectors, discussed in the foregoing, over 95% of the LC-analysis are performed in practice. A comparison is difficult because the performance of a detector depends on the analytes, on the sample matrix, and on the separation system. Still, some general trends can be observed. The UV-absorbance detector is used most frequently, because of its ease of operation and robustness, its reasonable selectivity (except at very low wavelengths), and its detection limits of near 1 ng.

When detection limits lower than 1 ng are required, a fluorescence detector is often chosen. The selectivity of fluorescence detection may be an advantage, but on the other hand, it often requires derivatization reactions performed before the separation. This seriously complicates the analytical procedure and may be an important source of experimental error. In comparison with UV detection, more attention must paid to the purification of solvents and the cleanup of samples to obtain adequate results.

A RI detector can be used when the concentrations to be determined are relatively high and when the selectivity requirements are low: in short, when the detection is easy. Under these circumstances, it is a robust and easy-to-use instrument. An additional advantage of its universality is that unexpected components in a sample are not easily overlooked.

For easily oxidizable analytes, electrochemical detection offers the lowest detection limits (0.01–0.1 ng). The major application of ECD is in the determination of catecholamines in body fluids. The operation and maintenance of an electrochemical detector is much more problematic than that of optical detectors. Electrode pollution necessitates frequent cleaning and recalibration. This is much less so in pulsed-amperometric detection. However, the detection limits with PAD are much higher than with constant-potential amperometric detection.

Conductivity detection is the norm in ion chromatography. For strong ions, its response is universal. The impossibility of obtaining any additional selectivity may be seen as a disadvantage.

Both UV and fluorescence detection are routinely combined with gradient elution. With ECD and RI detection, shifting baselines make this virtually impossible. Conductivity detectors can be combined with gradient elution, provided that an effective suppression system is used.

The effects of miniaturization of the separation system on the performance of the various detectors are quite divers. For RI detection microcells are unavailable. With UV detection, the signal/noise ratios decrease when the size of the flow-cell is decreased. The same is true for a fluorescence detector. However, by using a laser as an excitation source, this effect can be counteracted. An electrochemical detector can improve the signal/noise ratios in a miniaturized system.

Table 4 summarizes this comparison.

Table 4 Comparison of Detectors Generally Applied in LC

Detector type	UV-vis	Fluorescence	RI	ECD	Conductivity
Typical LOD (ng/injection)	1	0.01–0.1	100	0.01	1
Selectivity	Moderate[a]	Very high	No	High[b]	Low
Robustness	Excellent	High	High	Poor	High
Gradient elution	Yes	Yes	No	No	Yes[c]
Suitability for microsystems	Limited	High	No	Excellent	High

[a]Increases with increasing wavelength.
[b]Decreases with increasing detection potential.
[c]With a suitable suppression system.

REFERENCES

1. RE Majors, HG Barth, CH Lochmueller. Anal Chem 56:300R, 1984.
2. JC Sternberg, In: JC Gidings, RA Keller, eds., Advances in Chromatography, New York: Marcel Dekker, 1966, Chap. 6.
3. RE Majors. LC–GC Int 5:16, 1992.
4. CA Dorschel, JL Ekmanis, JE Oberholtzer, FV Warren Jr, BA Bidlingmeyer. Anal Chem 61:951A, 1989.
5. JW Dolan. LC–GC Int 5:16, 1992.
6. JB Li. LC–GC Int 10:856, 1992.
7. H Lingeman, WJM Underberg. Detection Oriented Derivatization Techniques in Liquid Chromatography. New York: Marcel Dekker. 1990.
8. H Jansen, RW Frei. In: K Zech, RW Frei, eds. Selective Sample Handling and Detection in High-Performance Liquid Chromatography Part B. Amsterdam: Elsevier, 1989 Chap. 5.
9. JM Elbicki, DM Morgan, SG Weber. Anal Chem 56:2560, 1984.
10. DA Roston, PT Kissinger. Anal Chem 54:429, 1982.
11. WT Kok. In: RW, Frei, K Zech, eds. Selective Sample Handling and Detection in HPLC. Part A. Amsterdam: Elsevier, 1988, pp. 309–363.
12. RW Murray. In: AJ Bard, ed. Electroanalytical Chemistry, Vol 13. New York: Marcel Dekker, 1984.
13. DC Johnson, WR LaCourse. Anal Chem 62:589A, 1990.
14. H Small, TS Stevens, WC Bauman. Anal Chem 47:1801, 1975.
15. DL Strong, PK Dasgupta. Anal Chem 61:939, 1989.
16. M Dreux, M Lafosse. Analusis 20:587, 1992.
17. P Kratochvil. In: MB Huglin, ed. Light Scattering from Polymer Solutions. London: Academic Press, 1972.
18. T Takagi. J Chromatogr 506:409, 1990.
19. PJ Wyatt, LA Papazian. LC–GC 11:862, 1993.
20. G Dollinger, B Cunico, M Kunitani, D Johnson, R Jones. J Chromatogr 592:215, 1992.
21. L Jeng, ST Balke, TH Mourey, L Wheeler, P Romeo. J Appl Polym Sci 49:1359, 1993.
22. PK Dutta, K Hammons, B Willibey, MA Haney. J Chromatogr 536:113, 1991.
23. C Fujimoto, K Jinno. Anal Chem 64:476A, 1992.
24. A Mannschreck. Chirality 4:163, 1992.
25. P Salvadori, C Bertucci, C Rosini. Chirality 3:376, 1991.
26. AR Reich, S Kucas-Reich, H Parvez. Drugs Pharm Sci 47:101, 1991.
27. UAT Brinkman, FA Maris. LC–GC Int 1:45, 1987.
28. VG Berezikin. Crit Rev Anal Chem 20:291, 1989.
29. CE Kientz, A Verweij, GJ de Jong, UAT Brinkman. J Chromatogr 626: 59, 1992.

4

Capillary Electrophoresis

Herbert E. Schwartz

FzioMed, Inc., Redwood City, California

Bart J. Wanders

Beckman Instruments, Inc., Fullerton, California

I. INTRODUCTION

Capillary electrophoresis (CE) has received increasing attention in recent years, as is evident from the exponential growth in the number of papers on the subject in the past decade. At present, more than half of the CE publications deal with life science applications (Fig. 1). Classic (slab-gel) electrophoresis techniques are well established in the biomedical sciences, particularly for the analysis of DNA and proteins. Electrophoretic techniques are based on the principle that charged particles migrate under the influence of an external electrical field. The velocity of this migration is proportional to the applied field strength, with a proportionality constant known as the electrophoretic mobility. The electrophoretic mobility is dependent on the medium in which the experiment is performed and on the properties of the analyte. The goal in electrophoresis is typically to separate sample components with sufficiently different effective mobilities.

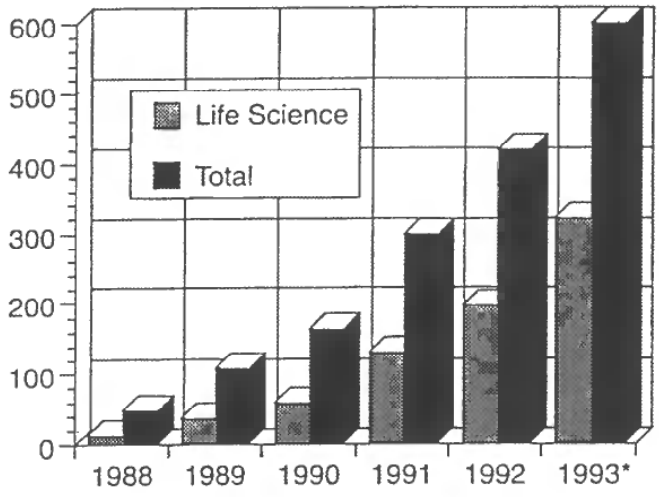


Figure 1 Number of CE articles per year from 1988 to 1993. *As of July 1993, the total was 256, of which 139 were in the life sciences.

A fundamental limitation in the performance of electrophoresis is the evolvement of heat during the run. Application of an electric field draws a current across a solution which, in turn, generates heat. Too much heat is detrimental to the separation efficiency and resolution. In classic electrophoresis, the primary purpose of the gel was to act as an anticonvective medium to limit the band dispersion caused by the generated heat. A capillary format for electrophoresis is extremely suitable for this because the evolved heat is easily dissipated through the capillary walls. Therefore, much higher field strengths can be applied in CE than in slab-gel electrophoresis which results in shorter analytical time and better resolution. Detection in slab-gel electrophoresis is performed mostly by staining the gel with a suitable (fluorescent) dye and subsequent densitometry or autoradiography. Although sensitive detection can be obtained in this manner, slab-gel techniques are generally labor-intensive, lack the precision of chromatographic methods, and are at best semiquantitative. The use of narrow-bore tubes and capillaries may solve these problems.

Capillary electrophoresis can be viewed as an instrumental approach, with many components adopted from the field of high-performance liquid chromatography (HPLC). Indeed, it can be argued that the chromatography–analytical instrumentation community is mainly responsible for the recent explosive growth of CE. As in HPLC, various separation modes are applicable in CE. Hence, CE represents a family of electrokinetic separation techniques: capillary zone electrophoresis (CZE), carried out in free solution, micellar electrokinetic chromatography (MECC), capillary isoelectric focusing (CIEF), capillary gel electrophoresis (CGE), and isotachophoresis (ITP).

A. Capillary Electrophoresis and HPLC: Complementary Techniques

The emergence of a new industry (i.e., biotechnology) has clearly increased the demand for sophisticated analytical instrumentation. In pharmaceutical biotechnology these instruments are used for the identification of chemicals and structures, control of purity, and assays of potency. Biomolecules, such as proteins, nucleic acids, and polysaccharides, are often present only in trace amounts, and sample sizes are small. In clinical and diagnostic applications, typically a few components must be analyzed at trace levels in the presence of many other matrix components. Miniaturized, microcolumn separation techniques, such as micro-HPLC, capillary gas chromatography, or capillary electrophoresis, are particularly suitable for the detection of analytes in very small (microliter) volumes.

Because many samples of biological origin are quite complex, two or more inherently different techniques must be used to perform qualitative and quantitative assays. For example, whereas in reversed-phase HPLC, species are typically separated on the basis of hydrophobicity, in CZE the charge/mass ratio is of premier importance. In addition, cleanup or purification of biomolecules is often done by preparative HPLC, which necessitates a second technique for purity control. The use of complementary methods provides more confidence in the analytical results. As the field of CE is maturing, both CE and HPLC may provide fully automated, computer-controlled, quantitative assays, as well as high-resolution separations with short analytical times (generally less than 1 h).

B. History of CE, Emergence of Commercial Instruments

The principles of electrophoresis were already known as early as the beginning of the last century; and a theoretical basis was formulated by Kohlrausch as early as 1897 [1]. In the 1930s, Tiselius, a Swedish researcher at the University of Uppsala, developed an analytical technique called "moving-boundary" electrophoresis. Although moving-boundary electrophoresis is not used much nowadays, an important milestone in biomedical sciences was reached in 1937 with Tiselius' separation of human serum components (i.e., albumin, α-, β-, and γ-globulin). Further work in Tiselius' laboratory by Hjerten [2] resulted in the development of

zone electrophoresis, which, in contrast to moving-boundary electrophoresis, allows complete separation of sample components.

As with many other techniques, it is difficult to pinpoint an "inventor" of CE. The technique evolved as a result of contributions from various researchers. For example, as early as 1953, Edstrom [3] employed 15 μm id fibers to separate tiny amounts of cellular RNA. Workers in "microelectrophoresis" in the 1950s and 1960s [4] also realized the advantages of capillaries for their heat properties, separation efficiency, and mass sensitivity. In his classic paper published in 1967 [2], Hjerten demonstrated that many electrophoretic separations could be carried out in free solution (i.e., in the absence of a gel) using narrow tubes (3-mm id) and on-tube detection. Zone stabilization was achieved by mechanically rotating the tube. Various applications of this technique, which he called "free zone electrophoresis," were demonstrated (e.g., inorganic ions, nucleotides, proteins, and even viruses). On the theoretical front, Giddings [5] showed that very efficient separations could be obtained if longitudinal diffusion was the only cause of dispersion in a capillary system. Experimentally this was verified by Everaerts et al. [6] in an ITP system with Teflon capillaries and also by Virtanen [7] in a CZE system with glass capillaries. However, from these early experiments, it became clear that further reduction of the capillary diameter would be practical only if suitable instrumentation for injection and detection of very small samples could be developed.

The detection problem was partly solved by Everaerts et al. [8] by using the displacement electrophoresis or ITP technique in conjunction with capillaries. In this technique, a double-electrolyte system, which sandwiches the sample, produces relatively narrow zones with self-focusing properties, thereby increasing the detectability. However, in spite of much progress in instrument development and theory, ITP never took off the way CE did in the late 1980s. In a sense, ITP was ahead of its time and in search of suitable applications (biotechnology had not yet emerged). Perhaps, also, the rather complicated buffer systems and the complex instrumentation, prevented widespread acceptance of ITP as a routine analytical tool.

Further progress in the field of CZE was made by Mikkers and associates [9,10], who demonstrated rapid and highly efficient separations of organic acids, approaching the theoretical predictions made earlier by Giddings. An important breakthrough was achieved in the early 1980s by Jorgenson's group [11,12]. They employed the flexible, gas chromatography (GC)-type fused-silica capillaries of 75-μm id and on-column detection for highly efficient separations of proteins. Modern commercial CE instrumentation, first introduced in 1988 by Brownlee and co-workers [13,14], has essentially the same key features as those described by Jorgenson. In 1994, more than a dozen vendors sold CE instrumentation, from stripped-down, modular versions, to fully integrated, automated systems [15]. Commercial instruments come standard with on-capillary UV absorbance detectors. Diode-array, (laser-induced) fluorescence, and mass-spectrometry interfaces also currently available from some manufacturers. In the future other detectors (e.g., conductivity, refractive index, electrochemical) are expected to become available. Figure 2 depicts a diagram of a modern CE instrument. The magnified view shows the electrical double layer at the capillary wall and an imaginary separation of anions, cations, and neutral molecules (see also Sec. III.A)

In the past decade, important advances have been made in the chemistry underlying separation mechanisms in CE. For example, an initial drawback was that, in principle, only charged species could be separated. In 1984, Terabe et al. [16] introduced micellar electrokinetic capillary chromatography (MECC). The micelles, for example, alkyl sulfonates aggregates, are charged and migrate electrophoretically in the capillary. A pseudostationary phase is thereby formed. Neutral compounds (e.g., many pharmaceuticals) can then be separated on the basis of different affinities for the micellar phase. Other research groups emphasized the importance of coatings to manipulate the electroosmotic flow (EOF) or to prevent undesirable adsorption of analyte on the capillary wall. Undoubtedly, in the near future; the number of commercially available coatings will increase, either as part of special applications kits, or as separate capillaries. After the initial phase of development, during which the focus was mainly on fundamental studies and the development of first-generation instrumentation, CE now en-

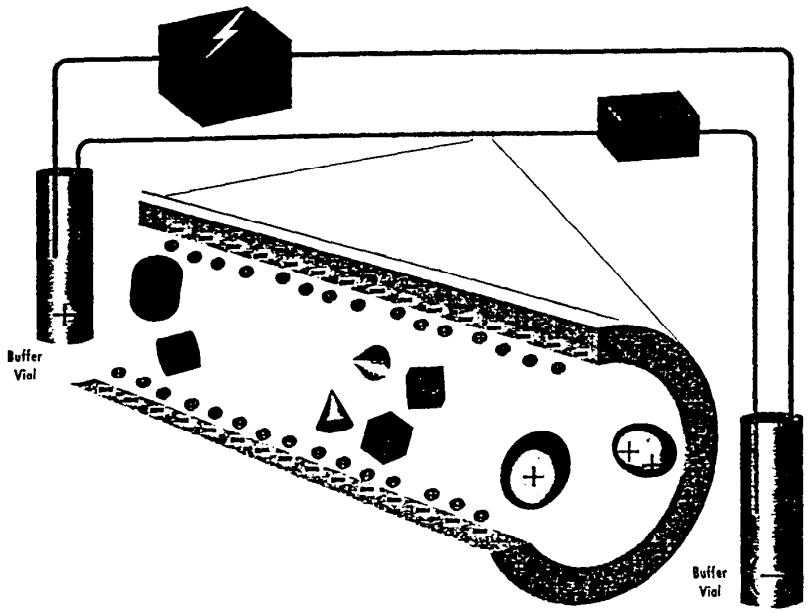


Figure 2 Block diagram of a basic CE instrument. The magnified view shows the interior of the capillary during a separation of anions, cations, and neutral molecules.

ters a second phase, in which it has to prove itself as a viable analytical tool for routine analyses, e.g., in quality control applications of the biopharmaceutical industry.

C. Scope of This Chapter

In this chapter, a brief introduction into the main principles of CE will be given. The concepts of electrophoretic mobility, origin of the EOF, and methods to measure and control the EOF are discussed from a theoretical perspective. This is followed by an examination of the factors affecting separation performance, including the sample introduction process, adsorption phenomena, and Joule heating. Finally, the various modes of CE (i.e., CZE, MECC, CIEF, CGE, and ITP) are discussed. Applications of CE, as well as instrumental designs, will not be discussed in detail in this chapter, but can be found in several recent textbooks [17–19]. A new journal (see *Journal of Capillary Electrophoresis*, Vol. 1, 1994) also focuses specifically on applications of CE.

II. PRINCIPLES OF CAPILLARY ELECTROPHORESIS

A. Electrophoretic Mobility

The term *electrophoresis* (from Greek: *ēlectro* + *phorēsis* [$\Phi o \rho \varepsilon \varepsilon \sigma \vartheta \alpha \iota$] = to be dragged) is used for a collection of separation techniques based on the difference in the velocity of charged particles when subjected to an external electric field. Under given experimental conditions the velocity v of each particle is proportional to the strength E of the electric field:

$$v = \mu E \tag{1}$$

The constant μ is the electrophoretic mobility.

The electrophoretic mobility of a given ion strongly depends on its environment. Therefore, a theoretical absolute mobility μ^0 is defined as the mobility under conditions of infinite dilution and complete ionization, when the species are unaffected by the solvent environment. Under these conditions, an expression for the electrophoretic mobility can be obtained by

equating, under steady-state conditions, the force exerted on a particle by an electric field with the opposing frictional force:

$$qE = f_c v \tag{2}$$

in which q is the electrical charge of the particle, E the electric field strength, and f_c the friction factor.
According to Stokes, the friction factor for a spherical particle is given by:

$$f_c = 6\pi\eta r \tag{3}$$

in which η is the viscosity of the solvent and r the radius of the particle. This leads to the following expression for the absolute mobility (μ^0):

$$\mu^0 = \frac{q}{6\pi\eta r} \tag{4}$$

At finite dilution, the situation alters because each ion will be surrounded by a cloud of counterions that tends to move in the "wrong" direction; thereby lowering the mobility. A correction factor γ is used to relate the mobility at finite dilution to the absolute mobility [20]:

$$\mu^c = \gamma\mu^0 \tag{5}$$

Separation of two species will be possible if the effective mobilities are sufficiently different. After a time (t) the difference in migration distance (Δd) will be:

$$\Delta d = |d_1 - d_2| = |\mu_1 - \mu_2|Et \tag{6}$$

An important factor determining the mobility of the species is the degree of dissociation, for example, of weak acids and bases. Here, the species will be in the ionized form only part of the time (dynamic equilibrium) and, therefore, the effective mobility μ_A of species A will depend on the mobility of the ion and on the dissociation constant. According to Tiselius [20] the effective mobility can be calculated from the summation of all products of the dissociation constant α, the correlation factor γ, and the mobility at infinite dilution μ^0:

$$\mu = \sum_i \alpha_i \mu_i^c = \sum_i \alpha_i \gamma_i \mu_i^0 \tag{7}$$

For a weak monovalent acid A the effective mobility μ_A can be calculated using

$$\mu_A = \mu_A^c \frac{[A^-]}{[HA] + [A^-]} = \mu_A^c \frac{K_A}{[H^+] + K_A} \tag{8}$$

where

$$K_A = \frac{[H^+][A^-]}{[HA]} \tag{9}$$

For two species A and B the separation will depend on the difference in effective mobilities and the pH.

$$\mu_A - \mu_B = \left(\mu_A^c \frac{K_A}{[H^+] + K_A}\right) - \left(\mu_B^c \frac{K_B}{[H^+] + K_B}\right) \tag{10}$$

The optimum pH for separation is then given by [8]

$$[H^+] = \left(\sqrt{\frac{\mu_A}{\mu_B}} - \sqrt{\frac{K_A}{K_B}}\right) \frac{\sqrt{K_A K_B}}{1 - \sqrt{\mu_A K_A}\sqrt{\mu_B K_B}} \tag{11}$$

B. Electroosmotic Flow

In CE the EOF serves multiple purposes. It has been used as a "liquid pump" in both CZE and electrokinetic chromatography (e.g., MECC). One of the major benefits for electrokinetic chromatography is the flat velocity profile of the flow compared with the parabolic profile created by mechanical, pressure-driven pumps used in HPLC (Fig. 3). Although Figure 3 perhaps gives an oversimplified picture—other factors are involved for comparable separations—peak broadening in CE is usually less than in HPLC. Theoretical plate numbers are often 10- to 100-fold higher in CE. The EOF is also used to generate a "bulk flow" to sweep all ions toward the detector, independent of their charge. Furthermore, the EOF, when oriented in a direction opposite that of the migration velocity of the compounds of interest, will increase the effective separation length of the capillary, resulting in improved resolution. Because of this strong influence of the EOF on the apparent mobility of the components in a separation process, fluctuations in this flow will directly influence the reproducibility of the analysis.

As will be discussed shortly in more detail, the EOF in capillaries originates from an electric double layer between the capillary wall and the electrolyte. When an electric field is applied across a capillary, the radial charge distribution in the double layer will result in a liquid flow, the EOF. However, simultaneously, other electrokinetic effects will occur and influence the electroosmotic flow (e.g., surface conductance, electrophoresis, electrolyte–wall interactions). Therefore, to predict, monitor, or control the EOF (and, hence, the run-to-run reproducibility), accurate measuring techniques are necessary that under separation conditions closely resemble the experimental ones.

1. Origin of the Electroosmotic Flow

The EOF in capillaries originates from an electric double layer between the capillary wall and the electrolyte present in the capillary. This double layer is produced when the surface of the capillary wall, as it comes in contact with an electrolyte, becomes charged. In fused-silica capillaries cations (e.g., hydrogen or alkali metal) will enter the solution, leaving a negative charge at the surface. The charge on the capillary wall will repel co-ions and attract counterions, resulting in the formation of a double layer with a radial potential gradient (see Fig. 2).

The most widely supported view on the electric double layer is the model of Stern [22]. According to this model the double layer consists of two parts. The first part, which has approximately the thickness of a single ion, remains almost fixed to the surface, and exhibits a sharp fall of potential. The second part is diffuse and extends some distance into the liquid. In this part of the double layer the ions can move freely, but the distribution between cations and anions is not uniform, for the residual negative charge at the surface will preferentially attract positive ions. As a result, this diffuse part of the double layer has a gradual fall of

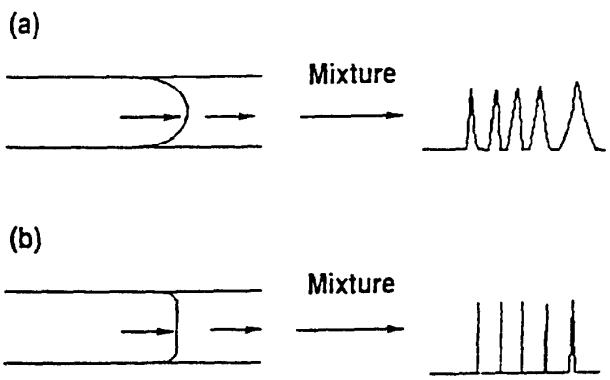


Figure 3 Flow profiles and resulting separations in HPLC (a) and CE (b).

potential into the bulk of the liquid where the charge distribution is uniform. Figure 4 gives a schematic view of this model.

Two potential differences are important in the description of the double layer: Π, the potential difference between the capillary wall and the bulk of the liquid and ζ, the potential drop in the diffuse part of the double layer.

If we assume that the diffuse part of the double layer is equivalent to an electrical condenser, then it is known from electrostatics that [23]:

$$\zeta = \frac{dq}{\varepsilon} \tag{12}$$

in which d is the distance between the plates, q the charge density on the plates, and ε the dielectric constant of the electrolyte.

When an axial electric field is applied over the capillary, the ions in the diffuse part of the double layer will move, dragging with them the electrolyte. This results in a bulk liquid flow, called electroosmotic flow (EOF), or electroosmosis. If we call v_{eo} the velocity of the EOF, then v_{eo}/d can be taken as the velocity gradient in the diffuse part of the double layer.

Because the EOF occurs at an uniform rate, the force caused by frictional effects must be equal to the electrical force causing the EOF. In Eq. (13)

$$Eq = \frac{\eta v_{eo}}{d} \tag{13}$$

E is the applied electric field and η the viscosity of the electrolyte.

A combination of Eqs. (12) and (13) leads to the following expression for the velocity of the EOF:

$$v_{eo} = \frac{\varepsilon \zeta E}{\eta} \tag{14}$$

This equation is known as the Helmholtz–Smoluchowski equation.

The assumption that the double layer is equivalent to an electrical condenser with parallel plates limits the use of this equation to cases in which the inner diameter of the capillary is considerably larger than the double-layer thickness [24]. With typical capillary i.d.'s (internal diameter) of 50 μm or more and a double-layer thickness of <0.01 μm or less, this is normally true in CE.

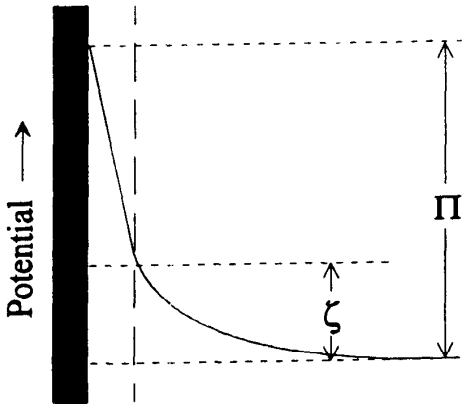


Figure 4 Schematic representation of the electric double layer: Shaded portion represents the capillary wall. The vertical broken line indicates the extent of the fixed part of the double layer. The ζ (zeta)-potential represents the potential decrease in the diffuse area of the double layer.

To estimate the velocity of the electroosmotic flow in a capillary, two approaches can be taken. The first, and most logical approach, is direct measurement of the EOF. The second is an indirect method, in which the zeta-potential is determined which, with Eq. (14), can be used to estimate the electroosmotic flow.

2. Methods to Measure the Electroosmotic Flow

One general method to measure the EOF is to include a neutral marker analyte in the sample. The marker migrates to the detector at a velocity equal to that of the EOF. The disadvantage of this method is that it gives only an average value of the electroosmotic flow. Another problem is finding a suitable molecule that shows no migration or retention behavior.

The technique of using streaming potentials to predict EOF values in capillaries, was first introduced by Reijenga et al. [25]. Although this is an indirect technique, the method is relatively simple and is suitable for fast characterization of different capillary–electrolyte combinations. It also allows the study of EOF fluctuations as a function of time.

Altria et al. [26,27] introduced a method based on weighing the amount of electrolyte leaving the capillary. Although the advantage is that the setup closely resembles the experimental conditions, the disadvantage is that only time-averaged results are obtained.

Huang et al. [28] replaced the electrolyte in one of the reservoirs by a similar electrolyte with a slightly different conductivity. This will result in a continuous change of the resistance over the capillary while the interface between the two buffers moves through the capillary, enabling calculation of the EOF.

Another approach for direct measurement of the EOF is to replace the outlet vial with a conductivity cell filled with water or with diluted electrolyte [29]. When an electric field is applied across the capillary, the EOF will transport undiluted electrolyte into the outlet vial, leading to an increase in conductivity with time. To convert this into actual velocity of the EOF, the system has to be calibrated using an off-line weighing method.

(*a*) *Indirect Measurement of the Electroosmotic Flow.* To estimate the EOF indirectly the streaming potential can be used. The *streaming potential* is the potential difference between the inlet and outlet of a capillary, which arises when a pressure gradient is applied over that capillary. This is basically the reverse phenomenon from the EOF, in which a flow is created by applying a voltage gradient over the capillary.

The streaming potential E_{ST}, similar to EOF, can be correlated with the ζ-potential [30]:

$$E_{ST} = \frac{\Delta P \varepsilon \zeta}{\eta \kappa} \tag{15}$$

in which ΔP is the pressure difference applied over the capillary, and κ the specific conductance of the electrolyte.

The ζ-potential obtained can be used to estimate the EOF by using Eq. (14).

(*b*) *Direct Measurement of the Electroosmotic Flow.* The mass of the flow leaving the capillary can be used to calculate the EOF. By determining the weight change of the outlet vial (ΔW) in a certain time interval (Δt), the velocity of the EOF can be calculated using:

$$v_{eo} = \frac{\Delta W}{\Delta t \rho A} \tag{16}$$

in which A is the cross-sectional area of the capillary and ρ the density of the electrolyte.

This method is suitable for on-line monitoring of the EOF, by placing the outlet vial on a microbalance and registering the weight change during an electrophoretic separation (Fig. 5)

3. Controlling the Electroosmotic Flow

Several methods may be used to change the magnitude or direction of the EOF; for example, the use of buffer additives [30], special capillary coatings [31], viscosity, and ionic strength

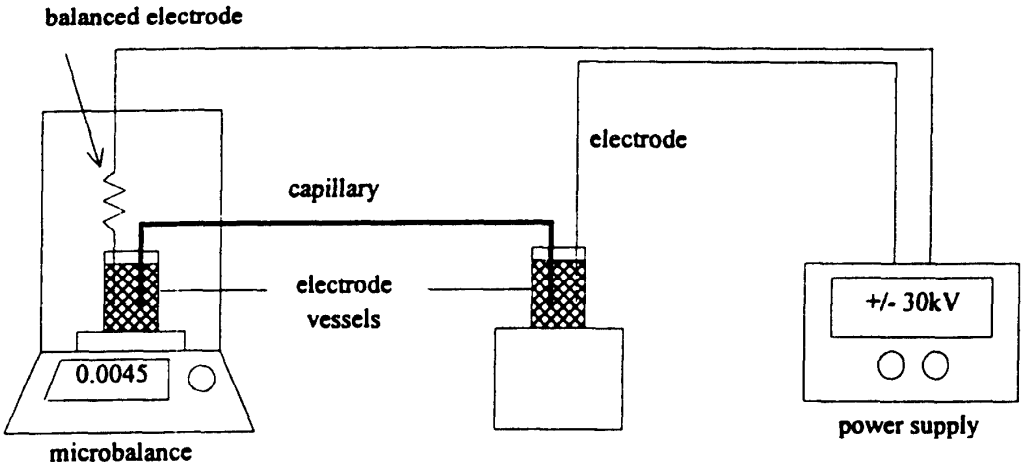


Figure 5 Experimental setup for measuring the EOF using a microbalance.

modifiers [32], or an external electric field [33,34]. Figure 6 shows schematically the reversal of the EOF achieved when a cationic surfactant, such as cetyltrimethylammonium bromide (CTAB), is added to the run buffer.

The exact concentration of surfactant at which EOF reversal takes place (i.e., at which the EOF = 0) is dependent on the type of surfactant. Increasing the surfactant concentration beyond this point increases the EOF (in reversed direction) and eventually, when exceeding the critical micelle concentration of the surfactant, will lead to MECC conditions. The EOF reversal generally requires a reversal of the polarity of the power supply, so that the bulk flow will again be in the direction of the detector.

C. Separation Efficiency and Resolution

The most important quantity measured in CZE is perhaps the migration time t_m, the time a sample component (zone) needs to migrate the distance l from injection point to detector.

$$t_m = \frac{l}{v + v_{eo}} \tag{17}$$

in which l is the effective length of the capillary (from injection side to the detector), v the

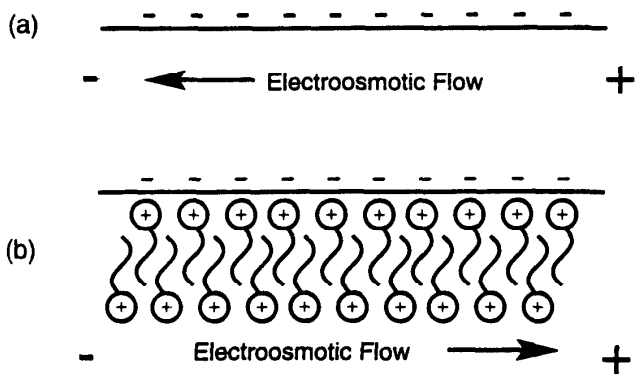


Figure 6 Schematic drawing of the reversal of the EOF: (a) no surfactant in the capillary, EOF is toward the cathode; (b) bilayer formation at the capillary wall, resulting in an EOF toward the anode.

electrophoretic velocity of the component and v_{eo} the velocity of the osmotic flow. From Eq. (1) this expression becomes

$$t_m = \frac{l}{(\mu + \mu_{eo})E} \tag{18}$$

With present-day apparatus the use of capillaries with a very small bore is possible, making longitudinal diffusion the main source of peak broadening. In the absence of other types of broadening, the variance σ_l^2 of the zone after time t is given by the Einstein equation:

$$\sigma_l^2 = 2Dt = 2D\frac{l}{(\mu + \mu_{eo})E} \tag{19}$$

where D is the molecular diffusion coefficient of the solute in the zone.

Giddings [5] postulated that the efficiency of a chromatographic system or, here, an electrophoretic system, can be expressed in terms of a number of theoretical plates, N, defined as

$$N = \frac{l^2}{\sigma_l^2} \tag{20}$$

By combining Eqs. (19) and (20), and by using $E = V/L$, where V is the applied voltage and L is the total length of the capillary, Eq. (21) can be obtained

$$N = \frac{(\mu + \mu_{eo})Vl}{2DL} \tag{21}$$

This equation shows that the number of theoretical plates is inversely proportional to the analyte diffusion coefficient. Small molecules (e.g., drugs or inorganic ions) generally yield lower plate numbers in CE than large molecules (e.g., proteins or DNA). For comparable separations, the separation efficiency in CE is typically far superior to HPLC. For large biomolecules, where D is relatively small, extremely high plate numbers may be generated. For example, with oligonucleotide samples Guttman et al. [36] calculated a plate number of 30 million/m. Figure 7 illustrates the high resolution achievable with CE. The electropherogram shows the separation of DNA-sequencing fragments in excess of 400 bases using a replaceable polymer network in the capillary (see also Sec. III.E).

The resolution R_S of two zones in CZE, according to Giddings, is given by

$$R_S = \frac{\sqrt{N}}{4}\frac{\Delta v}{\bar{v}} \tag{22}$$

where Δv is the velocity difference between the two zones, and $\bar{v}$ is the average velocity of the two zones.

Combining Eqs. (22) and (1) leads to

$$R_S = \frac{\sqrt{N}}{4}\frac{\Delta\mu}{\bar{\mu}} \tag{23}$$

For systems with an EOF, Eq. (24) can be obtained

$$R_S = \left(\frac{\sqrt{N}}{4}\right)\left(\frac{\Delta\mu}{\bar{\mu} + \mu_{eo}}\right) \tag{24}$$

After combining Eqs. (21) and (24) the result is

$$R_S = 0.18\,\Delta\mu\sqrt{\frac{Vl}{DL(\bar{\mu} + \mu_{eo})}} \tag{25}$$

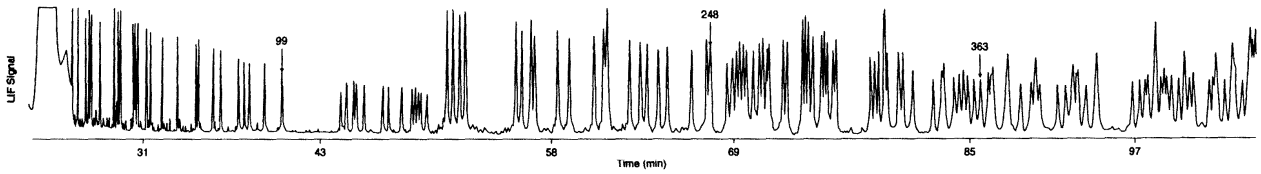


Figure 7 Electropherogram of fluorescently labeled DNA fragments, exemplifying the high-resolving power of CE. The pattern is readable beyond 400 bases. A replaceable, linear polyacrylamide-type polymer network was used in the capillary. Laser-induced fluorescence was used as detection method. (From Ref. 58.)

From this equation it can be seen that the resolution depends on the difference in electrophoretic mobilities of the sample components, the applied voltage, and the molecular diffusion coefficient of the solute. Also the sum of the electroosmotic flow and the average electrophoretic migration velocity influence the resolution. If $\overline{\mu}$ and μ_{eo} are equal, but of opposite sign, the resolution is maximal, infinite, but the net velocity through the capillary will be zero, which leads to extremely long run times.

D. Factors Influencing Performance

In using the Einstein equation (see Eq. 19), it was assumed that only longitudinal diffusion took place. In actual practice several other factors influence zone broadening. In CE, the total variance can be assumed, as a first approximation, to be a summation of the following statistically independent variances [37,38]:

$$\sigma_{tot}^2 = \sigma_l^2 + \sigma_D^2 + \sigma_J^2 + \sigma_E^2 + \sigma_{eo}^2 + \sigma_O^2 \tag{26}$$

in which the suffixes in the right hand terms represent the contributions of injection (l), diffusion (D), Joule heating (J), electrodispersion (E), electroosmotic flow (eo) and other effects.

All variances, except the injection, are proportional to the analytical time and can be expressed similarly to the Einstein equation for diffusion. The injection variance is determined only by the initial conditions. Its relative contribution to the overall variance will, therefore, decrease for longer analytical times.

The overall variance, as shown in Eq. (26) can now be rewritten as a summation of an analysis time-dependent and time-independent term:

$$\sigma_{tot}^2 = \sigma_l^2 + 2t(D_D + D_J + D_E + D_{eo} + D_O) \tag{27}$$

in which D_D, D_J, D_{eo}, and D_O are the dispersion coefficients of diffusion, joule heating, electrodispersion, electroosmotic flow, and other effects.

1. Injection

In the ideal case, in which a narrow pulse (width w) is injected, the variance caused by injection can be described as

$$\sigma_l^2 = \frac{w^2}{12} \tag{28}$$

As can be seen, the shorter the injection plug, the lower the injection variance. Practical reasons (e.g., the sensitivity of the detector), however, put a limit on the minimum injection volume.

Another limitation of Eq. (28) is that it is valid only when the ionic strength of the sample zone is equal to that of the background electrolyte. In practice, however, this is often not true, and additional effects, such as sample stacking and peak broadening caused by joule heating, will result in deviations from this equation.

2. Diffusion

The Einstein equation (see Eq. 19) describes the relation between the peak broadening caused by diffusion and the diffusion coefficient D. If this coefficient is unknown, it can be estimated from the mobility by the Nerst–Einstein equation for dilute solutions

$$D = \frac{RT\mu}{zF} \tag{29}$$

in which R is universal gas constant, T the absolute temperature, z the valence of the ion, and F the Faraday constant.

Equation (29) indicates that a small mobility value is favorable with respect to band broadening.

3. Joule Heating

The electric field applied during an electrophoretic experiment will draw a current and generate heat, depending on the conductivity of the solvent buffer. This heat is produced uniformly over the entire volume of capillary, but can be dissipated only at the capillary wall, resulting in a radial temperature gradient. For capillary columns, this profile can be approximated by a parabolic function [2,7,39]:

$$\Delta T = \frac{Wr^2}{4\lambda_T} \tag{30}$$

in which ΔT is the temperature changes, W is the electric power per unit of volume, r is the capillary radius, and λ_T is the thermal conductivity of the solvent buffer.

As the heat is generated over the entire volume of the capillary, the dispersion arising from joule heating is dependent on the applied voltage and the radius of the capillary. Virtanen [7] derived an equation for the dispersion coefficient showing that:

$$D_J \approx E^6 r^6 \tag{31}$$

It is clear that a low field and a small capillary bore are beneficial. However, a lower field lengthens the separation times and a reduction in capillary diameter will aggravate instrumental problems with injection and detection.

According to Jones et al. [39], there is no significant influence on the efficiency of a separation if the radial temperature gradient in the bore of the capillary is less than 1.5°C, corresponding to heat generation rates of over 10 Wm^{-1}. This means that under typical separation conditions, the contribution of the radial temperature gradient (joule heating) to the peak broadening in CE is negligible.

However, another effect that arises from the constant generation of heat in the capillary bore, is that the absolute temperature of the capillary can be significantly higher than the passive- or active-cooling environment. Terabe et al. [40] showed that, even in narrow-bore capillaries, the actual temperature in the bore can rise higher than 70°C without a proper-cooling method. This dramatic temperature increase in the bore of the capillary influences chemical equilibria, electrolyte viscosity and pH, sample stability, and most of the other physical and chemical parameters relevant to an electrophoretic separation. This means that to ensure optimal usage of the advantages inherent to CE separations—good reproducibility and repeatability—the temperature of the electrolyte and column have to be accurately and precisely controlled.

4. Electroosmosis

The driving force of the EOF is exerted on a very thin cylinder along the wall of the capillary (the thickness of the electric double layer) resulting in a characteristic plug-like flow. Only within the cylinder in which the velocity drops off to zero, will there be a gradient. Therefore, in an open-tubular system, on which the thickness of the double layer is negligible compared with the capillary diameter, the contribution to dispersion will be zero. Longitudinal variations in the double layer, however, may occur as a consequence of experimental conditions or of introduction of the sample, leading to a mismatch in osmotic flows, thereby causing dispersion [41]. In general, however, the contribution of these effects to band broadening will be small.

5. Electrodispersion

Electrodispersion may occur if the ionic strength of the sample is of the same order of magnitude as that of the background electrolyte and, at the same time, the effective mobilities of the two ions are different [42]. Under these conditions "tailing" or "fronting" occurs, de-

pending on which ion has the higher mobility. This process is comparable with the effects occurring in the moving-boundary method. As long as the concentration of the sample ion is kept low enough compared with that of the background ion (< 0.01) the effect of electrodispersion is negligible.

6. Surface Interaction

Control of the capillary's inner surface is of great importance to the separation performance in CE. For many CZE and MECC separations involving small molecules (including peptides), untreated (i.e., noncoated) fused silica capillaries can be used. Interaction between solute and surface has a direct effect on zone broadening; both electrostatic and van der Waals attraction are possible. The broadening can be minimized by choosing the optimum setup for the experiment; for example, by choosing the pH of the background electrolyte in a way such that the capillary wall and the analyte ions have the same charge sign, results in the ions being repelled from the wall. Biopolymers (e.g., proteins, polysaccharides, or DNA) generally require special capillary coatings to prevent adsorption or to moderate (or completely eliminate) the EOF [31].

E. Experimental Considerations

1. Sample Introduction (Injection)

Injection volumes in CE are extremely small, typically ranging from 10 to 50 nL, comparable with a moisture droplet in fog (approximately 10 nL). Injection valves, such as those used in HPLC, cannot be used in CE, for their internal dead volume would generate unacceptable band broadening. Therefore, special techniques have been developed in CE. During the sampling process, the capillary is temporarily moved from the buffer vial and positioned in a sample vial. After the sample is introduced into the capillary (either by hydrodynamic or electrokinetic means), the capillary is moved back to the buffer vial, after which the CE run can be initiated. In automated instruments, this process of sampling and electrophoresis is entirely automated.

Most commercial instruments offer both the electrokinetic and the hydrodynamic injection modes. Hydrostatic injection systems have been used mainly in homemade instruments. In the hydrodynamic injection mode, the sample vial is temporarily pressurized, allowing the sample to flow into the capillary. The same can be accomplished in a configuration in which a buffer vial is temporarily evacuated, allowing the sample to be sucked into the capillary.

(*a*) *Hydrodynamic Injection.* Hydrodynamic injection is generally preferred in quantitative work. The composition of the plug introduced into the capillary is exactly that of the sample vial. For example, consider quantitating a series of samples containing identical amounts of analyte, but varying in ionic strength. By using hydrodynamic injection, the same amount of analyte is introduced into the capillary, regardless of the ionic strength of the sample. In contrast, with electrokinetic injection, this is typically not true and the amount of analyte injected will vary (also see later discussion). The volume injected hydrodynamically V will be a function of the capillary diameter d, the applied pressure ΔP, the injection time t, and the viscosity of the buffer η, and can be calculated using the Hagen–Poisseuille equation [42]:

$$V = \frac{\Delta P d^4 \pi t}{128 \eta L} \tag{32}$$

The most difficult parameter to obtain is ΔP, because atmospheric conditions, aging of pressure or vacuum lines, or others, may influence the measurement. Compared with the fixed-loop injection systems used in HPLC, this can potentially lead to a higher run-to-run and, especially, day-to-day variability. However, with modern commercial instruments a precision comparable with that of HPLC can be obtained. Table 1 shows the injection volume and plug length obtained from a 1-s pressure injection with a commercial CE instrument (P/ACE—

Table 1 Injection Volumes and Plug Length for Different Standard-Sized Capillaries Using a Commercial Instrument (Beckman)[a]

Capillary dimensions	Injection (nL)	Plug length (mm)
50-μm id		
L = 20 cm	2.5	1.3
L = 50 cm	1.2	0.6
L = 100 cm	0.6	0.3
75-μm id		
L = 20 cm	12.5	2.7
L = 50 cm	5.9	1.3
L = 100 cm	3.1	0.7

[a]1.0-s, low-pressure (0.5 psi) injection; capillary and sample vial filled with water. η (water) = 0.798×10^{-2} at 30°C. Calculations based on Eq. (32).

Beckman Instruments) using different capillary lengths and internal diameters. It can be seen from Table 1 that the injection volume is strongly dependent on the capillary dimensions, with larger id capillaries giving larger volumes and plug lengths.

(*b*) *Hydrostatic Injection.* Hydrostatic injection can be considered as a special case of pressure injection. The sample is introduced by siphoning, under the influence of the hydrostatic pressure obtained by raising the sample an amount Δh above the other end of the capillary. Hydrostatic injection tends to be reproducible because most of the disturbing factors, mentioned earlier, are eliminated. However, the pressure range is rather limited. The injected volume can be calculated from Eq. (33).

$$V = \frac{\rho g \Delta h d^4 \pi t}{128 \eta L} \tag{33}$$

in which ρ is the density of the electrolyte, and g is the gravitational constant. This equation is similar to Eq. (32), but with a different expression for ΔP.

(*c*) *Electrokinetic Injection.* With electrokinetic injection, analytes are brought into the capillary by temporarily applying an electric field. The analytes can enter the capillary in two ways: passively by the force of the EOF (if present), or actively by the electrophoretic force of the ions themselves. As a first approximation, the apparent injection volume can be derived from:

$$V = (\mu + \mu_{eo})\, \pi r^2 E t \tag{34}$$

As mobility varies between different analytes, the amount injected will also be different. Therefore, electrokinetic injection will result in a biased representation of the sample in the capillary. A high value for μ_{eo} will decrease this bias. When the analytes have basically the same mass/charge ration (e.g., DNA restriction fragments), electrokinetic injection does not result in a biased sampling.

In practice, the exact calculation of the apparent injection volume in the electrokinetic mode is rather difficult, because it is dependent on the concentration and mobility of all the other ions in the system. For instance, variation in the ionic strength of the sample matrix greatly influences the electric field E in the sample during injection and, as a result, the injection volumes of the different analytes.

The electrokinetic injection mode is the only option for sample introduction when fixed (nonreplaceable), cross-linked, or high-viscosity gels (polymer networks) are used in the cap-

illary. Pressure injection would force the fixed gel out of the capillary. When the viscosity of the polymer solution is relatively high, introduction by pressure (or vacuum) becomes problematic, for extremely long injection times are required to force the sample into the highly viscous capillary contents. Occasionally, electrokinetic injection is very selective (i.e., only analytes with the right charge are introduced into the capillary, whereas others [undesirable sample components moving toward the opposite electrode] are not [43]). In other instances (e.g., with DNA fragments [44]), electrokinetic injection yields sharper peaks compared with hydrodynamic injection, for analytes are effectively stacked against the run buffer during the sampling.

2. Calculating Results from Experimental Parameters

(*a*) *Qualitative Results.* At the end of an electrophoresis experiment, the migration times of the analytes are known and their apparent mobilities can be calculated from

$$\mu_{app} = \frac{lL}{Vt_m} \tag{35}$$

where l represents the effective length of the capillary (from injection point to detection point), t_m the migration time, V the applied voltage, and L the total length of the capillary.

From μ_{app} the effective electrophoretic mobility can be obtained by subtracting μ_{eo}.

$$\mu = \mu_{app} - \mu_{eo} \tag{36}$$

The μ_{eo} can be obtained by using a so-called EOF marker. This marker, a neutral molecule that does not interact with the capillary wall, will migrate to the detector at a velocity equal to that of the EOF. From its migration time, the μ_{eo} can then be calculated from Eq. (35). The effective mobility is a characteristic quantity of an analyte under the given experimental conditions and, therefore, may be used for the identification of analytes.

(*b*) *Quantitative Results.* Quantitative information can be obtained from an electropherogram by integrating the signal over time, analogous with HPLC. However, there is a fundamental difference between the calculated peak areas in CE and HPLC. In contrast with HPLC, detection in CE is performed on-line. This means that the peak area will be dependent on the migration time, because different analytes pass the detector at different velocities. As a result, variation in migration times will cause variation in peak areas. To correct for this dependency, Hjerten suggested the use of the corrected peak area (A_C), which is equal to the peak area (A) divided by the migration time (t_m):

$$A_C = \frac{A}{t_m} \tag{37}$$

In some commercial instrumentation the software permits direct calculation of corrected peak areas.

(*c*) *Separation Efficiency.* To characterize the separation efficiency, the theoretical plate number in CE may be calculated in a way similar to that in HPLC. Assuming gaussian-type peaks, the theoretical plate number may be derived from the peak width after the analyte has traveled a certain distance in the capillary. In practice, it is convenient to take the peak width at half-peak height ($w_{0.5}$) at the time the peaks pass through the detector (t_m), both expressed in time units, as a measure for N [45]:

$$N = 5.54 \left(\frac{t_m}{w_{0.5}}\right)^2 \tag{38}$$

III. MODES OF CAPILLARY ELECTROPHORESIS

Five basic modes of operation can be distinguished, all based on electrophoretic principles.

1. Capillary zone electrophoresis (CZE)

2. Micellar electrokinetic capillary chromatography (MECC)
3. Capillary isotachophoresis (CITP)
4. Capillary isoelectric focusing (CIEF)
5. Capillary gel electrophoresis (CGE)

These CE techniques are shown schematically in Figure 8, and their operating principles will be briefly discussed in this section. For specific applications, the reader is referred to CE textbooks [17–19]. CZE, MECC, CIEF, and CITP, all are performed in free solution (i.e., no gel is present). With CGE, cross-linked, nonreplaceable gels, as well as replaceable, polymer network solutions can be used. The latter are relatively nonviscous polymer solutions (linear polyacrylamide, alkylcelluloses, and such that can be rinsed in and out of the capillary. MECC combines the principle of zone electrophoresis with partitioning chromatography, whereas CGE combines it with molecular sieving.

A. Capillary Zone Electrophoresis

Capillary zone electrophoresis (CZE) is perhaps the most basic and mature method of operation. The capillary is filled with a buffer, known as the background electrolyte. The sample is introduced as a small band into the background electrolyte and an electric field is applied. The components in the sample will begin migrating, each with its own velocity, depending on its effective mobility under the experimental conditions. After a certain time and given that the differences in effective mobility are large enough, the components will migrate in separate zones, giving CZE its name. The electrophoretic migration causes anions and cations to move in opposite directions. The superimposed EOF (if present) drives the analytes in the direction of the cathode (for fused silica capillaries), as illustrated in Figure 2. CE thus permits the separation of anions, cations, and neutral sample components in one run. The zone containing the cations with the highest mobility will be detected first, and the zone containing the anions with the highest mobility will be detected last. A zone with uncharged molecules

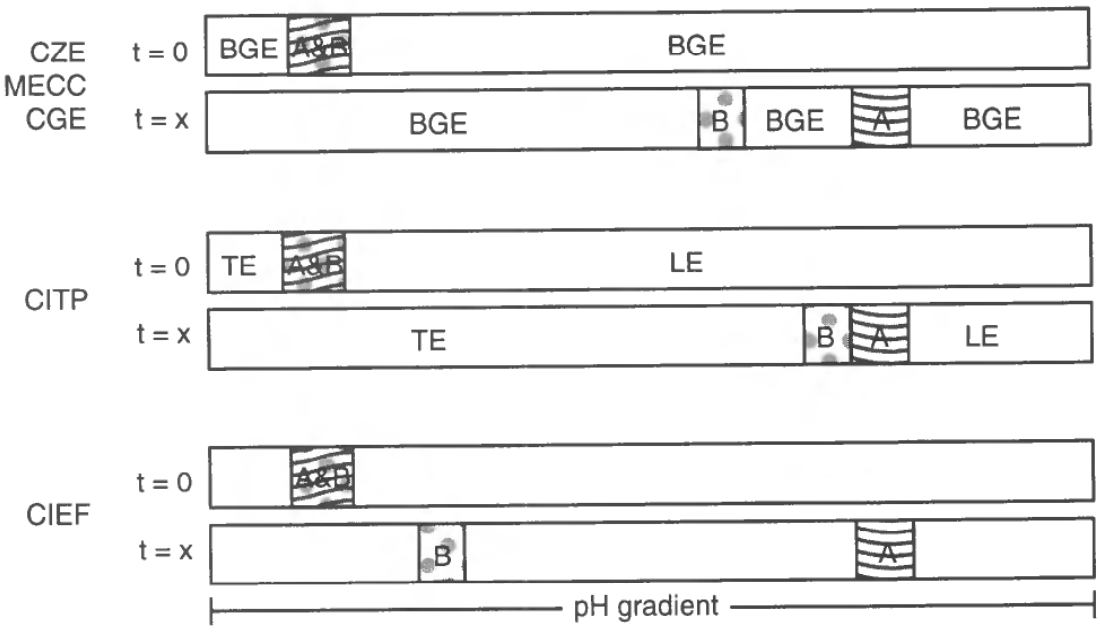


Figure 8 Modes of capillary electrophoresis: BGE, background electrolyte; LE, leading electrolyte; TE, terminating electrolyte. The top figure represents the CZE, MECC, and CGE modes, with a background electrolyte (CZE), a micellar pseudostationary phase (MECC), or a gel (CGE), respectively.

would migrate in between the zones of cations and anions (see Fig. 2). CZE has been applied to a wide variety of analytes; small ions, drugs, nucleosides, nucleotides, amino acids, peptides, proteins, and sugars.

B. Micellar Electrokinetic Capillary Chromatography

Use of MECC is similar to that of CZE in that the technique is performed in free solution. A surfactant (e.g., sodium dodecyl sulfate; SDS) is added to the background electrolyte in a concentration above its critical micellar concentration (CMC; typically 20–200 mM) [16]. The negatively charged micelles slowly migrate toward the anode. If the velocity of the EOF exceeds the absolute velocity of the micelles, the micelles will have a net velocity toward to cathode. In fact, two mobile phases are present: a fast-moving aqueous hydrophilic phase and a slower-moving hydrophobic phase created by the micelles (Fig. 9). MECC allows the separation of neutral solutes (pharmaceuticals, pesticides, drugs of abuse, chiral molecules, and others) based on differences in affinity for the hydrophobic phase inside the micelle. This method may also enhance the separation of charged analytes, because of the added separation capacity based on chromatographic principles (e.g., with separations of chiral drugs [46]). For all particles—ions as well as neutral species—the binding to the micelles reduces the migration velocity. Zone broadening, however, is minimal, owing to the high rate of association and dissociation.

C. Capillary Isotachophoresis

Isotachophoresis (ITP), or displacement electrophoresis, is an electrophoretic technique that can be used to concentrate dilute samples. Developed in the 1960s through 1970s in capillary format, it can be considered a front-runner to CE [8]. Many of the principles established and methods developed during that time were instrumental in the development of modern CE.

In capillary isotachophoresis (CITP) a discrete amount of sample is introduced at the interface between two electrolyte systems: the leading electrolyte and the terminating electrolyte (Fig. 8). Both these electrolytes contain one ionic species with the same charge sign as the components to be separated. The leading ion has a higher effective mobility, and the terminating ion has a lower effective mobility, than any of the components to be separated. As a practical consequence, only anions or cations can be separated in a single run. When the system has reached equilbrium, all the ions migrate with the same speed, but they are separated into discrete zones that are in direct contact with each other and arranged according

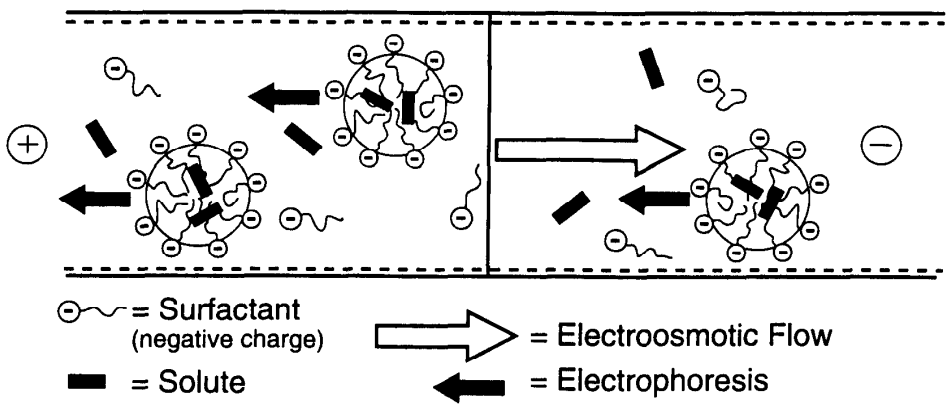


Figure 9 Schematic view of the MECC separation mechanism, using as negatively charged surfactant (e.g., SDS) and a noncoated capillary. EOF is toward the cathode and the detector. The capillary wall is negatively charged.

to their effective mobility. As all the zones move with constant and identical speed, a stepwise voltage gradient over the consecutive zones is established, each step being proportional to the effective mobility of the sample component in that zone. This potential gradient can be used for detection. According to Kohlrausch [1], the concentration in each zone is directly related to the concentration of the leading ions. Another important aspect of this arrangement is that the zones have self-correcting properties relative to zone broadening by dispersion. Within a zone, the concentration is constant; hence, the length of the zone provides quantitative information [47].

In combination with CE, ITP principles can often be used in a simple fashion to concentrate analytes during the sample injection process, (Fig. 10). This may be useful to increase the detectability of certain sample components [48]. When the sample is introduced in a low-conductivity solvent plug (e.g., pure water or a buffer of low concentration), the analytes are concentrated ("stacked") during application of the electric field. The field strength in the sample plug is higher than in the rest of the capillary, resulting initially in increased analyte velocities. When the analyte species cross the sample plug–buffer boundary, migration is slowed resulting in stacking of the ions. Typically, a two to five factor increase in detectability may be obtained using this stacking technique. Even larger concentration factors (nearly 100-fold) may be obtained by combining ITP with CZE, using either a separate precolumn or single-capillary configurations [49]. The ITP–CZE technique has been used for various small-ion separations (nucleotides), but recently, applications for proteins have also been described [50].

D. Capillary Isoelectric Focusing

In capillary isoelectric focusing (CIEF) amphoteric analytes are separated according to their isoelectric point (pI). Classic ITP techniques on slab gels are widely used for protein sepa-

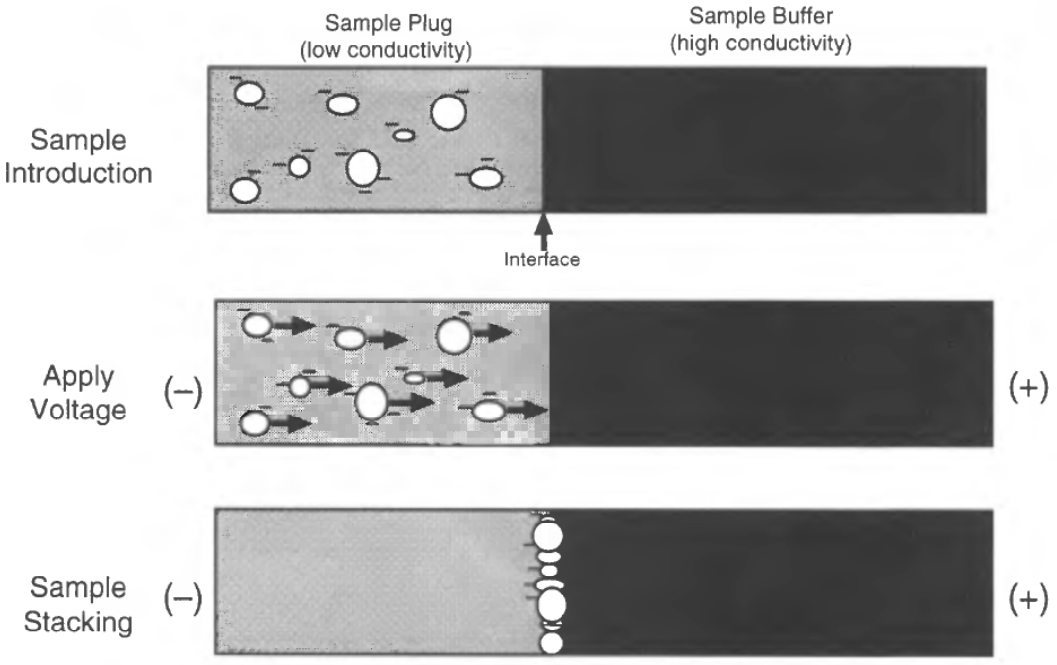


Figure 10 The mechanism of sample stacking: Sample ions (here, cations) are introduced in a relatively low-conductivity solvent. After a voltage is applied, the ions migrate with enhanced mobility through the sample–plug zone (high local field strength), until they encounter the zone of the sample buffer, where they are slowed down by the lower local field. The result is a stacking of ions at the interface between the sample plug and buffer. (From Ref. 59.)

rations. In CIEF, the capillary is filled with a background electrolyte containing ampholytes that span the desired pH range (see Fig. 8). When an electric field is applied, the analytes will migrate until they reach the pH that equals their pI. When all the components have reached their pI point, and their net velocities are zero and the conductivity is minimal. After the focusing step, the sample ions must be moved past the detector window, by pressure or vacuum [51], or by changing the composition of one of the buffer vials (pH or ionic strength) [52]. Alternatively, the EOF can be used to mobilize the focused protein zone [53]. These CIEF procedures are schematically outlined in Figures 11 and 12. For use in CIEF, the capillaries must be coated (e.g., with polyacrylamide) to suppress or moderate the EOF.

E. Capillary Gel Electrophoresis

In capillary gel electrophoresis (CGE), the selectivity of the separation is enhanced by filling the capillary with a polymeric gel. Historically, in slab gel electrophoresis, the gel functioned as a matrix to prevent zone broadening by thermal convection. In certain applications (protein or DNA separations), the gel also provides a molecular-sieving medium, through which the analyte molecules are separated according to size. Size-based separations can also be achieved in a capillary format, if a suitable, polymer matrix is used. For example, the frequently used electrophoresis technique (SDS–polyacrylamide gel or (SDS–PAGE) electrophoresis has an equivalent in CGE [54]. DNA separations in capillaries were first performed in 1988 [13] and, since then, optimization of sieving matrices has led to impressive, high-resolution separations, such as the analysis of polymerase chain reaction (PCR) products [44,57]. Even very large, chromosomal-type DNA has recently been resolved in capillaries, using pulsed-field techniques [55].

Use of CGE has definite advantages over conventional gel electrophoresis. Higher fields can be applied because Joule heat is more easily dissipated in the narrow-bore capillaries, allowing short-run times and high resolution. In addition, CGE allows full automation and one-line detection. With slab gels, a staining procedure typically needs to be performed to visualize the bands, making the entire sample preparation and separation procedure far more laborious and time-consuming.

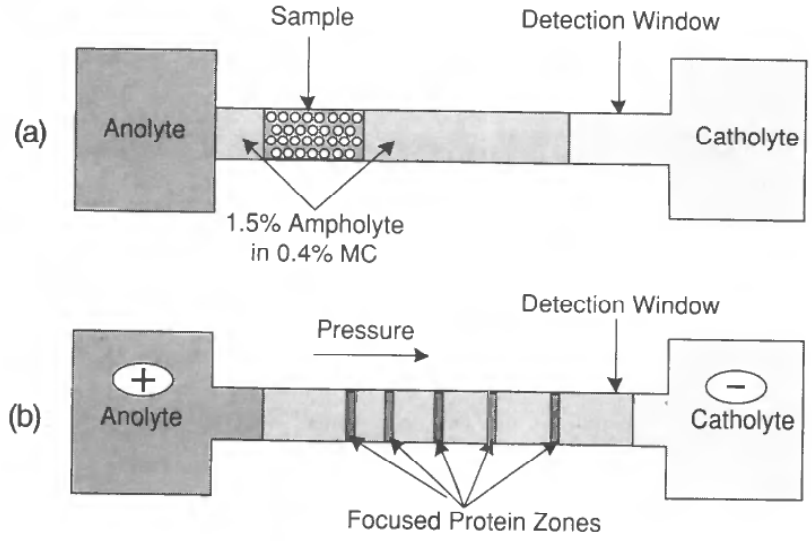


Figure 11 Principle of CIEF by simultaneous pressure–voltage mobilization: (a) (the electrolyte solution cathode is immersed) is backflushed past the detector point and a sample plug is introduced into the coated capillary (no voltage); (b) focusing of sample is complete and the sample components are driven toward the detector by a low-pressure rinse (at high voltage).

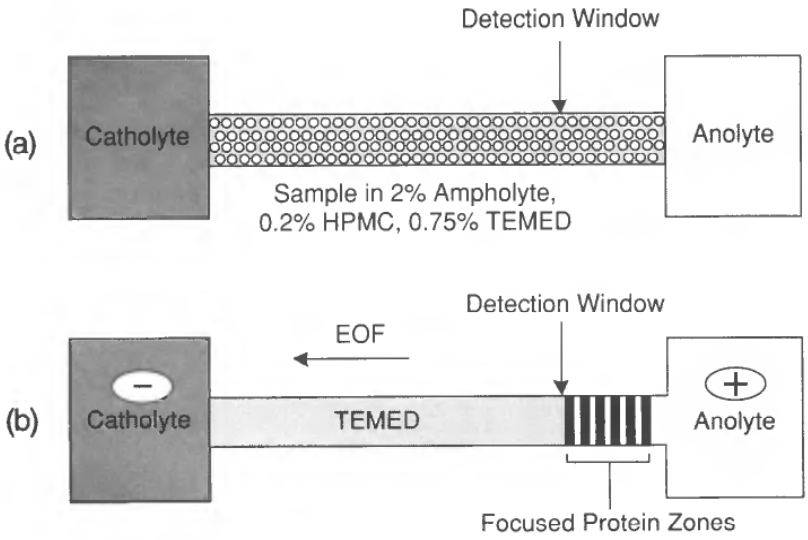


Figure 12 Principle of a CIEF method using the EOF to mobilize the focused sample zones: (a) coated capillary is filled with sample (no voltage); (b) proteins are focused in the short end of the capillary and mobilized past the detector point by the EOF (at high voltage).

The definition of a *gel* is perhaps somewhat vague: "a form of matter intermediate between a solid and a liquid" [56]. Gels may vary in consistency from viscous fluids to fairly rigid solids. In the electrophoresis literature, terms such as polymer solutions, polymer networks, entangled polymer solutions, chemical gels, physical gels, and liquid gels, have all been used to describe gel media. In CGE the sieving matrix is either a cross-linked gel ("chemical" gel, generally having a high viscosity) or a relatively low-viscosity, polymer network solution ("physical" gel). With both types of gels, precoated capillaries are required to eliminate the EOF.

The cross-linked gels have a well-defined pore structure and are rigid. Their pore size can be varied by adjusting the polymerization conditions (e.g., by varying the cross-linker concentration in the polyacrylamide gels). Typically, the gel matrix is covalently bonded to the walls of the capillary.

The non–cross-linked polymer networks have a dynamic pore structure and are more flexible. Low-viscosity, as well as high-viscosity polymer network solutions can be made by carefully selecting the concentration and chain length of linear polymers. With CGE, polymers solutions, consisting of linear polyacrylamide, alkylcellulose, and low-melting agarose, have been used. An important advantage of the polymer network solutions is that sufficiently low viscosity exists for the contents of the capillary to be rinsed in and out. The term "replaceable" gels has been used to describe the contents of these CE capillaries, which can be used for DNA or protein separations [44,54,57]. Thus, when desired, a fresh gel can be used for every sample injection. In addition, sample introduction is possible for either the pressure or the electrokinetic mode, in contrast with the chemical gels, for which only the electrokinetic mode is possible or the gel would be pushed out of the capillary. The availability of the pressure-injection mode can be important in quantitative work. An example of the high-resolving power of replaceable capillary gels for DNA-sequencing fragments was shown in Figure 7.

REFERENCES

1. F Kohlrausch. Ann Phys (Leipzig, 62:209, 1897.
2. S Hjerten. Chromatogr Rev 9:122, 1967.
3. JE Edstrom. Nature 172:908, 1953.

4. BM Turner. Nature 179:964, 1957.
5. JC Giddings. Sept. Sci., 4:181, 1969.
6. FM Everaerts, WML Hoving-Keulemans. Sci Tools 17:25, 1970.
7. R Virtanen. Acta Polytech Scand 123:1, 1974.
8. FM Everaerts, JL Beckers, TPEM Verheggen, Isotachophoresis: Theory, Instrumentation and Applications (Journal of Chromatography Library, Vol. 6). Amsterdam: Elsevier, 1976.
9. FEP Mikkers. TPEM Verheggen, FM Everaerts. J Chromatogr. 169:1, 1979.
10. FEP Mikkers. TPEM Verheggen, FM Everaerts. J Chromatogr, 169:11, 1979.
11. JW Jorgenson, KD Lukacs. Anal Chem., 53:1298, 1981.
12. JW Jorgenson, KD Lukacs. Clin Chem 27:1551, 1981.
13. RG Brownlee, SW Compton. AM Biotechnol Lab 20:10–17, 1988.
14. HE Schwartz, M Melera, RG Brownlee. J Chromatogr 480:129, 1989.
15. JP Landers. LCGC 12:50, 1994.
16. S Terabe, K Otsuka, A Ichikawa, A Tsuchiya, T Ando. Anal Chem. 56:111, 1984.
17. P Camillieri, ed. Boca Raton, FL: Capillary Electrophoresis: Theory and Practice. CRC Press, 1993.
18. JP Landers, ed. Handbook of Capillary Electrophoresis. Boca Raton, FL: CRC Press, 1994.
19. NA Guzman, ed. Capillary Electrophoresis Technology. New York: Marcel Dekker, 1993.
20. H Falkenhagen. Electrolyte, Leipzig: Verlag von S Hirzel, 1932.
21. Tiselius. Nova Acta Reg Soc Sve Sci Uppsala 4 (4):7, 1930.
22. O Stern. Z. Elektrochem. 30:508, 1924.
23. A Hudson, R Nelson. University Physics, New York: Harcourt Brace Jovanovich, 1982, p. 563.
24. S Glasstone. Textbook of Physical Chemistry. 2nd ed. New York: Van Nostrand, 1946, p. 1219.
25. JC Reijenga, GVA Aben, ThPEM Verheggen, FM Everaerts. J Chromatogr 260:241, 1983.
26. KD Altria, CF Simpson. Anal Proc 23:453, 1986.
27. KD Altria, CF Simpson. Chromatographia 24:527, 1987.
28. X Huang, MJ Gordon, RN Zare. Anal Chem. 60:1837, 1988.
29. BJ Wanders, TAAM Van de Goor, FM Everaerts. J Chromatogr 652:291, 1993.
30. T Tsuda. J Liq Chromatogr 12:2501, 1989.
31. SA Swerdberg. In: JP Londons, ed. Handbook of Capillary Electrophoresis. Boca Raton, FL: CRC Press, 1994, p. 513.
32. C Schwer, E, Kenndler. Anal Chem 63:1801, 1991.
33. CS Lee, WC Blanchard, CT Wu. Anal Chem, 62:1550, 1990.
34. CS Lee, D McManigill, CT Wu, B Patel. Anal Chem 63:1519, 1991.
35. MA Hayes, AG Ewing. Anal Chem. 64:512, 1992.
36. A Guttman, AS Cohen, DN Heiger, BL Karger. Anal Chem 62:137, 1990.
37. F Foret, M Deml, P Bocek. J Chromatogr 452:601, 1988.
38. F Foret, P. Bocek. Capillary Electrophoresis. In: A. Chrambach, MJ Dunn, BJ Radola, eds. Advances of Electrophoresis. Vol 3. Weinheim; VCH Verlaggesellschaft, 1989.
39. AE Jones, E. Grushka. J Chromatogr, 466:219, 1989.
40. S Terabe, K Otsuka, T, Ando. Anal Chem 61:251, 1989.
41. DS Burgi, RL Chien. Anal Chem 63:2042, 1991.
42. RH Sabersky, AJ Acosta, Hauptmann. Fluid Flow. 2nd ed. New York: Macmillan, 1971.
43. KD Altria, MM Rogan. Pharm Biomed Anal. 8:1005, 1990.
44. HE Schwartz, K Ulfelder, FJ Sunzeri, MP Busch, RG Brownlee. J Chromatogr 559:267, 1991.
45. CF Poole, SK Poole. Chromatography Today. Amsterdam: Elsevier, 1991.
46. M Novotny, H Soini, M Stefansson. Anal Chem 66:646A, 1994.
47. JL Beckers, FM Everaerts. J Chromatogr 470:277, 1989.
48. RL Chien, DS Burgi. Anal Chem 64:489A, 1989.

49. BJ Wanders, FM Everaerts. In: JP Landers, ed. Handbook of Capillary Electrophoresis. Boca Raton, FL, CRC Press, 1994, Chap. 5.
50. F Foret, E Szoko, BL Karger. J Chromatogr 608:3, 1992.
51. SM Chen, JE Wiktorowicz. Anal Biochem 206:84, 1992.
52. S Hjerten, M Zhu. J Chromatogr 346:265, 1985.
53. HE Schwartz, T Pritchett. Biotechnology 12:408, 1994.
54. K Ganzler, KS Greve, AS Cohen BL Karger, Al Guttman, NC, Cooke. Anal Chem 64:2665, 1992.
55. J Sudor, MV Novotny. Anal Chem 66:2446, 1994.
56. T Tanaka. Sci Am 244:124, 1981.
57. YF Pariat, J Berka, DN Heiger, T Schmitt, M Vilenchik, AS Cohen, F Foret, BL Karger. J Chromatogr 652:57, 1993.
58. HE Schwartz, KJ Ulfelder, FTA Chen, SL Pentoney Jr. J Capillary Electrophoresis 1:36, 1994.
59. RP Oda. In: JP Landers, ed. Handbook of Capillary Electrophoresis. Boca Raton, FL: CRC Press, 1994.

5
Programmed Analysis

Peter Schoenmakers

Shell Research and Technology Centre Amsterdam, Amsterdam, The Netherlands

I. INTRODUCTION

Analysis by column liquid chromatography (LC) basically requires (1) the elution of the components of interest (analytes), (2) the separation of these from each other and from the matrix, and (3) the measurement of the peak areas for quantification.

Little compromise is possible in the requirement of *eluting* the analytes. [In this chapter we will not consider thin-layer chromatography (TLC). In principle, nonmigrating analytes can be detected in TLC. However, they cannot be separated from other nonmigrating (matrix) components.] They will need to appear in the chromatogram, preferably as sharp, symmetrical peaks. There is an optimum elution window in which the separation power of the column is efficiently used, and detection sensitivity is not seriously imparted. Roughly, the optimum range of retention factors (k) is between 1 and 10 ($1 \leq k \leq 10$, or $2t_0 \leq t_R \leq 11t_0$, where t_R is the retention time and t_0 is the dead time or hold-up time of the column).

Separation of the analytes can be achieved through the usual chromatographic process, with retention (k), selectivity ($\alpha_{21} = k_2/k_1$) and efficiency (the plate number, N) all being essential factors. Column LC is rather limited in terms of the efficiency that can be conveniently attained. The plate numbers of typical LC columns will range from about 5,000 to about 20,000. In comparison, capillary gas-chromatography columns typically yield between 25,000 and 250,000 theoretical plates. Therefore, separations in LC cannot easily be achieved by brute force. Rather, knowledge, skill, and systematic procedures (see Sec. III.C) are required to develop LC methods. Sample-preparation techniques, to selectively remove matrix components from the sample, and specific or selective detection methods (see Chap. 3) are invaluable techniques to compensate for the moderate efficiency and peak capacity of LC columns.

Calibration for quantitative LC analysis is almost exclusively performed on a relative basis. This implies that the *peak areas* (occasionally, peak heights may be used) obtained for the analyte peaks in the sample are compared with areas obtained for reference mixtures under identical conditions. The main reason to do so is the type of detectors commonly used. Neither the prevalent ultraviolet (UV) detector, nor the most common alternatives (refractive-index detector or electrochemical detector) exhibit even approximately equal sensitivities for different compounds or groups thereof. Liquid chromatographers have learned to work with relative calibration methods using either internal or external standards. As long as suitable standard materials are available, calibration is not the most serious obstacle encountered in developing LC methods.

In order of importance, the two biggest problems encountered, therefore, are to find suitable conditions for elution of the analytes and to realize adequate separation. In this chapter we will focus our attention largely on the elution issue.

A. The General Elution Problem

Let us consider the chromatogram depicted as Fig. 1. The chromatogram features several peaks, separated by increasing time intervals. A sample that may typically give rise to such a chromatogram is a homologous series. The retention factors of the individual members of a homologous series increase by a constant factor. If n_c is the number of carbon atoms of an aliphatic chain this is usually described as

$$\log k_n = c + \alpha_{CH_2} n_c \tag{1}$$

where

$$\alpha_{CH_2} = \frac{k_{n+1}}{k_n} \tag{2}$$

is the selectivity between successive members.

In Fig. 1 five components elute in the optimum window, whereas at least five are discernible for which the retention factors are smaller than 1, and at least three components have retention factors greater than 10. Changing the elution strength of the mobile phase to another (constant) value does not improve the situation in the present example. [It is assumed here

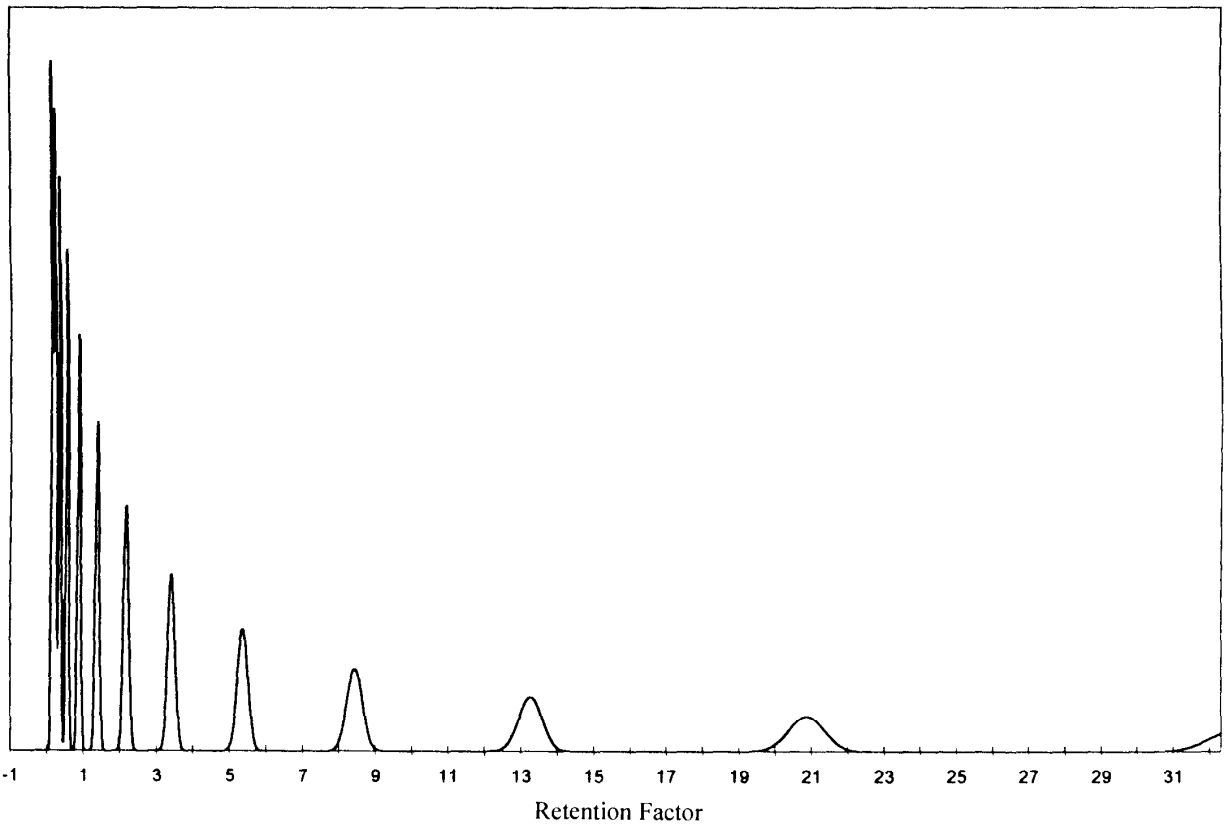


Figure 1 Chromatogram to illustrate the "general elution problem." Under isocratic conditions all the components present in the mixture cannot be eluted in the optimum range of retention factors.

that the elution strength can be varied without varying the selectivity. This is not strictly correct in LC, but it is a useful first-order approximation.] More components would either elute too early or too late. The number of components eluted in the optimum window can be increased by reducing the selectivity of the system, which may be achieved by choosing a different type of stationary phase (e.g., a shorter alkyl chain length in reversed-phase LC; RPLC). However, even with a reduced selectivity, the number of components of a series that can be eluted in a single isocratic run is limited. For example, on a column with 10,000 theoretical plates about 20 components may be separated in the optimum range ($1 \leq k \leq 10$) with equal selectivities, if the resolution (R_s) between the first two members equals 1.5.

It is not generally in the interest of chromatographers to reduce the selectivity (or separating power) of our systems. After all, we are in the business of separations. If we accommodate a greater range of components (e.g., homologues) in a chromatogram we increase the applicability of our system, at the expense of reducing the resolution between individual components. This is known as the *general elution problem.*

The most common solution of the general elution problem is the application of programmed elution methods, in which the conditions are varied during the run. When the composition of the mobile phase is programmed, we speak of *gradient elution.* This is the main subject discussed in the present chapter (see Sec. III). In contrast with gradient elution, we speak of *isocratic elution* if the composition of the mobile phase is kept unchanged during the analysis.

In a sense, it is also possible to program the composition of the stationary phase, by switching the eluent flow between various columns during the analysis. In Sec. II, we will investigate how and when column-switching methods can be used for analysis, rather than sample-preparation purposes. Other programming techniques, such as temperature programming, are briefly discussed in Sec. IV. In Sec. V The main programming methods are mutually compared, and their advantages and disadvantages are summarized.

B. The Place of Programmed Analysis

As will become evident during the course of this chapter, there are many sound reasons to apply programmed analysis, and there are many sound reasons not to apply programmed analysis unnecessarily. In short, when isocratic elution can be applied, it is usually more efficient, simpler, faster, and more reliable than a gradient-elution method. Therefore, the flow chart shown as Fig. 2 is generally valid. If the entire sample can be eluted under isocratic conditions and all analytes exhibit retention factors within a suitable range, then straightforward isocratic elution of the sample is clearly desirable.

If the analytes can be eluted conveniently under isocratic conditions, but other (matrix) components in the sample cannot, then it is sensible to address possible removal of the matrix components. Generally, components that are (approximately) unretained and elute from the column well before the analytes do not need to be removed. Matrix components that are not completely eluted before the analyte peaks start to emerge and late-eluting components typically give more reason for concern.

One practical consideration that has not been taken into account in the construction of the simple Fig. 2 is the purpose of the method. If only a few samples need to be analyzed, long analysis times will be a much smaller problem than if a routine method is being developed. In the latter instance, a significant effort to develop an elegant sample-preparation method is more likely to pay off.

Another complication is the use of programmed analysis with the very purpose of reducing the effect of matrix constituents on the analysis. The use of programmed (column-switching and gradient) methods for this purpose will not be discussed extensively in the present chapter. However, some general considerations will be incorporated in the discussion.

Figure 3 shows a schematic chromatogram, in which two highly distinctive groups of solutes appear. Under the conditions chosen, some of the components of the sample clearly

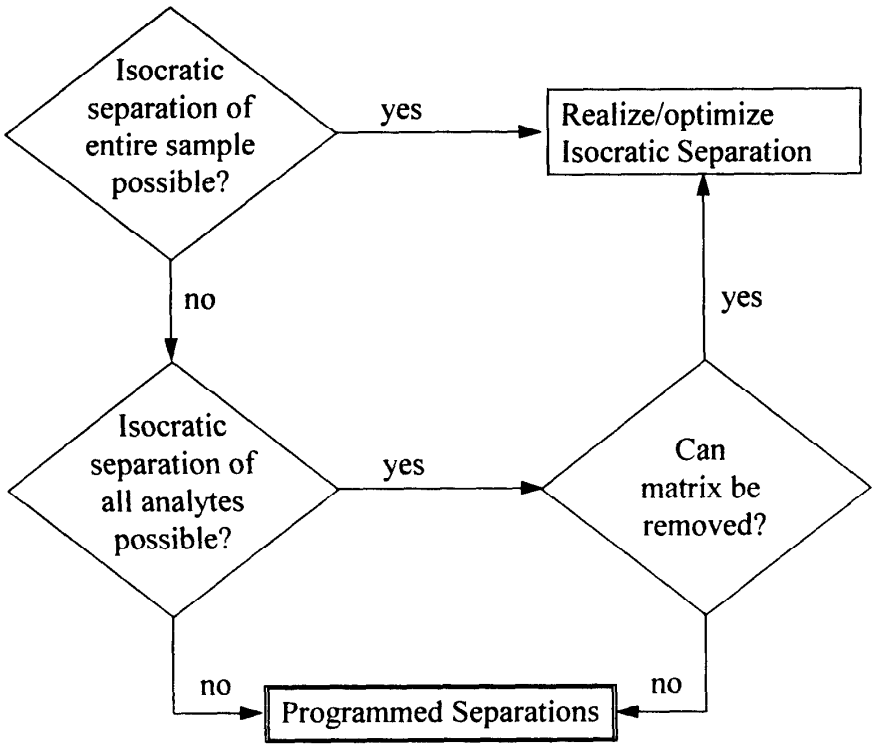


Figure 2 Schematic illustration of when programmed separations are required.

show little retention, whereas some others are highly retained. It is easy to envisage samples that can give rise to this type of chromatogram. One example is a reaction mixture, in which only part of the starting material has been transformed. If a group of relatively nonpolar components is partially oxidized, an RPLC separation will show the more polar oxidation products at the start of the chromatogram.

Three different situations may occur.

1. Only the second, late-eluting group of solutes contains relevant analytes, whereas the early-eluting components are of no interest. In this example the obvious approach is to (slightly) increase the eluent strength, to bring the analyte retention factors into the optimum range and to try and optimize the isocratic separation. This can be based on first principles (see Chaps. 1 and 2) or on systematic experimentation.
2. Only the first group of solutes consists of (relevant) analytes, whereas the second group represents matrix components that do not need to be analyzed. There are several different ways to deal with this situation.
   a. Remove the late-eluting components from the sample. A selective extraction using a liquid or solid-phase extraction medium may be found, given the distinction between the two groups.
   b. Remove the matrix components on-line, by incorporating a solid–phase extraction column as part of the instrument. The entire sample can be directed to this precolumn, while only the early-eluting analytes are directed to a second, analytical column. The late-eluting compounds are washed of the precolumn during the analysis, and sent to waste. [A very useful option is to use the backflush mode (see Sec. II.B.2 to wash late-eluting compounds from the column or precolumn.]
   c. Increase the retention of the early-eluting analytes (e.g., by decreasing the strength of the eluent), and wash the late-eluting matrix components from the column at the

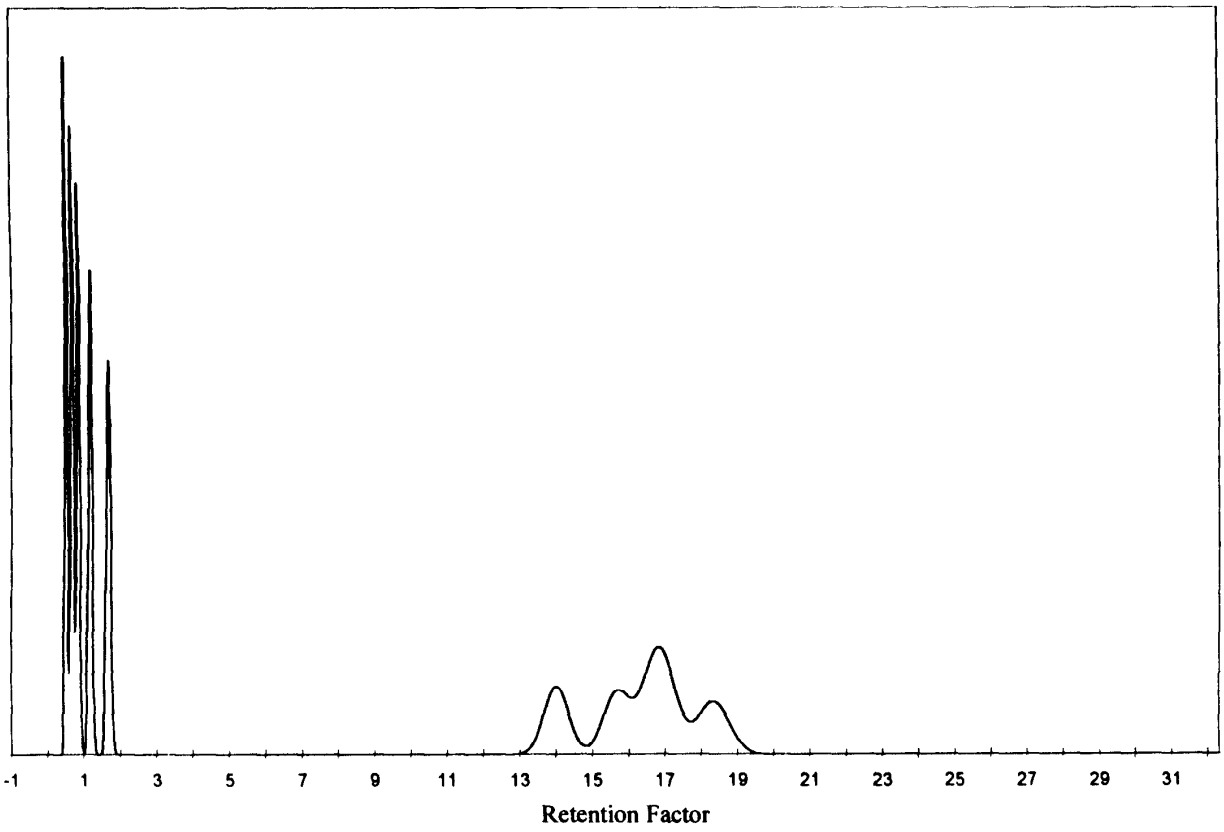


Figure 3 Chromatogram featuring two different groups of solutes. Such a separation provides an indication for the possible application of column-switching methods.

end of the analysis using a strong eluent [again the backflush mode may be used (see foregoing comment)]. Such a simple programmed analysis can be referred to as a *step gradient* (see Fig. 4).

d. Elute the entire sample with a continuously varying mobile-phase composition, using a linear or multisegment gradient.

3. Both groups of solutes are relevant. In this event, an equivalent set of approaches can be followed, namely

   a. Separate the sample (off-line) into two fractions, for example, by liquid or solid-phase extraction, and analyze the two fractions separately.
   b. Incorporate an on-line column-switching method, in which the late-eluting components are subjected to only a short (or otherwise low-retentive) column, while the early-eluting components are separated on a second column. Suitable conditions may be found to achieve adequate separations for both fractions.
   c. Create a step-gradient program, in which the mobile phase approaches the optimal composition for both fractions.
   d. Design an optimal linear or multisegment gradient to elute the entire sample.

The resulting analysis can involve a simple isocratic (1, 2a, or 3a), multicolumn isocratic (constant mobile-phase composition) (2b or 3b), or gradient method (2c,d or 3c,d). Indeed, it is frequently true that various solutions can be found for a given separation problem. Thus, it is worthwhile considering the advantages and disadvantages of the different approaches.

II. COLUMN-SWITCHING METHODS

Excellent switching valves are readily available for use in HPLC. Several manufacturers offer a great selection of valves that are sufficiently inert and robust, operate leak-free at pressures up to 400 bar, and give rise to acceptable extracolumn band-broadening when used in combination with columns of conventional diameters (≥4.6 mm). It is important to realize that the greatest sensitivity to extracolumn band-broadening occurs during the injection of a sample (i.e., when all sample bands are narrowest). Thus, extracolumn band-broadening is a more important issue for injection valves than it is for switching valves. Valves designed as injection valves can thus be readily used as switching valves.

Another general consideration is the possibility of stopping the flow for a time in (part of) the LC system. When the flow is stopped, solute bands will inevitably broaden owing to diffusion. However, diffusion coefficients in liquids are quite small. The contribution of stopping the flow to the total variance (σ^2; in area = length^2 units) can be estimated as

$$\sigma^2_{\text{stopped-flow}} = 2D_{\text{eff}}\, t_{\text{stopped-flow}} \tag{3}$$

which corresponds to a contribution to total plate height of

$$H_{\text{stopped-flow}} = \frac{\sigma^2_{\text{stopped-flow}}}{L} = \frac{2D_{\text{eff}}\, t_{\text{stopped-flow}}}{L} \tag{4}$$

In these equations D_{eff} is the effective diffusion coefficient of the analyte(s) under consideration. The binary diffusion coefficient of a small solute dissolved in the mobile phase can be used as an upper limit. When using a typical diffusion coefficient for a small (i.e., low molecular mass) solute of 10^{-9} m^2/s, stopping the flow for 500 s will result in a σ value of 1 mm, which in a 250-mm–long column corresponds to a contribution of 4 μm to the total plate height. This is considerably smaller than the sum of all intracolumn contributions to the plate height (see Chap. 2), and quite acceptable in most practical situations. [In practice, D_{eff} will be much smaller than in the example discussed here, because (1) a large fraction ($k_i/(1 + k_i)$) of the solute molecules will be in the stationary phase, where dispersion is much smaller; (2) diffusion is hindered in the small pores of the packing materials, where most of the analyte molecules will reside; and (3) molecular diffusion is much slower for solutes of higher molecular mass.]

A. Effects of the Column in LC

Different columns can be used to different effect in LC. For example, short (e.g., 50-mm) columns packed with very small (e.g., 3-μm) particles can be used for fast separations with moderate efficiency. Longer columns packed with somewhat larger particles may provide a greater number of theoretical plates in a longer analysis time. When column-switching methods are considered for solving separation problems, the prevailing issue is to what extent the retention times of the different (groups of) solutes can be made to vary by changing the column. The two groups of solutes in the chromatogram of Fig. 1 differ in retention factors by roughly one order of magnitude. Ideally, the first group of solutes should be somewhat more retained, whereas the opposite is true for the second group.

Various column properties can be used to alter the outcome of chromatographic experiments. A summary is provided in Table 1. Although various factors affect the observed retention times, only some of these affect the retention factors. If we want to increase the retention factors for the first group of solutes in Fig. 3, we may

1. Change the type of stationary phase (e.g., use silica instead of alkyl-modified silica). The difficulty here is that all aspects of the chromatography may be greatly affected. It may be difficult to find a mobile phase compatible with the different columns used. More subtle changes in column types are likely to result in only small changes in k. Roughly,

Table 1 Effect of Various (Column) Parameters on Five Different Chromatographic Observations (The Symbol ÷ Denotes Proportionality. A Small Effect is Indicated by Brackets. See Text for Further Explanation.)

	Effect on				
Parameter	Retention time	Retention factor	Peak width	Peak height	Sample capacity
Column length	$\div L$	Constant	$\div \sqrt{L}$	$\div 1/\sqrt{L}$	$\approx$ Constant
Column diameter[a]	Constant	Constant	Constant	$\approx$ Constant[d]	$\div d_c^{-2}$
Stationary phase:					
Type	Potentially large	Potentially large	Potentially large	Potentially large	Potentially large
Chain length[e]	Increase	Increase	Increase	Decrease	(Increase)
Particle size	Constant	Constant	$\div \sqrt{d_p}$	$\div 1/\sqrt{d_p}$	$\approx$ Constant
Surface area	$\div S$	$\div S$	$\div \sqrt{S}$	$\div 1/\sqrt{S}$	$\div S$
Flow	$\div 1/F$	Constant	Decrease[c]	(Decrease)	$\approx$ Constant
Flow reversal[b]	Large decrease	↓ "Zero"	Decrease	Increase	$\approx$ Constant
Mobile phase	Potentially huge	Potentially huge	Potentially huge	Potentially huge	Potentially huge

[a]When varying the column diameter, the linear velocity is assumed to be kept constant by adapting the flow rate ($F \div 1/d_c^2$).
[b]See Sec. II.B.2.
[c]The flow rate has a large effect (approximately $\div F^{3/2}$) on the peak width expressed in time units. The effect is much smaller (less than $\div F^{1/2}$) when the peak width is expressed in volume units.
[d]Reducing the column diameter is advantageous only in situations in which the amount of sample available is a limiting factor. If this is not the case, the injected volume should be adapted in proportion to d_c^{-2}. This implies that the column is loaded equally with sample. On decreasing the column diameter, care must be taken to minimize the extracolumn band-broadening. This may actually require changes to the detector (e.g., a reduction of the optical path length in UV detection) that cause a decrease in sensitivity on reducing the column diameter.
[e]Effects of increasing the chain length (e.g., from octyl to octadecyl) are listed.

the magnitude of the changes encountered in retention and selectivity will increase when a "standard" reversed-phase octadecyl-silica (ODS) column is replaced by one of the following:

A nominally identical ODS column from the same batch from the same manufacturer.
A nominally identical ODS column from a different batch from the same manufacturer.
A nominally identical ODS column from a different manufacturer.
A different type of ODS material (different carbon loadings, monomeric instead of polymeric phases) [Monomeric phases are prepared using monofunctional derivatizing agents, such as methoxy-dimethyl-octadecylsilane. In the preparation of polymeric phases, trifunctional reagents, such as trimethoxy-octadecylsilane, are used. The latter can bond to the surface and to each other, so that a "polymeric" layer can be formed on the surface.]
A modified silica with a different surface area of the stationary phase. Silica-based materials are available in a range of specific surface areas, covering about a factor of 10 (100–900 m^2/g), allowing a proportional variation in k. [If the specific area of a silica-support material changes, almost invariably, so does the pore size. The effect of the pore size in partition chromatography (RPLC, NPLC) tends to be underestimated. Size-exclusion effects do occur in the separation of all but very small solute

molecules on microporous materials, and these effects can be quite substantial. Electrostatic exclusion does occur for ionic species in mobile phases of low ionic strength.]

An alkyl-modified silica with a different chain length of the bonded phase. When using reversed-phase LC, the length of the alkyl chains on the surface may be altered. Increasing the chain length typically results in an increase in retention factors, until a certain "critical chain length" is reached [1].

A different type of silica-based chemically bonded stationary phase (e.g., cyano, phenyl).

A nonsilica-based packing material suitable for reversed-phase applications (e.g., polystyrene–divinylbenzene, porous carbon).

A normal-phase adsorbent, such as nonderivatized silica or alumina.

2. Changing the mobile phase allows drastic manipulation of the retention factors. This effect can also be used indirectly. For example, if a longer column is used, retention times will increase. If this is compensated by an increase in the eluent strength, the net result is a reduction of the retention factor at approximately constant retention time.

Clearly, there are many ways in which changes in the column can be used to affect the kind of changes needed to elute either of the two groups of analytes in Fig. 3 within the optimum range of retention factors. Other parameters, such as the detection sensitivity (peak height) or the sample capacity of the column, may be advantageously affected in the process, as is indicated in Table 1.

The effects of column length and diameter can (in principle) be predicted. To a smaller extent, this is true for the effects of the particle size, the surface area of the stationary phase, and the flow rate. The effects of changes in the chemistry of the chromatographic system (type of stationary phase and composition of mobile phase) are the least predictable.

Multicolumn LC methods are useful in a variety of areas, but their successful implementation is most commonly associated with the following conditions:

1. The chromatographic method is aimed for routine application for a substantial number of samples.
2. Only limited characterization of the sample is desired.

Examples in which the latter criterion is met include

The analysis of one (group of) solutes in the presence of a matrix

The separation of a sample into groups or classes of compounds (e.g., saturates, mono-, di-, and "tri-plus" aromatics)

Providing additional separation for part of the sample (e.g., separating one peak in a chromatogram into its isomers)

B. Valve-Switching Options and Requirements

1. Cutting

A selected fraction of a chromatogram obtained on a first column or precolumn can be "cut" and directed to a second column. Several options are illustrated in Fig. 4a–c. The selected fraction of the sample can be further separated on a second column. The advantage of incorporating a restrictor (see Fig. 4b) is that the pressure across the system remains constant on switching, so that the first column and the detector do not experience greatly different pressures during different parts of the run. This may increase the lifetime of the columns and enhance the stability of the baseline. In Fig. 4c, two columns have been drawn, that allow different fractions of the sample to be separated under different conditions, approaching optimum chromatography for each part of the sample.

The configurations shown readily allow various manipulations to be performed.

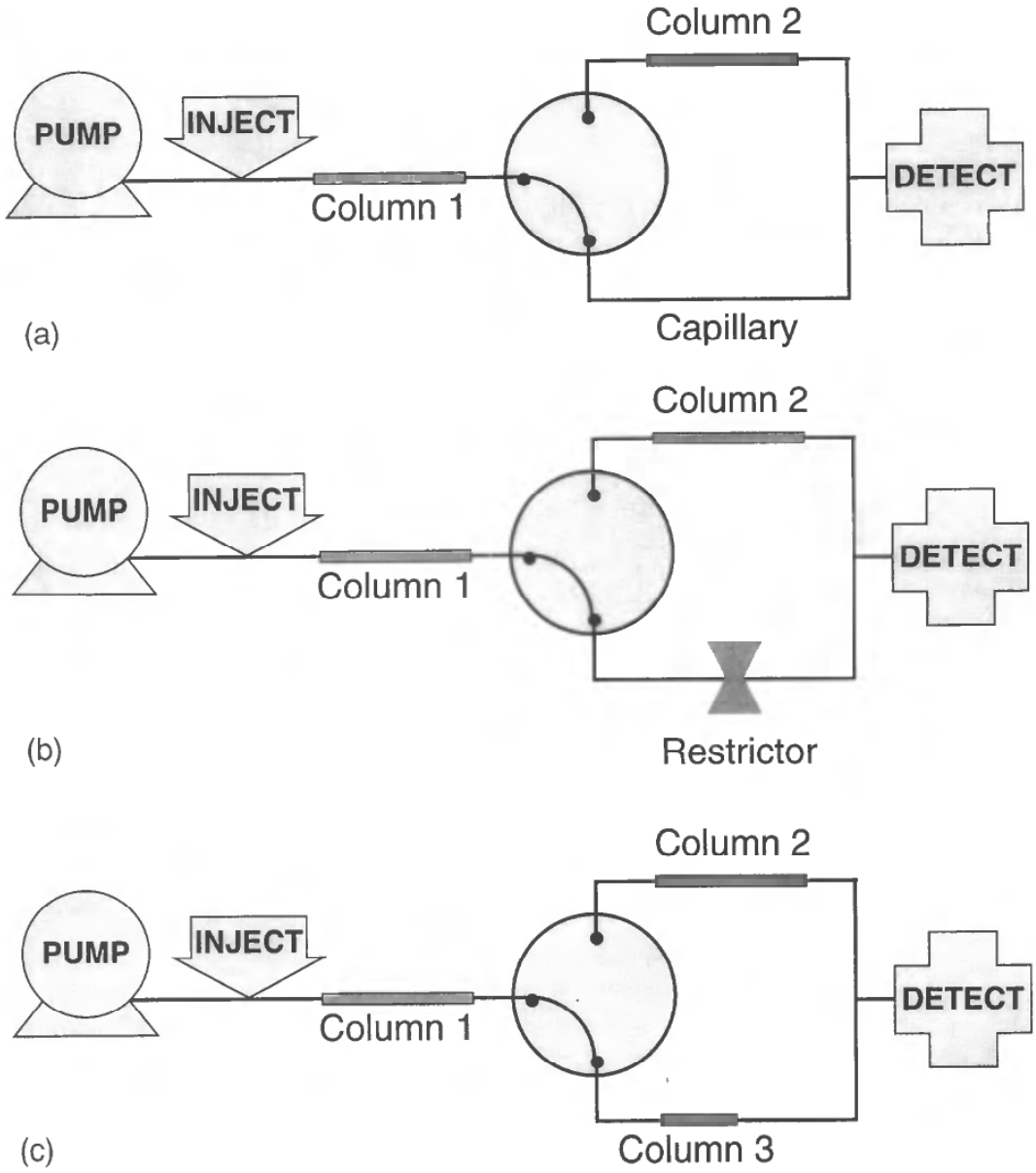


Figure 4 Simple two-column configurations that allow various cutting methods to be used for separations or for on-line sample preparation.

(a) *Front-cutting.* Early-eluting peaks can be directed to the second column. There they can be stored, while the flow is switched and late-eluting solutes are sent straight from the first column to the detector. After these peaks have been eluted, the valve can be switched again and the early-eluting solutes can be separated on the second column. This latter column may show higher retention factors for the early-eluting solutes based on one of the parameters mentioned in Table 1.

(b) *Heart-cutting.* A central part of the chromatogram may be directed to the second column. This may be a fraction that contains some or all of the relevant solutes if these are difficult to separate from each other or from the matrix on a single column. Again, this heart-cut fraction may be "stored" on the second column while first the early-eluting sample components and then the late-eluters are directed straight to the detector.

(c) *Back-cutting.* The late-eluting components from the sample may be separated on a first column with a low retentivity, keeping them away from the second, more-retentive col-

umn used to separate early-eluting solutes. If the components that elute late from the first column are matrix components that do not need to be analyzed, the backflush configuration described in Sec. II.B.2 may be more attractive.

2. Backflush

Reversing the flow through the column at some point after the injection allows the elution of very strongly retained compounds in a relatively short time in what is known as the "backflush" mode. This mode is ideal for cleaning up very "dirty" samples, but it is also possible to estimate the total amount of backflushed material from the total peak area (see Sec. II.B.3).

In broad terms backflush has the following characteristics:

1. In principle, all components will elute together (i.e., there is no resolution in the backflush mode) at a time double that of the loading time:

$$t_{BF} = 2 \times t_{FF} \tag{5}$$

   where the subscript BF denotes backflush, while FF denotes forward-flush.

2. Although in theory the chromatographic dispersion of a peak eluted in the backflush mode is quite small, in practice nonsymmetrical peaks are often observed. This is likely to be associated with (very) nonlinear adsorption (or distribution) coefficients for highly retained solutes. If the stationary phase is overloaded, the adsorption isotherm is convex and the apparent retention factor at high-solute concentrations (i.e., at the top of the peak) is lower than that at the edges. Thus, the tail of the peak elutes much slower than the top and tailing peaks.
3. Even in the backflush mode not all material will be eluted from the column. In theory, this should be true, but in practice, some highly retentive or hardly soluble materials may be virtually irreversibly adsorbed onto the column. Sometimes backflushing a column is accompanied with a step-gradient in the mobile phase to remove all sample materials from the column or precolumn.

In the context of this last point, in particular, the two-column configuration illustrated in Fig. 5b is more attractive than the one-column setup of Fig. 5a. Indeed, the two-column configuration is much more commonly used, with column 1 typically being a small, inexpensive precolumn (or cleanup column). This column serves to clean up the sample, by discarding late-eluting components. The relevant analytes are separated from each other on column 2. This column is typically longer and (much) more expensive, and enhancing its lifetime is one of the greatest benefits of the two-column configuration.

3. Example of Multivalve Configuration

One or two simple valves allow a multitude of different operations to be performed. Indeed, valve boxes that serve this purpose have been advocated [2] and commercialized.

There are many different ways in which valves and columns can be configured elegantly to achieve imaginative separations. Only one such scheme is discussed here, by way of an example. The application is the separation of complex hydrocarbon (oil) mixtures into several classes of compounds and the associated valve configuration is illustrated in Fig. 6.

The configuration shown in Fig. 6 can be used to separate a light hydrocarbon fraction (such as gasoline) or a middle-distillate fraction (diesel, kerosene) into three overall fractions: namely, the saturates (alkanes, branched alkanes, cyclic alkanes), olefins (alkenes, branched alkenes, cyclic alkanes, alkadienes), and aromatics (plus "polars," such as oxygenates). Saturates and olefins, on the one hand, can be separated from aromatics, on the other hand, using normal-phase LC. The stationary phase should be unmodified silica, with a high surface area, and the mobile phase should be a nonpolar solvent, such as *n*-heptane. A very attractive alternative eluent is carbon dioxide. Indeed, hydrocarbon group-type separations for light fractions and middle-distillates are often performed using supercritical-fluid chromatography.

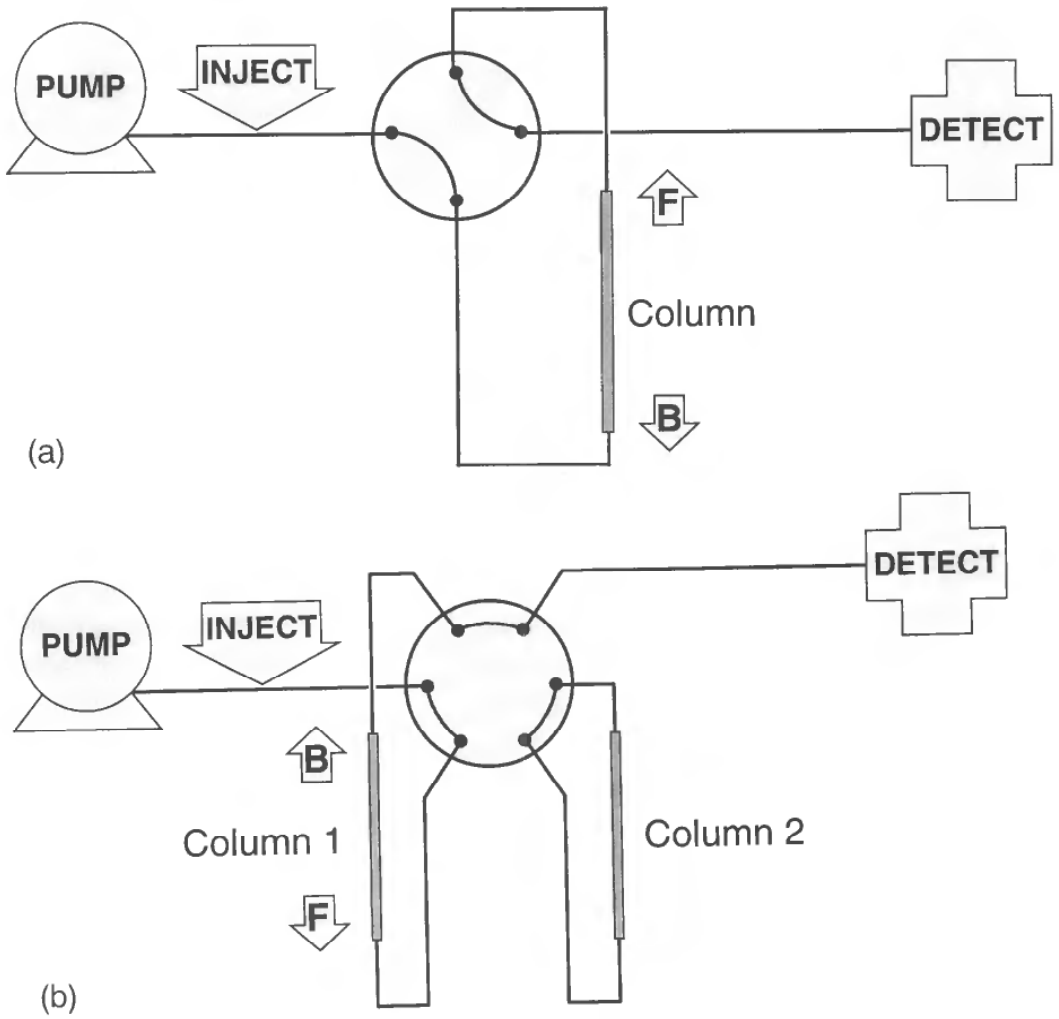


Figure 5 Simple valve configurations for backflush operations. (a) Backflush operation used for cleaning up a single column; (b) backflush operated on a precolumn.

For the saturates to be separated from the olefins, a special kind of column is needed, usually a silica or (preferably) an ion-exchange column impregnated with silver ions. However, it is highly undesirable to load the entire sample (including the aromatics and polars) onto a silver-loaded column. Thus, the sample is injected onto the silica column, from which the saturates and olefins are directed to the silver-loaded column. The aromatics are preferentially retained on the silica column and, subsequently, eluted in the backflush mode. The saturates can be eluted from the silver-loaded column in the forward-flush mode, either before or after the elution of the aromatics. Finally, the olefins are eluted from the silver-loaded column in the backflush mode. A chromatogram to illustrate the resulting separation is shown in Fig. 7.

From Fig. 7 some of the characteristics of backflush operation become clear. Although all aromatics (backflush from silica) are grouped into quite a sharp signal—a feat that cannot be achieved in the forward-flush mode—the olefins yield a highly nonsymmetrical peak, despite also being eluted in the backflush mode. However, there is ample separation in Fig. 7, and the olefins' signal can be readily integrated with excellent quantitative results.

4. Comprehensive Two-Dimensional Chromatography

Comprehensive two-dimensional liquid chromatography is a complex way to describe a type of separation that formerly was commonly performed in thin-layer chromatography. If a thin-

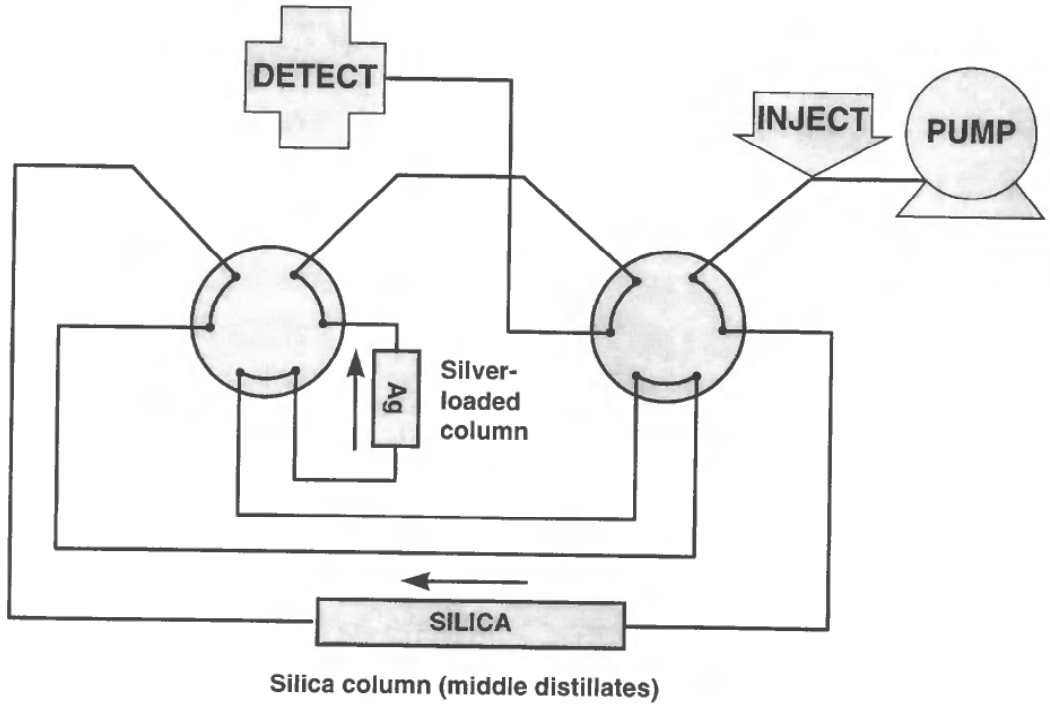


Figure 6 Two-way configuration for group-type separation of hydrocarbons. (Adapted from Ref. 3.)

layer plate is first developed in one direction using one mobile phase, and then, subsequently dried and developed in a perpendicular direction, all of the sample is subjected to two different chromatographic systems, and all the material present in the sample is presented as several separated components ("spots") in a two-dimensional surface.

Modern developments in column gas chromatography and liquid chromatography are giving rise to instrumental versions of such comprehensive systems. The great advantage of a comprehensive system, relative to a conventional column-switching (e.g., heart-cutting) approach, is that all of the sample can be characterized in a single run, whereas multiple heart-cuts would be required to characterize the entire sample. In fact, comprehensive systems can be envisaged as systems in which a large number of heart-cuts are performed and combined into a single two-dimensional contour plot (representing a TLC plate developed in two directions) or a pseudo–three-dimensional plot.

Ideally, in comprehensive two-column systems

All material is subjected to both columns.
The separation mechanisms on the two systems are completely independent ("orthogonal"). This implies that there is no correlation between the retention factors on the two different systems.
No band-broadening occurs in addition to the common dispersion on the two columns.
The peak capacity of the comprehensive two-dimensional system is then roughly equal to the product of the peak capacities of the individual columns.

For this latter reason we introduce the notation LC×LC, which distinguishes comprehensive systems from hyphenated LC-LC systems, which use conventional valve-switching (e.g., heart-cutting). One example is shown in Fig. 8. This concerns a copolymer of styrene (St) and butadiene (Bd) that is separated by normal-phase LC according to functionality (indicated as percentage Bd content) and by size-exclusion chromatography (SEC) according to molecular mass. The comprehensive two-dimensional chromatogram provides a much more detailed

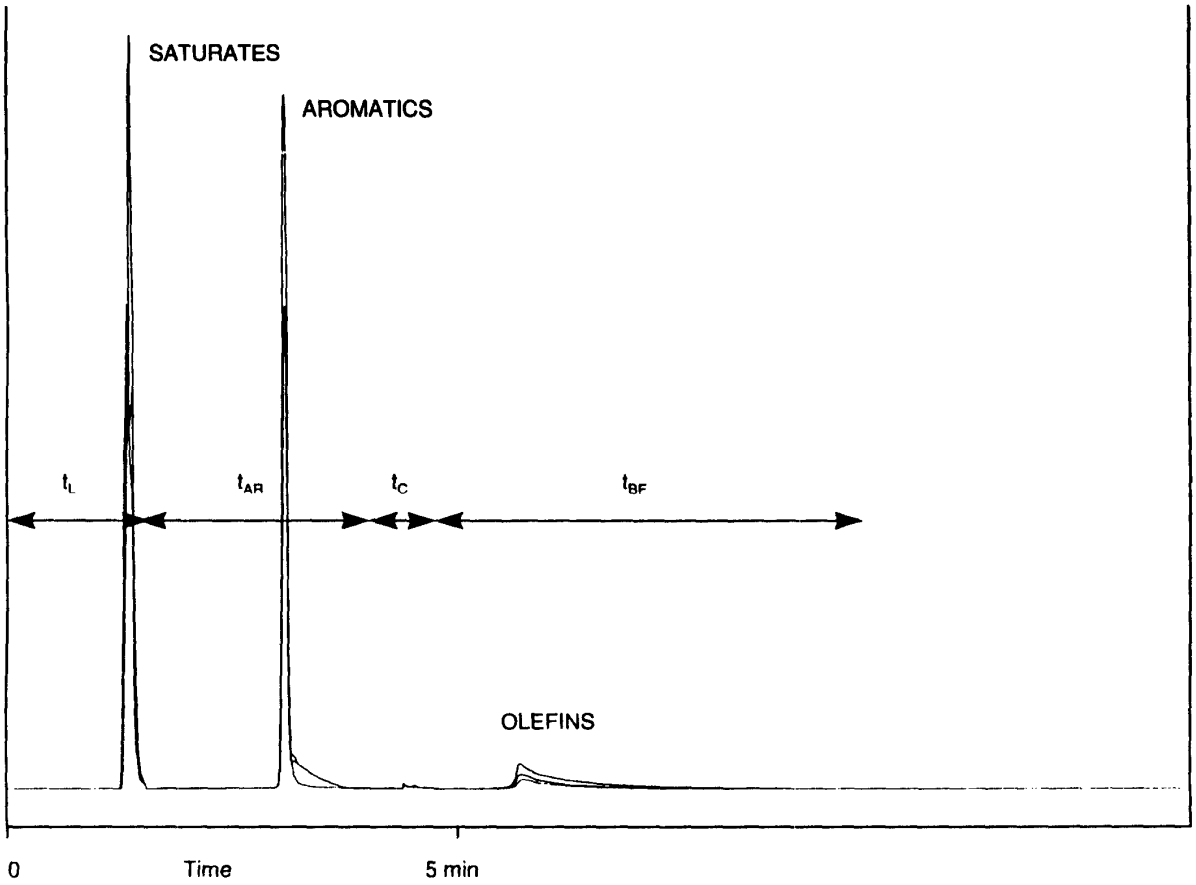


Figure 7 Chromatogram illustrating the separation of a gasoline into saturates, aromatics, and olefins, using the two-column setup shown in Fig. 6.

characterization of the block copolymer than either technique separately or, indeed, any linear two-dimensional (heart-cut) analysis can provide.

Jorgenson and co-workers [5] are in the process of developing various comprehensive two-dimensional separation systems, including combinations of RPLC with SEC and with capillary zone electrophoresis (CZE).

III. GRADIENT ELUTION

The word *gradient* can generally mean any kind of variation in the value of a certain parameter in space or time. Chemists are familiar with temperature gradients (variation of temperature with position) and concentration gradients (variation of composition with location). In LC gradient is short for *gradient elution* and both terms are commonly used as synonyms for solvent programming. *Solvent programming* refers to any kind of intentional variation of mobile-phase composition with time during the course of an analysis. Some ways in which this change of composition may be affected are illustrated in Fig. 9.

A. Migration Under Gradient Conditions

Changing the composition of the eluent during the run has several desired and some accidental effects, some of these latter being significant disadvantages of solvent programming in LC. Solvent programming should take place in such a way that the solvent strength is increased in time; in other words, the migration velocity of analytes is increased as a result of the

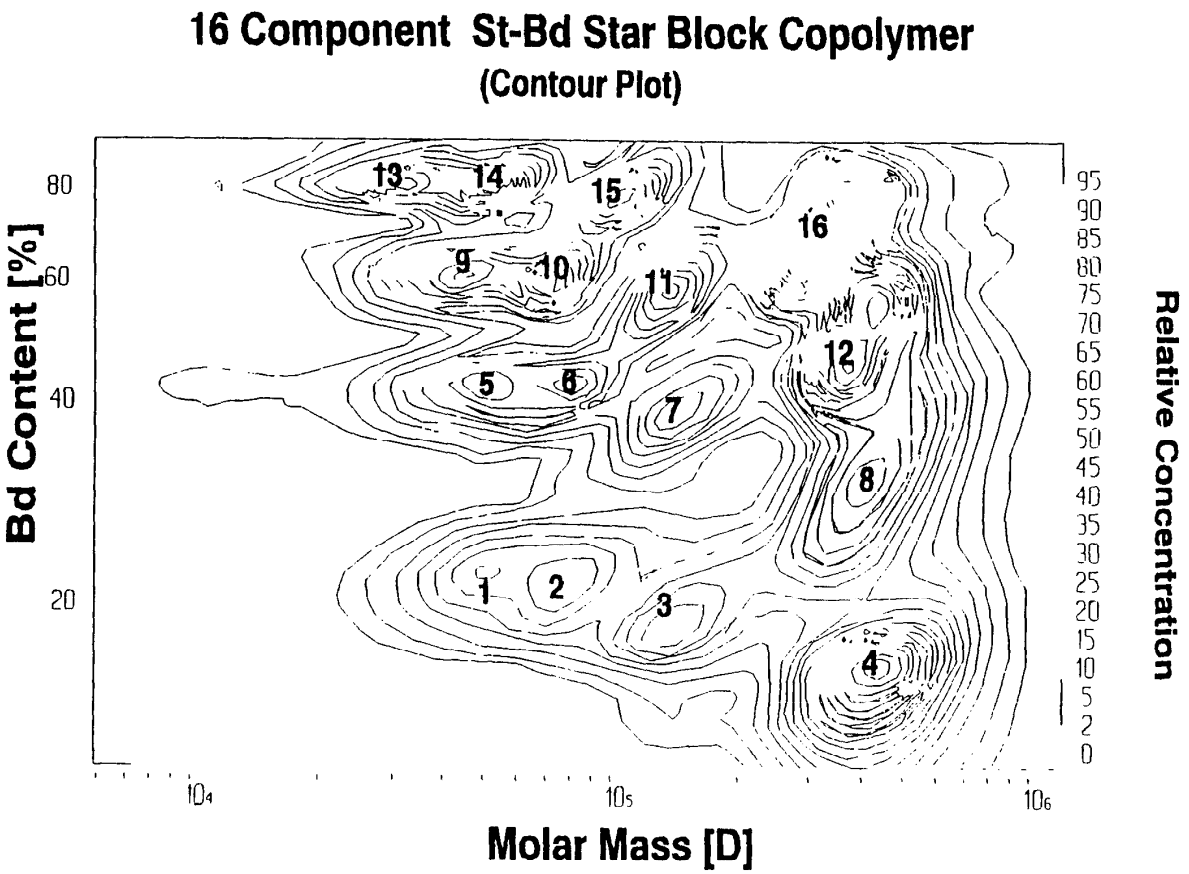


Figure 8 Example of comprehensive two-dimensional liquid chromatography (gradient NPLC×SEC) for the characterization of copolymers. (From Ref. 4.)

gradient. Programming in the opposite direction is senseless. [Reverse gradients turn all the common advantages of solvent programming into disadvantages. Fewer peaks can be adequately resolved in a single chromatogram than in an isocratic elution and peaks become broader than the width corresponding to their analysis time in isocratic elution. However, one intriguing application of solvent programming [5g] involves the injection of pulses of weak solvent at strategic moments to improve the separation of critical pairs of peaks.]

The intitial conditions at the start of the run are chosen such that the retention factor of the first (relevant) component is within the optimal window (typically $1 < k < 10$) or higher. Under these conditions, no relevant components are eluted too early in the chromatogram. However, some components may have very high k values under the initial conditions. When the solvent strength becomes higher, the retention factors of these components start to become smaller. Initially, these peaks move slowly through the column, but their migration speeds increase with time (see Fig 11).

The migration speed (u_i) of a zone i equals

$$u_i = \frac{u_m}{1 + k_i} \tag{6}$$

and the variation of u_i during the course of a gradient will be covered by two factors:

1. The variation of the solute retention factor as a function of composition [i.e., $k(\varphi)$]
2. The local composition of the mobile phase at the location of zone i [i.e., $\varphi(x,t)$].

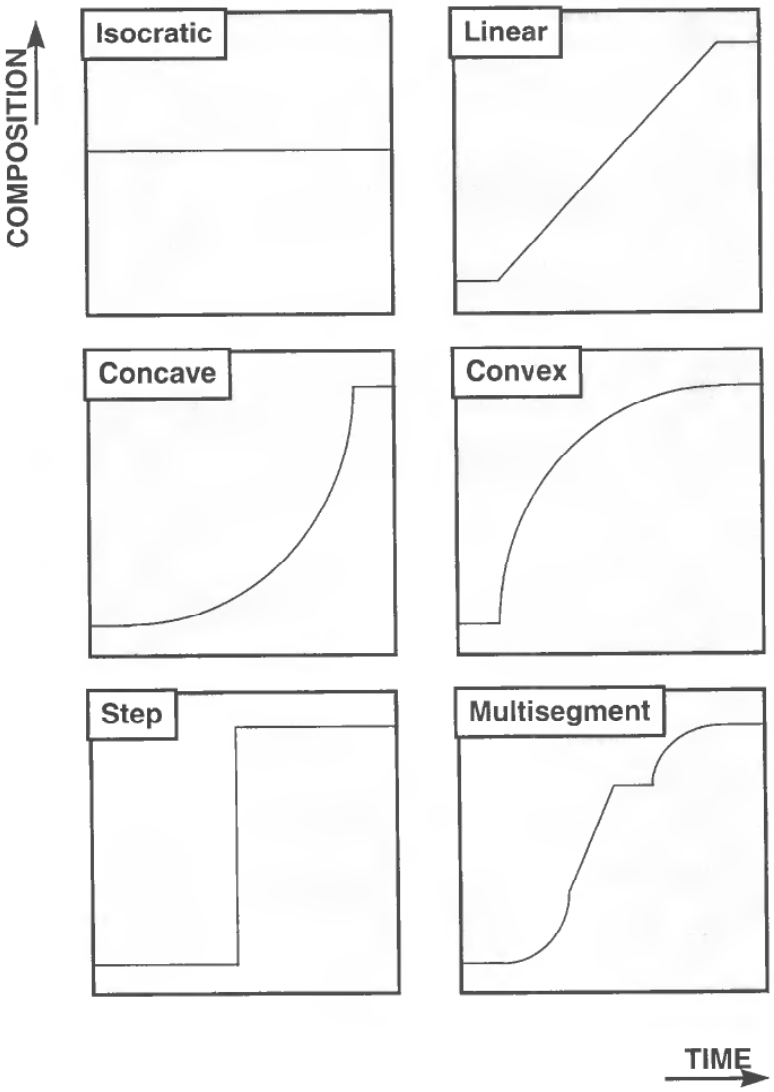


Figure 9 Possible shapes of gradients, illustrated as graphs of solvent composition versus time. The figure on the left top refers to isocratic elution (constant composition). All others represent solvent-programming (gradients).

Variations in mobile-phase composition, unlike variations in temperature, cannot be affected simultaneously throughout the entire column. A change made at the top of the column will take a time t_m to arrive at the detector; t_m is the mobile-phase time or hold-up time, i.e. the time it takes the average mobile-phase molecule to travel through the column. In general, the relation between the composition at the top of the column ($z = 0$) and at an arbitrary location (z) along the length of the column (L) is

$$\varphi(z,t) = \varphi\left[0,\left(t - \frac{zt_m}{L}\right)\right] \tag{7}$$

In addition to the retardation of the gradient owing to the column itself, there is a significant delay between the electronic implementation of a gradient, when the instruction to alter the mobile-phase composition is sent from the control system to the pumps or solvent-switching valve(s), and its arrival at the top of the column. This instrumental delay time is

usually referred to as the dwell time (t_D). The relation between the gradient specified in the (instrument) method $f(t)$ and the composition at an arbitrary position in the column is

$$\varphi(z,t) = f\left(t - \frac{zt_m}{L} - t_D\right) \tag{8}$$

The progression of a gradient through the column is more easily understood from a graphic illustration, such as provided by Fig. 10.

During a time t_D the composition of the eluent at the top of the column equals the initial composition of the gradient. [If the equilibration time is too short, it is actually possible that the eluent composition after injection is different from the specified initial composition. It is recommended that the equilibration time before any solvent program well exceeds t_D (to allow for deformation of the gradient) and that the equilibration time is kept constant (to obtain equal background signals in different runs).] During this time, solute bands will have progressed into the column to an extent dependent on their retention factors at the initial composition. Solutes that have high initial k values will essentially stick to the top of the column until they are overtaken by the gradient. Solutes with low initial k values may never be overtaken by the gradient.

This is illustrated in Fig. 11. This figure shows the calculated migration profiles (position in the column as a function of time) of several solutes [see e.g., Ref. 6]. The first solute shows a linear migration profile, which is indicative of isocratic analysis. The slope of the line equals the migration speed.

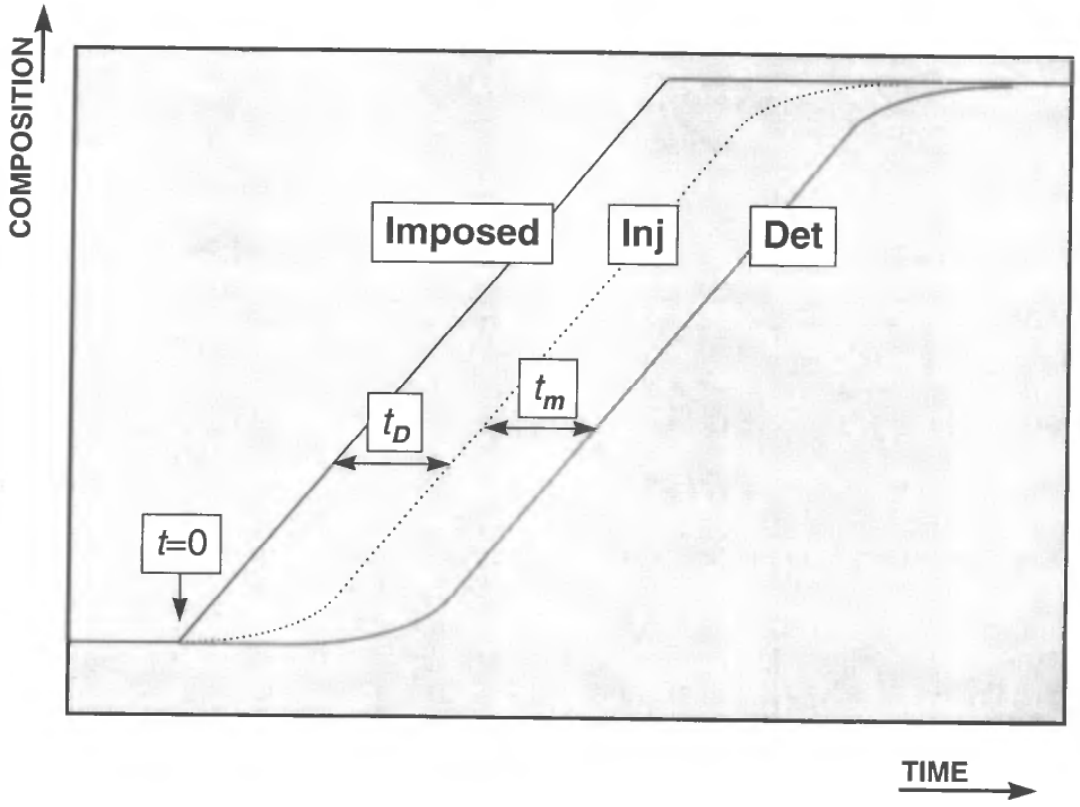


Figure 10 Schematic illustration of a linear gradient: The straight line indicates the imposed gradient (the user-defined solvent program). The second (dotted) curve (indicated by Inj) is the gradient delivered by the instrument to the top of the column (injector). The third (gray) curve represents the gradient program observed in the detector.

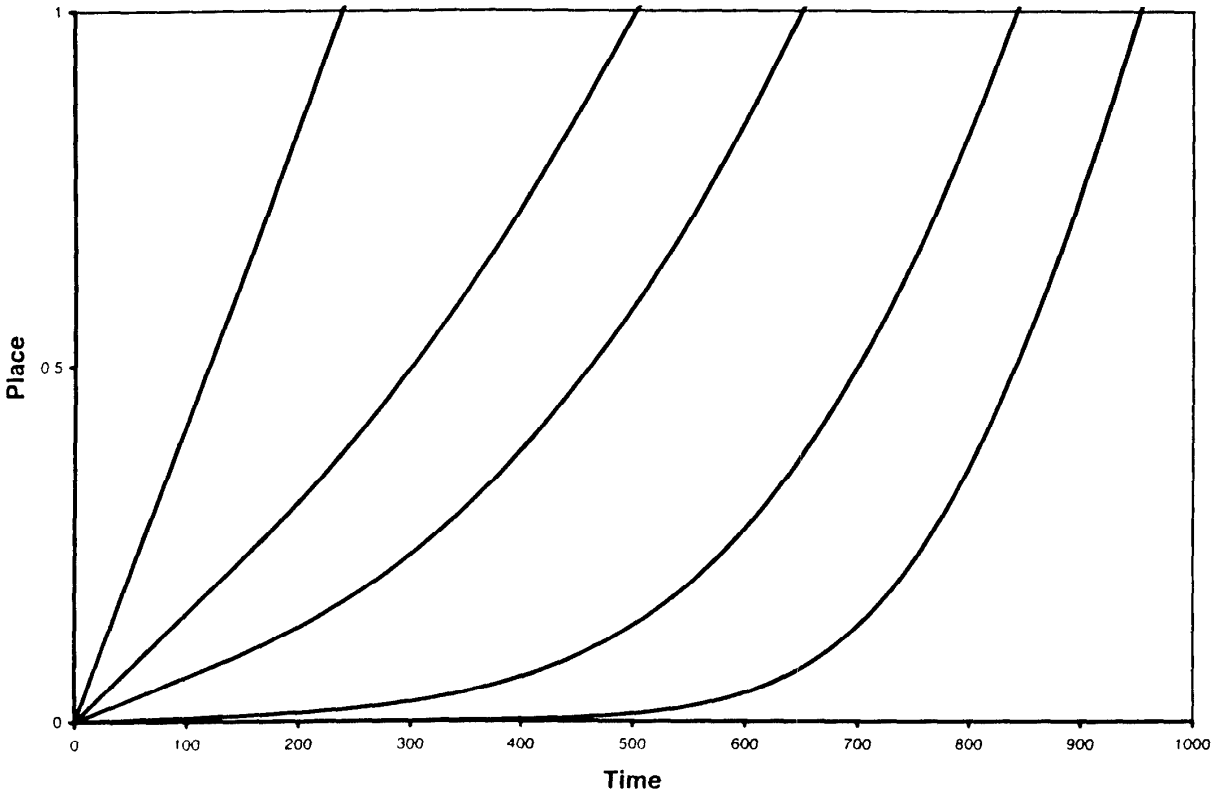


Figure 11 Calculated migration profiles of a series of solutes subjected to a linear gradient. Conditions: $L = 1$ (arbitrary units), $t_m = 120$ s, $t_D = 120$ s, linear gradient from 0 to 100% in 20 min. The ln k_0 and S_n values, respectively, for the individual solutes: are solute 1: 0 and 0; solute 2: 1.5 and −4; solute 3: 2.5 and −6; solute 4: 5 and −10; solute 5: 9 and −16.

$$\left(\frac{dz}{dt}\right)_i = u_i = \frac{u_m}{1 + k_i[\varphi(z,t)]} \tag{9}$$

A large slope corresponds to a rapid migration (low k value) and a constant slope indicates a constant k value. Once the gradient starts to overtake a solute band, its migration speed increases and its migration profile curves upward. Solutes with a large k_A value (denoting the initial value for k at the start of the gradient) are seen not to migrate significantly over a time period, but then progress rapidly through the column.

In fact, it is suggested by the curves in Fig. 11 that all solutes migrate through the column at similar speeds (similar slopes of the migration profiles). This is an important observation, that has practical consequences. The slope of the migration curve at the top of the figure (column length was assumed to equal unity) is the migration speed of the solute at the time of elution, which is the most important factor in determining the observed bandwidth. To a first approximation, the bandwidth under programmed conditions, such as the linear gradient underlying Fig. 11, is the same for all solute bands.

Thus, the linear gradient underlying Fig. 11 offers a beautiful solution to the general elution problem. Solutes of vastly different retentivities (different initial k values) can be made to elute in a single chromatographic run in a roughly optimal manner. However, the suggestion that "[gradient RPLC] offers the same broad applicability for non-volatile samples that temperature-programmed gas chromatography (GC) provides for volatile mixtures" [6] is a bit too emphatic. Unfortunately, many solutes (ionic compounds or carbohydrates) are insuf-

ficiently retained on typical (octadecyl-silica) RPLC columns even with 100% water as the mobile phase, many other solutes (large, apolar hydrocarbons and many polymers) cannot be eluted even with pure organic solvents, such as acetonitrile or tetrahydrofuran (THF). Also, gradient-elution RPLC does not yield the chromatographic efficiency (plate numbers) that can be routinely achieved in capillary GC. Finally, and perhaps most importantly, the detectability of analytes eluted under gradient-LC conditions is vastly inferior to that under temperature-programmed GC conditions.

Still, gradient-elution LC, particularly in the reversed-phase mode, is an invaluable separation technique for complex mixtures of nonvolatile solutes. In the next sections, retention and band-broadening will be quantitatively examined for certain types of gradients.

The most elegant way [7] to solve Eq. (9) is through the introduction of the inverse function $f^{-1}(\varphi)$. From Eq. (8) we find

$$t = t_D + \frac{z}{u} + f^{-1}(\varphi) \tag{10}$$

and

$$dt = \frac{dz}{u} + d[f^{-1}(\varphi)] \tag{11}$$

The combination of Eqs. (9) and (11) yields the fundamental equation for migration under gradient conditions

$$\frac{dz}{u} = \frac{d[f^{-1}(\varphi)]}{k(\varphi)} \tag{12}$$

Integration of this equation leads to

$$\int_0^L \frac{dz}{u} = \int_{-t_D}^{t_R - t_D} \frac{d[f^{-1}(\varphi)]}{k_i(\varphi)} = \int_{-t_D}^{0} \frac{d[f^{-1}(\varphi)]}{k_A} + \int_0^{t_R - t_D} \frac{d[f^{-1}(\varphi)]}{k_i(\varphi)} \tag{13}$$

and

$$t_m = \frac{t_D}{k_A} + \int_0^{t_R - t_D} \frac{d[f^{-1}(\varphi)]}{k_i(\varphi)} \tag{14}$$

Equation (14) may be solved analytically for several simple gradient shapes and k versus φ relations. [An extensive survey can be found in Ref. 8.] Numerical integration [9] is always possible, and increasingly easy using modern software toolkits for computations. However, analytical integration has some important advantages, the most important of which is the possibility to use gradient–elution retention data to establish the coefficients in the isocratic k versus φ relations.

Here, we will consider one very important example to illustrate the process. If a linear gradient is used, with starting composition A (volume fraction of strong solvent) and slope B, we can write

$$\varphi = f(t) = A + Bt \tag{15}$$

[because φ is a volume fraction and thus dimensionless, B is in min^{-1}; e.g., a gradient from 0 to 100% of strong solvent in 20 min (5%/min) has a B value of 0.05 min^{-1}] and inversely

$$t = f^{-1}(\varphi) = \frac{\varphi - A}{B} \tag{16}$$

Substitution in Eq. (14) yields

$$t_m = \frac{t_D}{k_A} + \frac{1}{B} \int_A^{A+B(t'_R - t_D)} \frac{d\varphi}{k_i(\varphi)} \tag{17}$$

This equation, which is valid for linear gradients, will be used later to describe retention behavior in reversed-phase LC.

B. Theory of LSS Gradients

1. Retention

The clearest way to describe the principles of LC gradients is the linear-solvent–strength (LSS) model, developed by Snyder [6,10,11]. The LSS concept is relatively simple, and it provides several useful analogies between isocratic and gradient elution. In practice, LSS gradients provide approximately constant peak widths for all peaks in the chromatogram and a regular spacing of a coherent group of analytes, such as a homologous series.

By definition, an LSS gradient is programmed such that the retention factors of the analyte decrease exponentially with time

$$\log k = \log k_{\text{init}} - b(t/t_0) \tag{18}$$

Here k_{init} is the initial retention factor (at time $t = 0$) and b is a constant. In the most common case of RPLC, retention approximately varies with mobile-phase composition, according to

$$\log k = \log k_0 - S\varphi \tag{19}$$

In this equation k_0 is the (extrapolated) retention factor in pure water (volume fraction of organic modifier $\varphi = 0$) and the slope S is a constant for a given solute, on a given column, using a given modifier. In reversed-phase LC an LSS gradient is clearly a linear gradient ($\varphi = A + Bt$). For mathematical reasons, it is more convenient to use natural logarithms in Eq. 19 [conventional decimal logarithms may be used, but this causes the occurrence of unnecessary constants (ln 10 = 2.3) to appear in several equations. Because $S_n = S \ln 10 = 2.303S$, all equations can readily be converted].

$$\ln k = \ln k_0 - S_n\varphi \tag{20}$$

$$k = k_0 e^{-S_n\varphi} \tag{21}$$

In combination with a linear gradient [see Eq. (15)] [for solutes that are overtaken by the gradient. If this is not so (i.e., if $t_D > [1 + k_A]t_m$), then $t'_R = k_A t_m$.] we find

$$t_m = \frac{t_D}{k_A} + \frac{1}{B} \int_A^{A+B(t'_R - t_D)} \frac{d\varphi}{k_0 e^{-S_n\varphi}} \tag{22}$$

an equation that can be readily integrated to yield

$$\begin{aligned} t_m &= \frac{t_D}{k_A} + \frac{1}{Bk_0S_n}[e^{S_n\varphi}]_A^{A+B(t'_R - t_D)} = \frac{t_D}{k_A} + \frac{e^{AS_n}}{Bk_0S_n}[e^{S_nB(t'_R - t_D)} - 1] \\ &= \frac{t_D}{k_A} + \frac{1}{Bk_AS_n}[e^{S_nB(t'_R - t_D)} - 1] \end{aligned} \tag{23}$$

or in terms of the net retention time t'_R

$$t'_R = \frac{1}{BS_n} \ln \left[1 + Bk_AS_n\left(t_m - \frac{t_D}{k_A}\right)\right] + t_D \tag{24}$$

It is equally straightforward to derive an equation for the retention time of a peak that

elutes after the completion of the gradient. If the gradient program takes a nominal time t_G to be completed, then the end of the gradient will have reached the end of the column at a time $t_F = t_G + t_D + t_m$. If the retention time of a solute exceeds this value (i.e., $t_R > t_F$ or $t'_R > (t_G + t_D)$, then the component elutes after the gradient has been completed. Here, the migration of the component through the column takes place in three distinct phases: (1) migration before the component being overhauled by the gradient, (2) migration during the gradient, and (3) migration after the completion of the gradient. These three phases are reflected in three separate integration terms.

$$\int_0^L \frac{dz}{u} = \int_{-t_D}^{0} \frac{d[f^{-1}(\varphi)]}{k_A} + \int_0^{t_G} \frac{d[f^{-1}(\varphi)]}{k_i(\varphi)} + \int_{t_G}^{t_R - t_G} \frac{d[f^{-1}(\varphi)]}{k_F} \tag{25}$$

or after integration

$$t'_R = k_F\left(t_m - \frac{t_D}{k_A}\right) - \frac{1}{BS_n}\left(1 - \frac{k_F}{k_A}\right) + t_G + t_D \tag{26}$$

One attractive simplification of Eq. (26) can be made if t_D is negligibly small. This is hardly ever true in practice [although t_D is usually significant, the term t_D/k_A is usually much smaller than t_m. In that case, t_D can simply be accounted for by subtracting its value from t'_R; that is, Eqs. (27), (29), and (30) can be used for not-too-early-eluting solutes with $t'_R = t_R - t_m - t_D$ on the left-hand side], but a realistic alternative is to inject the sample a time t_D after the start of the solvent program. Unfortunately, this fundamentally useful approach cannot easily be accommodated in many modern computerized data stations. The simplification yields

$$t'_R = \frac{1}{BS_n} \ln (1 + Bk_A S_n t_m) \tag{27}$$

Snyder's gradient–steepness parameter [$b_n = BS_n t_m$, see Eq. (18)] may be used in a number of different ways to describe and understand the effects of LSS gradients. Combining this group of parameters into b_n leads to

$$t'_R = \frac{t_m}{b_n} \ln \left[1 + \frac{b_n k_A}{t_m}\left(t_m - \frac{t_D}{k_A}\right)\right] + t_D \tag{28}$$

or with negligible t_D

$$t'_R = \frac{t_m}{b_n} \ln (1 + b_n k_A) \tag{29}$$

A final simplification is possible for all solutes that are highly retained under the initial conditions, such that $b_n k_A >> 1$ and

$$t'_R = \frac{t_m}{b_n} \ln (b_n k_A) \tag{30}$$

It is seen that despite some rather awkward mathematics, the resulting equations for retention under gradient conditions are quite simple.

2. Peak Width

The observed peak width under gradient conditions is determined mainly by the dispersion of the column and by the solute retention factor on leaving the column [k_e, see following Eq. (32)]. The chromatographic dispersion in volume units follows most of the rules described in Chapter 2. Some complications arise owing to the variation of solute migration with its position in the column. This is related to the variation of certain terms in the equations for the total plate height (e.g., the van-Deemter equation) with the retention factor k. Ideally, the

dispersion equations should be integrated along the column length using a calculated retention profile as illustrated in Fig. 11 [9]. However, thanks largely to the work of Snyder, several convenient simplifications have been described that allow us to present an adequate description of peak width under gradient conditions using simple mathematics.

The observed dispersion in time units (σ_t) is related to the true dispersion volume units (σ_V) as

$$\sigma_t = (1 + k_e)\frac{Gt_m}{\sqrt{N}} \tag{31}$$

where N is the column plate count observed under isocratic conditions. Note that it is grossly incorrect to estimate the plate height from a gradient–elution chromatogram using the retention time and peak width in time units in the same manner as in isocratic LC.

For LSS gradients, a simple expression can be derived for k_e [6]:

$$k_e = \frac{1}{b_n + (1/k_A)} \approx \frac{1}{b_n} \tag{32}$$

This equation illustrates quite clearly that the gradient–steepness parameter b_n plays a role in gradient–elution LC similar to that of the eluent strength in isocratic elution. It also shows that for all solutes for which $k_A >> 1$, the retention factor upon leaving the column, and thus the observed peak width, is similar.

Beside the conventional dispersion and the retention factor upon leaving the column, one other parameter appears in Eq. (31), (i.e., the band-compression factor G). This factor appears because under gradient conditions the tail of the peak experiences a stronger solvent than the front. The leading edge of the peak thus travels somewhat slower than the peak maximum, and the trailing edge travels a little faster. As a result, the band is compressed. However, this band-compression effect is relatively small. For optimum values of the gradient–steepness parameter ($0.5 < b_n < 1$) the theoretical gain is about 20% in peak width. Even for very steep gradients, peaks are narrowed by only about one-third. In practice, the theoretically predicted peak-compression effect is usually not quite achieved [12,13].

Jandera [8,14] presents a much more elaborate discussion on the peak width under gradient conditions, including several equations that are valid outside the domain of the LSS concept.

3. Resolution

Resolution in gradient elution can be described in very much the same way as under isocratic conditions; that is

$$R_s = \frac{(\alpha - 1)}{4}\sqrt{N}\frac{\bar{k}}{1 + \bar{k}} \tag{33}$$

However, the parameters in this equation have slightly different meanings from those under isocratic conditions: α is the separation factor for two adjacent bands, N is the plate number under isocratic conditions and $\bar{k}$ is an average or effective k value, usually taken as the local k value of the solute when passing the midpoint of the column. A very simple, but useful approximation for peaks eluting well after the start and before the end of an LSS gradient is

$$\bar{k} \approx \frac{1.8}{b_n} \tag{34}$$

This implies that the effective k value under gradient conditions is about twice as high as the retention factor of the solute on leaving the column ($k_e \approx 1/b_n$). The role of the column plate count under gradient conditions is clearly the same as it is under isocratic conditions.

This implies that doubling the plate count leads to a 40% higher resolution. Doubling the plate count can be achieved by doubling the column length (at the expense of an increase in the column pressure drop). The plate count can be somewhat increased (but rarely doubled) by reducing the flow rate. A third way of increasing the resolution under gradient elution is by increasing $\bar{k}$ through lowering b_n. Lowering the gradient slope leads to an increased resolution at the expense of an increased analysis time. Again, b_n appears to play a role very similar to that of the eluent strength in isocratic elution.

C. Gradient Optimization

1. Simple Optimization

Several sensible choices allow good gradient-elution LC to be performed in everyday practice. The following guidelines should be observed.

1. Initially, a low value of A (initial volume fraction of strong eluent; e.g., 0.05) and a high value of F (final volume fraction; e.g., 0.95) may be selected.
2. Aim for an optimal (or slightly lower) value of b_n in an initial experiment (i.e., $0.25 < b_n < 0.5$).
3. After the first run, it may be possible to increase the value of A, reducing the analysis time and the required reconditioning time for all subsequent runs. If no peaks are present in the beginning of the chromatogram, or if there is ample separation between the early-eluting matrix components and the first relevant solutes, the value of A may be increased.
4. For small solutes, when using methanol–water eluents, typical S_n values are between 5 and 10. On a column with $t_m = 1$ min a B value of 0.1 min^{-1} (10%/min increase of the concentration of strong solvent in the eluent) is optimal.
5. Larger (higher molecular mass) solutes show larger S_n values. Thus, such solutes require shallower gradients. For large, hydrophilic solutes, such as proteins, very shallow gradients, often covering only small ranges of compositions, are required [15].
6. Likewise, it may be feasible to reduce the value of F (final composition). However, a wider margin is suggested in tuning F, because

    a. Solutes may move to substantially higher compositions in faster gradients.
    b. If software programs for gradient optimization are used, it may be difficult to deal with components eluting after completion of the gradient.
    c. A high value of F (strong final solvent) helps in cleaning the column between analyses. At an early stage of method development, maintaining the column in good order may outweigh a possible reduction in the analysis time.

7. Perform a second experiment using a steeper gradient (e.g., double the slope).
8. Inspect the chromatograms for variations in the resolution. If substantial variations are observed for relevant peaks, proceed to optimize the slope of the gradient. In a first instance, such an optimization may be based on a few additional runs and visual inspection, but gradient-optimization software is certainly very useful at this stage.
9. If the resolution in the initial experiments is (1) not or hardly affected by the gradient slope and (2) the obtained resolution between one or more pairs of relevant peaks is judged to be inadequate, try to use a different strong solvent. For example, when methanol is replaced by acetonitrile significant selectivity affects are often observed.
10. Only resort to attempting multisolvent or multisegment gradients after more simple solvent programs have proved inadequate for the desired separation.

2. Computerized Optimization

When solvent programming is applied to large numbers of samples, the gradient program can be optimized to achieve desired separations in terms of resolution and analysis time. Many

literature reports deal with the subject, and several commercial software packages exist that have been designed mainly around the subject of gradient optimization.

At the heart of such strategies is the feasibility of calculating gradient–elution retention data (and peak widths) based on knowledge of the isocratic ln k versus φ relation (see Sec. B). This allows computation of the chromatogram as a function of the gradient program parameters and thus allows computer-assisted optimization. We will first address the former issue.

If the isocratic retention relation can be approximated by a straight line [or if by some kind of transformation, such as taking the logarithm of the retention factor, a straight-line relation can be obtained such as Eq. (20)], then two data points suffice to determine the coefficients. These two bits of information can be simply two retention factors under isocratic conditions. This way of determining the retention relation is computationally the most simple and experimentally the most precise, but it is practically the most difficult. The very reason to apply gradients ought to be that not all (relevant) components in the sample can be separated in a single isocratic run and, therefore, the sample may need to be eluted using a number (much larger than two) of different isocratic solvents, before two reliable retention factors are obtained for each solute.

Running the sample under two different sets of gradient conditions is much more convenient in practice. Good sets of starting conditions have been extensively discussed in the literature [16]. In principle, it is possible to calculate the two coefficients describing the straight line for ln k versus φ (or a straight line describing ln k versus ln φ) using any combination of two retention times obtained under isocratic or gradient conditions, no matter whether or not the components elute before the completion of the gradient run. The most prevailing requirement is that the solvent program used and the instrumental parameters, such as t_m and t_D, must be accurately known, but various other factors do play a role. Several studies have dealt specifically with the accurate determination of ln k_0 and S_n in RPLC gradient elution [17]. Baba [18] has dealt extensively with the equivalent problem in ion-exchange chromatography.

Here we will consider only the simplest case, in which a solute is eluted with the aid of two linear gradients of different steepness, but with identical starting compositions. The gradient–steepness parameter ($b_i = B_i S_n t_m$) for one solute subjected to two different linear gradients is directly proportional to the slopes B_i of the gradients in composition–time units, because S_n is a constant for a given solute and t_m is a constant throughout. If it is further assumed that the initial retention factors are large and that the solutes are eluted before completion of the gradient, then the simple Eq. (30) can be used. For the two different gradients (denoted by I and II) we have (with $t''_R = t_R - t_m - t_D$)

$$t''_{R,\mathrm{I}} = \frac{t_m}{b_{n,\mathrm{I}}} \ln (b_{n,\mathrm{I}} k_A) \tag{35}$$

and

$$t''_{R,\mathrm{II}} = \frac{t_m}{b_{n,\mathrm{II}}} \ln (b_{n,\mathrm{II}} k_A) \tag{36}$$

If we define the ratio of the slopes of the two gradients as

$$\beta = \frac{b_{n,\mathrm{II}}}{b_{n,\mathrm{I}}} \tag{37}$$

then we can simply calculate the absolute value of either of the two steepness parameters, for example

$$b_{n,\mathrm{II}} = \frac{t_m \ln \beta}{t''_{R,\mathrm{II}} - (t''_{R,\mathrm{I}}/\beta)} \tag{38}$$

and

$$b_{n,\mathrm{I}} = \frac{b_{n,\mathrm{II}}}{\beta} \tag{39}$$

from which

$$S_n = \frac{b_{n,\mathrm{II}}}{B_{\mathrm{II}} t_m} \tag{40}$$

$$k_A = \frac{1}{b_{n,\mathrm{II}}} \exp\left(\frac{t''_{R,\mathrm{II}} b_{n,\mathrm{II}}}{t_m}\right) \tag{41}$$

and finally

$$k_0 = k_A \exp(S_n \varphi_A) \tag{42}$$

Equation (38) is undetermined for $\beta \downarrow 1$ (i.e., when the slopes of the two gradients [and the resulting retention times] are equal). Indeed, to obtain reasonably precise values of ln k_0 and S, it is essential that the two different gradients vary greatly in slope, a difference of at least a factor of 3 being a typical recommendation.

The various software packages available for the optimization of LC gradients work along lines, such as the one outlined in the foregoing. From retention times for all individual components under two different sets of conditions, values of $k_{0,i}$ and $S_{n,i}$ can be established for each solute. The more-advanced programs [see Refs. 19,20] allow more difficult calculations to be performed than the one just outlined, including

Significant gradient-delay times (t_D), large enough to affect the migration patterns of early-eluting peaks ($t_D << t_m k_A$ is *false*)
Analytes eluting early in the gradient ($1 << b_n k_A$ is *false*)
Analytes eluting after completion of the gradient
Data from two gradient runs, two isocratic runs, or one gradient and one isocratic run

Obtaining the two required data points for each individual solute may be difficult. The elution order in two gradients of vastly different slope may be substantially different, and certain peak pairs may overlap in either run. This greatly complicates the assignment of the different peaks in the two chromatograms. On the other hand, if the two chromatograms are very similar, differing only in the time scale, then the optimization of the solvent program is not likely to be fruitful.

Another key issue is the minimization of errors [21,22] between the retention times (and peak widths) predicted by the model and those obtained experimentally. One source of errors is formed by the approximations inherent in the model. If the LSS model is used, assumptions are sometimes significant, but they are well understood and any complications are usually recognized. For example, if components elute early in the gradient, the initial retention factor k_A may not be much larger than $1/b_n$, so that the factor 1 in Eq. (29) needs to be maintained. A second, more significant problem is formed by discrepancies between the nominal conditions and the true values in practice. Although gradient instrumentation has been much improved in the last 10 years, emphasis has justifiably been on the repeatability and reliability of the delivered compositions (which is enhanced by adequate mixing), rather than on the accuracy of the delivered gradients (which is jeopardized by excessive mixing). Generally, the accuracy of the delivered gradient is better if larger columns (i.e., large V_m) and relatively slow gradients are used (e.g., $b_n = 0.1$ and $b_n = 0.3$, rather than $b_n = 0.3$ and $b_n = 1$ for the two initial gradients).

From the $k_{0,i}$ and $S_{n,i}$ values for all solutes the chromatogram for any given solvent pro-

gram can be predicted, with the purpose of establishing an optimum gradient program. The optimum program can simply be defined as that yielding the best separation (highest resolution) for the least-separated (critical) pair of peaks. However, various other so-called *optimization criteria* or *objective functions* have been selected in the literature. Such mathematical functions need to be treated with great care, because the word *objective* is often misplaced. The chromatographer is asked to make choices, the consequences of which are unclear.

Gradient-optimization packages feature algorithms of varying complexity that may be used for optimization of the solvent program. In the early days of computer-aided optimization in liquid chromatography the Simplex algorithm was popular [24,25]. This made it mathematically straightforward to optimize a number of parameters simultaneously. However, chromatographically some parameters (e.g., gradient slope and intercept) need a different approach to optimization than do others (e.g., flow rate).

With the rapid increase in available-computing power, a simulation approach was developed specifically for the optimization of LC gradients [26,27]. In this approach numerous gradients are simulated, based on the information gathered from two initial runs. The quality of the separation is calculated for each simulated chromatogram, typically in terms of the resolution of the least separated—*critical*—peak pair. This quality of separation can then be visualized (e.g., in a plot of minimum resolution vs. gradient steepness), and the optimum gradient can be selected.

The simulation approach is still the most popular way of optimizing gradient LC separations, but more-sophisticated optimization algorithms, such as strategies based on experimental design [28], Monte-Carlo search [29], and again, Simplex search [19,30], are now being combined with the simulation approach. In this way chromatographic knowledge can be paired with the most effective optimization strategies.

Contemporary gradient-optimization packages allow the generation of complex, multistep gradients in which the retention of all sample components is very precisely tuned to yield the best possible gradient separation [30]. Such multisegment gradients can be used successfully in LC. For example, Laemmerhofer et al. [31] have described such a solvent program for the separation of a mixture of 4-dinitrophenyl amino acids, establishing the gradient using a structured approach to method development. However, a warning is in place [see also Ref. 6]. The optimization of gradient programs is relevant in developing routine methods of analysis. In several situations, gradient elution LC is used on a routine basis, but isocratic elution, column-switching methods, and selective sample preparation methods (off-line or on-line), should be considered as alternatives if at all possible (see discussion in Sec. V). If gradient elution is required for a routine type of analysis, one should next question the wisdom of complex multisegment gradients. The more complex the gradient, the less robust the separation may be in practice, and the less accurate are the predictions obtained from computer-optimization programs. The latter is due to a summation of computational errors, but especially to greater differences between the imposed and true gradient profiles if the former contain a number of sharp edges and abrupt changes (steps).* Thus, the easy and efficient development of complex multisegment gradients allowed by sophisticated optimization packages tends to obscure the fact that they are but a small niche in the large area of gradient–elution RPLC.

---

*Any deformation of the gradient leads to an error in the descriptive models. Any "smearing out" of sharp edges leads to a reduced retention in RPLC. This is because mixing results in an arithmetic averaging of the composition, which corresponds to an arithmetic averaging of ln k values and, therefore, to a geometric averaging of k values. Because the arithmetic average of two positive numbers is always greater than the geometric average, retention is always reduced when the gradient is deformed. The effect may not be significant if the same model is used "back-and-forth" (i.e., if ln k_0 and S_n are determined with the aid of two gradients and the resulting coefficients are used to predict retention times under gradient conditions). However, if a complex multisegment gradient is devised, the cumulative error from gradient deformations may be mounting.

A similar question may be raised about the use of multisolvent gradients [32]. Modern HPLC equipment readily allows ternary gradients (made up from three solvents) or even quaternary gradients to be used. However, developing such separations in a structured manner is extremely difficult. It is equally difficult to justify the need for programming several solvents independently. Even though many applications of complex multisolvent gradients have been published, it is hardly ever documented that a binary gradient will not suffice. There are some good practical reasons to use ternary solvent programming. These are not aimed at realizing the full selectivity of ternary systems, but rather, at exploiting the full flexibility of the modern multisolvent HPLC instrument.

A ternary gradient can be used to maintain a constant level of certain additives in the mobile phase. For example, the ionic strength can be kept constant during a gradient if the ionic additives (salts) are added to only one solvent reservoir, the concentration of which is kept constant during the run. The actual result is a binary gradient of, for example, methanol and water, with a constant salt concentration, but three solvent reservoirs are used to create the program.

Another practical application of multisolvent gradients is in a succession of steps. For example, a methanol–water gradient can be followed by a segment in which methanol is gradually replaced by isopropanol or THF to elute very hydrophobic materials from the column.

Tools to develop optimal multisolvent gradients are just beginning to emerge [33]. Their proliferation may eventually lead to convincing applications of genuine multisolvent gradients.

3. Gradient Scouting

One very useful application of gradient analysis is during the development of isocratic methods. As mentioned in the previous section, applying a broad gradient to a sample is a practical way to obtain a great deal of information on its chromatographic behavior based on no more than two experiments. This approach can be followed successfully if

1. The analyte molecules can be detected by the gradient-compatible method of choice (typically a UV detector, but other detectors, such as the evaporative light-scattering detector [ELSD] may be selected).
2. All the peaks can be matched across the two chromatograms. This is necessary, because two retention times are required to calculate the values of $\ln k_0$ and S_n for each analyte.
3. Suitable software is available to perform the necessary calculations.

The first of these requirements is inevitable, but the other two may be needlessly complicated in some situations. If the result of an initial gradient run is a relatively simple chromatogram, with a single group of peaks bunched together in a small part of the gradient, then isocratic elution is indicated. The results from the gradient may be used to obtain a good first guess of possible isocratic conditions.

The easiest way to achieve this goal is the following

$$\varphi_{\text{iso}} = \varphi(t_{R,i} - 2t_m - t_D) = \varphi(t'_{R,i} - t_m - t_D) \tag{43}$$

where φ_{iso} is the isocratic composition recommended for the elution of analyte i, which has a retention time $t_{R,i}$ and a net retention time $t'_{R,i}$. As usual, $\varphi(t)$ is the applied gradient program. Under practical conditions ($0.1 < b < 1$) applying the foregoing rule leads to isocratic retention factors in the range $3 < k < 5$ [see Ref. 23; p. 195].

Another, somewhat more-sophisticated approach is based on the fact that in RPLC a strong correlation is often observed between the slopes and intercepts of $\ln k$ versus φ plots. Many studies have yielded linear correlations of the form

$$S = p + q \ln k_0 \tag{44}$$

In RPLC practice, both the retention in pure water and the rate at which retention de-

creases on adding a strong solvent, increase with increasing the size of the molecule [34,35]. Within a certain class of molecules Eq. (44) appears to be followed. However, different classes of molecules (e.g., small aromatic solutes [substituted benzenes] and proteins) may require different values of p and q to describe their retention behavior in RPLC. Typically, a set of p and q values is valid for a specified group of solutes, on a specified stationary phase, using a particular binary solvent mixture.

If the values of p and q are known for the problem at hand, only one experimental data point is required to estimate retention as a function of composition under isocratic conditions, or, indeed, to predict retention under any sort of solvent-programmed conditions, provided the two specified solvents are used.

The graph shown in Fig. 12 has been calculated using values of $p = 2.27$ and $q = 0.79$, obtained from experimental retention data for 32 small aromatic solutes using methanol–water eluents and an ODS column [36]. The figure applies to a linear gradient from 100% water to 100% methanol in 20 min, and t_m was taken as 125 s. This figure can be used irrespective of the column dimensions, because the flow rate can be adapted to match the value of t_m.

The figure can be used to predict the isocratic composition required to obtain a specified retention factor. For example, a component eluting at $t'_R = 9$ min is predicted to show a retention factor of 1 at a composition of 63% of methanol in water. If slightly less methanol is used, this component will be eluted in the optimum range ($1 < k < 10$). A last peak eluting at $t'_R = 13$ min is predicted to represent a component eluted at $k = 10$ at a composition of 59% methanol in water. Slightly more methanol will move this peak into the optimum range as well. If all peaks are eluted between 9 and 13 min under the specified gradient conditions, then all peaks are expected to be eluted in the optimum retention range if isocratic compositions between $\varphi = 0.59$ and $\varphi = 0.63$ are used. If necessary, the predicted isocratic composition can be improved mathematically based on the results of the first isocratic experiment performed after the scanning gradient [37].

Bartha et al. [38] have devised an ingenious way of characterizing solutes on the basis of retention data from initial gradient RPLC runs. Their scheme involves the injection of "slugs" of ion-pair reagent solutions together with the sample during some runs. By using slugs of positive- and negative-pairing ions at two pH values (high and low) in addition to two gradients without concurrent slugs (a total of six gradients), they are able to classify the components of a sample into weak acids, strong acids, weak bases, strong bases, and neutrals.

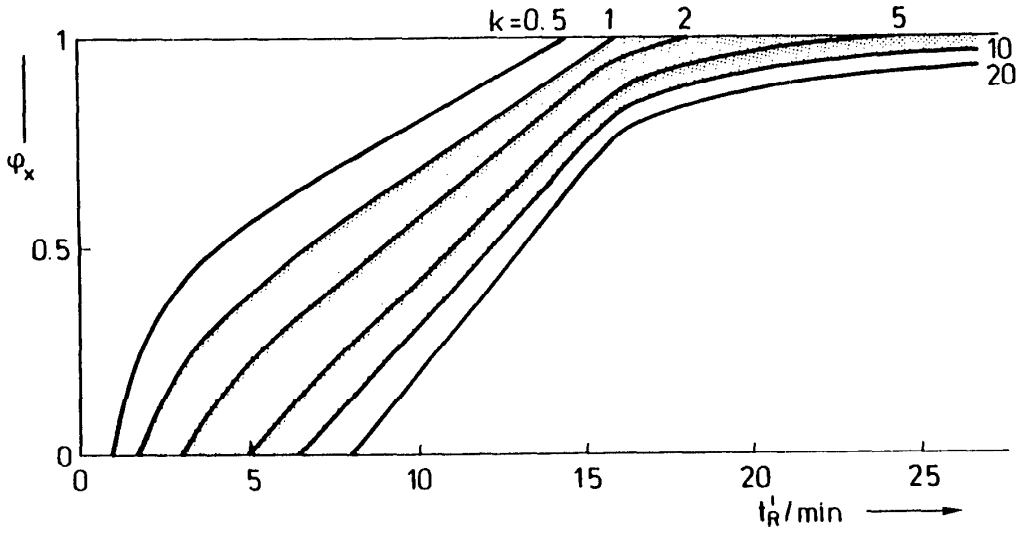


Figure 12 Curves relating the isocratic composition (φ_x) to the net retention time under gradient conditions for various desired values of the retention factor k.

For example, a weak acid, such as a carboxylic acid, with a typical pK_a of 4 will show little retention at pH 6, when it is essentially in the ionized form, and a much higher retention at pH 2, when it is essentially uncharged. In addition, when the elution of this solute at pH 6 is accompanied by that of a positively charged pairing ion its retention will increase significantly. The other three gradients accompanied with slugs (negative-pairing ions at pH 6 and either negative- or positive-pairing ions at pH 2) will have much less effect on the retention of this solute.

Serious attention has also been devoted in the literature to the optimization of step gradients [39,40,41]. Step gradients should be treated somewhat differently from linear gradients, with the integration being even simpler than for the linear gradients [see Eq. (22) and (25)], but the potential effects of instrumental deformation of the imposed program is much greater. Step gradients are particularly useful for on-line sample cleanup, often in combination with column-switching methods.

A final area in which gradient elution is important is in preparative liquid chromatography [42,43]. Some of the benefits of solvent programming weigh very heavy here, particularly the possibility to narrow down peaks in comparison with isocratic elution. Narrower peaks mean smaller volumes of solvent that need to be removed from the analyte(s) after fractionation. Optimization of the gradient is also of great importance in preparative LC, because it may result in some or all of the following benefits

More or better (purer) products
Shorter analysis times
Smaller volumes of solvent
Smaller columns

Preparative LC is an expensive technique, which is typically used for purifying valuable materials. Therefore, there are great potential profits associated with improvements and optimization.

D. Gradient Solvents

Gradients result from the mixing of two or more different solvents. The same restrictions apply to isocratic and gradient solvents (Table 2). In addition, certain considerations apply

Table 2 Solvent Considerations for Isocratic and Gradient Elution

Isocratic elution
Selectivity
Safety (toxicity, flammability, stability, reactivity)
Sample compatibility (reactivity)
Column compatibility
Detector compatibility (e.g., UV transparency)
Viscosity
Corrosivity
Plurity
Cost
Gradient elution
All the requirements that apply in isocratic elution, plus
Miscibility
Mutual compatibility
Insensitivity of detector for variations in composition

specifically when selecting gradient solvents. Miscibility of the different solvents is an obvious requirement. Even when solvents are considered to be well miscible, as in methanol and water, there may be a significant heat effect on mixing. In this particular example, there also is a significant contraction (i.e., a mixture of methanol and water has a smaller volume than the sum of the individually measured components).

When buffers or salts are added to (one of) the solvents, miscibility considerations become more urgent. Buffer solubility is typically much higher in water than it is in organic solvents, methanol being better than acetonitrile. In organic solvents organic buffers tend to be more soluble than typical inorganic buffers. When using gradient elution, on-line mixing of solvents must take place, and during this process local conditions may cause solubility problems. For example, when mixing an aqueous buffer with a pure organic solvent, buffer precipitation may occur more quickly than mixing.

Some useful practical rules are the following:

1. Always verify the miscibility of the individual solvents in an off-line (test-tube) experiment, especially when using buffers, salts, or other solid additives.
2. Keep a safety margin relative to the verified solubility. For example, keep the buffer concentration in on-line mixing well below that tried in the off-line experiment;
3. Use partially mixed solvents in the reservoirs when possible. Mixing solutions of 10% A in B and 10% B in A is much safer than mixing pure A with pure B.

Different eluents will interact with the column to a different extent. In RPLC, organic materials may be preferentially adsorbed or absorbed on the stationary-phase surface. This so-called solvent demixing slightly affects the composition of the gradient as it passes through the column, but the effect is typically minor. [The effects of solvents demixing may be more serious in systems other than RPLC. Whenever equilibration times on changing the solvent composition are known to be long, solvent demixing is likely to considerably affect the chromatographic system during the application of a gradient. This is true, for example, for normal-phase systems (especially when using underivatized silica) and for ion-pairing systems.]

The situation is more serious for organic contaminants present in the water. These will be concentrated at the top of the column during the time the weak eluent is pumped through the system (equilibration step). Any such contaminants will appear as peaks in the blank signal, the retention time being determined mainly by the molecular size and polarity of the contaminants and the peak height by their concentration, detector sensitivity, and the amount of weak solvent washed through the column.

The purity of all solvents, but especially the weak one(s), is a major source of concern in gradient-elution LC. Also, the equilibration step must be kept short and its duration must be constant.

E. Instrumental Aspects

There are three contemporary ways to generate gradients for HPLC. The most striking difference between the approaches is whether they are based on high-pressure mixing (after the HPLC pump) or low-pressure mixing (before the pump). Table 3 summarizes the advantages and disadvantages of such mixing. In the high-pressure mixing mode, several pumps are required. The resulting flows are mixed and the resulting eluent is fed through the injector to the column (Fig. 13a). There are two distinguishable methods of low-pressure mixing. In the first one several two-way valves (see Fig. 13b) or one multiway valve (see Fig. 13c) are incorporated in the inlet line of a single HPLC pump. By rapidly switching these valves, the desired eluent can be prepared in-line from the different reservoir flasks. In the second approach to low-pressure mixing, each solvent channel is equipped with an auxiliary metering pump, which delivers an exact volume into a mixing chamber (see Fig. 13d). Because there may be a substantial volume effect on mixing (e.g., mixing 60 mL of water and 40 mL of

Table 3 Relative Advantages and Disadvantages of High-Pressure and Low-Pressure Gradient Mixers

	Low-pressure mixers	
High-pressure mixers	Valve-switching	Metering
Advantages		
Simple control (flow proportional to composition)	Potentially cheap (one pump) Rather difficult to expand number of solvents	Moderately expensive Relatively easy to expand number of solvents Easy control Accurate control
Disadvantages		
Each solvent requires additional pump Pumps may be operated outside specifications at extreme compositions Pumps require calibration for each solvent Contraction affects flow	Complex switching patterns needed Operation of mixing valve(s) and check valves is critical Required mixing causes gradient delay and deformations Contraction may cause gas or vapor bubbles	Technically complex Performance difficult to verify Some gradient deformation owing to mixing

methanol yields 96 mL of mixed eluent) it is advantageous to meter a slight excess of the individual solvents into a low-pressure mixing chamber.

In all cases, some degree of mixing is required, either in a mixing chamber designed for the purpose, or in the pump itself (in case of low-pressure mixing). The more mixing takes place, the smoother will be the gradient, but the greater will be the delay time (or dwell time) that passes between the instruction to the instrument to deliver the gradient and its arrival at the top of the column (see Fig. 10). The deformation of the gradient (round edges in Fig. 10) will also be greater if the mixing volume is increased.

High-pressure mixing is a relatively fool-proof method, provided that the two (or more) pumps used are operating well and within their specified ranges. The latter is not usually true when extreme compositions are being mixed (i.e., a few percent of one solvent in a great excess of the other). For example, to add 2% methanol to an otherwise aqueous eluent at a (combined) flow rate of 1 mL/min, requires the methanol pump to perform reliably at a level of 20 μL/min. Such a value is low for most common LC pumps. If a specifically designed micro-LC pump were to be used, problems might arise when the methanol concentration would be increased to much higher values.

Another complication is the variability of the delivered flow rate with the eluent. Different solvents show different compressibilities and viscosities. These properties may have a fundamental and an empirical effect (respectively) on the resulting flow rates. Frequently pumps can be calibrated to allow for such effects.

Low-pressure mixing systems require advanced software control for the opening and closing of the valve(s). This is mainly because LC pumps are designed to deliver a flow that is as constant as possible. The suction (input) flow, however, is extremely variable. For the delivery stroke to be smooth, the suction (refill) stroke has to be very rapid. Yet, it is in this inlet flow stream that mixtures and gradients are being generated.

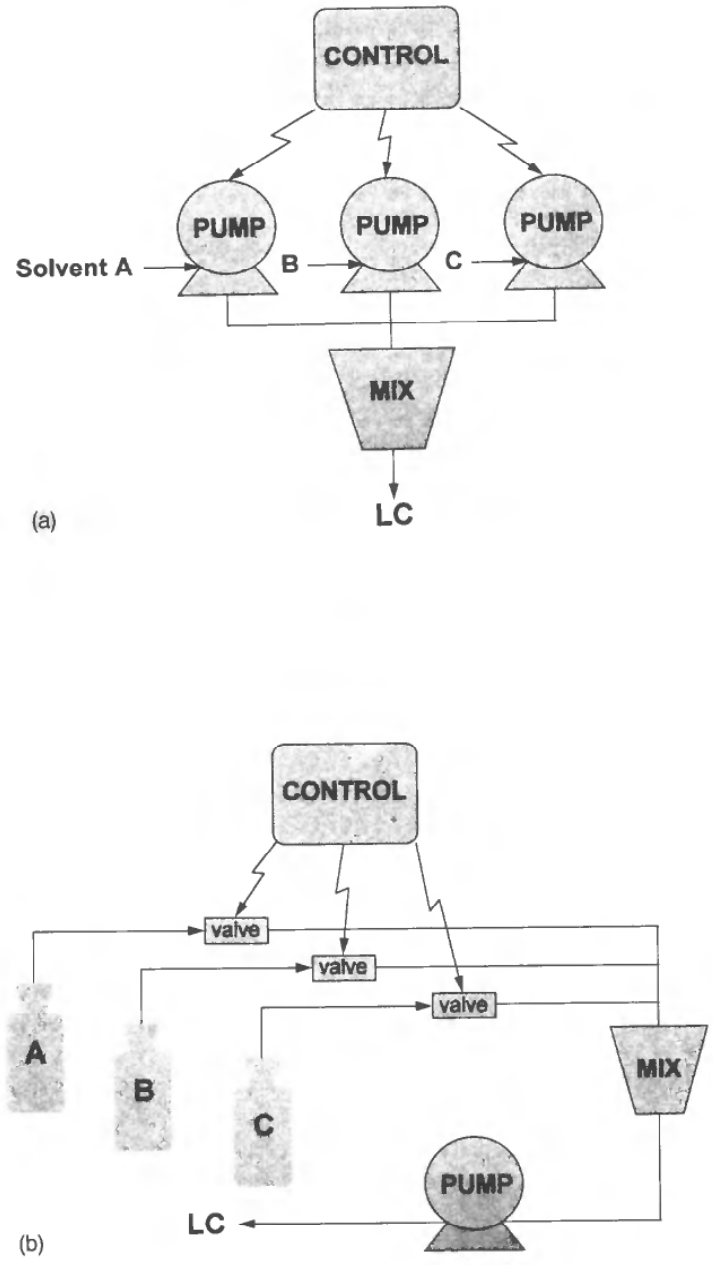


Figure 13 High-pressure (a) and low-pressure (b–d) gradient mixers: In the latter category the valve-switching (b) using a series of two-way valves; (c) using a single multiway valve; and (d) metering approaches can be distinguished.

A typical pump head of an LC pump may have a volume of 100 μL. To generate mixtures with an accuracy of 0.1%, the composition of the solvent entering the pump has to be controlled to within 100 nL.

The degasing of the solvents is a final subject that deserves attention. The heat effect on mixing solvents, especially water and organics, can be quite considerable. This may easily cause the emergence of dissolved gases in the form of bubbles. Thus, performance of the pump can be greatly affected. Extensive degasing of the individual solvents by helium purging has long been the method of choice, except for premixed mobile phases (mixtures of two or

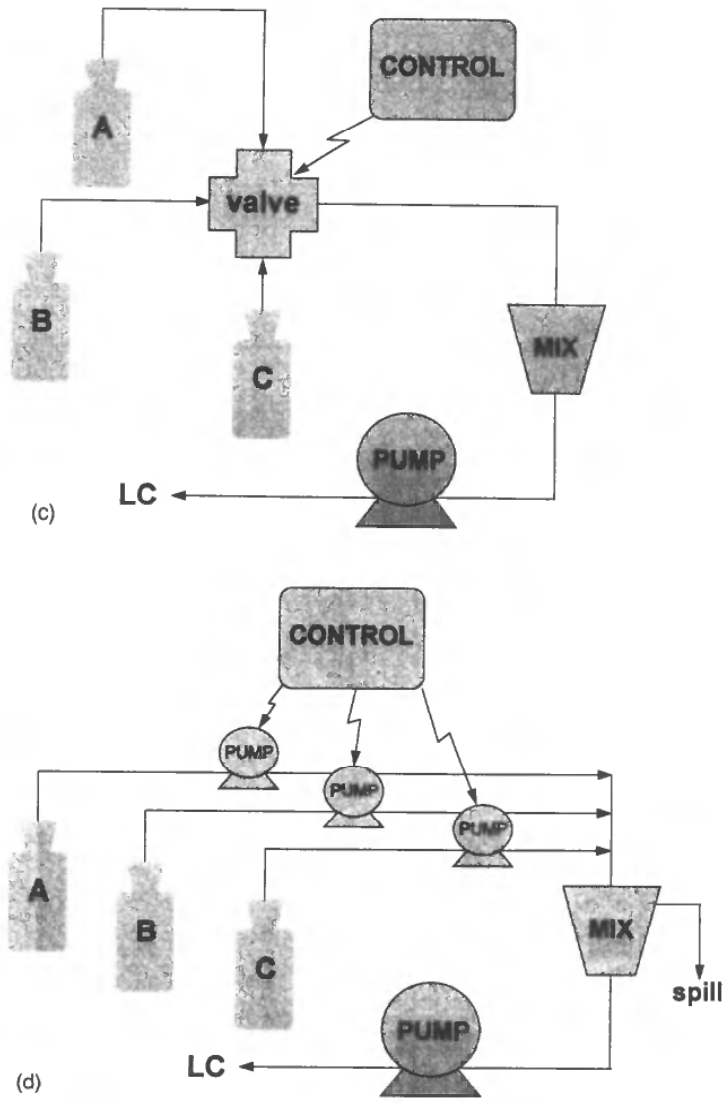


Figure 13 Continued

more solvents, salt or buffer solutions, and such). The composition of such mixed solvents may drift by continuous purging with helium. A quick burst of helium followed by leaving a helium cap (low flow of helium) in the bottle is then recommended. In recent years, in-line degasers have emerged, in which the mixed eluent passes alongside a membrane, the other side of which is pumped to a vacuum. In-line degasers allow effective degasing without affecting the composition of mixed eluents.

IV. OTHER PROGRAMMING METHODS

Gradient elution (solvent-programming) and column-switching are far and away the most important programming techniques applied in LC. Some other programming techniques are also used, however, and two of these will be described in some detail. Temperature programming will be described in Sec. IV.A and ionic-strength programming in Sec. IV.B.

Flow programming is occasionally used in LC [see, e.g., Ref. 44], but the possibilities to reduce retention significantly by increasing the flow rate are quite limited. The pressure drop across the column is too serious a limiting factor. Flow programming is used most commonly

on either very small or very large columns. When small (precolumns) are used for sample cleanup or for the introduction of large samples in weak eluents, increased flow rates during the sampling stages may be really advantageous. For example, the contaminants from a water sample may be concentrated on a precolumn by pumping the sample through the column at a high-flow rate. Before the eventual analysis takes place on the analytical column, the flow rate is then lowered.

A second situation for which flow rate programming is more common is in preparative LC. Here columns of increased (sometimes very large) diameter are used to fractionate a sample into one or more desired fractions and, usually, some undesired fractions. The particles used are typically larger than in analytical HPLC, and the pressure drop is usually significantly lower. This provides the possibility of using flow-rate programming to speed up the elution of the undesired fractions in particular.

Programming the pH of the mobile phase is interesting in principle, but extremely difficult in practice. The most common application of pH gradients is in isoelectric focusing. Here a pH gradient is immobilized in an electrophoresis column and the analytes (usually proteins) are made to migrate under the influence of an electric field to a position in the column corresponding to their isoelectric point (i.e., the pH value that corresponds to zero electric charge on the protein). Gradient chromatofocusing HPLC has also been devised [45].

A. Temperature Programming in LC

Generally, temperature is a much less powerful parameter in LC than it is in GC. Fundamentally (see Chap. 1), retention in LC is determined by the activity coefficients of the solute in the mobile and stationary phases, whereas in GC, retention is determined by the activity coefficient of the solute in the stationary phase and by the pure (solute) component vapor pressure. Vapor pressures vary much more strongly with temperature than do activity coefficients.

Besides being fundamentally less useful, variation of temperature is also less practical in LC than in GC. The process of heating or cooling an LC column is much less efficient than that encountered with typical GC columns. LC columns are thick-walled (because of the high pressures required) and the diameter of the typical (packed) columns used is of the order of several millimeters. If such a column is positioned in an air-circulation oven, it takes a long time to establish thermal equilibrium [46]. To achieve a better temperature control in LC columns, a reduction of their diameter will be required. In fact, in capillary electrophoresis and capillary electrochromatography (CEC), very small column diameters are required to allow dissipation of the heat generated in the column (or "conduit") under the influence of the strong electrical fields applied. Nevertheless, temperature does often affect selectivity and efficiency in LC. An area in which temperature is often found to dramatically affect selectivity is in the separation of optical isomers. Lowering the temperature often leads to a much needed increase in selectivity ($\alpha = k_2/k_1$). The effect of temperature on efficiency is particularly strong when dealing with ionic interactions, the kinetics of which can be significantly improved by increasing the temperature.

Thus, temperature is an important parameter in RPLC, but temperature programming is unlikely to be of great practical benefit. The most rewarding approach is probably to optimize the (isothermal) temperature at which solvent programming is performed [47]. Maintaining adequate temperature control can be extremely important if reliable data are to be obtained from gradient-elution LC [48].

Programmed temperature LC has been successfully applied in some particular instances. One niche technique is *temperature-rising elution fractionation* (TrEF) [49,50]. In this technique, a (hot) solution of a polymer is injected into an equally hot column. With the mobile-phase flow rate at a very low value, the temperature is reduced and different fractions of the polymer are successively deposited on the column. Finally, the flow rate is increased and the temperature is programmed slowly upward, dissolving and eluting the different fractions of

the polymer in order. A typical example is the separation of polyolefins according to molecular structure (isotactic, syndiotactic, and atactic).

Another, quite recent example of the application of temperature programming in LC involves the use of "superheated" water as the mobile phase in combination with flame-ionization detection (FID) [51,52]. The use of an FID prohibits the use of organic modifiers, as these would cause overwhelming background signals. The use of pure water as the eluent does allow the use of an FID, but solvent programming is no longer an option. Temperature programming has proved useful to some extent.

B. Ionic-Strength Programming

There are several instances in which ionic-strength programming is being used successfully in LC. The first example is a technique called hydrophobic-interaction chromatography (HIC) [53], which is specifically applicable to the separation of proteins. At a high ionic strength, the hydrophobic repulsion of nonpolar (parts of) molecules is increased. This is known as the "salting-out effect." If a reversed-phase column is used with short, nonpolar chains for the separation of a protein mixture and the initial conditions involve a mobile phase of high ionic strength, then the retention of the proteins is high. In time the ionic strength (salt concentration) of the eluent is gradually lowered, causing a migration of the proteins in a manner typical of that described for gradient elution (see Sec. III.A). The different proteins will be eluted in order of increasing hydrophobicity.

An ionic strength gradient in the opposite direction may be used in ion-exchange chromatography. Here retention is typically highest when the ionic strength of the mobile phase is lowest. Thus, a typical gradient would involve a gradual increase of the ionic strength. In recent years, sodium hydroxide gradients have gained popularity. The hydroxide ion is a weak eluent in ion-exchange chromatography, allowing other weak ions to be adequately retained when the mobile-phase ionic strength is low. By increasing the ionic strength to higher values, the different anions in a sample can be successively replaced. For this technique to become practically useful, adequate stationary phases (stable at very high pH values) and, especially, adequate suppressors, had to be developed. High concentrations of hydroxide are required to elute strong-binding ions. Large-capacity membrane suppressors and, lately, electrochemical suppressors have come in routine use to transform hydroxide ions into water before conductivity detection.

V. COMPARISON OF MAIN PROGRAMMING METHODS

Isocratic analyses, when applicable, are robust, cheap, and fast. Isocratic analysis requires by far the simplest equipment. However, isocratic elution is possible only if all the relevant analytes and the late eluters can be made to elute in the optimal retention window. Early irrelevant peaks are quite acceptable, for they do not disturb the analysis. Late-eluting peaks determine the analysis time, and peaks eluting well beyond the maximum acceptable k value cause the analysis time to be long. When late-eluting peaks occur in the chromatogram, solvent-programming can be used to reduce the analysis time. However, when comparing the retention time under gradient conditions with the isocratic values, one should realize that the analysis time in a series of runs is determined by the cycle time that expires between subsequent injections. When solvent-programming is used, the final eluent composition is different from the initial one. Before the next injection can take place, the system needs to be reequilibrated at the initial composition. This process requires a time that well exceeds the sum of t_m (mobile-phase time) and t_D (dwell time). It is usually recommended to return gradually to the initial composition if this differs greatly from the final one. This is thought to enhance the lifetime of the column and to improve the precision (repeatability) of the analysis. The time needed to return to the initial composition and to reequilibrate the system may be on the order of the gradient run time. Therefore, when comparing analysis times it is important

to use the cycle times between subsequent analyses. In several practical studies [54,55], it was shown that if gradient-elution methods were replaced by optimized isocratic methods, significantly reduced analysis times, increased method robustness, and easier transfer of methods between laboratories could be realized. Table 4 summarizes the advantages and disadvantages of the isocratic and gradient-elution methods. Several measures may help to promote the transferability of gradient methods [56].

Under gradient-elution conditions all peaks can be made to elute under roughly equal conditions, with final retention factors within the optimum range (see Sec. III.B). This implies that all peaks throughout the chromatogram can be sharp peaks. This is in contrast with isocratic analysis, in which the peak width increases proportionally with time. Early-eluting peaks are thus much sharper than late-eluting ones. The sensitivity (peak height) in case of UV detection is proportional to the concentration.

$$c_{max} = \frac{c_{inj}V_{inj}}{\sigma_V\sqrt{2\pi}} = \frac{c_{inj}V_{inj}\sqrt{N}}{(1 + k_e)GV_m\sqrt{2\pi}} \tag{45}$$

Here c_{max} is the analyte concentration at the peak maximum, c_{inj} and V_{inj} are the concentration of the analyte in the injected sample and the injection volume, respectively, and σ_V is the dispersion in the chromatographic system in volume units ($\sigma_V = F\sigma_t$). The dispersion in time units that is apparent in the chromatogram is inversely proportional to the speed of migration of the analyte on leaving the column. This gives rise to the factor $(1 + k_e)$ on the right-hand side of Eq. (45) [see also Eq. (31)].

Under gradient conditions, because k_e is approximately constant throughout the chromatogram, all peaks appear to be equally sharp. This is not to say that the sensitivity is also equal for all peaks. In UV detection the absorption a_i for analyte i is determined by three factors

$$a_i = \varepsilon_i(\lambda)lc_{max,i} \tag{46}$$

where l is the path length of the UV cell and $\varepsilon_i(\lambda)$ is the extinction coefficient of solute i at

Table 4 Relative Advantages and Disadvantages of Isocratic and Gradient-Elution LC Separations

Isocratic separations	Gradient elution
Advantages	
No time lost between analyses	Optimum elution conditions for most peaks
Best possible separation for any specified pair of peaks	Sharper (late-eluting) peaks
Most simple, cheapest, and most reliable	Increased sensitivity (for late-eluting peaks)
Disadvantages	
Limited range of analytes in one run	Time needed for column (re-) equilibration
Possible buildup of contaminants during each run	Limited choice of detectors
	Base-line drift on varying the eluent
	Lower signal-to-noise and signal-to-background ratios
	Spur peaks (contaminants in weak eluent)
	Increased instrument complexity

wavelength λ. The values for the extinction coefficients vary greatly between different (groups of) solutes, so that similar elution conditions do not necessarily lead to similar sensitivities. However, the contribution of chromatographic factors to the sensitivity is more constant under gradient conditions. The sensitivity for late-eluting solutes is usually much higher under gradient conditions than under isocratic conditions.

It is important not to confuse *sensitivity* with *detection limit* in this context. Although peak heights (sensitivity) often increase under gradient conditions, so do the noise and the detection background. Optical noise may be increased slightly if the background increases, but the chromatographic noise, caused by small variations in flow rate (the "pump profile" on the noise) and eluent composition may increase more significantly under gradient conditions. Ideally, all solvents used in gradient elution are compatible with the detection system under the conditions (e.g., wavelength) used. In practice, there is often a discernible baseline drift (see Sec. III.E). Also, even minute amounts of contaminants in the weak solvent may appear as peaks on the background, because these components are concentrated at the top of the column during the equilibration phase, from an eluent volume that is much larger than the volume of sample injected. In general, sensitivity may increase under gradient conditions, but *signal-to-noise* and, especially, *signal-to-background* ratios may go down [Ref. 57 discusses ways of minimizing the background in gradient LC].

An advantage of the use of solvent programming may be that the column is freshly conditioned for every run. Contaminations present in the mobile phase will reach a stationary (equilibrium) concentration on the stationary phase under isocratic conditions. Such a pollution of the column is unlikely to affect retention and selectivity dramatically, but it may give rise to the occurrence of *system peaks* (also known as *spur peaks* or *ghost peaks*). System peaks occur in any situation in which mixed eluents are used. If an additive is present in the mobile phase, but not in the sample, this gives rise to a negative "vacancy" peak in the chromatogram. The size of vacancy peaks is proportional to the concentration difference between sample and mobile phase; thus, minute contaminants will not lead to significant peaks under isocratic conditions. In addition, their size is proportional to the difference in detection response (e.g., extinction coefficients). As long as all the components (including contaminants) of the mobile phase are inactive under the detection conditions used (e.g., fully transparent at the selected UV wavelength), no vacancy peaks will be observed.

A more serious problem encountered in isocratic routine analysis may be fouling of the column by (components present in) the sample. If highly retained materials are present, they will build up at the top of the column, and this may easily result in a deterioration of the chromatographic separation. Frequently, this problem is alleviated in practice by washing the column after several isocratic runs. However, the analytical precision may be negatively affected by column fouling under isocratic conditions.

Column-switching methods do combine some of the advantages of isocratic and gradient methods (Tables 5 and 6). The cycle time between analyses is close to the retention time of the last peak. The time required to return the valves to the initial position is marginal, if it is not accompanied by a change in eluent composition. Several groups of solutes can be eluted under optimum retention conditions, ensuring high sensitivities. Immediately following the switching of a valve, or valves, there may be some distortion of the baseline, but in general, both the noise and the background are not significantly increased in comparison with isocratic chromatography. Buildup of contamination from the sample onto the column can be minimized, especially when the backflush mode is used for column cleanup. However, column-switching allows only a few groups of solutes to be eluted under optimal conditions, rather than the large numbers of peaks that may be accommodated in gradients. Column-switching methods are ideal for routine applications in which the nature of the sample and analytes is stable over very long periods. Flexibility is not a strong point of column-switching methods. It may be possible to change the method to compensate for changes in the samples or to meet new requirements for the analysis, but making the changes is sometimes difficult. Also, var-

Table 5 Relative Advantages and Disadvantages of Isocratic and Column-Switching LC Methods

Isocratic separations	Column switching
Advantages	
Simple setup	Optimum elution conditions for several groups of peaks
Relatively easy[a] method development	Short analysis (cycle) time
	Expensive columns can be kept clean or washed in backflush mode
Disadvantages	
Limited range of analytes in one run	Limited flexibility to cope with changing samples, matrices
Possible buildup of contaminants during each run	Time needed for method development
	(Programmable) valve-switching needed
	Pressure pulses may affect column lifetimes

[a]But not necessarily fast.

Table 6 Relative Advantages and Disadvantages of Gradient-Elution and Column-Switching LC Methods

Gradient elution	Column switching
Advantages	
Optimum elution conditions for most peaks	No time lost between analyses → short analysis (cycle) time
Flexibility in modifying methods	Best possible separation for specified pair(s) of analytes
Instrument can be used for different methods	Expensive columns can be kept clean or washed in backflush mode
Disadvantages	
Time needed for column (re-) equilibration	Limited flexibility to cope with changing samples, matrices
Limited in choice of detectors	Time needed for method development
Base-line drift on varying the eluent	(Programmable) valve-switching needed
Lower signal-to-noise and signal-to-background ratios	Pressure pulses may affect column lifetime
Spur peaks (contaminants in weak eluent)	
Increased instrument complexity	

iations in the column, for example, retention and selectivity differences between columns from different batches, can sometimes be difficult to deal with.

In comparison with gradient-elution methods column-switching methods are simpler and (potentially) faster, but less flexible and less suitable for separating very large numbers of solutes. For this latter application, the comprehensive systems described in Sec. II.B.3 ultimately offer the best solution.

We can summarize our comparison of programming methods as follows:

1. Simple, isocratic elution is the preferred method for relatively small numbers of solutes that are retained to a fairly similar extent.
2. Gradient elution is the preferred method for separating very large numbers of individual components and in situations that require flexibility (e.g., problem-solving work).
3. For routine separations of intermediate numbers of peaks, for separating a mixture into classes, and for on-line sample cleanup column-switching methods need to be considered.

REFERENCES

1. GE Berendsen, L de Galan. J Liq Chromatogr 2:12, 1980.
2. F Erni, HP Keller, C Morin, M Schmitt. J Chromatogr 204:65, 1981.
3. PE Anderson, M Demirbueker, LG Blomberg. J Chromatogr 595:301, 1992.
4. P Kilz, R-P Kruger, H Much, G Schulz. In: Characterization of Copolymers, Conference Proceedings, RAPRA, 1995.
5. a. TF Hooker, JW Jorgenson. Anal Chem 69:4134, 1997.
   b. DJ Jeffery, TF Hooker, JW Jorgenson. In JP Landers, ed. Handbook of Capillary Electrophoresis, 2nd ed., Boca Raton, FL: CRC Press, 1997, pp 765–790.
   c. KC Lewis, GJ Opiteck, JW Jorgenson, DM Sheeley. J Am Soc Mass Spectrom 8:495, 1997.
   d. GJ Opiteck, JW Jorgenson, RJ Anderegg. Anal Chem 69:2283, 1997.
   e. GJ Opiteck, KC Lewis JW Jorgenson, RJ Anderegg. Anal Chem 69:1518, 1997.
   f. AW Moore Jr, JW Jorgenson. Anal Chem 67:3456, 1995.
   g. VV Berry. J Chromatogr 321:33, 1985.
6. LR Snyder, JW Dolan, JR Gant. J Chromatogr 165:3, 1979.
7. PJ Schoenmakers, HAH Billiet, R Tijssen, L de Galan. J Chromatogr 149:519, 1978.
8. P Jandera, J Churácek. Gradient Elution in Column Liquid Chromatography, Theory and Practice. Amsterdam: Elsevier, 1985.
9. L Lajtar, S Sokolowski. Chem Anal (Warsaw) 26:199, 1981.
10. JW Dolan, JR Gant, LR Snyder. J Chromatogr 165:31, 1979.
11. LR Snyder. In CS Horvath, ed. HPLC, Advances and Perspectives, vol 1. New York: Academic Press, 1980, p 207.
12. MA Stadalius, HS Gold, LR Snyder. J Chromatogr. 327:27, 1985.
13. MI Aguilar, AN Hodder, MTW Hearn. J Chromatogr 327:115, 1985.
14. P Jandera. J Liq Chromatogr 12:117, 1989.
15. MA Quarry, MA Stadalius, TH Mourney, LR Snyder. J Chromatogr 358:1, 1986.
16. a. LR Snyder, JW Dolan. J Chromatogr 721:3, 1996.
    b. JA Lewis, LR Snyder, JW Dolan. J Chromatogr 721:15, 1996.
17. a. DD Lisi, JD Stuart, LR Snyder. J Chromatogr 555:1, 1991.
    b. JD Stuart, DD Lisi, LR Snyder. J Chromatogr 485:657, 1989.
18. a. Y Baba. J Chromatogr 485:143, 1989.
    b. Y Baba, MK Ito. J Chromatogr 485:647, 1989.
19. PJ Schoenmakers, Á Bartha, HAH Billiet. J Chromatogr 550:425, 1991.
20. P Chaminade, A Baillet, D Ferrier. J Chromatogr 672:67, 1994.
21. a. MA Quarry, RL Grob, LR Snyder. J Chromatogr 285:1, 1984.
    b. MA Quarry, RL Grob, LR Snyder. J Chromatogr 285:19, 1984.

c. MA Quarry, RL Grob, LR Snyder. Anal Chem 58:907, 1986.
d. LR Snyder, MA Quarry. J Liq Chromatogr 10:1789, 1987.
22. BFD Ghrist, BS Cooperman, LR Snyder. J Chromatogr 459:1, 1988.
23. PJ Schoenmakers. Optimization of Chromatographic Selectivity, A Guide to Method Development. Amsterdam: Elsevier, 1986.
24. MW Watson, PW Carr. Anal Chem 51:1835, 1979.
25. JC Berridge. J Chromatogr 485:3, 1989.
26. a. JW Dolan, DC Lommen, LR Snyder. J Chromatogr 485:91, 1989.
b. JW Dolan, LR Snyder, MA Quarry. Chromatographia 24:261, 1987.
c. JW Dolan, LR Snyder. LC–GC 5:970, 1987.
27. S Heinisch, JL Rocca, M Feinberg. J Chemom 3(suppl A):127, 1988.
28. a. N Lundell. J Chromatogr 639:97, 1993.
b. N Lundell, K Markides. J Chromatogr 639:117, 1993.
29. SV Galushko, AA Kamenchuk, GL Pit. Am Lab 27:33G, 1995.
30. R Cela, CG Barroso, C Viseras, JA Perez-Bustamante. Anal Chim Acta 191:283, 1986.
31. M Laemmerhofer, P Di Eugenio, I Molnar, W Lindner. J Chromatogr 689:123, 1997.
32. JJ Kirkland, JL Glajch. J Chromatogr 255:27, 1983.
33. a. S Heinisch, P Riviere, JL Rocca, Chromatographia 32:559, 1991.
b. S Heinisch, E Lesellier, C Podevin, JL Rocca, A Tchapla. Chromatographia 44:529, 1997.
34. LR Snyder, MA Stadalius, MA Quarry. Anal Chem 55:1421A, 1983.
35. a. BFD Ghrist, LR Snyder. J Chromatogr 459:25, 1988.
b. BFD Ghrist, LR Snyder. J Chromatogr 459:43, 1988.
36. PJ Schoenmakers, HAH Billiet, L de Galan. J Chromatogr 205:13, 1981.
37. DP Herman, HAH Billiet, L de Galan. J Chromatogr 463:1, 1989.
38. Á Bartha, HAH Billiet, L de Galan. J Chromatogr 458:371, 1988.
39. a. M Borowko, M Jaroniec, J Narkiewicz, A Patrykiejew, W Rudzinski. J Chromatogr 153: 309, 1978.
b. M Borowko, M Jaroniec, J Narkiewicz, A Patrykiejew. J Chromatogr 153:321, 1978.
40. P Jandera, J Churácek. J Chromatogr 170:1, 1979.
41. SM Gort, EA Hogendoorn, E Dijkman, P van Zoonen, R Hoogerbrugge. Chromatographia 42:17, 1996.
42. JE Eble, RL Grob, PE Antle, LR Snyder. J Chromatogr 405:51, 1987.
43. LR Snyder, JW Dolan, GB Cox. J Chromatogr 540:21, 1991.
44. JL Glajch, MA Quarry, JF Vasta, LR Snyder. Anal Chem 58:280, 1986.
45. Y Liu, DJ Anderson. J Chromatogr 762:47, 1997.
46. H Poppe, JC Kraak, JFK Huber, JHM van den Berg. Chromatographia 14:515, 1981.
47. a. PL Zhu, LR Snyder, JW Dolan, NM Djordjevic, DW Hill, LC Sander, TJ Waeghe. J Chromatogr 756:21, 1996.
b. PL Zhu, JW Dolan, LR Snyder, NM Djordjevic, DW Hill, JT Lin, LC Sander, L van Heukelem. J Chromatogr 756:63, 1996.
c. PL Zhu, JW Dolan, LR Snyder. J Chromatogr 756:41, 1996.
d. PL Zhu, JW Dolan, LR Snyder, DW Hill, J-T Lin, LC Sander, L van Heukelem, TJ Waeghe. J Chromatogr 756:51, 1996.
48. C Viseras, R Cela, CG Barroso, JA Perez-Bustamante. Anal Chim Acta 196:115, 1987.
49. L Wild. Adv Polym Sci 98:1, 1990.
50. G Glöckner. J Appl Polym Sci Appl Polym Symp 45:1, 1990.
51. RM Smith, RJ Burgess. Anal Commun 31:327, 1996.
52. DJ Miller, SB Hawthorne. Anal Chem 69:623, 1997.
53. S Hjerten. Adv Chromatogr 19:111, 1981.
54. SD Patterson. J Chromatogr 592:43, 1992.
55. D Hannak, F Scharbert, R Kattermann. J Chromatogr 728:307, 1996.
56. LR Snyder, JW Dolan. LC–GC 8:524, 1990.
57. PL Zhu, LR Snyder, JW Dolan. J Chromatogr 718:429, 1995.

6

Computers and Liquid Chromatography

J. Strasters

Nycomed, Inc., Wayne, Pennsylvania

I. INTRODUCTION

These days, computers play a role in every aspect of the liquid chromatographic (LC) process, apart from the physical separation of the compounds taking place in the column. As is true in other fields, this role can be viewed at various levels.

At the most elementary level, the computer is used to control the instrument and assist in the integration of signals in the time domain. Thus, the chromatographer is spared the execution of repetitive tasks, the flexibility of the instrumentation is extended, and the precision and efficiency of the overall process is improved. Most aspects of direct instrument control and elementary data analysis are discussed elsewhere in this volume. Here we will discuss general subjects relative to automation, such as robotics and coupling of instruments (see Sec. II).

At a higher level, the computer allows us to handle vast amounts of data and to reduce this information to an understandable format. Nowadays, numerical analysis of data implies the application of some form of digital analysis. In current LC practices this might occur both before and after the separation. Often the quantitative results of the chromatographic analysis will be further processed, both to achieve data reduction and to arrive at more meaningful conclusions. The versatility of hyphenated chromatographic techniques, such as LC–UV and LC–MS, would be but a fraction of the realized potential, were it not for the computer controlled data collection, data reduction and data presentation before human interpretation. This will be further discussed in Section VI. Additionally, retention behavior can be correlated with both chemical structure and biological activity to assist in either the prediction of retention or activity. This and related subjects will be touched on in Section III.

At the highest level, the computer itself becomes part of the decision making process as it relates to the experiments. In their most sophisticated forms, these approaches are often referred to as expert systems. However, less elaborate applications, such as the prediction of separations using simulations are currently more accessible to most users. The biggest effect of these approaches is found in the areas of method development (see Sec. IV) and method validation (see Sec. V). The scope varies from suggesting initial conditions for the separations to deriving optimal mobile-phase compositions to complete optimization of the chromatographic process.

In all of these implementations, the goal is to enhance the chromatographic separation process by joining the cognitive capabilities of the human mind and the number-crunching capabilities of computers.

II. AUTOMATION AND INSTRUMENT CONTROL

In this section we will review how the various aspects of chromatography have been influenced by digital control. In addition we will go into more detail of some specific examples for which chromatography has significantly profited from the technological advances provided by these types of control.

Rather than trying to define what is meant exactly by computer control, we will consider here the various forms of digital control that play a role in liquid chromatography in the widest sense. Currently, most equipment contains its own integrated circuits, sometimes referred to as firmware. This will be augmented by ways to interact with the environment through one or more of the available protocols, such as RS232 (a serial interface), IEEE, or HP-IB (parallel interfaces). These interfaces will allow input to or output from the instrument, depending on the configuration.

Ideally a central-processing unit or computer controls the functioning of the various elements that form the LC system. It provides setpoints and operational parameters as input to the instruments. On the other hand, the different elements provide output in the form of actual values of parameters and observations, such as detector signals, to the central controller. The advantage of using distributed processing through firmware is that the elements can work independently on the details of the operation. They provide the central-processing unit with a summary of the results and observations, thereby freeing it for other tasks. This is especially relevant in situations during which the elements are dealing with huge amounts of information. For instance, photodiode-array detectors can perform initial data manipulation, such as signal averaging and background subtraction, to avoid overloading the central controller.

Usually, the setpoints for an instrument can be provided through either an external device (computer), or locally through a keypad or switches. This provides additional flexibility when running the equipment as well as the possibility of running an instrument in the "stand-alone" mode, without external control. In addition, the flexibility of the firmware has been increased in the latest generations of instruments. In some equipment, reprogramming of the firmware is now possible through electronic means, rather than by manual replacement of the integrated circuits.

When implementing automation of multiple liquid chromatographs in a laboratory environment, a choice has to be made for the general organization. One solution is to maintain independent control of each of the instruments, generally in the form of a personal computer (PC) or equivalent. This provides great flexibility, but often implies that operators are confronted with different user interfaces and controls on instruments from different manufacturers. Another possibility is to implement central data collection and (limited) instrument control using a mainframe computer [1]. This setup is more rigid, and usually does not allow full central control of all the peripherals and all options of the instruments. Much depends on the support provided by the manufacturers. On the positive side, the same user interface applies to all instruments, thus decreasing the learning curve. In addition, data storage and backups are easily organized, it is easier to maintain the integrity of the data, and it is simpler to update to new versions of the software.

Combining the advantages of these two approaches is possible by implementing a local area network (LAN), linking the various computers controlling the individual instruments to a so-called server. The server provides a means for both data storage and software distribution, while the individual controllers perform the actual data collection and instrument control.

Although the advantages of automation may seem obvious, it is important to review them here before discussing the relevance of developments in this area. In addition, we will show that every aspect of the chromatographic process can benefit from these advantages. The first purpose of automation is to increase the efficiency. By partly automating the instrument control, operators are freed for tasks that require human attention and intervention. In LC, this increases the amount and the quality of analytical results generated. However, the improved quality is not just the result of fewer laborious and repetitive tasks. Under the right circum-

stances, computer control will result in improved precision, both in terms of repeatability and reproducibility. In the following sections of this chapter, several examples are described showing that automated instruments are able to repeat a programmed set of commands flawlessly over prolonged periods with a minimal variation in the operating conditions.

In addition to the foregoing, the computer may function as a tireless and meticulous bookkeeper. This applies not only to the samples and the corresponding results, but also to the conditions under which those results were obtained. This is especially important in heavily regulated environments, such as the pharmaceutical industry, in which great emphasis is placed on traceability and data integrity. The latter is generally achieved by allowing data manipulation only on copies of the raw data, while digitally safeguarding the original data.

There is no aspect of the chromatographic process that has escaped the effects of automation. Sampling and sample preparation in the form of preconcentration and precolumn derivatization can now be performed by robots, intelligent autosamplers, and preconcentration devices [2–4]. All operational aspects of the liquid chromatograph can be controlled and monitored by digital devices. Computers allow the execution of different calibration sequences and assist in further data manipulation, quantitation, and peak identification [5, 6, see Sec. V]. Most automated systems enable the user to develop customized reports that provide the best possible presentation of the relevant results for the application. An interface with a laboratory information management system (LIMS) allows the chromatographic results to be directly transferred and combined with other information. This may increase the sample throughput in the analytical laboratory.

Rather than trying to give an exhaustive list of all possible approaches to automation, we will focus here on some specific examples that highlight some of the aforementioned advantages.

A. Sample Preparation

Complete automation of the LC analysis extends beyond the operation of the chromatograph and the data analysis. Often the sample preparation takes as much time and effort as the actual analysis, exposes the analyst to potentially harmful vapors, and introduces additional sources of human error. Therefore, various more or less intelligent devices have been introduced to increase sample throughput and user friendliness, while reducing the amounts of solvents used.

Some of these devices are dedicated to certain aspects of the sample preparation and introduction process; for example, autosamplers. However, the current generation of autosamplers is able to do more than just inject defined volumes from subsequent sample vials. They provide rapid access to multiple vials in any order, enabling complex calibration sequences using a minimum number of vials. In addition, they can perform automatic dilutions to assist in the generation of calibration curves, add various reagents to the sample before injection, or inject different solutions simultaneously [see for instance Ref. 3]. Automated precolumn derivatization can thus be performed.

Preconcentration or extraction usually requires additional instrumentation. In general, solid-phase extractions are simpler, more robust, and easier to automate than liquid-liquid extractions. For instance, [2], the Prospekt (Spark Holland, Emmen, The Netherlands) automated sample preparation unit can be used for automated extractions, by controlling the timing of both the extraction and the LC analysis by using the computer of the high-performance (HP)LC. Also, the LC system itself can be used for automated sample clean-up and fractionation [6]. Again, the computer controls the valves and flows, regulating the flow through different columns. Desired fractions can be collected at the outlet.

More complicated forms of sample preparation, including liquid–liquid extraction, often require the use of robotics for complete automation. A robot is more flexible than the dedicated systems described earlier. The user can adapt its functionality to the task at hand. The downside is that use of such a system requires a significant investment in terms of time needed for setup, for validation, and to design methods for error checking [7].

A typical configuration for a robot is shown in Fig. 1 [8]. The robot itself consists of an arm to perform actions and to transfer items from one station to the next, surrounded by workstations that are dedicated to perform specific tasks that include recording weights, mixing, centrifuging, and crimping vials. In one of the commercially available robots, the Zymate (Zymark Corporation, Inc., Hopkinton, MA), the functionality of the robot arm can be adjusted by replacing the "hand" attached to the arm. The position of the hand is defined by three coordinates, and the robot's training consists of providing it with the proper coordinates and actions to be performed in order. This process can be further facilitated by locking the various stations into place (see Fig. 1). The robot can then be programmed by simply providing the segment corresponding to the desired action.

For a fully automated HPLC analysis, including robotic sample preparation, it is critical that there is communication between the computer controlling the robot, the workstations, and

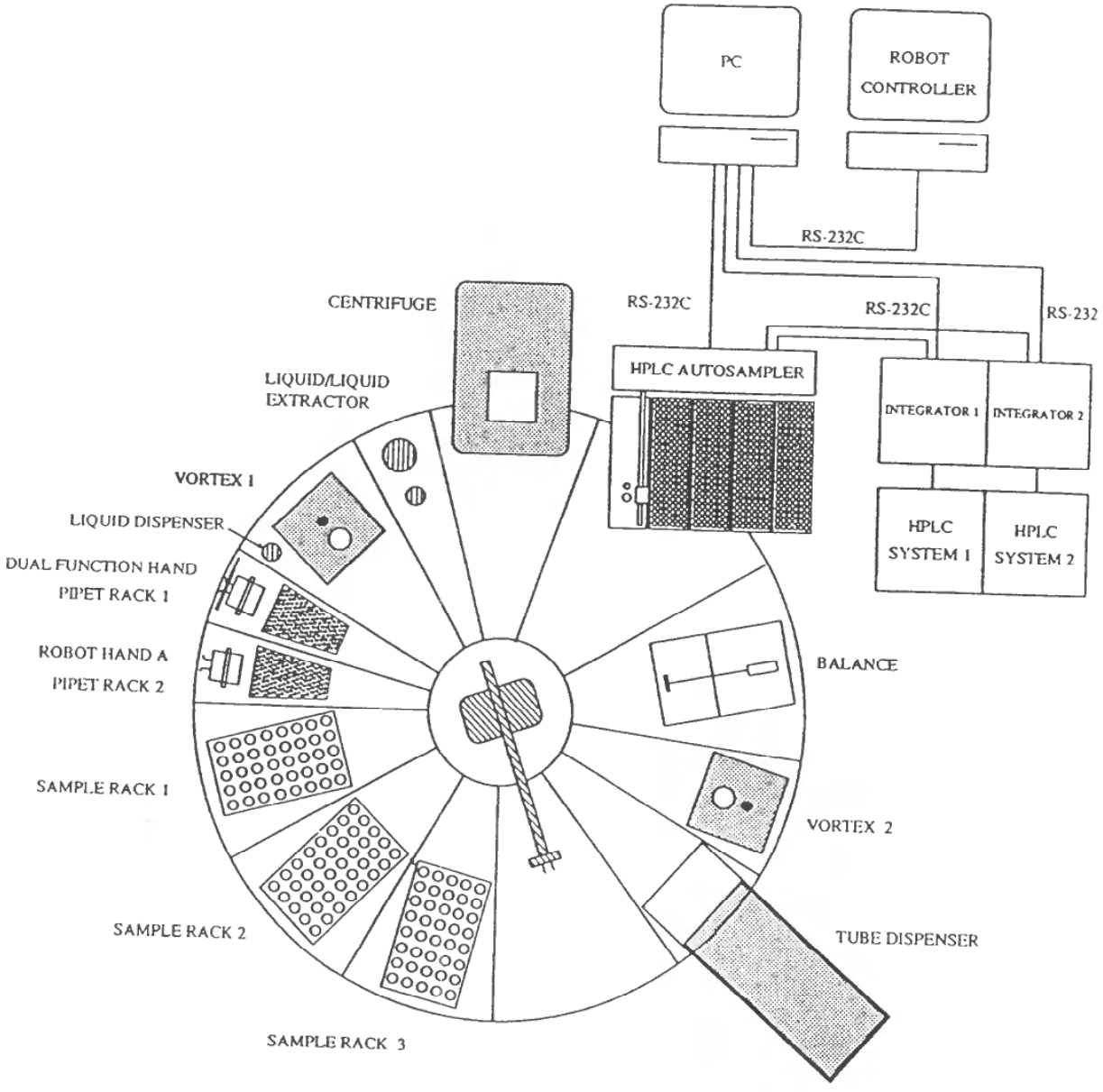


Figure 1 Overview of a robotic system used for sample preparation and sample introduction into an HPLC. (From Ref. 8.)

the controller of the HPLC [8]. If the samples are manually transferred from the robot to the HPLC, additional sources of human error are introduced. By providing the HPLC data analysis system with digitally recorded sample weights and sample identifications, transcription errors are avoided.

In its most advanced form, the interaction between the automated HPLC and the robot is used to regulate the functioning of the latter. This can be as simple as a command to discontinue the sample preparation when the chromatography shows too much baseline drift or when unexpected observations of an internal standard occur. However, it is also possible to use feedback to optimize the analysis by changing the operation parameters of the robot depending on the outcome of the HPLC experiments [4].

The attractiveness of a robot is highly dependent on the number of samples that will be analyzed with a given system, owing to the high costs of robotic systems, in terms of both initial investments and the time required for training and validation [9].

B. Column Coupling and Hyphenated Separation Techniques

As indicated earlier, automation can be a necessity when the timing of action is critical. One area in HPLC for which this is true involves the coupling of columns or separation techniques. Ideally, coupled techniques are orthogonal, which means that fundamentally different mechanisms cause differentiation between the analytes. Common combinations are ion-exchange and size-exclusion LC [10] and affinity and reversed-phase LC [11]. Coupling of orthogonal separation mechanisms is of great interest because of the enormous increase in peak capacity, compared with one-dimensional separations [12].

Two types of coupled column systems can be distinguished [11]. In the sequential approach, only the fraction of interest is transferred to the second column (heart-cut technique). The first column separates the analytes of interest from the matrix. The second column performs the actual separation of the analytes. In an automated system, the computer controls the position of the valves and regulates the flows through the columns. This ensures an efficient transfer, removes the risk of handling errors, and reduces the labor in comparison with a manual approach.

If the positions of the valves are exclusively based on timed events programmed into the computer, high demands are put on the reproducibility of the chromatography. Incorrect results will be obtained when the peak(s) of interest drift outside the heart-cut window. However, in an automated system, the chromatographic signal of the first separation can be used to trigger the switching of the valves (for instance, using signal thresholds or peak valleys); therefore, more variation in the chromatography can be tolerated [13]. This can be taken one step farther, to a point at which the computer assists in the development of the heart-cut procedure based on heuristic knowledge [14]. First, the time of the heart-cut is determined on the basis of the retention time of a standard compound on the first column. Next, the heart-cut window is optimized on the basis of the recovery from spiked samples. Additional modifications can be made if needed.

A second approach to coupled-column separations is truly multidimensional, in that multiple fraction are submitted to the second separation system. In the extreme case, all of the eluate is transferred to the second system. This requires either a stop-flow procedure, in which the first system is put on hold, while the separation on the second column takes place, or a rapid-sampling procedure, combined with appropriate combination of the flows through both systems. The latter method has been characterized as comprehensive two-dimensional (2D)-LC [10]. Rapid sampling of the first eluate requires accurate timing, both for the valve positions and the analytical time of the second separation.

Similar arguments can be made when discussing the coupling of various separation and detection techniques, such as HPLC–high-resolution gas chromatography (HRGC) [15], HPLC–Fourier-transform infrared spectrometry (FTIR) [16], HPLC–capillary electrophoresis

(CE) [17] or HPLC–amperometric detection [18], as well as other hyphenated systems such as LC–mass spectrometry (MS) and LC–UV (see also Sec. VI). Apart from the fact that these systems produce too much information not to have some form of automated data-reduction and data-analysis available, the transfer of the eluate from the LC system to the second technique is critical and often requires some form of computer control.

For instance in the coupling of LC with CE [17], data collection is suspended, and the voltage over the capillary is dropped during the transfer of eluate from the loop used for collection of fractions from the LC to the CE system. The voltage has to be lowered to avoid injection of excessive amounts of eluate by the electroosmotic flow. It takes some time for the voltage to reach the desired level, and this must also be taken into consideration. Especially, if the experimental conditions vary with the application, simultaneous control of voltage, of valves and of data collection requires digital control by a computer.

C. On-Line Monitoring and Control

One other aspect in instrument control and HPLC is when the LC is not only controlled by a computer, but the results of the LC analysis are also used in process monitoring and control; for instance, this has been described for biotechnological processes, such as fermentations [19–21].

In automated process monitoring, the results of the LC analysis are simply stored for future reference; for instance for further analysis of the process condition at a later stage. In general, HPLC is a preferred analytical technique when multiple analytes are monitored. However, it is also possible to use an array of sensors for this purpose. On-line sampling can be difficult in fermentation processes, because solid material must be removed from the sample before injection and because the sampling must occur in a fashion such that contamination or infection of the fermentor is avoided.

In its most advanced form, an automated on-line LC analysis can be applied to perform closed-loop control of a fermentation reaction [19]. The results of the analysis are used to adjust the feed of the fermentor so as to optimize the growth of biomass or the yield of the desired fermentation product (Fig. 2). On-line measurements will reduce the overall analytical time and, thereby, tighten the control; lower the personnel requirement; and reduce the chance of fermentor contamination.

When using LC for closed-loop control, a compromise must be found between the time needed for the LC analysis and the accuracy of the results. Obviously, the total time required for the chromatogram cannot be too long if a reliable estimate of the current status of the process is to be obtained. If the analytical time is excessively long, the necessary information is not obtained and the process cannot controlled. However, a shorter analysis time implies less resolution between the analyte(s) of interest and matrix interferences. This reduces the accuracy of the results. Clearly, if the analytes are completely unresolved, the process cannot be controlled. One other factor affecting the optimal analytical time, is the rate at which the process itself takes place. If the process is slow, one can spend more time on the analysis, whereas a rapid process will require a rapid response from the measurement. Thus, the control of the process is determined by the time constant of the process, the accuracy of the analytical results, and the sampling interval.

III. PREDICTION OF CHROMATOGRAPHIC PROFILES AND RETENTION

Although the fundamental knowledge of chromatography, in general, and liquid chromatography, in particular, has increased dramatically over the last decades, the science of liquid chromatography is still highly empirical. As a consequence it is often not possible to predict a priori the exact retention time of a component on the basis of its structure and the characteristics of the chromatographic system. Similarly, it is not always possible to derive exact

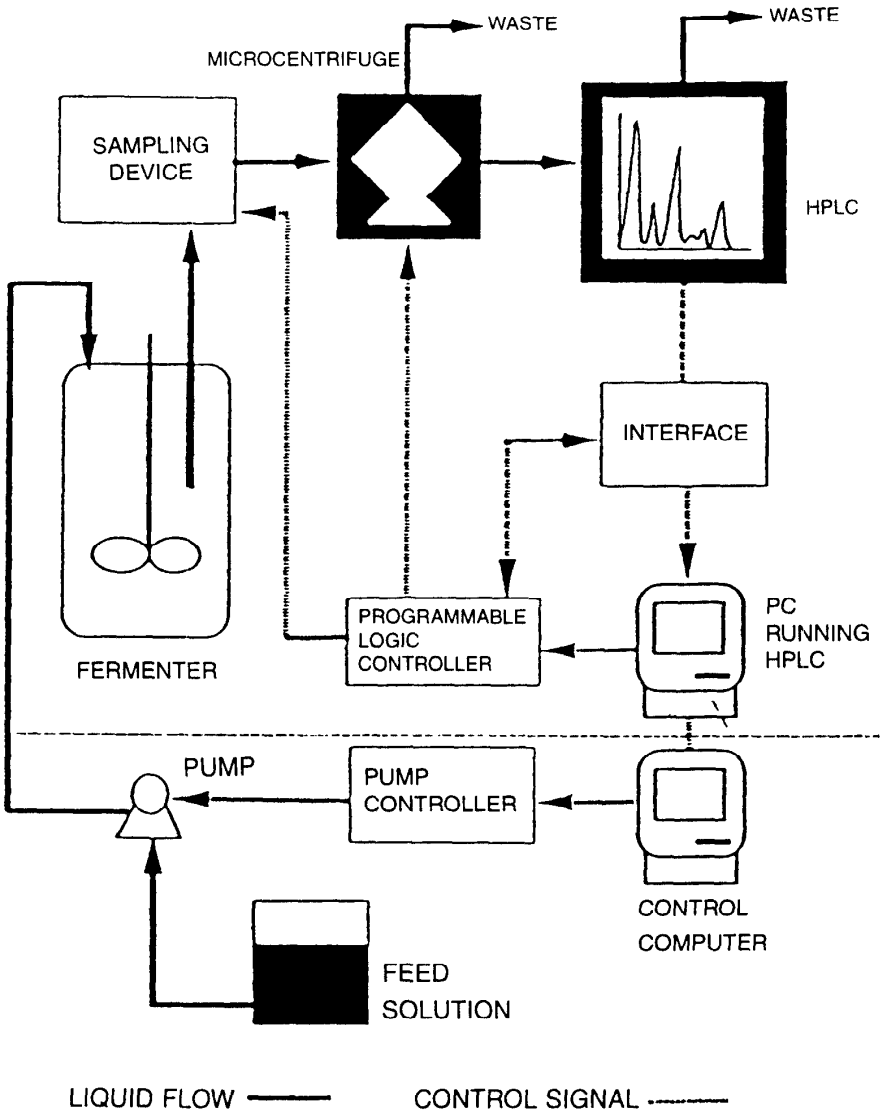


Figure 2 Layout of the monitoring and control components for automated sampling, analysis, and control of fermentation broth. (From Ref. 19.)

analytical solutions of the equations for the peak profile of a given solute injected at a given concentration and volume and a given column. The latter is particularly relevant for preparative LC.

The computer allows sophisticated numerical analyses to obtain more insight into the chromatographic process and the resulting retention of analytes. Attempts at exactly predicting retention times from statistical thermodynamics and related techniques are still at an early stage and will not be covered here. However, approximations of the chromatographic profile by empirical computer models are being employed more widely, and these will be discussed in Section III. A.

To describe retention behavior as a function of molecular structure, one uses so-called quantitative structure–retention models. Inversely, physical characteristics can be derived from chromatographic behavior. The computer is used both to derive models and to estimate the physical characteristics used as predictors. (see Sec. III. B).

Once models have been established to predict retention as a function of structure, they can be used to derive the chromatographic conditions needed for the separation of a given

mixture. As a rule, these models are approximations, at best, and it is not possible to predict conditions that yield optimal selectivity, nor even the optimal solvent strength. Therefore, such approaches are referred to as first-guess expert systems. General principles and some examples will be presented in Section III. C. Further steps to optimize selectivity and an overall approach to method development is covered in Section IV.

A. Simulation of Chromatographic Profiles

A better understanding of the principles underlying separation and band-broadening in LC is obtained when the development of the chromatographic profile in the column can be visualized. For analytical-scale LC, mathematical equations have been developed by means of either plate or rate models. Provided the number of theoretical plates is high enough, both types of models result in a gaussian-shaped profile with a variance increasing over time. Important assumptions are that the concentration of analytes is very small relative to the loading capacity of the column, and that the various solutes in a mixture behave independently of each other.

In analytical-scale chromatography, the foregoing assumptions are generally true. However, in preparative-scale LC, the amount of material loaded on the column will approach or exceed the loading capacity of the column. In that case the number of available adsorption sites on the stationary phase will vary significantly with the concentration of the solutes. In addition there will be significant interactions between different solutes and competition for the available adsorption sites. This can be mathematically expressed by a competitive Langmuir isotherm [22]:

$$C_{s,i} = \frac{a_i C_{m,i}}{1 + \sum_j b_a C_{m,j}} \tag{1}$$

where $C_{s,i}$ and $C_{m,i}$ refer to the concentrations of component i in the stationary and mobile phases, respectively. The mobile-phase concentrations of all other components are denoted by $C_{m,j}$ and a_i and b_j are numerical coefficients, the value of which depends on the nature of the solutes and the chromatographic system. In case of dilute solutions, the summation in the denominator becomes negligible and a_i can be thought of as the distribution coefficient.

The mathematical expression for the mass balance over a small segment of the column is given by:

$$\frac{\delta C_{m,i}}{\delta t} + \phi \frac{\delta C_{s,i}}{\delta t} + u \frac{\delta C_{m,i}}{\delta z} = D \frac{\delta^2 C_{m,i}}{\delta z^2} \tag{2}$$

Where ϕ represents the phase ratio, u the mobile-phase velocity, and D the apparent diffusion coefficient. The first two terms of the equation describe the variation of the concentration in the mobile and stationary phases as a function of the time t. The third term describes the transport of component i owing to convection along the column, described by the location variable z. Finally, the expression on the right-hand side of the equation describes the change in concentration owing to diffusing.

One of the consequences of the nonlinear nature of Eq. (1) is that it is not possible to obtain a simple mathematical solution for the resulting chromatographic profile. However, it is possible to use numerical methods to simulate it [see Ref. 22 and references therein]. For instance, the finite-difference approach transforms the differential Eq. (2) into a difference equation:

$$\frac{C_m^{j,n+1} - C_m^{j,n}}{\Delta t} + \phi \frac{C_s^{j,n+1} - C_s^{j,n}}{\Delta t} + u \frac{C_m^{j,n} - C_m^{j-1,n}}{\Delta z} = D \frac{C_m^{j+1,n} - 2\,C_m^{j,n} + C_m^{j-1,n}}{\Delta z^2} \tag{3}$$

(subscript i is left out for clarity). The column is divided in elements of length Δz, and the solute concentrations are determined for every time interval Δt. Thus, Eq. (3) refers to column

element j, between times $n\ \Delta t$ and $(n + 1)\ \Delta t$. After every step, the mobile phase (containing solute i) is transported along the column. This changes the concentrations; consequently, a reequilibration calculation has to be performed using Eq. (1). To perform this simulation, several boundary conditions must be imposed, which corresponds to an initialization of the various compartments at $t = 0$. The applied injection profile is also introduced in the form of a boundary condition, usually a plug of constant concentration.

The reliability of the resulting profile depends on the number of compartments and the size of the time interval relative to the time scale of the separation process. Therefore, these simulations are only possible thanks to the computer's ability to rapidly perform the enormous number of calculations involved. The small errors that are introduced by treating the continuous process as a series of discrete steps propagate as an additional dispersion process; thus, they can be corrected for by adjusting the apparent diffusion coefficient.

The results of the simulations of the profiles under overloading conditions have been used in various ways. Normally, a chromatographic profile is observed as the compounds are eluting from the column, along a time axis. However, the computer-generated profiles can be displayed while the components are migrating through the column, using the column coordinate z as the independent variable. This, in turn, allows an evaluation of the separation at any time, thereby enabling the selection of the optimal column length for complete separation [22].

Simulations also allow an easy evaluation of the effects on the separation process of various variables, such as the relative concentrations of the analytes, column dimensions, sample load, and such. The selectivity observed under analytical conditions can be related to preparative-scale separations. This allows optimization of the conditions to maximize the production rate [23,24].

Finally, simulations can be used to postulate hypotheses for fundamental aspects of the separation. For example [25], profiles observed when using a strong sample solvent were compared with simulated profiles. The simulated profiles resembled the observed profiles when oversaturated solutions were assumed to exist at the leading edge of the peak, suggesting that this is a possible explanation.

B. Quantitative Structure–Retention Relations

Chromatographic retention is characterized by change in free energy on the transfer of the solute from the mobile to the stationary phase. As such it is related to interactions between the solute and these phases. These interactions can be described as functions of molecular descriptors, such as the van der Waals volume, dipole moments, molecular electrostatic potentials, and others. Components can also be characterized by their hydrophobicity (lipophilicity) (i.e., their preference for a nonpolor solvent immiscible with water). In turn, the hydrophobicity can be expressed as a function of the foregoing molecular descriptors [26]. One of the traditional ways to do so is through the partition coefficient of a solute between water and octanol, P_{ow}.

Similar interactions play a role in the passive transport of compounds, such as drugs and toxins, in living organisms and thus affect their biological activity. Both aqueous compartments and structured lipophilic membranes are encountered in the organism. The distribution coefficients K for an analyte determined in various (similar) two-phase systems are related through the Collander equation [27].

$$\log K_1 = a \log K_2 + b \tag{4}$$

where a and b are constants for a set of similar analytes. The chromatographic process is also based on partitioning between two phases of different polarity, and is characterized by a distribution coefficient K_{chr}. By applying the Collander equation, we can relate the hydrophobicity of a component, as defined by its octanol–water partition coefficient P_{ow} to its chromatographic capacity factor k' [e.g., Ref. 28]:

$$\begin{aligned} \log P_{ow} &= a \log K_{chr} + b \\ &= a \left(\log k' - \log \frac{V_s}{V_m} \right) + b \\ &= a \log k' + c \end{aligned} \tag{5}$$

where V_s/V_m represents the phase ratio in a given chromatographic system and c is a constant.

It is shown by the foregoing that there are direct relations between parameters related to molecular structure, traditionally used to predict biological activity, and chromatographic retention. A symbolic representation of these relations is seen in Fig. 3. Quantitative structure–activity relations (QSAR) describe how the molecular structure, in terms of descriptors—hydrophobic, steric, and electronic—affects the biological activity of a component. Similarly, quantitative structure–retention relations (QSRR) relate these descriptors to chromatographic retention. Finally, the quantitative retention–activity relations (QRAR) imply that conclusions concerning biological activity can be based on chromatographic experiments.

The QRAR relations can be applied in various ways [29,30]. By determining which structural descriptors affect chromatographic retention, information is obtained on the separation mechanism [see e.g., Ref. 31]. This will also allow a comparison between different chromatographic systems to evaluate the orthogonality of their separation mechanisms. Similarly, by measuring the retention of unknown compounds, conclusions can be drawn about their molecular structure. This can be used to confirm hypotheses on the potential degradation products of a given compound [32], or to suggest the most likely sequence of the amino acids in small peptides [33].

Given the relation between chromatographic retention and molecular descriptors, it should also be possible to replace the latter by retention-related quantities in the prediction of biological activity. For instance, the use of reversed-phase LC retention data to replace P_{ow} as a measure of hydrophobicity has been discussed [see e.g., Ref. 34]. To obtain an unambiguous number, this usually entails an extrapolation to pure aqueous conditions, thereby removing the influence of organic modifiers that are added to adjust retention to within a workable range. The use of other forms of chromatography (e.g., micellar liquid chromatography) to predict either P_{ow} or biological activity, has also been proposed [29].

Numerical analysis plays an important role in various aspects of the foregoing processes. The relations themselves are usually based on correlation analysis. This can be a straightforward linear regression, to relate log P_{ow} with log k' [26] or log k' with the van der Waals volume [35]. Often the analysis involves multiple linear regression (MLR). In that event log

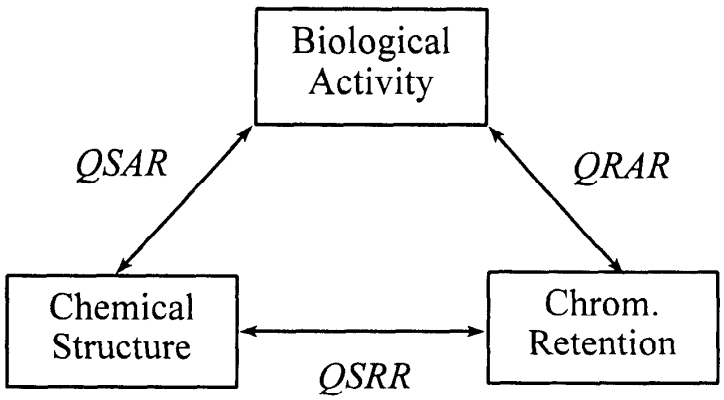


Figure 3 Symbolic representation of the three types of quantitative relations: QSAR; quantitative structure–activity relations: QRAR; quantitative retention–activity relations; and QSRR; quantitative structure–retention relations.

P_{ow} or log k' values are correlated with several molecular descriptors. By evaluating the error in the model in relation to the number of degrees of freedom, terms can be added (forward stepwise regression) or removed (backward stepwise regression) to arrive at a robust model that contains the maximum amount of information [36].

A more qualitative approach to evaluate the relation between structure and retention in various chromatographic systems, is hierarchical ascending classification [31]. This is a form of automatic classification in which the components are evaluated in a multidimensional space defined by the retention data observed in the various mobile-phase–stationary-phase combinations. The euclidean distance between the objects (components) is used to express the degree of similarity. The two most similar objects are replaced by an "average" object, and the process continues. This results in a branched structure, where analytes with similar retention characteristics are grouped together. A similar analysis is possible by considering the chromatographic systems as objects in a multidimensional space defined by the retention of the different analytes. New analytes can be classified on the basis of the observed retention characteristics, or alternative chromatographic systems can be evaluated relative to those previously examined.

Another form of computational analysis used for the correlation of biological activity, structure, and chromatographic retention is factor analysis (FA) or principal-component analysis (PCA) [37] (in chemical applications these two terms are used interchangeable). By using a multidimensional space similar to that described in the previous paragraph, a quantitative model is derived that transforms the axes of the system. The first principal component (PC) defines as much of the variation in the data as possible. The second PC describes the maximum amount of residual variation after the first PC has been taken into consideration, and so on. By using only a limited number of PCs, the dimensionality of the data space is reduced, thereby simplifying further analysis. In chromatography two principal components are often sufficient to describe most of the data's variation [31,38,40]. Although the PCs are abstract, one of them often shows some correlation with molecular size, steric factors, or hydrophobicity, whereas the other PC seems more strongly correlated with dipole–dipole interactions and electronic factors. Further confirmation of such a hypothesis can be obtained by relating known factors to the abstract factors (target factor analysis; TFA) [37]. A model based on principal components can be used to classify unknown solutes. For instance, Fig. 4 shows the classification of antihistamine drugs into H_1- and H_2-antagonists using a principal-component model derived from the retention times on different columns at different pH levels [38].

C. "First-Guess" Expert Systems

One important implication for knowledge of the relation between structure and retention is that it allows the prediction of retention for specific compounds. In theory, this opens the way toward defining an optimal set of conditions (column, mobile-phase) for the separation of a given mixture. Unfortunately, owing to the multitude of possible molecular interactions in liquid chromatographic systems, most quantitative structure–retention relations are derived empirically for a restricted set of compounds and a limited range of chromatographic conditions. Moreover, even if the appropriate relation is available, only an approximation of the retention time is generally obtained. Therefore, this approach is currently limited to determinating the appropriate elution strength. The prediction of selectivity (or resolution) is much more uncertain because of the small differences in energies of interaction between different solutes and the stationary and mobile phases [39]. Therefore, adjustments of the conditions to improve the selectivity are usually performed on the basis of several experimental observations (see Sec. IV).

Recognition of which relations apply requires involvement of an expert (i.e., somebody intimately familiar with the theory of liquid chromatography and the compound(s) under investigation). Apart from selecting the appropriate combination of a stationary and a mobile

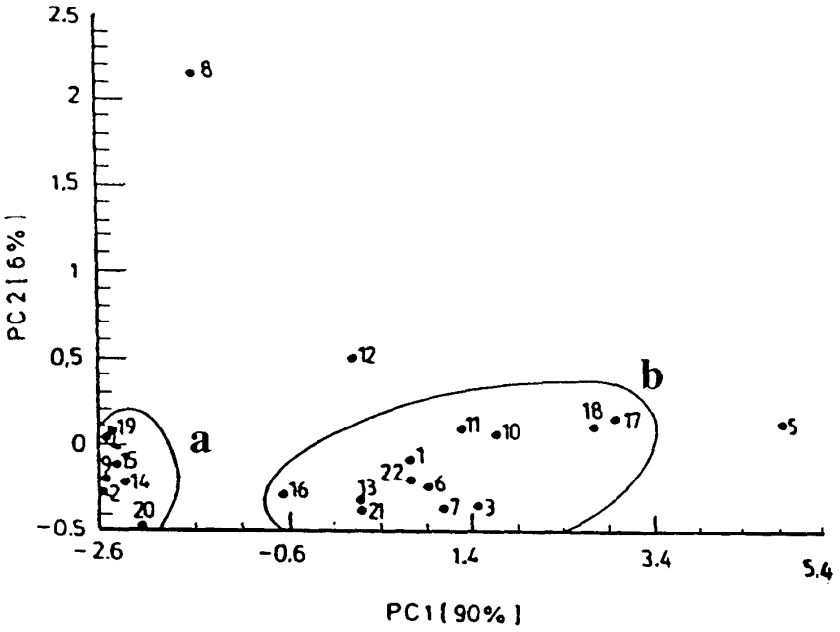


Figure 4 Classification of antihistamines on the basis of a principal component analysis using the retention data observed at different pHs and on different columns. The two classes are identified as H_2-antagonists (a) and H_1-antagonists (b). (From Ref. 38.)

phase, this expert must also decide on aspects of detection and sample preparation. To make this type of specific knowledge more widely available, one can try to capture the underlying reasoning of the expert for implementation in an expert system.

Hamoir and Massart present an overview of the structure of expert systems and their applications in chromatography [40]. In short, an expert system consists of a knowledge base, containing rules and facts, and an inference engine. The latter uses the rules and facts to derive conclusions. In addition to these two modules, an expert system will contain an explanation facility, to explain how conclusions were reached, and a user interface to obtain the necessary input and to present the results. Finally, there will often be links to other computer programs to perform calculations and statistical analyses (Fig. 5). The reasoning of such systems is either driven by the data toward the conclusions (forward chaining) or from the possible conclusions toward the prerequisites in the data (backward chaining). Many computer programs contain some of the elements of expert systems, without all the reasoning capabilities. These systems are sometimes referred to as knowledge-based systems. Examples include decision trees and hypertext applications.

The selection of the appropriate mode of chromatography in combination with the correct mobile-phase composition for a given sample is particularly suitable for implementation in expert systems, because the required knowledge involves a complex combination of heuristic rules (e.g., IF ionizable groups are present in one or more of the components, THEN the aqueous mobile phase should be buffered) and quantitative relations (e.g., the hydrophobicity of the components determines the required strength of the mobile phase). As indicated earlier, the results are only approximate and will often require adjustment based on subsequent experiments. This is why these types of expert systems are often referred to as first-guess systems. Over the last years several such systems have been discussed in the literature. Some examples are given in the following.

As part of the Applications of Expert Systems in Chemical Analysis (ESCA) project, various expert systems were developed and combined to assist in liquid chromatographic method development [41]. Two of these systems select initial separation conditions on the

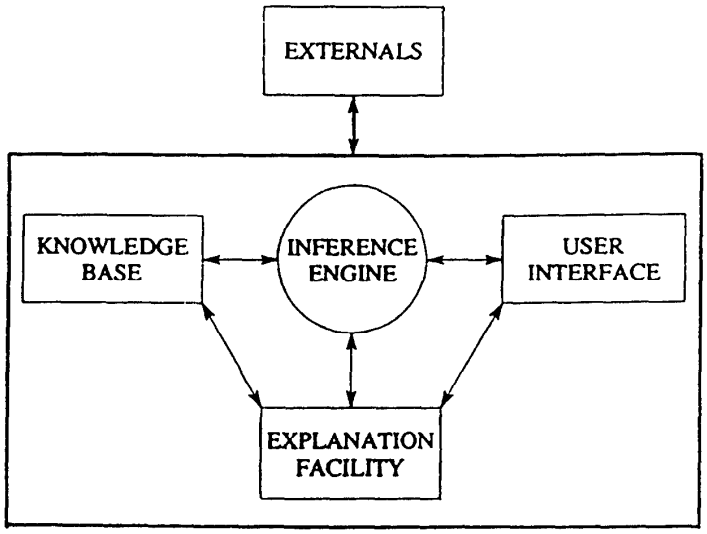


Figure 5 General structure of an expert system. (From Ref. 40.)

basis of the molecular structure. LABEL [described in Ref. 42] is used for the label claim analysis of drugs in pharmaceutical formulations using HPLC on a cyanopropyl column. The system provides advice for detection, type of chromatography (reversed-phase, reversed-phase with buffer, or normal-phase) and mobile-phase composition.The latter advice is based on the number of carbons in the analyte molecule as a measure of its hydrophobicity. DASH (drug analysis system in HPLC [43,44]) was developed for basic drugs. It determines the initial mobile-phase conditions to give k' values between 3 and 10. The required mobile-phase composition is estimated from the presence of polar and nonpolar groups. Each such group has a positive or negative contribution to the suggested percentage of methanol.

Alternatively, P_{ow} can be used as a predictor for the hydrophobicity and therefore, the retention behavior of a compound [45–47]. Several methods have been described to estimate the log P_{ow} value of a compound by using structural fragment constants [48–50]:

$$\log P_{ow} = \Sigma_i n_i F_i \tag{6}$$

where F_i is the fragment constant for a fragment i that occurs n_i times in a molecule. Correction terms are needed in certain cases. Commercially available computer programs analyze the structure of the molecule, which can be entered, for instance, in the form of a SMILES notation, a convention for representing molecular structures in the form of an ASCII string. The structure is divided in the appropriate fragments and the log P value is calculated. From an analysis of the retention behavior of many compounds in RPLC, the percentage acetonitrile (ϕ_a) or methanol (ϕ_m) that will result in a k' value of approximately 1 can be estimated as [45]:

$$\phi_a = 16 (\log P_{ow} + 26) \tag{7a}$$

$$\phi_m = 13 (\log P_{ow} + 42) \tag{7b}$$

The use of log P_{ow} is more suitable [47] for estimating retention than is the hydrophobicity, based on the number of carbons. However, the calculations required to determine P_{ow} are more involved.

Retention is not only a function of hydrophobicity, but also involves other interactions, such as dipole–dipole interactions, H-bonding, and other electronic contributions. Accurate estimates for retention under various chromatographic conditions can be obtained [51] by using two descriptors for fragments that constitute the analytes: partial molar volume in water

and increments of energy of interaction of bond dipoles in water. However, the improvement in prediction comes at the cost of a more extensive calibration of the chromatographic systems by running several selected standard compounds.

Although much progress has been made in the prediction of retention on the basis of molecular structure alone, the resulting expert systems are not yet widely available. In addition, modifications of the first-guess conditions are often required [41], and the correct elution strength does not guarantee adequate selectivity for the separation of a given mixture. However, computers can play an equally important role in the subsequent selectivity optimization, as described in the next section.

IV. COMPUTER-ASSISTED METHOD DEVELOPMENT: OPTIMIZATION OF THE SEPARATION

Method development for liquid chromatograph is a complex process that involves a number of steps (Fig. 6) [41]. Computer programs have been developed and investigated to assist in this process, either by addressing specific elements of the method development cycle, or by assisting the chromatographer with a number of the steps involved. Because of the complexity of the task, the latter approach will consist of a combination of algorithms and expert systems [41,52]. In recent years several excellent books and overviews have appeared in the literature that deal with the role of computers in LC method development [40,53–55].

As shown in Fig. 6, the method development process starts by selecting the appropriate procedure. We assume here that LC is the best technique for the given sample. Possible methods are reversed-phase, normal-phase, ion-exchange, and so on. The selected method, in combination with the available knowledge on the sample, will often dictate general parameter settings to obtain a reasonable peak-shape. In an isocratic method, the next step is an adjustment of the elution strength of the mobile phase such that all sample components will elute within an optimal range of k' values. Alternatively, the use of a gradient method will be indicated to achieve this goal. Computer assistance for these first steps can be provided by the first-guess expert systems discussed in Section III. C.

After the elution strength has been optimized, or appropriate gradient conditions have been established, there is still a high probability that some of the components will be only

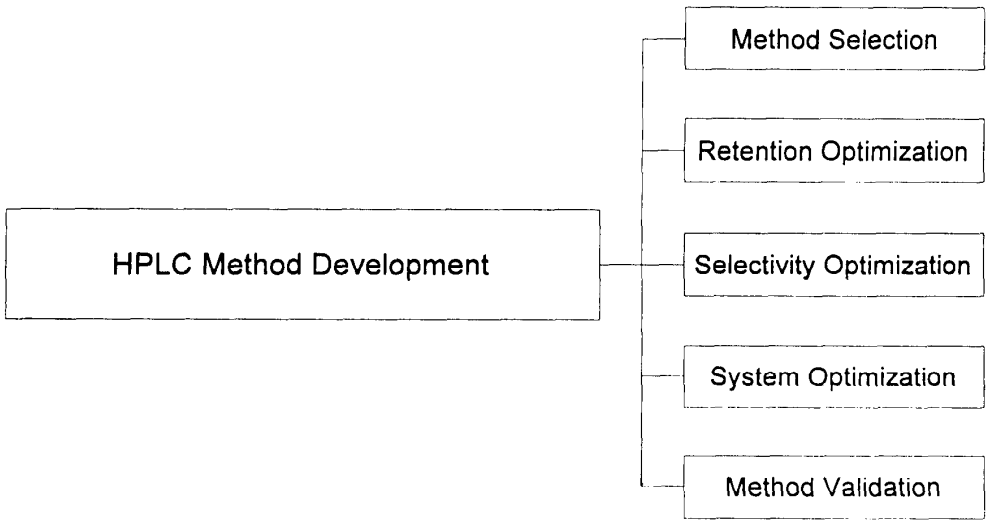


Figure 6 The different steps taken in the development and optimization of a liquid chromatography method.

partially separated. To improve the separation, it will then be necessary to optimize the selectivity of the method (i.e., adjust the separation conditions to obtain optimal band-spacing for adequate quantitation of all relevant analytes). The optimization of the band-spacing is often followed by further adjustment of instrument parameters to either improve the resolution by increasing the efficiency (increased column length, decreased particle size) or to decrease the analytical time by increasing the speed of the analysis (shorter column, higher flow rate). Computer-assisted approaches range from the use of simulations to predict how changing the conditions will affect the separation, to the consultation of expert systems designed specifically for this purpose. The last step in the method development cycle is the method validation, which will be discussed in Section V.

In Section IV, we will concentrate on those computer-assisted approaches that deal with adjustment of the elution strength or the establishment of appropriate gradient conditions, as well as with the optimization of selectivity on the basis of a limited number of initial experiments. These latter experiments result either from the advice of a first-guess expert system or from following a given experimental design. For the latter option the chromatographer has to select the appropriate parameters. The assistance of numerical analysis and artificial intelligence in this process is invaluable for the following (and other) reasons:

1. Because the optimization of an LC separation involves many potential parameters, a structured approach in both their selection and their adjustment is needed to avoid unnecessary experiments and to reduce the time required for method development.
2. Most mixtures contain more than two components, and changing the conditions may affect the retention of each of these in a different way. This will result in changing selectivities for each pair of analytes, and the computer is able to efficiently keep track of this.
3. When appropriate retention models are available, it is possible to predict chromatograms within a given range of parameter values. In this way, laboratory experiments are replaced by computer simulations that require only a fraction of the time to perform.
4. When it is known how the separation is affected by variations in the experimental conditions, the stability or ruggedness of the separation under the selected conditions can be estimated. In addition, it is often possible to predict how to change in instrumentation will affect the separation, thus assisting in technology transfer.

The foregoing considerations will be illustrated in the following sections. In Section IV. A we will emphasize the general principles and terminology underlying most computer-assisted approaches. One specific issue, the evaluation of chromatograms, will be dealt with in Section IV. B. Algorithms and applications involving gradient elution are discussed in Section IV. C, and the optimization of isocratic conditions is explored in Section IV. D.

A. General Considerations

During every optimization process, three aspects need to be considered: (1) the definition of the parameter space, (2) the definition of the response, and (3) the approach followed to search the parameter space for the conditions that result in the maximum response. These three elements are also encountered during the optimization of selectivity in liquid chromatography, as illustrated in Fig. 7 and 8.

The first step in the optimization process is the selection of the appropriate parameters. Some of the parameters typically considered in liquid chromatography are listed in Table 1 [92]. Typically, the selection is based on some knowledge of the sample. This may include analyte polarity, presence of ionizable groups, and such, as well as constraints imposed by the results of the method-selection step (Fig. 6). For instance, if the separation will be based on differences in the hydrophobicity of nonionizable compounds, the selected parameters for a reversed-phase separation will most likely be the type and percentage of organic modifier. If the presence of ionized compounds is expected, the type and concentration of an ion-pairing

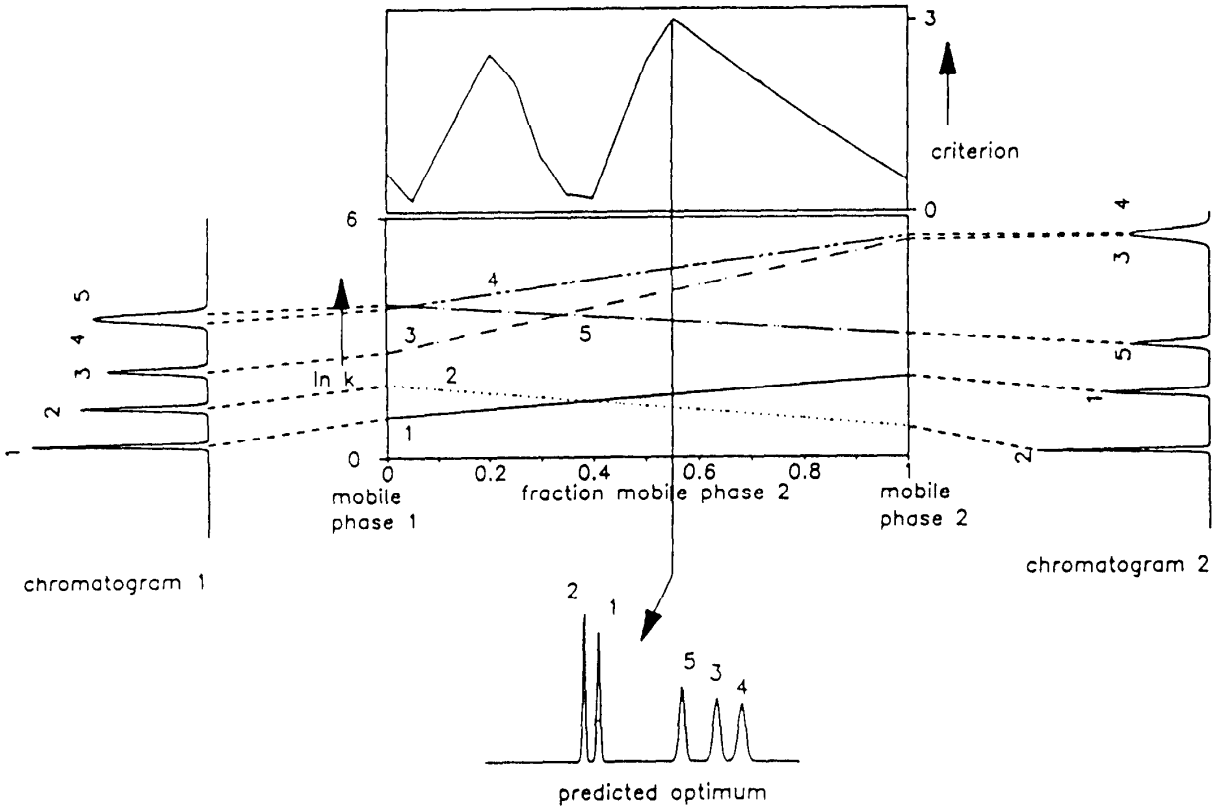


Figure 7 Example of a one-parameter optimization using an interpretive approach. By using the retention times observed in two chromatograms (numbered 1 and 2) and applying a linear model, retention times at other mobile-phase compositions are predicted. The quality of the predicted chromatograms is quantified using a criterion (minimum resolution in the chromatogram). This results in the response surface shown in the top panel. (From Ref. 155.)

reagent are appropriate parameters. The choice is ultimately made on the basis of whatever knowledge is available about the sample composition, combined with the experience of the chromatographer. A first-guess expert system may also be used.

The number of optimization parameters considered is an important characteristic because the amount of experimentation required to describe the retention behavior in a given system often increases exponentially with that number. Figure 7 illustrates an example of a one-parameter optimization. It shows how the retention of a set of compounds is expected to vary as a function of the mixing ratio of two mobile phases. Note that the dimensionality of this problem is 1, the only parameter being the fraction of mobile-phase 2 in the mixture. Figure 8 shows an example of a two-parameter optimization, taken from the area of micellar liquid chromatography (MLC) [56]. The two parameters are the concentration of the surfactant and the amount of organic modifier, 2-propanol. Because these two concentrations can be selected independently from each other, the dimensionality is 2.

The selection of the parameters is followed by the definition of a range of values that will be considered. The limits will be defined based on the expected behavior of the sample and practical considerations. Again, expert systems can assist less-experienced chromatographers. The set of all possible combinations of the parameter values evaluated in the optimization is generally referred to as the *parameter space*. Every point in the parameter space uniquely defines a set of chromatographic conditions that correspond to a chromatogram.

For example, the limits in Fig. 7 for the fraction of mobile phase 2 are 0 and 1, corresponding to pure mobile-phase 1 and pure mobile-phase 2, respectively. The parameter space

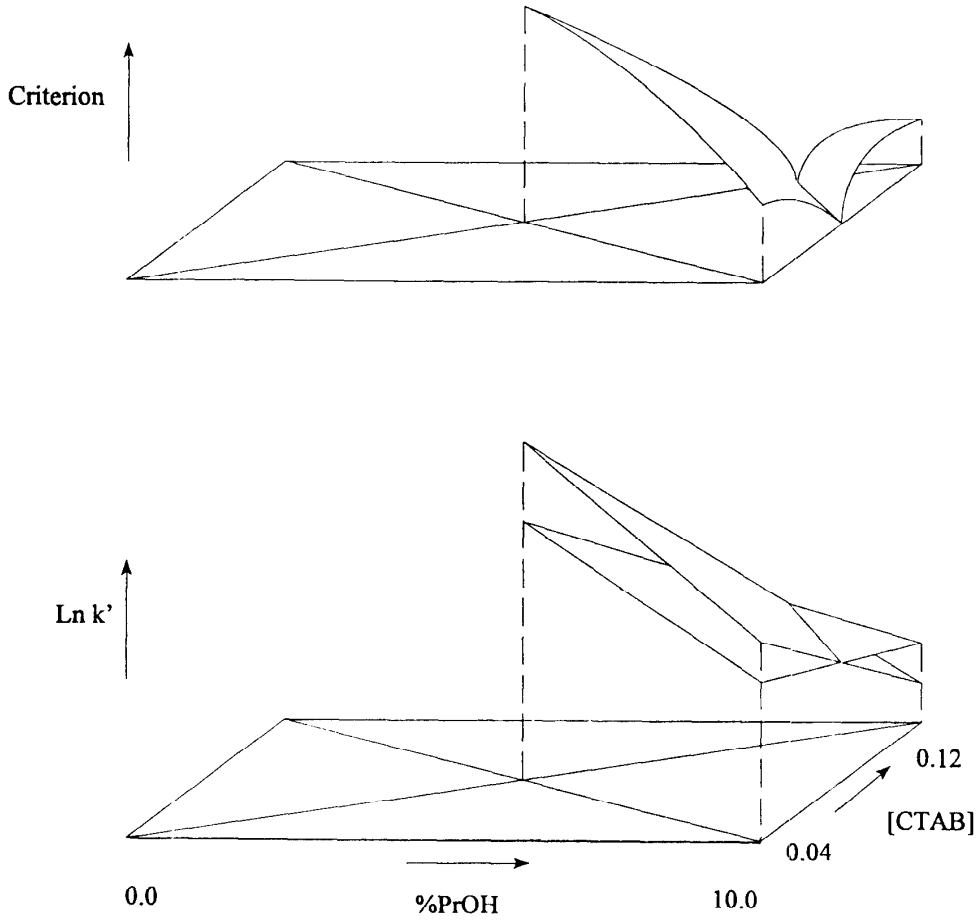


Figure 8 Example of (part of) a two-parameter optimization using an interpretive approach. The parameter space is defined by the concentrations of 2-propanol (%PrOH) and that of a cationic surfactant ([CTAB]). The bottom panel shows the expected retention behavior of two components in a section of the parameter space, based on three observations (dashed lines). The top panel shows the resulting response surface defined by a criterion (minimum resolution in the predicted chromatogram).

Table 1 Typical Parameters Considered for the Optimization of Selectivity in Liquid Chromatographic Separations

Type of organic solvent
Percentage of organic solvent or gradient profile
Column type (stationary phase)
Temperature
pH
Type and concentration of ion-pair reagent
Concentrations of additives (buffer, salt, amine modifier)

in Fig. 8 is defined to include surfactant concentrations from 0.04 to 0.12 mM, and organic modifier concentrations from 0 to 10% of isopropanol. These limits are based on practical considerations, such as the minimum required elution strength, the critical micelle concentration of the surfactant, the solubility of the surfactant, and the viscosity of the mobile phase.

The next aspect of computer-assisted optimization procedures is evaluation of the observed or predicted chromatograms. To use the results of experiments and to advise the user on the direction in which to adjust the conditions, the computer requires that the chromatograms be assessed in quantitative terms. It is often very difficult to establish that one chromatogram is "better" than another, let alone to derive a quantitative measure for the term *better*. This complication is partly because several considerations, such as resolution and analysis time, are considered. The measure for quality is generally referred to as a *criterion*, and the goal of the optimization procedure is to find those conditions that correspond to the maximum (or minimum) criterion value.

For instance, an often-applied criterion is the minimum resolution, $R_{s,min}$. This is the lowest resolution value encountered in the chromatogram. To optimize the separation, the process is aimed at maximizing $R_{s,min}$. The observed or expected criterion value is referred to as the *response* for a given set of chromatographic conditions. The collection of criterion values as they are located in the parameter space is called the *response surface*.

The top window of Fig. 7 shows the value of $R_{s,min}$ as a function of the fraction of mobile-phase 2, which represents a one-dimensional response surface. The complete coelution of compounds will give rise to an $R_{s,min}$ value of 0; consequently, to a minimum in the response surface. The top half of Fig. 8 displays a two-dimensional response surface for part of the parameter space of the MLC separation. Again, well-separated peaks result in a high criterion value, whereas coelution results in a minimum in the response surface.

The foregoing considerations are valid for every optimization procedure applied in liquid chromatography. The differences between the various approaches can be traced to how the response surface is estimated and to how the response surface is searched for either an acceptable separation or for the global optimum. The *global optimum* on a response surface is that set of conditions that corresponds to the maximum criterion value throughout the parameter space, as opposed to a local optimum, which corresponds to an optimal criterion value in a limited section of the parameter space. Because the elution order of the analytes often varies with the experimental conditions, local optima are a frequently encountered phenomenon in method development for liquid chromatography.

Some optimization procedures require a substantial amount of experimental work, which includes grid-search methods and sequential optimization procedures (see Sec. IV. D). The more versatile strategies applied for the optimization of liquid chromatographic separations require less experimental input. These are known as *interpretive* strategies. As indicated earlier, the order of peaks will change frequently when varying the experimental conditions. This results in local optima and minima on the response surface. However, the retention behavior of the individual analytes is much more regular and, therefore, is more amenable to modeling. The result is a retention surface for each analyte, as opposed to a response surface for the separation as a whole. If the retention of the components can be predicted at every point in the parameter space, it is possible to predict the chromatogram at every point. From the chromatogram the corresponding criterion value can be calculated. Thus, the response surface is estimated indirectly. Because of the regular nature of the retention surfaces, interperative strategies require far fewer experiments to obtain accurate estimates. The trade-off is the need to record ("interpret") the retention times of every analyte in every chromatogram. Because it is essential that the peaks in the various chromatograms are matched to each other, but it is not necessary to identify each analyte, this process is generally referred to as peak tracking. Some techniques for peak tracking will be discussed in Section VI.

The implementation of interpretive strategies is illustrated in Fig. 7 and 8. The window in the center of Fig. 7 shows the retention behavior of each individual analyte as a function of the mobile-phase composition. Because this is a one-parameter optimization, each analyte

is represented by a line. Each time two lines cross, there will be coelution of these two analytes, leading to a low criterion value (top window). This figure also illustrates the importance of peak tracking. If incorrect peaks are matched, the predicted retention times and, consequently, the predicted response surface will be incorrect. The bottom part of Fig. 8 shows the expected retention behavior for two components. Because this is a two-parameter optimization, each retention surface is now represented by a plane (often the retention surfaces cannot be represented by straight lines (as in Fig. 7) or planes (see Fig. 8); however, they are typically much smoother than response surfaces), and coelution of two analytes is observed along a line, rather than at a single point. In both cases, the computer steps through the parameter space in predefined small steps and evaluates the response at every point to generate the response surface. Chromatographic experiments are thus replaced by (much faster) computer simulations; the main limitation is the accuracy of the models applied for predicting the retention. The models used to describe retention range from very simple to complex, and from completely empirical to fundamentally correct. For instance, the model used in Fig. 8 is a simple linear model.

$$\ln k' = a_0 + a_1 * [\text{CTAB}] + a_2 * \%\text{PrOH} \quad (8)$$

where a_0, a_1, and a_2 are the constants of the model, [CTAB] is the concentration of the surfactant and %PrOH is the percentage of 2-propanol. Generally, the values of the constants are determined for each analyte by use of multiple linear regression. The advantage of simple models is that few experiments are required to establish the constants. The disadvantage is that simple models do not always provide an accurate description of the retention. In general, models that are based on some physical reality or theory will be more robust [92], especially for extrapolation purposes. In Sections IV. C and IV. D we will discuss some approaches for method development in liquid chromatography in terms of the experimental design and models used.

B. Optimization Criteria

An important aspect of computer-assisted strategies for the optimization of LC conditions is the evaluation of the quality of chromatograms. This forms the basis for creating the response surface. A thorough discussion on the subject of chromatographic optimization criteria is available [53,57,58]. The following is a brief overview of the most relevant aspects and considerations.

The first consideration is which quantity to use to express chromatographic separation, the so-called elementary criterion [58]. As in the foregoing example, resolution is often used for this purpose. The resolution function compares the difference in retention times with the widths of the individual peaks. Resolution can be calculated based on the assumption of simple symmetrical gaussian peak shapes, or their asymmetry and the height of individual peaks may be included [59,60]. If the analytes exhibit comparable efficiencies N, or if N is unknown, the separation factor S can be used. This is an expression for the difference in capacity factors relative to their absolute magnitude. These criteria can be applied when retention times or capacity factors are available across the complete parameter space, as is true in interpretive optimization strategies. Other more empirical elementary criteria are based on peak/valley ratios. These criteria can easily be determined from experimental chromatograms, but they cannot be easily predicted from data on the individual analytes.

The selected expression for separation is applied to all consecutive peak pairs in the chromatogram, resulting in a series of values. These values must be converted into a single number to achieve a workable response surface. In addition this information can be combined with other relevant aspects of the optimization, most commonly the sensitivity and the required analytical time. The easiest approach is to select one of the extreme values of the series, such as the minimum resolution, $R_{s,min}$. However, many other approaches have been proposed. These

include the resolution product and the normalized resolution product [53]. The latter will achieve its optimal value (equal to 1) when all peaks are spread evenly throughout the chromatogram. Criteria that consider only the resolution or separation of peaks are most suitable for those optimization procedures in which the overall analysis time does not vary greatly. This is achieved by a judicious choice of the parameter space, for instance, by using isoeluotropic mobile-phase compositions [57].

Special care must be taken if both separation and analysis time are considered in the optimization. These represent different aspects of the chromatogram which cannot be directly compared. One approach used to consider both aspects is the so-called threshold criterion. These criteria consider only one of the elements describing the chromatographic performance, provided that the other elements are fulfilling a given condition. For instance, the optimization procedure can aim to minimize the analysis time, but it considers only those chromatograms for which the minimum resolution exceeds a given value [58]. Alternatively, the procedure can be aimed at maximizing the number of peaks observed in the chromatogram, while not exceeding a predefined analytical time. Again, only those peaks that exhibit sufficient separation from their neighbors are counted [61,62]. By nature, threshold criteria will yield optima next to a steep drop in the criterion value. For example, the analysis time decreases and the criterion improves until the point that the resolution becomes unacceptable. Therefore, the threshold value must be carefully selected, otherwise a slight change in the conditions may result in unacceptable chromatographic results. Another problem with threshold criteria is that they provide little insight in how to improve the separation if the threshold value is not exceeded under any of the examined conditions. Therefore, this approach generally works best if the optimization is performed on the final analytical column, no adjustment of the particle size or the column length being anticipated [57]. If a system optimization step is planned after the selectivity optimization, additional factors affect the relation between analysis time and resolution.

Instead of a consecutive evaluation of the various characteristics of a chromatographic separation, such as applied in threshold criteria, a simultaneous evaluation can be performed. This is referred to as multicriteria decision making [63,64]. In this approach the optimal value of one aspect, for instance analysis time, is determined for every possible value of one of the other aspects, such as resolution. This provides the user with a firm understanding of the trade-offs between various choices. It is explicitly clear what sacrifice has to be made in terms of resolution to achieve a given analysis time. Because the concept involves a consideration of these trade-offs, part of the decision-making process is transferred back to the chromatographer.

In all of the foregoing approaches, it is possible to apply weights to the peaks in the various chromatograms. This indicates the relevance of achieving optimal separation of the corresponding analyte from other components in a mixture. The use of 1 and 0 for these weights can represent a simple yes or no decision. Thus, it is possible to identify a limited number of components in a mixture that will have to be separated. The weights can be used to identify which pairs of consecutive peaks should be considered. If either the first or the last peak of a pair has a weight of 1, the resolution must be considered. Otherwise it can be ignored. This concept can also be applied to account for system peaks and solvent peaks in a chromatogram. If one wishes to distinguish peaks in terms of relative importance, weights between 0 and 1 can be applied.

From the foregoing, it is clear that the selection and implementation of the appropriate criterion are complex processes. Therefore, it is a logical subject for implementation into an expert system [58,65]. This expert system can guide the user through the selection of the elementary criterion and the best overall "global" optimization criterion. It also advises on the applicability of corrections for nonideal peak shapes and on the use of weights. Required inputs are the selected approach for the optimization and the type of information available from the chromatograms.

C. Computer-Assisted Method Development for Gradient Separations

Software for computer-assisted method development in gradient elution is commercially available. Also, many applications are described in the literature, generally emphasizing a simulation approach [66–74]. Although the response surface, as defined by a simple criterion, such as $R_{s,min}$, is generally provided as a function of the gradient slope, the major purpose of the software is to provide the user with predicted chromatograms resulting from (simulated) changes in the gradient shape, the gradient slope, or the column dimensions. As before, laboratory experiments are replaced by computer experiments, which require far less time, but do provide insight for the relations between experimental conditions and retention, as well as in the ruggedness of a separation. Also, simulations can avoid fruitless investigations of conditions that cannot be expected to provide adequate separation, given the selected experimental constraints. Efforts can thus be directed toward viable alternatives. A true optimization of a gradient separation to determine the location of the global optimum for a given mixture is not easily accomplished. Such a process is usually not supported owing to the many aspects that determine the shape of a gradient (slope, initial and final concentrations of organic modifier, shape, and so on.) This is especially true for multisegmented gradients and for gradients involving more than one organic modifier.

Most of these approaches, including the well-known Drylab/G [see Ref. 66 for a review], are based on the assumption that the logarithm of the capacity factor of a component varies linearly with the concentration of the organic modifier, ϕ.

$$\log k' = \log k_0 - S(\phi - \phi_0) \tag{9}$$

where k_0 represents the capacity factor of the compound at the initial mobile-phase composition, and S is the slope of the linear relation. Equation (9) is valid for a large number of components, especially in the range of organic modifier concentrations for which the actual elution takes place during the gradient. The linear–solvent-strength approach, as developed by Snyder and co-workers [75] is based on a linear gradient, which defines the composition of the mobile phase at time t, $\phi(t)$, as

$$\phi(t) = \phi_0 + \left(\frac{\Delta\phi}{t_g}\right) t \tag{10}$$

$\Delta\phi$ is the difference between the final and initial (ϕ_0) concentrations of organic modifier and t_g is the gradient time (i.e., the time that elapses before the final concentration of the organic modifier is reached). Combining the two equations results in

$$\log k'(t) = \log k_0 - b\left(\frac{t}{t_0}\right) \tag{11}$$

with

$$b = \frac{V_m \Delta\phi S}{t_g F} \tag{12}$$

where V_m is the void or hold-up volume, t_0 the corresponding void time, and F the flow rate of the mobile phase. b is referred to as the gradient steepness. The retention of a component in a gradient method is largely determined by the gradient steepness. Equation (11) is an expression for the capacity factor of a component as a function of the elapsed time t. To predict the retention time, we will have to determine the progress through the column for each time segment dt. Because the time spent in the mobile phase during this time segment equals $dt/k'(t)$, the retention time under gradient conditions, t_r, can be found from the following integration:

$$\int_0^{tr-t0} \frac{1}{k'(t)}\,dt = t_0 \tag{13}$$

After substitution of Eq. (11), performing the integration and solving for t_r yields

$$\begin{aligned} t_r &= \frac{t_0}{b}\,[\log(2.3\,k_0\,b + 1)] + t_0 \\ &= \frac{t_0}{b}\,[\log(2.3\,k_0\,b)] + t_0 \end{aligned} \tag{14}$$

To accurately predict the gradient retention time for a component additional aspects of the chromatographic system must be taken into consideration. One such aspect is the dwell time (i.e., the time it takes for the gradient to arrive at the head of the column).

From these equations it follows that it is possible to predict the gradient retention time of a component on the basis of several instrument parameters, such as the void time (or void volume) and the dwell volume, and two characteristic values, k_0 and S, for each component in a mixture. Assuming the instrument parameters are known, it requires at least two experiments to define these two characteristic values. These experiments usually consist of two gradient runs with different slopes. To reduce the effect of experimental error on the values obtained for k_0 and S, the selected slopes should differ significantly. Generally a difference of a factor of 3 is recommended. The chromatographic separation can thus be predicted over a wide variety of experimental conditions on the basis of two initial experimental runs. If some of the instrumental parameters are not readily available, it is often possible to obtain a reasonable estimate by performing a third gradient run and by minimizing the difference between the predicted and observed retention values for this third run while varying the unknown instrument characteristics [74].

Once the values of k_0 and S have been established for the components in a mixture, more complex gradient shapes, such as segmented and step gradients can be simulated [69]. The retention under these conditions can be predicted, but these predictions may be less accurate than for simple linear gradients. This is due to deviations in the mobile-phase composition from the expected value because of dispersion of the gradient [76]. This dispersion is dependent on the mixing volume of the equipment, with smaller volumes resulting in more accurate predictions.

The parameter that is primarily optimized in gradient elution is the slope or steepness, represented by t_g in Eqs. (10) and (12) (a longer gradient time corresponds to a lower slope and results in longer retention). This parameter is the most logical choice, because it has the most profound effect on the retention and selectivity. A second parameter that can be considered is the initial percentage of the organic modifier, $\%B_i$. If the S values of all the components in a mixture are similar, increasing this percentage results in a reduction of the analytical time, while maintaining the separation. However, for certain samples, adjusting $\%B_i$ will also affect the separation. The simulation approach does not automatically provide the optimal $\%B_i$, but it does allow screening of the effect of this parameter to estimate a value that provides a dependable, rugged separation [77].

More formal approaches to simultaneously optimize the slope and the $\%B_i$ have also been described. For instance, a three-level factorial design was applied to establish the retention as a function of the two parameters [78]. The retention times of all mixture components are measured at three levels of both the gradient time and initial solvent composition, resulting in nine values for each component. An empirical model fitted through these nine observations is then used to predict the retention at other values of the two parameters, that is,

$$t_r = a_0 + a_1 \times t_g + a_2 \times \%B_i + a_{11} \times t_g^2 + a_{22} \times \%B_i^2 + a_{12} \times t_g\,\%B_i \tag{15}$$

where a_0, a_1, a_{11}, a_{22}, and a_{12} are the coefficients resulting from the fitting procedure. The last term of this equation involving both parameters is referred to as an interaction term. The

model of Eq. (15) or of a similar equation can also be used to optimize the resolution as a function of $\%B_i$ and t_g by providing a response surface that incorporates both parameters [79,80]. This approach was extended to optimize multisegmented gradients. First, the components in the chromatogram are divided into closely eluting groups. Second, the gradient segment used to separate the first group is optimized. Third, the next segment of the gradient is adjusted to optimize the separation of the second group of components, and so on. If no satisfactory separation of a group can be obtained, the algorithm can backtrack to investigate alternative parameters for earlier segments. Although this sequential approach does not result in a global optimum, it will achieve an acceptable separation, when possible.

The optimization of gradients involving more than one organic modifier can be very complex, owing to the many parameters that can be varied. The simulation approach described in the foregoing can be used to obtain some information on the effect of combinations of organic modifiers by using a mixture as the strong eluent. This can help direct the search toward the appropriate mobile-phase program [81], but it will not assist in determining the optimal mixing ratio. Alternative, more structured approaches have been described [80] but these are not easily implemented. The foregoing treatment was focused on gradients in reversed-phase liquid chromatography, but the principles can also be applied to other forms of liquid chromatography, such as ion-exchange [82] and micellar liquid chromatography [83].

D. Computer-Assisted Method Development for Isocratic Separations

During the last 10–12 years, several approaches to the computer-assisted optimization of isocratic separations has been described [40,53–55]. Again, some of these methods involve a simulation of the chromatographic separation at the various settings of the parameters within the parameter space examined. Other approaches aim to find the best separation possible in a given parameter space with little user interaction.

Often the optimization focuses on the mobile-phase composition. This can range from the concentration of a single organic modifier in an aqueous mobile phase (binary mixture) to mixtures involving two or three organic modifiers (ternary and quaternary mixtures, respectively). Optimization of binary mixtures by nature involves modification of the elution strength, along with possible variations in selectivity ("solvent strength selectivity"). For the ternary and quaternary mixtures it is possible to restrict the parameter space to mixtures that provide comparable elution strength (so-called isoeluotropic mixtures) Alternitively, the parameter space may cover a range of elution strengths (Fig. 9).

The distinction between the various approaches is the way in which the experiments are distributed over the parameter space. This determines whether a model (and which one) will be fitted through the observations.

A straightforward strategy that has been applied is a simple grid search [84]. The parameter space is spanned by a grid of experiments at specified intervals. The results of all experiments are evaluated separately, and the best conditions can be selected without implementing a retention model. The closer the points are on the grid, the higher the chance of finding the true global optimum. Although this method requires a fairly large number of experiments, the use of fully automated equipment and chromatography optimized for speed (employing short columns and high flow rates) have made its application feasible. In addition, there is less chance that a global optimum will be missed if the results of several selected experiments can be used as input in one of the more advanced modeling approaches. The results of a grid search can also be used to evaluate a method's ruggedness.

Sequential approaches, such as the simplex method, have also been investigated [85]. The results of a few experiments are used to locate the next experiment in the parameter space, in the direction in which the value of the criterion increases. This process continues until no further improvement in the separation is obtained. The quality of the separation is evaluated for each experiment, and no retention model is developed. Therefore, reversals in the elution

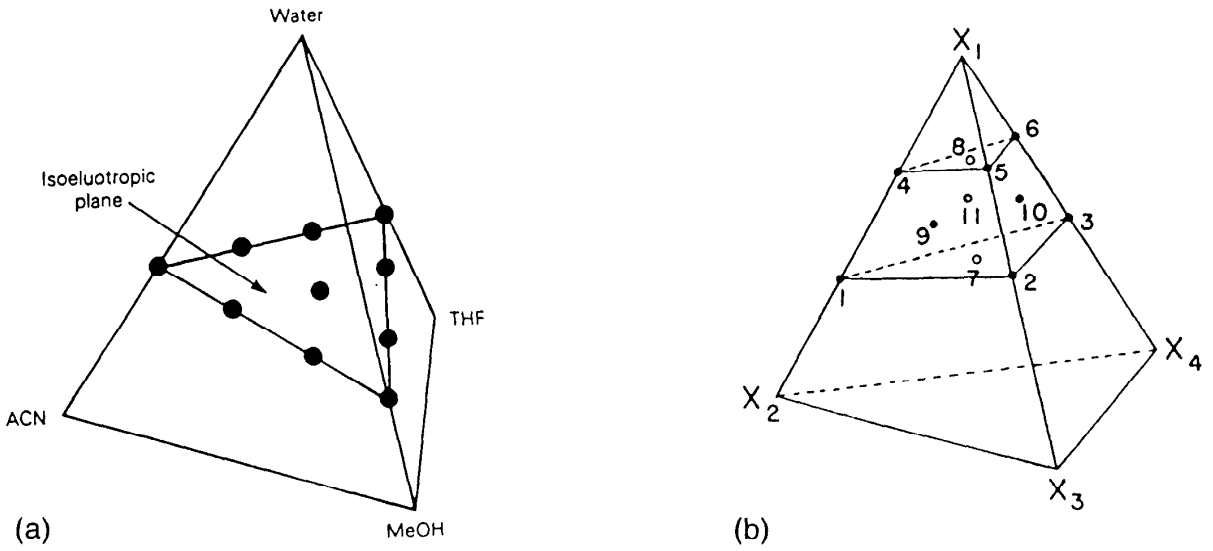


Figure 9 Two possible designs to model retention behavior as a function of mobile-phase composition: (a) All experiments use mobile-phase compositions of similar elution strength. (i.e., isoeluotropic mixtures). (b) The experiments are spread over a larger area of the parameter space so that the results will exhibit variation in both retention and selectivity. X1, water; X2, methanol; X3, ACN; and X4, THF. (From: (a) Ref. 98, (b) Ref. 88.)

order are not detected. This sort of method can require a fair number of experiments and is likely to result in a local, rather than a global, optimum.

As discussed in Section IV. A, interpretive methods involve fitting a retention model through the data obtained from a limited number of experiments covering the parameter space. Such a model is determined for each component in a mixture. The location of the experiments can be based on traditional experimental designs, such as a two-level factorial design. The two levels will correspond to a higher and lower concentration of each of the organic modifiers. Evaluation of other parameters, such as column temperature, is easily accomplished [86]. A two-level factorial design will allow linear models with interaction terms to be used. The more complex uniform shell, or Doehlert design, has also been applied in HPLC. This allows the fitting of second-order model [87]. In general, designs in which the experiments are defined by the mobile-phase compositions are referred to as mixture designs. The number of parameters related to the overall mobile-phase composition is always one lower than the number of components, because the concentration of the last component follows from that of the others. Some examples of mixture designs are shown in Fig. 9 [88–90].

The design and the selection of the associated retention model is affected by the type of chromatography and by the parameters being optimized. For instance, optimization of the organic modifier concentration in a binary mixture can be accomplished by applying the simple linear model of Eq. (9) [91–93]. Consequently, the experimental design can consist of two initial isocratic experiments to establish the values of k_0 and S for each solute. As indicated in Section VI. C, similar information can be obtained by running two initial gradient runs. Alternatively, the results from one gradient and one isocratic run can be combined to obtain these values [94]. However, when ternary or quaternary mixtures are being considered, higher-order polynomial models are generally applied [92,95,95]. These models require a larger number of initial experiments. Alternatively, empirical linear models with interaction terms have been applied [86,88].

One of the obstacles to fitting a higher-order polynomial model across the entire parameter space is the occurrence of significant errors in the predicted retention times. In addition, the

retention predicted at locations at which experiments have been performed does not necessarily equal the observed retention times [97]. To circumvent this problem, a simpler model can be used over a restricted area of the parameter space. This is referred to as piece-wise linear or quadratic interpolation and it is implemented in various approaches [98–100].

Piece-wise linear interpolation is often combined with iterative approaches [97,101,102]. Rather than trying to accurately describe the entire retention surfaces by using a number of experiments and a complex model, a minimum number of combined experiments and a simple model are used to approximate these surfaces. The most promising area of the response surface is then examined in more detail by performing additional experiments and by adjusting the model through linear interpolation. The process is repeated until no further improvement in the model can be expected.

The foregoing strategies have also been applied to optimize parameters other than mobile-phase composition. For some parameters the applied models can be based on theoretical or phenomenological models. For instance, by using the theory of acid–base equilibria a model can be derived that expresses the capacity factor k' of an acidic component as a function of pH [103,104].

$$k' = \frac{k_n + k_{-1}\,(K_a/[H^+])}{1 + (K_a/[H^+])} \tag{16}$$

where k_n is the capacity factor of the uncharged solute, k_{-1} is that of the ion, and K_a the dissociation constant in the mobile phase under consideration. Even though this model is strongly nonlinear, a reliable fit can be obtained from a few initial experiments, provided these experiments cover the appropriate section of the parameter space. Reliable values for the three constants in Eq. (16) can be obtained only if retention data are available for a component in all three regions of pH values: at least one measurement in the region at which the component is mostly uncharged, one measurement in the region at which the component is mostly dissociated, and one measurement in the region at which both species are present. If these criteria are met, a reliable model can be obtained and the retention times can be predicted over the entire practical range of pH values.

Optimization of the mobile phase can be combined with optimization of other parameters, such as the pH, ion-pairing reagent concentration, or temperature [104–110]. The major issue is whether interactions occur between these parameters: that is, does a change in the value of one of the parameters affect the system's responses to changes in another parameter? One way to deal with interactions is to increase the complexity of the design, adding a number of appropriately located experimental data points to the fitting procedure. This design must be combined with a more complex model [104,105] or with an iterative approach based on piece-wise linear interpolation (107). This will allow prediction of the retention times over a wide range of possible experimental conditions. Alternatively, the parameter space may be restricted to such a size that the interactions between the parameters can be neglected. Then, the number of experiments is reduced; for example, in a linear model for a given parameter only one additional experiment is needed to describe the behavior of a component in the proximity of an initial data point [109,110].

V. METHOD VALIDATION

The validation of a liquid chromatographic method is an integral part of the method development cycle (see Fig. 6). In general terms, the validation is intended to show that a method can be used within a specified range of conditions. This goal can be achieved by a systematic evaluation of the various characteristics and potential influences. The process involves the investigation and documentation of the selectivity, precision, accuracy, sensitivity, and ruggedness of a method. The level of detail in investigating these aspects will depend on the purpose of the method. If a method is part of the characterization of products that require a high level of quality control and regulation, such as pharmaceuticals, every aspect of the

method must be fully documented. Similarly, if a method will be applied at multiple sites by a variety of analysts, ruggedness testing is in order. In these circumstances, the cost involved in validating a method can become a major part of the overall costs of method development. Therefore, improving the efficiency of this process through computer-assisted data analysis or evaluation is actively pursued.

At a basic level, computer-assisted analysis is provided to perform the necessary calculations for various aspects of the validation process. This is mostly aimed at quantitative measures, such as precision, accuracy (recovery), robustness (retention reproducibility), resolution, or others. Most software packages used for the computer control of LCs contain routines for the calculation of system suitability parameters [111]. System suitability tests are designed to show that an instrument is functioning as required for a given application. Therefore, they can be viewed as a subset of the validation experiments. Computer control can also be used to extend system suitability testing to the actual time of the analysis [112]. When bracketed standards are run at 50, 100, and 150% of the normal level, the computer-generated quantitative results can be used to monitor all of the aforementioned method characteristics.

One of the issues encountered in establishing the selectivity of a method is the determination of peak purity. With the current generation of rapid-scanning UV detectors, the spectral data collected during the elution of a chromatographic peak can be subjected to various forms of multivariate analysis to establish whether coelution is occurring [see e.g., Ref. 113 and references cited therein]. This is discussed further in Section VI.

However, the method validation process is not just a quantitative exercise. The design of a validation test can be subdivided into the following steps [114,115]:

1. Definition of the method characteristics to be tested, such as precision, accuracy, or other.
2. Definition of the actual test to determine each method characteristic (e.g., repeatability testing to establish precision).
3. Selection and execution of an experimental design to obtain the necessary information.
4. Evaluation of the results of the experiments. This includes the application of pass/fail criteria and the diagnosis of problems that are encountered.

Again, the combination of heuristic knowledge and quantitative aspects in the form of well-defined algorithms needed to perform the foregoing steps is best handled by expert systems. This is especially true if the entire liquid chromatographic method is considered, including the sample preparation. As part of the Expert Systems Applied to Chemical Analysis (ESCA) project two expert systems were developed to assist in those aspects of the method validation process that are affected most by this combination of heuristic and algorithmic knowledge (i.e., repeatability testing and ruggedness testing) [114].

The system developed for repeatability testing [115] advises on the number and type of tests to be performed to characterize the precision of sample preparation or sample injection. The various factors that are considered involve the purpose of the method, the number of samples that will be run, the number of laboratories, and such. The real power of the expert system is in the evaluation of the results of the tests. It first calculates the relative standard deviation associated with the various chromatographic characteristics, such as peak area, peak height, retention time, and peak shape. Then, pass/fail criteria are applied, outlier tests are performed, and potential causes of observed problems are identified to assist the user in troubleshooting. The observed problems fall into either of two categories. Some problems, for instance insufficient resolution, will necessitate reoptimization of the method. In this case feedback to the system optimization routines is provided. Alternatively, the results may indicate that maintenance of the chromatographic system is required.

Ruggedness testing of a method is generally more involved, because it evaluates the performance of a method under the influence of macroscopic variations in the conditions. It is determined how the method is affected by slight variations in experimental conditions, such as mobile-phase compositions, temperature, and so on. Because a chromatographic method may be affected by a myriad of factors, a considerable amount of expertise is required to

design an efficient testing procedure. If systematic interpretive optimization procedures have been applied, such as those described in Section VI, the chromatographer will often be able to evaluate the ruggedness of a method, relative to the factors that have been varied during the optimization procedure, from an inspection of the computer-generated response surface. If the selected conditions are located in a flat region of the response surface, the effects of a slight variation in the parameters will be minimal. Conversely, if the selected optimum is on a sharp ridge it will be more difficult to maintain the quality of separation under practical conditions.

However, the optimization procedure will be limited to those parameters that have the strongest influence on the chromatographic behavior of the solutes in terms of the desired analytical criteria, such as resolution and analysis time. The robustness of the method ideally has to be established for all factors that might affect its performance. Although, with sufficient expertise, this number of factors can be reduced, it will still be much larger than the number considered in the optimization. Efficient experimental designs are required to minimize the amount of experimental work required. In this area, expert systems will be particularly useful, especially for less-experienced chromatographers [116–119]. The expert system assists in identifying the critical factors for all aspects of the liquid chromatographic analysis. It then advises on the most efficient experimental design to test the effect of variations in these factors. The latter requires a significant amount of knowledge in the area of statistics that will not be readily available to many practicing chromatographers. They will thus benefit from the assistance provided by an expert system.

VI. ADVANCED DATA ANALYSIS

As is true in many areas of analytical chemistry, the increased use of computers and digital analysis in HPLC has not only increased the efficiency and reduced the workload. It has also extended the capabilities of the technique by enabling more sophisticated data analysis. Modeling of the different steps of the analysis, ranging from the sample preparation [see e.g., Ref. 120], to detector response [see e.g., Ref. 121], facilitates the prediction of the performance under different conditions. This forms the basis for understanding and optimization. Modeling of the retention behavior of solutes under varying conditions can be used to derive chemical and physical characteristics, such as pK_a values [122]. The results of the HPLC analysis can be combined with those of other analytical techniques to detect patterns that are not immediately obvious from an examination of the data derived from any individual technique. Often, the identification of components is not necessary. Retention times and peak areas can be used in a correlation analysis of many samples to establish underlying relationships (or the lack thereof) in terms of origin, composition, and so forth [123–125].

The availability of fast and inexpensive computers has also enabled chromatographers to handle the enormous amounts of information that are generated by combining LC separations and multichannel detectors. These hyphenated systems extend the selectivity of the analysis, but they require full computer control if the maximum benefits are to be obtained from the generated data streams. Probably the most widely available form of hyphenation in liquid chromatography is the LC–UV combination employing a diode-array detector. The ability of these detectors to record complete UV spectra in the fraction of a second puts high demands on the digital control and even higher demands on the data reduction software. The latter is needed to present the results in a useful fashion to the chromatographer. Other forms of hyphenation are also available or under development, such as LC–MC and LC combined with potential swept electrochemical detection [126]. The methods used for data analysis will parallel those used for LC–UV, provided some requirements are fulfilled (as described in the following).

The data analysis applied to signals generated by a chromatographic system can be broadly divided into two areas. One approach is to concentrate on one domain at a time. This univariate approach can be applied to either the chromatographic trace, using time as the

domain, or the output of the detector at a given point in time. An example of the latter would be a further analysis of a UV spectrum generated by the diode array. Wavelength is then the domain examined. Alternatively, multiple domains can be investigated simultaneously, using advanced multivariate statistical analytical techniques.

A. Univariate Data Analysis

The reason for further manipulation of the recorded chromatographic trace in the time domain (the chromatogram) is to extract more or better qualitative and quantitative information, while simultaneously performing a data reduction step. The applied techniques range from a simple reduction of the noise component, by means of a digital filter, to deconvolution of strongly overlapping bands by means of curve fitting.

Detecting peaks in a chromatogram (or any other signal) is not a trivial matter [127], especially when the signal/noise (S/N) ratio is low. The latter can be improved either by time-averaging or by smoothing. Time-averaging is based on the principle that the addition of N measurements of a given signal will enhance the deterministic portion of the signal by a factor of N, whereas the noise components will increase by only a factor of $\sqrt{N}$. The result is an improvement in the S/N by factor of $\sqrt{N}$. Although this technique is more generally applied in spectroscopy, it can be used in LC as well [128]. By repeating the LC analysis a number of times and then adding the various chromatograms, the desired signal/noise improvement is achieved. A practical implementation of this approach is possible only if a very good retention time reproducibility is maintained, whereas the analytical time needed for each individual separation should be short.

Smoothing with a digital filter can be applied if the data have been collected at a predetermined, uniform sampling rate. A simple way to reduce the noise in the signal is to apply a moving average, in which each data point is replaced by the average of the surrounding observations:

$$Y_i = \frac{\sum_{j=-m}^{m} y_{i+j}}{2m + 1} \tag{17}$$

where Y_i represents the data point after the smoothing operation over $2m + 1$ original data points, denoted by y_i. This is, in fact, a special case of a convolution.

$$Y_i = \frac{\sum_{j=-m}^{m} (y_{i+j} h_j)}{\sum_{j=-m}^{m} h_j} \tag{18}$$

where h is the convolution function. In the case of a moving average, all element (h_j) of this function over the width of the window $2m + 1$ have the value of 1. Convolution functions aim to reduce the amount of noise as much as possible, without distorting the actual signal. Some well-known convolution functions that achieve this goal have been derived by Savitzky and Golay [129]. These functions are based on polynomial fits of a given degree and for a given width of the window. One of the great advantages of their approach is that higher-order derivatives of a signal can be obtained from the smoothing operation by selecting the proper convolution function.

Filtering in the frequency domain has also been described [130]. The chromatographic signal consists mainly of low frequencies. By means of a Fourier transformation it is separated from the noise component present in the higher frequencies. The result is an improved signal/noise ratio.

Digital analysis in the time domain can also be used for a numerical deconvolution of strongly overlapping peaks. A straightforward approach is to perform a least-squares curve-fitting procedure, using chromatographic profiles of the individual components. At any given time t, the observed detector signal $A_{p,t}$ can be written as a linear combination of the individual profiles A_1 and A_2.

$$A_{p,t} = (c_1 A_{1,t}) + (c_2 A_{2,t}) \tag{19}$$

Over all timepoints this is a set of equations, that can be rewritten in vector- and matrix-notation as:

$$\boldsymbol{A}_p = [\mathrm{A}]\, \boldsymbol{c} \tag{20}$$

where $\boldsymbol{A}_p$ represents the combined chromatographic profile, [A] is a matrix with the individual peak profiles as columns, and $\boldsymbol{c}$ is a vector defining the contributions of the individual profiles. As long as the number of time points t exceeds the number of components, this is an over-determined system. The calculated profile $\boldsymbol{A}_p$ can be compared with the observed profile $\boldsymbol{B}'_p$, and the difference can be expressed as a sum of squares, SS.

$$\mathrm{SS} = \sum_{t=1}^{n} (\boldsymbol{B}_{p,t} - \boldsymbol{A}_{p,t})^2 \tag{21}$$

The contributions of the individual profiles in $\boldsymbol{c}$ can now be adjusted such that SS is minimized. The solution to this least-squares problem is given by the so-called pseudo-inverse matrix.

$$\boldsymbol{c} = ([\mathrm{A}]^T [\mathrm{A}])^{-1} [\mathrm{A}]^T \boldsymbol{B}_p \tag{22}$$

The deconvolution is illustrated in Fig. 10. One of the assumptions made is that there is no variation in the peak shapes or the retention times of the components between the combined trace and the individual profiles. Through the least-squares minimization, any shift in the profiles will contribute to an error in the values found for $\boldsymbol{c}$, and thus in the estimated concentrations of the components. This can be partially circumvented by introducing an additional variable that represents the shift in profiles relative to the standard profiles [131]. However, a nonlinear algorithm is needed to determine the optimal value for this shift. Rotunno [131] describes an alternative approach to determine the optimal concentration values for a given shift in the profiles, using a so-called Kalman filter.

If the individual profiles are not known, a deconvolution of overlapping profiles is still possible. However, assumptions of a model for the peak shape must be made. A simple model is the gaussian one, which is defined by a standard deviation (or width) and a central moment, in our case the retention time. Because the gaussian model itself is a nonlinear function, fitting a combination of unknown gaussian profiles to an observed chromatographic profile is usually performed by means of a nonlinear least-squares procedure, for instance, the Marquardt algorithm [132]. Such an algorithm searches for the optimal combination of the parameters (peak widths and retention times for all components) by evaluating the change in a least-squares criterion [see Eq. (21)] as a function of changes in the parameter values. The assumption of a symmetrical gaussian peak shape, however, can introduce significant errors in the estimated values for plate count, and resolution. More complex, but more realistic, peak shapes have also been used, such as the exponentially modified gaussian profile (EMG) [133,134]. Obviously, the introduction of additional degrees of freedom in the shapes of the profile (i.e., the asymmetry introduced by the tailing factor in the EMG) further complicates the curve-fitting procedures.

Many of the techniques applied to chromatograms are used similarly in other domains, most notably on UV spectra obtained by scanning or photodiode-array UV detectors. Both smoothing and filtering have been applied, as well as spectral deconvolution using the spectra of the pure compounds (see also the next section). Because the distinctive features of UV spectra are somewhat limited, various methods have been applied to enhance minor features in the spectra. Examples include difference and second-derivative spectroscopy [135,136]. Again, higher-order derivatives can easily be calculated by means of convolution functions.

The use of UV spectra to identify LC peaks has created a need for library searching, for the retrieval of identical or similar spectra from a collection. Again, because of the limited number of distinctive features in UV spectra, the libraries will generally be smaller than the extensive (commercial) libraries available for infrared (IR) and nuclear magnetic resonance

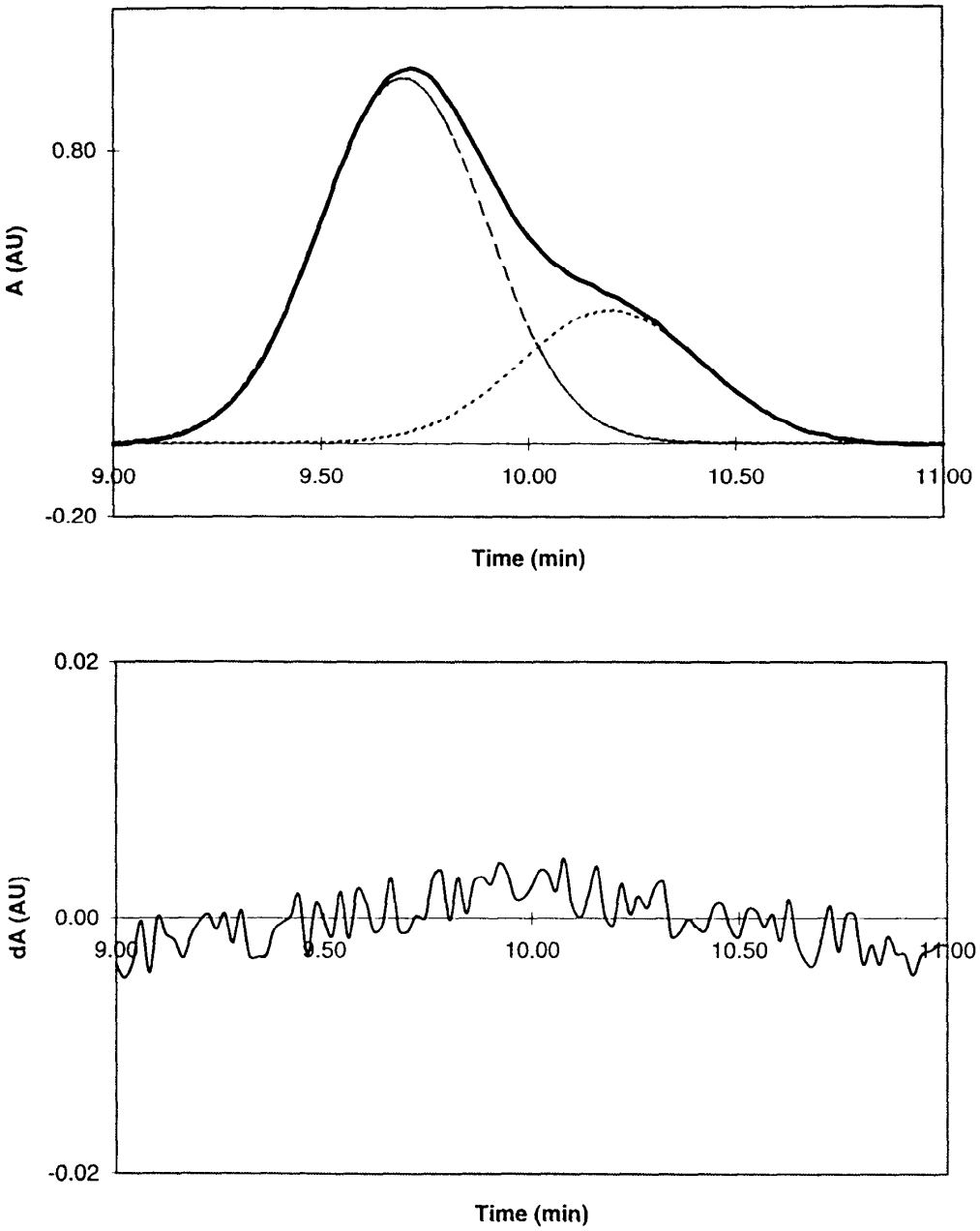


Figure 10 Two gaussian profiles (dashed lines) fitted to an observed chromatographic profile (solid line, top panel) to estimate the contributions of the individual components. The bottom panel shows the minimized difference d*A* between the observed profile and the sum of the two gaussian profiles.

(NMR) spectroscopy and for mass spectrometry (MS). The UV spectral libraries are usually dedicated to a specific sub-set of chemical substances. Thus, the emphasis on search algorithms is shifted from the efficient screening of large numbers of spectra, to a thorough comparison of complete spectra. The often minute differences between similar compounds need to be enhanced. The retrieval of UV spectra from a library for the identification LC peaks is further complicated because the experimental conditions can significantly impinge on the spectral characteristics. For instance, the type of organic modifier or the pH of the mobile phase can affect the location and intensities of the bands in the spectra. Library spectra have to be

recorded under similar circumstances to permit a correct identification. An excellent overview of the different ways to compare UV spectra and of the factors affecting the results is available [137].

A comparison of UV spectra usually involves some kind of point-to-point comparison of normalized spectra. The normalization has to take place to remove concentration effects. The results of the comparison are then summarized in one number to express the similarity (or dissimilarity) of the spectra. Often the similarity between spectra is expressed by means of a correlation coefficient [see e.g., Ref. 138]. Its value is calculated from the line resulting from a linear regression through the points representing the absorbances at the same wavelengths in the two spectra x and y values. Thus, the correlation coefficient r is given by:

$$r = \frac{\sum_{i=1}^{n} (a_i - a_{\text{avg}})(b_i - b_{\text{avg}})}{\sqrt{\sum_{i=1}^{n} (a_i - a_{avg})^2 \sum_{i=1}^{n} (b_i - b_{\text{avg}})^2}} \tag{23}$$

where a_i and b_i represent the absorbance observed in the two spectra at wavelength i, and a_{avg} and b_{avg} are the average absorbance values for each spectrum.

Another way to visualize this comparison is by representing the UV spectra as vectors in an n-dimensional space, where n equals the number of observations or wavelengths in the spectra. Each coordinate corresponds to the absorbance at a given wavelength. The comparison of two spectra is now equivalent to determining the angle between the two vectors. If the spectra are identical, this angle will be zero. The larger the difference, the farther the vectors will be apart and the larger the angle will be. The angle can be calculated from the dot product:

$$\cos(\boldsymbol{a}, \boldsymbol{b}) = \frac{\boldsymbol{a}\,\boldsymbol{b}}{|\boldsymbol{a}|\,|\boldsymbol{b}|} \tag{24}$$

where $\boldsymbol{a}$ and $\boldsymbol{b}$ are the vectors representing the spectra. The denominator in this equation again represents the normalization to remove concentration effects. The cosine is identical to the correlation coefficient for two mean-centered spectra.

Despite all efforts to distinguish and compare UV spectra, it is often not possible to make an unambiguous identification. However, by combining the UV spectral data with the observed retention time for a compound, it is often possible to reduce the possibilities sufficiently to make an identification. If retention models that describe the behavior of the compounds as a function of the organic modifier concentration are available, restrictions for the chromatographic conditions can be widened [139,140]. In peak tracking during optimization studies the retention times are intentionally varied owing to changes in the experimental conditions. For this the UV spectral data can be combined with peak areas to narrow the search. The latter principle has also been linked with a different approach to spectral comparison, the use of neural network [141].

B. Multivariate Data Analysis

The use of hyphenated forms of liquid chromatography, such as LC–UV, requires the availability of relatively powerful computers or distributed processing to handle the collection, storage, and retrieval of large amounts of data. In addition, to efficiently utilize the information, computer-assisted presentation and analysis of the data is a prerequisite. The presentation of data obtained using hyphenated LC methods ranges from the extraction of the signals in a single domain (i.e, the time domain or the domain related to the selected detection mode) to the representation of all the collected data in a three-dimensional plot or isometric plot. The latter usually consists of a projection of the data on a plane defined by the two domains. Areas with a similar response are shown in the same color or on a gray scale. However,

computer-assisted analysis of the data resulting from hyphenated runs can also be used to obtain (quantitative) hidden information. This includes the number of components contributing to a chromatographic profile, the individual peak profiles, or the detection characteristics (spectra) of these components.

In LC–UV, a relatively simple form of data manipulation is the calculation of the ratio of two signals recorded at different wavelengths [142]. When two or more components are coeluting to a significant extent, and the spectral characteristics of the components are different at the two wavelengths selected, this ratio will vary across the width of the peak. If this is not true, a constant plateau is observed.

Data manipulation can also involve a successive evaluation of the individual domains. Although this is not a true multivariate approach, the results can be used to deconvolute overlapping peaks. For instance, in LC–UV, one can perform a deconvolution in the wavelength domain on each spectrum observed during the elution of a chromatographic peak. By finding the optimal linear combination of a set of pure component spectra, one obtains relative concentrations for each of the components at each time point that a spectrum was recorded. This is followed by a reconstruction of the chromatograms for the individual components by evaluating the series of concentrations obtained from the previous step. The mathematical approach used to find the optimal linear combination of the reference spectra is called multicomponent analysis. The equations are similar to Eq. (19) and (22), but the combined signal ($A_{p,t}$) is replaced by the mixture spectrum, and the set of individual profiles ($\boldsymbol{c}$) is replaced by the set of reference spectra. One can use reference spectra obtained from an external source or from another chromatogram; however, the experimental conditions must be comparable, otherwise significant errors can be introduced [143]. Alternatively, one can use the pure component spectra observed in the two component upslope (front) and downslope (tail) sections of a peak to obtain an estimate of the true elution profiles [144].

A similar approach has been described for the quantitation of overlapping components, rather than for the reconstruction of the individual elution profiles [145]. For this, the peak areas observed at various wavelengths (corrected for intercepts of the calibration curves) are used as the response [vector $\boldsymbol{B}$ in Eqs. (21) and (22)], while the matrix [A] contains the slopes of the calibration curves for the different components at the given wavelengths. This approach requires that the calibration curves of the individual components at various wavelengths are available.

The most powerful approaches perform a simultaneous evaluation of the observations in both of the examined dimensions. As before, the major assumption is the applicability of independent linear relations; for instance, those described by Lambert–Beer's law for LC–UV. It is assumed that the observed absorbance is linearly dependent on the concentration of each of the components, and that the concentration of one component does not affect the spectroscopic behavior of any of the other absorbing species. If these assumptions are correct, the absorption ($A_{l,t}$) observed at a given time t and a given wavelength l can be expressed as:

$$A_{l,t} = \sum_{i=1}^{n} (e_{l,i}\, p_{i,t}) \tag{25}$$

where $p_{i,t}$ represents the (relative) concentration of component i at time t, and $e_{l,i}$ the extinction coefficient of component i at wavelength l. The summation is performed over the n components in a mixture. Over all $\boldsymbol{t}$ time points and all $\boldsymbol{w}$ wavelengths this can be expressed in a more general fashion using matrix notation.

$$[\mathrm{A}] = [\mathrm{E}]\,[\mathrm{C}]\,[\mathrm{P}] \tag{26}$$

[A] is a ($\boldsymbol{w} \times \boldsymbol{t}$) matrix containing all the spectra observed during the elution of a chromatographic peak as columns, [E] is a ($\boldsymbol{w} \times \boldsymbol{n}$) matrix with normalized UV spectra of the pure components as columns, [C] is a ($\boldsymbol{n} \times \boldsymbol{n}$) matrix with a measure of the total concentration (calibration factor) of each component in the mixture represented on the diagonal, and [P] is a ($\boldsymbol{n} \times \boldsymbol{t}$) matrix, with the normalized elution profiles of the individual components as rows.

The results of multivariate techniques, such as principal component analysis, factor analysis, or the singular value decomposition, performed on the matrix of observed absorbances [A] can all be written in a similar fashion.

$$[A] = [S]\,[V]\,[D] \tag{27}$$

The first n columns of the abstract ($w \times t$) matrix [S] can be thought of as linear combinations of the true spectra, and the first n rows of the ($t \times t$) abstract matrix [D] will be linear combinations of the true elution profiles. Columns in [S] beyond the first n columns and rows in [D] beyond the first n rows will be mostly representative of the experimental noise in the observations. The diagonal ($t \times t$) matrix [V] is related to the so-called eigenvalues of decomposition of [A]. The magnitude of these eigenvalues is related to the amount of variation described by each factor and thus to the significance of each factor. A much more detailed discussion of the foregoing is available [37,146].

A graphic illustration of the foregoing is provided in Fig 11. It represents the UV spectra observed during the elution of a chromatographic peak resulting from the partial coelution of two components. Every mixture spectrum is represented by a point, displayed in a three-dimensional space. Because each dimension corresponds to the absorption observed at a given wavelength, each spectrum is defined by the absorption at three wavelengths. In a graphic representation we are limited to three dimensions; however, the computational analysis can be applied to a higher number of dimensions; for instance, the number of recorded wavelengths.

Similar to the mixture spectra, the pure component spectra are represented by points in the data space. The UV spectra of the pure components will be located along the edges of the curve through the mixture spectra, and are represented here by two vectors e_1 and e_2 of unit length (one of the ways to normalize the spectra). The result of a principal component analysis is represented by the vectors s_1 and s_2, corresponding to the first two columns of matrix [S] in Eq. (27). Although s_1 and s_2 have no physical meaning, it can be demonstrated

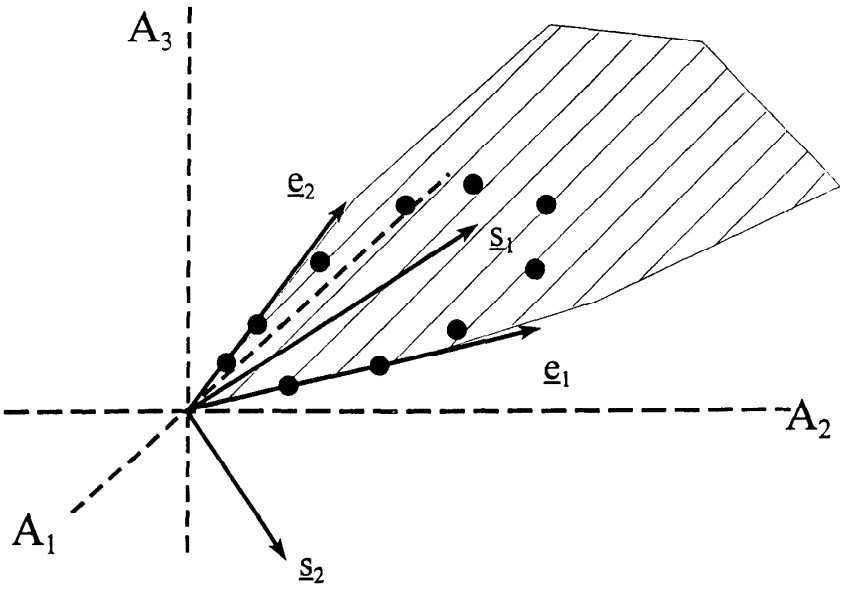


Figure 11 Graphic representation of the results of a multivariate analysis of a set of mixture spectra (heavy dots) in a three-dimensional space, defined by the absorbances observed at three wavelengths, A_1, A_2, and A_3. e_1 and e_2 are vectors representing the normalized pure component spectra and s_1 and s_2 are the first two principal components. The dashed area is a section of the plane containing all the mixture spectra and vectors.

that the pure component spectra are linear combinations of these abstract vectors. In other words, the pure component spectra are located in the plane defined by the two principal components.

The specific purpose of most chromatographic multivariate data analysis packages is to find the appropriate transformation that rotates the abstract vectors to coincide with the true spectra or with the elution profiles. Once the transformation for either domain has been established, the inverse transformation can be applied to the other domain to obtain the corresponding physical counterparts. In other words, once the true elution profiles have been determined, the corresponding UV spectra can be calculated, and inversely, when the true UV spectra are known, the elution profiles of the components can be determined. The abstract description provided by the principal components also provides a quick means to test whether a given component is contained in a peak cluster. If the UV spectrum of that component can be reconstructed as a linear combination of the principal components, then that component may be contributing to the peak. The inverse statement can be made with more certainty. If the UV spectrum of a component cannot be obtained as a linear combination of the principal components, then that component did not contribute to the peak cluster. This process is referred to as target factor analysis (TFA).

The first consideration in most forms of multivariate analysis is the determination of the correct dimensionality of the data space. In our case this translates into the determination of the number of coeluting components in a chromatographic peak. A factor analysis ranks the abstract factors in order of importance in terms of the amount of variability in the data described. Use of the correct number of factors allows reconstruction of the original data matrix within the experimental error:

$$[A] \simeq [A'] = [S'] [V'] [D'] \tag{28}$$

where the (′) indicates a reduced matrix; that is, a matrix with only the first n columns ([S′]), rows ([D′]), or both ([V′]). A simple test to determine the number of significant principal components is a reconstruction of the data matrix using increasing dimensionalities and determining the difference between [A] and [A′]. As soon as this difference remains within the experimental error, the true dimensionality has been established. This information is also contained in the eigenvalues resulting from a decomposition. However, in these methods it is assumed that the experimental error is known which is not always true. Various other statistical approaches exist to circumvent this problem [37,147]. However, the number of statistically significant components is not always the same as the number of components in a chromatographic peak. The statistical procedures identify any deviations from a uniform normal distribution in the noise as additional components. This may include nonlinearities observed in diode-array detection at higher absorbance values, or over broader wavelength ranges, as well as variations caused by baseline drift. Conversely, to distinguish a component in a cluster, there has to be some degree of separation from the other components and some degree of spectral dissimilarity to each of the other components. Otherwise the component will not introduce an additional variation in the data.

A practical way of estimating the number of components in LC is by evolving factor analysis (EFA) [148,149, and references cited therein]. A principal component analysis is performed on the first few spectra recorded during the elution of a peak and the eigenvalues are evaluated. The procedure is repeated after extending the data set with the next spectrum. This process continues across the width of the peak. Initially, only one eigenvalue will be significant, for only one component is eluting. If at some point a second component starts to elute and the spectrum of this component is different from the spectrum of the first component, the second eigenvalue calculated for the data matrix will also become significant. The peak can thus be diagnosed as impure. The published implementation of this approach [148] is especially impressive because the required intensive calculations are performed by dedicated processors in real-time, providing the chromatographer with peak purity information during the elution.

So far, it has been assumed that reconstruction of the elution profiles of the individual components requires information on the spectral characteristics of each of these components. However, multivariate data analysis also provides a means to obtain estimates of both the UV spectra and the elution profiles simultaneously. This so-called self-modeling curve resolution is based on several assumptions. It is assumed that the UV spectra do not contain negative extinction coefficients, and that the UV spectra do not contain negative extinction coefficients, and that the concentrations of all components are zero or positive at all times. This can be illustrated with Fig. 11. Only the mixture spectra (dots) are known. It is assumed that the pure spectra are located in the first quadrant of the data space if all extinction coefficients are at least zero. In addition, the pure component spectra cannot be located inside the envelop of mixture spectra, for this would require a negative concentration of one of the components to reconstruct some of the mixture spectra. In other words, not all mixture spectra can be composed by an addition of the normalized pure component spectra. In the two-component clusters, these restrictions generally narrow the number of possibilities to small regions in the data space. For mixtures of greater complexity, additional assumptions are required [150,151].

In LC–UV, very favorable results have also been obtained with a technique known as iterative target-transformation factor analysis (ITT-FA) [152,153]. Approximate values are obtained for the retention times of the individual components, either by an evaluation of the second derivative of the elution profile or by means of an abstract rotation. These approximate retention times are subsequently used to construct a simplified estimate of the elution profile, consisting of a 1 at the retention time and a 0 at all other time points in the cluster. This profile is then projected on the space defined by the abstract matrix resulting from the principal component analysis, and the resulting projection is corrected for negative concentrations and secondary maxima. This process is repeated until a stable profile is obtained. After this process is performed for each component present in the cluster, the corresponding UV spectra are obtained through the inverse transformation. Because LC profiles are generally simpler and better defined than UV spectra, this approach often provides reliable profiles and spectra. The performance of the ITT-FA process depends on the resolution, concentration, and spectral similarity of the analytes. ITT-FA is not restricted to LC–UV; it can also be applied to other combinations, such as LC with electrochemical detection [154]. The response of the detector must be a linear function of the concentrations of the analytes, and the response may not be affected by interactions between the different components.

The foregoing is a final illustration of how the use of computers in LC has grown beyond the straightforward control of instruments and peripherals. Computers can thus not only improve the efficiency and reliability of the liquid chromatographic analysis, but also they may actually increase the amount of information obtained. This results in improved chromatographic methods (as in computer-assisted method development) or more information on the analytes (as in sophisticated data analysis techniques).

REFERENCES

1. M Head, K Smith. Am Lab 24:50D, 1992.
2. J Slobodnik, MGM Groenewegen, ER Brouwer, H Lingeman, UAT Brinkman. J Chromatogr 642:359, 1993.
3. G Wu. J Chromatogr 641:168, 1993.
4. J Wieling, JHG Jonkman, J Hempenius, CK Mensius. Chem Intell Lab Syst 25:355, 1994.
5. T Rooney, C Chell, R Bell. Am Lab 22:28X, 1990.
6. K Dettmer, L Stieglitz. Chemosphere 29:1789, 1994.
7. J Wieling, J Hempenius, HJ Jeuring, JHG Jonkman, PMJ Coenegracht, DA Doornbos. J Pharm Biomed Anal 8:577, 1990.
8. JC van der Voorden, E Gout, OLT van Hulten, DEMM Vendrig. Chem Intell Lab Syst 17: 129, 1992.
9. RE Majors. LC–GC 13:742, 1995.

10. MM Bushey, JW Jorgenson. Anal Chem 62:161, 1990.
11. JB Wheatley, JA Montali, DE Schmidt Jr. J Chromatogr A 676:65, 1994.
12. JC Giddings. Anal Chem 56:1259A, 1984.
13. PW Willmott, I Mackenzie, RJ Dolphin. J Chromatogr 167:31, 1987.
14. PR Fielden, AJ Packham. Anal Chem 62:2594, 1990.
15. L Mondello, KD Bartle, G Dugo, P Dugo. J High Resolut Chromatogr 17:312, 1994.
16. PR Griffiths, AJ Lange. J Chromatogr Sci 30:93, 1992.
17. MM Bushey, JW Jorgenson. Anal Chem 62:978, 1990.
18. JC Hoogvliet, JM Reijn, WP van Bennekom. Anal Chem 63:2418, 1991.
19. C Turner, ME Gregory, NF Thornhill. Biotechnol Bioeng 44:819, 1994.
20. T Buttler, KAJ Johansson, LGO Gorton, GA Marko-Varga. Anal Chem 65:2628, 1993.
21. T Becker, R Kittsteiner-Eberle, T Luck, HL Schmidt. J Biotechnol 31:267, 1993.
22. Z Ma, G Guiochon. Anal Chem 62:2330, 1990.
23. LR Snyder, JW Dolan, GB Cox. J Chromatogr 540:21, 1991.
24. P Jageland, J Magnusson, M Bryntesson. J Chromatogr 658:497, 1994.
25. P Jandera, G Guiochon. J Chromatogr 588:1, 1991.
26. UB Nandihalli, MV Duke. J Agric Food Chem 41:583, 1993.
27. R Collander. Acta Chim Scand 5:774, 1951.
28. PP Csokan, F Darvas, F Csizmadia, K Valko. LC–GC 12:40, 1994.
29. ED Breyer, JK Strasters, MG Khaledi. Anal Chem 63:828, 1991.
30. R Kaliszan. Quantitative Structure Chromatographic Retention Relationships. New York: John Wiley & Sons, 1987.
31. L Morin-Allory, B Herbreteau. J Chromatogr 590:203, 1992.
32. H Kalasz, M Bathori, Z Tarjanyi, F Darvas. Chromatographia 30:95, 1990.
33. K Jinno, Y Ban. Chromatographia 30:51, 1990.
34. B Mester, N Hikichi, M Hanz, M Paulino de Blumenfield. Chromatographia 30:191, 1990.
35. T Hanai, H Hatano, N Nimura, T Kinoshita. Analyst 119:1167, 1994.
36. L Lawson, R Hanson. Solving Least Squares Problems. Englewood Cliffs, NJ:Prentice Hall, 1974.
37. ER Malinowski, DC Howery. Factor Analysis in Chemistry. New York:John Wiley & Sons, 1980.
38. R Gami-Yilinkou, A Nasai, R Kaliszan. J Chromatogr 633:57, 1993.
39. JH Park, MD Jang, JJ Chae, HC Kim, JK Suh. Chromatogr 656:69, 1993.
40. T Hamoir, DL Massart. In: PR Brown, E Grushka, eds. Advances in Chromatography, vol 53. New York:Marcel Dekker, 1993.
41. T Hamoir, M De Smet, H Pyrins, P Conti, N Vanden Driessche, DL Massart, F Maris, H Hindriks, PJ Schoenmakers. J Chromatogr 589:31, 1992.
42. M De Smet, G Musch, A Peeters, L Buydens, DL Massart. J Chromatogr 485:237, 1989.
43. H Hindriks, F Maris, J Vink, A Peeters, M De Smet, DL Massart, L Buydens. J Chromatogr 485:255, 1989.
44. F Maris, H Hindriks, J Vink, A Peeters, N Vanden Driessche, DL Massart. J Chromatogr 506:211, 1990.
45. PP Csokan, F Darvas, F Csizmadia, K Valko. LC–GC 12:40, 1994.
46. T Hamoir, B Bourguignon, DL Massart. Chromatographia 39:339, 1994.
47. T Hamoir, B Bourguignon, DL Massart, H Hindriks. J Chromatogr 633:43, 1993.
48. C Hansch, A Leo. Substituent Constants for Correlation Analysis in Chemistry and Biology. New York:Wiley, 1979.
49. RF Rekker. The Hydrophobic Fragmental Constant—Its Derivation and Application. Amsterdam:Elsevier, 1977.
50. RF Rekker, HM de Kort. Eur J Med Chem Chim Ther 14:479, 1979.
51. SV Galushko, AA Kamenchuk, GL Pit. J Chromatogr A 660:47, 1994.
52. PJ Schoenmakers, A Peeters, RJ Lynch. J Chromatogr 506:169, 1990.

53. PJ Schoenmakers. Optimization of Chromatographic Selectivity—A Guide to Method Development. Amsterdam:Elsevier, 1986.
54. JC Berridge. Techniques for the Automated Optimization of HPLC Separations. Chichester: Wiley, 1985.
55. JL Glajch, LR Snyder, eds. Computer-Assisted Method Development for High-Performance Liquid Chromatography. Amsterdam:Elseivier, 1990 (also published as special issue of the J Chromatogr vol 485).
56. JK Strasters, ED Breyer, AH Rodgers, MG Khaledi, J Chromatogr 511:17, 1990.
57. PJ Schoenmakers. J Liquid Chromatogr 10:1865, 1987.
58. A Peeters, L Buydens, DL Massart, PJ Schoenmakers. Chromatographia 26:101, 1988.
59. PJ Schoenmakers, JK Strasters, A Bartha. J Chromatogr 458:355, 1988.
60. S Sekulic, PR Haddad. J Chromatogr 485:501, 1989.
61. D Repka, P Sandra, J Krupcik. Analusis 20:555,1992.
62. S Hatrik, J Hrouzek, J Lehotay, J Krupcik. J Chromatogr 665:9, 1994.
63. AK Smilde, A Knevelman, DA Doornbos. J Chromatogr 369:1, 1986.
64. J Wieling, J Schepers, J Hempenius, CK Mensink, HG Jonkman. J Chromatogr 545:101, 1991.
65. B Bourguignon, P Vankeerbergen, DL Massart. J Chromatogr 592:51, 1992.
66. JW Dolan, DC Lommen, LR Snyder. J Chromatogr 485:91, 1989.
67. NG Mellish. LC–GC 9:845, 1991.
68. K Grogg-Sulser, HJ Helmlin, JT Clerc, J Chromatogr A 692:121,1995.
69. EA Hogendoorn, E Dijkman, SM Gort, R Hoogerbrugge, P van Zoonen, UAT Brinkman. J Chromatogr Sci 31:433, 1993.
70. L Wrisley. J Chromatogr 628:191, 1993.
71. TH Dzido, E Soczewinski, J Gudej. J Chromatogr 550:71, 1991.
72. W Markowski, TH Dzido, E Soczewinski. J Chromatogr 523:81, 1990.
73. R Bonfichi. J Chromatogr A 678:213, 1994.
74. H Fritsch, I Molnar, M Wurl. J Chromatogr A 684:65, 1994.
75. LR Snyder. In: Horvath, Ed. High-Performance Liquid Chromatography, vol 1. 1980, p. 207.
76. DD Lisi, JD Stuart, LR Snyder. J Chromatogr 555:1, 1991.
77. R Daeppen, I Molnar. J Chromatogr 592:133, 1992.
78. S Heinisch, JL Rocca, M Kolosky. Chromatographia 29:482, 1990.
79. QS Wang, RY Gao, BW Yang, DP Fan. Chromatographia 38:187, 1994.
80. P Jandera. J Chromatogr 485:113, 1989.
81. TH Dzido, HD Smolarz. J Chromatogr A 679:59, 1994.
82. Y Baba. J Chromatogr 485:143, 1989.
83. LS Madamba-Tan, JK Strasters, MG Khaledi. J Chromtogr A 683321, 1994.
84. JR Grant, FL Vandemark, AF Poile. Am Lab 22:15, 1990.
85. JC Berridge. J Chromatogr 485:3, 1989.
86. J Wei, J Wei, X Zhou. J Chromatogr 552:103, 1991.
87. Y Hu, DL Massart. J Chromatogr 485:311, 1989.
88. PMJ Coenegracht, AK Smilde, HJ Metting, DA Doornbos. J Chromatogr 485:195, 1989.
89. J Wieling, J Schepers, J Hempenius, CK Mensink, HG Jonkman. J Chromatogr 545:101, 1991.
90. R Lynch, G Meausres. Lab Pract 39:61, 1990.
91. LR Snyder, JW Dolan, DC Lommen. J Chromatogr 485:65, 1989.
92. JW Dolan, JA Lewis, WD Raddatz, LR Snyder. Am Lab 24:40D, 1992.
93. JD Stuart, DD Lisi. J Chromatogr 550:77, 1991.
94. P Chaminade, A Baillet, D Ferrier. J Chromatogr A 672:67, 1994.
95. S Heinisch, P Riviere, JL Rocca. Chromatographia 32:559, 1991.
96. C Zhou, N Mo, X Shu, H Wu, P Zhang, M Xie. J High Resolut Chromatogr 15:555, 1992.

97. PJ Schoenmakers, T Blaffert. J Chromatogr 384:117, 1987.
98. JC Pearce, A Churchill, AC Terry. Chemometr Intell Lab Syst 17:213, 1992.
99. SD Patterson. J Chromatogr 592:43, 1992.
100. R Faulstich, T Catalano LC–GC 9:776, 1991,
101. ACJH Drouen, HAH Billiet, L de Galan. J Chromatogr 352:127, 1986.
102. HAH Billiet, L de Galan. J Chromatogr 485:27, 1989.
103. JA Lewis, DC Lommen, WD Raddatz, JW Dolan, LR Snyder. J Chromatogr 592:183, 1992.
104. RM Lopes Marques, PJ Schoenmakers. J Chromatogr 592:157, 1992.
105. JA Lewis, JW Dolan, LR Snyder, I Molnar. J Chromatogr 592:192, 1992.
106. F Szokoli, Z Nemeth, J Inczedy. Chromatographia 29:265, 1990.
107. JK Starasters, ST Kim, MG Khaledi. J Chromatogr 586:221, 1991.
108. RP Tucker, AF Fell, JC Berrideg, MW Coleman. Chirality 4:316, 1992.
109. JW Dolan, DC Lommen, LR Snyder. J Chromatogr 535:55, 1990.
110. LR Snyder, JW Dolan, DC Lommen. J Chromatogr 535:75, 1990.
111. MW Dong, FL Vandemark, PV Passalacqua. Am Lab 24:36, 1992.
112. M Martin-Smith, DR Rudd. Acta Pharm Jugosl 40:7, 1990.
113. AA Fasanmade, AF Fell. Anal Lett 25:363, 1992.
114. M Mulholland, N Walker, JA van Leeuwen, L Buydens, F Maris, H Hindriks, PJ Schoenmakers. Mikrochim Acta 2:493, 1991.
115. M Mulholland, N Walker, F Maris, H Hindriks, L Buydens, T Blaffert, PJ Schoenmakers. J Chromatogr 550:257, 1991.
116. JA Van Leeuwen, BGM Vandeginste, G Kateman, M Mulholland, A Cleland. Anal Chim Acta 228:145, 1990.
117. JA van Leeuwen, LMC Buydens, BGM Vandeginste, G Kateman, PJ Schoenmakers, M Mulholand. Chemometr Intell Lab Syst 10:337, 1991.
118. JA van Leeuwen, LMC Buydens, BGM Vandeginste, G Kateman, PJ Schoenmakers, M Mulholland. Chemometr Intell Lab Syst 11:37, 1991.
119. JA van Leeuwen, LMC Buydens, BGM Vandeginste, G Kateman, A Cleland, M Mulholland, C Jansen, FA Maris, PH Hoogkamer, JHM van den Berg. Chemometr Intell Lab Syst 11: 161, 1991.
120. AJJ Debets, P van Wier, K-P Hupe, UAT Brinkman. Chromatographia 39:460, 1994.
121. P van der Meersen, J Vanderdeelen, L Baert. Anal Chem 64:1056, 1992.
122. P Chaminade, A Baillet, D Ferrier, B bourguignon, DL Massart. Anal Chim Acta 280:93, 1993.
123. RH Albert, C Zervos. Dev Food Sci 24:595, 1990.
124. DG Simpson, S Guo, J Sacks, JA Bietz, F Huebner, T Nelsen. Chemonetr Intell Lab Syst 10:155, 1991.
125. EPC Lai, RD Giroux, N Chen, R Guo. Can J Chem 71:968, 1993.
126. SP Kounaves, DD Lu. Comput Chem 16:29, 1992.
127. H Waetzig. Chromatographia 33:218, 1992.
128. P Jandera, B Prokes. J chromatogr 550:495, 1991.
129. A Savitzki, MJE Goley, Anal Chem 36:1627, 1964.
130. PJP Cardot, P Trolliard, S Tembely. J Pharm Biomed Anal 8:755, 1990.
131. T Rotunno. Chromatographia 34:56, 1992.
132. PR Bevington. Data Reduction and Error Analysis for the Physical Sciences. New York: McGraw-Hill, 1969, Chap. 11.
133. WW Yau, JJ Kirkland. J Chromatogr 556:111, 1991.
134. WW Yau, SW Rementer, JM Boyajian, JJ DeStegfano, JF Graff, KB Lim, JJ Kirkland. J Chromatogr 630:69, 1992.
135. AF Fell, TZ Woldemariam, PA Linley, JGe, MD Luc de Gastro, M Valcarcel. Anal Chim Acta 234:89, 1990.
136. AF Fell, JB Castledine, B SellBerg, R Modin, R Weinberger. J Chromatogr 535:33, 1990.

137. HP Sievert, ACJH Drouen. In: L Huber, SA Geroge, eds. Diode Array Detection in HPLC. New York:Marcel Dekker, 1993, Chromatographic Science Series 62:51.
138. WA Hardcastle, SG Lisseter, SG Hambling, P Bedson. Lab Microcomput 12:39, 1993.
139. K Jinno, M Hayashida, T Watanabe. J Chromatogr Sci 28:367, 1990.
140. M Hayashida, M Nihira, T Watanabe, K Jinno, J Chromatogr 506:133, 1990.
141. PMJ Coenegracht, HJ Metting, EM van Loo, GJ Snoeijer, DA Doornbos. J Chromatogr 631: 145, 1993.
142. L Huber, HP Fiedler. Drugs Pharm Sci 47:123, 1991.
143. JK Strasters, HAH Billiet, L de Galan, BGM Vandginste, G Kateman. J Chromatogr 385: 181, 1987.
144. T Hondo, M Kuwajima, Y Sato, K Okamura, Y Tanaka, H Eda, Y Okada, S Takamatu, M Saito. Anal Sci 7:235, 1991.
145. A Cladera, E Gomez, J Manual Esteda, V Cerda. J Chromatogr Sci 30:453, 1990.
146. JK Strasters. In: L Huber, SA Geroge, eds. Diode Array Detection in HPLC. New York: Marcel Dekker, 1993, Chromatographic Science Series, vol 62:127.
147. C Shen, TJ Vickers, CK Mann. J Chemometr 5:417, 1991.
148. J Schaefer. Am Lab 22:28N, 1990.
149. JA Gilliard, JL Cumps, BL Tilquin. Chemometr Intell Lab Syst 21:235, 1993.
150. JB Castledine, AF Fell, R Modin, B Sellberg. Anal Proc 29:100, 1992.
151. BGM Vandeginste, R Essers, T Bosman, J Reijnen, G Kateman. Anal Chem 57:971, 1985.
152. BGM Vandeginste, W Derks, G Kateman. Anal Chim Acta 173:253, 1985.
153. PJ Naish, RJ Lynch, T Blaffert. Chromatographia 27:343, 1989.
154. HZ Msimanga, PE Sturrock. Anal Chem 62:2134, 1990.
155. JK Strasters, HAH Billiet, L De Galan, BGM Vandeginste, G Kateman. J Liq Chromatogr 12:3, 1989.

7

Size Exclusion Chromatography

Howard G. Barth

DuPont Company, Wilmington, Delaware

I. INTRODUCTION

As compared with small molecules, which consist of single molecular weight species, synthetic polymers are comprised of hundreds to thousands of chains of differing molecular weights, each with a finite concentration. The characteristics of the molecular weight distribution of a polymer are governed by the polymerization mechanism, monomer reactivity ratios, monomer feed rates, initiator type, presence of chain-transfer agents, and polymerization and processing conditions. In addition to synthetic polymers, many naturally occurring polymers, such as polysaccharides, cellulosics, natural rubber, and some proteins, also have defined molecular weight distributions. These materials are considered polydisperse. Nucleic acids and most types of proteins, however, consist of a single, well-defined molecular weight structure, and they are defined as monodisperse.

The molecular weight and molecular weight distribution of polymers are key parameters that govern many of their physical properties, such as tacticity, tensile strength, melt flow, as well as solution properties. The shape, width, and magnitude of the molecular weight distribution are characterized in terms of statistical averages of the distribution. As shown in Figure 1, up to three average molecular weight parameters are typically used to define the distribution: number-average M_n, weight-average M_w, and z-average M_z molecular weights. Depending on the sample and baseline noise level, the $z + 1$ average molecular weight M_{z+1}, can also be used. The meaning and determination of these statistical averages are discussed in the Section III.

The most popular and convenient method of determining molecular weight distributions of polymers is size exclusion chromatography (SEC). The term "gel-permeation chromatography" (GPC) is also used, but refers to the separation of organosoluble polymers; whereas, the name "gel filtration" refers specifically to the separation of biopolymers. SEC separates on the basis of molecular hydrodynamic volume or size, rather than by enthalpic interactions with the stationary phase, as in other modes of chromatography. In SEC, high molecular weight material elutes first from an SEC column, followed by low molecular weight components.

Because gradient elution is not used in SEC, instrumentation is somewhat simpler compared with high-performance liquid chromatography (HPLC). The major differences are the

---

Dedicated to the memory of Professor J. Calvin Giddings.

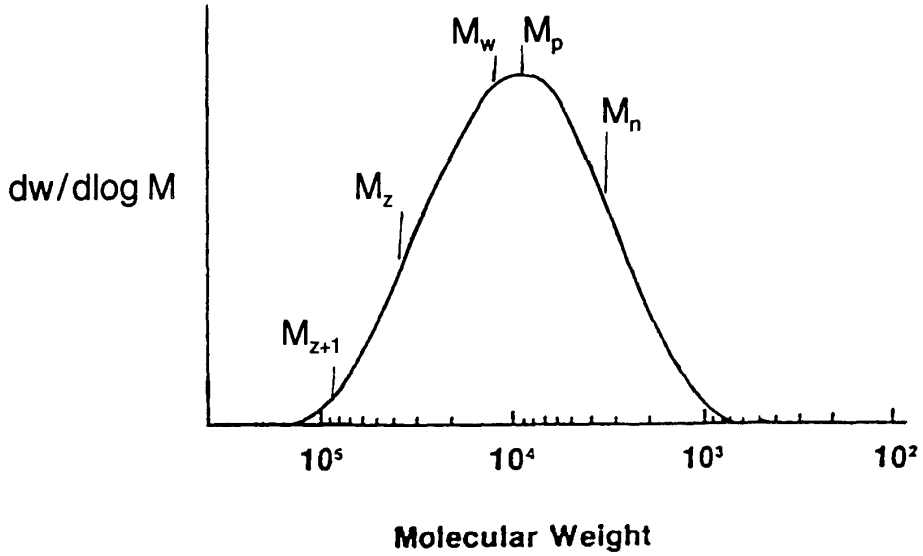


Figure 1 Representative molecular weight distribution of a polymer where M_n and M_w are the number- and weight-average molecular weights, M_p is the SEC peak maximum molecular weight, and M_z and M_{z+1} are higher molecular weight moments described in the text.

column required for the separation, molecular weight calibration, and a computer system for data acquisition and processing. Depending on the application, high-temperature conditions (e.g., 150°C) may be required, as in the analysis of polyolefins.

This chapter introduces the reader to the fundamentals of SEC, with emphasis on the mechanism of separation, calibration approaches, column and mobile-phase selection, and detection systems. General HPLC instrumentation is covered in other chapters of this volume. For more comprehensive treatment of SEC and associated techniques, please refer to Refs. [1–10]. References [11–18] are comprehensive reviews of SEC, published biennially in the Fundamental Review issues of *Analytical Chemistry*, which are an excellent source for selected and updated applications.

II. APPLICABILITY

The typical separation range of SEC is 10^2–10^6 g mol^{-1} thus, small molecules, as well as high molecular weight solutes, can be size separated, depending on the nature of the SEC column. In principle, any type of sample can be analyzed by SEC, provided it can be solubilized and there are no enthalpic interactions present between the sample and packing material, as discussed in Section IV.

In addition to being used for determining molecular weight distributions, SEC can be used to compare relative molecular weight differences among samples. Complex, unknown mixtures can be screened by SEC to determine the presence of small molecules, oligomers, and polymeric components. If there are sufficient molecular weight differences among solutes, SEC can be used in place of HPLC for the analysis of small molecules. Sample cleanup, in which low molecular weight components are isolated from complex matrices, as in biological or environmental samples, can be accomplished quite easily with SEC. Desalting biological compounds is typically performed with SEC.

Physiochemical properties of biopolymers and synthetic polymers can be studied with SEC, such as association and ligand binding, polymerization kinetics, and protein folding and conformation. For synthetic polymers, long-chain branching and polymer conformation, for example, can be determined by the use of molecular–weight-sensitive detectors. Composi-

tional heterogeneity of polymeric materials can be measured using SEC with on-line spectroscopic detection.

III. MOLECULAR WEIGHT AVERAGES

Of fundamental importance in SEC is the calculation of average molecular weights: M_n, M_w, M_z, and M_{z+1}. (M_p, also shown, is the molecular weight at peak maximum and is used only in conjunction with SEC.) The molecular weight distribution, shown in Figure 1, can be treated as a statistical population distribution, defined in terms of a number- and weight-average arithmetic mean. The number-average molecular weight is:

$$M_n = \frac{(N_1M_1 + N_2M_2 + \ldots N_iM_i)}{\sum N_i} \tag{1}$$

$$M_n = \frac{\sum(N_iM_i)}{\sum N_i} \tag{2}$$

where N_i is the number of molecules of molecular weight M_i; M_n is the average molecular weight per molecule. Because an SEC detector measures concentration or amount of eluting material, not the number or moles, the useful form of Eq. (2) is:

$$M_n = \frac{\sum W_i}{\sum(W_i/M_i)} \tag{3}$$

where W_i is the weight (or concentration) of M_i. Low molecular weight components have a pronounced affect on M_n, as compared with higher molecular weight chains.

The weight-average molecular weight, a *weighted* average, is defined as

$$M_w = \frac{(W_1M_1 + W_2M_2 + \ldots W_iM_i)}{\sum W_i} \tag{4}$$

or

$$M_w = \frac{\sum W_iM_i}{\sum W_i} \tag{5}$$

Compared with M_n, M_w values are sensitive to the presence of the high molecular weight components.

The next two moments of the distribution, M_z and M_{z+1}, focus on the high molecular weight end of the distribution (see Fig. 1) and are calculated from

$$M_z = \frac{\sum W_iM_i^2}{\sum W_iM_i} \tag{6}$$

$$M_{z+1} = \frac{\sum W_iM_i^3}{\sum W_iM_i^2} \tag{7}$$

These averages are sensitive to the presence of very high molecular weight species at the peak tail and, as such, can be difficult to measure reliably.

The width of a distribution, or polydispersity of a sample d, is the ratio of two molecular weight averages, usually M_w/M_n, although M_z/M_w or M_{z+1}/M_z can be used if the high molecular weight end of the distribution needs to be emphasized. For a monodisperse or single-molecular weight polymer, $d = 1$. For condensation polymers, $d = 2$; polymers made by anionic polymerization, d is close to 1, and d is greater than 2 for polymers made from free radical polymerization.

M_n values are highly sensitive to the presence of low molecular weight species, and influence properties that are affected by chain ends, such as colligative properties, refractive index, density, and the specific heat capacity of a sample. Polymer properties that are influenced by large chains, such as melt and solution viscosity, are best monitored by M_w measurements; whereas, viscoelastic properties (time-dependent mechanical properties), are sensitive to M_z or M_{z+1} values. For typical SEC experiments, M_n, M_w, and M_z are measured; M_{z+1} can be measured reliably only if baseline noise or drift is not a problem.

IV. SEPARATION MECHANISM

In SEC, a sample is injected into a chromatographic column packed with porous particles of defined pore size. As the sample elutes through the column, molecules that are too large to penetrate the pores of the packing elute in the interstitial volume of the column V_0, the total exclusion volume (Fig. 2). As the molecular size decreases, in comparison with the average pore size of the packing, polymer molecules penetrate into the pores, access more pore volume, and elute at a later elution volume. Smaller molecules, which can readily diffuse into and out of the pores, elute at the total elution volume of the column V_t. Polymers of intermediate molecular size elute between V_0 and V_t. The maximum separation volume of a given column is the difference between V_t and V_0, the pore volume V_i. The total elution volume of an SEC column is defined by its physical dimensions and the interstitial and pore volumes of the packing:

$$V_t = V_0 + V_i \tag{8}$$

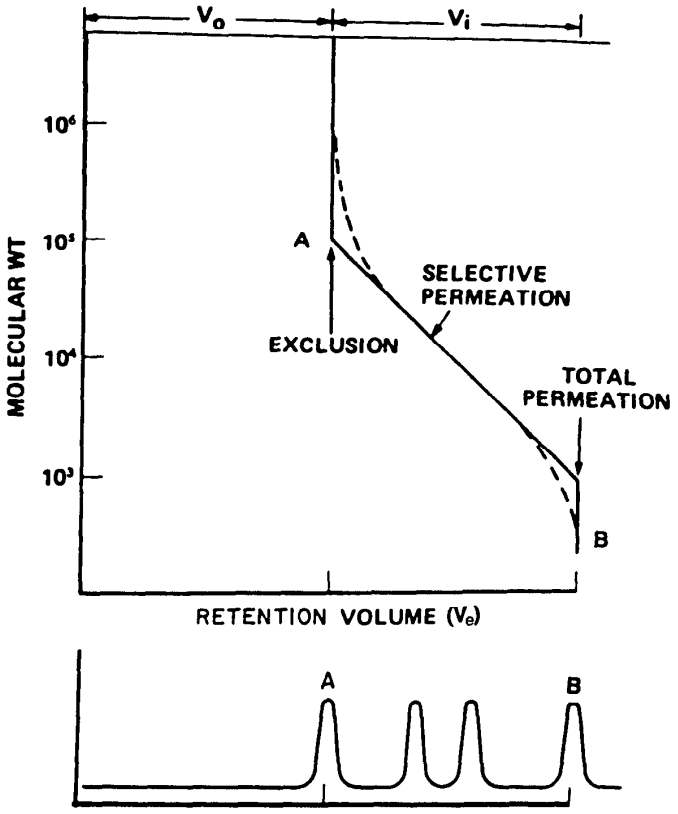


Figure 2 An SEC molecular weight calibration curve where V_0 is the interstitial or total exclusion volume of a column, and V_i is the pore volume or "working volume" of the column. (From Ref. 2.)

The elution volume of a sample V_e can be defined in terms of a chromatographic distribution coefficient K_d:

$$V_e = V_0 + K_d V_i \tag{9}$$

Thus, the elution volume of a sample is equal to the interstitial volume of the column plus the accessible pore volume $K_d V_i$. The SEC distribution coefficient K_d ranges from zero, for a totally excluded polymer, to unity, for a totally permeated polymer. The "working volume" of an SEC column is V_i. The goal in developing an SEC method is to ensure that the sample elutes between V_0 and V_t. If $K_d > 1$, enthalpic interactions are present between the polymer and packing, and the separation is no longer strictly governed by size exclusion.

There have been several theories proposed to describe the separation mechanism of SEC [2]; however, a thermodynamic explanation [19], rather than a kinetic model [20] has proved most useful. As shown in Eq. (10), any partition or distribution process is a function of both an entropic term and an enthalpic term:

$$K = e^{\Delta S/R} e^{-\Delta H/RT} \tag{10}$$

where ΔS and ΔH are the change in entropy and enthalpy, respectively, when solute is transferred from one phase to the other phase.

In SEC, however, enthalpic interactions are absent, and Eq. (10) becomes

$$K = e^{\Delta S/R} \tag{11}$$

Here, ΔS is the change of conformational entropy of a polymer [19]; the driving force being the concentration gradient between the pore volume of the packing and interstitial volume of the column. If there is a large decrease in conformational entropy, as in a high molecular weight polymer diffusing into small pores, K approaches zero, and the polymer elutes at V_0. For small molecules that can freely diffuse into and out of the pores of the packing, ΔS is zero, K approaches unity, and the solute elutes at V_t. Thus, according to thermodynamic considerations, K is independent of flow rate and temperature, and depends only on the size and shape (hydrodynamic volume) of a polymer relative to the average size and shape of the pores of the packing. Separation in SEC is governed by molecular size, which takes into account molecular weight *and* molecular conformation or shape. As discussed in Section V.D, molecular size is usually expressed in terms of a molecular hydrodynamic volume.

Unlike other modes of separation, there is no temperature dependency in SEC, as shown in Eq. (11), and the elution volume of a peak will be independent of column temperature. Obviously, column efficiency or peak broadening will be affected by temperature, but the peak position of the first moment will remain constant. Furthermore, changes in polymer hydrodynamic volume with temperature are generally small. Nevertheless, it is good practice to thermostat SEC columns to help maintain a constant flow rate and the baseline stability, especially when using a differential refractometer as the detector.

V. CALIBRATION

Size exclusion chromatography is a *relative*, not *absolute*, technique for determining molecular weight distribution. As such, the column must be calibrated with standards of known molecular weight to obtain a calibration curve, represented as a plot of logarithm of the molecular weight versus elution volume (see Fig. 2). The slope of the calibration curve is related to the conformation of the polymer: an extended or rod-like chain will have a much steeper slope, than that of a more compact structure, such as a branched polymer. The extrapolated intercept of the calibration curve is related to the molecular density or molecular mass per unit hydrodynamic volume of the polymer. Thus, a polystyrene calibration curve will be shifted upward when compared with that of polyethylene.

The calibration curve is used to convert detector output (response versus elution time) into a differential molecular weight distribution (Fig. 3). Because a molecular weight distri-

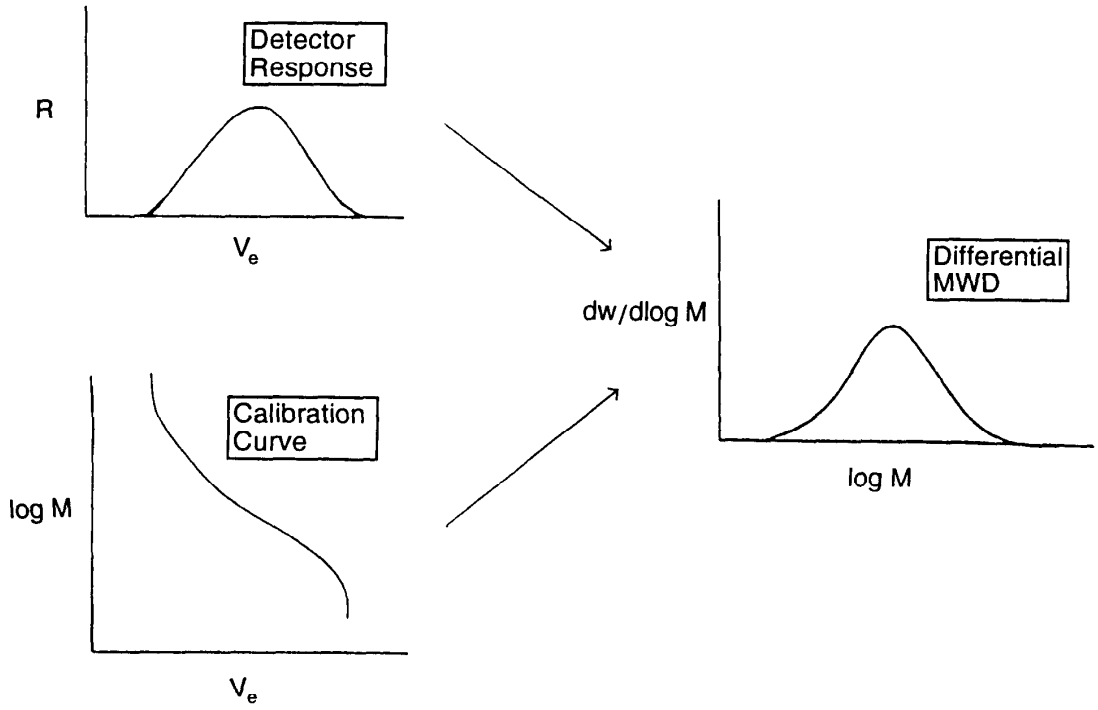


Figure 3 Transformation of the SEC detector output into a differential molecular weight distribution using a molecular weight calibration curve.

bution should represent a change in the amount or weight of a polymer relative to a change in molecular weight, $dw/d\log M$ is used as the ordinate, rather than the weight fraction w. To determine the weight fraction or a percentage of a sample at a given molecular weight, a cumulative distribution is used (Fig. 4), which represents the integrated form of the differential molecular weight distribution.

The four most commonly used calibration methods, described in the following, are (1) primarily calibration, (2) secondary calibration, (3) broad-molecular weight calibration, and (4) universal calibration (molecular–weight-sensitive detectors are discussed in Sec. XIII.C).

A. Primary Calibration

The most accurate approach to calibrate an SEC system is with monodisperse standards that are chemically and structurally similar to the samples being analyzed. The standards should cover the molecular weight separation range of the samples, should be well characterized in terms of molecular weight, and should be nearly monodisperse ($d < 1.05$). The number of standards used depends on the molecular weight range and the linearity of the calibration curve. Typically, between four and ten standards are required to define the calibration curve. All SEC software programs include curve-fitting routines for optimum calibration. The use of "mixed-bed" or "linear" columns give fairly linear calibration curves, and their application is highly recommended (see Sec. IX).

There are several low polydispersity standards that are available. The most common organosoluble calibrants are polystyrene, poly(methyl methacrylate), polyisoprene, and polybutadiene. Water-soluble standards include pullulan, poly(styrene sulfonate), poly(ethylene oxide), and poly(methacrylic acid; see Appendix A for suppliers).

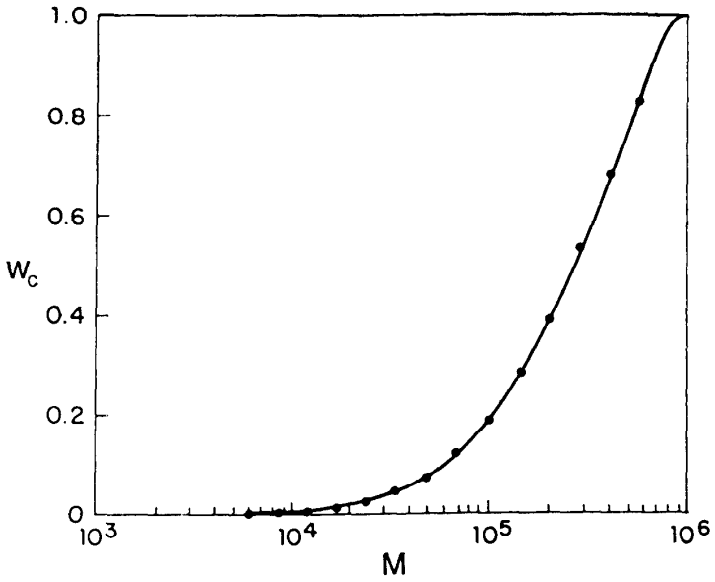


Figure 4 Cumulative weight fraction w_c molecular weight distribution: at a given molecular weight M, the corresponding w_c represents the total weight fraction of the sample having a molecular weight $\leq M$. (From Ref. 2.)

B. Secondary Calibration

Because of the limited availability of low-polydispersity standards that are structurally similar to samples, the aforementioned polymers can be employed as secondary standards. Because the molecular conformation and molecular density of a secondary standard will differ from those of the sample, calibration with these standards produces an *apparent molecular* weight distribution. This is an acceptable method of calibration that can be used to examine molecular weight trends or relative differences among samples. In reporting these data, one must explicitly state that the values were obtained using a secondary calibration curve; if not, absolute values may be inferred.

C. Broad-Molecular Weight Calibration

A very effective method to obtain absolute molecular weight values if narrow-molecular weight calibrants are not available, is to use a broad-molecular weight standard of known M_n and M_w values, or two broad standards of known M_n or M_w values if appropriate software is accessible. This procedure uses an iterative "search-and-find" approach whereby different calibration slopes and intercepts are tried until the correct M_n and M_w values are obtained [21]. To obtain accurate data, however, the polydispersity of the standard should encompass the molecular weight range of the samples being analyzed and, more importantly, the calibration curve must be linear over the entire molecular weight range.

D. Universal Calibration

Universal calibration is obtained by plotting log $(M[\eta])$, rather than log M, versus V_e, where $[\eta]$ is the intrinsic viscosity of the polymer measured at the same temperature and in the same solvent as used for the mobile phase [22]. In this manner, all polymers, regardless of their chemical composition or conformation, will fall on the same calibration curve when chromatographed under identical conditions. A well-known example of universal calibration is

shown in Figure 5. The reason universal calibration works is that the term $M[\eta]$ is proportional to the hydrodynamic volume of a polymer in solution. Because SEC separates on the basis of hydrodynamic volume, and not necessarily molecular weight, all polymers of the same hydrodynamic volume, irrespective of their composition, will elute at the same V_e.

To use universal calibration in the conventional manner, the Mark–Houwink coefficients of the sample must be known, as discussed later, and a series of nearly monodisperse standards of known molecular weight and intrinsic viscosity must be available. Furthermore, for universal calibration to be valid, enthalpic interactions between calibrants or samples and the SEC packing must be absent.

To use this approach, a universal calibration curve is first constructed using standards. The sample is then injected. At each given elution volume, the hydrodynamic volume of the sample, designated by subscript x, is equal to the hydrodynamic volume of the calibrant,

$$M_{\text{std}}\,[\eta]_{\text{std}} = M_x[\eta]_x \tag{12}$$

Substituting Eq. (13), the Mark–Houwink relation,

$$[\eta]_x = KM_x^a \tag{13}$$

where K and a are the Mark-Houwink coefficients of the sample, into Eq. (12), and solving for M_x, we arrive at

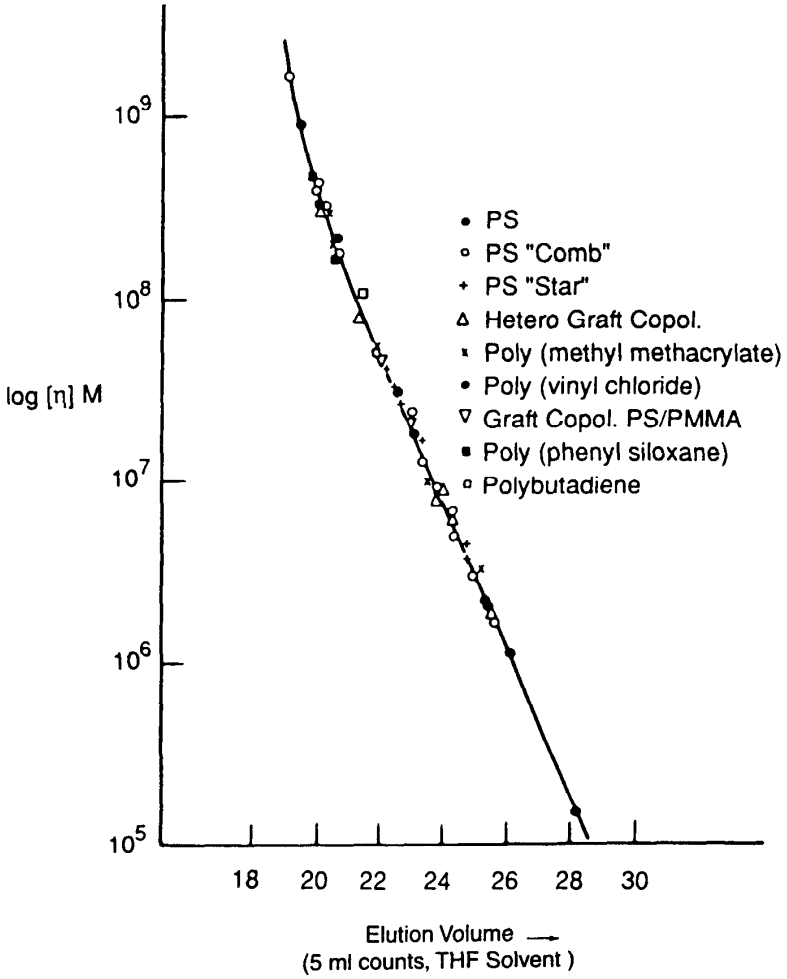


Figure 5 An SEC universal calibration in which $[\eta]M$ is the molecular hydrodynamic volume of the polymer. (From Ref. 22.)

$$\log M_x = \frac{[\log (M_{std}[\eta]_{std}) - \log K]}{(a + 1)} \tag{14}$$

(A comprehensive listing of Mark–Houwink coefficients can be found in Ref. [23].)

The major drawbacks of using universal calibration is the need to know accurate Mark–Houwink coefficients of the sample (and standards) at the SEC conditions. Unfortunately, these values are not always available, especially if the composition of the sample is unknown. Furthermore, the accuracy of many published coefficients are dependent on the polydispersity of the polymer standards and the method of measuring molecular weights. In view of these difficulties, on-line SEC viscometers are now used in conjunction with universal calibration, as discussed in Section XIII.C.1, to measure intrinsic viscosities of samples and standards.

VI. BAND BROADENING

In SEC, the shape and width of a polymer peak contains all the information related to its molecular weight distribution. As a result, band (peak) broadening and skewing are critical factors in obtaining reliable molecular weight data. Band broadening causes the polymer peak to spread out, leading to an overestimation of M_w and underestimation of M_n and an increase in polydispersity. Skewing can severely distort the molecular weight distribution. In essence, band broadening causes the SEC calibration curve to be rotated counterclockwise [2].

The sources of band broadening and skewing in SEC are similar to those found in other modes of HPLC. The major difference, however, is that the small diffusion coefficients of high molecular weight solutes result in a decreased rate of mass transfer of a polymer into and out of the pores of a packing. Furthermore, there can be additional band broadening, caused by the high viscosity of many mobile phases used in SEC. To help alleviate this added source of band broadening, SEC is commonly operated at an elevated temperature.

Before the advent of high-performance columns, mathematical approaches were used, with some success, to help correct for band broadening [24–28]. With the use of high-performance columns, typically about 10^4 plates, band-broadening corrections usually are not employed. Also, if the column set is calibrated using the broad standard approach, the resultant calibration curve helps compensate for band broadening. To maximize column performance, column sets should be constructed from columns that play a role in a given separation. Oftentimes an SEC column set will consist of columns outside the separation range—these extraneous columns add to band broadening. Lastly, as in HPLC, sample injection volumes should be kept to a minimum.

Depending on column efficiency, SEC viscometry with universal calibration may also be sensitive to band broadening [29]. This is because, although the correct intrinsic viscosity is measured at each elution volume increment, band broadening will shift the elution volume, and the corresponding molecular weight obtained from universal calibration curve will be incorrect. This incorrect viscosity–molecular weight relation will rotate the Mark–Houwink plot (log $[\eta]$ versus log M) counterclockwise, overestimating the Mark–Houwink exponent a. This effect, however, can be compensated by injecting a broad standard having well-defined Mark–Houwink coefficients and rotating the Mark–Houwink plot to give the correct a value. This rotation is accomplished by adjusting the interdetector volume, which now becomes an apparent value [30].

VII. RESOLUTION

The specific resolution R_s of an SEC system is obtained from the separation of two components differing by a decade of molecular weight [31]:

$$R_s = \frac{\Delta V_r}{4\sigma[1/\log(M_1/M_2)]} \tag{15}$$

where ΔV_r is the peak maximum separation and σ is the peak standard deviation proportional to peak width. This expression can be related to the slope of the SEC calibration curve D_2 [31]:

$$R_s = \frac{0.576}{\sigma D_2} \tag{16}$$

Thus, in SEC, resolution is dependent on both column efficiency (through σ), and the slope of the calibration curve. For maximum resolution, high-efficiency columns (low σ) are required containing packings of narrow pore size distribution and a high pore volume (low D_2).

As described by Yau and co-workers [2,31], the σD_2 term is a fundamental parameter in SEC that also can be related to the molecular weight error caused by band broadening (see Sec. VI). The error in M_n and M_w can be estimated from the following two equations assuming a gaussian dispersion function [30]:

$$M_n \text{ (error)} = e^{-(1/2)(\sigma D_2)^2} - 1 \tag{17}$$

$$M_w \text{ (error)} = e^{(1/2)(\sigma D_2)^2} - 1 \tag{18}$$

As explained in the previous section, band broadening leads to an underestimation of M_n and an overestimation of M_w, which are reflected in these two equations.

VIII. PACKING CHARACTERISTICS

For organosoluble polymers, either cross-linked polystyrene-based or silica-based packings may be used. For water-soluble polymers, there are various silica and hydrophilic polymeric packings from which to choose [32]. The most popular class of silica-based packings for aqueous SEC consist of a "diol"-type stationary phase (e.g., gycerolpropylsilane). For the analysis of cationic water-soluble polymers (see Sec. X.B), polyethyleneimine-coated silica is preferred [33]. There are many kinds of hydrophilic polymeric packings that have been introduced, which include cross-linked hydroxylated methacrylate copolymers, polyacrylamide, poly(vinyl alcohol), poly(styrene sulfonate), agarose, chitosan, and even a "glucose-treated" divinyl benzene. In addition, there are composite packings consisting of two phases, such as dextran–agarose, dextran–acrylamide, and agarose–acrylamide. Representative column suppliers are listed in Appendix B.

In general, silica-based packings are less hydrophobic and less expensive than polymeric packings. Furthermore, silica packings are more robust to high-temperature applications and can be used with virtually any organic mobile phase, without swelling or shrinking; however, the pore volume of silica columns tend to be lower than those of polymeric packings.

Particle sizes range from 3 to 20 μm, and corresponding column efficiencies go from about 20,000 to 4,000 plates per 25-cm column. Actual pore sizes of high-performance SEC packings extend from close to 30 Å to as high as 3000 Å, which corresponds to an effective separation range of approximately 100 to 10^6 g mol^{-1}, or higher, for linear, random coils. Pore sizes larger than 3000 Å are too fragile for use in high-performance SEC.

The "pore size" designations used for polystyrene packings are based on the extended chain length of a totally excluded polystyrene calibrant. To obtain the equivalent molecular weight of an excluded polystyrene calibrant, the column designation is multiplied by 40 g mol^{-1} Å^{-1}. For example, a "10^4-Å" column has an exclusion limit of approximately 400,000 g mol^{-1}, which corresponds to an actual pore size of near 500 Å.

IX. COLUMN SELECTION

For random coils, a single pore-sized packing can separate 1.5–2 decades of molecular weight [3]. Thus, in principle, a polydisperse sample containing a molecular weight range from 10^3 to 10^5 g mol^{-1}, would require, as a minimum, just a single "10^4-Å" polystyrene column. For

increased resolution and molecular weight accuracy, as shown in Eqs. (17) and (18), multiple columns of the *same* pore size should be used.

For samples that have a molecular weight distribution greater than two decades, multiple columns of different pore size are needed. For best calibration curve linearity, pore volumes of the columns should be matched. Alternatively, linear or mixed-bed columns, which contain packings of different pore sizes, can be employed, rather than a series of different pore-sized columns.

X. MOBILE SELECTION

A. Organosoluble Polymers

For organosoluble polymers, a good solvent is required that completely dissolves the polymer of interest at the SEC-operating temperature. To prevent adsorption of the polymer onto the packing, the solubility parameter of the mobile phase should be close to that of the packing. For cross-linked polystyrene, mobile phases, such as tetrahydrofuran, toluene, or chloroform, are good choices. If the polymer contains amino functionality, triethylamine or trifluoroacetic acid (typically about 0.1%) can be added to the mobile phase to prevent adsorption. For silica packings, a large range of mobile phases can be used; however, basic polymers will adsorb because of acidic silanol groups, and may require the addition of triethylamine or trifluoroacetic acid to the mobile phase.

B. Water-Soluble Polymers

Mobile-phase development for water-soluble polymers is oftentimes difficult because of hydrophobic or electrostatic interactions that can take place between the polymer and packing. The three most common types of interactions are ion-exchange, ion-exclusion, and hydrophobic [32]. As discussed in the following, mobile-phase composition must be fine-tuned to set $\Delta H = 0$, by adjusting mobile phase pH, ionic strength, and organic moderator content.

1. Ion-Exchange

Most polymeric packings contain residual ionic groups, predominantly carboxylate, inadvertently introduced during synthesis. For silica, residual silanol groups are the problem. These cationic exchange sites can ion-exchange with polymers containing a cationic functionality, resulting in either a highly tailed or irreversible adsorbed peak. The basic approaches to eliminate this effect are (1) reduce mobile phase pH to less than 4 to prevent dissociation of silanol or carboxylate groups; (2) increase the ionic strength of the mobile phase to help shield electrostatic interactions; (3) add a competitive compound to the mobile phase (e.g., triethylamine); (4) use a surface-modified silica packing to reduce the concentration of silanols; (5) use a polyethyleneimine-coated silica (commercially available through Micra Scientific, see Appendix B).

2. Ion Exclusion

Because of the presence of residual antionic groups on packings, anionically charged polymers tend to be excluded from the pores, owing to electrostatic repulsive forces. Furthermore, an electric double layer is formed that decreases the effective pore volume of the packing. As a result, anionic polyelectrolytes elute earlier than expected, causing an overestimation in molecular weight. As described earlier, the same approaches are employed as those used to eliminate on exchange, except for the use of polyethyleneimine-coated packings, to prevent ion exclusion.

3. Adsorption

Adsorption is a general term used to describe polymer elution in which enthalpic interactions play a role. The most commonly encountered adsorption mechanism in aqueous SEC is based

on hydrophobic interactions between hydrophobic groups on the polymer chain and hydrophobic regions on the packing. To eliminate these effects, the mobile-phase ionic strength should be reduced and an organic moderator added to the mobile phase, for example, methanol.

XI. SOLUTE CONCENTRATION EFFECTS

If the concentration of an injected sample is too high, the elution volume will increase and the peak may become distorted [34]. Increased elution volume is a result of a phenomenon called "molecular crowding," whereby polymer chains begin to overlap [35]. The conformational entropy of the chain is essentially decreased; the peak appears to have become smaller and elutes at a later elution time. This effect becomes more predominant with increasing molecular weight. The second mechanism involves a hydrodynamic effect termed "viscous fingering" [36]. Here, if the viscosity of an injected solution is somewhat greater than that of the mobile phase, the added resistance to flow will tend to decrease the velocity of the injected plug. The higher velocity mobile phase will be inclined to "finger" its way past the injected sample plug, distorting the peak shape. As with macromolecular crowding, viscous fingering will scale with the molecular weight of the sample.

To prevent concentration effects, the lowest possible sample concentration must be injected without compromising the signal/noise ratio of the detector. If detection limit becomes a problem, sample volume can be increased. Table 1 lists recommended injection concentrations for polymers of different molecular weights.

XII. SYSTEM EVALUATION

To ensure that there are no enthalpic interactions, a given sample *must* elute between V_0 and V_t; values of which are determined using an excluded high molecular weight calibrant, and a low molecular weight compound, typically a solvent. For a aqueous SEC, the elution volume of a sample should be constant within a narrow range of pH, ionic strength, or organic moderator content. Because the entropically controlled SEC process should be practically independent of temperature, the SEC analysis should be carried out at a slightly higher temperature to ensure that the peak does not shift. Finally, if a molecular weight-sensitive detector is being used and a sample of known or estimated molecular weight is available, the SEC system can be evaluated directly.

XIII. DETECTION

A. Concentration Detectors

1. Refractometry

The most popular detector used in SEC is the deflection-type differential refractometer (DRI). The detection limit, which depends on the specific refractive index and polydispersity of the

Table 1 Guidelines for Injected Polymer Concentration

Molecular weight	Concentration (%)
<10,000	<1
10,000–100,000	<0.5
100,000–500,000	<0.2
500,000–10^6	<0.1

sample, is in the parts per million (ppm) range using an injection volume of less than 100 μL. An interferometric DRI is also available that has much higher sensitivity [37]. For polymers larger than approximately 10,000 g mol^{-1}, the DRI response is independent of molecular weight; below this value calibration is required to correct for concentration. The DRI response also varies with composition; as a result, molecular weight distributions of blends and compositionally heterogeneous copolymers may be inaccurate, unless corrected for composition differences.

2. Ultraviolet Spectrophotometry

For homopolymers that are chromophoric, UV detection is the method of choice. Detection limits can be orders-of-magnitude lower than that of a DRI, which enables low concentration to be injected—an advantage in SEC, as treated in Section XI. Furthermore, molecular weight dependency on UV response is minimal. Other types of HPLC detectors, such as fluorescence and electrochemical, are not typically used in SEC.

3. Evaporative Light-Scattering Detection

One type of detector that is becoming more prevalent in SEC is the evaporative light-scattering detector (ELSD), also referred to as a "mass detector" [38]. Effluent from a chromatographic column is nebulized with a stream of inert gas, and the resulting aerosol passes through a heated tube to evaporate the mobile phase and to desolvate particles of polymer. The particles then pass across an incident beam of light. The intensity of scattered light, measured at a fixed angle relative to the forward direction of the incident beam, is proportional to polymer concentration.

When compared with a DRI, the ELSD has superior baseline stability, is insensitive to temperature fluctuations of the SEC system, and is less dependent on polymer composition [39]. Depending on the ELSD model used, these detectors can be significantly more sensitive than a DRI. A major limitation, however, is that the ELSD response is nonlinear (sigmoidal) relative to polymer concentration, because of different scattering regimens, and it must be calibrated to obtain reliable concentration information [38]. Recent studies have also demonstrated that the ELSD response decreases with molecular weight if the polymer is larger than approximately 600,000 g mol^{-1} [40]. The ELSD is also sensitive to operating parameters, such as nebulizing gas flow rate and solvent evaporation temperature, and must be optimized before analysis. Nevertheless, the ELSD is particularly useful for SEC of polymers that are either UV-transparent or isorefractive relative to the mobile phase. Furthermore, the ELSD is the detector of choice for gradient elution HPLC of nonchromophoric solutes, and for temperature-rising elution fractionation of polymers.

B. Composition Detectors

Many copolymers are compositionally heterogeneous in their molecular weights; that is, the composition can vary or drift with molecular weight. By adding a "composition-sensitive" detector in series with a concentration-sensitive detector, the composition drift or heterogeneity can be determined. This approach also is useful for the analysis of unknown polymeric materials or blends, or for determining the composition of block or graft copolymers. It is important to realize, however, that copolymers may be heterogeneous for *both* composition and molecular weight; that is, for a given molecular weight, there can be a range of compositions, and for a given copolymer composition, there can be a range of molecular weights. In this situation, a two-dimensional separation or cross-fractionation is required, such as HPLC followed by SEC or vice versa. Polymer cross-fractionation is beyond the scope of this chapter, and the reader is referred to References [6,41].

1. Ultraviolet Spectrophotometry

On-line UV diode-array detectors (DAD) are quite useful for measuring compositional heterogeneity and have been used in several SEC applications. The limitation of this detector is that comonomers or components must have characteristic UV spectra.

2. FT–IR Spectrophotometry

On-line Fourier-transform–infrared (FT–IR) detection has been reported, mainly for the determination of compositional heterogeneity of polyethylene copolymers, as well as for determining short-chain branching in polyethylene [42,43]. The major limitations of this detector are solvent interference and sensitivity; milligram quantities are typically required. To overcome these difficulties, a commercially available FT–IR detector "interface" has been introduced in which column effluent is sprayed onto an aluminum-backed, rotating germanium disk [44]. The mobile phase is evaporated, and the disk is placed onto a scanning turntable mounted within an FT–IR spectrophotometer in the reflection mode. Infrared spectra are taken along the polymer track, and FT–IR spectra recorded, essentially as a function of elution time.

This detector is most useful for qualitative analysis, especially for SEC analysis of unknown polymeric materials. With the availability of new instrumentation that focuses the effluent spray into a more narrow track, detection limits are in the submilligram range. Furthermore, FT–IR microscopy can also be employed to analyze the deposited polymer. For SEC analysis of polymers, however, a possible concern is spectral interference caused by the deposition of nonuniform films [45], although it may be possible to smooth out the deposit by solvent or thermal annealing.

3. Mass Spectrometry

Mass spectrometry (MS) is the ideal detector for chromatography because of its high sensitivity and its ability to provide structural information. MS is especially useful for analyzing the molecular weight and composition of oligomers, for identifying chain-end groups, and for determining the composition and molecular weight of unknown or multicomponent polymeric materials. With electrospray ionization, the most useful on-line ionization mode, analysis of polymers of molecular weight less than 1×10^4 g mol^{-1} is possible [46]. There are, however, several major concerns. Multiple charged species, insufficient resolution, and the presence of fragment ions can complicate spectral interpretation. Additionally, the total ion current may not reflect actual concentration, although a concentration-sensitive detector in series would solve this problem. Lastly, special mobile-phase conditions may be necessary to help induce ionization.

Matrix-assisted laser-desorption ionization–time-of-flight (MALDI-TOF) MS, an alternative "soft"-ionization mode, which has recently been introduced, holds great promise as an SEC detector. With this technique, molecular weights as high as 10^5 g mol^{-1} are possible. The formation of fragment ions and multiple charged molecules are minimized, which greatly simplifies spectral interpretation. In practice, SEC fractions are collected, mixed with a given matrix, and analyzed off-line. (In a typical experiment, less than 0.5 mg of polymer is fractionated and above 5-μg fractions taken for MALDI-TOF MS [47].) Two versions of automated microfraction collectors are now available commercially specifically for MALDI-TOF analysis (see Appendix C). Recently, the design and evaluation of an on-line SEC–MALDI-TOF system has been reported [48].

4. Nuclear Magnetic Resonance

For unambiguous structural determination, as well as for chain microstructural studies, on-line nuclear magnetic resonance (NMR) is required. Furthermore, if polymer end groups are well defined, NMR can also be used for determining molecular weights of less than 10^4 g mol^{-1} [49]. Flowthrough microprobes (60–250 μL) are now available [50,51]. When used in conjunction with 500-MHz instrumentation, with advanced shimming and solvent suppression features, sensitivity is in the microgram range for ^{1}H-NMR, and the milligram level for ^{13}C-

NMR [50]. The obvious limitation of on-line SEC–NMR is cost. Extracolumn band broadening is also a potential concern, because the SEC unit must be placed at a distance from the NMR probe.

C. Molecular-Weight-Sensitive Detectors

Although MS and NMR can be used under certain conditions to determine molecular weight, especially for oligomers and low molecular weight polymers, on-line viscometric and light-scattering detectors are the preferred instruments to be used. Furthermore, as described later, these "solution-property" detectors can also be used for measuring other molecular properties [52].

1. Viscometry

There are several different types of on-line viscometers available: single capillary [53], referenced dual-capillary [54], and a Wheatstone-bridge fluid-analogous design [55]. These detectors operate by measuring the pressure drop across a capillary situated at the exit of the column. The ratio of the pressure drop of an eluting component to the pressure drop of the mobile phase, at a given flow rate, is equal to the relative viscosity η_r of the polymer. If the concentration of the sample c at each elution volume increment is determined with a concentration-sensitive detector (usually a DRI) in series, the intrinsic viscosity $[\eta]$ can be measured using the following equation:

$$[\eta] = \left[\frac{\ln \eta_r}{c}\right]_{c\to 0} \tag{19}$$

Equation (19) assumes infinite dilution, which for all practical purposes is valid for a typical SEC experiment. With the use of universal calibration (see Sec. V.D), the molecular weight at each elution volume increment can be determined readily:

$$M = \frac{(M_{\text{std}}[\eta]_{\text{std}})}{[\eta]} \tag{20}$$

By assuming that each elution volume increment is nearly monodisperse, the average molecular weights of a sample are calculated from Eqs. (3) and (5) through (7). On-line SEC viscometry is essentially a *relative*, not *absolute* method for obtaining molecular weight information, and depends on the establishment and validity of universal calibration.

SEC viscometry is useful for determining several other molecular parameters in addition to molecular weight. By plotting log $[\eta]$ against log M, the Mark–Houwink coefficients (a and K) of a polymer can be determined [see Eq. (13)]. The slope a, which is related to the conformation of the polymer, can be used to evaluate polymer-branching differences among samples. A more quantitative parameter, the branching index g', can also be determined across the molecular weight distribution using

$$g' = \left(\frac{([\eta]_b)}{([\eta]_l)}\right)_M \tag{21}$$

where $[\eta]_l$ is the intrinsic viscosity of a linear polymer of the same molecular weight as the branched polymer of intrinsic viscosity $[\eta]_b$. It is also possible to calculate the radius of gyration for linear polymers at each elution volume increment using the modified Flory–Fox equation [56,57]:

$$R_g = \left(\frac{1}{\sqrt{6}}\right)\left(\frac{M[\eta]}{\Phi}\right)^{1/3} \tag{22}$$

where

$$\Phi = 2.55 \times 10^{21}(1 - 2.63\varepsilon + 2.86\varepsilon^2) \tag{23}$$

and

$$\varepsilon = \frac{(2a - 1)}{3} \tag{24}$$

where a is the Mark–Houwink exponent. (See Ref. [52] for a listing of other uses and applications of SEC viscometry.)

2. Light-Scattering Detection

In Rayleigh light scattering, a polymer solution is irradiated with a beam of coherent, monochromatic light. Light interacts with both dissolved polymer chains and solvent molecules and induces a temporary dipole moment that oscillates in-phase with the incident beam. Scattered light, which has the same wavelength as the incident beam, broadcasts scattered light in all directions. The intensity of scattered light i_s is dependent on several parameters, as described by the following equation:

$$i_s \propto \frac{Mc\ \alpha^2}{\lambda^4} \tag{25}$$

where α is the polarizability of a molecule and λ is the incident light wavelength. Thus, the greater the polarizability of a molecule (which is related to its refractive index), the more light will be scattered. As seen in this simple relation, if the concentration of a scatterer (polymer) is known, the molecular weight can be determined from first principles. As compared with viscometry, light scattering is an *absolute* technique for molecular weight measurements.

Equation (25) is the fundamental relation from which the following "working" light-scattering equation is derived [58]:

$$\frac{Kc}{\overline{R}_\theta} = \frac{1}{MP(\theta)} + 2A_2c \tag{26}$$

where:

K is the optical constant, comprised of constants and experimental parameters:

$$K = \frac{4\pi^2 n_0^2 (dn/dc)^2}{\lambda_0^4 N_A} \tag{27}$$

in which n_0 is the refractive index of the solvent, dn/dc is the specific refractive index of the polymer, and N_A is Avogadro's number.

$\overline{R}_\theta$, the excess Rayleigh ratio, is the scattered light intensity of the polymer (the scattered intensity of the solution minus the solvent), normalized relative to the incident beam intensity and the scattered volume geometry.

$P(\theta)$ is the particle-scattering function at the angle of measurement that takes into account angular dissymmetry of scattered light. If the hydrodynamic diameter of the polymer is $<0.05\lambda$, $P(\theta)$ is unity; at values $> 0.05\lambda$, $P(\theta)$ is less than unity, and must be evaluated.

A_2 is the second virial coefficient of the polymer solution that is related to polymer–solvent interaction. In a typical SEC light-scattering experiment, the A_2c term is close to zero and usually can be ignored.

There are now several different SEC light-scattering detectors available that differ in terms of cell design and measurement angles (see Appendix C). In general, however, if measurements are made at relatively low angles relative to the forward direction (i.e., less than about 15°), $P(\theta)$ is close to unity and Eq. (26) becomes

$$\frac{Kc}{\overline{R_\theta}} = \frac{1}{M} \tag{28}$$

and M can be calculated readily at each elution volume increment.

If scattered intensities are made at angles greater than 15°, at least several higher angles must be used. In this case, $Kc/\overline{R_\theta}$ is plotted against $\sin^2(\theta/2)$ and measurements extrapolated to zero angle; the correct molecular weight is obtained from the intercept. The molecular size (radius of gyration) of a polymer across the molecular weight distribution can also be obtained from the slope of this plot. The lower radius of gyration limit, however, is approximately 10 nm, which corresponds to approximately 1×10^5 g mol^{-1} relative to polystyrene in a good solvent. Multiangle light-scattering instruments use a diode-array detector configuration in which scattered intensities are measured simultaneously from various angles, depending on the number of diodes surrounding the cell [59,60]. (See Ref. [52] for a listing of other uses and applications of SEC light scattering.)

3. Light Scattering–Viscometry

For molecular–weight-sensitive detectors, the most useful system is the combination of both light-scattering and viscometry, in conjunction with a concentration-sensitive detector, sometimes referred to as a "triple detection system" [61–64]. In this manner, the molecular weight and intrinsic viscosity distributions of a polymer are determined simultaneously without the need of universal calibration. With this approach, Mark-Houwink coefficients, branching indices, and molecular size parameters can be calculated.

XIV. SUMMARY

With existing HPLC instrumentation and appropriate data acquisition and processing software, an SEC system can be set up easily. For organosoluble polymers, any appropriate good solvent may be used for the mobile phase, and cross-linked polystyrene is usually suitable for the packing. For synthetic water soluble polymers, however, mobile-phase optimization and SEC column evaluation may be required.

As an entropically controlled separation process, SEC has a peak capacity that is approximately an order of magnitude lower than that of gradient elution HPLC [65]. However, SEC is a useful method for screening complex, multicomponent oligomeric and polymeric materials. Because the elution order of components is directly related to molecular size, peak identification is facilitated.

Provided that the SEC system is properly calibrated, all the statistical average molecular weights of a polymer can be determined readily. In most laboratories, SEC has supplanted traditional methods of molecular weight measurements, such as osmometry and light scattering. Furthermore, if molecular–weight-sensitive detectors (light-scattering or viscometry) are employed, molecular parameters of a polymer, including branching an chain conformation, can be determined [52]. Lastly, by including an on-line composition-sensitive detector, for example an FT–IR, mass spectrometer, or NMR, compositional heterogeneity of polymeric materials can be obtained.

SUPPLIERS*

Appendix A: Polymer Standards

American Polymer Standards, P.O. Box 901, Mentor, OH 44061
National Institute of Standards and Technology, Gaithersburg, MD 20899

*Please note that these appendices list major suppliers and that this is by no means a comprehensive listing.

Polymer Laboratories Inc., 160 Old Farm Rd., Amherst, MA 01002
Polymer Standards Service, 13531 Cedar Creek Ln., Silver Spring, MD 20904
Polysciences, Inc., 400 Valley Rd., Warrington, PA 18976
Pressure Chemical Co., 3419-25 Smallman St., Pittsburgh, PA 15201
TosoHaas, 156 Keystone Dr., Montngomeryville, PA 18936
Waters Corporation, 34 Maple St., Milford, MA 01757

Appendix B: SEC Columns

Beckman Instruments, 2500 Harbor Blvd., Fullerton, CA 92634
Asahi Chemical, Kawasaki, Japan
Bio-Rad Laboratories, 2000 Alfred Noble Dr., Hercules, CA 94547
Jordi Associates, Inc., 4 Mill St., Bellingham, MA 02019
Mac-Mod Analytical, Inc., 127 Commons Ct., Chadds Ford, PA 19317
Micra Scientific, 1955 Techny Rd., Northbrook, IL 60062
Pharmacia Biotech Inc., 800 Centennial Ave., P.O. Box 1327, Piscataway, NJ 08855
Phenomenex, Inc., 2320 W. 205th St., Torrance, CA 90501
Polymer Laboratories Inc., 160 Old Farm Rd., Amherst, MA 01002
Polymer Standards Service, 13531 Cedar Creek Ln., Silver Spring, MD 20904
Showa Denko K.K., 13-9, Shiba Daimon, 1-chome, Minato-ku, Tokyo, 105, Japan
Supelco Inc., Supelco Park, Bellefonte, PA 16823
TosoHaas, 156 Keystone Dr., Montgomeryville, PA 18936
Waters Corporation, 34 Maple St., Milford, MA 01757

Appendix C: SEC Detectors

Differential Refractometers

Bio-Rad Laboratories, 2000 Alfred Noble Dr., Hercules, CA 94547
Hewlett-Packard 2850 Centerville Rd., Wilmington, DE 19808
JASCO Inc., 8649 Commerce Dr., Easton, MD 21601
Knauer GmbH, Hegauer Weg 38, 14163 Berlin, Germany
Waters Corporation, 34 Maple St., Milford, MA 01757
Wyatt Technology Corp., 802 East Cota St., Santa Barbara, CA 93103

Evaporative Light-Scattering (Mass) Detectors

Polymer Laboratories Inc., 160 Old Farm Rd., Amherst, MA 01002
Richard Scientific, 366-A Bel Marin Keys Blvd., Novato, CA 94949 (SEDEX Instrument)
Varex, 4000 Blackburn La., Burtonsville, MD 208966

Infrared Detectors

Foxboro Co., c/o Pioneer EDC, Inc., P.O. Box 7026, Wilmington, DE 19803
Lab Connections Inc., 5 Mount Royal Ave., Marlboro, MA 01752
Perkin-Elmer Corp., 761 Main St., Norwalk, CT 06859

Light-Scattering Detectors

LDC Analytical, 3681 Industrial Park Road North, Riviera Beach, FL 33404
Polymer Laboratories Inc., 160 Old Farm Rd., Amherst, MA 01002
Precision Detectors, Inc., 160 Old Farm Rd., Amherst, MA 01002
Tosoh Corp., 707, 1-chrome, Akasaka, Minato-ku, Tokyo, Japan
Viscotek Corp., 15600 West Hardy St., Houston, TX 77060
Wyatt Technology Corp., 802 East Cota St., Santa Barbara, CA 93103

MALDI-MS Fraction Collectors

LC Packings, 80 Carolina St., San Francisco, CA 94103
PerSeptive Biosystems, Inc., 500 Old Connecticut Path, Framingham, MA 01701

NMR Flow-Through Microprobes

Bruker Instruments Inc., 19 Fortune Dr., Manning Park, Billerica, MA 01821
Varian Instruments, P.O. Box 9000, San Fernando, CA 91340

Viscometers

Viscotek Corp., 15600 West Hardy St., Houston, TX 77060
Waters Corporation, 34 Maple St., Milford, MA 01757

REFERENCES

1. CS Wu, ed. Handbook of Size Exclusion Chromatography. New York: Marcel Dekker, 1995.
2. WW Yau, JJ Kirkland, DD Bly. Modern Size Exclusion Chromatography. New York: John Wiley & Sons 1979.
3. J Janca, ed., Steric Exclusion Liquid Chromatography. New York: Marcel Dekker, 1984.
4. BJ Hunt, SB Holding, eds. Size Exclusion Chromatography. New York: Chapman & Hall, 1989.
5. PL Dubin, ed. Aqueous Size Exclusion Chromatography. Amsterdam: Elsevier, 1988.
6. G Glöckner. Polymer Characterization by Liquid Chromatography. Amsterdam: Elsevier, 1987.
7. ST Balke. Quantitative Column Liquid Chromatography. Amsterdam: Elsevier, 1984.
8. EV Patton. In: BW Rossiter, JE Hamilton, eds., Physical Methods of Chemistry, Vol. IIIB. 2nd ed. New York: Wiley Interscience, 1989.
9. HG Barth, JW Mays, eds. Modern Methods of Polymer Characterization. New York: John Wiley, 1991.
10. AR Cooper, ed, Determination of Molecular Weight. New York: John Wiley & Sons, 1989.
11. GL Hagnauer. Anal Chem. 54:265R, 1982.
12. RE Majors, HG Barth, CH Lochmuller. Anal Chem 56:300R, 1984.
13. HG Barth, WE Barber, CH Lochmuller, RE Majors, FE Regnier. Anal Chem 58:211R, 1986.
14. HG Barth, WE Barber, CH Lochmuller, RE Majors, FE Regnier. Anal Chem 60:387R, 1988.
15. HG Barth, BE Boyes, Anal Chem 62:381R, 1990.
16. HG Barth, BE Boyes. Anal Chem. 64:428R, 1992.
17. HG Barth, BE Boyes, C Jackson. Anal Chem 66: 595R, 1994.
18. HG Barth, BE Boyes, C Jackson. Anal Chem 68:445R, 1996.
19. EF Cassasa, Y Tagami. Macromolecules 2:14, 1969.
20. EZ DiMarzio, CM Guttman. J Polym Sci Part B 7:267, 1969.
21. ST Balke, ARE Hamielec, BP LeClair, SL Pearce. Ind Eng Chem Prod Res Dev, 8:54, 1969.
22. Z Grubsic, P Rempp, H Benoit. J Polym Sci Polym Lett Ed 5:753 1967.
23. J Brandrup, EH Immergut, eds. Polymer Handbook. 3rd ed. New York: John Wiley & Sons, 1989.
24. LH Tung. J Appl Polym Sci 13:775, 1969.
25. Z He, X Zhang, R Cheng. J Liq Chromatogr 5:1209, 1982.
26. K Lederer, G Imrich-Scwarc, M Dunky. J App Poly Sci 32:4751, 1986.
27. J Billiani, I Amtmann, T Mayr, K Lederer. J Liq Chromatogr 13:2973, 1990.
28. J Billiani, K Lederer. J Liq chromatogr. 13:3013, 1990.
29. C Jackson, WW Yau. J Chromatogr 645:209, 1993.
30. CY Kuo, T Provder, ME Koehler, AF Kah ACS Symp Ser 352:130, 1987.
31. WW Yau, KK Kirkland, DD Bly, HJ Stoklosa. J Chromatogr 125:219, 1976.

32. HG Barth. Adv Chem Ser 213:31, 1986.
33. DL Gooding, MN Schumuck, KM Gooding. J Liq Chromatogr 5:2259, 1982.
34. HG Barth. ACS Symp Ser 352:29, 1987.
35. LH Tung, JC Moore. In: LH Tung, ed. Fractionation of Synthetic Polymers. New York: Marcel Dekker, 1977, p. 619.
36. JC Moore. Sep Sci. 5:723, 1970.
37. I Hagel. Anal Chem 50:569, 1978.
38. M Dreux, Lafosse. In ZE Rassi, ed Carbohydrate Analysis. Amsterdam: Elsevier, 1995, Chap. 13.
39. TH Mourey, LE Oppenheimer. Anal Chem 56:2427, 1984.
40. R Lew, HG Barth. Int J Polym Anal Charact (submitted).
41. G Glöckner. Gradient HPLC of Copolymers and Chromatographic Cross-Fractionation. Berlin: Springer-Verlag, 1991.
42. T Housaki, K Satoh, K Nishikida, Morimoto. Makromol Chem Rapid Commun 9:525, 1988.
43. K Nishikida, T Housaki, M Morimoto, T Kinoshita. J Chromatogr 517:209, 1990.
44. JN Willis, L Wheeler. Adv Chem Ser 247:253, 1995.
45. P Cheung, ST Balke, TC Schunk, TH Mourey J Appl Polym Sci Appl Polym Symp Ed 52: 105, 1993.
46. WJ Simonsick Jr, L Prokai. Adv Chem Ser 247:41, 1995.
47. G Montaudo, MS Montaudo, C Puglisi, F Samperi. Int J Polym Anal Charact 3:177, 1997.
48. X Fei, K Murray. Anal Chem 68:3555, 1996.
49. K Hatada, K Ute, M Kashiyama, M Imanari. Polym J 22:218, 1990.
50. K Albert. J Chromatogr 703:123, 1995.
51. H Pasch, W Hiller Macromolecules 29:6556, 1996.
52. C Jackson, HG Barth. In: C-S Wu, ed. Handbook of Size Exclusion Chromatography New York: Marcel Dekker, 1995, Chap. 4.
53. JL Ekmanis, RA Skinner. J Appl Polym Sci Appl Polym Symp Ed. 48:57, 1991.
54. WW Yau, SD Abbott, GA Smith, MY Keating. ACS Symp Ser 352:80, 1987.
55. MA Haney. J Appl Polym Sci, 30:3023, 3037, 1985.
56. PJ Flory, TG Fox JR. J Am Chem Soc, 73:1904, 1951.
57. B Ptitsyn, YE Eizner. Sov Phys Tech Phys 4:1020, 1960.
58. P Kratochvil. Classical Light Scattering from Polymer Solutions. New York: Elsevier, 1987.
59. PJ Wyatt, C Jackson, GK Wyatt. Am Lab 20(5):86, 1988.
60. PJ Wyatt, DL Hicks, C Jackson, GK Wyatt. Am Lab 20(6):108, 1988.
61. J Lesec, G Volet J Appl Polym Sci, Appl Polym Symp Ed 45:177, 1990.
62. J Lesec, G Volet, J Liq Chromatogr, 13:831, 1990.
63. C Jackson, HG Barth, WW Yau, Proceedings International Gel Permeation Chromatography Symposium 1991, San Francisco, 1993, p. 751.
64. WW Yau, DR Hill. Int J Polym Anal Charact, 2:151, 1996.
65. JC Giddings. Anal Chem, 39:1027, 1967.

8

Reversed-Phase HPLC: Preparation and Characterization of Reversed-Phase Stationary Phases

Charles A. Doyle

University of Cincinnati, Cincinnati, Ohio

John G. Dorsey

Florida State University, Tallahassee, Florida

I. INTRODUCTION

Reversed-phase liquid chromatography (RPLC) is applicable for separations of a wide variety of solutes with different functionalities. The chromatographic stationary phase contributes essential properties that influence the final outcome of a given chemical separation. Different supports and stationary phases are becoming available that are robust and provide uniquely selective retention behavior for certain particular types of solutes. A variety of physical characteristics of the chromatographic stationary phase affect its final chromatographic performance, including the type and physical properties of the support; the type, quantity, and functionality of the chromatographically active overlayer; and the conditions employed to synthesize the stationary phase. Several techniques have been developed both in the synthesis and characterization of these stationary phases to gain insight into which parameters affect separation quality, and by what mechanisms. This information is being used to develop better, more reproducible stationary phases, with more controlled and predictable retention characteristics.

This chapter covers the preparation and characterization of reversed-phase stationary phases. This topic has been thoroughly reviewed up to 1987 by Sander and Wise [1]. In addition, a useful source of updated information about this topic, as well as other aspects of both reversed- and normal-phase chromatography, can be found in each biannual Fundamental Review issue of *Analytical Chemistry* [2]. This chapter is intended to be a resource covering the present state-of-the art of stationary phases for reversed-phase liquid chromatography. Additionally, a review of the literature from 1987 to early 1995 is also presented. Subjects covered in other chapters of this text (e.g., bioseparations, enantiomeric separations, and so on) have been purposely omitted from this chapter.

II. SILICA

The most common type of stationary phase employed for RPLC consists of nonpolar, hydrophobic organic species (e.g., octyl, octadecyl, or phenyl groups) attached by siloxane (or silyl ether) bonds (—Si—O—Si—) to the surface of a silica support. These stationary phases are prepared by reacting organochlorosilanes (or organoalkoxysilanes) with reactive silanol (SiOH) groups on the surface of the silica. The inorganic network silica (SiO_2) is the most common support material because of its many beneficial properties. Small, spherical particles of silica are available in a variety of particle diameters (typically 3, 5, or 10 μm) and pore

sizes (typically 60–300 Å) of narrow distribution. The mechanical strength of silica allows porous particles with very large surface areas (typically 60–500 m^2 g^{-1}) to be used at high mobile-phase pressures, which yields fast mass-transfer conditions during chromatographic separations. In addition, the silica surface is easily modified owing to reactive SiOH sites. Several recent reviews discuss the properties of silica [3–5].

Unfortunately, there is as yet no "ideal" support material available. Thus, even with the foregoing list of advantageous properties of silica, there are several properties of silica that limit its usefulness under certain experimental conditions: namely, the limited pH stability of silica-based stationary phases and the presence of unreacted silanols and metal impurities that can interfere with certain solutes during chromatographic separations. Silica-based stationary phases are limited to operating within the relatively narrow pH range of approximately 2–8 [6–11] because siloxane bonds hydrolyze at low pH and silica dissolves at high pH, especially in mobile phases with high aqueous content and at elevated temperatures. Bare silica dissolves at about pH 7 [12], whereas the useful range of modified silica can be extended in both the low- and high-pH regions by employing different bonded and polymer-coated phases.

Because of stearic hinderance, only about 25–50% of the silanol groups present on the silica surface (approximately 8 ± 1 μmol m^{-2} on chromatographic-grade silica [9,13,14]) react with organosilanes. Trimethylsilyl (TMS) groups are one of the smallest groups that have been bonded to silica for chromatographic purposes, and thus the highest-bonding densities achieved to date (e.g., 5.43 μmol m^{-2}) [15] have used TMS groups because of their reduced stearic constraints. Silanol groups are weakly acidic (pK_a typically 5–7); thus, they are able to undergo hydrogen-bond and dipole–dipole interactions with polar compounds. Therefore, the unreacted, or residual silanols remaining after surface modification of the silica cause peak tailing and loss of chromatographic resolution, especially for basic solutes [3,4,9,15–17]. Amines have been used to measure the number of reactive silanols [4,18,19] and as tailing-reducing agents [20].

There are several types of surface silanols (Fig. 1) that have their own unique properties that affect both chemical derivatization reactions and adsorptive interactions with solutes. The relative distribution of these different types of silanols may affect the characteristics of silica-based stationary phases more than the absolute number of surface silanol groups [21–28]. The

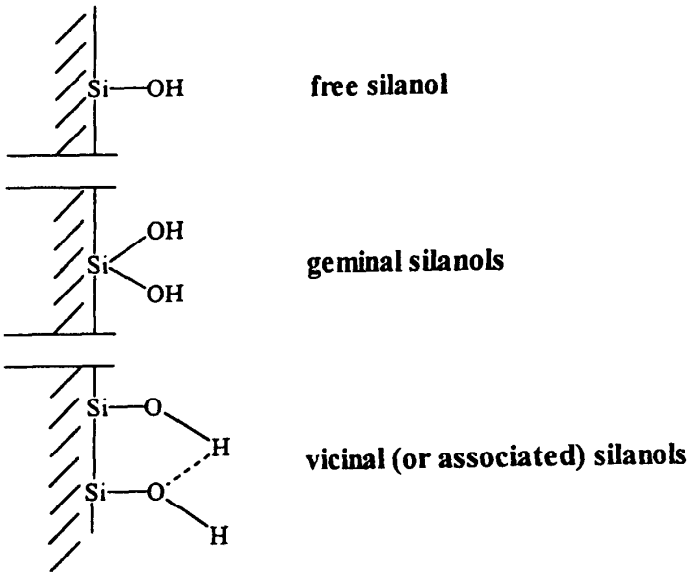


Figure 1 The types of surface silanols present on chromatographic silica gel.

relative importance of each of these different types of silanols has not yet been unambiguously established. Different studies have indicated that each one of these different silanol groups prevails over the other two as the primary reaction and adsorption sites; free, isolated silanols [21,24,25], internally hydrogen-bonded vicinal silanols [28], and geminal silanols [22,23, 26,27], all have been implicated as the primary reaction and adsorption sites.

Depending on which type of silanol group is considered to be contributing the most to derivatization and adsorption, different approaches, especially silica pretreatments, have been proposed to produce phases with reduced silanol activity. Methods to fully hydroxylate the silica surface before derivatization have been employed, as well as methods to reduce the number of surface silanols so that after derivatization the remaining silanols will have all reacted with the silanes. Köhler and Kirkland [17] selectively rehydroxylated the silica surface to produce a homogeneous distribution of associated silanols, whereas van den Driest and Ritchie [23] produced silica with a large population of germinal silanols by rehydroxylation. Reduction in the number of surface silanols before derivatization can be accomplished by either thermal pretreatment or by selective deactivation. Marshall and co-workers [29,30] demonstrated that improved chromatographic efficiencies resulted from the selective deactivation of the more reactive silanols using trimethylmethoxysilane before bonded-phase synthesis.

Thermal pretreatment, followed by either low- or high-temperature silylations, has also been employed [21,25]. High-temperature silylation appears to produce bonded phases that are more efficient and demonstrate little or no residual silanol interactions. Boudreau and Cooper [21] partially dehydroxylated silica by thermal pretreatment to remove the less reactive, associated silanols, resulting in the presence of only the more reactive free, unassociated silanols. These remaining free, unassociated silanols were then nearly completely derivatized by high-temperature silylation owing to the reduction of steric hindrance that resulted from the thermal removal of the associated silanols.

In addition to silanols, metal impurities (Table 1), typically present at about 0.1–0.3% for chromatographic-grade silica, are another source of peak tailing and loss of chromatographic resolution [3,4,15,16,31–35] by the metals acting as adsorption sites themselves, or by enhancing the activity of adjacent silanols. The quantities and types of metal impurities also affect the pH of silica particles. Theoretically, pure silica should have a pK_a of 7.1 ± 0.5, but pK_as ranging from 1.5 to 10 have been reported [3]. Differences in silica-manufacturing methods appear to contribute to the types and quantities of metal impurities found [3,35], as well as to the observed pH of the silicas. The pH values of irregularly shaped silicas are typically relatively neutral, whereas the lowest and highest pH values are found for spherical silica particles [3]. The observed acidity is usually a function of the amount of metal impurities found in the silica. Although there is no exact correlation, silica acidity usually increases with increasing metal content. Different metals contribute unequally to the overall silica acidity and to the acid strengths of different sites on the support. Multivalent metals, such as the lanthanides, aluminum, titanium, and zirconium, can generate sites of high acidity [3], whereas sodium appears to have an opposite effect. The high pH observed for LiChrospher silica gel (pH = 9.2) was attributed to its high sodium content (see silica 10 of Table 1) [15].

Many of the surface metal sites can be removed by acid treatment before derivatization. Compare, for instance, the metal contents of silicas 3, 4, 5, and 6; 14 and 15; 16 and 17; 21 and 22; and 23 and 24 of Table 1, which gives data for pairs of the same silicas before and after different acid-washing procedures. Acid washing reduced the metal content of some silicas by as much as 70% (e.g., see silicas 3, 5, and 6 of Table 1). Köhler et al. [15] report that washing the support with ethylenediaminetetraacetic acid (EDTA) resulted in silica that was completely free of metal impurities, according to inductively coupled plasma–atomic emission spectroscopy (ICP–AES) measurements (compare silicas 12 and 13 of Table 1). In contrast, Nawrocki [3] notes that others have found acid washing more effective than EDTA for removing metal impurities. Complete removal of all metal impurities by washing is un-

Table 1 Trace Metal Analyses of Silica Gel Particles

Metal[a]	1 Nucleosil RP18	2 Partisil ODS-1	3 Herrmann untreated	4 Herrmann washed	5 Herrmann 2 × 1 N HCl	6 Herrmann H_2SO_4 HNO_3	7 Merck	8 Woëlm	9 BASF 4 × 1 N HCl	10 LiChrospher Si-200	11 Nucleosil 5-100	12 Zorbax PSM-60	13 Zorbax PSM-60 EDTA
Li	*	*	*	*	*	*	*	*	*	no	<5	<5	no
Na	5.9	23	650	264	5.0	102	812	740	12.7	2900	56	105	no
Mg	78	79	265	259	69	78	119	<110	25	*	*	*	*
Al	100	80	120	122	86	91	260	1090	820	1100	no	no	no
Cl	570	700	160	40	190	16.0	60	24	43	*	*	*	*
K	3	7	<100	<70	<70	<110	<110	<450	4	*	*	*	*
Ca	123	216	1430	1430	350	305	740	<36	14	no	130	no	no
Ti	61	246	94	97	76	70	220	370	170	235	57	41	no
V	<0.07	<0.06	0.28	0.32	0.06	0.08	0.70	1.70	<0.11	*	*	*	*
Cr	0.662	2.47	0.64	0.60	0.129	0.26	0.70	0.42	1.00	no	no	115	no
Mn	0.24	0.27	0.20	0.12	0.06	<0.10	<0.10	<0.14	0.38	31	no	no	no
Fe	12.0	8.4	35	43	6.7	7	42	61	82	445	76	68	no
Co	0.029	0.057	0.36	0.33	0.023	0.014	0.116	0.004	0.055	*	*	*	*
Ni	<1.7	<1.1	<1.9	<1.7	<0.8	<2	<3	<2	<2.1	*	*	*	*
Cu	*	*	*	*	*	*	*	*	*	no	9	245	no
Zn	5.9	1.30	1.86	1.60	0.38	0.70	0.43	0.24	17.1	*	*	*	*
Rb	<0.1	<0.07	<0.16	<0.16	<0.06	<0.16	<0.2	<0.16	<0.1	*	*	*	*
Zr	9.8	3.5	18	24	22	5.0	36	36	115	no	no	<25	no
Pd	*	*	*	*	*	*	*	*	*	no	no	no	no
Sb	49.0 ppb	64 ppb	88 ppb	94 ppb	84 ppb	86 ppb	138 ppb	136 ppb	126 ppb	625	no	no	no
Ba	0.85	1.8	28	29	1.06	<1.7	37	62	2.6	81	6	no	no
La	52 ppb	49 ppb	550 ppb	560 ppb	130 ppb	170 ppb	530	1070	280 ppb	*	*	*	*
Dy	0.008	<0.005	0.008	0.012	0.008	<0.015	0.010	0.026	0.030	*	*	*	*
Hf	0.379	0.198	0.89	0.90	0.90	0.260	1.47	1.04	3.04	*	*	*	*
U	<0.002	0.0140	0.13	0.15	<0.10	<0.08	<0.1	<0.10	0.113	*	*	*	*
(ppb)[a]													
Sc	14.0	1.50	10.8	11.3	2.80	3.6	11.6	16.6	97	*	*	*	*
As	16.6	9.5	<200	<200	<150	<100	<180	<200	<3.7	*	*	*	*
Cs	<5	<2.8	<4	<3	<1	<4	6	4	7	*	*	*	*
Ce	70	79	720	860	170	212	640	1860	730	*	*	*	*
Sm	9.2	5.8	33	32	9.5	11.9	31	64	80	*	*	*	*
Eu	0.8	0.7	3.8	4.3	1.9	2.2	5.0	12.8	7.5	*	*	*	*
Tb	<6	<4	4	5	2	<3	4	15	8	*	*	*	*
Yb	1.0	<1.8	<50	<60	<40	<30	<40	<40	67	*	*	*	*
Lu	0.165	0.32	*	*	*	*	*	*	12.9	*	*	*	*
Ta	65	157	46	49	47	73	84	98	152	*	*	*	*
W	2.6	250	<150	<150	<100	<70	<130	<120	31	*	*	*	*

Metal[a]	1 Nucleosil RP18	2 Partisil ODS-1	3 Herrmann untreated	4 Herrmann washed	5 Herrmann 2 × 1 N HCl	6 Herrmann H_2SO_4 HNO_3	7 Merck	8 Woëlm	9 BASF 4 × 1 N HCl	10 LiChrospher Si-200	11 Nucleosil 5-100	12 Zorbax PSM-60	13 Zorbax PSM-60 EDTA
Au	0.26	0.11	*	*	*	*	*	*	0.36	*	*	*	*
Th	24.4	14.1	79	84	20	22	87	240	205	*	*	*	*
Σ (ppm)	~950	~1400	~3000	~2400	~850	~900	~2450	~3000	~1300	5417	<339	<604	0

Metal[a]	14 Shimadzu S-I untreated	15 Shimadzu S-I acid washed	16 Shimadzu S-III untreated	17 Shimadzu S-III acid washed	18 Develosil 5 μm 330 m^2/g	19 Kromasil 5 μm 330 m^2/g	20 Kieselgel acid washed	21 Porasil B untreated	22 Porasil B acid washed	23 Porasil C untreated	24 Porasil C acid washed	25 Porasil E untreated
Na	308	no	6	no	25	25	no	194	7.7	294	45	1295
Mg	11	8	0.1	no	51	<0.1	1.3	no	no	no	no	no
Al	264	188	8	6	54	<1	no	673	306	923	598	620
K	42	no	no	no	<0.5	<0.5	*	*	*	*	*	*
Ca	16	13	1	no	215	<1	348	469	189	484	320	380
Ti	230	162	10	7	38	2	16.4	83.1	43.3	173	126	134
Cr	*	*	*	*	*	*	no	no	no	6.4	2.2	9.3
Mn	*	*	*	*	*	*	no	0.8	1.0	2.1	1.6	1.1
Fe	154	33	15	1	<0.2	<0.2	no	615	288	545	371	402
Zr	11	13	3	3	5	<0.2	*	*	*	*	*	*
Mo	*	*	*	*	*	*	no	0.8	0.4	0.8	no	0.4
La	*	*	*	*	*	*	16.1	194	119	175	133	257
Σ (ppm)	1036	417	43.1	17	<389	<30.0	382	2230	954	2603	1597	3099

*, not determined; no, not observed.

[a]The metal contents are in parts per million (ppm) in the upper portion of the table (for Li to U), unless otherwise specified, they are in parts per billion (ppb) for the lower portion of the table (Sc to Th).

Trace metal contents for silica gels 1–9 [35] and 20–25 [32] were obtained by neutron activation analysis (NAA), whereas the contents for silica gels 10–13 [15], 14–17 [33], and 18–19 [31] were obtained by inductively coupled plasma-atomic emission spectroscopy (ICP-AES).

Silica gels 3–6 were Herrmann-DBR silica particles that have been (3) untreated, (4) washed, (5) boiled twice in 1 N HCl for 15 h, and (6) heated at 150°C for several hours with stirring in a 10:1 mixture of sulfuric and nitric acids. The BASF silica gel (9) was boiled four times in 1 N HCl for 15 h. This BASF silica gel contained a total of 5000 ppm metal impurities before acid treatment. Zorbax PSM-60 silica gel (13) was suspended in a 1% Na_2EDTA solution for 1 h, washed with fresh EDTA solution, and then with water to neutrality. Silica gels 14 and 15 were from a batch of silica from Shimadzu (S-I) containing a considerable amount of metal impurities that was (14) untreated and (15) washed with 2 M HCl at reflux temperature for 16 h, respectively. Silica gels 16 and 17 were from a purer batch of silica from Shimadzu (S-III) that was also (16) untreated and (17) acid washed. The Develosil silica (18) and the Kromasil silica (19) were both refluxed in 6 M HCl for 2 h. Silica gel 20, Kieselgel 60, was extracted with 20% HCl. Silica gels 21, 23, and 25 were untreated Porasil B, C and E, respectively. Silica gels 22 and 24 were acid-extracted (20% HCl) Porasil B and C, respectively.

likely because, although there are some metal impurities at and near the silica surface, there are others that are secluded [34], or are buried within the silica particles and, therefore, are inaccessible.

Some acid-washing procedures appear to have little effect on the surface area and pore size of the silica [33], and even on the organic-bonded material [35]. The efficiency of metal impurity removal by washing appears to depend on the surface area and the wall thickness of the silica support, with the efficiency increasing as the surface area increases or the wall thickness decreases [3,32]. The high purity of the Kieselgel silica (see silica 20 of Table 1) after acid washing was attributed, at least in part, to its high specific surface area (442 m^2 g^{-1}), which permitted the leaching of more impurities from the surface and near-surface regions of the support [32]. Different acid-washing procedures are more effective at removing certain metal impurities than other procedures. Certain multivalent elements, such as aluminum and titanium, are very strongly held by the silica matrix, and only limited quantities can be removed by acid washing [3]. For instance, hydrochloric acid and sulfuric acid removed almost all of the iron contamination (90%), but only a little aluminum and titanium [35]. Also, zirconium was affected by sulfuric acid, but not by hydrochloric acid [35].

The advantageous properties of silica have made it the most commonly employed reversed-phase support material. Research is ongoing to further improve silica-based stationary phases and alleviate the problems inherently associated with siliceous materials. In addition, the problems associated with silica have also been the driving force, in part, for the pursuit of more stable bonded phases. Alternative approaches to conventional silica-based stationary phases have included using other support materials (e.g., other metal oxides, polymer-based, and carbon-based supports) and/or coating the surface of the support with an organic polymer.

III. CHEMICALLY BONDED SILICA-BASED PHASES

Chemically bonded silica-based stationary phases are typically synthesized by reacting an organochlorosilane with the silica gel support material in an appropriate organic solvent. The organosilane ($X_{3-n}SiRR'_n$) consists of an organic ligand (R; e.g., saturated *n*-alkyl, alkylphenyl, or alkylcyano) that, ideally, acts as the chromatographic stationary-phase material with which solutes and solvents interact; *n* is the number of other organic ligands (R′; typically methyl groups) bound to the silicon atom (where $n = 0$, 1, or 2); and at least one reactive leaving group (X); e.g., chloro, alkoxy, or dialkylamino). The leaving groups react with the surface silanols of the siliceous support material to yield an organic stationary phase covalently bonded to the silica support through silyl ether (or siloxysilane) linkages (—Si—O—Si—). A variety of organic solvents have been employed for stationary phase syntheses (e.g., a mixture of pyridine and toluene [36], dichloromethane [37,38], methylene chloride, or *N*,*N*-dimethylformamide (DMF) [38]), but chlorinated solvents have been recommended over hydrocarbon reaction solvents when chlorosilanes are used [39,40]. A scavenger-base, or catalyst (e.g., imidazole [38,41], 2,6-lutidine [38], or 4-dimethylaminopyridine [42]), is added to the mixture to neutralize the acidic reaction by-product and drive the reaction equilibrium to the product side. This reaction slurry is typically refluxed for several hours, filtered, rinsed, and then dried. Alternatives to refluxing have included sonication of the reaction mixture [42,43] and the application of fluidized bed technology [44–46]. The methods and mechanisms of stationary-phase syntheses have not been completely explored in a systematic approach; thus, there is room for further improvement through optimization of parameters, such as the selection of silane, solvent, and scavenger-base, as well as other reaction conditions, such as temperature and reaction time.

Recent approaches to silica-based stationary phase synthesis have been directed toward (1) reducing the interaction of silica silanols and metal impurities with solutes, especially basic solutes; (2) improving the hydrolytic stability of the stationary phases in aqueous mobile phases; and (3) synthesizing stationary phases with more predictable and controllable selectivities toward different types of solutes. Many of the synthetic schemes have made improve-

ments in at least one of these areas. Although various ligands (R) have been used for RPLC, the most popular reversed-phase materials are still saturated hydrocarbon chains of 8 (C_8) or 18 (C_{18}) carbons in length. These phases are able to separate hydrophobic compounds as well as most hydrophilic compounds, owing to differing free energies of solutes' partitioning, and because the alkyl chains of the stationary phase lack functional groups; thus they do not provide any strong, specific interactions with solutes.

Depending on the number of leaving groups initially attached to the organosilane, these chemically bonded stationary phases are referred to as either *monomeric* (or monofunctional) (Fig. 2A) when one leaving group is present, or *polymeric* (or polyfunctional) (see Fig. 2B) if two or three leaving groups are attached to the organosilane reactant. Under carefully controlled reaction conditions, monomeric syntheses yield well-defined, reproducible, single-layer coverage of the stationary phase, with only one tie-down point on the support surface per organosilane. The bonding in polymeric syntheses, on the other hand, is more complicated and more difficult to reproducibly control. Multifunctional (e.g., di- and trichloro) organosilanes are capable of multiple attachment to the support surface (one or two tie-down points; three tie-down points are improbable because of steric constraints). In addition, and even more importantly, in the presence of trace quantities of water, the leaving groups can hydrolyze without interacting with the support surface, to form a polymeric network (see Fig. 2B) that extends away from the silica surface.

A. Monomeric Stationary Phases

A great majority of commercially available reversed-phase stationary phases are made by a monomeric process. Typical bonding densities achieved in monomeric syntheses of C_{18} materials are between 2.5 and 3.0 μmol m^{-2}, and are somewhat higher for shorter alkyl chains. Thus, only a fraction of the silanol groups at the silica surface available for bonding (approximately 8 μmol m^{-2}) are derivatized. Because of the steric effects, the maximum coverage obtainable using an octadecyldimethylsilane, for example, is considered to be approximately 4.0–4.7 μmol m^{-2}. Sentell and Henderson [47] recently obtained one of the highest bonding densities reported for a monomeric C_{18} stationary phase (4.4 μmol m^{-2}). One of the highest-bonding densities reported to date (5.43 μmol m^{-2}) [15] for a monofunctional stationary phase was obtained using a trimethylsilane. Smaller ligands on the silane allow the silica surface to be more densely covered owing to the reduced stearic hindrance, compared with larger, bulkier ligands. The pursuit of stationary phases with higher-bonding densities is driven by the fact that they allow improvements in all three areas mentioned previously. Specifically, higher-bonding density phases (1) shield residual silanols from interactions with solutes more efficiently [48], (2) are more stable toward hydrolysis [41], and (3) yield different selectivities than low-bonding density phases, owing to increased alkyl chain ordering and steric constraints [44,49]. In addition, sample loadability is also improved with higher-bonding density phases, as well as by the surface area of the support.

There are several recent examples in the literature of different approaches to synthesizing monofunctional silica-based stationary phases with improved characteristics. A recent approach to increasing the bonding density has employed alkyldihydrosilanes [50,51] as the derivatizing agent to reduce the steric hindrance around the silicon atom caused by the methyl side chains of the more typically employed alkyldimethylsilanes. Unfortunately, this is not a true monomeric synthesis because the Si–H bond is hydrolyzable, and thus some oligomers were detected by nuclear magnetic resonance (NMR) spectroscopy [50].

A method of reducing the number of silanols present in bonded stationary phases is termed endcapping [52]. Following the synthesis of a chemically bonded stationary phase with the desired alkyl silane, several residual surface silanols are still accessible to solute molecules (see Fig. 2). To reduce the number of surface silanols present on the derivatized stationary phase, the stationary phase may be further reacted with small organosilanes (e.g., trimethylchlorosilane, hexamethyldisilazane, or trimethylsilylphosphine) [52–55]. The residual silanols

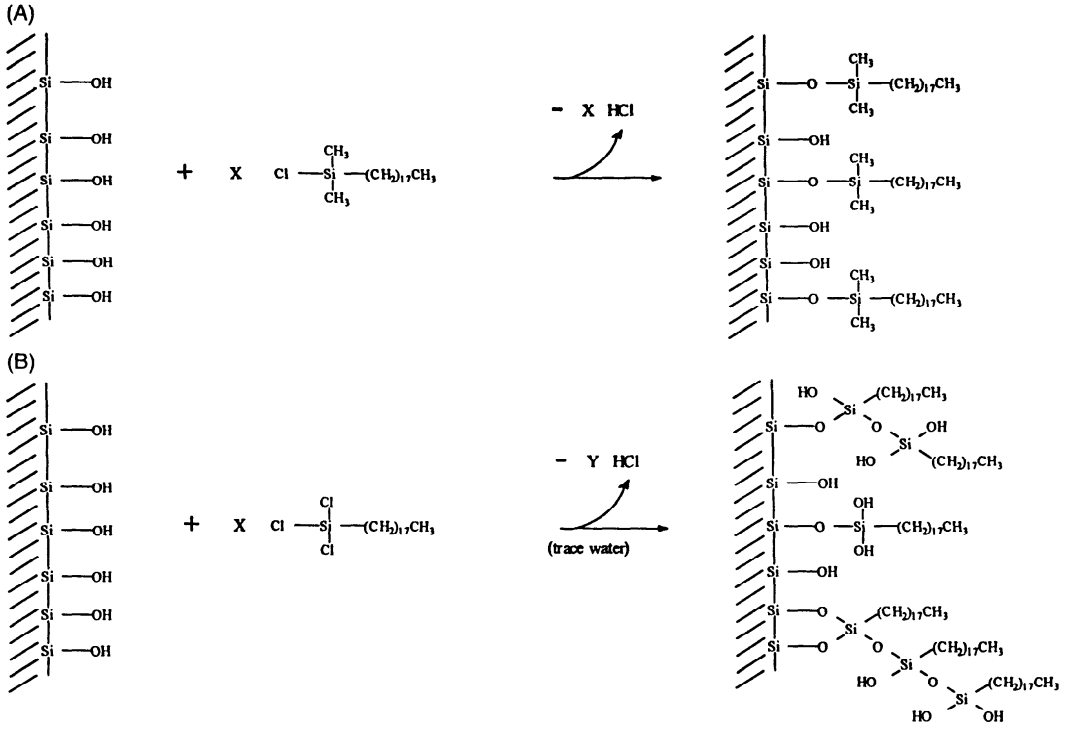


Figure 2 The synthetic schemes for producing (A) monomeric and (B) polymeric silica-based stationary phases. The synthesis of the polymeric phase is illustrated by reaction of silica gel with trichlorosilanes, but similar results are also obtained with dichlorosilanes. The variable *X* represents the number of silanes that react to form the bonded stationary phase, whereas *Y* (where $Y > X$ in the presence of even trace amounts of water) denotes the number of hydrolyzed chlorosilane bonds in polymeric phases (panel B). The remaining silanols, both on the silica surface and on the bonded silanes in polymeric phases (panel B), can be reduced (but not completely eliminated) by further reaction with an "endcapping" reagent, such as trimethylchlorosilane.

are not completely removed, but there is the possibility that the remaining silanols are at least partially shielded by the combination of alkylsilyl groups and endcapping linkages to the surface. Buszewski warns of the risks involved in using hexamethyldisilazane because of ammonolysis of the stationary phase [54].

In addition to endcapping, another approach to shielding residual silanol sites from solute interactions has been to use silanes with bulky ligand groups. Kirkland and co-workers [6,56–58] replaced the two methyl side chains of the silane with bulky isobutyl groups. In addition to sterically protecting residual silanol sites, the bulky ligands also protect the siloxane bond anchoring the alkyl group to the silica surface, resulting in stationary phases with increased hydrolytic stability at low pH, as well as at high temperatures. By using ^{29}Si cross-polarization magic-angle-spinning NMR spectroscopy (^{29}Si CP–MAS NMR), Scholten et al. [59] determined that a diisobutyl-*n*-octadecylsilylated silica-based stationary phase yielded significantly decreased hydrogen bonding of residual silanols to the oxygen atoms of the ligand siloxane bonds than did a conventional dimethyl-*n*-octadecylsilylated phase. They concluded that this observation accounts for the increased chromatographic stability at low pH of the diisobutyl-*n*-octadecylsilylated phases, because the siloxane bond is protected from contact with aggressive, hydrolyzing eluents. Lower-bonding densities are typically obtained when silanes with these bulky isobutyl groups are employed for stationary-phase synthesis, as compared with phases produced using methyl side chains. As a result of these lower-bonding densities, the silica support of these diisobutyl-*n*-octadecylsilylated phases are more susceptible to dissolution at high pH than more densely bonded, conventional dimethyl-*n*-octadecylsilylated phases [58,59]. Gisch et al. [60] found that a *t*-butyl-bonded stationary phase sterically protected residual silanol sites from basic small molecules better than an *n*-butyl-bonded stationary phase. In addition, Hetem and co-workers [61,62] demonstrated that chemical stability of stationary phases increased with increasing alkyl chain length of the organosilane.

Montes et al. [63] have developed a unique synthetic approach to produce chemically bonded silica-based stationary phases with direct Si–C linkages, as compared with the Si–O–SiC linkages of conventional chemically bonded stationary phases. These phases were prepared through olefin hydrosilylation on a hydride–silica intermediate to produce C_8- and C_{18}-modified silicas. In general, the chromatographic behavior of these stationary phases was identical with that of conventional phases produced by organosilanization, but their hydrolytic stability was significantly increased compared with the conventional phases, presumably as a result of the mode of ligand surface attachment.

Several stationary phases have been synthesized in which multiple, monofunctional silicon atoms are present in the derivatizing agent, providing for multiple attachment to the silica surface. Jinno and co-workers [64,65] synthesized *p*-bis(dimethylphenyl)-1,3,5-tris(dimethylphenyl)-, *p*-bis(dimethylbiphenyl)-, and 1,1′,1″-tris(dimethylquaternaryphenyl)-bonded silicas, referred to as P, TP, BP, and QP, respectively. In comparing the retention behavior of polycyclic aromatic hydrocarbons (PAHs) of comparable size [65]; the TP phase demonstrated an enhanced retention of small nonplanar PAHs (three rings), whereas the QP phase selectively retained larger planar PAHs (nine rings). The retention behavior of the BP phase was intermediate between TP and QP. The size and shape recognition abilities of these multidentate phases were attributed to the differences in the space made by cavity-like structures formed by the methyl groups and the phenyl rings of the different bonded phases. Kirkland et al. [6] synthesized a variety of stationary phases using bidentate silanes in which the two monofunctional silicon atoms per silane, joined by methylene [$(CH_2)_n$ where $n = 2$ or 6] or ether spacers, formed two bonds with the silica surface per silane. The extent of bidentate reaction was investigated by ^{29}Si CP–MAS NMR. They concluded that bidentate linkages with the support occurred for the bidentate silanes with methylene spacers. For the bidentate silanes with ether spacers, bidentate linkages with the support were observed when small R groups (i.e., methyls) were attached to the silane silicone atoms, but a mixture of both bidentate and single bonding to the support occurred when bulkier R groups (i.e., iso-

propyl) were attached to the silane silicone atoms. Gilpin and Gangoda [66] proposed several other structures that may result from the reaction of bidentate silanes with silica under different reaction conditions.

Itoh et al. [67] used C_{18}-derivatized nonporous silica for the separation of small molecules. Gradient elution provided rapid separations of various solutes. The sample loadability is greatly reduced on nonporous stationary phases compared with porous stationary phases owing to the reduced surface area of nonporous materials.

Smith and Miller [68] found selectivity differences among three commercially available cyanopropyl-bonded columns, which were generally thought to behave similarly to short alkyl–silyl-bonded columns. In addition, the stability of sterically protected, diisobutylcyanopropyl-derivatized stationary phases was also investigated [6,69]. Houbenová et al. [69] found that the sterically protected phases were more hydrolytically stable than conventional cyanopropyl-modified phases when exposed to aggressive eluents at both low and high pH, although occasionally, alkaline eluents did start to dissolve the silica substrate.

Also, investigations of the chromatographic behavior of a variety of aromatic and cyclic stationary phases produced by both monomeric- and polymeric-bonding schemes have been reported. Examples of these stationary phases include the following: phenylmethyl-, nitrophenylethyl-, diphenyl-, triphenyl-, naphthylethyl-, and pyrenylethyl-bonded silica [70–74] as well as norpinyl-, decadiynyl-, phenylbutyl- and β-naphthyl- [75], and adamantyl-bonded [75,76] silica-based stationary phases.

B. Polymeric Stationary Phases

The bonding in polymeric syntheses typically varies from one synthesis to the next owing to the presence of multiple, easily hydrolyzable leaving groups attached to the organosilane. Thus, with increasing polymerization, the polymeric network extends farther away from the silica surface (see Fig. 2B) and, simultaneously, the bonded mass, or carbon content, also increases. The surface coverage of these stationary phases is difficult to define. The concept of bonded chain density employed for monomeric stationary phases is incalculable for polymeric stationary phases because the *bonding density* is defined as the number of chains per unit *surface* area. Comparison of monomeric and polymeric stationary phases is, therefore, typically based on the carbon contents of the phases to approximately represent the differences in stationary phase loadings. For ease of comparison only, *bonding densities* of polymeric stationary phases are reported in this chapter to allow a convenient means of comparing monomeric and polymeric stationary phases. Polymeric phases tend to give higher retention values because of the increased mass of the stationary phases. Additionally, the thick polymeric layers partially shield residual silanols and result in stationary phases that are more hydrolytically stable than monomeric stationary phases.

Sander and Wise [77] have demonstrated that, under carefully controlled reaction conditions, such as water content, reproducible polymeric stationary phases can be produced. They prepared a polymeric C_{18} phase with a relative standard deviation of only 0.96% in surface coverage over four trials. Wirth and Fatunmbi [78] horizontally polymerized a mixture of C_{18}- and C_3-trichlorosilanes such that significant Si–O–Si bridging of the silanes occurred parallel to the silica surface. The chromatographic behavior of the resulting stationary phase was more similar to that of conventional monomeric stationary phases than polymeric stationary phases. Simpson and co-workers [45] synthesized oligomeric and polymeric stationary phases using the fluidized bed technique. They were able to control the polymerization by performing stepwise silanization reactions alternating with the hydrolysis of unreacted chlorine atoms to produce oligomeric layers of the derivatizing agent. In addition, Den and Lee [79] synthesized a series of oligomeric and polymeric stationary phases using 1,8-disilyloctanes.

C. Selectivities of Monomeric and Polymeric Stationary Phases

Chromatographic selectivity α is an expression of the relative retention of two solutes in a chromatographic separation, and it is a useful experimental parameter for examining the solute retention process. Selectivity reflects the difference in the Gibbs free energy of transfer from the mobile phase to the stationary phase of two solutes a and b:

$$\alpha = \frac{k'_b}{k'_a} \qquad \text{and} \qquad \ln \alpha = \frac{-\Delta(\Delta G)}{RT} \tag{1}$$

where k'_a and k'_b are the solute capacity factors, ΔG is the Gibbs free energy, R is the gas constant, and T is the absolute temperature. Identification and optimization of the relevant interactions that affect selectivity has been an ongoing topic of interest in the chromatographic literature because small improvements in selectivity can result in substantial improvements in both resolution and time of analysis.

The improvement in resolution R_s with enhanced selectivity can be illustrated through the use of the fundamental resolution equation:

$$R_s = \left[\frac{\sqrt{N}}{4}\right]\left[\frac{\alpha - 1}{\alpha}\right]\left[\frac{k'_b}{1 + k'_b}\right] \tag{2}$$

where R_s is a measure of the degree of separation between two peaks; N is the column efficiency or number of theoretical plates, and k'_b is the capacity factor for the later of the two eluting solutes. This expression can be derived by assuming gaussian peak shapes and that the two peaks are closely spaced and thus have equal peak widths. Should the peaks be cut and collected at the valley between them, an R_s value of 1.0 corresponds to solute purities of about 97.73% in each of the two gaussian peaks, whereas baseline resolution is achieved at $R_s = 1.5$ and the peaks are now about 99.87% pure. As indicated in Eq. (2), resolution depends on the square root of efficiency, which implies that, to double the resolution, the efficiency must be quadrupled. This fourfold increase in efficiency would require fourfold increases in column length, time of analysis, pressure drop, and solvent consumption, as well as further dilution of the solutes. Additionally, it may be very difficult to obtain such an increase in efficiency; therefore, increasing the efficiency is not typically a convenient means of adjusting the resolution.

Rearrangement of Eq. (2) to give the number of theoretical plates required (N_{req}) for a given separation is a more convenient means of evaluating selectivity contributions:

$$N_{req} = 16R_s^2\left[\frac{\alpha}{\alpha - 1}\right]^2\left[\frac{1 + k'_b}{k'_b}\right]^2 \tag{3}$$

By solving Eq. (3) for different values of α, while keeping R_s and k'_b at fixed typical values, demonstrates the ease with which a particular separation can be accomplished with increasing selectivity. For fixed values of $R_s = 1.0$ and $k'_b = 2.0$, an α value of 1.01 requires 367,000 theoretical plates. Increasing α to 1.05 reduces the number of theoretical plates required by about 96% to a value of $N_{req} = 16{,}000$. A further increase in α to 1.10 results in an additional 73% reduction in the number of theoretical plates required ($N_{req} = 4{,}400$) to achieve this separation. Considering that a typical analytical column is able to generate only 10,000–15,000 theoretical plates, the foregoing example illustrates the substantial contribution that even small improvements in selectivity can have on chromatographic separations.

Typically, selectivity is adjusted by changing either the mobile-phase composition (solvent strength optimization) [80] or the mobile-phase organic modifier (solvent selectivity optimization) [81]. Alternatively, employing the same mobile-phase composition when comparing different stationary phases allows stationary phase contributions to be selectivity examined [82]. The latter approach has been employed for alkyl-bonded, silica-based stationary phases

to investigate how changes in stationary-phase properties, such as chain length, bonding density, and substrate pore size, influence solute retention. For convenience of organization only, discussion of the studies investigating these stationary-phase properties are divided into the categories of retention and selectivity behavior.

1. Retention Behavior

With the same starting silica, Hennion et al. [83] synthesized polymeric phases varying in chain length from C_4 to C_{18} at a constant phase-loading equivalent to about 2.1 μmol m^{-2}. They observed that log k' increased linearly with bonded chain length for nonpolar PAHs, whereas k' increased linearly with bonded chain length for polar phenols. They interpreted these results as indicating that the total length of the bonded chain interacts with the solute.

Lork and Unger [84] investigated the effects of bonded alkyl chain length and ligand density on the capacity factors of benzoic acid esters and anilines, with two different series of monomeric bonded phases synthesized using the same starting silica: stationary phases with alkyl chain lengths from C_1 to C_{20} at a constant ligand density of 3.5 $\pm$ 0.2 μmol m^{-2}, as well as C_1, C_4, C_6, C_8, and C_{18}-bonded phases, with ligand densities varied between 0 and 4.1 μmol m^{-2} for each of the alkyl chain lengths. The capacity factors increased linearly as a function of either alkyl chain length or ligand density up to a critical value, beyond which the capacity factors remained constant. The critical chain length was observed between C_{11} and C_{14}, whereas the critical ligand density was between 2.3 and 3.2 μmol m^{-2}, and both values depended on the size of the polar solute. Higher critical chain lengths, but smaller critical ligand densities, were observed for larger solutes. The observance of these critical values was explained by a restricted intercalation of the solutes into the stationary phase.

Sentell and Dorsey [44] have also observed a plateau in solute retention as a function of monomeric C_{18} chain density. They further investigated this phenomenon relative to the lattice interphase model of partitioning by Dill and co-workers [85–87]. This model predicts that, at bonding densities below a critical value (predicted to be 2.7 μmol m^{-2} for C_{18} phases), partitioning and retention will increase linearly with increasing surface density. Above the critical-bonding density, chain-packing constraints become increasingly severe, leading to an entropic expulsion of the solute from the stationary phase; thus, partitioning is expected to decrease. This decrease in partitioning was confirmed experimentally [44], for which a maximum in the partition coefficient was observed at a bonding density of about 3.1 μmol m^{-2}. In addition, the observed plateau in retention was determined to be due to compensating changes in the partition coefficient and the stationary phase volume.

2. Selectivity Behavior

Methylene group selectivity refers to the retention behavior of solutes of a homologous series of methylene units. Plots of ln k' versus the number of carbon atoms in the alkyl chain of the homologue yields a straight line. The slope of this line is the natural logarithm (ln) of methylene selectivity and is a measure of the free energy of transfer of one methylene group from the mobile phase to the stationary phase. The retention of solutes in a homologous series is driven solely by nonspecific hydrophobic interactions between the alkyl chain of the solute and alkyl chains of the stationary phase. Therefore, their retention is expected to be influenced only minimally by the properties of the stationary phase and largely by the mobile phase.

Tchapla et al. [88] examined methylene selectivity for C_1, C_6, C_8, C_{14}, and C_{18} monomeric-bonded phases as a function of solute carbon number n_c. They observed a gradual decrease in selectivity up to a certain solute carbon number n_{crit}, which corresponded to the chain length of the stationary phase n_{bp}, at which a large step decrease in selectivity occurred. Their explanation of this phenomenon was that the stationary-phase–bonded chains solvate the alkyl chain of the solute molecule and, as long as the length of the solute alkyl chain was less than that of the bonded phase, increasing the number of methylene groups in the solute causes a constant stationary-phase contribution to selectivity. Once the length of the solute alkyl chain exceeds that of the bonded phase, the remaining solute methylene groups no longer penetrate

the chains; they undergo weaker dispersive interactions than those that penetrate, causing a sharp decrease in selectivity. This behavior was not observed with the C_1-bonded phase, for solutes will not penetrate it. Tchapla and Héron [89] expanded on this investigation of methylene selectivity and observed a second break in the curve, referred to as the saturation value, n_{sat}. For solutes with $n_c \leq n_{crit}$, the value of the methylene selectivity was dependent on the functionality of the different homologous series tested. For solutes with $n_{crit} \leq n_c \leq n_{sat}$ and $n_c \geq n_{sat}$, the value of the methylene selectivity was the same, regardless of the series, but was lower when $n_c \geq n_{sat}$. Additionally, the value of n_{sat} decreased with increasing stationary phase-bonding density.

Shape selectivity refers to the discriminate retention of solutes based on their three-dimensional structure. Sander and Wise [90], in their review of a series of investigations, examined the retention behavior of rigid, nonpolar PAHs, relative to their overall structure, on a variety of monomeric and polymeric alkyl-bonded stationary phases. They determined that polymeric C_{18} phases are typically more shape-selective than monomeric C_{18} phases, and that polymeric phases are better able to separate complex mixture of PAHs, especially isomeric mixtures. Wise and Sander [91] investigated the ability of a monomeric C_{18} column (2.52 μmol m^{-2}) and six polymeric C_{18} columns, with coverages between 2.7 and 5.9 μmol m^{-2}, to separate 11 PAH isomers of molecular weight 278. The monomeric column gave poor resolution of the mixture. The resolution was much better on the polymeric phases, but only the high-load columns (above about 5.1 μmol m^{-2}) were able to resolve all of the isomers. In general, the elution order of the solutes followed the trend of increased retention with increasing "length/breadth ratio" (L/B) [92], which is a descriptor of the two-dimensional structure of the solutes. Nonplanar isomers eluted earlier than predicted based on L/B values.

Wise and Sander [91] also investigated the ability of four C_{18} columns to differentiate between linear versus nonlinear solutes and planar versus nonplanar solutes of comparable molecular weights, overall shapes, and molecular dimensions. They compared a monomeric phase with a bonding density of 3.01 μmol m^{-2} and three polymeric phases with bonding densities of 3.55, 4.67, and 4.91 μmol m^{-2}. They observed that nonplanar solutes were eluted before planar solutes and that the selectivity between these solutes increased with increasing planarity/nonplanarity differences between the solutes. Similarly, nonlinear solutes were eluted before linear solutes, and selectivity increased with greater linearity/nonlinearity solute differences. They also observed that the selectivity of these compounds increased with increasing stationary-phase-bonding density.

Several studies [77,93] have found that certain planar and nonplanar PAHs exhibit different elution behavior on monomeric versus polymeric C_{18} columns. These observations have led to the development of a mixture of three PAH compounds by the National Institute of Standards and Technology (NIST) as a Standard Reference Material (SRM) for the empirical characterization of the shape selectivity of C_{18} reversed-phase columns [94–96]. The elution order of this mixture (SRM 869) is indicative of the type of phase. SRM 869 contains benzo[*a*]pyrene (BaP), phenanthro[3,4-*c*]phenanthrene (PhPh), and 1,2:3,4:5,6:7,8-tetrabenzonaphthalene (TBN). BaP is planar, whereas PhPh has a helical structure and is the most nonplanar of the three test solutes, and TBN is a nonplanar saddle-shaped solute (Fig. 3). The elution order for monomeric C_{18} phases is usually BaP $\leq$ PhPh $<$ TBN, whereas for polymeric phases, it is usually PhPh $<$ TBN $\leq$ BaP. The selectivity of TBN to BaP ($\alpha_{TBN/BaP}$) is a convenient means of classifying phase selectivity. Polymeric C_{18} phases yield $\alpha_{TBN/BaP} \leq 1$ and for monomeric C_{18} phases $\alpha_{TBN/BaP} \geq 1.7$, whereas phases that give $1 < \alpha_{TBN/BaP} < 1.7$ (elution order of PhPh $<$ BaP $<$ TBN) are termed intermediate and are often either lightly loaded polymeric phases, such as oligomeric phases [77], or densely loaded monomeric phases.

The greater shape selectivity of polymeric C_{18} phases has been explained in terms of an empirical "slot model" [91] in which the spaces between the bonded alkyl chains of the stationary phase are considered to be slots into which solute molecules penetrate during retention. The size of the slots narrows with increasing phase loading. Thus, planar solutes

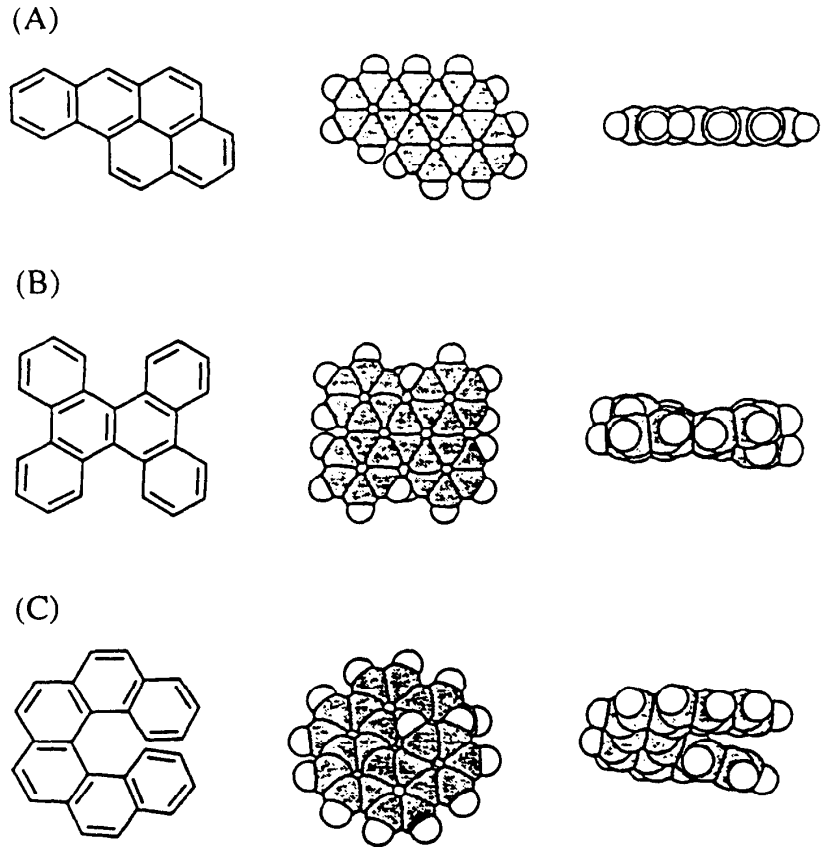


Figure 3 Structures and space-filling models of the compounds in the NIST SRM 869 shape selectivity test mixture: (A) benzo[*a*]pyrene (BaP); (B) 1,2:3,4:5,6:7,8-tetrabenzonaphthalene (TBN); (C) phenanthro[3,4-*c*]phenanthrene (PhPh). (From Ref. 96.)

penetrate narrower slots more readily than nonplanar solutes. Furthermore, long, narrow solutes (larger L/B) penetrate deeper into the slots, permitting more interaction with the stationary phase than bulkier, "square" solutes (smaller L/B). The increased shape selectivity of polymeric phases with increasing phase loading is attributed to the phases becoming more extended and rigid as a result of polymerization.

Sentell and Dorsey [49] examined shape selectivity differences for phenyl compounds, four-ring PAHs, and SRM 869 as a function of monomeric C_{18}-bonding density over the range 1.74–4.07 μmol m^{-2}. Phenyl selectivity, determined in a similar fashion as methylene selectivity, was observed to increase with increasing bonding density. Also, the shape selectivity for the four-ring PAHs generally increased with increasing bonding density, and the solute elution order generally corresponded with increasing L/B of the solutes. The higher bonding density phases (3.60 μmol m^{-2} and above) in this study behaved as oligomeric phases [77] according to $\alpha_{TBN/BaP}$ values of the shape selectivity test mixture SRM 869. Thus, increased selectivity does not appear to be an inherent property of polymeric phases. The enhanced shape selectivity with increasing bonding density was attributed to increased anisotropic chain ordering of the stationary phase.

The selectivity of TBN to BaP ($\alpha_{TBN/BaP}$) is also useful for characterizing whether a particular column is behaving more "polymeric-like" or more "monomeric-like" under a given set of conditions. Sander and Wise [97] synthesized different monomeric and polymeric phases varying in chain length from C_8 to C_{30}. They observed that shape selectivity increased with increasing chain length for both monomeric and polymeric phases. For any given chain

length, the polymeric phases were more shape selective than monomeric phases. Monomeric phases exhibited a gradual change in shape selectivity with alkyl lengths between C_8 and C_{22}, but a large increase in shape selectivity was demonstrated by the monomeric C_{30} phase. The monomeric C_{30} phase exhibited polymeric-like behavior similar to that of polymeric C_{18} phases. The C_{16} to C_{30} polymeric phases exhibited similar polymeric-like selectivity behavior, but the C_{12} and C_8 polymeric phases demonstrated increasingly monomeric-like shape selectivities. These results were explained in terms of the "depth" of the "slots" with which the solutes could interact. Longer alkyl chain lengths result in deeper slots and thus increased solute retention, especially for long, narrow PAHs. In addition, Sander et al. [98] developed a polymeric C_{30} stationary-phase column that is particularly applicable to the separation of carotenoid isomers.

Sander and Wise [99] investigated the effect of substrate pore size on the shape selectivity behavior of both monomeric and polymeric C_{18} stationary phases. For monomeric phases, they generally observed that retention decreased with increasing pore diameter, owing to an accompanied decrease in surface area and thus a decrease in phase loading. However, the shape selectivity behavior of the monomeric phases was essentially unaffected by changes in pore size. Unlike monomeric phases, the polymeric phases demonstrated increased shape selectivity with increasing pore size of the silica support. They explained this observation in terms of a size-limited exclusion of polymerized solution silanes from smaller substrate pores during bonded-phase synthesis for the polymeric phases. The polymeric solution reaction mixture consists of silane monomers as well as silane polymers of various size, which compete for accessible reactive sites on the silica surface. Smaller pore substrates (smaller than about 150 Å) result in phases with reduced polymeric character owing to the easier access of silane monomers in comparison with the excluded silane polymers. Larger substrate pores allow easier access of the larger silane polymers and, thus, an increased polymeric-phase character results. This, in turn, leads to stationary phases with enhanced shape selectivity.

The effect of temperature on shape selectivity has also been investigated. Sentell and Henderson [47] observed linear plots of $\ln k'$ versus $1/T$ (referred to as van't Hoff plots) for several PAHs and polyphenyl compounds on a low-bonding density (1.5 μmol m^{-2}) monomeric C_{18} stationary phase over the temperature range -20 to $+70$°C, but a distinct curvature in these plots at temperatures between 25° and 30°C for the same solutes on a high-bonding density (4.4 μmol m^{-2}) monomeric C_{18} stationary phase. They also observed that the shape selectivity for both columns increased at temperatures lower than 25°C, but that the increases in selectivity were much larger for the high-bonding density column at any given temperature. They explained the behavior of the high-bonding density column in terms of a phase transition occuring between 25° and 30°C in which the bonded alkyl chains become more ordered and rigid at and below this temperature range. The implication of a phase transition is that the bonded alkyl chains undergo a change from a more "liquid-like" behavior above the transition temperature to a more "solid-like" behavior below the transition temperature. The experimental evidence in support of phase transitions and the effect this ordering has on the retention process has been reviewed by Wheeler et al. [100].

Sander and Wise [101] investigated changes in shape selectivity as a function of temperature (-20° to $+100$°C) for commercial monomeric and polymeric C_{18} columns. They observed that selectivity varied continuously over this temperature range for both types of phases, and that shape selectivity was highest at subambient temperatures. Categorizing the selectivity behavior of these columns in terms of $\alpha_{TBN/BaP}$, they observed that both types of phases exhibited increasingly polymeric-like behavior as the temperature was reduced, whereas they approached similar monomeric-like behavior at the high end of the temperatures investigated. In addition, they examined the van't Hoff behavior of these stationary phases and found that the polymeric stationary phase exhibited linear behavior over the temperature range studied, whereas the monomeric stationary phase exhibited a break in the van't Hoff plots occurring in the range 40°–50°C. Because no sharp, distinct changes in selectivity as a function of temperature were observed for either the monomeric or the polymeric phases, they did not

attribute any increase in the selectivity of the monomeric phase to the occurrence of a phase transition. The increased selectivity of both phases at lower temperatures, however, was attributed to increased alkyl chain rigidity and reduced chain mobility, which results in the phases having more liquid crystal-like retention properties at the lower temperatures. Sentell and Henderson [47] pointed out, however, that the greatest selectivity changes for the monomeric phase of Sander and Wise [101] occurred below the transition temperature, whereas the polymeric phase exhibited a more constant change in selectivity with temperature over the entire temperature range studied.

D. Characterization Techniques

A variety of different techniques have been employed to characterize support materials as well as stationary phases. Several of the techniques, including NMR spectroscopy and infrared (IR) spectroscopy, have been employed in many of the papers cited in this chapter. A listing of these techniques and their uses follows, along with selected references of investigations that have used them.

Typically, nitrogen adsorption isotherms measured at 77 K are used to determine specific surface areas, pore volumes, and pore size distributions of both bare and modified chromatographic support materials [102,103]. Specific surface areas obtained from nitrogen adsorption are typically referred to as S_{BET} values because they are determined by methods developed by Brunauer, Emmett, and Teller (BET) [104]. Additional methods of determining pore sizes include mercury intrusion porosimetry [9] and size-exclusion chromatography (SEC) [105]. Particle size distributions can be determined by the Coulter counter method [9,106]. The specific surface area can also be estimated by the quantity of methyl red that adsorbs on silica gel [107]. Giddings and co-workers employed sedimentation–steric field-flow fractionation (FFF) [108] and flow–hyperlayer FFF [109] to determine particle density, porosity, and size distributions (average particle diameters and polydispersities) of chromatographic supports. They also emphasize that the type of mean particle diameter (e.g., area, mass, or number averages) examined affects the measured values and should thus be specified [109]. The use of scanning electron microscopy (SEM) has been employed to examine the particle size, overall shape, and surface morphology of bare and modified support materials [108–110], whereas Tanaka et al. [111] have reviewed the use of transmission electron microscopy (TEM) to examine the internal structure of supports. The types and concentration of hydroxyl groups (silanol groups for silica) associated with support materials has been determined by ^{29}Si CP-MAS NMR [15,112] as well as diffuse-reflectance and transmission infrared spectroscopic techniques [15,113]. Trace metal impurities have been measured by inductively coupled plasma–atomic emission spectroscopy (ICP–AES) [15,33] and neutron activation analysis [3,32,35].

Modified support materials (examples are typically given for alkyl-bonded silicas, but in general are not limited to them) have been characterized by various techniques. The quantity of bonded material is typically calculated from data obtained by carbon, hydrogen, and nitrogen (CHN) elemental analysis and surface area measurements. CHN elemental analysis gives a measure of the amount of carbon, or carbon content, associated with a bonded stationary phase, but this information alone is not a useful descriptor of bonded chain density. Carbon content is only informative if used in conjunction with the surface area of the underivatized support material to give the chain density *on the surface* of the support (typically reported in units of micromoles per square meter, $\mu mol\ m^{-2}$).

A number of different spectroscopic techniques have been employed to investigate the molecular dynamics and interactions that occur at the bonded, silica-based, stationary phase surface. NMR and electron spin resonance (ESR) spectroscopic studies have been reviewed by Sentell [114]. Gilpin [115] reviewed the extensive work by his group using infrared, ESR, and NMR techniques. Fluorescence and UV-visible spectroscopic investigations were reviewed by Rutan and Harris [116]. These investigations have provided insight into the organization,

orientation, and polarity of the bonded alkyl chains. The spectroscopic techniques often provide complementary information, and sometimes, the same behavior is observed by different techniques, further validating the results. Some of the results from these investigations are summarized in the following:

1. Cross-linking of adjacent alkyl ligands on polymeric stationary phases continues to occur after synthesis, and is accelerated under normal RPLC experimental conditions.
2. The mobility of the bonded alkyl chains can approach liquid-like behavior over a wide temperature range, with local viscosities similar to relatively viscous liquids. However, the chain mobility is still anisotropic, and for carbon segments within individual chains, the mobility increases as the segment becomes increasingly distal from the point of attachment. Very short or very long ligands are less mobile than ligands of intermediate length, and the first four carbons from the point of surface attachment in any ligand are very rigid and motionally restricted.
3. Interactions with the surface or neighboring ligands restricts chain motion, and in ligand–ligand interactions, ligand extension is more pronounced at high-bonding densities.
4. Ligand mobility increases in the presence of solvents with increasing wetting ability and results in a more-organized, extended chain configuration. This effect is greater for methylene units near the silica surface than for segments near the chain terminus. In addition, wetting, or solvation, strongly affects the dipolarity and polarizability of the stationary-phase microenvironment. In nonaqueous mobile phases, the stationary phase, and the mobile phase have very similar polarities.
5. Solvents with greater bulk solvent structure, such as methanol or methanol–water mixtures, induce more chain ordering than less-ordered bulk solvents. However, random ligand motions are greatly decreased in the presence of water owing to hydrophobic clustering of the ligands to form a "collapsed" chain structure. Additionally, bulk solvent effects are dependent on the phase length. The alkyl chains of C_{18} phases are capable of protecting the solute from exposure to bulk solvent through solute partitioning, whereas shorter ligands appear to adsorb solutes, and C_8 phases tend to demonstrate intermediate behavior.
6. Also, the surface-attached ligands are inhomogeneously distributed across the silica surface, and the extent of aggregation depends on the stationary-phase bonding density and the nature of the overlying solvent.

Sanders et al. [117] used small-angle neutron scattering to determine bonded-phase thicknesses. They found that the average thickness for a monomeric C_{18} phase is 17 Å, as opposed to the length of fully extended octadecane (23 Å). Ilg et al. [118] employed magnetic resonance imaging (MRI) to examine band profiles in real-time noninvasively, and were able to confirm the "wall effect" in solute elution. Diffuse-reflectance and transmission infrared spectroscopic techniques have also been used to characterize bonded phase supports [7,21,106,119]. The method of gas-phase titration has been used to estimate the number of strongly interacting sites in a chromatographic column [4]. Acid digestion of bonded phases, followed by analysis of reaction products, by techniques such as gas chromatography, NMR, and mass spectrometry, has been used to identify bonded ligands [120,121] and to investigate stationary-phase stability under acidic mobile-phase conditions [7,41,121].

There have been several chromatographic investigations using selected test solutes to characterize the chromatographic performance of experimental as well as commercially available columns. Pauls and McCoy [122] discuss procedures for determining plate heights, peak asymmetry, and silanol and trace metal activity, whereas Sander [95] discusses tests for assessing silanol and trace metal activity, hydrophobicity, stationary phase functionality, and pore size of silica-based stationary phases. Smith [123] recommends the use of alkyl aryl ketones to characterize the retention behavior of reversed-phase supports. As discussed in Section III.C.2, the NIST Standard Reference Material (SRM 869) (see Fig. 3) has been implemented for the classification of commercial columns according to their shape selectivity

behavior toward three polyaromatic hydrocarbons [90,96]. Engelhardt and co-workers [124–126] employed several test mixtures to evaluate the applicability of particular silica-based columns to the separation of basic solutes. Ying and Dorsey [127] employed an $E_T(30)$ solvent polarity scale for characterizing the retentivity of commercially available reversed-phase columns and found that surface area, affecting the volume phase ratio, is the most important parameter in predicting retention. Kimata et al. [16] have devised a chromatographic scheme to evaluate properties of standard packing materials, including surface coverages, types of silanes, and the extent of endcapping. In addition, chemometric methods [128–130] have been employed for the comparison of stationary phases.

IV. POLYMER-COATED SILICA-BASED PHASES

Polymer-coated stationary phases incorporate the mechanical stability of the underlying support material with the chemical stability of the polymerized material. In addition to silica, other metal oxides, including alumina and zirconia, have been coated with polymers and employed for reversed-phase separations (see also sections VII.B and VII.C.3, respectively). Metal oxides are more mechanically rugged than polymers, allowing higher mobile-phase flow rates to be used, and thus, in general, faster separations to be achieved. On the other hand, the polymer overlayer, ideally, provides the chemical stability so that polymer-coated stationary phases may be employed in strongly acidic and strongly basic mobile phases and, in addition, isolates solutes from interactions with chemically reactive groups (e.g., silanol groups for silica gel) present at the surface of the underlying support material. Cross-linking and immobilization of the polymer layers has been catalyzed by thermal treatment with peroxides or by gamma irradiation. The resulting polymer layers can either be physically adsorbed to the support surface or chemically bonded. A variety of polymer coatings have been employed to provide improvements in chemical stability or solute retention. The current status of polymer-coated stationary phases for the reversed-phase separation of small molecules has been reviewed by Schomburg [131], Hanson et al. [132], and Petro and Berek [133]. In addition, Schomburg [131] and Petro and Berek [133] also reviewed some of the other modes of chromatographic separations for which polymer-coated stationary phases have been employed.

Hetem et al. [112] compared the performance of cross-linked polymethyloctadecylsiloxane coatings on silica, with and without trimethylsilane precapping of the substrate, to a monofunctional octadecylsilane-bonded silica (ODS) synthesized from the same batch of silica. For the nonprecapped stationary phase ($PMSC_{18}$), the polymethyloctadecylsiloxane was immobilized by cross-linking, as well as chemical bonding to the silica surface. For the precapped stationary phase ($C_1/PMSC_{18}$), the polymethyloctadecylsiloxane was only physically adsorbed at the hydrophobic, presilanized silica surface. These stationary phases were characterized using multiple techniques before and after different artificial-aging experiments. The polymer-coated phases were more effective at reducing silanophilic interactions than the ODS stationary phase, but exhibited greater interactions with polar solutes, presumably as a result of solute interactions with siloxane bonds in the polymer coatings. $PMSC_{18}$ was the least effective stationary phase at shielding the silica surface during exposure to extreme mobile-phase conditions. Precapping substantially improved the stability of the $C_1/PMSC_{18}$ stationary phase compared with the $PMSC_{18}$ stationary phase. Also, surface shielding of the $C_1/PMSC_{18}$ phase improved considerably in the presence of organic mobile phases. In high pH-buffered aqueous mobile phases containing methanol, this shielding was superior to that of the conventional ODS phase. However, in high pH-buffered aqueous mobile phases without organic modifier, the ODS phase exhibited better shielding properties than the $C_1/PMSC_{18}$ stationary phase.

Ohtsu and co-workers [33,134,135] coated silica with a homogeneous silicone layer by polymerizing silicone monomers (1,3,5,7-tetramethylcyclotetrasiloxane) on the silica surface. Octyl or octadecyl groups were then attached to the silicone polymer by the hydrosilation of

the appropriate 1-alkene in the presence of a soluble platinum catalyst. These stationary phases (commercially available as Capcell-C_8 and -C_{18}) are highly nonpolar, have separating characteristics similar to those of ODS–silica gels, efficiencies typical of silica-based packing materials, and are stable under alkaline conditions. The Capcell-C_{18} stationary phase was compared with ODS and TMS-endcapped ODS phases, all of which were prepared on silicas of varying pretreatment and metal impurity content, for the suppression of undesirable peak tailing caused by hydrogen-bonding, ion-exchange, and chelate formation processes [33]. The silicone polymer coating was more effective at suppressing secondary retention processes than trimethylsilylation of ODS phases. The Capcell-C_{18} stationary phase was compared with different stationary phases in which the C_{18}-modified silicone polymers were prepared before immobilization of the polymer on the silica support [134]. The mobility of the octadecyl groups of the Capcell-C_{18} phase were similar to that of ODS phases based on ^{29}Si CP-MAS NMR results. In addition, the selectivity behavior of the Capcell-C_{18} phase toward aromatic compounds resembled that of conventional ODS phases, rather than the phases produced from the premodified silicone polymers.

Szabó et al. [136,137] compared the chromatographic performance of phenylmethylpolysiloxane-, phenylpropylpolysiloxane-, and diphenylpolysiloxane-coated silicas with that of a chemically derivatized phenylmethyl silica gel. The polarity of the phenylpolysiloxane phases increased in the order phenylmethyl- < phenylpropyl- < diphenylpolysiloxane, and were all less polar than the bonded phenyl phase. In general, the normalized retention (k'/S_{BET}) of a series of polycyclic aromatic hydrocarbons was higher on the more hydrophobic phase (phenylmethylpolysiloxane) and decreased with increasing polarity of the stationary phase.

Hanson et al. [138] coated nonporous silica with polybutadiene (PBD). The stationary phase was characterized by separating small molecules as well as peptides and proteins. The lipophilicity of the stationary phase was evaluated using a mixture of *n*-alkylbenzenes, and the residual adsorptivity of the silica was evaluated using a polarity test mixture. An approximately 1% (w/w) coating of PBD on the silica resulted in a stationary phase with lipophilic character, similar to an octadecyl-bonded derivative on the same type of silica. The residual adsorptivity of the silica support for solutes such as *n*-octylpyridine was eliminated with a minimum PBD load of about 1–3% (w/w). Rapid separations of peptides and proteins were achieved under gradient elution conditions with this stationary phase.

Engelhardt et al. [139,140] produced stationary phases that are more stable than conventional silanized phases and suppress residual silanol interactions by reacting the silica surface with trichlorovinyl silane, and then polymerizing the bonded vinyl groups with acrylic acid derivatives. The acrylic acid derivatives can be varied for different modes of chromatography in addition to reversed-phase separations. An acrylic acid *n*-butylester-coated stationary phase exhibited typical reversed-phase behavior for several test mixtures, but required about a 5–10% increase in water content of the mobile phases to obtain approximately the same retention as with conventional C_{18} reversed phases.

Polar stationary phases were prepared by coating silica with poly(vinylpyrrolidone) (PVP) [141,142] or poly(vinylimidazole) (PVI) [142]. Köhler [141] immobilized various molecular weight PVPs on silica by thermal treatment, γ-radiation, or peroxide-initiated polymerization. The performance of these stationary phases was compared with other phases, including a pyrrolidone ethyl dimethylchlorosilane-derivatized silica stationary phase and a multilayer-coated stationary phase produced by coating a PVP-coated silica with an additional layer of poly(methyloctadecylsiloxane). The hydrolytic stability of the polymerized stationary phases was much greater than that of the silanized stationary phase. The polymerized stationary phases were employed for reversed-phase separations as well as other chromatographic modes. The retention behavior of the multilayer stationary phase was influenced by one or the other of the layers, depending on the separation conditions. Kou et al. [142] reacted the silica surface with γ-methacryloxypropyltrimethoxysilane, and then used this phase as is, or reacted it further with either 1-vinyl-2-pyrrolidone or 1-vinylimidazole in the presence of benzoyl peroxide

to form the polymerized phases. The chromatographic behaviors of all three of these stationary phases were evaluated for a variety of solutes in both reversed- and normal-phase modes.

V. POLYMER-BASED PHASES

The overall performance of polymer-based stationary phases is still typically lower than that of silica-based stationary phases, especially for the separation of small molecules, and this is partly attributed to the microporous structure of the polymer resins [143]. Individual polymer-based phases may offer advantageous properties, such as pressure stability, chemical stability, column efficiency, or beneficial selectivity characteristics, but only rarely are a combination of more than a few of these properties offered in one polymer-based stationary phase simultaneously. Thus, the current status of polymer-based stationary phases is generally as an alternative phase when silica-based stationary phases are inadequate. Because of their chemical stability, polymer-based supports are generally used in place of silica-based supports under extremely acidic or alkaline conditions. The synthesis of polymer gels [144] usually involves suspending the monomers, a cross-linking reagent, and a polymerization initiator in a suitable organic, porogenic diluent by rapidly stirring the mixture in the presence of water to produce organic-phase droplets, the size of which defines the size of the resulting polymer beads. If necessary, a suspension stabilizer is also added to this reaction mixture to prevent the organic phase droplets from coalescing during polymerization. Polymerization proceeds within the organic phase droplets until a critical size is reached, at which time the polymer chains precipitate. The cross-linking reagent allows the polymer to form a rigid three-dimensional structure. The porogen provides the macroporous structure to the gel, and thus, proper selection of the porogen allows the size, distribution, and geometry of pores to be optimized.

A wide variety of polymer-based supports are currently commercially available or are under development. Tanaka and Araki [143] have reviewed the use of polymer-based supports in RPLC. Typically, the polymers employed for RPLC are either hydrophobic or have been derivatized with hydrophobic functional groups. Depending on the circumstances, derivatization renders a hydrophilic polymer hydrophobic, or it is an attempt to produce polymeric stationary phases with retention characteristics similar to those of the commonly employed C_8- and C_{18}-derivatized silica-based stationary phases. Although most of the polymer-based stationary phases are much more stable than silica under stringent mobile-phase conditions (pH 1–13), some types of polymers are not without their own inherent active sites for particular types of solutes. Therefore, even though polymers offer an improvement over silica-based stationary phases as far as pH stability is concerned, their solute-retention characteristics may introduce different problems.

Polystyrene–divinylbenzene (PS-DVB) is probably the most commonly employed polymeric stationary phase. The chromatographic behavior of PS-DVB generally resembles that of ODS silica-based stationary phases [145]. However, PS-DVB shows increased retentivity of aromatic solutes, presumably due to π–π interactions between these solutes and the benzene rings of the polymer [146–148]. Additionally, the retention characteristics of PS-DVB, as well as many other polymer phases, depends on the mobile phase employed. In hydrophilic mobile phases, such as methanol, the polymer shrinks and asymmetric peaks result. However, hydrophobic mobile phases capable of solvating polymer phases (e.g., tetrahydrofuran) cause the polymer to swell, and concomitantly, improved peak symmetries and efficiencies are observed [149–152] along with decreased retention times for aromatic solutes [149]. This improved chromatographic behavior, which is similar to that of bonded silica phases, could be due to the shielding of solutes from active sites on the polymer surface by the adsorbed mobile phase, or because the swelling of the polymer reduces the size of the micropores, restricting the access of solutes to the micropores, resulting in improved mass-transfer characteristics [150,151,153]. An interesting study using PS-DVB was reported by Wang et al. [154]. They performed a free radical polymerization reaction within a chromatographic column to produce

a continuous porous PS-DVB rod that was free of interstitial void volume and had an unusual pore size distribution.

In addition to PS-DVB, the chromatographic behavior of several other underivatized polymers have been investigated recently. Gawdzik [155] varied the ratio of monomers of different polarities to produce three di(methacryloyloxymethyl)naphthalene–divinylbenzene copolymer stationary phases with different retention characteristics. Hosoya et al. [156] employed different diluents in the copolymerization of methyl methacrylate with a divinyl monomer. The sizes and volumes of both micropores and macropores, and thus the retention characteristics of the copolymer, were dependent on the type of diluent used. Diluents that did not solvate the growing polymer during synthesis (e.g., alkanes and *n*-alkyl alcohols) yielded polymer gels that preferentially retained rigid, compact solutes owing to size-exclusion effects that resulted from the production of smaller micropores. In contrast, better solvation by cyclohexanol during the synthesis yielded polymer gels that preferentially retained bulky molecules because larger micropores were produced.

PS-DVB has been modified by hydrophobic alkyl groups [157,158] to induce solute partitioning into the alkyl chains to yield chromatographic behavior resembling bonded silica phases, and by hydrophilic groups [157,159] to produce unique retention characteristics. Recent investigations of the chromatographic behavior of other alkyl-derivatized polymer-based stationary phases have included polyvinyl alcohols (PVA) [150,160–162]; poly(hydroxyalkyl acrylates or methacrylates (PHA) [150,161]; poly(vinyl ethers) (PVE) [163]; *N*-alkyl [164–166] and *N,N*-dialkyl polyacrylamides (PAA) [164,165]; and poly(alkylmethacrylates) (PAM) [150]. Each of these polymer-based phases exhibited their own unique retention characteristics. In general, they were all fairly stable in acidic and alkaline media, especially compared with silica-based supports. The C_{18}-PVA [166], C_{18}-PVE [163], and *N,N*-dialkyl PAA [164,165] typically demonstrated better chromatographic performance than ODS silica-based stationary phases for the separations of bases, such as amines. The performance of many of these stationary phases depended on the mobile phase employed, the microporosity, and where appropriate, the ratio of monomers used to synthesize the polymer phases.

Tanaka et al. [150,161] compared the retention characteristics of PS-DVB, several alkyl-derivatized polymers, and a C_{18}-bonded silica stationary phase for a variety of solute classes. Although each of the polymers had their own unique retention characteristics, in general, the polymer phases preferentially retained structurally rigid, aromatic compounds, whereas the silica-based phase preferentially retained bulky, flexible solutes. The solute retention order on the polymer-based phases was opposite that on the silica-based stationary phase, and generally increased in the order: linear alkanes, cycloalkanes, flexible aromatic compounds, PAHs. The derivatized polymers tended to provide much better column efficiencies than the PS-DVB. This is probably due to the different solute retention mechanisms that the two different types of stationary phases undergo to achieve separations. The alkyl-derivatized polymers interact with solutes through a partitioning mechanism, which is weaker in energy than the adsorption mechanism of solute retention operating in the case of underivatized PS-DVB. Therefore, a faster solute exchange is occurring between the stationary and mobile phases in the alkyl-derivatized polymers, and thus higher column efficiencies are achieved.

Increased retention of certain types of solutes by specific polymer-based stationary phases can be attributed to particularly strong interactions of these solutes with active sites on the surfaces of the different polymers. Polar and aromatic solutes may interact with the π electrons of the benzene rings of PS-DVB. Aromatic solutes may also undergo π–π interactions with the triallylisocyanurate groups used as cross-linking agents for the production of certain PVAs [163,167–169]. *N*-Alkyl PAA [166] contains amide moieties (CONH) which can hydrogen bond with carbonyl groups of certain solutes (e.g., alkyl benzoates), resulting in asymmetric chromatographic peaks [164,165]. *N,N*-Alkyl PAAs [164,165] and the vinyl ether (PVE) derivatives [163] lack amide moieties as well as aromatic moieties; therefore they do not exhibit the aforementioned difficulties.

VI. CARBON-BASED PHASES

Carbon-based phases have lower sample-loading capacities and are typically not as efficient as conventional ODS phases, but they offer the advantages of increased chemical stability and the possibility of performing separations that are difficult on conventional ODS stationary phases. Currently, the most commonly used form of carbon for reversed-phase chromatographic applications is porous graphitic carbon (PGC). The production of PGC consists of the impregnation of a porous silica template with a phenol–formaldehyde resin, graphitization of the organic resin by pyrolysis, followed by the dissolution of the silica template. The resulting carbonaceous material consists of "intertwined two-dimensional graphitic ribbons" [170] that are essentially free of functional groups, having adequate mechanical strength to withstand typical solvent pressures employed in HPLC, and a pore structure defined by the formerly present silica template. Knox and Kaur [170] reviewed the different forms and properties of carbon that have been employed for chromatographic applications.

The PGC is chemically stable in both strongly acidic and strongly basic eluents. Kaur [171] lists recommended solvents according to the type of functional groups present on the solutes. PGC is more retentive than typical silica-based bonded phases and thus requires the use of stronger mobile phases to achieve elution comparable with silica-based bonded phases [172]. The homogeneity of PGC makes it suitable for the separation of basic substances, such as amines, without peak tailing [171]. Also, PGC is uniquely selective for the separation of stereoisomers and geometric isomers [170–172]. The retention mechanisms of PGC are not yet completely understood. The unique selectivity of PGC has been attributed to nonspecific, dispersive interactions of solutes with the hydrophobic, essentially flat surface of PGC [170]. In addition, the electronic structure of graphite allows electron donor–acceptor interactions to contribute to the retention of electron-rich solutes. These electronic interactions are maximized by solutes changing the orientation with which they interact with the graphite surface, depending on the solvent polarity conditions [172]. The method of principal component analysis was employed by Kaliszan et al. [173] for a set of noncongeneric aromatic solutes and by Forgács and co-workers for ring-substituted phenols [174,175], ring-substituted anilines [176], and monoamine oxidase inhibitory drugs [177] to characterize the retentive behavior of porous graphitic carbon supports.

Deinhammer et al. [178] used both spherical nonporous glassy carbon and PGC stationary phase particles as working electrodes in a three-electrode system to electrochemically manipulate the capacity factors of aromatic sulfonates both before and during elution from the chromatographic column, without changes in mobile-phase composition. This separation mode, termed electrochemically modulated liquid chromatography, provided potentially useful differences in retention that are not easily obtained through changes in mobile-phase composition. Also, Engel et al. [110] employed a new, low-temperature method of producing glassy carbon to coat silica particles and demonstrated this phase's applicability for RPLC.

VII. METAL OXIDE SUPPORTS OTHER THAN SILICA

Metal oxide reversed-phase supports other than silica have included alumina (Al_2O_3), zirconia (ZrO_2), and to a much lesser extent titania (TiO_2). The main advantage of these supports over silica is their greater alkaline stability. Alumina-based matrices measurably start to dissolve outside the pH range of 2–12 [179–181], with significant degradation at pH 13 [179], whereas zirconia-based matrices are completely stable over the pH range 0–14 and, additionally, at temperatures from ambient to 100°C [182,183]. In addition, the refractory nature of zirconia allows it to be heated to high temperatures (>500°C), with less change in pore structure than either silica or alumina [183]. The syntheses and properties of metal oxides have been reviewed by Unger and Trüdinger [184].

Even though alumina and zirconia show greater alkaline stability than silica, they are not without their own inherent difficulties. The chromatographic efficiency of some types of alu-

mina particles is much lower than that of silica because standard alumina consists of a bimodal pore size distribution, with most of its surface area hidden in small pores [185]. Residual sites on alumina tend to interact with phosphate and carboxylate functional groups [180]. The zirconia matrix undergoes interactions with basic and acidic solutes, inorganic and organic orthophosphates, and other polyoxy anions [179,180,186,187]. Acidic and basic interactions can be reduced by using competing agents (e.g., tartrate ions) in the eluent, whereas interactions with polyoxy anions can be reduced in the presence of phosphate ions.

The quantity of experimental data under reversed-phase conditions for these metal oxides is now limited. However, the existing data does illustrate the potential applicability of these supports to a variety of separations. Further investigations are needed to examine alternative metal oxide supports, to study a variety of pore and particle sizes, to continue the development of new and improved bonding and coating procedures, and to collect more chromatographic information about the interactions of these phases with a variety of solutes under various experimental conditions.

A. Chemically Bonded Alumina-Based Phases

Reversed-phase functional groups have been chemically bonded to alumina by reaction with organosilanes [188,189], organolithium compounds [190], and phosphorous-containing organic materials [191,192].

Knox and Pryde were the first to chemically bond stationary phases to alumina for HPLC [189]. For RPLC, they reacted 2-cyanoethylchlorosilane with the hydroxyl groups of the alumina surface to form an Al–O–Si–R linkage. Hirata et al. [188] used a similar linkage by an in situ reaction of a 150-μL injection of a 2% octadecyltriethoxysilane solution in toluene with alumina surfaces in a packed microcapillary column. This column was employed for the separation of a test mixture of PAHs and also for the separation of a mixture of basic compounds.

The Al–O–Si bond is more polar and, therefore, more easily hydrolyzed than the Si–O–Si bond of silica-based-bonded stationary phases [190,193]. Laurent et al. [193] found that most chemical reagents that have been successfully employed to modify silica show no reactivity toward alumina, including trimethylchlorosilane (TMCS). They were, however, able to bond the highly nucleophilic hexamethyldisilazane (HMDS) to the alumina surface, but the HMDS was rapidly displaced when contacted with polar solvents, such as methanol and, especially, water.

Pesek and Lin [190] tried several approaches to bonding organic species to alumina, the most successful being a two-step reaction approach involving the initial chlorination of surface Al–OH groups by thionyl chloride, followed by the reaction of the resulting Al–Cl sites with *n*-butyllithium to yield a bonded phase of the type Al–R. This *n*-butyl alumina stationary phase exhibited reversed-phase behavior for alkyl aryl ketones and was also successfully used to separate several common proteins.

Monomeric octyl and octadecyl aluminas (OCA and ODA, respectively) were produced by reaction of either a phosphonic acid [$RPO(OH)_2$] or a phosphinic acid [RR'PO(OH)] with alumina [191,192]. The porous alumina particles (Unisphere) employed for these stationary phases (as well as for several studies using polybutadiene-coated alumina [PBDA; see Sec. VII.B]) were developed by Wilhelmy [194], and consist of microplatelets fused together to form symmetric, spheroidal particles. Haky et al. employed octadecyl-bonded Unisphere alumina (ODA) particles for lipophilicity studies [195]; for the separation of small organic molecules [191]; for the separation of proteins and peptides [196]; and ODA, OCA, as well as other support and stationary-phase combinations, for mobile-phase flow-resistance studies [197]. ODA was compared with two ODS columns for the separation of small organic molecules [191]; it has selectivities similar to the ODS columns, as well as giving more efficient separations of organic bases.

B. Polymer-Coated Alumina-Based Phases

Schomburg and co-workers [131,198] developed several approaches to coating alumina particles with polymers, such as polybutadiene and polymethyloctadecylsiloxane, (see also Sec. IV). The column performance of a PBD-coated alumina column was observed to be essentially unchanged after more than 100 h of use with an alkaline mobile phase of pH 12.3 in both isocratic and gradient-elution modes. In addition, they demonstrated the absence of interactions between some basic solutes and surface hydroxyls. Most of the polymer-coated alumina columns employed in other studies have used coating methods similar to those developed by Schomburg and co-workers. Haky et al. employed PBD-coated Unisphere alumina particles for lipophilicity studies [195], for the separation of proteins and peptides [199], and for mobile-phase flow-resistance studies [197]. Other PBD-coated alumina investigations have included lipophilicity studies using Spherisorb alumina [181,200]; solvent strength, selectivity, and retention mechanism studies using Unisphere alumina and experimental PBD-coated alumina columns from Millipore [201]; and evaluation of the correlation between the chromatographic performance and the structure (as characterized by solid-state ^{13}C NMR) of a series of polybutadiene derivatives immobilized on Unisphere alumina [202].

C. Zirconia- and Titania-Based Phases

The concentration of hydroxyl groups on the zirconia surface has been determined to be approximately 9.8 μmol m^{-2} [182], and consists of at least two types of hydroxyl groups: free zirconium–hydroxyl groups, Zr–OH; and bridging zirconium–hydroxyl groups, Zr–(OH)–Zr [203,204]. These hydroxyl groups are available for surface modification by reaction with organosilanes, although the mechanism is not well understood. In addition, the relative chemical reactivity of these surface hydroxyl groups has not been fully investigated. The zirconia surface also contains hard Lewis acid sites [179] that interact strongly with oxyanions, such as phosphates, carboxylic acids, sulfates, and nitrates [182,183]. Nawrocki et al. [205] reviewed the physical and chemical properties of zirconia and its use as a support for RPLC and other separation modes.

1. Carbon-Clad Zirconia

Weber and co-workers [183,206] investigated carbon-clad zirconia stationary phases. Microporous zirconia was coated with carbon by chemical vapor deposition (CVD) of both 1-butanol [206] and toluene [183], resulting in carbon coverages of over 90 and 97% of the available zirconia surface area, respectively. The carbon film passivates the zirconia surface so that it no longer interacts with oxyanions. These phases were, in general, much more retentive, as well as more selective for the separation of both nonpolar and polar geometric isomers than a conventional ODS support. In addition, although the chromatographic efficiency of the carbon-clad zirconia support was lower than that of a conventional ODS column, the zirconia column had better resolving power and provided faster separations than did the ODS column [206]. Increases in solute dipolarity increase retention on the carbon-clad zirconia column, as opposed to decreasing retention on the ODS column, and thus the carbon-clad zirconia column may be useful for separations of compounds that are not retained or well separated on conventional ODS columns. The carbon-clad phase prepared from toluene consists of a heterogeneous surface, and was thus further passivated by treatment with hydrogen at elevated temperatures to remove residual, exposed high-energy adsorption sites on the carbon surface [183]. The carbon-clad zirconia supports were chemically stable even when exposed to stringent mobile-phase conditions: stable in mobile phases to pH 12, as well as being exposed to 5 M nitric acid solution for short periods (100–200 column volumes) and to temperatures as high as 80°C [183]. The sample loading capacities of these carbon-clad and hydrogen-treated carbon-clad zirconia supports are much lower than for conventional-bonded phases, which limits their usefulness for general reversed-phase chromatographic applications [183].

2. Chemically Bonded Zirconia- and Titania-Based Phases

Rigney et al. [180] found that zirconia-bonded phases produced by reaction with organosilanes, organozirconium compounds, and organophosphonates were not stable in alkaline environments. Trüdinger et al. [207], however, reacted *n*-octadecyltrimethoxysilane with zirconia and titania to give bonding densities in the range 1.2–1.4 μmol m^{-2}. The retention and selectivity of these phases were reported to be similar to those of silica-based supports. In addition, the titania-based support was stable up to pH 11, and the zirconia-based support was stable even after 500 h at pH 12. Yu and El Rassi [186] synthesized TMS-endcapped monomeric and polymeric octadecyl-bonded zirconia-based stationary phases, with surface coverages similar to those of octadecyl–silica sorbents, by reaction of nonporous, microspherical zirconia particles with organochlorosilanes. The polymeric phase exhibited higher retention, reduced metallic interactions with basic and acidic solutes, and higher stabilities in the pH range 2–12 than the monomeric C_{18}-zirconia stationary phase. Both phases were effective at separating PAHs, alkylbenzene, and phenyl alkylalcohol homologous series, as well as biological solutes.

3. Polymer-Coated Zirconia-Based Phases

Polybutadiene (PBD) was coated onto zirconia [179,190] and onto carbon-clad zirconia [183] and then immobilized by cross-linking reactions initiated by either chemically generated free radicals or by electron-beam irradiation. Rigney et al. [180] synthesized stationary phases with various levels of polymer loading and found that acidic solutes were still able to strongly interact with the zirconia surface, even in the presence of a thick polymer layer. The use of phosphate ions in the mobile phase reduced these interactions, and enabled the PBD-coated zirconia to give retention characteristics for small molecules comparable with those of alkyl-bonded silica-based stationary phases. These interactions were further reduced by employing carbon-clad zirconia as the support material for the PBD [183]. PBD-coated zirconia improved the peak shapes of basic solutes, such as amines, compared with the tailing peaks obtained on silica-based stationary phases [179]. Amine solutes eluted as sharp, symmetric bands from PBD-coated zirconia under acidic, neutral, or alkaline mobile-phase conditions. The pH stability, especially under alkaline conditions, is one of the biggest advantages of polymer-coated, as well as other zirconia-based supports. These stationary phases were stable over the pH range 0–14 [183].

VIII. ADDITIONAL REVERSED-PHASE SUPPORTS AND STATIONARY PHASES

Additional supports and stationary phases employed for the reversed-phase separation of small organic molecules include the following: controlled porosity glass supports [208–210]; fluoropolymers and fluorocarbon-bonded phases [211–215]; liquid-crystal-bonded phases [216–218]; cyclodextrin- [219] and tetraphenylporphyrin-bonded stationary phases [220,221]; a poly(vinylbenzo-18-crown-6)-immobilized silica-based stationary phase [222]; and a mixed-bed stationary phase combining reversed-phase and anion-exchange modes [223].

IX. SUMMARY

Octadecyl- and octyl-derivatized silica-based stationary phases are still the most widely used reversed-phase liquid chromatographic stationary phases owing to their applicability to the separation of a wide variety of solutes. Although the lot-to-lot reproducibility of stationary phases from any given manufacturer has improved in recent years, ideally identical stationary phases from different manufacturers can yield entirely different separation attributes. These wide variations in the performance of ostensibly the same stationary phases limits the comparison of results from different laboratories and may cause irreproducibility in a standard separation method protocol if a similar stationary phase, from a different lot or manufacturer,

is employed other than the phase used to develop the protocol. This problem is particularly important in the pharmaceutical industry and manufacturing quality control laboratories, where standard methods have been developed, and possibly certified to obtain a desired, consistent, separation result on a routine basis. If the synthetic scheme of a particular column has been altered, or it becomes necessary to obtain a column from a different manufacturer, the separation obtained from the standard method may be altered in an unpredictable way. Determining that the stationary phase has changed, and not the monitored procedure for which the chromatographic method was developed, may not be so easy.

Further understanding of the properties that affect the performance of stationary phases can help avoid the foregoing situation of column irreproducibility and also allow phases with unique retention characteristics to be tailor-made to suit the separation required. Chemically bonded silica-based phases are becoming more rugged, especially with the advent of different bonding schemes. Some of the deficiencies that exist for silica-based phases have stirred the development of alternative supports and overlying phases that can handle harsh aqueous conditions and provide their own selectivity characteristics. Many of these alternative phases need further characterization, and at this point are generally used as substitute phases when conventional ODS phases are inadequate. None of these phases are without their own characteristics and active sites that may or may not be applicable for a particular separation. An understanding of what stationary phase properties are available and required for a particular separation, will aid in the further development of the phases discussed in this chapter and possibly other types of phases that have not yet been discovered.

ACKNOWLEDGMENTS

The authors are grateful to NIH and AFOSR for support during the preparation of this chapter. We also thank Pfizer and Merck Research Laboratories for continued support of our research.

REFERENCES

1. LC Sander, SA Wise. CRC Crit Rev Anal Chem 18:299, 1987.
2. JG Dorsey, WT Cooper, JF Wheeler, HG Barth, JP Foley. Anal Chem 66:500, 1994.
3. J Nawrocki. Chromatographia 31:177 1991.
4. J Nawrocki. Chromatographia 31:193, 1991.
5. A Berthod. J Chromatogr 549:1, 1991.
6. JJ Kirkland, JL Glajch, RD Farlee. Anal Chem 61:2, 1989.
7. NJ Sagliano, RA Hartwick, RE Patterson, BA Woods, JL Bass, NT Miller. J Chromatogr 458:225, 1988.
8. JL Glajch, JJ Kirkland, J Köhler. J Chromatogr 384:81, 1987.
9. KK Unger. Porous Silica, Amsterdam: Elsevier, 1979.
10. A Wehrli, JC Hildenbrand, HP Keller, R Stampfli, RW Frei. J Chromatogr 149:199, 1978.
11. C Horváth, W Melander, I Molnár. Anal Chem 49:142, 1977.
12. RE Majors. In: C Horváth, ed. High-Performance Liquid Chromatography: Advances and Perspectives. New York: Academic Press, p. 79, (1980).
13. RK Iler. J Chromatogr 209:341, 1981.
14. LR Snyder, H Poppe. J Chromatogr 184:363, 1980.
15. J Köhler, DB Chase, RD Farlee, AJ Vega, JJ Kirkland. J Chromatogr 352:275, 1986.
16. K. Kimata, K Iwaguchi, S Onishi, K Jinno, R Eksteen, K Hosoya, M Araki, N Tanaka. J Chromatogr. Sci. 27:721, 1989.
17. J Köhler, JJ Kirkland. J Chromatogr 385:125, 1987.
18. J Nawrocki. J Chromatogr 407:171, 1987.
19. J Nawrocki. Chromatographia 23:722, 1987.
20. E Bayer, A Paulus. J Chromatogr 400:1, 1987.

21. SP Boudreau, WT Cooper. Anal Chem 61:41, 1989.
22. B Pfleiderer, E Bayer. J Chromatogr 486:67, 1989.
23. PJ van den Driest, HJ Ritchie. Chromatographia 24:324, 1987.
24. M Mauss, H Engelhardt. J Chromatogr 371:235, 1986.
25. T Welsch, HJ Frank. J Chromatogr 267:235, 1983.
26. DW Sindorf, GE Maciel. J Am Chem Soc 105:1487, 1983.
27. DW Sindorf, GE Maciel. J Phys Chem 86:5208, 1982.
28. LR Snyder, JW Ward. J Phys Chem 70:3941, 1966.
29. DB Marshall, KA Stutler, CH Lochmüller. J Chromatogr Sci 22:217, 1984.
30. DB Marshall, CL Cole, DE Connolly. J Chromatogr 361:71, 1986.
31. K Kimata, N Tanaka, T Araki. J Chromatogr 594:87, 1992.
32. J Nawrocki, DL Moir, W Szczepaniak. Chromatographia 28:143, 1989.
33. Y Ohtsu, Y Shiojima, T Okumura, J Koyama, K Nakamura O Nakata, K Kimata, N Tanaka. J Chromatogr 481:147, 1989.
34. PC Sadek, CJ Koester, LD Bowers. J Chromatogr Sci 25:489, 1987.
35. M Verzele, M De Potter, J Ghysels. J High Resolut Chromatogr Chromatogr Commun 2: 151, 1979.
36. K Jinno, S Shimura, N Tanaka, K Kimata, JC Fetzer, WR Biggs. Chromatographia 27:285, 1989.
37. KD Lork, KK Unger, JN Kinkel. J Chromatogr 352:199, 1986.
38. JN Kinkel, KK Unger. J Chromatogr 316:193, 1984.
39. K Jones. J Chromatogr 392:1, 1987.
40. K Jones. J Chromatogr 392:11, 1987.
41. NJ Sagliano, TR Floyd, RA Hartwick, JM Dibussolo, NT Miller. J Chromatogr 443:155, 1988.
42. KB Sentell, KW Barnes, JG Dorsey. J Chromatogr 455:95, 1988.
43. JG Dorsey, KB Sentell, KW Barnes. US Patent 4,919,804, 1989.
44. KB Sentell, JG Dorsey. Anal Chem 61:930, 1989.
45. RPW Scott, CF Simpson. J Chromatogr Sci 30:59, 1992.
46. TM Khong, CF Simpson. Chromatographia 24:385, 1987.
47. KB Sentell, AN Henderson. Anal Chim Acta 246:139, 1991.
48. B Buszewski, Z Suprynowicz, P Staszczuk, K Albert, B Pfleiderer, E Bayer. J Chromatogr 499:305, 1990.
49. KB Sentell, JG Dorsey. J Chromatogr 461:193, 1989.
50. F Meiouet, G Felix, H Taibi, H Hommel, AP Legrand. Chromatographia 31:335, 1991.
51. RD Golding, AJ Barry, MF Burke. J Chromatogr 384:105, 1987.
52. NHC Cooke, K Olsen. J Chromatogr Sci 18:512, 1980.
53. Z Matus, R Ohmacht. Chromatographia 30:318, 1990.
54. B Buszewski. Chromatographia 28:574, 1989.
55. DB Marshall, CL Cole, AD Norman. J Chromatogr Sci 25:262, 1987.
56. JJ Kirkland, CHJ Dilks, JE Henderson. LC-GC 11:290, 1993.
57. JJ Kirland, JW Henderson. J Chromatogr Sci 32:473, 1994.
58. JJ Kirkland, MA van Straten, HA Claessens. J Chromatogr A 691:3, 1995.
59. AB Scholten, JW de Haan, HA Claessens, LJM van de Ven, CA Cramers. J Chromatogr A 688:25, 1994.
60. DJ Gisch, R Ludwig, LA Witting. J High Resolut Chromatogr Chromatogr Commun 12: 409, 1989.
61. MJJ Hetem, JW de Haan, HA Claessens, LJM van de Ven, CA Cramers, JN Kinkel. Anal Chem 62:2288, 1990.
62. MJJ Hetem, JW de Haan, HA Claessens, LJM van de Ven, CA Cramers, PWJG Wijnen, JN Kinkel. Anal Chem 62:2296, 1990.
63. MC Montes, C van Amen, JJ Pesek, JE Sandoval. J Chromatogr A 688:31, 1994.

64. K Jinno, K Yamamoto, H Nagashima, T Ueda, K Itoh. J Chromatogr 517:193, 1990.
65. K Jinno, K Yamamoto, T Kuwamoto, H Nagashima, T Ueda, S Tajima, E. Kimura, K Itoh, JC Fetzer, WR Biggs. Chromatographia 34:381, 1992.
66. RK Gilpin, ME Gangoda. J Chromatogr Sci 28:227, 1990.
67. H Itoh, T Kinoshita, N Nimura. J Liq Chromatogr 16:809, 1993.
68. RM Smith, SL Miller. J Chromatogr 464:297, 1989.
69. A Houbenová, HA Claessens, JW de Haan, CA Cramers, K Stulík. J Liq Chromatogr 17: 49, 1994.
70. K Kimata, K Hosoya, N Tanaka, T Araki, DGJ Patterson. J Chromatogr 595:77, 1992.
71. G Szabó, E Csató, K Offenmüller, M Dévai, A Borbély-Kuszmann, G Liptai. Chromatographia 26:255, 1988.
72. K Jinno, T Ibuki, H Lamparczyk, M Okamoto, N Tanaka, JC Fetzer, WR Biggs. Chromatographia 25:483, 1988.
73. K Jinno, T Nagoshi, N Tanaka, M Okamoto, JC Fetzer, WR Biggs. J Chromatogr 392:75, 1987.
74. K Jinno, T Nagoshi, N Tanaka, M Okamoto, JC Fetzer, WR Biggs. J Chromatogr 386:123, 1987.
75. AM Stalcup, DE Martire, LC Sander, SA Wise. Chromatographia 27:405, 1989.
76. SS Yang, RK Gilpin. Anal Chem 59:2750, 1987.
77. LC Sander, SA Wise. Anal Chem 56:504, 1984.
78. MJ Wirth, HO Fatunmbi. Anal Chem 65:822, 1993.
79. TG Den, CH Lee. Fresenius Z Anal Chem 330:683, 1988.
80. LR Snyder, MA Quarry, JL Glajch. Chromatographia 24:33, 1987.
81. ACJH Drouen, HAH Billiet, L de Galan. J Chromatogr 352:127, 1986.
82. CH Lochmüller, ML Hunnicutt, JF Mullaney. J Phys Chem 89:5770, 1985.
83. MC Hennion, C Picard, M Caude. J Chromatogr 166:21, 1978.
84. KD Lork, KK Unger. Chromatographia 26:115, 1988.
85. KA Dill. J Phys Chem 91:1980, 1987.
86. KA Dill, J Naghizadeh, JA Marqusee. Annu Rev Phys Chem 39:425, 1988.
87. JG Dorsey, KA Dill. Chem Rev 89:331, 1989.
88. A Tchapla, H Colin, G Guiochon. Anal Chem 56:621, 1984.
89. A Tchapla, S Héron. J Chromatogr A 684:175, 1994.
90. LC Sander, SA Wise. J Chromatogr 656:335, 1993.
91. SA Wise, LC Sander. J High Resolut Chromatogr Chromatogr Commun 8:248, 1985.
92. SA Wise, WJ Bonnet, FR Guenther, WE May. J Chromatogr Sci 19:457, 1981.
93. SA Wise, WE May. Anal Chem 55:1479, 1983.
94. LC Sander SA Wise. J High Resolut Chromatogr Chromatogr Commun 11:383, 1988.
95. LC Sander. J Chromatogr Sci 26:380, 1988.
96. LC Sander, SA Wise. LC-GC 8:378, 1990.
97. LC Sander, SA Wise. Anal Chem 59:2309, 1987.
98. LC Sander, KE Sharpless, NE Craft, SA Wise. Anal Chem 66:1667, 1994.
99. LC Sander, SA Wise. J Chromatogr 316:163, 1984.
100. JF Wheeler, TL Beck, SJ Klatte, LA Cole, JG Dorsey. J Chromatogr 656:317, 1993.
101. LC Sander, SA Wise. Anal Chem 61:1749, 1989.
102. KK Unger, N Becker, P Roumeliotis. J Chromatogr 125:115, 1976.
103. SJ Gregg, KSW Sing. Adsorption, Surface Area and Porosity. New York, Academic Press, 1967.
104. S Brunauer, PH Emmett, E Teller. J Am Chem Soc 60:309, 1938.
105. FV Warren Jr., BA Bidlingmeyer. Anal Chem 56:950, 1984.
106. SO Akapo, CF Simpson. J Chromatogr 557:515, 1991.
107. I Wouters, I Quintens, E Roets, J Hoogmartens. J Liq Chromatogr 13:253, 1990.
108. JC Giddings, MH Moon. Anal Chem 63:2869, 1991.
109. SK Ratanathanawongs, JC Giddings. Chromatographia 38:545, 1994.

110. TM Engel, SV Olesik, MR Callstrom, M Diener. Anal Chem 65:3691, 1993.
111. N Tanaka, K Kimata, T Araki, H Tsuchiya, K Hashizume. J Chromatogr 544:319, 1991.
112. MJJ Hetem, JW De Haan, HA Claessens, CA Cramers, A Deege, G Schomburg. J Chromatogr 540:53, 1991.
113. SG Bush, JW Jorgenson, ML Miller, RW Linton. J Chromatogr 260:1, 1983.
114. KB Sentell. J Chromatogr 656:231, 1993.
115. RK Gilpin. J Chromatogr 656:217, 1993.
116. SC Rutan, JM Harris. J Chromatogr 656:197, 1993.
117. LC Sander, CJ Glinka, SA Wise. Anal Chem 62:1099, 1990.
118. M Ilg, J Maier-Rosenkranz, W Müller, E Bayer. J Chromatogr 517:263, 1990.
119. SG Bush, JW Jorgenson. J Chromatogr 503:69, 1990.
120. K Miyabe, N Orita. Talanta 36:897, 1989.
121. TR Floyd, NJ Sagliano, RA Hartwick. J Chromatogr 452:43, 1988.
122. RE Pauls, RW McCoy. J Chromatogr Sci 24:66, 1986.
123. RM Smith. Anal Chem 56:256, 1984.
124. H Engelhardt, H Löw, W Götzinger. J Chromatogr 544:371, 1991.
125. H Engelhardt, M Jungheim. Chromatographia 29:59, 1990.
126. H Engelhardt. Pure Appl Chem 61:2033, 1989.
127. PT Ying, JG Dorsey. Talanta 38:237, 1991.
128. MF Delaney, AN Papas, MJ Walters. J Chromatogr 410:31, 1987.
129. SJ Schmitz, H Zwanziger, H Engelhardt. J Chromatogr 544:381, 1991.
130. BA Olsen, GR Sullivan. J Chromatogr A 692:147, 1995.
131. G Schomburg. LC-GC 6:36, 1988.
132. M Hanson, A Kurganov, KK Unger, VA Davankov. J Chromatogr 656:369, 1993.
133. M Petro, D Berek. Chromatographia 37:549, 1993.
134. O Shirota, Y Ohtsu, O Nakata. J Chromatogr Sci 28:553, 1990.
135. Y Ohtsu, H Fukui, T Kanda, K Nakamura, M Nakano, O Nakata, Y Fujiyama. Chromatographia 24:380, 1987.
136. G Szabó, E Csató, P Keresztes, JP Pallos. J Chromatogr 463:345, 1989.
137. G Szabó, E Csató, P Keresztes, JP Pallos. J Liq Chromatogr 12:2839, 1989.
138. M Hanson, KK Unger, G Schomburg. J Chromatogr 517:269, 1990.
139. H Engelhardt, H Löw, W Beck, W Gotzinger. In: HA Mottola, JR Steinmetz, ed. Chemically Modified Surfaces. Amsterdam: Elsevier, 1992, p. 225.
140. H Engelhardt, H Löw, W Eberhardt, M Mauss. Chromatographia 27:535, 1989.
141. J Köhler. Chromatographia 21:573, 1986.
142. CR Kou, HD Luoh, CC Huang, TG Den. Fresenius Z Anal Chem 336:409, 1990.
143. N Tanaka, M Araki. Adv Chromatogr 30:81, 1989.
144. DC Sherrington. In: P Hodge, DC Sherrington, eds. Polymer Supported Reactions in Organic Synthesis. New York: Wiley, 1980, Chap. 1.
145. S Coppi, G Blo, A Betti. J Chromatogr 388:135, 1987.
146. JR Benson, A Woo. J Chromatogr Sci 22:386, 1984.
147. A Sugii, N Ogawa, K Harada, I Sato. J Chromatogr 294:185, 1984.
148. DS Dieter, HF Walton. Anal Chem 55:2109, 1983.
149. S Pedigo, LD Bowers. J Chromatogr. 499:279, 1990.
150. N Tanaka, T Ebata, K Hashizume, K Hosoya, M Araki. J Chromatogr 475:195 1989.
151. HW Stuurman, J Köhler, SO Jansson, A Litzén. Chromatographia 23:341, 1987.
152. LD Bowers, S Pedigo. J Chromatogr 371:243, 1986.
153. F Nevejans, M Verzele. Chromatographia 20:173, 1985.
154. QC Wang, F Svec, JMJ Fréchet. Anal Chem 65:2243, 1993.
155. B Gawdzik. J Chromatogr 549:77, 1991.
156. K Hosoya, S Maruya, K Kimata, H Kinoshita, T Araki, N. Tanaka. J Chromatogr 625:121, 1992.
157. JJ Sun, JS Fritz. J Chromatogr 522:95, 1990.

158. D MacBlane, N Kitagawa, JR Benson. Am Lab News 19:24, 1987.
159. JJ Jagodzinski, GT Marshall, BJ Poulsen, G Raza, WA Rolls. J Chromatogr 591:89, 1992.
160. T Ohtani, Y Tamura, M Kasai, T Uchida, Y Yanagihara, K Noguchi. J Chromatogr 515: 175, 1990.
161. N Tanaka, K Hashizume, M Araki. J Chromatogr 400:33, 1987.
162. M Hirukawa, Y Arai, T Hanai. J Chromatogr 395:481, 1987.
163. C Hirayama, H Ihara, S Nagaoka, H Makise. Chromatographia 33:19, 1992.
164. C Hirayama, H Ihara, S Nagaoka. J Liq Chromatogr 16:647, 1993.
165. S Nagaoka, H Ihara, C Hirayama. Polym J (Tokyo) 25:609, 1993.
166. JV Dawkins, NP Gabbott, LL Lloyd, JA McConville, FP Warner. J Chromatogr 452:145, 1988.
167. S Coppi, A Betti, C Bighi, GP Cartoni, F Coccioli. J Chromatogr 442:97, 1988.
168. RM Smith, DR Garside. J Chromatogr 407:19, 1987.
169. RK Gilpin, MF Burke. Anal Chem 45:1383, 1973.
170. JH Knox, B Kaur. Chem Anal (NY) 98:189, 1989.
171. B Kaur. LC-GC 8:468, 1990.
172. BJ Bassler, RA Hartwick. J Chromatogr Sci 27:162, 1989.
173. R Kaliszan, K Osmialowski, BJ Bassler, RA Hartwick. J Chromatogr 499:333, 1990.
174. E Forgács, T Cserháti, K Valkó. J Chromatogr 592:75, 1992.
175. E Forgács, K Valkó, T Cserháti. J Liq Chromatogr 14:3457, 1991.
176. E Forgács, T Cserháti. J Chromatogr 600:43, 1992.
177. E Forgács, K Valkó, T Cserháti, K Magyar. J Chromatogr 631:207, 1993.
178. RS Deinhammer, E-Y Ting, MD Porter. Anal Chem 67:237, 1995.
179. DA Hanggi, NR Marks. LC-GC 11:128, 1993.
180. MP Rigney, TP Weber, PW Carr. J Chromatogr 484:273, 1989.
181. R Kaliszan, J Petrusewicz, RW Blain, RA Hartwick. J Chromatogr 458:395, 1988.
182. MP Rigney, EF Funkenbusch, PW Carr. J Chromatogr 499:291, 1990.
183. TP Weber, PW Carr, EF Funkenbusch. J Chromatogr 519:31, 1990.
184. KK Unger, U. Trüdinger. Chem Anal (NY) 98:145, 1989.
185. I Halász, K Martin. Angew Chem Int Ed Engl 17:901, 1978.
186. J Yu, Z El Rassi. J Chromatogr 631:91, 1993.
187. CB Ampheltt, LA McDonald, MJ Redman. J Inorg Nucl Chem 6:236, 1958.
188. Y Hirata, M Novotny, T Tsuda, D Ishii. Anal Chem 51:1807, 1979.
189. JH Knox, A Pryde. J Chromatogr 112:171 (1975).
190. JJ Pesek, HD Lin. Chromatographia 28:565, 1989.
191. JE Haky, S Vemulapalli, LF Wieserman. J Chromatogr 505:307, 1990.
192. LF Wieserman, et al. US Patents 4,786,628, 1988; 4,788,176, 1988; 4,904,634, 1990.
193. C. Laurent, HAH Billiet, L de Galan. Chromatographia 17:253, 1983.
194. RB Wilhelmy, et al. US Patents 4,822,593, 1989; 4,900,537, 1990.
195. JE Haky, S. Vemulapalli. J Liq Chromatogr 13:3111, 1990.
196. JE Haky, AR Raghani, BM Dunn, LF Wieserman. Chromatographia 32:49, 1991.
197. JE Haky, ND Ramdial, AR Raghani, LF Wieserman. J Liq Chromatogr 14:2859, 1991.
198. U Bien-Vogelsang, A Deege, H Figge, J Köhler, G Schomburg. Chromatographia, 19:170, 1984.
199. JE Haky, A Raghani, BM Dunn. J Chromatogr 541:305, 1991.
200. R Kaliszan, RW Blain, RA Hartwick. Chromatographia 25:5 1988.
201. RV Arenas, JP Foley. Anal Chim Acta 246:113, 1991.
202. JR Garbow, J Asrar, CJ Hardiman. Chem Mater 5:869, 1993.
203. W Hertl. Langmuir 5:96, 1989.
204. PA Agron, EL Fuller, HF Holmes. J Colloid Interface Sci 52:553, 1975.
205. J Nawrocki, MP Rigney, A McCormick, PW Carr. J Chromatogr A 657:229, 1993.
206. TP Weber, PW Carr. Anal Chem 62:2620, 1990.
207. U Trüdinger, G Müller, KK Unger. J Chromatogr 535:111, 1990.

208. H Nagasawa, Y Matsumoto, N Oi, S Yokoyama, T Yazawa, H Tanaka, K Eguchi. Anal Sci 7:181, 1991.
209. M Okamoto, I Yoshida, M. Utsumi, K Nobuhara, K Jinno. J Chromatogr 515:43, 1990.
210. Z Suprynowicz, R Lodkowski, AL Dawidowicz, B Buszewski. J Chromatogr 395:145, 1987.
211. M-P Krafft, F Jeannaux, M Le Blanc, JG Riess, A Berthod. Anal Chem 60:1969, 1988.
212. E Csato, N Fulop, G Szabo. J Chromatogr 511:79, 1990.
213. ND Danielson, LG Beaver, J Wangsa. J Chromatogr 544:187, 1991.
214. AD Kataev, VV Saburov, OA Reznikova, DV Kapustin, VP Zubov. J Chromatogr A 660: 131, 1994.
215. K Jinno, H Nakamura. Chromatographia 39:285, 1994.
216. K Jinno, Y Saito, RMN Chopra, JJ Pesek, JC Fetzer, WB Biggs. J Chromatogr 557:459, 1991.
217. JJ Pesek, EJ Williamsen. Trends Anal Chem 11:259, 1992.
218. Y Saito, K Jinno, JJ Pesek, YL Chen, G Luehr, J Archer, JC Fetzer, WR Biggs. Chromatographia 38:295, 1994.
219. CE Lin, H Cheng, CH Lin, MH Yang, JC Jiang. J Chromatogr Sci 27:665 1989.
220. CE Kibbey, ME Meyerhoff. J Chromatogr 641:49, 1993.
221. CE Kibbey, ME Meyerhoff. Anal Chem 65:2189, 1993.
222. H Harino, K Kimura, N Tanaka, T Shono. J Chromatogr 522:107, 1990.
223. PJ Davis, RJ Ruane, ID Wilson. Chromatographia 37:60, 1993.

9

Normal-Phase Liquid Chromatography

Marcel Caude and Alain Jardy

Ecole Supérieure de Physique et de Chimie de Paris, Paris, France

I. INTRODUCTION

Normal-phase (NP) chromatography is a powerful complement to the more popular reversed-phase–high-performance liquid chromatography (RP–HPLC) method for separating nonionic compounds with moderate molecular weight. Recent surveys show that about one-fifth of all HPLC separations now are realized by NP–HPLC [1].

In this method, the stationary phase is more polar than the mobile phase. Liquid chromatography systems include as stationary phases unmodified silica and other solid adsorbents (adsorption chromatography) and polar-bonded phases (normal partition chromatography). All these phases are operated with nonaqueous, nonpolar, or moderately polar mobile phases; this is an advantage because of the high solute solubility in totally organic solvents.

II. ADSORPTION CHROMATOGRAPHY

A. Stationary Phases

Although materials such as alumina, zirconia, titania, and Florisil receive attention as alternative phases, bare silica is still, by far, the most commonly used support material.

1. Bare Silica

In contrast with the widespread use of silica as LC column packings, its physicochemical structure and chemical properties are often neglected by chromatographers. The books by Unger [2] and Snyder [3] can still be considered basic references, in addition to a recent review [4]. The chemistry of silica is extensively described in the books by Iler [5] and by Scott.

The silica used for LC column packings is essentially porous and noncrystalline with the general formula:

$$[SiO_{2-x/2}(OH)_x]_n \cdot H_2O_p$$

The Si-OH silanol groups are responsible for the polar character of silica packings used in normal phase. Figure 1 shows the possible types of surface silanols. One can distinguish isolated or free silanol groups (having the highest adsorption ability); bonded silanols (interaction by hydrogen bonding between two neighboring silanols also called vicinal silanols or between two OH groups borne by the same silicon atom, known as geminal groups); siloxane

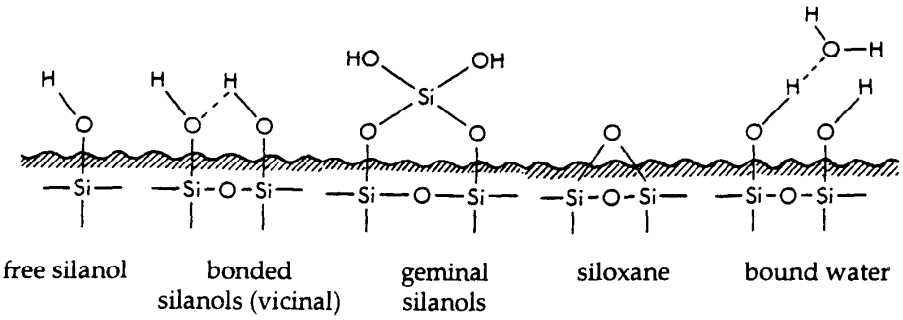


Figure 1 Surface groups on silica gel.

groups (Si–O–Si) are also present, but the activity of these essentially hydrophobic sites is so low that they are not considered of any consequence (a silica completely dehydroxylated by prolonged heating at 1300°C is hydrophobic).

The actual existence and relative quantities of these bound and free silanols on a silica gel surface are strongly dependent on the thermal and chemical history of the silica. Because bare silica gel surface is extremely heterogeneous, deactivation of the strongest active group—free silanols—is necessary. This is the role of water: free silanol groups exist in a different state when covered with a water molecule. This state is energetically close to that of bonded silanols: there is a "levelling effect."

The percentage of free silanols covered with a water molecule, so-called silica activity, depends on the mobile-phase's water content. Reproducible separations require constancy of the silica surface activity. The most effective procedure to stabilize this surface activity is to control the level of water adsorbed on the silica surface. The best method to reach this objective is to adjust the mobile-phase's water content (isohydric mobile phase; see Sec. II.B.3.b).

(*a*) *Water Solubility and Acid–Base Properties.* The water temperature and pH change the solubility of silica. The solubilization equation is

$$SiO_2 + 2H_2O \rightleftharpoons Si(OH)_4$$

The solubility of crystalline and glass forms is in the parts per million (ppm) range. The solubility of silicic acid $Si(OH)_4$ is largely dependent on the pH of the mobile phase. The silanol groups on the silica surface also have an acidic character according to the equation

$$\equiv Si\text{–}OH \rightleftharpoons \equiv SiO^- + H^+$$

The pK_a value of this reaction is about 6.8 (± 0.5), which is 3 pH units lower than the free silicic acid's first ionization constant ($Si(OH)_4$, $pK_{a2} = 9.8$, $pK_{a1} = 12$). The most common explanation is that the tendency for splitting off a proton from a particular silanol group is markedly promoted by its environment, particularly the presence of hydrogen bonds. Consequently, the mobile-phase pH should not exceed 7.5. This slow and insidious solubilization silica can be reduced by the use of a guard, or by a precolumn situated between the pump and the injection valve to saturate the mobile phase in soluble silica.

(*b*) *Density of Silanol Groups.* The density of total silanols on chromatographic-grade silica is about 8 ± 1 μmol m^{-2} (about 4.8 SiOH nm^{-2}). The ratio R of free silanol groups/bonded silanol groups depends mainly on the hydrothermal treatment of the silica (i.e., its specific surface area). The higher the specific surface area, the smaller the mean pore diameter and, consequently, the lower the R ratio (interactions by hydrogen bonding between two free silanol groups are favored).

Silicas with a high population of free silanol groups generally are more acidic and can entail tailing peaks with basic compounds. Bonded silanols are less acidic and a smaller problem for such solutes [6]. According to the percentage of free silanol groups, Kirkland [7,8] arbitrarily classified silicas into two types: type A silicas have a higher R value; are more adsorptive, acidic, and less purified; and consequently, they can exhibit tailing, misshapen peaks, with more polar or basic solutes. Type B silicas, with a lower R value, are more highly purified (metal contamination), are less acidic, and often preferred by users.

2. Miscellaneous Adsorbents

Despite the many desirable properties of silica, it still has one main drawback: its limited range of pH stability (between 2 and 7.5).

Several approaches have been developed to overcome this difficulty for partition chromatography (normal and reversed phases). For adsorption chromatography, there is only one possibility: to choose a different inorganic material that has both the desirable physical properties of silica and is resistant to hydrolysis over a wider pH range. Among these inorganic materials, alumina, titania, and zirconia are less frequently used as packing materials.

1. *Alumina*: The potential of alumina has been reinvestigated by De Galan and co-workers [9,10]. Recently, an alkaline-stable stationary phase for HPLC has become commercially available [11]. This packing shows a high chemical stability over a wide pH range (2–12) and, after an alkaline treatment, the separation of a mixture of organic bases, including aniline, pyridine, and some of their derivatives, are easily obtained without peak tailing.
2. *Titania and zirconia* [12–15]: Both titania and zirconia are basic oxides; therefore they are insoluble in alkaline media; in addition, they are stable in acidic media down to pH 1 (these two new ceramics did not dissolve in either 1 M hydrochloric acid or 0.5 M sodium hydroxide solution on shaking at 40°C for 48 h, whereas silica gel dissolved completely in 0.5 M sodium hydroxide solution).

Consequently, basic solutes can easily be resolved with very symmetrical peaks (no tailing) on calcinated titania and zirconia packings, with water containing dichloromethane as eluent. Their chromatographic properties under normal-phase conditions demonstrated that there was no main difference in the solvent strength sequence determined for silica or alumina.

In the same way, the solute capacity depends mainly on the mobile-phase water content. The specific surface area of these new porous ceramic packings are relatively low (between 50 and 300 $m^2\ g^{-1}$); the porosity is generated by the controlled crystal growth of amorphous precursors. Sophisticated sintering processes yield a network of interconnected microcrystals, creating the outstanding mechanical stability of these phases. Consequently, the narrow and symmetrical pore size distribution and the absence of internal micropores provide the fast mass-transfer rate, thereby providing high efficiencies. Although not commercially available in fine granulometry, Florisil (porous magnesium silicate) has received attention as a possible alternative stationary phase [16,17].

B. Retention Mechanisms

1. Snyder–Soczewinski Model

The most successful models of retention in LSC (i.e., the models having the greatest predictive usefulness) are those of Snyder et al. [3,18] and Soczewinski [19]. From a practical point of view, these models are quite similar and can be brought into essential agreement through small modifications. Both models assume that retention is the product of competitive adsorption between solute and solvent molecules for active sites on the stationary-phase surface. Each assumes a surface monolayer of solute or solvent molecules, but the model of Snyder et al. further assumes a homogeneous surface (adsorption energies of both solvent and solutes molecules are constant). This assumption is verified when the silica activity remains constant (i.e., when the number of silanol groups associated with a water molecule does not vary and,

consequently, the number of free silanol groups not covered with a water molecule is also constant). Under these conditions, a *mean distribution constant* can be defined taking into account the adsorption energy of the solute on each site types (free, bound, water-deactivated free silanol groups).

Then, the stoichiometry of solute–solvent competition can be expressed by:

$$S_{(MP)} + nM_{(a)} \rightleftharpoons S_{(a)} + 2M_{(MP)}$$

where (MP) and (a) refer to solute (s) and solvent (M) molecules in the mobile and stationary phases, respectively. The coefficient n takes into account different adsorption cross-sectional areas for solutes and solvents. In Figure 2, adsorption of a solute molecule takes place through the displacement of two solvent molecules in the adsorbed monolayer. This corresponds to the *adsorption displacement process.*

Snyder [3] formulated the following relation to predict the solute retention factor k':

$$\log k' = \log \frac{V_a W_a}{V_M} + \beta (E_0 - A_s \varepsilon_0) \tag{1}$$

where $k' = KV_s/V_m$; K is the mean distribution coefficient, and V_s is the stationary-phase volume inside the column.

V_M = mobile phase volume inside the column.
V_a = volume of the adsorbed solvent per gram of stationary phase (mL g^{-1}).
W_a = weight of adsorbent within the column (g).
β = adsorbent activity, a dimensionless number reflecting the percentage of free silanol groups associated with water.
E_0 = adsorption free energy of the solute onto the adsorbent surface.
ε_0 = solvent strength, defined as adsorption free energy of the solvent per unit area of the adsorbent.
A_s = adsorption area of the solute molecule.

The following conventions were chosen by Snyder [3]:

Standard adsorbent ($\beta = 1$): dry alumina
Standard solvent ($\varepsilon_0 = 0$): n-pentane
Standard solute area ($A_s = 6$): benzene

This convention for A_s implies that 1 unit in A_s corresponds to approximately 8.5 Å^2. Moreover E_0 and ε_0 are expressed as reduced energies (dimensionless parameters).

Equation (1) describes retention in adsorption chromatography in terms of separate parameters for the adsorbent (V_a, β) the solute (E_0, A_s) and the solvent (ε_0). As such, it is a useful tool for the interpretation of retention and selectivity phenomena in adsorption chromatogra-

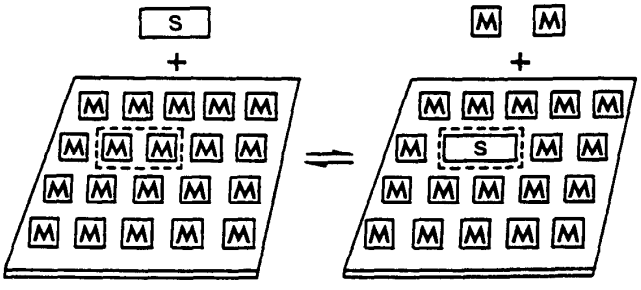


Figure 2 Schematic representation of the adsorption displacement process (a solute molecule arbitrarily displaces two solvent molecules in the adsorbed monolayer).

phy. For instance, the effect of a change in the solvent using the same adsorbent and solute can easily be understood in terms of a variation in ε_0.

Secondary solute–polar solvent interactions have been incorporated into the revised model of Snyder et al. [20] by adding an extra term ΔE_s in Eq. (1). It is clear that ΔE_s should depend on the nature of both the solute and the solvent.

2. Localized and Delocalized Interactions

In a more recent model [21,22] Snyder considers that solute and solvent adsorption energies may depend mainly on their structure. Because of the presence of discrete adsorption sites on the surface of the adsorbent, optimum interaction between a solute molecule and the adsorbent surface occurs when solute polar functional groups exactly overlap these adsorption sites, as a hand fits a glove. This overlapping *localized interaction* is easily possible for monofunctional solutes. For polyfunctional ones, each polar group cannot interact directly with an active site in the same way for various reasons (too low density of active sites on the adsorbent surface, special arrangement of solute polar groups, or intramolecular interaction of the solute). For instance, for a bifunctional solute, a double-localized interaction requires that, in the solute molecule, the distance between the two polar groups is exactly the same as that between two silanol groups and that there is no steric hindrance.

As a result, for these groups—in *delocalized interaction*—the adsorption energy is lower than when the same groups are in localized interaction. Both apolar or weakly polar solvents and such solutes as aliphatic and aromatic hydrocarbons are always in delocalized interaction. Moreover one can easily imagine that certain polyfunctional solutes will be better matched to the adsorbent surface than their isomeric counterparts, leading to a preferential retention of the isomers that best fit the active sites. In practice, adsorption chromatography is often the best method for separation of geometric isomers, the selectivity being sometimes surprisingly high. Figure 3 schematically depicts the various interactive modes.

3. Main Parameters Governing the Retention, Selectivity, and Loadability of Solutes

(*a*) *Specific Surface Area.* The higher the specific surface area of the adsorbent is, the higher is the solute retention. In a first approximation, the mobile-phase adsorbed volume V_a is proportional to the specific surface area, as demonstrated in Figure 4. The resolution be-

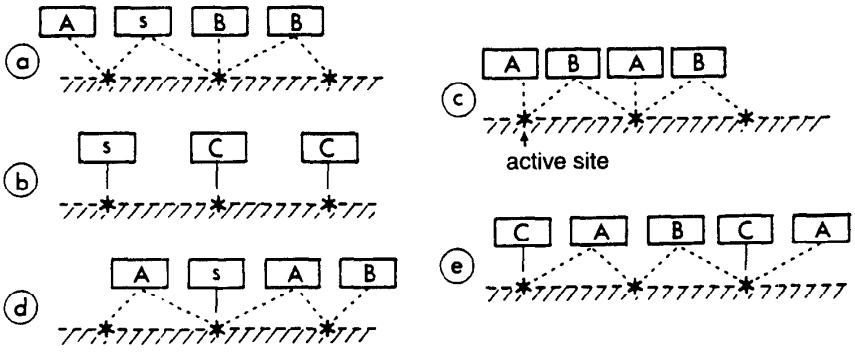


Figure 3 Schematic representation of the solute and solvent adsorption on the adsorbent silica surface: (a) solute (s) and A (polar) and B (weakly polar) solvent molecules in delocalized interaction; (b) solute (s) and C (polar) solvent molecules in localized interaction; (c) A and B solvent molecules in delocalized interaction; (d) solute (s) in localized interaction, and A and B solvent molecules in delocalized interaction; (e) C solvent molecules in localized interaction and A and B solvent molecules in delocalized interaction. Dashed lines symbolize delocalized interactions and solid lines localized ones. (From Ref. 22.)

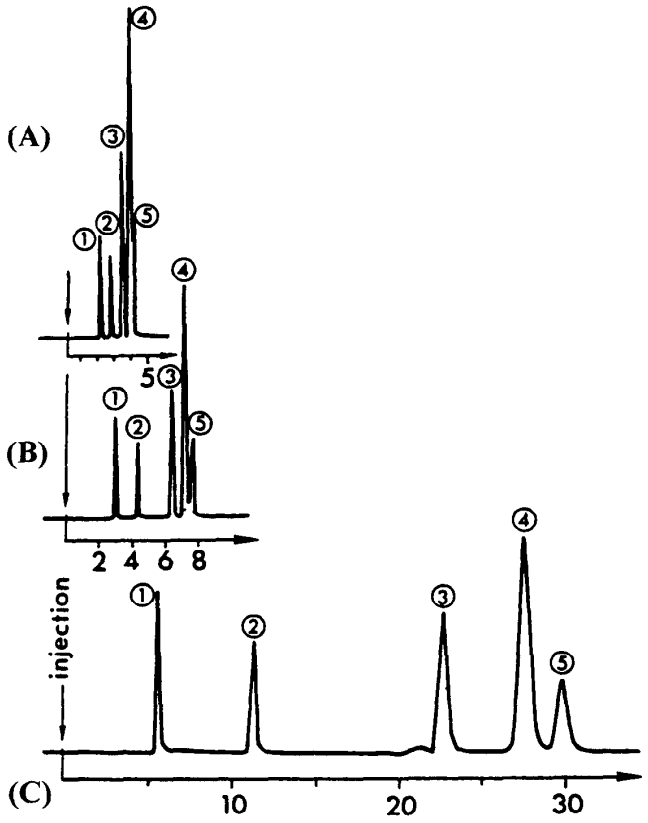


Figure 4 Variation of aromatic hydrocarbon retentions versus specific surface area of silica (Spherosil): Column: length 10 cm; internal diameter 0.4 cm. Stationary phase: Spherosil 4.6 μm, specific surface area: A = 470 $m^2\ g^{-1}$; B = 590 $m^2\ g^{-1}$; C = 900 $mg^2\ g^{-1}$. Mobile phase, dry hexane: Flow rate, 0.9 mL min^{-1}; room temperature; solutes: 1, toluene; 2, naphthalene; 3, biphenyl; 4, anthracene; 5, phenanthene. (From Ref. 42.)

tween all adjacent solute pairs increases with the specific surface area of silica. This effect results from a simultaneous increase in retention and selectivity (both are governed by the number of active sites contained in the chromatographic column).

In the same way, the loadability is proportional to the specific surface area. However, high values of specific surface area (S_p) entail a decrease of pore diameters according to the relation:

$$\overline{D}_{(nm)} = \frac{4V_p\ (cm^3\ g^{-1})}{S_p\ (m^2\ g^{-1})}\ 10^3$$

$\overline{D}$ is the mean pore diameter, assuming a monodisperse distribution of perfectly cylindrical pores, and V_p is the porous volume.

If the pore size is too small, large solute molecules cannot enter the porous volume: a steric exclusion effect occurs. Consequently, adsorbents that have S_p values higher than 800 $m^2\ g^{-1}$ cannot easily be used in practice. In addition, the number of free silanol groups per surface unit decreases—owing to the increase in the concentration of bonded silanol groups—when the S_p value is increasing (Table 1). Practically, silicas that have a specific surface area between 100 and 600 $m^2\ g^{-1}$ are commonly used.

(*b*) *Silica Activity and Mobile Phase Water Content.* Numerous studies have demonstrated that controlled deactivation of the unmodified silica surface is required for reproducible separations with reliable column efficiency and sample loadability.

Table 1 Variation of Free Silanol Group Numbers Versus the Specific Surface Area of Silicas

Adsorbent	Specific surface area ($m^2\ g^{-1}$)	Number of total silanol groups (per nm^2)	Number of free silanol groups (per nm^2)
Lichrosorb Si 100	309	4.6	2.95
Partisil 5	412	4.6	2.80
Lichrosorb Si 60	482	4.6	2.20

Source: Ref. 23.

Water, which is always present—often at a very low level—in all solvents, is the best deactivating agent, even though maintaining the proper water level in water-immiscible solvents is often deemed inconvenient. We must emphasize that reproducible results require the constancy of the adsorbent activity, and this can be reached only by using isohydric solvents (defined as solvents having water contents such that when they are equilibrated, one after another with an adsorbent, there is no change in activity; that is one maintains the adsorbent water concentration constant [24]).

Several methods have been described to determine the water content of isohydric solvents by using either an adsorption isotherm [25] or frontal analysis [24,26]. The water contents of isohydric solvents are summarized in Table 2. The values refer to ethyl acetate containing 0.06% water as the standardization solvent. The resulting water content of silica *is kept rigorously constant for each isohydric solvent series*, but its absolute value depends on the choice of water content for the standardization solvent and the silica's nature (mainly its specific surface area). From a practical perspective, the range of water contents for those classic silica gels, that are well suited for adsorption chromatography, lies between 1 and 3% w/w. (It is generally admitted that for a silica content higher than 5% w/w, partition chromatography on

Table 2 Water Contents of Pure Isohydric Solvents

	Water content % (v/v)	
Solvent	Spherosil XOA 600	Spherosil XOA 800
Methanol	5.2	5.2
Dimethylformamide	4.7	—
Isopropanol	0.7	0.3
Acetonitrile	0.22	0.18
Dioxan	0.14	—
Tetrahydrofuran	0.13	—
Ethyl acetate[a]	0.060	0.060
Isopropyl ether	0.008	0.010
Dichloro-1,2-ethane	0.007	0.009
Chloroform (0.5% ethanol)	0.006	0.006
Cyclohexane	<0.0005	—
n-Heptane	<0.0005	<0.0002
Isooctane	<0.0005	<0.0002

[a]Standardization solvent

Source: Ref. 27.

adsorbed multilayer water governs mainly the solute's retention.) It is obvious that water contents of the isohydric solvents mainly depend on the solvent polarity. The higher the isohydric water content, the higher is the solvent polarity.

The use of isohydric solvents allows:

1. A rapid equilibration of a column
2. A change of eluting solvent in a minimal time
3. A change of activity of the adsorbent

Isohydric solvents are a practical means to not only keep the silica activity constant, but also to vary it in known and reproducible ways. This can be done by changing from one series of isohydric solvents to another with different water concentrations for the same solvents.

As an example, Table 3 shows the reproducibility of the retention times for the analysis of a complex mixture obtained with gradient elution using isohydric solvents. (The isohydric water concentration of a solvent mixture is calculated by using the mixture rule.) These results are excellent, considering that these analyses were performed by different operators over a 2-month period [24], and the eluting gradient is realized on a very wide polarity scale.

In practice, for solvents in which water solubility is low (apolar and medium polar solvents), control of the water content is easily obtained through mixing the dry solvent (kept on a molecular sieve) and water-saturated solvent (for which the water content is fixed by its solubility) in appropriate volumes. The water content/water solubility ratio is also known as reduced water content.

Table 3 Reproducibility of Various Solute Retention Times

	Solute							
Parameter	a	b	c	d	e	f	g	h
Number of measurements[a]	20	20	20	12	5	20	20	6
Mean value of retention time (min)	3.40	5.71	6.71	8.72	9.38	10.35	16.01	18.33
Standard deviation	0.08	0.12	0.15	0.19	0.22	0.34	0.35	0.19
Relative standard deviation (%)	2.4	2.1	2.2	2.2	2.4	3.3	2.2	1.0

[a]Analysis performed by two different analysts over 2 months.

Chromatographic conditions. Column: 4 × 0.73 cm Spherosil XOA 600, 5 μm. Nonpolar solvent A: 2,2,4-trimethylpentane–diisopropyl oxide–ethyl acetate–acetonitrile–acetic acid (50:37.5:7.5:5:0.2); isohydric water content 0.037%. Polar solvent B: methanol–diisopropyl oxide–ethyl acetate–acetonitrile–acetic acid (50:37.5:7.5:5:0.2); isohydric water content 5.2%. Multilinear elution gradient (see below). Flow-rate: 2 mL min^{-1}.

Step	Duration (min)	Initial B (%)	Final B (%)
1	8	8	12
2	4	12	15.2
3	6	15.2	21.2
4	4	21.2	21.2

Solutes: a, fluorocortisone 21-acetate; b, fluorocortisone; c, 9α-fluoroprednisolone; d, 16α-hydroxyfluorocortisone; e, fluorocortisone 21-acetamide; f, triamcinolone; g, 9α-fluoro-11β,16α,17aα-trihydroxy-17aβ-hydroxymethyl-D-homoandrost-4-ene-3,17-dione; h, 9α-fluoro-11β,16α,17aα-trihydroxy-17aβ-hydroxymethyl-D-homoandrost-1,4-diene-3,17-dione.

Source: Ref. 24.

When the water percentage in the silica is too high, 2,2-dimethoxypropane has been proposed as a reagent to reactivate silica columns: it removes water adsorbed on silanol groups by a chemical reaction, with formation of methanol. A convenient activation mixture has the following composition: hexane–dichloromethane–methanol–2,2-dimethoxypropane (30:30:20:20 v/v). Because it takes a lot of water to hydrolyze all the reagent, this mixture can be recycled many times. This treatment is easier than the classic thermal procedure under vacuum.

(*c*) *Solvent Strength.* The solvent strength parameter ε_0 controls the k' values of all solutes. An increase in ε_0 means a stronger solvent and smaller k' values for all solutes: an increase in ε_0 value by 0.05 unit usually decreases all k' by a factor from two to four.

Pure Solvents. Table 4 lists several useful solvents for adsorption chromatography, classified in order of increasing ε_0 values for silica and alumina as adsorbents. Values of ε_0 for silica are slightly lower than those for alumina, being about 0.8-fold smaller on average. Such a series is called an eluotropic series.

Experimental Measurement of Solvent Strength. Let us consider two solvents S_1 and S_2 that have an eluent strength equal to ε_1 and ε_2. If k'_1 and k'_2 are the retention factors for a given solute, then

$$\log \frac{k'_2}{k'_1} = \beta A_s(\varepsilon_2 - \varepsilon_1) \tag{2}$$

A solvent's strength can be determined in two ways:

1. The use of one reference solvent and of a solute having a known adsorption cross-sectional area; for example, polyaromatic hydrocarbons, such as phenanthrene, known to be nonlocalizing, lie flat on the adsorbent surface, and their adsorption cross sections can be predicted accurately from molecular dimensions [28].
2. The use of a third solvent, for which solvent strength is known (ε_3). The following relation is then obtained:

$$\frac{\log k'_1 - \log k'_2}{\log k'_2 - \log k'_3} = \frac{\varepsilon_2 - \varepsilon_1}{\varepsilon_3 - \varepsilon_2}$$

It can be seen that this relation is independent of β and A_s values. However, it depends on the following assumptions:

- Solute: mobile-phase interactions can be neglected in comparison with solute–stationary-phase interactions (no secondary solvent effects).
- The adsorbent activity (water content) must be kept constant (i.e., all the solvents have to be isohydric).
- The three solvents must have the same or a close adsorption cross-sectional area ($n = A_s/A_M$ [A_M being the adsorption area of a solvent molecule (mobile-phase)] will be about the same for the three solvents). For instance, the eluent strength of MTBE was equal to 0.47 ± 0.03 when using five different test solutes and dichloromethane and chloroform as reference solvents [29].

Solvent Mixtures

Snyder's model without localization. Continuous variations in ε_0 can be obtained only by using solvent mixtures in various proportions. In the binary mixture A/B (B stronger than A), the solvent strength does not vary linearly with the percentage of volume B. There is a competition between A and B solvents on the active sites of the adsorbent; hence, the stronger solvent B will be preferentially adsorbed and, consequently, more concentrated in the adsorbed solvent layer. This is represented in Figure 5, which shows the dependence of solvent strength for several binaries on alumina as adsorbent. At low concentrations of the polar solvent, small increases in its concentration produce large increases in solvent strength; at the other extreme,

Table 4 Eluotropic Series Including Useful Solvents Used in Adsorption and Normal-Phase Chromatography

Solvent	ε_0 silica	ε_0 alumina
FC 78	—	−0.25
FC 75	—	−0.25
FC 43	—	−0.25
FC 113	0.02	—
Isooctane	—	0.01
n-Heptane	0	0.01
n-Hexane	0	0.01
Cyclohexane	—	0.04
Carbon tetrachloride	0.11	0.17
Isopropylether	0.32	0.28
Chloroform	0.26	0.36
1,2-Dichloroethane	0.34	0.44
Methyl-*tert*-butyl ether	0.47	—
Tetrahydrofuran	0.53	0.51
Ethyl acetate	0.48	0.60
Triethylamine	—	0.36
Acetonitrile	0.52	0.55
Dioxane	0.51	0.61
tert-Butanol	—	0.70
n-Butanol	—	0.82
Isopropanol	0.60	0.82
Ethanol	—	0.88
Methanol	0.70	0.95
Water	—	>0.95

FC, fluoroalkanes.

a relatively large change in the concentration of the polar solvent affects the solvent strength of the mobile phase to a lesser extent.

The value of ε_0 for a binary mixture (ε_{AB}) can be related to the ε_0 values of the pure solvents A and B (ε_A, ε_B) and to the molar fraction of B (N_B) in the binary mixture

$$\varepsilon_{AB} = \varepsilon_A + \frac{\log(N_B \cdot 10^{\beta n_B(\varepsilon_B - \varepsilon_A)} + 1 - N_B}{\beta n_B} \tag{3}$$

where β is the silica activity, n_B is the reduced area of the cross section of molecule B, which varies (from 4 to 6) with the molecular size of B. In Figure 5, the solid curves are from Eq. (3), and the points are experimental values.

Snyder's model with solvent localization. In practice, it was sometimes found that Eqs. (2) and (3) are most reliable for less polar solvents and solute molecules [21,30]. The reasons for these deviations from Eqs. (2) and (3) fall into two categories:

1. Hydrogen bonding or other interactions between solute and solvent molecules can appear in the mobile phase and lead to the secondary solvent effect.
2. The experimental deviation from Eqs. (2) and (3) is due to the localization of solvent molecules in the adsorbed phase. When a solvent has a polar substituent group within the

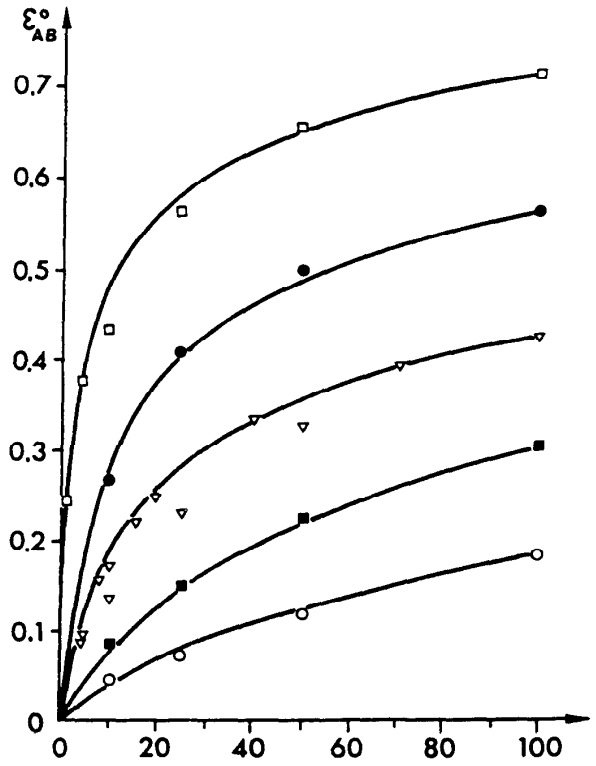


Figure 5 Variation of solvent strength as a function of binary solvent composition: binary solvent ε_0 value versus solvent composition for adsorption onto alumina. Apolar solvent: pentane (A). Solvents B added: ○ CCl_4, ■ *n*-propyl chloride, △ CH_2Cl_2, ● acetone, □ pyridine. (From Ref. 3.)

molecule, this polar group will attempt to adsorb directly on the silanol sites. An important consequence of the solvent localization is the change in apparent solvent strength value ε_0^B of a polar solvent (B) versus its content, for instance, in a binary mixture A–B (A being an apolar or weakly polar solvent.)

Thus, localization of solvent B will be possible as long as the fractional surface coverage on the adsorbent θ_B is lower than 0.75 [21]. For larger values of θ_B (corresponding to larger values of N_B in the mobile phase) the coverage of the remaining surface by *B* implies a delocalization of molecule B.

The plot of ε_0^B versus θ_B permits us to visualize the capability of solvent B to localize on the adsorbent surface. For a nonlocalizing solvent B (carbon tetrachloride, benzene, or methylene chloride) a horizontal graph is obtained (ε_0^B does not vary with its concentration in a mixture; Fig. 6a). For localizing solvents (diisopropyl ether, diethyl ether, acetone, or alcohols) the graph will be nonlinear (see Fig. 6b).

At a low solvent B level, B will adsorb with localization, the effective solvent strength ε_B, under these conditions, is large. However, with increasing coverage of the adsorbent surface by B (up to about 0.75) a point is reached at which preadsorbed molecules of B interfere with the localized adsorption of additional B molecules. Further adsorption of B then occurs without localization. This is the restricted-access delocalization of the solvent, meaning that later molecules of B adsorb in a delocalized state. Consequently, the effective solvent strength of B for large values of θ_B (i.e., for a high content of B in a binary mixture) is smaller than that for low contents of B. The ε_0 values gathered in Table 4 correspond, in Figure 6, to a value of θ_B equal to 1 for localizing solvents.

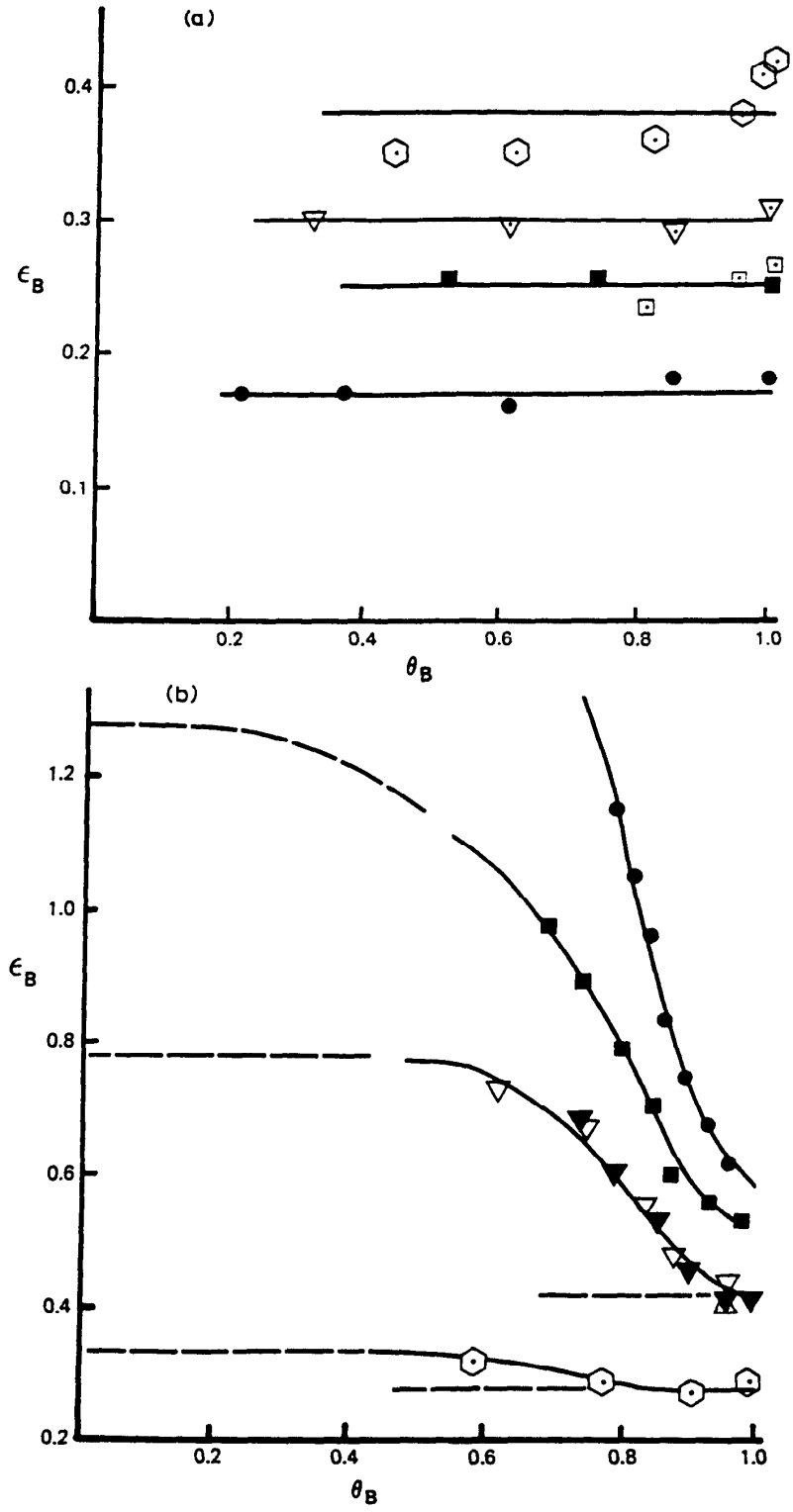


Figure 6 Variations of the apparent solvent strength ε_0^B versus calculated values of the fractional surface coverage θ_B on the adsorbent (silica or alumina): (a) nonlocalizing solvent B: ●, carbon tetrachloride + pentane/alumina; ■ benzene + pentane/silica; ⊡, benzene + hexane/silica; ▽, methylene chloride + pentane/silica; ⊙, methylene chloride + pentane/alumina. (b) Localizing solvent B: ⊙, diisopropyl ether + pentane/alumina; ▼, diethylether + pentane/silica; diethylether + hexane/silica; ■, acetone + hexane/silica; ●, isopropanol + hexane/silica. Experimental values of ε_0^B from Ref. 22. (From Ref. 21.)

For a practical use, graphic methods have been developed to obtain the percentage volume composition of mobile phases having a similar solvent strength ε_0, but different solvent constituents and, therefore, possible different selectivities.

A recent version using classic solvents and taking into account the polar solvent localization is given in Figure 7 [31]. The dashed vertical line was added for explanatory purposes:

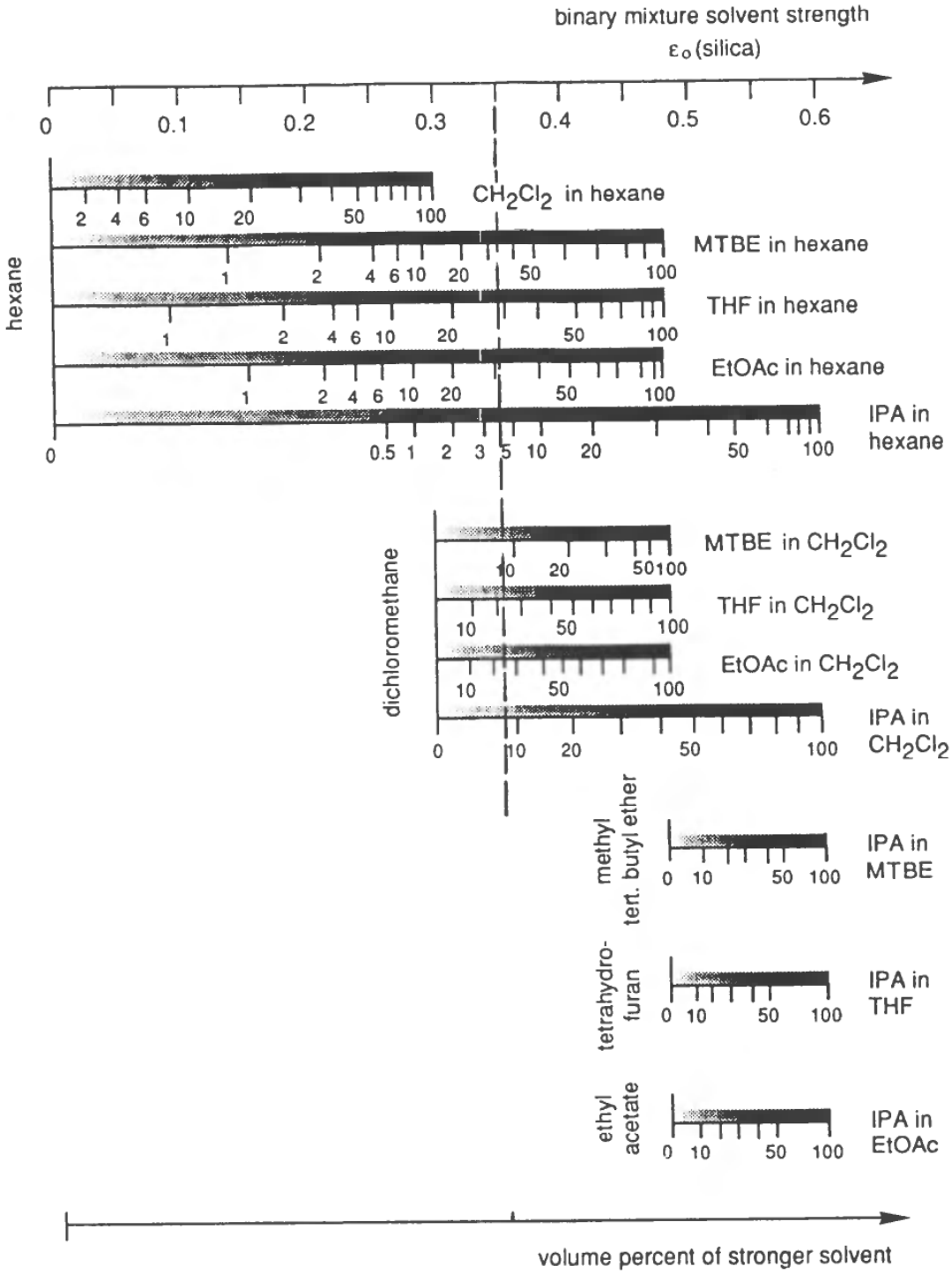


Figure 7 Solvent strength variations for binary mixtures of hexane, dichloromethane, MTBE, tetrahydrofuran, ethyl acetate, and isopropanol.

to obtain a mixture with $\varepsilon_0 = 0.35$ it is possible to choose, for example, 33% MTBE in hexane, 4% isopropanol (IPA) in hexane, 25% ethyl acetate (EtOAc), or 8% IPA in CH_2Cl_2.

(*d*) *Solute Adsorption Energy.* The solute adsorption energy E_0 depends on numerous factors. It is mainly determined by the nature of functional groups present in the molecule and by the total number of groups in the molecule. If the solute molecule contains i groups, the E_0 value can be calculated according to:

$$E_0 = \Sigma_i Q_i^0 \tag{4}$$

where Q_i^0 is the dimensionless free energy of adsorption of the sample group i.

However, the interaction of one group i with the adsorbent surface may restrict the surface interaction of some other group j in the same solute molecule, thereby affecting E_0. This is illustrated in Figure 8 for the hypothetical compounds X-benzene, Y-benzene, and *para*-X,Y-benzene (X and Y corresponding to strongly adsorbing groups). In the monosubstituted derivatives, X or Y groups can easily overlap active sites on the silica: they are in localized interactions. This is not possible for the solute *para*-X,Y-benzene (unless the distance between two active sites on the silica surface fortuitously matches the distance between X and Y in the solute molecule). Only the strongest adsorbing group, X, will be in localized interaction so that the adsorption energy of the weakest group Y, which is in delocalized interaction, will be less than its value in the corresponding monosubstituted derivative.

In addition, two groups in the same solute molecule may interact sterically, electronically, or chemically; in turn, changing their individual interactions with the silica surface and lowering their contributions to E_0. The values of Q_i^0 are summarized in Table 5.

For monofunctional solutes, their adsorption energy can be calculated according to Eq. (4).

For polyfunctional solutes, Eq. (4) has to be corrected for the loss in solute adsorption energy of delocalized groups in the solute molecule:

$$E_0 = \sum^i Q_i^0 - f(Q_k^0) \sum^{i \neq k} Q_i^0 \tag{5}$$

which is equivalent to:

$$E_0 = Q_k^0 + (1 - f(Q_k^0)) \sum^{i \neq k} Q_i^0$$

Because all groups i except k are assumed to be delocalized, the loss in adsorption energy owing to delocalization must be summed over all groups except k*. [For solutes with an aromatic ring attached directly to k, the summation $\Sigma^{i \neq k} Q_i^0$ does not include the six aromatic carbons in this ring (by convention). These groups may be delocalized, but their delocalization energy loss has already been taken into account in the calculation of Q_k^0.]

The f values, so-called localization function, depend on the Q_k^0 value and the relative position of the localizing and delocalizing groups in the solute molecule. Table 6 summarizes values of the localization function f versus Q_k^0 and solute structure. For aliphatic molecules the $f(Q_k^0)$ values decrease when the length p of the alkyl chain connecting the two groups increases. Moreover the relative delocalization of groups other than k is less on silica than on alumina and $f(Q_k^0)$ values are smaller; one can take with a good approximation: $f(Q_k^0)_{\text{silica}} = 0.4\, f(Q_k^0)_{\text{alumina}}$.

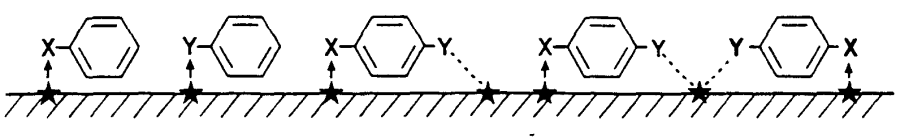


Figure 8 Differences in the interactions of polyfunctional solute molecules on the adsorbent surface: localized and delocalized interactions, ★, interaction site; X, group having the stronger adsorption energy; Y, group having the lower adsorption energy.

Table 5 Group Adsorption Energies (Dimensionless) for Adsorption on Alumina and Narrow Pore Silica

	Q_i^0					
	Alumina			Silica		
Group	X, Y = Ar	X = Al, Y = Ar	X, Y = Al	X, Y = Ar	X = Al, Y = Ar	X, Y = Al
X—CH_3	0.06		−0.03	0.11		0.07
X—CH_2—Y	0.12	0.07	0.02	0.07	0.01	− 0.05
—C= aromatic or ethylenic carbon	0.31	(0.31)	(0.31)	0.25	(0.25)	(0.25)
X—F	0.11		1.64	−0.15		1.54
X—Cl	0.20		1.82	−0.20		1.74
X—Br	0.33		2.00	−0.17		1.94
X—I	0.51		2.00	−0.15		1.94
X—SH	8.70		2.80	0.67		1.70
X—S—S—Y		~ 1.1	2.70		0.94	1.90
X—S—Y	0.76	1.32	2.65	0.48	1.29	2.94
X—O—Y	1.04	1.77	3.50	0.87	1.83	3.61
X_2—N—Y		2.48	4.40		2.52	~5.8
X—CHO	3.35		4.73	3.48		4.97
X—NO_2	2.75		5.40	2.77		5.71
X—C≡N	3.25		5.00	3.33		5.27
X—CO_2—Y	4.02	3.40	5.00	4.18	3.45	5.27
X—CO—Y	4.36	3.74	5.00	4.56	4.69	5.27
X—OH	7.40		6.50	4.20		5.60
X—CH=N—Y	4.14	4.46	6.00			
X—NH_2	4.41		6.24	5.10		8.00
X—SO—Y		4.0	6.70		4.2	7.2
X—COOH	19		21	6.1		7.6
X—$CONH_2$	6.2		8.9	6.6		9.6

Ar refers to an aromatic substituent and Al to an aliphatic substituent.

In addition to its relative delocalization, the adsorption energy of the group i may be altered in additional ways by the presence of another group j in the solute. Typical interactions are: intramolecular electronic interactions, negative interactions (steric hindrance), or hydrogen bonding.

1. The energy of interaction Q_i^0 of group i with a polar adsorbent is a function of the electronic configuration of i (i.e., its net electron density). Thus, it can be affected by other groups present in the solute molecule. This entails a significant isomeric effect for many solute molecules (LSC is well known as a good chromatographic method for separating positional isomers). These electronic interactions occur in both aliphatic and aromatic solutes, but are often more important for the aromatic ones.
2. The optimum adsorption of solute group i, corresponding to a maximum value of Q_i^0, requires the close proximity of i to an active site on the silica surface. A bulky adjacent group j in the same molecule can interfere with this process by steric hindrance, leading to a decrease in the adsorption energy. Such a phenomenon is encountered with the polysubstituted benzenes (for disubstituted benzenes of the type R-ø-i, where R is an alkyl

Table 6 Localization Function $f(Q_k^0)$ Versus Adsorption Energy of Localizing Group k and Solute Molecular Structure

	$f(Q_k^0)$					
Q_k^0	$p = 0$	$p = 1$	$p = 2$	$p = 3$	$p = 5$	$p = 10$
0.00	0.00	0.29	0.13	0.00	0.00	0.00
0.20	0.00	0.31	0.16	0.02	0.00	0.00
0.40	0.00	0.35	0.19	0.08	0.00	0.00
0.60	0.00	0.36	0.22	0.12	0.05	0.00
0.80	0.00	0.37	0.25	0.16	0.09	0.00
1.00	0.00	0.39	0.27	0.19	0.11	0.01
1.20	0.01	0.40	0.29	0.21	0.14	0.04
1.40	0.04	0.41	0.31	0.23	0.17	0.07
1.60	0.09	0.42	0.33	0.25	0.19	0.09
1.80	0.13	0.43	0.35	0.27	0.21	0.11
2.00	0.17	0.43	0.36	0.28	0.22	0.13
2.5	0.26	0.46	0.40	0.32	0.26	0.17
3.0	0.34	0.48	0.41	0.34	0.28	0.20
3.5	0.42	0.51	0.44	0.37	0.32	0.23
4.0	0.45	0.53	0.46	0.39	0.34	0.25
5.0	0.45	0.57	0.52	0.44	0.39	0.31
6.0	0.45	0.62	0.57	0.49	0.45	0.36

$p = 0$ refers to aromatic molecules where i and k are separated by an aromatic ring; $p = 1$, $p = 2$ . . . refers to molecules of type i-$(CH_2)_p$-k.

group, i a polar group, and ø stands for an aromatic ring, it is very often observed that the *ortho*-isomer is less adsorbed than the *para*-isomer).

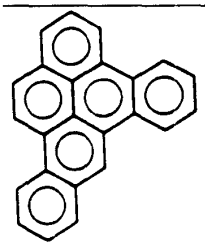
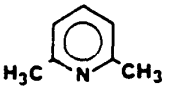
3. When two adjacent groups i and j are present in the same solute molecule, the possibility of intramolecular hydrogen bonding must be considered in addition to electronic interactions. If one of the two groups is a proton donor and the other a proton acceptor, an intramolecular hydrogen bond will be formed that competes with similar interactions between each group and the adsorbent-active sites. As a result, the adsorption energy will be less than when hydrogen bonding is absent [3].

(*e*) *Solute Molecular Surface Area.* According to Eq. (1), the effect of a change in solvents on the retention is related to the size of the solute molecule A_s. This suggests that the selectivity can be modified by a simple change in solvent strength, whenever the A_s values of the two solutes are different. An experimental instance is shown in Table 7. After changing the mobile phase from pentane to benzene, the change in distribution coefficient is greater for the larger dibenzopyrene than for the smaller dimethylpyridine. The effect is large enough to invert the elution order [3].

4. Mobile Phase Choice and Optimization

Retention in liquid chromatography depends on the strength of the solute interactions with both the mobile and stationary phases. Consequently, after an intelligent choice of the stationary phase, the selection of the mobile phase is very important. Some broad generalizations can be made about the selection of certain preferred solvents from the numerous solvents available. A suitable solvent will have the following properties: low viscosity, compatibility with the detection system, availability in a pure state, low flammability and toxicity, and highly inert. A short list of useful solvents for normal-phase HPLC is given in Table 8 (mobile-phase constituents and modifiers).

Table 7 Influence of the Solvent Strength on the Distribution Coefficient and the Selectivity for Two Solutes (1,2,4,5,-Dibenzopyrene and 2,6-Dimethylpyridine) Having Different Sizes

	K mL g^{-1}	
Solute	Benzene ($\varepsilon_0 = 0.32$)	Pentane ($\varepsilon_0 = 0.00$)
	0.6	365
	2.0	46
	$\alpha = 0.3$	$\alpha = 7.9$

Source: Ref. 3.

(*a*) *Solvent Selection.* The solvent properties of critical chromatographic interest are strength and selectivity. The solvent strength must be chosen to maintain solute retention factors k' within an optimum range of $1 \leq k' \leq 5$ for classic samples, and the selectivity values must be sufficient to reach a satisfactory resolution. The most common strategy is to adjust the solvent strength first and, then, while holding the latter constant, modify the solvent nature until the required sample resolution is reached.

A means of classifying solvents according to their strength and predicting solvent strength of mixtures was discussed earlier with ε_0 values. Let us now consider a scheme for classifying solvents according to their specific interactions with solutes and stationary phases [32].

The principal intermolecular forces responsible for describing the properties of nonelectrolytic solvents are dispersive, dipole, and hydrogen-bonding interactions. Dispersive interactions in mixtures of solvents that have a medium degree of polarity appear to play an unimportant role in contributing to solvent selectivity; consequently, they will be neglected (hydrocarbon solvents produce only dispersive forces and, therefore, entail no selectivity variation versus their nature).

The three most important selectivity properties of a solvent are its proton–acceptor, proton–donor, and dipole–donor affinities. To evaluate each contribution the overall polarity P' (related to their chromatographic strength or polarity) is divided into three parameters:

x_e = proton acceptor
x_d = proton donor
x_n = dipole

These parameters—P', x_e, x_d, and x_n—have been experimentally determined from distribution coefficients of test solutes: ethanol, dioxane, and nitromethane, respectively [33].

For instance, for chloroform, which is a medium polar solvent ($P' = 4.31$), the x values given in Table 8 are $x_e = 0.31$, $x_d = 0.35$, and $x_n = 0.34$: that means that polar interaction properties of chloroform involve 31% proton acceptor, 35% proton donor, and 34% dipole interactions.

If the x values of the solvents are plotted on a triple coordinate system (Fig. 9) according to the chosen solvents, they can be grouped into eight classes, with different,

Table 8 Classification of Solvents According to Their Specific Properties

Solvent	ε_0 silica	P'	x_e	x_d	x_n	Selectivity group
FC 78[a]	—	—	—	—	—	
FC 75[a]	—	—	—	—	—	
FC 43[a]	—	—	—	—	—	
FC 113[a]	0.02	—	—	—	—	
Isooctane[a]	—	−0.03	—	—	—	
n-Heptane[a]	0	—	—	—	—	
n-Hexane[a]	0	−0.14	—	—	—	
Cyclohexane[a]	—	0.17	—	—	—	
Carbon tetrachloride	0.11	1.56	0.26	0.40	0.34	
Isopropylether	0.32	1.83	0.51	0.10	0.39	I
Chloroform	0.26	4.31	0.31	0.35	0.34	VIII
Methylene chloride[b]	0.30	4.29	0.27	0.33	0.40	VII
Methyl *tert*-butyl ether	0.47	—	0.41	0.19	0.40	I
Tetrahydrofuran	0.53	4.28	0.36	0.22	0.42	III
Ethyl acetate	0.48	4.24		—	—	
Triethylamine	—	2.19	0.66	0.08	0.26	—
Acetonitrile	0.52	5.64	0.33	0.25	0.42	VI
Dioxane	0.51	5.27	0.37	0.23	0.40	II
tert-Butanol	—	4.03	0.56	0.20	0.24	II
n-Butanol	—	4.11	0.54	0.18	0.28	II
Isopropanol	0.60	3.92	0.57	0.17	0.26	II
Ethanol	—	4.40	0.52	0.19	0.29	II
Methanol	0.70	5.10	0.48	0.22	0.31	II
Water	—	10.2	0.37	0.37	0.26	VIII

[a]These solvents have a value for P' that is too small to obtain reliable x_e, x_d, and x_n values.
[b]This solvent, formerly set in group V, is now affiliated with group VII [34].

selectivities—called selectivity groups by Snyder [32]. Each class comprises solvents having similar selectivity. Consequently, the choice of a second solvent belonging to the same selectivity class cannot give substantial variation in the obtained chromatographic separation. Therefore, solvents that are as close to the apices of the triangle as possible will be chosen to reach the maximum selectivity effect in normal-phase HPLC (Fig. 10). [Sometimes to increase the solvent strength a small amount of alcohol, such as methanol (group II), can be added.] The chosen solvents are

Isopropyl ether, MTBE (group I)
Methylene chloride, 1-2-dichloroethane (group VII)
Chloroform and fluoroalcohols (group VIII)

In a general way, mixtures of solvents are used as mobile phases and the polarity or elution strength is adjusted by adding a nonselective solvent, such as hexane or other saturated hydrocarbons, for normal-phase HPLC [solvent mixtures having the same elution strength, but a different selectivity are called isoeluotropic mobile phases].

(*b*) *Mobile-Phase Optimization.* Binary mobile phases (mixture of an alkane with one of the recommended selective solvents) provide a simple means for governing mobile-phase strength, but have only limited abilities for controlling mobile-phase selectivity. Therefore, ternary and even quaternary mobile phases are now often used to achieve the required selec-

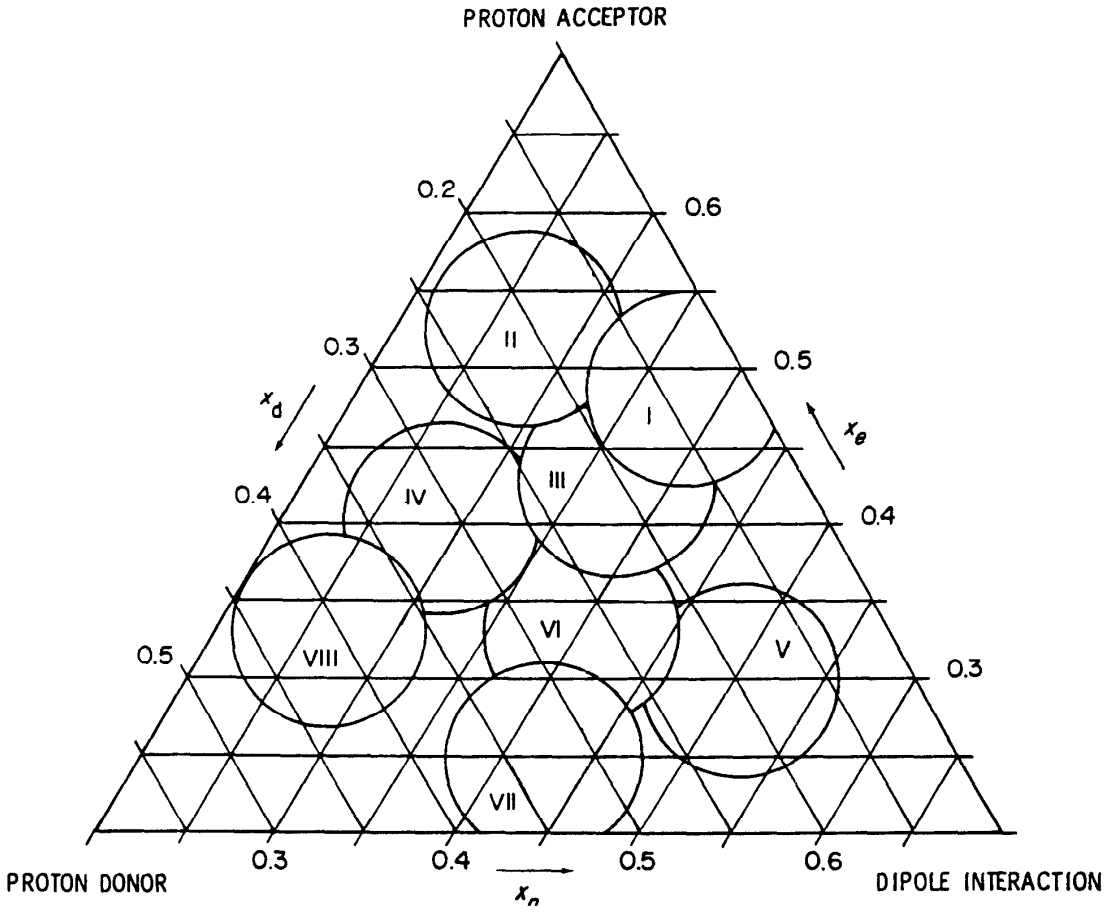


Figure 9 Snyder's selectivity triangle for solvents.

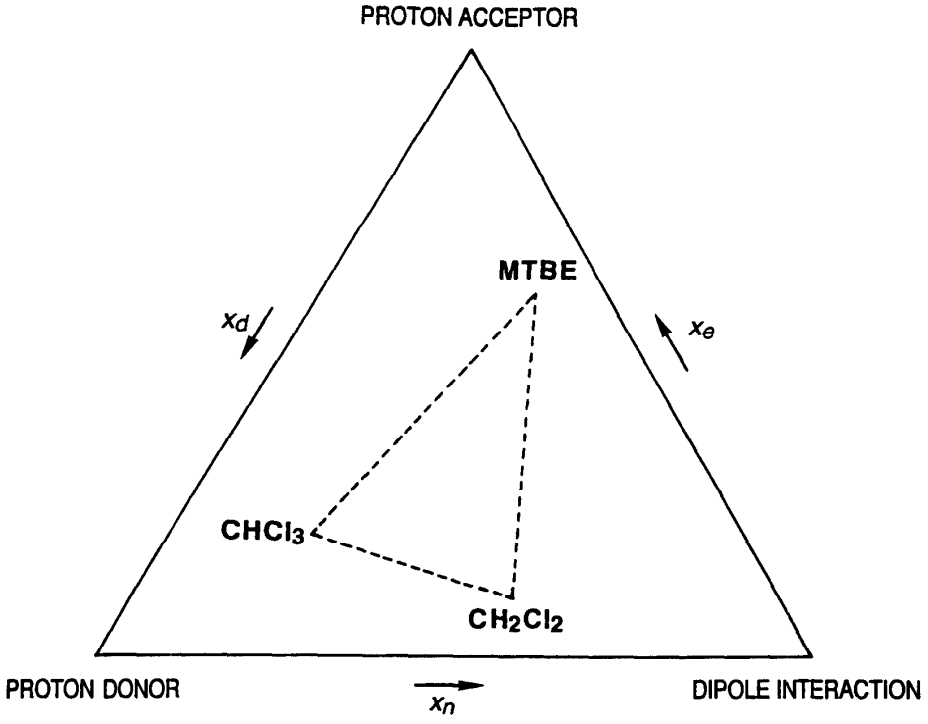


Figure 10 Selected solvents for the mobile phase optimization in NP–LC.

tivity; however, the choice of the optimal mobile phase is not easy and is time consuming if a trial-and-error procedure is used. Numerous procedures describing selectivity optimization are used; their detailed presentation is outside the scope of this chapter (interested readers will find full information in the book written by Schoenmakers [35]).

We will present only a simple method founded on Snyder's solvent selectivity triangle concept, combined with a statistical approach [36–38]. The corresponding mixture design is illustrated in Figure 11. A seven-run design is used as follows: A primary binary solvent mixture, with a solvent strength that is convenient for the separation is selected: for example, hexane–MTBE. This binary mixture defines one corner, for instance, A, of the triangle (Fig. 11). The two other binary mixtures (hexane–CH_2Cl_2 and hexane–$CHCl_3$), the composition of which is calculated to obtain the same solvent strength, are then tested. The area bound by the sides of the triangle defines the selectivity domain in which the optimum mobile-phase composition will be found.

The optimization is carried out by mixing an equal volume each of the binary solvents, producing three ternary mobile-phase systems (experimental points 4, 5, and 6 set in the middle of the triangle sides). Finally, run 7 is carried out by mixing in the ratio 1/3:1/3:1/3 the three binary mixtures. Visual comparison of the seven chromatograms will often allow the selection of the optimum solvent composition for the separation. Optimization procedures can also be pursued either mathematically or manually. In the first example, runs 1–7 are used to estimate, by regression analysis, the six coefficients used in a quadratic model describing the response surface. This equation, in turn, allows the location of areas in the triangle within which the optimum solvent composition lies.

In the last example, the same procedure is repeated, starting from a smaller triangle, for instance 2, 4, 5, the apices of which correspond to the area where the resolution is the highest (the triangle reduction method).

We must again emphasize that to obtain reproducible results use of isohydric solvents as a mobile phase is required. Consequently, all solvents chosen in the foregoing must have an adjusted water content.

5. Applications

Solutes that dissolve only sparingly in water, in water-organic solvent mixtures, and that are not compatible with the aqueous mobile phase typically used in reversed-phase chromatography can be resolved by normal-phase chromatography, particularly, by adsorption chromatography.

Liquid–solid chromatography is also most useful for the separation of positional isomers and for the resolution of solutes with different numbers of functional groups (Table 9). We can see the separation of quinoline from isoquinoline is trivially easy by LSC (α = 3.44), but rather difficult by reversed-phase HPLC. In the same manner, it is easy to separate *m*- and *p*-dibromobenzenes (α = 1.8 in pentane).

For maximum interaction the adsorbed molecule must orient itself parallel to the adsorption surface. Bulky alkyl groups adjacent to the polar group decrease the retention. The *cis*-isomer of a compound is always retained more strongly than the *trans*-isomer.

Adsorption chromatography has been applied in various fields for analyses of petroleum products, drugs and pharmaceuticals, food products, propellants, and explosives. We have chosen to describe here two examples: separation of a phenothiazine mixture and separation of tocopherols in cereal crops.

(*a*) *Separation of a Phenothiazine Mixture.* The separation of these pharmaceutical drugs has been developed by Thomas et al. [27]. To cover a wide range of both polarity and selectivity, a ternary mixture obtained from two selected binary mixtures, introduced in various proportions, was used. These two mixtures of solvents, which allowed a satisfactory miscibility of every mixture, are the following:

1. Mixture A (not very polar): isooctane–diisopropylether (1:1 v/v)

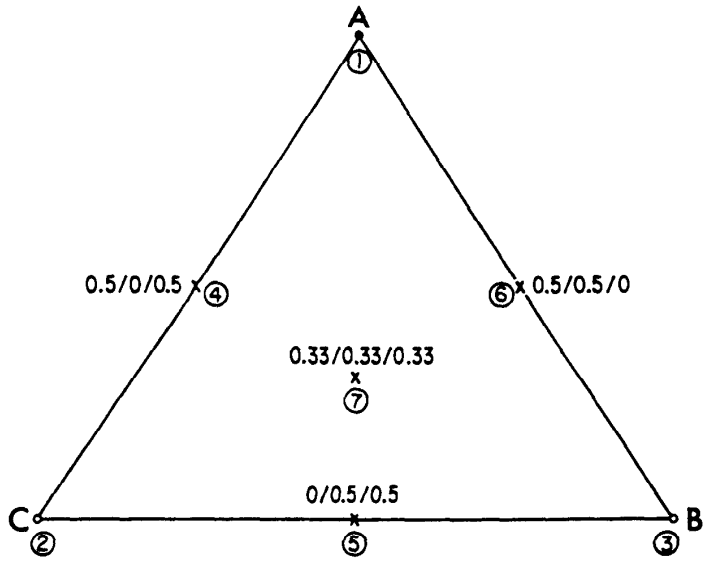


Figure 11 Simplex design for three solvents (A, B, and C) and mixtures. Values for each point are trilinear coordinates of A/B/C.

2. Mixture B (polar): diisopropylether–methanol (1:1 v/v).

Again, the control of the water content of these mixtures is essential to maintain the silica activity constant: the water contents of isohydric ternary mixtures for the silica used and equilibrated with ethyl acetate containing 0.06% of water (standardization solvent) are given in Table 10. For example, primary mixture A must be adjusted to 0.0041% water and primary

Table 9 Selectivity in Adsorption Chromatography

Compound	Support	Mobile phase	Value of k'
2-Methoxynaphthalene	Silica	23% CH_2Cl_2 in pentane	0.6
1-Nitronaphthalene	Silica	23% CH_2Cl_2 in pentane	1.8
1-Cyanonaphthalene	Silica	23% CH_2Cl_2 in pentane	2.7
1-Acetonaphthalene	Silica	23% CH_2Cl_2 in pentane	5.5
2-Methoxynaphthalene	Silica	23% CH_2Cl_2 in pentane	0.6
1,7-Dimethoxynaphthalene	Silica	23% CH_2Cl_2 in pentane	1.4
1-Nitronaphthalene	Silica	23% CH_2Cl_2 in pentane	1.8
1,5-Dinitronaphthalene	Silica	23% CH_2Cl_2 in pentane	6.1
Acetophenone	Silica	60% CH_2Cl_2 in pentane	1.1
3-Nitroacetophenone	Silica	60% CH_2Cl_2 in pentane	1.6
m-Dibromobenzene	Alumina	Pentane	3.8
p-Dibromobenzene	Alumina	Pentane	6.9
Quinoline	Alumina	Benzene	5.4
Isoquinoline	Alumina	Benzene	18.6
1,2,3,4,-Dibenzanthracene	Alumina	CH_2Cl_2	0.6
Picene	Alumina	CH_2Cl_2	12.0

Source: Ref. 39.

Table 10 Water Contents of the Ternary Mixtures A + B of Isohydric Solvents

	System isooactane diisopropyl oxide methanol	
B (%)	Water (%)	$1/N^a$
0	0.0041	2873.6
1	0.0301	398.1
2	0.0560	217.0
3	0.0820	150.5
4	0.1079	116.1
5	0.1339	94.9
6	0.1599	80.7
7	0.1858	70.4
8	0.2118	62.7
9	0.2377	56.6
10	0.2637	51.7
15	0.3935	37.0
20	0.5233	29.6
25	0.6531	25.2
30	0.7829	22.2
35	0.9127	20.0
40	1.0425	18.4
45	1.1723	17.2
50	1.3021	16.2
60	1.5616	14.7
70	1.8212	13.6
80	2.0808	12.8
90	2.3404	12.2
100	2.6000	11.7

[a]Corresponding values of $1/N^{isoh}_{H_2O}$, $N^{isoh}_{H_2O}$ being the water molar fraction. Adsorbent: Spherosil XOA 600.

mixture B to 2.6% water. However, in practice, because chromatographic-grade solvents contain only a few 10s ppm of water, the accurate adjustment of the water content of mixture A is not necessary if more than 5–10% of solvent B is used, because the water content of mixture B is much higher than that of mixture A.

Because the dielectric constant of the ternary mixture cannot be neglected, ion dissociation phenomena can occur, and a small amount of triethylamine is added to control the mobile-phase acidity. This addition has two chromatographic consequences:

1. It defines conditions under which the solutes are chromatographed: to prevent peak tailing, phenothiazines, which have basic properties, are used in their uncharged molecular form.
2. At the adsorbent surface, the triethylamine neutralizes the most active sites and the peak tailing is reduced.

More generally, acids such as acetic acid, are used to keep the acidic solutes in their molecular form, and aliphatic bases, such as mono-, di-, or triethylamine are used to keep the basic solutes in that form; these are known as "modulators."

A linear relation between the retention factors (k') of solutes and the inverse of the molar fraction of water in isohydric solvents ($1/N^{isoh}_{H_2O}$) has been previously demonstrated [24]. This linear relation allows the retention times (t_R) in the whole polarity range of solvents A and B to be predicted from a few trials: only two mixtures are needed. The straight lines obtained are then used to optimize the resolution.

From the standard equations that define the chromatographic resolution R_s and column efficiency N:

$$R_S = 2\left(\frac{t_{R_2} - t_{R_1}}{\omega_2 + \omega_1}\right), \qquad N_1 = 16\left(\frac{t_{R_1}}{\omega_1}\right)^2, \qquad \text{and} \qquad N_2 = 16\left(\frac{t_{R_1}}{\omega_2}\right)^2$$

Assuming that $N_2 \approx N_1 = N$, R_s is defined as

$$R_s = \frac{\sqrt{N}}{2}\left(\frac{t_{R_2} - t_{R_1}}{t_{R_2} + t_{R_1}}\right)$$

With this equation, it is not necessary to measure the peak width, and incomplete separations can be used to predict the relation between resolution and the polarity of the mobile phase. Curves of $t_R = f(1/N^{isoh}_{H_2O})$ are used to predict, from a limited number of trials, retention times for other mixtures of solvents A and B. With experimental and calculated values, curves of $t_{R_2} - t_{R_1}/t_{R_2} + t_{R_1}$ for each pair of peaks are plotted against, $1/N^{isoh}_{H_2O}$, which can be considered as a measurement of the polarity of the mobile phase.

Preliminary trials were carried out with two mixtures containing 50 and 20% of B and 0.2% of triethylamine, respectively. The stationary phase had a water content corresponding to that obtained with ethyl acetate containing 0.06% of water as standardizing solvent. The straight lines obtained when plotting t_R versus $1/N^{isoh}_{H_2O}$ are represented in Figure 12; there is an inversion in retention times between peaks f and g for about $1/N^{isoh}_{H_2O} = 25$, corresponding to about 25% of B (upper axis). The retention times were rapidly determined when using a short column (5 × 0.6 cm).

These determinations lead to the calculated curves $t_{R_2} - t_{R_1}/t_{R_2} + t_{R_1} = f(1/N^{isoh}_{H_2O})$ (Fig. 13); there are two possibilities for separating all of the phenothiazines. The first takes place when $1/N^{isoh}_{H_2O} \approx 38$ (about 15% of B) and the second when $1/N^{isoh}_{H_2O} \approx 20$ (about 35% of B). The latter was chosen so that the separation could be performed in a much shorter time, whereas the condition on the number of theoretical plates within the column necessary to achieve a convenient resolution ($N > 2500$ for $R_s > 2$) could be easily satisfied. The separation obtained is represented in Figure 14.

More recently, the separation of a similar mixture of phenothiazines was optimized, using a computed multiparameter optimization procedure. The primary mixtures A and B and the stationary phase (Spherosil XOA 600, $d_p = 6$ μm) remained the same; the constraints were the shortest analytical time, a resolution between any two peaks better than 2, and a pressure drop less than 200 bar. The parameters to be optimized were the column length, the flow rate, the percentage of the strongest solvent (B mixture), and the temperature [40].

Figure 15 shows a comparison between the experimental and the simulated chromatograms under the operating conditions suggested by the optimization program. Despite peak tailing, arising mainly from a combination of the dead volumes, detector response time (1 s) and recorder response time (0.4 s), the overall result is satisfactory; when using a multiparameter optimization procedure the analytical time was reduced by a factor of 5.

(*b*) *Analysis of Tocopherols in Cereal Crops.* The separation of tocopherols in corn oil (Fig. 16), which are oil-soluble vitamins, is representative of an appropriate use of adsorption chromatography in food analysis. We have chosen this example to illustrate the influence of

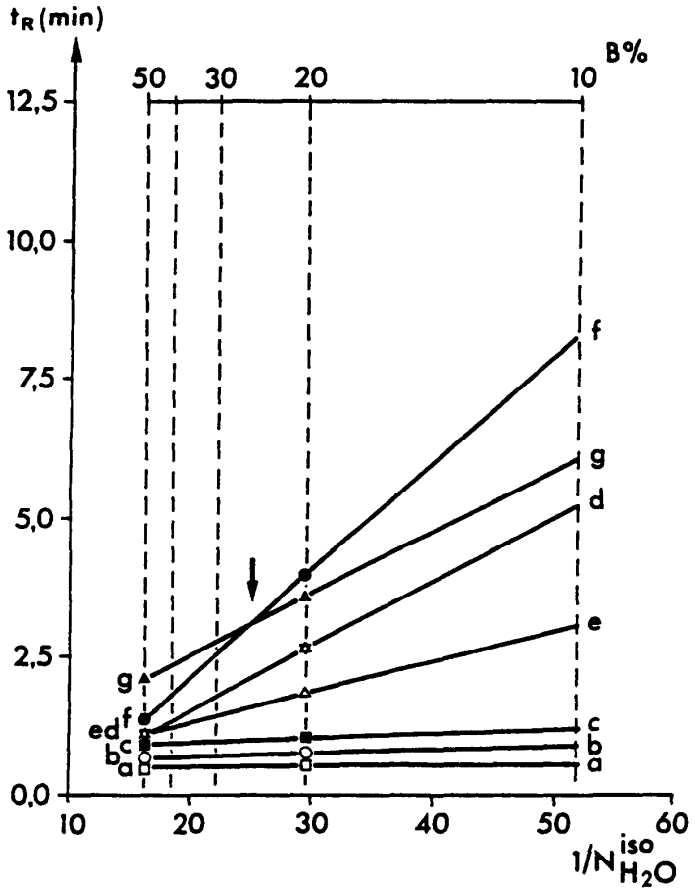


Figure 12 Variations in the retention times of phenothiazines versus $1/N^{isoh}_{H_2O}$ (lower axis) and the percentage of B in the mobile phase (upper axis). Column: 5 × 0.6-cm Spherosil XOA 600, 6 μm. Mobile phase A: isooctane–diisopropyl oxide (1:1). Mobile phase B: diisopropyl oxide–methanol (1:1). Acidity modulator: 0.2% triethylamine in A and B. Flow-rate: 3 ml/min. Solutes: (a) 3-chlorophenothiazine; (b) levomepromazine; (c) chlorpromazine; (d) dimethothiazine; (e) propericiazine, (f) pipothiazine; (g) oxomemazine.

steric hindrance around a polar functional group (phenol group) on retention. α-Tocopherol is eluted first because the two methyl groups, both *ortho* to the OH group, imparted an important steric hindrance toward the interaction (hydrogen bonding) between the silanol groups and the phenol function. Conversely, δ-tocopherol in which the phenol function is free from steric hindrance (no adjacent alkyl group) is eluted last. The separation of β- and γ-tocopherols, which eluted intermediately, shows a lower resolution because they differ only by the position of one methyl group.

III. POLAR-BONDED-PHASE CHROMATOGRAPHY

Although bare silica was the first LC stationary phase, extensive trials to synthesize polar-bonded phases to enhance and govern the selectivity in normal-phase chromatography were realized. Attempts were also made to replace and mimic the polar liquid stationary phases

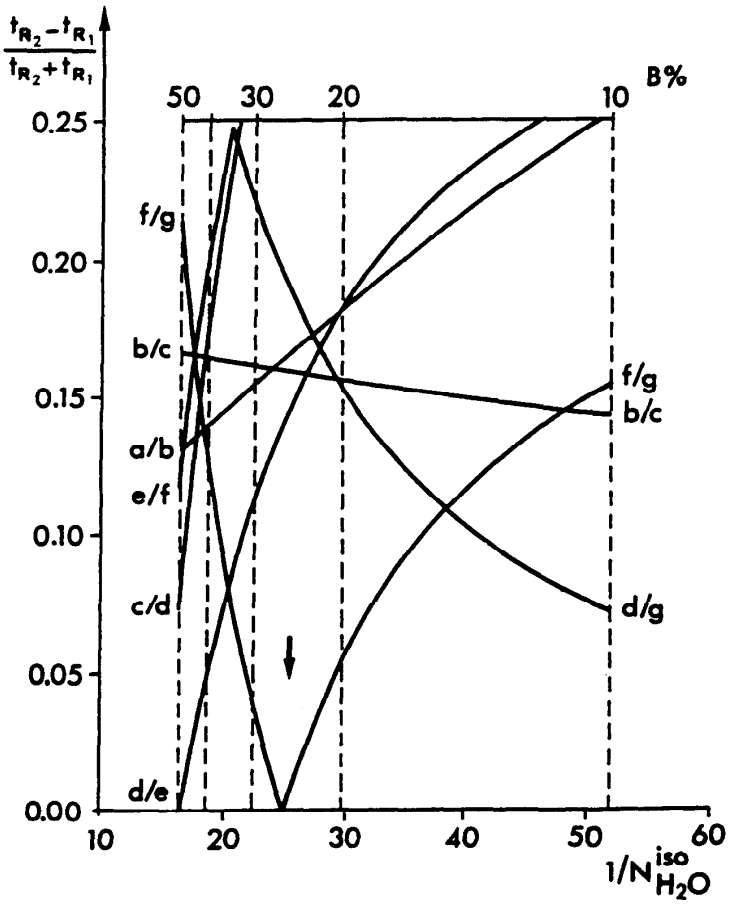


Figure 13 Optimization of the resolution between adjacent peaks of phenothiazines: variations of $t_{R_2} - t_{R_1}/t_{R_2} + t_{R_1}$ versus $1/N^{isoh}_{H_2O}$ (lower axis) and percent B (upper axis) (calculated curves from the values deduced from the straight lines plotted in Figure 12).

used in liquid–liquid partition chromatography.* Moreover, the heterogeneity of the silica surface entails some problems in the routine use of this material:

1. Variation of the apparent acidity of commercial silicas that causes a product-specific retention behavior toward acidic and basic solutes (although the acid or basic modifier addition at trace levels allows reduction of these undesirable interactions).
2. Irreversible adsorption of strongly polar analytes, which is generally attributed to the heterogeneity of the silica surface.
3. Control of the mobile-phase water content is necessary to obtain reproducible results (isohydric solvents).
4. Slow reequilibration occurred when changing the mobile phase composition.

Nevertheless, the time needed for reequilibration of a chromatographic column is highly reduced by using isohydric solvents, which permits the water content of the silica to be kept constant, independently of the mobile-phase composition.

*In this old technique, separations were founded on the partition of solutes between two immiscible liquid phases, one immobilized on an inert solid support and the other one acting as mobile phase. This method was discarded because of irreproducible results due to the solubility of a solvent in another one, even very low, is never zero: there was a slow, but gradual, dissolution of the stationary phase, leading to a capacity loss and a decrease of retention characteristics with time.

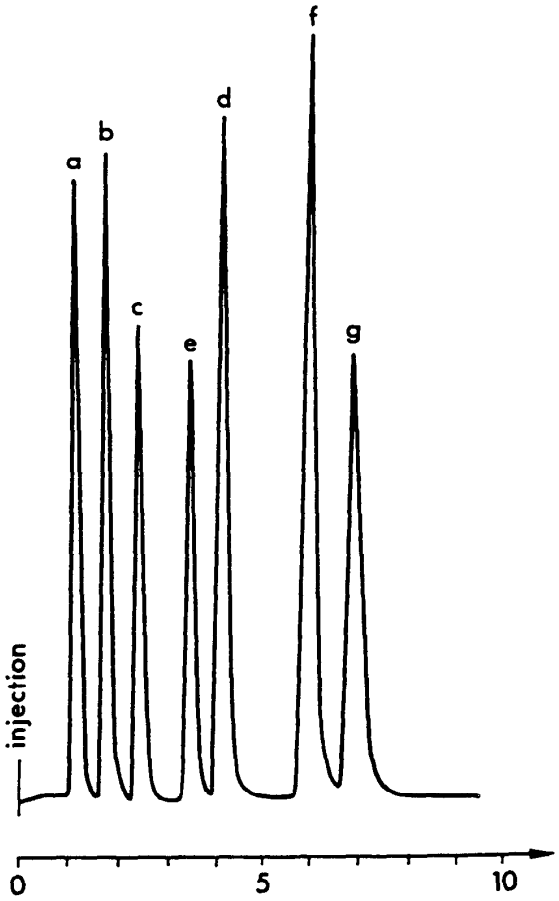


Figure 14 Optimized separation of phenothiazines: Column: 15 × 0.6-cm Spherosil XOA 600, 6 μm. Mobile phase: 35% B (i.e., isooctane–diisopropyl oxide–methanol [32.5:50:17.5], containing 0.2% triethylamine and 0.91% water). Flow-rate: 3 mL min^{-1} ΔP: 80 bar. Detection: UV, 254 nm. Solutes: as in Figure 12.

Polar-bonded phases, containing diol, cyano, amino, and mixed cyano–amino functional groups, are commercially available; typical structures are shown in Table 11. Akylnitrile- and alkylamine-substituted stationary phases are the most widely used. With a low polarity mobile phase—for example, an alkane or a chlorinated solvent containing a small amount of a polar modifier—their behavior is quite similar to the adsorbents discussed in the preceding section: the retention of solutes increases with their polarity, and an increase in the eluent polarity, for instance, by an increase of the modifier content, reduces the solute retention.

However these polar-bonded phases are generally less retentive than adsorbents.

A. Bonding Reactions

The full description of wide variety of bonding reactions used to produce an LC bonded phase is outside the scope of this chapter; interested chromatographers are referred to Refs. [43,44] for detailed discussions.

The grafting of polar functional groups onto the silica surface is generally realized by silanization. This can be accomplished by two methods. In the first, the ligand coupling is performed in one step by reacting the silanol groups with a convenient silane. In the second, the polar-bonded phase is obtained in two consecutive steps. An intermediate is formed by

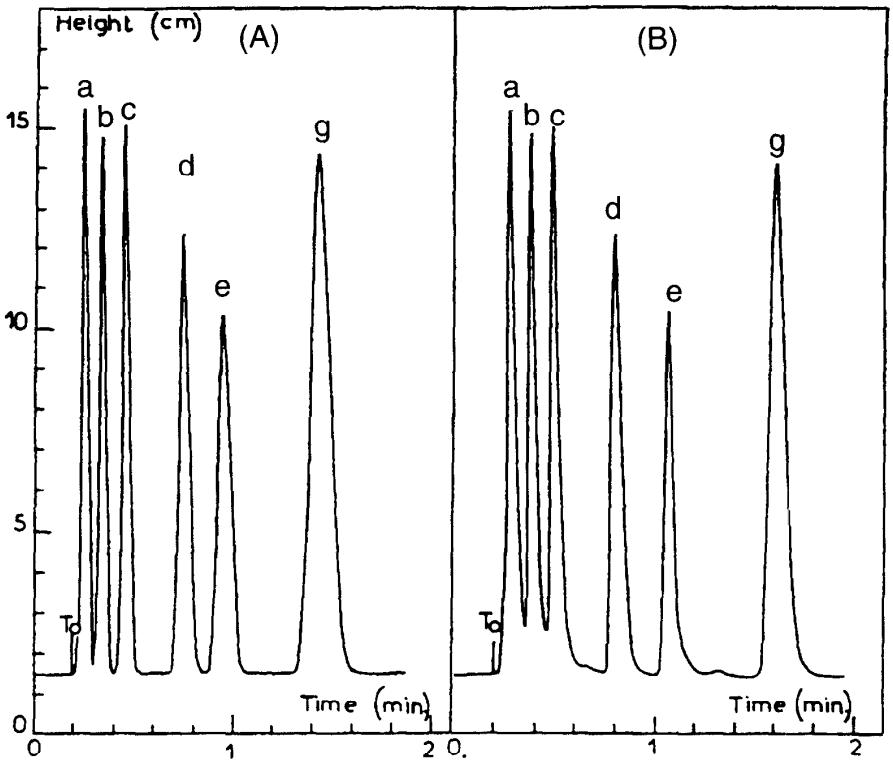


Figure 15 Multiparameter optimization. Comparison between computer simulation and the actual chromatogram. Chromatogram (A): computer simulation of the chromatogram after optimization. Required conditions: shortest analysis time; resolution between any two peaks to be greater than 2; pressure drop to be less than 200 bar. Parameter optimized: column length, flow-rate, volume fraction of the strongest solvent, temperature. Optimum conditions: L = 5 cm; u = 0.45 cm s^{-1}; φ_B = 0.25; T = 30°C; t_a = 1.65 min. Chromatogram (B): chromatogram obtained experimentally. Peak identification a = 3-chlorophenothiazine; b = levomepromazine; c = chlorpromazine; d = dimethothiazine; e = propericiazine; g = oxomemazine.

bonding a silane to the silica surface and, after that, the polar functional groups are fixed by the well-known substitution reactions. The direct route, according to the first method, is prevailing, and commercially available stationary phases are exclusively prepared by this reaction.

Generally, for the alkyl bonded-phase synthesis, alkylchlorosilanes and alkoxysilanes are used. They react directly with silanol groups after desorption of adsorbed water by heating the silica at 200°C under vacuum for about 12 h.

With an alkylmonochlorosilane the reaction can be written

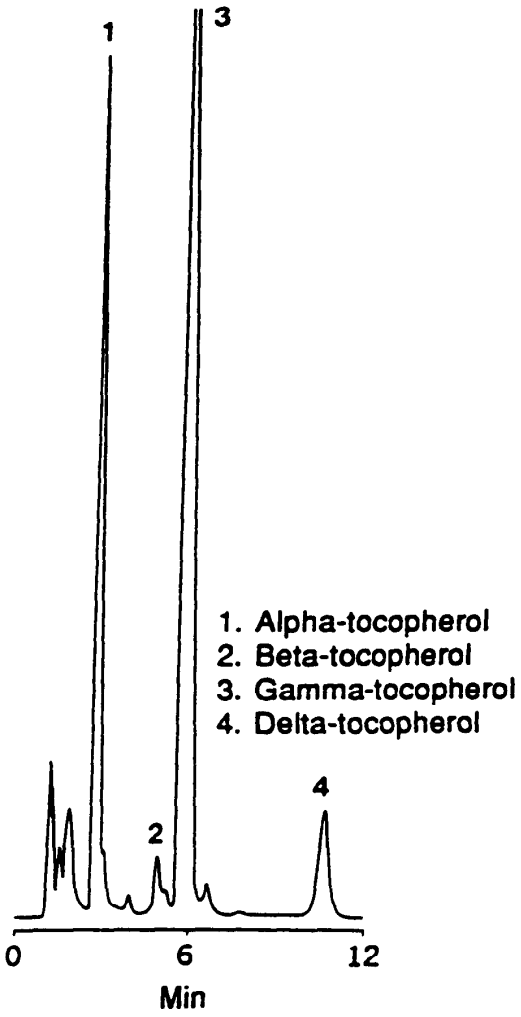
$$\equiv SiOH + Cl\text{–}SiR_3 \rightleftharpoons \equiv Si\text{–}O\text{–}SiR_3 + HCl$$

With an alkylmonochlorosilane or an alkylmonoalkoxysilane used in a dry solvent (water must be excluded systematically during phase preparation) "monomeric" bonded phases are obtained. With these phases only a monomolecular layer of alkyl chain is grafted to the surface (sometimes these phases are called "bristle type" or "brush-type" bonded phase).

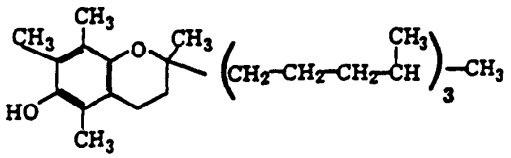
With trichlorosilane the reaction is

$$\equiv SiOH + R\text{–}SiCl_3 \rightleftharpoons \equiv Si\text{–}O\text{–}SiRCl_2 + HCl$$

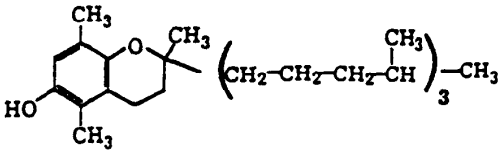
and



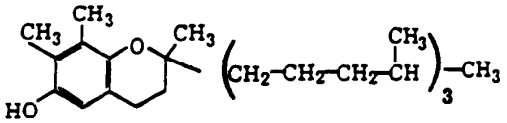
α-Tocopherol



ß-Tocopherol



γ-Tocopherol



δ-Tocopherol

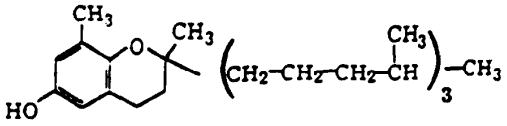
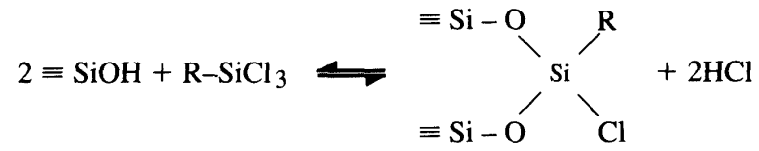


Figure 16 Separation by adsorption chromatography of corn oil tocopherols. Sample: 10 μL of corn oil in 100 μL of mobile phase. Column, Nova Pak Silica (4 μm), 3.9-mm id × 150 mm; mobile phase, 0.3% isopropyl alcohol in isooctane; flow rate, 1.0 mL min^{-1}; detection, fluorescence 290-nm excitation and 335-nm emission. (From Ref. 41.)

Table 11 Main Polar-Bonded Phases

Type	Typical functional group	Structure
Diol	Glyceropropyl	$-(CH_2)_3-O-CH_2-\underset{\displaystyle OH}{\underset{\displaystyle \vert}{CH}}-\underset{\displaystyle OH}{\underset{\displaystyle \vert}{CH_2}}$
Cyano	Cyanopropyl	$-(CH_2)_3-CN$
Amino	Aminopropyl	$-(CH_2)_3-NH_2$



(Because of sterical reasons the third chloro group cannot react with the surface directly). Consequently, trace amounts of water may hydrolyze some Si–Cl bonds according to

$$\equiv Si\text{–}O\text{–}SiRCl_2 + 2H_2O \rightleftharpoons \equiv Si\text{–}O\text{–}Si(OH)_2R + 2HCl$$

and so on. A polymer layer is then generated. These polymeric phases give higher retention owing to the larger volume of the bonded stationary phase, but they have the main drawback of giving a slower speed of mass transfer in the thick polymeric layer compared with the monomeric bonded phase.

To prepare stationary phases bearing polar functional groups in one step, it is necessary to first prepare an appropriate silane. According to several authors, because of the high reactivity of chlorosilanes, the introduction of polar groups into a silane is easier when using the less reactive alkoxysilanes [44,45]. However, according to Engelhardt and Orth [46], this low reactivity and the presence of polar functional groups require different operating conditions to attach these alkoxysilanes to the silica surface. These authors have described the conditions allowing the preparation of polar-bonded phases with reproducible chromatographic characteristics and optimum surface coverage. Important points are

1. Surface pretreatment of silica: the cleaning procedure removes organic and metallic impurities and gives a homogeneous, fully hydroxylated surface.
2. Use of an aromatic hydrocarbon as the reaction solvent: solvents that are too polar prevent the silane adsorption, whereas it is the first step of the binding reaction.
3. Use of catalysts: Although acidic or basic groups in the silane act autocatalytically for the reaction, the addition of catalysts (triethylamine, for example, for amino groups) is advantageous: the reaction is accelerated and the surface coverage is increased.
4. Wash with dilute hydrochloric acid: this achieves hydrolysis of alkoxygroups and desorption of the reactive silane from the silica surface.

Under these conditions, using a trialkoxysilane, for example, triethoxypropylamine silane, the surface coverage is about 4.7 μmol m^{-2}, which corresponds roughly to the maximum achievable without oligomerization, assuming a monomolecular layer. Therefore, the proportion of reacted silanol groups is slightly greater than 50%.

On the average, 1.5 alkoxy groups of the trialkoxysilane are able to react with the silica surface sites: because the third alkoxy group cannot react directly with the surface owing to steric hindrance, 50% of the silanes are bonded with one siloxane bond to the surface and 50% are bonded by two siloxane bonds.

B. Retention Mechanisms

In the normal-phase mode, the stationary phases, summarized in Table 11, exhibit chromatographic properties similar to bare silica, but they offer four main important advantages:

1. No irreversible fixation of very polar solutes.
2. Faster column equilibration.
3. Less importance of water content of the mobile phase; in others words, the use of isohydric solvents is not needed to obtain reproducible results.
4. Distinct selectivities can be obtained by varying the polar functional group nature of the stationary phase.

However, predicting solute retention in normal-bonded-phase liquid chromatography (NBP-LC) is more difficult than when silicas are used. This is largely because of the complexity of associations possible between solvent molecules and the chemically and physically heterogeneous bonded phase surface. Several models of retention in NBP-LC have been advocated [3,18,22,47], but their validity, particularly when mixed-solvent systems are used as mobile phase, can be questioned.

The most commonly accepted retention mechanisms is Snyder's model [3,18,22], which assumes competitive adsorption between solutes and solvent molecules on the active sites of the silica surface. Several studies showed that this model also holds true on diol- [48,49], cyano- [48,50], and aminopropyl-bonded silica [51,52]. For example, at a low polar modifier concentration, the competitive adsorption onto an aminopropyl-bonded phase may be symbolized as:

$$-\overline{NH_2}P + s \rightleftharpoons -\overline{NH_2}s + P$$

where $-\overline{NH_2}$, P, and s stand for an amino group, the polar modifier, and the solute, respectively. However, when increasing the polar modifier content, molecules of the latter tend to accumulate on the stationary phase in concentrations far beyond a monolayer; consequently, the hypothesis of competitive monolayer adsorption on the stationary phase is no longer valid at high modifier concentrations (60% v/v) [53]. In this second example, the dominant retention process is a partitioning mechanism (*partitioning* implies the solute is approximately fully embedded within the stationary phase, whereas *adsorption* implies the solute is only in surface contact with the stationary phase and not fully embedded).

Thus, for a polar modifier content lower than 60% v/v, the phenomenon of restricted access delocalization of the polar solvent appears. Polar modifier molecules will adsorb with localization and effectively disrupt solute localization; the effective solvent strength of the modifier will be relatively large. When increasing coverage of the stationary phase, additional polar modifier molecules interfere with further polar modifier localization, and further adsorption occurs without localization. The effective polar modifier strength decreases with increasing coverage. This behavior is shown in Figure 17: we can see that the position of

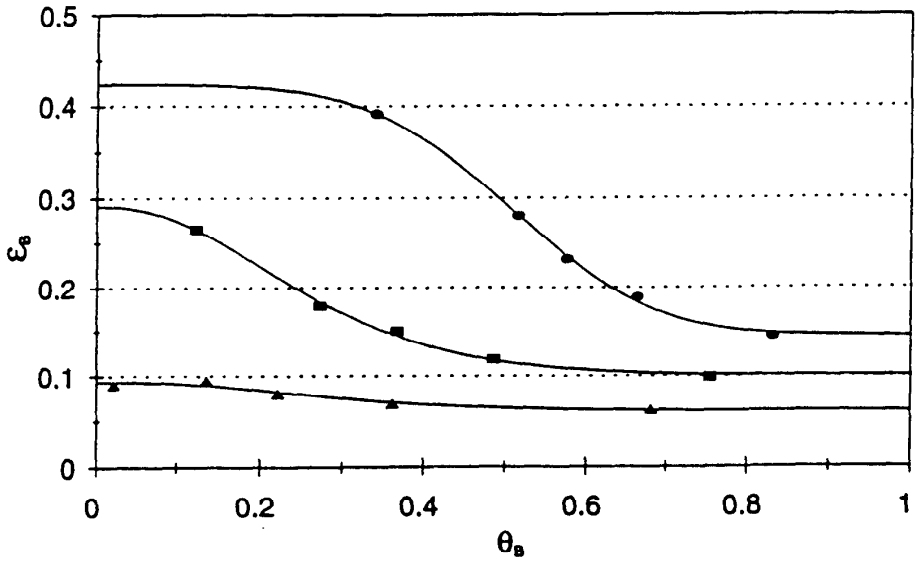


Figure 17 Variation of diethyl ether solvent strength ε_B versus the fractional surface coverage θ_B of the stationary phases: Column, 25 × 0.46-cm id; stationary phase, ■ diol, ▲ cyano, ● amino; mobile phase, pentane-diethyl ether; flow rate, 1.5 mL min^{-1}; detection, refractometry; hexane was used as the t_0 marker. (From Ref. 54.)

inflection depends on the bonded group type (θ_B = 0.25 [diol], 0.27 [cyano], and 0.51 [amino]). These fractional surface coverage values correspond to polar modifier levels in the mobile phase from 5 to 15% v/v [54].

For higher polar modifier concentrations in the mobile phase, the stationary phase can be considered as a randomly mixed bulk stationary phase (it has been advocated [55] that polar modifier molecules can accumulate close to the polar surface of the stationary phase, giving a polar stagnant layer) and the solute retention is described as partitioning, rather than adsorption.

The effects of the polar modifier content in the mobile phase on the column void volume, and the length of the alkyl chain on log k' have recently been studied. For a polar modifier concentration higher than 60% v/v, partitioning, rather than adsorption, is the dominant retention mechanism. Figure 18 shows the variations of log k' versus solute size of alkylaryl-ketone (propio, butyro, hexa, heptano, and octanophenone) homologues for an aminopropyl stationary phase. For modifier contents (MTBE) greater than 60% we can observe a strong linear relation between log k' and n_c [53]. This dependence of retention on molecular volume in partitioning systems has already been demonstrated [56,57].

Finally we must add that hydrogen bonding can occur between cyano groups (and probably also hydroxy and amino groups) and residual silanols, and these interactions can influence the retention characteristics [58].

C. Mobile-Phase Selection

The rational selection of the mobile-phase composition obeys the same rules as for adsorption chromtography, except the water content (the use of isohydric solvents is unnecessary). One generally uses a mixture of an alkane with small quantities of one or several polar solvents

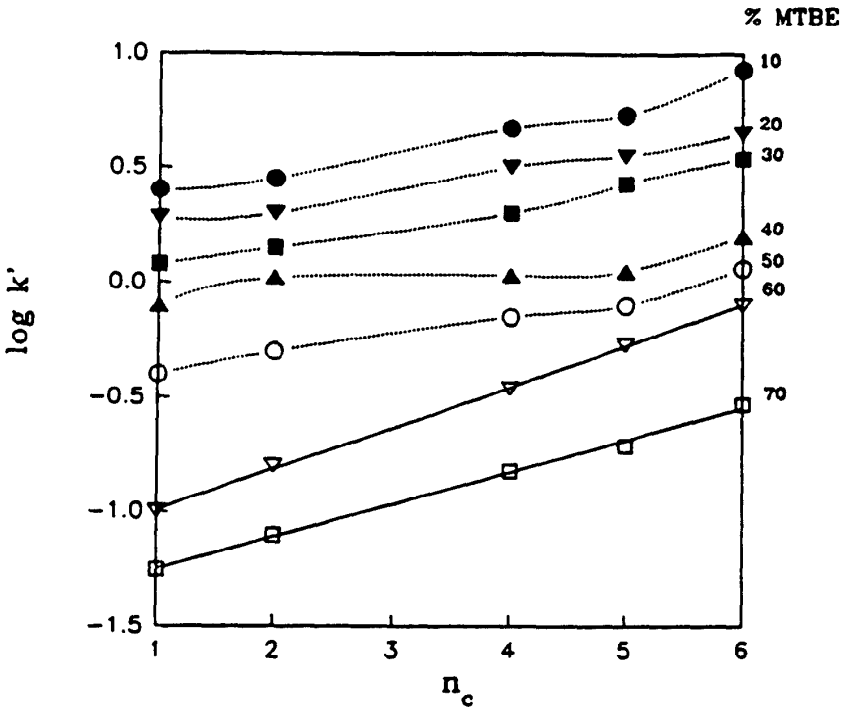


Figure 18 Variation of solute capacity factor logarithm versus the size of the solute molecule for various MTBE contents: column, 25 × 0.46-cm id; stationary phase, aminopropyl-bonded silica 5 μm (EM Science); mobile phase, hexane–methyl *tert*-butyl ether (MTBE); flow rate; 0.5 mL min^{-1}; detection; UV at 254 nm; hexane was used as the t_0 marker. (From Ref. 53.)

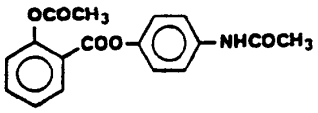
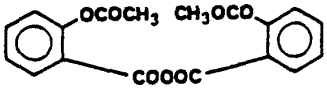
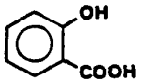
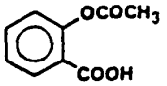
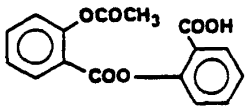
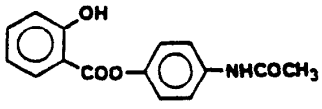
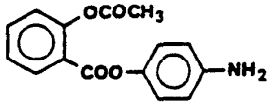
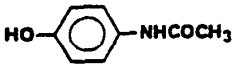
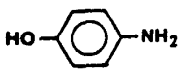
belonging to different selectivity groups (see Sec. II. B.4.a). These polar modifiers govern the selectivity, whereas the alkane content is adjusted to give a convenient retention for the solutes of interest.

When the mobile phase is a mixture of an apolar solvent with a strongly polar solvent present at a low concentration (typically less than 0.2% v/v), the inverse of the retention factor varies linearly with the polar solvent content in the eluent [59].

D. Applications

The analysis of highly hydrolyzable compounds is a typical example of the applications of NBP-LC. Let us consider the identification and the quantitation of impurities that may be encountered in benorylate, which is an ester of aspirin. For quality control of the manufactured drug, a method was needed to allow determination of several possible impurities (Table 12; some are suspected of being responsible of causing allergic reactions) [60]. Because of the

Table 12 Benorylate and Possible Impurities

Impurity	Structure
p-Acetamidophenylacetylsalicylate (benorylate)	
Acetylsalicylic anhydride	
Salicylic acid	
Acetylsalicylic acid (aspirin)	
Acetylsalicylsalicylic acid	
p-Acetamidophenyl salicylate (phenetsal; acetarminosalol)	
p-Aminophenylacetyl salicylate	
p-Acetamidophenol (paracetamol; acetaminophen)	
p-Aminophenol	

presence of acetylsalicylic anhydride, the use of water as a mobile phase constituent is prohibited; therefore, ion-exchange, ion-pair, or reversed-phase chromatography cannot be implemented. Owing to the variety of functional groups and the relatively high polarity of some of them, NBP-LC on an alkylnitrile-bonded silica as stationary phase (Micropak CN) was selected.

Preliminary trials carried out to optimize the selectivity led to the ternary mixture: hexane–dichloromethane–methanol, containing 0.2% of pure acetic acid (to prevent the ionization of acidic functions and deactivate residual silanol groups). The choice of methanol as a polar modifier can be considered the result of both its high eluting strength and its specific properties: it acts as an H-bond acceptor toward carboxylic acids and as donor toward *p*-aminophenol.

Because paracetamol (acetaminophen) and *p*-aminophenol are far more strongly retained than the first-eluting solutes, a separation under isocratic conditions is not possible: a very low methanol content is required to separate the early-eluting peaks with an appropriate resolution, but the elution of the last two peaks would require a prohibitively long time. Therefore, a methanol gradient elution was carried out, according to the profile shown in Figure 19.

Routine analyses are possible in these conditions: the reproducibility of the retention times is good (coefficient of variation in the order of 1%), the sensitivity allows the detection of the most harmful impurities at their critical levels (the limits of detection lie between 2 nmol of *p*-aminophenol and 40 pmol of acetaminosalol [phenetsal]), and the repeatability of the concentration determinations is satisfactory (coefficient of variation 0.54% for the main product over seven successive injections).

Another typical application of NBP-LC is the class separation of solutes, such as the separation of polynuclear aromatic hydrocarbons (PAHs)—based on the number of condensed rings—that is required, for example, in the petroleum industry. Reversed-phase chromatography is well suited for the PAH analyses; however, alkyl substitution significantly increases PAH retention so that alkyl-substituted PAHs with low ring numbers have retention times close to some unsubstituted higher-ring–number PAHs, giving coelution phenomena. Wise et al. reported [61] that aminopropylsilica-bonded phases yield a separation sequence according to the conjugated ring number, regardless of the type of alkylsubstitution. Furthermore, a study showed that a diaminosilica-bonded phase seems even better: on this $-R(NH_2)_2$-bonded silica, alkyl PAHs elute near the parent PAHs, and separations based on the number of conjugated rings are achieved for up to four-ring aromatics [62].

Similarly, a scheme has been described that permits the identification of different kinds of anilines by a two-phase analysis [63]. The systematic separation into structural types (tertiary, secondary, and primary anilines) is achieved by normal-phase chromatography on a nitrile stationary phase, whereas individual compounds within each group are identified mainly by reversed-phase chromatography, for which the elution order is governed by the alkyl carbon number. On the nitrile phase, the elution order is tertiary, secondary, and primary anilines and, within each group, the retention is determined mainly by the size of the alkyl group substituted at the nitrogen atom (Fig. 20).

Because isooctane containing 0.2% (v/v) of 2-propanol is used as mobile phase, the competitive adsorption mechanism is preponderant; hence, the classic rules for the prediction of solute retention in adsorption chromatography can be advocated to explain the retention order. Steric hindrance effects in the vicinity of the nitrogen atom of the amine group are clearly apparent:

1. *In the elution order*: tertiary, secondary, and primary anilines
2. *Within each group*: each *ortho*-substituted aniline is less retained than its *para*-substituted homologue; moreover, the primary anilines fall into three groups according to the number of *ortho*-substituents, non-*ortho*-, mono-*ortho*-, and di-*ortho*-substituted species, respectively (these groups are separated by the broken lines in Fig. 20).

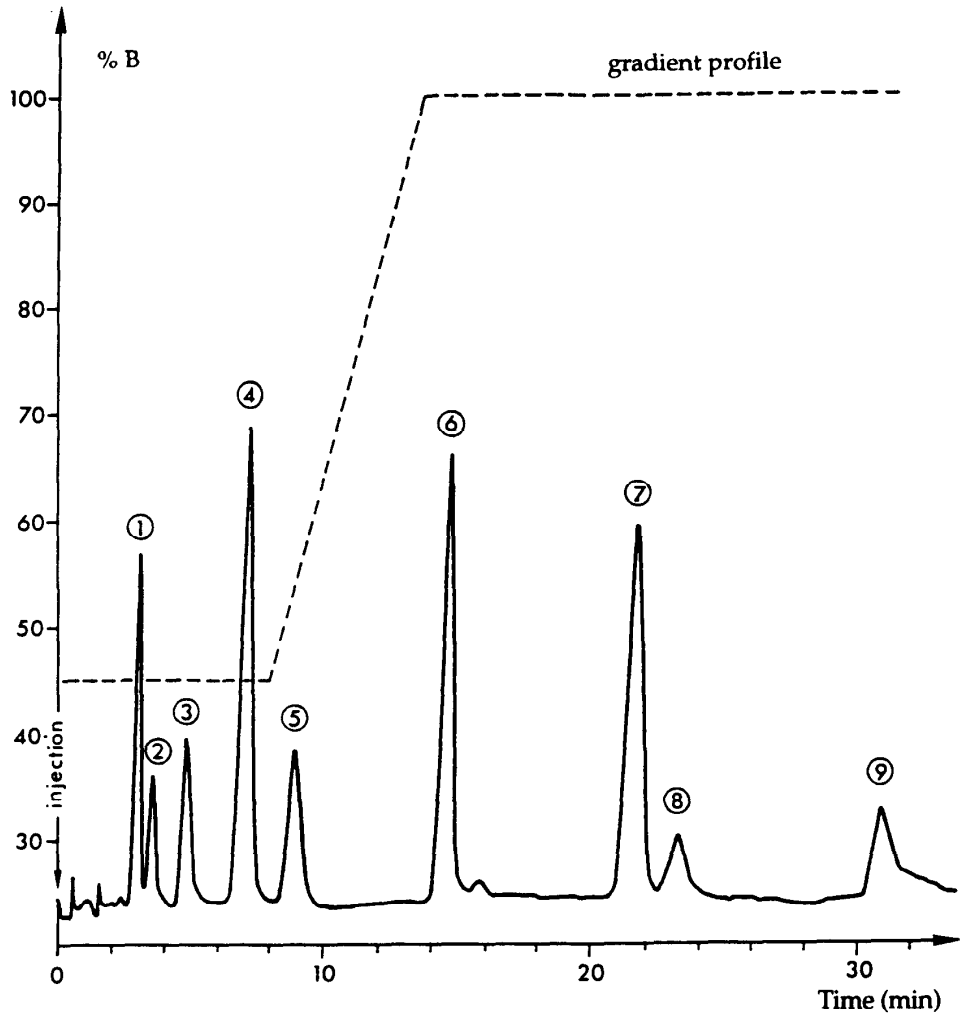
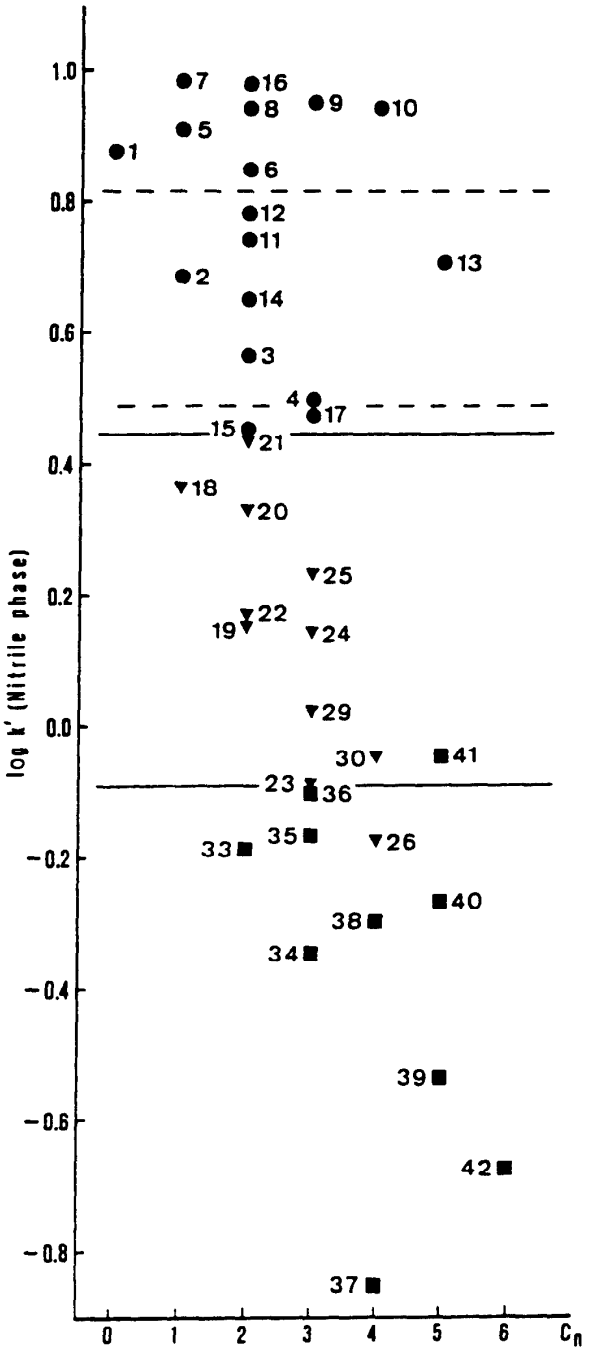


Figure 19 NBP–LC separation of impurities that may be present in benorylate tablets: column, −25 × 0.21-cm; stationary phase, Micropack CN, 10 μm; mobile phase; solvent A; hexane–dichloromethane–acetic acid (94.8:5:0.2 v/v); solvent B, hexane–dichloromethane–methanol–acetic acid (89.8:5:5:0.2 v/v); gradient profile as shown; flow rate, 1.5 mL min^{-1}; pressure drop, 70 bar; detection, UV 254 nm; injection volume; 3 μL; sample solvent, dichloromethane; solutes 1, acetylsalicylic anhydride (1 mg mL^{-1}); 2, aspirin (1.5 mg mL^{-1}); 3, acetylsalicylsalicylic acid (1.5 mg mL^{-1}); 4, phenetsal (0.5 mg mL^{-1}); 5, *p*-aminophenylacetylsalicylate (1 mg mL^{-1}); 6, benorylate (0.5 mg mL^{-1}); 7, paracetamol (0.5 mg mL^{-1}); 8, unknown impurity; 9, *p*-aminophenol (1.5 mg mL^{-1}). (From Ref. 60.)

The systematic separation of alkylanilines into primary, secondary, and tertiary anilines and the individual compounds are illustrated in Figures 21 and 22. The first separation, according to class, is carried out on the nitrile phase, whereas the three classes are then analyzed separately on a C_{18} phase, for which the separation is achieved accordingly to alkyl carbon number.

NBP-LC has also acquired numerous applications in the field of carbohydrate analysis. Recent reviews [64–66] mention that these separations of sugars are carried out using stationary phases, such as alkylamine-, diol-, or polyol-bonded silicas. Alkylamino-bonded silicas are commonly used for the separation of saccharides and oligosaccharides in various media, such as foods or biological fluids. Mobile phases often contain water as polar constituent (typical eluents are methanol–water, acetonitrile–water binary mixtures, or acetonitrile–



	Primary anilines
1	None
2	2-Methyl
3	2-Ethyl
4	2-Isopropyl
5	3-Methyl
6	3-Ethyl
7	4-Methyl
8	4-Ethyl
9	4-Isopropyl
10	4-*n*-Butyl
11	2,3-Dimethyl
12	2,4-Dimethyl
13	2-Methyl-4-*n*-butyl
14	2,5-Dimethyl
15	2,6-Dimethyl
16	3,4-Dimethyl
17	2,4,6-Trimethyl
	Secondary anilines
18	N-Methyl
19	N-Methyl-2-methyl
20	N-Methyl-3-methyl
21	N-Methyl-4-methyl
22	N-Ethyl
23	N-Ethyl-2-methyl
24	N-Ethyl-3-methyl
25	N-Ethyl-4-methyl
26	N-Ethyl-2-ethyl
27	N-Acetyl
28	N-Acetyl-4-methyl
29	N-Propyl
30	N-*n*-Butyl
31	N-Phenyl
32	N-Benzyl
	Tertiary anilines
33	N,N-Dimethyl
34	N,N-Dimethyl-2-methyl
35	N,N-Dimethyl-3-methyl
36	N,N-Dimethyl-4-methyl
37	N,N-Dimethyl-2,6-dimethyl
38	N,N-Diethyl
39	N,N-Diethyl-2-methyl
40	N,N-Diethyl-3-methyl
41	N,N-Diethyl-4-methyl
42	N,N-Diethyl-2-ethyl
43	N,N-Diphenyl

Figure 20 Relation between alkyl carbon number (C_n) and log k' of alkylanilines on the nitrile stationary phase (Nucleosil CN): mobile phase, 0.2% (v/v) isopropanol in isooctane; ●, primary anilines; ▼, secondary anilines; ■, tertiary anilines. (From Ref. 63.)

methanol–water ternary mixtures). Nevertheless, such systems cannot be classified as reversed-phase systems: retention decreases when water content increases, and carbohydrates are eluted in the order of increasing polarity and, more precisely, with the number of hydroxyl groups on the same molecule side. As shown by Koizumi et al. [67], the use of a 3-μm aminopropyl silica allows the resolution of *d*-glycooligosaccharides up to DP (degree of polymerization) 30–35 under isocratic conditions, with a binary mixture acetonitrile–water [67]; similarly, the use of a polyamine polymer resin-bonded silica or of an amido-bonded

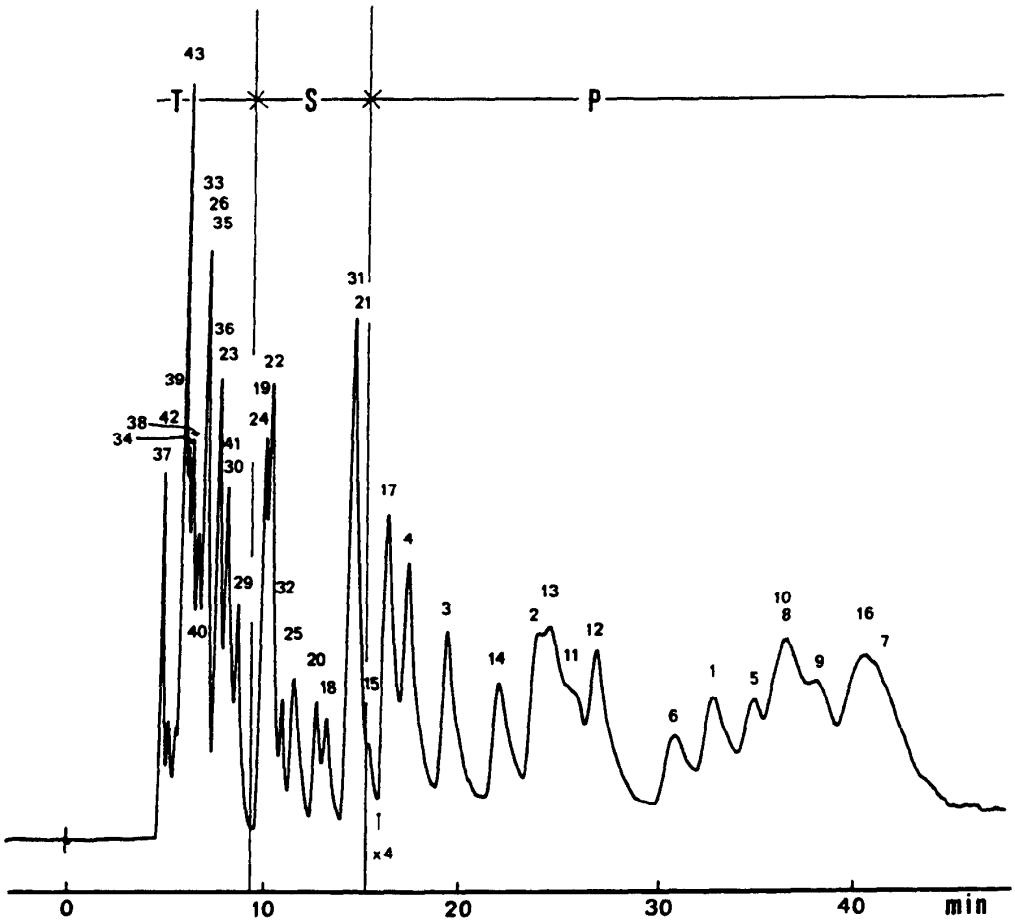


Figure 21 Class separation of a mixture of primary (P), secondary (S), and tertiary (T) alkylanilines by NBP–LC on the nitrile phase: column, 20 × 0.44 cm; stationary phase, Nucleosil CN, 5 μm; mobile phase, 0.2% (v/v) isopropanol in isooctane; flow rate, 0.75 mL min^{-1}; solutes, the numbers refer to Fig. 20. (From Ref. 63.)

silica, containing carbamoyl instead of aminopropyl groups, permits the analysis of maltooligosaccharides up to DP 28 [68].

However, two drawbacks occur when using amino phases:

1. Reducing sugars react with amino groups, by carbonyl-amine condensation yielding a Schiff base. This reaction causes a deterioration in column performance on prolonged use. Some authors recommend the use of secondary amino groups, which are less reactive.
2. Amino groups hydrolyze in the presence of water and, consequently, the life time of columns is rather limited [69]. Indeed, hydrolysis increases with water content in the eluent. Diol-bonded silica represents an alternative to aminopropyl silica, without the complication of glycoxylamine formation, but because of a partial resolution of anomers, an addition of amine to the acetonitrile–water eluents is necessary to prevent peak broadening, and this can be detrimental to the stability of silica-based packings.

A recent paper [70] has shown that mobile phases consisting of an acetonitrile–methanol–water ternary mixture, when reducing the water content, significantly improve the life time of amino columns. Moreover, the interest in the use of the light-scattering detector, which is compatible with an elution gradient, was clearly demonstrated in the oligosaccharide analysis.

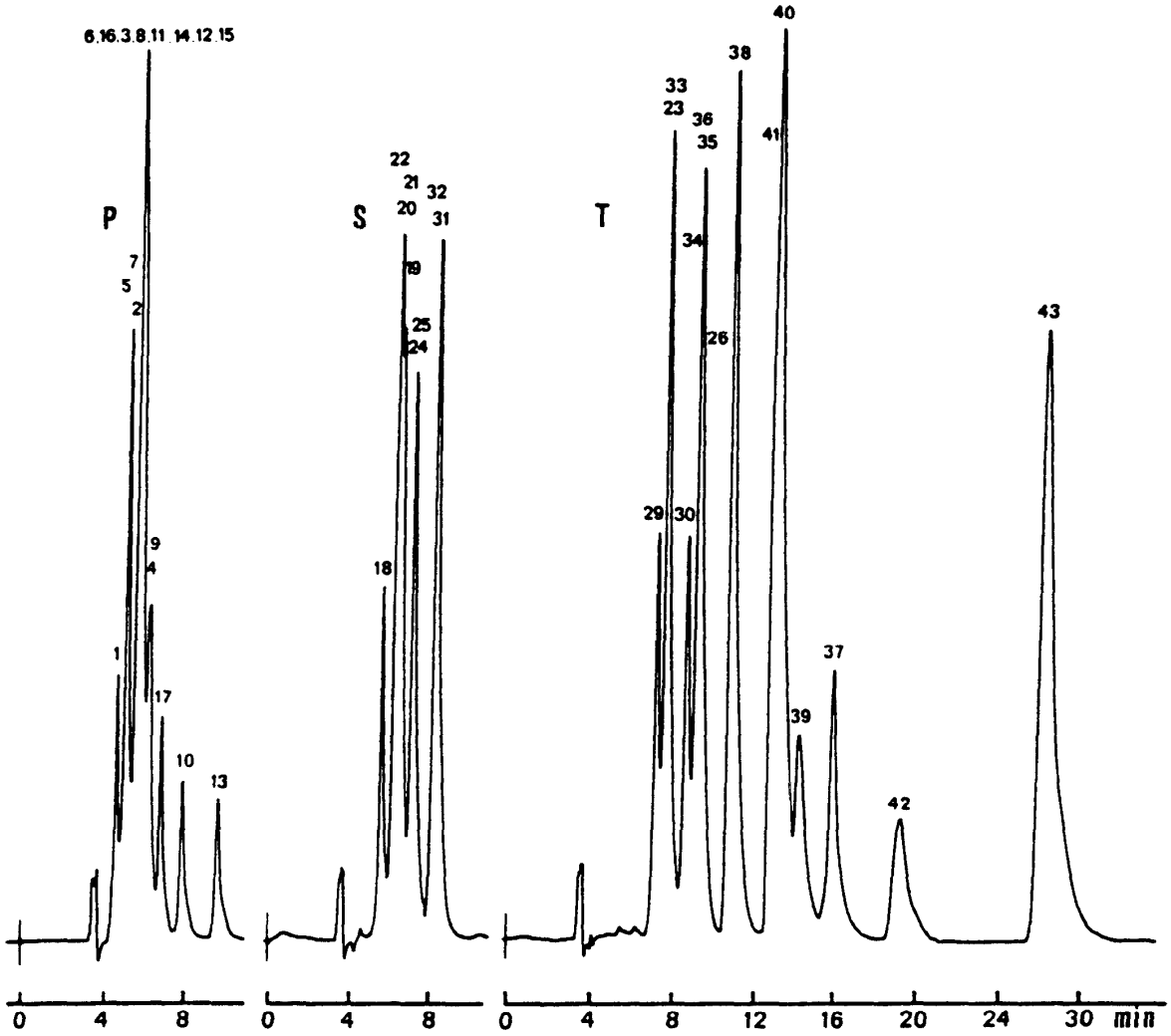


Figure 22 Carbon number separation, by reversed-phase chromatography, of primary (P), secondary (S), and tertiary (T) anilines isolated by class separation, according to Fig. 21: column, 20 × 0.44 cm; stationary phase, Nucleosil C_{18}, 5 μm; mobile phase, methanol–aqueous phosphate buffer, pH 7.0 (80:20 v/v); flow rate, 0.75 mL min^{-1}; solutes, the numbers refer to Fig. 20. (From Ref. 63.)

REFERENCES

1. RE Majors. LC–GC 9:686, 1991.
2. KK Unger. Porous silica. Journal of Chromatography Library, Vol. 16. Amsterdam; Elsevier, 1979, 2nd rep. 1986.
3. LR Snyder. Principles of Adsorption Chromatography. New York: Marcel Dekker, 1968.
4. A Berthod. J Chromatogr 549:1, 1991.
5. RK Iler. The Chemistry of Silica. New York: Wiley, 1979.
6. JJ Kirkland, CH Dilks Jr, JJ Destefano. J Chromatogr 635:19, 1993.
7. J Köhler, DB Chase, RD Farlee, AJ Vega, JJ Kirkland. J Chromatogr 352:275, 1986.
8. J Köhler, JJ Kirkland. J Chromatogr 385:125, 1987.
9. C Laurent, H Billiet, L de Galan. Chromatographia 17:253, 1983.
10. H Billiet, C Laurent, L de Galan. Trends Anal Chem 4:100, 1985.
11. K Cabrera, D Lubda, G Jung. Kontakte (Darmstadt) 12, 1992.
12. M Kawahara, H Nakamura, T Nakajima. J Chromatogr 515:149, 1990.

13. U Trüdinger, G Müller, KK Unger. J Chromatogr 535:111, 1990.
14. J Nawrocki, MP Rigney, A McCormick, PW Carr. J Chromatogr. 657:229, 1993.
15. JJ Pesek, VH Tang. Chromatographia 39:649, 1994.
16. M Waksmundzka-Hajnos, T Wawrzynowicz, TH Dzido. J Chromatogr 600:51, 1992.
17. M Waksmundzka-Hajnos. J Chromatogr 623:15, 1992.
18. LR Snyder. Anal Chem 46:1384, 1974.
19. E Soczewinski. Anal Chem 41:179, 1969.
20. LR Snyder, JL Glajch, JJ Kirkland. J Chromatogr 218:299, 1981.
21. LR Snyder. J Chromatogr 255:3, 1983.
22. LR Snyder, JL Glajch. J Chromatogr 248:165, 1982.
23. C Souteyrrand, M Thibert, M Caude, R Rosset. J Chromatogr 262:1, 1983.
24. JP Thomas, A Brun, JP Bounine. J Chromatogr 139:21, 1977.
25. M Thibert, M Caude, R Rosset. Analusis 7:454, 1979.
26. JP Thomas, M Caude, A Brun, JP Bounine. Analusis 5:205, 1977.
27. JP Thomas, A Brun, JP Bounine. J Chromatogr 172:107, 1979.
28. JG Dorsey, WT Cooper. Anal Chem 66:857A, 1994.
29. C Dumas, M Caude, R Rosset. Analusis 14:131, 1986.
30. LR Snyder, JL Glajch. J Chromatogr 214:1, 1981.
31. VR Meyer, MD Palamareva. J Chromatogr 641:391, 1993.
32. LR Snyder. J Chromatogr Sci 16:223, 1978.
33. L Rohrschneider. Anal Chem 45:1241, 1973.
34. SC Rutan, PW Carr, WJ Cheong, JH Park, LR Snyder. J Chromatogr 463:21, 1989.
35. PJ Schoenmakers. Optimization of Chromatographic Selectivity. Journal of Chromatography Library, Vol. 35. Amsterdam: Elsevier, 1986.
36. JL Glach, JJ Kirkland, KM Squire, JM Minor. J Chromatogr 199:57, 1980.
37. JL Glach, JJ Kirkland. Anal Chem 55:319 A, 1983.
38. R Lehrer. Int Lab 11(8):76, 1981.
39. LR Snyder, JJ Kirkland. Introduction to Modern Liquid Chromatography. New York: Wiley Interscience, 1979.
40. JP Bounine, G Guiochon, H Colin. J Chromatogr 298:1, 1984.
41. BA Bidlingmeyer. Practical HPLC Methodology and Applications. New York: John Wiley & Sons, 1992.
42. CL Guillemin. J Chromatogr 158:21, 1978.
43. KK Unger, FE Regnier, RE Major, eds. Liquid Chromatography Packings. J Chromatogr 544: 1991.
44. H Engelhardt, D Mathes. J Chromatogr 142:311, 1977.
45. H Engelhardt, D Mathes. J Chromatogr 185:305, 1979.
46. H Engelhardt, P Orth. J Liq Chromatogr 10:1999, 1987.
47. RPW Scott, P Kucera. J Chromatogr 142:213, 1977.
48. PL Smith, WT Cooper. J Chromatogr 410:249, 1987.
49. AW Salotto, EL Weiser, KP Caffey, RL Carty, SC Racine, LR Snyder. J Chromatogr 498: 55, 1990.
50. EL Weiser, AW Salotto, SM Flach, LR Snyder. J Chromatogr 303:1, 1984.
51. LD Olsen, RJ Hurtubise. J Chromatogr 479:5, 1989.
52. LR Snyder, TC Schunk. Anal Chem 54:1764, 1982.
53. CW Hsu, WT Cooper. J Chromatogr 603:63, 1992.
54. M Lübke, JL le Quere, D Barron. J Chromatogr 690:41, 1995.
55. RPW Scott. J Chromatogr Sci 18:297, 1980.
56. H Colin, AM Krustulovic, MF Gonnord, G Guiochon, Z Yun. Chromatographia 17:9, 1983.
57. GE Berendsen, L de Galan. J Chromatogr 196:21, 1980.
58. JG Dorsey, WT Cooper. Anal Chem 66:857A, 1994.
59. MC Hennion, C Picard, C Combellas, M Caue, R Rosset. J Chromatogr 210:211, 1981.
60. G Chevalier, P. Rohrbach, C Bollet, M Caude. J Chromatogr 138:193, 1977.

61. SA Wise, SN Chesler, HS Hertz, LR Hilpert, WE May. Anal Chem 49:2306, 1977.
62. J Chmielowiec. AE George. Anal Chem 52:1154, 1980.
63. LA Truedson, BEF Smith. J Chromatogr 214:291, 1981.
64. M Verzele, G Simoens, F Van Damme. Chromatographia 23:292, 1987.
65. SC Churms. J Chromatogr 500:555, 1990.
66. B Herbreteau, Analusis 20:355, 1992.
67. K Koizumi, T Utamura, Y Okada. J Chromatogr 321:145, 1985.
68. K Koizumi, T Utamura, Y Kubota, S Hizukuri. J Chromatogr 409:396, 1987.
69. M Lafosse, B Herbreteau, M Dreux, L Morin-Allory. J Chromatogr 472:209, 1989.
70. B Herbreteau, V Villette, M Lafosse, M Dreux. Fresenius J Anal Chem 351:246, 1995.

10

HPLC of Ions: Ion-Exchange Chromatography

Robert E. Smith

Midwest Research Institute, Kansas City, Missouri

I. INTRODUCTION

Ion-exchange chromatography has been the subject of many books, conference proceedings, and reviews [1–13]. This chapter will attempt to highlight theories discussed in detail by others. Also, advances in the past 2–3 years will be described, with special emphasis on biomedical applications and mass spectrometry, which were not emphasized in other reviews. An attempt is made to divide the subject into low molecular weight (< 1000 Da) and high molecular weight analytes, such as proteins.

The history of ion-exchange chromatography was described by Small [1]. As he pointed out, Adams and Holmes [14] were the first to demonstrate synthetic ion exchangers by making cross-linked, insoluble polymers from phenols, phenylene diamines, and formaldehyde. Bauman and Eichhorn [15] and Kunin and Myers [16] introduced mass action concepts into ion exchange and described ion-exchange equilibria. Boyd, and coauthors [14] described the diffusional nature of the ion-exchange process. Possibly the most significant event to follow in this field was the development of automated amino acid analysis by Moore and Stein [18,19], which led to their receiving the Nobel prize in chemistry in 1972. This work was continued by others, including Hamilton and co-workers [20–22], who demonstrated the power of coupling ion-exchange separation with a continuous flow-through detector. During this time, Glueckauf described the relation between column performance and the fundamental properties if ion-exchange resins [23]. Small described the development of the chromatography of inorganic ions as moribund in the early 1970s [1]. In late 1971, he started research at the Dow Chemical Company that eventually led to the adoption of conductimetric detection as a universal means of detecting inorganic ions, and many organic ions [1]. In 1975 Small and coworkers described the use of chemically suppressed conductivity detection [24]. They put a second column, called a stripper column, past the anion-exchange separator column. This stripper column removed the background eluent, but allowed the analyte ions to remain, often with enhanced conductivity. Earlier in 1975, the Dow Chemical Company applied for patents and granted a license to the Dionex Corporation to manufacture and market instruments that

Prepared for the United States Department of Energy by AlliedSignal, Kansas City Division, under contract number DE-AC04-76-DP00613.

used the stripper columns, which were renamed suppressor columns. The term ion chromatography was coined to designate the use of chemically suppressed conductivity detection.

As the marked for ion chromatographs grew, other methods were developed and more manufacturers appeared. In 1979, conductimetric methods that did not use a suppressor device were described [25–26] and were first commercialized by the Wescan Company [3], and later by Waters, Shimadzu, Metrohm, and others. In the February, 1994 issue of *American Laboratory* [27], 62 different companies were in the product listings under "Chromatography, Ion, Systems." There has been an evolutionary change in the concept of ion chromatography to where it now embraces a much wider combination of separation and detection methods. Ion chromatography is often thought of as any chromatographic method applied to ions [1].

While many people were developing methods to determine low molecular weight analytes, others focused on high molecular weight compounds, especially proteins or polypeptides. Often the goal was not to quantitate a protein, but to purify it from a complex biological matrix containing active proteases. This required rapid, preparative-scale methods. Instead of using pumps, carefully prepacked columns and flow-through detectors, hand-poured columns packed with ion-exchange materials and gravity-fed flow of eluent at low temperature were used to preserve the biological activity of the protein being purified. Although much of the theory and nomenclature used for low molecular weight analytes is useful, additional concepts were developed for describing the retention of polyelectrolyte proteins on ion-exchange materials [28–32]. In the next section, some of the basic nomenclature and theory that applies to ion exchange and ion interaction are discussed. Then, electrostatic models for protein retention and concepts important in preparative-scale ion-exchange chromatography are described.

II. PRINCIPLES OF ION EXCHANGE

A. The Ion-Exchange Process for Low Molecular Weight Ions in Analytical-Scale Chromatography

The basic definitions required for an understanding of chromatographic processes are presented in various books [1–5]. Especially recommended is Chapter 2 of Small's book [1]. Most definitions and equations that follow are used commonly in the chromatographic literature, although the letters of the alphabet used to denote various parameters will vary from one author to the next. As Small described in his book [1], a key element in an ion chromatograph is the column. It is usually a tube packed with some sort of finely divided spherical solids called the stationary phase. There is a small interstitial or void volume V_0, which is the space between the stationary phase particles. A liquid, called the mobile phase, is continuously being pumped through the column. The void volume is filled with the mobile phase. The mobile phase is also called the *eluent*. The fluid that exits out the bottom of the column is called the *effluent* or *eluate*. The verb *elute* is defined as the process of washing solutes off the column. Definitions relating to ion-exchange chromatography will be noted when describing the thermodynamics, kinetics, and retention mechanisms of ion-exchange chromatography.

The distribution of solutes between stationary and mobile phases depends on the thermodynamic distribution equilibria involved. The exchange of ions between a monofunctional ion exchanger preequilibrated with eluent ion E, with a charge of x and a low molecular weight sample ion S with a charge of y can be represented by the equilibrium expression [1]:

$$y(RE^x) + xS^y = x(RS^y) + yE^x \quad (1)$$

where RE^x is eluent with charge of x bound to ion-exchange resin and RS^y is sample ion bound to ion-exchange resin.

Charges are omitted on S and E so that the expression can apply to anion or cation exchange. An equilibrium constant for this ion exchange, $K_{S,E}$, is given by:

$$K_{S,E} = \frac{(RS^y)^x(E^x)^y}{(S^y)^x(RE^x)^y} \tag{2}$$

where parentheses indicate activities of the eluent and sample ions.

In analytical-scale ion-exchange chromatography, the eluent ion E^x is abundant, whereas the sample ion S^y is at much lower concentrations. Thus, RE^x tends to be equal to the ion-exchange capacity of the resin C_R. This is the quantity of exchangeable ions per unit quantity of exchanger. It can be expressed as milliequivalents of exchangeable ions per column or per gram of dry resin.

Ion exchange is also characterized by a distribution or partition coefficient. Small [1] defines a *concentration-based partition coefficient* K_D:

$$K_D = \frac{C_s}{C_m} \tag{3}$$

where C_s is the concentration of solute in the stationary phase and C_m is the concentration of solute in the mobile phase.

Haddad and Jackson [2] define a *weight-based distribution coefficient*, which is the weight of solute in the stationary phase divided by the weight of solute in the mobile phase. Small described thermodynamic aspects of a chromatographic separation [1]. Similarly, Haddad and Jackson [2] described it as a retention model for ion exchange. The goal of these and other authors [3–6] was to relate the thermodynamics of ion exchange to easily measured quantities in an ion-exchange chromatogram. These experimentally determined quantities include the retention time t_r, or retention volume V_r, of an analyte and the void volume V_0, or time, t_0. The *retention time* or *volume* of an analyte is obtained from the peak that the analyte produces, measured in time or volume. The *void volume* or *time* is the volume or time it takes to elute a solute that is not retained on the column. From these values, a capacity factor k', can be calculated:

$$k' = \frac{(t_r - t_0)}{t_0} = \frac{(V_r - V_0)}{V_0} \tag{4}$$

The capacity factor, an easily measured value can be directly related to the partition coefficient or ion-exchange equilibrium constant in what Haddad and Jackson [2] called a fundamentally important equation. It is rewritten here using the definitions presented in Eqs. (1) through (4).

$$\log k = \left(\frac{1}{x}\right) \log K_{S,E} + \left(\frac{y}{x}\right) \log \left(\frac{C_R}{x}\right) + \log \left(\frac{w}{V_m}\right) - \left(\frac{y}{x}\right) \log E^x \tag{5}$$

where w is the weight of the stationary phase and V_m is the volume of the mobile phase.

This equation provides a relation between capacity factor and easily measurable column and eluent parameters [2]. Equation (5) predicts that the capacity factor for an analyte is determined by the ion-exchange equilibrium constant, $K_{S,E}$, (or selectivity coefficient), the ion-exchange capacity of the column C_R, the ratio of stationary to mobile phases w/V_m, and the concentration of the eluent ion E^x. This assumes that there is only one eluent species. Increases in $K_{S,E}$, C_R, or w/V_m lead to increased capacity factors and, therefore, retention time and volume of the analyte. Increasing eluent concentration E^x, decreases the capacity factor. Also, increased charge on the eluent leads to decreased capacity factor. Thus, carbonate anion CO_3^{2-}, is a stronger eluent than bicarbonate HCO_3^-. A common experiment in ion chromatography is to increase the concentration of eluent E^x, and measure the analyte's retention time or volume and void time or volume so that the capacity factor k', can be calculated. In this experiment the charges on the analyte y, and eluent x, along with the resin weight w, and ion-exchange capacity C_R, and ion-exchange equilibrium constant $K_{S,E}$, are all constant. Thus, the

first three terms in Eq. (5) are constants that can be combined into what is sometimes called an isocratic constant I.

$$\log k' = \log I - \left(\frac{y}{x}\right) \log E^x \tag{6}$$

Equation (6) predicts that a plot of the log k' versus log of the eluent activity E^x, should be a straight line, with a slope equal to $-(y/x)$. For example, in anion-exchange chromatography, if the eluent has a -1 charge, the slope of such a plot would be equal to the charge on the analyte. One important implication of Eq. (6) is that an increase in eluent concentration will have much more effect on the k' of polyvalent ions than on monovalent ions. Thus, a gradient elution in which the eluent concentration is increased can pull peaks together that would be widely separated in an isocratic elution. The increasing concentration gradient will decrease the elution time of the polyvalent ions much more than that of the monovalent ions.

The ion-exchange equations become more involved when using a mixture of eluent species, such as the very common HCO_3^- plus CO_3^{2-} used with chemically suppressed conductivity detection. This will be discussed later in this chapter, and conductivity principles are discussed in Chapters 4 and 17. The ion-exchange equations for a mixture of HCO_3^- plus CO_3^{2-} were solved recently by Hajos et al. [34]. They measured the retention of halide anions and oxoanions and found that their equations predicted their retention and accounted for the degree of protonation of the analytes.

The resin's ion-exchange capacity is a key factor in determining ion retention. The capacity factor k' is related to the distribution coefficient K_D, by the equation:

$$k' = \frac{K_D V_R}{V_m} \tag{7}$$

where V_R is the volume of the resin and V_m is the volume of the mobile phase

If a column is packed with spherical particles in which the whole particle carries functionality, the volume of the stationary phase is about 65% of the column volume, i.e., $V_m = 0.65\ (V_R)$ and $V_R/V_m = 1.86$ [1]. On the other hand, if the functionality is only on the surface of the particle, the ratio is much smaller. Such particles are called *pellicles*. Small stated that he knows of no case in which the volume of the pellicle has been measured, but he estimated it from the capacities of low- and high-capacity resins [1]. The volume of the mobile phase V_m is unchanged, but the volume of the pellicular resin $V_{R,pell}$ is lower than in a fully functionalized porous resin. Thus k' is lower, so the analyte will elute sooner, and a lower eluent concentration will be needed. This lowers the contribution of eluent to the detector response and allows faster run times.

Most of the earlier ion chromatography articles described the use of pellicular ion-exchange resins in which ion exchange was the only retention mechanism. In the past few years, though, mixed-mode chromatography has been made possible by the introduction of a latex-bonded ion-exchange packing material that is compatible with organic solvents [35–37]. Mixed-mode chromatography enables the separation of analytes not easily separated on single-mode columns. Ionic and nonionic analytes can be separated using mixed-mode chromatography. This latex-bonded ion-exchange material consists of three regions: a highly cross-linked poly(ethylvinylbenzene/divinylbenzene) or EVB/DVB core, a highly reactive surface on the EVB/DVB core particle, and an aminated anion-exchange pellicular latex phase that comprises poly(vinylbenzylchloride–divinylbenzene) or VBC–DVB, which is covalently attached to the core. The VBC–DVB latex polymer is functionalized by reaction with a tertiary amine to form quaternary ammonium groups, which act as anion-exchange sites [35–36]. The EVB–DVB core particle has about 300 $m^2\ g^{-1}$ of adsorption surface area and 60-Å pores in one of the columns, called the Omni-Pac PAX-500. The PAX-500 will adsorb nonionic compounds, such as alkylphenones, by a solvophobic mechanism similar to reverse-phase high-performance liquid chromatography (HPLC) [36] (see also Chap. 10). There is also a PCX-

500 column that has the same core particle pore size and adsorption surface area as the PAX-500, but it has cation-exchange groups. An even newer dual-mode column is the AS-10 (Dionex, Sunnyvale, CA) that has an 8.5-μm–diameter macroporous (2000-Å pores) EVB–DVB core particle to which a layer of 65-nm–Micro-Bead latex particles are bonded. The latex particles contain quaternary ammonium anion-exchange sites. Similar to the PAX-500, the AS-10 is capable of nonionic retention as well as ion exchange [37].

The most common objective in chromatography is the separation of analytes. Resolution R is the term used to describe the quality of a chromatographic separation. It is defined as

$$R = \frac{2(V_2 - V_1)}{(W_1 + W_2)} \tag{8}$$

where V_1 is the retention volume of the first analyte eluted and V_2 is the retention volume of the second analyte and W_1 is the width of the first peak at half maximum and W_2 is the width of the second peak at half maximum.

Small stated that resolution is the result of two opposing effects: thermodynamic effects causing the peaks to move apart and kinetic effects that cause the peaks to overlap [1]. The thermodynamic aspects were described briefly earlier and are discussed in more detail by others [1–5], especially by Small. The kinetics can be described by the van Deemter equation [1], but for the exchange of small, fast ions on pellicular resins the most important factor in determining column performance is proper packing of the column [1].

A chromatographic separation factor $\alpha_{1,2}$, for analytes A and B can be defined, similar to the description by Haddad and Jackson [2]:

$$\alpha_{A,B} = \frac{k'_A}{k'_B} \tag{9}$$

where k'_A is the capacity factor for the first analyte and k'_B is the capacity factor for the second analyte.

They defined a selectivity coefficient, or ion-exchange equilibrium constant, between analytes A and B.

$$zRA^y + yB^z = zA^y + yRB^z \tag{10}$$

where RA^y represents analyte A with charge of y retained on the column, B^z is analyte B with charge of z dissolved in the mobile phase, A^y is A dissolved in the mobile phase, and RB^z is B retained on the column. The equilibrium binding constant $K_{AB} = (zA^y)(yRB^z)/(zRA^y)(yB^z)$.

The separation factor $\alpha_{A,B}$ is related to the weight of the stationary phase w, the volume of the mobile phase V_m, the charges on the analyses y and z, and the capacity factor of the later eluting component k'_B:

$$\log \alpha_{A,B} = \left(\frac{1}{z}\right) \log K_{A,B} + \left[\frac{(y - z)}{z}\right] \log \left(\frac{k'_B V_m}{w}\right) \tag{11}$$

A similar equation can be written that relates the resolution factor to the capacity factor of the earlier eluting component k'_A. If the two analytes have the same charge, Eq. (10) reduces to

$$\log \alpha_{A,B} = \left(\frac{1}{y}\right) \log K_{A,B} \tag{12}$$

If the analytes have the same charge, the separation factor depends only on the selectivity coefficient $K_{A,B}$, and on the charge of the solute ions [2].

The discussion presented so far applies to the ion exchange of low molecular weight ions on an ion-exchange medium containing fixed, or almost permanent, ion-exchange sites. The concentration of analytes is low; that is, the analyte's retention time (and k') are independent

of concentration. This stoichiometric model for ion exchange assumes that the electrolytes (analytes and eluent) obey ideal solution laws. There is no significant interaction between ions in solution. Activities of ions are assumed to be equal to concentrations, and no ion pairs are formed.

An alternative to ion-exchange chromatography is ion-interaction chromatography (IIC), also called ion-pair chromatography (IPC), in which the column packing material is nonionic. It is often octadecylsilica (ODS) or poly(styrene–divinylbenzene). A temporary ion-exchange surface is formed by including an ion-pair reagent in the mobile phase. Alkane sulfonic acids, such as hexane sulfonic acid, will form ion pairs with cations, whereas tetraalkyl ammonium compounds, such as tetramethylammonium hydroxide, will form ion pairs with anions. Different theories have been developed to describe IIC or IPC, which will be discussed in Section C. These theories do not assume ideal solution behavior. They allow the formation of ion pairs. One of these theories, is called the Gouy-Chapman theory [38]. The strength of electrostatic interactions is determined from the electrostatic potential between oppositely charged ions.

The same Gouy-Chapman theory was used recently by Stahlberg [39] and Bartha [40] to describe an electrostatic model for ion-exchange chromatography. Unlike the model described by Small [1], Haddad and Jackson [2], and others [3–5], Stahlberg and Bartha's model is not stoichiometric and does not assume ideal solution behavior. Interactions between solute ions and electrolyte ion in the ion-exchange medium (or resin phase) are determined from the electrostatic potential [39]. The stationary phase is considered as a rigid wall with a fixed number of charged groups per unit surface area. The theory can predict retention times of ions in ion-pair chromatography [40]. A relation was derived that separates the contributions from the type and concentration of ion-pairing reagent. Their theory was used to account for the effect of the accumulation of solute ions in an electric double layer on the capacity factor. The term *electrostatic ion chromatography* was used by Hu and others [41–42] to describe a method of separating ions based on simultaneous attraction and repulsion interactions between solute ions and zwitterionic bile salts attached to an ODS column, and deionized water was the eluent. They found that retention of ion pairs was determined by the species of the anion and the charge of the cation. The theory is best applied to the retention behavior on rigid column materials, and not to soft gel ion exchangers that shrink and expand with changes in ionic strength. Theories describing retention on soft gels are usually based on Donnan exclusion and osmotic pressure coefficients [5,43].

Stahlberg and Barta's model [39,40] considers a surface on which negatively charged groups are chemically bound and in contact with an electrolyte solution, or mobile phase. The positively charged counterions are not bound as a stoichiometric 1:1 ratio with the fixed charges, but are distributed in a diffuse double layer close to the surface. The distribution of electrolyte ions in the double layer was estimated by using the Gouy-Chapman theory, for which the charges on the stationary phase surface are considered to be evenly distributed and the electrolyte ions are approximated as point charges. Compared with another model called the Stern model [44], Stahlberg's model for low molecular weight ions assumes that the Poisson–Boltzmann equation holds from the bulk solution up to the ion-exchange resin surface.

The Gouy-Chapman theory solves the Poisson–Boltzmann equation for the interaction between a charged planar surface and a symmetric electrolyte [39,45]. The variation of the surface charge density with the surface potential was calculated [39]. The concentration of counterions decreases monotonically with the distance from the oppositely charged surface. The electrolyte coions are expelled from the double layer. The electrolyte ions are distributed so that their electrochemical potential is equal at every point in the system. The fixed charge groups on the surface were proposed to create a difference in electrostatic potential between the surface and the ionic bulk solution. It is the change in electrostatic potential as a function of distance from the surface that determines the concentration profile. Because the amount of

eluent is much greater than that of the analyte, the distribution of analyte ions is determined by the potential profile created by the excess eluent ions.

Stahlberg then calculated the electrostatic potential profile of systems containing eluent and charged stationary phase with trace amounts of analyte ions. He calculated retention from the distribution of solute ions in the double layer and to the ion-exchange resin surface [39]. Retention was proposed to be partly due to the accumulation of analyte ions in the diffuse double layer close to the stationary-phase surface. This differs from other models that assume that retention is due to the distribution of analyte ions between only two distinct phases. Stahlberg plotted counterion concentration as a function of the distance from the surface with charge density of -0.1 C m^{-2} and the electrostatic potential as a function of distance from that surface in the presence of 1-, 100-, and then 500-mM eluent. The concentration of solute ion relative to its bulk concentration as a function of the distance from the surface was also calculated and plotted [39]. Terms for both the specific adsorption of analyte and its accumulation in the double layer were included in the expression for the capacity factor for analyte. The concentration of electrolyte in the mobile phase affects the analyte's capacity factor through its influence on the double layer, the surface potential, and the surface concentra- of free fixed resin surface charges. The analytical solution of the linearized Poisson–Boltzmann equation for a planar charged surface with a low surface potentials gave a linear relation between surface potential Ψ, and surface charge density σ, as

$$\Psi = \frac{\sigma}{(\kappa\varepsilon_0\varepsilon_r)} \tag{13}$$

where ε_0 and ε_r are the dielectric permittivity of the solution and resin, respectively, and κ is called the Debye length.

This was used to write a second-order differential equation relating electrostatic surface potential and the association constant of the eluent counterion, its concentration in the mobile phase, and the surface concentration of fixed charges on the stationary phase. From that, they obtained an analytical solution for the capacity factor as a function of electrolyte concentration in the eluent and the association constants for the analyte and eluent counterion [39]. Theoretical plots of log k' versus log of eluent concentration for a monocharged analytes with different association constants were presented for columns with charge density of -0.15 and -0.05 C m^{-2}. The plots were linear with slope of -1 for counterion concentrations of 10–100 mM, but slight nonlinearities appeared at higher eluent concentrations. Thus, experimentally reported linearities between log k' versus log eluent concentrations support Stahlberg's theory as well.

B. The Ion-Exchange Process for High Molecular Weight (> 1000) Da Ions or Proteins

Ion-exchange is used primarily to separate peptides, proteins, and glycoproteins, although some ion-exchange methods for DNA are used [46–48]. Brown and Brown [46] described the strong anion-exchange purification of synthetic DNA (up to degree of polymerization of 40) on a Partisil P 10 SAX column using a KH_2PO_4 gradient elution. Similarly, Ng and Mitra [47] used a DEAE-Sepharose, strong anion-exchange column to remove DNA contaminants from protein preparations. In another study, Tebbe and Vajen extracted DNA from soil samples, and then further purified it using anion-exchange chromatography [48]. DNA fragments up to 200 base pairs (bp) were separated on the porous anion-exchange supports called Mono Q and Mono P by Westman et al. [49]. Kato et al. [50] used nonporous particles to which diethylaminoethyl groups were attached. Stege et al. [51] compared different porous and nonporous anion-exchange packings. DNA fragments up to 1000 bp, typically generated by the polymerase chain (PCR), which is a major tool in recombinant DNA technology, have

been successfully separated using nonporous anion-exchange particles [52]. A major disadvantage of anion exchange is the sequence-dependent retention of DNA fragments, because fragments with higher AT content tend to cause double-stranded DNA to be retained longer than would be expected, based simply on their size [53]. Huber et al. [54] recently introduced a method based on ion-pair chromatography on alkylated nonporous poly(styrenedivinylbenzene) for the rapid sizing of DNA fragments. DNA is usually purified by other methods, with kits that use a silica-based matrix that selectively binds single- or double-stranded DNA [55], or with glass beads or alcohol precipitation, or by binding to complementary bases (cDNA) to form base pairs. Individual nucleotides, nucleic acids, and small oligomers are often separated by ion exchange, based on theory described in the foregoing for low molecular weight ions. DNA fragments are often separated by electrophoresis. Polypeptides, proteins, and glycoproteins with molecular weights over 1000, are frequently separated by ion exchange, and theories have been described for them. Some are discussed in the following.

1. Mass Action Ion-Exchange Model

In the mass action model, considered by Kopiewicz et al. [56], there are only two phases, the stationary phase and the mobile phase (or electrolyte solution). Strict ion exchange between a multivalent protein ion and a stationary-phase surface was considered. The protein valency corresponds to the number of ions displaced on the stationary-phase surface. The ion-exchange process was described as being governed by electrostatic interactions. The attractive force F between two oppositely charged bodies, with charges of q_1 and q_2, separated by a distance, r can be represented by Coulomb's law:

$$F = \frac{q_1 q_2}{Dr^2} \tag{14}$$

where D is the dielectric constant of the medium. Although the protein and support are not point charges, the proportionality of the relation was proposed to be valid. Because there are acidic and basic amino acid side chains within the same protein, a net charge was considered; it is pH-dependent. At high pH, the protein charge decreases, whereas at low pH it increases. At some intermediate pH, called the *isolectric point* (pI), the net charge is zero, and the protein will not migrate in an electric field (the basis for the electrophoretic technique called isoelectric focusing).

This amphoteric nature of a protein is best examined by a titration curve. Because a protein can exhibit net positive, neutral, or negative charge, depending on its pI and the solution pH, Kopaciewicz et al. evaluated a net charge concept to predict retention on ion-exchange columns [56]. The net charge was labelled Z in their equation relating capacity factor k' to NaCl eluent concentration:

$$k' = \frac{K_z}{(D_0 C_i)^z} \tag{15}$$

where D_0 is the displacing ion concentration in the mobile phase and C_i is the concentration of counterions contributed by the protein.

Under conditions where $D_0 = C_i$, and when the mobile phase contains NaCl, the numerator in Eq. (10) becomes $(C_i)^2$, so

$$k' = \frac{K_z}{(C_1)^2} = \frac{K_z}{([\text{NaCl}])^{2z}} \tag{16}$$

where [NaCl] is the NaCl concentration in the eluent.

Taking the log of both sides:

$$\log k' = 2Z \log\left(\frac{1}{[\text{NaCl}]}\right) + \log K_z = -2Z \log[\text{NaCl}] + \log K_z \tag{17}$$

This equation is similar to Eq. (6), only the isocratic constant I in Eq. (6) is log K_z, and the charge x, on the eluent E^x, is 1, and E is NaCl. Thus, this equation extends the basic equation for ion exchange of small ions to proteins by treating the protein as if had a net charge, or Z number, equal to the number of ions displaced when it adsorbs onto the stationary phase. This concept of Z number was used to characterize the binding of inositol polyphosphates and other polyvalent low molecular weight anions on pellicular anion-exchange resins as well [57,58]. In another study, Roush et al. [59] described Z as the apparent number of binding sites in the contact region between a protein and the ion-exchange medium. They also described a stoichiometric displacement model that assumed a mass action consisting of an exchange equilibrium between the counterions associated with the protein and displacing ions associated with the ion-exchange surface, and an equilibrium between the bound protein and free protein. The anion-exchange behavior of rat cytochrome b_5 on Mono Q HR 5/5, or Q Sepharose Fast Flow, was investigated as a function of temperature and NaCl concentration. They observed positive Van't Hoff enthalpies of adsorption, indicating an entropically driven spontaneous adsorption [59].

Kopaciewicz et al. [56] measured the retention of β-lactoglobulin to the Pharmacia anion-exchange resin Mono Q and the cation-exchange resin Mono S as a function of pH. They found that β-lactoglobulin was retained on the Mono Q column at about 1 pH unit below its pI (5.1) and on the Mono S 0.5 pH unit above its pI. These results do not fit the net charge concept. Thirteen other commercially available proteins were tested, and similar results were found. Only three of them had zero retention at their pI, as predicted by the net charge concept. These Pharmacia columns have little, if any, hydrophobicity, so retention was not based on a solvophobic effect. Instead, they considered the influence of charge asymmetry. The interaction of a protein with an ion-exchange column does not occur at point sources, so Eqs. (11) or (6) are not complete. Areas of electrostatic potential exist on the surface of a protein adjacent to areas rich in anionic and cationic amino acids.

2. Electrostatic Interaction Model for Proteins

A theory for the electrostatic interaction chromatography of proteins was proposed by Stahlberg and co-workers [29], based on the solution to a linearized Boltzmann–Poisson equation for two oppositely charged planar surfaces in contact with a salt solution. They predicted a linear relation between the log of the capacity factor and the reciprocal square root of the ionic strength of the eluent. They plotted retention data for several proteins as ln k' versus $1/\sqrt{I}$, where I was the ionic strength. The slopes of such plots compared well with the protein charges calculated from titration curves.

Haggerty and Lenhoff described the relation between protein electrostatics and ion-exchange (and electrophoretic) behavior [60]. Their model described a charge distribution comprising a set of point charges inside the protein because some of the amino acids are charged. The Poisson equation

$$\nabla^2\Psi = \frac{-\rho}{\varepsilon_1} \tag{18}$$

for the potential Ψ was solved inside the protein, where ρ is the charge density, comprising a set of point charges, and ε_1 is the dielectric constant. Experimental values for the dielectric constant of proteins with a range of water contents are in the range of 2–4 [61–64]. The solvent is an electrolyte solution, and the governing equation accounts for free ions in solution by assuming that they redistribute themselves according to the Boltzmann distribution in the potential field. This Poisson–Boltzmann equation is

$$\nabla^2\Psi = -\left(\frac{e}{\varepsilon_0}\right) \sum z_i e n_{i0} \exp(-z_i e\Psi/kT) \tag{19}$$

where ε_0 is the dielectric constant of the solvent, taken by Haggerty and Lenhoff as 80, the

dielectric constant of water n_{i0} is the bulk concentration of ion i, z_i is the charge on an ion species i, and e is the electronic charge [60].

The boundary conditions for the system are that the potential goes to zero far from the protein and that, at the interface, the potentials in the solvent and the protein are equal, and the normal components of the dielectric displacement are continuous.

Defining the location of the surface of the protein for the dielectric boundary is difficult because it is unclear how the boundary is formed at the molecular level [60]. If one considers the folded polypeptide chain, there are folds, bumps, holes, and pockets. There are also tightly bound water molecules, the number of which depends on the definition. New NMR methods for characterizing bound waters in macromolecules based on how long they are in contact with the protein were reported [65]. Water oxygens detected by X-ray crystallography appear on most Brookhaven Protein Data Bank files. Some of these are lost when a protein binds a ligand. For example, it was estimated that hemoglobin, with a surface area of 18,964 A^2 has 258 water molecules per tetramer, 60 of which were involved in the allosteric regulation of hemoglobin [66–68]. Similarly, there must be a change in the hydration number of a protein as it binds to an anion-exchange column. Thus, it is useful to consider two or more types of water. The high dielectric solvent water may not be able to come in contact with many atoms or parts of atoms, even at the surface of the protein.

A useful concept is that of the solvent-accessible surface [69], in which a sphere with a radius of about 1.4–1.5 A (corresponding to the radius of water) is rotated along the surface of a biopolymer. This definition usually includes the contact surface of the sphere and the smooth curves, or reentrant surfaces, over the crevices [70]. This is taken to be the van der Waals surface, and can be calculated using an algorithm developed by Connolly [71]. It is this algorithm that was recently used to construct a stereolithographic model of subtilisin (Fig. 1) for the Smithsonian Institution Museum of American History in the Science in American Life exhibit.

The electrostatic information about a protein can be obtained experimentally from electrophoretic mobility measurements. These are based on the balance between the electrical driving force and the hydrodynamic drag. Electrophoretic mobilities are related to the ζ-potential [72], considered to be representative of the potential at the surface of shear, close to, but not at, the particle surface. The ζ-potential can give a lower boundary to the surface potential. Haggerty and Lenhoff [60] used the electrophoretic mobilities of several proteins to calculate their ζ-potentials. They then calculated the proteins' surface potentials. Haggerty and Lenhoff [60] plotted Kopaciewicz's data [56] of protein retention time on cation-exchange resins versus protein surface potential for ten proteins. As shown in Figure 2, there is an excellent correlation between mean surface potential and ion-exchange retention.

In another study, the surface charge of subtilisin was altered by genetic engineering and the effects on ion-exchange and electrophoretic behavior were determined [74]. Stronger subtilisin absorption on the cation-exchange column was seen as the number of surface charges on subtilisin increased. By using a novel monolithic ion-exchange column, Fang and Howell [75] developed a model incorporating axial dispersion. They estimated the hydrodynamic volume and internal porosity of conalbumin and lysozyme.

The surface potential of a protein is a map taken from a set of atomic coordinates from the Brookhaven Protein Data Bank. There is a charge distribution, comprising a set of point charges inside the proteins occurring at charged amino acid side chains. The equations in their model were solved by a finite difference scheme, using the DelPhi program from Honig's group at Columbia University [76,77]. It included the full three-dimensional protein structure, with discrete charges realistically distributed in an electrolyte solution described by the nonlinear Poisson–Boltzmann equation.

The DelPhi program places the molecule within a cubic grid with potential, dielectric constants, and ionic strength or charge, defined at each grid point. The finite difference form of the governing equations is set up based on the values of these grid points. The input parameters were used to tailor the calculation to include the size of the three-dimensional

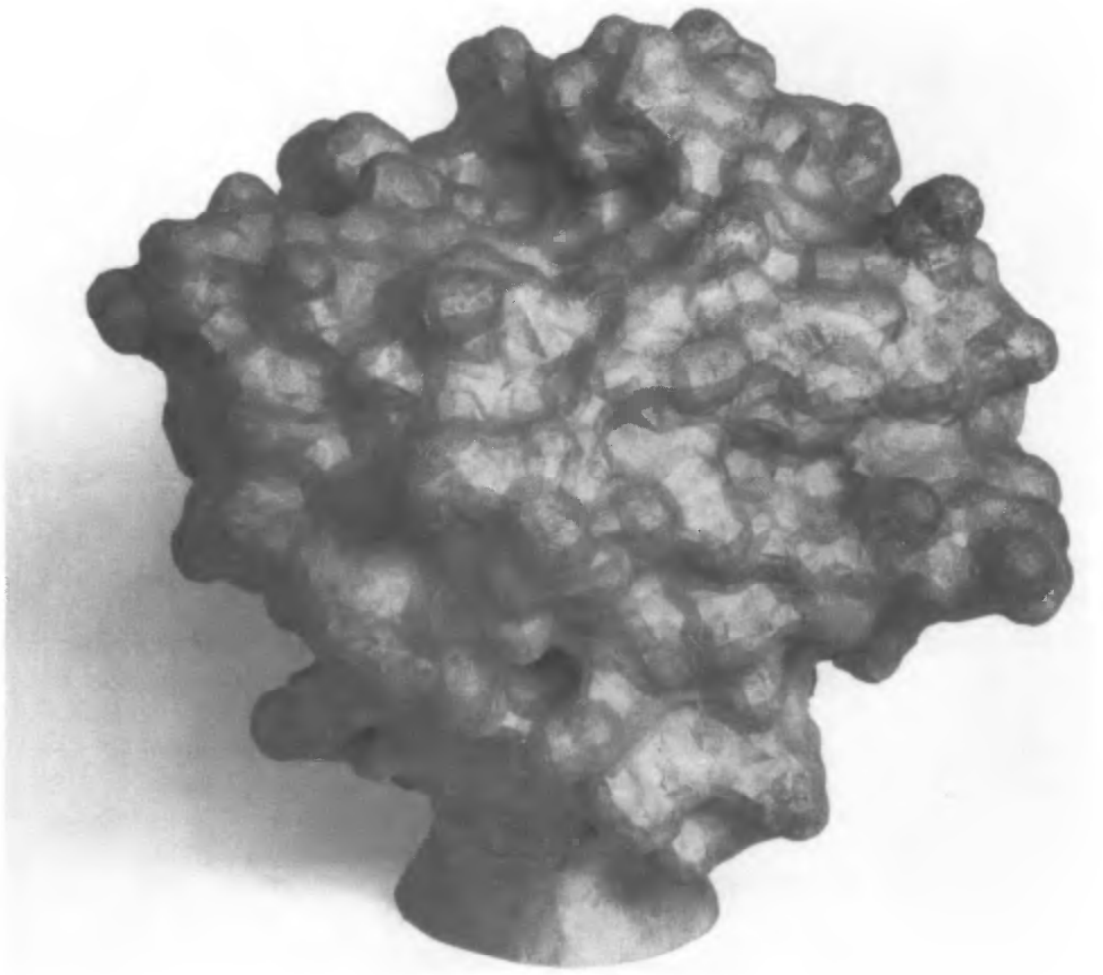


Figure 1 Stainless steel model of the solvent accessible surface of subtilisin. A colorized version of this model, showing the distribution of positive and negative charges on its surface, is on display in the Smithsonian Institution Museum of American History Exhibit, Science in American Life.

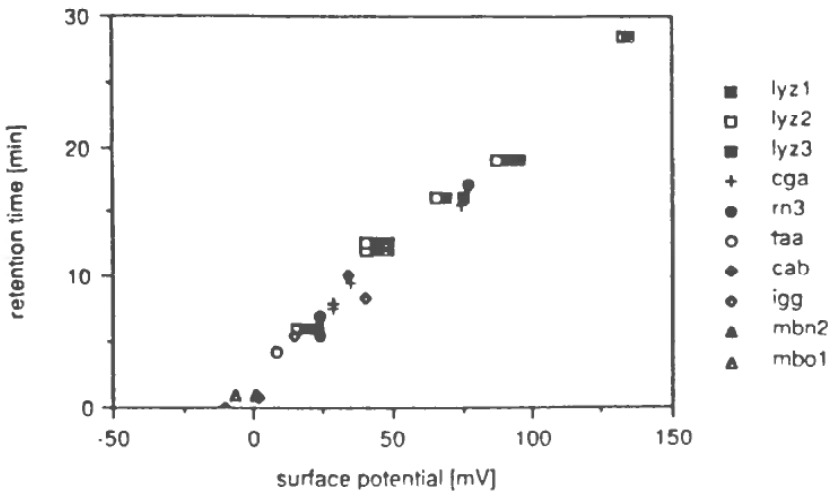


Figure 2 Comparison between computed mean surface potential and cation-exchange retention data of Kopaciewicz et al. [56]. Abbreviations in the key are for proteins listed in the Brookhaven Protein Data Bank [73]. (From Ref. 60.)

array, the scale of the protein in relation to this grid, and the probe radius. DelPhi provided the potential at all grid points. They used a protein dielectric constant of 4, a solution dielectric constant of 80, an ionic strength of 0.01 M, and a grid size of 65 × 65 × 65 with the protein occupying 60% of each side of the grid. To obtain surface potentials, the potential was calculated at each surface point generated by the Connolly program [71]. The mean surface potential was calculated by averaging the local surface potential values covering a very wide range. For example, lysozyme has a range of potentials from −2800 to 4100 mV and a standard deviation of 236 mV. Thus, the excellent correlation (see Fig. 2) found by Haggerty and Lenhoff [60] between chromatographic retention time and a protein's mean surface potential is striking. The surface potential is also related to the thermodynamic activity of molecules in the Debye-Huckel theory and thus to solubility and retention.

In addition, electrostatic interactions can depend on how a protein orients itself toward the charged surface. Yoon and Lenhoff [78] computed the electrostatic interaction between a positively charged ribonuclease A and a negatively charged surface at various separations and orientations. The strongest attraction was when the ribonuclease active site was pointed toward the surface, whereas some orientations could be repulsive. More recently, Roth and Lenhoff [30] calculated protein–surface equilibrium constants at low surface coverage, including both van der Waals and electrostatic contributions to protein adsorption. The values of the equilibrium constants depend on the protein and surface net charge, Hamaker constant (which characterizes dispersion forces), and protein size. By using the Brookhaven Protein Data Bank coordinates for lysozyme and chymotrypsinogen A, a triangulated protein boundary was calculated [79] and an equivalent sphere drawn with the charge distribution represented by a monopole moment at the center [78]. To obtain free energies from equilibrium constants, integrations relative to orientation and distance were performed. Free energies caused by electrostatics and van der Waals forces were plotted as a function of gap distance between lysozyme and surface with a charge density $\sigma = -4.6\ \mu C\ cm^{-2}$. They then calculated equilibrium constants for lysozyme adsorption on this charged surface at different ionic strengths of the mobile phase and found some curvature. At very low ionic strength, there is repulsion owing to mismatched surface charges, because the electric double layer extends farther out from the charged ion-exchange surface. At higher ionic strength, this effect decreases until the double-layer repulsion is confined to a distance so small that it becomes insignificant, and only electrostatics cause retention.

In another study, Noinville and co-workers [80] studied the adsorption of α-lactalbumin and hen egg white lysozyme on a poly(vinylimidazole) stationary phase. They calculated protein–polymer interaction energies using a model that explicitly considers all the atoms. A set of parameters was obtained for each atom and energies calculated for 2592 configurations, scanning the whole space of possible orientations. Preferred orientations were found for the proteins, and effective net charges were calculated [80].

Gerstner and co-workers [81] estimated the Gibbs free energy of adsorption (ΔG^0_{ads}) for several amino acids, peptides, and proteins in a cation-exchange system using a steric mass action formalism. Values for seven globular proteins ranged from −5.7 to −13.9 kcal mol^{-1}. The average bond energy (total ΔG^0_{ads} divided by the number of bonds between the protein and the cation-exchange surface) of the proteins ranged from −1.1 to −1.7 kcal mol^{-1}, comparable with those observed for individual amino acids (lysine and arginine). In contrast, protamine and two other peptides had a higher average bond energy (−2.6 kcal mol^{-1}), indicating that synergistic binding is involved in unstructured peptides, but not for globular (structured) proteins.

Mechanistic questions of protein retention by ion exchange have been addressed by Hearn and co-workers [82–87]. The adsorption behavior of several proteins on various gels was best correlated with a model that includes three mass-transfer resistances: film mass transfer, pore diffusivity, and the dynamics of the interaction step between protein and ion-exchange stationary phase [87]. A considerable resistance to mass transfer was observed when the ratio of stationary-phase pore size to protein size is small [85]. Pore diffusivity can be up to 100 times

as slow as bulk diffusivity, resulting in band broadening. Other factors affecting protein retention include the nature of the displacer salt, flow rate, gradient time, and buffer concentration. The effects of these parameters on the retention of carbonic anhydrase isoforms was compared by determining the *Z*-numbers (i.e., the average number of electrostatic interactions between the protein and the stationary phase) [82]. An increase in apparent *Z*-value was observed when the cation and anion of the displacer salt in the mobile phase contained a combination of chaotropic and kosmotropic ions. The effect of different displacer salts on the *Z*-number of hen egg white lysozymes was explained on the basis of their interactions with acidic amino acids located around the enzyme's catalytic cleft; both the concentration and nature of the displacing salts affected the dynamics of the cleft region.

In another model by Malmquist and Lundell [88], the effects of displacer salts on retention are protein-specific. The major contribution of displacing salts is through differences in an apparent *gradient slope*, defined as the rate of increase in elution strength per unit volume and elution strength of the buffer.

The ion-exchange chromatography of membrane-bound proteins offers a further complication, for they are often solubilized with detergents, such as sodium dodecyl sulfate (SDS), which remains attached to the protein. Various factors affect the retention of such proteins on hydroxyapatite columns, which contain negatively charged phosphate groups (P-sites) and positively charged calcium ions (C-sites). The higher the molecular weight of the membrane-bound protein and the greater its hydrophobicity, the more detergent is bound. If the detergent is SDS, which is anionic, the larger, more hydrophobic proteins will have a more negative charge and be retained longer [89–91].

In another approach, membrane lipids, such as dimyristylphosphatidylcholine, were chemically bonded to a silica surface [92] and used for immobilized artificial membrane chromatography of membrane proteins [93].

3. Preparative Chromatography of Proteins

All the discussion to this point has been on analytical-scale ion-exchange chromagraphy, in which the analyte concentration is low. That is, the retention time (and capacity factor) of the analyte is independent of analyte concentration, and chromatographic peak shapes are gaussian. A very important application of ion exchange, though, is the preparative-scale chromatography of proteins. Although the bulk of the discussion will be on packed columns, ion-exchange membranes can be useful when very fast flow rates are desired. Reif and Freitag [94] characterized Sartobind cation- and anion-exchange membranes made of a proprietary synthetic copolymer with a thickness of 170–190 μm and an average pore size of 0.45 μm. Flow rates up to 65 mL min^{-1} were used. The time required to separate some protein mixtures was less than 1 min. Appropriate conditions were established for the separation of human serum proteins and for the isolation of subtilisin Carlsberg and β-galactosidase from cell culture supernatants [94].

As described by Guiochon and Colin [95], there is a fundamental difference between preparative-scale and analytical chromatography. Up to now, it has been assumed that the size of the peak produced by an analyte is directly proportional to its concentration in the sample. The fraction R of analyte in the mobile phase was assumed to be the same, regardless of the analyte concentration. This fraction can be calculated from the capacity factor k' by:

$$R = \frac{1}{1 + k'} \tag{20}$$

If the concentration of the protein is relatively low, a plot of the analyte's concentration in the stationary phase versus its concentration in the mobile phase is a straight line and the analyte's capacity factor (and retention time) does not change as a little more protein is added to the sample. Such a plot is called a Langmuir adsorption isotherm. As the concentration of protein increases even more, its retention time (and capacity factor) decreases. In this region

of the adsorption isotherm, the plot deviates slightly from a straight line. Quantitative analysis is difficult, if not impossible, but protein throughput increases. The protein may not be as well resolved from other proteins in the sample, but further purification steps can be used. However, as throughput is further increased by loading more protein on the column, larger deviations from a linear adsorption isotherm occur, and resolution decreases and may eventually reach zero, causing a drop in yield. Thus, it becomes important to determine the adsorption isotherm for the protein of interest so that the highest volume and concentration can be injected on the ion-exchange column. In this way, the column saturation capacity, or the production rate of fractions at a certain degree of purity, can be determined [95].

The production rate as a function of throughput, described by Guiochon and Colin [95], is shown in Figure 3.

Eventually the production rate passes through a maximum and starts to decrease when the amount of protein injected becomes so large that the peaks or bands produced by the proteins interfere strongly and are poorly separated. This is illustrated by showing the shapes of the peaks produced at three representative points in Figure 3. The concentration of protein (or other material being isolated in large quantity) in the stationary phase versus the concentration in the mobile phase is shown in Figure 4.

At low protein concentration, the plot is linear, and analytical chromatography is possible, but protein yield is very low. The linear region is the Langmuir adsorption isotherm. In preparative chromatography, the volume and concentration of sample injected increases. The ratio of the amount of protein adsorbed onto the stationary phase to its concentration in the mobile phase decreases, and the peak produced in the chromatogram changes (Fig. 5). For very large protein concentrations, the band begins almost as soon as the nonretained compounds and lasts until the retention time of a very dilute protein solution.

Jungbauer [96] calculated the peak profiles of biopolymers based on an external mass balance theory. They measured the retention time of human superoxide dismutase on a DEAE–Sepharose fast-flow column at various NaCl eluent concentrations. From the retention time and column parameters, they calculated distribution coefficients and plotted them against NaCl concentration. Excellent correlation between predicted and observed peak profiles were obtained [96].

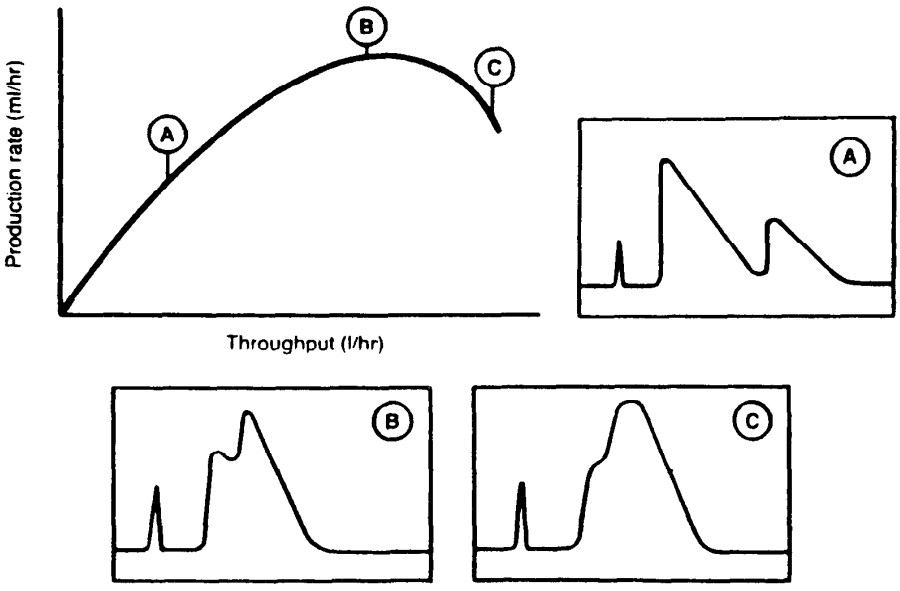


Figure 3 Production rate as a function of throughput. The insets show the band profiles for three representative points A, B, and C on the curve. (From Ref. 95.)

proteins (removed in the first step). An alternative to doing the first step is to use a precolumn [95].

In a recent study, Brooks and Cramer (97) described using a mixture of salt and larger polyions, called displacers, not only to purify proteins, but also to concentrate them. They described a mass-action model of nonlinear ion-exchange model to predict the effects of salt concentration and displacer equilibria to predict retention and the observed concentration of proteins in displacement zones. The use of relatively low salt concentration, with displacers having high steric factor, enabled concentration of the protein [97].

Velayudhan and Horvath [28] described a theory for preparative chromatography of proteins. They considered a Velcro fastener, consisting of many eyes and hooks to be analogous to the binding of a biopolymer to an ion-exchange surface. Each functional group of the biopolymer binds to the column with a small Gibbs free energy (ΔG) of binding just as each eye and hook make a weak bond. However, the ΔG for binding of the protein will have contributions from the ΔGs for all the interacting amino acid charged groups. Because the capacity factor is exponentially related to the free-energy change on binding, the retention factor for the protein is equal to the product of the individual retention factors for all the groups; therefore, it increases geometrically with the number of groups that bind to the ion-exchange column. In this model, a mobile-phase modifier, such as NaCl in ion-exchange chromatography, plays a role analogous to heat on the Velcro fastener. The resistance to releasing the eyes and hooks is drastically reduced, because the bond between eyes and hooks is weakened. Likewise, the multipoint binding of proteins to the ion-exchange material means that increasing the mobile-phase modifier concentration decreases the binding of each charged amino acid group, and the same geometric dependence causes retention of the protein to be greatly reduced.

Velayudhan and Horvath [28] used the classic ion-exchange formalism for multivalent ions, but distinguished three types of binding, strong, intermediate, and weak, on the basis of the strength of interaction with the ion-exchange column. This formalism was used to calculate multicomponent protein isotherms. The equations are highly nonlinear because of the multivalent nature of the protein. The number of amino acid residues in contact with the fixed ion-exchange sites was called the characteristic charge. In ion exchange, the stationary phase must always be electrically neutral, so the binding of any molecule to the surface must be accompanied by the expulsion of an equivalent number of counterions. If Λ is the concentration of stationary-phase binding sites, φ is the phase ratio (i.e., the ratio of Λ to the mobile phase volume V_0), the capacity factor for the protein is given by

$$\log k' = \log(\varphi K^{1/n}) + \left(\frac{m}{n}\right) \log\left(\frac{\Lambda}{n}\right) - \left(\frac{m}{n}\right) \log [\mathrm{S}] \tag{21}$$

where m is the protein's characteristic charge, n is the valence of the salt in the mobile phase, and [S] is the concentration of the salt.

Thus, plots of $\log k'$ versus $\log [\mathrm{S}]$ should produce a straight line, with slopes equal to $-m/n$. Unlike Eqs. (16) and (17), this equation by Velayudhan and Horvath [28] does not include the factor of 2. The similar equation by Haddad and Jackson [2] also does not have this factor of 2 (rewritten as Eqs. (5) and (6) in Sec. II.A). This is because they neglect the coion concentration in the ion-exchange process. If the process is one of counterion exchange, the coion concentration can be ignored. They consider that the coions of the protein are of two types. The first type are stripped away from the protein when it binds to the column, whereas those of the second type remain tightly bound to the protein, even when it is retained on the column. The protein along with the second type of coions is regarded as a polyion. Because the first type of coions are thermodynamically unchanged in the ion-exchange process, they cancel out of the equilibrium relation. The experimental characteristic charges were found to agree with this version in which the factor of 2 was not included [28].

Velayudhan and Horvath [28] then proposed that, because of multipoint binding, the Langmuir formalism is incapable of predicting the sensitive dependence of protein retention on mobile-phase modifier (salt) concentration. Over a very small range of NaCl (mobile-phase modifier) concentration, a protein goes from being strongly retained to being eluted quickly. They calculated various isotherms and found that only isotherms resulting from the multivalent ion-exchange formalism exhibited the characteristic features of protein binding under strong-binding conditions, but reduce to concave down forms at intermediate and low binding. They described different domains of binding to an ion-exchange column. Weak binding of a small molecule is characterized by a capacity factor k' less than 1. The binding of biopolymers with more negative charges and higher equilibrium constants (and thus a higher k') is characterized by intermediate and strong retention at low mobile-phase modifier (MPM) concentration. Absorption isotherms of proteins are different if there is more than one protein in the sample. When only one protein is considered, more of it will be adsorbed onto the stationary phase. When there are two proteins in the sample, they compete for binding, so less is present in the stationary phase. The more strongly retained protein has a higher initial slope because it has a higher charge. Its saturation concentration is lower than that of the protein with a lower charge. Velayudhan and Horvath [28] represented irreversibility in their equilibrium formalism as a limiting case in which the ion-exchange equilibrium binding constants are very high. The hyperbolic shape of the multicomponent isotherm indicated that competition between proteins A and B causes a departure from the irreversible limit to the more common reversible forms found in regions of weak and intermediate binding [28].

They used this theory [98] to interpret a systematic characterization of ion-exchange and adsorption isotherms in preparative chromatography. They described homovalent and heterovalent isotherms for ion exchange and adsorption. The shielding effect of macromolecular adsorbates on the binding of other macromolecules was discussed. They applied the general adsorptive formalism to reverse-phase chromatography and obtained two equations relating retention factor and eluent (or modifier) concentration. At one extreme, characteristic of small molecules, the log of the capacity factor is directly proportional to the eluent charge. At the other extreme, which is characteristic of large molecules, the log of the capacity factor is proportional to the log of the eluent concentration [98].

Huang et al. [99] measured adsorption isotherms for conalbumin, myoglobin, and gamma globulin on TSK-DEAE 5PW anion exchanger and found that the column saturation capacity varied considerably from one protein to another. The data were well accounted for by a bi-Langmuir isotherm model, corresponding to two types of adsorption sites with different adsorption energies [99].

C. Retention of Low Molecular Weight Ions by Ion-Interaction Chromatography or Ion-Pair Chromatography

In the technique called either IIC or IPC, a hydrophobic ion is added to the mobile phase in relatively high concentration to increase the retention of analyte ions of opposite charge onto a nonionic stationary phase. As described by Walton and Rocklin [3], singly charged ions that approach closer than 0.37 nm, or 3.7 A, in water (dielectric constant = 80) at 25°C are considered ion pairs. For ions of higher charge, the distance is larger by the product of their charges. It should be added that liquid water has a definite structure, with hydrogen bonding directed tetrahedrally around the oxygen atoms. When a large ion or molecule dissolves in water, it must create a cavity in the water, an energy-requiring process. For two large ions of opposite charge, it takes less energy for them to share the same cavity, rather than create two separate cavities.

Octadecylsilica (ODS) and poly(styrene–divinylbenzene) are popular stationary phases. If the hydrophobic ion is SDS, or larger, the technique is called micellar liquid chromatog-

raphy, because micelles form in the mobile phase. In this kind of chromatography, the pairing ion is sorbed onto the stationary phase. The analytes are retained by dynamic ion exchange, rather than ion-pair sorption [35]. The sorption of an organic ion onto a reverse-phase sorbent was explained quantitatively in terms of the Stern–Gouy–Chapman model of an electric double layer [100].

Some of the counterions are bound up in the Stern layer next to the charged ion-exchange surface. However, some are in a diffuse layer that includes oppositely charged ions (eluent and sample coions). This is the electric double layer in which dynamic ion exchange can occur. Cantwell and co-workers derived in detail a model for ion-pair retention of a sample ion in the presence of a reversibly sorbed pairing ion. The model includes both surface adsorption and dynamic ion exchange in the electric double layer [35,100,101]. This model was evaluated using tetra-*n*-butylammonium cation (TBA^+) as the ion-pair reagent and *p*-nitrobenzenesulfonate anion (NBS^-) as the sample ion or analyte. TBA^+ was added to the eluent as tetra-*n*-butylammonium chloride, so the counterion was chloride. They defined a dimensionless distribution constant, $K_{NBS,s}$, as being the sum of distribution constants for NBS^- ion exchange $K_{iex,NBS}$, and for NBS^- adsorption K_{ads}. The expression for the absorption of NBS^- is

$$K_{ads,NBS} = \exp\left(-ZF\Psi_0/RT - \mu^0_{ads,NBS}/RT\right) \tag{22}$$

where $\mu^0_{ads,NBS}$ is the standard chemical potential in units of joules per mole (J/mol) for the transfer of NBS^- from the bulk mobile phase to the surface when the electric potential at the charge surface, in (volts) is Ψ_0, F is 96,487 C mol^{-1}, R = 8.314 J $(mol\ K)^{-1}$, and T = 298 K. The numerator in the exponential (*exp*) term is an electrochemical potential.

Values of Ψ_0 were calculated from experimentally determined distribution coefficients for NBS^- at trace concentration (1.49 μM) in the presence of TBA^+ at five different ionic strengths [35]. As Cantwell and Puon discussed [100], the activity of TBA^+ (a_{TBS}) is calculated from the concentration of TBA^+ and its activity coefficient, so that $K_{NBS,s}$ can be plotted versus c at constant a_{TBA}, where c is the ionic strength of the bulk solution. Experimentally determined values of $K_{NBS,s}$ agreed well with those calculated according to Eq. (17), in support of the theory.

Stahlberg [102–104] also presented an electrostatic theory for ion-pair chromatography in which the capacity factor k' is related to the column phase ratio φ, the Gibbs free energy of sorption, and Ψ_0, the difference in electrostatic potential between the surface of the stationary phase and the mobile phase. The solution to the Poisson–Boltzmann equation was solved for a cylindrical surface. The model was evaluated using tetrabutylammonium as the ion-pair reagent and by analyzing several aromatic sulfonates on an ODS column. The capacity factors for the analytes on ODS without ion-pair reagent (i.e., $\Psi_0 = 0$) were defined as k'_0. The capacity factors of analytes in the presence of ion-pair reagent, k' were determined for various amounts of either tetraethylammonium, tetrabutylammonium, tetrapentylammonium, and sodium octyl sulfate ion concentrations in the mobile phase. As a test of the approximate form of the electrostatic theory, the ratio of capacity factor in the presence of ion-pair reagent to the capacity factor when $\Psi_0 = 0$ as a function of the concentration of ion-pair reagent is the same for different analytes with charge = −1. This was experimentally observed [103].

Further experimental support for the formation of ion pairs was given by Hwang and Lyle [105], who used the anionic spin label 1-oxyl-2,2,5,5-tetramethylpyrrolidine-3-carboxylate as the analyte and either *n*-hexyadecyltrimethylammonium bromide (CTAB) or tri-*n*-dodecylmethylammonium iodide (TLMAI) as ion-pair reagents on cross-linked poly(styrene) XAD-2 and XAD-4 resins. Electron paramagnetic resonance (EPR) spectral line shape analysis, with appropriate temperature controls, was performed. The nitrogen hyperfine coupling constants were measured and plotted versus $1/T$ (T varied from 124.1 to 244.2 K) so that activation energies for rotation of the label could be calculated. They developed a theoretical analysis based on a parameter d, to estimate anisotropy of rotation of the probe from the intensities of the low field, $I(-1)$, central, $I(0)$, and high-field lines, $I(+1)$:

$$d = \frac{C}{B} = \frac{[R(-) + R(+) - 2]}{[R(-) - R(+)]} \tag{23}$$

where the constants C and B are functions of the magnetic parameters of the EPR and the rotational correlation times of the label [104].

The $[d]$ values were 2.22 for TLMAI on XAD-4; 2.55 for CTAB on XAD-2; and 7.22 for CTAB on XAD-4, indicating anisotropic motion of the label. The EPR spectra were due to a combination of slow and fast movements, owing to the two different surroundings that the label experiences. One region includes the first two to three layers of strongly immobilized water in which the spin-label experiences local viscosities that are high enough to induce slow motion, whereas the other region is farther from the stationary phase in lower-viscosity solvent, with higher mobility. They assumed that the cavities in the stationary-phase resin are approximately cylindrical and calculated the area occupied by the ion pairs. The probe, or spin label, is negatively charged with the charge located about 3 Å from the spin-free *N*-oxyl group. The hydrocarbon chain of CTAB is about 24 Å long and is 16 Å long in TLMAI. The pore diameter of the XAD-4 was taken to be about 50 Å. The polar groups of the CTAB or TLMAI and the probe occupied a cylinder coaxial with the resin cavity, which would also accommodate any water present. Only in the XAD-4, with its smaller pores, would there be any interaction between polar heads. The anion probe was visualized as being positioned above the XAD framework and anchored to the framework through the hydrocarbon chains of the cation ion pair [105].

The correlation between the log of the *n*-octanol/water partition coefficient (often called log *P*) and both the Hammett's constant (σ) and extrapolated IPC capacity factor for 11 substituted benzoic acids was evaluated by Zou et al. [107]. They concluded that the electronic effect described by the Hammett constant plays an important role in describing the retention by IPC.

D. Ion-Exclusion Chromatography of Small Ions

As described by Small [1], when a water-swollen ion-exchange resin is placed in contact with a solution, there is a natural tendency for all mobile substances to reach the same level in both phases. For example, when a macroporous cation-exchange resin in the hydrogen form is placed in a dilute solution of HCl, diffusional forces try to level the large difference in hydronium ion concentration between the resin phase (about 3 mol L^{-1}) and the dilute solution phase. However, the anionic sulfonate groups on the resin are immobile, and electroneutrality must be preserved. When hydronium ions start to leave the resin phase, the electroneutrality is disturbed, and any further loss is opposed by an electrostatic potential that develops between the resin and solution phases. This is called the Donnan potential after F. G. Donnan, who first described the behavior of electrolyte solutions separated by membranes impermeable to one of the ions in the system [108]. Small [1] provided a thermodynamic explanation of ion exclusion. At equilibrium, the chemical potentials of all mobile species must be the same in the stationary phase and the mobile phase, or solution. When the concentration of strong acids such as HCl is low in the mobile phase, their distribution coefficient in the stationary phase is low, for conventional resins have a capacity on the order of 3 mol L^{-1}. Qualitatively, anions of strong acids that are fully dissociated at a pH of less than 3 are repelled by the negatively charged sulfonates on the macroporous cation-exchange resin. However, weak acids, such as carboxylic acids, are only slightly dissociated, are electrically neutral, and can fit into the pores of the resin and be retained. Thus, retention in ion-exclusion chromatography is based on the pK_a of the weak acids analytes. Anions of strong acids, such as Cl^-, NO_3^-, and SO_4^{2-}, elute in the void volume, whereas acids with a higher pK_a are retained.

Haddad and Jackson [2] gave a more detailed description of ion-exclusion chromatography. Other names used for ion-exclusion chromatography include ion chromatography exclusion (or ICE), ion exclusion partition chromatography. Donnan exclusion chromatography, and

ion-moderated partition chromatography. The stationary phases used are characterized by their particle size (ranging from 5 to 180 μm), ion-exchange capacity (ranging from 0.17 to 5 mEq g^{-1}), and degree of cross-linking (from 2 to 30%, with 8% being most common). Retention is based not only on the pK_a of the analyte and the pH of the eluent, but also on the molecular size and hydrophobicity of the analyte. For example, aromatic carboxylic acids will have strong hydrophobic interaction with the resin and be strongly retained. Others have reduced hydrophobic interactions by adding some methanol or acetonitrile to the eluent [109,110]. Haddad and Jackson presented a retention model for ion exclusion chromatography. The distribution coefficient D_A, for analyte A with an acid dissociation constant K_a at concentration c, is given by

$$D_A = \frac{(1 + 2c/K_a - (1 + 8c/K_a)^{0.5}}{(2c/K_a - 2)} \tag{24}$$

This equation was tested by plotting log D_a for 33 analytes (or solutes) as a function of c/K_a [111]. Agreement between experiment and theory was good [2]. Haddad and Jackson also present detailed listings of applications using ion-exclusion chromatography, mostly for aliphatic carboxylic acids [2].

E. Ion-Exchange HPLC Theories: Synopsis

Quantitative descriptions of the processes involved in ion exchange have existed for some time. Because an understanding of these theories can help in many ways. Manufacturers of columns can predict the effects of changing the chemical composition of ion-exchange sites, thereby producing newer and sometimes better columns. The analyst can use ion-exchange theories to help identify constituents in unknown mixtures. For example, the analyst can increase the strength of the eluent and measure the decrease in retention of analytes in a mixture. The net charge on the analytes can be obtained from plotting log k' versus log E as shown in Eqs. (5) and (6). For a univalent eluent (such as NaOH), the slope of such a plot gives the charge on the analyte. In mixtures containing ions of many different charges, these equations tell the analyst that an increase in eluent strength will decrease the retention of polyvalent ions much more than monovalent ions. Thus, gradient elution can pull together analyte peaks that are very widely separated using an isocratic elution. Equations such as (8) and (9) provide the analyst with exact definitions of resolution and separation factor. The analyst can use these equations to calculate these parameters for different columns to compare their efficiency. They can also be used to compare new and old columns to help determine when a column needs to be replaced.

It is important to remember that ion exchange of biopolymers (such as proteins) is somewhat different than that of low molecular weight ions. Biopolymers should not be approximated as point charges (unlike small inorganic ions). Biopolymers usually contain a distribution of charges over a relatively large surface area. One similarity with small ions, though, is that it is often useful to increase the concentration of eluent and measure the decrease in biopolymer retention. Plots of log k' versus log E can give a measure of the apparent charge of the biopolymer. For a more complete description of ion-exchange behavior, the electrostatic potential of the biopolymer should be considered. Electrostatic interactions between a protein and the ion-exchange sites on a column can depend on how the protein orients itself toward the charged surface of the ion-exchange sites.

When doing preparative scale chromatography, the goals are different. Instead of emphasizing resolution and quantitation, sample throughput is optimized. Much more sample is injected on the column, even though resolution decreases. The production rate depends on the throughput (see Fig. 3). The goal is to load as much sample onto the column as possible, until the production rate reaches a maximum. Quantitation may be impossible, but large quantities of valuable protein can be obtained.

Other methods related to ion exchange, including ion-pair chromatography and ion-exclusion chromatography, use different retention mechanisms. An understanding of the theory will help the analyst in methods development. For example, in ion-exclusion chromatography, decreasing the concentration of H_2SO_4 eluent decreases the retention of anions of weak acids. This is the opposite of what occurs in ion exchange, when an increase in eluent concentration decreases the retention of analyte ions. On the other hand, addition of organic solvents, such as acetonitrile or methanol, will decrease the retention of ion pairs in ion-pair chromatography.

Thus, an understanding of the mechanisms of retention and separation may help the analyst in methods development and help column manufacturers develop new columns.

III. OPERATING VARIABLES

A. Ion-Exchange Stationary Phases

1. Poly(styrene)-Based Phases

There are many types of ion-exchanging materials, but the most popular are those based on poly(styrene) cross-linked with divinylbenzene [3]. Poly(styrene)-based exchangers have good mechanical strength, so they can be used in high-pressure and gradient elution. The percentage cross-linking is defined as the mole percent divinylbenzene reacted with styrene. Alternatively, ethylvinylbenzene can be used, so the cross-linked resin is poly(ethylvinylbenzene–divinylbenzene), or EVB–DVB [35–36]. To introduce functional groups, a substance such as nitrobenzene, is added to the resin beads to make them swell [3]. Then concentrated or fuming sulfuric acid is added along with a catalyst such as a silver salt to produce sulfonic acid groups. The product is a cation exchanger. The beads of ion-exchange resin swell when placed in water and are called gel-type or conventional ion exchangers [3]. Walton and Rocklin [3] also describe the preparation of anion-exchange resins by reacting the polymer with chloromethyl ether, then with a tertiary amine, such as trimethylamine, to yield quaternary ammonium anion-exchange sites. Pellicular anion-exchange stationary phases are made by attaching aminated latex polymer to the sulfonated core polymer. They can be attached tightly through numerous salt, or electrostatic, bonds, or by convalent linkage in some of the organic solvent-compatible columns [35,36]. Latex-based columns are popular because they combine the internal homogeneity of gel-type exchangers with fast mass transfer [3]. Surface agglomeration is the term used to describe the attachment of colloidal latex ion-exchange resin to a much larger core particle of opposite charge [1]. A suspension of colloidal anion exchange particles is added to beads of surface sulfonated styrene–DVB. The positively charged quaternary ammonium groups on the small particles bind tightly to the negatively charged sulfonate groups on the core particle. The small latex beads are prepared by emulsion copolymerization of vinylbenzyl chloride (VBC) with DVB using an emulsifier and a catalyst, such as potassium persulfate [1]. The size of the final polymer, or latex bead, is controlled by the amount of emulsifier used. Then, the VBC–DVB beads are reacted with tertiary amine to form quaternary ammonium functionality. Several advantages of the surface agglomeration were listed by Small [1]. Column capacity and degree of cross-linking can be controlled, resin properties are highly reproducible, there are no partially functionalized regions, the layer of active resin has a uniform degree of solvation throughout its thickness, and surface agglomeration is safer because hazardous chloromethyl reagents are not needed [1].

For proteins, porous poly(styrene–divinylbenzene), or PS–DVB, is useful. In ion exchange of low molecular weight ions, ions move to the outer surface of the ion-exchange particles by rapid convective flow through the column bed. However, transport to the inner surface within the pores of macroporous particles occurs by molecular diffusion, which is slow for larger biopolymers. If the time required for diffusion into the pores is much greater than the time to flow past the particle, resolution and capacity can decrease. To overcome this problem, PerSeptive Biosystems (Framingham, MA) patented a bimodal pore structure for

their POROS columns in what is called perfusion chromatography [112]. Flow-through particles are engineered with two classes of pores to enhance mass transport. Microspheres are interadhered to create through pores with mean diameters of 600–800 nm. Connected to them are short, diffusive pores of 80–150 nm. The composition, flow density, and flow characteristics of POROS particles make it easy to self-pack a column. A PS–DVB support matrix is coated with a hydroxylated polymer that is cross-linked to the PS–DVB backbone, creating an uncharged surface with many hydroxyl groups. This hydrophilic surface coating is then reacted with the ionic functional groups to create the ion-exchange sites [112]. Particle sizes of 10 and 20 μm are recommended for analytical and high-performance preparative chromatography. The flow-through particles of 50 μm are used for larger-scale, low-pressure process chromatography with flow rates of 1000 cm h^{-1} and have a dynamic capacity for proteins of >70 mg mL^{-1} for strong (quaternary ammonium) anion exchange (HQ) and for strong (sulfopropyl) cation (HS) exchange.

Other macroporous PS–DVB-based ion-exchange resins for preparatory chromatography have pore sizes of 1000 Å, particle size of 50 μm, and ionic capacities ranging from 160 to 400 μEq mL^{-1} (dynamic binding capacities of 15–30 mg bovine serum albumin [BSA] for anion exchange or 20–55 mg human IgG per milliliter mL). They are available in weak anion exchange (DEAE), strong anion exchange ($-N^+-(CH_3)_3$), weak cation ($-COO^-$), and strong cation ($-SO_3^-$) exchange sites [113].

In addition, a large family of chelating resins can be prepared from poly(styrene) by nitration followed by reduction to poly(aminostyrene), followed by treatment with sodium nitrite and HCl to give a diazo resin [3,114]. The diazo resin can be coupled to a wide variety of compounds to add functional groups having special selectivities for different metals [3]. The diazo coupling can be broken by reduction with sodium dithionite ($Na_2S_2O_4$). An amino group remains that can be diazotized and coupled with a new ligand. A detailed review of the preparation of chelating resins is presented by Shani and Reedijk [115]. The main analytical use for chelating resins is to collect and preconcentrate metal ions at low concentrations. For example, Srafion or Monviex resins contain isothiouronium and sulfoguanidine groups and are selective for gold and platinum metals (116,117). Another popular chelating resin contains iminodiacetate groups (Chelex-100 resins, Bio-Rad Corp.; and MetPac CC-1, Dionex Corp.) and has been used to preconcentrate transition metals from seawater, followed by separation on a pellicular cation-exchange column and postcolumn reaction with the colorimetric reagent 4-(2-pyridylazo)resorcinol (PAR) with visible spectrophotometric detection [118]. Because the mechanisms of chelation are quite different from those of ion exchange, it is a useful addition to the analyst's tools.

In a different approach, Li and Schlenoff [119] developed a cation-exchange material that included a scintillating polymer for the direction determination of radioisotopes. They sulfonated the surface of a poly(styrene)-based scintillator to produce an ultrathin cation-exchange layer. The thickness of the layer (0.2–10,000 nm) was a function of the concentration of SO_3 in the sulfonating reagent. Radioisotopes absorbed into this layer caused efficient scintillation, permitting in situ measurement of ions content, selectivity coefficients, and exchange kinetics. Self-exchange was demonstrated using radiolabeled calcium ($^{45}Ca^{+2}$), a β-emitter. This system performs preconcentration and detection simultaneously [119].

2. Acrylic Polymer-Based Phases

After the poly(styrenes), acrylic polymers are the next most important ion-exchanging polymer according to Walton and Rocklin [3]. Metyl methacrylate is polymerized in the presence of a difunctional cross-linking agent, such as DVB, divinyl malonate, or ethylene glycol dimethacrylate. The product is hydrolyzed to give cross-linked poly(methacrylic acid) to give Bio-Rex 70 or Zeo-Karb 226. Another class of resins called Spheron is made by copolymerizing 2-hydroxyethyl methacrylate with ethylene glycol dimethacrylate. Sulfonic acid cation-exchange sites are added by reacting with sodium chloroacetate plus NaOH, followed by

chlorosulfonic acid. Weakly basic anion exchangers can be made by reacting the Spheron polymer with $ClCH_2CH_2NEt_2HCl$ and NaOH to produce $C_2H_4OC_2H_4NEt_2$ anion-exchange sites [3]. The acrylic acid polymers are softer that poly(styrene), so they are unsuited for closed columns operating under pressure, but they are less hydrophobic, making them more suited for the chromatography of proteins. Another important difference is that the acrylic polymers have little or no aromatic character, so they do not absorb nonionic aromatic analytes as do the poly(styrenes).

Another acrylic polymer, based on a copolymer of 2-hydroxyethylmethacrylate (HEMA) and ethylene dimethacrylate, is extensively cross-linked and is produced in the form of macroporous beads with 1000-Å pores [120]. The biocompatibility of this copolymer is demonstrated by its widespread use in soft contact lenses. The anion-exchange column described in this paper is called Tessek Separon HEMA-S 1000 Q-L [120]. Other column capacities vary from 0.4 to 1.6 mEq g^{-1} and are available in strong anion (Q; quaternary ammonium), weak anion (DEAE; diethylaminoethanol), strong cation (SB or $-SO_3^-$), and weak cation (CM; carboxymethyl). The selectivity of the hydroxyethylmethacrylate-based sorbent, Separon HEMA-S 1000 Q-L for small anions was reported by Saari-Nordhaus and others [121]. A similar resin, Tessek Separon HEMA-BIO 1000 DEAE was used in the preparative separation of gangliosides and in the separation of bovine hemoglobin from serum albumin [122].

A uniformly sized 10-μm porous copolymer of glycidyl methacrylate and ethylene dimethacrylate (60:40 vol%) was used as a starting material by Smigol and co-workers [123] to make a stationary phase (beads) with both ion-exchange and reverse-phase capabilities. The inner pores contain octadecyl groups for reverse-phase capabilities. The inner pores contain octadecyl groups for reverse-phase retention, and the outer pores contain diethylamino groups for cation exchange. Pore–size-specific hydrolysis of epoxide groups in the copolymer was performed using an aqueous (1%) solution of poly(styrene sulfonic acid) with MW 5000 containing 0.054 mol L^{-1} sulfonic groups [123]. Beads containing both the vicinal hydroxyl groups in large pores and unreacted epoxide in small pores were treated with molten octadecylamine (70°C), to convert the epoxides to amines (0.35-mmol amino groups per gram of beads). This was reacted with epichlorohydrin to produce epoxidized beads (1.12-mmol epoxide groups per gram of beads). Diethylamine was used for aminolysis of the epoxide groups to produce diethylamino functionality (0.62 mmol g^{-1}) in the small outer pores. The large inner pores had the octadecyl groups. Proteins were retained in dilute (10 mM Tris-HCl) eluent by their interactions with the charged diethylamino groups on the surface of the beads. The hydrophobic inner pores are inaccessible to the large proteins, but small, hydrophobic anticonvulsants reach the inner pores and are retained by reverse-phase chromatography in an aqueous eluent. Proteins were eluted by increasing the salt concentration, and small organic compounds are eluted by adding acetonitrile to the eluent [123]. Thus, small molecules can be separated from each other and biopolymeric proteins using pore–size-specific functionality on an acrylic polymer [123].

Another useful resin is made by cross-linking vinylpyridine with DVB to give a weakly basic anion exchanger that binds metals as their anion complexes from HCl solutions [3,124]. They can be used to recover copper from seawater [124]. Chelating resins can also be made by copolymerizing ethylene imine with phenylene diisocyanate or polymethylene polyphenyl isocyanate to obtain a poly(amine)–poly(urea) into which carboxyl and dithiocarbamate groups can be introduced [3].

B. Dextran- and Cellulose-Based Phases

Another important class of stationary phases for separating proteins is based on dextran or cellulose, which are carbohydrates containing many hydroxyl groups [3]. Sephadex adsorbents are made by cross-linking dextran with epichlorohydrin [125]. They are polar adsorbents with no ionic groups, but with a range of pore sizes. Ionic functional groups, such as diethylaminoethyl, can be added by reaction with $ClCH_2CH_2NEt_2$ to give the anion-exchanger DEAE-

Sephadex [3]. The same kind of anion exchanger can be made from cellulose to give DEAE-cellulose. Similarly, cation exchangers can be made by attaching carboxymethyl groups to dextran or cellulose to give CM-Sephadex or CM-cellulose. These are soft materials that must be used in open columns, but are still widely used in protein purification. They have been described in more detail by others [9,10]. The use of cellulosics as ion-exchange materials was reviewed by Levison [126]. Noel and co-workers [127] described a monolithic ion-exchange material with high capacity, fast kinetics of adsorption–desorption, and high flow rates at low pressures that can purify proteins directly from dirty feedstocks, such as cell homogenates and cheese whey.

Cross-linked chitosan, is another biopolymer that is used as a matrix on which ion-exchange sites are attached. It is derived from crab shells. The product name is Kurimover I and II (YMC, Inc., Wilmington, NC). Kurimover I is designed for early process cleanup and Kurimover II is recommended for later cleanup of endotoxins and DNA from protein preparations.

Another resin that is popular for anion-exchange chromatography is the Mono Q column. It has been used recently to purify an α-tocopherol-binding protein from rat liver and heart [128], a recombinant endoglucanase [129], and a recombinant antigen being evaluated as a vaccine against malaria [130]. The purification of the antigen, an apical membrane antigen, PF83/AMA-1, from the malarial protozoan *Plasmodium falciparum* required the inclusion of nonionic detergent in the eluent, because of hydrophobic interactions between the protein and the Mono Q 10/10 [130]. Mazur et at. [131] used Q-Sepharose to purify a recombinant protein, ornatin E, a potent glycoprotein IIb-IIIa antagonist, and blood platelet aggregation inhibitor.

Schulte and Stoffel (132) used DE-52 cellulose to purify ceramide UDP-galactosyltransferase from myelinating rat brain, a membrane-bound enzyme, requiring the addition of 0.5% Triton X-100 detergent. Interestingly, instead of using a packed column, they stirred the sample in a slurry containing 50 g of DE-52 cellulose, followed by filtration in a rapid purification step [132]. An entire protein complex, the prasinoxanthin–chlorophyll *a/b* light-harvesting complex, was purified using DEAE–cellulose with 0.1% dodecyl maltoside detergent [133].

Large-scale human albumin purification was reported by several workers [134–136] using both DEAE and CM-Sepharose Fast Flow anion-and cation-exchange materials in two separate steps. The processing of 5000 L of blood plasma required 24 runs on 200-L columns [135]. One plant was designed to process at least 250 tons of plasma per year to yield at least 98% pure human serum albumin, with 25–28 g of albumin produced per liter of plasma [134]. This plant was designed as a completely closed and automated system, hard-piped, able to be cleaned in place, and capable of meeting all the Australian and New Zealand blood requirements [134]. The anion-exchange step (with DEAE-Sepharose) was done at pH 5.2. The first fractions, containing mostly gamma globulins and transferrin were discarded [136]. Endotoxins were also removed in this step. The albumin was eluted directly onto a CM-Sepharose column using 0.025 M sodium acetate, pH 4.5. Hemoglobin could be eluted at pH 8 [136].

1. Tentacle Ion-Exchange Phases

In a recent study, Muller [137] introduced a new group of ion exchangers in which the ion-exchange groups are located on linear polymer chains attached to the macroporous support material, Fractogel TSK, a vinyl polymer (E. Merck). Chains consisting of 5–50 monomers form brush-like layers or tentacles up to 50-μm thick, located in the pores of the Fractogel to produce EMD, or tentacle-type Fractogel. Chymotrypsinogen A, cytochrome *c*, and lysozyme were separated better on stationary phases with the oligomeric chains attached, than with conventional Fractogel TSK cation exchangers. Similarly, conalbumin, ovalbumin, and human serum albumin were separated better on Fractogel EMD anion-exchange resins with the attached oligomeric tentacles, than by conventional Fractogel TSK anon exchangers. DNA restriction fragments were separated on silica-based LiChrosphere 4000 DMAE (5 μm)

tentacle-type anion-exchange resin. The tentacle-type ion exchangers exhibited faster mass transfer of biopolymeric analytes as well as changes in selectivity [137]. In agreement with previously discussed theories, protein analytes can interact with only a conventional ion exchanger with a certain, distinct area of its surface. In tentacle-type exchangers the flexibility of the charge arrangement on the tentacles allows additional protein orientations or other electrostatic interactions that may account for the change in selectivity [137]. Jacob and co-workers [138,139] used Fractogel for scale-up purification of proteins from egg white.

One type of tentacle ion-exchange medium, described by EM Science [140], consists of an insoluble matrix obtained from copolymerizing oligoethyleneglycol, glycidyl methacrylate, and pentaerythritoldimethacrylate, to which are grafted polymerized chains of acrylamide derivatives that are 15–50 units (-mers) in length. An average of 18 charged tentacles have been attached to these tentacles. Both anion- and cation-exchange columns, with capacities of about 100 mg BSA, lysozyme, or hemoglobin, have been used. There is also a Fractogel EMD Heparin that is useful in purifying antithrombin III and other coagulation protein factors, as well as several DNA-binding proteins. Fractogel EMD with either epoxy or azalactone, can be used for purifying lower molecular weight ligands or for coupling proteins [140].

On the opposite extreme are the hydrophobic fluorocarbon exchangers, the best known being Nafion, which has a fluorocarbon ($-CF_2-CF_2-$) backbone and sulfonic acid functional groups. It can be fabricated into thin membranes that are mechanically strong and chemically resistant [3].

Another useful column is a polymeric poly(ethyleneimine), or PEI, reported by Frenz et al. [141] in the separation of recombinant human deoxyribonuclease I (rhDNase) glycoforms. The different glycoforms vary in the positions and extent of phosphorylation in *N*-linked oligosaccharides. This enzyme, rhDNase, is an endonuclease that nonspecifically hydrolyzes double-stranded DNA to oligonucleotides and is undergoing clinical evaluation for the treatment of cystic fibrosis (CF) [142]. The rhDNase was expressed in Chinese hamster ovary (CHO) cells [141,142], then was purified by loading 0.02–1.0 mg of rhDNase on a 7.8 × 100-mm, 10-μm particle size HP-PEI column (Interaction Chemicals, Inc.) preequilibrated with 100 mM NaCl, 10 mM *N*-2-hydroxyethylpiperazine-*N'*-2-ethanesulfonic acid (HEPES) with 1 mM $CaCl_2$, pH 7.0 [141]. Glycoforms of rhDNase differing in the extent and position of mannose phosphorylation were separated. This enables workers to evaluate the role of glycosylation on enzyme function by site-directed deglycosylation (using endo H digestion) and separation of the glycoforms on the PEI column [141]. McNeff and co-workers [142] developed a high-performance anion exchanger for small anions by coating porous zirconia with polyethyleneimine. Yu and El Rassi [143] developed a partially quaternized polyethyleneimine-coated zirconia and reported separation of small anions and acidic proteins.

Ion exchangers can be either micro- or macroporous. Macroporous ion exchangers and absorbents appear milky or opaque, not clear and translucent, like microporous gel-type exchangers. Macroporous beads are made up of many much smaller beads some tens of manometers in diameter. The primary microbeads are connected loosely to give an aggregate with some mechanical stress, and with channels (or pores) up to 500 nm in diameter [3]. They allow ions and molecules in solution to move rapidly, so ion exchange is faster than with microporous resins. They do not swell or shrink appreciably as the ionic strength of the mobile phase changes. Macroporous resins without ionic groups are often used as absorbents to remove trace organics from water. The Amberlite XAD resins from Rohm and Haas [3] include styrene–DVB-based resins with pore diameters of 5 nm (XAD-4) to 20 nm (XAD-1) and acrylate-based resins with pore diameters of 8 nm (XAD-7) or 25 nm (XAD-8). Lightly sulfonated styrene–DVB polymers have been used for cation chromatography.

2. Silica-Based Stationary Phases

Ion exchangers can also be silica-based. Porous silica beads for liquid chromatography are made by the hydrolysis of ethyl orthosilicate in the presence of solvents [3,145]. The surface

silanol, SiOH, groups are weakly acidic, and can be reacted with a chlorosilane, ClSiR, to form reverse-phase packings. When R=$C_{18}H_{37}$, an octadecyl silica (ODS) packing is formed. To make a bonded ion exchanger, the R group must contain a reactive center, such as a vinyl, amino, or epoxy group [3]. Silica-based ion exchangers are used in single-column ion chromatography (i.e., no suppressor device) with neutral or weakly acidic eluents. The silica packings are attacked by solutions having a pH less than 3 or greater than 8.

Porous silica, or controlled pore glass, was used as a starting material by Regnier and co-workers in the preparation of stationary phases called Glycophases [146,147]. Glycophase G, used for size-exclusion chromatography, has no ion-exchange sites, but has a terminal $-CH(OH)-CH_2OH$. To make ion-exchange materials, they first reacted Glycophase G with a di- or trifunctional epoxy, such as diglycidylglycerol, to introduce cross-linking and to coat the silica or glass with chemically bound glycerol [3], which is hydrophilic. When diethylaminoethanol was added in the reaction mixture, a weakly basic DEAE anion exchanger was produced. To make a weak cation exchanger, allyl glycidyl ether was added, then the $-CH_2-CH=CH_2$ was oxidized to $-CH_2-COOH$ using alkaline permanganate or periodate [3]. To make a strong cation exchanger, sodium bisulfite was used instead to introduce sulfonate groups.

Silica has been used as the core for several immobilized proteins, including BSA, α_1-acid glycoprotein, ovomucoid, cellobiohydrolase I, and hen egg white lysozyme [148–153]. They have been especially useful in separating enantiomers, including *N*-aroyl D,L-amino acids [148], racemic barbiturates [149], and other drugs [150], and in the separation of *N*-acetylglucosamine, and the α- and β-anomers of di-*N*-acetylchitobiose [153]. The effects of eluent pH, which affects the immobilized lysozyme's aspartate-101, were discussed [153].

In another series of reactions, Alpert [154–156] bound poly(aspartic acid) to silica to make a weak cation exchanger. A strong cation exchanger was made using taurine, $H_2N-C_2H_4-SO_3H$ [156].

Not only are there many different ion-exchange media, but also different ways of making the sample and eluent flow through a column. Almost all the papers described so far use axial flow; that is, the eluent and samples flow down the length of a vertical column. However, Sepragen Corporation (San Leandro, CA) use a radial flow, enabling much faster flow rates for scaling-up to a larger preparative scale [157]. The column size, sample size, and flow rate can be increased linearly without affecting separation. Thus, it is not necessary to reoptimize conditions for each scale-up. The radial flow columns have three annular channels. The outer and inner channels have equal cross-sectional area and conduct the fluid flow to the outlet. The middle channel contains the chromatographic packing material, which can be any material, including soft gels, rigid media, or packings that swell and shrink. The sample is introduced at the sample inlet where it is distributed evenly throughout the outer channel. The sample then flows through a porous tube and into the packing material where sample constituents are bound. After elution, the sample components pass through the inner porous tube and out the column outlet. For a 60-L column, a flow rate of 200 L h^{-1} can be used.

3. Biological Ion Exchangers

Also, ion exchangers can be biological [158]. The membranes of most cells contain strong acid anion centers such as $-OSO_3^-$, $-COO^-$, and $-OPO_3^{2-}$ attached to sugars, proteins, and phospholipids, in a viscous, yet fluid matrix. These acid anion centers bind weakly to monovalent cations, but do bind to divalent cations, the most common being Ca^{2+} and Mg^{2+}. However, if exposed to Zn^{2+}, Cd^{2+}, Pb^{2+}, or other heavy metals, they will take them up readily. In this way, lichens can act as detectors of air pollution. In animals, ion exchange is also at work. The blood or other body fluids can be considered the eluent, the input solutions are from the digestive system, and the output is the various excretory mechanisms. The outer cellular membranes acts as a $Ca^{2+}-Mg^{2+}$ exchanger with a surplus of dispersed negative charges neutralized in a Gouy–Chapman double layer by Na^+. It is necessary to strictly

maintain ion concentrations in the cells and the blood to stay alive and healthy. Another example is the crystalline biominerals, such as calcite (shells) and hydroxyapatite (bone). They have a high surface area, being made of microcrystals; they are composed of oxyanions of carbon and phosphorus; and they are avid collectors of divalent cations, including Ca^{2+} and Mg^{2+}. Their morphology is affected by the amount of Mg^{2+}. In sea animals there is more magnesium in the aragonite, whereas in land animals, the bones are made of calcite. Moreover, the whole morphology of the cell is under some ion-exchange control. As cations bind the cell membrane, the lipids will phase-separate, causing the membranes to curve [158]. Cells also expend considerable energy in the selective moment of cations in and out of their cytoplasm. Many important processes from neurotransmission to regulation of growth and development are controlled by changes in cellular Ca^{2+} concentration [159]. Proteins can have very specific pockets for the selective binding of Ca^{2+} or other ions. Proteins contain positive and negative charges, so they can bind anions, such as mononucleotides (cAMP, ATP, GDP, GTP, and others), to regulate their activities or that of other proteins. Changes in the amount of charged groups (especially phosphate) in a protein can turn an enzyme off or on. The other major class of biopolymers, poly(nucleic acids), are polyanions, but bind inorganic cations such as K^+ and Mg^{2+} weakly. They bind polycations, such as polyamines and histone proteins, very tightly. For example, DNA is wrapped around polycationic histone proteins in eukaryotic chromosomes. For a piece of DNA in a chromosome to be transcribed into RNA, it must be separated from the histone core, and this is done by DNA-binding proteins [160]. Thus, binding of ions and their movement in biological systems is an important part of life.

C. Eluents

As described by Haddad and Jackson [2], the role of the eluent in ion exchange is to compete with the analyte or solute ions for the fixed ions on the stationary phase and to separate the mixture of analytes into well-resolved bands. The detection mode to be used is the major factor in determining the type of eluent used. Also important is the nature of the sample matrix, the types of analytes, and the type of column to be used. The choice of eluent is made with these factors in mind. More information about detection is provided in the next section, but some information is provided here to help better describe the choice of eluents.

With detection by chemically suppressed conductivity suppression, the eluent is converted to a low-conductivity form. In earlier forms, this was accomplished with a second column, placed after the separator column. For anion analysis, this second column was a higher-capacity cation-exchange column that exchanges protons for cations in the eluent and the sample. Thus, NaOH in the eluent could be converted to water, whereas NaCl in the sample was converted to HCl. Then, cation-exchange membranes were developed, and these were called membrane (or micromembrane) suppressors. Now, there are several ways to suppress the eluent's conductivity, including electrochemical suppression. This is discussed in more detail in Chapters 4 and 13 of this handbook. Anion micromembrane suppressors exchange H^+ for cations in the eluent. They will require an eluent that contains the anion of a weak acid, such as carbonate or bicarbonate, which will be converted to carbonic acid. Other common eluents include NaOH, which is converted to H_2O; sodium borate, converted to boric acid; and sodium 4-cyanophenolate, which is converted to 4-cyanophenol. It is also possible to add organic modifiers, such as acetonitrile or methanol. The final choice of eluent and column will depend on the sample matrix and the analytes of interest. A mixture of about 3 mM $NaHCO_3$ plus 2.4 mM Na_2CO_3 is a common eluent for the separation of mono- and divalent anions on several different pellicular anion-exchange columns [2,161,162]. Manufacturers are continuously improving their columns, so there are reports of $NaHCO_3$ plus Na_2CO_3 being used over the years on AS-1, AS-3, AS-4, AS-4A, up through AS-10 columns from Dionex [37,161,162]. Some columns, such as the AS-10, have higher capacity (170 mEq per column), so a stronger eluent is preferred for all but the separation of very weakly retained monovalent anions. There is a limit to how much $NaHCO_3$ or Na_2CO_3 can be effectively

suppressed, because the product of the suppression reaction, H_2CO_3, does have some conductivity. On the other hand, NaOH is converted to H_2O, so much more NaOH can be suppressed. This makes NaOH an excellent eluent for gradient anion-exchange chromatography when chemically suppressed conductivity detection is used [161,162] (Fig. 6).

The high pH of a NaOH eluent is needed for the anion-exchange chromatography of sugars and oligosaccharides, because these carbohydrates have pK_a values of 13–14. With other eluents with lower pH, they would be uncharged and not retained on an ion-exchange resin. More will be presented on carbohydrate analysis under the sections on electrochemical detection and mass spectrometry. It should be remembered, though, that silica-based columns will be damaged and slowly dissolve in NaOH, so an alkali-resistant polymeric column (with moderate capacity) is needed. The eluent concentration is much higher than that of the analytes, so the eluent pH can affect the state of ionization of the analytes. For example, $H_2PO_4^{2-}$ is the predominant form of phosphate in 3 mM $NaHCO_3$ plus 2.4 mM Na_2CO_3, but in NaOH eluent, it is PO_4^{3-}. As with the trivalent PO_4^{3-}, phosphate is retained longer and elutes well past SO_4^{2-} in a NaOH eluent, but it elutes before SO_4^{2-} in the $NaHCO_3$ eluent [37]. Polyanions will have different charges as eluent pH varies owing to the many pK_a values of the anionic sites. For example, the location of the three phosphates in inositol triphosphate isomers will affect their pK_a values. In the region of pH 7–9, the titration curves of inositol tri- and other polyphosphates isomers are different [163], and anion chromatography with a 4-cyanophenolate eluent will resolve them if the pH is properly controlled [164]. Thus, by changing the pH of the eluent, the analyst can change the charge on some analytes, thereby changing retention. This and other effects of eluent pH have been a subject of extensive review [1–3].

One limitation with NaOH is that it is a very weak eluent. Even though a micromembrane suppressor can suppress as much as 200 mM NaOH, this still may not be enough to elute strongly retained polyvalent anions, such as inositol hexaphosphate, more commonly known as phytic acid. Instead, a much stronger eluent, sodium 4-cyanophenolate, can be used to elute

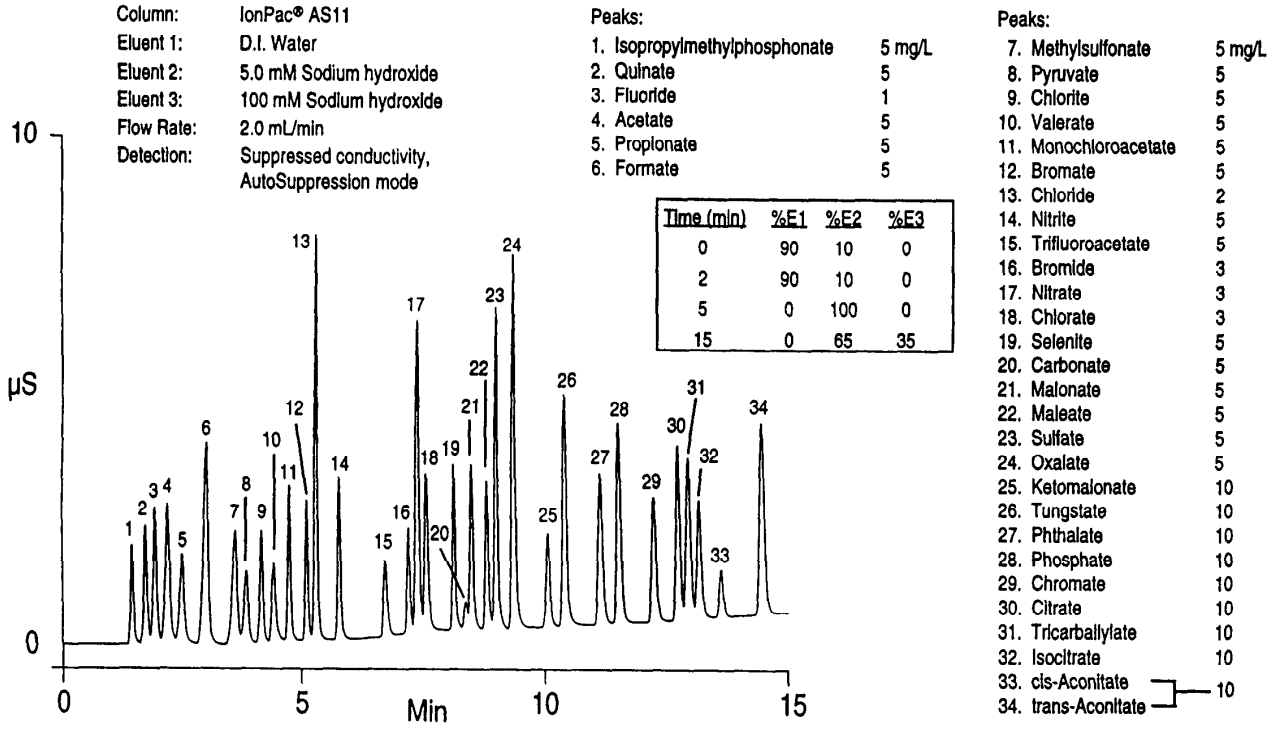


Figure 6 Gradient separation of inorganic and organic acid anions.

phytic acid and other inositol polyphosphates off an AS-4A column [58]. In addition, sodium 4-cyanophenolate was capable of eluting polyvalent anions off the medium-capacity AS-10 column, which has very different selectivity compared with the AS-4A [37].

Cation micromembrane suppressors require an eluent that can be converted to either water or a nonionic molecule with low conductivity. The cation micromembrane suppressor exchanges OH^- for anions in the eluent, converting strong acids, such as HCl, to H_2O and 2,3-diaminopropionic acid (DAP) to the free amine, which has low conductivity. Mixtures of HCl plus DAP are used in the separation of alkaline and alkaline earth metals before chemically suppressed conductivity detection using a cation micromembrane suppressor (CMMS). The exact amounts of DAP plus HCl depend on the type of cation-exchange column used. Campbell et al. [165] used 0.23 mM DAP plus 13.5 mM HCl with the Fast Cation I and CG-3 columns (from Dionex) for the determination of these metal cations plus ammonium and morpholine in ultrapure water for the semiconductor and electrical power industries. On the other hand, 4 mM DAP plus 40 mM HCl is recommended for the same separation using the CS-10 (Dionex) column when using a CMMS. HCl is not suitable for use with the newer electrochemical suppression device, the CSRS, because chlorine gas will be produced. Instead, methanesulfonic acid (MSA) in a mixture of acetonitrile (ACN) and water can be used with the CS-14 (Dionex) column to separate inorganic and organic mono- and divalent cations (Fig. 7). Acetonitrile and methanol can be included in the PCX-100, PCX-500, CS-14 (Dionex), and other solvent-compatible columns.

Chemically suppressed conductivity detection for anion analysis provides an effluent containing the analytes as anions in either deionized water or a dilute salt solution with volatility suited for mass spectrometric detection. Addition of sodium acetate up to 0.1 M to the effluent off the membrane suppressor provides a suitable matrix for thermospray mass spectrometry [166], or liquid chromatography–mass spectrometry (LC–MS). Because each analyte exiting the suppressor is ionic, they can be "evaporated" directly from the eluent phase into the gas phase for MS detection. A limit of detection of 40 pg injected on-column for tetrapropylam-

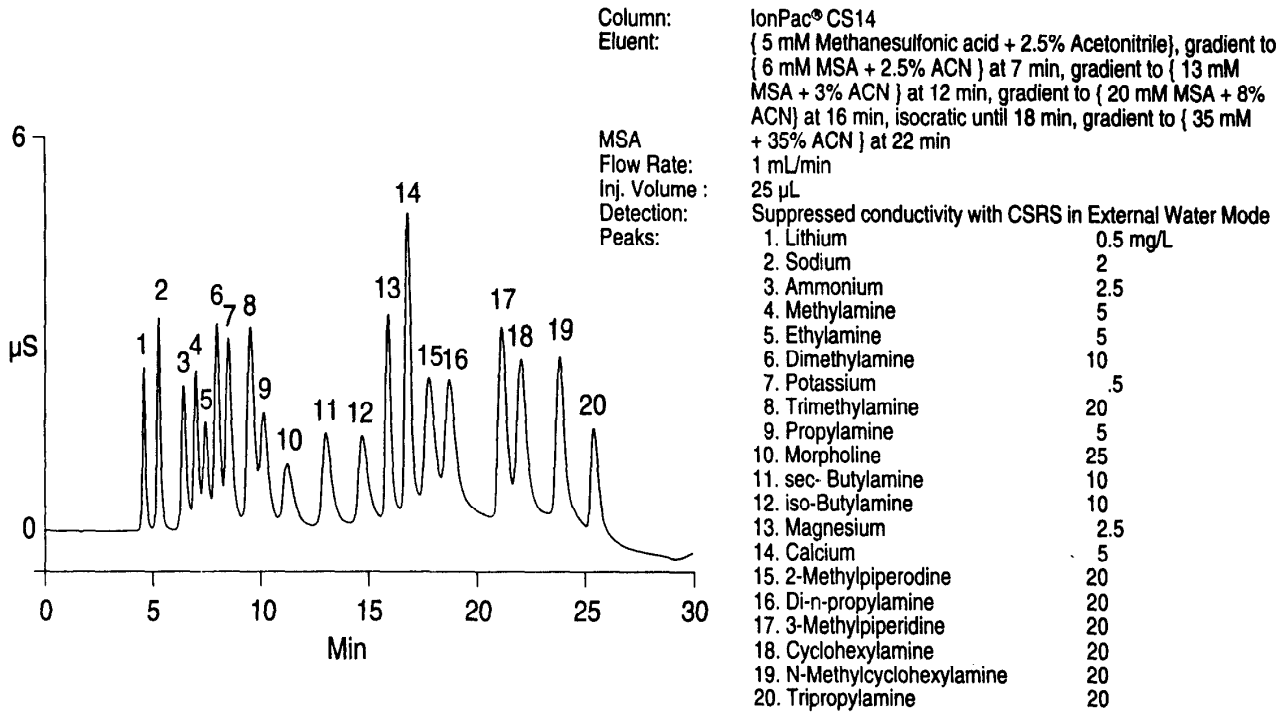


Figure 7 Gradient elution of alkylamines and the group I and II cations on IonPac CS14.

monium cation was reported [166]. The total electrolyte concentration cannot be very high, so the anion micromembrane suppressor was used [166–169].

The eluent requirements for single-column ion chromatography are not so strict. The term single-column ion chromatography implies that no chemically suppressed conductivity detection is used. Instead, aromatic carboxylic acids, which have low limiting equivalent ionic conductances, are quite popular, as described by Haddad and Jackson [2]. These same eluents are quite well suited for indirect UV detection, which will be discussed in greater detail in a later section. An extensive list of eluents for nonsuppressed on chromatography is given by Haddad and Jackson, together with a description of the effects of eluent pH, and system peaks in nonsuppressed ion chromatography [2]. Extensive data for the nonsuppressed ion chromatography of 17 different anions on three different stationary phases using seven different eluent types were reported by Sosimenko and Haddad [170].

The eluent requirements for UV-visible spectrophotometric detection in liquid chromatography have been described [2,7; see also Chap. 12]. When detecting an analyte chromophore, the eluent should not absorb at the wavelength of the chromophore. In the chromatography of ions, the chromophore or fluorophore is often a postcolumn derivative of the analyte [1–4,161,162]. The selection of eluent is driven by the type of analyte and the sample matrix. For example, transition metals have ion-exchange equilibrium binding constants very similar to cation-exchange resins. There is more difference in their binding to chelating agents, such as oxalate, citrate, and others. On the other hand, amino acids do have different binding strength to anion- and cation-exchange resins. They are zwitterionic, so their charge depends on the eluent pH. Here, the choice of eluent will be driven by the column. For cation-exchange chromatography, a low pH is needed to keep the analytes cationic. For anion exchange, a high pH is needed, so that as many of the amino acids as possible will be anions. The ion-exchange capacity of the column and the nature of the ion-exchange sites will dictate eluent selection [1]. One example is shown in Figure 8, in which 44 physiological amino acids were separated, then detected after postcolumn reaction with ninhydrin.

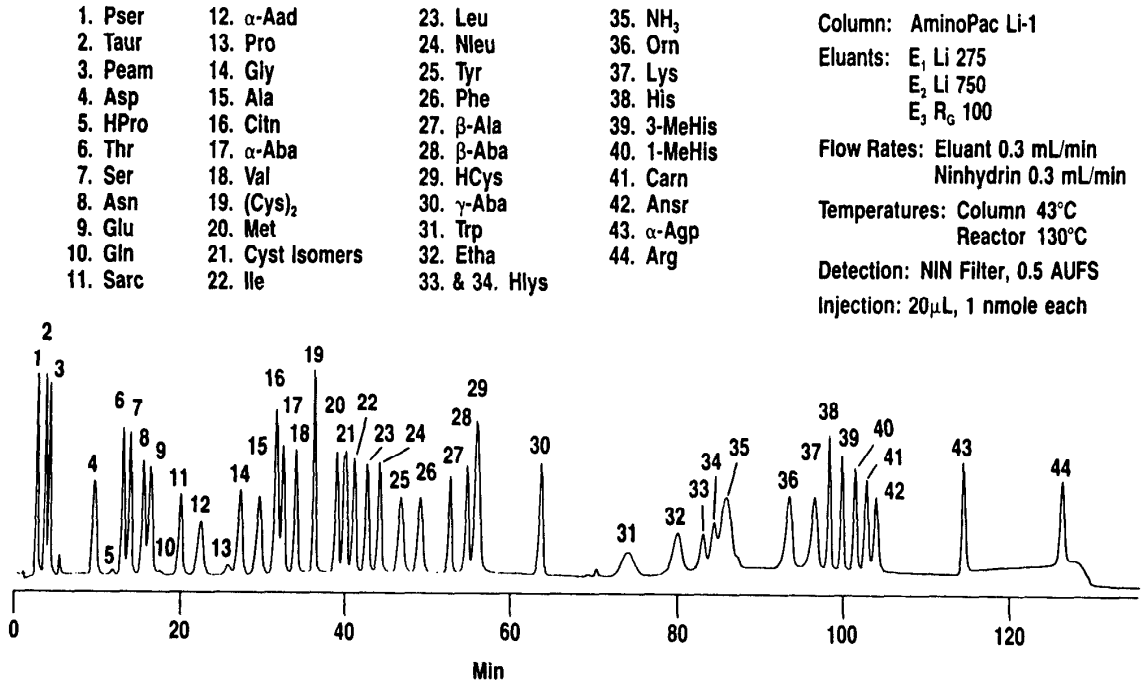


Figure 8 Fast physiological fluid amino acid separation.

Sometimes eluents for protein elution contain polymeric (polyionic) displacers. Patrickios and co-workers [171] used low molecular weight methacrylic triblock copolymers containing a block of negative-charged residues, a sequence of positively charged residues, and a middle nonionic, hydrophobic block, to resolve a mixture of β-lactoglobulins into A and B isoforms. These triblock polyampholytes (containing many positive and negative charges) enable easy column regeneration and the polymers can be recycled [171].

D. Detection

1. Conductivity or Conductimetric Detection

Conductimetric detection has been thoroughly described by several authors [1–4,152,172; and see Chap. 12). Only brief highlights are presented here.

Conductivity is measured by a cell containing two electrodes, to which an alternating voltage is applied, as described by Rocklin and others [152,172]. The measured conductivity is the sum of the individual ions' contributions, as described by Kohlraush's law [172]. The solution conductivity depends on the concentration and limiting equivalent conductivity of the ions in solution. The hydrogen ion has the highest, with a limiting equivalent conductivity of 350 S · cm^2/Eq, with OH^- at 198 S · cm^2/Eq also much higher than alkali metals or halides [3,172]. Thus, when a chemical suppressor device converts anions to their acidic form or cations to their hydroxyl form, they increase the conductivity of the analyte (i.e., NaCl → HCl or NaCl → NaOH) as well as reduce the conductivity of the eluent. The conductivity is affected by the degree of ionization of the ion. Protonation of a weak acid makes it less ionic. Addition of organic solvent (i.e., methanol to 80% or acetonitrile to 60% or higher) can dramatically decrease the conductivity of an electrolyte. For example, the high level of methanol needed to keep phospholipids in solution limits usefulness of conductivity detection for them. However, sugar phosphates, which are water-soluble, are easily detected to 20- to 40-pmol sensitivity [57,58].

Chemically suppressed conductivity detection is suited for gradient elution [4,161,162, 173–175]. In linear gradient elution, the instantaneous capacity factor k' is related to the concentration of the eluent E at that instant by Eq. 25:

$$\log k' = I - \left(\frac{y}{x}\right) \log E^x \tag{25}$$

The value of E at any instant during a linear gradient elution is given by

$$E = E_0 + \left(\frac{t\Delta E}{t_g}\right) \tag{26}$$

where E_0 is the initial eluent concentration, ΔE is the total change in eluent concentration during the gradient, and t_g is the length of time the gradient has been on. The apparent capacity factor of an analyte in a gradient is predicted by a gradient constant K_G by

$$\log k' = \log K_G - Z \log E \tag{27}$$

where K_G is related to the isocratic constant I the charge or Z-value of the analyte, and the charge of the eluent by

$$K_G = \left(\frac{E}{Z+E}\right)^{-E/(Z+E)} t^{-Z/(Z+E)} I^{E/(Z+E)} \tag{28}$$

The values of gradient constants for 28 anions on a pellicular anion exchange column were reported [57] in the development of a gradient method for the separation of organic acids, nucleotides, and inositol polyphosphates [58].

There are many applications using conductivity detection that have been summarized in previous books [1–4,161–162] and in the next chapter. Process, or on-line, ion chromatography using conductivity detection has also been described [176–179]. It provides an effective, reliable, and accurate method for continuous monitoring of inorganic anions and cations, and of morpholine in electrical power plant water [177]. At least 17 sample streams can be controlled at once. Sample preconcentration or dilution is possible. Data handling and reporting is automated according to operator specifications. Maximum concentration alarms can be set to alert key-operating personnel about any out-of-specification situations [176]. Results of long-term testing of an automated process ion chromatograph setup was reported by Sasturain and Schwedt [178]. Wojtusic [179] reviewed on-line ion chromatography for the chemical and petrochemical industries. Van der Merbel and co-workers [180] monitored amino acids during fermentation processes using on-line ion-exchange and postcolumn derivatization using *o*-phthalaldehyde. They studied the metabolism of recombinant *Escherichia coli* and were able to improve the productivity about 35% by optimizing the growth media [180].

2. Electrochemical and Pulsed Amperometric Detection (PAD)

Electrochemical detection in liquid chromatography enables sensitive and selective determinations of many electroactive organic and inorganic ions [1–4,161,162]. This subject is reviewed as well in Chapters 12 and 16. Another review is focused on the theory and use of multistep waveforms (E–t) for direct, sensitive, and reproducible detection of alcohols, glycols, carbohydrates, alkanolamines, amino acids, and sulfur compounds at Au and Pt electrodes [181].

Most aliphatic alcohols and amines are not electroactive under conditions of amperometric detection at constant (dc) applied potentials unless noble metal (e.g., Au or Pt) electrodes are used [181]. However, the Au and Pt electrodes can become fouled by the accumulation of reaction products that are strongly absorbed onto the electrode surface. However, electrode activity can be regenerated using a large positive potential, which oxidizes the reaction products. The final stable AuO and PtO are then cathodically redissolved by a negative potential excursion to restore the native reactivity of the clean metal surfaces [181].

The potential–time waveforms for anodic detection, oxidative cleaning, and cathodic reactivation were presented by Johnson and LaCourse [181] (Fig. 9).

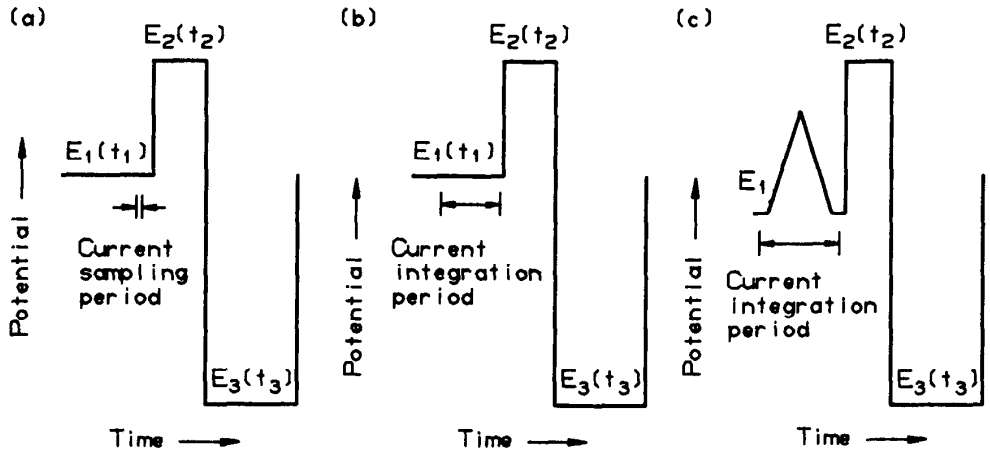


Figure 9 Potential–time waveforms: processes: E_1, anodic detection; E_2, oxidative cleaning; E_3, cathodic reactivation. Waveforms: (a) pulsed amperometric detection (PAD) with a short current sampling period (e.g., 16.7 ms); (b) PAD with a long current integration period (e.g., 200 ms); and (c) integrated PAD with a long integration period (e.g., 200 ms). (From Ref. 181.)

The chronamperometric response ($I - t$) following a potential step from the third voltage (E_3) to the first voltage (E_1) was presented by Johnson and LaCourse [181] and are shown in Figure 10. Two different detection modes are shown, with responses in the absence and then in the presence of analyte shown.

All aldehydes, simple alcohols, glycols, polyalcohols, and carbohydrates can be detected by PAD, which is also known as pulsed electrochemical detection (PED), at a Au or Pt electrode, although Au is more convenient [181]. The maximum anodic signal for polyalcohols and carbohydrates in 0.1 M NaOH is obtained at E = 0.1–0.2 V versus SCE (saturated calomel electrode), so a value in this range is chosen for E_1 in the PAD waveform (see Figs. 9 and 10). Alkanolamines can be detected this way also, but with a different eluent. When acetonitrile is added it interferes with the oxidation of the alcohol groups, but not the amines. The influence of acetonitrile added postcolumn to the effluent stream during separation can be used to distinguish between peaks (when no acetonitrile is present) owing to alcohols, as opposed to amines. Sugar amines can be detected as either sugars or amines, but when detected as sugars, sensitivity is better, unless acetonitrile is added. Peaks for sugar amines are not attenuated by acetonitrile when the amine groups are sterically free to adsorb at the electrode surface. Amino acids also can be detected at Au or Pt electrodes by this mode, which the authors call IPAD. The Au electrode is preferred to minimize interference from dissolved oxygen. Numerous organic and inorganic sulfur compounds can be adsorbed at the electrode surface as well, enabling their detection by IPAD, but adsorption is a prerequisite to detection [181]. In a more recent study, the adsorption and desorption of aliphatic amines at a gold electrode in 0.1 N NaOH were studied to optimize the PED wave form applied [182]. Proper choice of the potential for oxide reduction (E_{RED}) enables simultaneous preadsorption of amines, resulting in improved sensitivity [182].

The details of the multimode electrochemical detector were described by Rocklin et al. [183]. Conductivity detection is accomplished using a bipolar pulsed waveform. The dc amperometry of electroactive species is accomplished using a dc potential, which causes a re-

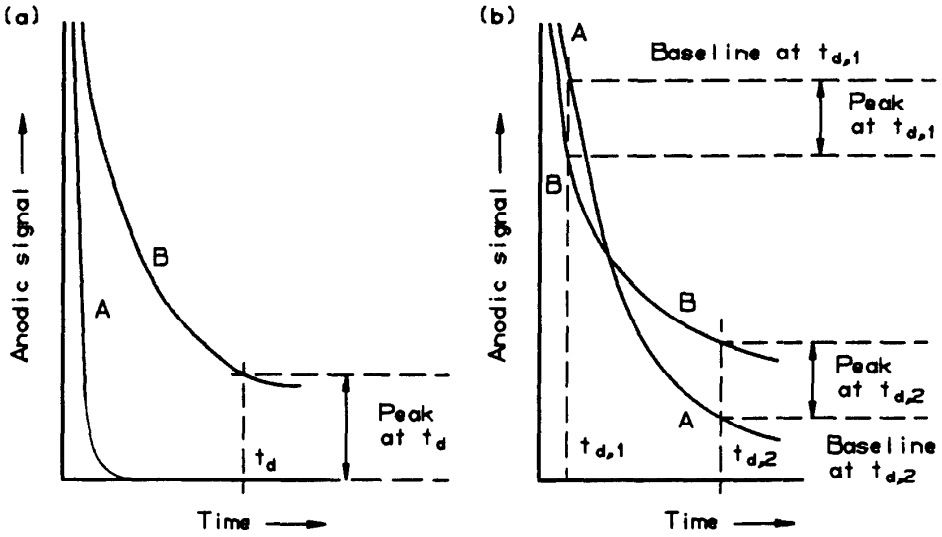


Figure 10 Chronamperometric response (i-t) following a potential step from E_3 to E_1 in the PAD waveform to illustrate the origins of chromatographic baseline and peak signals in LC–PAD. Detection: (a) mode I and (b) mode II. Curves: (A) background response in the absence of analyte and (B) in the presence of analyte. Note that the delay after the step to E_1 is indicated by t_d; LC baselines are indicated by the labeled dashed lines, and LC–PAD peak signals are indicated by arrows.

duction or oxidation of the species. Integrated and pulsed amperometry use a programmed waveform with a frequency of 0.5–2.0 Hz. Pulsed amperometry uses the sequence of pulses shown in Figure 9. The current is integrated at a single potential following a pulse. With integrated amperometry, the current is integrated while the potential is swept across the metal oxide formation wave. Positive and negative cleaning potentials are added to the potential versus time program following the integration period as shown in Figure 10. The advantage of integrated amperometry, especially for amines and sulfur species, is that by cancelling the change from oxide formation and reduction, baseline drift is minimized. Also, the detector output is less sensitive to changes in oxide formation and reduction potentials caused by a change in pH [182]. The reference electrode in the pulsed electrochemical detector (PED) is a combination of pH–Ag/AgCl electrode. Either half cell may be used as the reference electrode. The pH half can be used if a pH gradient elution is used and the baseline drift will be minimized [183–185].

Organosulfur compounds do not react with either methods shown in Figure 9. Instead, a unique waveform is required, as described by Vandeberg and Johnson [185]. Cysteine, methionine, and the tripeptide, glutathione, both in its reduced state (GSH) and its oxidized state (GSSG), were separated on a Dionex OmniPac PCX-500 column and detected at 0.90 to 3.1-pmol limit of detection (LOD), or 18- to 62-nM–concentration limit of detection. The PCX-500 column has both cation-exchange and reversed-phase (nonionic) properties. Similar to the PAX-500 column described in Section II.A., the PCX-500 resin has an 8-μm–macroporous EVB–DVB [poly(ethylvinylbenzene–divinylbenzene)] core particle with about 300 $m^2\ g^{-1}$ of adsorption surface area and 60-A pores that will adsorb nonionic compounds. But the PCX-500 has cation-exchange sites (40 μEq per column), so an acidic eluent, 0.10 M $HClO_4$ plus 0.15 M $NaClO_4$ in 95:5 H_2O:CH_3CN, was used [186].

The main application for the PAD or PED detector, for which few other methods exist, is the determination of sugars, oligosaccharides, and related compounds. Maltooligosaccharides were separated by anion exchange on an AS-6 column with an on-line immobilized enzyme reactor followed by PAD [187]. The molar sensitivities for maltooligosaccharides increase with each additional glucose on the carbohydrate chain. However, immobilized glucoamylase was capable of converting maltooligosaccharides to glucose to improve sensitivity. For example, the limit of detection of maltoheptaose, after conversion to glucose, was 0.1 nmol [187].

The CarboPac PA-1, also known as the AS-6A, column was used to separate positional isomers of oligosaccharides and glycopeptides, followed by PAD [187]. The accessibility of the oxyanions of the oligosaccharides to the functional groups of the stationary phase enables superior resolution of positional isomers, defined as oligosaccharides having the same number, type, sequence, and anomeric configurations of monosaccharides, but differing in linkage position of a single sugar. Splitting of peaks caused by mutarotation was not observed. Linkage of Fuc(α1-3) to GlcNAc of oligosaccharides decreased retention times. Picomolar quantities of underivatized oligosaccharides were detected. Quantification of two triantennary glycopeptides from bovine fetuin compared well to ^{1}H NMR results. The *N*-glycanase-catalyzed release of two 1–4 and 1–3 positional isomers of an undecasaccharide from a tryptic glycopeptide of bovine fetuin was observed [188].

Campbell et al. [189] used two newer columns in series (i.e., two CarboPac PA-100 [Dionex]) columns, to separate neutral, reduced oligosaccharides that are not retained on other columns. They analyzed standards purified from glycoproteins extracted from human meconium. The standards were obtained as their alditols after alkaline borohydride degradation. Trisaccharide isomers differing only in their $\beta(1 \rightarrow 3)$- and $\beta(1 \rightarrow 4)$-linked terminal galactose were separated. Using this dual column method, the two acetamido sugar alditols, D-GalNAcol and D-GlcNAcol were well resolved past the void volume. Linear neutral disaccharide alditols of the same composition, but varying in linkage position of the sugars ($\beta 1 \rightarrow 3$, $\beta 1 \rightarrow 6$, and $\beta 1 \rightarrow 4$) were separated. The presence of branched isomers and the progressive extension of

the oligosaccharide alditol side chains generally increased retention on the PA-100 column [189].

Anumula and Taylor [190] reported the use of enzymes to cleave oligosaccharides from the asparagines to which they were attached. The oligosaccharides were separated on the AS-6 or PA-1 column and detected by PAD. Ion-exchange Econo-Columns filled with AG50-X2 resin from BioRad were used to purify the oligosaccharides from the glycoprotein digests. The oligosaccharides were released from heat-denatured and trypsin-treated glycoproteins. Bovine fetuin, human transferrin, and α_1-acid glycoprotein were analyzed. Alkaline sodium acetate gradients were used in the production of oligosaccharide maps in which separated oligosaccharides eluted in the order of neutral, mono-, di-, and tri-, and tetrasialylated species, on charge, size, and structure. Baseline separations were obtained for neutral oligosaccharide mixtures, but high-mannose and complex oligosaccharides were poorly resolved. The high-mannose peaks were eliminated by digesting with α-mannosidase. Treatment with β-galactosidase, β-*N*-acetylglucosaminidase, and α-mannosidase resulted in more detailed maps as the individual sugars were hydrolyzed off from the oligosaccharides [190].

Strang et al. [191] analyzed glycopeptides from *Trypanosoma brucei* produced by Pronase digestion and found high-mannose–type oligosaccharides with the structure. $Man_{7-9}GlcNAc_2$; (mannose heptamer through nonamer attached to *N*-acetylglucosamine) linked to asparagine-alanine-threonine (Asn-Ala-Thr) on the variant surface glycoprotein. Another glycopeptide fraction contained glycosylphosphatidylinositol (GPI)-type oligosaccharides.

This subject was reviewed by Spellman [192] who described the treatment of a glycoprotein with endo-β-*N*-acetylglucosaminidase H (endo H) followed by peptide:*N*-acetylglucosaminidase F (PGNase F) can be used to distinguish sites that are not glycosylated from those carrying high-mannose structures and from those containing complex oligosaccharaides. After individual glycosylation sites have been identified by this series of reactions, the resulting peptides can be sequenced. This technology is especially useful in characterizing recombinant glycoproteins of pharmaceutical interest.

The same AS-6A column was reported by Dionex [193] in the separation of neomycins A,B, and C aminoglycoside antibiotics, followed by PAD (or PED) detection with a detection limit (signal/noise of 3:1) of 5 ng.

The same AS6A column was used with PAD detection by Pollman [194] in his development of an Association of Official Analytical Chemists (AOAC) method for the determination of lactose, galactose, and dextrose in grated cheese. The AS-6 column was used by Lamb et al. [195] to determine glucose, fructose, and sucrose in raw and processed vegetables. Garbarino [196] used the PA1/S-6 column with PAD to determine thickening and gelling agents in food. Nair [197] determined trace levels of cyanamide in a potassium channel activator bulk drug, using PED at a Ag electrode. Sarzanini and co-workers [198] developed an automated method for determining urinary free-catecholamines. An internal standard, 3,4-dihydroxybenzylamine, was used. Simultaneous cleanup and separation was done using an on-line purification on a microcolumn, followed by column switching to an analytical cation exchanger. Two different working electrodes, set at 500 mV for sample cleanup and 700 mV for detection were used [198]. Sullivan and Douek [199] determined monosaccharides in H_2SO_4 hydrolysates of wood, pulp, Mg-spent sulfite liquor, kraft weak black liquor, and newsprint paper machine white water, using PED. First, hydrolysates were partly purified by a solid-phase extraction using cross-linked poly(*N*-vinylpyrrolidone) and a strong anion-exchange resin [199]. Taha and Deits [200] used PED to detect and quantitate three major metabolites (6-phosphogluconate, 2-keto-3-deoxy-6-phosphogluconate, and pyruvate) in the Entner–Doudoroff metabolic pathway.

To aid the analyst in selecting an ion chromatographic method, Haddad and co-workers have compiled a database [2,201]. The properties of a method that were used for rule-building were solute names and number of solutes, separation mechanism, application, ion class, halide type, presence of sulfate or nitrate, and whether a suppressor or postcolumn detection was

used. They built an expert system to choose the property that maximizes the amount of information obtained. By examining properties that pertain to a given class, C4.5 operates a top-down induction process. A tree with 62 rules was derived from this database [201].

3. Mass Spectrometry Detection

Although mass spectrometry (MS) has traditionally avoided the analysis of aqueous samples and is usually used with gas chromatography, many nonvolatile and ionic compounds and biopolymers have been analyzed recently by liquid chromatography in conjunction with mass spectrometry (LC–MS). This subject has been described in a recent book by Niessen and van der Greef [202] and has been reviewed [203,204]. MS has been described as the most sensitive detector for organic ions [205].

(a) LC–MS Interfaces. To couple an LC or ion chromatograph (IC) to an MS requires an interface device that will convert the dissolved analyte's liquid phase to a gas in the presence of a vacuum (see also Chap. 19). Several types of commercial interfaces have been developed. Thermospray, electrospray, ion spray, direct interface probe (DIP), and continuous flow probes (CFP) with fast-atom bombardment (FAB) are suited for ionic analytes [202–233].

In thermospray MS, the dissolved analytes are heated in a vaporizer, then directed into a heated probe. The book by Niessen and van der Greef [202] describes thermospray and other interfaces in detail. Nebulization occurs as a result of the disruption of the liquid by the expanding vapor that is formed on evaporation in a heated vaporizer tube. With sufficient pumping, up to 2 mL min^{-1} of aqueous solution can be introduced into the MS vacuum system. The analytes ionize by chemical ionization reactions and ion evaporation processes. Heat sources can include laser, hydrogen flame, electrical heating, and others [202]. Nonvolatile salts in the mobile phase can be removed by a membrane suppressor before being sent to the MS [207,208].

In ion spray interfaces, the dissolved analyte exiting a membrane suppressor is evaporated by the application of a high-voltage (about 3 kV) to a capillary. Preformed ions are desorbed from rapidly shrinking, highly charged droplets, resulting in quasimolecular precursor ions. Typically, ions are generated in solution by a proton addition ($[M + H^+]$) in the positive-ion mode and proton loss ($[M - H^-]$) in the negative-ion mode. The ion spray interface is operated at ambient temperature under mild conditions, virtually guaranteeing molecular ion formation [204]. The ion spray interface is described in more detail by Niessen and van der Greef [202], with a schematic diagram of the interface and a detailed description of the electrospray process and ionization mechanisms. Phosphate buffers can severely compromise performance, but acetate and formate buffers work well. Ion spray, which uses a nebulizing gas in the ion spray interface, permits stable operation at flow rates as high as 200 μL min^{-1}, is used frequently for the analysis of low molecular weight (< 1000-Da) compounds.

Niessen and van der Greef [202] described electrospray interface and ionization mechanisms in detail. Ikonomou et al. [216] compared electrospray and ion spray. Ion spray works better at higher water content. They described ion spray as a modification of electrospray in which the nebulization of the liquid effluent is assisted by a turbulent gas (N_2) flow. Droplet dispersion is obtained by two different means. In electrospray, ions are completely dissociated in the column effluent. When the MS capillary is the positive electrode, some cations in the effluent will drift toward the liquid surface and some anions will drift away from it. This is called the electrophoretic mechanism. The positive charge at the liquid surface leads to surface destabilization, and the surface is drawn out so that a cone forms. At higher capillary voltage, the tip of the cone begins to emit small, positively charged droplets. Karlsson [206] described the use of deuterium oxide as a reagent for the modification of mass spectra in electrospray microcolumn LC–MS. Deuterium oxide induces peak shifts that provide the number of heteroatoms carrying hydrogens.

In ion spray, charges separate in an electrophoretic mechanism, but the droplet formation is due to the turbulent flow of the nitrogen gas. Thus, a fine mist of droplets can be observed,

even in the absence of capillary voltage [216]. This allows greater freedom in choosing eluents and flow rates. Pure electrospray is restricted to lower-flow rates ($< 10\ \mu L\ min)^{-1}$ [204]. Although the mass spectra of basic analytes produced by ion spray and electrospray are similar, ion spray will give a higher analyte, BH^+, signal as shown by Ikonomou et al. [216].

Niessen and van der Greef [202] also described continuous-flow fast-atom bombardment (FAB) for LC–MS. FAB is one of the most frequently used of the soft ionization techniques for MS. Ionization is produced by bombarding the analyte dissolved in a nonvolatile matrix, such as glycerol, with a Xe-atom beam of 5–8 kV. The nonvolatile matrix is needed primarily to serve as a transport medium to replenish the bombarded surface. More details, along with a schematic of an FAB interface were described [202].

The particle beam interface was also described in detail by Niessen and van der Greef [202]. The column effluent is nebulized into an almost atmospheric pressure desolvation chamber that is connected to a momentum separator where the high molecular weight analytes are transferred to the MS ion source, while the low molecular weight solutes are pumped away. The analytes are transferred in small particles to a conventional electron ionization (EI) or chemical ionization (CI) source. Schematics of a monodisperse aerosol generator, a monodisperse aerosol-generating interface for chromatography (MAGIC), and a momentum separator were presented [202].

The four basic types of mass analyzers are magnetic sector, quadrupole, ion trap, and time of flight [202]. Magnetic sector analyzers use a magnetic field to alter the paths of the ionized molecules. To scan the mass range, the magnetic field strength is changed over time. Quadrupole mass analyzers are based on the interaction between the ionized molecule and an oscillating electric field. Four pencil-shaped electrodes are electrically connected. The ionized molecule is directed through the quadrupole by the electric potential applied to the electrodes. By varying the dc and ac applied potential, only ions of a selected mass will oscillate in a stable path and reach the detector. They are relatively cheap and have made the use of GC–MS and LC–MS possible for environmental and clinical applications. Ion trap analyzers also use an electric field interaction, but ions are trapped in a cell. They are detected when they are released from the cell. The time of flight mass spectrometer measures the amount of time it takes for ions to reach the detector. The variations in mass of the ions result in different velocities and different times to reach the detector [202].

(*b*) *Ion Chromatography–Mass Spectrometry.* The first coupling of an ion chromatograph to an MS was accomplished by Pacholec et al. [206] using a thermospray LC–MS interface. In thermospray MS, the mobile phase containing analytes is sprayed into the vacuum region, forming a fine mist [202]. Some droplets will carry charges when they leave the nozzle. The solvent evaporates rapidly in the vacuum, resulting in a charged molecule devoid of solvent [202].

Van Leuken et al. described the behavior of volatile long-chain carboxylic acid ion-pairing reagents for LC–thermospray–MS [230]. They determined amino acids and amino acid amides this way. Lemiere et al. [232] evaluated LC–thermospray–MS for the determination of some phenyl glycidyl ether-2-deoxynucleoside adducts. Their results helped understand the basis for epoxide mutagenicity. Gelpi and Abian [233] used reverse-phase HPLC with a thermospray MS to determine long-chain fatty acids (arachidonic acid and its lipoxygenase metabolic profile of leukotrienes) containing conjugated triene and tetraene groups, which are weak UV chromophores. Extracts from human polymorphonuclear leukocytes (PMNL) were incubated with arachidonic acid and analyzed without any derivation methods required for GC–MS analysis. Several sample components were unequivocally identified by their molecular ions produced by the soft ionization technique [233].

Alternatively, the analyte exiting a membrane suppressor is evaporated in an ion spray LC–MS interface [207,208] in which microsized droplets formed from the effluent of the suppressor were subjected to field-assisted ion evaporation by the application of a 3-kV electrical field to a capillary [202]. The flow rate to the MS is kept below 100 $\mu L\ min^{-1}$. Field-

assisted evaporation readily occurs if the charge density of the analytes in the evaporating microdroplet appears to reach a maximum, whereupon the ejection of the ion takes place by coulombic explosion [205,210]. The gas-phase ions were sampled through an atmospheric pressure ionization (API) tandem quadrupole mass spectrometer to obtain both molecular weight and structural information on organic ammonium and sulfate compounds [211]. The ion-sampling cone was bathed in a dry nitrogen curtain gas, which facilitated the declustering of solvent–ion adducts and desolvating the droplets. LC–MS can be performed on a triple quadrupole, or LC–MS–MS system, to obtain more information about the precursor ions generated from the LC–MS interface. For quantitative analysis, the multipole reaction-monitoring (MRM) mode can be used [215]. The first quadrupole is set at the precursor ion's m/e value, allowing only the precursor ions to pass through the first quadrupole mass filter. The second quadrupole is where the collisions with argon gas take place. The third quadrupole is set to the mass of a specific fragment ion, selected from a fragment ion mass spectrum. This procedure reduces the chemical background, especially useful when analyzing urine, plasma, soil extracts, or other difficult sample matrices.

Although the term LC–MS is used much more often than IC–MS, often it is ionic compounds that are separated and detected. In pharmacology, biotransformations of drugs, such as oxidation, reduction, glucuronidide, and other adduct formation can be measured [213]. Glutathione conjugates of chlorambucil were identified [203,211].

Gilbert et al. [212] developed an LC–MS–MS method in the MRM mode for the determination of a cholecystokinin receptor agonist, L-365,260, in blood plasma for pharmacokinetic studies during phase I clinical trials. Mean concentrations of 2–200 ng mL^{-1} in plasma were found in various times after oral doses of 2.5–50 mg [204,213].

Fouda et al. [213] used a heated nebulizer interface, negative-ion detection, and single-ion monitoring to determine a tripeptide renin inhibitor, CP-80, 794 that may be an effective drug for treating hypertension. They used a structural analogue of CP-80, 794 as an internal standard and reported a minimum limit of detection of 50 pg mL^{-1} of human serum with satisfactory accuracy and precision ($r^2 > 0.995$) over the 50 pg mL^{-1} to 10 ng mL^{-1} range [204,213].

Subramanyam et al. [214] used LC–MS with the ion spray interface to study the metabolism of haloperidol (a 1,4-disubstituted piperidine derivative used to treat schizophrenia). They showed that it was metabolized into a potentially neurotoxic pyridinium compound that might be responsible for debilitating side effects. Human urinary levels as low as 330 pg mL^{-1} were detected [214].

Weidolf and Covey used an ion spray LC–MS method to study the metabolism of the thermally labile drug omeprazole, used to treat acid-related disorders [204,215]. Full-scan mass spectra were used to identify at least 40 metabolites in rat urine. Chait et al. [217] reviewed mass spectrometry of peptides and proteins. They stated that sensitivity is usually limited by sample handling before mass spectrometry, but concentrations as low as 10^{-7} to 10^{-9} M could be detected.

Ling et al. [218] analyzed tissue plasminogen activator (TPA), produced by recombinant DNA expression, for use in treating coronary disease. TPA was digested with trypsin to produce smaller peptides. Nebulizer gas-assisted electrospray MS of the LC effluent was used to characterize the peptides. Accurate mass measurements enabled rapid identification of peptides from this already sequenced TPA. Two-dimensional plots of m/z versus HPLC elution time enabled the detection of families of glycopeptides containing the same peptide, but with heterogeneous carbohydrates [218]. Phosphoproteins, which play a key role in biochemical signal transduction and the regulation of cell division, were analyzed by Chivia et al. [219] using electrospray HPLC–MS. The α (catalytic) subunit of murine cAMP-dependent protein kinase was expressed in *E. coli* with a mixture of isoforms, differing in the degree of phosphorylation. The number of phosphates attached to each isoform was established by accurate MS mass measurements [219].

Thermospray was demonstrated by Simpson et al. [168] for use with the AS-6/PA-1 anion-exchange column and an AMMS for carbohydrate analysis. Sodium acetate (to 0.1 M) was added to the effluent after the AMMS. The vaporizer was at 190°C, the probe was at 125°C, the source block was at 200°C, and the vapor jet was at 250°C. The AMMS was needed to remove nonvolatile alkaline salts from the mobile phase before introduction into the MS. Isocratic and gradient separations of a three-component mixture of *N*-acetylated mono- and disaccharides were demonstrated, with sensitivity in the microgram range.

Thermospray LC–MS was used by Korfmacher et al. [220] and compared with electrospray for the analysis of rifamycin antibiotics. They obtained different mass spectra in the electrospray versus the thermospray modes, and reported that thermospray was more readily interfaced with an MS.

Van der Hoeven et al. [167] used the same AS-6/PA-1 anion-exchange column and AMMS followed by thermospray MS to characterize sugar oligomers. The detection of β-1,4-xylose oligomers with a degree of polymerization up to 25 was demonstrated. They also analyzed mixed oligomers of hexoses, pentoses, and uronic acids with a degree of polymerization up to 10.

Vreeken et al. [221] used a trapping column packed with polymeric PLRP-S to couple LC with thermospray MS by phase switching. Phase switching removed nonvolatiles from the eluent before it entered the MS. The analytical system was optimized for the determination of chlorinated phenoxy acids in the Rhine river.

Barr et al. [222] developed a general strategy for determining the structural class (oligomannose, hybrid, or complex), branching-type (biantennary or triantennary), and location of *N*-linked oligosaccharides using AS-6/PA-1 anion-exchange column with AMMS, followed by fast-atom bombardment (FAB) and methylation analysis. It was used on the CD4 receptor glycoprotein, to which the human immunodeficiency virus (HIV) binds. The glycoprotein was reduced and alkylated. One aliquot was subjected to proteolytic cleavage into peptides plus glycopeptides, which were analyzed by FAB–MS to obtain a map of the protein, excluding regions around the glycosylation sites. Another aliquot was subjected to PGNase F digestion, then proteolytic cleavage to produce peptides plus free carbohydrates for IC–FAB–MS analysis.

Krotkiewski et al. [223] used IC–FAB–MS to analyze mouse monoclonal IgG antibody OKT3. Sialic acid, galactose, mannose, fucose, and *N*-acetylglucosamine were identified. These *N*-linked carbohydrate chains were isolated as alditols after alkaline sodium borohydride degradation. They were further fractionated on a concanavalin A–Sepharose column and an AS-6/PA-1 anion-exchange column with PAD detection. Structural analysis was performed by FAB–MS and by 500-MHz ^{1}H NMR.

Basa and Spellman [224] used the same AS-6/PA-1 column with PAD detection, followed by FAB–MS analysis to separate and detect 19 different high-mannose, hybrid, and complex type oligosaccharides isolated after peptide:*N*-glycosidase F or endo-β-*N*-acetylglucosaminidase H digestion of glycoproteins. The FAB–MS analysis was done after conversion of the oligosaccharides (after the AMMS) to permethyl derivatives or after reductive amination.

Karlsson [225] demonstrated the use of deuterium oxide (D_2O) as a reagent for the modification of mass spectra in electrospray microcolumn LC–MS. The D_2O caused a mass shift to identify heteroatoms with attached hydrogens.

Al-Omair and Todd [226] used a continuous-flow probe (CFP), which allowed a continuous flow of sample to be introduced into a FAB source. The CFP consisted of a hollow shaft terminated with a hemispheric gold-plated tip through which a 0.4-mm hole was drilled. A 3-cm–long insulating section made of Vespel polyamide electrically insulated the tip of the probe from the probe shaft. A 0.075-mm–id capillary tube was passed through the shaft and allowed to protrude about 0.2 mm beyond the probe tip. The probe was adjusted to obtain the optimum position in the ionization chamber using a 2-cm–range micrometer. A valve was used to split the anion-exchange column effluent so that 0.5 μL was injected into the FAB

source. Positive-ion FAB spectra using a xenon atom beam were recorded [226]. The eluent contained 5% (vol) glycerol. A mixture of water-soluble vitamins, ascorbic acid, thiamine hydrochloride, pyridoxine hydrochloride, and riboflavin, were separated and detected. A mixture of gluconic acid, glucose, and gluconolactone were also separated and detected by FAB [226].

Brown et al. [227] described a series of methods using a particle beam (electron ionization, or EI) LC–MS interface for environmental analyses. Aromatic chlorinated sulfonic acids at the Stringfellow hazardous waste site were analyzed. The source temperature was 250°C, a 70-eV electron energy for EI or 200-eV for chemical ionization (CI) using isobutane, and a helium gas for the particle beam interface were used. Chlorinated phenoxy acid herbicides were determined after ethyl acetate extraction from soil and water samples, followed by hydrolysis to the free carboxylic acids. They were separated by reversed-phase HPLC, quantitated by UV absorption and confirmed by particle beam MS. The capability of particle beam MS to give conventional EI spectra with diagnostic fragment ions was called invaluable for analyte confirmation [227].

Hsu [228] interfaced ion chromatography with particle beam MS for the determination of organic anionic compounds in hazardous waste samples. The mixed-mode PAX-500 column was used to separate the anions, and an AMMS was used to remove sodium salts from the eluent, before introduction into the particle beam interface. The effluent was passed through a capillary and nebulized at the exit end by a surrounding flow of helium gas. The dispersion of helium, vapor, and liquid droplets formed was then passed at high speed through a nozzle. While the solvent evaporated, the nonvolatile solutes concentrated further down in the droplets and aggregated to form solid particles. The central beam of particles traversed the length of the transfer tube to reach the MS ion source. Mono-, di-, and trisulfonic acids from aqueous leachates at hazardous waste dump sites were separated on the PAX-500 using a simultaneous acetonitrile and NaCl gradient. Characteristic EI spectra were used to confirm the structures of the analytes [228].

Alexander and Quinn [229] used ion-exclusion chromatography with a particle beam interface to an MS to determine organic acids, using both EI and CI. Isobutane CI produced protonated molecular ions, which, combined with structural information from EI, allowed identification of weak acids in juice and wine samples.

Van Leuken et al. [230] used volatile ion-pairing reagents, heptafluorobutanoic acid, tridecafluoroheptanoic acid, and nonadecafluorodecanoic acid with a thermospray MS interface to analyze amino acids and amino acid amides. The sensitivity was enhanced by postcolumn addition of HO_2CCF_3 and ionization with NH_3 gas.

Kassel et al. [231] used a packed capillary perfusion column in LC–MS–MS for the rapid mapping and sequencing of enzymatic digests. An electrospray interface was used. Separation of tryptic digests of human growth hormone were separated using capillary ODS columns. By using a modified PE-Sciex API III collision cell, they fully sequenced several of the tryptic peptides from a 25-pmol injection. Methods for improving sensitivity using ion spray were proposed.

Lemiere et al. [232] evaluated an LC–thermospray–MS interface for the determination of some phenylglycidyl ether-2′-deoxynucleoside adducts, using a 10 RP Select B column for separation. The 2′-deoxycytidine–PGE adduct was deaminated by hydrolysis to the 2′-deoxyuridine adduct. A detection limit of 500 pg in a multiple ion-monitoring mode was reported.

Thus, interfacing IC or LC with MS is one of the most important recent advances in the detection of ionic compounds and biopolymers.

4. Atomic Absorption and Inductively Coupled Plasma Detection

Atomic absorption (AA) and inductively coupled plasma (ICP) have been used to detect metals after IC separation. Sarzanini et al. [234] separated methyl mercury, ethyl mercury, and in-

organic mercury as cysteine complexes, then used on-line cold vapor AA for detection. An on-line continuous flow cell coupled with a sodium tetrahydroborate reduction system was used. The influences of the pH, ionic strength, and cysteine concentration, as well as stripping-gas flow rate were evaluated. Using an on-line preconcentration column and 100-mL samples, detection limits of 2, 10, and 4 ng for Hg, methylmercury, and ethylmercury were reported. Synthetic mixtures and tap water were analyzed.

Ion-exchange separation and enrichment techniques for ultratrace elemental analysis with ICP detection was reviewed by Bloerdorn [235]. He described chelating compounds immobilized on a cellulose support, enabling the use of both ion-exchange and chelation. ICP enabled simultaneous multielement detection. Finely divided cellulose has a large surface area with a hydrophilic structure and is suited for enrichment. This enables the sorption of trace elements in the picogram to microgram per milliliter range. As chelating agents, EDTrA (ethylenediamine triacetic acid) and oxine-modified cellulose were used. Limits of detection from 1 to 150 pg mL^{-1} were reported for 21 elements [235].

Hexavalent chromium (Cr^{6+}) is a human respiratory carcinogen. As described by Sheehan et al. [236] airborne Cr^{6+} emissions are associated with various industrial sources. To date, only the workplace sampling and analytical NIOSH Method 7600 have been validated for measuring airborne Cr^{6+}. Its limit of detection is 500 ng m^{-3}. They described the field evaluation of a method using ICP detection with a detection limit of 0.1 ng m^{-3}. They used three 500-mL Greenberg-Smith impingers in series, filled with 200 mL of 0.02 M $NaHCO_3$ buffer, and operating at 15 L min^{-1} for 24 h. As described by others [237–239], Cr^{+6} can be separated from the noncarcinogenic Cr^{+3} on an AS7 anion-exchange column using a 250-mM (NH_4), SO_4 plus 100-mM NH_4OH eluent, in which the Cr^{+6} exists as the CrO_4^{2-} anion. When post-column reaction with 2 mM diphenylcarbizide plus 1 N H_2SO_4 in 9:1 H_2O:CH_3OH (v/v) is used with UV/vis detection at 530 nm, the detection limit is not so low, but this method has been validated as EPA Method 218.6. Urasa and Nam [237] used the AS-7 column, but with a direct-current plasma emission spectrometer at 425.4 nm for the determination of Cr^{6+} in NBS (formerly called the National Bureau of Standards, but now called the National Institute for Standards and Technology; NIST) standard reference material, or SRM 909, in a human serum matrix. They also showed that Cr^{+6} could be separated as a cation on the CS-2 column. Arar et al. [238] used a VG PlasmaQuad Type I ICP–MS, equipped with a water-cooled spray chamber, a nebulizer, and peristaltic pump to distinguish ^{50}Cr from ^{53}Cr. A 0.75-mm nickel skimmer cone and 1-mm nickel sampling cone were used to facilitate ion extraction from the plasma. Chromium isotope ratios were determined by scanning over the 48–55 amu range [238]. When Cr isotope speciation was not required, they used a Jarrell-Ash Atomcomp spectrometer, Model 1160-Mark III, equipped with a Model HFP2000D Plasma-Therm RF generator, Models FC260 and FC 262 Tylan Corp. mass flow controllers, and a Model Miniplus 2 Gilson Electronics peristaltic pump.

Garcia-Alonso [239] used ICP–MS to detect tin in butyltin species that were separated by ion exchange on a Zorbax SCX column. Mono-, di-, and tributyltin were separated, and ICP–MS detected the tin in them. Betti et al. [240] also used ICP–MS, but they analyzed highly radioactive liquid samples. An Elan 5000 ICP–MS (Sciex, Canada) was modified to handle radioactive samples in a glove box. It was coupled to a Dionex ion chromatograph (Sunnyvale, CA) containing a CS-3 and a CS-5 cation separator column. Heavy fission products, Cs, Ba, and lanthanides, were separated by ion chromatography before ICP–MS detection. Separation was needed because of the mixture of fission products present in spent fuels, some of which have the same nominal mass (i.e., ^{137}Cs and ^{137}Ba, ^{148}Nd and ^{148}Sm). By using a CS3 column, which has only cation-exchange sites, and α-hydroxyisobutyric acid eluent, lanthanides eluted in a series beginning with Lu^{+3} to La^{+3}, but with the mixed-bed CS-5, the elution order was reversed, and even Ba^{+2} could be eluted with a strong enough eluent (700 mM HNO_3). This enabled the determination of fuel burn-up based on ^{148}Nd, free from interference from ^{148}Sm [240].

Seubert [241] described on-line coupling of ICP and ion chromatography for the determination of 21 elements that can be detrimental to microelectronic industry. Absolute detection limits were at the low nanogram level. The combination of a high number of theoretical plates and element-specific detection allowed the measurement of different retention times of normally coeluting cations. The reproducibility was not significantly lowered by the coupling, but the sensitivity improved tenfold compared with similar off-line methods (241).

Thus, ICP is another powerful detection method available to the chromatographer.

REFERENCES

1. H Small. Ion Chromatography. New York: Plenum Press, 1989.
2. PR Haddad, PF Jackson. Ion Chromatography. Amsterdam: Elsevier, 1990.
3. HF Walton, RD Rocklin. Ion Exchange in Analytical Chemistry. Boca Raton: CRC Press, 1990.
4. J Weiss. Ionenchromatographie. Weinheim: VCH, 1993.
5. F Helffrerich. Ion Exchange. New York: McGraw-Hill, 1962.
6. PK Dasgupta. Anal Chem 64:775A, 1992.
7. A Dyer, MJ Hudson, PA Williams. Ion Exchange Processes: Advances and Applications. London: Royal Society of Chemistry, 1993.
8. K Dorfner, ed. Ion Exchange. Berlin: Walter de Gruyer & Co., 1991.
9. S Yamamoto. Ion Exchange Chromatography of Proteins. New York: Marcel Dekker, 1988.
10. KM Gooding, FE Regnier, eds. HPLC of Biological Macromolecules. New York: Marcel Dekker, 1990.
11. JG Dorsey, WT Cooper, JF Wheeler, HG Barth, JP Foley. Anal Chem 66:500R, 1994.
12. J Chromatogr 645:1, 1993.
13. J Chromatogr 670:1, 1994.
14. BA Adams, EL Holmes. J Soc Chem Ind (Lond.) 54:1T, 1935.
15. WC Bauman, J Eichhorn. J Am Chem Soc 69:2830, 1947.
16. R Kunin, RJ Myers. J Am Chem Soc 69:2874, 1947.
17. GE Boyd, AW Adamson, LS Myers Jr. J Am Chem Soc 69:2836, 1947.
18. S Moore, WH Stein. J Biol Chem 176:367, 1948.
19. S Moore, WH Stein. J Biol Chem 192:663, 1951.
20. PB Hamilton. Anal Chem 32:1779, 1960.
21. PB Hamilton, DC Bogue, RA Anderson. Anal Chem 32:1782, 1960.
22. PB Hamilton. Anal Chem 35:2055, 1963.
23. E Glueckauf. Ion Exchange and Its Applications. London: Society of Chemical Industry, 1954.
24. H Small, TS Stevens, WC Bauman. Anal Chem 47:1801, 1975.
25. DT Gjerde, JS Fritz, G Schmuckler. J Chromatogr 186:509, 1979.
26. TH Jupille, DW Togami, DE Burge. Ind Res Dev 25(2):151, 1983.
27. B Howard, ed. Am Lab 26(4):56–58; 113–114; 199–240, 1984.
28. A Velayudhan, C Horvath J Chromatogr 443:13, 1988.
29. J Stahlberg, B Jonsson, C Horvath. Anal Chem 63:1867, 1991.
30. CM Roth, LM Lenhoff, Langmuir 9:962, 1993.
31. LA Haff. Chromatogr Forum 2(2):25, 1987.
32. MTW Hearn. Chromatographia 24:769, 1987.
33. S Borman. Anal Chem 59:99A, 1987.
34. P Hajos, O Horvath, V Denke. Anal Chem 67:434, 1995.
35. A Siriraks, CA Pohl, M Toofan. J Chromatogr 602:89, 1992.
36. RE Smith, RA MacQuarrie. J Chromatogr Sci 29:232, 1991.
37. RE Smith, D Yourtee, T Bean, RA MacQuarrie. J Chromatogr Sci 31:366, 1993.
38. J Stahlberg. J Chromatogr 356:231, 1986.
39. J Stahlberg. Anal Chem 66:440, 1994.

40. A Bartha, Stahlberg. J Chromatogr A 668:255, 1994.
41. W Hu, H Tao, and H Haraguchi. Anal Chem 66:2514, 1994.
42. W Hu, T Takeguchi, H Haraguchi. Anal Chem 65:2204, 1993.
43. J Marinsky. J Chromatogr 201:5, 1980.
44. H Liu, FF Cantwell. Anal Chem 63:2032, 1991.
45. J Stahlberg. J Chromatogr 356:231, 1986.
46. T Brown, DJS Brown. Methods Enzymol 211:20, 1992.
47. P Ng, G Mitra. J Chromatogr 658:459, 1994.
48. CC Tebbe, W Vahjen. Appl Environ Microbiol 59:2657, 1993.
49. E Westman, S Eriksson, T Laas, PA Pernamalm, SE Skold. Anal Biochem 166:158, 1987.
50. Y Kato, Y Yamasaki, A Onaka, T Kitamura, T Hashimoto, T Murotsu, S Fukushige, K Matsubara. J Chromatogr 478:264, 1989.
51. MA Strege, A Lagu. J Chromatogr 555:109, 1991.
52. J Wages, ED Katz. In: ED Katz, ed. HPLC: Methods and Principles in Biotechnology. New York: John Wiley & Sons, 1995, p. 351.
53. R Hecker, M Coplan, D Riesner. J Chromatogr 326:251, 1985.
54. CG Huber, PJ Oefner, GK Bonn. Anal Chem 67:578, 1995.
55. BioRad. One Prep-A-Gene Master Kit. US Bulletin 1890, 1994.
56. W Kopaciewicz, MA Rounds, J Fausnaugh, FE Regnier. J Chromatogr 266:3, 1983.
57. RE Smith, RA MacQuarrie. Anal Biochem 170:308, 1988.
58. RE Smith, RA MacQuarrie, RS Jope. J Chromatogr Sci 27:491, 1989.
59. DJ Roush, DS Gill, RC Wilson. J Chromatogr 653:207, 1993.
60. L Haggerty, LM Lenhoff. J Phys Chem 95:1472, 1991.
61. SC Harvey. Proteins 5:78, 1989.
62. S Takashima, HP Schwan. J Phys Chem 69:4176, 1965.
63. BD Penncock, HP Schwan. J Phys Chem 73:2600, 1969.
64. SC Harvey, P Hoekstra. J Phys Chem 76:2987, 1972.
65. RW Kriwacki, RB Hill, JM Flanagan, JP Caradonna, JH Prestegard. J Am Chem Soc 115: 8907, 1993.
66. LA Kuhn, MA Siani, ME Pique, CL Fisher, ED Getzoff, JA Tainer. J Mol Biol 228:13, 1992.
67. MF Colombo, DC Rau, VA Parsegian. Science 256:655, 1992.
68. D Bulone, PL, San Biaio, MB Palma-Vittorelli, MU Palma. Science 259:1335, 1993.
69. B Lee, FM Richards. J Mol Biol 55:379, 1971.
70. FM Richards. Annu Rev Biophys Biochem 6:151, 1977.
71. ML Connolly. Science 221:709, 1983.
72. RJ Hunter. Zeta Potential in Colloid Science. London: Academic Press, 1981.
73. FC Bernstein, TF Koetzle, GJB Williams, EF Meyer, MD Brice, JR Rogers, O Kennard, T Shimanouchi, MJ Tasumi. J Mol Biol 112:535, 1977.
74. MR Egmond, WP Anthenhuisse, CJ van Bemmel, P Ravestein, J deVlieg. Protein Eng 7: 793, 1994.
75. M Fang, JA Howell. Food Bioprod Process 71(C4): 267, 1994.
76. I Klapper, R Hagstorm, R Fine, K Sharp, BH Honig. Proteins 1:47, 1986.
77. D Jayaram, K Sharp, BH Honig. Biopolymers 28:975, 1989.
78. BJ Yoon, AM Lenhoff. J Phys Chem 96:3130, 1992.
79. ML Connolly. J Appl Crystallogr 18:499, 1985.
80. V Noinville, VM Claire, B Seville. J Phys Chem 99:1516, 1995.
81. JA Gerstner, JA Bell, SM Cramer. Biophys Chem 52:97, 1994.
82. AN Hodder, MI Aguilar, MTW Hearn. J Chromatogr 506:17, 1990.
83. AN Hodder, KJ Machin, MI Aguilar, MTW Hearn. J Chromatogr 517:317, 1990.
84. AN Hodder, KJ Machin, MI Aguilar, MTW Hearn. J Chromatogr 507:33, 1990.
85. A Johnston, MTW Hearn. J Chromatogr 512:101, 1990.
86. MTW Hearn, AN Hodder, FW Fang, MI Aguilar. J Chromatogr 548:117, 1991.

87. A Johnston, MTW Hearn. J Chromatogr 557:335, 1991.
88. G Malmquist, N Lundell. J Chromatogr 627:107, 1992.
89. P Lundahl, Y Watanabe, T Tagaki. J Chromatogr 604:95, 1992.
90. T Hiranuma, T Horigome, H Sugano. J Chromatogr 515:399, 1990.
91. T Horigome, T Hiranuma, H Sugano. Eur J Biochem 186:63, 1989.
92. C Pidgeon, UV Venkataram. Anal Biochem 176:36, 1989.
93. C Pidgeon, J Stevens, S Otto, C Jefcoate, C Marcus. Anal Biochem 194:163, 1991.
94. OW Reif, R Freitag. J Chromatogr 654:29, 1994.
95. G Guiochon, H Colin. Chromatogr Forum 1:21, 1986.
96. A Jungbauer, S Hackl, S Yamamoto. J Chromatogr 658:399, 1994.
97. CA Brooks, SM Cramer. J Chromatogr A 693:187, 1995.
98. A Velayudhan, C Horvath. J Chromatogr 663:1, 1994.
99. JX Huang, J Schudel, G Guiochon. J Chromatogr Sci 29:122, 1991.
100. FF Cantwell, S Puon. Anal Chem 51:623, 1979.
101. FF Cantwell. J Pharm Biomed Anal 2:153, 1984.
102. J Stahlberg. J Chromatogr 356:231, 1986.
103. J Stahlberg. Chromatographia 24:820, 1987.
104. J Stahlberg. Chromatographia 24:783, 1987.
105. JS Hwang, SJ Lyle. J Phys Chem 94:8727, 1990.
106. AS Li, JS Hwang. J Phys Chem 89:2556, 1985.
107. H Zou, Y Zhang, M Hong, P Lu. J Liq Chromatogr 16:3433, 1993.
108. FG Donnan. Z Elektochem 117:572, 1911.
109. K Tanaka, JS Fritz. J Chromatogr 361:151, 1986.
110. K Tanaka, T Ishizuka. J Chromatogr 190:77, 1980.
111. BK Glod, W Kemula. J Chromatogr 366:39, 1986.
112. Perseptive Biosystems. Perfusion Chromatography. Framingham; MA, 1995.
113. BioRad, Guide to Ion Exchange, Catalog No. 140-9997, Hercules, CA, 1993.
114. F Vernon, H Eccles. Anal Chim Acta 63:403, 1973.
115. SK Sahni, J Reedijk. Coord Chem Rev 59:1, 1984.
116. G Koster, G Schmuckler. Anal Chim Acta 38:179, 1967.
117. A Warshawsky, MMB Frieberg, P Mihalik, TG Murphy, YB Rao. Sep Purif Methods 9:209, 1980.
118. A Siriraks, HM Kingston, JM Riviello. Anal Chem 62:1185, 1990.
119. M Li, JB Schlenoff. Anal Chem 66:824, 1994.
120. I Vins, R Saari-Nordhaus. J Chromatogr 640:49, 1993.
121. R Saari-Nordhaus, JM Anderson Jr, K Ravichandran. J Chromatogr 602:15, 1992.
122. J Coupek, I Vins. J Chromatogr 658:391, 1994.
123. V Smigol, F Svec, JMJ Frechet. Anal Chem 66:4308 1994.
124. A Sugii, N Ogawa, Y Ilinuma, H Yamamura. Talanta 28:551, 1981.
125. JC Janson. Chromatographia 23:361, 1987.
126. PR Levison. Cellulosics 1:25, 1993.
127. R Noel, A Sanderson, L Spark. Cellulosics 1:17, 1993.
128. AK Dutta-Roy, DJ Leishman, MJ Gordon, FM Campbell, GG Duthie. Biochem Biophys Res Commun 196:1108, 1993.
129. T Mosolova, SV Kalyuzhnyi SD Varfolomeyev, GA Velikodorskaya. Appl Biochem Biotechnol, 42:9, 1993.
130. DL Narum, G Welling, AW Thomas. J Chromatogr 657:357, 1993.
131. P Mazur, MS Dennis, JL Seymour, RA Lazarus. Protein Expression Purif 4:282, 1993.
132. S Schulte, W Stoffel. Proc Natl Acad Sci USA 90:10265, 1993.
133. MW Fawley. Biochim Biophys Acta 1183:85, 1993.
134. V Micucci, IF Young, HB Yap, JR Davies, RW Herrington, BR White, G Naylor, PJ Turner. Colloq INSERM 227:155, 1993.

135. HB Yap, IF Young, V Micucci, RW Herrington, PJ Turner, JR Davies. Colloq INSERM 227:143, 1993.
136. SB Marrs. Colloq INSERM 227:169, 1993.
137. W Muller. J Chromatogr 510:133, 1990.
138. L Jacob, G Rathgeber, M Mack. Chim Oggi 12:25, 1994.
139. L Jacob, M Mack, G Rothgeber. Am Biotechnol Lab 12:37, 1994.
140. EM Science. EM Separations Technology. Gibbstown, NJ: Author, 1995, pp. 71–81.
141. J Frenz, CP Quan, J Cacia. C Democko, R Bridenbaugh, T McNerney. Anal Chem 66:335, 1994.
142. C McNeff, Q Zhao, PW Carr. J Chromatogr A 684:201, 1994.
143. J Yu, Z El Rassi. J High Resolut Chromatogr 17:705, 1994.
144. S Shak, DJ Capon, R Hellmiss, SA Masters, CL Baker. Proc Natl Acad Sci USA 87:9188, 1990.
145. RL Smith, DJ Pietrzyk. Anal Chem 56:610, 1984.
146. SH Chang, R Noel, FE Regnier. Anal Chem 48:1839, 1976.
147. FE Regnier, KM Gooding. Anal Biochem 103:1, 1980.
148. S Allenmark, B Bomgren. J Chromatogr 264:63, 1983.
149. S Allenmark, B Bomgren, H Boren. J Chromatogr 316:617, 1984.
150. MT Aubel, LB Rogers. J Chromatogr 392:415, 1987.
151. S Andersson, S Allenmark. J Liq Chromatogr 12:345, 1989.
152. J Hermansson. J Chromatogr 269:71, 1983.
153. W Su, RB Gregory, RK Gilpin. J Chromatogr Sci 31:285, 1993.
154. AJ Alpert. J Chromatogr 266:23, 1983.
155. AJ Alpert. J Chromatogr 359:85, 1986.
156. AJ Alpert, PC Andrews. J Chromatogr 443:85, 1988.
157. Sepragen Corporation. SUPERFLO Radial Flow Chromatography. San Leandro, CA: Sepragen Press, 1992.
158. RJP Williams. In: PA Williams, MJ Hudson, eds. Recent Developments in Ion Exchange. New York: Elsevier, 1990, p. 3.
159. PP Foa. Ion Channels and Ion Pumps. New York: Springer-Verlag, 1993.
160. PJ Mitchell, R Tjian. Science 245:371, 1989.
161. RE Smith. Ion Chromatography Applications. Boca Raton: CRC Press, 1988.
162. J Weiss. Handbook of Chromatography. Sunnyvale, CA: Dionex, 1987.
163. AB Reitz, ed., Inositol Phosphates and Their Derivatives. Washington, DC: American Chemical Society, 1991.
164. RE Smith, RA MacQuarrie, RS Jope. J Chromatogr Sci. 29:528, 1991.
165. DL Campbell, J Stillian, S Carson, R Joyce, S Heberling. J Chromatogr 546:229, 1991.
166. JJ Conboy, JD Henion, MW Martin, JA Zweigenbaum. Anal Chem 62:800, 1990.
167. RAM van der Hoeven, WMA Niessen, HA Schols, C Bruggink, AGJ Voragen, J van der Greef. J Chromatogr 627:63, 1992.
168. RC Simpson, CC Fenselau, MR Hardy, RR Townsend, YC Lee, RJ Cotter. Anal Chem 62: 248, 1990.
169. J Hsu. Anal Chem 64:434, 1992.
170. AD Sosimenko, PR Haddad. J Chromatogr 546:37, 1991.
171. CS Patrickios, SD Gadam, SM Cramer, WR Hertler, TA Hatton. Biotechnol Prog 11:33, 1995.
172. RD Rocklin. J Chromatogr 546:175, 1991.
173. RD Rocklin, CA Pohl, JA Schibler. J Chromatogr 411;107, 1987.
174. DL Strong, P Dasgupta, K Friedman, JR Stillian. Anal Chem 63:480 1991.
175. A Velayudhan, MR Ladisch. Anal Chem 63:2028, 1991.
176. Dionex. Series 8200 OnLine Ion Analyzer. Sunnyvale, CA: Dionex Press, 1993.
177. ME Potts, JR Stillian. J Chromatogr Sci 26:315, 1988.

178. J Sasturain, G Schwedt. Vom Wasser 80:221, 1993.
179. MJ Wojtusik, J Berthold, EQ Kaiser. Adv Instrum Control 48:(Pt.1)305, 1993.
180. NC van der Merbel, P Zuur, M Frijlink, JJM Holthius, H Lingeman, UAT Brinkman. Anal Chim Acat 303:175, 1995.
181. DC Johnson, WR LaCourse. Anal Chem 62:589A, 1990.
182. DA Dobberpuhl, DC Johnson. Anal Chem 67:1254, 1995.
183. RD Rocklin, A Henshall, RD Rubin. Am Lab 22(3):34, 1990.
184. WR LaCourse, DA Mead Jr, DC Johnson. Anal Chem 62:220, 1990.
185. GG Neuberger, DC Johnson. Anal Chem 60:2288, 1988.
186. PJ Vandeberg, DC Johnson. Anal Chem 65:2713, 1993.
187. LA Larew, DC Johnson. Anal Chem 60:1867, 1988.
188. MR Hardy, RR Townsend. Proc Natl Acad Sci USA 85:3289, 1988.
189. BJ Campbell, MJ Davies, JM Rhodes, and EF Hounsell. J Chromatogr 622:137, 1993.
190. KR Anumula, PB Taylor. Eur J Biochem 195:269, 1991.
191. AM Strang, AK Allen, AA Holder, H vanHalbeek. Biochem Biophys Res Commun 196: 1430, 1993.
192. MW Spellman. Anal Chem 62:1714, 1990.
193. Dionex, Neomycin in Transderm Application Note AN66, 1990.
194. RM Pollman. J Assoc Off Anal Chem 72:425, 1989.
195. JD Lamb, GS Myers, N Edge. J Chromatogr Sci 31:353, 1993.
196. M Garbarino. Boll Chim Ig Parte Sci 44:99 1993.
197. JB McNair. J Chromatogr A 671:367 1994.
198. C Sarzanini, E Mentasi, M Nerva. J Chromatogr A 671:259, 1994.
199. J Sullivan, M Douek. J Chromatogr A 671:339, 1994.
200. TSM Taha, TL Deits. Anal Biochem 219:115, 1994.
201. M Mulholland, DB Hibbert, PR Haddad, C Sammut. Chemom Intell Lab Syst 27:95, 1995.
202. W Niessen, J van der Greef. Liquid Chromatography–Mass Spectrometry. New York: Marcel Dekker, 1993.
203. P Newton. LC–GC 8:706, 1990.
204. MH Allen, BI Shushan. LC–GC 11:112, 1993.
205. JJ Conboy, JD Henion, MW Martin, JA Zwiegenbaum. Anal Chem 62:800, 1990.
206. F Pacholec, DR Eaton, DT Rossi. Anal Chem 58:2581, 1986.
207. AP Bruins, TP Covey, and JUD Henion. Anal Chem 59:2642, 1987.
208. TR Covey, ED Lee, AP Bruins, and JD Henion. Anal Chem 58:1451A, 1986.
209. JV Iribane, PJ Dziedzic, BA Thompson. Int J Mass Spectrom Ion Phys 50:331, 1983.
210. G Schmelzeisen-Redeken, FW Rollgen, H Writz, F Vogtle. Org Mass Spectrom 20:752, 1985.
211. DM Dulik, OM Colvin, C Fenselau. Biomed Environ Mass Spectr 19:248, 1990.
212. JD Gilbert, EL Hand, AS Yuan, TV Olah, TR Covey. Biol Mass Spectrom 21:63, 1992.
213. H Fouda, M Nocerini, R Schneider, C Gedutis, J Am Soc Mass Spectrom 2:164, 1991.
214. B Subramanyam, SM Pond, DW Eyles, HA Whiteford HG Fouda, N Castagnoli Jr Biomed Biophys Res Commun 181:573, 1991.
215. L Weidolf, TR Covey. Rapid Commun Mass Spectrom 14:573, 1991.
216. MG Ikonomou, AT Blades, P Kebarle. Anal Chem 63:1989, 1991.
217. BT Chait, SBH Kent. Science 257:1885, 1992.
218. V Ling. Anal Chem 63:2909, 1991.
219. JC Chivia, MD Uhler, GS McKnight. J Biol Chem 263:5739, 1988.
220. W Korfmacher, J Bloom, MI Churchwell, TA Getek, EB Hansen Jr, CL Holder, KT McManus. J Chromatogr Sci 32:498, 1993.
221. RJ Vreeken, RT Ghijsen, RW Frei, GJ deJong, UAT Brinkman. J Chromatogr 654:65, 1993.
222. JR Barr, KR Anumula, MB Vettese, PB Taylor, SA Carr. Anal Biochem 192:181, 1991.
223. H Krotkiewski, G Gronberg, B Krotkiewski, B Nilsson, S Svensson. J Biol Chem 265: 20195, 1990.

224. LL Basa, MW Spellman. J Chromatogr 499:205, 1990.
225. KE Karlsson. J Chromatogr 647:31, 1993.
226. AS Al-Omair, JFJ Todd. Rapid Commun Mass Spectrom 3:405, 1989.
227. MA Brown, RD Stephens, IS Kim. TRAC 10:330, 1991.
228. J Hsu. Anal Chem 64:434, 1992.
229. JN Alexander Jr, CJ Quinn. J Chromatogr 647:95, 1993.
230. RGJ van Leuken, GTC Kwakkenbos, ALL Duchateau. J Chromatogr 647:131, 1993.
231. DB Kassel, B Shushan, T Sakuma, JP Salzmann. Anal Chem 66:236, 1994.
232. F Lemiere, EL Esmans, W Van Dongen, E Van den Eeckhout, H Van Onckelen. J Chromatogr 647:211, 1993.
233. E Gelpi, J Abian. LC–GC 9:122, 1991.
234. C Sarzanini, G Sacchro, M Aceto, O Abollino, E Mentasti. Anal Chim Acta 284:661, 1993.
235. W Bloedorn. Nachr Chem Tech Lab 41:1252, 1993.
236. P Sheehan, R Ricks, S Ripple, D Paustenbach. Am Ind Hyg Assoc J 53:57, 1992.
237. IT Urasa, SH Nam. J Chromatogr Sci 27:30, 1989.
238. EJ Arar, SE Long, TD Martin, S Gold. Environ. Sci Technol 26:1944, 1992.
239. JI Garcia-Alonso, A Sanz-Medel, L Ebdon. Anal Chim Acta 283:261, 1993.
240. M Betti, JI Garcia-Alonso, P Arbore, L Koch, T Sato. Spec Publ R Soc Chem 124:205, 1993.
241. A Seubert, R Meinke. Fresenius J Anal Chem 348:510, 1994.

11
Ion Chromatography by HPLC

Donald J. Pietrzyk

University of Iowa, Iowa City, Iowa

I. INTRODUCTION

A. Historical

Although the properties of ion exchangers, the fundamentals of the ion-exchange process, and the applications of ion-exchange toward the separation of inorganic and organic analytes were well understood [1–5; see Chap. 11], ion exchange and its applications in high-performance liquid chromatography (HPLC) were not widely practiced as high-efficiency LC was emerging as a major separation technique. This was particularly true in applications directed toward the separation of inorganic analyte ions.

New, efficient ion exchangers were being synthesized, but the objectives in these studies were not specifically tied to addressing the problem of separating inorganic analyte ions. Also, availability of a method for the sensitive detection of the separated inorganic analyte ions remained a problem. Only the separation of inorganic cations for which postcolumn reactions, which usually involved complex formation and absorption measurements, was practical and sensitive. In 1975 Small and associates [6] described a clever and novel strategy that accomplished both the separation and the conductometric detection of anionic and cationic analytes at favorable detection limits. This was accomplished by employing ion-exchange principles in both the separation and the detection steps. First, they improved the quality of the ion exchangers needed to bring about the separation. Second, and most importantly, they used ion exchange to reduce the contribution of the eluent conductivity, which significantly enhances the conductometric detection of the separated analyte ions. This technique was subsequently licensed to Dionex Corporation and was further developed and marketed under the terminology "ion chromatography."

Ion chromatography (IC) and its applications [4,7–13] grew rapidly following the work of Small et al. [6] because, for the first time, it offered a method for the determination of many simple inorganic and organic analyte anions and cations at detection limits that were not easily obtained by other methods. This was particularly important from the standpoint of the determination of inorganic anions because sensitive atomic absorption and emission spectroscopic techniques were already available for inorganic cation determinations. Furthermore, IC provided a high degree of sensitivity that was obtained rapidly at a high degree of accuracy and reproducibility, and with confidence.

Modern IC is applicable to a wide range of samples, IC procedures and areas of application are discussed in Chapter 25 of this handbook and in other sources [4,7–13], and the

complexity of the samples subjected to IC continues to increase. Typically, IC detection limits for inorganic anions and cations are about 10 ppb for a 50-μL sample, and many factors have contributed to this improved detection limit compared with what was obtained by Small et al. [6]. Acceptance of IC is indicated by the fact that many methods have been approved by the American Society for Testing Materials (ASTM) and by the United States Environmental Protection Agency (EPA).

The scope of IC also quickly changed, and the narrow definition of IC that was appropriate in its early stages of development as a method for the ion-exchange separation and conductometric determination of inorganic analyte anions and cations was no longer applicable. Currently, IC encompasses other allied strategies for the separation and detection of analyte ions and extends beyond the separation of simple inorganic anions and cations. Development of better ion exchangers; improved suppression techniques; elimination of the suppression step; improved methods for sample cleanup; separation of weak organic acids and bases as ions and by ion-exclusion techniques; improvement in conductivity detectors; incorporation of detection techniques other than conductivity; and including postcolumn and indirect detection strategies into the separation procedure; development of ion interaction reagents as mobile-phase additives in combination with reversed-phase columns; development of ion exclusion techniques; and improvements in computer optimization, all have contributed to a broader interpretation of IC. It is within this broad description that suppression and nonsuppression IC is discussed in this chapter.

B. Ion Exchange: Basic Principles

Ion exchangers are typically insoluble, solid substances, containing fixed charge centers (ionogenic groups) and exchangeable counterions of opposite charge associated with each ionogenic group. The exchanger framework is held together by lattice energy or chemical bonds and contains either cation or anion ionogenic groups. The charges at these groups are satisfied by the diffuse, freely moving counterions, and they can be replaced by other counterions of the same charge on a stoichiometric basis. The exchanger resembles a porous, insoluble electrolyte. When it is placed in an aqueous solution, containing an electrolyte, the exchanger is composed of three phases: the solid polymeric matrix, the imbibed solution within exchanger particles, and the free solution between the exchanger particles. The polymeric network acts as a semipermeable membrane between the two liquid phases. The ion exchanger counterions, for which the charges are opposite the ionogenic group, freely move from the exchanger phase to the solution phase and are simultaneously replaced by counterions of the same charge from the electrolyte solution. Ions of the same charge as the ionogenic group do not freely move into the exchanger phase because of Donnan exclusion. This phenomenon, although preventing movement of the strong electrolyte from entering the imbibed phase, allows movement of weak electrolytes or nonelectrolytes between the two phases, and this process accounts for retention of weak and nonelectrolytes by ion exchangers. Separations based on this behavior are called ion-exchange exclusion separations. In addition, analytes may interact with the polymeric matrix by adsorption processes, whereas other analytes may undergo a partitioning process between the two liquid phases.

A typical cation-exchange process, in which H^+ and K^+ counteractions compete for the ionogenic site, is defined by Eq. (1).

$$H^+M^-(s) + K^+Cl^-(aq) \rightarrow K^+M^-(s) + H^+Cl^-(aq) \quad (1)$$

A typical anion-exchange process where OH^- and Cl^- counteranions compete for the ionogenic group is defined by Eq. (2).

$$M^+OH^-(s) + N^+Cl^-(aq) \rightarrow M^+Cl^-(s) + Na^+OH^-(aq) \quad (2)$$

In Eqs. (1) and (2) M is the insoluble ion exchanger matrix or structural unit that contains the ionogenic group and a stoichiometric quantity of the counterion of opposite charge, (s)

represents the solid-phase exchanger, and (aq) is the aqueous phase, containing the electrolyte. The exchanger matrix is often an organic polymeric matrix, such as the cross-linked polystyrene divinylbenzene copolymer [5,14]; however, other insoluble materials, for example, alumina [15], silica [16], and other inorganic salts and oxides [17,18], can exhibit useful ion-exchange behavior, or can be used to prepare ion exchangers by chemically bonding a group containing the ionogenic group to the material. This is done for the commercially available silica-based bonded-phase ion exchangers.

The general ion-exchange process represented by Eqs. (1) and (2) describes a distribution of the two counterions between the internal pore liquid and the external bulk solution. When equilibrium is reached, the ionogenic group establishes a preference for one counterion over another and, under a specified set of experimental conditions, this preference is expressed numerically as the ion-exchange selectivity. Thus, it is possible to tabulate selectivities for anions toward anion exchangers and cations towards cation exchangers. Typical selectivities for anions and cations are listed in Table 1. The ion-exchange selectivities are particularly valuable in optimizing ion-exchange separations, because these data indicate both the elution order and the eluent strength. The larger the ion-exchange selectivity value, the greater is its retention and power as an eluent counterion.

In optimizing the ion-exchange strategy for IC, ion-exchange selectivity is only one of the key properties that must be considered; others include the following:

1. Ion-Exchanger Capacity

The capacity is a measure of the quantity of exchangeable ions per unit amount of ion exchanger and influences chromatographic performance through sample loading. Analyte ion sample sizes should involve only a small percentage of the available exchange capacity; such that the exchange isotherm is linear. For pellicular and latex-derived ion exchangers, in which the ionogenic groups are located primarily on the outer surface of the exchanger particle, and for silica-bonded phase ion exchangers, exchange capacities are much lower than for exchangers in which the ionogenic groups are located within the bead interior as well as on the surface.

2. Swelling

When an organic polymeric-type ion exchanger is placed in a solution of an electrolyte, the exchanger takes up the solution within its framework, causing the exchanger polymeric matrix to swell. The swelling can be significant, and the extent of the swelling is influenced by the cross-linking within the polymer. Furthermore, column chromatographic performance can be affected by exchanger swelling, because it influences the availability of the inner portions of the particle framework and, thereby access to the ionogenic groups located within the interior of the exchanger. Exchanger swelling will also influence packing of the exchanger into a column. Swelling is a more serious problem in polymeric gel and porous-type ion exchangers and less of a problem in pellicular and latex-type exchangers, for which the particle core is nonporous or low in porosity, and the ionogenic groups are located on the outer surface of the particle, or for silica-bonded–phase ion exchangers.

3. Rates of Exchange

Exchange rates are controlled by diffusion within the exchanger particle and by film diffusion at the bead surface. Thus, exchanger swelling and the porous nature of the exchanger framework, which influences the availability of the ionogenic group, will affect the exchange rate. The rate of exchange will generally be slower for the exchanger that is more porous or swells to a greater extent. Usually, the pellicular, the latex type, and the silica-bonded–phase ion exchangers will have the faster rate of exchange.

4. Reversibility

Ion exchange, as described by Eqs. (1) and (2) are reversible and stoichiometric. For dilute solutions, low concentrations of counterions to maintain a linear isotherm and low ion-

Table 1 Ion-Exchange Selectivities[a]

Cation	Anion
Li^+	OH^-
H^+	F^-
Na^+	$C_2H_3O_2^-$
NH_4^+	IO_3^-
K^+	Cl^-
Rb^+	NO_2^-
Cs^+	BrO^-
Mg^{2+}	HSO_3^-
Ca^{2+}	Br^-
Sr^{2+}	NO_3^-
Ba^{2+}	ClO_3^-
Zn^{2+}	HSO_4^-
Cu^{2+}	Phenolate
Ni^{2+}	Benzenesulfonate

[a]Listed in order of increasing selectivity.

exchange capacities—Eqs. (1) and (2)—when at equilibrium, also define the ion-exchange selectivity. Under these conditions the selectivity value can be viewed as a constant.

5. Ionogenic Group

Organic polymeric, pellicular, latex, and silica-bonded–phase ion exchangers can be prepared as strong or weak acid- or base-type ion exchangers [4,5,10,13,14]. The strong acid or a cation exchanger contains the $-SO_3^-$ ionogenic group, whereas the strong base or an anion exchanger contains the $-NR_3^+$ ionogenic group. Weak acid- and weak base-type ion exchangers typically contain $-CO_2H$, $-PO_3H_2$, $-OH$, or SH; and $-NH_2$, $-NHR$, or $-NR_2$ ionogenic groups, respectively. Their ability to function as ion exchangers is dependent on dissociation of the ionogenic group and, therefore, on the pH of the environment. Exchangers containing chelating and oxidation–reduction groups can also be prepared [4,5,10,13,14].

6. Stability

Ion exchangers should have physical strength to withstand the rigors of modern LC and eluents that are required for ion-exchange separations. Bead fracture should not occur as a result of column inlet pressure or of particle swelling or contracting as the polarity or ionic strength of the eluents are changed. The exchangers should be stable over a wide range of eluent composition. Organic polymeric- and latex-based ion exchangers containing weak or strong acid or basic ionogenic groups are generally stable over the entire pH range. In contrast, silica-based–bonded phase ion exchangers are stable throughout the pH range of 2 to about 9 because of the reactivity of the silica toward a strong acidic on basic environment. This factor seriously limits the application of the silica-based ion exchanger in ion-exchange separations, even though the exchangers are efficient, show excellent retention toward ionic analytes, and provide good resolution. Bead fracture may be a problem with the polymeric ion exchangers, particularly if they are minimally cross-linked. It is less serious with latex-derived ion exchangers, and of usually not a problem with the silica-based ion exchangers. The strong acid cation-exchange group, $-SO_3^-$, is more stable than the strong base anion-exchange group, $-R_4N^+$, both for temperature and the chemical environment. The $-R_4N^+$ ionogenic group charged in the OH^- form has the lowest level of stability, particularly when the exchanger particles are dry.

7. Ion Exchanger Matrix

For organic polymeric ion exchangers the polymeric matrix, its composition, cross-linking, and porous- or gel-like properties influence the availability (surface or interior) of the ionogenic groups, the rate of ion exchange, and compatibility with mixed or nonaqueous solvents. It can also participate in interactions with nonionic analytes. For silica-bonded–phase ion exchangers residual silanols can influence ion exchange, because the silanol is a weak acid site and can participate in cation exchange [19]. Anion and cation latex-derived ion exchangers are capable of participating in both cation and anion exchange [20].

Ion exchangers developed for IC must satisfy these basic ion-exchange properties, and they must also provide other stationary-phase properties required by modern LC, such as availability of small, physically strong, uniform-sized, microparticles that can be reproducibly packed into efficient columns. Several types of ion exchangers are commercially available that exhibit a broad range of these essential ion-exchange properties. Both porous- and pellicular-type cation and anion exchangers are available. Typical commercially available ion exchangers for ion chromatography are strong acid and weak acid anion exchangers, containing the $-SO_3H$ and $-CO_2H$ ionogenic groups, respectively; and strong base and weak base cation exchangers, containing the quaternary ammonium and amine ionogenic groups, respectively. These ionogenic groups are bonded to an organic polymeric matrix, such as a gel or macroporous polystyrene divinylbenzene copolymer or methacrylate polymer; to latex-modified polymer; or to silica. Advances in the synthesis of ion exchangers for IC are discussed elsewhere [4,5,8,10,12–14]. Successful application of ion exchangers in IC and related separation strategies require the selection of the appropriate exchanger, an understanding of the scope of the eluting conditions, and manipulation of these two to establish detector compatibility that delivers the desired detection limit.

C. Conductivity Detection in Ion Chromatography

All ions are electrically conducting, and the measurement of conductivity offers a unique and universal method for the detection of inorganic and organic analyte ions following their chromatographic separation, including separations on ion exchangers. In addition conductivity detectors are simple devices that can be constructed to have a very low cell dead volume (typically, about 1–3 μL), provide a rapid reproducible response, and easily operated, and are reproducible and accurate.

Consider an aqueous eluent containing an electrolyte that provides a counteranion of fixed concentration and anion-exchange selectivity suitable for elution of an analyte anion that is flowing through an anion-exchange column. The eluent will have a conductance that is determined by the concentration of the electrolyte, its degree of dissociation into ions, and the limiting ionic equivalent conductance for the different ions that are present in the eluent. As long as these factors remain constant, the conductance of the cell used to monitor this value for the flowing mobile phase will also remain constant, providing the temperature is constant and there is no physical change in the cell that alters the cell constant.

When the analyte enters the anion-exchange column, the anion is retained by the column, and a stoichiometric amount of anion exchanger counteranion [see Eq. (1)] is released in its place into the mobile phase. This exchanger counteranion with the analyte anion's cocation migrates down the column with continued passage of eluent as a band, the conductance of which is the sum of the conductance of the eluent and that of the analyte anion co-cation–exchanger counteranion, and it appears in the chromatogram as the injector or void volume.

The analyte anion also slowly moves down the column as eluent flows, according to the anion-exchange process between the analyte anion, the counteranion in the eluent, and the anion-exchange site. As the analyte anion emerges from the column, the anion-exchange capacity that it occupied in the column is replaced by a stoichiometric amount of eluent

counteranion. The cocation concentration remains constant during this entire process to maintain electroneutrality. Thus, the analyte band that passes through the conductivity detector provides a total conductance that represents the analyte anion, its cocation, and a decrease in the amount of the eluent counteranion that remains on the column owing to a stoichiometric replacement of the analyte anion. The analyte band that passes through the conductance cell is measured as a conductance change compared with the background conductance. The degree of the change is determined by dissociation of the eluent electrolyte and the analyte and by the limiting ionic equivalent conductances of the ions involved.

If the eluent electrolyte and the analyte are fully ionized, the conductance change is then proportional to the analyte anion concentration and to the difference in the limiting ionic equivalent conductances between the analyte anion and the mobile-phase electrolyte counteranion. The conductometric detection of analyte cations would be explained similarly, based on cation exchange [see Eq. (2)] in the column. If the eluent electrolyte and the analyte are completely ionized, the conductance would be proportional to the analyte cation concentration and to the limiting ionic equivalent conductance difference between the analyte cation and the eluent electrolyte counteraction. In both cases the conductance change for the chromatographic analyte peak can be positive or negative, depending on the limiting ionic equivalent conductance difference. Also, an extraneous or nonanalyte peak, which can be positive or negative, often appears in the chromatogram. It is generally called a system peak, and its location and appearance is dependent on the eluent conditions, as well as other factors [10].

To obtain reproducible and accurate conductance detection in ion-exchange separations at low-detection limits, the conductance change must be enhanced relative to the background conductance. The greater the enhancement, the better is the detection limit. This is illustrated in Figure 1. In Figure 1a a typical chromatogram for the separation of analyte anions on an

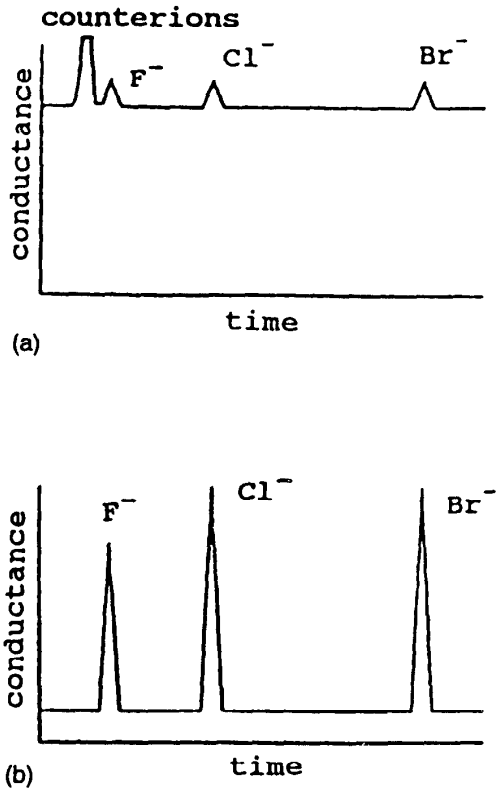


Figure 1 Enhanced analyte conductivity signal caused by suppression: (a) no suppression; (b) suppression.

anion exchanger is shown, using a highly conducting eluent and conductivity detection. Attempts to magnify the signal for the chromatographic peaks are handicapped by the large background conductance and the signal/noise ratio (S/N) effects. If the contribution of the background eluent electrolyte to conductance can be sharply reduced (see Fig. 1b), than the S/N for each analyte is sharply enhanced and detection limits are improved significantly. Clearly, one way to accomplish this is to use an eluent electrolyte that provides an eluent counterion that differs substantially in limiting ionic equivalent conductance compared with that from the analyte ions. Another way is to enhance the conductivity signal of the analyte ion postcolumn. It is strategies of this type that are emphasized within the main body of this chapter. Space does not allow a discussion of LC conductivity detection and the design of conductivity detectors, and these topics are reviewed in detail elsewhere [4,6–10,13,21]. Although conductivity detection probably accounts for well over 50% of the detection techniques used in IC, the more common LC detector strategies, including absorption, fluorescence, and electrochemistry, are also important to IC applications. This, and other LC detection instrumentation applicable to IC, is also reviewed in detail elsewhere [9,10,13,21; and see also Chaps. 3 and 15].

II. SUPPRESSED ION CHROMATOGRAPHY

A. Ion-Exchange Column Suppression

Conductivity detection is an attractive mode for detection in the separation of analyte ions on ion exchangers. However, eluting conditions in ion-exchange separations, as indicted by Eqs. (1) and (2) require that the eluent contains an appreciable concentration of an electrolyte for the elution. Thus, under these conditions, a small change in conductivity caused by the analyte ion must be determined on a highly conducting background when using conductivity as the detection mode. The approach taken by Small et al. [6] to solve this problem was to effectively minimize the background conductance by the eluent, but not the conductance of the analyte ions. Figure 2 illustrates the arrangement that was used to achieve these objectives. In this example of the instrumental setup, anions are separated by using an aqueous NaOH eluent. The first column in which the separation takes place, which is often called the separator column, is an anion-exchange column. The effluent from this column is passed directly into the second column, which is packed with a cation exchanger charged in the H^+ form. The second column is usually referred to as the suppressor column, and its role is to reduce the conductivity of the flowing stream caused by the eluent. Once this is accomplished, the flowing stream passes into the conductivity detector, and the conductance from each analyte anion is determined. The extent to which the conductivity of the eluent is reduced by the suppressor column depends on the type of electrolyte used in the mobile phase to bring about the separation of the analyte anions.

In Figure 2, a mixture of F^-, Cl^-, and Br^- is introduced into the separator column, which is packed with a strong base anion exchanger of modest anion-exchange capacity charged in the OH^- form. The NaOH eluent brings about the separation of the halides, and the elution order is consistent with the anion-exchange selectivities (see Table 1), or F^- is eluted first, followed by Cl^-, and then Br^-. Each analyte anion in the NaOH eluent passes through the suppressor column, which is packed with a strong acid cation exchanger with a high cation-exchange capacity charged in the H^+ form. The following cation exchange occurs in the suppressor column:

$$NaOH + ResSO_3^-H^+ \rightarrow HOH + ResSO_3^-Na^+ \quad (3a)$$

$$M^+X^- + ResSO_3^-H^- \rightarrow H^+X^- + ResSO_3^-M^+ \quad (3b)$$

where X^- is the halide ion and Res is the resin polymeric matrix of the cation exchanger.

All cations are converted to H^+. Thus, the eluent electrolyte or NaOH is converted to water, and each halide analyte anion emerges from the suppressor as the acid in a water

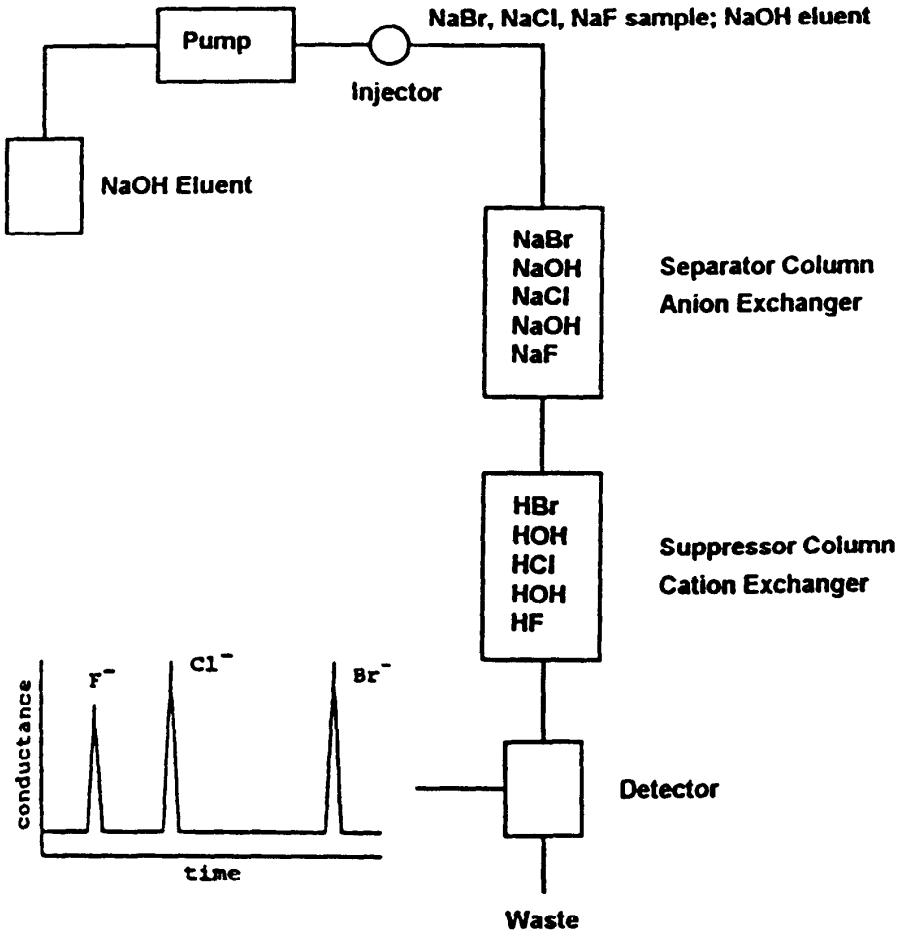


Figure 2 Ion chromatographic system for the separation of analyte anions on an anion exchanger using a cation-exchange column suppressor. (According to Ref. 6.)

background. Accordingly the conductivity from the NaOH eluent background is sharply reduced, and the conductivity from each analyte is significantly enhanced, because the ionic equivalent conductance of H^+ is exceptionally high. The net effect is a considerable improvement in the S/N and the detection limit.

If cations are to be separated, then the separator column in Figure 2 is a strong acid cation exchanger, with a low cation-exchange capacity, and the suppressor column is packed with a strong base anion exchanger, with a large anion-exchange capacity, and is charged in the OH^- form. Therefore, to separate cations (e.g., alkali metal ions), a dilute HNO_3 solution can be used as the eluent. The elution order of the cations would follow the cation-exchange selectivities (see Table 1) and would pass into the suppressor column in a HNO_3 eluent. As the eluent containing the separated cations flows through the suppressor, all the anions are converted to OH^- as shown in Eq. (4a) and (4b).

$$H^+NO_3^- + ResNR_3^+OH^- \rightarrow HOH + ResNR_3^+NO_3^- \quad (4a)$$

$$M^+NO_3^- + ResNR_3^+OH^- \rightarrow M^+OH^- + ResNR_3^+NO_3^- \quad (4b)$$

where Res is the polymeric matrix of the anion exchanger and M^+ is an alkali metal cation analyte.

The HNO_3 in the eluent is thus converted to water, and the analyte cation salts are converted to hydroxide salts. The conductivity of the eluent background is sharply reduced, whereas conductivity for the analyte cations, as the hydroxides, is enhanced because the

hydroxide ion has an exceptionally high ionic equivalent conductance. Consequently, the analyte cation conductance is determined by the detector on a background that is poorly conducting. Application of suppression in analyte cation separations has limitations because the cations being separated must form hydroxides that are soluble.

Eluents and eluent strength in suppression IC are not limited to strong bases for the separation of anions and strong acids for the separation of cations, nor for changes in their concentration in the mobile phase. For example, salts of weak acids can be used in eluents for the separation of anions, and suppression to enhance conductivity detection can still be obtained. Therefore, it is possible to use eluents with eluent strengths that vary widely from that provided by OH^-, the counteranion provided by a strong base eluent.

A $NaHCO_3$–Na_2CO_3 eluent is widely used in IC [6,10,13,22]. The HCO_3^- counteranion is a weak eluent counteranion similar to OH^-, whereas CO_3^{2-} is a much stronger eluent counteranion in terms of anion-exchange selectivity. Use of an $NaHCO_3$–Na_2CO_3 mixture has several advantages: The ratio can be changed by altering the pH, which provides a range of eluent strengths. A more basic pH increases the CO_3^{2-} concentration in the eluent, which increases its strength as an eluent; therefore, this kind of eluent can be used to separate anions that are more highly retained on an anion exchanger. A lower pH, which increases the HCO_3^- concentration in the eluent, yields a weaker eluent and would be used to elute more weakly retained anions. Second, the mixture is buffered; therefore, it is more resistant to sample matrix effects that may influence the mobile-phase pH. Because of these factors a HCO_3^-–CO_3^{2-} eluent is widely used for analyte anion separations.

Analyte anions are separated on an analytical anion-exchange column (see Fig. 2) according to the competition between the HCO_3^-–CO_3^{2-} and the analyte anions for the anion-exchange sites. As the separated analyte anions pass through the suppressor, the following exchange takes place:

$$Na^+HCO_3^- + ResSO_3^-H^+ \rightarrow H_2CO_3 + ResSO_3^-Na^+ \quad (5a)$$

$$2Na^+CO_3^{2-} + 2ResSO_3^-H^+ \rightarrow H_2CO_3 + 2(ResSO_3^-Na^+) \quad (5b)$$

$$Na^+X^- + ResSO_3^-H^+ \rightarrow H^+X^- + ResSO_3^-Na^+ \quad (5c)$$

where Res is the anion-exchange matrix, and the HCO_3^-, CO_3^{2-}, and halide analyte anions X^-, are used as the Na^+ salts.

Conductivity of the analytes is enhanced because the analytes are converted to acids, as before, but here, suppression of the conductance by the $NaHCO_3^-$–Na_2CO_3 eluent occurs because the poorly dissociating weak acid H_2CO_3 is formed. When different salts of weak acids are used in the eluent, the degree of suppression or reduction of background conductance is, therefore, influenced by the dissociation (K_a) of the weak acid formed which, in turn, influences detection limit. The greater the dissociation of the weak acid, the greater will be the concentration of H^+ in the suppressed environment. Because H^+ has an exceptionally high, limiting ionic equivalent conductance; the background conductance is less suppressed; therefore, the detection limit will be less favorable.

The ion-exchange column suppression strategy described in the foregoing, and illustrated in Figure 2, was an especially valuable contribution to inorganic anion analysis, and this strategy rapidly became the method of choice for these problems in the late 1970s. Few other methods were available that allowed a rapid and sensitive determination of inorganic anions in complex mixtures. Although cation separations by suppressed IC were equally rapid and sensitive, particularly for alkali metal and alkaline earth cations, other sensitive methods, such as atomic absorption and emission, were available and were often preferred for cation analysis.

Suppressed IC as described by Small et al. [6] has several limitations. The lifetime of the suppressor column is limited by the exchange capacity for the suppressor ion-exchange column and depends on the eluent electrolyte concentration. Periodically, the suppressor column must be removed from the chromatographic system to be regenerated, which prevents continuous operation of the system. Second, the ion-exchange suppression column contributes a signifi-

cant dead volume because of its size; therefore, increased band dispersion and broadening occur which, in turn, affect the detection limit. Earlier-designed ion-exchange column suppressors contributed up to 1500 μL in dead volume. Initially, this was not a serious problem because of the lack of highly efficient ion-exchange analytical columns and the limitations in conductivity detector designs. As column technology and conductivity detector design was improved, this level of dead volume became excessive, and it seriously handicapped the ability to obtain better detection limits. Third, weak acid analyte anions eluted from the analytical column may undergo retention as undissociated weak acids on the strong acid ion-exchanger–suppressor column by ion-exclusion effects. The extent of this effect is influenced by the degree of exhaustion of the suppressor column; therefore, the reproducibility of elution time for a weak acid analyte anion will be affected. Nevertheless, suppressed IC was recognized as a powerful analytical separation and detection strategy that was applicable to a broad range of analytical problems, and many other workers initiated studies to improve various aspects of the technique.

From an applied perspective, modern suppressed IC employs anion or cation micromembrane suppressors, or the more recently developed anion or cation self-regenerating suppressor. (These are discussed in the following sections.) However, the ion-exchanger–type suppression concept has been recently reintroduced commercially [23]. It is designed specifically for the detection of anions and employs a strong-type cation exchanger in the suppressor. Continuous operation for suppressed IC is achieved by using two cation-exchange columns as replaceable cartridges in the setup (see Fig. 2) and a switching valve to shift from one to the other when the exchange capacity of the first is exhausted. The design also permits both cartridges to be in equilibrium with the mobile phase, which simplifies the cartridge switch to maintain continuous operation and to replace the spent cartridge with a new one. Furthermore, the see-through cartridges, which have low dead volume, contain an inert dye that undergoes an easily seen color change, signifying that the exchanger is exhausted. A typical chromatogram illustrating the separation and the quality of the suppression of a mixture of inorganic anions—using an HCO_3^-–CO_3^{2-} eluent—is shown in Figure 3. It is suggested [23] that chromatographic efficiency and peak area reproducibility for the separation of the common inorganic anions is comparable with that obtained by a micromembrane suppressor.

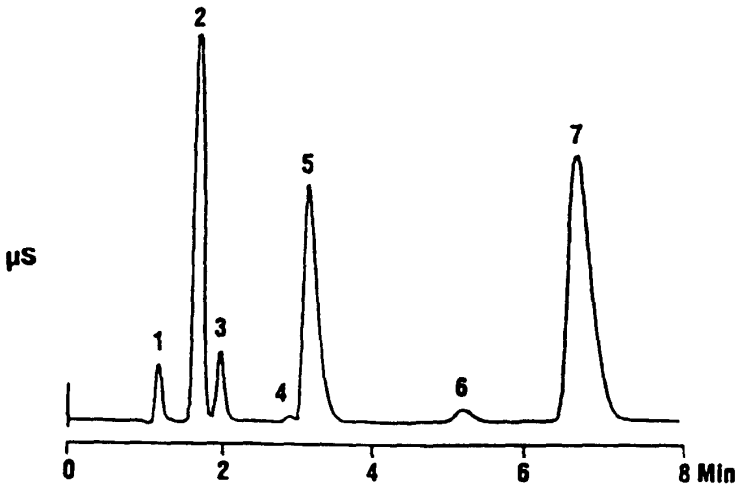


Figure 3 Separation of inorganic analyte anions in a water matrix with suppression by a cation-exchange column and conductivity detection according to US EPA method 300.0. Analytes: (1) F^- (2 ppm); (2) Cl^- (20 ppm); (3) NO_2^- (2 ppm); (4) Br^- (2 ppm); (5) NO_3^- (10 ppm); (6) PO_4^{3-} (2 ppm); (7) SO_4^{2-} (60 ppm). Eluent: 1.7 mM $NaHCO_3$/1.8 mM Na_2CO_3 at 2.0 mL mm^{-1}. Column: Dionex AS4A. (From Ref. 23.)

The chromatography, suppression, detection, and sensitivity with a modern ion-exchange column suppression system are improved over that obtained by earlier versions of the ion-exchanger column suppression system. The revised column suppression system accounts for some of this improvement; but also contributing is the current availability of improved ion exchangers specifically designed for analytical IC and for use in a suppressor column. The ion-exchange column type of suppression should still be considered a practical and viable signal-enhancement strategy in analytical IC.

B. Hollow-Fiber Membrane Suppressor

Ion-exchange suppression columns are used less often today and have mostly been replaced by advances in suppression technology. The goals in the development of newer suppression techniques were still essentially those of Small et al. [6]. That is, the conductance contribution of the mobile phase eluent electrolyte was to be minimized, while the conductance by the analyte was to be maximized. Additional goals for the newer developed suppressors were to allow continuous operation of the chromatographic apparatus and to ensure that dead volume in the suppression system was as low as possible.

The first major improvement in suppressor technology was the development of the first membrane-based suppressor device, or the hollow-fiber membrane-type suppressor, in 1981 [24,25]. This device replaces the ion-exchange column suppressor between the column and the conductivity detector (see Fig. 2) and consists of a long, hollow fiber(s), made of a semipermeable ion-exchange material, that the column effluent passes through. The hollow fibers in the suppressor unit (Fig. 4) contain ion-exchange sites on the interior wall that would be in contact with the separator column effluent on the interior side. The regenerate is passed over the exterior wall of the fiber in direction opposite that of the eluent flow. Thus, if anions are being separated, the ionogenic sites within the hollow fiber are $SO_3^-H^+$ groups, and cations in the flowing eluent stream are converted to H^+ whereas the analytes are converted to the corresponding acids, as in Eqs. (3a) and (3b). Suppression is continuous because the regenerate solution, for example, a H_2SO_4 solution, replaces the cations with H^+. For a cation hollow-fiber suppressor, the inner fiber ionogenic groups are cation groups, the regenerate is a strong base solution, and anions in the eluent stream are converted to OH^-, according to Eq. (4a) and (4b). In both cases, the analyte ions are excluded from passing through the fiber walls because of Donnan equilibrium.

The hollow fiber suppressor offered two major advantages over the ion-exchange column suppressor. First, the hollow-fiber suppressor could be used continuously because regeneration was no longer necessary. Consequently, the suppressor was more compatible with automation.

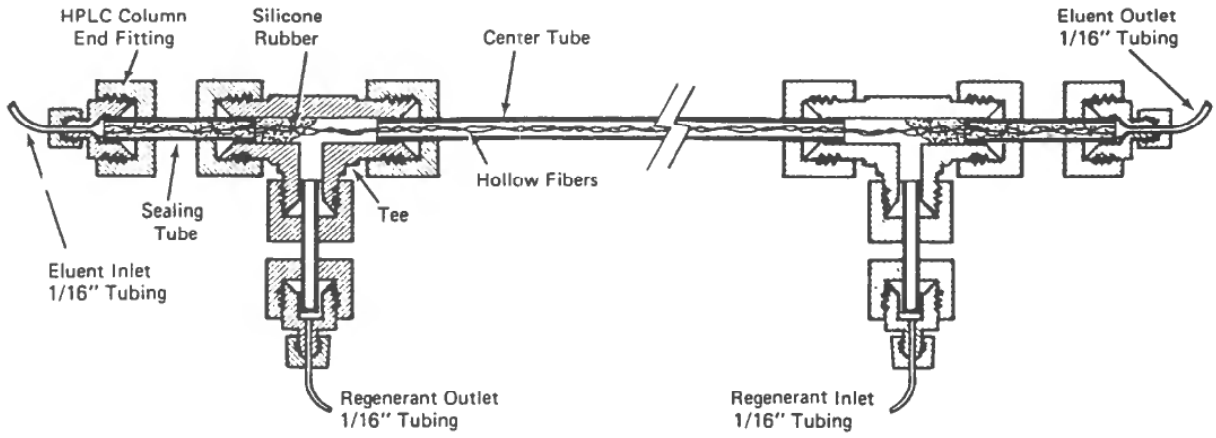


Figure 4 A diagram of the first reported hollow-fiber suppressor. (From Ref. 24.)

Second, the hollow-fiber suppressor had considerably less dead volume, compared with the ion-exchange column suppressor; thus, it was more compatible with the improved analytical ion-exchange columns that had been developed through advances in ion-exchange technology. This resulted in a significant improvement in detection limit.

To keep band-broadening effects of the suppressor as small as possible, the inner diameter of the hollow fiber also must be comparatively small. Although initial designs were based on truly hollow fibers, subsequent studies demonstrated that a packed hollow fiber provided less band dispersion and broadening, higher eluent flow rates could be suppressed, and higher eluent concentrations could be suppressed. However, the suppressor was still limited to suppressing a maximum eluent flow rate of about 2 mL min^{-1} and an eluent concentration of less than 5 mM. Either a filament or beads to fill the fiber was successfully employed. Other designs to improve efficiency of the regeneration, provide physical strength, alter the flow pattern through the fiber to ensure better suppression, and a discussion of transport at the membrane are described and reviewed in detail elsewhere [25].

The hollow-fiber membrane suppressor was effective in IC separations to enhance conductivity detection. However, it still did not allow achievement of the full potential of enhanced conductivity detection with the advanced analytical ion-exchange columns that were being developed. Furthermore, neither the ion-exchange column nor the hollow-fiber suppressors worked well with gradient elution. Workers in the field quickly recognized these limitations, but also recognized the advantages of membrane suppression, and attention was directed to the development of a membrane sandwich-type suppressor device, which is discussed in the following section.

C. Micromembrane Suppressor

In 1985 the micromembrane suppressor (MMS) was introduced [26]; it was immediately recognized as being superior to the hollow-fiber membrane suppressor and overcame the limitations of the ion-exchange column suppressor. Consequently, the commercially available micromembrane suppressor quickly replaced both the ion-exchange column suppressor and the hollow-fiber–type suppressor in most suppressor type applications [10,13]. A diagram for a MMS for suppression and conductivity detection enhancement for analyte ion separations is shown in Figure 5.

In Figure 5 two semipermeable ion-exchange membranes are sandwiched between two ion-exchange screens. A third ion-exchange eluent screen separates the two membranes, and this region between the membranes constitutes the internal volume. The eluent ion-exchange screen reduces internal volume, provides additional ion-exchange capacity, and creates a tortuous flow path for the eluent stream, to enhance mass transfer. Regenerate solution flows on the exterior sides of the membranes across and through the ion-exchange screens in a flow direction opposite that of the column effluent flow, which is on the interior side or between the two ion-exchange membranes. The regenerate ion-exchange screens serve two key purposes. First, the screens provide a tortuous path for regenerate flow, which aids the mass transfer of the regeneration process. And second, they are functionalized and, therefore, act as reservoirs for the ions involved in the suppression process. For an anion MMS, the ionogenic groups within the suppressor are $-SO_3^-H^+$ groups, and the regenerate is a strong acid, such as H_2SO_4; for the cation MMS the groups are the strong base $R_4N^+OH^-$ groups and the regenerate is a $R_4N^+OH^-$ solution, typically tetrabutylammonium hydroxide solution. The internal volume of the commercially available MMS [26] is compatible with typical 4-mm–id analytical ion-exchange columns used in IC and often is not the limiting device in determining the peak efficiency or detection limit for the instrumentation and columns typically used in IC applications.

Consider the IC chromatographic system shown in Figure 2 that is now modified so that the ion-exchange suppressor column between the analytical column and the conductivity de-

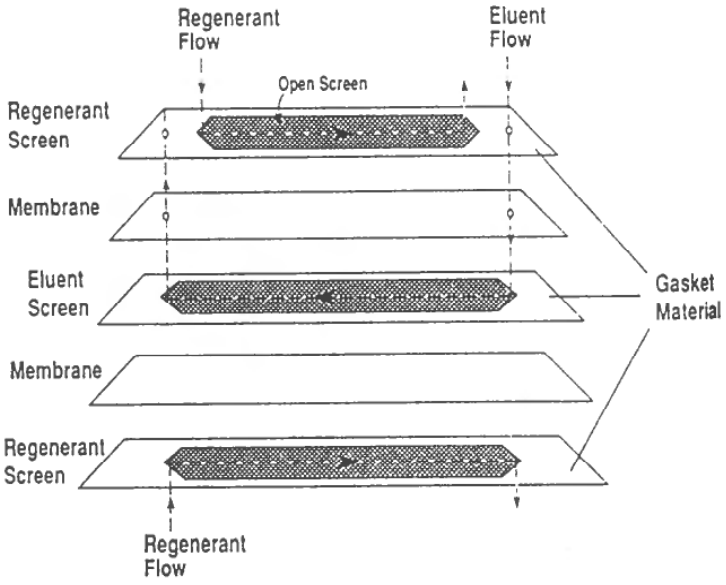


Figure 5 A diagram showing the internal components of a micromembrane suppressor. (From Ref. 27.)

tector is replaced with the anion MMS. The halide anions, which are separated in the analytical column by the NaOH eluent, individually pass through the anion MMS in the NaOH solution. In the suppressor the eluent flows through a small narrow internal volume of about 50 μL, which is about 15% of the internal volume provided by the commercially available hollow-fiber membrane suppressor, sandwiched between two semipermeable cation-exchange type membranes (see Fig. 5). All cations in the mobile phase on the interior side of the membrane are removed by the membrane and replaced by H^+ as in Eqs. (3a) and (3b). Simultaneously, these cations are replaced on the membrane by H^+ stoichiometrically because on the exterior side of the membrane H_2SO_4 solution flows along the membrane in a direction opposite that of the eluent flow and serves as the regenerate for the cation exchange membrane. Again, Donnan equilibrium prevents the analyte anions from passing from the interior side of the membrane to the exterior side. Thus, the conductivity detector, which is placed following the anion MMS, responds to H^+Cl^-, H^+Br^-, and H^+I^- in water, just as in the ion-exchange column suppression system described by Small et al. [6].

As long as the H_2SO_4 regenerate solution is passed over the membrane, usually at a rate of three to ten times the eluent flow rate, suppression occurs. Thus, (1) the suppression capacity is approximately 25 times that obtained by a hollow-fiber membrane suppressor and corresponds to about 250 μEq min^{-1}. (2) The functionalized screens contribute to this increased capacity as fixed sites, reduce leakage, and create a more tortuous flow path, which aids mass transfer. (3) The suppression is continuous from sample to sample and, only occasionally, is cleaning of the membrane required. (4) Band dispersion and broadening effects are very small because of low dead volume and improved mass transfer in the MMS. With efficient analytical columns and appropriate instrumentation, the MMS is capable of providing more than 8000 plates per column. (5) The MMS is compatible with a wide range of isocratic and gradient eluents, including those that contain modest amounts of organic solvents. (6) IC detection limits obtained with the MMS are excellent. For example, for many analyte anions, detection limits often approach 10 ppb, depending on the sample matrix.

An MMS suitable for suppression with microbore IC columns (2-mm and smaller id) is commercially available. Its design [27] is similar to the MMS device shown in Figure 5, except the key internal dimensions, which determine the internal volume, are almost halved

in size. This results in an internal volume of about three to four times less than the internal volume of the regular MMS device. Furthermore, suppression capacity is not sacrificed, even though the microbore MMS device is smaller.

When salts of weak acids are used in the eluent, the corresponding weak acid is produced in the anion MMS step, and its contribution to background conductance will depend on its degree of dissociation, as discussed previously. Figure 6 illustrates a typical separation of inorganic anions on an anion exchanger using an anion MMS, conductivity detection, and a HCO_3^-–CO_3^{2-} eluent [28]. The effect of an eluent pH change depends on the degree of change. For a small pH change only phosphate ion retention time is affected, because of its K_a values. Retention times for the other analyte anions are not affected unless there is an appreciable change in the CO_3^{2-} concentration because the CO_3^{2-} is a strong eluent counteranion.

The same principle is applied to the cation MMS. Here, the two semipermeable membranes around the eluent screen contain strong base ionogenic groups and are sandwiched between two similar cation-exchange regenerate screens (see Fig. 5). Cations in the column effluent as it passes through the suppressor are excluded, and anions freely move from the flowing eluent stream containing the separated cation analytes into the regenerate. Simultaneously, a stoichiometric amount of OH^- moves from the regenerate through the membrane-exchange sites into the flowing stream. Cation analytes are converted by the cation MMS to hydroxides, and the eluent electrolyte, for example HCl, is converted to water [see Eqs. (4a) and (4b)]. Thus, the conductivity detection of the analyte cations is enhanced and regeneration of the suppressor is completed by a quaternary ammonium hydroxide solution.

The MMS is not without limits in terms of eluent electrolyte that can be suppressed, but far surpassed the capabilities of previously designed suppressors. Although the flow pattern within the suppressor is manipulated into a flow that promotes mass transfer across its

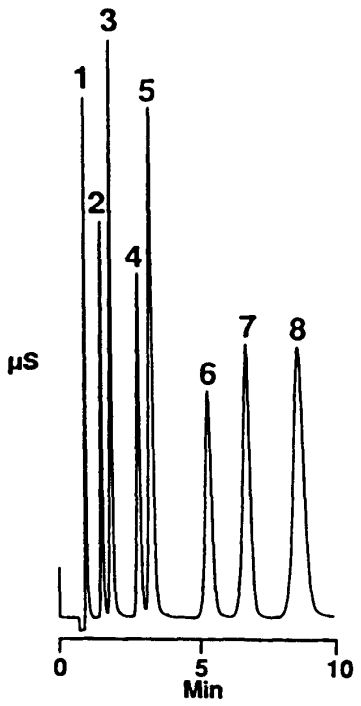


Figure 6 Separation of inorganic analyte anions on an anion exchanger using an anion micromembrane suppressor and conductivity detection. Analyte: (1) F^- (1.5 ppm); (2) Cl^- (2.8 ppm); (3) No_2^- (7.5 ppm); (4) Br^- (7.5 ppm); (5) No_3^- (10 ppm); (6) HPO_4^{2-} (15 ppm), (7) SO_4^{2-} (10 ppm), (8) $C_2O_4^{2-}$ (15 ppm). Eluent: 1.8 mM Na_2CO_3/1.7 mM $NaHCO_3$ at 2.0 mL min^{-1}. Column: Dionex AS4A. (From Ref. 28.)

membrane surface, the ion-exchange capacity of the membrane–screen system within the suppressor and the concentration and flow rate of the regenerate are key parameters that need to be controlled when using the MMS. With commercially available MMS, the range of useful regenerate conditions are established and provided by the manufacture. In general, eluents up to the lower 100-mM range at 1 mL min^{-1} can be readily suppressed.

The most serious problems encountered when using the anion MMS are penetration of the anion MMS membrane by the acid regenerate and the effects of dissolved CO_2 in non-HCO_3^-–H_2CO_3 eluents. Penetration of the acid regenerate, although small owing to Donnan equilibrium, can be further reduced by using a regenerate solution of a strong organic acid, such as polystyrene sulfonic, *p*-toluenesulfonic, naphthalenetrisulfonic, or dodecylbenzenesulfonic acids [29–32]. The mass or the multiple charge of these acids provide a lower diffusion and a better electrostatic exclusion. The interference of dissolved CO_2 in anionic suppression IC, particularly when using a strong base eluent, is due to the formation of trace levels of H_2CO_3 in the suppression step [see Eqs. (5a) and (5b)]. The partial ionization of H_2CO_3 contributes to a conductive background even though the strong base eluent is converted to water [see Eqs. (3a) and (3b)]. Two techniques that have been successfully used to minimize the effects of the CO_2 and, consequently, improve detection limits in anion separations are (1) to remove the CO_2 postcolumn before the suppression step and (2) to electrolytically generate a CO_2-free strong base eluent. Both of these strategies are described in Section II.G of this chapter.

The amount of regenerate solution required for the MMS, although relatively inexpensive, can be significant over time and replenishing the supply can be inconvenient in automated and on-line IC applications. To deal with this problem, Dionex (since 1987) has made available a unit that continuously regenerates the exhausted regenerate solution. Thus, large, stored volumes of the regenerate solution are not required because recycle, on-line, and automated IC applications require less operator time. The recycle device takes advantage of ion-exchange principles. For example, with the anion MMS the H_2SO_4 regenerate is converted to $NaHSO_4$ in the regeneration step. In the recycle this is converted back to H_2SO_4 by passing the exhausted regenerate through a large-volume, high-exchange capacity, strong acid cation exchanger charged in the H^+ form, which is then pumped back as fresh regenerate through the MMS. Typically, the recycle cation-exchange column will last about 2 weeks under normal use before it needs to be regenerated.

The MMS offers many advantages over the ion-exchange column suppressor, hollow-fiber membrane suppressor, and other chemical-type suppression techniques and is widely used in a broad range of applications. The more important advantages are outlined in the following:

1. Continuous operation of the IC instrumentation with automation is possible, including on-line analysis, because regeneration is continuous.
2. Internal volume of the MMS is small and its contribution to band-broadening is usually not the limiting factor.
3. Suppression is efficient, rapid, and reproducible.
4. The upper limit of eluent electrolyte concentration is high, provided regenerate conditions are maintained within MMS limits.
5. The MMS is compatible with gradient elution.
6. The MMS is resistant to organic solvents and most common mobile-phase additives.
7. The MMS is physically strong and requires only a periodic cleaning, depending on the kinds of samples and sample matrices that are analyzed, to maintain good performance.
8. The MMS can be used to reduce electrolyte background, if required, in other types of LC separations.

D. Self-Regenerating Suppressor

The need for a separate and continuous supply of regenerate as required by the anion and cation hollow-fiber and MMS suppressers, can be eliminated [27,33–39]. This can be accom-

plished by producing the regenerate ions in situ through the electrolysis of water at electrodes conveniently placed on the exterior side of ion-exchange membranes that separate the eluent stream from the regeneration side. Thus, a pumping system, flow control, and other supporting instrumentation for the regenerate can be eliminated. This device, which is also commercially available as a "self-regenerating suppressor" (SRS), provides a continuous supply of regenerate [38,39]. A diagram illustrating the internal structure of the SRS, which is similar to the MMS except for placement of the electrodes, is shown in Figure 7.

Figure 8 illustrates the suppression that takes place within the SRS. Column effluent containing the separated anions (or cations) passes within the interior side of the ion-exchange membranes. For anion analyte separations the membrane is a strong acid cation exchanger (see Fig. 8a), and for analyte cation separations, the membrane is a strong base anion exchanger (see Fig. 8b).

First consider the anion SRS. Water on the exterior side of the membranes or the regenerate sides is electrolyzed at the electrodes to produce H^+ at the anode and OH^- at the cathode, according to Eq. (6a) and (6b):

$$\text{Anode:} \quad 3H_2O \rightarrow 2H_3O^+ + \tfrac{1}{2}O_2 + 2e^- \tag{6a}$$

$$\text{Cathode:} \quad 2H_2O + 2e^- \rightarrow 2OH^- + H_2 \tag{6b}$$

The H^+ of the regenerate and the Na^+ and other cations in the eluent side pass through the membrane at the anode side and cathode side, respectively, through the exchange sites simultaneously and stoichiometrically as described by Eqs. (3a) and (3b), thus enhancing the conductance signal for the analyte anions. Donnan equilibrium prevents coanions from passing through the membrane. The cations that pass into the cathode regenerate side are swept away as the hydroxides, thereby maintaining stoichiometry and electroneutrality. The SRS is directional because of the electrolysis reactions at the anode and cathode; that is, H^+ is made available at only the anode membrane, whereas Na^+ and other eluent cations pass through the cathode membrane. This is unlike the MMS, for which the suppression reaction in the MMS is uniform throughout the two membrane surfaces that constitute the suppression chamber.

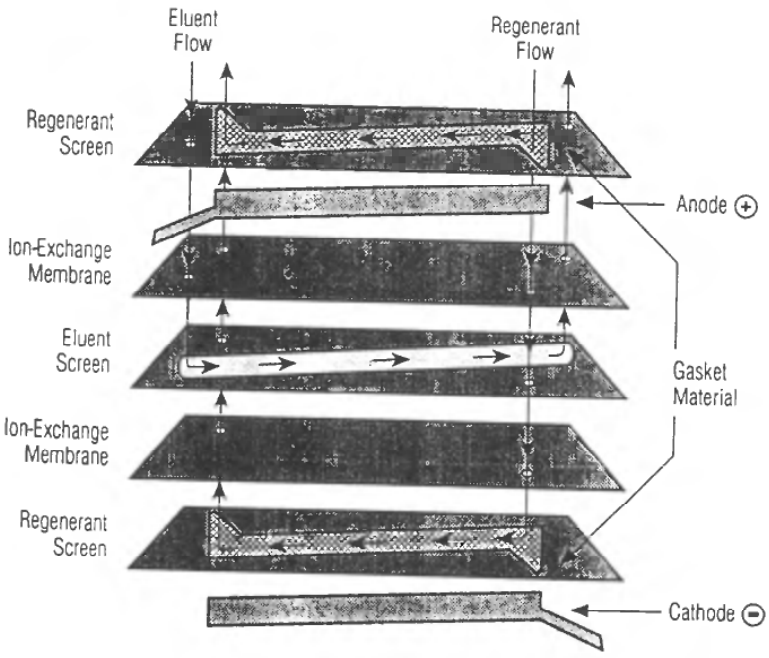
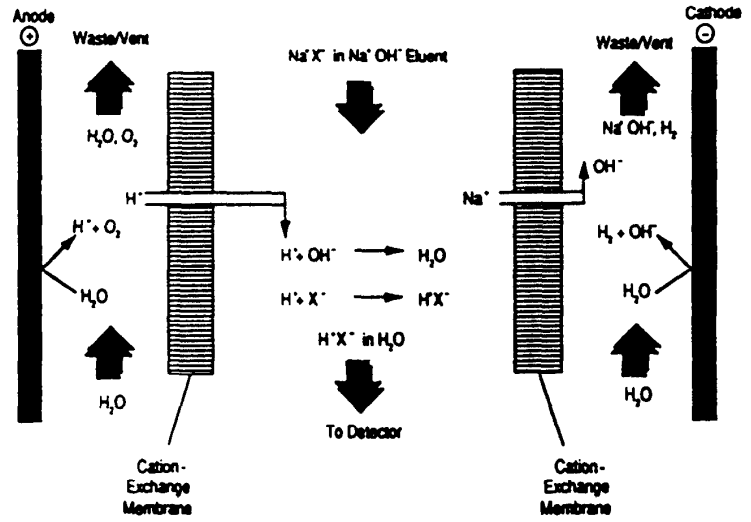
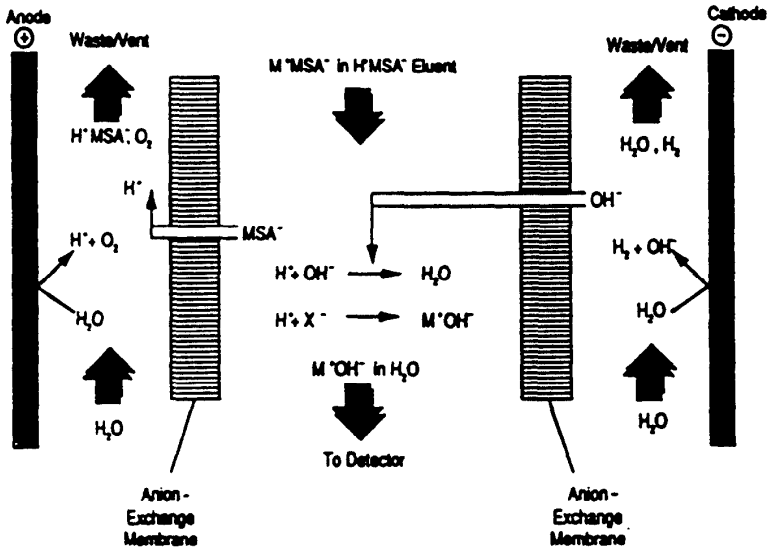


Figure 7 A diagram showing the internal components of a self-regenerating suppressor. (From Ref. 27.)



(a) **Anion SRS**



(b) **Cation SRS**

Figure 8 (a) Suppression within the anion self-regenerating suppressor and (b) within the cation self-regenerating suppressor. (From Ref. 27.)

The water that is required to maintain the electrolysis can be replenished by diverting the eluent stream from the conductivity detector from waste into the regenerant chamber [27,38,39]. When operated in this manner, no external solutions are needed for the SRS regeneration.

The cation SRS (see Fig. 8b) operates essentially the same way, producing an enhanced conductance signal for the analyte cations, except that the OH^- developed in the cathode chamber passes into the flow stream through an anion-exchange membrane, whereas anions in the eluent pass into the anode chamber through an anion-exchange membrane, with the exclusion of the cocations. As with the anion SRS, the cation SRS is also directional. Both

the anion and cation SRS require mild electrolytic conditions of only a few volts and milliamperes of current for their operation, and they are capable of handling eluents up to about 50 mM at 1 mL min^{-1} [38,39], similar to the anion and cation MMS.

In addition to simplifying the regeneration step, the SRS offers other advantages. The SRS dead volume is even smaller than that of the MMS, and the SRS is more readily adaptable to small-bore–type analytical separation columns. As with the MMS, suppression by the SRS is rapid, efficient, reproducible, and applicable to a wide range of eluents typically used in IC at isocratic and gradient conditions. Figure 9 illustrates the on-line separation of inorganic and organic anions in a powerplant cooling-water sample on a anion exchanger using a strong base eluent, conductivity detection, and a SRS. The original sample contained 1.2% boric acid, and the trace analytes were concentrated by a precolumn before the separation.

E. Eluents in Suppression Ion Chromatography

Eluent strength can be varied by using different salts of weak acids as the eluent electrolyte and source for the eluent counterion. Often, the experimentally obtained detection limit may vary according to the dissociation of the weak acid. Several different salts of weak acids can be used in the eluent for suppressed IC, and a summary of the more widely used eluents are listed in Table 2. Eluent strength, in general, increases from top to bottom, although differences can be small, depending on concentration.

The eluent counteranions in Table 2, which provide a wide range of eluent strength because of their own anion-exchange selectivities and are converted to water or poorly dissociated weak acids in the suppression step, are applicable to the elution of weak to strongly retained anions. In addition, eluent strength can be increased by modestly increasing eluent counteranion concentration, providing suppression capacity is not exceeded. Selecting the counteranion and its concentration are key factors in optimizing IC separations with conductivity detection. Choosing the optimum anion exchanger for the application is also important. A description of available anion exchangers for IC is provided in the previous chapter and

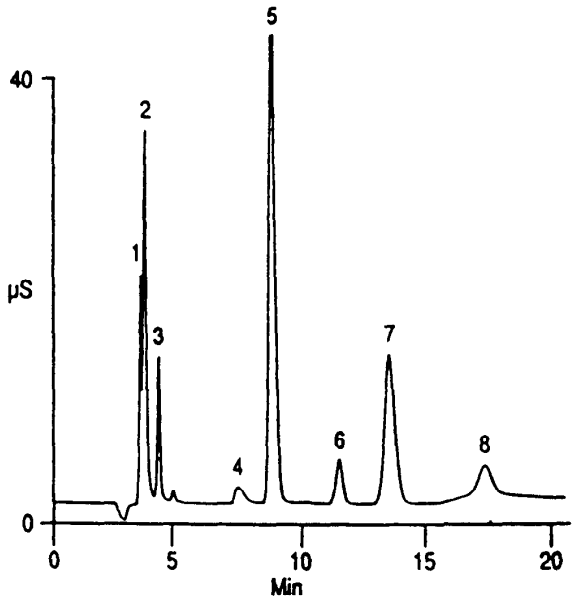


Figure 9 On-line separation of analyte anions in a 1.2% boric acid powerplant cooling-water solution with SRS conductivity detection. Analytes: 8 ppb except where noted; (1) F^- (4 ppb); (2) $C_2H_3O_2^-$; (3) HCO_2^-; (4) BO_3^{3-}/CO_3^{2-}; (5) Cl^-; (6) NO_2^-, (7) SO_4^{2-}; (8) $C_2O_4^{2-}$. Eluent: 85 mM NaOH at 0.25 mL min^{-1}. Column: Dionex Ion Pac AS-10. (From Ref. 38.)

Table 2 Eluents Used in Suppressed Ion Chromatography

Eluent	Ref.
$Na_2B_4O_7$	36,38
NaOH	6,24,36,41,42
$NaHCO_3$	36,41,43,44
Na_2CO_3	36,38,41,43,44
$NaHCO_3$–Na_2CO_3	20,24,36,41,45–47
Sodium phenolate	6
Sodium *p*-cyanophenolate	42
Disodium adipate	48
Disodium succinate	48
Tyrosine	24

elsewhere [4–13]. Examples of the separation of inorganic anions on an anion exchanger with suppression to enhance conductivity detection are illustrated in Figures 6 and 9. Figure 10 demonstrates the separation of weakly retained monoprotic organic acids on an anion-exchange column using a $Na_2B_4O_7$ eluent and suppression.

For cation exchange and suppression, the number of eluent counteractions that are also suppressor-compatible is small for several reasons. First, if the suppressor is used in the OH^- form, as shown in Eqs. (4a) and (4b), many metal cations that can be separated on action exchangers will form hydroxide precipitates that can interfere with operation of the suppressor or with the response or operation of the conductivity detector. Second, many analyte cations,

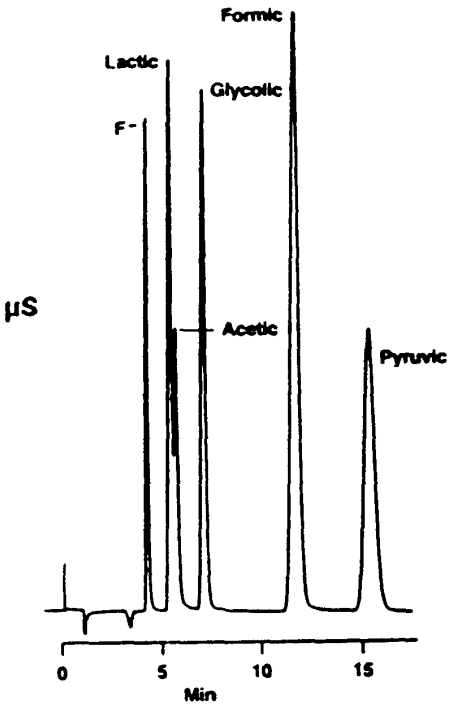


Figure 10 On-line separation of monoprotic acids on an anion exchanger. Analyte: 1 μg of each acid. Eluent: 20 mM $Na_2B_4O_7$ at 1.5 mL/min^{-1}. Column: Dionex AS6. (From Ref. 42.)

particularly multivalent cations, have high cation-exchange selectivities; therefore, elution of these cation analytes requires a strong eluting condition of either a high eluent electrolyte concentration or an eluent countercation of high cation-exchange selectivity. To overcome this elution problem, eluents for multivalent cations generally include complexing agents in the mobile phase, and formation constants for the metal ion-complexing agent complex(es) also become a key factor in the cation elution behavior as well as in the suppression.

For the separation of alkali metal cations, other univalent cations, and alkaline earth cations, strong mineral acid eluents [6,49–51], or methanesulfonic acid [52], and eluents containing protonated forms of organic bases, such as anilinium salts [6], ethylenediammonium salts [53,54], phenylenediammonium salts [20,49], and salts of 2,3-diaminopropionic acid (DAP) [52,55], are used most often. A stronger-eluting condition suitable for the separation of alkaline earth and other multivalent cations is obtained with the last three eluents. Retention of these analyte cations can also be reduced by using a carboxylic acid-type cation exchanger [52,54,56], which has lower cation-exchange selectivities compared with a strong acid-type cation exchanger, or by including a complexing agent, such as citrate, tartrate, EDTA, 2-hydroxybutyrate, or pyridine-2,6-dicarboxylate [49,57–63], in the eluent.

Figure 11 compares the eluent strength for several strong acid, Pb^{2+} and Ba^{2+} [64,65], and amine salt eluents in the absence of chelating agents. For the Pb^{2+} and Ba^{2+} eluents, precipitation suppression, which is discussed in the next section, was used, rather than column or membrane suppression. If a chelating agent is included, eluent strength can be altered, and the analyte cation elution order is dependent on the formation constants for the complexes that are formed.

An example of a cation separation using membrane suppression to enhance conductivity detection is illustrated in Figure 12. In this example, trace cations at the parts per billion level in ultrapure water are separated and determined using an aqueous 13.5 mM HCl–0.23 mM

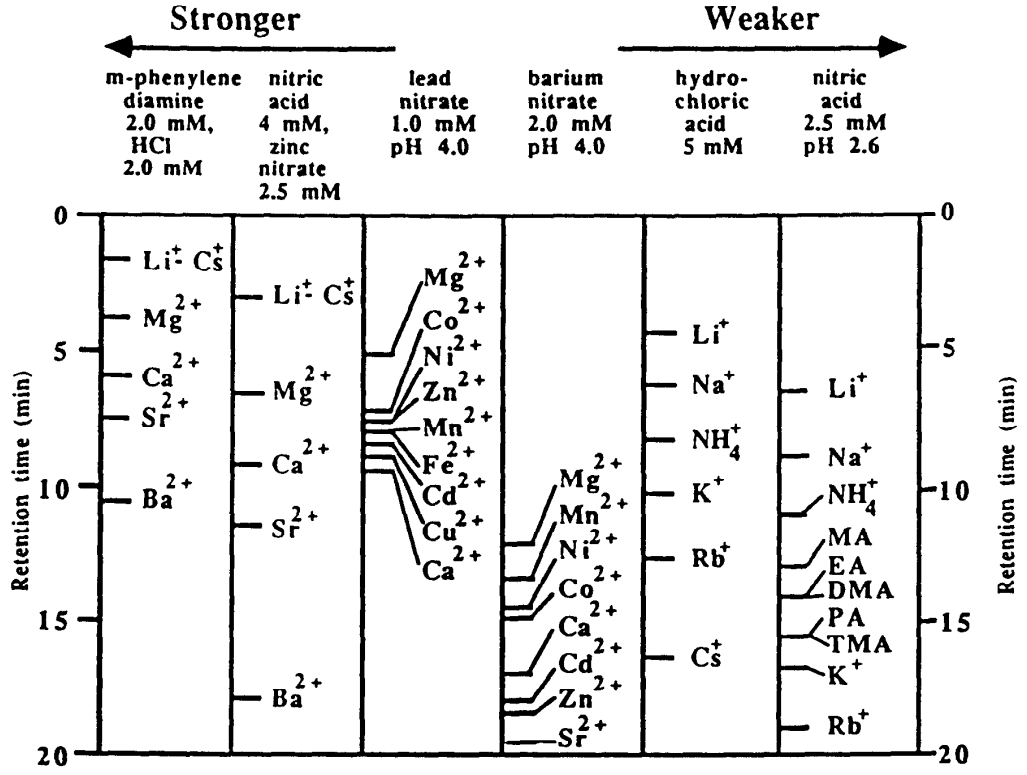


Figure 11 Comparison of analyte cation retention for a series of eluents used in suppressed ion chromatography. (From Ref. 10.)

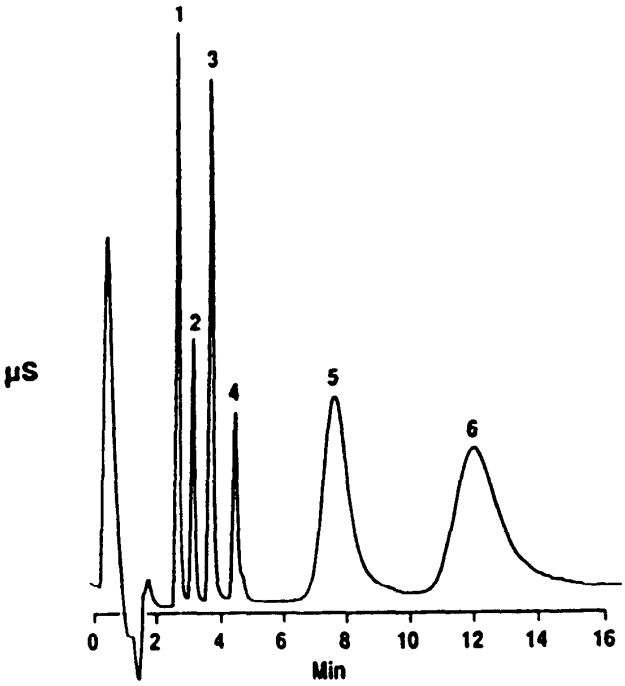


Figure 12 Separation of trace cations in ultrapure water using precolumn concentration and column switching. Analytes: a 10-mL sample that is concentrated; (1) Li^+ (1 ppb); (2) Na^+ (1 ppb); (3) NH_4^+ (3 ppb); (4) K^+ (3 ppb); (5) Mg^{2+} (5 ppb); (6) Ca^{2+} (10 ppb). Eluent: 13.5 mM HCl/0.23 mM DAP at 2.0 mL/min^{-1}. Column: Dionex Fast Cation I/CG3 and Fast Cation II. (From Ref. 51.)

DAP eluent, a small preconcentrating column, and analytical column switching [52]. The column switching allows both the less-retained alkali metal cations and the more highly retained alkaline earth cations to be conveniently separated on cation-exchange columns designed for these separations. Column switching has also been used to eliminate interferences [66,67] and to determine Cr^{6+} and other common anions in a single run [68].

A typical gradient elution in ion-exchange separations would involve an increase in the eluent counterion concentration with time. A similar-type gradient would be employed in IC when analyte ions that differ widely in retention are being separated. If conductivity detection is used, the background conductance in the IC separation would change accordingly, detection of the analyte would become difficult, and the detection limit would suffer. Suppression will overcome this problem; thus, conductivity is a viable and sensitive detector for gradient separations when the MMS or SRS is used for suppression [27,55,69–71]. This is particularly true for strong base gradient elution in analyte anion separations [27,69–71] or strong acid gradient elution in analyte cation separations [55]. For both of these cases, suppression converts the acid or base to water or a low-conducting background, depending on the efficiency of the suppression and the capacity of the suppression device. As the eluent acid or base concentration increases, which is necessary to increase eluting power, these two properties become more critical.

Salts of weak acids or bases can also be used in gradient elution of analyte anions and cations, respectively. Weak acids or weak bases are formed in the suppression step, respectively. Because these are partially dissociated, a conductance change in the background will occur as the gradient takes place, for weak acid or base concentration formed in the suppressor will increase during the gradient run. The weaker the acid or base formed in the suppressor, the smaller the change will be in the conductivity background. For analyte anion separations

salts of weak acids, such as *p*-cyanophenolate and borate salts, are used successfully in gradient elution with suppression, with only minor effects from background conductivity change [70].

Figure 13 illustrates a gradient elution separation of 36 anions on an anion-exchanger using a NaOH gradient, for which the NaOH changes from 0.75 to about 85 mM in 30 min, with a MMS and conductivity detection. By initially running the 0.75 mM NaOH isocratically, the weakly retained anions are eluted and resolved. As the NaOH concentration is increased rapidly, the highly retained anions are eluted and resolved. Only a small change in conductance background occurs as the NaOH is increased, even though the change in NaOH concentration in the gradient is over 100-fold in about 25 min. Furthermore, detection limits are not sacrificed. Without the gradient three separate runs at three different isocratic elution conditions would be required for a satisfactory separation [70].

F. Other Suppression Techniques

Other postcolumn suppression strategies have been proposed. The objectives remain essentially the same as with the suppression techniques already discussed. That is, the electrolyte properties in the eluent are altered following the separation so that the electrolyte's influence on detection is minimized. Therefore, the analyte ion detection signal can be obtained with greater ease and with better sensitivity and accuracy.

The ion exchanger suppressor column can bring about suppression through a precipitation reaction that takes place within the suppressor column [6]. This approach is generally most useful in special types of applications or when stronger-type eluents are required for the separation. It has been applied in both analyte anion and cation separations to enhance con-

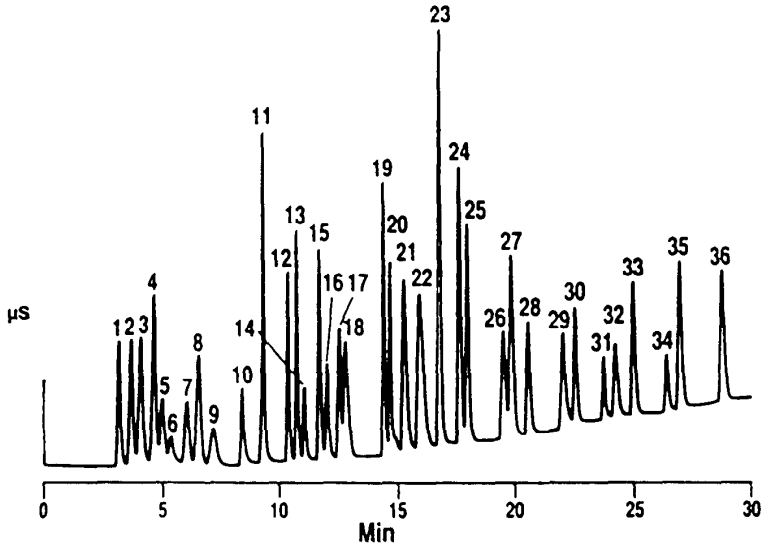


Figure 13 Gradient separation of 36 analyte anions with anion micromembrane-suppressed conductivity detection. Analytes: 10 ppm except where noted; (1) F^- (1.5 ppm); (2) α-hydroxybutyrate; (3) acetate; (4) glycolate; (5) butyrate; (6) gluconate; (7) α-hydroxyvalerate; (8) formate (5 ppm); (9) valerate; (10) pyruvate; (11) monochloroacetate; (12) BrO_3^-; (13) Cl^- (3 ppm); (14) galacturonate; (15) NO_2^- (5 ppm); (16) glucoronate; (17) dichloroacetate; (18) trifluoroacetate; (19) PO_3^{3-} (20) selenite; (21) Br^-; (22) NO_3^-; (23) SO_4^{2-}; (24) $C_2O_4^{2-}$; (25) selenate; (26) α-ketoglutarate; (27) fumarate; (28) phthalate; (29) oxalacetate; (30) PO_4^{3-}; (31) AsO_4^{3-}; (32) CrO_4^{2-}; (33) citrate; (34) isocitrate; (35) *cis*-aconitate; (36) *trans*-aconitate. Eluent: 0.75 mM NaOH constant for 5 min and a gradient to 85 mM NaOH in 30 min at 1.0 mL min^{-1}. Column: Dionex AS5A. (From Ref. 70.)

ductometric detection. Major limitations are the following: the precipitate as it forms in the column may interfere in normal mobile-phase flow before exhaustion of the exchange capacity of the suppressor column, the suppressor column period of use is still limited by the suppressor exchanger capacity, the suppressor column may require more rigorous treatment to remove the precipitate than usually required in recharging an ion-exchange column, and the precipitate may escape the suppressor column and interfere in the detection.

In the application of precipitation as the suppression step in analyte anion separations the eluent counteranion must form a precipitate with the displaced cation from the cation-exchange suppressor, while the analyte anion does not precipitate with the displaced cation from the cation-exchanger suppression column. For example, a ClO_4^- analyte can be retained, eluted, and its conductivity signal enhanced using and aqueous NaI eluent [22]. The ClO_4^- is highly retained on an anion exchanger and a strong eluent counteranion, such as I^-, is required for its elution from the exchanger. The suppression column is an Ag^+-charged cation exchanger. The Na^+ from the eluent and the ClO_4^- cocation exchange with Ag^+, yielding an AgI precipitate, which remains within the suppression column while the ClO_4^- as the soluble Ag^+ salt passes on to the conductivity detector where it is detected almost free of the background electrolyte.

To use precipitation suppression in analyte cation separations the eluent countercation must form a precipitate with the displaced anion from the anion exchanger suppressor column, whereas the analyte cation does not precipitate with the displaced anion. Aqueous Ba^{2+} and Pb^{2+} [64] or Pb^{2+} [65] eluents were used with either a SO_4^{2-} or IO_4^--charged anion exchanger suppression column, respectively, to separate alkaline earth and transition metal cations on a cation exchanger. The eluent strength of the Ba^{2+} or Pb^{2+} countercation is required to achieve this separation. The suppression occurs because of the formation of $PbSO_4$, $BaSO_4$, or $Pb(IO_4)_2$ precipitates in the anion exchanger suppression column, while the analyte cations as the soluble sulfate or iodate salts pass on to the conductivity detector. An aqueous eluent of HNO_3 and a soluble Zn^{2+} salt were used to separate alkaline earth cations on a cation exchanger by precipitation suppression [50]. For this, an anion exchanger charged in the OH^- form is used as the suppressor and the HNO_3 and Zn^{2+} are converted to H_2O and insoluble $Zn(OH)_2$, respectively, which allows the separated cations to be detected in the conductivity detector as the nitrate salts.

Chelation has been employed to aid the suppression step in the separation of anions on anion exchangers. In one approach [72] a solution of tris(hydroxymethyl)amino methane (Tris) and nitrilotriacetic acid (NTA) is used as the eluent for the separation of analyte anions. NTA is the principal counteranion that results in the analyte anion separation. The effluent from the anion-exchange column containing the separated anions is combined with a solution containing CaO and boric acid. The Ca^{2+} undergoes a reaction with the NTA to form a Ca $(NTA)^-$ complex, whereas H^+ and $HTris^+$ are converted into the poorly dissociated H_3BO_3 and Tris base form. Thus, when this combined column effluent–postcolumn solution mixture passes through the conductance detector, the eluent conductance is reduced by a factor of about three as a result of these reactions. This reduction in eluent background conductance, therefore, allows the analyte anions to be detected with higher sensitivity. For this suppression, peak heights of analyte anions are about twice those obtained in the absence of the suppression.

In a second strategy involving coordination, Sato and Miyanga [72] used a solution of dipotassium ethylenediamnine-*N*,*N*′-diacetate (K_2EDDA) as the eluent for the separation of analyte anions on an anion-exchange column. The $EDDA^{2-}$, which has chelating properties and serves as the eluent counteranion, passes through the analytical column and carries the separated anions into a suppression column packed with a cation exchanger charged in the Cu^{2+} form. The K^+ is exchanged for Cu^{2+} to form the stable CuEDDA complex and the Cu^{2+} salts of the separated anions, which are then detected by conductance on the CuEDDA background. The suppression corresponds to about an 80-fold decrease in the conductance by the background eluent. Figure 14 illustrates the separation of a mixture of common anions

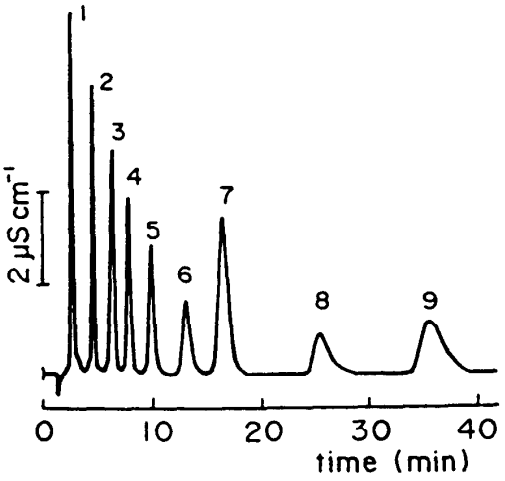


Figure 14 Separation of inorganic analyte anions using chelation for separation. Analyte: each ion is 10^{-4} M, 100-μL sample; (1) F^-, (2) Cl^-, (3) NO_2^-; (4) Br^-; (5) NO_3^-; (6) HPO_4^{2-}; (7) SO_4^{2-}; (8) I^-; (9) $S_2O_3^{2-}$. Eluent: 2mM K_2EDDA at 1.0 mL min^{-1}. Column: Tosoh IC anion PW. (From Ref. 72.)

and the enhancement in detection owing to the suppression. The peak heights are higher by more than two times those obtained in the absence of suppression.

In a third suppression scheme involving coordination [72], a solution of a borate or carbonate salt of ethylenediamine or other polyamine is used as the eluent for the separation of analyte anions on an anion exchanger. The suppression column is packed with a Cu^{2+} charged cation exchanger. In the suppression column the cations replace the Cu^{2+}, which forms the Cu–amine complex and the poorly dissociated H_2CO_3 or H_3BO_3. Thus, the background conductance is reduced and the analyte anions are detected on this background. When the eluent composition is optimized from both the standpoint of the separation and the suppression, background conductance is reduced by a factor of more than 20 by the suppression. If an ethylenediamine solution is used as the eluent, OH^- is the eluent counteranion owing to the ionization of the amine, and reduction in conductance by the Cu^{2+}-charged cation exchanger suppression column is almost 80-fold. But, OH^- is a weak eluent counteranion, and this limits which anions can be conveniently separated on the analytical column. One of the useful features of the Cu^{2+}-charged suppressor column is that one can visually determine when the column is exhausted and recharging is required. As the Cu^{2+} is removed from the cation exchanger, the exchanger loses its bluish coloration.

Gjerde and Benson [73], similarly to Small et al. (6), used a cation exchanger for suppression in the separation of analyte anions. The difference is that Gjerde and Benson introduced a slurry of a strong acid cation exchanger continuously postcolumn into the column effluent and before the conductivity detector to obtain suppression. This kind of suppression has been termed solid-phase suppression. The strong acid-type cation exchanger is insoluble, and it stays suspended during the chromatographic run because it is used as small, colloidal (< 7-μm) microparticles charged in the H^+ form. The suspended particles do not interfere in detection by conductance. The reactions describing the suppression are the same as if an H^+-charged cation exchanger suppressor column was used [see Eqs. (3a) and (3b)]. That is, the eluent stream is converted into a low-conducting background, and the analyte conductivity signal is enhanced. However, because a column is not used for the suppression, peak dispersion and broadening effects are reduced and dispersion and broadening are primarily due to the postcolumn mixing chamber. Also, this ion-exchange slurry suppression system can be used continuously, unlike the cation-exchange suppressor column strategy, and is compatible with

gradient elution [74]. The effectiveness of the slurry suppression system is indicated by considering a typical HCO_3^-–CO_3^{2-} eluent. For a 2.8 mM/2.2 mM ratio at 1 mL min^{-1} eluent, background conductance was 624 $\mu s\ cm^{-1}$ and was reduced to 18 $\mu m\ cm^{-1}$ when the slurry suspension was used [73]. Other practical applications of solid-phase suppression are described elsewhere [74].

G. Postsuppression Strategies

A postsuppressor device can be used to enhance the detection or increase the number of detection options in suppressed IC by placing the device between the suppressor and the column (see Fig. 2). Consider the HCO_3^-–CO_3^{2-} eluent, which is widely used in suppressed analyte anion separations. As indicated in Eqs. (5a) and (5b), H_2CO_3 is formed in the suppressor and partial dissociation of the H_2CO_3 affects background conductance. Furthermore, H_2CO_3 dissociation is also influenced by the acid form of the analyte anion, which subsequently, affects conductance detection of the analyte anion. Formation of CO_2 can cause degasing problems and changes in the eluent stream, for the CO_2 can partially diffuse through the suppressor membrane.

The presence of CO_2 in basic eluents, particularly strong base eluents, provides a low conductivity background after suppression and affects the detection limit [37]. The CO_2 can permeate a basic eluent if not protected, or can permeate the eluent through porous tubing used to transport the eluent. Figure 15 illustrates the extent that CO_2 can permeate Tefzel tubing. The CO_2 permeation of water was determined by IC as a function of residence time of the water within the tubing [37].

Removal of the H_2CO_3 before conductivity detection or its removal from the strong base eluents will, therefore, improve both the chromatographic performance and the detection limit. Postsuppression devices have been designed to remove CO_2 before conductivity detection; strategies for the removal of CO_2 from strong basic eluents are described later. The basic idea

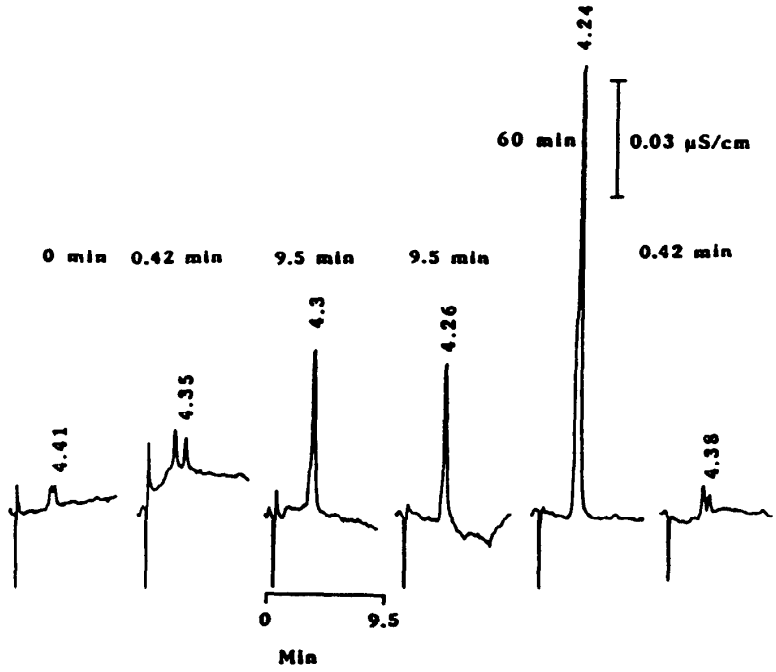


Figure 15 Ion chromatographic determination of CO_2 permeation through Tefzel tubing of 0.5-mm-wall thickness as a function of water residence time within the tube. (From Ref. 36.)

is to pass the suppressed eluent through a tubing, of suitable length and small dead volume, that is permeable to CO_2. Postsuppressor devices devised from porous Teflon tubing [75], silicone rubber [76], and a composite tubing made from polypropylene and silicone rubber packed with a nylon filament [77] have been used for H_2CO_3 removal.

A postsuppressor device can be used to extend IC to other kinds of detectors. For example, consider a typical suppressed IC systems for separating analyte anions or cations, except that a Li^+-charged postsuppressor device, such as a Li^+-charged cation exchanger [78] or a Li^+-charged fiber [79] is inserted between the suppressor and the detector (see Fig. 2). Instead of conductivity, a flame photometer set to detect Li^+ is used for detection. For analyte anion separations and detection, the suppressed analyte anions are acids in a water background when a strong acid eluent is used [see Eqs. (3a) and (3b)]. These are subsequently converted stoichiometrically into Li^+ salts by the Li^+ charged postsuppressor device, which allows the detection of the analyte anions as the Li^+ salt by the flame photometer. In analyte cation separations and detection using a strong acid eluent [see Eqs. (4a) and (4b)] the suppressed analyte cations in a water background and pass through the Li^+-charged postsuppressor device and are stoichiometrically converted into Li^+ salts, which are detected by flame photometry. If an IO_3^- or NO_3^--charged anion exchanger fiber device is used as the postsuppressor, then the separated anions or cations can be detected by UV absorbance at a wavelength at which IO_3^- or NO_3^- absorb [79]. A useful feature of this approach to detection in IC is that one calibration curve is suitable for all anions or cations separated and detected, because the detection is based on a stoichiometric exchange of the analyte ion for Li^+, IO_3^-, or NO_3^- [78–80]; the experimental factors affecting this calibration are discussed in detail elsewhere [80].

Membrane postsuppressor devices have been used to facilitate analyte anion detection by fluorescence or UV absorption [77]. A strong base eluent is used for the separation of the anions and the analytes for the acids following suppression are converted to anthranilic acid or Ce^{3+} salts by passing the analyte across a membrane where the outer surface is flushed continuously with an aqueous anthranilate or Ce^{3+} salt solution, respectively, before passage through the fluorescence or UV detector. A postsuppressor strategy has also been used following the detector to provide additional detection options or useful information about the analyte [78].

H. Other Applications of Suppressors

Suppression or suppression-like devices can be used precolumn to improve IC separations and postcolumn to enhance detection in non-IC–LC separation strategies. One key precolumn application is to employ membrane devices to do sample cleanup before completing the IC separation and determination. Sample matrix cleanup in both anion [83–85] and cation [86] samples is possible. Elevated NaOH concentrations in anion samples can be removed by passing the sample through a strong acid cation-exchange fiber that is bathed in an H^+-donating medium [83]. Another approach demonstrated by these workers is to use a membrane-based dialysis device to convert the NaOH to H_2O, and the analyte anions can then be determined by IC free of the NaOH interference. The SRS can be used to remove the effects of an NaOH sample matrix [84,85]. For example, trace inorganic anions in samples that are 48% in NaOH can be determined accurately by IC. In the presence of the NaOH sample matrix, the OH^- chromatographic peak interferes in the determination of many trace inorganic analyte anions. When the anion SRS is used precolumn, the NaOH is, or is nearly completely removed, depending on NaOH concentration, and the trace anions are readily determined. Figure 16a and b show chromatograms for the separation of trace inorganic anions and cations obtained after pretreatment of a 48% NaOH analyte solution [84].

Electrolytic devices have been used to generate a highly purified NaOH eluent solution suitable for IC separations of anions [37,87,88]. The eluent, which is electrolytically made

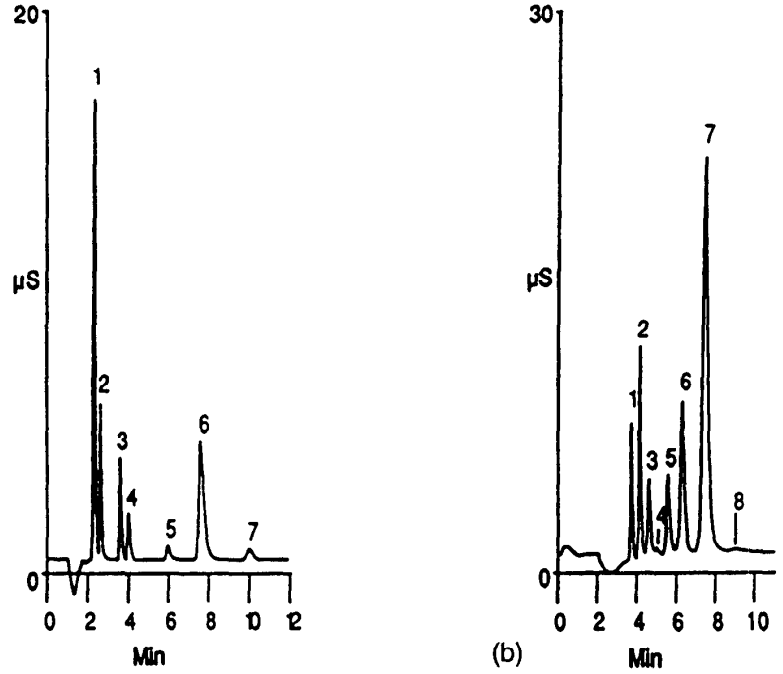


Figure 16 Separation of (a) inorganic analyte anions and (b) cations in a 48% NaOH sample after sample cleanup by a cation self-regenerating suppressor with micromembrane suppressed conductivity detection. (a) Analytes: (1) Cl^-; (2) NO_2^-; (3) Br^-; (4) NO_3^-; (5) PO_4^{3-}; (6)SO_4^{2-}; (7) $C_2O_4^{2-}$. Eluent: 1.7 mM $NaHCO_3$/1.8 mM Na_2CO_3 at 0.50 mL min^{-1}. Column: Dionex Ion Pac AS4A SC. (b) Analytes: (1) Li^+; (2) Na^+; (3) NH_4^+; (4) unknown; (5) K^+; (6) Mg^{2+}; (7) Ca^{2+}; (8) unknown. Eluent: 22 mM HCl at 1.0 mL min^{-1}. Column: Dionex Ion Pac CS12. (From Ref. 84.)

from a clean water source [see Eqs. (6a) and (6b)], is free of CO_2 as well as ultratrace levels of Cl^- and SO_4^{2-}, which can be introduced into the eluent by a solid NaOH source. This precolumn-prepared NaOH eluent, in combination with suppression following the IC separation, lowers background conductivity and noise and, therefore, yields better detection limits. When combined with a SRS device [37], both NaOH isocratic and gradient elutions at very high analyte anion sensitivity and response linearity are obtained. The sensitivity is particularly favorable for CO_2–HCO_3^-–CO_3^{2-} analytes.

Suppression devices can be used to enhance conductivity detection in other LC-types separations. Anionic surfactants, such as alkane sulfonates, alkyl sulfates, linear alkylbenzene sulfonates, sulfonated ethers, and related compounds can be separated on reversed stationary phases. Retention, efficiency, and consequently, resolution and detection limits of complex mixtures of the anionic surfactants are sharply increased when the mobile phase is at a high ionic strength. Under these conditions, conductivity background is very high, and conductivity is not a very sensitive detection method, even though the anionic surfactants have favorable limiting ionic equivalent conductances. If a salt of a weak acid or a strong base is used as the mobile-phase ionic strength electrolyte, its influence on the conductivity background can be minimized by a suppression device. Thus, the best column chromatography is obtained, and sensitive detection by conductivity is possible. Both solid-phase reagent suppression [89] and the MMS [90,91] have been employed in this type of application.

III. NONSUPPRESSED ION CHROMATOGRAPHY

A. Introduction

The quality of conductivity detectors was being improved as suppressed IC was undergoing development. Two major improvements broadened the scope of conductivity detection in IC: (1) Electronic suppression was improved; and (2) temperature control of the conductivity cell was also improved. The former increased the range over which background conductance could be electronically zeroed, whereas the latter contributed to reproducibility of the analyte signal and the electronically suppressed background signal. With these improved conductance detectors it was possible to maximize the difference in the limited ionic equivalent conductances between the eluent counterions and the analyte ions. Under these conditions, the conductivity detector becomes a viable detector for IC without suppression.

B. Nonsuppression

Fritz and co-workers [92–94], in a series of studies, demonstrated how to manipulate the parameters of an ion-exchange separation so that the separation would be efficient and detection by conductivity would be sensitive. With these modifications suppression is not required and low detection limits can be obtained. This approach has been identified by several different names, with the most common being nonsuppressed ion chromatography (NSIC) and single-column ion chromatography. NSIC will be used in this chapter.

Two major features of ion exchange were exploited to improve conductivity detection in the absence of suppression [92–94]. First, the ion exchanger for the separation must have a low ion-exchange capacity. Because the exchanger capacity is low, the eluent can be dilute, which means the background conductance is low and is easily compensated by the conductivity-offset capabilities. The low exchanger capacity also requires that the sample size not be too large, or a mass overload would occur. This is usually not a problem in NSIC, because the conductivity detector, as well as many other types of detectors suitable for NSIC, have low detection limits and are compatible with small sample masses. If the sample is injected in a large volume, a volume overload may occur, and this should also be avoided.

A second key factor is that an eluent electrolyte should be used that provides a counterion with a high-exchange selectivity and one that has a large difference in limited ionic equivalent conductance, compared with the analyte ion. The strong eluent counterion also allows its eluent concentration to be low.

The net effect of using a dilute eluent solution containing a strong eluent counterion with a limited ionic equivalent conductance that differs from the analyte ion is a reduction in the background conductance. Because the background conductance can also be offset, a large difference between the background conductance and the analyte ion conductance is obtained. With this kind of ion-exchange column and eluent optimization and the availability of quality conductivity detector with appropriate offset capabilities, good detector temperature control, and low internal volume, detection limits by NSIC are often comparable with those obtained by SIC. Also of importance is that NSIC is compatible with other types of detection, including absorption, fluorescence, and electrochemical detection as well as with postcolumn reactions, thereby broadening the scope of NSIC. This is one of the main advantages offered by NSIC [8,10,13].

In the initial work of Fritz [92–94], low-capacity ion exchangers were prepared with capacities of 7–40 mmol g^{-1} of exchanger. This capacity range is typical of many of the currently commercially available ion exchangers for NSIC, including the organic polymeric, silica-based, latex-based, and other pellicular-type ion exchangers [8,10,13].

Improvements in conductivity detectors and the compatibility of NSIC with other detection strategies allow higher-capacity ion exchangers to be used, and these are also commercially available for NSIC. One advantage of the higher-capacity exchangers is that they can

be used with more concentrated eluents or with weaker-strength eluents, thereby increasing the number of eluent counterions for NSIC.

C. Eluent Counterion for Nonsuppressed Ion Chromatography

A wide range of inorganic counteranions, organic acids, and their salts have been used for the separation of analyte anions on anion exchangers by NSIC. Table 3 lists many of the more common eluent counteranions that have been used to separate analyte anions by NSIC. Several have relatively low, limiting ionic equivalent conductances, particularly salts of the organic acids, and dilute solutions of these counteranions, are compatible with conductivity detection. For other samples, other types of detection provide better detection limits. The eluent electrolytes in Table 3 (which are not listed in order of eluting strength) represent a wide range in eluent strengths. The multiprotic electrolytes can be converted into multicharged counteranions of even greater eluent strength by raising the eluent pH. Naphthalene trisulfonate eluents have been used for the separation of multivalent inorganic and organic analyte anions, such as polyphosphates and polycarboxylates [95], and an acidic 1,3-cyclohexanedionate eluent was especially useful for a F^-–Cl^- separation [96]. Figure 17 compares the eluent strength of several of the carboxylate-type counteranions toward analyte anion retention on a methacrylate polymeric-based quaternary ammonium-type anion exchanger. A detailed discussion of eluent strength for other organic and inorganic eluent electrolytes and the scope of application are provided elsewhere [7–13].

A strong base eluent, such as KOH solution, can be used in NSIC separations, but this eluent does not provide the best detection limit if conductivity detection is used because of the high-limited ionic-equivalent conductance for OH^-. Because OH^- is also a weak eluent

Table 3 Electrolytes for Anion Separations in Nonsuppressed Ion Chromatography

Carboxylic acids	Sulfonic acids	Inorganic
Monoprotic	Monoprotic	KOH
		Phosphate buffer
Formic acid	Benzenesulfonic acid	$NaClO_4$
Acetic acid	Toluenesulfonic acid	Na_2SO_4
Benzoic acid	Substituted benzenesulfonic	HCl
Substituted benzoic acids	acids	HNO_3
Multiprotic	2-Naphthylamine-1-sulfonic	HCO_3^-/CO_3^{2-}
	acid	Borate-hydroxy
o-Phthalic acid	Substituted naphthylamine-	compound
Citric acid	sulfonic acids	Metal–EDTA complexes
Tartaric acid	Methanesulfonic acid	
Succinic acid	Alkanesulfonic acids	
Fumaric acid		
1,3,5-Tricarboxybenzene	Multiprotic	
(trimesic acid)		
1,2,4,5-Tetracarboxybenzene	Sulfobenzoic acids	
(pyromellitic acid)	1,2-Dihydroxybenzene-3,5-	
Ethylenediaminetetraacetic	disulfonic acid	
acid (EDTA)	Sulfophthalic acids	
	Naphthalene trisulfonate	

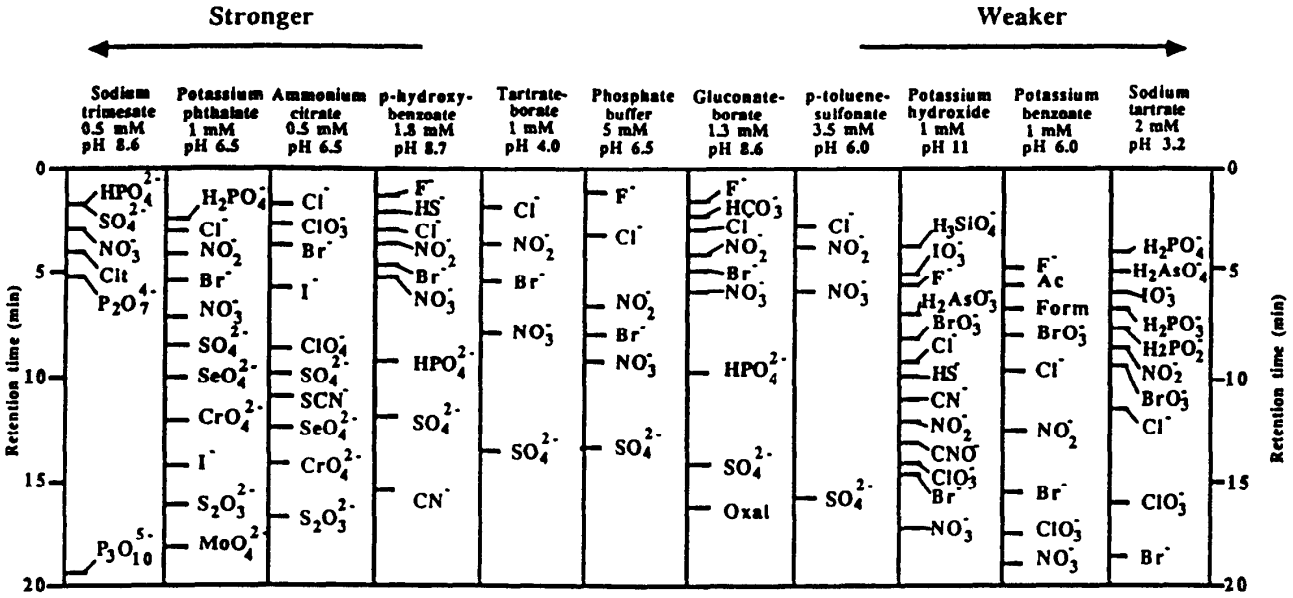


Figure 17 Comparison of retention data of analyte anions for different eluents used in nonsuppressed ion chromatography. (From Ref. 10.)

counteranion and its eluent strength is low, KOH concentration is used at a higher level, and this also limits conductivity detection. The OH^- eluent, however, is compatible with many other detection strategies. The major use of the OH^- eluent counteranion is for the anion-exchange separation of anions derived from very weak acids, such as CN^-, BO_3^-, and others [97]. The high pH is required to ensure analyte ionization. Because the analyte anions are also poorly retained on anion exchangers, a weak-eluting counteranion, such as OH^-, is required. A second counteranion can also be added to the OH^- eluent to increase eluent strength. A sodium phenoxide eluent can also be used for these kinds of separations.

Boric acid and borate salts form a series of complexes with polyhydroxy compounds; for example, neutral compounds, such as sugars and glycols, or acidic compounds, such as tartaric acid, gluconic acid, and glucuronic acid, and these mixtures provide an unique eluent for NSIC anion separations [98–101]. Depending on the borate and polyhydroxy compound concentration, their ratio, type of polyhydroxy compound, and pH, the charge on the complex can be varied. In alkaline pH at which borate and the polyhydroxy compound are about equal in concentration a mononegative 1:1 complex is the major species. This complex is a weak eluent counteranion and provides a low-conductivity background. Consequently, this eluent is very useful in NSIC with conductivity detection. A much stronger eluent is obtained by forming mutivalent-charged borate:polyhydroxy compound complexes by changing the pH or concentration and ratio of the two.

EDTA is a versatile reagent in NSIC applications. On one hand, it can be a very strong eluent counteranion, because it is a tetraprotic acid and can be converted into a -4 anion at a basic pH. This eluent has been applied to the elution of strongly retained anions, such as polyphosphates [102]. Alternatively, EDTA will convert transition metal ions into anionic metal–EDTA complexes that can be separated on anion exchangers [103–105]. Metal complexes of EDTA have also been used as eluent counteranions [106,107].

Modifications of cation exchanger column capacity and eluent countercation concentration to separate analyte cations by NSIC with conductivity detection is performed much the same as that for analyte anion NSIC. Low-capacity cation exchangers and a stronger, dilute eluent countercation, differing in limiting ionic equivalent conductance from the analyte cation, are

required. If other detectors are employed, higher-capacity cation exchangers and additional eluent countercations can be used, which increases the scope of cation NSIC.

A major difference between anion NSIC and cation NSIC is that the number and versatility of eluting conditions are more restricted in cation NSIC. For a low-capacity cation exchanger the eluent can be a dilute solution of a strong acid [94,108–110], where H^+ is the eluent countercation, or a pH-controlled solution of an organic base, or where the eluent countercation is the organo ammonium cation. Buffered solutions of pyridine, aniline, benzylamine, and their substituted derivatives, ethylenediamine and phenylenediamine, have been used [111–114].

Buffered solutions of polyamines provide a wide range of eluent strengths because they can be converted into multivalent cations, depending on their pK_b through pH control. For example, ethylenediamine is frequently used as a divalent eluent countercation. The disadvantage of polyamine cations is that they have high, limited ionic-equivalent conductances, and this limits their scope of applications or detection limits in NSIC with conductivity detection. This is not a limitation with other forms of detection.

Quaternary ammonium salts can be used as an eluent countercation in analyte cation separations by NSIC and have the advantage of a low, limited ionic-equivalent conductance. However, quaternary ammonium salts tend to be retained by polymeric cation exchangers by processes other than cation exchange. These interactions between the quaternary ammonium cations and the polymeric matrix affect the eluent strength of the quaternary ammonium electrolyte solution, provide sites on the stationary phase surface for interactions with anions, and generally, broaden analyte cation chromatographic peaks. The lower the cation exchanger capacity and the higher the hydrocarbon carbon number within the quaternary ammonium group, the more extensive the interaction is between the cation exchanger polymeric surface and the quaternary ammonium cation. Because of these limitations H^+ and organic bases are used more often as the eluent countercations in analyte cation NSIC.

Retention times for monovalent inorganic cations and organic bases on a sulfonated-type cation exchanger suitable for cation NSIC are consistent with the cation-exchange selectivities found on conventional strong acid-type cation exchangers (see Table 1). Figure 18 compares eluent strength for an HNO_3 solution to stronger and weaker eluents derived from organic bases. Monovalent inorganic cations, such as the alkali metal cations, alkaline earth cations, and simple organic amines, can be separated by several of the eluents listed in Figure 18. A major separation problem occurs when the two groups are in a mixture, for the divalent alkaline earth cations require a stronger eluent for their elution from a cation exchanger. However, separations of this kind can be significantly improved by using a carboxylic acid-type cation exchanger. Particularly useful is a polybutadiene–maleic acid-type cation-exchange column [115–117].

Separation of transition metals and other multivalent cations, which are typically more highly retained on a cation exchanger, require a ligand in the eluent. A ligand in the eluent, such as a crown ether, can also improve the separation of alkali metal and alkaline earth cations [115]. The competing equilibria for the complexes formed between the cation and the ligand and the effects of these equilibria on the cation exchange are responsible for the separation. Although conductivity is an effective detector for these separations, other detector modes are more frequently used, particularly postcolumn reactions with absorbance or fluorescence detection. These latter detection strategies often increase the range of eluent conditions that can be used to improve the resolution of the separation.

Inorganic cations are useful as eluents in NSIC, usually with nonconductometric detection modes. For example, Cu^{2+} [118] and Ce^{3+} [118,119] were good eluents for the separation of mono- and divalent analyte cations. The Ce^{3+} is a stronger eluent and, therefore, the Ce^{3+} eluent concentration can be less, which aids detection. Although conductivity detection is possible, indirect absorbance (Cu^{2+} or Ce^{3+}) or indirect fluorescence (Ce^{3+}) provides a more sensitive detection [120]. Other stable metal complexes carrying a positive charge can be

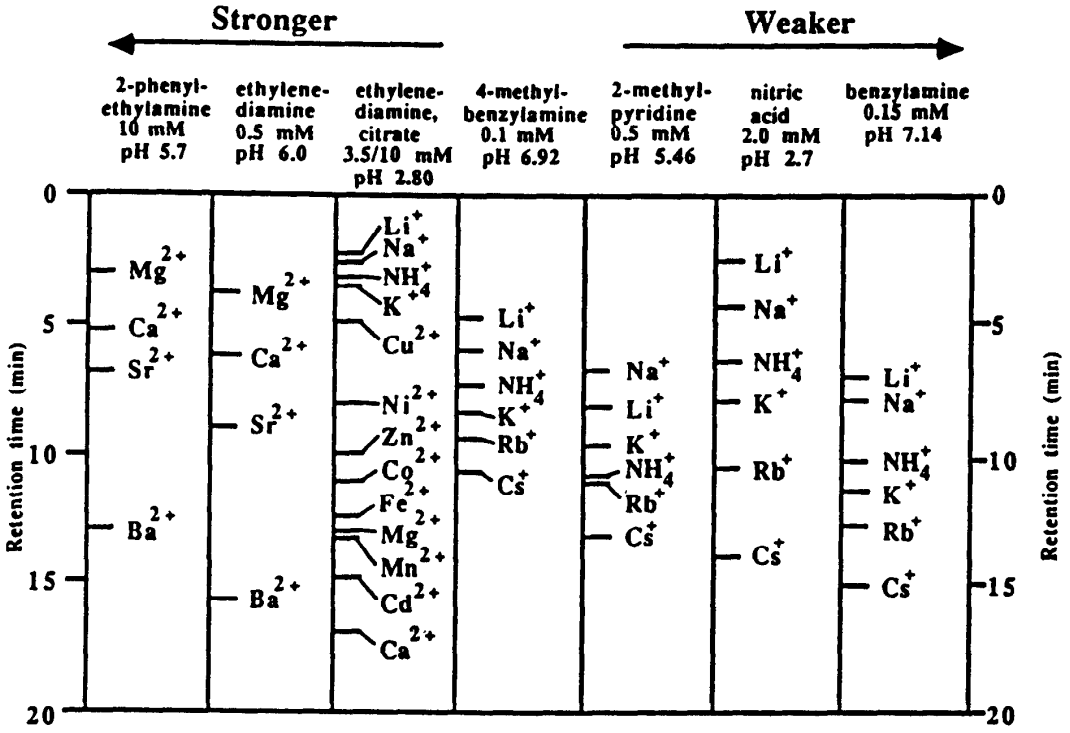


Figure 18 Comparison of retention data of analyte cations for different eluents used in nonsuppressed chromatography. (From Ref. 10.)

useful eluent countercations and, if the complex absorbs, indirect absorbance detection can often be employed with excellent detection limits.

Fewer eluents are suitable for gradient elution in NSIC than for SIC, particularly when conductivity detection is employed. In the NSIC separation of analyte anions, for example, eluents will always have a conducting background, and although it may be small, the background will change, because the gradient will involve a concentration change in the eluent counteranion during the elution time. If a detector that does not respond to the eluent background is used, then the flexibility of the gradient and the type of the gradient components that can be used are significantly increased. Thus, many of the eluents routinely used in NSIC are better with other detectors, if possible, when the separation requires a gradient elution.

Gradient elution with conductivity detection is feasible at favorable detection limits and minor baseline interference if the conductivity remains constant during the gradient; that is, it is isoconductive during the gradient elution. In an isoconductive gradient, two eluents differing in eluent strength are combined precolumn so that the eluent strength increases with time, while the conductivity of the combined mixture remains constant. Eluents for gradient NSIC separation of anions that are isoconductive have been reported [121,122]. Figure 19 illustrates the isoconductive gradient separation of series of inorganic anions that differ widely in retention on an anion exchanger. In the absence of the gradient, this separation would not be possible in the time frame indicated in Figure 19, or by a single-column run. The isoconductive gradient is achieved by using concentration changes in buffered solutions of boric acid, gluconic acid (a polyhydroxy compound), CsOH, and LiOH [121]. Other isoconductive cation combinations that can be effectively used are Rb^+–tetrabutylammonium salts and K^+–Li^+ combinations [122].

Computer cancellation of the background conducting signal caused by the gradient change is possible, providing the change can be stored in a reproducible form. This strategy in general is applicable to most types of detection used in NSIC.

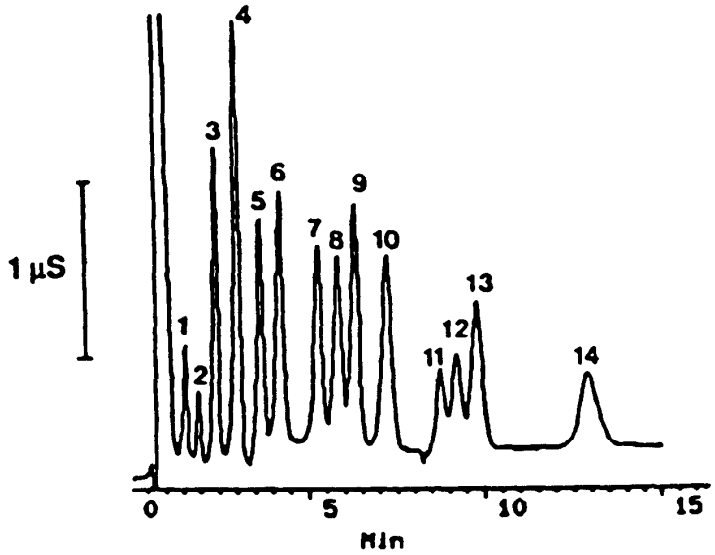


Figure 19 Separation of an inorganic analyte anion mixture using a isoconductive gradient. Analytes: (1) F^- (5 ppm); (2) CO_3^{2-} (20 ppm); (3) Cl^- (15 ppm); (4) NO_2^- (20 ppm); (5) Br^- (20 ppm); (6) NO_3^- (20 ppm); (7) PO_4^{3-} (30 ppm); (8) PO_3^{3-} (20 ppm); (9) SO_4^{2-} (20 ppm); (10) $C_2O_4^{2-}$ (20 ppm); (11) tungstate (25 ppm); (12) CrO_4^{2-} (25 ppm); (13) molybdate (25 ppm); (14) SCN^- (25 ppm). Eluent: conversion of eluent A 8.25 mM boric acid, 1.11 mM gluconic acid, 3.08 mM CsOH, 0.48 mM glycerin, 12% CH_3CN to eluent B 12.65 mM boric acid, 1.70 mM gluconic acid, 4.72 mM LiOH, 0.75 mM glycerin, 12% CH_3CN at 1.2 mL min^{-1} for 8 min and then increased in a gradient to 1.7 mL min^{-1}. Column: waters IC-Pac Anion HR. (From Ref. 121.)

D. Detection by Postcolumn Reaction

A postcolumn reaction (PCR) is a reaction between an analyte following its separation on a column with a reagent or a series of reagents on-line, and it is the product of the reaction that is detected by a suitable detector. PCR offers several advantages as a detection strategy: (1) analytes that are not easily detected can be converted into products that are detected, (2) the number of detection options may be increased, (3) sensitivity can be increased by detecting the analyte as the reaction product, and (4) a PCR procedure can often be used to improve the specificity of the detection. PCR has been widely used in HPLC and many excellent reviews and reference books [7–10,13,25,123–126] survey this important and useful method of detection in LC. PCR strategies are also important in IC, and it can be argued that suppression techniques in IC are a special type of PCR. The following briefly outlines the scope of PCR in IC.

The major type of PCR (excluding suppression techniques) used in IC is one in which the column effluent and the PCR reagent are combined on-line in a postcolumn mixing chamber. The mixture on-line may be heated or provided additional reaction time to ensure a favorable reaction before entry into the detector. A second type that can be used is to pass the column effluent through a postcolumn, packed-bed reactor, in which the analytes undergo a reaction with reagent that is physically absorbed or chemically bonded to the packed-bed material. The reaction may also be heated and or provided with additional reaction time before entering the detector. The postcolumn suppression column packed with ion exchanger, although not providing a reactive reagent, nevertheless, can still be considered a type of packed-bed reactor. In general and excluding suppression, the packed-bed reactor-type PCR is more widely used to aid in the detection of organic analytes. In the IC separation of simple inorganic anions and cations solution, PCR is used more often in the detection of inorganic analyte cations. Although the PCR approach is a viable and sensitive aid to detection in IC, because

it increases the number of detector options, the method is not as widely used as conductivity with or without suppression.

A typical instrumental setup for solution PCR is shown in Figure 20. For a packed-bed reactor-type PCR the mixing unit and PCR pump in Figure 20 would be replaced by the packed-bed reactor, so the reaction can still be carried out on-line. The mixing chamber or the coil may be heated, and the coil length can be lengthened to increase the reaction time. The keys to successfully using PCR is to have available an appropriate reaction that yields a detector-active product that can be detected with good sensitivity. The percentage conversion of the analyte into the PCR product need only be reproducible, although a 100% conversion is preferred. And finally, the reaction must be controllable and cause little or no band dispersion and broadening owing to reaction or mixing of the reagents.

Ultraviolet and visible absorption, fluorescence, and electrochemical detection are frequently used with PCR in IC separations. However, PCR is not limited to only these modes of detection [7–10,13,123–126]. Although PCR detection is compatible with a wide variety of detectors, it requires more rigid control and operator attention to obtain a sensitive, reproducible, and accurate detection. For example, solution PCR is likely to require the following:

1. The reaction between the analyte and the postcolumn reagent must be rapid, complete, or reproducible, and provide a species suitable for detection.
2. Efficient mixing of the reagent and column effluent must be obtained so that the reaction occurs as in item 1 and quickly provides a homogeneous solution.
3. Heat may be required and eluent, reagent, and analyte must be stable at the required temperature.
4. Extra tubing or coils may be required between the mixing chamber and detector to provide the necessary reaction time.
5. Each of these steps have to be optimized to produce baseline uniformity and thus obtain a good, reproducible S/N and at the same time prevent excessive contributions to band dispersion and broadening, which would also affect detection limits.

Even though detection limits by PCR can be low, IC with or without suppression and conductivity detection is often the preferred method, because these latter approaches do not demand such rigid control and operator attention.

Most PCR methods are based on complex formation between the PCR reagent and the inorganic analyte ion; this is particularly true for inorganic analyte cations. In general, these reactions have been widely used in other areas of analytical chemistry, and the chemistry of these reactions are often well understood. Therefore, in applying the reaction to aid detection in IC, it is the on-line postcolumn reaction conditions that must be optimized to satisfy the IC application.

Table 4 lists several PCR reagents that can be used to detect inorganic analyte anions. Most reagents for inorganic anions tend to be selective, whereas those for cations tend to be more general. One of the more general PCR reagents for inorganic anions is Fe^{3+}, which is used as the perchlorate salt. The Fe^{3+} forms weak complexes with many anions, and these

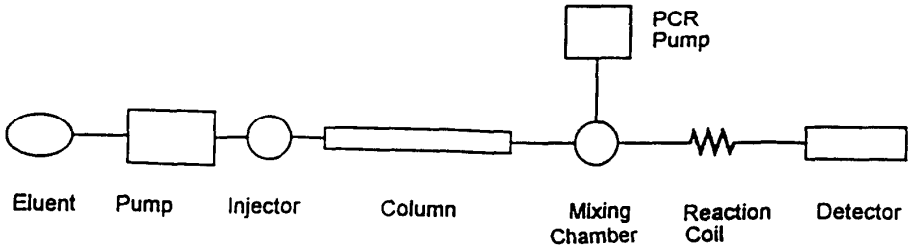


Figure 20 A diagram of the basic instrumentation required to aid detection by a postcolumn reaction.

Table 4 Reagents for the Postcolumn Detection of Inorganic Anions Used in Nonsuppressed Ion Chromatography

Analytes	Postcolumn reagent
Aminocarboxylic acids, polyphosphates	Ca-methylthymol blue
Aminocarboxylic acids, polyphosphates	$Fe(NO_3)_3$
CN^-,SCN^-	Pyridine-barbituric acid
EDTA, NTA,	$Fe(ClO_4)_3$
I^-, Br^-	Chloramine T + 4,4′-bis(dimethylamino)diphenylmethane
Inorganic anions (see Table 5)	$Fe(ClO_4)_3$
NO_{2-},NO_3^-	UV photolysis
NO_2^-, NO_3^-, $S_2O_3^{2-}$, I^-	Cd^{4+} in H_2SO_4
Phosphonic acids	$Fe(ClO_4)_3$
Phosphonic acids	Al–morin
Phosphorous anions	Al–morin
Phosphorous anions	Mo^{5+}/Mo^{6+}
Phosphorous anions	$Fe(ClO_4)_3$
Polyphosphates	$(NH_4)_6Mo_7O_{27}$ + NH_4VO_3
SiO_3^{2-}	Na_2MoO_4
Sulfur anions	$Fe(ClO_4)_3$
Sulfate	Ba–chloroanilate

Source: Ref. 10.

can be detected by absorption [127]. A $Fe(ClO_4)_3$–$HClO_4$ solution is combined with the column effluent postcolumn and the separated analyte anions form complexes with the Fe^{3+} in the mixing chamber. Heat is not required. Table 5 lists anions detected by the $Fe(ClO_4)$–$HClO_4$ postcolumn reaction. Usually, detection is at 300 to 340 nm and detection limits range from about 1 to over 100 nM.

An example of a more selective PCR reagent is the Al–morin complex. This complex, which is highly fluorescent, is used to detect separated phosphorous oxo acids [128,129] or F^- [130] using an indirect fluorescent detection. The Al–morin is introduced postcolumn, which provides a fluorescent background that is monitored by the fluorescence detector. When either the phosphorous-oxo acid or F^- analyte emerge from the column and is combined with the Al–morin complex the fluorescence decreases because the P–analyte–Al or Al–F complex is more stable than the Al–morin complex. Therefore, the P–analyte or F^-–analyte chromat-

Table 5 Inorganic Anions Detected by a Fe(III)–$HClO_4$ Postcolumn Solution

CrO_4^{2-}	I^-	IO_3^-
SCN^4	S^{2-}	CO_3^{2-}
$Fe(CN)_6^{4-}$	$S_2O_3^{2-}$	Br^-
$Fe(CN)_6^{3-}$	NO_2^-	$B_4O_7^{2-}$
SO_4^{2-}	PO_4^{3-}	BrO_3^-
Cl^-	SO_3^{2-}	SiO_3^{2-}
$P_2O_7^{4-}$	PO_3^{3-}	

Source: Ref. 124.

ographic band is detected as a negative peak on a fluorescent background. Few other anions interfere in the detection, unless they complex with Al^{3+}. Heat is not required, but the reaction time and pH must be carefully controlled. The detection is sensitive, selective, and also demonstrates that a postcolumn, indirect fluorescence detection strategy is feasible, reproducible, and accurate.

Table 6 lists several PCR reagents that can be used to detect inorganic cations. In general, PCR reagents used to detect cations are complexing agents. Because complexing agents are also frequently used in the eluent to elute inorganic analyte cations, an additional important requirement for the PCR reagent is that it forms a more stable complex with the analyte cation than the complex that is formed between the cation and the eluent-complexing agent.

Several complexing agents are good general PCR reagents for detecting analyte cations. For example, the reagent 4-(2-pyridylazo)resorcinol (PAR), which forms stable complexes with many inorganic cations, has been used extensively to detect a variety of analyte cations [131–133]. It is used postcolumn as a NH_3/NH_4^+-buffered solution. The reactions with cations are rapid, permitting direct mixing, and cation–PAR complexes are detected by absorption in the 500- to 540-nm–wavelength range. Typical detection limits are in the 1- to 25-ng range, depending on the cation.

IV. ION-EXCLUSION CHROMATOGRAPHY

A. Background

Ion exchangers are capable of retaining weak or nonelectrolytes by processes other than ion exchange as briefly described in Section I.B. If a column of a cation exchanger charged in the H^+ form is eluted with water or an aqueous strong acid eluent, such as an HCl solution, an aqueous phase is maintained within the ion exchanger particles. The HCl, if in the eluent, is excluded from the imbibed liquid phase within the cation exchanger by Donnan equilibrium. However, weak or nonelectrolytes are able to distribute between the imbibed liquid and the water eluent or the HCl eluent solution surrounding the exchanger particle. The distribution of the weak or nonelectrolytes, if they are introduced into the column as a sample, are retarded in their movement down the column as the eluent flows, and separation occurs because of

Table 6 Reagents for the Postcolumn Detection of Inorganic Cations Used in Nonsuppressed Ion Chromatography

Analytes	Postcolumn reagent
Al^{3+}	8-Hydroxyquinoline-5-sulfonate
Al^{3+}	Tiron
Ca^{2+}, Mg^{2+}	Arsenazo I
Ca^{2+}, Mg^{2+}	Neo-thorin
Co^{2+}	Luminol
Cr^{3+}, Cr^{4+}	Diphenylcarbohydrazide
Fe^{2+}, Fe^{3+}	PAR
Fe^{2+}, Fe^{3+}	Bathophenanthroline disulfonic acid
Di-, tri-, and tetravelent cations	8-Hydroxyquinoline
Transition metal cations	Na pyrrolidinedithiocarbamate
Transition metal cations	Dithizone
Transition metal cations	Eriochrome Black T
Transition metal cations	PAR
Rare earth cations	Arsenzao I and III

Source: Ref. 10.

differences in the ability of the weak or nonelectrolyte to undergo the distribution process. Weakly ionized acids are separated on high-capacity cation exchangers, and weakly ionized bases are separated on anion exchangers. Nonelectrolytes can be separated on both types of exchangers. This kind of chromatography is called ion-exclusion chromatography (IEC).

Factors that influence the analyte migration through the column are the degree of ionization of the analyte (the more ionized the analyte is, the faster it travels), polar interactions between the analyte and the ionogenic groups, interactions between the analyte and the imbibed solvent, and interactions between the analyte and the polymer matrix of the exchanger. Clearly, the difference between a true exclusion process and partitioning or adsorption is not large. Recent work, for example, has compared retention of simple short-chain aliphatic carboxylic acids on a lightly sulfonated porous polymeric stationary phase with one without the sulfonic acid groups, using an acid-free mixed solvent [134]. Retention was independent of the sulfonic acid groups and was more dependent on the *n*-butanol that was in the acid-free mobile phase. It is suggested that the light sulfonation or the presence of the *n*-butanol in the absence of the sulfonation makes the stationary phase more hydrophilic, and this factor determines the differences in retention of the carboxylic acid analytes.

Exclusion in gravity-flow ion exchange has been recognized for some time, and this background is reviewed elsewhere [1–4,7–10,13,134–137]. Modern IEC uses efficient ion-exchange columns and improved instrumentation, and complements anion and cation IC. IEC is often an effective strategy for the separation of weakly acidic compounds, such as phosphates, condensed phosphates, organo ammonium salts, aromatic and aliphatic carboxylic acids, and biologically important compounds containing weak acidic or basic groups. IEC can also be used to separate alcohols, carbonyl compounds, carbohydrates, and other nonionic compounds, as well as for separating ionics from nonionics; many of these procedures are also reviewed elsewhere [1–4,7–10,13,134–137].

IEC requires regular LC instrumentation and eluents that are simple in composition. A typical instrumental setup for IEC of weak organic acids includes a column of a strong acid cation exchanger, charged in the H^+ form; a water or strong acid eluent; and a standard HPLC instrument equipped with a universal detector, such as a refractive index detector, a conductivity detector, or any other detector capable of monitoring the analytes in the sample. The column can be used repeatedly and regeneration is not required, except in those instances in which the column can be affected by sample matrices. Polymeric- and latex-based cation exchangers are preferred over silica-based bonded-phase cation exchangers when using acidic eluents because of the instability of the silica-based cation exchangers in the acidic solution. Cation exchangers for IEC are microparticles to ensure good column efficiency, and usually the exchangers have higher exchange capacities than those typically used in cation IC separations.

B. Ion-Exclusion Chromatography: A Brief Survey of Applications

Tanaka et al. [138], using modern LC instrumentation, rather than gravity-flow, determined the elution behavior of strong and weak acid analytes on a H^+-charged cation exchanger using water as an eluent. These elution data are summarized in Table 7 and are consistent with previous gravity-flow studies [1–4,7–10,13,139,140]. Strong acid analytes are excluded and travel with the void volume through the column, whereas the weak acids travel at slower rates and exhibit retention times that, in general, increase as their pK_a values increase. More recently, a quantitative relation correlating retention time to pK_a values has been derived [141,142].

When a mineral acid solution, such as HCl, rather than water, was used as the eluent, retention and resolution in the separation of weak acid analytes was improved [143]. This improvement was attributed to the mineral acid's suppression of the weak acids. Because of the better chromatographic performance with the acidic eluent, water is now less often used as an eluent in IEC applications. Figure 21 shows a chromatogram obtained for the separation

Table 7 Retention Order in Ion Exclusion Chromatography[a]

HCl, HBr, HI, $HClO_4$, H_2SO_4, HNO_3
$H_2C_2O_4$
H_3PO_3
H_3PO_4
H_2SO_3
HF
CH_3CO_2H
Phenol
H_2CO_3,HCN, H_3BO_3
$CH_3CH_2CO_2H$
H_2S

[a]Listed in increasing order of retention.
Source: Ref. 135.

of the citric acid cycle acids using this eluent and UV detection. As with the water eluent analyte, retention time in general followed the pK_a values for the weak acid analytes. Subsequently, IEC has been applied to a wide variety of analytical problems involving organic weak acid determinations in the food industry, the beverage industry, biological samples, water treatment, and others.

IEC can be applied to the separation and determination of inorganic anions derived from weak acids. The retention order for selected inorganic analyte anions on a cation exchanger is listed in Table 7. Table 8 lists the elution order for weak organic acids on a strong acid cation exchanger prepared specifically for IEC applications.

IEC is compatible with most HPLC detection modes, although universal detectors, such as conductivity or refractive index, are used most often. When water is the eluent, the background conductivity is nil, and the conductivity by the analyte can be detected with sensitivity, even though the weak acid analytes are only partially ionized. When a strong mineral acid solution is the eluent, dissociation of the weak acid analytes are suppressed owing to the high H^+ concentration. Conductivity of the background is high, conductivity from analyte is low; therefore, sensitivity of the detection is poor. MMS and other membrane suppression techniques can be used to alleviate this S/N problem, thereby allowing the conductivity signal of the analyte to be enhanced. For this a suppressor with a cation-exchange–type membrane is used, and the regenerating solution for the MMS is a $R_4N^+OH^-$, NaOH, or K_2SO_4 solution. The mineral acid eluent, for example HCl or H_2SO_4, is converted to the corresponding salt, the conductance of which is much less than for HCl, and the weak acid analytes that may have been introduced as the salts are converted to the weak acids. An added driving force is the neutralization of the H^+ by the regenerating solution. This is the reverse of the process used in membrane suppression when doing suppressed anion IC separations. Weak acid detection by conductivity is still feasible because of partial dissociation of the weak acid to produce H^+, which has a very high, limiting ionic-equivalent conductance. Thus, the analyte conductivity is higher than if it were detected as the salt. However, as the pK_a value for the weak acid analytes increases, the sensitivity of the conductivity detection decreases.

Water or aqueous solutions of strong mineral acids, such as HCl and H_2SO_4, are usually used as the eluent. However, conductivity detection can be further enhanced by using a strong acid that provides an anion that has a low, limiting ionic-equivalent conductance. Use of aliphatic and aromatic sulfonic acids [144–148] satisfies this goal. Figure 22 illustrates the isocratic separation of 20–500 ppm aliphatic carboxylic acids and 5–50 ppm aromatic car-

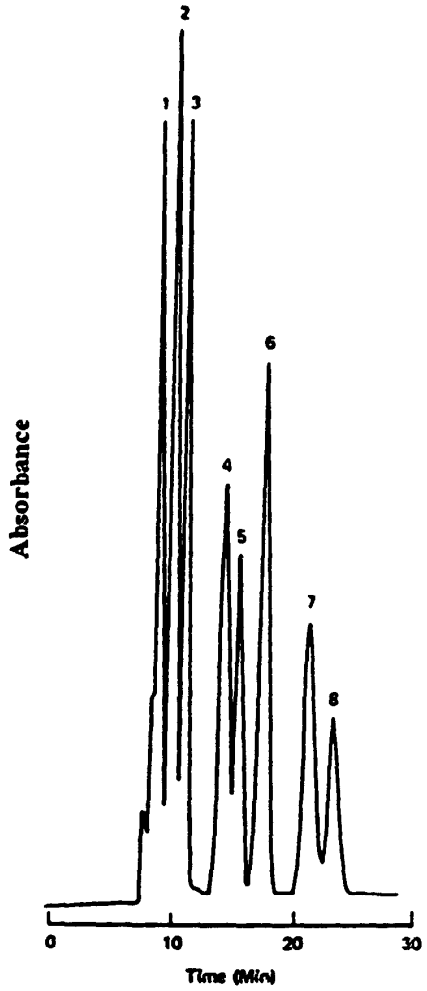


Figure 21 Separation of citric acid cycle acids by ion exclusion chromatography. Analytes: (1) *cis*-aconitic (30 ppm); (2) α-ketoglutaric (190 ppm); (3) oxaloacetic (260 ppm); (4) citric (1220 ppm); (5) isocitric (1770); (6) malic (1650 ppm); (7) fumaric (9 ppm); (8) succinic (1340 ppm). Eluent: 1.0 mM HCl at 1.0 mL min^{-1}. Column: BioRad Aminex 50W-X4. (From Ref. 143.)

boxylic acids on a strong cation exchanger using a 10-mM methanesulfonic acid eluent and UV detection at 210 nm.

Weak acids, which also provide a low-conductivity background, such as carbonic acid, phosphoric acid, fluorinated aliphatic carboxylic acids, aliphatic carboxylic acids, and benzoic acids, have also been used. Often the suppression step can be omitted when the lower-conducting background eluents are employed in IEC. Including organic solvent in the IEC eluent will influence retention because of its effect on the interactions between the analyte and the polymer matrix of the ion exchanger and its effect on analyte ionization. The effect of carboxylic acid retention on cation exchangers also depends on the cation form of the exchanger [149] and decreases in the order

$$K^+ > Cs^+ > NH_4^+ > Na^+ > Li^+ > H^+ \tag{7}$$

which also indicates the complex nature of the exclusion process in IEC.

Table 8 Retention of Organic Acids on an Ion Exclusion Column[a]

Organic acid	k'
Ketoglutaric acid	0.23
Maleic acid	0.34
Pyruvic acid	0.38
Isocitric acid	0.39
Citric acid	0.42
Tartaric acid	0.47
Glyoxylic acid	0.65
Malic acid	0.68
Malonic acid	0.71
Ascorbic acid	0.86
Fumaric acid	1.21
Succinic acid	1.24
Lactic acid	1.26
Glycolic acid	1.30
Formic acid	1.45
Acetic acid	1.72
Glutaric acid	1.78
Adipic acid	2.39

[a]A Benson polymeric OA850 strong acid cation exchange column and a 0.5 mM H_2SO_4 eluent.
Source: Ref. 136.

Suppression in IEC is not limited to membrane-type suppression devices. For example, an HCl eluent can be suppressed with a column packed with a Ag^+ form cation exchanger (see Sec. II.F). The H^+ in the eluent replaces Ag^+, which precipitates as AgCl, and the weak acid analytes are converted to Ag^+ salts, thereby enhancing the conductivity detection. The conductivity detection of HCO_3^-, which is separated by IEC, is enhanced with two ion-

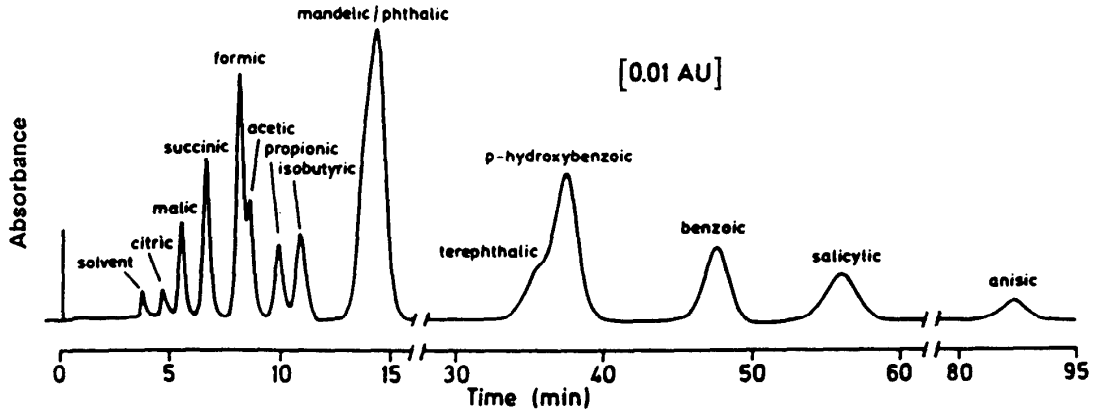


Figure 22 Ion exclusion chromatographic separation of carboxylic acids. Analytes: aliphatic carboxylic acids (25–500 ppm); aromatic carboxylic acids (5–50 ppm). Eluent: 99:1 H_2O:CH_3CN, 10 mM methanesulfonic acid. Column: BioRad Aminex HPX-87H. (From Ref. 148.)

exchange, packed suppressor columns [150]. The first (a K^+-charged cation exchanger) converts the carbonic acid analyte from the IEC column to $KHCO_3$ and the second (a OH^--charged anion exchanger) converts the $KHCO_3$ to KOH, which is detected by the conductivity detector, with enhanced sensitivity. A redox suppression was also used to enhance the conductivity detection of carboxylic acid derivatives separated by IEC [151]. In this study, HI was the eluent and it was combined with H_2O_2 postcolumn to yield I_2 and H_2O, which allows a more sensitive conductivity detection of the separated carboxylic acids.

IEC was successfully coupled with IC to improve resolution [152]. The IEC cation-exchange column on-line is the first column and performs a group separation initially by retaining the weakly acidic analytes while the highly dissociated analytes travel with the void volume into the second column, which is an anion-exchange separator column. The weakly dissociated analytes are resolved on the first column by IEC and, following suppression, they are detected by conductivity, while the strongly dissociated analytes are separated on the second column and, following suppression, are also detected by conductivity.

V. ION INTERACTION CHROMATOGRAPHY

A. Background

Addition of an ionic, lipophilic reagent to an eluent will often increase the retention of an analyte ion of opposite charge on a reversed stationary phase. This strategy is known by several terms; the major ones being ion interaction chromatography (IIC) and ion-pair chromatography. This strategy and its variations are widely employed to broaden the scope of the separation and determination of organic analyte ions, including biological molecules containing acidic or basic groups. Increased retention, better selectivity, improved resolution, and enhanced detection are chromatographic properties gained by this approach. These advantages are realized in the separation and determination of inorganic analyte ions, and this separation strategy is equally important in this application. Because of the conditions under which inorganic analyte ions are separated by this technique, which suggests that ion pairs are not the principle species, the strategy is referred to as IIC in this chapter. IIC does not involve an ion exchanger as the stationary phase but does require the control of equilibria, which resemble ion-exchange–like processes.

B. Equilibria

The interactions between analyte ions, the ionic lipophilic IIC reagent, and the reversed stationary phase have been studied extensively [4,10,12,13,20,25,153, and references within]. Clearly, the interactions are influenced by properties of the mobile-phase components, particularly the lipophilic reagent, and the stationary phase. It is these properties that determine the mode of retention on the reversed stationary phase. An excellent review that critically describes the proposed models for these interactions is available elsewhere [153].

If it is assumed that all species in the eluent are highly dissociated, micelle and aggregate formations are absent, and the solvent is mostly water, which favors dissociation, the major equilibria describing the retention of the analyte ion on the reversed stationary phase A, can be described by Eqs. (8a) and (8b) for retention of the analyte X^-, in the presence of a cationic IIC reagent R^+C^-, and by Eqs. (9a) and (9b) for the retention of an analyte cation X^+, in the presence of an anionic IIC reagent R^-M^+.

$$A + R^+C^- \rightarrow A \cdots R^+C^- \tag{8a}$$

$$A \cdots R^+C^- + X^- \rightarrow A \cdots R^+X^- + C^- \tag{8b}$$

$$A + R^-M^+ \rightarrow A \cdots R^-M^+ \tag{9a}$$

$$A \cdots R^-M^+ + X^+ \rightarrow A \cdots R^-X^+ + M^+ \tag{9b}$$

Thus, the analyte ion in this double-layer type model [153] competes in an ion exchange like selectivity with the eluent counterion, which is present as the IIR reagent coion, added as a buffer to control pH, or provided by an ionic strength salt. If the R^+C^- IIC reagent is a quaternary ammonium salt, $R_4N^+C^-$, then the selectivity toward inorganic analyte anions, according to Eq. (8b), would be expected to be similar to anion exchangers that contain the R_4N^+ ionogenic group. Similarly, for alkyl or aryl sulfonates or sulfates of high carbon number as the IIC reagent, selectivity for inorganic analyte cations [see Eq. (9b)] is similar to sulfonated cation exchanger selectivities.

This description of anion and cation IIC is a simplification of the processes that occur [153]. However, it is still useful because the parameters that affect analyte ion retention are identified. Furthermore, it provides the chromatographer a basis for semiquantitatively predicting chromatographic behavior and optimization of IIC separations.

IIC, compared with ion exchange, involves more equilibria that must be controlled and, therefore, is more complex than ordinary ion exchange. This complexity, however, can be an advantage, because more parameters in IIC can be manipulated to alter retention, resolution, and influence detection [20]. In applications of IIC these are the parameters to be optimized. The major ones are outlined in the following, assuming the eluent contains the lipophilic reagent at a fixed concentration and the pH and ionic strength are controlled.

1. As the IIC reagent carbon number of hydrophobicity increases, the equilibria in Eqs. (8a) and (9a) shift to the right, increasing the ion-exchange–like capacity and, hence, analyte ion retention.
2. As the concentration of the IIC reagent increases, the equilibria in Eqs. (8a) and (9a) shift to the right, increasing the ion-exchange–like capacity, causing analyte retention to increase. However, counterion concentration owing to the IIC reagent also increases, and this reduces the ion-exchange–like capacity, causing analyte ion retention to decrease. Thus, analyte retention passes through a maximum as IIC reagent concentration increases because of these opposing effects.
3. An increase in the concentration of eluent organic modifier shifts the equilibria in Eqs. (8a) and (9a) to the left. This reduces the equilibrium amount of the IIC reagent maintained on the stationary phase, the ion-exchange–like capacity decreases, and analyte ion retention drops. The type of organic modifier also influences Eqs. (8a) and (9a) consistent with solvent effects in reversed-phase retention.
4. An increase in the concentration of the counterion provided by the IIC reagent, the buffer, and the ionic strength salt shifts the equilibria in Eqs. (8a) and (9a) to the right and the equilibria in Eqs. (8b) and (9b) to the left. Over a wide change in counterion concentration, retention of the analyte ion will pass through a maximum.
5. When comparing eluent counterions, the one with the higher ion-exchange selectivity shifts the equilibria in Eqs. (8a) and (9a) to the right, increasing the ion-exchange–like capacity, resulting in higher analyte ion retention and shifts the equilbria in Eqs. (8b) and (9b) to the left, which decreases analyte retention. The second of these two opposing effects generally is the dominate one; thus, the analyte anion retention will decrease for the stronger eluent counterion.
6. Mobile-phase pH, although providing H^+ or OH^- eluent counterions, plays a larger role in determining the degree of dissociation of weak acid and base analytes to produce the ionic forms of the two.
7. The reversed-phase properties of the stationary phase influences the equilibria in Eqs. (8a) and (9a). For a given IIC reagent, retention of the IIC reagent and hence, the analyte ion increase as the hydrophobicity of the stationary phase increases.

C. Ion Interaction Chromatographic Eluents

Lipophilic cations, such as symmetrical R_4N^+ salts, in which the alkyl group is C_1 to C_5;

unsymmetrical alkyltrimethyl quaternary ammonium salts, in which the long-chain alkyl group is more than C_{10}; alkylaryl quaternary ammonium salts; and alkyl pyridinium salts are used to separate analyte anions [4,10,12,13,20,25]. Complexes, such as Fe(II) and Ru(II) 1,10-phenanthroline, and 1,1-bipyridyl complexes [154–156] and crown ethers [25,157; and references therein], are good IIC reagents for the separation of analyte anions. In addition to enhancing retention and resolution of the analyte anions, IIC reagents that contain a chromophoric or other detector-active group allow indirect detection of the analyte anions; this is briefly discussed in section V.E.

In general, inorganic analyte anion elution order follows the elution order for a strong base anion exchanger. This is illustrated in Figure 23. Occasional observed reversals in elution order have been attributed to the reversed stationary phase [158]. Figure 24 illustrates a typical separation of analyte anions using an intermediate lipophilic $(butyl)_4N^+$ salicylate salt as the eluent IIC reagent [159]. This reagent has a low conductance and analyte anions are detected directly with good sensitivity on the low-conducting background.

Alkane sulfonates for which the alkane group is C_4 to C_{10}, alkyl sulfates of similar carbon number, and aromatic sulfonates are common lipophilic IIC eluent additives for analyte cation separations [4,10,12,13,20,25]. Similar to cation exchange on strong acid-type cation exchangers, elution of multivalent cations requires a complexing agent in the eluent, which plays a major role in determining the analyte cation elution order. Figure 25 illustrates the separation of rare earth cations and related cations with octane sulfonate as the lipophilic ion eluent additive and α-hydroxybutyric acid as a ligand to improve elution and selectivity of the separation [160]. The cations are detected by PCR with Arsenazo III.

The usual procedure is to equilibrate the reversed stationary phase with eluent composed of an ionic lipophilic IIC reagent of known concentration, an aqueous–organic solvent mixture, a buffer to control pH (particularly if anions or cations derived from weak acids and bases, respectively, are being separated), and often an electrolyte to control ionic strength. The choice

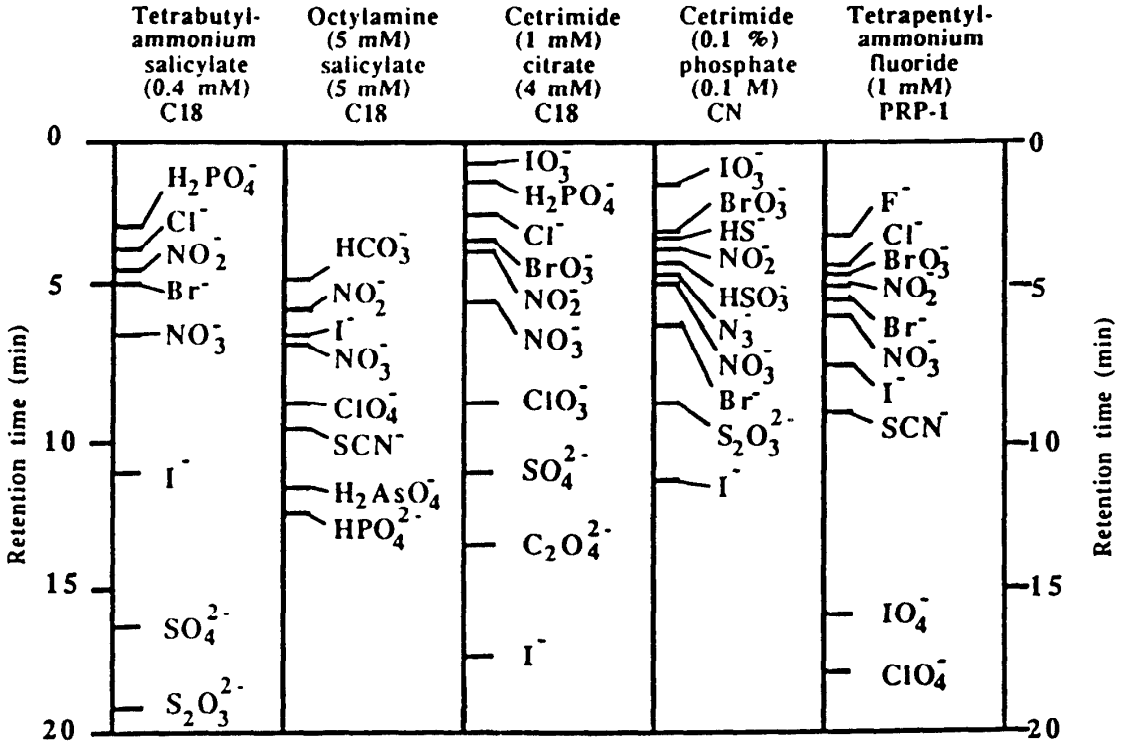


Figure 23 Retention times for several analyte anions on silica and polymeric reversed stationary phases for eluents containing different quaternary ammonium IIC reagents. (From Ref. 10.)

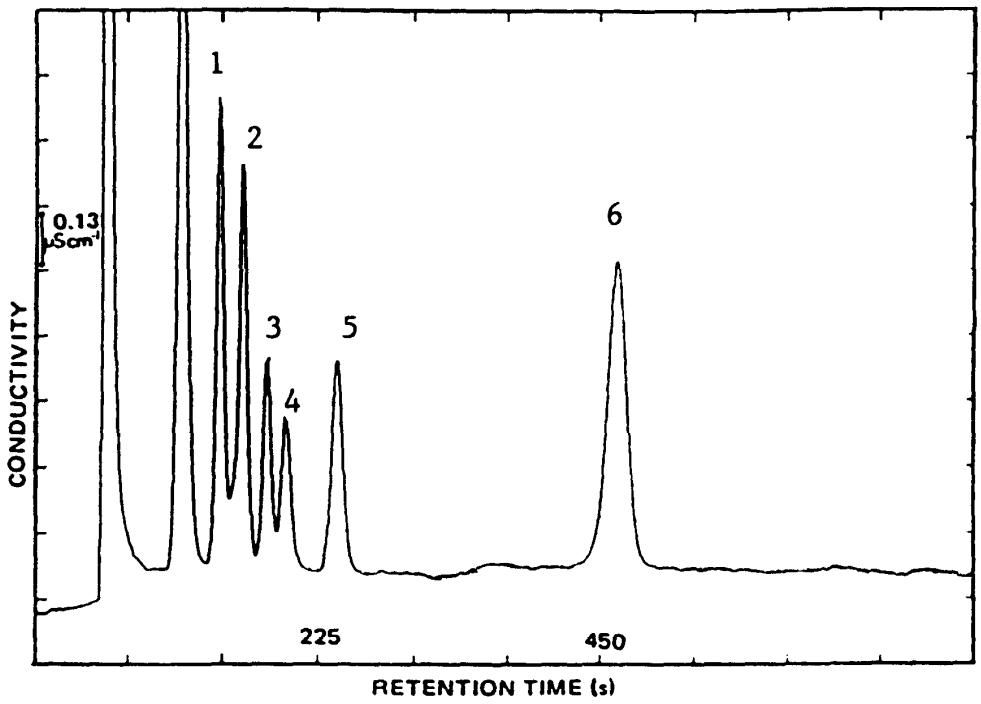


Figure 24 Separation of inorganic analyte anions by IIC. Analytes: all at 10 ng except where noted; (1) F^-; (2) Cl^-; (3) NO_2^-; (4) Br^-; (5) NO_3^-; (6) SO_4^{2-} (20 ng). Eluent: 7:93 H_2O:CH_3CN, 0.75 mM tetrabutylammonium salicylate at 1.0 mL min^{-1}. Column: Hamilton PRP-1. (From Ref. 159.)

of the eluent counterion supplied by the lipophilic salt, the buffer, the ionic strength salt, or their combination can be critical. After the column reaches equilibrium with an equilibrium amount of the lipophilic ion and its coion maintained on the stationary phase surface, the analyte mixture is introduced, and the separation is completed by a continued flow of the eluent. If eluent conditions are changed, column reconditioning at the new condition is required. The lipophilic ion can be removed from the stationary phase column by washing with an organic solvent, such as CH_3CN.

An alternative way to carry out the separation is to use a lipophilic IIC reagent that is tightly held by the reversed stationary phase [159,161,163]. These are also quaternary ammonium salts and alkane sulfonates and alkyl sulfates in which the sizes of the hydrocarbon groups are large. Their level of retention is high, and studies [159,161,162] have demonstrated that the stationary phase is permanently coated relative to the eluting conditions required for the IIC separations. If the lipophilic ion slowly elutes from the column when using an eluent free of the lipophilic ion, the column can be reconditioned with fresh lipophilic reagent.

D. Stationary Phases in Ion Interaction Chromatography

The reversed stationary phase has little or no effect on elution order, although there are exceptions [158]. The reversed stationary phase does, however, play an important role in determining the amount of lipophilic ion and its coion that is maintained on its surface [see Eqs. (8a) and (9a)] at a fixed eluent condition. Generally, the more hydrophobic the reversed stationary phase is, the greater the retention of the lipophilic salt. Poly(styrene–divinylbenzene) copolymeric phases, C_{18} and other alkyl-bonded phases of varying carbon loadings, and phenyl-bonded phases are reversed stationary phases routinely used in IIC.

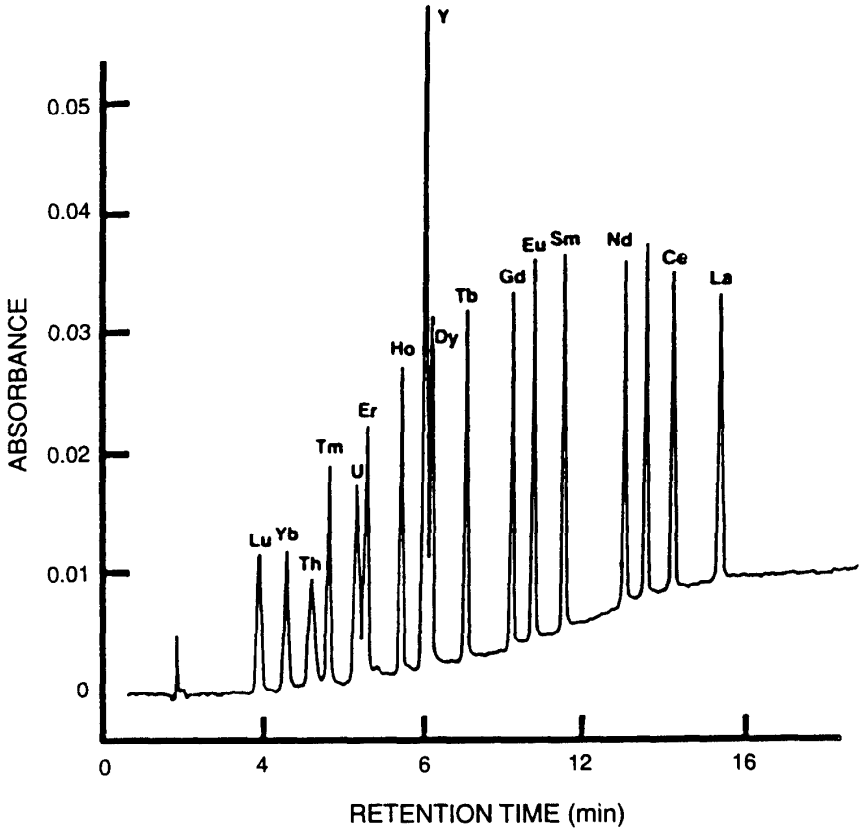


Figure 25 Separation of rare earths, Y^{3+}, Th^{4+}, and U^{6+} by IIC. Analytes: 25 ng of each rare earth and 50 ng of Y^{3+}, Th^{4+}, and U^{6+}. Eluent: 30 mM $C_8SO_3^-$ with a gradient of 50–400 mM α-hydroxybutyric acid at 1.0 mL min^{-1}. Column: Supelcosil LC-18. (From Ref. 160.)

E. Detection in Ion Interaction Chromatography

If the IIC eluent solution is optically transparent or provides a very low absorbance background and the analyte ions are not transparent, then absorbance detection of the analyte ions is a viable detection mode. Similarly, conductivity detection is applicable when the background conductivity of the eluent is low and the ionic equivalent conductances of the analyte ions differ significantly from the background ions. If the lipophilic salt in anion separations contains a counteranion, such as F^-, OH^-, or Cl^-, absorption detection is often suitable, whereas if the counteranion is phthalate, benzoate, or salicylate, conductance is often suitable.

Suppression systems enhance conductivity detection; both ion-exchange column [163] and membrane suppression [164] have been demonstrated to be effective in IIC applications. In both cases, anions are separated with a quaternary ammonium hydroxide eluent. The suppression system, as explained earlier, converts the IIC eluent additive to water and the anion analytes to acids, thereby enhancing the conductivity detection of the analyte anions. Direct detection in IIC is feasible by other detection modes, providing the IIC eluent is detector-inactive or only provides a low detector background response compared with the analyte ion. However, absorption, conductivity, and PCR (see Fig. 25) are employed the most in IIC separations.

Indirect detection of analyte ions in IIC can be very sensitive, providing the background signal is maintained within the offset limits of the detector. Two types of IIC reagents have been effective and sensitive for indirect detection in IIC separations.

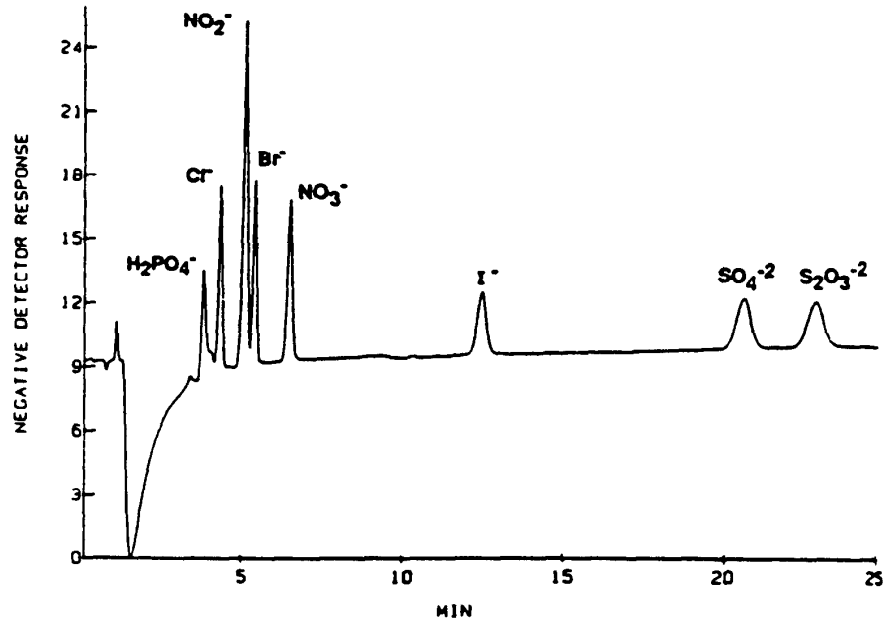


Figure 26 Separation of inorganic anions by IIC with indirect absorbance detection when the lipophilic reagent counteranion absorbs. Analytes: 200 ng of each except 100 ng for Cl^- and 300 ng for SO_4^{2-} and $S_2O_3^{2-}$. Eluent: 0.4 mM tetrabutylammonium salicylate at 2.0 mL min^{-1}. Column: waters resolve C-18 Radial Pak. Detection: 288 nm. (From Ref. 165.)

In one strategy, the IIC additive provides a counterion that is detector-active. For example, when using tetrabutylammonium salicylate as the eluent IIC reagent for the separation of analyte anions, the salicylate will absorb (also fluoresce), and a change in absorbance (fluorescence) indicates the presence of analyte anions [165]. Because the eluent flows continuously through the detector a background absorbance (fluorescence) is obtained. When the analyte anions emerges from the column it displaces a stoichiometric amount of the salicylate in the analyte band [see Eqs. (8a) and (8b)] causing a decrease in the band absorbance (fluorescence). It is the salicylate concentration decrease in the band, which is proportional to the amount of the analyte present, that is detected; not the analyte anion itself, resulting in a negative chro-

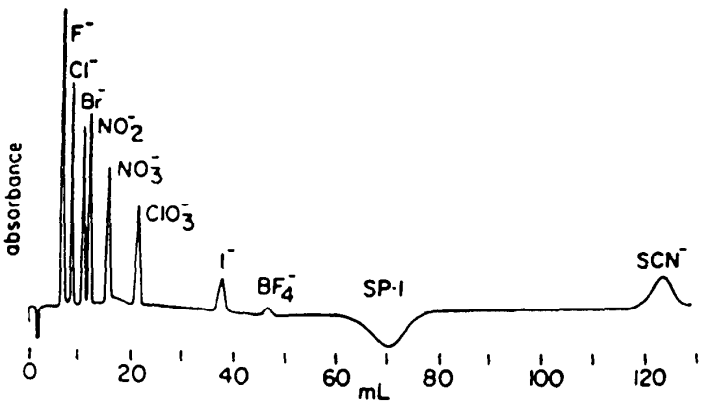


Figure 27 Separation of analyte anions by IIC using indirect absorbance detection when the lipophilic ion absorbs. Analytes: about 1 μg each. Eluent: 0.10 mM $Fe(phen)_3SO_4$, 0.10 mM succinate, pH 6.1. Column: Hamilton PRP-1. (From Ref. 154.)

matographic peak. Other chromophoric or detector-active counterions can be used, which allows eluent strength to be changed or detection sensitivity to be altered. Figure 26 illustrates an anion separation by IIC with a tetrabutylammonium salicylate eluent additive for which the anions are detected by indirect absorbance detection [165].

An alternative indirect detection strategy is based on the lipophilic ion being detector-active. For example, quaternary ammonium salts in which one or more of the groups are chromophoric [166], or Fe(II) or Ru(II) 1,10-phenanthroline, or 1,1-bipyridyl complexes [154–156] are IIC reagents that affect both the separation of analyte anions and also allow their detection by indirect absorbance detection [154,155,166] or indirect fluorescence detection [156]. In these examples, the indirect detection is due to ionic strength and counteranion effects within the analyte band [167]. Analyte bands can be negative or positive, depending on how the ionic strength and counteranion affect the equilibrium amount of the detector-active lipophilic ion maintained on the stationary-phase surface within the analyte band. The detector is set at a wavelength at which the lipophilic on absorbs, and a change in its concentration that is proportional to the amount of the analyte anion present is detected on the absorbing background. Figure 27 illustrates the separation and indirect absorption detection of analyte anions when a Fe(II)–1,10-phenanthroline salt is the IIC eluent additive. Detection limits are about 10 ng, depending on the analyte anion. If the Ru(II)–1,10-phenanthroline salt is the IIC reagent, indirect fluorescence detection at about 0.4 ng is possible [156].

REFERENCES

1. F Helfferich. Ion Exchange. New York: McGraw Hill, 1962.
2. J Inczedy. Analytical Applications of Ion Exchangers. [Eng. trans.] Pergamon Press: M Williams, 1966).
3. W Rieman III, HF Walton. Ion Exchange in Analytical Chemistry. New York: Pergamon Press, 1970.
4. HF Walton, RD Rocklin. Ion Exchange in Analytical Chemistry. Boca Raton; CRC Press, 1990.
5. DJ Pietrzyk. In: J Cazes, ed. Packings and Stationary Phases in Chromatographic Techniques. New York: Marcel Dekker; 1990, p. 585.
6. H Small, TS Stevens, WC Bauman. Anal Chem 47:1801, 1975.
7. RE Smith. Ion Chromatography Applications. Boca Ration, FL. CRC Press, 1988.
8. DT Gjerde, JS Fritz. Ion Chromatography, 2nd ed. Heidelberg; Huthig, 1987.
9. J Tarter, ed. Ion Chromatography. New York: Marcel Dekker, 1987.
10. PR Haddad, PE Jackson. Ion Chromatography: Principles and Applications. Journal of Chromatography Library, vol 46. Amsterdam: Elsevier, 1990.
11. PK Dasgupta. Anal Chem 64:775A, 1992.
12. PR Haddad, AL Heckenberg. J Chromatogr 300:357, 1984.
13. J Weiss. Ion Chromatography, 2nd ed. Weinheim; VCH, 1995.
14. RM Wheton, MJ Hatch. Synthesis of ion exchange resins. In: JA Marinsky, ed. Ion Exchange, vol 2. New York: Marcel Dekker, 1969, p. 191.
15. GL Schmitt, DJ Pietrzyk. Anal Chem. 57:2247, 1985.
16. RL Smith, DJ Pietrzyk. Anal chem 56:610, 1984.
17. MJ Fuller. Chromatogr Rev 14:45, 1971.
18. A Clearfield. Inorganic Ion Exchange Materials. Boca Ration: CRC Press, 1982.
19. RL Smith, Z Iskandarani, DJ Pietrzyk. J Liq Chromatogr 7:1935, 1984.
20. DJ Pietrzyk, DM Brown, D Yuan, SH Edelmuth, P Rigas, GL Schmitt, RL Smith. In: P Jandik, RM Cassidy, eds. Advances in Ion Chromatography, vol 1. Franklin, MA: Century International, 1989, p. 35.
21. ES Yeung, ed. Detectors for Liquid Chromatography. New York, John Wiley & Sons 1986.
22. CA Pohl, EL Johnson. J Chromatogr Sci 18:442, 1980.
23. R Saari-Nordhaus, JM Anderson Jr. Am Lab 26(Jan):28C, 1994; 28(Feb):33N, 1996.

24. TS Stevens, JC Davis, H Small. Anal Chem 53:1488, 1981.
25. PK Dasgupta. In: JG Tarter, ed. Ion Chromatography. New York: Marcel Dekker, 1987, p. 191.
26. J Stillian. LC Mag 3(9):802, 1985.
27. S Rabin, J Stillian, V Barreto, K Friedman, M Toofan. J Chromatogr 640:97, 1993.
28. HF Walton, RD Rocklin. Ion Exchange in Analytical Chemistry. Boca Raton, FL: CRC Press, 1990, p. 64.
29. Y Hanaoka, M Takeshi, S Muramoto, M Tamizo, A Nanba. J Chromatogr 239:537, 1982.
30. S Rokushiko, ZY Qi, H Hatano. J Chromatogr 260:81, 1983.
31. PK Dasgupta, RQ Bligh, VD Agostino, J Lee. Anal Chem 57:253, 1985.
32. S Gupta, PK Dasgupta. J Chromatogr 26:34, 1988.
33. KH Jansen, KH Fischer, B Wolf. US Patent, 4,459,357, 1984.
34. ZW Tian, RZ Hu, HS Lin, JT Hu. J Chromatogr 439:159, 1988.
35. DL Strong, PK Dasgupta. Anal Chem 61:939, 1989.
36. DL Strong, CV Joung, PK Dasgupta. J Chromatogr 546:159, 1991.
37. C Pohl, RW Slingsby, JR Sillian, R Gajek. US Patent 4,999,098, 1991.
38. A Henshall, S Rabin, J Statler, and J Stillian. Am Lab 24(Nov):20R, 1992.
39. S Rabin, J Stillian, V Barreto, K Friedman, M Toofan. J Chromatogr 640:97, 1993.
40. DP Hautman, M Bolyard. J Chromatogr 602:65, 1992.
41. Y Hanaoka, T Murayama, S Muramoto, T Masuura, A Nanba. J Chromatogr 239:537, 1982.
42. RD Rocklin, RW Slingsby, CA Pohl. J Liq Chromatogr 9:757, 1986.
43. SA Bouyoucos. J Chromatogr 242:170, 1982.
44. M Nonomura. Anal Chem 59:2073, 1987.
45. RD Rocklin, CA Pohl, JA Schibler. J Chromatogr 411:107, 1987.
46. RJ Williams. Anal Chem 55:851, 1983.
47. R Saari-Nordhaus, JM Anderson Jr, K Ravichandran. J Chromatogr 602:15, 1992.
48. MJ van Os, J Slanina, CL deLigny, WE Hammers, J Agterdenbos. Anal Chim Acta 144: 73, 1982.
49. RW Slingsby, JM Riviello. LC 1:354, 1980.
50. JW Wimberley. Anal Chem 53:2137, 1981.
51. DL Cambell, J Stillian, S Carlson, R Joyce, S Heberling. J Chromatogr 546:229, 1991.
52. D Jensen, J Weiss, M Rey, C Pohl. J Chromatogr 640:65, 1993.
53. GJ Sevenich, JS Fritz. Anal Chem 55:12, 1983.
54. J Morris, JS Fritz. J Chromatogr 602:111, 1992.
55. RD Rocklin, M Rey, JR Stillian, D Campbell. J Chromatogr Sci 27:474, 1989.
56. LM Nair, R Saari-Nordhaus, JM Anderson Jr. J Chromatogr 671:43, 1994.
57. GJ Sevenich, JS Fritz. J Chromatogr 347:147, 1985.
58. H Saitoh, K Oikawa. J Chromatogr 329:247, 1985.
59. B Kondratjonok, G Schwedt. Fresenius Z Anal Chem 332:333, 1988.
60. D Yan, G Schwedt. Fresenius Z Anal Chem 320:325, 1985.
61. OA Shipgun, OD Choporova, Yu A Zolotov. Anal Chim Acta 172:341, 1985.
62. PR Haddad, PW Alexander, M Trojanowicz. J Chromatogr 324:319, 1985.
63. S Reiffenstuhl, G Bonn. Fresenius Z Anal Chem 332:130, 1988.
64. FR Nordmeyer, LD Hansen, DJ Eatough, DK Rollins, JD Lamb. Anal Chem 52:852, 1980.
65. JD Lamb, LD Hansen, GG Patch, FR Nordmeyer. Anal Chem 53:749, 1981.
66. SR Villasenor. J Chromatogr 671:11, 1994.
67. H Kumagai, T Sakai, K Matsumoto, Y Hanaoka. J Chromatogr 671:15, 1994.
68. C Umile, JFK Huber. Talanta 41:1101, 1994.
69. JG Tarter. Anal Chem 56:1264, 1984.
70. RD Rocklin, CA Pohl, JA Schibler. J Chromatogr 411:107, 1987.
71. MW Martin, RA Giacofel. In: P Jandik RM Cassiday, eds. Advances in Ion Chromatography, vol 1. Franklin, Ma: Century International, 1989, p. 119.
72. H Sato, A Miyanga. Anal Chem 61:122, 1989.

73. DT GJerde, JV Benson. Anal Chem 62:612, 1990.
74. PE Jackson, P Jandik, J Li, J Krol. J Chromatogr 546:189, 1991.
75. T Sunden, A Cedergren, DD Siemer. Anal Chem 56:1085, 1984.
76. DD Siemer, VJ Johnson. Anal Chem 56:1033, 1984.
77. H Shintani, PK Dasgupta. Anal Chem 59:802, 1987.
78. SW Downey, GM Hieftje. Anal Chim Acta 153:1, 1983.
79. LG Galante, GM Hieftje. Anal Chem 59:2293, 1987.
80. LG Galante, GM Hieftje. Anal Chem 60:995, 1988.
81. H Shintani, P Dasgupta. Anal Chem 59:1963, 1987.
82. I Berglund, P Dasgupta. Anal Chem 63:2175, 1991.
83. S Laksana, PR Haddad. J Chromatogr 602:57, 1992.
84. A Siriraks, J Stillian. J Chromatogr 640:151, 1993.
85. PR Haddad, S Laksana, RG Simons. J Chromatogr 640:135, 1993.
86. Y Okamoto, N Sakamoto, M Yamamoto, T Kumamaru. J Chromatogr 539:221, 1991.
87. DL Strong, PK Dasgupta, K Friedman, JR Stillian. Anal Chem 63:480, 1991.
88. DL Strong, PK Dasgupta. J Membr Sci 57:321, 1991.
89. JB Li, P Jandik. J Chromatogr 546:395, 1991.
90. D Zhou, DJ Pietrzyk. Anal Chem 64:1003, 1992.
91. S Chen, DJ Pietrzyk. J Chromatogr 671:73, 1994.
92. DT Gjerde, JS Fritz, G Schmuckler. J Chromatogr 186:509, 1979.
93. DT Gjerde, G Schmuckler, JS Fritz. J Chromatogr 187:35, 1980.
94. JS Fritz, DT Gjerde, RM Becker. Anal Chem 52:1519, 1980.
95. SA Shamsi, ND Danielson. J Chromatogr 653:153, 1993.
96. N Hirayama, M Maruo, A Shiota, T Kuwamoto. J Chromatogr 707:384, 1995.
97. T Okada, T Kuwamoto. Anal Chem 57:258, 1985.
98. T Okada. J Chromatogr 403:27, 1987.
99. C Erkelens, HAH Billiet, L DeGalan, EWB DeLeer. J Chromatogr 404:67, 1987.
100. JE Girard, N Rebbani, PE Buell, AHE Al-Khalidi. J Chromatogr 448:355, 1988.
101. TH Walter, DJ Cox In: P Jandik, RM Cassidy, eds. Advances in Ion Chromatography, vol 2. Franklin, MA: Century International, 1990, p. 179.
102. T Nakamura, T Yano, A Fujita, S Okashi. J Chromatogr 130:384, 1977.
103. M Yamamoto, H Yamamoto, Y Yamamoto, S Matsushita, N Baba, T Ikushiga. Anal Chem 56:832, 1984.
104. S Matsushita. Anal Chim Acta 172:249, 1985.
105. G Schwedt, B Kondratjonok. Fresenius Z Anal Chem 332:855, 1989.
106. K Wayakawa, T Sawada, K Simbo, M Miyazaki, Anal Chem 59:2241, 1987.
107. K Hayakawa, M Miyazaki. LC–GC 6:509, 1988.
108. DT Gjerde, JS Fritz. J Chromatogr 188:391, 1980.
109. D Wong, P Jandik, WR Jones, and A Hagenaars. J Chromatogr 389:279, 1987.
110. DT Gjerde. J Chromatogr 439:49, 1988.
111. RCL Foley, PR Haddad. J Chromatogr 366:13, 1986.
112. PR Haddad, RC Foley. Anal Chem. 61:1435, 1989.
113. T Miller Jr. Adv Instrum 38:347, 1983.
114. NE Fortier, and JS Fritz. Talanta 32:1047, 1985.
115. G Schomburg, P Kolla, MW Läubli. Am Lab 21(May):92, 1989.
116. LM Nair, R Saari-Nordhaus, JM Anderson Jr. J Chromatogr 640:41, 1993.
117. MW Läubli, B Kampus. J Chromatogr 706:103, 1995.
118. H Small, TE Miller Jr. Anal Chem 54:462, 1982.
119. JH Sherman, ND Danielson. Anal Chem 59:490, 1987.
120. JH Sherman, ND Danielson. Anal Chem 59:1483, 1987.
121. WR Jones, P Jandik, AL Heckenberg. Anal Chem 60:1977, 1988.
122. WR Jones, P Jandik. Res. Dev Sept:92, 1988.
123. RS Deelder, MGF Kroll, AJB Beeren, JHM Van den Berg. J Chromatogr 149:669, 1978.

124. IS Krull, EP Lankmayr. Am Lab 14(May):18, 1982.
125. SJ van der Wal. J Liq Chromatogr 6:37, 1983.
126. RB Rubin, SS Heberling. Am Lab. 19(May):46, 1987.
127. T Imanari, S Tanabe, T Toida, T Kawanishi. J Chromatogr 250:55, 1982.
128. SE Meek, DJ Pietrzyk. Anal Chem 60:1397, 1988.
129. DJ Pietrzyk, MJ Lovdahl. In: P Jandik, RM Cassidy, eds. Advances in Ion Chromatography, vol 2. Franklin, MA: Century International, 1990, p. 255.
130. MJ Lovdahl, DJ Pietrzyk. J Chromatogr 602:197, 1992.
131. RG Anderson, G Nickless. Analyst 92:207, 1967.
132. JS Fritz, JN Story. Anal Chem 46:825, 1974.
133. RM Cassidy, S Elchuk. J Liq Chromatogr 4:379, 1981.
134. J Morris, JS Fritz. Anal Chem 66:2390, 1994.
135. PE Buell, JE Girard. In: JG Tarter, ed. Ion Chromatography. New York: Marcel Dekker, 1987, p. 235.
136. D Gjerde, H Mehra. In: P Jandik, RM Cassidy, eds. Advances in Ion Chromatography, vol 1. Franklin, MA: Century International, 1989, p. 139.
137. JS Fritz. J Chromatogr 546:111, 1991.
138. K Tanaka, T Ishizuka, H Sunahara. J Chromatogr 174:153, 1979.
139. RM Wheaton, WC Bauman. Ind Eng Chem 45:228, 1953.
140. P Jandera, J Churacek. J Chromatogr 86:351, 1973.
141. BK Glod, W Kemula. J Chromatogr 366:39, 1986.
142. BK Glod, A Piasecka, J Stafiej. J Chromatogr 457:43, 1988.
143. VT Turkelson, M Richards. Anal Chem 50:1420, 1978.
144. PR Haddad, PE Jackson. J Chromatogr 447:155, 1988.
145. MH Dunn. LC–GC 7:138, 1989.
146. WR Jones, P Jandik, MT Swartz. J Chromatogr 473:171, 1989.
147. HF Botte, L Joergensen. J Chromatogr. 602:27, 1992.
148. R Widiastuti, PR Haddad, PE Jackson. J Chromatogr 602:43, 1992.
149. KK Kihara, S Rokushika, H Hatano, J Chromatogr 410:103, 1987.
150. K Tanaka, JS Fritz. Anal Chem 59:708, 1987.
151. T Okada. Anal Chem 60:1666, 1988.
152. W Rich, F Smith, L McNeill, T Sidebottom. In: JD Mulik, E Sawicki, eds. Chromatographic Analysis of Environmental Pollutants, vol. 2. Ann Arbor, MI: Ann Arbor Science Publisher, 1979, p. 17.
153. JG Chen, SG Weber, LL Glavina, FF Cantwell. J Chromatogr 656:549, 1993.
154. PG Rigas, DJ Pietrzyk. Anal Chem 58:2226, 1986.
155. PG Rigas, DJ Pietrzyk. Anal Chem 59:1388, 1986.
156. PG Rigas, DJ Pietrzyk. Anal Chem 60:1650, 1988.
157. JD Lamb, RG Smith, J Jagodzinski. J Chromatogr 640:33, 1993.
158. DF Hilton, PR Haddad. J Chromatogr 361:141, 1986.
159. RM Cassidy, S Elchuk. J Chromatogr 262:311, 1983.
160. DJ Barkley, DJ Blanchette, RM Cassidy, S Elchuk. Anal Chem 58:2222, 1986.
161. RM Cassidy, S Elchuk. Anal Chem 54:1558, 1982.
162. E Papp, A Fehervari. J Chromatogr 447:315, 1988.
163. CA Pohl. US Patent 4,265,634, 1981.
164. PK Dasgupta. Anal Chem 56:769, 1984.
165. BA Bidlingmeyer, CT Santasania, FV Warren Jr. Anal Chem 59:1843, 1987.
166. PW Carr, WE Barber. J Chromatogr 260:89, 1983.
167. PG Rigas, DJ Pietrzyk. Anal Chem 60:454, 1988.

12

Hydrophobic Interaction Chromatography of Biopolymers

Ziad El Rassi

Oklahoma State University, Stillwater, Oklahoma

I. INTRODUCTION

Hydrophobic interaction chromatography (HIC), employing weakly hydrophobic sorbents and descending salt gradients, is exclusively used in the separation of large biomacromolecules and, in particular, proteins. Solute retention is based on the noncovalent association between the nonpolar moieties of the biopolymer solute and the weakly hydrophobic ligand of the stationary phase. This association is driven by the use of aqueous mobile phases of high-ionic strengths. Usually, the stationary phase consists of a highly hydrophobic organic layer to which widely spaced, short alkyl or small aryl functions are attached. This rather "friendly environment" induces little or no irreversible protein unfolding, thereby making HIC a nondenaturing chromatographic method highly suited for the purification of bioactive proteins. In other words, the energetically "soft" stationary phases usually do not undergo strong interactions with internal hydrophobic residues in the protein molecule.

This chapter is aimed at (1) providing a brief accounting for the fundamentals of retention, (2) describing the chromatographic system, including the stationary and mobile phases, (3) discussing the operating conditions that apply to HIC of biopolymers at large, and (4) providing typical recent applications.

II. SOME FUNDAMENTALS OF RETENTION

Only a brief summary of the underlying retention is given here. For more rigorous and detailed treatments, the interested reader may consult the referenced literature.

In HIC, the retention process involves an interaction between two nonpolar groupings: the hydrophobic moiety of the solute and the weakly hydrophobic ligand bonded to the surface of the solid support. According to the thermodynamic model of Horváth et al. [1–6], which is based on the solvophobic theory of Sinanoglu [7], the free-energy change on solute binding is related to the process of the solvation of the solute, the stationary phase ligands, and the complex of the two. The solvation process of the solute involves two distinct steps. First, a cavity in the solvent is created of the same shape and size as the incoming solute. Second, the solute enters the cavity and subsequently interacts with its surroundings through electrostatic and van der Waals forces. The free-energy for cavity formation is of particular importance, for it is mainly responsible, together with the van der Waals interaction, for the hydrophobic effect.

In chromatography, solutes undergo a series of sorption–desorption while moving down the column. According to the hydrophobic theory [1], the net free-energy related to the reduction of the cavity size as a result of solute binding or sorption ΔG_c^0 increases with the contact area between the solute and the stationary phase ligand ΔA, and with the microthermodynamic surface tension of the mobile phase. In HIC, ΔG_c^0 is given by [5]

$$\Delta G_c^0 = -\Delta A \sigma m + \text{constant} \tag{1}$$

which reflects the direct proportionality of ΔG_c^0 on the salt molality m and the molal surface tension increment σ of the salt. ΔA is given by [6]

$$\Delta A = (A_l + A_x) - A_{xl} \tag{2}$$

where A_l is the surface area of the stationary phase ligand, A_x the surface area of the cavity (i.e., surface area of the solute), and A_{xl} is the surface area of the solute–stationary phase complex. Thus, ΔA represents the molecular surface area by which the total cavity area is reduced after solute binding to the stationary phase ligand. In other words, ΔA is the surface area no longer accessible to the solvent when the complex formation occurs (i.e., the nonpolar contact area between the two species in the complex).

According to the hydrophobic theory [1–6], the higher the value of the surface tension γ, the greater the retention. In HIC with aqueous buffer solutions containing neutral salts, γ increases linearly with increasing the molal concentration m of the salt in the eluent as follows [1,5]

$$\gamma = \gamma^0 + \sigma m \tag{3}$$

where γ^0 is the surface tension of pure water. Therefore, the capacity factor k' increases with increasing salt concentration in the eluent. The solutes are retained in HIC in an aqueous mobile phase containing a high salt concentration. Because of the weak hydrophobic character of the stationary phase, plain water is usually employed as a strong eluent to elute the solutes.

The retention behavior of proteins in HIC as a function of the salt concentrations in the eluent follows the trends predicted by the solvophobic theory [5,8,9]. The capacity factor k' first decreases with increasing salt concentration because the electrostatic effect of the salt weakens solute binding. With further increase in the salt concentration, hydrophobic interaction becomes predominant so that k' increases, and the dependence of log k' on salt molality becomes linear at sufficiently high salt concentration, according to the following relation [5]:

$$\log k' = \lambda m + C \tag{4}$$

where C is an amalgam of the salt-independent terms and λ is the limiting slope of the plot of log k' versus salt molality m. The limiting slope λ, termed the hydrophobic interaction parameter, is given in the simplest cases by

$$\lambda = \sigma \Delta A \tag{5}$$

This slope correlates with the molecular weight of the biopolymer, when a given column was used, and with the hydrophobic character of the stationary phase when a given set of proteins was used under otherwise identical conditions [8]. In other words, λ was strongly influenced by ΔA. Also, λ was largely affected by σ, and the slopes of the lines (i.e., plots of log k' versus m) for sodium sulfate (larger σ) were greater than for ammonium sulfate for various model proteins [10]. With certain salts, such as $MgCl_2$ and $CaCl_2$, owing to specific salt binding by the protein [11], the observed retention behavior is different from that predicted by the surface tension argument [12].

The effect of salt on protein adsorption in HIC has also been treated by applying Wyman's thermodynamic theory of linked functions for equilibrium reactions [13,14]. The linked functions approach [15] allowed the correlation of HIC adsorption to preferential interactions of

the salts with the stationary phase and the protein analyte [16,17] (see Ref. [18] for further details).

In addition to van der Waals interactions with both the stationary and the mobile phases, the solute undergoes polar interaction (e.g., electrostatic interaction) with the mobile phase. Thus under a given set of conditions, the introduction of polar groups into the solute molecule usually results in decreasing retention. Also, the ionization of the solute with mobile phase pH strongly affects solute retention. Usually, solute retention decreases with increasing ionization owing to increasing polar interactions with the mobile phase. Thus, the control of pH of the eluent is an important means to adjust the retention of the analytes.

Increasing column temperature is normally accompanied by an increase in retention [19]. This is because HIC is an entropy-driven process. Since HIC employs weakly hydrophobic stationary phases and aqueous eluents, both the protein and the stationary phase ligands are associated with structured water molecules. On solute binding, the surfaces of the solute molecule and the stationary-phase ligands release the structured water; consequently, the entropy of the bulk solution increases. In addition, because van der Waals forces are the major nonpolar interaction forces and the contact area of the protein with the surface is small, ΔH^0 may also be a small positive or negative value. According to the following equation:

$$\Delta G^0 = \Delta H^0 - T\Delta S^0 \tag{6}$$

the Gibbs free energy ΔG^0 is controlled by a large positive entropy change and, therefore, increases with temperature. According to the following equation

$$\ln k' = \ln \varphi - \left(\frac{\Delta G^0}{RT}\right) \tag{7}$$

where R is the gas constant, φ is the phase ratio, and T is the absolute temperature, the capacity factor would increase with increasing temperature. This may be considered an advantage for proteins, in the sense that subambient temperature can be used to achieve weaker interaction and bring about elution and separation of proteins under mild conditions, with little or no denaturation of the analytes. (For other recent treatments of the fundamentals of HIC, see Refs. [18,20–22].

III. THE CHROMATOGRAPHIC SYSTEM

A. Stationary Phase

Numerous sorbents have been used in HIC. They are based on hydrophilized silica gels or, more often, on hydrophilic organic gels, such as cross-linked or non–cross-linked agarose, methacrylate gel, and TSK gel. HIC was originally introduced (in the early 1970s [19,23]) for protein separation using low ligand-density alkyl– or aryl–agarose gels. This type of gel is still used in traditional HIC, when separation is carried out at low mobile-phase flow velocity using either gravity-driven flow or low-pressure pumping systems.

To adapt the HIC technique to high-performance ligand chromatography (HPLC), rigid microparticulate silica- or organic-based stationary phases were developed. This usually involves covering the surface of the rigid support with a hydrophilic coating that becomes highly hydrated when in contact with aqueous mobile phases. The hydrophobic ligands, usually widely spaced, short alkyl or aryl functions, are attached to the strongly hydrophilic surface layer. This sublayer (i.e., hydrophilic surface layer) also serves as an inert spacer, so that the incoming solute would interact with the hydrophobic ligands and not with the support proper. This mimics the inertness and highly hydrated nature of polysaccharide gels (i.e., agarose) that are used as the support in traditional low-pressure HIC.

Silica and polymeric supports having surface-bound hydrophilic layers, which were originally designed for size-exclusion chromatography of biopolymers, were further derivatized through their hydroxyl groups with butyl, phenyl [24], or polyether functions [25]. Weakly

hydrophobic polyamide ligands [26,27], as well as methyl, hydroxypropyl, propyl, benzyl, or pentyl [28], were attached to silica to produce HIC sorbents. Ether ligands [29] as well as polyethylene glycol (molecular weight, MW 400) [30], were covalently attached to microparticulate silica supports. A series of poly(alkylaspartamide)–silica stationary phases were also introduced for HIC of proteins [31]. Silica gels with surface-bound polyvinyl alcohol or oligoaminoalcohol ligands [8], or amide functions [32] are useful for HIC of proteins. Hjertén et al. [33] introduced rigid microparticulate highly cross-linked agarose that may be used in HIC of proteins under HPLC conditions. Separon HEMA materials, which are copolymers of 2-hydroxyethyl methacrylate (HEMA) and ethylene dimethacrylate, are rigid materials that can be used under HPLC conditions as HIC sorbents, without any modification [34]. However, for enhanced separation efficiency and selectivity toward proteins, simple modification of Separon HEMA with benzoyl chloride and especially with 1,2-epoxy-3-phenoxypropane was later recommended [35]. In another approach reversed-phase chromatography (RPC) columns were transformed dynamically to HIC column by coating the RPC column with nonionic surfactant of polyoxyethylene type [36].

Recently, polyvinylpyrrolidone (PVP)-coated silica sorbents were prepared by reacting a copolymer of vinylmethyldiethoxysilane and vinylpyrrolidone with wide-pore silicas [37]. Physicochemical measurements (e.g., nitrogen adsorption, porosimetry, and inverse size-exclusion) have shown that the coating with PVP retains the wide-pore structure. Besides exhibiting good selectivity and separation ability toward proteins and peptides in the HIC mode with high ionic strength eluents, the PVP-coated silica was also useful in the size-exclusion mode when low ionic strength or straight water was used as the eluent.

A novel concept for HIC of proteins is the performance of separations on continuous beds [38]. This method is based on polymerization of the monomers, including the interacting ligands, directly in the chromatographic tube [38–40]. This single-step gel bed process yields a more homogeneous bed than the one obtained by conventional packing. The net result is a higher resolution. The bed is typically formed by introducing into the tube a mixture of *N,N'*-methylenebisacrylamide, butylacrylate, ammonium persulfate, and TEMED, and allowing the bed to polymerize for 5 h. It is thought that the compressed gel plug (i.e., the chromatographic bed) consists of intercommunicating "channels," the "walls" of which are impermeable to proteins. The gel plug is then compressed 10 to 15-fold, which decreases the average diameter of the channels. The gel bed formed shows a resolution that, at constant gradient volume, is independent of or increases with an increase in flow rate, similar to the behavior of compressed nonporous agarose bed. As shown in Figure 1, this type of gel permits the separation of four different proteins by HIC.

As for other modes of chromatography (e.g., RPC, ion-exchange and affinity), several nonporous HIC column materials have been introduced for the rapid separation of proteins on the time scale of few seconds and minutes. Monodisperse nonporous silica columns with surface-bound amide or ether [41] were introduced for rapid HIC. As expected, differences in selectivity were observed between the amide and the ether phase. Hjertén and Liao [42] and Hjertén et al. [43] converted macroporous agarose beads into nonporous particles by shrinkage and cross-linking in organic solvents, and showed that these beads could be used for high-performance HIC without derivatization, because the 1,4-butanediol diglycidyl ether, used as cross-linker, gives relatively hydrophobic bridges. These particles have the advantage over silica-based materials of being stable up to pH 14. Kato et al. [44] modified a nonporous hydrophilic resin of 2.5-μm–diameter particle into an HIC sorbent by covalently attaching butyl functions to the surface of the rigid particles, and the resulting packing is commercially available under the trade name TSKgel Butyl-NPR. Recently, Kalghatgi [45] introduced a silica-based HIC column by modifying 2.0-μm particle with polyether functions. A mixture of four proteins could be separated in less than 2 min.

HIC has been used extensively in the area of proteins, and only in few instances in the area of nucleic acids [46–58]. Since the early attempts of applying HIC to the purification of nucleic acid fragments (e.g., tRNAs), which were performed at low pressure, the importance

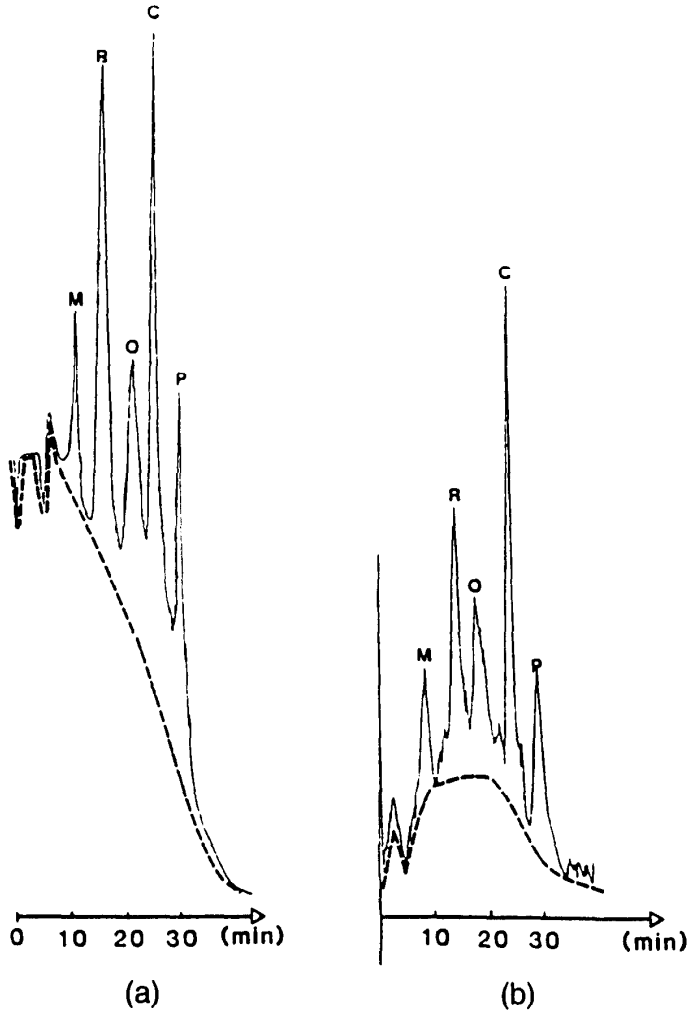


Figure 1 Microcolumn HIC with (a) on-tube and (b) off-tube detection. Bed dimensions, 70 × 0.3-mm id. The sample contained 0.4 μg each of the proteins myoglobin (M), ribonuclease (R), ovalbumin (O), α-chymotrypsinogen A (C), and phycoerythrin (P); sample volume, 1 μL. A linear 35-μL gradient from 0.01 M sodium phosphate (pH 7.0), containing 2.25 M ammonium sulfate, to 0.01 M sodium phosphate (pH 7.0), containing 0.25 M ammonium sulfate, was used at a flow rate of 1-μL min^{-1}. (From Ref. 38.)

of the nature of the stationary phase [48] was readily appreciated. For example, Sepharose 4B (i.e., nonderivatized agarose used for gel filtration) proved more effective in tRNA fractionation than Sepharose 2B, and the cross-linked agarose gel Sepharose 4B CL [48]. Similarly, phenyl-Sepharose 4B CL and Spheron 1000 gave some resolution, but they were inferior to Sepharose 4B. On the other hand, Ultrogel, which is a composite of agarose and polyacrylamide gel, was useful for the further resolution of Sepharose 4B fractions. According to the author [48] the mechanism of retention seems to be adsorption, rather than hydrophobic interaction, because the retention decreased as temperature was increased. This means that the retention process is exothermic, and the free-energy change is primarily enthalpic, rather than entropic. The explanation that the retention is based on adsorption may be favored because Sepharose 4B had no hydrophobic sites and it is used for gel filtration. Although Ultrogel and phenyl-Sepharose have surface-bound hydrophobic sites, they showed the same temperature dependence as the Sepharose 4B. This may suggest that the polysaccharide matrix (i.e., agarose support) of Ultrogel and phenyl-Sepharose still has some effects on retention, and it

may be that a dual retention mechanism is involved, with adsorption being the primary component. Other mechanistic studies were conducted to explain the binding mechanisms of tRNAs on neutral polysaccharide columns [53–55]. These authors suggested that the mechanism of retention involves two distinct steps. First, the high ionic strength of the initial buffer induced "interfacial precipitation" of tRNAs, which could be released as the salt concentration was reduced. Second, solubilized tRNAs experienced "adsorptive retardation" through hydrophobic interaction with the stationary phase as they were eluted from the column.

Different adsorbents are thought to separate according to different principles, thus complementing each other. In fact, naphthoyl-Sepharose CL-6B [47] was useful in the fractionation of tRNAs using descending salt gradient. This adsorbent offered different selectivity (different elution order) than Sepharose 4B. Other functionalities were needed for DNA fragments or for poly(A^+)mRNA. These involved trityl-agarose or trityl-cellulose [49]. Polynucleotides that associate with the trityl sorbents are thought to do so through the formation of hydrophobic bonds between themselves and the trityl groups anchored to the resin. However, the "unpredicted specificity for poly A tracts that tritylated sorbent exhibits is thought to be based on the more open, partially unstacked, and hence more accessible management of this polypyrine's bases" [49]. A similar-binding mechanism was postulated for denatured DNA [49].

Using HPLC approach for HIC of nucleic acid fragments, Pearson et al. [56] have shown that RPC columns based on silica supports can be used for the fractionation of tRNAs using decreasing salt gradient. Because unsubstituted Sepharose proved useful for HIC of tRNAs, the authors [56] thought that a short *n*-alkyl–chain-bonded silica should be more useful than the regular C_{18} column. The C_1, C_2, and C_4 type all worked well on macroporous, microparticulate silica gels to affect RNA separation, and a very low concentration of organic modifier, such as propanol, ethanol, or methanol, enhanced the fractionation process. Other variables, such as initial salt concentration, temperature, and pH, also affected the selectivity.

El Rassi and Horváth [57,58] introduced microparticulate-bonded stationary phases for the separation of nucleic acid fragments by either HIC or ion-exchange chromatography using gradient elution, with decreasing or increasing salt concentration in the eluent, respectively. These stationary phases were based on silica gels having weak cationic- or hydrophobic-binding sites. The logarithmic retention factor of $tRNA^{Val}$ versus the concentration of salt in the eluent obtained on the various columns are shown in Figure 2. As can be seen in this figure, although log k' increased linearly with the concentration of phosphate in the eluent for the purely HIC column (e.g., HI-300 I column and HI-1000 column), the log k' versus concentration of phosphate decreased, first at low-ionic strength and then increased linearly at higher-ionic strength with the column having both cationic and hydrophobic sites on the surface (e.g., IE-300 I and IE-300 II columns). In these studies, the decrease in retention with increasing salt concentration at low-ionic strength suggests that retention is governed by electrostatic interactions. However, at high-ionic strength the increase in retention with salt concentration indicates the predominance of hydrophobic interaction in the mechanism of retention. The dual-retention mechanism is illustrated in Figure 3, in which Figure 3a and b show that electrostatic interactions are the driving forces for retention and separation, and in Figure 3c hydrophobic interactions are responsible for retention. Frequently, isocratic elution was sufficient to separate tRNAs on these columns (see Fig. 3a and b). Also, purely HIC column provided the separation of at least seven tRNAs either isocratically at high salt concentration or by decreasing salt gradient.

In another report by El Rassi and Horváth [8], various stationary phases, with purely hydrophobic ligands, were introduced for HIC of proteins and tRNAs. This study demonstrated that the HIC of proteins and nucleic acids necessitated a set of stationary phases having appropriate hydrophobic ligands that are suited for each type of compounds. The separation of tRNAs is best carried out on stationary phases that are more hydrophobic than those optimal for HIC of proteins. Stationary phases with covalently bound polyether chains at the surface were most suitable for HIC of proteins and tRNAs. As shown in Figure 4, for tRNAs, the POE 4C stationary phase with shorter polyether chains, exhibits higher retentivity and gives

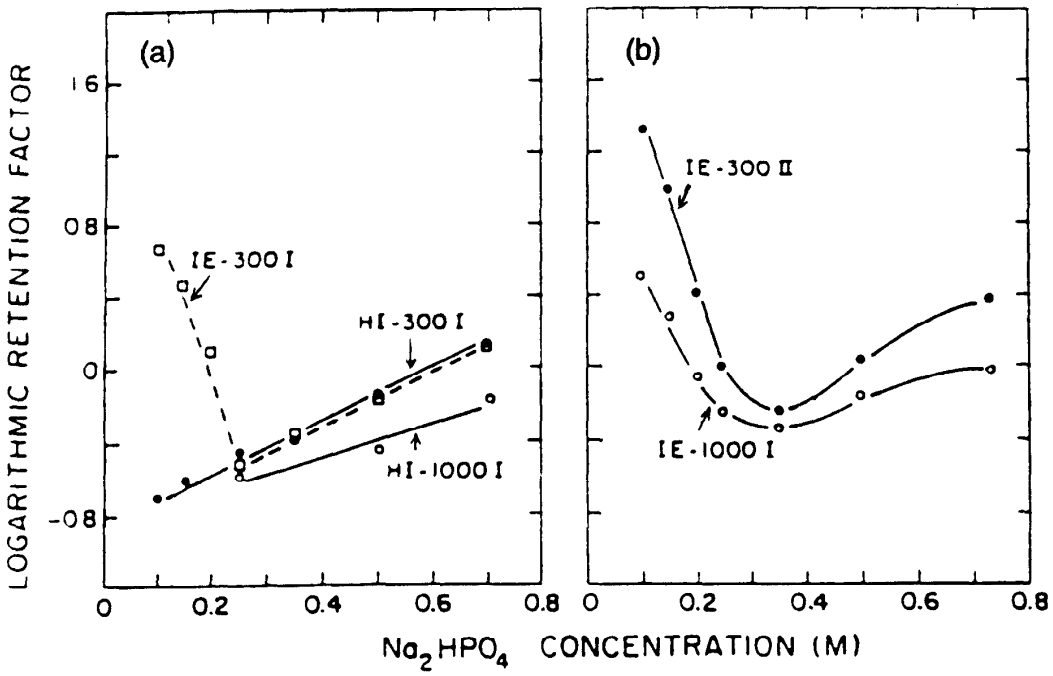


Figure 2 Plots of logarithmic retention factor of $tRNA^{Val}$ on different stationary phases against disodium hydrogen phosphate concentrations in the eluent at pH 6.3. (From Ref. 57.)

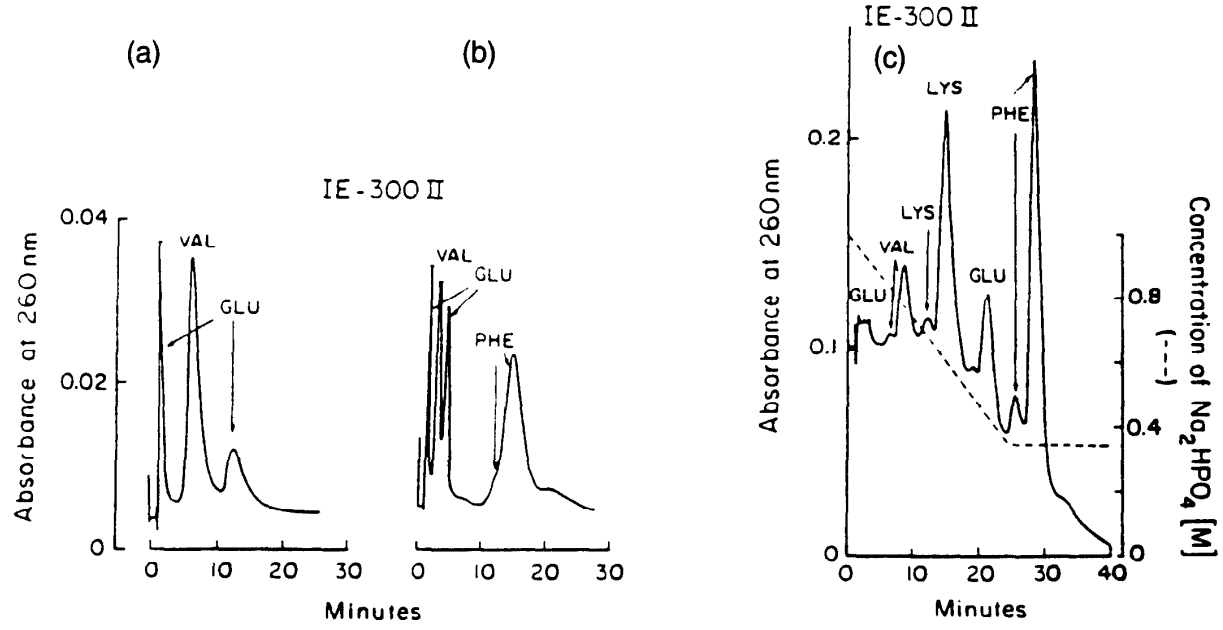


Figure 3 Chromatograms of tRNAs: Column, 100 × 4.6-mm id, 5-μm IE-300 II; flow-rate, 1 mL min^{-1}; temperature, 25°C. Isocratic elution (ion-exchange mode) in (a) and (b): eluent, 0.15 M disodium hydrogen phosphate, pH 6.3, (a) containing 10 mM Mg^{2+}, (b) containing 3.75 mM *n*-decylbetaine. Descending salt gradient (HIC mode) in (c): linear gradient in 25 min from 0–100% (v/v) gradient former followed by 15 min of isocratic elution. Starting eluent, 1.0 M disodium hydrogen phosphate, pH 6.3; gradient former, 0.35 M disodium hydrogen phosphate, pH 6.3. (From Ref. 57.)

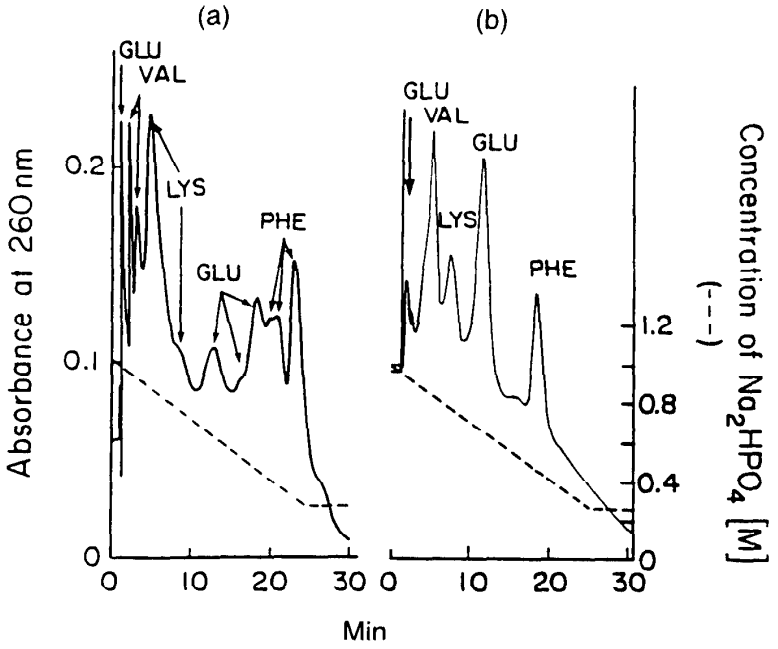


Figure 4 Separation of tRNAs by HIC. Column, 100 × 4.6 mm, (a) POE 4C and (b) POE 4M (POE stands for polyethylene oxide, 4C = 400 MW; 4M = 4000 MW); flow-rate, 1 mL min^{-1}, temperature, 25°C. Linear gradient in 25 min from 1.0 M to 0.25 M phosphate buffer, pH 6.3. (From Ref. 8.)

higher resolution than the POE 4M with ten times longer polyether chains (i.e., less hydrophobic) bound to the surface.

Among the stationary phases available for HIC of proteins, the more hydrophobic are those bearing a short alkyl chain at the surface of the support, followed by phenyl, polyether, and glycol phases [59]. Although the overall efficiencies of most HIC columns were broadly similar relative to most proteins, some proteins did chromatograph with enhanced efficiency on some packing. The elution order of individual proteins was, with one or two exceptions, similar for all columns tested using comparable mobile phases. In an earlier report [29] concerning polyether stationary phases, the retention increased, with no significant change in selectivity, when the alkyl end group was varied from methyl to ethyl. Stationary phases with a butyl end group irreversibly adsorbed proteins, which were not eluted, even with a dilute buffer [29]. On the other hand, for poly(alkylaspartamide)–silica, not only did changing the length of the ligand from ethyl to propyl increase protein retention, but the selectivity of the separation was affected significantly [31].

The widely differing sorbents now available for HIC, have recently prompted researchers [60–62] to provide ways for characterizing the various stationary phases in the aim of generating some guidelines on how to select the desired column for a given separation problem.

It is possible to use the same column for performing more than one mode of chromatography? In other words, with a multiliganded column, is it possible to turn on and off each mode of chromatography independently? Several attempts have been made in this direction, and researchers have exploited the composite nature of some of the available packing to accomplish at least two modes of chromatography. Typical examples include (1) columns with weak cation- and hydrophobic-binding sites could be used for the separation of tRNAs (as discussed earlier) by either HIC or ion-exchange chromatography [57]; (2) a column designed for metal interaction chromatography works in HIC by changing the composition of the mobile phase [63]; (3) polyether columns allow size exclusion as well as HIC when operated either with low ionic strength mobile phases or with high ionic strength eluents [29]; (4) silica-

based stationary phases which were originally designed for size-exclusion chromatography of proteins, have the potential to separate proteins by HIC at high salt concentration [64]; and (5) ion-exchange columns were also useful at high salt concentration in the eluent to perform HIC of proteins [65].

Very recently, the concept of pore-size-specific functionalization of porous polymers to prepare media in which the surface of pores within different size ranges may be endowed with different chemistries [66] was developed. This concept, which resembles that of the internal-surface reversed-phase media advanced by Hagestam and Pinkerton [67], relies on the use of catalysts with defined molecular volumes that are able to perform a chemical modification process only in those pores large enough to allow their access. The net result of this modification is the formation of particles of different chemistries, segregated in different size pores. The concept was employed in the preparation of a single packing in which hydrophobic interaction chromatography of proteins and reversed-phase chromatography of small molecules can proceed consecutively. This bimodal distribution of chemistries in the pores consists of four steps, and used monodisperse 10-μm poly(glycidylmethacrylate–coethylene dimethacrylate) beads. Briefly, the large pores of each bead were provided with phenyl groups interspersed among hydrophilic functionalities, while a much higher surface concentration of hydrophobic phenyl groups was introduced into the small pores. Because of this distribution, no protein interaction with any highly hydrophobic surface was observed during chromatography. The use of such columns in the separation of small hydrocarbon or drug molecules by RPC followed by the separation of proteins by HIC is shown in Figure 5. The dependence of the logarithmic retention factor on salt concentration followed the normal behavior observed

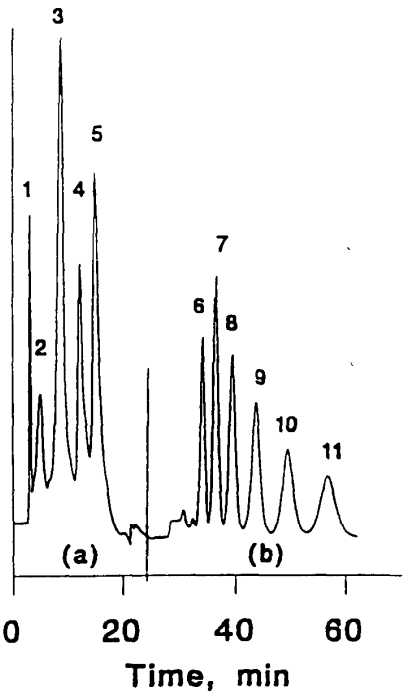


Figure 5 Separation of proteins and alkylbenzenes in consecutive hydrophobic interaction and reversed-phase chromatographic modes: column size, 100 × 8 mm id; HIC, mobile-phase gradient decreasing from 1.7 to 0 M ammonium sulfate in 20 mM phosphate buffer (pH 7) in 15 min; RPC, mobile phase of 0.02 M phosphate buffer solution (pH 7)–acetonitrile mixture (65:35 v/v); flow-rate, 1 mL min^{-1}; UV detection; peaks, cytochrome *c* (1); ribonuclease A (2); conalbumin (3); lysozyme (4); soya bean trypsin inhibitor (5); benzene (6); toluene (7); ethylbenzene (8); propylbenzene (9); butylbenzene (10); and amylbenzene (11). (From Ref. 66.)

in HIC (linear at high salt concentration) while the log k' versus the percentage acetonitrile in the eluent was linear, as normally encountered in RPC.

B. Mobile Phase

The HIC separations are usually carried out with eluents containing relatively high salt concentrations. The sample is first loaded onto a column that is equilibrated with a mobile phase of relatively high salt concentration. Subsequently, the adsorbed proteins are eluted by stepwise or gradient elution at decreasing salt concentration in the eluent. In this adsorption–desorption process, the nature and concentration of the neutral salt play an important role in determining the magnitude of retention and selectivity.

Generally, and in the absence of specific interactions between the salt and the protein, the effectiveness of the salt in promoting hydrophobic interaction follows the Hofmeister series, which is based on the ability of the salt to cause precipitation of proteins from aqueous solutions. Protein retention is stronger with kosmotropic salts (also called antichaotropic salts; i.e., water structure makers) that increase the surface tension of aqueous solutions (e.g., phosphates, sulfates, and citrates) than with chaotropic salts (water structure breakers) such as perchlorates and thiocyanates.

The neutral salt must be highly soluble (solubility > 1.0 M) so that it can be added in relatively high concentration to the eluent to induce hydrophobic interaction. Other important factors for choosing the neutral salt are (1) viscosity, (2) UV transparency, and (3) stability at alkaline pH. Among the useful salts, ammonium sulfate is the least viscous, whereas sodium sulfate and sodium phosphate are characterized by a higher molal surface tension increment. On this basis, sodium sulfate and sodium phosphate exhibited higher retention, whereas ammonium sulfate provided a better separation efficiency and sharper peaks [68] under otherwise identical conditions. Although ammonium sulfate has a very high solubility and is available in high purity, the chromatography at alkaline pH is accompanied by decomposition of the salt and liberation of ammonia. Here, monosodium glutamate or sodium sulfate is an alternative salt [69].

The choice of the salt and its concentration in the eluent is dictated by the hydrophobic character of the proteins and that of the stationary phase. Very recently, the effect of different salts on the separation of proteins on an alkyl-Superose column was examined using gradient elution measurements [70]. The salts had different effects on the retention of the hydrophobic and hydrophilic proteins. Whereas sodium acetate, in comparison with ammonium sulfate, increased the retention of the hydrophobic and decreased those of the hydrophilic proteins, sodium citrate exhibited the reverse behavior.

When the protein or the stationary phase are relatively hydrophobic, the inclusion of small amount of organic solvent (ethanol or propanol) is recommended to bring about better mass recovery of the protein [19]. Also, the addition of denaturing agents, such as urea and guanidine chloride, may also be useful in eluting strongly bound proteins [71]. For hydrophobic and insoluble proteins, the addition of ionic or nonionic surfactants at concentrations below their critical micelle concentration should be considered if mild conditions do not suffice to elute the proteins [72]. In some instances, the detergent is added to solubilize the solutes, such as membrane proteins, and to keep the biomolecules from forming molecular aggregates in the eluent [73]. In addition, zwitterionic detergents, which have less tendency to denature proteins, have been suggested as useful mobile-phase additives in gradient elution HIC. They modulate the selectivity of separations of globular proteins [74].

Recently, a novel approach has been introduced for the elution and separation of proteins by HIC [75]. It involved the use of binary and ternary salt gradients with mixtures of chaotropic and antichaotropic salts as well as organic salts. At constant eluent surface tension, a gradient with two or three aqueous salt solutions was superior to a single-salt gradient in modulating HIC retention and selectivity. The effect was attributed to the competitive salt-specific binding to the protein molecule or the stationary phase. In general, with

chaotropic–antichaotropic salt gradient systems, the retention of basic protein increased, whereas that of acidic proteins either decreased or remained unchanged with the use of chaotropic salts. At the same surface tension of the eluent, KSCN and $KClO_4$ yielded different selectivity. The addition of organic salts, such as tetrabutylammonium bromide, was suitable for the separation of proteins having a wide range of isoelectric points [75].

IV. SOME GENERAL ASPECTS OF HIC OF PROTEINS AND SELECTED APPLICATIONS

Hydrophobic interaction chromatography is virtually nondenaturing for proteins, because organic solvent is not required for elution, and the stationary phases, which are mildly hydrophobic, would not cause any substantial change in the conformation of the protein molecule. As a typical example, ceruloplasmin that was denatured in RPC was recovered from an HIC column in its native structure [76]. Also, β-2-glycoprotein I, which binds lipid because it is a constituent of lipoprotein, showed two distinct peaks in HIC versus a single peak in RPC. This behavior was explained by the fact that some of the molecules are associated with lipids that can be washed by the organic solvent used in RPC, thereby yielding a single peak [76]. The low-denaturing potential of HIC was proposed to be used as a tool for protein refolding [77]. For instance, strong denaturing conditions are often used for harvesting recombinant proteins from cells. Guanidine hydrochloride denatured recombinant human interferon gamma that was extracted from *Escherichia coli*. When injected on an HIC column, the protein refolded and was purified with high bioactivity recovery [77].

However, depending on the actual structure of the ligands of the stationary phase, denaturation can also be observed on HIC columns. Wu et al. [78] found that polypropyl HIC columns caused human growth hormones to denature. By employing intrinsic fluorescence spectroscopy, Oroszlan et al. [79] studied the kinetics and unfolding of bovine α-lactalbumin on two HIC columns; namely, a methyl ether (C_1) and an ethyl ether (C_2) column. The rate of unfolding of the protein was about four times faster with the C_2 than with the C_1 phase, indicating that the more hydrophobic the column, the stronger its denaturing propensity.

The detection of proteins after HIC separation is mainly achieved by UV, relying on absorption of light of aromatic amino acids, such as tyrosine, tryptophan, and phenylalanine, or on absorption by the peptide bond. Recently, Dou et al. [80] described the use of on-line, postcolumn photolysis, for the electrochemical (EC) detection of proteins at microgram per milliliter levels. The compatibilities of various modes of HPLC including HIC with photolysis–electrochemical detection was demonstrated with the analytical figures of merit. Because of the high salt concentration used in HIC, the postcolumn photolytic derivatization did not work under high potentials because serious baseline drift prevented detection. The chromatogram shown in Figure 6 was obtained at an applied potential of +0.90 V at which, in the absence of irradiation, the EC showed no peaks. Briefly, the mechanism of detection is based on the photochemistry of proteins, which is more complicated than that of amino acids and peptides. The photochemical reactions with proteins may involve the cleavage of disulfide bonds, the photolysis of side-chain amino acids, the aggregation of irradiated proteins, or the change of conformation of proteins [81]. All these factors combined would probably account for the increase of the detectability of proteins in EC by irradiation [80].

Although rigid microparticulate stationary phases are now commercially available for high-performance HIC from several column manufacturers, most of the applications are still carried out by classic low-pressure HIC using aryl– or alkyl–agarose gel as the sorbents. Some of the recent applications (from 1990 to 1994) that used rigid or quasi rigid microparticulate HIC columns are summarized in Table 1. Earlier applications (before 1990) of high-performance HIC have been discussed in recent reviews [18,21,22,82]. Also, the applications of the technique to isolation of glycoproteins [83] has been reviewed recently by the author [20,84].

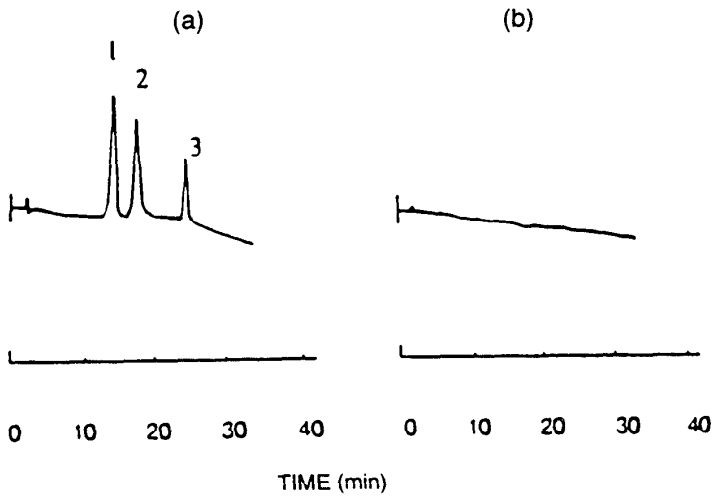


Figure 6 HIC-hv-EC of proteins: on-line, postcolumn photolysis with EC detection using HIC for separation. Peaks: 1, ribonuclease A; 2, lysozyme; 3, α-chymotrypsinogen A. (a) Lamp on; (b) lamp off. (From Ref. 80.)

As can be seen in Table 1, HIC is useful not only for the isolation of proteins, but also for their characterization. Typical examples including characterization of the hydrophobicity of proteins [85–88], assessment of denaturation of proteins [89] or microenvironmental changes in genetically engineered proteins [90], monitoring deamidation or oxidation in the amino acid residues of the protein solute [91], evaluating protein microheterogeneity [91], determination of protein [92] and others. Also important is the use of HIC for method development for protein purification by means of partitioning in aqueous two-phase systems (i.e., liquid–liquid partitioning strategies [93]), which have been known for more than 30 years [94].

Besides its numerous analytical applications, the main area of application of HIC is preparative separation. A typical example of preparative HIC is illustrated in Figure 7, which demonstrates the separation of 1 g crude lipoxidase on a 20 × 5.5-cm–id phenyl-5PW column [95]. The fractionated lipoxidase peak, which is delimited by two vertical lines on Figure 7, showed 84% recovery in terms of enzymatic activity, and was obtained in considerably pure form, revealed by analyzing the fraction by various modes of analytical HPLC, including RPC, HIC, ion-exchange, and size-exclusion chromatography [95]. The usefulness of HIC in preparative work is facilitated by the following: (1) expensive organic solvents are not required for elution in HIC so that pure materials are obtained at minimum cost; (2) the nondenaturing feature of HIC; and (3) the relatively high mass recovery. In preparative work, HIC is a convenient form of chromography after a high salt precipitation step, and is often used in serial manner with other chromatographic techniques (e.g., ion-exchange, hydroxylapatite, size-exclusion, and affinity chromatography) to carry out a given purification (see Table 1). The position of the HIC step in the consecutive chromatographic stages depends on the problem to be solved and the type and source of the protein. In general, it precedes an affinity chromatography step.

Preparative chromatography, including preparative HIC, has made important progress owing to recent advances in instrumentation and column technology, as well as to better understanding of the underlying phenomena. The *Journal of Chromatography* has recently published a special thematic issue on this important area of chromatography [96]. Guidelines related to column concepts, stability, and packing procedures, as well as some specific problems in the practice of preparative HPLC (e.g., column size selection and optimum use, sample solubility in the mobile phase, and packing solubility) were recently reviewed [97]. Also, advanced

Table 1 Selected Applications of High-Performance HIC[a]

Protein	Comments	Ref.
Acidic fibroblast growth factor (*E. coli*)	Phenyl-Superose column. The elution position in HIC was dependent on the exposure of hydrophobic regions in the folded state of protein.	88
Carbonic anhydrase isoenzymes (human erythrocytes and rat stomach)	TSK gel phenyl-5PW column. The isoenzymes could be separated by HIC with very high recovery of protein and retention of enzymatic activity.	100
Catalase (human)	Synchropack propyl-HIC column. Sequential LC on DEAE–cellulose, propyl agarose, chromatofocusing, and HIC resulted in the isolation of a 60-kDa protein.	101
Complement inhibitor (CI) (*Aspergillus fumigatus*)	Pheynl-Superose column. This allowed the separation of the active inhibitory component of CI from contaminating materials in crude CI preparations. The active material proved to be extremely hydrophobic desorbing from the column only during elution with ethanol. This material contained only 15% protein and 5% polysaccharides.	85
Cytochrome P-450 enzyme geraniol 10-hydroxylase (G10H, *Catharanthus roseus*)	TSK gel phenyl-5PW column. An efficient separation of G10H from contaminating proteins was achieved by HIC using TSKgel phenyl-5PW column saturated with a nonionic detergent. The isolated fraction showed a single band of M_r 56,000 on SDS–PAGE.	72
DNA polymerases (*Bacillus* species)	Phenyl-Superose HR 5/5 column. Besides traditional chromatography, fast-flow HIC and ion-exchange as well as sucrose density-gradient centrifugation were needed to obtain the enzymes in the form of homogeneous 95-kDa proteins.	102
Endoglycosidases F (*Flavobacterium meningosepticum*)	TSK-butyl column. Endo F preparations have been resolved by HIC into at least three activities designated F_1, F_2, and F_3, each with unique substrate specificity. The 32-kDA endo F_1 is the principal component representing in excess of 95% of most endoglycosidase preparations.	103
Epidermal growth factor (EGF, human urine)	TSK gel phenyl-5PW column. HIC yields four fractions: only 3% of the 6000 Da EGF from human coeluted with the biosynthetic EGF and the rest was separated into three different peaks. These forms may lack one or two NH_2- or COOH-terminal amino acids from the 53 amino acids present in EGF, or they may be the product of deamidation or oxidation of amino acids.	91

Table 1 Continued

Protein	Comments	Ref.
Foaming proteins (Champagne base wine)	Fractogel TSK butyl 650 column: 12 proteins were detected. More hydrophobic proteins were found in the foam, whereas hydrophilic proteins have greater percentage in the remainder wine than in the foam.	104
Glucokinase (*Propionibacterium shermanii*)	TSK gel Ether-5PW column. The protein was readily purified and homogeneous preparations containing both the ATP and poly(P) glucokinase activities could be produced.	105
Glutathione reductase (pea seedings)	Phenyl-Superose HR 5/5 column. Glutathione reductase was purified by serial chromatography, including HIC. The purified protein yielded six isoforms by chromatofocusing.	106
Glycoprotein hormones (human)	Separon HEMA BIO 1000n phenyl column. Because the glycoprotein hormones were relatively hydrophobic, their elution necessitated the addition of small amounts of ethanol in the gradient former.	107
Granulocyte–macrophage colony-stimulating factor (recombinant human)	Phenyl Sepharose fast-flow column. Three-step chromatography was performed to isolate the protein involving HIC, ion-exchange, and gel filtration. The overall purification factor was about 4.6.	108
Hemoglobin (Hb) (bovine)	Butyl-Sepharose hydrophobic interaction HPLC column. HIC can assess the increase in hydrophobicity after partial unfolding (or denaturation) during exposure of protein to radical ·OH.	89
Human growth hormone (rhGH, recombinant DNA)	Several HPLC columns were examined. TSK-ether column gave the best results in the analysis of rhGH samples at different temperatures, as well as allowing an efficient separation of methionyl-hGH from rhGH.	78
Immunoglobulin (Ig) G (human sera)	Alkyl- and phenyl-Sepharose fast-flow columns were used.	109
IgM (human)	Phenyl-Superose HR 5/5 column. A two-step purification involving HIC and gel filtration was developed. It could be readily scaled-up to isolate milligram to gram amounts of antibody.	110
Legunin-like storage protein (white lupin seeds)	TSK gel phenyl-5PW column. HIC and titration with the hydrophobic 8-anilino-1-naphthalenesulfonate indicate that the legunin is less hydrophobic than the prolegunin.	87

Table 1 Continued

Protein	Comments	Ref.
Lipoxygenase (rabbit reticulocytes)	TSK gel phenyl-5PW column. Serial HPLC using HIC, hydroxyapatite and cation-exchange columns yielded a homogeneous enzyme with >98% purity.	111
Microtubule-associated protein (MAP) kinase (pheochromocytoma cells)	Phenyl-Superose column. HIC (similar to ion exchange) resolved MAP kinase into two peaks, one of which has no detectable phosphotyrosine, whereas the other showed some overlap with phosphoprotein 40.	112
Milk growth factor (MGF, bovine)	Butyl-polyol Si500 HIC column. HIC in combination with SCX and size-exclusion chromatography yielded a total purification of 10^6 to 10^7-fold with good yield. The combination of ethanol and volatile ammonium acetate salt facilitated the detection of biological activity.	113
Monoclonal antibodies (MAbs) (mouse hybridomas)	TSK gel phenyl-5PW column. HIC could discriminate a small difference in hydrophobicity between light chains from spleen and NS-1 cells.	114
Pancreatic juice proteins (canine)	TSK gel phenyl-5PW column. Amylase, lipase, and trypsinogen present in dog pancreatic juice were separated by high-performance HIC during a four-stage gradient of decreasing sodium sulfate. The enzymatic activity of the proteins was preserved during the separation process.	115
Pancreatic kallikrein (porcine)	TSK gel phenyl-5PW column. HIC profile of all batches of the enzyme showed four different peaks indicating the presence of multiple forms. The HPLC column provided quantitative recovery, and the minimum injectable amount that can be detected in HPLC was 2.5 U.	116
Proteoglycans (human skin fibroblasts)	Octyl-Sepharose column. The proteoglycans were isolated by isopycnic density gradient centrifugation, size-exclusion, ion-exchange, and HIC.	117
3PG-PP72 (bovine brain)	TSK gel phenyl-5PW column. Ammonium sulfate fractionation, hydroxylapatite chromatography, and HIC allowed the purification of the protein from a substrate protein and a kinase.	118
Serine proteases	TSK gel phenyl-5PW column. A method is described for the simultaneous determination of two serine proteases by HIC. It is based on the specific and direct measurements of the stable complexes that proteases form with aprotinin.	92

Table 1 Continued

Protein	Comments	Ref.
Sialic acid-binding protein (saprophytic bacteria)	Butyl-Toyopearl and poly(*N*-butylacrylamide)-coated porous glass (Butyl-WPG) columns were compared in the HIC of the lectin. HIC with Butyl-WPG yielded better resolution of nonactive contaminants from the active lectin. One step provided 98% purification of the lectin, which retained 65% of its initial hemagglutinating activity.	119
Sperm membrane glycoprotein (rat)	Propylaspartamide-silica column. The protein could be purified by a single-step HIC.	83
Subtilisin (*Bacillus amyloliquebaciens*)	TSK gel phenyl-5PW column. Genetically engineered variants of subtilisin were used to show how microenvironmental changes in the S1 substrate-binding subsite of subtilisin contribute to the HIC behavior of the proteins. HIC could separate proteins varying by one amino acid, and the technique was much superior to RPC.	90
1.3 subunit of transcarboxylase (*E. coli*)	TSK ether-5PW column. After avidin–agarose affinity chromatography, the HIC separation of biotinylated and apo-1.3S subunits was achieved by a linear negative gradient of ammonium sulfate at pH 6.8. The biotinylated subunit was more retarded, suggesting that this subunit is more hydrophobic.	120
Tumor protein CAP-2 (human)	Hydropore HIC column. HIC with other HPLC modes resulted in the isolation and separation to homogeneity of this novel CAP-2 protein.	121
Venom fibrinolytic enzymes	Propyl-aspartamide column. HIC was the first step in the purification of snake venom blood clot-dissolving enzymes. Fractions containing the fibrinolytic activity were then concentrated and applied to a hydroxylapatite column.	122
Yeast cell surface proteins (*Candida albicans*)	TSK gel phenyl-5PW column. HIC was used to assess the origin of yeast cell hydrophobicity. It appears that the hydrophobicity is not determined by differences in surface hydrophobic proteins, but by the presence of hydrophilic, surface fibrils.	86

[a]Listed alphabetically according to the name of the proteins.

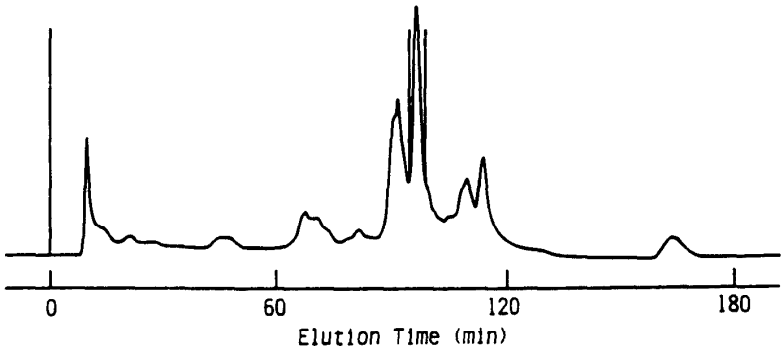


Figure 7 Separation of 1-g crude lipoxidase obtained from commercial source on a phenyl-5PW preparative column of 20 × 5.5-cm id. (From Ref. 95.)

sorbents for preparative protein separation purposes, including those used for HIC have been reviewed [98]. In this recent review, besides describing the effect of the packings on selectivity, efficiency, capacity, and productivity, a discussion is provided on sorbent deterioration and cleaning aspects in preparative chromatography.

Because of proteins' importance in the biotechnology area, the efficient purification of recombinant proteins on a large scale is currently an important research topic. The scale-up of HIC was recently described using human recombinant superoxide dismutase as a model protein [99]. The scale-up was performed by keeping the height/diameter (H/D) ratio of the column constant. The column was a phenyl-Sepharose; fast-flow, and the purification was performed with a decreasing salt gradient. Under this condition, the scale-up of HIC by keeping H/D constant was shown by the authors [99] to lead to the same product purity as observed in the laboratory-scale experiments.

ACKNOWLEDGMENTS

The current financial support from the Cooperative State Research Service, US Department of Agriculture, under Agreement 94-37102-0989 and Agreement 96-35201-3342 are gratefully acknowledged.

REFERENCES

1. C Horváth, WR Melander, I Molnár. J Chromatogr 125:129, 1976.
2. C Horváth, WR Melander, I Molnár. Anal Chem 49:142, 1977.
3. C Horváth, WR Melander. J Chromatogr Sci 15:393, 1977.
4. C Horváth, WR Melander. Am Lab 10:17, 1978.
5. WR Melander, C Horváth. Arch Biochem Biophys 183:200, 1977.
6. WR Melander, C Horváth. In: C Horváth, ed. High Performance Liquid Chromatography: Advances and Perspectives, New York, Academic Press, 1980, p. 114.
7. O. Sinanoglu. Advances in Chemical Physics. New York: John Wiley & Sons. 1967.
8. Z El Rassi, C Horváth. J Liq Chromatogr. 9:3245, 1986.
9. M Kunitani, D Johnson, LR Snyder. J Chromatogr 371:313, 1986.
10. JL Fausnaugh, FE Regnier. J Chromatogr 359:131, 1986.
11. T Arakawa, N Timasheff. Biochemistry 23:5912, 1984.
12. L Szepesy, C Horváth. Chromatographia 26:13, 1988.
13. BF Roettger, JA Myers, MR Ladisch, FE Regnier. Biotechnol Prog 5:79, 1989.
14. S-L Wu, K Benedek, BL Karger. J Chromaogr 359:3, 1986.
15. J Wyman. Protein Chem 19:223, 1964.

16. T Arakawa, SN Timasheff. Biochemistry 21:6536, 1982.
17. T Arakawa, SN Timasheff. Biochemistry 21:6545, 1982.
18. RE Shansky, S-L Wu, A Figueroa, BL Karger. In KM Gooding, FE Regnier, eds. HPLC of Biological Macromolecules. Methods and Applications. New York: Marcel Dekker, 1990, p. 95.
19. S Hjertén, J Rosengren, S Pahlman. J Chromatogr 101:281, 1974.
20. Z El Rassi. In: Z El Rassi, ed. Carbohydrate Analysis: High Performance Liquid Chromatography and Capillary Electrophoresis. Amsterdam: Elsevier Science Publishers, 1995, p. 41.
21. Z El Rassi, AL Lee, and C Horváth. In: JA Asenjo, ed. Separation Process in Biotechnology. New York: Marcel Dekker, 1990, p. 447.
22. D Haidaccher, C Horváth. In: F Dondi, G. Guiochon, eds. Theoretical Advancement in Chromatography and Related Separation Techniques. Dordrecht: Kluwer Academic Publishers, 1992, p. 443.
23. Z Er-el, Y Zaidenzaig, S Shaltiel. Biochem Biophys Res Commun 49:383, 1972.
24. Y Kato, T Kitamura, T Hashimoto. J Chromatogr 26:49, 1983.
25. Y Kato, T Kitamura, T Hashimoto. J Chromatogr 360:260, 1986.
26. JL Fausnaugh, E Pfannkoch, S Gupta, FE Regnier. Anal Biochem 137:464, 1984.
27. JL Fausnaugh, LA Kennedy, FE Regnier. J Chromatogr 317:141, 1984.
28. DL Gooding, MN Schmuck, KM Gooding. J Chromatogr 296:107, 1984.
29. NT Miller, B Feibush, BL Karger. J Chromatogr 316:519, 1985.
30. J-P Chang, Z El Rassi, C Horváth. J Chromatogr 319:396, 1985.
31. AJ Alpert. J Chromatogr 359:85, 1986.
32. H Engelhardt, U Schön. J Liq Chromatogr 9:3224, 1986.
33. S Hjertén, K Yao, KO Eriksson, B Johansson. J Chromatogr 359:99, 1986.
34. I Kleinmann, J Plicka, P Smidl, V Svoboda. J Chromatogr 479:334, 1989.
35. P Smidl, I Kleinmann, J Plicka, and V Svoboda. J Chromatogr 523:131, 1990.
36. YLK Sing, Y Kroviarski, S Cochet, D Dhermy, O Bertrand. J Chromatogr 598:181, 1992.
37. A Kurganov, Y Puchkova, V Davankov, F Eisenbeiss. J Chromatogr A 663:163, 1994.
38. J-L Liao, R Zhang, S Hjertén. J Chromatogr 586:21, 1991.
39. S Hjertén, J-L Liao, R Zhang. J Chromatogr 473:273, 1989.
40. S Hjertén, K Nakazato, J Mohammad, D Eaker. Chromatographia 37:287, 1993.
41. R Janzen, KK Unger, H Giesche, JN Kinkel, MTW Hearn. J Chromatogr 397:91, 1987.
42. S Hjertén, J-L Liao. J Chromatogr 457:165, 1988.
43. S Hjertén, J Mohammad, K-O Eriksson, J-L Liao. Chromatographia 31:85, 1991.
44. Y Kato, T Kitamura, S Nakatani, T Hashimoto. J Chromatogr 483:401, 1989.
45. K Kalghatgi. J Chromatogr 499:267, 1990.
46. WM Holmes, RE Hurd, BR Reid, RA Rimerman, GW Hatfield. Proc Natl Acad Sci USA 72:1068, 1975.
47. S Hjertén, U Hellman, I Svensson, J Rosengren. J Biochem Biophys Methods 1:263, 1979.
48. CJOR Morris. J Chromatogr 159:33, 1978.
49. P Cashion, A Javed, D Harrison, J Seeley, V Lentini, G Sathe. In: JG Chirikijian, TS Papas, eds. Gene Amplification and Analysis. Amsterdam: Elsevier, 1981, p. 551.
50. S Hjertén. Methods Biochem Anal 27:89, 1981.
51. P Cashion, G Sathe, A Javed, J Kuster. Nucleic Acids Res 8:1167, 1980.
52. C Schafer-Nielsen, C Rose. Biochim Biophys Acta 696:323, 1982.
53. M Spencer, MM Binns. JK Chromatogr 238:297, 1982.
54. M Spencer. J Chromatogr 238:307, 1982.
55. M Spencer. J Chromatogr 238:317, 1982.
56. JD Pearson, M Mitchell, FE Regnier. J Liq Chromatogr 6:141, 1983.
57. Z El Rassi, C Horváth. J Chromatogr 326:79, 1985.
58. Z El Rassi, C Horváth. Chromatographia 19:9, 1984.
59. JA Smith, M O'Hare. J Chromatogr 496:71, 1989.

60. P Kårsnäs, T Lindblom. J Chromatogr 599:131, 1992.
61. G Rippel, E Alattyani L Szepesy. J Chromatogr A 668:301, 1994.
62. L Szepesv, G Rippel. J Chromatogr A 668:337, 1994.
63. Z El Rassi, C Horváth. J Chromatogr 359:241, 1986.
64. D Corradini, R Filippetti, C Corradini. J Liq Chromatogr 16:3393, 1993.
65. WR Melander, Z El Rassi, C Horváth. J Chromatogr 469:3, 1989.
66. V Smigol, F Svec, JMJ Fréchet. Anal Chem 66:2129, 1994.
67. IH Hagestam, TC Pinkerton. Anal Chem 57:1757, 1985.
68. Y Kago, T Kitamura, T Hashimoto. J Chromatogr 298:407, 1984.
69. LO Narhi, Y Kita, T Arakawa. Anal Biochem 182:266, 1989.
70. G Rippel, L Szepesy. J Chromatogr A 664:27, 1994.
71. R Bigelis, HE Umbarger. J Biol Chem 250:4315, 1975.
72. AH Meijer, A De Waal, R Verpoorte. J Chromatogr 635:237, 1993.
73. Y Kato, T Kitamura, A Mitsui, Y Yamasaki, T Hashimoto. J Chromatogr 391:395, 1987.
74. J J Buckley, DB Wetlaufer. J Chromatogr 518:99, 1990.
75. Z El Rassi, LF DeOcampo, MD Bacolod. J Chromatogr 499:141, 1990.
76. N Takahashi, FW Putnam. In: KM Gooding, FE Regnier, eds. HPLC of Biological Macromolecules. New York: Marcel Dekker, 1990, p. 571.
77. X Geng, X Chang. J Chromatogr 599:185, 1992.
78. SL Wu, WS Hancock, B Pavlu, P Gellerfors. J Chromatogr 500:595, 1990.
79. P Oroszlan, R Blanco, X-M Lu, D Yarmush, and BL Karger. J Chromatogr 500:481, 1990.
80. L Dou, A Holmberg, IS Krull. Anal Biochem 197:377, 1991.
81. AD McLaren. Photochemistry of Proteins and Nucleic Acids, Oxford: Peragmon, 1964.
82. N Cooke, P Shieh, N Miller. LC–GC 7:954, 1989.
83. ED Eccleston, TW White, JB Howard, DW Hamilton. Mol Reprod Dev 37:110, 1994.
84. Z El Rassi. J Chromatogr A 720:93, 1995.
85. RG Washburn, DJ DeHart, DE Agwu, BJ Bryant-Varela, NC Julian. Infect Immun 58:3508, 1990.
86. KC Hazen, BW Hazen. Infect Immun 60:1499, 1992.
87. M Duranti, N Guerrieri, P Cerletti, G Vecchio. Eur J Biochem 206:941, 1992.
88. T Arakawa, TP Horan, LO Narhi, DC Rees, SC Schiffer, PL Holst, SJ Prestrelski, LB Tsai, GM Fox. Protein Eng 6:541, 1993.
89. RE Pacifici, Y Kono, KJA Davies. J Biol Chem 268:15405, 1993.
90. RM Chicz, FE Regnier. J Chromatogr 500:503, 1990.
91. K Pesonen. J Chromatogr Biomed Appl 568:226, 1991.
92. G Rapsi, A Lo Moro, M Spinetti. Chromatographia 35:381, 1993.
93. JG Huddleston, R Wang, A Lyddiatt. Biotechnol Bieng 44:626, 1994.
94. PÅ Albertsson. Nature 181:709, 1958.
95. Y Kato, T Kitamura, T Hashimoto. J Liq Chromatogr 15:3209, 1986.
96. G Guiochon, ed. Preparative Chromatography. J Chromatogr 658: 1994.
97. B Porsch. J Chromatogr A 658:179, 1994.
98. E Boschetti. J Chromatogr A 658:207, 1994.
99. K Vorauer, M Skias, A Trkola, P Schulz, A Jungbauer. J Chromatogr 625:33, 1992.
100. H Abou-Rebyeh, D Josiac, K Gottschall, K Schubert-Rehberg, F Körber. J Chromatogr 566: 351, 1991.
101. PA Sandstrom, TM Buttke. Proc Natl Acad Sci USA 90:4708, 1993.
102. E Sellmann, K-L Schröder, I-L Knoblich, P Westermann. J Bacteriol 174:4350, 1992.
103. BT Trimble, AL Tarentino. J Biol Chem 266:1646, 1991.
104. F Brissonnet, A Maujean. Am J Enol Vitic 44:297, 1993.
105. NFB Phillips, PJ Horn, HG Wood. Arch Biochem Biophys 300:309, 1993.
106. NR Madamanchi, JV Anderson, RG Alscher, CL Cramer, JL Hess. Plant Physiol 100:138, 1991.

107. MA Chlenov, EI Kandyba, LV Nagornaya, IL Orlova, YV Volgin. J Chromatogr 631:261, 1993.
108. M Belew, Y Zhou, S Wang, L-E Nyström, J-C Janson. J Chromatogr A 679:67, 1994.
109. P Bridonneau, F Lederer. J Chromatogr 616:197, 1993.
110. D Roggenbuck, U Marx, ST Kiessig, G Schroeherr, S Jahn, T Porstmann. J Immunol Methods 167:207, 1994.
111. DL Sloane, MF Browner, Z Dauter, K Wilson, RJ Fletterick, E Sigal. Biochem Biophys Res Commun 173:507, 1990.
112. T Miyasaka, DW Sternberg, J Miyasaka, P Sherline. Proc Natl Acad Sci USA 88:2653, 1991.
113. DA Cox, RR Bürk. Eur J Biochem 197:353, 1991.
114. N Abc, K Inouye. J Biochem Biophys Methods 27:215, 1993.
115. K Yamadera, P DiMagno. Pancreas 9:32, 1994.
116. G Raspi, A Lo Moro, M Spinetti. J Chromatogr 593:119, 1992.
117. G Westergren-Thorsson, A Schmidtchen, B Särnstrand, LÅ Fransson, A Malmström. Eur J Biochem 205:277, 1992.
118. H Morino, C Fischer-Bovenkerk, PE Kish, T Ueda. J Neurochem 56:1049, 1991.
119. LS Zhigis, AE Ivanov, EM Rapoport, EA Kovalenko, EI Getman, VP Zubov. Biotechnol Tech 7:667, 1993.
120. BC Shenoy, WJ Magner, GK Kumar, NFB Phillips, FC Haase, D Samols. Protein Expression Purif 4:85, 1993.
121. R Serrano, Y Yiangou, R Solana, JA Sachs, J Pena. J Immunol 145:3516, 1990.
122. AD Retzios, FS Markland. Protein Expression Purif 1:33, 1990.

13
Affinity Chromatography

David S. Hage

University of Nebraska, Lincoln, Nebraska

I. PRINCIPLES OF AFFINITY CHROMATOGRAPHY

A. Introduction

Affinity chromatography is a liquid chromatographic technique that uses a specific-binding agent for the purification or analysis of sample components [1–4]. Solute retention in this method is based on the types of selective and reversible interactions that occur in biological systems, such as the binding of an enzyme with a substrate or a hormone with its receptor. These interactions are used in affinity chromatography by immobilizing one of a pair of interacting molecules onto a solid support and placing it into a column. The immobilized molecule is referred to as the *affinity ligand*. This makes up the stationary phase of the affinity column.

Figure 1 shows a typical scheme used to perform affinity chromatography. A real-life example based on this scheme is shown in Figure 2. In this approach, a sample containing the compound of interest is injected onto the affinity column in the presence of a mobile phase that has the proper pH, ionic strength, and solvent composition for solute–ligand binding. This solvent, which represents the weak mobile phase of an affinity column, is referred to as the *application buffer*. As the sample passes through the column under these conditions, compounds that are complementary to the affinity ligand will bind. However, owing to the high selectivity of this interaction, other solutes in the sample will tend to wash or elute from the column as a nonretained peak.

After all nonretained components have been washed from the column, the retained solutes are then eluted by applying a solvent that displaces them from the column or that promotes dissociation of the solute–ligand complex. This solvent, which represents the strong mobile phase for the column, is known as the *elution buffer*. As the solutes of interest elute from the column, they are either quantitated directly or collected for later use. The application buffer is then reapplied to the system and the column is allowed to regenerate before the next sample injection [4].

Owing to the strong and selective binding that characterizes many affinity ligands, solutes that are quantitated or purified by these ligands can often be separated with little or no interferences from other sample components. Frequently, the solute of interest can be isolated in only one or two steps, with purification yields of 100- to several thousand-fold being common [2–4]. In work with hormone receptors, purification yields approaching 1 million-fold have even been reported with affinity-based separations [3].

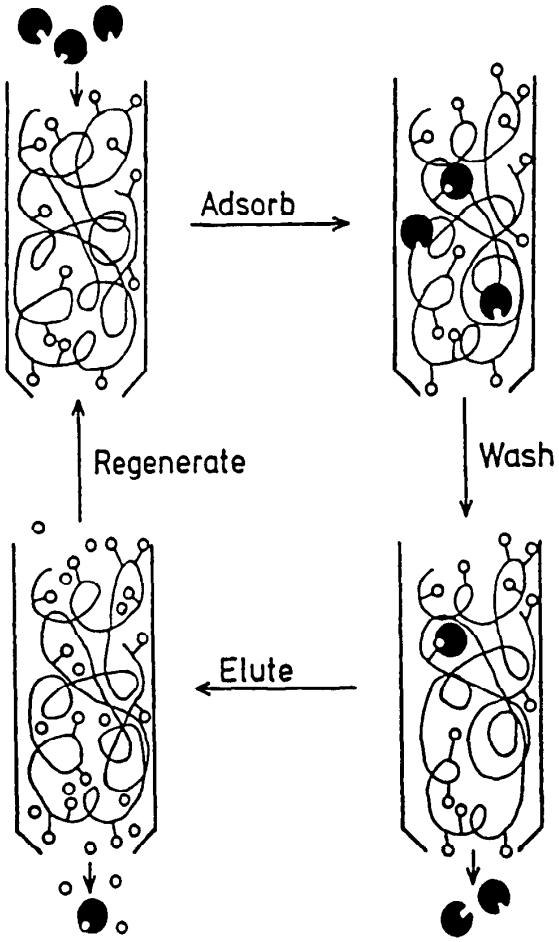


Figure 1 Typical separation scheme for affinity chromatography. (Adapted from Ref. 4.)

The wide range of ligands available for affinity chromatography make this method a valuable tool for the purification and analysis of compounds present in complex samples. Areas in which affinity chromatography has been used include biochemistry, pharmaceutical science, clinical chemistry, and environmental testing. Some specific applications of this technique will be examined later in this chapter.

B. Theoretical Basis

Several factors are important in determining the retention and elution of a compound in an affinity column. These factors include the strength of the solute–ligand interaction, the amount of immobilized ligand present in the column, and the kinetics of solute–ligand association and dissociation. In the case of a solute A that has a single-site binding to a ligand L, the following equations can be used to describe the interactions between the solute and ligand in a column:

$$A + L \underset{k_d}{\overset{k_a}{\rightleftharpoons}} A\text{–}L \tag{1}$$

$$K = \frac{k_a}{k_d} \tag{2}$$

$$= \frac{\{A\text{–}L\}}{[A]\{L\}} \tag{3}$$

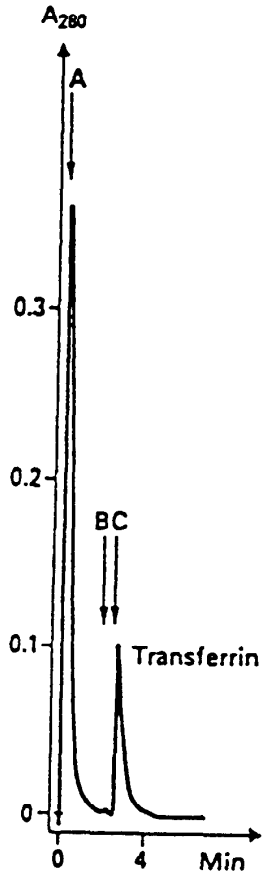


Figure 2 Determination of transferrin in serum by HPAC using an immobilized anti-transferrin antibody column at 3 mL min^{-1}. (From Ref. 67.)

In these equations, K is the association constant for the binding of A with L, A–L is the resulting solute–ligand complex, [A] is the mobile phase concentration of A at equilibrium, and {L}/{A–L} represent the surface concentrations of the ligand and solute–ligand complex. The term k_a is the second-order association rate constant for solute–ligand binding, and k_d is the first-order dissociation rate constant for the solute–ligand complex.

At equilibrium, the retention of solute in the foregoing system is given by the expressions shown in Eqs. (4) and (5):

$$k' = \frac{K\, m_L}{V_m} \tag{4}$$

$$= \left(\frac{t_r}{t_m}\right) - 1 \tag{5}$$

In these equations, k' is the capacity factor for the injected solute, t_r is the solute retention time, and t_m is the void time of column. The term m_L represents the moles of active ligand in column and V_m is the column void volume. Equations (4) and (5) indicate that the capacity factor of a solute, or its retention time, will depend on both the strength of solute–ligand binding (i.e., the association equilibrium constant K) and the amount of ligand in the column (i.e., m_L/V_m).

The strong retention of solutes seen on many types of affinity columns can be illustrated using Eqs. (4) and (5). For example, for a porous silica-based column containing immobilized polyclonal antibodies, the association equilibrium constant would generally be in the range of

10^8–10^{10} M^{-1} [6], and the concentration of active immobilized ligand would be about 10 μM or greater [7]. Use of these values with Eqs. (4) and (5) results in a capacity factor of 1,000–100,000. For a 10-cm × 4.1-mm–id column operated at 1.0 mL min^{-1}, this would represent a mean elution time of about 1–90 days. The only way in which solutes could be eluted from this column on a reasonable time scale would be to change the system conditions to lower the effective equilibrium constant for solute–ligand binding. This is the purpose of the elution buffer used in Figure 1.

Although "on/off" or "step-gradient" elution, as shown in Figures 1 and 2, is a common practice in affinity chromatography, it is also possible to use isocratic or linear gradient methods. An example of this is shown in Figure 3. This approach can be used if the value of the solute's association constant (and capacity factor) are small enough that elution can occur on the time scale of minutes, instead of days or hours. Fast association and dissociation kinetics are also desirable to allow a large number of solute–ligand interactions, thereby producing good plate heights and narrow solute peaks. This approach, sometimes referred to as *weak affinity chromatography*, can easily be performed if the value of a solute's association equilibrium constant is less than or equal to 10^4 M^{-1} [8–9]. Isocratic elution can also be used with affinity systems having association constants up to 10^6 M^{-1}, provided that the ligand concentration in the column (m_L/V_m) is sufficiently small [10–11].

C. Types of Affinity Ligands

The key factor in determining the success of any affinity separation is the type of ligand used within the column. Several ligands that are commonly used in affinity chromatography are listed in Table 1. Many of these ligands are of biological origin, but a wide range of natural

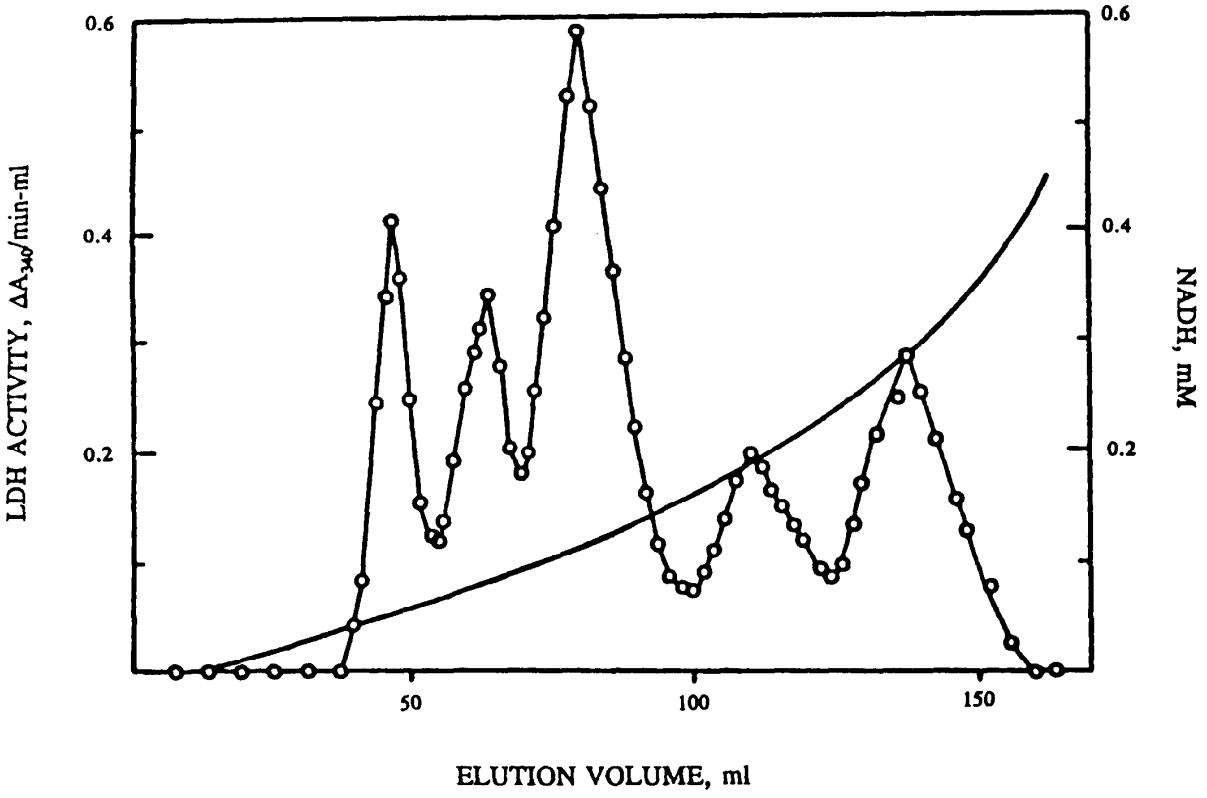


Figure 3 Purification of lactate dehydrogenase isoenzymes on an AMP-analogue Sepharose column using a concave gradient of NADH at 3.4 mL h^{-1}. (From Ref. 93.)

Table 1 Common Ligands Used in Affinity Chromatography

Ligand	Retained solutes
Biological ligands	
Antibodies	Antigens (drugs, hormones, peptides, proteins, viruses, cell components)
Inhibitors, substrates, cofactors, and coenzymes	Enzymes
Lectins	Sugars, glycoproteins, and glycolipids
Nucleic acids	Complementary nucleic acids and DNA/RNA-binding proteins
Proteins A/protein G	Antibodies
Nonbiological ligands	
Boronates	Sugars, glycoproteins, and diol-containing compounds
Triazine dyes	Nucleotide-binding proteins and enzymes
Metal chelates	Metal-binding amino acids, peptides, and proteins

and synthetic molecules of nonbiological origin can also be used. Examples of specific applications for many of these ligands will be presented later.

All of the compounds listed in Table 1 can be placed into one of two categories: (1) high-specificity ligands and (2) general, or group-specific, ligands [4]. The term *high-specificity ligands* refers to compounds that bind to only one or a few closely related molecules. This type of ligand is used in chromatographic systems for which the goal is to analyze or purify a specific solute. Typical high-specitivity ligands include antibodies (for binding antigens), substrates or inhibitors (for separating enzymes), and single-stranded nucleic acids (for the retention of a complementary sequence). As this list suggests, most high-specificity ligands tend to be biological compounds. These ligands also tend to have relatively large association constants for solutes and are generally eluted by a step gradient (e.g., see Fig. 2).

General, or *group-specific*, *ligands* are compounds that bind to a family or class of related molecules. These ligands are used in methods for which the goal is to isolate a class of structurally similar solutes. General ligands can be of either biological or nonbiological origin. Examples given in Table 1 include proteins A and G, lectins, boronates, triazine dyes, and immobilized metal chelates. Many of these compounds have weaker binding for solutes than that seen with high-specificity ligands. However, there are exceptions to this. For example, protein A has an equilibrium association of over 10^8 M^{-1} for some types of antibodies [12]. Also, some molecules that are usually considered to be high-specificity ligands, such as antibodies, can be used to retain an entire class of solutes if they recognize a feature that is common to all of the desired analytes [13].

D. Support Materials

Another important factor to consider in affinity chromatography is the material used to hold the ligand within the column. Ideally, the support material should have low nonspecific binding for sample components, but should be easy to modify for ligand attachment. This material should also be stable under the flow rate, pressure, and solvent conditions to be used in the final application. In addition, the support should be readily available and simple to use in method development [1–4,14]. A wide variety of materials have been employed as supports in affinity chromatography. Table 2 lists some commercial matrices that are currently available. Suitable affinity supports can also be made in-house using underivatized agarose and silica or a variety of other materials [1,2,14–15].

Table 2 Commercial Supports for Affinity Chromatography

Type of material	Trade names (suppliers)
Carbohydrate-based supports	
Agarose and cross-linked agarose	Affinica Agarose (Schleicher & Schuell); AminoLink/CarboLink/SulfoLink/Reacti-Gel 6x (Pierce); AvidGel Ax (BioProbe); Bio-Gel A/Affi-Gels (BioRad); Matrix Gel (Amicon); Sepharose/Sepharose Fast Flow (Pharmacia LKB, Sigma); Superose (Pharmacia LKB); Ultrogel (IBF); Generic brands (ICN, Pierce, Sigma)
Cellulose and modified cellulose	Reinforced cellulose (Memtek); Nalgene Affinity Matrix (Nalge); Generic brands (BioRad, Schleicher & Schuell, Sigma, Whatman)
Modified inorganic supports	
Silica/glass	AvidGel CPG (BioProbe); HiPAC (ChromatoChem); Glutaraldehyde P (J.T. Baker); Protein-Pak Affinity Packing (Waters); Ultraaffinity-EP (Bodman)
Synthetic organic-based supports	
Agarose–acrylamide copolymer	Ultrogel AcA and Magnogel AcA (IBF)
Azalactone beads	Emphaze (3M Corp./Pierce)
Dextran–acrylamide copolymer	Sephacryl (Pharmacia LKB)
Hydroxylated polystyrene matrix	POROS (PerSeptive Biosystems)
Polyacrylamide derivatives	AvidGel T (BioProbe); Bio-Gel P/Affi-Gels (BioRad); Reacti-Gel GF-2000 (Pierce); Trisacryl (IBF)
Polyethersulfone matrix	UltraBind US450 (Gelman)
Polymethacrylate derivatives	Affinica Polymeric Support (Schleicher & Schuell); AvidGel F (BioProbe); Eupergit (Richard Sci./Spect. Med.); Fractogel (EM Separations); HEMA-AFC/HEMA-AFC Bio (Alltech); TSK-Gel Toyopearl (TosoHaas)

Source: Ref. 14 and information provided by the manufacturers.

From the type of support material used, affinity chromatography can be characterized as being either a low- or high-performance technique. In *low-performance* (or *column*) *affinity chromatography*, the support is usually a large-diameter, nonrigid gel. Many of the carbohydrate-based supports and synthetic organic materials fall within this category. An example of a separation performed with such materials is given in Figure 3. The low backpressure of these supports means that they can be operated under gravity flow or with a peristaltic pump. This makes these gels relatively simple and inexpensive to use for affinity purifications. Disadvantages of these materials include their slow mass-transfer properties and their limited stability at high-flow rates and pressures. These factors limit the usefulness of these supports in analytical applications, where both rapid efficient separations are often desired [4].

In *high-performance affinity chromatography* (HPAC), the support consists of small, rigid particles capable of withstanding the high-flow rates or pressures that are characteristic of high-performance liquid chromatography (HPLC) [4,16]. Supports that can be used for this include modified silica or glass, azalactone beads, and hydroxylated polystyrene media. Specific examples of these materials are listed in Table 2. A typical separation based on a silica support is shown in Figure 2. The mechanical stability and efficiency of these supports allows

them to be used with standard HPLC equipment. Although the need for more sophisticated instrumentation does make HPAC more expensive to perform than low-performance affinity chromatography, the better speed and precision of this technique makes it the method of choice for analytical applications [4].

E. Immobilization Methods

A third item to consider in using affinity chromatography is the way in which the ligand is attached to the solid support, or the *immobilization method*. Several techniques are available for this. For a protein or peptide, this generally involves coupling the molecule through free amine, carboxylic acid, or sulfhydryl residues present in its structure. Immobilization of a ligand through other functional sites (e.g., aldehyde groups produced by carbohydrate oxidation) is also possible.

Table 3 summarizes various immobilization methods used in affinity chromatography. Each of these methods involves at least two steps: (1) an *activation step*, in which the support is converted to a form that can be chemically attached to the ligand, and (2) a *coupling step*, in which the affinity ligand is attached to the activated support. With some techniques, a third step, in which remaining activated groups are removed, is also required. The methods listed in Table 3 can be performed either in-house (see references provided) or can be used in the form of preactivated supports available from commercial suppliers.

The choice of immobilization method is important because it can affect the actual or apparent activity of the final affinity column. If the correct procedure is not used, a decrease in ligand activity can result from multisite attachment, improper orientation, or steric hindrance. *Multisite attachment* refers to the coupling of a ligand to the support through more than one functional group. Although multisite attachment does create a more stable linkage than single-site immobilization, this phenomenon can also lead to distortion and denaturation of the ligand's active region. This effect can be minimized by coupling the ligand through functional groups that occur in only a few places in its structure or by using a support with a low density of activated sites.

Improper orientation can lead to a similar loss in ligand activity. This can be avoided by coupling the ligand through groups that are distant from its active region. An example would be the use of oxidized carbohydrate residues for the attachment of antibodies to a solid support [39]. If the actual location of the ligand's active site is not known or if no appropriate functional groups are available, it is sometimes possible to minimize this problem by empirically varying the procedure or conditions used for ligand attachment.

Steric hindrance refers to the loss of ligand activity owing to the presence of a nearby support or neighboring ligand molecules. Steric hindrance produced by neighboring ligands can be minimized by using a low ligand coverage. Steric hindrance produced by the support can be reduced by adding a *spacer arm*, or tether, between the ligand and supporting material [18]. The presence of a spacer arm is particularly important when using small ligands for the retention of large analytes. Examples of common spacer arms used in affinity chromatography include 6-aminocaproic acid, diaminodipropylamine, 1,6-diaminohexane, ethylenediamine, and succinic acid (anhydride) [14].

F. Application Conditions

The application buffer is another parameter that must be considered in the use of an affinity column. Most application buffers in affinity chromatography are solvents that mimic the pH, ionic strength, and polarity experienced by the solute and ligand in their natural environment. Any cofactors or metal ions required for solute–ligand binding should also be present in this solvent. Under these conditions, the solute will probably have its highest association constant for the ligand and its highest degree of retention on the column.

Table 3 Immobilization Methods for Affinity Chromatography

Group/compound	Immobilization technique	Refs.
Amines	Azalactone method (for Emphaze supports)	14
	Cyanogen bromide (CNBr) method	17–19
	N,N'-Carbonyl diimidazole (CDI) method	14,20–22
	Divinylsulfone method	23
	Epoxy (bisoxirane) method	15
	Ethyl dimethylaminopropyl carbodiimide (EDC) method	24,25
	Fluoro methylpyridinium toluenesulfonate (FMP) method	26
	N-Hydroxysuccinimide ester (NHS) method	27,28
	Schiff-base (reductive amination) method	14,15
	Tresyl chloride–tosyl chloride method	14,15,29–31
Sulfhydryls	Azalactone method (for Emphaze supports)	14
	Divinylsulfone method	23
	Epoxy (bisoxirane) method	14,15
	Iodoacetyl/bromoacetyl methods	14
	Maleimide method	14
	Pyridyl disulfide method	18,32,33
	TNB-thiol method	34
	Tresyl chloride–tosyl chloride method	14,15,29–31
Carboxylates	Ethyldimethylaminopropyl carbodiimide (EDC) method	24,25
Hydroxyls	Cyanuric chloride method	14,35
	Divinylsulfone method	23
	Epoxy (bisoxirane) method	14,15
Aldehydes	Hydrazide method	36–39
	Schiff-base (reductive amination) method	14,39
Nucleic acids	Carbodiimide (CDI) method	40
	Carboxymethyl method (for cellulose)	41
	Cyanogen bromide (CNBr) method	42,43
	Cyanuric chloride method	44
	Diazonium (azo) method	14
	Epoxy (bisoxirane) method	14,15
	Hydrazide method	36–39
	Schiff-base (reductive amination) method	14,39
	UV irradiation (for cellulose)	45,46

Source: Refs. 14 and 15.

The proper choice of an application buffer can help minimize any nonspecific binding caused by undesired sample components. For example, coulombic interactions between solutes and the support can often be decreased by altering the ionic strength and pH of the application buffer. In addition, surfactants and blocking agents (e.g., Triton X-100, Tween-20, bovine serum albumin, gelatin, or others) may be added to the buffer to prevent nonspecific retention of solutes on the support or affinity ligand.

The activity of the immobilized ligand should be considered in determining how much sample can be applied to the affinity column with each use. A rough indication of the maximum possible column-binding capacity can be made by assaying the total amount of ligand present. However, a better approach is to actually measure the ligand's activity. This can be done by continuously applying a known concentration of solute to the affinity column (i.e.,

breakthrough curves) or by combining the immobilized ligand with a known excess of solute and measuring the amount of free solute that remains after binding has occurred.

With some affinity systems, it is possible to see a large amount of nonretained solute during the application step, even when the amount of injected sample is significantly less than the known column-binding capacity [28]. This phenomenon, known as the *split-peak effect*, is caused by the presence of slow adsorption or mass-transfer kinetics within the column. This effect has been reported with many types of affinity ligands [1,7,14,28], but tends to occur with high-performance supports because of the more rapid flow rates often used with these materials. Ways in which this effect can be minimized include reducing the flow rate used for sample injection, increasing the column size, or placing a more efficient support within the column. Occasionally, changing to a different immobilization method may also help by providing a ligand with more rapid-binding kinetics [28].

G. Elution Conditions

The conditions used for removal of retained solutes is another item that should be considered in the design of an effective affinity separation. Just as the application conditions are selected to maximize specific solute–ligand interactions, the elution conditions are chosen to promote fast or gentle removal of solute from the column. The elution buffer used in affinity chromatography can be either a solvent that produces weak solute–ligand binding (i.e., a small association constant) or a solvent that decreases the extent of this binding by using a competing agent that displaces solute from the column. These two approaches are known as *nonspecific elution* and *biospecific elution*, respectively.

Biospecific elution is the gentler of these two elution methods, for it is carried out under essentially the same solvent conditions as those used for sample applications. This makes this approach attractive for purification work, for which a high recovery of active solute is desired. Biospecific elution may be performed either by adding an agent to the eluting solvent that competes with ligand for solute (i.e., normal role elution) or by adding an agent that competes with solute for ligand-binding sites (i.e., reversed-role elution). In both conditions, retained solutes are eventually eluted from the column by displacement and mass action.

The main advantage of biospecific elution is its ability to gently remove analyte from the column. The main disadvantages of this method include its typically slow elution times and its broad solute peaks. Another limitation is the need to remove the competing agent from the eluted solute. A further difficulty that may be encountered in analytical applications is the need to use a competing agent that does not produce a large background signal under the conditions used for analyte detection.

Many of these problems can be overcome by using nonspecific elution. This approach involves changing the column conditions to weaken the interactions between retained solutes and the immobilized ligand. This can be done by changing the pH, ionic strength, or polarity of the mobile phase. The addition of denaturing or chaotropic agents to the running buffer can also be used. This results in an alteration in the structure of the solute or ligand, leading to a lower association constant and lower solute retention.

Nonspecific elution tends to be much faster than biospecific elution in removing analytes from affinity columns. This results in sharper peaks which, in turn, produce lower limits of detection and shorter analysis times. For these reasons, nonspecific elution is commonly used in analytical applications of affinity chromatography. This elution method can also be used in purifying solutes, but there is a greater risk of solute denaturation with this approach than there is with biospecific elution. Also, care must be taken in nonspecific elution to avoid using conditions that are too harsh for the column. If this is not considered, it may result in long column regeneration times or an irreversible loss of ligand activity.

II. TYPES OF AFFINITY CHROMATOGRAPHY

A. Bioaffinity Chromatography

Bioaffinity chromatography, or *biospecific adsorption*, refers to affinity methods that use a biological molecule as the affinity ligand. This was the first type of affinity chromatography developed and represents the most diverse category of this technique. The earliest known use of bioaffinity chromatography was in 1910, when Starkenstein used insoluble starch to purify the enzyme α-amylase [47]. However, it was not until the development of beaded agarose supports [48] and the cyanogen bromide immobilization method [17] that bioaffinity chromatography came into common use [49].

Table 1 lists several ligands that are used in bioaffinity applications. These, and many other biological compounds, can be attached to chromatographic supports using the materials and methods given in Tables 2 and 3. Many commercial suppliers even provide these ligands already coupled to supports or packed in columns. Several hundred different types of immobilized biological molecules are presently available in this fashion [4].

The earliest application of bioaffinity chromatography involved its use in enzyme purification [47]. Enzyme purification has continued to be a major use of this technique (e.g., see Fig. 3). Some ligands used for this purpose are enzyme inhibitors, coenzymes, substrates, and cofactors. Examples include methods that use nucleotide mono-, di-, and triphosphates for the purification of various kinases, the use of NAD for collecting dehydrogenases, the use of pyridoxal phosphate for the isolation of tyrosine and aspartate aminotransferases, and the use of RNA or DNA for the purification of polymerases and nucleases [3]. The importance of bioaffinity chromatography in enzyme purification is illustrated by a recent review that listed almost 300 different applications in this area [50].

Lectins represent a class of general ligands that are common in bioaffinity chromatography. These are nonimmune system proteins that have the ability to recognize and bind certain types of carbohydrate residues [51]. Two lectins often used in affinity chromatography are concanavalin A, which binds to α-D-mannose and α-D-glucose residues, and wheat germ agglutinin, which binds to D-*N*-acetylglucosamines. Other lectins that can be employed are jackalin and lectins found in peas, peanuts, or soybeans. These ligands are used in the separation of many carbohydrate-containing compounds, such as polysaccharides, glycoproteins (e.g., immunoglobulins or cell membrane proteins) and glycolipids [1–4,14].

Another useful class of bioaffinity ligands are bacterial cell wall proteins, such as protein A from *Staphylococcus aureus* and protein G from group G streptococci [12,52,53]. These ligands have the ability to bind to the constant region of many types of immunoglobulins. This makes them useful in antibody purification. Protein A and protein G have their strongest binding to immunoglobulins at or near neutral pH, but readily dissociate from these solutes when placed into a lower pH buffer. These two ligands differ in their ability to bind to antibodies from different species and classes [12,54]. However, a recombinant protein that blends the activities of these compounds, known as protein A/G, is now also available [55].

Nucleic acids and polynucleotides can act as either general or specific ligands in bioaffinity chromatography. For instance, as high-specificity ligands they can be used to purify DNA- or RNA-binding enzymes and proteins or to isolate nucleic acids that contain a sequence that is complementary to the ligand [56]. As a group-specific ligand, an immobilized nucleic acid can be used to purify solutes that share a common nucleotide sequence. An example is the use of immobilized oligo(dT) for the isolation of nucleic acids containing poly(A) sequences [57].

B. Immunoaffinity Chromatography

In methods based on *immunoaffinity chromatography* (IAC), the ligand is an antibody or antibody-related reagent [58]. Because the ligand is a biological compound, this technique

represents a special subcategory of bioaffinity chromatography. Other methods sometimes included under the heading of immunoaffinity chromatography are those that use immobilized antigens for antibody purification [59]. Depending on the nature of the antigen, the ligand used in this latter approach may or may not be of biological origin [50,59].

The high selectivity of antibody–antigen interactions and the ability to produce antibodies against a wide range of solutes has made immunoaffinity chromatography a popular tool for biological purification and analysis. Examples include methods developed for the isolation of antibodies, hormones, peptides, enzymes, recombinant proteins, receptors, viruses, and subcellular components [50,58–64]. The strong binding constants of many antibodies requires that nonspecific elution be used with most immunoaffinity columns [59]. However, isocratic elution methods can also be used with low-affinity antibody systems [8].

The first known use of immunoaffinity chromatography was reported by Campbell et al. in 1951, when an antigen immobilized to *p*-aminobenzyl cellulose was used for antibody purification [65]. Many current applications are still based on the use of low-performance supports, particularly agarose [58]. However, recent work has also been performed using derivatized silica, glass, and perfusion media. The use of these supports along with an antibody or antigen ligand is referred to as *high-performance immunoaffinity chromatography* (HPIAC) [59].

The use of immunoaffinity chromatography in analytical methods has received increasing attention in recent years. Of particular interest is the use of immobilized antibody columns in performing immunoassays, a technique known as a *chromatographic* or *flow-injection immunoassay*. An example of a chromatographic immunoassay is given in Figure 4. This approach has already been used in several different formats, such as those involving simple analyte adsorption–desorption [66–68], sandwich immunoassays [69,70], competitive-binding immunoassays [71–74], and multianalyte methods [7]. Typical advantages of these methods include decreased analysis times and improved precision over manual immunoassays [6,66–74].

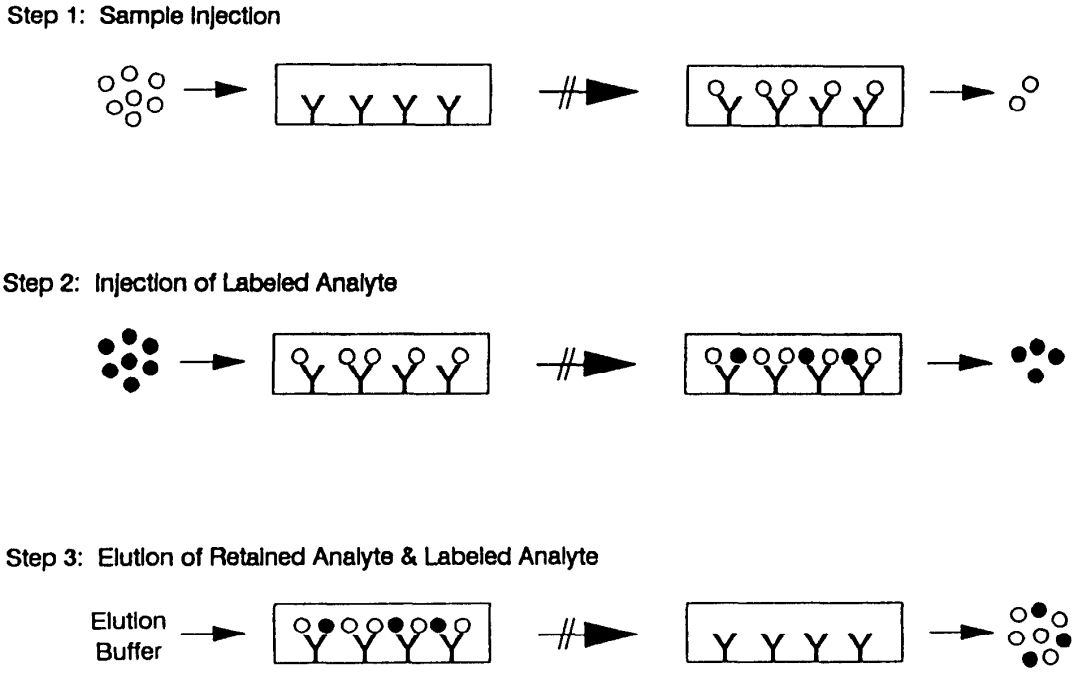


Figure 4 Scheme for a sequential injection, competitive binding immunoassay performed by high-performance immunoaffinity chromatography. (From Ref. 73.)

Although antibodies are usually thought of as being high-specificity ligands, they can also be used to bind a general class of compounds that share a common structural feature. When used in this way, the resulting immunoaffinity column can serve either as a screening tool for the desired compound class, or as a specific absorbent for the extraction and concentration of compounds before analysis by a second separation method. Several methods have been recently developed using this approach for the quantitation of solutes in biotechnology, clinical chemistry, and pharmaceutical research [see Ref. 13 for review].

C. Dye–Ligand Affinity Chromatography

Another category of affinity chromatography is the technique known as dye–ligand affinity chromatography. In this method, a synthetic triazine or triphenylmethane dye is used as the immobilized ligand. One triazine dye often used in this method is Cibacron blue F3G-A (see structure given in Fig. 5). Note that the triazine portion of this dye is similar to the purine or pyrimidine bases of nucleotides. This makes this type of dye useful as a ligand for the purification of enzymes and other biomolecules that bind to nucleotides or related factors [75].

The first use of dye–ligand affinity chromatography was described in 1974 [76]. Since that time it has become an extremely popular tool for enzyme and protein purification [1–4,76]. At present, over 500 such compounds have been isolated by this technique [4]. This list includes kinases, dehydrogenases, restriction endonucleases, polynucleotides synthetases, CoA-dependent enzymes, hydroxylases, glycolytin enzymes, phosphodiesterases, decarboxylases, clotting factors, serum lipoproteins, interferons, transferrin, and serum albumin [50,76].

D. Immobilized Metal Ion Affinity Chromatography

In *immobilized metal ion affinity chromatography* (IMAC), the ligand is a metal ion complexed with an immobilized chelating agent. Another term for this technique is *metal chelate affinity chromatography*. This approach was initially used to separate proteins and peptides that contained amino acids with electron donor groups, such as histidine, tryptophan, or cysteine. Proteins and peptides that contain these residues are retained by interactions between the amino acids and the immobilized metal chelate [77–78].

This type of affinity chromatography was first described by J Porath and co-workers in 1975 [77]. Since that time, various peptides, proteins, and amino acids have been purified by

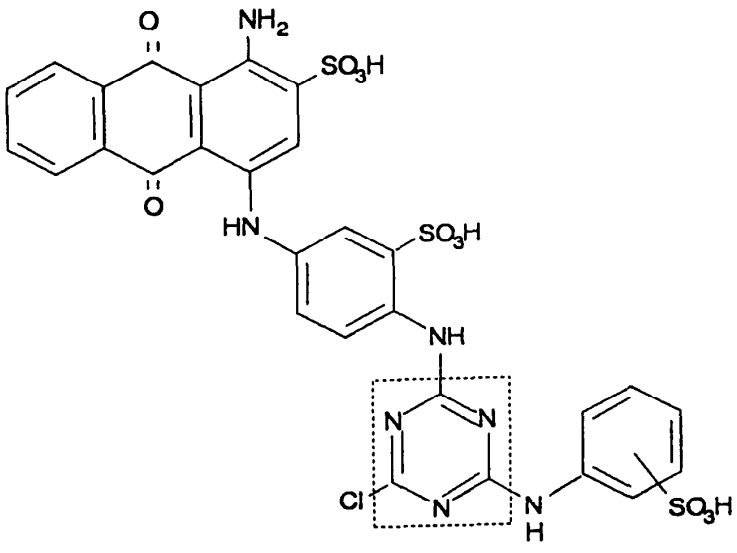


Figure 5 Structure of Cibacron blue F3G-A (triazine ring shown in box).

this method. Selectivity in IMAC is determined by the chelating group and metal ion used to make up the affinity ligand. Iminodiacetic acid is the most common chelating agent employed. Metal ions used with this agent and other chelating groups include Cu^{2+}, Zn^{2+}, Ni^{2+}, Co^{2+}, and Fe^{3+} [79].

E. Analytical Affinity Chromatography

Besides its use in separating molecules, affinity chromatography can also be employed as a tool for studying solute–ligand interactions. This particular application of affinity chromatography is called *analytical*, or *quantitative*, *affinity chromatography*. By using this technique, information can be acquired about both the equilibrium and rate constants for biological interactions [5].

Information on equilibrium constants can be obtained by using the methods of *zonal elution* or *frontal analysis* (i.e., breakthrough curves). Zonal elution involves the injection of a small amount of solute onto an affinity column in the presence of a mobile phase that contains a known concentration of competing agent. The equilibrium constants for binding of the ligand with the solute (and competing agent) can then be obtained by examining how the solute's retention changes with competing agent concentration. A typical zonal elution experiment is shown in Figure 6. This technique was first used to study biological interactions by Andrews et al. in 1974 [80] and Dunn and Chaiken in 1975 [81]. Since that time it has been used to examine various systems, such as enzyme–inhibitor binding, protein–protein interactions, and drug–protein binding [see Ref. 5 for review].

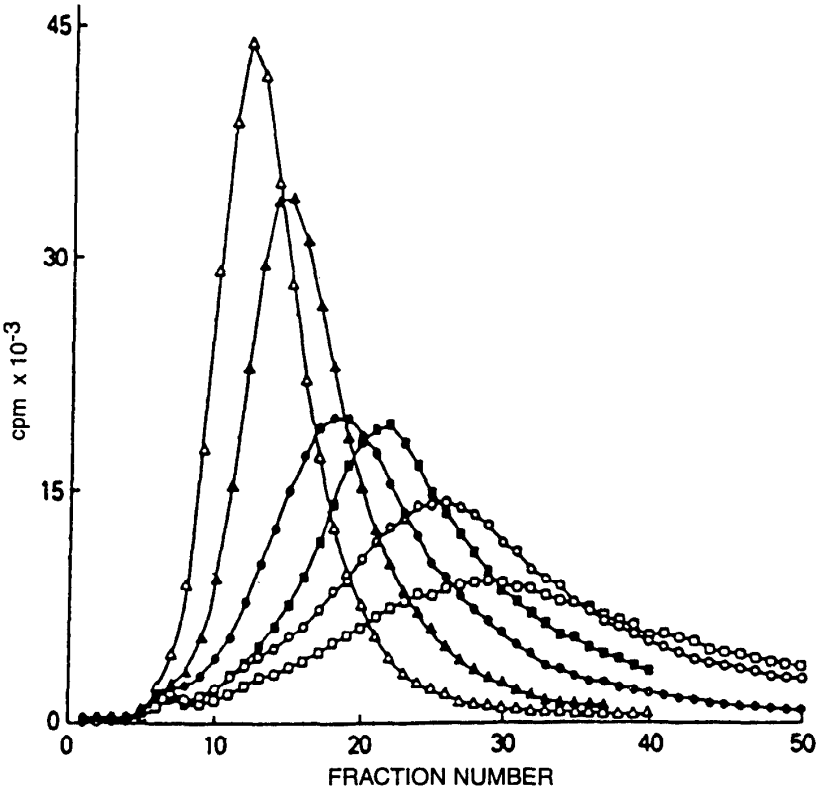


Figure 6 Zonal studies examining the competitive binding of injected neurophysin II with various concentrations of LVP on a Met-Tyr-Phe-AB-A affinity column under gravity flow. The mobile phase concentrations of LVP (from left to right) were 64.2, 42.8, 27.9, 17.1, 9.3, and 0 μM. (From Ref. 94.)

Frontal analysis is performed by continuously applying a known concentration of solute to an affinity column at a fixed flow rate. The moles of analyte required to reach the mean point of the resulting breakthrough curve is then measured and used to determine the equilibrium constant for solute–ligand binding. This method was used first by Kasai and Ishii in 1975 to examine the interactions of trypsin with various peptide ligands [82]. It has since been used in many other applications [5]. One advantage of this approach over zonal elution is that it simultaneously provides information on both the equilibrium constants and number of active sites involved in analyte–ligand binding. The main disadvantage of this method is the need for a larger quantity of solute than is required by zonal elution.

Information on the kinetics of solute–ligand interactions can also be obtained using affinity chromatography. Various methods have been developed for this, including techniques based on band-broadening measurements [83–85], the split-peak effect [28,73], and peak decay analysis [5]. These methods are generally more difficult to perform than equilibrium constant measurements, but represent a powerful means of examining the rates of biological interactions. Systems that have been studied by these techniques include the binding of lectins with sugars [5,84,85], protein A with immunoglobulins [28], and antibodies with antigens [5,73].

F. Miscellaneous Ligands and Methods

Besides the specific methods already discussed, several other ligands and techniques are often placed under the category of affinity chromatography. For example, boronic acid and its derivatives represent a class of general ligands that are usually considered to be affinity ligands. At a pH of 8 or higher, these ligands have the ability to form covalent bonds with compounds that contain *cis*-diol groups in their structure. This makes these ligands useful for the purification and analysis of many compounds that contain sugar residues, such as polysaccharides, glycoproteins, ribonucleic acids, and catecholamines [86,87]. One important clinical application of immobilized boronate ligands is their use in the analysis of glycosylated hemoglobin in diabetic patients [88].

Other methods that are related to affinity chromatography include *hydrophobic interaction chromatography* (HIC) and *thiophilic adsorption*. Hydrophobic interaction chromatography is based on the interactions of proteins, peptides, and nucleic acids with short nonpolar chains on a support. This was first described in 1972 [89,90] following work that examined the role of spacer arms on the nonspecific adsorption of affinity columns [90]. Thiophilic adsorption, also known as *covalent* or *chemisorption chromatography*, makes use of immobilized thiol groups for solute retention [91]. Applications of this method include the analysis of sulfhydryl-containing peptides or proteins and mercurated polynucleotides [92].

REFERENCES

1. J Turkova. Affinity Chromatography. Amsterdam: Elsevier Scientific, 1978.
2. WH Scouten. Affinity Chromatography: Bioselective Adsorption on Inert Matrices. New York: John Wiley & Sons, 1981.
3. I Parikh, P Cuatrecasas. Chem Eng News 63:17, 1985.
4. RR Walters. Anal Chem 57:1099A, 1985.
5. IM Chaiken, ed. Analytical Affinity Chromatography. Boca Raton, FL: CRC Press, 1987.
6. DP Stites, JD Stobo, HH Frudenberg, JV Wells. Basic and Clinical Immunology, 5th ed. Los Altos, CA: Lange Medical Publications, 1984.
7. DS Hage, RR Walters. J Chromatogr 386:37, 1987.
8. D Zopf, S Ohlson. Nature 346:87, 1990.
9. M Wikstroem, S Ohlson. J Chromatogr 597:83, 1992.
10. J Yang, DS Hage. Anal Chem 66:2719, 1994.
11. B Loun, DS Hage. Anal Chem 66:3814, 1994.

12. R Lindmark, C Biriell, J Sjoquist. Scand J Immunol 14:409, 1981.
13. M de Frutos, FE Regnier. Anal Chem 65:17A, 1993.
14. GT Hermanson, AK Mallia, PK Smith. Immobilized Affinity Ligand Techniques. New York: Academic Press, 1992.
15. P-O Larsson. Methods Enzymol 104:212, 1984.
16. S Ohlson, L Hansson, P-O Larsson, K Mosbach. FEBS Lett 93:5, 1978.
17. R Axen, J Porath, S Ernback. Nature 214:1302, 1967.
18. P Cuatrecasas. J Biol Chem 245:3059, 1970.
19. SC March, I Parikh, P Cuatrecasas. Anal Biochem 60:149, 1974.
20. GJ Bartling, HD Brown, SK Chattopadhyay. Nature 243:342, 1973.
21. MTW Hearn. Methods Enzymol 135:102, 1987.
22. SC Crowley, KC Chan, RR Walters. J Chromatogr 359:359, 1986.
23. J Porath. Methods Enzymol 34:13, 1974.
24. CR Lowe, PDG Dean. Affinity Chromatography. New York: John Wiley & Sons, 1974.
25. JM Stewart, JD Young. Solid Phase Peptide Synthesis, 2nd ed. Rockford, IL: Pierce Chemical Co, 1984, pp. 20, 33.
26. TT Ngo. Biotechnology 4:134, 1986.
27. M Wilchek, T Miron. Appl Biochem Biotechnol 11:191, 1985.
28. DS Hage, RR Walters, HW Hethcote. Anal Chem 58:274, 1986.
29. K Nilsson, K Mosbach. Eur J Biochem 112:397, 1980.
30. K Nilsson, K Mosbach. Biochem Biophys Res Commun 102:449, 1981.
31. K Nilsson, K Mosbach. Methods Enzymol 135:65, 1987.
32. K Brocklehurst, J Carlsson, MPJ Kierstan, EM Crook. Methods Enzymol 34:531, 1974.
33. J Porath, R Axen. Methods Enzymol 34:41, 1974.
34. C Jayabaskaran, PF Davison, H Paulus. Prep Biochem 17:121, 1987.
35. TH Finaly, V Troll, M Levy, AJ Johnson, LT Hodgins. Anal Biochem 87:77, 1978.
36. WL Hoffman, DJ O'Shannessy. J Immunol Methods 112:113, 1988.
37. EA Bayer, H Ben-Hur, M Wilchek. Anal Biochem 161:123, 1987.
38. PF Ruhn, S Garver, DS Hage. J Chromatogr 669:9, 1994.
39. DJ O'Shannessy, M Wilchek. Anal Biochem 191:1, 1990.
40. A Weissbach, M Poonian. Methods Enzymol 34:463, 1974.
41. H Potuzak, U Wintersberger. FEBS Lett 63:167, 1976.
42. U Lindberg, T Persson. Eur J Biochem 54:411, 1971.
43. MS Poonian, A Schlabach, A Weissbach. Biochemistry 10:424, 1971.
44. S Biagioni, R Sisto, A Ferraro, P Caiafa, C Turano. Anal Biochem 89:616, 1978.
45. RJ Britten. Science 142:963, 1963.
46. RM Litman. J Biol Chem 243:6222, 1968.
47. E Starkenstein. Biochem Z 24:210, 1910.
48. S Hjerten. Arch Biochem Biophys 99:446, 1962.
49. P Cuatrecasas, M Wilchek, CB Anfinsen. Proc Natl Acad Sci USA 61:636, 1968.
50. M Wilchek, T Miron, J Kohn. Methods Enzymol 104:3, 1984.
51. IE Liener, N Sharon, IJ Goldstein. The Lectins: Properties, Functions and Applications in Biology and Medicine. London: Academic Press, 1986.
52. PL Ey, SJ Prowse, CR Jenkin. Immunochemistry 15:429, 1978.
53. L Bjorck, G Kronvall. J Immunol 133:969, 1984.
54. B Akerstrom, L Bjorck. J Biol Chem 261:10240, 1986.
55. M Eliasson, A Olsson, E Palmcrantz, K Wibers, M Inganas, B Guss, M Lindberg, M Uhlen. J Biol Chem 263:4323, 1988.
56. H Potuzak, PDG Dean. FEBS Lett 88:161, 1978.
57. PT Gilham. J Am Chem Soc 86:4982, 1964.
58. GJ Calton. Methods Enzymol 104:381, 1984.
59. TM Phillips. LC Mag 3:962, 1985.
60. H Ehle, A Horn. Bioseparation 1:94, 1990.

61. TM Phillips. Receptor Biochem Methodol 14:129, 1989.
62. P Bailon, SK Roy. ACS Symp Ser 427:150, 1990.
63. KE Howell, J Gruenberg, A Ito, GE Palade. Prog Clin Biol Res 270:77, 1988.
64. M Nakajima, I Yamaguchi. Kagaku Seibutsu 29:270, 1991.
65. DH Campbell, E Luescher, LS Lerman. Proc Natl Acad Sci USA 37:575, 1951.
66. JR Sportsman, GS Wilson. Anal Chem 52:2013, 1980.
67. S Ohlson, BM Gudmundsson, P Wikstroem, P-O Larsson. Clin Chem 34:2039, 1988.
68. TM Phillips. Clin Chem 34:1689, 1988.
69. PF Ruhn, JD Taylor, DS Hage. Anal Chem 66:4265, 1994.
70. U De Alwis, GS Wilson. Anal Chem 59:2786, 1987.
71. DS Hage, PC Kao. Anal Chem 63:586, 1991.
72. M Nilsson, H Haakanson, B Mattiasson. Anal Chim Acta 249:163, 1991.
73. SA Cassidy, LJ Janis, FE Regnier. Anal Chem 64:1973, 1992.
74. DS Hage, DH Thomas, MS Beck. Anal Chem 65:1622, 1993.
75. CH Pollema, J Ruzicka, GD Christian, A Lernmark. Anal Chem 64:1356, 1992.
76. CR Lowe, JC Pearson. Methods Enzymol 104:97, 1984.
77. RL Easterday, JM Easterday. In: RB Dunlap, ed. Immobilized Biochemicals and Affinity Chromatography. New York: Plenum Press, 1974, p. 123.
78. J Porath, J Carlsson, I Olsson, G Balfrage. Nature 258:598, 1975.
79. ES Hemdan, J Porath. J Chromatogr 516:333, 1985.
80. J Porath. Trends Anal Chem 7:254, 1988.
81. P Andrews, BJ Kitchen, D Winzor. Biochem J 135:897, 1973.
82. BM Dunn, IM Chaiken. Proc Natl Acad Sci USA 71:2382, 1974.
83. K-I Kasai, S-I Ishii. J Biochem 77:261, 1975.
84. IM Chaiken. Anal Biochem 97:1, 1979.
85. AJ Muller, PW Carr. J Chromatogr 284:33, 1984.
86. DJ Anderson, RR Walters. J Chromatogr 376:69, 1986.
87. M Glad, S Ohlson, L Hansson, M-O Mansson, K Mosbach. J Chromatogr 200:254, 1980.
88. RR Maetas, JR Prieto, GD Kuehn, JH Hagemann. J Chromatogr 189:225, 1980.
89. AK Mallia, GT Hermanson, RI Krohn, EK Fujimoto, PK Smith. Anal Lett 14:649, 1981.
90. RJ Yon. Biochem J 126:765, 1972.
91. S Shaltiel. Methods Enzymol 104:69, 1984.
92. K Brocklehurst, J Carlsson, MPJ Kierstan, EM Crook. Biochem J 133:573, 1973.
93. P Mohr, K Pommerening. Affinity Chromatography: Practical and Theoretical Aspects, New York: Marcel Dekker, 1985.
94. P Brodelius, K Mosbach. FEBS Lett 35:223, 1973.
95. S Angal, IM Chaiken. Biochemistry 21:1574, 1982.

14

Mobile-Phase Delivery Systems for HPLC

Robert L. Stevenson

Abacus Group, Lafayette, California

I. INTRODUCTION

In a recent survey of high-performance liquid chromatography (HPLC) users, over 40% rated the pump as the component that required the highest scrutiny [1]. In the early days of HPLC, the percentage probably would have been much higher, because the pumps were the most troublesome module. Reliability and ease of use have improved tremendously, but potential customers are still wary: and they should be. The goal in writing this chapter is to help the user understand the sources of trouble and error that can originate in the mobile-phase system. A secondary goal is to explain the evolution of HPLC pumps, especially if this reinforces the first goal. This chapter will assume that the reader is familiar with the basic operation of an HPLC.

The solvent delivery system is required to force the mobile phase through the injector, column and detector(s), and from there on out. The concept is simple, but the details are important. In the early days, HPLC systems used pumps with prices less than 1000 dollars. These were quickly replaced by more sophisticated metering pumps that commanded prices higher than good new automobiles. In 1993, the prices of pumps were about the same in current dollars, but inflation has increased the price of automobiles by a factor of three, or more.

II. ISOCRATIC ELUTION

Starting with the simplest case, isocratic elution of the sample components from the column under constant pressure, temperature, and flow rate will be considered. The mobile phase carries the sample components down the column and into a detector. The output of the detector is fed to a data collection device, such as a recorder or data station. Most data collection devices measure the deviation from the anticipated baseline as the quantitative signal and the elution time as the primary index of peak identity.

HPLC is performed on a relative basis, always comparing current data with data obtained with authentic standards. Chromatography involves balancing so many delicate forces, most of which are too complex for estimation by calculation. Thus, it is not possible to determine or predict a chromatogram from first principles. Therefore, reproducibility, especially run-to-run reproducibility, is essential for HPLC, especially in quantitative analysis.

A. Constant-Pressure Pumps

In the first decade of HPLC, pump design was the primary sales determinant. Some pumps relied on constant pressure for control of flow rate. Looking at the fluid mechanics, the pressure required to force the liquid through the column is given by Eq. (1).

$$\Delta P = \frac{\eta L v}{\theta d_p^2} \tag{1}$$

where η is the viscosity of the mobile phase, L is the length of the column, v is the flow velocity, θ is a dimensionless constant that has a value of about 500 for well-packed columns, and d_p^2 is the diameter of the column-packing particle.

Once the column has been selected, the values of length and particle diameter have been set. In a pump that applies a constant pressure, only the viscosity and the flow velocity can change, and these must change inversely. In fact, one of the earliest pump designs held the pressure constant, but failed to control the column temperature. Viscosity changes about 2% per degree centigrade; hence, as the room temperature increased, the retention times decreased. (In some modes there is also an enthalpic, ΔH component to retention, which may change retention time with increasing column temperature.) Also, constant-pressure pumps could not respond to partial plugging of the column. Although this was a major problem in the 1970s, chromatographers are much more aware of it now and take steps to avoid plugging columns in sample preparation or by the use of guard columns, eluent filters, or other such.

Such changes were not important in the early 1970s, for most data was processed manually, and peak height provided adequate precision. Peaks were assigned on the basis of retention order, not time. Today things are highly automated. Most peaks are identified on the basis of the retention time and tolerance window, thus it is necessary to control the flow rate sufficiently that the computer can assign the identity. Typically, the data station searches for a peak to occur within a narrow window close to an expected value that has been determined on previous runs. Consequently, constant-pressure pumps have disappeared from the scene, except for packing HPLC columns.

B. Constant Flow Rate Pumps

All HPLC pumps on the market in 1995 strived to provide constant flow rate, even when the pressure varied. Some did better than others. Because the common detectors all measure the concentration as a function of time, having constant flow can eliminate a contribution to the variance of the analysis. For example, take any isocratic chromatogram, and then double the flow rate. The peaks comes out in half the time. However, if the data station had not been told that the flow rate had been doubled, it would not know that conditions had changed, and might assign an inappropriate response factor to a peak, because most data tables are set up on a time base. In addition, the peaks would also be expected to spend half the time in the detector cell. If the quantitative analysis is performed with peak area, the detector response (measured in microvolts) times the time in seconds (giving peak area in microvolt seconds) will be halved. If quantitation by peak height is used, the peak height may be reduced by the decreased efficiency of the column, or slow response time of the detector and data output device.

Changing the flow rate by a factor of two is obvious and predictable. However, a smaller change, say by 1%, could escape notice, especially if it were a short-lived random event. Check valve failure, leaking seals, and such can cause such flow variations. This explains why experienced users look for specifications on flow rate constancy. This may include "reproducibility of retention time," "flow rate precision," and so on. Modern pumps for HPLC can provide flow rate precision much smaller (better) than 0.1% in retention time. Figure 1 demonstrates an example of the precision that can be obtained.

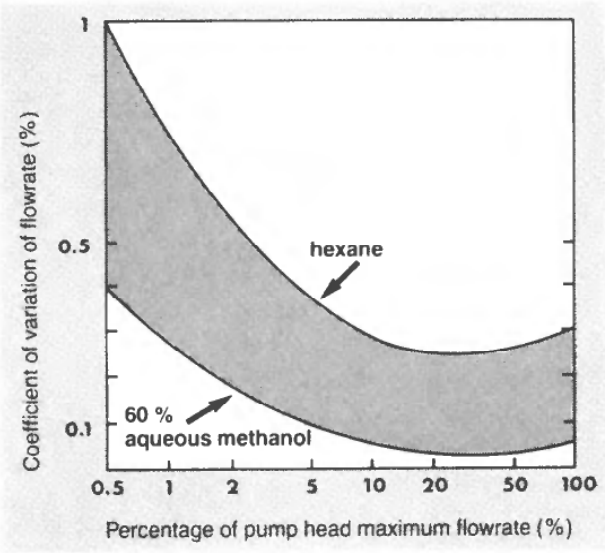


Figure 1 Reproducibility of Gilson pump heads: this graph illustrates the precision range of Gilson pump heads with water, aqueous solutions, and hydroorganic solvent mixtures (lower curve) and with hydrocarbon and chlorinated volatile solvents (upper curve). The range—the shaded area—is valid for all models of interchangeable heads from 5SC to 200WTi at ambient temperatures and within the full pressure range specified for each model. (Courtesy of Gilson Medical Electronics, Inc., Middleton, WI.)

The accuracy of the flow rate is much less important, because the measurements are usually made on the same instrument. However, flow rate accuracy can be important when trying to copy a method worked out on one instrument to another instrument. If the flows are different, the retention time (T_r) should be different. The effect could be even stronger in gradient elution, during which the solvent composition could be affected. Most pumps for HPLC now set the flow rate electronically, with an accuracy of 1% or better. Accuracy is determined using some specified test. The tests vary from one manufacturer to another.

C. Reciprocating Pumps

By the 1980s, all commercial HPLC units used constant flow rate pumps. And almost all of these were continuous reciprocating pumps. The simplest design uses a piston and check valves (Fig. 2).

If only one piston is used, there can be no flow during the refill portion of the cycle (see Fig. 2a). One popular model in the earliest days of HPLC adjusted the flow by limiting the refill stroke. For example, if 60% of maximum flow was desired, the refill stroke was terminated at 60% of travel. Thus, the periods between flow pulses could be very long. In practice, the system contained compliant or compressible elements, such as pulse dampers, that acted to smooth out (but not eliminate) these effects. The function of pulse dampers is discussed later in Section VI of this chapter. However, many HPLC detectors are flow-sensitive. That is, the detector can sense the changes in flow rate and add that to the signal from the sample. Modern detectors are designed to be much less flow-sensitive, but variations in flow are still a major source of detector noise.

In automobiles, adding pistons improves smoothness, and this is true in HPLC. Two pistons are better than one because one can be refilled while the other is delivering the mobile phase (Fig. 3b). And if two pistons are better, would three be better yet? What about four, five, or six? Obviously, three pistons cost more than two pistons, which cost more than one.

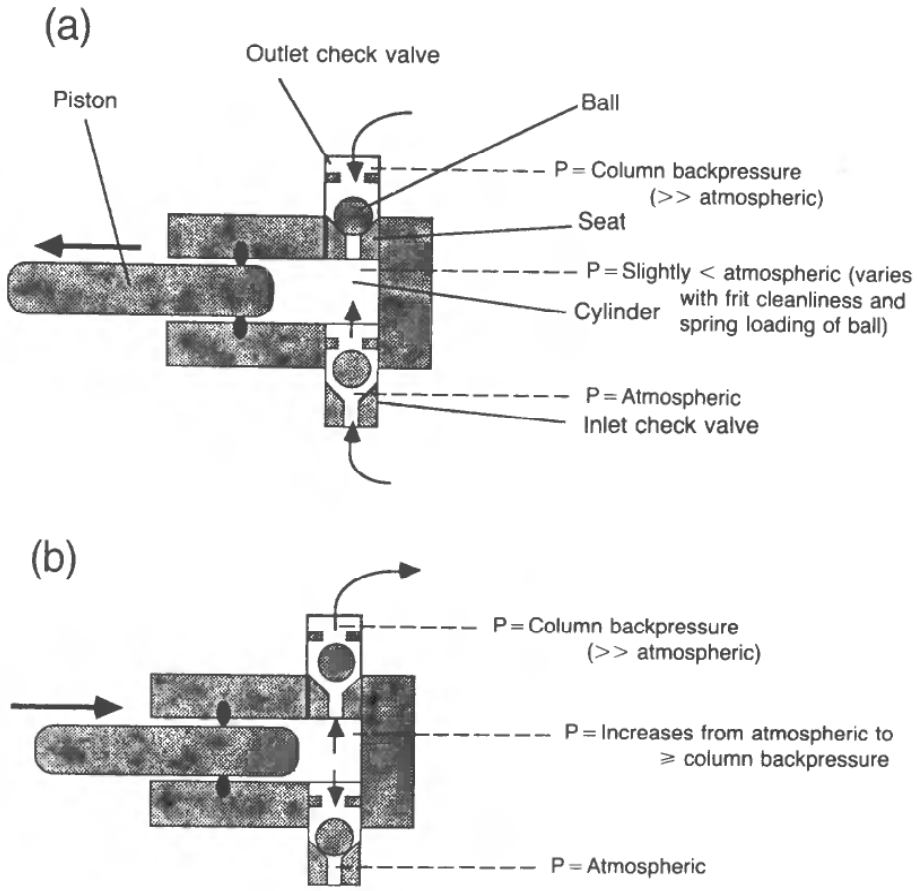


Figure 2 Piston and check valve reciprocating pump: the inlet check valve is open during the suction segment of the stroke, but closes during the exhaust segment, which forces open the outlet check valve. The liquid is thus displaced toward the column during the exhaust stroke. (From Ref. 2.)

Some manufacturers [notably, DuPont and Jasco] did market three-piston pumps, but the improvement in the baseline stability was not sufficient to merit the increased price, plus the problems and expense of diagnosing check valve failure were magnified.

The flow from even single-piston pumps can be remarkably uniform and refill interruptions are very short (see Fig. 3c). Indeed single-piston pumps incorporating rapid refill cycles (less than 200 ms) were popular in the late 1970s and are still marketed by Varian and Beckman. The concept was to make the refill cycle so short that it was not seen by the detector. This was possible with some of the slower detectors of the day. However, today, detectors are faster, and these pumps are declining in market acceptance. Today, dual-piston reciprocating pumps are the most popular, and almost all of these use complex microprocessor-controlled fill and delivery cycles. (For more detailed information on particular pumps, please see the Appendix at the end of this chapter).

In the simplest design, the flow rate is determined by the piston displacement (piston diameter × length of travel) and the frequency of pumping. For instance, if the piston displaces 0.1 mL/stroke, then for a flow rate of 1 mL min^{-1}, ten strokes per minute are required. This would be fine, except that liquids are compressible. However, users want the retention times to be reproducible, even if the column is starting to plug, or the room temperature changes. Column plugging usually manifests itself as increased system pressure.

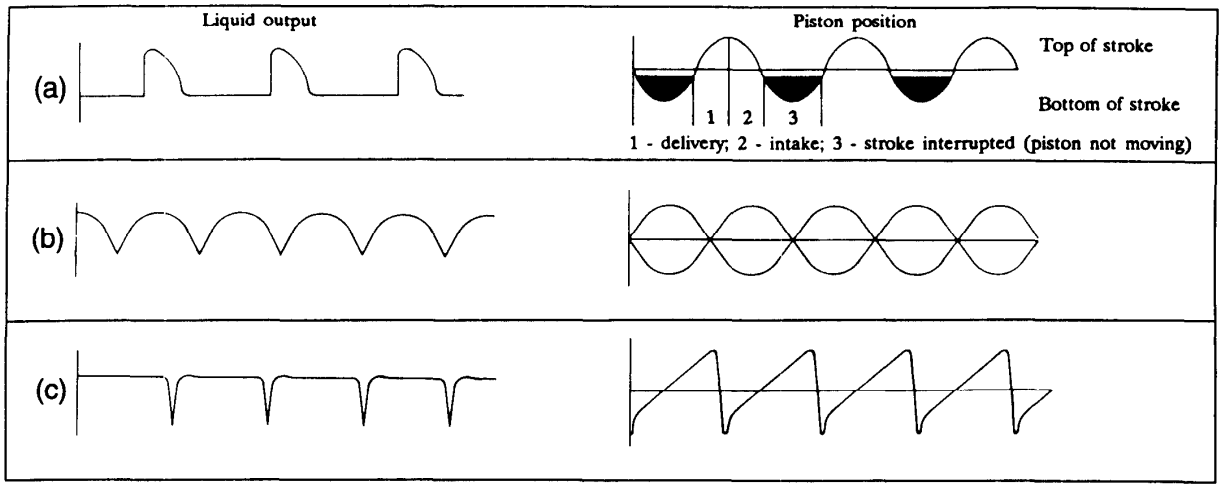


Figure 3 Comparison of the piston and flow profiles for three different designs of reciprocating pumps (also see Appendix). (a, left) The output profile from a single-piston pump at 60% of maximum flow. The flow is reduced by interrupting the refill stroke at 60% of maximum. The drawing on the right shows the corresponding position of the piston. The black area is omitted from the refill cycle to reduce the flow rate from maximum. The motor runs at a constant RPM. (b, left) The pressure profile from a two-piston pump with 180° out-of-phase sinusoidal stroke. The plot on the right shows that as one piston is delivering, the other is refilling. Flow rate is adjusted by changing the motor speed. (c, left) The flow output from a single-piston pump using a linear cam with a fast intake. Liquid is metered during the long delivery cycle. The refill is very rapid, minimizing both the duration and magnitude of the flow interruption. Most reciprocating pumps, even those with two pistons, use some adaptation of this design. (Illustration provided by Isco, Lincoln, NE.)

1. Solvent Compressibility

Pumps were designed to adjust the flow rate to compensate for the changes in system pressure [Eq. (2) and (3)].

$$\kappa = \frac{1}{V[dV/dP]_t} \tag{2}$$

where V is the volume of liquid and P is the pressure in pascals.

$$\begin{aligned}\text{Flow rate} = \{&(\text{piston diam})(\text{piston travel}) - \Delta P\ (\kappa \times \text{volume in cylinder}) \\ &- \Delta P\ (\text{seal compressibility}) \\ &- (\text{volume of bubbles})\}(\text{pump frequency}).\end{aligned} \tag{3}$$

Generally, the pump frequency was increased slightly to add back the product of solvent compressibility [see Eq. (2)] times the pressure. Solvents differ by about a factor of four in compressibility (Table 1), so for optimum results, it is necessary to adjust a compression compensation circuit, depending on the solvent. This is illustrated for a pump cycle in Figure 4. The pump alternates between filling compression and delivery. The filling and compression cycle ends when the pressure in the pump reaches the pressure measured on the previous stroke at point M1. This causes the pump electronics to shift from the refill mode to the delivery mode, minimizing the effect of bubbles and changes in system pressure.

Later, with microprocessors, a compressibility number was entered, or even more recently, the pump can go through a self-optimization routine when started up. The compressibility

Table 1 Isothermal Compressibility of Some Solvents Used in HPLC

Solvent	$\kappa/(10^{-11}\ Pa^{-1})$
Methanol	120
Water	45
n-Hexane	150
n-Octane	100
Isopropanol	100
Chloroform	105
Diethylether	185

Source: Ref. 4.

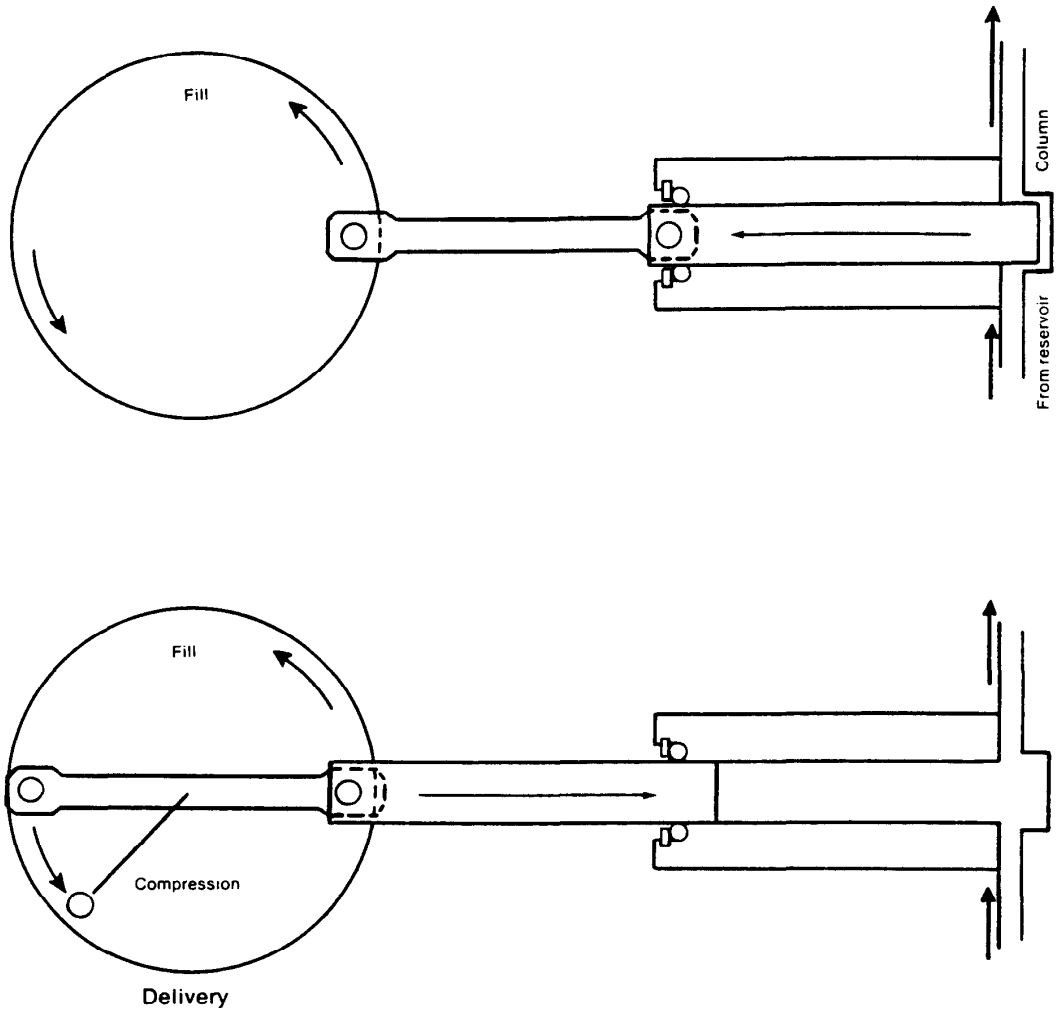


Figure 4 Timing diagram for a single-piston pump: as the crank rotates, the piston completes the delivery stroke and refills. During refill, the liquid, seals, and bubbles, if any, must be compressed before liquid can flow out of the cylinder chamber. (From Ref. 3.)

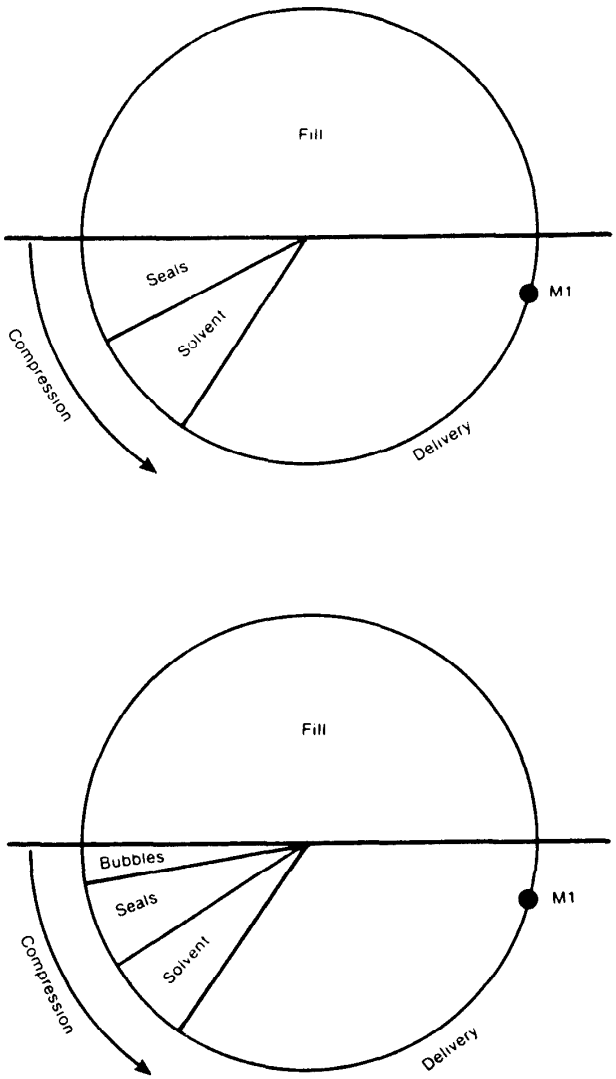


Figure 4 Continued.

compensation circuits were then useful in minimizing the detector noise, originating from the refill cycle, and transfer to the pumping mode. With careful adjustment, the compensation can be very good (Fig. 5).

The compressibility of liquids changes when mixed with others. Thus, the compressibility may change during gradient elution. If the proportioning is done in the low-pressure side of the pump, the compensation parameters may change during the run. Few, if any, pumps have the memory or optimization schemes to perform this compensation during gradient elution. Gradients formed by high-pressure mixing, with multiple reciprocating pumps (each pumping a constant liquid), avoid the problems of changing compressibility in the pressurization stroke. (For more on gradient elution, see Sec. III of this chapter).

The flow rate lost during the compression of the solvent is minimized by minimizing the volume in the cylinder surrounding the piston. This leads to designs with very small clearance between the piston and the cylinder wall. These small clearances often increase the problems with clearing bubbles. Some seals, such as those around the piston, are also compressible. In good designs, these are backed up with firm retainers that minimize this correction. Thus, the flow rate is usually empirically calibrated to be accurate to within 1% of set flow at the sweet

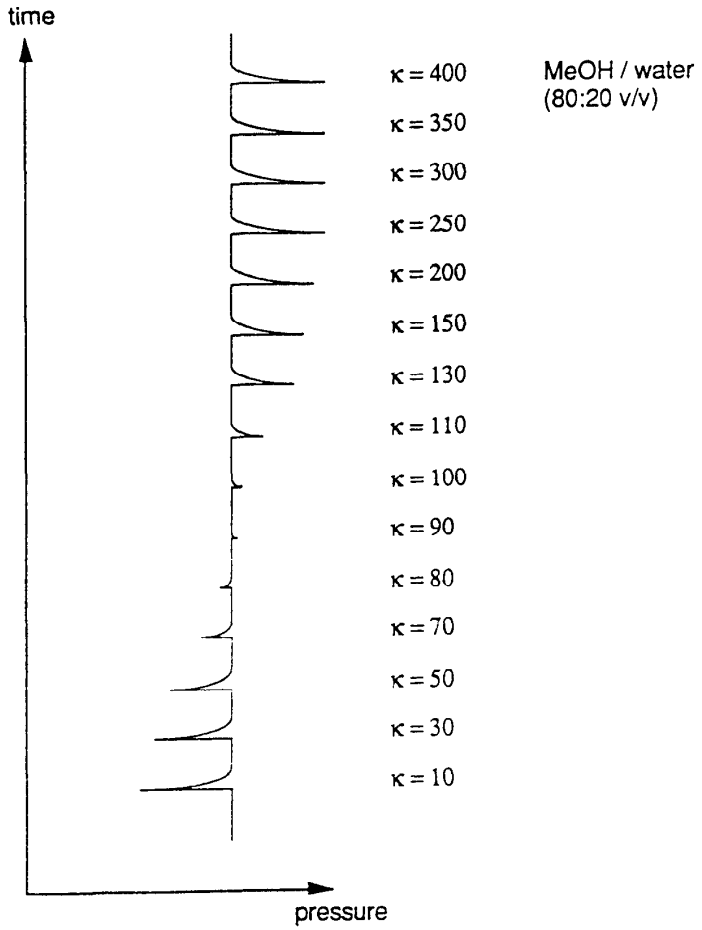


Figure 5 Effect of compressibility adjustment on the pressure for a reciprocating pump [4]. By entering the appropriate value, the pressure pulse occurring during the refill and repressurization cycle can be minimized. Note that the minimum pulse is obtained from a κ that is intermediate between either pure solvent in Table 1. (Courtesy of Bischoff Analysentechnik Undgeräte GmbH, Leonberg, Germany.)

point (i.e., the point at which it operates the best) of the system. For analytical pumps this is usually 1 mL min^{-1}.

However, in syringe pumps (discussed in Sec. II.D), which have a large volume (typically 250 mL) under pressure, compressing the solvent can require a few milliliters of piston displacement if the system pressure is high, say 400 atm or more. This can present problems in gradient elution as discussed later.

Compressibility circuits are not desirable in certain cases. For instance, in size exclusion chromatography (SEC) of large polymers, the viscosity of the sample is a strong function of elution time. If the polymer is sufficiently concentrated, and that may not require much, a pressure increase can be expected as the sample passes through the column inlet frit, followed by a decrease as the sample is diluted in the column, followed by an increase in pressure as the larger polymers pass through the exit frit of the column. These changes in flow can be important in polymer characterization, which rely on measurement of higher moments of the peak envelope.

2. Check Valves

When check valves are nice, they can be very nice, but when they are bad, they are horrid. Check valves are designed to let liquid pass in only one direction (Fig. 6). When the pressure

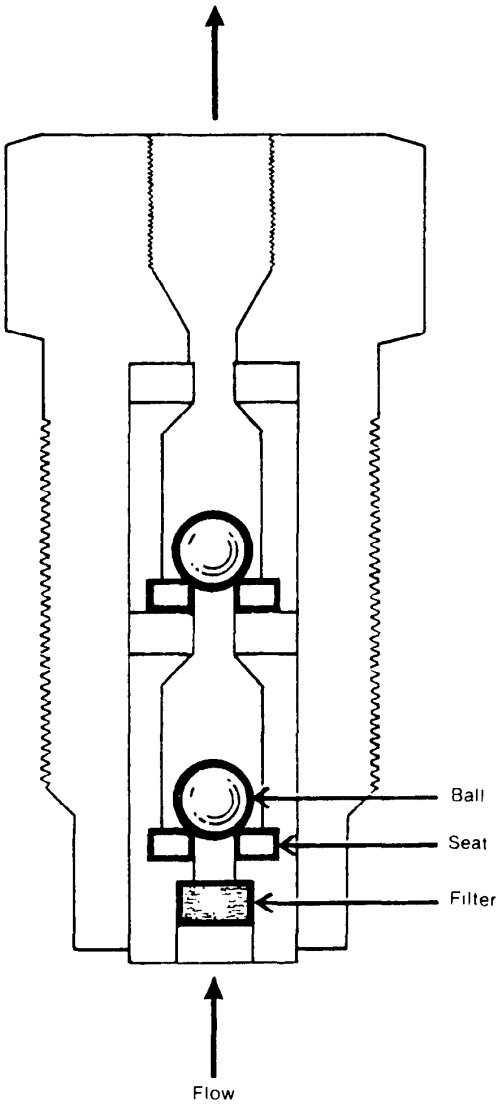


Figure 6 Outlet check valve of the Altex 110 pump. (Altex is now part of Beckman Instruments, Fullerton, CA.) (From Ref. 3.)

is high enough, the ball is forced up by the liquid flow. When the flow decreases, such as during the refill stroke, the high upstream pressure slams the balls against the seat, thus stopping or "checking" the flow. Check valves are expected to perform flawlessly on every cycle, under changing conditions (high salt, to water, to acetonitrile, to chloroform) for months or even years. It is a fact of life that they do not meet this expectation. Check valves have one problem: They leak. It is only the magnitude of the leak that changes. If the leak is a small and a constant portion of the flow rate, the pump is considered to be working well. However, even the best of pumps will have trouble with check valve leaks at flow rates in the low microliter per minute range or less, which is of interest in capillary HPLC.

Diagnosing a check valve problem is usually a matter of experience. Pump manufacturers will usually have diagnostic procedures in the troubleshooting section of the operating manual. Typically, these are specific to the pump and control circuit being used.

Occasionally, one may encounter trouble with poor reproducibility of flow rates, and thus suspect a leak. Leaks are usually obvious, but not always, and there can be other causes of poor precision in T_r. To test for leaks, the column should be replaced with an empty column

with an internal volume of about 1.5 mL. After filling the column with mobile phase, the outlet end of the column is capped, and the flow turned on slowly until a pressure of 300 atm is reached. Then the pump is stopped, and the pressure decay with time is recorded. If the pressure changes slowly, say within 2 atm min^{-1}, the pump is probably not the source of the problem. If the decay rate is larger, then a leak is indicated. If none is found externally, it may be necessary to replace the check valves or piston seals [6].

3. Bubbles and Degasing

In mammals, air bubbles in the heart chamber can cause the heart to lose the ability to pump, with fatal results. This is also true in HPLC pumps, which are said to lose their "prime." If a pump cylinder has a gas bubble, the gas is the first thing to compress on the delivery stroke. However, nothing passes the check valve until the pressure in the cylinder chamber is slightly greater than the system pressure. If the bubble is large enough, this pressure increase never happens, and the pump fails to operate. The bubble simply expands and contracts out of phase to the piston stroke. Good design can nearly eliminate this problem, at least so that some pumps can pump carbonated beverages without losing the prime. One way to minimize this problem is to decrease the degree of gas saturation for the solvent. Thus, if a bubble forms, it is dissolved rapidly, for the thermodynamics favors the solvent adsorbing the gas.

Several methods can be used to degas the mobile phase:

1. Continual purging of the mobile phase with helium (also known as helium sparging) is generally the best method for lowering the level of dissolved nitrogen and oxygen in the mobile phase. It also has the advantage of replacing gases that are problems in detection (such as oxygen) with an inert gas that has much lower solubility.
2. Boiling the liquid was one of the early methods of reducing the level of dissolved gas, but as the temperature was lowered, saturation was usually very rapid. Many laboratories shy away from handling boiling solvents for reasons of safety.
3. Vacuum degasing is another popular method, but it is also relatively expensive. Many plastics, such as Teflon, are permeable to atmospheric gases. Thus, if one places a vacuum on the outside of a tube containing a liquid, the gases are able to permeate the membrane and are sucked into the vacuum, and expelled. One study shows that degasing improves the relative standard deviation (RSD) by about a factor of 2 (Table 2).

The foregoing data show that degasing improves (lowers) the RSD compared with non-degased mobile phases. The data in Table 2 also show that blending in a pump is less reproducible than premixed solvents. Although this data is valid only for the pumps used in the study [7], it is my experience that these effects are general and typical.

The choice of method, particularly between vacuum and helium sparging, is largely a matter of personal preference. I prefer helium because it is easy, inexpensive, and compatible with most detectors.

Table 2 Effect of Degasing on the Retention time (T_r) Reproducibility

Mobile-phase conditions	T_r	% RSD	Peak area	% RSD
Premixed, degased	5.113	0.52	26,863	0.34
Premixed, nondegased	5.076	1.09	27,254	0.46
Blended and degased	5.264	1.42	27,511	1.21

Source: Ref. 7.

D. Syringe Pumps

In the early days of HPLC, syringe pumps were believed to be the most accurate and reproducible, on almost an intuitive basis. When compared with the reciprocating pumps of the day, they were more reproducible because if the check valve seated, it would generally hold tight until the next refill, which might be tens of runs away. However, the flow rate consistency of reciprocating pumps improved, and deficiencies were discovered in syringe pumps [8], especially during gradient elution [9]. Cost, size, and weight were other factors that limited the market acceptance of syringe pumps. Syringe pumps are generally more expensive than reciprocating pumps and require refilling, which could occur in the middle of a run. It if was necessary to refill the cylinder when a peak was in the detector, then the flow through the detector ceased, and the microvolt seconds continued to accumulate, throwing off the results for that run (Fig. 7).

In 1992, syringe pumps were used when very high pressure (typically 600 atm) at low flow was required, such as with capillary columns. This took advantage of the inherent design advantages of syringe pumps to deliver liquids at flow rates lower than about 50 μL min^{-1}.

E. Flow Programming

All too frequently in isocratic elution, there is a pair of peaks in the beginning of the chromatogram with poor resolution. Also, later in the chromatogram, the last peaks have excessive resolution, which means that the time between the peaks is large. Consequently, the total run time is longer than desired. As has been discussed in earlier chapters of the handbook (see Chap. 2) the efficiency of columns generally improves with decreasing flow rate. Thus, one can start with a low flow rate for the first part of the chromatogram, to maximize efficiency and, thereby, resolution. However, later in the chromatogram, there is no need for a large plate count, and thus, the flow rate can be increased to save time (Fig. 8). This is called flow programming. It has been used all too rarely, perhaps owing to the ignorance of users.

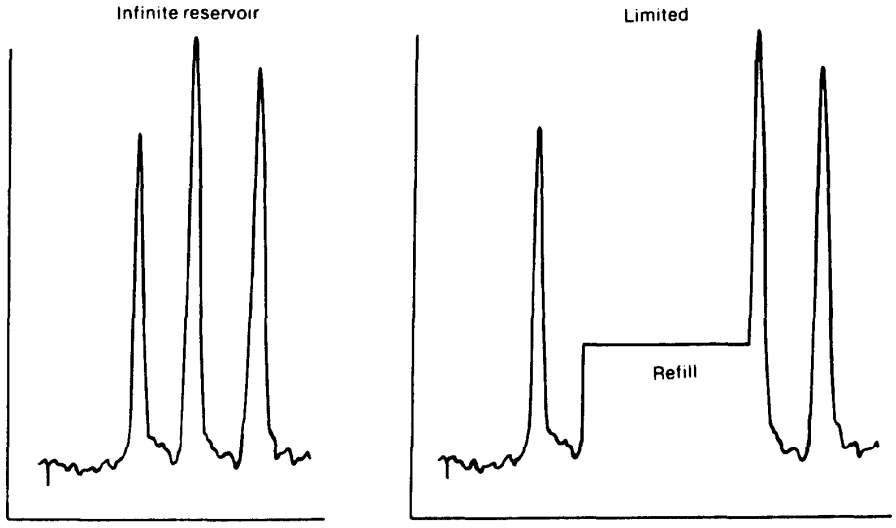


Figure 7 The effect of a refill stroke occurring during a run with a syringe pump. The sample component stays in the detector cell because there is no flow through the column during refill. Although this could be avoided by using two pumps, one in stand-by or refill, the expense is too high. (From Ref. 3.)

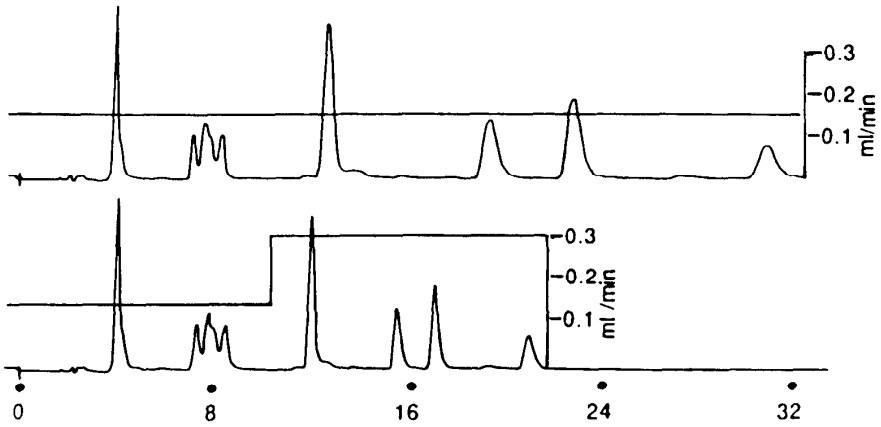


Figure 8 A rare example [10] of flow programming to optimize resolution in the initial segment of the chromatogram, and save time in the later part. (Illustration provided by Isco, Inc., Lincoln, NE.)

F. Recycle Chromatography

Resolution can be increased by increasing the number of plates. (Recall that the resolution is proportional to the square root of the number of plates.) Conceivably, this could be accomplished by increasing the length of the column, if all other parameters were held constant. In the early 1970s one firm successfully made up for a lack of efficient columns by promoting the practice of recycling the poorly resolved components of a mixture back through the column set. Thus, in each pass, the resolution improved a bit. Although in analytical runs in which many peaks were of interest, the task of keeping track of all the peaks soon became a problem; recycle in preparative chromatography makes more sense. In preparative LC, one is often interested in purifying only one component, so the unwanted material can be discarded once it begins to become a problem. Indeed, at least one instrument designed for preparative separations using recycle is offered commercially [11].

III. GRADIENT ELUTION

Gradient elution is a technique of programming the strength of the mobile phase as a function of time. The initial composition of the mobile phase is chosen to be a poor eluent under the mode selected; therefore, most of the components of the sample are retained on the column. The eluting power of the mobile phase is increased by mixing with a miscible stronger solvent, which elutes the more strongly retained components from the column. Gradient elution is used in many separations when the number of the sample components is large or covers a wide range in retention.

The eluting strength of the mobile phase is directly related to the composition of the mobile phase. Perhaps the simplest idea is to control the composition by changing the speeds of the pumps, each metering one solvent. One can start with 100% of the flow from the pump with the weaker solvent and then increase the flow from the pump with the stronger solvent as shown in Figure 9.

There are several ways that mobile-phase gradients can be generated [13,14]. The two most popular methods proportion the solvents on the high-pressure side of the pump, as shown in Figure 9, or on the low-pressure side, as in Figure 10. The latter are often called "prepump" gradients. The performance of the gradients differs, primarily because of the larger dwell time associated with the prepump gradients. These are generally much less expensive, however.

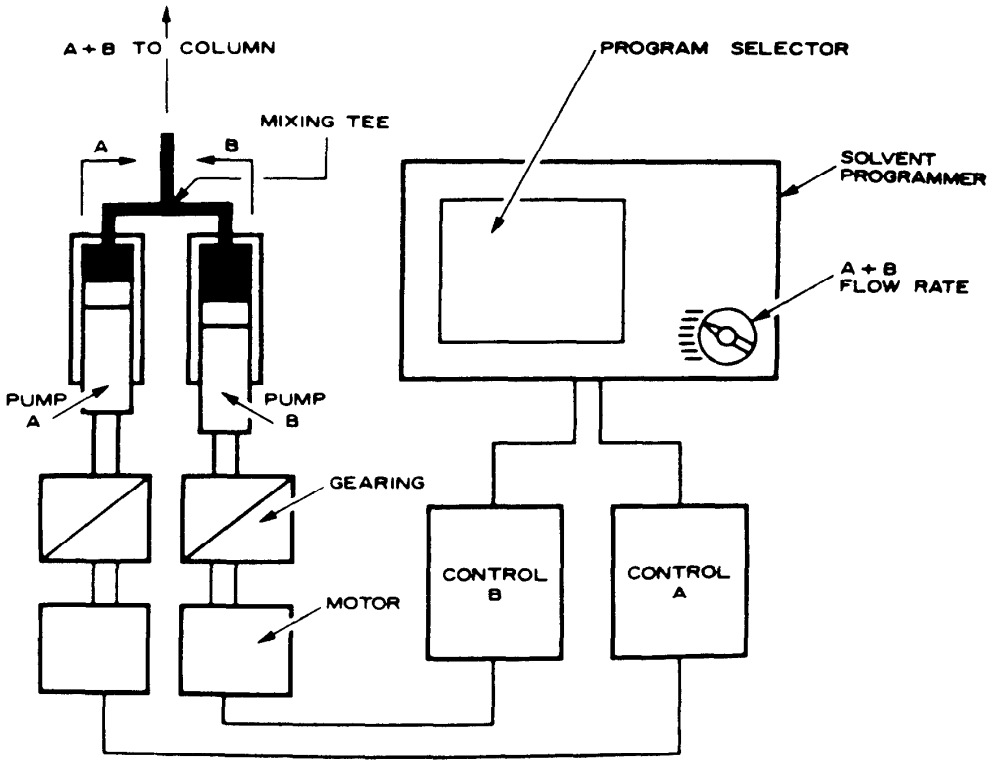


Figure 9 Schematic of gradient elution HPLC. One cylinder delivers the weak solvent (usually refered to as "A") and the second delivers the stronger solvent (often called "B"). (From Ref. 14.)

The dwell or delay time is especially important in transferring a method from one instrument design to another. For instance, many research-grade systems use multiple pumps because these are used for method development and the analyst wants the most flexible system. However, when the method is transferred to the quality control laboratory, controlling cost is often a major concern. The volume from the mixer to the top of the column may be only a few hundred microliters for the multipump system, and ten times larger for the single-pump gradient. Thus, the solvent change is delayed significantly with the single-pump system. To some extent this can be compensated by changes in the gradient program. The highly useful chromatogram simulation software developed by LC Resources (Walnut Creek, CA) has a specific entry for the solvent delay line in gradient separations. In short, gradient delay volume is an important parameter to control, especially for different models of instruments.

In 1978, Varian introduced a single-piston pump that performed the proportioning in the pump head. The goal was to lower the cost by using a single one-piston pump, and reduce the delay time by coupling the proportioning very closely to the piston. Despite significant engineering problems, which were overcome, the pump worked well. Varian ran an advertisement showing that this pump could pump fresh champagne. However, the cost reduction did not lead to a strong competitive advantage. Today, these pumps account for an insignificant percentage of sales. The reviewer of this chapter offered the opinion that this design "may well be the pump design of the future." Varian's patents expire shortly. It will be interesting to see if this changes anything.

Conceptually, the simplest system involves multiple pumps, each pumping a single solvent. By varying each pump speed, it is possible to control the composition [15]. For instance, if 25% of the total flow is delivered by the acetonitrile pump, then the composition should

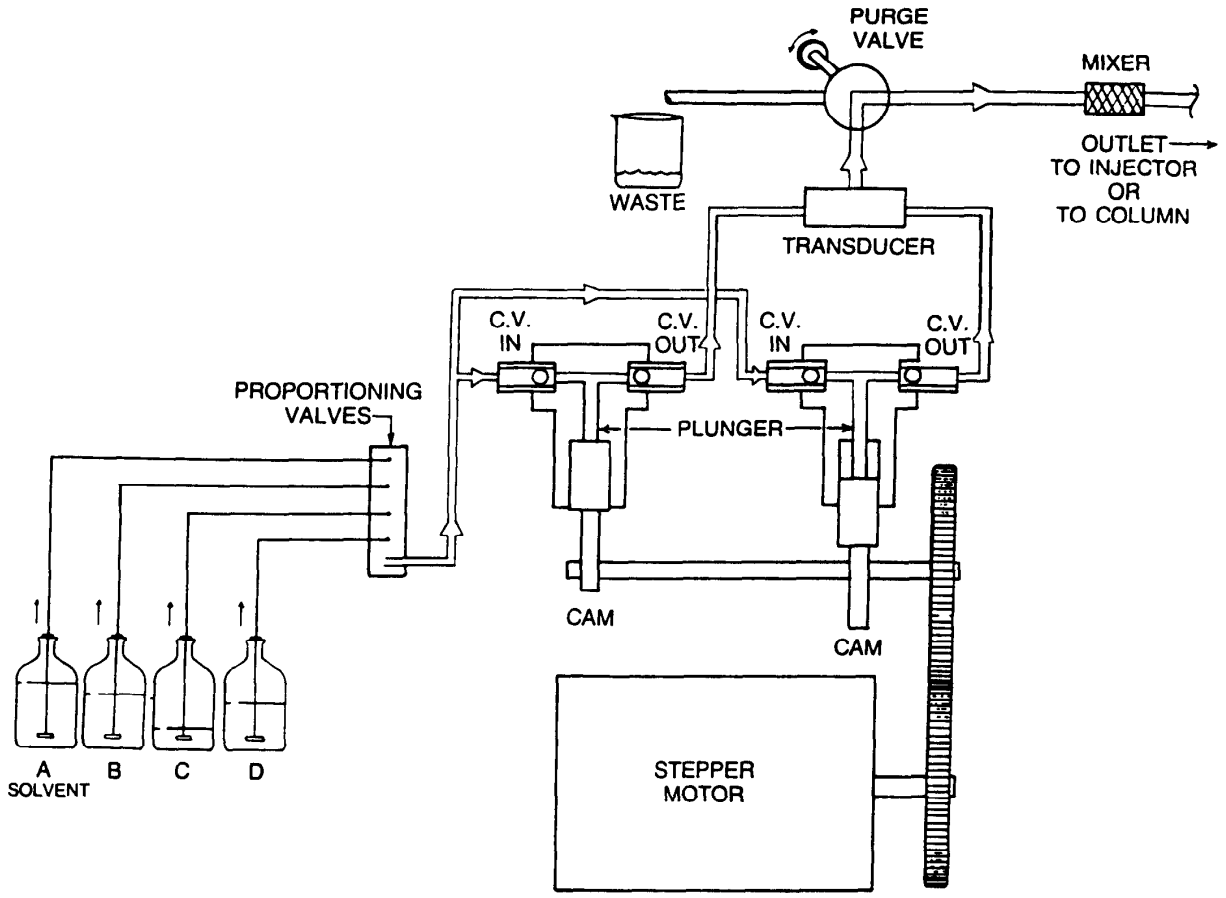


Figure 10 Schematic of typical prepump gradient elution system. (Courtesy of LDC Analytical, Riviera Beach, FL.)

be 25% acetonitrile. The remainder is delivered by the other pump. Today, multiple pump systems for gradient elution are considered to be a premium performance option as shown in Table 3.

Some of the problems that were encountered are listed in Table 4, along with the remedies.

Many gradient elution systems are used in method development to scout for solvent conditions for isocratic separations. This takes advantage of the very convenient and rapid changes in solvent composition that are possible, especially with multiple pump designs. This is analogous to temperature-programmed gas chromatography (GC), which is often used to hunt for isothermal conditions. Both isothermal GC and isocratic LC are usually more reproducible and trouble-free than the gradient counterparts of temperature programming or gradient elution. This is illustrated in some data from Varian, which compares the RSD for the retention time for premixed and proportioned isocratic runs and gradient elution (Table 5).

The data in Table 5 show that for the best precision in retention time, one should use isocratic elution with premixed solvents. Experience shows that good volumetric techniques are required as well as A grade glassware. The trend in percentage RSD for gradient elution probably is caused by the difficulty in metering-in small amounts of one solvent during the early part of the gradient. Because the modifier is usually chosen to have a large effect, a small variation in composition can show up as a larger variance in retention time. The data also show that it is possible to obtain very good precision from HPLC. With careful adjustment and optimization, RSD of less than 0.1% can be achieved in retention time and peak area or height, which makes HPLC high-precision liquid chromatography.

Table 3 Comparison of Attributes of Various Gradient Elution Designs

Design	Advantages	Disadvantages
Multiple pumps	Lowest dead volume, can be used with narrow or short columns, fast analysis	Highest price
	Quickest response	Syringe pump systems may have problems with wide changes in viscosity
	Most flexibility	Takes lots of bench space
	Degasing seldom required	
	Lower solvent consumption	
	Easiest to troubleshoot	
Single pump with mixing valves	Lower price for system	Minimum-delay volume is often several milliliters, slowing chromatography and wasting solvent
	Flexible: up to 4 solvents can be proportiond	Mixing solvents can release dissolved gas, causing pump to stall
	Compact compared to multipump system	Troubleshooting is moderate to difficult

IV. BIOCOMPATIBILITY AND MATERIALS OF CONSTRUCTION

Generally, pumps and the high-pressure flow path are made from stainless steel, usually 316 grade. Stainless steel resists corrosion by forming a dense oxide surface over the metal, which renders the metal inert for most applications. The slight risk of corrosion with halides can be managed by occasional passivation by flushing the system with nitric acid, which can be a practical option for the routine user of HPLC. [Consult your owner's manual for details on the specific protocols for passivation.] The other elements in the flow path are listed in Table 6.

It is hard to separate the need for pumps made from other materials from the marketing hype that some firms used in promoting their pumps. In the early days of HPLC, Nester-Faust marketed syringe pumps with glass walls and Teflon pistons. Few found them to be required, and the option was dropped after the firm was purchased by Perkin-Elmer. About a decade later, Pharmacia introduced an integrated glass and plastic system specifically designed and marketed for protein chromatography. Pharmacia was very successful in communicating to prospects the potential problems of metal contamination from stainless steel systems or adsorption of proteins on metal oxides. The claim was that only glass and plastic were "biocompatible." Other firms continued using stainless steel or offered other materials, such as sapphire, titanium, polyetheretherketone (PEEK), and others.

Ion chromatography (IC) is another mode for which stainless steel has not been well accepted, owing to the potential problems with corrosion. Dionex, the leading manufacturer, has consistently avoided using metals in the liquid flow paths of IC instruments. Metrohm [17] has found few, if any, problems with pumps with stainless steel in the flow path.

Use of PEEK is quickly becoming the most popular alternative to stainless steel. It is a strong and relatively inert plastic that can be machined into complex shapes, almost as a

Table 4 Problems, Causes, and Remedies in Multipump Gradient Elutions

Problem	Cause and remedy
Bubbles form in the pump or detector	Mobile phases prepared from blended solvents may have lower solubility limits for atmospheric gases, which form bubbles. Helium sparging or vacuum degasing usually eliminate the problem.
Retention time reproducibility is worse than isocratic elution	In general, this is true even for the best systems. Apparently the control of the mobile-phase composition is not developed. One should be able to obtain a relative standard deviation (RSD) of about $\pm 0.5\%$ in retention time with care.
Methods are very instrument-dependent	The biggest problem in transferring a method from one instrument to one with a different design is that the mixing and dead volumes can be very different. This makes it difficult to transfer methods unless one controls the dead volume, and mixing volume [12].
Problems with check valves and other pump failures are more frequent	Mixing solvents in the piston chamber, as is done in prepump mixing, can lead to degasing and precipitation. Both will cause problems with maintaining the flow rate and, thus, the composition from run to run.
Pressure can change by a large factor	The viscosity of some mixed solvents such as methanol and water can be more than twice as high as either pure solvent. This can cause problems with set pressure limits of a pump.
Pumps can lose control of the solvent composition	Syringe pumps have large volume under pressure. Under certain conditions, it is possible for a solvent and pressure oscillation to occur as the viscosity decreases during a run. The oscillation can be eliminated by minimizing the liquid volume of the most compressible solvent [8,9].

Table 5 Comparison of Retention Time Reproducibility of a Varian[a] HPLC Using Premixed and Proportioned Solvents

	Isocratic			
Peak No.	Premixed (%)	Proportioned binary (%)	Proportioned ternary (%)	Gradient elution
1	0.19	0.17	0.43	0.28
2	0.19	0.20	0.42	0.28
3	0.21	0.22	0.42	0.20
4	0.20	0.29	0.61	0.19

[a]Pump is single-piston design with proportioning via microprocessor controlled metering valves on pump inlet. All values are % RSD.
Source: Ref. 16.

Table 6 Materials of Construction for HPLC Parts in the Liquid Flow Path

Component	Standard material	Optional
Cylinder body	Stainless	Sapphire Glass Titanium PEEK[b]
Piston	Sapphire	
Check valve ball	Ruby or sapphire	
Check valve seat	Machinable ceramics or glass filled polymer[a]	KEL-F[c] PEEK
Piston seal	Spring-loaded polymer	
Liquid lines	Stainless steel	PTEE[d] Titanium PEEK

[a]The polymers are carefully selected by each manufacturer to provide long life with the piston and check valve. The selection is generally empirical. If problems are encountered, contact the service staff of the vendor. They may know of seals with improved compatibility with your work.
[b]Polyetheretherketone (PEEK)
[c]Product of 3M, St. Paul, MN
[d]Polytetrafluoroethelene (PTFE) is the generic name for Teflon (Dupont, Wilmington, DE)

metal. PEEK is not inert to all solvents [18]. For example, 1/16-in. tubing was allowed to soak in various solvents for 3 weeks and then burst tested (Table 7). The data show that PEEK tubing, and to a lesser extent, PEEK parts, should be carefully handled, especially with mobile phases containing acetonitrile and tetrahydrofuran. Other mobile phases should be investigated before prolonged use.

At 500 psi below the listed pressure, the tubing did not burst. This data lists burst pressure, so it is strongly recommended that an appropriate safety factor be used before plumbing a system with this tubing.

In general, the materials of construction should be as inert as practical for the application of interest. Despite hundreds of human years of searching by engineers in many firms, no

Table 7 Burst Pressure (psi) for 1/16-od (0.0625-od) Tubes After Exposure for 3 Weeks to the Indicated Mobile Phase

Bore (in.)	0.007	0.010	0.020	0.030
Solvent				
Water	> 6000	> 6000	> 6000	> 6000
1:1 Acetonitrile/water	> 5500	5500	4500	3500
Acetonitrile	4000	3500	300	3000
Isopropanol	> 5000	5000	4000	4000
Tetrahydrofuran	2500	2500	1500	1500

Source: Ref. 18.

universally inert materials have been found. Even plastics and glass adsorb, leach, or even denature some analytes. A proficient chromatographer knows the system, and checks both methods and instrument frequently to make sure it is operating as desired. Trouble often begins shortly after an assumption is made.

V. FLOW RATE RANGE

Engineers designing pumps must make compromises in their design. The flow rate of a pump can be varied by about a factor of ten from the design point, but outside the range, the performance starts to decline rapidly. Some manufacturers can extend the range by changing parts of the pumps, such as the pump head. If the motor is strong enough, this effectively increases the dynamic range of the pump.

Pumps designed for a particular purpose will usually be capable of operation in a broader range, but the performance, or perhaps the reliability, will begin to degrade.

As the size of the column increases, it is necessary to change the pump. The common HPLC pump is designed for operation at about 1 mL min^{-1} and at pressures of 150 atm or less. The specifications cover a wider range, but experience shows that operating at the extreme, often increases maintenance problems. As of 1995, few pumps or other system components are designed for routine operation at the extreme pressures and flows listed in the specifications. This is unfortunate, because column technology is perhaps 15 years ahead of the design of the instrumentation.

Liquid chromatography–mass spectrometry (LC/MS) and amino acid sequencing and peptide mapping are driving the interest in capillary HPLC columns. The need to conserve solvents to decrease disposal costs also favors using smaller-diameter columns. There are not many instruments capable of delivering these low flow rates with the same performance that has become standard with pumps designed for the analytical range in Table 8. The problem is how to obtain low flow rates from existing instrumentation? Some chromatographers use splitters to decrease the flow through the analytical column. This is an expedient design, but still wastes small amounts of solvent. Future system designs will probably have total flow rate ranges in the 1–50 μL min^{-1}. Figure 11 shows how an LC–MC can be interfaced with small-bore columns and Figure 12 compares the results of MS and UV detection for a tryptic map.

Preparative modes listed in Table 8 are somewhat arbitrary, but useful, for they demonstrate that, as the sample size increases, the column diameter increases also (see also Chap. 2). Theory and practice demonstrate that the best utilization of a preparative column is to use frequent short cycles at high linear velocity. Some would argue that one can scale-up the analytical column directly by just increasing the flow rate, as required, to keep the linear velocity the same. In practice, this works up to columns in the range of about 2- to 4-cm id, and then the game changes. In large-scale preparative LC, one seldom needs the very high

Table 8 General Categories of Mode, Column Diameter, and Pressure Range for HPLC Operation

Mode/purpose	Column id	Flow rate range	Pressure range (atm)
Capillary	< 1 mm	10–500 μL min^{-1}	50–400
Analytical	2–8 mm	0.5–2 mL min^{-1}	20–150, 400 atm max
Laboratory preparation	7–22 mm	2–10 mL min^{-1}	< 100
Pilot plant	20 mm–10 cm	10–200 mL min^{-1}	< 100
Perfusion	20 mm–10 cm	100–2 L min^{-1}	< 50
Process	5 cm and larger	> 200 mL min^{-1}	< 50

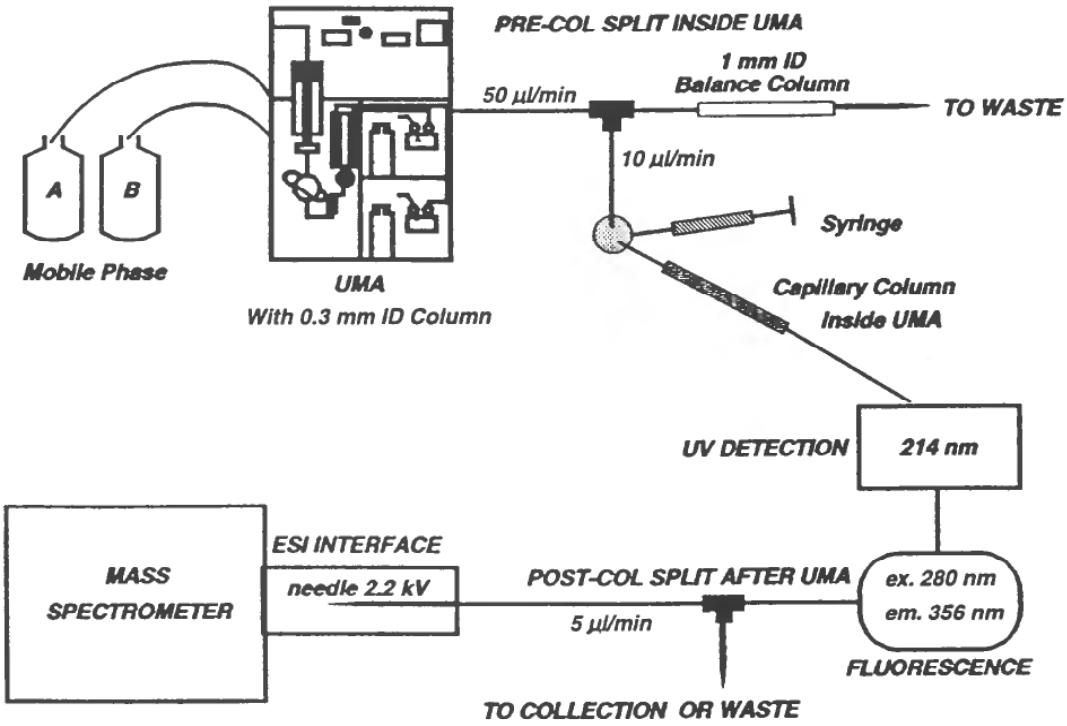


Figure 11 Schematic of HPLC with two columns: the capillary column feeds the mass spectrometer, while a minibore balancing column is used to take the excess flow rate from the HPLC pumps [19]. This wastes about 90% of the solvent, but does permit the use of capillary columns. Larger diameter balancing columns have been used with conventional HPLC instruments. (Courtesy of Michrom BioResources, Inc., Pleasanton, CA.)

resolution that is found in the analytical column. Also, if one increases the column diameter further, the wall thickness and other design problems start to become significant. Thus, larger-scale preparation often uses larger-diameter particles than found in analytical columns, which lowers the pressure requirements. Another factor is that the beds in narrow columns are held up by the wall, but as the column diameter increases the wall has less influence, and beds are often less robust as the diameter increases. Chromatographers compensate for this by decreasing the linear velocity and, thereby, the force on the column bed. This decreases the pressure drop across the column as predicted in Eq. (1).

VI. PULSE DAMPERS

It is an unfortunate fact that many detectors for HPLC are flow-sensitive; that is, the detector signal output changes with the flow rate through the detection cell. The mechanisms for the flow dependence are complex and are covered in the detector chapters. Syringe pumps had the advantage that the flow was very uniform because the mobile phase, once compressed, was displaced very smoothly. The proponents of metering pumps found that by adding springy elements (engineers call this compliance) into the flow path, it was possible to smooth out the extremes in the pressure profile and thereby improve the signal/noise ratio of the system as seen in the detector output.

The simplest pulse dampers were coiled tubes, which expanded and contracted with pressure, much like a Boudon tube in a pressure gauge. If the metal was thin, the pressure change could cause the volume to change by bending coil. However, these metal pieces had to be made out of thin metal to be deformable, and thus they had low pressure ratings. As a consequence, pulse dampers were frequent sources of leaks. It did not help when one major

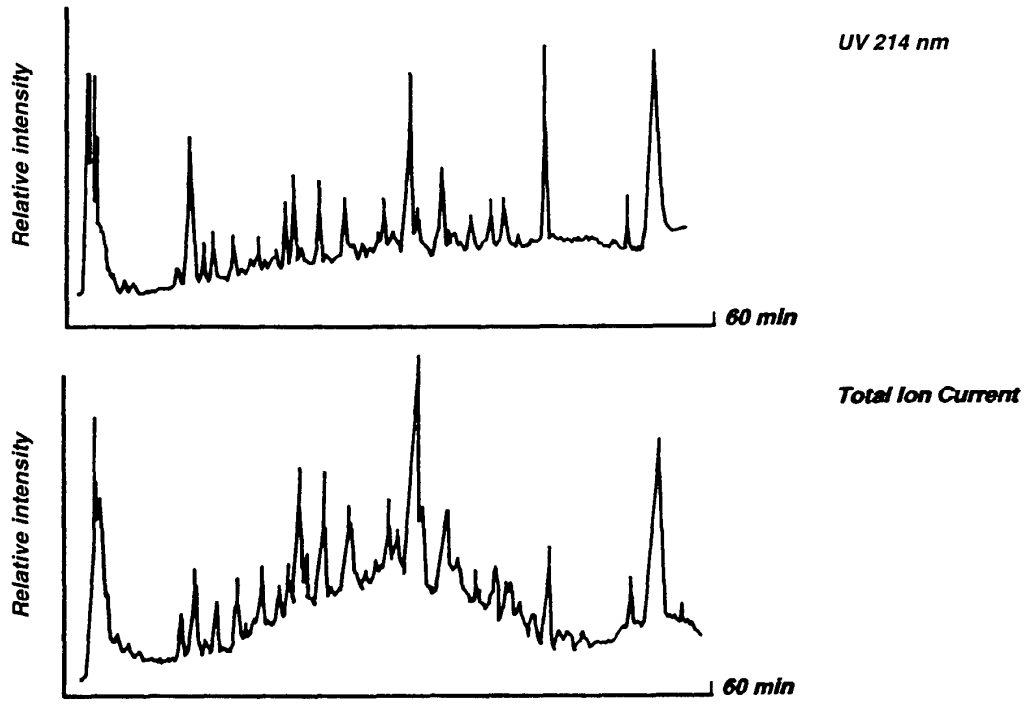


Figure 12 Comparison of electrospray MS and UV detection at 214 nm for tryptic digest of bovine serum albumin (BSA). Separation conditions: RPLC with acetonitrile/water gradient with trifluroacetic acid (0.1%). (Courtesy of Michrom BioResources, Inc., Pleasanton, CA.)

vendor used a different metal in the damper, which set up an electrochemical cell, and could not be cleaned with acid or base. Consequently, engineers have tried to develop designs that did not require pulse dampers.

To get around the low-pressure limit, Varian developed a pulse damper that relied on the compressibility of some solid plastics. The damper was a plastic rod encased in a metal column housing. The column housing could take pressure of over 10,000 psi. The pressure pulses simply compressed the plastic rod.

Pulse dampers are problems because they change volume to compensate for the pressure fluctuation. The volume change is probably of little consequence in isocratic work, but in gradient elution, the pressure excursion can be larger than a factor of three, which can cause a change in the solvent composition, especially in two-pump systems. Also, pulse dampers do increase the delay time for responding to a change in solvent composition in single-pump gradient systems.

More recently, microprocessor-controlled pumps have been taught to minimize the pressure pulses by fine tuning the refill and decompression cycles of the pump cycle.

VII. TROUBLESHOOTING

As with most repairs, the first step is to locate the problem. Occasionally, it is easy because of previous experience, or recurring failures. However, in general, one should use the repairman's approach: look at the problem, select and change one variable and see if the symptom is affected. Work systematically. In this way, it is possible to focus attention on increasingly smaller parts of the system, until the culprit is located. The repair is then much easier. The other tool is a suspicious mind.

First, with today's instrumentation, over half of the problems will probably be chemical. New reagents, unexpected components in the sample, or a new vendor of mobile phase, all are new variables in the experiment. Chromatography is based on a very delicate balance of forces. Thus, small changes can have a large effect on the outcomes (Table 9).

Gradient elution usually adds several more variables, each of which can become out of control unexpectedly (Table 10). For instance, solvents that are suitable for isocratic work can

Table 9 Troubleshooting Isocratic Elution

Symptom	Possible cause	Remedy
Retention times are not reproducible (isocratic elution)	Flow rate through column is not constant	Monitor pressure: if pressure is not constant, suspect: plugged solvent inlet filter; check valve malfunction; bubble in cylinder chamber; leak (s), owing to pump, high column inlet pressure, pulse dampers.
	Temperature of column is changing.	Confirm by insulating column to see if situation improved, or use column temperature control such as oven, water bath, or thermostated room.
	Uncontrolled variations in mobile phase composition	Improve technique for preparation of mobile phase. For example: 1. Use volumetric glassware. 2. Reduce helium sparge rates, if using helium sparging.
Retention times show definite trend (higher or lower)	Column temperature is not controlled. Suspect if the period corresponds to changes in laboratory temperature.	Control column temperature.
	Material is being added or removed from column, changing selectivity or capacity	Add guard column between pump and injector. If improvement, suspect mobile phase contaminants. Plot the change in retention versus the number of samples injected, but vary the time between injections. If strong correlation with sample number, revise sample preparation protocol to remove problem origin.

Table 9 Continued

Symptom	Possible cause	Remedy
Pressure changes randomly	Flow rate is changing	Check if valves are dirty: wash with detergent or replace. Leak around piston: replace seal. Leak in high-pressure lines or fittings: repair. Bubble in cylinder: use degased or helium-sparged mobile phase.
Pressure is too high	Flow rate is too high, especially with pumps controlled by panel and computer	Reset flow
	Solvent improperly made	Check composition or prepare new batch
	Column is plugging	Replace inlet filter or replace column. If plugged column, see column troubleshooting sections.
	Injector failure or misposition	See injector section
Pressure is too low	Leak	Locate and repair
	Bubble in pump	Sparge with helium or degas
	Check valve failure	Wash with detergent or replace valves
	Inlet filter is plugged, starving the pump	Replace filter, discard old filter
	Flow rate set incorrectly, especially with pumps with panel and computer control.	Reset flow.
	Broken piston	Replace piston: Look for primary cause

be the source of ghost peaks as shown in Figure 13. In isocratic separations, small amounts of contaminants in the mobile phase may not be a significant problem, especially if guard columns are used. However, in gradient elution, the bands can be concentrated and give a bad blank run.

Table 10 Troubleshooting in Gradient Elution

Symptom	Possible Cause	Remedy
Retention times are not reproducible	Flow rate through column is not constant	Pump malfunction owing to leak: repair. Bubble in cylinder or proportioning valve: sparge or degas (low pressure mixing). Plugged solvent inlet filter: replace. Check valve malfunction: wash with detergent or replace.
	Pressure limit set too low	Set pressure limit higher. Find cause for increased pressure.
Noisy baseline	Mixer not functioning (high-pressure and low-pressure mixing)	Confirm by turning off mixer power; if no change, mixer is not operating: repair mixer.
	Proportioning valves in pre-pump gradient not operating	Use only one solvent: if noise decreases, proportioning valves may need repair.
	Ghost peaks	Confirm by making run but injecting nothing: if peaks persist at about same height, suspect contamination of mobile phase or injectors, or corrosion of system. Locate source of contaminants (see below). If peaks are smaller or absent, suspect injector malfunction, or excessive column loading.
Ghost peaks	Impurities in mobile phase	Determine which phase by systematically varying the flow at compositions below elution. For instance, if pumping twice the volume of water increases the height of the peaks, the water may be the source. Also try changing sources of solvent or buffer components.
	Polymers trapped in column packing	Some polymers (proteins) have narrow elution windows: decrease gradient slope to increase time for elution; decrease particle size of packing, or use perfusion chromatography.
	Solvent decompression oscillation (syrine pumps only)	Consult manufacturer. Avoid mixed solvents with large viscosity changes.

Table 10 Continued

Symptom	Possible Cause	Remedy
	Injector contamination	Clean injector with a strong solvent, possibly including nitric acid.
Excessive shift in baseline.	Impurity in mobile phase	Locate source of impurity by making up fresh mobile-phase components from different batches of reagents. Vary flow volumes of reagents at compositions favoring retention on column, then run gradient to see which is the source; obstruction in the sample or reference cell of the detector.

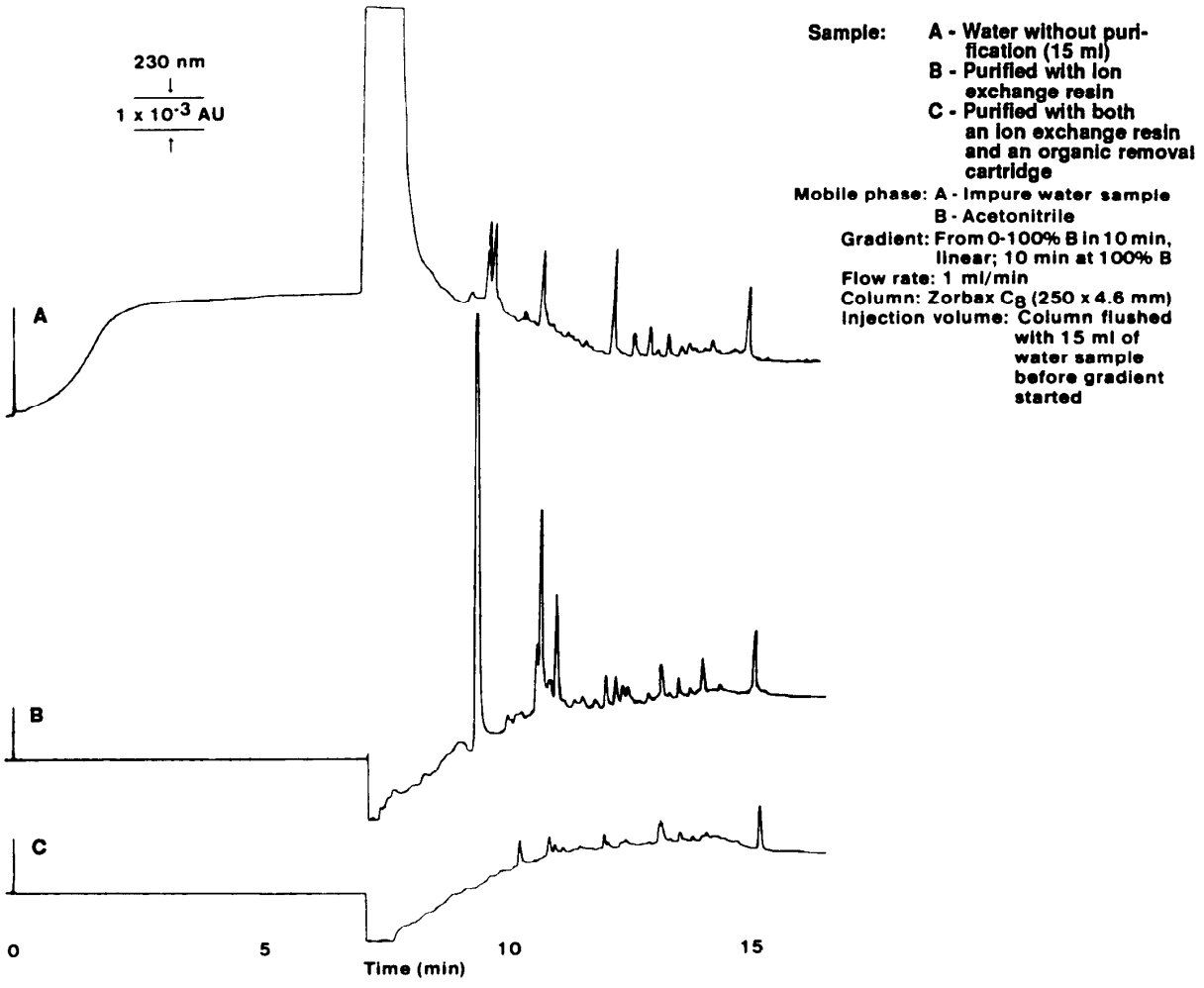


Figure 13 Comparison of runs obtained with water purified by three different techniques. Changing the water source can be important in identifying the source of peaks in chromatograms when no sample is injected. Similar studies with modifiers (such as acetonitrile for RPLC or buffers in IEX) are important steps in method validation. (Illustration provided by Isco, Inc., Lincoln, NE.)

Appendix Pump Vendors and Models

Vendor and model	Flow rate range (mL/min)	P_{max} (atm)	No. Pistons	SS?	Ti?	Plastic/bio	Glass	Gradient	Comments
Bischoff 2250	(0.001–0.999) or (0.01–4.99) or (0.1–19.9)	600	2-piston and check valves	Std.	Opt	PEEK, opt.		Low-pressure prepump and multipump high pressure	3 interchangeable pump heads
Dionex GP 40 Standard bore	0.04–10	333	2	Std.	No	Opt.	No	Quaternary	Optional degasing
Dionex GP 40 Microbore	0.01–25	333	2	Std.	No	Opt.	No	Quaternary	Optional degasing.
Dionex GP 40 Standard bore	0.04–10	333	2	Std.	No	Opt.	No	Isocratic	Optional degasing
Dionex GP 40 Standard bore	0.01–2.5	333	2	Std.	No	Opt.	No	Isocratic	Optional degasing
Eldex 9600	0.01–10	400	2	Yes	No	No	No	Preppump	Metal-free model available
Eldex MicroPro	0.001–0.500	670	Syringe	Yes	No	No	No	Multiple pump high pressure	Syringe pump for capillary HPLC
Flux Rheos 4000	0.005–4.0	400	2-piston serial		Opt			Quaternary prepump	Unique sandwich design; low pulse
Gilson, Inc. Model 305	0.010–200	592	1	Yes	Yes	No	No	Yes	Stand alone programmability or remote control from Gilson software
Gilson, Inc. Model 306	0.010–200	592	1	Yes	Yes	No	No	Yes	Remote control from 305 master pump or Gilson software
Gilson, Inc. Model 307	0.010–5	592	1	Yes	Yes	No	No	No	Stand alone programmability or remote control from Gilson software

Appendix: Continued

Vendor and model	Flow rate range (mL/min)	P_{max} (atm)	No. Pistons	SS?	Ti?	Plastic/bio	Glass	Gradient	Comments
Hitachi/Merck L-7100	0.001–9.999	400	2-piston serial	Std	—	—	—	Low-pressure prepump and multipump high pressure	Electronic pulse suppression
HP 1100 series binary pump	0.001–5.0	400	4	Yes	No	No	No	High-pressure binary mixing	Optimized design—only 180–480 μL internal volume and highest composition stability
HP 1100 series isocratic pump	0.001–10.0	400	2	Yes	No	No	No		Designed to meet the needs of QA/QC applications
HP 1100 series quaternary pump	0.001–10.0	400	2	Yes	No	No	No	Low-pressure quaternary mixing	Provides highest flexibility in solvent mixing
Jasco PU 980i	0.001–10.0	250	Single			Std		Prepump quaternary or 2-pump high pressure	Pump module for biocompatible system
Jasco PU-980	0.001–10.0	500	Single	Std.	—	See PU 980i	—	Prepump quaternary or 2-pump high pressure	Small profile
Jasco PU-986	0.001–20.0	400	Dual	Std.	—	—	—	2-pump high pressure	Small profile
Jasco PU-987	0.001–50.0	150	Dual	Std.	—	—	—	2-pump high pressure	Small profile
Jasco PU985	0.1–5.0	350	Single	—	—	—	—	Constant pressure	For pumping reagent in postcolumn derivitization detectors
Metrohm 709	0.1–5.0	500	2-piston and check valves	Std.	—	PEEK Std.	—	—	Optimized for ion chromatography

Micro-Tech Scientific Ultra-Plus 200 M	0.0001–0.5	689	Single	Yes	Yes	Yes	Yes	Multiple pumps	High-pressure gradient with integrated feed-back close-loop control
Micro-Tech Scientific Ultra-Plus 200 M	0.001–5	550	Single	Yes	Yes	Yes	Yes	Multiple pumps	High-pressure gradient with integrated feed-back close-loop control
Perkin-Elmer Series 200	0.01–10.0	420	2	Std.	Opt.	No	No	Prepump	Isocratic binary, and quaternary gradient
Rainin Instrument SD-1	0.01–3200	680	2	Yes	Yes	Yes	—	2 or more pumps, high pressure	Choice of 4 pump heads covering flow range
Rainin Instrument SD-200	0.01–200	590	1	Yes	Yes	Yes	—	2 or more pumps, high-pressure	—
Rainin Instrument SD-300	0.01–200	590	1	Yes	Yes	Yes	—	1 or more pumps, high-pressure	Prep version of the SD-200
Sykam S 1121	(0.1–9.95 or (0.02–4.0) or (0.4–40)	400	2-piston serial	Std.	—	—	—	Low-pressure prepump	Economical pump for general HPLC.
Thermo Separation P4000 Narrow Bore Quaternary Analytical Gradient pump	0.01–5.0	400	2-piston serial	Std.	No	No	No	Low-pressure/gradient	—
Thermo Separation P4000 Quaternary Gradient Analytical pump	0.01–10.0	400	2-piston serial	Std.	No	Total inert version	No	Low-pressure/isocratic	—
Thermo Separation Products P1000 Isocratic Analytical Pump	0.01–10.0	400	2-piston serial	Std.	No	Total inert version	No	N/A	—
Thermo Separation Products P1500 Binary Isocratic Analytical Pump	0.01–10.0	400	2-piston serial	Std.	No	Total inert version	No	N/A	—

Appendix: Continued

Vendor and model	Flow rate range (mL/min)	P_{max} (atm)	No. Pistons	SS?	Ti?	Plastic/bio	Glass	Gradient	Comments
Thermo Separation Products P2000 Binary Gradient Analytical Pump	0.01–10.0	6000 psi	2-piston serial	Std.	No	Total inert version	No	Low pressure/gradient	
Waters 515 HPLC pump	0.001–10.00 0.001–22.500	4008 204	2 2	Yes Yes	No No	No No	No No	No[a] No[a]	Standalone: Isocratic, with controller: binary or ternary gradient. Analytical flow rate range with 100 μL standard heads. Semiprep range with optional 225 μL heads. Flow precision: 0.1% RSD or 2-SD. Flow accuracy: $\pm$1.0% or 30 μL/min. whichever is greater.
Waters 600 E Multisolvent Delivery System	0.01–20.00 0.01–45.00	408[b] 68[b]	2 2	Yes Yes	No No	No No	No No	Yes Yes	408 atm at 20.0 mL/min., 68 atm at 45.00 mL/min. Single-pump quaternary gradient, analytical to semiprep flow rates. Flow precision: 0.1% RSD. Composition precision: $\pm$0.15% absolute and composition accuracy: $\pm$0.5 absolute (both independent of backpressure).

Waters 616 LC System	0.01–10.00	340	2	Yes	No	No	No	Yes	Single-pump quaternary gradient, narrowbore to analytical flow rates. Low dispersion (< 400 μL). Flow precision: 0.1% RSD. ± Composition precision: ±0.15 absolute and composition accuracy: ±0.5% absolute (both independent of backpressure). SILK microflow control.
Waters 626 LC System	0.01–10.00	272	2	No	No	Yes	No	Yes	Single-pump quaternary gradient, narrow bore to analytical flow rates in a nonmetallic flow path. Low dispersion (< 400 μL). Flow precision: 0.1% RSD. Composition precision: ±0.15% absolute and composition accuracy: ±0.5% absolute (both independent of back pressure). SILK microflow control.

Appendix: Continued

Vendor and model	Flow rate range (mL/min)	P_{max} (atm)	No. Pistons	SS?	Ti?	Plastic/bio	Glass	Gradient	Comments
Waters 650 Advanced Protein Purification System	0.01–45.0[c] 0.5–80.0[d]	51	2	No	No	Yes	No	Yes	Single-pump quaternary gradient, analytical to semiprep flow rates in a nonmetallic flow path. Composition accuracy: ±0.5% absolute, 225-μL heads, Composition accuracy: ±1.0% absolute; 400-μL heads (both independent of backpressure).
Waters Delta Pump® 4000	0.50–150.00	272	2	Yes	No	No	No	No	Single-pump quaternary gradient, analytical to preparative flow rates. Composition accuracy: Better than 3.0%.
Waters 2690 Separations Module	0.001–10.000	340	2	Yes	No	No	No	No	Quaternary, microbore-narrow bore analytical solvent and sample management system. Independent, software-controlled piston motors and serial flow path. Low dispersion (< 650 μL, including sample management system). Flow precision: 0.075% RSD or 0.02 min.

Std., Standard; Opt., optional; Prep, preparative; N/A, not available.

REFERENCES

1. Strategic Directions, Report on HPLC, June 1992.
2. Sheehan, TL, Tschida, J. Am Lab 1989; August: 22.
3. Stevenson, R, Henry, R, Magnussen, H, Mansfield, P. Am Lab 1978 (Jan) p. 32.
4. HPLC Pump Model 2200, Bischoff analysentechnik und gerate, Gmbh, Leonberg, Germany, p. 13. Jan 6, 1991.
5. Bischoff Model 2200, Illustrations, Fig. 3. Jan 6, 1991.
6. HPLC Pump Model 2200, Bischoff analysentechnik und gerate, Gmbh, Leonberg, Germany, p. 24. Jan 6, 1991.
7. Advanced Technology for Intelligent HPLC, Zymark Corp. December 1992.
8. Martin, M, Blu, G, Eon, C, Guichon, G. J Chromatogr 1975;112:399.
9. JC Helmer. Anal Chem 1976;48:1741.
10. ISCO catalog 27, p. 47 (1991). Used with permission.
11. Japan Analytical Industry Co., Ltd. Model LC-20 and LC 908. (See also, Kubo L, Nakatsu T. LC-GC 1990;8:933.
12. Snyder, LR, Dolan, JW. LC-GC 1990;8:524.
13. Scott, RPW. Contemporary Liquid Chromatography, New York: John Wiley & Sons, 1976: 106.
14. Johnson, EL, Stevenson, R. Basic Liquid Chromatography. Varian Associates, 1977:249.
15. Allington, RW, ISCO, US Patent 3,398,689, Aug. 27, 1968.
16. Varian Star LC System, Pub. 800870-003 March 1991.
17. Systems for IC, Technical Specifications, Model 697 IC Pump 02.90, Metrohm CH-9101 Herisau, p. 3.
18. Sample injectors and accessories for liquid chromatography. Rheodyne, p. 7, 1991.
19. Nugent, K. Personal communication, 1993.

15

Liquid Chromatography Detectors

Raymond P. W. Scott

Birkbeck College, University of London, London, England, and Georgetown University, Washington, D.C.

I. INTRODUCTION

The lack of a sensitive, linear detector was probably the greatest single impediment to the evolution of liquid chromatography (LC) in the years past. The development of LC detectors proved to be far more difficult than their gas chromatography (GC) counterparts. Unfortunately, very low concentrations of solute vapor in a gas modify the physical properties of the gas to a far greater extent than the same concentration of solute will modify the physical properties of a liquid. Nevertheless, despite the sensitivity problems, many LC detectors have been developed over the past 30 years, based on a variety of different sensing principles. During the 1950s, 1960s, and 1970s a considerable number of sensing methods were examined with a view to their being developed into an LC detector. However, the field has narrowed, and today, most LC separations are monitored by one of four detectors: the UV detector, the fluorescence detector, the electrical conductivity detector, and the refractive index detector. Other detectors have found certain areas of application; the high sensitivity of the electrochemical detector to those substances that readily oxidize or reduce has been used for certain types of trace analysis; the so-called molecular weight detector that functions on the basis of scattered light measurement has also found use in the detection of large molecular weight biopolymers. However, the four detectors mentioned satisfy the needs of most contemporary analytical separations.

A *detector* consists essentially of two parts, the sensor and the associated electronics. The performance of the overall detector is almost exclusively determined by the properties of the sensor, the associated electronics usually serving as an impedance converter or, in some cases, as a signal modifier. Detectors have been classified in various ways [1], but the most common method of classification is into two basic classes: *bulk property* detectors and *solute property* detectors. Bulk property detectors function by measuring some bulk physical property of the column eluate such as dielectric constant, conductivity or refractive index. In contrast solute property detectors function on some physical or chemical property that is unique to the solute, for example, UV absorption. However, this classification is not completely precise. The UV detector, for example, is usually classed as a solute property detector, but when used with a *n*-heptane–ethyl acetate mixture as the mobile phase, it will also give a background signal arising from absorption by the ethyl acetate. Furthermore, any fluctuation in the ethyl acetate content of the mobile phase will appear as noise or drift on the sensor output. It follows that, under these circumstances, the UV detector, although a solute property detector, behaves as a

hybrid between a solute property detector and a bulk property detector. Nevertheless, despite the overlap, the design and function of the detectors will be discussed under these two classes.

The analyst must be able to determine the suitability of a given detection device for a particular application and also be able to compare the performance of one specific detector with that of another, so that a rational choice can be made between the two. This can be achieved only if the detector performance specifications are readily available. Unfortunately, even today, useful detector performance data can be difficult to obtain, particularly in a form that is useful to the analyst. Often, the analyst may be compelled to obtain the necessary information in an instrument evaluation trial. A list of detector suppliers is given in the Appendix.

II. DETECTOR SPECIFICATIONS

There are seven major detector specifications that are important to the analyst and that should be provided by the manufacturer:

Linearity
Linear dynamic range
Noise level
Sensitivity, or minimum detectable concentration
Pressure sensitivity
Flow sensitivity
Temperature sensitivity

These specifications have been selected because they constitute the minimum necessary for the satisfactory selection of an appropriate detector.

A. Detector Linearity and the Response Index (α)

Detector linearity is probably the most important specification, for it determines the accuracy that is attainable in quantitative analysis. True detector linearity is, in fact, a theoretical concept, and despite the claims by many manufacturers, all detectors can only *tend* to this ideal response. Because the detector linearity will determine the analytical accuracy, it is important to have some method for measuring linearity that can be given in numeric terms and, thus, can be used to correct the detector response. A method for linearity measurement was proposed by Scott and Fowlis [2] for LC detectors, but the procedure can be used for detectors in general. Scott and Fowlis assumed that, for a nearly linear detector, the response could be expressed by the following simple relations.

$$\phi = \psi c^{\alpha} \tag{1}$$

where ϕ is the output from the detector, c is the concentration of solute in the detector, ψ is a constant, and α is the *response index*.

The response index α will be unity for a truly linear detector, and the numeric value of α will provide an accurate measure of the proximity of the detector response to strict linearity. The value of α, if known, can also be used to correct for any nonlinearity that might exist and, thereby, improve the accuracy of the analysis. Equation (1) can be expressed in the form,

$$\log \phi = \log \psi + \alpha \log c \tag{2}$$

It is seen that a numeric value for α can be obtained from an experimentally determined set of values for ϕ and c, as the slope of the curve relating the log ϕ to the log c, such as that shown in Figure 1.

The necessary data can be obtained by injecting samples of differing concentrations onto the column and measuring the respective area or height of the peaks obtained. Duplicate samples should be employed, and the average should be used to construct the graph. If the

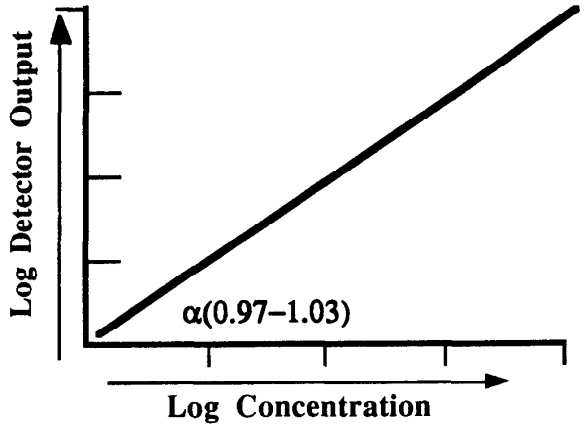


Figure 1 Graph of log ϕ against log c.

results are presented on a potentiometric recorder, then the peak *height* must be corrected for the detector sensitivity settings as they are changed. If a computer data acquisition and processing system is used, then the peak *area* can be obtained directly from the printout and be used as an alternative to the peak height. True linearity can be assumed only if the response index α lies between 0.98 and 1.02, as shown in Figure 1. If the response index is outside this range, then it will be necessary to use the numerical value of α to correct for the nonlinearity.

The curves relating detector output to solute concentration for detectors having different response indexes are shown in Figure 2. When examined individually, all the curves appear to be linear, and any one of the five curves might be considered to give accurate quantitative results. However, the actual results that would be obtained from the analysis of a binary mixture containing 10% of one component and 90% of the other, and employing detectors with each of the five response factors, is shown in Table 1.

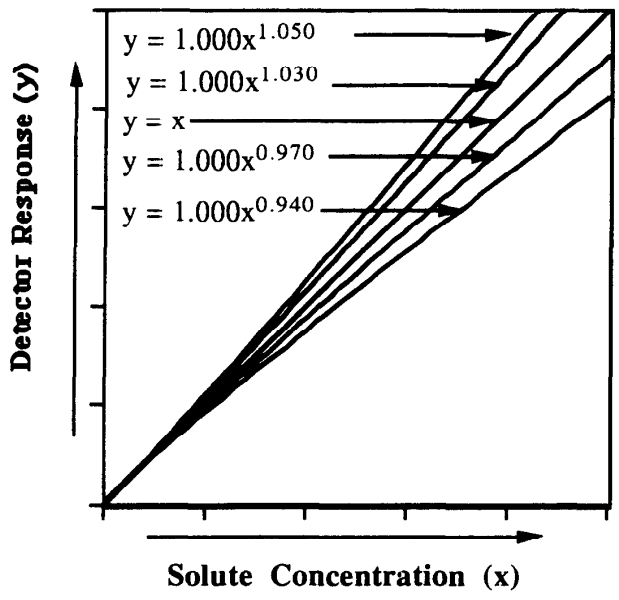


Figure 2 Graph of detector output against solute concentration for different response indices.

Table 1 Analysis of a Binary Mixture Employing Detectors with Different Response Indexes

Solute	$\alpha = 0.94$	$\alpha = 0.97$	$\alpha = 1.00$	$\alpha = 1.03$	$\alpha = 1.05$
1	11.25%	10.60%	10.00%	9.42%	9.05%
2	88.75%	89.40%	90.00%	90.58%	90.95%

It is seen that for a response index of 0.94, errors in the smaller component can be as great as 12.5% (1.25% absolute). Nevertheless, on examining the curve for a response index of 0.94 in Figure 2, the nonlinearity is scarcely apparent. In a similar manner, a response index of 1.05 gives an error of 9.5% (0.95% absolute) and, again, the poor linearity is not obvious from the curve shown in Figure 2. Once again, if accurate results are to be obtained without employing a correction factor, *the response index should lie between 0.98 and 1.02.* Most GC detectors can be designed to meet this criteria over a concentration range of at least two to three orders of magnitude.

B. Linear Dynamic Range

The *linear dynamic range* of a detector is not the same as the *dynamic range*, for detector linearity usually deteriorates at high solute concentrations. The linear dynamic range of a detector is that range of solute concentration over which the numeric value of the response index falls within defined limits. For example, the linear dynamic range D_L of a detector might be specified as

$$D_L = 1 \times 10^{-10} \text{ to } 1 \times 10^{-5} \text{ g mL}^{-1} \ (0.98 < \alpha < 1.02)$$

In contrast, the dynamic range, which is that range over which the detector continues to respond to changes in solute concentration, may be as large as 1×10^{-10} to 1×10^{-3}.

C. Detector Noise Level

Detector noise is extremely important as it determines the ultimate detector *sensitivity* or *minimum detectable concentration*. There are three different types of detector noise: short-term noise, long-term noise, and drift. These noise sources combine to give the composite noise of the detector. The different types of noise are depicted in Figure 3.

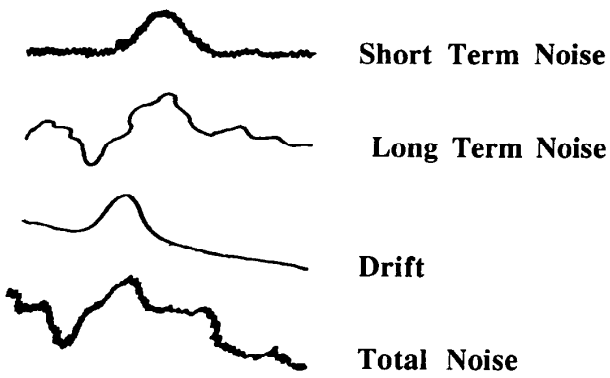


Figure 3 Different types of detector noise.

1. Short-Term Noise

Short-term noise consists of baseline perturbations that have a frequency that is significantly higher than the eluted peak. Short-term detector noise is not often a serious problem, for it can be easily removed by appropriate noise filters without significantly affecting the profiles of the peaks. Its source is usually electronic, originating from either the detector sensor system or the amplifier.

2. Long-Term Noise

Long-term noise consists of baseline perturbations that have a frequency that is similar to that of the eluted peak. This type of detector noise is the most significant and deleterious, for it is indiscernible from very small peaks in the chromatogram. Long-term noise cannot be removed by electronic filtering without affecting the profiles of the eluted peaks. In Figure 3, it is clear that the peak profile can easily be discerned above the high frequency noise, but is lost in the long-term noise. Long-term noise usually arises from temperature, pressure, or flow rate changes in the sensing cell. It is largely controlled by detector cell design and ultimately limits the detector sensitivity or the minimum detectable concentration.

3. Drift

Drift results from baseline perturbations that have a frequency that is significantly larger than that of the eluted peak. Drift is almost always due to either changes in ambient temperature, changes in mobile phase flow rate, or pressure or solvent composition. As a consequence, baseline drift can become very significant at high temperatures. Drift is easily constrained by choosing operating parameters that are within the detector and column specifications.

A combination of all three sources of noise is shown by the trace at the bottom of Figure 3. In general, the sensitivity of the detector should never be set above the level at which the combined noise exceeds 2% of the full-scale deflection (FSD) of the recorder (if one is used), or appears as more than 2% FSD of the computer simulation of the chromatogram.

D. Measurement of Detector Noise

The *detector noise* is defined as the maximum amplitude of the combined short- and long-term noise, measured in appropriate units (e.g., millivolts; mV) over about 15 min. The detector noise is obtained by constructing parallel lines embracing the maximum excursions of the recorder trace over the defined time period as shown in Figure 4. The distance between the parallel lines, measured in millivolts, is taken as the noise level.

E. Detector Sensitivity or the Minimum Detectable Concentration

Detector sensitivity, or the *minimum detectable concentration*, has been defined as the minimum concentration of an eluted solute that can be discerned unambiguously from the noise. The ratio of the signal to the noise for a peak that is considered decisively identifiable has



Figure 4 Method for measuring detector noise.

been traditionally chosen to be 2. This ratio originated from electronic theory and has been applied directly to chromatography. Nevertheless, the ratio is realistic, and any peak having a signal/noise ratio of less than 2 is seriously obscured by the noise and is difficult to identify.

Thus, the minimum detectable concentration is that concentration that provides a signal equivalent to twice the noise level. Unfortunately, the concentration that will provide a signal equivalent to twice the noise level will usually depend on the physical properties of the solute used for measurement. Consequently, the detector sensitivity, or minimum detectable concentration, must be quoted in conjunction with the solute that is used for measurement.

F. Pressure Sensitivity

The pressure sensitivity of a detector is important because it will be one factor that determines the long-term noise. It is usually measured as the change in detector output for unit change in sensor pressure. Pressure sensitivity and flow sensitivity, to some extent, are interdependent, subject to the manner in which the detector functions. Pressure sensitivity is particularly important when using two-dimensional liquid chromatography.

G. Flow Sensitivity

Flow sensitivity is another factor that determines the long-term noise of the detector and thus will influence the sensitivity, or minimum detectable concentration of the detector. It is usually measured as the change in detector output for unit change in flow rate through the sensor.

H. Temperature Sensitivity

Temperature sensitivity of the sensor is another factor that can cause long-term noise and thus reduces the detector sensitivity or minimum detectable concentration. It is usually measured as the change in detector output for unit change in sensor temperature.

III. BULK PROPERTY DETECTORS

There are various bulk property detectors developed over the years; the refractive index detector, the thermal lens detector, the differential viscometer detector, the interferometer detector, the density detector, the density balance detector, and the electrical conductivity detector. With the exception of the electrical conductivity detector, they all have relatively low sensitivity. Two detectors from this group, however, have survived and are in common use today: the refractive index detector, which is a catholic detector and very useful for monitoring these compounds that are nonionic, do not absorb in the UV, or do not fluoresce; the other is the electrical conductivity detector, which is widely used in ion chromatography.

A. The Refractive Index Detector

The refractive index detector is sensitive to changes in ambient temperature, pressure, and flow rate and, because it is a bulk property detector, it cannot be used for gradient elution. As a consequence, it is important to ensure good chromatographic stability for its effective use. There are several different optical systems used in refractive index detectors [1], but the simplest and probably the most common, is the differential refractive index detector, shown diagrammatically in Figure 5.

The differential refractometer responds to the deflection of a light beam that is caused by the differing refractive index between the contents of the sample cell and that of the reference cell. A beam of light from an incandescent lamp (usually a tungsten filament lamp) passes through an optical mask that confines the beam to the region of the cell. A lens collimates

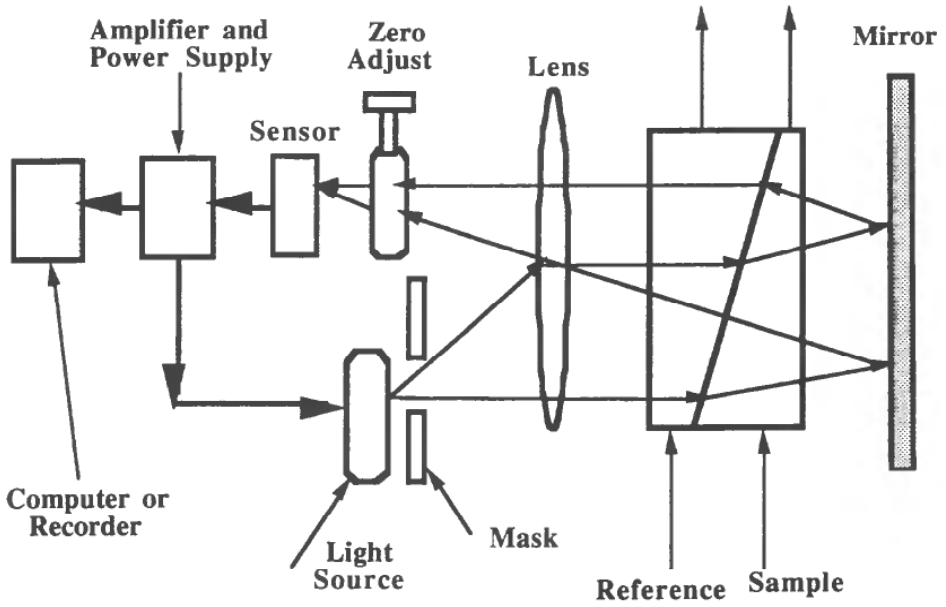


Figure 5 The differential refractometer. (Courtesy of Waters Chromatography.)

the light beam, which then passes through both the sample and reference cells to a plane mirror. The mirror reflects the beam back through the sample and reference cells and is focused by another lens onto a photocell. The location of the beam, rather than its intensity, is determined by the angular deflection of the beam caused by the refractive index difference between the contents of the two cells. As the beam changes its position of focus on the photoelectric cell, the output changes and the resulting difference signal is electronically modified to provide a signal proportional to the concentration of solute in the sample cell.

The refractive index detector, although not in common use, has certain areas of application for which it is specially useful, one being for the separation and analysis of polymers. If a polymer contains more than six monomer units, the refractive index becomes directly proportional to the concentration of the polymer and is nearly independent of its molecular weight. Consequently, because there is no need for individual solute response factors, a polymer mixture can be analyzed by *peak area normalization*. The refractive index has sensitivity (e.g., benzene) of about 1×10^{-6} g mL^{-1}, a linear dynamic range of about 1×10^{-6} to 1×10^{-4} g mL^{-1}, and a response index that ranges between 0.97 and 1.03 over the linear dynamic range.

A typical example of the use of the refractive index detector is in the separation of carbohydrates. Carbohydrates have no UV chromophores, they do not fluoresce, nor do they contain ions; thus, unless derivatives are made, an appropriate and commercially available detector would be the refractive index detector. The separation of such a mixture is shown in Figure 6. The refractive index detector is still frequently used in the separation of carbohydrates, aliphatic alcohols, the hydrolysis products of starch and those natural products that do not have chemical groups that permit other methods of detection. The catholic nature of the response of the refractive index detector would make it far more popular if it could only tolerate gradient elution.

B. The Electrical Conductivity Detector

The first conductivity detector was developed by Martin and Randall as long ago as 1951 [3], and the basic sensor, being so simple, has changed little in the intervening period. The de-

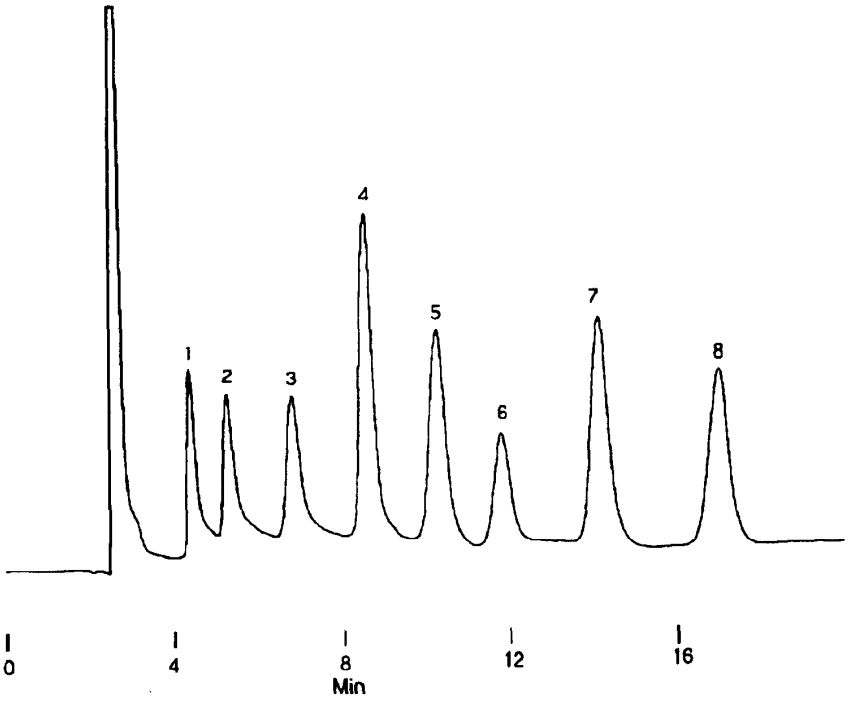


Figure 6 The separation of some carbohydrates: 1, ribose; 2, arabinose; 3, galactose; 4, sucrose; 5, maltose; 6, isomaltose; 7, melezitose; 8, raffinose. The column used was Supelcosil LC-NH_2, an aminopropyl-bonded phase that exhibits fairly strong polar interactions in addition to the dispersive interactions from the propyl chains. The support used is a spherical silica with a mean pore size of 100 Å. The column was 25 cm long, 4.6 mm id, and the particle size of the packing was 5 μm. The mobile phase consisted of a mixture of 75% v/v acetonitrile and 25% v/v water; the flow rate was 1 mL min^{-1}. The sample consisted of 20 μL of a solution containing 10 μg mL^{-1} of each analyte in deionized water. It is seen that the carbohydrates are well resolved in little over 16 min. (Courtesy of Supelco Inc.)

tecting volume has become much smaller, but it still consists of two electrodes situated in the column eluate, the resistance (or more strictly the impedance) of which is measured by a suitable electronic circuit. A diagram of a simple conductivity sensor is shown in Figure 7.

The basic sensor is, indeed, very simple and, if well designed, can have an effective sensing volume of only a few nanoliters. Consequently, it is often used as a detector in capillary electrophoresis. The sensor is usually placed in one arm of a Wheatstone bridge and the out-of-balance signal that occurs when ions pass between the electrodes is amplified and fed to a recorded or computer. The signal will be proportional to a change in electrical resistance between the electrodes, which will not necessarily be linearly related to the ion concentration. As a consequence, an appropriate signal-modifying amplifier must be used to provide an output that is directly proportional to solute concentration. As a bulk property detector the conductivity detector responds to any electrolytes present in the mobile phase (e.g., buffers), as well as the solutes. It follows that the mobile phase must be either nonconducting, which is frequently difficult, if not impossible to achieve, or the mobile phase buffer electrolytes must be removed before the sensor. The technique of buffer ion removal is called *ion suppression*. The first type of ion suppression involved the use of a second ion-exchange column, subsequent to the analytical column, that removed the buffer cations, replacing them with hydrogen ions.

Conversely, if cations were being separated, a suitable anion exchanger would replace the buffer anions with hydroxyl ions. Ion suppression works well, providing the ion suppressor

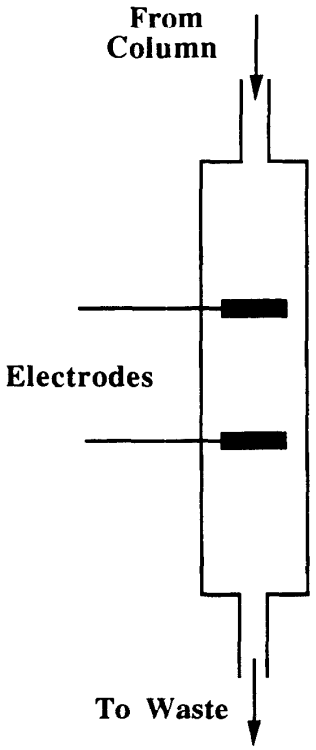


Figure 7 The electrical conductivity detector.

(ion remover) does not produce significant peak dispersion and consequent loss of resolution. Alternatively, an organic buffer, such as methane sulfonic acid, can be used and then removed subsequent to the column in a short length of reversed-phase column. The methyl sulfonate is absorbed almost irreversibly onto the reversed phase, leaving the ions of interest to enter the sensor in the absence of any buffer ions. The suppressor column will have a limited lifetime, but can be regenerated by passing acetonitrile through the suppressor column followed by water. An example of a separation employing an ion suppression procedure is shown in Figure 8.

Ion suppression is frequently used in ion-exchange chromatography, but depending on the nature of the separation, a specific type of ion suppression column or exchange membrane will be required that will be appropriate for the phase system that is chosen. A wide variety of ion suppression columns are available for this purpose. Any suppressor system introduced between the column and the detector that has a finite volume will cause band dispersion; consequently, connecting tubes and the suppression column itself must be very carefully designed to reduce it to an absolute minimum. A detailed discussion of ion suppression systems is given in Chapters 10 and 11. The conductivity detector should have a sensitivity of about 5×10^{-9} g mL^{-1} (chlorine ions), a linear dynamic range from 5×10^{-9} to 1×10^{-6} g mL^{-1}, and a response index over that range of about 0.97–1.03.

IV. SOLUTE PROPERTY DETECTORS

Among the solute property detectors are found the most sensitive and those with the widest linear dynamic range. In general, however, even the solute property detectors have very poor sensitivities compared with their counterparts in GC. The sensitivity of LC detectors is between three and four orders of magnitude less than that of GC detectors (e.g., the electron capture detector and the triode argon detector). Nevertheless, LC solute property detectors can be used very effectively for trace analysis and with high-efficiency columns. Today, the most

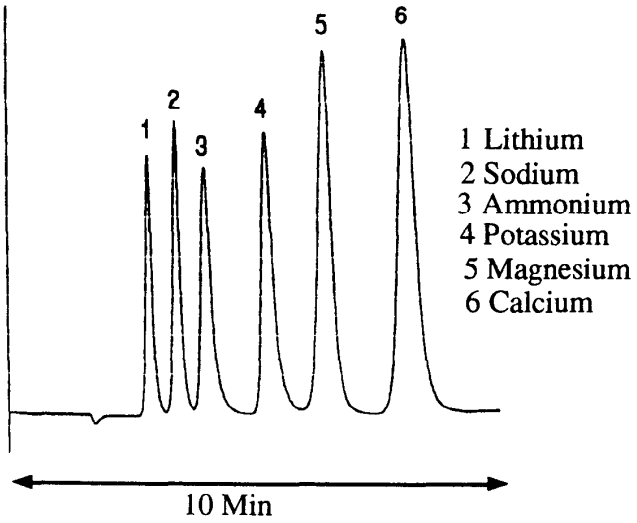


Figure 8 Determination of alkali and alkaline earth cations. A proprietary ion-exchange column, IonPacCS12, was used and the mobile phase consisted of a 20 nM methanesulfonic acid solution in water. A flow rate of 1 mL min^{-1} was employed and the sample volume was 25 μl. (Courtesy of Dionex Inc.)

popular detectors are the UV detector, the fluorescence detector, and the electrochemical detectors. However, several other detectors have a somewhat restricted area of interest, but are very important; therefore some of these will also be discussed.

A. The Ultraviolet Detectors

There are three types of ultraviolet (UV) detectors: the *fixed wavelength detector*, the *variable wavelength detector*, and the *diode array detector*. Each of these detectors, although measuring the amount of UV light absorbed by the column eluent, are quite different in design and will be discussed separately.

1. The Fixed-Wavelength Detector

The fixed-wavelength detector operates with light emitted at a single wavelength. In fact, this is not entirely true. Although most of the light may be emitted at one wavelength, with most single-wavelength UV lamps, other wavelengths are also always present, although often at a much lower intensity. In fact, it is more correct to say that the "single-wavelength lamp" emits light at a specific wavelength that is at a very high intensity compared with that emitted at the same wavelength by broad-spectrum emission lamps. Thus, the fixed wavelength UV detector has a propensity for a much higher sensitivity, but as will be seen, at the expense of detector versatility. A diagram of the optical system of a fixed wavelength UV detector is shown in Figure 9.

Light from the low-pressure mercury vapor lamp is focused through two adsorption cells onto two photoelectric sensors. The sensor output is electronically modified and fed to a recorder or a computer data acquisition system. One absorption cell carries the column eluent and the other is a reference cell containing pure mobile phase. The cell volume must be kept as small as possible to reduce band dispersion and maintain the integrity of the separation. Modern high-efficiency LC columns restrain the peak volume to a few microliters; thus, if the cell volume is too large, more than one peak can enter the cell at one time and the resolution would be completely lost. The sensing volume of a modern LC detector cell should be no greater than 5 μL and preferably about 2 μL or less. In addition connecting tubes

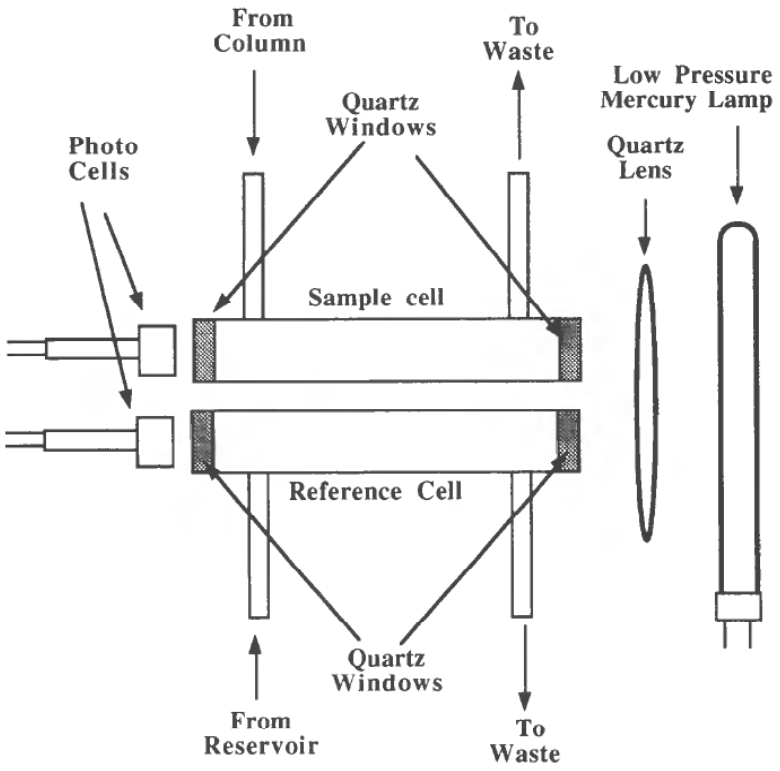


Figure 9 The fixed-wavelength UV detector.

between column and detector should be kept as short as possible. The intensity of the UV light absorbed in the cell is given as a function of the concentration of the solute in the cell by Beer's law,

$$I_T = I_0 e^{-klc} \text{ or } \ln I_T = \ln I_0 - klc \tag{3}$$

where

I_0 is the intensity of light entering the cell.
I_T is the intensity of light transmitted through the cell.
l is the path length of the cell.
c is the concentration of solute in the cell.
k is the molar absorption coefficient of the solute at the specific wavelength of the UV light.

If Eq. (3) is put in the form,

$$I_T = I_0\, 10^{-k'lc} \tag{4}$$

then k' is termed the molar extinction coefficient.

Differentiating Eq. (1),

$$\frac{\partial\,(T_T/T_0)}{\partial c} = -kl \tag{5}$$

It is seen that the sensitivity of the detector, as measured by the transmitted light, will be directly proportional to the extinction coefficient k and the path length of the cell l. It follows that to increase the sensitivity of the system, l must be increased. However, l cannot be enlarged without the radius being also reduced because the total volume of the cell must be kept small. In addition, reduction in cell radius reduces the amount of light falling on the

photocell increasing the noise and, consequently, reducing the signal/noise ratio. The two effects oppose one another and the process of increasing detector sensitivity by lengthening the cell is limited. Most modern UV cells have path lengths lying between 1 and 10 mm and internal diameters of 1 mm or less.

From Eq. (2),

$$\log \frac{I_T}{I_0} = k'lc = A \tag{6}$$

where A is the *absorbance*.

ΔA is commonly employed to define the detector sensitivity if the value of ΔA is the change in absorbance that produces a signal/noise ratio of 2. Thus,

$$\Delta A = k'l\Delta c \qquad \text{and} \qquad \Delta c = \frac{\Delta A}{k'l} \tag{7}$$

where Δc is the detector concentration sensitivity or the minimum detectable concentration, which is the parameter of importance to chromatographers.

It follows that two detectors having the same sensitivity, defined as the minimum detectable change in absorbance, will not necessarily have the same sensitivity relative to solute concentration. Only if the path length of the two cells are identical will they also exhibit the same concentration sensitivity. This can cause some confusion for the chromatographer who might expect that instruments that are defined as having the same spectroscopic sensitivity will have equivalent chromatographic sensitivity. To compare the sensitivity of two detectors given in units of absorbance, the path lengths of the cells in each instrument must be taken into account.

An example of the use of a fixed wavelength UV detector is afforded by the determination of trimethoprim in blood serum (Fig. 10). The sensitivity of the fixed-wavelength UV detector

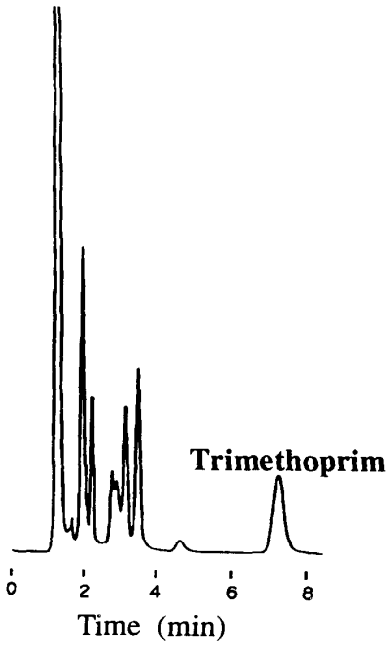


Figure 10 The determination of trimethoprim in blood serum. Column: Hisep, 15 cm × 4.6 mm id packed with 5-μm particles. Mobile phase: 180 mM ammonium acetate:acetonitrile (95:5). Flow rate 1.0 mL min^{-1}. Sample: 10 μL serum containing 0.025 mg mL^{-1} of trimethoprim. (Courtesy of Supelco Inc.)

should be approximately 5×10^{-8} g mL^{-1} (toluene), with a linear range of 5×10^{-8} to 5×10^{-4} g mL^{-1} and a response index of about 0.98–1.02.

2. The Variable-Wavelength Detector

The variable-wavelength detector employs a lamp that emits light over a wide range of wavelengths and, by using a monochromator, light of a particular wavelength can be selected for detection purposes. Alternatively, the flow rate can be arrested, the solute trapped in the detection cell, and by scanning through the different wavelengths, an absorption spectrum of the solute can be obtained. A diagram of a variable wavelength detector is shown in Figure 11. Light from a deuterium lamp is focused by two curved mirrors onto a diffraction grating and the selected wavelength is reflected back onto the second curved mirror. The light then passes to a third curved mirror and is focused by a plane mirror and a quartz lens through the absorption cell. After leaving the absorption cell, the transmitted light is focused by a second quartz lens onto the photocell. Rotating the grating allows the wavelength of the light passing through the cell to be selected to provide the maximum sensitivity. There are three basic advantages to a variable wavelength detector.

1. A UV absorption spectrum can be obtained for any, or for all the eluted solutes. Such spectra can sometimes help confirm solute identification.
2. To confirm peak purity, the spectra of a solute can be taken at various points across a peak as it is slowly moved through the cell; consistent spectra indicates the peak is pure.
3. The variable-wavelength detector can be used as a wavelength selector to increase sensitivity by employing optimum wavelengths for detection.

The sensitivity of the variable-wavelength detector is significantly less than that of the fixed-wavelength detector, but should still be about 1×10^{-7} g mL^{-1}. This will depend on

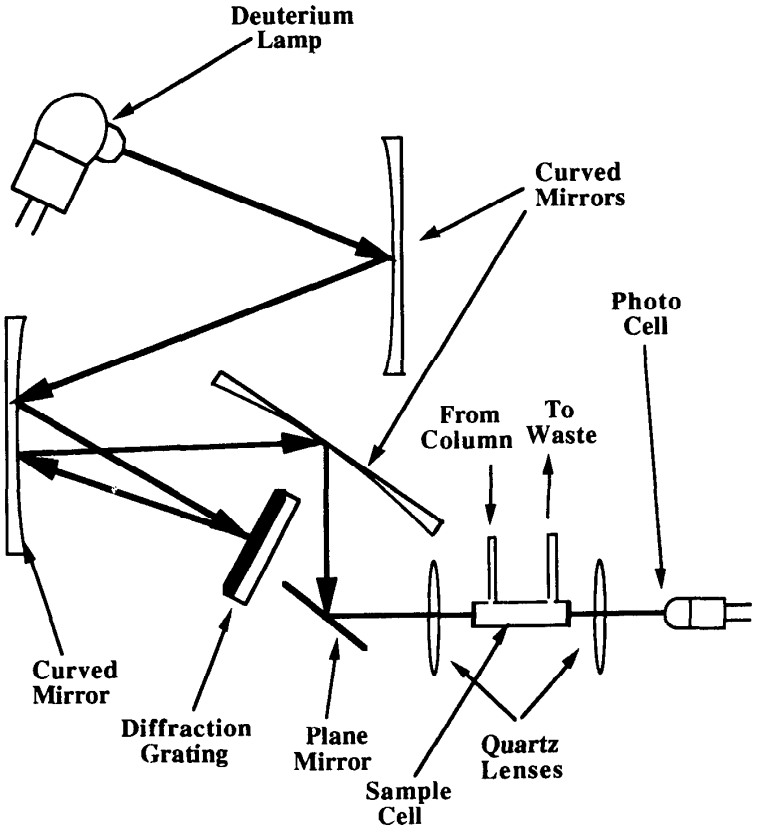


Figure 11 The variable wavelength detector.

the magnitude of the extinction coefficient of the respective solute and will vary from one substance to another. The linear dynamic range is about 1×10^{-7} to 5×10^{-4} g mL^{-1}, with a response index of 0.98–1.02.

The use of the variable-wavelength detector to select a wavelength that provides the maximum response for a specific solute is given in Figure 12. The separation was monitored by UV absorption at 280 nm, at which tryptophan has a high absorption. It is seen that an excellent separation was obtained and the tryptophan was unambiguously detected even at the relatively low concentration.

3. The Diode-Array Detector

The diode-array detector is also a multiwavelength UV detector, but functions on an entirely different principle. A diagram of a UV diode-array detector is shown in Figure 13. A deuterium or xenon lamp is employed that emits light over the whole UV spectrum range. Light from the lamp is focused by an achromatic lens through the sample cell and onto a holographic grating. The dispersed light from the grating is arranged to fall on a linear diode array.

The resolution of the detector ($\Delta\lambda$) will depend on the number of diodes n in the array (which is determined by the semiconductor manufacturer), and on the range of wavelengths covered ($\lambda_2 - \lambda_1$; defined by the optical arrangement and the grating that is used). Thus,

$$\Delta\lambda = \frac{\lambda_2 - \lambda_1}{n} \tag{8}$$

The diode-array detector takes a UV spectrum of the eluent continuously throughout the complete development of the chromatogram, which can be used to a great advantage.

It follows that a chromatogram can be reconstructed by monitoring at a specific wavelength [strictly ($\Delta\lambda$) a narrow group of wavelengths]; thus, depicting only those substances

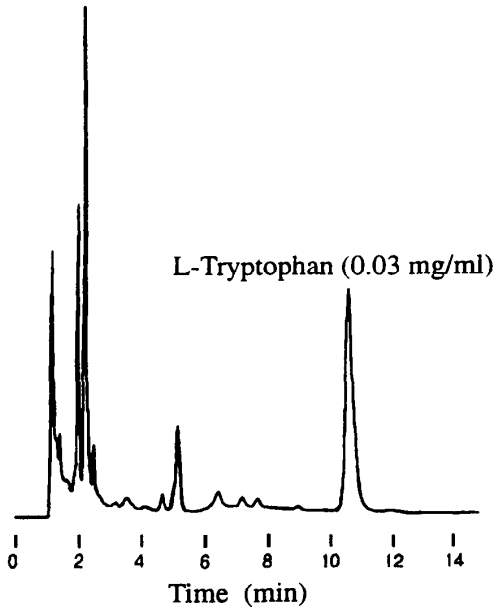


Figure 12 The determination of L-tryptophan in poultry meal. Column: Supelcosil LC 18, 15 cm × 4.6 mm id packed with 5-μm particles. Mobile phase: 0.0085 M sodium acetate, pH 4.0 with acetic acid. Flow rate: 15 mL min^{-1}. Sample: 10 μL of the meal hydrolysate. (Courtesy of Supelco Inc.)

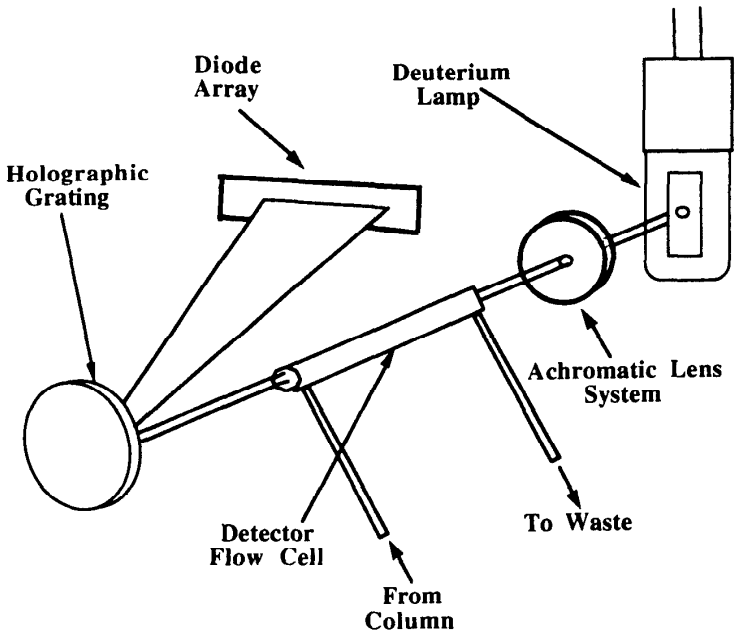


Figure 13 The UV photo diode-array detector.

that adsorb UV light at the chosen wavelength. Consequently, the chromatogram can be arranged to display only those substances that have unique absorbance characteristics. The diode-array detector can be used in various other unique ways, and an example of its use to verify the purity of a given solute is shown in Figure 14. The separation monitored at 274 nm is shown in the upper part of the figure. Because a diode-array detector was employed, with suitable software, it was possible to ratio the output from the detector at different wave-

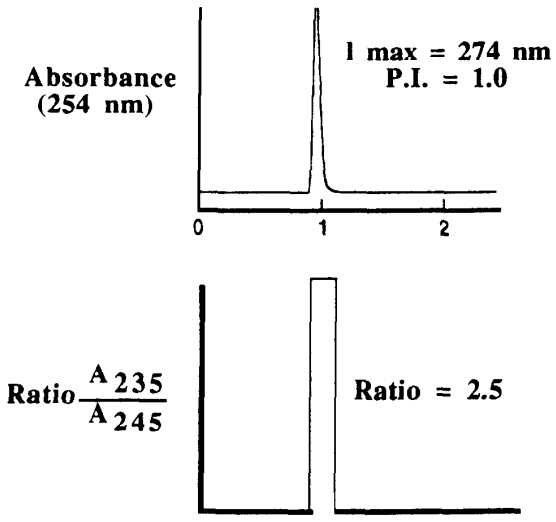


Figure 14 Dual channel curves from a diode-array detector for chlorthalidone showing the separation and confirming peak purity. The chlorthalidone was isolated from a sample of tablets and separated by a reverse-phased (C_{18}) column 4.6-mm id, 3.3 cm long, using a solvent mixture consisting of 35% methanol and 65% aqueous acetic acid solution (water containing 1% of acetic acid). The flow rate was 2 mL min^{-1}. (Courtesy of the Perkin Elmer Corporation.)

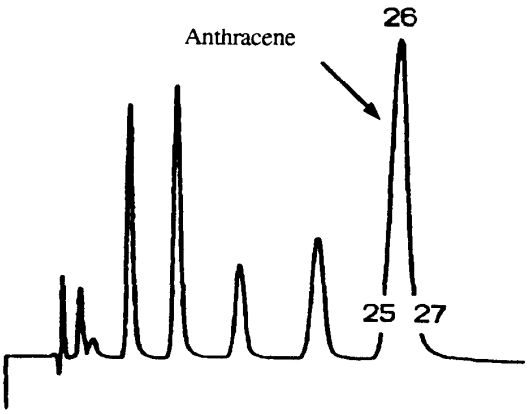


Figure 15 The separation of a series of aromatic hydrocarbons. This separation was carried out on a column 3 cm long, 4.6 mm in diameter and packed with a C_{18} reversed phase on particles 3-μm in diameter. (Courtesy of the Perkin Elmer Corporation.)

lengths and plot the ratio simultaneously with the chromatogram monitored at 274 nm. Now, if the peak was pure and homogeneous, the ratio of the adsorption at the two wavelengths (those selected being 225 and 245 nm) would remain constant throughout the elution of the entire peak.

The lower diagram in Figure 14 shows this ratio plotted on the same time scale, and a clean rectangular peak is obtained that unambiguously confirms the purity of the peak for chlorthalidone. Note that the wavelength chosen to provide the confirming ratio will depend on the UV absorption characteristics of the substance concerned, relative to those of the most likely impurities to be present.

Another interesting example of the use of the diode-array detector to confirm the integrity of an eluted peak is afforded by another application, published by the Perkin Elmer Corporation, showing the separation of a mixture of aromatic hydrocarbons. The separation they examined is shown in Figure 15. The separation appears to be good and all the peaks represent individual solutes. However, by plotting the adsorption ratio, 250 nm/255 nm, for the anthracene peak, it became clear that the peak tail contained an impurity. The absorption ratio peaks are shown in Figure 16. The ratio peaks in Figure 16 clearly show the presence of an impurity

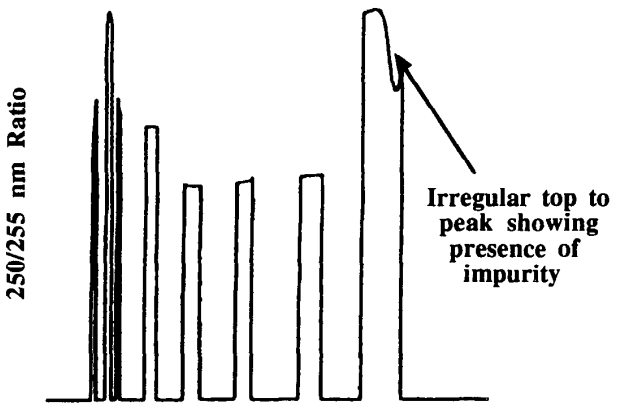


Figure 16 Curves relating the adsorption ratio 250 nm/255 nm, to time. (Courtesy of the Perkin Elmer Corporation.)

by the sloping top of the anthracene peak, and further work identified the impurity as *t*-butylbenzene at a level of about 5%.

The characteristics of both the variable-wavelength and the diode-array detector are very similar; consequently, they have very comparable specifications. The sensitivity of the diode-array detector, expressed as the minimum concentration that can be detected, will again depend on the extinction coefficient of the solute. A mean value for the sensitivity can be taken as about 1.5×10^{-7} g mL^{-1}. The linear dynamic range is very similar to that of the variable wavelength detector about 1.5×10^{-7} to 5×10^{-4} g mL^{-1} for a response index range of 0.97–1.03.

B. The Fluorescence Detector

The fluorescence detector is one of the most sensitive LC detectors, but unfortunately, far less versatile. By definition, the fluorescence detector will detect only those materials that will fluoresce or, by appropriate derivatization can be made to fluoresce. Nevertheless, because of its sensitivity, it is one of the most important detectors for use in trace analysis both in environmental and forensic analysis. A diagram of a simple form of fluorescence detector is shown in Figure 17. The UV lamp that provides the excitation radiation is often a low-pressure mercury lamp, for it is comparatively inexpensive and provides relatively high-intensity UV light at 253.7 nm. Many substances that fluoresce will, to a lesser or greater extent, be excited by light at this wavelength. The light is focused by a quartz lens through the cell, and another lens situated normal to the incident light focuses the fluorescent light onto a photocell. The fluorescence detector can have a sensitivity of about 1×10^{-9} g mL^{-1}, over a linear dynamic range of 1×10^{-9} to 5×10^{-6} g mL^{-1}, with a response index that ranges from about 0.96 to 1.04.

A far more sophisticated fluorescence detector is shown in Figure 18. The diagram depicts the basic fluorescence *spectrometer* but, because it incorporates two distinctly different light paths, the optical system appears quite complicated. If the different light paths are considered separately—that is, the path of the excitation light and the path of the fluorescent light—the

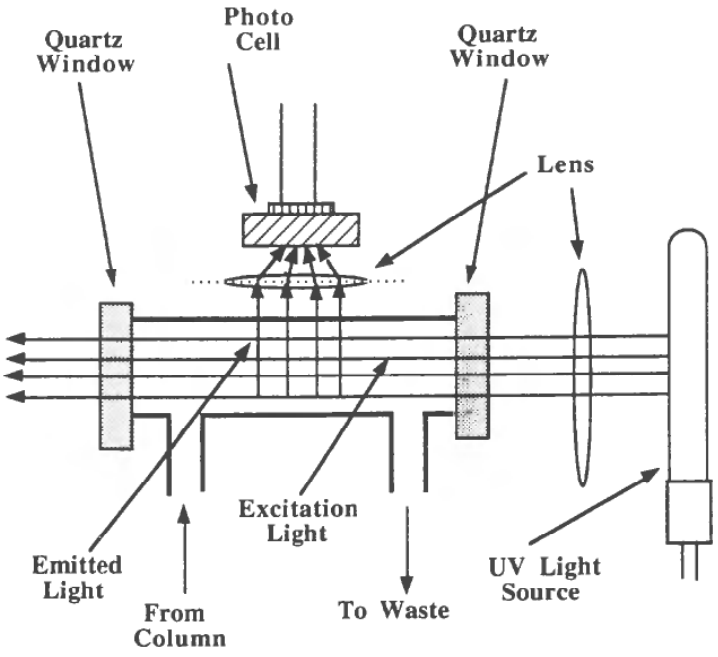


Figure 17 The simple fluorescence detector.

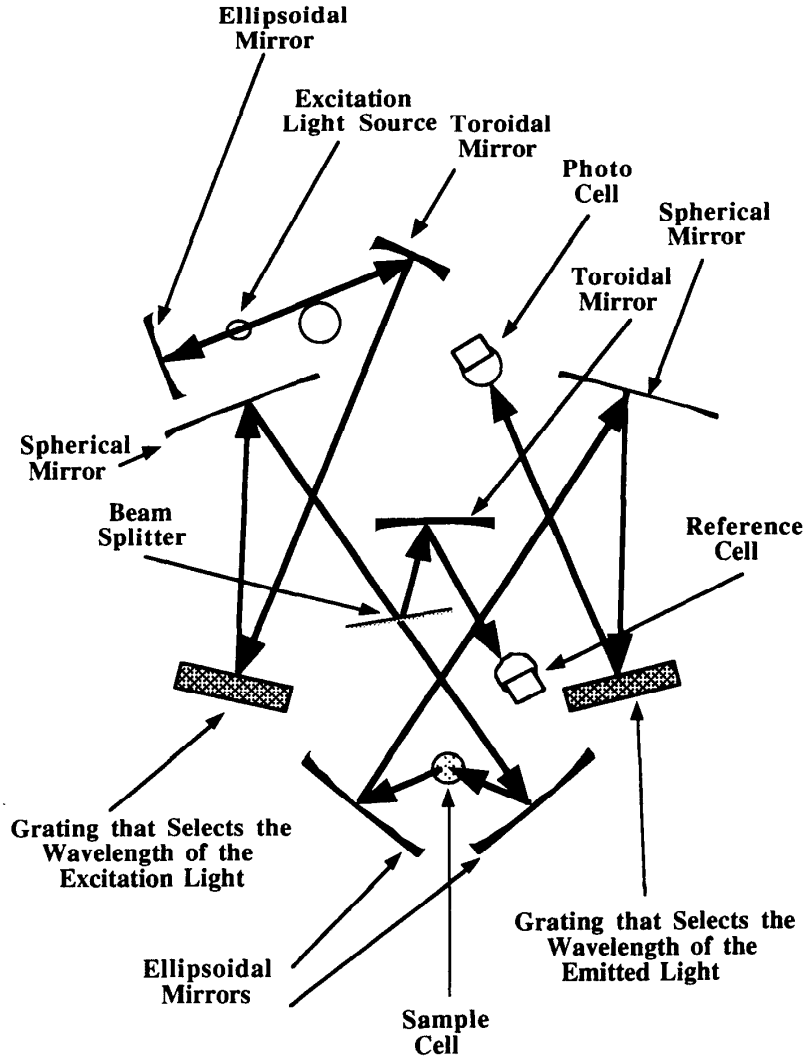


Figure 18 The fluorescence spectrometer detector.

diagram is easier to understand. The excitation source that emits UV light over a wide range of wavelengths (usually a deuterium lamp) is situated at the focal point of an ellipsoidal mirror, shown at the top left-hand corner of the diagram. The parallel beam of light is arranged to fall on a toroidal mirror that focuses it onto a grating on the left-hand side of the diagram. This grating allows the frequency of the excitation light to be selected or the whole spectrum scanned, providing a complete range of excitation wavelengths. The selected wavelength then passes to a spherical mirror and then to an ellipsoidal mirror at the base of the diagram, which focuses it onto the sample. The excitation light path is largely situated on the left-hand side of the diagram.

Between the spherical mirror and the ellipsoidal mirror, in the center of the diagram, is a beam splitter that reflects a portion of the incident light onto another toroidal mirror. This toroidal mirror focuses the portion of incident light onto the reference photocell, providing an output that is proportional to the strength of the incident light. The path of the fluorescent light is largely on the right-hand side of the diagram. Fluorescent light from the cell is focused by an ellipsoidal mirror onto a spherical mirror at the top right-hand side of the diagram.

This mirror focuses the light onto a grating situated at about center right of the figure. This grating can select a specific fluorescent wavelength to monitor or scan the fluorescent

light and provide a fluorescence spectrum. Light from the grating passes to a photoelectric cell that monitors its intensity. The instrument is extremely complex and, as a result, rather expensive; however, for measuring fluorescence it is extremely versatile. An excellent example of its use is given in Figure 19, which depicts the separation of a group of priority pollutants using programmed fluorescence detection.

The separation was carried out on a column 25 cm long, 4.6 mm in diameter, and packed with a C_{18} reversed-phase. The mobile phase was programmed from a 93% acetonitrile/7% water, to 99% acetonitrile/1% water over a period of 30 min. The gradient was linear and the flow rate was 1.3 mL min^{-1}. All the solutes are separated and the compounds, numbering from the left are given in the table. The separation illustrates the clever use of wavelength programming to obtain the maximum sensitivity. The program used for this particular mixture was rather complex. During the development of the separation, both the wavelength of the excitation light and the wavelength of the emission light that was monitored were changed. This ensured that each solute, as it was eluted, was excited at the most effective wavelength and then, consequently, monitored at the strongest fluorescence wavelength. The program that was used is also shown following the figure. It is seen that the analysis is an elaborate procedure carried out with a very complex and expensive instrument. Nevertheless, if the analysis is sufficiently important it may be necessary to resort to this type of solution.

The system can also provide fluorescence spectra, should it be required, by arresting the flow of mobile phase when the solute resides in the detecting cell and scanning the fluorescent light as with the variable wavelength detector.

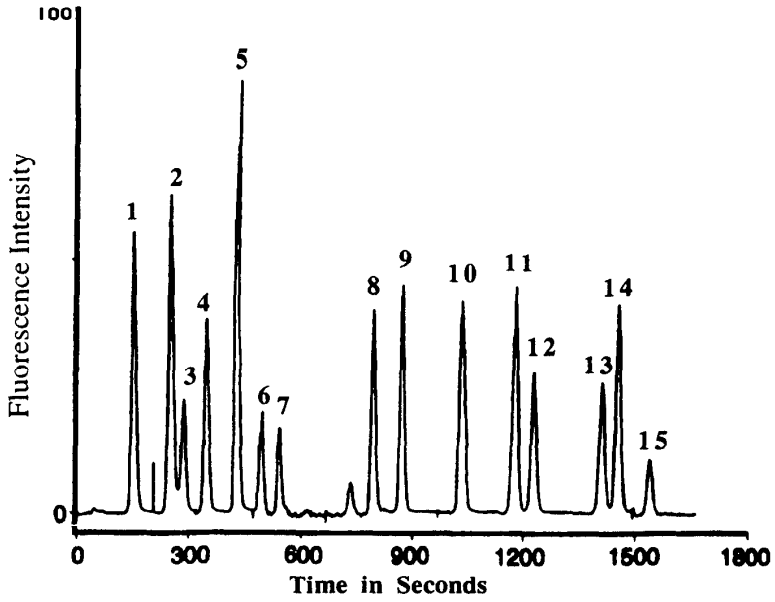


Figure 19 Separation of a series of priority pollutants with programmed fluorescence detection. Fifteen priority pollutants: 1, naphthalene; 2, acenaphthene; 3, fluorene; 4, phenanthrene; 5, anthracene; 6, fluoranthene, 7, pyrene; 8, benz[*a*]anthracene; 9, chrysene; 10, benzo[*b*]fluoranthene; 11, benzo[*k*]fluoranthene; 12, benzo[*a*]pyrene; 13, dibenz[*a,h*]anthracene; 14, benzo[*ghi*]perylene; 15, indeno[123-*cd*]pyrene. (Courtesy of the Perkin Elmer Corporation.)

Fluorescence Detector Program

Time (s)	Wavelength of excitation light (nm)	Wavelength of emitted light (nm)
0	280	340
220	290	320
340	250	385
510	260	420
720	265	380
1050	290	430
1620	300	500

C. The Electrochemical Detector

The electrochemical detector is one of the most sensitive and responds to substances that are either oxidizable or reducible. The electrical output results from an electron flow caused by reactions that take place at the electrode surface. If the reaction is allowed to proceed to completion, exhausting all the reactant, then the current falls to zero, and the total charge passed will be proportional to the total mass of material that has been reacted. This process is called *coulometric* detection.

If, on the other hand, the electrolyte flows past the electrodes, the reacted solute will be continuously replaced as the peak passes through the detector. Although solute is present between the electrodes, a current will be maintained, albeit varying in magnitude. This is the most common procedure employed and is called *ampiometric* detection. Normally, three electrodes are employed, the working electrode (at which the oxidation or reduction takes place), the auxiliary electrode and the reference electrode (which compensates for any changes in the background conductivity of the mobile phase). The reaction is extremely rapid, resulting in the layer close to the electrode being completely depleted of reacting material.

Thus, the output will depend on the rate at which solute reaches the electrode surface and, as this is by diffusion, which is concentration-driven, it will be proportional to the concentration of solute in the mobile phase. There are various electrode configurations that have been satisfactory [4] and one example of these is shown in Figure 20. A simplified form of the circuit that is used is shown in Figure 21.

The auxiliary electrode (A) is held at a fixed potential by the first amplifier, the voltage being selected by the potentiometer (P) that is connected to a regulated power supply. The current flowing through the working electrode (W) is processed by the second amplifier, and the output is fed to the recorder or data acquisition system.

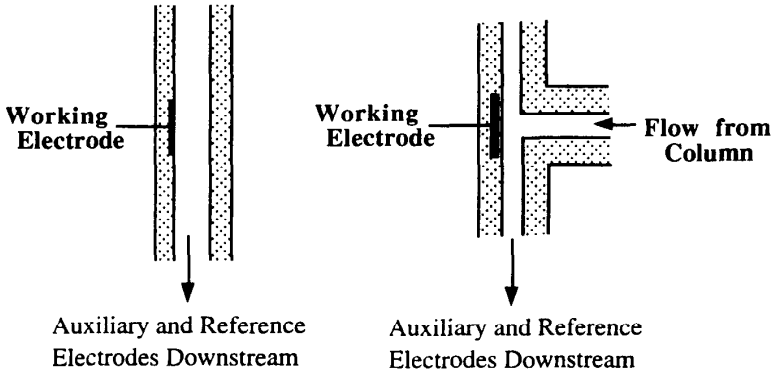


Figure 20 Electrode configurations for the electrochemical detector.

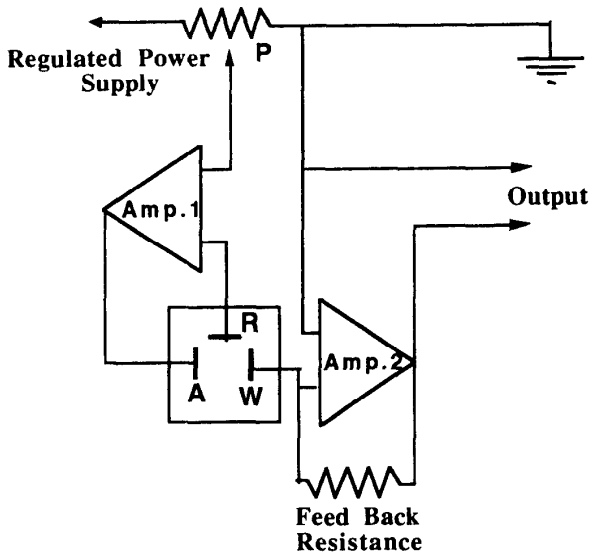


Figure 21 Basic circuit used with the electrochemical detector.

The electrochemical detector is extremely sensitive, but suffers from several drawbacks. First, the mobile phase must be extremely pure and, in particular, free of oxygen and metal-ions. A more serious problem arises, however, from the adsorption of the oxidation or reduction products on the surface of the working electrode. The consequent electrode contamination requires that the electrode system be frequently calibrated to ensure accurate quantitative analysis. Ultimately, the detector must be disassembled and cleaned, typically by the use of abrasives. The contamination can be diminished by careful design and operation but, so far, not eliminated. The low-sensing volume of the detector, usually a fraction of a microliter, makes it very suitable for use with small-bore columns.

D. The Light-Scattering Detector

If the column eluate is atomized and allowed to evaporate into small droplets, the solutes finally remaining are left as fine particulate matter suspended in the atomizing gas. The atomizing gas may be air or an inert gas if so desired. In the light-scattering detector, the suspended particulate matter is allowed to pass through a light beam, and the light, scattered by the particles, is viewed at an angle of about 45° to the incident beam using a pair of optical fibers. The scattered light entering the fibers is conducted internally to a photomultiplier and is then electronically processed. The detector signal from the processor is then passed either to a computer or to a potentiometric recorder. A diagram of the light-scattering detector is shown in Figure 22. The detector responds to all solutes that are not volatile and because the light dispersion is largely Raleigh scattering, the response is consequently proportional to the mass of solute present. To ensure good linearity the droplets' size must be carefully controlled because they, in turn, control the particle size of the dried solute fragments. The sensitivity of the detector is claimed to be between 10 and 20 ng of solute. However, in these terms it is difficult to compare its performance with other detectors.

If the solute is assumed to be eluted at a k' of unity from a column 15 cm long, 4.6 mm in diameter, and packed with 5-μm particles, then this would indicate a sensitivity, in terms of concentration, of about 2×10^{-7} g mL^{-1}, which is equivalent to the response of a fairly sensitive refractive index detector. The detecting conduits inevitably involve considerable dead volume, and this will contribute to peak dispersion. However, it would appear that the extent of peak dispersion that occurs with such detectors has not been reported.

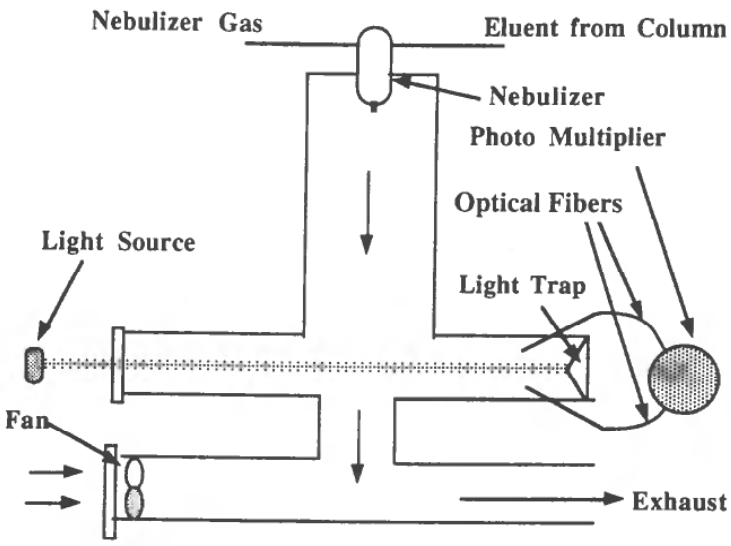


Figure 22 A diagram of the light-scattering detector. (Courtesy of Polymer Laboratories Inc.)

There are two advantages claimed for this detector. First, it has a catholic response and, second, its response is linearly related to the *mass* of solute eluted. It is, in fact, claimed to be a *mass detector*. An example of its use is shown in Figure 23 [5]. Estimation of the minimum detectable concentration from this chromatogram was again made to be about 10 ng of solute. To some extent, this detector provides a replacement for the transport detector as it detects all substances, irrespective of their optical or electrical properties.

E. The Tridet Multifunctional Detector

The popularity of the UV detector, the electrical conductivity detector, and the fluorescence detector motivated Schmidt and Scott [6] to develop a trifunctional detector that detected solutes by all three methods simultaneously in a single low-volume cell.

A diagram of their detector is shown in Figure 24. The UV adsorption system, employed single-wavelength detection and consisted of a low-pressure mercury lamp emitting light at 254 nm and a solid state photocell with quartz windows allowing the photocell to respond to light in the UV region. The detector cell was about 3 mm long and was terminated at one end by a cylindrical quartz window and at the other by a quartz lens that focused the transmitted light on to the photocell. In contact with each quartz windows were two stainless steel disks separated by 3 mm of Pyrex tube. The mobile phase entered and left the detector cell through radial holes in the stainless steel disks. The stainless steel disks also acted as the electrodes for conductivity detection. At right angles to the Pyrex tube was situated another photocell that receives any fluorescent light emitted normal to the UV excitation light. The output from each sensor passed to an appropriate amplifier that modified the signal from the sensor to provide an output that was linearly related to solute concentration. In this way, the column eluate was continuously and simultaneously monitored by UV adsorption, fluorescence, and electrical conductivity.

Chromatograms demonstrating the simultaneous use of all three detector functions are shown in Figure 25. The mixture contained benzene, toluene, ethyl benzene, isopropyl benzene, *t*-butylbenzene, anthracene, and sodium chloride.

It is seen that the anthracene is clearly picked out from the mixture of aromatics by the fluorescence detector, and the chloride ion, not shown at all by the UV adsorption or fluorescence detectors, is clearly shown by the electrical conductivity detector.

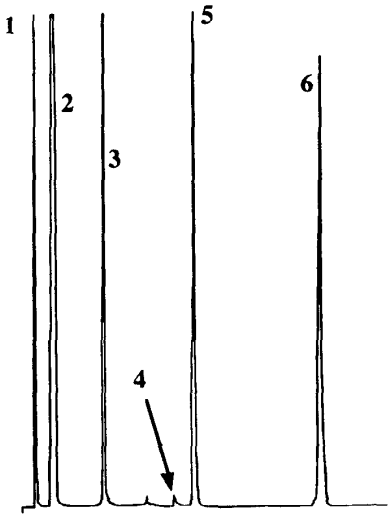


Figure 23 An LC separation monitored by the light-scattering detector. (Courtesy of Polymer Laboratories Inc.)

Peak	Compound	Mass (μg)	Retention time (min)
1	Cholesterol ester	5	0.717
2	Triglyceride	18	1.746
3	Cholesterol	10	4.687
4	Unknown	—	8.860
5	Phosphatidylcholine	10	10.028
6	Phosphatidylethanolamine	10	17.390

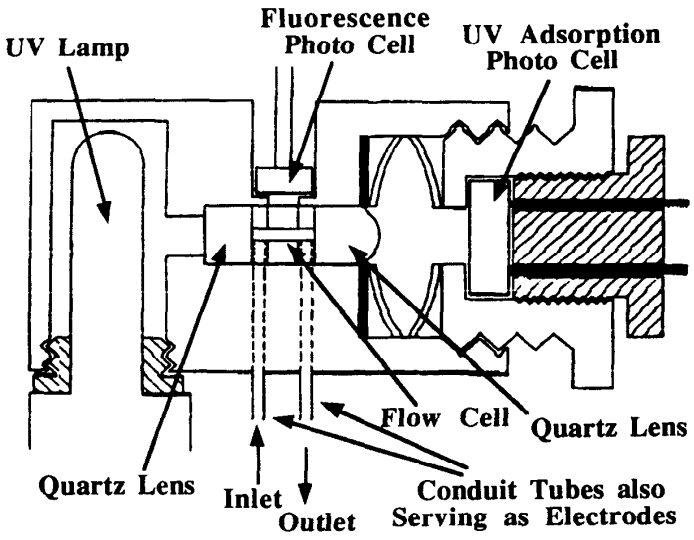


Figure 24 The tridet detector cell.

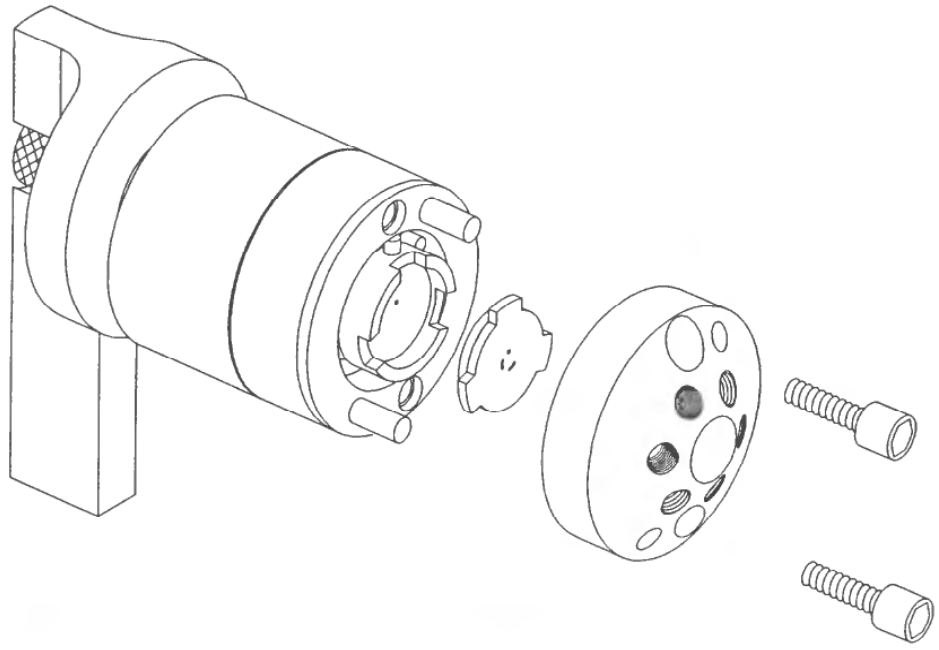


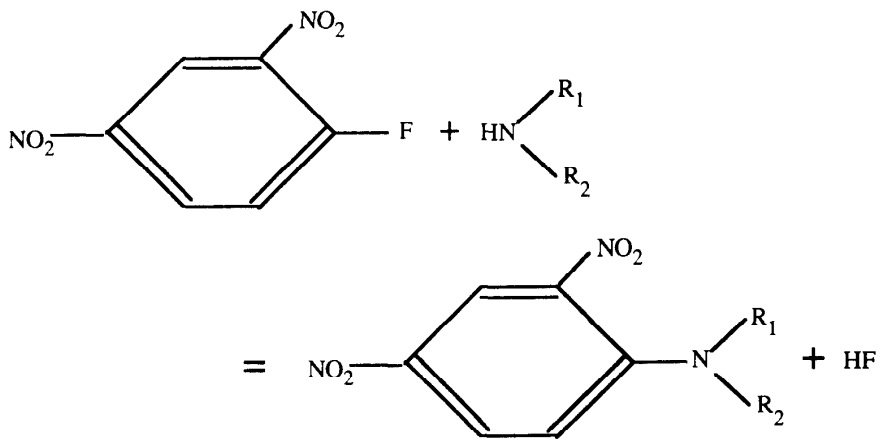


Figure 3 Two-position rotary injection valve exploded to show body, rotor, and stator where tube connections are made (Model C1). (Courtesy of Valco Instruments Co., Inc.)

When sample waste must be avoided, the laminar flow effect can be minimized by blowing the loop dry before the filling operation, or by pulling a small air gap into the dispensing syringe to act as a bubble that sweeps the mobile phase in the loop, effectively preventing it from diluting the sample. In this manner, nearly all of the sample can be introduced up to the nominal loop volume without significant waste [10]. The injection of a few microliters of air into the column will normally not be harmful. Another approach to con-

also been used for the same purpose. Nitrobenzoyl reagents are also effective reagents to insert a strong UV-adsorbing group into an amine.

An interesting reaction of 1-fluoro-2,4-dinitrobenzene with secondary amines is used for derivatizing such compounds as neomycin [12], fortimicin [13], and amikacin [14]. The reaction proceeds as follows.



Benzoyl chloride [15] and *p*-nitrobenzoyl chloride [16] are also used for derivatizing hydroxy compounds. The most common reagent for derivatizing carbonyl groups is 2,4-dinitrophenylhydrazine [17], which introduces the very strong 2,4-dinitrophenyl UV-absorbing group into the molecule.

Fluorescence reagents are also widely used to assist in the detection of amino acids. One of the first to be used effectively was *o*-phthalaldehyde (commonly known as the reagent Fluoropa) [18–20] and this was followed by Fluorescamine (4-phenylspiro[furan-2(3*H*),1′-phthalan)-3,3′-dione) which gave enhanced fluorescence, but was less stable after reaction, thus, measurements must be made immediately after reaction.

An excellent book by Blau and Halkert [7] gives a comprehensive description of the various derivatization procedures and includes experimental details.

VI. CHOICE OF DETECTORS

One of the four detectors, the UV detector, the electrical conductivity detector, the fluorescence detector, or the refractive index detector will meet the needs of over 95% of all LC analyses. The UV detector will probably be suitable for 85% of all analyses and is, by far, the most commonly used detector. The diode-array UV detector, the most popular of all the UV detectors, is the most versatile, easy to operate, and gives accurate quantitative results. The fixed-wavelength UV detector is the least expensive, also the simplest to operate, has excellent sensitivity, and has the widest linear dynamic range; in addition the fixed-wavelength detector gives good quantitative accuracy. Coupled with appropriate derivatization techniques, the fixed-wavelength UV detector is probably the most sensitive, versatile, and economical of all the LC detectors and might be the first choice for someone entering the field of LC analysis. The fluorescence detector is the most sensitive general detector and is also easy to operate. The fluorescence detector with the fixed-wavelength excitation lamp, employed with appropriate derivatization techniques, can be used for almost all trace analyses for which high sensitivity is essential. The electrical conductivity is the detector of choice for the separation and analysis of ions of all types and can also be relatively inexpensive. In my opinion, the refractive index detector is the detector of last resort. It is relatively insensitive, cannot be used with gradient elution but, because it is a catholic detector, it can often be successful when all other detection methods fail.

It is important to choose a detector that has a linear dynamic range that will extend over the concentration range of the solutes being analyzed. The dynamic range of a particular sample may exclude certain detectors and force the operator to choose from a particular group that has the necessary linear capacity.

If trace components are being analyzed, it is best to employ a selective detector because, in general, it will give a higher sensitivity. In addition, because there will be components of the mixture to which it does not respond, it will also simplify the separation process.

In general, LC detectors are relatively simple in design, inexpensive to construct, and are overpriced for what they are; consequently, low-cost alternatives should not be rejected without serious consideration.

VII. THE OPERATION OF LC DETECTORS

Detailed operating instructions are usually given with all commercial detectors. It is extremely important to operate the detector inside these specifications if optimum performance and accurate quantitative results are to be realized. Sensor pressures and flow rates must be controlled to within specifications, and the sensor temperature must be maintained constant within the limits recommended by the suppliers.

The maximum detector sensitivity should never be used unless there is limited sample available, trace components are being determined, or the type of column demands the minimum sample size. Under normal circumstances, the sensitivity should be set at midscale and the sample size adjusted appropriately so that the solutes of interest provide peaks that can be accurately measured. Only under extreme circumstances should the sensitivity be set at the point the noise is apparent on the recorder trace or the reconstructed chromatogram.

One common problem with an LC detector is the presence of bubbles in the sensor cell. These can cause extreme signals that can be positive or negative and violent instability. Bubbles usually arise from dissolved air in the mobile phase. It is best removed by degasing, either under vacuum or by sparging with helium. Helium is much less soluble in solvents than other gases and can displace nitrogen and oxygen from the mobile phase without becoming a source of bubbles itself. The removal of a bubble once present in the sensor cell can sometimes be difficult. Increasing the flow rate can sometimes remove it. Applying a slight backpressure on the cell by restricting the detector outlet can increase the pressure in the cell, reduce the size of the bubble, and on releasing the restriction, the bubble often flows out of the cell. Care must be taken not to cause too high a backpressure on the cell or the cell gaskets may be distended, causing leakage. If the bubble is particularly recalcitrant, the union between the column and the cell can be loosened and acetone forced back through the cell by means of a syringe, forcing the bubble out through the loosened union. The latter procedure rarely fails.

APPENDIX: LC DETECTOR SUPPLIERS

Alltech, Inc. P.O. Box 641326 San Jose, CA 95164 (408) 435-9160	Supplies moderately priced UV detectors.
ATI UNICAM 1001 Fourier Drive Madison, WI 53717 (608) 831-5515	General supplier of popular detectors.

Beckman Instruments Inc. 2500 Harbor Boulevard Fullerton, CA 92634-3100 (800) 742-2345	Specializes in UV absorption detectors.
CAMAG Scientific Inc. 515 Cornelius Harnett Drive Wilmington, NC 28401 (800) 334-3909	Supplies TLC scanners.
ESA, Inc. 22 Alpha Road Chelmsford, MA 01824-4171 (508) 250-7090	Specializes in electrochemical detectors, in particular the electrode array detector.
GOW-MAC Instrument Co. P.O. Box 2544 Lehigh Valley, PA 18002-5444 (610) 954-9000	Specializes in a wide range of reliable, low-cost detectors.
Hewlett Packard Rockville, MD (301) 670-4300	Offers a wide range of LC detectors, specializing in spectroscopic detectors.
JM Science Inc. Grand Island Industrial Park P.O. Box 250/355 Lang Boulevard Grand Island, NY 14072-0250 (716) 774-8706	Supplies chiral detectors.
LDC Analytical P.O. Box 10235 Riviera Beach, FL 33419 (407) 844-5241	Specializes in moderately priced detectors of the more popular range.
Packard Instruments 800 Research Parkway Meriden, CT 06450 (800) 323-1891	Specializes in radio-activity detectors.
Perkin Elmer Corporation Analytical Instruments Main Avenue Norwalk, CT 06859-0012 (203) 762-1000	Specializes in a wide range of detectors including quadrapole mass spectrometers.
Polymer Laboratories Amherst Fields Research Park 160 Old Farm Road Amherst, MA 01002 (413) 253-9554	Specializes in light scattering detectors for HPLC and GPC including low-angle light-scattering detectors.
Valco Instruments Co. Inc. P.O. Box 55603 Houston, TX 77255 (713) 688-9345	Specializes in high-sensitivity gas discharge detectors.

Wyatt Technology Inc.
802 East Cota Street
Santa Barbara, CA 93103-9931
(805) 963-5904

Specializes in multiangle light-scattering detectors.

REFERENCES

1. RPW Scott. Liquid Chromatography Detectors. Amsterdam: Elsevier, 1986.
2. IA Fowliss, RPW Scott. J Chromatogr 11:1, 1963.
3. AJP Martin, SS Randall. Biochem J 49:293, 1951.
4. H Poppe. In: JFK Huber (ed) Instrumentation for High Performance Liquid Chromatography. Amsterdam: Elsevier, 1978.
5. WW Christie. J Lipid Res 26:507, 1985.
6. GJ Schmidt, RPW Scott. Analyst 110:757, 1985.
7. K Blau, JM Halket. Handbook of Derivatives for Chromatography. New York: John Wiley & Sons, 1993.
8. SL Wellons, MA Carey. J Chromatogr 154:219, 1978.
9. JW Redmond, A Tseng. J Chromatogr 170:479, 1979.
10. CR Clark, MM Wells. J Chromatogr Sci 16:33, 1978.
11. NE Larsen, K Marinelli, AM Heilesen. J Chromatogr 221:182, 1980.
12. K Tsuji, JF Goetz, W Vanmeter, KA Gusciora. J Chromatogr 175:141, 1979.
13. L Elrod Jr, LB White, CW Wrong. J Chromatogr 208:357, 1981.
14. LT Wong, AR Beaubien, AP Pakuts. J. Chromatogr 231:45, 1982.
15. FA Fitzpatrick, S Siggia. Anal Chem 45:2310, 1973.
16. F Nachtmann, KW Budna. J Chromatogr 136:278, 1977.
17. MA Carey, AF Persinger. J Chromatogr Sci 10:537, 1972.
18. TP Davis, GW Gehrke Jr, CW Gehrke, TD Cunningham, KC Kuo, KO Gerhardt, HD Johnson, CH Williams. Clin Chem 24:1317, 1978.
19. J Reisch, HJ Kommert, D Clasing. Pharm Zig 115:754 1970.
20. HJ Klimisch, DK Ambrosius. J Chromatogr 121:93 1976.

16
Injection Devices

Richard A. Henry

Keystone Scientific, Inc., Bellefonte, Pennsylvania

I. INTRODUCTION

Liquid chromatography (LC) and high-performance LC (HPLC) will be used as equivalent terms in this chapter. The results obtained from any liquid chromatographic system are dependent on and limited by the performance of all independent system components. A primary concern of the chromatographer is to prevent the sample from spreading owing to factors other than the column separation mechanism as it travels through the chromatograph. A properly designed injection valve, operated in the correct manner, ensures that the sample begins the separation process as a narrow band. Without proper injection, optimum chromatographic performance can never be achieved.

Developments in injection technology over the past decade have resulted in improved performance characteristics measured by precision, accuracy, and contribution to system band-broadening [1–8]. However, improvements have also resulted in a wide variety of products, and selection of the most suitable device can still be a primary factor in determining system performance. An informed chromatographer must possess an understanding of the operating parameters and features of valves and the requirements of the column and separation. The following discussion will present the user with a description of injection valves and factors affecting performance and optimization of the chromatographic system. It will also address maintenance and troubleshooting of injection devices and other valves. A recent, comprehensive method development book [9] also contains much useful information that complements the material presented here.

II. MANUAL SAMPLE INJECTION VALVES

Since the early development of LC instrumentation in the 1960s, it has been clear that syringe–septum injectors of the type usually employed for gas chromatography (GC) would not be suitable for LC because of the requirements of high pressure and continuous solvent exposure. Instead, precision valves have been employed to meet most of the requirements for LC sample introduction. The basic-operating principle of LC injection involves the transfer of a sample, by means of a syringe, from atmospheric pressure to a sample chamber. While the syringe remains in place, a rotary action of the valve diverts the flow of mobile phase through the loaded sample chamber and carries the sample onto the column. The accuracy, precision, and amount of sample necessary are inherently dependent not only on the injection valve design, but also on the loading technique [4]. The act of filling the loop, or zone, that

will eventually be pressurized will be referred to as *load*, which is usually carried out by a low-pressure syringe that has a larger volume than the amount to be injected. The act of turning the valve to pressurize and introduce the sample volume and mass to the column will be called *inject*. Although many valve manufacturers exist, most of all LC rotary valves are made by Rheodyne, L.P. and Valco Instruments Co., Inc. (VICI).

A typical two-position, six-port valve, with an external sample loop is diagrammed in Fig. 1. In the load position, the sample is introduced to the loop at low pressure by a calibrated syringe with a blunt tip. Figure 2 shows a popular variation on the design that employs a center port for the loading syringe to connect internally to the sample loop. This results in virtually no sample waste. When the loop has been partially or completely filled, the sample is introduced to the column by manually turning the knob to the inject position, which turns the rotor and directs mobile phase through the sample loop carrying the sample onto the LC column. Unlike GC, the syringe is not removed until the valve is turned to inject to avoid pulling sample back out of the loop before injection and to prevent loss of sample from the loop by siphon action. Samples as small as 0.1 μL may be injected in this manner with an appropriate valve and syringe. Injection may be accomplished at pressures as high as 7000 psi (483 bar, 48 MPa) at ambient temperature, although requirements higher than 3000 psi are rare. Operation at elevated temperature reduces the maximum pressure rating and shortens

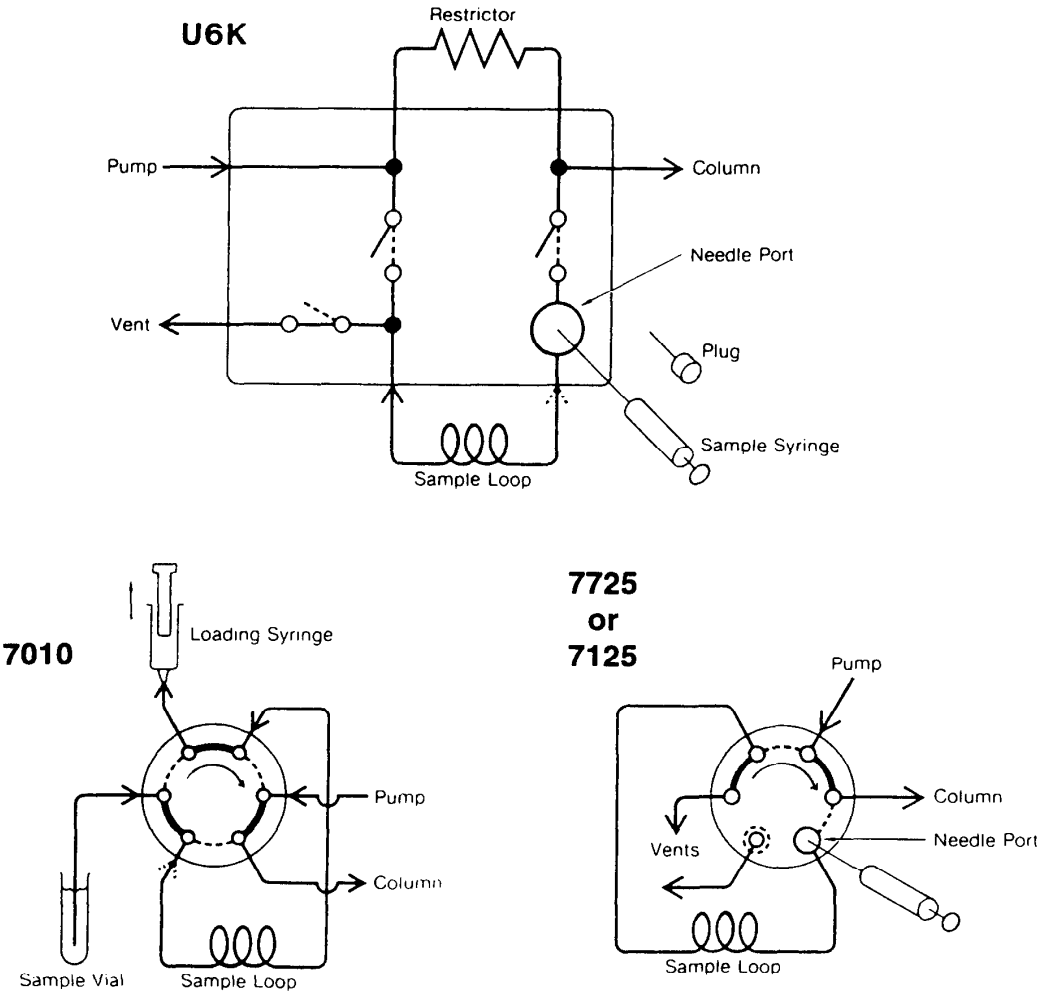


Figure 1 Two-position, six-port rotary injection valve with external sample loop (Model 7010). (Courtesy of Rheodyne, L.P.)



Figure 1 Continued

the seal rotor lifetime. In a typical six-port, two-position injection valve with sample loop, only the pump and column valve ports are always at high pressure, whereas the column is under flowing condition. The two loop ports are at high pressure only during sample injection. The two ports used for syringe filling are never pressurized in normal operation; therefore, the syringe may be left installed in the valve port while the sample is injected. This is usually desirable, because withdrawal of the syringe before injection may remove some sample from the loop and create very poor precision of injection, especially for small samples. The injection valve may be kept in the inject position until the end of the analysis, or it may be returned to load after the sample is safely swept into the column (normally, only a few seconds). In either event, it is advisable to flush the needle port to avoid trace carryover from a previous sample. Manufacturers will be able to supply accessories and directions for proper flushing and cleaning (also see Sec. V of this chapter on maintenance and troubleshooting). A new

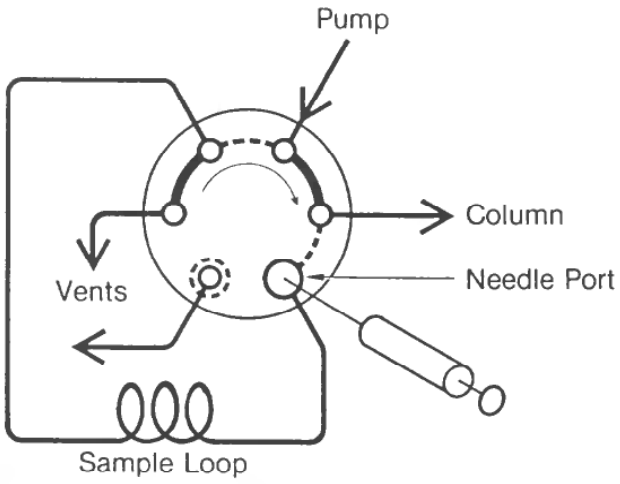




Figure 2 Two-position rotary injection valve with center port for very efficient loop filling (Model 7125 or 7725). (Courtesy of Rheodyne, L.P.)

model of the popular valve shown in Fig. 2 has been recently introduced. The Model 7725 has all of the features of the 7125 plus several additional ones; including continuous flow during switching (no interrupt), front-end pressure adjustment, improved access to fittings for easy connection, and an internal loop option for very small samples. The feature of continuous flow or make-before-break flow path addresses a significant problem that is especially important with manual injectors. Most injector valves in service at the time of this writing are designed so that flow is interrupted between load and inject positions. A slow movement of the handle can cause pressure to rise rapidly and release suddenly each time a sample is injected. This pressure pulse can damage the column and cause finger-tight fittings to slip and develop gaps that cause band-spreading. An automatic actuator or brisk manual movement of the valve handle is recommended to avoid the problem with valves that do not employ this new design feature.

Certain physical and chemical properties must be considered in the design and manufacture of any valve used for sample injection. Interaction with either the mobile phase or the sample must be avoided by building the entire flow path with inert materials. Both reactivity and adsorption must be avoided. The most common material for construction of valve bodies and tubing is type 316 stainless steel, although Hastelloy C and other materials have been substituted for extreme-operating conditions. Recently, valves constructed of polyetherether-

ketone (PEEK) have been introduced for applications that require the absence of metal surfaces. The rotor or rotating inner portion of the valve is typically polymide, although PEEK has been used to give a somewhat greater degree of chemical resistance, especially at high pH. All internal volumes must be minimized, and all flow passages must be smooth and regular, with diameters optimized for flow rate and sample size to prevent excessive band-broadening. Diameters, often called thru-holes, in each of the valve ports must also be matched to each other by the rotor and to the connecting tubing to avoid band-tailing from eddy formation. Hole and tubing inside diameters can be as large as 1 mm for preparative applications and as small as 0.25 mm or less for microbore column applications. Very small holes greatly increase valve production costs. Figure 3 shows an exploded view of a typical center-port injection valve in which the small holes and grooves in the rotor can be seen. Table 1 lists typical specifications for rotary injection valves and other similar valves.

A. Sample-Loading Techniques

The sample chamber may be loaded either by complete filling or by partial filling. The accuracy and precision of these two methods are governed by the characteristics of liquid flow through narrow tubes. When a sample is transferred at atmospheric pressure to the sample chamber by means of a syringe inserted through a sleeve seal in an injection port, it displaces the mobile phase already present in the loop, creating a parabolic boundary layer caused by the laminar flow of the liquid (Fig. 4). The velocity at the center of the tube is twice the average, whereas at the walls it is nearly zero. It is important to realize that an open tube can be a good mixing chamber, and the extent of mixing or dispersion becomes greater as flow and the tube internal diameter (id) increase, as shown by an equation for dispersion under laminar flow conditions.

$$\sigma^2_{\text{tubing}} = \frac{1.36(10^{-3}\, d_t^4 L_t\, F)}{D} \tag{1}$$

where σ^2 is variance (μL^2), d_t is the tubing inside diameter (mm), L_t is the tubing length (mm), F is the flow rate (mL/min), and D is the diffusion coefficient (cm^2/s) [8].

Figure 5 shows a plot of sample response versus dispensed volume from a syringe indicating three distinct regions resulting from the laminar flow behavior. In the first region, results are dependent on the syringe design and skill of the analyst. Good linearity can be achieved if the volume dispensed is less than half of the loop volume. If the operator uses the full-scale volume of the syringe, accuracy of nearly 1% relative standard deviation (rsd) can be attained with great care. Precision of sample introduction typically ranges from 1 to 2% rsd in this partial-filling mode. Poor technique can result in much lower precision. It is advisable to avoid dispensing a volume between half the loop volume and about two-loop volumes when the loop is filled with mobile phase. Dispensing a volume equal to the volume of the loop places you in the least desirable region, in terms of quantitative performance. Sample spillover from the loop will result, causing poor accuracy and precision. If the sample is not limited, complete filling with about five-loop volumes is desirable. Under these conditions, residual mobile phase is almost completely displaced from the sample loop, leaving only pure sample. Under these overfill conditions, the mass injected is independent of the volume dispensed from the syringe, and accuracy is determined by the loop itself. Precision of 0.5% or better can be achieved, depending on the volume loaded. Precision can be improved when the sample is limited and only a few loop volumes can be dispensed, by carefully loading the same volume at every injection and introducing the sample at the same speed. Unless specifically calibrated, indicated loop volumes are only estimations and should be considered nominal. Variation of approximately ± 0.001 in. in the internal diameter of tubing used in the construction of sample loops is typical and can cause relatively large differences in the actual volume injected when loops or injectors are changed or when results are compared between instruments.

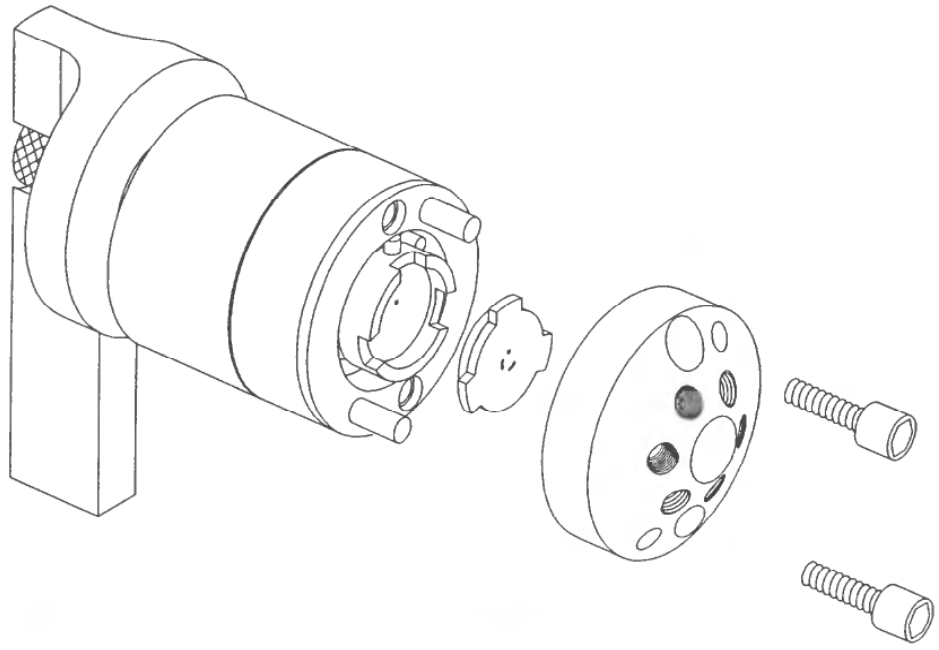




Figure 3 Two-position rotary injection valve exploded to show body, rotor, and stator where tube connections are made (Model C1). (Courtesy of Valco Instruments Co., Inc.)

When sample waste must be avoided, the laminar flow effect can be minimized by blowing the loop dry before the filling operation, or by pulling a small air gap into the dispensing syringe to act as a bubble that sweeps the mobile phase in the loop, effectively preventing it from diluting the sample. In this manner, nearly all of the sample can be introduced up to the nominal loop volume without significant waste [10]. The injection of a few microliters of air into the column will normally not be harmful. Another approach to con-

Table 1 Valve Performance Characteristics

Item	Typical values	Comments
Pressure	5000–7000 psi (345–483 bar)	Rating drops as temperature increases
Materials	Stainless steel (type 316) Hastalloy C PEEK	Determines suitability for extreme sample and mobile-phase operation
Loop size	External loop (5 μL up) Internal loop (<5 μL)	Determines range of possible injection volumes
Thru-hole (in valve body)	0.3 mm (microbore) 0.5 mm (standard) 1.0 mm (prep)	Determines suitability for microbore, standard bore, and preperative LC. Should match closely with connection tube id.
Autoactuator (for autosampler or autoswitching)	Pneumatic or electric motor connected to valve stem or shaft	Pneumatic typically faster, but electric more convenient. Interchangeable in most situations.
Valve port geometry	3-, 4-, 6-, and 10-port valves are common. Can be clustered in the center or located on the perimeter of a valve body.	Location of ports often determines convenience of installation. Nuts and ferrules for different brands are typically not interchangeable.

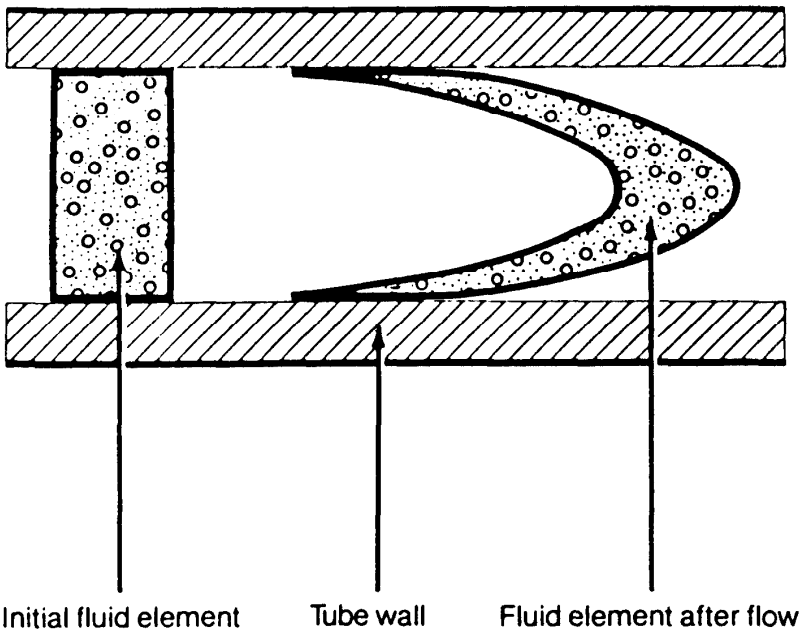


Figure 4 Laminar flow profile of liquid in an open tube. (Courtesy of Rheodyne, L.P.)

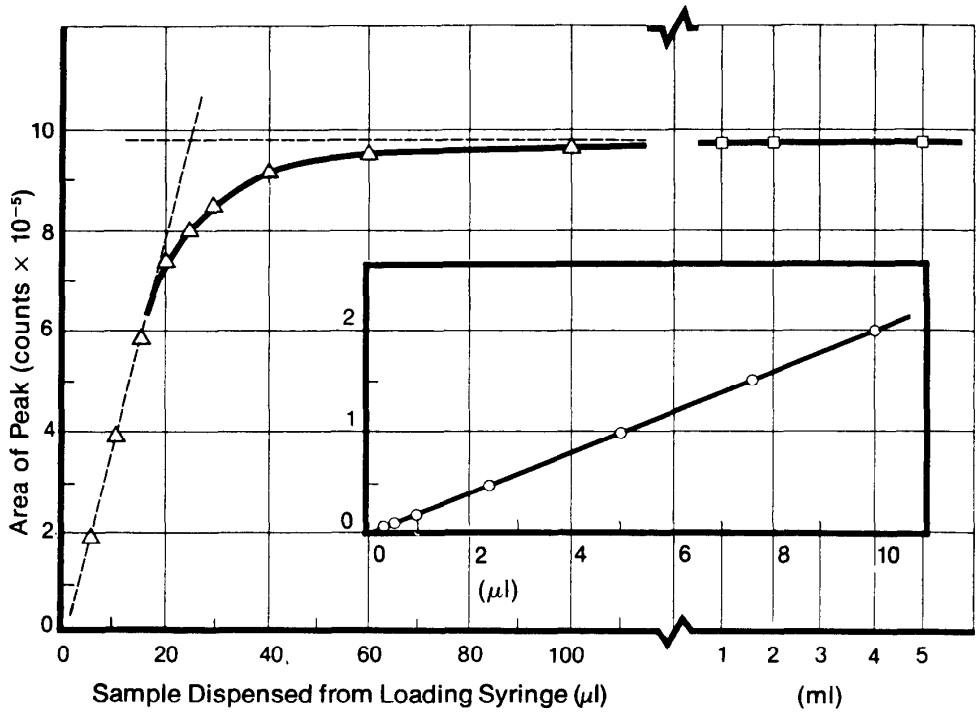


Figure 5 Sample response versus amount loaded into an external-loop injection valve. (Courtesy of Rheodyne, L.P.)

serving sample involves changing the more common 10- or 20-μL loop supplied by manufacturers to a 50- or 100-μL loop or larger. In this fashion, up to half of the loop volume or more can be introduced without loss from the laminar flow effect. When larger loops are employed, it is very important to be sure that the valve ports are connected so that sample is backflushed from the loop into the column (i.e., in a direction opposite that by which the sample was loaded). It is easy to inadvertently interchange pump port and column port during installation or maintenance, which will sweep the loop in the same direction as the filling operation and cause unnecessary band-spreading during partial loop filling.

A variation on the rotary valve with large sample loop has been made popular by one manufacturer and may still be encountered in older instruments. Called the Waters U6K, it employs three shut-off valves activated by a single lever (Fig. 6). When the lever is open, the valves close causing pump flow to travel through a bypass capillary tube and restrictor to the column, while the sample is back-filled through a syringe port into a large 2-mL loop of capillary tubing. When the sample is deposited and the plug replaced in the filling port, the lever is closed and flow is diverted by the restrictor to sweep the sample into the column. Although very reliable because there are no valve rotors with small, precision grooves and holes to wear out, the U6K suffers from two important disadvantages. It is limited to partial loop injection and precision of the syringe-filling and dispensing technique, and it is not a low-dispersion injector that can be used with small-bore and microbore columns without very significant loss of resolution, compared with optimized rotary valves. This injector is no longer manufactured.

B. Small-Volume Sample Injection

Dispersion (band-spreading) outside of the column is not the only variable that can degrade performance. To maintain high efficiency and resolution when column internal diameter is reduced, it is important to also reduce the volume of sample injected so that it occupies the

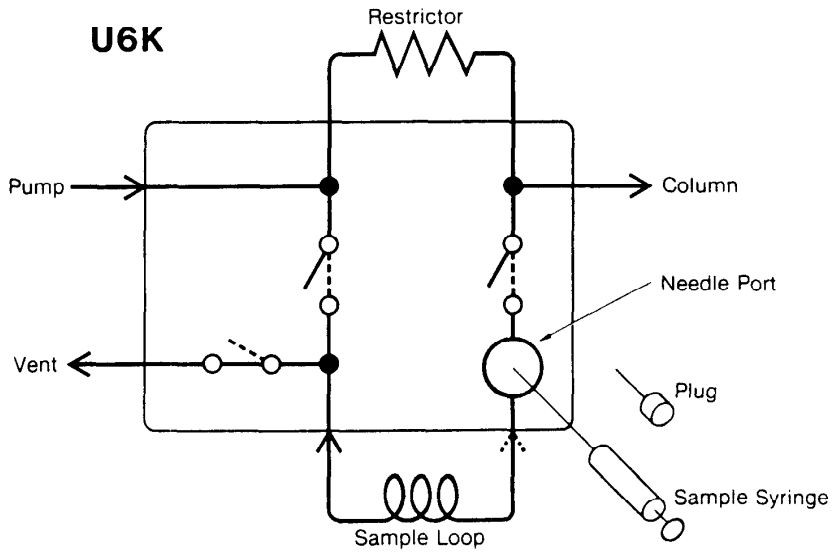


Figure 6 Diagram of the U6K injector. (Courtesy of Waters Associates, Inc.)

same percentage of the column volume or length at the inlet, before separation begins to take place owing to differential migration of species. Figure 7 illustrates this effect for 4.6-, 2.1-, and 1.0-mm–id columns from a very comprehensive paper on the subject of scaling-down while maintaining high resolution [11]. Sample volume (and flow rate) must be reduced in proportion to the column cross-sectional area (πr^2) to maintain performance when the packing bed conditions (particle size, uniformity, length, and such) are otherwise identical. For ex-

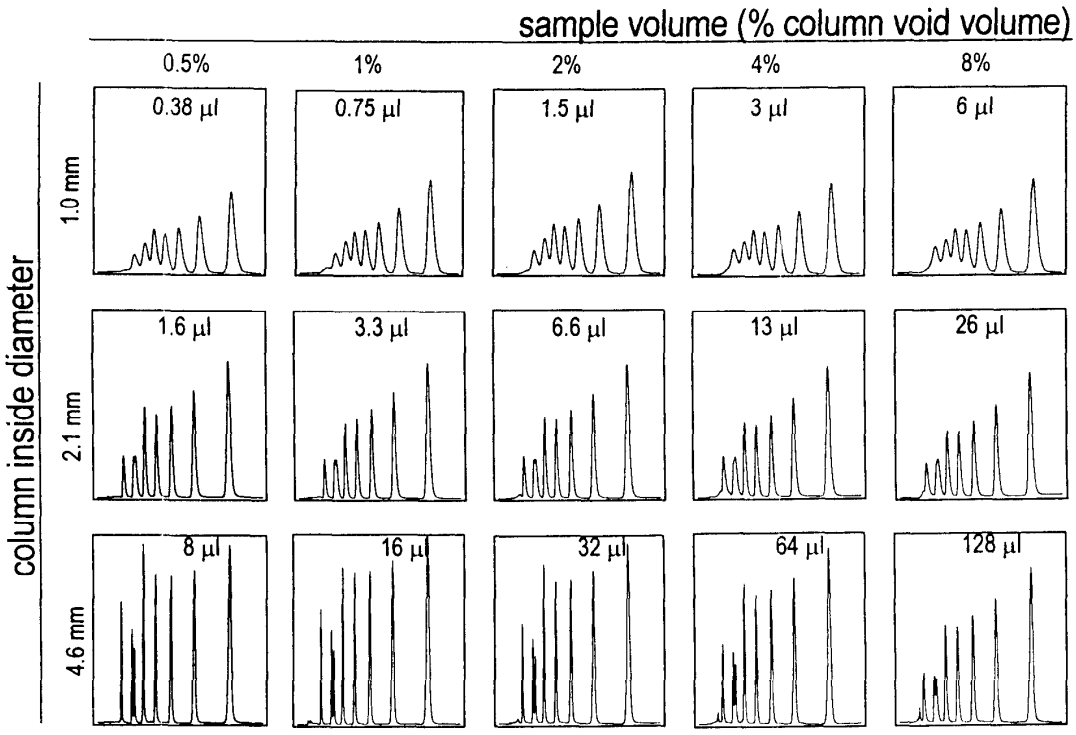
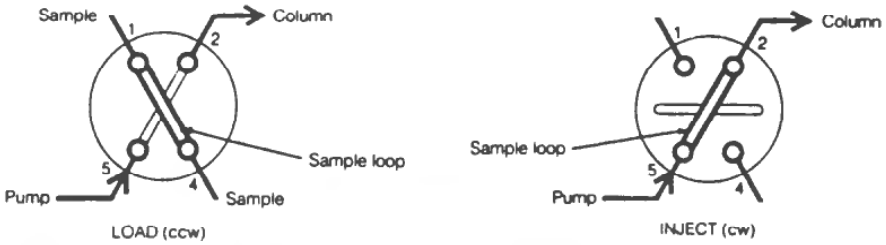
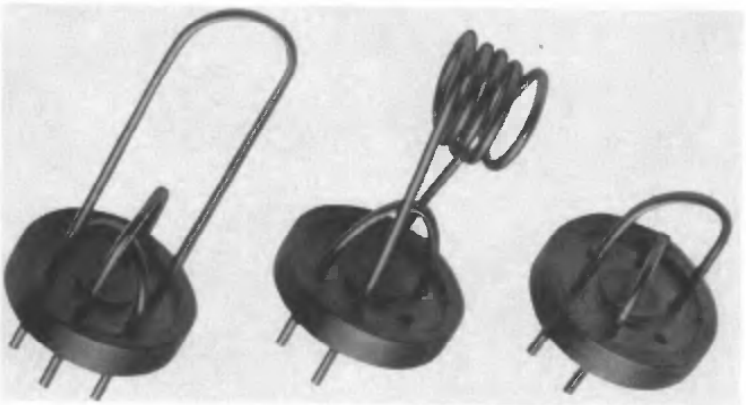


Figure 7 Optimum sample volume for different column inside diameters. (From Ref. 11.)

ample, only about 0.1 μL can be introduced to a 0.3-mm–id packed capillary LC column without serious loss of resolution, to extend the example shown in Fig. 7. It is apparent from the poor resolution for a 1-mm–id column that system dispersion parameters, other than injection volume, were dominant.

When samples as small as 1 μL or less must be introduced for small-bore, microbore, or packed capillary LC, special valves with very small-diameter sample passages are required. Although six-port, external-loop valves with very small holes and low dispersion have been designed to allow sample introduction to a wide range of columns, the external loop valve is often replaced with an internal loop design when columns having 2-mm id or less are employed. A diagram of a typical four-port injection valve with internal loop is shown in Fig. 8. In most four-port injection valves, the injection volume is changed by installing new rotors, which are designed so that this operation can be done quickly. In some designs, small-volume injection can be varied precisely by timing the period in which the valve is in the inject position. This is feasible only when the valve is electrically or pneumatically actuated and timed by an electronic controller or computer [3].





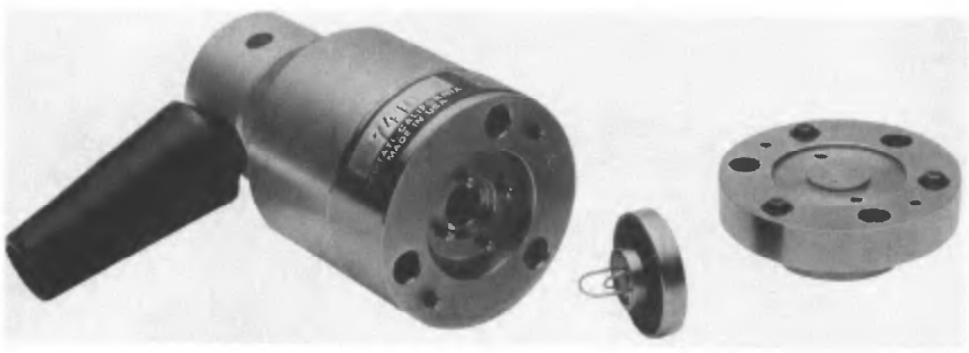


Figure 8 Two-position, four-port rotary injection valve for small sample volumes (Model 7410). (Courtesy of Rheodyne, L.P.)

III. AUTOSAMPLERS

Virtually all manufacturers of LC equipment have an autosampler that allows unattended introduction of samples from vials that are usually arranged in a rectangular or circular tray. When operating properly, an autosampler removes human error and increases precision and accuracy of injection. Manufacturers commonly report precision values of ± 0.5% in partial-loop filling and ± 0.25% in complete-loop filling methods. A complete description of all autosampler designs is beyond the scope of this chapter; however, a few general comments may be helpful to the autosampler user.

Autosamplers can be divided into two major categories. Both types employ mechanized valves as part of their design. Type 1 employs a simple mechanism to pierce the septum cap of a sample vial and then displace liquid by gas pressure or plunger action to the inlet port of a typical six-port manual injector that has been fitted with an electric or pneumatic actuator to turn the shaft. In this manner, the action of filling a loop and turning the valve from load to inject by the operator can be simulated by the electromechanical device. Type 1 autosamplers were the first ones to appear in the 1970s and are still reliably employed when excess sample is available and lowest cost is desired. Type 1 autosamplers are practical only for complete-loop filling; therefore, at least five times the volume of the valve loop and connecting tube to the valve sample inlet should be displaced. Even more displacement volume may be needed to completely eliminate carryover from the previous sample, especially if a wash cycle is not employed between sample vials. Simple diagrams of two type 1 autosamplers are shown in Fig. 9.

Type 2 autosamplers are designed to allow much smaller samples to be injected without waste and are much more versatile in their attempt to duplicate all operations that are possible with a manual injector. They typically include motorized sample syringes to draw from the sample vial and deposit the sample into the loop of an automated injection valve. Both complete-loop and partial-loop filling may be employed with some limitations caused by the design of the sampling syringe device. Several type 2 designs employ a mechanism whereby the syringe needle mechanism that pierces the sample vial actually becomes part of the injection loop. This design has one important advantage in that very low sample volumes can be introduced to the column without waste. Disadvantages include the need for another high-pressure–sealing mechanism at the filling tip, which can become a maintenance problem, and loss of flexibility for larger-volume injections and complete-loop–filling applications. Type 2 autosamplers are typically much more expensive than type 1 and can be more complicated to troubleshoot and maintain. A diagram of a type 2 autosampler is shown in Fig. 10.

One major disadvantage of many autosampler designs is that the injector valve is not readily accessible for inspection and maintenance or replacement. A related disadvantage is that many autosamplers do not allow convenient override so that the chromatographer can employ simple manual load and inject experiments during method development and trouble-shooting to verify proper operation. Another disadvantage is that autosamplers typically introduce excessive band-spreading by the time the sample reaches the column. Most designs are not suitable for interface to reduced-bore columns without changing components or employing special techniques, such as weak sample solvent focusing or gradient elution. When gradient elution is employed with an autosampler installed, it is important to recognize that the extra tubing can add significant time to gradient arrival at the column and equilibration between gradient runs. Special autosampler designs with low-dispersion valves and tubing are required for optimum interface with microbore and packed capillary LC columns.

IV. COLUMN-SWITCHING VALVES

In addition to sample injection, valves can be used to connect more than one column to a liquid chromatograph. A different column is selected for use by turning the valve handle. This has several advantages: selection is immediate, fittings are not subjected to the wear of re-

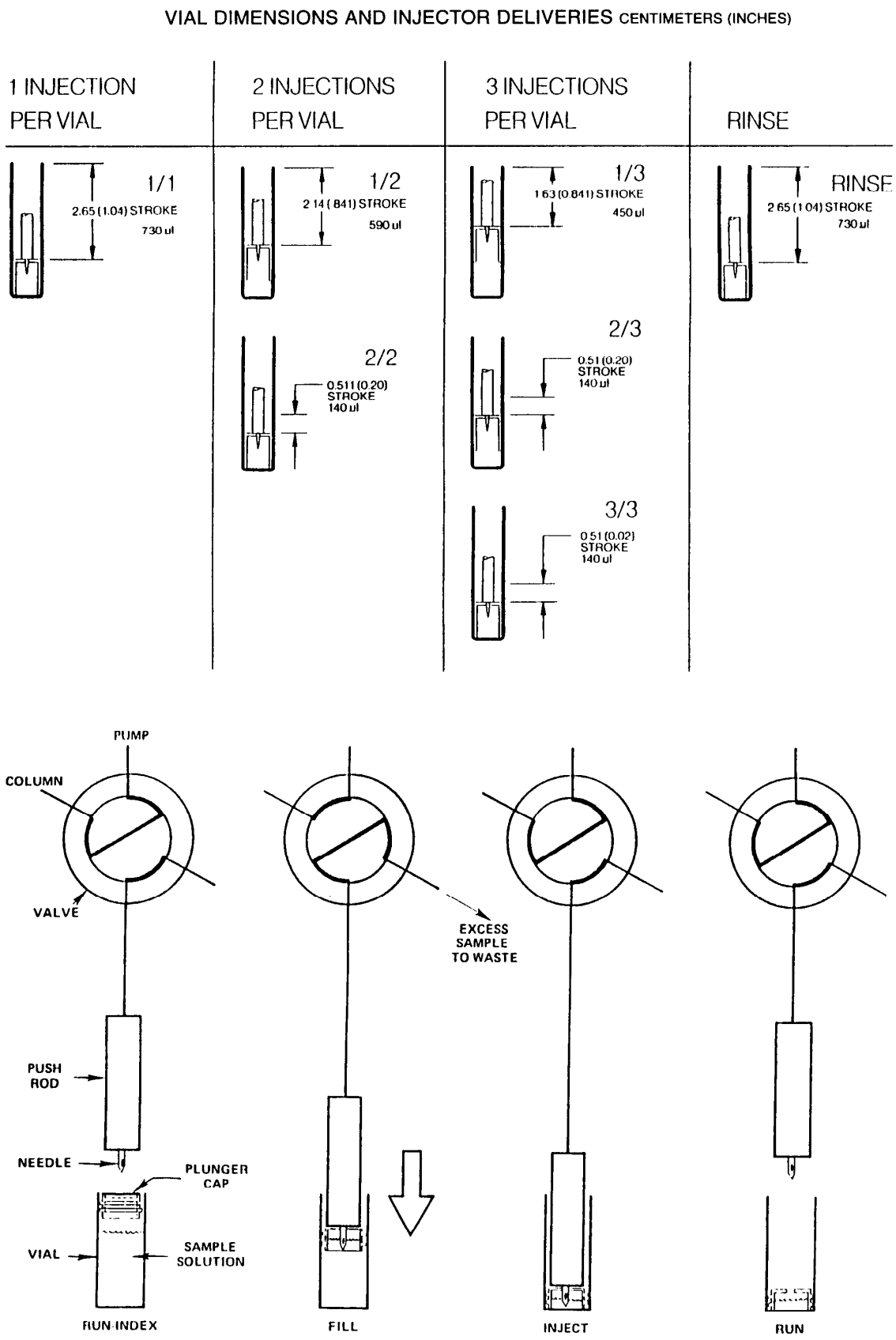


Figure 9 Type 1 autosamplers that use sample displacement and the full-loop–filling method. (Courtesy of Allcott Chromatography and Scientific Glass Engineering.)

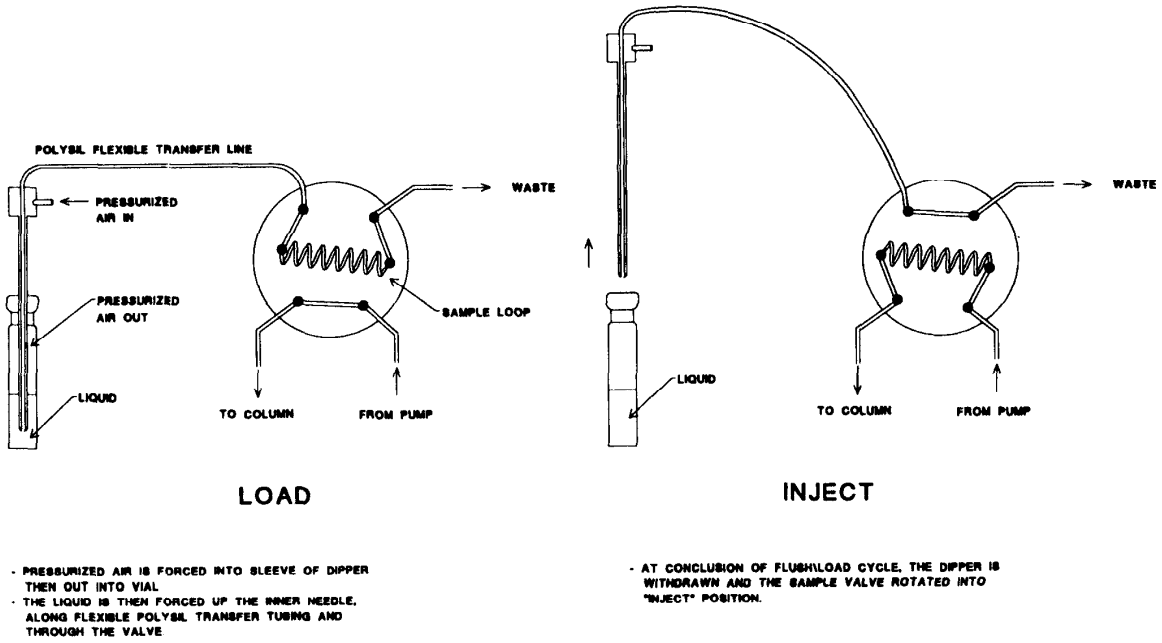


Figure 9 Continued

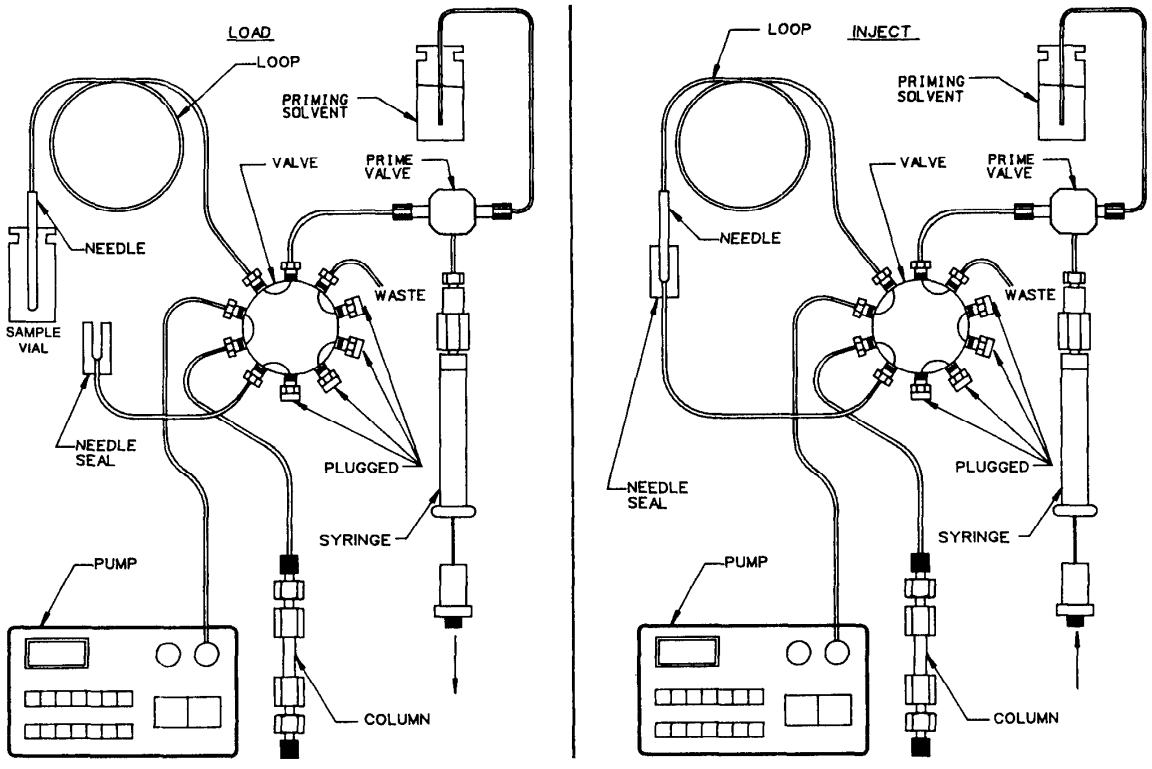


Figure 10 Type 2 autosampler that can use partial-loop methods (Model 718). (Courtesy of Allcot Chromatography.)

peated tightening, the valve seals the off-line columns at both ends and keeps them on standby for future use, and columns can be changed for any reason, even when the operator is not present, by the use of a controller and autoactuator. Switching valves may be fitted with a bypass line that permits rapid mobile-phase changeover, without exposing any column to adverse mobile-phase conditions. A bypass line can also be useful for checking detector response to sample and mobile phase without the column in line. Figure 11 shows simple two-column selection using a single, six-port valve, and Fig. 12 shows a more elaborate arrangement for five columns and a bypass line using two, six-position valves. Both configurations require an injection valve in addition to the switching valve assemblies. There are many other uses for valves beyond injection and column selection including column back-

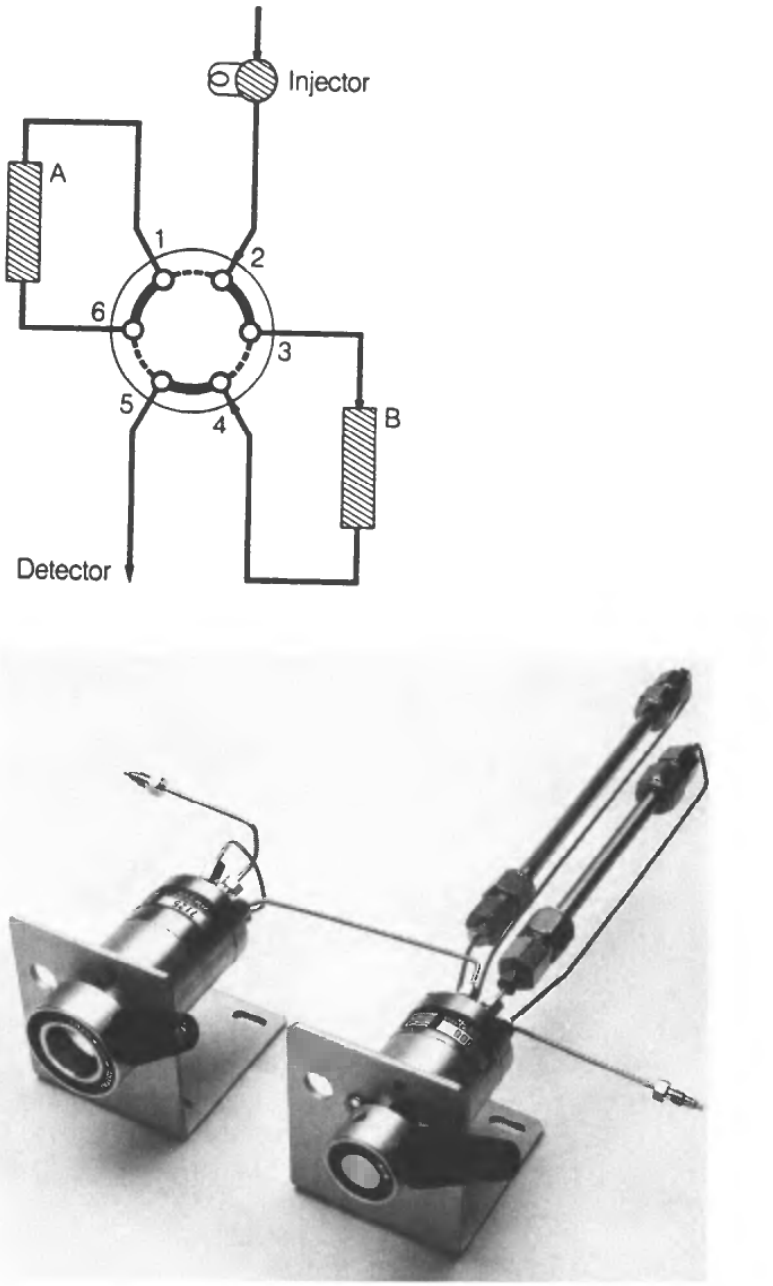


Figure 11 Two-column selection using a single, six-port, two-position rotary valve (Model 7000). (Courtesy of Rheodyne, L.P.)

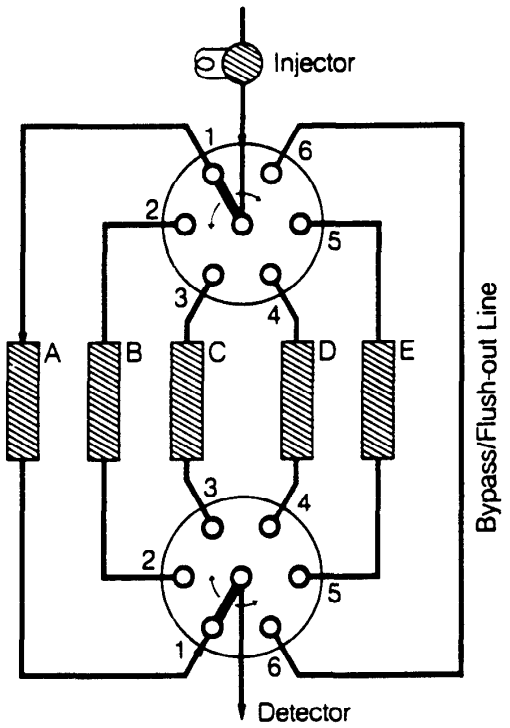


Figure 12 Five-column selection and bypass using two, six-position rotary valves (Model 7060). (Courtesy of Rheodyne, L.P.)

flushing, sample trace enrichment, or column–stationary-phase programming (an alternative to gradient elution), and stream switching in multidimensional chromatography. The reader is referred to other texts and the valve manufacturer for more information on these valve applications.

Every valve and related connecting tube reduces peak resolution by zone-spreading caused by laminar flow effects, as described in Eq. (1) and Ref. [8]. Loss of resolution will be significant only if valve and tubing dispersion is large compared with that caused by the column. Dispersion after the column is equally important to dispersion before the column [8]. Resolution loss from extracolumn effects will be negligible when chromatographic column peak widths in volume units are large, and will be significant when peak widths are small. Loss of resolution caused by differences in valves and connectors can be negligible with 4.6-mm–id columns, but can be very noticeable with 2-mm–id columns and smaller (see Fig. 7). Table 2 summarizes typical values for volumetric peak widths for various column geometries. As a rule, the total volume of valves and tubing should not exceed 10% of the smallest column peak volume measured by base width (4σ), to maintain resolution achieved in the column. The use of volume can be misleading, however, because smaller id valves and tubing will always show much less dispersion than larger id, even when the two systems contain equal volume. With careful valve selection and use of 0.005-in.–id tubing, relatively complex systems can be installed, even with 2-mm–id columns, without significant degradation of performance.

V. MAINTENANCE AND TROUBLESHOOTING

Problems with injector or autosampler probably account for a large percentage of the errors that can affect HPLC analysis. Injection problems typically manifest themselves as poor reproducibility of peak heights and areas. Injection devices normally do not affect retention

Table 2 Typical Peak Width Values[a]

Column diameter (mm)	Column length (mm)	Packing diameter (μm)	4 σ peak width (μL)	σ variance (μL^2)	Plate number ($H = 3\ d_p$)
4.6	250	5	167	1,751	16,670
	100	5	106	701	6,670
	100	3	82	420	11,110
	30	3	45	126	3,330
3	250	5	72	324	16,670
	100	5	45	126	6,670
	100	3	35	81	11,110
2	250	5	32	63	16,670
	100	5	20	26	6,670
	100	3	15	15	11,110
1	250	5	8	3.9	16,670
	100	5	5	1.5	6,670
	100	3	4	0.9	11,110

[a]Values were calculated for worst-case situations of short retention ($k = 1$) and a well-packed column ($H = 3\ d_p$)
Source: Ref. 8.

times unless a severe leak occurs, which would be easily observed at all but the very low flows used in microbore and packed capillary LC. If retention time variation occurs, other LC components, such as the solvent delivery system or column, should be suspected before the injector. Some of the problems, such as external leaks, are easily diagnosed and corrected, whereas others can be more difficult. A troubleshooting guide [12] from one of the valve manufacturers contains much information of a general nature that pertains to all valves.

The most common problems can be divided into four main categories for easy discussion: operator technique, valve rotor malfunction, poor connections, and valve contamination or blockage.

A. Operator Technique

The injection valve may be operating perfectly, but poor reproducibility of peak heights and areas can be caused by poor injection technique. Some of the most common problems follow:

1. Syringe is removed before turning valve from load to inject: This pulls some sample back into the needle port and can be very irreproducible, especially with small samples. Always leave the syringe in the needle port until the valve is turned to inject.
2. Valve is not allowed to remain in inject long enough: After turning to inject, remain in this position long enough for the pumped mobile phase to flush all sample from the loop. This provides maximum precision and eliminates the need for any further flushing of the loop. Pump at least ten sample volumes. For example, if you load 20 μL into a 100-μL loop, and pump at 1 mL/min, stay in inject at least 12 s.

$$\frac{(20\ \mu\text{L/sample vol})(10\ \text{sample vol})(60\ \text{s/min})}{1000\ \mu\text{L/min}} = 12\text{s} \tag{2}$$

You can then return to load, or you can stay in inject until ready to load the next sample. Remove the syringe from the needle port at any time before returning to load.

3. Syringe is filled with a volume too close to the loop volume: Remember from the earlier discussion that one should inject less than 50% of the loop or more than 500% of the loop for maximum precision.

4. Syringe is not properly filled or does not have the correct dimensions: Learn how to clean and remove air bubbles from a syringe and keep it in good-operating condition. If the needle does not have the correct length and od, it will not fit the port geometry. Sample will flow around the needle, avoid the loop, and contaminate the port. Separate syringes must be used for best precision in partial-loop and complete-loop–filling methods. One very attractive aspect of an autosampler is that it virtually eliminates this type of error and many other operator variables.

B. Rotor Malfunction

The rotor is the only part in most rotary valves that must be replaced regularly, even if the valve does not receive excessive use, the rotor should be inspected annually and replaced if worn. It is easy to visually compare a new rotor with a used one to detect grooves or channels between the holes or ports. The flat stationary part or stator that seals to the rotor is typically constructed of highly polished steel or ceramic. If the stator is scratched or cracked, it must also be replaced with the rotor. Stains or deposits on the stator can be removed by gently rubbing with toothpaste or any mild abrasive. Maximum rotor life can be expected when samples and mobile phase are filtered to remove small hard particles. Autoactuators can also be helpful to extend rotor seal life because, unlike human operators, they apply very uniform torque to the valve shaft. Some of the most common rotor problems include the following:

1. Leaks are observed continuously through the needle port or vent tube, or at the bottom of the valve: Occasionally, this can be corrected by tightening the tension adjustment nut on the valve, but usually the flow is due to cross-port leakage caused by a scratch on the rotor, which must be replaced. Leaking of mobile phase at the rotor seal will also cause a decrease in operating pressure. Depending on where the scratch is located, leaks and loss of system pressure can be observed in either or both valve positions.

2. Ghost peaks or artifact peaks are present during sample and blank injection: This condition can be caused by a rotor groove or scratch that does not cause a leak but can hide small amounts of previous sample. More commonly, unexpected peaks will be caused by contamination of the sample, syringe, or needle port.

3. Tailing peaks are persistent even when a simple calibration sample is tested: Although poorly shaped peaks can usually be corrected by attention to column or mobile phase conditions, a worn rotor can also be at fault. Figure 13 illustrates how this condition can be easily diagnosed by clipping the tailing end of the injection [13]. First, make an injection by leaving the valve in inject for at least five-loop volumes, then make a second injection by turning the valve back to load before the sample is totally flushed from the loop (usually a few seconds will be effective). If the rotor is in perfect condition and alignment, the clipped injection will be virtually identical with the full-loop injection, but the peaks will be somewhat smaller. If the clipped injection eliminates the tail, the rotor should be replaced and the procedure repeated to verify correction. A clipped or timed injection can also be useful for efficient introduction of viscous samples. Tailing and loss of resolution induced by a worn rotor can be quite common with small-volume injections required by reduced-bore HPLC [11].

C. Poor Connections

Peak-tailing is commonly caused by poor connections that leave a gap or unswept area in the valve ports or column connection, as shown in Fig. 14. This condition should be checked before changing a valve rotor because it is easier. Many new fittings are very convenient because they can adjust to different seat geometries and can be installed without wrenches

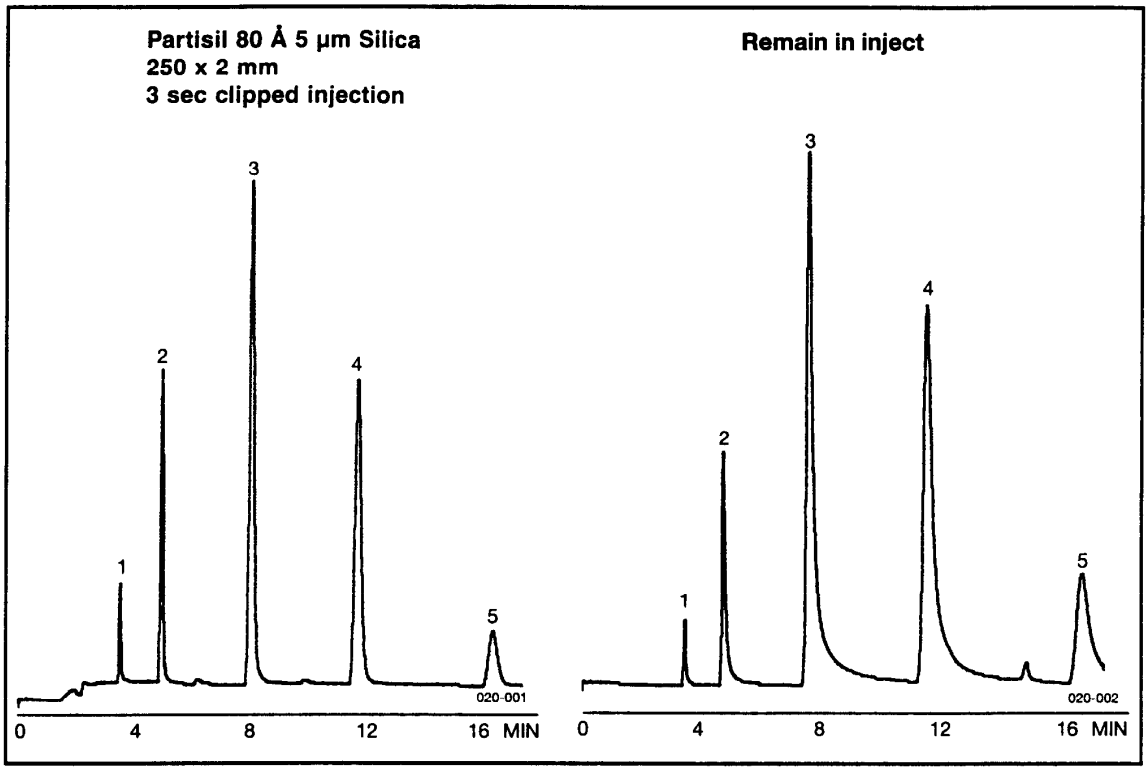


Figure 13 Use of a clipped injection to detect a worn rotor valve.

(Fig. 15). but some are prone to slipping, especially at high pressures and temperatures. Be sure to regularly inspect each fitting that has an adjustable ferrule design to be sure that it is properly seated. Connecting tubes and sample loops that are not square cut and free of burrs will also cause problems with peak shape, especially with reduced-bore column applications for which very small sample peak volumes are employed. PEEK tubing has become very popular in LC, but it is very difficult for the user to make a clean, square cut with any tubing. The use of tubing that is cut by the manufacturer is recommended for best results, especially with reduced-bore columns.

D. Valve Contamination

This last, major problem category can be one of the most detrimental to good analytical performance and one of the hardest to diagnose. To test for contamination, one typically makes a blank injection of mobile phase or sample solvent. A contaminated needle port will be indicated by small peaks that should appear at retention times that are related to previous samples. Flushing the needle port after every injection to prevent cross-contamination is normally not necessary, but frequent flushing with a large-volume syringe without a needle, or with a short needle, minimizes inadvertent introduction of old sample traces. Direct-connection port designs connect the tip of the syringe needle directly to the end of the sample loop so there is no connecting passage that traps sample, which would then be pushed into the loop when the next sample is loaded. Make sure that you are not inadvertently creating a connecting passage by

1. Using a needle that is too short, so that the needle tip does not touch the stator face. Minimum length from hub to the needle tip should be specified by the manufacturer.

Loss of Efficiency Due to Excess Tubing Volume

Column Dimensions	Tubing Dimensions	Volume	Efficiency (N/m)	% Loss of Efficiency
150 x 4.6 mm	0.006"x 6 cm	1.1 µL	98,096	–
150 x 4.6 mm	0.020"x 10 cm	20.3 µL	93,388	4.8
150 x 1 mm	0.006"x 6 cm	1.1 µL	56,551	–
150 x 1 mm	0.020"x 10 cm	20.3 µL	19,481	66

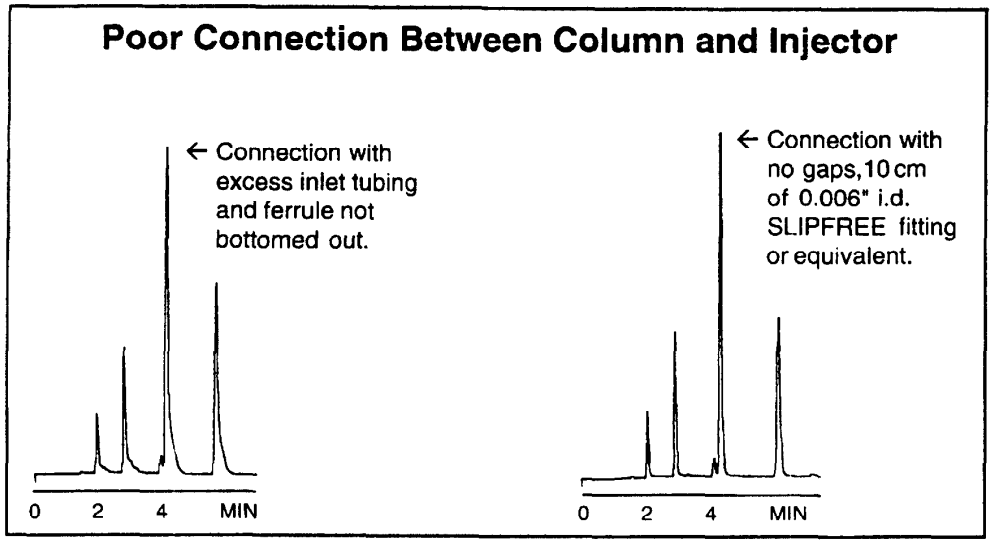


Figure 14 Peak-tailing caused by a poor connection.

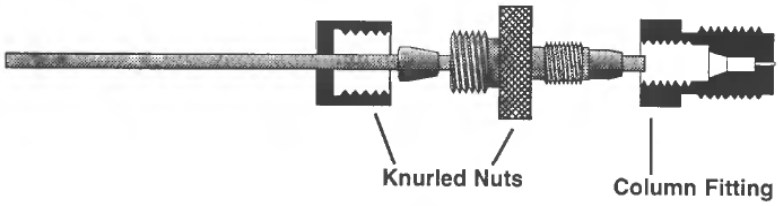
2. Not fully inserting the syringe into the needle port.
3. Introduction of dirt particles or needle seal shavings into the needle port, which prevent the needle tip from touching the stator face.

Even when cross-contamination is not a concern, it is good practice to flush the needle port every 10 or 20 injections. This keeps liquid in the needle port tube, which bathes the syringe needle and dilutes any sample that contaminates this region during movement of the syringe into or out of the port. It also keeps the needle port and vent tube filled with solvent, preventing air from inadvertently entering the sample loop. If none of the obvious causes can be determined and the usual flushing with large amounts of solvent from a special syringe with a short blunt tip does not clean the liner and needle port, then complete disassembly and cleaning or rotor replacement may be needed. Stubborn stains or deposits on the metal or ceramic face plate (stator) of the injector can often be removed by gently wiping with a cotton swab and small amount of toothpaste.

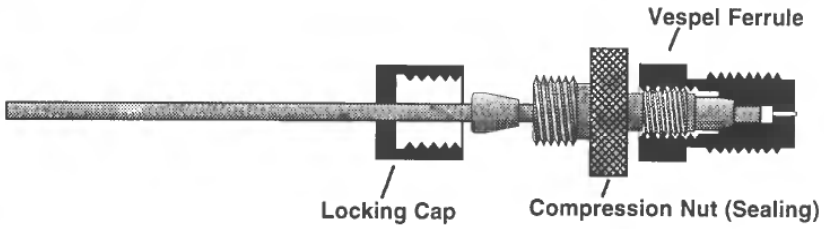
E. Preventative Maintenance

Although it is important to develop skill and experience in each of the foregoing problem categories, there is no substitute for prevention. Some ideas for prevention measures include the following:

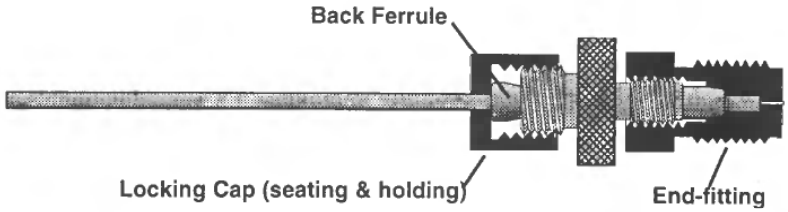
(1) Loosen both knurled nuts.



(2) Seat the Vespel® ferrule by turning the larger, front compression nut using firm finger action.



(3) Tighten the smaller, back locking cap until it meets the factory-set stationary back ferrule. Since the front ferrule seals, the locking cap requires only modest finger pressure to seat the tube.



The SLIPFREE connector comes standard with a replaceable Vespel® ferrule. PEEK and Kel-F® are optional for applications in which Vespel is not suitable, such as with strong acids or bases.

Figure 15 Fitting designed to facilitate installation and avoid gaps between tubing and valve or fitting seat (SLIPFREE Fitting). (Courtesy of Keystone Scientific, Inc.)

1. Flush the needle port where sample is introduced at the beginning and end of each day.
2. Flush all buffers and additives from the valve and LC system when downtime is expected. Solid crystals resulting from evaporation can harm the rotor. If mobile-phase additives are inadvertently left in the LC system, flush all valve ports and tubing thoroughly before high-pressure operation to dissolve and remove any residue from evaporation. This is easily accomplished by replacing the LC column with an empty length of tubing (sometimes called a dummy column).
3. Check all fittings that are made up with steel nuts and ferrules to be certain they are seated exactly and are square and clean. Check all fittings with adjustable ferrules at the beginning or end of each day.
4. On a regular basis, test a simple mixture with a known good column for peak efficiency and symmetry. If more than one instrument is in service, test and compare each one with the same reference sample and column under identical isocratic conditions to become familiar with their characteristics when functioning properly.
5. On a regular basis, schedule each injector and autosampler for routine cleaning and maintenance. If possible, this should be planned at least annually. The availability of a spare device that can be rotated into service eliminates downtime and acts as a substitute in an emergency. Because it can be scheduled, only one or two individuals with the best skill

and experience should be used for routine maintenance to keep systems in identical, proper-working order.

Even though there are many excellent HPLC texts with helpful sections on hardware design, one of the best sources of current information will always be the valve manufacturers and the instrument companies who employ the valves in their HPLC systems.

ACKNOWLEDGMENT

The valuable assistance of Virginia A. McKay, Keystone Scientific, Inc., Matthew V. Piserchio, Restek Corporation, and Stephen R. Bakalyar, Rheodyne, L.P. is acknowledged and greatly appreciated.

REFERENCES

1. A Schmid. Chromatographia 12:825–831, 1979.
2. MC Harvey, SD Stearns. HPLC sample injection and column switching. In: JF Lawrence, ed. Liquid Chromatography in Environmental Analysis. Humana Press, 1983.
3. MC Harvey, SD Stearns. J Chromatogr Sci 21:473, 1983.
4. SR Bakalyar, B Spruce. Achieving accuracy and precision with rheodyne injectors. Technical Notes 5 December, 1983.
5. MC Harvey, SD Stearns. Anal Chem 56:837–839, 1984.
6. NHC Cooke, K Olsen, BG Archer. LC Mag 2 (7): July/Aug, 1984.
7. SR Bakalyar, B Spruce. How to use column selection valves for HPLC. Technical Notes 8: Feb, 1987.
8. SR Bakalyar, K Olsen, B Spruce, and BG Bragg. How to make tube connections between injectors, columns, and detectors in liquid chromatography. Technical Notes 9: Aug 1988.
9. LR Snyder, JJ Kirkland, JL Glajach. Practical HPLC Method Development, 2nd ed. New York: Wiley-Interscience, 1997.
10. MC Harvey, SD Stearns. J Chromatogr Sci 20:487, 1982.
11. SR Bakalyar, C Phipps, B Spruce, K Olsen. J Chromatogr A 762:167–185, 1997.
12. SR Bakalyar, B Spruce. Troubleshooting Guide For HPLC Injection Problems, 3rd ed. Rheodyne, L.P., 1993.
13. M Kaminski, J Reusch. J Chromatogr 356:47, 1986.

17

Tandem Liquid Chromatography Systems

Raymond P. W. Scott

Birkbeck College, University of London, London, England, and
Georgetown University, Washington, D.C.

I. INTRODUCTION

The need to employ ancillary techniques, to confirm the identity of peaks eluted from a column, was recognized early in the development of chromatography. It was soon found, however, that the process of collecting and transferring a sample of the column eluent, containing a solute peak to an appropriate spectrometer, was tedious, clumsy, and often very inefficient. As a result, the concept of connecting the chromatograph directly to an appropriate spectrometer, to eliminate the tedious manual solute transfer, was developed. Various interfacing techniques have been explored for directly coupling the liquid chromatograph with a spectrometer. Today, the mass spectrometer, infrared (IR) spectrometer, the nuclear magnetic resonance (NMR) spectrometer, and the atomic emission (AE) spectrometer, all have been combined with the liquid chromatograph (LC) with varying degrees of success. It would appear that the mass spectrometer (MS) has emerged as the most useful ancillary technique to LC for structure elucidation and solute identification. Consequently, in this limited treatment of tandem systems the LC–MS combination of instruments will receive greater emphasis.

The first LC–MS tandem instrument was described by Baldwin and McLafferty as early as 1973 [1]. The authors connected the outlet of an LC column directly to the mass spectrometer employing a split inlet, and demonstrated the feasibility of the system. The major problem encountered, when associating a liquid chromatograph with a mass spectrometer, is the relatively high volume of vapor that is generated by the evaporation of the mobile phase and, consequently, the need for high-capacity pumps in the source of the mass spectrometer. Nevertheless, the problems associated with coupling the liquid chromatograph to the mass spectrometer have largely been overcome by the use of low-dispersion conduits, unique interfaces, and a range of different ionization techniques.

In any LC tandem system, the interface must incorporate some form of conduit, usually a small-diameter tube. It has been shown (2), that unless the tube is kept as short as possible, and the minimum internal diameter is employed (but not so small as to render the conduit liable to blockage) serious peak dispersion can occur, and the separation achieved in the column destroyed in the interface. Unfortunately, it is sometimes difficult to arrange the combination such that these specifications are met, and under such circumstances, low-dispersion tubing can sometimes be used.

II. LOW-DISPERSION CONNECTING TUBES

Dispersion in open tubes results from the parabolic velocity profile that occurs across the tube under conditions of Newtonian flow, and results in the mobile phase, close to the wall, moving very slowly, and that at the center, to move at the maximum velocity. This effect causes significant band dispersion. To reduce this dispersion, the parabolic velocity profile of the fluid must be disrupted to allow rapid radial mixing. The velocity profile can be ruptured and secondary flow can be introduced by deforming the regular geometry of the tube. The dispersion in geometrically distorted tubes (squeezed, twisted, and coiled) has been extensively studied by Halasz [3–5], and the effect of radial convection (secondary flow) on the dispersion introduced into tightly coiled tubes has been examined, both theoretically and experimentally, by Tijssen [6]. The effect of secondary flow produced by employing serpentine-shaped tubes has also been examined by Katz and Scott [7]. The dispersion characteristics of serpentine tubing, were far superior to those of coiled tubes. Furthermore, the dispersion that takes place in serpentine tubing, is practically independent of the mobile-phase linear velocity; consequently such tubes can be used over a wide range of flow rates. Katz and Scott first examined the effect of secondary flow on band dispersion that took place in tubes of different radii, coiled to different diameters. They applied the theory of Tijssen [6] to qualitatively describe the relation between the variance per unit length of the serpentine tube H and the mobile-ogase velocity.

The equations that Tijssen derived for radial dispersion in a coiled tube are given, as follows in terms of conventional chromatographic terminology. At relatively low linear velocities (but not low relative to the optimum velocity for the tube) Tijssen derived the equation,

$$H = \frac{jr^2 u}{D_m} \tag{1}$$

where:

u is the linear velocity of the fluid.
r is the radius of the tube.
D_m is the diffusivity of the solute in the mobile phase.
j is a constant over a given velocity range.

It is seen that the band variance is directly proportional to the square of the tube radius. At high linear velocities, Tijssen deduced that

$$H = \frac{bD_m^{0.14}}{\phi u} \tag{2}$$

where b is a constant for a given mobile phase, and ϕ is the ratio of the tube radius to the coil radius ($\phi = r_{tube}/r_{coil}$), and was given the term the *coil aspect ratio.*

It can be seen from Eq. (2) that, at high linear velocities, the value of H depends directly on D_m taken to the power of 0.14, and is inversely dependent on the coil aspect ratio and the linear velocity. According to Eqs. (1) and (2), at low velocities the band dispersion *increases* with u, whereas at high velocities, the band dispersion *decreases* with u. It follows that a plot of H against u should exhibit a maximum at a certain value of H. By combining Eqs. (1) and (2), an equation can be obtained, that predicts the value of u at which H is a maximum, and is given by

$$u = \frac{c}{r\sqrt{\phi}} \tag{3}$$

where c is a constant for a given solute and given mobile phase.

Table 1 Physical Dimensions of Coiled Tubes Examined

Tube	r (cm)	L (cm)	R (coil; cm)	ϕ	L (coil; cm)
1	0.019	365.8	0.5	0.038	18.5
2	0.020	365.0	0.085	0.235	65.8
3	0.0127	998.0	0.0765	0.166	128.0
4	0.0127	337.5	0.0498	0.255	73.7

The foregoing equations were employed to explain the effect of tube radius and coil aspect ratio on the onset of radial mixing in coiled tubes. The dimensions of the coiled tubes examined are given in Table 1, and the curves relating H and u in Figure 1.

It can be seen that at low linear velocities, at which radial mixing is still poor, H increases as u increases. Furthermore, the dispersion in coiled tubes 1 and 2 of larger radii is greater than that in tubes 3 and 4, which have smaller radii. At high linear velocities, at which radial mixing commences, H decreases as u increases. As the range of linear velocities is approached at which radial mixing dominates, the solute dispersion becomes independent of the linear velocity u. It is also seen that the maximum value of H for the four coils, occurs at different values of u, depending on the relative values of r and ϕ. In general, it would seem that a high coil aspect ratio reduces both the maximum value of H and the value of u at which it occurs.

A. Serpentine Tubes

The low-dispersion serpentine tube, developed by Katz et al. [7] was an alternative approach to the coiled tube and was designed to increase secondary flow by actually *reversing* the direction of flow at each serpentine bend. A diagram of a serpentine tube is shown in Figure 2. In practice, the serpentine tube is encased in an outer sheath to protect the tube and provide some rigidity.

A graph relating the variance per unit length of the tube to flow rate is shown in Figure 3 for a serpentine tube having the dimensions given in Figure 2. The flow rate is employed as the independent variable, an alternative to the more usual linear velocity, because the flow rate is defined by the column with which the low-dipersion tubing is to be used. A curve is

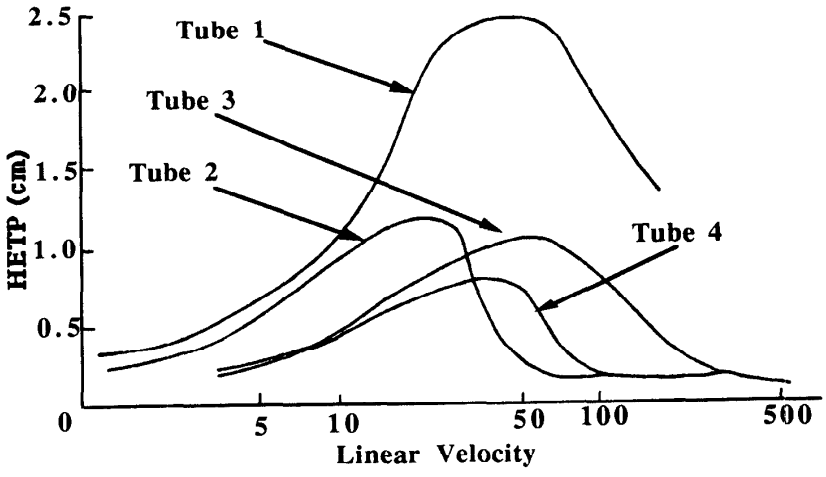


Figure 1 Curves relating H against u for different coiled tubes.

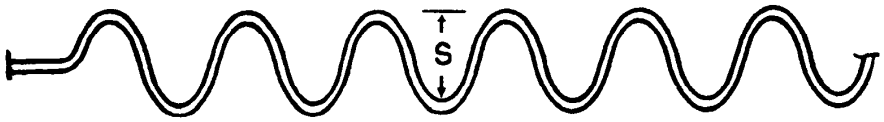


Figure 2 The low dispersion serpentine tube. Dimensions r_i, internal, 0.0127-cm (0.010-in) id; r_e; external, 0.025 cm (0.020 in) od linear length of tube 42.5 cm; linear length of coil 38.5 cm; S, serpentine amplitude 0.05 cm.

obtained for the serpentine tube similar to that for the coiled tube, but the maximum value of *H* is reached at a flow rate much lower than that with the coiled tube. Furthermore, the variance remains more or less constant over a wide range of flow rates that encompass those usually employed in normal LC separations.

It is interesting to compare the dispersion characteristics of a straight tube with that of a serpentine tube. The variances of a straight tube and serpentine tube are plotted against flow rate in Figure 4. The values of the variance for the straight tube were theoretical and were calculated from the Golay equation. The dispersion from the serpentine tube is drastically reduced in comparison with that from the straight tube. According to the graph, the numerical value of the peak variance per unit length for the serpentine tube (0.010-in. id) is 0.05 μL^2 cm^{-1} and, consequently, a tube 10 cm long would contribute a variance of 0.5 μL^2. In contrast, the dispersion of a straight tube having the same internal diameter, and only 1 cm in linear length, would be 5.5 μL^2, which is an order of magnitude larger.

Low-dispersion connecting tubes are still not in common use in LC equipment today, although at least one manufacturer provides serpentine tubing as a standard column and detector connection in a combined sample valve–column–detector instrument. Low-dispersion tubing has another feature that, in fact, could be anticipated from its principle of operation. The secondary flow that results from its serpentine form also greatly improves its thermal transfer properties; thus, serpentine tubes can be used as highly efficient heat exchangers. In fact, another instrument manufacturer uses serpentine tubing as a heat exchanger between a thermostating medium and the inlet tube carrying mobile phase to the column. Only a few centimeters of serpentine tubing were necessary to achieve complete thermal equilibrium between the thermostating medium and the mobile phase. Another interesting property of the

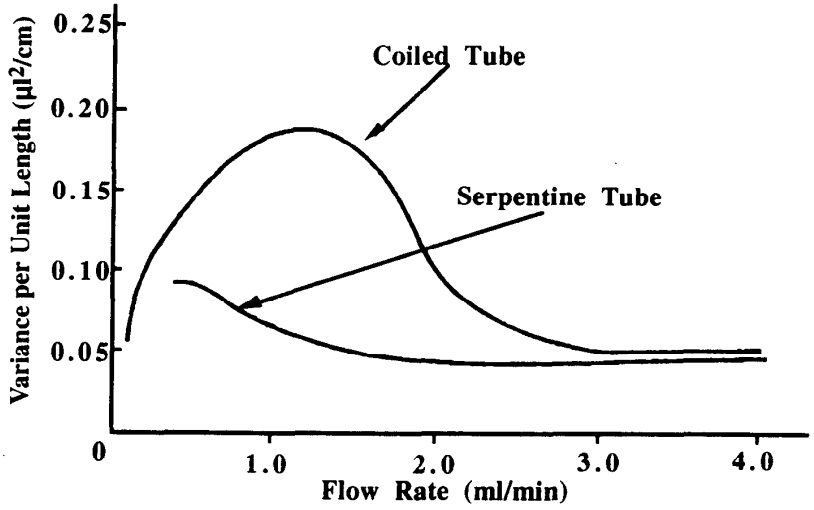


Figure 3 Graphs of peak variance against flow rate for coiled and serpentine tubes.

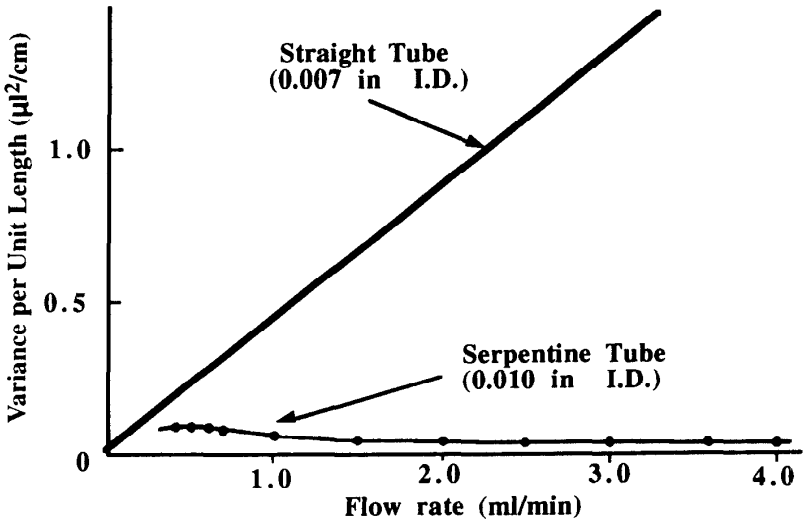


Figure 4 Graphs of peak variance against flow rate for a straight and serpentine tube.

serpentine tube is its excellent mixing capabilities. As a consequence, serpentine tubes could be used very effectively as postcolumn reactors. Not only would there be very little peak dispersion in the reactor, but the reagents would be exceedingly well mixed and provide ideal conditions for reaction to proceed rapidly to completion. It will be seen later, that serpentine tubing has been successfully used in an LC–flame AAS tandem system.

III. LIQUID CHROMATOGRAPHY–MASS SPECTROMETRY SYSTEMS

Solutes separated by LC are often very polar, or have very high molecular weights; thus, they have very low volatility. As a result, quite different ionization techniques are frequently required than those employed in GC–MS. The most common ionization analyzers are *electron impact ionization* and *chemical ionization.* Electron impact ionization results from the collision of electrons of appropriate energy with the sample molecules in vapor form and requires relatively low source pressures. In contrast, chemical ionization takes place at relatively higher pressures than electron impact ionization (about 1 torr) and results from the collision of the sample molecules with the reagent ions. The reagent ions are themselves produced by electron impact ionization and so chemical ionization is often a two-stage process. Chemical ionization produces sample ions close in molecular weight to that of the uncharged molecule (often M + H, M + CH_3, or similar, if methane is being used as the reagent gas) and usually very few smaller fragments. Because chemical ionization can take place at significantly higher pressures than electron impact ionization, it is a convenient ionization process to use with GC tandem systems, because the demands made on the pumping system to remove the carrier gas or mobile-phase vapor are not so stringent. However, although electron impact and chemical ionization are often used in LC–MS systems, the ionization of solutes eluted from LC columns can, in general, be very difficult. In 1976 Benninghoven et al. [8], demonstrated that high-energy primary ions, at low-current densities, could be used to produce intact molecular ions from organic compounds adsorbed on surfaces, and this procedure was given the term *secondary ion mass spectrometry* (SIMS). A similar technique, *fast-atom bombardment* (FAB), uses a neutral primary atom beam aimed at a liquid sample matrix containing the solute of interest to produce ionization [9,10]. *Laser desorption ionization* (LDI) [11], another ionization method, was improved by Kistemaker [12], who demonstrated that submicrosecond laser pulses could be used to generate pseudomolecular ions from solid surfaces. Unfortunately,

however, these ionization techniques require a fairly complicated interface for their successful use and their employment in LC–MS is confined to relatively high molecular weight solutes.

There are various types of mass spectrometers that can be employed in tandem with the liquid chromatograph. The two most commonly used mass spectrometers are the single- and triple-quadrupole mass spectrometer, and the time-of-flight mass spectrometer. Neither of these instruments can be classed as high-resolution instruments, but the triple-quadrupole spectrometer can be used to provide mass spectra of selected ions (LC–MS–MS), which can be almost as powerful for structure elucidation as the high resolution mass spectrometer.

In LC–MS systems, the mobile phase must be eliminated, either before entering, or from inside the mass spectrometer, so that the production of ions is not unfavorably affected. The volatilization of all the mobile phase from an LC column generates a considerable volume of solvent vapor. The problem can be reduced by using a splitting system, a small portion of the column eluent is allowed to pass directly into the mass spectrometer, together with the eluting solutes. As a result, the solvent ions produce chemical ionization spectra of the eluates. The difficulties involved in coping with the eluting solvent have evoked several different types of LC–MS interfaces. One approach has been to take the eluate, remove the solvent, and transport the residue to the mass spectrometer for examination. This approach is only rarely used today, and will be only briefly mentioned.

A. Transport Interfaces

In 1974 Scott et al. [13], developed a transport system for transferring the solute from the LC column to the mass spectrometer. This interface allowed electron impact spectra to be obtained and so all the expected ion fragments were present to facilitate interpretation of the spectra. The basic principle is similar to that of the moving wire LC transport detector. The eluent from the column passes over a moving stainless steel wire, coating it with a film of column eluate. The wire then passes through two jeweled orifices that separate two differential pumping chambers. A current of a few milliamperes is passed continuously through the wire, which becomes hot only when it enters the high vacuum of the ion source, where it can no longer lose heat to its surrounding. The temperature of the wire rises rapidly to about 250°C in the ion source, vaporizing the sample directly into the electron beam. The total ion current chromatogram of a sample of the mother liquor from the crystallization of vitamin A acetate, using the wire transport interface, is shown in Figure 5. The total ion current is taken as proportional to the sum of all the mass peaks in a specific spectrum.

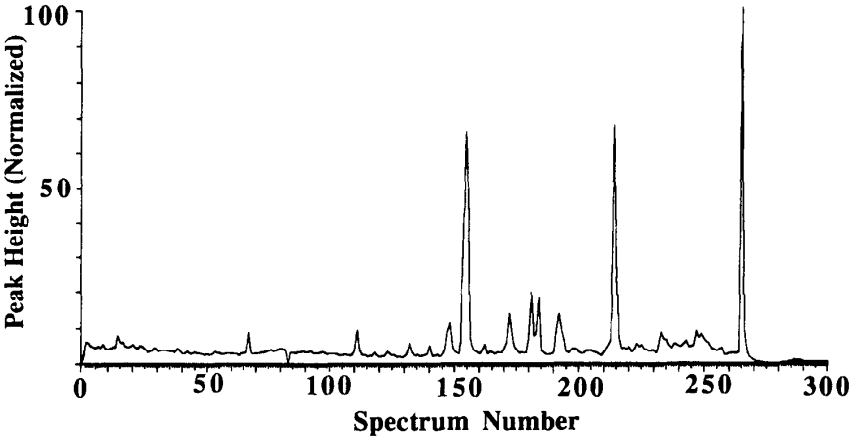


Figure 5 The total ion current chromatogram of a sample of mother liquor from a vitamin A acetate crystallization.

The wire transport interface was later modified by McFadden et al. [14], the wire being replaced by a continuous belt, made from a high-temperature plastic, which could be thermally cleaned after passing through the ion source, and before reentering the coating device. The belt was actuated by a motor-driven pulley. A diagram of the McFadden interface is shown in Figure 6.

The column eluate was taken up on the high-temperature plastic ribbon (about 3.2 mm wide and 0.05 mm thick) and transported through the vacuum locks by the moving belt. On the way to the vacuum locks, the coating was heated by an infrared heater, to facilitate the evaporation of the solvent. The remaining solvent was removed in the vacuum locks, and about 10^{-7} g s^{-1} enters the mass spectrometer. The first pump removes air at a rate of 500 L min^{-1}, and the second at about 300 L min^{-1}. The pressure in the first vacuum lock is maintained at about 1–20 torr, and that in the second, at about 0.1–0.5 torr. As a consequence, the mass spectrometer source can be easily operated at about 10^{-6} torr. Flash vaporization of the solute occurs by radiant heating in a small chamber that butts directly onto the solid probe entrance to the ionization chamber, and the solute vapor passes through a small hole directly into the ion source.

The flash heater is either a Nichrom coil or a quartz heater tube. The slots in the vacuum locks are made of sapphire strips. An example of the use of the belt interface to monitor the separation of a pesticide mixture is shown in Figure 7. It is seen that there is little loss of resolution in the interface, and very little cross-contamination occurs between the peaks, owing to incomplete removal of each solute from the belt before the next coating. The sensitivity of the system to carbaryl was claimed to be about 1 ng, but the actual sensitivity in grams per milliliter was not possible to calculate from the data available.

B. The Thermospray Interface

The thermospray interface is a development from the direct inlet system of McLafferty. The successful use of the thermospray interface, a diagram of which is shown in Figure 8, was first reported by Covey and Henion [15]. The device consisted of a central stainless steel tube, (0.004-in id), that passes through a heated copper block containing a cartridge heater. In the

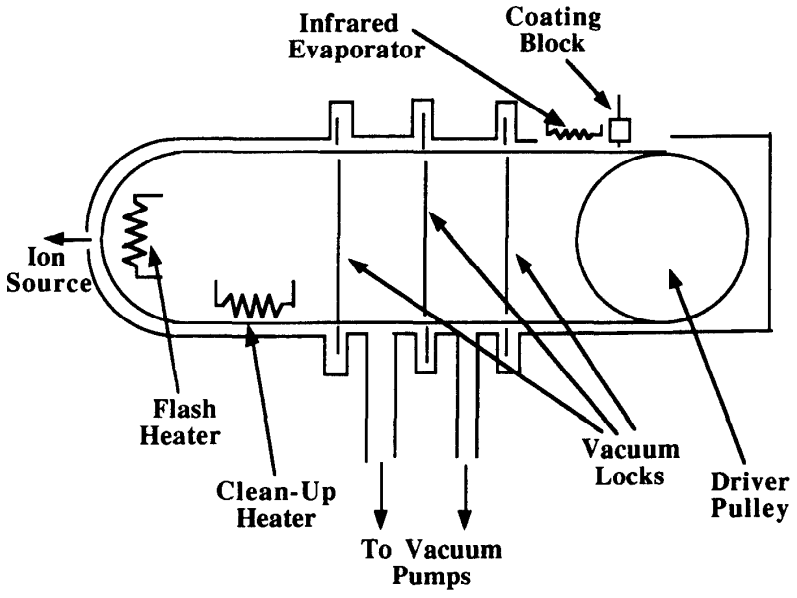


Figure 6 The belt LC–MS interface.

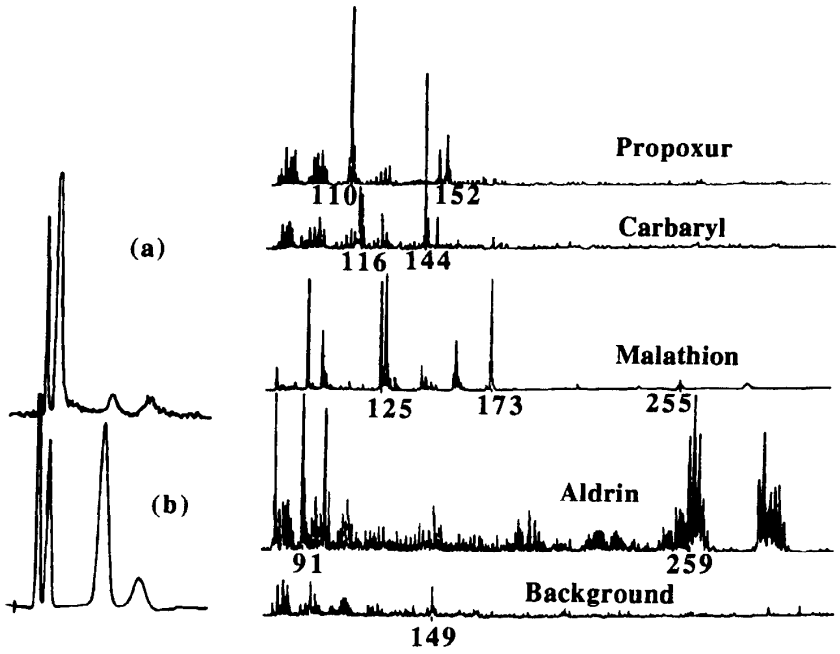


Figure 7 The separation of some pesticides using the belt interface: (a) separation monitored by total ion current; (b) separation monitored by UV detector.

block was embedded a thermocouple that monitored the temperature and provided an output to actuate the temperature controller. At the end of the tube was a pinhole through which the heated solute was vaporized. The use of the thermospray system was further developed by Voyksner et al. [16]. They noted that the LC–MS thermal spray system frequently produced molecular weight information (parent ions), and exhibited lower detection limits, than the other forms of LC–MS interfaces. When they used a thermal spray system with a 0.1-M ammonia acetate buffer and a mobile phase that contained a high proportion of water, high senstivities were achieved. The optimum interface temperature varied with solvent composition, and could be determined by maximizing the solvent buffer ion intensities.

The system produces protonation, ammonium addition, and proton-bound solvent molecular clusters. The ionization procedure with this system was reported to be very soft, resulting in very few molecular fragment ions being formed. The system was used very successfully

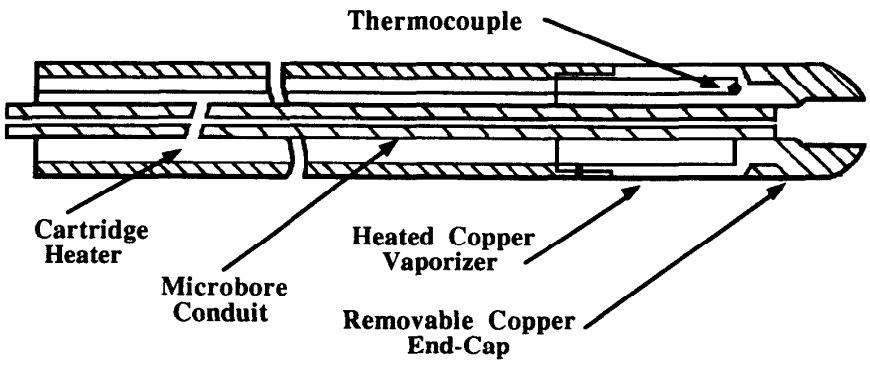


Figure 8 The thermospray LC–MS interface.

in the analysis of triazine herbicides and organophosphorus pesticides. Excellent specificity and sensitivity were achieved.

C. The Electrospray Interface

Another ion-producing inlet system that is now commonly used in LC–MS, is *electrospray ionization*, reported by Whitehouse et al. [17] The explanation given for the formation of ions is as follows. The column eluate, usually containing ions of some type, is sprayed into a dry gas such as nitrogen. This process produces a cloud of droplets that rapidly evaporate and, as a consequence, become smaller. The accompanying increase in charge density and the reduced radius of curvature of the droplets result in strong electric fields being formed that are sufficient to cause the droplets to explode, producing ions, many of which can contain multiple charges. A diagram of the Hewlett-Packard Electrospray Ionization LC–MS interface is shown in Figure 9. The column eluate is mixed with a nebulizing gas, and the spray jet is directed onto a disk target. In the center of the target is a pinhole entry into the interface, and the jet is directed to the side of this aperture. The fine droplets at the periphery of the spray are drawn through the pinhole aperture into a chamber that is held at a reduced pressure. Inside the chamber, the droplets are entrained in a stream of hot nitrogen gas that rapidly evaporates the solvent, producing ions in the manner described earlier. The core of the jet is skimmed by conical screens to remove the drying gas, and the ions then pass directly into the mass analyzer. Because ions with multiple charges can be produced, each charge being provided by an associated proton, in effect, this increases the mass range of the spectrometer.

For example, an ion with a of molecular weight 1000, carrying three charges, will appear on the spectrum at about a 'mass' (m/z value) of 333. The total ion current chromatogram of a sample from the tryptic digest of lysozyme, is shown in Figure 10. The total column eluate was passed into the interface, but as seen in the foregoing, because of the nature of the ionization process, only a portion of the solute actually enters the mass analyzer. The mass spectrometer employed was the Hewlett-Packard MS Engine Quadrupole Mass Spectrometer. The mass spectrum of the peak eluted at 30.35 min is shown in Figure 11. The figure shows three peaks at m/z values of 554.1, 876.0, and 1106.8. It is seen from Figure 11, that the peak was not completely resolved from its neighbors; thus, it was necessary to decide whether

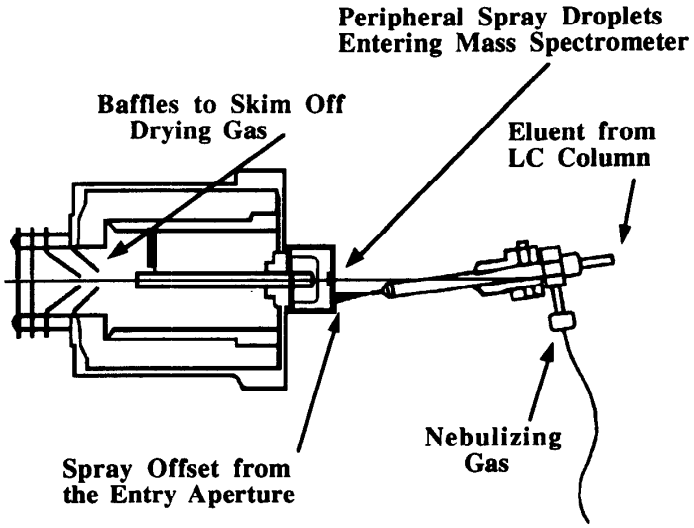


Figure 9 The Hewlett-Packard electrospray ionization LC–MS interface. (Courtesy of the Hewlett-Packard Company.)

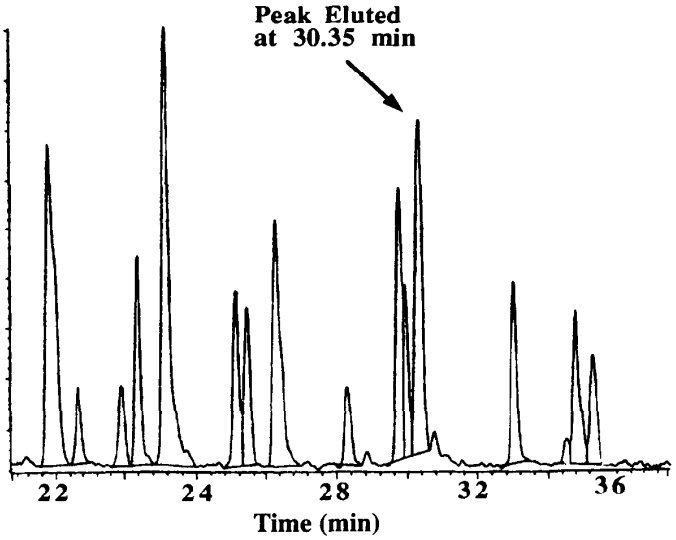


Figure 10 The total ion current chromatogram of a sample from the tryptic digest of lysozyme. (Courtesy of the Hewlett-Packard Company.)

all three peaks originated from the same solute, and whether any pair of the peaks resulted from multiple charges on the same molecule. A program is included in the Hewlett-Packard data-handling software that tests the interrelation between the individual mass peaks of the mass spectrum.

The software determines whether the m/z values of any pair or group of peaks are linearly related. If the respective m/z values of the peaks increase or decrease proportionally with one another, then they must originate from the same parent molecule and probably represent multiple charges on the same molecule. The peaks in Figure 11 were tested in this manner and the results are shown in Figure 12.

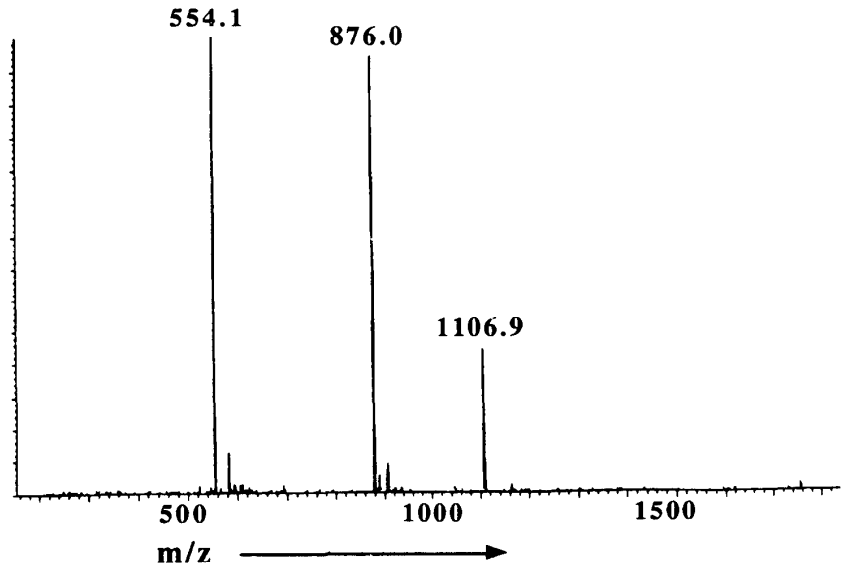


Figure 11 The mass spectrum of the peak eluted at 30.35 mins in the tryptic digest chromatogram of lysozyme. (Courtesy of the Hewlett-Packard Company.)

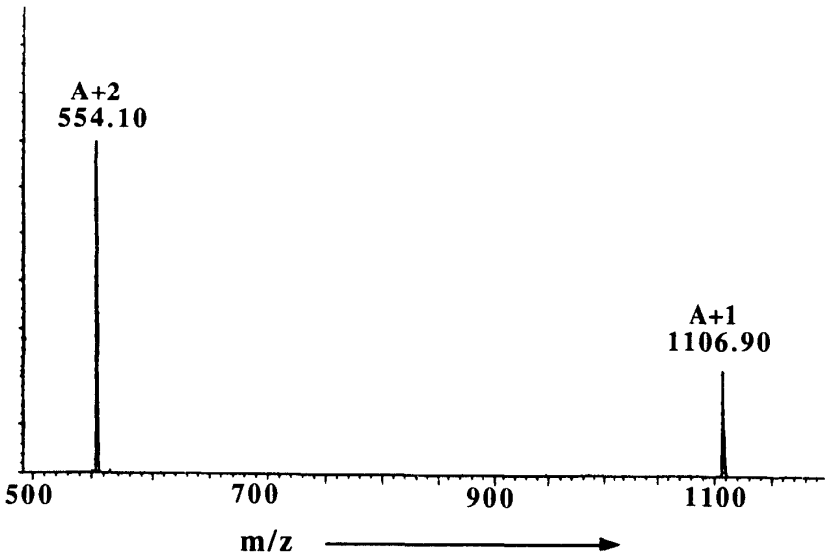


Figure 12 Mass spectrum showing multiple charged peaks of a parent molecule. (Courtesy of the Hewlett-Packard Company.)

The data-processing demonstrated that the peak at 876.0 m/z was not related to the other two and, furthermore, the peaks at 554.1 and 1106.9 were doubly and singly charged species of the same molecule. For example

$$\frac{1106.9 - 1(H^+)}{2} + 2(H^+) = 554.95 \text{ c.f. } 554.1 \text{ (from spectrum)} \quad (4)$$

A recent report [18] discusses the various LC–MS interfaces that have been employed in the analysis of carotenoids. Carotenoids, many of which are brightly colored, are primarily C_{40} polyisoprenoid compounds, with extensive double bonds. The carotenoids produce the red of tomatoes (lycopen), the yellow of sweet corn (lutein and zeaxanthin), and the orange of carrots, (α- and β-carotene). Carotenoids are also associated with bird plumage, and the pink color of flamingoes and salmon, is largely due to the carotenoid astaxanthin. They are also involved in the synthesis of vitamin A, an essential metabolite for vision, cellular differentiation, and embryological development. Carotenoids are the product of photosynthesis; hence, all carotenoids used by mammals must be obtained by the consumption of plants or other organisms. An example of the separation of raw carrot extract using the electrospray interface is shown in Figure 13.

The separation was carried out using reversed-phase chromatography; there was 20 ng of the isomers of each carotenoid present in the mixture. The chromatogram on the left was monitored using the single-ion m/z = 536, which was the doubly charged protonated molecular ion. This chromatogram is very similar to that produced by the absorbance detector operating at 450 nm. This would indicate that little or no chromatographic resolution was lost in the interface. The spectrum on the right is for β-carotene, and shows the peak for the doubly charged protonated molecular ion. The spectrum is very simple, contains little or no fragment ions, leaving the m/z peak for the β-carotene as the only peak of any significance in the spectrum.

D. The Atmospheric Ionization Interface

Another popular and efficient inlet system for the LC–MS combination is the *atmospheric pressure chemical ionization* process. This system has some similarity to the electrospray

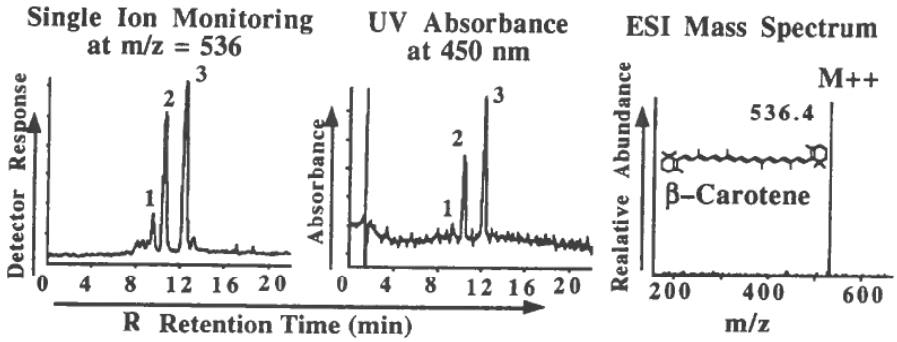


Figure 13 Electrospray ionization LC–MS analysis of raw carrot extract: 1, *cis*-isomers of α-carotene and β-carotene; 2, all-*trans*-isomers of α-carotene; 3, all-*trans*-isomers of β-carotene.

interface, and can also cope with flow rates of up to 2 mL min^{-1}, and thus the total column eluent can be used without splitting the flow. However, as with the electrospray interface, only a small portion of the eluent actually provides ions that enter the mass spectrometer. A diagram of the atmospheric pressure chemical ionization interface is shown in Figure 14. The sample is first vaporized in the heated center tube of two coaxial tubes, the outer tube carrying a nitrogen stream. The sample then drifts through a chamber containing a corona discharge, set up by a potential difference of about 2000 Volts, which is applied between a simple two-electrode arrangement. The reactant ions formed in the corona discharge, collide with the sample molecules, and give sample molecule plus proton ions (hydrogen-positive ions); i.e., $[M + H]^+$. This is a process very similar to chemical ionization. The ions so formed then pass through two differentially pumped chambers to reduce the pressure sufficiently to allow the ionized sample to enter the mass spectrometer. In the first chamber the ions are elctrically focused through two apertures, and the excess un-ionized material is skimmed off to waste.

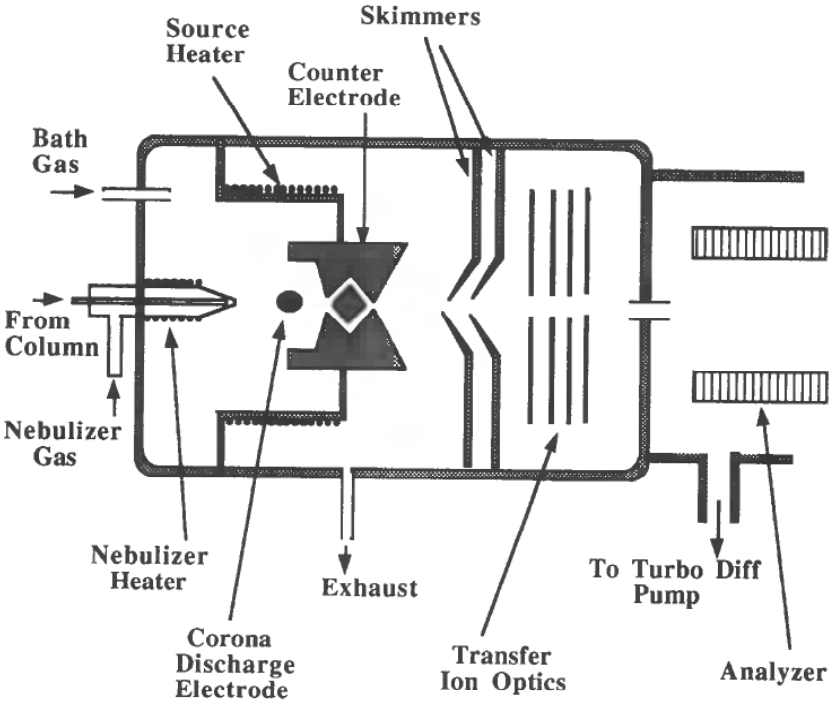


Figure 14 The atmospheric pressure chemical ionization interface.

In the second chamber, more gas is removed, the pressure is reduced further, and the ions are electrically focused onto the entrance aperture of a quadrupole mass spectrometer. The sample then enters the electron beam of the electron impact ionization source of the mass spectrometer, and fragmentation takes place. As the sample entering the mass spectrometer is virtually a parent ion already, the fragmentation pattern is very similar to that obtained in MS–MS. In this way, the system differs fundamentally from the electrospray interface. The ionization process is soft, very sensitive, and gives good characteristic spectra that can be used both for sample identification and structural elucidation.

An example of the use of the atmospheric ionization interface in the analysis of carotenoids, reported by Breeman [18], is shown in Figure 15. The separation was performed employing a reversed-phase column, and the whole of the column eluate (flow rate 300 μL min^{-1}) was passed through the interface. The chromatograms were obtained by single-ion monitoring (m/z = 537 for α- and β-caritone and 569 for lutein) and by UV absorbance at 450 nm. With use of the appropriate m/z value, each solute can be exclusively monitored, and the two isomers of the carotene are clearly separated. The mass spectrum of β-carotene exhibits little fragmentation and could be confidently used for solute identification.

A recent modification of the atmospheric pressure ionization technique, involving a special low dead volume interface, was described by Thomson et al. [19]. They employed packed microbore columns, 170 μm, 320-μm id, and 500-μm, with lengths ranging from 5 to 15 cm, in conjunction with a low-volume, wall-coated capillary column as the conduit. The total ion current chromatogram of the tryptic digest sample, from about 1 pmol of human growth hormone is shown in Figure 16.

The column was packed with an octadecyl-bonded phase, having a mean pore size of 300 A and a particle diameter of 7 μm. A gradient from 20% solvent A (0.1% TFA in water), to 80% solvent B (75% 0.1% TFA and 25% acetonitrile), was employed, over a period of about 1 h. Flow rates of about 80–100 μL min^{-1} were used, with about 3 μL passing to the capillary column and entering the interface. An excellent separation was obtained, and apparently little resolution was lost in the capillary conduit. The mass spectrum of the peak marked T2 in the chromatogram is shown in Figure 17. Good quality spectra can be obtained up to m/z values of nearly 900. Such a combination of techniques can be invaluable for the structure elucidation of compounds generated in biochemical research.

E. Laser Desorption Mass Spectrometry

The laser can be used for two purposes: first, to desorb the sample as vapor into the ionizing system; and second, to actually produce the sample ions. However, ions that are produced by pulsed lasers produce bursts of ions, and are obviously unsuitable for use with the scanning spectrometer. Intermittent ion production, however, is compatible with the time-of-flight mass spectrometer, which can record all the ions produced by each laser pulse. Another advantage

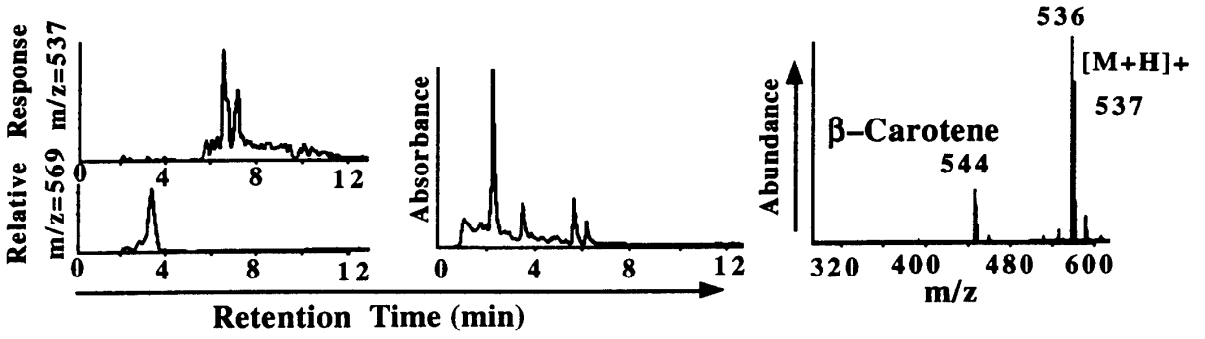


Figure 15 The analysis of a mixture of lutein and β-carotene by atmospheric ionization LC–MS.

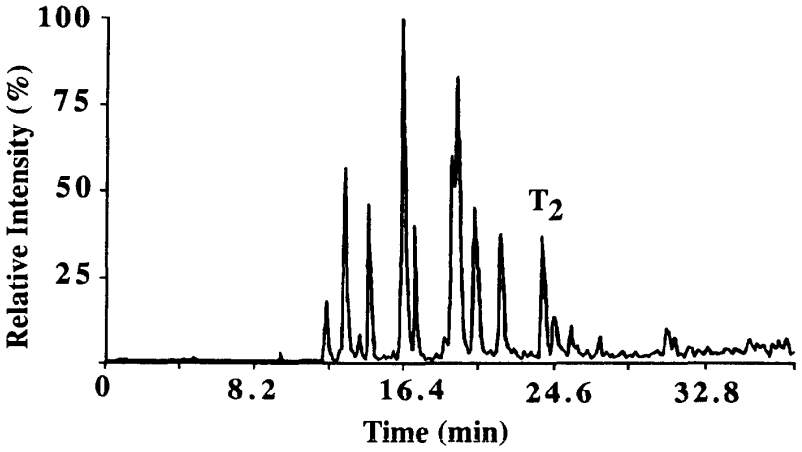


Figure 16 Total ion current chromatogram of a tryptic digest sample of human growth hormone. (Courtesy of the Perkin Elmer SCIEX Corporation.)

of this combination is the nearly unlimited mass range of this particular type of mass spectrometer. A diagram of the basic laser desorption–time-of-flight mass spectrometer association, employing probe sampling, is shown in Figure 18.

The description of the function of the time-of-flight mass spectrometer is not pertinent to this chapter, but a brief description of the procedure that is used is as follows. The sample is placed on a probe that received high-energy laser pulses from a carbon dioxide laser. The bursts of vaporized sample are propelled by an expanding argon stream from a 100-μm orifice, through a skimmer, into the accelerating section of the mass spectrometer. In this section, the molecules are again subjected to a high-energy laser light beam, this time from a dye laser, which produces ions by photoionization. The ions formed are immediately accelerated through the region into a drift section, where they are deflected by an ion reflector to an electron multiplier detector. It is seen that to desorb and ionize a sample from a liquid chromatograph, a fairly complicated transport system would again be necessary.

Such a transport system was described by Fan et al. [20] for use with the quadrupole mass spectrometer. They developed a belt interface system for LC–MS that could provide

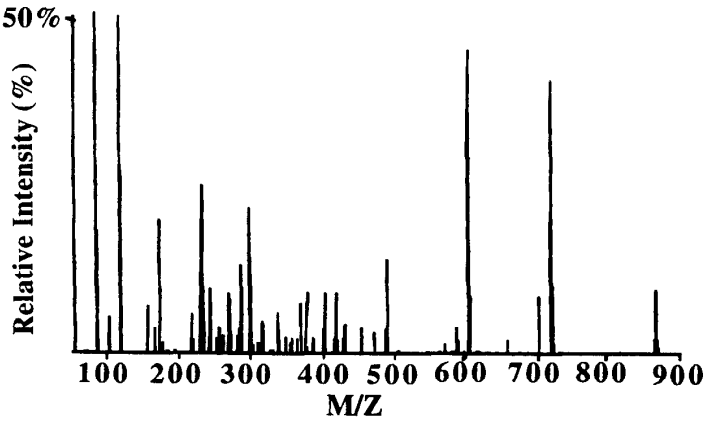


Figure 17 Spectrum of a product from the tryptic digest of human growth hormone obtained from a low dead volume atmospheric ionization interface. (Courtesy of the Perkin Elmer SCIEX Corporation.)

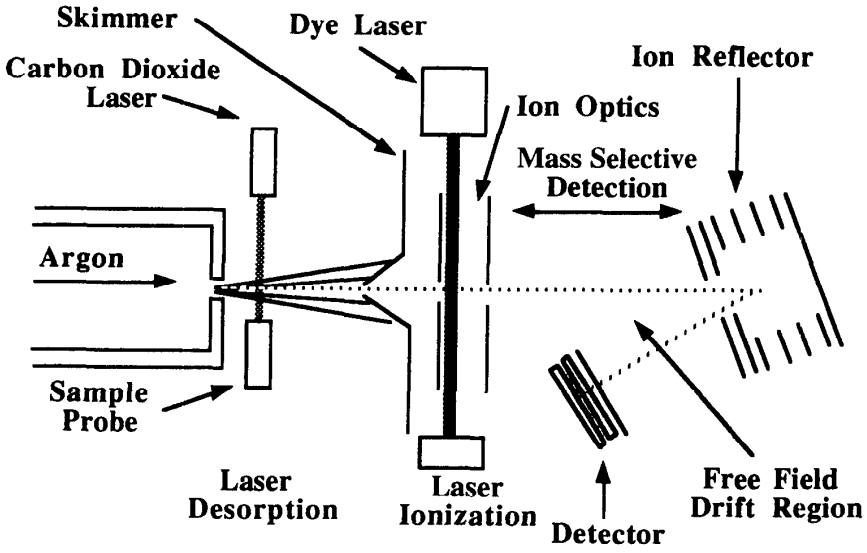


Figure 18 The laser desorption–mass spectrometer combination.

both secondary ion mass spectrometry and laser desorption mass spectrometry and, if required, matrix-assisted laser desorption mass spectrometry (MALDI–MS). Matrix-assisted laser desorption mass spectrometry involves the use of a substance, or substances, that are normally incorporated in the mobile phase. Consequently, the reagents are mixed with the solute when exposed to the laser beam. The materials assist in the expulsion of the solute molecules from the surface, and thus evoked the term matrix-assisted desorption. A diagram of the transport interface, and the dual ionization source, is shown in Figure 19.

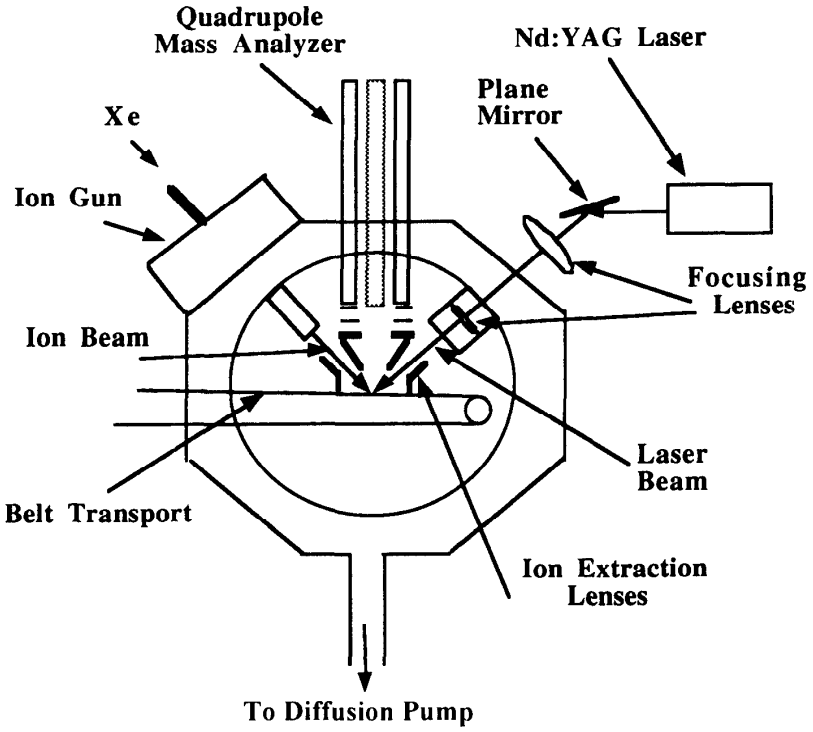


Figure 19 The dual ionization transport interface.

It consisted of a quadrupole mass spectrometer with a moving belt and a Finnigan/INCOS data system. Samples were deposited on the belt by a type of thermospray process. Both the ion beam and the laser light were aligned to strike the belt at 45° and normal to each other. Xenon gas, ionized by electron impact, was used as the source of primary ions, which are focused by an Einzel lens and steering plates, through an aperture, onto the belt, forming a spot covering an area of about 5 mm^2. The beam strikes the belt with an energy of about 3 keV. The laser light can be focused on the same spot by a suitable set of mirrors and lenses. Ultimately, as the transport medium, the authors employed a carbon steel belt that had a blackened surface and, consequently, absorbed more energy from the laser beam. When laser energies were kept reasonably low, there was no degradation of the surface.

When one compares the results from the two methods of ionization, laser desorption has the advantage that it provided more reliable molecular weight information. Furthermore, by varying the power of the laser, different degrees of fragmentation could be achieved; consequently, more structural information could be obtained. However, because it is difficult to control the laser energy absorbed, the mass spectra are less reproducible. In contrast, continuous ionization by primary ion bombardment provides more characteristic fragment peaks, without losing molecular weight information, and both the mass spectra and the chromatograms are less noisy and more reproducible.

IV. OTHER LC TANDEM SYSTEMS

The liquid chromatograph has, at one time or another, been combined with most other spectroscopic techniques, including flame atomic absorption spectroscopy (AAS), inductively coupled plasma atomic emission spectroscopy, infrared spectroscopy, and nuclear magnetic resonance spectroscopy. Initially, these tandem systems gave relatively poor results, hardly justifying the construction of the apparatus for their operation. However, over the last decade, great improvements in all four tandem combinations have taken place and, for specific problems, they can provide a real service to the analyst. Some examples of these tandem systems, together with a typical application, will be given to indicate the analytical possibilities of the combined techniques.

A. Liquid Chromatography–Atomic Absorption Spectroscopy Systems

The association of an atomic absorption spectrometer with the liquid chromatograph (LC–AAS) is usually employed to detect specific metal and semimetallic compounds at high sensitivity. The technique is frequently used to determine element speciation in biological materials and in environmental samples for toxicity assessment. In most studies, it is not sufficient, for example, to detect the mere presence of the elements lead, mercury, or chromium, but also one must be able to identify the form in which they are present. Depending on the chemical form of a mercury compound, it may, or may not, be highly toxic. Chromium, present in the tertiary form, is not particularly dangerous; however, in its sixth valency state, it is strongly carcinogenic. It follows, that the liquid chromatograph can be employed to separate the different species, and the atomic absorption spectrometer can identify and confirm the presence of a specific element eluted at a particular retention time.

Most LC–AAS combinations involve the use of a flame atomic absorption spectrometer or an atomic spectrometer fitted with a graphite furnace. Nevertheless, the combination of the liquid chromatograph with the inductively coupled plasma atomic emission spectrometer is also quite frequently used.

Katz and Scott [21], used a low-dispersion serpentine tubing as the conduit between the exit from the UV detector of the liquid chromatograph, and the spectrometer. A diagram of their interface is shown in Figure 20. The principal of low-dispersion tubing has already been

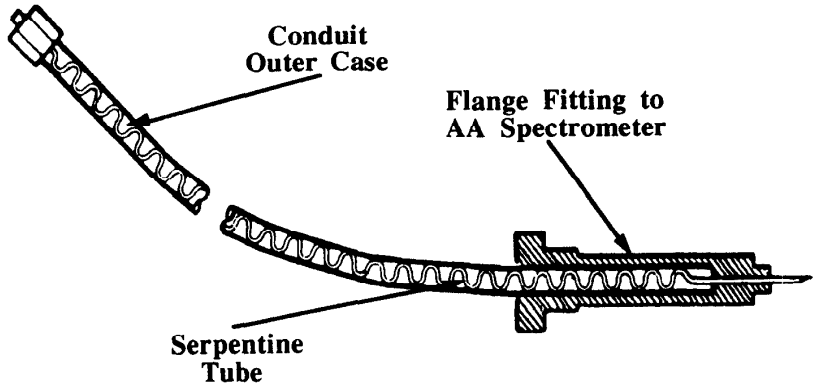


Figure 20 The LC–AAS serpentine tubing interface.

discussed, and it is sufficient to say that the outer interface tube was 49 cm long, 0.25-cm id, and merely protected the serpentine tube contained inside. The inner serpentine tube had a peak-to-peak amplitude of 1 mm.

An example of the chromatograms obtained from a blood sample, monitored by both a UV detector and the AAS spectrometer employing the serpentine interface, is shown in Figure 21. The AAS unambiguously picks out the peak containing iron, and the width of the iron peak clearly substantiates the efficacy of the serpentine interface.

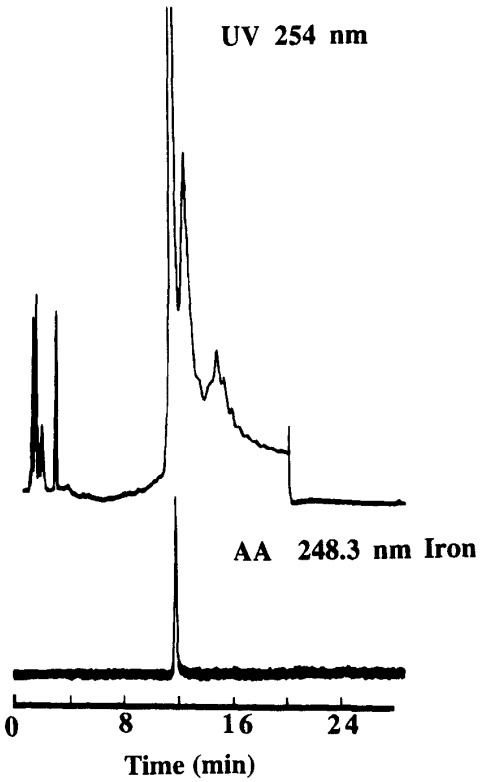


Figure 21 Chromatograms of a blood sample monitored by UV detector and atomic absorption spectrometer with the serpentine tube interface.

Another example of the LC–AAS tandem system is afforded by the work of Robinson and Boothe [22], who used the selectivity of the LC–AAS system to monitor the alkyl lead compounds in seawater. In addition, Messman and Rains [23] separated the four alkyl leads, tetramethyl lead (TML), trimethylethyl lead (TMEL), dimethyldiethy lead (DMDEL), methyltriethyl lead (MTEL) and tetraethyl lead (TEL) in gasoline. An example of their separation is shown in Figure 22. It is seen that excellent selectivity can be obtained, eliminating the need for high-resolving power columns because the multitude of interfering hydrocarbons present in gasoline are not detected.

Zhang et al. [24] developed a moving wheel transport interface that combined the liquid chromatograph with a helium microwave-induced plasma atomic emission spectrometer. The wheel' transport system was used in conjunction with an atmospheric pressure helium plasma interface, which was specifically designed for halogen-selective detection. The layout of their apparatus is shown in Figure 23.

The apparatus involved a standard LC pump, column, and nebulizer. The output from the nebulizer passed through the transport interface, which will be discussed separately, and then into the microwave-induced plasma torch, which was driven by an appropriate microwave generator. Light from the torch passed through an optical system to the spectrometer, and thence, to a photomultiplier and its associate electronics. The halides and oxyhalogenated materials were separated by ion-exchange chromatography, and the column eluent was directed as a mist onto a continuously moving wheel interface. The aqueous solvent was evaporated in a stream of hot nitrogen, leaving the solute as a solid residue on the surface of the wheel.

The moving wheel transporter (shown in detail in Fig. 24) then carried the dry sample

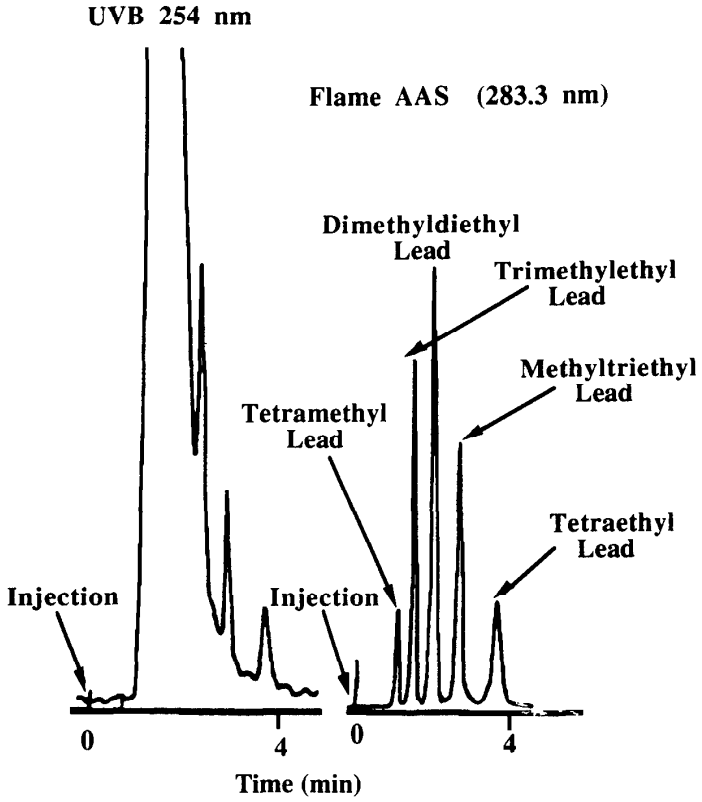


Figure 22 An example of a separation of lead compounds demonstrating the selectivity of the LC–AAS system.

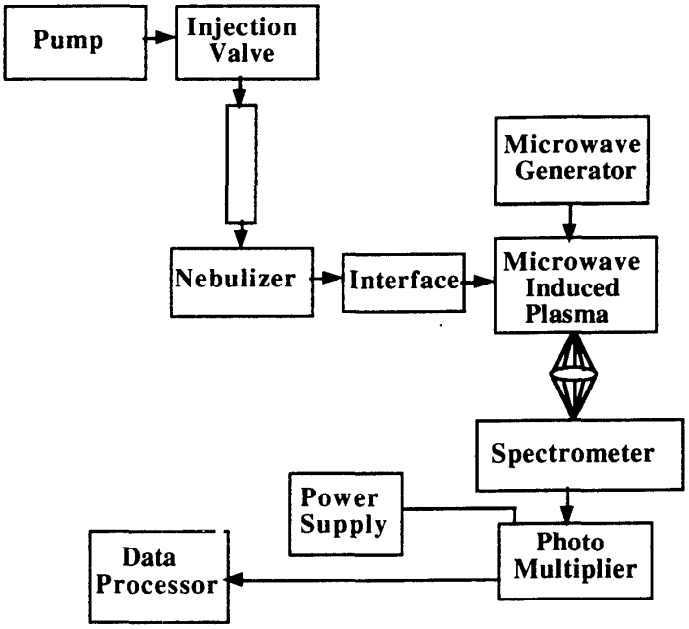


Figure 23 The moving wheel LC–helium microwave-induced plasma interface.

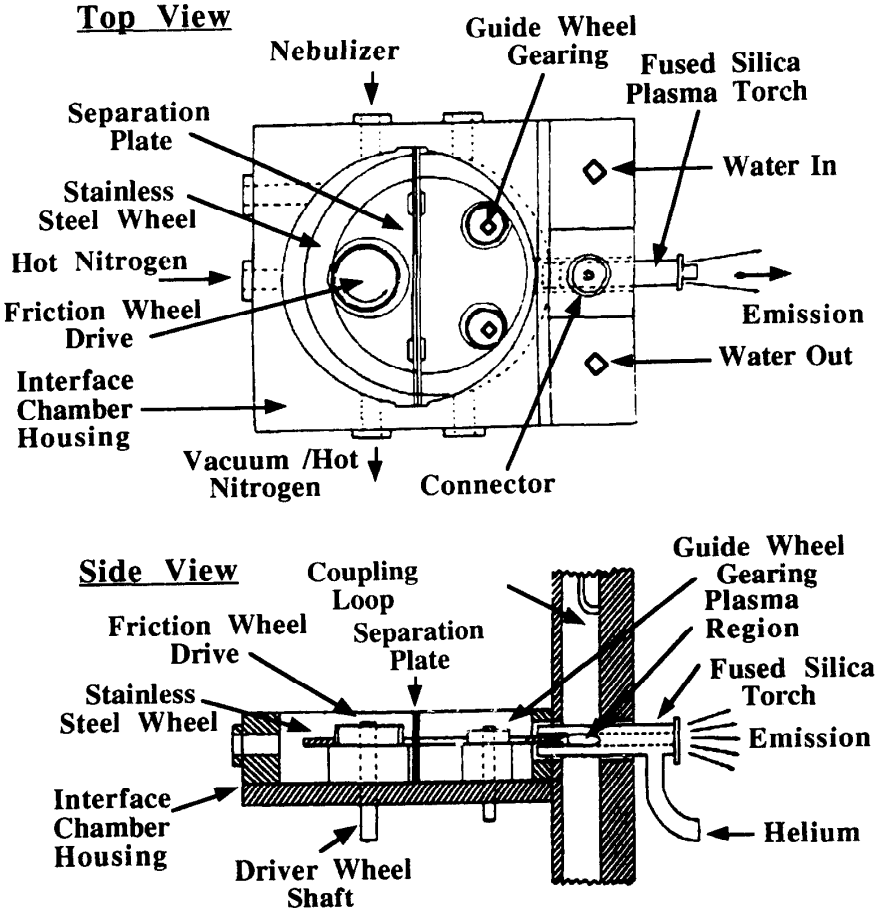


Figure 24 The wheel transport interface.

into the plasma, where it was volatilized, atomized, and excited. The plasma was a small-volume helium microwave-induced plasma, and was operated at 100 W, with a helium support gas flow of 3.1 L min^{-1}. The interface consisted of a stainless steel wheel 77.7-mm od, 62.9-mm id, and 1.5 mm thick. The wheel was friction-driven by a high-torque electric motor. The microwave resonant cavity was connected at right angles to the interface, in such a way that the edge of the wheel penetrated into the resonant cavity structure. The plasma was produced by a low-power microwave generator, and the torch was constructed from a fused silica tube, 7-mm od, and 2.5-mm id. Some examples of the results that were obtained from the transport interface are shown in Figure 25.

The chromatograms show the separation of a range of different halogen and oxyhalogen ions. The sensitivity ranged widely from 4 ng s^{-1} for sodium iodide, to 300 ng s^{-1} for sodium bromide. These limits of detection do not approach those of ion chromatography, but the system does offer selectivity, which would allow the halogen peaks of interest to be picked out from a complex group of coeluting ions containing different elements.

B. Liquid Chromatography–Infrared

The association of the IR spectrometer with the liquid chromatograph is more difficult than with the mass spectrometer because of the inherent IR absorption characteristics of the solvents normally employed in LC, and the relative insensitivity of the IR spectrometer. In fact, most useful solvents absorb light in the infrared range and, more importantly, those ranges are frequently the most informative in structure elucidation and sample identity confirmation. This means that, either the solvent needs to be removed before measurement, or an infrared-transparent solvent must be employed. Unfortunately, of the few solvents that are transparent to the IR over the wavelength range that is important, many are not compatible with the mobile-phase requirements of LCD. As a result of the introduction of the Fourier transform IR (FTIR) spectrometers, the problem of sensitivity was partly solved. Furthermore, because the spectra could be stored, the problem of solvent absorption was also partly solved. In

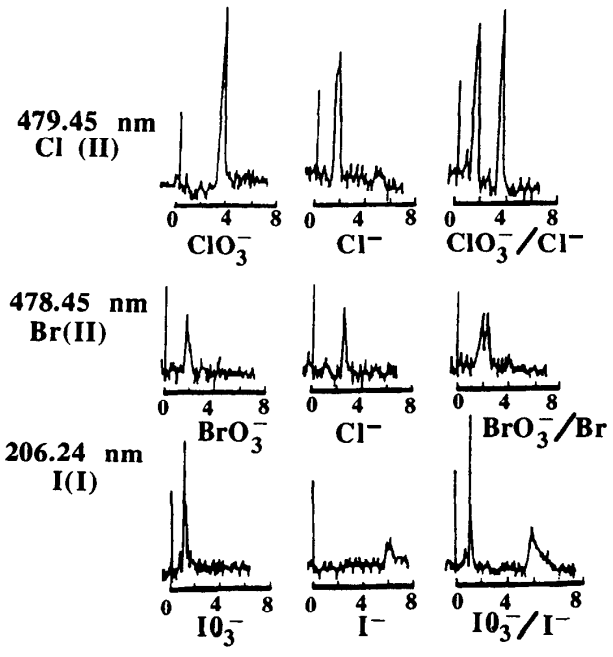


Figure 25 Chromatograms obtained using the moving wheel LC–helium microwave–induced plasma interface.

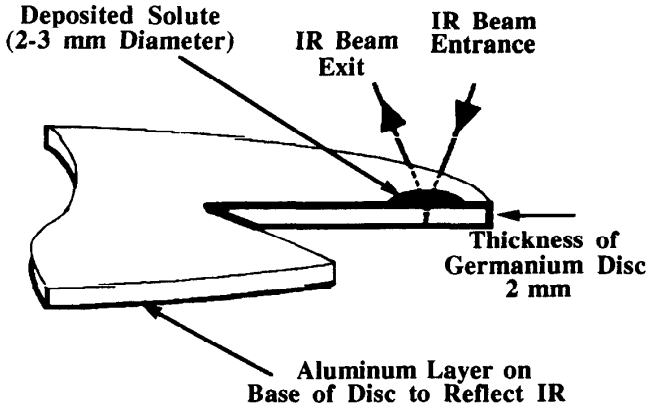


Figure 26 Section of the germanium disk transport system. (Courtesy of Lab Connections Inc.)

theory, the background spectrum of the solvent could be subtracted from the spectrum obtained for the solute, leaving the actual spectra of the solute as a difference value.

Unfortunately, this involves subtracting two very large signals, and thus the signal to noise of the difference spectrum is rather low. One of the more successful commercial LC–IR interfaces is that developed by Lab Connections Inc. The device is unique in the sense that it is a transport-type interface, but uses a germanium disk that is transparent to IR light, as the carrier. A section of the germanium disk is shown in Figure 26. The disk is about 2 mm thick, and the lower surface is coated with aluminum to reflect any IR light that passes through it. The total interface consists of two modules, the coating module and the optical module. Diagrams of the two modules are shown in Figure 27.

The LC column is connected to the chromatography module and eluent from the column passes into an ultrasonic nebulizer. The nebulizer sprays the solvent, in a tightly focused jet, onto the surface of a monocrystalline germanium sample-collection disk. The temperatures of

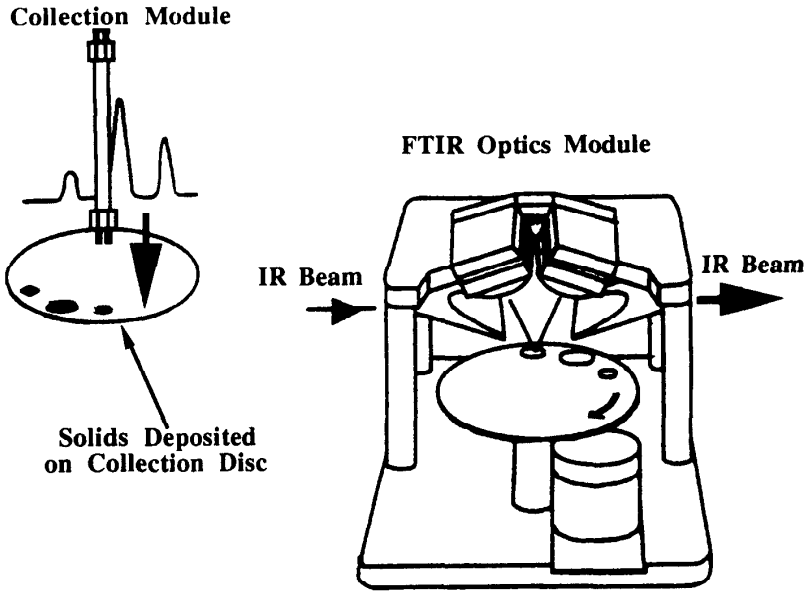


Figure 27 The coating and optical modules of the interface. (Courtesy of Lab Connections Inc.)

both the ultrasonic nebulizer and the collection disk are carefully controlled. The disk rests on a heated stage in an evacuated compartment that rotates slowly during the elution of the sample. All the solvents evaporate, leaving a deposit of solvent-free solutes on the disk surface. After the separation is complete, the disk is removed and placed on the stage of the optical module, which is located the sample compartment of the FTIR bench. The compartment is purged with carbon dioxide-free air. The stage rotates and the incoming IR beam passes though the sample, through the disk, and is reflected back though the sample by the layer of aluminum on the underside of the disk and back to the spectrometer. This procedure produces a two-pass transmission spectrum of the sample. The FTIR spectra obtained from a calibration sample of benzyl benzoate and testosterone cypionate are shown in Figure 28.

It is claimed that satisfactory spectra can be obtained for identification purposes from 100 ng of sample. This level of sensitivity is quite satisfactory and represents an advance in the technique for drug process control. However, it might not be so suitable for biological samples, such as blood and urine.

C. Liquid Chromatography–Nuclear Magnetic Resonance Systems

There are several difficulties in the association of the liquid chromatograph with the NMR spectrometer. The four main problems that must be solved were outlined, many years ago, by Bayer et al. [25]. First, the intensity of the NMR signal depends on the flow rate and, as the flow rate increases, the signal decreases. Second, to realize high NMR resolution, the magnetic field throughout the sample must be very homogeneous and, to achieve this, the sample tube is usually spun at fairly high speeds. So far, this procedure has proved impossible in flow-through cells, and, consequently, considerable resolution has been lost in these types of cell. Third, the solvent itself usually contains protons or ^{13}C nuclei, and thus can interfere with the spectrum of the solute. For proton spectroscopy, solvents may be chosen that do not contain protons, such as carbon tetrachloride or deuterated solvents, but the former restricts chromatographic performance, and the latter can become very expensive. Nevertheless, over the years with improved techniques, such as higher-resolution NMR spectrometers operating at 500 and 800 MHz, using superconducting magnets, coupled with ^{13}C spectroscopy, practical LC–NMR systems have been successfully developed and are now commercially available. Modern high-resolution NMR instruments have superconducting magnets and, consequently, must have

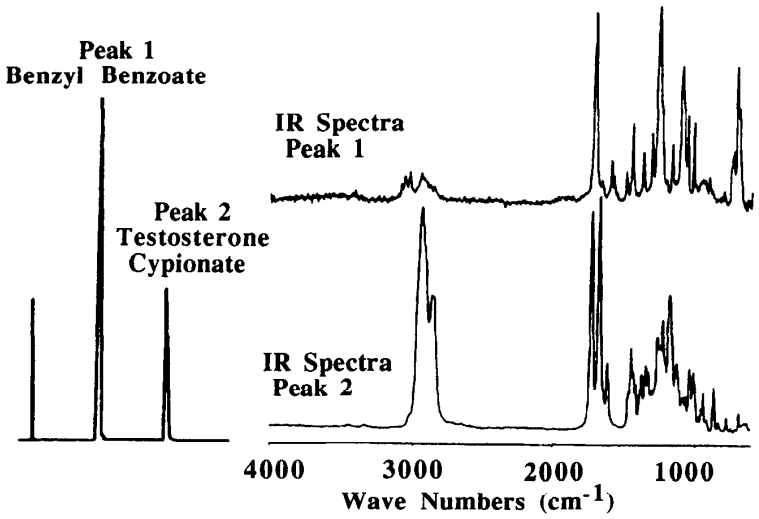


Figure 28 Infrared spectra of benzyl benzoate and testosterone cypionate obtained from the LC–IR interface.

special sensing coils and flow cells to fit into the probe cavity. The coils are not usually wound concentrically on the sample tube, but are in the Helmholtz configuration. The eluate from the column normally passes through a U-shaped conduit, one limb of which will be the actual sample cell. Modern flow cells have volumes ranging from 20 to 50 μL, but recently, Sweedler et al. [26] have claimed the successful use of sample tubes with capacities that are measured in nanoliters, with an improved signal/noise ratio of about two orders of magnitude. The sensing coil is only 1 mm long, 0.5-mm od and the capillary running through the coil has a sample capacity of 5 nL. The secret appears to be in surrounding the coil–capillary assembly in a commercial perfluorinated organic liquid that has the same magnetic susceptibility as the copper microcoil. This is claimed to provide a more uniform magnetic field in the sample region, leading to improved resolution and peak shape. A diagram of a modern LC–NMR tandem system is shown in Figure 29.

For the most part, modern LC–NMR systems are not in-line devices, but actually function as automatic fraction collectors that pass the sample to the NMR spectrometer for examination by a normal static procedure. They are unique in that the cell is designed for a flow-through function and for small-sample volume. They also have special valving arrangements to direct the column and solvent flows appropriately. Nevertheless, the spectra are generally run on a stop-flow principle; the sample being held in the cell while the spectra are obtained. The sample cell must be small enough not to destroy the chromatographic resolution, but be large enough that it contains sufficient sample to allow the spectrometer to acquire valid data in the residence time available. These two criteria have not yet been very efficiently achieved. As seen in Figure 29, the tandem system is basically a liquid chromatograph and a NMR spectrometer, joined by a valving system. The valving system allows any given peak to be passed directly to the spectrometer, or it can be stored in sample loops until the spectrometer is available. A diagram of the flow control and sampling unit is shown in Figure 30.

The flow control and the sampling unit sustain three alternative methods of operation. First, the eluent from the column can flow directly from the UV detector, to the NMR sample tube, and the spectra can be continuously monitored during the development of the separation. The success of this procedure will depend on the volume of the cell, the sample size, the column flow rate, the resolution of the NMR spectrometer, and the rate of data acquisition by the computer. In general, unless the new microcell facilities mentioned earlier are exploited,

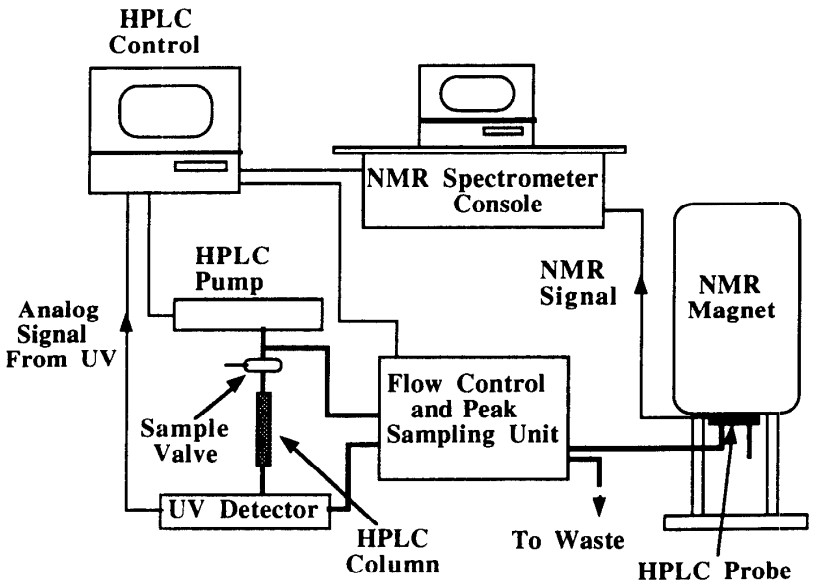


Figure 29 The layout of modern LC–NMR tandem system.

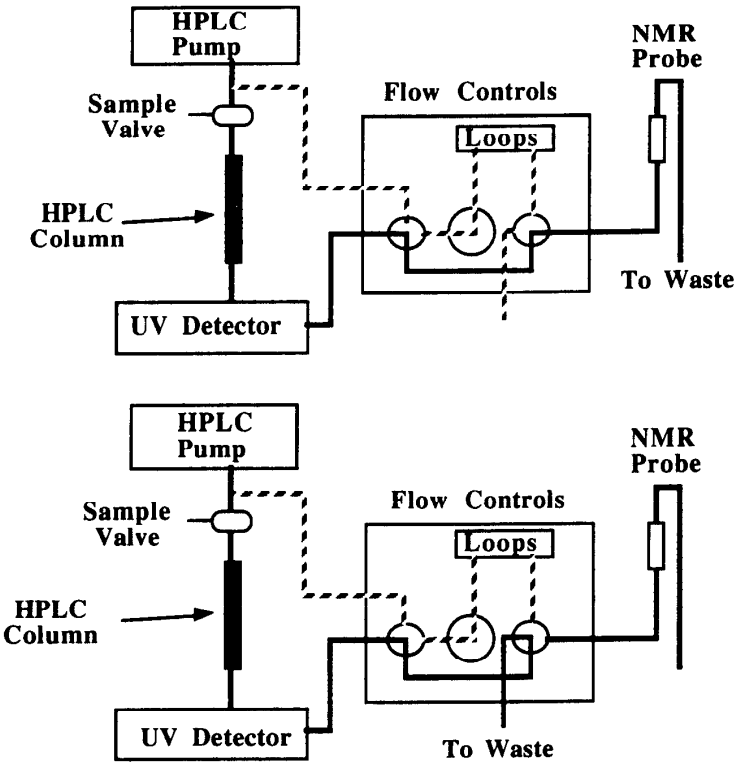


Figure 30 The flow control and peak sampling unit for a LC–NMR system.

this procedure will rarely be successful, particularly if microbore columns are used and multicomponent mixtures are being examined. The second alternative is to direct specific samples to the NMR spectrometer that are of particular interest. The sample can then be trapped in the cell, and data can be acquired from an adequate number of pulses to provide the required resolution. Subsequently, the sample can be expelled from the cell, using solvent supplied directly from the chromatography pump. The third alternative is to direct the eluate from the column to the sample loops, where each solute can be stored in its respective loop, until the spectrometer is available to take data. If necessary, the solutes can be stored in the loops for extended periods and then examined when convenient. Samples that have been examined can either be displaced to waste, or be collected for further examination.

An interesting example of the use of the Varian LC–NMR system in handling two unresolved peaks is shown in Figure 31. The spectra were obtained using their new LC–NMR Microflow probe, which was designed to maintain good chromatographic resolution and also to provide the necessary high NMR sensitivity. The cell had a sensor volume of 60 μL, which is a little large for microbore columns, but can be used with columns of wider bore. The spectra were obtained by stopping the column flow when the peaks were in the sensor cell, and running the spectra in the normal way. With this technique, it is clear that a multiple peak can be scanned. It is seen from the insert chromatogram obtained from the UV detector, that there are two unresolved solutes present in the peak, and the NMR spectra taken across the peak clearly differ, as shown in Figure 31.

Even though the components are not resolved, a shoulder on the main component peak yields an identifiable spectrum that is quite different from that taken from the front portion of the peak. The ares of the NMR spectra that demonstrate the change that results during the final elution of the first peak and the start of the elution of the second peak, are indicated by arrows.

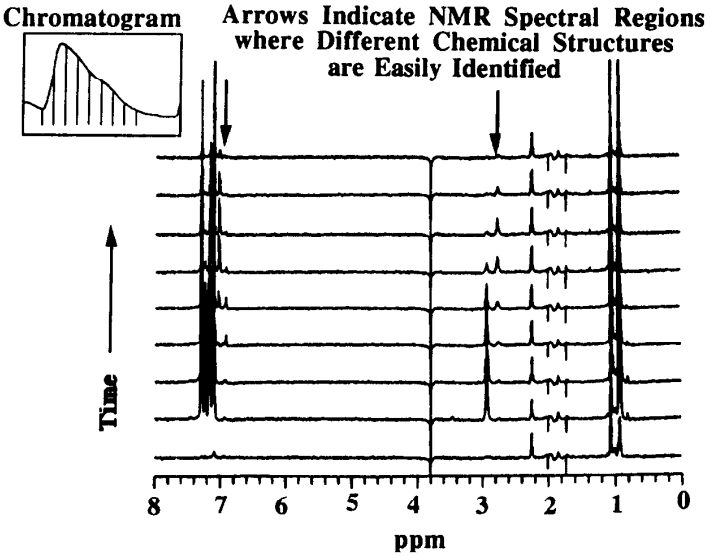


Figure 31 The NMR spectra taken across an unresolved peak using the Varian interface system, the LC–NMR system. (Courtesy of Varian Inc.)

V. SYNOPSIS

The tandem instrument, combining the liquid chromatograph with an appropriate spectrometer, was evoked by the need to identify the substances separated from hitherto unknown mixtures, and to confirm, unambiguously, the identity of certain substances for forensic purposes. Most spectroscopic techniques have been successfully combined with liquid chromatograph but LC–MS appears to be the most frequently employed. It is important to eliminate any dispersion that might take place in conduits between the chromatograph and the spectrometer, and in any interface that might be used. Either very short tubes, of very small diameter, or low-dispersion tubing, must be employed. Low-dispersion tubing is designed in such a way that it disrupts the parabolic flow profile and, thus, inhibits dispersion. Serpentine tubing can act efficiently as low-dispersion conduit in tandem interfaces. In LC–MS there are several different ionizing procedures available: secondary ion mass ionization, fast atom bombardment, laser desorption ionization, and matrix-assisted laser desorption ionization. The most commonly used mass spectrometers are the single- and triple-quadrupole mass spectrometer and the time-of-flight mass spectrometer, the latter being particularly useful for providing spectra of very high molecular weight materials. There are basically two types of interfaces used in LC–MS: transport interfaces and direct inlet interfaces. Transport interfaces collect the eluate as a film on the surface on a moving transport medium, which may be a wire, belt, disk, or wheel, passes it through an evaporation unit to remove the chromatographic solvent, and then into the ionization unit, where the dry solute is ionized in an appropriate manner. The direct inlet interface may be a heated jet that sprays the eluate into the ion source, or an electrospray that forms droplets under a strong electric field. The droplets rapidly evaporate and, as a consequence, become smaller. The accompanying increase in charge density and the reduced radius of curvature of the droplets, result in strong electric fields being formed that cause the droplets to explode, producing ions. Finally, there is atmospheric ionization, for which the column eluate is sprayed into a corona discharge at atmospheric pressure, and the ions formed are electrostatically guided either into the ion source of a guadrupole, or into a time-of-flight mass spectrometer. LC–MS has a wide field of application, but the combination of the electrospray interface, or the atmospheric ionization interface, with the time-of-flight mass spectrometer, has found particular use in the biotechnology field in the separation and analysis of

biopolymers. The liquid chromatograph has also been combined with the flame atomic absorption spectrometer and microwave-induced plasma atomic emission spectrometer, for elemental analysis and element speciation. By employing an IR transparent germanium disk as a transport medium, the IR spectrometer has also been linked with the liquid chromatograph, providing good spectra, but the spectra are actually obtained off-line. In a similar way the NMR spectrometer has been combined with the liquid chromatograph, but the spectra are obtained, either by a stop–start procedure, or the solutes are stored in sample tubes and examined off-line.

REFERENCES

1. MA Baldwin, FW McLafferty. Biomed Mas Spectrom 7:1111, 1973.
2. RPW Scott. Chromatography Detecters. New York: Marcel Deeker, 1996:42.
3. I Halasz, HO Gerlach, KF Gutlich, P Walking. US patent 3,820,660, 1974.
4. K Hofmann, I Halasz. J Chromatogr 173:211, 1979.
5. K Hofmann, I Halasz. J Chromatogr 199:3, 1980.
6. R Tijssen. Separ Sci Technol 13:681, 1978.
7. ED Katz, RPW Scott. J Chromatogr 268:169, 1983.
8. A Benninghoven, D Jaspers, W Lidtermeann. Appl Phys Lett 11:35, 1976.
9. KL Rinehart Jr. Science 218:254, 1982.
10. M Barber, RS Bordoli, RD Sedgwich, AN Tyler. J Chem Soc Chem Commun 7:325, 1981.
11. FJ Vastola, AJ Pirone. Adv Mas Spectrom 167, 1968.
12. MA Pothumus, PG Kistemaker, HLC Menzelaar. Anal Chem 50:985, 1978.
13. RPW Scott, CG Scott, M Munroe, J Hess Jr. The Poisoned Patient: The Role of the Laboratory. New York:Elseiver, 1974:395.
14. WM McFadden, HL Schwartz, S Evens. J Chromatogr 122:389, 1976.
15. T Covey, J Henion. Anal Chem 55:2275, 1983.
16. RD Voyksner, JT Bussey, JW Hines. J Chromatogr 323:383, 1985.
17. CM Whitehouse, RN Dreger, M. Yamashita, JB Fenn. Anal Chem 573:675, 1985.
18. RB van Breeman. Anal Chem News Features May:299A, 1996.
19. B Thomson, T Covey, B Shushanm, M Allen, T Sakuma. Perkin Elmer Corporation. Personal Communication.
20. TP Fan, AE Schoem, RG Cooks, PH Hemberger. J Am Chem Soc 103:1295, 1981.
21. ED Katz, RPW Scott. Analyst March:253, 1985.
22. JW Robinson, ED Boothe. Spectroscopy Lett 17:689, 1984.
23. JD Messman, TC Rains. Anal Chem 53:1632, 1981.
24. L Zhang, J Carahan, RE Winnans, PH Neill. Anal Chem 61:895, 1989.
25. E Bayer, K Albert, M Nieder, E Grom, T Keller. J Chromatogr 186:497, 1979.
26. V Sweedler. Science 270:1967, 1995.

18

Temperature Control in Analytical High-Performance Liquid Chromatography

Joel K. Swadesh

University of Massachusetts, Amherst, Massachusetts

I. INTRODUCTION

Temperature is a variable that affects sample stability, chromatographic resolution, and detection. Control of temperature at each step, therefore, is essential in high-performance liquid chromatography (HPLC). The advent of automatic injection has meant that samples are often stored in solution for periods of hours to days awaiting injection, as is discussed in Chapter 16. Many samples are stable indefinitely; however, some samples, particularly those of biological origin, are highly labile. For example, proteins decompose by hydrolysis of amides, by oxidation of residues, such as cysteine and methionine, and by aggregation [1]. Even simple synthetic compounds can decompose while waiting for injection. Accordingly, testing sample stability is essential to HPLC method development. Because sample stability is a very extended topic, this section will instead focus on temperature effects on retention, efficiency, detection, and other parameters of system performance. Control of these parameters ensures optimal HPLC performance. Devices for control of temperature will also be described.

II. EFFECTS OF TEMPERATURE ON RETENTION

The capacity factor k' is a function of temperature. In many forms of chromatography, retention tends to be reduced at elevated temperatures [2–7], although there are numerous exceptions to this general observation. Certain stationary phase–analyte interactions, such as those of hydrophobic interaction chromatography, may actually be stronger at higher temperature. Because acid–base ionization constants are functions of temperature, retention of ionizable compounds might either increase or decrease through that mechanism.

One common example in which retention increases with an increase in temperature is in the reversed-phase (RPLC) or ion-exchange (IEC) chromatography of proteins. Here, elevated temperature leads to unfolding and a concomitant increase in potential contact sites for adsorption. In gel permeation chromatography, the increase in hydrodynamic volume associated with unfolding would be expected to decrease retention.

III. EFFECTS OF TEMPERATURE ON COLUMN EFFICIENCY

Temperature effects on column efficiency are often extremely pronounced in reversed-phase liquid chromatography (RPLC), but they are also observed with other chromatographic mechanisms. The plate height of a column can be written as

$$H = \left[\frac{c_1 + c_2 f(T)}{u}\right] + \left[\frac{c_3 u}{f(T)}\right] + \left\{c_4 \left[\frac{u}{f(T)}\right]^{2/3}\right\} + \left[\frac{U}{g(T)}\right]$$

where H is the plate height, $f(T)$ is the temperature-dependent solute diffusivity, $g(T)$ is the temperature-dependent desorption rate constant, k' is the capacity factor of the column, u is the chromatographic velocity, $U = uk'/(1 + k')^2$, and the coefficients c_i are positive constants, dependent principally on particle size [8]. Temperature, therefore, enters into the longitudinal diffusion (second term), intraparticle mass transfer (third term), interfacial mass transfer (fourth term), and the kinetics of sorption (fifth term). Because $f(T)$ and $g(T)$ are functions that increase with increasing temperature, higher temperature reduces band broadening through effects on the third, fourth, and fifth terms, but increases band broadening through the effects on longitudinal diffusion. In other words, elevated temperature generally improves the kinetics of adsorption and desorption, but band broadening from mixing is increased. Because of the complex interplay of these different factors, a decrease of plate height has been observed with increasing temperature in small-molecule separations [9], whereas the reverse has been observed in macromolecular separations [8]. In gel permeation chromatography (GPC), an increase in efficiency has been reported [10,11]. In ion-exchange separations, elevation of temperature generally improves efficiency through an acceleration of local ionic equilibria [7,12].

IV. TEMPERATURE EFFECT ON VISCOSITY

Elevation of temperature reduces solvent viscosity and the observed backpressure. The rate of solute diffusion is increased, a factor that favors band broadening and the loss of chromatographic resolution. In some chromatographic systems, the loss of resolution is small, or can be compensated through flow rate. Because pump flow rate control may be dependent, to some degree, on solvent viscosity, flow rate adjustment may be necessary for precise comparison of chromatograms obtained at different temperatures.

V. TEMPERATURE EFFECTS ON THE STATIONARY PHASE

The characteristics of the stationary phase are also affected by temperature. Alkyl-bonded phases are subject to irreversible changes by hydrolytic release of the bonded phase from the support. Hydrolysis is accelerated at elevated temperature. However, there may also be *reversible* thermally induced changes in stationary phase characteristics. This is most easily illustrated by consideration of a liquid crystalline stationary phase [13,14]. Liquid crystals undergo sharp, well-defined, reversible transitions on heating. A densely packed smectic phase can, for example, undergo a transition to a less-dense nematic phase. Similarly, bonded phases can become more solvent-exposed at higher temperatures. In polymeric phases, there may be increased penetration of solvent into the particle as a consequence of swelling, which can lead to irreversible degradation [15]. In gel permeation chromatography, a reduction in retention may be due either to an expansion of the physical components of the column, or be due to an expansion in pore volume [10]. Because the molecular weight distributional values of synthetic polymers, as obtained by retention versus standards in GPC, are *extremely* sensitive to small changes in retention, temperature control is advisable.

VI. TEMPERATURE EFFECTS ON ANALYTE CONFORMATION

Many molecules, particularly large biological molecules, exhibit a defined conformation that is a function of temperature. At low temperatures, a globular protein, for example, is typically in a compact conformation, with hydrophobic residues not exposed to the solvent. As the temperature is raised, the protein denatures, and the hydrophobic core is exposed. The denatured form may elute with a different retention time than the native form. If interconversion is slow, two distinct peaks may be resolved. If interconversion is more rapid, one broad peak may be observed between the native and the denatured retention times.

Even relatively small molecules, such as peptides, exhibit conformational exchange and, indeed, conformational exchange is probably a major contributor to band broadening in chromatography of macromolecules. Conformational change is especially important in the chromatography of proteins on adsorptive hydrophobic phases [16,17].

VII. DETECTOR PERFORMANCE

The effects of temperature on detector response can be divided into various categories. Detector response may, in turn, be dependent on the temperature of the detector components, which is why detectors are normally allowed to equilibrate before taking measurements. The analyte contribution to response may be dependent on conformation, temperature-dependent solvation, or analyte ionization, all of which, in turn, may be dependent on temperature. Analyte response may also be dependent on the composition of the solvent in which the analyte is eluted, so changes in selectivity may affect response.

Refractive index detectors (RI) are extremely sensitive to changes in temperature. The refractive index changes by about 1 mRI unit per degree centigrade [18,19]. Even if the sample and reference cells are isothermal relative to each other, changes in temperature affect detector response [20]. Because most RI detectors are used to measure changes in refractive index of about 1 μRI, temperature is a critical variable. Most RI detectors use a heat sink ahead of the detection cell to minimize fluctuations in temperature of the mobile phase entering the detector cell. A recent design for a refractive index detector, based on a 5-mW HeNe laser, an optical fiber, and a graded refractive index lens to measure the *radial* concentration gradient has been presented [21]. This design appears to be suitable for thermal gradient chromatography.

Commercial ultraviolet–visual light (UV–VIS) spectrophotometers have also been designed with tapered cell configurations to be relatively insensitive to refractive index effects [22,23]. Because refractive index changes alone can cause a change in absorbance of 100 μAU/°C [18], temperature control is proportionately important in UV–VIS detection at high sensitivity. Temperature can also shift the UV absorbance spectrum, resulting in changes in relative extinction coefficients. Therefore, the wavelength used for detection should be near a peak maximum or valley.

Conductivity cells require precise temperature control for maximal stability [24–27]. The change in conductivity is about 2%/°C [28], so accuracy of calibration and baseline stability are dependent on temperature control. Electrochemical (EC) detectors also have been reported to exhibit variability related to temperature changes [29,30], although the magnitude of the effect is substantially less than observed in conductivity [27]. Temperature affects detector performance principally through the reference electrode, with the temperature coefficients for silver–silver chloride electrodes and calomel electrodes being reported to be -1 mV/°C and -0.3 mV/°C, respectively [31]. Changes in temperature during the run can cause baseline drift. Other detectors are also sensitive to temperature effects, although the magnitude of the change in response may be substantially less than those of the RI or conductivity detectors. For example, fluorescence efficiency is a function of temperature. Collisional quenching of a fluorophore by solvent molecules, which increases at elevated temperatures, tends to decrease

fluorescence. Fluorescence may be indirectly affected by the column temperature in gradient chromatography, because fluorescence efficiency is strongly dependent on solvent composition [32].

VIII. TEMPERATURE EFFECTS IN ON-LINE REACTORS

Pre- and postcolumn reactors are another area of chromatography in which temperature control is critical. Some examples of the importance of the effects of temperature on derivatization efficiencies include the following. In a postcolumn detector for alanine-based surfactants detected by hypochlorite oxidation and reaction with iodide to form triiodide, the relative response for one compound varied by a factor of three over 30°C, apparently owing to reaction kinetics [33]. In a 3,5-dinitrobenzoylation reactor, reaction efficiency increased by a factor of about ten from ambient to 60°C [34]. In the reaction of butylamine with 9-fluorenylmethoxycarbonyl, the reaction efficiency reached a maximum near 5°C and declined at both higher and lower temperatures [35]. In the derivatization of propylamine in the presence of three amine-derivatizing reagents, temperature was used to shift the distribution of products [36]. Run-to-run temperature stability is essentially for repeatability.

IX. TEMPERATURE CONTROL DEVICES

Temperature control devices include water baths, column ovens, and thermal tape. Conventional resistance-heating column ovens are capable of temperature control only well above ambient temperature. Peltier devices capable of operating at subambient temperatures are also available. Water baths are useful for subambient work.

In examining the specifications for temperature control devices, the following parameters are important:

1. The operating range
2. Basis and accuracy of calibration
3. The temperature stability
4. Temperature uniformity across the heating or cooling cavity
5. The time to stabilize on heating and on cooling
6. The number of columns accommodated

Because most chromatographic applications involve the use of ovens to control column temperature, some examples of commercially available devices are presented in Table 1. For very precise temperature control, it may be desirable to incubate the solvent bottles and connecting tubes in a temperature-controlled water bath to reduce the thermal gradient on entering a thermostated column.

It is also possible to construct a relatively inexpensive temperature control device by using resistance heat tape, a thermistor, and a controller equipped with a power source for the heating tape. Omega Engineering offers a wide variety of controllers, thermistors, and configurations of heating tape. Proportional control reduces the temperature fluctuations associated with turning the heater on and off. Water baths are available from several vendors, including Brinkmann Instruments, Forma Scientific, Haake Instruments, Lab-Line Instruments, and Neslab Instruments. The principal disadvantage of using a water bath to control column temperature is that the thermal inertia of large volumes of water may mean long equilibration times. Also, it is difficult to inspect column fittings for leaks. However, to preheat the solvent reservoir, a large-capacity water bath may be advantageous. A column oven can be used to heat the solvent ahead of the injector. There may be an associated increase in gradient delay time and a rounding of the gradient, unless dead volume in the preheating line is kept to a minimum.

Table 1 Operating Characteristics of Some Commercially Available Column Ovens

Manufacturer and model	Operating range and precision (°C)	Stabilization time	Number of columns	Comments
Perkin-Elmer Model 101 LC	3–99 + 0.1	30 min	4	Calibration is accurate to ±2°C and may be adjusted. The oven preheats solvent using low dead-volume serpentine tubing.[a]
Eldex CH-150	30–150 ± 0.1	10 min at 60°C	4	—
Chrompack	30–99 ± 0.1	16 min at 60°C	2	A vapor detector capable of shutting off the oven in the event of a leak is supplied as a safety device.
Anspec Croco-Cil	Ambient–99°C ± 0.1	5°C/min heating 4°C/min cooling	Various	Some models are equipped with forced air or liquid cooling devices to permit subambient operation.
Anspec Euramark 225	5–85°C ± 0.1	2–3°C/min	Compartment is 18″ × 6″ × 2″	Peltier device for temperature control, including programmed operation.

[a]The very low dead volume of serpentine tubing allows rapid temperature equilibration without a large corresponding increase in precolumn void volume.

X. EXAMPLES OF TEMPERATURE EFFECTS

Temperature may not be an important variable in many routine chromatographic separations, because the fluctuations and drift in ambient temperature are small enough that the effect on the separation is imperceptible. Under several circumstances, however, temperature control is critical. If the ruggedness of a separation is paramount, as occurs in analysis of regulated substances, such as pharmaceuticals, control of temperature will minimize assay variability. Very labile compounds may require temperature control to avoid on-column decomposition. In the analysis of peptides and proteins, temperature control is almost always recommended, because conformational changes can lead to multiple peaks or erratic retention.

An example of how elevation of temperature can be used to increase column efficiency while decreasing analysis time is shown by a high-speed RPLC separation in Figure 1 [37]. In the figure, the peptides generated from tryptic hydrolysis of rabbit cytochrome *c* were separated at 26°C and 0.5 mL min^{-1} (panel A), at 42°C and 0.7 mL min^{-1} (panel B), and at 70°C and 1.1 mL min^{-1} (panel B). Under these conditions the column backpressures were identical. Elevating the temperature served to reduce solvent viscosity and permit more rapid separation. The separation in panel A is poor. In panel B, the separation is considerably better. In panel B, the four peaks at 1.6–2.2 min have been resolved from two peaks at 3–3.2 min in panel A. The column peak capacity at 70°C is *double* that at ambient temperature. In addition, the separation time has been reduced by a third.

One example of the importance of temperature control for labile compounds was seen in the RPLC of *o*-phthaldehyde–2-mercaptoethanol derivatives of amino acids. In one chromatographic system, these derivatives could not be chromatographed above 35°C without decomposition [38]. For chiral chromatography, enantioselectivity is often a strong function of temperature. Reduction of temperature increased enantioselectivity and decreased retention time in the separation of β-blockers on an *N*-3,5-dinitrobenzoyl-α-amino phosphonate chiral stationary phase [39]. Retention and resolution decreased in the RPLC of compounds such as naphthalene and biphenyl [40]. Derivatives of simple carbohydrates, such as α-mannoside, α-galactoside, and 4-nitrophenyl cellobioside, exhibited an increase in retention at low tem-

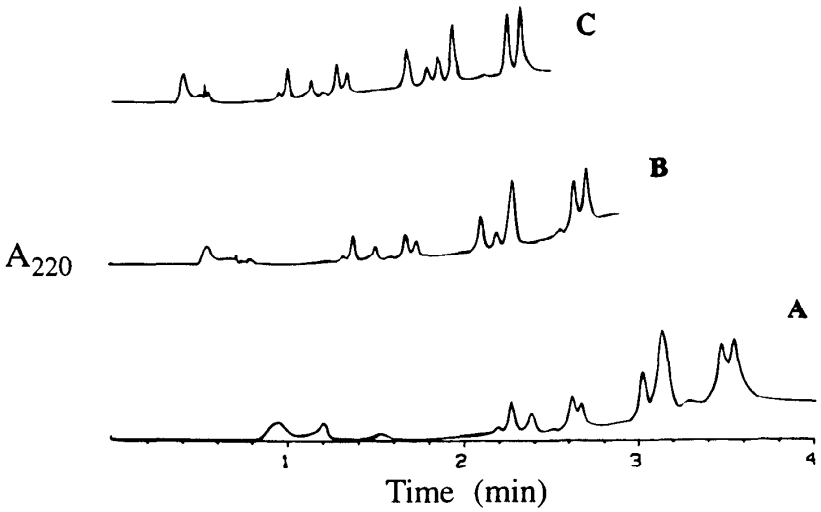


Figure 1 The separation of the tryptic peptides of rabbit cytochrome *c* as a function of flow rate and temperature. Separation is performed on a 15 × 0.2-cm poly(styrene/divinyl benzene) column packed with 3-μm, 300-Å particles by gradient reversed-phase HPLC. Detection is by UV absorbance at 220 nm. The mobile phase is 99% water:1% isopropanol:0.1% trifluoroacetic acid versus 99% acetonitrile:1% isopropanol:0.1% trifluoroacetic acid. (A) 26°C and 0.5 mL min^{-1}; (B) 42°C and 0.7 mL min^{-1}; (C) 70°C and 1.1 mL min^{-1}.

perature on reversed-phase chromatography at elevated pH [41]. Retention of thymine was observed to show a 2%/°C decrease on RPLC [3]. The efficiency of the sodium and potassium forms of a cation-exchange column increased to a maximum near 70°C in the separation of glucose and its derivatives [42]. A study of the micellar reversed-phase chromatography of anthracene and its derivatives showed that the entropy of retention was correlated with the analyte polarity [43]. Several carboxylic acids were separated on a Bio-Rad Aminex HPX-87H column using a programmed increase of temperature to accelerate the elution of the more strongly retained components [5]. One detailed study of temperature effects in ion chromatography concluded that detection was noticeably affected only in nonsuppressed systems [44]: retention was observed to increase. Epimeric pairs of C_{24} alkylsterols were separated at subambient temperatures by RPLC [45].

Conformational effects are often important factors in the chromatographic behavior of peptides and proteins. In RPLC, organic mobile-phase constituents may induce nonnative conformation [46]. Ribonuclease, which eluted as a broad peak on RPLC at 25°C, eluted as a sharp peak at 40°C, indicating a conformational transition to a denatured form [47,48]. Temperature effects in the RPLC of histones have also been examined [49]. In anion-exchange of rat cytochrome b_5, the *Z*-number (a measure of the apparent number of contacts between analyte and stationary phase) increased with temperature, resulting in stronger retention [50].

Peptides can also exhibit conformational effects as a function of temperature, particularly owing to *cis–trans* isomerization of proline [51]. Elevated temperature will accelerate the rate of isomerization and tend to stabilize the higher-energy conformer. Temperature effects were demonstrated in the separation of captopril, a proline-containing compound [52]. A cyclic peptide containing proline and a number of linear peptides containing proline were observed to exhibit temperature-dependent elution [53]. RPLC separation of diprotin B, elastin chemotactic fragment, bradykinin, morphiceptin, β-casomorphin, and proctolin also exhibited temperature-dependent elution [54]. Ramipril, an angiotensin-converting enzyme inhibitor and its metabolite, ramiprilate, exhibited multiple peaks at ambient temperature on RPLC caused by proline isomerization [55]. Entropy effects may be important in selectivity of peptide diastereomers [56]. On RPLC, the retention of tryptophan, ACTH 1-24, and ribonuclease decreased with increasing temperature, whereas the retention of bovine serum albumin and of prolactin increased [57]. An analysis of how retention is related to adsorption kinetics has been presented [58]. Elevated temperature improved resolution and reduced analysis time in peptide mapping [59].

XI. SUMMARY

Temperature control may be necessary in sample autoinjection, elution, and detection. Temperature control on autoinjection is principally important for reduction of sample degradation. Temperature affects elution through effects on column efficiency and selectivity, and on analyte conformation. Temperature effects in detection are most pronounced in refractive index and conductivity detection, but may affect other detectors as well.

ACKNOWLEDGMENT

The useful suggestions provided by Dr. Kálmán Benedek are gratefully acknowledged.

REFERENCES

1. SE Zale, AM Klibanov. Biochemistry 25:5432, 1986.
2. HJ Issaq, M Jaroniec. J Liq Chromatogr 12:2067, 1989.
3. RC Simpson, PR Brown, MK Schwartz. J Chromatogr Sci 23:89, 1985.
4. WC Mahoney, MA Hermodson. J Biol Chem 255:11199, 1980.
5. G Chiu. J HRC CC 9:410, 1986.

6. G Chiu. J HRC CC 9:57, 1986.
7. CG Horváth, BA Preiss, SR Lipsky. Anal Chem 39:1422, 1967.
8. FD Antia, CS Horváth. J Chromatogr 435:1, 1988.
9. FV Warren Jr, BA Bidlingmeyer. Anal Chem 60:2821, 1988.
10. T Takeuchi, S Matsuno, D Ishii. J Liq Chromatogr 12:987, 1989.
11. CN Renn, RE Synovec. Anal Chem 64:479, 1992.
12. J Korkisch. Handbook of Ion Exchange Resins, Vol. 1. Boca Raton, FL: CRC Press, 1989; 49.
13. BK Klein, J Springer. J Liq Chromatogr 14:1519, 1991.
14. BK Klein, J Springer. J Liq Chromatogr 14:1539, 1991.
15. MR Haddon, JN Hay. In BJ Hunt, SR Holding, eds., Size Exclusion Chromatography: Glasgow: Blackie, 1989:57.
16. FE Regnier. Science 238:319, 1987.
17. G Vanacek, FE Regnier. Anal Biochem 109:345, 1980.
18. RL Stevenson. In: TM Vickrey, ed., Liquid Chromatography Detectors, Vol. 23. New York: Marcel Dekker, 1983: 33.
19. H Colin, A Jaulmes, G Guichon, J Corno, J Simon. J Chromatogr Sci 17:485, 1979.
20. S Mori. J Liq Chromatogr 6:813, 1983.
21. CN Renn, RE Synovec. J Chromatogr 536:289, 1991.
22. A Trisciani, F Andreolini. J High Resol Chromatogr 13:270, 1990.
23. JE Steward. Anal Chem 53:1125, 1981.
24. RM Cassidy, S Elchuk. J Chromatogr Sci 21:454, 1984.
25. JA Glatz, JE Girard. J Chromatogr Sci 20:266, 1982.
26. DR Jenke, GK Pagenkopf. Anal Chem 54:2603, 1982.
27. PR Haddad, AL Heckenberg. J Chromatogr 300:357, 1984.
28. CA Pohl, EL Johnson. J Chromatogr Sci 18:442, 1980.
29. JT Bretz, PR Brown. J Chromatogr Sci 26:310, 1988.
30. PT Kissinger. In: TM Vickrey, ed. Liquid Chromatography Detectors, Vol. 23. NY: Marcel Dekker, 1983; Chap. 4.
31. HW van Rooijen, H Poppe, J Liq Chromatogr 6:2231, 1983.
32. JR Lakowicz. Principles of Fluorescence Spectroscopy. New York: Plenum, 1983: Chap. 7.
33. J Kawase, H Ueno, K Tsuji. J Chromatogr 264:415, 1983.
34. F-X Zhou, J Wahlberg, IS Krull. J Liq Chromatogr 14:1325, 1991.
35. H-M Zhang, F-X Zhou, IS Krull. J Pharm Biomed Anal 10:577, 1992.
36. ME Szulc, IS Krull. Biomed Chromatogr 6:269, 1992.
37. JK Swadesh. Biotechniques 9:626, 1990; reprinted in Peptide Res 3:282, 1990.
38. JDH Cooper, G. Ogden, J McIntosh, DC Turnell. Anal Biochem. 142:98, 1984.
39. WA Pirkle, JA Burke III. J Chromatogr 557:173, 1991.
40. HJ Issaq, SD Fox, K Lindsey, JH McConnell, DE Weiss. J Liq Chromatogr 10:49, 1987.
41. M Stefansson, D Westerlund. Chromatographia 35:55, 1993.
42. DW Togami, BJ Poulsen, CW Batalao, WA Rolls. Biotechniques 10:650, 1991.
43. PR Bedard, ML Cotton. L Liq Chromatogr 14:1113, 1991.
44. PE Jackson, JP Romano, BJ Wildman. J Chromatogr A 706:3, 1995.
45. DJ Chitwood, GW Patterson. J Liq Chromatogr 14:151, 1991.
46. AJ Sadler, R Micanovic, GE Katzenstein, RV Lewis, CR Middaugh. J Chromatogr 317:93, 1984.
47. KA Cohen, K Schellenberg, K Benedek, BL Karger, B Grego, MTW Hern. Anal Biochem 140:223, 1984.
48. SA Cohen, K Benedek, Y Tapuhi, JC Ford, BL Karger. Anal Biochem 144:275, 1985.
49. H Lindner, W Helliger. Chromatographia 20:518, 1990.
50. DJ Roush, DS Gill, RC Willson. J Chromatogr A 653:207, 1993.
51. DE Henderson, CS Horváth. J Chromatogr 368:203, 1986.
52. J Kirschbaum, S Perlman, RB Poet. J Chromatogr Sci 20:336, 1982.

53. JC Gesquierre, E Diesis, MT Cung, A Tartar. J Chromatogr 478:121, 1989.
54. DE Henderson, JA Mello. J Chromatogr 499:79, 1990.
55. S Gustaffson, B-M Eriksson, I Nilsson. J Chromatogr 506:75, 1990.
56. H Zou, Y Zhang, M Hong, P Lu. J Liq Chromatogr 15:2289, 1992.
57. MJ O'Hare, MW Capp, EC Nice, NHC Cooke, BG Archer. Anal Biochem. 126:17, 1982.
58. K Benedek, S Dong, BL Karger. J Chromatogr 317:227, 1984.
59. K Kalghatgi, Cs Horváth. J Chromatogr 443:343, 1988.

19
Collection Devices

Gordon S. Hunter

Gilson, Inc., Middleton, Wisconsin

I. PURPOSES AND USES OF FRACTION COLLECTORS

The enormous growth of high-performance liquid chromatography (HPLC) in recent years has prompted significant interest in preparative liquid chromatography (LC) as a tool for purifying organic compounds in complex liquid mixtures. On any scale, preparative LC implies separation of target compounds and subsequent collection of the column eluate, containing the compounds, in appropriate vessels for their isolation. This frequently occurs in complex mixtures containing both major and minor peaks. Identification of the isolated compound is then usually performed by complementary techniques, such as mass spectroscopy (MS), nuclear magnetic resonance (NMR), or infrared (IR) spectroscopy. In protein purification, biological activity of the isolated fractions is often assessed by immunoassay tests, such as radioimmunoassay (RIA) and enzyme immunoassay (EIA).

If only several fractions are to be collected from the liquid chromatograph and only a few samples are to be purified, then the eluate from the column can sometimes be collected manually. However, a fraction collection device is recommended if the the analyst has many samples to process or if there are many fractions to collect. Fraction collectors are especially useful in applications involving unattended, overnight, and automated chromatographic purification schemes.

The goals of preparative HPLC are different from those of analytical and trace analyses [1]. In analytical applications, the goal is to obtain information about the sample; therefore, important chromatographic parameters include resolution, sensitivity, and fast analysis times. With preparative HPLC, the goal is to isolate and purify compounds from complex mixtures. Preparative liquid chromatography traditionally meant fast flow rates, large id columns, and relatively large column particles to isolate and purify milligram to gram quantities of compounds of interest. In recent years, however, preparative liquid chromatography has been "scaled down" to analytical (4.6-mm id) and narrow-bore ($\leq$20-mm id) column proportions as biopharmaceutical and biomedical research focuses on trace analytes at the picogram level or lower [2].

Preparative liquid chromatography and fraction collectors are widely used to purify target compounds for applications found in many areas:

1. Pharmaceuticals: Determination of drug metabolite structure in drug therapy and development studies; end-product and intermediate purification

2. Organic chemistry: Preparation of standards; purification of starting materials; identification of impurities in end products; determination of intermediate structures during organic synthesis
3. Biotechnology and biomedical: Identification of molecular structures in genetic-engineering applications; end-product and intermediate purification; isolation and purification of enzymes, proteins, nucleic acids, carbohydrates, lipids, and other biomolecules; polymerase chain reaction (PCR) products and monoclonal antibody purifications
4. Food and beverage: Additive purification; determination of intermediate structures during fermentation processes

II. OPERATIONAL CONSIDERATIONS OF FRACTION COLLECTORS IN LIQUID CHROMATOGRAPHY

The purification of compounds by preparative liquid chromatography is performed by a wide spectrum of laboratories. Purification and isolation techniques have evolved from low-resolution to high-resolution separations, led by developments in column technologies and packing materials, and followed by adaptations to pumps, detectors, injectors, and fraction collectors [3]. Low-resolution, large-particle columns still have their place for crude or preliminary purifications, but the trend is clearly toward high-resolution, small-particle column separations. As a result, small-scale preparative LC is performed today even on "analytical-scale" HPLC columns and systems.

The functional requirements of the fraction collector have changed, therefore, as purification techniques evolved from low-pressure (low-resolution) to high-pressure (high-resolution) techniques. The following section describes some of the key operational considerations of fraction collection devices. Representative fraction collectors that are commercially available are summarized in Table 1.

A. Low-Resolution Techniques

Classic low-pressure LC is a relatively simple technique developed in the 1950s, but still commonly used today by organic chemists and biochemists. It is very effective as a crude purification step, especially before preparative HPLC, to remove contaminants and interferences, even though it is slow and offers low resolution. For many laboratories studies using classic low-pressure LC, requirements are generally for simple *time and drop* mode fraction collectors. The entire chromatographic eluate is automatically collected by selecting equal fractions based on time per tube or drops per tube (Fig. 1). The residence time above each collection vessel is the same, so equal fractions are achieved from a constant flow rate. Similarly, when performing drop-counting protocols, the user will obtain fractions of equal volume if the viscosity of the mobile phase remains constant.

If the elution time(s) of peaks of interest are known and reproducible, the user can program most microprocessor-based fraction collectors to automatically collect only the peaks of interest and discard the between-peak eluate or peaks of noninterest. This is variable time window programming mode, also known as *time program* plus *time* (or *drop*) mode, involves a sequence of time-based collection and drain steps (Fig. 2). Each collection step is commonly referred to as a collection time window. It conveniently allows the user to define time intervals during which the column eluate is either collected into fractions or discarded into waste. Each selected peak will be subfractionated by equal slices, based on time-counting or drop-counting. Column void volumes, equilibration volumes, and peaks of no interest are discarded. Time window collection is appropriate for both classic LC and HPLC purifications.

B. Separations of Complex Mixtures

The development of microparticle chemically bonded packings in the 1970s was a major breakthrough in obtaining high-resolution separations not possible with classic LC techniques

Table 1 Summary of Representative Fraction Collectors

Features	Bio-Rad Econo 2110	Bio-Rad 2128	Eldex Universal FC	Gilson 203/204	Gilson 205	ISCO Retriever IV	ISCO FOXY 200	Pharmacia FRAC 200	Pharmacia GradiFrac
Collection modes	Time, drop, manual	Time, drop, volume, peak, manual	Time, drop, manual	Time, drop, peak, manual	Time, drop, manual	Time, drop, volume, manual	Time, drop, volume, peak, manual	Time, drop, volume, peak, manual	Time, drop, volume, peak, manual
Collection windows per run	Not available	Up to 20	Not available	Up to 10	Up to 10	Not available	Up to 25	Not available	Not available
Maximum number of tubes	80 13 mm	138 12–13 mm	200 18 mm	128 12 mm (203); 432 10 mm (204)	128 12 mm	190 10–18 min	288 12–13 mm	175 12 mm	175 12 mm
Types of tubes and vessels	13-mm, 1.5-mL micro-test tubes	12–18 mm; 96-well microtiter plate	13, 18, and 25 mm	10–17 mm (203); 10–18 mm (204); micro-test tubes; microtiter plates	10–17 mm; micro-test tubes; microtiter plates	10–18, 25, and 28 mm	12–18 mm; 25 and 28 mm; micro-test tubes	10–18 mm; 28 mm; micro-test tubes	12, 18, and 28 mm
Rack design	Carousel	Fixed	Carousel	Fixed	Fixed	Carousel	Fixed	Carousel	Carousel
Weight	11 kg	5.7 kg	8 kg	203: 5kg 204: 11 kg	5 kg	12 kg	11 kg	6 kg	4 kg
Size (W × D × L)	24 × 33 × 25 cm	31 × 42 × 24 cm	25 × 20 × 29 cm	203: 32 × 29 × 28 cm	32 × 29 × 28 cm	32 × 61 × 10 cm	29 × 38 × 61 cm	30 × 39 × 29	30 × 39 × 29 cm
Special features		Optional diverter valve and prep adapter		Optional diverter valve (standard with 204)	Optional diverter valve	Optional diverter valve	Optional diverter valve and prep rack	Optional diverter valve	Remote control of pump; method storage

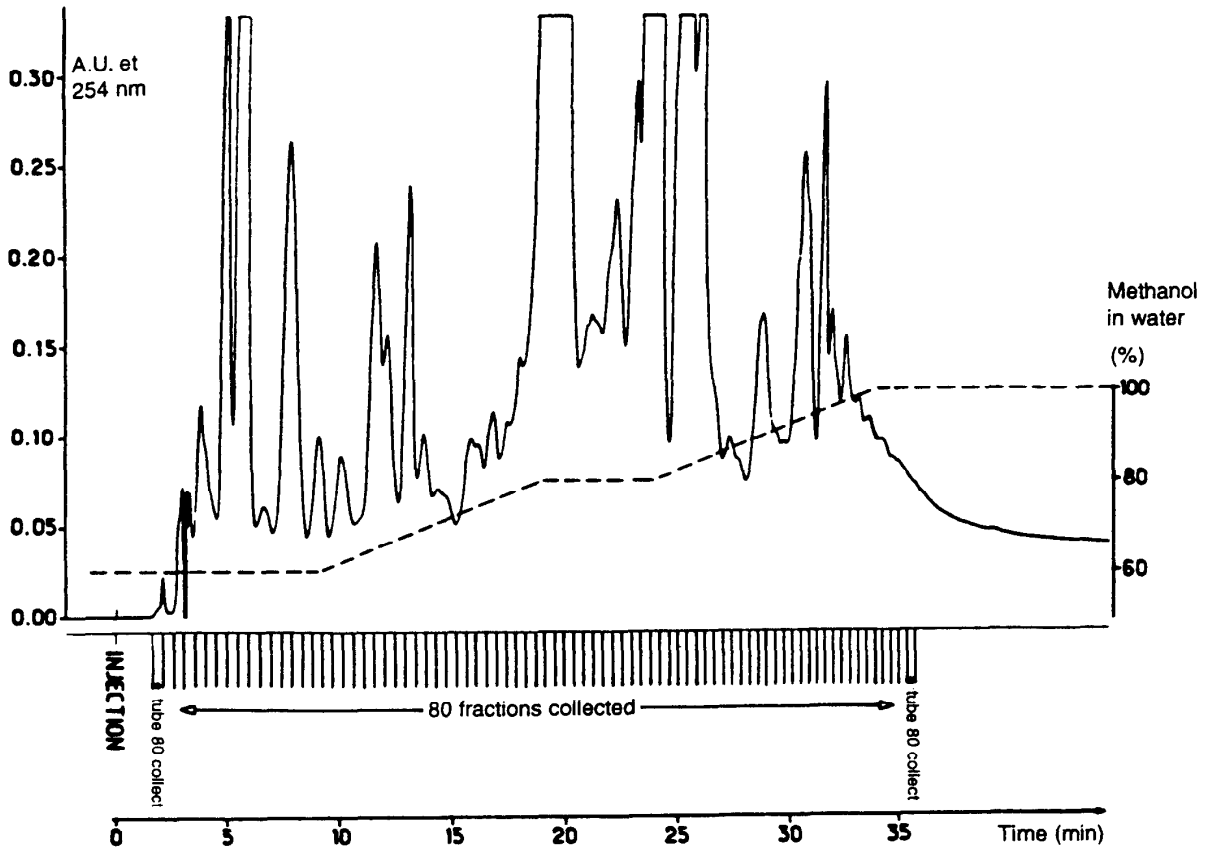


Figure 1 Examples of several fraction collection modes. Collection in *drop* mode: the entire run is collected by selecting equal fractions based on drops per tube.

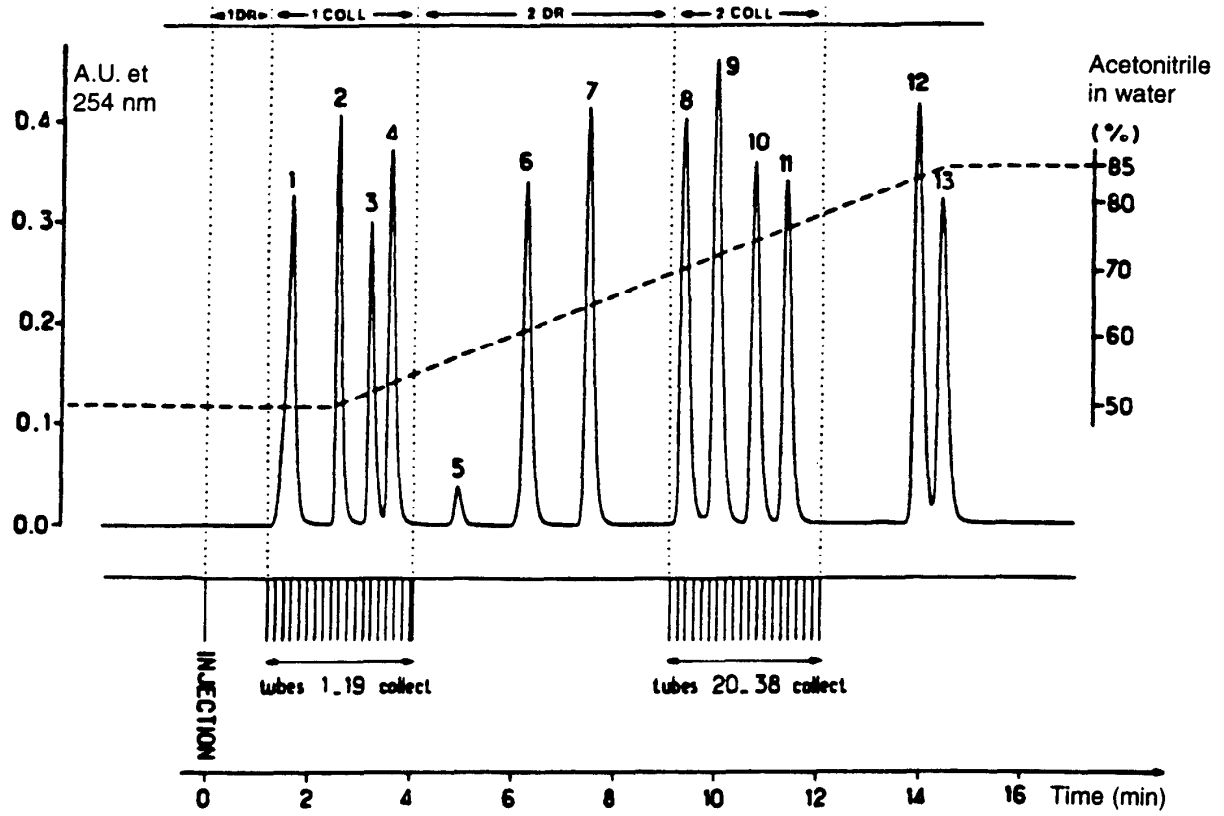


Figure 2 Collection in *time program* plus *time* mode. Two collection time windows are subfractionated into equivalent fractions based on time per tube.

[1]. Small-particle packing materials (≤15 μm) are effective for isolation and purification of difficult to separate mixtures [4]. Recent advances in column technology, especially in small-bore (≤2-mm id) columns, has enabled small-scale preparative chromatography using "analytical-scale" HPLC columns, pumps, injectors, and detectors [2]. But the resultant high-resolution chromatograms are frequently very complex and require fraction collectors capable of "cutting" pure peaks of less than 20 s duration.

The very high chromatographic efficiency and selectivity of present HPLC columns has created a need for a new generation of flexible fraction collectors capable of sophisticated collection, based on the detector output signal that corresponds to the target compound(s). The fraction collector responds to various chromatographic parameters, such as preset threshold signal levels and peak slope. When very high purity levels are required, peaks of interest containing target compounds should not be contaminated by neighboring peaks or diluted with mobile phase, which would occur if the collector were to collect equal fractions throughout the run, based simply on time or drop counts (see Fig. 1). These high-purity requirements are usually found in small-scale laboratory studies for which optimum purity of fractions (sometimes ≥99.9%) is critical.

Fraction collection based on detection of chromatographic peaks enables isolation of the purest part of each peak into a single tube. This is sometimes referred to as *peak cutting*. An example of fraction collection based on the detector signal is summarized in Figure 3. Each fraction corresponds to a peak detected by the collector. Unwanted peaks, between-peak eluate, column void volumes, and equilibration volumes are discarded to waste. Because the chromatographer is not collecting the entire column eluate from beginning to end, there is no need

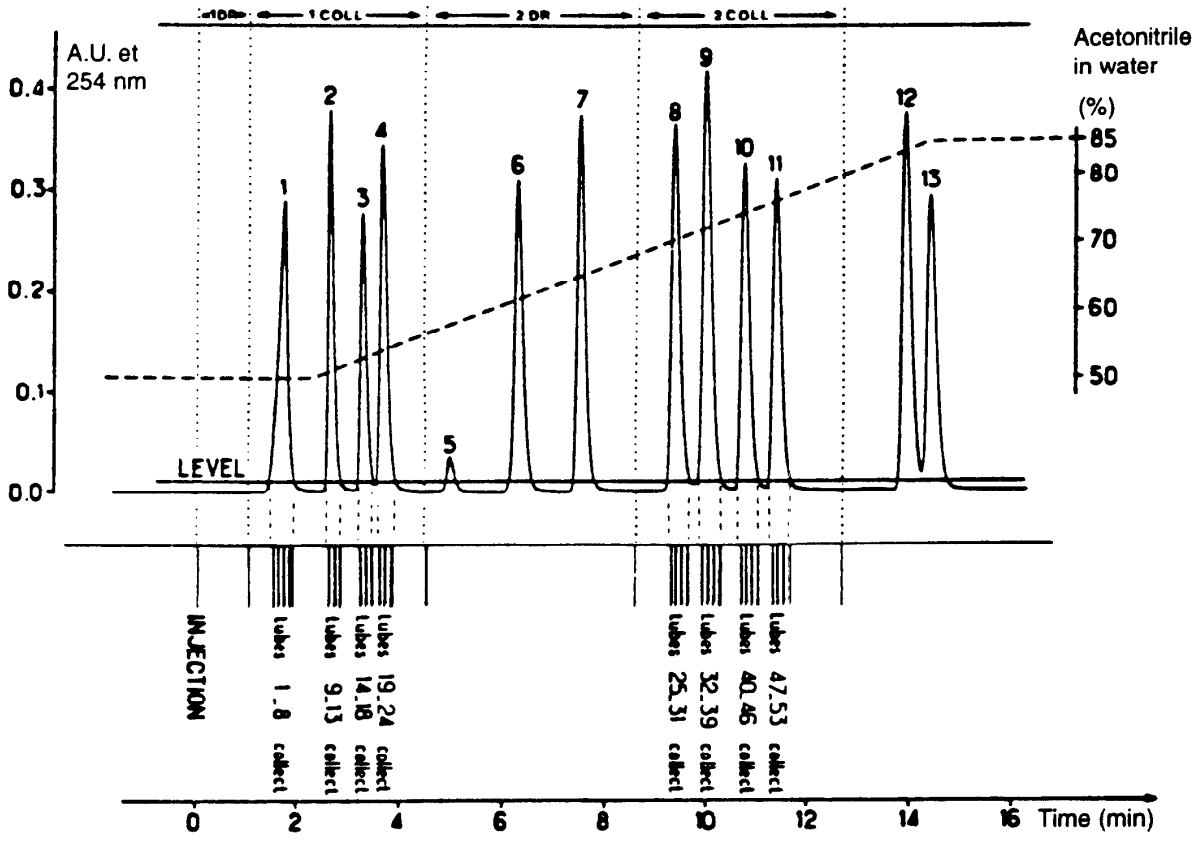


Figure 3 Collection in *time program* plus *peak* plus *time* mode. This multimode protocol involves two collection time windows, peak detection (based on slope) within those time windows, and subfractionation of the peaks by time per tube.

to stop the system and change tubes or racks, thereby enabling automated, unattended operation.

Detection of peaks by the fraction collector is determined by the collector's calculation of a minimum baseline *slope*. In the *peak* mode, a two-parameter algorithm is typically used to calculate a master slope: (1) the height of the smallest peak of interest (in millivolt), and (2) the width of an average peak, measured at half-peak height. The master slope enables the fraction collector to distinguish the baseline from the smallest detectable peak. All calculated baseline slopes below the master slope value are considered as baseline drift and are not collected. The collector can also identify merged peaks by recognizing that the falling slope of one peak is directly adjacent to the rising slope of the next.

As an alternative to peak collection, based on slope, fraction collectors can also collect by a user-specified millivolt *level* of the detector's output. This is sometimes referred to threshold-based collection. Peaks above the specified millivoltage level are collected, whereas peaks below the level are directed to waste. This enables collection of only the most concentrated part of the peak, or when partially resolved peaks are to be collected in a single fraction. Peak width parameters are used to filter noise and to determine the width of a safety window so that the fraction collector does not miss the specified eluate volume. As shown in Figure 4, the shaded peak areas and event marks in the chromatogram plot show how setting the level at different millivoltage values affects the amount of effluent collected for peaks.

III. APPLICATIONS

In preparative HPLC, fraction collection is likely to be employed for two extreme applications: (1) the purification of one or a few major components; or (2) the isolation of trace components or impurities in the presence of main components [5]. The first problem is generally solved by the millivolt level (threshold) collection mode with time or drop "subfractionation" of each peak. Slope-detecting peak collection mode with equal time slices is often the best solution to the second problem.

An example of the isolation of several minor components is given in Figure 5 [5]. Impurities and by-products in a triazine fungicide preparation were isolated for identification purposes. The zone of the major component was screened out by the use of programmable time windows, as was the zone between fractions 7 and 8. In the remaining collection zones, eight fractions were collected, including fraction 1 on the down side of the major component. These by-products were subsequently identified by gas chromatography coupled with mass spectrometry (GC–MS).

A specialized collection technique involves purifications of large volumes of crude samples using high-resolution, small-particle HPLC columns. Because the loading capacities of these columns are typically small (microgram range), and throughput and purity requirements are frequently very high, relatively small volumes of the crude sample need to be repetitively injected and collected to obtain the desired quantity of material. Typically, the entire system is automated for unattended, overnight runs. In this case the fraction collector would operate in a "multicycle" mode. Starting each injection → chromatography → collection cycle at tube 1, the peak (or peaks) of interest are repetitively collected into the same set of vessels. This convenient "autopreparative" technique enables the chemist or technician to collect gram to multigram quantities of target product, yet still use high-resolution columns for complex chromatographic separations.

IV. OTHER TYPES OF FRACTION COLLECTION DEVICES

Process-scale preparative liquid chromatography involves large flow rates and column diameters to meet high-throughput goals commonly seen in many pharmaceutical and biotechnology production laboratories. For these large-volume collection applications, it is sometimes advantageous to use one or several switching valves to divert the column eluate from the

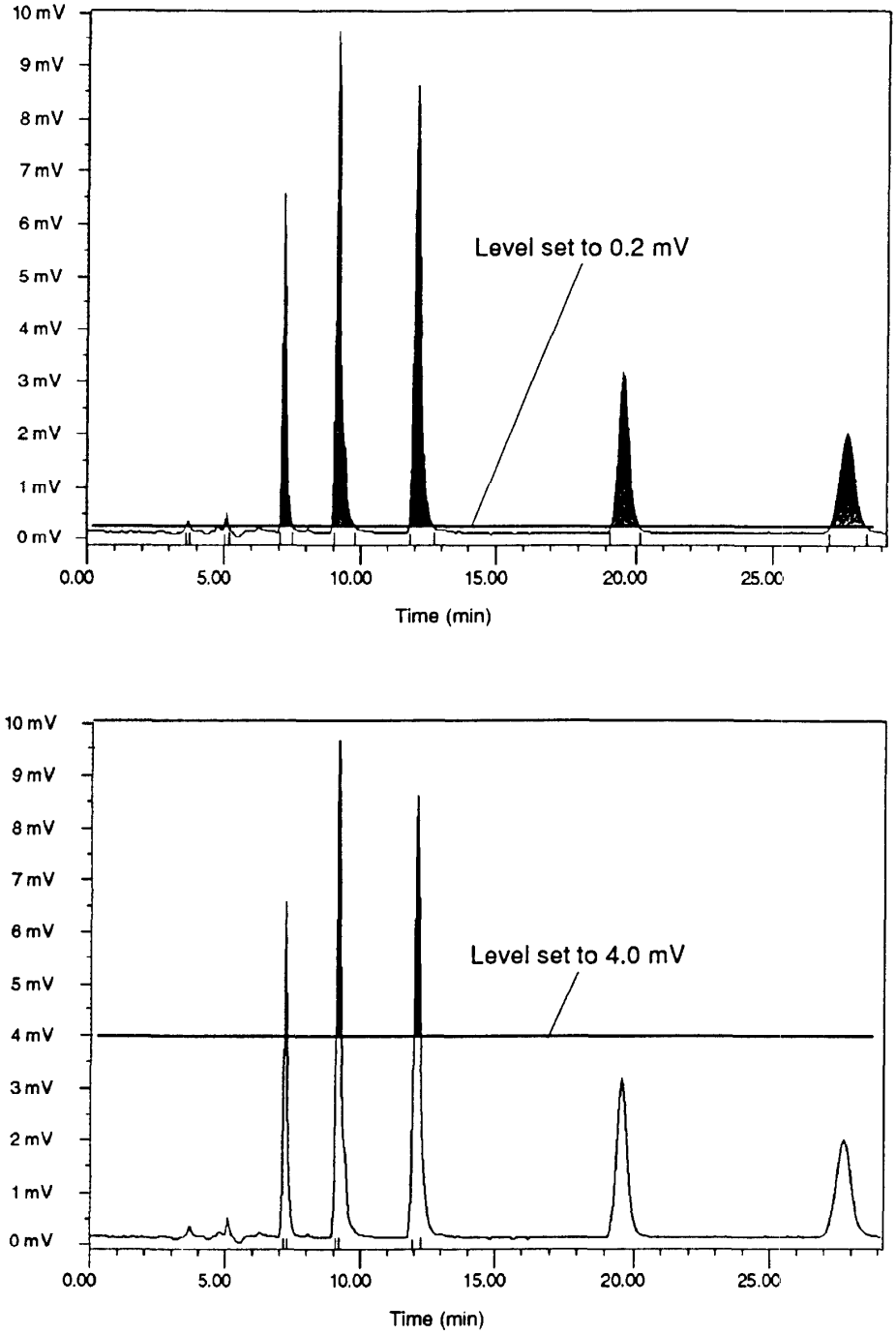


Figure 4 Peak collection based on millivolt (mV) level. The shaded peak areas and event marks in the following chromatograms show how setting the detector input level at different millivolt values affects the amount of eluent collected for peaks.

detector to the appropriate collection vessels (Fig. 6). The low-pressure valves are usually switched by an actuation device in response to a master controller. Valve actuation is initiated on a time window basis or by a peak detection component in the system that monitors the detector signal. In the latter, collection can be performed by either peak-detecting slope algorithms or by user-specific millivolt threshold level settings.

Another valve-switching technique enables injection of the sample and fraction collection on the same instrument. This allows unattended purifications from injection to chromato-

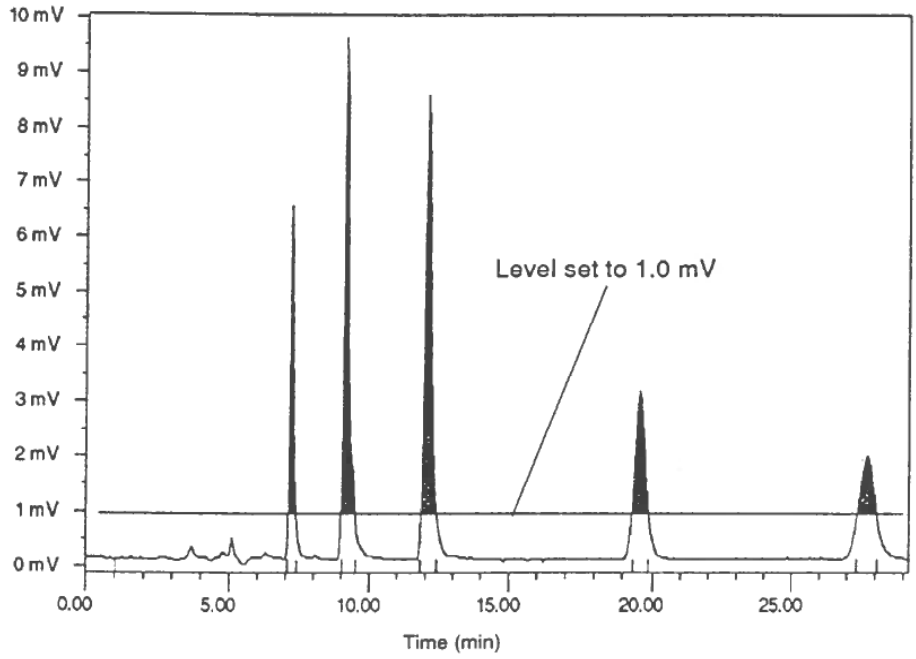


Figure 4 Continued

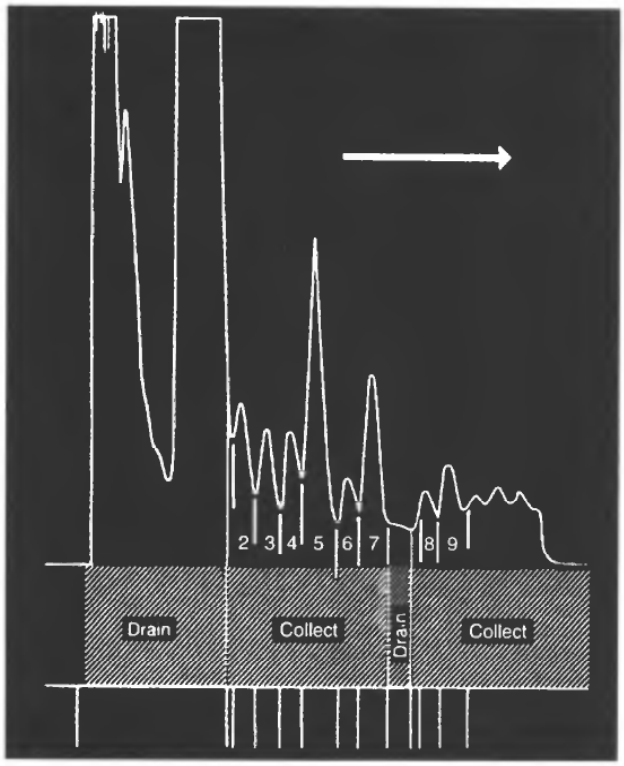


Figure 5 Isolation of several minor impurities in a complex chromatogram. The early-eluting component was screened out with programmable collection time windows. The remaining peaks were collected in peak mode and subfractionated by time per tube.

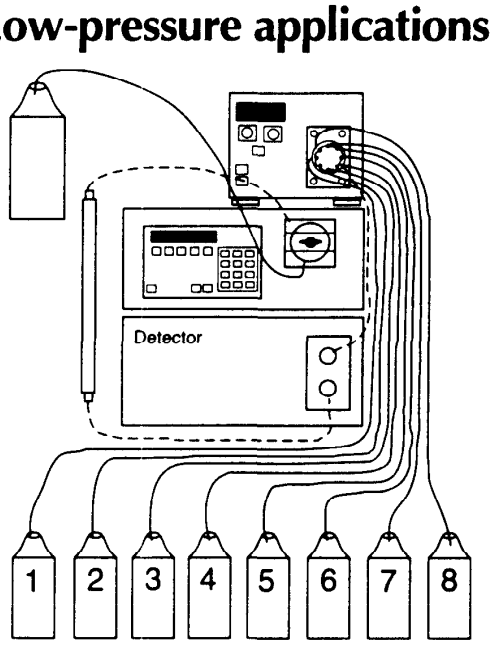


Figure 6 Large-volume fraction collection with a valve-switching device. The eluate from the detector automatically diverts fractions into appropriate collection vessels.

graphic separation to fraction collection, and if desired, reanalysis of the purified target compounds. HPLC autoinjectors with a dual valve design can use one valve for sample injection and the second valve as a switching and collection valve. Figure 7 shows a schematic diagram of the dual valve system for injection and fraction collection. After injection of the sample and when the peak is detected, the switching valve turns so that the band is diverted through the injection needle to a collection vial in which the pure compound is deposited. Fraction collection is determined by the detector signal and is performed by either threshold- or time-based modes. Collection of multiple bands per injection is possible. Collection into sealed vials helps protect fragile biomolecules from evaporation or contamination by oxygen, metal ions, heat, or light. The collected fractions can even be reinjected on the same column for purity checks.

V. TROUBLESHOOTING

Fraction collectors are very reliable and easy to operate, but as with any laboratory instrument, occasional malfunctions can occur. Listed in Table 2 are some of the more common problems and possible solutions.

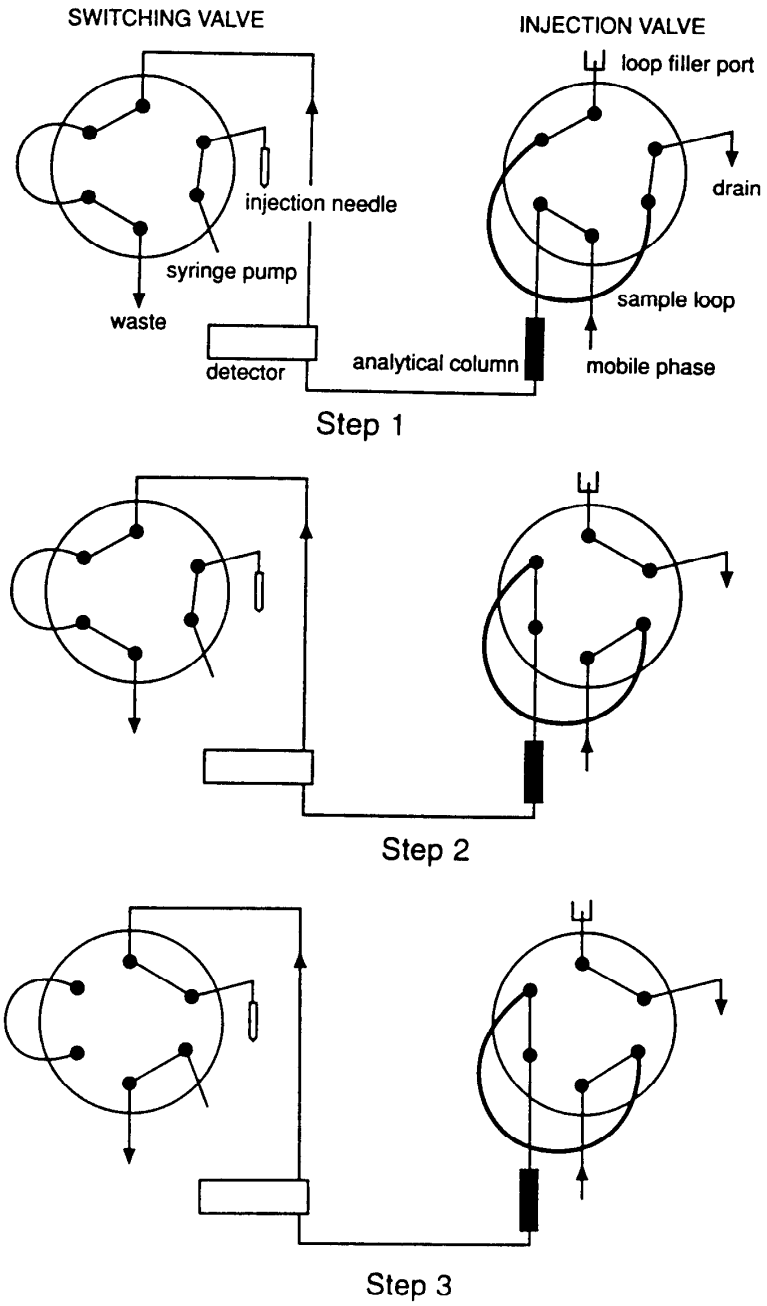


Figure 7 Injection and fraction collection in sealed vials with a dual valve HPLC autoinjector. This schematic illustrates the three steps of the process. (Step 1) sample is loaded in the loop of the injection valve. (Step 2) the sample is injected and the separation starts. The switching valve remains unchanged until detection of the first peak. (Step 3) fraction collection begins when the peak is detected. The switching valve turns so that the peak eluate is diverted through the needle into a collection vial. The valve is switched back after peak elution and the system is ready for the next injection.

Table 2 Troubleshooting Fraction Collectors

Problem	Solution
Drops missing test tube	Check to be sure rack (or carousel) in program matches rack (or carousel) you are using Check rack (or carousel) location. It may be out of position on tray or locator base Check for crimp in effluent tubing. Replace tubing into dispense head Check mechanical arm assembly for alignment. Contact factory for realignment
Drop detector not counting drops, or unreliable counting	Check for bent tubing in dispenser head's drop detector Be sure the inlet tubing fitting is completely tightened Clean or replace glass collar in drop detector Replace drop detector assembly
Not recognizing peaks in peak mode	Check detector input voltage. Should be less than 100 mV full scale Check peak parameters Check polarity. Connections from detector may be incorrect
Input–output functions not operating	Make sure connections to terminal block connector are secure Make sure terminal block connector is secure Check connections for proper pin assignments Confirm that source supplying input to fraction collector is working
Unit is completely dead	Make sure power is ON Check AC power cord connections Try different AC outlet Check fuse(s); replace if necessary. Contact factory if unit continues to blow fuses

20

HPLC Application of Drugs in Biological Samples

James T. Stewart

College of Pharmacy, University of Georgia, Athens, Georgia

I. INTRODUCTION

High-performance liquid chromatography (HPLC) continues to be a very popular analytical technique for the analysis of drugs and related compounds in biological samples. Its popularity resides in its ease of operation and its ability to separate closely related analytes with excellent selectivity and sensitivity. The cost of purchasing HPLC equipment is within the budget of almost all laboratories, and the instrumentation is highly reliable and can be easily maintained by most laboratory personnel. There are environmental concerns with the quantities of organic waste associated with HPLC, but the use of narrow-bore and microbore columns and, more recently, the introduction of a 1.5-μm nonporous silica column will enable the analyst to use even less mobile phase for a given separation.

A biological sample is a unique material of biological orgin that is prepared in a reproducible manner and includes samples such as blood, plasma, serum, feces, saliva, sputum, tissue, and hair. Chamberlain has addressed the issues of special problems associated with biological samples [1]. Detection of a drug or related substance in a biological sample is usually complicated by the matrix. Therefore, cleanup procedures are employed to effectively separate drugs from endogenous materials. The ultimate sensitivity and selectivity of an assay may be limited by the efficiency of the cleanup methods. The *sensitivity* or *limit of detection* (LOD) of a given assay for a drug in a biological sample is related to the lowest levels of drug that the process can reliably differentiate from background levels. *Specificity* concerns the ability of an assay to measure only what it is intended to measure. The *limit of quantitation* (LOQ) for a particular analyte is that concentration that can be measured with an agreed on level of confidence. Precision and accuracy are inherent factors in any biological sample assay. *Precision* is the closeness of replicate measurements by an assay, and *accuracy* is the closeness of the measured value to the true value. The use of fluorescence (FL), chemiluminescence, and electrochemical (EC) detection, and the development of pre-and postcolumn irradiation, chemical derivatization, and ion-pair methods have definitely affected HPLC by increasing the limits of detection and creating improvements in specificity. McDowall et al. have discussed the future role of automation in HPLC assay of biological samples [2].

Analytical method validation is an important step in biological sample assays. It includes all of the procedures required to demonstrate that an assay method for the quantitative analysis of an analyte(s) in a particular matrix is reliable. The parameters necessary to ensure the acceptability of an analytical method are stability of the analyte in the matrix, accuracy, precision, specificity, and reproducibility [3].

Usually samples are frozen immediately after collection and thawed before assay. When drugs are susceptible to plasma esterases, esterase inhibitors, such as sodium fluoride, are added to the sample before freezing. Although most drugs can be conveniently stored at −20°C, a few drugs must be stored at −60°C or lower to prevent degradation. The storage container is an important entity in any biological sample assay. Glass is usually recommended because loss of drug and leaching of plastic components have occurred with plastic containers. Because some drugs can also be adsorbed onto a glass surface, many investigators silylate glass surfaces before their use as storage containers or in the actual assay method.

Sample preparation is essential in the HPLC analysis of analyte(s) in biological samples. Often, there is the necessity to concentrate the analyte to the detection range, or to greatly improve specificity by removing or separating the many endogenous components, or to free the analyte from matrix components such as proteins or other macromolecules. A perusal of the current drug literature indicates that there is a growing interest in the use of solid-phase extraction (SPE) in the disk and cartridge form as a biological sample cleanup technique and in the use of direct biological sample injection into the HPLC flowing stream [4]. The latter procedure is especially popular among those analysts who have less than 500 μL of total samples. Krishnan and Ibraham have written a review on the solid-phase extraction technique in assay of biological samples [5].

In this chapter, HPCL assays of drugs and related substances in biological samples are discussed. The HPLC applications are discussed in terms of individual drugs, listed in alphabetical order, and not therapeutic categories. Because literally, there has been an explosion of HPLC literature in bioanalysis over the past 10 years, this discussion will center on newer methods that have been reported in the last 6 years. There is no intention to imply that these drugs are more important than the thousands of other biologically active compounds. The reader is referred to Marcel Dekker books on *HPLC in Clinical Chemistry* [71] and *Therapeutic Drug Monitoring and Toxicology* [72] for additional information on this subject.

II. ACYCLOVIR

An assay for acyclovir in serum using ultrafiltration was reported by Nebinger and Koel [6]. Acyclovir is a nucleoside that demonstrates strong and selective activity against herpes simplex and varicella–zoster virus. The assay included a heat inactivation step at 56°C to prevent risk of infection to the analyst. Ultrafiltration was employed before injection of the sample onto a 12.5-cm × 4-mm–id octylsilane column. The ion-pair separation was achieved using a mobile phase of 5:95 v/v methanol–0.1-M phosphate buffer, pH 3.0, containing 0.05 M of 1-octanesulfonic acid. The flow rate was 1 mL min^{-1} and detection was at 254 nm with guanosine as internal standard. A 97–100% recovery from serum was reported, with linearity in the 0.5–100 μg mL^{-1} range. Precision was in the 1–8% range and the LOD was 50 ng mL^{-1}. The method should be excellent for therapeutic drug monitoring and could also be used to measure the drug in a wide range of clinical situations.

III. ALCLOFENAC

Delbeke et al. have reported an HPLC determination of alclofenac in equine plasma and urine [7]. Alclofenac is a nonsteroidal anti-inflammatory drug that has both analgesic and antipyretic actions. The assay method used liquid–liquid extraction with diethyl ether for plasma samples and a solid-phase extraction (SPE) method for urine employing C_{18} cartridges. A 2-mL portion of plasma was treated with internal standard solution (diclofenac, 50 μg mL^{-1}) followed by 250 μL of 1-M hydrochloric acid. The mixture was extracted with 5 mL of diethyl ether for 15 min, centrifuged, and the organic layer evaporated to dryness at 36°C. The extraction was repeated and the combined residues were dissolved in 200 μL of mobile phase and 20 μL injected onto the analytical column. The SPE method consisted of adding a 0.5-mL urine

sample containing pH 6 phosphate buffer to a preconditioned C_{18} SPE cartridge. The cartridge was then washed with buffer, and the alclofenac and internal standard were eluted with 80:20 v/v methanol–water. Twenty microliters were injected into the liquid chromatograph. Linearity of the method for plasma and urine samples was 0–10 and 0–20 μg mL^{-1}, respectively. The LOD was 0.1 μg mL^{-1}, based on a 2-mL–plasma sample. The LOQ was 1 μg mL^{-1}, based on a 0.5-mL–plasma sample. The UV detector was set at 220 nm. A 100-cm × 3-mm–id octadecylsilane column was used for the separation. The mobile phase for plasma samples was a 99:1 v/v acetonitrile–aqueous 1% acetic acid mix. The mobile phase for urine samples was 45:55 v/v acetonitrile–aqueous 1% acetic acid. The flow rate for both types of samples was 0.5 mL min^{-1}. Extraction recoveries were in the 76–77% range for plasma and 95–97% range for urine. Retention times for alclofenac and diclofenac internal standard from plasma samples were 2.9 and 5.7 min, respectively. In urine samples, the retention times for alclofenac and diclofenac were 3.4 and 7.3 min, respectively.

IV. AMFENAC

Kato et al. have reported the simultaneous determination of amfenac sodium and its metabolite, 7-benzoyl-2-oxindole, in human plasma by HPLC (8). Amfenac sodium is used to treat chronic articular rheumatism, arthritis deformans, and lumbago. A 100-μL–plasma sample containing 100 μL of water, 0.2 g of ammonium sulfate and 100 μL of ethanol with 100 μg mL^{-1} of fenbufen (internal standard) were mixed and centrifuged. Twenty microliters of the ethanol layer was directly injected onto a 25-cm × 4.6-mm–id octadecylsilane column. The mobile phase consisted of a gradient system of various proportions of acetonitrile and pH 7 phosphate buffer. The UV detector was set at 245 nm. The retention times for drug, metabolite, and internal standard were less than 10 min. Recoveries of drug and metabolite from plasma were 92–95% (0.5–10 μg mL^{-1}) and 93–98% (40–400 ng mL^{-1}), respectively. Intraday and interday variabilities were 4.5 and 4.2% and 3.6 and 4.2% for drug and metabolite, respectively. The LOD for drug and metabolite were 100 and 20 ng mL^{-1}, respectively.

V. AMOXICILLIN

An HPLC assay for amoxicillin in human plasma was reported by Krauwinkel and co-workers [9]. Amoxicillin is a widely used broad-spectrum antibiotic of the β-lactam family. A 150-μL–plasma sample was mixed with 1.5 mL of phosphate buffer pH 7.0, and 20 μL of water. The sample was passed through an SPE C_8 cartridge and eluted on-line into the 25-cm × 4.6-mm–id octadecylsilane analytical column maintained at 30°C. The mobile phase was 80:20 v/v phosphate buffer pH 7.6–methanol containing tetrabutylammonium (TBA) dihydrogenphosphate at a flow rate of 1 mL min^{-1}. The on-line elution from the C_8 SPE cartridge was near quantitative. The TBA counterion was necessary for extraction of amoxicillin, but penicilloic acids were also obtained, which interfered with the HPLC separation of amoxicillin on the C_{18} analytical column. If TBA was omitted, the amoxicillin recovery decreased, but was reproducible (63–64%). The LOD was reported to be 25 ng ml^{-1} (signal to noise ratio; S/N = 3). Accuracy was excellent (<5%) and the intra- and interday precisions are in the 0.02–0.38% and 0.08–0.82% ranges, respectively.

Another HPLC method for amoxicillin in urine was reported by Chulavatnatol and Charles [10]. Urine sample cleanup used a C_{18} solid-phase extraction cartridge. To 1 mL of urine was added 100 μL of 0.5-M aqueous tetrabutylammonium bromide. The sample was applied to the SPE cartridge and 9 mL of a 3% acetonitrile on 0.01-M phosphate buffer pH 7.1 was used to elute the drug. After adjustment to 10 mL, 30 μL was injected into the LC. The separation was achieved on a 25-cm × 4.6-mm–id octadecylsilane column using a mobile phase of 32.5:67.5 v/v acetonitrile–0.01-M phosphate buffer pH 7.1, at a flow rate of 1.2 mL min^{-1}. With UV detection at 229 nm, the method was linear in the 5–500 μg mL^{-1} range.

Recovery from urine was more than 94%. No internal standard was used. The LOQ was 7.5 $\mu g\ mL^{-1}$. Intra-and interday precision were in the 3–16% range, and accuracy of the method was less than 7.1%.

VI. ASCORBIC ACID

Watson et al. have reported the HPLC measurement of ascorbic acid in human aqueous humor and plasma and in bovine aqueous humor using electrochemical detection [11]. A 200-μL volume of 30% trichloroacetic acid was added to 50-μL samples of bovine or human aqueous humor (preserved with metaphosphoric acid). After centrifugation, 1 μg of hydroquinone (internal standard) was added to the supernatant and the mixture diluted to 1 mL with mobile phase. A 50-μL aliquot was injected into the HPLC system. The same procedure was also applied to sample preparation with human plasma samples. The analytical column was a 10-cm × 4.6-mm–id octadecylsilane, and the mobile phase was 5:95 v/v acetonitrile–water containing 0.08 M of sodium acetate and 0.001 M of cetyltrimethylammonium bromide (pH adjusted to 4.2 with glacial acetic acid). The flow rate was 1 mL min^{-1}, and the potential of the amperometric detector was set at +0.6 V versus Ag/AgCl. The retention times of ascorbic acid and internal standard were approximately 4 and 6 min, respectively. Linearity of the procedure was in the 0.5 to 5-$\mu g\ mL^{-1}$ range. The precision of replicate measurements was 1.49% (n = 5). The reproducibility of five separate assays of the same sample was 1.63%.

VII. BAY y3118

Schaefer has reported an HPLC method to determine BAY y3118, a novel 4-quinolone, in biological fluids using a photothermal postcolumn derivatization step [12]. The chemical structure of the compound is shown in Fig. 1. The compound has outstanding antimicrobial activity against gram-negative and gram-positive pathogens, as well as anaerobic and intracellular bacteria. A direct injection of a plasma sample (diluted with 0.05-M phosphoric acid) or urine sample (diluted with 0.1-M phosphate buffer pH 7.5) was made onto a 25-cm × 4.6-mm–id octadecylsilane column. The mobile phase was 19:81 v/v acetonitrile–water, containing tetrabutylammonium bromide, adjusted to pH 2 with phosphoric acid. At 1-mL min^{-1} flow, the column temperature was maintained at 50°C. The postcolumn derivatization involved the passing of the analytical column eluate through PTFE capillary tubing wrapped around a mercury UV lamp. Either photolysis or a combination of thermolysis and photolysis gave a derivatized compound. The excitation and emission wavelengths used for the fluorometric detector were 277 and 418 nm cutoff filter, respectively. The LOD was reported to be 10 ng mL^{-1}.

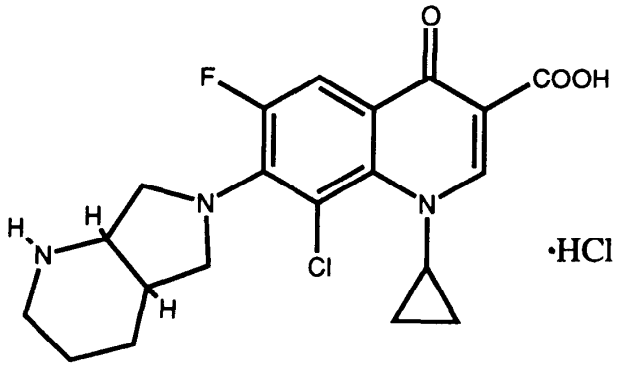
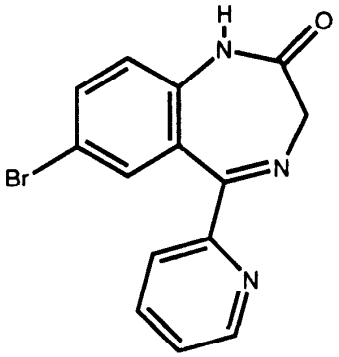


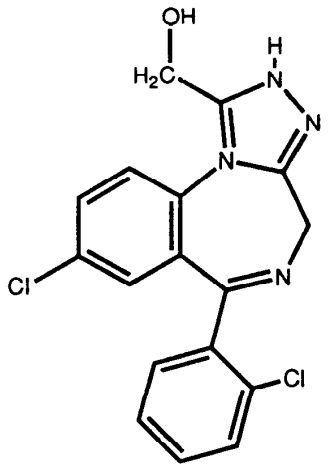
Figure 1 Chemical structure of Bay y3118.

VIII. BROMAZEPAM

Solleu et al. have reported an HPLC method for bromazepam in plasma [13]. Bromazepam belongs to the 1,4-benzodiazepine class of antianxiety agents. It has been extensively used in anxiolytic therapeutics. The drug and internal standard (α-hydroxytriazolam) were extracted from alkalinized plasma using diethyl ether. The chemical structures of bromazepam and the internal standard are shown in Fig. 2. The ether was separated, evaporated to dryness, the residue dissolved in 100 μL of mobile phase, and 20 μL was injected into the HPLC system. The separation was achieved on a 15-cm × 3.9-mm–id octadecylsilane column, using a 700:300:4 v/v/v acetonitrile–water–triethylamine pH 7.4 mobile phase. Typical chromatograms of blank and spiked plasma samples are shown in Fig. 3. The LOD was 50 ng mL^{-1} based on UV detection at 240 nm (S/N = 3). Inter- and intraday precisions were less than 6%. Recovery of drug from urine was 97–104%. The limit of quantitation (LOQ) was established at 50 ng mL^{-1} (S/N = 10). Accuracy of the method was in the 94–103% range (intraday) and 91–102% (interday). The method allowed the separation of bromazepam from most of the other benzodiazepines or structural analogues.



Bromazepam



α - Hydroxytriazolam

Figure 2 Chemical structures of bromazepam and internal standard α-hydroxytriazolam. (From Ref. 13.)

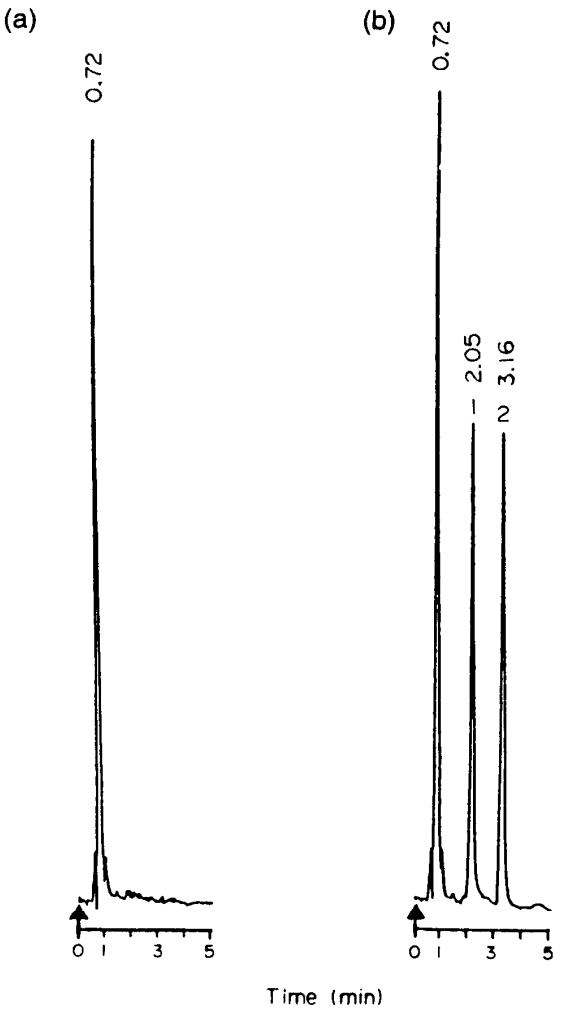


Figure 3 Typical chromatograms of (a) human drug-free plasma; (b) human plasma, after extraction, containing 2 μg mL^{-1} of bromazepam (peak 1 corresponds to bromazepam and peak 2 to internal standard). (From Ref. 13.)

IX. BUPRENORPHINE AND NORBUPRENORPHINE

A column-switching, solid-phase trace enrichment HPLC method for the measurement of buprenorphine and norbuprenorphine in human plasma and urine was reported by Schleyer et al. [14]. Buprenorphine is a relatively new analgesic with morphine-like action. It is chemically derived from thebaine and shows agonistic and antagonistic activity at the micro-opiate receptor. It exceeds the potency of morphine by 25- to 40-fold. The trace enrichment was accomplished on a 4-cm × 4-mm–C_{18} cartridge using an eluent of 0.05 M of phosphate buffer pH 8.5 with 20% acetonitrile for elution of buprenorphine and 10% acetonitrile for metabolite elution. The flow rate in the trace-enrichment system was 2 mL min^{-1} at ambient temperature. A 30-cm × 4-mm–id C_{18} column was sufficient for the chromatography using a 75:25 v/v phosphate buffer–acetonitrile mixture for the drug and an 80:20 v/v phosphate buffer–acetonitrile mixture for the metabolite. The flow rate was set at 0.8 mL min^{-1} and the electrochemical detector (glassy carbon) was set at +0.48 V versus Ag/AgCl. The total analysis time was 16 min. The LOD was 40 pg mL^{-1}. Recoveries of drug and metabolite from plasma and urine were 77–83 and 70–76% and 75–81 and 73–81%, respectively. Intra-assay RSDs were in the 6–17% range.

X. CANRENONE

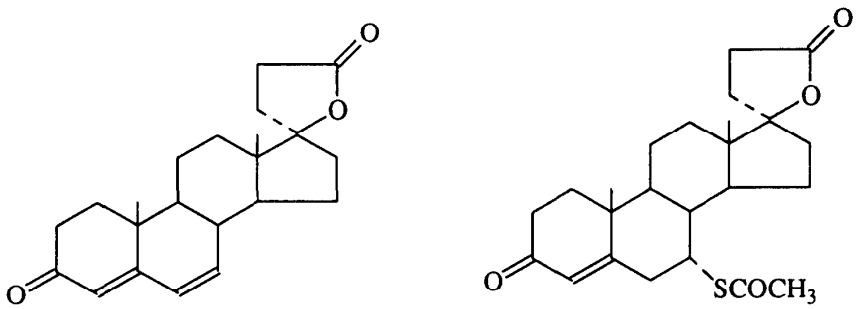
Zhang and Stewart have reported an HPLC method for the determination of canrenone in human serum [15] Canrenone is a dethioacetylated derivative of spironolactone, a steroidal compound that has properties consistent with specific competitive antagonism of aldosterone and other mineralocorticoids. Canrenone appears to play an important role in the pharmacological activity of spironolactone, even though it is not the principal metabolite. Because canrenone has a relatively long half-life, there is considerable accumulation during long-term therapy of spironolactone; thus, canrenone can be used as a monitor of spironolactone levels. The chemical structures of canrenone and spironolactone are shown in Fig. 4. A 1-mL–serum sample containing internal standard (5-adrostan-17-ol-3-one) was passed through a 1-mL–C_{18} SPE using vacuum. After washing with water, the analytes were eluted using 2 to 500-μL aliquots of acetonitrile. After evaporation to dryness, the residue was dissolved in mobile phase and duplicate 100-μL injections were made into the LC system. Chromatography was achieved on a 25-cm × 4.6-mm–id octadecylsilane analytical column, equipped with a ODS guard column and maintained at ambient conditions. The model phase was 50:50 v/v acetonitrile–water at a 1-mL min^{-1}–flow rate and UV detection at 280 nm. Retention times for canrenone and internal standard were 10.9 and 11.9 min, respectively (Fig. 5). Linearity was reported to be in the 10–340 ng mL^{-1} range in serum. The LOQ was determined to be 10 ng mL^{-1} and the LOD was 3 ng mL^{-1} (S/N = 2). Intra- and interday precision and accuracy were in the 2–4 and 0–4% and 0.2–2.4 and 4.4–5.9% ranges, respectively.

XI. CARBAMAZEPINE

A direct-injection HPLC approach to the analysis of carbamazepine and its active 10,11-epoxide metabolite in plasma was reported by He et al. [16]. The stationary phase consisted of an octadecylsilane ligand as a hydrophobic inner phase and a polyoxyethylene network as a hydrophilic outer phase (semipermeable surface column, Regis Chemical Co.). A 5-μL aliquot of plasma was injected onto the column. The mobile phase was 4:1 v/v pH 7.1 phosphate buffer (ionic strength 0.1)–acetonitrile at a flow rate of 1 mL min^{-1}. On this 15-cm × 4.6-mm–id column, the plasma proteins were size-excluded, but the drug and metabolite were retained. Chromatograms illustrating the separations are shown in Fig. 6. The assay time was 17 min and recoveries from plasma were essentially quantitative. The method linearity was in the 1- to 70-μg mL^{-1} range for drug and metabolite which was favorable because the therapeutic plasma levels of carbamazepine were in a relatively narrow range (4–12 μg mL^{-1}).

XII. CARBAMAZEPINE, PHENYTOIN, PHENOBARBITAL, AND PRIMIDONE

A simultaneous determination of carbamazepine, phenytoin, phenobarbital, and primidone and their principal metabolites by HPLC with photodiode-array detection was reported by Liu et al. [17]. A 100-μL–serum or saliva sample was treated with 200 μL of acetonitrile to denature the proteins in the sample. For urine, no protein denaturation was needed. However, a SPE method for urine was developed using a 2-mL urine sample passed through a C_{18} Sep-pak and 0.5 mL of acetonitrile was used as eluent. A 2-μL aliquot of the denatured serum or saliva sample or the urine eluate was directly injected onto a 25-cm × 2-mm–id octadecylsilane column maintained at 40°C. The drugs and metabolites were separated using a mobile phase of 110:50:30 v/v/v phosphate buffer–acetonitrile–methanol at a flow rate of 0.2 mL min^{-1}. The recovery of the analytes from the biological samples was in the 95–104% range. The retention times were all within 15 min. Intra- and interday variability, as measured by percentage RSD were less than 5% and 2.3–4.8%, respectively.



CANRENONE SPIRONOLACTONE

Figure 4 Chemical structures of canrenone and spironolactone. (From Ref. 15.)

XIII. CATECHOLAMINES

A general determination of catecholamines (norepinephrine [NE], epinephrine [E], and dopamine [DA]) in urine or plasma by on-line sample pretreatment, using an internal surface boronic acid gel, was reported by Soga and Inoue [18]. The new internal surface support was designed with a carboxymethylcellulose-bonded external surface that was nonadsorptive to

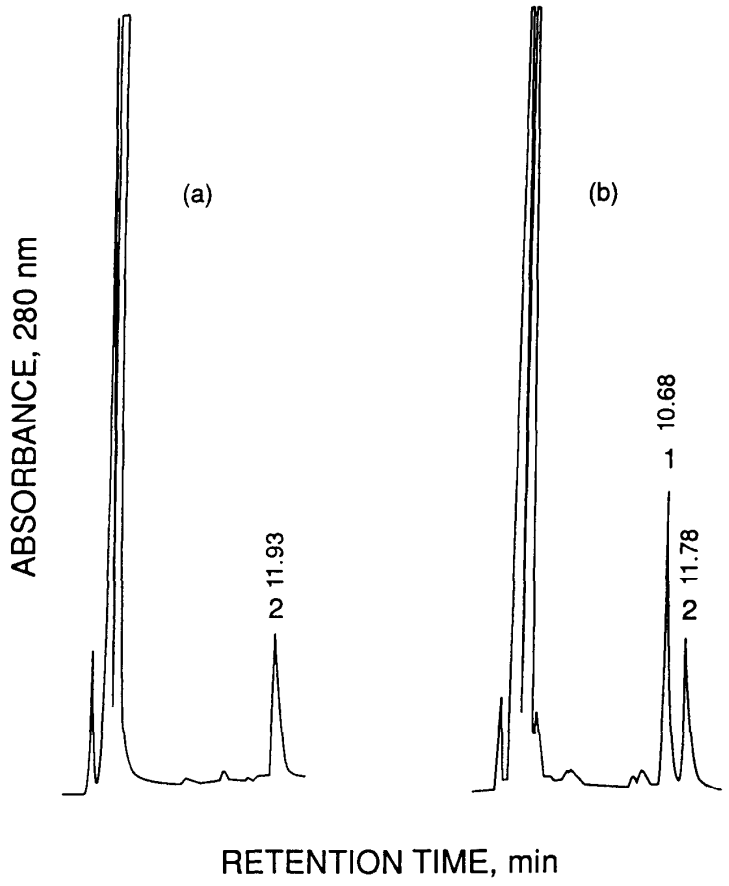


Figure 5 Typical chromatograms of (a) blank serum and (b) serum spiked with 195 ng mL^{-1} of canrenone. Peak 1 is canrenone and peak 2 is the internal standard at 100 μg mL^{-1}. (From Ref. 15.)

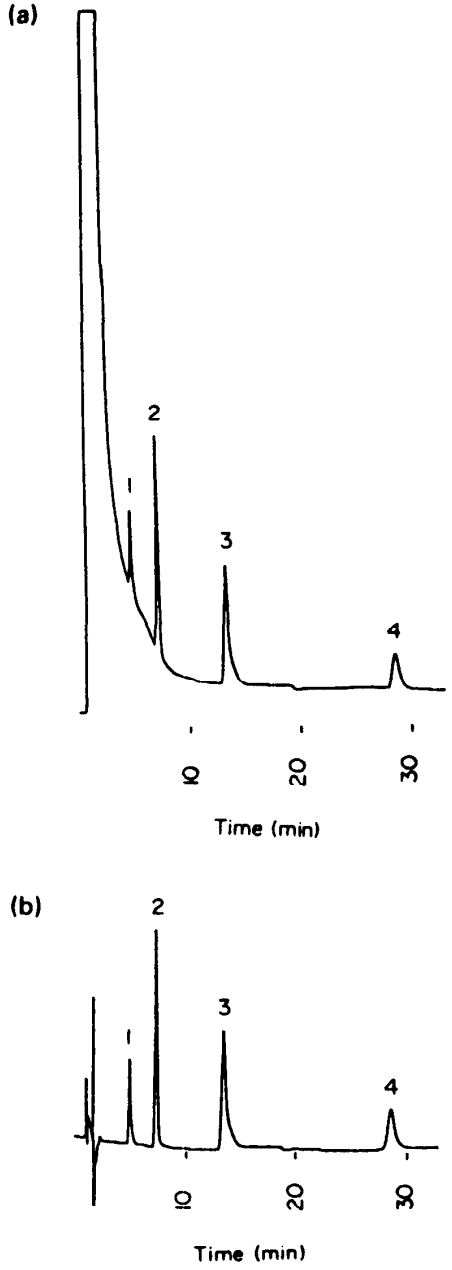


Figure 6 Chromatogram of (a) spiked plasma and (b) standard solution samples; 1, EPO; 2, PB; 3, CBZ; and 4, DPH. HPLC conditions: column, SPS C_{18} (15-cm × 4.6-mm–id); mobile phase, phosphate buffer (pH 7.1, ionic strength 0.1)–acetonitrile (4:1, v/v); flow rate, 1.0 mL min^{-1} for 0–17 min, 1.5 mL min^{-1} after 17 min; detection, UV, 214 nm; injection volume, 5 μL; column temperature, 30°C. (From Ref. 16.)

proteins and a phenylboronic acid-bonded internal surface that retained only catecholamines. Urine or plasma samples were transported to the internal surface column using a buffered mobile phase. The catecholamines formed boronic acid complexes and adsorbed onto the column, thereby allowing other compounds to elute to waste. After washing the column, a valve was switched and the eluate was eluted to the analytical column using the mobile phase, which dissociated the catecholamine–boronic acid complexes. The analytical column for urine was a 25-cm × 4.6-mm–id octadecylsilane column and for plasma was a 15-cm × 4.6-mm–id

cation-exchange column. An electrochemical detector was employed. The mobile phase for urine samples was 50 mM of phosphate buffer, pH 3–200 mM potassium nitrate, and 0.07 mM EDTA at a flow rate of 1.2 mL min^{-1}. The plasma mobile phase consisted of 15 mM citric acid, 65 mM sodium nitrate, 0.07 mM EDTA, pH 2.2, at a flow rate of 1 mL min^{-1}. The LODs for NE, E, and DA were 10, 15, and 11 pg mL^{-1}, respectively. The LOQs were 1–3 ng mL^{-1} in urine and 10–15 pg mL^{-1} in plasma (S/N = 3). The reproducibilities of analyte peak areas were 2.9% for NE and 3.5% for E and DA.

XIV. CELIPROLOL AND DILTIAZEM

Rutledge and co-workers reported an HPLC assay for celiprolol and diltiazem and its metabolites in human plasma [19]. An increased interest in coadministration of celiprolol (β-adrenergic blocking agent) and diltiazem (calcium channel antagonist) led to the development of the method. The drugs were extracted by a backextraction procedure using hexane–isopropanol and 5 mM of sulfuric acid. A portion of the aqueous acidic solution was injected into the HPLC system. The chromatography was performed using a 25-cm × 4.6-mm–id short–alkyl-chain silanol-deactivated column (SCD 100, SynChrom, Lafayette, IN) at ambient temperature. The mobile phase consisted of 50:50 v/v 0.04-M dibasic potassium phosphate, pH 5.5–methanol. The flow rate was set at 1 mL min^{-1} with UV detection at 237 nm. The curves for celiprolol and diltiazem or its two principal metabolites were linear over 50–3000 ng mL^{-1} and 20–400 ng mL^{-1}, respectively. Mean extraction efficiencies for the analytes were in the 60–85% range, except for celiprolol (= 18%). The low recovery for celiprolol was due to the use of a high 8.9 pH during the liquid–liquid extraction. The LODs for celiprolol and diltiazem were 4.5 and 3.0 ng mL^{-1}, respectively. The metabolite LODs were also in the same range. Within-day and between-day precisions were in the 3.4–9.6% range (n = 10).

XV. CHLOROQUINE AND CHLOROGUANIDE

The simultaneous determination of chloroquine, chloroguanide (proguanil), and their metabolites in human plasma, erythrocytes, and urine was reported by Chaulet et al. [20]. Chloroquine has been the most prescribed drug for the treatment of malaria for more than 50 years. Chloroguanide has been used since 1946. It forms an active metabolite, cycloguanil, in vivo. Before extraction, whole blood and erythrocytes were diluted with distilled water (1:2 v/v), lysed by ultrasonication, and deproteinated with acetonitrile. Urine was diluted with water (1:99 v/v). A 3-mL–C_8 SPE cartridge was used for sample cleanup. *N*-(2-6 Dichlorobenzylidene amino)guanidine was added to each sample as an internal standard. Elution of the analytes from the SPE cartridge was accomplished using 2 mL of methanol containing 0.1% hydrochloric acid. After evaporation to dryness with a nitrogen stream, the residue was reconstituted in 200 μL of water and 50 μL was injected. The chromatographic separation was achieved on a 25-cm × 4-mm–id octylsilane column. The mobile phase was 78:28:4 v/v/v water–acetonitrile–methanol, with 0.05-M ammonium formate and 0.075-M perchloric acid, at a 0.5-mL min^{-1}–flow rate. The eluate was monitored by UV detector set at 254 nm. The LOQs for chloroquine and chloroguanide and their metabolites were near 6 and 9 ng mL^{-1}, respectively. There were no interferences from endogenous compounds or other antimalarial agents. The inter- and intra-assay RSDs were less than 6–8% for plasma samples. The chromatographic procedure took about 35 min for separation of each drug and their two metabolites.

XVI. CHLORZOXAZONE

An improved HPLC method for chlorzoxazone and its 6-hydroxy metabolite in human serum and urine was reported by Zhang and Stewart [21]. Chlorzoxazone is a potent skeletal muscle

relaxant that is effective in the treatment of skeletal muscle spasms with no significant side effects. The serum procedure used C_{18} SPE cleanup with injection of the eluent onto a 25-cm × 4.6-mm–id ethylsilane analytical column (Fig. 7). The urine method used a buffer dilution of the urine followed by direct injection onto the analytical column (Fig. 8). Ultraviolet detection of the analyte peaks was at 280 nm (serum) and 295 nm (urine). Recoveries of drug and metabolite from serum and urine were in the 85–103% range. Drug/internal standard peak height ratios were linear in the 0.5- to 50- and 5 to 100-μg mL^{-1} ranges for serum and urine, respectively. The LOQs for chlorzoxazone in serum and urine were 0.12 μg mL^{-1} and 0.62 μg mL^{-1}, respectively. The LOQs for the metabolite in serum and urine were 0.23 and 0.029 μg mL^{-1}, respectively. Accuracy and precision for both serum and urine were in the 0–5% ranges.

XVII. CLOBAZAM AND DIAZEPAM

The monitoring of benzodiazepines, namely clobazam, diazepam, and their active metabolites, in human plasma by column-switching HPLC was reported by Lacroix et al. [22]. Clobazam is often prescribed as an anticonvulsant drug in the treatment of minor seizure disorders in epilepsy. Diazepam is the recommended treatment for controlling status epilepticus or febrile convulsions in children. In the assay procedure, a 100- to 200-μL–plasma sample was subjected to gel filtration. After a wash step with phosphate buffer, the retained analytes were backflushed onto a 7.5-cm × 4.6-mm–id octadecylsilane analytical column, and the separation was achieved using a mobile phase of 33:66:1 v/v/v acetonitrile–phosphate buffer–diethylamine (pH adjusted to 5.4). The UV detector was set at 230 nm and the flow rate was 1 mL min^{-1}. Recoveries of all drugs and metabolites were 90–100%. Intra- and interday precision were 0.9–7.7% (n = 5) and 2.8–12% (n = 7), respectively.

XVIII. CLOZAPINE

Olesen and Poulsen have reported an on-line fully automated determination of clozapine and desmethylclozapine in human serum by SPE on exchangeable cartridges and HPLC using a methanol buffer mobile phase on unmodified silica [23]. The SPE used a cyanopropyl cartridge and elution of the analytes with methanol–ammonium acetate pH 8 mix. Clozapine is a high-dose neuroleptic drug that was developed as an antidepressant agent some 30 years ago. It does not induce extrapyramidal side effects. The most common side effects are sedation, orthostatic hypotension, and hypersalivation, with convulsions reported if serum concentrations of the drug are higher than 1 μg mL^{-1}. A separate liquid–liquid extraction procedure was also developed in which 1 mL of serum was mixed with 0.1-M sodium hydroxide and internal standard (trifluoperazine or imipramine) and extracted with 5 mL of a 99:1 v/v heptane–isoamyl alcohol. After centrifugation, the organic layer was evaporated to dryness at 50°C with the aid of a nitrogen stream. The residue was dissolved in 75 μL of mobile phase and 65 μL was injected. The mobile phase used with the 15-cm × 4.6-mm–id silica analytical column was 85:15 v/v methanol–50 mM ammonium acetate pH 9.9 at a flow rate of 1.4 mL mL^{-1}. There was good agreement between the SPE and liquid–liquid extraction methods. Recoveries of clozapine and imipramine were around 90% and desmethylclozapine and trifluoperazine were about 80%. The UV detector was set at 261 nm and total analysis time was approximately 13 min. The method was linear in the 30- to 3000-ng mL^{-1} range. Interday variability was less than 6 and 8% for clozapine and desmethylclozapine, respectively.

XIX. COCAINE

An HPLC method to determine cocaine, benzoylecgonine, ecgonine methyl ester, and ethyl cocaine in human urine was reported by Roy et al. [24]. Although ecgonine methyl ester is

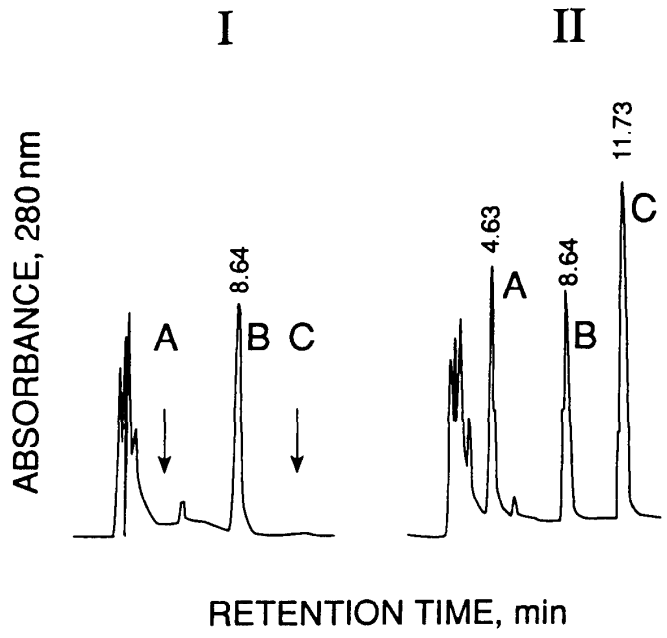


Figure 7 Typical HPLC chromatograms of (I) blank human serum and (II) spiked human serum containing 5 μg mL^{-1} each of (A) 6-hydroxychlorzoxazone and (C) chlorzoxazone. Peak B is the internal standard phenacetin. (From Ref. 21.)

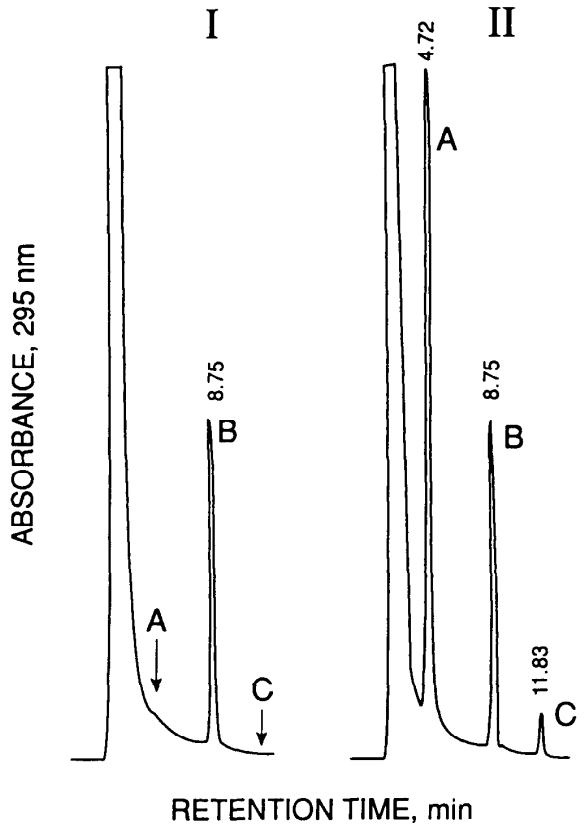


Figure 8 Typical HPLC chromatogram of (I) blank human urine and (II) spiked human urine containing 20 μg mL^{-1} each of (A) 6-hydroxychlorzoxazone and (C) chlorzoxazone. Peak B is the internal standard phenacetin. (From Ref. 21.)

a major metabolite of cocaine, it is rare to see it included in a cocaine assay method owing to poor UV detection and difficult recovery from aqueous-based samples, such as urine. The urine samples were subjected to SPE (Bond-Elut Certify) and the analytes were eluted with 1.5% ammonium hydroxide in 80:20 v/v dichloromethane–isopropanol. Recoveries of 85% for ecgonine methyl ester, 97% for cocaine, 106% for benzoylecgonine, and 80% for ethylcocaine were obtained from urine. The ecgonine methyl ester, benzoylecgonine and norcocaine were derivatized with *N*-methyl-*N*-(*tert*-butyldimethylsilyl)trifluoroacetamide. These derivatives had improved retention and detection sensitivity. The silylated ecgonine methyl ester was stable in HPLC mobile phase for up to 1 week. The HPLC separation occurred on a 25-cm × 2.1-mm–id deactivated octadecylsilane column using an acetonitrile step-gradient from 11–30% acetonitrile in 0.05-M phosphate buffer (pH 4) at 0.4 mL min^{-1} at 7-min postinjection and returned to 11% at 25 min. A postcolumn ion-pair extraction system was developed to ion-pair the analytes with sodium 9,10-dimethoxyanthracene sulfonate (Fig. 9). Methylene chloride was then pumped (0.6 mL min^{-1}) into the mobile phase to extract the ion-pair and the organic solvent routed to a fluorescence detector set at 383-nm excitation and 465-nm emission. Linearity of the method was in the 200- to 1000-ng mL^{-1} range (r = >0.99) for all analytes. LODs of 59, 95, 46, and 81 ng mL^{-1} were obtained for cocaine, ethyl cocaine, benzoylecgonine, and ecgonine methyl ester, respectively.

XX. COUMARIN

A new HPLC method for the assay of coumarin in plasma was reported by Millart and Choisy [25]. Coumarin is a naturally occurring substance widely used at low doses (5–10 mg day^{-1}) as a vascular protectant in the treatment of venous insufficiency symptoms. More recently, higher doses of coumarin (100–400 mg day^{-1}) have been reported. The single-step extraction

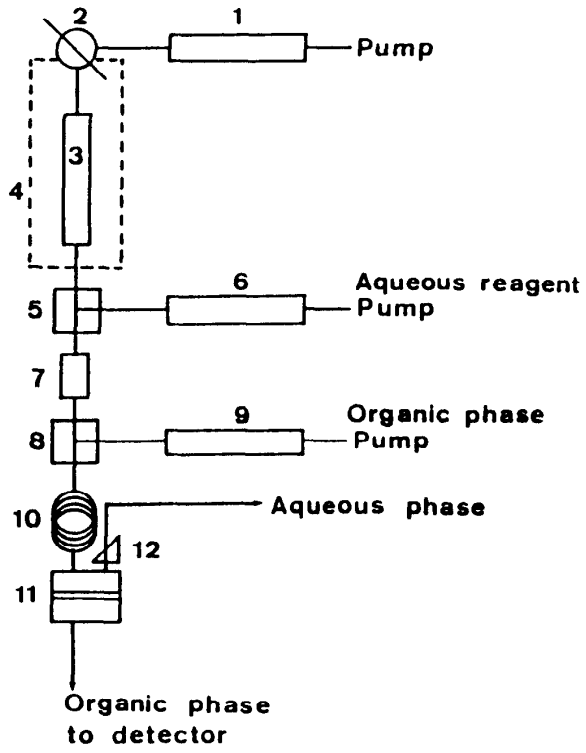


Figure 9 Schematic diagram of HPLC postcolumn system: 1, 6, and 9, in-line columns; 2, injection valve; 3, analytical column; 4, oven; 5 and 8, T-connectors; 7, mixing column; 10, extraction coil; 11, phase separator; and 12, microneedle valves. (From Ref. 24.)

of a 1-mL alkalinized plasma sample with 6 mL of hexane and subsequent evaporation of the organic layer in the presence of 50 μL of 0.2-M hydrochloric acid was followed by chromatography on a 25-cm × 4-mm–id octylsilane column. The UV detector was set at 275 nm, and flunitrazepam was employed as internal standard. The mobile phase was a 60:40 v/v acetonitrile–0.01M phosphate buffer pH 3, containing 0.02-M tetramethylammonium chloride at a flow rate of 1.2 mL min^{-1}. Retention times for coumarin and the internal standard were 5.5 and 9.0 min, respectively. The extraction efficiency for both compounds was approximately 80%. Intra- and interday precisions were in the 5–10% and 14–16% ranges, respectively. The LOD was 0.3 ng mL^{-1} for coumarin.

XXI. DANAZOL

Danazol is a steroidal isoxazole that inhibits output of gonadotropins and suppresses the pituitary–ovarian axis. Selinger et al. have reported an HPLC method for the determination of danazol in human serum [26]. Sample pretreatment involved the extraction of the drug from serum with pentane–methylene chloride (4:1 v/v). The organic layer was evaporated to dryness and the residue dissolved in 200 μL of mobile phase. An internal standard 1,4-androstandiene-3,17-dione was used in the assay. Reversed-phase 15-cm × 3.9-mm–id octyl and 15-cm × 3.9-mm–id octadecylsilane analytical columns were used with a column-switching valve and isocratic elution with 18:22 v/v water–acetonitrile at a 1.6-mL min^{-1}–flow rate and UV detection at 285 nm (Figs. 10 and 11). Retention times for danazol and internal standard were 9.5 and 4.2 min, respectively. The total run time was 14 min at ambient temperature. Linearity of the method was in the 1-to 150-ng mL^{-1} range. Recoveries of the drug and internal standard from serum were 100–108% and 100%, respectively. Within-run and between-run precision were in the 4–15 and 1–4% ranges, respectively. Accuracy of the method was in the 100–108 and 95–98% for within and between runs, respectively.

XXII. DEBRISOQUINE

Debrisoquine is an antihypertensive drug that undergoes oxidative metabolism in humans. The major metabolite is the 4-hydroxy compound and it displays genetic polymorphism. Bozkurt et al. have reported an HPLC assay to measure drug and metabolite levels in urine using solid-phase extraction and fluorescence detection [27]. The extraction of urine samples used a SPE cartridge containing silica modified with carboxylic acid ion-exchange functional groups. A 1-mL–urine sample was applied to a cartridge, followed by washes with water, 50:50 v/v acetonitrile–water, water and 0.5 mL of 0.1-M hydrochloric acid. The analytes were eluted using 3 mL of 40:60 v/v acetonitrile–0.1-M hydrochloric acid. An aliquot of the eluate (60 μL) was injected onto a 30-cm × 4-mm–id octadecylsilane column. The separation was accomplished using a mobile phase of 87:13 v/v 0.1-M aqueous sodium dihydrogen phosphate–acetonitrile at a flow rate of 1 mL min^{-1}. The fluorescence detector was set at 210-nm excitation and 290-nm emission. Retention times for debrisoquine and metabolite were 5.4 and 13.2 min, respectively. The mean recoveries from urine for drug and metabolite were 93.8 and 76.9%, respectively. It was determined that the SPE cartridges could be reused for up to 13 extractions before discard. Linearity of the method was in the 0.1 to 20-μg mL^{-1} range for both analytes. The LODs based on S/N = 2.5 were 25 and 12.5 ng mL^{-1} for drug and metabolite, respectively. The within-day and interday reproducibilities were less than 7% for both analytes. No internal standard was used, so the method was based on the external standard technique.

XXIII. DEXFENFLURAMINE

An HPLC method to assay for dexfenfluramine and nordexfenfluramine (metabolite) levels in urine was reported by Gross et at. [28]. The dextrorotatory or (+) enantiomer of fenfluramine

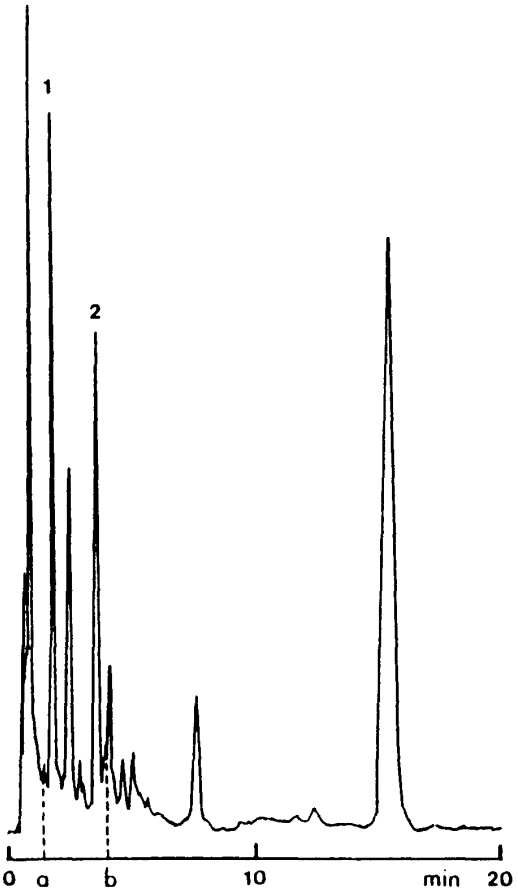


Figure 10 Chromatography of extracted danazol (100 ng mL^{-1}) after C_8 column only. Portion of the eluate between points "a" "b" was sent to C_{18} column, where the danazol peak was well resolved from other peaks. In the meantime, the endogenous peak at 15.5 min was eluted from the C_8 column and next sample is injected. (From Ref. 26.)

is widely used as a pure anoretic drug. A 1-mL sample of urine was treated with aqueous sodium hydroxide and extracted with diethyl ether. The ether extract was separated from the aqueous layer and reextracted with 0.5-M sulfuric acid (120 μL). The acid extract (100 μL) was then injected into the HPLC system. Extraction recoveries were in the 96–99% range for drug and metabolite. No internal standard was used, so quantitation was performed using the external standard method. The separation of the analytes was achieved on a 30-cm × 3.9-mm–id octadecylsilane column using a mobile phase of 27:75 v/v acetonitrile–50 mM aqueous dibasic potassium phosphate, at a flow rate of 1.3 mL min^{-1} with UV detection at 210 nm. The LOD was calculated to be 10 ng mL^{-1} for both analytes and is appropriate to measure drug and metabolite in urine for up to 5 days after a single 30-mg dose. The method was linear in the 120 to 1500-ng mL^{-1} range. Intra- and interday precision was in the 4.2–15% range and accuracy for both analytes was less than 8%.

XXIV. DICLOFENAC

Avgerinos et al. reported an nonextraction HPLC method for diclofenac in human plasma and urine [29]. Diclofenac is a nonsteroidal anti-inflammatory (NSAI) agent that combines high therapeutic efficacy with improved tolerability. A 0.5-mL–plasma sample was treated with 1.5 mL of dilute methanol, and indomethacin (internal standard) was added. After mixing and centrifugation, a 20-μL direct injection was made into the liquid chromatograph. A 1.0-

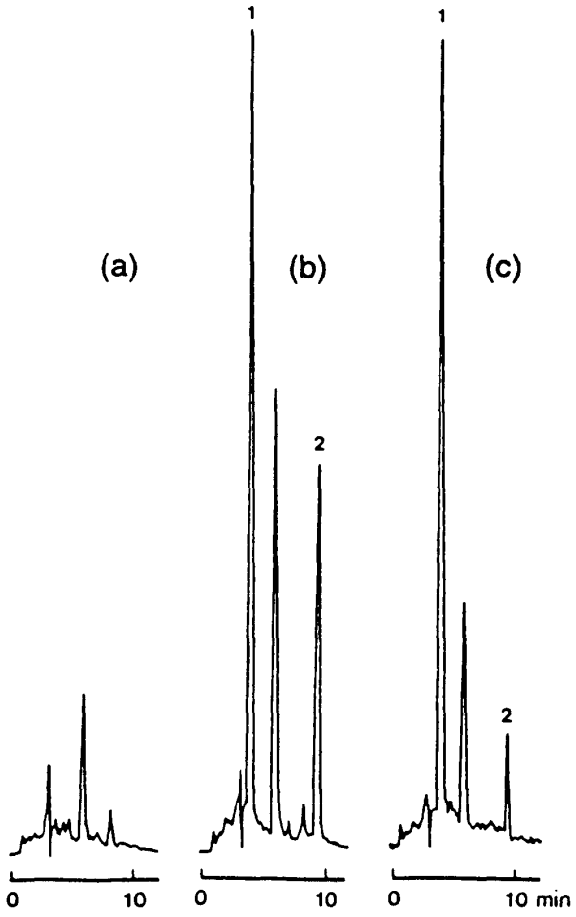


Figure 11 Representative chromatograms of the danazol in serum (two-column system): (a) drug-free serum, (b) serum obtained 4 h after 200 mg danasol administration, (c) standard 10 ng mL^{-1}. Chromatographic conditions; wave-length, 285 nm, 0.005 AUFS; mobile phase, water–acetonitrile (45:55, v/v); flow rate, 1.6 mL min^{-1}. 1, internal standard; 2, danazol. (From Ref. 26.)

mL–urine sample was hydrolyzed with 4-M hydrochloric acid by allowing the mixture to stand for 10 min at ambient temperature. The internal standard was added and, after mixing, a 20-μL direct injection was made. The separation occurred on a 25-cm × 4.5-mm–id octadecysilane column using a 35:65 v/v acetonitrile–0.1-M aqueous sodium acetate pH 6.3 mobile phase and a 2.8-mL min^{-1}–flow rate. Using UV detection at 278 nm, the LOD was 0.2 μg mL^{-1}. Linearity of the procedure was 0.5–6 and 0.5–30 μg mL^{-1} for plasma and urine, respectively. The total run time was less than 5 min and the retention times for diclofenac and indomethacin were 2.8 and 3.6 min, respectively. The method was successfully applied to a pharmacokinetic study during which a single oral dose of 100 mg of diclofenac sodium was administered to a human volunteer and the plasma and urine levels measured out to 12 h.

XXV. DMP 811

DMP 811 is chemically (4-ethyl-2-propyl-1-[(2′-(1*H*-tetrazol-5-yl) biphenyl-4-yl) methyl] imidazole-5-carboxylic acid (Fig. 12) and is used to lower blood pressure in conscious renal hypertensive rats and furosemide-treated dogs. An HPLC method in plasma has been reported [30]. A 500-μL–plasma sample was extracted with 13 mL of 95:5 v/v diethylether–isopropanol. The organic layer was separated and extracted with aqueous sodium hydroxide

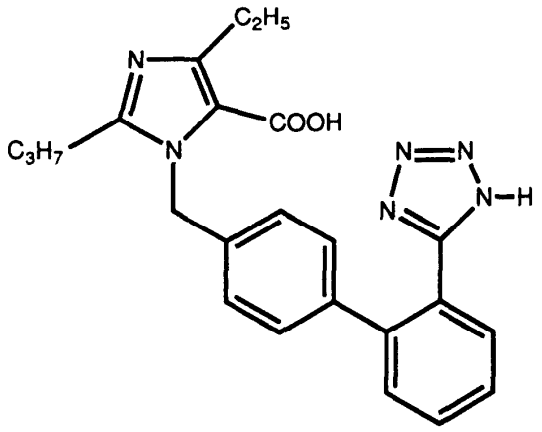


Figure 12 Chemical structure of DMP 811.

to back-extract the drug. After evaporation of residual organic solvent in the aqueous sample, 50 μL was injected. The separation occurred on a 25-cm × 4.6-mm–id octylsilane column at 35°C, using a mobile phase of 78:22 v/v 0.05-M ammonium acetate, pH 3.75–acetonitrile, using fluorescence detection with excitation and emission of 235 and 370 nm, respectively. The method showed linearity in the 2- to 2000-ng mL^{-1} range. Intraday and interday variability were in the 2.7–16.5 and 0.9–5.2% ranges, respectively. The LOQ was reported to be 2 ng mL^{-1}. Recovery of drug from plasma was 111 ± 6.4%.

XXVI. DOBUTAMINE

Dobutamine is a synthetic catecholamine with a structural resemblance to isoprenaline and dopamine. A rapid and sensitive HPLC assay of the drug in plasma has been reported by Husseini et al. [31]. With the external standard method, a plasma sample containing 0.1 mL of EDTA–glutathime was diluted on ice with 0.2 mL 5% trichloroacetic acid (TCA) solution. After mixing and centrifugation, a 30-μL aliquot was directly injected into the LC. The chromatographic separation was achieved on a 15-cm × 3.9-mm–id octadecylsilane column using a 80:20 v/v 0.1-M phosphate buffer–acetonitrile mobile phase containing 1-octanesulfonic acid and triethylamine, with the pH adjusted to 2.7. Electrochemical detection was employed in the method. The direct injection method was linear in the 1- to 400-ng mL^{-1} range. The LOD was reported to be 100 pg mL^{-1} of plasma.

XXVII. DROTAVERINE

An HPLC method for the analysis of drotaverine in human plasma and urine was described by Bolaji et al. [32]. Drotaverine is a benzylisoquinoline derivative, similar to papaverine, with excellent smooth muscle relaxant properties. The method consists of the alkalinization of plasma or urine with sodium hydroxide, followed by extraction with diethyl ether. The ether extract was then extracted with 0.1-M hydrochloric acid. After centrifugation, a 10-μL injection was made. The separation of drotaverine and internal standard (imipramine) was achieved on an 30-cm × 4-mm–id octadecylsilane column using a mobile phase of 30:70-v/v aqueous 0.02-M monobasic sodium phosphate–methanol containing 70-mM L^{-1} perchlorate ion and the pH adjusted to 3.2. The flow rate was set at 1.2 mL min^{-1}, with UV detection of the analytes. The LOD was 6 ng mL^{-1} (S/N = 3). The method was linear in the 0.025- to 1.0-μg mL^{-1}, and absolute recoveries of drotaverine and internal standard were 85–93%. The retention times of the drotaverine and imipramine (IS) were about 8 and 10 min, respectively.

XXVIII. E-1100

Tokumura and Horie have reported an HPLC assay for a novel β-lactam antibiotic in rat plasma [33]. The compound, E-1100, is (+) (6*R*, 7*R*)-[(*z*)-2-(2-aminothiazol-4-yl)-2-hydroxyiminoacetamido]-3-*N*,*N*-dimethylcarbamoyloxymethyl-8-oxo-5-thia-1-azabicyclo[4.2.0]-oct-2-ene-2-carboxylic acid and has a wide spectrum of antibacterial activity. Methanol (200 μL), containing 0.2% perchloric acid and 50 μL of sodium cefteram (internal standard) solution, was added to 100 μL of plasma cooled in an ice bath. After mixing and centrifugation at 4°C, 20 μL of the supernate was directly injected into the liquid chromatograph. The separation was achieved on a 15-cm × 6-mm–id octyldecylsilane column (column temperature at 40°C) using a mobile phase of 156:844:1:5 v/v/v/v acetonitrile–water–60% perchloric acid–sodium perchlorate at a flow rate of 1 mL min^{-1} and detection set at 254 nm. The absolute recoveries of E-1100 were 76, 70, and 76% at 1-, 10-, and 100-μg mL^{-1} levels. Interday precision of the assay was less than 10%.

XXIX. EM523

A sensitive HPLC determination of a new erythromycin, EM523, in human plasma and urine with UV detection and the column-switching technique was reported by Yamashita [34]. The chemical structure of EM523 is shown in Fig. 13. The drug has strong gastrointestinal tract (GIT)-stimulating activity with antibiotic activity. It has a biological mechanism similar to motilin and is expected to be useful in the treatment of GIT disorders. A 1-mL alkalinized plasma or a 200-μL urine sample diluted with 1-mL pH 11 buffer was extracted twice with 4 mL of a 6:1 v/v hexane–acetone mix. After separation of the organic layer and evaporation to dryness, the residue was dissolved in 200 μL of 1:1 v/v 20-mM monobasic potassium phosphate–acetonitrile. After injection of an aliquot onto the first 15-cm × 4.6-mm–id C_{18} analytical column, column switching of the heart-cut fraction onto a second 15-cm × 4.6-mm–id C_{18} analytical column gave further separation of the drug peak at a 200-nm detector setting. The first C_{18} column used a mobile phase of 1:1 v/v 20-mM monobasic potassium phosphate–acetonitrile, containing 3.5-mM sodium dodecyl sulfate (SDS) and the pH adjusted to 4.0. The second C_{18} column used the same mobile phase, without the sodium dodecyl sulfate component. Column temperature of the second C_{18} column was 40°C, with a 1-mL

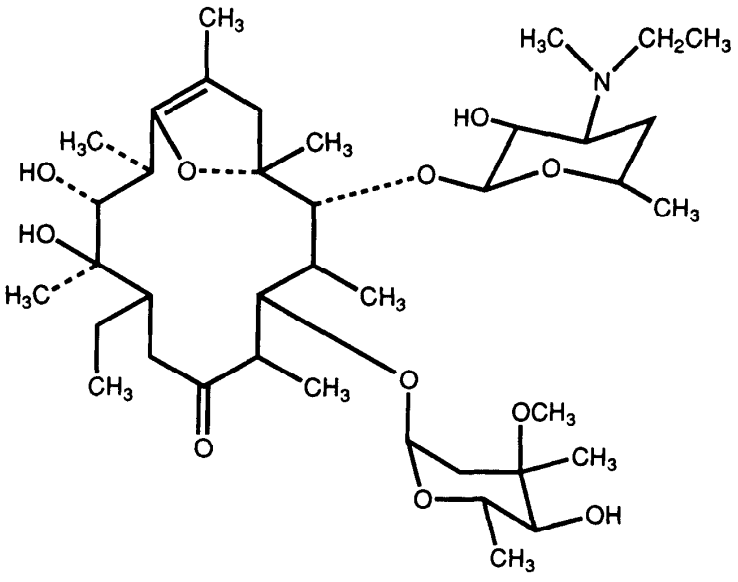


Figure 13 Chemical structure of EM523.

min^{-1} flow rate. Recoveries of EM523 from plasma and urine were 96.5 and 95.1%, respectively. The LODs in plasma and urine were 1 ng mL^{-1} and 10 ng mL^{-1}, respectively, based on a 150-μL injection on column.

XXX. ETHYNYLESTRADIOL

A rapid assay for ethynylestradiol in rabbit plasma was reported by Fernadez et al. [35]. Ethynylestradiol is a widely used component of oral contraceptive pills. The procedure consisted of extracting 1 ml of plasma with 5 mL of diethyl ether, followed by evaporation of the organic layer to dryness. The residue was redissolved in mobile phase and a 50-μL sample injected onto a 15-cm × 3.9-mm–id octadecylsilane column. The mobile phase was 10:7:3 v/v/v 50-mM potassium dihydrogen phosphate pH 3.6–acetonitrile–methanol, and the flow rate was 1.6 mL min^{-1}. The analytes were detected using an electrochemical detector set at +1V versus Ag/AgCl. The naturally occurring estrogens did not interfere with the method. The retention time for ethynylestradiol was 2.94 min. Recovery of the estrogen from plasma was 74.5% and the LOD was calculated to be 10 pg on column (50 pg mL^{-1}). Interday precision was listed in the 8–15% range.

XXXI. ETOPOSIDE

An HPLC procedure for the determination of etoposide in blood using electrochemical detection was reported by Eisenberg and Eickhoff [36]. Etoposide is a semisynthetic epipodophyllotoxin derivative that is active against a variety of malignancies. It is the most active single agent for treatment of small cell lung cancer and is approved by the US Food and Drug Administration (FDA) for the treatment of testicular carcinoma. A 200-μL–plasma sample was extracted with 1 mL of a methylene chloride–hexane mixture containing 0.5 mg mL^{-1} of teniposide (internal standard). After mixing and centrifugation, the organic layer was separated and evaporated to dryness at 40°C. The residue was reconstituted with an aqueous acetonitrile solution, pH 4, and 30 μL was injected into the chromatograph. Etoposide and internal standard were eluted on a 15-cm × 3.9-mm–id phenyl column, using a mobile phase (A) of 77:573:350 v/v/v 0.65-M sodium citrate–water–acetonitrile for 7 min, then a 4-min wash with a mobile phase (B) of 77:273:700 v/v/v 0.65-M sodium citrate–water–acetonitrile followed by reequilibration with mobile phase A for 9 min before a new sample injection. The electrochemical detector employed a glassy carbon electrode and was set at +0.7 V versus Ag/AgCl. The mobile phase flow rate was 2 mL min^{-1} and the HPLC system was operated at ambient temperature. The extraction recoveries of etoposide and internal standard were 78–94%. Linearity of the method was in the 2.4- to 5000-ng mL^{-1} range with accuracy of 97–103% for etoposide. The LOD was 7.5 ng mL^{-1} (S/N = 3). Intraday and interday precision were in the 2–8 (n = 5) and 3–8% (n = 15) ranges, respectively.

XXXII. FLUMAZENIL AND MIDAZOLAM

The simultaneous determination of flumazenil, midazolam, and their metabolies in human plasma and urine was reported by Chan and Jones [37]. Flumazenil is a benzodiazepine antagonist that is used for reversal of benzodiazepine-induced anesthesia, sedation, and intoxication. Midazolam is a water-soluble benzodiazepine that is widely used in anesthesia and for sedation of artifically ventilated patients in intensive care units (ICU). The drugs and metabolites were extracted from plasma or urine using 40:60 v/v methylene chloride–diethylether. The organic layer was evaporated to dryness with the aid of a nitrogen stream, and the residue was redissolved in 80 μL of absolute methanol. A 30-μL injection was made into the following stream consisting of 32:68 v/v acetonitrile–0.04-M sodium monohydrogen phosphate pH 7.2, containing 1 mL of triethylamine, at a flow rate of 1.5 mL min^{-1}. The 10-cm × 8-mm–id octylsilane column was operated at ambient temperature, and

detection was at 220 nm. The mean recoveries of flumazenil, midazolam, and metabolites were in the 80–96% range, with LODs of 4 ng mL^{-1} for flumazenil and 10 ng mL^{-1} for midazolam.

XXXIII. FLUOROQUINOLINES AND THEOPHYLLINE

Davis et al. have reported a simultaneous HPLC assay for fluoroquinolines and theophylline in plasma [38]. The fluoroquinolines studied were ciprofloxacin, enoxacin, and norfloxacin. These drugs are antibiotics that are effective against a wide range of infections. There have been reports that there is a pharmacokinetic interaction between the fluoroquinolines and theophylline. Buffer and internal standard (β-hydroxypropyltheophylline) solutions were added to 100 μL of plasma and extracted with chloroform–isopropanol or methylene chloride–isopropanol. The organic layer was evaporated to dryness, reconstituted in 100 μL of mobile phase, and 25 μL was injected into the liquid chromatograph. Extraction efficiencies for all the analytes were greater than 80%. The separation of the theophylline, fluoroquinolines, and internal standard was performed on a 25-cm × 4.9-mm–id ethyl silane (C_2) column using a mobile phase of 15:85 v/v acetonitrile–pH 3 phosphate buffer containing 4.4 mM of tetrabutylammonium acid sulfate (ion-pair reagent), at a 1.3-mL min^{-1}–flow rate with UV detection at 280 nm. Retention times for all analytes were less than 10 min. Linearity of the method was in the 0.2 to 20-μg mL^{-1} range and the LOQ was 0.5 μg mL^{-1}.

XXXIV. FUROSEMIDE

An automated HPLC method for furosemide in dog plasma was reported by Matsuura et al. [39]. The plasma sample was directly injected onto a precolumn consisting of C_{18} particles coated with bovine serum albumin (BSA). Furosemide remained trapped on the precolumn, whereas proteins were washed to waste. Then furosemide was washed onto a 15-cm × 4.6-mm–id octadecylsilane analytical column using 1:1 v/v acetonitrile–water. The method was linear in the 0.1 to 10-μg mL^{-1} range and required no extraction and denaturation of plasma proteins. The mobile phase for the assay was 69:31 v/v 2.5-mM phosphate buffer pH 2.5–acetonitrile. The flow rate was 1.2 mL min^{-1}, with an average chromatographic run taking less than 20 min. The LOD in plasma was 0.1 μg mL^{-1} of furosemide.

XXXV. GALOCITABINE

The simultaneous determination of the anticancer drug galocitabine and its three metabolites has been reported by Funaki et al. [40]. A 100-μL–blood sample was mixed with internal standard (5-bromouracil) and acetonitrile. After mixing and centrifugation, the upper layer was evaporated to dryness, the residue redissolved in 100 μL of 2:98 v/v acetonitrile–water, and 20 μL was injected into the HPLC system. The chromatographic separation was achieved on a 10-cm × 5-mm–id octadecylisilane column. The 5-FU, 5′-DFCR, 5′-DFUR, and galocitabine (Fig. 14) were resolved using these mobile phases in order: 2:98 v/v acetonitrile–water for 1.3 min, a linear gradient to 5.4:94.6 v/v acetonitrile–water for 3.7 min, a linear gradient to 50:50 v/v acetonitrile–water from 1 min and maintained for 2.5 min. Representative chromatograms of the separations are shown in Fig. 15. Linearity was in the 0 to 100-μg mL^{-1} range. The recoveries of drug, metabolite, and internal standard from blood were more than 95%. Retention times for all analytes were less than 8 min using UV detection at 270 nm. The RSD for interday precision was less than 10% for all analytes. The LODs were 6.9 μg mL^{-1} for galocitabine, 3 μg mL^{-1} for 5′-DFCR, 4 μg mL^{-1} for 5′-DFUR, and 3.7 μg mL^{-1} for 5-FU.

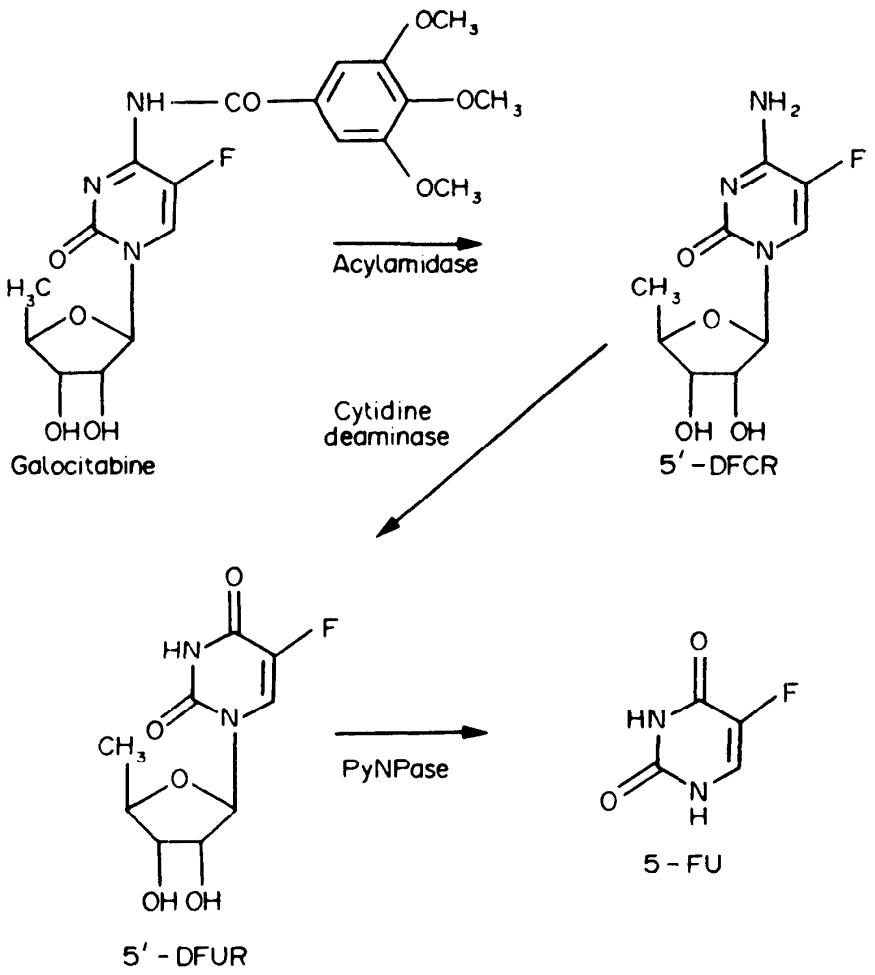


Figure 14 Structures of galocitabine (N^4-trimethoxybenzoyl-5′-deoxy-5-fluorocytidine; RO 09-1390), 5′-deoxyfluorocytidine (5′-DFCR), 5′-deoxyfluorouridine (5′-DFUR), and 5-fluorouracil (5-FU), and metabolic pathway of galocitabine. (From Ref. 40.)

XXXVI. GUAIFENESIN

An HPLC method to determine guaifenesin in human plasma in the presence of pseudoephedrine was reported by Alvin and Stavchansky [41], A need to assay guaifenesin levels at the nanogram per milliliter level in human plasma is important to establish a pharmacokinetic profile of the drug in humans. In the method, guaifenesin was extracted from plasma at pH 7 using 5:95 v/v methanol–methylene chloride, containing mephenesin (internal standard) and pseudoephrine. After separation of the organic layer and evaporated to dryness, the residue was dissolved in the mobile phase of 11:11:78 v/v/v methanol–acetonitrile–0.05-M phosphate buffer containing 4-mM of heptanesulfonic acid and 1% glacial acetic acid. The chromatographic separation was achieved on a 30-cm × 3.9-mm–id octadecylsilane column, using 1-mL min^{-1} flow rate (Fig. 16). Retention times for guaifenesin and internal standard were 7.9 and 15.7 min, respectively. Linearity was in the 50 to 1000-ng mL^{-1} and 1 to 4-μg mL^{-1} ranges. Inter- and intraday accuracy were within 15.4% of true values. Precision (% RSD) ranged from 4.8–8.7% (intraday) to 5–8.4% (interday). Recovery of drug from plasma was 89–98%. The LOQ for guaifenesin was 50 ng mL^{-1} of plasma (S/N = 10). The LOD was set at 25 ng mL^{-1} of plasma (S/N = 3). The assay was particularly selective for pseudoephedrine; however, it was remarkedly free of interference from endogenous plasma compo-

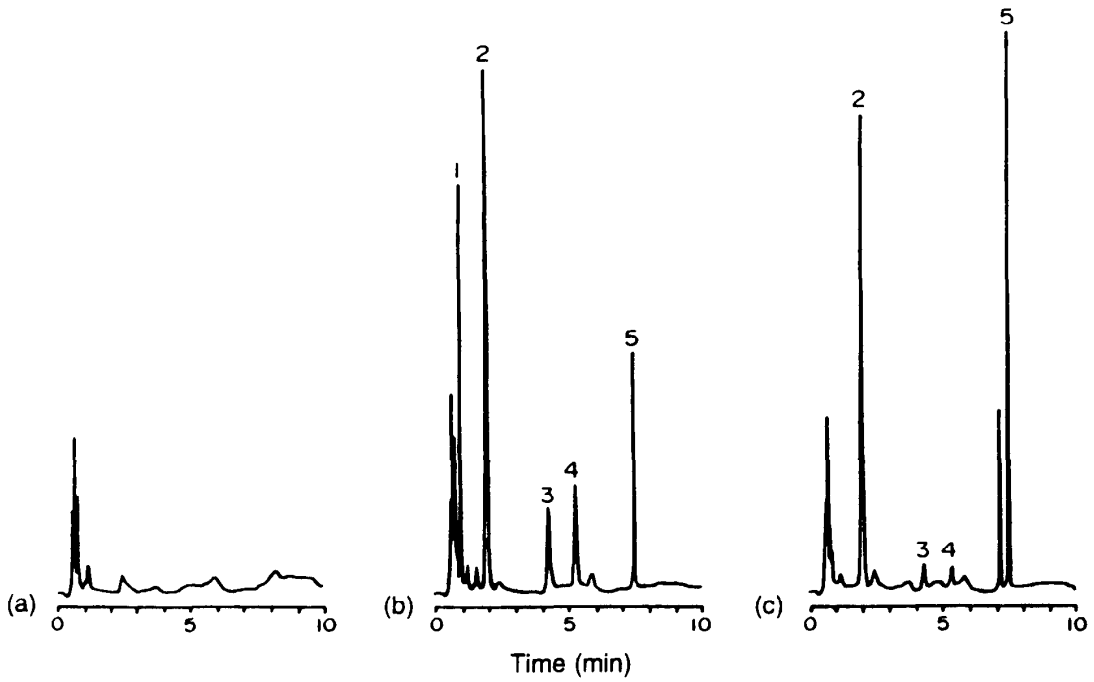


Figure 15 Representative chromatograms showing retention times (min) for galocitabine (peak 5), 5′-DFCR (peak 3), 5′-DFUR (peak 4), 5-FU (peak 1) and IS (peak 2). (a) Blood sample blank; (b) blood sample spiked with 25 μg mL^{-1} galocitabine, 5′-DFCR, 5′-DFUR, and 5-FU; (c) 1-h postdosed blood sample. The chromatograms were obtained at 0.32 AUFS. (From Ref. 40.)

nents. The method was applied to a bioequivalence study of sustained-release formulations of guaifenesin tablets (600 mg) in humans.

XXXVII. HYDROCHLOROTHIAZIDE

Miller and Amestoy reported an HPLC assay for hydrochlorothiazide in human plasma [42]. The drug is an antihypertensive–diuretic agent that is indicated in the management of hypertension, either as the lone therapeutic drug or to enhance the effect of other antihypertensive agents. A 0.5-mL–plasma sample was treated with internal standard in phosphate buffer followed by 1 M of sodium carbonate and then mixing. The analytes were extracted with ethyl acetate and, after shaking for 15 min and centrifugation, the organic extract was evaporated to dryness and the residue dissolved in 300 μL of mobile phase. A 100-μL aliquot was injected onto the HPLC system. The separation was performed on a 15-cm × 4.6-mm–id octylsilane column using a 90:6:4 v/v/v 10-mM monobasic sodium phosphate–acetonitrile–methanol mobile phase at a flow rate of 1.2 mL min^{-1}. The UV detector was set at 273 nm. The method was linear over a 2 to 1000-ng mL^{-1} range (S/N = 4). Recoveries of drug and internal standard were in the 95–98% range. The retention times for drug and internal standard were approximately 11 and 13 min, respectively. The overall chromatographic run time was 15 min. The intra- and interday precision were less than 12%, and accuracy was within 14% even at the LOQ of 2 ng mL^{-1}.

XXXVIII. IMIPENEM

Imipenem is a stabilized amidine derivative of thienamycin. It belongs to a class of β-lactam antibiotics, the carbapenems, which possess a desthiocarbapenem nucleus. Carlucci et al. have reported an HPLC assay for imipenem in human plasma, urine, and tissue [43]. Plasma (0.5

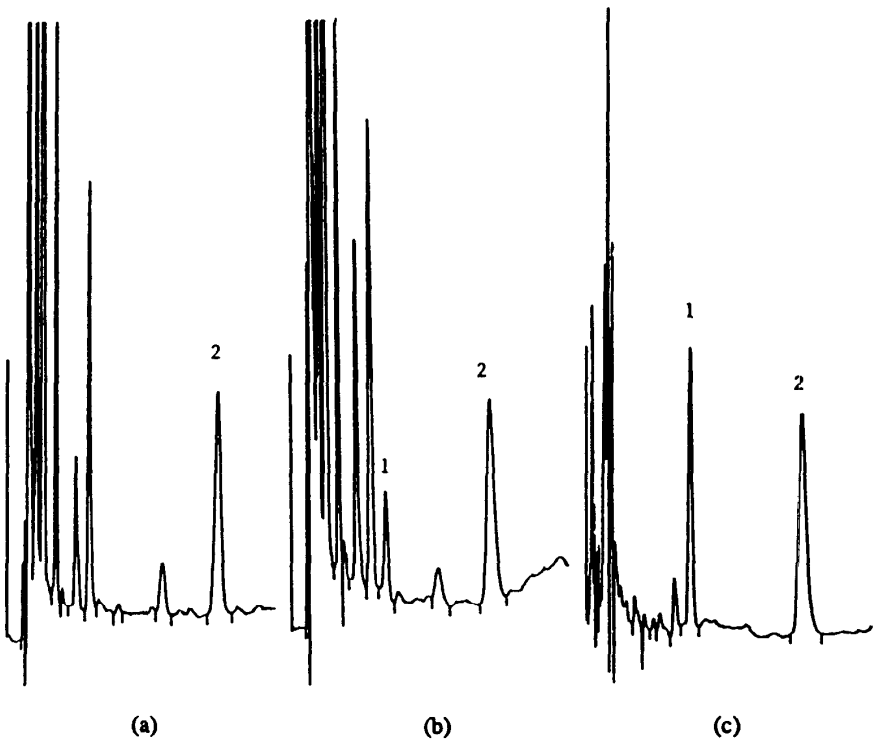
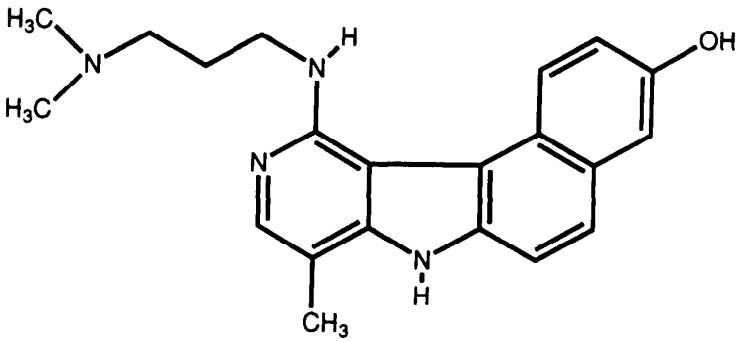


Figure 16 Chromatograms of (a) blank plasma spiked with mephenesin; (b) plasma standard: guaifenesin (50 ng mL^{-1}), mephenesin; (c) plasma sample from clinical study: guaifenesin (375 ng mL^{-1}), mephenesin; concentration of mephenesin was 300 ng mL^{-1}. 1, guaifenesin; 2, mephenesin. (From Ref. 41.)

mL) was treated with methanol and then centrifuged and the supernatant collected. An aliquot of the supernatant was directly injected onto the LC column. The same procedure was followed for urine samples. For tissue, the sample was homogenized with a 4-(2-hydroxyethyl)-piperazine-1-ethanesulfonic acid buffer and centrifuged. The supernatant was then treated with methanol, centrifuged, and an aliquot injected onto the LC column. The separation was performed on a 25-cm × 4.6-mm–id octylsilane column using a mobile phase of 90:10 v/v sodium borate buffer, pH 7.2–methanol, at a flow rate of 1.2 mL min^{-1}. The column was maintained at ambient temperature and the analytes were detected at 313 nm. Linearity of the method was 0.5–70 and 0.5–100 $\mu g\ mL^{-1}$ in plasma and urine, respectively. The LODs were 0.4 $\mu g\ mL^{-1}$ for plasma and 0.3 $\mu g\ mL^{-1}$ for urine (S/N = 3). An internal standard was not used in the method. Precision for a plasma calibration curve ranged from 1.2 to 3.5% RSD, and for urine the calibration curve precision ranged from 1.4 to 3.8% RSD.

XXXIX. INTOPLICINE

Van Gijn et al. have reported an HPLC method for intoplicine, a new antitumor drug, in human feces [44]. The drug is chemically 11-(3-dimethylaminopropylamino)3-hydroxy-8-methyl-7*H* benzo[*e*]pyrido[4, 3-*b*]indole dimetanesulfonate (Fig. 17). It is currently in phase I clinical evaluation in the United States and Europe. After a patient received a 1080-mg dose of the drug as a 24-h infusion, feces samples were collected and stored at −30°C until assay. After thawing the sample, homogenization of the feces with water gave a homogenate, to which was added 50 μL of 0.1 N hydrochloric acid and 10 mL of hexane. After mixing and centrifugation, the organic layer was discarded and 6% borate buffer pH 9 and 10 mL of methylene chloride were added. After shaking and centrifugation, 8 mL of the organic layer



$2CH_3SO_3H$

Figure 17 Chemical structure of intoplicine dimethanesulfonate. (From Ref. 44.)

was transferred to a clean tube and evaporated to dryness at 40°C using a nitrogen stream. The residue was dissolved in 1 mL of mobile phase, and 10 μL was injected into the LC. The separation was achieved on a 10-cm × 3-mm–id glass column packed with 5-μm silica at ambient temperature using a 40:40:1 v/v/v methylene chloride–2-propanol–10% ammonia mobile phase at 0.6 mL min^{-1}. The HPLC chromatograms of blank and feces samples are shown in Fig. 18. The peaks were detected using a fluorescence detector set at excitation 275 nm and emission 425 nm. The absolute recovery of intoplicine was 60.1 ± 4.9% (n = 3). The LOD was 10 ng g^{-1} based on 1000 μL of the fecal homogenate. The LOQ was 50 ng g^{-1}. No internal standard was used in the method. Linearity of the procedure was in the 50-ng g^{-1} to 10-μg g^{-1} range. Intra- and interday precision were in the 1.6–7.1 and 1.0– 2.1% ranges, respectively (n = 5). Accuracy of the method was in the 91–116% range.

XL. IODOBENZYLGUANIDINE

An HPLC method for *m*-iodobenzylguanidine (IBG) in the urine of cancer patients was developed by Wafelman et al. [45]. Iodine-131 labeled IBG is used in scintigraphy and in the treatment of neuroectodermally derived tumors, such as malignant pheochromocytoma, neuroblastoma, and carcinoid. A cyanopropyl SPE cartridge was used for the extraction step. After conditioning and application of a 50-μL–urine sample, the analyte was eluted with 1 mL of 0.1-M hydrochloric acid in methanol. The eluate was evaporated to dryness at 60°C and 200 μL of mobile phase was used to redissolve the residue. An injection of 100 μL was made. The analytical column was a 30-cm × 3.9-mm–id μ-Bondapak octadecylsilane using a mobile phase of 75:25 v/v 25-mM aqueous ammonium phosphate, pH 3–acetonitrile, with UV detection at 254 nm and a flow rate of 1 mL min^{-1}. Overall recovery of IBG from urine was 95.8 ± 3.6%. The LOD and LOQ were 0.1 μg mL^{-1} and 0.2 μg mL^{-1}, respectively, using a 500-μL–urine sample and a 100-μL injection. Accuracy was in the 2–13% range, and intra- and interday precisions were 0.9–3.7 and 2–8.3%, respectively, based on n = 10–20.

XLI. LISURIDE

A quantitative assay for the dopamine agonist lisuride in plasma was reported by Wolthers et at. [46]. Lisuride is an ergot compound that has strong dopaminergic properties. It is ten times as potent as bromocryptine and is used as adjuvant therapy in parkinsonian patients and in the treatment of hyperprolactonemia. Ergotamine tartrate was used as internal standard. A 2-mL–plasma sample was extracted twice with diethyl ether. The ether extract was evaporated to dryness and the residue dissolved in methanol. An aliquot was injected into a 10-cm ×

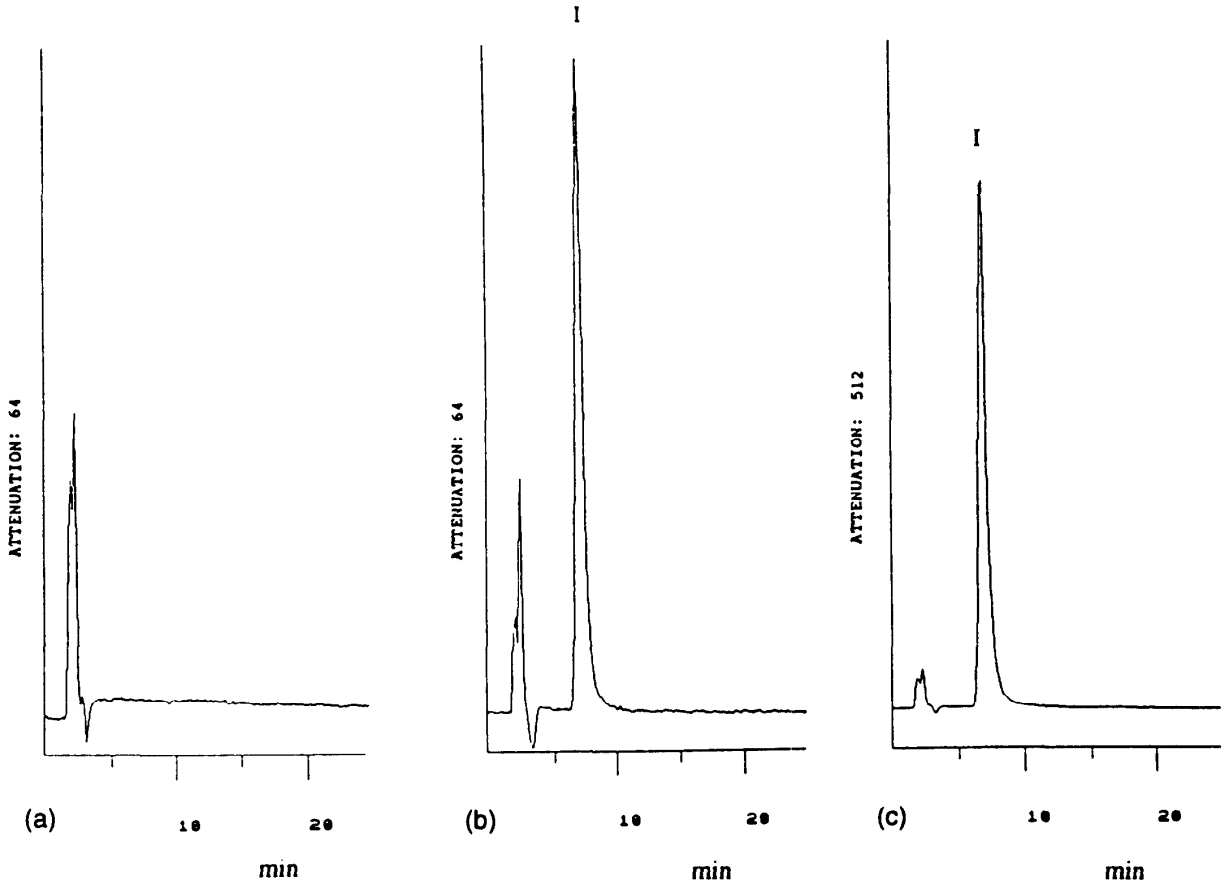
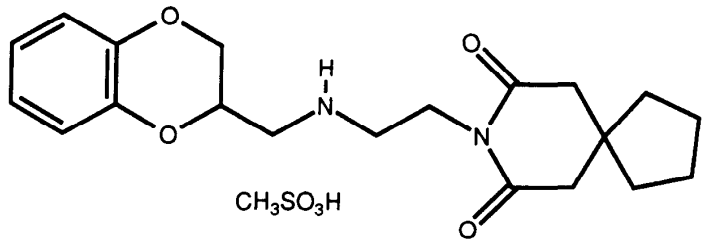


Figure 18 (a) HPLC of blank feces; (b) a calibration sample (concentration of intoplicine = 500 ng g^{-1}); and (c) a feces sample (concentration of intoplicine, 6.7 μg g^{-1}) of a patient receiving 1080 mg as a 24-h intravenous infusion. The retention time of intoplicine (I) is 6.5 min. (From Ref. 44.)

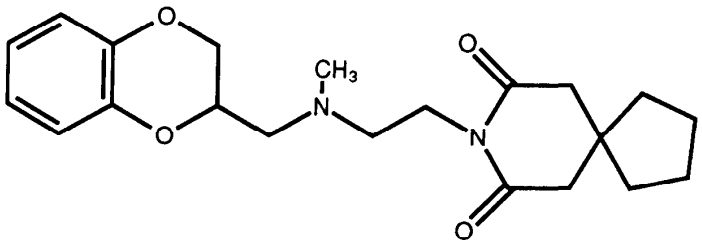
4.6-mm–id silica column for separation and detection. The mobile phase was 40:2:10 v/v/v methanol–aqueous acetic acid–acetonitrile at a flow rate of 1 mL min^{-1} with fluorescence detection (excitation at 322 nm and emission at 405 nm). Extraction recovery was near quantitative, and the LOD was reported to be 20 pg mL^{-1}. The HPLC procedure was linear over a 70 to 4500-pg mL^{-1} range.

XLII. MDL 73,005EF (BINOSPIRONE MESYLATE)

A new antianxiety agent for humans (MDL 73,005EF) is classified as a serotonin ($5\text{-}HT_{1A}$) partial receptor agonist owing to its pharmacological activity in animal models. Chemically, the MDL compound is 8-azaspiro[4,5]decane-7,9-dione-8-[2[[2,3-dihydro-1,4-benzodioxin-2-yl)methyl]amino]ethyl]monomethanesulfonate (Fig. 19). Recently, an HPLC method was reported by Chan et al. [47]. The drug was unstable in water and at basic pH. It was most stable at pH 2 and plasma was acidified to 2 after collection of the sample. Sample cleanup was achieved using a cyanopropyl SPE cartridge. An internal standard numbered MDL 74,348 was added to a 1-mL–plasma sample along with 100 μL of 2-M hydrochloric acid. After the sample was applied to the SPE cartridge, the cartridge was washed with water, followed by a methanol–water wash. After drying under vacuum for 5 min, the analytes were eluted with 3- to 100-μL aliquots of 0.1% perchloric acid in acetonitrile. A 75-μL injection was made into the HPLC. Chromatography was achieved on a 25-cm × 4.6-mm–id octadecylsilane



MDL 73005EF



MDL 74348

Figure 19 Chemical structures of MDL 73005EF (binospirone mesylate) and internal standard MDL 74348. (From Ref. 47.)

column using a mobile phase of 50:50:0.05 v/v/v acetonitrile–aqueous 0.02-M monobasic potassium phosphate pH 2.5 with triethylamine, at 1-mL min^{-1}–flow rate at an ambient column temperature. The analytes were detected at 274 nm. The retention times for drug and internal standard were 8.9 and 11.4 min, respectively. The extraction efficiency was 89.1% at 50 ng mL^{-1}. Interday accuracy and precision were 96.4–102.9 and 1.7–5%, respectively.

XLIII. 6-METHYLEN-ANDROSTA-1,4-DIENE-3,7-DIONE

6-Methylen-androsta-1,4-diene-3,7-dione is a new aromatase inhibitor. Its major metabolite in plasma is the 17-dihydro compound. A new HPLC method for the drug and metabolite has been reported by Breda et al. [48]. The analytes were extracted from 1 mL of plasma, using a methylene chloride–isooctane mix. The organic layer was evaporated to dryness, and the residue was reconstituted in aqueous acetonitrile. Norgestrel was used as internal standard and was added to the plasma sample before extraction. The chromatographic separation was achieved on a 12.5-cm × 4.6-mm–id octadecylsilane column, using a mobile phase of 35:65 v/v acetonitrile–0.05-M monobasic potassium phosphate pH 4.5, at 1.5 mL min^{-1} with the detector set at 247 nm. Retention times were 10, 14, and 17 min for the metabolite, drug, and internal standard, respectively. Linearity of the method was in the 10- 1000-ng mL^{-1} range. Recoveries of drug and metabite from plasma were 67–79 and 69–78%, respectively. The recovery of the internal standard was 76%. Intra- and interday precisions of the method were 3.2–16.8 and 1.3–3.9%, respectively. Accuracy of the method was 94–103% for the drug and 85–100% for the metabolite.

XLIV. METOCLOPRAMIDE

El-Sayed and co-workers have reported a rapid and sensitive HPLC method for assay of metoclopramide in plasma [49]. Metoclopramide is a dopamine receptor antagonist that is used as an antiemetic and a stimulant of upper gastrointestinal tract motility. With diazepam

as internal standard (IS), the drug and IS were extracted from an alkalinized 0.5-mL–plasma sample with 5 mL of diethyl ether. The ether extract was evaporated to dryness and the residue redissolved in mobile phase consisting of 55:45-v/v acetonitrile–pH 3 buffer. The flow rate was 1.3 mL min^{-1} and the analytes were detected at 273 nm. Retention times for metoclopramide and diazepam were 8.2 and 6.2 min, respectively, on the 10-cm × 8-mm–id octadecylsilane column. The LOD was 5 ng mL^{-1}. Relative and absolute recoveries of the metoclopramide were 94–95 and 93–97%, respectively. Intra- and interday precisions were 3–4.4 and 4.1–5.7%, respectively, at three different concentration levels. The HPLC method showed linearity in the 0 to 120-ng mL^{-1} range.

XLV. MITOMYCIN

An assay of mitomycin in human aqueous humor and serum by HPLC was reported by Li et al. [50]. Mitomycin is one of several antibiotic substances, produced by *Streptomyces caespitosus*, possessing antineoplastic activity. It is currently used in the palliative treatment of disseminated adenocarcinoma of the stomach and pancreas that is unresponsive to other treatment modalities. The analysis method for aqueous humor samples was based on direct injection of the sample into the LC without sample pretreatment steps. A 5-cm × 4.6-mm–id octadecylsilane column was used with a mobile phase of 28:72 v/v methanol–10-mM ammonium dihydrogenphosphate adjusted to pH 7.0 with diluted ammonia solution and detection set at 365 nm. The procedure was linear in the 6.3 to 50-ng mL^{-1} range. The human serum samples were initially subjected to SPE cleanup using a C_{18} cartridge before chromatography on a 15-cm × 4.6-mm–id octadecysilane column with the same mobile phase as before. Linearity was reported to be in the 10 to 500-ng mL^{-1} range. Mean recoveries of mitomycin and internal standard (4-aminoacetophenone) were 73.7 ± 4.9 and 74.2 ± 2.5%, respectively.

XLVI. MIZOLASTINE

Ascolone et al. have reported an assay for mizolastine in human plasma [51]. Mizolastine is a benzimidazole derivative that is a potent and selective antagonist of histamine H_1 receptors. It is completely free of sedative effects. They compared the use of liquid–liquid extraction to solid-phase extraction and column-switching with on-line solid-phase extraction. The separation was accomplished on a 15-cm × 4.6-mm–id octylsilane column, using a phosphate buffer–acetonitrile mobile phase with UV detection at 285 nm and a 1-mL min^{-1}–flow rate. A chlorinated derivative of mizolastine was used as the internal standard. The LOD of the assay using liquid–liquid extraction, solid-phase extraction, and column-switching–SPE were 0.5, 1.0, and 2.5 ng mL^{-}, respectively. Absolute recoveries at the 10- and 100- ng mL^{-1} levels were 75.8 ± 5.7 and 72.7 ± 3.6%, respectively. Precision of the liquid–liquid extraction was in the 3–6% range with an accuracy (percent error) of 2–3%. The precision and accuracy of the column-switching–SPE method were in the 2–3% and 1–2% ranges, respectively. The method was successfully applied to a mizolastine pharmacokinetic study, and levels of drug were detected in plasma up 60 h after a single 10-mg–oral dose to a human volunteer.

XLVII. MORPHINE

An ion-pair extraction and HPLC assay of morphine in rat brain and plasma was reported by Borg et at. [52]. They report that electrochemical (EC) detection is now accepted as being better suited for morphine analysis in biological samples. Newer EC assays report have focused on higher sensitivities or lower interferences from matrix components. This EC method used a two-step liquid–liquid extraction for morphine in brain and plasma samples using the liquid cation-exchanger di(ethylhexyl)-phosphoric acid (DEHPA). A 25-cm × 4.6-mm–id strong cation-exchange analytical column was used with a mobile phase of 15:85 v/v acetonitrile–76-mM orthophosphoric acid–ammonia buffer, pH 3.0. At a 3-mL min^{-1}–flow

rate, the column temperature was 28°C and mobile phase was continuously recycled and prepared fresh every 2 days. In the assay method, trunk blood from sacrificed rats was mixed with heparin and then centrifuged to obtain plasma. Brain tissue was homogenized with methanol containing 30 ng mL^{-1} of internal standard nalbuphine hydrochloride and then centrifuged. The supernate from either preparation was evaporated to dryness and reconstituted with ethyl acetate contining 10 mM of DEHPA. The ethyl acetate was washed with 1 mL of 50-mM dibasic sodium phosphate pH 7. After centrifugation, the organic phase was placed in a clean tube and extracted with 500 μL of 170-mM phosphoric acid. The acidic extract was adjusted to pH 2–3 with ammonia solution and 100 μL was injected into the HPLC system. It was clearly shown that DEHPA helped to eliminate interfering peaks in the chromatograms from either blood or brain samples. The electrochemical detector used a glassy carbon electrode and was set at +0.95 versus Ag/AgCl. The RSD of the slope of the calibration curve for morphine in brain samples for 5 consecutive days was 5.8% and plasma for 3 consecutive days was 8.6%.

An HPLC assay for morphine and its metabolites in plasma using diode array detection was reported by Wielbo et al. [53]. In the procedure, morphine and its metabolites, codeine, normorphine, morphine-3-glucuronide, and morphine-6-glucuronide, were determined from a single plasma sample. Solid-phase extraction was used for sample cleanup before injection into the HPLC system; 1 mL of plasma was treated with 2-mL 10-mM phosphoric acid and the mix added to a pre-conditioned silica SPE cartridge. The analytes were eluted with 3 mL of 2% ammonia in methanol. After evaporation of the eluate to dryness at 45°C, the residue was redissolved in 50 μL of mobile phase. The separation was achieved on a 20-cm × 4.5-mm–id diol column using a mobile phase of 20:80 v/v 0.05-M monobasic sodium phosphate–acetonitrile, pH adjusted to 3.0. A 20-μL injection of eluate from the SPE cartridge was made onto the column and the analytes were detected at 230 nm. The estimated retention times for codeine, morphine, normorphine, morphine-6-glucuronide, and morphine-3-glucuronide were 6, 7, 8, 10, and 12.5 min, respectively. The recovery of analytes from the SPE column was greater than 90%. The LODs were 1 ng mL^{-1} for morphine, codeine, and morphine-3-glucuronide and 10 ng mL^{-1} for normorphine and morphine-6-glucuronide. The intra- and interday precision were less than 10%.

XLVIII. NICORANDIL

An HPLC method for nicorandil in rat plasma was reported by Bachert and Fung [54]. Nicorandil is a unique vasodilator that combines the action of a potassium channel activator with a nitrovasodilator. To a 180-μL–plasma sample was added internal standard [*N*-(3-hydroxypropyl) nicotinamide nitrate ester] and 0.1-M sodium hydroxide. The mixture was extracted twice with 1 mL of ethyl acetate. The combined extracts were evaporated to dryness and water was added to redissolve the residue. An injection of the aqueous residue was made onto a 30-cm × 3.9-mm–id μ-Bondapak C_{18} column. The mobile phase was 45:55 v/v methanol–water at 1 mL min^{-1} with detection at 254 nm. Retention times of the drug and internal standard were 5.5 and 6.7 min, respectively. Absolute recovery of nicorandil was 95 ± 0.03%. The method was linear in the 0.3- to 100-μg mL^{-1} range and the LOD was 0.3 μg mL^{-1} or 8.7 ng on-column. Intra- and interday precisions were less than 5% in the 5- to 50-μ mL^{-1} range.

XLIX. NICOTINE

Nicotine and four metabolites were determined in the serum of smokers using an HPLC method reported by Zuccaro et al. [55]. The metabolites were cotinine, *trans*-3′-hydroxycotinine, norcotinine, and cotinine-*N*-oxide. At the time this method was reported, only a radiometric HPLC assay was available for these analytes in biological fluid. A 1.5-mL–serum sample containing 100 μL of *N*-ethylnorcotinine (internal standard) was mixed

with 1.4 mL of 0.5-M sodium hydroxide and transferred to a Extrelut-3 glass column that had been preconditioned with 12 mL of methylene chloride for 24 hs. After 15 min on the column, nicotine and its metabolites were eluted under gravity feed with 10 mL of 9:1 v/v methylene chloride–isopropanol. Methanol (300 μL) was added to the eluate and the entire volume evaporated to dryness with a nitrogen stream. The residue was redissolved in 100 μL of water and 20 μL was injected. Two HPLC systems were used. System 1 used a 25-cm × 4.6-mm–id octylsilane column, with a binary gradient mobile-phase system at a flow rate of 1.5 mL min^{-1}. Solvent A consisted of 96.4:3.6 v/v water–acetonitrile containing 2 mL L^{-1} of triethylamine and 0.012-M sodium heptanesulfonate and citric acid, pH 4.7. Solvent B consisted of 80.3:19.7 v/v water–acetonitrile, containing 2 mL L^{-1} of triethylamine and 0.012-M sodium heptanesulfonate and citric acid pH 5.2. System 2 used a 25-cm × 4.6-mm–id suplex pKb-100 basic column and a binary gradient mobile-phase system at a flow rate of 0.3 mL min^{-1}. Solvent C consisted of 95:5 v/v 0.014-M monobasic potassium phosphate–water and Solvent D was 5:95-v/v 0.014-M monobasic potassium phosphate–acetonitrile. The UV detector was set at 254 nm in both system 1 and 2. The LODs for nicotine and cotinine-*N*-oxide were 10 and 3 ng mL^{-1}, respectively. The LODs for the remaining metabolites were 5 ng mL^{-1}.

L. NIFEDIPINE

An HPLC analysis of nifedipine in human plasma has been reported by Thongnopnua [56]. Nifedipine is a calcium channel blocker and is used as a potent arterial vasodilator in the management of angina and various cardiovascular diseases. Pretreatment of the plasma sample with urea was used to denature the plasma proteins. The samples were then extracted with ethyl acetate for about 1 min. After evaporation of the organic phase, the residue was dissolved in 200 μL of methanol and 20 μL was injected into the liquid chromatograph. The chromatographic separation was performed on a 25-cm × 4.6-mm–id octadecylisilane column using a mobile phase of 62:38 v/v methanol–aqueous 0.01 M ammonium acetate pH 6.1, at a flow rate of 1 mL min^{-1}. Ultraviolet detection was carried out at 247 nm with butamben as an internal standard. The LOQ for nifedipine was 7 ng mL^{-1} of plasma. Linearity of the method was in the 7 to 240-ng mL^{-1} range. Precision and accuracy were in the 0–10 and 1–8% ranges, respectively. The mean extraction recovery of nifedipine was 93.3 ± 6%. Studies indicated that plasma samples containing nifedipine could be stored frozen up to 7 days without loss or deterioration of sample.

LI. PACLITAXEL

Willey et al. have reported an HPLC procedure for the quantitative assay of paclitaxel (Taxol) in human plasma [57]. Paclitaxel is a novel antimitotic and anticancer agent. It is a natural product extracted from the bark of the western yew tree (*Taxus brevifolia*). It was first isolated and identified in 1971 and has been licensed to Bristol Myers-Squibb Co. by the National Cancer Institute. Epitaxol, a biologically active stereoisomer, and baccatin III, a degradation product, were also separated and detected by this method. Plasma (0.5 mL) was mixed with 0.5 mL of 0.2-M ammonium acetate pH 5 and added to a preconditioned 1-mL cyanopropyl SPE cartridge. The analyte was eluted from the cartridge and the eluate evaporated to dryness. After reconstitution of the residue in mobile phase, an aliquot was injected. The separation was achieved within 10 min on a 25-cm × 4.6-mm–id octyl silane column using a mobile phase of 4:1:5 v/v/v acetonitrile–methanol–water, containing 0.01-M ammonium acetate pH 5, at a flow rate of 1 mL min^{-1} and UV detection at 227 nm. The linearity of the method was 10- to 1000-ng mL^{-1}. Extraction recovery of paclitaxel on the cyanopropyl SPE cartridge was 83%. Intra-assay accuracy and precision were 18 and 2–15%, respectively. The LOQ was 10 ng mL^{-1}.

LII. PHENYTOIN

Kouno et al. reported a simple and accurate HPLC method for the measurement of phenytoin, phenobarbital, and carbamazepine in serum [58]. Individual maintenance doses of epileptics should be determined on the basis of therapeutic drug monitoring before patients are discharged from the hospital. Serum was extracted with methylene chloride and the extract injected onto a 12.5-cm × 4-mm–id silica analytical column using a syringe-type minicolumn (Extrashot–silica) packed with diatomaceous earth granules. The mobile phase was *n*-hexane containing 0.2% glacial acetic acid, 2% ethanol, and 15% methylene chloride at a flow rate of 1 mL min^{-1} and UV detection at 240 nm. The method was linear in the 1- to 20-μg mL^{-1} range for carbamazepine and in the 5- to 40-μg mL^{-1} range for phenytoin and phenobarbital. The analytical results were comparable with those obtained with enzyme immunoassays. Serum samples as small as 5 μL were analyzed using this method.

An isocratic HPLC method has been reported for the assay of phenytoin in plasma and 5(4-hydroxyphenyl)-5-phenylthydantoin in urine [59]. Phenytoin is a very efficacious and widely prescribed drug for treatment of epilepsy. The purpose of this study was to develop a rapid, simple, and sensitive procedure that could be used in a comparative bioavailability study in humans. Plasma samples (0.5 mL) were extracted with ethyl acetate and, after mixing and centrifugation, the organic layer was evaporated to dryness and the residue dissolved in 100 μL of mobile phase. Urine samples (0.5 mL) were applied to an Extrelut-1 column and the analyte eluted with chloroform. Evaporation of the chloroform to dryness and redissolving the residue in 75 μL of mobile phase followed. Aliquots of both plasma and urine eluate were injected onto the HPLC system. The analytes were separated on a 15-cm × 3.9-mm–id octadecylsilane column using for plasma a mobile phase of 60:40:4 v/v/v water–methanol–tetrahydrofuran, at a flow rate of 1.2 mL min^{-1}, and for urine, a mobile phase of 60:40 v/v 0.2-M acetate buffer pH 4–methanol at a flow rate of 1 mL min^{-1}. Linearity of the method was 0.4–4 μg mL^{-1} for phenytoin in plasma and 0.1–1.2 μg mL^{-1} for phenytoin and hydroxy metabolite in urine, respectively. Mean relative recovery for phenytoin in plasma was in the 94–104% range. In urine, the recovery range was 97–108% for both analytes. Between-day precision ranged from 1.9 to 4.5% for phenytoin in pooled plasma and 1.2 to 2.6% for drug and metabolite in pooled urine.

LIII. PHYSOSTIGMINE

Quinn and Stewart have reported on an HPLC postcolumn fluorescent ion-pair extraction system and its application to physostigmine and its metabolite eseroline in human serum [60]. Physostigmine is a potent acetylcholinesterase inhibitor and has been suggested as a useful agent in the treatment of Alzheimer's disease. In this method, an HPLC postcolumn extraction system was designed for the analysis of quaternary ammonium and amine drugs in serum. A new fluorescent ion-pair reagent, sodium(3,4-dimethoxyphenyl)cinnamonitrile-2′-sulfonate, was synthesized specifically for this purpose. The postcolumn extraction system was composed of a three-dimensional knitted Teflon mixing coil and a membrane phase separator as shown in Fig. 20 and 21. Neostigmine was used as the internal standard. The physostigmine and neostigmine were extracted from serum using a C_{18} SPE cartridge. The ion-pair reagent was added into the serum sample before extraction. The analytes were eluted using a 200-μL aliquot of 95% methanol. After evaporation to dryness, the residue was dissolved in mobile phase and a 50-μL sample injected into the LC. The compounds were chromatographed on a 25-cm × 4.6-mm–id diol column, using a mobile phase of 80:20 v/v, pH 4 phosphate buffer–absolute methanol at a flow rate of 1 mL min^{-1}. Methylene chloride was used as the on-line extraction solvent for the ion pairs formed. After postcolumn separation of the methylene chloride from any aqueous component, the methylene chloride was sent to the fluorometric detector (excitation 243 nm and emission 418 nm cutoff filter) for measurement of the ion-pair physostigmine and neostigmine peaks. Linearity was calculated to be 2–100 ng mL^{-1}

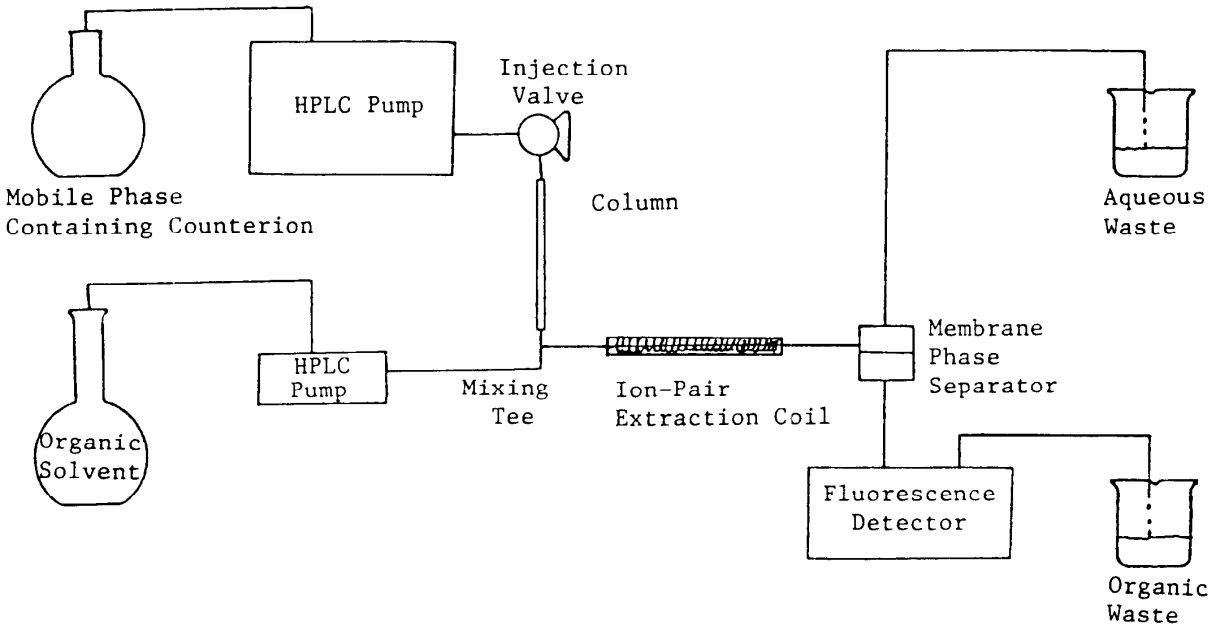


Figure 20 Schematic of HPLC postcolumn fluorescence ion-pair extraction system. (From Ref. 60.)

for physostigmine and 5–100 ng mL^{-1} for neostigmine. LODs were 2 and 5 ng mL^{-1} for physostigmine and neostigmine, respectively (S/N = 2). Precision of the method was 1.5–3% and accuracy 1.5–7% for both analytes.

LIV. PYRONARIDINE

Saleh and Loh have described an HPLC assay for pyronaridine, a new antimalarial drug, with high activity and low toxicity, in plasma [61]. To a 200-μL–plasma sample was added 500

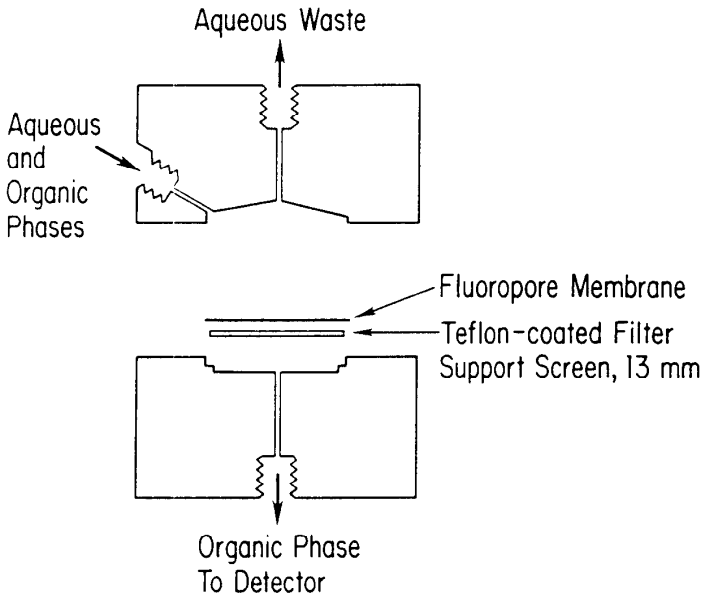


Figure 21 Diagram of membrane phase separator.

μL of buffer, followed by extraction with 3 mL of diethyl ether. After centrifugation, the ether extract was evaporated to dryness and the residue dissolved in 100 μL of mobile phase. A 50-μL aliquot was injected into the LC system. The drug was separated on a 25-cm × 4.6-mm–id octadecylsilane column, using a mobile phase of 85:15 v/v 0.08-M monobasic potassium phosphate–acetonitrile, containing 1% triethylamine. Triethylamine was used as a masking agent and was a very important component of the mobile phase for chromatographic separation of the pyronaridine, even though the C_{18} analytical column used was end-capped. The UV detector was set at 278 nm. The LOD was 70 ng on-column. Typical sample preparation and analysis time per sample was 130 min.

LV. QUINIDINE

A simple direct injection HPLC method for quinidine in plasma was reported by Huang and Morgan [62]. A 2-μL aliquot of the plasma sample containing the drug was directly injected onto a large-pore (300-A) 25-cm × 4.6-mm–id octadecylsilane column. The mobile phase was 85.4:13:1:0.6 v/v/v/v water–acetonitrile–triethylamine–phosphoric acid pH 3.0, at a flow rate of 1 mL min^{-1} with fluorescence detection (excitation of 250 nm and emission of 430 nm). The LOQ was 0.01 μM of quinidine (S/N >4). Intraday variability showed a RSD range of 0.7–2% at 0.2-, 1-, and 100-μM concentrations. There was little or no column deterioration noted during the investigation.

LVI. R023-9424

The assay of a new antibacterial agent R023-9424 has been reported by Szuna and Blain [63]. The novel compound (Fig. 22) consists of a cephalosporin linked by an ester bond at the 3′-position to a fluoroquinoline. The drug encompasses the antibacterial spectrum of both components. The assay was complicated because the metabolite fleroxacin is formed not only in vivo, but also nonenzymatically by hydrolysis of the ester bond. The HPLC method used both direct injection of plasma coupled with multidimensional chromatography. The first dimension was a size-exclusion column that allowed plasma proteins to elute with the column void volume. The second dimension was a reversed-phase column that allowed a high-resolution separation of the analyte and metabolites based on the hydrophobic nature of the sample. The 4-cm × 6-mm–id size-exclusion column used at 10:90 v/v isopropanol–0.03-M dibasic potassium phosphate buffer, pH 6.2, at a flow rate of 0.6 mL min^{-1}. The reversed-phase column was a 25-cm × 4.6-mm–id octylsilane column that used a 18:82 v/v acetonitrile–0.05-M

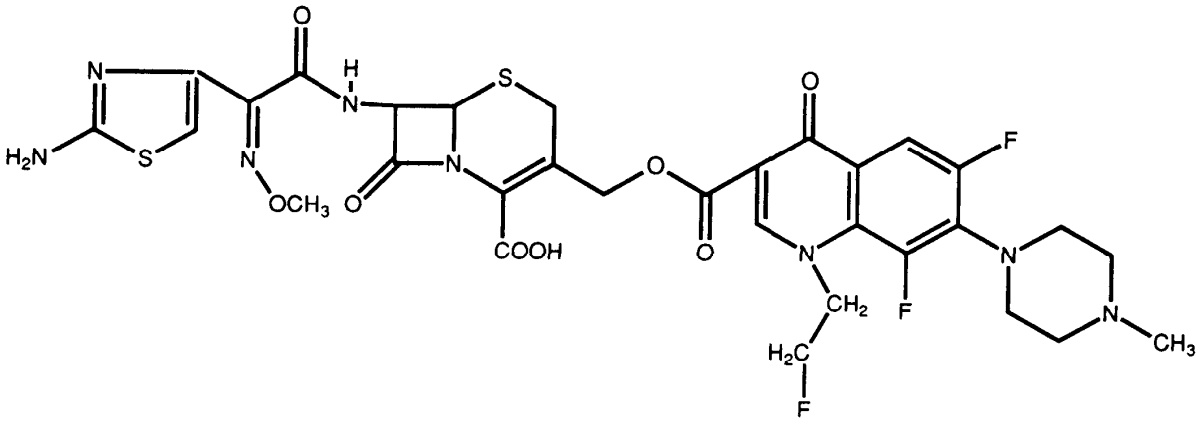


Figure 22 Chemical structure of RO23-9424.

dibasic potassium phosphate, pH 2.7, mobile phase at 1 mL min^{-1}. Detection of the analytes was at 287 nm. The LOQ was 0.35 $\mu g\ mL^{-1}$ for the drug and 0.27 $\mu g\ mL^{-1}$ for the metabolite. The recoveries of drug were 103 and 129% on the size-exclusion and reversed-phase columns, respectively.

LVII. RIVASTATIN

An HPLC procedure for the separation and induced fluorometric detection of rivastatin in plasma was reported by Kool et al. [64]. Rivastatin is a synthetic, enantiomerically pure HMG-CoA reductase inhibitor that is about 100-fold more active than lovastatin and is administered in the active free acid form. High reductase inhibitory activity facilitates a low oral dose, which gives very low plasma concentrations (0.05–5 ng mL^{-1}). To 1 mL of plasma was added 0.5 mL of an internal standard (analogue of rivastatin) and 1-mL pH 5.5 phosphate buffer. The mixture was extracted for 20 min with 4 mL of 3:1 v/v ether–hexane. After centrifugation, the organic layer was evaporated to dryness at 50°C under a nitrogen stream. The residue was reconstituted in 0.3 mL of the aqueous component of the mobile phase. An 80 to 90-μL injection was made into a 25-cm × 4.6-mm–id octadecylsilane column, using a mobile phase of 10:4:10 v/v/v acetonitrile–absolute methanol–aqueous 0.01-M monobasic potassium phosphate, pH 2.5. The flow rate was 1.4–1.6 mL min^{-1} at a column temperature of 54–55°C. Postcolumn irradiation of the column eluate gave a fluorescent signal, which was 75-fold more intense than the nonirradiated drug. Excitation and emission wavelengths of the irradiated drug peak were 290–295 and 390 nm, respectively. The linearity of the method was 0.025–8 ng mL^{-1}. Mean recoveries of the drug and internal standard were 88%. The LOQ was 25 pg mL^{-1} after 100 to 400-μg oral doses (S/N = 5). The percentage RSD at 25 pg mL^{-1} and 8 ng mL^{-1} were 3.6–13.5 and 0.7–3.6%, respectively. Intra- and interday variability were 0.4–5% (n = 6) and less than 10% (n = 6000), respectively.

LVIII. SCE-2787 (CEFOZOPRAN)

A method for a new cephalosporin antibiotic cefozopran (SCE-2787; Fig. 23) in serum and urine by HPLC was reported by Borner et al. [65]. Cefozopran is an injectable broad-spectrum antibiotic. After a serum sample was treated with acetonitrile to denature proteins, the supernate after centrifugation was extracted with methylene chloride (20-μL injection). With urine samples, dilution with HPLC mobile phase was the sole pretreatment step followed by a 5-μL injection. Chromatography was performed on an 12.5-cm × 4-mm–id octadecylsilane column, using a mobile phase of 4.5:95.5 v/v acetonitrile–phosphate buffer pH 3.2, containing 15 mM of sodium heptane-sulfonate. The UV detector was set at 235 nm. Retention time for cefozopran under these parameters was about 5.3 min. The LODs in serum and urine were 0.6 and 3.5 $\mu g\ mL^{-1}$, respectively. Overall recovery from serum was in the 84–103% range and recovery from urine in the 82–105% range. Linearity of the method for serum and urine

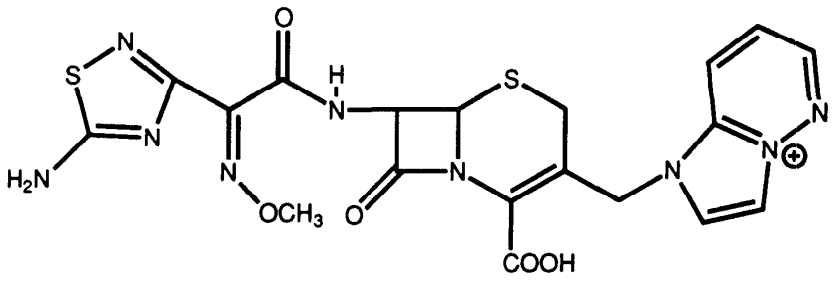
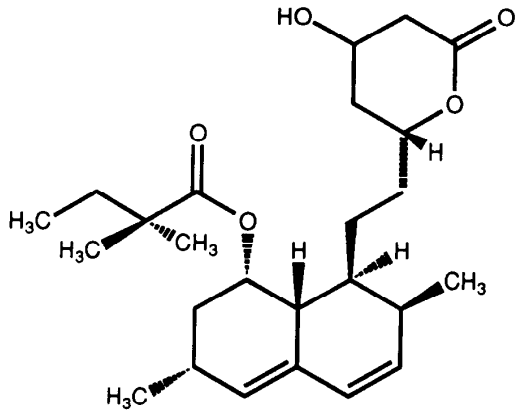


Figure 23 Chemical structure of SCE-2787 (cefozopran).

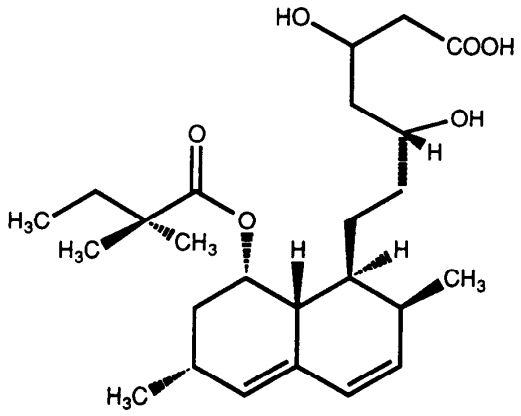
was 1–200 and 5–1000 $\mu g\ mL^{-1}$, respectively. A comparison of the HPLC assay with a reported microbiological assay showed no significant statistical difference in slopes of the standard curves.

LIX. SIMVASTATIN

Simvastatin is an orally active cholesterol-lowering agent in animals and humans. An HPLC method to measure the drug and its hydroxy acid form (formed on hydrolysis) in human plasma was reported by Carlucci et al. [66]. The chemical structures of the two analytes are shown in Fig. 24. Plasma (1 mL) was mixed with 50 μL of 60:40 v/v acetonitrile–water mix. After centrifugation, the supernatant is again treated with the acetonitrile–water mixture. The combined extracts are evaporated to dryness and the residue reconstituted in 25:75 v/v acetonitrile–water. Aliquots of the reconstituted solution were chromatographed. The separation was achieved on a 25-cm × 4.6-mm–id octadecylsilane column using a mobile phase of 35:65 v/v 0.025-M sodium dihydrogenphosphate pH 4.5–acetonitrile at a flow rate of 1.5 mL min^{-1} (Fig. 25). The column was at ambient temperature, and the analytes were detected at



Simvastatin



Hydroxy Acid Form

Figure 24 Chemical structures of simvastatin and its hydroxy acid form. (From Ref. 66.)

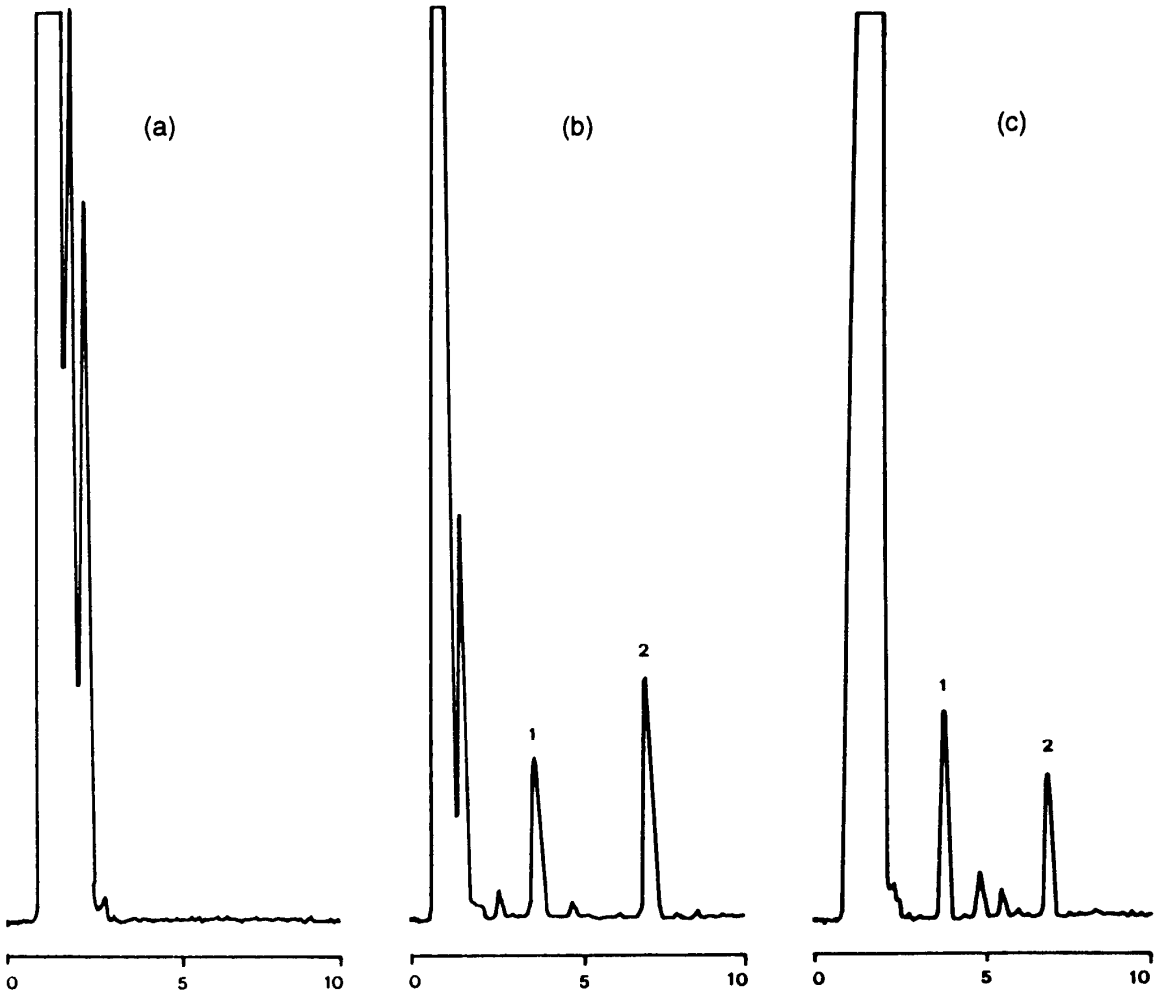


Figure 25 Chromatograms from human plasma extract: (a) blank plasma; (b) blank plasma spiked with 200 ng mL^{-1} of SV (2) and 200 ng mL^{-1} of SVA (1); (c) plasma sample collected 1 h after a dose of 10 mg of simvastatin. All concentrations refer to sample extracts. (From Ref. 66.)

238 nm. Linearity of the method was in the 20- to 1000-ng mL^{-1} range. Extraction efficiences were 95 and 96% at 50 and 250 ng mL^{-1}, respectively, for simvastatin and at 93 and 95%, respectively, for the hydroxy acid form of the drug. The LOD (S/N = 3) was 15 and 20 ng mL^{-1} for drug and hydroxy acid form, respectively. The accuracy of the method was ±5%. No internal standard was used in the procedure. Assay precision was ±2.3%, based on RSDs obtained from spiked plasma samples of the drug.

LX. SULFAMETHAZINE

A fully automated HPLC assay of sulfamethazine and its N^4-acetyl metabolite in ovine plasma was developed by Hubert et al. [67]. Sulfamethazine is most commonly used in veterinary medicine for therapeutic and prophylactic purposes in diseases of food-producing animals. The plasma samples were placed in a robotic autosampler that had been programmed to perform SPE. The plasma samples were applied to SPE C_{18} cartridges and the analytes were eluted with methanol. The eluate was mixed with a small amount of pH 6.4 phosphate buffer, and 20-μL was injected. The 12.5-cm × 4-mm–id octadecylsilane analytical column used a mobile phase of 25:75 v/v methanol–pH 6.4 phosphate buffer, with UV detection at 262 nm.

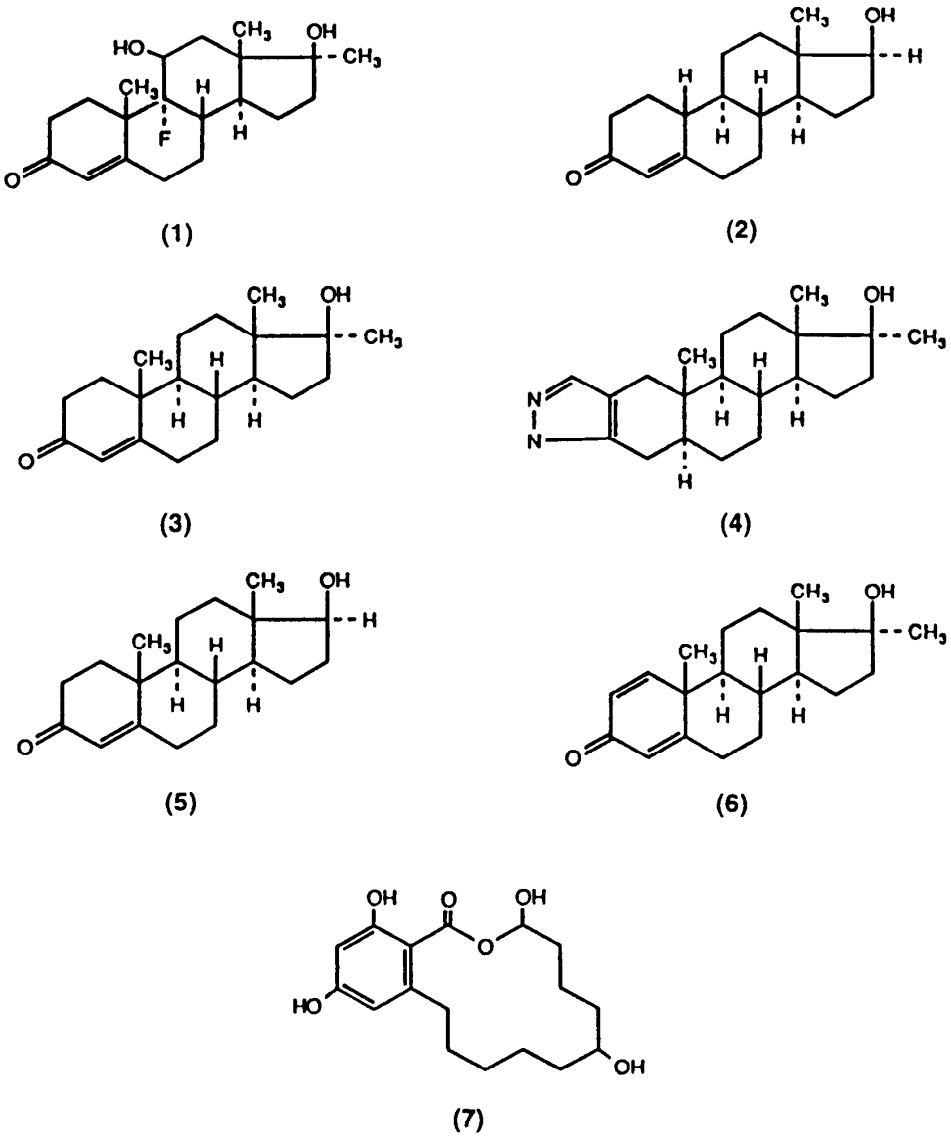


Figure 26 Structures of anabolic steroids and the anabolic agent zeranol: fluoxymesterone (**1**), 19-nortestosterone (**2**), methyltestosterone (**3**), stanozolol (**4**), testosterone (**5**), methandrostenolone (**6**), and zeranol (**7**). (From Ref. 68.)

The method was linear in the 2 to 250-μg mL^{-1} range. Extraction recovery from plasma was greater than 90%. The intra- and interday precisions of the method were 0.7 and 2%, respectively, at 50-μg mL^{-1} levels. The LOD and LOQ for sulfamethazine were 1.1 and 3.7 μg mL^{-1}, respectively. The LOD and LOQ for the N^4-acetyl metabolite were 1.5 and 5.0 μg mL^{-1}, respectively.

LXI. TESTOSTERONE-RELATED COMPOUNDS

Lampert and Stewart have reported a procedure for anabolic steroids and zeranol in human serum by isocratic reversed-phase HPLC on silica [68]. Apart from their legal use as growth-promoting agents and as androgen replacement therapy, anabolic drugs are widely abused in humans and animals. In the method, the anabolic drugs (fluoxymesterone, 19-nortestosterone, testosterone, methandrostenolone, methyltestosterone, stanozolol, and zeranol), shown in Fig.

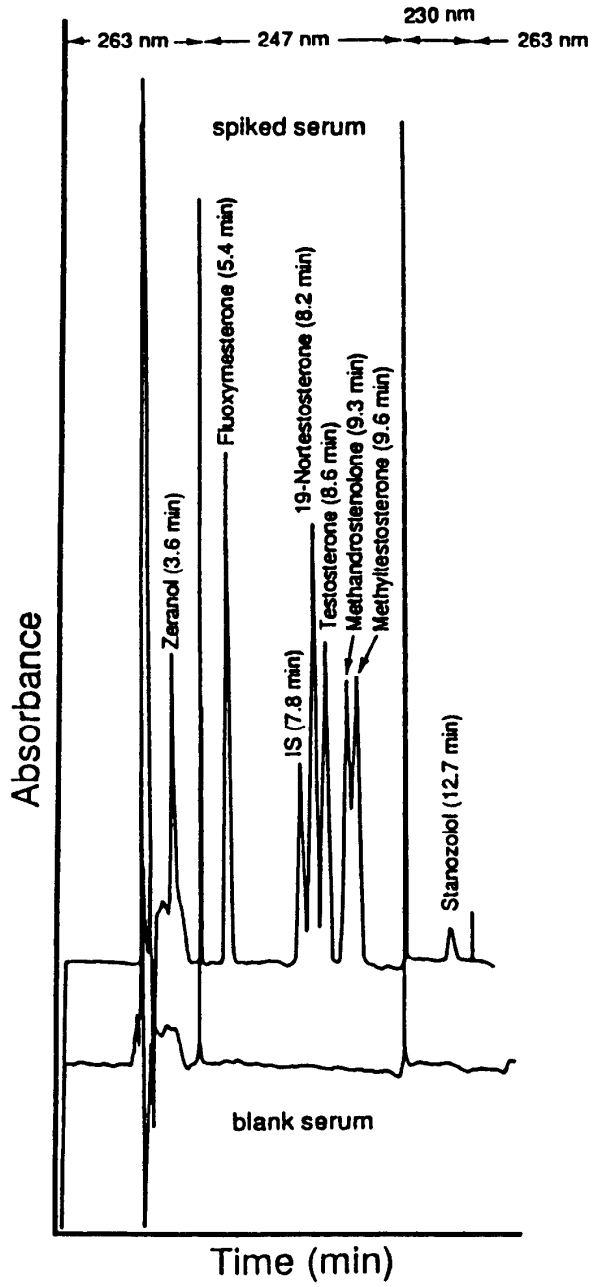


Figure 27 Typical chromatograms of blank and spiked human serum (0.5 mL) fortified with 30 ng mL^{-1} of each analyte and 125 ng internal standard (spironolactone). (From Ref. 68.)

26, were extracted from 0.5-mL–serum samples, using methylsilane SPE cartridges. Spironolactone (5 μg mL^{-1}) was added as internal standard. The analytes were eluted from the C_1 SPE cartridge using 45% aqueous acetonitrile at low vacuum. The eluate was reduced to low volume with a nitrogen stream and 50-μL injected into the HPLC. Separation of the drugs was performed on a 22-cm × 4.6-mm–id silica column using 86:15 v/v 0.1-M phosphate buffer pH 2.5–acetonitrile at a flow rate of 1 mL min^{-1} and 60°C column temperature (Fig. 27). The LOQs were 5 ng mL^{-1} for all analytes, except stanozolol (10 ng mL^{-1}). The LODs were 3 ng mL^{-1} for all drugs except stanozolol (7 ng mL^{-1}). Linearity was in the 0 to 1000-ng mL^{-1} range, with good accuracy (96–103%) and precision (RSD 2.8–10.9%).

LXII. TETRACYCLINE, CHLORTETRACYCLINE AND OXYTETRACYCLINE

A rapid direct-indirect determination of tetracyclines in serum was reported by Iwaki et al. [69]. Tetracyclines are widely used as antimicrobial agents. The method was developed for tetracycline (TC), chlortetracycline (CTC), and oxytetracycline (OTC). The initial cleanup step involved protein precipitation using trichloracetic acid (TCA) in methanol. A 100-μL–serum sample was treated with TCA and a 25-mM EDTA buffer was added followed by mixing and centrifugation. A whole-blood sample was kept at ambient temperature for 30 min, followed by centrifugation. The serum obtained would be treated as in the following. Chromatography was achieved on a 25-cm × 4.6-mm–id octadecylsilane column at 1-mL min^{-1} with fluorescence detection (excitation of 390 and emission of 512 nm). Recoveries of TC, CTC, and OTC were 99.5–100.3, 94.3–101.2, and 100–103%, respectively. Linearity of the method for TC, CTC, and OTC was 0.01–10, 0.04–10, and 0.04–10 μg mL^{-1}, respectively. The LOD for all three drugs was 10–35 ng mL^{-1}. Intraday and interday precision were in the 0.77–1.94% and 1.7–2.3% range, respectively at 0.05–5 and 1.0 μg mL^{-1}, respectively.

LXIII. ZIDOVUDINE

A method to determine serum zidovudine levels using ultrafiltration and HPLC was reported by Nebinger and Koel [70]. Zidovudine is a thymidine analogue that is a common drug in the treatment of acquired immunodeficiency syndrome (AIDS) or AIDS-related complex. Before assay, serum samples were heat inactivated for 1 h at 56°C. An internal standard (adenine, 100 μg mL^{-1}) was added to the 500 μL mL^{-1} serum sample, and the sample was subjected to ultrafiltration for sample cleanup. The ultrafiltrate was diluted 1:20 with HPLC eluent buffer and 50 μL was directly injected into the LC. The separation was achieved on a 12.5-cm × 4-mm–id octylsilane column, using a 20:80-v/v methanol–50-mM octanesulfonic acid in 0.1-M phosphate buffer pH 2.3 at a flow rate of 1 mL min^{-1} and UV detection at 268 nm. The zidovudine recovery was in the 98–100% range at concentrations of 1, 5, and 25 μg mL^{-1}. An LOD of 500 ng mL^{-1} was achieved at a S/N = 5. Overall method reproducibility was good with intra- and interday precisions in the 2.3–6.9 and 3.2–8.1%, respectively.

REFERENCES

1. J Chamberlain. Analysis of Drugs in Biological Samples. Boca Raton, FL: CRC Press, 1985.
2. RD McDowall, E Doyle, GS Murkitt, VS Picot. J Pharm Biomed Anal 7:1087, 1989.
3. VP Shah, KK Midha, S Dighe, IJ McGilveray, JP Skelly, A Yacobi, T Layloff, CT Viswanathan, CE Cook, RD McDowall, KA Pittman, S Spector. Pharm Res 9:588, 1992.
4. TC Pinkerton. J Chromatogr 544:13, 1991.
5. TR Krisnan, I Ibraham. J Pharm Biomed Anal 12:287, 1994.
6. P Nebinger, M Koel. J Chromatogr Biomed Appl 619:342, 1993.
7. FT Delbeke, J Landuyt, M Debackere. J Chromatogr Biomed Appl 621:209, 1993.
8. Y Kato, M Shimokawa, T Yokoyama. J Chromatogr Biomed Appl 616:67, 1993.
9. WJJ Krauwinkel, NJ Volkers-Kamermans, J Van Zijtveld. J Chromatogr Biomed Appl 617: 334, 1993.
10. S Chulavatnatol, BG Charles. J Chromatogr Biomed Appl 615:91, 1993.
11. DG Watson, Z Iqbal, JM Midgley, H Pryce-Jones, L Morrison, GN Dutton, S Karditsas, W Wilson. J Pharm Biomed Anal 11:389, 1993.
12. HG Schaefer. J Chromatogr Biomed Appl 616:87, 1993.
13. H LeSolleu, F Demotes-Mainard, G Vincon, B Bannwarth. J Pharm Biomed Anal 11:771, 1993.
14. E Schleyer, R Lohmann, C Rolf, A Gralow, CC Kaufmann, M Unterhalt, and W Hiddemann. J Chromatogr Biomed Appl 614:275, 1993.

15. H Zhang, JT Stewart. J Pharm Biomed Anal 11:1341, 1993.
16. J He, Shiukawa, T Nakagawa. J Pharm Biomed Anal 10:289, 1992.
17. H Liu, M. Delgado, LJ Forman, CM Eggers, JL Montoya. J Chromatogr Biomed Appl 616: 105, 1993.
18. T Soga, Y Inoue. J Chromatogr Biomed Appl 620:175, 1993.
19. DR Rutledge, AH Abadi, LM Lopez. J Pharm Biomed Anal 12:135, 1994.
20. JT Chaulet, G Greland, P Bellemin-Magninot, C Mounier, JL Bazier. J Pharm Biomed Anal 12:111, 1994.
21. H Zhang, JT Stewart. Anal Lett 26:675, 1993.
22. C Lacroix, F Wojciechowski, and P Danger. J Chromatogr Biomed Appl 617:285, 1993.
23. OV Olesen, B Poulsen. J Chromatogr Biomed Appl 622:39, 1993.
24. IM Roy. TM Jefferies, MD Threadgill, GH Dewar. J Pharm Biomed Anal 10:943, 1992.
25. H Millart, H Choisy. J Chromatogr Biomed Appl 620:273, 1993.
26. K Selinger, HM Hill, JA Anslow, D Gash. J Pharm Biomed Anal 8:79, 1990.
27. A Bozkurt, NE Basci, A Isimer, SO Kayaalp. J Pharm Biomed Anal 11:745, 1993.
28. AS Gross, AC Phillips, J. Boutagy, GM Shenfield. J Chromatogr Biomed Appl 621:115, 1993.
29. A Avgerinos, T Karidas, S Malamataris. J Chromatogr Biomed Appl 619:324, 1993.
30. AM Agra, S Huang. J Chromatogr Biomed Appl 620:205, 1993.
31. H Husseini, V Mitrovic, M Schlepper. J Chromatogr Biomed Appl 620:164, 1993.
32. OO Bolaji, CO Onyeji, FO Ogungbamila, FA Ogunbona, EO Ogunlana. J Chromatogr Biomed Appl 622:93, 1993.
33. T Tokumura, T Horie. J Chromatogr Biomed Appl 620:153, 1993.
34. K Yamashita, M Motohashi, T Yashiki. J Chromatogr Biomed Appl 616:144, 1993.
35. N Ferandez, JJ Garcia, MJ Diez, MJ Teran, M Sierra. J Chromatogr Biomed Appl 619:143, 1993.
36. EJ Eisenberg, WM Eickhoff. J Chromatogr Biomed Appl 621:110, 1993.
37. K Chan, RDM Jones. J Chromatogr Biomed Appl 619:154, 1993.
38. JD Davis, L Aarous, JB Houston. J Chromatogr Biomed Appl 621:105, 1993.
39. A Matsuura, T Nagayama, T Kitagawa. J Chromatogr Biomed Appl 617:339, 1993.
40. T Funaki, H Onodera, K Ogawa, S Ichihara, H Fukazawa, I Kurima. J Pharm Biomed Anal 11:379, 1993.
41. JB Alvin, S Stavchansky. J Pharm Biomed Anal 11:803, 1993.
42. RB Miller, C Amestoy. J Pharm Biomed Anal 10:541, 1992.
43. G Carlucci, L Biordi, C Vicentini, M Bologna. J Pharm Biomed Anal 8:283, 1990.
44. R Van Gijn, S. Kruijs, H Rosing, AC Dubbelman, O Van Tellingen, WW Ten Bokkel Huinink, HM Pinedo, JH Beijnen. J Pharm Biomed Anal 11:1345, 1993.
45. AR Wafelman, YLM Nortier, H Rosing, WJM Underberg, RAA Maes, JH Beijen. J Chromatogr Biomed Appl 622:71, 1993.
46. BG Wolthers, WDJV Kamerbeek, CM Van Beusekom, F Elshof, AW deRuyter Buitenhius, EPR Brunt, JPWF Lakhe. J Chromatogr Biomed Appl 622:33, 1993.
47. KY Chan, DK Satonin, LK Cheng, RA Okerholm. J Pharm Biomed Anal 11:1337, 1993.
48. M Breda, E Pianezzola, MS Benedetti. J Chromatogr Biomed Appl 620:225, 1993.
49. YM El-Sayed, SH Khidr, EM Niazy. Anal Lett 27:55, 1994.
50. WY Li, SKL Seah, RT Koda. J Chromatogr Biomed Appl 619:148, 1993.
51. V Ascalone, P Guinebault, A Rouchouse. J Chromatogr Biomed Appl 619:275, 1993.
52. PJ Borg, BR Sitoram, DA Taylor. J Chromatogr Biomed Appl 621:165, 1993.
53. D Wielbo, R Bhat, G Chari, D Vidyasagar, IR Tebbett, A Gulati. J Chromatogr Biomed Appl 615:164, 1993.
54. EL Bachert, HL Fung. J Chromatogr Biomed Appl 619:336, 1993.
55. P Zuccaro, I Altieri, M Rosa AR Passa, S Pichini, G Ricciarello, R Pacific. J Chromatogr Biomed Appl 621:257, 1993.
56. P Thongnopnua, K Viwatwongsa. J Pharm Biomed Anal 12:119, 1994.

57. TA Willey, EJ Bekos, RC Gaver, GF Duncan, LK Tay, JH Beijen, RH Farmen. J Chromatogr Biomed Appl 621:231, 1993.
58. Y Kouno, C Ishikura, M Homma, K Oka. J Chromatogr Biomed Appl 622:47, 1993.
59. MT Maya, AR Farinha, AM Lucas, JA Morais. J Pharm Biomed Anal 10:1001, 1992.
60. KD Quinn, JT Stewart. Biomed Chromatogr 5:8, 1991.
61. MI Saleh, HK Loh. Anal Chem Acta 282:559, 1993.
62. JL Huang, DJ Morgan. J Chromatogr Biomed Appl 620:278, 1993.
63. AJ Szuna, RW Blain. J Chromatogr Biomed Appl 620:211, 1993.
64. GJ Kool, GW Beck, W Ritter, JT Lettieri. J Pharm Biomed Anal 11:1269, 1993.
65. K Borner, E Borner, H Lode. J Chromatogr Biomed Appl 615:174, 1993.
66. G Carlucci, P Mazzeo, L Biordi, M Bologna. J Pharm Biomed Anal 10:693, 1992.
67. P Hubert, P Chiap, B Evard, L Delattre, J Crommen. J Chromatogr Biomed Appl 622:53, 1993.
68. BL Lampert, JT Stewart. J Liq Chromatogr 12:3231, 1989.
69. K Iwaki, N Okumura, M Yamazaki. J Chromatogr Biomed Appl 619:319, 1993.
70. P Nebinger, M Koel. J Pharm Biomed Anal 12:141, 1994.
71. IN Papadoyannis, HPLC in Clinical Chemistry. New York, NY: Dekker, 1990.
72. SHY Wong, Therapeutic Drug Monitoring and Toxicology. New York, NY: Dekker, 1985.

21

HPLC Applications for Chiral Pharmaceutical Analysis

Curt Pettersson

University of Uppsala, Uppsala, Sweden

Bengt-Arne Persson

Astra Hässle AB, Mölndal, Sweden

I. INTRODUCTION

A. Enantioselectivity in Biological Systems

Biological systems are predominantly homochiral, which means that enantiomers of drugs given in a racemic mixture normally will behave as two different compounds. For pharmacological activity the two enantiomers of a drug may have a similar effect and potency, but most often there are great differences, in one respect or both, between their interactions with enzymes or receptors within the organism.

Enantioselectivity in pharmacodynamics may be due to differences in pharmacokinetics and metabolism between the two enantiomers. Each step of the pharmacokinetic pathway may discriminate between the enantiomers; that is, absorption, protein binding, metabolism, and renal clearance. It must be anticipated, that somewhere along the road the enantiomers will behave differently.

Chiral drugs of natural and semisynthetic origin are almost exclusively available as single isomers, whereas among those from synthetic origin almost all are applied as racemic mixtures or with fixed ratios between the stereoisomers. For the future, chiral drugs will, to a much greater extent, appear as single isomers. Stereoselective methods for analysis of drugs are then needed (e.g., to examine whether an administered enantiomer is racemized).

The interest for chiral separations has developed along with the increased access of useful separation methods, in particular owing to new chiral stationary phases. Moreover the application field is enormous owing to all the synthetic chiral drugs sold as racemates on the drug market. Nowadays, there is a generally accepted view that a racemate provides not only mirror images, but also two different individuals in the organism relative to pharmacodynamics and pharmacokinetics. This new awareness, combined with the increased access of tools for enantioselective separation by liquid chromatography, has generated a most rapidly growing application field in bioanalytical chemistry. The contribution from the fast development in enantioselective synthesis of reference compounds must not be forgotten in this context. Even drugs established for several years have, in recent time, been subjected to pharmacodynamic and pharmacokinetic studies concerning metabolism and interaction with other drugs of the individual enantiomers.

B. Separation of Enantiomers by HPLC

Enantioselective analysis of drug substances in pharmaceutic formulations and in biological material is primarily performed by liquid chromatographic techniques. Gas chromatography has found some use, but the lack of chiral stationary phases with sufficient stability at high temperatures hampers the applicability. Lately, chiral selectors previously used in liquid chromatography have been employed in capillary electrophoresis, with great success. For liquid chromatographic assay of drugs in biological samples there are some differences relative to nonchiral separations, although general conclusions cannot be drawn. As a rule, the chiral stationary phases show lower column efficiency in terms of plate count. Also their capability to handle impurities in applied samples seems to be lower and so does the long-term stability, requiring more caution and protection. Provided that enantioselectivity is achieved, racemic drugs will give one peak for each enantiomer, and their metabolites may also appear in multiples. Analogues or homologues as internal standards may elute as two peaks, provided an enantiomeric form is not used. Together this means, that the peak capacity and the space in the chromatogram are insufficient to give room for both the compounds related to the drug, such as metabolites, and to regular impurities in samples from biological objects. This may put extra demand on the efficiency of the sample preparation procedure, including the use of coupled-column systems. Coupled-column chromatography has also been applied to sharpen the peaks from a chiral column with limited performance. For this, gradient elution has been employed as in achiral chromatography.

Chiral separation methods are either indirect, based on chiral derivatization before chromatographic separation of the diasteromeric products on a nonchiral stationary phase or, with the same kind of solid phase directly, when a chiral additive in the mobile phase is inducing enantioselectivity. However, for a couple of years the dominating technique is direct separation employing chiral stationary phases; those that are commercially available and used for separation of drug enantiomers are discussed relative to biomedical and pharmaceutical applications.

II. CHIRAL STATIONARY PHASES (CSPs)

A. Polysaccharides

Phenylcarbamate derivatives of polysaccharides, amylose, and cellulose, coated onto macroporous silica have lately found wide use within enantioselective separation of drugs. Most of these chiral stationary phases are attributed to Okamoto and co-workers [1–5]. As a rule, they are used with nonpolar mobile phases of hexane, with some alcohol as modifier. The cellulose-based phase Chiralcel OD has been used for β-adrenoceptor-active compounds such as atenolol [3,6], metoprolol [7,8], nadolol [9], bisoprolol [10], propranolol [3,11,12], bevantolol [13], timolol, and celiprolol [14], and for other drugs, such as dihydroipyridine derivatives [15], tropane alkaloids [3], mexiletine [16], and flosequinan [17]. Chiralcel OJ is often preferred for dihydropyridines, such as felodipine [18,19], nimodipine, nitrendipine [20], and manidipine [21], and was also used for acidic antidiabetic drugs [22]. Disopyramide was resolved on Chiralcel OF [23,24], and diltiazem [3,25,26] and warfarin [3,27] on Chiralcel OC. The separation of warfarin enantiomers in a plasma sample is demonstrated in Fig. 1.

The different nature and position of the substituents introduced in the phenyl ring of the carbamate derivatives have a major influence on the chiral recognition ability of the stationary phases [4]. Hydrogen-bonding interaction with the carbamate moiety is considered to be crucial for the chiral resolution. One of the cellulose materials Chiralcel OD-R is used with polar aqueous mobile phases [28–33] for which the organic modifier, ionic strength, and counterions present in the mobile phase influence retention and the chromatographic performance. Compounds such as propranolol, verapamil, and quaternary tropane alkaloids have been resolved.

Amylose-based chiral stationary phases, in some instances, provide chiral separations similar to the corresponding cellulose ones, but in other applications, complementary prop-

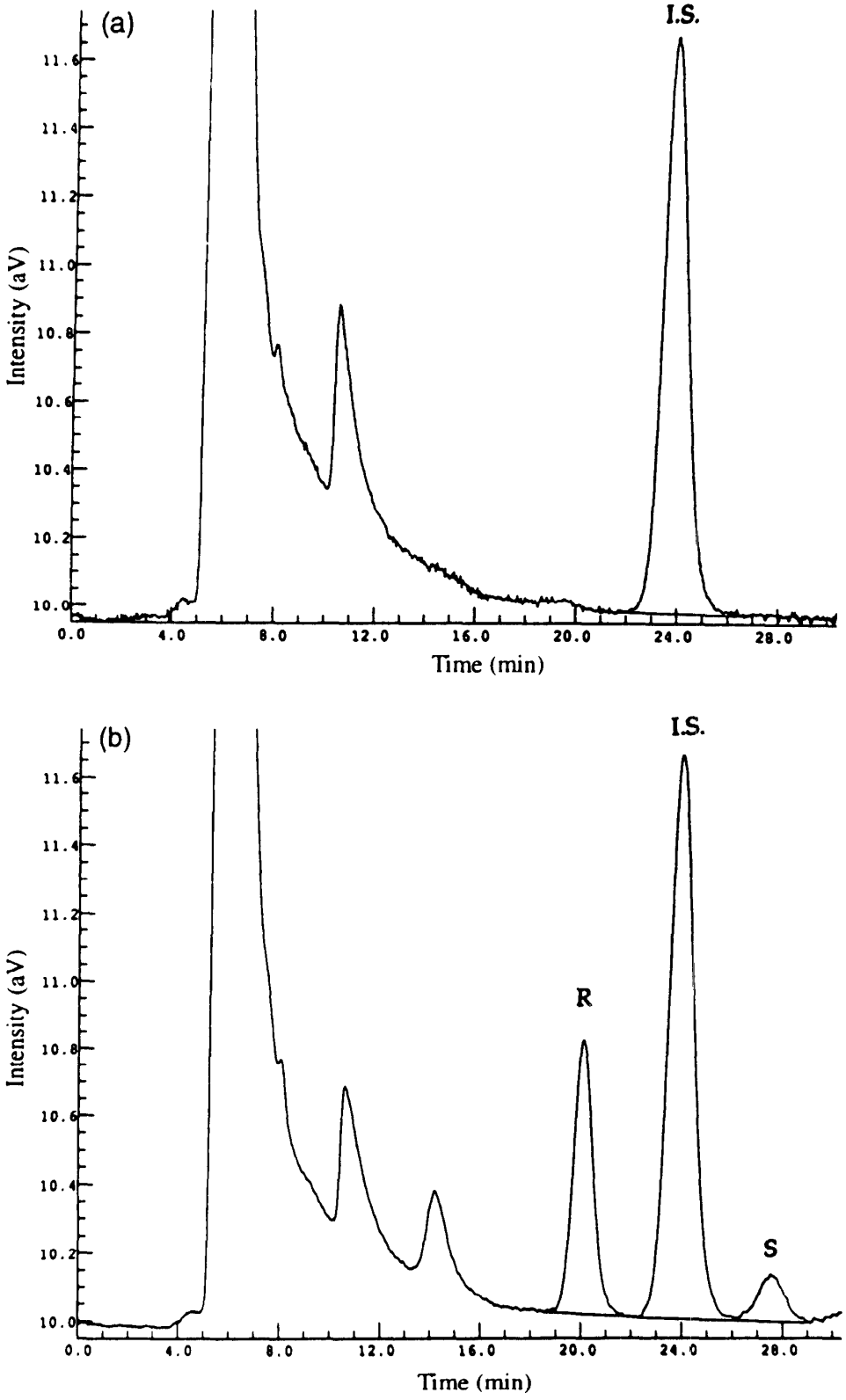


Figure 1 Enantioselective assay of warfarin in blood plasma by liquid chromatography on Chiralcel OC. Sample: extracts from authentic plasma samples (a) before and (b) 120 h after a single dose of 25 mg of (*R*,*S*)-warfarin. The latter sample contained 950 nmol L^{-1} (*R*)-warfarin and 240 nmol L^{-1} (*S*)-warfarin. (From Ref. 27.)

erties are found. Most studies have been made with tris (3,5-dimethyl-phenylcarbamate)-substituted amylose coated on silica, Chiralpak AD. Amidotetralins were separated both on this material and on Chiralcel OD [34] and so were an aminoalcohol, almokalant (Fig. 2) [35], compactin [36], and an analgesic drug tramadol [37]. Sulfoxide-substituted benzimidazoles [38,39], verapamil and norverapamil [40,41], the four isomers of nadolol [42], and cannabinoids [43] were resolved on Chiralpak AD. Isradipine [44], isoflavanones [45], and phthalimides [46] were separated on Chiralpak OT, a chiral phase not based on amylose, but on poly-(triphenylmethyl-methacrylate) coated on silica. Most of the polysaccharide phases have been developed for use with nonpolar mobile phases and, typically, mixtures of hexane and propanol or of any other alkane and organic modifier. Apart from control of temperature, which is important for consistent results as in all other chiral separation systems, the composition of the mobile phase can influence chromatographic performance, retention, and selectivity.

The manufacturer recommends the presence of an aliphatic amine (e.g., diethylamine) in the mobile phase for separation of organic bases such as most drugs. Peak shape is then improved, but the effect may be more pronounced for primary and secondary amines relative to tertiary ones and be due to the steric exposition of the amino function.

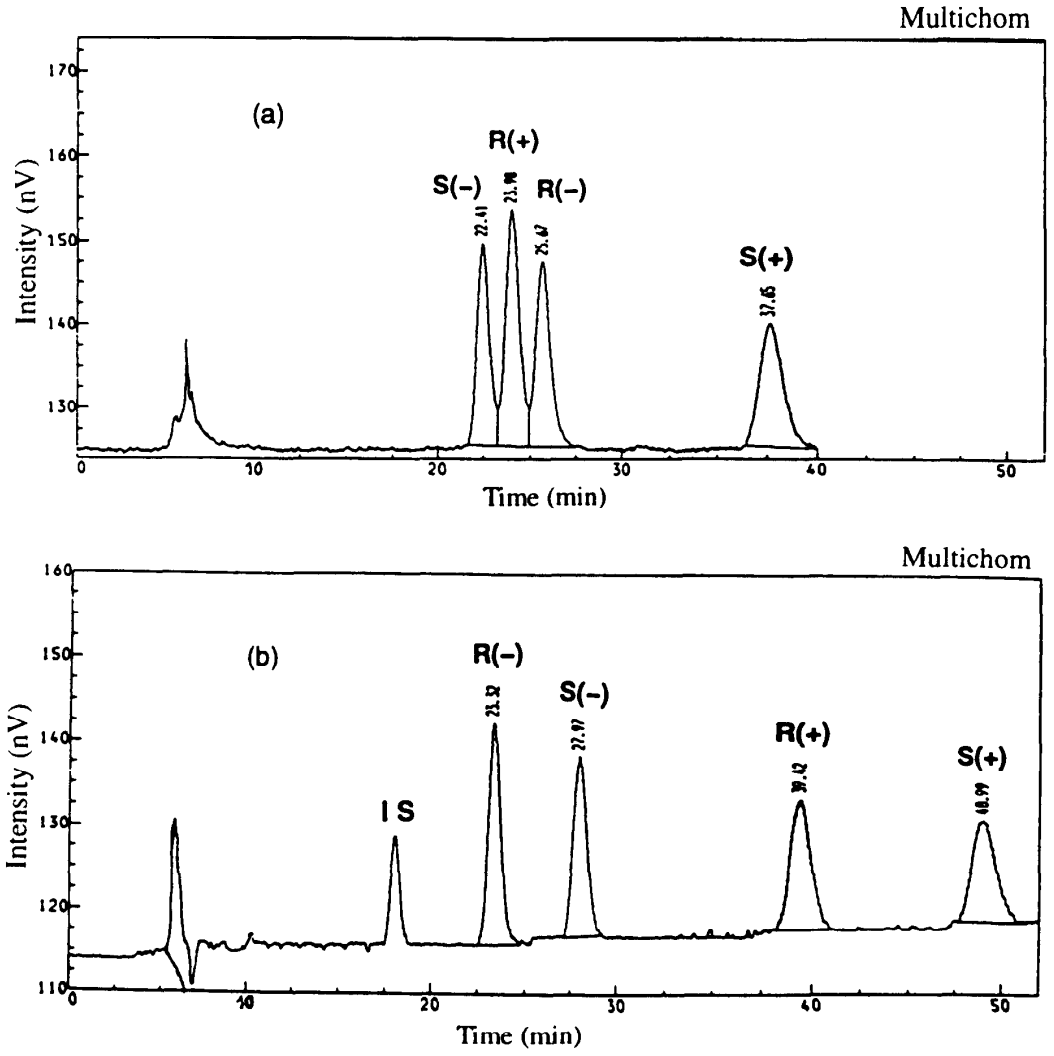


Figure 2 Liquid-chromatographic separation of isomers of almokalant using nonpolar mobile phase on (a), Chiralcel OD and (b) Chiralpak AD (IS, internal standard). (From Ref. 35.)

Increased content of propanol or other organic modifier in the alkane mobile phase will, as a rule, decrease retention. Varying the nature of the alcohol's lipophilic and steric properties may influence the peak performance, but even more importantly the enantioselectivity [47]. In a few instances it has been reported, that switching from one alcohol to another has reversed the retention order of a pair of antipods [38,47]. Other kinds of modifiers, such as acetonitrile, ethyl acetate, methyltertbutylether, and tetrahydrofuran have been employed alone or in combination with an alcohol to affect selectivity and efficiency. There is no simple way to explain the effects seen, because even the structure of the alkane bulk solvent may affect the chiral and retention properties of the stationary phase [46].

The presence of water in the nonpolar mobile phase, may influence both enantioselectivity and retention [8,48]. This is most often overlooked and is of no concern, if a sufficient and satisfactory resolution of two enantiomers is achieved. If this is not valid, or if more stereoisomers are involved through additional asymmetric centers, control of the water content may be decisive for the success of the separation [8,35]. Reversed retention order caused by changed water content has also been reported [49]. Retention effects by modifiers such as alcohols and by water content may be related to temperature, which then has to be controlled and investigated [49].

The chiral stationary phases, based on polysaccharides such as cellulose and amylose, in pharmaceutical and biomedical applications show excellent stability. Most often one or more of the different substituted variants will provide sufficient selectivity for a certain enantioselective separation.

B. α_1 Acid Glycoprotein

Orosomucoid, or α_1-acidglycoprotein (AGP), is a plasma protein that was introduced as a chiral stationary phase on silica in 1983 by Hermansson [50]. This phase, first as Enantiopac and later on as CHIRAL-AGP, has appeared as probably the most widely used chiral stationary phase in the drug field. Many drugs are amines, and AGP is well-suited for these although neutral and acidic compounds are also separated. There are a few review articles in the literature by Hermansson and Schill [51–53]. Among amino compounds β-adrenoceptor-blocking agents are separated in most instances in intact form [54–58], but also as phosgen derivatives [59] or after acetylation [60]. Other examples are local anestethics, such as bupivacaine and mepivacaine [61,62], atropine-related compounds [63,64], verapamil [65], terbutaline [66], disopyramide [67,68], mefloquine [69], and trimipramine [70]. Neutral kinds of compounds that have been resolved, are dihydropyridines and calcium antagonist drugs [71–73], warfarin and other coumarin anticoagulants [74], an alkylating agent ifosfamide [75], and sulfoxide-substituted benzimidazoles used against acid-related diseases [76]. Barbiturates [56] and anti-inflammatory agents (NSAIDs) [77–79] may represent acidic drugs, for which AGP has found use as a chiral stationary phase. Numerous other applications of this phase are given in the review articles [51–53].

Temperature may influence both retention and selectivity [52] and must be controlled. Because, often, only minor effects are needed to improve an insufficient resolution or to change retention, temperature is a useful variable. The pH of the mobile aqueous phase can be varied between 2 and 7 and will affect both retention and selectivity. A lower pH will elute bases earlier, as in reversed-phase liquid chromatography. The choice of pH buffer components may also influence the elution of both the acid anion and the cation [78]. Retention by ion-exchange and ion-pair formation has been suggested, in addition to chiral recognition [64,78]. Therefore, charged additives may displace analytes of the same charge and increase retention of analytes of opposite charge; as in reversed-phase chromatography. Charged organic modifiers may have a significant effect on the enantioselectivity, as shown both for cationic and anionic solutes [51,52] and illustrated in Fig 3.

Uncharged organic modifiers, such as propanols and acetonitrile, are used to regulate retention. For hydrophilic or moderately hydrophobic compounds low, if any, content is

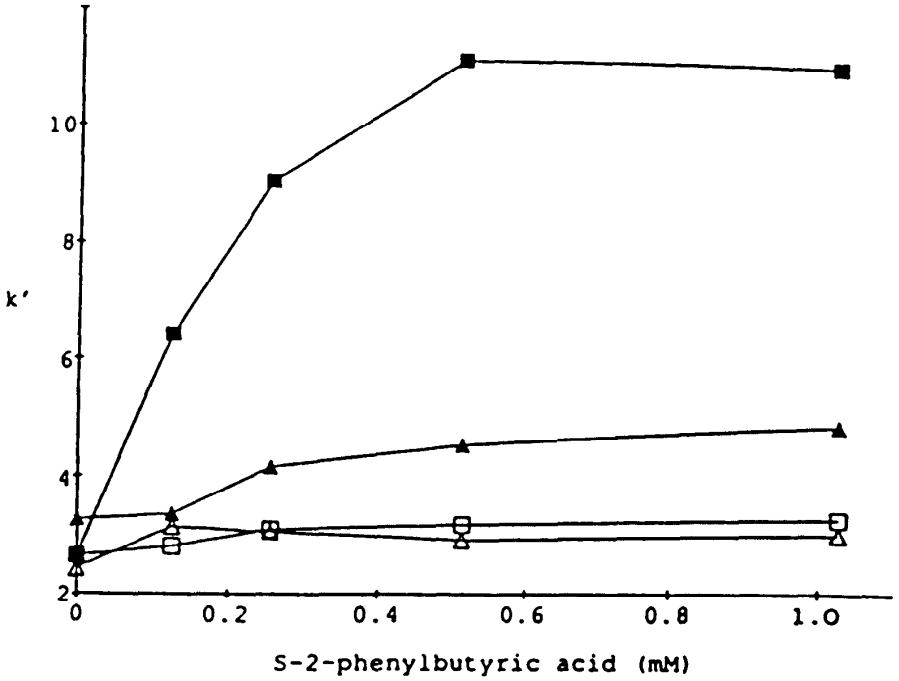


Figure 3 Influence by addition of (*S*)-2-phenylbutyric acid on capacity factors for the enantiomers of atropine (□, ■) and homatropine (△, ▲) on CHIRAL-AGP. (From Ref. 64.)

needed, whereas for hydrophobic calcium channel blockers, 20% or more organic modifier has been added. Besides the effect on retention, selectivity will naturally be influenced, for it must be anticipated that the chiral recognition structure of the protein will be affected by most additives. Gradient elution may be advantageous in terms of peak sharpness and is preferably performed by a successive increase of the content of the organic modifier [80]. However, a pH gradient may be as useful if the pH buffer capacity of the stationary phase is taken into account (Fig. 4). The application of the AGP phases to enantioselective assay of drugs in

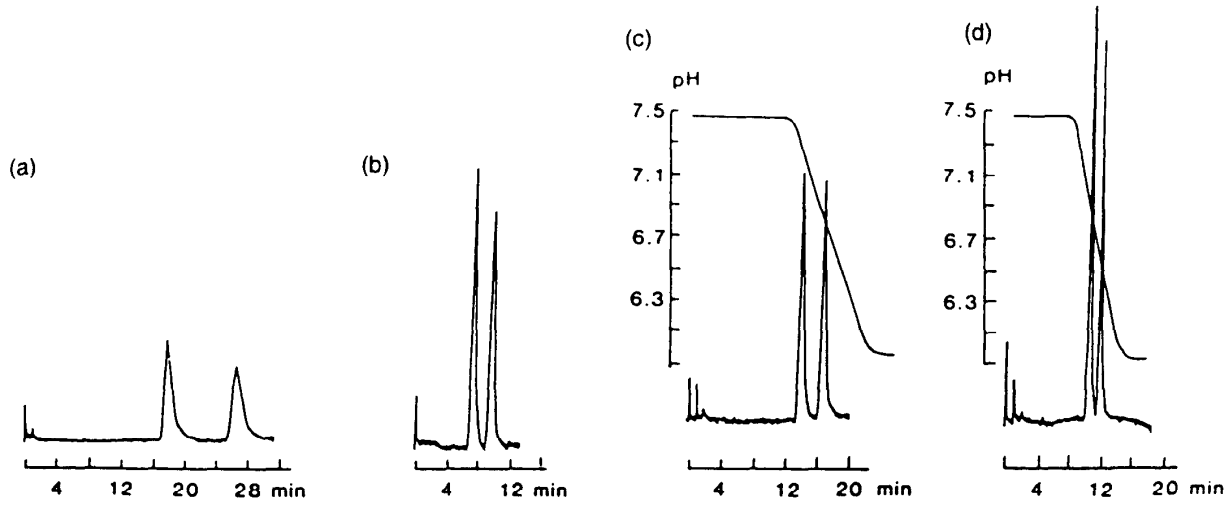


Figure 4 Influence on pH by isocratic and gradient elution of metoprolol enantiomers on CHIRAL-AGP: (a) pH 7.5, (b) pH 6.40, (c and d) pH-gradients. (From Ref. 80.)

biological material often demands careful sample preparation and selective detection (e.g., by fluorescence) if low concentrations have to be measured [81]. Coupled column systems have also been employed [82]. Guard columns and prevention of particles from entering the packing will prolong the life of the column and, at least a few hundred, biological extracts can be run provided precautions are taken.

C. Ovomucoid-Bonded Stationary Phase

Ovomucoid protein-based chiral columns have shown about the same application field in drug analysis as the AGP-phase. That means these columns can be tested and used for most kinds of drugs whether basic, neutral, or acidic [83]. Drugs with amino function, such as verapamil [84–86] or chlorpheniramine [87–89]; β-adrenoceptor-blocking agents, such as oxprenolol, pindolol, propranolol [83,90–91], and homochlorocyclizine [92], have been resolved on Ultron ES-OVM, which is the trade name for the ovomucoid column. Neutral drug compounds are represented by warfarin [83], oxazepam [83], nimodipine, nicardipine [93,94], econazole [95], and omeprazole [76]; and acidic ones by mephenytoin, thalidomide, hexobarbital, ibuprofen, ketoprofen; and ketorolac [87–89,96]

The enantiomeric resolution on the ovomucoid column is greatly influenced by pH of the mobile aqueous phase. Basic drugs are most often separated at neutral pH, whereas acids are run at pH 4–5. The content of an organic modifier (e.g., methanol, acetonitrile, or propanol) is used to regulate retention and may also influence the resolution of an enantiomeric pair. Certain hydrophobic drugs, such as dihydropyridine calcium channel blockers, have strong affinity for the ovomucoid phase, and a high concentrations 25–30% of the organic modifier will be required for reasonable retention times [93,94]. In other respects there are similarities, but also differences, between the performance of the ovomucoid and AGP chiral phases, not the least of which is the enantioselective properties. Verapamil [84,85] and propranolol [91] have been assayed in biological samples using column-switching during which the ovomucoid-bonded phase has enabled the enantioselective separation. Drug enantiomers of chlorpheniramine, ketoprofen, and oxazepam in serum were injected directly on to this kind of stationary phase [88].

D. Serum Albumin Phases

Bovine serum albumin (BSA), was the first protein to be immobilized on silica and used for enantiomer separation. It was introduced as a stationary phase by Allenmark and co-workers in 1982–1983 [97,98]. In recent years, human serum albumin (HSA) has also been covalently bonded to silica and used as a chiral stationary phase [99]. The albumin phases have found use for enantioselective separation of acidic and neutral compounds; however, these phases are not as well suited for basic drugs with aliphatic amino function. Ketoprofen and suprofen are carboxylic acids that have been resolved [100] and, among neutral compounds, warfarin [101], methaqualone [102], oxazepam and other benzodiazepinones [102,103], tryptophan [104], and sulfoxide-substituted benzimidazoles, such as omeprazole [105], will illustrate the applicability of this kind of chiral stationary phase in the drug field. The resolution of omeprazole on an albumin phase and two other protein columns is shown in Fig. 5.

The pH of the aqueous mobile phase is most often near neutral, with or without a few percent of added organic modifier, usually propanol; but acetonitrile and methanol have also been used [106]. Besides pH, temperature, buffer components, and added charged, organic modifiers may influence the enantioselectivity and retention [107].

E. Cyclodextrin Stationary Phases

β-Cyclodextrin, in intact or derivatized form, has been employed as a chiral selector bonded to silica. Armstrong and co-workers have made major contributions in the development and

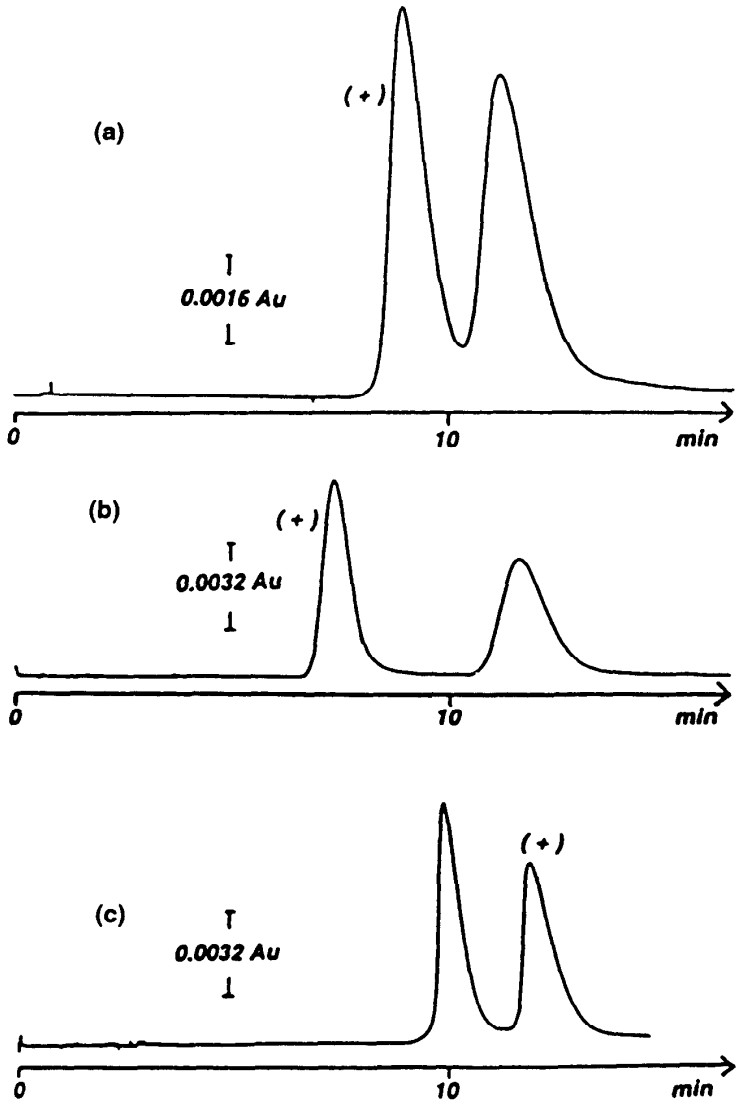


Figure 5 Enantioselective separation of omeprazole on protein-based columns at pH 7.0 (a) CHIRAL-AGP; (b) BSA-DSC; (c) Ultron ES-OVM. (From Ref. 38.)

exploitation of this kind of stationary phases [108–110]. Columns with native cyclodextrin are used under reversed-phase conditions with a polar aqueous mobile phase, and both normal and reversed-phase modes are used with stationary phases of derivatized cyclodextrin on silica [108–112]. Applications in the drug field concern amines, such as chlorpheniramine [110], terbutaline [113], scopolamine [114], terodiline [112], nicotine and analogues [115], and β-adrenoceptor blockers, such as propranolol, metoprolol, atenolol, and timolol [116,117]. Weakly acidic drugs, such as ibuprofen, ketoprofen, mephenytoin, and hexobarbital [118], and more neutral compounds, such as nisoldipine and chlorthalidone [119], oxazepam, bendroflumethiazide, glutethimide, and indapamide [112], complete the picture of a versatile chiral stationary phase, for which, however, the enantioselectivity generally seems to be lower, compared with the protein phases. Coupled column liquid chromatography combined with mass-spectrometric detection was employed for the enantioselective assay of terbutaline in biological samples [113,117].

F. Pirkle Phases

Pirkle and co-workers introduced *N*-(3,5-dinitrobenzoyl) amino acids as chiral selectors ionically or covalently linked to aminopropyl silica [120]. Through the years this group has made several contributions to this type of chiral stationary phases, but also others have developed useful and commercially available material [121–123]. These selectors are based on charge-transfer complexation, and the retention is mediated by $\pi-\pi$ interaction along with hydrogen bonding in the nonpolar solvent used as mobile phase. To improve the chiral recognition of the solutes, derivatization by acylation or carbamoylation and introduction of a 3,5-dinitrophenyl or a naphthyl group were often used.

Applications within the pharmaceutical field are numerous (e.g., mephenytoin [124], benzodiazepinones [125], propranolol [126], pindolol [127], nadolol [128], and ibutilide [129]). The β-adrenoceptor-blocking agents and ibutilide were separated after derivatization with phosgene [126] or alkyl or aryl isocyanates [127–129]. Other applications are dihydropyridines [119], β-adrenoceptor blockers without prior derivatization [131,132] and naproxen [133]. Most recently, an extensive survey on the applicability of Pirkle-concept chiral stationary phases in the pharmaceutical field has been presented [134].

There are not many applications of the Pirkle-type columns to the enantioselective assay of drugs in biological samples. Phenprocoumon, an anticoagulant, was determined in human plasma and urine [135], albruterol in serum [136], and ibuprofen [137] and fenfluramine [138] in biological material after derivatization.

III. CHIRAL MOBILE-PHASE ADDITIVES (CMPAs)

Direct separation of enantiomers can be obtained by adding a chiral molecule to the mobile phase; a chiral mobile-phase additive (CMPA). The mechanisms of chiral recognition by CMPAs have previously been reviewed [139–142]. In principle, the CMPA gives labile diastereomeric complexes with the enantiomeric analytes in the mobile phase. The two diastereomeric complexes differ in energy content and in physical and chemical properties; they can be separated by an achiral solid phase. A chiral separation obtained by a CMPA is due to (1) an enantioselective complexation in the mobile phase, (2) a selective distribution of labile diastereomeric complexes to the stationary phase, or (3) because the CMPA is dynamically coated on the solid phase and forms a chiral stationary phase with the possibility to discriminate between enantiomers (i.e., the stationary phase is operating as an ordinary CSP.) Clearly, a combination of these different separation mechanisms is also possible. The chromatographic enantioselectivity ($\alpha = k_2'/k_1'$) may be improved or impaired by the presence of several simultaneously operating enantioselective mechanisms [see 142,143]. A drawback of the separation technique based on a CMPA is that the presence of a chiral additive in the mobile phase may restrict the choice of detection systems and the labile diastereomeric complexes may have different detector response [144].

However, the approach of CMPAs offers some advantages over the use of CSPs. The conventional solid phases used (e.g., achiral reversed-phase and silica supports) generally have high column efficiency and are less expensive and more robust than CSPs. The use of CMPAs for promotion of chiral separation is a flexible method, because the chiral selector in the mobile phase can easily be changed when exploring new chiral selectors during the development of an enantioselective separation method. Chromatographic systems based on CMPAs, offer a wide range of variables (e.g., its chirality and concentration as well as the nature of the achiral solid phase) to optimize the enantioselective separation. CMPAs have been used in studies of qualitative control of active components and intermediates as well as in determination of pharmacokinetic and pharmacodynamic effects of enantiomers. Occasionally, CMPAs have also been used for the isolation of pure enantiomers at a semipreparative scale. Gaskell et al. used (+)-tartaric acid as counterion in chiral ion-pair chromatography to separate

up to 17 mg of an aminoalcohol per injection on a 1 in ID column packed with silica particles [145].

A. Ligand-Exchange Chromatography

In the late 1960s Davankov and co-workers introduced ligand-exchange chromatography for the separation of enantiomers [146]. The original studies of enantioselective separation of amino acids were made using a resin with a chemically immobilized ligand that had been saturated with copper (i.e., a chiral stationary phase was used). Later, Lindner et al. introduced chiral triamines, L-2-alkyl-4-octyldiethylenetriamine in combination with Zn(II) as CMPAs for separation of dansyl derivatives of D- and L-amino acids [147]. The solid phase was a conventional C_8 support. The principle of chiral ligand-exchange chromatography is based on the formation of diastereomeric ternary complexes between the selector ligand, a transition metal (both are present in the mobile phase), and the solute enantiomers. In a recent review Davankov discussed the use of ligand-exchange chromatography in the CMPA mode for the enantioselective analysis of amino acids and their derivatives [148].

The amino acid profile of cerebrospinal fluid (CSF) from a patient with meningitis was determined using ligand-exchange chromatography [149]. The mobile phase was 20% acetonitrile in a buffer containing 5 mM of L-histidine methyl ester, 2.5 mM of $CuSO_4$, and 2.0 g of ammonium acetate per liter of deionized water, pH 7.0. A ligand based on tartaric acid, (*R,R*)-tartaric acid mono-*n*-octylamide, was introduced by Lindner et al. [150] as a chiral selector in ligand-exchange chromatography for separation of amino acids. The enantioselectivity depended on the transition metal used for complexation.

An enantioselective method based on ligand-exchange chromatography has been developed for determination of a chiral impurity in L-dopa [151] and could also be applied for the stereoselective analysis of tryptophan, methyldopa, and carbidopa. The enantiomers of penicillamine have also been analyzed using the ligand-exchange principle [152]. The enantiomers had to be derivatized with formaldehyde to give dimethylthiazolidinecarboylic acid before the analysis. Resolution of enantiomers of ofloxacin (Fig. 6) and pyridone carboxylic acid was accomplished using a mobile phase containing 6 mmol L^{-1} of L-phenylalanine and 3 mmol L^{-1} of Cu(II) [153].

Lam applied the commercially available sweetner asparatame, in coordination with copper, as a CMPA to monitoring the concentrations of D- and L-pipecolic acid in urine of hyperlysinemic patients [149]. The pharmacokinetics of the enantiomers of thyroxine were studied, using as a CMPA a coordination complex of L-proline and Cu(II) [154]. A chiral metabolic study of the a prochiral drug phenytoin was performed using the hydrophobic ligand L-proline-octylamide coordinated with Ni(II) in the mobile phase to promote the enantioselective separation. The enantiomers of the phenytoin metabolite, *p*-hydroxyphenylhydantoin, were measured [155,156].

B. Chiral Counterions

The counterion should have a complementary structure to the enantiomeric solutes to be separated. Generally, the presence of functional groups in the vicinity of the chiral center in the counterion is important to give the diastereomeric ion-pairs different stability or distribution properties [157]. Enantiomeric solutes that have possibilities for giving additional intermolecular interactions (e.g., hydrogen bonding) besides the electrostatic attraction to the counterion gave high enantioselectivities [143,158]. Compounds having no polar functions other than the acidic or basic function are generally difficult to resolve by use of a chiral counterion.

Drugs that have been separated using 10-camphorsulfonic acid are alprenolol, metoprolol, and propranolol [159,160]. Apolar mobile phases were selected, for they promote a high degree of ion-pair formation. Most studies have been performed with dichloromethane, con-

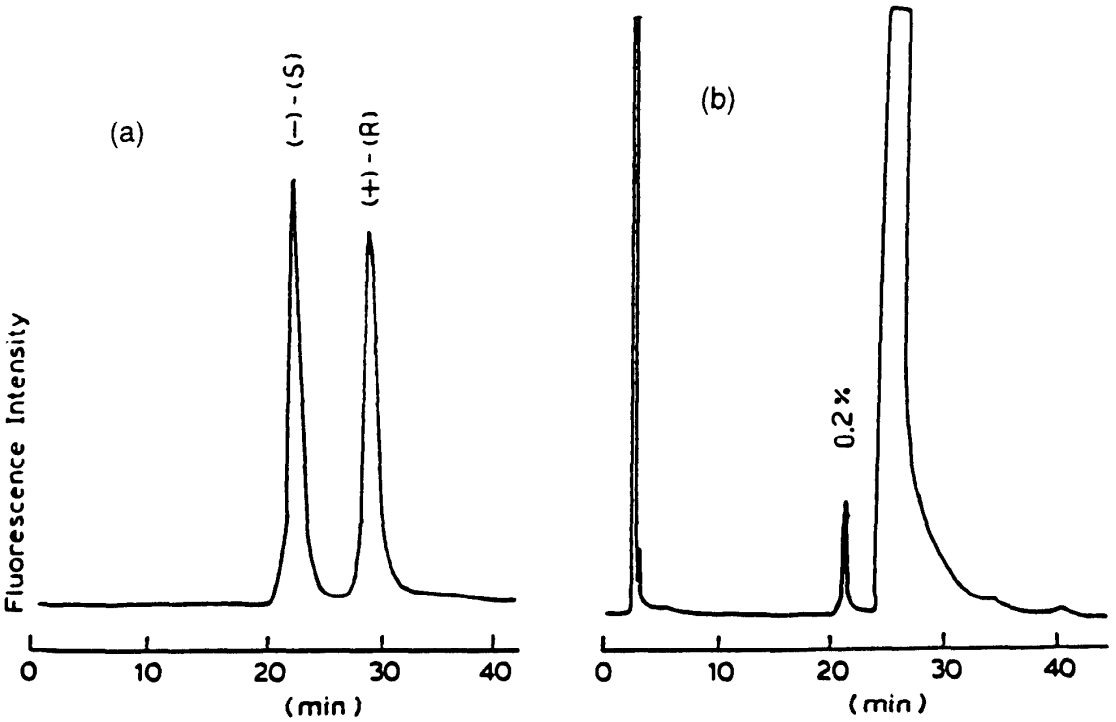


Figure 6 Separation of (*R*)- and (*S*)-ofloxacin by ligand-exchange chromatography with L-phenylalanine and Cu(II) in the mobile phase. Sample: (a) 200 ng as a racemic mixture; (b) 3 μg as the (*R*)-enantiomer containing 0.2% (*S*)-enantiomer. (From Ref. 153.)

taining a small amount of an alcohol. As retaining phase LiChrosorb DIOL gives the highest enantioselectivities and the best chromatographic performance (column efficieny and peak symmetry). The main regulators of retention and enantioselectivity in chiral ion-pair chromatography with nonpolar mobile phases are the concentration of counterion and the nature as well as concentration of a mobile phase additive having the same protolytic character as the enantiomeric analytes [157]. The retention of the enantiomers generally decreases as the counterion concentration is increased. A significant improvement in chromatographic performance (peak shape) of amines and amino alcohols has been observed when triethylamine was present in the mobile phase [143,158]. Addition of an alcohol to dichloromethane reduced the analysis time but impaired the enantioselectivity [160]. 10-Camphorsulfonic acid as counterion has also resolved ergot peptide and eburnane [140,161,162] and amino steroids [163]. The chiral acid was dissolved in a mixture of apolar, medium polar, and polar solvents. The solid phase was cyanopropyl silica and silica, respectively. Mobile phases containing *N*-benzoxycarbonyl-glycyl-L-proline (L-ZGP), triethylamine, and dichloromethane successfully separated enantiomers of various β-adrenoceptor-blocking agents on a LiChrosorb DIOL column [143,164]. Later, a novel basic antihypertensive agent, *trans*-3,4-dihydro-2,2-dimethyl-2*H*-1-benzopyran was resolved using the same counterion [165]. Karlsson and co-workers have applied chiral ion-pair chromatography with L-ZGP as the counterion for the determination of (*R*)- and (*S*)-propranolol in plasma [166]. Figure 7 shows the chromatograms from a healthy volunteer before and after intake of 80 mg propranolol (Inderal). A similar separation system was applied to assay the enantiomers of metoprolol and its metabolites in blood, urine, and human liver microsomal preparations [167]. Determination of the enantiomeric purity of both antipodes of 8-hydroxy-2-(dipropylamino)-tetralin, a highly potent 5-hydroxytryptamine (5-HT)-receptor agonist, has been performed by using ZGP as counterion in the mobile phase [168]. To facilite the determination of the small peak of the enantiomeric impurity, either the

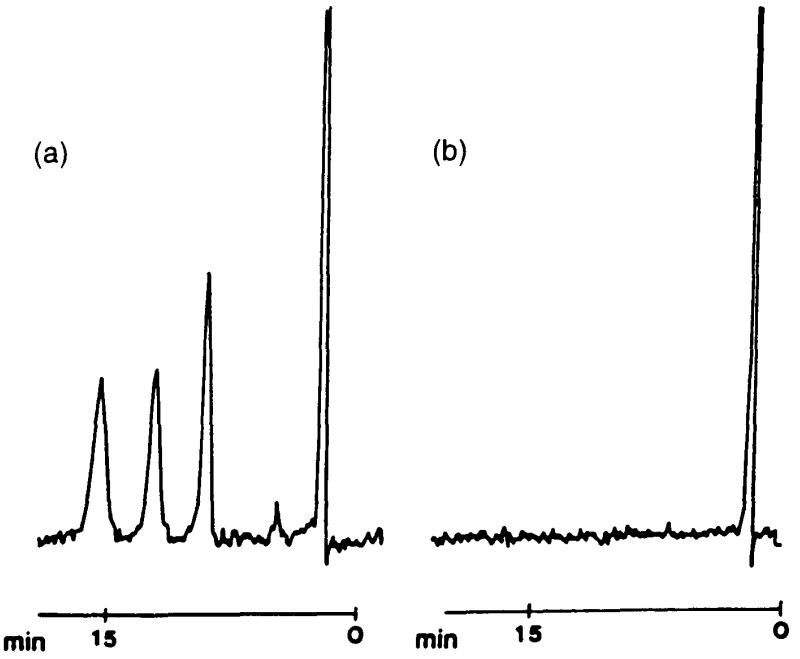


Figure 7 Determination of (*S*)- and (*R*)-propranolol in blood plasma by ion-pair chromatography. Sample: (a) plasma sample 45 min after and (b) before drug intake. (From Ref. 166.)

(−)-enantiomer or (+)-enantiomer was directed to be the first eluted peak by using either D- or L-ZGP as CMPA.

The introduction of porous graphitic carbon (PGC) as the achiral adsorbing phase in chiral ion-pair chromatography greatly extended the type of compounds that could be resolved. Enantiomers of alprenolol, metoprolol, oxprenolol, atenolol, and other amino alcohols [158,169], tocainide, mexilitine, prilocaine, and chlorthalidone [158] were separated using L-ZGP as counterion in apolar mobile phases and PGC as solid phase. Quinine and other cinchona alkaloids as counterions have promoted enantioselective separation of acids (e.g., naproxen [169,170], ketoprofen, and ibuprofen [169]). The amine counterion was dissolved in dichloromethane, and an acid (e.g., acetic acid) was also added to the organic solvent to control the chiral separation. Both LiChrosorb DIOL [170] and Hypercarb (PGC) [169] have been used as the solid phase. The inherent UV-absorption properties of quinine and analogues as counterions have been used for improvement in detection sensitivity of acidic enantiomers [169–171].

The PGC-based solid phase Hypercarb has enabled the use of chiral counterions in polar mobile phases (e.g., mixtures of water and methanol) for the separation of enantiomers [158,172]. L-ZGP has been employed as counterion for enantioselective separation of propranolol, 2′-methylpropranolol, promethazine [158]. (−)-2,3:4,6,-di-*O*-isopropylidene-2-keto-L-gulonic acid have been used as counterion for chiral separation of bupivacaine, remoxipride, sotalol, oxprenolol, alprenolol, and mefloquine [172]. In reversed-phased chiral ion-pair chromatography, the separation is mainly regulated by the counterion concentration and the mobile-phase content of organic modifier [172,173]. In an analytical assay of mefloquine enantiomers in plasma, L-ZGP in acetonitrile–methanol–acetate buffer, pH 4.6 (48:20:32) was applied as mobile phase and Hypercarb as the achiral solid phase [174].

C. Cyclodextrins

In the pharmaceutical field, traditionally cyclodextrins (CDs) have been used to solubilize drugs that are relatively insoluble in water. Cyclodextrins have also proved useful as chiral

selectors for enantioselective analysis of drugs in several separation systems. As discussed previously, β-cyclodextrin and analogues have been immobilized on solid supports and used as chiral stationary phases in liquid chromatography [108–110] and gas chromatography [175]. The successful use of cyclodextrins as chiral additives in aqueous mobile phases in liquid chromatography [176] and in capillary electrophoresis [177] is well documented. Several enantiomeric separations of drugs have been reported, where α-, β-, or γ-cyclodextrins were used as mobile phase additives. Occasionally, a combination of several different cyclodextrins in the eluent were applied to promote the enantioselectivity [178]. Another eluent used by Szepesi and co-workers was based on a mixture of the counterion 10-camphorsulfonic acid and α-, β-, and γ-cyclodextrins [140].

β-Cyclodextrin is the most frequently used, and enantiomeric separations of drugs includes barbiturates, and mephenytoin [179,180], chiral hydantoins [181], trimeprazine (alimemazine) [182], chlorthalidone [183,184], oxazepam [185], lorazepam [186], and propranolol [187]. In bioanalytical studies Edholm et al. used β-cyclodextrin as a CMPA for the enantioselective determination of oxazepam and terbutaline [188]. The overall selectivity in the analysis was improved by using a coupled column system.

Mephenytoin, an antiepileptic drug, was studied relative to metabolic levels of the enantiomers in urine (Fig. 8). A mobile phase that contained β-cyclodextrin and a C_8 achiral column gave a baseline resolution with an analysis time of just under 10 min [189]. β-

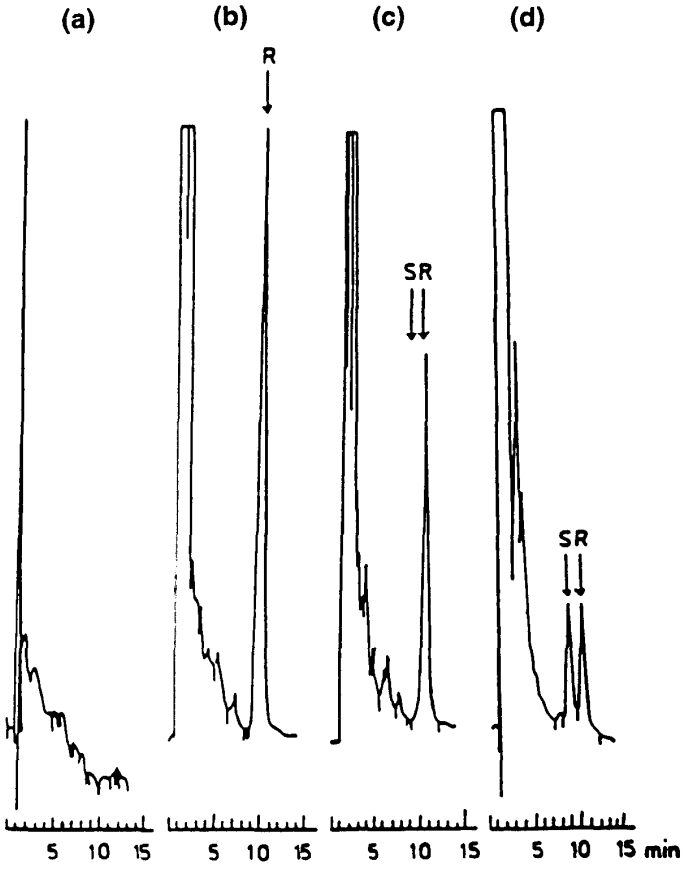


Figure 8 Liquid chromatographic determination of enantiomers of mephenytoin in urine employing β-cyclodextrin as a mobile phase additive. Sample: (a) drug-free urine; (b) standard sample containing 20.0 μg mL^{-1} (*R*)-mephenytoin; (c) an extensive and (d) a poor metabolizer. (From Ref. 189.)

Cyclodextrin is relatively inexpensive and can be used in high concentrations without disturbing the UV-detection of the analytes.

The α- and γ-cyclodextrins are less frequently used as chiral additives. The enantiomers of norgestrel were resolved by Gazdag et al. using γ-cyclodextrin in the mobile phase and different C_{18} phases [190]. β-Cyclodextrin can be modified to give more a hydrophobic dextrin molecule; for example, heptakis (2,3,6-tri-*O*-methyl)-β-cyclodextrin (TM-β-cyclodextrin). Addition of methylated CDs to the mobile phase resulted in a dynamic modification of the support, creating a CSP. Zukowski and co-workers, in their studies of enantioseparation of various barbiturates, have investigated several different modified cylcodextrins such as heptakis(2,6-*O*-dimethyl)-β-cyclodextrin and TM-β-cyclodextrin [180,191]. Another modified β-cyclodextrin, peracylated β-cyclodextrin, also gave enantioselective recognition of barbiturates, methylphenobarbital, and glutethimide [192].

D. Miscellaneous

Marle et al. used albumin from different species as CMPAs for enantioselective separation of acids and tryptophan [193]. The solid phase was a modified silica support LiChrosorb RP 2. The enantiomer with the highest binding affinity to albumin, L-tryptophan, eluted first. The reversed elution order for the tryptophan enantiomers have been observed when using a chiral stationary phase based on immobilized albumin [194].

The chromatographic retention and selectivity is dependent on the binding constants of the enantiomers to the protein, as well as the protein concentration in the mobile phase. Thus, the binding affinity constant for the enantiomers to albumin could be determined from the capacity factors recorded at different concentrations of albumin in the mobile phase [195]. The protein binding of omeprazole and tryptophan to albumin was studied.

When working with high concentration of albumin in the mobile phase, it was not possible to measure the UV response of the enantiomeric analytes at a wavelength at which albumin also has absorption. Thus, the indirect detection technique using 1-ethylquinilinium as a probe and measuring at a wavelength at which albumin has low UV absorption, was introduced to monitoring enantiomers in the eluate [193]. Later, Clark et al. applied the same system for separation of enantiomers of kynurenine [187] and Gaskell et al. for separation of methotrexate analogues [196]. α-$Acid_1$-glycoprotein has also been used as mobile-phase additive for chiral separation of tertiary amines (e.g., promethazine, trimeprazine (alimemazine), disopyramide, trimipramine [197], and hexabarbitone [187]. The stability of chromatographic systems with high concentrations of proteins in the mobile phase is rather limited [195], LiChrosorb DIOL gives the most robust chromatographic systems.

An uncharged derivative of tartaric acid, dicyclohexyl tartrate (DCHT), was introduced by Heldin et al. as a CMPA for separation of enantiomers [198]. DCHT has high affinity for Hypercarb and gives a dynamically modified stationary phase. Phosphate buffer containing DCHT and a low content of isopropanol were used to elute the enantiomers from the column. Enantioselective separations have been obtained for ephedrine and pseudoephedrine [198], norephedrine, atropine, homoatropine [198,199], and ipratropine [198], (*2S,3S*)-DCHT as the CMPA enabled determination of 0.5% of the enantiomeric impurity (*R*)-atropine in (*S*)-atropine. The enantiomeric purity of (S)-atropine depot tablets was analyzed (Fig. 9) [199]. Dihexanyl-*trans*-1,2-cyclohexanediamide was used by Sinibaldi et al. as a CMPA for resolving oxazepam enantiomers [200]. Underivitazed silica was the support, and the mobile phase was composed of the CMPA dissolved in a mixture of hexane and chloroform.

IV. INDIRECT SEPARATION OF ENANTIOMERS AS DIASTEREOMERIC DERIVATIVES

Indirect separation of enantiomers (i.e., formation of diastereomeric derivatives) has been performed for many years and is still commonly used, especially in pharmacokinetic studies

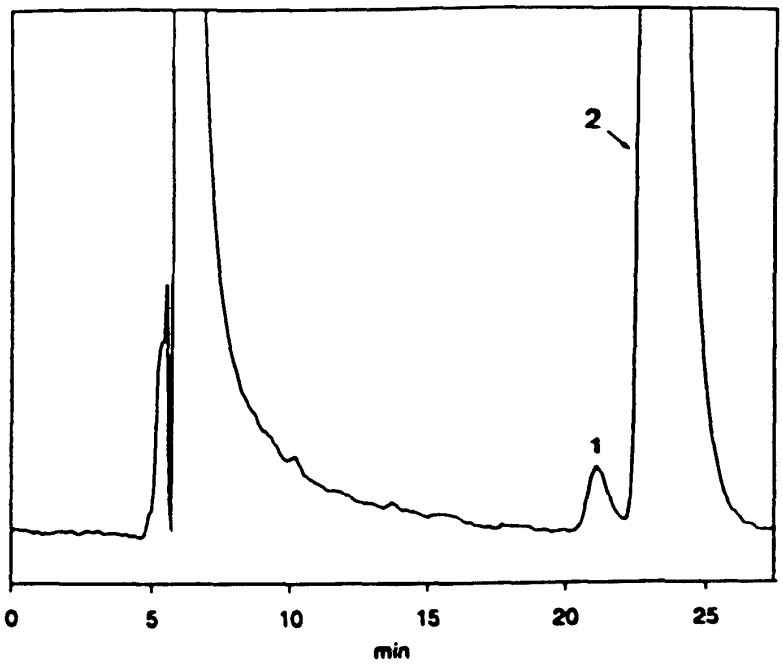


Figure 9 Determination of enantiomeric purity of (*S*)-atropine in depot tablets using a mobile phase of (2*S*,3*S*)-dicyclohexyl tartrate in phosphate buffer pH 2.8. Peaks: 1, (*R*)-atropine, 10.5%; 2, (*S*)-atropine. (From Ref. 199.)

and for preparative purposes. Drug molecules often have functions that are easy to derivatize (i.e., an alcohol, amine, or carboxylic acid) and are thus suitable for making diastereoisomers. The drug enantiomers are converted to diastereomeric derivatives using one enantiomer of a chiral derivatization reagent (CDR). Unlike the enantiomers, the corresponding diastereoisomers have different physiochemical properties and can be separated in an achiral chromatographic system.

The approach of indirect separation has some advantages: (1) wide applicability for a variety of functional groups can be derivatized, and there is a large pool of CDRs available; (2) method development is rather straight-forward; (3) inexpensive conventional achiral columns with high efficiency can be used; (4) by selection of an appropriate CDR having a strong chromophor or fluorophor, the detection sensitivity of the enantiomers can be improved considerably. Although the separation of enantiomers as diastereomeric derivatives is popular and widely used, one has to consider the limitations of the method before applying it to a specific analytical problem. A disadvantage is the negative effect of an enantiomeric impurity in the reagent; one should use a CDR with a high optical purity, especially when determining the enantiomeric purity of a solute. Another drawback of the method is that the derivatization procedure might be time-consuming and give rise to formation of several reaction products, especially if the enantiomeric solute has different functional groups. As discussed in review articles [201,202], the problem of kinetic resolution and racemization during derivatization, and that diastereoisomer may have different detector response, which might complicate the quantitative evaluation, must be considered when applying the indirect separation method.

A short survey of some of the CDRs that have been used for formation of distereoisomers of drugs is given in the following, but further applications are given in review articles and books [e.g., 201–208].

A. Derivatization of Alcohols

Generally, enantiomeric solutes with a hydroxyl group are converted to diastereomeric esters or carbamates by derivatization with a chiral acid or an isocyanate. The enol hydroxy group in warfarin has been esterified with (−)-(1*S*,2*R*,4*R*)-endo-1,4,5,6,7,7-hexachlorobicyclo[2,2,1]-hept-5-ene-2-carboxylic acid, and dicyclohexylcarbodiimide (DCC) was used as the condensing agent. The separation was obtained on a reversed-phase column, with fluorimetric detection after an on-line (postcolumn) pH adjustment of the mobile phase, (Fig. 10) [209]. The analysis of warfarin enantiomers in biological samples has been accomplished by using carbobenzoxycarbonyl-L-proline as a chiral derivatization regent [210], and the diastereoisomers were separated in a normal-phase chromatographic system. Postcolumn reaction of the diastereomeric derivatives to form fluorescent compounds improved the detection sensitivity. Later, the enantiomers of acenoumarol (nicoumalone) were separated using the same method [211].

The alcohol function of venlafaxine was reacted with (+)-*S*-naproxen chloride to form diastereoisomers for the analysis of venlafaxine enantiomers in plasma using reversed-phase chromatography [212]. A similar reagent, flunoxaprofen chloride, was used by Liebmann et al. for the stereoselective analysis of ciclotropium [213]. Conversion of the alcohol group in proxyphylline with camphanic acid chloride resulted in diastereomeric esters that could be separated in reversed-phase chromatography [214]. The menthoxyacetic acid chloride was used for enantioselective separation of nipradilol [215]. Determination of the enantiomeric purity of a calcium antagonist drug diltiazem was performed in reversed-phase chromatography after conversion of the enantiomers to diastereomeric derivatives *S*(−)*N*-1-(2-naphthylsulfonyl)-2-pyrrolidine carbonyl chloride [216], a reagent that is not commercially available.

1-Phenylethyl isocyanate and 1-(1-naphythyl)ethyl isocyante, frequently used for derivatization of amines, can also be used to form diastereomeric derivatives of alcohols by con-



Figure 10 Determination of warfarin enantiomers after derivatization with (1*S*, 2*R*, 4*R*)-endo-1,4,5,6,7,7-hexachlorobicyclo[2.2.1]-hept-5-ene-2-carboxylic acid. Solid phase: LiChrosorb C_{18}. Sample: extract from 1 mL of plasma spiked with 10 ng racemic warfarin. (I, *S*-warfarin ester; II, *R*-warfarin ester; and III, *R*-chlorowarfarin ester (IS). (From Ref. 209.)

version of the hydroxy groups to carbamates, although more vigorous conditions generally are required [207]. Williams used 1-phenylethyl isocyanate in his study of the pharmacokinetics of the enantiomers of misonidazole [217].

Lindner et al. have introduced *O,O,*-disubstituted tartaric acid anhydrides for separation of enantiomeric amino alcohols (β-adrenoceptor-blocking agents). Only the hydroxy group of the amino alcohol reacts with the anhydride to produce a monoester [218]. The diastereomeric derivatives become zwitterions, and ion-pair formation within the diastereoisomers is claimed to contribute to the separation of the diastereoisomers.

B. Derivatization of Amines

Drugs often have an amino group, and because this group is relatively easy to derivatize, several methods for enantioselective analysis based on formation of diastereomeric derivatives have been published. Chiral amines have been separated as diastereomeric amides, carbamates, ureas, and thiureas. One of the most used methods is the derivatization of amines by use of an activated chiral acid to give amides. α-Methoxy-α-trifluoromethylphenylacetyl chloride (MTPA) and *O*-methylmandelic acid chloride are commerically available in high enantiomeric purity and as both antipodes. The latter acid chloride has been used for separation of the enantiomers of tocainide [219], whereas MTPA has been applied for determine the enantiomers of amphethamine [220]. Lately, naproxen chloride was used for separation of tocainide enantiomers [221]. The diastereoisomers of tocainide were resolved in normal-phase chromatography and measured by fluorescence detection. Beside naproxen, other nonsteroidal antiinflammatoric acids have been used as derivatization agents owing to the good fluorescent and chromatographic properties of the diastereomeric amides formed. Both (+)-naproxen and (+)-benoxaprofen chloride separated enantiomers of baclofen butyl ester [222]. (+)-Flunoxaprofen chloride enabled separation of amino acids in normal-phase chromatography [223] and propranolol in reversed-phase chromatography [224].

Two popular isocyanates used for formation of diastereomeric derivatives of amines are 1-phenylethyl isocyanate and 1-(1-naphthyl)ethyl isocyanate. They react rapidly, and under mild condition, selectively, with the amine function, but not with the hydroxy group. Enantiomers of pindolol [225], propranolol [226,227], and flecainide [228] in biological fluids have been determined using 1-phenylethyl isocyanate. The 1-(1-naphthyl)ethyl isocyanate converted the enantiomers of betaxolol [229], tertatolol [230], propafenone [231], and tocainide [232] into separable diastereoisomers. Alternatively it is possible to use isothiocyanates, which are more stable than isocyanates. 2,3,4,6-Tetra-*O*-acetyl-β-D-glucopyranosyl isothiocyanate (GITC) and 2,3,4-tri-*O*-acetyl-α-D-arabinopyranosyl isothiocyanate (AITC) are frequently used to derivatize primary and secondary amines into diastereomeric thioureas [236]. Nimura et al. introduced GITC as a chiral derivatization reagents for the chiral separation of amino acid esters [233]. GITC has also been applied for enantioselective analysis of various drugs (e.g., tretoquimol [trimetoquinol; 234], bevantolol [235], norepinephrine [236], mexiletine [237], carvedilol [238], hydroxypropranolol sulfate [239], and metoprolol [240]).

A new approach, formation of diastereoisomers of amines by use of 9-fluorenylmethoxychloroformate (FMOC)-L-proline in solid-phase derivatization, is worth mentioning [241,242]. The diastereoisomers contain the FMOC moiety, which has excellent fluorescent properties and can be used to determine enantiomers in the picomolar range. The enantiomers of amphetamine have been investigated using this CDR.

An important method for producing diastereoisomers of chiral amines and amino acids is the reaction with *o*-phthalaldehyde (OPA) and a chiral thiol to form isoindole derivatives. L-N-Acetylcystein and *o*-phthalaldehyde gave fluorescent diastereoisomers and were applied for the analysis of baclofen, (Fig. 11) [243] and amino acids [244]. The same procedure was used for the analysis of thyroxine, applying electrochemical detection [245]. Jegorov et al. used D-1-thio-β-galactose [246], D-1-thio-β-glucose [246,247], or D-1-thio-β-mannose [246] in combination with *o*-phthalaldehyde to separate enantiomers of amino acids. Another highly

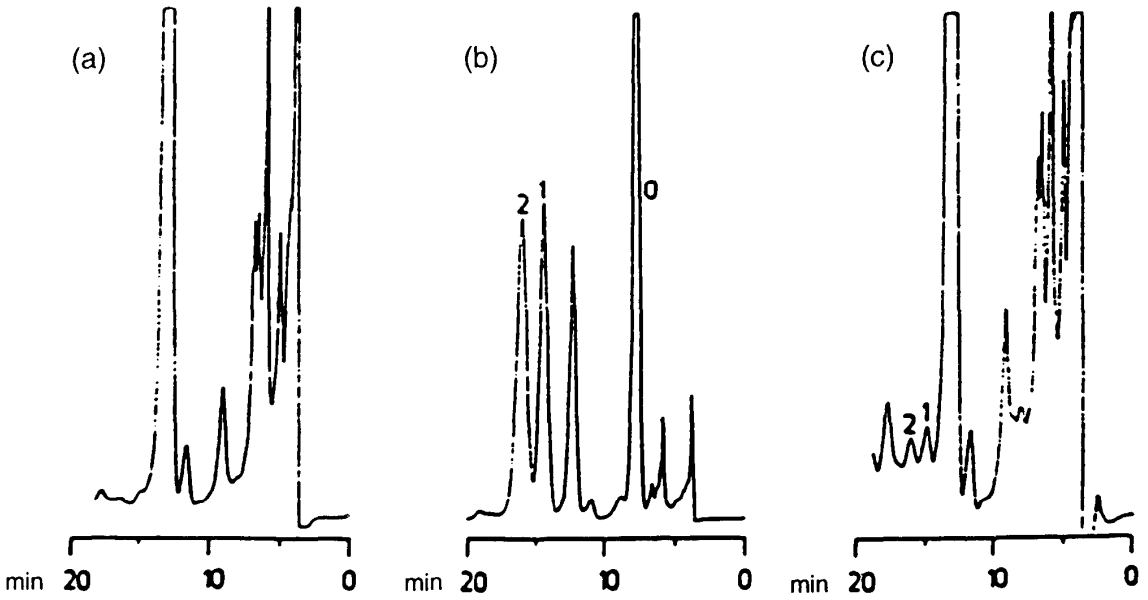


Figure 11 Enantiomeric determination of baclofen after derivatization with a chiral adduct of *o*-phthaldialdehyde. Solid phase: Chrompack Cp-Spher C_8. Sample: (a) 0 ng (blank); (b) 410 ng; and (c) 4.0 ng of (*R*,*S*)-baclofen. (From Ref. 243.)

efficient reagent for enantioselective analysis of amino acids is 1-(9-fluorenyl)ethyl chloroformate (FLEC). An enantiomeric impurity as low as 0.06% of D-glutamine in L-glutamine has been determined [248]. The FLEC reagent is commercially available, and the derivatization is easy to perform. FLEC has also been used for enantioselective analysis of propranolol [249] and atenolol [250].

C. Derivatization of Carboxylic Acids

Most of the studies involving chiral separations of acids have been performed on 2-arylpropionic acids (e.g., naproxen, ibuprofen, or fenoprofen). For most of these nonsteroidal anti-inflammatory drugs, the enantiomers give different biotransformation in humans [251]. Thus, several stereoselective analytical methods, including indirect separations, have been developed for the determination of enantiomers of 2-arylpropionic acids in various biological materials. The preferred method, based on formation of diastereoisomers, is the conversion of the acids into diastereomeric amide by use of a chiral amine. Several of the 2-arylpropionic acids—ketoprofen [252,253], fenoprofen [252,253], benoxaprofen [253], ibuprofen [254], naproxen [254], flurbiprofen [254], cicloprofen [254] carprofen [254], suprofen [254], and pirprofen [255]—have been separated in normal-phase chromatography as diastereomeric derivatives with (*R*)- or (*S*)-1-methylbenzylamine. The same reagent was applied for determination of enantiomers of flunoxaprofen [256] in reversed-phase chromatography. To improve the detection of enantiomeric acids, fluorescent reagents such as 1-(4-dimethylaminonaphthalen-1-yl)ethylamine) [DANE; 257] have been introduced. DANE was applied for determination of (*R*)- and (*S*)-loxoprofen and metabolites in urine samples, (Fig. 12) [258].

Björkman introduced a different method to form diastereomeric derivatives of 2-arylpropionic acids [259]. The acid (indoprofen) was mixed with ethylchloroformate to form a carboxylic–carbonic mixed anhydride, which was later mixed with L-leucineamide to form diastereomeric derivatives. A reversed-phase system was used to assay the enantiomers of indoprofen [259] and ketoprofen [260] in plasma samples. Previously, stereoselective analysis of carboxylic acids was also performed after conversion of the acids to esters by using (+)-

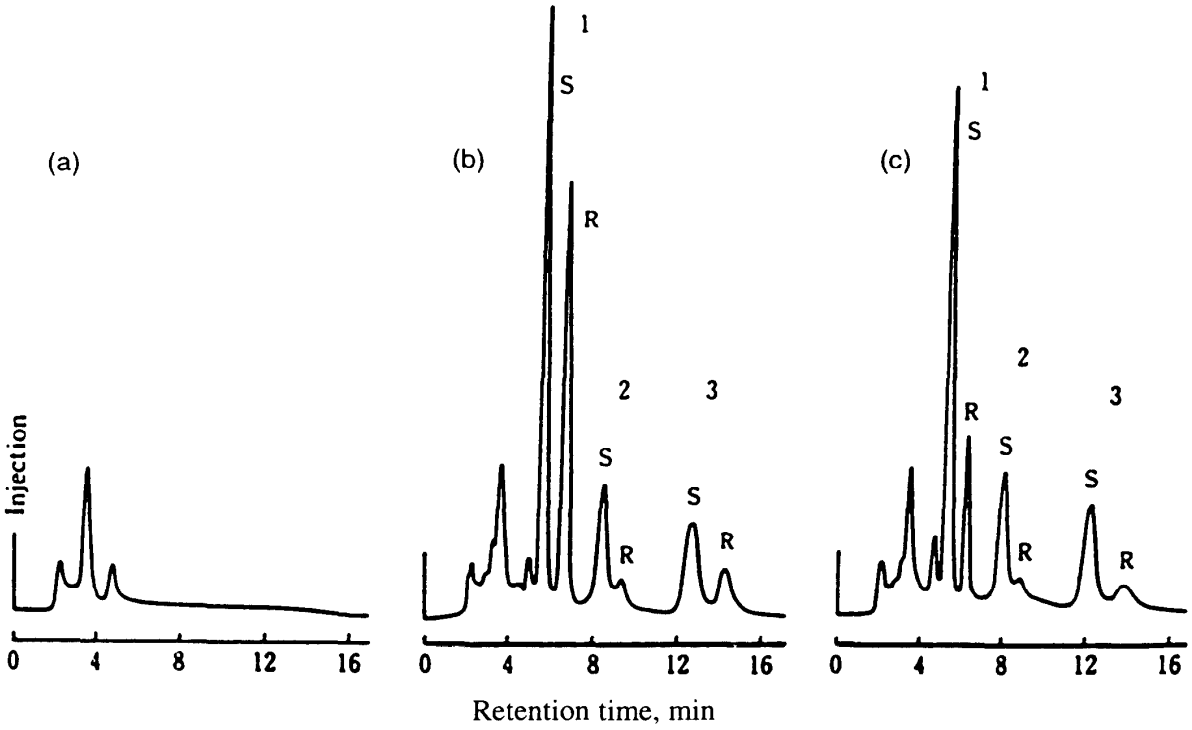


Figure 12 Chiral determination of loxoprofen and its monohydroxy metabolites in human urine after extraction and derivatization with DANE reagent. Solid phase: μ Porasil. Sample: (a) control urine; (b) 0 to 2-h and (c) 2 to 4-h urine after oral administration of 80 mg of loxoprofen sodium. (From Ref. 258.)

octanol [261]. However, derivatization with amines is preferale, for the diastereomeric amides are more stable than the esters. Furthermore, introducing the rigid amide group between the chiral centers is generally considered to be a way to facilitate the chromatographic separation of diastereoisomers [207].

REFERENCES

1. Y Okamoto, M Kawashima, R Abreratani, K Hatada, T Nishiyama, M Masuda. Chem Lett 1237, 1986.
2. Y Okamoto, M Kawashima, K Hatada. J Chromatogr 363:173, 1986.
3. Y Okamoto, R Aburatani, K Hatano, K Hatada. J Liq Chromatogr 11:2147, 1988.
4. Y Okamoto, Y Kaida. J High Resolut Chromatogr 13:708, 1990.
5. Y Okamota, Y Kaida. J Chromatogr A 666:403, 1994.
6. B Kofahl, D Henke, E Mutschler. Chirality 5:479, 1993.
7. MS Lelous. Biomed Chromatogr 6:99, 1992.
8. K Balmér, A Persson, P-O Lagerström, B-A Persson, G Schill. J Chromatogr 553:391, 1991.
9. CR Lee, J-P Porziemsky, M-C Aubert, AM Krstulovic. J Chromatogr 539:55, 1991.
10. T Suzuki, Y Horikiri, M Mizobe, K Noda. J Chromatogr 619:267, 1993.
11. VL Herring, JA Johnson. J Chromatogr 612:215, 1993.
12. CB Ching, BG Lim, EJD Lee, SC Ng. Chirality 4:174, 1992.
13. HY Aboul-Enein, V Serignese. Biomed Chromatogr 8:22, 1994.
14. HY Aboul-Enein. Anal Lett 26:271, 1993.
15. T Ohkubo, T Uno, K Sergawara. Chromatographia 33:287, 1992.
16. H Fieger, IW Wainer. J Pharm Biomed Anal 11:1173, 1993.

17. E Kashiyama, M Osomi, T Shimizu. J Chromatogr B 652:179, 1994.
18. PA Soons, MCM Roosemalen, DD Breimer. J Chromatogr 528:343, 1990.
19. T Sakamoto, Y Ohtake, M Itoh, S Tabata, T Kuriki, K Uno. Biomed Chromatogr 7:99, 1993.
20. C Fischer, F Schönberger, W Müch, K Heuch, M Eichelbaum. J Pharm Sci 82:244, 1993.
21. M Yamaguachi, K Yamashita, I Soki, T Tabata, S-I Hirai, T Yashiki. J Chromatogr 575: 123, 1992.
22. R Neidlein, Th Heitzmann, K Strein, C Volland. J Chromatogr 616:129, 1993.
23. H Takahashi, A Tamura, H Ogata, K Masuhara. J Chromatogr 529:347, 1990.
24. H Echizen, K Ochiai, Y Kato, K Chiba, T Ishizaki. Clin Chem 36:1300, 1990.
25. K Johii, K Banno, T Miyamoto, T Kakimoto. J Chromatogr 564:338, 1991.
26. K Ishii, K Minato, N Nishimura, T Miyamoto, T Sato. J Chromatogr 686:93, 1994.
27. C Andersen, K Balmér, P-O Lagerström. J Chromatogr 615:159, 1993.
28. Y Okamoto, R Aburatini, Y Kaida, K Hatada. Chem Lett P. 1125, 1988.
29. K Ikeda, T Hamasaki, H Kohmo, T Ogawa, T Matsumoto, J-I Sahai. Chem Lett 1089, 1989.
30. A Ishikawa, T Shibata. J Liq Chromatogr 16:859, 1993.
31. TRE Hampe, J Schlüter, KH Brandt, J Nagel, E Lamparter, G Blaschke. J Chromatogr 634: 205, 1993.
32. C Facklam, A Modler. J Chromatogr A 664:203, 1994.
33. L Miller, R Bergerson. J Chromatogr 648:381, 1993.
34. D Witte, F Bruggeman, JP Franke, S Copinga, JM Jansen, RA De Zeeuw. Chirality 5:545, 1993.
35. K Balmér, P-O Lagerström, S Larsson, B-A Persson. J Chromatogr 631:191, 1993.
36. A Kunath, B Henkel, J Wagner. J Chromatogr 634:119, 1993.
37. B Elsing, G Blaschke. J Chromatogr 612:223, 1993.
38. K Balmér, B-A Persson, P-O Lagerström. J Chromatogr A 660:269, 1994.
39. P Camilleri, DJ Livingston, JA Murphy, DT Manallack. J Comput Aided Mol Design 7:61, 1993.
40. A Shibukawa, IW Wainer. J Chromatogr 574:85, 1992.
41. H Fieger, G Blaschke. J Chromatogr 575:255, 1992.
42. JP Mc Carthy. J Chromatogr A 685:349, 1994.
43. S Levin, S Abre-Lafi, J Zahalka, R Mechoulan. J Chromatogr A 654:53, 1993.
44. E Küsters, C Dosenbach, G Gerber. J High Resolut Chromatogr 14:769, 1991.
45. S Antus, R Bauer, A Gottsegen, H Lotter, O Seligmann, H Wagner. J Chromatogr 603:133, 1992.
46. EG Sundholm. J Liq Chromatogr 15:2111, 1992.
47. M Gaffney, R Stiffin, IW Wainer. Chromatographia 27:15, 1989.
48. LW Nicholson, CD Pfeiffer, GT Boralski, B Singoram, GB Fisher. J Chromatogr A 687: 241, 1994.
49. K Balmér, P-O Lagerström, B-A Persson. J Chromatogr 592:331, 1992.
50. J Hermansson. J Chromatogr 269:71, 1983.
51. J Hermansson. Trends Anal Chem 8:251, 1989.
52. J Hermansson, G Schill. In: PR Brown, RA Hartwick eds. High Performance Liquid Chromatograph. New York: John Wiley & Sons, 1989, Chap. 8.
53. G Schill, IW Wainer, SA Barkan. J Chromatogr 365:73, 1986.
54. G Schill, IW Wainer, SA Barkan. J Liq Chromatogr 9:641, 1986.
55. L Le Garrec, E Delee, JC Pascal, I Juillien. J Liq Chromatogr 10:3015, 1987.
56. M Enquist, J Hermansson. J Chromatogr 519:271, 1990.
57. C Vandenbosch, T Hamoir, DL Massart, W Lindner. Chromatographia 33:454, 1992.
58. F Li, SF Cooper, M Côté, C Ayotte. J Chromatogr B 660:327, 1994.
59. J Hermansson. J Chromatogr 325:379, 1985.
60. M Enquist, J Hermansson. Chirality 1:209, 1989.

61. J Hermansson, K Ström, R Sandberg. Chromatographia 24:520, 1987.
62. JJ Butter, JC Kraak, H Poppe. J Pharm Biomed Anal 3:225, 1993.
63. E Arvidsson, SO Jansson, G Schill. J Chromatogr 506:579, 1990.
64. E Arvidsson, SO Jansson, G Schill. J Chromatogr 591:55, 1992.
65. G de Lorenzi, AF Fell, G Cacialanze, G Massolini, M Kitsos. J Pharm Biomed Anal 10: 909, 1992.
66. A Walhagen, LE Edholm. J Chromatogr 473:371, 1989.
67. J Hermansson, M Eriksson, O Nyqvist. J Chromatogr 336:321, 1984.
68. P Le Corre, D Gibassier, P Sado, R Le Verge. J Chromatogr 450:211, 1988.
69. L Wallén, Ö Ericsson, I Wikström, U Hellgren. J Chromatogr 665:153, 1994.
70. D Haupt, C Pettersson, D Westerlund. Chirality 5:224, 1993.
71. JM Evans, RJ Smith, G Stemp. J Chromatogr 623:163, 1992.
72. RJ Smith, D Smith, J Evans, G Stemp. Chromatographia 36:115, 1993.
73. V Chapeau, A Moulin, M Caude, A Dufour. J Chromatogr B 660:341, 1994.
74. JX de Vries, E Schmitz-Kummer. J Chromatogr 644:315, 1993.
75. SA Corlett, H Chrystyn. J Chromatogr B 654:152, 1994.
76. K Balmér, B-A Persson, P-O Lagerström. J Chromatogr A 660:269, 1994.
77. JX De Vries, E Schnitz-Kummer, D Siemon. J Liq Chromatogr 17:2127, 1994.
78. J Hermansson, I Hermansson. J Chromatogr A 666:181, 1994.
79. DJ Jones, AR Bjorksten. J Chromatogr B 661:165, 1994.
80. K Balmér, B-A Persson, G Schill. J Chromatogr 477:107, 1989.
81. B-A Persson, K Balmér, P-O Lagerström, G Schill. J Chromatogr 500:629, 1990.
82. J Iredale, IW Wainer. J Chromatogr 573:253, 1992.
83. KM Kirkland, KL Neilson, DA McCombs, JJ DeStefano. LC–GC 10:322, 1992.
84. Y Oda, N Asakawa, T Kajima, Y Yoshida, T Sato. J Chromatogr 541:411, 1991.
85. Y Oda, N Asakawa, T Kajima, Y Yoshida, T Sato. Pharm Res 8:997, 1991.
86. SM Lankford, SA Bai. J Chromatogr B 663:91, 1995.
87. T Miwa, H Kuroda, S Sakashita, N Asakawa, Y Miyake. J Chromatogr 511:89, 1990.
88. J Haginaka, T Murashima, H Fujima, H Wada. J Chromatogr 620:199, 1993.
89. J Haginaka, C Seyama, T Murashima, H Fujima, H Wada. J Chromatogr A 600:275, 1994.
90. G Tamai, M Edani, H Imai. Biomed Chromatogr 4:157, 1990.
91. J Haginaka, C Seyama, H Yasuda, K Takahashi. J Chromatogr 598:67, 1992.
92. M Nishikata, A Nakai, H Fushida, K Miyake, T Arita, K Iseki, K Miyazaki, A Nomura. J Chromatogr 612:239, 1993.
93. E de Lorenzi, AF Fell, G Caccialanza, G Massolini, M Kitsos. J Pharm Biomed Anal 10: 905, 1992.
94. E de Lorenzi, AF Fell, AL Holmes, G Caccialanza, G Massolini, C Candini, K Kitsos, C Ponci. Chirality 5:622, 1993.
95. M Lämmerhofer, W Lindner. Chirality 6:261,1994.
96. MJ Diaz-Perez, JC Chen, A-F Aubry, IW Wainer. Chirality 6:283, 1994.
97. S Allenmark. Chem Sci 20:5, 1982.
98. S Allenmark, B Bomgren, H Borén. J Chromatogr 264:63, 1983.
99. E Domenici, C Bertucci, P Salvadori, G Felix, I Chahagne, S Montellier, IW Wainer. Chromatographia 25:170, 1990.
100. TAG Noctor, IW Wainer, DS Hage. J Chromatogr 577:305, 1992.
101. Y-Q Chu, IW Wainer. Pharm Res 5:680, 1988.
102. S Andersson, RA Thompson, SG Allenmark. J Chromatogr 591:65, 1992.
103. E Domenici, C Bertucci, P Salvadori, IW Wainer. J Pharm Sci 80:164, 1991.
104. RK Gilpin, SE Ehtesham, RB Gregory. Anal Chem 63:2825, 1991.
105. S Allenmark, B Bomgren, H Borén, PO Lagerström. Anal Biochem 136:293, 1984.
106. S Allenmark, B Bomgren, H Borén. J Chromatogr 316:617, 1984.
107. S Allenmark, S Andersson. Chirality 1:154, 1989.

108. K Fujimura, T Ueda, T Ando. Anal Chem 55:446, 1983.
109. WL Hinze, TE Riehl, DW Armstrong, W Demond, A Alak, T Ward. Anal Chem 57:237, 1985.
110. DW Armstrong, TJ Ward, RD Armstrong, TE Beesley. Science 323:1132, 1986.
111. AM Stalcup, S-C Chang, DW Armstrong. J Chromatogr 540:113, 1991.
112. DW Armstrong, CD Chang, SH Lee. J Chromatogr 539:83, 1991.
113. L-E Edholm, C Lindberg, J Paulson, A Walhagen. J Chromatogr 424:61, 1988.
114. AM Stalcup, JR Faulkner Jr, Y Tang, DW Armstrong, LW Levy, E Regalado. Biomed Chromatogr 5:3, 1991.
115. JI Seeman, HV Secor, DW Armstrong, KD Timmons, TJ Ward. Anal Chem 60:2120, 1988.
116. DW Armstrong, S Chen, C Chang, S Chang. J Liq Chromatogr 15:545, 1992.
117. J He, A Shibukawa, T Nakagawa, H Wada, H Fujima, E Imai, Y Go-oh. Chem Pharm Bull 41:544, 1993.
118. W Naidong, JW Lee. J Pharm Biomed Anal 12:551, 1994.
119. AM Stalcup, S-C Chang, DW Armstrong, J Pitha. J Chromatogr 513:181, 1990.
120. WH Pirkle, DW House, JM Finn. J Chromagr 192:143, 1980.
121. WH Pirkle, CJ Welch. J Org Chem 49:148, 1984.
122. H Hyun, WH Pirkle. J Chromatogr. 393:357, 1987.
123. N Oi, H Kitahara, Y Matsumoto, H Nahajrina, Y Horikawa. J Chromatogr 462:382, 1989.
124. ZY Yang, S Barkan, C Brummer, JD Weber, TD Doyle, IW Wainer. J Chromatogr 324:444, 1985.
125. WH Pirkle, A Tsipouras. J Chromatogr 291:291, 1984.
126. IW Wainer, TD Doyle, KH Dome, JR Powell. J Chromatogr 306:405, 1984.
127. E Küsters, D Girou. J High Resol Chromatgr Commun 9:531, 1986.
128. AM Dyas, ML Robinson, AF Fell. J Chromatogr 586:335, 1991.
129. CL Hsu, RR Walters. J Chromatogr. 550:621, 1991.
130. T Ohkubo, T Uno, K Sugawore. J Chromatogr A 659:467, 1994.
131. M Ohwa, M Akioshi, S Mitamura. J Chromatogr. 521:122, 1990.
132. WH Pirkle, JA Burke. J Chromatogr 557:173, 1991.
133. WH Pirkle, CJ Welch. J Liq Chromatogr 14:3387, 1991.
134. T Cleveland. J Liq Chromatogr 18:649, 1995.
135. J Leaver, G Foster. Biotechnol Tech 3:179, 1989.
136. AG Adams, JT Stewart. J Liq Chrom 16:3863, 1993.
137. H-Y Ahn, GK Shiu, WF Trafton, TD Doyle. J Chromatogr B 653:163, 1994.
138. J-N Zeng, L Dou, M Duda, HH Stuting. J Chromatogr B 654:231, 1994.
139. C Pettersson. Trends Anal Chem 7:209, 1988.
140. G Szepesi, M Gazdag. J Pharm Biomed Anal 6:623, 1988.
141. C Pettersson, E Heldin. In: G Subramanian, ed. A Practical Approach to Chiral Separations by Liquid Chromatography. Weinheim: VCH, 1994, Chap 9.
142. VA Davankov. Chromatographia 27:475, 1989.
143. C Pettersson, M Josefsson. Chromatographia 21:321, 1986.
144. R Corradini, G Sartor, R Marchelli, A Dossena, A Spisni. J Chem Soc Perkin Trans 2:1979, 1992.
145. RM Gaskell, B Crooks. In: D Stevenson, IW Wilson, eds. Chiral Separations. New York: Plenum, 1988 p. 65.
146. SV Rogozhin, VA Davankov. Russ Pat Appl, 1968, Chem Abstr 72:90875c, 1970.
147. W Lindner, JN Lepage, G Davies, DE Seitz, BL Karger, J Chromatogr 185:323, 1979.
148. VA Davankov. In: D Cagniant ed. Complexation Chromatography. New York: Marcel Dekker 1992, p. 197.
149. S Lam. J Chromatogr Sci 22:416, 1984.
150. W Lindner, I Hirschböch. J Liq Chromatogr 9:551, 1986.
151. LR Gelber, JL Neumeyer. J Chromatogr 257:317, 1983.
152. E Busker, K Günther, J Martens. J Chromatogr 350:179, 1985.

153. T Aria, H Koike, K Hirata, H Oizumi. J Chromatogr 448:439, 1988.
154. ID Hay, CA Gorman, KD Burman, N-S Jiang. Metabolism 34:266, 1985.
155. JD Huang, C-Y Hsieh. Chirality 3:454, 1991.
156. C-Y Hsieh, JD Huang. J Chromatogr 575:109, 1992.
157. C Pettersson. In: AM Krstulovic, ed. Chiral Separations by HPLC: Chichester: Ellis Horwood, 1989, Chap. 6.
158. A Karlsson, C Pettersson. J Chromatogr 543:287, 1991.
159. C Pettersson, G Schill. J Chromatogr 204:179, 1981.
160. C Pettersson, G Schill. Chromatographia 16:192, 1982.
161. G Szepesi, M Gazdag, R Ivancsics. J Chromatogr 241:153, 1982.
162. G Szepesi, M Gazdag, R Ivancsics. J Chromatogr 244:33, 1982.
163. L Ladanyi, I Sztruhar, A Vedres, G Vereczkey-Donath. J Chromatogr 353:27, 1986.
164. C Pettersson, A Karlsson, C Gioeli. J Chromatogr 407:217, 1987.
165. V de Biasi, MB Evans, WJ Lough. In: D Stevenson, ID Wilson; Eds. Recent Advances in Chiral Separations. New York: Plenum, 1991 p. 93.
166. A Karlsson, C Pettersson, S Björkman. J Chromatogr 494:157, 1989.
167. T Leeman, P Dayer. In: D Stevenson, ID Wilson, eds. Chiral Separations. New York: Plenum, 1988, p. 71.
168. A Karlsson, C Pettersson, S Sundell, L-E Arvidsson, U Hacksell. Acta Chem Scand B 42: 231, 1988.
169. A Karlsson, C Pettersson. Chirality 4:323, 1992.
170. C Pettersson. J Chromatogr 316:553, 1984.
171. C Pettersson, K No. J Chromatogr 282:671, 1983.
172. C Pettersson, C Gioeli. Chirality 5:241, 1993.
173. N-H Huynh, A Karlsson, C Pettersson. J Chromatogr A 705:275, 1995.
174. Y Bergqvist, J Kabbani, C Pettersson, N-H Huynh. J Chromatogr 620:217, 1993.
175. V Schurig. J Chromatogr A 666:111, 1994.
176. D Sybilska, J Zukowski. In: AM Krstulovic, ed. Chiral Separations by HPLC. Chichesterr: Ellis Horwood, 1989, p. 147.
177. R Vespalee, P Boček, Electrophoresis, 18:843, 1997.
178. M Gazdag, G Szepesi, L Huszár. J Chromatogr 436:31, 1988.
179. D Sybilska, J Zukowski, J Bojarski. J Liq Chromatogr 9:591, 1986.
180. J Zukowski, D Sybilska, J Bojarski. J Chromatogr 364:225, 1986.
181. J Zukowski, Phd Thesis, 1989, Polish Academy of Sciences.
182. AD Cooper, TM Jefferies. J Pharm Biomed Anal 8:847, 1990.
183. AM Rizzi, C Plank. J Chromatogr 557:199, 1991.
184. K Cabrera, G Schwinn. Int Lab 20(6):28, 1990.
185. A Yamamoto, K Hayakawa, A Matsungag, E Mizukami, M Miyazaki. Anal Sci 7:149, 1991.
186. AF Fell, TAG Noctor, JE Mama, BJ Clark. J Chromatogr 434:377, 1988.
187. BJ Clark, JE Mama. J Pharm Biomed Anal 7:1883, 1989.
188. A Wahlhagen, L-E Edholm. Chromatographia 32:215, 1991.
189. K Röna, I. Szabó. J Chromatogr 573:173, 1992.
190. M Gazdag, G Szepesi, L Huszf. J Chromatogr 351:128, 1986.
191. J Zukowski, D Sybilska, J Bojarski, J Szejtli. J Chromatogr 436:381, 1988.
192. M Pawlowska, J Zukowski. Microchim Acta 3:55, 1990.
193. C Pettersson, T Arvidsson, A-L Karlsson, I Marle. J Pharm Biomed Anal 4:221, 1986.
194. S Allenmark, B Bomgren, H Borén. J Chromatogr 237:473, 1982.
195. I Marle, C Pettersson, T Arvidsson. J Chromatogr 456:323, 1988.
196. RM Gaskell, B Crooks. In: D Stevenson, ID Wilson, eds. Recent Advances in Chiral Separations. New York: Plenum, 1990, p. 85.
197. J Hermansson. J Chromatogr 316:537, 1984.
198. E Heldin, N-H Huynh, C Pettersson. J Chromatogr 585:35, 1991.
199. E Heldin, N-H Huynh, C Pettersson. J Chromatogr 592:339, 1992.

200. M Sinibaldi, F Federici, S Fanali, A Messina. J High Resolut Chromatogr Commun 10:206, 1987.
201. W Lindner. Indirect separation of enantiomers by liquid chromatography. In: M Zief, LJ Crane, eds. Chromatographic Science Series, vol. 40. New York: Marcel Dekker, 1988, Chap 4.
202. J Gal. Indirect chromatographic methods for resolution of drug enantiomers, synthesis and separation of diastereomeric derivatives. In: IW Wainer, DE Drayer, eds. Drug Stereochemistry. New York: Marcel Dekker 1988, Chap 4.
203. W Lindner, C Pettersson. Resolution of optical isomers by liquid chromatographic techniques. In: IW Wainer, ed. Liquid Chromatography in Pharmaceutical Development, An Introduction. Springfield: Aster Publishing 1985, Part 1.
204. S Görög. In: H Lingeman, WJM Underberg, eds. Detection-Oriented Derivatization Techniques in Liquid Chromatography. New York: Marcel Dekker, 1990 p. 193.
205. J Gal. LC–GC Mag 5:106, 1987.
206. NR Srinivas, LN Igwemezie. Biomed Chromatogr 6:163, 1992.
207. M Ahnoff, S Einarsson. Chiral derivatization. In: WJ Lough, ed. Chiral Liquid Chromatography. New York: Chapman & Hall, 1989, Chap 4.
208. S Görög, M Gazdag. J Chromatogr B 659:51, 1994.
209. SR Carter, CC Duke, DJ Cutler, GM Holder. J Chromatogr 574:77, 1992.
210. C Banfield, M Rowland. J Pharm Sci 73:1392, 1984.
211. TS Gill, JK Hopkins, M Rowland. J Pharm Pharmacol 36(suppl):12, 1984.
212. CP Wang, SR Howell, J Scatina, SF Sisenwine. Chirality 4:84, 1992.
213. B Liebmann, D Henke, H Spahn-Langguth, E Mutschler. J Chromatogr 572:181, 1991.
214. M Ruud-Christensen, B Salvesen. J Chromatogr 303:433, 1984.
215. M Yoneda, M Shiratsuchi, M Yoshimura, Y Ohkawa, T Muramatsu. Chem Pharm Bull 33: 2735, 1985.
216. R Shimizu, T Kakimoto, K Ishii, Y Fujimoto, H Nishi, N Tsumagari. J Chromatogr 357: 119, 1986.
217. KM Williams. Clin Pharmacol Ther 36:817, 1984.
218. W Lindner, C Leitner, G Uray. J Chromatogr 316:605, 1984.
219. K-J Hoffman, L Renberg, C Bäärnhielm. Eur J Drug Metab Pharmacokinet 9:215, 1984.
220. KJ Miller, J Gal, MM Ames. J Chromatogr 307:335, 1984.
221. H Spahn. Arch Pharm 321:847, 1988.
222. H Spahn, D Krauss, E Mutschler. Pharm Res 5:107, 1988.
223. P Langguth, H Spahn, HP Merkle. J Chromatogr 528:55, 1990.
224. H Spahn, B Podkowik, E Stahl, E Martin, E Mutschler. J Anal Toxicol 15:209, 1991.
225. P-H Hsyu, KM Giacomini. J Pharm Sci 75:601, 1986.
226. HG Schaefer, H Spahn, LM Lopez, H Derendorf. J Chromatogr 527:351, 1990.
227. S Laganiere, E Kwong, DD Shen. J Chromatogr 488:407, 1989.
228. L Lie-A-Huen, RM Stuurman, FN Ijdenberg, JH Kingma, DKF Meijer. Ther Drug Monit 11:708, 1989.
229. A Darmon, JP Thenot. J Chromatogr 374:321, 1986.
230. T Lave, C Efthymiopoulos, JC Koffel, L Jung. J Chromatogr 572:203, 1991.
231. R Mehvar. J Chromatogr 527:79, 1990.
232. RA Carr, RT Foster, D Freitag, FM Pasutto. J Chromatogr 566:155, 1991.
233. N Nimura, H Ogura, T Kinoshita. J Chromatogr 202:375, 1980.
234. H Nishi, N Fujimura, H Yamaguchi, T Fukuyama. J Chromatogr 539:71, 1991.
235. SE Rose, EJ Randinitis. Pharm Res 8:758, 1991.
236. N Nimura, Y Kasahara, T Kinoshita. J Chromatogr 213:327, 1981.
237. O Grech-Bélanger, J Turgeon, M Gilbert. J Chromatogr 337:172, 1985.
238. EJ Eisenberg, WR Patterson, GC Kahn. J Chromatogr 493:105, 1989.
239. T Walle, DD Christ, UK Walle, MJ Wilson. J Chromatogr 341:213, 1985.
240. D Schuster, MW Modi, D Lalka, FM Gengo. J Chromatogr 433:318, 1988.

241. C-X Gao, IS Krull. J Pharm Biomed Anal 7:1183, 1989.
242. F-X Zhou, IS Krull. Chromatographia 35:153, 1993.
243. EW Wuis, EWJ Beneken Kolmer, LEC Van Beijsterveldt, RCM Burgers, TB Vree, E Van Der Kleyn. J Chromatogr 415:419, 1987.
244. N Nimura, T Kinoshita. J Chromatogr 352:169, 1986.
245. G Lovell, PH Corran. J Chromatogr 525:287, 1990.
246. A Jegorov, V Matha, T Trnka, M Cerný. J High Resolut Chromatogr 13:718, 1990.
247. A Jegorov, K Triska, T Trnka, M Cerný. J Chromatogr 434:417, 1988.
248. S Einarsson, B Josefsson, P Möller, D Sanchez. Anal Chem 59:1191, 1987.
249. A Roux, G Blanchot, A Baglin, B Flouvat. J Chromatogr 570:453, 1991.
250. MT Rosseel, AM Vermeulen, FM Belpaire. J Chromatogr 568:239, 1991.
251. AJ Hutt, J Caldwell. Clin Pharmacokinet 9:371, 1984.
252. BC Sallustio, A Abas, PJ Hayball, YJ Purdie, PJ Meffin. J Chromatogr 374:329, 1986.
253. SW McKay, DNB Mallen, PR Shrubsall, BP Swann, WRN Williamson. J Chromatogr 170: 482, 1979.
254. JM Maître, G Boss, B Testa. J Chromatogr 299:397, 1984.
255. A Sioufi, D Colussi, F Marfil, JP Dubois. J Chromatogr 414:131, 1987.
256. S Pedrazzini, W Zanoboni-Muciaccia, C Sacchi, A Forgione. J Chromatogr 415:214, 1987.
257. J Goto, N Goto, A Hikichi, T Nishimaki, T Nambara. Anal Chim Acta 120:187, 1980.
258. H Nagashima, Y Tanaka, R Hayashi. J Chromatogr Biomed Appl 345:373, 1985.
259. S Björkman. J Chromatogr 339:339, 1985.
260. S Björkman. J Chromatogr 414:465, 1987.
261. EJD Lee, KM Williams, GG Graham, RO Day, GD Champion. J Pharm Sci 73:1542, 1984.

22

HPLC Applications in Biotechnology

John C. Ford

Indiana University of Pennsylvania, Indiana, Pennsylvania

I. INTRODUCTION, SCOPE, AND ORGANIZATION

"Biotechnology" is considered by many chemists to describe the manufacture of recombinant proteins for pharmaceutical use. Certain agricultural applications, such as freeze-resistant strawberries, are also commonly associated with the term. However, the field is much broader. A partial list of the areas using biotechnology and representative applications is given in Table 1. An on-line search of *Chemical Abstracts* yielded 13 references indexed to the keyword "biotechnol?" before 1976; between 1991 and mid-1994, 2172 references are indexed to that keyword (Fig. 1). Clearly, the field has undergone enormous growth, and concurrent with that growth has been an increase in new separation problems. Just as biochemistry has played an important role in the development of chromatography [e.g., 1], it is appropriate that high-performance liquid chromatography (HPLC) is playing an increasingly important role in the development of this new technology.

As Table 1 shows, biotechnology not only encompasses virtually all of biochemistry, but may involve many other fields as well. Given this enormous breadth, it is impossible in a review such as this to detail even the most representative applications. Many important areas must be omitted or underrepresented. Other sections of this handbook will be of interest, depending on the specific emphasis of the reader. The chapters on chiral separations (Chap. 21), pharmaceuticals (Chap. 20), food and nutritional analysis (Chap. 23), and polymers (Chap. 26) may all offer insight to particular biotechnological problems. This review is restricted to those biological molecules most common in the development of biotechnological systems, (i.e., amino acids, peptides, proteins, nucleic acids, and oligosaccharides). Simple carbohydrates, nucleotides, and similar species are only briefly mentioned, for these are seldom the focus of biotechnological work. The vast number of secondary metabolites that might be relevant to a particular problem and the multitude of substances that might serve as substrates for biotechnological transformations are omitted.

Many texts are useful resources for the practitioner of chromatography, who may desire practical information beyond that typically available in introductory texts. Two specifically written on methods development are those by Bidlingmeyer [2] and by Snyder et al. [3]. Both contain valuable information on developing rugged separation protocols as well as excellent information on troubleshooting. These may be especially useful to those workers primarily interested in applying HPLC and will provide guidance when faced with a new and perplexing problem. Although the texts overlap, each has its own merit and both are recommended for laboratory reference. Likewise, certain literature reports [e.g., 4] deal with the issues of de-

Table 1 Representative Applications of Biotechnology

General area	Biotechnological applications in area (1987–1994)
Medical	Fundamental studies; diagnostics; seroculture; vaccine development; and disease model development
Pharmaceutical	Medicinal plant production; antibiotics; immunomodulators; interferon; plasminogen activator; and growth hormone
Agricultural	Weed and insect control; animal breeding, including poultry and dairy; crop improvement, including soybeans, rice, ornamentals, flowers, woody plants, sunflowers, potatoes, rapeseed, canola, trees, grapevines, fruits, and vegetables; and veterinary medicine
Paper	Wood pulp bleaching; processing lignocellulosics
Textiles	Improvement of cotton; cellulosic fibers; and silk
Energy	Hydrogen production; methane production; and fossil fuels, including coal desulfurization
Food	New foods; cheese; coffee; milk; safety and spoilage; fish sauce; flavors, colors, and aromas; vitamins; beer production and modification; wine production; and alcohol production
Material science	Mining and ore processing; gold and noble metal extraction; ceramics; and polymers, including synthetics and aerospace matrix resins.
Environmental	Drinking water purification; wastewater cleanup, including from electroplating and uranium mining; air pollution detection and control; hazardous waste treatment; and groundwater decontamination
Leather	Production and waste treatment
Aquaculture	Fish; algae and microalgae; and seaweed
Forensics	DNA fingerprinting
Cosmetics	Shampoos; skin rejuvenators; and emollients
Chemicals	Commodity and fine-chemical production; alkaloids; starches; hormones; proteins and peptides; fats, oils, and lipids; lectins; organics; surfactants; fluorinated fine chemicals; and pigments

veloping rugged HPLC procedures and the regular column by Dolan in the journal *LC–GC* provides valuable guidance in troubleshooting problems.

Several texts covering chromatographic applications in biotechnology have been published recently [e.g., 5–10]. Not only do these serve to indicate the rapid growth in and importance of this area, but they are valuable to the worker desiring additional resources. The current format for the liquid chromatography methodology fundamental review, published by the journal *Analytical Chemistry* in even-number years contains a section on biopolymer separations that can be helpful. The application reviews published in odd-numbered years may also prove useful, particularly the clinical chemistry review. Notably, commencing with the 1993 application reviews issue, *Analytical Chemistry* now includes a review section concerned with peptides and proteins [11]. Again, this indicates the growing importance of the area as well as serves as a valuable resource for workers.

This chapter is organized primarily by chemical species. It is hoped that, in this way, the reader can more easily find relevant information on a particular problem. In view of the availability of so many excellent monographs [5–10], it seemed appropriate to focus on the 1989–1994 literature. The chapter starts with a brief overview of the operations of biotechnology, to provide a sense of context to chromatographers, as well as to indicate the scope of separation problems involved. Next a brief discussion of chromatographic developments of

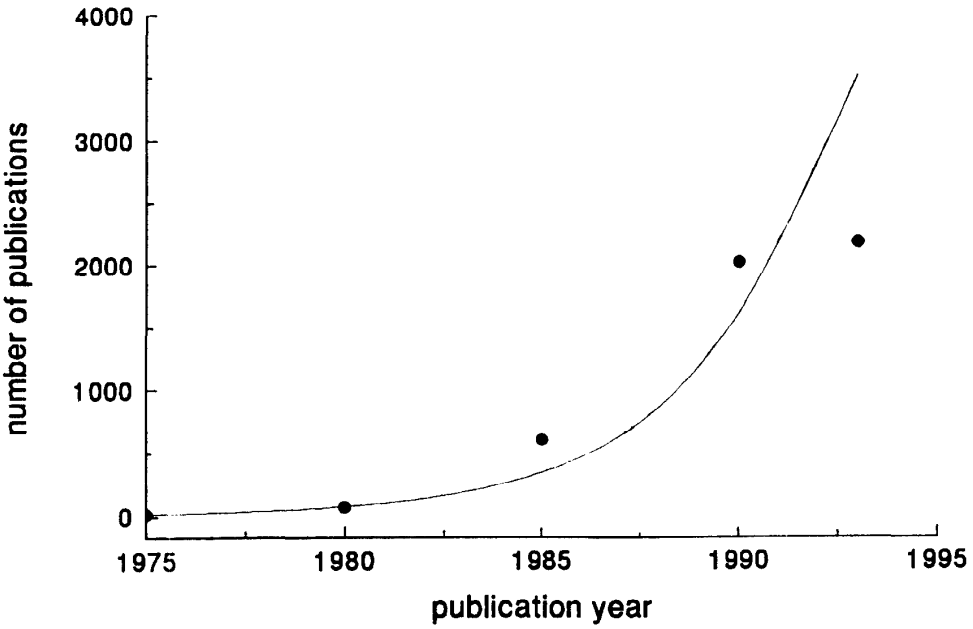


Figure 1 Number of publications indexed to "BIOTECHNOL?" in Chemical Abstracts as a function of time. Each point is the number of publications for the preceding years and including the indicated year (i.e., point at 1975 represents all publications before 1976, the point at 1980 represents all publications from 1976 through 1980, and so on). The point at 1995 represents citations (2207) at the time of the search (January 1995).

general interest to biotechnologists is presented, followed by specific applications to the various classes of biomolecules.

II. OVERVIEW OF BIOTECHNOLOGICAL METHODOLOGY

Broadly defined, *biotechnology* is the use of biological systems for the benefit of mankind. Modern biotechnology uses the techniques of molecular biology and genetics to develop organisms having increasingly desirable properties (e.g., synthesizing high levels of desirable materials). Although many important areas (e.g., clinical diagnostics) focus on developing molecules to interact specifically with selected genes, much biotechnology is concerned with increasing the production of a desired protein. With apologies for inaccuracies, this process is now briefly summarized.

The desired protein must be *cloned* (i.e., the DNA coding for the protein must be isolated). To do this, the protein must first be isolated in sufficient quantity to allow at least partial sequence determination. At this stage, protein purification techniques must preserve biological activity, because the purification effectiveness is monitored by the ratio of activity to total protein. Frequently, total protein is measured by amino acid analysis, although dye-binding or spectrophotometric assays are also common. Even though successful results have been obtained from picomolar quantities of protein, nanomolar (i.e., tens of micrograms for a 30-kDa protein) quantities are more practical.

Following purification to homogeneity (typically as judged by polyacrylamide electrophoresis with silver-stain detection), the desired protein is sequenced. As the NH_2-terminal information is particularly useful, frequently sequence determination of the intact protein is attempted. Chemical or enzymatic proteolysis is also used to generate several short (i.e., 10- to 20-residues) peptides. The resultant mixture is purified into individual peptides without

concern for biological activity (which, in all probability, will have been lost by the fragmentation), and the individual peptides are subjected to both sequence determination and amino acid analysis. Matsudaira has produced an excellent monograph on these subjects [12].

As first used in 1950, protein sequence determination still largely relies on successive applications of the Edmund degradation [13]. In classic protein sequencing, the goal was to generate overlapping sets of peptides by the use of two or more proteases with differing specificities. By sequencing these sets, the sequence of the entire original protein could be pieced together. The current approach is to obtain sufficient sequence information to allow the design of a synthetic oligonucleotide "probe," which can be used in the isolation of the gene coding for the protein. Because sequencing DNA is faster than sequencing proteins and isolation of the gene is necessary for the development of an expression system, this approach has become common.

Each amino acid residue is determined by one or more triplets (codons) of DNA bases; knowing the peptide sequence and the genetic code, one can write the gene sequence. However, because most amino acids have two or more codons encoding them (i.e., are degenerant), one cannot necessarily determine a unique gene sequence, but rather, several possibilities. Figure 2 illustrates this problem. For highest efficiency in the isolation of the gene, it is desirable to reduce the number of possibilities. Thus, not all peptide sequence information is equally useful in the design of the probes; regions of high degeneracy (many possible DNA sequences) are undesirable. Further discussion of probe design is given in Sambrook et al. [14] and references therein. Following determination of the desired nucleotide sequence, the oligonucleotide probe is synthesized. For many applications, it is desirable to purify the de-

(a) The genetic code

	Second position in codon				
	U	C	A	G	
U	Phe	Ser	Tyr	Cys	U
	Phe	Ser	Tyr	Cys	C
	Leu	Ser	stop	stop	A
	Leu	Ser	stop	Trp	G
C	Leu	Pro	His	Arg	U
	Leu	Pro	His	Arg	C
	Leu	Pro	Gln	Arg	A
	Leu	Pro	Gln	Arg	G
A	Ile	Thr	Asn	Ser	U
	Ile	Thr	Asn	Ser	C
	Ile	Thr	Lys	Arg	A
	Met	Thr	Lys	Arg	G
G	Val	Ala	Asp	Gly	U
	Val	Ala	Asp	Gly	C
	Val	Ala	Glu	Gly	A
	Val	Ala	Glu	Gly	G

(b) Two-fold degenerant amino acid sequence

Met - Trp - Cys - Trp

possible DNA sequences

AUG-UGG-UGU-UGG
AUG-UGG-UGC-UGG

(c) Eight-fold degererant amino acid sequence

Met - Val - His - Trp

possible DNA sequences

AUG-GUU-CAU-UGG
AUG-GUC-CAU-UGG
AUG-GUA-CAU-UGG
AUG-GUG-CAU-UGG
AUG-GUU-CAC-UGG
AUG-GUC-CAC-UGG
AUG-GUA-CAC-UGG
AUG-GUG-CAC-UGG

Figure 2 The origins of degeneracy in the determination of the codon sequence corresponding to a protein sequence. The situation arises because, although each codon maps to precisely one amino acid, the reverse is not true. (a) The genetic code, mapping codon sequences to amino acids; (b) an example of an amino acid sequence that is twofold degenerant (i.e., can be generated by two distinct polynucleic acids); (c) an example of an amino acid sequence that is eightfold degenerant.

sired probe from partially deblocked and failed sequences that are also produced. Subsequent to (or concurrent with) synthesis, the probe is labeled (e.g., radioactively).

The probe is used to detect the desired DNA sequence in a *library*, a collection of vectors, each containing genetic information relevant to the problem at hand. Libraries are of two types: genomic and cDNA. A *genomic library* is constructed by isolating the genomic DNA from an organism, fragmenting it into appropriately sized pieces, and combining these pieces with DNA (a *vector*) that will allow the propagation of the foreign DNA in a selected host (e.g., *Escherichia coli*). The collection of *E. coli* colonies then contains the complete genomic information of the original organism (i.e., it is the genomic library). A *cDNA* (complementary DNA) library is constructed similarly, although the first step is the isolation of messenger RNA (mRNA) from the organism, followed by the synthesis of DNA complementary to that RNA using a reverse transcriptase.

Although, in principle, a genomic library contains the complete genetic information of the source organism, it is not the optimal choice for all cloning efforts. Such a library may contain a single copy of the desired gene among millions of nucleotides of other information. Likewise, the DNA coding for the desired protein may be separated in the gene by regions of DNA (*introns*) that do not code for the desired protein and are not carried into the mRNA. On the other hand, although a cDNA library eliminates the problem of introns and, if the original tissue is selected wisely, may have multiple copies of the target DNA, handling RNA is technically more difficult than manipulating DNA. Interesting proteins usually correspond to rare mRNAs, and many novel approaches to selective enrichment of desired mRNAs before library construction have been developed. The HPLC-based enrichment of desired mRNAs seems a potentially fruitful area for exploration.

Next, the desired gene is isolated by replica plating of the library, followed by colony hybridization. A sufficient number of colonies of the library are plated to ensure a high probability that the gene of interest is present. Sterile membranes (e.g., nitrocellulose filters) are carefully laid on the plate, and some cells of each colony adhere to the membrane. The membrane is marked so that it can be unambiguously reoriented on the plate and then removed. The cells adhering to the membrane are lysed and the DNA is denatured and irreversibly bound to the membrane. The membrane is next saturated ("blocked") with short DNA fragments (e.g., from salmon sperm DNA) to minimize nonspecific binding of the probe to the membrane. The labeled probe is added to the blocking solution, and the probe is allowed to bind (*hybridize*) to the membrane-bound DNA under conditions sufficiently stringent to minimize the binding to partially complementary regions (i.e., to minimize false-positives). Following hybridization, the probe remaining on the membrane is detected. Because the membrane can be oriented onto the original plate, those colonies that contain DNA binding the probe can be isolated.

Isolation of the foreign DNA from the organism must be followed by careful characterization. The method described does not ensure that the complete sequence of the desired protein will result. Protein synthesis stop points are unambiguous, but starts are not; thus, NH_2-terminal sequence information is valuable. Any DNA fragment isolated by the foregoing process contains part, but not necessarily all, of the desired gene. It may also contain extra information. Consequently, cloning requires additional steps to "trim" the fragment from extraneous DNA and to assemble the gene in a fashion that allows the host organism to synthesize the desired protein. These steps are termed *subcloning*.

When one assumes that the gene of interest yields a functional protein, it is next used to develop an *expression system*—a combination of that gene inserted into a vector containing regulatory and signaling information, a host organism, and a protocol for growing the host in a fashion such that it causes the synthesis of large quantities of the protein of interest. In addition to the issue of maintaining biological activity, issues such as toxicity to the host organism, solubility in the host and medium, and ease of purification, also must be considered. When synthesized (*expressed*) at high levels in foreign hosts, many proteins form insoluble (and inactive) inclusion bodies. Although recovery of active protein from inclusion bodies is

possible for some proteins, this is not always so. For pharmaceutical applications, in particular, purification of the active recombinant protein from the proteins of the host organism is necessary. Isolation of pure, active protein must be followed by the development of appropriate formulations for the delivery of the material. This involves measurement of the stability of the formulation, not only toward chemical modification of the protein, but also toward denaturation and aggregation.

However, isolation of the correct gene and development of an expression system does not ensure the synthesis of functional protein. Proteins are frequently not simply linear polypeptide chains. Higher-order structure from associations between similar or dissimilar chains, proteolytic processing, and a variety of other modifications (collectively termed posttranslational modifications) can be critical in determining the precise biological activity. Interest in the characterization of posttranslationally modified proteins has grown rapidly with the recognition of the importance of these modifications to the functionality of proteins. Again, pharmaceutical products need be thoroughly characterized relative to possible microheterogeneities arising from variations in posttranslational modifications.

Hence, biotechnologists must not only verify that the desired product is free from contaminants, but also that any factor influencing the structure and activity has acted correctly. Less precisely but more pragmatically, the desired product must be characterized not only chemically, but also structurally. Complete characterization of a recombinant product may require characterization of glycosylation, lipoylation, hydroxylation, phosphorylation, methylation, acetylation, acylation, or other such modifications. A summary of methods for approaching these problems is provided by Graves et al. [15].

This brief outline shows clearly that a wealth of biotechnological separation problems exist. The following sections describe selected approaches (and their limitations) for the application of HPLC techniques to these problems.

III. GENERAL CHROMATOGRAPHIC DEVELOPMENTS

There have been many general perspectives surveying various aspects of the role of chromatography in biotechnology published [e.g., 16–26]. Likewise, some general developments in chromatographic instrumentation, column technology, and such, are of great interest to biotechnologists. Moreover, some publications describe methodology that, although directed to a particular category of molecules, is of rather general usefulness. The following section describes several such reports.

For example, although nucleic acids and related compounds were their focus, the discussion by Jang and Brown [27] on peak identification is of broader interest. Whereas mass spectrometry (MS) is undoubtedly the preferred technique for unambiguous assignments, many laboratories do not have routine access to this technique. Hence, identification methods based on retention, spectral properties, and chemical behavior, are discussed. As the authors describe, the arsenal of on-line spectroscopic and electrochemical detectors, if applied appropriately, can result in a high degree of confidence in peak assignment.

Similarly, Hansen and Emborg [28] used precolumn, *o*-phthaldehyde derivatization-based amino acid analysis as a model for systematic method development by two-level factorial design. The statistical optimization method is more far-reaching and deserves a broader audience.

A. Bioprocess Control

Process control is an issue of interest in any industry, including biotechnology. Cooley and Stevenson [29] described the use of HPLC as a process monitor in biotechnology. The production of recombinant human insulin was monitored by an on-line, isocratic HPLC system. Techniques to minimize the effect of the system's response time on the process were devel-

oped, as was an on-line dilution–dissolution technique. However, the emphasis of the report is on the process control aspects and the chromatographic details are sketchy.

Such process control applications can place stringent demands on the analytical method if real-time (i.e., continuous sampling) or nearly real-time control (i.e., fast, discontinuous sampling) is to be achieved. If the process is relatively slow, then slow sampling may be acceptable. Nadler et al. [30] followed the production of recombinant interferon gamma (rIFN-γ) by cultured cells, sampling approximately every 2 h. Cells were grown to confluency and moved to a serum-free medium. Samples of this medium were tested to determine the production of glycosylated and nonglycosylated IFN-γ.The analytical procedure involved analysis of samples before and after passage through an anti-IFN-γ affinity column; thus, the IFN-γ was determined by subtraction. Total protein analysis was performed on a 100 × 4.6-mm POSROS Q/M anion-exchange column; mobile-phase conditions were not reported. Nonglycosylated IFN-γ was also added to the samples for standard addition quantitation. As much as 1 mL of conditioned medium was injected in each analysis. The production of glycosylated IFN-γ paralleled the production of nonglycosylated material over the 60-h monitoring period, although the glycosylated IFN-γ was produced at a higher level. The low sampling frequency was appropriate for this slowly changing process.

Faster processes require more rapid monitoring. As already revealed, biomolecules are frequently eluted with gradient techniques. However, conventional gradient elution chromatography does not lend itself to nearly real-time control of a process requiring sampling every 1–2 min. This is due to the time required for reequilibration before injection of the next sample, as well as because current gradient generator designs are simply incapable of reproducibly creating 60-s gradients at 5 mL min^{-1}. Thévenon-Emeric and Regnier [31] addressed this problem, using two exponential mixing chambers and a ten-port valve (Fig. 3). In position 1, chamber A is filled with the starting solvent and column C1 is equilibrating (or equilibrated) for injection; chamber B is filled with the final solvent, and column C2 is being washed. Following injection of a sample at valve V1, the ten-port valve is changed to position 2. Now, chamber A begins filling with the final solvent; however, this forms an exponential mixing chamber, so that column C1 experiences a gradient (albeit nonlinear) from the starting solvent to the final solvent. At the same time chamber B and column C2 are being returned to the starting conditions. C1 and C2 were custom-made, 5-mm–long, 6-mm–id columns packed with 8-μm Polymer Laboratories PLRP-S 1000 resin. Detection was at 225 and 440 m simultaneously. Gradient shape could be modified by changes in either the flow rate or the composition of the starting and final solvent. The retention volumes of each of six different proteins gave percentage relative standard deviations of less than 5%. Note that this configuration allows not only rapid gradient generation, but also eliminates failure-prone proportioning valves. It also requires two pumps and a single detector and is, thus, less equipment-intensive than two separate systems. The model process studied was the preparative anion-exchange purification of a crude extract from *Cyanobacterium anabaena* PCC7120, corresponding to the 50–90% ammonium sulfate precipitate (after dialysis). The preparative isolation was performed on a 300 × 2.54-mm column packed with 20-μm SynChroprep AX 200 resin. Samples were acquired every 90 s throughout the preparative separation. A significant baseline offset and artifactual peaks occurred when the ten-port valve was switched; this is likely due to the pressure surge and may be attenuated by detector cell design. (The report indicates that three different detectors were used in the work; this idea apparently occurred to the authors also.) Alternatively, a pressure by-pass configuration may be possible. The authors noted that the effect was greatly diminished at 440 nm, although that wavelength would not be generally useful. A ghost peak (carryover, not previously reported on poly(styrene–divinylbenzene) columns), was observed following samples that significantly overloaded either of the analytical columns. One clear benefit from this design is the nearly 50% reduction in time between samples, achieved without doubling the instrumentation cost. The authors also state, "A second advantage of the dual column approach is that when prob-

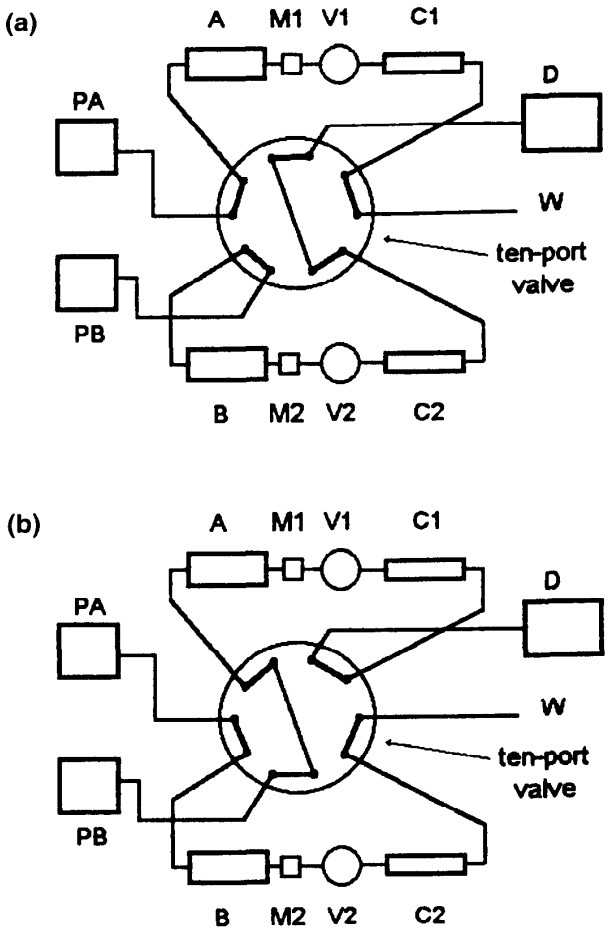


Figure 3 Parallel column gradient elution system: PA, pump for starting solvent; PB, pump for final solvent; V1, V2, six-port valves, sampling process stream; C1, C2, analytical columns; A, B, gradient mixing chambers; M1, M2, high-pressure mixers; D, detector; W, waste exit port. (a) Position 1, chamber A and column C1 in starting solvent, chamber B and column C2 in final solvent, before injection onto column C1. (b) Position 2, chamber A and column C1 in final solvent, chamber B and column C2 in starting solvent, before injection onto column C2. Switching the ten-port valve from position 1 to position 2 generates a nonlinear gradient from starting to final solvent on column C1 and a similar gradient from final to starting solvent on column C2. (Adapted from Ref. 31.)

lems or questions are encountered relative to the analytical system, they are more easily diagnosed. It is seldom that both columns fail or experience the same problems at the same time," [31]. This work demonstrates the potential for the use of gradient HPLC methods in process control.

B. Column Technology

Diffusion has long been recognized as being critical in chromatography [e.g., 32]. To achieve highly efficient separations, it is necessary to minimize distances traveled by diffusion. Because the peptides, proteins, nucleic acids, and carbohydrates of most interest in biotechnology are fairly large (i.e., >1000 Da), it follows that their diffusion coefficients are small. Consequently, diffusional path lengths must be reduced for these species to achieve chromatographic performance equivalent to that of smaller molecules. This problem has been addressed in various ways. The following reports focus on peptides and proteins; however, the improve-

ments achieved should also be relevant for other macromolecules. Developments in these areas will undoubtedly continue.

The most direct approach is to reduce the particle size. Given that the diffusion coefficients for the species of interest are an order of magnitude smaller than that of a typical small molecule, particles of 1 μm or smaller should offer equivalent chromatographic performance. Consequently, several workers have evaluated the use of smaller particles.

Totally porous 1- to 2-μm, wide-pore (20-nm) silica microspheres were examined by Danielson and Kirkland [33]. The columns used were 33 $\times$ 4.6 and 33 $\times$ 6.2 mm, packed with butylsiyl-modified microspheres. The primary mobile phase was 30:70 ACN–water with 0.1% trifluoroacetic acid (TFA) for the isocratic work and a 25:75–100:0 ACN–water (both with 0.1% TFA) gradient. Commercial HPLC equipment was used, although a 2.5-μL flow cell and 0.007-μm–id tubing were used to minimize extracolumn band-broadening. The reduced plate-height of insulin was comparable with that of small molecules, although the dependence of reduced plate height on reduced velocity showed a much higher contribution from mass transfer, as expected. Separations of relatively simple mixtures of peptides and proteins were obtained in less than 1 min. Excellent (95–114%) recoveries of proteins were observed for ribonuclease A, insulin, lysozyme, and myoglobin; the recovery for ovalbumin was 62%. These latter studies were performed at relatively high reduced velocities; lowering the flow rate should provide increased performance. This material is not commercially available, however.

Unger et al. have used nonporous 1-μm–silica microspheres for the HPLC of proteins [34–38]. Ethyl-, butyl-, phenyl-, octyl-, and octadecyl-silyl-modified particles were evaluated, using column dimensions of 35 $\times$ 8 mm and water–ACN–TFA mobile phases. The chromatographic performance was quite satisfactory. Although a nonporous material might not be expected to provide adequate retention capacity, this was not so. In common with porous particles, few, if any, selectivity differences were observed between the various phases; in contrast to porous particles, the slope of the plot of the logarithm of the capacity factor versus organic modifier concentration (the S value) did not significantly vary with protein molecular weight. MICRA Scientific has introduced such a material with an octadecylsilyl-modified surface.

An alternative method of reducing diffusional path lengths is to use pellicular or superficially porous particles. Pellicular materials consist of a thin shell of microparticles agglomerated around a nonporous core. Superficially porous particles are similar, possessing a thicker layer of microparticles around the solid core. Both materials are historically important in the development of HPLC [39–42], although these 20- to 50-μm materials lost favor as smaller than 10-μm, totally porous spherical particles became available. However, pellicular and superficially porous particles provide very short diffusional path lengths and have been reexamined for use in macromolecular separations.

Kalghatgi and Horvath developed 2-μm–micropellicular silica-based particles [43,44]. These permit very fast (20-s) separations of proteins. However, pellicular materials have a low surface area, thereby limiting their use to analytical applications. Such particles also require extremely small dead volumes and specialized detectors, injectors, and connectors needed to benefit from their potential. These particles are not currently commercially available. In addition to reversed-phase supports, affinity [45], and displacement [46] chromatographies on the same substrate have been reported.

Kirkland [47] produced superficially porous silica particles with a 5-μm core and a 1-μm–thick shell of 44-nm microbeads, giving about 30-nm pores. The dimensions were a compromise; the thickness of the layer was calculated to provide adequate mass capacity and sufficient void volume to allow the use of conventional instrumentation, yet still minimize the diffusional path length. He states, "The intent was to minimize limitations imposed by totally porous 3–5 μm particles and the new 1–2 μm totally porous and pellicular particles." The approximately 7-μm superficially porous (SP) particles were compared with 8.7-μm totally porous (TP) particles treated in the same fashion as the superficially porous materials. The

SP and TP particles showed similar van Deemter plots for a 2-kDa styrene; the SP particles were superior in both maximum efficiency and mass transfer characteristics for a 207-kDa styrene. Indeed, as judged from the rate of increase in plate height with velocity, the SP particles exhibited equivalent mass transfer characteristics for both solutes. Both materials showed equivalent degradations in efficiency as a function of mass injected. In the range of 1–100 μg for the 2-kDa sample, the SP particle was marginally superior for the 200-kDa sample. These results were obtained using the size-exclusion chromatographic (SEC) mode; thus, overload of the stationary phase was not examined. Diisopropyl-*n*-octyl-silyl–modified particles of both types were compared in the RPLC mode. Both gave equivalently efficient separations of a mixture of small molecules, although the TP particles provided more retention (i.e., required a higher percentage of organic modifier to provide similar retention times). The *S* values of small molecules were essentially the same on both materials. A gradient separation of RNaseA, cytochrome *c*, lysozyme, ovalbumin, and carbonic anhydrase (using a water–ACN–0.1% TFA system) shows that the elution from the SP particles occurred at lower ACN concentrations. The peak shape of RNaseA was also better on the SP particles, and the lysozyme–ovalbumin separation improved. The author suggests that this material might be attractive for hydrophobic proteins, such as membrane proteins, for the lower surface area requires lower ACN concentrations for elution. The larger particles are also expected to generate lower hydrodynamic sheer forces at equivalent velocities. Again, this material is not commercially available.

A completely different approach is being explored by Svec et al. [48,49]. Columns packed with particulate materials necessarily have interparticle voids. In a column of length L and radius r, approximately 80% of the empty column volume (i.e., of $\pi r^2 L$) is empty when that column is packed with totally porous particles. Approximately 40% of the empty column volume is the interparticle void volume—the empty space between particles. By polymerizing a macroporous polymer within the column, no such interparticle void exists. As described by Svec and Fréchet, "The main advantage . . . is that the separation occurs as all the mobile phase flows *through* the porous structure of the separation medium. This reduces the elution pathway and facilitates diffusion in and out of small porous areas" [48]. In the first study, the polymers were formed by reacting a mixture of glycidyl methacrylate and ethylene dimethacrylate with azobisisobutyronitrile (AIBN) in the presence of cyclohexanol and dodecanol at 70°C in situ in the column. The cyclohexanol and dodecanol act to create macroscopic pores within the polymer matrix. This material was functionalized by acid-induced epoxide ring opening to yield a diol-functionalized rod (diol column) or by reacting diethylamine with the epoxide to yield an 1-*N*,*N*-diethylamino-2-hydroxypropyl rod (amino column). (Testing was performed to confirm that the polymer reacted uniformly to generate an apparently homogeneous amino surface.) The diol columns gave linearly increasing pressures with increasing flow rates for both water and THF. Switching between these solvents did not change the column properties, indicating that the phase neither collapses nor swells in these solvents. The HETP for benzene (THF mobile phase) was about 9 μm, quite respectable. The diol columns were usable to 20 mL min^{-1} in these solvents. The amino columns showed a much steeper increase in pressure with flow, using 10 mM Tris, pH 7.6, as the eluent. This was attributed to swelling, which in this situation must decrease the porosity, rather than increase the rod diameter. Nonetheless, the column was usable to 2 mL min^{-1}. Ion-exchange results using the amino column show reasonable potential for this technique. Recoveries were better than 95% for the tested proteins, and the columns were chromatographically stable "over a period of 5 weeks of daily use." The manufacturing reproducibility was reported to be reliable.

Wang and associates used the same in situ polymerization process to generate a styrene–divinylbenzene column [49]. Again, a 1:1 mixture of the monomers, AIBN, and dodecyl alcohol (the porogenic solvent) were mixed, placed in a column, and polymerized at 70°C. THF was pumped through the column to remove the dodecyl alcohol. The pore size distribution was bimodal, with large (500–1000 nm) pores providing the largest contribution to the total pore volume (70% of the total); small pores (7–20 nm) made the next largest

contribution (13%). The smallest pores provided the main contribution to the specific surface area, however. SEC data also support the bimodal pore size distribution. The pore volume of the rod composed 69% of the empty column volume. The pressure increased linearly with increasing flow with THF; with 20:80 ACN–water, there was some curvature to the relation. In both cases, the column was usable to 25 mL min^{-1}. The pressure drop was slightly less than half that of an equivalent column packed with Polymer Laboratories 8-μm–PLRP-S 1000 resin operated under the same conditions. Thus, hydrodynamically, the column behaves as if it is packed with 12-μm particles. The van Deemter plot shows an unusual *S* shape with a slowly rising slope from about 400 to 2000 cm h^{-1}. Estimating the data from the published figure, using the estimated effective particle size of 12 μm, and assuming a diffusion coefficient of 1.5×10^{-6} cm^2 s^{-1} for cytochrome *c* (the tested molecule), a more conventional reduced plate height versus reduced velocity curve can be constructed (Fig. 4). This shows that the study was performed at relatively high, reduced velocities, far from the expected optimum of 3–5. There is a sharp drop at the lowest point, but that may be artifactual. Regardless, the range of velocities over which the column operates at a reduced plate height near 20 is quite broad. The authors attribute this behavior to improved mass transfer owing to short diffusional path lengths and possibly to enhancement by convection. The excellent mass transfer is also demonstrated by the near flow-rate invariance of the breakthrough curve of ovalbumin. The loading capacity was 1.2 mg/column. In terms of protein chromatography, the *S* values for cytochrome *c*, RNaseA, and ovalbumin in ACN–water were determined to be approximately as predicted by the empirical equation of Snyder [50]. This is somewhat surprising because the equation was developed using data generated using conventional alkyl–silyl-modified silica particles. The *S* value for myoglobin was approximately 2.5 times higher than that predicted. Excellent separations of cytochrome *c*, myoglobin, and ovalbumin were obtained in less than 1 min and acceptable separations of all four mentioned proteins demonstrated in less than 2 min. Although still developmental, this in situ column-generation process appears to have much to offer.

In some sense, this in situ process described in the foregoing is an extension of high-performance membrane chromatography (HPMC) [51–54]. Here too, the separation media consists of a single, macroporous entity. Typically, HPMC is performed using a 2- to 3-

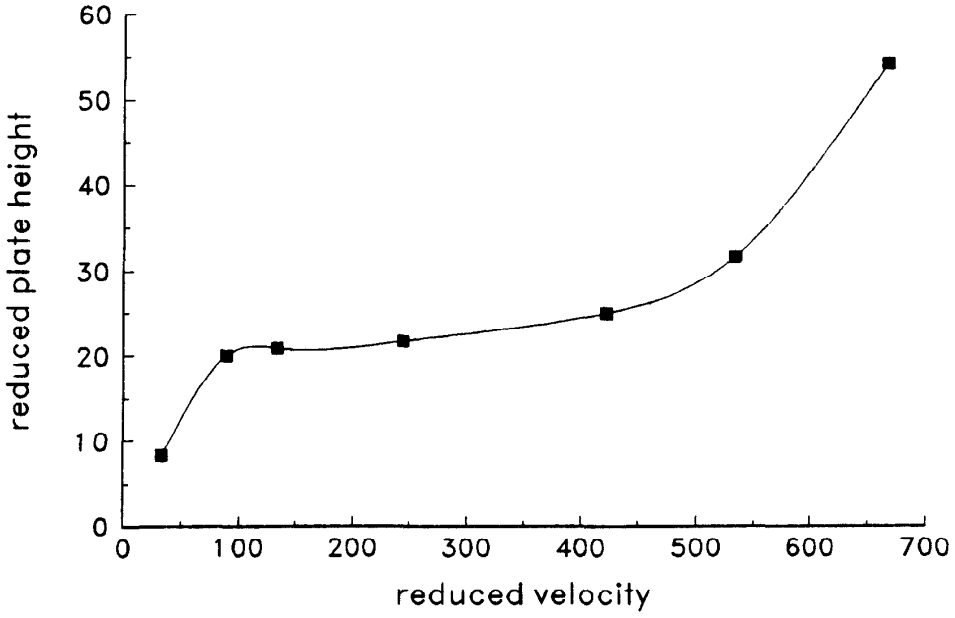


Figure 4 Reduced plate height versus reduced velocity relation for cytochrome *c* on an in situ polymerized column. (Estimated from Ref. 49.)

mm–thick membrane as the stationary phase, again with no interparticle void volume. Early work with totally porous silica-based materials showed that frequently the efficiency of a gradient peptide or protein separation did not depend on column length; hence, the interest in membranes acting as extremely short, well-packed columns. Loading capacity is achieved by making the diameter large relative to the length. The system's extramembrane dead volume is likely to be large compared with the membrane pore volume. HPMC "columns" are commercially available (Säulentechnik Knauer, Berlin, Germany).

Tennikova and Svec [55] described the preparation, treatment, and uses of poly(glycidyl methacrylate–*co*-ethylene dimethacrylate) (PGM), poly(glycidyl methacrylate-*co*-dodecylmethacrylate-*co*-ethylene dimethacrylate) (PDM), poly(glycidyl methacrylate-*co*-octylmethacrylate-*co*-ethylene dimethacrylate) (POM), and poly(styrene-*co*-divinylbenzene) membranes (PSV). The PGM membranes were treated with diethylamine to provide an anion-exchange (AE) material. The PDM and POM membranes were treated with sulfuric acid to create diol materials, the PDM containing dodecyl groups and the POM containing octyl groups. These were used for hydrophobic interaction (HI) membrane separations. The PSV membrane was used as a reversed-phase (RP) material, although its properties were only briefly described. The membranes' properties were examined using the conventional chromatographic parameters k' and σ, because as the authors note, ". . . the differences" between HPLC and HPMC "seems [*sic*] not to be in the art but more likely in the degree." The HI and AE membranes generally followed the retention and bandwidth trends predicted, but the retention was smaller in AE-HPMC than in HPLC under similar conditions. The bandwidths were independent of velocity over the range 0–125 cm h^{-1} (roughly 6 mL min^{-1}). The authors summarize by saying, ". . . HPMC obeys the rules typical of column chromatography. . . . Owing to the unique absence of interparticular voids in the membrane, all the mobile phase flows through the pores of the separation medium. This results in an increase in diffusivity by several orders of magnitude augmented by the convective flow."

Josic et al. addressed the issue of efficiently using the available surface in HPMC [56]. Although titled *High-performance membrane chromatography of serum and plasma membrane proteins*, most of the report is devoted to solving the dead volume problem and evaluating the influence of membrane geometry on efficiency in HPMC. The dead volume problem arises because the sample is introduced in a narrow stream, whereas the membrane is rather wide and typically quite short. For example, the inlet tubing may be 0.01-in. (0.025-cm) id whereas the membrane is from 10 to 50 mm in diameter. Distribution of the sample over this surface typically results in excessive dead volume preceding the membrane. The use of compressed air to drive the sample into the membrane (held in an Amicon filtration device) minimized the dilution of the sample, but resulted in poor gradient reproducibility. This technique was recommended for affinity chromatography, however. A variety of sample distribution configurations were evaluated, with the most successful appearing as a series of concentric circles. Thicker disks generally gave better performance, although the current thickness limit was 10 mm. As much as 10 mg of conalbumin (ovotransferrin) could be separated from trypsin inhibitor in less than 10 min using a 50 mm–diameter, 4-mm–thick DEAE poly(glycidyl methacrylate) membrane. Such a membrane had an adsorption capacity of 300 mg of bovine serum albumin.

The high speed and efficiency of HPMC will undoubtedly attract workers to the field. Whether in the membrane format or the in situ column format of Svec et al. [48,49], the improved mass transfer and the chemical and mechanical stability of the membranes indicate increased applications of HPMC in biotechnological separations.

Another approach to minimizing diffusional path lengths is perfusion chromatography [57–61]. The particles employed for this technique contain a network of large pores (600–800 nm) as well as diffusive pores (30 nm). When operated at sufficiently high velocities, movement in the large pores is convective. Hence, the diffusional path lengths are reduced in comparison with those experienced by solutes in conventional, totally porous particles. Perfusion chromatography materials are available from PerSeptive Biosystems (Cambridge, MA).

Liapis and McCoy have developed a theoretical description of perfusion chromatography [62]. Their work indicates that relatively fast adsorption–desorption kinetics are still necessary to provide improved performance. Applications of perfusion chromatography to a variety of chromatographic retention modes have been described [63–65].

In addition to these developments, many new stationary phases based on silica, polymers, and other materials have been reported. It sometimes seems that the variety of HPLC stationary phases is approaching the number of stationary phases used in gas chromatography in the late 1950s and 1960s. Because these are surveyed elsewhere [11,66], they will not be treated here.

IV. AMINO ACIDS

In biotechnology, the quantification of amino acids following hydrolysis of a polypeptide or protein is most commonly termed *amino acid analysis*—the determination of the amino acid composition of a protein or peptide. This quantification is important in protein purification and sequencing as well as required by the US Food and Drug Administration (FDA) for recombinant polypeptide pharmaceuticals; thus, amino acid analysis is an important application of HPLC in biotechnology. Detailed discussions of amino acid analysis are available [67,68]. The review by Moinãr-Perl [69] also presents much information of general interest.

Note that although the analysis of a hydrolysate or Edmund reaction product is largely restricted to approximately 20 common α-amino acids, physiological samples may contain many others. The analysis of physiological amino acids is more complex, given this wider variety of species. In 1981, Dreshcher et al. [70] described a lithium citrate buffer system for this application, showing the separation of some 40 species in about 5 h. Improvements have been made; Grunau and Swiader [71] provide retention data for 99 amino acids and other ninhydrin-reactive compounds, focusing on compounds found in plants. In their report, they illustrate the separation of 59 such species in about 2 h.

However, these species are generally of little interest in biotechnology. A review by Kazmierczak [72] discusses amino acids related to metabolic disorders, but no analytical information is presented. Reviews are available on the topic of quantifying physiological amino acids [73–75]. The review by Qureshi [76] discusses of the uses of HPLC in the determination of physiological amino acids as well as a great deal of practical information. Generally, precolumn derivatization methods are applied to either type of sample without specific differentiation (i.e., authors reporting precolumn methods do not usually refer specifically to physiological amino acid samples, even if they are presenting relevant [i.e., physiological] amino acid data).

A. Classic Amino Acid Analysis

The typical instrument sold as an "amino acid analyzer" is based on the work of Spackman et al. [77]. It is an automated liquid chromatograph, equipped with a postcolumn reaction detector. Underivatized amino acid samples are separated by cation-exchange chromatography using sulfonated resins. A variety of buffer systems have been used [78]. The eluent is mixed with ninhydrin, heated to promote the color-forming reaction, and monitored at 570 and 440 nm. Except for proline, which shows a maximum absorbance at 440 nm, the products of amino acids absorb at 570 nm. In spite of generally longer analysis times and relatively complex operation, these instruments have proved quite reliable, are still routinely and widely used, and have the advantage of a very large set of retention data available.

B. Hydrolysis of Polypeptides

Although instrumental amino acid analysis has been performed for nearly 40 years, there remain certain difficulties not associated with the speed of the separation or the sensitivity of the detection instrumentation, but rather, with the hydrolysis reaction. Amino acid contami-

nation of equipment and reagents must be addressed and controlled. Groups of aliphatic acids are resistant to hydrolysis and, consequently, low values of valine, isoleucine, alamine, and leucine are frequently obtained. Asparagine and glutamine are hydrolyzed in the common acidic method to aspartate and glutamate, respectively; consequently, Asx (Asp + Asn) and Glx (Glu + Gln) values are reported. Cysteine, tyrosine, tryptophan, serine, methionine, and threonine, are all susceptible to degradation during the hydrolysis. A common practice is to perform several hydrolyses of the same sample, each for a different length of time, and to extrapolate the results—extending those of sensitive residues back to 0 hydrolysis time and extending those of aliphatic residues forward. This is clearly a frustrating situation. An alternative method that uses the individual maximum value obtained for each amino acid in the time-course series and thus compile an "optimum response," is hardly more satisfying.

These difficulties and approaches to dealing with them have been discussed by Pickering and Newton [79]. The review by Molnãr-Perl [69] also contains useful discussion of these problems. Although vapor-phase hydrolysis minimizes problems associated with the purity of the hydrolysis acid, it limits the protective additives available to minimize the destruction of, for example, methionine. Elevated temperatures (e.g., 150°C) not only increase the hydrolysis of aliphatic regions, but also increase the destruction of more sensitive residues. At least four hydrolysis instruments are offered commercially, although only one is automatic. Manual liquid and vapor-phase hydrolysis are currently the most common techniques and are generally accurate and reliable. Newer methods have yet to meet the test of time. As Pickering and Newton [79] state, ". . . although time savings are always desired in research, they are of little value if the standards for accuracy and reliability are not met."

Microwave digestion has been used to generate high temperatures (e.g., 180°C) quickly and should minimize the problem of degradation caused by prolonged heating, although in some reports, the losses are somewhat higher than those for manual hydrolysis [80]. In contrast, Chen et al. [81] obtained recoveries the same as or higher than conventional hydrolysis for native and oxidized RNaseA and insulin B after 5 min of microwave hydrolysis.

Tatãr et al. [82] have examined the use of microwave hydrolysis in some detail, using egg white lysozyme as a model and comparing the microwave hydrolysis results with those obtained using a vapor-phase method (VPM). Acceptable yields were found for all residues—unfortunately, not under the same conditions. Yields varied with time and pressure (which is used to regulate temperature) and were generally lower than those obtained from the VPM. Tryptophan was generally the most poorly recovered amino acid (53–92% of the VPM). Although the authors indicate that tyrosine showed the greatest sensitivity to hydrolysis conditions, their yields appear to indicate otherwise (the recovered Tyr was 69–115% of the VPM; compared with the cited Trp values). It was not possible to achieve optimum conditions for all the essential amino acids simultaneously. The work was performed at 90 and 100 psig; at higher pressures, reproducibility worsened. Microwave hydrolysis has not yet proved sufficiently reliable to convince most workers to adopt this method.

Tryptamine was used as a protective agent for tryptophan during vapor-phase acid hydrolysis [83]. The addition of 30 μg of tryptamine (dissolved at 2 mg mL^{-1} in water) to the sample before vapor-phase hydrolysis did not interfere with the phenylisocyanate precolumn derivatization-based determination; did not reduce the yields of other amino acids; and increased the yield of tryptophan to 76, 84, 98, and 95% of the theoretical value for α-chymotrypsin, bovine albumin, human albumin, and lysozyme, respectively. Phenol, at 1–3% [84], and tryptamine [85] had been used previously to provide similar protection during liquid-phase acid hydrolysis, and did not interfere with other precolumn derivatization techniques.

Alternative approaches to acid hydrolysis have been attempted, but have met with limited success. Alkaline hydrolysis can provide virtually complete recovery of Trp (perhaps the amino acid most sensitive to acid hydrolysis-induced destruction), although Arg, Ser, Thr, and Cys are destroyed. Enzymatic hydrolysis suffers from irregular kinetics (i.e., substrate-dependent), complex incubation procedures, and contamination [68]. Improved alternatives would be of enormous value, given the critical nature of the hydrolysis step and the importance

of amino acid analysis. However, the stability of the peptide bond and the wide range of functionalities of the amino acid residues make it unlikely that a convenient, less destructive chemical alternative to acid hydrolysis will be developed.

C. Detection of Underivatized Amino Acids

Hancock and Harding [86] discussed the direct detection of amino acids, pointing out that the detection limit for direct spectroscopic monitoring at 190–210 nm is 10 ng in favorable cases, but is typically 100 ng or more. This is generally unacceptable, and when coupled with the difficulties caused by the numerous possible interferences at these lower wavelengths, results in few, if any, laboratories relying on direct detection. Direct fluorometric detection is even more restricted, for only phenylalanine, tyrosine, and tryptophan fluorescence under common conditions. Indirect spectroscopic detection has been applied [87,88], but has attracted little attention.

Luo et al. [89] demonstrated electrochemical detection of underivatized amino acids. A copper electrode was used and, although both neutral and alkaline conditions were examined, alkaline (0.15-M NaOH) conditions gave superior results. The detection limits were in the 1- to 50-pmol range, comparable with those obtained by Johnson and LaCourse [90] with pulsed amperometric detection at a gold electrode, all 20 common amino acids were detectable. The chromatogram presented is hardly inspiring; the authors [89] admit "the separation conditions here were not completely optimized for amino acids." However, their primary focus in this publication was the electrochemical behavior of amino acids at this electrode surface. Coupling this detection system to an efficient chromatographic system and evaluating the performance has not yet been done.

D. Postcolumn Reaction Detection Methods

Postcolumn alternatives to ninhydrin include *o*-phthalaldehyde (OPA) and fluorescamine [91]. Lewis [92] has described the use of OPA and fluorescamine, including many practical considerations. Both reagents provide fluorescent products when reacted with primary amines and thus cannot directly quantitate proline. A ring-opening reaction with *n*-chlorosuccinimide can provide proline detection for fluorescamine, but not OPA, which reacts with the reagent. OPA also requires the presence of a mercaptan to develop the fluorescent product.

Judging from the number of publications, new development in postcolumn reaction-based detection is less favored than in precolumn derivatization techniques. A possible explanation for this is apparent by examining one such report: Saurina and Hernãndez-Cassou [93] used 1,2-naphthoquinone-4-sulfonate as a postcolumn derivatization reagent for detection of amino acids following ion-pairing liquid chromatography. The product was detected by absorbance at 305 nm. The response was linear up to approximately 40 nmol, but the detection limits were rather high (90 pmol for lysine). The ion-pairing separation required 90 min and an additional 15 min to stabilize the baseline for a subsequent injection.

With modern autosamplers, the automated amino acid analysis performed in many core facilities could use either the pre- or postcolumn approach, provided the results were reliable and sufficiently rapid and sensitive. Although the work just cited [93] is satisfactory, the current postcolumn technology is quite reliable, and a new method needs to be significantly better to encourage current users to switch. Postcolumn derivatization technology has proved reliable and is used in many laboratories. Postcolumn methods involving absorbance and fluorescence have been extensively explored. Thus, precolumn methods are receiving more attention. However, it may still be attractive to explore new postcolumn derivatization chemistries, perhaps using alternative detectors.

Along these lines, Dou et al. [94–97] have used photochemical postcolumn derivatization coupled with electrochemical detection (HPLC-hv-EC) for the determination of a variety of amino acids. Low picomoles of Tyr, Phe, Trp, Met, and Cys were detected using a reaction

system consisting of a Teflon-knitted coli irradiated by a low-pressure mercury lamp. Selective detection of di- through hexapeptides containing these residues was also demonstrated, suggesting the possible usefulness in peptide mapping.

In something of a hybrid system, Lee and Nieman [98] used postcolumn reaction chemiluminescent detection (CLD) of dansylated amino acids using tris(2,2′-bipyridyl)ruthenium(II) [Ru(bpy)] as the derivatization reagent. Their detection limits (2 pmol for Dns-Glu) were superior to a similar detection system employed for underivatized amino acids. Unfortunately, it was ten times higher than that reported using fluorescence and 200-fold higher than CLD using bis(2,4,6-trichlorophenyl)oxalate [99]. The authors [98] point out that the Ru(bpy) reagent is more stable than the oxalate reagent, is more compatible with RPLC solvent systems, and may be usable as an immobilized regenerable reagent. They also state, "Furthermore it is likely that significantly improved Ru(bpy) detection could be achieved with a dansyl-like derivation reagent designed specifically for Ru(bpy) CL."

These reports indicate that continued exploration of postcolumn detection methods has the potential for yielding a major advance in amino acid analysis. Alternatives to fluorescence and absorbance detection may offer enhanced sensitivity and selectivity.

E. Precolumn Derivatization Techniques

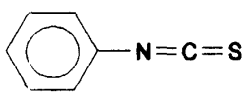
With the advent of sophisticated autosampling and robotic technologies, precolumn derivatization techniques have gained increased popularity. Although many laboratories still use the classic ion-exchange separation and ninhydrin-based detection, precolumn derivatization techniques are used in most publications describing newer and more sensitive alternatives. A wide variety of reagents have been used, and the development of new derivatization reagents has been a fruitful area for chemists.

In spite of this effort, a perfect derivatization chemistry does not exist. The perfect agent would (1) react only with the species of interest; (2) rapidly form a single, stable compound with that species; (3) provide a highly detectable product with that species; (4) do all these in a wide range of conditions, with insensitivity to contaminants; (5) the excess reagent would not be a detectable material; (6) be completely safe to handle and generate nontoxic derivatives; and (7) be free or at least inexpensive. These last serve to remind us that "perfect" is akin to Plato's "ideal universe"—our real world contains imperfections that limit the degree of perfection obtainable. And although our "imperfect" methods have become quite good, implementing any published, complex procedure as a routine laboratory method is a frustrating task. Workers facing this will find the discussion of Krok and Seaver [100] concerning the practicalities of implementing one such "quite good" method worthwhile.

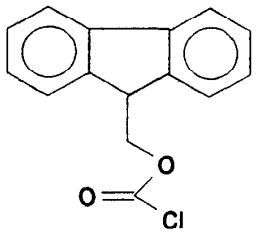
Currently, the most popular precolumn derivatization techniques are the phenyl isothiocyanate (PITC; Fig. 5, compound **1**) method, the 9-fluorenylmethyl chloroformate (FMOC; compound **2**) method, the 6-aminoquinolyl-*N*-hydroxysuccinimidyl carbamate (AQC; compound **3**) method, the 1-dimethylaminonapthalene-5-sulfonyl (dansyl) chloride (compound **4**) method, the 4-dimethylaminoazobenzene-4′-sulfonyl (dabsyl) chloride (compound **5**) method, and the *o*-phthaldialdehyde (OPA; compound **6**) method. These methods are described in the following sections.

1. PITC Derivatization

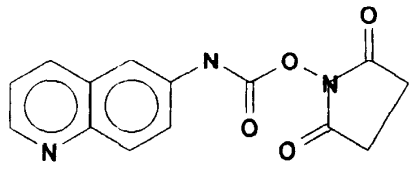
Widely used as a precolumn derivatization reagent, PITC yields a phenylthiocarbamate (PTC). The method was originally used for the analysis of amino acids liberated by carboxypeptidase Y digestion [101]. It was adapted to the determination of amino acids in hydrolysates by Bidlingmeyer et al. [102] and commercialized as the Pico-Tag system (Waters Associates, Milford, MA). The amino acid sample is dried and 10–20 μL of ethanol–water–triethylamine (TEA) (2:2:1 by volume) is added. The drying step is repeated, then 20 μL of a freshly (not more than 1-day old) mixture of ethanol–TEA–water–PITC (7:1:1:1 by volume) is added to the dried amino acid sample. The mixture is reacted for 20 min at room temperature; followed



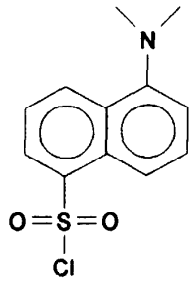
(1)



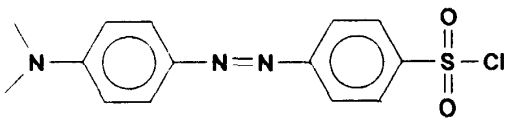
(2)



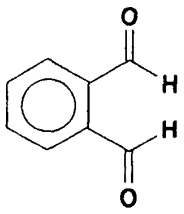
(3)



(4)



(5)



(6)

Figure 5 Structures of commonly used, precolumn derivatization reagents for amino acid analysis: (**1**) phenylisothiocyante; (**2**) 9-fluorenylmethyl chloroformate; (**3**) 6-aminoquinolyl-*N*-hydroxysuccinimidyl carbamate; (**4**) 1-dimethylaminonaphthalene-5-sulfonyl chloride; (**5**) 4-dimethylaminoazobenzene-4′-sulfonyl chloride; (**6**) *o*-phthaldialdehyde.

by a third drying. The dried samples can be stored frozen "for several weeks" with no significant degradation. The following chromatographic description is based on the publication cited, which is one of the early reports. The review by Molnăr-Perl [69] provides 25 alternative separation protocols. Bidlingmeyer et al. [102] performed the analysis using application-specified 150 × 3.9-mm Pico-Tag columns, although many workers have used octadecylsiyl-modified silica (i.e., C_{18}) columns from a variety of manufacturers. A gradient elution was used, with the weak eluent (A) being 0.14-M sodium acetate containing 0.5 mL L^{-1} TEA adjusted to pH 6.35 with glacial acetic acid, and the strong eluent (B) was 60% ACN in water. The program was a convex curve (number 5 on the Waters M720 controller) from 10 to 51% B in 10 min, followed by a washing step at 100% B before returning to initial conditions (10% B). Linear gradients and other solvent systems have been used by other workers with

other equipment; the 12-min separation in the original report is quite impressive, however (Fig. 6). The detection limit obtained with 254-nm absorbance detection is approximately 1 pmol. More recent descriptions of the separation use a somewhat more complex mobile-phase system [103] The PTC derivatives are unstable and convert to phenylthiohydantoin (PTH) analogues. Molnãr-Perl states that the maximum storage time at 4°C is 7 h [69]. The sensitivity of the derivatization step to salts, the need to remove excess PITC by vacuum drying, and difficulties with the quantitation of cysteine [104] are also drawbacks to this method.

Palladino et al. [105] described the use of PITC precolumn derivatization for the determination of amino acid composition of glycoproteins. The low recovery of amino acids during the liquid-phase hydrolysis of glycoproteins is well documented [106]. In this work [105], the amino acid recoveries from hydrolysates of ovalbumin (OA)—approximately 4% by weight carbohydrate—and soluble intercellular adhesion molecule 1 (IAM)—approximately 30% by weight carbohydrate—were compared with that from a nonglycosylated model protein, BSA. A second control was hydrolysates of samples of BSA spiked with approximately 10% by weight of each of mannose, *N*-acetylglucosamine, and galactosamine. Vapor-phase hydrolysis of different levels (all between 30 and 185 μg) of each protein was performed at 150°C for 0.5, 0.75, 1.0, 1.5, and 2.0 h in a series of separate experiments. Quantitation was by PITC precolumn derivatization, followed by RPLC, essentially as described earlier. The results were discussed in the context of compositional agreement CA, defined by

$$CA = 100\% \times [N_p - (\Sigma|n_e - n_p|)]N_p$$

where N_p is the predicted (known) total number of moles of all amino acids in one mole of polypeptide; n_e is the experimentally determined number of moles of a specific amino acid in 1 mol of polypeptide; n_p is the predicted (known) number of moles of that specific amino acid in 1 mol of polypeptide; and the summation is performed across all amino acids. This is equivalent to the percentage correct composition [107]. Compositional agreement values for 14 samples of BSA hydrolysates gave an average agreement of 91% and ranged from 88 to 95%. OA gave compositional agreement values ranging from 87 to 89% and averaging

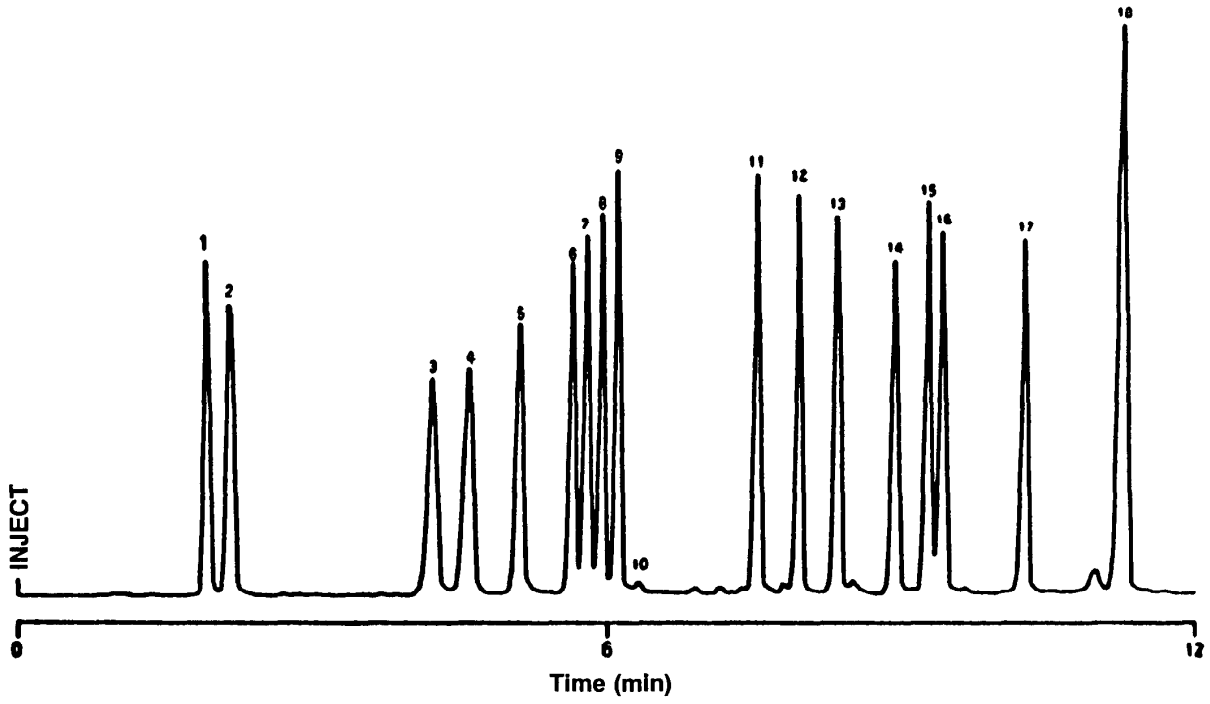


Figure 6 Separation of phenylthiocarbamyl-derivatized amino acids. (From Ref. 102.)

88%. The carbohydrate-spiked BSA gave a compositional agreement ranging from 88 to 95% and averaging 92%. IAM gave an average compositional agreement of 92%. Compositional agreement decreased at increased (1.5- and 2-h) hydrolysis times. The authors concluded that there is no significant loss of amino acids owing to the presence of carbohydrate in this system. This was interpreted as being due to immobilization of the reactants (the amino acids and carbohydrates) on the surface of the hydrolysis tubes in the vapor-phase system. Although demonstrated for only PITC-based derivatization, this same conclusion is likely to be true for any of the sensitive, precolumn derivatization methods, provided vapor-phase hydrolysis is used.

Other isothiocyanate-based derivatization reagents have been used, but none have proved entirely satisfactory [e.g., 108,109].

2. FMOC Derivatization

The original descriptions of derivatization with FMOC involved extraction of the excess reagent with pentane to prevent interference [110–112]. This can be avoided by adding an excess of 1-aminoadamantane to react with the excess derivatization reagent, but that complicates the chromatography [113,114]. Another approach is described by Haynes et al. [115] in which alkaline hydroxylamine is used to destroy the excess FMOC-Cl. The derivatization solution is 4.16 mg mL^{-1} FMOC-Cl in ACN; the alkaline cleavage reagent consists of a mixture of 680 μL of 850 mM sodium hydroxide, 300 μL of 500 mM hydroxylamine hydrochloride, and 20 μL of 2-(methylthio)ethanol; the quenching reagent was ACN–water–acetic acid (20:3:2 by volume). The dried hydrolysate sample was dissolved in 50 μL of 200 mM borate buffer, pH 8.5. To this was added 50 μL of the derivatization reagent and the tube agitated. After 90 s, 30 μL of the cleavage reagent was added; after an additional 3.5 min, 50 μL of quenching reagent was added, and the solution was used directly for analysis. Several different columns were tested, with a 150 × 4.6-mm, 3-μm–Spherisorb ODS-2, and a 150 × 4.6-mm–Goldpak, 3-μm–Hypersil ODS-2, providing the best results. Guard columns were used. The column was maintained at 43°C and a flow rate of 1 mL min^{-1}. The best mobile phase system used as the weak eluent (A) 50 mM sodium acetate, 7 mM TEA, pH 6.5, 10% ACN, and as the strong eluent (B) ACN–water, 90:10 by volume. The gradient profile was: 0–1.5 min, 12% B; 1.5–2.0 min, 12–18% B; 2.0–9.0 min, 18–25% B; 9.5–12.5 min, 25% B; 12.5–13.0 min, 25–30% B; 13.0–16.0 min, 30% B; 16.0–17.0 min, 30–40% B; 17.0–20.0 min, 40% B; 20.0–22.0 min, 40–50% B; 22.0–23.0 min, 50% B; 23.0–24.0 min, 50–99% B. Detection was by monitoring emission at 313 nm following excitation at 263 nm. Einarsson et al. [112] reported detection limits in the range of 25 fmol. The FMOC-OH and FMOC-NOH elute late in the described system and do not interfere. The alkaline cleavage reagent cleaves any disubstituted histamine and tyrosine to produce primarily the monosubstituted derivative; the N-FMOC derivative is the primary form for tyrosine. This production of multiple derivatives is a common criticism of FMOC methods [104]. The 2-(methylthio)ethanol acts as an antioxidant to minimize the formation of methionine sulfone and sulfoxide. Dithiothreitol and 2-mercaptoethanol are unsuitable for this purpose because they react with FMOC-Cl.

3. AQC Derivatization

Cohen and Michaud [116] described the synthesis and use of AQC as a precolumn derivatization reagent. This reagent has been commercialized by Millipore as Accu-Tag. The derivatization is performed by adding 1 vol of 3.0 mg mL^{-1} AQC in ACN to 4 vol of sample dissolved in 200 mM borate buffer, pH 8.8. The reaction is carried out at 50°C for 10 min. This is necessary to speed the formation of a monoderivatized product of tyrosine, which otherwise forms an unstable, presumably diderivatized form involving an *O*-adduct. This unstable form converts to the more stable form with a half-life of approximately 1 h at room temperature; the mildly elevated temperature speeds the conversion. The chromatography was performed on a 150 × 3.9-mm–Waters Nova-Pak 4-μm–C_{18} column thermostated at 37°C

and operated at 1 mL min^{-1}. The weak eluent (A) was 140 mM sodium acetate, 17 mM TEA, pH 5.05; the strong eluent (B) was ACN–water, 60:40 by volume. The gradient program was 0 min, 0% B; 0.5 min, 2% B; 15 min, 7% B; 19 min, 13% B; 33 min, 32% B; followed by a 5-min wash with 100% B and a 10-min reequilibration interval. Detection was by monitoring emission at 395 nm following excitation at 245 nm. The emission maxima of the derivatives is somewhat blue-shifted from that of the reagent; this in part, allows the use of a large excess of the reagent without severe interference. Detection limits were from 40 to 320 fmol, except for cysteine, for which the detection limit was 800 fmol. The authors interpret this as being due to internal quenching of the fluorescence by the diderivatized cysteine. Analysis of 2.5- to 200-μM standards yielded excellent linearity. The derivatization reaction has a broad pH optimum and was insensitive to the presence of disodium hydrogen phosphate, sodium citrate, sodium acetate, sodium dodecyl sulfate, and sodium chloride. Phosphate did generate an additional peak, but it did not interfere with the quantitation. Tris at low levels (4 mM) did not prevent derivatization, but the peak of derivatized Tris interfered with the quantitation of proline. The derivatives were stable for at least 1 week at room temperature.

In addition to hydrolysates, AQC has been used for some physiological determinations (intravenous solutions) and glycoproteins [117]. The modified amino acids and other potential interferences did not affect the method. Liu [118] showed that detection by UV absorbance at 248 nm provided detection limits in the 150- to 300-fmol range. However, there are more potential interferences in this method because it does not possess the additional selectivity afforded by fluorescence techniques.

4. Dansyl Derivatization

The method for derivatization of amino acids with dansyl chloride is well established [119]. The amino acid mixture in 40 mM of lithium carbonate, pH 9.5, is mixed with dansyl chloride. The reaction proceeds at room temperature for 35 min, followed by quenching with methyl- or ethylamine. A variety of elution protocols have been used. The product can be detected by absorbance at 254 nm or by fluorescence at 475 nm with excitation at 385 nm. Detection limits in the 100-fmol range are possible; higher sensitivities can be achieved with a postcolumn reaction detection system [99], although that negates the advantages of precolumn derivatization. Wilkinson suggests a sensitivity of 100 pmol is more practical [120]. Under the conditions of Tapuhi et al. [119], derivatization of aspartic acid is problematic. The derivatives are not photochemically stable and must be protected from light under laboratory conditions. The dansyl derivatives have been used extensively for chiral separations [e.g., 121], discussed elsewhere in this book. However, multiple derivatives of histidine are possible, rendering quantitation questionable [104].

5. Dabsyl Derivatization

Similar to dansyl derivatization, dabsyl amino acids are also formed by reacting an acid chloride with the free amino acids [122]. The amino acid mixture in pH 8.3 sodium bicarbonate buffer is mixed with dabsyl chloride in ACN. The samples are heated for 12–14 min at 70°C and diluted in 1:1 ethanol–water before analysis. Dabsyl amino acids are photochemically stable. Again, a variety of separations protocols have been employed. Absorbance at 436 nm is employed; the low-energy absorbance maxima affords this derivative a high degree of selectivity against many possible interferences. Sensitivities are in the 10-pmol range. However, the derivatization is not quantitative for all amino acids [122], and multiple derivatives have been reported [123].

Dabsylation was used for the amino acid analysis of synthetic phosphopeptides and glycopeptides by Gorbics et al. [124]. Earlier work [125] had shown dabsylation to be the most appropriate method for determining the acid-labile phosphoamino acid species. Vapor-phase hydrolysis was performed on two phosphoserine-containing pentapeptides, two *N*-acetylglucosamine-containing peptides, and appropriate model amino acids. For the separations shown, the phosphorylated dabsyl-amino acids and dabsyl-saccharides would interfere

with dabsyl-amino acid analysis. The authors [124] conclude that hydrolysis times of 1 h at 110°C for glycopeptides and of 1.5 h at 110°C for phosphopeptides are most appropriate. Yields for glucosamine and phosphoserine are approximately 23 and 10%, respectively, at these times.

This work clearly shows the need for additional development of methods for determining modified amino acids. The analytical methodology for the actual determination of the amino acids seems adequate; it is recovering the modified residue intact that is currently the limiting step. Again, an improvement in the hydrolysis is needed. As our understanding of the importance of posttranslational modification increases, so will the use of modified residues in biotechnological products and the need for appropriate analytical procedures.

6. OPA Derivatization

Postcolumn derivatization with OPA was developed in 1971 [126]. OPA reacts with primary amines in the presence of thiols (mercaptans) to yield a fluorescent product. Thus, proline is not detected as such and amine buffers or ammonia cause high background responses in postcolumn detection systems. Precolumn derivatization with OPA avoids the latter problem; the failure to derivatize proline remains, however. A typical procedure follows [127]. The derivatization reagent consists of 270 mg of OPA dissolved in 5 mL of 99.5% ethanol, 200 μL of 2-mercaptoethanol, and sufficient 0.4-M boric acid, pH 9.5, to bring the total volume to 50 mL. The reagent is "aged" 24 h before use, and an additional 20 μL of 2-mercaptoethanol were added every 3–4 days. Derivatization is performed by mixing 20 μL of the sample with 100 μL of the reagent. After precisely 2 min, 5–10 μL of sample is injected. The derivatives are unstable; accurate quantitation requires high precision in the time between forming the derivative and performing the analysis. A variety of chromatographic protocols have been employed; detection is by monitoring the emission at 420 nm following excitation at 330 or 230 nm. Detection limits are near 100 fmol. Electrochemical detection lowers this somewhat [128]. Although modern autosamplers make the stability of the derivative less of an issue, the inability to quantitate proline is a serious disadvantage.

Attempting to overcome the stability problem, other dialdehyde reagents have been explored, including naphthalene-2,3-dicarboxaldehyde (NDA) [129,130]. The NDA derivatives are more stable than the OPA analogues. Detection limits were in the 100-fmol range, using excitation at 246 nm with a conventional deuterium source [130] and in the 500-amol (10^{-18}–mol) range with laser-induced fluorescence [129]. Oates and Jorgenson [131] used precolumn derivatization with NDA, open tubular columns, and electrochemical detection to determine amino acids in neurons, with detection limits in the 100-amol range. They attribute the improved mass detection limit to the use of capillary columns. However, this reagent still fails to derivatize proline.

Use of a chiral thiol in the OPA procedure results in the formation of diastereomeric isoindol derivatives following treatment of samples containing both D- and L-amino acids. This has been explored by Buck and Krummen [132] and Brückner et al. [133,134]. Although the separation of chiral materials are discussed in Chapter 21, the growing recognition of their importance justifies specific mention of the brief review by Brückner et al. [135]. These workers show the use of *N*-isobutyryl-L-cysteine (IBLC) and *N*-isobutyryl-D-cysteine (IBDC) as a chiral thiol for precolumn OPA derivatization of amino acids. Fluorescence detection at 445 nm with 230-nm excitation gave detection limits of 1–2 pmol and linearity from 25 to 1000 pmol. The separation was performed using a 250 × 4-mm, 5-μm–Shandon Scientific Hypersil ODS column. A 20 × 2.1-mm guard column packed with the same material was necessary to ensure a reasonable column life; the guard column was replaced approximately every 70 injections. The weak eluent was 23 mM sodium acetate adjusted to pH 5.95 with 10% acetic acid. The strong eluent was 474 g of MeOH and 39 g ACN (roughly 600 and 50 mL, respectively). A linear gradient of from 0 to 53.5% strong eluent over 75 min was used, followed by a 10-min reequilibration time. OPA–IBLC derivatization permitted the analysis of a 41-component standard containing the 17 optically active common amino acids, glycine,

DL-cysteic acid, L-*homo*-arginine, DL-isovaline, and α-aminoisobutyric acid. Chromatograms of derivatized samples from bacteria, fungi, higher plants, invertebrates, mammals, and a meteorite were presented. Various practical considerations are also discussed, many of which are of interest to anyone involved in amino acid analysis.

F. Commentary

This variety of methods for amino acid analysis exists because no method is perfect. Certain various residues are problematic for each procedure; sensitivity to or interference from common reagents exists; several procedures require additional steps to prevent interference from excess derivatization reagent. The AQC method appears to combine the most favorable properties with the fewest problems, but that may partly be due to the limited use this method has yet experienced.

Furthermore, raw sensitivity alone does not solve the problem. As stated by Cohen and Michaud [116]: "Although the femtomole level detection limits would allow the composition of nanogram amounts of protein to be determined, this has as yet not proven to be practical due to background levels of amino acids in the 0.1- to 1.0-pmol range in hydrolyzed blank control samples even in the best of circumstances." Isolation of proteins by electrophoretic transfer onto nitrocellulose, nylon, PDVF, or other membranes is a common procedure; how effectively the aforedescribed amino acid analysis procedures handle this type of sample is, in most cases, unproved. Given the ubiquitous nature of amino acid contamination, one can envision obtaining accurate results from only the most highly purified materials; imagine the number of such reagents necessary to carry out an electroblot and subsequent amino acid analysis. Moreover, the problem of preserving modified amino acids, notably phosphorylated amino acids, remains unsolved. These are issues of real interest to biotechnologists.

V. PROTEIN SEQUENCING

Here, protein sequencing is considered to be performed by repetitive applications of the Edmund degradation [13]. Alternative methods, such as COOH-terminal sequencing, will not be addressed, and although MS sequence analysis is an area of very active research, it is beyond the scope of this chapter.

The reactions used in protein sequencing are shown in Fig. 7. PITC (see Fig. 7, compound **1**) reacts with the free NH_2-terminus to generate a phenylthiocarbamyl (PTC) peptide (see Fig. 7, **2**). This is reacted under anhydrous conditions to yield an anilinothiazolinone (AZT) amino acid (see Fig. 7, **3**). The AZT is hydrolyzed to yield a PTC amino acid intermediate (see Fig. 7, **4**), which cyclizes to a phenylthiohydantoin (PTH) amino acid (see Fig. 7, **5**). In sequencing terminology, these steps are coupling (see Fig. 7, reaction a), cleavage (b), and conversion (c and d), respectively. The identity of each residue is established by retention in standardized RPLC chromatographic conditions, although other techniques have been and are used.

The analysis of PTH-amino acids was one of the first major applications of HPLC in biotechnology [136,137]. The speed and sensitivity of the method quickly rendered HPLC the dominant technique. Detection limits of 5 pmol may be obtained by UV detection at 254 nm. Discussions of PTH-amino acid analysis including extensive listings of chromatographic conditions are available [e.g., 138,139]. The compilation of Wittmann-Liebold et al. [140] also has chapters on PTH-amino acid analysis as well as many other aspects of protein sequencing, as does the text by Findlay and Gelsow [141].

Just as for amino acid analysis, the fact that many proteins are not simply linear polymers of the 20 common α-amino acids gives rise to many problems in protein sequencing. The variety of modified amino acids can result in seeming "blank" cycles, because the standard chromatographic protocols are typically developed with primarily the common PTH-amino acids in mind. Glycosylated, phosphorylated, or other hydrophilically modified residues may

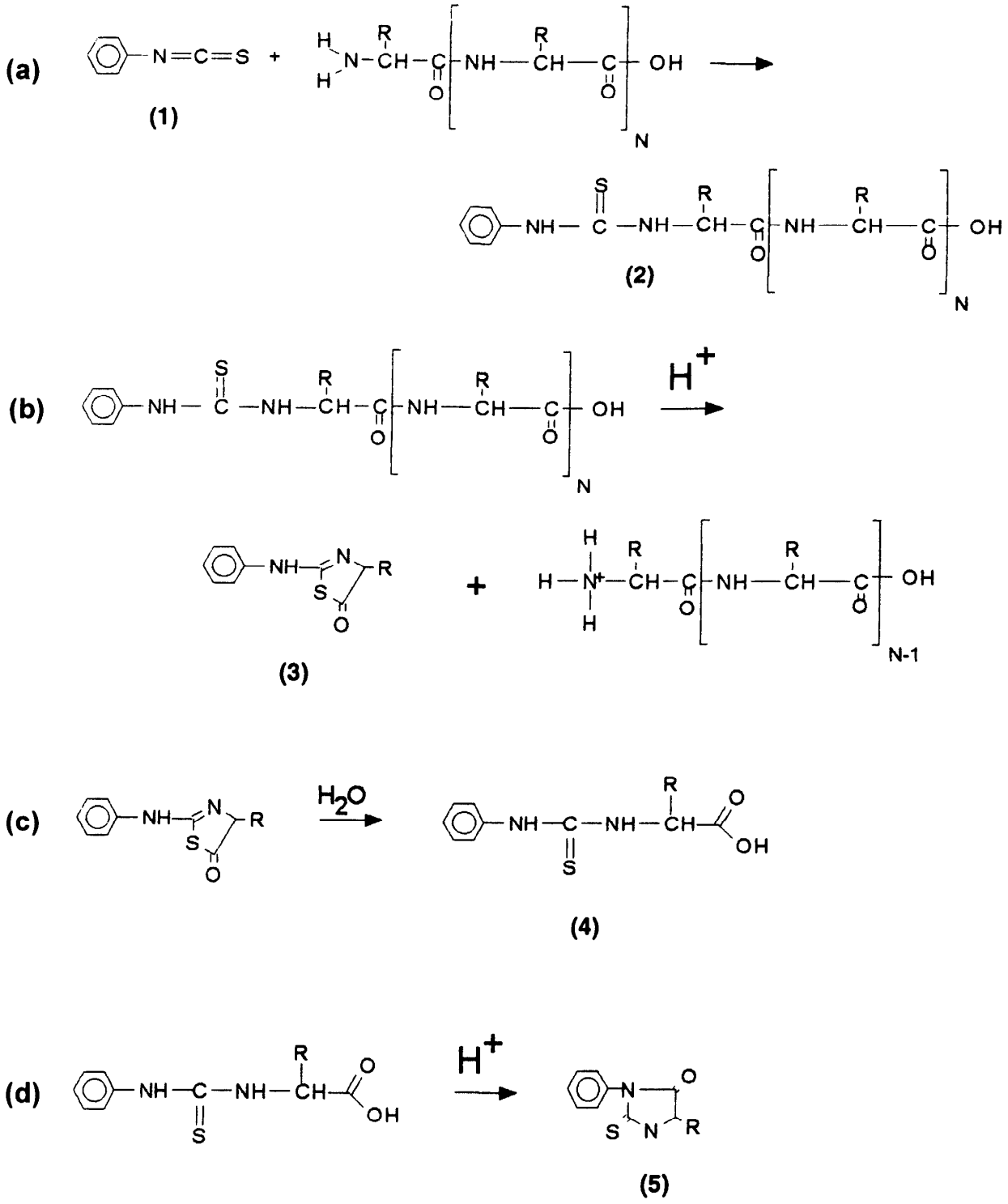


Figure 7 Reactions occurring during protein sequencing by the Edmund method: (a) coupling; (b) cleavage; (c,d) conversion. Compounds: **(1)** phenylisothiocyanate; **(2)** phenylthiocarbamyl-peptide; **(3)** anilinothiazolinone; **(4)** phenylthiocarbamyl amino acids; **(5)** phenylthiohydantoin amino acid derivative.

be missed or confused with the "system" peaks in common systems. Strydom [142] has addressed this difficulty and developed a separation protocol compatible with a 34-min sequencer cycle time that allows additional space for hydrophilically modified PTH–amino acids. The column was a 250 × 4.6-mm–Supelcosil LC-18-DB; a guard column of the same material was used. The weak eluent (A) was 0.33% TEA, 9.5% MeOH, 10.5% ACN (all percentages are v/v). The pH of the A eluent was adjusted to 3.55 with phosphoric acid before the addition of the organic solvents. The strong eluent (B) was MeOH–isopropanol–water (60:20:20). The gradient program was: 0 min, 5% B at 1 mL min^{-1}; 7 min, 5% B; 22 min, 67% B; 23 min, 100% B; 25 min, 100% B at 1 mL min^{-1}; 25.5 min, 100% B at 1.2 mL min^{-1}; 28 min, 100% B at 1.2 mL min^{-1}; 29 min, 5% B at 1.2 mL min^{-1}; 33 min, 5% B at 1.2 mL min^{-1}; 33.5 min, 5% B at 1 mL min^{-1}. Absorbance detection at 269 nm allows 1- to 4-pmol sensitivity. The resultant separation also provides early elution of PTH–histadine and PTH–arginine, improving their detectability. Sequencer by-products are well resolved from the PTH–amino acids. There is space in the chromatogram for various modified PTH–amino acids, including glycosylated aspartic acid, γ-carboxy-glutamic acid and β-OH-aspartic acid. Phosphotyrosine overlaps with arginine and serine. Although the system does not solve all possible problems, it offers several advantages, particularly to the worker involved with glycoproteins.

A second common problem is the existence of NH_2-terminally blocked proteins, which are unamenable to PITC-based sequencing. Acetylation is the most common modification, although other modifications, including pyroglutamylation, formylation, and acylation, are also known. It has been estimated that 80% of eukaryotic soluble proteins are acetylated; to the frustrated researcher, it sometimes seems that estimate is approximately 20% too low. LeGendre et al. [143] present a systematic approach to the problem. Nonetheless, obtaining NH_2-terminal information from a blocked peptide or protein is an area of active research. Enzymatic methods involving acylamino acid-releasing enzyme (AARE) are available, but AARE cannot act on peptides larger than 20 residues nor on electroblotted proteins [144]. AARE has also been reported to have a high degree of substrate specificity [145].

Kawakami and Ohmori [145] reported a method capable of detecting the blocked residue at the 100-pmol range. In their procedure the blocked peptide is completely digested by successive treatments with pronase E, proteinase K, and carboxypeptidase Y. The released amino acids are derivatized at the free COOH-group with 9-anthryldiazomethane. The resultant highly fluorescent compounds are separated by RPLC. The blocked residues have characteristic retention times allowing detection and identification in the complex mixture. They demonstrated the technique for proteins containing *N*-acetylated Ser, Ala, Met, Gly, Tyr, and Pro, as well as *N*-myristoyl Gly. The method destroys the peptide of interest; thus, although it allows identification of the blocked residue, does not allow further sequencing. Additionally, the time required to perform the procedure is rather significant.

Mass spectrometric sequencing of blocked peptides is possible, but it first requires isolation of the peptide containing the blocked terminus. Gorman and Shiell [146] have described a cation-exchange–RPLC technique for isolating COOH- and blocked NH_2-terminal peptides. Quoting the authors, "This strategy exploits the fact that most tryptic peptides derived from the carboxyl-termini or blocked amino-termini of proteins have a single positive charge at acid pH and are barely retained by cation exchangers." This strategy was used earlier by Titani et al. [147] and Kawasaki et al. [148] for selectively isolating blocked NH_2-terminal peptides. The model proteins used by Gorman and Shiell [146] were ovalbumin (OA), the matrix protein (MP) of Newcastle disease virus (NDV), and the nucleocapsid protein (CP) of NDV. The reduced and alkylated protein was digested with trypsin (which cleaves at basic residues). The digest was desalted and chromatographed on a 200 × 4.6-mm–PolyLC PolySulfoethyl Aspartamide column. The weak eluent (A) was 10 mM disodium hydrogen phosphate, adjusted to pH 3.0 with phosphoric acid, and 40% (v/v) ACN. (The ACN concentration was varied for samples from different proteins.) The strong eluent (B) was the same containing an additional 76 mM of sodium sulfate. The gradient was 0 min, 0% B; 50 min, 20% B; 60 min,

100% B; 65 min, 100% B; and 70 min, 0% B; all at 1 mL min^{-1}. Detection was by monitoring UV absorbance at 210 nm. The amount of protein digest loaded was not specified. The cation-exchange (CE) fractions were rechromatographed using a 250 × 4.6-mm–Vydac C_{18} column and a 0.1% TFA–water–ACN gradient. Fractions from this step were subjected to amino acid analysis and sequence determination by MS or chemical means. The first two CE fractions of the OA digest contained 11 RPLC-resolvable fractions, including the acetylated NH_2-terminal peptide and the COOH-terminal peptide. Similarly, the early CE fractions of the MP digest contained NH_2-terminal and COOH-terminal peptides, resolvable by RPLC. The early CE fractions of the CP digest contained the COOH-terminal peptide; the NH_2-terminal peptide eluted in a later CE fraction. This anomaly was due to the failure to cleave at an Arg–Pro bond, resulting in a peptide containing three basic residues. This last result points to the greatest weakness in this approach. Although it does, in favorable cases, enrich the desired fragments into the early CE fractions, it falls whenever the ability to generate singly charged peptides from the COOH- or NH_2-terminal regions is compromised. Moreover, the early CE fractions contained peptides other than those from the COOH- or NH_2-terminal regions. It would be hazardous to assume that one of the peptides so recovered from an unknown protein necessarily corresponded to either termini of that protein. It does provide a relatively rapid method for increasing the likelihood of securing the desired fragments and certainly tryptic digestion followed by chromatographic purification and characterization of the fragments is common in any event. The low-pH CE step provides an additional selectivity, and multidimensional techniques necessarily provide higher peak capacities.

Akiyama et al. [149] proposed a method for selectively isolating NH_2-terminally blocked peptides, which would then be submitted to MS analysis. The protein was first succinylated (which blocks reactive side-chain groups), then desalted and digested with chymotrypsin (which cleaves at hydrophobic residues). Each peptide of the resulting mixture contains a free NH_2-terminus, excepting the peptide from the original, blocked NH_2-terminus. The mixture was reacted with cyanogen bromide-activated Sepharose (100 mg/80 μg protein) which couples to the free NH_2-termini, binding them to the beads. The peptide containing the original, blocked NH_2-terminus was recovered by rinsing the beads with several aliquots of the 0.1-M sodium hydrogen carbonate, pH 8.3, coupling buffer. The recovered peptide was purified and concentrated by RPLC on a 250 × 4.6-mm TSK ODS 80TM column using a 0.1% TFA–water–ACN gradient. As in the preceding method, this method isolates the peptide from the blocked NH_2-terminus; unlike the preceding method, it does not depend on presumed charge differences. It does appear to require somewhat more sample than the preceding method. These workers have successfully applied the technique to 1 nmol of starting protein, recovering 45% of the blocked peptide. The use of RPLC following the selection process also allows purification of multiple blocked peptides, such as would result from partial digestion or the presence of multiple, blocked subunits in the starting protein. However, the preceding approach allows recovery of many peptides from a single digest, whereas this technique allows recovery of only the blocked peptide(s).

Other methods directed at selective detection or concentration of peptides from a digest include the use of immobilized anhydrochymotrypsin by Ohta et al. [150,151] to select for peptides having an aromatic COOH-terminal amino acid, the use of immobilized anhydrotrypsin by Ohta et al. [152] to select for peptides containing a COOH-terminal arginine or lysine, and detection of NH_2-terminally blocked peptides by selective labeling with FMOC [153].

Shao and Chin [154] have described a method for detecting glycopeptides in HPLC peptide maps. The glycoproteins were reduced, *S*-alkylated with vinylpyridine, digested with TPCK-treated trypsin, and fractionated by RPLC on a 250 × 4.6-mm Dynamax wide-pore C_8 column with a water–0.1% TFA–ACN gradient. Fractions were biotinylated with an excess of reagent [sulfosuccinimidyl 6-(biotinamido) hexanoate], then subjected to an enzyme lectin-linked glycopeptide assay. Briefly, the biotinylated peptides were placed in wells of a 96-well plate previously coated with streptavidin. The biotinylated peptides bound to the bound strep-

tavidin. After washing, the peptides were tested with a variety of horseradish peroxidase-labeled lectins, followed by development. Selected lectins bound to the glycopeptides, and the type of oligosaccharide involved could be characterized by which lectins were bound and by enzymatic treatment before testing. The method required less than 1 pmol of peptide.

The advantages to selective concentration or identification of peptide fragments corresponding to "interesting" regions of the protein appear obvious. Knowledge of the NH_2-terminal sequence is enormously useful in the cloning process. Likewise, prior knowledge of glycosylation sites is useful in a sequencing effort. Also note from Fig. 2 that the aromatic residue tryptophan is specified by single codon; phenylalanine and tyrosine are specified by two codons each. Peptides rich in aromatic residues will generally be coded for by fewer possible codons than, for example, a peptide containing Ser, Ala, Leu, or Val residues (i.e., the possible DNAs are less degenerant for such peptides). Consequently, the oligonucleotide probe used for cloning can be of lower degeneracy, and the concentration of the effective probe is higher. The wash stringency can also be higher. The net result is a more selective method for isolating the gene.

VI. PEPTIDES

Peptide purification is extensively discussed in many of the recent texts [5–10] and reviews [11]. Here, the discussion is limited to general, mostly chromatographic considerations.

Peptides are either of direct interest (i.e., many hormones, growth factors, and such, are considered peptides) or are generated as a step in protein characterization. If a peptide is of direct interest, then the maintenance of biological activity is a relevant issue. The classification of a biologically active polypeptide as a peptide or a protein is nearly arbitrary; consequently, such so-called peptides are discussed with proteins in the following section.

However, if the peptides are fragments of a larger protein, generated as part of a sequencing effort, the issue of biological activity is most probably irrelevant. Here, the central concerns are to purify each fragment to homogeneity while minimizing any inadvertent structural changes. Because the product peptides are to be sequenced, this is a preparative purification, although the scale is far smaller than the more common uses of that description. Likewise, tryptic mapping—the generation of peptide fragments by enzymatic or other means to create an electrophoretic or chromatographic profile characteristic of a particular protein (*fingerprinting*)—does not require biological activity. In this situation, reproducibility is the most important consideration.

Matsudaira [12] has published an excellent monograph on the isolation of peptides for sequence analysis, complete with representative protocols for enzymatic and chemical digestion as well as electrophoretic and chromatographic purification. Likewise, much of the information presented in Section V concerns isolation of peptides for sequencing from digests. RPLC is the most common mode of operation, either solely [e.g., 155,156] or as part of a multidimensional approach [e.g., 157]. Alkylsilyl-modified, 5- to 10-μm, wide-pore silica is the most common packing; the alkyl group and the column size preferred vary. Although phenylsilyl-modified silica provides a somewhat different selectivity than, for example, butylsilyl-modified silica, the difference is much less than that provided by an alternative chromatographic mode (e.g., ion-exchange). The most common mobile-phase system is a 0.1% TFA–water–ACN gradient; the gradient rates and ranges vary widely. Propanol and isopropanol are also common, particularly for peptides generated from more hydrophobic proteins. Hydrochloric, phosphoric, acetic, and formic acids have been used in place of TFA. The reviews by Frenz et al. [158] and by Schoneich et al. [11] contain much additional information on columns, mobile-phase systems, an instrumentation used for peptide separations.

Although many groups have reported that short columns yield higher performance, this is a result of the fundamental nature of gradient operation. The critical parameter is the ratio of the gradient volume (i.e., the volume during which the change in composition occurs) to

the column void volume. Snyder et al. have shown that peptides undergoing gradient RPLC generally follow the linear strength solvent model of gradient elution [49, and references therein], and that the observed effects of column size are consistent with the predictions of that model. However, extremely short or hydrophilic peptides may not be sufficiently retained to exhibit the behavior typical of large molecules.

In practice, the time expended in separating the peptides is small compared with the total time required to isolate and characterize the protein. Although methods exist for determining the optimum gradient [e.g., 49], most workers simply apply a long, slow (e.g., 0–50% ACN in 60- to 120-min) gradient and collect the resultant peaks. Many groups routinely reserve separate columns for each project; again, the cost of a column is small compared with the total project cost. In peptide mapping (fingerprinting), optimizations, such as those described by Snyder [49], may be more practical.

VII. PROTEINS

Two approaches are generally recognizable for HPLC-based protein purification. Some groups develop new supports and attempt to demonstrate their general applicability, whereas other groups are primarily interested in the isolation of a specific protein. A decade ago, very few groups successfully evaded that categorization. Now, however, the number of these is increasing as biochemists become better acquainted with the power of HPLC and as chromatographers develop a better understanding of the important problems in biotechnology.

A second generalization concerning protein purification is that biochemists are more likely than chromatographers to exploit biospecific interactions in developing a separations protocol. This generalization is also becoming less true as the usefulness of dye–ligand, histidine–ligand, lectin, immobilized metal ion, and other, less specific forms of affinity chromatography have become available. One chromatographic text [9], directed at biochemists, contains 7 of 20 chapters describing such forms and another 7 describe more specific affinity chromatographic modes. Only 4 chapters are devoted to other chromatographic modes—SEC, chromatofocusing, ion-exchange, and displacement. Notable by their absence are RPLC and HIC, likely because of extensive discussions elsewhere and because of the relatively universal method of application of these techniques.

The origins of these generalizations are primarily that, although every protein is different, the number of proteins in an organism is enormous, and the differences may be quite subtle. Consequently, generally applicable techniques, such as SEC, RPLC, and HIC can purify some proteins, but not others, and certainly not all. The discussion here is limited to some general issues and some selected examples because of the uniqueness of each purification procedure and because HPLC-based protein purification is extensively reviewed elsewhere [5–10].

A. General Interest

A question of some interest in protein isolation is the maintenance of biological activity. Such issues as column-packing material, mobile-phase composition, materials used for the chromatographic equipment, temperature, and so on, have been offered as possible sources of inactivity or denaturation. Anecdotal "information" abounds. Herrold et al. [159] examined the issue of the recovery of biologically active enzymes using three different HPLC systems (two were stainless steel, one was titanium) and 12 different columns. The modes used, enzymes and columns tested, and results are summarized in Table 2. The data in Table 2 (all obtained using a titanium system) show that the mass and activity recovery vary more according to the specific enzyme than to the mode of separation. Statistical analysis of the results shows the activity recoveries to be slightly higher on the steel columns, although this too varied significantly with the actual enzyme tested (Fig. 8; 80% confidence). Similarly, a comparison of the mass losses and activities recovered among the titanium HPLC system and the two stainless steel systems showed no significant effect of construction materials (see Fig.

Table 2 Mass Losses and Activity Recoveries of Enzymes Subjected to HPLC

Chromatographic mode[a]	Column	Tested enzyme[a]	Mass loss (μg)	Activity recovery (%)
Anion-exchange	TSK 5PW DEAE steel	CAT	< 0.1	94
		hLDH	< 0.1	99
	PL-1000-SAX glass	CAT	< 0.2	94
		hLDH	< 0.1	96
	Mono Q glass	CAT	< 0.1	92
		hLDH	< 0.1	95
	Merck TMAE glass	CAT	< 0.1	97
		hLDH	< 0.1	100
Cation-exchange	TSK 5PW SP steel	CHY	< 0.1	88
		mLDH	< 0.2	94
	PL-1000-SCX glass	CHY	< 0.1	92
		mLDH	< 0.2	95
	Mono S glass	CHY	< 0.1	93
		mLDH	1.5	70
	Merck SO_3 glass	CHY	< 0.5	97
		mLDH	< 0.1	87
Size-exclusion	TSK 2000 SWXL steel	ADH	< 0.1	86
		mLDH	< 0.1	96
	Superose 12 glass	ADH	< 0.1	86
		mLDH	< 0.1	98
HIC	TSK Phenyl TPW steel	PK	< 0.2	92

[a]ADH, yeast alcohol dehydrogenase; CAT, bovine catalase; CHY, bovine α-chymotrypsin; HIC, hydrophobic interaction chromatography; hLDH, porcine heart lactate dehydrogenase; mLDH, porcine muscle lactate dehydrogenase; PK, rabbit pyruvate kinase.
Source: Ref. 159.

8). The authors conclude that, usually, the deactivation of enzymes by contact with either support or HPLC equipment materials is negligible compared with the deactivation by storage conditions. They state, "It became clear that the stainless steel instruments were as well suited for the separation of active proteins as . . . titanium instruments. Titanium, however, clearly shows superior corrosion resistance against the highly corrosive mobile phases that are commonly used in biochromatography." Again, however, the effect of column material varied according to the specific enzyme involved. Perhaps the most significant conclusion is that poor recoveries for an enzyme may be associated with a particular chromatographic substrate, rather than with a particular chromatographic mode. Thus, it is worthwhile to compare several manufacturers' packings when attempting to maximize recovery.

Peptide mapping by HPLC has been widely used in characterizing a single protein. Similar attempts to map chromatographically complex mixtures of proteins such as exist in a cell, fail because of the very complexity of the sample. *Escherichia coli*, for example, contains in excess of 3000 different proteins. Two-dimensional (2-D) gel electrophoresis provides additional resolution compared with one-dimensional chromatographic approaches, but is limited owing to the multiple step, manual handling necessary. Isobe et al. [160] have described an automated two-dimensional HPLC system for mapping proteins. The system consisted of two low-pressure gradient systems (stages) controlled by a single computer. The effluent of the first, HPAE stage could be applied directly to the second RPLC stage by a four-way valve.

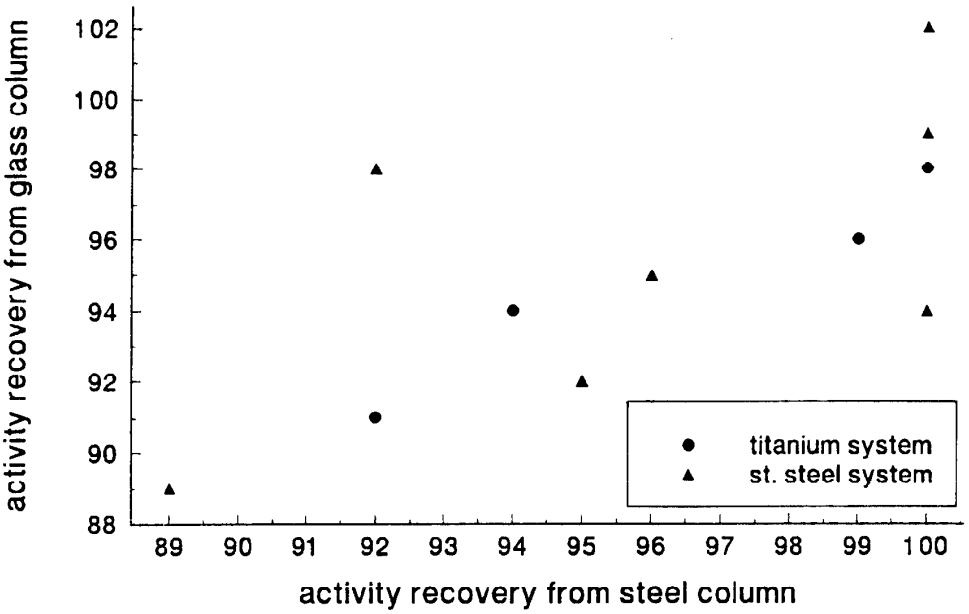


Figure 8 Enzymatic activity recovered following chromatography on a glass column versus that recovered following chromatography on a stainless steel column for bovine catalase, porcine heart lactate dehydrogenase, bacterial glucose-6-phosphate-dehydrogenase, and rabbit pyruvate kinase. The first three enzymes were chromatographed in the anion-exchange mode; pyruvate kinase was chromatographed in the hydrophobic interaction mode. (From Ref. 159.)

The first stage used a 75 × 7.5-mm–TSK DEAE-5PW column operated at 1 mL min^{-1}. The weak eluent (A1) for this stage was 25 mM Tris-HCl, pH 7.5; the strong eluent (B1) was the same, containing 400 mM NaCl. The second stage used a 75 × 4.6-mm–TSK phenyl 5PWRP column also operated at 1 mL min^{-1}. The weak eluent (A2) for the second stage was 20% ACN, 0.1% TFA in water; the strong eluent (B2) was 60% ACN, 0.1% TFA in water. Initially, both systems are equilibrated in their respective A solvents; during this phase, the valve connecting the two columns directs the first-stage effluent to waste, rather than into the second stage. After 40 min of equilibration time, the second-stage pump is stopped, the sample is injected onto the first-stage column, and the valve between the columns directs the effluent onto the second-stage (RPLC) column. After 20 min, the first-stage pump is stopped, the second-stage pump started, and the RPLC column is eluted with a 40-min linear gradient from A2 to B2. The RPLC column is reequilibrated for 15 min with A2 before stopping the second-stage pump and restarting the first-stage pump. At each successive step, the amount of B1 in the first-stage eluent is stepwise increased. The result is a series of RPLC chromatograms, each representing an HPAE fraction of the mixture, (i.e., a 2-D HPLC map of the protein mixture). Figure 9 illustrates such a map for a soluble extract of bovine cerebellum. The number of peaks resolved was a function of the number of HPAE-steps performed. With 4 steps, approximately 75 peaks were resolved, whereas 10 and 20 steps resolved about 200 and 250 peaks, respectively. The times required were approximately 5, 12, and 24 h, respectively. The same sample analyzed by 2-D gel electrophoresis with Coomassie staining yielded about 400 proteins. Although the time required for 2-D HPLC analysis of a single sample compares favorably with 2-D gel electrophoresis, multiple samples can be run in parallel in electrophoresis without a significant increase in equipment costs. Thus, 2-D gel electrophoretic mapping is currently faster. Although the number of resolved peaks was lower for 2-D HPLC, the precision of the technique was judged better. More importantly, the precision of the 2-D HPLC approach is determined by the instrument, rather than by operator skill. Although the application of crude extracts tended to increase the system backpressure, these columns tol-

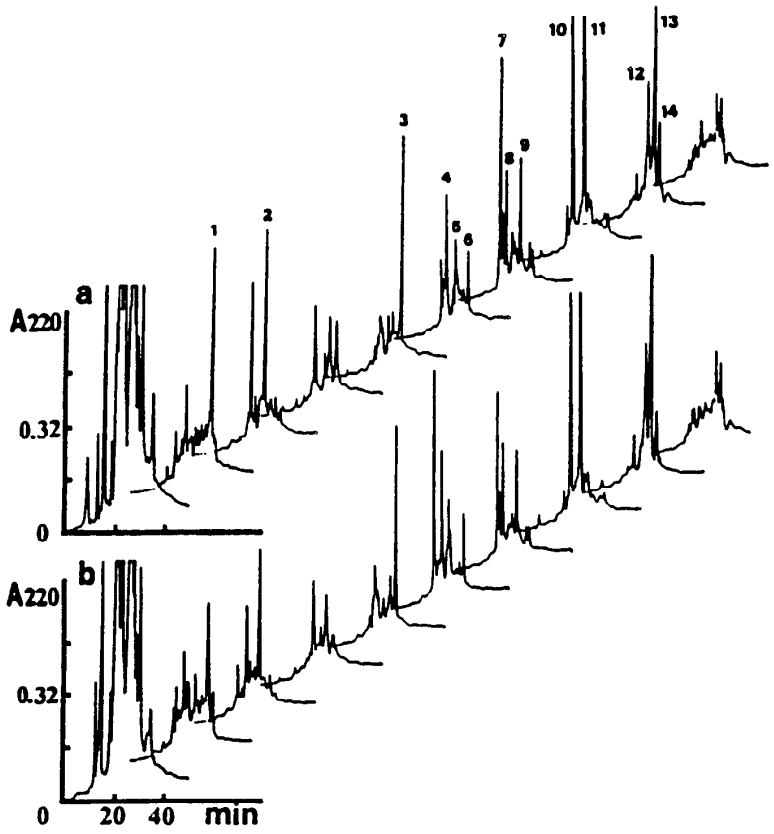


Figure 9 Two-dimensional high-performance liquid chromatographic map of soluble bovine cerebellum proteins: (a) and (b) are two separate experiments that illustrate the reproducibility of the method. (From Ref. 160.)

erated cleaning with 0.5 M sodium hydroxide. The application of about 10 mg of protein allowed 1–100 μg of each protein to be isolated in a single run. For mapping, the sensitivity could be increased by increasing the detector sensitivity, allowing analytical mapping with 100 μg extracts. The authors noted that a cation-exchange first stage was more effective for mixtures of basic proteins. The RPLC second stage was viewed as somewhat limiting the applicability, because this mode is strongly denaturing, particularly for larger proteins. However, they state, ". . . as a tool for preparative purposes, the 2D-HPLC system presented here is thought to be most suitable for use in protein chemical studies such as microscale sequencing or the purification of a protein to produce a specific antibody."

A specific example of the power of genetic engineering and HPLC-based purification is the purification and characterization of recombinant tropomyosins (rTMs) by Ferraz et al. [161]. Tropomyosin (TM) is involved in the regulation of muscle contraction. It is a long, fibrous protein found wound along the grooves of the F-actin helix. TM possess various functional properties (troponin binding, actin binding, and such), none of which are understood in detail. To investigate the molecular mechanism of action of TM, Ferraz et al. developed an *E. coli*-based expression system for human TM and generated deletion mutants of TM. The wild-type and mutant rTMs were isolated by disrupting the cells in a French press and heating the extract in a boiling water bath for 5 min, followed by centrifugation at 10,000 *g* for 15 min. The heat treatment removed most of the bacterial proteins. Although TM denatures at 50°C, no loss was observed. Thus, the solubilization must be due to an efficient and rapid renaturation. The TM was concentrated from the supernatant as the 35–60% ammonium sulfate fraction. The resuspended pellet was dialyzed against 20 mM of Tris-HCl, 0.5 mM DTT,

pH 7.5, and further purified by HPAEC, performed using a 150 × 21.5-mm–DEAE TSK column and eluting with an ammonium acetate gradient to 0.6 M. Typically, 260 mg of crude material was injected. Recombinant TM-containing fractions from the HPAEC were identified by sodium dodecyl sulfate–polyacrylamide gel electrophoresis (SDS–PAGE) and further purified by low-pressure hydroxyapatite chromatography (HAC) on a 100-mL–HA-Ultrogel column or HPHAC on a 100 × 12.5-mm Hypatite-C column. Although the conditions varied according to the specific system, in both cases, an increasing phosphate gradient was used for elution. In spite of poorer resolution in the HAC step than in the HPAEC, the rTMs were significantly purified (as judged by SDS–PAGE) by the HAC. Further purification by HPSEC was possible, but gave low recoveries. The HPAEC and HPHAC required 80 and 120 min, respectively. This report also provides two additional interesting features. First, although one might expect the chromatographic profiles of the crude extracts to be quite similar, excepting the expressed rTM, that was not true. Even using the same expression hosts, the profiles varied from batch to batch. Second, the authors developed a program to simulate the tryptic digestion pattern, based on the algorithm of Meek [162] as modified by Guo et al. [163]. The agreement between the experimental profile and the simulation was good for long peptides.

B. Immunoglobulins

Immunoglobulins (Igs) have a wide range of applications in biotechnology, including use as purification, detection, and characterization agents, as well as direct use as a product. Consequently, purification of Igs has been an area of long-standing interest. Although most monoclonal antibodies (MAbs) are in the IgG class, IgA, IgM, and bispecific MAbs are also of commercial interest. Whether from cell culture (which is frequently supplemented with bovine serum) or ascites, it is desirable to purify the Ig from nonimmunoglobulin proteins secreted by the cells, from proteins used in the supplementation, or for ascites, from host polyclonal Igs. Nau has published an extensive discussion of the purification of Igs by HPLC [164]. High-performance anion- and cation-exchange, hydrophobic-interaction, size-exclusion, affinity chromatography, and hydroxyapatite chromatography, all have been successfully applied to Ig purification. RPLC tends to irreversibly bind or to denature Igs and is generally unacceptable for the recovery of active Igs.

Gaillard et al. [165] applied the micropellicular particles developed by Kalghatgi and Horvath [43,44] to the determination of proteins in mammalian cell cultures. Two HPLC methods were employed, RPLC using the micropellicular particles and high-performance affinity chromatography (HPAC) using a 50 × 5.6-μm—Perstorp Biolytica Selectispher material covalently linked to a proprietary Fc receptor. The HPLC methods were sequentially used to monitor the IgG production of a hybridoma line in serum-free medium. The cell growth medium was supplemented with insulin, transferrin, and BSA, among other factors. RPLC was performed with a water–ACN–0.1% TFA gradient from 0 to 57% ACN in 5 min at 1.5 mL min^{-1} and 80°C; 25-μL samples were used. Analyses required approximately 7 min. HPAC used a 100-mM citric acid, pH 5.0, solution for binding and a 100-mM citric acid, pH 1.6, solution for elution. The flow rate was 3 mL min^{-1}; the 250-μL sample was injected into the column equilibrated with binding solution, followed by 2 min of washing with the binding solution, and 2 min of elution solution. Unfortunately, 45 min of equilibration is required before subsequent analysis. The insulin and transferrin could be quantitated directly from the RPLC results; the BSA and IgG coeluted, and the BSA had to be quantitated by difference, using the HPAC results to quantitate the IgG. The insulin, transferrin, and BSA concentrations were stable over the 140-h–growth period, although somewhat (and to differing degrees) reduced from the supplementation level. The IgG increased nearly linearly to a final concentration of 50 μg mL^{-1} after 140 h.

Chauret et al. [166] used high-performance size exclusion chromatography (HPSEC) to determine the amount of monoclonal IgM produced in cell culture. HPSEC was seen as useful because it is nondenaturing and provides molecular weight information about the species

present. IgM, however, is sufficiently large (950,000 Da) that it is excluded from most commercially available HPSEC materials. Flapper et al. [167] had earlier shown that coupled TSK-Gel 4000SW and TSK-Gel 3000SW columns allowed the analysis of IgM and other serum proteins. With TSK-Gel $4000SW_{XL}$ and TSK-Gel $3000SW_{XL}$ columns connected in series (size unspecified), and a 0.2-M sodium chloride, 0.2-M sodium phosphate, pH 6.8, eluent, Chauret et al. [166] analyzed supplemented and serum-free growth media by HPSEC and compared the results with those from an enzyme-linked immunosorbent assay (ELISA). The HPSEC analysis required approximately 70 min for each sample, and retention volumes larger than the pore volume were observed for some small molecules. IgM eluted in approximately 29 min. Using a 50-μL direct injection of the culture medium, the HPSEC detection limit for IgM was 0.3 $\mu g\ mL^{-1}$, with an RSD of about 2%. The ELISA assay required approximately 150 min following overnight binding of the antigen to the plate. Eight samples were run on a single plate, making the ELISA technique faster. HPSEC results correlated well with the ELISA results; the precision of the HPSEC assay (2%) was better than that of the ELISA assay (1020%). However, HPSEC allows no estimate of the quality or specificity of the immunoglobulins produced.

The selective purification of bispecific monoclonal antibodies (biMAbs) was addressed by Tarditi et al. [168]. The current method for producing biMAbs by hybrid hybridomas requires purification of the biMAbs from parental MAbs and inactive or partially active (monospecific) MAbs [169]. Tarditi et al. applied the IgG isolation method of Mariani et al. [170] which uses both protein A affinity chromatography and high-performance hydroxyapatite chromatography (HPHAC). Pretreatment of the ascites-derived samples was necessary to preserve the HPLC columns [168]. Ascites fluid was first adjusted to 1 mM in calcium chloride and stored at room temperature for 2 h, then, at 4°C for 16–22 h to convert fibrinogen to fibrin. The clot was removed; then the sample was centrifuged at 10,000 *g*, followed by heat inactivation at 56°C for 40 min. The sample was clarified by spinning at 100,000 *g* for 60 min and precipitated at 50% ammonium sulfate, pH 6.5, saturation. The pellet resulting from a 10,000-*g*, 25-min centrifugation was dissolved in water and dialyzed against a 1.5-M glycine, 3.0-M sodium chloride, pH 9, buffer. This same buffer served as the loading buffer for affinity chromatography using a 100 × 25-mm–Affi-Prep protein A column. The sample was applied at 5 $mL\ min^{-1}$ and the total IgG fraction was eluted with 0.1-M citrate, pH 3.0, buffer, followed by immediate neutralization with 1-M Tris, pH 8.5. Following dialysis against 10-mM sodium phosphate, pH 6.8, buffer, the optimum HPHAC gradient was chosen using a 100 × 7.8-mm Bio-Rad HPHT column at 0.4 $mL\ min^{-1}$ with 10-mM phosphate, pH 6.8, (A) and 350-mM phosphate, pH 6.8, (B) buffers. Preparative purification was performed on a 50 × 25-mm–HPHT column at a flow rate of 4 $mL\ min^{-1}$ using the same buffers. Although the precise conditions varied according to the biMAbs being isolated, generally, the elution conditions were a 40- to 60-min isocratic wash at 10% B, followed by a linear gradient to 60% B over 60 min. (Note that these conditions are estimated from Fig. 1 in the report; the authors describe the conditions as 100- to 120-min–linear gradients from 10–20% B to 40–80% B.) The desired fraction was identified by radioimmunoassay (RIA). HPHAC separates IgGs by charge; thus, the desired biMAb was invariably between peaks corresponding to the parental MAbs. Indeed, the authors state, "Thus, a consistent gap between the retention times of parental Mabs becomes a condition that cannot be overlooked in order to obtain a satisfactory separation of biMAbs." The fraction containing the desired biMAb were dialyzed against the A buffer and rechromatographed under the same conditions to provide the desired purity. The overall yield (determined relative to the initial total IgG content of the ascites fluid) for six biMAbs varied from 12 to 31% and averaged 19%.

C. Membrane Proteins

The first successful HPLC protein separations involved primarily well-characterized, soluble proteins such as insulin, serum albumin, RNaseA, and such. Traditional isolation of these

proteins involved, e.g., ammonium sulfate or organic solvent fractionation, size exclusion or ion-exchange fractionation, performed with aqueous buffers. Because the proteins were reasonably soluble, the incorporation of additives, such as glycerol or EDTA, tended to be directed toward stabilizing the protein conformation, but not typically toward preventing aggregation. Membrane proteins, in contrast, generally have large hydrophobic regions and aggregate readily. Purification schemes frequently incorporate surfactants to prevent this behavior. Goheen [171] and Welling et al. [172] have both provided excellent summaries of the peculiarities of membrane proteins, the extraction procedures used, and typical HPLC applications for this important class of proteins. Rather than duplicate that information, two rather novel approaches are presented here.

The HPMC study by Josic et al. [56] cited earlier, also included membrane proteins. The detergents reduced Triton X-100, reduced Triton X-114, octyl glucoside, decanoyl- and octanoyl-*N*-methyglucamide, 3-[(3-chloro)dimethylammonio]-1-propane sulfonate (CHAPS), and sodium dodecyl sulfonate (SDS) were tested and were generally compatible with HPMC. However, certain technical problems, such as foaming and poor detergent solubility at high salt concentrations, did arise. All the detergents could be washed from the column following use. Freeze-thaw and detergent extracts of kidney plasma membranes were analyzed on a DEAE poly(glycidyl methacrylate) disk. The mobile phase contained 0.25% reduced Triton X-100. Dipeptidyl peptidase IV and nucleotide pyrophosphatase activity recoveries were approximately 80 and 85%, respectively; the total protein recovery was approximately 90%. Similarly, anion-exchange HPMC of annexin CBP 65/67 from rat liver plasma membranes resulted in a 95% recovery of protein; EDTA and 0.25% octyl glucoside were added to ensure solubility. This is particularly notable because 50% formic acid is needed to elute this protein under RPLC conditions, and annexin could not be recovered from silica or polymeric HPLC anion-exchange supports. Heparin and collagen were also used to prepare affinity membranes and membrane protein separations shown using these supports. Clearly, HPMC appears to be a promising approach for membrane protein separation.

Pidgeon and co-workers [173–176] have described "immobilized artificial membrane chromatography" (IAMC), and have applied the technique to purifying proteins, small peptides, and deoxynucleotides, as well as membrane proteins [177]. IAMC is characterized by the nature of the stationary phase, which is a monolayer of membrane lipid molecules covalently bound to silica through the lipid's alkyl chain. The lipid's polar head groups form the exposed surface. The only IAMC phase so far described uses a dimyristylphosphatidylcholine analogue [173] and is commercially available through the Regis Chemical Company. The isolations of cytochrome P-450 isozymes (P-450s) from rat liver, kidney, and adrenal microsomes, and of NADH oxidoreductase from rat liver plasma membrane were the model systems studied [177]. Retention in IAMC appears to be due to nonspecific dispersion interactions between the protein and the stationary phase, as well as the hydrophobic effect. As such, IAMC shares similarities with RPLC and HIC, although the elution conditions are much milder than for RPLC. Unlike HIC, retention in IAMC occurs at a relatively low ionic strength (the weak eluent was 0.1-M potassium phosphate, pH 7.25, 20% glycerol, 1-mM EDTA, 0.6% sodium cholate). The glycerol was incorporated to stabilize the P-450s. Elution is achieved by a gradient in detergent, using as the strong eluent the same mobile phase, but containing 2.0% Lubrol PX. The choice and concentration of detergents used appears critical. Omission of sodium cholate rendered Lubrol PX ineffective in eluting the P-450s. Higher (1%) sodium cholate concentrations improved the peak shape, but reduced the total recovery by approximately 50%. (This was attributed to an elevated conversion of P-450 to P-420, which did not bind to the support under these conditions.) The nonionic surfactant Emulgen 911 was much less effective than Lubrol PX, even in combination with sodium cholate. Substituting CHAPS for the sodium cholate gave elution profiles similar to those with the Lubrol PX gradient, although the total recovery was again lower, apparently owing to decreased binding of P-450 to the IAM support. In contrast, NADH oxidoreductase was unretained by the IAMC support in the presence of sodium cholate, although the detergent was necessary for elution. Substi-

tution of 0.1-M Tris-HCl for the phosphate also reduced yields, again indicating the sensitivity of the technique to mobile-phase conditions. Preparative isolations of P-450s were performed using a 100 × 21-mm–IAM column and sample loads in excess of 200 mg of crude microsomes. Activity yields were on the order of 50% of that applied; specific activities increased 3- to 26-fold.

IAMC is in its infancy. It is intuitively satisfying to mimic the natural environment of a membrane, thereby maintaining the desired protein in its active conformation. However, the results show that the system is quite complex. IAMC is probably not suited to giving high selectivities—the "generic" dispersion interactions apparently giving rise to retention may preclude this. Its true strength may be as an early purification step, for which careful selection of operating parameters may yield a fraction highly enriched in the desired activity. Indeed, Pidgeon et al. [177] demonstrate a two-step purification of P-450IIB isozymes from rat liver microsomes by following IAMC, as described in the foregoing, with anion exchange on a 75 × 7.5-mm–TSK 5PW DEAE column. The recovered P-450s were separated from cytochrome b_5 and from P-420, yielding essentially pure isozymes from crude material in two, 2-h chromatographic steps, with a dialysis step between them. It is worth noting that, thus far, only IAMC using a dimyristylphosphatidylcholine phase has been performed; other membrane lipids may provide, if not differing selectivities, different retentive strengths. A complete understanding of the retention and elution mechanisms will require a more detailed understanding of the interaction between the proteins and surfactants in solution as well as on the lipid-like surface. Even without that detailed model, IAMC holds promise as a generally useful approach to selectively purify a wide variety of membrane proteins.

Closely related to the purification of membrane proteins is the purification of viral proteins, particularly coat proteins. This is because many viruses exit an infected cell by a process called budding—the assembled viral particle gathers a lipid bilayer as it moves through the cell membrane. Consequently, viral coat proteins frequently are anchored in the bilayer by a hydrophobic transmembrane region and are structurally similar to membrane proteins. The coat proteins are of interest for vaccine production. The purification of viral proteins was reviewed by Welling et al. [178], who cite more than 50 examples of HPLC-based purification of viral proteins. A partial list of these is given in Table 3. Although immunoaffinity techniques are most commonly used, other, less selective chromatographic modes have also proved useful.

Table 3 High-Performance Liquid Chromatographic (HPLC) Modes Used for the Purification of Viral Proteins

HPLC mode	Source virus
Ion-exchange	Adenovirus, bovine viral diarrhea virus, rubella virus, sendai virus
Size-exclusion	Borna disease virus, equine infectious anemia virus, influenzavirus, Sendai virus, tick-borne encephalitis virus
Reversed-phase	Adenovirus, bovine leukemia virus, cytomegalovirus, hepatitis A virus, herpes simplex virus, influenzavirus, Moloney murine leukemia virus, poliovirus, Sendai virus, tick-borne encephalitis virus
Hydroxyapatite	Murine hepatitis virus
Immunoaffinity	Borna disease virus, bovine herpesvirus type 1, canine distemper virus, cytomegalovirus, Epstein–Barr virus, foot-and-mouth disease virus, hepatitis A virus, hepatitis B virus, herpes simplex virus, human immunodeficiency virus, infectious bronchitis virus, measles virus, Moloney murine leukemia virus, Rous sarcoma virus, Sendai virus, varicella–zoster virus

Source: Ref. 172.

VIII. NUCLEIC ACID AND RELATED COMPOUNDS

Although frequently of central interest in biochemistry, biotechnological projects seldom involve studies of the purine or pyrimidine bases, or the nucleosides or simple nucleotides. Consequently, these species are mentioned only briefly here.

However, oligonucleotides and larger nucleic acids are the key ingredients in biotechnology. The in vitro manufacture or manipulation of synthetic DNA and RNA fragments (oligos) is possibly the defining factor in differentiating modern genetic engineering from more classic approaches to manipulating living organisms. Given this importance, it is not surprising that HPLC methods have been used in purifying both synthetic and naturally occurring nucleic acids. The extent of application seems to lag behind proteins. For the synthetic oligos, frequently the crude material is sufficiently pure for the desired application. When it is not, gel electrophoretic [179] and solid-phase extraction methods [180,181] are generally preferred by biotechnologists, perhaps owing to greater familiarity and less stringent technical demands. The larger naturally occurring nucleic acids pose complex separation problems owing to the difficulties of achieving adequate selectivity while maintaining the structural integrity of the fragment—which is not only sensitive to nucleases, but also to hydrodynamic sheer. Moreover, frequently, contamination of the desired nucleic acid with material from previous runs is unacceptable; hence, methods that rely on "disposable" separation media are generally favored.

A. Simple Nucleotides and Related Compounds

Separations of the bases, nucleosides, nucleotides, and related compounds are well documented [182,183]. Generally, in complex mixtures of ribonucleosides, ribonucleotides, deoxyribonucleosides, and deoxyribonucleotides, a group separation is first carried out. Zhao et al. [184] have published a method for the separation of 21 purine and pyrimidine bases, ribonucleotides, ribonucleosides, deoxyribonucleotides, and deoxyribonucleosides in a single run. The method uses a simple sample preparation (filtration), followed by RPLC on a 100 × 8-mm–Waters Resolve C_{18} column, using a weak eluent of 0.02-M potassium phosphate (pH 6.30) and an MeOH gradient for elution. However, the methods do not separate isomers of nucleotides.

For laboratories involved with quality assurance of nucleotides, Coniglio et al. [185] showed the use of an isocratic microbore system appropriate for evaluating the purity and (in conjunction with scintillation counting) the specific activity of various ^{32}P-nucleotides. The system consisted of a 150 × 2-mm–C_8 Ultrasphere column operated with a 20% MeOH, 5-mM tetrabutylammonium hydroxide, 50-mM potassium phosphate, 10-mM tricine, pH 7.0, mobile phase. The detector was a Waters Model 440 fitted with a 2-μL–microbore flowcell and was operated at 254 nm. Sample volumes between 2.5 and 15 μL and flow rates from 10 to 100 μL min^{-1} were used. The authors state, "We now use this procedure here at DuPont NEN Research Products for routine specific activity quality control analysis of a variety of ^{32}P-nucleotide products including [α-^{32}P]dCTP, [α-^{32}P]dATP, [α-^{32}P]dGTP, [α-^{32}P]dTTP, [γ-^{32}P]dATP, and [α-^{32}P]dUTP." This suggests that the application is relatively robust. The minimal dilution associated with microbore techniques, coupled with the relatively large sample capacity and the strong absorbance at 260 nm, allows small (10- to 60-pmol)–sample sizes to provide adequate quantitation. [A cautionary note to those considering establishing such a system: the chromatograph was shielded with 1/4″ Plexiglas and effluent wastes (albeit reduced by the low flow) are radioactive as well as chemical waste.]

B. Synthetic and Small Oligodeoxyribonucleotides

A variety of chemical methods are used in the solid-phase synthesis of oligonucleic acids, varying in the coupling methods employed. In common, the resultant product contains the

desired sequence and a multitude of closely related failed sequences. Although the deprotected crude product is frequently adequate for many uses, purification of the desired sequence from the failures is always desirable. Two general approaches are employed for purification: purification before removal of the protecting group ("trityl-on"), frequently using RPLC, and purification after deprotection ("trityl-off"), most commonly using high-performance anion-exchange (HPAEC).

Germann et al. [186] demonstrated the usefulness of the PRP-1 resin for the purification of DNA oligonucleotides with secondary structure. The alkaline stability of this support allows the use of pHs above 12, which offers two advantages. Aqueous ammonia is used to cleave the crude oligo from the synthesis support; because the PRP-1 resin is compatible with this solution, no time is lost transferring the crude reaction mixture to a less aggressive solvent. Also, such high pHs eliminate secondary structure from oligos, preventing self-association. This latter feature also prevents association (and copurification) of the desired sequence strands with undesirable, incompletely deblocked or failed sequence strands.

Hobbs and Yarem [187] refined this approach, retaining the use of the PRP-1 resin and alkaline mobile phases, but substituting 100-mM triethylammonium hydroxide (TEAH) for 50-mM sodium hydroxide. This provided some ion-pairing interactions that increased the retention of the protected DNA oligo, allowing a higher sample capacity and, consequently, a higher purity product. In a typical application, 5 μmol of a crude 22-mer were dissolved in 100 mM of TEAH (or the equivalent amount of TEAH was added to the ammoniacal solution of crude oligo). This was applied to a 30 $\times$ 7.0-mm Hamilton PRP-1 column, equilibrated in 15% acetonitrile (ACN) in 100 mM of TEAH at 4 mL min^{-1}. The elution protocol was (1) 6 min in the starting conditions; (2) 4 min in 15% ACN, 85% 100 mM aqueous triethylammonium bicarbonate (TEAB), pH 7.0; (3) 6 min in 0.5% aqueous trifluoroacetic acid; (4) 4 min in 100 mM of aqueous TEAB; and (5) a gradient from 0 to 50% ACN, remainder 100 mM aqueous TEAB over 12 min (Fig. 10). Unlike the procedure of Germann et al. [186], failed sequences are retained during loading in this protocol [187] and eluted during the first wash. Step 3 removes the trityl protective group, although "occasionally, this 60 min treatment fails to detritylate a small fraction (< 5%) of the product." The final gradient separates the full-length product for any nondetritylated oligonucleotides and the dimethoxytrityl alcohol. The purification provided by this protocol was demonstrated by mixing a crude tritylated 18-mer [$d(CT)_9$] with a crude nontritylated 20-mer [$d(AG)_{10}$-OH]. The 20-mer represented a failed sequence that would interact strongly with the desired product. Although conventional (nondenaturing) HPLC purification resulted in a mixed product (as judged by HPCE), the TEAH/TEAB protocol yielded only the desired 18-mer. As much as 10 μmol of a 6-mer were purified in a single run.

Warren and Vella [188] have compared the use of HPCE and HPAEC in the analysis of synthetic DNA oligos. Their emphasis was the analytical usefulness, rather than preparative uses, although both techniques have been used for preparative applications involving oligos. Both techniques provided *N*/*N*-1 resolution (i.e., separated $p(T)_{24}$ from $p(T)_{23}$) at low loads and both techniques showed a loss in resolution as the sample load increased. For HPCE, a 5-s, 5-kV injection of a 660-ng μL^{-1} sample was sufficient to cause loss of resolution, whereas the HPAEC system tolerated as much 5 μg of the mixed oligos. Because the Gen-Pak FAX 100 $\times$ 4.6-mm anion-exchange column used is generally considered an analytical column and because microgram quantities of oligonucleotides are frequently adequate, this shows that analytical-scale systems can function as preparative instruments in oligonucleotide purification. HPAEC also showed advantages in the separation of self-complementary oligonucleotides, when operated at an elevated temperature (80°C); in the resolution obtainable by modifying the gradient steepness (Fig. 11); in separating failed sequences from the desired 20-mer sequence in a phosphorothioate reaction mixture; and in the robustness and reproducibility of the separation. HPCE was superior for large (>50 bases) oligos. The oligonucleotide sequence influenced retention in both methods (i.e., TGT-CAA-GAC-CGT-GTA-C did not

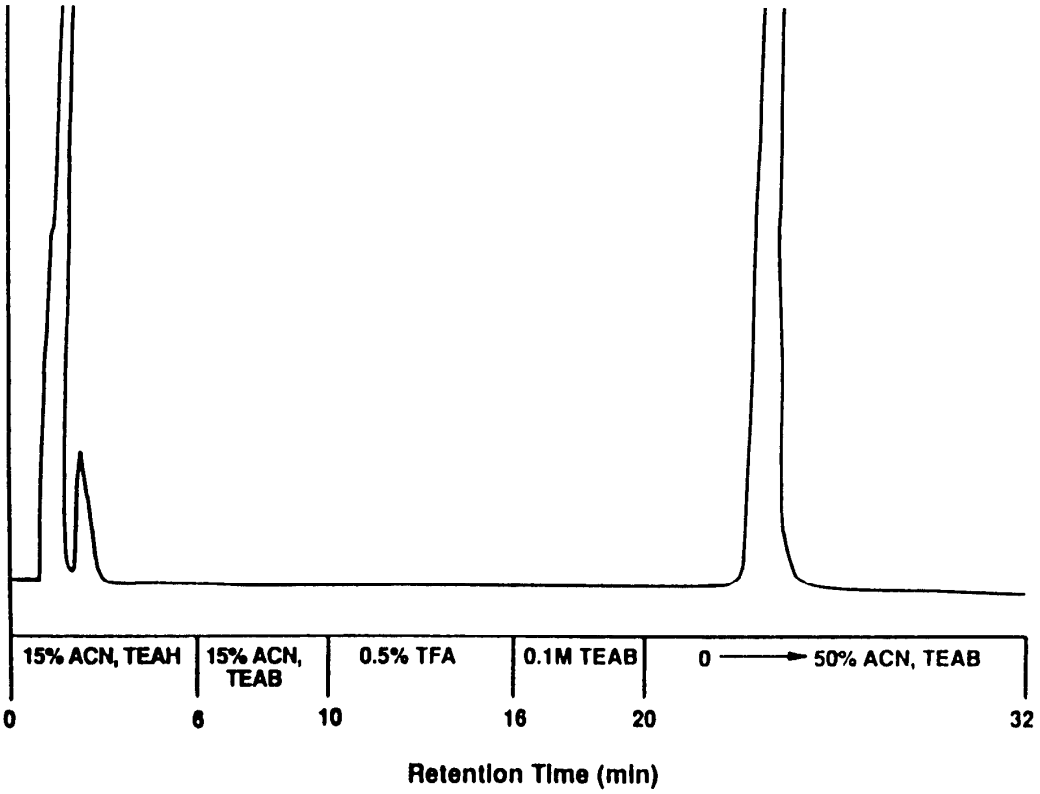


Figure 10 Denaturing, trityl-on purification of a self-complementary oligodeoxynucleotide by the method of Hobbs and Yarem. The sample represents approximately 5 μmol of crude d(CCTGAGTCAGGCCTGACTCAGG). Failure sequences eluted just after the solvent front. Detritylation occurs during the 0.5% TFA step (10–16 min) and the detritylated, full-length product was collected from 24–25 min. (From Ref. 187.)

coelute with CAT-GTG-CCA-GAA-CTG-T although the number of each nucleotide is the same in each oligo).

C. Synthetic and Small Oligoribonucleotides

Small RNA molecules appear to be involved in many cellular regulatory roles, including RNA process, transcription, and translation control. Hence, many biotechnological problems involve manipulating small RNAs. However, RNA is notoriously more difficult to handle than DNA, because of the ubiquitous presence of (and relative robustness of) RNA-degrading RNases. Additionally, synthetic methods for the production of oligo-RNAs faced the difficulty of protecting the 2′-OH group on ribose. This latter problem has been surmounted, and synthetic RNAs can be produced nearly as readily as synthetic DNAs. Again, following cleavage of the crude product from the synthesis resin, the product is deprotected and the resultant crude material contains failed sequences as well as partially deprotected sequences. Gel filtration is the most common method of purification although this method does not separate partially protected oligoribonucleotides from the fully deprotected product.

Webster et al. [189] have developed an RPLC/HPAEC method for the large-scale purification of synthetic oligoribonucleotides (i.e., RNA oligonucleotides). The crude material from a 1-μmol synthesis (following 4- to 6-h deprotection in 1-M tetrabutylammonium fluoride (TBAF) in THF) was concentrated, diluted with 0.1 M of triethylammonium acetate

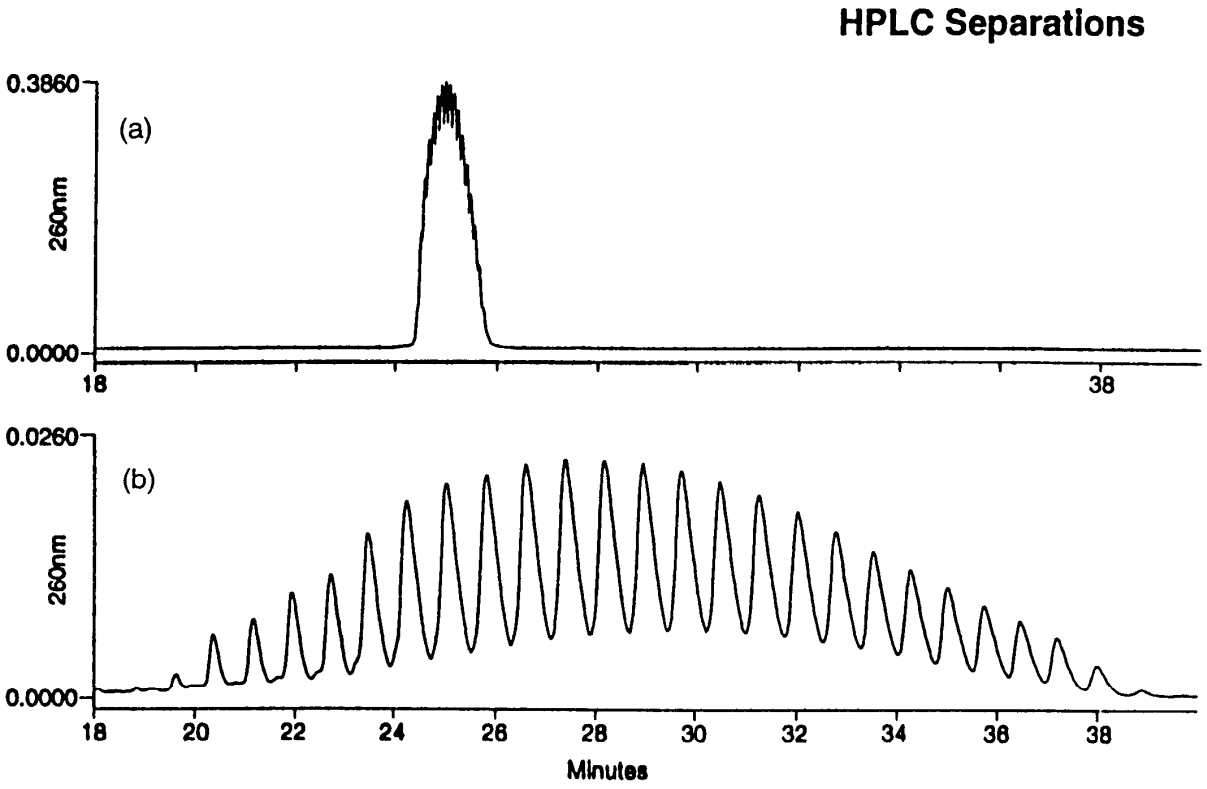


Figure 11 Effect of gradient program on oligonucleotide separation by anion-exchange HPLC: (a) 3 μg of a mixture of polydeoxyadenosines, ranging from 40 to 60 bases, were separated using a linear gradient from 0.1- to 1.0-M sodium chloride in 30 min; (b) same sample, with a 0.1–0.5-M sodium chloride gradient in 0.01 min, followed by a 0.5- to 0.6-M sodium chloride gradient over 30 min. Both separations performed at 0.75 mL min^{-1}, 80°C, on a 100 × 4.6-mm–Gen-Pak FAX column. (From Ref. 188.)

(TEAA), pH 6.8, and separated on a 250 × 4.6-mm–Vydac C_4 column using 0.1-M TEAA, pH 6.8, and a gradient from 0 to 40% ACN at a flow rate of 1 mL min^{-1}. Fully deprotected material eluted before the partially deprotected sequences. Peak fractions were concentrated and pooled before application to a 125 × 4-mm–Nucleogen DEAE-60-7 column equilibrated with 20% ACN, 20 mM of sodium acetate, pH 6.5, at a flow rate of 2 mL min^{-1}. Elution was performed with a 0–1.5 M potassium chloride gradient over 50 min. The 98% or higher purity of the resultant material was demonstrated by polyacrylamide electrophoresis of ^{32}P end-labeled samples, followed by autoradiographic analysis. Overall yields ranged from 30 to 50% for oligoribonucleotides ranging from 12 to 30 residues. The overall yield for a 10-μmol synthesis of a 12-mer was less than the yield for a 1-μmol synthesis (27 vs. 41%, respectively). However, it is not specified that the 12-mers were the same; hence, this may not be a general trend.

D. Large Deoxyribonucleotides

A variety of techniques have been used for the isolation of plasmids, which are extrachromosomal double-stranded, circular nucleic acids commonly used in biotechnology. Plasmid preparations are frequently contaminated with host nucleic acids in the form of various RNA species and fragments of the host chromosomal DNA. Isopycnic cesium chloride gradient centrifugation, in the presence of ethidium bromide, is the classic purification method [190];

other methods include lithium chloride and polyethylene glycol precipitation [190] as well as size-exclusion chromatography [191], hydroxyapatite chromatography [192], and other chromatographic procedures [193–196]. Many laboratories have adopted some variant of a solid-phase extraction protocol, using proprietary resins (e.g., the Wizard preparation systems from Promega), and HPLC procedures are not likely to compete successfully with these convenient, single-use devices for routine use. However, there may be applications—extremely large-scale or high-purity—that are still appropriate for HPLC.

Hines et al. [197] applied HPAEC for the large-scale (e.g., as much as 36-mm–total nucleic acids loaded onto the column) purification of plasmids. Using a 100 × 10-mm–Waters Protein-Pak DEAE 8HR anion-exchange column and a 25-mM Tris-HCl, pH 8.0, 1-mM EDTA, buffer, with a sodium chloride gradient, they removed detectable RNA species from the crude lysate. The transfection efficiencies, as monitored by CAT activity, obtained for three trials using purified plasmid pRNH147 had an RSD of 16%; three trials using purified plasmid pRSVcat yielded an RSD of 6.5%. Although the authors described these results as "highly reproducible," they failed to provide the proper controls to demonstrate that conclusion convincingly. The results are quite favorable, however.

Plasmids exist in a number of conformational states (relaxed and linear monomers, supercoiled monomers, dimers, and concatemers), and many purification schemes do not fully resolve these forms. The method of Hines et al. [197], for example, provides little, if any, change in the relative abundance of the coiled and concatemeric forms. However, the authors noted the presence of an endonuclease-resistant, apparently supercoiled form that "eluted on the trailing edge of the plasmid peak." Although, in most circumstances, these multiple forms are of little concern, some fundamental studies on plasmid structure require highly purified, single forms. Likewise, studies on transfection, transformation, and similar phenomena are best performed with well-characterized materials.

The HPSEC of crude plasmid-containing lysates generally elute the plasmid with the excluded volume [198]. Consequently, the peak contained both supercoiled and relaxed circular forms. Even though small (2–20 kbp, or approximately 1.3–13 MDa) in comparison with, for example, chromosomes, plasmids are huge compared with most molecules routinely chromatographed. With retentive separations, very wide pore sizes are desirable. Using HPAEC on a 125 × 6-mm–Nucleogen DEAE-4000 column, Colpan and Riesner [199] separated supercoiled, relaxed, and linear forms of the plasmid pBR322. The mobile phase was 20-mM potassium phosphate, 5-M urea, pH 6.6, with a gradient from 0.75- to 1.50-M potassium chloride for elution. However, the separation was performed with 4 μg of pBR322 and the relaxed and supercoiled forms were not completely resolved. Higher loadings, such as for a preparative isolation, would have further deteriorated the separation quality. Rapid purification of a single plasmid form is still an issue. Thus, the efficient separation of the various conformational forms of plasmids may be an area of some interest to separation scientists.

Likewise, although the plasmids routinely used in biotechnology are considered small, many interesting functionalities are associated with large (>125-kbp) plasmids found, for example, in *Pseudomonas*, and certainly the separation of chromosomes is of great interest. Currently, pulsed-field gel electrophoresis and in-well lysis techniques are used to study such large oligonucleotides. Indeed, sensitivity to hydrodynamic sheer may completely preclude chromatographic isolation of these species; however, alternatives (e.g., FFF techniques) may prove useful.

E. Large Ribonucleotides

Traditionally, mRNA is isolated by affinity selection of poly(adenylated) [poly(A)] RNAs on poly(thymidylated) [poly(T)] or poly(uridylated) cellulose, agarose, or Sepharose supports using a step elution procedure. Goss et al. [200,201] have evaluated poly(T)-modified silica as a support, seeking to improve the speed and resolution. RNA is notoriously susceptible to the nearly ubiquitous RNase activities; increased speed of isolation could result in longer

transcripts, with less technical demands. The poly(T)-modified silica was prepared by an in situ reaction of amino-$(dT)_{50}$ with *N*-hydroxysuccinylmidyl ester–silica packed in a 30 × 4.6-mm cartridge. In one protocol, 8.6 units of the oligo dT were dissolved in pH 7.5 buffer and continuously recirculated through the column for 1 h. In a second protocol, 6 units of oligo dT were dissolved in 85 μL of 0.2-M sodium phosphate, pH 5.0, buffer and injected into the activated column. The flow was stopped and the column removed from the system, the ends sealed, and the column was incubated at 50°C for 3 h. The coupling efficiencies were 27 and 73%, respectively. Good chromatographic performance was observed for both columns. At room temperature and with a mobile phase containing 1 M of sodium chloride, both columns quantitatively bound 0.5 unit (about 15 μg) of a mixture of poly-A of lengths 19–24, or of average length 5000. Neither species was bound on either column when the column was equilibrated at 40°C in water or 5-mM sodium chloride. This suggests a binding capacity of approximately 300 μg of poly(A) RNA. While formamide gradients could be used to elute the bound poly(A) (and provided resolution of each of the 19- to 24-base species), the high UV absorbance of formamide made the use of salt and temperature preferable. Lithium chloride-precipitated yeast RNA was fractionated by first equilibrating a $poly(T)_{18}$ column with 1 M of sodium chloride, 10 mM sodium phosphate, pH 7, at 1 mL min^{-1}, injecting approximately 200 μg of the crude RNA dissolved in the same buffer onto the column, then performing a step-wise elution. The nonpoly(adenylated) mRNA and ribosomal RNA (rRNA) eluted unretained. The column was then brought to 40°C, which caused the elution of mRNAs having short poly(A) stretches. Switching to 5-mM sodium phosphate, pH 7, buffer caused elution of the bulk of the poly(A) RNA (approximately 28% of the total cellular RNA). Finally, heating the column to 55°C caused elution of very long poly(A) tail mRNA. The third fraction (the major poly(A) RNA fraction) was further fractionated on the $poly(T)_{50}$ column, again using temperature and salt concentration changes to effect elution. Interestingly, poly(A) length analysis of these further-resolved fractions revealed a quite unequal distribution of tail lengths. All fractions contained material corresponding to a poly(A) region of length 12–18; each fraction also contained material that corresponded to longer poly(A) regions. The length of this latter poly(A) stretch increased as the retention of the fraction increased. Lengths of about 20, 30, and 80 were observed, but lengths of, for example, between 25 and 30 were uncommon. The authors [201] speculate that the 12–18 poly(A) region actually represents genomically coded poly(A), as has been observed in *Dictyostellum*. Regardless, the results indicate the usefulness of the technique in the analysis of mRNA.

Attempts to use SEC [e.g., 202] or RPLC [e.g., 203] to purify mRNAs have not generally provided adequate resolution. For RPLC, the separation is influenced more by base composition (hence, hydrophobicity) than by size. Results improved when poly(A) material is first selected before HPLC. The method described in the foregoing [201] offers the ability to fractionate by poly(A) length directly.

IX. CARBOHYDRATES

Simple sugars and related compounds are of limited interest in biotechnology. Most often, monosaccharides, amino sugars, and their acetylated forms are of interest primarily as standards in determining the structure of a complex carbohydrate. Thus, the analysis of simple carbohydrates and related compounds is only briefly mentioned. It is important in food analysis and conceivably certain biotechnological projects may be interested in, for example, increasing the glucose content of a particular engineered crop.

In contrast to this, oligosaccharides are of great interest because glycosylation is a common protein modification. Varki [204] has reviewed the biological roles of oligosaccharides. The details of carbohydrate structures known to occur, and methods for studying protein glycosylation, are beyond the scope of this review; more information can be found in Graves et al. [15] or Ginsburg [205–207]. Here, it is sufficient to note that carbohydrates can be attached to various amino acids (Asn, Thr, or Ser being most common). These are frequently

branched structures resulting from multiple posttranslational steps. Asparagine-linked carbohydrates are characterized as belonging to one of three categories: high-mannose type, complex type, and hybrid type. High-mannose oligosaccharides contain only mannose in the outermost branches; the outermost branches of complex oligosaccharides contain *N*-acetylglucosamine, galactose, and sialic acid; hybrid types contain branches of both of the other types. To characterize such a material, a mapping or fingerprinting procedure, analogous to peptide mapping, is useful. Variations in the carbohydrate map indicate differences between samples. Variation in degree and extent of glycosylation is a frequent source of protein microheterogeneity. Takahashi and Putnam [208] state the difficulty this way, ". . . when dealing with glycoproteins by use of HPLC we are often put into a dilemma; the more the separation power of the column is increased, the more the separation becomes ambiguous."

A. Simple Carbohydrates and Related Compounds

Ball [209] reviewed the analysis of simple sugars in foods. Similarly, the applications review issue of *Analytical Chemistry* published every odd-numbered year contains a section on carbohydrates in the food review; certain topics in the clinical chemistry review may also prove valuable.

Togami et al. [210] have examined the retention of 21 simple carbohydrates and carbohydrate derivatives in high pH cation- and anion-exchange chromatography. Both Na^+ and K^+ forms of cation-exchange resins were evaluated. Figure 12 summarizes their findings. Although the cation-exchange system did retain the carbohydrates and did provide selectivities different from the anion-exchange method, note that the scales for capacity factors in the figure differs for the two modes; retentions were, in general, significantly less in the cation-exchange mode. Given that robust separation procedures are more likely for capacity factors

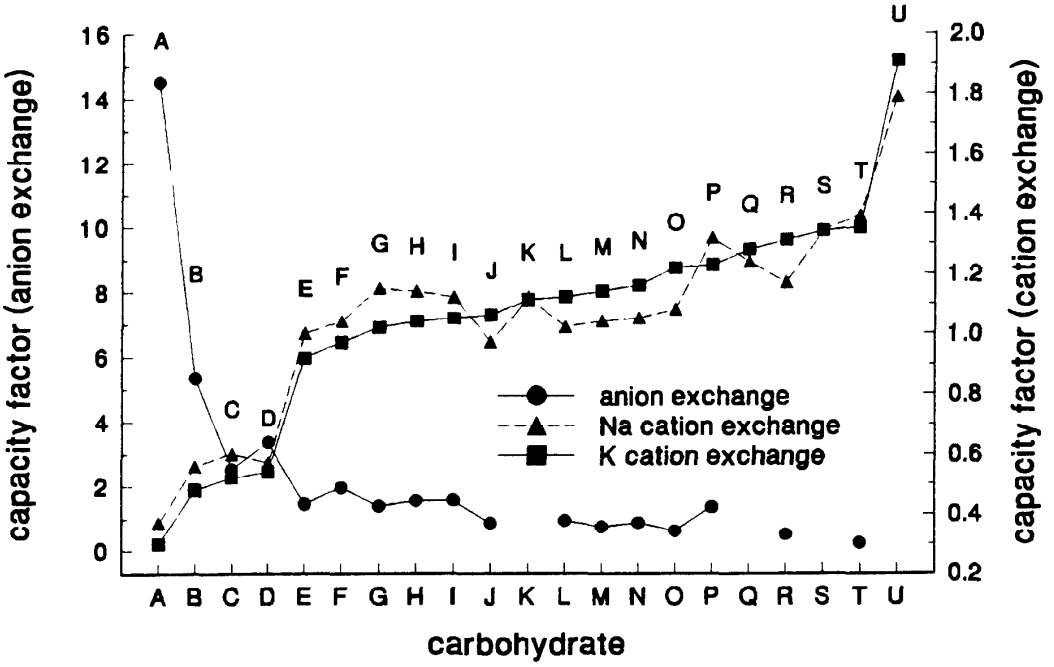


Figure 12 Capacity factors for carbohydrates and related compounds in anion- and cation-exchange HPLC: A, maltotriose; B, maltose; C, lactose; D, sucrose; E, glucose; F, fructose; G, mannose; H, galactose; I, xylose; J, mannitol; K, monoacetone glucose; L, dulcitol; M, adonitol; N, sorbitol; O, arabitol; P, arabinose; Q, diacetone glucose; R, xylitol; S, monoacetone xylofuranose; T, *myo*-inositol; U, diacetone xylofuranose. (From Ref. 210.)

between 2 and 10, rather than less than 1 (as many of the cation-exchange values are), it appears that the cation-exchange mode is not well suited for robust, routine work.

B. Complex Carbohydrates

Spellman [211] has reviewed complex carbohydrate characterization relative to recombinant glycoproteins. This review includes a brief discussion of the importance of carbohydrates in determining biological activities as well as an introduction to the techniques used to characterize glycoproteins. The author sums up the complexity of carbohydrate characterization as follows:

> The following elements define the complete primary structure of an oligosaccharide: the glycosyl residue composition; the positions of glycosidic bonds; the anomeric configurations (*a* or *b*), absolute configurations (D or L) and ring forms (furanose or pyranose) of the constituent sugars; the sequence of glycosyl residues; and the attachment positions of any non-carbohydrate substituents (e.g., phosphate or sulfate). When a glycoprotein is expressed in a mammalian cell line, it is reasonable to assume that all residues are in the pyranose (six-membered) ring form and that all residues except fucose have the D absolute configuration. The remaining structural features must be determined by physical, chemical, or enzymatic methods [211].

Commercial reagent systems are available to assist in oligosaccharide characterization (e.g., from Oxford GlycoSystems, Rosedale, NY). In addition to specialized columns, Dionex (Sunnyvale, CA) offers a specialized analysis system (Glycostation); Oxford GlycoSystems offers an automated hydrazinolysis system (GlycoPrep 1000) and an automated oligosaccharide-sequencing system (RAAM 1000 GlycoSequencer). As the methods become more mature, it is likely that other such instruments will become available. Just as for amino acid analysis, the laboratory with a smaller workload (or budget) will likely adapt a general-purpose HPLC system for these purposes.

Kobata et al. [212] introduced the sequential use of exoglycosidase digestion coupled with SEC for the characterization of the carbohydrate moieties of glycoproteins. Perhaps the most notable feature of this approach was that instead of determining which monosaccharide was released by the exoglycosidase, Kobata determined what size change occurred in the oligosaccharide portion. Chromatographic retentions were determined as *glucose units* (i.e., the retention was specified as being equivalent to a particular [and frequently fractional] glucose oligomer). This is somewhat analogous to the Kováts retention index used in gas chromatography. The work described was performed on two 20 × 1000-mm, low-pressure BioGel P-4 (< 400 mesh) columns connected in series and operated at 55°C with refractive index detection. Although not high-performance conditions, modern SEC columns and PAD should provide equivalent results at higher sensitivities and in far less time.

Hardy and Townsend [213] used HPAEC and pulsed amperometric detection (PAD) to study the composition, size, and linkage of oligosaccharide units. Picomolar quantities of underivatized isomeric oligosaccharides were separated. The method differentiated 1–3, 1–4, and 1–6 positional isomers of neutral oligosaccharides, 1–3 and 1–4 positional isomers of tetrasaccharides, and 1–6 and 1–4 positional isomers of two branched nonasaccharides.

Townsend et al. [214] extended this work, using HPAEC-PAD to characterize sialylated oligosaccharides from bovine fetuin (BF). The multisialylated branched oligosaccharides of BF were previously characterized using one- and two-dimensional high-field nuclear magnetic resonance (NMR) and methylation analysis. A 250 × 4.9-mm–Dionex CarboPac PA-1 column was used; 0.3 M of sodium hydroxide was added to the eluent stream at 1 mL min^{-1} to minimize PAD baseline drift during gradient analyses. A binary gradient was used for the neutral separation of sialylated oligosaccharides. The weak eluent (A) was 10 mM of acetic acid adjusted to pH 6.0 with 50% sodium hydroxide. The strong eluent (B) was 500 mM of acetic acid also adjusted to pH 6.0. The neutral gradient program was: 0 min, 0% B; 10 min,

0% B; linear gradient to 100% B over 60 min; followed by a 15-min equilibration time in the starting solvent before subsequent injection. A ternary gradient system was employed for the alkaline separation of sialylated oligosaccharides with the following eluents: A, 200 mM of sodium hydroxide; B, water; C, 600 mM of sodium acetate. The program used was: 50% A, 33% B, and 17% C for 5 min; linear gradient to 50% A, 17% B, 33% C, over 60 min; linear gradient to 50% A, 50% C, over 20 min; followed by a return to starting conditions over 10 min. Under neutral chromatographic conditions, the mono-, di-, tri-, tetra-, and pentasialylated oligosaccharides separated into classes, but little resolution of each class was obtained. Chromatography in alkaline conditions resolved the oligosaccharides into approximately 20 peaks (Fig. 13). The chromatographic profile of oligosaccharides released from BF by *N*-glycanase treatment was qualitatively similar to that of glycopeptides obtained from a tryptic digest of BF. Response factors and retention times allowed estimation of oligosaccharides for which standards were not available. The glycosylation patterns differed for BF samples from different sources.

Watson and Bhide [215] characterized the carbohydrate portion of recombinant erythropoietin (EPO). EPO is a small (about 30-kDa) glycoprotein (approximately 40% glycosylation) involved in regulating the level of circulating red blood cells. The *N*-linked carbohydrates at Asn-38 or Asn 83 and *O*-linked carbohydrate at Ser-126 are critical for biosynthesis and secretion. The work cited evaluated a pH of 12 or higher and pH 5.0 gradient elution anion-exchange methods. The N-linked complex oligosaccharides were isolated by (1) denaturing the protein in a mildly alkaline buffer containing 1% mercaptoethanol and 1% SDS; (2) incubating with *N*-glycanase for 18 h; (3) applying the sample to a C_{18} solid-phase extraction column; (4) eluting the carbohydrate with water; and (5) desalting on a Biogel P-2 column. In some experiments, sialic acid and fucose were removed by separate digestions with neuraminidase and 2-fucosidase; similarly unreduced and sodium borohydride-reduced oligosaccharides were both examined. Dionex 250 × 4-mm and 250 × 9-mm AS-6 HPAEC columns were used for the high- and low-pH work, respectively, at a flow rate of 1 mL min^{-1} with PAD. High-pH anion-exchange was the most effective technique for asialo-oligosaccharides (which are uncharged at neutral pHs); a gradient from 2.5 mM to 300 mM sodium acetate over 60 min, with both phases being 75-mM NaOH (approx. pH of 13), was used. Low-pH (5.0) anion-exchange proved more effective for the complex oligosaccharides, and the reduced forms produced superior peak shape and resolution (Fig. 14). This gradient was from 2.5-mM sodium acetate, pH 5.0, to 125-mM sodium acetate, pH 5.0, over 60 min. PAD was again employed with a postcolumn mixing system to raise the eluent pH. Retentions of the complex oligosaccharides were approximately determined by the number of sialic acid residues; within

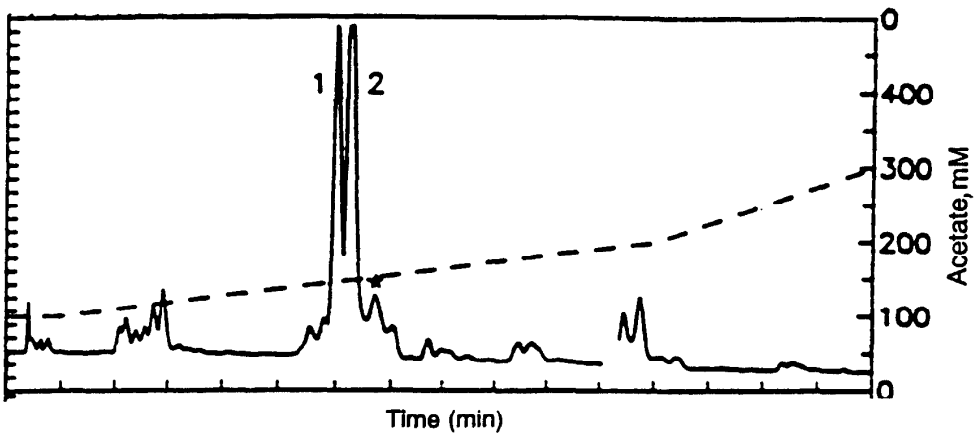


Figure 13 Anion-exchange HPLC separation of sialylated oligosaccharides from bovine fetuin using pulsed amperometric detection. (From Ref. 214.)

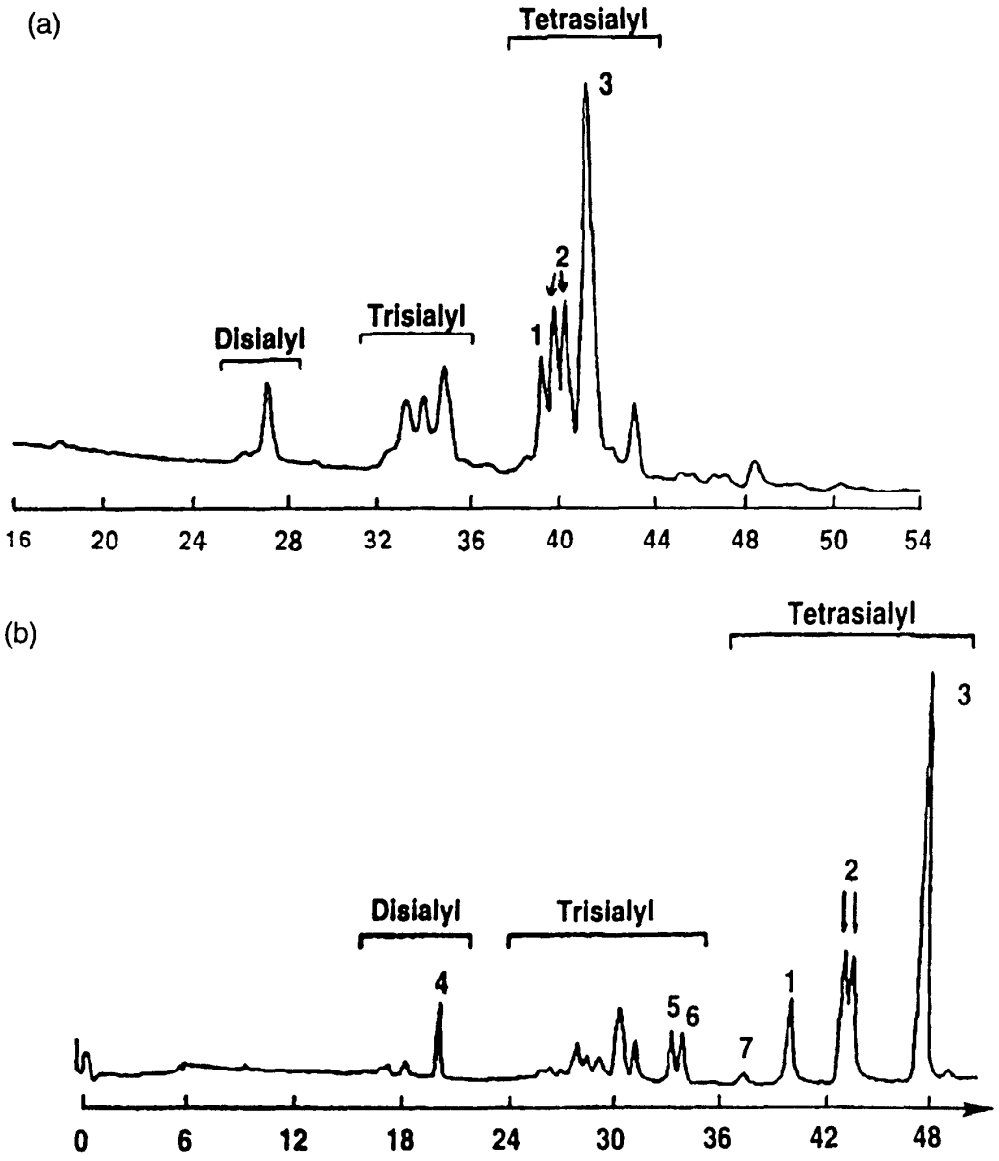


Figure 14 Anion-exchange HPLC separation of complex oligosaccharides from recombinant human erythropoietin: (a) unreduced oligosaccharides, 75 mM sodium hydroxide, pH 13; (b) reduced oligosaccharides, pH 5.0. (From Ref. 215.)

each group, retention decreased with increasing number of lactosamine units in the oligosaccharide. Resolution of fucosylated and nonfucosylated carbohydrates at pH 5.0 was possible, which was interpreted as possibly being due to fucose-induced conformational states. Such resolution in high pH HPAEC is attributed to oxyanion formation by the nonfucosylated compounds resulting in a consequently stronger interaction with the column. The authors indicate that there is a need for a wider variety of carbohydrate standards with authenticated structures, to allow structure prediction based on chromatographic retention.

Leonard et al. [216] characterized the glycosylation sites of the envelope glycoprotein (gp120) of the human immunodeficiency virus HIV-1. Recombinant gp120 has a polypeptide mass of approximately 60 kDa, is approximately 50% by weight carbohydrate, and contains 24 potential *N*-glycosylation sites. Tryptic digests of reduced, carboxymethylated gp120 contain polypeptides with two, three, and four glycosylation sites. Successive treatments with *endo-β-N*-acetylglycosaminidase H (endo H) and peptide:*N*-glycosidase F (PNGase F), fol-

lowed by sequence analysis, allows differentiation of the glycosylation sites. Endo H treatment hydrolyzes high-mannose and hybrid oligosaccharides, leaving *N*-acetylglucosamine (GlcNAc) at the glycosylation site. PNGase F hydrolyzes complex oligosaccharides, leaving an aspartic acid at the site. Subsequent sequence analysis showed GlcNAcAsn at high-mannose or hybrid glycosylation sites, aspartate at complex glycosylation sites, and asparagine at nonglycosylated sites.

Weitzhandler et al. [217] applied a similar analysis to glycoproteins separated by SDS–PAGE and electroblotted onto PVDF membrane. The Coomassie blue-stained bands were excised from the dried membrane, wet with MeOH, and incubated at 100°C in 350 μL of water and 60 μL of TFA (about 2 M) to hydrolyze the carbohydrates to monosaccharides. Carbohydrates from bovine fetuin (BF), RNaseB (RB), and recombinant erythropoietin (EPO) were released as monosaccharides in an average yield of 72% in 4 h. The authors state that more saccharides can be released with 6-N HCl if the sample is not limiting. Analysis of the composition by HPAEC-PAD yielded results in good agreement with expectations. Similarly, oligosaccharides were released and classified by single or sequential digestion with the endoglycosidases endo H, endo F2, or *endo*-β-galactosidase, or the amidase PNGase. Small amounts (0.1%) of reduced Triton X-100 were added to these digestions. Analysis of the released carbohydrates and sialic acids was performed by HPAEC-PAD. The buffer used for the digestions was compatible with direct HPAEC-PAD analysis, thereby minimizing handling. Oligosaccharide analysis of electroblotted BR, RB, EPO, and recombinant plasminogen activator yielded results in excellent agreement with those obtained from solution samples. The presence of the detergent in the digestion buffer was necessary, presumably to prevent adsorptive losses of the enzymes onto the membrane. The technique was applied to the analysis of the cloned α- and β-subunits of a gastric H^+,K^+-ATPase. The α-subunit was not glycosylated, in agreement with expectations based on the suspected cytoplasmic location and certain experimental data. The β-subunit contained *N*- and *O*-linked oligosaccharides and was devoid of sialic acids.

Protein blots have become a powerful tool in the analysis and characterization of protein structure and function as well as in protein isolation. Sequencing, amino acid analysis, and a variety of chemical and enzymatic procedures have already been shown to be compatible with blotting techniques; the work [217] cited in the foregoing adds oligosaccharide analysis to the list of methods available.

C. Microheterogeneity of Glycoproteins

Guzzetta et al. [218] used LC–MS with selected ion extraction to identify carbohydrate structures in glycoprotein peptide maps. The protein of interest was recombinant tissue plasminogen activator (rtPA), a 527-residue protein containing four known glycosylated sites. rtPA yields 51 peptides on tryptic digest, 4 of which bear carbohydrate structures. Asn-184 in peptide T17 is glycosylated in approximately 50% of the native rtPA (i.e., type I and type II isozymes); thus peptide T17 is present in two forms. Although tryptic mapping of proteins by RPLC is well-established, such maps of glycoproteins frequently have broad peaks owing to carbohydrate microheterogeneity [219]. Guzzetta et al. [218] separated tryptic digests of rtPA and of neuraminidase-treated rtPA on a 250 × 2.1-mm–Vydac C_{18} column using a 0.05% TFA-water–0.05% TFA–AN gradient (0–25% AN in 50 min at a flow rate of 200 μL min^{-1}). The sample size was 100 μg, although a 1:15 split into the nebulizer resulted in only about 6 μg of sample reaching the MS. Electrospray ionization was used. Figure 15 shows total ion current chromatograms of the treated and untreated rtPA tryptic digests, illustrating the level of complexity of this sample. Comparison of the contour plots of m/z versus elution time for these reveal characteristic "streaks" for the glycosylated peptides; the appearance of these streaks varies significantly between the untreated and treated samples (Fig. 16). By comparison of selected ion profiles, the extent and nature of the microheterogeneity of the glycosylated peptides was established. This required some prior knowledge of the carbohydrate structures

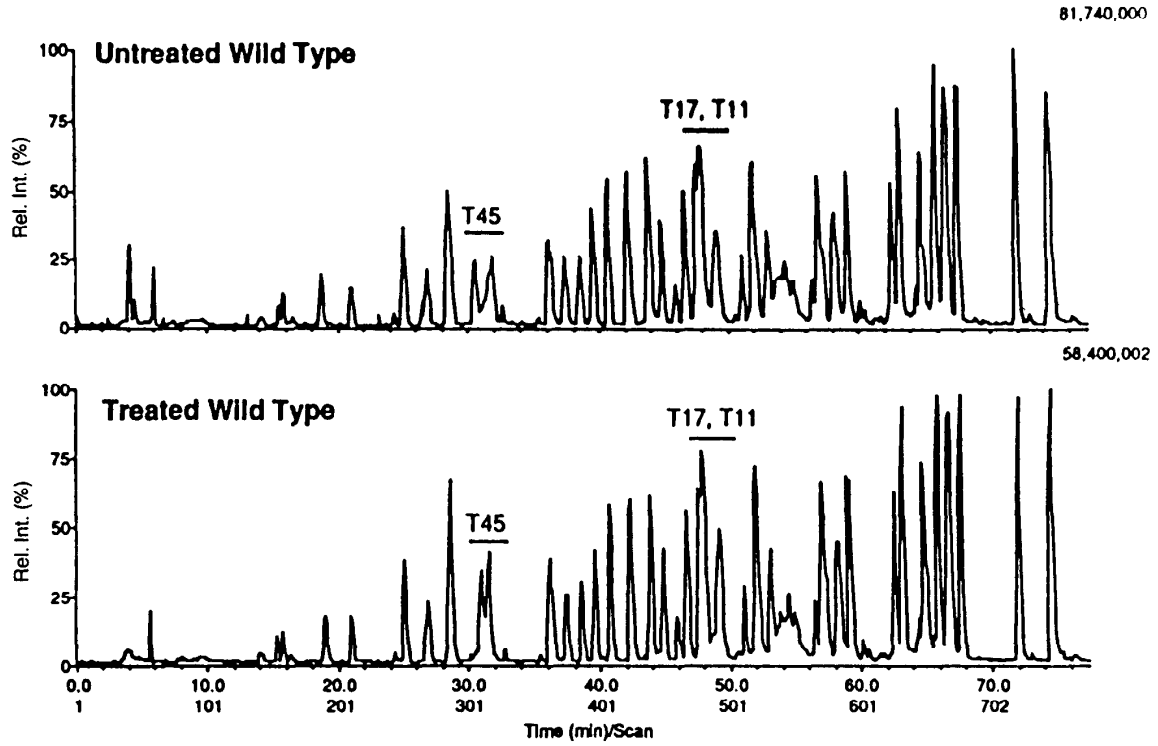


Figure 15 Electrospray total ion current chromatograms of tryptic digests of untreated and neuraminidase-treated recombinant tissue plasminogen activator. (From Ref. 218.)

involved. This procedure revealed three different carbohydrate structures in the high-mannose-type structure on peptide T11C; five to seven different structures were found in the sialic-oligosaccharides on peptides T45 and T17. The same method was applied to an rtPA mutant, created by site-specific mutagenesis. This mutant had an additional consensus glycosylation site at position 103, as well as some other modifications. The mutant was glycosylated at the new site as well as the previous sites. The degree of microheterogeneity at the new site was comparable with that previously found at Asn-117. However, glycosylation at Asn-117 in the mutant changed from the high-mannose type found in the wild-type protein to a complex type. The work described here extends an earlier application of LC/ESI-MS to the characterization of the tryptic map of rtPA [220].

Microheterogeneity is also addressed by Frenz et al. [221] in an examination of recombinant human DNase I (rhDNase). rhDNase contains two glycosylation sites, both capable of bearing complex oligosaccharides; rhDNase also contains zero to two mannose-6-phosphate (Man-6-P) groups. The degree of microheterogeneity possible is dauntingly high. Narrow range (pH 3–5) isoelectric focusing (IEF) could not resolve the isoforms containing Man-6-P from those containing sialic acid. Treatment with neuraminidase removed sialic acid groups; alkaline phosphatase digestion removed phosphate groups. Thus, untreated (UT), neuraminidase-treated (NAT), alkaline phosphatase-treated (APT), and neuraminidase–alkaline phosphatase-treated (NAAPT) rhDNase samples provide a set of presumably decreasingly complex proteins. Anion-exchange on a 75 × 7.5-mm–TPK DEAE-5PW column using an NaCl gradient at pH 6.0 gave only broad smeared bands for UT, NAT, and APT samples. However, anion-exchange on a 100 × 7.8-mm–Interaction Chemicals HP-PEI column using a mobile phase of 100 mM NaCl, 10 mM *N*-2-hydroxyethyl-piperazine-*N*′-2-ethanesulfonic acid, 1 mM $CaCl_2$, pH 7.0, at 1 mL min^{-1}, and a gradient to 1.5 M NaCl over 47 min provided distinctly different patterns for the UT, NAT, and APT samples (Fig. 17). The striking difference between the UT profile (five fractions) and the APT profile (single peak eluting at the

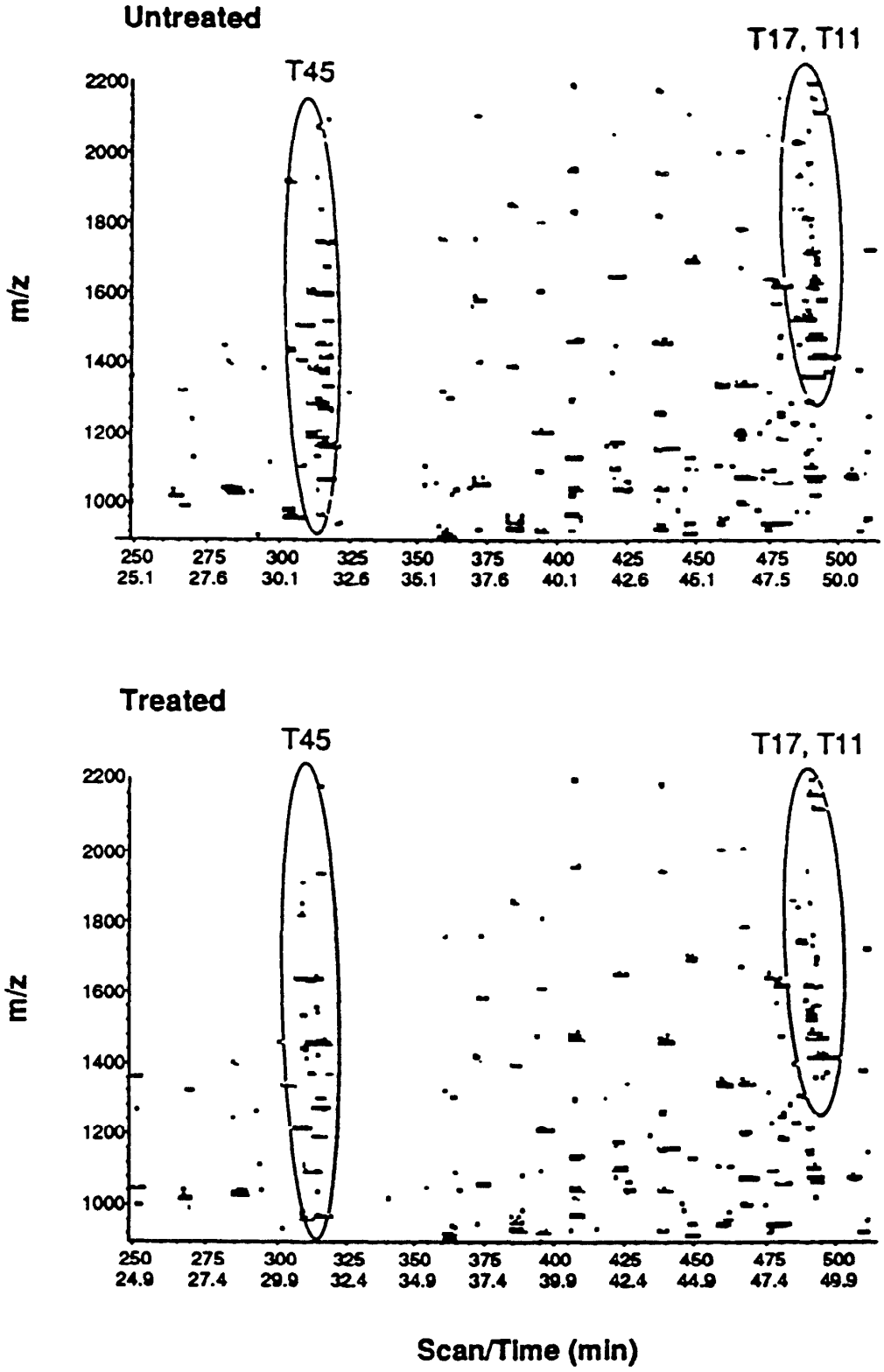


Figure 16 Contour plots of m/z versus elution time for electrospray total ion current chromatograms of tryptic digests of untreated and neuraminidase-treated recombinant tissue plasminogen activater. The circled "streaks" are characteristic of glycosylated peptides. (From Ref. 218.)

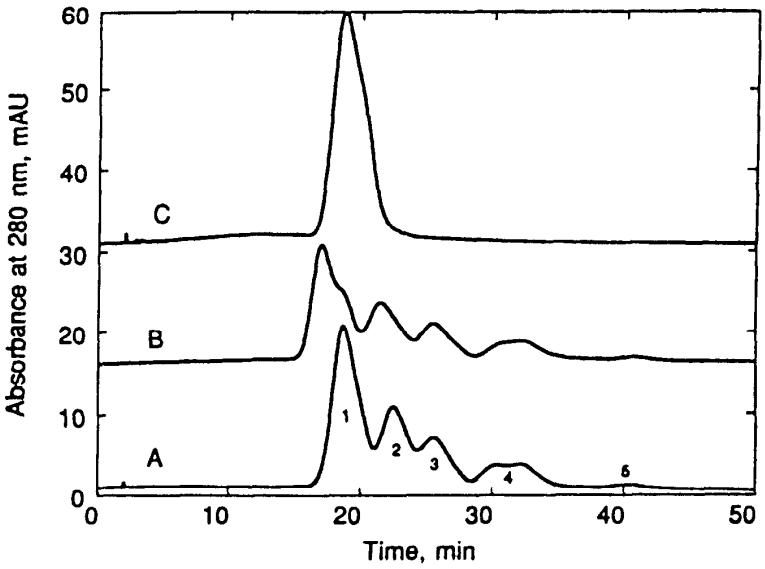


Figure 17 Anion-exchange HPLC on a 100 × 7.8-mm–interaction Chemicals HP-PEI column of (A) untreated; (B) neuraminidase-treated; and (C) alkaline phosphatase-treated recombinant human DNase I. The differences between the untreated and alkaline phosphatase-treated samples are due to a strong selectivity for phosphate differences. Peaks 1–5 contained 0, 1, 1, 2, and 3 mannose-6-phosphate residues, respectively. (From Ref. 221.)

position of the first peak of the UT sample) was interpreted as being due to a strong selectivity for phosphate differences exhibited by the PEI column. Because the UT and NAT profiles were quite similar, the PEI column is relatively insensitive to sialic acid differences in these samples. Moreover, phosphate analysis of the five fractions from the UT sample indicated approximately 0, 1, 1, 2, and 3 mol of phosphate per mole of rhDNase, respectively. IEF of these fractions revealed considerable heterogeneity. IEF of the same fractions following neuraminidase treatment indicated a single major component in each fraction. Because the removal of sialic acids by neuraminidase would leave charge heterogeneity by phosphate, the PEI-resolved fractions clearly correspond to rhDNase isoforms having differing degrees of phosphorylation. Tryptic mapping of untreated and endo H-treated samples of each fraction revealed the distribution of Man-6-P residues in the rhDNase, as well as the presence of considerable residual, presumably complex, oligosaccharide glycosylation. (Again, endo H removes high-mannose and hybrid oligosaccharides, but not complex oligosaccharides.) As for rtPA, extensive microheterogeneity of the carbohydrate moiety is indicated. The authors describe a procedure using PEI-based purification followed by endo H treatment for generating various, well-characterized isoforms of rhDNase for detailed studies of the functional role of glycosylation.

The rapid solution to problems of such structural complexity as glycoproteins requires sophisticated tools, such as MS and NMR, although well-designed experiments involving enzymatic digests, liquid chromatography, and electrophoresis can yield a surprising amount of information, albeit more slowly. More information concerning the retention behavior of complex carbohydrates needs to be acquired to allow more confident structural predictions to be made from chromatographic data. However, this also requires well-characterized complex carbohydrate standards.

X. DOWNSTREAM PROCESSING

The isolation and characterization of a recombinant material in the research laboratory is demanding; the development of methods for commercial production of that material is even

more demanding, and subject to constraints not generally applicable to research consideration, such as the expenses of waste disposal, energy, regulatory issues, and so on. The term *downstream processing* is used to encompass the purification and processing steps applied in the creation of a marketable product. The overviews by Fair and by Hoare and Dunnill [222,223] provide excellent introductions to many of the issues involved in developing a commercially attractive purification process. The series by Becker [224–226] focuses primarily on chromatographic issues in downstream processing, but is also an excellent introduction.

As Humphrey [227] points out, biotechnology involves primarily two distinct scales of culture: those low-value (10 dollars/kg), high volume (100 kton/year production) products, such as biochemicals, antibiotics, or enzymes; and very high-value (1 million dollars/g), low-volume (1 kg/year production) products, such as interferons, interleukins, erythropoietin, and the like. Although much of the recent focus has been on these latter materials, it remains true that the commercial value of the low-value products exceeds that of the high-value products by an order of magnitude. Humphrey cites three examples—one from plant cell culture, one from antibiotic production, and one from biotechnology monitoring and control—that illustrate the importance of basic chemical engineering considerations of mass transfer, sheer, aseptic design, and so forth, in biotechnological production. Although beyond the scope of this review, each is worthwhile reading.

Commercial production also requires complete validation of the production process. This problem was thoroughly described by Werner et al. [228]. Among the aspects addressed are validation of the equipment used, the raw materials, the fermentation process, the recovery and purification processes, support systems, and the consistency of the final products.

Closely related to validation is the commonly held belief that bioprocesses are inherently irreproducible, or at least far less reproducible than conventional chemical processes. Sonnieitner and Flechter [229] described the use of automated control systems to obtain a higher degree of reproducibility than is generally expected. The authors state, "Bioprocess automation is mandatory to boost biotechnology from an empirical discipline to a natural science." Schugerl [230] and Locher et al. [231,232] also address on-line monitoring and process control in biotechnology. Again, although beyond the scope of this review, these articles are worthwhile for individuals involved in the development of downstream-processing procedures.

The Applied Chemistry Division Commission on Biotechnology of IUPAC has published a technical report on purification techniques for recombinant products, primarily focusing on proteins [233]. This report is notable in the breadth of scale considered (from alcohol or citric acid production to vaccine production) and for its overview of typical expression systems used. Advantages and disadvantages of *E. coli*, *Bacillus subtilis*, yeast, mammalian cell, and baculovirus expression systems are summarized in Table 4. Gel filtration (GFC), ion-exchange (IEC), hydrophobic interaction (HIC), biospecific affinity (AC), and immobilized metal ion affinity (IMIAC) chromatographies are briefly reviewed for their use in downstream protein purification. This last technique is particularly interesting in that genetic engineering can be used to generate histadine fusion products, rendering IMIAC appropriate for highly selective purification of the desired product. The report concludes

> However, the most exciting development in downstream processing was made possible by genetic engineering. Genetic engineering now provides means to tailor a protein in such a way that it can be purified more efficiently. Genetic techniques can be used, on one hand, to modify and control the location of a protein in the host cell (e.g., periplasm, culture medium) and, on the other hand, to produce fusion proteins which can be purified by specific chromatographic techniques. Many of these methods can be expected to be included in future manufacturing procedures [233].

Table 4 Comparison of Expression Systems

Expression system host	Advantages	Disadvantages
Escherichia coli	Well-characterized host; high levels of expression possible; easy to grow; grow quite rapidly	Prokaryotic host; NH_2-terminal processing may not be correct; reducing environment may not fold Cys-rich proteins correctly; proteolytic degradation of foreign proteins
Bacillus subtilis	Well-characterized host; high level of product secretion possible; easy to grow; grow quite rapidly	Prokaryotic host; proteases secreted into medium; some products not secreted efficiently
Yeast	Eukaryotic host; grow rapidly; high levels of expression possible	Lysis more difficult than for bacteria; many proteases in host vacuoles may not process product correctly or completely
Mammalian cell cultures	Eukaryotic host; efficient secretion; efficient processing	Expensive and difficult to grow; slow growing; generally low product titers
Baculovirus system	Eukaryotic host; secretion of products; efficient processing	Processing pathway different from mammalian system

Scawen and Hammond [234] have also provided a summary of protein purification techniques, including GFC, IEC, HIC, and AC, as they apply to downstream processing. They stress the importance of support selection in large-scale purification, with hydrophilic, macroporous, rigid, spherical, chemically stable, and reusable materials being the most desirable. Macrosorb—a kieselguhr coated with cross-linked agarose, available from Sterling Organics, UK—and DuPont's Teflon-based Perflex are of particular interest, because these are not commonly described in the analytical separations literature. The perfluoroalkyl surface of Perflex interacts strongly with ligands having perfluoroalkyl tails; proper ligand choice allows the creation of AC media. The authors also provide much practical advice concerning the sequence of chromatographic operations. For example, HIC can conveniently follow IEC because most proteins require a high-ionic strength to bind in HIC. Similarly, IMIAC can frequently follow IEC, provided appropriate buffers are chosen for the first step. Because many of the affinity ligands used are chemically "fragile," AC in general is recommended for later stages in purifications to minimize contamination of the support with hard-to-remove materials, thereby avoiding the need to expose the ligands to harsh environments. Magnetic separations (i.e., batchwise absorption onto iron-bearing resins followed by magnetic recovery of the resin), aqueous two-phase partitioning, and electrophoresis as downstream-processing methods are also briefly considered.

Purification and recovery costs can amount to 80% of the total manufacturing cost for a recombinant product [235]. Savings of only a few percent can represent significant absolute cost savings. Fulton et al. [236] performed calculations to show that preparative perfusion chromatography would allow higher throughput at lower operational cost than conventional chromatographic media. Because perfusive media allow significantly higher speeds, a given sample volume can be processed faster on the same-sized column, or it may be processed in the same time on a much smaller column as a series of injections. This lies at the heart of the comparison. By using perfusive media, smaller columns can provide throughputs equivalent to larger columns packed with conventional media. Savings are due to the less expensive

equipment outlay and to the reduced separation media costs. The savings in total-operating costs according to their model range from 6 to 16%.

Membrane-based affinity separations for commercial-scale purification have been described by Brandt et al. [237]. These commercially available (Sepracor, Marlborough, MA) systems provide advantages similar to perfusive media, in that mass transfer is largely due to convection, rather than diffusion. With a hollow-fiber affinity device, IgG was protein A-affinity purified at a rate sufficient to produce 15 g/day of IgG from 300 L of feed.

Several groups have approached increased throughput by using radial-flow techniques. In common, the sample is applied to the entire outer surface and flows radially through the bed to a collection duct. In effect, the radius of the column becomes the bed height and the length of the column determines the "cross-sectional area." Such devices are available commercially (e.g., ZetaPrep from Cuno Inc, Meriden, CT, and Superflo from Sepragen, San Leandro, CA). Although the ZetaPrep system is primarily for low- and medium-pressure laboratory purifications, the Superflo systems are available in column volumes from 100 mL to 20 L. When describing the Superflow system, Saxena and Weil [238] state, ". . . if a separation is optimized on a bench scale, it can be predictably scaled-up in a linear fashion as much as 50 fold in one step, unlike conventional column methodologies where several reoptimization steps may be necessary." The isolation of an unspecified plasma component by heparin affinity chromatography from 350 L of partially purified plasma in a single, 6-h run shows the preparative potential of the technique. This particular isolation required a 60-L radial-flow column; the traditional mode required a 180-L conventional column and 24 h. The savings in media alone amounts to approximately 240,000 dollars.

Although conventional and high-performance chromatography offers the advantages of relatively easy scale-up and extensive experience, alternatives, such as perfusion, membrane, and radial-flow chromatographies and magnetic separations, offer attractive features that drive their increasing use. Particularly for downstream processing, we are likely to see continuing development of alternatives to conventional chromatographic procedures.

XI. CLOSING REMARKS

The complexities of biomolecular structure are being gradually uncovered by increasingly sophisticated, sensitive, and selective analytical methods, including high-performance separations. Questions can now be answered that only a decade ago would either be enormously difficult or even impossible to address. For example, the glycosylation microheterogeneity studies cited earlier involved recombinant human proteins expressed in Chinese hamster ovary cells. One cannot help but wonder to what degree the microheterogeneity is influenced by the evolutionary distance between the host organism and the source of the target protein. Glycosylation patterns of human recombinant interferon-1b are known to vary according to host [239] and rtPA expressed in various cell lines contained populations of oligosaccharides differing significantly from one another [240–243]. The extent to which this behavior is due to clonal variation, culture conditions, purification processes, or fundamental biochemical differences remains to be determined.

Perhaps illustrative of the fractal quality of nature, as we gain the ability to resolve species of ever-finer differences or to quantitate ever-smaller amounts, we reveal increasing levels of complexity. There clearly remains an embarrassing wealth of separation problems in biotechnology.

ACKNOWLEDGMENT

This work was supported in part by a Senate Research Committee Award, provided by the Provost's Scholarly Activities Fund, Indiana University of Pennsylvania.

REFERENCES

1. G Guiochon. Anal Chim Acta 283:309, 1993.
2. BA Bidlingmeyer. Practical HPLC Methodology and Applications. New York: John Wiley & Sons, 1992.
3. LR Snyder, JL Glajch, JJ Kirkland. Practical HPLC Method Development. New York: John Wiley & Sons, 1988.
4. KM Gooding, MN Schmuck. Biotechniques 11:232, 1991.
5. KM Gooding, FE Regnier, eds. HPLC of Biological Macromolecules: Methods and Applications. New York: Marcel Dekker, 1990.
6. WS Hancock, ed. High Performance Liquid Chromatography in Biotechnology. New York: John Wiley & Sons, 1990.
7. C Horvath, LS Ettre, eds. Chromatography in Biotechnology. Washington, DC: American Chemical Society, 1993.
8. J-C Janson, L Ryden, eds. Protein Purification: Principles, High Resolution Methods, and Applications. New York: VCH Publishers, 1989.
9. A Kenney, S Fowell, eds. Practical Protein Chromatography. Totowa, NJ: Humana Press, 1992.
10. MTW Hearn, ed. HPLC of Peptides, Proteins, and Polynucleotides: Contemporary Topics and Applications. New York: VCH Publishers, 1991.
11. C Schoneich, SK Kwok, GS Wilson, SR Rabel, JF Stobaugh, TD Williams, DG Vander Velde. Anal Chem 65:67R–84R, 1993.
12. P Matsudaira, ed. A Practical Guide to Protein and Peptide Purification for Microsequencing, 2nd ed. San Diego, CA: Academic Press, 1993.
13. P Edman. Acta Chem Scand 4:283, 1950; for a brief review of the history of sequencing, see G Allen. Sequencing of Proteins and Peptides. Amsterdam: Elsevier, 1989.
14. J Sambrook, EF Fritsch, T Maniatis. Molecular Cloning: A Laboratory Manual, 2nd ed. Cold Spring Harbor, NY: Cold Spring Harbor Laboratory Press, 1989, Chap. 12.
15. DJ Graves, BL Martin, JH Wang. Co- and Post-translational Modification of Proteins: Chemical Principles and Biological Effects. New York: Oxford University Press, 1994.
16. LL Evans, MA Burns. Biotechnology 13:46, 1995.
17. BJ Compton, L Kreilgaard. Anal Chem 66:1175A, 1994.
18. MEP McNally, AC Barefoot. Am Lab 26(18):28N, 1994.
19. WH Velander, U Snow, P Hedman. Downstream 17:12, 1994.
20. S-L Wu. LC–GC, 10:430, 1992.
21. PR Brown. Anal Chem 62:995A, 1990.
22. RM Chicz, RE Regnier. In: MP Deutscher ed. Methods in Enzymology, vol 182. New York: Academic Press, 1990.
23. N Cooke, P Shieh, N Miller. LC–GC 7:954, 1989.
24. MTW Hearn. Aust J Biotechnol 3:183, 1989.
25. JF Kennedy, ZS Rivera, CA White. J Biotechnol 9:83, 1989.
26. DF Samain. Adv Chromatogr. 29:77, 1989.
27. N-I Jang, PR Brown. LC–GC 10:526, 1992.
28. HA Hansen, C. Emborg. J Chromatogr 626:171, 1992.
29. RE Cooley, CE Stevenson. Process Control Quality 2:43, 1992.
30. TK Nadler, SK Paliwal, FE Regnier, R Singhvi, DIC Wang. J Chromatogr 659:317, 1994.
31. G. Thévenon-Emeric, FE Regnier. Anal Chem 63:1114, 1991.
32. JC Giddings. Dynamics of Chromatography. New York: Marcel Dekker, 1965.
33. ND Danielson, JJ Kirkland. Anal Chem 59:2501, 1987.
34. KK Unger, G Jilge, JN Kinkel, MTW Hearn. J Chromatogr 359:61, 1986.
35. KK Unger, G Jilge, R Janzen, H Giesche, JN Kinkel. Chromatographia 22:379, 1986.
36. G Jilge, R Janzen, H Giesche, KK Unger, JN Kinkel, MTW Hearn. J Chromatogr 397:71, 1987.

37. R Janzen, KK Unger, H Giesche, JN Kinkel, MTW Hearn. J Chromatogr 397:81, 1987.
38. R Janzen, KK Unger, H Giesche, JN Kinkel, MTW Hearn. J Chromatogr 397:90, 1987.
39. C Horvath, BA Preiss, SR Lipsky. Anal Chem 39:1422, 1967.
40. C Horvath, BA Preiss, SR Lipsky. Anal Chim Acta 38:305, 1967.
41. JJ Kirkland. Anal Chem 41:218, 1969.
42. JJ Kirkland. J Chromatogr Sci 7:7, 1969.
43. K Kalghatgi, C Horvath. J Chromatogr 443:343, 1988.
44. K Kalghatgi, C Horvath. J Chromatogr 398:335, 1987.
45. L Varady, K Kalghatgi, C Horvath. J Chromatogr 458:207, 1988.
46. K Kalghatgi, I Fellegvari, C Horvath. J Chromatogr 604:47, 1992.
47. JJ Kirkland. Anal Chem 64:1239, 1992.
48. F Svec, JMJ Fréchet. Anal Chem 64:820, 1992.
49. QC Wang, F Svec, JMJ Fréchet. Anal Chem 65:2243, 1993.
50. LR Snyder. In: KM Gooding, FE Regnier, eds. HPLC of Biological Macromolecules. New York: Marcel Dekker, 1990.
51. Y Kikumoto, YM Hong, T Nishida, S Nakai, Y Masui, Y Hirai. Biochem Biophys Res Commun 147b:315, 1987.
52. A Upshall, AA Kumar, MC Baley, MD Parker, MA Favreau, KP Lewinson, ML Joseph, JM Maragnore, GL McKnight. Biotechnology 5:1301, 1987.
53. S Brandt, RA Groffe, SB Kessler, JL O'Conner, SE Zale. Biotechnology 6:779, 1988.
54. SH Huang, S Roy, KC Hou, GT Tsao. Biotechnol Prog 4:159, 1988.
55. TB Tennikova, F Svec. J Chromatogr 646:279, 1993.
56. D Josic, J Reusch, K Loster, O Baum, W Reutter. J Chromatogr 590:59, 1992.
57. FE Regnier. Nature 350:634, 1991.
58. NB Afeyan, N Gordon, I Maszaroff, I Varady, SP Fulton, Y Yang, FE Regnier. J Chromatogr 519:1, 1990.
59. NB Afeyan, SP Fulton, FE Regnier. J Chromatogr 544:267, 1991.
60. SP Fulton, NB Afeyan, NF Gordon, FE Regnier. J Chromatogr 547:452, 1991.
61. L Dughan. Biotechnology 12:1090, 1994; provides an interesting perspective on some legal issues involving "perfusion confusion."
62. AI Liapis, MA McCoy. J Chromatogr 599:87, 1992.
63. AT Salzman. Biotechnol Forum Eur 9:442, 1992.
64. NB Afeyan, NR Gordon, SP Fulton, FE Regnier. In: RH Angeletti, ed. Techniques in Protein Chemistry III. New York: Academic Press, 1992.
65. S Fulton, M Meys, J Protentis, NB Afeyan, J Carlton, J Haycock. Biotechniques 12:742, 1992.
66. JG Dorsey, WT Cooper, JF Wheeler, HG Barth, JP Foley. Anal Chem 66:500R, 1994.
67. S Hunt. In: GC Barret, ed. Chemistry and Biochemistry of the Amino Acids. London: Chapman & Hall, 1985.
68. S Blackburn. In: S Blackburn, ed. Amino Acid Determination Methods and Techniques, 2nd ed. New York: Marcel Dekker, 1978.
69. I. Molnãr-Perl. J Chromatogr 661:43, 1994.
70. MJ Drescher, JE Medina, DG Drescher. Anal Biochem 116:280, 1981.
71. JA Grunau, JM Swiader. J Chromatogr 594:165, 1992.
72. SC Kazmierczak. Anal Chem 65:401R, 1993.
73. G Sawar, HG Botting. J Chromatogr Biomed Appl 615:1, 1993.
74. RS Ersser, JF Davey. Med Lab Sci 48:59, 1991.
75. IM Moodie, GS Shephard, D Labadarlos. J High Resolut Chromatogr 12:509, 1989.
76. GA Qureshi. In: MTW Hearn, ed. HPLC of Proteins, Peptides, and Polynucleotides: Contemporary Topics and Applications. New York: VCH Publishers, 1991, Chap. 16.
77. DH Spackman, S Moore, WH Stein. Anal Chem 30:1190, 1958.
78. G Robinson. In: S Blackburn, ed. Amino Acid Determination Methods and Techniques, 2nd ed. New York: Marcel Dekker, 1978.

79. MV Pickering, P Newton. LC–GC, 8:778, 1990.
80. LB Gilman, C Woodward. Current Research in Protein Chemistry. San Diego, CA: Academic Press, 1990.
81. ST Chen, SH Chiou, YH Chu, and KT Wang. Int J Pept Protein Res 30:572, 1987.
82. E Tatăr, Mohamed Khalifa, G. Zăray, I Molnăr-Perl. J Chromatogr 672:109, 1994.
83. I Molnăr-Perl, M. Pintér-Szakăcs, M Khalifa. J Chromatogr 632:57, 1993.
84. K Muramoto, H Kamiya. Anal Biochem 189:223, 1990.
85. LC Gruen, PW Nicholls. Anal Biochem 47:348, 1972.
86. WS Hancock, DRK Harding. In: WS Hancock, ed. CRC Handbook of HPLC for the Separation of Amino Acids, Peptides, and Proteins; vol I. Boca Raton, FL: CRC Press, 1984.
87. M Eslami, P Hashemi, MN Sarbolouki. J Chromatogr Sci 31:480, 1993.
88. D Yuan, DJ Pietrzyk. J Liq Chromatogr 14:2835, 1991.
89. P Luo, F Zhang, RP Baldwin. Anal Chem 63:1702, 1991.
90. DC Johnson, WR LaCourse. Anal Chem 62:589A, 1990.
91. GW Robinson. In: S Blackburn, ed. Amino Acid Determination Methods and Techniques, 2nd ed. New York: Marcel Dekker, 1978.
92. RV Lewis. In: WS Hancock ed. CRC Handbook of HPLC for the Separation of Amino Acids, Peptides, and Proteins, vol I. Boca Raton, FL: CRC Press, 1984.
93. J Saurina, S Hernăndez-Cassou. J Chromatogr 676:311, 1994.
94. L Dou, J Mazzeo, IS Krull. Biochromatography 5(2):74, 1990.
95. L Dou, IS Krull. Anal Chem 62:2599, 1990.
96. IS Krull, L Dou. Curr Sep 11(1–2):7, 1992.
97. L Dou, IS Krull. Electroanalysis 4:381, 1992.
98. W-Y Lee, TA Nieman. J Chromatogr 659:111, 1994.
99. S-I Kobayashi, K Imai. Anal Chem 52:424, 1980.
100. KA Krok, SS Seaver. Biotechniques 10:664, 1991.
101. DR Koop, ET Morgan, GE Tarr, MJ Coon. J Biol Chem 257:847, 1982.
102. BA Bidlingmeyer, SA Cohen, TL Tarvin. J Chromatogr 336:93, 1984.
103. DJ Strydom, SA Cohen. Anal Biochem 222:19, 1994.
104. P Fürst, L Pollack, TA Graser, H Godel, P Stehle. J Chromatogr 499:557, 1990.
105. DEH Palladino, RM House, KA Cohen. J Chromatogr 599:3, 1992.
106. A Gottschalk. In: A Gottschiak, ed. Glycoproteins: Their Composition, Structure, and Function, Part A. Amsterdam: Elsevier, 1972.
107. D Atherton. In: TE Hugli, ed. Techniques in Proteins Chemistry. San Diego, CA: Academic Press, 1989.
108. SA Cohen. J Chromatogr 512:283, 1990.
109. K-L Woo, S-H Lee. J Chromatogr 667:105, 1994.
110. S Einarsson, B Josefsson, S Lagerkvist. J Chromatogr 282:609, 1983.
111. S Einarsson. J Chromatogr 348:213, 1985.
112. S Einarsson, S Folestad, B Josefsson, S Lagerkvist. Anal Chem 58:1638, 1986.
113. I Betner, P Foldi. Chromatographia 22:381, 1986.
114. B Gustavsson, I Betner. J Chromatogr 507:67, 1990.
115. PA Haynes, D Sheumack, J Kibby, RW Redmond. J Chromatogr 540:177, 1991.
116. SA Cohen, DP Michaud. Anal Biochem 211:279, 1993.
117. SA Cohen, KM DeAntonis. J Chromatogr 661:25, 1994.
118. H-J Liu. J Chromatogr 670:59, 1994.
119. Y Tapuhi, DE Schmidt, W Lindner, BL Karger. Anal Biochem. 115:123, 1981.
120. JM Wilkinson. In: WS Hancock, ed. CRC Handbook of HPLC for the Separation of Amino Acids, Peptides, and Proteins, vol I. Boca Raton, FL: CRC Press, 1984.
121. Y Tapuhi, N Miller, BL Karger. J Chromatogr 205:325, 1981.
122. JY Chang, R Knecht, DG Braun. Biochem J 199:547, 1981.
123. J Vendrell, FX Aviles. J Chromatogr 358:401, 1986.
124. L Gorbics, L Urge, L Otvos Jr. J Chromatogr 676:169, 1994.

125. L Gorbics, L Urge, E Lang, GI Szendrel, L Otvos Jr. J Liq Chromatogr 17:175, 1994.
126. M Roth. Anal Chem 43:880, 1971.
127. P Lindroth, K Mopper. Anal Chem 51:1667, 1979.
128. LA Allison, GS Mayer, RE Shoup. Anal Chem 56:1089, 1984.
129. MC Roach, MD Harmony. Anal Chem 59:411, 1987.
130. P de Montigy, JF Stobaugh, RS Givens, RG Calrson, K Srinivasachar, L Sternson, T Higuchi. Anal Chem 59:1096, 1987.
131. MD Oates, JW Jorgenson. Anal Chem 61:432, 1989.
132. RH Buck, K Krummen. J Chromatogr 315:279, 1984.
133. H Brückner, R Wittner, H Godel. J Chromatogr 476:73, 1989.
134. H Brückner, R Wittner, H Godel. Chromatographia 32:383, 1991.
135. H. Brückner, S Haasman, M Langer, T Westhauser, R Wittner, H Godel. J Chromatogr 666: 259, 1994.
136. G Frank, W Strubert. Chromatographia 6:522, 1973.
137. CL Zimmerman, E Appella, JJ Pisano. Anal Biochem 77:569, 1977.
138. F Lottspeich, A Henschen. In: A Henschen, K-P Hupe, F Lottspeich, W Voelter, eds. High Performance Liquid Chromatography in Biochemistry. VCH, Winheim: VCH, 1985.
139. WD Annan. In: JM Rattenbufy, ed. Amino Acid Analysis Symposium Proceedings. Chichester: Horwood, 1981.
140. B Wittmann-Liebold, J Sainikow, VA Erdmann, eds. Advanced Methods in Protein Microsequence Analysis. Berlin: Springer-Verlag, 1986.
141. JBC Findlay, MJ Geisow, eds. Protein Sequencing: A Practical Approach. Oxford: IRL Press at Oxford University Press, 1989.
142. DJ Strydom. J Chromatogr 662:227, 1994.
143. N LeGendre, M Mansfield, A Weiss, P Matsudaira. In: P Matsudaira, ed. A Practical Guide to Protein and Peptide Purification for Microsequencing, 2nd ed. San Diego, CA: Academic Press, 1993.
144. H Hirano, S Komatsu, H Takakura, F Sakiyama, S Tsunasawa. J Biochem 111:754, 1982.
145. Y Kawakami, S Ohmori. Anal Biochem 220:66, 1994.
146. JJ Gorman, BJ Shiell. J Chromatogr 646:193, 1993.
147. K Titani, K Narita, K Okunuki. J Biochem 51:350, 1962.
148. H Kawasaki, S Imajoh, K Suzuki. J Biochem 102:393, 1987.
149. TH Akiyama, T Sasagawa, M Suzuki, K Titani. Anal Biochem 222:210, 1994.
150. T Ohta, K Ishimura, S Takitani. J Chromatogr 637:35, 1993.
151. T Ohta, K Ishimura, S Takitani. Chromatographia 33:113, 1992.
152. T Ohta, T Inoue, Y Fukumoto, S Takitani. Chromatographia 30:410, 1990.
153. ET Buttimer, F Barry. Biochem Soc Trans 18:332, 1990.
154. M-C Shao, CCQ Chin. Anal Biochem 207:100, 1992.
155. FE Regnier, KM Gooding. Anal Biochem 103:1, 1980.
156. WS Hancock, JT Sparrow. In: Horvath, ed. High-Performance Liquid Chromatography, vol 3. New York: Academic Press, 1983.
157. N Takahashi, N Ishioka, Y Takahashi, FW Putman. J Chromatogr 326:407, 1985.
158. J Frenz, WS Hancock, WJ Henzel, C Horvath. In: KM Gooding, FE Regnier, eds. HPLC of Biological Molecules: Methods and Applications. New York: Marcel Dekker, 1990, Chap. 6.
159. M Herold, GP Rozing, JL Curtis. Biotechniques 10:656, 1991.
160. T Isobe, K Uchida, M Tanka, F Shinkai, T Manabe, T Okuyama. J Chromatogr 588:115, 1991.
161. C Ferraz, J Sri Widada, J-P Liautard. J Chromatogr 539:465, 1991.
162. J Meek. Proc Natl Acad Sci USA 77:1632, 1980.
163. D Guo, C Mant, A Tanega, R Parker, RJ Hodges. J Chromatogr 359:499, 1986.
164. DR Nau. In: WS Hancock, ed. High Performance Liquid Chromatography in Biotechnology. New York: John Wiley & Sons, 1990, Chap. 15.

165. I Gaillard, A Martial, A Marc, J-M Engasser, M Fick. J Chromatogr 679:261, 1994.
166. N Chauret, J Cote, J Archambault, G Andre. J Chromatogr 594:179, 1992.
167. W Flapper, AGM Theeuwes, JTG Kierkels, J Steenbergen, HJ Hoenders. J Chromatogr 533: 47, 1990.
168. L Tarditi, M Camagina, A Parisi, C Vassarotto, LB DeMonte, M Letarte, F Malavasi, M Mariani. J Chromatogr 599:13, 1992.
169. LB DeMonte, P Nistico, R Tecce, P Dellabona, M Momo, A Anichini, M Mariani, PG Natali, F Malavasi. Proc Natl Acad Sci USA 87:2941, 1990.
170. M Mariani, F Bonelli, L Tarditi, R Calogero, M Camagna, E Spranzi, E Seccamani, G Deleide, GA Scassellati. Biochromatography 4:149, 1989.
171. SC Goheen. In: MTW Hearn, ed. HPLC of Proteins, Peptides, and Polynucleotides: Contemporary Topics and Applications. New York: VCH Publishers, 1991.
172. GW Welling, R van der Zee, S Welling-Wester. In: KM Gooding, FE Regnier, eds. HPLC of Biological Macromolecules: Methods and Applications. New York: Marcel Dekker, 1990.
173. C Pidgeon, UV Venkataram. Anal Biochem 176:36, 1989.
174. C Pidgeon. Enzyme Microb Technol 12:149, 1990.
175. RJ Markovich, JM Stevens, C Pidgeon. Anal Biochem 182:237, 1989.
176. JM Stevens, RJ Markovich, C Pidgeon. Biochromatography 4:193, 1989.
177. C Pidgeon, J Stevens, S Otto, C Jefcoate, C Marcus. Anal Biochem 194:163, 1991.
178. GW Welling, R van der Zee, S Welling-Wester. In: MTW Hearn, ed. HPLC of Proteins, Peptides, and Polynucleotides: Contemporary Topics and Applications. New York: VCH Publishers, 1991.
179. WJ Efcavitch. In: D Rickwood, BB Hames, eds. Gel Electrophoresis of Nucleic Acids: A Practical Approach. New York: IRL Press at Oxford University Press, 1990.
180. BA Johnson, SG McClain, ER Doran, G Tice, MA Kirsch. Biotechniques 8:424, 1990.
181. LJ McBride, C McCollum, S Davidson, JW Efcavitch, A Andrus, SJ Lombardi. Biotechniques 6:362, 1988.
182. PR Brown. In: PR Brown, ed. HPLC in Nucleic Acid Research, Part I. New York: Marcel Dekker, 1984.
183. A Fallon, RFG Booth, LD Bell. Applications of HPLC in Biochemistry. New York: Elsevier, 1987.
184. J Zhao, B Todd, GH Fleet. J Chromatogr 673:167, 1994.
185. C Coniglio, G Pappas, WJ Gill, M Kashdan, M Maniscalco. Biotechniques 10:452, 1991.
186. M Germann, RT Pon, JH van de Sande. Anal Biochem 165:399, 1987.
187. FW Hobbs, JA Yarem. Biotechniques 14:584, 1993.
188. WJ Warren, G Vella. Biotechniques 14:598, 1993.
189. KR Webster, Y Shamoo, W Konigsberg, EK Spicer. Biotechniques 11:658, 1991.
190. T Maniatis, EF Fritsch, J Sambrook. Molecular Cloning: A Laboratory Manual, 2nd ed. Cold Spring Harbor, NY: Cold Spring Harbor Laboratory Press, 1989, Chap. 1.
191. N Moreau, X Tabary, F LeGoffic. Anal Biochem 166:188, 1987.
192. TR Johnson, J. Ilan. Anal Biochem 132:20, 1983.
193. PAD Edwardson, T Atkinson, CR Lowe, DAP Small. Anal Biochem 152:215, 1986.
194. JK McClung, RA Gonzales. Anal Biochem 177:378, 1989.
195. M Merion, W Warren. Biotechniques 7:60, 1989.
196. MP Weiner, TW Thannhauser, JH Laity, ME Benning, DP Lee, HA Scheraga. Nucleic Acids Res 16:8185, 1988.
197. RN Hines, KC O'Connor, G Vella, W Warren. Biotechniques 12:430, 1992.
198. Pharmacia FPLC Application File. Plasmid DNA, 1987.
199. M Colpan, D Riesner. In: A Neuberger, LLM van Deenen, eds. New Comprehensive Biochemistry: Modern Physical Methods in Biochemistry, vol 11B. Amsterdam: Elsevier, 1988.
200. TA Goss, M Bard, HW Jarrett. J Chromatogr 508:279, 1990.
201. TA Goss, M Bard, HW Jarrett. J Chromatogr 588:157, 1991.
202. T Ogishima, Y Okada, T Omura. Anal Biochem 138:309, 1984.

203. S Garcia, JP Liautard. J Chromatogr 296:355, 1984.
204. A Varki. Glycobiology 3:97, 1993.
205. V Ginsburg, ed. Methods in Enzymology, vol 179. New York: Academic Press, 1989.
206. V Ginsburg, ed. Methods in Enzymology, vol 138. New York: Academic Press, 1987.
207. V Ginsburg, ed. Methods in Enzymology, vol 83. New York: Academic Press, 1982.
208. N Takahashi, FW Putnam. In: KM Gooding, FE Regnier, eds. HPLC of Biological Macromolecules: Methods and Applications. New York: Marcel Dekker, 1990, Chap. 21.
209. GFM Ball. Food Chem 35:117, 1990.
210. DW Togami, BJ Poulsen, CW Batalao, WA Rolls. Biotechniques 10:651, 1991.
211. MW Spellman. Anal Chem 62:1714, 1990.
212. K Yamashita, T Mizuochi, A Kobata. In: V Ginsburg, ed. Methods in Enzymology, vol 83. New York: Academic Press, 1982, p 105, and references therein.
213. MR Hardy, RR Townsend. Proc Natl Acad Sci USA 85:3289, 1988.
214. RR Townsend, MR Hardy, DA Cumming, JP Carver, B Bendiak. Anal Biochem 182:1, 1989.
215. E Watson, A Bhide LC–GC 11:216, 1993. [Errata in LC–GC 11:369, 1993.]
216. CK Leonard, WW Spellman, L Riddle, RJ Harris, JN Thomas, TJ Gregory. J Biol Chem 265:10373, 1990.
217. M Weitzhandler, D Kadlecek, N Avdalovic, JG Forte, D Chow, RR Townsend. J Biol Chem 268:5121, 1993.
218. AW Guzzetta, LJ Basa, WS Hancock, BA Keyt, WF Bennett. Anal Chem 65:2953, 1993.
219. RC Chloupek, RJ Harris, CK Leonard, RG Keck, BA Keyt, WM Spellman, AJS Jones, WS Hancock. J Chromatogr 463:375, 1989.
220. V Ling, AW Guzzetta, E Canova-Davis, JT Stuits, WS Hancock, TR Covey, BI Shushan. Anal Chem 63:2909, 1991.
221. J Frenz, CP Quan, J Cacia, C Democko, R Bridenbaugh, T McNerney. Anal Chem 66:335, 1994.
222. JR Fair. Chem Eng Prog 85:38, 1989.
223. M Hoare, P Dunnill. Philos Trans R Soc Lond B 324:497, 1989.
224. C Becker. Aust J Biotechnol 2:34, 1988.
225. C Becker. Aust J Biotechnol 2:116, 1988.
226. C Becker. Aust J Biotechnol 3:18, 1989.
227. AE Humphrey. Perspectives in chemical engineering: research and education. Adv Chem Eng 16:463, 1991.
228. RG Werner, H Langlouis-Gau, F Walz, H Allgaier, H Hoffmann. Drug Res 38(I):855, 1988.
229. B Sonnleitner, A Flechter. Adv Biochem Eng Biotechnol 46:143, 1992.
230. K Schugerl. Pure Appl Chem 64:205, 1992.
231. G Locher, B Sonnleitner, A Flechter. J Biotechnol 25:23, 1992.
232. G Locher, B Sonnleitner, A Flechter. J Biotechnol 25:55, 1992.
233. E Hochuli. Pure Appl Chem 64:169, 1992.
234. MD Scawen, PM Hammond. J Chem Technol Biotechnol 46:85, 1989.
235. TC Ransohoff, MK Murphy, HL Levine. BioPharm 3:20, 1990.
236. SP Fulton, AJ Shahidi, NF Gordon, NB Afeyan. Biotechnology 10:635, 1992.
237. S Brandt, RA Goffe, SB Kessler, JL O'Connor, SE Zale. Biotechnology 6:779, 1988.
238. V Saxena, AE Weil. Biochromatography 2:90, 1987.
239. Y Kagawa, S Takasaki, J Utsumi, K Hosoi, H Shimizu, N Kochibe, A Kobata. J Biol Chem 263:17506, 1988.
240. MW Spellman, LJ Basa, CK Leonard, JA Chakel, JV O'Connor, S Wilson, J Van Halbeek. J Biol Chem 264:14100, 1989.
241. RB Parekh, RA Dwek, PM Rudd, JR Thomas, TW Rademacher, T Warren, T-C Wun, B Herber, B Reitz, M Palmier, T Ramabhadran, DC Tiemeir. Biochemistry 28:7670, 1989.
242. RB Parekh, RA Dwek, JR Thomas, G Opdenakker, TW Rademacher, AJ Wittwer, SC Howard, R Nelson, NR Siegel, MG Jennings, NK Harakas, J Feder. Biochemistry 28:7644, 1989.
243. G Pohl, L Kenne, B Nilsson, M Einarsson. Eur J Biochem 170:69, 1987.

23

HPLC Applications in Food and Nutritional Analysis

Kenneth A. Berg and Carlos E. Canessa

The PQ Corporation, Conshohocken, Pennsylvania

I. INTRODUCTION

Food analysis by high-performance liquid chromatography (HPLC) is one of the most massive subjects in chromatographic literature. Several large books on food HPLC have appeared recently [1–3]. Investigators analyzing just foods may need to access in-depth resources such as these. This review endeavors to provide an overview with enough detail to begin measurements, but without encumbering the reader with the detail that may be necessary for difficult analyses. The literature from 1991 has been examined, although just the articles easily obtained were used.

For one reason or another, almost every compound imaginable has been found or sought in food. Consequently, extensive discussion will center on only topics not covered elsewhere in this handbook. These are carbohydrates, lipids, vitamins, and polyphenols. Other classes of compounds found in foods will be discussed by referencing appropriate recent reviews on the subject. Some examples of HPLC analyses of oils and beer samples will be provided from our own work that has not been previously published.

II. CARBOHYDRATES

Carbohydrates are the most important source of dietary calories, if not the largest source of calories for all people. The nutritional value of food is going to be strongly dependent on the source of calories.

The type of carbohydrates captivates equal interest because it can also determine the nutritional value. Complex carbohydrates such as starches are considered longer-lasting and more important than sugars, even though starches are broken down to sugars by amylases on digestion. Sugar alcohols are indigestible for humans and are able to contribute texture and flavor without adding calories. (The flip side of this benefit is that intestinal flora can digest these sugar alcohols and create gas.)

Previously referenced books have chapters on carbohydrate analysis by Galensa [2] and Scott [3]. A recent review of the analysis of carbohydrates in foods covers the use of HPLC in addition to other techniques [4]. A review by Porretta [5] looks at Maillard reaction products, which are due to the nonenzymatic reaction of carbohydrates with proteins owing to heat, uncontrolled diabetes, or other.

Table 1 lists recent articles reporting new methods of carbohydrate analysis.

23

HPLC Applications in Food and Nutritional Analysis

Kenneth A. Berg and Carlos E. Canessa

The PQ Corporation, Conshohocken, Pennsylvania

I. INTRODUCTION

Food analysis by high-performance liquid chromatography (HPLC) is one of the most massive subjects in chromatographic literature. Several large books on food HPLC have appeared recently [1–3]. Investigators analyzing just foods may need to access in-depth resources such as these. This review endeavors to provide an overview with enough detail to begin measurements, but without encumbering the reader with the detail that may be necessary for difficult analyses. The literature from 1991 has been examined, although just the articles easily obtained were used.

For one reason or another, almost every compound imaginable has been found or sought in food. Consequently, extensive discussion will center on only topics not covered elsewhere in this handbook. These are carbohydrates, lipids, vitamins, and polyphenols. Other classes of compounds found in foods will be discussed by referencing appropriate recent reviews on the subject. Some examples of HPLC analyses of oils and beer samples will be provided from our own work that has not been previously published.

II. CARBOHYDRATES

Carbohydrates are the most important source of dietary calories, if not the largest source of calories for all people. The nutritional value of food is going to be strongly dependent on the source of calories.

The type of carbohydrates captivates equal interest because it can also determine the nutritional value. Complex carbohydrates such as starches are considered longer-lasting and more important than sugars, even though starches are broken down to sugars by amylases on digestion. Sugar alcohols are indigestible for humans and are able to contribute texture and flavor without adding calories. (The flip side of this benefit is that intestinal flora can digest these sugar alcohols and create gas.)

Previously referenced books have chapters on carbohydrate analysis by Galensa [2] and Scott [3]. A recent review of the analysis of carbohydrates in foods covers the use of HPLC in addition to other techniques [4]. A review by Porretta [5] looks at Maillard reaction products, which are due to the nonenzymatic reaction of carbohydrates with proteins owing to heat, uncontrolled diabetes, or other.

Table 1 lists recent articles reporting new methods of carbohydrate analysis.

Table 1 Methods for the Analysis of Carbohydrates

Target class	Compound	Food	Stationary phase	Mobile phase	Detector[a]	Ref.
	Amadori compounds	—	—	—	—	*16*
Carbohydrates				—	—	*16*
Cyclamates	*N,N*-Dichlorocyclo-hexylamine	Fruit beverages	—	—	—	*17*
Polyols		Sugarcane juice	Micropak NH2 IOP/N	Isocratic acetonitrile–water	UV	*7*
Polyols	Glycerol	Wine, grape juice	—	—	—	*18*
Polyols	Glycerol	Wines	ION-300 cation-exchanger H^+ form	10-mM sulfuric acid	—	*2*
Polyols	Glycerol	Wines, grape must	ION-300 cation-exchanger	13-mM sulfuric acid	RI	*6*
Saccharides	Aminosaccharides	Alfalfa	CarboPac PA1 anion-exchanger	Gradient 50-mM NaOH in sodium acetate vs. water	Pulsed amperometric detection	*9*
Saccharides	Glycuronic acids	Alfalfa	CarboPac PA1 anion-exchanger	Gradient 50-mM NaOH in sodium acetate vs. water	Pulsed amperometric detection	*9*
Saccharides	Lactose, fructose, glucose	Mustard extract, white wines, beverages	Microparticulate Ca^{2+} form ligand exchanger (Waters)	Water	Postcolumn derivatization + fluorescence or ELSD or RI	*20*
Saccharides	Maltooligosaccharides	Standards	TSK gel SAX	Sodium acetate buffer	Postcolumn enzyme reaction, pulsed amperometric detector	*10*
Saccharides	Neutral saccharides	Alfalfa	CarboPac PA1 anion-exchanger	Gradient 50-mM NaOH in sodium acetate vs. water	Pulsed amperometric detection	*9*
Starches	Natural and modified	Standards	Micro-Hydrogel 2000 and 250 GPC columns	50-mM NaOH	RI or post column deriv. with KI, visible detection	*11*

Sugar	—	Beet sugar	Column-switching	—	Pulsed amperometric detector	*19*
Sugar	—	Orange juice	Column-switching	—	Pulsed amperometric detector	*19*
Sugars	—	—	—	—	ELSD + RI	
Sugars	—	Orange juice	Anion-exchange	—	Pulsed amperometric detector	*14*
Sugars	—	Sugarcane juice	Micropak NH_2 IOP/N	Isocratic acetonitrile–water	UV	*7*
Sugars	Disaccharides		TSK-G2000 SW; G-Oligo-Pw; Protein-Pak 60	Isocratic 75% acetonitrile–water	Pulsed amperometric detector	*3*
Sugars	Fructose	Peanut	Sugar-Pak column	Water	RI	*8*
Sugars	Fructose	Soybean, potato, banana, apple	TSK gel SCX	0.1 M phosphate pH 7.0–100-μM NADH	Postcolumn enzyme reaction, flourescence detection	*12*
Sugars	Galactose	Cheddar cheese	Aminex HPX-87H	Ioscratic 9-mM sulfuric acid	RI	*1*
Sugars	Galacturonate	Grapefruit, radish, cucumber, celery	BioLC anion-exch.	Sodium acetate buffer	Pulsed amperometric detection	*13*
Sugars	Galactose	Corn, syrup, pear juice	Supelcosil LC18, LiChrospher ODS	0.2-M phosphate pH 6.4 gradient with water	Postcolumn enzyme reaction, amperometric detection	*5*
Sugars	Glucosamine	Peanut	Sugar-Pak column	Water	RI	*8*
Sugars	Glucose	Cheddar cheese	Aminex HPX-87H	Isocratic 9-mM sulfuric acid	RI	*1*
Sugars	Glucose	Corn syrup, pear juice	Supelcosil LC18, LiChrospher ODS	0.2-M phosphate, pH 6.4 gradient with water	Postcolumn enzyme reaction, amperometric detection	*5*

Table 1 Continued

Target class	Compound	Food	Stationary phase	Mobile phase	Detector[a]	Ref.
Sugars	Glucose	Peanut	Sugar-Pak column	Water	RI	*8*
Sugars	Glucose polymers		TSK-G2000 SW; G-Oligo-Pw; Protein-Pak 60	Isocratic 75% acetonitrile–water	Pulsed amperometric detector	*3*
Sugars	Lactose	Cheddar cheese	Aminex HPX-87H	Isocratic 9-mM sulfuric acid	RI	*1*
Sugars	Monosaccharides		TSK-G2000 SW; G-Oligo-Pw; Protein-Pak 60	Isocratic 75% acetonitrile–water	Pulsed amperometric detector	*3*
Sugars	Monosaccharides	Grape musts	Carbopac PA1 anion-exchanger	Isocratic 20-mM NaOH	Ultramicroband electrode	*23*
Sugars	Monosaccharides	Grapefruit, radish, cucumber, celery	BioLC anion-exchanger	Sodium acetate buffer	Pulsed amperometric detection	*13*
Sugars	Monosaccharides	Soft drinks, orange juice, sports drink	3-Morpholinopropyl-modified silica	10-mM imidazole–acetonitrile–borate, pH 6.5	RI	*22*
Sugars	Monosaccharides	Wines	Aminex A-25 borate anion-exchanger	0.4-M borate, pH 9.35	Postcolumn derivitization + fluorescence	*4*
Sugars	Monosaccharides	Wines, grape must	ION-300 cation-exchanger	13-mM sulfuric acid	RI	*6*
Sugars	Raffinose	Peanut	Sugar-Pak column	Water	RI	*8*
Sugars	Rhamnose, xylose, fructose, glucose, sucrose, maltose, melibiose, melezitose, and raffinose	Standards, pine buds	LiChrospher 100 NH2	Isocratic or gradient: acetonitrile–water	ELSD or RI	*15*

Sugars	Rhamnose, xylose, fructose, glucose, sucrose, maltose, melibiose, melezitose, and raffinose	Standards, pine buds	Aminex carbohydrate HPX-87C	Water	ELSD or RI	*15*
Sugars	Rhamnose, xylose, fructose, glucose, sucrose, maltose, melibiose, melezitose, and raffinose	Standards, pine buds	Polyspher CH-Pb	Water	ELSD or RI	*15*
Sugars	Sorbose	Soybean, potato, banana, apple	TSK gel SCX	0.1-M phosphate, pH 7.0–100-μM NADH	Postcolumn enzyme reaction, flourescence detection	*12*
Sugars	Stachyose	Peanut	Sugar-Pak column	Water	RI	*7*
Sugars	Sucrose	Peanut	Sugar-Pak column	Water	RI	*7*
Sugars	Sucrose	Soybean, potato, banana, apple	TSK gel SCX	0.1-M phosphate, pH 7.0–100-μM NADH	Postcolumn enzyme reaction, flourescence detection	*12*

[a]ELSD, evaporative light-scattering detector; MS, mass spectrometer; RI, refractive index; UV, ultraviolet.
Note: Table references can be found at the end of this chapter under the heading "Table References."

III. LIPIDS

A versatile and useful procedure to identify or separate components in lipids is HPLC. The elution of the lipids from the column may be carried out either by gradient elution, stepwise elution with either binary or ternary solvent systems, or isocratically. The conditions used are described in the tables. Usually the lipid eluates are collected for further tests. This section focuses on the latest techniques in HPLC detection of lipids (since 1991). Complete books on earlier HPLC techniques for oils and fats already exist [6].

A. Detectors

There are hundreds of papers of different HPLC methods to identify lipid components. This section will focus on the latest HPLC methods (1991 and up). Because the type of lipid component dictates the detector used, the literature will be grouped by detectors. Although there are many different types of HPLC detectors used for lipids, only those used in the latest publications are mentioned.

1. Ultraviolet Detectors

The most sensitive, versatile, and inexpensive detector used with lipids, which are deficient in specific absorption peaks, is the variable wavelength ultraviolet (UV) detector [7]. Lipids can be detected by "end absorption" [8] in the region of 200–215 nm owing to double bonds in the fatty acyl groups, or to functional groups, such as phosphatidic, phosphate, carboxyl, carbonyl, quaternary ammonium, and amino groups [9]. Detection at such wavelengths has disadvantages. Many chromatography solvents (e.g., acetone, toluene, chloroform–methanol mixtures, and ethyl acetate) show strong absorption below 240 nm and cannot be used in mobile phases. This problem has been overcome by the use of mixtures, such as acetonitrile–methanol–water [9] and hexane–2-propanol–water [10], which are transparent above 200 nm. Solvents must be meticulously purified of contaminants that absorb in this region. Solvent impurities seriously impair baseline stability and have high background absorption. Natural substances, such as tocopherols, can also give disproportionately large peaks that obscure other lipid components in the HPLC trace.

Nevertheless, UV detection at this low range has been widely used in lipid analysis, mainly in the separation of phospholipids and glycolipids. These compounds can be detected by UV absorption after suitable derivatization (e.g., benzoylation) in chloroform- or methanol-containing solvent mixtures [11].

Researchers have found some versatility in UV detection, even though not many solvents can be used in mobile phases [12]. In phospholipid separation, hexane–isopropanol–water or acetonitrile–methanol–water mixtures are used. The order of elution of the neutral phospholipids is not greatly affected by the type of mobile phase employed, but acidic phospholipids, such as phosphatidylinositol and phosphatidylserine, have a tendency to elute earlier when the solvent acetonitrile is present.

Direct quantitation of lipids is difficult. Relatively saturated lipids might even be overlooked, because variation in the unsaturation level causes a substantial difference in the extinction coefficient. By determining the apparent extinction coefficient for each component in a standard mixture very similar to that being analyzed, quantitation of lipid components has been attempted by many analysts [13]. Some of the latest uses of UV detectors include the analysis and fractionation of diacylglycerols [14]; separation of monoacylglycerols on nitrile-bonded stationary phase [15]; analysis of triacylglycerol autoxidation products [16]; and separation of wax esters [17]. Table 2 summarizes the latest HPLC procedures with UV detectors.

2. Evaporative Light-Scattering Detectors

An evaporative light-scattering detector (ELSD) is widely use these days for lipid analysis. This is an optical detection system that is also called a "universal detector," "mass detector,"

Table 2 HPLC Analysis of Lipids Using Ultraviolet Detectors

Compound	Food	Stationary phase	Mobile phase	Solvent	Ref.
Wax esters	Olive oils	Supelcosil LC-Si	Gradient	Hexane–diethyl ether	*24*
Monoacylglycerols	Soybean oil	Nitrile-bonded phase, LIChrospher 100	Isocratic	Hexane–dichloroethane–ethanol	*25*
Autoxidation products of triacylglycerol	Edible oils	Nova-Pak C_{18}	Ioscratic	Acetonitrile–dichloromethane–methanol	*26*

or "evaporative analyzer." Such instruments are made by Varex Corporation, Cunow S.A., Sedere, and Applied Chromatography Systems Ltd., among others. The solvent emerging from the column is evaporated in a stream of air or nitrogen in a heated chamber. Nonvolatile eluates, such as lipids do not evaporate but are nebulized into minute droplets that pass through a light beam, which is reflected and refracted. The scattered light produced by the nonvolatile components is measured by a photomultiplier tube. A good description of the process is presented by Pomeranz and Meloan [7]. Solvents, such as ketones, esters, aromatic compounds, and others, can be used in complex gradients without interference with the signal. The sensitivity of this detector is as good as the best refractive index detectors, and is better than transport flame ionization detectors or UV detectors operated at short wavelengths. An additional advantage in ELSD is that it is not affected by temperature changes or small variations in the flow rate of the mobile phase. The disadvantages of the evaporative light-scattering detector are that the sample is destroyed and that the solvent cannot contain nonvolatile buffers.

In the 1990s many HPLC lipid analyses use ELSD. These include determination of the positional distribution of fatty acids [18]; analysis of lipid classes [19]; characterization of triacylglycerols in complex mixtures of milk fat [20]; quantitative determination of mono- and diglycerides [21]; analysis of lecithins and phospholipids [22,23]; analysis of tocopherols and phytosterols [24]; and autoxidation of unsaturated glycerols [25]. Evaporative light-scattering detectors are being used for separation and quantitation of hydroxy and epoxy fatty acids. Gerard et al. [26] reported that ELSD can discriminate between monohydroxy, epoxy, epoxyhydroxy, dihydroxy, and trihydroxy fatty acids. It can also be used to identify compound monoglycerides synthesized with lipases [27]. These are only some examples in which ELSD maximizes detection. A summary of the latest HPLC procedures using ELSD is presented in Table 3.

3. Refractive Index Detectors

Refractive index (RI) detectors are commonly used with lipids. There are different kinds of RI detectors. The most common ones use deflection, interference, and Fresnel optics. RI detection can be used for all lipid compounds, although it is not as sensitive as UV detection. As a general rule, the sensitivity in milligrams of sample is almost equal to the reciprocal of the difference in refractive index between the solvent and the lipid component. RI detectors are difficult to use with gradient elution systems, and temperature control of the solvents is critical. Lipid samples should be dissolved in a fresh mobile phase just before injection onto the HPLC column because the RI detector is very sensitive to temperature fluctuations. Accurate results with lipid separations often require temperature programming systems [28]. The American Oil Chemists' Society official method for the determination of polymerized triglyc-

Table 3 HPLC Analysis of Lipids Using Evaporative Laser or Light-Scattering Detectors

Compound	Food	Stationary phase	Mobile phase	Solvent	Ref.
Triacylglyerols	Butterfat	Spherisorb-ODS-2	Isocratic	Chloroform–acetonitrile	*27*
Tocopherols	Vegetable oils	Waters Ch. 'resolve'	Isocratic	Acetonitrile–tetrahydrofuran–water	*28*
Phytosterols	Vegetable oils	Waters Ch. 'resolve'	Isocratic	Methanol–water	*28*
Monoglycerides	Glycerols	Ultrasphere-ODS	Isocratic	Acetone–acetonitrile	*29*
Hydroxy and epoxy fatty acids	Plants, animals, microbes	Lichrosorb Si60	Gradient	Hexane–acetic acid-isopropanol	*30*
Phospholipids	Vegetable oils	Lichrosorb Si-60	Gradient	Chloroform–tetrahydrofuran; methanol–ammonium hydroxide–water	*31*
Lipid classes	Fats, edible oils	PLGEL 100–50 A	Isocratic	Tetrahydrofuran	*32*
Phospholipid lecithins	Beef, soybean	Zorbax	Gradient	Isooctane–tetrahydrofuran–isopropanol–chloroform–water	*33*
Monoglycerides diglycerides	Vegetable oils, emulsifiers	Chromegasphere SI-60	Gradient	Hexane: hexane–2-propanol: ethylacetate–formic acid	*34*
Autoxidation products of triacylglycerol	Butter, rapeseed oil	PLGEL 100–50 A	Isocratic	Tetrahydrofuran	*35*
Autoxidation products of triacylglycerol	Edible oils	Nova-Pak C18	Isocratic	Acetonitrile–dichloromethane–methanol	*36*
Tocopherols	Vegetable oils	Beckman Ultrasphere 5 μm	Isocratic	Hexane–isopropanol	*37*
Sucrose polyester	Cooking oils	Beckman ODS 5 μm	Gradient	Methylene chloride–acetonitrile–isopropanol	*38*
Triacylglycerol	Vegetable oils	LiChrospher 100 RP-18	Gradient	Acetone–acetonitrile	*39*

erides (AOCS method Cd 22-91) [29], dictates the use of a refractive index detector, but it mentions that a constant temperature must be maintained to obtain satisfactory results. The Official Method of the International Union of Pure and Applied Chemistry (IUPAC) [30] also dictates the use of an RI detector for polymers detection. My own experience (CEC) with RI detectors is that they are not sufficiently sensitive or suitable for gradient elution procedures. RI detectors were once relatively common in lipid laboratories and have been used, especially for preparative-scale chromatography and gel-filtration, but their use is diminishing.

A refractive index detector was used in my laboratory (CEC) to determine the effect on oil polymers of an oil treatment powder. Used cooking oil was analyzed for polymer by an HPLC size-exclusion method, Official American Oil Chemists' Society method Cd 22-91 (Fig. 1). Polymerized triglycerides elute before the triglyceride trimer, which is a clearly separated peak at 7.53 min. After treatment with a powder containing silica and alumina (BRITESORB R100), the polymer content of the oil is greatly reduced, as shown by the HPLC peak (Fig. 2). Reduction of polymers in cooking oil is expected to reduce plating on cooking surfaces and to reduce oil dragout on the food.

Flor et al. developed a criterion for determining grades of commercial oils based on RI detection [31]. Other methods were developed for: fatty acid distribution of fats and oils without derivatization [32]; identification of thermooxidative and hydrolytic alterations of oils [33]; and identification of adulterated oils [34,35]. A summary of the latest HPLC procedures using refractive index is presented in Table 4.

4. Photodiode Array Detector

The photodiode array (PDA) or diode array detector is now commonly used in lipid HPLC. Instruments are made by Hewlett-Packard, Perkin Elmer, Waters, and others. The latest work with PDA detectors include identification and quantitation of oryzanol components and simultaneous assessment of tocols [36], measurement of chlorophyll [37], analysis of conjugated diene fatty acids [38], and identification of the composition and distribution of individual molecular species of major glycolipids [39]. A summary of these procedures and others that involve photodiode array detection in lipids separations is presented in Table 5.

5. Other Detectors

There are many other types of HPLC detectors used in the identification and analysis of lipids. These methods are presented in Table 6. A new technique that uses electrochemical detection is described by Akasbi and coworkers [40]. This technique has been developed to separate and quantitate the major phenolic compounds of olive oils. Electrochemical detection provides selectivity as well as good sensitivity.

B. HPLC for Lipid Separation Without a Detector

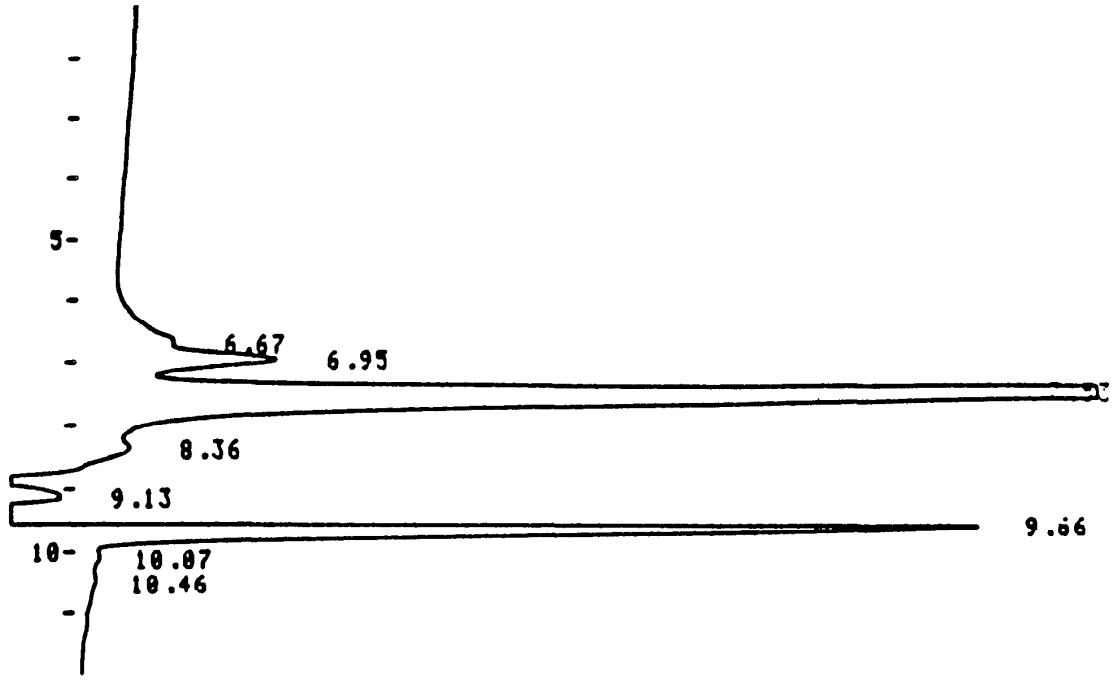
Other HPLC techniques do not require a detector. Some techniques are described in Table 7 for separation of lipid components. Singleton described a technique for enrichment of phospholipids from neutral lipids [41].

IV. VITAMINS AND MINERALS

Federal labeling regulations require food packaging to contain a list of analyses that include all the vitamins, seven minerals, fiber, fat, carbohydrate, and sugar.

Although these values may be based on calculations from the food ingredients, the original values may be determined. Many of the assays are biological. Because of their complexity, there is a need for quick, automatable measurements of the battery of nutritional parameters. HPLC is the obvious choice, providing adequate sensitivity can be achieved.

Several books discuss the HPLC of vitamins. An extensive chapter on vitamin HPLC analysis by Mladek can be found [see Ref. 2] Fat-soluble and water-soluble vitamins are examined separately in chapters of Nollet's book [3].



D-2000 11/16/92 15:40

METHOD: POLYMERS TAG: 8 CH: 1

FILE: 6 CALC-METHOD: AREA% TABLE: 0 CONC: AREA

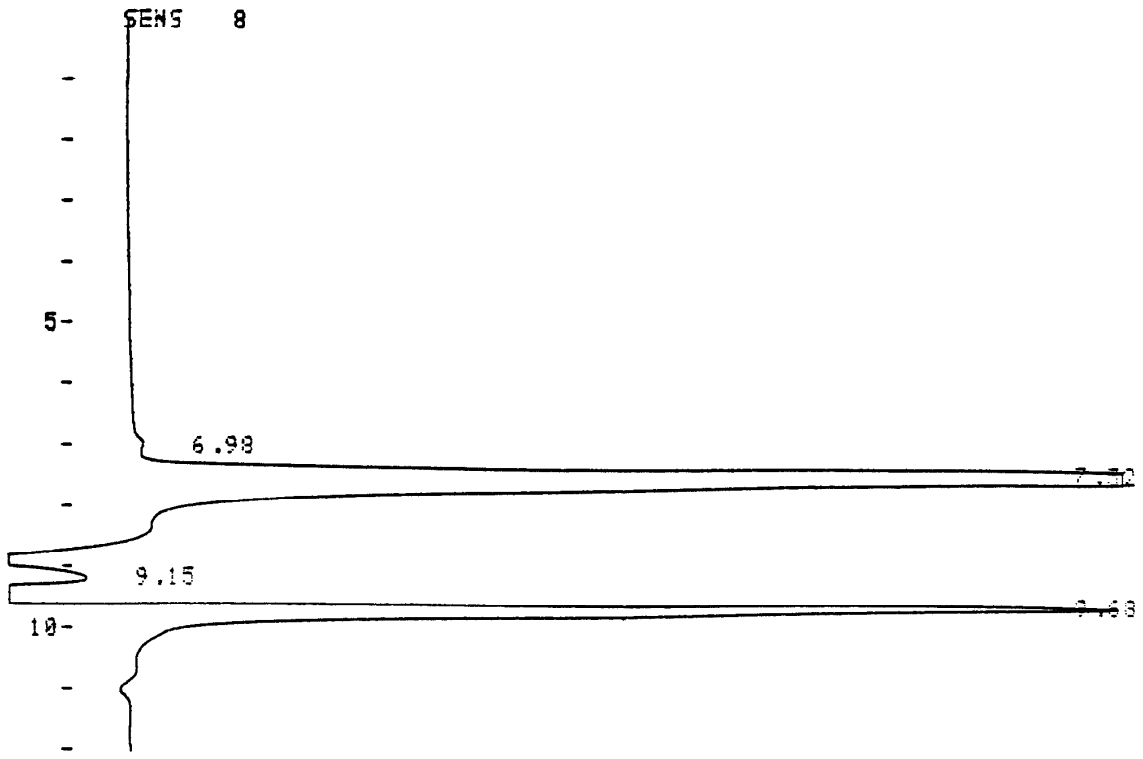
NO.	RT	AREA	PERCENT	BC
1	6.67	98068	3.374	BV
2	6.95	167079	5.749	VV
3	7.53	1185647	40.801	VV
4	8.36	122217	4.205	TBV
5	9.13	250243	8.611	TVB
6	9.66	1081277	37.210	BV
7	10.07	491	0.016	TBB
8	10.46	847	0.029	TBB
TOTAL		2905860	100.000	

PEAK REJ : 0

Figure 1 Size-exclusion chromatography of used cooking oil. Detector: RI; column: Beckman U-Spherogel 1000-A (10-μm), (300 × 7.7 mm); mobile phase: tetrahydrofuran at 1 mL min^{-1}, according to the AOACS method Cd 22-91. Polymerized triglyceride: 6.67 and 6.69 min; triglyceride monomer: 7.53 min; free fatty acids: 8.36 min.

Various reviews of vitamin analysis by HPLC have recently appeared: general reviews [42–44]; water-soluble vitamins [45–47]; and HPLC analyses of the carotenoid isomers (vitamin A precursors) [48].

Table 8 lists recent articles reporting new methods of vitamin analysis.



D-2000

METHOD: TAG: 12 CH: 1

FILE: 0 CALC-METHOD: AREA% TABLE: 0 CONC: AREA

NO.	RT	AREA	CONC	BC
1	6.98	65534	2.488	BV
2	7.52	1411553	53.604	VV
3	9.15	441556	16.768	VB
4	9.68	714635	27.138	BB
TOTAL		2633278	100.000	

PEAK REJ : 0

Figure 2 Size-exclusion chromatography of used and treated cooking oil. Conditions: as in Fig. 1. Oil treatment: silica–alumina-based adsorbent. Polymerized triglyceride: 6.98 min; monomer triglyceride: 7.52 min; free fatty acids.

V. OTHER FOOD COMPONENTS

A. Proteins

The subject of protein HPLC has already been discussed in Chapter 22. Many of these techniques are transferrable to foods.

On the other hand, foods pose a different matrix from most fermentation broths, in that they are often the whole organism or organ, either plant or animal. This involves structure, structural components that can complicate extraction of a single compound, and a host of diluting materials that may or may not interfere with the target analysis.

Table 4 HPLC Analysis of Lipids Using Refractive Detectors

Compound	Food	Stationary phase	Mobile phase	Solvent	Ref.
Triacylglycerols	Olive oil	Supelcosil LC-18	Isocratic	Acetone–acetonitrile	*40*
Polar components	Sunflower oil	Ultrastyragel 100–500 A	Isocratic	Tetrahydrofuran	*41*
Triglycerols	Olive oil, canola oil	Supelcosil LC-18	Isocratic	Acetone–acetonitrile	*42*
Polar compounds	Sunflower oil	HP pL gel 10–50 μm	Isocratic	Tetrahydrofuran	*43*
Fatty acids	Soap-related fats and oils	Radial Pak 8 mm	Isocratic	Acetonitrile–tetrahydrofuran–water–glacial acetic acid	*44*
Triacylglycerols	Bovine butterfat	LiChrospher 100 RP-18	Isocratic	Acetone–acetonitrile	*45*
Triacylglycerol	Vegetable oils	LiChrospher 100 RP-18	Gradient	Acetone–acetonitrile	*46*

Table 5 HPLC Analysis of Lipids Using Photodiode Array Detectors

Compound	Food	Stationary phase	Mobile phase	Solvent	Ref.
Glycolipids	Wheat flour	ODS Supelco Hypersil	Gradient	Hexane–propan-2-ol–water	*47*
Oryzanols	Rice bran oil	ODS HP Hypersil	Gradient	Acetonitrile–methanol–isopropanol–water	*48*
Chlorophyll	Canola seed and oil	ODS 5	Isocratic	Water–methanol–acetone	*49*
Conjugated diene fatty acids	Partially hydrogenated fat	HP C18 ODS Hypersil	Isocratic	Acetonitrile–water–acetic acid–ammonium acetate	*50*

Table 6 HPLC Analysis of Lipids Using Other Detectors

Detector	Compound	Food	Stationary phase	Mobile phase	Solvent	Ref.
Fluorescence	Tocopherols, tocotrienols	Rice bran oil	ODS HP Hypersil	Gradient	Acetonitrile–methanol–isopropanol–water	*51*
Fluorescence	Tocopherols	Vegetable oils	Beckman Ultrasphere 500 A	Isocratic	Hexane–isopropanol	*52*
Flame ionization	Triacylglycerols	*Crepis alpina*	Silver Ion-HPLC Chromsphere	Isocratic	Acetonitrile–hexane	*53*
Flame ionization	Fatty acids	Vegetable oils	Zorbax C18	Gradient	Acetonitrile–methylene chloride	*54*
Fluorescence	Fatty acids	Fish oil	200-μm–id Hewlett-Packard	Isocratic	Methanol–acetonitrile–water	*55*

Table 7 HPLC Uses with Lipids Without Detection

Compound	Food	Stationary phase	Mobile phase	Solvent	Ref.
Phospholipids	Peanut oil	Supelco 5-μm Si	Gradient	Hexane, isopropanol–hexane–water	*56*

Several reviews exist that cover the breadth of techniques examined to date. A review by Bietz on the HPLC analysis of wheat proteins discusses all methods, including size-exclusion, ion-exchange, and reversed-phase chromatographies [49]. Many techniques involving grain should be applicable to other foodstuffs.

Our laboratory (KAB) has studied the HPLC chromatography of whole beer samples, which include proteins, polyphenols, salts, and polymers of these. One of the methods examined was size-exclusion chromatography (SEC) using a variety of detectors. Untreated beer was chromatographed and the effluent was monitored for protein by combining the column output with a second stream containing Bradford reagent (Fig. 3). (The signal, therefore, represented protein exceeding 3000 MW). The column effluent was also monitored using UV absorption and a universal mass detector: an evaporative light-scattering detector. It observes nonvolatile components as a dust, the light scattering of which is proportional to total nonvolatile weight. Notice that there is not much agreement between the peaks. This means that there are a variety of materials here (proteinaceous and nonproteinaceous). The materials differ in color and amount. There are many more peaks when UV detection is used.

The conditions used to run the SEC column are critical to results that are meaningful. Some UV-absorbing material is hydrophobic enough to be retained on the packing coating. This can be reduced by adding methanol to the eluent (Fig. 4).

Buffer concentration is also important for SEC on this column. As the buffer concentration is decreased, "proteins" seem to aggregate and chromatograph as larger units (Fig. 5). The binding in the aggregates that is broken up by a higher buffer concentration may be ionic. Chromatograms with buffer concentrations higher than 20 mM looked similar to those at 20 mM.

A review by Strange et al. discusses the analysis of milk proteins by anion-, cation-, reversed-phase, SEC, and affinity chromatographies [50]. Although already a liquid, milk poses the added problem of being a colloidal suspension of lipid droplets in an aqueous medium, a phase that contains different components from the aqueous phase.

The affinity chromatography of proteins in foods is discussed in a review by Phillips et al. [51]. The stationary-phase is a protein-bound epoxy-activated Protein-Pak affinity column. Proteins purified by this method include glycoproteins, immunoglobulins, enzymes, and lectins.

Small variations in HPLC methods have been discussed in terms of their effect on the chromatography of food proteins. Alternative mobile phases have been reviewed [52]. Temperature gradients and column brand do make a difference in separations [53]. Protein separations are especially sensitive to free silanol groups, making C_{18} columns generally unsuitable for use with proteins. Free silanols in other types of columns can be masked by alkyl ammonium salts such as triethylammonium phosphate [53].

B. Phenolics

The variety of plant-derived phenolic compounds is impressive. They serve as defenses against microorganisms and predators [Table Refs. *98,121*], as colorants [54], and flavors in plants.

Table 8 Methods for the Analysis of Vitamins

Target class	Compound	Food	Stationary phase	Mobile phase	Detector[a]	Ref.
Biotin	Biotin	Almonds	Supelcosil LC-8-DB	Hexanesulfonic acid–triethylamine–methanol	UV	*70*
Biotin	Biotin	Royal jelly	—	—	—	*76*
Biotin	Biotin	Vitamin preparations	TSK gel ODS-80TM	Acetontrile–phosphate buffer–1-butanesulfonate	Postcolumn fluorescence with thiamin	*74*
Folic acid	Folate	Orange juice, grapefruit juice	Zorbax ODS	Methanol gradient in phosphate–acetate buffer–pH 5.0–5-mM tetrabutylammonium bromide (TBAB)	Selective amperometric detection	*77*
Folic acid	Folic acid	—	—	—	UV	*66*
Niacin	Niacin	Almonds	Supelcosil LC-8-DB	Hexanesulfonic acid–triethylamine–methanol	UV	*70*
Niacin	Niacin	Legumes	Micro-Bondapak C_{18} or ODS2 Spherisorb	5-mM (TBAB) in methanol–10-mM acetate buffer	UV	*59*
Niacin	Niacin	Pork	Micro-Bondapak C_{18} or ODS2 Spherisorb	5-mM TBAB in methanol–10-mM acetate buffer	UV	*59*
Niacin	Niacin	Vinegar, strawberry jam	Asahipak NH 2P-50	Acetonitrile–water–sodium acetate	UV/vis	*69*

Niacin	Nicotinamide	Elemental diet	Capcellpak C_{18}	Acetonitrile–water–pH 2.1 with phosphoric acid	UV	*86*
Riboflavin	FAD	Bovine milk	Capcell Pak C_{18}	Gradient: 90% MeOH-water vs. 10-mM sodium phosphate, pH 5.5	Fluorescence	*60*
Riboflavin	FAD	Milk	C_{18}	—	Fluorescence	*87*
Riboflavin	FMN	Bovine milk	Capcell Pak C_{18}	Gradient: 90% MeOH–water vs. 10-mM sodium phosphate, pH 5.5	Fluorescence	*60*
Riboflavin	FMN	Milk	C_{18}	—	Fluorescence	*87*
Riboflavin	Riboflavin	Bovine milk	Capcell Pak C_{18}	Gradient: 90% MeOH–water vs. 10-mM sodium phosphate, ph 5.5	Fluorescence	*60*
Riboflavin	Riboflavin	Foods	—	—	—	*85*
Riboflavin	Riboflavin	Infant formula	—	—	—	*82*
Riboflavin	Riboflavin	Milk	C_{18}		Fluorescence	*87*
Riboflavin	Riboflavin 5′-P	—	MicroBondapak C_{18}	10 mM potassium–methanol	UV/vis	*88*
Thiamine	Thiamine	Almonds	Supelcosil LC-8-DB	Hexanesulfonic acid–triethylamine–methanol	UV	*70*

Table 8 Continued

Target class	Compound	Food	Stationary phase	Mobile phase	Detector[a]	Ref.
Thiamine	Thiamine	Infant formula	—	—	—	*82*
Vitamin A	Vitamin A	Calf liver	Normal phase	—	Fluorescence	*61*
Vitamin A	Vitamin A	Chicken liver	Normal phase	—	Fluorescence	*61*
Vitamin A	Vitamin A	Lamb liver	Normal phase	—	Fluorescence	*61*
Vitamin A	Vitamin A	Milk	RP-18	100-mM $LiClO_4$–MeOH–water	Electrochemical detection	*67*
Vitamin A	Vitamin A	Ox liver	Normal phase	—	Fluorescence	*61*
Vitamin A	Vitamin A	Pig liver	Normal phase	—	Fluorescence	*61*
Vitamin A	Vitamin A	Turkey liver	Normal phase		Fluorescence	*61*
Vitamin A	α-Carotene	Vegetables	Phenomenex with Ultramex C_{18}	Acetonitrile–methanol–ethyl acetate	Photodiode array	*62*
Vitamin A	Ascorbate	Potatoes, strawberries	Aminex HPX-87H ion-exclusion	4.5-mM sulfuric acid	UV	*68*
Vitamin A	β-Carotene	Vegetables	Phenomenex with Ultramex C_{18}	Acetonitrile–methanol–ethyl acetate	Photodiode array	*62*
Vitamin A	β-Cryptoxanthin	Vegetables	Phenomenex with Ultramex C_{18}	Acetonitrile–methanol–ethyl acetate	Photodiode array	*62*
Vitamin A	Dehydroascorbate	Potatoes, strawberries	Aminex HPX-87H ion-exclusion	4.5 mM sulfuric acid	UV	*68*
Vitamin B_{12}	B_{12} precursors	Nonfoods	—	—	—	*63*
Vitamin B_2	FAD	Foods	—	—	—	*85*
Vitamin B_2	FMN	Foods	—	—	—	*85*
Vitamin B_6	5s-*O*-(β-D-glucopyranosyl) pyridoxine	Grains	Ultrasphere ion-pair (IP)	Gradient of isopropanol vs 8-mM octane sulfonic acid pH 2.2 in 33-mM phosphate	Fluorescence	*80*

Vitamin B_6	Vitamin B_6	—	—	—	Postcolumn derivatization	*79*
Vitamin B_6	Vitamin B_6	Grains	Ultrasphere ion-pair (IP)	Gradient of isopropanol vs. 8-mM octane sulfonic acid pH 2.2 in 33-mM phosphate	Fluorescence	*80*
Vitamin B_6	Carbamoyl derivatives	Standards with liver extract	Supelcosil LC-18	Potassium phosphate–methanol	UV	*71*
Vitamin B_6	Glycosylated B_6	Grains	Ultrasphere ion-pair (IP)	Gradient of isopropanol vs. 8-mM octane sulfonic acid pH 2.2 in 33 mM phosphate	Fluorescence	*80*
Vitamin B_6	Pyridoxal-5′-P	Standards with liver extract	Supelcosil LC-18	Potassium phosphate–methanol	UV	*71*
Vitamin B_6	Pyridoxamin-5′-P	Standards with liver extract	Supelcosil LC-18	Potassium phosphate–methanol	UV	*71*
Vitamin B_6	Pyridoxine	Elemental diet	Capcellpak C_{18}	Acetonitrile–water–pH 2.1 with phosphoric acid	UV	*86*
Vitamin B_6	Pyridoxine	Infant formula	—	—	—	*82*
Vitamin B_x	Vitamin B	Milk	C_{18}	—	Fluorescence	*87*

Table 8 Continued

Target class	Compound	Food	Stationary phase	Mobile phase	Detector[a]	Ref.
Vitamin C	Ascorbate	Tomato, kiwi, camu-camu	Micro-Bondapak C_{18} ion-pair	MeOH–water–cetrimide–potassium phosphate buffer pH 4.59	UV	*57*
Vitamin C	Isoascorbate	Tomato, kiwi, orange juice, camu-camu	Micro-Bondapak C_{18}	Methanol–water–5 mM cetrimide–50 mM potassium phosphate	UV	*89*
Vitamin C	Ascorbate	Diet supplement	Inertsil ODS-2	1 mM EDTA–100 mM potassium phosphate pH 3.0	Electrochemical detection	*65*
Vitamin C	Ascorbate	Fruits, vegetables	Spheri-5 PP-18	2% potassium phosphate, pH 2.3	Photodiode array	*58*
Vitamin C	Ascorbate	Milk, yogurt	PRP-1	Acetonitrile–potassium phosphate–1-propane-sulfonate	Fluorescence	*73*
Vitamin C	Ascorbate	Plasma	Micro-Bondasphere	Acetonitrile–water	UV/vis	*75*
Vitamin C	Ascorbate	Tomato, kiwi, orange juice, camu-camu	Micro-Bondapak C_{18}	Methanol–water–5 mM cetrimide–50-mM potassium phosphate	UV	*89*

Vitamin C	Ascorbate, K_2 ascorbyl-2-sulfate dihydrate, L-ascorbyl-2-phosphate sodium	Shrimp	Novapak	1.3-uM *n*-octylamine–0.6 mM EDTA–pH 5.0 with acetic acid–0.1-M sodium acetate	UV	*81*
Vitamin C	Ascorbate, K_2 ascorbyl-2-sulfate dihydrate, L-ascorbyl-2-phosphate sodium	Shrimp	Novapak	0.1-mM EDTA–tetrabutyl-ammonium phosphate–80-mM sodium acetate, pH 4.0	UV	*81*
Vitamin C	Ascorbate, K_2 ascorbyl-2-sulfate dihydrate, L-ascorbyl-2-phosphate sodium	Shrimp	Shodex NH pak	70-mM potassium phosphate–2-mM EDTA 20–mM NH_4Cl	UV	*81*
Vitamin C	Ascorbic acid	—	—	—	Postcolumn derivitization + fluorometric detection	*71*
Vitamin C	Ascorbic acid	Wine, beer	—	—		*83*
Vitamin C	Dehydroascorbate	—	PRP-1	Acetonitrile–potassium phosphate–1-propanesulfonate	Fluorescence	*73*

Table 8 Continued

Target class	Compound	Food	Stationary phase	Mobile phase	Detector[a]	Ref.
Vitamin C	Dehydroascorbate	Fruits, vegetables	Spheri-5 PP-18	2% potassium phosphate, pH 2.3	Photodiode array	*58*
Vitamin C	Dehydroascorbate	Tomato, kiwi, camu-camu	Micro-Bondapak C_{18} ion-pair	MeOH–water–cetrimide–potassium phosphate buffer pH 4.59	UV	*57*
Vitamin C	Dehydroascorbate	Tomato, kiwi, orange juice, camu-camu	Micro-Bondapak C_{18}	Methanol–water–5 mM cetrimide–50 mM potassium phosphate	UV	*89*
Vitamin C	Dehydroascorbic acid	—	—	—	Postcolumn derivitization + fluorometric detection	*78*
Vitamin C	Isoascorbate	Tomato, kiwi, camu-camu	Micro-Bondapak C_{18} ion-pair	MeOH–water–cetrimide–potassium phosphate buffer pH 4.59	UV	*57*
Vitamin C	Isoascorbic acid	Wine, beer	—	—	—	*83*
Vitamin E	Vitamin E	Milk	RP-18	100-mM $LiClO_4$–MeOH–water	Electrochemical detection	*67*

[a]UV, ultraviolet; UV/vis, ultraviolet/visual.

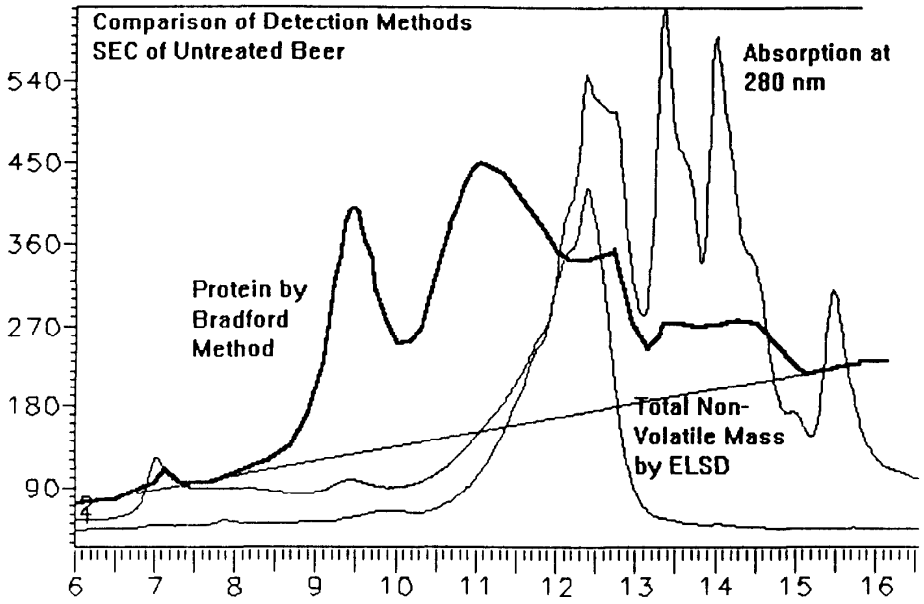


Figure 3 Size-exclusion chromatography (SEC) of whole beer sample. Detection of total mass by an evaporative light-scattering detector; protein by Bradford reagent; and UV absorption at 280 nm. Column: Beckman Ultraspherogel SEC 2000 (300 × 7.5 mm); mobile phase: 20% methanol in water (v/v); flow rate: 1 mL min^{-1}.

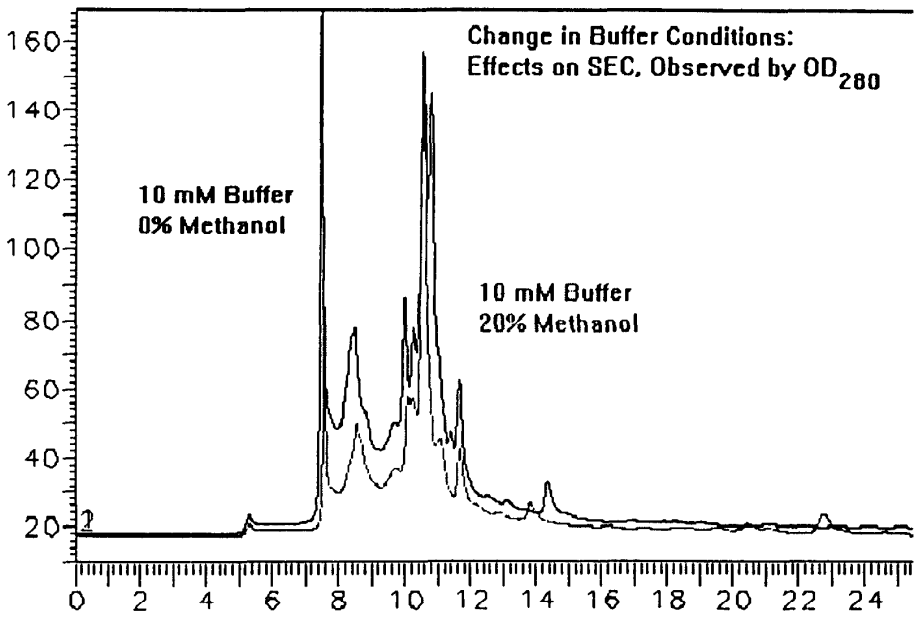


Figure 4 Effect of solvent polarity on size-exclusion chromatography of whole beer. Mobile phase: 10 mM of phosphate buffer, pH 4.4; 0% methanol (upper curve); 20% methanol (lower curve). Otherwise the sample was chromatographed as described in Fig. 3; detection of UV chromophores at 280 nm.

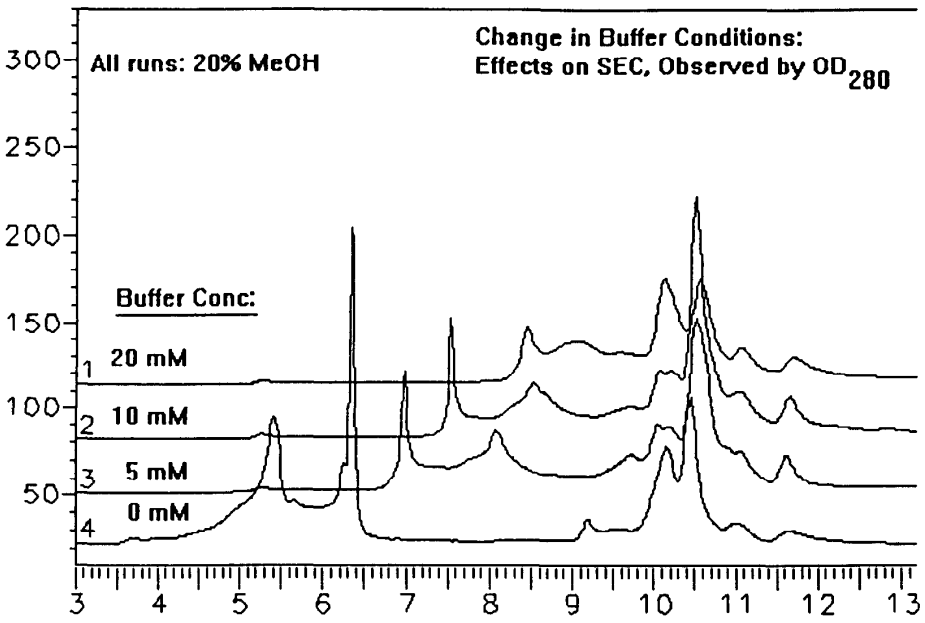


Figure 5 Size exclusion chromatography (SEC) of whole beer. Column conditions described above. Mobile phase: phosphate buffer (concentration indicated on graph). pH 4.4, 20% methanol (v/v). Detection by UV absorption at 280 nm.

The analysis of polyphenols in food is important because of the variety of effects they have on foods. They contribute color and flavor, especially bitterness and astringency [see Table Ref. *108*]. Polyphenols become especially important when they affect the quality and age stability of the food. An example is the level of tannins in barley. These compounds survive intact through the malting process, brewing, and fermentation steps of beer production into finished beer [55]. They are normally hydrogen-bonded to a class of proteins having a high percentage of proline residues and no attached carbohydrate. Over time, these complexes combine to form aggregates that are soluble at room temperature, but insoluble at refrigerator temperatures. This beer defect is called chill haze, and is actively countered by every major brewer.

Various HPLC systems have been reported to separate polyphenols. A review by Lew and Hong [68] discusses the analyses of many anthocyanins in berries, apples, and wine.

C. Pesticides and Herbicides

The measurement of pesticides and herbicides in foods has become more important recently as the public has become aware of their presence and of the ability of food producers to avoid residues in foods. An entire industry has appeared to attempt to provide "organically grown" food, specifically to avoid the residues of agricultural chemicals.

The large-scale production of high-quality food, however, does seem to require judicious use of certain chemicals. These products are changing constantly as longevity and toxicity are reduced without sacrificing efficacy against pests.

An often overlooked fact is that the "disease-resistant" plant strains produce their own pesticides, often in amounts exceeding residues of commercial products. Analysis of these "natural" toxins may lead to a more rational agricultural program.

The extent of the agricultural chemical industry and the level of public concern has generated a significant body of literature specific to food analysis. Chapter 31 on pollutant analysis discusses the chromatography of agricultural and industrial products in environmental

Table 9 Methods for the Analysis of Phenolics

Target class	Compound	Food	Stationary phase	Mobile phase	Detector[a]	Ref.
Anthocyanins	Cyanidin 3-glucoside	Red raspberry juice	Spherisorb ODS II	Methanol gradient in 15% acetic acid–water	UV/vis	*123*
Anthocyanins	Cyanidin 3-glucosylrutinoside	Red raspberry juice	Spherisorb ODS II	Methanol gradient in 15% acetic acid–water	UV/vis	*123*
Anthocyanins	Cyanidin 3-rutinoside	Red raspberry juice	Spherisorb ODS II	Methanol gradient in 15% acetic acid–water	UV/vis	*123*
Anthocyanins	Cyanidin 3-sophoroside	Red raspberry juice	Spherisorb ODS II	Methanol gradient in 15% acetic acid–water	UV/vis	*123*
Anthocyanins	Pelargonidin-3-glucorutinoside	Red raspberry juice	Spherisorb ODS II	Methanol gradient in 15% acetic acid–water	UV/vis	*123*
Anthocyanins	Pelargonidin-3-sophoroside	Red raspberry juice	Spherisorb ODS II	Methanol gradient in 15% acetic acid–water	UV/vis	*123*
Anthocyanins	—	Berries	LiChrospher RP-18	Gradients with water–methanol or acetonitrile or THF–formic or acetic acids	UV/vis	*101*
Anthocyanins	(*p*-Hydroxyphenyl) butan-2-one	Raspberry	—	—	—	*93*
Anthocyanins	Cyanidin 3-glucoside	Cranberry, blackberry	Chemcopak, Capcellpak C_{18}	Isocratic 4% phosphoric acid–acetonitrile	UV/vis	*111*
Antohcyanins	Cyanidin 3-glucosylrutinoside	Cranberry, blackberry	Chemcopak, Capcellpak C_{18}	Isocratic 4% phosphoric acid–acetonitrile	UV/vis	*111*

Table 9 Continued

Target class	Compound	Food	Stationary phase	Mobile phase	Detector[a]	Ref.
Anthocyanins	Cyanidin 3-rutinoside	Cranberry, blackberry	Chemcopak, Capcellpak C_{18}	Isocratic 4% phosphoric acid–acetonitrile	UV/vis	*111*
Anthocyanins	Cyanidin 3-sophoroside	Cranberry, blackberry	Chemcopak, Capcellpak C_{18}	Isocratic 4% phosphoric acid–acetonitrile	UV/vis	*111*
Catechins	—	Grape seed	CO: PELL ODS + Nucleosil C_{18}	Gradient of 10% acetic acid vs. water	Photodiode array	*106*
Flavonoid aglycons	—	Bean pods	Li Chrospher 100 RP-100	Isocratic methanol–5% formic acid	Photodiode array	*118*
Phenolics	—	Fruit juices	—	—		*114*
Phenolics	—	Grapes	SEC	—		*109*
Phenolics	—	Olive oil	Erbasil (C_{18})	2% acetic acid	Photodiode array	*116*
Phenolics	—	Olive oil	Reversed phase	—	UV	*110*
Phenolics	—	Olive oil	—	—	—	*94*
Phenolics	—	Olive oil	—	—	—	*96*
Phenolics	15 free phenolic acids	Wines, sherry	Spherisorb ODS2	Gradient of methanol–water–phosphoric acid	UV	*102*
Phenolics	3-Flavanols, low MW phenolics	Fruit juices	C_{18} Nova-Pak	Methanol gradient in acetic acid–water	Photodiode array	*92*
Phenolics	39 phenols	Beer, wines, lemon juice, soya	HR 80 (PTFE-lined ODS)	SDS–sodium phosphate–nitriloacetic acid–methanol; gradient in SDS	Coulometric electrode array system	*90*
Phenolics	7 phenols	Apples	Spherisorb ODS2	Dilute HCl gradient in methanol	UV	*100*

Phenolics	9 phenols	Olive oil	Erbasil (C_{18})	Gradient between 2% acetic acid and methanol	Photodiode array	*113*
Phenolics	Caffeic acid	Potato	Zorbax ODS	Acetonitrile gradient in acetic acid–water	UV	*99*
Phenolics	Caffeine	Coffee	TSK 3000-SW	0.05% sodium azide in water	UV	*107*
Phenolics	Chlorogenic acid	Coffee	TSK 3000-SW	0.05% sodium azide in water	UV	*107*
Phenolics	Chlorogenic acid	Potato	Zorbax ODS	Acetonitrile gradient in acetic acid–water	UV	*99*
Phenolics	Chlorogenic acid	Potato products	Ultrasphere Octyl	Methanol–0.5% formic acid in water	UV	*97*
Phenolics	Chlorogenic acid	Potatoes			UV	*122*
Phenolics	Ferulic acid	Potato	Zorbax ODS	Acetonitrile gradient in acetic acid–water	UV	*99*
Phenolics	Flavanol glycosides	Fruit juices	C_{18} Nova-Pak	Isocratic 2.5% acetic acid–THF–water–acetic acid	Photodiode array	*92*
Phenolics	Flavonol aglycons	Fruit juices	C_{18} Nova-Pak	Isocratic methanol–water–acetic acid	Photodiode array	*92*
Phenolics	Hydroxytyrosol	Olives	Spherisorb ODS-2	Acetonitrile gradient in water pH 2 with phosphoric acid	Photodiode array	*115*

Table 9 Continued

Target class	Compound	Food	Stationary phase	Mobile phase	Detector[a]	Ref.
Phenolics	Low-MW phenolics	—	—	—	Thermospray LC/MS	*91*
Phenolics	Oleuropein	Olives	Spherisorb ODS-2	Acetonitrile gradient in water pH 2 with phosphoric acid	Photodiode array	*115*
Phenolics	*p*-OH-benzoic acid	Carrots, apple, artichoke	Rosil C_{18}	Gradient of methanol–acetonitrile in water, pH 2.6, with phosphoric acid	UV	*121*
Phenolics	*p*-OH-benzoic acid esters	Carrots, apple, artichoke	Rosil C_{18}	Gradient of methanol–acetonitrile in water pH 2.6 with phosphoric acid	UV	*121*
Phenolics	*p*-Coumaric acid	Olives	Spherisorb ODS-2	Acetonitrile gradient in water, pH 2 with phosphoric acid	Photodiode array	*115*
Phenolics	*p*-Coumaric acid	Potato	Zorbax ODS	Acetonitrile gradient in acetic acid–water	UV	*99*
Phenolics	*t*-5′-Caffeoylquinic acid	Carrots, apple, artichoke	Rosil C_{18}	Gradient of methanol–acetonitrile in water, pH 2.6 with phosphoric acid	UV	*121*

Phenolics	Tyrosol	Olives	Spherisorb ODS-2	Acetonitrile gradient in water, pH 2 with phosphoric acid	Photodiode array	*115*
Phenolics	Vanillic acid	Olives	Spherisorb ODS-2	Acetonitrile gradient in water, pH 2 with phosphoric acid	Photodiode array	*115*
Phenolics	Verbascoside	Olives	Spherisorb ODS-2	Acetonitrile gradient in water, pH 2 with phosphoric acid	Photodiode array	*115*
Phenolics	4-Methylcatechol	Apple	Chrompack C_{18}	Isocratic methanol–2.5% acetic acid in water	UV	*112*
Phenolics	Catechin	Apple	Chrompack C_{18}	Isocratic methanol–2.5% acetic acid in water	UV	*112*
Phenolics	Chlorogenic acid	Apple	Chrompack C_{18}	Isocratic acetonitrile–water, pH 2.6 by phosphoric acid	UV	*112*
Phenolics	Epicatechin	Apple	Chrompack C_{18}	Isocratic acetonitrile–water, pH 2.6 by phosphoric acid	UV	*112*
Polyphenolics	Caffeine	Tea	—	—	—	*105*
Polyphenolics	Flavanols	Tea	—	—	—	*105*
Polyphenolics	Gallic acid	Tea	—	—	—	*105*

Table 9 Continued

Target class	Compound	Food	Stationary phase	Mobile phase	Detector[a]	Ref.
Polyphenolics	Theaflavic acids		Hypersil ODS or Hypersil octyl wide-pore or Hamilton PRP-1	Acetonitrile gradient in 2% acetic acid and 1% citric acid	Photodiode array	*103*
Polyphenolics	Theaflavins	Black tea	Hypersil ODS or Hypersil octyl wide-pore or Hamilton PRP-1	Acetonitrile gradient in 2% acetic acid and 1% citric acid	Photodiode array	*103*
Polyphenolics	Thearubigins	Black tea	Hypersil ODS or Hypersil octyl wide-pore or Hamilton PRP-1	Acetonitrile gradient in 2% acetic acid and 1% citric acid	Photodiode array	*103*
Polyphenolics	Theogallin	Tea	—	—	—	*105*
Polyphenolics	Tocopherols	Paprika	—	—	—	*104*
Polyphenolics	Desgalloyl	Black tea	—	—	—	*120*
Polyphenolics	Humulones	Hops	PMSCL cyanopropyl	Gradient of acetonitrile in water–0.05% phosphoric acid	UV	*117*
Polyphenolics	Hydroxycinnamic acid esters	—	—	—	—	*95*
Polyphenolics	Lupulones	Hops	PMSCL cyanopropyl	Gradient of acetonitrile in water–0.05% phosphoric acid	UV	*117*
Polyphenolics	Polyphenol esters and glycosides	—	—	—	—	*95*
Polyphenolics	Polyphenols	Fruit juice	—	—	—	*95*
Polyphenolics	Theaflavonin	Black tea	—	—	—	*120*
Polyphenolics	Theogallin	Black tea	—	—	—	*120*

Proanthocyanidins		Grade seed	CO: PELL ODS + Nucleosil C_{18}	Gradient of 10% acetic acid vs. water	Photodiodc array	*106*
Proanthocyanidins	8 phenols	Sainfoin leaf	LiChrospher 100 RP-18	Gradient from 1% acetic acid to methanol	Photodiode array	*98*
Procyanidins	Catechin, epicatechin, procyanidins B1, B2, B5, C1, chlorogenic acid, *p*-coumaroylquinic acid, phoridzin	Apple pulp	Nova Pak C_{18}	Acetonitrile–water gradient	UV	*108*
Tannins	—	Black tea	—	—	—	*128*
Volatile phenols	4-Ethylgaiacol	Wines	LiChrospher 100 RP-18	Isocratic acetonitrile–acetic acid–triethylamine pH 5	UV	*119*
Volatile phenols	4-Ethylphenol	Wines	LiChrospher 100 RP-18	Isocratic acetonitrile–acetic acid–triethylamine pH5	UV	*119*
Volatile phenols	Vinylguiacol	Wines	LiChrospher 100 RP-18	Isocratic acetonitrile–acetic acid–triethylamine pH 5	UV	*119*
Volatile phenols	Vinylphenol	Wines	LiChrospher 100 RP-18	Isocratic acetonitrile–acetic acid–triethylamine pH 5	UV	*119*

[a]UV, ultraviolet.

water samples. Many of these techniques are applicable to foodstuffs. Several book reviews exist on this subject: pesticide analysis in foods [56] and pesticide residues [57]. There is, in fact, an entire journal devoted to the topic: *Journal of Food Additives and Contaminants.*

Several excellent articles review pesticide analysis. Various chromatographic methods are discussed by K. Fodor-Csorba [58]. Agarwall [59] and Guggisberg et al. [60] review sulfonamide chromatography; herbicide analyses [61], and pesticide residues found specifically in oils and fat by gel-permeation chromatography [62] have also been reviewed [60].

D. Drugs

The pharmaceutical industry has generated a significant volume of literature specific to the analysis of their products. These analysis techniques permit not only further drug development, but also drug testing in foodstuffs. They also allow their measurement in situations of potential abuse (e.g., the Olympics).

Drugs are never far from the news, owing to the underground economy of illicit drugs, the invention of new products, and the attempt to reduce the recreational use of drugs in our society. Because of this awareness, the public is sensitive to drug use in livestock and the food-borne residues that could result. Because some of the drugs are growth-inducing hormones, they may be impossible to detect apart from naturally occurring hormones secreted at natural levels. In such cases, quantitative precision becomes important. In other situations, selectivity is more valuable. Assays for synthetic drugs must be able to detect their subtle structural differences from their natural analogues.

Chapter 20 discusses pharmaceutical analysis. The books previously discussed have chapters on drug analysis (i.e., drugs used in animals [1], residues and contaminants [63], and antimicrobials in meats [64].

The literature also includes a review on antibiotics [65] and one on antibacterials in foods of animal origin [66]. Tetracyclines are also specifically reviewed [67].

REFERENCES

1. W Baltes, ed. Rapid Methods for Analysis of Food and Food Raw Material. Lancaster: Technomic Publishing, 1990.
2. R Matissek, R Wittkowski, eds. High Performance Liquid Chromatography in Food Control and Research. Hamburg: Springer-Verlag, 1992.
3. LML Nollet, ed. Food Analysis by HPLC. New York: Marcel Dekker, 1992.
4. FW Scott. Food Sci Technol 52:259–274, 1992.
5. S Porretta. J Chromatogr 624:211–220, 1992.
6. WW Christie. High Performance Liquid Chromatography and Lipids. Oxford: Pergamon Press, 1987.
7. Y Pomeranz, C Meloan. Food Analysis: Theory and Practice. New York: Van Nostrand Reinhold, 1987.
8. WW Christie. Advances in Lipid Methodology—One. Great Britain: Oil Press, 1992.
9. FB Jungalwala, JE Evans, RH McCluer. Biochem J 155:55–60, 1976.
10. WSM Geurts van Kessel, WMA Hax, RA Demel. J Biochim Biophys 486:524, 1977.
11. JE Evans, RH McCluer. J Biochim Biophys 270:565, 1972.
12. WW Christie. High Performance Liquid Chromatography and Lipids. Oxford: Pergamon Press, 1987.
13. R Vercaemst, et al. Atherosclerosis 78:245–250, 1989.
14. B Semporé, J. Bézard. J Chromatogr 547:89–103, 1991.
15. T Takagi, Y Ando. J Am Oil Chem Soc 71:459–461, 1994.
16. E Vinanen, A Hopia. J Am Oil Chem Soc 71:537–540, 1994.
17. M Amelio, R Rizzo, F Varazini. J Am Oil Chem Soc 70:793–796, 1993.

18. S Kermasha, S Kubows, M Safari, A Reid. J Am Oil Chem Soc 70:169–173, 1993.
19. A Hopia, V Piironen, P Koivistoinen, L Hyvönen. J Am Oil Chem Soc 69:772–776, 1992.
20. G Spanos, S Schwartz, R van Breemen, C-H Huang. Lipids 30:85–90, 1995.
21. J Liu, T Lee, E Bobik, H Guzman. J Am Oil Chem Soc 70:343–348, 1993.
22. S Melton. J Am Oil Chem Soc 69:784–788, 1992.
23. T Mounts, S Abidi, K Kennick. J Am Oil Chem Soc 69:438–442, 1992.
24. K Warner, T Mounts. J Am Oil Chem Soc 67:827–831, 1990.
25. A Hopia, A Lampi, V Piironen, L Hyvonen, E Koivistoinen. J Am Oil Chem Soc 70:779–784, 1993.
26. H Gerard, R Moreau, W Fett, S Osman. J Am Oil Chem Soc 69:301–304, 1992.
27. C Akoh, C Cooper, C Nwosu. J Am Oil Chem Soc 69:257–260, 1992.
28. E Frede, H Thiele. J Am Oil Chem Soc 64:521–528, 1987.
29. American Oil Chemists' Society. Official Methods and Recommended Practices. Chicago: American Oil Chemists' society, 1994.
30. International Union of Pure and Applied Chemistry. Official Procedures. Oxford: International Union of Pure and Applied Chemistry, 1985.
31. R Flor, L Hecking, B Martin. J Am Oil Chem Soc 70:199–204, 1993.
32. E George. J Am Oil Chem Soc 71:789–791, 1994.
33. R Arroyo, C Cuesta, C Garrido-Polonio, S Lopez-Varela, F Sanchez-Muniz. J Am Oil Chem Soc 69:557–563, 1992.
34. E Salivaras, A McCurdy. J Am Oil Chem Soc 69:935–938, 1992.
35. F Sanchez-Muniz, C Cuesta, G Garrido-Polonio. J Am Oil Chem Soc 70:235–240, 1993.
36. E Rogers et al. J Am Oil Chem Soc 70:301–307, 1993.
37. K Ward et al. J Am Oil Chem Soc 71:931–934, 1994.
38. S Banni et al. J Am Oil Chem Soc 71:1321–1326, 1994.
39. J Prieto, A Ebri, C Collar. J Am Oil Chem Soc 69:1019–1022, 1992.
40. M Akasbi, D Shoeman, A Saari. J Am Oil Chem Soc 70:367–370, 1993.
41. J Singleton. J Am Oil Chem Soc 70:637–639, 1993.
42. AP DeLeenheer, WE Lambert, MGM De Ruyter. Modern Chromatographic Analysis of the Vitamins, Chromatographic Science Series, Vol. 30, NY: Marcel Dekker, 1985.
43. ID Lumley, PR Lawrance. J Micronutr Anal 7:301–313, 1991.
44. A Rizzolo, S Polesello. J Chromatogr 624:103–152, 1992.
45. WE Lambert, A deLeenheer. Food Sci Technol 52:341–369, 1992.
46. R Macrae. J Microntur Anal 7:247–260, 1990.
47. A Polesello, A Rizzolo. J Micronutr Anal. 8:105–158, 1990.
48. CA O'Neil, SJ Schwartz. J Chromatogr 624:235–252, 1992.
49. JA Bietz, DG Simpson. J Chromatogr 624:58–80, 1992.
50. ED Strange, EL Malin, DL van Hekken, JJ Basch. J Chromatogr 624:81–102, 1992.
51. DJ Philips, B Bell-Alden, M Cava, ER Grover, WH Mandeville, R Mastico, W Sawlivich, G Vella, A Weston. J Chromatogr 536:95–106, 1991.
52. BS Welinder, HH Sørensen. J Chromatogr 537:181–199, 1991.
53. S Linde, BS Welinder. J Chromatogr 536:43–55, 1991.
54. BF De Simon, J Pérez-Ilzanbe, T Hernández, C Gómez-Cordovés, I Estrella. J Agric Food Chem 40:1531–1535, 1992.
55. JW Gramshaw. MBAA Tech Q 6:239–251, 1969.
56. R. Naiisch, H Heasinger, Analysis of Residue and Contaminants, pp. 299–346, in: R Matissek, R Wittkowski, eds. High-Performance Liquid Chromatography in Food Control and Research. Hamburg: Springer-Verlag, 1992, pp 326–332.
57. RJ Bushway. In: LML Nollet, ed. Food Analysis by HPLC. New York: Marcel Dekker, 1992, p 57.
58. K Fodor-Csorba. J Chromatogr 624:353–367, 1992.
59. VK Agarwall. J Chromatogr 624:411–424, 1992.
60. D Guggisberg, AE Mooser, H Koch. J Chromatogr 624:425–438, 1992.

61. J Tekel', K Kovačičova'. J Chromatogr 643:291–303, 1993.
62. Food Sci Lab. Analyst (Lond) 117:1451–1455, 1992.
63. R Malisch, H Heusinger. In: R Matissek, R Wittkowski, eds. High-Performance Liquid Chromatography in Food Control and Research. Hamburg: Springer-Verlag, 1992.
64. NA Botsoglou, DC Kufidis. In: LML Nollet, ed. Food Analysis by HPLC. New York: Marcel Dekker, 1992.
65. DR Bobbitt, KW Ng. J Chromatogr 624:153–170, 1992.
66. B Shaikh, WA Moats. J Chromatogr 643:369–378, 1993.
67. SA Barker, CC Walker. J Chromatogr 624:195–209, 1992.
68. HS Lee, V Hong. J Chromatogr 624:221–234, 1992.

TABLE REFERENCES

1. J Bouzas, CA Kantt, F Bodyfelt, JA Torres. J Food Sci 56:276–278, 1991.
2. M Calull, E. López, RM Marcé, JC Olucha, F Borrull. J Chromatogr 589:151–158, 1992.
3. AS Feste, I Khan. J Chromatogr 607:7–18, 1992.
4. MJ Del Nozal, JL Bernal, FJ Gomez, A Antolin, L Toribio. J Chromatogr 607:191–198, 1992.
5. R Mögele, B Pabel, R Galensa. J Chromatogr 591:165–173, 1992.
6. M Calull, E López, RM Marcé, F Borrull. J Chromatogr 590:215–222, 1992.
7. C Vicente, JL Mateos, MM Pedrosa, M Legaz. J Chromatogr 553:271–283, 1991.
8. SM Basha. J Agric Food Chem 40:780–783, 1992.
9. DA Martens, WT Frankenberger Jr. J Chromatogr 546:297–309, 1991.
10. N Kiba, K Shitara, M Furusaw, Y Takata. J Chromatogr 537:443–448, 1991.
11. T Suortti, E Pessa. J Chromatogr 536:251–254, 1991.
12. N Ciba, R Matsushita, M Furusawa. Anal Chim Acta 259:15–18, 1992.
13. KA Garleb, LD Bourquin, GC Fahey Jr. J Food Sci 56:423–426, 1991.
14. KW Swallow, NH Low, DR Petrus. J Assoc Off Anal Chem 74:341–345, 1991.
15. A Clement, D Yong, C Brechet. J Liq Chromatogr 15:805–817, 1992.
16. A Olano, G Santa-Maria, N Corzo, MM Calvo, I Martinez-Castro, ML Jimeno. Food Chem 43:351–358, 1992.
17. M Lehr, W Schmid. Z Zebensm. Unters Forsch 192:355–358, 1991.
18. A Caputi Jr, E Christensen, N Biedenweg, S Miller. J AOAC Int 75:379–383, 1992.
19. DR White, PF Cancalon. J AOAC Int 75:584–587, 1992.
20. A Coquet, J-L Veuthey, W Haerdi. Chromatographia 34:651–654, 1992.
21. MS Gentleman, HM Burt, DD Kitts, KM McErlane. J Chromatogr 633:105–110, 1993.
22. S Akiyama, K Nakashima, K Yamada. J Chromatogr 626:266–270, 1992.
23. P Pastore, I Lavagnini, G Versini. J Chromatogr 634:47–56, 1993.
24. M Amelio, R Rizzo, F Varazini. J Am Chem Soc 70:793–796, 1993.
25. Y Takaagi, Y Ando. J Am Chem Soc 71:459–461, 1994.
26. E Viinanen, A Hopia. J Am Chem Soc 71:537–540, 1994.
27. S Kermasha, S Kubow, M Safari, A Reid. J Am Chem Soc 70:169–173, 1993.
28. K Warner, T Mounts. J Am Chem Soc 67:872–831, 1990.
29. C Akoh, C Cooper, C Nwosu. J Am Chem Soc 69:257–260, 1992.
30. H Gerard, R Moreau, W Fett, S Osman. J Am Chem Soc 69:301–304, 1992.
31. T Mounts, S Abidi, K Rennick. J Am Chem Soc 69:438–442, 1992.
32. A Hopia, V Piironen, P Koivistoinen, L Hyvönen, J Am Chem Soc 69:772–776, 1992.
33. S Melton. J Am Chem Soc 69:784–788, 1992.
34. J Liu, T Lee, E Bobik, M Guzman-Harty, C Hastilow. J Am Chem Soc 70:343–348, 1993.
35. A Hopia, A Lampi, V Piironen, L Hyvönen, P Koivistoinen. J Am Chem Soc 70:779–784, 1993.
36. E Viinanen, A Hopia. J Am Chem Soc 71:537–540, 1994.
37. W Chase, C Akoh, R Eitenmiller. J Am Chem Soc 71:877–880, 1994.

38. W Chase, C Akoh, R Eitenmiller. J Am Chem Soc 71:1273–1276, 1994.
39. A Carelli, A Cert. J Chromatogr 630:213–222, 1993.
40. R Flor, L Hecking, B Martin. J Am Chem Soc 70:199–203, 1993.
41. R Arroyo, C Cuesta, C Garrido-Polonio, S Lopez-Varela, F Sanchez-Muniz. J Am Chem Soc 69:557–563, 1992.
42. E Salivaras, A McCurdy. J Am Chem Soc 69:935–938, 1992.
43. F Sanchez-Muniz, C Cuesta, C Garrido-Polonio. J Am Chem Soc 70:235–240, 1993.
44. E George. J Am Chem Soc 71:789–791, 1994.
45. C Maniogui, J Gresti, M Bugaut, S Gauthier, J Bezard. J Chromatogr 543:81–103, 1991.
46. A Carelli, A Cert. J Chromatogr 630:213–222, 1993.
47. J Prieto, A Ebri, C Collar. J Am Chem Soc 69:1019–1022, 1992.
48. E Rogers, S Rice, R Nicolosi, D Carpenter, C McClelland, L Romanczyk. J Am Chem Soc 70:301–307, 1993.
49. K Ward, R Scarth, J Daun, C Thorsteinson. J Am Chem Soc 71:931–934, 1994.
50. S Banni, B Day, R Evans, F Corongiu, B Lombardi. J Am Chem Soc 71:1321–1326, 1994.
51. E Rogers, S Rice, R Nicolosi, D Carpenter, C McClelland, L Romanczyk. J Am Chem Soc 70:301–307, 1993.
52. W Chase, C Akoh, R Eitenmiller. J Am Chem Soc 71:877–880, 1994.
53. W Neff, R Adlof, M El-Agaimy. J Am Chem Soc 71:853–856, 1994.
54. H Konishi, W Neff, T Mounts. J Chromatogr 629:237–241, 1993.
55. J Shin Yoo, V McGuffin. J Chromatogr 627:87–96, 1992.
56. J Singleton. J Am Chem Soc 70:637–638, 1993.
57. S Zapata, J-P DuFour. J Food Sci 57:506–511, 1992.
58. MO Nisperos, BS Busling, PE Shaw. J Agric Food Chem 40:1127–1130, 1992.
59. C Vidal-Valverde, A Reche. J Agric Food Chem 39:116–121, 1991.
60. C Kanno, K Shirahuji, T Hoshi. J Food Sci 56:678–681, 1991.
61. MJ Scotter, SA Thorpe, SL Reynolds, LA Wilson, DJ Lewis. Food Addit Contam 9: 237–242, 1992.
62. BFH Chen, JR Chuang, JH Lin, CP Chiu. J Food Prot 56:51–54, 1993.
63. SH Ford, J Gallery, A Nichols, M Shambee. J Chromatogr 537:235–247, 1991.
64. H Hasegawa. J Chromatogr 605:215–220, 1992.
65. H Iwase. J Chromatogr 606:277–280, 1992.
66. H Iwase. J Chromatogr 609:399–401, 1992.
67. MM Delgado Zamarreño, A Sánchez Pérez, G Gómez Perez, J Hernández Méndez. J Chromatogr 623:69–74, 1992.
68. WD Graham, D Annette. J Chromatogr 594:187–194, 1992.
69. S Hirayama, M Maruyama. J Chromatogr 58:171–175, 1991.
70. A Rizzolo, C Baldo, A Polesello. J Chromatogr 553:187–192, 1991.
71. L Terzuoli, R Pagiani, R Leoncini, D Vannoni, E Marinello. J Chromatogr 547:472–477, 1991.
72. K Takamura, H Hoshino, T Sugahra, H Amano. J Chromatogr 545:201, 1991.
73. N Bilic. J Chromatogr 543:367–374, 1991.
74. T Yokoyama, T Knoshita. J Chromatogr 542:365–372, 1991.
75. E Kisnida, Y Nishimoto, S Kojo. Anal Chem 64:1505–1507, 1992.
76. P Nandhasri, AK Htoon, J Chaivmol, C Phunchaisri. ASEAN Food J 6:163–164, 1991.
77. DR White Jr, HS Lee, RE Krueger. J Agric Food Chem 39:714–717, 1991.
78. M Capellmann, HM Bolt. Fresenius J Anal Chem 342:462–466, 1992.
79. A Bognar. Fresenius J Anal Chem 343:155–156, 1992.
80. JF Gregory III, DB Sartain. J Agric Food Chem 39:899–905, 1991.
81. KM Hoffman, PR Brown, PD Maugle. J Liq Chromatogr 15:2581–2610, 1992.
82. GW Chase, WO Landen, RR Eitenmiller, A-G M Soliman. J Assoc Off Anal Chem 75: 561–565, 1992.
83. B Seiffert, H Swaczyna, I Schaefer. Dtsch Lebensm Rundsch 88:38–40, 1992.

84. MG Sliva, AE Green, JK Sanders, JR Euber, JR Saucerman. J AOAC Int 75:566–571, 1992.
85. LF Russell, JT Vanderslice. Food Chem 43:151–162, 1992.
86. H Iwase. J Chrom 625:377–381, 1992.
87. C Kanno, K Shirahuji, T Hoshi. J Food Sci 56:678–681, 1991.
88. AS Huang, DS Byerly. J Food Sci 57:245–248, 1992.
89. S Zapata, J-P Dufour. J Food Sci 57:506–511, 1992.
90. G Achilli, GP Cellerino, PH Gamache, GVM d'Eril. J Chromatogr 632:111–117, 1993.
91. GC Galletti, J Eagles, FA Mellon. J Sci Food Agric 59:401–404, 1992.
92. B Fernández de Simon, J Pérez-Ilzarbe, T Hernández, C Gómez-Cordovés, I Estrella. J Agric Food Chem 40:1531–1535, 1992.
93. W Borejsza-Wysocki, SK Goers, RN McArdle, G Hrazdia. J Agric Food Chem 40: 1176–1177, 1992.
94. G Montedoro, M Servili, M Baldioli, E Miniati. J Agric Food Chem 40:1571–1576, 1992.
95. B Fernandez de Simon, J Perez-Itzarbe, T Hernandez, C Gomez-Cordoves, I Estrella. J Agric Food Chem 40:1531–1535, 1992.
96. G Montedoro, M Servili, M Baldioli, E Miniati. J Agric Food Chem 40:1577–1580, 1992.
97. L Dao, M Friedman. J Agric Food Chem 40:2152–2156, 1992.
98. MR Koupai-Abyazani, J McCallum, BA Bohm. J Chromatogr 594:117–123, 1992.
99. MS Ramamurthy, B Maiti, P Thomas, PM Nair. J Agric Food Chem 40:569–572, 1992.
100. E Delage, G Bohuon, A Baron, J-F Drilleau. J Chromatogr 555:125–136, 1991.
101. J-P Goiffon, M Brun, M-J Bourrier. J Chromatogr 537:101–121, 1991.
102. GP Cartoni, F Coccioli, L Pontelli, E Quattrucci. J Chromatogr 537:93–99, 1991.
103. RG Bailey, NE Nursten, I McDowell. J Chromatogr 542:115–128, 1991.
104. P Vinas, N Campillo, M Hernandez Cordoba. Mikrochim Acta 106:293–302, 1992.
105. S Kuhr, UH Engelhardt. Z Lebensm. Unters Forsch 192:526–529, 1991.
106. E Revilla, M Bourzeix, E Alonso. Chromatographia 31:465–468, 1991.
107. LC Trugo, CAB de Maria, CC Werneck. Food Chem 42:81–87, 1991.
108. FJ Pérez-Ilzarbe, V Martínez, T Hernández, I Estrella. J Liq Chromatogr 15:637–646, 1992.
109. J Cacho, J Enrique Castells. Am J Enol Vitic 42:327–335, 1991.
110. M Tsimidou, G Papadopoulos, D Boskou. Food Chem 44:53–60, 1992.
111. A Chandra, MG Nair, A Iezzoni. J Agric Food Chem 40:967–969, 1992.
112. FC Richard, PM Goupy, JJ Nicolas, JM Lacombe, AA Pavia. J Agric Food Chem 39: 841–847, 1991.
113. G Montedoro, M Servilli, M Baldioli, E Miniati. J Agric Food Chem 40:1577–1580, 1992.
114. BF De Simon, J Pérez-Ilzarbe, T Hernandez, C Gomez-Cordoves, I Estrella. J Agric Food Chem 40:1531–1535, 1992.
115. M Brenes-Balbuena, P García-García, A Garrido-Fernandez. J Agric Food Chem 40: 1192–1196, 1992.
116. G Montedoro, M Servili, M Baldioli, E Miniati. J Agric Food Chem 40:1571–1576, 1992.
117. M Verschuere, P Sandra, F David. J Chromatogr 30:388–391, 1992.
118. FA Tomas-Barberan, MM Garcia-Grau, F Tomas-Lorente. J Agric Food Chem 39:256–258, 1991.
119. J Siegrist, C Salles, P Etiévant. Chromatographia 35:50–54, 1993.
120. F Hashimoto, G Nonaka, I Nishioka. Chem Pharm Bull 40:1383–1389, 1992.
121. I Babic, MJ Amiot, C Nguyen-The, S Aubert. J Food Sci 58:351–356, 1993.
122. L Dao, M Friedman. J Agric Food Chem 40:2152–2156, 1992.
123. LM Withy, TT Nguyen, RE Wrolstad, DA Heatherbell. J Food Sci 58:190–192, 1993.

24
HPLC Analysis of Surfactants

Thomas M. Schmitt

BASF Corporation, Wyandotte, Michigan

I. INTRODUCTION

Surfactants (surface active substances) are compounds that have chemical structures incorporating both hydrophilic and hydrophobic functions. As their name implies, they congregate at interfaces, where they function in various useful ways. The predominant use of synthetic surfactants is in detergents for cleaning fabrics, food utensils, and buildings. There are also thousands of food, cosmetic, and industrial applications of these compounds, which are found everywhere as adjuvants and formulation aids.

High-performance liquid chromatography (HPLC) is the technique most broadly applicable to surfactant analysis [1]. Analysis of pure surfactants and their solutions is easily accomplished by HPLC. More challenging is the determination of surfactants in complex matrices, because HPLC alone is not particularly selective for surfactants. It is often necessary to make preliminary separations to isolate the surfactants from interfering compounds. The dictum that the analytical chemist must be familiar with the chemistry of the entire system is nowhere more true than in surfactant analysis.

For trace analysis, care must be taken that the concentration of surfactants in solution is not decreased with time because of adsorption to laboratory apparatus, even to the surfaces of sample bottles. Sample filtration will usually result in the loss of surfactant, because its concentration is enriched on the surface of particulates [2]. A common strategy to minimize this problem is addition of a second surfactant of similar functionality in much higher concentration.

Surfactants form micelles: aggregates of molecules that function as a unit. Although these are functionally very important, allowing solubilization of soil and stabilization of hydrophile and hydrophobe mixtures, they can make analysis difficult. The chromatographer must always be aware that micelle formation can occur at relatively low concentration whenever aqueous solutions are used.

A few HPLC systems have been developed for general qualitative and quantitative analysis of unknown mixtures of surfactants. These are effective when the list of possibilities is short. They consist of reversed-phase systems with a salt added to the mobile phase, usually sodium perchlorate [3–5]. The methods have been adapted to the analysis of, for example, toothpaste and shampoo.

II. HPLC OF IONIC SURFACTANTS

Anionic and cationic surfactants are compounds in which the hydrophilic portions of the molecules are anionic and cationic, respectively. Anionics form the most widely used class of surfactants. They are moderately strong organic acids, and HPLC analysis is often based on this property. Cationic surfactants are used in much smaller quantities than anionics. Their chief applications are as fabric softeners and disinfectants. There are wide variations in basicity among these compounds.

Amphoteric surfactants are a smaller group of compounds that contain both cationic and anionic functions in the same molecule. Many can be analyzed by the HPLC systems similar to those applied to cationics.

A. General Principles

The HPLC analysis of ionic surfactants is almost always performed either by paired-ion reversed-phase chromatography, with a mixed solvent system, or by ion-exchange chromatography, including ion chromatography. In conventional paired-ion chromatography (also called ion-interaction chromatography), an organic counterion is used to form a hydrophobic ion pair, which is retained on the reversed-phase column. For shorter retention times, an inorganic salt may be used, such as sodium perchlorate. Reversed-phase retention of anionic surfactants may be increased by lowering the pH of the mobile phase to suppress ionization [6]. Cationic surfactants of low water solubility, such as the dialkyldimethyl compounds used as fabric softeners, are often analyzed by normal-phase chromatography.

Detection is usually performed with one of the more "universal" detectors, such as ultraviolet (UV) absorption at about 200 nm, evaporative light-scattering, or differential refractive index (RI). Ion-exchange chromatography applications use conductivity detection, perhaps after a second ion-exchange reaction to enhance the conductivity of the analyte or suppress that of the mobile phase [7]. Detection by postcolumn reaction is highly sensitive, although a substantial time investment is required to set up the necessary hardware. For example, cationic surfactants (as well as amphoterics at low pH) may be selectively detected by formation and extraction of ion pairs with a colored or fluorescent anion [8–10]. Often, a detection system of such selectivity greatly eases the requirements for sample pretreatment and for HPLC separation.

B. Anionic Surfactants

1. Alkyl Sulfates and Alkanesulfonates

Aliphatic sulfates and sulfonates are readily separated according to increasing alkyl chain length on a reversed-phase column with a water–acetonitrile gradient and a counterion such as tetrabutylammonium ion [7]. Retention is affected mainly by alkyl chain length (including both the analyte chain length and the counterion chain length [11], with secondary effects from isomeric configuration. Conductivity detection is suitable after chemical suppression of the eluent conductivity. More often, detection is by inverse UV absorbance, using a UV-absorbing counterion [12]. Residual alkanol in alcohol sulfates may be determined by reversed-phase HPLC of the naphthylisocyanate derivatives, using UV detection [13].

Ion-exchange separation is used less often. Retention increases with higher alkyl chain length and decreases with higher eluent ionic strength and with higher concentrations of organic solvents. The salt functions to increase the affinity of the surfactant for the stationary phase. Most efficient separation of complex mixtures is performed with a gradient in which the concentration of the salt decreases while the organic content of the eluent increases [14]. In ion-exchange separation, inverse UV detection may be accomplished by using an eluent containing a UV-absorbing anion, such as naphthalenesulfonate [15]. If the number of hom-

ologues is limited, sulfonates and sulfates can be separated from each other. Commercial mixtures are usually complex and will normally exhibit overlapping peaks.

Example 1. Alcohol sulfates are separated by chain length on a Wakosil 5C4 reversed-phase C_4 column with 50:50 acetonitrile–water, both in 0.1 M in sodium perchlorate, with RI detection [16].

Example 2. Alcohol sulfates and alkanesulfonates are separated by chain length on a Novapak C_{18} column with water–acetonitrile gradient, each 0.005 M in tetrabutylammonium borate. Detection is by conductivity after chemical suppression [7] (Fig. 1).

Example 3. Hexadecane monosulfonates are separated according to position of the sulfonate group by paired-ion chromatography on three C_{18} columns. Gradient elution: A = water, 0.0003 M in *N*-methylpyridinium chloride; B = 50:50 acetonitrile–water 0.0003 M in *N*-methylpyridinium chloride; 60% B to 90%B in 53 min. Detection by inverse UV absorbance at 260 nm [12] (Fig. 2).

2. Alkylarylsulfonates

Alkylbenzenesulfonate may be produced with linear or (rarely) branched alkyl chains (LAS and ABS, respectively). HPLC retention of the compounds is little affected by branching or by the position of attachment of the sulfophenyl group. Alkylbenzenesulfonate is one of the few common anionic surfactants that absorbs light in the 254-nm range. Detection at the wavelength more specific for arylsulfonates at about 225 nm gives greater specificity and sensitivity than 254 nm, where the absorbance is relatively weak. Fluorescence detection is suitable for determination of low levels of LAS and is widely used in environmental analysis.

Most investigators use paired-ion chromatography with acetonitrile–water or methanol–water and detection at about 220 nm. It is usually best to choose conditions such that isomers are not separated, but that instead peaks are obtained for only individual alkyl chain lengths [16]. Reversed-phase packings with shorter alkyl chains are more suitable for this purpose than are C_{18} packings. For example, Matsutani and Endo report that a C_8 column with methanol–water will given the distribution of LAS methyl esters according to only alkyl chain length, whereas a C_{18} column also differentiates the esters according to point of attach-

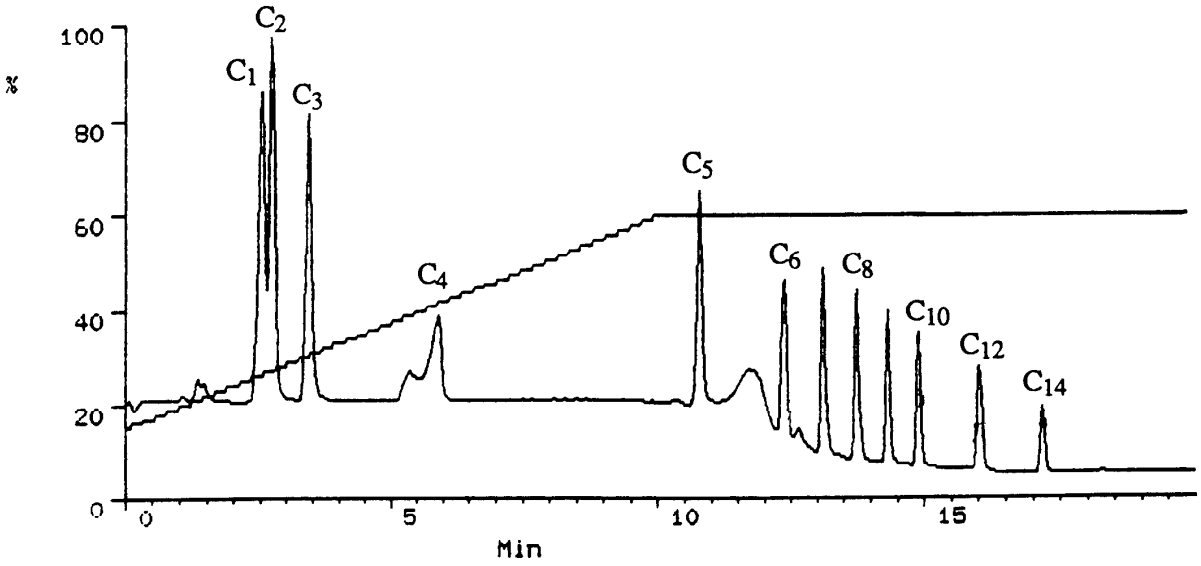


Figure 1 Reversed-phase separation of linear alkyl sulfates and alkanesulfonates with conductivity detection using Waters' Solid Phase Reagent. (From Ref. 7.)

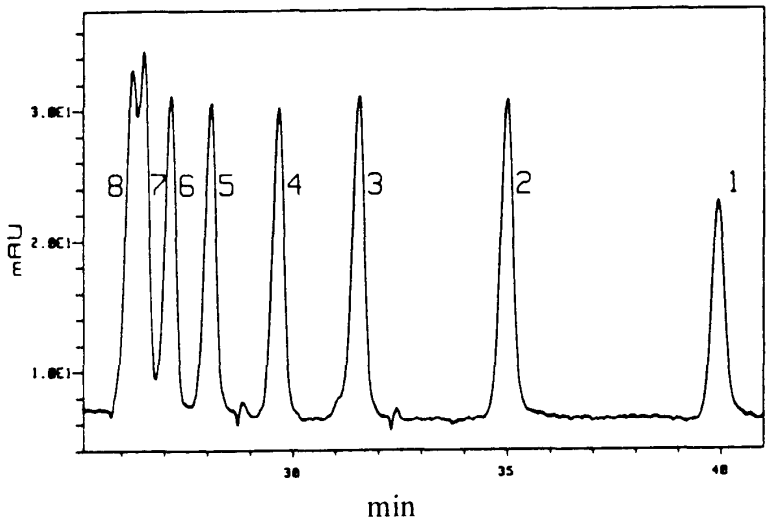


Figure 2 Reversed-phase separation of isomers of *n*-hexadecanesulfonate. Numbers refer to the carbon position to which the sulfonate group is attached. (From Ref. 12. Reprinted by permission of Preston Publications, a division of Preston Industries, Inc.)

ment, making quantification difficult [17]. Addition of a salt, such as sodium chloride, to the mobile phase will increase retention times [18].

Example 1. LAS is determined in river water by concentration and purification on an anion-exchange precolumn, then HPLC on a Wakosil 5C4 reversed-phase C_4 column with 50:50 acetonitrile–water, both 0.1 M in sodium perchlorate: UV detection is at 220 nm; separation is by alkyl chain length [16] (Fig. 3).

Example 2. LAS is determined in sewage and river water by concentration on various precolumns and HPLC on a C_8 or C_{18} column, 80:20 methanol–water, 0.1 M in sodium perchlorate; detection by fluorescence with 225-nm excitation and 290-nm emission [19–21].

3. Ether Sulfates

These are the sulfate esters of ethoxylated alcohols and alkylphenols, having the general formula $C_nH_{2n+1}O(C_2H_4O)_xSO_3H$ or $C_nH_{2n+1}C_6H_4O(C_2H_4O)_xSO_3H$. Ether sulfates are generally analyzed with the same systems as alkanesulfonates and alkyl sulfates. In a paired-ion chromatography or ion-exchange chromatography system, more highly ethoxylated materials are retained longer, and the alkylethoxysulfate elution pattern is superimposed on that of other sulfates and sulfonates [11]. Resolution according to alkyl chain length by paired-ion chromatography is generally not possible for alkylether sulfates [22]. A normal-phase gradient system was demonstrated for separating sulfated and unsulfated dodecylphenolethoxylates according to increasing degree of ethoxylation. The separation is made during a single analysis, with the entire unsulfonated distribution eluting before the anionic distribution [23]. A similar separation, but with the order of elution inverse to degree of ethoxylation, was demonstrated with a reversed-phase paired-ion system [24]. For environmental analysis, mass spectrometric (MS) detection is required for discrimination of homologues [25].

Example 1. A normal-phase system based on a Shandon Hypersil 5-CPS cyanopropyl column and 70:30 hexane–ethanol, containing 0.01-M tetramethylammonium chloride as an ion-pairing agent, separated alkylphenolether sulfate according to increasing degree of ethoxylation; detection by UV absorbance was at 220 nm [26].

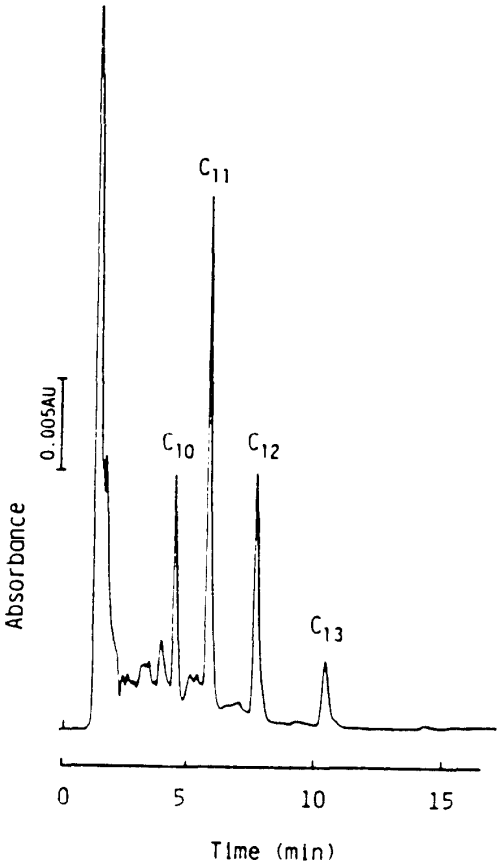


Figure 3 Reversed-phase determination of LAS in river water. Labeled peaks correspond to C_{10}–C_{13} alkyl chain lengths. (From Ref. 16.)

Example 2. Alkyl ether sulfates were separated by rapid reversed-phase HPLC on a 2.5-cm–C_{18} column using a tetrahydrofuran (THF)–water gradient and backflush into three peaks for inorganic salt, ether sulfate, and unsulfated ethoxylate using evaporative light-scattering detection [27]. The backflush technique aids quantification by giving sharper peaks [28].

Example 3. Nonylphenolether sulfates are separated according to degree of ethoxylation by a mixed mode (ion-exchange and reversed-phase) system consisting of an Alltech RP8/Anion 100-A column and a mobile phase gradient: A = 0.02-M potassium dihydrogen phosphate, pH 4.7; B = acetonitrile; 60% B to 80% B in 20 min; 60 min hold; UV detection at 223 nm. Elution is in reverse order of ethoxylate chain length; unsulfonated material elutes first [29].

4. α-Olefin Sulfonates

α-Olefin sulfonates are mixtures of alkenesulfonates and hydroxyalkanesulfonates of varying alkyl chain lengths. Reversed-phase HPLC separates the individual components in the order disulfonates, hydroxyalkanemonosulfonates, and alkenemonosulfonates. Compounds are simultaneously separated according to increasing alkyl chain length, with some resolution of the hydroxy isomers. Quantitative analysis of commercial mixtures is thus difficult because of incomplete resolution and the difficulty of positively identifying peaks [30–32] (Figs. 4 and 5).

5. Other Anionic Surfactants

Alkylethercarboxylic acids and alkylphenolethercarboxylic acids can be separated according to alkyl chain length on a C_{18} column with a mobile phase of 75:15:10

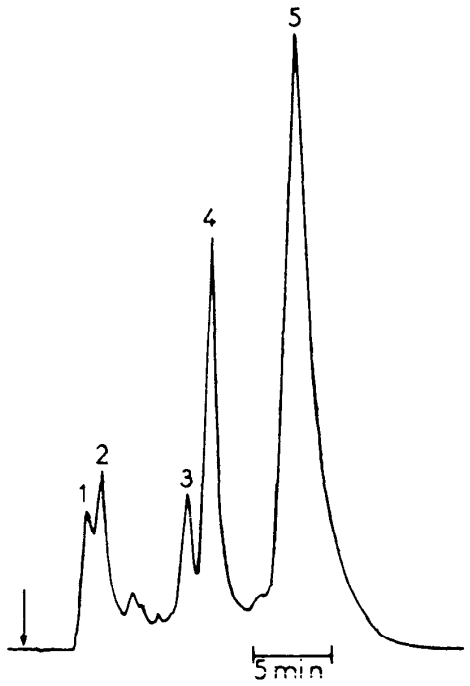


Figure 4 Reversed-phase separation of a C_{16} α-olefin sulfonate using a moving-wire flame ionization detector. Peaks 1, 2, disulfonates; 3, 4-hydroxysulfonate; 4, hydroxysulfonate; 5, alkenesulfonates. (From Ref. 31.)

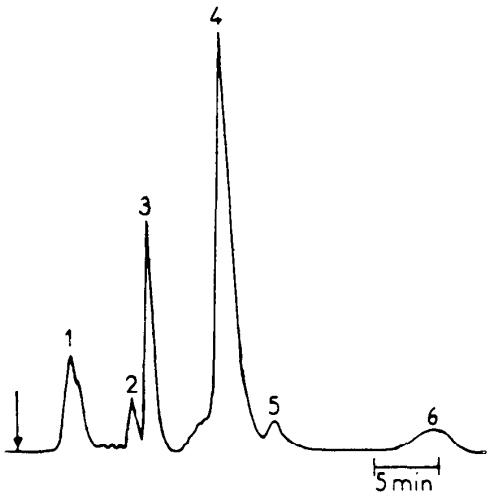


Figure 5 Separation of a C_{14} and C_{16} α-olefin sulfonate. Peak 1, disulfonates; 2, C_{14} 4-hydroxysulfonate; 3, C_{14} 3-hydroxysulfonate; 4, C_{14} alkenesulfonates; 5, C_{16} 3-hydroxysulfonate; 6, C_{16} alkenesulfonates. (From Ref. 31.)

methanol–water–acetonitrile containing 0.004-M tetramethylammonium bisulfate and 0.001-M tetramethylammonium hydroxide [33]. A similar system, with double the usual column length, permits resolution by both alkyl and ethoxy chain length in a single run [34].

Phosphate esters of ethoxylated nonylphenol (NPE) can be separated into monoesters, diesters, and free NPE, respectively, by chromatography on a C_{18} column, with a gradient from 90:10 water–methanol to acetonitrile, with UV detection at 230 nm [35].

Sulfosuccinate esters are separated by paired-ion reversed-phase chromatography according to the length of the alkyl substituents. Separation from other anionics is possible, providing that their alkyl substituents differ substantially from the combined total chain length of the sulfosuccinates [36].

Petroleum sulfonates may be separated into mono-, di-, and higher sulfonates by HPLC on an anion-exchange column [37]. In a two-dimensional approach, petroleum sulfonates are first separated from crude oil by passage through a C_{18} column, then separated into mono- and disulfonates by passage through an anion-exchange column [38].

Lignin sulfonates have been analyzed only by size-exclusion chromatography. Aqueous eluents are used, and care is necessary to minimize secondary separation effects. A suitable system consists of a silica-based hydrophilic TSK G3000SW column, with a mobile phase of 0.2-M sodium acetate, pH 7 [39].

α-Sulfo fatty acid esters can be analyzed by reversed-phase HPLC of the methyl ester derivatives, with separation according to alkyl chain length [17].

C. Cationic Surfactants

Any difficulty encountered in analysis of cationic surfactants is mainly a function of concentration. In the many formulations containing no other organic cations, any of several straightforward ion-exchange or paired-ion chromatographic methods are suitable. For environmental analysis, some form of preconcentration is necessary. Solid-phase extraction and liquid–liquid extraction are widely used for this purpose. For example, benzalkonium compounds are readily preconcentrated from aqueous solution on reversed-phase solid-phase extraction devices [40].

To avoid solubility problems, ditallowdimethylammonium compounds are often analyzed by normal-phase HPLC. Under these conditions, elution is in order of decreasing alkyl character (i.e., in the order trialkylmethyl-, dialkyldimethyl-, alkyltrimethylammonium). Under the proper conditions, there will be partial resolution of the components under the dialkyldimethylammonium peak, with the more fatty materials again eluting first [41] (Fig. 6).

Example 1. Alkyltrimethylammonium compounds are separated by alkyl chain length on a Wakosil 5C4 reversed-phase C_4 column with 50:50 acetonitrile–water, both 0.1 M in sodium perchlorate, with RI detection [16]. Elution is in order of increasing chain length.

Example 2. Separation of stearyltrimethyl-, distearyldimethyl-, and tristearylmethylammonium chloride from each other, with elution in reverse order to the number of fatty substituents, is accomplished on a Partisil 5 PAC column, with a mobile phase of 89:10:1 chloroform–methanol–acetic acid and conductivity detection [42]. A similar system was applied to environmental analysis [43].

Example 3. Alkylbenzyldimethylammonium chlorides were separated according to increasing alkyl chain length (C_8–C_{18}) by reversed-phase HPLC on a CN column with 605:375:20 aqueous 0.1-M triethylammonium acetate (pH 3.8)–acetonitrile-tetrahydrofuran; UV detection is at 262 nm [44] (Fig. 7).

Example 4. Cetylpyridinium chloride is determined in mouthwash without prior workup by HPLC on a cyano-bonded column with sodium acetate–methanol–water mobile phase and UV detection. Other reversed-phase columns give excessively long run times [46].

Example 5. Alkyltrimethyl-, dialkyldimethyl-, and alkyldimethylbenzylammonium chlorides, as well as a cationic imidazoline derivative, were separated from sewage and sludge by paired-ion extraction, purified by adsorption on alumina, and analyzed on a Merck Diol 100 column with 50:50:10 methanol–THF–water mobile phase, 0.0002 M in HCl, using conductivity detection [47]. Elution was in order of decreasing hydrophobic character.

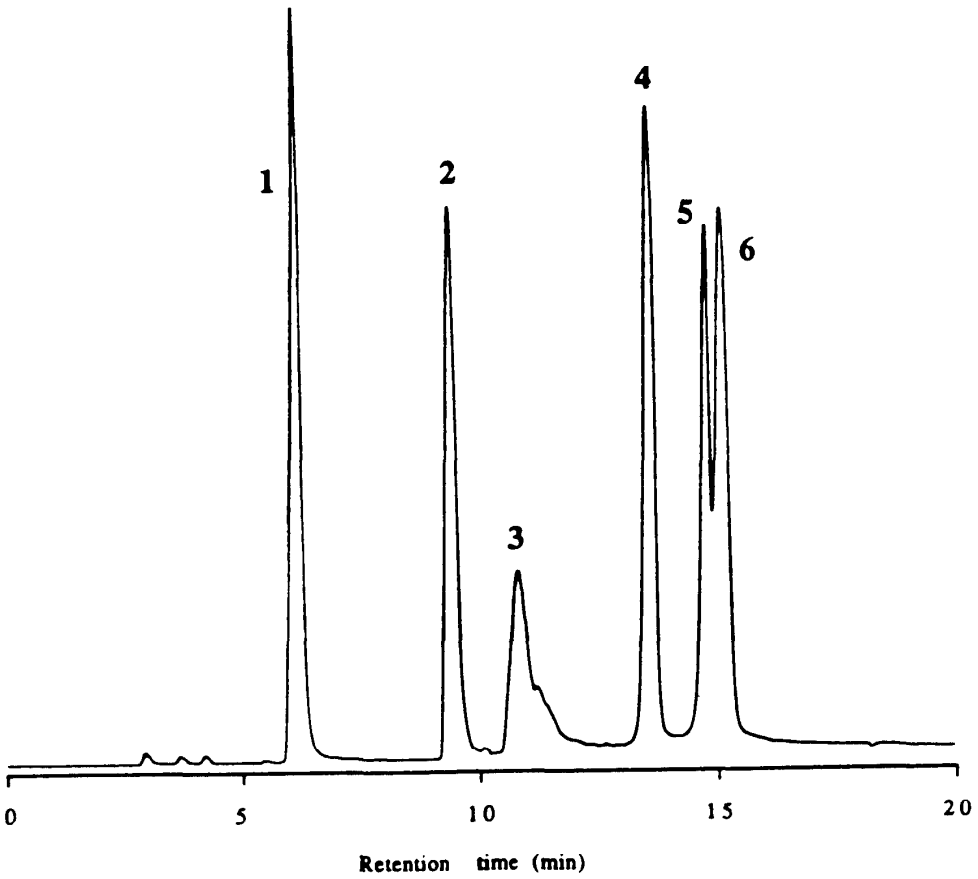


Figure 6 Normal-phase separation of quaternary amines: 1, trialkylmethylammonium salt; 2, dialkyldimethylammonium salt; 3, imidazolinium salt; 4, benzylhexadecyldimethylammonium salt; 5, octadecyltrimethylammonium salt; 6, hexadecyltrimethylammonium salt. Column: Bio-Rad RSil polyphenol, 4.6 × 250 mm. Gradient elution from 98:2 to 78:22 *n*-hexane (0.005-M trifluoroacetic acid)–methanol. (From Ref. 45.)

D. Amphoteric Surfactants

Amphoteric surfactants can usually be analyzed in the same way as cationic materials if the pH is sufficiently acidic. An alternative approach is to perform the analysis at neutral pH, at which the compounds behave similarly to nonionic surfactants [48]. Carboxybetaines may be first derivatized with 4-bromomethyl-7-methoxycoumarin, permitting UV detection and gradient elution [49].

Lecithin is an amphoteric surfactant in a class of its own. Lecithin is most often analyzed by normal-phase HPLC, which shows the main phosphatide constituents: phosphatidylcholine, phosphatidylethanolamine, phosphatidylinositol, and neutral lipids [50,51]. Reversed-phase HPLC may be used to further characterize fractions from normal-phase HPLC. For this, the acyl substitution of each of the phosphatides is determined [52]. Because the degree of unsaturation of the fatty acid substituents varies, the specific response of phosphatides to low-wavelength UV varies greatly. Consequently, RI detection is most often used, with the flame ionization detector and evaporative light-scattering detector also frequently employed. For high accuracy, phosphatide standards should have the same acyl composition as the samples [53]. Very rapid progress is being made in analysis of phosphatides because of their biological importance. Current research on LC–MS techniques may result in methods for the rapid characterization of these materials [54].

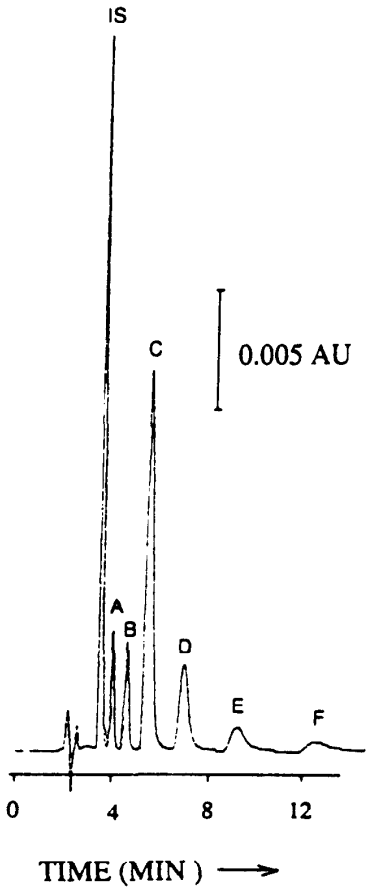


Figure 7 Reversed-phase separation of benzylalkyldimethylammonium chlorides: IS, dibenzyldimethylammonium chloride internal standard; A–F are benzylalkyldimethylammonium chlorides of varying alkyl chain lengths: A, C_8; B, C_{10}, C, C_{12}; D, C_{14}; E, C_{16}; F, C_{18}. (From Ref. 44.)

Example 1. Phosphatidylcholine, phosphatidylglycerol, and their hydrolysis products are determined in a liposome dispersion by HPLC on a Zorbax NH_2 column, with a mobile phase of 64:28:8 acetonitrile–methanol–0.01-M ammonium dihydrogen phosphate solution, pH 4.8, with RI detection [55] (Fig. 8).

Example 2. Phosphatidylcholine, phosphatidylethanolamine, and phosphatidylinositol are individually separated according to fatty acid substituents by reversed-phase chromatography on a C_{18} column, with a mobile phase of 70:28:2 acetonitrile–methanol–water, 0.025 M in tetramethylammonium phosphate; detection is by UV absorbance at 208 nm [56].

Phosphatidylserine is analyzed with a mobile phase of 70:22:8 acetonitrile–methanol–water, 0.005 M in a tetraalkylammonium phosphate salt [57] (Fig. 9).

Example 3. Several carboxybetaine and sulfobetaine derivatives, as well as amine oxides, were separated according to increasing carbon chain length by isocratic reversed-phase HPLC at neutral pH, with RI detection, a technique recommended for qualitative as well as quantitative use [48].

Example 4. Alkylamidopropylbetaine is determined in cosmetic and detergent formulations, with elution according to increasing alkyl chain length (C_8–C_{18}), by separation on a mixed mode C_8–cation-exchange column with 75:25 acetonitrile–water mobile phase and detection by evaporative light-scattering or by UV absorbance at 214 nm. The separation is relatively insensitive to pH [58].

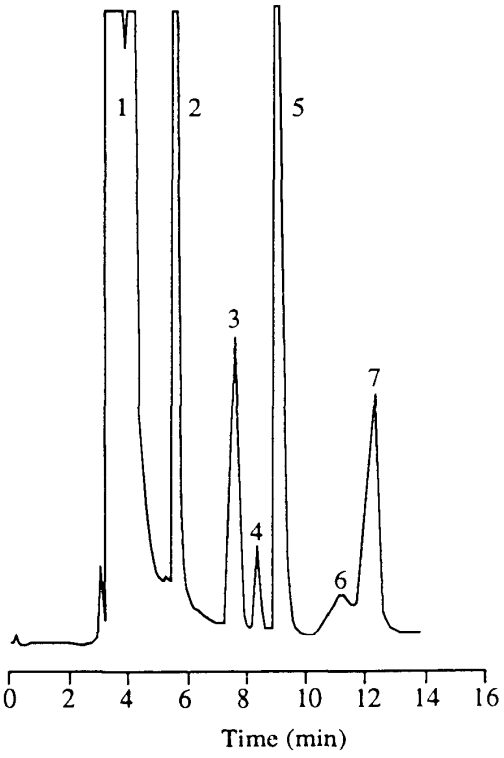


Figure 8 Analysis of phospholipids on an NH_2 column. Peak 1, solvent front: 2, phosphatidylcholine; 3, phosphatidylglycerol; 4, 2-acyl lysophosphatidylcholine; 6, 2-acyl lysophosphatidylglycerol; 7, 1-acyl lysophosphatidylglycerol. (From Ref. 55.)

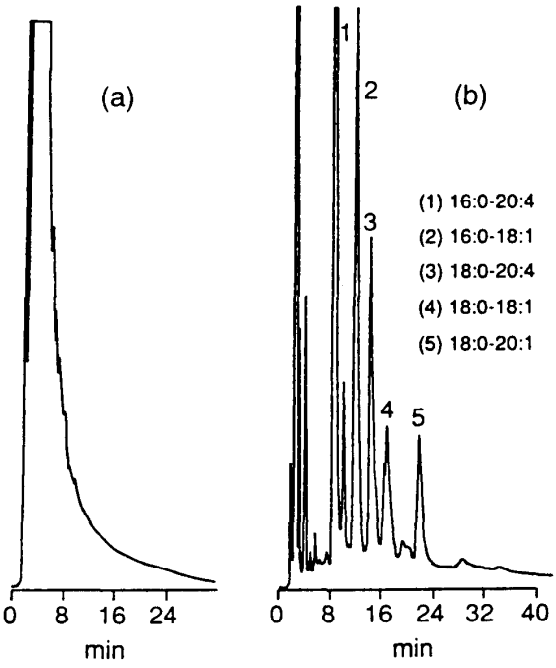


Figure 9 Reversed-phase separation of phosphatidylserine components according to fatty acid constitution. The eluent for (a) contained no salt; that for (b) contained 0.005-M tetraethylammonium phosphate. (From Ref. 57.)

III. HPLC OF NONIONIC SURFACTANTS

A large proportion of commercial nonionic surfactants are produced by addition of ethylene oxide (EO) to an alkyl or alkylphenol compound, giving an ether or ester of polyethylene oxide. The product consists of a series of homologues of varying polyethylene oxide chain length. Typically, the hydrophobic starting material itself consists of various compounds; hence the product actually has a two-dimensional distribution of homologues. This complexity is either a challenge or a nuisance to the analyst, depending on whether the objective is complete characterization of the surfactant or simply the determination of its total concentration. An HPLC system may be optimized to resolve nonionic surfactants by the hydrophobe's distribution, by the hydrophile's distribution, or simply to give a single peak for all congeners of a certain type.

A. General Principles

All ordinary reversed-phase systems separate nonionic surfactants according to their hydrophobe (typically, according to alkyl chain length). In addition, reversed-phase HPLC conditions can be found that can separate nonionics according to either increasing degree of ethoxylation or decreasing degree of ethoxylation. Usually, reversed-phase conditions are selected such that EO chain length plays no part in the separation, only the hydrophobe's chain length. These conditions are usually in the range of 80:20 to 90:10 methanol–water for alcohol ethoxylates and EO–PO copolymers [59]. If these conditions are not chosen, ethoxylates will be retained according to increasing hydrophobe's chain length and also according to increasing or decreasing ethoxy chain length, making for a difficult chromatogram [60].

Reversed-phase HPLC is well suited to routine determination of the content of free polyethylene glycol (PEG) impurity of ethoxylated surfactants. The PEG elutes first as a single peak and is readily measured with RI detection [61]. Such a simple method, coupled with a backflush technique, will also permit rapid determination of total ethoxylates in commercial samples [28].

Normal-phase HPLC is effective in separating according to length of the ethylene oxide chain (Fig. 10). As with reversed-phase chromatography, the mobile phase must be optimized to minimize mixed-mode separation [62]. Usually, gradient elution is required. If less than baseline resolution is acceptable, an isocratic system can sometimes be devised to satisfy the needs of a specific analysis [63]. A rigorous analysis frequently requires collecting of individual peaks from one separation for reanalysis by the complementary separation mode.

Analysis of nonionics according to ethylene oxide chain length can also be performed on a cation-exchange column, using the ability of alkoxylate chains to form complexes with alkali metal cations such as K^+ [64]. In this case, conductivity detection may be used as well as RI.

Although not usually a convenient method for trace analysis, size-exclusion chromatography (SEC) is very often used for characterization of pure nonionics. Although it is possible to obtain baseline resolution of lower molecular weight compounds, higher ethoxylates usually elute as a single broad peak [65]. For many commercial purposes, this resolution is sufficient to assure the identity and gross purity of the product.

Trace analysis of nonionic surfactants in environmental samples is a challenging task because of the great variety of natural and synthetic compounds that interfere with the determination. A reading of the full text of methods proposed for HPLC determination of, for example, alcohol ethoxylates [66] or alkylphenolethoxylates [67,68] is mandatory to appreciate the rigorous attention to detail required to obtain specificity from this type of HPLC analysis.

Detector choice is limited for nonionic surfactants. Of common nonionics, only the alkylphenol ethoxylates can be readily determined by UV absorbance. Refractive index or low-wavelength UV detection is often used, but these methods are incompatible with gradient elution. UV-absorbing derivatives are often made to permit solvent programming. Newer detection methods based on flame ionization or on evaporative light-scattering are sometimes

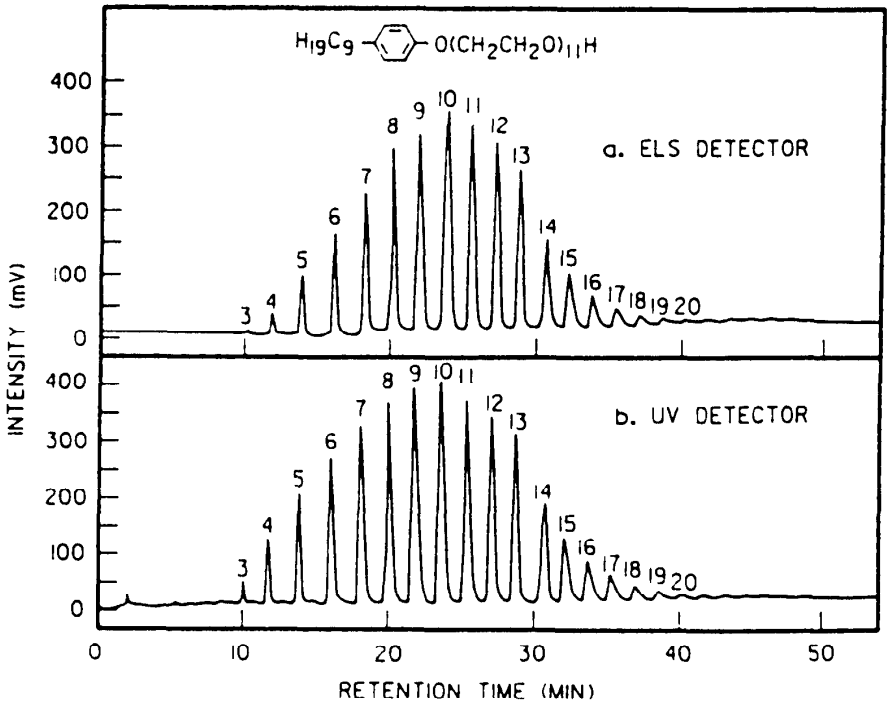


Figure 10 Separation on a Zorbax NH_2 column of a nonylphenol ethoxylate using a hexane–2-propanol (3% H_2O) gradient. (From Ref. 27.)

applied. MS detection is feasible, but because of the lack of volatility of higher homologues, LC–MS may give an apparently lower molecular weight distribution for an ethoxylate than the true value [69]. Several specialized detection methods are used. For example, esters can be detected by hydrolyzing in a postcolumn reactor and forming the violet 2-nitrophenylhydrazide derivatives of the resulting fatty acids [70].

B. Analysis of Individual Nonionic Surfactants

1. Alkylphenol Ethoxylates

There is an abundant literature on the HPLC analysis of alkylphenol ethoxylates (APE). This is because they are easily detected by UV absorbance or by fluorescence; hence, they are amenable to gradient elution methods.

Most commercial products are homogeneous for the alkylphenyl portion of the molecule, the most frequently encountered compounds being based on octylphenol, nonylphenol, or dodecylphenol. Thus, reversed-phase HPLC is often used to give a single peak for easy quantification of total alkylphenolethoxyolate [68,71]. Sometimes, small impurity peaks are also seen, presumably owing to the presence of *o*-alkylphenol in the predominantly *p*-alkylphenol starting material [72].

A collaborative study of normal-phase HPLC analysis of nonyl- and dodecylphenol 5- and 6-mole ethoxylates showed a reproducibility between laboratories of 9–12% for quantification of individual ethoxy homologues [73]. This study was performed with various NH_2 and diol columns, with *n*-hexane–isopropanol–water mobile phase and detection by UV or RI.

Lower molecular weight ethoxylates may be characterized according to ethoxy chain length on a NH_2 column with a mobile phase of A = isooctane; B = 50:50 isopropanol–2-methoxyethanol; 5% B to 30% B in 30 min; nonlinear [69]. A generally useful system for determination of higher APE homologues consists of a NH_2 column with an *n*-

heptane–isopropanol gradient, such as A = 90:10 heptane–isopropanol; B = 90:10 isopropanol–water; 15% B to 40% B in 20 min; linear. Detection by UV absorbance [69,74].

Example 1. APE was determined after isolation from sewage by HPLC on a Partisil 5 PAC column, with a solvent gradient: A = ethyl *t*-butyl ether, 0.1% acetic acid; B = 95:5 acetonitrile/methanol, 0.1% acetic acid; 0% B to 100% B in 30 min; fluorescence detection, 230-nm excitation; 302-nm emission. A similar chromatogram was obtained using UV absorbance detection at 280 nm and a micro-Porasil column with gradient: A = hexane; B = 95:5 chloroform–DMSO; 0% B to 45% B in 30 min. Separation is by ethoxy chain length [42].

Example 2. APE was separated according to alkyl chain length on a C_{18} column with a mobile phase of 83:14:3 hexane–THF–water. Separation by ethoxy chain length was accomplished on a Merck LiChrosorb Diol column with gradient elution: A = 95:5 hexane–methylene chloride; B = 50:40:10 hexane–methylene chloride–isopropanol; 30% B to 60% B in 15 min. Detection in each case was by UV absorbance at 275 nm [62].

Example 3. A simple and sensitive determination of nonylphenol-9-mole ethoxylate in biological fluids, giving a single peak for the surfactant, consists of chromatography on an Alltech R-SIL-amine NH_2 column with 95:5 THF–acetonitrile. Detection is by fluorescence with 275-nm excitation and 575-nm emission [2].

2. Alcohol Ethoxylates

The ethoxy distribution of alcohol ethoxylates (AE) is easily determined by gradient-elution normal-phase HPLC of the phenylisocyanate derivatives, with UV detection [75]. Okada demonstrated complete characterization of an AE (as the dinitrobenzoate ester) by an initial reversed-phase separation by alkyl chain length, after which the fractions corresponding to individual chain lengths were trapped on short styrene–divinylbenzene copolymer columns, mixing water with the mobile phase before the trapping column to prevent elution of the AE. The trapped fractions were then eluted into a cation-exchange column in the K^+ form to give the corresponding ethoxy distributions [76].

Example 1. After several cleanup steps, AE is determined in sewage samples by HPLC of the phenylisocyanate derivative. Reversed-phase HPLC on a microBondapak C_{18} column with a gradient from 80:20 methanol–water to 100% methanol is used for quantification and to determine the alkyl chain distribution. Octanol and eicosanol are used as internal standards and a degree of ethoxylation of 8 is assumed. Optionally, normal-phase HPLC is used to determine the ethoxylate chain distribution with a microBondapak NH_2 column and gradient from 35:15 hexane–ethylene dichloride to 185:65 acetonitrile–isopropanol (800 μL acetone per liter), 0–35% in 50 min. Detection is by UV absorbance at 240 nm [66,77].

Example 2. A 20-mole ethoxy adduct of C_{16} and C_{18} alcohols is separated according to ethoxy chain length by chromatography of the 3,5-dinitrobenzyoyl derivatives on a diol column, with gradient elution from 92.6:4.9:2.5 to 66.5:3.5:30 *n*-heptane–methylene chloride–isopropanol. There is some discrimination according to the alkyl chain length [78].

3. Ethoxylated Acids

Acid ethoxylates are prepared by addition of ethylene oxide to fatty acids, and thus have a range of homologues of varying alkyl and varying ethoxy chain length. The homologue distribution may be determined in a manner similar to the methods described for analysis of alcohol ethoxylates.

These compounds can be considered to be esters of PEG and a fatty acid. As such, they may contain, in addition to the monoester main component, low levels of diester and free PEG. These components can be separated by normal-phase HPLC on a diol column. The order of elution is diester, monoester, and PEG [78]. Reversed-phase HPLC is more suitable for determining the minor diester component [80].

4. Fatty Acid Alkanolamides and Their Ethoxylates

The most common products in this category are fatty acid ethanolamides and diethanolamides. Similar to other nonionics, these can be separated by alkyl chain length using reversed-phase HPLC [81]. Reversed-phase HPLC also serves to separate free fatty acid and a few other impurities. Crude reaction mixtures containing oil are best analyzed by normal phase HPLC. The elution order in the latter is: triglycerides, diglycerides, free acids, amine esters, monoglycerides, and finally, the alkanolamides [82]. The ethoxy chain length of ethoxylated alkanolamides is also determined by normal-phase HPLC [83].

5. Ethoxylated Alkylamines

Alkylamine ethoxylates are easily separated according to alkyl chain length by reversed-phase chromatography, and according to degree of ethoxylation by normal-phase HPLC. Although these are usually classified as nonionic compounds, they have enough cationic character at low pH to be determined by a postcolumn extraction system using a fluorescent anionic-pairing agent [84].

6. Esters and Ethoxylated Esters

The ester and ethyoxylated ester category includes esters of polyhydroxy compounds. Reversed-phase HPLC is suitable for separating fatty acid esters according to the number and the size of the acyl groups [85,86]. Residual free fatty acids interfere by overlapping with the ester peaks; addition of triethylamine to the mobile phase eliminates the interference, causing the acids to elute before the esters [70]. Little has been published on separation of ethoxylated esters other than characterization by SEC.

Example 1. Esters of sucrose and sorbitan are separated individually according to number of ester groups by chromatography on a Hitachi gel 3057 C_{18} column, with a gradient of A = 85:15 methanol–water, 0.0057-M triethylamine; B = 75:25 ethanol–methanol, 0.0057-M triethylamine; complex step gradient from 0% B to 100% B in 25 min. Detection is based on the color reaction of fatty acids after hydrolysis [70].

Example 2. Sucrose monoesters are separated according to the nature of the fatty acid group by HPLC on two C_{18} columns, with a mobile phase of 70:30 acetone and water; DRI detection [87].

7. Block Copolymers of Ethylene Oxide and Propylene Oxide

Because of their complex structure, block copolymers have so far resisted characterization by HPLC analysis. By choosing a reversed-phase system that does not discriminate by ethoxy chain length, it is possible to measure the homologue distribution of the propoxy chain [88]. Fractions may be trapped and subsequently analyzed for ethoxy distribution by HPLC or other techniques. However, the high molecular weight of block copolymers in the surfactant range is such that they are better characterized by spectroscopic techniques in conjunction with SEC.

8. Amine Oxides

Amine oxides can be analyzed according to conventional reversed-phase HPLC, with retention according to alkyl chain length [48].

IV. CONCLUDING REMARKS

At the time of this writing, HPLC is the most generally useful technique for determination of ionic surfactants. It is also suitable for their characterization, although derivatization GC or GC–MS is a strong competitor.

Although HPLC gives less information than GC or GC–MS in the analysis of nonionic surfactants, it is often preferred. This is because HPLC conditions can be found that give a

single peak for the surfactant, whereas the GC methods separate the compound into many homologues.

REFERENCES

1. TM Schmitt. Analysis of Surfactants. New York: Marcel Dekker, 1992.
2. GJ Beck, D Kossak, SJ Saxena. J Pharm Sci 79:1029–1031, 1990.
3. H König, W Strobel. Fresenius Z Anal Chem 331:435–438, 1988.
4. K Nakamura, Y Morikawa. J Am Oil Chem Soc 59:64–68, 1982.
5. K Nakamura Y Morikawa. J Am Oil Chem Soc 61:1130–1135, 1984.
6. A Marcomini, A Di Corcia, R Samperi, S Capri. J Chromatogr 644:59–71, 1993.
7. JB Li, P Jandik. J Chromatogr 546:395–403, 1991.
8. M Shoester, G Kloster. Vom Wasser 77:13–20, 1991.
9. C De Ruiter, JCHF Hefkens, UAT Brinkman, RW Frei, M Evers, E Matthijs, JA Meijer. Int J Environ Anal Chem 31:325–339, 1987.
10. M Kanesato, K Nakamura, O Nakata, Y Morikawa. J Am Oil Chem Soc 64:434–438, 1987.
11. T Takeda, S Yoshida, T Ii. Chem Express 7:441–444, 1992.
12. G Eppert, G Liebscher. J Chromatogr Sci 29:21–25, 1991.
13. G Czichocki, P Müller, D Vollhardt, M Krüger. J Chromatogr 604:213–218, 1992.
14. D Zhou, DJ Pietrzyk. Anal Chem 64:1003–1008, 1992.
15. SA Maki, J Wangsa, ND Danielson. Anal Chem 64:583–589, 1992.
16. Y Yokoyama, H Sato. J Chromatogr 555:155–162, 1991.
17. S Matsutani, Y Endo. Yugagaku 40:566–573, 1991.
18. S Chen, DJ Pietrzyk. J Chromatogr A 671:73–82, 1994.
19. A Di Corcia, M Marchetti, R Samperi, A Marcomini. Anal Chem 63:1179–1182, 1991.
20. E Matthijs, H De Henau. Tenside Surfactants 24:193–199, 1987.
21. E Matthijs, M Stalmans. Tenside Surfactants Deterg 30:29–33, 1993.
22. YL Hofman, HP Angstadt. Chromatographia 24:666–670, 1987.
23. JA Pilc, PA Sermon. J Chromatogr 398:375–380, 1987.
24. P Jandera, J Chromatogr 449:361–389, 1988.
25. DD Popenoe, SJ Morris III, PS Horn, KT Norwood. Anal Chem 66:1620–1629, 1994.
26. REA Escott, SJ Brinkworth, TA Steedman. 282:655–661, 1983.
27. GR Bear, J Chromatogr 459:91–107, 1988.
28. H Yoshimura, T Sugiyama, T Nagai. J Am Oil Chem Soc 64:550–555, 1987.
29. T Austad, I Fjelde. Anal Lett 25:957–971, 1992.
30. RO Johannessen, WJ DeWitt, RS Smith, ME Tuvell. J Am Oil Chem Soc 60:858–861, 1983.
31. V Castro, J Canselier. J Chromatogr 325:43–51, 1985.
32. A Beranger, T Holt. Tenside Deterg 23:247–254, 1986.
33. H König, W Strobel, Fresenius J Anal Chem 338:728–731, 1990.
34. Y Mengerink, HCJ De Man, S Van der Wal, J Chromatogr 552:593–604, 1991.
35. JD Frazier, RD Johnson, CG Wade, DJ O'Leary. Comun J Com Esp Deterg 22:99–110, 1991.
36. B Steinbrech, D Neugebauer, G Zulauf. Fresenius Z Anal Chem 324:154–157, 1986.
37. GR Bear, CW Lawley, RM Riddle. J Chromatogr 302:65–78, 1984.
38. J Shengxiang, C Liren. Anal. Sci. 7:129–131, 1991.
39. ERE Van der Hage, WMGM van Loon, JJ Boon, H Lingeman, UAT Brinkman. J Chromatogr 634:263–271, 1993.
40. L Elrod, TG Golich, JA Morley. J Chromatogr 625:362–367, 1992.
41. DL Lawrence. J Am Soc Mass Spectrom 3:575–581, 1992.
42. E Matthijs, EC Hennes. Tenside Surfact Deterg 28:22–27, 1991.
43. L Nitschke, R Müller, G Metzner, L Huber. J Anal Chem 342:711–713, 1992.
44. JE Parkin. J Chromatogr 635:75–80, 1993.
45. AJ Wilkes, G Walraven, J Talbot. J Am Oil Chem Soc 69:609–613, 1992.

46. D Murawski. J Chromatogr 546:351–367, 1991.
47. M Emmrich, K Levsen. Vom Wasser 75:343–349, 1990.
48. H König, W Strobel. Proceedings 2nd World Surfactants Congress, Paris, 3:108–122, 1988.
49. Y Kondoh, S Takano. Anal Sci 2:467–471, 1986.
50. MD Grieser, JN Geske. J Am Oil Chem Soc 66:1484–1487, 1989.
51. SL Melton. J Am Oil Chem Soc 69:784–788, 1992.
52. TL Mounts, SL Abidi, KA Rennick. J Am Oil Chem Soc 69:438–442, 1992.
53. P Van der Meeren, J Vanderdeelen, G Huyghebaert, L Baert. Chromatographia 34:557–562, 1992.
54. H Kim, TL Wang, Y Ma. Anal Chem 66:3977–3982, 1994.
55. M Grit, DJA Crommelin, J Lang. J Chromatogr 585:239–246, 1991.
56. SL Abidi, TL Mounts. J Chromatogr 598:209–218, 1992.
57. SL Abidi, TL Mounts. J Liq Chromatogr 15:2487–2502, 1992.
58. AJ Wilkes, G Walraven, J Talbot. Comun J Com Esp Deterg 25:209–220, 1994.
59. B Trathnigg, B Maier, D Thamer. J Liq Chromatogr 17:4285–4302, 1994.
60. PL Desbene, B Desmazieres, JJ Basselier, A Desbene-Monvernay. J Chromatogr 461: 305–313, 1989.
61. I Zeman, M Paulovic. Proceedings 2nd World Surfactants Congress, Paris, 1988, 3:384–398.
62. C Zhou, A Bahr, G Schwedt. Anal Chim Acta 236:273–280, 1990.
63. N Marquez, RE Anton, A Usubillaga, JL Salager. Sep Sci. Technol 28:1769–1782, 1993.
64. T Okada. Anal Chem 63:1043–1047, 1991.
65. L Mikolajczyk, W Leukefeld, E Döring. Tenside Surfact Deterg 30:34–38, 1993.
66. TM Schmitt, MC Allen, DK Brain, KF Guin, DE Lemmel, QW Osburn. J Am Oil Chem Soc 67:103–109, 1990.
67. E Kubeck, CG Naylor. J Am Oil Chem Soc 67:400–405, 1990.
68. MJ Scarlett, JA Fisher, H Zhang, M Ronan. Water Res. 28:2109–2116, 1994.
69. Z Liang, AG Marshall, DG Westmoreland. Anal Chem 63:815–818, 1991.
70. Y Kondoh, A Yamada, S Takano. J Chromatogr 541:431–441, 1991.
71. BB Sithole, LH Allen. J Assoc Off Anal Chem 72:273–276, 1989.
72. DF Anghel, M Balcan, A Voicu, M Elian. J Chromatogr A 668:375–383, 1994.
73. I Zeman. J Chromatogr 509:201–212, 1990.
74. P Jandera, J Urbanek, B Prokes, J Churacek. J Chromatogr 504:297–318, 1990.
75. MC Allen, DE Linder. J Am Oil Chem Soc 58:950–957, 1981.
76. T Okada. J Chromatogr 609:213–218, 1992.
77. L Nitschke, L Huber. Fresenius J Anal Chem 345:585–588, 1993.
78. PL Desbene, B Desmazieres, V Even, JJ Basselier, L. Minssieux. Chromatographia 24: 857–861, 1987.
79. I Zeman, J Silha, M Bares. Tenside 23:181–184, 1986.
80. N Parris, JK Weil. J Am Oil Chem Soc 56:775, 1979.
81. K Nakamura, Y Morikawa, I Matsumoto. J Am Oil Chem Soc 58:72–77, 1981.
82. AA Ben-Bassat, T Wasserman, A Basch. J Liq Chromatogr 7:2545–2560, 1984.
83. I Zeman. Abh Akad Wiss DDR Abt Math Naturwiss Tech (1N):603–608, 1986.
84. RH Schreuder, A Martijn, H Poppe, JC Kraak. J Chromatogr 368:339–350, 1986.
85. VR Kaufman, N Garti. J Liq Chromatogr 4:1195–1205, 1981.
86. N Garti, E Wellner, A Aserin, S Sarig. J Am Oil Chem Soc 60:1151–1154, 1983.
87. MC Torres, MA Dean, FW Wagner. J Chromatogr 522:245–253, 1990.
88. H Pasch, C Brinkmann, H Much, U Just. J Chromatogr 623:315–322, 1992.

25

HPLC Applications to the Analysis of Ions and Inorganic Species

Charles A. Lucy

University of Calgary, Calgary, Alberta, Canada

I. INTRODUCTION

The use of ion exchangers for inorganic analysis dates back to the 1917 method of Folin and Bell [1] for the determination of ammonia in urine. The first chromatographic determination of an inorganic species was that of alkaline earths and transition metals by Schwab in 1937 [2]. However, the use of HPLC for the analysis of ions and inorganic species should truly be dated from the introduction of ion chromatography with suppressed conductivity detection, by Hamish Small in 1975 [3]. Ion chromatography (IC) represented by first analytical technique that could provide rapid and sensitive analyses of multiple anions simultaneously.

The instrumental aspects of ion chromatography have been described in Chapter 12, and in recent texts [4–6] and review articles [7,8]. The text by Haddad and Jackson [4] is extremely comprehensive for both ion chromatographic methodology and applications and is highly recommended for any practitioner in the field. In addition the *International Ion Chromatography Symposium Proceedings* are a rich source of the latest innovations and applications of this technique [9–15].

Other HPLC methods that can be used for the determination of inorganic species include ion-interaction and reversed-phase chromatography. These alternative methods have also been reviewed [16–18].

II. SEPARATION OF IONS AND INORGANIC SPECIES

A. Mode of Separation

The determination of ions and inorganics species by chromatography begins with the selection of the mode of separation and detection. Although there are a wide variety of methods to choose among the selection process can be simplified by considering a few of the intrinsic characteristics of the analytes. Figure 1 shows a flowchart that uses properties of anionic species to guide selection of the separation mode. The first consideration is whether the analyte is hydrophilic or hydrophobic. A hydrophilic anion is retained only by its coulombic interaction with the ion-exchange sites on the stationary phase, whereas hydrophobic ions are retained by both these coulombic interactions and by nonspecific dispersive interactions with the resin backbone. Thus, Figure 1 splits the anions into hydrophilic and hydrophobic groupings, not because different modes of separation are necessarily required for the two groups, but simply as a reminder that, with hydrophobic anions, consideration must be given to the

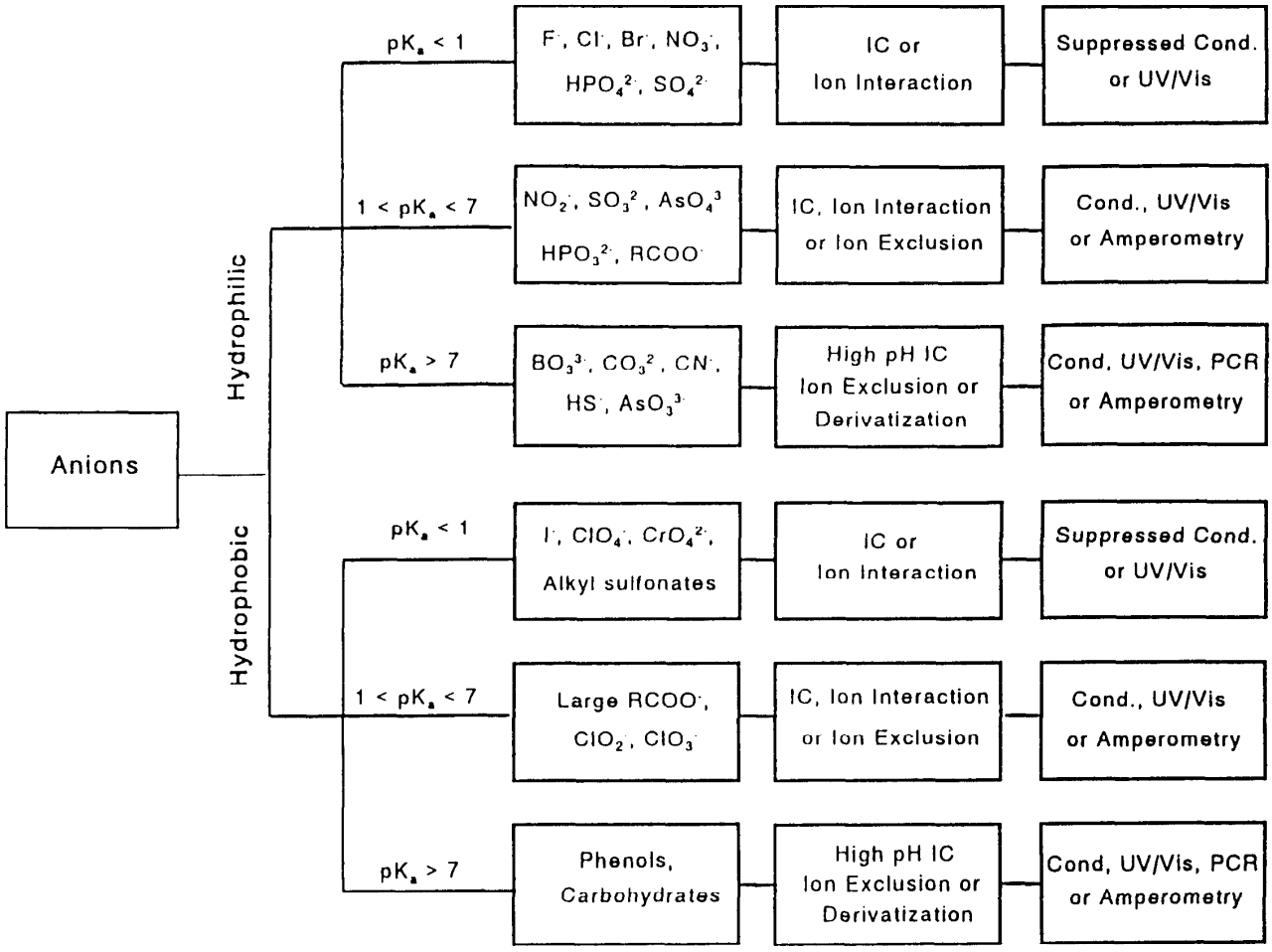


Figure 1 Flowdiagram for selection of separation and detection mode for anions. Abbreviations: IC, ion chromatography; PCR, postcolumn reaction; UV/Vis, direct or indirect UV/visible spectrometry. (Modified from Refs. 4 and 62.)

hydrophobic characteristics of the stationary phase as well as the ion-exchange characteristics. Hydrophobic interactions are greatest with reversed-phase supports, less intense, but nonetheless important, for polymeric ion-exchangers, and of minimal importance on inorganic ion-exchangers. If a sample contains both hydrophilic and hydrophobic anions, the hydrophobic interactions will influence the ultimate success of the separation; thus, the mixture should be classed as hydrophobic in using Fig. 1.

The second important characteristic is the acid dissociation constant, pK_a, of the analyte, which will strongly affect the mode of detection. The most common mode of detection for anions in ion chromatography is suppressed conductivity. Suppressed conductivity is less sensitive to weakly acidic anions; therefore, other detection modes, such as direct UV–Vis, amperometry, and postcolumn reaction detection must be considered. Illustrative examples of the separation and detection modes available for each anion group and specific anions are given in Secs. III and IV, respectively.

Figure 2 displays a flowchart for method selection based on properties of cationic species. The first characteristic that must be considered is the lability of the cation of interest. For kinetically inert ions or those that exist in a multitude of oxidation states, the best approach is to derivatize the metal before the separation, and then use reversed-phase, normal-phase,

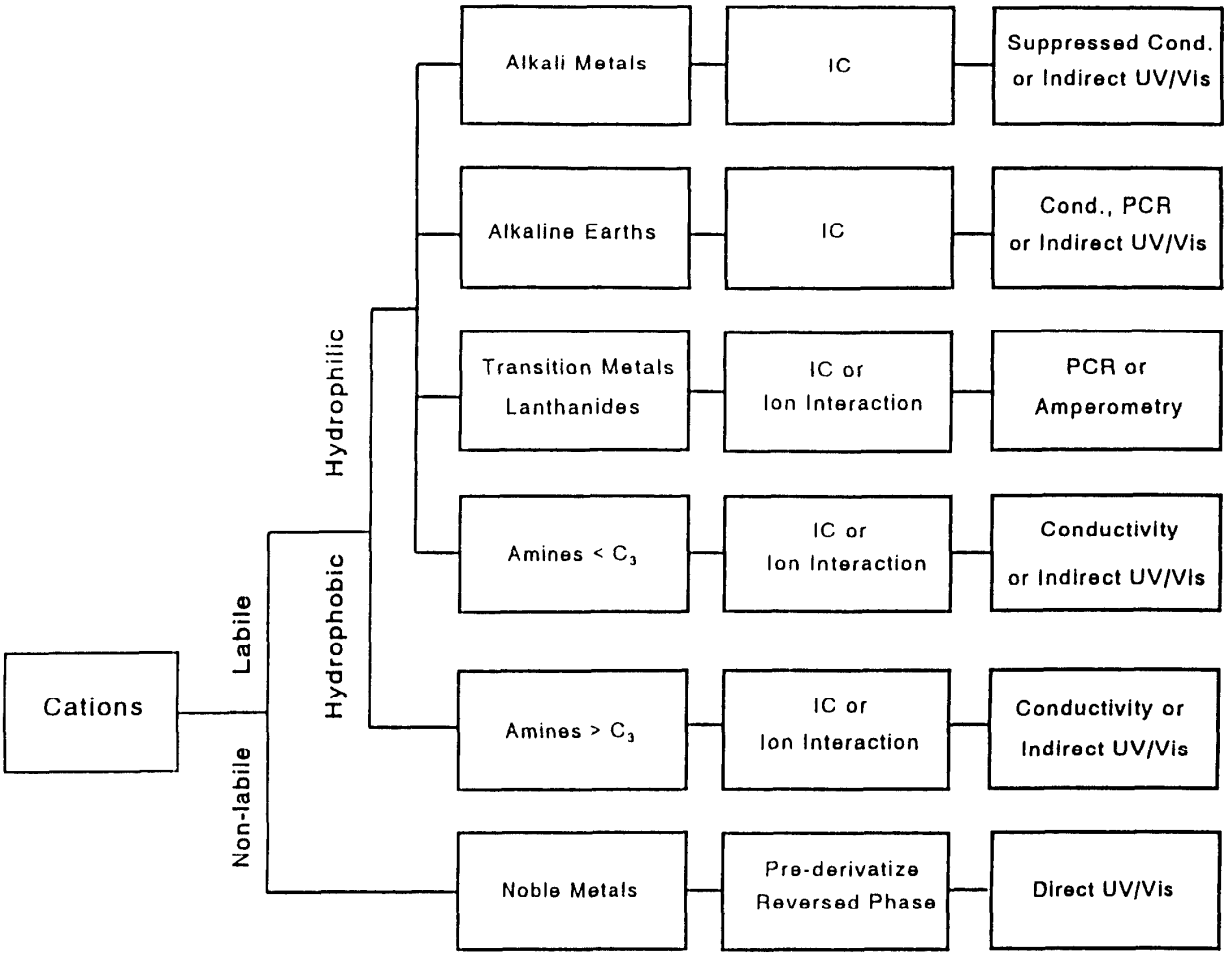


Figure 2 Flowdiagram for selection and detection mode for cations. Abbreviations: IC, ion chromatograph; PCR, postcolumn reaction; UV/Vis, UV/visible spectrometry. (Modified from Refs. 4 and 62.)

or size-exclusion chromatography to separate and analyze the stable chelate. Prederivatization techniques for metals analysis will be discussed in more detail in Sec. V.

As with anionic analytes, the hydrophobic nature of some analytes will play a role in their retention. It is important to realize that the classification of cations into hydrophobic and hydrophilic ions in Fig. 2 is only approximate, and that hydrophobic behavior may still play a role in the separation of hydrophilic ions. For example, uranium can be separated from lanthanide and actinide metals based on the hydrophobic nature of its complexes [19]. Illustrative examples of the determination of common cation groups are given in Sec. V.

B. Practical Aspects of Ion Chromatographic Separations

1. Water

Water used in the preparation of standards and eluants should be freshly distilled and deionized and meet the specifications for American Society for Testing and Materials (ASTM) type I water [20]. However, even with such water, the ionic impurities in the water can be significant in trace analyses because 18 MΩ·cm water may contain several parts per billion (ppb) of anion and cation impurities. Modern deionization systems using nuclear-grade ion-exchange resins

to "polish" out inorganic impurities can provide water containing down to 20 ppt chloride, 100 ppt sodium, and 50–60 ppt ammonium [21]. High-purity water should be used fresh, as the water will leach inorganic [22] and organic [23] impurities from the storage vessel.

2. Contamination

(a) During Sample Preparation. High-purity water samples can easily be contaminated during collection, storage, or even while sitting on the laboratory bench. The ASTM methods recommend TFE-fluorocarbons, FEP, linear polyethylene, conventional polyethylene, or polycarbonate containers and caps for trace metals; and polycarbonate, polystyrene, polypropylene, and polymethyl pentane for trace inorganic ions [24]. Sterilized culture bottles are another recommended storage container [25]. However, such polymeric materials release significant quantities of acetate (3 ppb) and formate (2 ppb) [26], and so should be avoided in trace measurements of carboxylic acids. The container should always be prerinsed with type I water before use. For trace analyses more extensive pretreatment may be required [24].

Precolumn cartridges and filter units are commonly used for sample cleanup before ion chromatographic analysis. These devices, as well as any syringes and vials used, can be additional sources of contamination, particularly when working in the ppb range for nitrate, chloride, sulfate, zinc, and lead [27]. The contamination levels can be reduced by prerinsing the cartridges and filters with type I water before use. However, some filter materials, such as cellulose esters, and to a much lesser degree nylon, will continue to liberate nitrate apparently indefinitely [28]. Gelman polysulfone, Nuclepore polycarbonate, and Nuclepore polyester are acceptable for low-level determinations of nitrate, chloride, phosphate, and sulfate [28].

Laboratory air is another source of sample contamination. Measurements of ammonium ions at a few ppb can be erroneous because of dissolution of trace amounts of ammonia from the atmosphere. Indeed, the ammonium ion content has been observed to increase from 1 to 49 ppb over 9 h of exposure to ambient air in a clean-air bench [29]. Similar difficulties have also been encountered with trace fluoride, acetate, and formate [26,30], and possibly lead [31].

Reagents used for stabilization of samples should be ACS reagent grade or the equivalent. Other grades may be used, provided it has been demonstrated that the reagent is of sufficient purity to permit its use without compromising the accuracy of the determination.

Losses of analyte can occur during storage owing to a variety of mechanisms, including sorption onto the storage material, biological activity, and oxidation. Specific means to avoid these losses are discussed in Secs. IV and V. Regardless of the ions of interest, however, it is advisable to run blanks and control standards, particularly when working in the low-ppb range.

(b) From System. Contamination of eluents as a result of corrosion of the stainless steel components of a chromatographic system are an obvious area of concern. Iron concentrations of 10–320 ppb and smaller concentrations of other components of 316-stainless steel have been measured in oxidizing and complexing buffers eluting from a stainless steel chromatographic system [31]. The major source of the corrosion products is the frits on the column, which possess a very high surface area relative to the rest of the chromatographic system. Thus, simply replacing the column with a metal-free column reduces the iron impurity levels to about 2 ppb, which is within the impurity levels expected from the eluant reagents [31].

Recent years have seen a movement to ion chromatographic systems constructed of poly(etheretherketone) (PEEK). PEEK is extremely chemically inert, flexible, inexpensive, and capable of withstanding high pressures, all of which make it ideal for ion chromatography. As yet, there have been no reports of leaching of ions from PEEK. However, some carryover between injections was observed in our laboratory when determining hydrophobic anions, such as iodide using a PEEK sample loop [32].

(c) Of the Column. One of the primary causes for deterioration in column performance is contamination of the ion-exchange sites or the surface matrix by the sample or the eluant

[33,34]. This contamination can take many forms, including irreversible retention of highly retained ions (e.g., ClO_4^- and $Fe(CN)_6^{4-}$); hydrophobic organics, ionic organics; humic and other colloidal materials; and polyvalent (transition) metal ions. Protocols for cleaning the column will depend on the nature of the column and the contaminant; consequently, it is necessary to refer to the manufacturer's literature.

The best way to prevent contamination of the analytical column is to use a guard column. A guard column is a short column packed with the same material as the analytical column and placed between the analytical column and the injector. The less expensive guard column will then be contaminated, rather than the separation column. Increasing backpressure or decreasing sample retention times indicate that the guard column has been significantly contaminated and should be cleaned or replaced.

C. Sample Pretreatment

1. Matrix Elimination

Bulk components of the sample can interfere with the analysis of the analytes of interest in various ways, including coelution, column overload, baseline disruption, or through masking of the analytes. Matrix components, such as strongly retained ions and hydrophobic material may also foul the separation column, limiting the column life. In such cases, it is obviously essential that the matrix components be removed. Solid-phase extraction (SPE) is a convenient means of eliminating such interferences [35]. SPE cartridges are prepared from cation-exchange resin in the H^+ form to reduce sample pH, in the Ag^+ form to selectively precipitate halides, and the Ba^{2+} form to precipitate sulfate. Cartridges are also available containing anion-exchange resin in the OH^- form to neutralize acidic samples, and polystyrene packing to remove hydrophobic matrix components. Care must be taken to avoid loss of the analytes of interest through coprecipitation, particularly with the Ba^{2+}-loaded resins. Furthermore, pretreatment cartridges can be a source of contamination [27].

Alternatively, excessive sample acidity [36] or basicity [37] can be eliminated using dialysis. In effect, the sample is passed through a membrane suppressor before analysis. Both chemical- and electrochemical-based [38] dialysis systems can be used. A similar approach has also been used to remove chloride from brine samples before ion chromatographic analysis [39].

A second means of removing the sample matrix is the "heart-cut" or "recycle" method in which the sample with matrix is injected onto a precolumn, and the portion of the precolumn eluate containing the component of interest is directed onto the separation column by a column-switching valve [40–42]. This procedure works best when the sample matrix is of a consistent composition and does not permanently affect the column performance.

2. Preconcentration

The most common form of pretreatment is to pass the sample through a small ion-exchange precolumn that concentrates the ions of interest and allows the matrix material to pass through unretained. The ions from the "concentrator" column are then eluted onto the analytical column for separation and quantification. If the concentrator column capacity is less than 40% that of the separation column, then the same eluant may be used for stripping the concentrator column and for the separation [43].

Increasing the sample volume will increase the quantity of analyte that is ultimately delivered to the separation column and thus the sensitivity. However, if too large a volume is loaded onto the concentrator column, the sample will be eluted from the concentrator by the sample matrix. The maximum sample volume that can be concentrated will thus be a function of the sample matrix. For instance, more than 45 mL of deionized (DI) water or 1 ppm ammonium water can be reliably concentrated on an anion concentrator, but 20 mL of 1.2 ppm boric acid is the maximum that can be concentrated [44].

To establish the maximum sample volume for a new application, prepare a plot of the peak height of the most weakly retained component of interest versus the volume concentrated. Negative deviation on such a plot indicates the volume at which the sample matrix is beginning to elute the analytes from the column. The maximum permissible concentration volume for reliable quantitative analysis is 80% of the volume at which the deviation is observed.

As an alternative to ion-exchange concentrator columns, columns possessing chelating functionality, such as iminodiacetate can be used. Chelation chromatography has been used to preconcentrate transition metals and lanthanides from complex matrices, such as seawater and digested biological, botanical, and geological materials, before ion chromatographic [45] or atomic spectroscopic analysis [46].

3. Solid Samples

The recommended procedure for preparation of solid samples for the determination of leachable ions is to slurry the sample in ten times its mass of reagent water, mix the slurry for 10 min [47] to 24 h [48] using a magnetic stirrer or rotation apparatus, and then filter the slurry using a 0.45-μm–membrane filter before injection. The use of 1:9 ethanol/water as the slurry solvent is also used in standard procedures [49]. Recovery studies should be performed using spikes of the analytes of interest.

If it is the concentration of a component of the bulk insoluble matrix that is of interest, then it is necessary to dissolve the solid, preferably in distilled water, although dissolution with water-miscible organic solvents, such as methanol followed by dilution with water, can be used [50]. Standard dissolution media, such as strong acids or bases, are unsuitable for sample preparation for ion chromatography because of their highly ionic matrix. Solid matrices are most commonly rendered compatible with ion chromatographic analysis through combustion in either a Parr oxygen bomb or a Schöniger oxygen flask. Combustion-ion chromatography is most commonly used to analyze total sulfur and chlorine, but has also been applied to the other halogens, total nitrogen, and total phosphorus, in matrices which include organic chemicals [51,52], pulp and paper [53], plant material [54], silicate rocks [55], catalyst [56], edible oils [57,58], fuel oil [59], coal, and oil shale [60]. Recovery of sulfur, nitrogen, and phosphorus is improved by addition of hydrogen peroxide to the receiver solution [54], whereas bromine and iodine are improved by addition of hydrazine [60]. Care must be taken to avoid contamination of nitrogen from N_2 from the air dissolved in the sample and present in the bomb if proper flushing with oxygen has not been performed [58,60].

4. Gaseous Samples

Gas samples containing species such as SO_2, HNO_3, and HONO are filtered to removed particulate material and collected in a dilute peroxide solution for subsequent IC determination. The collection device may be a classic impinger system or a diffusion denuder-based system [8].

III. METHODS FOR COMMON ANION MIXTURES

When searching for procedures for determining common anion mixtures, regulatory methods [61] and manufacturers' application notes [62] offer the highest degree of confidence. Application notes will not be covered in general, but will be cited for specific applications when appropriate. Listings of application notes are available from the column manufacturers.

A. Regulated Methods for Anion Determination

Regulatory agencies, such as the US Environmental Protection Agency (EPA) and the American Society for Testing and Materials (ASTM) have approved methods for several ion mixtures. These are summarized in Table 1. EPA Method 300.0 A [47] and ASTM 4327 [63] are approved for analysis of F^-, Cl^-, NO_2^-, Br^-, NO_3^-, HPO_4^{2-}, SO_4^{2-} in drinking- and

Table 1 Regulated Methods for Anion Analysis

Method number	Ions determined (MDL; ng)[a]	Separation mode (eluant)	Detection mode	Ref.
EPA 300.0A; ASTM D4327	F^-(0.6), Cl^-(1), NO_2^-(0.7), Br^-(0.5), NO_3^-(0.5), HPO_4^{2-}(0.5), SO_4^{2-}(1)	Anion-exchange (HCO_3^-/CO_3^{2-})	Suppressed conductivity	47, 63, 229
EPA A-1000	F^-(4), HCO_3^-(30), Cl^-(2) NO_2^-(4), Br^-(6), NO_3^-(4) HPO_4^{2-}(15), SO_4^{2-}(10)	Anion-exchange (borate/gluconate, pH 8.5)	Nonsuppressed conductivity	65
EPA B-1011	NO_2^-(0.9), NO_3^-(0.2)	Anion-exchange (LiOH)	Direct UV (214 nm)	65, 230, 231
EPA 300.0 B	ClO_2^-(0.5), BrO_3^-(1), ClO_3^-(0.2)	Anion-exchange (HCO_3^-/CO_3^{2-})	Suppressed conductivity	47
	ClO_2^-(0.2), BrO_3^-(0.4), NO_2^-(0.2), Br^-(0.4), ClO_3^-(0.6) NO_3^-(0.4)	Anion-exchange (OH^-/BO_3^{3-})	Suppressed conductivity	67
	ClO_2^-(0.5), BrO_3^-(0.5), NO_2^-(0.3), Br^-(0.4), NO_3^-(0.5)	Anion-exchange (OH^-/BO_3^{3-})	Direct UV (196 nm)	67
ASTM D5257	CrO_4^{2-}(0.1)	Anion-exchange $(NH_4)_2SO_4/NH_4OH$	PCR:diphenylcarbohydrazine (520 nm)	68, 69

[a]Method detection limits (MDL) are given in nanograms of the anion in the form shown in the table.

wastewaters using a Dionex AS4A anion separator column (or equivalent [64]) with 1.7 mM sodium bicarbonate–1.8 mM sodium carbonate eluant and suppressed conductivity detection. EPA 300.0 also includes approved procedures for determining anion content in solids and leachates. EPA method A-1000 has been approved for determination of chloride and sulfate using nonsuppressed ion chromatography [65], and will separate the other ions discussed earlier.

Nitrate and nitrite in drinking- and wastewater can be determined either using suppressed conductivity detection (EPA 300.0 A) or nonsuppressed direct UV detection (EPA B-1011 for drinking water [65] and B1012 for wastewater [66]).

Disinfection of drinking water results in the formation of oxyhalide by-products (ClO_2^-, ClO_3^-, BrO_3^-). EPA 300.0 B [47] describes a suppressed conductivity method using 0.2 mM HCO_3^-–1.4 mM CO_3^{2-} eluant on a Dionex AS9 separator column. Application of this method to drinking water, has experienced interferences from background levels of chloride, carbonate, and nitrate. A new eluant, 30 mM NaOH–120 mM H_3BO_3, has been proposed to eliminate these interferences [67].

The acute toxicity of hexavalent chromium [Cr(VI)] has led to the development of standard procedures for its analysis in water by anion exchange with postcolumn reaction detection with diphenylcarbazide and detection of the colored complex at 520 nm [68,69]. Sample water is adjusted to pH 9–9.5 using concentrated $(NH_4)_2SO_4$–NH_4OH eluant and is analyzed within 24 h, although Cr(VI) remains stable in reagent and drinking waters for up to 15 days [69]. No approved ion chromatographic procedure exists for determination of Cr(VI) in solid samples.

B. Alternative Methods for Common Anion Mixtures

The regulated methods offer the highest degree of confidence, and are thus the recommended starting point for method development. However, frequently, the recommended instrumentation is not available or the regulated method is unsuitable for a specific analysis. In these cases, alternative procedures must be used to analyze the sample. Table 2 presents some illustrative examples of alternative separation and detection procedures that can be used for inorganic anion mixtures.

C. Methods for Various Sample Matrices

Inorganic anions within a wide range of sample matrices can be determined using the ion chromatographic methods described in Secs. III.A and III.B by combining these determination

Table 2 Other Methods for Anion Analysis

Ions determined (MDL; ng)[a]	Separation mode (eluant)	Detection mode	Ref.
F^-(3), Cl^-(2.5), NO_2^-(4), Br^-(5), NO_3^-(4), HPO_4^{2-}(6), SO_4^{2-}(8)	Anion-exchange (*p*-hydroxybenzoic)	Nonsuppressed conductivity	232
F^-(1), Cl^-(1), NO_2^-(3), (Br^-, propionate), $H_2PO_4^-$(21), NO_3^-(4), SO_4^{2-}(4)	Anion-exchange (phthalate, pH 6.8)	Indirect UV (265 nm)	233
$H_2PO_4^-$, Cl^-(0.25), NO_2^-, Br^-(1), NO_3^-(0.2), ClO_3^-, I^-, BF_4^-, SO_4^{2-}(0.8), (ClO_4^-, $S_2O_3^{2-}$), SCN^-	IIC (Bu_4N^+) (naphthalene-1,5-disulfonate, pH 4.3)	Indirect UV (300 nm)	234

[a]Method detection limits (MDL) are given in nanograms of the anion in the form shown in the table.

procedures with the sample preparation procedures described in Sec. II.C. Table 3 presents application of EPA method 300.0 A (anion exchange with a HCO_3^-–CO_3^{2-} eluant and suppressed conductivity detection) to a wide variety of matrices through the use of various sample preparation techniques.

IV. METHODS FOR SPECIFIC ANIONIC SPECIES

A. Halides, Pseudohalides, and Oxyhalides

Difficulties in fluoride analysis arise largely from the weak retention of this anion in anion-exchange chromatography. Interference by the water dip can be minimized by the addition of eluant to the sample [63]. The interference from other weakly retained anions (e.g., propionate or butyrate) can be eliminated by using a higher-capacity column [70]. In a comparison of six commercially available columns, based on the fluoride-acetate peak resolution and total run time for a standard anions mixture, the Dionex AS10, Sarasep, AN2, and Waters IC-PAK Anion HR were deemed to be acceptable, although no column met every requirement [71]. Specific detection of fluoride can be achieved by postcolumn fluorescence [72] and absorbance [73], with detection limits of 0.2 $\mu g\ L^{-1}$ and 50 $\mu g\ L^{-1}$, respectively.

As chloride and bromide are target anions of the regulatory methods described in Sec. III.A, a wide range of columns are available that provide excellent separations of these ions from other common anions [71]. However, chloride retention is generally low ($k' < 1$), and so interference can result from large concentrations of weakly retained species, such as acetate, formate, and carbonate. Aspects of the extraction and ion chromatographic determination of chloride in coal have been reviewed [74]. Bromide, along with other anions, such as iodide, nitrate, and nitrite, absorb in the 210- to 220-nm range and so can be detected down to nanogram levels using direct UV-absorption [75]. Other common anions, such as chloride and sulfate, do not absorb.

Table 3 Anion Analysis in Various Sample Matrices[a]

Matrix	Anions	Sample preparation	Ref.
Ultrapure water	F^-, acetate, formate, Cl^-, NO_2^-, Br^-, NO_3^-, HPO_4^{2-}, SO_4^{2-}, oxalate	Anion-exchange; preconcentration	71
Atmospheric precipitation	Cl^-, NO_3^-, SO_4^{2-}	None	235
Ultraclean surfaces	Anionic and cationic inorganic residues	Distilled water rinse	236
Smoke aerosols	Acetate, formate, Cl^-, NO_2^-, NO_3^-	Electrostatic precipitation; methanol leaching	237
HF	HPO_4^{2-}, SO_4^{2-}	Anion-exchange; preconcentration	238 239
HCl, HNO_3, H_3PO_4, H_2SO_4	Cl^-, NO_3^-, HPO_4^{2-}, SO_4^{2-}	Heart-cut/recycle	240
NaOH	F^-, Cl^-, NO_2^-, Br^-, ClO_3^-, NO_3^-, HPO_4^{2-}, SO_4^{2-}	SPE in H^+-form	241

[a]The separation is based on EPA Method 300.0A: anion-exchange with a HCO_3^-/CO_3^{2-} eluant and suppressed conductivity detection.

Iodide is a strongly polarizable, hydrophobic anion, and as such, the most efficient separations for iodide are achieved using hydrophilic silica-based anion exchangers. Detection limits are 50 ng by suppressed conductivity, 5 ng by UV detection at 226 nm [76], and 1.3 ng by amperometric detection at +0.155 V [77]. Iodide and bromide catalyze the reaction between chloramine-T and 4,4′-bis(dimethylamino)diphenylmethane. This system has been used as an extremely sensitive detection system for iodide (0.02 ng) [78]. Bromide also responds, but with a detection limit of only 15 ng.

Cyanide is a very weak acid (pK_a = 9.2), making detection by suppressed conductivity insensitive. Oxidation of cyanide by hypochlorite produces cyanate ion (pK_a = 3.66), which elutes similarly to nitrite, which is the only interferant. Resultant calibration curves are linear from 0.05 to 1.0 mg L^{-1} with a precision of 1.1% [78]. Prederivatization with quinoline and benzoyl chloride allows cyanide to be determined using reversed-phase chromatography with nanogram detection limits by direct UV (225 nm) [80]. Sensitive (MDL = 0.1 μg L^{-1}) and selective determination of cyanide is achieved by ion-exclusion separation, followed by postcolumn fluorescence derivatization of CN^- with *o*-phthaldehyde or naphthalenedicarboxylic acid in the presence of an amino acid [81].

The EPA method 300.0 B refers to the determination of oxyhalides present as by-products of water disinfection. The recommended carbonate–bicarbonate eluant does not provide complete separation of BrO_3^-, NO_2^-, and ClO_3^- from typical background levels of chloride, carbonate, and nitrate. Tetraborate–boric acid eluants yield much better separations (see Table 1) [67]. Although the other oxyhalides are stable, chlorite is rapidly lost from samples. Addition of 50 mg L^{-1} ethylenediamine to samples preserves chlorite for 15 days. Bromate is believed to be a potential carcinogen, even at the low ppm level. Detection limits of 1 μg L^{-1} can be achieved by eliminating the background chloride using an Ag^+-loaded cation-exchange column and preconcentrating 5 mL of sample using a concentrator column [82].

Recently, inductively coupled plasma–mass spectroscopy (ICP–MS) has been coupled to an ion chromatographic system for the determination of IO_3^-, BrO_3^-, Cl^-, ClO_3^-, Br^-, and I^-, with detection limits of 25 ng for I species, 0.8 ng for Br species, and 36 ng for Cl species [83].

B. Nitrogen-Containing Anions

The EPA method 300.0 recommends that water samples for nitrate and nitrite analysis be kept at 4°C and analyzed within 48 h [47]. Samples acidified with sulfuric acid to a pH < 2 and stored at 4°C can be held for 28 days. However, environmental samples stored in this fashion may undergo nitrate oxidation to nitrate by nitrogen-fixing bacteria. Preservation of samples under highly basic conditions (pH 12 with sodium hydroxide) inhibits the bacteria, and no conversion of nitrite was observed during a 37-day period [84].

Azide elutes between bromide and nitrate. The separation has been investigated for Waters, Hamilton, and Dionex columns, with the best resolution being achieved using a Dionex AS4A column with 16 mM tetraborate eluant [85]. Using suppressed conductivity, the calibration was linear from 0 to 15 ppm with a detection limit of 30 ppb. The method was validated for the assays of several proteins.

C. Sulfur-Containing Anions

With low-capacity columns, such as used in the regulatory methods described in Sec. III.A, sulfate elutes near the end of the chromatogram, between phosphate and oxalate. However, if a moderate capacity column (e.g., Dionex AS10) is used with correspondingly stronger eluants, the retention of dianions, such as sulfate, are more strongly reduced than for monoanions, resulting in sulfate eluting in the middle of the standard anion mixture between nitrite and

bromide. Rapid sulfate determination (<1 min) can be achieved using just a guard column [86].

Sulfite is determined by anion-exclusion chromatography using electrochemical detection [87,88], with a detection limit of 0.1 mg L^{-1} and a linear range to 15 mg L^{-1}. Extraction of foods and beverages with a buffer of pH higher than 9 yields both "free" sulfite and sulfite that is bound to carbonyl compounds, whereas extraction with pH 2.0 will result in the determination of only the "free" form [89]. Mannitol, glycerol, and fructose are effective for stabilization of samples against oxidation by dissolved oxygen [90]. Alternatively, sulfite can be converted to hydroxymethanesulfonate by the addition of excess formaldehyde and then separated on an anion exchanger using a bicarbonate eluant containing 0.2% formaldehyde. The linear range is 0.1–12 mg L^{-1} by suppressed conductivity detection.

Ion chromatographic methods for the determination of SO_2, SO_4^{2-}, and $S_2O_6^{2-}$ have been compared with other methods of analysis [91]. In the latest of a series of papers on the separation of sulfur-species, hydroxymethanesulfinate ($HOCH_2SO_2^-$), the product of the reaction between formaldehyde and dithionite ($S_2O_4^{2-}$), and other S-species such as HS^-, SO_3^{2-}, and $S_2O_3^{2-}$ or $S_2O_3^{2-}$, $S_4O_6^{2-}$, $S_5O_6^{2-}$, and $S_6O_6^{2-}$ have been separated by ion interaction with tetrabutylammonium with direct UV detection at 215 nm [92].

Thiocyanate is strongly retained by anion-exchange chromatography, and so experiences no interferences from common anions or other forms of sulfur. Suppressed conductivity detection has been used for determination of 0.02–10 mg L^{-1} SCN^- in soil extracts [93]. Direct UV detection at 195 nm has been used for 0.01–40 mg L^{-1} SCN^- in serum [94].

D. Phosphorus-Containing Anions

As evidenced by the retention orders in Table 2, phosphate's order of elution can vary much more than that of any of the other standard anions. This is a function of both its weak acidic character and its high charge. Hypophosphite, phosphite, and orthophosphate can be separated by anion exchange with direct conductivity, yielding detection limits of 0.2 ppm [95]. Detergent mixtures containing orthophosphate, pyrophosphate, tripolyphosphate, as well as organophosphates and chelating agents can be determined by anion exchange with a nitric acid step-gradient and absorbance detection at 340 nm after postcolumn reaction with Fe(III) [65]. The separation of phosphate and polyphosphates up to $P_4O_{12}^{4-}$ can be achieved using gradient elution with hydroxide eluants and suppressed conductivity detection [96]. Phosphates and polyphosphates can also be detected spectrophotometrically at 820 nm after postcolumn formation of the heteropolyacid with molybdenum as the derivatizing agent [97].

E. Arsenic, Selenium, and Tellurium Anions

Arsenite is a very weak acid and so cannot be detected by conductivity. Anion-exchange separations yield method detection limits of 0.11 mg L^{-1} for As(III) with electrochemical detection, and 0.026 mg L^{-1} for Se(IV), 0.029 mg L^{-1} for Se(VI), and 0.12 mg L^{-1} for As (V) with suppressed conductivity detection [98]. A 50-fold excess of common anions does not cause an interference. Greater tolerance of interferents is gained by using direct UV detection (195 nm). The background absorbance of the carbonate eluant is reduced using a suppressor. The detection limits are 0.1 mg L^{-1} for As(III), 0.1 mg L^{-1} for Se(IV), 0.25 mg L^{-1} for Se(VI), and 0.25 mg L^{-1} for As (V) [99].

Neither anion exchange with suppressed conductivity nor UV spectroscopy detection meet the detection limits required by the National Primary Drinking Water Standards (0.05 mg L^{-1} for As and 0.01 mg L^{-1} for Se). Ion interaction with inductively coupled plasma–atomic emission spectroscopic (ICP–AES) detection has yielded detection limits of 3 ng for methylarsonic acid, 5 ng for demethylarsonic acid, 10 ng for arsenobetaine, and 14 ng for arsenocholine [100]. ICP–mass spectroscopy (ICP–MS) has yielded detection limits of 0.16 ng for

As(III), 0.032 ng for dimethylarsonic acid, 0.18 ng for monomethylarsonic acid, and 0.26 ng As(IV) [101]. Other applications of ICP–MS for chromatographic detection have recently been reviewed [102].

ICP–MS has also been used for selective detection of $HTeO_4^-$ and TeO_3^{2-} anion exchange and organic tellurium species after reversed-phase chromatography [103].

F. Molybdate, Tungstate, and Chromate

Molybdate [104] and tungstate [105] in soil have been determined by nonsuppressed anion exchange with detection limits of 0.045 mg L^{-1} MoO_4^{2-} and 0.17 mg L^{-1} for WO_4^{2-}. Tungstate and molybdate can be separated by ion-interaction separation of their tiron chelates [106]. Detection is by direct UV (315 nm), with detection limits of 3.3 ng for tungsten and 2.4 ng for molybdenum. The presence of Fe^{3+}, V^{5+}, Cr^{6+}, Ti^{4+}, and Sn^{2+} cause serious interference.

Direct UV determination of Cr(VI) at 365 nm has yielded results comparable with the approved diphenylcarbohydrazide postcolumn derivatization detection in the concentration range of 8–1000 μg L^{-1} [61].

G. Inorganic Complexes

Metallocyanide complexes such as $Ag(CN)_2^-$ and $Pd(CN)_4^{2-}$ can be separated either by anion exchange [107] or by ion interaction on a reversed-phase column in the presence of a tetra-alkylammonium in the mobile phase [108,109]. Detection limits in the low to sub-ppm range are achieved by direction UV detection at 214 nm.

Total EDTA is typically performed by formation of the copper(II) [110] or the iron(III) [111] complex before separation by anion-exchange or ion-interaction chromatography. Both of these complexes can be sensitively monitored using direct UV detection at ~250 nm. Other metal complexes such as $Pb(EDTA)^{2-}$ and $Ni(EDTA)^{2-}$ can also be monitored at 250 nm, although the sensitivity of $Ni(EDTA)^{2-}$ is only about a 1/10 that of the Cu or Pb complexes. $Zn(EDTA)^{2-}$, $Cd(EDTA)^{2-}$, and $Co(EDTA)^{2-}$ show appreciable absorbance only in the short UV. Postcolumn addition of 0.1 mM $CuSO_4$ in 0.3 M acetic acid yields $Cu(EDTA)^{2-}$, which can be sensitively monitored at 250 nm, with detection limits for each of the metal–EDTA complexes of 30–50 ng and linearity up to 5 μg [112].

H. Miscellaneous Inorganic Anions

Boric acid is an extremely weak acid (pK_a = 9.2) and so requires a strongly alkaline eluant (pH > 10) to be separated by anion exchange [113]. Borate can also be determined by ion exclusion chromatography with a detection limit of 8 ng B using refractive index detection [114]. Polyols, such as fructose, complex with borate making it a much stronger acid. Use of 0.1 M fructose as the eluant for ion-exclusion chromatography allows direct conductometric determination of boric and germanic acid with detection limits of 0.5 ppb (B) and 1.5 ppb (Ge) [115].

Bicarbonate/CO_2 can be determined by ion exclusion with distilled water as eluant or by single column anion exchange. Direct conductometric detection results in nonlinear calibration curves over the 0.1- to 1-mM range owing to the inherent nonlinear response of conductivity detector to weak acids [116]. Postseparation conversion of carbonic acid to K^+OH^- using a cation-exchange column in the K^+ and an anion-exchange column in the OH^- form improves the signal-to-noise and linearity [117]. Both procedures have a detection limit of 2–3 μM.

Silicate can be determined down to 2 ppb using anion-exchange chromatography with a 0.5-mM KOH eluant and nonsuppressed conductivity [65]. Silica can also be determined by postcolumn reaction with molybdate to produce the molybdenum blue, which is monitored at 410 nm [118]. Reliable quantification (<10% RSD) can be made down to 10 ppb silica.

I. Carboxylic Acids

Carboxylic acids can be separated by reversed-phase, anion-exchange and ion-exclusion chromatography. Reversed-phase chromatography with direct UV detection at 210 nm has been used for determination of organic acids present in wines at the 50- to 5000 mg L^{-1} range [119,120]. Reversed-phase separations can be made more sensitive and selective by prederivatizing the carboxylic acids with reagents, such as phenacyl bromide, and monitoring at 254 nm [121]. Anion-exchange chromatography with suppressed detection will provide detection limits in the ppb range [122]. Monoprotic acids such as formic, glycolic, and pyruvic acid can be separated on a moderate-capacity column (0.36 mEq) using a weak eluant such as 20-mM borate. Most diprotic acids, such as tartaric and succinic acid, must be separated on the same column using a stronger carbonate–hydroxide eluant. Strongly retained diprotic acids and triprotic acids must be separated on a lower capacity column (0.028 mEq) using a carbonate/hydroxide eluant. If a mixture of mono-, di-, and triprotic acids is to be analyzed an ion-exclusion column can be used. The separation in ion exclusion is largely determined by the Donnan exclusion of the acids; thus, the acids will elute in order of pK_a. Hydrophobic and steric effects also play a part in retention. If carboxylic acids and strong inorganic acids are all to be determined, gradient elution anion-exchange chromatography can be used. With this technique up to 36 anions have been separated in 30 min [123].

An assessment of ion-exclusion and isocratic and gradient anion-exchange methods for the determination of common inorganic and organic acids [124] found that gradient anion exchange was best if only one method were to be used. However, to adequately cover all of the common acids, it was recommended that two methods be used. Gradient anion exchange was most reliable for formate, methanesulfonate, and the inorganic anions, whereas ion exclusion was best for acetate and lactate, as well as giving corroborating analyses for other organic acids of interest. Detection limits for gradient (0.01–0.08 mg L^{-1}) and isocratic (0.01–0.25 mg L^{-1}) anion exchange were superior to those for ion exclusion (0.1–0.4 mg L^{-1}). The isocratic procedure however provided the best precision.

Iminodiacetic acid [125] and nitrilotriacetic acid (NTA) [126] have been determined by ion exclusion with suppressed conductivity. Detection limits of 0.05 mg L^{-1} and 1 mg L^{-1} were achieved in clean samples, and 0.23 and 11 mg L^{-1} in cell-free extracts for iminodiacetate and NTA, respectively. Free NTA has been determined by anion exchange with a nitric acid eluant followed by amperometic (MDL = 100 ng) or potentiometric detection (MDL = 500 ng) [127]. Ethylenediaminetetraacetic acid (EDTA) can be determined by the formation of the Cu^{2+} [110] or Fe^{3+} [111] complex, separation by ion-interaction chromatography and direct UV detection at 254 or 300 nm. Using Cu^{2+} and 300 nm, linear calibration was observed for 20 μL injections of 7–178 mg L^{-1} EDTA with a detection limit of 1.4 mg L^{-1} [128]. EDTA and other hexedentate chelating ligands have been determined fluorometrically by postcolumn generation of fluorescent (lutetium)-(ligand)-(8-hydroxyquinoline-S-sulfonic acid complexes [243]. Detection limits were 0.5 picomoles (10 nM). This detection scheme has also been applied to metal-EDTA-complexes [244] and other chelating ligands such as NTA and diethylenetriaminepentaacetic acid (DTPA) [245].

J. Sugars

Carbohydrates are weakly acidic ($pK_a \sim 12$). Thus, anion-exchange separations of carbohydrates can be performed using sodium hydroxide or sodium hydroxide–sodium acetate eluants of pH 12 or higher [129]. The anion-exchange retention increases with molecular size; sugar alcohols, monosaccharides, disaccharides. Retention is also a function of the eluant pH and temperature.

V. CHROMATOGRAPHIC METHODS FOR CATIONIC SPECIES

A. Alkali and Alkaline Earth Metals

Alkali metals are eluted in order of increasing atomic mass from cation-exchange columns by noncomplexing eluant. Detection limits of 5 ppb can be achieved with suppressed conductivity detection. Indirect absorbance detection can also be used for the alkali metals, but with inferior detection limits [130]. Simultaneous determination of alkali and alkaline earth metals can be difficult owing to the large difference in retention between the monovalent and the divalent metals. Column switching allows rapid analyses of the two groups of cations by eluting each group from a column for which ion-exchange capacity has been optimized for the respective group. For example, the mixed cations can be injected onto a low-capacity Dionex Fast Cation II column. The monovalent cations rapid pass through the Fast Cation II column and onto a higher-capacity Fast Cation I column. At this point, while the divalent cations are still on the Cation II column, the column order is switched. The monovalent cations now elute from the Cation I column and, once again, the Cation II column, before the divalent cations eluting from the Cation II column. With this technique combined with preconcentration (10 mL), linear ranges of 0.5–10 ppb sodium and 1–15 ppb magnesium were achieved using suppressed conductivity [131].

An alternative means of simultaneously determining the alkali and alkaline earth metals is to use cation-exchange and a gradient of noncomplexing eluant. Use of a 30-mM HCl–0.5 mM 2,3-diaminopropionic acid (DAP) to 50 mM HCl–2 mM DAP step-gradient allows all alkali metal and alkaline earth metals up to calcium to be separated on a Dionex CS-10 column in 12 min [131]. A third means of simultaneously determining the alkali and alkaline earth metals is to use cation-exchange with a complexing eluant. For instance, addition of 0.1 mM EDTA to a 3.0 mM HNO_3 eluant allows the alkali metals and alkaline earths to barium to be separated on a Waters IC-Pak C column in 22 min (15 min for calcium) [65].

In addition to conductivity detection, alkaline earth metals can be determined by post-column reaction detection [132]. Arsenazo I [133] and Zn-EDTA-PAR [134] have been used with absorbance detection. The latter of these reagents has been more extensively used because it also responds to a wide variety of transition and lanthanide metals. 8-Hydroxyquinoline-5-sulfonic acid has been used for fluorescence postcolumn reaction of Mg^{2+} and Ca^{2+} [135].

Beryllium has been determined in the 50- to 5000-ppb range using a Dionex CS3 column with 190-mM HCl eluant and absorbance postcolumn reaction detection with Beryllon II [136]. Alternatively conductimetric detection can be used for beryllium after cation-exchange separation with a pyridine-2,6-dicarboxylic acid (PDCA)–citric acid eluent [137].

B. Group IIIA (B, Al, Ga, In, Tl)

Aluminum–ligand reactions are kinetically slow. Thus, most chromatographic methods for aluminum involve cation exchange with a noncomplexing eluant. Detection is commonly postcolumn reaction with Tiron with absorbance detection at 310 nm [138–140] or pyrocatechol violet with absorbance detection at 570 nm [140]. Cation-exchange followed by fluorescent postcolumn reaction detection with 8-hydroxyquinoline-5-sulfonic acid (HQS) yields linear response from 5 to 10,000 ppb for aluminum, with a detection limit of 1 ppb [141]. These techniques can be used for speciation of fluoro-, oxalato-, citrato-, and free aluminum [138,142].

Prederivitization with 8-hydroxyquinoline (HQ) allows reversed-phase separation and absorbance (370 nm) detection of Al(III), Cu(II), Ga(III), Fe(III), and In(III) [143]. Gallium, indium, and thallium have been separated in 15 min using a bonded-phase cation-exchanger with 0.1 M tartrate–0.12% NaCl (pH 2.25) eluant. Postcolumn absorbance detection with Zn-EDTA-PAR yields quantification in the 0.004–0.1% range for each of the metals [144].

C. Group IVA (Si, Ge, Sn, Pb)

Germanium and tin can be simultaneously analyzed using a bifunctional column with detection limits of 0.5–1.5 $\mu g\ L^{-1}$ using postcolumn reaction detection with phenylfluorone and absorbance detection at 520 nm [145]. Addition of CTAB micelles enhances the sensitivity. Tetraalkyltin compounds are separated by reversed-phase chromatography [146], whereas organotin chlorides are separated by ion-exchange or ion-interaction chromatography [147]. Organotin chlorides undergo secondary interactions with silica-based supports; thus, polymeric-based columns yield superior sensitivities [148]. Detection limits of 2000 ng have been achieved for organotin chlorides using flame atomic absorption [146], 200–1700 ng for ICP–AES [147], and 0.002 ng for ICP–MS [148].

Speciation of inorganic Pb^{2+} and organolead compounds, such as the trialkyllead chlorides and tetraethyllead, have been performed using reversed-phase, ion-interaction, and ion-exchange chromatography [149]. On-line detectors and their associated detection limits are direct UV (>140 ng) [150], flame atomic absorption spectroscopy (10 ng) [150], ICP–AES (74–320 ng) [149], and ICP–MS (low picograms) [149,151].

D. Transition Metals

Table 4 presents several procedures for determining mixtures of transition and noble metals. The most common means of separating the first-row transition metals by HPLC is on reversed-phase columns dynamically coated with $C_8SO_3^-$ [152], or on low-capacity ion exchangers

Table 4 Methods for Determining Inorganic Cation Mixtures by HPLC

Transition metals determined (MDL; ng)[a]	Separation mode (eluant)	Detection mode	Ref.
Fe^{3+} (dead vol.), Cu^{2+} (0.5), Pb^{2+} (1.5), Zn^{2+} (0.5), Ni^{2+} (1), Co^{2+} (0.5), Cd^{2+} (1.5), Fe^{2+} (2.5), Mn^{2+} (1)	Ion-interaction (tartrate–acetonitrile (pH 3.65)–octanesulfonate)	PCR: PAR (500 nm)	65
Pb^{2+}, Fe^{3+}, Cu^{2+}, Ni^{2+}, Zn^{2+}, Co^{2+}, Cd^{2+}, Mn^{2+}, Fe^{2+}, Hg^{2+}	Anion-exchange CS-5 (pyridine-2,6-dicarboxylic acid)	PCR: PAR (520 nm)	6, 242
Ni^{2+} (0.2), Co^{2+} (0.1), Cr^{3+} (1.0), Cu^{2+} (0.8), Hg^{2+} (8)	Derivatization with diethylcarbamate; reversed-phase (MeOH–water)	Direct UV (254 nm)	162
Cu^{+}, Ag^{+} (1.9), Fe^{2+}, Co^{3+}, Fe^{3+}, Au^{+} (2.6), Pd^{2+} (0.8), Pt^{2+} (0.9)	Prederivatization with CN^-; ion-interaction C_{18} (acetonitrile–water–tetramethylammonium)	Direct UV (214 nm)	108
Ru^{3+}, Pt^{2+} (0.25), Pd^{2+} (0.2), Rh^{3+} (0.25)	Prederivatization with diethyldithiocarbamate C_{18} (acetonitrile–water)	Direct UV (260 nm)	163
Cd(10), Pb(3.6), Se(2.4), Cr, Ni(8), Sb(22), Hg(15), Cu(9), Co, Cr	Prederivatization with dibenzyldithiocarbamate C_{18} (methanol, THF, acetonitrile, pH 5 acetate)	Direct UV (254 nm)	164
Co^{3+}(<17), Be^{2+}(<110), Rh^{3+}(<10), Cr^{3+}(<20), Ru^{3+}(<10), Ir^{3+}(<5), Pd^{2+}(<10), Pt^{2+}(<5)	Prederivatization with acetylacetone C_{18} (methanol/water)	Direct UV (254 nm)	165

[a]Method detection limits (MDL) are given in nanograms of the anion in the form shown in the table.

[153], using a complexing eluant. Postcolumn reactions detection with 4-(2-pyridylazo)resorcinol (PAR) responds to a wide range of metal ions, including Pb^{2+}, Fe^{3+}, Cu^{2+}, Ni^{2+}, Zn^{2+}, Co^{2+}, Cd^{2+}, Mn^{2+}, Fe^{2+}, and Hg^{2+}, with detection limits in the low ppb range for typical injection volumes. This is more than 100 times the sensitivity achievable with conductivity [154]. Concentration detection limits can be reduced using either ion-exchange or chelation [45] preconcentration. The iminodiacetate resin used in chelation preconcentration retains only transition and lanthanide metals. Thus, the alkali and alkaline earth metals that compose the sample matrix are eliminated during the sample preconcentration step. This technique, known as chelation ion chromatography, has recently been used for the determination of sub-ppb levels of Cu^{2+}, Ni^{2+}, Zn^{2+}, Co^{2+}, and Mn^{2+} [155]; low ppb levels of Cd^{2+} and Pb^{2+} [156] in seawater; and low ppt Mn^{2+} in nuclear power plant waters [157].

Metalloluminescent reagents are useful only for metals ions with the most stable electron configurations (i.e., either completely full or empty electron shells). Thus, fluorescent reagents are useful for only a limited number of transition metals. Cadmium and zinc can be determined in the picomole range using buffered 8-hydroxyquinoline-5-sulfonic acid (HQS) as eluant and subpicomole detection limits if the HQS is added as a postcolumn reagent [158]. Addition of $MgEDTA^{2-}$ or $MgCDTA^{2-}$ to HQS yields a reagent with detection limits in the 33- to 140-pmol range for a wide variety of alkaline earth, transition, and lanthanide metal ions [159,160].

Precolumn derivatization is an effective means of determining kinetically inert metal ions by HPLC, and when resources or the number of sample ions militates against assembling a postcolumn reaction detection system. In precolumn derivatization, discrete neutral metal complexes are formed before the separation. To be effective the complexation or derivatization reaction must produce only one complex with each metal ion and the complex must be highly stable and nonlabile. Normal-phase, reversed-phase, anion-exchange, and ion-interaction chromatography, all have been used to separate metal ions after derivatization, with reversed-phase HPLC being most common [18,161,162]. Dithiocarbamates react with a wide range of transition metals [162–164]. Decomposition of this reagent can cause additional chromatographic peaks, but is minimized by protecting the reagent from oxygen, maintaining the eluant pH above 4, and minimizing the stainless steel in the flow path (i.e., eliminate any metal frits). Other ligands that have been used successfully include β-diketones [165], 8-hydroxyquinoline [166], and pyridylazoresorcinol [167].

E. Noble Metals

The separation and determination of the noble metals is difficult owing to their similar chemical properties and their complicated and variable speciation in solution. Most commonly, these elements are prederivatized with a complexing agent, followed by anion-exchange, ion-interaction, or reversed-phase chromatographic separation. Complexing agents that have been used include cyanide [108], halides [168], pyridylazo-reagents [169], and thiocarbamates [163].

F. Lanthanides and Actinides

Lanthanides have been determined using paper, thin layer, adsorption, partition, cation-exchange, anion-exchange, and extraction chromatography [18]. The most common procedure is the cation-exchange separation using an α-hydroxycarboxylate eluant and postcolumn reaction detection with a metallochromic reagent. Reversed-phase C_{18} columns dynamically coated by the $C_8SO_3^-$ mobile-phase additive [152] provides a high efficiency medium for the separation of lanthanides in order of decreasing atomic mass (Lu⟶La) using gradient elution with α-hydroxyisobutyric acid (HIBA). Postcolumn reaction detection with Arsenazo III with detection at 658 nm yields 1- to 5-ppb–detection limits using a 20-μL injection [65,170]. This procedure has been used for the determination of lanthanides in a wide variety of ma-

trices, including irradiated nuclear fuels [170], urine [171], and nuclear-grade uranium [172]. Alternatively the lanthanides can be separated in order of increasing atomic mass (La⟶Lu) using an isocratic oxalic acid eluant to separate the anionic lanthanide complexes on a reversed-phase C_{18} column dynamically coated with tetra-*n*-butylammonium [173]. Simultaneous separation of transition and lanthanide metals has been achieved based on the charge of the metal–pyridine-2,6-dicarboxylate (PDCA) complexes [174]. Transition metals form monovalent or divalent anionic complexes with PDCA and so can be separated with a PDCA eluant on the anion-exchange CS5 column. Once all of the transition metals have eluted, the lanthanides, which form strongly retained trivalent anionic complexes with PDCA, are eluted with a oxalate–diglycolate eluant. Detection limits of 20–40 ppb are observed for postcolumn reaction detection with PAR.

Uranium, and to a smaller extent other actinides, are retained by reversed-phase C_{18} supports through the hydrophobic adsorption of their HIBA complexes [175]. Transition metals and lanthanides are not retained under these conditions. This selective retention has been used for the determination of uranium and thorium in samples from refining processes [19], in the preconcentration and determination of uranium in natural ground waters [176], in the determination of uranium in irradiated nuclear fuel [177], and in the determination of thorium in plutonium [178]. Mandelic acid, an aromatic homologue of HIBA, has also been used for the separation of the actinides [179].

G. Ammonium and Organic Amines

Ammonium (NH_4^+) elutes between Na^+ and K^+ from cation-exchange columns with the typical eluants used for alkali metals. Detection limits of 24 ppb are achieved using nonsuppressed conductivity detection for a 100-μL injection [65]. Much lower detection limits can be achieved with cation-exchange enrichment, but care must be taken to avoid sample contamination from the laboratory air [29]. Determination of the isotopic ratio of ^{15}N in ammonium was achieved by cation exchange through exploitation of the isotope effect on the acid dissociation constant of NH_4^+ [180].

Alkylamines and alkanolamines can be separated using the same columns and eluants used for the alkali metals. Addition of methanol or acetonitrile reduces peak tailing caused by reversed-phase interaction between the amines and the column [181]. Amine-based corrosion inhibitors, such as NH_4^+, 2-amino-2-methylpropanol (AMP), 5-aminopentanol (5-AP) [182], and morpholine [132], can be determined by cation exchange with conductimetric detection. Pulsed amperometric detection has been used for monitoring of alkanolamines in the low-ppm range and projected detection limits of 1 ppb [183].

VI. SEPARATION OF ORGANOMETALLIC COMPOUNDS

Often, HPLC can be used to separate and quantify organometallic and metal coordination compounds when other separation methods are unsuitable. HPLC is generally performed at ambient temperature with oxygen-free eluants, which are distinct advantages with thermally unstable or reactive compounds. The availability of a variety of separation modes is also an advantage of HPLC over other separation techniques. The use of normal-phase, reversed-phase, ion-interaction, ion-exchange, and size-exclusion chromatography for HPLC separations of organometallic and metal coordination complexes has been reviewed through to the end of 1981 [184]. More recent HPLC separations of mono- and polynuclear metal carbonyls, including their phosphine-, arene-, and cyclopentadiene-substituted derivatives, metallocenes, metallocene dichlorides, and cyanometallated anions have also been reviewed [185]. The use of chiral HPLC separations in organometallic chemistry has also been reported [186].

VII. SIMULTANEOUS DETERMINATION OF ANIONS AND CATIONS

The simultaneous determination of anions and cations with one sample injection has the potential of increasing the analysis throughput of a laboratory. Various approaches have been used to simultaneously analyze both anionic and cationic analytes. Sample can be simultaneously injected into multiple ion chromatographic systems, each operating under different separation conditions [187,188]. An instrumentally simpler means of determining both anions and cations is column switching [189]. In this procedure, the anions and cations are injected onto an anion-exchange column. The cations elute rapidly from the anion-exchange column and onto a cation-exchanger, which is then switched off-line. Once all of the anions have eluted from the anion-exchange column, the cation-exchange column is switched back into the flow stream. Using 5 mM phthalate and nonsuppressed conductivity detection, inorganic anions and alkaline earth metals can be determined in less than 40 min with detection limits in the low to mid-ppb range [190]. Finally, anions and cations can be analyzed simultaneously using a single column either by using a bifunctional column that contains both anion- and cation-exchange functionality [191,192] or by converting the cations into anionic species using chelating agents, such as EDTA, and separated on an anion-exchange column [193].

VIII. APPLICATIONS OF HPLC ANALYSIS OF INORGANIC SPECIES TO SPECIFIC INDUSTRIES

Applications of inorganic anion, cation, and heavy metal analysis by ion chromatography related to agricultural research have been reviewed [194]. Given the recent concerns over sulfites in foods, the analyses of foodstuffs has seen great activity [195–197]. Chromatographic analyses related to the brewing industry have also been reviewed [198,199]. Two brief reviews of the use of ion chromatography in clinical analysis have also appeared [200,201].

Applications of ion chromatography for environmental analyses [202,203] and aspects of the cost and quality assurance [204] of the technique have been discussed. The use of hyphenated techniques for environmental speciation have also been reviewed [205–207]. A short overview of recent advances in the determination of atmospheric gases by IC has also been given [8]. The use of ion chromatography in petroleum and coal analyses is discussed in several reviews [59,74,208].

IX. CAPILLARY ELECTROPHORESIS

Since its inception, capillary electrophoresis (CE) has been used primarily for biochemical applications because of its high efficiencies and mild separation conditions. The high efficiencies of CE holds significant potential for the separation of inorganic ions, as evidenced recently by the separation of the isotopes of chloride [209]. However, it is other characteristics of CE that make it attractive for inorganic analyses. These advantages include reduced reagent consumption, inexpensive columns, and quick and easy switching between separation conditions. More significant than all of these is the simple fact that CE separations use a totally different separation process from ion chromatography.

The separation selectivity of CE is based on the ionic mobilities of the sample ions. Therefore, the order of elution of ions is significantly altered from that traditionally seen in IC. For example, fluoride is a difficult ion to quantify in complex matrices by IC because it is weakly retained and so is often obscured by the weakly retained carboxylic acids and the water dip. The ionic mobility of fluoride, however, is significantly different from that of the carboxylic acids, and so in CE fluoride is well resolved from these interferences. Thus, the two techniques can be viewed as complementary, for an analysis that is difficult on one may well be straightforward using the other technique [210].

Several reviews of CE for the analysis of inorganic and other small ions are available [210–214].

A. Anions

In typical capillary zone electrophoresis operating conditions, anions migrate toward the positive electrode, but are overwhelmed by the electroosmotic flow, such that the anions, as well as neutrals and cations, are detected at the negative end of the capillary. Although this approach is recommended for large, low-mobility ions, such as proteins and peptides, it is not appropriate for the high-mobility inorganic anions. The inorganic anions migrate more rapidly than the electroosmotic flow and thus would not be detected using the typical capillary zone electrophoresis conditions. Thus, in CE of inorganic and other highly mobile anions, the sample is injected at the cathode and detection occurs at the amode, a reversal of the typical configuration. Cationic surfactants, such as cetyltrimethylammonium bromide (CTAB), tetradecyltrimethylammonium (TTAB), diethylenetriamine (DETA), and hexamethylammonium bromide are added to the electrolyte to reverse the electroosmotic flow and thus accelerates the overall analysis.

Under these conditions the earliest detected anions are small inorganic mono- and divalent anions, with those inorganic species that possess larger Stokes radii eluting later. The migration rates of ions can be predicted using the ionic equivalent conductances of the ions [215]. The selectivity and resolutions achieved for inorganic ions is affected by the concentration of the background electrolyte, the pH, the concentration of the electroosmotic flow modifier, and the mobility of the primary electrolyte component [215,216]. If the electrolyte mobility differs significantly from that of the analyte, peak distortion will be observed [217]. Thus, the optimal electrolyte should match the mobility of the analytes of interest: chromate and pyromellitic [216] acid for most common inorganic anions that possess high electrophoretic mobilities; *p*-hydroxybenzoate for moderate mobility anions; and sorbate for slow-migrating anions (i.e., those eluting after bicarbonate) [218].

Detection is typically accomplished using indirect UV absorption, wherein the decrease in absorbance observed when an analyte ion displaces a chromophoric ion in the electrolyte is monitored. Thus, strongly absorbing buffers, such as chromate, are most commonly used as the electrolyte. Methods for the determination of sub-ppm to ppm quantities of fluoride, chloride, bromide, nitrite, phosphate, and sulfate in drinking water, wastewater, and reagent water [219] and for 0.5- to 50-ppb quantities of the same anions in high-purity deionized water and nuclear reactor moderator water [220] have been submitted to regulatory agencies for approval. For specific applications of CE for inorganic ion analysis, the reader is referred to the review articles [210–214] and to the annual proceedings of the International Ion Chromatography Symposium [9–15].

B. Cations

Inorganic and low molecular weight cations are separated by capillary electrophoresis using the typical electrophoretic configuration—injection at the anode and detection at the cathode. By using untreated capillaries, the cation migration is in the same direction as the electroosmotic flow and rapid high-efficiency separations result. Thus, the relative migration rates for the cations can be deduced from the associated equivalent conductances [221]. Many metal cations possess similar ionic mobilities, making their separation difficult. In such cases modification of the mobilities through weak complexation of the metal with a complexing agent, such as α-hydroxyisobutyric acid (HIBA), can be used to achieve resolution [222]. The migration rate of amines can be adjusted by altering the electrolyte pH [221].

As with the anion analysis by CE, detection is most commonly achieved using indirect UV detection, typically with an aromatic base. Typical detection limits are about 200 ppb,

and the linear dynamic range extends almost two orders of magnitude higher than the detection limit [221]. Indirect fluorescence [223,224], indirect amperometry [225], and prederivatization [226,227] also have been used for cation detection, but are much less common.

X. CONCLUSIONS

In a classic editorial Herb Laitinen described "The Seven Ages of an Analytical Method" [228]. These ages are: first, the conception; second, the validation; third, the development of commercial equipment; fourth, the detailed studies of the principles and mechanisms; fifth, the development of standard applications; sixth, the extension of the standard applications into new areas; and seventh, the period of senescence as other methods of greater speed, economy, sensitivity, and such, become available.

As evidenced by the applications discussed in this review, the determination of ions and inorganic species by HPLC is currently in the sixth age. Meanwhile, capillary electrophoresis instruments became available only in 1989 (third age), but are already entering into the fifth age with the submission of a regulatory method for the determination of anions in drinking [219] and high-purity waters [220]. As to whether capillary electrophoresis will force ion chromatography into the seventh age (obsolescence), or whether the two instruments will remain complementary [210], only time will tell. Regardless, the present, as described in this chapter, holds great power for the separation of ions and inorganics, and the future holds the promise of even greater capabilities to come.

REFERENCES

1. O Folin, R Bell. J Biol Chem 29:329, 1917.
2. G-M Schwab. Naturwissenschaften 25:44, 1937.
3. H Small, TS Stevens, WC Bauman. Anal Chem 47:1801, 1975.
4. PR Haddad, PE Jackson. Ion Chromatography: Principles and Applications, New York: Elsevier, 1990.
5. DT Gjerde, JS Fritz. Ion Chromatography, 2nd ed. Heidelberg: Hüthig, 1987.
6. RE Smith. Ion Chromatography Applications. Boca Raton, FL: CRC Press, 1988.
7. JS Fritz. Anal Chem 59:335A, 1987.
8. PK Dasgupta. Anal Chem 64:775A, 1992.
9. PR Haddad, ed. International Ion Chromatography Symposium 1990 Proceedings. J Chromatogr 546: 1991.
10. JD Lamb, ed. International Ion Chromatography Symposium 1991 Proceedings. J Chromatogr 602: 1992.
11. GK Bonn, ed. International Ion Chromatography Symposium 1992 Proceedings. J Chromatogr 640: 1993.
12. RM Cassidy, ed. International Ion Chromatography Symposium 1993 Proceedings. J Chromatogr 671: 1994.
13. C Sarzanini, ed. International Ion Chromatography Symposium 1994 Proceedings. J Chromatogr 706: 1995.
14. DJ Pietrzyk, ed. International Ion Chromatography Symposium 1995 Proceedings. J Chromatogr 739: 1996.
15. P Jones, ed. International Ion Chromatography Symposium 1996 Proceedings. J Chromatogr 770: 1997.
16. JC MacDonald, ed. Inorganic Chromatographic Analysis. New York: Wiley, 1985.
17. IS Krull, ed. Trace Metal Analysis and Speciation. J Chromatogr Libr, vol 47, Amsterdam: Elsevier, 1991.
18. K Robards, S Clarke, E. Patsalides. Analyst 113:1757, 1988.
19. DJ Barkley, M Blanchette, RM Cassidy, S Elchuk. Anal Chem 58:2222, 1986.

20. D1193-91, Annual Book of ASTM Standards, vol. 11.01 Water (I): Water and Environmental Technology. Philadelphia: American Society for Testing and Materials, 1993.
21. Technical Brief TB015. Bedford, MA: Millipore Corporation, 1990.
22. Technical Brief TB006. Bedford, MA: Millipore Corporation, 1991.
23. R Gabler, R Hegde, D Hughes. J Liq Chromatogr 6:2565, 1983.
24. D4453-91, Annual Book of ASTM Standards, vol 11.01 Water (I): Water and Environmental Technology. Philadelphia: American Society for Testing and Materials, 1993.
25. DT Gjerde, JS Fritz. Ion Chromatography, 2nd ed. Heidelberg: Hüthig, 1987, p 126.
26. C Saigne, S Kirchner, M Legrand. Anal Chim Acta, 203:11, 1987.
27. R Bagchi, PR Haddad. J Chromatogr 351:541, 1986.
28. JA Grunau, JM Swaider. In: P Jandik, RM Cassidy, eds. Advances in Ion Chromatography, vol 1, Franklin, MA: Century International, 1989, p 361.
29. M Legrand, M de Angelis, RJ Delmas. Anal. Chim. Acta 156:181, 1984.
30. AD Hewitt, JH Cragin. Atmos Environ 25A:453, 1991.
31. PR Haddad, RCL Foley. J Chromatogr 407:133, 1987.
32. CA Lucy, SL Mitchell. AECL Research, unpublished results, 1991.
33. DT Gjerde, JS Fritz. Ion Chromatography, 2nd ed. Heidelburg: Hüthig, 1987, 111.
34. DR Eubanks, JR Stillian. LC Mag 2:74, 1984.
35. IK Henderson, R Saari-Nordhaus, JM Anderson, Jr. J Chromatogr 546:61, 1991.
36. WR Jones, P Jandik. J Chromatogr Sci 27:449, 1989.
37. S Laksana, PR Haddad. J Chromatogr 602:57, 1992.
38. A Siriraks, J Stillian. J Chromatogr 640:151, 1993.
39. PE Jackson, WR Jones. J Chromatogr 538:497, 1991.
40. SR Villaseñor. J Chromatogr 602:155, 1992.
41. PF Subosa, K Kihara, S Rokushika, H Hatano, T Murayama, T Kubota, Y Hanaoka. J Chromatogr Sci 27:680, 1989.
42. M Murayama, M Suzuki, S Takitani. J Chromatogr 466:355, 1989.
43. PE Jackson, PR Haddad. J Chromatogr 439:37, 1988.
44. Application Note 56. Sunnyvale, CA: Dionex Corporation, 1988.
45. A Siriraks, HM Kingston JM Riviello. Anal Chem 62:1185, 1990.
46. Application Note 76. Sunnyvale, CA: Dionex Corporation, 1992.
47. JD Pfaff, CA Brockhoff, JW O'Dell. Test Method: The Determination of Inorganic Anions in Water by Ion Chromatography—Method 300.0. Cincinnati, OH: US Environmental Protection Agency, December 1989.
48. Deutsche Industrienorm (DIN) 38405, Teil 19. Weinheim: VCH, 1988; B Gade. J Chromatogr 640:227, 1993.
49. VDI-Richtlinie 3497/4 (Entwurf). Messen partikelgebundener Anionen in der Aussenluft. Düsseldorf: VDI-Verlag, 1989; H Schumann, M Ernst. J Chromatogr 640:241, 1993.
50. HL Tucker, TK Smith, SJ Van Hook III. J Chromatogr 640:355, 1993.
51. JF Colaruotolo, RS Eddy. Anal Chem 49:884, 1977.
52. JR Kreling, K Block, GT Louthan, J DeZwaan. Microchem J 34:158, 1986.
53. M Douek, J Ing. J Pulp Paper Sci 15:J72, 1989.
54. LM Busman, RP Dick, MA Tabatabai. Soil Sci Soc Am J 47:1167, 1983.
55. KL Evans, CB Moore. Anal Chem 52:1908, 1980.
56. RP Singh, K Alam, DS Redwan, NM Abbas. Anal Chem 61:1924, 1989.
57. RC Wijesundera, RG Ackman, V Abraham, JM deMan. J Am Oil Chem Soc 65:1526, 1988.
58. RC Wijesundera, RG Ackman. J Am Oil Chem Soc 65:1531, 1988.
59. M Andrew, IMV Burholt, NJ Kernoghan, TP Lynch, R Mackison, D Mealor, JA Price, P Schofield. J Chromatogr 640:111, 1993.
60. RA Nadkarni, DM Pond. Anal Chim Acta 146:261, 1983.
61. JP Romano, J Krol. J Chromatogr 602:205, 1992.
62. RA Wetzel, CA Pohl, JM Riviello, JC MacDonald. In: JC MacDonald, ed, Inorganic Chromatographic Analysis. New York, Wiley, 1985, chap 9.

63. D4327-91, Annual Book of ASTM Standards, vol 11.01 Water (I). Philadelphia: American Society for Testing and Materials (ASTM), 1993.
64. R Saari-Nordhaus, JM Anderson Jr, R Ravichandran. J Chromatogr 602:15, 1992.
65. AL Heckenberg, PG Alden, BJ Wildman, J Krol, JP Romano, PE Jackson, P Jandik, WR Jones. Waters Innovative Methods for Ion Analysis. Millipore, MA: Millipore Corp., 1989.
66. WS Tweet, SL Hoeffner. In: P Jandik, RM Cassidy, ed. Advances in Ion Chromatography, vol 2. Medfield, MA: Century International, 1990, p 321.
67. DP Hautman, M Bolyard. J Chromatogr 602:65, 1992.
68. D5257-92, Annual Book of ASTM Standards, vol 11.01 Water (I). Philadelphia: American Society for Testing and Materials (ASTM), 1993.
69. EJ Arar, JD Pfaff. J Chromatogr 546:335, 1991.
70. LJ Lewis, JD Lamb, DJ Eatough, LD Hansen, RJ Paxton, EA Lewis. J Chromatogr Sci 28: 490, 1990.
71. MW Martin, RA Giacofei. J Chromatogr 644:333, 1993.
72. P Jones. Anal Chim Acta 258:123, 1992.
73. NW Barnett, P Jones, HW Handley. Anal Lett 26:2525, 1993.
74. JA Cox. Coal Sci Technol 17:31, 1991.
75. PR Haddad, AL Heckenberg. J Chromatogr 300:357, 1984.
76. GA Ubom. Water Res 22:1455, 1988.
77. RK Chadha, JF Lawrence. J Chromatogr 518:268, 1990.
78. W Buchberger. J Chromatogr 439:129, 1988.
79. M Nomomura. Anal Chem 59:2073, 1987.
80. L Madungwe, MF Zaranyika, RC Gurira. Anal Chim Acta 251:109, 1991.
81. K Gamoh, S Imamichi. Anal Chim Acta 251:255, 1991.
82. RJ Joyce, HS Dhillon. Part-per-billion level determination of bromate in ozonated drinking water using ion chromatography. Presented at the International Ion Chromatography Symposium, Baltimore, September 1993.
83. VV Salov, J Yoshinaga, Y Shibata, M Morita. Anal Chem 64:2425, 1992.
84. M Roman, R Dovi, R Yoder, F Dias, B Warden. J Chromatogr 546:341, 1991.
85. PL Annable, LA Sly. J Chromatogr 546:325, 1991.
86. W Frenzel, A Rauterberg. Mikrochim Acta 106:175, 1992.
87. HJ Kim, YK Kim. J Food Sci 51:1360, 1986; Application Note AN54, Sunnyvale, CA: Dionex Corporation, 1987.
88. DC Johnson, D Dobberpuhl, R Roberts, P Vandeberg. J Chromatogr 640:79, 1993.
89. HJ Kim. J Assoc Off Anal Chem 72:113;266, 1989; HJ Kim, YK Kim. Food Technol 41: 85, 1987.
90. L Campanella, M Majone, R Pocci. Talanta, 37:201, 1990.
91. LM Petrie, ME Jakel, RL Brandvig, JG Kroening. Anal Chem 65:952, 1993.
92. R Steudel, V Münchow. J Chromatogr 623:174, 1992.
93. PD Brown, MJ Morra. J Agric Food Chem 39:1226, 1991.
94. Y Michigami, T Takahashi, F He, Y Yamamoto, K Ueda. Analyst 113:389, 1988.
95. DS Ryder. J Chromatogr 354:438, 1986.
96. IonPac AS11 Anion Exchange Column. Sunnyvale, CA: Dionex Corporation, 1992.
97. P Linares, MD Luque de Castro, M Valcárcel. J Chromatogr 585:267, 1991.
98. SL McGeehan, DV Naylor. J Environ Qual 21:68, 1992.
99. SS Goyal, A Hafez, DW Rains. J Chromatogr 537:269, 1991.
100. KA Francesconi, P Micks, RA Stockton, KJ Irgolic. Chemosphere 14:1443, 1985.
101. BS Sheppard, JA Caruso, DT Heitkemper, KA Wolnik. Analyst 117:971, 1992.
102. NP Vela, LK Olson, JA Caruso. Anal Chem 65:585A, 1993.
103. H Klinkenberg, S Van der Wal, J Frusch, L Terwint, T Beeren. Atmos Spectrosc 11:198, 1990.
104. HC Mehra, WR Frankenberger. Analyst 114:707, 1989.
105. HC Mehra, WR Frankenberger. Anal Chim Acta 217:383, 1989.

106. H Yamada, T Hattori. J Chromatogr 320:403, 1985.
107. Application Note 55. Sunnyvale, CA: Dionex Corporation, 1989.
108. DF Hilton, PR Haddad. J Chromatogr 361:141, 1986.
109. PR Haddad, C Kalambaheti. Anal Chim Acta 250:21, 1991.
110. CCT Chinnick. Analyst 106:1203, 1981.
111. DL Venezky, WE Rudzinski. Anal Chem 56:315, 1984.
112. W Buchberger, PR Haddad, PW Alexander. J Chromatogr 558:181, 1991.
113. DP Lee. J Chromatogr Sci 22:327, 1984.
114. WR Jones, AL Heckenberg, P Jandik. J Chromatogr 366:225, 1986.
115. T Okada, T Kuwamoto. Fres Z Anal Chem 325:683, 1986.
116. JR Kreling, J DeZwaan. Anal Chem 58:3028, 1986.
117. K Tanaka, JS Fritz. Anal. Chem 59:708, 1987.
118. S Harvey. J Chromatogr 546:209, 1991.
119. D Tusseau, C Benoit. J Chromatogr 395:323, 1987.
120. RM Marcé, M Calull, RM Manchobas, F Borrull, FX Rius. Chromatographia 29:54, 1990.
121. E Mentasti, MC Gennaro, C Sarzanini, C Baiocchi, M Savigliano. J Chromatogr 322:177, 1985.
122. RD Rocklin, RW Slingsby, CA Pohl. J Liq. Chromatogr 9:757, 1986.
123. RD Rocklin, CA Pohl, JA Schibler. J Chromatogr 411:107, 1987.
124. V Cheam. Analyst 117:1137, 1992.
125. RP Schneider, F Zürcher, G Hamer. J Chromatogr 462:293, 1989.
126. RP Schneider, F Zürcher, T. Egli, G Hamer. Anal Biochem 173:278, 1988.
127. W Buchberger, PR Haddad, PW Alexander. J Chromatogr 546:311, 1991.
128. J de Jong, A van Ponanen, JJM Driessen. J Chromatogr 553:243, 1991.
129. DP Lee, MT Bunker. J Chromatogr Sci 27:496, 1989.
130. Application Note 52. Sunnyvale, CA: Dionex Corporation, 1986.
131. DL Campbell, J Stillian, S Carson, R Joyce, S Heberling. J Chromatogr 546:229, 1991.
132. RM Cassidy, BD Karcher. In: IS Krull, ed. Reaction Detection in Liquid Chromatography. Chromatographic Science Series, vol 34; New York: Marcel Dekker, 1986, Chap 3.
133. MD Arguello, JS Fritz. Anal Chem 49:1595, 1977.
134. CA Lucy, HN Dinh. Anal. Chem. 66:793, 1994.
135. T Williams, NW Barnett. Anal Chim Acta 259:19,1992.
136. M Betti, S Cavalli. J Chromatogr 538:365, 1991.
137. B Kondratjonok, G Schwedt. Fres Z Anal Chem 337:332, 1988.
138. S Motellier, H Pitsch. J Chromatogr A 660:211, 1994.
139. Application Note A0008. Deerfield, IL: Alltech Associates, 1992.
140. Application Note 42. Sunnyvale, CA: Dionex Corporation, 1987.
141. P Jones, L Ebson, T Williams. Analyst 113:641, 1988.
142. PM Bertsch, MA Andeson. Anal Chem 61:535, 1989.
143. Y Shijo, A Saitoh, K Suzuki. Chem Lett 181, 1989; H Onashi, N Uehara, Y Shijo. J Chromatogr 539:225, 1991.
144. D Yan, J Zhang, G Schwedt. Fres Z Anal Chem 331:601, 1985.
145. S Mou, H Wang, Q Sun. Presented at the International Ion Chromatography Symposium, Baltimore, 1993.
146. L Ebdon, SJ Hill, P Jones. Analyst 110:515, 1985.
147. H Suyani, J Creed, T Davidson, JA Caruso. J Chromatogr Sci 27:139, 1989.
148. UT Kumar, JG Dorsey, JA Caruso, EH Evans. J Chromatogr 654:261, 1993.
149. A Al-Rashdan, D Heitkemper, JA Caruso. J Chromatogr Sci 29:98, 1991.
150. JD Messman, TC Rains. Anal. Chem 53:1632, 1981.
151. SCK Shum, H-M Pang, RS Houk. Anal Chem 64:2444, 1992.
152. RM Cassidy, S Elchuk. Anal Chem 54:1558, 1982.
153. Technical Note 10. Sunnyvale, CA: Dionex Corporation, 1985.
154. Application Notes A0009 and A0010. Deerfield, IL: Alltech Associates, 1992.

155. R Caprioli, S Torcini. J Chromatogr 640:365, 1993.
156. N Cardellicchio, S Cavalli, JM Riviello J Chromatogr 640:207, 1993.
157. A Siriraks, J Stillian, D Bostic. J Chromatogr 640:371, 1993.
158. K Soroka, R Vithanage, DA Phillips, B Walker, PK Dasgupta. Anal Chem 59:629, 1987.
159. T Williams, NW Barnett. Anal Chim Acta 264:297, 1992.
160. CA Lucy, L Ye. J Chromatogr A 671:121, 1994.
161. AR Timerbaev, OM Petrukhin, IP Alimarin, TA Bol'shova. Talanta 38:467, 1991.
162. S Dilli, PR Haddad, AK Htoon. J Chromatogr 500:313, 1990.
163. BJ Mueller, RJ Lovett. Anal Chem 59:1405, 1987.
164. JH Shofstahl, JK Hardy. J Chromatogr Sci 28:225, 1990.
165. RC Gurira, PW Carr. J Chromatogr Sci 20:461, 1982.
166. C Baiocchi, G Saini, P Bertolo, GP Cartoni, G Pettiti. Analyst 113:805, 1988.
167. AR Timerbaev, OM Pertrukhim, VI Orlov, AA Aratskova. J Liq. Chromatogr 15:1443, 1992.
168. P Jones, G Schwedt. Anal Chim Acta 220:195, 1989.
169. YS Nikitin, NB Morozova, SN Lanin, TA Bol'shova, VM Ivanov, EM Basova. Talanta 34: 223, 1987.
170. CH Knight, RM Cassidy, BM Recoskie, LW Green. Anal Chem 56:474, 1984.
171. S Elchuk, CA Lucy, KI Burns. Anal Chem 64:2339, 1992.
172. CA Lucy, L Gureli, S Elchuk. Anal Chem 65:3320, 1993.
173. EA Jones, HS Bezuidenhout, JF Van Staden. J Chromatogr 537:277, 1991.
174. SS Heberling, JM Riviello, M Shifen, AW Ip. Res Dev 29:74, 1987.
175. H Fuping, PR Haddad, PE Jackson, J Carnevale. J Chromatogr 640:187, 1993.
176. A Kerr, W Kupferschmidt, M Attas. Anal Chem 60:2729, 1988.
177. RM Cassidy, S Elchuk, LW Green, CH Knight, FC Miller, BM Recoskie. J Radioanal Nucl Chem Art 139:55, 1990.
178. VT Hamilton, WD Spall, BF Smith, EJ Peterson. J Chromatogr 469:369, 1989.
179. S Elchuk, KI Burns, RM Cassidy, CA Lucy. J Chromatogr 558:197, 1991.
180. WS Gardner, LR Herche, PA St John, SP Seitzinger. Anal Chem 63:1838, 1991.
181. J Krol, PG Alden, J Morawski, PE Jackson. J Chromatogr 626:165, 1992.
182. JC Greene, RM Donaldson. J Chromatogr 640:303, 1993.
183. DL Campbell, S Carson, D Van Bramer. J Chromatogr 545:381, 1991.
184. H Veening, BR Willeford. Adv Chromatogr 22:114, 1983.
185. A Casoli, A Mangia, G Predieri, E Sappa, M Volante. Chem Rev 89:407, 1989.
186. Y Yamazaki, N Morohashi, K Hosono. J Chromatogr 542:129, 1991.
187. V Cheam, ASY Chau. Analyst 112:993, 1987.
188. E Dabek-Zlotorzynska, JF Dlouhy. J Chromatogr 640:217, 1993.
189. R Saari-Nordhaus, JM Anderson Jr. J Chromatogr 549:257, 1992.
190. R Saari-Nordhaus, L Nair, JM Anderson Jr. J Chromatogr 602:127, 1992.
191. DM Brown, DJ Pietrzyk. J Chromatogr 466:291, 1989.
192. S Mou, H Wang, Q Sun. J Chromatogr 640:161, 1993.
193. D Yan, G Schwedt. J Chromatogr 516:383, 1990.
194. AA Hafez, SS Goyal, DW Rains. J Chromatogr 546:387, 1991.
195. MR Marshall, RH Schmidt, BL Walker. Food Sci Technol 45:39, 1991.
196. C Fernández Pereira. J Chromatogr 624:457, 1992.
197. ND Danielson, JH Sherman. Food Sci Technol 52:713, 1992.
198. CJ Dale. J Inst Brew 97:187, 1991.
199. H Klein, R Leubolt. J Chromatogr 640:259, 1993.
200. GK Grimble. Anal Proc 29:468, 1992.
201. GK Grimble. Lab Pract 41:41, 1992.
202. WT Frankenberger Jr, HC Mehra, DT Gjerde. J Chromatogr 504:211, 1990.
203. S Mou. J Chromatogr 546:317, 1991.
204. P Papoff, A Giacomelli, M Onor. Microchem J 46:385, 1992.
205. OFX Donard, FM Martin. TRAC 11:17, 1992.

206. DT Gjerde, HC Mehra, IS Krull, eds. Trace Metal Analysis and Speciation. J Chromatogr Libr vol 47, Amsterdam: Elsevier, 1991, pp 213–237.
207. SJ Hill, MJ Bloxham, PJ Worsfold. J Anal At Spectrom 8:499, 1993.
208. D Mealor. In: GB Crump, ed. Petroanalysis '87: Developments in Analytical Chemistry in the Petroleum Industry. Chichester: Wiley, 1988, p 221.
209. CA Lucy, TL McDonald. Anal. Chem 67:1074, 1995.
210. PE Jackson, PR Haddad. TRAC 12:231, 1993.
211. P Jandik, G Bonn. Capillary Electrophoresis of Small Molecules and Ions. New York: VCH Publishers, 1993.
212. WR Jones. In: JP Landers, ed. Handbook of Capillary Electrophoresis. Boca Raton, FL: CRC Press, 1993.
213. WR Jones. In JP Landers, ed. Handbook of Capillary Electrophoresis, 2nd ed. Boca Raton, FL: CRC Press, 1997.
214. P Jandik, WR Jones, A Weston, PR Brown. LC–GC 9:40, 1991.
215. WR Jones, P Jandik. J Chromatogr 546:445, 1991.
216. MP Harrold, MJ Wojtusik, J Riviello, P Henson. J Chromatogr 640:463, 1993.
217. FEP Mikkers, FM Everaerts, ThPEM Verheggen. J Chromatogr 169:1, 1979.
218. WR Jones. J Chromatogr 640:387, 1993.
219. JP Romano, J Krol. J Chromatogr 640:403, 1993.
220. JP Romano. Presented at International Ion Chromatography Symposium, Baltimore, Maryland, September 1993; Paper 72.
221. A Weston, PR Brown, P Jandik, WR Jones, AL Heckenberg. J Chromatogr 593:289, 1992.
222. A Weston, PR Brown, AL Heckenberg, P Jandik, WR Jones. J Chromatogr 602:249, 1992.
223. L Gross, ES Yeung. Anal Chem 62:427, 1990.
224. K Bächmann, J Boden, I Haumann. J Chromatogr 626:259, 1992.
225. W Lu, RM Cassidy. Anal Chem 65:1649, 1993.
226. DF Swaile, MJ Sepaniak. Anal Chem 63:179, 1991.
227. T Saitoh, H Hoshino, T Yotsuyanagi. J Chromatogr 469:175, 1989.
228. HA Laitinen. Anal Chem 45:2305, 1973.
229. R Saari-Nordhaus, JM Anderson Jr, K Ravichandran. J Chromatogr 602:15, 1992.
230. WS Tweet, SL Hoeffner. In: P Jandik, RM Cassidy, eds. Advances in Ion Chromatography. vol 2. Medfield, MA: Century International, 1990, p 321.
231. Application Note A0019. Deerfield, IL: Alltech Associates, 1992.
232. Alltech Application A0002. Deerfield, IL: Alltech, 1992.
233. N Chauret, J Hubert. J Chromatogr 469:329, 1989.
234. J Zou, S Motomizu, H Fukutomi. Analyst 116:1399, 1991.
235. D5085-90, Annual Book of ASTM Standards, vol 11.03. Atmospheric Analysis and Occupational Health and Safety. Philadelphia: American Society for Testing and Materials (ASTM), 1992.
236. F1374-92, Annual Book of ASTM Standards, vol 10.05. Electronics (II). Philadelphia: American Society for Testing and Materials (ASTM), 1992.
237. EJ Nanni, ME Lovette, RD Hicks, KW Fowler, MF Borgerding. J Chromatogr Sci 28:432, 1990.
238. G Vanderford. J Chromatogr 602:75, 1992.
239. A Siriraks, CA Pohl, M Toofan. J Chromatogr 602:89, 1992.
240. H Schäfer, K Budde. Presented at International Ion Chromatography Symposium. Baltimore, MD, September 1993, Paper 48.
241. Application Note 51. Sunnyvale, CA:Dionex Corporation.
242. Application Update 101. Sunnyvale, CA: Dionex Corporation, May 1987.
243. CA Lucy, L Ye. Anal Chem 67:79, 1995.
244. L Ye, CA Lucy. Anal Chem 67:2534, 1995.
245. L Ye, CA Lucy. J Chromatogr A 739:307, 1996.

26

HPLC Application to Polymer Analysis

Sadao Mori

Mie University, Tsu, Mie, Japan

I. INTRODUCTION

A polymer, especially a synthetic polymer, is a large molecule built up by the repetition of small, simple chemical units. The repeating units of the polymer are usually equivalent to the monomer or the starting material composing the polymer. The length of the polymer chain is specified by the number of the repeating units in the chain, which is called the *degree of polymerization*. The molecular weight (MW) of the polymer is the product of the MW of the repeating unit and the degree of polymerization. A synthetic polymer contains molecules having many different chain lengths and, unlike many small molecules and biopolymers, it has a distribution of the different chain lengths (the different MW). A *biopolymer*, such as protein, is an assembly of several amino acids connected by peptide linkage and consists of molecules having the same chain length (the same MW).

For a given polymer composition, molecular weight averages and a molecular weight distribution (MWD) of a synthetic polymer are some of molecular characteristics that determine its properties. In copolymers, the chemical composition and the chemical composition distribution are other molecular characteristics of the copolymers. Several other molecular characteristics can be considered, and they are measured by several techniques of instrumental analysis. Molecular characteristics measured by high-performance liquid chromatography (HPLC) are listed in Table 1.

Size-exclusion chromatography (SEC) is a technique that separates materials according to the differences in their molecular sizes (hydrodynamic volumes in a solution). Non-exclusion liquid chromatography (NELC) is a technique that separates molecules by separation modes (adsorption and partition) other than size exclusion. Hyphenated techniques such as SEC–viscometry can give the information on branching and a branching distribution of synthetic polymers. Microgels in polymers eluting at or earlier than the exclusion limit of an SEC column system are, because of a small amount of microgels in the polymers compared with the main component, almost impossible to detect with a refractomer, which is usually used as detector for SEC. SEC–LS (light scattering) can detect such small amounts of microgels. Temperature-rising elution fraction (TREF) is a technique to fractionate crystalline polymers or stereo regular polymers, such as polyethylene and polypropylene by raising the column temperature to increase the solubility of the polymers adsorbed on the surface of packings in a column. Field-flow fractionation (FFF) is a technique to separate polymers and particles in the order of increasing MW or size and is different from other HPLC modes on

26

HPLC Application to Polymer Analysis

Sadao Mori

Mie University, Tsu, Mie, Japan

I. INTRODUCTION

A polymer, especially a synthetic polymer, is a large molecule built up by the repetition of small, simple chemical units. The repeating units of the polymer are usually equivalent to the monomer or the starting material composing the polymer. The length of the polymer chain is specified by the number of the repeating units in the chain, which is called the *degree of polymerization*. The molecular weight (MW) of the polymer is the product of the MW of the repeating unit and the degree of polymerization. A synthetic polymer contains molecules having many different chain lengths and, unlike many small molecules and biopolymers, it has a distribution of the different chain lengths (the different MW). A *biopolymer*, such as protein, is an assembly of several amino acids connected by peptide linkage and consists of molecules having the same chain length (the same MW).

For a given polymer composition, molecular weight averages and a molecular weight distribution (MWD) of a synthetic polymer are some of molecular characteristics that determine its properties. In copolymers, the chemical composition and the chemical composition distribution are other molecular characteristics of the copolymers. Several other molecular characteristics can be considered, and they are measured by several techniques of instrumental analysis. Molecular characteristics measured by high-performance liquid chromatography (HPLC) are listed in Table 1.

Size-exclusion chromatography (SEC) is a technique that separates materials according to the differences in their molecular sizes (hydrodynamic volumes in a solution). Non-exclusion liquid chromatography (NELC) is a technique that separates molecules by separation modes (adsorption and partition) other than size exclusion. Hyphenated techniques such as SEC–viscometry can give the information on branching and a branching distribution of synthetic polymers. Microgels in polymers eluting at or earlier than the exclusion limit of an SEC column system are, because of a small amount of microgels in the polymers compared with the main component, almost impossible to detect with a refractomer, which is usually used as detector for SEC. SEC–LS (light scattering) can detect such small amounts of microgels. Temperature-rising elution fraction (TREF) is a technique to fractionate crystalline polymers or stereo regular polymers, such as polyethylene and polypropylene by raising the column temperature to increase the solubility of the polymers adsorbed on the surface of packings in a column. Field-flow fractionation (FFF) is a technique to separate polymers and particles in the order of increasing MW or size and is different from other HPLC modes on

Table 1 Molecular Characteristics Measured by HPLC and Separation Modes Applied

Molecular characteristic	Separation mode applied[a]
Molecular weight	
Molecular weight average and distribution	SEC
Chemical composition	
Average composition	NELC
Chemical heterogeneity	NELC, (SEC)
Composition distribution	NELC
Fine structure	
Branching	SEC with VIS
Stereoregularity	TREF
End group	SEC, NELC
Crystallinity	TREF
Microgel	SEC with LS
Monomer and oligomers remained	SEC, NELC
Additives	SEC, NELC

[a]SEC, size exclusion chromatography; NELC, nonexclusion liquid chromatography; TREF, temperature-rising elution fractionation; LS, light-scattering; VIS, viscosity.

several points: no packing in a column; hence, no interactions of solutes with the so-called stationary phase.

It is my intention to present, rather briefly in this chapter, HPLC applications to polymer analysis. For readers who require detailed information, it is recommended that they refer to many excellent previously published textbooks and chapters for SEC and NELC of polymers [1–6].

II. SEPARATION BY SIZE

A. Introduction

Size-exclusion chromatography is a mode of liquid chromatography in which the separation is carried out according to the differences among the hydrodynamic volumes (the molecular sizes) of the solute molecules in solution. It is essential that the separation of polymers by SEC be accomplished solely by the differences in their hydrodynamic volumes in solution and that, in principle, there are no secondary effects, such as adsorption and ion-exclusion, between polymer samples and the stationary phase if one uses SEC as a technique to measure MW averages and MWD of various polymers. It becomes possible by this restriction to determine MW averages of polymer samples other than polystyrene (PS) using a calibration curve constructed with PS standards.

The retention volume V_R of a polymer sample in SEC is expressed as

$$V_R = V_0 + K_{SEC} V_i \tag{1}$$

where V_0 is the interstitial liquid volume between the packing particles in the column, V_i is the internal pore volume of the packing material in the column, and K_{SEC} is the distribution coefficient for SEC, which is defined as

$$K_{SEC} = K_D K_P \tag{2}$$

where K_D is the distribution coefficient for size exclusion and K_P is the distribution coefficient for solute–stationary phase interaction effects [7]. The value K_P becomes unity when no secondary effects can be considered.

The term K_P is defined as [8]

$$\log K_P = B\,(\delta_{mobile} - \delta_{stationary})\,(\delta_{mobile} - \delta_{solute}) \tag{3}$$

where δ_{mobile}, $\delta_{stationary}$, and δ_{solute} are solutibity parameters for mobile phase, stationary phase, and a solute, respectively. B is constant. This equation means that when $\delta_{mobile\ phase} = \delta_{stationary\ phase}$, or $\delta_{mobile\ phase} = \delta_{solute}$, then $K_P = 1$.

The solubility parameter of PS is 19.1 ($J^{1/2}cm^{-3/2}$) and the parameter for PS gel is estimated to be the same as the value for non–cross-linked PS. Therefore, if the solubility parameter of the mobile phase is close to this value, then K_P becomes unity. For example, the solubility parameter for tetrahydrofuran (THF) is 19.4, and in the system of PS gel–THF for SEC, the separation would be mainly be size exclusion and the secondary effects would be small. Equation (3) is effective for nonionic polymers with PS gel.

Columns packed with PS gel are commonly used for SEC. This is because columns packed with PS gel, having high numbers of theoretical plates, are commercially available, and the properties of PS gel as the stationary phase are adequate for polymer separation. Other than PS gel, silica gel and trimethylsilylated silica gel are used for nonaqueous SEC, and polyvinyl alcohol gel, polyacrylamide gel, polyhydroxymethacrylate gel, and diol-bonded silica gel are used as the packing materials for aqueous SEC.

Solvents used as the mobile phase for SEC must dissolve polymer samples. Among these solvents, those that satisfy Eq. (3) are preferable: that is, good solvents for the polymer samples or good solvents for the non–cross-linked PS. The former solvents mostly have solubility parameters similar to the polymer samples, and the latter solvents have solubility parameters similar to the PS gel.

Chloroform, THF, toluene, and methylene chloride are commonly used as mobile phases for nonaqueous SEC. Dimethylformamide is used as the mobile phase for SEC of polyacrylonitrile, polyamides, and poly(ethylene terephthalate); and fluoroalcohols, such as tetrafluoro-2-propanol, for the latter two. However, when these latter two solvents are used as the mobile phases, small amounts of inorganic electrolytes must be added in the mobile phase to prevent abnormal elution behavior of the polymer samples. For aqueous SEC, buffer solutions are normally used. The ionic strength of the mobile phase plays an important role for the elution of the ionic polymer samples.

Polyolefins, such as polyethylene and polypropylene are dissolved in *o*-dichlorobenzene and 1,2,4-trichlorobenzene at temperatures higher than 100°C, and they readily solidify from the solution on cooling. Therefore, the SEC measurement for such polyolefins is carried out at 130–140°C, and the whole SEC system from the injection port (preferably from the solvent reservoir) to the detector outlet must be maintained at this elevated temperature. A high-temperature size-exclusion chromatograph is used for this purpose.

B. Molecular Weight Measurement of Polymers

1. Calibration of Columns

Molecular weight measurement by SEC is a relative method compared with other techniques, such as light scattering and membrane osmometry, which are so-called absolute methods for MW determination. Any SEC system must first be calibrated for MW against retention volume using standard polymers of known MW. The use of a light-scattering detector makes the calibration of the SEC system unnecessary for homopolymer analysis and for copolymer analysis when there is minimal composition drift with MW.

The calibration of the SEC system is usually performed by measuring peak retention volumes of polymer standards of known MW having relatively narrow MWD and a calibration curve of log MW versus peak retention volume is constructed. As the polymer standards for the calibration of the SEC system, a very wide range of MWs should be available. For nonaqueous SEC, PS and poly(methyl methacrylate) are used as calibration standards. For aqueous SEC, poly(ethylene oxide) and poly(ethylene glycol), pullulan, dextran, sodium poly(styrenesulfonate) are commercially available as calibration standards. Several proteins such as myoglobin and egg albumin are also used as calibration standards for protein measurements.

The reason to use narrow MWD standards for calibration of the SEC system is as follows: Because a synthetic polymer is normally a mixture of components having different MW, number-average molecular weight (M_n) and weight-average molecular weight (M_w) are not the same [for definition of these averages, see Eqs. (7) and (8)]. The ratio of both averages is the measure of polydispersity or MWD. Peak MW of such polymers is neither M_n nor M_w, and it would probably be between them. Moreover, sensible estimation of the peak retention volume will not be obtained when the SEC chromatogram is broad. For narrow MWD standards, the peak retention volume can be easily estimated precisely and peak MW is taken as a mean of both molecular weight averages: $(M_w + M_n)/2$ or $(M_w M_n)^{1/2}$. Sometimes peak MW is roughly estimated as M_w or M_n.

Examples of a semilogarithmic plot of peak MW versus peak retention volume for PS in THF are shown in Fig. 1. Molecular weight is on the ordinate (logarithmic scale) and retention volume is on the abscissa (regular scale). Molecular weight at the exclusion limit of column, M_I, is defined as the lowest MW of the solutes that cannot enter the pore of the packing materials in the column and elute through the outside of the packing particles in the column. Retention volume at the exclusion limit corresponds to the interstitial volume V_0. The exclusion limit of a Shodex KF-801 column has 2000 as PS MW, that of a Shodex KF-803 column is 8×10^4, and that of a Shodex KF-80M column has over 1×10^7 by extrapolation. Therefore, a Shodex KF-801 column can be used for the separation of low MW materials of less than 2000 MW as PS, and a Shodex KF-803 column for the separation of low MW polymers less than 8×10^4 MW. A Shodex KF-80M column is used for the polymer separation.

When a data-handling system is used, the calibration curve is approximated as a linear fit or a third-order polynomial. For a linear fit

$$M = D_1 \exp(-D_2 V_R) \tag{4}$$

or

$$\log M = a - D_2 V_R \tag{5}$$

For a third-order polynomial

$$\log M = A + BV_R + CV_R^2 + DV_R^3 \tag{6}$$

where D_1, D_2, a, A, B, C, D are constants. The value $-D_2$ corresponds to the slope of the calibration curve.

2. Calculation of Molecular Weight Averages and Molecular Weight Distribution

Most commercially available data-handling systems can construct a calibration curve and calculate MW averages automatically. All one must do is inject solutions of polymer standards and polymer samples concerned. However, to estimate whether or not the calculated values are correct and precise, it is necessary to know how to calculate MW averages.

Calculation procedures for PS samples are as follows: An SEC chromatogram of a PS sample is first measured. A baseline to the chromatogram is drawn and the chromatogram is sliced into equal portions (30–40 points or more are preferable). The height H_i from the

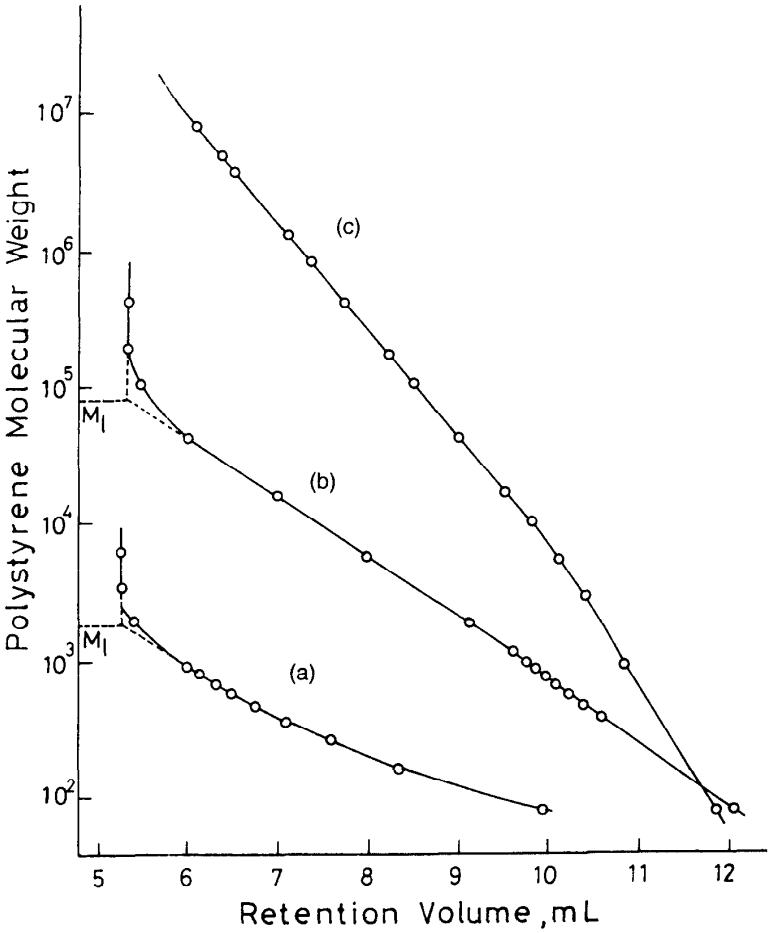


Figure 1 Examples of calibration curves for polystyrene. Columns 8-mm id × 300 mm, (a) Shodex KF-801, (b) Shodex KF-803, (c) Shodex KF-80M; mobile phase: THF; sample: polystyrene standards. (Data courtesy of Shodex group, Showa Denko, Ltd.)

baseline to the chromatogram trace at each divided point i is measured. Molecular weight M_i at each divided point is obtained from the calibration curve constructed in Sec. II. B.1 and MW averages are calculated using the equations:

$$M_n = \frac{\sum H_i}{\sum (H_i/M_i)} = \frac{\sum (N_iM_i)}{\sum N_i} = \frac{\sum w_i}{\sum N_i} \tag{7}$$

$$M_w = \frac{\sum (H_iM_i)}{\sum H_i} = \frac{\sum (N_iM_i^2)}{\sum (N_iM_i)} = \frac{\sum w_iM_i}{\sum w_i} \tag{8}$$

$$M_v = \left[\frac{\sum (H_i M_i^a)}{\sum H_i}\right]^{1/a} \tag{9}$$

$$M_z = \frac{\sum (H_i M_i^2)}{\sum (H_i M_i)} \tag{10}$$

where M_v is viscosity-average MW, M_z Z-average MW, a the exponent of the Mark–Houwink equation, and w_i weight of ith component.

When a calibration curve is linear, then number-average and weight-average molecular weights can be calculated using Eqs. (4), (7), and (8) as

$$M_n = \frac{D_1 \sum H_i}{\sum [H_i \exp (D_2 V_{R,i})]} \tag{11}$$

$$M_w = \frac{D_1 \sum [H_i \exp (-D_2 V_{R,i})]}{\sum H_i} \tag{12}$$

The shape of an SEC chromatogram of a polymer is similar to a differential molecular weight distribution curve of the polymer, but both are different. A differential molecular weight distribution curve is a plot of log M (abscissa) versus dW/d (log M) (ordinate). Here W is a weight fraction and M is molecular weight. The curve is normalized as

$$\int_0^\infty W_{\log M} \, d(\log M) = 1 \tag{13}$$

On the other hand, an SEC chromatogram is a plot of retention volume V_R (abscissa) versus dW/dV_R (ordinate).

To obtain a differential molecular weight distribution curve from an SEC chromatogram, $dW/d(\log M)$ at each divided point i must be calculated as follows.

$$\frac{dW_i}{d(\log M_i)} = \frac{dV_{R,i}}{d(\log M_i)} \cdot \frac{H_i}{\sum H_i} \cdot \frac{1}{\text{division interval}} \tag{14}$$

where $dV_R/d(\log M)$ is a reverse slope of the calibration curve used for the SEC system and a term $H_i/(\Sigma H_i) \times$ (division interval) equals $dW_i/dV_{R,i}$. Division interval means the space between each data point expressed in milliliters. For example, when retention volume is indicated by a milliliter unit, and if height is measured every 0.25 mL, then the division interval is 0.25 mL.

An integral molecular weight distribution curve is a plot of the area percentage of a differential molecular weight distribution curve up to molecular weight M_i integrated from a low molecular weight region versus log M_i.

3. Conversion of Molecular Weight

Molecular weight averages and MWD of polymers other than PS can also be calculated in the same manner as mentioned in Secs. II. B.1 and II. B.2. However, calculated values are not real ones for the polymers of interest, but are polystyrene equivalent molecular weight averages. To obtain actual MW of the polymers, conversion methods must be applied. The simplest method is to use "Q factors," but it lacks accuracy, because it assumes the extended chain length of the polymer in solution. Most flexible polymers are not extended, but are randomly coiled in solution.

The more realistic and reliable method is to use the concept of "the hydrodynamic volume" [9]. For two polymers A and B that elute at the same retention volume, Eq. (15) is valid, provided that these polymers are separated by size only, without any secondary interactions.

$$[\eta]_A M_A = [\eta]_B M_B \tag{15}$$

where $[\eta]_A$ and $[\eta]_B$ are the intrinsic viscosities and M_A and M_B are MW of polymers A and B eluted at the same retention volume. If the parameters, K and a, from the Mark-Houwink equation, $[\eta] = K M^a$, are known for both polymers in the same solvent and at the same temperature, MW of polymer B, M_B, for any given retention volume can be calculated from Eq. (16) by knowing MW of polymer A, M_A, and the parameters of the Mark-Houwink equations for polymers A and B as

$$\log M_B = \frac{1}{1 + a_B} \log \frac{K_A}{K_B} + \frac{1 + a_A}{1 + a_B} \log M_A \tag{16}$$

When polymer A is polystyrene, for example, M_A at given retention volume can be obtained from a PS calibration curve. This procedure is called the universal calibration method. Importantly if secondary interactions between the polymer of interest and the column packing materials exist, the procedure cannot be applied to the system. Polar polymers require careful observation of their elution behavior before one applies the hydrodynamic volume concept to the system. For example, a secondary effect for the elution of polyacrylonitrile in dimethyl formamide–lithium bromide at 60°C with PS gel columns was observed; therefore, the universal calibration method cannot be applied to polyacrylonitrile in this system [10]. A list of frequently encountered Mark-Houwink parameters is given in Table 2.

When the parameters from the Marke-Houwink equation are not known for polymer B or for both polymers A and B, then a differential viscometer can be connected to the SEC system. The intrinsic viscosity of a polymer fraction eluted from the SEC columns at a retention volume i is obtained as

$$[\eta]_i = \frac{1}{C_i} \cdot \frac{\Delta P_i - \Delta P_0}{\Delta P_0} \tag{17}$$

where ΔP_i is the pressure drop of the polymer fraction across the capillary of the differential viscometer, ΔP_0 the pressure drop of the mobile phase across the capillary, and C_i the sample

Table 2 Examples for Mark-Houwink Parameters

Polymer	Solvent[a]	Temperature (°C)	$K \times 10^4$ (dL g^{-1})	a	Ref.
Polystyrene	THF	25	1.60	0.706	11
Polyvinyl chloride	THF	25	1.63	0.766	11
Polymethyl methacrylate	THF	25	1.48	0.677	12
Polyisoprene	THF	25	1.77	0.735	13
Polybutadiene	THF	25	1.6	0.776	14
Polyethylene	TCB	135	4.34	0.724	15
Polypropylene	TCB	135	1.37	0.75	15
Polystyrene	TCB	135	1.21	0.707	15
Polyethylene oxide	DMF[b]	60	5.0	0.653	10
Polyacrylonitrile	DMF[b]	60	0.146	0.897	10
Polyethylene oxide	Water[c]	25	5.88	0.65	16
Pullulan	Water[c]	25	1.79	0.67	16

[a]THF, tetrahydrofuran; TCB, 1,2,4-trichlorobenzene; DMF, dimethylformamide.
[b]With 0.01 M LiBr.
[c]With 0.1 M NaCl.

concentration at retention volume i. The value $M_{B,i}$ at given retention volume i is easily calculated from Eq. (15).

The other approach to calibrate an SEC system is to use a single, broad MWD polymer of interest or use two such. A pair of M_n and M_w, M_n and $[\eta]$, or M_w and $[\eta]$ for a single, broad MWD polymer of interest or a pair of M_w, M_n, or $[\eta]$ for two broad MWD polymers of interest must be known. A calibration curve is assumed to be linear [17] or a quadratic equation [18].

An alternative approach by which assumption of any formula for the calibration curve is not required uses one or two broad MWD polymers as secondary standards for which two of three molecular weight averages are known and a calibration curve of log molecular weight versus retention volume constructed with PS standards as primary standards [19]. At first, molecular weight $(M_B)_i$ of a species of polymer B eluted at retention volume i is related to molecular weight $(M_A)_i$ of a species of polymer A eluted at the same retention volume i by the expression

$$(M_B)_i = s(M_A)_i^t \tag{18}$$

where s and t are constants. Polymer A is PS and polymer B is a polymer of interest. Suppose that the weight-average molecular weight $(M_w)_t$ and the number-average molecular weight $(M_n)_t$ of polymer B used as a secondary standard are known. A chromatogram of the secondary standard is measured, and from the chromatogram and a calibration curve for PS standards, the weight- and number-average molecular weight, $(M_w)_c$ and $(M_n)_c$, can be calculated by Eqs. (19) and (20).

$$(M_w)_c = \frac{\sum [h_i s(M_A)_i^t}{\sum h_i} \tag{19}$$

$$(M_n)_c = \frac{\sum h_i}{\sum [h_i / s(M_A)_i^t]} \tag{20}$$

where h_i is height of the chromatogram from baseline at retention volume i.

Guess value t first, then the molecular weight averages of the secondary standards are calculated by Eqs. (19) and (20) as follows:

$$(M_w)_c = k_1 s \tag{21}$$

$$(M_n)_c = k_2 s \tag{22}$$

where k_1 and k_2 are numerical values obtained from h_i and $(M_A)_i^t$. Let us assume

$$(M_w)_t = (M_w)_c, \qquad (M_n)_t = (M_n)_c \tag{23}$$

then we obtain two values of s, which may be unequal at the beginning. The goal of this calculation is to find a value t where a value of s from Eq. (21) equals that of s from Eq. (22). The process may be repeated with other values of t until an absolute value of [s of Eq. (21) − s of Eq. (22)] becomes sufficiently small.

4. Molecular Weight Measurement for Copolymers

Most synthetic copolymers have both MWD and a chemical composition distribution (CCD). SEC is the technique to separate polymers according to the sizes of the molecules in solutions, not their MW. Copolymers of the same molecular size are not necessarily the same in MW, and those eluted at the same retention volume are an assembly of species having different MW. Therefore, determination of MW for copolymers by SEC lacks only accuracy of the value. Accurate determination of MW for copolymers is limited to the case when the copolymer has the homogeneous composition across the whole range of MW. SEC is, however, a rapid and simple technique used to obtain MW averages of polymers and, therefore, if it is

possible to consider that molecular sizes of copolymers are roughly proportional to MW, then it is not meaningless to determine MW averages of copolymers by SEC.

Construction of a calibration curve for copolymers is rather complicated compared with homopolymers. At first, composition of copolymers is assumed to be the same over the whole range of MW, or the average composition at each retention volume is determined, and then MW of the species is estimated. For a copolymer consisting of components A and B, a calibration curve of log MW versus retention volume V_R for the copolymer can be constructed from those for two homopolymers A and B. For the styrene–butadiene block copolymers, molecular weight $M_{c,i}$ at retention volume i was estimated as [20]

$$\log M_{c,i} = W_{c,i} \log M_{s,i} + W_{b,i} \log M_{b,i} \tag{24}$$

where $M_{s,i}$ and $M_{b,i}$ are MW for PS and polybutadiene at retention volume i, which can be measured from calibration curves for these two homopolymers, and $W_{s,i}$ and $W_{b,i}$ are weight fractions of styrene and butadiene in the copolymer at retention volume i.

The use of the so-called universal calibration technique is a theoretically reliable procedure for calibration. Equation (15) can be applied here. If a copolymer and a polystyrene are eluted at the same retention volume, then

$$M_c [\eta]_c = M_s [\eta]_s \tag{25}$$

where M_c and M_s are molecular weights for the copolymer and the polystyrene, and $[\eta]_c$ and $[\eta]_s$ are intrinsic viscosities for the copolymer and the polystyrene [21]. To apply this equation, Mark-Houwink parameters for both homopolymers and their copolymer must be known. For ethylene–propyrene copolymers, the parameters for the copolymer are estimated as [22]

$$a_{EP} = (a_{PE}\, a_{PP})^{1/2} \tag{26}$$

$$K_{EP} = K_{PE}\, W + P_{PP}\,(1 - W) - 2(K_{PE}\, K_{PP})^{1/2}\, W(1 - W) \tag{27}$$

where subscripts EP, PE, and PP mean ethylene–propylene copolymer, polyethylene, and polypropylene, and W is the weight fraction of ethylene in the copolymer. When Mark-Houwink parameters are not known, then one can use a differential viscometer to obtain the value of $[\eta]_{c,i}$ at each retention volume i.

The application of light-scattering detectors, such as a low-angle laser light-scattering detector (LALLS) and a multiangle laser light-scattering detector (MALLS) for the measurement of absolute MW eluted from SEC columns is not generally applicable to copolymers, because the intensity of light-scattering is a function not only of the molecular weight of the copolymer, but also of the specific refractive index in the solvent used as the mobile phase.

The apparent weight average MW of a copolymer $(M_w)_a$ is expressed with the true weight average molecular weight $(M_w)_t$ and the heterogeneity parameters P and Q as follows:

$$(M_w)_a = (M_w)_t + 2Pb + Qb^2$$

$$b = \frac{(\nu_a - \nu_b)}{\nu} \tag{28}$$

where ν is the specific refractive index increment of the copolymer, and ν_a and ν_b are the specific refractive index increments of the homopolymers A and B [23]. [For a detailed discussion on calibration approaches for copolymers, see Ref. 24.]

5. Absolute Molecular Weight Measurements

Values of M_n and M_w can be independently measured by several physical methods. The number-average MW is determined by one of the colligative property methods. The relation between the colligative properties and MW for infinitive dilute solutions rest on the fact that the activity of the solute in a solution becomes equal to its mole fraction as the solute concentration becomes sufficiently small. When a polymer solution is contacted with pure solvent

through a semipermeable membrane at temperature T, the pressure difference between the two phases is defined as the osmotic pressure π, which relates to M_n as

$$\pi = RT\left[\left(\frac{C}{M_n}\right) + A_2C + A_3C^2 + \cdots\right] \tag{29}$$

where C is the solute concentration, A_2 and A_3 are the osmotic second and third virial coefficients and R is a gas constant. If C is supposed to be very dilute, Eq. [29] is regarded as

$$\frac{\pi}{C} = \frac{RT}{M_n} \tag{30}$$

This is the principle of membrane osmometry.

When the polymer solution is placed under an atmosphere of saturated vapor phase and both phases are in equilibrium, the vapor pressure P of the solvent component in the solution is smaller than the vapor pressure of the pure solvent P_0 and their ratio is expressed as

$$\ln\left(\frac{P}{P_0}\right) = V_0\left[\left(\frac{C}{M_n}\right) + A_2C^2 + A_3C^3 + \cdots\right] \tag{31}$$

where V_0 is the molar volume of solvent. The technique of the indirect measurement of the vapor pressure is known as vapor-pressure osmometry, where the small temperature difference results from different rates of solvent evaporation from and condensation onto droplets of pure solvent and polymer solution maintained on respective thermistors in an atmosphere of solvent vapor is measured. The temperature difference in the steady state $(T - T_0)$ is expressed as

$$\frac{(T - T_0)}{C} = \frac{K_s}{M_n} \tag{32}$$

where K_s is a calibration constant depending on the combination of solute and solvent and on the dimensions of the apparatus. The other methods for determining M_n by using the colligative property of the polymer solution are ebulliometry and cryoscopy. Ebulliometry measures the boiling-point elevation of the polymer solution compared with the pure solvent, and cryoscopy measures the freezing-point depression.

Chemical methods can also be applied to determine M_n. Condensation polymers such as polyamides and polyesters are good examples. Polyamides have a carboxyl group and an amino group at either end of the chain. The mole numbers of the carboxyl [COOH] and the amino [NH_2] groups per 1 g of the sample are measured by titration with base or acid and M_n is given by

$$M_n = \frac{2}{([\text{COOH}] + [\text{NH}_2])} \tag{33}$$

The weight-average M_w is determined from LS measurements. The reduced-scattering intensity (Rayleigh's ratio) at a scattering angle θ, $R(\theta)$, of a dilute solution of a polymer with M_w is measured by changing the scattering angles and it is expressed as

$$\frac{KC}{R(\theta)} = \left[\left(\frac{1}{M_w}\right) + 2A_2C + 3A_3C^2 + \cdots\right]\left[\frac{1}{P(\theta)}\right] \tag{34}$$

where K is the optical constant and $P(\theta)$ is the function of polymer size and the scattering angle. When $\theta = 0$ and $C = 0$, then

$$\frac{KC}{R(\theta)} = \frac{1}{M_w} \tag{35}$$

By plotting data of $KC/R(\theta)$ and $\sin^2(\theta/2)$ at several θ and C and by extrapolating θ and C to 0, the reciprocal value at the intercept of the ordinate $KC/R(\theta)$ gives M_w. Several LS instruments are commercially available. Among them, some LS instruments can also be used for SEC detectors: multiangle laser light-scattering (MALLS), triple-angle LS (TALLS), dual-angle LS (DALLS), right-angle LS (RALLS), and low-angle LS (LALLS).

The intrinsic viscosity of a polymer is proportional to the hydrodynamic size of the polymer and can be used as the measure of the polymer MW. Recently, several capillary viscometers have become commercially available. When the pressure drop of the mobile phase across a capillary is ΔP_0, the difference, $\Delta\Delta P$, between the pressure drop of the polymer solution, ΔP, and ΔP_0 is expressed as

$$\Delta\Delta P = \Delta P - \Delta P_0 = \frac{8\, l\, Q(\eta - \eta_0)}{\pi r^4} \tag{36}$$

where r is the capillary radius, l the capillary length, Q the fluid flow rate and η and η_0 the fluid viscosities of the sample solution and the mobile phase, respectively. For very dilute polymer solutions, such as those in SEC, the intrinsic viscosity $[\eta]$ of the polymer sample is defined as

$$\begin{aligned}[\eta] &= \lim_{c \to 0} \left(\frac{1}{C}\right) \frac{(\eta - \eta_0)}{\eta_0} = \left(\frac{1}{C}\right) \frac{(\eta - \eta_0)}{\eta_0} \\ &= \left(\frac{1}{C}\right) \frac{(\Delta P - \Delta P_0)}{\Delta P_0} = \left(\frac{1}{C}\right) \left(\frac{\Delta\Delta P}{\Delta P_0}\right)\end{aligned} \tag{37}$$

C. Application

1. Branching

There are two types of branching, short-chain branching (SCB) and long-chain branching (LCB). SCB is a chain of one or two monomer units and high-density polyethylene (HDPE) and linear low-density polyethylene (LLDPE) have it. HDPE has about 25 SCB per 1000c. High-pressure, low-density polyethylene (LDPE) includes LCB of which the minimum length lies between 6 and 16 carbons [25].

A branching parameter g is defined as the ratio of the mean-square radii of gyration $<s^2>$ of branched (denoted by subscript br) and linear (subscript l) molecules of the same MW and of the same chemical composition.

$$g = \frac{<s^2>_{br}}{<s^2>_l} \tag{38}$$

A branched molecule has smaller dimensions in solution and lower intrinsic viscosity than a linear molecular of the same MW. The reduction in intrinsic viscosity resulting from branching gives Eq. (39).

$$g^b = \frac{[\eta]_{br}}{[\eta]_l} \tag{39}$$

The exponent b is a value ranging between 0.5 and 1.5, depending on the type of branching. The value of b is 0.5 for star-branched polymers and 1.5 for comb-like polymers.

Linear and branched polymers eluted at the same retention volume have the same hydrodynamic volume

$$[\eta]_{br} M_{br} = [\eta]^* M^* \tag{40}$$

Superscript * means a linear polymer eluted at the same retention volume as the branched polymer. In general, $M_{br} > M^*$ and $[\eta]_{br} < [\eta]^*$.

2. Specific Polymers

m-Cresol and *o*-chlorophenol can be used as the mobile phase for SEC of polyamides, but these solvents are acidic and viscous and the handling is rather complicated. Fluoroalcohols, such as trifluoroethanol (TFE) and hexafluoroisopropanol (HFIP) dissolve most polyamides at room temperature and can be used as the mobile phase for SEC. Although these fluoroalcohols do not swell a polystyrene gel packing, recent high-performance SEC columns can tolerate the use of these solvents as the mobile phase [26]. Trifluoroacetic acid was added to the mobile phase to suppress the early elution near the exclusion limit. A system of silica gel–TFE was also applied for SEC of polyamides [27]. Poly(methyl methacrylate) standards are used for the construction of a calibration curve.

Poly(ethylene terephthalate) (PET) is insoluble in solvents commonly used for SEC and is soluble in HFIP. A system of PS gel–HFIP was used for SEC of PET [28]. Although HFIP is a very expensive solvent, recycling the solvent reduces the cost. The effluent from the columns was collected and distilled for reuse. When HFIP is used as the mobile phase, note safety because it is hazardous.

Polyacrylonitrile is soluble in dimethylformamide (DMF). Although DMF is a poor solvent for polystryene, it is possible to use DMF as the mobile phase for SEC with PS gel [10]. Polyethylene glycols and polyethylene oxides were used as standards for a calibration curve and lithium bromide was added to the mobile phase to suppress the early elution near the exclusion limit.

High-temperature SEC needs the use of a high-temperature apparatus in which components from the injector (preferably from the solvent reservoir) to the outlet of the detector(s) are kept at higher temperature, mostly over 100°C. This apparatus is exclusively applied for SEC of polyolefins, such as polyethylene and polypropylene and these polyolefins are soluble in *o*-diclorobenzene (ODCB) or 1,2,4-trichlorobenzene (TCB) over 100°C. On cooling below 100°C, these polymers solidify from the solution.

Polyethylene (PE) and polypropylene (PP) are determined at 135°C or 145°C using ODCB or TCB as the mobile phase. Irganox 1010 (tetrakis[methylene(3,5-dibutyl-4-hydroxyhydrocynamaate)] methane) or BHT (2,6-di-*t*-butyl-*p*-cresol) is added as an antioxidant. A calibration curve is constructed using PS and the next equations are used for calculation of MW averages.

For PE, TCB at 135°C [14]

$$\log M_{PE} = -0.329 + 0.99 \log M_{PS}$$

For PE, ODCB at 135°C [29]

$$\log M_{PE} = -0.332 + \log M_{PS}$$

For PP, TCB at 145°C [30]

$$\log M_{PP} = -0.0308 + 0.975 \log M_{PS}$$

Ethylene–vinyl acetate (EVA) copolymers were measured at 135°C using TCB as the mobile phase and a refractometer and a differential viscometer as detectors [31]. A Mark-Houwink equation for EVA at 135°C in TCB was

$$[\eta] = K M^{0.7}$$

and

$$K = 0.053 (1 - 0.56 W) \qquad \text{for } 0 \leq W \leq 0.45$$

or

$$K = 0.053\ (1 - 0.46W - 0.32W^2) \qquad \text{for full range}$$

where W is weight fraction of vinyl acetate in EVA.

Poly(ether ether ketone) (PEEK) is insoluble in most organic solvents at room temperature. At high temperature, closer to its melting point, PEEK dissolves in benzophenone or diphenyl sulfone. SEC analysis was performed at 115°C in a mixture of phenol–trichlorobenzene (1:1) [32]. Poly(phenylene sulfide) (PPS) is also insoluble in most organic solvents below 200°C, and it has been measured by SEC with 1-chloronaphthalene as the mobile phase at 210°C [33].

D. Separation of Oligomers

1. SEC

Although in the SEC separation of synthetic polymers, the SEC chromatogram usually shows just a broad and continuous elution pattern, chromatograms of oligomers have several distinct peaks. Therefore, in the oligomer analysis, the separation into individual species (different degrees of polymerization) is an objective as well as the determination of MW averages.

In the separation of oligomers by SEC, the selection of pore sizes of packing materials in columns is very important. Among seven or eight different pore sizes that are now commercially available, three to four sizes can be used for the oligomer separation. Chromatograms shown in Fig. 2 represent the different elution profiles of epoxy resins with different pore sizes of packing materials. Epikote 1001 had higher MW averages than Epikote 828. A column of Shodex A801 has the exclusion limit of 2000 as PS and that of Shodex A 803 has 8×10^4 (see Fig. 1). Epikote 828 was separated well with columns of Shodex A801, but

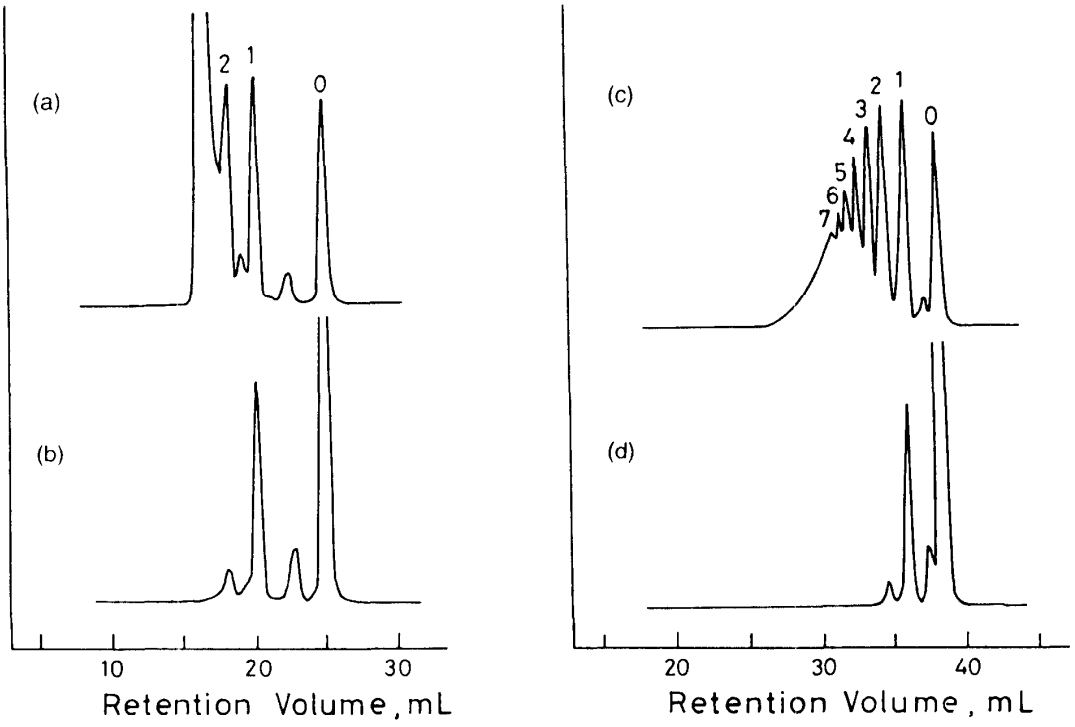


Figure 2 Separation of epoxy resins with different porosity polystyrene gels. Sample: (a) and (c) Epikote 1001; (b) and (d) Epikote 828; column: (a) and (b) Shodex A-801 × 2; (c) and (d) Shodex A-803 × 2; mobile phase: THF. (Data courtesy of Shodex group, Showa Denko, Ltd.)

resolution was worse with columns of Shodex A803. On the other hand, most of Epikote 1001 eluted at the exclusion limit when columns of Shodex A801 were used because of smaller pore sizes of the columns. The resin was separated well with columns of Shodex A803. Figures on the chromatograms represent the degree of polymerization; that is, the number of monomeric repeating units.

In peak separation, it is possible to construct a calibration curve of peak retention volume versus MW for the oligomer of interest. The higher MW region can be extrapolated. Elution order of different oligomers of the same molecular size changed with mobile phase change because of the change of molecular sizes in different solvents and the adsorption effect. The examples are shown in Figs. 3 and 4 [34]. *p*-Cresol novolak resin oligomers in THF (see Fig. 3) eluted earlier than oligostyrenes in contrast with their elution in chloroform (see Fig. 4).

When the resolution between two adjacent peaks is poor, even though the selection of columns of appropriate pore sizes has been made, then one may couple together more columns of the same pore size [35] or use recycled SEC [36] to improve resolution. An example is shown in Fig. 5. Both chromatograms were obtained with the same packing materials having the same pore size, but the column lengths were different. Figure 5a was obtained with 16 columns of 1.5-mm id × 25 cm for which the number of theoretical plates was 103,000, and

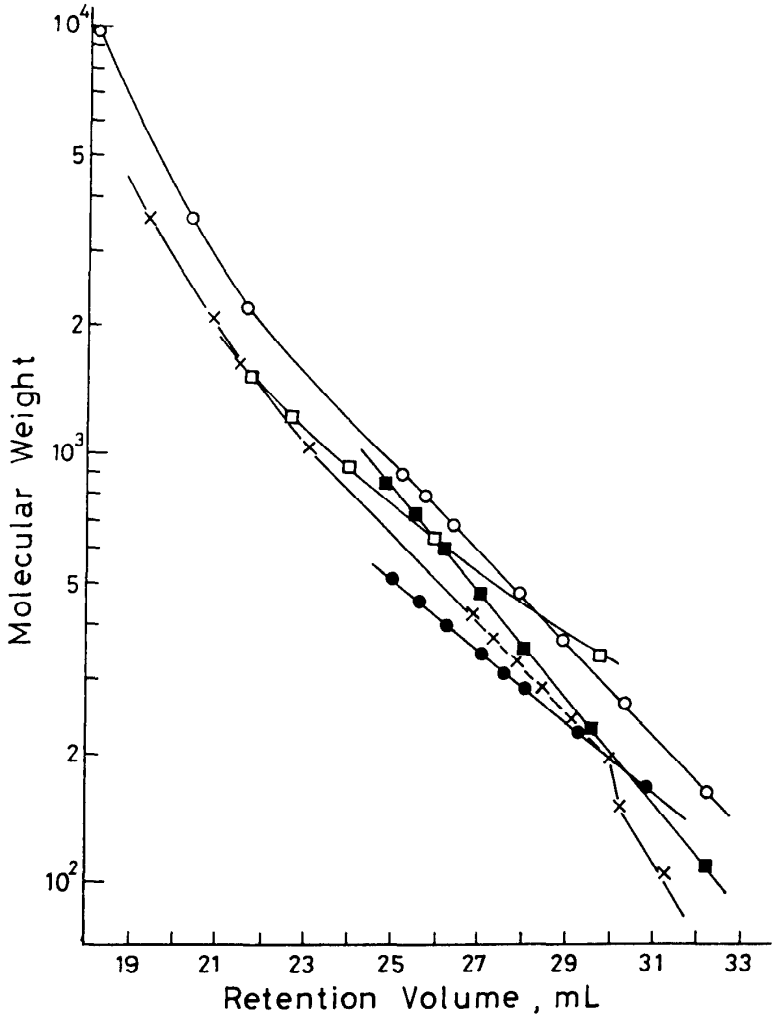


Figure 3 Elution order of oligomers in THF mobile phase. Column: Shodex A-802 × 2; sample: (○) polystyrene, (●) *n*-hydrocarbon, (□) epoxy resin, (■) *p*-cresol novolak resin, (x) polyethylene glycol. (From Ref. 34.)

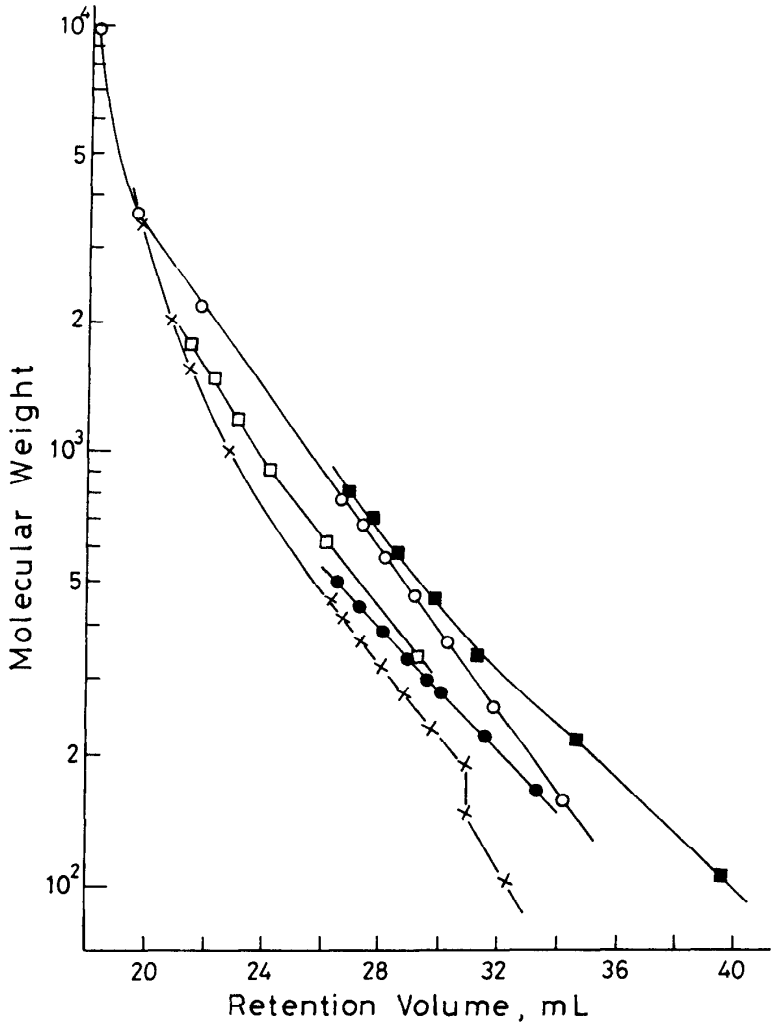


Figure 4 Elution order of oligomers in chloroform mobile phase. Column: Shodex A-802 × 2; sample: (○) polystyrene, (●) *n*-hydrocarbon, (□) epoxy resin, (■) *p*-cresol novolak resin, (x) polyethylene glycol. (From Ref. 34.)

Fig. 5b was obtained with two columns of 8-mm id × 30 cm for which the number of theoretical plates was 35,000.

A differential refractometer, which is the most widely used detector for SEC, detects the difference in refractive index between a reference mobile phase and the mobile phase containing the sample as it elutes from the column. Although refractive index of a polymer is generally assumed to be constant for the calculation of MW averages from the SEC chromatograms, it changes with MW for oligomers, because of end-group effects.

Therefore, the response correction is required for the calculation of MW averages for oligomers. Refractive indexes of oligoethylene glycols increased with increasing MW [37]. Response correction factors for oligoethylene glycols in THF at 25°C against pentadecamer (n = 15) are as follows: n = 2, 1.487; n = 3, 1.260; n = 4, 1.177; n = 6, 1.105; n = 8, 1.063; n = 10, 1.043; n = 12, 1.025. These values were calculated by taking pentadecamer as a reference. Similarly, response correction factors for polyethylene glycols in THF at 25°C against polyethylene glycol of MW 20,000 are as follows: MW 500, 1.141; MW 1000, 1.066; MW 2000, 1.030; MW 5000, 1.009; MW 8000, 1.003. Although refractive index increased with increasing MW, its increase was small over 1000 MW.

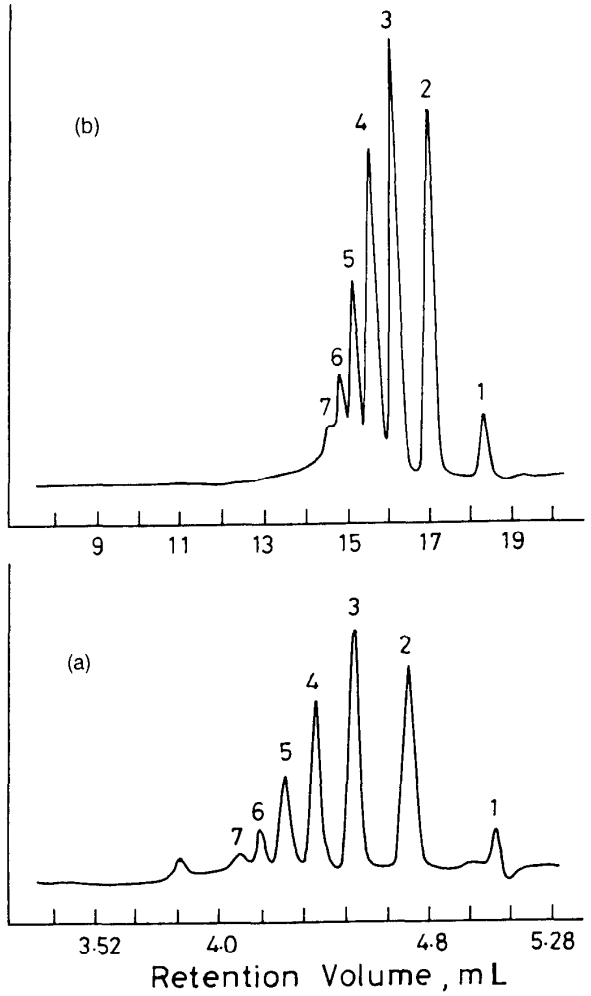


Figure 5 SEC chromatograms of oligostyrene obtained at different column lengths. Sample: oligostyrene A-300 (molecular weight 300). (a) Semimicro SEC; column: packed with Shodex A-802 polystyrene gel in 1.5-mm id × 25 cm × 16; sample: 0.5%, 4 μL injected; flow rate: 40 μL min^{-1} THF. (b) Conventional SEC; column: packed with Shodex A-802 polystyrene gel in 8-mm id × 30 cm × 2; sample: 0.5%, 30 μL injected; flow rate: 1 mL min^{-1} THF. (From Ref. 35.)

Phenol–formaldehyde resin prepolymers of the novolak and resol type contain a variety of components, depending on the reaction conditions. Mono-, di-, and trinuclei of the novolak- and resol-type resins could be observed and identified by SEC [35]. The results are shown in Fig. 6. The 2,4′- and 4,4′-dihydroxy diphenyl methanes (DPM) could not be separated from each other. Similarly, 2,2′,6′,4″-, 2,2′,4′,2″-, and 2,2′,6′,2″-trimer appeared as one peak and 4,2′,4′,4″-, and 4,2′,6′,4″-trimer eluted at the same retention volume. 2-Methyl phenol (MP), 4-MP (and, 2,6-DMP), 2,4-dimethylol phenol (DMP), 2,4,6-trimethylol phenol (TMP) of the resol type resin could be separated into individual peaks.

Melamine–formaldehyde resin is insoluble in THF and chloroform and is slightly soluble in water. The resin is also soluble in dimethylformamide (DMF). Therefore, it could be separated with the system of PS gel–DMF, and up to five nuclear melamines were detected, which contain five melamines bridged by methylene ether or methylene linkages [38]. Methyl ether derivatives of polynuclear methylol melamines obtained by the reaction of the methylol group with methanol were soluble in THF and were separated by SEC of PS gel–THF [35].

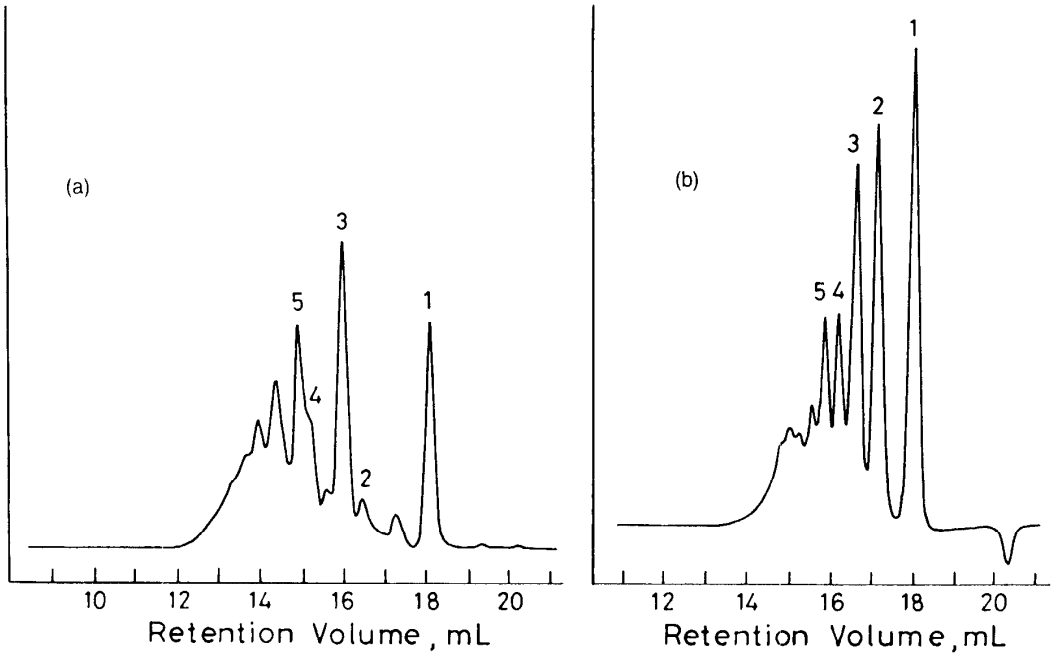


Figure 6 SEC chromatograms of phenol–formaldehyde resin prepolymer (a) novolak type (b) resol type. Column: Shodex KF-802 (8-mm id × 30 cm) × 2; mobile phase: THF, 1 mL min^{-1}; detector: UV at 254 nm. (a) (1) Phenol: (2) 2,2′-DPM; (3) 2,4′- and 4,4′-DPM; (4) 2,2′,6′,4″-, 2,2′,4′,2″- and 2,2′,6′,2″-trimer; (5) 4,2′,4′,4″- and 4,2′,6′,4″-trimer. (b) (1) Phenol; (2) 2-MP; (3) 4-MP and 2,6-DMP; (4) 2,4-DMP; (5) 2,4,6-TMP. (From Ref. 35.)

2. Interactive HPLC

The separation of oligomers by SEC is primarily dependent on the pore size of packing materials in a column and not on the nature of the mobile phase and the stationary phase. If more resolution is needed, other separation modes such as adsorption mode in HPLC should be considered.

Oligostyrene of average MW 800 was separated into peaks up to pentadecamer with the system of silica-ODS–THF–water [39]. Gradient elution was applied and the condition was from 60% THF in water to 75% THF in water in 75 min. Oligostyrenes of higher average molecular weights such as 2200 and 4000 were separated with nitrile-bonded silica gel by the gradient elution procedure of 60% THF in water to 85% THF in water, or 3% THF in *n*-hexane to 23% THF in *n*-hexane. Excellent steroisomer separation as well as the separation by the degree of polymerization was provided by the gradient elution of acetonitrile–water (80:20) to acetonitirile in 30 min and then to acetonitrile–dichloromethane (50:50) in 30 min with alkyl-bonded or phenyl-bonded silica gel [40].

Epoxy resins were separated with a system of silica-ODS–50% *p*-dioxane in water to 85% *p*-dioxane [41] and silica–ODS–55% acetonitrile in water to 100% acetonitrile [42]. Oligomers up to $n = 16$ could be separated completely. Phenol–formaldehyde resins of the novolak and resol types were separated with silica-ODS–10% methanol in water to 90% methanol in water [43]. The order of separation for one to two nuclei was as follows: 2,4-DMP, 4-MP, 2,6-DMP, 2-MP, phenol, 4,4′-DPM, 2,4′-DPM, 2,2′-DPM. *p*-Cresol novolak resin was separated with a system of silica-ODS–10% THF in water–55% THF in water and oligomers up to $n = 13$ were identified [41].

Polycarbonate oligomers were separated with silica-ODS–65% acetonitrile in water to 100% acetonitrile [44]. Cyclic oligoamides of nylon 6 were separated with a system of silica-

ODS–5 mM acetic acid–water (7:3)—UV at 210 nm [45]. Similarly, cyclic oligoamides of nylon 6 and nylon 66 were separated with RP8–40% trifluoroethanol in water—UV at 205 nm—50°C [46]. Poly(ethylene terephthalate) oligomers were separated with silica-ODS–15% hexafluoroisopropanol (HFIP) in water to 90% HFIP in water and the oligomers up to n = 15 were identified [41]. The oligomers up to n = 25 were identified by the gradient elution of 25% HFIP in water to 98% HFIP in water.

E. Hydrophilic Polymers

There are three types of hydrophilic polymers: synthetic polymers, such as polyethylene oxide(glycol), polyacrylamide, and sodium polystyrene sulfonate (NaPSS); natural polymers, such as polysaccharide, dextran, and cellulose; and biopolymers, such as proteins. The former two types will be discussed briefly in this section.

Nonionic polymers can be easily separated with a system of aqueous SEC column–water mobile phase. Columns packed with hydrophilic polymer-based packings are preferable. Ionic polymer gels, such as polystyrene sulfonate gels that are used on ion-exchange chromatography can also be used as the SEC packing material for nonionic polymers such as polyethylene oxides and polysaccharides.

Secondary effects, such as ion-exclusion and adsorption effects are observed when polvinyl pyrrolidone and polyacrylamide are sample polymers. For these, the addition of electrolytes, such as sodium chloride or sodium nitrate in 0.05–0.1 M concentration, to the water mobile phase is effective to suppress the secondary effects. When tailing or leading of a chromatogram is observed, the addition of polar organic solvents, such as methanol and acetonitrile, to the salt solution in 5–10% concentration is also effective to obtain a normal chromatogram. Care must be taken when MW averages of polymers are calculated using a calibration curve constructed with polymer standards other than polymers of interest and a universal calibration concept is applied. Nonionic natural polymers usually have a small amount of ionic groups. Therefore, the addition of electrolytes to a water mobile phase is preferable.

Hydrophilic nonionic polymer-based packings, such as polyhydroxymethacrylate gel, have a small amount of anionic groups in a chain. Therefore, when anionic polymers are separated with only pure water as the mobile phase, most of the anionic polymers elute at the exclusion limit because of ion-exclusion between sample polymers and the stationary phase. The addition of an electrolyte, such as sodium chloride, suppresses the early elution of anionic polymers. Elution behavior of NaPSS on several commercially available columns was studied at varying ionic strengths of phosphate buffer at pH 8.0 [47]. Ion exclusion was the only secondary effect on porous glass columns, and this effect was suppressed at high ionic strength. Elution of NaPSS on diol-bonded silica columns at low ionic strength was governed by the ion-exclusion effect, and with an increasing in the ionic strength, the ion-exclusion effect decreased, and hydrophobic interactions between NaPSS and the packings became remarkable. Adsorption of NaPSS on hydrophilic nonionic polymer-based packings was predominant even with the mobile phase of high ionic strength. The addition of organic solvent to the mobile phase in 10–20% concentration was useful to prevent this secondary effect [48].

A high concentration of electrolytes in the mobile phase is required for cationic polymers [48]. A combination of aqueous acetic acid and an electrolyte is also effective to elute some cationic polymers.

III. SEPARATION BY COMPOSITION

A. Introduction

Size-exclusion chromatography with dual detectors is well known as one of the methods of determining CCD of copolymers, although this is not really a CCD, but rather, composition

as a function of molecular size in solution. When one component in a copolymer has ultraviolet (UV) absorption, but the other is transparent, then a UV-RI (refractometer) dual-detector system can be used to measure CCD of the copolymer [49]. When an infrared detector is employed, two different wavelengths are selected to detect both components at each elution interval [50].

However, SEC separates copolymers according to the sizes of molecules in solution, not according to their MW nor composition. Therefore, the elution order of the copolymers by SEC is not proportional to compositional difference, and components eluted at the same retention volume from SEC columns may have different compositions of the same molecular size. Therefore, only the average composition at each retention volume can be measured by SEC [51]. A mixture of equal amounts of three styrene–methyl methacrylate copolymers (42, 26, and 15% styrene) was separated by SEC, and the UV and RI chromatograms were measured [51]. The styrene weight fractions at each retention volume were nearly 0.275 and the mixture seemed to have a relatively uniform composition for molecular size. If composition difference (chemical heterogeneity) of a copolymer is observed by SEC, then it can be said that the copolymer is chemically heterogeneous. However, even if a uniform CCD of a copolymer is observed by SEC, it is impossible to conclude that the copolymer is homogeneous in composition [52].

To separate copolymers by composition, interactive LC must be employed. SEC is one type of HPLC in which solute molecules are separated by the size-exclusion mechanism. The separation mechanisms of HPLC except SEC are based on interactions between the stationary phase and the solute molecules. Besides these interactions, the solubility difference of copolymers in the mobile phases is also one of the separation mechanisms for the copolymers. Besides these two mechanisms, there are others for the separation of copolymers according to composition. Therefore, NELC is defined as all kinds of HPLC except SEC for the separation of copolymers according to composition. Hyphenated techniques, such as SEC-NELC are required to characterize both MWD and CCD of copolymers in detail and accurately.

B. Separation Mechanisms by Composition

Liquid adsorption chromatography (LAC) is one mode of interactive LC, and silica gel is mostly used as the stationary phase. Hydrogen bonding between silanol groups at the silica surface and appropriate groups on the copolymer molecules is the main mechanism for adsorption. The initial mobile phase is a good solvent for the copolymer molecules that have to first adsorb on the surface of silica gel. Gradient elution is performed to increase the content of a displacer in the mobile phase, which decreases the adsorption power of the stationary phase for the absorbed copolymer molecules.

Solubility difference of copolymers in the mobile phase plays the important role for separation of the copolymers, and NELC used in this category is defined as liquid precipitation chromatography (LPC). The initial mobile phase is a nonsolvent for sample copolymers, so that the copolymers injected into a column precipitate on the inlet of the column. Subsequent gradient elution is performed by increasing the content of a good solvent for the copolymers in the mobile phase, so that the copolymers precipitated in the inlet of the column are redissolved into the mobile phase when it reaches a specific composition and elute from the column. Solubility of the copolymers in the mobile phase governs the separation of the copolymers. The influence of the types of the stationary phase on the separation is small.

In LAC, the mobile phases during elution from the beginning until the complete elution of the copolymers must be good solvents for the copolymers. In LPC, the copolymers injected into the column must precipitate at first in the inlet of the column and redissolve in the mobile phase by increasing the amount of a good solvent in the mobile phase. If the separation mechanism is unclear, or if no adsorption to the stationary phase or no precipitation on the column are expected at the beginning of the sample elution, then the techniques should be classified by other separation modes. They are normal-phase (NPLC) and reversed-phase

(RPLC) liquid chromatography depending on the polarity of the mobile phase and the stationary phase.

Besides these four different separation modes, there are two other techniques to separate copolymers according to composition. They are explained in Sec. III.F.

C. Separation by Liquid Adsorption Chromatography

1. Survey of the Literature

Nonexclusion LC was first applied for the separation of styrene–methyl acrylate copolymers according to composition by Teramachi in 1979 [53]. Silica gel was the stationary phase, and a gradient elution from 7% methyl acetate in carbon tetrachloride to 31% methyl acetate in carbon tetrachloride was applied. Styrene–methyl methacrylate copolymers, P(S-MMA), were separated by a gradient elution method from 3% THF in dichloroethane to 20% THF with silica gel as the stationary phase [54]. Polyacrylates, polymethacrylates, and their copolymers were separated with a combination of silica gel–toluene–methyl ethyl ketone (MEK) [55]. An evaporative light-scattering detector was used to monitor the polymers. A gradient elution condition was 2% MEK in toluene to 100% MEK (for polyacrylates, polymethacrylates, and their copolymers) or 50% MEK (for styrene copolymers of acrylates and methacrylates).

In LAC, the mobile phases including the initial and the final mobile phases in gradient elution should be good solvents for the sample copolymers. All solvents described in the foregoing are good solvents for these polymers and copolymers. At least they can dissolve them. When carbon tetrachloride, dichloroethane, and toluene, including a small amount of displacers, are used as the initial mobile phases, these copolymers adsorb on the surface of silica gel, and methyl acetate, THF, and MEK are used as displacers. Both mobile phase and stationary phase play important roles for the separation of the copolymers according to composition. Hydrogen bonding between carbonyl groups of the copolymers (or acrylate and methacrylate polymers) and silanol groups of silica surface is the main interaction. Elution of these styrene copolymers is in the order of decreasing styrene content and that of polyacrylates and polymethacrylates is in the order of butyl, ethyl, and methyl acrylates and methacrylates.

2. A System of Chlorinated Hydrocarbon and Ethanol as the Mobile Phase

Among several techniques for LAC with silica gel as the stationary phase, a system of chloroform and ethanol or 1,2-dichloroethane (DCE)–ethanol used as the mobile phase is explained rather in detail in this section.

Silica gel with a pore diameter of 30 Å and a mean particle size of 5 μm was packed in 4.6-mm id $\times$ 50 mm in length stainless-steel tubing and was thermostated at a specified temperature. Gradient elution was performed with a mixture of chloroform and ethanol or DCE and ethanol. An example of gradient conditions is as follows: the initial mobile phase (A) was a mixture of chloroform and ethanol (99:1), the final mobile phase (B) was a mixture of chloroform and ethanol (93:7), and the composition of the mobile phase was changed from 100% A to 100% B in 30 min. At column temperature 40–70°C, styrene copolymers of acrylates and metacrylates were separated in the order of decreasing styrene content in the copolymers [56]. Ethanol was used as a displacer.

DCE was transparent at wavelengths over 230 nm and methacrylate and acrylate homopolymers and copolymers as well as their styrene copolymers could be monitored with a UV detector at about 230 nm [57]. An example is shown in Fig. 7 [58].

Styrene copolymers of acrylates and methacrylates as well as acrylate and methacrylate homopolymers and their copolymers were retained in the column with pure chloroform and DCE. Only PS could be eluted from the column. By adding ethanol in the mobile phase, the copolymers were eluted from the column in the order of decreasing styrene content in the copolymers. Copolymers having much acrylate or methacrylate required much ethanol in the mobile phase to elute from the column [56,59]. The copolymers tended to absorb on the

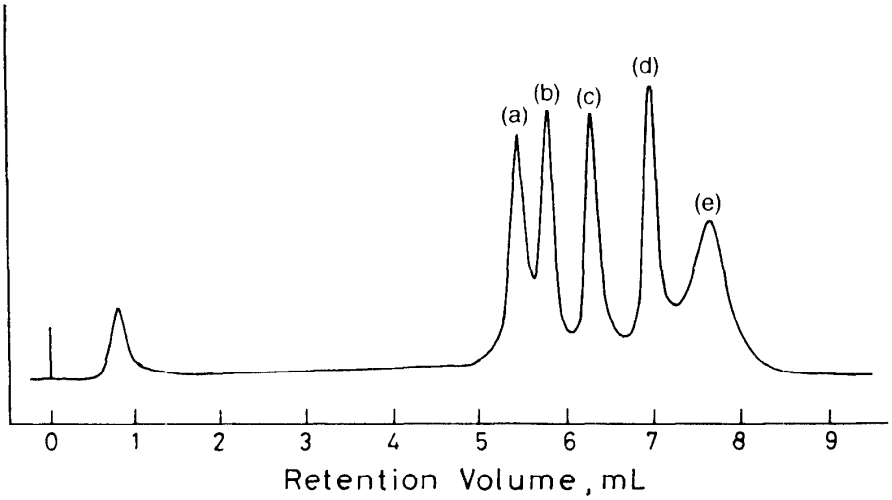


Figure 7 LAC chromatogram of polyethyl methacrylate (e), poly-*n*-butyl methacrylate (a) and their copolymers. Copolymer: (b) poly(ethyl methacrylate–*n*-butyl methacrylate), (25:75); (c) (50:50); (d) (75:25); column temperature: 60°C; detector: UV at 233 nm; gradient condition: 100% DCE–ethanol (99:1) to 100% DCE–ethanol (90:10) in 20 min; flow rate: 0.5 mL min^{-1}. (Reprinted with permission from Ref. 58. Copyright (1990), American Chemical Society.)

surface of silica gel in a column at higher column temperature, and those having much acrylate or methacrylate required a lower column temperature for elution. At the same gradient elution condition, the copolymers were more retained and retarded at higher column temperature. The results are shown in Fig. 8 [60].

The main interaction of the copolymers with the stationary phase is hydrogen bonding of carbonyl groups in the copolymers to silanol groups of the silica surface. Ethanol is feasible to form hydrogen bonding to silanol groups and can control the content of the free silanol groups on the silica surface [61]. Free silanol groups decrease in proportion to the ethanol content in the mobile phase. At higher column temperature, ethanol which formed hydrogen bonding to silanol groups desorbs; consequently, free silanol groups on the silica surface increase. Lower ethanol content in the mobile phase and higher column temperature result in the same phenomenon: free silanol groups on the silica surface increase and the copolymers tend to adsorb on the silica surface.

Plots of the relations between the styrene content and retention volume for the styrene copolymers of acrylate and methacrylate having the same ester groups [e.g., poly-(styrene–methy methacrylate) and poly(styrene–methyl acrylate)] lie roughly on the same line, indicating that a pair of styrene copolymers having the same ester groups and the same styrene content could not be separated [62]. On the other hand, styrene copolymers of methyl acrylate, ethyl acrylate, *n*-butyl acrylate (or methacrylate) having the same styrene content could be separated and the elution was in the order of *n*-butyl, ethyl, and methyl acrylates (or meth-acrylates). The example is shown in Fig. 9 [63].

To determine the molecular weight dependence of retention volume, the copolymers were fractionated by SEC, and fractions were subjected to LAC. The example is shown in Fig. 10 [64]. Peak retention volume of each fraction was almost the same, explaining negligible molecular weight dependence. Fractionation by SEC followed by LAC gave information on both MWD and CCD [65].

The method presented in this section can be applied to other styrene copolymers for which hydrogen bonding to the silica gel is feasible. Styrene–methyl methacrylate block copolymers [66] and styrene–vinyl acetate block copolymers [67] were characterized by SEC–LAC.

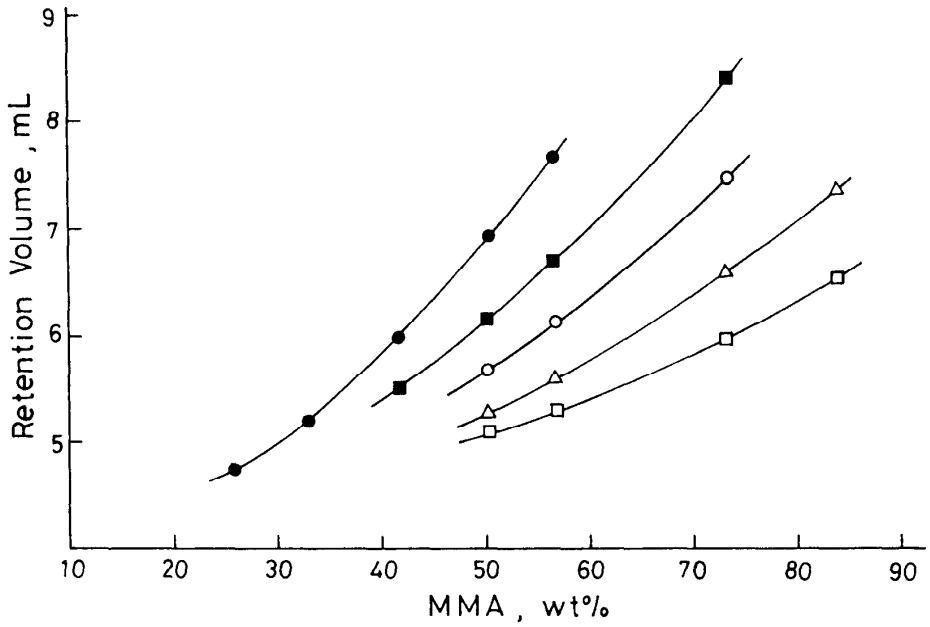


Figure 8 Relation of retention volume versus MMA content of P(S-MMA) at different column temperatures. (●) 80°C, (■) 60°C, (○) 50°C, (△) 40°C, (□) 30°C; gradient condition: 100% chloroform–ethanol (99:1) to 100% chloroform–ethanol (95.5:4.5) in 15 min; flow rate: 0.5 mL min^{-1}. (Reprinted with permission from Ref. 60. Copyright (1987) John Wiley & Sons.)

D. Separation by Liquid Precipitation Chromatography

Liquid precipitation chromatography (LPC) was developed by Glöckner and his co-workers and applied for the separation of styrene–acrylonitrile copolymers, P(S-AN) [68]. A mixture of THF and *n*-hexane was used as the mobile phase and *n*-hexane, which was a nonsolvent for the copolymers was the initial mobile phase. Gradient elution was performed to increase the THF content in the mobile phase. Styrene-rich copolymers eluted first from the column. Redissolution of the initially precipitated copolymer molecules according to their solubility differences is the main mechanism of LPC.

P(S-AN) copolymers were separated on a silica–ODS column by gradient elution from 10% THF in isooctane to 90% THF [69]. Methanol was added to THF in 10% concentration in advance to adjust UV absorbance during elution. Gradient elution from *n*-heptane to dichloromethane (DCM–methanol (8:2) on a silica–ODS column, or from 20% DCM in *n*-heptane to 100% DCM with 2.75% methanol on a silica gel column, was also applied for the separation of P(S-AN) copolymers [70]. P(S-MMA) copolymers were separated on a silica gel column by gradient elution from 10% THF in isooctane to 100% THF [71]. THF used in this separation included 10% methanol in advance. Styrene–methyl acrylate and styrene–butyl acrylate copolymers were separated on a silica gel column by gradient elution from 10% DCM or DCE in *n*-heptane to 100% DCM or DCE [72]. Ten percent methanol was added to DCM or DCE in advance.

E. Separation by Other Separation Modes in HPLC

In this type of separation, the mobile phases during elution, including the initial and the final mobile phases, should be good solvents for the sample copolymers. When the stationary phase is hydrophobic, such as silica–ODS, the initial mobile phase is polar, and the content of the less polar solvent is increased in the mobile phase. This is called reversed-phase LC (RPLC).

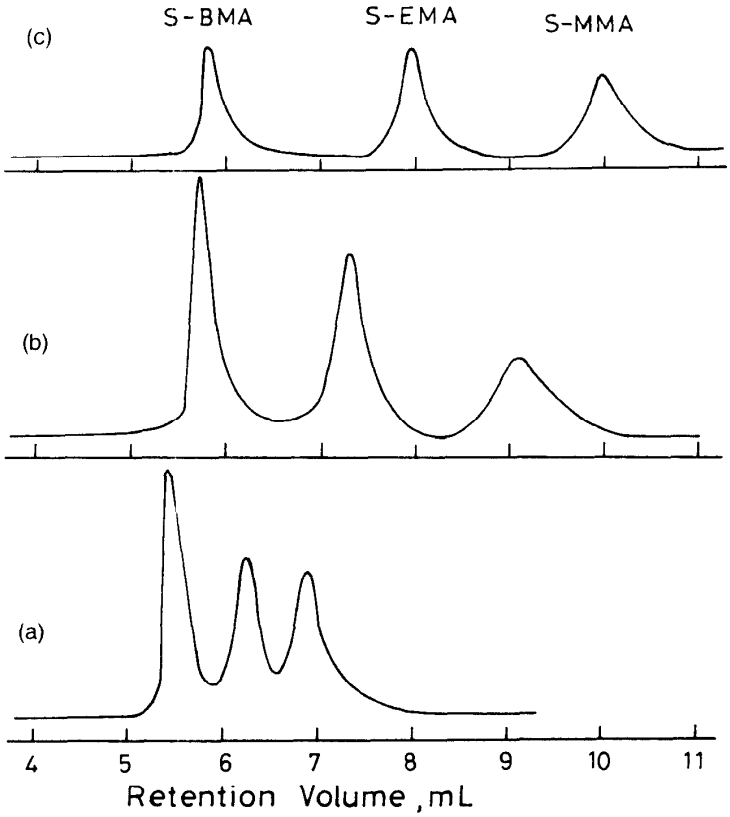


Figure 9 LAC chromatograms of mixtures of styrene–methacrylate copolymers. Sample: (a) styrene-*n*-butyl methacrylate (S–BMA) (50.3% styrene); S–ethyl methacrylate (S–EMA) (50.2%S); and S–MMA (47.3% S); (b) S–BMA (30.7%); S–EMA (30.4%); S–MMA (28.7%); (c) S–BMA (14.5%); S–EMA (15.5%); S–MMA (14.7%). Column temperature: 50°C; flow rate: 0.5 mL min^{-1}; gradient condition: 100% DCE–ethanol (99:1) to 100% DCE–ethanol (93:7) in 30 min; detector: UV at 233 nm. (From Ref. 63.)

When the stationary phase is hydrophilic, such as silica-CN, the initial mobile phase is less polar and the content of polar solvent in the mobile phase is increased. This is called normal-phase LC (NPLC). Several examples are shown in Table 3. In NPLC, elution is in the order of decreasing styrene content, and in RPLC, it is in the order of increasing styrene in the copolymers. For SBR, the elution in NPLC is in the order of increasing styrene content. These differences are dependent on the solubility differences of the copolymers.

F. Separation by Other Techniques

Orthogonal chromatography has been developed by Balke [77] and applied to the separation of styrene–butyl metacrylate copolymers P(S–BMA). PS gel for SEC was used as the stationary phase, and THF and a mixture of THF and *n*-hexane were the first (SEC) and the second (NELC) mobile phases, respectively. Orthogonal chromatography is a hyphenated technique (SEC–NELC) and uses the same column for both separation modes. Fractions separated by SEC were subjected to NELC to separate fractions according to composition. Isopropanol was also used instead of *n*-heptane for the separation of P(S–BMA) [78]. This NELC is classified as RPLC. As the second column (NELC), it is also possible to use a column different from the first column (SEC). Polyacrylamide gel was also used as the second column [78].

Liquid adsorption chromatography at the critical point (LACCP) is especially useful for the determination of the functionality type distribution of oligomers and polymers. Because

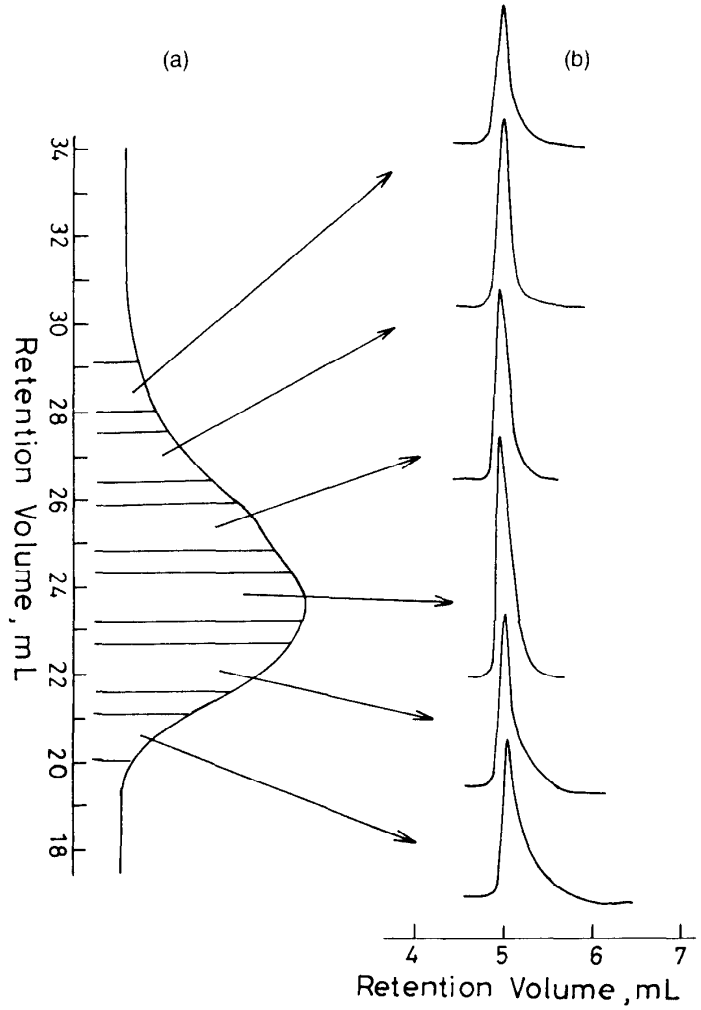


Figure 10 SEC chromatogram (a) of P(S-MMA) and LAC chromatograms (b) of their SEC fractions. SEC: column, Shodex A-80M, mobile phase: chloroform containing 1% ethanol; LAC: gradient condition the same as in Fig. 8; column temperature, 30°C. (Reprinted with permission from Ref. 64. Copyright (1988) The Japan Society for Analytical Chemistry.)

it operates in the region between the size-exclusion and the adsorption modes of LC by changing the composition of a binary mobile phase, retention becomes independent of polymer size, and the separation is attained by the number and type of functional groups [79]. This technique was applied to the characterization of poly(ethylene oxide–propylene oxide) block copolymers [80].

IV. SEPARATION BY OTHER FUNCTIONS

A. Temperature-Rising Elution Fractionation

Temperature-rising elution fractionation (TREF) is a type of column fractionation technique and separates polymers according to the solubility difference by increasing column temperature. Inert materials, such as glass beads or diatomaceous earth (Chromosorb-P) are packed in a fractionation column for which temperature is controlled in a column oven or in a circulating oil bath. The polymer to be investigated is dissolved in a suitable solvent, such as xylene or 1,2,4-trichlorobenzene, at elevated temperature and the hot sample solution is in-

Table 3 Separation System for Normal-Phase and Reversed-Phase Liquid Chromatography

Type	Column	Gradient condition[a]	Copolymer[a]	Ref.
Normal	Silica-NH_2	28% THF in CHX to 78% THF	S-MMA	73
Normal	Silica-CN	10% THF in CHX to 60% THF	S-MMA	73
Normal	Silica gel	35% THF in HX to 85% THF	S-MMA	74
Normal	An gel	35% chloroform in HX to 85% chloroform	S-MMA	74
Normal	AN gel	10% chloroform in HX to 45% chloroform	SBR	75
Reversed	Silica-phenyl	15% THF in ACN to 65% THF	S-MMA	73
Reversed	Silica-ODS	5% THF in ACN to 55% THF	S-MMA	73
Reversed	PS gel	20% DCM in ACN to 80% DCM	S-MMA	76

[a]THF, tetrahydrofuran; CHX, cyclohexane; HX, *n*-hexane; ACN, acetonitrile; DCM, dichloromethane; AN, polyacrylonitrile; PS, polystyrene; SBR, styrene–butadiene rubber.

troduced into a heated column. The temperature of the column is cooled slowly and the polymer sample is deposited onto the surface of the column packing. Elution is started with the same solvent by raising the column temperature gradually. The amorphous component that is more soluble at lower column temperature elutes first, followed by more crystalline components.

TREF was first performed by Wild and his co-workers [81]. It is useful to characterize the degree of short-chain branching, which is related to the degree of crystallinity of polyethylene. Nakano and Goto have developed an automatic cross-fractionation system (analytical TREF–SEC) which had a crystallizability fractionation device before a commercially available SEC apparatus [82]. The fractionation technique involves loading a sample onto a column packed with glass beads and slow cooling the sample solution in *o*-dichlorobenzene [83]. Linear low-density polyethylene (LLDPE) has been examined by eluting stepwise from the column at 40–140°C. Each eluted polymer solution was automatically introduced into the SEC part of the system, which had an infrared detector. Chromatograms of elution temperature versus concentration were recorded and the biomodal distribution of LLDPE was observed.

A similar apparatus has also been developed by Hazlitt and applied for the measurement of the short–chain-branching distribution in ethylene–olefin copolymers [84]. Mirabella prepared a TREF apparatus and characterized a commercial impact-grade polypropylene with a melt flow rate of 6 [85]. This impact copolymer was composed of about 75% isotactic polypropylene, about 17% of a highly noncrystalline ethylene–propylene rubber, and about 8% of semicrystalline ethylene–propylene copolymers.

B. Field-Flow Fractionation

Field-flow fractionation (FFF) was invented by Giddings and has been developed by him and his group. It can be applied for the separation of macromolecules, colloids, and particles of diverse types extending over a mass range from a few hundred to 10^{18} Da [86]. Separation in FFF takes place in a narrow tube or channel through which a solvent or a carrier liquid is

flowing. The separated components are subsequently eluted from the flow system and subjected to a detector. Because of the close relation to LC, FFF has instrumentation similar to that of LC. The only difference between FFF and HPLC (and SEC) is that FFF is carried out in an open tube or channel, and there are no support particles in the channel.

The FFF process is carried out in a thin open channel with externally generated fields applied across the thin dimension of the channel, in a direction perpendicular to flow. The applied field interacts with components of interest, driving them toward one of the walls. The larger particles are primarily driven toward the wall, resulting in a later elution than the smaller ones. There are several applied fields, and the FFF techniques of each different applied field has a different name: thermal FFF, sedimentation FFF, flow FFF, electrical FFF, and magnetic FFF. The particular field chosen depends on the material one wishes to separate.

Therma FFF (TFFF) is a successful and powerful subtechnique for polymer separation. The temperature drop between the walls provides the driving force necessary for the transport of polymeric materials across the channel thickness. Under the influence of a temperature gradient, polymer molecules of a given size and type will be driven to the accumulation (cold) wall and they form a stead-state layer of effective thickness. The larger this thickness (smaller molecules), the faster the elution from the channel. Sedimentation FFF (SFFF) employs centrifugation in a mechanical centrifuge. Flow FFF (FFFF) uses two semipermeable membranes as the walls and the field is a cross-flow of the carrier liquid moving transversely from one wall of the channel to the other. FFFF has the widest dynamic range of separation than other subtechniques.

For details on the use of FFF several reference books [87–90] should be consulted.

REFERENCES

1. WW Yau, JJ Kirkland, DD Bly. Modern Size-Exclusion Liquid Chromatography. New York: John Wiley & Sons, 1979.
2. S Mori. Chromatographic determination of copolymers In: JC Giddings, E Grushka, J Cazes, PR Brown, eds. Advances in Chromatography, Vol 21. New York: Marcel Dekker, 1983, p 187.
3. J Janča, ed. Steric Exclusion Liquid Chromatography of Polymers. New York: Marcel Dekker, 1984.
4. BJ Hunt, SR Holdings, eds. Size Exclusion Chromatography. Glasgow: Blackie & Son, 1989.
5. G Glöckner. Gradient HPLC of Copolymers and Chromatographic Cross-Fractionation. Heidelberg: Springer-Verlag, 1991.
6. TH Mourey, TC Schunk. In: E Heftmann, ed. Chromatography, 5th ed. Part B Amsterdam: Elsevier, 1992, p B475.
7. JV Dawkins, M Hemming. Makromol Chem. 176:1795, 1975.
8. S Mori. Anal Chem 50:745, 1978.
9. Z Grubisic, P Rempp, H Benoit. J Polym Sci B Polym Lett 5:753, 1967.
10. S Mori. Anal Chem 55:2414, 1983.
11. T Provder, EM Rosen. Sep Sci 5:437, 1970.
12. KK Chee. J Appl Polym Sci 30:1323, 1985.
13. C Kraus, CJ Stacy. J Polym Sci Part A-2 10:657, 1972.
14. WS Park, WW Graessley. J Polym Sci Polym Phys Ed 15:71, 1977.
15. H Coll, DK Gilding. J Polym Sci Part A-2 8:89, 1970.
16. S Mori. Size Exclusion Chromatography [in Japanese]. Tokyo: Kyoritsu Shuppan, 1991, p 181.
17. BB Log, J Polym Sci Polym Chem Ed 14:232, 1976.
18. FL McCrackin. J Appl Polym Sci 21:191, 1977.
19. S Mori. Anal Chem 53:1817, 1981.
20. JR Runyon, DE Barnes, JF Rudd, LH Tung. J Appl Polym Sci 13:2359, 1969.
21. WW Smitt. J Appl Polym Sci 18:3685, 1974.

22. T Ogawa, T Inaba. J Appl Polym Sci 21:2979, 1977.
23. FB Malihi, C-Y Kuo, T Provder. J Appl Polym Sci 29:925, 1984.
24. S Mori. Copolymer analysis. In: BJ Hunt, SR Holding, eds. Size Exclusion Chromatography. Glasgow: Blackie & Son, 1989, p 100.
25. A Rudin, V Grinshpun, KF O'Driscoll. J Liq Chromatogr 7:1809, 1984.
26. S Mori, Y Nishimura. J Liq Chromatogr 16:3359, 1993.
27. CA Veith, RE Cohen. Polymer 30:942, 1989.
28. S Mori. Anal Chem 61:1321, 1989.
29. JV Dawkins, JW Maddock. Eur Polym J 7:1537, 1971.
30. V Grinshpun, A Rudin. Makromol Chem Rapid Commun 6:219, 1985.
31. D Lecacheux, J Lesec, C Quivoron, R Panaras, H Benoit. J Appl Polym Sci 29:1569, 1984.
32. J Devaux, D Delimony, D Daoust, R Legras, FJ Mercier. Polymer 26:1994, 1985.
33. CJ Stacy. J Appl Polym Sci 32:3959, 1986.
34. S Mori, A Yamakawa. J Liq Chromatogr 3:329, 1980.
35. S Mori, J Liq Chromatogr 9:1329, 1986.
36. S Mori. J Chromatogr 156:111, 1978.
37. S Mori. Anal Chem 50:1639, 1978.
38. T Matsuzaki, Y Inoue, T Ookubo, S Mori. J Liq Chromatogr 3:353, 1980.
39. MC Curtis, JW Webb, DC Warren, VO Brandt, FG Gerberich, KB Raut, LB Logers. Sep Sci Technol 15:1413, 1980.
40. JJ Lewis, LB Rogers, RE Pauls. J Chromatogr 299:331, 1984.
41. FPB van den Maeden, MEF Biemond, PCGM Janssen. J Chromatogr 149:539, 1978.
42. S Shiono, I Karino, A Ishimura, J Enomoto. J Chromatogr 193:243, 1980.
43. V Preussler, K Šlais, J Hanuš. Angew Makromol Chem 150:179, 1987.
44. C Bailly, D Daoust, R Legras, JP Mercier, M deValch. Polymer 27:776, 1986.
45. V Krajnik, P Bozek, J Kondelikova, J Kralicek. J Chromatogr 240:539, 1982.
46. C Guaita. Makromol Chem 185:459, 1984.
47. S Mori. Anal Chem 61:530, 1989.
48. Y Kato, T Hashimoto. J Chromatogr 332:39, 1985.
49. HE Adams. Sep Sci 6:259, 1971.
50. S Mori, A Wada, F Kaneuchi, A Ikeda, M Watanabe, K Mochizuki. J Chromatogr 246:215, 1982.
51. S Mori. J Chromatogr 411:355, 1987.
52. S Mori. J Appl Polym Sci Appl Polym Symp 43:65, 1989.
53. S Teramachi, A Hasegawa, Y Shima, M Akatsuka, M Nakayama. Macromolecules 12:992, 1979.
54. M Danielewicz, M Kubin. J Appl Polym Sci 26:951, 1981.
55. TH Mourey. J Chromatogr 357:101, 1986.
56. S Mori, M Mouri. Anal Chem 61:2171, 1989.
57. S Mori. J Chromatogr 541:375, 1991.
58. S Mori. Anal Chem 62:1902, 1990.
59. S Mori, Y Uno. Anal Chem 59:90, 1987.
60. S Mori, Y Uno. J Appl Polym Sci 34:2689, 1987.
61. S Mori. J Liq Chromatogr 12:323, 1989.
62. S Mori. J Appl Polym Sci Appl Polym Sump 45:71, 1990.
63. S Mori. J Liq Chromatogr 13:3039, 1990.
64. S Mori, Anal Sci 4:365, 1988.
65. S Mori. Anal Chem 6:1125, 1988.
66. S Mori. J Appl Polym Sci 38:95, 1989.
67. S Mori. J Chromatogr 503:411, 1990.
68. G Glöckner, H Kroschwitz, C Meissner. Acta Polym 33:614, 1982.
69. G Glöckner, JHM van den Berg, NLJ Miejerink, TG Scholte, R Koningsveld. Macromolecules 17:962, 1984.

70. R Schultz, H Engelhardt. Chromatographia 29:325, 1990.
71. G Glöckner, JHM van den Berg. J Chromatogr 352:511, 1986.
72. RW Sparidans, HA Claessens, GHJ van Doremale, AM van Herk. J Chromatogr 508:319, 1990.
73. S Teramachi, A Hasegawa, K Motoyama. Polym J 22:489, 1990.
74. H Sato, H Takeuchi, Y Tanaka. Macromolecules 19:2613, 1986.
75. H Sato, H Takeuchi, S Suzukli, Y Tanaka. Makromol Chem Rapid Commun 5:719, 1984.
76. H Sato, K Mitsutani, I Shimizu, Y Tanaka. J Chromatogr 447:387, 1988.
77. ST Balke, RD Patel. In: CD Crave, ed. Polymer Characterization. Advances in Chemistry Series, No. 203, Washington DC: American Chemical Society, 1983, p 281.
78. JV Dawkins, AMC Montenegro. Br Polym J 21:31, 1989.
79. G Schulz, H Munk, H Krüger, C Wehrstedt. J Liq Chromatogr 13:1745, 1990.
80. H Pasch, C Brinkmann, H Munk, V Just. J Chromatogr 623:315, 1992.
81. L Wild, TR Ryle, DC Knobeloch, IR Peat. J Polym Sci Polym Phys Ed 20:441, 1982.
82. S Nakano, Y Goto. J Appl Polym Sci 26:4217, 1981.
83. T Usami, Y Gotoh, S Takayama. Macromolecules 19:2722, 1986.
84. LG Hazlitt. J Appl Polym Sci Appl Polym Symp 45:25, 1990.
85. FM Mirabella Jr. J Appl Polym Sci Appl Polym Symp 51:117, 1992.
86. JC Giddings. Anal Chem 53:1170A, 1981.
87. KD Caldwell. In: HG Barth, ed. Modern Methods of Particle Size Analysis. New York: John Wiley & Sons, 1984.
88. J Janča. Field-Flow Fractionation. New York: Marcel Dekker, 1988.
89. JC Giddings. In: BJ Hunt, SR Holding, eds. Size Exclusion Chromatography. Glasgow: Blackie & Son, 1989.
90. KD Caldwell. In: HG Barth, JW Mays, eds. Modern Methods of Polymer Characterization. New York: John Wiley & Sons, 1991.

27

HPLC Applications in Physicochemical Measurements

Klára Valkó

GlaxoWellcome Medicines Research Center, Stevenage, Hertfordshire, England

I. INTRODUCTION

Chromatography is used essentially for separation of compounds in various mixtures. The application of chromatography for physicochemical measurements, however, is not new. For example two excellent books [1,2] discuss the applications of gas chromatography (GC) for such measurements. The applications of high-performance liquid chromatography (HPLC) for physicochemical measurements, however, is not so widespread. The quantitative relation between the chemical structure, physicochemical properties, and chromatographic retention have been discussed in detail [3]. The quantitative correlations can be used for the estimation of several physicochemical properties from the measured retention data of compounds. The application of HPLC for the determination of molecular interactions has also been reviewed [4].

The theoretical basis for using HPLC for physicochemical measurements is that the solute retention in chromatography is determined by the strength of solute—stationary-phase interactions, modulated by the solute–mobile-phase interactions. The retention parameter k', derived from the retention time or retention volume is proportional to the average solute distribution between the mobile and the stationary phases. The relative strength of the solute stationary-phase interactions, or more precisely the relative solute distribution, can easily be determined by measuring the retention parameters of a given solute series in the same chromatographic system, or in a series of slightly modified chromatographic systems. The retention mechanisms in HPLC (i.e., the type of interactions between the solute and the stationary phase) can be divided into six major groups: namely, reversed-phase, adsorption, ion-exchange, gel filtration, hydrophobic interaction, and chiral chromatography.

In reversed-phase HPLC, when a nonpolar hydrocarbon stationary phase and a hydroorganic mobile phase are applied, the retention of the solute is governed mostly by hydrophobic forces (the strength of the solute–stationary-phase interaction is determined by the hydrophobicity of the compounds).

In adsorption chromatography the strength of the solute–stationary-phase interaction is determined by adsorption forces. The adsorption interaction is the result of various types of forces, such as dispersive, inductive, or hydrogen-bond formation.

In ion-exchange chromatography the stationary phase has an ion-exchanger group, which interacts with the solute molecules, and the interaction is modulated by the presence of other displacing ions in the mobile phase.

In gel-filtration chromatography the separation takes place according to the size of the molecules. The smaller molecules elute later from the column, because they spent more time

in the pores of the stationary phase. Gel-filtration chromatography can be applied to determine the size of the molecules. The method can be applied only for large molecules (over 1000 MW).

In hydrophobic-interaction chromatography, which is mostly applied in the analytical or preparative separation of biomolecules, the solute–stationary-phase interaction (which is basically hydrophobic, as in reversed-phase) is modulated by the gradually decreasing concentration of salt molecules in the mobile phase.

In chiral chromatography, the mechanism of the solute–stationary-phase interaction can be of various types, but it should be enantioselective. Usually, at least three interacting points between the solute and the stationary phase should be present close to the chiral center of the molecule. These interactions can be hydrophobic, adsorptive, H-bonding, steric, or π-π interactions.

It can be concluded that the stationary phases can be designed to interact with the solute molecules by various mechanisms. In practice the stationary phases are designed for certain separation problems. What can a chemist do when he or she wants to use chromatography for physicochemical measurements? On the basis of the different mechanisms of solute–stationary-phase interaction, he or she can select among the commercially available stationary phases, or it is possible to apply various mobile-phase additives, by which a so-called dynamically coated stationary phase can be prepared. The peak shape and the efficiency of the column should always be checked. An imprecise peak shape can reveal secondary equilibria or multiple retention mechanisms. When we use the retention data for the determination of molecular interactions or physicochemical measurements we always have to know the type of interactions and the retention mechanism to be able to draw valid conclusions. The retention will always be the result of a combination of all the solute–stationary phase interactions.

Reversed-phase chromatography provides the simplest way to determine solute–stationary-phase interactions that will indicate the hydrophobic character of the solute. Commercially available reversed-phase columns provide good efficiency, excellent reproducibility, and a long lifetime for accurate retention determination. Therefore, the most widespread application of HPLC for physicochemical measurements is the determination of partition coefficients; in other words, the hydrophobic properties of compounds. Depending on the chemical-bonding technology and the amount of coating, reversed-phase columns can be considered as inert phases, and only the hydrophobic interactions govern the retention, although in special cases, the presence of the free silanol groups might cause a dual retention mechanism. The methods for the application of RP-HPLC for hydrophobicity determination of compounds will be discussed in detail. The application of HPLC for adsorption isotherms, molecular weight, shape and size, and molecular interactions will be briefly summarized.

II. DETERMINATION OF HYDROPHOBICITY BY HPLC

A. The Role of Hydrophobicity in Biomedical Sciences

Overton [5] and Meyer [6] first recognized the role of hydrophobicity of compounds in their pharmacological activity. They described a correlation between the narcotic effect and the partition of compounds between an aqueous and a lipid layer. Since then, several thousand papers have discussed the correlations between the hydrophobicity of the compounds and their pharmacological activity. The absorption of compounds from soil by plants [7]; the distribution of drug molecules in the body, and their probability of reaching the active site of a receptor [8]; or the bioaccumulation of the chemicals in soil, natural waters, fish [9] and so on, depend on the hydrophobic nature of the compound. These correlations are based on the fact that both the soil and the living systems contain hydrophobic and hydrophilic compartments, among which the molecules should be partitioned. In drug–receptor interactions or enzyme–substrate interactions, hydrophobic forces may play an important role, which can be

predicted from the hydrophobic character of certain substituents at certain positions in the drug or substrate molecule. The hydrophobic nature of a compound is its inherent property, and it can be characterized easily by its partition coefficients. The distribution or partition of a molecule between two nonmiscible liquids depends on the types and the strength of weak interactions between the solute molecule and the two types of solvent molecules.

Tremendous efforts have been taken to find the best partition system (two nonmiscible liquids) that can be a reliable model for describing the biological distribution of the compounds, and also for establishing standard methods for the determination of hydrophobicity.

The partition coefficient of a compound can be a characteristic, such as the melting point, and it depends on only the type of the two liquid phases and the temperature; thus, it can be easily tabulated.

In 1951, Collander, a Swedish botanist, studied the absorption of certain compounds in plants [7] and underlined the importance of the partition coefficients of compounds in higher alcohols in relation to their absorption from the soil. This pioneering work inspired Hansch and Fujita [8] in selecting the 1-octanol–water partition system as a reference system for modeling the biological partitioning processes. Although 1-octanol is not an "easy" solvent to work with—it smells, is relatively soluble in water, easily makes emulsion and such—it has a very special property; namely, the hydrogen-bonding ability through its hydroxyl group. This functional group makes the 1-octanol especially good for modeling the biological membrane distributions, because they also contain polar functional groups able to form hydrogen bonds.

In the same time, much criticism appeared against the 1-octanol–water partition system as a model for biological partition process. Sometimes water–c-hexane partition coefficients showed better correlation with the pharmacological activity data, especially for drugs acting on the central nervous system [10]. Because none of the models can be perfect enough to completely describe another partition process, we have to accept the 1-octanol–water system. The logarithmic value of the 1-octanol–water partition coefficients (log P) were compiled in a huge database [11]. The accurate and standardized determination of log P value is more and more important. For any biologically active molecules or chemicals used in agriculture, the log P values should be measured and provided.

B. Determination of Partition Coefficients

The most obvious method is the use of a traditional shake-flask filled with water and 1-octanol. After adding the compound to the partitioning solvents and shaking to accelerate the equilibrium procedure, the concentrations of the solute in the two phases should be determined. The c_o and c_w values (the concentration of the molecule in the octanol and the water phase, respectively) are divided (c_o/c_w) and the quotient gives the P value for which the logarithm is taken. The procedure seems very simple, but, in practice, many questions and problems may arise. The most important complications are to define the temperature, determine the length of the equilibration procedure, design the volumes of the two phases and the amount of partitioning compound, develop an analytical method for the concentration determination in the two phases, determine the pH of the aqueous phase, and separate the two phases by centrifuging if an emulsion is formed.

Theoretically, it is also possible to calculate log P values from the group contributions. Hansch and Fujita [12] explored the possibility of deriving additive group contributions to the partition coefficients that would allow this to be calculated even for not yet synthesized compounds. These group contributions, often called "π values" can be calculated according to Eq. (1):

$$\log P_R - \log P_H = \pi_R \tag{1}$$

where R stands for a substituent, log P_R is the log P value of a molecule containing the R substituent, log P_H is the log P value of a molecule containing H instead of the R substituent,

and π_R is the hydrophobicity contribution of the R substituent. The π values for a large set of substituents are compiled by Hansch and Leo [11], and they also developed a computer program [13] for the calculation of log P values based on substituent contributions (so called clog$P$). Despite evidence [14] that π values are not always additive, usually for steric reasons, but sometimes through electronic and hydrogen-bonding effects, the clog$P$ program can be very useful for the estimation of log P values, because many of the aforementioned correction factors are built into it.

A slightly different approach was developed by Rekker [15], who did not consider the hydrophobicity contribution of the hydrogen as zero (which is the case when Eq. (1) is used), and his hydrophobic fragments relate to special molecular fragments that are not necessarily substituents. He included the effect of neighboring fragments as well. The Rekker approach can be also computerized, which makes the calculation much easier.

A combined approach was developed by Compudrug Ltd. (Budapest, Hungary) for the calculation of log P values by their ProLogP [16] expert systems. The possibilities of the calculation of log P values by personal computers have been summarized [17]. These calculation methods are mentioned here because they were used in the correlation studies with the chromatographic hydrophobicity values.

C. Theoretical Background of Using HPLC for Hydrophobicity Determination

As early as 1941 Martin and Synge [18] showed that the thin-layer chromatographic (TLC) R_f values can be related to P according to Eq. (2):

$$P = \text{constant} \cdot \left(\frac{1}{R_f - 1}\right) \tag{2}$$

In 1963 Green and Marcinkiewicz [19] pointed out that the R_M values, which can be defined by Eq. (3) are linearly related to the log P values and, therefore, R_M values are analogous to these values.

$$R_M = \log\left(\frac{1}{R_f - 1}\right) \tag{3}$$

The first exploitation of this relation in biological context was by Boyce and Milbarrow [20], who showed a relation between the molluscicidal activity of some *N*-alkyltritylamines and their R_M values on TLC plates.

The applicability of chromatographic methods for characterizing the hydrophobicity of the compounds can be supported by two facts. First, the chromatographic retention (log k' values in HPLC or R_M values in TLC) is proportional to the solute distribution in the mobile and the stationary phases and, therefore, analogous to the distribution or partition in two nonmiscible solvents. Second, Collander [7] in 1951, found linear correlations between partition coefficients obtained in two different partition systems, described by Eq. (4).

$$\log P_1 = a \log P_2 + b \tag{4}$$

where 1 and 2 refer to two liquid–liquid partition systems, a and b are constant.

Leo [21], however, demonstrated the limitations of the Collander type [Eq. (4)] relation by investigating the partition coefficients of more than 300 compounds in 12 various liquid–liquid partition systems. He found that the linear relation between log P values obtained in two different partition systems was valid only when the partitioning solvents in the two systems were chemically related. When the partition coefficients obtained in octanol–water and in hexane–water were compared, the linear correlation was valid only when he divided the compounds into proton donor and proton acceptor groups. The values of the a and b parameters were different in the two cases. The deviation was explained by the fact that,

although 1-octanol is able to form hydrogen bonds, the hexane is not; therefore, different weak interactions dominate the partition process in the two systems. So, he stated that Eq. (4) can be valid only when either the compounds or the partitioning liquids are similar in character. These limitations are valid also when the partition coefficients (or analogous retention parameters) obtained by chromatographic and shake-flask method are compared. We can expect linear correlations for only structurally related compounds, or when directly 1-octanol and water is applied in the chromatographic partition system.

Chromatographic methods can be applied for characterizing the molecular hydrophobicity only when the chromatographic retention (i.e., distribution) is governed mostly by hydrophobic forces. This means that the chromatographic system (the mobile and the stationary phases) should contain aqueous and nonpolar phases. Therefore, only reversed-phase HPLC can be used when the stationary phase is usually a chemically bonded *n*-paraffin hydrocarbon silica and the mobile phase is water or a mixture of water and organic solvent. (In TLC the silica plates can be impregnated by paraffin or octanol; also, a hydroorganic solvent can be used for the development.)

In HPLC, the most frequently used chromatographic retention parameter for characterizing hydrophobicity is the logarithmic value of the retention factor ($\log k' = \log (t_R - t_M)/t_M$, were t_R and t_M are the retention times of the compound and an unretained compound, respectively), which can be related to the chromatographic partition coefficient (K_{chr}) according to Eq. (5).

$$\log k' = \log K_{chr} + \log\left(\frac{V_s}{V_m}\right) \tag{5}$$

where V_s and V_m are the volume of the stationary and the mobile phases, respectively, and V_s/V_m is the so-called phase ratio. The phase ratio can be considered as constant, but it is difficult to determine its exact value. Therefore, it is necessary to determine the log k' values of a few standard compounds with known log P values, and by plotting their log k' values against their log P values, the parameters a and b of Eq. (4) can be determined. It might cause differences that, whereas the shake-flask method refers to a static equilibrium, chromatography provides a "dynamic" equilibrium system. This means that during the chromatographic process, the compound actually is never in equilibrium, it always goes through numerous local equilibrium processes.

Another question is the mobile-phase composition. The pH of the hydroorganic mobile phase can be very important for ionizable compounds. The appearance of more than one species of a compound (ionized and neutral) often results in nonsymmetric peak shapes, which might also influence an accurate retention determination. Therefore, it is even more important to use a mobile-phase pH in which the solute is in neutral form, than it is with the shake-flask method. As the practical log k' values range between -1 and 2, compounds with only a narrow range of hydrophobicity could be determined by using water as the mobile phase. The application of a water-miscible organic modifier in the mobile phase makes it possible to use RP–HPLC for hydrophobicity determination of compounds with much wider range of hydrophobicity. When only the log k' values are applied for characterizing the hydrophobicity of the compounds, the parameters of Eq. (5) should be determined for each concentration of the organic phase in the mobile phase by using standard reference compounds with known log P values.

When the mobile-phase composition has to be changed for the measurement of a compound series, the log k' versus organic phase concentration ϕ should also be taken into consideration. Let us suppose that the log k' versus ϕ plot is linear. Then by measuring the log k' values at various mobile-phase compositions the linearity of the plot can be tested. It was suggested [22] that the extrapolated log k' value to the zero concentration of the organic modifier (log k'_w; i.e., log k' values referring to only water as the mobile phase) can then be

correlated with the log P values, it can be considered a measure of hydrophobicity. However, the log k'_w values are different if they are obtained from acetonitrile–water or methanol–water mobile-phase mixtures [23,24]. Schoenmakers et al. [25] describe the solute retention over the full range of mobile-phase composition in RP–HPLC, with special emphasis on mobile phases with a high water content. A quadratic relation between the logarithm of the capacity factor and the volume fraction of organic modifier is generally valid for mobile phases containing less than 90% water; however, when more water is added to the mobile phase, a quadratic equation is insufficient.

Good correlations were generally found between log k'_w and log P values only for structurally related compounds [26–28]. Dissimilar compounds (noncongeners) usually showed poorer correlations between the log P and log k'_w values [29–33]. Figure 1 shows the plot of the log k'_w (obtained in a regular RP–HPLC system using acetonitrile as an organic modifier in the mobile phase) and log P values of structurally unrelated compounds. When the compounds are subdivided into congeneric groups, the correlation can be improved. The explanation for this is that the limitation of the Collander-type relation revealed by Leo [21], is a differential hydrogen-bonding effect that is qualitatively similar to that observed when 1-octanol–water partition coefficients are correlated with alkane–water systems. The usual RP–HPLC system, as well as the alkane–water systems, exhibit greater hydrogen-bonding selectivity than does the octanol–water system.

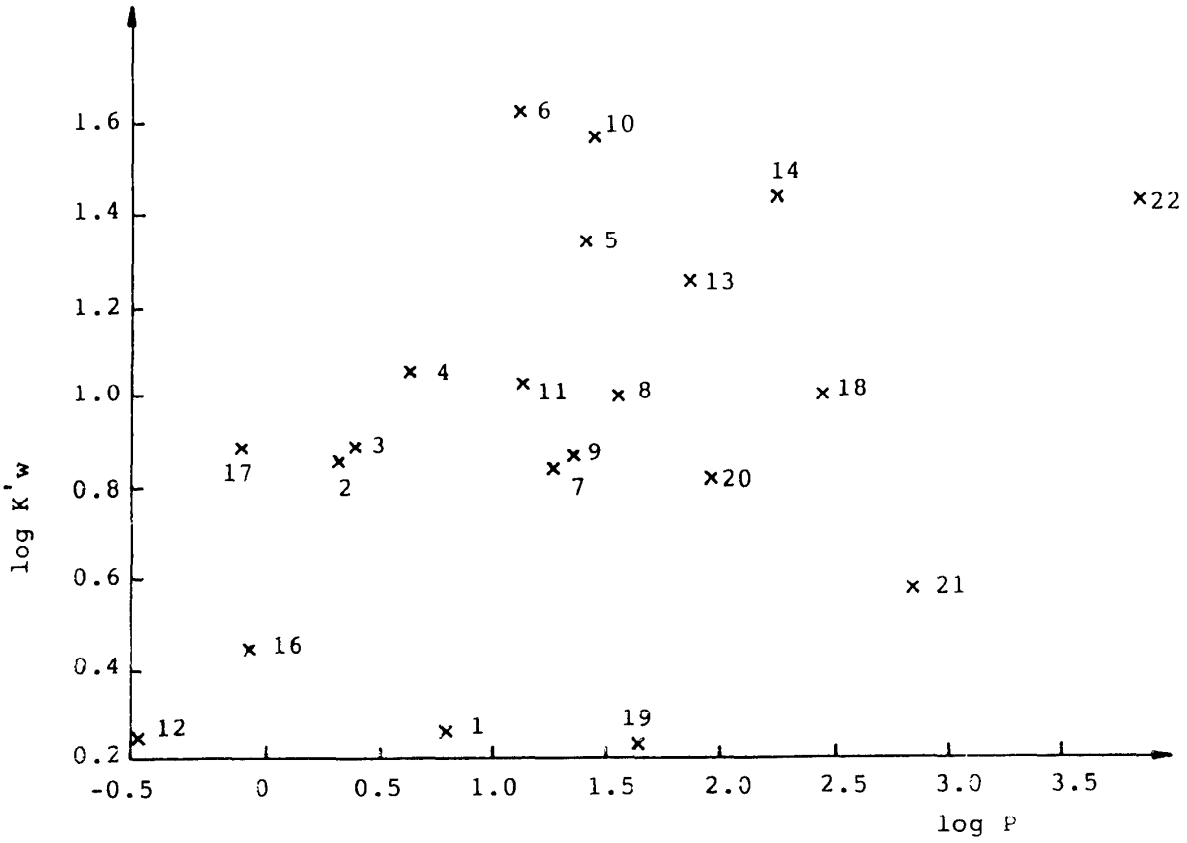


Figure 1 The plot of the log k'_w values against the log P values of structurally unrelated drug molecules. (From Ref. 33.)

D. Practical Aspects of Using HPLC for Hydrophobicity Determination

As early as 1976, Mirrlees et al. [34] described a thin-layer chromatographic method for modeling the log P values of noncongeneric compounds by using octanol-saturated Kieselguhr as the stationary phase and octanol-saturated water as the eluant. Unger et al. [35] obtained very good correlations between log P values of noncongeneric compounds and their log k' values by applying octadecyl silica gel dynamically coated by 1-octanol and octanol-saturated water as the mobile phase. This approach can be considered to be the most straightforward to produce a chromatographic partition system that is most similar to that of 1-octanol–water. However, this approach suffers from practical disadvantages. The stationary phase reproducibility is very poor. We cannot define exactly the adsorbed volume of octanol on the stationary phase and, therefore, the reproducibility of the measurements is rather poor. To increase the reproducibility, the measurements of log k' values of several reference compounds with known log P values are necessary. The more difficult problem in this approach is that we cannot adjust these chromatographic systems for a wide range of compounds (exerting a wide range of hydrophobicity), because the mobile-phase composition cannot be varied.

Minick et al. [36] reported a polycratic procedure for estimating hydrophobicity constants by RP–HPLC that largely eliminates the discrimination arising from the differences in hydrogen-bonding capacity of noncongeners. This method used mixtures of aqueous buffer, methanol, octanol, and decylamine as eluants and octyl-modified silica as the stationary phase to obtain extrapolated capacity ratios (log k'_w). This approach included trace amounts of octanol and alkylamine in the eluant, and showed little differential hydrogen-bonding effects, presumably owing to enrichment of these components in the stationary phase. The advantage of this approach is that noncongeners with hydrophobicities varying between -0.20 and 5.2 could be measured. Additionally, the net hydrogen-bonding property of any solute molecule can be predicted from the chromatographic experiment.

A more theoretical approach was presented by Terada [37] and Myake [38] who obtained good correlations between log P and log k' values for sets of noncongeners by including hydrogen-bonding indicator variables in their regression equations.

E. General Approach of Using HPLC for Hydrophobicity Determination

Another approach [39] is to measure the log k' values of the compounds by using various concentrations of organic modifier in the mobile phase and calculating the slope (S) and the intercept (log k'_w) of the log k' versus organic-phase concentration plots. Good correlation was found for structurally unrelated compounds between the log P values and both the slope and intercept values as two independent variables. The following equations reveal the meaning of the application of the two independent variables (slope and intercept) in the correlation study. We can describe Eq. (4) (the Collander-type relation between partition coefficients obtained in two different partition systems) considering the 1-octanol–water and the chromatographic partition system (chromatographic mobile and stationary phases), shown by Eq. (6).

$$\log P = a \log K_{chr} + b \tag{6}$$

where a and b are constant, P and K_{chr} refer to partition coefficients in the 1-octanol–water and the chromatographic partition systems, respectively. As shown by Eq. (5) the chromatographic partition coefficient (log K_{chr}) is linearly related to the log k' (retention parameter) values. The relation contains a constant [log (V_s/V_m)] that is the volume ratio of the mobile and stationary phases, a characteristic value of the given chromatographic system. By expressing log K_{chr} from Eq. (5) and introducing it to Eq. 6, Eqs. (7) and (8) can be obtained.

$$\log K_{chr} = \log k' - \log\left(\frac{V_s}{V_m}\right) \tag{7}$$

$$\log P = a \log k' - a \log\left(\frac{V_s}{V_m}\right) + b \tag{8}$$

The dependence of the retention ($\log k'$) on the organic phase concentration of the mobile phase (ϕ) can be described by Eq. (9) considering only the linear section of the plot.

$$\log k' = S\phi + \log k'_w \tag{9}$$

where the S and the $\log k'_w$ values are the slope and the intercept values of the straight line. We can now introduce the right side of Eq. (9) to Eq. (8) instead of the $\log k'$ values, and Eq. (10) can be set up.

$$\log P = aS\phi + a \log k'_w - a \log\left(\frac{V_s}{V_m}\right) + b \tag{10}$$

In Eq. (10), the S and the $\log k'_w$ values can be calculated from the experimental data (the slope and the intercept values of the straight line obtained by plotting the measured $\log k'$ values of the compounds against the organic phase concentration of the mobile phase), and the other parameters can be considered to be constant. When we set up a linear regression equation in which the dependent variable is the $\log P$ value, and the two independent variables are the measured slope S and the intercept values $\log k'_w$, the calculation of the regression coefficients means an optimization of the constant parameters of Eq. (11).

$$\log P = p_1 S + p_2 \log k'_w + p_3 \tag{11}$$

As a, b, and the $\log(V_s/V_m)$ are constants, characteristic for the applied chromatographic system, the only variable is the ϕ, by which the optimization can be carried out. Introducing the measured S and $\log k'_w$ values of 140 compounds (the data are listed in Tables 1–6 in the Appendix) as the two independent variables into Eq. (11) and their calculated $\log P$ values, Eq. (12) was obtained.

$$\log P = 185.4(\pm 13.7)\, S + 2.57(\pm 0.12) \log k'_w + 3.5 \tag{12}$$
$$n = 140 \quad s = 1.16 \quad r = 0.89$$

The chromatographic retention parameters S and $\log k'_w$ were obtained by using acetonitrile as the organic modifier in the eluant. The plot of the original $\log P$ values and the estimated $\log P$ values from Eq. (12) can be seen in Fig. 2. It can be seen that only a few compounds can be considered as outliers (their data points are out of the 95% confidence interval lines). When comparing Eqs. (10) and (11), it also can be seen that the quotient of p_1 and p_2 parameters gives the optimum ϕ value [Eq. (13)].

$$\frac{p_1}{p_2} = \frac{a \cdot \phi}{a} = \phi_{opt} \tag{13}$$

It follows that this approach results in a backward extrapolation method, when the $\log k'$ values are not extrapolated to the zero percent organic modifier concentration in the mobile phase (which is the $\log k'_w$ value), but to an optimum mobile-phase composition by which the octanol–water partition system could be best modeled. The optimum mobile-phase concentration was close to 40% acetonitrile and buffer [40]. Only slight differences in the optimum mobile-phase compositions were observed by using various commercially available reversed-phase columns [40]. The advantages of the method are that there is no need to use special mobile-phase additives or to dynamically coat the stationary phases, and also it can be used to model not only the 1-octanol–water partition, but directly a biological partition process [41]. We must be careful, however, when using this method if the slope and the intercept

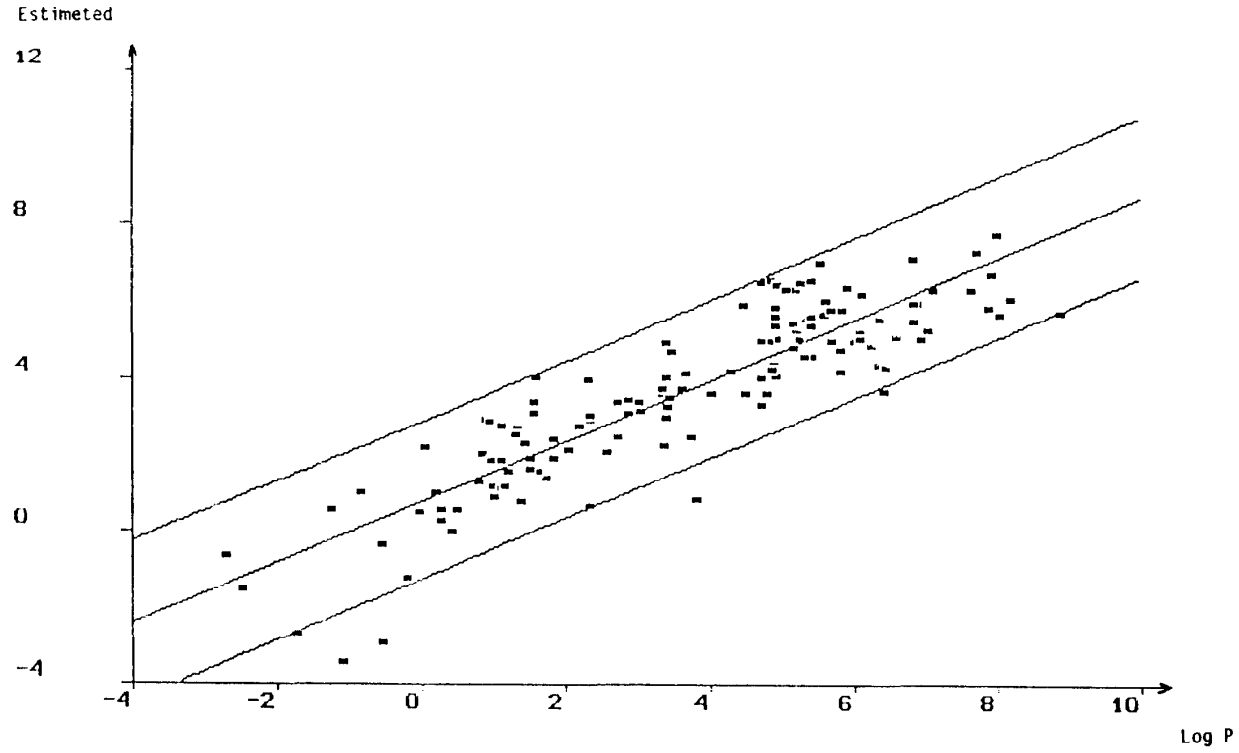


Figure 2 The plot of the calculated log P values as a function of the ones estimated by Eq. (12). The chromatographic retention parameters (S and log k'_w) values of the compounds were obtained by using acetonitrile as the organic modifier in the mobile phase.

values show high correlation, because then they cannot be considered two independent variables. Also, the slope and the intercept values showed high correlations only when structurally related compounds were investigated [42]. Figure 3 shows the theoretical log k' versus organic modifier concentration plots for structurally related and unrelated compounds. But if that is true, then we do not have to adjust the chromatographic partition system to be similar to the octanol–water partition system, and we can expect good correlations between log k' values obtained by any mobile-phase compositions or log k'_w values. Figure 4 illustrates graphically the backward extrapolation method for calculating the log k' values for an optimum organic phase concentration for modeling the 1-octanol–water partition [see Eq. (10)]. The application of the slope and intercept values in correlation with the log P values for structurally unrelated compounds mathematically means to move a vertical straight-line (see line A in Fig. 4) to an optimum organic-phase concentration, and the intersection points of that straight-line with the log k' versus straight-lines for each compound give the log k' values extrapolated to the optimum organic-phase concentration.

F. Chromatographic Hydrophobicity Index

Mathematically the aforementioned straight-line can also be positioned horizontally (see Line B; Fig. 4). Then the straight-line represents a certain log k' value (the same retention time for each compound) and the intersection points represent an organic-phase concentration in the mobile phase from which a log k' value can be obtained. It was suggested [43] to use log k' values equal to zero (i.e., the horizontal straight-line at log $k' = 0$). It means that the solute distribution in the chromatographic mobile and stationary phase is exactly 1:1, when the log k' equals zero. From the intersection of log $k' = 0$ straight-line and the log k' versus plot,

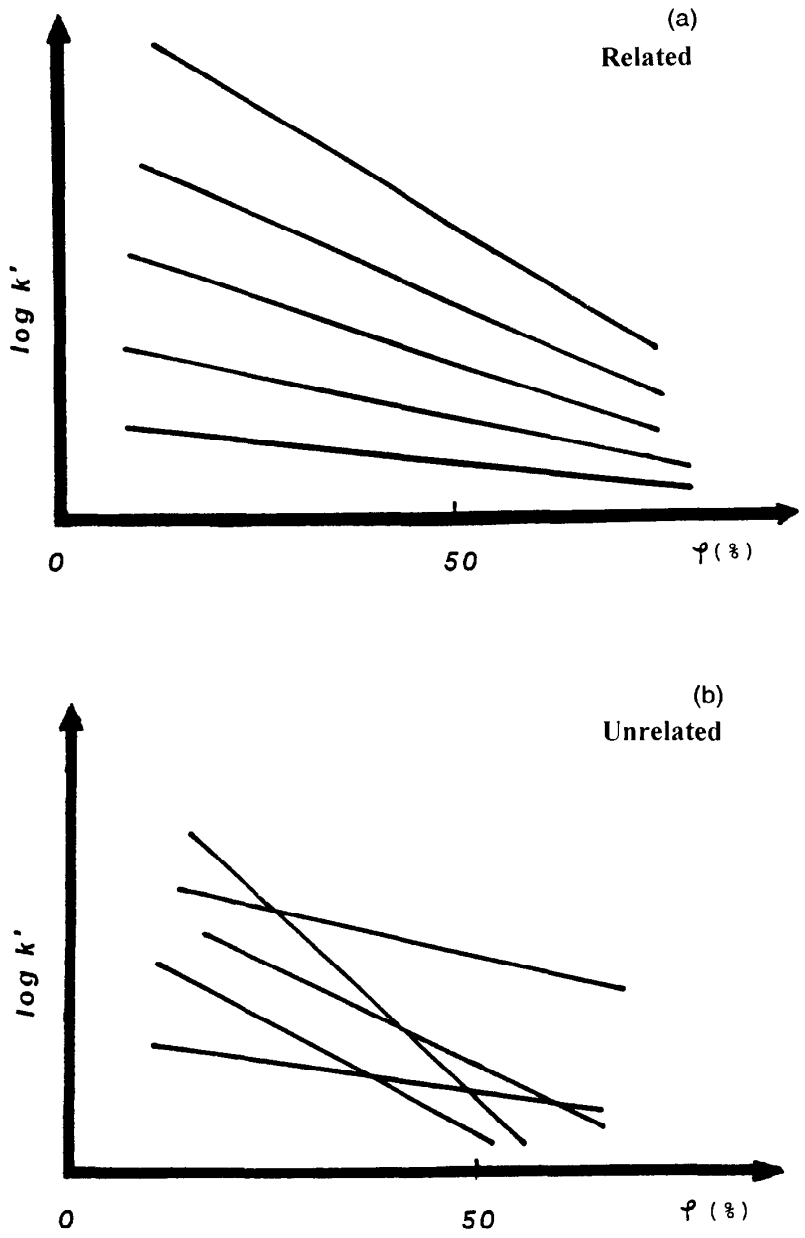


Figure 3 The hypothetical plot of the log k' versus straight-lines for structurally related and unrelated compounds. (From Ref. 42.)

we can derive an organic modifier concentration that will show good correlation with the log P values of structurally unrelated compounds. As follows from Eq. (9) this value includes both the slope and the intercept values in one value. From Eq. (9) we can express a ϕ value by which the log $k' = 0$, which gives ϕ_0 value as shown by Eq. (14).

$$\phi_0 = \frac{-\log k'_w}{S} \tag{14}$$

where S and log k'_w are the slope and the intercept values of the log k' versus organic-phase concentration (ϕ) plot, and ϕ_0 is the organic modifier concentration by which the solute distribution in the mobile and the stationary phase is 1:1. Graphically, it can be seen in Fig.

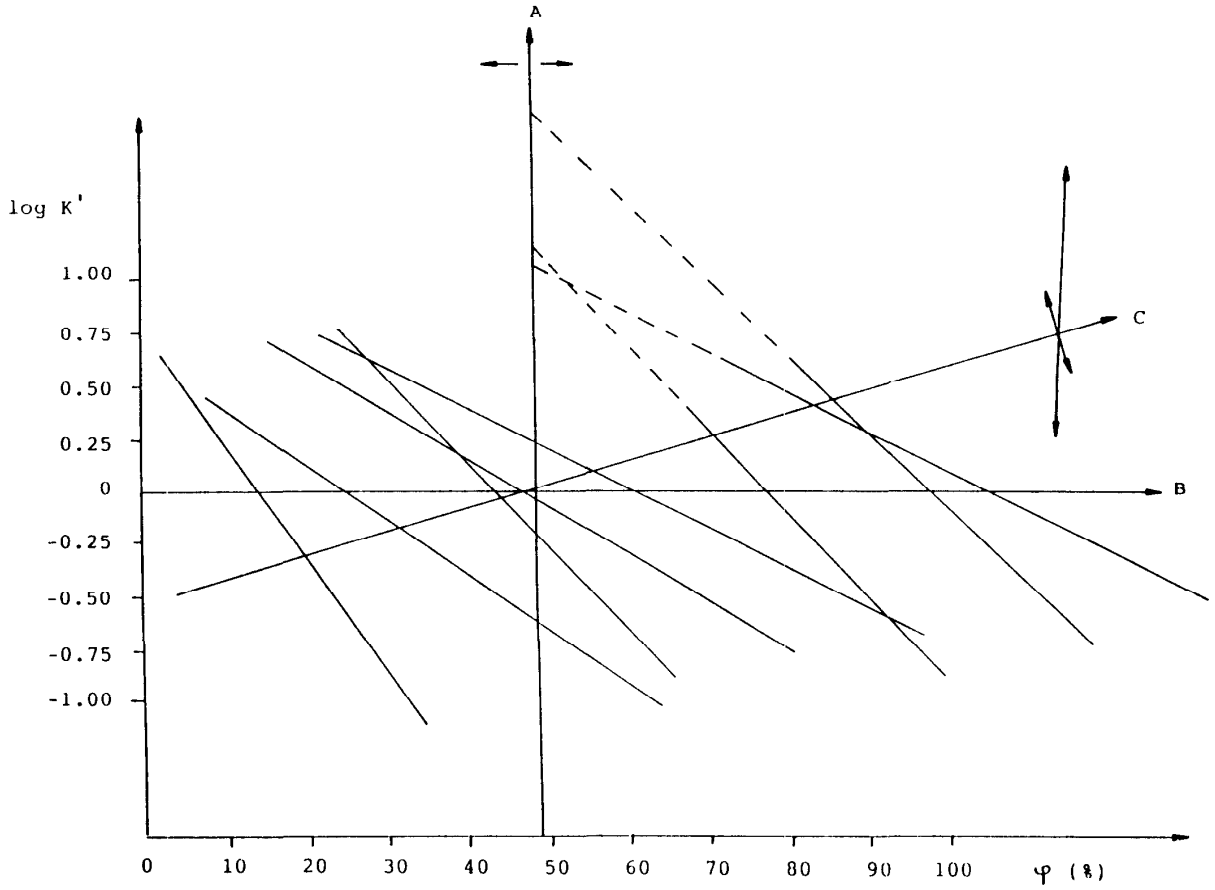


Figure 4 The graphic illustration of the possible optimization procedures for modeling the 1-octanol–water partition by the reversed-phase chromatographic partition. By the slope and intercept approach the position of straight-line A is optimized. Straight-line B determines the mobile-phase composition by which log k' = 0. The intersection points of straight-line B and log k' lines give the chromatographic hydrophobicity index. The position of straight-line C can be optimized by allowing various angles and moving along the Y axis.

4 that the ϕ_0 values are also the intersection points of the log k' versus ϕ straight-lines and a horizontal straight-line positioned at log k' = 0. These ϕ_0 values were suggested as a general chromatographic hydrophobicity index values [43].

To prove that ϕ_0 values are independent from the column constant (V_s/V_m) the following consideration can be made. The k' is proportional to the distribution constant K, according to Eq. (15):

$$k' = K\left(\frac{V_s}{V_m}\right) \tag{15}$$

The logarithmic form of this equation was shown by Eq. (5) [log k' = log K + log (V_s/V_m)]. The log k' values are also dependent on the organic-phase concentration, and for the sake of simplicity, we can consider a linear relation (a properly small portion of any suggested curves can be regarded as linear, after all), which can be described by Eq. (16):

$$\log k' = \log K + \log\left(\frac{V_s}{V_m}\right) = S\,\phi + \log k'_w \tag{16}$$

where S and log k'_w are the slope and the intercept values of the straight line. The intercept value theoretically means the log k' value extrapolated to the neat water mobile phase and can be expressed by the distribution constant and the phase ratio as shown by Eq. (17):

$$\log k'_w = \log K_w + \log \left(\frac{V_s}{V_m}\right) \tag{17}$$

The S slope value can be written as the log k' change caused by changing the organic-phase concentration of the mobile phase by 1%, which can be formulated by Eq. (18):

$$S = \log K_{x+1} - \log K_x \tag{18}$$

x and x + 1 refer to x% and (x + 1)% volume fraction of organic modifier, respectively. The volume fraction of the organic phase in the mobile phase by which the log k' value equals zero (ϕ_0) can be described by Eq. (20) on the basis of Eq. (16)–(19):

$$\log k' = 0 = \log K_x + \log \left(\frac{V_s}{V_m}\right)$$

$$= \phi_0(\log K_{x+1} - \log K_x) + \log K_w + \log \left(\frac{V_s}{V_m}\right) \tag{19}$$

$$\phi_0 = \frac{\log K_x - \log K_w}{\log K_{x+1} - \log K_x} \tag{20}$$

With the help of Eq. (14), the ϕ_0 values can be calculated from the experimental data. When the measured log k' values are close to zero, the application of the linear fit to the log k' versus ϕ plot for the calculation of ϕ_0 does not result in high error. In those cases in which basic compounds are investigated, for example, as published by Tayar et al. [42], two ϕ_0 values can be obtained. The correct ϕ_0 value is what can be obtained at a lower organic-phase concentration, when only hydrophobic interactions govern the retention. The ϕ_0 value belonging to the higher organic-phase concentration is caused by dual retention mechanism (hydrophobic and silanophilic), so it cannot be considered the chromatographic hydrophobicity index.

The graphic illustration of the calculation of ϕ_0 values for various compounds can be seen in Fig. 5. The hypothetical example shows that the log k' versus ϕ plots may be a straight-line (compound 1), quadratic function (compound 2), cross each other (compound 2 and 3), or they may be the result of dual retention mechanism (compound 4). When the mobile-phase compositions are such that the measured log k' values are close to 0, the error of the linear extrapolation for the calculation of ϕ_0 values is negligible.

As the ϕ_0 values are dependent only on the distribution constants of the compounds in a given hydroorganic mixture, the value will depend only on the type of organic phase and the temperature. For ionizable compounds, the pH also influences the distribution constant, so ϕ_0 will also depend on the pH. Consequently, the proper way of expressing ϕ_0 values is:

$$\phi_{0,op,T,\mathrm{pH}}$$

where *op* stands for the type of organic phase, T stands for temperature. The literature data for the slope and log k'_w values and the calculated chromatographic hydrophobicity index values can be found in the Appendix.

Retention data (log k') values obtained in various mobile-phase compositions were collected from the literature. The retention data of 22 nicotinate esters were published by Reymond et al. [44]. The measurements were carried out on LiChrosorb RP-18 (10 μm) column. The mobile phase were aqueous methanol or acetonitrile, in various proportions (v/v) buffered with 3-morpholinopropanesulfonate (0.02 M, pH 7.4). The retention data of 35 monohydroxyl aromatics were reported by Cooper and Hurtubise [45]. The measurements were carried out

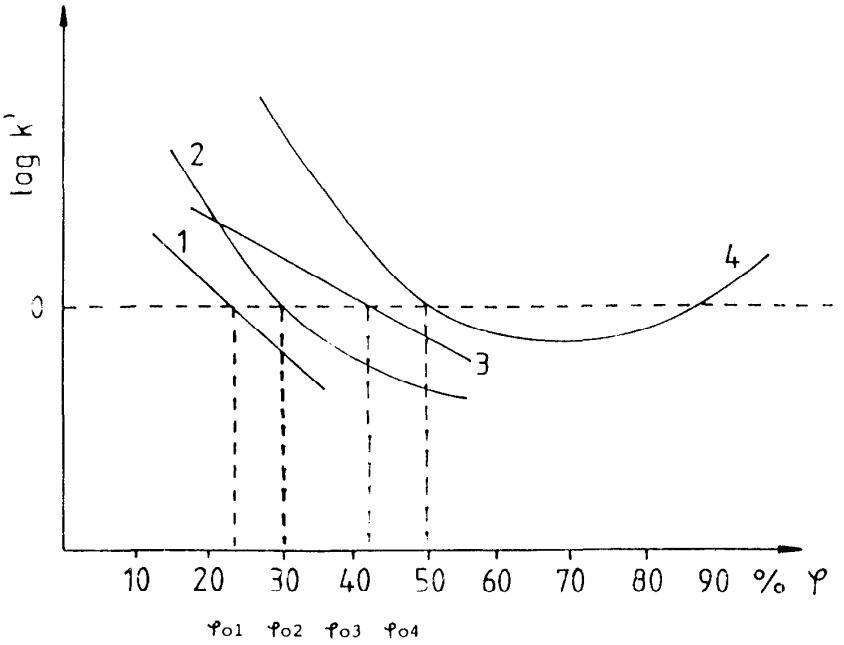


Figure 5 A graphic illustration of the determination of the new chromatographic hydrophobicity index (ϕ_0). Numbers refer to hypothetical compounds for which the log k' versus plots are straight-line (1), cross each other (2 and 3), or show dual retention mechanism (4). (From Ref. 43.)

on μ Bondapak C_{18} column with various mixtures of water and methanol. Braumann et al. [46] published the data of 30 pesticides. The retention data of the pesticides were obtained by varying the methanol concentration in the mobile phase. Schoenmakers et al. [47] published retention data of 45 phenoxycarbonic acid derivatives, which were measured in water–acetonitrile mobile phases and Lichrosorb RP-18 (10 μm) column was used. The acidic derivatives were measured with mobile phases that contained 0.5-M acetate buffer pH 2.9, to decrease dissociation. The retention data of 113 aromatic hydrocarbons were measured by Opperhuizen et al. [48] on Hypersil ODS (5 μm) column with methanol–water mixtures as mobile phases. The data of 143 acidic, basic, and neutral drugs were published by Roos and Lau-Cam [49]. Three types of columns were used (μ Bondapack C_{18} 10 μm, Zorbax ODS 5 μm, and Ultrasphere ODS 5 μm). The mobile phases were variable portion of methanol, 1.5 parts acetic acid, 0.5 parts triethylamine and water to yield 100 parts by volume. The pH of the mobile phase was not given. The retention data of 26 drug molecules were published by Valkó [39,42], both acetonitrile–buffer and methanol–buffer mobile phases. The pH of the mobile phase was adjusted according to the molecules investigated. A pH of 2 was used for the measurements of acidic compounds to reduce dissociation, whereas the mobile-phase pH was adjusted to 8 for the measurements of basic compounds. The retention data referring to acetonitrile–buffer plus butanesulfonic acid mobile phases for 11 morphine derivatives were reported by Valkó et al. [41]. The same ion-pair chromatographic system was used for the measurements of 11 tricyclic drugs published by Kálmán et al. [50]. The data of 19 benzodiazepine derivatives were published by Valkó et al. [51] by varying the acetonitrile concentration in the mobile phase. Valkó and Slégel [52] published the ϕ_0 values referring to methanol for 10 deoxyuridine derivatives. The slope and intercept values of 8 aniline and 8 phenol derivatives were published by Gullner et al. [53] by changing the methanol concentration in the mobile phase. The ϕ_0 values of 42 adenosine monophosphates, 12 barbiturates, and 10 penicillins and cephalosporins were also calculated on the basis of the published retention data of Braumann and Jastorff [54], Toon et al. [55] and Yamana et al. [56], respectively.

The linearity of the log k' versus ϕ plots were checked at the proper concentration range. The slope S and the intercept log k'_w values were used for the calculation of ϕ_0 values when the correlation coefficient of the fit was higher than 0.998. The published slope and intercept values were used for the calculation of the chromatographic hydrophobicity index, when the authors revealed acceptable high correlation coefficients for the linear fit. The log P values of 500 compounds were calculated by ProLogP Version 4.1 software package (CompuDrug Chemistry Ltd., Budapest, Hungary). The correlation analysis was carried out by the Drugidea program system developed for drug design (Chemicro Ltd., Budapest, Hungary).

Table 1 in the Appendix contains the calculated chromatographic hydrophobicity indices ($\phi_{0,AcN}$, $\phi_{0,MeOH}$) and the calculated log P values of 22 nicotinate esters. The calculated log P and ϕ_0 values referring to methanol for 35 monohydroxyl aromatics are presented in Table 2. The log P and ϕ_0 values of 30 pesticides and 45 phenoxycarbonic acid derivatives are summarized in Table 3 and 4. The calculated log P and $\phi_{0,MeOH}$ values of the 113 aromatic hydrocarbons are shown in Table 5. The obtained ϕ_0 and log P data of 143 acidic, basic, and neutral drugs can be seen in Table 6. The $\phi_{0,AcN}$ and the $\phi_{0,MeOH}$ data and log P values of 16 drug molecules are presented in Table 7. Table 8 contains the calculated data of morphine and tricyclic derivatives obtained from their ion-pair chromatographic retention data.

The calculated hydrophobicity index data of the benzodiazepine, deoxyuridine, and aniline derivatives are shown in Tables 9–11, respectively. Tables 12–14 show the chromatographic hydrophobicity index values for adenosine monophosphate, barbiturate, and β-lactam antibiotic derivatives, respectively.

The correlation between $\phi_{0,MeOH}$ and $\phi_{0,AcN}$ values for the compounds in Table 1, 4, and 7 was also investigated. These two values refer to isoelutropic eluant mixtures, as they both mean mobile-phase composition by which the same retention (log $k' = 0$) can be obtained. Significant correlation between the two types of chromatographic hydrophobicity indices was found for 72 compounds as described by Eq. (21).

$$\phi_{0,MeOH} = 0.82\ \phi_{0,AcN} + 20.46 \qquad (21)$$
$$n = 72 \quad r = 0.96 \quad s = 5.0$$

where n stands for the number of compounds, r is the correlation coefficient, s shows the standard error of the estimate. Equation (21) suggests a calculation method for converting the hydrophobicity indices from acetonitrile to methanol. The standard error of the estimate shows that, in spite of the fact that the data of the 72 compounds were obtained by different columns and buffers or neat water, the hydrophobicity index values obtained with acetonitrile can be calculated to methanol with ±5% error.

The correlation of $\phi_{0,AcN}$ hydrophobicity index values with the calculated log P values for the data of 140 compounds can be described by Eq. 22:

$$\phi_{0,AcN} = 9.31 \log P + 37.94 \qquad (22)$$
$$n = 140 \quad r = 0.88 \quad s = 12.8$$

Equation (22) shows the significant correlation between the two parameters, although because the relatively low correlation coefficient r and the high standard error of the estimate s, it cannot be used for the measurements of the log P values. The plot of the $\phi_{0,AcN}$ values against the log P values can be seen in Fig. 6. Similarly, statistically significant correlation could be found between the $\phi_{0,MeOH}$ and the log P values for the data of 448 compounds:

$$\phi_{0,MeOH} = 7.08 \cdot \log P + 42 \qquad (23)$$
$$n = 448 \quad r = 0.787 \quad s = 13.48$$

On the basis of Eq. (23) the exact measurements of log P cannot be carried out by the measurements of the chromatographic hydrophobicity index, but the good correlation shows that, even for a large set of compounds, the relation exists. The high standard error of the

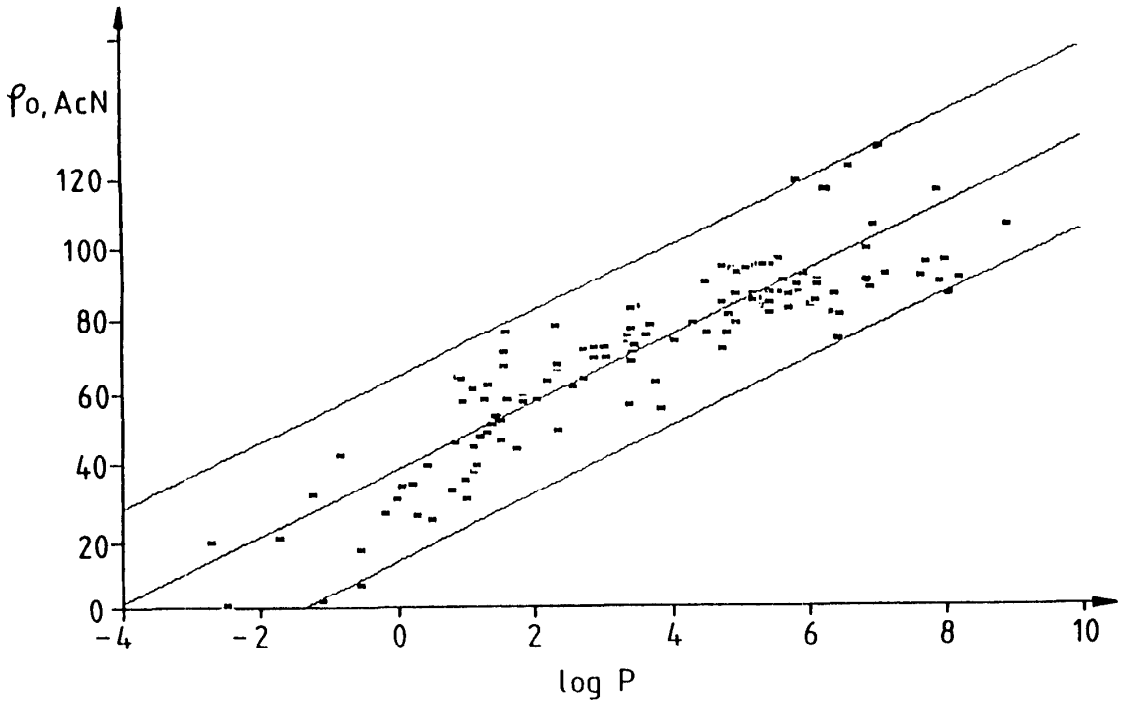


Figure 6 The plot of log P values and $\phi_{0,AcN}$ values for 140 compounds listed in the Appendix [Tables 1, 4, 7–10, and 15] [Eq. (22)]. (From Ref. 43.)

estimate (± 13%) can be due to error in the calculation of partition coefficients, to error in the measurements of ϕ_0 values, and also to error caused by differences in the applied chromatographic conditions. The main reason, however, for the lack of high correlation coefficients (higher than 0.99) is that we cannot expect to properly model from the reversed-phase chromatographic partition coefficients another partition system, such as 1-octanol–water, for structurally unrelated compounds.

The advantages of using ϕ_0 values as a measure of hydrophobicity of the compounds are that they are valid for structurally related and unrelated compounds, they have a physical meaning (i.e., a certain eluant composition by which a certain retention can be achieved) so it can also be used for HPLC method development, and these values are relatively independent from the reversed-phase columns obtained from different manufacturers. The hydrophobicity index value ranges from 0 to 100, and the higher the value is the more hydrophobic the compound is.

Mathematically it is possible to calculate the intersection points of the log k' versus ϕ straight-lines and a straight-line positioned in an optimum place in the plot as seen from Fig. 4. According to the calculations [57] the optimum position was very close to the log $k' = 0$ value, and it showed only a small slope in comparison with the horizontal value (zero slope). The improvement of the mathematical statistical parameters (correlation coefficient, Fisher-test value, standard error of the estimate) for the correlation of the log P and intersection points, however, was not significant.

G. Conclusions for HPLC Application in Hydrophobicity Measurements

In all of the aforementioned mathematical approaches the experiments were carried out by applying mobile-phase pH for obtaining the compounds in a nonionized form. For the acidic

compounds (such as salicylic acid), pH = 2 was used; for slightly basic compounds (such as caffeine) pH = 7.8 was used.

The hydrophobicity measurements of protonated basic compounds is still problematic, whatever approach is used, because the silica-based reversed-phase columns are not stable when using buffers with a high pH value. Basic compounds will then be partially or fully protonated in the chromatographic system. Tayar et al. [58] presented the determination of hydrophobic properties of a series of basic neuropharmacological compounds by RP–HPLC. They measured the apparent log k' values (referring to pH = 7.5 mobile phase) at various methanol concentrations, and they extrapolated the log k' values to 100%. They used the solute ionization correction and both linear and parabolic fit on the experimental values for calculating the log k'_w values for the correlation with the log P values. Another approach can be the application of low pH and ion-pair reversed-phase chromatography for the log k' measurements of basic compounds, as has already been suggested [41,59]. In these cases, it can be supposed that the log k' values express the chromatographic distribution of a neutral associate of the protonated basic compound and the anionic ion-pair molecule. The role of solute hydrophobicity and charges in reversed-phase ion-pair liquid chromatography has been discussed in detail [60]. If the same ion pair is always used for the measurements of a series of compounds, the increased hydrophobicity (by the hydrophobicity of the ion-pair molecule) of the associate will be manifest only in the value of the constant of the log P versus log k' relation.

The relation between the 1-octanol–water partition coefficients, determined by the traditional shake-flask method, and the biological partition and the various chromatographic approaches are summarized in Fig. 7. The theoretical limitation of the application of RP-HPLC retention data for the general characterization of the 1-octanol–water partition coefficients is that the chromatographic partition system is not the same as the 1-octanol–water partition system. Therefore, good correlations between a simple log k' values and log P values can be expected only for structurally related compounds. When structurally unrelated compounds, having a wide range of hydrophobicity values, are considered, the reversed-phase chromato-

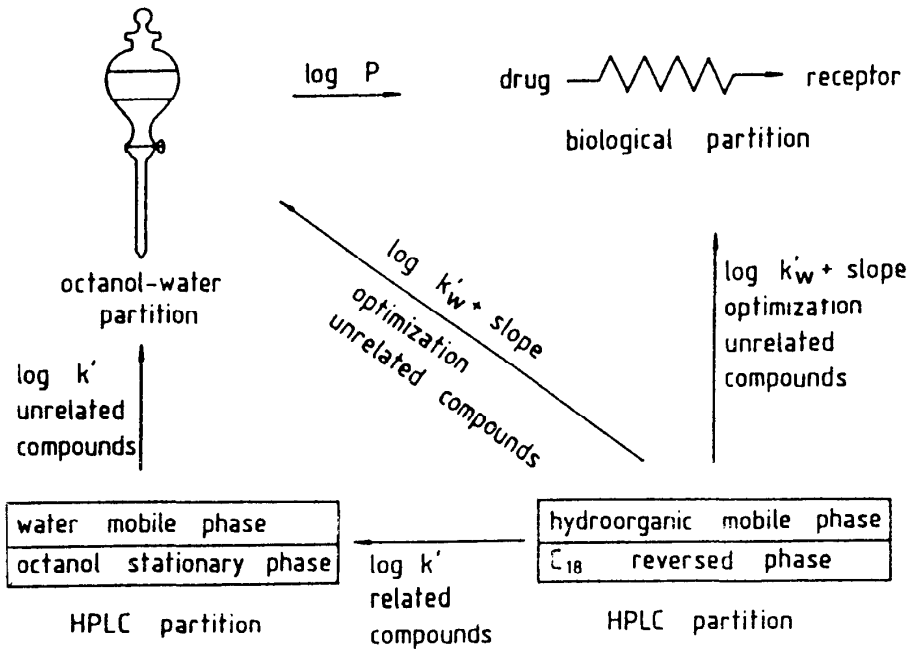


Figure 7 The summary of the possibilities of using HPLC for modeling partition properties of compounds. (From Ref. 60.)

graphic partition system should be modified to be more similar to the 1-octanol–water partition system.

The aforementioned procedures cannot be directly applied for the hydrophobicity determination of amino acids, peptides, and proteins, although it would also be very important to measure a kind of hydrophobicity for these molecules. Because they are amphoteric molecules and tend to associate with each other, even the application of the shake-flask method is problematic. There are several approaches to calculate and estimate the hydrophobicity of the amino acid side chains. The calculations can provide erroneous results because owing to the secondary and tertiary structure of the proteins, the overall hydrophobicity cannot be estimated by a simple sum of the side chain hydrophobicities. To measure the actual hydrophobicity on the surface of the molecule, reversed-phase chromatography is promising, because the retention is governed only by the real solute–stationary phase interactions, so hydrophobic amino acid side chains that cannot interact with the stationary phase will not manifest in the retention. Because a protein molecule always has charges on the surface at every pH value, we can measure only the distribution coefficients. Many protein molecules cannot be eluted from the reversed-phase column by applying a certain mobile-phase composition, but only by using a gradient method. When the organic phase concentration is gradually increased in the mobile phase, the retention factor will not be dependent on only the solute–stationary phase interactions. In these cases we cannot use the log k' values, we cannot extrapolate to the zero organic-phase concentration, and the slope and intercept method also cannot be applied. The change of the mobile-phase composition can also change the secondary or tertiary structure of the protein molecule; consequently, its hydrophobic surface will not be the same as in the natural conditions. Therefore, the determination of molecular hydrophobicity of biopolymers is still an exciting field of research.

In conclusion, the advantages of using HPLC for the estimation of hydrophobicity of compounds are the following: a much smaller amount of compound with less purity requirements is sufficient to carry out the analysis. The HPLC procedure can be completely automatized by using computer-controlled HPLC equipment. The conditions of the measurements (temperature, mobile phase pH, ionic strength) can be controlled and maintained constant for a large number of compounds. There is no need to develop an analytical method for the concentration determination of the compounds in the two phases. In general, it is less time-consuming to measure retention data, than concentration.

III. DETERMINATION OF EQUILIBRIUM CONSTANTS BY HPLC

Chromatography was developed for the separation of compound mixtures. The separation takes place by different migration patterns of the molecules. The different velocity of each type of compound is due to the different strength of the interaction with the mobile phase. The strength of the solute–stationary-phase interaction depends on the equilibrium constant of the distribution of the solute between the mobile and the stationary phase. Although during chromatography the system is never in equilibrium, the velocity of the molecules can be directly related to the equilibrium constant. Therefore, from the retention behavior of compounds, the so-called dynamic equilibrium constants can be determined. That was also the basis of the previously discussed hydrophobicity determination. When the solute stationary-phase distribution depends only on hydrophobic forces, the retention will refer only to the hydrophobicity of the molecules. When the solute stationary-phase interaction depends on complex formation, the retention will be proportional to the complex stability constants.

A. Determination of Complex Stability Constants by HPLC

Theoretically, there are two possibilities for the application of HPLC for the determination of complex stability constants. When the complex-forming agent (for example, cyclodextrin) is

chemically bonded to the stationary phase, the solute retention will be proportional to the complex stability constant K, according to Eq. (24).

$$\log K = \log \left[\frac{(t_R - t_0)}{t_0} \right] - \log \left(\frac{V_s}{V_m} \right) \tag{24}$$

where t_R is the retention time of the solute, t_0 is the retention time of another solute that has no interaction with the chemically bonded complexing agent. V_s/V_m is the volume of the stationary and the mobile phases. K is the stability constant of the complex, which can be expressed by Eq. (25):

$$K = \frac{[C]\,[X]}{[CX]} \tag{25}$$

where [C] and [X] are the concentration for the complex forming two molecules, [CX] is the concentration of the complex. When the complex-forming agent C is chemically bonded to the stationary phase, the complex molecule cannot move at all. Only the free X molecules can move by the mobile phase, and then the new equilibrium distribution takes place. Through this series of equilibrium distributions the X molecules go through the column. The velocity of the migration will be proportional to the concentration of X molecules in the mobile phase. The higher portion of the molecules are in the mobile phase (i.e., the lower the stability constant is, the lower will be the retention time). This general theory was applied, for example, for the determination of the interaction of β-cyclodextrin and some drugs by Sebille et al. [61]. The β-cyclodextrin polymer was prepared by reacting mono-6-*O*-tosyl-β-cyclodextrin with poly(ethyleneimine). The β-cyclodextrin content of the polymer was 60% w/w. A 5% solution of polymer was stirred with silica gel for 24 h at room temperature. Another stationary phase was similarly prepared that contained the poly(ethyleneimine) polymer, but without the cyclodextrin molecule, to compare the retention of the drug molecules on the two stationary phases. This is necessary because types of interactions other than the inclusion complex formation are also possible. The presence of immobilized β-cyclodextrin makes the retention of the solute higher as the association constant becomes stronger. The relation between the elution volume of the solute and its affinity for β-cyclodextrin can be described by Eq. (26):

$$V_A - V_A^* = V_S(X)\, n_i K_i \tag{26}$$

This equation is valid only if the amount of solute A is very small. V_A is the elution volume of A molecule; V_A^* is the elution volume of A on a stationary phase that does not contain the cyclodextrin molecule; V_S is the volume of the stationary phase; X is the molar concentration of immobilized cyclodextrin (considered to be uniformly distributed through the volume accessible to the solute); K_i is the equilibrium constant; n is the number of the interacting sites. Figure 8 shows the chromatograms obtained for several drug molecules on the stationary phases containing the β-cyclodextrin in the stationary phase. The same method can also be applied for the determination of other complex stability constants. The only difficulty is in the preparation of the HPLC stationary phases, which needs special skill and technology.

A much easier approach is the application of the complex-forming agent in the mobile phase. Then the retention determination should be carried out with and without the complexing agent in the mobile phase. The complex stability constant is in relation to the change of the retention. Many HPLC methods have been developed for determination of the stability of various inclusion complexes of cyclodextrin using different theoretical and practical considerations. From the different distribution of the uncomplexed X and complexed CX molecules between the mobile and the stationary phases the complex stability constant can be determined according to Eq. (27).

$$K = \frac{[CX]_m}{[X]_m,\, [C]_m} \tag{27}$$

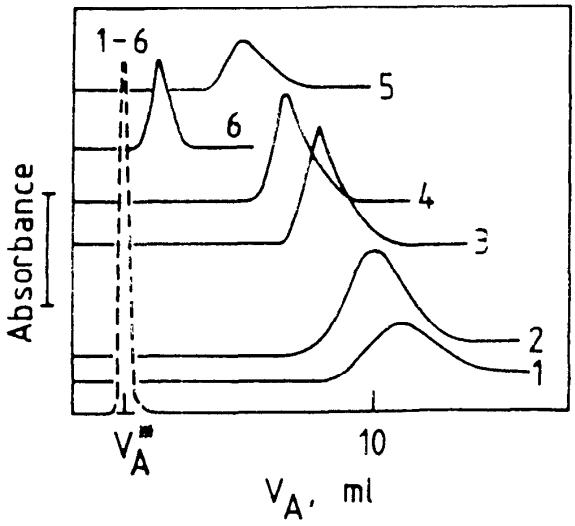


Figure 8 Elution of drugs on 10-cm columns filled with polymer-coated silica (broken line: support without β-cyclodextrin; solid lines support with β-cyclodextrin). (1) warfarin; (2) indomethacin; (3) propranolol; (4) furosemide; (5) diazepam; (6) phenylbutazone. (From Ref. 61.)

where m and s refer to the mobile and the stationary phase, respectively. [C], [X], and [XC] refer to the cyclodextrin, guest molecule, and the cyclodextrin–guest molecule complex concentration, respectively. K is the stability constant of 1:1 cyclodextrin–guest molecule complex. The apparent concentration distribution can be expressed by Eq. (28).

$$D_{obs} = \frac{[X]_s + [CX]_s}{[X]_m + [CX]_m} \tag{28}$$

By combining Eqs. (27) and (28), Eq. (29) can be obtained:

$$D_{obs} = \frac{D_x + (D_c\, K\, [C]_m)}{1 + (K\, [C]_m)} \tag{29}$$

where D_x and D_c are the distribution of the guest and the cyclodextrin molecule in the mobile and stationary phases, respectively.

When the addition of cyclodextrin to the mobile phase does not significantly change the void volume of the column, the distribution ratios can be calculated from the retention times according to Eqs. (30)–(32).

$$D_x = \left(\frac{t_x - t_0}{t_0}\right)\left(\frac{V_m}{V_s}\right) \tag{30}$$

$$D_c = \left(\frac{t_{cx} - t_0}{t_0}\right)\left(\frac{V_m}{V_s}\right) \tag{31}$$

$$D_{obs} = \left(\frac{t_{obs} - t_0}{t_0}\right)\left(\frac{V_m}{V_s}\right) \tag{32}$$

where t_s, t_c, and t_{cx} are the retention times of the guest molecule, the cyclodextrin molecule, and the complexed molecules at a given cyclodextrin concentration in the mobile phase, respectively. The t_{obs} means the retention time of the X molecule at a given cyclodextrin concentration in the mobile phase. The t_0 refers to the dead time, and the V_s/V_m is the phase ratio. By substituting Equations (30)–(32) into Eq. (29) Eq. (33) can be obtained:

$$t_{obs} = \frac{(t_x + t_{xc})\,(K\,[C])}{1 + (K\,[C]_m)} \tag{33}$$

By rearranging Eq. (33), Eq. (34) can be obtained:

$$\frac{[C]_m}{t_x - t_{obs}} = \frac{[C]_m}{t_x - t_{xc}} + \frac{1}{K\,(t_x - t_{xc})} \tag{34}$$

Equation (34) provides the possibility for determination of the K stability constant and t_{cx} values from the slope and the intercept of the plot $[C]_m/(t_m - t_{obs})$ versus $[C]_m$ plot. When the retention times are long or t_x is unknown, the retention time of the X molecule can be determined at various cyclodextrin concentrations in the mobile phase. Several cyclodextrin complex stability constants have already been determined by these chromatographic methods [62–70].

In general, the HPLC method for the determination of cyclodextrin complex stability constants or, more exactly, relative strength of the interactions, can be applied when only one species of the solute (i.e., the neutral molecule) is exclusively present, only 1:1 is the stoichiometry of the complex formation, and the cyclodextrins do not influence the properties of the stationary phase. Under the circumstances, the HPLC method offers a precise determination of complex stability constants in solution. Unlike other methods, HPLC can be applied with relatively impure samples without further purification, as separation takes place during the measurements. Because of the low concentrations in the eluant, the low solubility of the molecules cannot disturb the measurements, whereas poor sample solubility often limits the use of traditional techniques. However, the HPLC method can be applied for the association constant measurements only when the rate of equilibration in the mobile phase is rapid, compared with the time of the chromatographic run. Otherwise poor peak shape and peak splitting can cause difficulties in the retention determination.

B. Determination of Drug–Protein-Binding Constants by HPLC

The most important binding constants characterize drug–protein interactions. It has been well recognized for more than 40 years that the pharmacological activity of a drug molecule depends on the concentration of the free molecule in biological compartments. The binding of drugs to a protein influences its pharmacokinetics. Basically, the drug–receptor interaction also can be considered as drug–protein binding. Acidic drugs mostly bind to albumin in plasma, whereas basic drugs preferentially bind to ϕ_1-acid glycoprotein. Stereoselective binding of racemic mixtures of drugs has been frequently established [71,72], and its importance in storage and transport processes has been reviewed [73]. Numerous methods, such as equilibrium dialysis, fluorescence spectroscopy [74], circular dicroism [75], and gel column centrifugation [76–80], have been used to study drug–protein binding. In general, the methods can be divided into spectroscopic and nonspectroscopic ones. The nonspectroscopic methods usually involve separation of the free ligands from the bound species. They included soft-gel chromatography, HPLC, ultrafiltration, ultracentrifugation, and equilibrium dialysis. These methods can be applied as complementary, rather than competitive, and it is always advisable to use more than one method for the binding measurements. Sebille et al. [81] have published a concise review about the separation procedures to reveal and follow drug–protein binding. The applications of HPLC for the determination of drug–protein binding has been discussed in detail [82].

Basically, two types of chromatographic approaches can be considered: either all the species at equilibrium are dissolved in the mobile phase, or one of them is immobilized, as a stationary phase, on the chromatographic support. The latter is the well-known affinity chromatographic technique. When none of the species to be studied is immobilized, the quan-

titation of the drug–protein complex can be determined by zonal elution, by the Hummel and Dreyer method, by frontal elution, or by vacancy peak method.

1. Zonal Elution

A small sample volume containing a mixture of the drug and the protein is injected onto the column and is eluted by aqueous buffer solution. A size-exclusion mechanism or an ion-exchange one can be used for the separation of the free and complexed drug molecules. The quantitative measurements of the complex and the free ligand concentrations allow the calculation of the binding parameter. The validity of the results depends on the interaction kinetics, for the complex may be dissociated by the dilution resulting from the elution transfer, as well as by the drug retention on the stationary phase. The theoretical aspects of this process have been analyzed [83], and the conditions of complex stability that allow the application of the method have been calculated. When the association constant is higher than 10^7 M^{-1}, the dissociation rate is small enough to keep the ligand–protein complex intact during the chromatographic elution. In general, the quantitative analysis of peak areas in zonal chromatography may be used when the eluted sample is moderately diluted and the protein–ligand dissociation kinetics are slower than the chromatographic elution process.

2. Hummel and Dreyer Method

The chromatographic method most widely used for measuring drug–protein interactions was first described by Hummel and Dreyer [84] in 1962. The method requires a column that separates the drug and the protein. At the beginning only a size-exclusion mechanism was used with soft gels, but gradually the use of rigid supports and HPLC equipment allowed the development of the method by decreasing the analysis time. Ion-exchange columns have recently been introduced [85]. The basic principle of the method is that the mobile phase contains the drug molecule to be studied dissolved at a given concentration. Then a small amount of protein is injected onto the column. As a result, a positive peak will appear corresponding to the ligand–protein complex, and a negative one emerges at the drug retention volume, indicating the decrease of the drug concentration at that retention time interval. The negative peak area depends directly on the amount of bound drug. An example of the obtained chromatogram can be seen in Fig. 9 obtained by Sun et al. [86]. The number of bound molecules per macromolecule is fixed by the applied drug concentration in the mobile phase and, therefore, it is constant during elution. The exact determination of the positive and negative peak area can cause some problems, because the integrators are not able to calculate the negative peak area. The various techniques for peak area determination (planimeter, geometry, and integrator) were studied and evaluated by Sun and Hsiao [87] quite recently. They also developed two types of Hummel–Dreyer elution pattern, one with a positive peak followed by a negative peak, and the other with two positive peaks. The several calibration methods (external, internal calibrations and so on) were also compared.

A good resolution between the protein peak and the negative drug peak is the main requirement of the method, and erroneous measurements may result mostly from protein peak tailing. This tailing can appear owing to the slow kinetic processes or may occur from self-association induced by the ligand interaction. In principle, drug adsorption on the chromatographic gel does not interfere with the drug–protein-binding measurements. When the column is saturated with an eluant containing the drug, the drug concentration in the mobile phase is actually the free ligand concentration, which is in equilibrium with the protein. The Hummel–Dreyer method is useful for studying the competitive interactions of two drugs toward the same protein.

The method is mostly applied to drugs that are weakly retained in an aqueous medium on size-exclusion supports. The use of ion-exchangers can give better peak resolution.

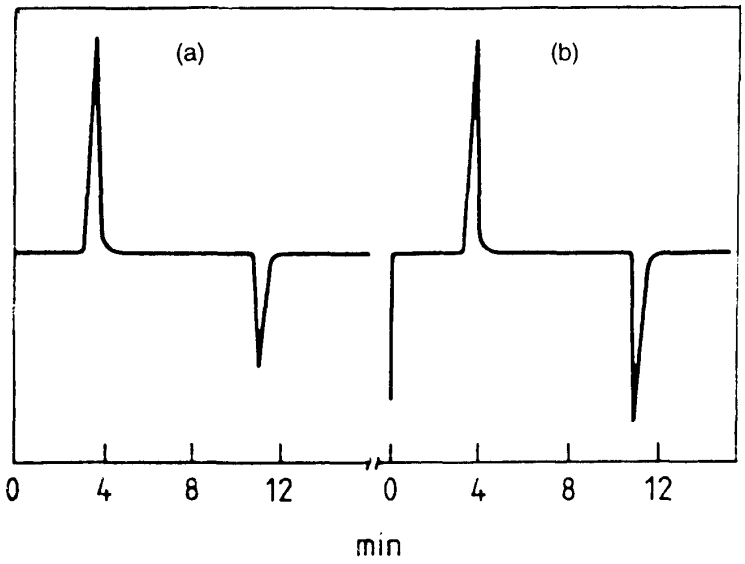


Figure 9 Chromatogram of binding of warfarin to human serum albumin (HSA). UV at 313 nm, 0.4 AUFs. Flow rate 2.0 mL/min^{-1}. Chart speed: 5 cm 10 min^{-1}. Mobile phase: 37.0 μM warfarin in 0.067 M sodium phosphate buffer, pH 7.4. (a) Sample: 500 μL 114.0 μM protein stock solution + 750 μL 86.3 μM warfarin stock solution; (b) sample: 500 μL 114.0 μM protein stock solution + 500 μL 86.3 μM warfarin stock solution. (From Ref. 86.)

3. Frontal Elution

In frontal chromatography, a solution is applied continuously to the column until the column is equilibrated. The elution profile at the column outlet reaches a plateau equal to the input concentration. At the beginning, only gel chromatographic columns were applied. The use of soft gels limited the extension of this technique because of the low-flow rates and because of gel shrinkage observed with large concentrations of proteins. Now that rigid supports and HPLC techniques have been introduced, frontal analysis has again become popular. The first HPLC application was given by Morrid and Brown [88], who measured the binding of methyl orange to albumin using rigid beads and a medium-range inlet pressure. With frontal chromatography the typical chromatogram can be seen in Fig. 10, obtained by Sebille et al. [89]. The chromatographic profile can be divided into three parts. The α-plateau is related to the unbound protein concentration; a region (β) shows the complex plus free species concentration; and a region (γ) corresponds to the free-ligand concentration. By carefully measuring the height of the last plateau one can determine the free-ligand concentration and the r can be calculated according to Eq. (35):

$$r = \frac{[B]}{[P]} = \sum_{i=1}^{m} n_i \frac{k_i[F]}{1 + k_i[F]} \tag{35}$$

where r is the fraction of bound ligand molecules per protein molecule; [F], [B], and [P] are the concentrations of free drug, bound drug, and protein, respectively, n_i is the number of sites of class i and k_i is the corresponding association constant.

The advantage of the frontal elution method is that it gives results at known and constant concentrations for all the species in equilibrium.

4. Vacancy Peak Method

Sebille et al. [90] introduced the method, which is based on an equilibrium-saturation procedure using standard HPLC equipment. In a typical experiment, a size-exclusion column is

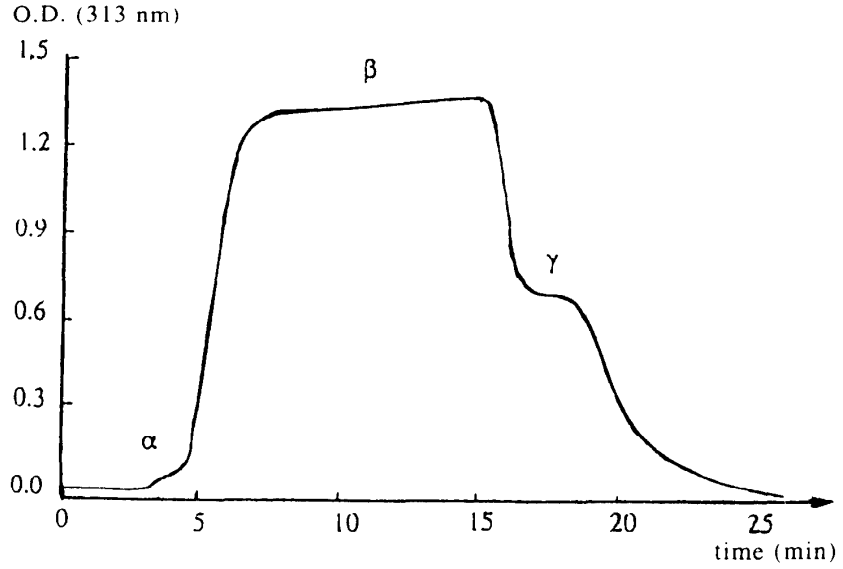


Figure 10 Elution profile in frontal analysis of a mixture of warfarin (10^{-4} M) and HSA (2 g L^{-1}). Eluent, warfarin (10^{-4} M) and HSA (2 g L^{-1}) in 0.067 M phosphate buffer (pH 7.4). (From Ref. 89.)

eluted with a solution containing a mixture of protein and drug in an aqueous buffer. After injection of a few microliters of pure buffer, two negative peaks are detected at the column outlet as can be seen in Fig. 11. The first peak corresponds to a vacancy in the ligand–protein complex, and the second peak to the free-drug concentration in the mixture. With the help of an appropriate calibration procedure (external or internal) the r ratio and the binding equilibrium parameters can be calculated according to Eq. (35). Because the eluant contains the protein and the drug, the background absorbance is high and an internal standard method is recommended because of the nonlinearity of the detector response. As with the frontal elution method, the concentrations of free and bound species are kept constant during the whole chromatographic process, and this aspect is the main advantage of both methods. This method is especially advantageous for drugs that are weakly soluble in water. The presence of both the protein and the ligand in the eluant increases the ligand solubility. The method is also applicable for studying competitive binding of several ligands to the same protein site, provided that the column can resolve the different components with an eluant containing the protein.

In conclusion, an HPLC method can be applied for measuring equilibrium constants. One approach is to measure the equilibrium constant of a solute interaction with the stationary phase. In these cases, the retention properties of the solute will be directly proportional to the equilibrium constants. The advantage of this approach is the fast and simple measurements, whereas the disadvantage is that previously one of the interacting molecules should be immobilized on the stationary phase surface. The second approach is to use conventional HPLC stationary phases (mostly gel filtration or ion-exchange) and the two interacting species should be applied to the chromatographic system in various ways. The detection and quantitation of the free and bound species needs special approaches, depending on the methods applied.

In general, the application of a chromatographic method is faster, it can be automated, and there is no need for radiolabeling. They are useful to identify the interacting components in a complex mixture, because usually, separation also takes place during the measurements.

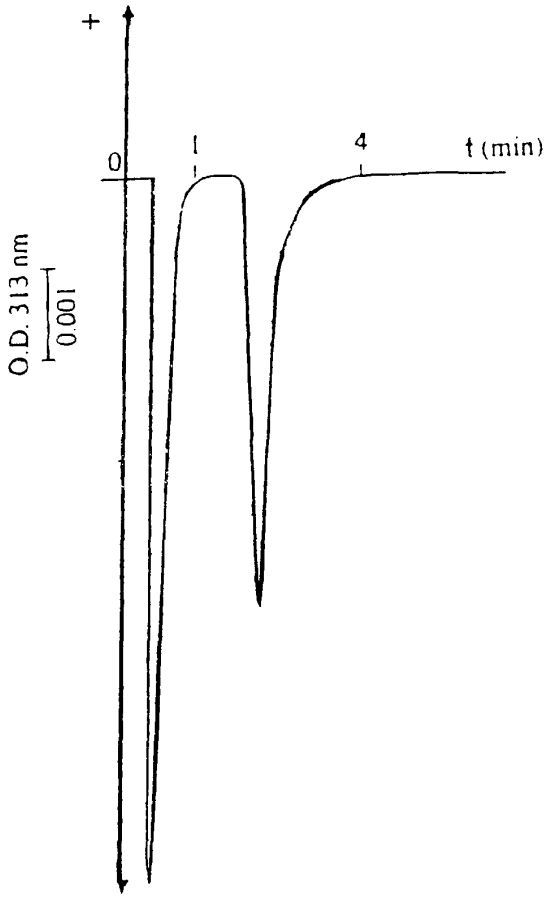


Figure 11 Vacancy peak chromatographic method. Eluent, HSA (2 g L^{-1}) and diazepam (5×10^{-5} M) in 0.067 M phosphate buffer (pH 7.4). Injection volume, 50 μL of buffer; flow rate, 0.5 mL min^{-1}. (From Ref. 89.)

IV. DETERMINATION OF THERMODYNAMIC PARAMETERS BY HPLC

A. Temperature Dependence of the Retention: Determination of Enthalpy or Entropy Effects by HPLC

The magnitude of chromatographic retention is determined by the energetics of the solute interactions with both the mobile and the stationary phases. The close relations between the retention factor and equilibrium constant (referring to the equilibrium distribution of the solute between the mobile and the stationary phases) allows us to extract from the chromatogram thermodynamic information that may be useful in a context other than chromatography. As discussed earlier, several equilibrium constants of pharmacological interest can be obtained from the chromatographic retention data. As for every equilibrium, the chromatographic equilibrium also depends on the temperature. The effect of temperature on retention has been studied less extensively in RP–HPLC than the effect of solvent composition. Over a temperature range from 5° to 100°C one can expect a roughly tenfold decrease in the retention factor if the enthalpy of solute–stationary phase interaction is -5 kcal mol^{-1}, which is a typical value in RP-HPLC. A retention change of similar magnitude occurs when the organic-phase component of the mobile phase is changed by approximately 30%. Melander et al. [91] described a quantitative relation of the log k' values on the temperature and the mobile phase-composition as shown by Eq. (36).

$$\log k' = A_1 X\left(\frac{1 - T_c}{T}\right) + \frac{a_2}{T} + A_3 + A_4 f(X,T) \tag{36}$$

where X is the volume fraction of the organic cosolvent in the hydroorganic mobile phase, T is absolute temperature, and T_c is the so-called compensation temperature, derived by taking advantage of the enthalpy–entropy compensation [92]. The temperature effects can be more important in determining the column inlet pressure, analysis time, and resolution. The flow rate can be increased with no change in operating pressure if the mobile-phase viscosity is decreased. This can be easily achieved by increasing the temperature. The temperature can also affect the efficiency of the chromatographic system, because the diffusion coefficient of a solute increases with the temperature. The effect of temperature on retention is largely determined by the enthalpy of the solute–stationary phase interaction. The enthalpy can be calculated from the slope of plots of log k' versus the reciprocal of the absolute temperature, which are called van't Hoff plots. Usually the enthalpies do not differ greatly among the several solutes, although relatively large differences in retention factors are observed. In many physicochemical interactions that are subject to the same intrinsic mechanism, the free-energy change is proportional to the enthalpy. If it is true, in reversed-phase chromatography, the logarithm of the retention factor increases linearly with the enthalpy and the slope of the van't Hoff plot. Published results indicate [93–94] that the logarithm of the retention factor is linearly related to the enthalpy; however, it is much greater than expected. This is due to changes in binding enthalpy, which are accompanied by corresponding changes in the binding entropy caused by the structural modifications of the solute molecule or changes in the mobile phase composition. A linear relation has been found in RP–HPLC between the enthalpy and the entropy for reversible solute binding to the hydrocarbon stationary phases [94]. The effect is called enthalpy–entropy compensation. The slope of the plot is called the compensation temperature [T_c in Eq. (36)]. Comparison of the compensation temperatures obtained from the slopes of the van't Hoff plots can be used to investigate the retention mechanism, whether or not they are identical in two different chromatographic systems. The nonlinearity of the van't Hoff plots can also show if there is more than one kind of solute species, such as when the solute is partly ionized, and both are present in significant quantities. The secondary equilibria are usually, but not necessarily, manifest in the peak shape as well. It depends on the kinetics of the retention and the secondary equilibrium process. A more recent investigation about the temperature dependence in reversed-phase retention was published by Cole et al. [95,96]. They used the method for studying the retention mechanism in reversed-phase chromatography from the stationary- and the mobile-phase point of view.

In conclusion, the investigation of the temperature dependence of the HPLC retention through van't Hoff plots can reveal the mechanism of retention, and the number of molecular species in the solute stationary-phase and mobile-phase interactions. These types of physicochemical measurements are used mostly for understanding the chromatographic process more deeply to improve the development of new stationary phases or new separation methods.

B. Determination of Adsorption Isotherms by Displacement Chromatography

Chromatographic retention depends on the solute–stationary phase interactions modified by the mobile phase. The solute–stationary phase interaction can also be considered an adsorption process. Adsorption isotherms have attracted greater attention as a fundamental tool for investigation of the physical process involved in chromatographic retention. The adsorption isotherm quantitatively describes the equilibrium distribution of a solute between the two phases involved in the chromatographic process over a wide range of concentrations. Usually, in elution chromatography, we work at the linear portion of the adsorption isotherms; but in preparative- or process-scale chromatography, the column is usually overloaded, and we can

reach the nonlinear part of the adsorption isotherms. This is true in overloaded preparative elution chromatography and displacement chromatography [97]. This is called nonlinear chromatography. In many instances, measurement of adsorption isotherms is the only way of obtaining data for the design of a chromatographic purification process. Therefore, a need exists for a technique of isotherm measurement that offers high speed, accuracy, and convenience. Isotherms have been measured traditionally by the static method, in which the change in concentration of a solute is measured by adding the adsorbent to the solution, and the points of the isotherms are calculated from this measurement. The disadvantages of the static method are that it is very slow, there is uncertainty in reaching equilibrium, and the large amounts of solute and adsorbent required for the measurements.

Jacobson et al. [98] introduced frontal chromatographic method for the determination of adsorption isotherms by HPLC. A miniaturized liquid chromatographic system was constructed to measure milligram quantities of material by frontal development. Two types of chromatographic methods can be applied for the determination of adsorption isotherms. They involve changing the concentration of the solute at the column inlet in a step-wise fashion, either up or down. When the concentration is increased, the step develops into a sharp front at the column outlet as shown in Fig. 12, whereas when it decreased, it becomes a tailing boundary at the outlet as shown in Fig. 13. The method that employs the front boundary (see Fig. 12) is called frontal analysis method. By the application of a mass balance equation the surface concentration can be calculated, which is in equilibrium with solute concentration, c. Thus, one experiment as in Fig. 12, gives one point on the isotherm. The second method, frontal analysis by characteristic point, calculates the entire isotherm from the concentration profile of the rear boundary (see Fig. 13). The theoretical background for the calculations and the comparison of the various methods have been discussed in detail [98]. Frontal analysis with HPLC system, incorporating a narrow-bore column, 50.00 × 1.18 or 40.5 × 1.18 mm, provided the most rapid, precise, and accurate measurements [98]. It needs a small amount of the solute for the measurements, by which the isotherm determination of rare and expensive compounds is also possible. The isotherms measured by frontal analysis were of a langmuirian or quasi-langmuirian shape. The langmuirian parameter (a) yielded a linear Van't Hoff relation when plotted as log s versus $1/T$. The relation between parameter a and the retention factor k' was linear. This relation can be used to determine the phase ratio or predict the Langmuir parameter from the measured retention factors. With the help of the adsorption isotherms, the

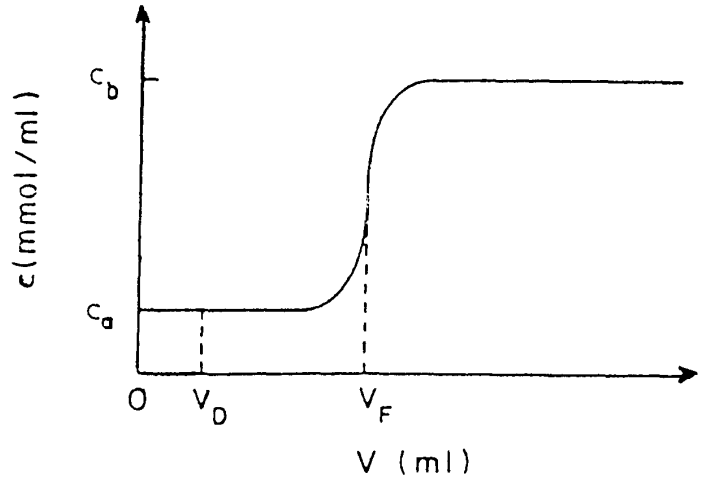


Figure 12 Self-sharpening boundary in frontal analysis. V_D is the system dead-volume, including column hold-up volume, V_F is the retention volume of the front, c_a is the solute concentration, which is changed to c_b. (From Ref. 98.)

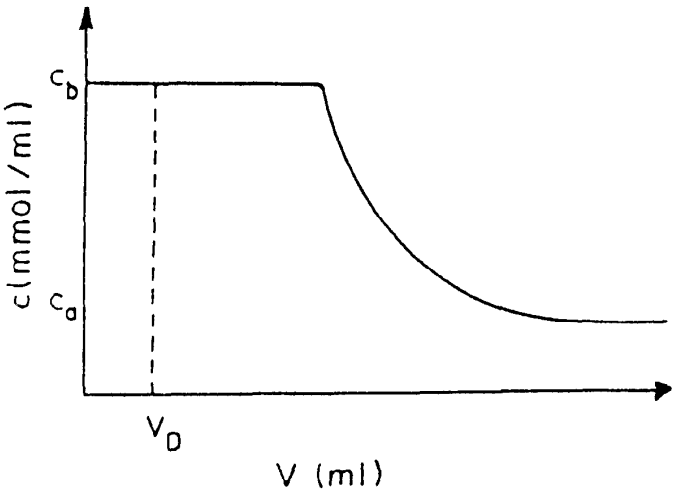


Figure 13 Illustration of the diffuse rear boundary used in "frontal analysis by characteristic point" measurements. (From Ref. 98.)

peak shape and the retention at overloaded concentrations can be predicted. Levin et al. [99] studied another method for isotherm determination through system peaks. They compared the frontal analysis method and the system peak method for measuring the adsorption isotherms of phenylalanine, and they obtained identical results. They suggest the system peaks method, especially for multicomponent systems for which mixed isotherms are needed for rational formulation of a preparative separation. The theoretical background of the method has been described [100]. With a multicomponent mobile phase in which one or more components are adsorbed on the stationary phase, injection of a sample different in any sense from the mobile phase itself induces system peaks. Identification and quantitative treatment of these peaks allow the calculation of the retention factors of the mobile phase components and column void volumes. The adsorption isotherm of a particular mobile phase component can be calculated from the corresponding system peak.

Because the peak shape is also determined by the adsorption isotherms of the compounds, its analysis can help in the adsorption isotherm determination. Guiochon et al. [101] described a new method for determining equilibrium isotherms from chromatographic peak shape. In the new method, initial estimates of the parameters of an isotherm equation are refined by finding simulated chromatographic peak shapes that most nearly approximate the experimental peak shapes. A method of successive approximation to the physical isotherm can be designed, given a means of computing chromatographic peak shapes from a given isotherm and plate number; a score measuring the similarity of this simulated peak shape to the experimental shape; and an algorithm that generates new isotherms with increasing similarity scores and that recognizes convergence of the series of new isotherms to a single best isotherm.

The foregoing three methods are most commonly used for the adsorption isotherm determination of compounds by HPLC. The parameters of the isotherm provides help mostly for designing preparative HPLC separations, when the adsorption isotherms are no longer linear. It also helps predict the peak shape in overloaded conditions.

V. CONCLUSIONS

The application of HPLC for determination of physicochemical parameters is not as widespread as gas chromatography. The distribution process during the liquid chromatographic separation is more complicated because the solute–stationary phase interaction is always modulated by the mobile phase, which can also be multicomponent. The most common physi-

cochemical application of HPLC is the determination of partition coefficients, more exactly the hydrophobic (or lipophilic) nature of compounds. This is understandable, for the solute distribution takes place between the mobile and the stationary phase. The distribution of a solute between a hydrophobic stationary phase and an aqueous mobile phase is proportional to the partition coefficient. In spite of the simple theoretical basis, the application of HPLC for the determination of the biologically most important octanol–water partition coefficients is still not straightforward. Because the two partition process are not identical, various approaches can be applied for structurally related and unrelated compounds. These approaches were discussed in detail.

The application of interacting molecules in the mobile phase makes possible the use HPLC techniques for determination of molecular interactions, and several biologically important binding parameters. The various methods were discussed in detail. Several other approaches have been developed for the determination of drug–protein-binding constants by HPLC method.

The application of HPLC for thermodynamic measurements is not as widespread, but is very useful, especially for the design of preparative chromatographic separations of biologically important compounds. In these instances the chromatographic stationary phase is overloaded, and the separation process takes place at the nonlinear part of the adsorption isotherms.

The general advantages of the HPLC methods for physicochemical measurements are that it can be easily automated; it requires much smaller amounts of compounds; usually, the compounds need not be pure, for separation from impurities also takes place during the measurements; and in general, HPLC methods are faster and more accurate.

APPENDIX

Table 1 The Calculated log P, $\phi_{0,AcN}$, and $\phi_{0,MeOH}$ Values for 22 Nicotinates Based on the Published Retention Data

Ser. No.	Name of the compound	log P	$\phi_{0,AcN}$	$\phi_{0,MeOH}$
1.	Methyl	0.830	31.75	44.93
2.	Ethyl	1.339	42.91	54.93
3.	*n*-Propyl	1.868	50.04	64.92
4.	*i*-Propyl	1.868	49.21	62.86
5.	*n*-Butyl	2.387	59.69	71.67
6.	*i*-Butyl	2.387	58.91	67.50
7.	*t*-Butyl	2.387	58.30	67.24
8.	*n*-Hexyl	3.425	77.24	81.73
9.	*n*-Octyl	4.463	84.93	87.64
10.	Cyclohexyl	3.061	74.23	78.51
11.	TTMCH	4.618	81.66	84.40
12.	2-Methoxyethyl	0.833	21.56	43.10
13.	2-Butoxyethyl	2.390	54.27	67.91
14.	THF	1.507	39.62	52.53
15.	2-Chloroethyl	1.784	43.24	57.27
16.	3-Hydroxypropyl	0.216	−5.29	33.64
17.	Carbamoylmethyl	−0.487	4.35	12.88
18.	MCM	0.032	11.47	23.15
19.	Benzyl	2.488	54.37	70.90
20.	*p*-Chlorophenyl	2.991	62.18	76.30
21.	*p*-Nitrophenyl	2.014	58.31	67.92
22.	2-Phenoxyethyl	2.568	53.23	68.93

Source: Ref. 44.

Table 2 The Calculated log P and $\phi_{0,MeOH}$ Values for 35 Hydroxyl Aromatics Based on the Published Retention Data

Ser. No.	Name of the compound	log P	$\phi_{0,AcN}$	$\phi_{0,MeOH}$
23.	1-Acenaphthenol	2.296	—	65.82
24.	5*H*-Dibenzo[*a*,*d*]cycloheptene-5-ol	3.200	—	71.65
25.	7,12-Dimethyl-9-hydroxybenz[*a*anthracene	6.643	—	83.65
26.	2-Hydroxybenzo[*c*]phenanthrene	5.557	—	80.16
27.	3-Hydroxybenzo[*c*]phenanthrene	5.557	—	82.04
28.	1-(1-Hydroxymethyl)pyrene	5.739	—	81.29
29.	1-(Hydroxymethyl)benzo[*a*]pyrene	5.816	—	85.77
30.	4-Hydroxymethylpyrene	5.739	—	76.52
31.	9-Hydroxyphenanthrene	4.332	—	76.55
32.	13-Hydroxypyrene	7.456	—	90.23
33.	1-Hydroxypyrene	5.220	—	81.32
34.	4-Hydroxypyrene	5.220	—	81.12
35.	1-Indanol	1.542	—	53.89
36.	5-Indanol	2.690	—	64.68
37.	1-Naphthol	2.770	—	64.77
38.	2-Naphthol	2.770	—	62.67
39.	3-Phenylphenol	3.444	—	70.83
40.	1,2,3,4-Tetrahydro-4-hydroxy-4-methylphenanthrene	3.853	—	78.16
41.	1,2,3,4-Tetrahydro-1-naphthol	2.061	—	62.77
42.	5,6,7,8-Tetrahydro-1-naphthol	3.209	—	71.28
43.	5,6,7,8-Tetrahydro-2-phenantrol	3.334	—	82.35
44.	*o*,*o*′-Biphenol	2.919	—	61.13
45.	*p*,*p*′-Biphenol	2.919	—	55.40
46.	1,2-Dihydroxybenzene	0.972	—	28.65
47.	1,3-Dihydroxybenzene	0.972	—	20.69
48.	1,4-Dihydroxybenzene	0.972	—	23.72
49.	1,3-Dihydroxynaphthalene	2.245	—	54.79
50.	1,6-Dihydroxynaphthalene	2.245	—	48.39
51.	1,7-Dihydroxynaphthalene	2.245	—	54.03
52.	2,3-Dihydroxynaphthalene	2.245	—	56.33
53.	2,6-Dihydroxynaphthalene	2.245	—	45.09
54.	2,7-Dihydroxynaphthalene	2.245	—	49.69
55.	2,5-Dihydroxynaphthalene	2.245	—	64.69
56.	2,6-Dihydroxytoluene	1.491	—	24.74
57.	3,5-Dihydroxytoluene	1.491	—	35.25

Source: Ref. 45.

Table 3 The Calculated log P and $\phi_{0,MeOH}$ Values for 30 Herbicides Based on the Published Retention Data

Ser. No.	Name of the compound	log P	$\phi_{0,AcN}$	$\phi_{0,MeOH}$
58.	Fenuron	1.18	—	50.47
59.	Metoxuron	1.98	—	56.62
60.	Monuron	1.91	—	62.96
61.	Monolinuron	1.99	—	67.21
62.	Chlortoluron	2.55	—	69.24
63.	Metobromuron	2.37	—	69.49
64.	Diuron	2.68	—	72.37
65.	Linuron	2.76	—	75.28
66.	Chloroxuron	3.65	—	77.70
67.	Neburon	4.31	—	80.29
68.	Simazine	1.51	—	66.48
69.	Atrazine	2.05	—	71.81
70.	Propazine	2.59	—	76.05
71.	Prometryn	1.91	—	85.30
72.	Desmetryn	2.46	—	86.16
73.	Terbutryn	2.56	—	87.55
74.	2,4-D	2.22	—	54.24
75.	MCPA	2.30	—	57.25
76.	2,4,5-T	2.99	—	62.00
77.	Dichlorprop	2.75	—	62.23
78.	Mecoprop	2.83	—	64.40
79.	Fenoprop	3.52	—	68.21
80.	MCPB	3.53	—	73.67
81.	2,4-D-M	2.64	—	77.44
82.	MCPA-M	2.72	—	78.51
83.	Dichlorprop-M	3.17	—	81.30
84.	Mecoprop-M	3.25	—	81.76
85.	2,4,5-T-M	3.41	—	82.82
86.	MCPB-M	3.95	—	85.90
87.	Fenoprop-M	3.94	—	85.99

Source: Ref. 46.

Table 4 The Calculated log P, $\phi_{0,AcN}$, and $\phi_{0,MeOH}$ Values for 45 Substituted Aromatic Compounds Based on the Published Retention Data

Ser. No.	Name of the compound	log P	$\phi_{0,AcN}$	$\phi_{0,MeOH}$
88.	Acetophenone	1.66	62.28	70.33
89.	Aniline	1.10	—	58.74
90.	Anisole	2.11	70.99	80.83
91.	Benzaldehyde	1.48	61.26	67.92
92.	Benzene	2.13	72.37	84.38
93.	Benzonitrile	1.56	63.11	67.30
94.	Benzophenone	3.18	78.26	84.68
95.	Benzyl alcohol	1.10	43.01	58.33
96.	Biphenyl	4.02	88.62	91.96
97.	*n*-Butylbenzene	4.26	90.72	95.15
98.	Chlorobenzene	2.81	77.41	85.62
99.	*p*-Chlorophenol	2.39	59.86	71.67
100.	*p*-Chlorotoluene	3.33	83.06	89.63
101.	*o*-Cresol	1.96	58.17	68.30
102.	*o*-Dichlorobenzene	3.38	83.28	90.06
103.	Diethyl phthalate	3.15	71.43	78.38
104.	2,4-Dimethylphenol	2.30	64.60	74.76
105.	Dimethyl phthalate	2.11	62.45	68.63
106.	*m*-Dinitrobenzene	1.49	64.81	72.90
107.	*o*-Dinitrobenzene	1.58	64.17	69.66
108.	*p*-Dinitrobenzene	1.46	64.95	69.08
109.	2,4-Dinitrotoluene	1.98	68.85	79.00
110.	Diphenyl ether	4.20	82.67	90.09
111.	Ethylbenzene	3.15	78.34	90.34
112.	*m*-Fluoronitrobenzene	1.99	68.93	78.02
113.	*p*-Fluoronitrobenzene	1.99	67.27	73.63
114.	*p*-Fluorophenol	1.77	51.20	60.00
115.	*p*-Hydroxybenzaldehyde	1.35	37.33	53.28
116.	*p*-Methoxybenzaldehyde	1.68	60.43	70.61
117.	*p*-Methylbenzaldehyde	2.04	68.11	73.63
118.	Methyl benzoate	2.12	69.73	79.44
119.	Naphthalene	3.37	81.73	89.94
120.	*p*-Nitroacetophenone	1.53	63.40	70.40
121.	*p*-Nitrobenzaldehyde	1.20	60.87	63.94
122.	Nitrobenzene	1.85	67.67	75.19
123.	*m*-Nitrophenol	2.00	54.48	66.18
124.	*o*-Nitrophenol	1.79	64.40	74.80
125.	*p*-Nitrophenol	1.91	53.02	63.44
126.	Phenol	1.46	48.40	57.02
127.	2-Phenylethanol	1.36	50.00	64.06
128.	p-Phenylphenol	3.20	68.18	80.65
129.	3-Phenylpropanol	1.88	58.02	71.57
130.	*n*-Propylbenzene	3.68	86.02	92.05
131.	Toluene	2.69	77.55	86.35
132.	2,3,5-Trichlorotoluene	2.92	85.63	91.65

Source: Ref. 47.

Table 5 The Calculated log P and $\phi_{0,MeOH}$ Values for the 113 Substituted Aromatic Hydrocarbons Based on the Published Retention Data

Ser. No.	Name of the compound	log P	$\phi_{0,AcN}$	$\phi_{0,MeOH}$
133.	Benzene	2.022	—	56.10
134.	Toluene	2.541	—	67.67
135.	Ethylbenzene	3.060	—	75.83
136.	Propylbenzene	3.579	—	81.44
137.	Butylbenzene	4.098	—	85.88
138.	Pentylbenzene	4.617	—	89.05
139.	Hexylbenzene	5.136	—	91.53
140.	Heptylbenzene	5.655	—	103.01
141.	Octylbenzene	6.174	—	95.31
142.	Nonylbenzene	6.693	—	96.80
143.	Decylbenzene	7.212	—	98.08
144.	Monochlorobenzene	2.762	—	66.20
145.	1,2-Dichlorobenzene	3.502	—	73.82
146.	1,3-Dichlorobenzene	3.502	—	77.50
147.	1,4-Dichlorobenzene	3.502	—	75.02
148.	1,2,3-Trichlorobenzene	4.242	—	81.50
149.	1,2,4-Trichlorobenzene	4.242	—	82.98
150.	1,3,5-Trichlorobenzene	4.242	—	86.96
151.	1,2,3,4-Tetrachlorobenzene	4.982	—	87.68
152.	1,2,3,5-Tetrachlorobenzene	4.982	—	90.00
153.	1,2,4,5-Tetrachlorobenzene	4.982	—	89.09
154.	Pentachlorobenzene	5.722	—	93.81
155.	Hexachlorobenzene	6.462	—	98.10
156.	2-Monochlorotoluene	3.281	—	76.08
157.	3-Monochlorotoluene	3.281	—	75.90
158.	4-Monochlorotoluene	3.281	—	75.22
159.	2,4-Dichlorotoluene	4.021	—	83.93
160.	2,5-Dichlorotoluene	4.021	—	82.54
161.	2,6-Dichlorotoluene	4.021	—	84.17
162.	3,4-Dichlorotoluene	4.021	—	80.78
163.	3,5-Dichlorotoluene	4.021	—	84.18
164.	2,4,5-Trichlorotoluene	4.761	—	88.43
165.	1-Monochloronaphthalene	4.035	—	73.64
166.	2-Monochloronaphthalene	4.035	—	82.15
167.	1,2-Dichloronaphthalene	4.775	—	81.12
168.	1,3-Dichloronaphthalene	4.755	—	87.21
169.	1,4-Dichloronaphthalene	4.755	—	89.04
170.	1,5-Dichloronaphthalene	4.755	—	89.06
171.	1,8-Dichloronaphthalene	4.755	—	84.59
172.	2,3-Dichloronaphthalene	4.755	—	86.11
173.	2,7-Dichloronaphthalene	4.755	—	85.93
174.	1,3,7-Trichloronaphthalene	5.515	—	93.43
175.	2,3,6-Trichloronaphthalene	5.515	—	89.53
176.	1,2,3,4-Tetrachloronaphthalene	6.255	—	98.64
177.	1,2,3,5-Tetrachloronaphthalene	6.255	—	98.32
178.	1,3,5,7-Tetrachloronaphthalene	6.255	—	99.87
179.	1,3,5,8-Tetrachloronaphthalene	6.255	—	97.88
180.	Octachloronaphthalene	9.215	—	112.06

Table 5 Continued

Ser. No.	Name of the compound	log P	$\phi_{0,AcN}$	$\phi_{0,MeOH}$
181.	Biphenyl	3.969	—	74.68
182.	2-Monochlorobiphenyl	4.709	—	81.86
183.	3-Monochlorobiphenyl	4.709	—	85.29
184.	4-Monochlorobiphenyl	4.709	—	84.68
185.	2,2′-Dichlorobiphenyl	5.449	—	80.95
186.	2,4-Dichlorobiphenyl	5.449	—	88.30
187.	2,4′-Dichlorobiphenyl	5.449	—	89.55
188.	2,5-Dichlorobiphenyl	5.449	—	82.18
189.	2,6-Dichlorobiphenyl	5.449	—	85.39
190.	2,2′,5-Trichlorobiphenyl	6.189	—	86.37
191.	2,3,4-Trichlorobiphenyl	6.189	—	90.63
192.	2,3′,4′-Trichlorobiphenyl	6.189	—	90.14
193.	2,3′,5-Trichlorobiphenyl	6.189	—	90.59
194.	2,3,6-Trichlorobiphenyl	6.189	—	113.06
195.	2,4,5-Trichlorobiphenyl	6.189	—	92.82
196.	2,4′,5-Trichlorobiphenyl	6.189	—	90.27
197.	2,4,6-Trichlorobiphenyl	6.189	—	90.93
198.	2,2′,3,3′-Tetrachlorobiphenyl	6.929	—	87.46
199.	2,2′,3,5′-Tetrachlorobiphenyl	6.929	—	89.02
200.	2,2′,4,4′-Tetrachlorobiphenyl	6.929	—	91.62
201.	2,2′,4,5′-Tetrachlorobiphenyl	6.929	—	90.99
202.	2,2′,4,6-Tetrachlorobiphenyl	6.929	—	90.06
203.	2,2′,5,5′-Tetrachlorobiphenyl	6.929	—	90.28
204.	2,2′,5,6′-Tetrachlorobiphenyl	6.929	—	87.03
205.	2,2′,6,6′-Tetrachlorobiphenyl	6.929	—	82.31
206.	2,3′,4,4′-Tetrachlorobiphenyl	6.929	—	93.48
207.	2,3,4,5-Tetrachlorobiphenyl	6.929	—	95.71
208.	2,3′,4′,5-Tetrachlorobiphenyl	6.929	—	93.17
209.	2,3′,4,6-Tetrachlorobiphenyl	6.929	—	92.82
210.	2,3′,5,5′-Tetrachlorobiphenyl	6.929	—	94.90
211.	2,3,5,6-Tetrachlorobiphenyl	6.929	—	93.07
212.	2,4,4′,6-Tetrachlorobiphenyl	6.929	—	92.89
213.	3,3′,4,4′-Tetrachlorobiphenyl	6.929	—	93.67
214.	2,2′,3,4,5′-Pentachlorobiphenyl	7.669	—	93.84
215.	2,2′,3′,4,5-Pentachlorobiphenyl	7.669	—	97.85
216.	2,2′,3,5,6-Pentachlorobiphenyl	7.669	—	92.09
217.	2,2′,4,5,5′-Pentachlorobiphenyl	7.669	—	94.21
218.	2,2′,4,5,6-Pentachlorobiphenyl	7.669	—	91.47
219.	2,3,4,5,6-Pentachlorobiphenyl	7.669	—	97.07
220.	2,2′,3,3′,4,4′-Hexachlorobiphenyl	8.409	—	94.60
221.	2,2′,3,3′,5,5′-Hexachlorobiphenyl	8.409	—	96.35
222.	2,2′,3,3′,6,6′-Hexachlorobiphenyl	8.409	—	89.55
223.	2,2′,3,4,4′,5′-Hexachlorobiphenyl	8.409	—	95.18
224.	2,2′,3,4,5,5′-Hexachlorobiphenyl	8.409	—	96.53
225.	3,3′,3,5,5′,6-Hexachlorobiphenyl	8.409	—	94.00
226.	2,2′,4,4′,5,5′-Hexachlorobiphenyl	8.409	—	96.82
227.	2,2′,4,5,5′,6′-Hexachlorobiphenyl	8.409	—	95.98
228.	2,2′,4,4′,6,6′-Hexachlorobiphenyl	8.409	—	95.49

Table 5 Continued

Ser. No.	Name of the compound	log P	$\phi_{0,AcN}$	$\phi_{0,MeOH}$
229.	2,3,3′,4,4′,5-Hexachlorobiphenyl	8.409	—	98.84
230.	2,3,3′,4,5,6-Hexachlorobiphenyl	8.409	—	96.72
231.	3,3′,4,4′,5,5′-Hexachlorobiphenyl	8.409	—	94.26
232.	2,2′,3,3′,4,4′,6-Heptachlorobiphenyl	9.149	—	96.63
233.	2,2′,3,4,4′,5,6-Heptachlorobiphenyl	9.149	—	98.00
234.	2,2′,3,4,4′,5′,6-Heptachlorobiphenyl	9.149	—	97.44
235.	2,2′,3,4,5,5′,6,6′-Octachlorobiphenyl	9.889	—	97.26
236.	2,2′,3,3′,4,4′,5,5′-Octachlorobiphenyl	9.889	—	100.19
237.	2,2′,3,3′,4,4′,5,6-Octachlorobiphenyl	9.889	—	98.97
238.	2,2′,3,3′,4,4′,6,6′-Octachlorobiphenyl	9.889	—	99.00
239.	2,2′,3,3′,4,5,5′,6-Octachlorobiphenyl	9.889	—	99.15
240.	2,2′,3,3′,5,5′,6,6′-Octachlorobiphenyl	9.889	—	97.49
241.	2,2′,3,4,4′,5,6,6′-Octachlorobiphenyl	9.889	—	99.84
242.	2,2′,3,3′,4,4′,5,5′,6-Nonachlorobiphenyl	10.629	—	101.38
243.	2,2′,3,3′,4,4′,5,6,6′-Nonachlorobiphenyl	10.629	—	100.97
244.	2,2′,3,3′,4,5,5′,6,6′-Nonachlorobiphenyl	10.629	—	100.50
245.	Decachlorobiphenyl	11.369	—	103.52

Source: Ref. 48.

Table 6 The Calculated log P and $\phi_{0,MeOH}$ Values for 143 Drug Molecules Based on the Published Retention Data

Ser. No.	Name of the compound	log P	$\phi_{0,AcN}$	$\phi_{0,MeOH}$
246.	Acetanilide	1.131	—	45.28
247.	Acetophenazine	2.779	—	67.38
248.	Acetyl sulfisoxazole	−2.192	—	50.48
249.	Aminopromazine	4.189	—	68.77
250.	Amitriptyline	5.993	—	68.26
251.	Amodiaquin	4.468	—	60.04
252.	Amphetamine	1.969	—	27.65
253.	Antazoline	3.233	—	52.94
254.	Antipyrine	0.551	—	44.52
255.	Atropine	2.119	—	37.02
256.	Atropine methyl	2.679	—	35.78
257.	Benzatropine (benztropine)	4.064	—	69.35
258.	Bromodiphenhydramine	4.243	—	65.91
259.	Bromopheniramine	3.960	—	60.90
260.	Bupivacaine	4.846	—	54.12
261.	Butacaine	4.287	—	47.53
262.	Butaperazine	4.393	—	77.70
263.	Caffeine	0.681	—	37.59
264.	Carbinoxamine	2.748	—	57.47
265.	Chlorcyclizine	3.792	—	66.29
266.	Chloroprocaine	3.010	—	28.73
267.	Chlorpromazine	4.713	—	71.90
268.	Cinchonidine	3.034	—	52.38
269.	Cinconine	3.034	—	51.23
270.	Clemizole	4.709	—	68.46
271.	Cyclizine	3.052	—	49.85
272.	Cyclothiazide	1.691	—	47.74
273.	Cycrimine	4.390	—	49.55
274.	Desipramine	4.166	—	56.27
275.	Dextromethorphan	4.730	—	48.96
276.	Dibucaine	3.779	—	62.95
277.	Dienestrol	5.883	—	61.85
278.	Diethylstilbestrol	6.247	—	61.84
279.	Dihydrocinchonidine	3.398	—	55.41
280.	Dihydrocinchonine	3.398	—	54.34
281.	Dihydroergocornine	2.339	—	52.46
282.	Dihydroergocristine	2.959	—	56.82
283.	Dihydroergocryptine	2.858	—	56.37
284.	Dihydroquinidine	3.467	—	57.68
285.	Dihydroquinine	3.467	—	58.85
286.	Diphenhydramine	3.294	—	46.99
287.	Diphenylpyraline	3.390	—	51.07
288.	Doxylamine	2.527	—	38.60
289.	Dyphylline	−1.049	—	24.91
290.	Ephedrine	1.178	—	19.59
291.	Ergonovine	1.750	—	30.92
292.	Ergotamine	1.846	—	63.40

Table 6 Continued

Ser. No.	Name of the compound	log P	$\phi_{0,AcN}$	$\phi_{0,MeOH}$
293.	Estradiol	4.960	—	73.05
294.	Estradiol benzoate	6.953	—	87.66
295.	Estradiol cypionate	8.610	—	91.60
296.	Estradiol valerate	7.417	—	87.51
297.	Estriol	3.865	—	59.91
298.	Estrone	4.424	—	72.22
299.	Ethinyl estradiol	5.270	—	71.68
300.	Fluphenazine	4.339	—	75.07
301.	Homatropine	1.889	—	28.16
302.	Hydrochlorothiazide	−0.070	—	21.47
303.	Hydrocortisone	2.029	—	62.92
304.	Hydroxyamphetamine	1.444	—	6.79
305.	Hyoscyamine	2.119	—	38.54
306.	Imipramine	4.532	—	68.16
307.	Isoproterenol	0.647	—	−5.23
308.	Lidocaine	3.134	—	35.53
309.	Meclizine	5.696	—	84.74
310.	Medroxyprogesterone acetate	5.027	—	78.13
311.	Mephentermine	2.792	—	34.80
312.	Mesoridazine	3.635	—	60.46
313.	Mestranol	5.864	—	82.59
314.	Methamphetamine	2.273	—	31.88
315.	Methapyriline	3.394	—	49.83
316.	Methotrimeprazine	4.561	—	66.65
317.	Methoxyamphetamine	1.969	—	37.21
318.	Methoxypromazine	4.042	—	65.61
319.	Methyldopate	0.650	—	26.71
320.	Methylparaben	1.586	—	55.04
321.	Methyltestosterone	5.331	—	76.64
322.	Naphazoline	2.629	—	43.56
323.	Norethindrone	4.603	—	71.36
324.	Nortriptyline	5.627	—	69.43
325.	Oxyphencyclimine	3.990	—	65.95
326.	Perphenazine	3.930	—	74.59
327.	Phenacetin	1.719	—	54.44
328.	Phenindamine	4.532	—	61.07
329.	Pheniramine	3.011	—	46.70
330.	Phenothiazine	3.764	—	73.78
331.	Phenoxybenzamine	5.401	—	61.27
332.	Phentermine	2.488	—	35.32
333.	Phentolamine	3.147	—	49.25
334.	Phenylpropanolamine	0.874	—	118.19
335.	Phenylephrine	0.134	—	−20.1
336.	Phenyltoloxamine	4.425	—	60.71
337.	Phthalylsulfathiazole	1.359	—	43.44
338.	Physostigmine	2.067	—	34.55

Table 6 Continued

Ser. No.	Name of the compound	log P	$\phi_{0,AcN}$	$\phi_{0,MeOH}$
339.	Prednisolone	1.954	—	62.41
340.	Prednisone	1.418	—	58.11
341.	Procaine	2.270	—	21.13
342.	Prochlorperazine	4.506	—	82.87
343.	Progesterone	4.508	—	79.49
344.	Promazine	3.973	—	65.96
345.	Promethazine	4.551	—	65.04
346.	Pyrantel	2.790	—	45.35
347.	Pyrilamine	2.780	—	55.27
348.	Pyrvinium	7.992	—	78.19
349.	Quinidine	3.103	—	55.14
350.	Quinine	3.103	—	55.59
351.	Salicylamide	0.206	—	40.64
352.	Salicylic acid	1.225	—	42.75
353.	Scopolamine	0.752	—	26.96
354.	Scopolamine aminoxide	0.941	—	26.07
355.	Spironolactone	5.053	—	70.03
356.	Succinylsulfathiazole	0.156	—	34.38
357.	Sulfabenzamide	1.896	—	43.24
358.	Sulfachlorpyridazine	−0.293	—	39.06
359.	Sulfadiazine	−0.783	—	25.59
360.	Sulfadimethoxine	−0.645	—	50.36
361.	Sulfamerazine	−0.264	—	32.52
362.	Sulfamethazine	0.255	—	37.52
363.	Sulfamethizole	0.405	—	27.11
364.	Sulfamethoxazole	0.262	—	39.90
365.	Sulfamethoxypyridazine	0.400	—	37.50
366.	Sulfanilamide	−0.726	—	−0.20
367.	Sulfanilic acid	−1.690	—	−18.19
368.	Sulfaphenazole	1.999	—	46.52
369.	Sulfapyridine	0.325	—	28.93
370.	Sulfathiazole	0.050	—	27.08
371.	Sulfisomidine	0.255	—	26.45
372.	Sulfisoxazole	−0.210	—	40.52
373.	Testosterone	4.812	—	74.34
374.	Testosterone cypionate	8.462	—	92.31
375.	Testosterone enanthate	8.307	—	91.70
376.	Testosterone propionate	6.231	—	84.28
377.	Tetracaine	3.414	—	57.65
378.	Theobromine	0.162	—	22.57
379.	Theophylline	−0.020	—	26.78
380.	Thioridazine	5.765	—	74.22
381.	Trichlormethiazole	0.872	—	42.64
382.	Trimeprazine	4.492	—	66.53
383.	Tripelennamine	2.711	—	54.24
384.	Triprolidine	4.707	—	58.94
385.	Tropic acid	0.829	—	39.12

Source: Ref. 49.

Table 7 The Calculated log P, $\phi_{0,MeOH}$, and $\phi_{0,AcN}$ Values for 26 Drug Molecules Based on the Published Retention Data

Ser. No.	Name of the compound	log P	$\phi_{0,AcN}$	$\phi_{0,MeOH}$
386.	Resorcin	0.80	17.27	24.39
387.	Sulfadimidinine	0.32	30.57	40.55
388.	Sulfamethoxypyridiazine	0.40	31.30	40.77
389.	Barbital	0.65	26.44	39.76
390.	Phenobarbital	1.42	42.04	53.14
391.	Chloramphenicol	1.14	39.25	51.89
392.	Salicylamide	1.28	34.16	46.72
393.	Phenacetin	1.58	44.34	58.83
394.	Vanillin	1.37	35.49	47.61
395.	Benzaldehyde	1.45	51.98	—
396.	Acetanilide	1.16	37.78	53.44
397.	Nicotinamide	−0.57	6.57	21.77
398.	Benzoic acid	1.87	44.08	56.20
399.	Salicylic acid	2.25	47.34	59.93
400.	Acetylsalicylic acid	1.23	39.60	—
401.	Caffeine	−0.07	18.46	43.44
402.	Hydrochlorothiazide	−0.07	1.95	25.79
403.	Cortexolone	2.46	54.87	—
404.	Dexamethasone	1.99	40.98	—
405.	Deoxycortone	2.88	76.35	—
406.	Sulfaguanidine	−1.22	0.41	—
407.	Isoniazid	−1.14	1.59	—
408.	Methylsalicylate	2.46	70.63	81.68
409.	Hydrocortisone	1.61	33.80	—
410.	Progesterone	3.87	95.36	—
411.	Testosterone	3.31	75.87	—

Source: Refs. 39 and 42.

Table 8 The Calculated log P and $\phi_{0,AcN}$ Values for 12 Morphine Derivatives Based on the Published Retention Data

Ser. No.	Name of the compound	log P	$\phi_{0,AcN}$	$\phi_{0,MeOH}$
412.	Azidomorphine	1.694	31.35	—
413.	Azidocodeine	2.288	77.97	—
414.	*N*-Cyclopropylmethylazidomorphine	2.887	63.93	—
415.	Azidoethylmorphine	2.807	97.95	—
416.	*N*-Phenylmethylazidoethylmorphine	4.465	86.56	—
417.	*N*-Phenylmethylazidomorphine	3.352	74.93	—
418.	Acetylazidomorphine	1.638	119.25	—
419.	Norazidoethylmorphine	2.441	83.74	—
420.	*N*-Cyclopropylmethylazidoethylmorphine	4.000	84.74	—
421.	Norazidomorphine	1.328	31.40	—
422.	Normorphine	1.497	12.42	—
423.	Morphine	1.863	15.57	—

Source: Ref. 41.

Table 9 The Calculated log P and $\phi_{0,AcN}$ Values for 11 Tricyclic Drug Molecules Based on the Published Retention Data

Ser. No.	Name of the compound	log P	$\phi_{0,AcN}$	$\phi_{0,MeOH}$
424.	EGYT-2347	5.713	86.64	—
425.	EGYT-2509	3.980	88.00	—
426.	EGYT-2474	4.499	84.41	—
427.	EGYT-2541	3.832	90.85	—
428.	RL-205	3.011	74.08	—
429.	RL-215	3.773	93.62	—
430.	RL-218	3.197	74.33	—
431.	Peritol	6.587	88.38	—
432.	Hybernal	4.772	114.49	—
433.	Pipolphen	4.551	89.25	—
434.	Melleril	5.790	111.33	—

Source: Ref. 59.

Table 10 The Calculated log P and $\phi_{0,AcN}$ Values for 18 Benzodiazepine Derivatives Based on the Published Retention Data

Ser. No.	Name of the compound	log P	$\phi_{0,AcN}$	$\phi_{0,MeOH}$
435.	7-Aminonitrazepam	0.950	51.41	—
436.	Bromazepam	1.649	73.32	—
437.	Uxepam	0.981	62.10	—
438.	Oxazepam	1.180	62.48	—
439.	Lorazepam	3.466	64.67	—
440.	Nitrazepam	1.726	71.24	—
441.	Clonazepam	2.466	68.87	—
442.	Chlordiazepoxide	2.443	79.08	—
443.	Alprazolam	3.609	84.53	—
444.	Desmethyldiazepam	2.726	75.75	—
445.	Flunitrazepam	1.814	75.34	—
446.	Clorazepat	−0.638	77.23	—
447.	Diazepam	2.597	84.01	—
448.	Midazolam	4.345	74.18	—
449.	Medazepam	4.007	91.88	—
450.	Prazepam	3.790	87.55	—
451.	Clobazam	1.994	76.68	—
452.	Tofizopam	3.647	81.37	—

Source: Ref. 51.

Table 11 The Calculated log P and $\phi_{0,MeOH}$ Values for 19 Deoxyuridine Derivatives Based on the Published Retention Data

Ser. No.	Name of the compound	log P	$\phi_{0,AcN}$	$\phi_{0,MeOH}$
453.	Deoxyuridine	−0.544	—	16.00
454.	Ethyldeoxyuridine	0.494	—	24.68
455.	*i*-Propyldeoxyuridine	1.013	—	30.27
456.	*sec*-Butyldeoxyuridine	1.532	—	46.06
457.	*tert*-Butyldeoxyuridine	1.532	—	46.46
458.	Pentyldeoxyuridine	2.051	—	57.82
459.	Hexyldeoxyuridine	2.570	—	61.24
460.	Vinyldeoxyuridine	0.285	—	25.14
461.	Butenyldeoxyuridine	1.323	—	48.41
462.	Pentenyldeoxyuridine	1.842	—	58.40
463.	Hexenyldeoxyuridine	2.361	—	67.40
464.	Heptenyldeoxyuridine	2.880	—	72.19
465.	Octenyldeoxyuridine	3.399	—	77.17
466.	Propynyldeoxyuridine	0.285	—	25.97
467.	Butynyldeoxyuridine	0.804	—	32.73
468.	Hexynyldeoxyuridine	1.842	—	56.89
469.	Heptynyldeoxyuridine	2.361	—	48.86
470.	Octynyldeoxyuridine	2.880	—	69.24
471.	Methyldeoxyuridine	0.016	—	21.19

Source: Ref. 52.

Table 12 The Calculated log P and $\phi_{0,MeOH}$ Values for 16 Aniline and Phenol Derivatives Based on the Published Retention Data

Ser. No.	Name of the compound	log P	$\phi_{0,AcN}$	$\phi_{0,MeOH}$
472.	*o*-Nitroaniline	1.129	—	60.77
473.	*m*-Nitroaniline	1.447	—	52.87
474.	*p*-Nitroaniline	0.840	—	45.79
475.	2,4-Dinitroaniline	0.894	—	64.23
476.	2,4,6-Trinitroaniline	0.948	—	63.48
477.	2-Cl-4-nitroaniline	1.582	—	67.11
478.	4-Cl-3-nitroaniline	2.189	—	62.77
479.	2,6-DiCl-4-nitroaniline	2.324	—	78.05
480.	*p*-Nitrophenol	1.291	—	57.60
481.	2,4-Dinitrophenol	1.345	—	61.69
482.	2,6-Dinitrophenol	1.634	—	57.72
483.	2,4,6-Trinitrophenol	1.399	—	50.76
484.	3,5-Dinitro-4-cyanophenol	0.987	—	57.41
485.	3-Nitro-4-cyano-5-chlorophenol	2.341	—	71.72
486.	3-Nitro-4-cyano-5-bromophenol	2.725	—	63.30
487.	3-Nitro-4-cyano-5-iodophenol	3.367	—	55.86

Source: Ref. 53.

Table 13 The Calculated log P and $\phi_{0,MeOH}$ Values for 42 Adenosine Monophosphate Derivatives Based on the Published Retention Data

Ser. No.	Name of the compound	log P	$\phi_{0,AcN}$	$\phi_{0,MeOH}$
488.	2-*n*-Hexyl	—	—	65.70
489.	8-PCTP	—	—	60.13
490.	6-Bezyloxy	—	—	62.23
491.	Dibutyryl	—	—	55.69
492.	2-Phenyl	—	—	51.39
493.	2-*n*-Butyl	—	—	51.29
494.	2′-DNP	—	—	54.04
495.	2-Thiopropyl	—	—	52.20
496.	6-(S_p)-DMA-*S*	—	—	46.28
497.	2-*n*-Propyl	—	—	42.47
498.	6-(R_p)-DMA-*S*	—	—	41.65
499.	6-Thiomethyl	—	—	41.49
500.	6-DMA	—	—	40.21
501.	2-Ethyl	—	—	34.78
502.	2-Thiomethyl	—	—	34.88
503.	Monobutyryl	—	—	38.07
504.	8-Bromo	—	—	30.99
505.	8-Thioethyl	—	—	29.62
506.	(S_p)-cAMPS	—	—	26.89
507.	6-MA	—	—	29.65
508.	8-OH-*i*-P	—	—	27.77
509.	1′N^6-Etheno	—	—	26.41
510.	8-Methoxy	—	—	25.54
511.	2-Chloro	—	—	31.77
512.	(R_p)-cAMPS	—	—	23.75
513.	6-Methoxy	—	—	31.91
514.	6-Chloro	—	—	31.10
515.	8-MA	—	—	23.61
516.	cAMP	—	—	21.96
517.	(S_p)-cGMPS	—	—	19.28
518.	cPuMP	—	—	20.91
519.	3′NH-cAMP	—	—	21.10
520.	5′NH-cAMP	—	—	18.15
521.	2-Methyl	—	-	16.99
522.	8-Thio	—	—	13.46
523.	8-Amino	—	—	14.89
524.	8-DMA	—	—	14.90
525.	cIMP	—	—	13.52
526.	cGMP	—	—	13.13
527.	N^1-Methoxy	—	—	12.76
528.	N^1-Oxide	—	—	10.42
529.	8-Hydroxy	—	—	7.04

Source: Ref. 54.

Table 14 The Calculated log P and $\phi_{0,MeOH}$ Values for 10 β-Lactame Antibiotics Based on the Published Retention Data

Ser. No.	Name of the compound	log P	$\phi_{0,AcN}$	$\phi_{0,MeOH}$
530.	Carbenicillin phenyl	3.14	—	50.57
531.	Dicloxacillin	2.83	—	47.92
532.	Floxacillin	2.58	—	47.56
533.	Cloxacillin	2.48	—	48.23
534.	Phenethicillin	2.19	—	45.80
535.	Penicillin V	1.62	—	43.78
536.	Penicillin G	1.30	—	34.48
537.	Ampicillin	0.94	—	37.60
538.	Amoxicillin	0.48	—	8.89
539.	Sulbenicillin	0.20	—	3.51

Source: Ref. 56.

Table 15 The Calculated log P and $\phi_{0,AcN}$ Values for 12 Barbiturate Derivatives Based on the Published Retention Data

Ser. No.	Name of the compound	log P	$\phi_{0,AcN}$	$\phi_{0,MeOH}$
540.	5-Ethylbarbituric acid	1.52	−2.93	—
541.	5-Ethyl-5-methylbarbituric acid	0.02	−0.14	—
542.	Barbital	0.68	3.92	—
543.	5-Ethyl-5-*n*-propylbarbituric acid	0.87	10.65	—
544.	Butethal	1.70	18.33	—
545.	5-Ethyl-5-*n*-hexylbarbituric acid	3.08	32.44	—
546.	5-Ethyl-5-*n*-heptylbarbituric acid	3.64	35.35	—
547.	5-Ethyl-5-*n*-octylbarbituric acid	3.85	41.98	—
548.	5-Ethyl-5-*n*-nonylbarbituric acid	4.13	46.26	—
549.	Pentobarbital	2.13	22.35	—
550.	Amobarbital	2.11	23.98	—
551.	Phenobarbital	1.42	14.58	—

Source: Ref. 55.

REFERENCES

1. RJ Laub, RL Pecsok. Physicochemical Applications of Gas Chromatography. New York: Wiley Interscience.
2. JR Conder, CL Young. Physicochemical Measurements by Gas Chromatography. Chichester: Wiley, 1979.
3. R Kaliszan. Quantitative Structure—Chromatographic Retention Relationships. New York: Wiley, 1987.
4. T Cserháti, K Valkó. Chromatographic Determination of Molecular Interactions, Applications in Biochemistry, Chemistry, and Biophysics. Boca Raton, FL: CRC Press, 1993.
5. E Overton. Z Physikal Chem 22:189, 1897.
6. H Meyer. Arch Exp Pathol Pharmakol 42:109, 1899.
7. R Collander. Acta Chem Scand 5:774, 1951.
8. C Hansch, T Fujita. J Am Chem Soc 86:1616, 1964.
9. CV Eadsforth, P Moser. Chemosphere 12:1459, 1983.
10. JK Seydel, KJ Schaper. Chemische Struktur und Biologische Aktivitat von Wirkstoffen. New York: Verlag Chemie, 1979.

11. C Hansch, A Leo. Substituent Constants for Correlation Analysis in Chemistry and Biology. New York: Wiley, 1979.
12. C Hansch, WJ Dunn. J Pharm Sci 61:1, 1972.
13. CLOGP, MedChem Software, Pomona, CA.
14. C Hansch, SM Anderson. J Org Chem 32:2583, 1967.
15. RF Rekker. The Hydrophobic Fragmental Constant. Its Derivation and Application. A Means of Characterizing Membrane Systems. Amsterdam: Elsevier, 1977.
16. ProLogP. An expert system for the calculation of log P. Budapest: CompuDrug Chemistry, 1991, Version 4.1.
17. H Van de Waterbeemd. In: F Davvas, ed. Hydrophobicity of Organic Compounds. How to calculate it by PC's. Booksoft Series. Vienna: CompuDrug International, 1986.
18. AJP Martin, RLM Synge. Biochem J 35:1358, 1941.
19. S Marcinkiewicz, J Green. J Chromatogr 10:372, 1963.
20. CBC Boyce, BV Milbarrow. Nature 208:537, 1965.
21. AJ Leo. In: RF Gould, ed.: Biological Correlations—The Hansch Approach. Advances in Chemistry Series. No. 114. Washington, DC: American Chemical Society, 1972, p. 51.
22. T Yamana, A Tsuji, E Miyamoto, O Kubo. J Pharm Sci 66:747, 1977.
23. PJ Schoenmakers, HAH Billiet, R Tijssen, L de Galan. J Chromatogr 149:519, 1978.
24. PJ Schoenmakers, HAH Billiet, L de Galan. J Chromatogr 185:179, 1979.
25. PJ Schoenmakers, HAH Billiet, L de Galan. J Chromatogr 282:107, 1983.
26. A Brent, JJ Sabatka, DJ Minick, DJ Henry. J Med Chem 26:1014, 1983.
27. SE Krikorian, TA Chorn, JW King. Quant Struct Activ Relat 6:65, 1987.
28. F Gaspari, M Bonati. J Pharm Pharmacol 39:252, 1987.
29. CV Eadsforth. Pestic Sci 17:311, 1986.
30. JE Haky, AM Young. J Lig Chromatogr 7:675, 1984.
31. T Braumann, G Weber, LH Grimme. J Chromatogr 261:329, 1983.
32. WE Hammers, GJ Meurs, CL de Ligny. J Chromatogr 247:1, 1982.
33. K Valkó. In: H. Kalász, LS Ettre, eds. Chromatography, The State of the Art. Budapest: Akadémia, 1985, p 739.
34. MS Mirrlees, SJ Moulton, CT Murphy, PJ Taylor. J Med Chem 19:615, 1976.
35. SH Unger, JR Cook, JS Hollenberg. J Pharm Sci 67:1364, 1978.
36. DJ Minick, J Frenz, MA Patrick, DA Brent. J Med Chem 10:1923, 1988.
37. H Terada. Quant Struct Activ Relat 5:81, 1986.
38. K Miyake, N Mizuno, H Terada. J Chromatogr 439:227, 1988.
39. K Valkó. J Lig Chromatogr 7:1405, 1984.
40. K Valkó. In: Chromatography 84. H Kalász, LS Ettre, eds. Budapest: Adadémiai Kiadó, 1986, p. 73.
41. K Valkó, T Friedmann, J Báti, A Nagykáldi. J Lig Chromatogr 7:2073, 1984.
42. K Valkó. J Lig Chromatogr 10:1663, 1987.
43. K Valkó, P Slégel. J Chromatogr 631:49, 1993.
44. D Reymond, GN Chung, JM Mayer, B Testa. J Chromatogr 391:97, 1987.
45. HA Cooper, RJ Hurtubise. J Chromatogr 360:313, 1986.
46. T Braumann, G Weber, LH Grimme. J Chromatogr 261:329, 1983.
47. PJ Schoenmakers, HAH Billiet, L de Galan. J Chromatogr 218:261, 1981.
48. A Opperhuizen, TL Sinnige, JMD van der Steen. J Chromatogr 388:51, 1987.
49. RW Roos, CA Lau-Cam. J Chromatogr 370:403, 1986.
50. A. Kálmán, L Párkányi, K Valkó, G Mátray, J Batke, J Gaál. Acta Biochim Biophys Hung 24:143, 1989.
51. K Valkó, S Olajos, T Cserháti. J Chromatogr 499:361, 1990.
52. K Valkó, P Slégel. J Chromatogr 592:59, 1992.
53. G Gullner, T Cserháti, B Bordás, K Valkó. J Liq Chromatogr 12:957, 1989.
54. T Braumann, B Jastorff. J Chromatogr 350:105, 1985.
55. S Toon, J Mayer, M Rowland. J Pharm Sci 73:625, 1984.

56. T Yamana, A Tsuji, E Miyamoto, O Kubo. J Pharm Sci 66:747, 1977.
57. K Valkó, G Csonka. Magy Kém Lap 25:134, 1986.
58. NE Tayar, H Van de Waterbeemd, B Testa. J Chromatogr 320:293, 1985.
59. HF Zou, YK Zhang, MF Hong, PC Lu. Chromatographia 32:329, 1991.
60. K Valkó. Trends Anal Chem 6:214, 1987.
61. B Sebille, N Thuaud, J Piquion, N Behar. J Chromatogr 409:61, 1987.
62. I Uekama, F Hirayama, S Nasu, N Matsuo, T Irie. Chem Pharm Bull 26:3477, 1978.
63. J Zukowski, D Sybilska, J Jurczak. Anal Chem 57:2215, 1985.
64. M Seno, M Lin, K Iwamoto. J Chromatogr 508:127, 1990.
65. RM Mohseni, RJ Hurtubise. J Chromatogr 499:395, 1990.
66. J Debowski, D Sybilska, J Jurczak. J Chromatogr 237:303, 1982.
67. D Sybilska, J Lipkowski, J Woycikowski. J Chromatogr 253:95, 1982.
68. D Sybilska, J Debowski, J Jurczak, J Zukowski. J Chromatogr 286:163, 1984.
69. J Debowski, D Sybilska. J Chromatogr 353:409, 1986.
70. K Fujimura, T Ueda, M Kitagawa, H Takayanagi, T Ando. Anal. Chem 58:2668, 1986.
71. J Visy, M Simonyi, T Láng. In: HC van der Plaas, M Simony, FC Alderweireldt, JA Lepoivre, eds. Bio-Organic Heterocycles. Amsterdam: Elsevier, 1986, p 269.
72. J Visy, M Simonyi. Chirality 1:271, 1989.
73. M Simonyi, I Fitos, J Visy. Trends Pharmacol Sci 7:112, 1986.
74. A-K Johansen, N-P Willassen, G Sager. Biochem Pharmacol 43:725, 1992.
75. S Watanabe, T Saito. Biochem Pharmacol 43:931, 1992.
76. WD Singer, RT Hersh, RH Himes. Biochem Pharmacol 37:2691, 1988.
77. WD Singer, RH Himes. Biochem Pharmacol 43:545, 1992.
78. V Colotta, L Cecchi, F Melani, G Filacchioni, C Martini, S Gelli, A Lucacchini. Il Farmaco 46:1139, 1991.
79. I Kovács, G Maksay, Z Tegyei, J Visy, I Fitos, M Kajtár, M Simonyi, L Otvos. In: HC van der Plaas, L Otvos, M Simonyi, eds. Bio-Organic Heterocycles. Amsterdam, Budapest: Elsevier-Akademia Kiado, 1984, p 239.
80. I Fitos, J Visy, M Simony. Biochem Pharmacol 41:377, 1991.
81. B Sebille, R Zini, C-V Madjar, N Thuaud, J-P Tillement. J Chromatogr 531:51, 1990.
82. T Cserháti, K Valkó. Chromatographic Determination of Molecular Interactions. Boca Raton, FL: CRC Press, 1993, p 173.
83. IA Nimmo, A Bauermeister. Biochem J 169:437, 1978.
84. JP Hummel, WJ Dreyer. Biochim Biophys Acta 63:530, 1962.
85. G Berger, G Girault, JM Galmiche. J Liq Chromatogr 12:535, 1989.
86. SF Sun, SW Kuo, RA Nash. J Chromatogr 288:377, 1984.
87. SF Sun, CL Hsiao. J Chromatogr 648:325, 1993.
88. MJ Morris, JR Brown. J Pharm Pharmacol 29:642, 1977.
89. B Sebille, N Thuaud, JP Tillement. J Chromatogr 167:159, 1978.
90. B Sebille, N Thuaud, J Tillement. J Chromatogr 180:103, 1979.
91. WR Melander, B-K Chen, C Horváth. J Chromatogr 318:1, 1985.
92. WR Melander, DE Campbell, C Horváth. J Chromatogr 158:315, 1978.
93. H Colin, JC Diez-Masa, G Guiochon, T Czajkowsa, I Medziak. J Chromatogr 167:41, 1978.
94. JH Knox, G Vasvári. J Chromatogr 83:181, 1973.
95. LA Cole, JG Dorsey. Anal Chem 64:1317, 1992.
96. LA Cole, JG Dorsey, KA Dill. Anal Chem 64:1324, 1992.
97. J Frenz, C Horváth. AIChE. J. 31:400, 1985.
98. J Jacobson, J Frenz, C Horváth. J Chromatogr 316:53, 1984.
99. S Levin, S Abu-Lafi. J Chromatogr 556:277, 1991.
100. S Golshan-Shirazi, G Guiochon. Anal Chem 62:923, 1990.
101. EV Dose, S Jacobson, G Guiochon. Anal Chem 63:833, 1991.

28

HPLC Applications in Art Conservation

Susana M. Halpine*

National Gallery of Art, Washington, D.C.

I. INTRODUCTION

A. Background

The concept of the modern public museum began with the opening of the British Museum, London, in 1759, which displayed natural history specimens, manuscripts, art pieces, and collections of ethnographic, numismatic, and classical artifacts [1]. Since then, museums worldwide have unveiled holdings as diverse as contemporary toy collections, local historical artifacts, NASA spacesuits and airships, modern video art, outdoor sculpture, and architectural sites. The physical maintenance of these collections has been entrusted to conservators, whose tasks include examination, treatment, storage, and display of the artifacts for optimal preservation.

Conservators are responsible for stabilizing a wide range of materials and minimizing their natural course of degradation. A single museum piece may comprise several different materials, each material reacting independently to environmental stresses and, not infrequently, entirely incompatible with the other elements [2]. Other museum pieces may have been prepared in ways that weaken the structural integrity of the materials, such as the process of dyeing textiles [3].

In 1888, the first conservation laboratory was opened at the Staatliche Museen in Berlin, thereby acknowledging the importance of maintaining a dedicated conservation staff within a museum [4]. Scientific investigation was soon required to help the conservators understand how factors such as light, temperature, and humidity fluctuations, as well as human and biological activity could affect inherent rates of degradation. In 1896, 1 year after the discovery of the X-ray, radiography was being used to detect alterations in an oil painting, and in 1928 the Fogg Art Museum at Harvard University established the first scientific museum laboratory [4]. The analytical interests of the field of art conservation science have subsequently grown to encompass nearly every type of material, both natural and synthetic, as well as the environmental factors that may affect these materials.

Until recently, conservation science has had to rely on techniques developed for analytical applications in other fields. With such a wide range of materials to investigate, a similarly wide range of disciplines had to be tapped from the appropriate fields of interest. More

**Current affiliation*: Consultant, Playa del Rey, California.

important, the paucity of funds available to most museums made it difficult to fund conservation research. Therefore, museum conservators have periodically collaborated with universities and industries that were able to provide support as time and funding allowed. In the past two decades, however, there has been an increasing interest in the conservation of artistic and cultural property, with a concomitant rise in the number of analytical support facilities associated with museums. Most major museums now have in-house laboratories or have access to regional centers with scientific equipment. The instrumentation generally includes light and phase-contrast microscopes, gas chromatographs (GC), infrared (IR) and ultraviolet–visible (UV–Vis) spectrophotometers, X-ray radiography, diffraction (XRD) and fluorescence (XRF) equipment, accelerated-aging chambers, and in the larger facilities, scanning electron microscopes (SEM), and mass spectrometers (MS).

High-performance liquid chromatography (HPLC) was introduced into conservation in the 1980s to identify organic pigments and proteinaceous paint binders. These materials had been previously characterized using more laborious methods requiring larger sample sizes or, more frequently, were simply left unidentified. At the same time, size-exclusion chromatography was being applied to the degradation of natural artists' materials and ion chromatography was monitoring inorganic corrosion products. The success of these analytical techniques has encouraged other areas of HPLC research.

The HPLC is ideally suited to manage the range of analytical approaches needed in the field of conservation science. Variations in column chemistry, solvent systems, and detectors give HPLC an adaptability that has barely begun to be tapped [5]. Of equal importance is the instrument's sample size flexibility. Most samples taken for analysis of an art object are as small as is humanly possible to manipulate. Estimating the exact amounts of components can be difficult with unique, unknown samples. HPLCs are able to maintain resolution over a wider range of sample sizes than other column chromatography systems [6]. A standard analytical HPLC column (C_{18} 4.6 × 150 mm) used to identify proteinaceous art materials can accommodate most samples sizes submitted for binder analysis, ranging from 37 ng to 4.5 μg [7]. Microbore columns offer greater detection sensitivity and small-sample capacity, while decreasing the consumption of mobile phase [5]. Large-scale or preparative columns may be helpful in "cleaning up" or separating complex samples before further analytical steps. Certainly another advantage in using HPLC, regardless of column size, is that unique samples can be collected after nondestructive HPLC techniques and submitted to other analytical methods.

This chapter will describe how art conservation science, referred to herein as art conservation, is continuing to explore a variety of HPLC techniques to assist conservators in the preservation of our cultural and historical legacy. The discussion will focus primarily, but not exclusively, on the conservation of art work in the general categories of painting, drawing, sculpture, and textiles.

B. General Areas of Investigation in Art Conservation

If you have to take care of something it helps to know what it is made of.
Max Saltzman [8]

Most museum objects have undergone some alteration of their original state, either by the natural course of deterioration or by human intervention. The primary goal of the conservator is to minimize further deterioration. Actual restoration of the object to some presumed state is usually avoided because it can often be very intrusive and ultimately misguided. Therefore, conservation treatment may include a simple cleaning, treating the object to arrest further deterioration, carrying out repairs for stabilization, and optimizing the display and storage conditions. To assist the conservator with these tasks, the conservation scientist may be asked to identify the materials involved in the object, propose alternative treatments, develop products more compatible than those traditionally used, and to isolate harmful environmental

factors. As we shall see, HPLC instrumentation is now being used in each of these phases of investigation.

Conservators are able to select the most appropriate treatment only when they can base their judgment on accurate identification of the constituent materials [9]. For example, paintings have been damaged in the past when they were cleaned using solvents that inadvertently dissolved the paint surface [10]. Accurate identification of the paint binders could have averted these problems. Classification of the materials used in an artifact may also indicate the geographic location, available resources, technical advances, and cultural priorities of the original craftspeople. In some cases, dating of the artifact can be done by identifying the incorporated materials, such as synthetic or imported pigments available only after a specific date. This historical art information enhances the appreciation and the overall value of the object.

The materials in an artifact may be incompatible with traditional treatment methods. In such instances the scientist may be consulted on novel solvent systems, enzyme preparations, and gel-poultice applications. For example, enzyme preparations have been used to remove old paste or glue accretions from paper documents and paint supports [11]. Furthermore, when new treatments are developed, it is often necessary to monitor the progress of the object during the treatment to verify that the desired outcome is underway. Accelerated aging studies are used to predict the outcome of natural aging and to test proposed treatments before applying them to the actual objects under study.

Finding more permanent materials than those currently in use is also of great interest to the field. The most commonly used natural resin varnishes are known to darken and change their solubility over time, requiring periodic cleanings and revarnishings, approximately every 50 years, that progressively weaken the paint layers [12,13]. A varnish with the desired optical and handling properties, without the negative-aging properties, is currently being sought [14].

Optimal display and storage conditions are as important as any conservation work, because a well-considered environment will minimize any need for further handling, whereas poor conditions can quickly reverse the benefits of the best treatment. Excessive heat and high humidity are fairly obvious hazards, but recommended levels for temperature and humidity may have to be tailored to the requirements of a single object or set of objects [15]. The effects of light, especially from the ultraviolet spectral region, may be extremely detrimental to some organic materials, such as fugitive lake pigments, whereas they leave other materials, such as some inorganic pigments, largely unaffected [16]. Similarly, the effects of airborne pollutants on organic and inorganic materials are only now beginning to be fully understood [17].

Analytical results must be interpreted within the proper historical context. To this end, extant records on artistic practices, such as artisan handbooks, logbooks, and pictorial records can be very helpful. Tracts written by Pliny the Elder [18], Cennino Cennini [19], and Theophilus [20], among others [21–23], provide an excellent foundation of early European artistic practices. Some artistic techniques, such as hide glue binders, cross cultural barriers and time frames [24]. On the other hand, ethnographic studies offer information on localized materials and traditions that may have survived only in isolated cultures.

II. PRIMARY HPLC APPLICATIONS IN ART CONSERVATION

A. Identification of Natural and Early Synthetic Dyestuffs

The analysis of dye components can be important in determining the color permanence of a textile artifact, in establishing its approximate date and geographic origin, and in providing insight into its original cultural value. Cochineal, a red insect dye, became an important red dye in Europe after its importation from the Americas in the 16th century [8]. The identification of cochineal in textiles will have a direct bearing on the conservation of the object,

because it is more permanent than other red dyes such as brazilwood [8]. Dye and lake pigment identification may also indicate the original color in faded areas of textiles and paintings, respectively (Fig. 1). The color of garments often indicated hierarchical rank within societies [25]; blue, purple, and scarlet dyestuffs were used along with gold and silver as religious offerings [26].

Although spectrophotometric [8,27–30] and thin-layer chromatographic (TLC) [30,31] techniques have been developed for the identification of organic pigments in museum artifacts, HPLC is generally considered the most effective means of characterizing natural and synthetic dyes as well as lake pigments [32,33]. Walker and Needles realized this potential and developed a reverse-phase (RP) HPLC system for the separation of natural dyes, based on the Snyder solvent selectivity triangle concept [33]. Using an isocratic four-solvent, single-wavelength detector system, they relied on fingerprint matching with reference material, but were hampered by impurities and minor components coeluting with the primary dyestuff. A dye extraction scheme was also developed to minimize flavonoid polymerization into complex

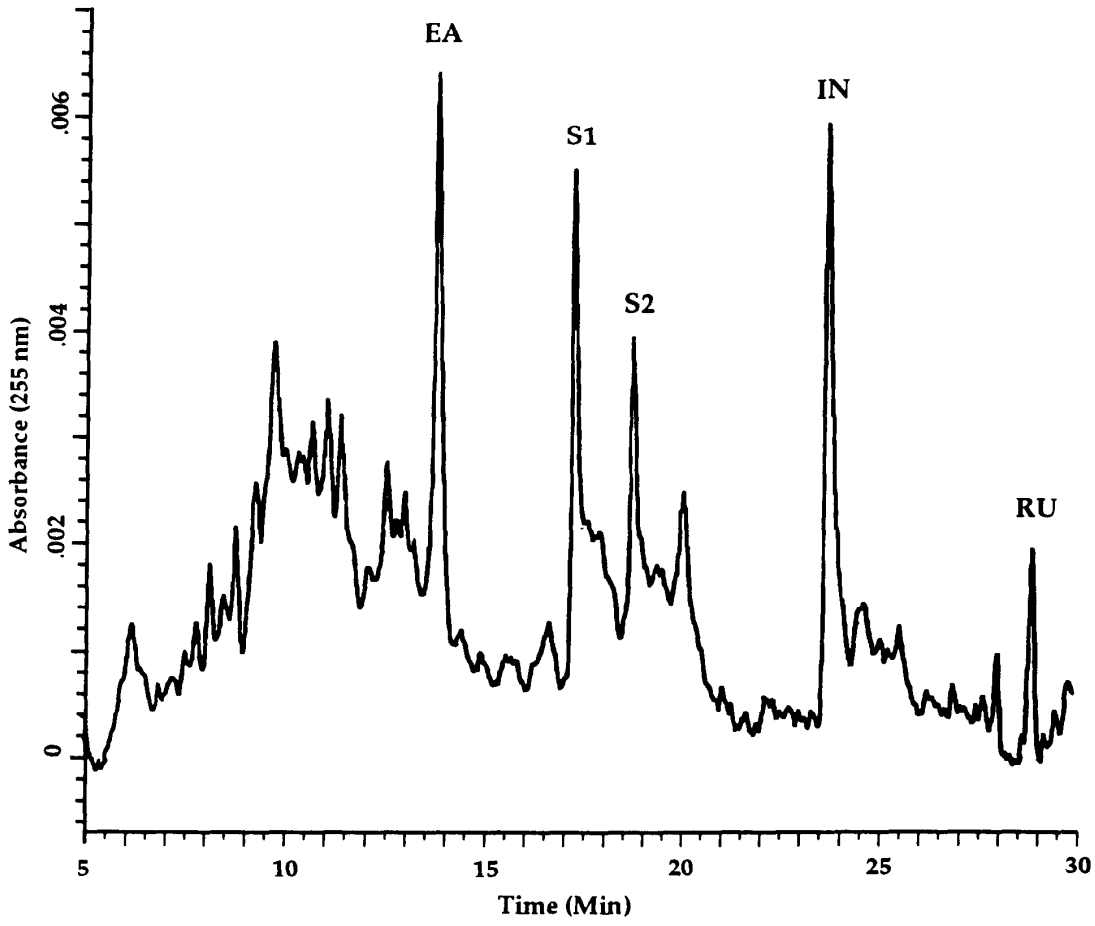


Figure 1 Clear blue dye on early woven Indian silk textile, presumed 15th–17th century, flushing weft fiber, in the collection of Association pour l'Etude et la Documentation des Textiles d'Asie, Paris, accession no. AEDTA 3110. Chromatogram monitored at 255 nm. S1 and S2 represent the synthetic dyes CI acid orange 7 and CI acid orange 5, respectively. Ellagic acid (EA), indigotin (IN), and rubiadin (RU) were also detected. Both synthetic dyes were discovered in 1876. According to textile's curator, original yarns were sampled. Therefore, this textile should be dated no earlier than the last quarter of the 19th century. The original hue probably would have been rather green, but has turned to blue after the early synthetic dyes faded. (Courtesy of Jan Wouters, Institut Royal du Patrimoine Artistique [IRPA/KIK], Brussels, Belgium.)

tannins. White used a microbore column and a single-wavelength detector to identify lake pigments in paint samples at the National Gallery, London [34,35].

Wouters took full advantage of the HPLC capabilities by using a solvent gradient and a diode-array detector (DAD), thereby effectively combining the chromatographic separation and the spectrophotometric analysis used in earlier techniques [25,36] (see Fig. 1). This reverse-phase method uses a 4.6 × 100-mm C_{18} column and a three-solvent system: (a) water, (b) methanol, and (c) 5% (w/v) phosphoric acid in water. The gradient program starts with 66 a/24 b/10 c and runs to 0 a/90 b/10 c over 32 min with the column kept at ambient temperature between 20° and 22°C [37]. The detection wavelength is selected according to the analysate, with insect red dyes monitored at 275 nm, vegetal red and yellow dyes at 255 nm, and indigoid dyes at 288 nm. Spectral information is collected from 200 to 700 nm with the DAD and a suitable data-handling system. For the retention times of the primary dyes and lake pigments separated using Wouters' phosphoric acid–methanol method, see Table 1, column A.

Halpine developed a reverse-phase separation method using a narrow-bore C_{18} column, a DAD, and a water and acetonitrile gradient system with 0.1% trifluoroacetic acid (TFA) added to both solvents [38–41]. Acetonitrile was selected over methanol because its lower UV cutoff decreases baseline rise caused by solvent absorbance, and its lower viscosity gives a lower backpressure within the system [42–46]. TFA, a volatile acid, reduces the chance of salt precipitation in the instrument and is compatible with many liquid chromatography–mass spectrometry interface techniques (LC–MS) [47]. The 40-min gradient starts at 5% and extends to 100% acetonitrile to allow the separation of dyes and a range of lake pigments, such as Indian yellow—the salts of euxanthic acid—and gamboge—a water-insoluble natural resin—both used as yellow watercolor pigments [38]. See Table 1, column B, for the retention times of the primary dyes and lake pigments using Halpine's TFA–acetonitrile system.

The colorant is extracted from fiber samples with methanol–3 N HCl (1:1, v/v) heated at 100°C in an open Pyrex tube for approximately 10 min, using 400 μL of solution per milligram of fiber [37,38]. The extract is rapidly cooled down and filtered by centrifugal force in a Vac-Elut tube (Analytichem, USA), and the filtrate dried in a vacuum desiccator over sodium hydroxide pellets [37]. The extracted colorant is then redissolved in an appropriate volume of methanol–water (1:1, v/v), and 20 μL of the solution are injected for analysis on the HPLC [37]. Alternately, the extract can be dried in a Pico-Tag vacuum-hydrolysis workstation (Waters Corporation), dissolved in methanol–water (1:1), and centrifuged to precipitate particulates before injection [38,39].

With use of a mass spectrometer rather than a UV-Vis detector, Shibayama et al. have begun to apply thermospray LC–MS to the identification of natural dyes [48–50]. Samples were extracted with 20% formic acid in methanol and dissolved in 20% dimethylformamide (DMF) in methanol for analysis on a Shimadzu LC–MS QP-1000. This method of extraction may increase the yield of glycosilated flavonoids. Two column sizes were used, Shimadzu CLC-ODS 150 × 4.6 mm and 150 × 60 mm, with three different isocratic mobile phases, consisting of methanol, 0.1 M ammonium acetate, and acetic acid, depending on dyestuffs being analyzed. A portion of the dye extract is analyzed separately using a UV-Vis spectrophotometer. This method was successfully used to characterize natural dyes in ancient Egyptian, 19th-century European, and Japanese textiles.

The red colorants were usually the first to be studied because of the fairly characteristic color-imparting components [8,36]. Often a single compound, such as carminic acid, kermesic acid, or alizarin, for example, will indicate the dye source as cochineal, kermes, or madder root, respectively. Identification of the minor components has also been investigated [51]. The precision of Wouters' dye analysis results, however, traces the source of the dye to specific plant and insect species, placing the dyed artifact within a more accurate time frame and geographic region [52–60] (see Table 1, column A).

The yellow colorants are frequently made up of varying ratios of flavonoid components and, until recently, were nearly impossible to characterize with any accuracy [8]. HPLC sep-

Table 1 Retention Times of Primary Organic Colorants

Natural dye component	(A) Methanol/phosphoric acid system, retention times (min)	(B) Acetonitrile/TFA system, retention times (min)
Gallic acid	—	0.9
Protocatechuic acid	2.5	1.7
Euxanthic acid (Indian yellow)	4.0	1.8
Maclurin	—	4.7
Safflower yellow A[a]	—	6.4
Laccaic acid B	6.5	9.2
dcII[b]	8.5	—
Carminic acid	9.0	10.2
Lawsone	9.5	10.6
Brazilwood[c]	10.0	5.7
dcIII[b]	10.6	—
lcI[b]	11.3	—
Ellagic acid	11.4	10.7
Laccaic acid A	11.6	13.4
kvIa[b]	12.3	—
kvIb[b]	12.3	—
Quercitrin	—	13.0
Fisetin	12.4	13.8
Safflower yellow B[a]	—	14.5
Morin	12.4	14.8
3′,4′,6-Trihydroxyaurone	14.0	—
dcIV[b]	14.1	—
Quercetin	14.5	17.9
Laccaic acid E	15.0	16.8[d]
Genistein	15.0	19.7
Luteolin	15.5	17.6
dcVII[b]	16.6	—
Kaempferol	17.0	21.0
Anthragallol	17.4	—
Apigenin	17.6	20.8
Flavokermesic acid	18.1	19.9
Kermesic acid	18.6	21.4
Carthamin (safflower carmine)	—	23.1
Alizarin	19.3	24.4
Rhamnetin	20.1	25.1
Munjistin	20.3	20.3
Pseudopurpurin	20.5	22.6
Indigotin	22.1	28.1
Rhamnazin	22.5	—
Xanthopurpurin	22.6	27.4
Curcumin	22.9	29.3
Purpurin	23.4	28.7
Indirubin	24.7	29.1
Rubiadin	26.7	29.5
Alkannin	27.3	31.5
Alkannan	—	35.3
Emodin	27.3	29.5

Table 1 Continued

Natural dye component	(A) Methanol/phosphoric acid system, retention times (min)	(B) Acetonitrile/TFA system, retention times (min)
Shikonin	27.3	—
6,6'-Dibromoindigotin	29.5	—
Gambogic acid	—	38.0

Retention times of organic colorants using chromatographic conditions described in text. (A) Eluents consisting of phosphoric acid, water, and methanol [37]; and (B) eluents consisting of 0.1% TFA–water and 0.1% TFA–acetonitrile [38]. Some deviation in elution times should be expected owing to changes in chromatographic instrumentation as well as the column temperature, age, and batch of packing. This table is meant to serve as a general guide; reference standards should be run to determine the elution characteristics of each HPLC setup. For absorbance maxima of colorants, see reference 38. (Courtesy of Jan Wouters, Institut Royal du Patrimoine Artistique [IRPA/KIK], Brussels, Belgium, and Susana M. Halpine, National Gallery of Art, Washington, D.C.)

[a]Safflower yellow-A, primary colorant and safflower yellow-B, secondary colorant of water extract from *Carthamus tinctorius* [38].

[b]Red dye components from *Coccoidea* insect, chemically uncharacterized to date [54,55,57,195].

[c]The red dye brazilwood, from the *Caesalpinia* species, is more easily identified by a degradation product of brazilin, called "brazilwood" for the purposes of this table, which is much more easily traced in aged brazilwood dyeings than the fugitive brazilin [196].

[d]Product of acid hydrolysis of lac dye; identification as laccaic acid E is as yet unconfirmed [38].

aration technology had provided the best analytical approach for organic yellow colorants [37–39,48–50,61–64]. Although full characterization of both the color-imparting constituents and, for faded articles, colorless identifiers in flavonoid dyestuffs has yet to be completed, Halpine has compiled the retention times and absorbance maxima for the most common yellow colorants [38], Wouters has collect UV-Vis spectral information on luteolin and luteolin-like products [37], and Shibayama has assembled the retention times and mass numbers of several yellow colorants [67].

The blue indigoid dyes are difficult to extract into a solution and, therefore, are somewhat problematic for characterization using HPLC. Nevertheless, indigoids have been separated using the foregoing methods [38,65–67]. After a pyridine extraction [68], Wouters showed the conversion of dibromoindigotin, a main component in Tyrian purple, to monobromoindigotin and indigotin when exposed to UV radiation in an alkaline environment [65]. Warm acetonitrile dissolved indigo paint pigment for HPLC analysis [38]. Another extraction method uses a sodium hydrosulfite (sodium dithionite) solution similar to that used in dye vat recipes [69] to reduce and solubilize the indigo dyes [39,70]. The sodium hydrosulfite extraction was used for TLC [70], but may also be applicable to HPLC.

Tannins have also been investigated using HPLC [71–76]. Wouters analyzed tannins extracted from new and aged leather samples and has proposed a parameter for determining the age of leathers based on the percentage of monomers in total extractable tannins [71,76].

Future research may focus on fully characterizing the yellow and blue natural dyes as well as synthetic dyes and colorants [77]. A novel dyestuff separation technique involving relatively aggressive solvent plugs may have interesting applications here, although it seems inherently less reproducible [78]. Studies of the products formed during aging and fading of dyes will be especially helpful in identifying fugitive material [79,80]. The foregoing methods may be further exploited for lake pigment identification in painting samples [34,35,38,41,81–84]. Ink identification techniques developed for forensic applications may also find a use in conservation [85]. Although DAD–MS may become the preferred method of detection, RP–HPLC with either a multiwavelength detector or a DAD is quickly estab-

lishing itself as the analytical instrument of choice for the identification of small samples of organic colorants.

B. Proteinaceous Materials in Conservation

1. Binder Identification Using Amino Acid Analysis

Proteinaceous binders have been used extensively as paint media (egg yolk tempera, egg white or glair, casein, and animal glue or distemper) and as adhesives (casein, animal hide, bone, and blood or albumin glues) [24]. These binders vary in permanency from very stable egg yolk paint films to moisture-sensitive animal glues [7]. Despite their prevalence, these proteinaceous materials have only recently been identified in works of art. The presence of egg tempera for example, was usually deduced from fatty acid composition [86], which can be confounded by factors such as pigment–element interference [87], possibility of egg–oil emulsions [86], and the finding of similar fatty acid compositions in animal glues [35,88]. The conservation field had to wait until amino acid analysis technology caught up with its requirements for small-sized samples.

Early work by Keck and Peters, who used a dedicated ion-exchange analyzer at a local hospital, showed that amino acid composition could be used to identify the principal proteinaceous paint binders [89]. A similar instrument was used by Von Endt to study disease states in prehistoric bones [90]. This and other early work was not incorporated into the conservation field because of the large sample size requirements (1–4 mg) and the limitations of a single-purpose instrument. For a review of early articles on this subject see ref. 7.

Transferring amino acid biotechnology to the study of early Italian Renaissance panel paintings, Halpine was able to show that artists combined different proteinaceous binders for distinct visual effects within the same panel painting [7,24,41,91]. The use of animal-skin glue (gelatin or collagen) for binding blue and green pigments on egg-tempera on panel paintings had been described in a 15th-century artists' handbook [19] and was first confirmed using this technique [7]. These two proteinaceous media, animal glue and egg tempera, have distinct optical characteristics and, because animal glue is very water-soluble compared with egg yolk, they require very different conservation treatments. Blue areas in early European paintings are frequently damaged, in part because previous restorers were not aware that animal glue was often used as a paint binder for blue pigments. Amino acid analysis of paint binders can provide a more informed conservation treatment, while giving insight into the artist's technique.

For the foregoing results, Halpine used the Pico-Tag amino acid analysis method (Waters Corporation), which involves a vapor-phase acid hydrolysis and precolumn derivatization with phenylisothiocyanate (PITC; Fig. 2) [7,24]. This method has also been used by Ronka, by Shi, and by Sinkai et al. to identify proteinaceous binders and adhesives used in European, Chinese, and Japanese cultural artifacts, respectively [92–95]. The phenylthiocarbamyl (PTC)–amino acids are separated on a 4.6 × 150 mm C_{18} column at 38°C using an (a) aqueous sodium acetate buffer and (b) 60% acetonitrile buffer system monitored at 254 nm [7,96–98]. A programmed gradient from 0 to 46% b gives a good separation of the proteinaceous amino acids in 12 min. The sample sizes range from approximately 30 ng to 2 μg for conservation materials [7]. This method can be easily adapted to identify specific amino acids, such as those derived from posttranslation modification or converted by sample pretreatment, and amino acids from physiological fluids [24,98].

A newly developed derivative, 6-aminoquinolyl-*N*-hydroxysuccinimidyl carbamate (AQC), may provide the same advantages as PITC with less sample preparation time [99]. Other derivatizing reagents can provide similar sensitivity and handling properties [100–103]. It is strongly suggested, however, that the method selected be able to identify secondary amino acids. Proline and hydroxyproline are important components of proteinaceous artists materials: 4-hydroxyproline alone can often indicate the presence of collagenous animal glues in complex mixtures and may also be an important component of certain gums and resins [24,41,93,104].

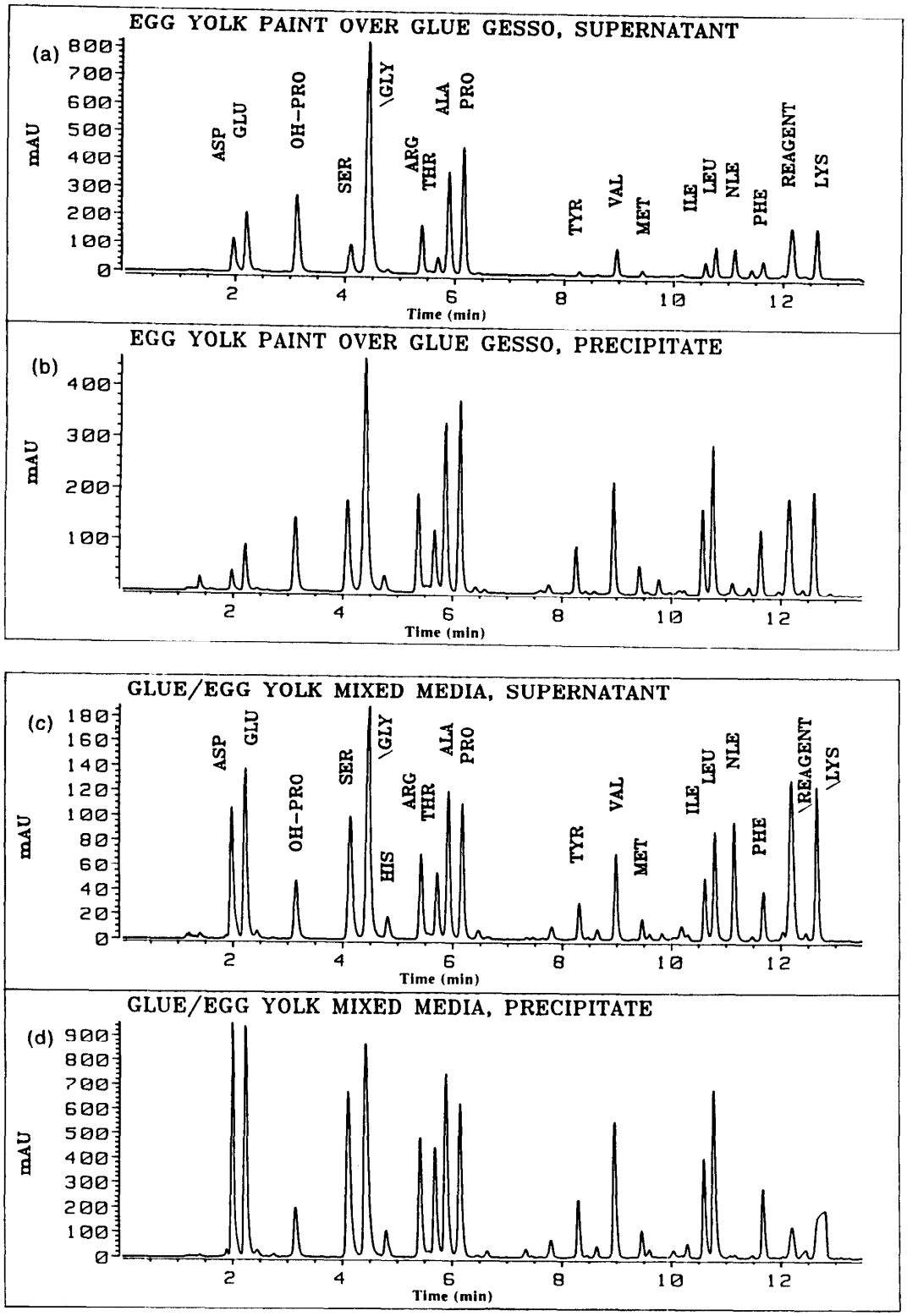


Figure 2 Chromatograms showing differences in extracts from egg yolk and animal glue paint binders prepared as adjacent layers (a and b), and in a combined egg–glue mixed media paint film (c and d). A sample of egg tempera paint on an animal glue gesso ground, from a traditionally prepared test panel painting, extracted into (a) a water-soluble supernatant fraction and (b) a water-insoluble precipitate fraction. The two different proteinaceous binders separated into distinct phases, with glue predominantly in the supernatant fraction, and egg yolk predominantly in the precipitate. Ratios of amino acids, serine/glycine peaks at 4 min, for example, are markedly different between the two extracts.

An egg yolk–animal glue (1:1 by volume) mixed medium paint film was extracted into (c) a supernatant fraction and (d) a precipitate fraction. Approximately the same ratio of egg yolk to animal glue appear in both fractions (note similar serine/glycine ratios). (For amino acid compositions see Refs. 7 and 24.) (From Ref. 24.)

In fact, 4-hydroxyproline constitutes 25% of the amino acids in extensin, the main protein in plant cell walls [105,106], and approximately 10% of collagen, the most abundant protein in the animal kingdom [7,107].

Vapor-phase hydrolysis is indispensable for the small-sized samples encountered in conservation because it reduces sample handling and contamination [7,98]. A glass desiccator can be adapted as an economical alternative to the Pico-Tag vacuum-hydrolysis workstation (Waters Corporation) [108].

A simple 1-h water extraction procedure was developed by Halpine to facilitate analytical interpretation when complex mixtures, adjoining paint layers, or interfering pigments are present in samples [24] (see Fig. 2). Using this procedure, a red brocade paint was shown to be composed of adjoining layers of animal glue paint and an egg yolk glaze: the animal glue layer easily dissolved in the water-soluble supernatant fraction and the egg yolk layer remained in the water-insoluble precipitate fraction [24,41,91]. The findings were confirmed with cross-sectional analysis. Furthermore, pigments, such as copper-containing azurite, malachite, and verdigris, which may cause up to a 60% decrease in yield [7], possibly through catalytic effect or complex formation [109], can be isolated in the precipitate fraction.

The results of sample analyses were compared with the amino acid compositions of known artists' materials. Beside the published composition of proteinaceous binders within the field [7,24,89,92,93], the US Department of Agriculture publications [110,111], and the Protein Information Resource International databases [112] can provide more detailed compositions, including the tryptophan and cysteine content of proteins.

As mentioned earlier, Halpine and others have recently found amino acids in "nonproteinaceous" gums [24,104,93], pastes [24,101,104,113], and resins [24,41,104,114,115]. Although amino acid analysis has been used for botanical investigations [104,116–120], plant exudates used as artists' materials have not been analyzed with this technique. Amino acids can be relatively permanent materials compared with fatty acids, carbohydrates, and terpenoids, and may assist in the identification of aged nonproteinaceous artists' materials [24,41,104]. For example, the amino acid composition of paint coatings on 4000-year-old ancient Egyptian objects match the compositions of unaged animal glue (collagen) and the trace amino acids found in natural resins [41,104,113–115]. Therefore, nonproteinaceous reference materials should be analyzed along with proteinaceous binders to potentially characterize unknown materials as well as to account for the interference of trace amino acids in the analytical results. Trace amino acids in nonproteinaceous materials will likely play an even greater role using the more sensitive amino acid analysis methods (detecting 50 ng or less).

Amino acid analysis is a valuable tool for the identification of paint binders, adhesives, and coatings, confirming published painting techniques, and uncovering innovative applications. It is best used in conjunction with other analytical techniques, such as fatty acid and resin analysis using GC–MS and cross-sectional analysis using microscopy [41,121,122]. Systematic approaches have been proposed to evaluate fats, proteins, and carbohydrates in museum samples [123,124]

2. Degradation Assessment: Amino-Terminal Analysis and Amino Acid Analysis of Silk and Leather

Before a conservator proceeds with an object's conservation treatment or prepares it for display, its state of deterioration must be assessed. Will the object be able to withstand a cleaning treatment or the necessary light exposure required for exhibition, or will these exposures pose too great a risk for the long-term preservation of the piece? Although morphology, color, and breaking strength give a general indication of the state of deterioration for silk and leather artifacts, more sensitive methods are needed to assess specific hazards, such as light, heat, and chemical contamination, for these materials [103].

Larsen, Becker, and others have investigated the possibility of using subtle changes in the amino acid composition of leather, silk, and wool to assess deterioration and estimate the

age of museum artifacts [102,103,109,125–128]. The preparation of these materials, from skin to tanned leather and from cocoon fibroin to silk, may predispose certain constituent amino acids to accelerated hydrolytic and oxidative changes [129]. Larsen proposed a method to classify leather as being new or historical by using variance–covariance analysis of the resulting changes in amino acid composition over time [125–128]. The amino acids were analyzed by ion-exchange chromatography using a fluorescence detector after postcolumn derivatization with orthophthaldialdehyde (OPA). For heat-aged and naturally aged (historical) leather samples, small increases were seen in glutamate, aspartate, and ammonia, compared with new leather, while similar decreases were seen in lysine, proline, and arginine. The changes in aged leather appear to slow down after the initial alterations [127], indicating that the compositional changes may be partly due to the type of tanning treatment used [129] as well as exposure to some environmental pollutants.

Exposure to light is the single most important factor in silk deterioration [103]. Silk aged by light exposure showed a decrease in tyrosine, followed by decreases in amino acids with hydroxylated and ionizable side chains, compared with the more stable aliphatic amino acids. Using an ion-exchange postcolumn OPA analytical system, similar to the one just mentioned, Becker found the glycine/ammonia ratio to be a useful means of assessing the overall state of preservation of silk material [109].

Becker also used a gas-phase protein sequencer for NH_2-terminal analysis of peptide cleavage points in silk fibroin [109]. The NH_2-terminal residues were converted to phenylthiohydantoin (PTH)–amino acids using an automated Edman degradation instrument, and separated using an on-line reverse-phase HPLC. Although the results showed both random cleavage in naturally aged and specific cleavage sites in artificially aged silk samples, protein sequencers are most effective when purified peptide samples are used, rather than aggregates of proteins and peptides.

Vilmont analyzed several leather samples using the Edman degradation chemistry adapted for the NH_2-terminal analysis by Ilse and Edman [130–132]. PITC-treated leather samples were exposed to acid to convert the NH_2-terminal PTH-residue and simultaneously hydrolyze the remaining peptide. The PTH derivatives were then separated using an ammonium acetate–acetonitrile gradient on a Ultrasphere (Altex) reverse-phase C_{18} column. Results showed disproportionately high serine, alanine, and threonine NH_2-terminal residues in both naturally and artificially aged leather, indicating peptide cleavage at these sites. Yamamoto et al. used a dinitrophenyl (DNP) derivative and reverse-phase chromatography for NH_2-terminal analysis of hair, wool, and silk [133].

3. Amino Acid Racemization Dating

Amino acid racemization is used for dating bones, shells, and fossils [134] and has been proposed as a method for dating art work. Despite its use in anthropology, archeology, and geology over the past 30 years on samples too small for radiocarbon dating, it is still considered a controversial technique, with results "regarded only as preliminary estimates unless corroborated by other independent dating criteria" [135].

The method is based on the fact that most amino acids, although found as L-amino acids in proteins, will equilibrate to a D/L ratio of 1 over a given time period [134,136]. As a protein begins to break down, the L-amino acids at the cleaved ends rotate to their D-enantiomers and back again until equilibrium is reached. The specific rates of racemization for each amino acid at a given temperature are used to determine the relative age of a material. Because of variables, such as temperature, humidity, pH, and metal ion catalysis, the rate of racemization for a site must be "calibrated" by either radiocarbon dating, geographic information, or with historical records. Once the rate is determined, the D/L values of other objects within the same site can be used for comparative dating.

Amino acid racemization dating may be applicable to art objects because confounding factors such as large temperature differences, leaching, and changes of environmental pH may not apply. For example, the fact that a given painted artifact has survived to the present attests

that the temperature and humidity were kept relatively constant, because fluctuations even within museum environments can cause extensive peeling of paint [137]. Therefore, the stability of an object would be a fair indication of its previous environments. The effect of metal ions could be determined by comparing different pigments mixed with the same binder.

Conversely, art objects may require considerations different from fossils because of the relatively short time span involved, since art objects are dated to hundreds, rather than millions, of years. Amino acids with faster rates of racemization—serine, for example—may be more indicative of aging over a shorter period [134]. Additionally, the preparation of the materials by the artisan, such as heating animal glue, may accelerate the rate of racemization. A database sorting the various factors should be instituted before this method is relied on for placing artifacts within a chronological context.

A variety of techniques can be used to identify amino acid enantiometers. After hydrolysis, Bada separated and collected aspartate using ion-exchange chromatography, and the D/L ratios were determined by reacting aspartate with L-leucine-*N*-carboxyanhydride (L-leu-NCA) [138]. The resulting dipeptides, L-leu-L-aspartate and L-leu-D-aspartate, were separated with an automatic amino acid analyzer using a ion-exchange column and a postcolumn ninhydrin reaction. Hardial and Simpson similarly separated aspartate, but quantify the recovered amino acid on a "chiral-generated column," that is, a reverse-phase C_{18} column coated for 3 h with a L-phenylalanine–copper(II) acetate mobile phase [139]. New methods are being developed that separate enantiometers with novel derivatives or special column chemistries; these methods may facilitate racemization dating of art work.

C. The Study of Degradation and Polymerization Reactions with Size Exclusion Chromatography

1. Gel-Permeation Chromatography and the Varnish Problem

Egg tempera and oil paintings have traditionally been varnished with a transparent coating to enhance their color saturation, give a uniform gloss to the patient surface, and offer some protection from surface accumulations [14,140]. Varnishes usually consist of natural resins such as sanderac, gum mastic, and rosin boiled in linseed or walnut oil (oil varnishes) or dissolved in a volatile solvent, such as oil of turpentine (spirit varnishes). Dammar resin and gum mastic spirit varnishes have predominated in the 19th and 20th centuries [14].

Natural varnishes are known to break down over time, eventually obscuring the painting by hazing, cracking, and yellowing [14]. Therefore, a conservator must regularly "clean" a painting by removing and replacing the varnish layer. The organic solvents usually used to redissolve, remove, and reapply the varnish can cause swelling and leaching, even in the most permanent paint applications [12,13], and more sensitive paint applications may dissolve along with the aged varnish. A great deal of a painting conservator's time is taken up with this cycle of varnish application and removal, which ultimately leads to a rougher, leaner, and weaker paint surface [14].

By studying the factors causing varnish breakdown, such as autoxidation reactions accelerated by UV light, new additives and light filters have been proposed that inhibit oxidation and slow the yellowing process brought about by the oxidation products. Similarly, by relating molecular characteristics to the desirable and undesirable qualities of commonly used varnishes, new synthetic resins have been proposed as more stable varnish alternatives [14].

De la Rie used gel-permeation chromatography (GPC) to determine the molecular weights of various traditional and modern varnish materials and related them to the resin's characteristic viscosity and appearance [141]. Two 30-cm PL–Gel 5-μm columns (Polymer Laboratories, Ltd.) with pore sizes of 10,000 and 500 A were used in series for these studies, with a tetrahydrofuran (THF) eluent and a refractive index (RI) detector. Calibration was performed using polystyrene molecular weight standards. Low molecular weight and relatively high refractive indexes were found to be the primary characteristics of natural resins, such as dammar, giving a highly desirable saturated appearance to paintings [141].

During photochemical and thermal degradation studies, changes in the molecular weight distribution of dammar resin films were determined using RI and UV detectors in series on the foregoing GPC system [14,142]. Dammar's triterpenoid fraction nearly disappears during light-aging studies, with a shift to higher molecular weight fractions, possibly to highly oxidized triterpenoids and triterpenoid dimers (Fig. 3a.) Heat aging had similar, but less dramatic, effects. Most important autooxidation in films of dammar resin and the ensuing yellowing can be significantly inhibited with the addition of a hindered amine light stabilizer (HALS) to the varnish and by removing the UV component from light sources [142]. GPC traces showed the molecular weight distribution of stabilized dammar virtually unchanged after 900 h of UV-filtered accelerated-light aging. Because many museum galleries have eliminated the ultraviolet component of their light sources, these additives may prolong the life of a dammar varnish coating on museum paintings by a factor of 20 or more [14,143]. Several low molecular weight synthetic resins, including reduced ketone and hydrogenated hydrocarbon resins, are considerably more stable than natural resins [144]. The addition of HALS to these synthetic resins offers enhanced stability even when the UV component is included in light-aging tests [144] (see Fig. 3b).

2. Gel-Filtration Chromatography of Cellulose and Water-Soluble Organics

Cellulose is the main component of paper, linen, and cotton. The breakdown of cellulose has a direct bearing on the structural integrity of manuscripts, painting supports, and textiles. There is considerable interest in studying the effect of conservation treatments on these materials, and to correlate chain length with physical parameters, such as breaking strength, toughness, and fold endurance [145,146].

Converting cellulose to nitrocellulose and other soluble forms allows for GPC analysis using organic solvents, such as THF [147,148] and ethyl acetate [149], but it may also cause substantial breakdown of the cellulose polymer [145,149,150]. Instead, Burgess used a fluorescent label, dichlorotriazinylaminofluorescein (DTAF), and the resulting DTAF–cellulose complex was dissolved in Cadoxen solvent (triethylenediamine hydroxide) [145,151]. This method used a gravity-fed cross-linked agarose gel column, but it may also apply to HPLC gel filtration chromatography (GFC) methods using Superose gel columns (Pharmacia) [152]. The results showed that "new" and "old" cellulose fibers reacted differently to a stabilized peroxide treatment, suggesting a potential danger in using unaged reference materials.

Bose separated underivatized cellulose using a RI detector and sodium hydroxide or sodium chloride eluent on a Sepharose CL-6B column (Pharmacia) [153]. Dextrans and polystyrene sulfonates were used for calibration. Additionally, Bose made recommendations for future cellulose investigations [153].

Gel-filtration and ion-exchange chromatography were used to purify osteocalcin, a protein extracted from fossil bones [154]. The antigenic activity of osteocalcin was intact in bones that were 13 million years old. The active bone fractions eluted in a sodium chloride buffer from a Mono-Q anion-exchange column (Pharmacia) were pooled, concentrated, and applied to a TSK-125 SE column (TosoH Corporation) with a sodium chloride–Tris buffer [154]. The samples thus prepared could be further characterized by amino acid sequencing.

3. Monitoring Reactions with SEC and Other Separation Techniques

Waterlogged wooden archeological finds, such as Viking ships and a Roman river barge, are frequently treated with polyethylene glycols (PEG) [155,156]. PEGs are gradually infiltrated into old timbers to reduce the enormous shrinkage that occurs on drying. The stabilization treatment can be optimized by monitoring the penetrability, degradation, and diffusion velocity of PEG incorporated into the wood. Barka and Hoffmann used two reverse-phase C_8 columns in series, LiChrosorb RP-8 (7 μm, 100 A) and Hypersil MOS WP (10 μm, 300 A) (Dr. H. Knauer KG), to analyze the degree of polymerization (DP) of PEGs within archeological

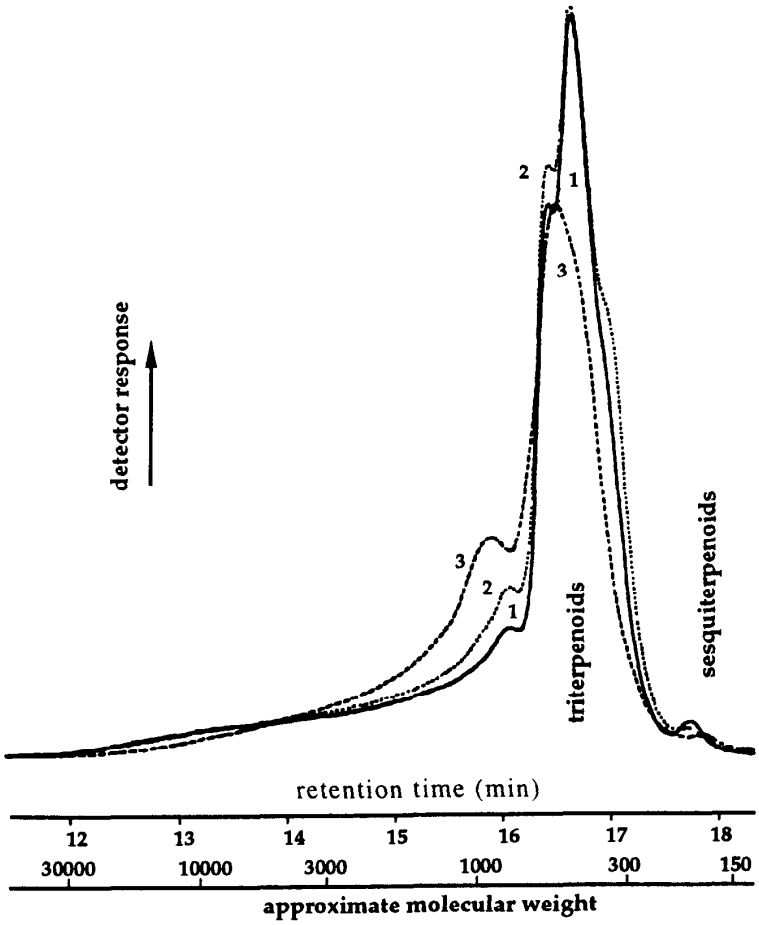


Figure 3a GPC traces from aged natural and synthetic resin films. (a) GPC traces from samples of dammar resin films: 1, dammar film unstabilized and unaged; 2, dammar film aged with 2% Tinuvin 292 and 3% Tinuvin 328; and 3, aged without additive. Both 2 and 3 were aged approximately 900 h in a xenon arc fadeometer behind a UV filter. (From Ref. 143.)

timbers [155,156]. The water and acetonitrile gradient system was monitored at 190 nm with a variable wavelength detector, and mono-, di-, tri-, and polyethylene glycols were used as reference standards. PEGs with a DP from 1 to 110 can be separated with this system, allowing PEG extracts from treated wood to be characterized by molecular weight. This system had advantages over early SEC and reverse-phase systems in specificity and range of molecular weight distribution. Monitoring at 190 nm, however, may present some problems with baseline disturbances and drifting [156].

Ishiguro et al. investigated recently developed GFC column packings for the separation of PEGs of similar molecular weight distribution [157]. Two OHPAK KB-802.5 columns (Shodex) set up in series, using a RI detector and water as the eluent, separated a PEG standard mixture with a molecular weight distribution of 200–7500 [157].

Acryloid B-72, an ethylmethacrylate–methylacrylate copolymer used as a coating and adhesive in art conservation, showed increases in both higher and lower molecular weight fractions after natural aging, indicating both polymerization and molecular breakdown [158]. For this study, Druzik and Lansing employed an Ultrastyragel column (Waters Corporation) with a RI detector, THF as eluent, and polystyrene standards to calibrate the GPC system.

Wheeler used GPC to monitor polymerization rates of four alkoxysilanes systems for possible use as stone consolidants [159]. GPC confirmed the faster reaction time of one alkoxysilane system over the others. The large molecular weight reaction products (over 9000

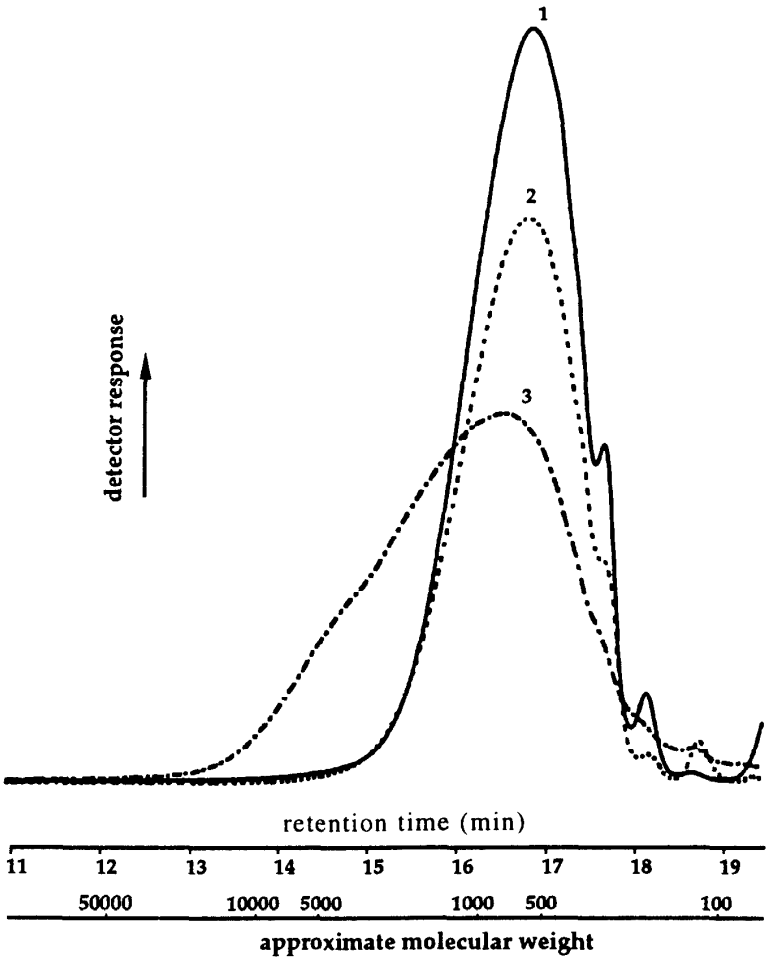


Figure 3b GPC traces from samples of Regalrez 1094 hydrogenated hydrocarbon resin films: 1, Regalrez 1094 film unstabilized and unaged; 2, Regalrez 1094 film aged with 0.5% Tinuvin 292 for 6580 h; 3, aged without additive for 2904 h in an Atlas Weather-ometer without filter. (Courtesy of E. René de la Rie and Stephen L. Funk, National Gallery of Art, Washington, D.C.)

number-average molecular weight) could not have been analyzed using other instrumentation [159]. Care must be taken, however, when studying polymerization rates of resins and consolidants, to prevent cross-linking within the instrument.

The antioxidant Irganox 565, proposed as a resin varnish stabilizer, was monitored in extracts of dammar resin films during accelerated light-aging [160]. Using a normal-phase HS-5 silica column (Perkin Elmer), 98% hexane–2% methanol isocratic elution, and a variable wavelength UV detector set at 300 nm, de la Rie showed nearly a 100% drop in the concentration of Irganox 565 within 24 h, which made it an unsuitable antioxidant for a varnish coating. A slower decrease occurred when a UV filter was placed in front of the sample, but increased yellowing would still be expected during natural aging [160].

Hersh et al. used an ion-exchange HP × 8 heavy-metal cationic resin column (Bio-Rad) to separate water-soluble degradation products of artificially and naturally aged cotton fabrics [161,162]. The water eluant was mixed with a developing agent, bicinchonic acid (BCA), and monitored with a variable wavelength detector at 560 nm. The nonlinearity at higher concentrations and the high signal/noise ratio suggest that BCA may not be the best labeling agent for cello-oligomer detection on HPLC, but the results of extractions and other procedures may be useful in applying HPLC to textile degradation studies.

Doshi and Vaickus outline several HPLC techniques used in the textile industry to monitor product development and quality control, including PEG and formaldehyde analysis and polymer-monitoring systems [163].

D. Ion Chromatography for Monitoring Inorganic Contaminants and Corrosion Products

Ion chromatography (IC) has been used to monitor inorganic contaminants in a variety of materials. Wouters measured anions in aged leathers, specifically sulfate and nitrate ions, which are good indicators of the acidity and leather deterioration [71–76]. After a 24-h water extraction, the leather extracts were diluted in the potassium phthalate buffer, pH 5.8, and injected onto a Ionosphere-A low-capacity ion-exchange column (Chrompack). The conductivity detector was a Model 430 (Waters Corporation) [71]. With this method, new leathers were found to be free of acids from the processing conditions; the ionic contaminants were due to sulfate and nitrate atmospheric pollutants [71–76]. This system was also used to study the acidification in limestone sculptures, with the sulfate anion indicating the concentration of calcium sulfate formation [164].

Tennent et al. used IC to characterize efflorescence products and salt residues in museum artifacts [165]. A Dionex 4000i instrument was used to identify the anions (acetate, formate, chloride, nitrate, and sulfate ions) and cations (sodium, ammonium, potassium, magnesium, and calcium ions) present in efflorescence products. These included Byne's disease in mollusca specimens, calclacite, "thecotrichite" (efflorescence X), and acetate efflorescence on bronze antiquities.

Water washings of objects must be carefully monitored to remove undesirable contaminants without disturbing the water-soluble components. IC has been used to monitor the rinse water after cleaning treatments of tapestries [166], bronzes [167,168], and fresco murals [169]. For example, Matteini et al. used a Dionex 20001/sp instrument to study the patina and surface corrosion on outdoor Florentine bronzes [167]. IC may also provide insight into the chemical treatments of photographs, such as intensification treatments and electrochemical cleaning of daguerreotypes [170]. Reconfiguring the system to monitor transition metals can also give information on the metallic salts used in photographs [170].

Ion chromatography is also used to monitor corrosion products from organic pollutants in museum environments, as will be discussed in the following section.

E. Monitoring Organic Pollutants in the Museum Environment

Organic acids and carbonyl pollutants pose a serious hazard for museum artifacts, causing corrosion and eventually complete degradation of calcareous shell or limestone artifacts; metal objects made of lead, bronze, and zinc; as well as glass, ceramics, and enamels [17,171,172]. A major source of these pollutants are the wood and adhesives used in making the storage and display cases that hold the artifacts.

Monitoring for organic pollutants generally involves trapping the compounds of interest on specially prepared surfaces, such as badges or cartridges, then collecting the reacted compounds and analyzing them quantitatively on an HPLC. The collection device may use passive diffusion or may actively pump air into a filtering chamber. Less sensitive devices may use a color reaction to estimate the amount of pollutant present [173].

Tennent et al. tested storage and display environments, constructed of various types of wood, for acetate and formate off-gasing [171]. Lead foil and borax-impregnated silica gel strips were exposed to the test environments and were then analyzed for organic carbonyl corrosion products using a Dionex 4000i [165,171]. The results showed considerable variation among wood types.

Druzik et al. collected air samples using pretreated C_{18} SEP-Pak cartridges (Waters Corporation) attached to a pump [17,172,174–176]. For aldehyde and ketone pollutants, the cartridges were impregnated with 2,4-dinitrophenylhydrazine (2,4-DNPH) then rinsed with acetonitrile to collect the DNPH-derivatives. The carbonyl products were analyzed isocratically, 55:45 acetonitrile–water, by reverse-phase and monitored at 365 and 415 nm using a diode array UV-Vis detector. For carboxylic acid pollutants the cartridges were washed with methanolic potassium hydroxide and the resulting salts collected with water. These organic salts were analyzed by ion-exclusion chromatography, using 0.5 mM sulfuric acid, and monitored at 210 nm [172,174–176]. The analytical detection limits were 0.2 ppb for carbonyl pollutants and 0.5 ppb for carboxylic acids in a 0.4 m^3 air sample [174,177]. A replaceable reactive adsorption cartridge unit has been developed to reduce these pollutants and has been tested in display cases with low air circulation where high concentrations of pollutants tend to accumulate [177].

Grosjean et al. evaluated passive monitors specifically targeted for formaldehyde and ozone, and found fairly good correlation with active monitors based on the same chemistry [173,178].

III. FUTURE APPLICATIONS

A. Carbohydrate Analysis of Gums and Cellulose

There is considerable interest in characterizing plant exudates and cellulosic fibers found in museum articles [179,180], but recent HPLC techniques for carbohydrate characterization have not yet been fully implemented in the field. Several methods for sugar analysis using HPLC may hold promise for the identification of gums used in aqueous paint binders as well as for degradation studies of paper and textile fibers.

Eggert and Jones obtained higher yields of sugars after mild hydrolysis with 2 M TFA for 6–10 h at 105°C than with 2 M HCl [181].

Precolumn derivatization of saccharides offers the highest analytical sensitivity [182], while underivatized analysis using UV detection at lower wavelengths is generally more sensitive than RI detection [183]. Lin and Wu [182] and Muramoto et al. [184] compared two main derivatizing reagents, dansylhydrazine (DNS-hydrazine) [181,185–187] and dabsyl hydrazine (DABS-hydrazine) [182,184]. Both reagents give sensitivity in the picomole range, but the DABS-hydrazine reaction requires less reagent than DNS-hydrazine (eightfold excess [184] compared with 20-fold excess [187]) and generally affords better chromatographic separation. DABS-hydrazine is monitored in the visible range at either 426 or 485 nm [182,184], while DNS-hydrazine is somewhat unstable as a fluorophore label [182] and detection at 350 nm is comparable with fluorescence detection [184]. Good separations with water and either acetonitrile or acetone solvents were reported [181–187]. Acetic acid, formic acid, and triethylamine were often added to the solvent systems to increase resolution [181,187]. DABS-hydrazine derivatives were separated by Lin and Wu using a concave water–acetonitrile gradient on a reverse-phase C_{18} Nova-Pak column (Waters Corporation) [182], and by Muramoto et al., using an isocratic 25% aqueous acetone–0.08 M acetic acid on a reverse-phase ODS Hypersyl column (Shandon Southern Products) [184] with comparable success.

B. Fatty Acid Analysis and Hybrid Techniques

Gas chromatography (GC or GC–MS) is usually used for fatty acid and resin analysis of samples from museum collections. However, derivatized or underivatized fatty acids analyzed using HPLC can provide information omitted by GC owing to incomplete conversion to methyl ester derivatives or undesirable chemical transformations before analysis [188]. More importantly, fatty acid analysis techniques [189,190] may be combined with analytical meth-

ods used for other types of materials. For example, a hybrid phenacyl bromide–PITC method for oil–protein analysis is now being developed [191] that could be extremely useful in characterizing emulsions and other mixtures of materials encountered in art conservation. Considering the potential of hybrid techniques [192], fatty acid analysis should be investigated for possible applications in the conservation field.

Passi et al. analyzed free fatty acids and triglycerides extracted from 1500-year-old Mediterranean amphorae using HPLC because it offered higher sensitivity (in the nanogram range) and less interference from secondary components than GC analysis [193]. The fatty acids were derivatized with phenacyl bromide and the *p*-bromophenacyl esters separated on reverse-phase RP-18 column (Brownlee Laboratories) with a phosphoric acid (H_3PO_4)–acetonitrile gradient, and monitored at 254 nm. Derivatized fatty acids and underivatized secondary peaks were differentiated using an online scanning spectrophotometer. The results indicated the presence of olive and sesame oil in the amphorae and showed the effects of leaching and oxidation that occurred during the ensuing 15 centuries.

King et al. studied saponified fatty acids from industrial oils and alkyd resins with an isocratic mixture of acetonitrile, water, THF, and acetic acid using a uBondapak fatty acid analysis column (Waters Corporation) and a refractive index detector [188]. The emphasis was on good separation within a 10-min analysis time, rather than on sensitivity. Nevertheless, the observations on mobile-phase variations and peak resolution may be helpful for tailored method development.

C. Liquid Chromatography–Mass Spectrometry

Many of the HPLC techniques described earlier, such as the analysis of carbohydrates, amino acids, and fatty acids in paint binders, would be greatly enhanced with the addition of a mass spectroscopic detector (MS). To date, with the exception of the dye identification work by Shibayama et al., liquid chromatography–mass spectrometry (LC–MS) has not been widely used in art conservation because of inherent methodological shortcomings as well as financial considerations. Nevertheless, as LC–MS becomes more widely available it is sure to offer insight in the analysis of complex mixtures of materials.

IV. DISCUSSION

HPLC techniques have only begun to be fully exploited in the field of art conservation. For example, given the uniqueness of samples taken from museum artifacts, collecting effluent fractions after nondestructive HPLC analysis and resubmitting these to further instrumental analysis may prove especially useful. Many of the techniques described in the foregoing, for example, could be combined to provide richer information on a single paint sample.

Increased instrumental sensitivity may allow natural materials to be characterized by trace components: for example, the composition of trace amino acids in plant gums and resins and the trace fatty acid profiles in proteinaceous animal glues. Similarly, investigations into the degradation products of organic colorants could indicate the original appearance of long-faded paintings and textiles.

Research is underway on the interaction between constituent materials, both organic and inorganic, and the reactive or buffering effects they have on one another. A large-scale study of aged leather has used HPLC techniques both to determine the breakdown of structural proteins as well as to measure the exposure to inorganic pollutants [71–74, 76, 126–128,130–132].

Art conservation offers interesting opportunities for HPLC applications and the field will undoubtably continue to benefit from other scientists reflecting on its inherent challenges. At the same time, the findings in conservation research may also contribute to the fields from which it previously borrowed. New viewpoints on common problems may help more traditional lines of research. For example, the characterization of insect dyes used in textiles has

contributed to entomological studies [54,55,57], the extensive but short-lived use of blood glue was of interest to forensic investigators [24], and papers on the composition and aging of resin varnishes have been presented to polymer chemists [104,194].

The recent introduction of HPLC techniques to art conservation has been suffused with the enthusiasm and informed speculation accompanying any emerging field of research. Most of the analytical techniques described here are still in the developmental stages. By discussing potentially useful HPLC techniques, investigators within the field will be encouraged to experiment, while HPLC users previously unfamiliar with the field may propose helpful suggestions that will lead to methodological improvements.

With the insight garnered through scientific investigation, the beautiful and compelling objects from our common cultural heritage are experienced in a new light, promoting a greater appreciation for the original artisans' craftsmanship and ingenuity while simultaneously assisting in the preservation of these treasures for future generations.

REFERENCES

1. GD Lewis. The New Encyclopedia Britannica. 24:482, 1993.
2. T Raphael. In: R Barclay, M Gilberg, JC McCawley, T Stone, eds. Symposium 86, The Care and Preservation of Ethnological Materials, Proceedings. Ottawa: Canadian Conservation Institute, 1986, pp 68–73.
3. JS Crighton. Silk: a study of its degradation and conservation. Preprints of Conservation Science in the U.K., Glasgow, 1993, pp 96–98.
4. JH Stoner. Academic American Encyclopedia 2:204–206, 1993.
5. RR Jones. R&D Mag 33(1):54, 1991.
6. JM Miller. Chromatography: Concepts and Contrasts, New York: John Wiley & Sons, 1988, pp 278–279.
7. SM Halpine. Stud. Conserv 37:22, 1992.
8. M Saltzman. Analysis of dyes in museum textiles or, you can't tell a dye by it's color. In: CC McLean, P Cornell, eds. Textile Conservation Symposium in Honor of Pat Reeves. Los Angeles: Los Angeles County Museum of Art, 1986, pp 27–39.
9. A Moncrieff, G. Weaver. Cleaning, Science for Conservators Book 2. London: Craftscouncil, 1983, pp 14–15, 21–22.
10. P Mora, L Mora, P Philippot. Conservation of Wall Paintings. London: Butterworths, 1984, pp 213–214, 285.
11. PC DeSantis. J Am Inst Conserv 23:7, 1983.
12. R Feller, N Stolow, EH Jones. On Picture Varnishes and their Solvents. Washington, DC: National Gallery of Art, 1985, pp 47–116.
13. J-S Tsang, D Erhardt. J Am Inst Conserv 31:87, 1992.
14. ER de la Rie. Anal Chem 61:1228A, 1989.
15. D Erhardt, M Mecklenburg. Relative humidity re-examined. In: Preventive Conservation: Practice, Theory and Research. Preprints of the Ottawa Congress, International Institute for Conservation of Historic and Artistic Works, London, 1994, pp 32–38.
16. G Thomson. The Museum Environment. London: Butterworths, 1986, pp 10–16, 184–186.
17. F Preusser, JR Druzik. Restaurator 10:160, 1989.
18. Pliny the Elder, (WHS Jones, trans., H Rackam, ed.) Natural History. Cambridge: Harvard University Press, 1963.
19. C Cennini. (DV Thompson Jr, trans.) The Craftsman's Handbook 'Il Libro dell'Arte', Mineola, NY: Dover Publications, 1966, pp 24–36, 54–55, 68.
20. Theophilus. (JG Hawthorne, CS Smith, trans.) On Divers Arts. Mineola, NY: Dover Publications, 1979.
21. G Vasari. On Technique. Mineola, NY: Dover Publications, 1960.
22. B Cellini. The Treatise of Benvenuto Cellini on Goldsmithing and Sculpture. Mineola, NY: Dover Publications, 1967.

23. RJ Gettens, GL Stout. Painting Materials, A Short Encyclopedia. Mineola, NY: Dover Publications, 1966, p 90.
24. SM Halpine. Conservation Res, Stud History Art, Ser II, vol 51. Washington, DC: National Gallery of Art, 1995, pp 28–69.
25. J Wouters. Analyse des colorants des tapisseries brugeoises des XVIe et XVIIe siecles. In: Bruges et la tapisserie, Bruges, Mouscron, Belgium: 1987, pp 515–526.
26. Exodus 25.4. The Bible. New York: American Bible Society, 1970, p 67.
27. R Kumar. Analysis for Organic Pigments Using Solution Spectrophotometry. Dissertation, Rensselaer Polytechnic Institute, Troy, NY, 1981.
28. J Kirby. Natl. Gallery Tech. Bull 1:35, 1977.
29. GW Taylor. Stud Conserv 28:153, 1983.
30. JH Hofenk-De Graaff. Natural Dyestuffs—Origin, Chemical Constitution, Identification. International Council of Museums—Committee for Conservation, Plenary Meeting, Amsterdam, 1969.
31. H Schweppe. Handbuch der Naturfarbstoffe. Landsberg, Germany: Ecomed Fachverlag, 1992, pp 640–648.
32. LJ Papas. In: K Venkataraman, ed. The Analytical Chemistry of Synthetic Dyes. New York: John Wiley & Sons, 1977, pp 93, 135.
33. C Walker, HL Needles. In: HL Needles, SH Zeronian, eds. Historic Textiles and Paper Materials: Conservation and Characterization. Washington, DC: American Chemical Society, 1986, pp 176–185.
34. D Saunders, J Kirby. Natl Gallery Tech Bull 15:79, 1994.
35. C Brown, D Bonford, J Plesters, J Mills. Natl Gallery Tech Bull 11:60, 1987.
36. J Wouters. Stud Conserv 30:119, 1985.
37. J Wouters, N Rosario-Chirinos. J Am Inst Conserv 31:237, 1992.
38. SM Halpine. An improved dye and lake pigment analysis method using high performance liquid chromatography and diode-array detector. Stud. Conserv 41:76, 1996.
39. SM Halpine. Report on Gobelin and Croome Court Commission Tapestry Upholsteries. Scientific Research Department, National Gallery of Art, Washington, D.C., March 5, 1993; unpublished.
40. C Bremer-David. Systematic Catalog of European Decorative Arts. Washington, DC: National Gallery of Art, (in press).
41. SM Halpine. Analysis of artists' materials using high-performance liquid chromatography. In: A Bakkenist, R Hoppenbrouwers, H Dubois, eds. Early Italian Painting Techniques and Analysis. Maastricht, The Netherlands: Strichting Restauratie Atelier Limburg, 1997.
42. C Seaver, P Sadek. LC–GC Mag 12:742, 1994.
43. C Seaver, J Przybytek, LC–GC Mag 13:220, 1995.
44. Optima Solvent Handbook, Bulletin 878. Pittsburgh, PA: Fisher Scientific Co., 1987, pp 7, 12–17, 36–41, 67.
45. C Seaver. Today's Chemist at Work January:17, 1994.
46. T Studt. R&D Mag December: 43, 1994.
47. V Ling, AW Guzzetta, E Canova-Davis, JT Stults, WS Hancock. Anal Chem 63:2909, 1991.
48. R Yamaoka, N Shibayama, T Yamada, M Sato. Mass Spectrom 37:249, 1989.
49. N Shibayama, R Yamaoka, M Sato, J Iida. Mass Spectrom 39:123, 1991.
50. N Shibayama. The Separation and Identification of Natural Dyestuffs Used in Archeological Fabrics Using Chromatography/Mass Spectrometry. Dissertation, Kioto Institute of Technology, Kioto, Japan, 1992.
51. J Wouters, A Verhecken. Tetrahedron Lett 28:1199, 1987.
52. A Verhecken, J Wouters. Bull. KIK22 1888–'89:207, 1990.
53. J Wouters, A Verhecken. Stud. Conserv 34:189, 1989.
54. J Wouters, A Verhecken. Ann Soc Entomol Fr 25:393, 1989.

55. J Wouters. Dyestuff analysis of scale-insect species by high-performance liquid chromatography. Proceedings of the Sixth International Symposium of Scale Insect Studies, Krakow, Poland, 1990, pp 61–70.
56. J Wouters, A Verhecken. Dyes Hist Archeol Textil 6:32, 1987.
57. J Wouters, A Verhecken. Belg J Zool 121:211, 1991.
58. J Wouters. In: Peeters ed. De Analyse van de Kleurstoffen, Clenodia Tungrensis. Leuven, Belgium, 1988, pp 100–106.
59. GW Taylor. Text Hist 18:143, 1987.
60. J Wouters, S Florquin. Dyes Hist Archeol Textil. 6:28, 1987.
61. DJ Daigle, EJ Conkerton. J Liq Chromatogr 11:309, 1988.
62. JP Goiffon, M Brun, MJ Bourrier. J Chromatogr 537:101, 1991.
63. P Pietta, P Mauri, C Gardana, RM Facino, M Carini. J Chromatogr 537:449, 1991.
64. T Vogt, PG Gulz. J Chromatogr 537:453, 1991.
65. J Wouters, A Verhecken. J Soc Dyers Color 107:266, 1991.
66. J Wouters. Dyes Hist Archeol 10:17, 1992.
67. N Shibayama. Dye analysis of historic textiles by high-performance liquid chromatography and high-performance thin layer chromatography. Textile Conservation Studios, Hampton Court Palace, East Molsey, Surrey, UK, 1993, unpublished.
68. GW Taylor. Stud Conserv 28:153, 1983.
69. R Buchanan. A Weaver's Garden. Loveland, CO: Interweave Press, 1987, pp 118–120.
70. JH Hofenk-De Graaff. Stud Conserv 19:54, 1974.
71. J Wouters. High-performance liquid chromatography of vegetable tannins extracted from new and old leathers. Preprints of Proceedings of ICOM Committee for Conservation. Washington, DC, 1993, pp 669–673.
72. J Wouters. Tannin and ion analysis of 20 historical and 2 artificially aged leathers. STEP Leather Project–First Progress Report, Commission of the European Communities, 1992, pp 153–187.
73. J Wouters. Evaluation of small leather samples following successive analytical steps. ICOM Committee for Conservation, Conservation of Leathercraft and Related Objects Interim Symposium, London, England, UK, pp 3–33.
74. J Wouters. Tannin and ion analysis of naturally and artificially aged leather. STEP Leather Project—Second Progress Report, Commission of the European Communities, 1993, pp 175–189.
75. M Verzele, P Delahaye. J Chromatogr 268:469, 1983.
76. J Wouters. In: STEP Leather Project: Evaluation of the Correlation Between Natural and Artificially Ageing of Vegetable Tanned Leather and Determination of Parameters for Standardization of an Artificial Aging Methods. Copenhagen: Bjarnholt Repro, 1994, pp 91–105.
77. JW Wegener, JC Klamer, H Govers, UAT Brinkman. Chromatographia 24:865, 1987.
78. JC Gluckman, K Slais, UAT Brinkman, RW Frei. Anal Chem. 59:79, 1987.
79. K Jorgensen, LH Skibsted. Food Chem 40:25, 1991.
80. JP Luttringer, P Dussy. Melliand Textilber 62:84, 1981.
81. PWF Brinkmann, L Kockaert, L Maes, EMM Thielen, J Wouters. Bull. KIK22 1988–'89: 26, 1990.
82. J Wouters. De Kruisoprichting van Pieter Paul Rubens. Ministerie van de Vlaamse Gemeenschap—Bestuur voor Monumenten en Landschappen, Brussels, Belgium, 1992, p 181.
83. SM Halpine. Report on lake pigment identification of samples from two Toulouse-Lautrec paintings. Scientific Research Department, National Gallery of Art, Washington, DC, January 8, 1991, unpublished.
84. SM Halpine. Report on lake pigment identification of sample from Brazilian polychrome sculpture. Scientific Research Department, National Gallery of Art, Washington, DC, November 11, 1993, unpublished.
85. IR Tebbett, C Chen, M Fitzgerald, L Olson. J Forensic Sci 37:1149, 1992.

86. J Mills, R White. The Organic Chemistry of Museum Objects. London: Butterworths, 1987, pp 142–143.
87. J Mills. Stud Conserv 11:92, 1966.
88. B Skans, P Michelsen. Maltech Restauro 92:63, 1986.
89. S Keck, T Peters. Stud Conserv 14:75, 1969.
90. DW Von Endt, DJ Ortner. Am J Phys Anthropol 59:377, 1982.
91. SM Halpine. Amino acid analysis of two brocade areas on an Agnolo Gaddi triptych. American Institute of Conservation of Historic and Artistic Works (AIC) Meeting, Denver, CO, 1993, pp 50–51.
92. T Sinkai, R Sugista. Sci Papers Jpn Antiq Art Crafts 35:1, 1990.
93. T Sinkai, I Nagasawa, T Shida, R Sugista. Sci Papers Jpn Antiq Art Crafts 37:1, 1992.
94. L Shi. Dunhuang Res 2:11, 1993.
95. F Ronka. Stud Conserv 39:107, 1994.
96. BA Bidlingmeyer, SA Cohen, TL Tarvin. J Chromatogr 336:93, 1984.
97. SA Cohen, BA Bidlingmeyer, TL Tarvin. Nature 320:769, 1986.
98. SA Cohen, M Meys, TL Tarvin. The Pico-Tag Method, A Manual of Advanced Techniques for Amino Acid Analysis. Milford, MA: Millipore Corporation, Waters Chromatography Division, 1989, pp 2–3, 11–12.
99. SA Cohen, DP Michaud. Anal Biochem 211:279, 1993.
100. P Furst, H Godel, TA Graser, L Pollack, P Stehle. J Chromatogr 499:557, 1990.
101. BW Singer. The analysis of proteinaceous media and adhesives by HPLC. Conservation Science in the UK Preprints, Glasgow, Scotland, addendum, 1993.
102. TB van Oosten. Research on the influence of 19th-century silk weighting on the accelerated aging of silk. ICOM Committee for Conservation Preprints, Washington, DC, 1993, p 909.
103. M Becker, N Tuross. MRS Bull 27:39, 1992.
104. SM Halpine. In: K. Anderson, J Crelling, eds. Amber, Resinite, and Fossil Resins. Washington, DC: American Chemical Society, pp. 234–254, 1995.
105. M-N Miege. In: D Boulter, B Parthier, eds. Encyclopedia of Plant Physiology, New Series: Nucleic Acids and Protein in Plants I, vol 14A. 1982, pp 142, 331–333.
106. NAM Eskin. Plant Pigments, Flavors and Textures: The Chemistry and Biochemistry of Selected Compounds. New York: Academic Press, 1979, pp 176–179.
107. DW Martin Jr, PA Mayes, VW Rodwell, DK Granner. Harper's Review of Biochemistry, 20th ed. Los Altos, CA: Lange Medical Publications, 1985, p 493.
108. N Meltzer, GI Tous, S Gruber, S Stein. Anal Biochem 160:356, 1987.
109. MA Becker. The Characterization of the Initial Degradative Alterations of *Bombyx mori* Silk Fibroin. Dissertation, Johns Hopkins University, Baltimore, MD, 1993, pp 40, 60–67, 101–189.
110. Composition of Foods, Dairy and Egg Products. Agricultural Handbook 8-1. Washington, DC: US Department of Agriculture, 1976.
111. Composition of Foods, Cereals, Grains, and Pasta. Agricultural Handbook 8-20. Washington, DC: US Department of Agriculture, 1976.
112. WC Barker, DG George, H-W Mewes, F Pfeiffer, A Tsugita. Nucleic Acids Res 21:3089, 1993.
113. SM Halpine. Second report on amino acid composition of ancient Egyptian paint samples from the Boston Museum of Fine Arts. Scientific Research Department, National Gallery of Art, Washington, DC, March 5, 1992, unpublished.
114. SM Halpine. Report on amino acid composition of ancient Egyptian paint samples from the Boston Museum of Fine Arts. Scientific Research Department, National Gallery of Art, Washington, DC, June 27, 1991, unpublished.
115. SM Halpine. Third report on amino acid composition of ancient Egyptian paint samples from the Boston Museum of Fine Arts. Scientific Research Department, National Gallery of Art, Washington, DC, December 3, 1993, unpublished.

116. G Rosenthal. Plant Nonprotein Amino and Imino Acids: Biological, Biochemical, and Toxicological Properties. New York: Academic Press, 1982, pp 2, 187–189.
117. S Hunt. In: GC Barrett, ed. Chemistry and Biochemistry of Amino Acids. London: Chapman & Hall, 1985, pp 59, 103.
118. J Van Die, PML Tammes. In: MH Zimmermann, JA Milburn, eds. Encyclopedia of Plant Physiology, New Series: Transport in Plants I vol 1. Berlin: Springer-Verlag, 1975, p 202.
119. TW Goodwin, EI Mercer. Introduction to Plant Biochemistry. New York: Pergamon Press, 1983, pp 336–349.
120. L Taiz, E Zeiger. Plant Physiology. Redwood City, CA: Benjamin/Cummings Publishing, 1991, pp 156, 151.
121. R Newman, SM Halpine. Ancient Egyptian paint binders. American Institute of Conservation of Historic and Artistic Works (AIC) Preprints, Buffalo, New York, 1992, p 17.
122. M Saito, F Morioka, M Kashiwagi. Sci Papers Jpn Antiq Art Crafts 33:1, 1988.
123. D Erhardt, W Hopwood, M Baker, D von Endt. A systematic approach to the instrumental analysis of natural finishes and binding media. American Institute for Conservation of Historic and Artistic Works (AIC) Preprints, New Orleans, LA, 1988, pp 67–84.
124. D Stulik, H Florsheim. J Am Inst Conserv 31:275, 1992.
125. R Larsen, V Barkholt, K Nielsen. Das Leder 40:53, 1989.
126. R Larsen. The STEP Leather Project, background and first results. Conservation of Leathercraft and Related Objects Interim Symposium, ICOM Committee for Conservation, London, 1992, pp 3–6.
127. R Larsen, M Vest, K Nielsen, AL Jensen. Amino Acid Analysis. STEP Leather Project—Second Progress Report, Commission of the European Communities, 1993, pp 29–60.
128. R Larsen, M Vest, K Nielsen, AL Jensen. In: STEP Leather Project: Evaluation of the Correlation Between Natural and Artificially Ageing of Vegetable Tanned Leather and Determination of Parameters for Standardization of an Artificial Aging Method. Copenhagen: Bjarnholt Repro, 1994, pp 39–57.
129. HA Gruber, EF Mellon. Oxidation products of amino acids and collagen. Anal Biochem 66:78, 1975.
130. LB Vilmont. Etude du vieillissement des cuirs de tannage vegetal: dosage par chromatographie liquide des groupements N-terminaux. Preprints of Proceedings of ICOM Committee for Conservation, Washington, DC, 1993, pp 662–668.
131. LB Vilmont. N-Terminal group analysis. STEP Leather Project—Second Progress Report, Commission of the European Communities, 1993, pp 105–114.
132. LB Vilmont. Determination of the N-terminal groups in vegetable tanned leathers by high performance liquid chromatography. Conservation of Leathercraft and Related Objects Interim Symposium, ICOM Committee for Conservation, London, England, 1992, pp 10–15.
133. S Yamamoto, Y Morikawa, M Sakamoto. [N-Terminal amino acids in protein fibers by high-performance liquid chromatography.] Seni Gakkaishi 41:78, 1985.
134. DW Von Endt. In: RL Humphrey, D Stanford, eds. Pre-Llano Cultures of the Americas: Paradoxes and Possibilities. Washington, DC: The Anthropological Society of Washington, 1979, pp 71–100.
135. GH Miller, PE Hare. In: PE Hare, TC Hoering, K King, eds. Biogeochemistry of Amino Acids. New York: John Wiley & Sons, 1980, pp 415–443.
136. JL Bada, M-Y Shou. In: PE Hare, TC Hoering, K King, eds. Biogeochemistry of Amino Acids. New York: John Wiley & Sons, 1980, pp 235–255.
137. GL Stout. The Care of Pictures. Mineola, NY: Dover Publications, 1975, pp 78–82.
138. JL Bada. Annu Rev Earth Planet Sci 13:269, 1985.
139. R Hardial, CF Simpson. Anal Proc 26:57, 1989.
140. R Perry. Problems of dirt accumulation and its removal from unvarnished paintings: a practical review. Conference on Dirt and Pictures Separated, United Kingdom Institute of Conservation and the Tate Gallery, London, England, 1990, pp 3–10.

141. ER de la Rie. Stud Conserv 32:1, 1987.
142. ER de la Rie. Stud Conserv 33:53, 1988.
143. ER de la Rie, CW McGlinchey. Stud Conserv 34:137, 1989.
144. ER de la Rie, CW McGlinchey. New synthetic resins for picture varnishes. International Institute of Conservation Congress on Cleaning, Retouching, and Coatings, Preprints, Brussels, Belgium, 1990, pp 168–173.
145. H Burgess. The use of gel permeation chromatography in investigating the degradation of cellulose during conservation bleaching. International Institute for Conservation Congress Preprints, Washington, DC, 1981, pp 85–88.
146. L Segal. Adv Chromatogr 12: 32, 1975.
147. M Chang, TC Pound, RStJ Manley. J Polym Sci Polym Phys Ed 11:399, 1973.
148. RStJ Manley. J Polym Sci Polym Phys Ed 12:1347, 1974.
149. C Holt, W Mackie, DB Sullen. Polymer 19:1421, 1978.
150. AL Kvernheim, E Lystad. Acta Chem Scand 43:209, 1989.
151. H Burgess. In: HL Needles, SH Zeronian, eds. Historic Textiles and Paper Materials: Conservation and Characterization. Washington, DC: American Chemical Society, 1986, p 363.
152. H Burgess. The use of GPC to characterize the MWD of cellulose. Meeting of Cellulose, Paper and Textile Division of the American Chemical Society, Chicago, Illinois, no. 56, 1985.
153. A Bose. Aqueous size exclusion chromatography of nonderivatized cellulose: applications of excluded volume concepts to calibration. PhD dissertation, Purdue University, Lafayette, IN 1980.
154. MMW Ulrich, WRK Perizonius, CF Spoor, P Sandburg, C Vermeer. Biochem Biophys Res Commun 149:712, 1987.
155. G Barka, P Hoffmann. J Chromatogr 389:273, 1987.
156. P Hoffmann. HPLC for the analysis of polyethylene glycols (PEG) in wood. Conservation of Wet Wood and Metal, Proceedings of the ICOM Conservation Working Groups on Wet Organic Archeological Materials and Metals, Freemantle, 1987, pp 41–58.
157. S Ishiguro, R Takahashi, H Yabe, M Komuro, T Takada, S Moriguchi. New columns for high-speed aqueous gel permeation chromatography, International GPC Symposium '89, Newton, Massachusetts, 1989, pp 589–603.
158. C Druzik, H Khanjian, S Lansing. Monitoring the weathering of polymers used in the conservation of cultural objects by GPC. International GPC Symposium, Newton, MA, 1989, pp 584–588.
159. GE Wheeler. The chemistry of four alkoxysilanes and their potential for use as stone consolidants. PhD dissertation, University Microfilms International, Ann Arbor, MI 1987.
160. ER de la Rie. Stud Conserv 33:109, 1988.
161. SP Hersh, JK Hutchins, N Kerr, PA Tucker. In: F Pertegato, ed. Conservazione e Restauro dei Tessili, Milan: C.I.S.S.T., 1982, pp 87–95.
162. JK Hutchins. The soluble components of degraded cellulose. MS dissertation, University Microfilms International, Ann Arbor, MI, 1981.
163. RP Doshi, MJ Vaickus. Use of HPLC in the textile laboratory. AATCC, Book of Papers, 1986, p 231.
164. J Wouters. Conservation Scientist, Royal Institute for Cultural Heritage, Brussels, Belgium, personal communication, 1993.
165. NH Tennent, BG Cooksey, D Littlejohn, BJ Ottaway. Some Applications of ion chromatography to the study of the deterioration of museum artifacts. In: PB Vandiver, JR Druzik, GS Wheeler, IC Freestone, eds. Materials Issues in Art and Archeology III. MRS Symposium Proceedings, Pittsburgh, PA, 267: 869–882, 1992.
166. L Dolcini, LM Nicolai, M Matteini, CM Pradel, CP Da Zarra, I Tosini. OPD Restauro 2: 46, 1987.
167. M Matteini, C Lalli, I Tosini. OPD Restauro 3:40, 1987.

168. GP Bernardini, M Corazza, C Lalli, M Matteini, A Moles, MR Nepoti, F Olmi, C Sabelli, I Tosini, R Trosti-Ferroni. In: L. Dolcini, ed. Verrocchio's Christ and St. Thomas. New York: Metropolitan Museum of Art and Harry N. Abrams, 1992, pp 119–123.
169. G Lanterna, M Nepoti, M Rizzi, I Tosini. OPD Restauro. 4:117, 1992.
170. S Rempel. Conservation science for conservators—computer assisted chemistries. Conservation of Archival Materials Seminar, H Ransom Humanities Research Center, Austin, TX, 1985, pp 124–126.
171. NH Tennent, BG Cooksey, L Gibson, D Littlejohn. Simple monitors for carbonyl pollutants, Preprints of Conservation Science in the UK, Glasgow, Scotland, 1993, pp 119–122.
172. C Druzik, and Taketomo. Standard operating protocol: analysis of airborne aldehydes, ketones, and carboxylic acids using HPLC. Getty Conservation Institute Scientific Program Report, Marina del Rey, CA 1988, pp 1–70.
173. D Grosjean, EL Williams II, CMG Druzik. Development and evaluation of passive monitors for measuring airborne formaldehyde in museums. Final Report to the Getty Conservation Institute, Marina del Rey, CA 1991, pp 1–46.
174. C Druzik, D Grosjean, A Van Neste, S Parmar. Int J Environ Anal Chem 38:495, 1990.
175. C Druzik, D Stulik, F Preusser. Carbonyl and carboxylic acid pollutants in the museum environment. Preprints of American Chemical Society Meeting, Division of Environmental Chemistry, Miami, FL, no. 70, 1989.
176. CM Grzywacz, NH Tennent. Pollution monitoring in storage and display cabinets: carbonyl pollutant levels in relation to artifact deterioration. Preventive Conservation: Practice, Theory and Research. Preprints of the Ottawa Congress, International Institute for Conservation of Historic and Artistic Works, London, England, 1994, pp 164–170.
177. CM Grzywacz, DC Stulik. Scot Soc Conserv Restor J 4:16, 1993.
178. CM Grzywacz. Detecting pollutants in the museum environment with passive sampling devices. Preprints of ICOM Committee for Conservation, Washington, DC, 1993, pp 610–615.
179. J Twilley. In: J Lambert, ed. Advances in Chemistry Series 205, Archeological Chemistry III. Washington, DC: American Chemical Society, 1984, pp 357–394.
180. KV Kharbade, GP Joshi. Stud Conserv 40:1995 (in press).
181. FM Eggert, M Jones. J Chromatogr 333:123, 1985.
182. J-K Lin, S-S Wu. Anal Chem 59:1320, 1987.
183. DW Armstrong, HL Jin. J Chromatogr 462:219, 1989.
184. K Muramoto, R Goto, H Kamiya. Anal Biochem. 162:435, 1987.
185. WF Alpenfels. Anal Biochem 114:153, 1981.
186. M Takeda, M Maeda, A Tsuji. J Chromatogr 244:347, 1982.
187. K Mopper, L Johnson. J Chromatogr 256:27, 1983.
188. JW King, EC Adams, BA Bidlingmeyer. J Liq Chromatogr 5:275, 1982.
189. R Wood, T Lee. J Chromatogr 254:237, 1983.
190. HD Durst, M Milano, EI Kikta Jr, SA Connelly, E Grushka. Anal. Chromatogr 47:1797, 1975.
191. SM Halpine. Report on fatty acid analysis by HPLC. National Gallery of Art, Washington, DC, December 10, 1991, unpublished.
192. W Nowik. Stud Conserv 40:1, 1995.
193. S Passi, MC Rothschild-Boros, P Fasella, M Nazaro-Porro, D Whitehouse. J Lipid Res 22: 778, 1981.
194. ER de la Rie. Degradation and stabilization of varnishes for paintings. 13th International Conference on Advances in Stabilization and Degradation of Polymers, Luzern, Switzerland, May 22–24, 1991, pp 129–139.
195. J Wouters. In Fils Renoues—Tresors Textiles du Moyen Age en Languedoc-Roussillon. Musee des Beaux-Arts de Carcassonne, 1993, pp 158–165.
196. A Quye, J Wouters. Dyes Hist Archaeol 10:48, 1991.

29

Sample Handling and Analysis of Organic Pollutants (Pesticides and Phenols) in Water Matrices by HPLC

Sílvia Lacorte, David Puig, and Damià Barceló

Centro de Investigacion y Desarollo, Consejo Superior de Investigaciones Científícas, Barcelona, Spain

I. INTRODUCTION

The high-performance liquid chromatography (HPLC) determination of organic micropollutants, such as pesticides and phenolic compounds, is of environmental concern because they are toxic and persistent. Organic micropollutants can suffer biotic and abiotic degradation [1], with the subsequent formation of transformation products (TPs) that are more toxic than their parent compounds [2,3]. Such are the oxo derivatives and sulfoxides. Also chloro- and nitrophenols are the main degradation products of many chlorinated phenoxyacid herbicides and organophosphorus pesticides, respectively [4,5]. Several organic micropollutants were included in different water monitoring programs, such as the National Pesticide Survey (NPS) and the Commission of the European Communities (CEC). The EEC Directive on the Quality of Water Intended for Human Consumption (CEC 76/464/EEC) has included different pesticides and phenolic compounds (e.g., parathion, methyl-azinphos, fenitrothion, malathion, pentachlorophenol, and 2,4-dinitrophenol) to be monitored in the environment and has already elucidated the need for analyzing organic micropollutants and TPs at levels less than 0.1 $\mu g\ L^{-1}$ [6]. Moreover, the NPS has published a list that includes all pesticides and their TPs that have been detected in groundwater [7,8]. Therefore, the achievement of an analytical method that accomplishes such needs is comprehensive.

For the isolation of organic contaminants from water samples, dichloromethane liquid–liquid extraction (LLE) methods have been reported in the literature, covering several groups of pesticides and are also recommended by the US Environmental Protection Agency (EPA) through their NPS [9,10]. As an alternative to LLE, solid-phase extraction (LSE) procedures have been implemented in the last few years. LSE methods can be easily converted into fully automated on-line systems coupled to LC. Such systems, also referred to as "pre-column technology," show additional advantages, such as lower detection limits (analysis of eluate instead of an aliquot), no evaporation losses, no contamination, and easy automation. Moreover, the EPA has pointed out the need to develop on-line LSE methods to minimize sample manipulation, analyte losses, and the use of toxic solvents.

Traditionally, most pollutants, which include pesticides of different families and phenolic compounds, have been analyzed by gas chromatographic (GC) techniques using a selective detector such as the nitrogen–phosphorus (NPD) or the electron capture (ECD). Classically, identification of the analytes was performed through retention time comparison with a standard

solution. Errors and lack of reproducibility often appeared owing to variations in the response of the detector. This is especially relevant when GC–NPD or GC–ECD is used and, therefore, duplicate analysis using two columns of different polarity or the addition of internal standards or surrogates is needed to meet quality control requirements [11]. The use of GC with mass spectrometric (MS) detection is a valid alternative to confirm the results obtained by other techniques. However, GC-based techniques are unsuitable for the analysis of polar, nonvolatile, and thermolabile compounds, because for these compounds, a derivatization step before GC analysis is compulsory. The use of two different techniques and the difficulty of analyzing both the degradation products along with the parental pesticides limit the applicability of GC-based techniques for environmental analysis. To mention an example, GC of underivatized phenols using capillary columns with conventional phases is difficult because phenols and, in particular nitrophenols, tend to tail, even when using highly deactivated columns [12]. However, EPA methods for phenols may often lead to incorrect results because derivatization of phenols, especially nitrophenols, it is not straightforward. Recently, the EPA has reported a new protocol (method 8041) [13] that recommends the derivatization to methylated phenols instead of to pentafluorobenzoyl ether derivatives. However, this method requires the use of diazomethane, which is carcinogenic and explosive, and the potential hazards associated with its use are well known. For these reasons, there is a general trend to change to liquid chromatography (LC) methods that can overcome the foregoing limitations.

Liquid chromatographic techniques are preferred for the analysis of organic pollutants because they cover a wide range of polarities and permit the identification of pesticides and phenolic compounds along with their transformation products. LC with diode-array detection (LC–DAD) or fluorescence has been successfully used to monitor pesticides of various natures, such as organophosphorus [14,15], carbamates [16], phenoxyacids [17], and phenolic compounds [18]. The main advantages of LC–DAD are its easy use and that it renders some structural information that can be used to identify parent organic compounds through spectral comparison. However, limitations arise for compounds that exhibit a poor chromophore, and the impossibility of identifying unknowns in real water samples. These problems are solved when using LC with mass spectrometric detection (LC–MS). Coupling LC to MS has been achieved through many interfaces: thermospray interface (TSP), which produces scarce fragmentation; and particle beam (PB), which gives high-detection limits and poor reproducibility of the results, are the most common ones. The advent of atmospheric pressure (API) liquid chromatography–mass spectrometry interfaces has overcome the disadvantages of GC–MS and other LC–MS interfacing devices, such as TSP, because they can provide structural information similar to chemical ionization.

II. SAMPLE HANDLING STRATEGIES

The presence of interfering materials in the water sample, mainly humic and fulvic acids, should always be taken into consideration because they will notably affect analytical performance. Humic matter can bind organic contaminants [19]; for instance, up to 50% decay on recovery was found for 4-nitrophenol and 2,4-dinitrophenol, but 27% for 2-nitrophenol at neutral pH [20]. Acidification of the sample is a common practice in environmental analysis because it can avoid the deprotonation of the most acidic compounds and inhibits microbiological degradation. However, if the sample is acidified, adsorption of humic material into the sorbent is increased, so a large unidentified complex matrix (UCM)-interfering peak appears somewhere in the chromatogram [21]. Figure 1 shows the chromatographic profiles of three different water matrices spiked with some phenolics at 4 $\mu g\ L^{-1}$ and analyzed using the sorbent PLRP-S: drinking water (a), groundwater (b) and river water (c). When working with drinking water, it is no problem to detect and quantify all target compounds, but for analyzing groundwater, quantification of cathecol is quite difficult at this level because of early elution of the matrix peak. Furthermore, alkyl-substituted phenols generally showed an inverse ten-

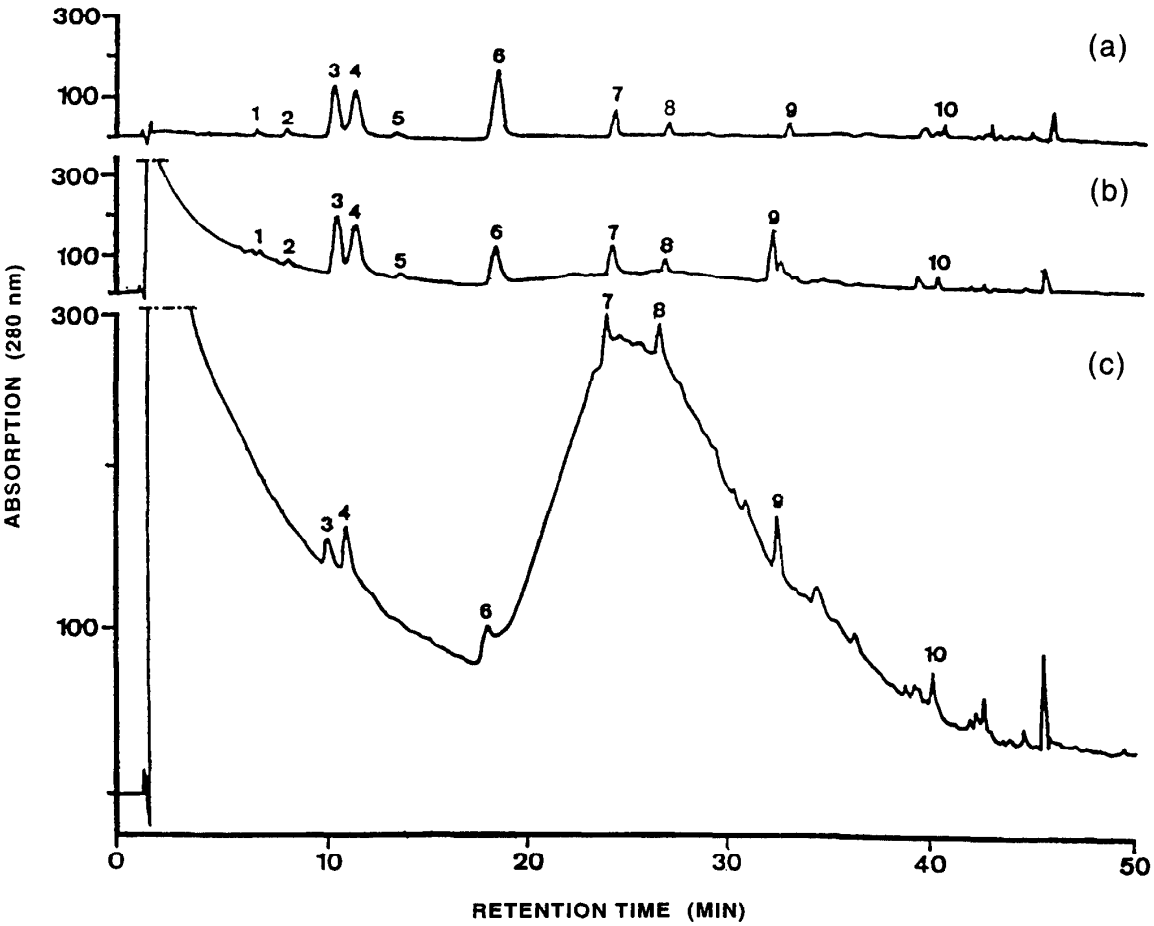


Figure 1 LC–DAD chromatographic profile at 280 nm of phenolic compounds spiked at 4 μg L^{-1} level after on-line LSE of 100 mL of sample using PLRP-S sorbent. (a) HPLC water; (b) groundwater, (c) river water. Peak identification (1) 4-nitrophenol, (2) 4-methylphenol, (3) 2,4-dinitrophenol, (4) 2-nitrophenol, (5) 4-chlorophenol, (6) 2,4-dimethylphenol, (7) 4-chloro-3-methylphenol, (8) 2,4-dichlorophenol, (9) 2,4,6-trichlorophenol, (10) pentachlorophenol.

dency, and slight losses in recovery were obtained when working at acidic pH, thus showing that optimal extraction pH should be checked carefully and will depend on the target phenol.

However, because organic micropollutants are found in the environment at very low concentrations, it becomes necessary to perform a preconcentration step before the chromatographic analysis. Briefly, sample pretreatment involves the extraction of organic pollutants from the water matrix and the elution of such traces with an adequate solvent. Afterward, the extract is evaporated to a small volume of 0.1–1 mL, and finally it is ready to be analyzed. Traditionally this was carried out by LLE, but nowadays, there is a general trend to change to LSE procedures. Both approaches will be discussed in the following two sections.

A. Liquid–Liquid Extraction

Liquid–liquid extraction (LLE) is still the sample preparation technique preferred by the environmental analyst because of its extensive implementation in official methods. Most of the current EPA methods for the analysis of priority pollutants in water samples involve sample acidification to pH 2 and extraction with various solvents, such as dichloromethane, butyl acetate [22], or hexane [23]. On the other hand, a different approach using an ion-pair tech-

nique has been described by adjusting the pH to a basic value and addition of tetrabutyl ammonia [24]. Table 1 shows the average percentage recovery values obtained at spiking levels of 1–5 $\mu g\ L^{-1}$ into 1 L of river water using LLE according to the National Pesticide Survey (NPS) method 4 [25]. For a complete extraction of the more acidic pesticides, sulfuric acid at pH 2 and 50 mL of dichlormethane were added to the water sample, which was shaken again and extracted. Recoveries of most of the compounds were within the NPS EPA range, who accept recoveries between 70 and 130% for samples analyzed at microgram per liter levels. However, most of the polar compounds, such as sulfoxides and sulfones, were not recovered. The LLE approach has some drawbacks, such as it requires a large amount of generally toxic and inflammable organic solvents, emulsions can be generated and further cleanup is often necessary. All these factors lead to losses during the concentration step, which results in poor recoveries and bad reproducibility, with risk of sample contamination. Moreover, its automation requires the use of expensive robots. Hence, there is a general trend to substitute current LLE procedures with LSE protocols.

B. Liquid–Solid Extraction

1. Off-Line Versus On-Line

Liquid–solid extraction (LSE) has been successfully applied to extract organic pollutants from environmental matrices. The procedure is based on extracting the pesticides from water by percolating the water sample through a sorbent material in which the organic compounds are effectively trapped while water is eliminated to waste. After preconcentration, the analytes are

Table 1 Average Percentage Recovery (av) and Coefficient of Variation (CV) of Pesticides in River Water Using C_{18} Empore Extraction Disks and Dichlormenthane LLE

	Empore disks		LLE	
Pesticide	av	CV	av	CV
Aldicarb	83	7	62	10
Aldicarb sulfoxide	35	21	18	24
Aldicarb sulfone	30	20	36	18
Aldrin	51	10	n.d.	n.d.
Atrazine	100	5	99	4
Bentazone	77	6	81	7
Carbaryl	87	8	109	2
Carbofuran	74	7	90	4
Chlorpyrifos	94	4	86	3
Cyanazine	84	7	92	14
Deethylatrazine	76	13	90	9
Fenamiphos	95	5	87	9
Fenamiphos sulfoxide	97	11	98	10
Fenamiphos sulfone	100	5	97	6
3-Ketocarbofuran phenol	60	19	89	6
Linuron	96	6	94	5
Propanil	95	7	94	3
Simazine	80	10	97	8
Tetrachlorvinfos	96	6	92	4

eluted with an organic solvent. LSE methods include extraction using off-line methods with cartridges [26,27], using Empore extraction disks both off-line [28] and on-line [25], or using precolumn technology [29,30]. The principle of LSE is the same for both off- and on-line extraction methods and is shown in Fig. 2. The method involves a condition step with an organic solvent, sample loading, washing to remove the more polar matrix interferences, and final elution of trapped analytes. With off-line methods, the preconcentration, elution, and chromatographic analysis are performed in discrete steps. To eliminate residual water, such methods require complete drying of the sorbent (under vacuum) before proceeding to the elution step. Elution is performed with 10–20 mL of solvent, which must be evaporated before obtaining a final extract of 0.1–1 mL, from which an aliquot is injected into the LC. Table 1 reports the recovery values after preconcentrating 1 L of river water spiked at 1–5 $\mu g\ L^{-1}$ onto Empore extraction disks. Values are similar to those obtained with LLE, indicating that the method offers recoveries similar to those of the NPS method 4; thus, it can be recommended for monitoring studies, owing to its simplicity and easy use. Aldrin was not recovered because of losses during prefiltration, since this compound has high log P_{ow} values and will have a strong affinity for adsorption on the particulate matter of the filter. In general, however, off-line practices are well-accepted owing to the large variety of packing materials available in the market, with different sizes and volumes, which permits a great operational flexibility. In the cartridge format, the sorbent (40- to 150-μm–particle size) is usually packed in a Teflon

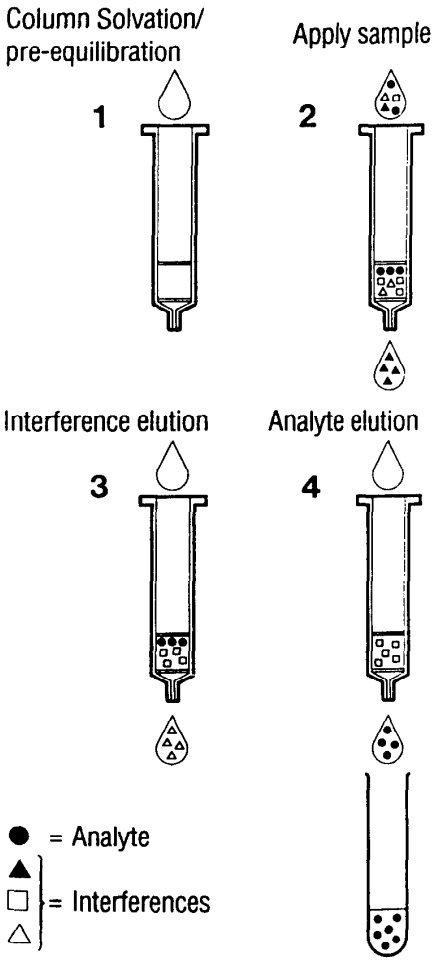


Figure 2 LSE process that includes (1) conditioning of the precolumn, (2) sample preconcentration, (3) elimination of the interferences, and (4) elution of the analytes.

syringe and percolation of water samples must be performed with a special device. Nowadays, however, off-line extraction with cartridges can be automated by using the ASPEC XL from Gilson (France) or the Zymark system (Germany), making the technique useful for routine analysis. With Empore disks, the sorbent particles are meshed in Teflon fibrils to form strong sheets or membranes that can be used in standard filtration equipment. Because the channeling phenomenon does not occur in the disk format, higher sample flow rates can be applied in comparison with cartridges. This induces a very efficient adsorption as a result of the reduction of the linear velocity of the water by the particle size and high packing density, although automation is not straightforward.

The main advantage of off-line methods is that the final extract can be analyzed with various techniques. However, when the technique is not automated, off-line methods are tedious and fail, with risk of contamination owing to intense sample manipulation, and losses of the most volatile analytes can occur during the concentration of the extract. Hence, a soft evaporation process is usually recommended, and in some cases, dryness should be avoided to prevent important analyte losses. For phenolic compounds, some authors suggest pH adjustment to a basic value to obtain phenolate ions [31], but excessive basification of the extract can lead to the degradation of the nitrophenols [32].

Most of the problems that appear when using off-line methods are solved with the on-line approach. The setup is very simple and is illustrated in Fig. 3. The trace enrichment is performed on a small precolumn, which is placed at the loop position of a six-port valve. After preconcentration of the water sample, the valve is electrically switched to the injection position and the pesticides are eluted by the mobile phase and the analytes are separated in the analytical column. The most common fully automated devices include the Prospekt (Spark Holland, The Netherlands) and the OSP-2 (Merck, Germany). The two systems differ in that, although the former has only one position for each precolumn, the OSP-2 can be operated in

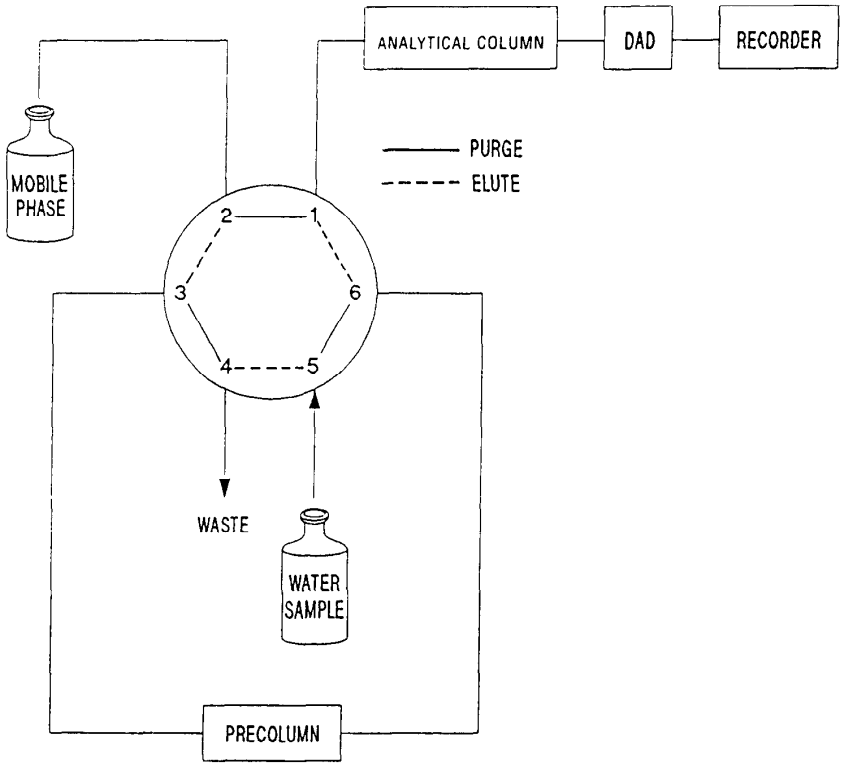


Figure 3 General diagram of the system used for on-line preconcentration and determination of organic micropollutants in water samples.

such a way that while one sample is preconcentrated in the "preparation" position, another precolumn is being eluted. This option is very interesting because it saves time. The two systems have their own precolumn design, which covers a large variety of packing materials and includes the possibility of eluting in normal and backflush mode. However, to achieve optimal performance with on-line LSE, the sorbent of the precolumn should be as similar as possible to the analytical column packing in terms of type of packing, particle size, and such. Band-broadening can be minimized by using a suitable gradient that causes peak compression on the top of the analytical column. The size of the precolumn is also of importance because the elution profile of the analytes should be as narrow as possible, especially at the beginning of the separation, where the high water content tends to cause peak distortion. For a classic analytical column of 15 × 0.46-cm, common sizes are 2 mm long and 2–3 mm internal diameter, and are packed with 10- to 60-mm sorbent material which efficiently traps the analytes while precolumn clogging is prevented.

In general, better detection limits (LODs) and reproducibility values can be obtained by using the on-line approach because the entire sample is transferred to the analytical column and losses during sample manipulation are minimized. However, the problem of enrichment of the more polar compounds, which exhibit low breakthrough volumes, is originated by the restricted size of the precolumns [20,33–35]. For phenolic compounds, LODs below 0.7 $\mu g\ L^{-1}$ have been reported when working with on-line LSE using Lichrolut EN precolumns and UV detection [20]. However, for polar phenols, values below 0.25 $\mu g\ L^{-1}$ have been obtained using off-line LSE [27] because no limitation on the amount of sorbent exist, so better LODs are usually achieved [36–38], as can be seen in Table 2.

An additional advantage of using coupled technologies is that degradation studies can be followed with almost no manipulation of the water sample; therefore, the modification of the original matrix is minimized. As a result, further degradation of pesticides does not occur during the extraction procedure, as compared with off-line methods, and formation of transformation products during sample manipulation is avoided. At the same time, on-line methods are more sensitive because it is possible to analyze pesticides at a nanograms per liter level with only 100 mL of sample. Even though in routine analysis there is a tendency to replace off-line methods with automated methods, the former method will still be preferred in some specific applications owing to its higher versatility.

2. Breakthrough Volumes

Because of the large variety of packing materials, sizes, and formats, the extraction efficiency, both off- and on-line will vary, depending on the nature of the analytes. It is of prime importance to establish which compounds can be successfully analyzed with each type of sorbent and what the optimum analytical conditions are to attain maximum sensitivity. The most critical parameter in LSE efficiency is the breakthrough volume, or the maximum volume of water that can be preconcentrated on an adsorbent without producing losses of any particular analyte. The breakthrough volume is different for each analyte, and it depends mainly on the analyte's polarity and on the affinity for a particular type of sorbent and on the amount of sorbent. Different methods for calculating the breakthrough volumes are described in a recent review and involve the study of the breakthrough curves [39], empirical estimation from elution chromatography [40], or measuring the peak areas or heights after on-line preconcentration of increasing volumes of water spiked with a decreased concentration, so that in each analysis the amount of analytes preconcentrated is the same [41]. The estimation of the breakthrough volumes, either with on-line or off-line techniques, offers information about the optimal sample volume that can be percolated through the sorbent to gather optimal sensitivity. When 100% recovery is required, the percolated volume must be lower than the breakthrough volume. However, in environmental analysis, it is a common practice to surpass the breakthrough volume; in such case, the total amount of analyte preconcentrated is higher and, therefore, the sensitivity is increased at the expense of recovery.

Table 2 Detection Limits (μgL^{-1}) of Several Phenolic Compounds in Groundwater Using On-Line and Off-Line LSE with Lichrolut Sorbent Followed by LC–UV and Using On-Line LSE with C_{18} Sorbent for Pesticides

	On-line		Off-line	
Compound	A	B	A	B
Phenol	0.7	3.5	0.8	3
Catechol	2	9	0.5	6
4-Methylphenol	0.4	2	0.25	1.7
2,4-Dimethylphenol	0.03	0.5	0.1	1
2-Nitrophenol	0.05	0.8	n.d.	n.d.
4-Nitrophenol[a]	0.01	0.08	0.05	0.25
2,4-Dinitrophenol[a]	0.09	0.3	0.1	0.8
4-Chloro-3-methylphenol	0.05	1	0.5	1.3
2-Chlorophenol	0.2	1.2	0.1	1
3-Chlorophenol	0.2	1.2	0.1	0.9
4-Chlorophenol	0.2	1.4	0.2	1.4
2,4-Dichlorophenol	0.1	0.8	0.1	0.5
2,4,6-Trichlorophenol	0.08	0.3	0.1	0.6
2,3,5-Trichlorophenol	0.07	0.3	0.1	0.2
2,3,4-Trichlorophenol	0.08	0.3	0.1	0.1
Pentachlorophenol[a]	<0.01	0.02	0.1	0.2
Azinphos-methyl	0.06	0.14	n.r.	n.r.
Dichlorvos	0.09	0.25	n.r.	n.r.
Fenitrothion	0.04	0.09	n.r.	n.r.
Malathion	0.15	0.3	n.r.	n.r.
Fenthion	0.06	0.09	n.r.	n.r.
Parathion-methyl	0.05	0.09	n.r.	n.r.
Parathion-ethyl	0.04	0.08	n.r.	n.r.

A, groundwater; B, river water; [a]310 nm.
n.d., not detected; n.r., not reported.
Sample: on-line, 100 mL; off line, 1000 mL.

Matrix composition affects the analytical performance and should be considered when calculating breakthrough volumes. Because the water matrix accounts for variations in method performance, it is expected that differences in quality parameters will be found. Consequently, it is advisable to perform calibration of the system using the same water matrix as the unknown water sample and the same analytical method should always be applied. A change in the type of water can lead to considerable variations of breakthrough volumes and LODs [42]. Moreover, adsorption of analytes onto humic substances can result in a decrease of breakthrough volumes and recoveries, because only the dissolved fraction will be enriched [20,21]. This can be partially solved by acidifying the sample at low pH, but adsorption of humic substances into the sorbent is increased, because their hydrophobic character is raised. Therefore, this can result in a decrease of breakthrough volume of analytes that lack strong affinity for the sorbent because there is strong competition between analytes and humic substances. For instance, important differences in working at pH 7 or pH 2.5 were found when analyzing river water samples spiked with priority phenols, driving which cresols or 2,4-dimethylphenol were displaced with humic substances, so their breakthrough volume and recoveries were reduced. Conversely, higher recoveries than expected were found when analyzing polar pesticides such

as aldicarb sulfoxide or aldicarb sulfone in drinking water. This could be explained by the fact that absorbed humic and fulvic substances increases the surface of the sorbent, thereby raising recoveries of some polar analytes. As a result of the variations found in the recovery of the different organic pollutants in the different types of waters, before HPLC analysis the extraction pH should be optimized to maximize analyte recovery and detection limits. Quantitation in real samples is, in any event, difficult because humic substances appear during the earlier minutes, making identification and quantification of low-retention time analytes troublesome, as shown in Fig. 4. In conclusion, when breakthrough volumes, recoveries, or detection limits need to be calculated, their determination should be carried out in a water matrix similar to that of the final analysis.

When analyzing samples with a high percentage of humic material another relevant parameter to be optimized is the cleanup step. Humic material can be partially removed from the sorbent by passing a small amount of water through the sorbent bed, thereby providing a chromatographic profile void of interferences. But the water volume should be carefully optimized, especially when working with low breakthrough volume analytes such as phenol.

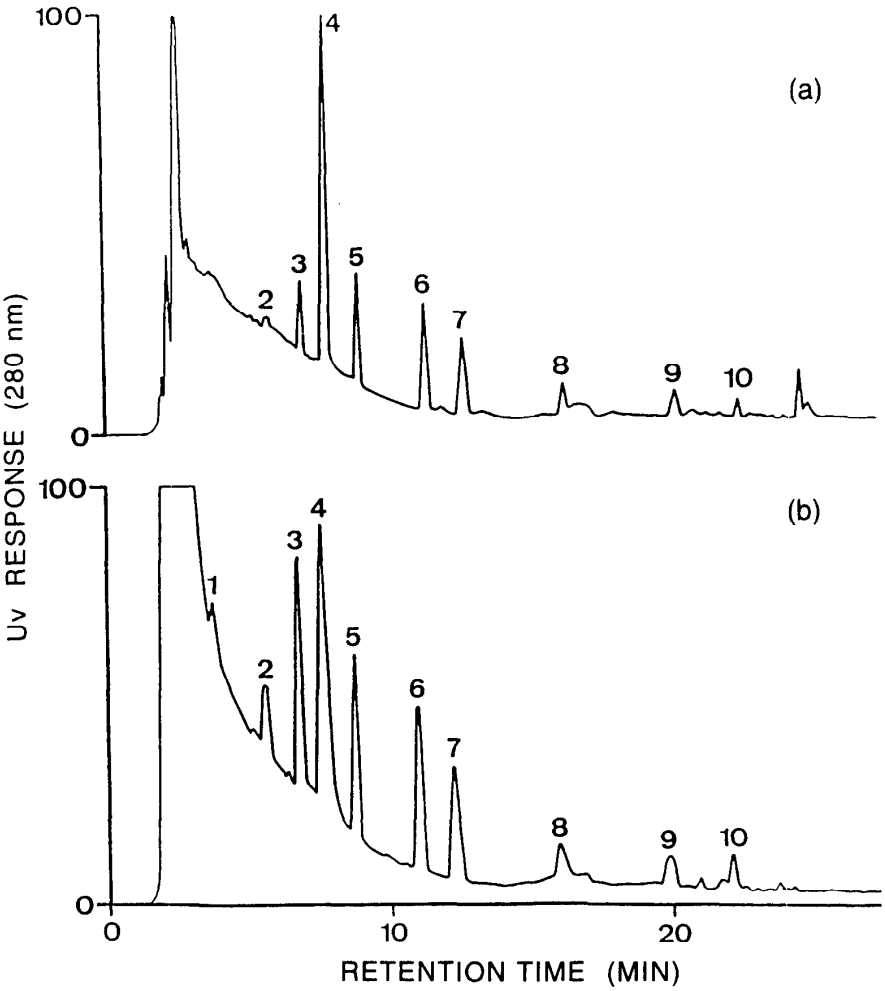


Figure 4 LC–UV (280 nm) chromatograms of phenolic compounds spiked at 4 μg L^{-1} in groundwater after on-line LSE using a 10 × 2 stainless steel precolumn using different polymeric sorbents. (a) PLRP-S, (b) LiChrolut EN. Sample volume: 50 mL. Peak identification: (1) cathecol, (2) phenol, (3) 4-nitrophenol, (4) 2,4-dinitrophenol, (5) 4-chlorophenol, (6) 2,4-dimethylphenol, (7) 4-chloro-3-methylphenol, (8) 2,4-dichlorophenol, (9) 2,4,6-trichlorophenol, (10) pentachlorophenol.

When using an on-line approach, precolumns are normally packed with about 20 mg; thus, no more than 1–1.5 mL are required. On the other hand, it should be taken into consideration that some analytes can be adsorbed onto humic substances, which at the same time, are adsorbed onto the sorbent. This is especially true when acidification of river samples rich in humic substances is carried out before the analysis. In this situation, the washing step will lead to a decrease in recovery because when removing humic material the analytes will also be removed.

3. Sorbents

Today, a wide range of sorbent materials are available in different configurations, such as cartridges, Empore extraction disks, packed in small precolumns for on-line approach. Even though bonded silicas such as C_{18} or C_8 are still the most used material for environmental applications [43,44], styrene divinylbenzene-based sorbents have gained popularity in the last few years [20,35]. A comparative study among various available sorbent materials were carried out to determine which one globally provides the best performance. Lower breakthrough volumes were found for the most polar pesticides (mevinphos, dichlorvos, and fenamiphos) owing to their high polarity, which leads to an increased affinity toward the water phase in comparison to the C_{18} material [45]. Table 3 shows the breakthrough volumes of phenolic compounds calculated at 4 μg L^{-1} [33]. Good results were achieved for the most apolar analytes, such trichlorophenol and pentachlorophenol, when using bonded silicas, but volumes of less than 10 mL were obtained for the rest of the target compounds. Values were slightly improved using monofunctional C_{18} (C_{18}/OH). This sorbent allows a better interaction with the free silanol groups because silanization is done by using trichloroorganosilanes instead of the monochloroorganosilanes currently used. Because the percentage of free silanol groups is increased, the polarity of the sorbent raises. Cyclohexyl sorbent has a medium polarity that allows the achievement of high breakthrough volumes for moderately polar compounds such as phenols. The best results, with breakthrough volumes higher than 100 mL, were achieved for trichlorophenols and pentachlorophenol. The good compromise of the breakthrough volumes with the low band-broadening suggests that it can be a reasonable approach for the trace enrichment of phenolics in environmental waters.

Table 3 Breakthrough Volumes (mL) of Several Phenolic Compounds in Groundwater Calculated by On-Line LSE–LC–UV (280 nm) at 4 μgL^{-1} Level with Different Types of Sorbents[a]

Sorbent	C_{18}	C_{18}(MF)	—CH	PLRP-S	LiChrolut EN	Isolute ENV
Catechol	<10	<10	<10	<10	25	25
Phenol	<10	<10	<10	<10	35	30
4-Methylphenol	<10	<10	<10	50	55	60
2,4-Dimethylphenol	<10	<10	30	180	>200	>200
2-Nitrophenol	<10	<10	<10	60	75	70
4-Nitrophenol	<10	<10	<10	45	70	80
2,4-Nitrophenol	<10	<10	<10	>200	>200	>200
4-Chloro-3-methylphenol	<10	<10	<10	100	110	100
4-Chlorophenol	<10	<10	30	70	85	75
2,4-Dichlorophenol	20	40	50	100	120	130
2,4,6-Trichlorophenol	40	60	100	>200	>200	>200
Pentachlorophenol	>200	>200	>200	>200	>200	>200

[a]C_{18}(MF), C_{18} monofunctional; CH, cyclohexyl.

Polymeric sorbents have become an acceptable alternative to bonded silica for effective preconcentration of moderately to polar organic compounds [21,33,46] because better recoveries, especially for the more polar compounds, are obtained (see Table 3). Disposable prepacked columns, cartridges, or Empore disks are available from most manufacturers under various trade names, such Envi-chrom, PLRP-S, Lichrolut EN, and Isolute ENV, had have few differences among them. XAD resin has been used for extraction and stabilization of phenols [47] and pesticides [48] from water. However, this sorbent needs an extensively cleanup before the preconcentration step [49]. On the other hand, recoveries higher than 90% for priority pollutants were found using Amberchrom resins [12] and higher than 80% were obtained when using column-switching systems and PLRPs sorbent [50]. The main problem of this sorbent material when the on-line approach is used, is that band-broadening can appear, especially when normal flush elution is used.

New phases such as Lichrolut EN or Isoelute ENV have recently appeared in the market. They are highly cross-linked and have an open structure (highly porous material), which maximizes the active surface compared with other sorbents such as PLRP-S; thus, leading to better breakthrough volumes. Recoveries higher than 80% and detection limits below 0.5 and 2 $\mu g\ L^{-1}$ were obtained for all listed phenols using off- and on-line approaches, respectively [20,26] when using Lichrolut EN, although there was considerable band-broadening with the column switching technology [20]. This can be seen in Fig. 4 which shows chromatographic profiles obtained using PLRP-S and LiChrolut EN.

A few modifications, such acetylation [51] or sulfonation [52], led to increase recovery values. A comparative study between an unmodified polymer (SDB) and a sulfonated one (SDB-RPS) in Empore disk format [53] showed the excellent performance of the modified sorbent, giving recoveries for phenol and cathecol ranging from 80 to 86%, when processing 1 L of water. These values are sizeable improvements in data obtained when using the SDB disks (from 40 to 50%). The sulfonated disks have a mixed retention mechanism that includes hydrophobic and ionic interactions which facilitates the trapping of the most polar phenols. Unfortunately, it is now available only in the Empore disk format, although development in other configurations more suitable for automation can be expected in the near future.

Graphitized carbon black (GCB), available in cartridge format, has been described by several authors [54,55], and recoveries higher than 90% were found, except for phenol. However, the excessive retention makes the desorption of the trapped phenols difficult, and some of them (e.g., 2,4-dimethylphenol) were irreversibly adsorbed. Elution in backflush mode can overcome this problem, but the automation in off-line mode is not straightforward [32]. The poor mechanical stability of GCB cartridges has prevented their routine application in the on-line approach. This problem was overcome by the development of porous graphite carbon (PGC) for which the graphite is immobilized on a silica structure and the phase is pressure-resistant; thus, it shows better stability [56]. This sorbent has been successfully applied for on-line trace enrichment of aminophenols and catechols, but recoveries for phenol were lower than those obtained with polymeric sorbents [57]. In general, the PGC precolumns must be coupled with a PGC analytical column to prevent band-broadening. However, excessive retention occurs for most of the listed phenols, even when working with mobile phases with methanol ratios up to 80% [20]. Hence, the use of this sorbent will be restricted to the most polar phenols (e.g., catechols), and other sorbent materials will be preferred for the other phenolic compounds.

Combination of various sorbent materials, such C_{18}, GBC, or PLRP-S, with an anion exchanger has also been described, using both on-line and off-line procedures. Even though it allows monitoring of a broad range of analytes, with recoveries higher than 90% for all of them [18], complex designs are required, and the application is uncommon. Hence, an anion exchanger will be applied for the analysis of very polar analytes, as such aminophenols and polyhydroxyphenols, which are not trapped using polymeric phases. Analyses with the two phases should be carried out together to determine analytes of different polarities [18].

On-line preconcentration using a two-step approach with a PRP-1 in combination with an ion-exchange precolumn has allowed the determination of various chlorotriazines and urons in water at a 10 ng L^{-1} level [58]. In this way, PRP-1 acts as a filter to remove many of the neutral interference compounds present in drinking water samples.

Some attempts to couple LSE with supercritical fluid extraction (SFE) have been carried out [59]. This has the advantage against on-line LSE-LC that, by using CO_2 as a desorption agent, a more selective elution can be achieved. With LSE–SFE, identification and quantification of polar phenols can be achieved, with LODs ranging from 2 to 6 $\mu g\ L^{-1}$ with a UV detector. Even though this data is far lower than those obtained with on-line LSE–LC–DAD, the method can be successfully applied to analyze wastewater, with cleaner chromatographic profiles.

However, a really promising feature is the development of immunoaffinity sorbents for LSE. By taking advantage of cross-reactivity, trapping capacity, and selectivity, a family of compounds can be selectively extracted, thereby avoiding the matrix interferences. This approach has been recently applied for pesticide analysis [60] and the breakthrough volumes obtained with different sorbents are reported.

III. CONVENTIONAL DETECTORS (LC–UV, LC–DAD, LC–EC, LC–FD)

The absence of derivatization requirements and the possibility of on-line coupling with LSE without very sophisticated instrumental requirements has made LC the most applied separation technique for the analysis of organic micropollutants that basically include the polar, thermolabile, and nonvolatile pesticides. Universal analytical columns are C_{18}- or C_8-bonded silica, which may differ in sizes, internal diameter, particle size, and so on, covering the great demand for environmental analysis. The most usually detectors that can be used with LC are ultraviolet (UV), with fixed or variable wavelengths diode array detection (DAD), and fluorescent (FD), or electrochemical (EC).

A. Liquid Chromatography with Diode-Array Detection Analysis

Modern organic pollutants cover a wide range of compounds that differ in their chemistry. Pollutants susceptible to absorb at UV wavelengths are those that present a suitable chromophore, with molecular extinction coefficients that may vary from 40,000 to 100,000. This characteristic permits their detection by a UV detection, provided a proper sample preconcentration technique has been carried out. Most pesticides present a typical UV spectra, with UV maxima between 230 and 280 nm, whereas phenolic compounds are preferably detected at 280 nm, except for nitrophenols and pentachlorophenol, which show a better signal at 310 nm [27]. Pesticide transformation products can also be detected by UV spectra owing to absorbance similarities to the parental compound. Peak identification with LC–DAD is usually carried out by means of retention time, in comparison with a standard, and by spectral match through a library search, which is an option that is now included in most software. Selectivity enhancement is obtained through UV selection and can be used to identify and quantify pesticides with very close retention times. In this case, it is recommended that quantitative analysis be performed at the wavelength that provides better calibration adjustment. To reduce quantification errors, modern software includes the peak purity analysis of each compound, which permits the detection of a potential coelution problem with another pesticide or with matrix interferences.

As a result of variations of the results reported by the various laboratories, method testing, based on repeatability, reproducibility, and calibration data should be performed routinely to evaluate the performances of an analytical method and should be specifically aimed to provide

reliable quantitative results. Most important sources of method error concern the sample pretreatment step and method of quantification. In general, for environmental analysis the long-term reproducibility should not exceed a 10% variation, and the triplicate analysis should have a maximum error of 3%. It is clear that the use of on-line devices decreases the percentage of variation because the risks of sample losses or contamination are minimized. However, the type of water and analytical method have a direct influence on the results obtained. A recent project that involved various European countries was aimed at examining the performances of the SAMOS system for pesticide monitoring. The SAMOS system includes a sample preconcentration unit (Prospekt, Spark Holland, The Netherlands) connected on-line with a Hewlet Packard model 1090 equipped with a diode array detector. The whole setup is programmed with a workstation. This system is extensively described [61] and has been applied to monitor pesticides in European rivers. The performance of the system has recently been tested in industrial effluent water, and errors varying from 1 to 15% have been encountered after preconcentration of 100 mL of surface water spiked at 1 ng mL^{-1} through PLRPs precolumns of Prospekt. The authors concluded that the highest errors were due to breakthrough of the more basic compounds and to the presence of interferences. The repeatability and reproducibility of on-line LSE–LC–DAD using the SAMOS system were tested with Milli-Q and river water involving the preconcentration of 100 mL of sample onto C_{18} precolumns. The repeatability and reproducibility of the method are closely linked to the type of water. The overall values, measured as the percentage coefficient of variation, were less than 10% error, indicating the suitability of the method for water control analysis. Better values were obtained with Milli-Q water than river water because in the former, matrix interferences were not present. The higher error of simazine was due to a matrix coeluting peak at the interval.

To sum up, the system testing with Milli-Q water indicate the method's capabilities, but did not provide quantitative data that could be extrapolated to field measurements. A more realistic approach is gathered if method performance is first evaluated with surface water because the complexity of the determination of pesticides is increased owing to the water matrix, presence of particles, and presence of humic and fulvic material. Because water matrix accounts for variations in a method's performance, it is expected that differences in quality parameters will be found. Consequently, it is advisable to perform calibration of the system using the same water matrix as the unknown water sample. On the other hand, comparison with direct injection is not advisable when performing on-line experiments because band-broadening always occurs, although imperceptibly. Pichon et al. [62] have already indicated a 5% error if quantification of on-line samples was contrasted with direct injection. Table 4 reports the calibration data of eight pesticides obtained after the preconcentration of effluent river waters. Linearity was observed for all the compounds studied over a concentration level from 0.3 to 1.5 ng mL^{-1}. Coefficients of correlation were close to 0.99, which are acceptable if one takes into consideration that river water was used. The worst values were for diazinon and chlorpyrifos, which eluted at a high percentage of acetonitrile, together with the more lipophilic components in the water matrix. The high LODs of diazinon contributed to the low coefficient of correlation of this compound. Desethylatrazine and simazine could not be detected owing to early elution during the interval at which humic and fulvic substances abound.

B. Liquid Chromatography with Electrochemical Detection

Electrochemical (EC) detectors include various devices, such as conductivity detector and amperometric, coulometric, and polarographic detectors. The main advantage of this approach is that a great improvement in sensitivity can be obtained. This can be seen in Table 5, which shows LODs obtained using UV (280 nm), EC (1000 mV), and coulometric detection (E1: 300 mV; E2: 650 mV). For instance, one order of magnitude enhancement on sensitivity was found with amperometric detection, as compared with UV [63,64]. Moreover, the high sensitivity of EC allows one to reduce the sample volume, thus avoiding the percolation of low

Table 4 Calibration Data Using Llobregat River Water Spiked with a Mixture of Triazines and Organophosphorus Pesticides at a Level from 0.3 to 1.5 ng mL^{-1} [a]

Compound	nm	Calibration curve	R^2	Rep (%)	Repro (%)	LOD (ngL^{-1})
Desethylatrazine	215	n.d.	n.d.	3	10	120
Simazine	215	n.d.	n.d.	23	50	89
Atrazine	215	$Y = 485603X-14495$	0.997	4	4	10
Propazine	215	$Y = 657625X+16098$	0.996	9	13	10
Parathion	275	$Y = 177910X-4062$	0.994	4	5	13
Fenitrothion	275	$Y = 168103X+23745$	0.987	5	6	18
Diazinon	250	$Y = 83159X+11072$	0.972	5	10	105
Chlorpyrifos	215	$Y = 92692X+16050$	0.974	4	10	22

[a]nm, wavelength used for quantitation; R^2, coefficient of correlation; Rep, repetitivity ($n = 5$, spiked sample at 1 ng mL; Repro, reproducibility ($n = 5$, spiked sample at 1 ng mL^{-1}); LOD, limit of detection; n.d. not determined

breakthrough volume analytes, such as phenol. LODs of 0.02 $\mu g\ L^{-1}$ were found when processing 10 mL of river water, which could not be accomplished by UV [65]. This can be seen in Fig. 5, in which by reducing the sample volume it was possible to detect phenol, although nitrophenols could not then be monitored because the optimal working potential is slightly higher for these compounds.

Table 5 Detection Limits (ngL^{-1}) of Phenolic Compounds Obtained After On-Line LSE Followed by Spectrophotometric (UV), Amperometric (EC), and Coulometric (Screen-Out Mode) Detection

Compound[a]	UV (280 nm)	EC (1 V)	Screen-out mode (E1:350 mV) (E2:650 mV)
Phenol	1200	20	1.5
Catechol	n.d.	—	1.2
4-Methylphenol	1500	10	1.6
2,4-Dimethylphenol	800	30	
2-Nitrophenol	1200	2000	2
4-Nitrophenol	800	3000	2.3
2,4-Dinitrophenol	500	3000	3
4,6-Dinitro-2-methylphenol	n.d.	—	2.5
2-Chlorophenol	1500	50	2.5
3-Chlorophenol	1700	50	5.4
4-Chlorophenol	1500	40	0.6
2,4-Dichlorophenol	2000	30	0.9
4-Chloro-3-methylphenol	2000	25	2.4
2,4-Dichlorophenol	2000	30	n.d.
2,4,6-Trichlorophenol	2000	50	n.d.
Pentachlorophenol	1000	30	n.d.

[a]Sample volume 5 mL (10 mL for amperometric detector).

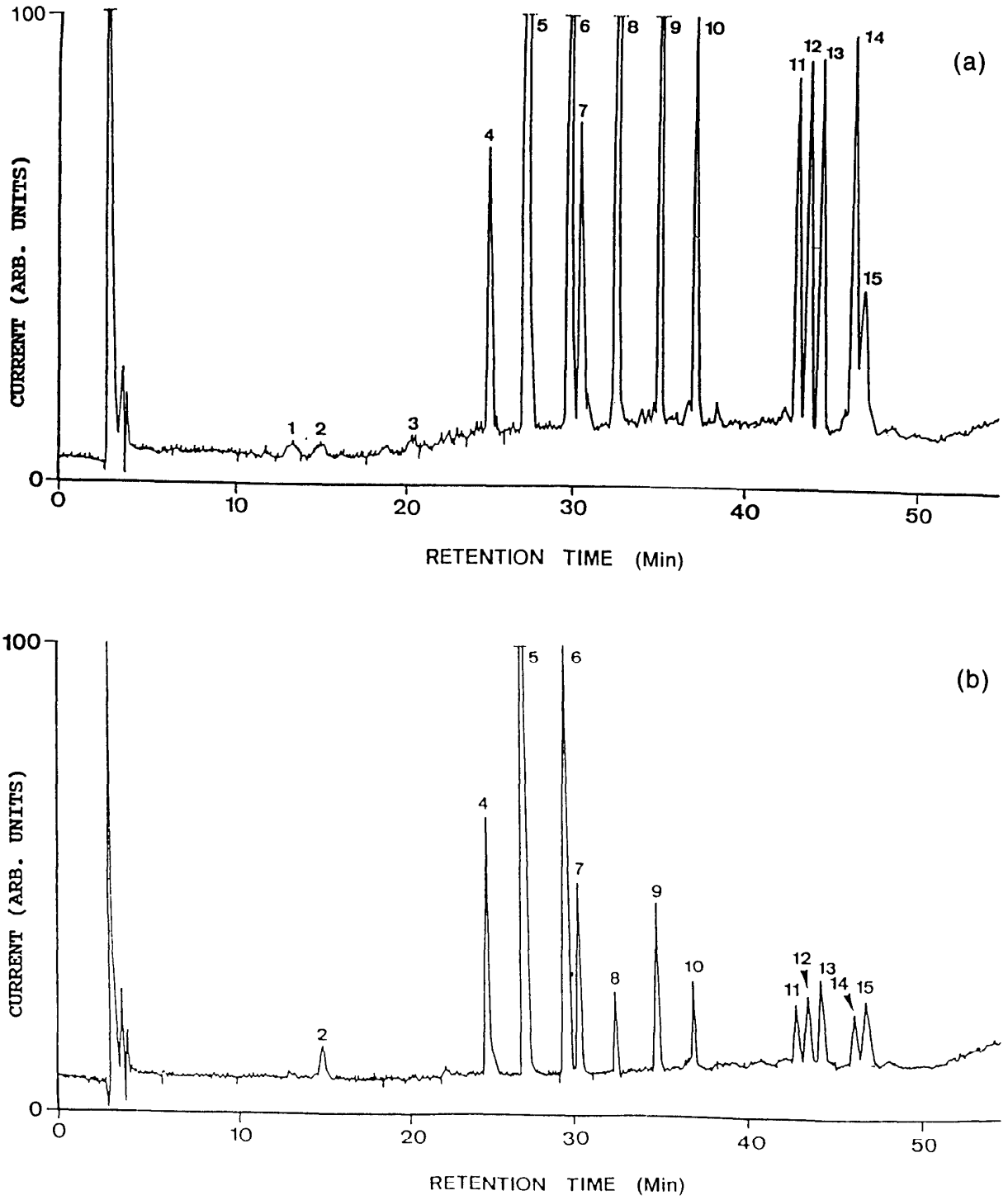


Figure 5 LC–EC (1 V) chromatograms of phenolic compounds spiked at 1 μg L^{-1} after on-line LSE of groundwater onto PLRP-S sorbent. (a) 50 mL and (b) 10 mL. Peak identification: (1) 4-nitrophenol, (2) phenol, (3) 2-nitrophenol, (4) 2,4-dinitrophenol, (5) 4-methylphenol, (6) 4-chlorophenol, (7) 3-chlorophenol, (8) 2,4-dimethylphenol, (9) 4-chloro-3-methylphenol, (10) 2,4-dichlorophenol, (11) 2,3,4-trichlorophenol, (12) 2,4,6-trichlorophenol, (13) 2,4,5-trichlorophenol, (14) 2,3,5-trichlorophenol, (15) pentachlorophenol.

Despite all these obvious advantages, a problem arises from the cleaning requirements of the electrochemical cell, which results in response instability. EC detection of phenolics requires the use of high applied potentials (about 1 V), which introduces the possibility that other matrix components can be oxidized, thereby increasing the background current, leading to lower reproducibility values compared with UV detection. The development of amperometric detectors (PAD) has improved signal stability. However, even here, the working electrode should be cleaned regularly to obtain the initial response, especially when processing dirty samples. Because this is sometimes very difficult to achieve, new calibration of the system should often be carried out. This is especially true when working in on-line LSE where the amount of interferences introduced into the chromatographic system is higher. This is obviously time-consuming and makes EC detectors less suitable for unattended use, which should be taken into consideration when many samples have to be monitored. Conversely, UV detection shows better performance for signal stability. However, higher sample volumes are required for the LSE step because of the lower sensitivity of the system. The problem involved is the risk of overcoming breakthrough volume of the more polar phenols. In summary, EC detection is a good choice to monitor relatively clean samples, such as drinking water, for which electrode fouling is not a critical problem. However, for the analysis of complex samples, such as river or wastewater, the more robust UV will be preferred, although EC may be required to detect the low breakthrough volume analytes.

Recently, coulometric array detectors have been introduced. Unlike common electrochemical detectors in which electrodes typically react at 10% or less of the injected sample, coulometric sensors convert 100% of the analyte because oxidation of phenols occurs in a high porosity electrode. Even though this obviously leads to higher background currents, sensitivity was one order of magnitude higher than for amperometric devices. In those systems the detector cells are designed so that the eluate flows through a porous graphite electrode, rather than flowing by the electrode as in traditional electrochemical detectors. This leads to large cell constants, which means that even if a significant portion of the electrode surface is contaminated, the response will remain constant. Consequently, cleaning requirements are less critical, and better reproducibility values are obtained. In their most sophisticated approach, a serial array of electrodes at increasing potentials provides three-dimension chromatograms (similarly to diode-array detectors) for which analyte voltammogram facilitates peak identification. Up to three orders of magnitude increase in sensitivity was obtained, compared with diode-array detectors, and LODs ranging from 0.03 to 0.38 ng L^{-1} were obtained when combined with LSE [66], although the high price of such systems has prevented spread of their application. Less sophisticated devices are available that are equipped with only two electrodes connected in series. In general, they can be operated in two main operational modes, usually called screen-out and redox mode. When using the screen-out approach, the first electrode (E1) is set a low potentials to eliminate interferences and only the second one (E2) is used for analytical purposes. Alternatively, the system can be run in redox mode. In this case E1 is set at high positive potentials to ensure all compounds of interest are oxidized. Afterward, the oxidation product is reduced in a second step. This approach is interesting for analytes that require high oxidative potentials, such as phenols, because these can be reduced by using potentials of about −200 mV, at which background and chromatographic interferences are reduced [67]. When combined with on-line LSE LODs below 100 ng L^{-1} were obtained for all priority phenols when processing 5 mL of water (see Table 5), which largely overcomes the data found with other detection devices [68]. However, this approach has been successfully used in the food and pharmaceutical industry, but few applications have been reported for environmental samples, mainly because their use for multiscreening purposes is unsuitable because gradient elution is not feasible. Hence, even though data are apparently really promising, careful studies devoted to reproducibility and robustness should be still carried out.

C. Liquid Chromatography and Fluorescence Detection

Similarly to electrochemical detection, the high sensitivity of fluorescence detectors (FD) allows reduction of the preconcentrated water volume, thereby preventing the breakthrough of the more polar compounds. However, the main drawback of this approach is that only a few compounds show fluorescence phenomena; hence, postcolumn derivatization is generally required, but obviously a high degree of selectivity is then obtained. This approach has been applied for the analysis of several types of pesticides as well of phenolic compounds.

Postcolumn derivatization with fluorescence has been applied for the determination of *N*-methylcarbamates and *O*-(methylcarbomoyl)-oxyme pesticides, and it is the official EPA method for the determination of these compounds [69]. For the higher sensitivity of these devices, water volume can be reduced to 10 mL, thereby avoiding percolation of the low breakthrough volume analytes [70]. Even though peak interferences can also occur, because the proposed system also detects substances with natural fluorescence (e.g., 1-naphthol), the postcolumn fluorescence detection system was extremely selective compared with LC–UV at 229 nm. This, explains the lack of matrix peak interferences at the beginning of the gradient elution. Figure 6a corresponds to the analysis of 10 mL of river water spiked at 0.2 $\mu g\ L^{-1}$ without any kind of cleanup. Figure 6b corresponds to the analysis of 10 mL of river water spiked at 0.2 $\mu g\ L^{-1}$ with a trifluoroacetic acid mobile phase (pH 3), and the switching valve system was removed after 10 min of gradient elution. The chromatogram front and the peak tailing was reduced and the peak shape was enhanced.

Fluorescence detection was also applied to monitoring phenolic compounds using direct [71] or indirect [72] fluorescence detection. LODs of less than nanogram per liter level were obtained in both cases, but derivatization to dansyl derivatives was required for the former approach and tubular flow through the reactor for indirect detection.

D. Liquid Chromatography and Mass Spectrometric Analysis

The LC–MS method has become a good approach for the analysis of polar contaminants that are difficult to analyze by GC. Moreover, it can provide useful structural information that can be used for unequivocal identification of contaminants and their degradation products in environmental matrices. The coupling of LC–MS is not as obvious as with GC–MS, because the mobile phase has to be eliminated before entering the MS, and at the same time, ions have to be generated. There are two main types of interfaces: trace enrichment (particle beam and moving belt) and nebulization (thermospray and atmospheric pressure interfaces). Trace enrichment interfaces have the advantage that they can provide electron-impact mass spectra, but their application in the environmental field has been prevented by their low sensitivity. Therefore, these interfaces will not be treated in this work and all the discussion will be focused toward nebulization devices.

1. Liquid Chromatography and Mass Spectrometry with Thermospray Interface

Liquid chromatography–TSP–MS has been widely used to determine organic contaminants in water matrices [53,73,74] and has been adopted by the EPA (method 8321) [75] for the analysis of pesticides in different types of water matrices. The LC–TSP–MS interface consists in sample nebulization and ionization through a heated capillary that renders molecular peak spectra and lacks fragment ions. Because it is a soft ionization technique, identification of unknowns becomes difficult. To enhance fragmentation, additives, mainly ammonium acetate or formate, are added to the mobile phase. Ionization is due to gas-phase protonation reactions between the analyte and the ammonium [76–78]. Filament-on or discharge-assisted ionization generates solvent-mediated ionization similar to direct TSP ionization (without additives), but sensitivity is enhanced [79]. The best choice to enhance fragmentation is the use of

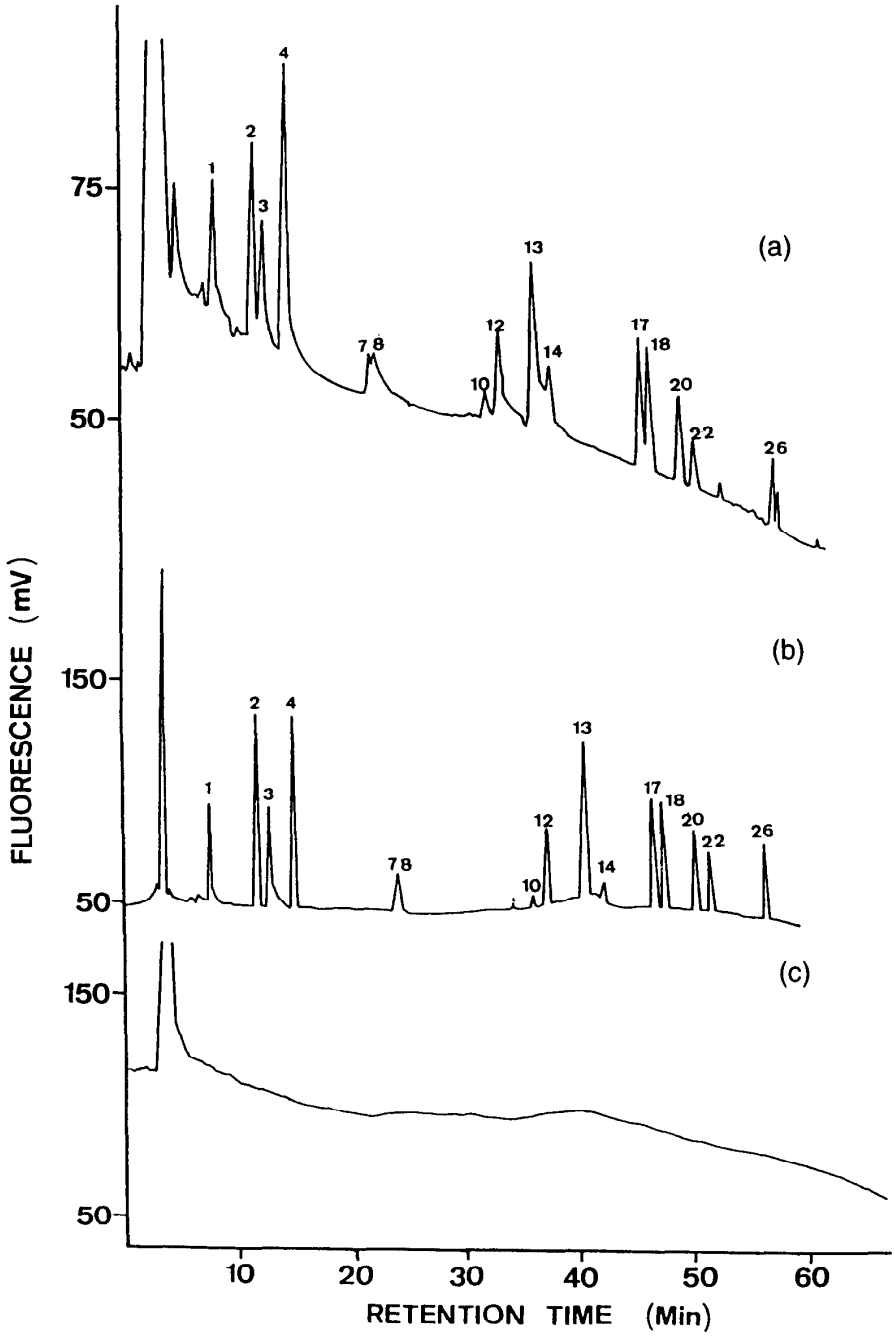


Figure 6 LC postcolumn fluorescence derivatization chromatograms obtained after preconcentration on ten C_{18} Empore disks of Ebro river water spiked at 0.2 μg L^{-1}. (a) Without any sample pretreatment, (b) after sample pretreatment, and (c) water blank. Peak identification (1) aldicarb sulfoxide, (2) aldicarb sulfone, (3) oxamyl, (4) methomyl, (7) 3-hydroxycarbofuran, (8) methiocarb sulfoxide, (10) methiocarb sulfone, (12) butocarboxim, (13) aldicarb, (14) 3-ketocarbofuran, (17) baygon (propoxur), (18) carbofuran, (20) carbaryl, (22) 1-naphthol, (26) methiocarb.

LC–TSP–MS–MS [80,81], which renders collision-induced dissociation (CID) spectra and is used both for identification and quantification purposes.

(a) LC–TSP–PI. Common trends in ion formation in TSP in positive mode are the favored formation of $[M + NH_4]^+$ as base peak for pesticides, which indicates that the proton affinity for these compounds is slightly lower than of ammonia (858 kJ mol^{-1}). The formation of $[M + H]^+$ ion as the second abundant ion with relative abundances varying from 12 to 93% indicates that these compounds exhibit intermediate basicity, with equal or less proton affinity values than ammonia, favoring both the formation of $[M + NH_4]^+$ and $[M + H]^+$ ions. Reverse-phase LC–TSP–MS is often carried out with acetonitrile or methanol–water mixtures. The addition of a volatile buffer, mainly ammonium acetate or formate is a common practice that leads to an increased ionization efficiency and generates solvent-mediated chemical ionization mass spectra [82]. Nicotinic acid can also be used, but not fragmentation from nicotinic acid adducts occurs. In positive mode of operation, adducts with methanol or acetonitrile can be formed and $[M + H + CH_3OH]^+$, $[M + CH_3OH]^+$ or $[M + H + CH_3CN]^+$, $[M + CH_3CN]^+$, respectively, are generated. It has been reported that using this ionization mode can increase the fragmentation of many carbamate pesticides [77]. Adduct formation is closely linked to the ion source and vaporizer temperature. High temperatures can be used to produce thermally assisted degradation, that occasionally can be used for identification purposes [78]. However, thermolabile pesticides undergo degradation, and their detection is impossible. An additional problem that comes up at high source and vaporizer temperatures is related to the spray stability that affects ion reproducibility. Fragmentation is also related to the type of instrument, and different ion formation has been observed using different instruments [83].

Table 6 reports the characterization of several pesticides under LC–TSP–MS in positive and negative mode. Little or no fragmentation is observed for many of the pesticides. Translated to an environmental sample, identification of unknowns using this technique is rather difficult because at least three different ions are needed to unequivocally confirm the presence of a pesticides in a real water sample. Under full-scan conditions, instrument detection limits (IDL) are close to 1 ng for pesticides [84,85]. For some pesticides, such as the parathion group [86], sensitivity is higher in the positive-ionization (PI) than the negative-ionization (NI) mode; hence, these compounds cannot be detected under NI mode and scan detection. The poor formation of oxons in NI mode was expected because, for oxygen analogues, the oxo group enhances the proton affinity in comparison with the thio group.

(b) LC–TSP–NI. With the NI mode, the analytes that produced the strongest signal and fragmentation were the electronegative compounds. For these compounds, NI mode is advantageous, because it yields more structural information and it is usually more selective. For example phenols, in general, exhibit good response in TSP–NI, except for phenol, 4-methylphenol, and 2,4-dimethylphenol, because current buffers cannot deprotonate them even when working at high buffer concentration level [53].

Under the NI mode organophosphorus pesticides yield specific fragment ions as reported previously [87,88], which correspond to molecular ions or adducts with formate as base peaks. However, strong fragmentation was observed for most of these pesticides, rendering fragment ions as base peaks, as is shown in Table 6. This behavior has already been observed for some OP pesticides [89]. For fenamiphos, whereas the parent compound and its sulfone exhibited $[M–H]^-$ as a base peak, the sulfoxide presents an unidentified ion at m/z 169. However, adducts with fragments have been observed for this compound at m/z $[M + 16]^-$, which can be attributed to $[169 + HCOOH–CH_2O]^-$. Fenthion exhibited an ion at m/z 279, which corresponds to an $[M + H]^-$ ion similarly to that observed by Vreeken [89] for other pesticides. The base peak for fenthion was at m/z 340, which can be tentatively identified as $[M + 61]^-$ corresponding to $[M + HCOOH + HCOO–CO]^-$. The loss of CO from the original molecule has already been reported [89] for phenyl urea pesticides. The poor detectability of oxons in the NI mode is because the oxo group enhances the proton affinity in comparison

Table 6 Mass Fragments and Relative Abundances (%) Observed in Flow-Inject Thermospray LC–MS in PI and NI Modes and Filament-on Conditions[a]

Compound	MW	Ions (m/z) (% abundance) PI mode	Ions (m/z) (% abundance) NI mode
Chlorpyrifos	322	*323*(58) $[M + H]^+$ 340(100) $[M + NH_4]^+$	286(100) $[M\text{-}HCl]^-$
Diazinon	304	*305*(100) $[M + H]^+$	169(100) $[(C_2H_5O)_2POS]^-$ 303(4)$[M\text{-}H]^-$
Disulfoton	274	153(75) $[(CH_3CH_2O)_2PS]^+$ 275(100) $[M + H]^+$ *292*(26) $[M + NH_4]^+$	185(100) $[(C_2H_5O)_2PS_2]^-$
Disulfoton sultone	306	291(100) 324(44) $[M + NH_4]^+$	185(100) $[(C_2H_5O)_2PS_2]^-$
Disulfoton sulfoxide	290	159(73) 291(100) $[M + H]^+$ 308(15) $[M + NH_4]^+$	185(100) $[(C_2H_5O)_2PS_2]^-$
Fenamiphos	303	*304*(100) $[M + H]^+$ 321(17) $[M + NH_4]^+$	153(15) $[CH_3S\text{-}C_6H_3\text{-}CH_3O]$ 302(100) $[M\text{-}H]^-$
Fenamiphos sulfone	335	304(57) 336(30) $[M + H]^+$ 353(100)$[M + NH_4]^+$ 377(11) $[M + H + CH_3CN]^+$	185(65) 320(98) $[M\text{-}CH_3]^-$ 334(100) $[M\text{-}H]^-$ 380(42) $[M + HCOO]^-$
Fenamiphos sulfoxide	319	304(21) 320(93) $[M + H]^+$ 337(100) $[M + NH_4]^+$ 361(17) $[M + H + CH_3CN]^+$	169(100) 185(82) $[169 + HCOOH\text{-}CH_2O]^-$ 215(29) $[169 + HCOOH]^-$ 318(85) $[M\text{-}H]^-$
Fenthion	278	183(53) 279(25) $[M + H]^+$ 296(100) $[M + NH_4]^+$	153(28) $[M\text{-}(CH_3O)_2PS]^-$ 279(48) $[M + H]^-$ 340(100) $[M + HCOOH + HCOO\text{-}CO]^-$
Fenthion oxon	262	171(13) $[C_8H_9OS + NH_4]^+$ 263(24) $[M + H]^+$ 280(100) $[M + NH_4]^+$ 304(8) $[M + H + CH_3CN]^+$	153(100) 194(40)

Isophenfos	345	287(100) $[M\text{-}NHCH(CH_3)_2]^+$	344(100) $[M\text{-}H]^-$
		346(89) $[M + H]_+$	
Malathion	330	331(12) $[M + H]^+$	157(100) $[(CH_3O)_2PS_2]^-$
		348(100) $[M + NH_4]^+$	329(33) $[M\text{-}H]^-$
Malaoxon	314	315(54) $[M + H]^+$	172(100) $[(CO_2CH_2CH_3)_2\text{-}C_2H_2]^-$
		332(100) $[M + NH_4]^+$	230(48) $[172 + CH_3COO + H]^-$
			313(18) $[M\text{-}H]^-$
Metidathion	302	303(18) $[M + H]^+$	157(100) $[(CH_3O)_2PS_2]^-$
		320(100) $[M + NH_4]^+$	287(6) $[M\text{-}CH_3]d^-$
Pyridafenthion	340	*341*(100) $[M + H]^+$	169(100) $[(C_2H_5O)_2POS]^-$
			203(10) $[M\text{-}(C_2H_5O)_2PO]^-$
			340(11) $[M]^-$
Temephos	466	466(53) $[M]^+$	341(35) $[M\text{-}(CH_3O)_2PS]^-$
		484(100) $[M + NH_4]^+$	451(100) $[M\text{-}CH_3]^-$
Temephos sulfoxide	482	348(44)$[M\text{-}(OCH_3)_2P + CH_3CN]^+$	341(6) $[M\text{-}(CH_3O)_2POS]^-$
		482(45) $[M]^+$	373(22) $[M\text{-}(CH_3O)_2PO]^-$
		483(100) $[M + H]^+$	451(100) $[M\text{-}CH_3O]^-$

[a]Eluant: 50% acetonitrile–50% water with ammonium formate 0.05M. Amount injected = 200 ng.

with the thio group; therefore, the sensitivity is one order of magnitude better in PI compared with NI mode.

Phenolic compounds were extensively studied using TSP interface in NI [53,90]. High chlorinated phenols were deprotonated by the acetate ion with the subsequent formation of the $[M-H]^-$ ion, or underwent resonance electron capture to form the $[M]^-$ ion, which produces, by hydrogen abstraction from a solvent molecule, the $[M + H]^-$ ion that is usually the base peak of the spectra because of overlapping of the isotopic patterns. For pentachlorophenol, the $[M-Cl + H]^-$ ion (*m/z* 229) was detected with a relative abundance of 45%. Moreover, adduct formation of $[M + CH_3COO]^-$ (*m/z* 314) and $[M + (CH_3CN)_2]$ (*m/z* 347) was found for this compound, with relative abundances of 5 and 15%, respectively. Both adducts were also found for the trichlorophenols with relative abundances of 15% (*m/z* 255) and 12% (*m/z* 277), but no fragmentation was observed in these cases.

The low chlorinated phenols showed a different behavior, with the adduct $[M + CH_3COO]^-$ as base peak. $[M-H]^-$ ion (*m/z* 161) was detected for 2,4-dichlorophenol, but the relative abundance was only 50%. For the monochlorophenols it was impossible to detect $[M-H]^-$ ion owing to the restricted scan range (beginning with *m/z* 138), but from the general tendency of the chlorophenols, lower abundances of this ion can be expected.

For the nitrophenols, the mass spectra were dominated by $[M-H]^-$ ion, which indicates lower gas-phase acidity (GPA) than acetic or formic acid. $[2M-H]^-$ ion was detected for mononitrophenols (*m/z* 277), the relative abundance being higher for 2-nitrophenol than for 4-nitrophenol (60 vs. 35%), owing to stearic and electronic effects. However, because the abundance of this ion should be dependent on the analyte concentration, it is not likely that this adduct will be detected at low concentration levels. Also, $[M + CH_3COO]^-$ ion (*m/z* 198) was detected, with a relative abundance of 20%. None of these ions were observed for 2,4-dinitrophenol, but $[M-NO-H]^-$ ion (*m/z* 153) was obtained with an abundance of 15%.

In general, sensitivity is strongly dependent on the number of substituents capable of stabilizing the phenolate ion (Table 7). When working in full-scan mode, instrumental detection limits (IDLs) fall within a range of 180–500 ng. The best values were obtained for the high-chlorinated phenols (e.g., 2,4,6-trichlorophenol [80 ng] and pentachlorophenol [45 ng]). Moreover, sensitivity for 4-nitrophenol was higher than, for example, 4-chlorophenol because the former has a strong resonance effect. In general, no response was found for phenol, 4-methylphenol, and 2,4-dimethylphenol because current buffers cannot deprotonate them even when working at a high-buffer concentration [53].

Similarly to other detection techniques, LC–TSP–MS has been coupled on-line with LSE to enhance sensitivity, and has been applied for pesticide monitoring [74]. A linear relation between the area of each peak versus concentration was found with correlation coefficient (R^2) of about 0.99 calculated from the LD, implying that quantitation can be performed at levels of a few micrograms per liter. Only fenthion was degradated in aqueous solution during the preconcentration step owing to instability in water solution. Coelution problems between chlorpyrifos and pyridafenthion were the cause of a decreased linearity of the former pesticide (from 0.1 to 2 $\mu g\ L^{-1}$).

Special interest is given to the analytical techniques that allow simultaneous identification of pesticides and their TP in environmental matrices, and at the same time, they can be used for quantification purposes. In this line of research, the latest works concerning the analysis of pesticides of different nature with on-line LSE–LC–TSP–MS with positive mode of ionization include those of Bagheri [91] and those of Sennert [92]. Most recent works that have included various TPs in their analytical methods, such as Chiron]93], who characterized several phenylurea pesticide and triazines, along with their oxons and sulfoxides, and those of Lacorte [94], who included the identification of various degradation products of organophosphorus pesticides. Lacorte et al. [94] have applied on-line LSE–LC–DAD and on-line LSE–LC–TSP–MS to unequivocally identify the parental pesticides and the TPs formed by degradation under seminatural conditions (Ebre river water spiked at a low concentration, and exposed outdoors for 4 weeks). On-line LSE–LC–DAD was used to follow the degradation

Table 7 Instrumental Detection Limits (IDL) in SIM Mode Using Various LC–MS Interfaces

	IDLs (ng)		
Compound	TSP	APCI	INS
Catechol	2	0.004	0.740
2-Nitrophenol	1.5	0.050	0.045
4-Nitrophenol	0.4	0.002	0.120
2,4-Dinitrophenol	0.7	0.004	0.256
2-Amino-4-chlorophenol	3.1	0.050	0.500
2-Chlorophenol	5	0.085	3
3-Chlorophenol	4	0.045	2
4-Chlorophenol	4	0.040	2
2,4-Dichlorophenol	3	0.007	1.310
2,4,6-Trichlorophenol	0.95	0.004	0.330
2,3,5-Trichlorophenol	0.90	0.003	0.350
2,4,5-Trichlorophenol	0.90	0.003	0.330
3,4,5-Trichlorophenol	0.90	0.002	0.300
Pentachlorophenol	0.5	0.001	0.100
Chlorpyrifos-methyl	0.08	0.001	n.d.
Diazinon	0.01	0.002	n.d.
Fenamiphos	0.01	0.004	0.01
Fenitrothion	0.1	0.018	0.2
Dichlorvos	0.15	0.012	0.06
Malathion	0.03	0.002	n.d.

n.d., not determined.

of the pesticides. The half-life measured by $T_{1/2} = \ln 2/k$ indicated that pesticides persisted in the environment for 6–12 days. However, since degradation occurred, confirmatory analyses were carried out by means of MS detection with TSP interface. The oxons of chlorpyrifos-methyl, diazinon, isofenphos, pyridafenthion, and temephos were detected 4 weeks after exposure. In general, the oxygen analogues could be identified because they followed the same adduct formation as the parental pesticide and eluted before it. The presence of sulfoxide derivatives was found for disulfoton, fenamiphos, and fenthion.

Fenamiphos sulfoxide was formed after sunlight exposure, which is in accordance with reports [95] of the formation of this compound by photodegradation. Fenamiphos also presented an unidentified peak with a molecular weight of 288, which was tentatively identified as a loss of CH_3 from the original molecule. Chukwudube et al. [96] pointed out that after UV irradiation, dealkylation with losses of CH_3 could happen for phosphorothioate pesticides. Sulfones were not found in the water sample, because they are more difficult to form in the environment, since it implies another oxidation step.

Fenthion is a compound that can easily degradate in aqueous solution, but could still be identified at m/z $[M + H]^+$ 4 weeks after spiking. Its sulfoxide was also identified. Fenthion is actually a matter of controversy because it has been removed from the NPS–EPA list, so it is considered unstable in well-water solution over a period of 14 days.

Figure 7 shows the LC–DAD and LC–TSP–MS chromatograms of a water sample spiked with chlorpyrifos-methyl and analyzed after 4 weeks. Although DAD detected chlorpyrifos and a transformation product, not identified, TSP–MS confirmed the presence of chlorpyrifos and its oxon. These samples were analyzed under both PI and NI modes, to gain more struc-

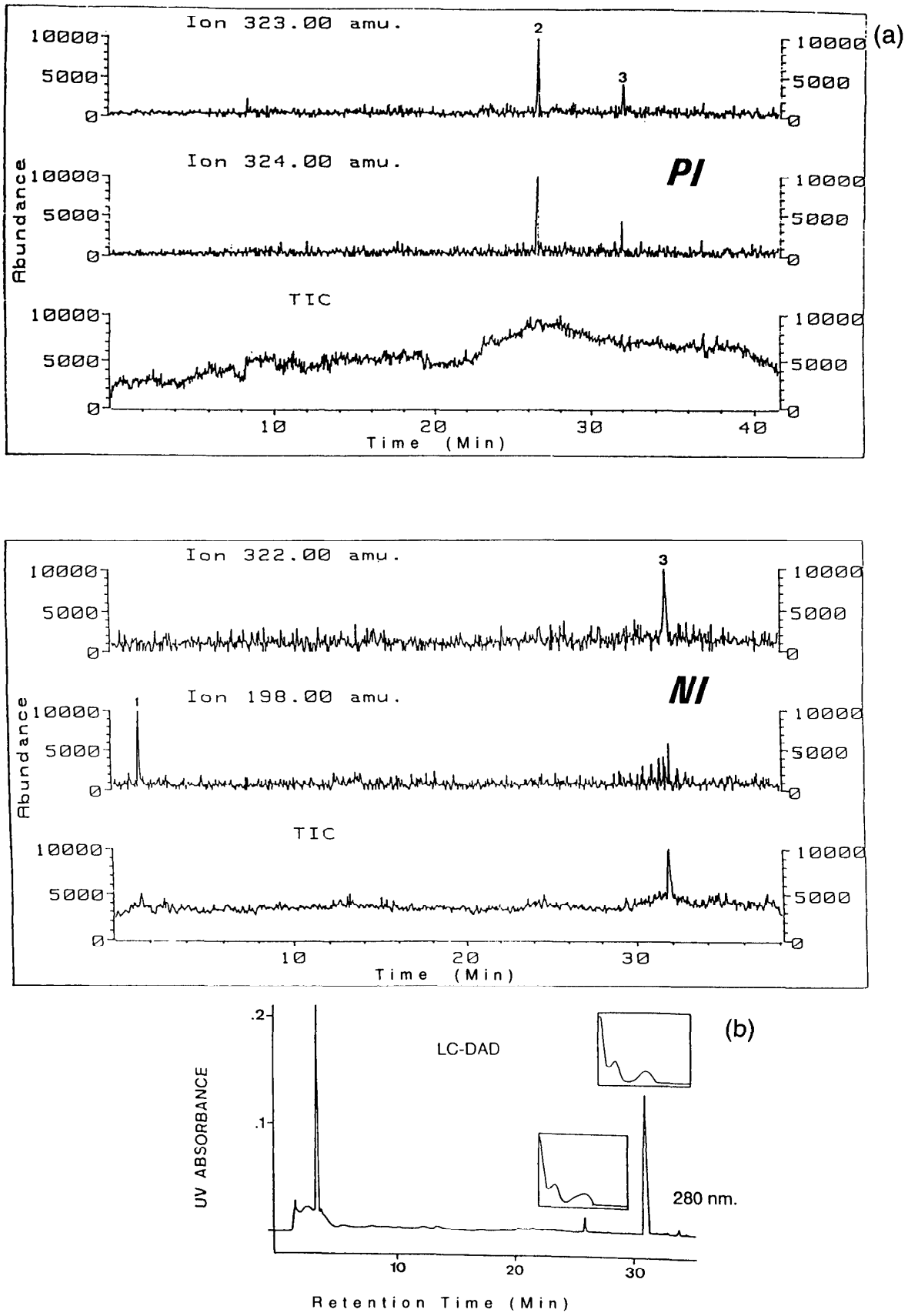


Figure 7 Reconstructed ion chromatogram obtained with (a) on-line LSE–LC–TSP–MS with PI and NI mode of ionization of an Ebre river water sample spiked with chlorpyrifos-methyl at 50 $\mu g\ L^{-1}$, and analyzing the water sample 4 weeks after spiking. Peak identification: (1) 3,5,6-trichloro-2-pyridinol, (2) chlorpyrifos-methyl oxon, (3) chlorpyrifos-methyl. (b) Same water sample analyzed by on-line SPE–LC–DAD at 280 nm.

tural information. The NI mode showed good sensitivity for chlorpyrifos-methyl, and chlorine losses could be determined. The TIC in the PI and NI ionization modes and the ion traces at *m/z* 323, 324, and 198 are presented, which correspond to the parental compound and the two TPs formed, chlorpyrifos-methyl oxon (*m/z* 324) and 3,5,6-trichloro-2-pyridinol (*m/z* 198). 3,5,6-Trichloro-2-pyridinol exhibited losses of chlorine atoms and proton abstraction, similar to the parent compound. The formation of 3,5,6-trichloro-2-pyridinol by hydrolysis has also been reported [97]. The toxicity of 3,5,6-trichloro-2-pyridinol is greater than that of chlorpyrifos, with EC_{50} values of 18.6 and 46.3 mg mL^{-1}, respectively, calculated with the Microtox system [98]. Also it has been reported that this compound is toxic to soil microorganisms and results in less mineralization and, therefore, enhanced persistence of chlorpyrifos in soil.

The presence of these compounds in water solution for at least 4 weeks means that, according to the NPS–EPA, they are stable for at least 14 days, and so their inclusion in the NPS–EPA list as toxic contaminants should be contemplated. Because the NPS–EPA stability study was conducted without the use of LC–MS, the TPs were probably also formed, but were not detected in water. These TPs are potential candidates to be included in future monitoring programs, (or they can be more toxic for the environment and can persist for a longer time period. LC–MS is a very useful technique for the identification of OP pesticide TPs. However, although LC–TSP renders structural information, often it is insufficient to identify unknowns, referring basically to transformation products of pesticides that might be present in real water samples. This problem can be approached from different perspectives that include MS–MS techniques, or by API techniques that produce spectra by collision-induced fragmentation, which aids the identification of unknowns.

2. Liquid Chromatography and Mass Spectrometry with Ionspray Interface

The advent of atmospheric pressure ionization (API) has opened a new window in environmental analysis. This heading includes several interfaces (i.e., electrospray [ESP]; the high-flow pneumatically assisted electrospray, commonly named ionspray [ISP]; the heated pneumatic nebulizer [HPN]; and atmospheric pressure chemical ionization [APCI]). The main advantage of these interfaces is their higher sensitivity compared with TSP or PB [99,100]. This can be seen in Table 7 in which the different sensitivities of phenolic compounds and pesticides obtained in the SIM mode using different interfaces are shown. API techniques have scarcely been used in environmental analysis, especially in the NI mode, as pointed out in the ASMS conference in Chicago [101]. Few applications using ESP or APCI for the analysis of organophosphorus [102,103], chlorophenoxy acids [104], triazines [105], or carbamates [106] were reported. The analysis of pentachlorophenol [107] and chloronitrophenols [108] using ESP was reported, but their performance for a wider range of priority phenols has not yet been investigated.

The main advantage of API techniques are related to the ionization efficiency because ionization of the molecules takes place at atmospheric pressure and, therefore, ions are efficiently formed in the liquid phase. Other advantages relate to the fact that no heat is applied to ionize the samples, eliminating thermal-assisted degradation, as happens when using a TSP interface. This allows the LC–MS analysis of thermolabile analytes, such as trichlorfon [109], which is a compound that suffers thermal degradation under TSP process caused by the probe tip and gas-phase temperatures higher than 200°C. Trichlorfon is converted to dichlorvos (Fig. 8) approximately 16% with a rearrangement and HCl elimination that was confirmed by isotopic abundance.

ESP consists in applying a voltage to a capillary that ionizes the sample, which emerges from the capillary as a spray. This spray contains microdroplets that are positively or negatively charged, depending on the difference of potential between the capillary and the counterelectrode. In the desolvation chamber, the droplets undergo ion evaporation and ions escape

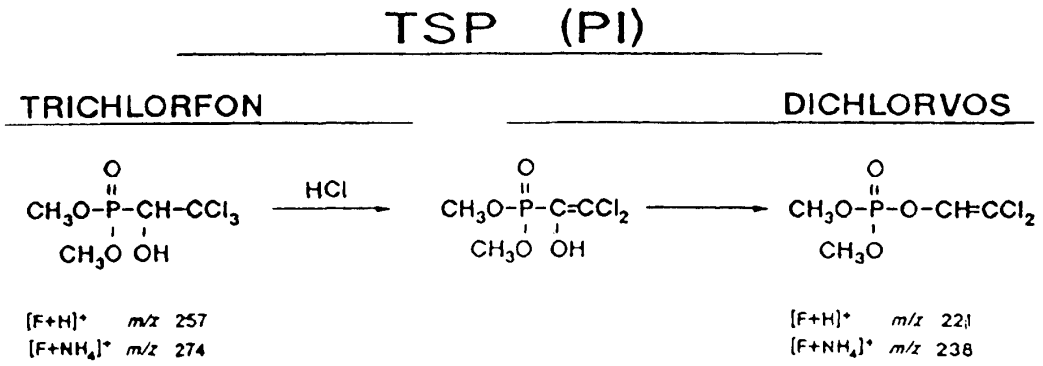


Figure 8 Degradation pathway of trichlorfon to dichlorvos under LC–TSP–MS conditions.

to the gas phase. Such ions are, therefore, focused toward the quadrupole of the mass spectrometer.

This technique has not been applied to the analysis of pesticides mainly because the interface design allows only reduced mobile-phase flow rates (10 mL min^{-1}) or otherwise a splitting device must be used. This obligates the use of a capillary analytical column, which makes the technique incompatible with HPLC. This results in a rather poor sensitivity of the ESP interface for pesticide analysis. Recently, high-flow ESP also called ionspray (ISP) has been developed, and it is commercially available. ISP has overcome these problems by applying a gas, normally nitrogen, that aids the formation of the spray on one hand, and on the other, solvent evaporation is facilitated by breaking the analyte–solvent clusters at the desolvation chamber. It has the advantage over conventional ESP that it does not require low flow rates (10 mL min^{-1}) that need either a split—when using conventional LC pumps—or syringe LC pumps, with the consequences of time consumption and extra cost. With ISP, ions emerge from the capillary owing to the simultaneous action of the nitrogen and the capillary voltage of 2–4 kV. As a result, flow rates up to 300 μL min^{-1} can be handled, in contrast with the original 10–80 μL min^{-1} with ESP interface. In ISP techniques, as the ions are transported through the desolvation chamber, ion evaporation takes place as a result of an increased coulombic repulsion forces that are superior to the superficial tension of the droplets, and ions escape to the gas phase. These ions have very little internal energy and, therefore, molecular ion spectra are obtained. To enhance fragmentation, an extraction potential of 20–100 V is applied at the extraction cone. This potential accelerates the ions and, as a result, the total ion current increases and fragmentation is induced by collision-induced dissociation (CID) and ions are focused toward the skimmer and finally to the mass spectrometer. This can be seen in Fig. 9 in which the mass spectra of deethylatrazine at 20 and 40 V cone voltage are shown. However, it should be noticed that increasing the cone voltage also leads to a decrease of sensitivity, as it can be seen for dimethoate (Fig. 10). Therefore, careful optimization of this parameter is required and generally a compromise between both factors (structural information and sensitivity) is achieved.

(a) ISP–PI. ISP was applied to the determination of organophosphorus pesticides in water samples [102,105]. The most volatile ones, such as trichlorfon, showed no degradation under ISP conditions. Table 8 shows the fragment ions of organophosphorus pesticides using extraction voltages of 20 and 40 V. Generally, an increased fragmentation is observed when working at 40 V, at the expenses of sensitivity, with the exceptions of fenamiphos, its metabolites, and fenitrooxon. When working at 20-V cone voltage $[M + Na]^+$ ion is obtained as base peak at 20 V. The Na^+ ions are due to the sodium ions present as impurity in the methanol solution, which means that more than 90% of the observed ions are due to ions present in solution. It has also been reported [105] that at increasing voltages, the fragmentation of some pesticides was done at expenses of $[M + H]^+$ ion, and the abundance of the adduct with Na

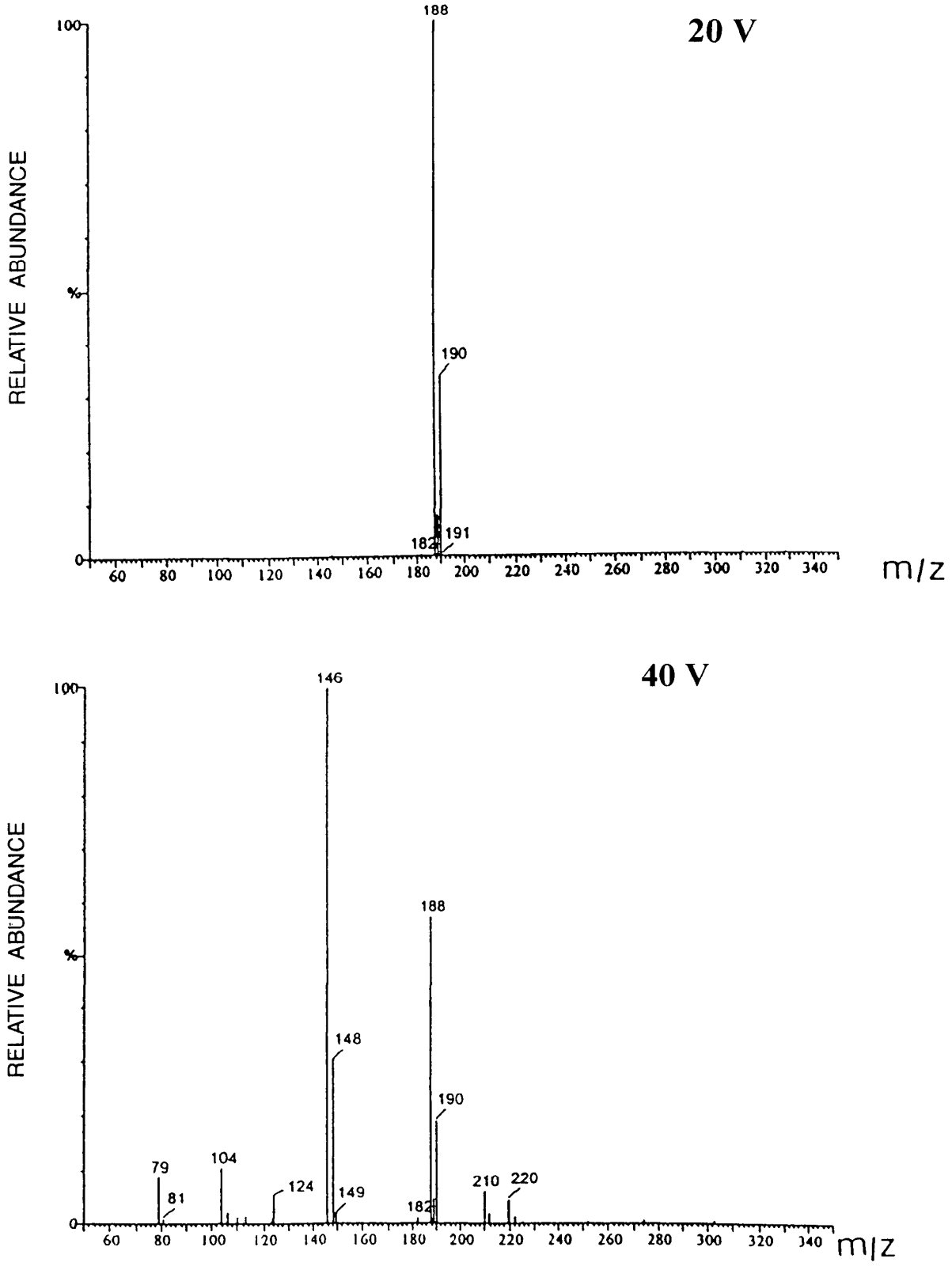


Figure 9 Mass spectra of deethylatrazine obtained using ISP interface at various cone voltages. Concentration 1 mg mL^{-1}. Carrier: methanol–water 1:1. Flow rate: 0.2 mL min^{-1}.

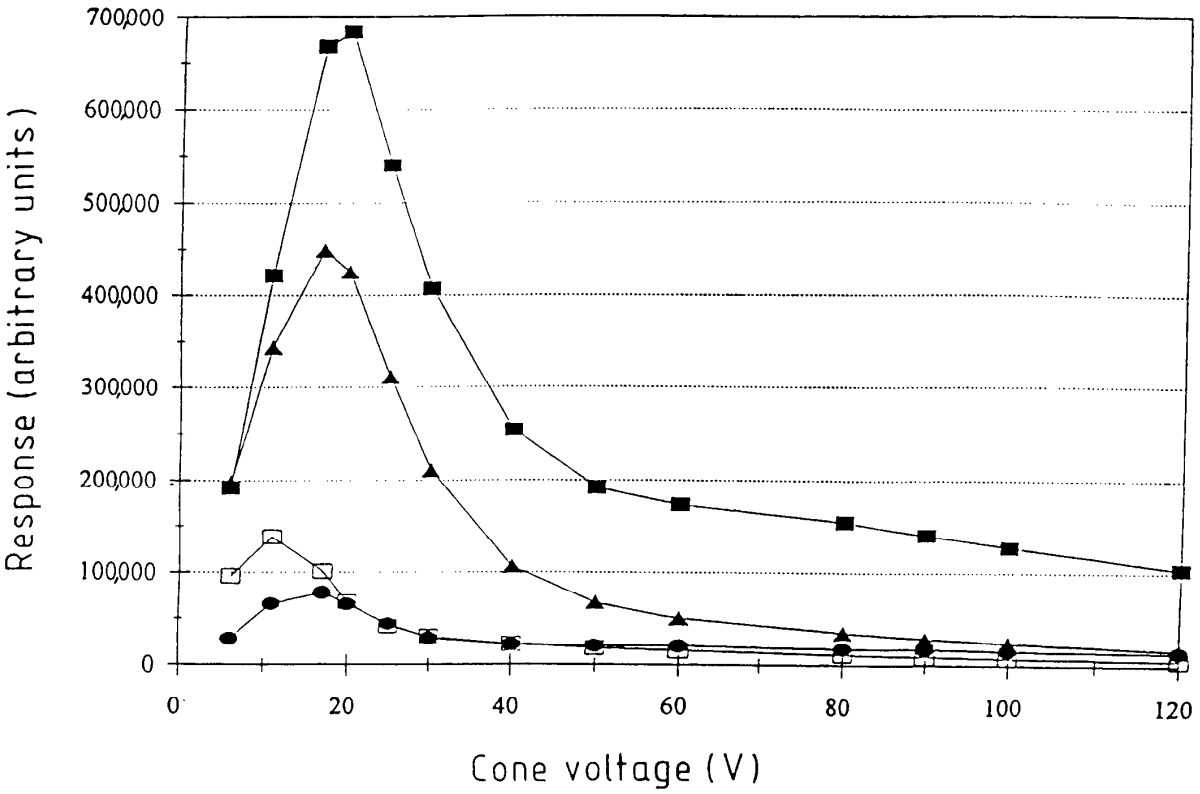


Figure 10 ISP response of dimethoate against cone extraction voltage. Ions registered were $[M + Na]^+$, $[M + H]^+$ with or without 0.5% of acetic acid in the mobile phase MeOH–water (1:1).

remained constant. This means that with ISP, a change of the extraction voltage is sometimes not sufficient to obtain fragmentation. In such cases, analytical conditions should be directed to obtain protonated molecules that can undergo fragmentation at high extraction voltages. High-flow pneumatically assisted electrospray (ESP) under the PI mode achieved LODs at the picogram levels for selected pesticides [105,106]. Sensitivity problems for the parathion group (parathion-methyl, parathion-ethyl, fenitrothion, and fenitrooxon) were noticed when using ISP or conventional ESP [102]. The ionization of these compounds under ESP conditions offers problems, and generally, it is difficult to achieve low nanogram per liter LODs in water samples.

A remarkable fact from the data observed in Table 8 is that typical diagnostic ions of organophosphorus pesticides under electron-impact ionization are observed in the data presented [110]. This corresponds to diagnostic ions at m/z 109, 110, 125, and 141, or to adducts of these diagnostic ions with Na^+, such as 133 and 164. This is a very important feature of ISP because it is a technique that can be used for identification of unknown pesticides, contrary to most of the TSPs that usually give very poor structural information; consequently, it is used for confirmation purposes of target analytes. Moreover, when working at a 40-V cone voltage more structural information its obtained compared with 20 V. Consequently, higher voltage will be recommended when identification of unknown pesticides in environmental samples is required.

By combining LC–ISP–MS with off-line LSE, the recovery at 0.1 $\mu g\ L^{-1}$ level of oxydemeton methyl, demeton-*s*-methyl, dimethoate, and fenamiphos in water was higher than 70%, which was an improvement over previous data.

The repeatability and the long-term reproducibility ($n = 9$) for the organophosphorus pesticides varied from 12–17% to 22–30%, respectively, when injecting 1 ng of each com-

Table 8 Important Mass Spectral Fragments, Relative Intensities (rel. intens.) of Organophosphorus Pesticides Using an LC Eluent of Methanol–Water (50:50) and Extraction Voltages (EV) of 20 and 40 V Under ISP/MS

MW	*m/z*	Compounds and ions tentative identification	Rel. intens. 20 V	Rel. intens. 40 V
246	164	Oxydemeton-methyl	—	30
	169	$[(CH_3O)_2POS + Na]^+$	—	19
	191	$[(CH_3O)_2POSC_2H_4]^+$	—	34
	269	$[C_2H_5SOC_2H_4S]^+$	100	100
		$[M + Na]^+$		
		Trichlorfon		
256	109	$[(CH_3O)_2PO]^+$	—	50
	133	$[(CH_3O)_2POH + Na]^+$	22	89
	279	$[M + Na]^+$	100	100
		Dimethoate		
229	125	$[(CH_3O)_2PS]^+$	—	28
	230	$[M + H]^+$		7
	252	$[M + Na]^+$	100	100
		Dichlorvos		
220	109	$[(CH_3O)_2PO]^+$	—	55
	243	$[M + Na]^+$	100	100
		Demeton-*s* methyl		
230	89	$[C_2H_5SC_2H_4]^+$	24	89
	109	$[(CH_3O)_2PO]^+$	—	20
	169	$[(CH_3O)_2POSC_2H_4]^+$	20	20
	253	$[M + Na]^+$	100	100
		Fenamiphos sulfoxide		
319	320	$[M + H]^+$	11	10
	342	$[M + Na]^+$	100	100
	358	$[M + K]^+$	41	20
		Fenitrooxon		
261	109	$[(CH_3O)_2PO]^+$	—	100
	284	$[M + Na]^+$	100	21
	320	$[M + H]^+$	38	21
		Fenamiphos sulfone		
335	358	$[M + Na]^+$	100	100
		Fenamiphos		
303	304	$[M + H]^+$	11	9
	326	$[M + Na]^+$	100	100

pound. Such values are acceptable because usually repeatability in LC–TSP–MS is performed by injecting higher amounts (e.g., 0.2 μg). Recently, it has been reported that for TSP, the reproducibility often exceeds 20% [111], which is in the range of the values obtained by using ESP.

(b) ISP–NI. The use of ISP in negative ion mode has been scarce owing the poor negative ion stability, and the problems of electric (corona) discharge, presumably caused by electrons emanating from the sharp edges of the ESP capillary needle held at a few thousand volts

negative relative to a counterelectrode. A breakdown to discharge at the tip of the capillary needle occurs at much lower field strength in the case of negative polarities than for positive polarities. Once the corona discharge occurs, the extraction efficiency of the ions from the solution to the gas phase decreases dramatically. This is because the plasma itself is a good electric conductor and the high electrical field for ion separation at the tip of the capillary disappears with the occurrence of the discharge. For aqueous solutions, it becomes very difficult to keep stable electrospray ionization (ESI) for negative polarities owing to the higher voltage needed to electrospray the liquid.

The signal instability of ESI can be reduced by adding chloroacetonitrile to the LC eluant which acts as an electron scavenger [104]. By adding these, there is a suppression of the electrical (corona) discharge phenomena leading to a stable ESI with finer-charged liquid droplets. Nevertheless, the improvements in ion stability are obtained at the expense of sensitivity (one order of magnitude less) owing to the $[M + Cl]^-$ adduct ion formation and to the higher cluster ions intensity. Chlorine attachment occurred in a way similar to TSP–MS for the phenoxy acid with a relative abundance of 8% in the best case. Because the major analytical requirements of environmental analysis is to achieve a low detection limit, cloroacetonitrile was not used for further analysis.

ISP in the negative ion mode was applied for the determination of phenolic compounds [53] and acidic pesticides [104] in water. However, because an acid pH is normally required for the LC separation of these compounds, post column addition of a 0.1 M solution of triethylamine (TEA) was necessary. Other authors reported the use of ion-pair chromatography, which allows the analytes to be separated as preformed ions [107], although this option is not so attractive because of the more-restricted chromatographic requirements.

The $[M–H]^-$ ion dominated the mass spectra of phenols and acidic herbicides, except benazolin and MCPB which exhibited $[M–COOH]^-$ and $[M–(CH_2)_3COOH]^-$ ions as base peaks at the optimal cone voltage (30 V). Benazolin displays extensive fragmentation, corresponding to $[M-45]^-$ and $[M-73]^-$ ions, which can be explained by the loss of the carboxylic acid moiety and the loss of NCH_2COOH group, respectively. However, few fragmentations were found for phenolic compounds; only the nitrophenols gave patterns similar to those obtained in APCI at 80-V cone voltage. Because ISP is a soft ionization technique, with no heat supply, the extent of fragmentation is lower.

As with TSP interface, no signal was obtained for phenol, 4-methylphenol, 2,4-dimethylphenol, and also 2-amino-4-chlorophenol had no response, even when raising the TEA concentration to 0.25 M or when using stronger bases such as 0.01 M KOH. However, it was reported that phenol was detected in FIA using ESP with pure methanol as eluant, using 5 mM KOH as additive [112]. Contrary to other interfaces, such as TSP or APCI, where an increase in the organic modifier ratio led to a decrease in the ion current, a great increase in sensitivity was found when raising the ratio of organic solvent. This was attributed to the lower solvation power and surface tension of methanol against water, which facilitates ion evaporation from the charged droplets. On the other hand, better sensitivity was found when using methanol instead of acetonitrile, as reported by other authors [102]. Because acetonitrile lacks of hydrogen-bonding capability, homoconjugation will occur, thereby leading to a decrease in sensitivity. Additionally, methanol shows lower surface tension than acetonitrile (0.0246 N m^{-1} vs. 0.0293 N m^{-1} respectively) which results in a more efficient ion evaporation process.

However, by raising the percentage of methanol, it was possible to detect phenol, 4-methylphenol, 2,4-dimethylphenol, and 2-amino-4-chlorophenol, which at high percentages of water could not be monitored because of their high pK_a and their hydrophilic character. This is particularly remarkable because, for these compounds, no response was obtained with the other interfaces. Especially the detection of phenol at low microgram per liter levels is still an unsolved problem, as shown by the results of an intercalibration exercise organized by Aquacheck, where only 1–2 laboratories out of 16–19 participants gave correct results for phenol. However, a problem arises from the need to use 100% methanol in the mobile phase

because in these conditions no retention on typical bonded silicas such as C_8 or C_{18} occurs. Porous graphitic carbon (PGC) analytical columns are an excellent alternative because they allow effective separation of polar phenolic compounds, using 100% methanol as a mobile phase (Fig. 11). Even though the restricted mobile phase conditions did not allow monitoring the entire range of analytes, and excessive retention occurs for some analytes, such as pentachlorophenol, to our knowledge it is the only reported way to monitor phenol in LC–MS experiments. Moreover, because ion evaporation is favored by low surface tension mobile phases, such as methanol, the use of PGC columns leads to significant increase in sensitivity for the rest of the target compounds. Hence, their use will be preferred when analyzing polar micropollutants with ISP interface.

On-line LSE–LC–ISP–MS coupling was developed for the determination of acidic herbicides [104] and phenolic compounds [113] in water samples. The best results were obtained with narrow-bore LC columns (3-mm id) using an eluant flow rate of 0.25 mL min^{-1} and the postcolumn addition of the buffer at a flow rate of 0.1 mL min^{-1}. In this way the final LC carrier stream does not exceed the critical values of 0.4 mL min^{-1} that will cause a relevant decrease in sensitivity in LC–ESP–MS. The use of 2.1-mm id narrow-bore LC columns appeared more suitable for flow rates of 0.3 mL min^{-1}. Unfortunately, extra peak band-broadening was observed when the analytical column was coupled on-line with a 2-mm–id OSP-2 precolumns, so this option was discarded. Under full-scan conditions, LODs for acidic herbicides ranged from to 1–3 $\mu g\ L^{-1}$ which combined with the abundant structural information makes the on-line LSE–LC–ESP–MS a powerful tool as an early warning system for the screening of polar pollutants in river water. Data for phenolic compounds was slightly worse, but values less than 0.1 $\mu g\ L^{-1}$ were found for all of them under SIM conditions. This is especially remarkable because the determination of priority phenols (especially phenol) at these levels is still unsolved, and because it is the only way to detect the presence of phenol,

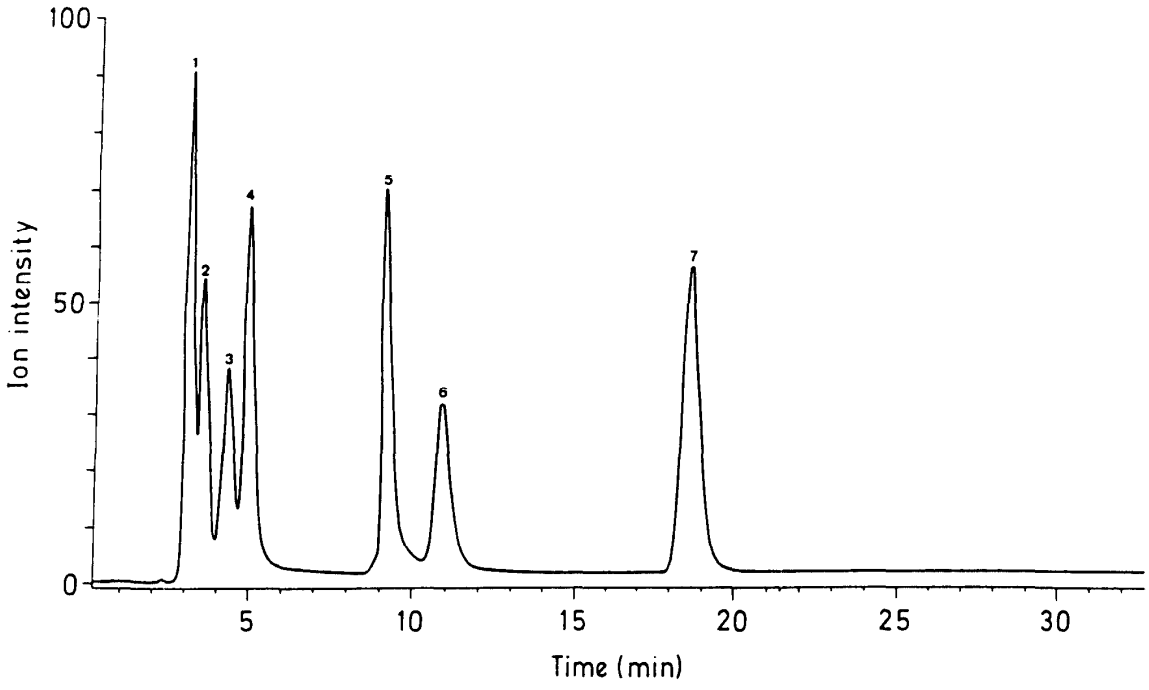


Figure 11 Reconstructed SIM chromatographic profile obtained using ISP interface and Hypercarb analytical column (id: 2 mm) which corresponds to a standard at 0.1 $\mu g\ L^{-1}$ of (1) phenol, (2) catechol, (3) 4-methylphenol, (4) 2,4-dimethylphenol, (5) 4-chlorophenol, (6) 4-nitrophenol, and (7) 2,4-dichlorophenol. Mobile phase: 100% methanol. Flow rate: 0.2 mL min^{-1} (postcolumn addition of 0.1 mL min^{-1} of 10 g L^{-1} triethylamine).

4-methylphenol, 2,4-dimethylphenol by LC–MS. RSD values are in the range of 20% (n = 6 at a spiking level of 0.2 $\mu g\ L^{-1}$) and are comparable with those obtained under on-line LSE LC–TSP–MS, although sensitivity, already cited earlier, and selectivity are considerably improved by the use of LC–ESP–MS compared with LC–TSP–MS.

3. Liquid Chromatography and Mass Spectrometry with Atmospheric Pressure Chemical Ionization

The atmospheric pressure chemical ionization (APCI) technique differs from ESP and ISP in that a spray is generated as a result of applying nitrogen gas and heat at the interface. The spray, which contains the mobile phase and the analytes, is afterward ionized at the nebulizing chamber after applying a corona discharge of 2–4 kV. Contrary to TSP in which high percentages of water increased sensitivity, in APCI no significant differences were observed when working at different ratios of water and organic modifier, and no buffer addition is required. On the other hand, no important variations in sensitivity were found working at different temperatures in the range from 350 to 550°C when analyzing phenolic compounds.

From the practical perspective, there are two main parameters to be optimized in APCI: the corona discharge voltage and the cone extraction voltage. For the corona discharge, a voltage between 2.5 and 3 kV is usually chosen, because at lower discharge voltages, weak ionization is achieved and above 2.5–3 kV the ionization efficiency decreases dramatically. Similar to the ISP interface, by raising the cone voltage, structural information can be obtained by collision-induced dissociation (CID) at the expense of sensitivity. This can be seen in Fig. 12 in which mass spectra of 2,4-dinitrophenol and pentachlorophenol obtained using APCI interface at 20 and 60 V are shown [53].

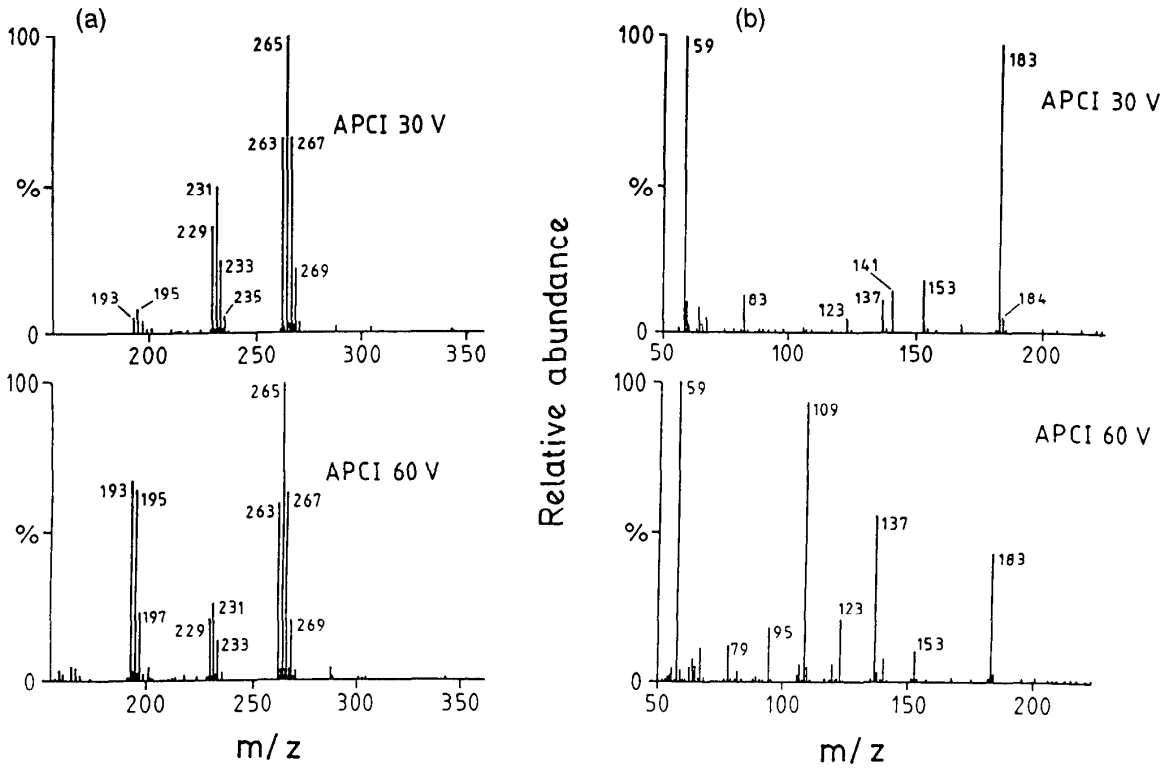


Figure 12 Mass spectra of (a) pentachlorophenol and (b) 2,4-dinitrophenol obtained using APCI interface at 30 and 60 V cone voltages. Corona discharge voltage: 2.5 kV. Concentration 1 $\mu g\ L^{-1}$. Carrier: methanol–water 1:1 (1% acetic acid). Flow rate: 1 mL min^{-1}.

(a) LC–APCI–PI. An APCI interface has been recently applied to monitor organic pollutants in drinking and ground water matrices. The main advantage of this technique is that it is totally compatible with conventional HPLC because flow rates of 1–2 mL min^{-1} can be employed, and conventional columns can be used. Moreover, most analytes can be ionized because ionization of the sample is facilitated by it taking place in the gas phase. The former works include those of Kawasaki et al. [114] who obtained structural information under APCI, but with poor limits of detection, varying between 2 and 50 ng under selected ion monitoring (SIM). These levels differ considerably from those obtained by Molina [105] with high-flow pneumatically assisted electrospray (ESP), who achieve LODs at the picogram levels under the PI mode for selected OP. Sensitivity problems for the parathion group (parathion-methyl, parathion-ethyl, fenitrothion, and fenitroxon) were noticed when using high-flow pneumatically assisted ESP or conventional ESP [104,115]. The ionization of these compounds under ESP conditions offers problems, and generally, it is difficult to achieve low nanogram per liter LODs in water samples. LODs below 100 ng L^{-1} are needed for pesticide compliance consistent with the Commission of the European Communities-Drinking Water Directive (CEC-DWD).

Table 9 summarizes the main ions and their relative abundances formed under different extraction voltage conditions for various pesticides and phenolic compounds in PI and NI modes. For organophosphorus pesticides, ion formation was compound-dependent, with the formation of $[M + H]^+$ as base peak for some of the compounds (e.g., diazinon and dichlorvos), whereas pesticides of the parathion group underwent stronger fragmentation at 20 V of extraction voltage and exhibited specific fragment ions as base peaks. Some pesticides differed in ion formation at cone voltages of 20 and 40 V and corona voltage of 3–4 kV. Dichlorvos and azinphos-methyl are representative of the behavior of most of the studied compounds: at higher cone and corona voltages higher fragmentation was obtained. However, the influence of the corona voltage is not as important as the sample cone voltage, because a low corona discharge is enough to ionize this molecules. Parathion-ethyl and its group behave in a different way and at low cone voltage the specific fragment ion is the base peak (at m/z 110). For such compounds, the increase in the voltage does not dramatically influence the fragmentation.

Even though information concerning the use of APCI interface for pesticide monitoring is scarce, it is clear that structural information is gathered at the expense of sensitivity, and that optimum analytical conditions must be selected to gain both structural and quantitative results. In this sense, the technique has recently been applied to the identification of unknowns, which include basic degradation products of some pesticides (temephos and fenthion). At a 40-V extraction voltage, oxo analogues, sulfoxides, and the isomeric forms of these pesticides were successfully identified. This means that in the near future, this technique can be implemented in routine work for the analysis of real water samples, because it can potentially detect both parental and transformation products of pesticides at nanogram per liter levels. However, more research is needed in the field of characterization of oxo analogues and other metabolites before optimal analytical conditions can be defined.

(b) LC–APCI NI. The main ions obtained for phenolic compounds [53] and organophosphorus pesticides [103] when working at 20, 40, and 60 V, respectively are shown in Table 9. For phenolic compounds at low cone voltages the mass spectra were similar to those obtained with TSP. At 20 V, the $[M–H]^-$ ion was the base peak, and no structural information was obtained except for the high chlorinated phenols and nitrophenols, from which $[M–HCl]^-$ and $[M–NO–H]^-$ ions were observed, respectively. Contrary to that, OP pesticides exhibited the fragment ion of the specific group as the base peak. Only the parathion group (parathion, methyl, parathion-ethyl, and fenitrothion) gave the $[M]^-$ ion, which was attributed to the aromatic moiety that stabilizes this ion by electron delocalization, and it is comparable with conventional negative chemical ionization mass spectrometry (NCI–MS) [116], DLI [117], and TSP–MS [87,118] of OP. Previous work of Kawasaki [114] did not observe the $[M]^-$ ion

Table 9 Relative Abundance of Main Ions Obtained in FIA Using APCI with Various Cone Extraction Voltages in Negative and Positive Ion Modes[a]

M_n	Compound	APCI (20 V)	APCI (40 V)	APCI (60 V)
NI mode				
110	Catechol			
	91 $[M\text{-}H_3O]^-$	n.d.	15	40
	108 $[M\text{-}2H]^-$	5	50	100
	109 $[M\text{-}H]^-$	100	60	70
139	4-Nitrophenol			60
	92 $[M\text{-}H\text{-}NO_2]^-$	3	25	100
	108 $[M\text{-}H\text{-}NO]^-$	20	80	35
	138 $[M\text{-}H]^-$	100	100	
184	2,4-Dinitrophenol			
	109 $[M\text{-}H\text{-}NO_2\text{-}CO]^-$	5	25	100
	137 $[M\text{-}H\text{-}NO_2]^-$	10	100	65
	153 $[M\text{-}H\text{-}NO]^-$	25	50	10
	183 $[M\text{-}H]^-$	100	60	35
198	4,6-Dinitro-2-methylphenol			
	109 $[M\text{-}H\text{-}NO_2\text{-}CH3\text{-}CO]^-$	n.d.	20	65
	122 $[M\text{-}H\text{-}NO\text{-}HNO_2]^-$	n.d.	45	70
	123 $[M\text{-}H\text{-}NO_2\text{-}CO]^-$	n.d.	60	100
	137 $[M\text{-}H\text{-}NI\text{-}CH3]^-$	5	20	40
	151 $[M\text{-}H\text{-}NO_2]^-$	5	100	35
	167 $[M\text{-}H\text{-}NO]^-$	25	50	10
	197 $[M\text{-}H]^-$	100	80	25
128	4-Chlorophenol			
	127 $[M\text{-}H]^-$	100	100	100
162	2,4-Dichlorophenol			
	127 $[M\text{-}Cl]^-$	10	40	100
	161 $[M\text{-}H]^-$	100	100	60
196	2,4,6-Trichlorophenol			
	123 $[M\text{-}H\text{-}2HCl]^-$	n.d.	n.d.	100
	159 $[M\text{-}H\text{-}HCl]^-$	15	80	70
	195 $[M\text{-}H]^-$	100	100	60
	193 $[M\text{-}Cl\text{-}HCl]^-$	n.d.	10	70
	229 $[M\text{-}Cl]^-$	45	50	30
	263 $[M\text{-}H]^-$	80	100	100
224	Mevinphos			
	79 $[(CH_3O)POH]^-$	n.d.	34	n.d.
	125 $[(CH_3O)_2PO_2]^-$	100	100	n.d.
263	Parathion-methyl			
	122 $[(C_6H_4)NO_2]^-$	12	14	n.d.
	138 $[(C_6H_4)NO_3]8^-$	100	63	n.d.
	141 $[(CH_3O)_2POS]^-$	93	100	n.d.
	248 $[M\text{-}CH_3]^-$	26	16	n.d.
	263 $[M]^-$	22	16	n.d.
303	Diazinon			
	167$[M\text{-}(C_2H_5O)(C_2H_5)PS$	100	100	n.d.

Table 9 Continued

M_n	Compound	APCI (20 V)	APCI (40 V)	APCI (60 V)
PI mode				
345	Azinphos-ethyl			
	77[$(C_2H_3O)PH]^+$	n.d.	54	n.d.
	132 [CH_2-N_3-$C_6H_4]^+$	37	100	n.d.
	160 [CH_3-N_3-CO-$C_6H_4]^+$	100	56	n.d.
	346 [M + H]$^+$	13	12	n.d.
221	Dichlorvos			
	109 [$(CH_3O)_2PO]^+$	10	100	n.d.
	221 [M]$^+$	100	18	n.d.
277	Fenitrothion			
	97 [$PS(OH)_2]^+$	n.d.	100	n.d.
	124 [M-$(CH_3O)_2$PS-CO]$^+$	100	33	n.d.
	248 [M-NO-H]$^+$	76	38	n.d.
	278 [M + H]$^+$	6	n.d.	n.d.
224	Mevinphos			
	127 [$(CH_3O)_2P(OH)_2]^+$	40	100	n.d.
	193 [M-$CH_3O]^+$	100	8	n.d.
	225 [M + H]$^+$	46	10	n.d.
291	Parathion-ethyl	51	n.d.	n.d.
	97 [$PS(OH)_2]^+$	100	100	n.d.
	110 [$(CH_3O)_2P(OH)]^+$	n.d.	90	n.d.
	262 [M-NO + H]$^+$	n.d.	10	n.d.
	292 [M + H]$^+$			

[a]Carrier stream, methanol/water containing (50:50) 1% acetic acid at a flow rate of 1 mL min^{-1}. M_n, nominal mass.
n.d., not determined.

for fenitrothion and parathion under LC–APCI–MS, although its nebulizer temperature was 250°C. However, he used ammonium acetate that can suppress the molecular peak (in the relative and absolute sense), in a way similar to that observed in TSP ionization [77].

Abundant fragmentation by CID was obtained for phenolic compounds when increasing the cone voltage to 60 V, usually giving fragmentation patterns similar to those obtained with MS–MS. For example, with 2,4-dinitrophenol (see Fig. 12), at cone voltage of 40 V (data not shown) the base peak was still $[M–H]^-$ ion (*m/z* 183), but an abundance of $[M–NO–H]^-$ ion (*m/z* 153), $[M–NO_2–H]^-$ ion (*m/z* 137), and $[M–H–NO_2–CO]^-$ ion (*m/z* 109) changed to 30, 70, and 32%, respectively, resulting in a 50% loss of sensitivity. However, there were no differences in the formation of fragment ions under the two different cone voltages (20 and 40 V) for the OP pesticides. This is probably because most of the OP studied already offered quite high fragmentation at 20-V cone voltage. Pesticides of the so-called parathion group underwent strong fragmentation at low extraction voltages, rendering fragment ions at low *m/z* as base peaks.

Response was linear for all compounds in the concentration range investigated (0.5–100 ng), and the repeatability values varied from 12 to 20%, when 100 ng of each compound was injected. However, the main operational problem of this interface and, in general in all API interfaces, arises from the frequent necessity to remove the sample cone and skimmer assembly for cleaning, especially when relatively dirty water samples are analyzed [107]. In such cases, the cleaning step should be done every 15–20 injections, and system response should be

corrected afterward. This represents a major drawback of these new API interfaces when applied to environmental analysis. Because the system offers high sensitivity, it should be calibrated very accurately; therefore, maximum cleaning is essential.

Similar to TSP, sensitivity strongly depends on the number of electron-attractive substituents capable of stabilizing the negative charge in the aromatic ring. Hence, for phenolic compounds, high chlorinated phenols and nitrophenols gave the best results. Also in APCI worse values were noticed for phenols substituted in the *ortho*-position than for the other isomers, similar in TSP. For example, IDLs for 2-chlorophenol and 4-chlorophenol in SIM were 0.085 and 0.040 ng, respectively. The difference was still more important for 2-nitro- and 4-nitrophenol with instrument limits of detection (IDLs) of 0.045 and 0.002 ng, respectively. This can be explained by the formation of a five- or six-unit ring by hydrogen bonding between the hydroxy group and the nitro group in 2-nitrophenol, which hinders the deprotonation of the analyte in the gas phase. This effect will be favored in molecules with electronegative *ortho*-substituents having the ability to obtain electronic density from the aromatic ring either by inductive or electron resonance effects. When there are more substituents on the aromatic ring, the electron density will be distributed among all electron-attractive groups, thereby preventing the formation of these rings.

Similarly to ISP, on-line coupling of LSE with APCI–MS has been successfully performed for the determination of pesticides [103] and phenolic compounds [113] using C_{18} and Lichrolut sorbent, respectively. A sample volume of 50–100 mL was used to avoid percolation of low breakthrough volume analytes. For phenolic compounds, recoveries ranging from 70 to 106% were found for all target phenols. However, coefficients of variation (CV) were higher than those currently obtained using on-line LSE–LC–UV. This was attributed to the frequent necessity (each 2–3 days) to remove the sample cone and skimmer assembly for cleaning, which represents a major drawback when applied to routine environmental analysis. However, initial response can usually be recovered if a careful cleaning protocol is applied [107]. In general, those CV values meet the Quality Acceptance Criteria of the EPA methods for phenols reported in method 604 which range from ± 14.1 (phenol) to ± 36 (2,4-dinitrophenol) [119].

Figure 13 shows a typical chromatographic profile of a 50-mL river water sample spiked with phenolic compounds at 10 $\mu g\ L^{-1}$. An interesting feature of the present system is that it can be operated under full-scan conditions for "alarm" of organic contaminants in water samples. This can be seen in Table 10 in which LODs of selected phenols and pesticides are shown in full-scan and SIM mode. The good data obtained in full-scan mode that, when combined with the abundant structural information provided by APCI interface, allowed the screening of unknown samples at concentration levels of 0.7–6 $\mu g\ L^{-1}$ for the phenolic compounds and less than 0.1 $\mu g\ L^{-1}$ for pesticides. On the other hand, values ranging from 0.05 to 65 ng L^{-1} were obtained when working in SIM mode.

In summary, future trends will lead to a more extensive use of API interfaces owing to their high sensitivity and the more structural information. However, the main operational problem of ISP and, in general, of all API interfaces arises from the frequent cleaning requirements of the sample cone and skimmer assembly and, in general, system response had to be corrected after every cleaning step, which leads to reproducibility values that often exceed 25%. However, this is a common problem in most of the LC–MS interfaces currently available, as reported recently for TSP giving values up to 44% [120].

IV. INTERLABORATORY TESTS USING ON-LINE LC

As new methods appear, validation becomes a key issue before method approval and implementation can be done. The analytical method should provide statistical documentation of its capacity to render accurate quantitative parameters. Interlaboratory validation studies are used to evaluate the performance of an analytical method by comparing the results of each laboratory with those of the rest of participants to reach a true value, with the aim of providing

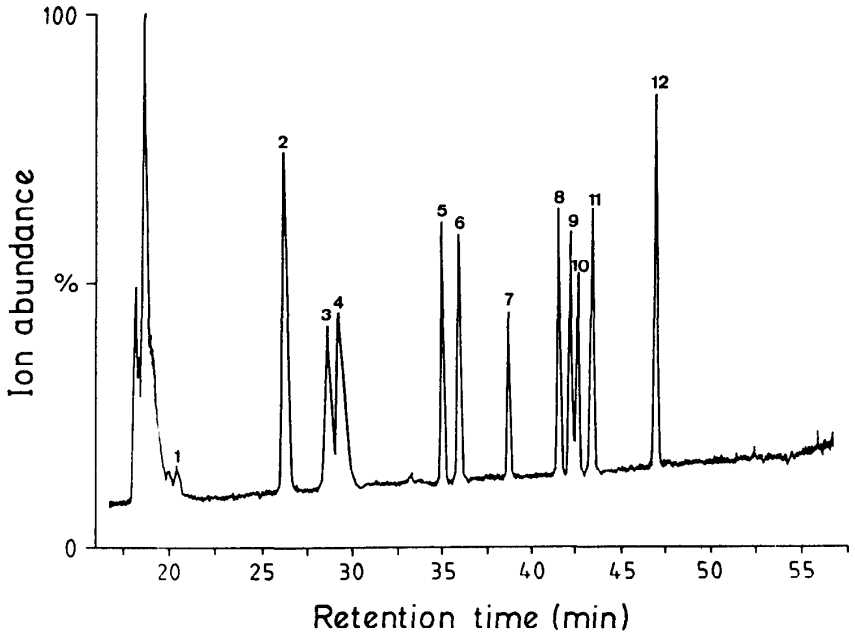


Figure 13 LC–APCI–MS chromatogram obtained after on-line LSE of 50 mL of water spiked at 5 $\mu g\ L^{-1}$ level using Lichrolut EN sorbent in full-scan mode. Peak identification (1) catechol, (2) 4-nitrophenol, (3) 2,4-dinitrophenol, (4) 2-dinitrophenol, (5) 4,6-dinitro-2-methylphenol, (6) 2,6-dinitro-4-methylphenol, (7) 2,4-dichlorophenol, (8) 2,3,4-trichlorophenol, (9) 2,4,6-trichlorophenol, (10) 2,4,5-trichlorophenol, (11) 2,3,5-trichlorophenol, (12) pentachlorophenol. Cone and corona voltages set at 30 V and 2.5 kV, respectively.

unanimity and reliability of the results provided by different laboratories. Various papers have published results on the validation of on-line LSE–LC–DAD for pesticides [14,121] and phenolic compounds [33,53]. As an example, Table 11 shows the results of the interlaboratory studies after analyzing spiked groundwater samples by on-line LSE–LC–DAD and on-line LSE–LC–APCI–MS, and the percentage error in comparison with the certified value from Aquacheck. Results were evaluated according to the AOAC [122], who indicate 22% as maximum permissible error among laboratories. Levels varying from 0.02 to 0.2 $\mu g\ L^{-1}$ were encountered for each individual pesticide. The presence of isomeric forms, matrix interferences, coelution of compounds, and poor chromophor were the main causes of error. In wastewater samples, levels varied from 0.15 to 0.8 $\mu g\ L^{-1}$, being the percentage of error from 4 to 65% (see Table 11). The method was unsuitable for detection of organophosphorus pesticides at such low levels, owing to matrix interferences and to an unresolved complex mixture (UCM) peak of an industrial source that appeared at the beginning of the chromatogram.

The results reported in the interlaboratory exercise suggested that on-line LSE coupled to LC–DAD is a robust method for the analysis of organophosphorus pesticides, and it is equivalent to conventional GC techniques in many aspects, as shown by flagged and double-flagged results given by many laboratories who used the well-known and widely applied GC-based techniques.

From the results obtained in the interlaboratory studies and from data published in the bibliography, it is evident that one of the major problems in the on-line analysis of pesticides at low levels in environmental waters is the presence of interfering substances. Such interferences—namely, humic and fulvic material—appear as an early eluting unresolved complex mixture (UCM) peak in the chromatogram, and are especially relevant in analyzing surface and estuarine river waters. The water type is a relevant parameter in the quantitation

Table 10 Detection Limits for Selected Phenols and Pesticides in River Water Using On-Line LSE–LC–(APCI/ISP)–MS in Negative and Positive Ion Mode[a]

	Full scan	SIM
	(μgL^{-1})	(ngL^{-1})
NI mode		
2-Nitrophenol	0.9	1
4-Nitrophenol	0.3	0.2
2,4-Dinitrophenol	0.7	0.8
4-Chlorophenol	13	60
2,4-Dichlorophenol	1	5
2,4,6-Trichlorophenol	0.5	0.5
Pentachlorophenol	0.1	<0.01
Phenol[b]	—	—
4-Methylphenol[b]	7	49
2,4-Dimethylphenol[b]	12	54
2-Amino-4-chlorophenol[b]	—	120
PI mode		
Melvinphos-cis	0.5	1
Mevinphos-trans	0.4	2
Dichlorovos	0.8	0.6
Azinphos-methyl	0.4	12
Parathion-methyl	0.6	9
Malathion	0.4	3
Fenitrothion	0.8	8
Azinphos-ethyl	0.3	14
Parathion-ethyl	0.5	15
Fenthion	0.3	10
Clorfenvinfos	0.2	1
Diazinon	0.2	2

[a]Volume of water preconcentrated = 100 mL
[b]Data obtained using ISP interface

of pesticides at these low levels, and differences in calibration and quantitation depend on the water type [25,62]. Figure 14 represents a UV chromatogram that corresponds to a river water extract at different wavelengths. At 220 nm, interferences are more significant, and they mainly correspond to humic and fulvic material. Depending on the water nature and on the gradient elution, this UCM can elute at different intervals during a chromatographic run and normally covers the more early-eluting polar compounds. The second problem that arises when analyzing pesticides at these low levels, is derived from the coelution of two compounds in a mixture. Because the LC runs usually contain a mixture of 30 compounds, it is difficult to achieve baseline separation between all analyte peaks and matrix interferences that appear at this low concentration level. The determination of coeluted pesticides is even more problematic in the analysis environmental waters at low concentrations (micrograms per liter) when on-line solid-phase preconcentration techniques are used. Then, interferents at very low concentrations and mobile-phase effects become more significant than for direct injection analysis of more concentrated samples ($\mu g/l$ level).

One way to solve coelution problems is by using a different LC column with different polarity and optimize all the parameters involved in the separation. This will probably improve

Table 11 Mean Concentration (ngL^{-1}) and Percentage of Mean Difference ($n = 4$) in Relation to Reference Values of Organophosphorus Pesticides from Three Intercalibration Studies[a]

	Groundwater LC-DAD		Wastewater LC–DAD		Groundwater LC–APCI–MS	
Compound	ngL^{-1}	% error	ngL^{-1}	% error	ngL^{-1}	% error
Phenol	1649	−15	n.r.	n.r.	3413	35
2,4,6-Trichlorophenol	4372	8	n.r.	n.r.	2381	−16
Pentachlorophenol	1120	12	n.r.	n.r.	2449	14
Azinphos-methyl	97.8	6	594	4	62.9	2
Dichlorvos	54.9	69	n.r.	n.r.	48.9	2
Fenitrothion	47.3	14	638	16	24.7	10
Malathion	94.2	24	391	21	60.2	10
Mevinphos-*trans*	74.3	4	n.r.	n.r.	51.1	12
Chlorfenvinfos	31.4	22	717	6	53.9	3
Diazinon	n.r.	n.r.	n.r.	n.r.	n.r.	n.r.
Azinphos-ethyl	100	12	446	55	48.2	0.5
Fenthion	n.r.	n.r.	n.r.	n.r.	38.8	30
Parathion-ethyl	78.0	6	342	40	9.09	63.5
Parathion-methyl	69.7	24	437	19	50.9	21.5

[a]Results are obtained from spiking groundwater with the certified material from Aquacheck.
n.r., not reported or unable to quantify.

a certain separation of analytes, but can affect other mixtures, and new coelution of analytes may appear. Multivariate self-modeling curve resolution [123–125] has been proposed to improve the resolution of strongly coeluting compounds in liquid chromatography–diode array detection. One coelution problem in the analysis of pesticides in water samples is the coelution of alachlor and metolachlor (Fig. 15) that have very similar spectra, and quantification through UV selectivity is not possible [25]. The problem is also enhanced by the fact that both compounds elute approximately at 100% of organic modifier and also by the presence of interfering compounds. Recently, the chemometric approach has been applied to improve the resolution and quantitation of coeluted alachlor and metolachlor, which have a spectral similarity of 0.9992 [123]. The analysis of these two compounds in river water involved on-line LSE–LC–DAD with preconcentration of 100 mL of river water spiked at 1.5 ng mL^{-1} and quantitation with the MSCR approach. This method permitted the deconvolution of the overlapped alachlor and metholachlor at levels from 0.4 to 2 $\mu g\ L^{-1}$, with complete resolution and recovery, and with errors lower than 10%. Figure 15 also represents the elution profiles of alachlor and metolachlor in two different C_8 analytical columns. A maximum of five different components were detected when river water was preconcentrated on-line (see Fig. 15a and c). A slight separation of the two herbicides was attributed to the preconcentration step. Of these five species, the two herbicides were identified plus a mobile-phase contribution and interferents from the preconcentration step [123]. With direct injection of the standards (see Fig. 15b and c), the overlapping of the two peaks was even more relevant, although only a small contribution of the mobile phase appeared. MSCR was extended to the determination of coeluting pesticides in certified water samples. The participation in interlaboratory exercises organized by Aquacheck (Medmenham, UK) [126] allowed the validation of on-line LSE–LC–DAD and MSCR by comparing the results with those obtained by other participants who used conventional GC-based techniques. The results reported errors between 0.7 and 20% when analyzing pesticides at levels between 0.27 and 0.61 $\mu g\ L^{-1}$. In view of these promising results, the chemometric approach seems a valid option for resolving overlapped peaks, even

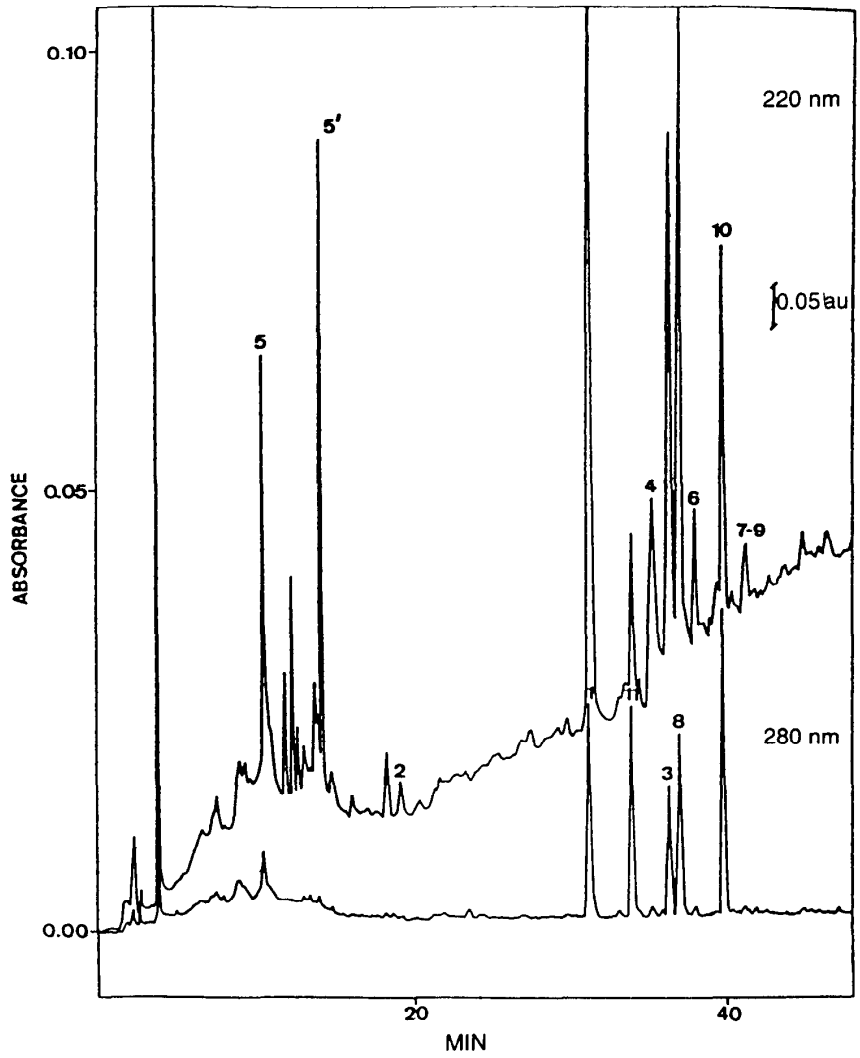


Figure 14 LSE–LC–DAD of a groundwater sample. A Superspher 60 RP-8 endcapped cartridge column of 250 × 4-mm id packed with 4 μm C_8. The gradient elution was: solvent A = 80% acetonitrile and 20% methanol; solvent B = HPLC water. From 10% A and 90% B to 40% A and 60% B in 10 min, isocratic for 5 min and to 90% A and 10% B in 33 min. Back to initial conditions in 5 min. Flow rate set at 1 mL min^{-1}. Peak identification number and peak retention times (min): (5) mevinphos-*cis*- (10.677), (5′) mevinphos-*trans* (14.112), (2) dichlorvos (19.112), (1) azinphos-methyl (31.245), (11) parathion-methyl (34.012), (4) malathion (35.345), (3) fenitrothion (36.412), (8) azinphos-ethyl (37.045), (6) chlorfenvinphos (38.043), (10) parathion-ethyl (39.812), (7) fenthion, and (9) diazinon (39.812).

when there was a strong influence of water matrix interferences, since the maximum error allowed within laboratories (22%) was not exceeded.

The development of such a software system that allows quantitation of peaks at these trace-levels is particularly relevant because this problem is not solved in the automated routine measurement of pesticides in water samples by automated LSE methods. The incorporation of such software systems into the diode-array detector (DAD) software will be a consideration for the future and would be of help for laboratories involved in the routine measurement of pesticides at trace levels using automated systems.

Other studies refer to the use of the automated on-line LSE followed by LC–MS using various interfaces, by participating in the Aquacheck interlaboratory exercise organized by the

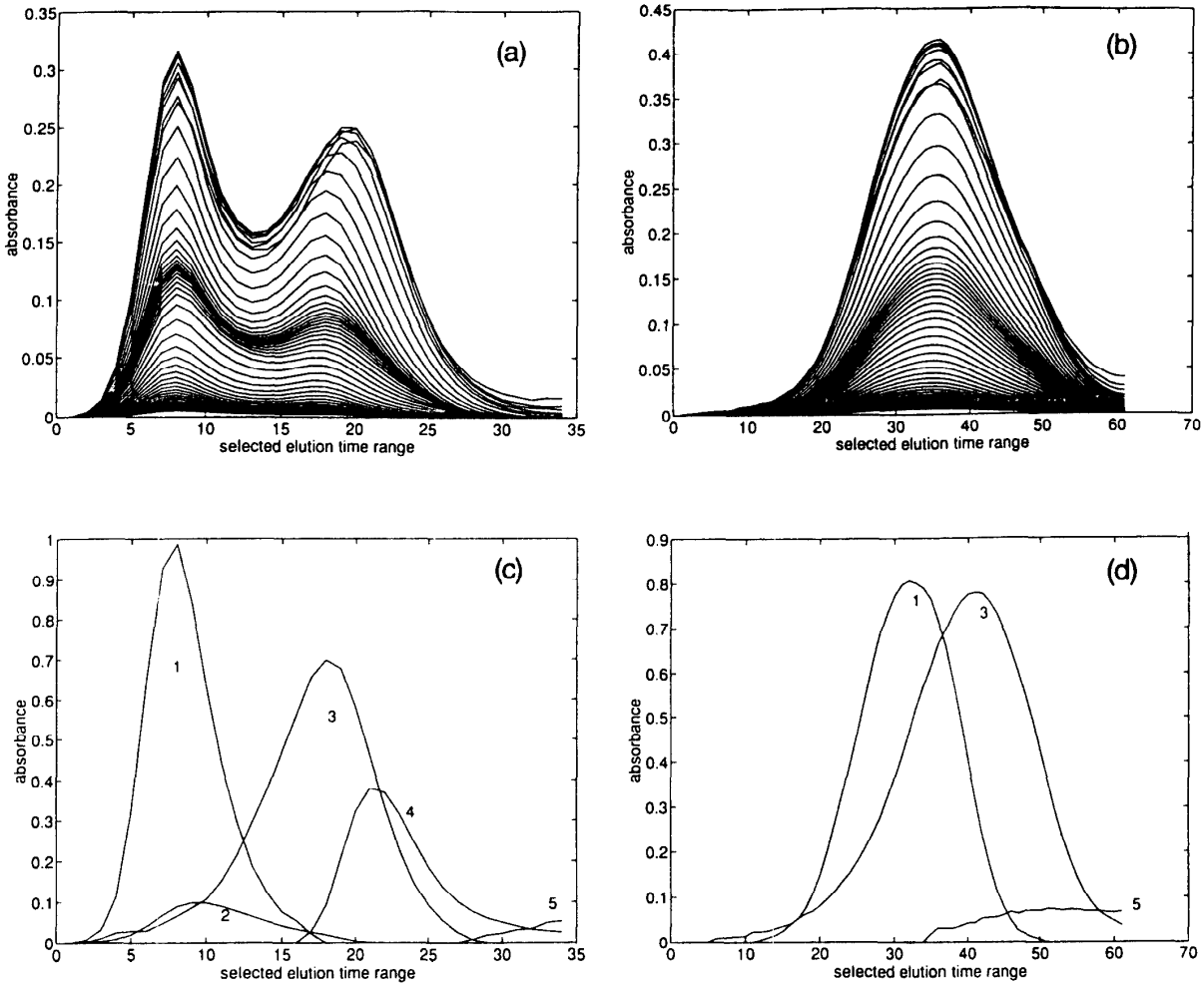


Figure 15 (a) Elution profile of Ebre delta water sample spiked with alachlor and metolachlor at a level of 1.5 ng mL^{-1} and analyzed by on-line LSE–LC–DAD and MSCR; (c) elution profiles of the three resolved species calculated through MSCR: 1, metolachlor; 2, interference due to the preconcentration step; 3, alachlor; 4, interference due to the preconcentration step; and 5, mobile-phase contribution.

Water Research Center, at Medmenham, UK. This is especially useful because until now API interfaces were not used in environmental analysis as commonly as TSP, PB, and other MS techniques. In Table 11, the results obtained in one of the interlaboratory exercises using both interfaces are reported. The percentage of error for the target values reported by Aquacheck is also indicated. In the PI mode, most of the compounds gave acceptable values (with standard deviation below 22%) with the exception of parathion-ethyl and fenthion. This can be attributed to the poor LODs of these two compounds compared with the other analytes for which the levels determined were close to the LOQs. Under the NI mode, parathion-ethyl gave better results compared with the PI mode, but fenthion could not be determined, which can be attributed to spiking values close to the LD. Fenthion exhibited additional problems caused by its poor stability in water during the preconcentration step and its degradation. Some of the other compounds (mevinphos-*trans*, dichlorvos, and chlorfenvinphos) could not be determined by NI, which was mainly attributed to a matrix effect that enabled quantification at a nanogram per liter level. For the determination of mevinphos-*cis* and dichlorvos under NI we need to use the m/z 125 ion which makes its quantitation difficult in real samples because of

the interferences with the matrix background. Figure 16 shows the chromatographic traces of the samples analyzed under the PI mode.

For phenolic compounds acceptable values for trichlorophenol and pentachlorophenol were obtained with all the MS interfaces. A high coefficient of variation (CV) was obtained for phenol using ISP interface, with a 28% deviation relative to the target value. However, it has been reported that interlaboratory results varied, depending on the analytical technique used. In general, for the analysis of chlorinated compounds in water, the overall CV varied from 5.5 to 38% and from 17 to 49% using either LC–UV or LC–MS (PB or TSP) [120]. According to this data we can conclude that the deviation obtained for phenol using LC–ISP–MS is within the limits expected when working with LC–MS.

V. CONCLUSIONS

In the last few years, new technologies based on HPLC systems have been developed to determine organic pollutants in the environment. The large variety of detectors that are available, such as DAD, fluorescence, or electrochemical, cover most of the priority pesticides as well as phenolic compounds that are monitored in environmental waters. Moreover, when an appropriate extraction technique is applied to the water samples, it is possible to achieve limits

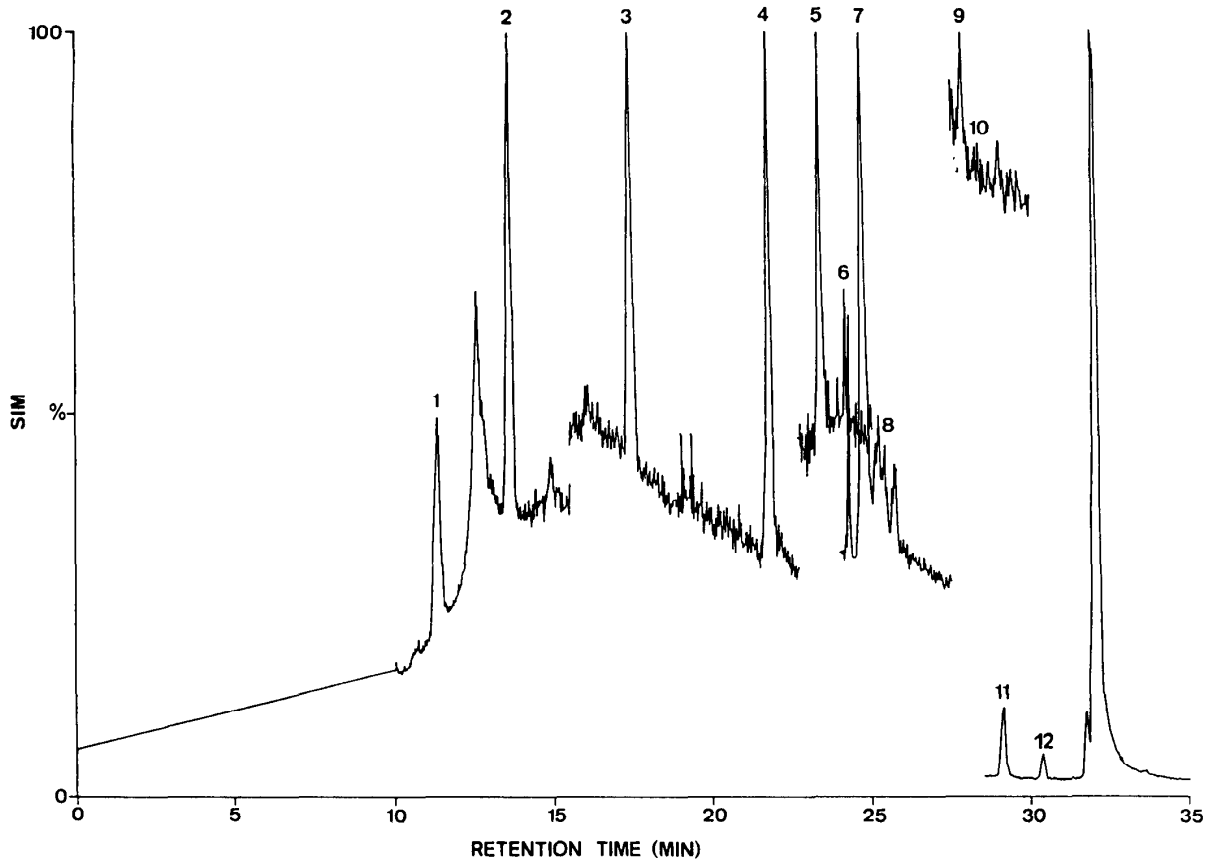


Figure 16 On-line LSE using the OSP-2 followed by LC–APCI–MS under time-scheduled PI mode of operation of 100 mL of groundwater sample spiked with a certified solution from Aquacheck containing 11 organophosphorus pesticides. Peak identification number: (1) mevinphos-*cis*, (2) mevinphos-*trans*, (3) dichlorvos, (4) azinphos-methyl, (5) parathion-methyl, (6) malathion, (7) fenitrothion, (8) azinphos-ethyl, (9) parathion-ethyl, (10) fenthion, (11) chlorfenvinphos, and (12) diazinon.

of detection at the sub-microgram per liter level. One of the main advantages to use LC-based techniques relies on the fact that there is no need to derivatize the water sample to detect the polar and nonvolatile compounds. As a consequence, it is becoming a highly robust technique and the preferred option by many laboratories.

As a result of the implementation of new regulations on water monitoring, there is a growing tendency to use automated methods for the surveillance of organic contaminants in surface waters. In this sense, HPLC has been efficiently coupled with liquid solid extraction by sophisticated equipment such as the Prospekt, the OSP-2, or the Aspec. Because the manipulation of the water samples is minimized, coupled techniques render extremely precise and accurate results. Moreover, there is a large variety of packing materials, that range from the so-called C_{18} precolumns, to the recently appeared Isolut ENV. As a consequence, polar compounds are effectively trapped on the polymeric sorbents, thus increasing the breakthrough volumes without producing an additional band-broadening.

For the identification of unknowns, or for confirmation purposes, HPLC has been coupled with MS detection. Although PB and TSP have long been used, the recent appearance of atmospheric pressure ionization interfaces for the first time allows the characterization of compounds of polar and thermolabile nature at nanogram levels. Sensitivity is enhanced when on-line coupling between LSE and LC–API–MS is performed, thus allowing the determination of several pesticides at the nanogram per liter level, even when scan mode is used. As a result, this technique appears highly powerful for the unequivocal determination of pesticides in water.

For quality assurance, all these new techniques, especially on-line LSE–LC–API–MS, have been validated to provide reliability of the results. This is important to meet quality control standards and to allow the comparison of the results provided by different laboratories. The analysis of certified water samples with HPLC techniques allowed the determination of different pesticides with an interlaboratory precision of less than 22%. This is an important feature to consider before these techniques can be implemented in routine monitoring programs concerning organic pollutants.

ACKNOWLEDGMENT

This work has been supported by the Environment and Climate Program of the European Commission [Contract No. ENV4 CT97-476].

REFERENCES

1. PH Pritchard, CR Cripe, WW Walter, AW Bourquin. Chemosphere 16:1509, 1987.
2. KE Day. Pesticide Transformation Products, Fate and Significance in the Environment. Washington DC: ACS Symp Ser 459. In: L Somasundaram and JR Coats, eds. 1991, chap 16.
3. J Miyamoto, N Mikami, K Mihara, Y Takimoto, H Kohda, H Suzuki. J Pestic Sci, 3:35, 1978.
4. L Marcheterre, GG Choudry, GRB Webster. Rev Environ Contam Toxicol 103:61, 1988.
5. S Lacorte, D Barceló. Environ Sci Technol 28:1159, 1994.
6. M Fielding, D Barceló, A Helweg, S Galassi, L Tortensson, P Van Zoonen, R Wolter, G Angeletti. Pesticides in ground and drinking water. Water Pollution Research Report 27. Brussels: Commission of the European Communities, 1992, pp 1.
7. DJ Munch, RL Graves, RA Maxey, TM Engel. Environ Sci Technol 24:1446, 1990.
8. DJ Munch, CP Frebis. Environ Sci Technol 26:921, 1992.
9. EPA Method 553. Methods for the Determination of Organic Compounds in Drinking Water, Suppl II, rev 1.1. Research Triangle Park, NC: US Environmental Protection Agency (EPA), 1993.

10. D Barceló. In: D Barceló, ed. Environmental Analysis: Techniques, Application and Quality Assurance. Amsterdam: Elsevier, 1993, chap 5.
11. D Barceló. J Chromatogr 643:117, 1993.
12. P Mubmann, K Levsen, W Radeck. Fres J Anal Chem 348:654, 1994.
13. EPA Method 8041. Phenols by Gas Chromatography: Capillary Column Technique. Washington DC, 1995, pp 1–28.
14. S Lacorte, D Barceló. Anal Chim Acta 296:223, 1994.
15. J Slobodnik, MGM Groenenwegen, ER Brower, H Lingeman, UAT Brinkman. J Chromatogr 642:359, 1993.
16. A de Kok, M Hiemstra, UAT Brinkman. J Chromatogr 623:625, 1992.
17. S Chiron, E Martínez, D Barceló. J Chromatogr 665:283, 1994.
18. MWF Nielen, UST Brinkman, RW Frei. Anal Chem 57:806, 1985.
19. J Porchmann, U Stottmeister. Chromatographia 36:207, 1993.
20. D Puig, D Barceló. J Chromatogr A 733:371, 1996.
21. I. Liska, ER Brouwer, H Lingeman, UAT Brinkman. Chromatographia 37:13, 1993.
22. BK Afgan, PE Belliveau, RH Larose, JF Ryan. Anal Chim Acta 71:355, 1974.
23. K Abrahamsson, TM Xie. J. Chromatogr 279:199, 1983.
24. PJM Kwakman, DA Kamminga, UAT Brinkman, GJ de Jong. J Chromatogr 553:345, 1991.
25. S Chiron, A Fernandez-Alba, D Barceló. Environ Sci Technol 27:2352, 1993.
26. HJ Borburgh, WE Hammers. Toxicol Environ Chem 35:79, 1992.
27. M Castillo, D Puig, D Barceló. J Chromatogr A 778:301, 1997.
28. G Durand, S Chiron, V Bouvot, D Barceló. Int J Environ Anal Chem 49:31, 1992.
29. UAT Brinkman. J Chromatogr A 665:269, 1994.
30. MW Nielen, RW Frei, UAT Brinkman. In: RW Frei, K Zech, eds. Selective Sample Handling and Detection in High Performance Liquid Chromatography, vol 39. New York: Elsevier, 1988, chap 1, p 5.
31. MT Galceran, O Jauregui. Anal Chim Acta 304:75, 1995.
32. A Di Corcia, S Marchese, R Samperi, G Cecchini, L Cirilli. J AOAC Int 77:446, 1994.
33. D Puig, D Barceló. Chromatographia 40: 435, 1995.
34. E Pocorull, RM Marcé, F Borrull. Chromatographia 40:85, 1995.
35. ER Brouwer, UAT Brinkman. J Chromatogr 678:223, 1994.
36. LH Keith, WA Telliard. Environ Sci Technol 13:416, 1979.
37. E Pocorull, M Calull, RM Marcé, F Borrull. Chromatographia 38:579, 1994.
38. C Molina, P Grasso, E Benfenatti, D Barceló. J Chromatogr 737:47, 1996.
39. D Barceló, MC Hennion. Anal Chim Acta 318:1, 1995.
40. MC Hennion, V Coquart. J Chromatogr 642:211, 1993.
41. P Subra, MC Hennion, R Rosset, RW Frei. J Chromatogr 456:121, 1988.
42. A Scott, TL Senseman, J Lavy, D Mattice. Environ Sci Technol 29:2647, 1995.
43. I Ferrer and D Barceló. J Chromatogr A 778:161, 1997.
44. DA Hickley, TF Bidleman. Environ Sci Technol. 23:995, 1989.
45. S Lacorte, D Barceló. J Chromatogr A 725:85, 1992.
46. MC Hennion, V Pichon. Environ Sci Technol 28:576, 1994.
47. CL Arthur, DW Potter, KD Buchholz, S Motlagh, J Pawllszyn. LC–GC 10:656, 1992.
48. K Berkane, GE Caissie, VN Mallet. J Chromatogr 139:386, 1977.
49. HA James, CP Steel, Y Wilson. J Chromatogr 208:89, 1981.
50. E Pocurull, G Sánchez, F Burrull, RM Marcé. J Chromatogr A 696:31, 1995.
51. MW Powell. J Chromatogr 697:101, 1995.
52. JS Fritz, PJ Dumont, LW Smith. J Chromatogr 691:133, 1995.
53. D Puig, I Silgoner, M Grasserbauer, D Barceló. J Mass Spectrom 31:1297, 1996.
54. A di Corcia, M Marchetti. Anal Chem 63:580, 1991.
55. A di Corcia, S Marchese, R Samperi. J Chromatogr 642:175, 1993.
56. E Forgacs, T Cserháti. Trends Anal Chem 14:23, 1995.

57. V Coquart, MC Hennion. J Chromatogr 600:195, 1992.
58. MWF Nielen, J de Jong, RW Frei, UAT Brinkman. Int J Environ Anal Chem 25:37, 1987.
59. E Pocorull, RM Marcè, F Borrull, ML Serna, L Toribio, JL Bernal. J Chromatogr (submitted).
60. V Pichon, L Chen, MC Hennion, R Daniel, A Martel, FL Goffic, J Abian, D Barceló. Anal Chem 67:2451, 1995.
61. UAT Brinkman, J Slobodnik, JJ Vreuls. Trends Anal Chem 13:373, 1994.
62. V Pichon, MC Hennion. J Chromatogr A 665:269, 1994.
63. J Ruana, I Urbe, F Borrull. J Chromatogr 655:217, 1993.
64. DA Baldwin, JK Debowski. Chromatographia 26:186, 1988.
65. D Puig, D Barceló. Anal Chim Acta 311:63, 1995.
66. G Achilli, GP Cellerino, GM Eril, S Bird. J Chromatogr 697:357, 1995.
67. G Galletti, R Piccaglia, V Concialini. J Chromatogr 507:439, 1990.
68. D Puig, D Barceló. J Chromatogr A 778:313, 1997.
69. RL Graves. US EPA method 531.1. Measurement of *N*-methylcarbamoyloxines and *N*-methylcarbamates in water by direct aqueous injection HPLC and post-column derivatization, revision 3.0. Cincinnati, OH: Environmental Monitoring Systems Laboratory Office of Research and Development, 1989.
70. S Chiron, D Barceló. J Chromatogr 645:125, 1993.
71. C Ruiter, JF Bohle, GJ de Jong, UAT Brinkman, RW Frei. Anal Chem 60:666, 1988.
72. G Lamprecht, JFK Huber. J Chromatogr 667:47, 1994.
73. D Barceló, G Durand, V Bouvot, M Nielen. Environ Sci Technol 27:271, 1993.
74. S Lacorte, D Barceló. J Chromatogr A 712:103, 1995.
75. Method 8321A. Solvent extractable non-volatile compounds by high performance liquid chromatography/thermospray/mass spectrometry (HPLC–TS/MS) or ultraviolet (UV) detection. Revision 1, January 1995. Environmental Protection Agency, EPA.
76. D Barceló, G Durand, RJ Vreeken, GJ de Jong, H Lingeman, UAT Brinkman. J Chromatogr 553:311, 1991.
77. M Honing, D Barceló, BLM van Baar, RT Ghisen, UAT Brinkman. J Am Soc Mass Spectrom 5:913, 1994.
78. D Volmer, K Levsen. J Am Soc Mass Spectrom 5:655, 1994.
79. D Volmer, A Preiss, K Levsen, G Wünsch. J Chromatogr 647:235, 1993.
80. KS Chiu, A van Langenhove, C Tanaka. Biomed Environ Mass Spectrom 18:200, 1989.
81. J Abián, G Durand, D Barceló. J Agric Food Chem 41:1264, 1993.
82. W Niesser, J Van der Greef. Liquid Chromatography–Mass Spectrometry: Principles and Applications. Chromatographic Science Series. New York: Marcel Dekker, 1002, pp 1–479.
83. D Volmer, K Levsen, M Honing, D Barceló, J Abián, JE Gelpí, BLM Van der Baar, UAT Brinkman. J Am Soc Mass Spectrom 6:656, 1995.
84. RD Voyksner, JT Bursey, ED Pellizzari. Anal Chem 56:1507, 1984.
85. G Durand, N De Bertrand, D Barceló. J Chromatogr 562:507, 1991.
86. G Durand, N De Bertrand, D Barceló. J Chromatogr 554:233, 1991.
87. D Barceló. Biomed Environ Mass Spectrom 17:363, 1988.
88. A Farran, J de Pablo, D Barceló. J Chromatogr 455:163, 1988.
89. RJ Vreeken, WD Van Dongen, RT Ghijsen, UAT Brinkman. In J Environ Anal Chem 54: 119, 1994.
90. RJ Vreeken, AUT Brinkman, GJ Jong, D Barceló. Biomed Mass Spectrom 19:481, 1990.
91. H Bagheri, ER Brower, RT Ghijsen, UAT Brinkman. J Chromatogr 647:121, 1993.
92. S Sennert, D Volmer, K Levsen, G Wunsch. Fres J Anal Chem 351:642, 1995.
93. S Chiron, S Dupas, P Scribe, D Barceló. J Chromatogr A 665:295, 1994.
94. S Lacorte, S Lartiges, P Garrigues, D Barceló. Environ Sci Technol 29:431, 1995.
95. D Barceló, G Durand, N De Bertrand. Toxicol Environ Chem 38:183, 1993.
96. A Chukwudebe, RB March, M Othman, TR Fukuto. J Agric Food Chem 37:539, 1989.

97. S Walia, P Dureja, SK Mukerjee. Arch Environ Contam Toxicol 17:183, 1988.
98. L Somasundaram, JR Coats, KD Racke, HM Stahr. Bull Environ Contam Toxicol 44:254, 1990.
99. R Straub, RD Voyksner, JT Keever. J Chromatogr 627:173, 1992.
100. S Pleasance, JF Anacleto, MR Bailiey. J Am Soc Mass Spectrom 3:378, 1992.
101. WL Budde. Proceedings, 42nd ASMS Conference on Mass Spectrometry and Allied Topics; Chicago, IL, May 29–June 3, 1994, p 782.
102. C Molina, M Honing, D Barceló. Anal Chem 66:4444, 1994.
103. S Lacorte, D Barceló. Anal Chem 68:2464, 1996.
104. S Chiron, S Papilloud, W Haerdi, D Barceló. Anal Chem 67:1637, 1995.
105. C Molina, G Durand, D Barceló. J Chromatogr 712:113, 1995.
106. M Honing, J Riu, D Barceló, BLM Van Baar, UAT Brinkman. J Chromatogr 733:283, 1996.
107. C Cresenzi, A Di Corcia, S Marchese, R Samperi. Anal Chem 67:1968, 1995.
108. BM Hughes, DE McKenzie, KL Duffin. J Am Soc Mass Spectrom 4:604, 1993.
109. LD Betowski, TL Jones. Environ Sci Technol 22:1430, 1988.
110. S Lacorte, C Molina, D Barceló. Anal Chim Acta 281:71, 1993.
111. TL Jones, LD Betowski, B Lesnik, TC Chiang, JE Teberg. Environ Sci Technol 25:1880, 1991.
112. JME Quirke, CL Adams, GJ Van Berkel. Anal Chem 66:1302, 1994.
113. D Puig, I Silgoner, M Grasserbauer, D Barceló. Anal Chem 69:2796, 1997
114. S Kawasaki, H Ueda, H Itoh, J Tadano. J Chromatogr 595:193, 1992.
115. A Di Corcia, C Crescenzi, R. Samperi. American Chemical Society, Division of Environmental Chemistry. 209 the ACS National Meeting, Anaheim, CA, April 2–7, 1995, pp 199–202.
116. HJ Stan, G Kellner. Biomed Mass Spectrom 9:483, 1982.
117. D Barceló, FA Maris, RA Geerdink, RW Frei, GJ De Jong, UAT Brinkman. J Chromatogr 394:65, 1987.
118. G Durand, F Sanchez-Baeza, A. Messeguer, D Barceló. Biol Mass Spectrom 20:3, 1991.
119. EPA method 604. Phenols. In: Federal Register, Friday October 26, 1984, Environmental Protection Agency, Part VIII, 40, CFR Part 136, pp 153–174.
120. KW Edgel. JAOAC 75:858, 1992.
121. S Lacorte, D Barceló. J Chromatogr A 725:85, 1995.
122. RJ Mesley, WD Pocklington, RF Walker. Analyst 116:975, 1991.
123. S Lacorte, D Barceló, R Tauler. J Chromatogr A 697:345, 1995.
124. R Tauler, D Barceló. Trends Anal Chem 12:319, 1993.
125. R Tauler, G Durand, D Barceló. Chromatographia 33:244, 1992.
126. R Tauler, S Lacorte, D Barceló. J Chromatogr A 730:177, 1996.

INDEX

A

Acid-base equilibria, 37-47

α_1-Acidglycoprotein (ACP) chiral stationary phase, 673-675

Acrylic polymer-based phase for ion-exchange chromatography, 386-387

Actinides, 820-821

Activity coefficients in mixed liquid phases, 7-14

Acyclovir, 630

Adsorption chromatography, 325-348

retention mechanisms, 327-348

applications, 344-348

localized and delocalized interactions, 322
main parameters governing solutes, 329-340
mobile phase choice and optimization, 340-344
Snyder-Soczewinski model, 327-329
stationary phases, 325-327
bare silica, 325-327
miscellaneous adsorbents, 327
Adsorption isotherms determination by displacement chromatography, 883-885
Advanced data analysis, computer-assisted, 259-267
Affinity chromatography (AFC), 483-498
principles, 483-491

application conditions, 489-491
elution conditions, 491
immobilization methods, 489, 490
support materials, 487–489
theoretical basis, 484–486
types of affinity ligands, 486–487
stationary phases, 32–33
types of AFC, 492–496
analytical affinity chromatography, 495-496
bioaffinity chromatography, 492
dye-ligand affinity chromatography, 494

immobilized metal ion affinity chromatography, 424-495
immunoaffinity chromatography, 492-494
miscellaneous ligands and methods, 496
Agricultural applications of biotechnology, 696
Aiclofenac, 630-631
Alcohol ethoxylates, 801
Alcohols, derivatization of, 684-685
Alkali metals, 818
Alkaline earth metals, 818
Alkanesulfonates, 790-791
Alkylarylsulfonates, 791-792

Alkylphenol ethoxylates, 800-801

Alkyl sulfates, 790-791

Alumina, 22, 24

adsorption chromatography and, 327

chemically bonded alumina-based phases, 315

polymer-coated alumina-based phases, 316

Amfenac, 631

Amine oxides, 802

Amines, derivatization of, 685-686
Amino acids, 707-716
classic analysis of, 707
detection of underivatized amino acids, 709
hydrolysis of polypeptides, 707-709
postcolumn reaction detection methods, 709-710
precolumn derivatization techniques, 710-716
Ammonium, 821
Amoxicillin, 631-632
Amphoteric surfactants, 796-798
Analytical affinity chromatography, 495-496

ion-exchange process for low molecular weight ions in, 366-371
Anionic surfactants, 790-795
alkylarylsulfonates, 791-792
alkyl sulfates and alkanesulfonates, 790-791
ether sulfates, 792-793
α-olefin sulfonates, 793
other anionic sulfonates, 793-795
Anions (*See* Ions and inorganic species)
Anion self-regenerating suppressor, 428, 429
Anion separation in nonsuppressed ion chromatography, 441
Arsenic anions, 815-816

Art conservation, 903-927
background, 903-904
future applications, 919-920
carbohydrate analysis of gums and celluloses, 919
fatty acid analysis and hybrid techniques, 919-920
LC-mass spectrometry, 920
general areas of investigation, 904-905
primary HPLC applications, 905-919
identification of natural and early synthetic dyestuffs, 905-909
ion chromatography for monitoring inorganic contaminants, 918
monitoring organic pollutants in museum environment, 918-919

proteinaceous materials in conservation, 910-914

study of degradation and polymerization reactions, 914-918

Ascorbic acid, 632

Atmospheric pressure chemical ionization (APCI) process, 591-593, 960-964

Atomic absorption (AA), 404-406

LC-atomic absorption spectroscopy (LC-AA) tandem systems, 596-600

Autosamplers, 569, 570-571

B

BAY y3118, 632

Benorylate, quantitation of impurities in, 356-357, 358

Bioaffinity chromatography, 492

Biological ion exchangers, 390-391

Biologically active compounds (See Drugs in biological samples)

Biomedical science, role of hydrophobicity in, 860-861

Biotechnology, 695-751

amino acids, 707-716

classic analysis, 707

detection of underivatized amino acids, 709

hydrolysis of polypeptides, 707-709

postcolumn reaction detection methods, 709-710

precolumn derivatization techniques, 710-716

carbohydrates, 734-742

complex carbohydrates, 736-739
microheterogeneity of glycoproteins, 739-742
simple carbohydrates and related compounds, 735-736
downstream processing, 742-745
general chromatographic developments, 700-707
bioprocess control, 700-702
column technology, 702-707
methodology, 697-700
nucleic acid and related compounds, 729-734
large deoxyribonucleotides, 732-733
large ribonucleotides, 733-734

Block copolymers of ethylene oxide and propylene oxide, 802

Bromazepam, 633

Bulk property detectors, 536-539

electrical conductivity detector, 537-539

refractive index detectors, 536-537

Buprenorphine, 634

C

Calibration for an SEC system, 277-281

broad-molecular weight calibration, 279

primary calibration, 278

secondary calibration, 279

universal calibration, 279-281
Cauroscne, 635
Capillary electrophoresis (CE), 44-46, 169-191, 822-824
emergence of commercial instruments, 170-172
HPLC and, 170
modes, 184-189
capillary gel electrophoresis, 188-189
capillary isoelectric focusing, 187-188
capillary isotachophoresis, 186-187
capillary zone electrophoresis, 185-186
micellar electrokinetic capillary chromatography, 186

principles, 172-184
electroosmotic flow, 174-177
electrophoresis mobility, 172-173
experimental considerations, 182-184
factors influencing performance, 180-182
separation efficiency and resolution, 177-180
Capillary gel electrophoresis (CGE), 170, 188-189
Capillary isoelectric focusing (CIEF), 170, 187-188
Capillary zone electrophoresis (CZE), 170, 185-186
Carbamazepine, 632
Carbohydrate analysis of gums and cellulose, 919

Carbohydrates, 734-742, 753-757

complex carbohydrates, 736-739

microheterogeneity of glycoproteins, 739-742

simple carbohydrates and related compounds, 735-736

Carbon-based phases for RPLC, 314

Carbon-clad zirconia, 316

Carboxylic acids, 817

derivatization of, 686-687

Catecholamines, 636-638

Cationic surfactants, 795

Cations (See Ions and inorganic species)

Cation self-regenerating suppressor, 428, 429

Celprolol, 638

Cellulose-based phases, 387-391

Check valves, 205-208

Chelation equilibria, 42-51

Chemically bonded alumina-based phases, 315

Chemically bonded silica-based phases for RPLC, 298-310

- characterization techniques, 308-310
- monomeric stationary phases, 299-302
- polymeric stationary phases, 302
- selectivities of phases, 303-308

Chemicals, application of biotechnology for, 606
Chemisorption chromatography, 496
Chiral pharmaceutical analysis, 669-693
chiral mobile-phase additives (CMPAs), 677-682
chiral counterions, 678-680
cyclodextrins, 680-682
ligand-exchange chromatography, 678
chiral stationary phases (CSPs), 670-677
α_1-acid glycoprotein, 673-675
cyclodextrin stationary phases, 675-676
ovomucoid-bonded stationary phase, 675

Pirkle phases, 677
polysaccharides, 670-673
serum albumin phases, 675
enantioselectivity in biological systems, 669
indirection separation of enantiomers, 682-687
derivatization of alcohol, 684-685
derivatization of amines, 685-686
derivatization of carboxylic acids, 686-687
separation of enantiomers by HPLC, 670
Chiral stationary phases (CSPs), 33-35, 670-677
Chloroguanide, 638

Chloroquine, 638

Chlortetracycline, 666

Chlorzoxazone, 638-639

Chromate, 816

Chromatographic hydrophobicity index, 867-873

Chromatographic profiles and retention, prediction of, 238-246

"first-guess" expert systems, 243-246

quantitative structure-retention relations, 241-243

simulation of profiles, 240-241

Clobazam, 639

Clozapine, 639

Cocaine, 639-641

Collection devices, 617-627

applications, 622

fraction collectors, 617-618

operational considerations of fraction collection, 618-622

low-resolution techniques, 618
separation of complex mixtures, 618-622
other types of fraction collection devices, 622-625
troubleshooting, 625-627
Column efficiency, effects of temperature on, 608
Column-switching methods, 198-205
effects of the column in LC, 198-200
relative advantages and disadvantages of gradient-elution LC methods and, 230
relative advantages and disadvantages of isocratic LC separations and, 230
valve-switching options and requirements, 200-205
Column-switching valves, 569-573

Complexation equilibria, 47-51
Complex carbohydrates, 736-739
Complex stability constants, determination of, 875-878
Compressibility effects on flow and plate weight, 118-120
Computers, 233-271
advanced data analysis, 259-267
multivariate data analysis, 263-267
univariate data analysis, 260-263
automation and instrument control, 234-238
column coupling and hyphenated separation techniques, 237-238
on-line monitoring and control, 238

sample preparation, 235-237
computer-assisted method development, 246-257
general considerations, 247-251
for gradient separations, 253-255
for isocratic separations, 255-257
optimization criteria, 251-252
interlaboratory tests using on-line LC, 964-970
method validation, 257-259
prediction of chromatographic profiles and retention, 238-246
"first-guess" expert systems, 243-246
quantitative structure-retention relations, 241-243

simulation of profiles, 240-241
Conductimetric detection, 395-396
Conductivity detection, 160-162
in ion chromatography, 417-419
principles of operation, 160-161
suppression systems, 161-162
Constant-flow rate pumps, 300-301
Constant-pressure pumps, 300
Cosmetics, applications of biotechnology for, 696
Coumarin, 641-642
Cyclamates, 754

Cyclodextrins (CDs), 680-682

D

Danazol, 642

Debrisoquine, 642

Deoxyribonucleotides, large, 732-733

Detectors (detection), 143-168, 531-558

bulk property detectors, 536-539

electrical conductivity detector, 537-538

refractive index detectors, 536-537

choice of detectors, 555-556

comparison of detector performances, 167-168

conductivity detection, 160-162
principles of operation, 160-161
suppression systems, 161-162
derivatization, 554-555
detectors for polymer analysis, 162-163
evaporative detectors, 163-164
light-scattering detection, 164-165
viscosity detectors, 165
effects of temperature on, 609-610
electrochemical detection, 156-160
electrode materials, flow-cells, and instrumentation, 158

pulsed-amperometric detection, 159-160
principles of operation, 156-158
selectivity enhancement, 159
fluorescence detection, 150-154
fluorescence yields, 152
instrumentation, 152-153

[Detectors (detection)]
postcolumn derivatization, 154
precolumn fluorescence labeling, 153
to identify lipid components, 758-761, 764, 765, 766
in ion interaction chromatography, 457-459
as operating variable in ion-exchange chromatography, 395-406
operation of LC detectors, 556
other detectors, 165-167
gas-phase detectors, 167
infrared detection, 165-166
optical activity detection, 166

radiochemical detection, 166
refractive index detection, 154-156
optical principles, 155
performance and application, 156
requirements for and characterization of detectors, 143-147
linearity, 146
peak broadening, 144
selectivity, 147
sensitivity and detection limits, 144-146
for the SEC system, 284-289
composition detectors, 285-287

concentration detectors, 284-285
molecular-weight-sensitive detectors, 287-289
solute property detectors, 539-554
electrochemical detector, 550-551
fluorescence detectors, 547-550
light-scattering detector, 551-552
tridet multifunctional detector, 552-554
UV detectors, 540-547
specifications for, 532-536
detector linearity and response index, 532-534
detector noise level, 534-535

detector sensitivity, 535-536
flow sensitivity, 536
linear dynamic range, 534
measurement of detector noise, 535
pressure sensitivity, 536
temperature sensitivity, 536
suppliers of LC detectors, 556-558
UV-vis absorbance detection, 147-150
multiple wavelength absorbance detection, 149-150
single- and variable-wavelength detectors, 148-149
Desfenfluramine, 642-643

Diclofenac, 643-644

Diltiazem, 638

Diode-array detector (DAD), 544-547

LC with diode-array detection (LC-DAD), 940-941

Displacement chromatography, determination of adsorption isotherms by, 883-885

Distribution coefficients:

in adsorption from solution, 4-7

chemical potentials in solution and, 4

retention factor and, 2-3

DMP 811, 644-645

Dobutamine, 645

Dominant solvation phenomena, 18-21

Downstream processing in biotechnology, 742-745

Drotaverine, 643

Drug-protein-binding constants, determination of, 878-881

frontal elution, 880

Hummel and Dreyer method, 879

vacancy peak method, 880-881

zone elution, 879

Drugs in biological samples, 629-668, 704

acyclovir, 630

aklofenac, 630-631

amfenac, 631

amoxicillin, 631-632

ascorbic acid, 632

BAY y3118, 632

bromazepam, 633

buprenorphine, 634

camrenone, 635

carbamazepine, phenytoin, phenobarbital, and primidone, 635

catecholamine, 636-638

celiprolol and diltiazem, 638

chloroquine and chloroguanide, 638

chlortetracycline, 666

chlorzoxazone, 638-639

clobazam and diazepan, 639

clozapine, 639

cocaine, 639-641

coumarin, 641-642

danazol, 642

debrisoquine, 642

dexfenfluramine, 642-643

diclofenac, 643-644

DMP 811, 644-645

DMP 811, 644-645

dobutamine, 645

[Drugs in biological samples]

drotaverine, 645

E-1100, 646

Ebd523, 646-647

ethynylestradiol, 647

etoposide, 647

flumazenil and midazolam, 647-648

fluoroquinolines and theophylline, 648

furosemide, 648

galocitabine, 648

guaifenesin, 649-650

hydrochlorothiazide, 620

imipenem, 650-651

intoplicine, 651-652

iodobenzylguanidine, 652

lisuride, 652-653

MDL 73,005EB (binospirone mesylate), 653-654

6-methylen-androsta-1,4-diene-3,7-dione, 654

metoclopramide, 654-655

mitomycin, 655

mizolastine, 655

morphine, 655-656

nicorandil, 656

nicotine, 656-657

nifedipine, 657

norbuprenorphine, 634

oxytetracycline, 666

paclitaxel, 657

phenytoin, 658

physostigmine, 658-659

pyronaridine, 659-660

quinidine, 660

rivastatin, 661

R023-9424, 660-661

SCE-2767 (cefoxoprazan), 661-662

simvastatin, 662-663

sulfamethazine, 663-664

testerone-related compounds, 664-665

tetracycline, 666

zidovudine, 666

Dye-ligand affinity chromatography, 494

Dyestuffs, natural and early synthetic, identification of, 905-909

E

E-1100, 646

Early synthetic dyestuffs, identification of, 905-909

Electrical conductivity detector, 537-539, 555

Electrochemical detection (ECD), 156-160, 396-400, 550-551

electrode materials, flow-cells, and instrumentation, 158

LC with electrochemical detection (LC-ECD), 941-944

principles of operation, 156-158

pulsed-amperometric detection, 159-160

selectivity enhancement, 159

Electrodrive chromatography (EDC), 120-121

Electrokinetic chromatography (EKC), 120-121

Electroosmotic flow (EOF), 174-177

Electrophoretic mobility, 172-173

Elution (eluter) (See also Gradient elution, Isocratic elution)

in affinity chromatography, 421

eluent counterion for nonsuppressed ion chromatography, 441-444

ion interaction chromatographed eluents, 454-456

role in ion exchangers, 391-395

in suppression ion chromatography, 430-434

EM523, 646-647

Enantiomers

indirect separation of, 682-687

derivatization of alcohol, 684-685

derivatization of amines, 685-686

derivatization of carboxylic acids, 686-687

separation of, 670

Environmental applications of biotechnology, 626

Equations for chromatographic eluent selection, 14-21

Equilibrium constants, determination of, 875-881

complex stability constants by HPLC, 875-878

drug-protein-binding constants by HPLC, 878-881

Esters, 802

Ether sulfate, 792-793

Ethoxylated acids, 801

Ethoxylated alkylamines, 802

Ethoxylated esters, 802

Ethylene oxide, block copolymers of, 802

Ethynylestradiol, 647

Etoposide, 647

Evaporative light-scattering detector (ELSD), 163-164, 285

to identify lipid compounds, 758-759, 760

Expert Systems in Chemical Analysis (ESCA) project, 244-246, 258

F

Fatty acid alkanolamides and their ethoxylates, 202

Fatty acid analysis of museum collection samples, 919-920

Field flow fractionation (FFF), 831-832, 835-836

  kinetic optimization of, 140

Fixed-wavelength detector, 340-343

Flame-ionization detector (FID), 226

Flow programming for isocratic elution, 209

Flumazenil, 647-648

Fluorescence detection (FD), 150-154, 347-350, 355

fluorescence yields, 152

instrumentation, 152-153

LC with fluorescence detector (LC-FD), 945

postcolumn derivatization, 154

precolumn fluorescence labeling, 153

Fluoroquinolines, 648

Food and nutritional analysis, 733-788

carbohydrates, 733-757

lipids, 758-761

detectors, 758-761, 764, 765, 766

other food components, 763-784

pesticides and herbicides, 776-784
phenolics, 767-776, 777-783
proteins, 763-767
vitamins and minerals, 761-762, 763, 768-774
Foods, applications of biotechnology for, 696
Fourier-transform-infrared (FT-IR) detection, 286
Fraction collectors, 617-618
applications, 622
operational considerations in LC, 618-622
low-resolution techniques, 618
separation of complex mixtures, 618-622

troubleshooting, 625-627

Furosemide, 648

G

Galocitabine, 648

Gas-phase detectors, 167

General elution problems, 194-195

Genetic engineering, downstream processing and, 743-744

Glycoproteins, microheterogeneity of, 739-742

Gradient elution, 205-225, 510-512, 513

comparison of designs, 513

gradient optimization, 214-218

gradient scouting, 218-220
gradient solvents, 220-221
instrumental aspects, 222-225
migration under gradient conditions, 206-211
multipump, problems, causes, and remedies in, 514
relative advantages and disadvantages of column switching LC methods and, 230
relative advantages and disadvantages of isocratic LC methods and, 227
theory of LSS gradients, 211-214
troubleshooting, 521-522
Gradient separations, computer-assisted, 253-255
Group IIIA metals, 212

Group IVA metals, 819

Guaifenesin, 649-650

H

Halides, 813-814

Herbicides, 776-784

Hollow-fiber membrane suppressor, 423-424

Host-guest complexation equilibria, 51

Hydrochlorothiazide, 629

Hydrodynamic chromatography (HDC), kinetic optimization of, 138-140

Hydrophilic polymers, SEC separation of, 848

Hydrophobic interaction chromatography (HIC), 463-482, 796

chromatographic system, 464-473

Mobile Phase, 472-473

Stationary Phase, 35-36, 465-472

fundamentals of retention, 463-465

general aspects of HIC of proteins and selected applications, 473-479

selected applications of high performance HIC, 475-478

Hydrophobicity, determination of, 860-875

chromatographic hydrophobicity index, 867-873

determination of partition coefficients, 861-862

general approach, 863-867

hydrophobicity in biomedical sciences, 860-861

[Hydrophobicity, determination of]

practical aspects, 865

theoretical background, 862-864

I

Imipenem, 630-631

Immobilized metal ion affinity chromatography (IMAC), 494–495

Immunoaffinity chromatography (IAC), 492–494

Immunoglobulins (Igs), 725-726

Inductively-coupled plasma (ICP) detection, 404–406

Infrared (IR) detection, 165-166

LC with infrared (LC-IR) tandem systems, 600-602

Injection devices, 339-379
autosamplers, 368, 370-371
column-switching valves, 369-373
maintenance and troubleshooting, 373-379
operator techniques, 374-375
poor connections, 375-376
preventative maintenance, 377-379
rotor malfunction, 375
valve contamination, 376-377
manual sample injection valves, 339-368
sample-loading techniques, 362-366

small-volume sample injection, 366–368
Inorganic complexes (See Ions and inorganic species)
Isoplicine, 631–632
Iodobenzylguanidine, 632
Ion chromatography, 413–462
basic principles of ion exchange, 414–417
conductivity detection in ion
chromatography, 417–419
historical background, 412–414
ion-exclusion chromatography, 448–453
background, 448–449

survey of applications, 442–453
ion interaction chromatography, 453–459
background, 453
detection, 457–459
eluents, 454–456
equilibria, 453–454
stationary phases, 456
nonsuppressed ion chromatography, 440–448
detection by postcolumn reaction, 445–448
eluent counterion, 441–444
nonsuppression, 440–441

suppressed ion chromatography, 419–439
eluents in suppression ion chromatography, 430–434
hollow-fiber membrane suppressor, 423–424
ion-exchange column suppression, 419–423
micromembrane suppression, 424–427
other suppression applications, 438–439
other suppression techniques, 434–437
postsuppression strategies, 437–438
self-regenerating suppression, 427–430
Ion-exchange chromatography, 365–411
operating variables, 385–406

detections, 395–406
dextran- and cellulose-based phases, 387-391
eluents, 391-395
ion-exchange stationary phases, 385-387
principles of ion exchange, 366-385
for high molecular weight ions or proteins, 371-381
ion-exchange HPLC theories, 384-385
ion-exclusion chromatography of small ions, 383-384
for low molecular weight ions, 366–371
retention of low molecular weight ions, 381-383
stationary phases for, 29-31

Ionic-strength programming, 226

Ionic surfactants, 790-798

amphoteric surfactants, 796-798

anionic surfactants, 790-795

cationic surfactants, 795

general principles, 790

Ion-pairing, 49-51

Ions and inorganic species, 805-829

capillary electrophoresis, 822-824

anions, 823

cations, 823-824

chromatographic methods for cationic species, 818-821

alkali and alkaline earth metals, 818

ammonium and organic amines, 821

group IIIA metals, 818

group IVA metals, 819

lanthanides and actinides, 820-821

noble metals, 820

transition metals, 819-820

HPLC analysis of inorganic species in specific industries, 822

[Ions and inorganic species]

methods for common anion mixtures, 810-813

methods for specific anionic species, 813-817

arsenic, selenium, and tellurium anions, 815-816

carboxylic acids, 817

halides, pseudohalides, and oxyhalides, 813-814

inorganic complexes, 816

miscellaneous inorganic anions, 816

molybdate, tungstate, and chromate, 816

nitrogen-containing anions, 814

phosphorus-containing anions, 817

sugars, 817

sulfur-containing anions, 814-815

separation of, 805-810

modes of separation, 806-807

practical aspects of ion chromatographic separations, 807-809

sample pretreatment, 809-810

separation of organometallic compounds, 821

simultaneous determination of anions and cations, 822

Isocratic elution, 499-510

comparison of column-switching LC separations and, 229

comparison of gradient-elution LC separations and, 227

computer-assisted methods for isocratic separations, 255-257
constant flow rate pumps, 500-501
constant-pressure pumps, 500
flow programming, 509
reciprocating pumps, 501-508
recycle chromatography, 510
syringe pumps, 509
troubleshooting, 519-520
Isotachophoresis (ITP), 170, 186-187
Iterative target-transformation factor analysis (ITT-FA), 267

K

Kinetic optimization, 123-133

particle size limitations, 127-129

pressure limitations, 125-127

of separation methods for macromolecules, 133-140

compressible supercritical fluid chromatographic methods, 134-136

field-flow fractionation, 140

hydrodynamic chromatography, 138-140

SEC, 136-138

using reduced variables, 129-130

L

Lanthanides, 620-621

Large deoxyribonucleotides, 732-733

Large ribonucleotides, 733-734

Laser desorption mass spectrometry, 593-596

Ligand-exchange chromatography, 678

Ligands in affinity chromatography, 486-487

Light-scattering detector, 164-165, 285-289, 551-552

Linear-solvent-strength (LSS) model of LC gradients, 211-214

Lipids, 758-761

detectors, 758-761, 764, 765, 766

Liquid adsorption chromatography (LAC), 850-851
Liquid chromatography (LC)-atomic absorption spectroscopy (LC-AAS) tandem systems, 596-600
Liquid chromatography with diode-array detection (LC-DAD), 940-941
Liquid chromatography with electrochemical detection (LC-ECD), 941-944
Liquid chromatography with fluorescence detection (LC-FD), 945
Liquid chromatography-infrared (LC-IR) tandem systems, 600-602
Liquid chromatography-mass spectrometry (LC-MS) tandem systems, 585-596
in analysis of organic pollutants in water, 945-964
with atmospheric pressure chemical ionization, 960-964
with ionspray interface, 953-960
with thermospray interface, 945-953

in art conservation, 920
atmospheric ionization interface, 591-593
electrospray interface, 589-591, 953-960
laser desorption mass spectrometry, 593-596
thermospray interface, 587-589, 945-953
transport interface, 586-587
Liquid chromatography-nuclear magnetic resonance (LC-NMR) tandem systems, 602-604, 605
Liquid-liquid chromatography (LLC), 1
distribution equilibria in, 7-14
in extracting organic pollutants from water, 931-932

Liquid precipitation chromatography (LPC), 852

Liquid-solid chromatography (LSC), 1

distribution equilibria in, 7-14

in extracting organic pollutants from water, 932-940

Lisunde, 652-653

Low-angle laser-light-scattering (LALLS) detectors, 164-165

Low-dispersion connecting tubes, 582-586

M

Macromolecular chromatography, kinetic optimization of separation methods for, 133-140

compressible supercritical fluid chromatographic methods, 134-136

field-flow fractionation 140

hydrodynamic chromatography, 138-140

SEC, 136-138

Manual sample injection valves, 339-368

sample-loading techniques, 363-366

small-volume sample injection, 366-368

Mass spectrometry (MS) (*See also* Liquid chromatography-mass spectrometry (LC-MS) tandem systems), 386, 400-404

laser desorption MS, 593-596

Matrix-assisted laser desorption mass spectrometry (MALDI-MS), 595

MDL 73,005EF (benpiroxne mesylate), 653-654

Mechanisms of zone-broadening, 69-107

alternative expressions and additional forms of broadening, 82-107
convective dispersion in the mobile phase, 71-79
longitudinal molecular diffusion, 69-70
sorption and desorption, 80-82
Medical applications of biotechnology, 696
Membrane proteins, 726-728
Metal oxide supports in RPLC, 314-317
chemically bonded alumina-based phases, 315
polymer-coated alumina-based phases, 316
zirconia- and titania-based phases, 316-317
6-Methylen-androsta-1,4-diene-3,7-dione, 654

Metoclopramide, 654-655
Micellar electrokinetic chromatography (MEKC), 51-52, 170, 186
Microcapillary hydrodynamic chromatography (MHDC), 138
Microheterogeneity of glycoproteins, 739-742
Micromembrane suppressor (MMS), 424-427
Midazolam, 647-648
Minerals, 761-762, 763, 768-774
Mitomycin, 655
Mitolactone, 655
Mobile-phase delivery systems, 499-529
    biocompatability and materials of construction, 513-516

flow rate range, 516-517
gradient elution, 510-512, 513
problems, causes, and remedies in multipump gradient elution, 514
troubleshooting, 521-522
isocratic elution, 499-510
constant flow rate pumps, 500-501
constant-pressure pumps, 500
flow programming, 509
reciprocating pumps, 501-508
recycle chromatography, 510
syringe pumps, 509

troubleshooting, 519-520
pulse dampers, 517-518
pump table, 523-528
troubleshooting, 518-522
Mobile phases of hydrophobic interaction chromatography, 472-473
Molecular-weight-sensitive detectors for SEC systems, 287-289
light-scattering detection, 288-289
light-scattering viscometry, 289
viscosity, 287-288
Molybdate, 816
Morphine, 655-656

Morphine, 655-656

Multiangle laser-light-scattering (MALLS) detector, 165

Multiple wavelength absorbance detection, 149-150

Multipump gradient elutions, problems, causes, and remedies in, 514

Multivariate data analysis, computer-assisted, 263-267

N

Natural dyestuffs, identification of, 905-909

Nicorandil, 656

Nicotine, 656-657

Nifedipine, 657

Nitrogen-containing anions, 814

Noble metals, 820

Nonionic surfactants, 799-802
analysis of individual surfactants, 800-802
general principles, 799-800
Nonsuppressed ion chromatography, 440-448
detection by postcolumn reaction, 445-448
eluent conversion, 441-444
nonsuppression, 440-441
Norbuprenorphine, 634
Normal-phase (NP) liquid chromatography, 325-363
adsorption chromatography, 325-348
retention mechanisms, 327-348

stationary phases, 325-327
polar-bonded-phase chromatography, 348-361
applications, 356-361
bonding reactions, 350-353
mobile-phase selection, 355-356
retention mechanisms, 353-355
stationary phases for, 26-28
Nuclear magnetic resonance (NMR), 286-287
LC-nuclear magnetic resonance (LCNMR) tandem systems, 602-604, 605
Nucleic acid and related compounds, 729-734
large deoxyribonucleotides, 732-733

large ribonucleotides, 733-734
simple nucleotides, 729
synthetic and small oligodeoxyribonucleotides, 729-731
synthetic and small oligoribonucleotides, 731-732

O

α-Olefin sulfonates, 725
Oligodeoxyribonucleotides, synthetic and small, 729-731
Oligomers, separation of, 843-848
Oligoribonucleotides synthetic and small, 731-732
On-line LC, interlaboratory tests using, 964-970
Optical activity detection, 166

Optimization of LC conditions, computer-assisted strategies for, 251-252

Organic amines, 821

Organic pollutants in the museum environment, monitoring, 918-919

Organic pollutants in water, 929-974

conventional detectors, 940-964

LC with diode-array detection analysis, 940-941

LC with electrochemical detection, 941-944

LC with fluorescence detection, 945

LC with mass spectrometric analysis, 945-964

interlaboratory tests using on-line LC, 964-970

sample handling strategies, 930-940

liquid-liquid extractions, 931-932

liquid-solid extraction, 932-940

Organic polymers, 24

Organometallic compounds, 821

Organosoluble polymers, 283

Ovomucoids-bonded stationary phase, 675

Oxyhalides, 813-814

Oxytetracycline, 666

P

Packed-column hydrodynamic chromatography (PHDC), 138

Paclitaxel, 657

Partition equilibria, 51-52

Peptides, 720-721

Pesticides, 776-784

pH influence on retention factor and selectivity coefficient, 41–46

Pharmaceutical applications of biotechnology, 696

Phenobarbital, 632

Phenolics, 767-776, 777-783

Phenytoin, 635, 638

Phosphorus-containing anions, 815

Photodiode array (PDA) detector, 761, 765

Physicochemical measurements, 855-902

determination of equilibrium constants by HPLC, 875-881
complex stability constants, 875-878
drug-protein-binding constants, 878-881
determination of hydrophobicity by HPLC, 860-875
chromatographic hydrophobicity index, 867-873
determination of partition coefficients, 861-862
general approach, 865-867
hydrophobicity in biomedical sciences, 860-861
practical aspects, 865
theoretical background, 862-864
determination of thermodynamic parameters by HPLC, 882-885

[Physicochemical measurements]
adsorption isotherms by displacement chromatography, 883-885
temperature dependence of the retention, 882-883
Physostigmine, 658-659
Particle phases, 677
Polar-bonded-phase chromatography, 348-361
applications, 356-361
bonding reactions, 350-353
mobile-phase selection, 355-356
retention mechanisms, 353-355
Polymer analysis, 831-858

detectors for, 162-165
evaporative detectors, 163-164
light-scattering detection, 164-165
viscosity detectors, 165
separation by composition, 848-854
separation by liquid adsorption chromatography, 850-851
separation by liquid precipitation chromatography, 852
separation by other techniques, 852-854
separation mechanisms, 849-850
separation by other functions, 854-856
field-flow fractionation, 855-856

temperature-rising elution fractionation, 854-855
separation by size, 832-848
applications, 841-843
hydrophobic polymers, 848
molecular weight measurements, 833-841
separation by oligomers, 843-848
Polymer-based phases for RPLC, 312-313
Polymer-coated alumina-based phases, 316
Polymer-coated silica-based phases for RPLC, 310-312
Polymer-coated zirconia-based phases, 317
Polyols, 754

Polypeptides, hydrolysis of, 707-709
Polysaccharide separation employing CSPs, 670-673
Poly(styrene)-based phases, 385-386
Porous graphitized carbon (PGC), 22, 24
Pressure-flow relations in zone spreading, 115-118
flow in capillaries, 115-117
flow through packed columns, 117-118
Primidone, 635
Programmed analysis, 193-232
column-switching methods, 198-205
effects of the column in LC, 198-200

valve-switching options and requirements, 200-205
comparison of main programming methods, 226-230
general elution problem, 194-195
gradient elution, 205-225
gradient optimization, 214-218
gradient scouting, 218-220
gradient solvents, 220-221
instrumental aspects, 222-225
migration under gradient conditions, 206-211
theory of LSS gradients, 211-214
other programming methods, 225-226

ionic-strength programming, 226
temperature programming in LC, 225-226
place of programming analysis, 195-198
Propylene oxide, block copolymers of, 802
Proteinaceous materials in art conservation, 910-914
Proteins, 721-728, 763-767
general interest, 721-725
hydrophobic interaction chromatography of, 473-479
immunoglobulins, 725-726
membrane proteins, 726-728
preparative chromatography of, 377-381

Protein sequencing, 716-720

Pseudohalides, 813-814

Pulsed-amperometric detection (PAD), 159-160, 396-400

Pulse dampers, 517-518

Pump design for isocratic elution: constant flow rate pumps, 500-501

constant-pressure pumps, 500

flow programming, 509

reciprocating pumps, 501-508

syringe pumps, 509

Pyromellitic, 659-660

Q

Quinidine, 660

R

Radiochemical detection, 166

Reciprocating pumps, 501-508

bubbles and degassing, 508

check valves, 505-508

solvent compressibility, 503-505

Recycle chromatography, 510

Refractive index (RI) detector, 134-136, 536-537, 555
to identify lipid compounds, 759-761, 764
optical principles, 155
performance and application, 156
Refractometry, 284-285
Retention and selectivity, 1-54
chemical structure of surfaces and retention, 21-31
ion-exchange chromatography, 29-31
normal-phase LC, 26-28
reversed-phase LC, 28-29
support materials in LC, 21-26

effects of temperature on retention, 607
equations for chromatographic elient selection, 14-21
principles of distribution and adsorption, 1-14
distribution coefficients and chemical potentials in solution, 4
distribution coefficients in adsorption from solution, 4-7
retention factor and distribution coefficients, 2-3
solvation of analytes 7-14
stationary phases of special types of chromatography, 31-36
affinity chromatography, 32-33
chiral-stationary phases, 33-35
hydrophobic-interaction chromatography, 35-36

size-exclusion chromatography, 36
use of secondary chemical equilibria, 36-52
acid-base equilibria, 37-47
complexation equilibria, 47-51
partition equilibria into pseudophases, 51-52
Reversed-phase stationary phases, 28-29, 293-323
additional reversed-phase supports and stationary phases, 317
carbon-based phases, 314
chemically bonded silica based phases, 298-310
characterization techniques, 306-310
monomeric stationary phases, 299-302

polymeric stationary phase, 302
selectivities of monomeric and polymeric phases, 303-308
metal oxide supports other than silica, 314-317
chemically bonded alumina-based phases, 315
polymer-coated alumina-based phases, 316
zirconia- and titania-based phases, 316-317
polymer-based phases, 312-313
polymer-coated silica-based phases, 310-312
silica, 293-298
Ribonucleosides, large, 733-734
Rivastatin, 661

R023-9424, 660-661

S

Saccharides, 754

SCE-2787 (cefozopran), 661-662

Secondary chemical equilibria, 36-52

acid-base equilibria, 37-47

complexation equilibria, 47-51

partition equilibria into pseudophases, 51-52

Selectivity (*See* Retention and selectivity)

Selenium anions, 815-816

Self-regenerating suppressor, 427-430

Serpentine tubes, low-dispersion, 383-385
Serum albumin phases, 675
Silica (*See also* Chemically bonded silica-based phases)
for adsorption chromatography stationary phases, 325-327
for ion-exchange chromatography stationary phases, 389-390
for RPLC stationary phases, 293-298
silica gel, 22, 23-24
Simvastatin, 662-663
Single-wavelength detector, 148-149
Size exclusion chromatography (SEC), 272-292, 831, 832-848
applications, 274-275, 841-843

band broadening, 281
calibration, 277-281
broad-molecular weight calibration, 279
primary calibration, 278
secondary calibration, 279
universal calibration, 279-281
column selection, 282-283
detection, 284-289
composition detectors, 285-287
concentration detectors, 284-285
molecular-weight-sensitive detectors, 287-289

[Size exclusion chromatography (SEC)]
hydrophobic polymers, 848
kinetic optimization of, 136-138
mobile selection, 282-284
organosoluble polymers, 283
water-soluble polymers, 283-284
molecular weight measurements, 275-276, 833-841
packing characteristics, 282
resolution, 281-282
separation by oligomers, 843-848
separation mechanism, 276-277

solute concentration effects, 284

stationary phases for, 36

study of degradation and polymerization reactions with, 914-918

system evaluation, 284

Small-volume sample injection, 366-368

Snyder-Soczewkinski retention model, 327-329

Solubility parameter model, 9-11

Solute property detectors, 539-554

electrochemical detector, 550-551

fluorescence detectors, 547-550

light-scattering detector, 551-552

trident multifunctional detector, 532-534

UV detectors, 540-547

Starches, 754

Stationary phases:

effects of temperature on, 608

for HIC, 465-472

for ion-exchange chromatography, 29-31

for ion interaction chromatography, 456

Sugars, 755-757, 817

Sulfamethazine, 663-664

Sulfur-containing anions, 814-815

Supercritical fluid chromatography (SFC), kinetic optimization of, 134-136

Support materials in LC, 21-26

inorganic materials, 24

modification of support materials, 24-26

organic polymers, 24

physical parameters, 22

silica gels, 23-24

Suppressed ion chromatography, 419-439

eluents in suppression ion chromatography, 430-434

hollow-fiber membrane suppressor, 423-424

ion-exchange column suppression, 419-423

micromembrane suppression, 424-427
other suppression applications, 438-439
other suppression techniques, 434-437
postsuppression strategies, 437-438
self-regenerating suppression, 427-430
Surfactants, 789-904
ionic surfactants, 790-798
amphoteric surfactants, 796-798
anionic surfactants, 790-795
cationic surfactants, 795
general principles, 790

nonionic surfactants, 799-802

analysis of individual nonionic surfactants, 800-802

general principles, 799-800

Synthetic dyestuffs, identification of, 905-909

Synthetic oligodeoxyribonucleotides, 729-731

Synthetic oligoribonucleotides, 731-732

Syringe pumps, 209

T

Tandem LC systems, 581-606

LC-mass spectrometry systems, 585-596

atmospheric ionization interface, 591-593

electrospray interface, 388-391
laser desorption mass spectrometry, 593-596
thermospray interface, 587-589
transport interface, 586-587
low-dispersion connecting tubes, 582-585
serpentine tubes, 583-585
other tandem LC systems, 596-604
LC-atomic absorption spectroscopy systems, 596-600
LC-infrared, 600-602
LC-nuclear magnetic resonance systems, 602-604, 605
Tellurium anions, 815-816

Temperature control, 607-615
detector performance and, 609-610
devices for, 610-611
effects of temperature
on analysis confirmation, 609
on column efficiency, 608
in on-line reactors, 610
on retention, 607
on the stationary phase, 608
on viscosity, 608
examples of temperature effects, 612-613

Temperature programming in LC, 225-226

Temperature-rising elution fractionation (TrEF), 226, 831, 854-855
Tentacle ion-exchange phases, 388-389
Testosterone-related compounds, 664-665
Tetracycline, 666
Textiles, applications of biotechnology for, 696
Theophylline, 648
Thermodynamic parameters, determination of, 882-885
  adsorption isotherms by displacement chromatography, 883-885
  temperature dependence of the retention, 882-883
Thiophilic adsorption, 496
Tissues, 316-317

in adsorption chromatography, 327
Transition metals, 819-820
Trident multifunctional detector, 552-554
Tungstate, 816
U
Ultraviolet (UV) detectors, 540-547, 553
diode-array detector, 544-547
fixed-wavelength detector, 540-543
to identify lipid compounds, 738, 739
variable-wavelength detector, 543-544
Ultraviolet (UV) spectrophotometry, 285, 286

UV-vis absorbance detector, 147-150
multiple wavelength absorbance detection, 149-150
single- and variable-wavelength detectors, 148-149
Underivatized amino acids, detection of, 709
Univariate data analysis, computer-assisted, 260-263
V
Valve-switching options and requirements, 200-205
backflush, 202
comprehensive two-dimensional chromatography, 204-205
cutting, 200-202
multivalve configuration, 202-204

Variable-wavelength detector, 148-149, 543-544

Viral proteins, 728

Viscosity, effects of temperature on, 608

Viscosity detector, 165

Vitamins, 761-762, 763, 768-774

W

Water, organic pollutants in, 922-974

conventional detectors, 940-964

LC with diode-array detection analysis, 940-941

LC with electrochemical detection, 941-944

LC with fluorescence detection, 945

LC with mass spectrometric analysis, 945-964
interlaboratory tests using on-line LC, 964-970
sample handing strategies, 930-940
liquid-liquid extractions, 931-932
liquid-solid extraction, 932-940
Water-soluble polymers, 283-284
Z
Zidovudine, 666
Zirconia, 316-317
in adsorption chromatography, 327
Zone spreading, 35-142

flow phenomena and compressibility effects, 113-121
compressibility effects on flow and plate height, 118-120
electrodrive and electrokinetic chromatography, 120-121
pressure flow relations, 113-118
measures of efficiency, 26-113
broadening and peak shape from nonideal and extracolumn processes, 107-113
mechanisms of zone-broadening, 69-107
peak shape, 56-59
random-walk processes, variance, diffusion, and plate height, 61-66
resolution and peak capacity, 66-69
theoretical plate concept, 59-61

optimization, 122-140

kinetic optimization, 123-133

kinetic optimization of separation methods for macromolecules, 133-140